ASPECTS OF COORDINATION CHEMISTRY

FRANK RICHARD KEENE

BSc (Hons I), PhD (University of Adelaide), FRACI

Submission to Faculty of Science, University of Adelaide

for the degree of

DOCTOR OF SCIENCE

March 1998

DEDICATED

To

Cheryl

Graeme

Tom

and all my postdocs and students

TABLE OF CONTENTS

DECLARATION

This submission contains material which arises from original research in which I have been involved or have supervised. As it comprises a compilation of published papers, the other contributors are acknowledged therein as co-authors. Unless specified, the submission contains no material which has been accepted for the award to me of any other degree.

I give consent to this copy of my submission, when deposited in the University Library, being available for loan and photocopying.

F. Richard Keene
March 9, 1998.

ABSTRACT

My early research activities included aspects of stereochemistry, electron transfer and ligand reactivity in transition metal complexes. These interests developed subsequently in my own research group (on occasions in collaboration with other groups), and were extended and combined with electrochemical and photochemical studies. *Inter alia,* three particularly significant contributions are noted:

- the elucidation of the mechanism of oxidation of ligands to ruthenium(II) and osmium(II) centres, and the establishment of two-electron processes resulting from the lowering of redox potential by deprotonation;
- the structural and bonding characteristics of complexes of tripodal ligands; and
- the establishment of techniques for control of the stereochemistry of polymetallic supramolecular assemblies, and the demonstration of a spatial dependence of intramolecular electron- and energy-transfer processes within such assemblies.

A majority of the publications that form the basis of this thesis have appeared in prestigious journals (such as *Journal of the American Chemical Society, Inorganic Chemistry* and *Journal of the Chemical Society, Dalton Transactions*).

ACKNOWLEDGMENTS

Over my career, there a number of people to whom I am indebted for various reasons. Firstly, my PhD supervisor (Graeme Searle) for his selfless dedication as a scientist and a teacher, and secondly my two postdoctoral supervisors (Alan Sargeson and Tom Meyer) for their continuing inspiration, counsel and humour.

I have had a number of valued collaborators over my research career and they are acknowledged in the Discourse section of this thesis, but I would particularly thank Tom Meyer and Alex von Zelewsky for their continued interest and for many stimulating scientific conversations. And although he and I have never actually done collaborative research together, I would like to thank my long-term inorganic colleague at James Cook University, Len Lindoy, for support.

It is a special pleasure to acknowledge and sincerely thank the members of my research group at JCUNQ over 20 years, who have have provided such valuable intellectual input and experimental skills to the various programs we have undertaken together. I have been privileged to work with you all: my postdoctoral fellows (Drs Nigel Surridge, Klaus Haarmann, Erik Jandrasics, Nick Fletcher, and Brett Yeomans), postgraduate students (Michael Ridd, Geoff Whebell, Ian Atkinson, Timo Karaiste, Jiaxiong Wang, Peter Anderson, Maria Pappalardo, Todd Rutherford, Laurie Kelso, and David Reitsma), Honours students (most of the the postgraduates above, plus Peter Adcock, David Gakowski, Tracy Hafeli, Toni Wright, Austin Schultz, Michael Quagliotto, and Brad Patterson), and a Research Assistant (Philip Stephenson).

And most of all I thank my wife Cheryl for her unstinting love and faith.

Listing of publications in journals and monographs

(Contribution given as percentage in parenthesis for each publication)

Stereochemical Studies of Cobalt(III) Complexes of Amine Ligands

NOT INCLUDED IN DSc APPLICATION - publications arising from postgraduate studies

1. "Geometric and Optical Isomers of the Bis(diethylenetriamine)cobalt(III) Ion", F.R. Keene, G.H. Searle, A. Imai, K. Yamasaki, and Y. Yoshikawa, *Chem. Commun.*, 784-786 (1970).

2. "The Circular Dichroism and the Chirality of the Unsymmetric-*cis*- and $(+)_D$-*trans*-Bis(diethylenetriamine)cobalt(III) Ion", F.R. Keene, S.F.Mason, and G.H. Searle, *Chem. Commun.*, 893- 894 (1970).

3. "The Isomers of the Bis(diethylenetriamine)cobalt(III) Ion and a New Source of Optical Activity", F.R. Keene and G.H. Searle, *Inorg. Chem.*, **11**, 148-156 (1972).

4. "Racemization and Hydrogen Exchange in the *trans*-Bis(diethylenetriamine)cobalt(III) Ion", G.H. Searle and F.R. Keene, *Inorg. Chem.*, **11**, 1006-1011 (1972).

5. " Isomers of the Bis(diethylenetriamine)cobalt(III) Cation. Dependence of Equilibrium Isomer Proportions on Environmental Parameters", F.R. Keene and G.H. Searle, *Inorg. Chem.*, **13**, 2173-2180 (1974). [70%]

6. "The Synthesis of 4,7-Dimethyltriethylenetetramine", G.H. Searle, M. Petkovic, and F.R. Keene, *Aust. J. Chem.*, **25**, 2045-2048 (1972). [30%]

7. "Cobalt(III) Complexes of 4,7-Dimethyl-1,4,7,10-tetraazadecane. Preparations, Stereochemistry, and Reactions and the Effect of N-Methylation on Relative Isomer Stabilities", G.H. Searle, M. Petkovic, and F.R. Keene, *Inorg. Chem.*, **13**, 399-408 (1974). [30%]

8. "Bis(tridentate)cobalt(III) Complexes with Diethylenetriamine and 2,2'-Methyliminodi(ethylamine) [2,2'-Methyliminodi(ethylamine]: Assignment of Geometric Configurations by ^1H and ^{13}C NMR Spectroscopy", G.H. Searle, S.F. Lincoln, F.R. Keene, S.G. Teague, and D.G. Rowe, *Aust. J. Chem.*, **30**, 1221-1228 (1977). [20%]

9. "Homogeneous and Charcoal-Catalyzed Isomerizations of the (Diethylenetriamine)(methyldiethylenetriamine)cobalt(III) and Bis(diethylenetriamine)cobalt(III) Ions", G.H. Searle, F.R. Keene, and S.F. Lincoln, *Inorg. Chem.*, **17**, 2362-2369 (1978). [30%]

10. "Polarographic Studies of the Geometric Isomers of the Bis(diethylenetriamine)cobalt(III) and -cobalt(II) Cations in Acetone", A.M. Bond, F.R. Keene, N.W. Rumble, G.H. Searle, and M.R. Snow, *Inorg. Chem.*, **17**, 2847-2853 (1978). [30%]

11. "Isomers of the Bis(1,4,7-triazacyclodecane)cobalt(III) Ion, and the Occurrence of Higher Cyclic and Non-Cyclic Amines in the Richman-Atkins Synthesis for Cyclic Amines", M.E. Angley, M. Dwyer, S.F. Lincoln, G.H. Searle, R.J. Geue, and F.R. Keene, *Inorg. Chim. Acta* , **45**, L91-L93 (1980). [30%]

12. "Pressure Studies on the Intramolecular Isomerization Reactions of (Diethylenetriamine)(methyldiethylenetriamine)cobalt(III) and Bis(diethylenetriamine)cobalt(III) Cations", F.R. Keene, I.A.S. McDonald, and G.H. Searle, *Aust. J. Chem.*, **34**, 1331-1335 (1981). [90%]

13. "Cobalt(III) Complexes with N-Methylethane-1,2-diamine (meen). Synthesis and Characterization of the Isomers of $[Co(meen)_3]^{3+}$, $[Co(meen)_2(en)]^{3+}$ and $[Co(meen)(en)_2]^{3+}$", G.H. Searle and F.R. Keene, *Inorg. Chim. Acta,* **155**, 125-138 (1989). [30%]

14. "Conformational Analyses of the Isomers of the $[Co\{(\pm)pn\}_n(en)_{3-n}]^{3+}$ Systems: A Re-Investigation (en = ethane-1,2-diamine; pn = propane-1,2-diamine; n = 0-3)", I.M. Atkinson, F.R. Keene, and G.H. Searle, *J. Mol. Struct.*, **240**, 313-329 (1990). [90%]

15. "Conformational Analyses of the Isomers of the $[Co(men)_n(en)_{3-n}]^{3+}$ Systems (men = N-methylethane-1,2-diamine, en = ethane-1,2-diamine; n = 1-3)", I.M. Atkinson, F.R. Keene, and G.H. Searle, *J. Chem. Soc., Dalton Trans.*, 45-51 (1991). [90%]

16. "A Molecular Mechanics Analysis of $[Co(medien)_n(dien)_{2-n}]^{3+}\{n = 0\text{-}2\}$ (dien = diethylenetriamine or 1,5-diamino-3-azapentane; medien = 3-methyl-1,5-diamino-3-azapentane), and X-ray Structural Studies of the *mer-* and *s-fac*-$[Co(medien)(dien)]^{3+}$ Cations", I.M. Atkinson, F.R. Keene, J.M. Gulbis, G.H. Searle, and E.R.T. Tiekink, *J. Mol. Struct.*, **265**, 189-213 (1992). [80%]

17. "Structure of the Stable Isomer of the Bis(ethane-1,2-diamine)(*N*-methylethane-1,2-diamine)cobalt(III) Cation, $[Co(meen)(en)_2]^{3+}$", G.H. Searle, E.R.T. Tiekink, I.M. Atkinson, and F.R. Keene, *Acta Cryst., C, Struct. Commun.*, **C49**, 13-16 (1993). [50%]

Studies of Ligand Reactivity

18. "The Base Hydrolysis of Coordinated Acetonitrile", D.A. Buckingham, F.R. Keene, and A.M. Sargeson, *J. Am. Chem. Soc.*, **95**, 5649-5652 (1973). [50%]

19. "Reactivity of Coordinated Nitriles", I.I. Creaser, J. McB. Harrowfield, F.R. Keene, and A.M. Sargeson, *J. Am. Chem. Soc.*, **103**, 3559-3564 (1981). [30%]

20. "Facile Intramolecular Hydrolysis of Dipeptides and Glycinamide", D.A. Buckingham, F.R. Keene, and A.M. Sargeson, *J. Am. Chem. Soc.*, **96**, 4981-4983 (1974). [50%]

21. "Intramolecular Hydrolysis of Glycinamide and Glycine Dipeptides Coordinated to Cobalt(III). Part I: Hg^{2+}, HOCl and Base Hydrolysis of the *cis*-$[Co(en)_2Br(glyNHR)]^{2+}$ Ions (R = H, $CH_2CO_2C_3H_7$, $CH_2CO_2^-$) and the Properties of *cis*- and *trans*-$[Co(en)_2(OH_2/OH)(glyNHR)]^{3+/2+}$", C.J. Boreham, D.A. Buckingham, and F.R. Keene, *Inorg. Chem.*, **18**, 28-38 (1979). [30%]

22. "Intramolecular Hydrolysis of Glycinamide and Glycine Dipeptides Coordinated to Cobalt(III). Part II: The Reactions of the *cis*- $[Co(en)_2(OH_2/OH)(glyNHR)]^{3+/2+}$ Ions (R = H, $CH_2CO_2C_3H_7$, $CH_2CO_2^-$) and the Effect of Buffer Species", C.J. Boreham, D.A. Buckingham, and F.R. Keene, *J. Am. Chem. Soc.*, **101**, 1409-1421 (1979). [30%]

23. "Oxidation of Coordinated Diamines in Bis(2,2'-bipyridine) Complexes of Ruthenium", G.M. Brown, T.R. Weaver, F.R. Keene, and T.J. Meyer, *Inorg. Chem.*, **15**, 190-196 (1976). [30%]

24. "Oxidation of Primary Amines Bound to Bis(2,2'-bipyridine)ruthenium(II)", F.R. Keene, D.J. Salmon, and T.J. Meyer, *J. Am. Chem. Soc.*, **98**, 1884-1889 (1976). [70%]

25. "Mechanism of Oxidation of an Amine Coordinated to Ruthenium", M.J. Ridd and F.R. Keene, *J. Am. Chem. Soc.*, **103**, 5733-5740 (1981). [100%]

26. "Oxidation of Isopropylamine Coordinated to Ruthenium", P.A. Adcock and F.R. Keene, *J. Am. Chem. Soc.*, **103**, 6494-6495 (1981). [100%]

27. "Investigations of the Nature of Dehydrogenation of the α-Carbon Atom in the Oxidation of Amines Coordinated to Ruthenium", F.R. Keene, M.J. Ridd, and M.R. Snow, *J. Am. Chem. Soc.*, **105**, 7075-7081 (1983). [90%]

28. "Oxidation of Isopropylamine and Related Amines Coordinated to Ruthenium. Formation of Monodentate Imine and Alkylideneamido Complexes of Ruthenium", P.A. Adcock, F.R. Keene, R.S. Smythe, and M.R. Snow, *Inorg. Chem.*, **23**, 2336-2343 (1984). [90%]

29. "Stabilization of Simple Imines by Coordination to Ruthenium(II), and Aspects of their Reactivity", G.W. Whebell and F.R. Keene, *Aust. J. Chem.*, **39**, 2027-2035 (1986). [100%]

30. "Mechanism of Oxidative Dehydrogenation of Alcohols Coordinated to Ruthenium", M.J. Ridd, D.J. Gakowski, G.R. Sneddon, and F.R. Keene, *J. Chem. Soc., Dalton Trans.*, 1949-1956 (1992). [80%]

31. "Mechanism of Oxidative Dehydrogenation of an Amine Coordinated to Osmium(II)", F.R. Keene, P.A. Lay, G.E. Sneddon, and G.W. Whebell, *Aust. J. Chem.*, **46**, 1763-1774 (1993). [80%]

32. "Disproportionation at the Ligand in Nitro Complexes of Ruthenium(III)", F.R. Keene, D.J. Salmon, and T.J. Meyer, *J. Am. Chem. Soc.*, **99**, 2384-2387 (1977). [60%]

33. "Nitro Complexes of Ruthenium(III) as Oxidation Catalysts. Chemically-Catalyzed Net Electrochemical Oxidation of Triphenylphosphine", F.R. Keene, D.J. Salmon, and T.J. Meyer, *J. Am. Chem. Soc.*, **99**, 4821-4822 (1977). [60%]

34. "Oxidation of the Ligand in Nitro Complexes of Ruthenium(III)", F.R. Keene, D.J. Salmon, J.L. Walsh, H.D. Abruna, and T.J. Meyer, *Inorg. Chem.*, **19**, 1896-1903 (1980). [40%]

Studies of Bonding, Structure, and Electron Transfer in Transition Metal Complexes and Electropolymerized Films

35. "Intervalence Transfer and Electron Transfer in the Mixed-Valence Ion $[(bpy)_2ClRu(pyz)RuCl(bpy)_2]^{3+}$", R.W.Callahan, F.R. Keene, T.J. Meyer, and D.J. Salmon, *J. Am. Chem. Soc.*, **99**, 1064-1073 (1977). [30%]

36. "Measurement of Rates of Electron Exchange between $Ru(bpy)_3^{3+}$ and $Fe(phen)_3^{2+}$, and between $Ru(phen)_3^{3+}$ and $Ru(bpy)_3^{2+}$ by Differential Excitation Flash Photolysis", R.C. Young, F.R. Keene, and T.J. Meyer, *J. Am. Chem. Soc.*, **99**, 2468-2473 (1977). [60%]

37. "Coordination Mode of Tris(2-pyridyl)carbinol to Cobalt(III): Crystal Structure of $Li[Co\{(2\text{-}py)_3COH\}_2](S_2O_6)_2.10H_2O$", D.J. Szalda and F.R. Keene, *Inorg. Chem.*, **25**, 2795-2799 (1986). [90%]

38. "Mode of Coordination of Tris(2-pyridyl)methanol to Ruthenium(II): Synthetic, Spectral and Stuctural Studies of the Bis(Ligand) Species", F.R. Keene, D.J. Szalda, and T.A. Wilson, *Inorg. Chem.*, **26**, 2211-2216 (1987). [90%]

39. "Tris(2-pyridyl)phosphine", F.R. Keene, M.R. Snow, and E.R.T. Tiekink, *Acta Cryst., C, Struct. Commun.*, **C44**, 757-758 (1988). [50%]

40. "Tris(2-pyridyl)methanol", F.R. Keene, M.R. Snow, and E.R.T. Tiekink, *Acta Cryst., C, Struct. Commun.*, **C44**, 937-938 (1988). [50%]

41. "Ruthenium(II) Complexes of C_{3v} Ligands Tris(2-pyridyl)amine, Tris(2-pyridyl)methane, and Tris(2-pyridyl)phosphine. 1. Synthesis and X-Ray Structural Studies of the Bis(ligand) Complexes", F.R. Keene, P.J. Stephenson, M.R. Snow, and E.R.T. Tiekink, *Inorg. Chem.*, **27**, 2040-2045 (1988). [90%]

42. "Synthetic and Characterization Studies of the Complexes $[Ru(NH_3)_3(Py_3X)]^{2+}$ (Py = 2-pyridyl; X = N, CH, COH, P) and the X-Ray Crystal Structure of $[Ru(NH_3)_3(Py_3COH\}]Br_2.H_2O$", P.S. Moritz, A.A. Diamantis, F.R. Keene, M.R. Snow, and E.R.T. Tiekink, *Aust. J. Chem. (invited contibution to D.R. Stranks Memorial issue),* **41**, 1353-1360 (1988). [40%]

43. "Stabilization of Cobalt(I) by Tripodal π-Acceptor Ligands Py_3X (Py = 2-pyridyl; X = N, CH, COH, P, P=O), and Preliminary Studies on the Reaction of Water and Carbon Dioxide with the Bis(ligand)cobalt(I) Complexes", T.A. Hafeli and F.R. Keene, *Aust. J. Chem. (invited contibution to D.R. Stranks Memorial issue),* **41**, 1379-1388 (1988). [100%]

44. "Tri(2-pyridyl)methane", F.R. Keene and E.R.T. Tiekink, *Acta Cryst., C, Struct. Commun.*, **C46**, 1562-1563 (1990). [50%]

45. "Ambidentate Coordination of the Tripyridyl Ligands 2,2':6',2"-Terpyridyl, Tris(2-pyridyl)amine, Tris(2-pyridyl)methane, and Tris(2-pyridyl)phosphine to Carbonylrhenium Centres: Structural and Spectroscopic Studies", P.A. Anderson, F. R. Keene, E. Horn, and E.R.T. Tiekink, *Appl. Organometallic Chem.,* **4**, 523-533 (1990). {Invited contribution}. [90%]

46. "Coordination of Bis(2-pyridyl)phosphinic Acid as a Tridentate Ligand. Crystal Structure of the {Bis(2-pyridyl)phosphinato}{tris(2-pyridyl)phosphine oxide}ruthenium(II) Cation, $[Ru\{py_2P(O)O\}\{py_3PO\}]BF_4{\cdot}2H_2O$", F.R. Keene, P.J. Stephenson, and E.R.T.Tiekink, *Inorg. Chim. Acta,* **187**, 217-220 (1991). [90%]

47. "Crystal Structure of Bis(nitrato)bis(tripyridylamine}copper(II), $C_{30}H_{24}CuN_{10}O_6$", P.A. Anderson, J.M. Gulbis, F.R. Keene, and E.R.T. Tiekink, *Z. Kristall.,* **206**, 275-278 (1993). [50%]

48. "Extended X-Ray Absorption Fine Structure, Crystal Structures at 295 and 173K, and Electron Paramagnetic Resonance and Electronic Spectra of Bis{tris(2-pyridyl)methane}copper(II) Dinitrate", T. Astley, P.J. Ellis, H.C. Freeman, M.A. Hitchman, F.R. Keene, and E.R.T. Tiekink, *J. Chem. Soc., Dalton Trans.,* 595-601 (1995). [25%]

49. "Crystal Structures and Electron Paramagnetic Resonance Spectra of $[Cu\{(C_5H_4)_3P\}_2]Br_2.8H_2O$ and Cu^{2+}-doped $[Zn\{(C_5H_4)_3P\}_2]Br_2.8H_2O$, Examples of a Dynamic Jahn-Teller Effect in Two Dimensions", T. Astley, H. Headlam, M.A. Hitchman, F.R. Keene, J. Pilbrow, Y. Zhong, and E.R.T. Tiekink, *J. Chem. Soc., Dalton Trans.,* 3809-3818 (1995). [50%]

50. "Structural, Spectroscopic and Angular-Overlap Studies of Tripodal Pyridine Ligands with Nickel(II) and Zinc(II)", T. Astley, M.A. Hitchman, F.R. Keene, and E.R.T. Tiekink, *J. Chem. Soc., Dalton Trans.*, 1845-1851 (1996). [40%]

51. "Stablization of Cobalt(I) by the Tripodal Ligands Tris(2-pyridyl)methane and Tris(2-pyridyl)phosphine. Structural, Spectroscopic and *Ab Initio* Studies of the $[CoL_2]^{n+}$ Species", K.R. Adam, P.A. Anderson, T. Astley, I.M. Atkinson, J.M. Charnock, C.D. Garner, T.W. Hambley, M.A. Hitchman, F.R. Keene, and E.R.T. Tiekink, *J. Chem. Soc., Dalton Trans.,* 519-530 (1997). [70%]

52. "Crystal Structure of Bis[tris(2-pyrazol-1-yl)methane]cobalt(II) nitrate (redetermination at 173K), $C_{20}H_{20}CoN_{14}O_6$", F.R. Keene, and E.R.T. Tiekink, *Z. Kristall.,* **209**, 548-549 (1994). [50%]

53. "Reduction of Carbon Dioxide by Tris(2,2'-bipyridine)cobalt(I)", F.R. Keene, C. Creutz, and N. Sutin, *Coord. Chem. Rev.*, **64**, 247-260 (1985). [60%]

54. "Thermodynamic, Kinetic and Product Considerations in Carbon Dioxide Reactivity", F.R. Keene, Chapter 1 in monograph *"Electrochemical and Electrocatalytic Reactions of Carbon Dioxide"* (B.P. Sullivan, K. Krist, and H.E. Guard, eds.); Elsevier (Amsterdam), 1993. [100%]

55. "Mechanisms of the Electrochemical Reduction of Carbon Dioxide Catalyzed by Transition Metal Complexes", F.R. Keene and B.P. Sullivan, Chapter 5 in monograph *"Electrochemical and Electrocatalytic Reactions of Carbon Dioxide"* (B.P. Sullivan, K. Krist, and H.E. Guard, eds.); Elsevier (Amsterdam), 1993. [50%]

56. "Reduction of Terminal Alkynes Mediated by Tris(2,2'-bipyridine)cobalt(I)", D.A. Reitsma and F.R. Keene, *Organometallics,* 13, 1351-1354 (1994). [100%]

57. "Site Dilution of Osmium Polypyridine Complexes in Three Electron Hopping-Conductive Polymer Films on Electrodes by Electrochemical Copolymerization of Osmium with Ruthenium and with Zinc Complexes", N.A. Surridge, F.R. Keene, B.A. White, J.S. Facci, M. Silver, and R.W. Murray, *Inorg. Chem.*, **29**, 4950-4955 (1990). [30%]

58. "Effects of Mixed-Valent Composition and Bathing Environment on Solid-State Electron Self-Exchanges in Osmium Bipyridine Redox Polymer Films", N.A. Surridge, M.E. Zvanut, F.R. Keene, C.S. Sosnoff, M. Silver, and R.W. Murray, *J. Phys. Chem.*, **96**, 962-970 (1992). [20%]

59. "Synthesis of 4-[ω-(3-thienyl)alkyl]pyridines and 4-[ω-(3-thienyl)alkyl]-2,2'-bipyridines", J. Wang, M. Pappalardo, and F.R. Keene, *Aust. J. Chem.*, **48**, 1425-1436 (1995). [100%]

60. "Electrochemical Properties of Poly-[3-(ω-4-pyridylalkyl)thiophenes]", J. Wang and F. R. Keene, *J. Electroanal. Chem.*, **405**, 59-70 (1996). [100%]

61. "Synthesis and Electrochemical Properties of Poly-[3-{ω-[4-(2,2'-bipyridyl)]alkyl}thiophenes], P{B(n)T}, and of Poly-[Ru(II){B(n)T}$_3^{2+}$], J. Wang and F.R. Keene, *J. Electroanal. Chem.*, **405**, 71-83 (1996). [100%]

62. "Mechanism of Mediation of the Electrocatalytic Oxidation of $K_4Fe(CN)_6$ at Poly-[*tris*-(3-{ω-[4-(2,2'-bipyridyl)]alkyl}thiophene)]iron(II)-Film Modified Electrodes in Aqueous Solutions", J. Wang and F.R. Keene, *Electrochim. Acta,* **41**, 2563-2569 (1996). [100%]

Spectroscopy of Laser Desorbed Molecules

63. "CO_2-Laser Desorption and Multiphoton Ionization of Tris(2,2'-bypyridyl)ruthenium", R. Beavis, J. Lindner, J. Grotemeyer, I.M. Atkinson, F.R. Keene, and A.E.W. Knight, *J. Am. Chem. Soc.*, **110**, 7534-7535 (1988). [40%]

64. "Low Fragmentation Laser Desorption of Thermally Labile Molecules", I.M. Atkinson, J.A. Shorter, R.T.T. Karaiste, F.R. Keene, J.I. Steinfeld, and A.E.W. Knight, *Materials Research Society, Conference Proceedings,* **201** (Surface Chemistry. Beam-Solid Interactions), 459-461 (1991). [50%]

65. "Molecular Beam Spectroscopy of Molecules with Low Volatility via Laser Desorption from Thin Films containing Particulate Silver", R.T.T. Karaiste, I.M. Atkinson, J.A. Shorter, A.E.W. Knight, and F.R. Keene, *Anal. Chem.*, **65**, 2776-2783 (1993). [60%]

Artificial Photosynthesis

66. "Synthesis of Polypyridyl Complexes of Ruthenium(II) Containing Three Different Bidentate Ligands", G.F. Strouse, P.A. Anderson, J.R. Schoonover, T .J. Meyer, and F.R. Keene, *Inorg. Chem.*, **31**, 3004-3006 (1992). [80%]

67. "Diastereoisomeric Forms of Ligand-Bridged Dimetallic Diruthenium(II) and Ruthenium(II)-Osmium(II) Species Containing Bidentate Polypyridyl Ligands", D.A. Reitsma and F.R. Keene, *J. Chem. Soc., Dalton Trans.*, 2859-2860 (1993). [100%]

68. "Black MLCT Absorbers", P.A. Anderson, G.F. Strouse, J.A. Treadway, F.R. Keene, and T.J. Meyer, *Inorg. Chem.*, **33**, 3863-3864 (1994). [50%]

69. "Stereochemistry in Tris(bidentate)ruthenium(II) Complexes containing Unsymmetrical Polypyridyl Ligands", T.J. Rutherford, D.A. Reitsma, and F.R. Keene, *J. Chem. Soc., Dalton Trans.*, 3659-3666 (1994). [100%]

70. "Chiral $[Ru(pp)_2(CO)_2]^{2+}$ Species (pp = Bidentate Polypyridyl Ligand) and their Use in the Stereoselective Synthesis of Ligand-Bridged Dinuclear Complexes", T.J. Rutherford, M.G. Quagliotto and F.R. Keene, *Inorg. Chem.*, **34**, 3857-3858 (1995). [100%]

71. "Designed Synthesis of Mononuclear Tris(Heteroleptic) Ruthenium Complexes containing Bidentate Polypyridyl Ligands", P.A. Anderson, G.B. Deacon, K.H. Haarmann, F.R. Keene, T.J. Meyer, D.A. Reitsma, B.W. Skelton, G.F. Strouse, N.C. Thomas, J.A. Treadway, and A.H. White, *Inorg. Chem.*, **34**, 6145-6157 (1995). [90%]

72. "Effect of Delocalization and Rigidity in the Acceptor Ligand on MLCT Excited-State Decay", J.A. Treadway, B. Loeb, R. Lopez, P.A. Anderson, F.R. Keene, and T.J. Meyer, *Inorg. Chem.*, **35**, 2242-2246 (1996). [30%]

73. "Spectral and Electrochemical Properties of the Diastereoisomeric Forms of Azobis(2-pyridine)-Bridged Diruthenium Species", L.S. Kelso, D.A. Reitsma, and F.R. Keene, *Inorg. Chem.*, **35**, 5144-5153 (1996). [100%]

74. "Preparation of 7,8-Diazaphencyclone and its Use in the Construction of Rigid, Space-Separated 1,10-Phenanthroline Donor-Acceptor Systems: New ligands for Metal Complexation", R.N. Warrener, M.A. Houghton, A.C. Schultz, F.R. Keene, L.S. Kelso, R. Dash, and D. N. Butler, *Chem. Commun.*, 1151-1152 (1996). [30%]

75. "Space-Separated 1,10-Phenanthroline, 4,5-Diazafluorene or 3,6-Di(2-pyridyl)pyridazine Units as Ligands in Diruthenium Complexes: Preliminary Studies of Metal-Metal Interactions", R.N. Warrener, A.B.B. Ferreira, A.C. Schultz, D.N. Butler, F.R. Keene, and L.S. Kelso, *Angew. Chem. Int. Ed. Engl.*, **35**, 2485-2487 (1996). [30%]

76. "Synthesis of and Properties of Mononuclear Tris(Heteroleptic) Osmium(II) Complexes containing Bidentate Polypyridyl Ligands", E.Z. Jandrasics and F.R. Keene, *J. Chem. Soc., Dalton Trans.*, 153-159 (1997). [100%]

77. "Stereochemistry and Polymetallic Ligand-Bridged Molecular Assemblies", F.R. Keene, *Coord. Chem. Rev.*, **166**, 121-159 (1997). *(Invited contribution).* [100%]

78. "The Synthesis and Characterization of New Optically Active 'Dimeric' 'Pineno'-[4,5]-Fused 2.2'-Bipyridines Linked without a Spacer or by Small Spacer Groups", N.C. Fletcher, F.R. Keene, M. Ziegler, H. Stoeckli-Evans, H. Viebrock, and A. von Zelewsky, *Helv. Chim. Acta*, **79**, 1192-1202 (1996). [20%]

79. "Molecular Architecture of Polynuclear Ruthenium Bipyridyl Complexes with Controlled Metal Helicity", N.C. Fletcher, F. R. Keene, H. Viebrock, and A. von Zelewsky, *Inorg. Chem.*, **36**, 1113-1121 (1997). [20%]

80. "Isolation of the stereoisomers of $[\{Ru(bpy)_2\}_2\{Os(bpy)_2\}(\mu\text{-HAT})]^{6+}$ (HAT = 1,4,5,8,9,12-hexaazatriphenylene; bpy = 2,2'-bipyridine)", T.J. Rutherford and F.R. Keene, *Inorg. Chem.*, **36**, 3580-3581 (1997). [100%]

81. "Stereoisomers of Mono-, Di- and Tri-ruthenium(II) Complexes Containing the Bridging Ligand 1,4,5,8,9,12-Hexaazatriphenylene (HAT), and Studies of their Photophysical and Redox Properties", T.J. Rutherford, O. Van Gijte, A. Kirsch - De Mesmaeker, and F.R. Keene, *Inorg. Chem.*, **36**, 4465-4474 (1997). [80%]

82. "Stereochemical Control of Donor and Acceptor Groups in a Monomeric Chromophore-Quencher Complex of Ruthenium(II)", T.J. Rutherford and F.R. Keene, *Inorg. Chem.*, **36**, 2872-2878 (1997). [100%]

83. "Mapping Electron Transfer Pathways in a Chromophoric-Quencher Triad", J.A. Treadway, T.J. Rutherford, P. Chen, F.R. Keene, and T.J. Meyer, *J. Phys. Chem. A*, **101**, 6824-6826 (1997). [30%]

84. "Chromatographic Separation of Stereoisomers of Dinuclear Ligand-Bridged Polypyridyl Complexes of Ruthenium(II)", N.C. Fletcher, P.C. Junk, D.A. Reitsma, and F.R. Keene, *J. Chem. Soc., Dalton Trans.*, 133-138 (1998). [100%]

85. "Isolation of Geometric Isomers within Diastereoisomers of Dinuclear Ligand-Bridged Complexes", B.T. Patterson and F.R. Keene, *Inorg. Chem.*, **37**, 645-650 (1998). [100%]

PUBLICATIONS IN PRESS: no reprints included.

86. "'Black Absorbers" and Fuzzy Stereochemistries'", F.R. Keene, in *"Electrochemistry at the Edge"* {Proceedings of 10th Australasian Electrochemistry Conference (Surfers Paradise, 1997)}, in the press. [100%]

87. "Stereoisomers in Heterometallic (Ru_2Os) and Heteroleptic Homometallic (RuRu'Ru") Trinuclear Complexes Incorporating the Bridging Ligand HAT (1,4,5,8,9,12-hexaazatriphenylene), T.J. Rutherford and F. Richard Keene, *J. Chem. Soc., Dalton Trans.*, in the press. [100%]

88. "Isolation and Characterisation of Stereoisomers in Di- and Tri-nuclear Complexes", F.R. Keene, *Chem. Soc. Rev.*, in the press. *(Invited contribution).* [100%]

PUBLICATIONS submitted: no reprints included.

89. "Synthesis of Mixed-Metal Dinuclear Complexes via the Stereoselective Coupling of Alicyclic Mononuclear Ru(II) and Os(II) Complexes", R.N. Warrener, A.C. Schultz, L.S. Kelso, M.R. Johnston, D. Margetic, and F.R. Keene, submitted to *Angew. Chem. Intl. Edn. Eng.* [60%]

90. "The Importance of Second-Sphere Anion Interactions in the Separation of Stereoisomers of Ligand-Bridged Polymetallic Assemblies", N.C. Fletcher and F.R. Keene, submitted to *J. Amer. Chem. Soc.* [100%]

91. "Isolation of Enantiomers of a Range of Tris(bidentate)ruthenium(II) Species using Chromatographic Resolution and Stereoretentive Synthetic Methods", T.J. Rutherford, P.A. Pellegrini, J. Aldrich-Wright, P.C. Junk, and F.R. Keene, submitted to *Eur. J. Inorg. Chem.* [80%]

92. "A New Synthetic Route to Monocarbonyl Polypyridyl Complexes of Ruthenium: Their Stereochemistry and Reactivity", N.C. Fletcher and F.R. Keene, submitted to *J. Chem. Soc., Dalton Trans.* [100%]

Other

93. "Energy and Chemistry", Australian Chemistry Resource Book, Volume 11, (C.L. Fogliani, ed.); Mitchell Printery (Charles Sturt University, Bathurst), 1992, pps 197-209. *{Invited contribution of 1991 R.A.C.I. Queensland Schools' Chemistry Lecture.}* [100%]

DISCOURSE ON PUBLISHED WORK

1. PREAMBLE

The thesis details research undertaken by the author and his coworkers within the general field of the coordination chemistry of transition metal compounds. It incorporates studies in a number of areas, including

- synthetic organic and inorganic chemistry;
- reactivity of coordinated ligands, including kinetic and mechanistic studies of proton exhange processes, electron transfer reactions, intermolecular and intramolecular ligand hydrolyses, oxygen transfer reactions, oxidative dehydrogenation of ligands;
- stereochemistry of coordination compounds;
- electrochemistry and the modification of electrode surfaces;
- photochemistry;
- spectroscopy and the volatilisation of samples for spectroscopic studies;
- catalysis of carbon dioxide reactivity by transition metal centres;
- bonding, structural and stability studies in metal complexes.

The work has been divided into a number of sections, each with a particular theme of study, although some papers would fit equally well into a number of the categories. An outcome of this arrangement is that the papers are not necessarily described in a chronological order, since work within some of the categories continued over a long period of time.

2. BIOGRAPHICAL PERSPECTIVE

During the period 1968-1971, I undertook postgraduate research in the Department of Physical and Inorganic Chemistry at the University of Adelaide, under the supervision of (the late) Dr Graeme Searle. Four of the papers included here (acknowledged in the appropriate section) arose from that candidature, but the collaboration with Graeme Searle continued actively until his untimely death in July, 1992. For the following two years, I held a Postdoctoral Fellowship in the Research School of Chemistry at Australian National University, Canberra working with Professor Alan M. Sargeson and Dr David A. Buckingham. Subsequently, from early 1974 until late 1976, I was a Research Associate at the University of North Carolina in Chapel Hill working with Professor Thomas J. Meyer. After a short period as a Senior Tutor in Inorganic Chemistry in the School of Chemistry, University of Melbourne in 1977, I accepted in 1978 an appointment to the position of

Lecturer in Inorganic Chemistry at James Cook University of North Queensland. I currently hold a Personal Chair, awarded by the University in 1997 on the basis of my research achievements.

During my appointment at James Cook University, I have undertaken a number of periods of study leave. In 1983-84, I spent twelve months at the Brookhaven National Laboratory, New York working with Drs Norman Sutin and Carol Creutz. In 1988, another six month period was spent in the U.S.A., divided between Stanford University (working with Professor Henry Taube) and the University of North Carolina at Chapel Hill (working with Professors Royce W. Murray and Thomas J. Meyer). In 1992, I was invited as a Troisième Cycle Lecturer and Visiting Professor at the Université de Fribourg Suisse, where I spent a three month period. In 1994-95, another six month study leave was taken, divided between the Université Louis Pasteur de Strasbourg in France (working with Professor Jean-Pierre Sauvage), and the Université de Fribourg Suisse (working with Professor Alex von Zelewsky). I will return to the Université Louis Pasteur de Strasbourg in 1998 for 6 weeks to continue a collaborative project with Professor Sauvage.

Because of the relative physical and academic isolation of North Queensland, I have actively pursued collaborations with other groups, both in Australia and overseas. The purpose of this philosophy is two-fold: primarily it has enabled a more scientifically complete and efficient execution of the problems at hand. Secondly, in some cases such collaborations have allowed visits by myself and my students to these other centres for research, and by the collaborators and their students to James Cook University. Such cooperation with the following institutions and individuals is acknowledged in this context:

- University of North Carolina at Chapel Hill (Professor T.J. Meyer)
- Université de Fribourg Suisse (Professor A. von Zelewsky)
- Université Libre de Bruxelles (Professor A. Kirsch-De Mesmaeker)
- Université Louis Pasteur de Strasbourg (Professor J.-P.Sauvage)
- University of Adelaide (Drs G.H. Searle, E.R.T. Tiekink, M.R. Snow, A.A. Diamantis, G.S. Laurence)
- Griffith University (Professor A.E.W. Knight)
- University of Tasmania (Dr M.A. Hitchman)
- University of Melbourne (Dr P.A. Tregloan)
- University of Central Queensland (Professor R.N. Warrener)
- University of Western Sydney, Macarthur (Dr Janice Aldrich-Wright)

It is emphasised that in a majority of these studies, the collaborations served to expand investigations that were primarily conceived and executed at James Cook University, but for which the required facilities and/or expertise were not available locally. In fewer cases, which are noted in the discussion, the origins the collaborations were somewhat different. I

4. DISCUSSION OF INDIVIDUAL SECTIONS

4.1 *Stereochemical Studies of Cobalt(III) Complexes of Amine Ligands*

Papers **#1-4** arose from my postgraduate studies, undertaken at the University of Adelaide under the supervision of Dr Graeme Searle, and are based on work reported in my PhD thesis entitled *"The Bis(diethylenetriamine)cobalt(III) Complex System: Stereochemical and Kinetic Studies"*. The studies in paper **#5** were commenced during my PhD studies, but completed subsequently. I was significantly involved in the writing of these respective papers, particularly in paper **#5** where I was totally responsible for its presentation and production. These papers were concerned with the synthesis and stereochemistry of the cation bis(diethylenetriamine)cobalt(III), $[Co(dien)_2]^{3+}$. The system has three geometric isomers, one of which is highly symmetrical *(s-fac),* one of which is dissymmetric (*u-fac;* point goup symmetry $\mathbf{C_2}$) and the third *(mer)* which has configurational $\mathbf{D_{2d}}$ point group symmetry, but because of the orientation of the two N-H bonds from the (central) secondary amine donors it is potentially chiral ($\mathbf{C_2}$) as long as there is no inversion at those two nitrogen centres.

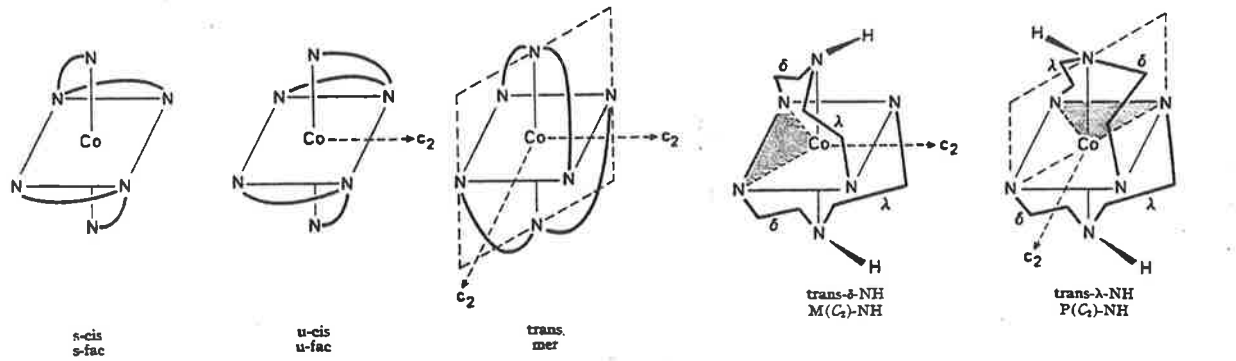

The three isomers were isolated and the dissymmetric forms optically resolved and differentiated by the racemisation of the *mer* form under basic conditions. The nature of the chirality observed in this isomer was novel at the time of its disclosure. Papers published dealt with the optical activity (papers **#2-3**), the synthesis and characterisation of the isomers (papers **#1** and **#3**), the nature of the proton exchange reactions in the *mer* geometric isomer (**#4**), and the dependence of the relative thermodynamic stabilities of the three isomers on environmental parameters (such as solvent, counter-anion, temperature etc.; paper **#5**).

Subsequent studies were carried out on this system, but were initiated by myself and conducted independently - *viz.* an electrochemical study of the $[Co(dien)_2]^{n+}$ system, which enabled a comparison of the relative thermodynamic stabilites of the geometric isomers in the cobalt(II) and cobalt(III) states (paper **#10**). Also, as part of a series of conformation analysis studies on cobalt systems with amine ligands, detailed molecular mechanics calculations were done on this system (paper **#16**), as described below.

During the period of postgraduate study, I was also involved in a collaborative capacity on a project involving another postgraduate student (M. Petkovic) and dealing with cobalt(III) complexes containing the tetradentate ligand 4,7-dimethyltriethylenetetramine: papers **#6-7** resulted from these studies.

Following the completion of my PhD degree, I maintained close ties with Adelaide, and with projects that arose from my postgraduate work. In particular, studies involving complexes of the ligand medien (= 3-methyl-1,5-diamino-3-azapentane) were undertaken to extend the earlier detailed work on the dien system. I made some experimental and writing contribution to the initial two papers involving this ligand (papers **#8-9**), and then independently undertook a study of the pressure dependence on the isomerisation of the $[Co(dien)_2]^{3+}$ and $[Co(medien)(dien)_2]^{3+}$ systems (paper **#12**) during my period in Melbourne. Subsequently, as part of a series of detailed conformational analysis studies (see below), the $[Co(dien)_2]^{3+}$ and $[Co(medien)(dien)_2]^{3+}$ systems were revisited by my own research group (paper **#16**), with a number of the structures of the geometric isomers of the latter complex being determined. The structural studies in the Section were undertaken in collaboration with Dr Edward Tiekink (University of Adelaide)

At my instigation, Graeme Searle started work using the ligand tacn (1,4,7-triazacyclodecane) when I provided him with a sample of the ligand and the cobalt(III) complex. Initial studies are reported in paper **#11**; Graeme Searle went on in the following years to publish a number of studies on complexes involving this (and related) ligands, but I was not involved in those further studies.

Jointly, Graeme Searle and I undertook a study on the cobalt(III) complexes involving the bidentate ligand N-methylethylenediamine (meen). Because of the unsymmetrical nature of the ligand, the chiral nature of the coordinated secondary amine group, the conformation of the chelate rings, and the configurational chirality of a tris(bidentate) octahedral species, systems incorporating this ligand have a very large number of isomeric forms. Papers **#13** and **#17** reported synthetic, characterisation and structural studies on isomers of the $[Co(meen)_3]^{3+}$, $[Co(meen)_2(en)]^{3+}$ and $[Co(meen)(en)_2]^{3+}$ (en = ethylenediamine).

Within the postgraduate studies of one of my own students, the limitations of molecular mechanics calculations were investigated. It was decided that the systems $[Co(pn)_n(en)_{3-n}]^{3+}$ (n = 1-3; pn = 1,2-diaminopropane), $[Co(meen)_n(en)_{3-n}]^{3+}$ (n = 1-3), $[[Co(medien)_n(dien)_{2-n}]^{3+}$ (n = 1-2) constituted an excellent test of the calculation method because of the large number of closely related isomers in the first two systems, and the more limited number of isomers with significant structural differences in the last example. In all three cases, our own work and the work of others meant that substantial thermodynamic and structural information was available. Our molecular mechanics calculations of the thermodynamic relationships between the isomers and the structural calculations of geometric forms for the first two systems were in excellent agreement with the observed

values; the results in the last systems were also successful but gave a valuable salutary warning about comparisons of calculated energies of isomers with significant structural differences (papers **#14-16**).

4.2 Studies in Ligand Reactivity

Studies on the hydrolysis of coordinated nitriles were undertaken in association with Professor Alan Sargeson while I was a Postdoctoral Fellow at the Australian National University. The first study involved the elucidation of the mechanism of the base hydrolysis of coordinated acetonitrile, for which I did the experimental work and had a substantial role in the writing of the paper (paper **#18**). Other work was undertaken on the hydrolysis of other coordinated nitriles (particularly malononitrile), and aspects of that work which were unfinished at the time of my departure were completed and published subsequently (paper **#19**).

A study of the mechanism of the intramolecular hydrolysis of coordinated dipeptides was also undertaken during this period in Canberra. While initial details were published at that time (paper **#20**), a number of avenues opened by my original work formed the basis of the postgraduate studies of Christopher Boreham. Three years later, on my return from the U.S.A., I assisted Dr David Buckingham in writing the two major manuscripts describing the work (papers **#21-22**).

A detailed study of the oxidative dehydrogenation of coordinated amines and alcohols had its origins during my period as a Research Associate at the University of North Carolina (Chapel Hill). During that period in the laboratory of Professor Thomas Meyer, I investigated the stoichiometry of the chemical and electrochemical oxidative dehydrogenation of 1,2-diamines and primary monodentate amines, which show substantial promotion when coordinated to ruthenium centres. Papers **#23 -24** resulted from those studies - I had substantial role in all aspects of the latter paper (paper **#24**), and in the writing of paper **#23**, although my experimental contribution to the latter was lower.

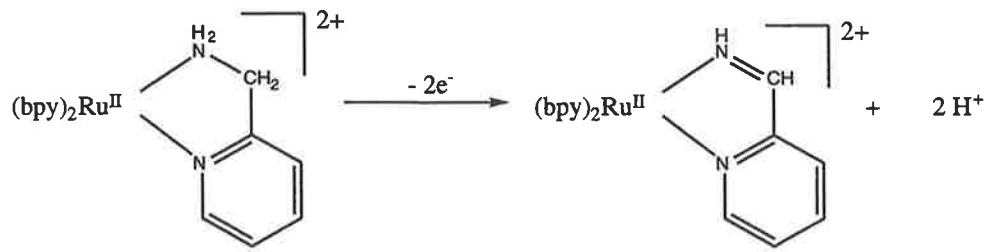

On taking up my position at James Cook University, the first program undertaken was the elucidation of the mechanism of these dehydrogenation reactions of coordinated amines and alcohols. The first target molecule was the complex $[Ru(bpy)_2(ampy)]^{2+}$ {bpy = 2,2'-

bipyridine; ampy = 2-(aminomethyl)pyridine}. The intramolecular redox process subsequent to initial oxidation of the metal centre was followed using flash photolysis and electrochemical techniques and revealed a mechanistic path which included the disproportionation of 2Ru(III) → Ru(II) + Ru(IV), with the Ru(IV) intermediate allowing a two-electron process to occur without involving a radical intermediate. The particular efficacy of the ruthenium centre in promoting this reaction is related to the stabilisation of the high oxidation state on deprotonation of the coordinated amine group. The initial disclosure of this mechanistic study (paper **#25**) was the first formulation of this mechanistic path, although a number of other research groups have since confirmed the features of the scheme. A second associated paper (paper **#27**) was published subsequently which explained some further details of the dehydrogenation process, based on stereochemical and deuterium isotope effect studies of the kinetics of the reaction.

In further investigations of the essential features of this reaction, we undertook related studies on the osmium analogue (paper **#31**) and the ruthenium complex in which the non-participatory ligands were ammine groups, i.e. $[Ru(NH_3)_4(ampy)]^{2+}$ (M.J. Ridd, F.R. Keene, V.E. Alvarez. P.C. Ford, T. Matsubura, and G.M. Brown, unpublished work). These two studies were chosen as the change in metal and the ligand environment modified features of the dehydrogenation process relating to the acidity of the amine group and the rate of electron exhange processes (in the disproportionation step).

A detailed mechanistic study was also carried out on the oxidative dehydrogenation of the analogous alcohol ligand 2-(hydroxymethyl)pyridine in the complex $[Ru(bpy)_2(hmpy)]^{2+}$ using stopped-flow kinetic and electrochemical techniques. This work provided valuable confirmation to the principles of the mechanistic scheme developed for the amine, but established the importance of base-assisted removal of the hydrogen atom from the α-carbon atom in the rate-determining step. This work was published in paper **#30**.

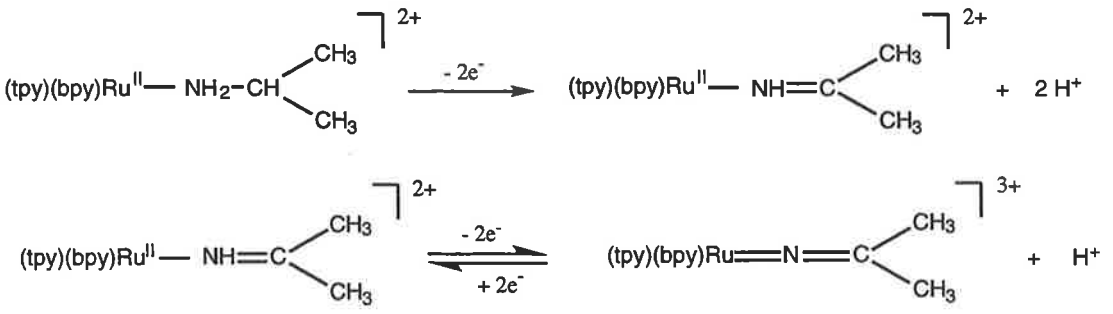

The final aspect of this program related to the dehydrogenation of *iso*-propylamine and secondary amines. The oxidation of *iso*-propylamine was of interest since the dehydrogenation of this monodentate primary amine should stop at the imine stage, and we established that this simple imine was stabilised by coordination. However, its further oxidation produced what was formally a Ru(II) complex of the deprotonated imine (*iso*-

propyleneimide), established by an X-ray structure. This discovery was also timely, since the $Ru^{IV/III}$ redox couple for this complex was cathodic of that for the $Ru^{III/II}$ couple for the non-deprotonated ligand, verifying our earlier assertion about the Ru^{IV}-imido intermediate formed by disproportionation in the dehydrogenation processes. This work was published in papers **#26** and **#28**.

In order to avoid this subsequent process, a further study was undertaken on secondary amines, so that the dehydrogenation process was constrained to stop at the imine stage. The dehydrogenation of coordinated pyrrolidine to 1-pyrroline and of piperidine to 2,3,4,5-tetrahydropyridine, and the stabilisation of those products by coordination, achieved the original aims of this part of the project. We extended this work to demonstrate that the technique could be used to stabilise 1-aza-1,3-butadienes (by dehydrogenation of the corresponding amine, in this case N-methylallylamine), which generally are particularly unstable due to polymerisation. For this case, we were able to undertake a Diels Alder cyclisation of the coordinated 1-aza-1,3-butadiene to produce the corresponding six-membered N-heterocyclic ring system. This work was published in paper **#29**.

While at Chapel Hill as a postdoctoral Research Associate, I initiated a study on the reactivity of the nitrite ion coordinated to ruthenium(III), which undergoes oxide transfer reactions - to an organic substrate if it is present, or otherwise in the form of disproportionation to produce the corresponding nitrosyl and nitrato complexes. Since the coordinated nitrosyl ion may be reconverted to the nitrite ion in basic media, this reaction can be made catalytic under selected conditions; i.e. to allow the chemically-catalysed electrochemical oxidation of an organic substrate, or the quantitative formation of the nitrato species in the absence of such a substrate. Both of these reactions were studied in detail to elucidate the mechanistic aspects of the process, and these results were published in papers **#32-34**. It might be noted that there were some disadvantages to the use of these species as catalytic oxidants, but the study in part provoked the development of the oxo-ruthenium (ruthenyl) and oxo-osmium (osmyl) chemistry that has since been such a major thrust within the group at the University of North Carolina, and within other research groups.

4.3 Studies of Bonding, Structure , and Electron Transfer in Transition Metal Complexes and Electropolymerized Films

While working as a Research Associate at the University of North Carolina, I undertook some kinetic studies on electron transfer reactions within a dinuclear complex, as part of the elucidation of intervalence transfer processes in ligand-bridge dimers (paper **#35**). At that time, I also devised a technique for establishing a numerical value for the self-exchange electron transfer rate for $[Ru(bpy)_3]^{3+/2+}$ using flash photolysis methods. This

important study was undertaken with a postgraduate student in the group (Roger Young) and the results were published in paper **#36**. It is noted that the technique was used by a subsequent student (Jeffrey Nagle) as the basis for his entire PhD studies, although that work was undertaken subsequent to my departure from Chapel Hill.

In 1985, I instigated a research program to study a number of aspects of complexes of C_{3v} tripodal ligands containing π-acceptor donor groups. The aims of this study included the elucidation of aspects of bonding and structure within this class of compounds, and their use in catalysis studies.

X = N, CH, COH, P, P=O

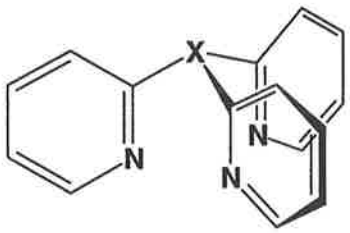

The initial studies were directed to complexes of tris(2-pyridyl)methanol. The ligand $(2\text{-py})_3\text{COH}$ may coordinate as a tridentate either via the three py-N atoms (N,N',N") or via two py-N and the alcohol-O (N,N',O).

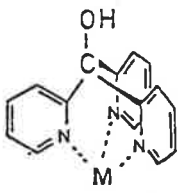

$(py)_3COH$-*N,N',N"*

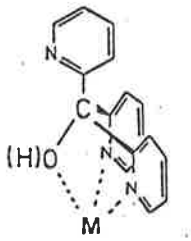

$(py)_3CO(H)$-*N,N',O*

For the bis(ligand)cobalt(III) complex, two linkage isomers were identified: *viz.* a symmetrical $(N,N',N")_2$ form and an unsymmetical form, (N,N',N")(N,N',O), and both were characterised from their spectral, electrochemical and structural features (paper **#37**). The corresponding bis(ligand) species of ruthenium(II) shows only unsymmetrical coordination, with protonation occurring at the coordinated alcohol group ($pK_a = 3.8$). Aspects of the synthesis, structure, and chemical and electrochemical properties of the $[Ru(py_3COH)(py_3CO(H)]^{+/2+}$ species have been published in paper **#38**. A mono(ligand) species, $[Ru(NH_3)_3\{(2\text{-py})_3COH\}]^{2+}$, has been synthesized and its crystal stucture determined and reported along with spectral and electrochemical studies (paper **#42**). The ligand shows (N,N',O)-coordination, with $pK_a = 6.5$ for the coordinated alcohol group. For comparison with structural effects on bonding in these ligands, the structure of the free ligand has also been determined (paper **#40**), as well as the structures of the $(2\text{-py})_3P$ and $(2\text{-py})_3CH$ analogues (papers **#39** and **#44**).

We have also undertaken a comprehensive study of complexes involving the analogous ligands tris(2-pyridyl)amine {$(2\text{-py})_3N$}, tris(2-pyridyl)methane {$(2\text{-py})_3CH$}, tris(2-pyridyl)phosphine {$(2\text{-py})_3P$}, and tris(2-pyridyl)phosphine oxide {$(2\text{-py})_3P{=}O$} with a number of metal centres (*viz.* cobalt, iron, nickel, copper, zinc, ruthenium. rhodium, rhenium and molybdenum).

The bis(ligand) complexes of cobalt have been synthesized in oxidation states I, II and III, and electrochemical studies undertaken (paper **#43**). The electrochemistry of the series of complexes $[Co\{(2\text{-py})_3X\}_2]^{n+}$ (X = N, CH, COH, P, P=O) and $[Co(bpy)_3]^{n+}$ (bpy = 2,2'-bipyridine) revealed the comparable stabilities of the Co(I) species. The stabilisation of Co(I) by polypyridyl ligands such as bpy has generally been attributed to $d\rightarrow\pi^*$ backbonding. The opportunity for similar interactions in the tripodal ligands is less obvious, since delocalisation of the accumulated electron density in the ligand is not as likely. Accordingly, the precise nature of the π-acceptor behaviour of these tripodal ligands was of particular interest. Theoretical studies of the bonding in $[Co\{(2\text{-py})_3CH\}_2]^{n+}$ and $[Co\{(2\text{-py})_3P\}_2]^{n+}$ (n = 1, 2 and 3) were undertaken (paper **#51**), in collaboration with Dr Michael Hitchman (spectroscopy - University of Tasmania), Dr Edward Tiekink (X-ray crystallography - University of Adelaide), Dr Trevor Hambley (X-ray crystallography - University of Sydney), Professor C.D. Garner (EXAFS - University of Manchester, U.K.), and Drs Ken Adam and Ian Atkinson (*ab initio* calculations - JCUNQ). These studies have provided a detailed understanding of the metal-ligand interactions in these systems, and confirm the description of the $[Co\{(2\text{-py})_3CH\}_2]^{+}$ and $[Co\{(2\text{-py})_3P\}_2]^{+}$ complexes as "d^8 cobalt(I)-ligand" rather than "d^7 cobalt(II)-ligand radical" species.

The characterisation of the ruthenium(II) complexes of this series of ligands was achieved by a combination of spectral (electronic, NMR), electrochemical, and X-ray structural methods. The structures {undertaken in collaboration with Drs E.R.T. Tiekink and M.R. Snow (University of Adelaide)} show increasing distortion from ideal $\mathbf{D_{3d}}$ symmetry as the bridgehead(X)-C(py) bond distance increases (X = N<C<P) (paper **#41**). Mono(ligand) complexes have also been studied. The reaction of $[Ru(NH_3)_3(OH_2)_3]^{2+}$ with $(2\text{-py})_3X$ produces $[Ru(NH_3)_3\{(2\text{-py})_3N\}]^{2+}$ for X = N, whereas for X = CH de-ammination occurs and $[Ru(NH_3)_2(OH_2)\{(2\text{-py})_3CH\}]^{2+}$ is isolated (paper **#42**).

In the synthesis of the bis{tris(2-pyridylphosphine oxide)}ruthenium(II) cation, $[Ru(py_3P{=}O)_2]^{2+}$, a species {bis(2-pyridyl)phosphinato}{tris(2-pyridyl)phosphine oxide}ruthenium(II), $[Ru\{py_3P{=}O\}\{py_2P(O)O\}]^{+}$, was also isolated. The latter cation has been characterised by a structural determination and is the first example of a tridentate phosphinate anion. The electrochemical and spectral properties of both cations are reported (paper **#46**).

The bis(ligand)rhodium(III) complexes have been synthesized and characterised, and their electrochemical behaviour investigated. The ligand tris(2-pyridyl)phosphine, $(2\text{-py})_3P$,

displays an unusual ability to stabilize a reduced form {Rh(II) or Rh(I)} of the metal centre. This work is yet to be published.

The reactions of $[Re(CO)_5Cl]$ with the ligands $(2\text{-py})_3N$, $(2\text{-py})_3CH$ and $(2\text{-py})_3P$ in toluene solution realise compounds with the general formulation $[Re(ligand)(CO)_3Cl]$, in which the tri-pyridyl ligands are bidentate. If the synthetic procedure is undertaken under irradiation by visible light, for the ligand $(2\text{-py})_3N$ a species $[Re\{(2\text{-py})_3N\}(CO)_2Cl]$ (characterised by infrared spectroscopy and conductance measurements) is also formed, and in which the ligand $(2\text{-py})_3N$ is tridentate. No analogous tridentate species is formed with the ligands tpy or $(2\text{-py})_3P$, although there is evidence that it also forms for $(2\text{-py})_3CH$ (paper #**45**). Studies of the analogous molybdenum complexes have demonstrated similar tendencies for bidentate coordination with molybdenum (F.R. Keene, M.J. Ridd, and A.G. Wedd, unpublished results).

A study (papers #**47-51**) of the first-row transition complexes involving these tripodal ligands was instigated in collaboration with the research groups of Dr M.A. Hitchman (University of Tasmania) and Dr E.R.T. Tiekink (University of Adelaide).

The case of the copper complexes is particularly interesting. For $(2\text{-py})_3N$, the bis(ligand) complex had the ligands in bidentate mode with aqua groups in the *trans* positions of the coordination sphere (paper #**47**). For $(2\text{-py})_3CH$, the X-ray structure of $[Cu\{(2\text{-py})_3CH\}_2](NO_3)_2$ indicated that all six Cu-N bonds were crystallographically equivalent at both 173K and 295K, although the electronic spectra implied the presence of a tetragonally-elongated ligand field (Jahn-Teller distortion). This distortion was confirmed by the EXAFS of the compound (paper #**48**). The apparent trigonal symmetry revealed by the X-ray analysis is due to disorder of the short and long Cu-N bonds about the three-fold axis. The EPR spectrum shows an isotropic signal at 295K, but a signal charactersitic of a tetragonally-distorted octahedral complex at 150K, suggesting that the directions of the long and short bonds interchange rapidly on the EPR timescale at room temperature, but the complexes become frozen into particular orientations on cooling (paper #**48**). `For $(2\text{-py})_3P$, a bis(ligand)copper(II) complex was formed in which the ligands were tridentate and the X-ray structure show two Cu-N bonds are shorter than the other four. However, temperature-dependent EPR studies suggested the complex has a tetragonally-elongated octahedral geometry with two possible orientations in the crystal lattice, differing by the interchange of the directions of the long and intermediate Cu-N bonds. The bonding parameteres derived from the electronic spectra are consistent with the proposed tetragonal elongation (paper #**49**). We also undertook similar structural and spectroscopic studies of the corresponding zinc(II) and nickel(II) complexes, which confirm the previous results on the bonding characteristics of the pyridine groups of these ligands, and established a way of assessing the effect of the bridging atom (paper #**50**).

As part of the collaborative effort on the stuctural studies of complexs of these tripodal ligands with Dr Tiekink, we also re-determined a stucture of bis{tris(2-pyrazol-1-

yl)methane]cobalt(II) nitrate (at 173K - paper **#52**) to provide more precise structural information (than an earlier structure at 275K) to support calculations associated with spectroscopic observations on the system by Dr Hitchman and his coworkers.

While on study leave at Brookhaven National Laboratory (New York) in 1983-84, I became interested in studies of the promotion of the reactivity of carbon dioxide by transition metal complexes. In association with Drs Norman Sutin and Carol Creutz, a mechanistic study was undertaken of the interaction of $[Co(bpy)_3]^+$ with carbon dioxide in aqueous solution (paper **#53**). Subsequent studies in my own "tripodal ligands" program on the reactivity of the $[Co^I\{(2\text{-}py)_3X\}_2]^+$ species (X = CH, P) with water and HCO_3^- indicated that water underwent reduction to H_2 but no reduction of HCO_3^- occurred. The mechanism of water reduction by $[Co(bpy)_3]^+$ is generally proposed to occur via formation of an hydridocobalt species, following ligand dissociation: in addition, CO_2 (HCO_3^-) reduction occurs via the same intermediate but coordination by the substrate is thought to be required. For the reaction of $[Co\{(2\text{-}py)_3P\}_2]^+$ with water, while total dissociation of a ligand does not occur there may well be dissociation of a single pyridine moiety allowing formation of an hydrido species and leading to water reduction: however simultaneous CO_2 (or HCO_3^-) coordination is precluded, inhibiting its reduction (paper **#43**). Since that time, we have maintained an interest in carbon dioxide reactivity, and I was invited to contribute two chapters to a monograph on this subject (papers **#54-55**). Such catalytic studies are still part of our activities, and in particular the study of multi-electron reduction of carbon dioxide (e.g. to methanol and methane) using polynuclear metal complexes and metal cluster species. We have also examined the more general usage of $[Co(bpy)_3]^+$ as a catalyst for reduction of organic species using alkynes as substrates (paper **#56**).

In a period of study leave in the laboratory of Professor Royce Murray (University of North Carolina at Chapel Hill, U.S.A.) during 1988-89, I was involved in work directed at elucidating structural and environmental effects on electron and ion transfer in films made from electroreductive polymerisation of monomeric osmium complexes containing vinyl-substituted pyridyl and polypyridyl ligands.

In the first of these studies, a series of films were investigated in which the electron-transport-active osmium metal centres were isostructurally diluted with analogous centres of either ruthenium or zinc. For these films, the correspondence between the composition of the monomer feed and the that of the films was tested using X-ray photoelectron spectroscopy (XPS), and electron transport studies undertaken by measuring electron diffusion rates through the various copolymer films (paper **#57**).

In the second study, rate constants for the electrical gradient driven, bimolecular electron self-exchange reaction between Os^{III} and Os^{II} sites in dry, mixed-valent electropolymerized films of poly-$[Os(bpy)_2(vpy)_2](BF_4)_m$ and poly-$[Os(vbpy)_3](BF_4)_m$ {vpy = 4-vinylpyridine; vbpy = 4-methyl-4'-vinyl-2,2'-bipyridine} were determined as a function of m. Linear

potential sweep and a.c. impedance measurements showed that the electron exhange followed bimolecular characteristics. Comparison of the self-exchanges driven by electrical and concentration gradients in a variety of bathing environments showed that electron-hopping rates were affected by the rigidity of the matrix (paper **#58**).

Since that time, within my laboratory we have pursued a continuing program on chemically modified electrodes with particular interest in the use of 2,2'-bipyridine ligands functionalised with thiophene (thiophene is known to undergo anodic electropolymerisation to form conducting films). We developed a synthetic methodology for thiophene-functionalised 4-methylpyridine and 4-methyl-2,2'-bipyridine in which the linking alkyl chain length has been varied from n = 2-11 (paper **#59**). Electropolymerized films of the ligands (paper **#60**) and their ruthenium complexes (paper **#61**) were studied by electrochemistry (cyclic voltammetry, chronoamperometry, and a.c. impedance spectroscopy) and scanning electron microscopy measurements of surface structure. The porous nature of the films and their electrochemical behaviour was shown to be dependent on the length of the alkyl chain, and charge transfer was influenced in oxidative and reductive regions by differing proportions of kinetic factors and diffusion (papers **#60-61**).

As a preliminary investigation of the catalytic properties of metal-containing films made from these ligands, the kinetics of the electrochemical oxidation of $K_4Fe(CN)_6$ at poly-[tris(3-{ω-[4-(2,2'-bipyridyl)]alkyl}thiophene)iron(II)]-film modified electrodes was investigated in aqueous solutions, using cyclic voltammetry and rotating disk electrode voltammetry. The retro-electrocatalytic reaction of the substrate at the polymer-coated electrodes was dependent on the alkyl chain length between the thiophene and 2,2'-bipyridine moieties and on the concentration of the substrate (paper **#62**).

4.4 Spectroscopy of Laser Desorbed Molecules

Laser-based spectroscopy coupled to molecular beam technology has, over the past decade, proved a powerful tool for studying the photophysics and dynamics of polyatomic molecules. The spectroscopy of molecules studied in this fashion is greatly simplified by the cold, rarefied environment of the molecular beam. A lack of thermal and matrix congestion in molecular beams means that spectra can be recorded with dramatic clarity compared with measurements taken in more traditional media. However, these experiments are restricted by the need for the sample molecules to be volatile to allow introduction into a molecular beam.

In a study undertaken in collaboration with Professor Alan Knight (Griffith University), we addressed the problem of evaporating intrinsically involatile materials by laser desorption (papers **#64 -65**). A new polymer matrix containing particulate silver was developed for the introduction of analytes with low or negligible volatility into molecular beams via laser desorption (LD) - the process by which the interaction between a laser and a

solid can cause the evaporation of molecules (and their fragments) from the solid surface. These silver-containing film matrices (SCFM) permit stable desorption to proceed for extended periods (*ca.* ~10 hours), and were applied successfully to the non-destructive volatilisation of a number of amino acids and a transition metal compound ($[Ru(bpy)_3]^{n+}$, where bpy = 2,2'-bipyridine). Analytes were extracted directly from solution on to the SCFM surface by simply dipping the film into the solution and then air-drying the film. The laser desorption apparatus, when coupled to a supersonic molecular beam/laser ionisation time-of-flight mass spectrometer (TOF-MS), permitted the detection of the analytes at femtogram levels. Furthermore, we developed a reel-to-reel tape transport device that allowed extended usage of the analyte-loaded SFCM, thereby permitting the measurement of wavelength-scanned mass-selected resonance-enhanced multiphoton ionization spectra of analytes with low or negligible volatility. We demonstrated this application for the two examples below.

Firstly, with the biologically significant aromatic amino acids *l*-tryptophan and *l*-phenylalanine, the degree of cooling achieved in the molecular expansion was shown to be comparable with that achieved using conventional beam sources, and the desorption yield was sufficiently stable for high quality spectra to be measured. The resonance enhanced multiphoton ionization (REMPI) spectrum of laser desorbed *l*-phenylalanine revealed that the molecule exists in a number of distinct conformational forms, and the low frequency structure present in the electronic spectra of *l*-phenylalanine was interpreted as arising in part from vibronic transitions associated with hindered rotation of the carboxylic acid moiety within the amino acid grouping. Various semi-empirical molecular orbital calculations were employed to rationalise these structures and motions (papers **#64- 65**).

Transition metal complexes have not been the subject of high resolution spectroscopic interrogation using molecular beam conditions. The potential of such measurements is enormous: it would allow detailed interrogation of the excited state properties of metal complexes, which is an important, but often poorly understood, area of inorganic chemistry. The principle reason for this yet untapped application of molecular beam spectroscopy is largely pragmatic; most metal coordination complexes are simply not volatile, and therefore cannot be introduced into molecular beam expansions. While our work stopped short of measuring the LD/REMPI spectrum of a metal complex, an intense molecular beam of $[Ru(bpy)_3]^{n+}$ was generated, as shown by time-of-flight mass spectrometry (TOF-MS). Signal instability prevented the associated electronic spectra being recorded (paper **#63**).

4.5 Artificial Photosynthesis

Present activities in my laboratory are primarily devoted to the development of polymetallic molecular assemblies which will allow the harvesting of light energy and its conversion to high energy chemicals - termed "artificial photosynthesis". In the early

stages, the research was directed to the development of synthetic strategies to allow controlled design of photophysical and redox characteristics of chromophores for such assemblies (particularly polypyridyl complexes of Ru^{II}). Further, we have developed synthetic strategies for modification of polypyridyl (and related) ligands to incorporate electron (and energy) transfer groups, in which the spacing, stereochemistry and electronic communication between the quencher and the metal centre may be systematically varied and tested by photophysical measurements. We are also devising ligand-bridged assemblies to assess factors affecting inter-metal communication as a function of the stereochemistry of the metal centres and the structure of the ligand-bridge assembly.

Initially, we established a general synthetic method for heteroleptic tris(bidentate) complexes of ruthenium(II), $[Ru(pp)(pp')(pp'')]^{2+}$ {pp, pp' and pp" are polypyridyl ligands} based on the sequential addition of the ligands to the oligomer $[Ru(CO)_2Cl_2]_n$, which has allowed the systematic control of the ground and excited state properties of these monomeric complexes by variation of the ligand environment (papers **#66**, **#68**, **#71**).

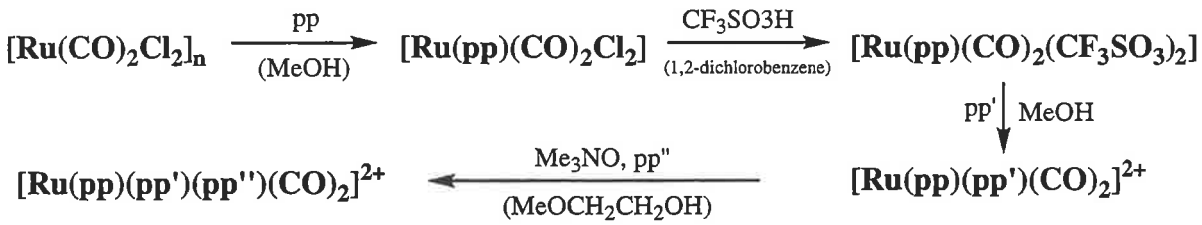

Detailed photophysical investigations of a number of such $[Ru(pp)(pp')(pp'')]^{2+}$ species have been undertaken using transient emission and absorbance studies, and resonance Raman techniques, to probe excited and ground state properties. By controlled variation of the π^* levels of the ligands and the $d\pi$ levels of the metal centre, it has proved possible to extend the absorptivity into the red region of the visible spectrum and enhance the absorbance over the entire visible range ("black absorbers"). All mixed ligand complexes were found to be much less prone to undergo photoinduced ligand loss than the parent compound $[Ru(bpy)_3]^{2+}$ (papers **#68** and **#71**). We have also identified (paper **#72**) the possibility that metal complexes containing ligands with extended delocalization may exhibit enhanced excited state lifetimes (despite the low energy gap between the $d\pi$ and π^* levels, and in contravention of the "energy gap law").

We have also recently developed an analogous synthetic methodology for the tris(heteroleptic) species of osmium(II) (paper **#76**). Another study has also realised a new photosynthetic route to complexes of the type $[Ru(ppp)(pp)(CO)]^{2+}$ {ppp = a tridentate ligand such as tpy (2,2':6',2"-terpyridine); pp = a bidentate ligand}, which is a promising precursor for a range of complexes in which the sixth corrdination position may be widely varied by replacement of CO with X under decarbonylation conditions (paper **#92**).

The methodology described above also provides avenues for the development of polymetallic molecular assemblies. The key intermediate in the scheme is the $[Ru(pp)(pp')(CO)_2]^{2+}$ species, which undergoes reaction with the pp'' ligand under decarbonylation conditions to form the ultimate product. In cases where the third ligand is a bridge which is part of another complex {e.g. BL = 2,2'-bipyrimidine or 2,3-bis(2-pyridyl)pyrazine}, further work has shown that the technique may be extended to dinuclear and higher nuclearity species using a "complexes as ligands" strategy (paper **#67**).

$$\mathbf{[Ru(pp)(pp')(CO)_2]^{2+}} \xrightarrow[Me_3NO/MeOCH_2CH_2OH]{\mathbf{[Ru(pp'')(pp''')(BL)]^{2+}}} \mathbf{[Ru(pp)(pp')(BL)Ru(pp'')(pp''')]^{4+}}$$

We have now demonstrated that the decarbonylation reactions proceed under certain conditions with retention of the stereochemical integrity of the metal centre (papers **#69-70**). In the first of these studies, the formation of the species $[Ru(Me_2bpy)(pmb)_2]^{2+}$ was studied in detail, where 4,4'-dimethyl-2,2'-bipyridine (Me_2bpy) is a symmetrically-substituted ligand, and 4-methyl-4'-*neo*-pentyl-2,2'-bipyridine (pmb) is non-symmetrically substitituted. The target complex in such a case has three possible geometric isomers.

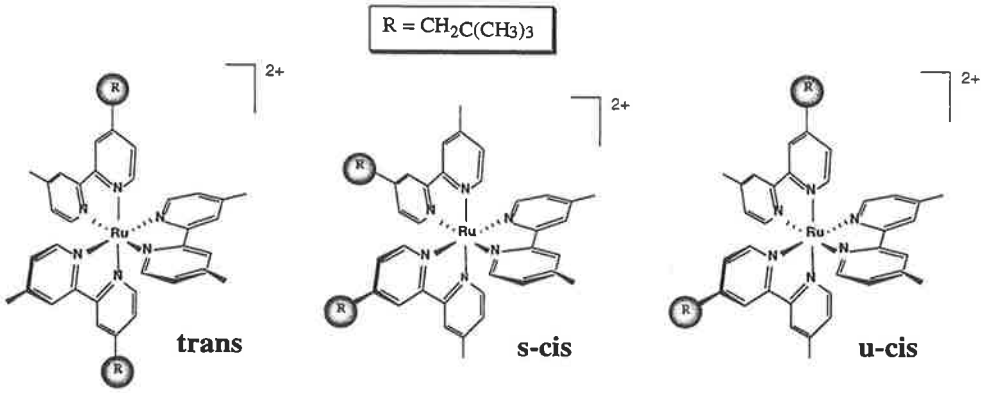

There are two alternative synthetic approaches to the target molecule - either reaction of Me_2bpy with $[Ru(pmb)_2(CO)_2]^{2+}$ or reaction of pmb with $[Ru(Me_2bpy)(pmb)(CO)_2]^{2+}$. The respective dicarbonyl complexes were separated into their geometric isomers and the stereochemical course of the final decarbonylation reaction studied. Under appropriate conditions, it was observed that the stereochemical integrity of the dicarbonyl species was completely retained (paper **#69**).

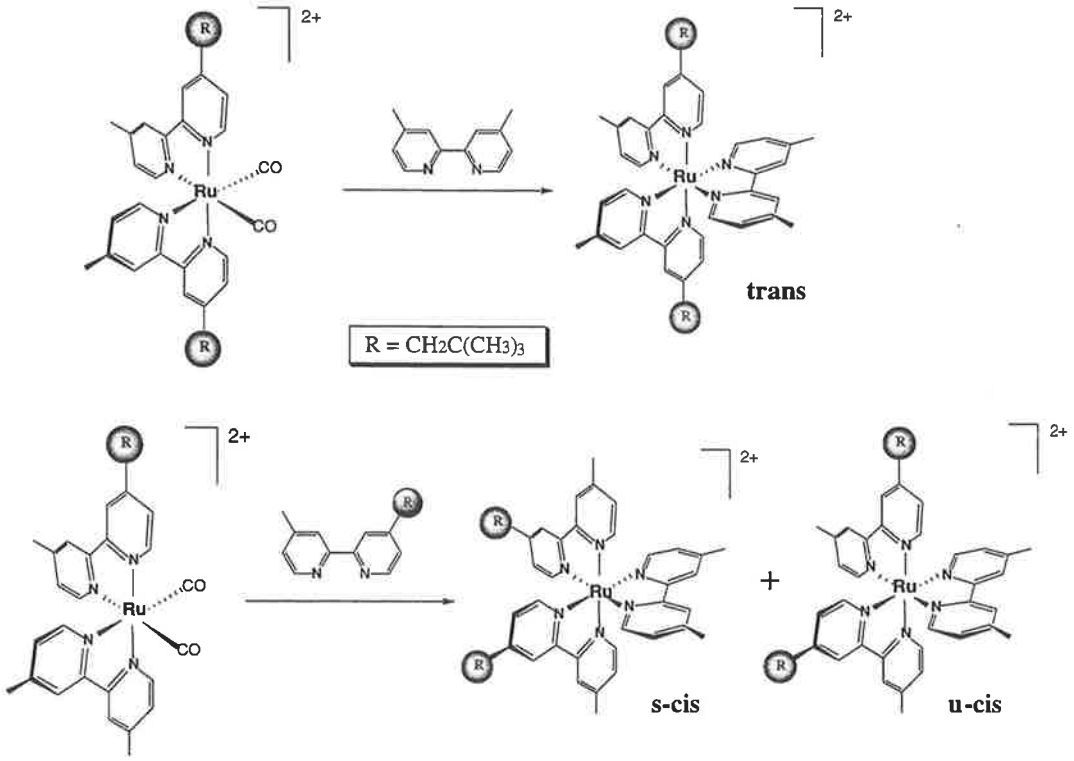

In the second study, the chiral integrity of the dicarbonyl species was observed during the decarbonylation process (papers **#70** and **#91**) This enabled the isolation of specific stereoisomers of mononuclear and dinuclear species, as shown in the example below {Me_4bpy = 4,4',5,5'-tetramethyl-2,2'-bipyridine; phen = 1,10-phenanthroline}.

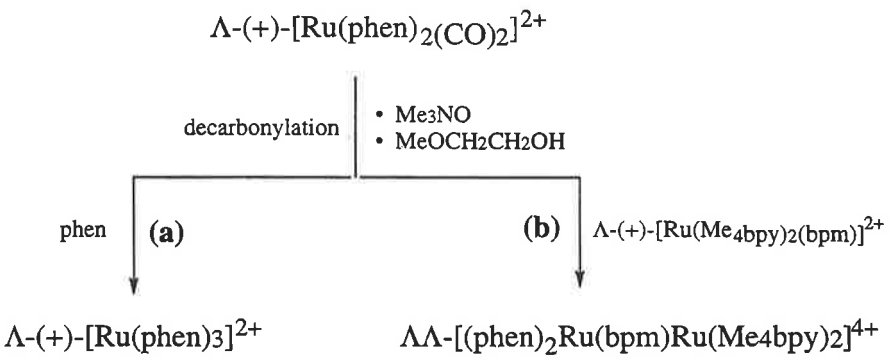

The conclusions are extremely significant. The synthetic methodology allows not only the controlled variation of the spectral, photophysical and redox characteristics of the metal centres, but also predetermination of the stereochemistry in mononuclear and oliogonuclear species by appropriate choice of the stereochemistry of the precursor. We have exploited the techniques to isolate stereoisomers of a number of mono-and poly-nuclear species with the aim of identifying differences in photophysical and electrochemical characteristics between isomers of the same compound.

In a monouclear complex, we isolated the four geometric isomers of the system $[Ru(bpy)(bpy\text{-}D)(bpy\text{-}A)]^{4+}$ (paper **#82**), shown below (where D and A are donor and acceptor redox-active groups respectively).

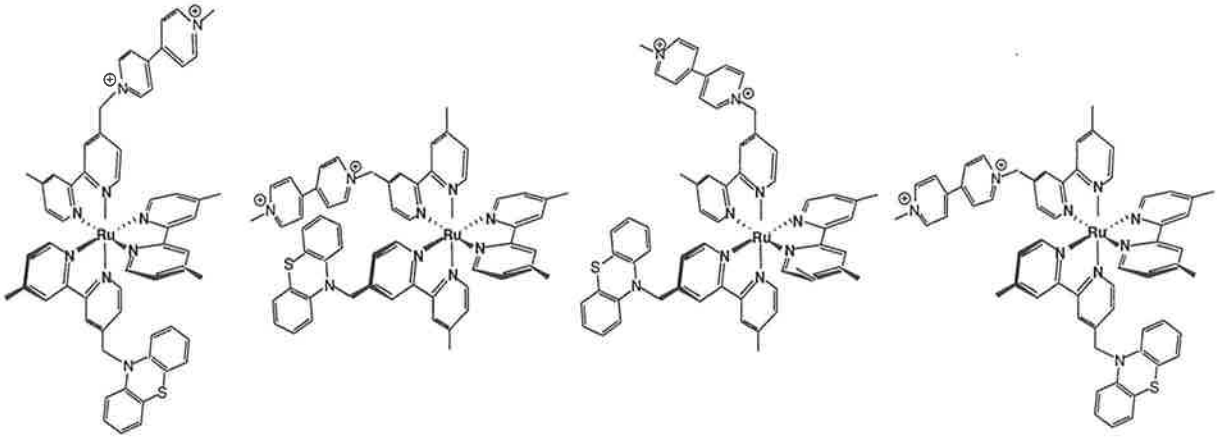

trans *cis (1)* *cis (2)* *cis (3)*

The assignment of the stereochemistry was achieved by NMR spectroscopy. We have undertaken comparative photophysical studies of the isomers and established for the first time that the emission lifetimes of the charge-separated states formed on light absorption are distinguishable. These variations are not totally understood at this stage but probably reflect differences between the isomers in solvent and vibrational barriers and electronic coupling, as well as subtle differences in their orbital pathways for electron transfer (paper **#83**). Further studies are in progress of analogues in which the bridge between the ligating group and the PTZ subsitituent are extended.

For ligand-bridged dinuclear species, there are two diastereoisomeric forms, each comprising of an enantiomeric pair. The two stereoisomers are represented schematically below, where the terminal ligands on each metal centre are identical.

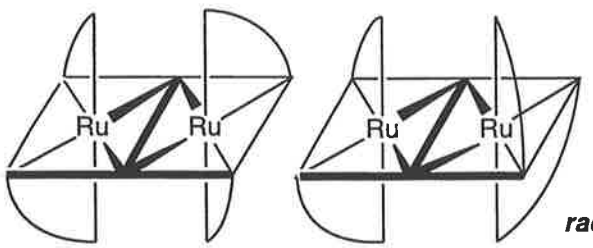

meso {ΛΔ} ***rac*** {ΛΛ, ΔΔ}

A significant difference in the relative ligand orientations may be discerned in the two diastereoisomeric pairs: the terminal polypyridyl ligands "above" and "below" the plane of the bridging ligand are approximately parallel in the ΔΔ/ΛΛ form, whereas they are perpendicular in the ΔΛ/ΛΔ stereoisomer. We have synthesised a range of complexes of types $[\{Ru(pp)_2\}_2(\mu\text{-}BL)]^{4+}$, $[\{Ru(pp)_2\}\{Ru(pp')_2\}(\mu\text{-}BL)]^{4+}$, $[\{Ru(pp)_2\}\{Os(pp)_2\}(\mu\text{-}BL)]^{4+}$, and $[\{Ru(pp)_2\}\{Os(pp')_2\}(\mu\text{-}BL)]^{4+}$ {pp, pp' are bidentate ligands, BL = bridging ligand; paper **#67**), and chromatographically separated and characterised the diastereoisomers. For the

situation where there are two different terminal ligands on each metal centre, $[\{Ru(pp)(pp')\}_2(\mu\text{-BL})]^{4+}$, geometrical isomerism is also possible, and we have separated and characterised geometric isomers in such systems (paper #**85**).

In investigating higher nuclearity species (papers #**80-81, 87**), using a combination of our synthetic and chromatographic techniques we have synthesized the separate diastereoisomers of the homometallic and heterometallic dinuclear and trinuclear complexes of the ligand 1,4,5,8,9,12-hexaazatriphenylene (HAT).

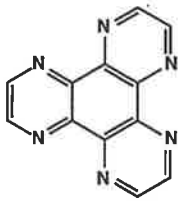

HAT

In the homometallic dinuclear case where the metal centres are equivalent, two diastereoisomers are possible:

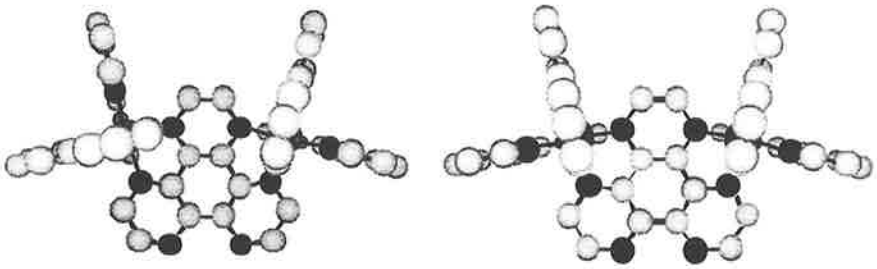

$\Delta\Delta$–$[\{Ru(bpy)_2\}_2(\mu\text{-HAT})]^{4+}$ *(rac)* $\Lambda\Delta$-$[\{Ru(bpy)_2\}_2(\mu\text{-HAT})]^{4+}$ *(meso)*

and similarly in the trinuclear case.

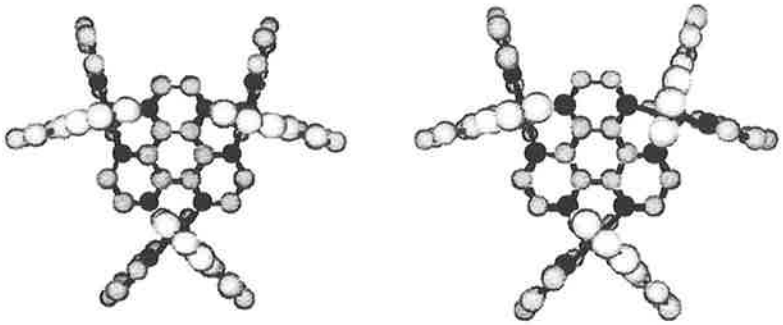

$\Lambda\Lambda\Delta/\Delta\Delta\Lambda$–$[\{Ru(bpy)_2\}_2(\mu\text{-HAT})]^{6+}$ $\Delta\Delta\Delta/\Lambda\Lambda\Lambda$-$[\{Ru(bpy)_2\}_2(\mu\text{-HAT})]^{6+}$

The effect of the variation in relative ligand orientation on intramolecular electron and energy transfer in these complexes was probed by photophysical techniques in collaboration with a research group at the Université Libre de Bruxelles (Belgium). For the dinuclear species at room temperature, the relative luminescence quantum yields and the emission lifetimes showed a significant drop for the *meso* compared with the *rac* diastereoisomers. Moreover in a glass at low temperature (77 K), the luminescence lifetimes of the trinuclear heteronuclear diastereoisomer were slightly shorter than those of the homonuclear form. No significant differences were detected at room temperature in the diastereoisomeric forms of the trinuclear compounds. Electrochemical and electronic absorption spectroscopic

studies of both the dinuclear and trinuclear series showed minimal differences in the properties of the diastereoisomeric pairs (paper #**81**)

We have also isolated all possible stereoisomers of the analogous heterometallic trinuclear species $[\{Ru(bpy)_2\}_2\{Os(bpy)_2\}(\mu\text{-HAT})]^{6+}$ (papers #**80** and #**87**), and a heteroleptic homometallic trinuclear species $[\{Ru(bpy)_2\}\{Ru(Me_2bpy)_2\}\{Ru(phen)_2\}(\mu\text{-HAT})]^{6+}$ (paper #**87**).

Other systems reveal spatial consequences of energy and electron migration patterns in polynuclear species. In a recent study, we isolated the diastereoisomers of the ligand-bridged species $[(bpy)_2Ru(\mu\text{-apy})Ru(bpy)_2]^{4+}$ (apy = 2,2'-azopyridine) and the methylated congeners in involving Me_2bpy (4,4'-dimethyl-2,2'-bipyridine) and Meapy {2,2'-azobis(4-methylpyridine} (paper #**73**).

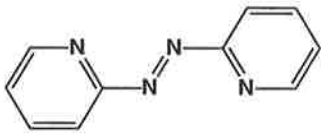

apy = azopyridine

The diastereoisomer pairs show differences in their electrochemical and electronic spectral characteristics, which indicates a spatial dependence for the inter-metal communication.

In collaboration with the research group of Professor R.N. Warrener (Central Queensland University), we have been seeking the design of ligand-bridges and quencher-functionalised ligands in which the geometry and electronic characteristics of the linkage between the ligating groups and the functionalities may by deliberately controlled using the "molrac" methodology established in Professor's Warrener's laboratory. Thus far, we have achieved the linkage of the 1,10-phenantholinyl ligating group to quinone (acceptor) and dimethoxyphenyl (donor) groups (paper #**74**),

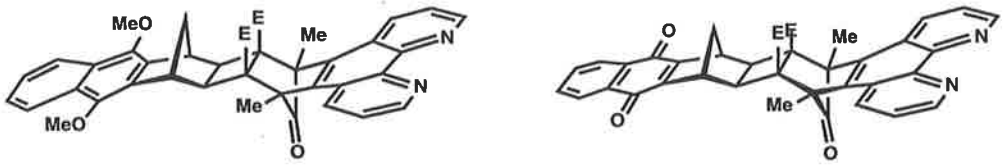

as well as various bridges with 1,10-phenanthrolinyl, 4,5-diazafluorenyl or 3,6-di(2-pyridyl)pyridazinyl moieties (paper #**75**). A number of complexes have been made and preliminary photophysical studies have been undertaken.

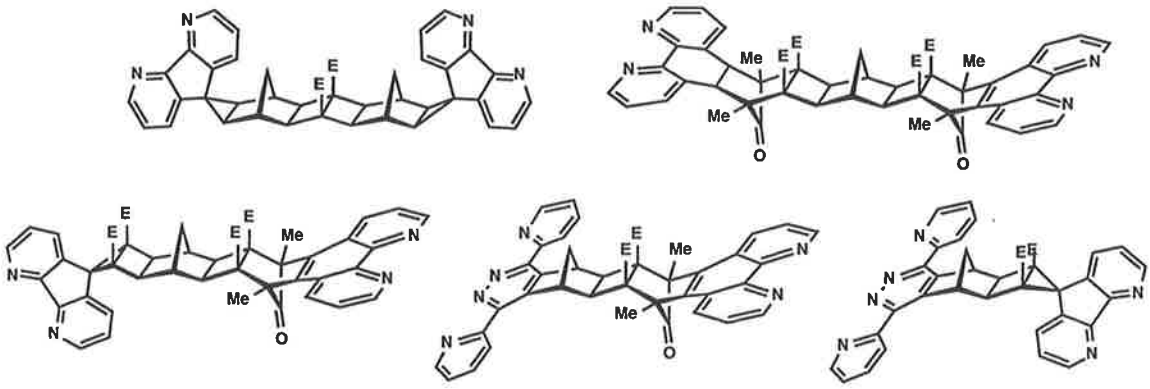

We have also developed a synthetic methodology for formation of dinuclear complexes which the metals are bridged by a rigid alicyclic (morac) framework by coupling mononuclear species with molrac ligands functionalised with epoxide and olefinic groups paper #**89**). The technique provides a superior route to heterometallic dinuclear species, whose synthesis is difficult using the pre-constructed ligand. We have also linked ruthenium complexes containing polypyridyl ligands with metal-containing porphyrin species using this technique (paper #**89**).

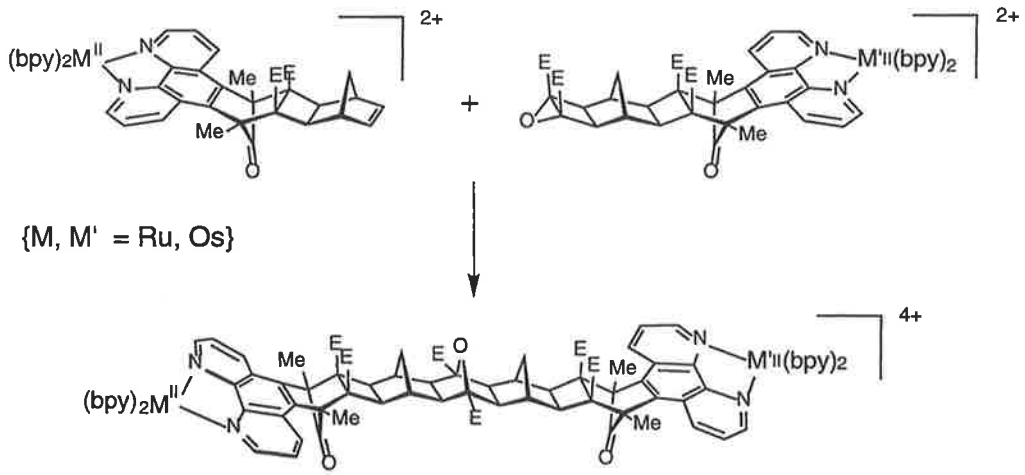

As part of the stereochemical studies, we have developed general cation-exchange chromatographic methods of separating stereoisomers (geometric isomers, enantiomers and diastereoisomers) of mono- and polynuclear complexes containing polypyridyl ligands (paper #**84**). The work indicates that there are significant second sphere interactions between the complexes and the counter-ions in the electrolyte, and that those associations may differ between stereoisomeric forms of the same species. In order to enhance the separation technique we invesigated specific associations of aliphatic and aromatic organic anions with simple monomeric and dinuclear species. Using NMR techniques, a strong edge-to-face π-π interaction between the anion and the the bidentate ligands (such as bpy) is suggested, but the studies with the aliphatic anions also indicate a hydrophobic interaction is important (paper #**90**).

There are other important implications in these observations. There has been considerable interest in the interaction of polypyridyl complexes of ruthenium with DNA, which may include electrostatic interactions, hydrogen bonding, covalent binding, and intercalation or insertion of planar hetereocylic aromatic groups into clefts in the double helix. With their luminescent properties, the complexes are of particular interest in terms of determination of DNA structure for sequencing studies and as site-specific cleavage reagents. One of the exciting prospects for our work is that the program provides a range of complexes with hitherto unavailable subtle stereochemical variations, and studies of the mechanism of their interactions with polynucleotides are being undertaken in collaboration with the research groups of Professors Andrée Kirsch-De Mesmaeker and Jaques Riesse (Université Libre de Bruxelles, Belgium), and Dr Janice Aldrich-Wright (University of Western Sydney). Using our chromatographic technique, we have chirally resolved a wide range of homoleptic and heteroleptic tris(bidentate)ruthenium(II) complexes for this purpose (paper #**91**).

In the last five years, our program has made a major contribution to the area of stereochemistry in polynuclear assemblies, and I was recently invited by *Coordintation Chemistry Reviews* to contribute a review on this topic (paper #**77**). A review in the area was also sought by *Chemical Society Reviews,* and is currently in press (publication in May 1998; paper #**88**). A review of aspects of our work in this area was also sought for a presentation at the 10th Australasian Electrochemistry Conference, the substance of which has been published as paper #**86**.

Although a there are a number of research groups who have now begun to recognise the importance of stereochemistry in polymetallic supramolecuar assemblies, we are aware of only one other research group in the world which was pioneering this area in the early 1990's. Professor A. von Zelewsky and his coworkers (Université de Fribourg Suisse) have adopted a different approach to ours to achieve a similar aim, and in 1994-5 I spent five months of study leave in that laboratory. I was involved experimentally in aspects of their program during this period, and I initiated some work on a new sub-set of a ligand type used by this group to to promote stereoselective formation of polypyridyl complexes of ruthenium. That work was continued in Fribourg after my departure, and has resulted in two joint publications (papers #**78-79**).

4.6 Other

In 1991, I was invited by the Queensland Branch of the Royal Australian Chemical Institute to be the "Schools' Chemistry Lecturer". During a number of trips throughout the state, I addressed nearly 4,500 secondary school students - that presentation was sought for publication (paper #**91**) in the Australian Chemistry Resource Book (Volume 11).

5. SUMMARY

My early research activities as a postgraduate student and postdoctoral fellow included aspects of stereochemistry, electron transfer and ligand reactivity in transition metal complexes. In the programs developed subsequently within my own research group (on occasions in collaboration with other groups), such interests have been extended and combined with electrochemical and photochemical studies. *Inter alia,* particular contributions are noted to

- the elucidation of the mechanism of oxidation of ligands to ruthenium(II) and osmium(II) centres, and the establishment of two-electron processes resulting from the lowering of potential by deprotonation;
- the structural and bonding characteristics of complexes of tripodal ligands; and
- the establishment of techniques for control of the stereochemistry of polymetallic supramolecular assemblies, and the demonstration of a spatial dependence of intramolecular electron- and energy-transfer processes within such assemblies.

It is noted that a majority of the publications that form the basis of this thesis (which are described above, and listed in the next section) have appeared in prestigious journals (such as *Journal of the American Chemical Society, Inorganic Chemistry* and *Journal of the Chemical Society, Dalton Transactions*).

F. R. KEENE

PUBLISHED PAPERS

Geometric and Optical Isomers of the Bis(diethylenetriamine)cobalt(III) Ion

By F. R. Keene and G. H. Searle*
(*Department of Physical and Inorganic Chemistry, The University of Adelaide, South Australia*, 5001)
and Y. Yoshikawa, A. Imai, and K. Yamasaki*
(*Department of Chemistry, Faculty of Science, Nagoya University, Nagoya* 464, *Japan*)

Reprinted from

Chemical Communications 1970

The Chemical Society, Burlington House, London W1V OBN

Geometric and Optical Isomers of the Bis(diethylenetriamine)cobalt(III) Ion

By F. R. KEENE and G. H. SEARLE*

(*Department of Physical and Inorganic Chemistry, The University of Adelaide, South Australia*, 5001)

and Y. YOSHIKAWA, A. IMAI, and K. YAMASAKI*

(*Department of Chemistry, Faculty of Science, Nagoya University, Nagoya* 464, *Japan*)

Summary All the geometric and optical isomers possible for the $[Co(dien)_2]^{3+}$ system have been isolated and characterised, and the geometric configurations have been assigned from the difference in racemisation behaviour of the optical forms of the *u-cis*- and *trans*-isomers and from the ^1H n.m.r. spectra.

IN co-ordinating to metals, diethylenetriamine (dien) can adopt either facial (*cis*) or meridional (*trans*) dispositions, so that a bis-complex $[M(dien)_2]^{n+}$ can exist in three topological isomers, *s-cis* (symmetrical-*cis*), *u-cis* (unsymmetrical-*cis*), and *trans* (Figure 1). Also, the *u-cis*- and *trans*-isomers can exist in optical forms. The complex $[Co(dien)_2]Cl_3$ was described many years ago[1] but the isomers have not previously been reported.

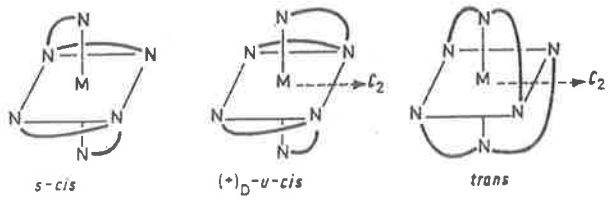

FIGURE 1. *Topological isomers of* $[M(dien)_2]^{3+}$

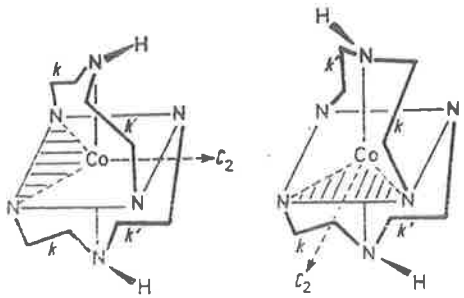

FIGURE 2. *Optical isomers of* trans-$[Co(dien)_2]^{3+}$

The isolation and characterisation of these isomers has been carried out separately and concurrently in our two laboratories. Some sections of the work are accredited to one of our laboratories; these are denoted by Adelaide or Nagoya in parentheses.

The complexes were prepared as mixtures of isomers by the following methods:

(1) $CoX_2 + HX + O_2 + dien + C^* \xrightarrow[\text{or } 80°]{20°} [Co(dien)_2]^{3+}$ (Adelaide);

(2) $[Co(NH_3)_5X]X_2 + dien + H_2O + C^* \rightarrow [Co(dien)_2]^{3+}$;

(3) $K_3[Co(CO_3)_3]^3 + dien + H_2O + C^*$ at 0—3° with precipitation of the complex by addition of bromide ion (Nagoya);

(4) direct mixing of dien with *trans*-$[Co(dien)Cl_2]^{3,4}$ at room temperature (Nagoya). This is not an equilibrium method.

The resulting mixtures contained the *trans*- and *u-cis*-isomers as main components, and a small amount of the *s-cis*-isomer was formed in the reactions (1)—(3) with bromide as anion. No *s-cis*-isomer has been isolated from preparations (2) and (4) involving chlorides. The *s-cis*-isomer was separated cleanly as the least soluble bromide. The *trans*- and *u-cis*-isomers could then be separated from the filtrates by fractional crystallisation as iodides, with *trans* being the less soluble (Adelaide). The first and final fractions thus obtained were isomerically pure.

The mixtures could also be partially separated by paper chromatography, cellulose t.l.c., and ion-exchange. These

procedures (Adelaide) were useful in monitoring the *u-cis/trans* separation by fractional crystallisation and in determining isomer ratios in equilibrium solution mixtures. The equilibrium isomer proportions (Table) indicate that previously determined,[9] supported by a study of ion-pairing effects, allows the absolute configuration to be assigned as that shown in Figure 1. A more detailed analysis of the dichroism will be reported elsewhere.

TABLE

		s-cis	*u-cis*	*trans*
Isomer proportions in equilibrium solution mixtures	20°	5%	30%	65%
of bromides	80°	8%	40%	52%
Visible absorption spectra maxima (nm)	..	ϵ_{461} 68·5; ϵ_{333} 65·0	ϵ_{468} 96·4; ϵ_{338} 94·1	ϵ_{468} 134; ϵ_{341} 103
^{1}H n.m.r. spectra in deuteriated dimethyl sulphoxide		single NH_2 peak at 4·80 p.p.m. (downfield from Me_4Si)	two NH_2 peaks at 5·08 and 4·68 p.p.m.	two NH_2 peaks at 4·75 and 4·18 p.p.m.
^{1}H n.m.r. spectra in D^+/D_2O	.. ..	*s-cis* and *trans* similar; *u-cis* spectrum more complex consistent with its lower symmetry		
Rotations of optical isomers from less soluble diastereoisomers with the resolving agents indicated		optical isomers not possible	$(+)_D$-SbO tartrate $[M]_D$ +164°	$(+)_D$-$[Co(en)(mal)_2]^-$ $[M]_D$ +28·8°

the *trans*-configuration of the ligand is preferred, which is the configuration assigned to the complexes $[Co(dien)Cl_3]$,[4] $[Co(dien)(NO_2)_3]$,[5] and $[Cu(dien)_2]Br_2,H_2O$[6] on the basis of i.r. spectra[4] and *X*-ray structural analysis.[5,6] These results demonstrate that bond-angle strain is not the dominant factor in determining relative stabilities of isomers in amine systems of this type.[7]

The mixture of the three geometric isomers was also completely separated by column chromatography (Nagoya). A solution of the mixture in water-saturated n-butanol was poured on to a column of P-cellulose,[8] and the isomers were eluted by a mixture of n-butanol, concentrated HCl, and water (volume ratio 200 : 15 : 15). The *trans*-isomer was eluted first, followed by the *s-cis* and *u-cis* successively. The final eluted fractions (*u-cis*) were optically active, indicating partial resolution.

The isomers differ in their i.r. and electronic spectral properties (Table) and while these served to characterise and distinguish the isomers they were not particularly useful in assigning these configurations. The ^{1}H n.m.r. spectra, however, (Table) clearly differentiated the *u-cis*-isomer from the two more symmetrical forms. Whereas the four primary amine groups are equivalent in the *s-cis*-isomer (one NH_2 resonance observed) they are not equivalent in the *u-cis*- and *trans*-isomers (two peaks observed), the two NH_2 groups on each dien ligand being in different environments. The *k/k'* designations of the chelate ring conformations in the *trans*-isomer (Figure 2) follow Sargeson's nomenclature.

The isomeric products (8% *u-cis*, 92% *trans*) from method (4) involving *trans*-$[Co(dien)Cl_3]$ are consistent with the topological assignment to the *trans*-$[Co(dien)_2]^{3+}$ isomer, provided extensive isomerisation does not occur in this reaction.

The *u-cis*-isomer was completely resolved into optical isomers by two methods.

(1) An aqueous solution was adsorbed on a column of SE-Sephadex C-25 and eluted by 0·15 M-sodium (+)-tartrate solution (Nagoya). The $(+)_D$-isomer was eluted first. Details of this resolution will be published elsewhere.

(2) Diastereoisomer formation with $(+)_D$-antimonyl tartrate and recrystallisation of the active iodides to maximum rotation gave the results shown in the Table (Adelaide). A solution of the complex at pH 8 showed no measureable change in rotation after 2 weeks at 20°.

A comparison of the c.d. spectrum of $(+)_D$-*u-cis*-$[Co(dien)_2]^{3+}$ (Figure 3) with that of $(+)_D$-$[Co(penten)]^{3+}$ as

Optical activity in the *trans*-$[Co(dien)_2]^{3+}$ isomer arises predominantly from chirality of the N^2–H bonds about the C_2 axis (Figure 2). It does not arise from a configurational effect, and Figure 1 implies two planes of symmetry for this isomer. Sargeson *et al.*[10] have demonstrated that such N^2–H bonds in cobalt(III) complexes are rendered sufficiently inert towards hydrogen exchange in acid conditions to allow separation of optical isomers whose dissymmetry arises from this source. In solutions of higher pH the N–H exchange process becomes facilitated and leads to racemisation at rates which are proportional to hydroxide ion concentration.

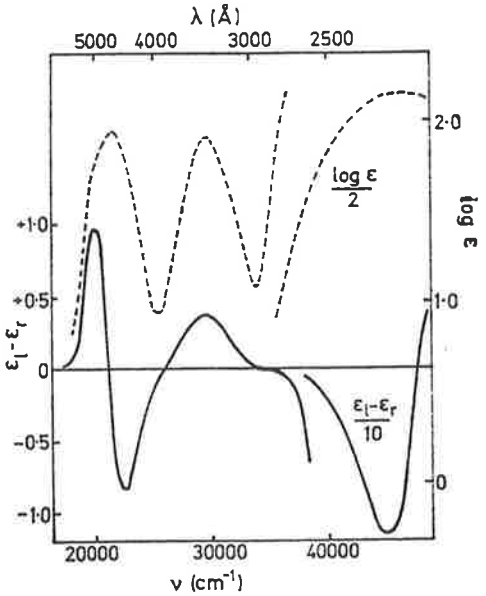

FIGURE 3. *Absorption* (– – – –) *and c.d.* (———) *spectra of* $(+)_D$-*u-cis*-$[Co(dien)_2]Cl_2.2H_2O$ *in water.*

The *trans*-isomer was resolved with the $(+)_D$-$[Co(en)(mal)_2]^-$ ion in acid conditions (Adelaide). The optical isomer obtained from the less soluble diastereoisomer as the perchlorate had rotation $[\alpha]_D$ +3·4°, and on fractional recrystallisation the highest rotation obtained (least soluble fraction) was $[\alpha]_D$ +5·1°, $[M]_D$ +28·8°. The optical purity is probably high, but the diastereoisomer

crystallises with difficulty and only a small amount of the active perchlorate has so far been obtained. The active *trans*-isomer was optically stable in solution pH 2 at 20°, but on raising the pH of this solution to pH 10 by addition of lithium hydroxide, complete racemisation had occurred within 5 min. This behaviour contrasts with the optical stability of the *u-cis*-isomer where the activity is ascribed predominantly to a configurational effect, and these results unequivocally assign the geometric configurations to these complexes. The kinetics of this racemisation of *trans*-[Co(dien)$_2$]$^{3+}$ are at present being studied (Adelaide).

The *X*-ray determination of the crystal structures of the *s-cis*-, optically active *u-cis*-, and racemic *trans*-[Co(dien)$_2$]$^{3+}$ isomers is in progress (Professor Y. Saito, University of Tokyo). The absolute *X*-ray structural analysis of optically active *trans*-[Co(dien)$_2$]$^{3+}$ will be undertaken at the University of Adelaide, and the c.d. of this isomer will also be reported later.

(*Received, January 27th*, 1970; *Com.* 125.)

[1] F. G. Mann, *J.Chem. Soc.*, 1934, 466.
[2] M. Mori, M. Shibata, E. Kyuno, and T. Adachi, *Bull. Chem. Soc. Japan*, 1956, **29**, 883; M. Shibata, M. Mori and E. Kyuno, *Inorg. Chem.*, 1964, **3**, 1573.
[3] P. H. Crayton and J. A. Mattern, *J. Inorg. Nuclear Chem.*, 1963, **13**, 248.
[4] H. H. Schmidtke and D. Garthoff, *Inorg. Chim. Acta*, 1968, **2**, 357.
[5] Y. Kushi, W. Watanabe, and H. Kuroya, *Bull. Chem. Soc. Japan*, 1967, **40**, 2985.
[6] F. S. Stephens, *J. Chem. Soc.* (*A*), 1969, 883 and 2233.
[7] F. P. Dwyer, *Austral. J. Sci.*, 1961, **24**, 97.
[8] Y. Yoshikawa and K. Yamasaki, *Inorg. Nuclear Chem. Letters*, 1968, **4**, 697.
[9] Y. Yoshikawa, E. Fujii, and K. Yamasaki, *Proc. Japan Acad.*, 1967, **43**, 495; A. Muto, F. Marumo, and Y. Saito, *Inorg. Nuclear Chem. Letters*, 1969, **5**, 85; S. F. Mason and B. J. Peart, *ibid.*, p. 491.
[10] B. Halpern, A. M. Sargeson, and K. R. Turnbull, *J. Amer. Chem. Soc.*, 1966, **88**, 4680; D. A. Buckingham, L. G. Marzilli, and A. M. Sargeson, *ibid.*, 1967, **89**, 825 and 3428; D. A. Buckingham, P. A. Marzilli, and A. M. Sargeson, *Inorg. Chem.*, 1967, **6**, 1032.

The Circular Dichroism and the Chirality of the Unsymmetric-*cis*- and the *trans*-(+)$_D$-Bis(diethylenetriamine)cobalt(III) Ion

By F. R. Keene and G. H. Searle*

(*Department of Physical and Inorganic Chemistry, The University of Adelaide, Adelaide, South Australia* 5001)

and S. F. Mason

(*School of Chemical Sciences, University of East Anglia, Norwich*)

Reprinted from

Chemical Communications 1970

The Chemical Society, Burlington House, London W1V OBN

The Circular Dichroism and the Chirality of the Unsymmetric-*cis*- and the *trans*-(+)$_D$-Bis(diethylenetriamine)cobalt(III) Ion

By F. R. Keene and G. H. Searle*

(*Department of Physical and Inorganic Chemistry, The University of Adelaide, Adelaide, South Australia* 5001)

and S. F. Mason

(*School of Chemical Sciences, University of East Anglia, Norwich*)

Summary The circular dichroism of the systems u-*cis*-(+)$_D$-[Co(dien)$_2$]$^{3+}$ and *trans*-(+)$_D$-[Co(dien)$_2$]$^{3+}$ indicates the stereochemical configuration of the former, and indicates in the latter a new type of chirality which has hitherto not been realized, but which will be present in metal–polyamine complexes.

The three geometric isomers of [Co(dien)$_2$]$^{3+}$ have been isolated recently, and the unsymmetrical *cis* (u-*cis*) (I) and the *trans* isomer (II), each having only C_2 symmetry, have been resolved into optical antipodes.[1] The third isomer,[1] symmetrical *cis* (s-*cis*), is not dissymmetric (C_{2h} symmetry).

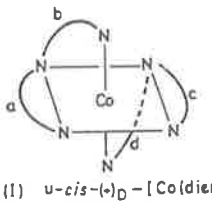

(I) u-*cis*-(+)$_D$-[Co(dien)$_2$]$^{3+}$

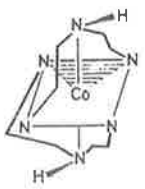

(IIa) *trans* – δ–NH

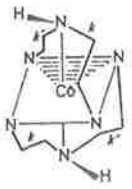

(IIb) *trans* – λ–NH

The c.d. spectra of the u-*cis*-(+)$_D$- and the *trans*-(+)$_D$-[Co(dien)$_2$]$^{3+}$ optical isomers have now been measured (Figure) in order to determine the stereochemical configuration of the former and to evaluate the optical effect of a new type of chirality in the latter. The results show (Figure) that u-*cis*-(+)$_D$-[Co(dien)$_2$]$^{3+}$ in aqueous solution gives a major positive and a minor negative c.d. band, at a lower and a higher frequency, respectively, in the spectral region of the octahedral $^1A_{1g} \rightarrow {}^1T_{1g}$ absorption of the

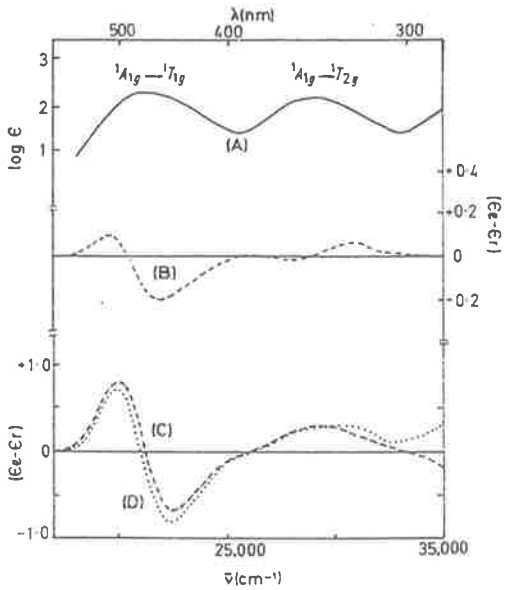

FIGURE. *The absorption spectrum* (A) *and the c.d.* (B) *of trans*-(+)$_D$-[Co(dien)$_2$]$^{3+}$ *in* 0·1 M-$HClO_4$ *and the c.d. of* u-*cis*-(+)$_D$-[Co(dien)$_2$]$^{3+}$ (C) *in water and* (D) *in* 0·2 M-*sodium selenite.*

$Co^{III}N_6$ chromophore, the areas of these c.d. bands being diminished and enhanced, respectively, by the addition of a polarisable oxyanion. The signs and relative frequencies and magnitudes of the lower-energy c.d. bands of u-*cis*-$(+)_D$-$[Co(dien)_2]^{3+}$, and the changes in band area on the addition of selenite are similar[2] to the corresponding properties of the analogous c.d. bands of $(+)_D$-$[Co(en)_3]^{3+}$, $(+)_D$-*cis*-$[Co(en)_2(NH_3)_2]^{3+}$, and $(+)_D$-$[Co(penten)]^{3+}$, and it is concluded that the former complex has the same configuration (I) as that of the latter group of complex ions, which also contain the $Co^{III}N_6$ chromophore.

Crystal structure analysis by the anomalous *X*-ray scattering method shows[3,4] that both $(+)_D$-$[Co(en)_3]^{3+}$ and $(-)_D$-$[Co(penten)]^{3+}$ have the Λ configuration, in terms of the ring-pairing nomenclature of the IUPAC commission.[5]

The application of the ring-pairing procedure to u-*cis*-$(+)_D$-$[Co(dien)_2]^{3+}$ indicates that whilst the chelate rings *b* and *d* of (I) have a mutual Δ chirality, both of the pairs *a* and *d*, and *b* and *c*, have a mutual Λ chirality. Thus the overall configuration of (I) is Λ, like that[4] of $(+)_D$-$[Co(penten)]^{3+}$ where the ring-pairing relations are closely analogous,[6] the two complex ions differing only in that a fifth chelate ring, joining the nitrogen atoms which are secondary in the former (I), is present in the latter complex.

Hitherto the optical activity of dissymmetric metal complexes has been ascribed to two principal sources,[7-9] firstly, the configurational effect due to the chiral disposition of two or more chelate rings (which may be planar) around the metal ion, and secondly, the conformational and vicinal effect due to a preferred dissymmetric conformation of non-coplanar chelate rings augmented by a vicinal perturbation from the asymmetric carbon or nitrogen centre or centres which determine the ring conformation. For *trans*-$(+)_D$-$[Co(dien)_2]^{3+}$ (II) the configurational and the conformational or vicinal effects are vanishing. The stereochemical disposition of the chelate rings about the metal ion in (II) is non-chiral, the symmetry of the complex being D_{2d} if the atoms of each ring are taken to be coplanar. For each dien ligand the conformational effect is internally compensated in (II), one chelate ring having the *k* and the other the *k'* conformation in the Corey and Bailar nomenclature,[10] or the δ and the λ conformation in the IUPAC system.[5]

However *trans*-$(+)_D$-$[Co(dien)_2]^{3+}$ gives a minor positive and a major negative c.d. band at a lower and a higher frequency, respectively, in the spectral region of the $^1A_{1g} \rightarrow {}^1T_{1g}$ absorption of the octahedral $Co^{III}N_6$ chromophore (Figure), these bands having the same sign and similar magnitudes to those given by[9] [Co-(+)-(pn)$(NH_3)_4$]$^{3+}$ or by[11] $(-)_D$-$[Co(NMe\text{-}en)(NH_3)_4]^{3+}$, where the optical activity derives in each case, from a single asymmetric centre in the ligand and a single puckered chelate ring. The sole element of chirality in the complex ion, *trans*-$[Co(dien)_2]^{3+}$ is the stereochemical relationship between the two *trans* N–H bonds of the secondary nitrogen atoms in the ligands. These two N–H bonds form a segment of either a right-handed (IIa) or a left-handed helix (IIb), taking either N–H bond as the helix axis according to the IUPAC convention,[5] and they are designated the *trans*-δ-NH and the *trans*-λ-NH isomers, respectively. The c.d. spectrum of *trans*-$(+)_D$-$[Co(dien)_2]^{3+}$ (Figure) indicates that the *trans*-NH chiral element gives rise to optical effects comparable in magnitude to those of the conformational and vicinal effect of a single optically-active chelate ring, but the c.d. recorded does not distinguish between the structures (IIa) and (IIb) for this isomer. An absolute *X*-ray crystal analysis of an optical isomer of the *trans*-complex is in progress.

Although measurements were taken throughout the u.v. region down to 185 nm on a Jouan CD 185 Dichrographe (c.d. optical density detection limit 1 in 10^5), no c.d. response was recorded over this region for the *trans*-isomer. Thus the c.d. in this charge transfer region, where $\epsilon_{max} = 39{,}000$ at 222 nm cannot be larger than about 0·3, compared with -30 for $(+)_D$-$[Co(en)_3]^{3+}$ or $+12$ for *trans*-$[Co\text{-}(-)\text{-}(pn)_2(NH_3)_2]^{3+}$.[8] We take this to indicate that the conformational contribution to the optical activity is negligible (hence our assignment of the observed c.d. bands in the ligand field region to the N–H chiral effect).

A molecular model indicates some crowding in one quadrant of the *trans*-molecule (shown shaded in the diagram). Such crowding could be relieved by distortion of the conformation of one chelate ring of each dien ligand. Optical activity could then also arise from asymmetry of charge around the nitrogen (a small vicinal effect) together with a conformational effect since the *k'* helical contributions would not then completely cancel those of *k*. Such distortion will be checked in the *X*-ray structure analysis, although any distortion is evidently too small to be detectable from the dichroism.

Since this is the first complex observed to give no c.d. in the charge transfer region, this result lends support to the hypothesis[8] that configurational and conformational effects are the principal contributors to the c.d. of the charge transfer region in metal complexes.

A contribution to optical activity from this N–H chiral effect should also be present in complexes of all linear polyamines forming gauche five-membered chelate rings, such as triethylenetetramine, tetraethylenepentamine, and (linear) pentaethylenehexamine, but in these instances it would not be separately distinguishable from the conformational and vicinal effects.

(*Received, February 2nd*, 1970; *Com.* 149.)

[1] F. R. Keene, G. H. Searle, Y. Yoshikawa, A. Imai, and K. Yamasaki, *Chem. Comm.*, 1970, 784.
[2] S. F. Mason and B. J. Norman, *Chem. Comm.*, 1965, 73.
[3] K. Nakatsu, Y. Saito, and H. Kuroya, *Bull. Chem. Soc. Japan*, 1956, **29**, 428.
[4] A. Muto, F. Marumo, and Y. Saito, *Inorg. Nuclear Chem. Letters*, 1969, **5**, 85.
[5] IUPAC Bulletin, 1968, No. 33, 68; *Inorg. Chem.*, 1970, **9**, 1.
[6] S. F. Mason and B. J. Peart, *Inorg. Nuclear Chem. Letters*, 1969, **5**, 491.
[7] B. E. Douglas, *Inorg. Chem.*, 1965, **4**, 1813.
[8] S. F. Mason, A. M. Sargeson, R. Larsson, B. J. Norman, A. J. McCaffery, and G. H. Searle, *Inorg. Nuclear Chem. Letters*, 1966, **2**, 333; *J. Chem. Soc.* (*A*), 1968, 1304 and 1310.
[9] K. Ogino, K. Murano, and J. Fujita, *Inorg. Nuclear Chem. Letters*, 1968, **4**, 351.
[10] E. J. Corey and J. C. Bailar, *J. Amer. Chem. Soc.*, 1959, **81**, 2620.
[11] D. A. Buckingham, L. G. Marzilli, and A. M. Sargeson, *J. Amer. Chem. Soc.*, 1967, **89**, 825.

[Reprinted from Inorganic Chemistry, 11, 148 (1972).]

CONTRIBUTION FROM THE DEPARTMENT OF PHYSICAL AND INORGANIC CHEMISTRY,
THE UNIVERSITY OF ADELAIDE, ADELAIDE, SOUTH AUSTRALIA 5001

The Isomers of the Bis(diethylenetriamine)cobalt(III) Ion and a New Source of Optical Activity

BY F. R. KEENE AND G. H. SEARLE

Received March 29, 1971

The three geometric isomers of the $[Co(dien)_2]^{3+}$ ion s-cis, u-cis, and trans have been separated by various methods, and the u-cis and trans isomers have been resolved into optical isomers through diastereoisomer formation. The configurations have been unequivocally assigned to these geometric forms from the different racemization behavior of the u-cis and trans optical isomers. Factors determining relative isomer stabilities are discussed, and infrared and pmr criteria for assigning isomer configurations are examined.

Introduction

The problem of the existence of the three geometric isomers which are possible for a complex $[M(dien)_2]^{3+}$ (where dien designates the tridentate ligand diethylenetriamine)[1] has remained ever since the cobalt(III) complex ion of this formulation was first isolated as the iodide $[Co(dien)_2]I_3$ by Mann in 1934.[2] The corresponding chromium(III) complex $[Cr(dien)_2]I_3$ has also been prepared[3] and again isomers have not been isolated. This paper describes the isolation and characterization of all the geometric and optical isomers which

(1) Abbreviations used: en, ethylenediamine; *N*-Meen, *N*-methylethylenediamine; dien, diethylenetriamine; trien, triethylenetetramine; tetraen, tetraethylenepentamine; penten, pentaethylenehexamine (double branched chain isomer); sarc, sarcosinato; tart, tartrate; mal, malonato.

(2) F. G. Mann, *J. Chem. Soc.*, 466 (1934).

(3) V. O. Kling and H. L. Schlafer, *Z. Anorg. Allg. Chem.*, **313**, 187 (1961).

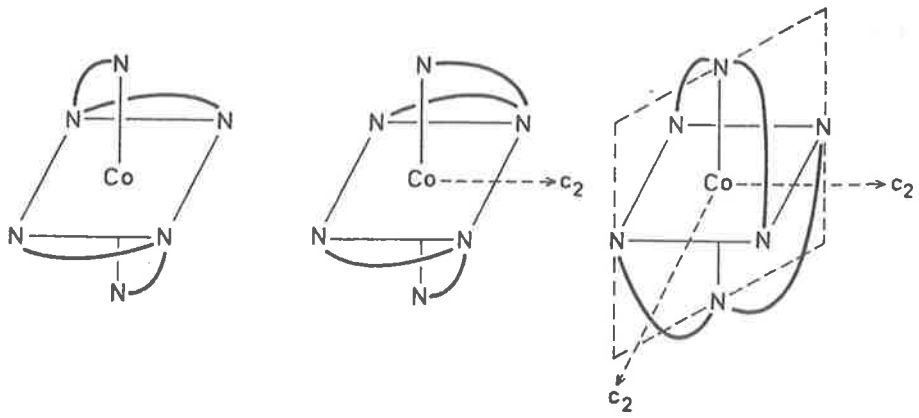

s-cis
s-fac

u-cis
u-fac

trans
mer

(+)D optical isomer
Λ absolute configuration

Figure 1.—Topological isomers of $[Co(dien)_2]^{3+}$.

are possible for the $[Co(dien)_2]^{3+}$ ion. The three geometric isomers are shown in Figure 1. These may be designated in terms of the facial or meridional disposition of the ligands or alternatively by the cis or trans positions of the primary amino donor groups of each dien ligand, and an additional specification s or u is necessary to distinguish the two cis forms. The u-cis (unsymmetrical) form has only a twofold rotation axis and should exist in optical isomers, with the dissymmetry arising primarily from a configurational effect. The s-cis (symmetrical) isomer with a center and planes of symmetry is not dissymmetric.

The facility of linear polyamine ligands (and related linear multidentate ligands) to coordinate in facial or meridional dispositions over each pair of interlocked five-membered chelate rings is well established. This facility for dien has been demonstrated by extensive studies of mono-dien complexes, and in a number of systems all the possible geometric isomers have been isolated.[4-8] On this basis it seems surprising that the two possible geometric forms of $[Co(dien)X_3]$ ($X^- = Cl^-, NO_2^-, NCS^-$) have not so far been prepared or separated.[5,6,9]

The bis-dien cobalt(III) complex has been used in studies by several workers,[9-13] and from the reported preparative methods it is now apparent that these materials were isomeric mixtures. In the only attempt to assign a configuration, Crayton and Mattern[9] implied that only the most stable isomer in such systems would be isolated. Partly on the basis of failure to resolve their $[Co(dien)_2]^{3+}$ with three resolving agents, they assigned the configuration as trans, and although the rationale for this proposal was invalid (failure to achieve a resolution does not prove that a compound is incapable of being resolved or is not dissymmetric) the present work shows that the trans isomer is indeed the most stable.

An aspect of particular interest in the $[Co(dien)_2]^{3+}$ system is the origin of dissymmetry and the resulting optical activity in the trans isomer. In principle, the configurational and conformational effects are vanishing for this isomer. Figure 1 indicates that if the atoms of each chelate ring are taken to be coplanar, the structure has two planes of symmetry and two C_2 axes (there is also an S_4 axis mutually perpendicular to the two C_2 axes shown in the figure) so that the stereochemical disposition of the chelate rings about the metal ion is nonchiral. Figure 2 shows the chelate ring conformations which must obtain in the optical isomers. When these ring conformations are considered the planes of symmetry in Figure 1 disappear and the S_4 axis is destroyed (although each coordinated ligand retains a mirror plane as in Figure 2), but one of the C_2 axes remains and relates the two ligands in the molecule. The point group is thus reduced from S_2 (ring atoms taken to be coplanar) to C_2 by the ring conformations. A vicinal effect should not arise since the two chelate rings constituting each dien ligand are mirror images. It is also evident that for each dien ligand the conformational effect is internally compensated, one chelate ring having

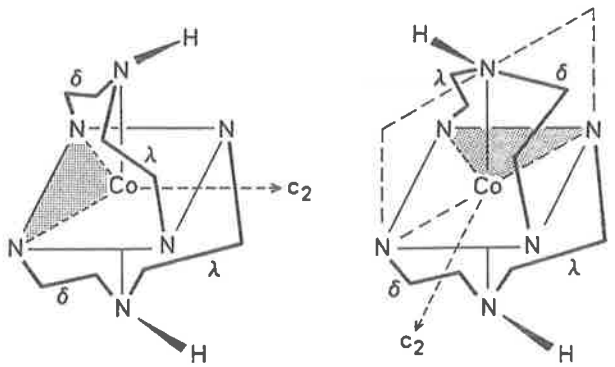

trans-δ-NH
M(C_2)-NH

trans-λ-NH
P(C_2)-NH

Figure 2.—Optical isomers of *trans*-$[Co(dien)_2]^{3+}$.

(4) J. I. Legg and D. W. Cooke, *Inorg. Chem.*, **5**, 594 (1966).
(5) D. A. House, *Inorg. Nucl. Chem. Lett.*, **3**, 67 (1967).
(6) H. H. Schmidtke and D. Garthoff, *Inorg. Chim. Acta*, **2**, 357 (1968).
(7) A. R. Gainsford and D. A. House, *ibid.*, **3**, 367 (1969).
(8) S. H. Caldwell and D. A. House, *J. Inorg. Nucl. Chem.*, **31**, 811 (1969).
(9) P. H. Crayton and J. A. Mattern, *ibid.*, **13**, 248 (1960).
(10) J. Brigando, *Bull. Soc. Chim. Fr.*, 211 (1957).
(11) G. A. Barclay and A. K. Barnard, *J. Chem. Soc.*, 2540 (1958).
(12) F. Basolo, J. W. Palmer, and R. G. Pearson, *J. Amer. Chem. Soc.*, **82**, 1073 (1960).
(13) H. Yoneda and Y. Morimoto, *Bull. Chem. Soc. Jap.*, **39**, 2180 (1966).

a δ conformation and the other the λ conformation (or k and k′, respectively, in the Sargeson–Bailar and Corey designation).[14] Thus the "conventional" sources of chirality, configurational and conformational and vicinal effects, are not present in this molecule.

The dissymmetry of the molecule is due to another chirality type which is exemplified and uniquely described by the stereochemical relationship between the two trans N^2H bonds of the secondary nitrogen atoms in the two ligands (Figure 2). These two NH bonds form a segment of either a right-handed or a left-handed helix taking either NH bond as the helix axis according to the IUPAC convention,[14] and we designate the absolute configurations of the optical forms of the *trans*-$[Co(dien)_2]^{3+}$ complex as trans-δ-NH and trans-λ-NH, respectively (Figure 2). We therefore describe this source of chirality in such amine complexes as the "NH chiral effect".

However the dissymmetry is not due solely to the presence of the N^2H bonds as the structure would retain dissymmetry even if such bonds were absent, for example if a sulfur donor replaced the secondary amine group. The same type of symmetry relationship holds between any of the C_2-related CH, NH, NC, or CC bonds in the two ligands and these individual bond chiralities should all contribute to the overall helicity of the molecule. The absolute configuration can therefore be described by any of these bond relationships (these are not all of the same skew, δ or λ) and we have chosen the N^2H bonds as the simplest description for this complex as this means of nomenclature lends itself more generally to a wider variety of potential ligands. With sulfur donors for example, the lone pair directions might be employed in an analogous stereochemical situation. An alternative designation for the absolute configurations of the *trans*-$[Co(dien)_2]^{3+}$ optical isomers could be in terms of the left-handed (minus) or right-handed (positive) helicity of the two N^2H bonds about the C_2 axis, M(C_2)-NH or P(C_2)-NH, respectively (Figure 2).

Such chiral effects as we have described have not hitherto been realized as contributing effects to optical activity in metal polyamine complexes, but should be present in complex systems such as $[Co(trien)X_2]^+$ in addition to the "conventional" sources of chirality.

It has been known for some time that NH bonds on coordinated nitrogen donor atoms are relatively inert toward hydrogen exchange in acid conditions. However, it has only recently been appreciated from the work of Sargeson, *et al.*,[15] that this inertness of N^2H bonds on coordinated *secondary* amine donor groups is sufficient to allow separation of optical isomers of complexes whose dissymmetry arises from this source. Optical isomers of a number of complexes containing the ligands *N*-methylethylenediamine (*N*-Meen) or sarcosinato (sarc) have been observed to racemize only very slowly in acid conditions, but in solutions of higher pH the NH exchange process becomes facilitated and leads to racemization following the rate law

$$\text{rate} = k_{rac}[\text{complex}][OH^-]$$

The situation in *trans*-$[Co(dien)_2]^{3+}$ is analogous to that in the $[Co(NH_3)_4(N\text{-Meen})]^{3+}$ and $[Co(NH_3)_4(sarc)]^{2+}$ complexes. In each of these complexes[16,17] the molecular dissymmetry arises from the alternative possible dispositions of the N^2H bond, and these alternative dispositions are interconvertible in basic solution. These racemization phenomena provide the basis of a method for unequivocally distinguishing the trans isomer from the other two geometric isomers in the $[Co(dien)_2]^{3+}$ system.

Although the contribution of "NH chiral effects" to optical activity of polyamine complexes has not previously been appreciated, the stereochemical basis is not new. An N^2H bond fixed in one of two alternative dispositions will confer isomerism providing these alternative dispositions can be distinguished. In *trans*-$[Co(dien)_2]^{3+}$ the alternative dispositions of one N^2H are distinguished with reference to one fixed disposition of the other N^2H bond in the molecule. Due to the particular symmetry properties of this molecule the "NH chiral effect" is the only contribution to the dissymmetry, since these coordinated nitrogen atoms themselves are not asymmetric. In all complexes of *N*-Meen and sarc, however, the secondary amine nitrogen becomes asymmetric on coordination (a situation described as donor atom asymmetry) and vicinal and conformational effects both contribute to optical activity. In these instances with only one N^2H bond the chiral effect does not arise, yet the kinetic aspects of the racemization should be closely similar.

A similar situation to that in *trans*-$[Co(dien)_2]^{3+}$ arises in the case where dien is coordinated meridionally in the system $[Co(en)(dien)Cl]^{2+}$, shown in Figure 3. Here the two alternative dispositions of the single

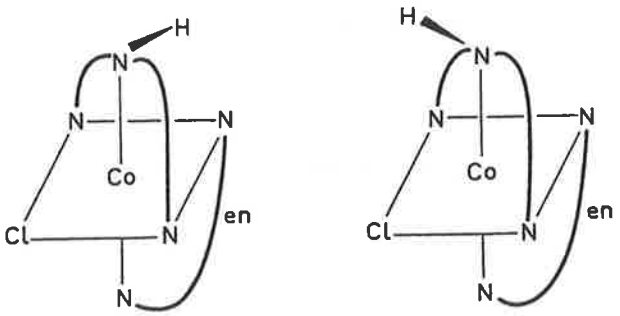

Figure 3.—Isomers of $[Co(en)(dien)Cl]^{2+}$ arising from dien coordinated meridionally.

N^2H bond can be distinguished by reference to the chloro ligand which is cis to the donor secondary nitrogen. This creates two geometric isomers,[7] but optical isomers are not possible as there is no "NH chiral effect" nor vicinal effect and the conformational contributions in the coordinated dien cancel as in *trans*-$[Co(dien)_2]^{3+}$.

The optical activity and circular dichroism of *trans*-$[Co(dien)_2]^{3+}$ have been discussed in a previous communication[18] and the kinetics of racemization and exchange will be reported in due course.

The factors which determine relative stabilities of isomers are not well understood, and the number of systems where equilibrium isomer proportions have

(14) *IUPAC Bull.* **No. 33**, 66 (1968); *Inorg. Chem.*, **9**, 1 (1970).
(15) A. M. Sargeson and G. H. Searle, *ibid.*, **6**, 787 (1967).
(16) B. Halpern, A. M. Sargeson, and K. R. Turnbull, *J. Amer. Chem. Soc.*, **88**, 4630 (1966).
(17) D. A. Buckingham, L. G. Marzilli, and A. M. Sargeson, *ibid.*, **89**, 825 (1967).
(18) F. R. Keene, G. H. Searle, and S. F. Mason, *Chem. Commun.*, 893 (1970).

been assessed experimentally is as yet very limited. Much further experimental data are necessary to compare with results from energy minimization computations. Some systems previously studied such as $[Co(trien)X_2]^{n+}$ [15] and $[Co(tetraen)X]^{n+}$ [19] involve factors arising from the acido ligands X, and the present system provides an opportunity to study isomer stabilities as a function of factors in the amine chelate rings only.

Experimental Section

Diethylenetriamine, from either Fluka (puriss) or Union Carbide Australia Ltd., was used without further purification.

Visible spectra were measured on a Unicam SP700 recording spectrophotometer in 1-cm cells against water as a reference. For estimating isomer proportions, spectra of elutes from chromatographic separations were measured at the first band maximum (*ca.* 466 nm) on a manual Shimadzu QR-50 spectrophotometer. The separate isomers in either water or in 0.3 *M* sodium tartrate solution gave identical visible spectra, and extinction coefficients obtained on the two instruments agreed.

Infrared spectra were obtained on a Perkin-Elmer 457 grating infrared spectrophotometer in KBr disks against air reference. Optical rotations were measured on a Perkin-Elmer 141-MC spectropolarimeter in a 1-dm tube at 20°. Signs of rotations refer to the sodium D line unless another wavelength is specified. ORD curves were obtained on a Perkin-Elmer P22 recording spectropolarimeter. Pmr spectra were obtained on a Varian HA-100 spectrometer or a 60-Mc Jeol spectrometer using sodium trimethylsilylpropanesulfonate as a reference.

Preparation of $[Co(dien)_2]^{3+}$ by Aerial Oxidation.—To a solution of $CoCl_2 \cdot 6H_2O$ (47.6 g, 0.20 mol) in water (250 ml) was added dien (34.5 g, 0.33 mol), dien·3HCl (14.5 g, 0.067 mol), and charcoal (25 g). Air was passed through the solution for 36 hr. After filtering, the solution was evaporated to a small volume using a rotary evaporator and the product was then precipitated as completely as possible by the addition of ethanol. The product was filtered off, washed with ethanol and acetone, and then air-dried; yield of $[Co(dien)_2]Cl_3 \cdot xH_2O$, 76.0 g (93% calcd for 2-hydrate).

The complex was prepared as the bromide in an analogous manner using anhydrous $CoBr_2$ (44.0 g, 0.20 mol), dien (34.5 g, 0.33 mol), and dien·3HBr (23.0 g, 0.067 mol) in water (500 ml). After aeration and filtration, the solution was evaporated almost to dryness, and the remaining product was precipitated with ethanol; yield 99.0 g (95% calcd for $[Co(dien)_2]Br_3 \cdot H_2O$).

Preparation of $[Co(dien)_2]^{3+}$ from $[Co(NH_3)_5X]X_2$.—A slurry in water was prepared of charcoal (20 g) and either $[Co(NH_3)_5Cl]Cl_2$ (100 g, 0.40 mol) or $[Co(NH_3)_5Br]Br_2$ (154 g, 0.40 mol). dien (91 g, 0.88 mol) was stirred in, and the mixture was heated on a steam bath for 4 hr. After filtering, the solution was evaporated almost to dryness and the product was precipitated as completely as possible with ethanol. The product was filtered off, washed with ethanol and acetone, and then air-dried; yield of $[Co(dien)_2]Cl_3 \cdot 2H_2O$, 153 g, 94%; yield of $[Co(dien)_2]Br_3 \cdot H_2O$, 200 g, 95%.

Separation of Geometric Isomers from Preparative Mixtures.—The above bromide preparations were recrystallized from warm water by allowing the solution to cool and stand until about 10% of the material had separated. This was filtered off and fractionally recrystallized again from warm water (3 times its weight). As each fraction was filtered off it was washed with 70% ethanol, and the filtrate was evaporated in a rotary evaporator to induce crystallization of the next fraction. The least-soluble fractions comprised pure *s-cis*-$[Co(dien)_2]Br_3$ as relatively large well-formed prisms, and the point at which the more soluble trans isomer commenced to crystallize could be recognized visually from the very much smaller thin needles of *trans*-$[Co(dien)_2]Br_3 \cdot H_2O$. This procedure allows essentially quantitative separation of the s-cis isomer from the mixture.

The trans and u-cis isomers in the remaining solution were separated by fractional precipitation by adding LiI in small amounts. The trans isomer is the less soluble, but the precipitated products appeared (halide analyses) to be mixed bromide–iodides. This separation was monitored by running thin-layer chromatograms on cellulose of the various fractions (developing solvent *sec*-butyl alcohol:water:concentrated HCl = 70:20:10). The first and last fractions were isomerically pure trans and u-cis, respectively, but middle fractions contained both isomers. The mixed halide precipitates of the separated isomers were converted to pure bromides or iodides using an anion exchanger. The trans and u-cis iodides are anhydrous. *Anal.* Calcd for *s-cis*-$[Co(C_4H_{13}N_3)_2]Br_3$: C, 19.0; H, 5.19; N, 16.6; Br, 47.5. Found: C, 19.4; H, 5.40; N, 16.7; Br, 47.7. Calcd for *trans*-$[Co(C_4H_{13}N_3)_2]Br_3 \cdot H_2O$: C, 18.4; H, 5.40; N, 16.1; Br, 45.8. Found: C, 18.0; H, 5.12; N, 16.1; Br, 45.7. Calcd for *u-cis*-$[Co(C_4H_{13}N_3)_2]Br_3 \cdot 0.5H_2O$: C, 18.7; H, 5.29; N, 16.3; Br, 46.6. Found: C, 18.6; H, 5.29; N, 16.2; Br, 46.5.

Isomeric purity was checked by chromatography on a column of SE-Sephadex C-25 cation exchanger (Na^+ form), column dimensions 40 × 0.9 cm. A dilute aqueous solution of a small portion (*ca.* 0.1 g) of a particular fraction was absorbed on the column and eluted with 0.3 *M* sodium tartrate solution. Two hours was required to ensure a clean separation on the column of the bands of the three isomers (if present), the band order being s-cis (fastest moving), u-cis, and trans (slowest).

Estimation of Equilibrium Isomer Proportions.—Solutions containing the three isomers were prepared by synthesis involving aerial oxidation as above, with equilibrium between the isomeric products being established by the presence of charcoal. The reaction mixtures in all cases involved the stoichiometry

$$\text{aqueous } CoX_2 + 1.67\text{dien} + 0.33(\text{dien}\cdot 3HX) \xrightarrow{\text{air, charcoal}} [Co(dien)_2]^{3+} + 3X^-$$

and air was passed through the solutions at 20° for 36 hr.

After filtering off the charcoal from such reaction mixtures a small sample of each solution (from which crystallization of products was prevented) was extracted, and in suitable dilution was applied to a column of SE-Sephadex C-25 as described earlier. The eluate bands (0.3 *M* sodium tartrate solution) were collected separately and made up to convenient exact volumes, and the relative amounts were estimated spectrophotometrically at the first absorption band maxima (4-cm cells).

For preparations involving quantities as described earlier, but with a solution volume of 500 ml in each instance, the isomer proportions (chloride or bromide preparation) obtained for equilibration at 20°, with [Co] = 0.4 *M*, were as follows: 65% trans, 28% u-cis, 7% s-cis. These figures were obtained from duplicate preparations of bromides and duplicate preparations of chlorides. Each preparation was analyzed by two chromatographic separations and spectral determinations. The above figures were reproducible to ±1 in the eight determinations. The charcoal used was freshly finely ground B.D.H. granulated activated charcoal for gas absorption, and before use in the equilibrations its catalytic ability was tested to ensure that it satisfied the criterion of causing racemization of $(+)[Co(en)_3]^{3+}$ within 2 min at 90°.[20]

Resolution of *u-cis*-$[Co(dien)_2]^{3+}$.—To a solution of *u-cis*-$[Co(dien)_2]Cl_3 \cdot 2H_2O$ (8.2 g, 0.02 mol) in warm water (200 ml) was added Ag(+)[SbOtart] (23.6 g, 0.06 mol). After shaking, the precipitated silver chloride was filtered off and the filtrate volume was made up to 250 ml. Scratching the beaker induced crystallization of the diastereoisomer $(+)$*u-cis*-$[Co(dien)_2](+)[SbO\ tart]_3 \cdot 2H_2O$, and after cooling at 0° for several hours it was filtered off, washed with 75% ethanol, absolute ethanol, and then acetone, and then air-dried; yield 9.2 g, 80% of one optical form. It was recrystallized from water (discarding the most soluble portions) until constant rotation was attained. $\alpha_D = +0.533°$ for a 0.44% solution in water, whence $[\alpha]_D = 121°$. *Anal.* Calcd for $(+)$*u-cis*-$[Co(C_4H_{13}N_3)_2](+)[SbO(C_4H_4O_6)]_3 \cdot 2H_2O$: C, 20.9; H, 3.65; N, 7.2. Found: C, 20.9; H, 3.65; N, 7.0.

This recrystallized diastereoisomer (2.6 g) was ground with NaI in an aqueous slurry, and the $(+)$*u-cis*-$[Co(dien)_2]I_3$ which separated was filtered off, washed with ice-cold NaI solution, ethanol, and acetone, and then air-dried. Recrystallization from hot water did not increase the rotation; yield 1.0 g (8%). $\alpha_D = +0.033°$ for a 0.13% aqueous solution, $[\alpha]_D = +25.6°$. *Anal.* Calcd for $(+)$*u-cis*-$[Co(C_4H_{13}N_3)_2]I_3$: C, 14.9; H, 4.06; N, 13.0. Found: C, 14.9; H, 3.95; N, 13.0.

The diastereoisomer remaining in the aqueous solution above was fractionally precipitated by gradually adding ethanol and

(19) M. R. Snow, D. A. Buckingham, I. E. Maxwell, and A. M. Sargeson, *J. Amer. Chem. Soc.*, **92**, 3610, 3617 (1970).

(20) F. P. Dwyer and A. M. Sargeson, *Nature (London)*, **187**, 1022 (1960).

cooling. The most soluble of these fractions (4.0 g) was ground with sodium iodide as before, and the (−)*u-cis*-$[Co(dien)_2]I_3$ obtained was recrystallized three times from water to give constant rotation. The optical isomer was less soluble than the racemate; yield 1.3 g (10%); $[\alpha]D = -24.9°$.

Resolution of *trans*-$[Co(dien)_2]^{3+}$.—*trans*-$[Co(dien)_2]Cl_3 \cdot 2.5H_2O$ (8.3 g, 0.02 mol) was dissolved in water acidified with acetic acid (100 ml of water containing 0.5 ml of glacial acetic acid, giving a solution of pH 3–4). Ag(+)$[Co(en)(mal)_2] \cdot 2H_2O$[15] (28 g, 0.06 mol) was added, and after shaking the solution in a stoppered flask, the precipitated silver chloride was filtered off. Water (100 ml) and methanol (200 ml) were added to the filtrate, then ethanol (about 500 ml) was added carefully to incipient crystallization. Crystallization of the diastereoisomer is somewhat difficult, but with the above conditions (+)*trans*-$[Co(dien)_2]$(+)-$[Co(en)(mal)_2]_3 \cdot 10H_2O$ crystallized on cooling the solution for several days in a refrigerator; yield 7.3 g, 52% of one optical form. The diastereoisomer was filtered off, washed with methanol, ethanol, and acetone, and then air-dried. Because of the difficulty with crystallization and the relatively poor discrimination between the two diastereoisomers with this resolving agent, optical purification of the diastereoisomer was difficult. *Anal.* Calcd for (+)*trans*-$[Co(C_4H_{13}N_3)_2]$(+)$[Co(C_2H_8N_2)(C_3H_2O_4)_2]_3 \cdot 10H_2O$: C, 27.1; H, 5.8; N, 11.9. Found: C, 26.7; H, 5.2; N, 12.1.

The dextro isomer was obtained by dissolving the diastereoisomer in 0.1 *M* HBr and absorbing the cation on a column of cation-exchange resin (Bio-Rad AG 50W-X2, 200–400 mesh, in H^+ form). The resolving anion was washed from the column with 0.1 *M* HBr, then the (+)$[Co(dien)_2]^{3+}$ cation was eluted with 3 *M* HBr. (+)*trans*-$[Co(dien)_2]Br_3 \cdot H_2O$ crystallized on evaporating the elute, and the product was recrystallized from 0.1 *M* HBr four times to constant rotation, the active bromide being less soluble than the racemate; yield 0.6 g. $\alpha_{546} = +0.089°$ for a 0.308% solution in 0.1 *M* HBr, whence $[\alpha]_{546} = +28.9°$.

Further diastereoisomer was crystallized from the cold solution by careful addition of further portions of ethanol over several days. The product was removed in fractions until the total diastereoisomer obtained was about 80% of the total (both optical forms). The solution which then contained essentially only (−)*trans*-$[Co(dien)_2]$(+)$[Co(en)(mal)_2]_3$ was passed through the cation exchanger as above, and (−)*trans*-$[Co(dien)_2]$-$Br_3 \cdot H_2O$ crystallized from the 3 *M* HBr elute. Recrystallization to constant rotation gave $[\alpha]_{546} = -29.2°$; yield 0.8 g. *Anal.* Calcd for (−)*trans*-$[Co(C_4H_{13}N_3)_2]Br_3 \cdot H_2O$: C, 18.4; H, 5.40; N, 16.1; Br, 45.8. Found: C, 18.4; H, 5.30; N, 15.9; Br, 44.7.

trans-$[Cu(dien)_2]Br_2 \cdot 0.5H_2O$.—A solution of $CuBr_2$ in ethanol was added to dien (2.1 molar ratio) in ethanol. After cooling the solution, the deep blue crystals were filtered off, washed with ethanol, and then air-dried. The product was recrystallized slowly from hot methanol; yield 70%. *Anal.* Calcd for *trans*-$[Cu(C_4H_{13}N_3)_2]Br_2 \cdot 0.5H_2O$: C, 21.9; H, 6.20; N, 19.2; Br, 36.4. Found: C, 21.7; H, 6.20; N, 19.0; Br, 36.4. The configuration of this product has been established as trans by X-ray structure analysis.[21]

$[Ni(dien)_2]Br_2 \cdot H_2O$.—A solution of $NiBr_2 \cdot 3H_2O$ in water was added to dien (2.1 molar ratio) in water. The product was precipitated by addition of ethanol, filtered off and washed with ethanol and acetone, and then air-dried. Slow recrystallization from hot water gave a yield of 70%. *Anal.* Calcd for $[Ni(C_4H_{13}N_3)_2]Br_2 \cdot H_2O$: C, 21.7; H, 6.37; N, 19.0; Br, 36.1. Found: C, 21.7; H, 6.33; N, 19.0; Br, 36.0.

Reaction *cis*-$[Co(dien)(H_2O)_3]^{3+}$ + dien.—*cis*-$[Co(dien)(H_2O)_3]^{3+}$ was prepared and purified chromatographically by methods given previously,[8,22] except that the complex was eluted from Bio-Rad AG 50W-X4 cation-exchange resin with a 2.9 *M* $NaClO_4$–0.1 *M* $HClO_4$ solution (replacing 3 *M* $HClO_4$,[22] to reduce the acidity).

dien was added dropwise to portions of the red-violet elute to adjust the pH to either 6 or 9; one set of these solutions was warmed on a steam bath (1 hr) and another set was allowed to stand at room temperature. The $[Co(dien)_2]^{3+}$ constituents of these yellow reaction mixtures were assessed by chromatography on Sephadex. A faster moving violet band of unreacted monodien species was also obtained from all reactions but was more prominent in the less complete reactions at pH 6.

(21) F. S. Stephens, *J. Chem. Soc. A*, 2233 (1969).

(22) P. Wilairat and C. S. Garner, *J. Inorg. Nucl. Chem.*, **32**, 2293 (1970).

Results and Discussion

$[Co(dien)_2]^{3+}$ was prepared as a mixture of the three geometric isomers by two general methods, the standard method of aerial oxidation of cobalt(II) chloride or bromide in the presence of dien, and by a substitution method involving reaction of dien with $[Co(NH_3)_5X]X_2$ (X = Cl, Br). All preparations were carried out in aqueous solution at room temperature in the presence of charcoal catalyst to establish equilibrium.

The resulting mixtures contained all three isomers; the trans isomer was the major component and the s-cis isomer was present in smallest proportion. The presence of the s-cis isomer in both chloride and bromide preparations was demonstrated by separations of the product mixtures by a chromatographic procedure using Sephadex (see later).

The three isomers could be separated by fractional crystallization, but the s-cis could be isolated only from the preparations involving bromides, as the least-soluble bromide. No s-cis isomer could be separated by fractional crystallization of the product mixtures from preparations involving chlorides. Even when the complex in a chloride solution was fractionally precipitated as complex bromide by adding lithium bromide, the least soluble fractions obtained were always predominantly the trans isomer. The inability to isolate s-cis by these methods from any preparation in the presence of chloride ion has also been noted by Yamasaki,[23] so that the presence of chloride evidently modifies the solubility relationships between the bromides of the three isomers. This may be due to crystallization as mixed chlorides–bromides, since this effect was noticed with iodide precipitation of the u-cis and trans isomers.

On a preparative scale the remaining trans and u-cis isomers (after removal of *s-cis*-$[Co(dien)_2]Br_3$) were separated from the mixtures by fractional crystallization as iodides, iodide giving a better discrimination than bromide. This separation required a chromatographic monitoring technique, and either thin-layer chromatography on cellulose or chromatography using a Sephadex column was suitable, although Sephadex was preferable for checking isomeric purity. The early and later fractions thus obtained were *trans*-$[Co(dien)_2]I_3$ and *u-cis*-$[Co(dien)_2]I_3$, respectively (these are actually mixed halides; see Experimental Section), and the intermediate mixed fractions were discarded.

A number of chromatographic procedures were examined for their ability to separate the three isomers, and a column of SE-Sephadex C-25 cation exchanger proved the most effective. The separation appears to be greatly dependent on the developing electrolyte, sodium (+)tartrate solution producing a clean separation in 2 hr. NaCl gave no separation, so that the mechanism is not purely ion exchange with Na^+ ion but some form of differential association between the complex cations and solvent anion $[Co(dien)_2]^{3+}$–(+)$tart^{2-}$ must be involved. The three bands we obtain are the three geometric isomers, since separate samples of (±)u-cis and (±)trans each give only one band when passed down the column. Yamasaki[23] reports that this chromatographic medium and eluent will separate the u-cis isomer into optical forms al-

(23) F. R. Keene, G. H. Searle, Y. Yoshikawa, A. Imai, and K. Yamasaki, *Chem. Commun.*, 784 (1970).

TABLE I

	s-cis	u-cis	trans
Sephadex C-25, elution order of isomers	1	2	3
TLC on cellulose, eluent *sec*-BuOH:H_2O:HCl = 70:20:10 Paper chromatography, eluent as above (30 hr) or 80:10:10 for sharper bands	1	2	1
Solubility order in water (chloride, bromide, or iodide)	3 (least soluble)	1 (most soluble)	2
Visible absorption maxima, nm	ϵ_{461}, 68.5; ϵ_{333}, 65.0	ϵ_{468}, 96.4; ϵ_{338}, 94.1	ϵ_{466}, 137; ϵ_{341}, 105
Rotations of optical isomers from less soluble diastereoisomers with the resolving agents indicated	Optical isomers not possible	(+)D SbO tartrate $[M]_D$ = +165° $[M]_{533}$ = +852° (peak) $[M]_{476}$ = −3540° (trough) $[M]_{415}$ = +506° (peak) Zero at 512, 435, 367 nm	(+)D $[Co(en)(mal)_2]^-$ $[M]_D$ = +84° $[M]_{546}$ = +153° (peak) $[M]_{482}$ = −675° (trough) $[M]_{423}$ = +382° (peak) Zero at 518, 456 nm

though the effective column length to achieve the resolution is many times the length we use for the above separation. Sephadex has a relatively low capacity and thus we do not find it particularly suitable for isomer separations on a large preparative scale.

Paper and thin-layer chromatography gave only partial separations of mixtures, yet tlc proved to be useful for monitoring fractional crystallization separations. Although a wide range of solvent mixtures and compositions and tl support media were examined, under no conditions was a suggestion of a third band obtained. On paper, *sec*-BuOH:H_2O:HCl (80:10:10) eluent and for tlc on cellulose *sec*-BuOH:H_2O:HCl (70:20:10) gave the best separations, but in both instances the s-cis and trans isomers ran together in the faster band.

The separated isomers were characterized by a number of methods (Table I) but of these only racemization behavior and pmr spectra allowed unequivocal assignment of the geometric configurations.

The u-cis isomer was resolved into optical isomers through diastereoisomer formation with antimonyl (+)tartrate, and the ORD curve of the (+) optical isomer is given in Figure 4. Comparison of the circular dichroism spectrum with that of (+)$[Co(pentene)]^{3+}$, supported by a study of ion-pairing effects,[18] allows the absolute configuration of (+)*u-cis*-$[Co(dien)_2]^{3+}$ to be assigned as Λ[14] as shown in Figure 1.

A solution of active u-cis isomer in pH 8 buffer showed no change in rotation after standing for 2 months. This isomer, like $[Co(en)_3]^{3+}$, is thus optically stable in base since the optical activity is ascribed predominantly to a configurational effect, and racemization would have to involve a gross rearrangement of the chelate rings.

The trans isomer was resolved with (+)$[Co(en)(mal)_2]^-$ ion. The active *trans*-$[Co(dien)_2]^{3+}$ complex should be handled in acid conditions to avoid racemization, and although in principle acid conditions are not essential to obtain the solid less soluble diastereoisomer, such conditions were used throughout the resolution procedure to avoid racemization of the more soluble diastereoisomer left in solution. Since both optical forms were obtained from the resolution and could be recrystallized to constant rotation, this was taken to indicate that optical purity had been achieved.

In contrast to the u-cis isomer, active trans racemizes in basic media according to the same rate law as observed previously for other systems involving racemization due to N^2H hydrogen exchange. For instance

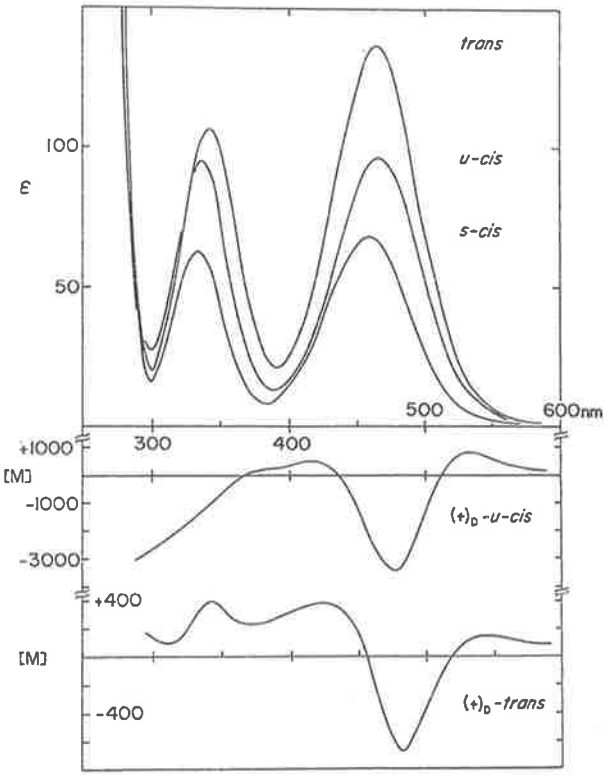

Figure 4.—Absorption and ORD spectra of the $[Co(dien)_2]^{3+}$ isomers.

the half-lives for racemization of aqueous buffer solutions (collidine–HNO_3) at 35° are 93 min at pH 7.42 and 17 min at pH 8.10. These observations allow the u-cis and trans assignments to these isomers.

The ORD (Figure 4) and CD spectra[18] of the active trans isomer in the spectral region of the $^1A_{1g} \rightarrow {}^1T_{1g}$ absorption of the $Co^{III}N_6$ chromophore are of similar forms to those of the u-cis isomer, and the ORD curves of the optically pure isomers indicate that the rotatory power of the "N^2H chiral effect" only (in trans) is an order of magnitude lower than the rotatory power due to the configurational effect (u-cis). The absolute configuration of the active trans isomer cannot be deduced from the ORD or CD at this stage since no suitable reference structures are available, and the assignment awaits our absolute X-ray crystal structure analysis.

Although the visible spectra are closely similar in form for the three isomers (although differing significantly in intensities) (Figure 4), the infrared spectra

are much more distinctive and are useful for characterizing the isomers. The region most useful for characterization is 800–300 cm^{-1} and peaks in this region are listed in Table II.

TABLE II

INFRARED FREQUENCIES[a] OF $[Co(dien)_2]Br_3$ ISOMERS IN THE 800–300-cm^{-1} RANGE (KBr DISKS)

s-cis	u-cis	trans
803 s	810 sh, 802 m	
779 m	777 w	761 s, 742 sh
758 s	755 mw, 743 sh	
	702 vw	
683 s, 671 sh	671 sh, 667 mw	675 vw
592 s	609 m	589 m
	581 m, 568 sh	575, 568 d, mw
	540 vw	
521 sh, 516 m	525 mw	528 m
	501 mw	487 w
	482 vw	472 w
460 sh, 451 w	457 mw	
	445 w	446, 438 d, mw
	432 w	
		414 vw
389 w	388 w	395 vw
374 s		375 sh, 370 m
	339 m	324 mw
307 sh, 301 m	310 m, 305 sh	

[a] Estimated intensities: s, strong; m, medium; w, weak; sh, shoulder; d, doublet.

Infrared criteria for assigning the configuration of a coordinated dien ligand as facial or meridional have been proposed[6–8] on the basis of experimental data for a number of monodiethylenetriamine complexes. We find that Schmidtke's criteria[6] at 1500–1400, 1250, and 850–700 cm^{-1} are not sustained in our bis-dien complexes, and it is likely that each dien ligand in $[M(dien)_2]^{n+}$ systems will be in a less symmetric environment due to interligand interactions than will dien in complexes of types $[M(dien)X_3]$, or $[M(dien)X]^+$ (planar). If this is so, greater splitting of absorbances would be expected in $[M(dien)_2]^{n+}$, and our spectra do appear more complicated than those on which the above criteria were established.

The 950–800-cm^{-1} region appears to be more distinctive, however. *trans*-$[Co(dien)_2]Br_3 \cdot H_2O$ and *trans*-$[Cu(dien)_2]Br_2 \cdot 0.5H_2O$ both show a band quartet in this region (attributed to CH_2–, NH_2–, and NH– rocking modes and CN skeletal vibrations) whereas both *cis*-$[Co(dien)_2]Br_3$ (facial) isomers exhibit either fewer peaks or broad unsymmetric absorptions (Figure 5). $[Ni(dien)_2]Br_2 \cdot H_2O$ (configuration undetermined) also shows the band quartet. This quartet–triplet distinction has also been noted in mono-dien systems.[6–8]

Our results support the observation[6] that the CH_2 stretching vibrations (3000–2800 cm^{-1}) are very weak for facial dien, but strong for meridional dien, in $[M(dien)X_3]$ (M = Rh, Co, Cr; X = Cl, Br). Figure 5 shows that the CH_2 bands are very weak for *s-cis*- and *u-cis*-$[Co(dien)_2]^{3+}$, but are quite pronounced for the trans isomers of $[Co(dien)_2]^{3+}$ and $[Cu(dien)_2]^{2+}$. On this criterion the corresponding nickel(II) complex may be assigned as trans, which is consistent with the quartet criterion above and also with trans appearing to be the most stable isomer in all these bis-dien systems.

It is of interest to consider the use of pmr spectra as a criterion to assign geometric configurations to these complexes. The solvent we investigated particularly was D_2O (neutral, or acidified with D_2SO_4), and the spectra have also been recorded in dimethyl-d_6 sulfoxide by Yamasaki.[23] We find that the three spectra run in one solvent do not in general distinguish all three isomers, but may allow one assignment to be made. Only from spectra taken under various conditions is it possible to assign all three configurations by this method alone.

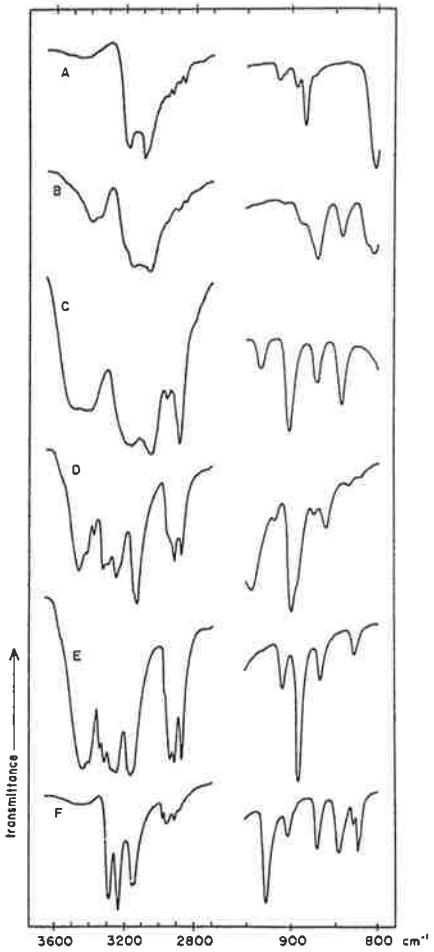

Figure 5.—Infrared spectral regions for characterizing facial or meridional coordination of dien in $[M(dien)_2]^{n+}$ complexes (KBr disks of bromides). A, *s-cis*-$[Co(dien)_2]^{3+}$; B, *u-cis*-$[Co(dien)_2]^{3+}$; C, *trans*-$[Co(dien)_2]^{3+}$; D, *trans*-$[Cu(dien)_2]^{2+}$; E, *trans*(?)-$[Ni(dien)_2]^{2+}$; F, *trans*-$[Co(dien)Cl_3]$.

In D_2O two of the isomers give a simple CH_2 resonance (Figure 6). The third isomer gives a complex splitting pattern and may therefore be assigned as the u-cis, having four nonequivalent methylene groups (Figure 1). The s-cis and trans isomers should have only two nonequivalent CH_2 groups, since in neutral solution the rapid conformational interchange in the trans isomer should make each chelate ring equivalent on a time average.

Spectra in acidic D_2O were all distinctive (Figure 6) with only one isomer showing a single NH_2 peak (4.73 ppm from TMP) whereas multiple NH_2 resonances were apparent for the other two isomers. These observations can be interpreted on the basis of chelate ring conformations.

Figure 6.—Pmr spectra of $[Co(dien)_2]Cl_3 \cdot xH_2O$ isomers: (a) in D_2O–D_2SO_4, and (b) in D_2O (containing trace of sodium carbonate), in ppm with respect to sodium trimethylsilypropanesulfonate. Spectra (a) are 100-Mc, obtained on a Varian HA-100 spectrometer. Spectra (b) were run on a 60-Mc Jeol spectrometer.

For the s-cis isomer there are (in principle) five possible types of combinations for the four ring conformations: $\lambda\delta$–$\lambda\delta$, $\lambda\delta$–$\delta\lambda$, $\lambda\lambda$–$\lambda\delta$, $\lambda\lambda$–$\delta\delta$, and $\lambda\lambda$–$\lambda\lambda$. Conformational interchange in this isomer is not dependent on N^2H dissociation, so that such interchange should be facile even in acid solution. On a time average therefore all four primary amine groups should be equivalent and on this basis this isomer may be regarded as having a center and planes of symmetry. The s-cis configuration may therefore be assigned to the isomer showing the single NH_2 resonance in D_2O/D^+, and a single resonance is also obtained from this isomer in dimethyl-d_6 sulfoxide.[23]

The NH_2 groups on each dien ligand are in nonequivalent environments in the u-cis and trans isomers, and this is apparent from Figures 1 and 2, respectively. Conformational interchange in trans must involve N^2H dissociation as discussed previously and will not take place in the acidic solvent, and multiple resonance could be expected. Although conformational interchange could take place in the u-cis isomer (as with s-cis discussed above) the two NH_2 groups of each ligand would still remain in nonequivalent environments due to the configurational symmetry being C_2, and this is consistent with the two resonances observed both in D_2O/D^+ (Figure 6) and in dimethyl-d_6 sulfoxide.[23]

The three spectra in trifluoroacetic acid were qualitatively similar, and were less useful as criteria for configurations.

The proportions of the three isomers at equilibrium were found to be independent of the anion being chloride or bromide. Replicate determinations of the isomer proportions (under standardized conditions) gave the ratios trans:u-cis:s-cis = 65:28:7. These figures demonstrate the stability of the trans or meridional arrangement over facial coordination of the dien ligand, but the proportions also indicate that there is an even greater difference in stabilities of the two cis isomers. It is now generally agreed that a number of structural factors affect relative isomer stabilities in metal complex systems.[19] In the present system these will include bond angle strain at the secondary nitrogens bridging chelate rings, and nonbonded atomic interactions. The above results clearly show that bond angle strain is not the major factor involved, since scale molecular models indicate that considerable strain exists between two adjacent en chelate rings when in the meridional disposition, as in *trans*-$[Co(dien)_2]^{3+}$ and *trans*-$[Co(trien)X_2]^+$. Nonbonded interactions are likely to be important, although it must be appreciated that the relative contributions from factors such as solvation energy are difficult to assess.

Preliminary experiments suggest that the isomer proportions in the $[Co(dien)_2]^{3+}$ system also depend to some extent on environmental factors such as temperature (the proportions of s-cis and u-cis increase at the expense of trans, with rise in temperature), cobalt concentration, and nature of the anion (other than chloride–bromide). We also find that charcoal samples differ in their capacity to establish equilibrium. The figures quoted above were obtained with a charcoal sample whose high catalytic efficiency was established by quantitative measurement of its effect on racemization of $[Co(en)_3]^{3+}$. These further results will be discussed along with energy minimization calculations in a subsequent article.

In seeking a method to obtain the *s-cis*-$[Co(dien)_2]^{3+}$ isomer in higher yield, the reaction of a solution claimed[8] to contain *cis*-$[Co(dien)(H_2O)_3]^{3+}$ with excess dien was examined under various conditions of pH. The reaction was most complete in alkaline conditions pH 8–9 (as judged by the color change), and product analysis by chromatography on Sephadex showed that the $[Co(dien)_2]^{3+}$ reaction products were almost all trans with only a trace of the u-cis isomer, with no evidence of any s-cis. This product proportion, while quantitatively similar to that obtained by synthesis, involves an even higher proportion of trans/cis. If the starting complex was in fact *cis*-$[Co(dien)(H_2O)_3]^{3+}$, these results would suggest that substitution of the second dien ligand on a cis-mono-dien arrangement evidently leads to substantial isomerization. This would accord with the greater stability of the trans configuration in the bis complex as indicated by all other preparative methods.[23]

The starting triaquo complex was obtained by the reaction sequence[8]

$$trans\text{-}[Co(dien)Cl_3] \xrightarrow{NaOH} trans\text{-}[Co(dien)(OH)_3] \xrightarrow{HClO_4} trans\text{-}[Co(dien)(H_2O)_3]^{3+}$$

and it is reported that on standing the trans triaquo

isomerizes completely to the cis.[22] The cis disposition of coordinated dien would thus appear to be considerably stabilized only by coordinated water. This might be attributed to more favorable hydrogen bonding between the aquo ligands all cis, as this factor may be used to rationalize the greater stability of β-$[Co(trien)(H_2O)(OH)]^{2+}$ compared with the α configuration.[24] The identity of the complex species purported to be *cis*-$[Co(dien)(H_2O)_3]^{3+}$ remains in some doubt however since it has been obtained only in solution.

(24) A. M. Sargeson and G. H. Searle, to be submitted for publication.

Acknowledgments.—We thank Professor K. Yamasaki and coworkers (Nagoya University) and Dr. H. H. Schmidtke (University of Frankfurt) for helpful discussions and the mutual exchange of information and data on this problem. We thank Union Carbide Australia Ltd. for the gift of dien and Dr. D. A. Buckingham (A.N.U.) for some pmr spectra.

[Reprinted from Inorganic Chemistry, 11, 1006 (1972).]

CONTRIBUTION FROM THE DEPARTMENT OF PHYSICAL AND INORGANIC CHEMISTRY, UNIVERSITY OF ADELAIDE, ADELAIDE, SOUTH AUSTRALIA 5001

Racemization and Hydrogen Exchange in the *trans*-Bis(diethylenetriamine)cobalt(III) Ion

BY GRAEME H. SEARLE* AND F. RICHARD KEENE

Received July 9, 1971

The rates of hydrogen exchange and racemization at the secondary N–H center in the *trans*-$[Co(dien)_2]^{3+}$ ion with coupled chelate rings have been measured, and rates and activation parameters are compared with previous results. The close correspondence of the kinetic results with those for the single chelate ring complex $[Co(NH_3)_4(N\text{-Meen})]^{3+}$ of identical cationic charge indicates that the coupling of chelate rings across the secondary N–H center in the dien complex has little effect on either process. It is still difficult however to decide on the details of the nitrogen inversion process. Comparisons with the other asymmetric nitrogen systems previously studied involve variations of more than one structural parameter, but it appears that the electronegative trans substituent X in *sym*-$[Co(trenen)X]^{2+}$ has a greater effect on the kinetics than does the extensive chelate ring coupling.

Introduction

The three geometric isomers of $[Co(dien)_2]^{3+}$ (dien = diethylenetriamine) have recently been separated, and the two dissymmetric forms u-cis[1a] and trans resolved into their optical isomers.[1b] The trans isomer (Figure 1) is of particular interest because the dissymmetry arises essentially from the chiralities of the C_2 related bond pairs in the two dien ligands, as typified and uniquely described[2] by the two secondary N–H bonds at the secondary nitrogen centers.

Coordination of amines to cobalt(III) considerably reduces the rate of nitrogen–hydrogen dissociation from that in corresponding organic quaternary ammonium salts. Coordination of an unsymmetrically substituted secondary amine NHR_1R_2 to a metal generates an asymmetric center at the donor nitrogen atom, and the proton-exchange rate is sufficiently slow at suitably low pH to restrict inversion at that nitrogen center. Optical resolution of the resulting asymmetric complex thus becomes feasible, and a number of such optical separations have now been achieved.

dien is a symmetrically substituted secondary amine so that *trans*-$[Co(dien)_2]^{3+}$ does not contain an asymmetric donor atom. However racemization will result if one of the secondary N–H bonds adopts the alternative disposition (Figure 1). This process is equivalent to inversion of configuration at the asymmetric nitrogen center in the situation $Co\text{–}NHR_1R_2$, and we henceforth use the term "inversion" to describe the analogous configurational change about a secondary nitrogen center in *trans*-$[Co(dien)_2]^{3+}$ despite the absence of asymmetry. This configurational change must involve N–H dissociation and will be accompanied by conformational inversion in each of the adjacent chelate rings.

These phenomena provide an unequivocal method for establishing the geometric configurations of the two dissymmetric forms, since the optical rotatory powers derive from different chiral sources in the u-cis and trans isomers. The u-cis, whose optical activity arises essentially from a configurational effect, should be optically stable in base, but the racemization of the trans isomer should be OH^- catalyzed. It was thus necessary to establish the OH^- dependence of the racemization of the trans isomer, and this prompted the present study of the kinetics of both racemization and hydrogen exchange under a variety of conditions in the hope of further elucidating the mechanistic steps involved in the racemization.

Recently the kinetics of racemization and deuteration have been studied by Buckingham and Sargeson and coworkers for several cobalt(III) complexes where the sole source of asymmetry resides in a coordinated secondary amine N atom. For the three complexes $[Co(NH_3)_4sarc]^{2+}$,[3] $[Co(NH_3)_4(N\text{-Meen})]^{3+}$,[4] and *trans*,*trans*-$[Co(N\text{-Meen})_2(NO_2)_2]^+$ [5] (sarc = sarcosinato anion; *N*-Meen = *N*-methylethylenediamine) the rates of proton exchange were several orders of magnitude faster than the respective rates of racemization, and both measured processes were described by rate laws of similar form, $R = k[\text{complex}][OH^-]$.

The two mechanisms which have been proposed by

(1) (a) The three geometric isomers of $[C(dien)_2]^{3+}$ have been designated s-cis (or symmetrical-facial), u-cis (or unsymmetrical-facial), and trans (or meridional). (b) F. R. Keene and G. H. Searle, *Inorg. Chem.*, 11, 148 (1972); F. R. Keene, G. H. Searle, Y. Yoshikawa, A. Imai, and K. Yamasaki, *J. Chem. Soc. D*, 784 (1970).

(2) F. R. Keene, G. H. Searle, and S. F. Mason, *ibid.*, 893 (1970).

(3) B. Halpern, A. M. Sargeson, and K. R. Turnbull, *J. Amer. Chem. Soc.*, 88, 4630 (1966).

(4) D. A. Buckingham, L. G. Marzilli, and A. M. Sargeson, *ibid.*, 89, 825 (1967).

(5) D. A. Buckingham, L. G. Marzilli, and A. M. Sargeson, *ibid.*, 89, 3428 (1967).

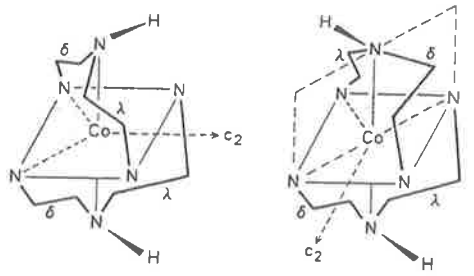

Figure 1.—Optical isomers of *trans*-$[Co(dien)_2]^{3+}$.[1,2]

the previous authors[4,5] to account for all these results are shown in Figure 2, where the part chelate ring indicated may be either *N*-Meen or sarc. The preferred scheme A involves abstraction of the N proton with OH^- (k_1). The alternative mechanism B proposes formation of an ion pair with OD^- (k_3) and ion–solvent dissociation (k_4). The two mechanisms are equivalent for the racemization step as given by inversion of the deprotonated intermediate k_2. In

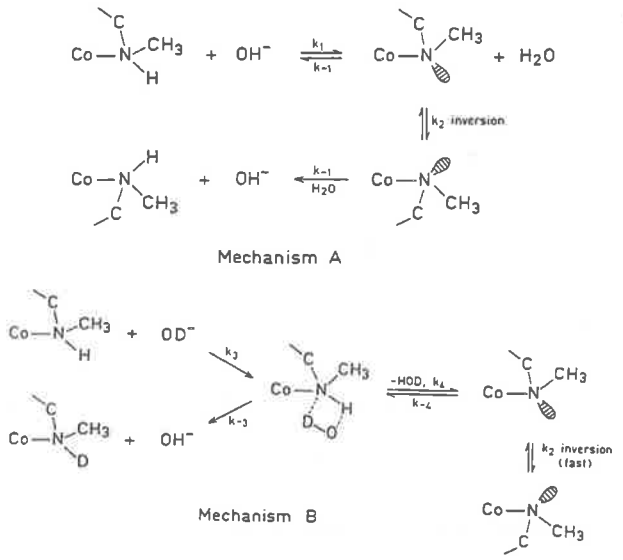

Figure 2.—Alternative mechanisms for hydrogen exchange and racemization at an asymmetric nitrogen center.

mechanism B ion–solvent pair separation is required for racemization for which k_4 could thus be the rate-determining step, but this step is not required for exchange to occur with retention of configuration k_{-3}. The absence of a substantial isotope effect $k_{deuteration}/k_{protonation}$ (k_D/k_H) for the exchanges, as would be expected for the step k_4,[5] gave support for the former mechanism, and circumstantial evidence also supporting mechanism A has been expounded.[4,5] Results of measurements of retention ratio $k_{protonation}/k_{racemization}$ during exchange in nonaqueous solutions have also been interpreted on the basis of mechanism A.[6]

The previous studies cited above are confined to complexes involving an asymmetric donor nitrogen center in the bidentate ligands *N*-Meen or sarc. The chelate ring in the sarcosine complex is essentially planar[7] so that a ring conformational change is not involved. Mechanisms A and B as drawn in Figure 2 do not specifically consider inversion of the single chelate ring conformation in the *N*-Meen complexes, and k_2 in Figure 2 refers only to the nitrogen inversion which is the essential step for racemization. The ring conformation must invert however if the methyl substituent is to remain in the preferred equatorial disposition with respect to the overall plane of the ring in the *N*-Meen complexes.[4,5] The increase in $\Delta H^{\ddagger}$ and in retention ratio for the *N*-Meen complexes compared to the sarc complex was attributed to the additional energy required to invert the *N*-Meen ring conformation as well as the N center.[4,5] In the studies mentioned, no decision could be made as to the time relationship between conformational interchange and inversion at the nitrogen atom during the observed racemization, and Figure 2 is noncommittal on whether the ring inversion precedes, postcedes, or is synchronous with k_2.[4,5]

A subsequent study of hydrogen exchange and racemization of (+)D-*sym*-$[Co(trenen)N_3]^{2+}$ (trenen = 4-(aminoethyl)-1,4,7,10-tetraazadecane) attempted to clarify the issue of the interaction between conformational interchange and nitrogen inversion.[8] This complex has coupled ring conformations (Figure 3, X

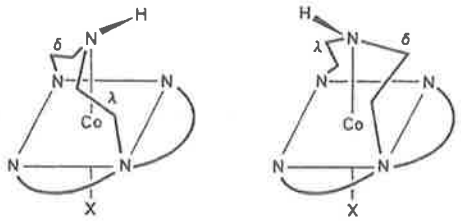

Figure 3.—Optical isomers of *sym*-$[Co(trenen)X]^{2+}$. This geometric isomer of the trenen complex may be alternatively designated $[Co(sec\text{-}trenen)X]^{2+}$ where X is trans to the secondary amine group.

= azido) and it was felt that the conformations of the two rings abreast of the asymmetric nitrogen (conformations designated δ and λ[9] in Figure 3) would invert synchronously with configurational inversion at the asymmetric center. The close correspondence between observed activation energies for racemization of this system and of $(+)_{480}[Co(NH_3)_4(N\text{-Meen})]^{3+}$ was then taken to imply that inversion at the N center and conformational interchange might coincide for puckered ring systems generally. However the trenen complex has multiple ring coupling at the tertiary nitrogen atom also, and this would confer some restriction on the conformational interchange in question (about the secondary N atom). The portion of the trenen ligand comprising the interlocked rings (δ and λ) about the asymmetric nitrogen in *sym*-$[Co(trenen)N_3]^{2+}$ should be closely similar stereochemically to each dien ligand in *trans*-$[Co(dien)_2]^{3+}$ (compare Figures 1 and 3). This latter complex is free of the restriction mentioned, however, and is also a better basis for comparison with $[Co(NH_3)_4(N\text{-Meen})]^{3+}$ on account of similar cation charge and the absence of the electronegative azido

(6) D. A. Buckingham, L. G. Marzilli, and A. M. Sargeson, *J. Amer. Chem. Soc.*, **90**, 6028 (1968).

(7) H. C. Freeman and I. E. Maxwell, *Inorg. Chem.*, **9**, 649 (1970).

(8) D. A. Buckingham, P. A. Marzilli, and A. M. Sargeson, *ibid.*, **8**, 1595 (1969).

(9) *Ibid.*, **9**, 1 (1970).

substituent. The comparison of the kinetic patterns for the dien and trenen complexes may be expected to give some further information on the effects of cation charge and azido substituent however.

Experimental Section

(+)D-*trans*-$[Co(dien)_2](NO_3)_3 \cdot H_2O$.—The racemic chloride was resolved with Ag(+)$[Co(en)(mal)_2] \cdot 2H_2O$ as described earlier.[1] The active bromide thus obtained was converted to the nitrate by passage of a solution in 0.01 *M* HNO_3 through an exchange resin in the nitrate form. The eluate was concentrated on a rotary evaporator, and crystallization was completed by the addition of ethanol. *Anal.* Calcd for (+)D-*trans*-$[Co(C_4H_{13}N_3)_2](NO_3)_3 \cdot H_2O$: C, 20.5; H, 6.0; N, 26.8. Found: C, 20.6; H, 5.7; N, 26.5.

Deuterated (±)-*trans*-$[Co(dien\text{-}d_5)_2]Cl_3 \cdot xD_2O$.—A sample of racemic chloride–2.5-water was dissolved in D_2O (99.8%), and after standing at 80° for 1 hr the D_2O–H_2O was evaporated off under vacuum. The process was repeated with fresh D_2O, and the pmr spectrum showed that deuteration was essentially complete.

Buffer Solutions.—The buffer solution for each pH was made up using 2,4,6-collidine (freshly distilled) and the appropriate amount of HNO_3,[10] and sufficient solid $NaNO_3$ was added to adjust the ionic strength of this solution to μ = 1.9 *M*. The solid complex, when added for each racemization run, contributed a further 0.1 *M* to the ionic strength.

Racemization Kinetics.—(+)-*trans*-$[Co(dien)_2](NO_3)_3 \cdot H_2O$ (0.075 g) was dissolved in collidine–HNO_3 buffers (10 ml) giving solutions 0.016 *M* in complex, with ionic strength adjusted to 2.0 *M* with $NaNO_3$. Racemization was conveniently followed at the Hg line 546.1 nm which is coincident with the first peak of the ORD curve.[1] Rotations were measured on a Perkin-Elmer 141 MC polarimeter in a 1-dm cell jacketed to ±0.1° from a water bath. Initial rotations were about α_{546} +0.14°, and individual measurements were accurate to ±0.002°. In the slower runs light was excluded between readings and each run was followed to at least 2 half-lives.

The pH of each solution was obtained with a Radiometer Model 22 pH meter (±0.005 pH unit) by measurement of the kinetic solution at the run temperature after each run was completed (the collidine buffer is temperature dependent). Rates were reproducible to ±5% with the accuracy limited by the pH determination.

Hydrogen-Exchange Kinetics.—The deuteration runs were carried out on racemic *trans*-$[Co(dien)_2]Cl_3 \cdot 2.5H_2O$ in D_2SO_4–D_2O, and the corresponding deuterated compound was used for the protonation studies in H_2SO_4 solutions. The stock acid solutions were titrated potentiometrically against sodium tetraborate. Pmr spectra were measured using a Varian T-60 nmr spectrometer with sodium trimethylsilylpropanesulfonate as the external reference standard. All solutions were 0.33 *M* in complex, whence μ = 2.0 *M*. The nmr tubes were kept in the probe of the spectrometer throughout the runs at 34.9° and in a constant-temperature water bath for the higher temperatures. In these latter runs the tubes were withdrawn from the bath at suitable times and cooled quickly to 35°, and the N–H region of the spectrum was recorded immediately.

It was not possible to assess peak areas using the instrument integrator due to its instability over the broad N–H peak and with time. Relative peak areas were obtained by making three tracings of the peak recorded at each time (smoothing out noise) onto paper of uniform thickness, sketching in the base line, and cutting out. The triplicate paper pieces were weighed together (weights corresponding to maximum peak areas were about 0.25 g). This procedure averaged out variations caused by subjective judgements in making the tracings.

Results

Hydrogen Isotope Exchange.—The pmr spectrum of *trans*-$[Co(dien)_2]Cl_3 \cdot 2.5H_2O$ in D^+–D_2O is given in Figure 4. The band assignments follow from the peak area ratios NH:NH_2:CH_2 = 1:4:8 as determined previously.[1] The >NH peak is also shown at the higher

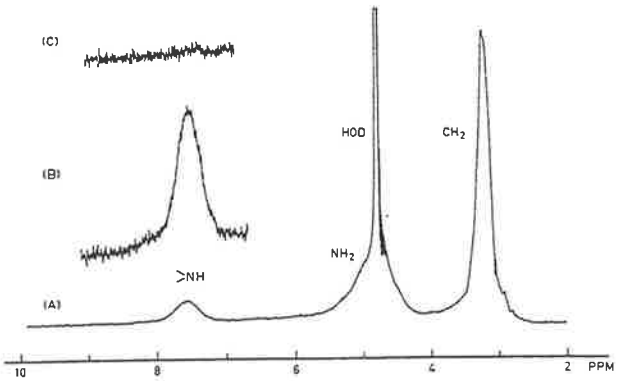

Figure 4.—Pmr spectrum of *trans*-$[Co(dien)_2]^{3+}$ in D^+–D_2O: (A) complete spectrum; (B) >NH peak at amplitude increased 8 times, initially; (C) after deuteration complete (10 half-lives).

amplitude at which the deuteration runs were followed, and it is evident (Figure 4C) that after ~10 half-lives exchange was essentially complete. The exchange was followed in both directions, by measurement of peak area of the >NH signal at appropriate times. Plots of log [(peak area)$_t$ − (peak area)$_\infty$] *vs.* *t* were linear (within the errors) over at least 2 half-lives for the deuteration runs in D_2SO_4–D_2O. Protonation runs of the deuterated sample in aqueous H_2SO_4 solutions were more difficult to measure due to the large HOD peak lying close to the >NH signal under these conditions. The HOD background tail under the NH had to be extrapolated subjectively for each recording, and the experimental points in the plot of log [(peak area)$_\infty$ − (peak area)$_t$] *vs.* *t* (peaks background corrected) were more scattered. All rate constants were computed by least-squares analysis of the experimental points up to 2 half-lives for each run. The number of points used in the computation was at least 8 but was usually about 12. Rate constants for the exchanges are listed in Tables I and II. k_D and k_H were obtained by k_D = $k_{obsd}/[OD^-] = k_{obsd}[D^+]/K_{D_2O}$ and $k_H = k_{obsd}[H^+]/K_w$. The constants used were $K_w = 2.11 \times 10^{-14}$ for 2 *M* KCl at 34.9°[11] and values of K_w for the other

TABLE I
RATE CONSTANTS FOR DEUTERATION IN D_2SO_4–D_2O OF SECONDARY N–H IN *trans*-$[Co(dien)_2]Cl_3 \cdot 2.5H_2O$[a]

$[D^+]$, *M*	Temp, °C	$10^{-3}k_D$, M^{-1} sec^{-1}	$[D^+]$, *M*	Temp, °C	$10^{-3}k_D$, M^{-1} sec^{-1}
0.100–0.00100	34.9	1.04 ± 0.05	0.0300	40.0	1.43
0.0100	34.9	0.60[b]	0.0300	45.0	2.23
0.0100	34.9	1.68[c]	0.0300	50.0	3.0

[a] [Co] = 0.33 *M*; μ = 2.0 *M* (no supporting electrolyte added). [b] [Co] = 0.167 *M*; μ = 2.0 *M*; [KCl] = 1.0 *M*. [c] [Co] = 0.167 *M*; μ = 1.0 *M* (no supporting electrolyte added).

TABLE II
RATE CONSTANTS FOR PROTONATION IN H_2SO_4 OF SECONDARY N–D IN DEUTERATED *trans*-$[Co(dien\text{-}d_5)_2]Cl_3 \cdot xD_2O$[a]

$[H^+]$, *M*	Temp, °C	$10^{-3}k_H$, M^{-1} sec^{-1}	$[H^+]$, *M*	Temp, °C	$10^{-3}k_H$, M^{-1} sec^{-1}
0.0098	34.9	0.35	0.098	45.0	0.80
0.098	40.0	0.71	0.098	50.0	1.10

[a] [Co] = 0.33 *M*; μ = 2.0 *M* (no supporting electrolyte added).

(10) R. M. C. Dawson, D. C. Elliott, W. H. Elliott, and K. M. Jones, "Data for Biochemical Research," 2nd ed, Oxford University Press, London, 1969, p 491.

(11) H. S. Harned and W. J. Hamer, *J. Amer. Chem. Soc.*, **55**, 2194 (1933).

temperatures were also calculated for 2 M KCl using data from the same source.[11] K_{D_2O} was taken as 0.195 K_w for zero ionic strength.[12] The assumption has been made that the ratio 0.195 does not change significantly with ionic strength or temperature, as zero ionic strength is the only condition for which strictly comparable values of K_{D_2O} and K_w have been determined.[13] The constancy of k_D over nine runs with D^+ concentration varied over the range 10^{-1} to 10^{-3} M at constant temperature (average value 1.04×10^8 M^{-1} sec^{-1} with spread ± 0.05 at 34.9°) establishes the rate law to be the same as that for the previously studied bidentate complexes, $R = k_D[\text{complex}][OD^-]$. The average value of k_H under the same conditions is 0.35×10^8 M^{-1} sec^{-1} at 34.9° giving the isotope effect as $k_D/k_H = 3.0$. Our results indicated that rate constants for the deuterations were reproducible to within 10%, all replicate values being within 5% of the mean. Data for a typical deuteration run are plotted in Figure 5.

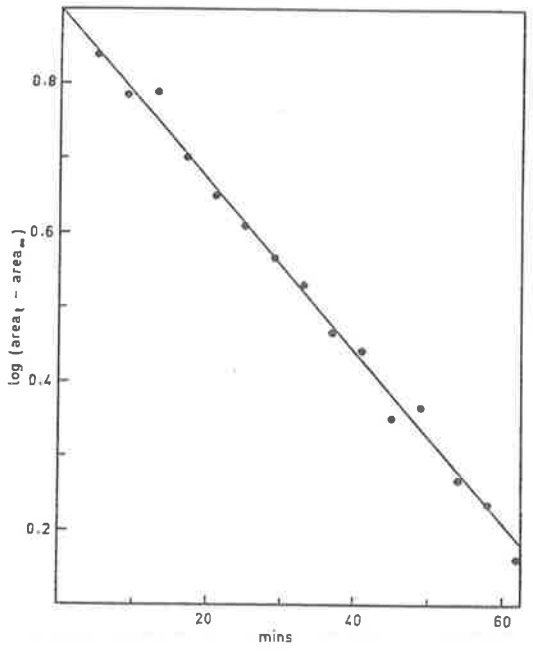

Figure 5.—Rate plot for a typical deuteration run ($[D^+] = 10^{-3}$ M, 34.9°, $k_{obsd} = 4.43 \times 10^{-4}$ sec^{-1}).

The accuracy and precision were less than this however for protonation (within 7% of the mean). All determinations were run in duplicate or triplicate, and Tables I and II list only the mean values.

Racemization.—The rates of racemization were measured in buffer solutions at constant ionic strength ($\mu = 2.0$ M) over almost the complete pH range 7.08–8.27 of the collidine–HNO_3 buffer system at various temperatures, Table III. Pseudo-first-order plots of log α_{546} *vs.* t were linear to at least 3 half-lives, and lines of best fit were drawn visually through the large number of points for each run. Several runs were followed to zero rotation over the visible range ($>10t_{1/2}$), and the constancy of the visible spectrum indicated that in the reaction times any hydrolysis or isomerization was insignificant. Chromatographic analysis on SP C-25 Sephadex[1] of a solution which had completely racemized

(12) W. F. K. Wynne-Jones, *Trans. Faraday Soc.*, **32**, 1397 (1936).
(13) *Chem. Soc., Spec. Publ.*, **No. 17**, 39 (1964).

TABLE III
RATE CONSTANTS FOR RACEMIZATION OF (+)-*trans*-$[Co(dien)_2](NO_3)_3 \cdot H_2O$ IN COLLIDINE–HNO_3 BUFFERS[a]

Temp, °C	pH	$10^4 k_{obsd}$, sec^{-1}	$10^{-2}k_R$, M^{-1} sec^{-1}	Temp, °C	pH	$10^4 k_{obsd}$, sec^{-1}	$10^{-2}k_R$, M^{-1} sec^{-1}
25	8.27	1.30	0.69	35	7.76	4.94	4.1[c]
30	7.51	0.586	1.23	35	7.68	2.84	2.9[d]
30	7.92	1.25	1.29	35	6.42	0.086	1.54[e]
35	7.20	0.769	2.3	40	7.31	2.89	4.7
35	7.42	1.24	2.3	40	7.55	4.87	4.6
35	7.46	1.51	2.5	40	6.44	0.297	3.6[e]
35	7.75	2.76	2.3	45	7.08	4.17	8.7
35	8.12	6.89	2.5	45	7.15	4.75	8.4
35	7.67	1.81	1.86[b]	45	6.45	0.865	7.7[e]
35	7.62	2.85	3.3[c]				

[a] [Co] = 0.016 M; $\mu = 2.0$ M (supporting electrolyte $NaNO_3$). [b] [Co] = 0.008 M; $\mu = 2.0$ M ($NaNO_3$). [c] [Co] = 0.016 M; $\mu = 1.0$ M ($NaNO_3$). [d] [Co] = 0.008 M; $\mu = 1.0$ M ($NaNO_3$). [e] Phosphate buffer HPO_4^{2-}, $H_2PO_4^-$; [Co] = 0.016 M; $\mu = 2.0$ M ($NaNO_3$).

failed to detect any other species. $k_R = k_{obsd}/[OH^-]$ was calculated using values of K_w as mentioned above. The constancy of k_R over the pH range 7.20–8.12 (average value with standard deviation $(2.36 \pm 0.09) \times 10^2$ M^{-1} sec^{-1} at 35°) confirmed that only the one reaction was being observed and that the rate law was as previously, $R = k_R[\text{complex}][OH^-]$.

Activation Parameters.—Activation energies E_a for the three processes were computed by least-squares analysis of the Arrhenius plots of k_R, k_D, and k_H, where these rate constants from the individual runs have been calculated allowing for the temperature variation of K_w or K_{D_2O}. Figure 6 shows the Arrhenius plots for the

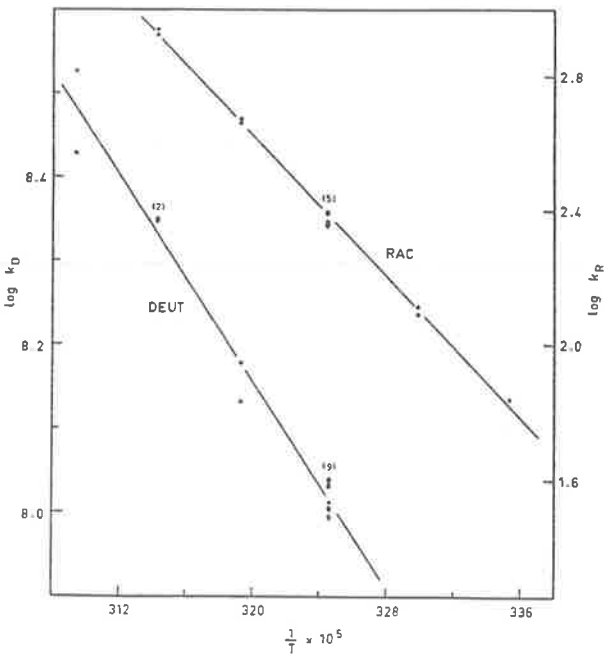

Figure 6.—Arrhenius plots for deuteration and racemization of *trans*-$[Co(dien)_2]^{3+}$. Figures in parentheses are the numbers of points at each temperature.

deuteration and racemization. The activation parameters calculated for the three processes ($\Delta H^{\ddagger} = E_a - 0.60$ kcal mol^{-1}) are given in Table IV. Errors listed were obtained from the standard errors in the least-squares analyses.

TABLE IV

RATE CONSTANTS AND ACTIVATION PARAMETERS FOR SECONDARY N–H HYDROGEN EXCHANGE AND RACEMIZATION

Reaction	Medium	Temp, °C	$k_{D,H,\text{ or }R}$, M^{-1} sec^{-1}	$\Delta H^{\ddagger}$, kcal mol^{-1}	$\Delta S^{\ddagger}$, eu
		trans-$[Co(dien)_2]^{3+}$			
Deuteration	D_2SO_4	34.9	1.0×10^8	13.5 ± 1	22 ± 3
Protonation	H_2SO_4	34.9	0.35×10^8	13.4 ± 2	20 ± 7
Racemization	Collidine–HNO_3	35.0	2.4×10^2	23.5 ± 0.4	29 ± 2
		$[Co(NH_3)_4(N\text{-Meen})]^{3+}$			
Deuteration	DCl	34.3	3.0×10^7	13.8	21
Protonation	HCl	34.3	1.0×10^7	15.4	24
Racemization	Collidine–HCl	34.3	2.5×10^2	24.3	31
	Acetate buffer	34.3	2.4×10^2	23.8	30
		sym-$[Co(trenen)Cl]^{2+}$			
Deuteration	DCl	34	5.6×10^9	13.7[a]	31
		sym-$[Co(trenen)N_3]^{2+}$			
Deuteration	DCl	34	1.3×10^9	...	...
Racemization	Tris–$HClO_4$ buffer	34	5.7×10^2	22.7	28

[a] Reference 8 states that $\Delta H^{\ddagger}$ for deuteration of the chloro and "activation energy" for racemization of the azido complexes are 28 and 36 kcal mol^{-1}, respectively. It appears from the context that these values are both $E_{a,obsd}$ and the $\Delta H^{\ddagger}$ and $\Delta S^{\ddagger}$ parameters in the above table have been calculated accordingly.

Discussion

The kinetic results obtained for the hydrogen exchanges and racemization follow the general pattern previously observed for the asymmetric nitrogen center complexes, and the OH^- catalysis of the racemization allows the geometric configuration of this particular geometric isomer of $[Co(dien)_2]^{3+}$ to be unequivocally assigned as trans.[1]

The close similarity in activation parameters between the dien, *N*-Meen, and trenen complexes, as compared in Table IV, strongly indicates a common mechanism. We are thus led to conclude that the coupling of two puckered chelate rings across the secondary N atom in Co(dien) confers no additional constraint on the nitrogen "inversion" over that in the single-ring case of Co(*N*-Meen). We infer also that the additional ring coupling around the tertiary N in the *sym*-$[Co(trenen)N_3]^{2+}$ complex (Figure 3) places no additional restriction on inversion at the secondary N center.

The present results do not allow a firm decision to be made as to whether nitrogen inversion and conformational interchange are synchronous processes or not. Certainly in the Co(*N*-Meen) case inversion and ring interchange are not required to be synchronous,[4] and conformational change or distortion could occur subsequent to deprotonation but prior to nitrogen inversion. In the present system, as in *sym*-$[Co(trenen)N_3]^{2+}$,[8] Dreiding models imply that it is difficult to invert at the N center without inverting at least one of the ethylenediamine (en) rings, but even this is not required by the results. However recent X-ray studies on coupled en ring systems[14] reveal departures from the idealized structures implied by Dreiding models (fixed bond angles) so that caution must be exercised in the use of such models for mechanistic predictions.

It might be argued that if synchronous conformational interchange does not occur in Co(*N*-Meen), the similarity in $\Delta H^{\ddagger}$ (racemization) for these three systems suggests inversion of only one ring in each of the dien and trenen complexes during the nitrogen inversions, equivalent to configurational interchange only of the methyl and hydrogen substituents in Co(*N*-Meen) (without conformational change). If ring conformational change does occur synchronously in the Co(*N*-Meen) system, then on this basis both rings would have to invert synchronously in Co(dien). While it seems likely therefore that one ring in Co(dien) inverts synchronously with the nitrogen inversion, the same uncertainties remain for the second ring as in the previous comments[4] on the $[Co(NH_3)_4(N\text{-Meen})]^{3+}$ results.

The concurrent inversion of both chelate rings in one dien ligand of *trans*-$[Co(dien)_2]^{3+}$ would produce a deprotonated intermediate having substantial eclipsing of these chelate rings.[8] From the known energy barriers between the staggered and eclipsed conformers of ethane and methylamine,[15] the energy barrier to formation of the eclipsed deprotonated intermediate for the dien complex may be assessed as $\sim$14 kcal mol^{-1}. On this basis alone we feel that this symmetrical intermediate is unlikely, and such an intermediate has been discounted also in the base hydrolysis of *sym*-$[Co(trenen)Cl]^{2+}$ where the product retains optical activity[8] and in the racemization of $[Pt(N\text{-Meen})(en)]^{2+}$ [16] where the high retention ratio k_D/k_R dictated against a symmetrical π-bonded intermediate.[17] We propose therefore that in the conformational interchanges associated with the nitrogen inversion in *trans*-$[Co(dien)_2]^{3+}$, the two coupled rings will not invert simultaneously. This consideration is distinct from whether or not the inversion of one of the rings is synchronous with nitrogen inversion.

In comparing racemization and exchange rates for the various complexes, account has to be taken of the number of active centers in each molecule and the relationship between inversion at each center and the observed racemization. The significant comparison should be between inversion rates related to a single center, k_i.

trans,*trans*-$[Co(N\text{-Meen})_2(NO_2)_2]^+$, with two reactive centers, requires inversion of one center in each

(14) D. A. Buckingham, P. A. Marzilli, I. E. Maxwell, A. M. Sargeson, and H. C. Freeman, *J. Chem. Soc. D*, 473 (1969); M. Dwyer and I. E. Maxwell, *Inorg. Chem.*, **9**, 1459 (1970); D. A. Buckingham, I. E. Maxwell, A. M. Sargeson, and H. C. Freeman, *ibid.*, **9**, 1921 (1970); M. R. Snow, *J. Amer. Chem. Soc.*, **92**, 3610 (1970).

(15) D. J. Millen, *Progr. Stereochem.*, **3**, 138 (1962).

(16) D. A. Buckingham, L. G. Marzilli, and A. M. Sargeson, *J. Amer. Chem. Soc.*, **91**, 5227 (1969).

(17) P. Haake and P. C. Turley, *ibid.*, **90**, 2293 (1968).

molecule to form the inactive meso form, so that $k_R = k_i$. However, with both *trans*-$[Co(dien)_2]^{3+}$ (two reactive centers) and $[Co(NH_3)_4(N\text{-Meen})]^{3+}$ (one asymmetric center) only one center per two molecules need invert to form racemate, so that $k_R = 2k_i$. The inversion rates k_i are thus essentially similar for these latter ions of identical charge (allowing for the [Co] and μ differences), while that for *sym*-$[Co(trenen)N_3]^{2+}$ ($k_R = 2k_i$) may be slightly higher (Table IV).

Statistical factors do not enter into the H-exchange rate measurements so that the deuteration rates for the two 3+ complexes differ threefold (Table IV) as do the retention ratios k_D/k_i, 2.5×10^5 for $[Co(NH_3)_4(N\text{-Meen})]^{3+}$ and 8×10^5 for *trans*-$[Co(dien)_2]^{3+}$. These ratios for the 3+ complexes are considerably less than for *sym*-$[Co(trenen)N_3]^{2+}$, $k_D/k_i = 4.6 \times 10^6$. This factor cannot be correlated with the charge difference and it is difficult to associate with some restriction on conformational interchange in the trenen complex since the k_i rates are similar, so that it is probably to be ascribed to the electronegative azido substituent. Although the two highly electronegative groups did not appear to increase the retention ratio in *trans,trans*-$[Co(N\text{-Meen})_2(NO_2)_2]^+$ [5] ($k_D/k_i = 9 \times 10^4$), the nitro groups are cis to the asymmetric centers in this instance. It seems likely that the azido group is exerting a *trans effect* in *sym*-$[Co(trenen)N_3]^{2+}$, enhancing k_D and k_D/k_i. This may not be a general effect however, since estimates of N–H exchange rates at both "angular" and "planar" secondary nitrogen donor sites in α-$[Co(trien)NH_3Cl]^{2+}$ [18] and the various configurations of β-$[Co(trien)gly]^{2+}$ [19] (trien = triethylenetetramine; gly = glycinato anion) indicate that both detailed ring geometry and position of electronegative substituent affect these rates, but so far few generalizations have emerged.

Other features found common with previous observations are an isotope effect for exchange similar to that in $[Co(NH_3)_4(N\text{-Meen})]^{3+}$ ($k_D/k_H \approx 3$)[4] and a decrease of racemization rate in phosphate buffers (Table III) associated with ion pairing.

A feature not observed previously[3,5] however is a small dependence of all rates on complex concentration, and the effect of ionic strength on all rates is larger than previously noted[3] (Tables I and II). These features may be rationalized on the basis of ion pairing. Ion association of Cl^- (or NO_3^-) may restrict access of the catalyzing base to the exchangeable proton or reduce the effective positive charge on the complex moiety, so that the ion pair would be less reactive toward exchange (on both mechanisms A and B) and the racemization rate would be consequently diminished also. Slower rates would thus result from increasing μ or by adding KCl to maintain μ constant when [complex] is reduced. Such interactions may be rather specific[20] so that the smaller effects noted by the previous workers need not be surprising, despite the larger specific effect of phosphate on the $[Co(NH_3)_4sarc]^{2+}$ system.[3]

The parallel effects of varying [complex] and μ on both the exchange and racemization rates are more consistent with mechanism A, involving a common intermediate for both processes, than with mechanism B (Figure 2), so that we concur with the remarks of the previous authors. The conceptual difference between the alternative mechanisms is small however.

Acknowledgment.—We are grateful to Drs. D. A. Buckingham (Australian National University) and M. Dwyer (University of Adelaide) for helpful discussions on this work.

(18) M. Dwyer, Ph.D. Thesis, Australian National University, Canberra, 1971.

(19) D. A. Buckingham, M. Dwyer, L. G. Marzilli, A. M. Sargeson, and K. R. Turnbull, unpublished results.

(20) S. F. Mason and B. J. Norman, *Proc. Chem. Soc., London*, 339 (1964); *Chem. Commun.*, 73 (1965); I. R. Lantzke and D. W. Watts, *Aust. J. Chem.*, **19**, 969 (1966); **20**, 2623 (1967).

Inorganic Chemistry, Vol. 13, No. 9, 1974 2173

Contribution from the Department of Physical and Inorganic Chemistry, The University of Adelaide, Adelaide, South Australia 5001

Isomers of the Bis(diethylenetriamine)cobalt(III) Cation. Dependence of Equilibrium Isomer Proportions on Environmental Parameters

F. RICHARD KEENE and GRAEME H. SEARLE*

Received December 18, 1973 AIC30900N

The equilibrium distribution of the three geometric isomers of $[Co(dien)_2]^{3+}$ depends considerably on the environmental parameters solvation, ion association, and temperature. Addition of a basic oxy anion such as phosphate, selenite, or sulfate profoundly modifies the isomer distribution through the differential specific associations between the anion and the three isomers. The relative magnitudes of the specific interactions with phosphate as deduced from isomer proportions measurements are correlated with the measured association constants of the three isomers with that anion, and they are rationalized in terms of the detailed molecular structures of the isomers. The equilibrium isomer distribution measurements carried out at different temperatures lead to quantitative assessment of the enthalpy and entropy differences between the isomers. These thermodynamic data allow the first comparison of experimental equilibrium results with the predictions from energy-minimized conformational analysis calculations for different topological forms of a multidentate ligand complex and indicate the limitations of the present calculative methods.

Introduction

It has been appreciated for many years that a number of factors may determine the relative stabilities of the various isomeric forms of a metal complex, where these forms differ in relative geometry, *i.e.*, geometric isomers, internal diastereoisomers, or conformational isomers.[1] These factors include ion association, solvation, temperature, intramolecular nonbonded atomic interactions, and statistical weighting factors. The quantitative evaluation of all these factors, either on an experimental or on a theoretical basis, has not been possible however since it is recognized that they are not all independent. Even the relative importance of intramolecular and intermolecular factors is not generally known.

Experimentally, the reliable quantitative data for equilibrium distributions of isomers are essentially confined to some cobalt(III) complexes, with equilibrium frequently

(1) E. J. Corey and J. C. Bailar, *J. Amer. Chem. Soc.*, 81, 2620 (1959).

being established by the presence of charcoal.[2] Frequently the relative isomer proportions have been determined under only one particular set of experimental conditions of temperature, solvent, pH, and counterion concentration, and few studies of isomer proportions as functions of variations in these environmental parameters are apparent in the literature.[3-6]

We here report a more comprehensive experimental study of the influence of these environmental factors on the complex system $[Co(dien)_2]^{3+}$, dien = diethylenetriamine. This system is particularly useful for such a study. It is inert and free of possible complications such as disproportionation or hydrolysis or ligand substitution reactions which are inherent with complex systems involving mixed-ligand or acido substituents. The three geometric isomers[7] shown in Figure 1 have been well characterized,[8-10] and the effects of variations in environmental parameters are manifested primarily as changes in the geometric isomer proportions (rather than on conformer populations) so that the various effects can be measured quantitatively by chromatographic separations of the isomers from admixtures.[9]

Previous studies of this type on systems of noncoupled chelate rings such as $[Co(en)_3]^{3+}$ have demonstrated the effects of variations in temperature or ion association on conformer distributions. In noncoupled chelate ring systems equilibrium conformer proportions have to be deduced indirectly however from circular dichroism[3,11-15] or pmr[15-17] measurements, so that the data are semiquantitative only and interpretation is less certain.

The quantitative data obtained in the present study allow some conclusions as to the practical usefulness of present conformational analysis calculative methods for geometric isomers of metal complexes. Conformational analysis calculations have been refined in the present energy minimization techniques[4,18] to include all intramolecular factors. Such calculations yield enthalpy differences between isomers, as well as the "energy-minimized" detailed molecular structures for the isolated (hypothetical gas state) complex ions. The calculated strain energies are based on unknown energy zeros however, so that the applications to date have been restricted to comparisons of conformational isomers or internal diastereoisomers.[4] For these isomer types the intermolecular effects might be expected to be similar and the zero energies may reasonably be assumed approximately constant. The agreements between the energy-minimized isomer ratios (and structures) and the experimentally determined ratios (and structures) found for several systems so far have given some confidence in the calculations, so that for these systems at least it would seem that variations in entropy or intermolecular factors between the closely similar isomers are small.[6]

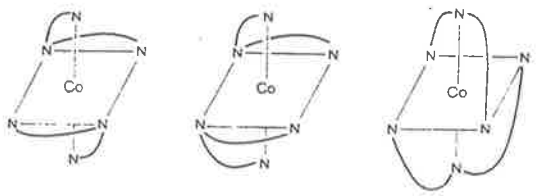

Figure 1. Topological isomers of $[Co(dien)_2]^{3+}$: left, *s-fac*; center, *Δ-u-fac*; right, *mer*.

For geometric isomers the zero levels for the minimized energies need not be similar.[19] Some experimental isomer equilibrium data obtained earlier for the $[Co(dien)_2]^{3+}$ system allowed the first test of the calculative method for geometric isomers.[19] This comparison, of experimental ΔG° with calculated ΔH° values, involved unknown entropy and intermolecular factors however, so that the uncertainty as to zero-level imbalances in the comparison has remained.

The isomer equilibrium measurements on this complex system have been extended in the present paper so that the more useful comparisons of calculated and experimental ΔH° values between the isomers can now be made. The experimental results also allow some assessment of the contribution of environmental or intermolecular factors (ion–ion and ion–solvent interactions) and show that intermolecular factors are of considerable importance in determining the isomer distribution in $[Co(dien)_2]^{3+}$.

Experimental Section

Equilibrium proportions of the three geometric isomers of $[Co(dien)_2]^{3+}$ were determined from separate aerial oxidation procedures carried out under a variety of conditions. The reaction stoichiometry involved in all runs was

$$CoX_2 + 2dien + HX + {}^1/_4O_2 \xrightarrow{C} [Co(dien)_2]^{3+} + 3X^- + {}^1/_2H_2O$$

All aerations were of 36-hr duration and were carried out in the presence of charcoal, either at room temperature (18 ± 1°) or over a steam bath (80 ± 1°). Analytical grade reagents (Co(II) salts, added salts, solvents, and acids) and freshly distilled dien were used throughout. Freshly finely ground "BDH granulated charcoal for gas absorption" from the same batch was used, and its catalytic activity was tested to ensure that it satisfied the criterion of causing racemization of $(+)[Co(en)_3]^{3+}$ within 2 min at 90°.[20] The equilibrium preparations were carried out under a variety of conditions (Table I) which included variation in the anion X^-, variation of X^- concentration by adding salts in some runs, and variations in the cation concentration, temperature, solvent, and pH.

(2) F. P. Dwyer in "Advances in the Chemistry of Coordination Compounds," S. Kirschner, Ed., Macmillan, New York, N. Y., 1961, p 21.
(3) A. M. Sargeson, *Transition Metal Chem.*, 3, 303 (1966).
(4) D. A. Buckingham and A. M. Sargeson, *Top. Stereochem.*, 6, 219 (1971), and references therein.
(5) S. F. Lincoln and D. R. Stranks, *Aust. J. Chem.*, 21, 1745 (1968).
(6) R. J. Dellaca, V. Janson, W. T. Robinson, D. A. Buckingham, L. G. Marzilli, I. E. Maxwell, K. R. Turnbull, and A. M. Sargeson, *J. Chem. Soc., Chem. Commun.*, 57 (1972); *J. Amer. Chem. Soc.*, 96, 1713 (1974).
(7) The geometric isomers of $[Co(dien)_2]^{3+}$ are designated *s-fac* (symmetrical-facial), *u-fac* (unsymmetrical-facial) and *mer* (meridional), or alternatively as s-cis, u-cis, and trans, respectively.
(8) F. R. Keene, G. H. Searle, Y. Yoshikawa, A. Imai, and K. Yamasaki, *Chem. Commun.*, 784 (1970).
(9) F. R. Keene and G. H. Searle, *Inorg. Chem.*, 11, 148 (1972).
(10) Y. Yoshikawa and K. Yamasaki, *Bull. Chem. Soc. Jap.*, 45, 179 (1972).
(11) T. S. Piper and A. G. Karipides, *J. Amer. Chem. Soc.*, 86, 5039 (1964).
(12) S. F. Mason and B. J. Norman, *Proc. Chem. Soc., London*, 339 (1964); *J. Chem. Soc. A*, 307 (1966).
(13). A. J. McCaffery, S. F. Mason, B. J. Norman, and A. M. Sargeson, *J. Chem. Soc. A*, 1304 (1968).
(14) P. G. Beddoe, M. J. Harding, S. F. Mason, and B. J. Peart, *Chem. Commun.*, 1283 (1971).
(15) J. K. Beattie, *Accounts Chem. Res.*, 4, 253 (1971).
(16) L. R. Froebe and B. E. Douglas, *Inorg. Chem.*, 9, 1513 (1970).
(17) J. L. Sudmeier and G. L. Blackmer, *J. Amer. Chem. Soc.*, 92, 5238 (1970); *Inorg. Chem.*, 10, 2010 (1971); J. L. Sudmeier, G. L. Blackmer, C. H. Bradley, and F. A. L. Anet, *J. Amer. Chem. Soc.*, 94, 757 (1972).
(18) M. R. Snow, *J. Amer. Chem. Soc.*, 92, 3610 (1970); M. Dwyer, R. J. Geue, and M. R. Snow, *Inorg. Chem.*, 12, 2057 (1973).
(19) M. Dwyer and G. H. Searle, *J. Chem. Soc., Chem. Commun.*, 726 (1972). The calculated strain energy figures for the $[Co(dien)_2]^{3+}$ isomers given in this reference were based on the 290 most significant interactions only. The strain energy figures quoted in the present paper are revised calculations utilizing a full force field: M. Dwyer, unpublished work.
(20) F. P. Dwyer and A. M. Sargeson, *Nature (London)*, 187, 1022 (1960).

Table I. Equilibrium Geometric Isomer Proportions in Aerial Oxidation Preparations of $[Co(dien)_2]^{3+}$ at 18° with Variations in Environmental Parameters

Solvent[a]	Co^{3+} anion	[Co], *M*	Added salt and [salt]	Isomer proportions, %		
				s-fac	*u-fac*	*mer*
Water	ClO_4^-	0.2, 0.02		8	30	62
Water	ClO_4^-	0.02	$NaClO_4$, 2 *M*	9	30	61
DMSO	ClO_4^-	0.01		6	14	80
DMA	ClO_4^-	0.005		7	14	79
DMA	ClO_4^-	0.005	$(Bu_4N)Cl$, 0.025 *M*	17	15	68
Water	NO_3^-	0.02		7	29	64
Water	NO_3^-	0.02	$NaNO_3$, 2 *M*	8	30	62
Water	CH_3COO^-	0.02		7	27	66
Water[b]	CH_3COO^-	0.02		14	42	44
Water	CH_3COO^-	0.02	$NaCH_3COO$, 2 *M*	12	31	57
Methanol	CH_3COO^-	0.02		18	29	53
t-C_4H_9OH	CH_3COO^-	0.02		20	45	35
Water	Br^-	0.4, 0.2, 0.02		7	28	65
Water	Br^-	0.2, 0.02	NaBr, 2 *M*	7	26	67
Water	Cl^-	0.4, 0.2, 0.02		7	28	65
Water[b]	Cl^-	0.02		12	41	47
Water	Cl^-	0.02	NaOH, 0.01 *M*; pH ~10	10	28	62
Water	Cl^-	0.2, 0.02	KCl, 2 *M*	7	28	65
Water	Cl^-	0.02	Na_2SeO_3, 2 *M*	59	28	13
Water	Cl^-	0.02	Phosphate buffer, 1 *M*; pH ~4	6	29	65
Water	Cl^-	0.02	Na_2HPO_4, 2 *M*	37	38	25
Water	Cl^-	0.02	Na_3PO_4, 0.01 *M*	16	31	53
Water	Cl^-	0.02	Na_3PO_4, 0.02 *M*	26	33	41
Water	Cl^-	0.02	Na_3PO_4, 0.04 *M*	37	33	30
Water	Cl^-	0.02	Na_3PO_4, 0.08 *M*	55	25	20
Water	Cl^-	0.02	Na_3PO_4, 0.4 *M* (satd)	59	29	12
Water	SO_4^{2-}	0.2, 0.02		19	34	47
Water[b]	SO_4^{2-}	0.02		22	44	34
Water	SO_4^{2-}	0.2, 0.02	K_2SO_4, 2 *M*	25	38	37

[a] DMSO = dimethyl sulfoxide, DMA = dimethylacetamide. [b] Temperature 80°.

Isomer Proportions in Aqueous Solution. The following procedure was typical of the runs in aqueous solution where anion was added in excess of that required by the reaction stoichiometry. $Co(NO_3)_3 \cdot 6H_2O$ (0.29 g, 0.0010 mol) was dissolved in water (30 ml) in a two-necked 100-ml round-bottom flask fitted with a reflux condenser to minimize evaporation during the aeration. To this solution $NaNO_3$ was added (8.5 g, 0.10 mol) and was dissolved as completely as possible before the addition of charcoal (2 g). A solution of dien (0.23 g, 0.0022 mol) and HNO_3 (1.1 ml of 1.0 *M*, 0.0011 mol) in water (20 ml) was then added. After aeration for 36 hr the charcoal was filtered off.

In the preparations involving phosphate or selenite ions the cobalt(II) salts of these anions were not used directly due to their low solubilities. Na_3PO_4 or Na_2SeO_3 was added to the solution of $CoCl_2$ as in the procedure above, and the aeration was carried out on the resulting suspension of the sparingly soluble cobalt(II) salt which precipitated along with some cobalt(II) hydroxide. This cobalt(II) salt dissolved as the reaction proceeded so that the preparation should have remained under equilibrium conditions throughout the process.

The filtrate from each preparation was diluted so that the concentration of the 1+ cations was less than 0.1 *M*, and aliquots (approximately one-fourth of the total volume) were applied to two columns (50 × 0.9 cm) of SP-Sephadex C-25 cation-exchange resin in the Na^+ form for duplicate isomer separations. The absorbed complex on each column was eluted with 0.3 *M* sodium (+)-tartrate solution to separate the isomers in the order *s-fac* (eluted first), *u-fac*, then *mer* (last).[9] The separated bands were collected and subsequently made up to standard volumes (25 or 50 ml) in volumetric flasks. The solutions were estimated either by cobalt atomic absorption or by spectrophotometry in 1- or 4-cm quartz cells. The optical densities of the eluted isomer bands from each chromatographic separation were measured at the first band maximum (*ca.* 466 nm)[9] on a manual Shimadzu QR-50 spectrophotometer against water reference, and it was established that each isolated isomer gave identical extinction coefficients in water and in 0.3 *M* sodium (+)-tartrate solution. The isomer proportion values given in Table I are the means from the duplicate separations for each run, and in separations where both analytical methods were used the analyses agreed. The percentage figures are each considered accurate to ±1.

Isomer Proportions in Nonaqueous Solvents. Modifications of the above procedure were necessary. For the runs in alcoholic solvents acetate counterion was used to confer solubility on the complex products. With the aprotic solvents, an aliquot of a dried (3-A molecular sieves) 0.1 *M* solution of $Co(ClO_4)_2 \cdot 6H_2O$ in the appropriate solvent (dimethyl sulfoxide or dimethylacetamide), charcoal, and (if required) added anion as the tetrabutylammonium salt were mixed. dien and dien·3$HClO_4$ in 1.67 and 0.33 molar proportions compared to cobalt were added, and subsequent treatment was as above.

Determination of the Ion Association Constants between the Isomers of $[Co(dien)_2]^{3+}$ and PO_4^{3-}. Aliquots of Na_3PO_4 solution (2×10^{-2} *M*) were added to separate solutions of the geometric isomers of $[Co(dien)_2]^{3+}$ (*ca.* 2×10^{-3} *M*) in a stirred cell (3.2 cm) thermostated at 25.0° and containing a pH electrode assembly. The optical density at 300 nm was followed as a function of phosphate concentration using a Cary 16K spectrophotometer, and the pH was maintained at 11.5 by addition of NaOH using an ABU-1 autoburet. The ionic strength of each solution was adjusted to $\mu = 0.12$ *M* with NaCl. The ion association constants K_{IP} were calculated using the reiterative graphical method of Newton and Arcand[21a] as elaborated by Davies.[21b] Constant K_{IP} values were obtained after about five reiterative graphical plots.

Results and Discussion

The equilibrium proportions of the three geometric isomers of $[Co(dien)_2]^{3+}$ under various conditions (given in Table I) were obtained by analyzing the solutions resulting from aerial oxidation of mixtures of cobalt(II) and dien in the presence of charcoal catalyst.

An alternative approach to obtaining this information, equilibration of each separate isomer to the mixture in the presence of charcoal, was also investigated.[22] It was found that equilibration of any one isomer at 18° required several months, so that it might be argued that the aerial oxidation preparations at that temperature should have been performed over a time scale similar to that of the equilibration experiments. However the isomer proportions obtained from the aerial oxidation procedures after 36 hr were identical with

(21) (a) T. W. Newton and G. M. Arcand, *J. Amer. Chem. Soc.*, 75, 2449 (1953); (b) C. W. Davies, "Ion Association," Butterworths, London, 1962, pp 56–58.

(22) G. H. Searle and F. R. Keene, unpublished results.

the equilibration results within the experimental errors, so that presumably the catalysis induced by charcoal is enhanced by the presence of the cobalt(II) in the aerial oxidation preparations.[20] At 80° the aerial oxidation preparations here reported and the charcoal-catalyzed equilibrations also gave identical values of the isomer proportions. It is also relevant to the present work that each isomer undergoes isomerization to this same mixture extremely slowly in the absence of charcoal (equilibration requires *ca.* 2 weeks at 80°).[22]

The crude $[Co(dien)_2]Cl_3$ complex (as an isomeric mixture) has been isolated in 94% yield from aerial oxidation preparations with charcoal,[9] so that it is assumed in the present isomer proportion studies that the complex was formed in solution in at least this amount. The maximum yield of cobalt(III) species anticipated would probably be ~96%, because ~4% reduction to cobalt(II) is known to occur from the analogous hexaamine system $[Co(en)_3]^{3+}$ in the presence of charcoal.[20] This isolation of the complex in high yield indicates that any errors in the determined isomer proportions arising from adsorption of the complex on the charcoal should be insignificant.

All these results, together with the observation that all charcoal-catalyzed preparations (aqueous solutions) of $[Co(dien)_2]^{3+}$ (both oxidative and substitutive) gave products of similar isomeric distribution,[8-10] provide substantial evidence that charcoal markedly catalyzes the attainment of a true thermodynamic equilibrium distribution of isomers in the $[Co(dien)_2]^{3+}$ preparations. It is generally accepted that charcoal catalyzes equilibration between cobalt(III) complexes and isomers in aqueous solution, although this function of charcoal in nonaqueous solvents has not been confirmed. For all runs by the aerial oxidation method the concentrations were adjusted to ensure that no product separated out, so that all the results correspond to equilibria in solution.

The isomer proportions were not affected by variation of cobalt concentration over the 20-fold range [Co] = 0.4-0.02 *M* (Table I).

Preference for the Meridional Configuration. The *mer* ligand arrangement has been indicated for the isolated mono(diethylenetriamine) complexes $[Co(dien)Cl_3]$,[23-26] $[Co(dien)(NO_2)_3]$,[23-27] $[Co(dien)(NO_2)_2Cl]$,[23] and $[Co(dien)(NO_2)_2(NH_3)]^+$,[23] and only in certain circumstances have facial mono(diethylenetriamine) complexes of cobalt(III) been observed. In the mixed bis(tridentate) systems $[Co(dien)(IDA)]^+$ [28] and $[Co(dien)(S\text{-}Asp)]^+$ [29] the predominance of the facial geometric forms was attributed to the strong preference by these amino acid ligands for the less strained facial coordination. Of the mono(diethylenetriamine)cobalt(III) complexes involving three monodentate ligands however, only in $[Co(dien)(H_2O)_3]^{3+}$ and $[Co(dien)(H_2O)_2Cl]^{2+}$ have facial arrangements been reported[26,30] although these two complexes have not been isolated as solids. It is possible that the aquo ligands might enhance the stability of facial dien coordination through intramolecular hydrogen bonding or through intermolecular hydrogen bonding involving bridging solvent water molecules.[31] It is noted however that $[Cr(dien)Cl_3]$ and $[Rh(dien)Cl_3]$ have each been isolated in facial and meridional forms.[32]

Thus, there appears to be a preference for meridional coordination by dien in the above cobalt(III) complexes, although the effect of the acido substituents is not really known. This accords however with the *mer*-$[Co(dien)_2]^{3+}$ isomer being favored over the two facial forms, at least under conditions where intermolecular interactions appear to be insignificant. Under the usual preparative conditions at 18° the proportions obtained were *s-fac:u-fac:mer* = 7:28:65 for aqueous solutions (with Cl^- or Br^- as anion) and 7:14:79 for aprotic solvents (with ClO_4^- counterion). These figures will be used as references with which the other data will be compared.

The *u-fac* isomer should be favored over the *s-fac* on statistical grounds; after one dien ligand has coordinated *facially* to the metal ion, the second ligand can subsequently attach in three possible ways, leading to the distribution *s-fac:u-fac* = 1:2. (The *u-fac* isomer can exist as enantiomers; the s-cis cannot.[9]) This statistical ratio is reflected in the observed proportions quoted above and particularly with the aprotic solvents.

Effect of Solvation. From preparations carried out in various solvents (water, alcohols, and dipolar aprotic solvents) it was evident that the equilibrium isomer proportions were significantly dependent on the solvent. In water, ion association with chloride or perchlorate anions seems to be unimportant (Table I), and with dimethyl sulfoxide and dimethylacetamide as solvents ion association would be expected to be minimal under the perchlorate anion conditions studied.[33] The observed differences in the proportions with these two solvent types should therfore be due predominantly to solvation effects.

These differences are not large however (*s-fac:u-fac:mer* = 7:28:65 in water, 7:14:79 in aprotic solvents), and this may reflect that none of the isomers is greatly polar, so that *specific* cation-solvent interactions would not be large. The increased stability of the *mer* form in the aprotic solvents implies that this isomer is more polar than the *u-fac* (both have molecular symmetry C_2).

The proportions in methanol (18:29:53) show the *mer* isomer to be relatively less stable here. There is a correlation between the *mer* proportions observed in aprotic solvents, water, and methanol (79, 65, and 53% respectively) and the solvating powers of these solvents for cations in the order DMA, DMSO > water > methanol,[34] although the possibility of specific interactions of the complex cations with acetate ion in these methanol runs cannot be dismissed.

Effect of Perchlorate, Nitrate, Bromide, and Chloride Anions. In aqueous solution runs at 18° with the above anions or acetate present in stoichiometric quantities, the equilibrium isomer composition was independent of the anion. This accords with the relatively small variations in association constants for outer-sphere complexes between a given cobalt(III)-hexaamine type cation and the above an-

(23) P. H. Crayton and J. A. Mattern, *J. Inorg. Nucl. Chem.*, 13, 248 (1960).
(24) H. H. Schmidtke and D. Garthoff, *Inorg. Chim. Acta*, 2, 357 (1968).
(25) D. A. House, *Inorg. Nucl. Chem. Lett.*, 3, 67 (1967).
(26) S. H. Caldwell and D. A. House, *J. Inorg. Nucl. Chem.*, 31, 811 (1969).
(27) Y. Kushi, K. Watanabe, and H. Kuroya, *Bull. Chem. Soc. Jap.*, 40, 2985 (1967).
(28) J. I. Legg and D. W. Cooke, *Inorg. Chem.*, 5, 594 (1966).
(29) J. I. Legg and D. W. Cooke, *J. Amer. Chem. Soc.*, 89, 6854 (1967).
(30) P. Wilairat and C. S. Garner, *J. Inorg. Nucl. Chem.*, 32, 2293 (1970).
(31) A. W. Adamson, *J. Amer. Chem. Soc.*, 80, 3183 (1958).
(32) A. D. Fowlie, D. A. House, W. T. Robinson, and S. S. Rumball, *J. Chem. Soc. A*, 803 (1970).
(33) W. A. Millen and D. W. Watts, *Aust. J. Chem.*, 19, 43 (1966).
(34) W. R. Fitzgerald, A. J. Parker, and D. W. Watts, *J. Amer. Chem. Soc.*, 90, 5744 (1968).

ions, although the tabulated data are limited.[35] The addition of a large excess of any of these anions (excepting acetate) did not change the isomer proportions of $[Co(dien)_2]^{3+}$, and pmr[16] and CD[12,36] evidence indicates that excesses of these anions do not greatly change the conformer compositions in systems such as $[Co(en)_3]^{3+}$. It seems therefore that these anions do not associate greatly with these complex ions in water, or at least they show no preferred orientations.

In dimethylacetamide the ion association with chloride should be larger than in water,[33,37] and the isomer proportions in $[Co(dien)_2]^{3+}$ were considerably altered on addition of excess chloride in this solvent. In particular the *s-fac* isomer was stabilized at the expense of the *mer* (Table I).

Effect of pH. The proportion of *s-fac*-$[Co(dien)_2]^{3+}$ was raised slightly (to 12%) with excess acetate ion. In all aqueous preparations involving the other singly charged anions, the solutions had pH ~4, but the pH of the acetate solution was ~8. That this was an effect of pH rather than of acetate ion specifically was checked by basifying a chloride preparation with added sodium hydroxide when a similar change in isomer proportions was observed (Table I). Basic conditions also obtained for the preparations involving phosphate and selenite, but the greater effects in these instances were due primarily to specific ion associations which swamped any pH effect.

Specific Ion Associations with Phosphate, Selenite, and Sulfate. The greatest effects on the equilibrium isomer proportions were shown on the addition of the oxy anions SO_4^{2-}, SeO_3^{2-}, PO_4^{3-}, or HPO_4^{2-} (but not $H_2PO_4^-$), with the effect of sulfate being less than that for the other species (aqueous solutions, Table I). Under these conditions the proportion of the *s-fac* isomer increased at the expense of the *mer*, with the *u-fac* proportion remaining nearly constant. As the PO_4^{3-} concentration was increased, the proportions of isomers changed continuously from *s-fac:mer* = 7:65 in the "reference case" to 59:12. These observations imply that there are specific interactions between the three $[Co(dien)_2]^{3+}$ isomers and phosphate anion and that the magnitudes of the interactions are in the order *s-fac* > *u-fac* > *mer*.

Of many anions tested, phosphate and selenite (and to a lesser extent sulfate) had particularly marked effects on pmr[15-17] and CD[12,36] spectra of $[M(en)_3]^{3+}$ ions. The spectral changes observed have been interpreted as the consequence of alterations of relative conformer populations,[3,12,15-17] although ion pairs formed should also contribute direct electronic effects to the CD.[12] Although larger association effects would be expected for these more highly charged oxy anions than for singly charged anions in any case, the results have indicated that specific interactions occur such that the tris-lel[1] conformer becomes more favored relative to the other three conformers. The tris-lel conformer of $[M(en)_3]^{3+}$ has two sets of three N-H bonds aligned nearly parallel to the molecular C_3 axis, a situation which does not obtain for any of the other conformers having ob[1] rings. Mason and Norman[12] suggested that these tetrahedral oxy anions could approach the tris-lel cation along the C_3 axis and associate by hydrogen bonding to the nearly parallel N-H bonds. The structure of the proposed specifically oriented ion pair $[Co(en)_3]^{3+}$. PO_4^{3-} is shown in Figure 2.[38,39] If the predominant conformation in solution was *not* originally tris-lel but was lel$_2$ob as indicated by recent pmr studies,[15,17] then the addition of these oxy anions would stabilize the tris-lel form and decrease the proportion of lel$_2$ob. The $-CH_2-$ resonances of the pmr spectrum should therefore be modified,[16] and the CD spectrum should change significantly.[12] The recent X-ray crystal structure analyses of $[Co(en)_3]_2(HPO_4)_3 \cdot 9H_2O$[40] and $[Co(en)_3]PO_4$[41] have shown the three chelate ring conformations to be lel and the phosphate ion to be positioned approximately on the C_3 axis of each molecule as proposed by Mason.

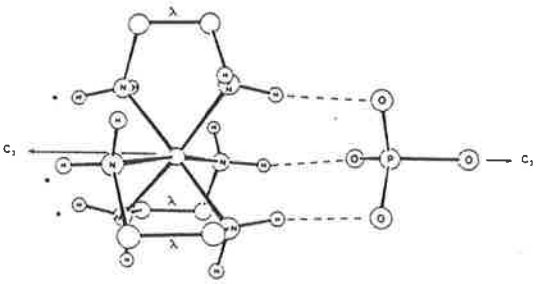

Figure 2. The structure of the ion pair between Δ-$[Co(en)_3]^{3+}$ (λλλ, tris-lel) and PO_4^{3-}, drawn using crystallographic data from G. L. Blackmer, G. H. Lin, J. L. Sudmeier, and R. M. Wing, unpublished work, private communication.

Such hydrogen-bonding capacity should depend on the basicity of the anion. Thus the reduced effect of sulfate, compared to the other oxy anions mentioned, on both $[Co(dien)_2]^{3+}$ and $[M(en)_3]^{3+}$ systems may be correlated with its being the poorest hydrogen-bond acceptor since it is the weakest base.

For the isomers of $[Co(dien)_2]^{3+}$, some association with oxy anions has been indicated previously. The CD of the *u-fac* isomer changes on addition of selenite, indicating some conformational change due to specific ion association.[42] Similarly, sulfate ion changes the CD of the *mer* form,[10] and phosphate decreases the racemization rate of this isomer.[43]

Dreiding molecular models show that the *s-fac*-$[Co(dien)_2]^{3+}$ ion has two sets of three N-H bonds (two from primary amine groups, one from secondary) appropriately disposed at opposite ends of the molecule (Figure 3) to allow hydrogen bonding in a manner analogous to that proposed above for $[M(en)_3]^{3+}$. The models indicate that while there may be some conformational flexibility within the *s-fac* arrangement, such conformational changes would not affect these N-H dispositions significantly. Figure 3[38] shows the particular conformer λδ-δλ[39] (point symmetry C_{2h}) which is that found in the crystal form[44] and which might be expected to be present in reasonable proportion in solution. Stabilization of this isomer could thus occur by ion-pair formation, with oxy anions specifically oriented through hydrogen bonding in the manner indicated in the figure.

(35) F. Basolo and R. G. Pearson, "Mechanisms of Inorganic Reactions," 2nd ed, Wiley, New York, N. Y., 1967, p 37.
(36) H. L. Smith and B. E. Douglas, *J. Amer. Chem. Soc.*, 86, 3885 (1964); *Inorg. Chem.*, 5, 784 (1966).
(37) W. A. Millen and D. W. Watts, *J. Amer. Chem. Soc.*, 89, 6858 (1967).

(38) The perspective structure representations in the figures were obtained using computer drawings of crystallographic structure data. Open circles are carbon or cobalt atoms. C-H bonds are omitted for clarity. In each diagram an alternative set of N-H bonds for association with PO_4^{3-} ion is denoted with asterisks.
(39) Λ and Δ refer to absolute chelate configurations about a metal atom, and λ and δ refer to chelate ring conformations, as defined in *Inorg. Chem.*, 9, 1 (1970).
(40) E. N. Duesler and K. N. Raymond, *Inorg. Chem.*, 10, 1486 (1971).
(41) G. L. Blackmer, G. H. Lin, J. L. Sudmeier, and R. M. Wing, unpublished work.
(42) F. R. Keene, G. H. Searle, and S. F. Mason, *Chem. Commun.*, 839 (1970).
(43) G. H. Searle and F. R. Keene, *Inorg. Chem.*, 11, 1006 (1972).
(44) M. Kobayashi, F. Marumo, and Y. Saito, *Acta Crystallogr., Sect. B*, 28, 470 (1972).

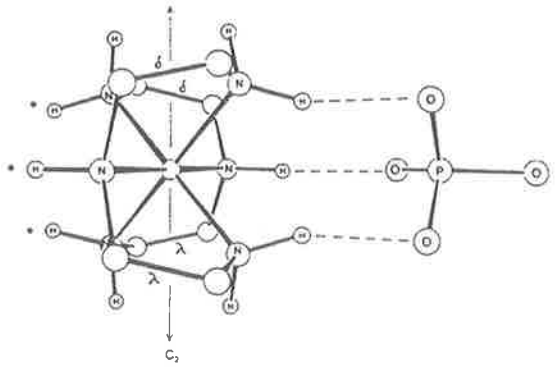

Figure 3. The proposed structure of the ion pair between *s-fac*-[Co(dien)$_2$]$^{3+}$ ($\lambda\delta$-$\delta\lambda$) and PO_4^{3-}. The cation structure was drawn using crystallographic data from M. Kobayashi, F. Marumo, and Y. Saito, *Acta Crystallogr., Sect. B*, 28, 470 (1972).

The *u-fac* isomer also has two such sets of three N-H bonds (all from NH_2 groups), these sets being related by the molecular C_2 axis. In this isomer however, these two potential sites for hydrogen bonding to PO_4^{3-} ion are in close proximity (they are effectively on two adjacent faces of the N_6 octahedron). Association with one PO_4^{3-} might therefore be expected to be intrinsically less favorable than for the *s-fac* isomer. In the latter isomer the two potential hydrogen-bonding sites are widely separated, so that we consider that there is a greater chance of a PO_4^{3-} ion locating one of these suitable sites. The Dreiding models suggest that for the *u-fac* isomer the orientations of the N-H bonds are more dependent on the particular chelate ring conformations than in the case of *s-fac*. Figure 4[38] shows the Δ-*u-fac*[39] isomer in the $\delta\lambda$-$\delta\lambda$[39] conformation (symmetry C_2) which we consider is favorable for hydrogen bonding, and this is one of the conformational forms present in the solid state.[45]

The *mer* form of the complex appears to have no such triple parallel N-H dispositions to favor strong specific association with tetrahedral oxy anions.

In [M(en)$_3$]$^{3+}$ systems, the effects of such associations are observed only as conformational changes. The [Co(dien)$_2$]$^{3+}$ system probably involves some conformational ordering also so that the particular N-H bonds in each isomer attain the most appropriate orientations for the maximum associative effects, but this is of minor importance compared with the preferential stabilization of geometric forms in the context of the present experiments. Such conformational changes probably account for the changes in CD of the *u-fac* and *mer* forms with added anions.[10,42]

We propose that these specific associations between oxy anions and the [Co(dien)$_2$]$^{3+}$ cations by hydrogen bonding through suitably disposed sets of N-H bonds can satisfactorily account for the present experimental proportions results. The study of models indicates that the existence of such N-H bond sets should lead to stabilizations of the isomers in the order *s-fac* > *u-fac* > *mer*, which is that deduced from the experimental proportions results.

If the *mer* isomer is stabilized on interaction with phosphate, to an extent designated $(\Delta G^\circ_{IP})_{mer}$, then it is clear that each of the facial isomers is stabilized even more on association as their proportions increase relative to the *mer* form. This additional stabilization of the facial isomers can

(45) Y. Saito, *Proc. Int. Conf. Coord. Chem.*, 14, 91 (1972); M. Konno, F. Marumo, and Y. Saito, *Acta Crystallogr., Sect. B*, 29, 739 (1973).

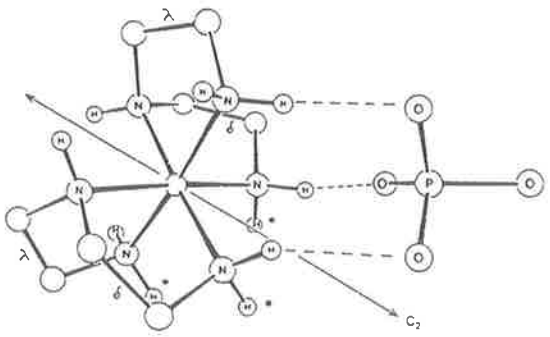

Figure 4. The proposed structure of the ion pair between *u-fac*-[Co(dien)$_2$]$^{3+}$ ($\Delta(\delta\lambda$-$\delta\lambda)$) and PO_4^{3-}. The cation structure was drawn using crystallographic data from M. Konno, F. Marumo, and Y. Saito, *Acta Crystallogr., Sect. B*, 29, 739 (1973).

Scheme I

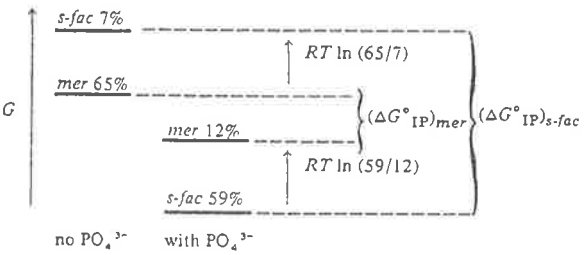

be evaluated from the isomer distributions already quoted (see Scheme I). $(\Delta G^\circ_{IP})_{s\text{-}fac} - (\Delta G^\circ_{IP})_{mer} = -RT \ln (59/12) - RT \ln (65/7) = -2.3$ kcal mol^{-1}. Similarly, $(\Delta G^\circ_{IP})_{u\text{-}fac} - (\Delta G^\circ_{IP})_{mer} = -1.0$ kcal mol^{-1}. The values of ΔG°_{IP} for the individual isomers cannot be evaluated from these data.

The ion association constants K_{IP} between the three isomeric cations and phosphate in aqueous solution were obtained spectrophotometrically ($\mu = 0.12$ *M* with NaCl, temperature 25.0°, pH 11.5). The values of K_{IP} thus determined for 1:1 [Co(dien)$_2$]$^{3+}$, PO_4^{3-} ion pairs of the geometric isomers are 5460 (*s-fac*), 850 (*u-fac*), and 84 (*mer*). These values indicate the same order of stabilizations of the three isomers with phosphate as that deduced above from the proportions results. From these K_{IP} results the ΔG°_{IP} values for the isomers are calculated as -5.1 kcal mol^{-1} for *s-fac*, -4.0 kcal mol^{-1} for *u-fac*, and -2.6 kcal mol^{-1} for *mer*. The differences between these values agree well with the corresponding differences calculated above from the proportions data, particularly considering the variations in ionic strength and pH involved in the comparison.

In dimethylacetamide, similar stabilization of *s-fac* at the expense of *mer* was observed with added chloride (Table I), suggesting ion association between chloride and suitable N-H bonds of the complex isomers. The effects of oxy anions on isomer proportions could not be reliably studied in the aprotic solvents due to the reduced solubilities of the oxy anion salts of [Co(dien)$_2$]$^{3+}$ in these media. Despite some precipitation of products, solution analyses did suggest that the *s-fac* isomer was again considerably enhanced in these solvents. (These results are not given in Table I.)

Effect of Temperature. The less stable facial isomers became more favored when the aeration preparations were carried out at 80°, compared with preparations at 18° but with conditions otherwise similar (Table I). However, as little is known concerning the relative contributions of enthalpy

Table II. Enthalpy and Entropy Contributions to Observed Isomer Equilibria in Aerial Oxidation Preparations of $[Co(dien)_2]^{3+}$

Anion	Temp, °C	K	$\Delta G°$, kcal mol^{-1}	$\Delta H°$, kcal mol^{-1}	$-T\Delta S$, kcal mol^{-1}	$\Delta S°$, eu
			Isomer Pair *mer-u-fac*			
Cl^-	18	2.32	−0.49 ± 0.03		1.8 ± 0.4	
				−2.3 ± 0.5		−6 ± 1
Cl^-	80	1.15	−0.10 ± 0.03		2.2 ± 0.5	
SO_4^{2-}	18	1.41	−0.20 ± 0.03		1.8 ± 0.4	
				−2.0 ± 0.5		−6 ± 1
SO_4^{2-}	80	0.77	+0.18 ± 0.04		2.2 ± 0.5	
			Isomer Pair *mer-s-fac*			
Cl^-	18	9.29	−1.3 ± 0.1		1.6 ± 1.0	
				−2.7 ± 1.2		−5 ± 3
Cl^-	80	3.92	−1.0 ± 0.1		1.9 ± 1.2	
SO_4^{2-}	18	2.67	−0.57 ± 0.05		1.2 ± 0.5	
				−1.8 ± 0.6		−4 ± 2
SO_4^{2-}	80	1.55	−0.31 ± 0.05		1.5 ± 0.6	
			Isomer Pair *u-fac-s-fac*			
Cl^-	18	4.00	−0.8 ± 0.1		−0.3 ± 1.0	
				−0.5 ± 1.1		+1 ± 3
Cl^-	80	3.42	−0.9 ± 0.1		−0.3 ± 1.2	
SO_4^{2-}	18	1.89	−0.34 ± 0.05		−0.7 ± 0.5	
				+0.3 ± 0.5		+2 ± 2
SO_4^{2-}	80	2.00	−0.49 ± 0.05		−0.8 ± 0.6	

and entropy to conformational and isomeric stability, the effect of temperature could not be predicted.

The isomer ratios determined for the system $[Co(dien)_2]^{3+}$ at these two temperatures allow the separation of the free energy differences between the isomers into the enthalpy and entropy contributions. The only experimental errors involved in these determinations were in the temperature interval (±2°) and in the isomer proportion percentages which were in general reproducible to ±1. While this error in the proportions might appear reasonably satisfactory, it results in appreciable uncertainty in the derived energy values, and the maximum errors are quoted with the calculated energies in Table II. The temperature uncertainty leads to relatively small errors only. Although the present results do not therefore allow the most accurate analysis, the possibilities and limitations of this experimental approach will be apparent.

The effects of temperature variations were studied in aqueous solutions with the three different counterions chloride, acetate, and sulfate. The equilibria between the isomers in the presence of chloride and acetate were essentially the same as shown by the observed proportions (Table I), so that the thermodynamic data are given only for chloride and sulfate in Table II. The results indicate large negative entropy differences (~−6 eu) for the equilibria *s-fac* ⇌ *mer* and *u-fac* ⇌ *mer*, but the entropy contribution to *s-fac* ⇌ *u-fac* is small. This is consistent with the *mer* form being the most ordered, which may be rationalized by the less conformational freedom than is possible in the two facial isomers of the complex. The pmr spectra[9] have also been interpreted on the basis of rapid conformational inversion in the facial forms, whereas such inversion would be restricted for the *mer* isomer under the acidic (pH 4) conditions obtaining in both the pmr spectra and the present work.

For the equilibrium in the presence of sulfate, where association occurs, the energy values suggest that the differences in proportions (compared to the chloride and acetate conditions where association is less important) may be due mainly to the enthalpy contributions. However because of the limited accuracy possible in the energy analysis this conclusion must at present be viewed with some caution. The greater associative effects shown by the anions selenite and phosphate could not be examined at 80° since the basic solutions containing these ions induced decomposition of the cobalt complex at this temperature.

Minimized calculations of the intramolecular enthalpies of the isomers of $[Co(dien)_2]^{3+}$ have predicted that on this basis the three geometric isomers should be of comparable stabilities.[19] The strain energies thus calculated are 9.6, 9.6 and 9.7 kcal mol^{-1} for the *s-fac*, *u-fac*, and *mer* isomers, respectively, but it is uncertain whether these minimization values relate to the same energy zero.[18,19]

While the differences ($\Delta H°$) between isomer pairs from these calculations are in qualitative agreement with the experimental isomer distribution ($\Delta G°$),[19] this correlation may be fortuitous as the present thermodynamics results show that both the entropy and enthalpy contribute significantly, but in opposition, to $\Delta G°$ for the *u-fac* ⇌ *mer* and *s-fac* ⇌ *mer* equilibria (Table II). The comparisons of the calculated intramolecular $\Delta H°$ values between isomer pairs with the present experimental (intramolecular and intermolecular) $\Delta H°$ values reveal some disparities outside the limits of our experimental errors. These disparities are probably a result of the comparisons of the calculated free ion and equilibrium measurements on the ion in its solution environment.

For these various reasons, present minimization calculations would not seem to be greatly reliable for predicting the relative stabilities of geometric isomers under practical solution conditions. Work is continuing on the calculative method and on the minimization assessment of interionic factors.[46]

Modified Preparation of the *s-fac* Isomer. The present work demonstrates that ion association might sometimes be applied to advantage in obtaining less stable isomers of metal complex systems. Such effects have also been noted previously.[47] For optimum yield (59%) of the *s-fac*-$[Co(dien)_2]^{3+}$ isomer the aerial oxidation preparation[9] with charcoal may be carried out in aqueous 0.1 *M* sodium phosphate at room temperature, the product solution being absorbed on a large column of SP-Sephadex C-25 and eluted with 0.3 *M* sodium tartrate solution. The first eluted *s-fac* band can then be reabsorbed on a short column of a weak-acid cation exchanger (Bio-Rex 70, analytical grade, 50–100 mesh, in the sodium form), washed with water, and eluted with 0.1

(46) M. Dwyer and M. R. Snow, work in progress.
(47) E. W. Gillow and G. M. Harris, *Inorg. Chem.*, 7, 394 (1968).

M hydrobromic acid. The eluate on evaporation yields crystals of *s-fac*-$[Co(dien)_2]Br_3$.

Acknowledgments. We are grateful for the use of facilities at the Research School of Chemistry, Australian National University, Canberra, to complete some of the experimental work (F. R. K.). We thank Dr. D. W. Watts (University of Western Australia) for valuable discussions and for advice on the ion association constants measurements and Dr. G. Gainsford (Australian National University) for assistance in preparing the figures. dien was kindly provided by Union Carbide (Australia) Ltd.

Registry No. *s-fac*-$[Co(dien)_2]^{3+}$, 38318-04-6; *u-fac*-$[Co(dien)_2]^{3+}$, 38318-05-7; *mer*-$[Co(dien)_2]^{3+}$, 38318-06-8; ClO_4^-, 14797-73-0; NO_3^-, 14797-55-8; CH_3COO^-, 71-50-1; Br^-, 24959-67-9; Cl^-, 16887-00-6; SO_4^{2-}, 14808-79-8; SeO_3^{2-}, 14124-67-5; HPO_4^{2-}, 14066-19-4; PO_4^{3-}, 14265-44-2.

THE SYNTHESIS OF 4,7-DIMETHYLTRIETHYLENETETRAMINE

By G. H. Searle,* M. Petkovic,* and F. R. Keene*

[Manuscript received 10 January 1972]

Studies of diacidocobalt(III) complexes of the facultative ligand triethylenetetramine (trien = 1,4,7,10-tetraazadecane), $[Co(trien)X_2]^{n+}$, have disclosed some intriguing features of the stereochemistry associated with coupled five-membered puckered ring systems.[1–4] To extend these studies the homologue of trien methylated at the secondary nitrogen centres (the 4 and 7 positions of the tetraazadecane chain) was required, since the configurational inversions which may occur by N–H exchange at these asymmetric donor nitrogens in the trien complexes[5,6] are avoided in the complexes $[Co(4,7\text{-dimethyltrien})X_2]^{n+}$.

The amine 4,7-dimethyl-1,4,7,10-tetraazadecane (4,7-dimethyltrien) has been mentioned in the patent literature[7] but details of its synthesis are not available. We now report a convenient synthesis of the amine as its tetrahydrochloride salt, starting from *N*,*N*′-dimethylethylenediamine and synthesizing the molecular chain with the reagent bromoethylphthalimide according to Scheme 1.

The overall yield of the final amine hydrochloride is about 25%. The method has the advantages of using readily available reagents and of simplicity; it can be used on a large scale. The isolation of 4,7-dimethyltriethylenetetraminediphthalimide from the corresponding dihydrobromide avoided mixed hydrochloride–hydrobromide being precipitated after the hydrolysis with hydrochloric acid.

Several methods were examined before the successful route was developed. The most direct method would seem to be direct methylation on the secondary nitrogens of the trien chain, following the method used to obtain 4-methyldiethylenetriamine.[8] However, the bis(phthalimide) derivative of trien could not be prepared

* Department of Physical and Inorganic Chemistry, University of Adelaide, P.O. Box 498D, Adelaide, S.A. 5001.

[1] Sargeson, A. M., and Searle, G. H., *Inorg. Chem.*, 1965, **4**, 45.
[2] Sargeson, A. M., and Searle, G. H., *Inorg. Chem.*, 1967, **6**, 787.
[3] Buckingham, D. A., Maxwell, I. E., Sargeson, A. M., and Freeman, H. C., *Inorg. Chem.*, 1970, **9**, 1921.
[4] Buckingham, D. A., Marzilli, P. A., Sargeson, A. M., Mason, S. F., and Beddoe, P. G., *Chem. Commun.*, 1967, 433.
[5] Buckingham, D. A., Marzilli, P. A., and Sargeson, A. M., *Inorg. Chem.*, 1967, **6**, 1032.
[6] Keene, F. R., Sargeson, A. M., and Searle, G. H., unpublished data.
[7] Earle, R. H., U.S. Pat. 3,240,664, 1966 (*Chem. Abstr.*, 1966, **64**, P19977f).
[8] Mann, F. G., *J. chem. Soc.*, 1934, 461.

in a pure state, and attempted methylations of the bis-benzylidene Schiff base of trien with excess methyl iodide under various conditions were unsuccessful.

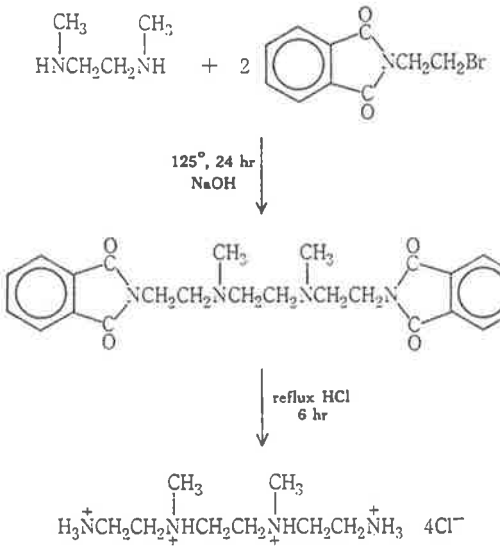

Scheme 1

An alternative approach, which has been employed in the synthesis of trien methylated on positions 1 and/or 5 of the tetraazadecane chain,[9,10] is shown in Scheme 2. The diamino diamide was obtained satisfactorily, but reduction of the amide could not be effected by use of lithium aluminium hydride[9–13] or by diborane[13–15] under a variety of conditions.

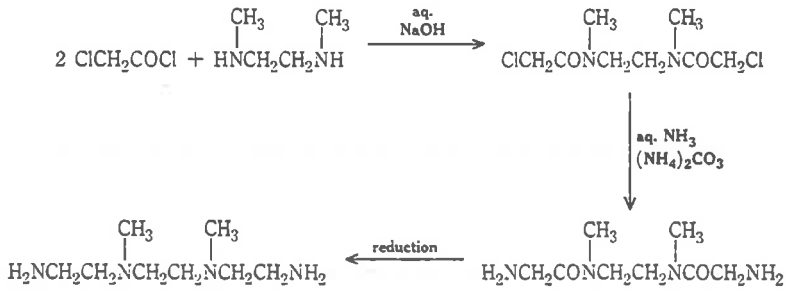

Scheme 2

Metal complexes of 4,7-dimethyltriethylenetetramine will be discussed in a subsequent article.

[9] Goto, M., Saburi, M., and Yoshikawa, S., *Inorg. Chem.*, 1969, **8**, 358.
[10] Goto, M., Okubo, A., Sawai, T., and Yoshikawa, S., *Inorg. Chem.*, 1970, **9**, 1488.
[11] Yoshikawa, S., Sekihara, T., and Goto, M., *Inorg. Chem.*, 1967, **6**, 169.
[12] Stetter, H., and Mayer, K., *Chem. Ber.*, 1961, **94**, 1410.
[13] Schenker, E., in "Newer Methods of Preparative Organic Chemistry." (Ed. W. Foerst.) Vol. 4, p. 196, 231. (Verlag Chemie–Academic Press: New York 1968.)
[14] Brown, H. C., and Heim, P., *J. Am. chem. Soc.*, 1964, **86**, 3566.
[15] Asperger, R. G., *Inorg. Chem.*, 1969, **8**, 2127.

Experimental

Reagents

N,N'-Dimethylethylenediamine from Koch–Light Laboratories, England, was fractionally distilled over sodium. The large middle fraction, b.p. 119·5–121°, was used in the synthesis. *N*-(2-Bromoethyl)phthalimide from Ralph N. Emanuel Ltd, England (97%, m.p. 81·5–82·5°) or from Eastman Organic Chemicals, New York (m.p. 82·5–83·5°) was used without further purification.

4,7-Dimethyltriethylenetetraminediphthalimide Dihydrobromide (1,8-Bis(phthalimido)-3,6-dimethyl-3,6-diazaoctane Dihydrobromide)

Bromoethylphthalimide (152·5 g, 0·60 mol) was completely melted on a steam bath. *N,N'*-Dimethylethylenediamine (26·4 g, 0·30 mol) was stirred into the melt in small portions over 15 min, with the mixture being stirred continuously over the steam bath. The orange oil which first formed as the amine was added dispersed to give a homogeneous brown liquid, which was heated in an oven at 125° for 24 hr with occasional stirring. The negligible weight loss was consistent with formation of the dihydrobromide of the product.

The dark brown mass was broken up while still hot, and on refluxing with ethanol (250 ml) the product crystallized from the brown solution. It was filtered off from the solution while still hot to avoid the separation of a viscous brown oil and washed with ethanol. It was further washed by suspending in boiling ethanol, filtered off, and washed with hot ethanol, then with ether, and dried at 100°. Yield 67·0 g, 37%; m.p. 250–251° (dec.) (Found: C, 48·8; H, 4·8; N, 9·4; Br, 27·2. $C_{24}H_{28}Br_2N_4O_4$ requires C, 48·4; H, 4·7; N, 9·4, Br, 26·8%). The product was essentially insoluble in ethanol, acetone, chloroform, benzene, dimethylformamide, and water.

Unchanged bromoethylphthalimide was recovered (33 g) from the brown ethanol filtrate by warming to redissolve the oil which had separated on cooling, precipitating the product by addition of water, and recrystallizing from hot ethanol, m.p. 81·5–82·5° (Found: C, 47·0; H, 3·2; Br, 31·2; N, 5·6. $C_{10}H_8BrNO_2$ requires C, 47·3; H, 3·2; Br, 31·4; N, 5·5%). N.m.r. ($CDCl_3$, TMS internal reference, on Varian T60): δ 3·61 (triplet, 2H, *J* 10 Hz; $N-CH_2$), 4·08 (triplet, 2H, *J* 11 Hz; CH_2Br), 7·51–8·00 (multiplet, 4H; aromatic protons).

4,7-Dimethyltriethylenetetraminediphthalimide

The above hydrobromide (59·6 g, 0·10 mol) was stirred with 10% NaOH solution (165 ml) and the slurry was extracted with chloroform (6 × 110 ml). The chloroform was removed, and the resulting yellow-brown oil was dissolved in boiling ethanol (280 ml), and the solution was filtered quickly. After cooling the solution for 2 days, the pale cream crystals which had precipitated were filtered off, washed with a small volume of ethanol then with ether, and dried. Yield 30·8 g, 71%, m.p. 113·5–116° (Found: C, 65·9; H, 6·2; N, 12·6. $C_{24}H_{26}N_4O_4$ requires C, 66·3; H, 6·0; N, 12·9%). N.m.r. ($CDCl_3$, TMS external lock reference, on Jeol 60 MHz spectrometer): δ 2·19 (singlet, 6H; $N-CH_3$), 2·57 (triplet, 8H, *J* 11 Hz; C3, C5, C6, and C8 methylene protons), 3·68 (triplet, 4H, *J* 11 Hz; C2 and C9 methylene protons), 7·41–7·80 (multiplet, 8H; aromatic protons) in the ratio 3 : 4 : 2 : 4.

4,7-Dimethyltriethylenetetramine Tetrahydrochloride (3,6-Dimethyl-3,6-diazaoctane-1,8-diamine Tetrahydrochloride)

The above diphthalimide (43·4 g, 0·10 mol) was hydrolysed by gently refluxing in concentrated HCl (210 ml). When all the material had dissolved (2 hr) more HCl was added (20 ml), and the heating was continued for a total of 6 hr. After cooling, the separated phthalic acid was filtered off and washed once with 6M HCl, and the combined filtrate was concentrated to a light yellow oil. This was dissolved in hot water (30 ml), and methanol was added (100 ml) with stirring. The product was crystallized by careful addition of acetone to incipient crystallization, and as the product slowly crystallized more acetone was added at intervals, and finally to excess (1 l.). After cooling, the product was filtered off, washed with ethanol and acetone, and dried at 100°. Yield 31·2 g, 97%. The hydrochloride was recrystallized by adding acetone to an aqueous methanol solution as above, m.p. 237–240° (Found: C, 30·2; H, 8·4; Cl, 44·1; N, 17·3.

$C_8H_{26}Cl_4N_4$ requires C, 30·0; H, 8·2; Cl, 44·2; N, 17·5%). N.m.r. (D_2O, TMS external lock, on Varian HA-100): δ 3·60 (singlet, 6H; N–CH_3), 3·92–4·27 (multiplet, 8H; C3, C5, C6, and C8 methylene protons), 4·35 (singlet, 4H; C2 and C9 methylene protons) in the ratio 3 : 4 : 2.

N,N′-Bis(chloroacetyl)-N,N′-dimethylethylenediamine

A solution of redistilled chloroacetyl chloride (86 g) in benzene (300 ml) was added dropwise to a stirred solution of *N,N′*-dimethylethylenediamine (30 g) in 5M NaOH (360 ml) cooled in an ice bath. The solution was kept below 5° with vigorous stirring and after 2 hr the white product was filtered off, washed successively with small volumes of ice-cold water, methanol, and acetone, and dried. The product was recrystallized from hot ethanol. Yield 62 g, 76%; m.p. 132–133° (Found: C, 40·4; H, 6·0; N, 11·5. $C_8H_{14}Cl_2N_2O_2$ requires C, 39·9; H, 5·9; N, 11·6%).

N,N′-Bis(glycyl)-N,N′-dimethylethylenediamine Dihydrochloride

A mixture of the above chloroamide (60 g) and ammonium carbonate (500 g) in 0·880 aqueous ammonia (1 l.) was left stirring at 40° for 2 days. The solution was concentrated to an oil. This was taken up in a little water, HCl was added to adjust the pH to 1, and the product was precipitated with ethanol. The product was filtered off, washed with ethanol and acetone, and dried. It was recrystallized from water by adding ethanol. Yield 45 g, 65%; m.p. 286° (dec.) (Found: C, 34·8; H, 7·3; N, 19·8. $C_8H_{18}N_4O_2$,2HCl requires C, 34·9; H, 7·3; N, 20·3%).

Benzylidene Schiff Base and Phthalimide Derivatives of Trien

The pale yellow bis-benzylidene Schiff base was obtained readily by reaction of benzaldehyde and trien in methanol and precipitation with water; m.p. 85–86°.

Reaction of trien with phthalic anhydride under various conditions (reactants neat, reaction in glacial acetic acid, variable proportions) gave a brown solid mass which on recrystallization from dimethylformamide or ethanol yielded first a white solid, m.p. 241° (dec.), yield up to 40%, followed by gummy material. Microanalyses of the solid indicated an empirical composition $C_{26}H_{24}N_4O_5$ (standardized to N_4 assuming preservation of the molecular chain, since acid hydrolysis gave only trien,4HCl). This is consistent with the product being a mixture of the bis- and tris-phthalimide derivatives (1 : 1 mixture requires $C_{26}H_{23}N_4O_5$), and all attempts to prepare the pure bis(phthalimide) derivative were unsuccessful.

Acknowledgment

We thank Union Carbide Australia Limited for the gift of triethylenetetramine and diethylenetriamine.

Contribution from the Department of Physical and Inorganic Chemistry, The University of Adelaide, Adelaide, Australia 5001

Cobalt(III) Complexes of 4,7-Dimethyl-1,4,7,10-tetraazadecane. Preparations, Stereochemistry, and Reactions and the Effect of N-Methylation on Relative Isomer Stabilities

GRAEME H. SEARLE,* MIRKO PETKOVIC, and F. RICHARD KEENE

Received March 8, 1973

The preparations of complexes $[Co(4,7\text{-dimetrien})X_2]^{n+}$ (4,7-dimetrien = 4,7-dimethyl-1,4,7,10-tetraazadecane; X = Cl, OH_2, NO_2; 2X = CO_3) are described. The configurations of the racemic geometric isomers are assigned as *RR,SS*-α or *RR,SS*-β from pmr spectra and from interconversion reactions in which configurational changes at the asymmetric nitrogen donor centers are precluded by the methyl substituents. The following conversions occurring with isomerization have been observed: β-dichloro → α-dichloro; β-dichloro → α-dinitro; β-chloroaquo → α-chloroaquo; β-diaquo → α-diaquo; β-diaquo → α-dinitro; α-dichloro → β-carbonato. From the tendency for β → α isomerizations to occur and from other comparisons with the corresponding $[Co(trien)X_2]^{n+}$ complexes, it is evident that the methyl substituents enhance the stabilities of the "angular" configuration at the central amine donor atoms (stability α > β) such that trans complexes with this ligand might not be obtainable.

Introduction

The chemistry of diacidocobalt(III) complexes with the flexible tetradentate ligand triethylenetetramine,[1] $[Co(trien)X_2]^{n+}$, and with homologs of trien, has attracted considerable interest and the field has been reviewed recently.[2]

Apart from the alternative trien ligand topologies,[3] alternative configurations are possible at the asymmetric secondary nitrogen donor centers giving rise to two possible configurational isomers *RR,SS* and *RS,SR*[4] for each of the β and trans topologies. Figure 1 shows all the possible isomers (one optical form of each) for complexes $[Co(trien)X_2]^{n+}$ having identical substituents X. In addition, further geometric isomers β_1 and β_2 are possible when the diacido substituents are not identical in $[Co(trien)XY]^{n+}$, and with the exception of *RS*-trans, all of these isomeric forms have now been isolated and characterized for various diacido and amino acid complexes of trien having the above formula types.[5-11] The less stable *RS*-trans configuration has however been obtained for the first time recently[12] in the complex *RS-trans*-[Co(*meso*-3*R*,8*S*-dimetrien)Cl_2]ClO_4[1] where the particular dispositions of the methyl substituents on the trien backbone impose stereospecificity at the coordinated secondary nitrogen centers.

The present paper examines the isomers which may be realized for cobalt(III) complexes when the trien ligand is modified by methyl substitution at the central nitrogen atoms to create two tertiary amine functions (Figure 1).

It has been shown that the secondary N-H bonds of coordinated trien may exert considerable effect in determining the stereochemical course of various reactions.[13] Thus formation of the diaquo,[7] amino acid,[10,11] chloroammine,[14] and dinitro[15] complexes in *RS*-β[4] forms requires inversion at the "planar" secondary nitrogen center of the *RR*-β configuration. These inversions occur by N-H hydrogen exchange favored by more alkaline conditions. Similarly racemization of Δ-*RR*-β-

(1) trien = triethylenetetramine = 1,4,7,10-tetraazadecane. It has become customary to designate alkyl-substituted derivatives according to the positions of substitution on the tetraazadecane chain for which the trivial designation trien is retained; thus 4,7-dimetrien = 4,7-dimethyl-1,4,7,10-tetraazadecane.

(2) G. R. Brubaker, D. P. Schaefer, J. H. Worrell, and J. I. Legg, *Coord. Chem. Rev.*, 7, 161 (1971).

(3) The three possible topological arrangements for coordination of trien about an octahedral metal center have usually been designated (arbitrarily) as α, β, and trans. The alternative nomenclature symmetrical cis and unsymmetrical cis for the α and β topologies in *cis*-diacido complexes has been suggested by J. H. Worrell and D. H. Busch, *Inorg. Chem.*, 8, 1563 (1969).

(4) The *R* or *S* specifications refer to the absolute configurations at asymmetric carbon atoms or at the secondary nitrogen centers of the coordinated trien ligand, according to the sequence rules of R. S. Cahn, C. K. Ingold, and V. Prelog, *Angew. Chem., Int. Ed. Engl.*, 5, 385 (1966). For β complexes the configuration at the normal trigonal nitrogen ("angular" nitrogen) is designated before the nitrogen center bridging the two coplanar chelate rings (the "planar" nitrogen). Δ and Λ refer to the absolute chelate configurations about the metal atom as defined in *Inorg. Chem.*, 9, 1 (1970).

(5) A. M. Sargeson and G. H. Searle, *Inorg. Chem.*, 4, 45 (1965).

(6) A. M. Sargeson and G. H. Searle, *Inorg. Chem.*, 6, 787 (1967).

(7) D. A. Buckingham, P. A. Marzilli, and A. M. Sargeson, *Inorg. Chem.*, 6, 1032 (1967).

(8) A. M. Sargeson and G. H. Searle, *Inorg. Chem.*, 6, 2172 (1967).

(9) D. A. Buckingham and L. G. Marzilli, *Inorg. Chem.*, 6, 1042 (1967).

(10) C. Y. Lin and B. E. Douglas, *Inorg. Nucl. Chem. Lett.*, 4, 15 (1968); *Inorg. Chim. Acta*, 4, 3 (1970).

(11) R. J. Dellaca, V. Janson, W. T. Robinson, D. A. Buckingham, L. G. Marzilli, I. E. Maxwell, K. R. Turnbull, and A. M. Sargeson, *J. Chem. Soc., Chem. Commun.*, 57 (1972); *Inorg. Chem.*, in press.

(12) M. Saburi and S. Yoshikawa, *Bull. Chem. Soc. Jap.*, 45, 1443 (1972).

(13) G. H. Searle and A. M. Sargeson, *Inorg. Chem.*, 12, 1014 (1973).

(14) M. Dwyer, unpublished work.

(15) G. H. Searle and F. R. Keene, unpublished work.

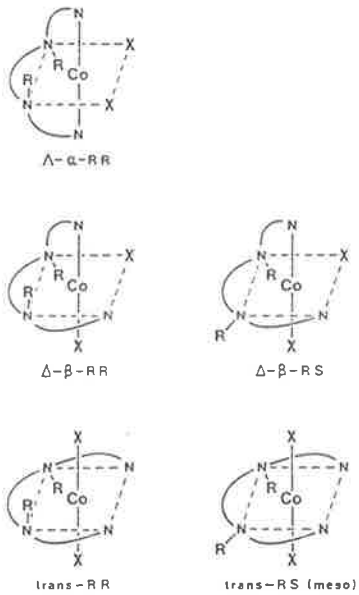

Figure 1. Geometric isomers and internal diastereoisomers of $[Co(trien)X_2]^{n+}$ (R = H) or $[Co(4,7\text{-dimetrien})X_2]^{n+}$ (R = CH_3).

$[Co(trien)(OH_2)_2]^{3+}$ requires inversion at this "planar" nitrogen center, although the inversion in this instance occurs in the *RR-trans*-diaquo isomer formed by initial isomerization.[13]

Clearly, the reactions of trien complexes in all conditions except aqueous acid can be complicated. In investigations of the mechanism of the hydrolysis reaction

$$\Lambda\text{-}RR\text{-}\alpha\text{-}[Co(trien)Cl_2]^+ \rightarrow \Delta\text{-}RR\text{-}\beta\text{-}[Co(trien)(OH)_2]^+$$

we encountered some difficulties due to concomitant inversion at the "planar" nitrogen center and three products were obtained which we believe to be the Λ-*RR*-α (with retention), Δ-*RR*-β (from ligand topological change only, Figure 2), and Δ-*RS*-β (ligand topological change and nitrogen inversion). To clarify these studies we required a system where the complications imposed by such nitrogen center inversions are avoided, and methyl substitution on the secondary nitrogen atoms of the parent trien provides a means of fixing the stereochemistry at these centers.

We accordingly synthesized 4,7-dimethyl-1,4,7,10-tetraazadecane,[16] hereafter abbreviated 4,7-dimetrien,[1] and the present article reports the preparations of some diacidocobalt(III) complexes in racemic forms with this ligand and the assignments of their isomeric configurations as *RR,SS*-α or *RR,SS*-β. No *RS,SR*-β isomers nor any *trans*-diacido compounds could be obtained. Interconversion reactions between these α and *RR,SS*-β complexes have been examined, and in the course of this work several isomerization reactions β → α have been observed for the first time and these should occur with concomitant configurational inversion Δ → Λ (Figure 2). Our results of more detailed investigations on some inversion reactions, employing optically active complexes, will be reported in subsequent articles.

Experimental Section

Instrumentation. Visible absorption spectra were measured on a Cary 14 spectrophotometer, and the infrared spectra in KBr disks (1.2 mg in 300 mg) were measured on a Perkin-Elmer 125 grating spectrophotometer. The pmr spectra were recorded on a Varian A-60A

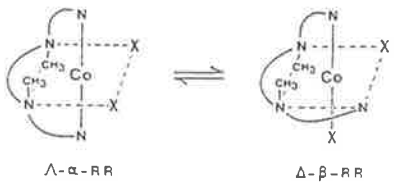

Figure 2. Possible α ⇌ β topological change, with Λ ⇌ Δ configurational inversion and preservation of the nitrogen configurations *RR*.

spectrometer (usually in D_2O or D_2SO_4 solutions using sodium trimethylsilylpropanesulfonate as internal reference), except that the diaquo spectra in $DClO_4$ (Figure 6) were recorded on a Jeol HA-100 spectrometer. The rate of aquation of α-$[Co(4,7\text{-dimetrien})Cl_2]ClO_4$ in $HClO_4$ solution was measured spectrophotometrically at 350, 400, 560, and 650 nm using Perkin-Elmer 402 and Cary 16K spectrophotometers.

4,7-Dimethyl-1,4,7,10-tetraazadecane Tetrahydrochloride. The ligand was synthesized as the tetrahydrochloride salt as described previously.[16]

α-Dinitro(4,7-dimethyl-1,4,7,10-tetraazadecane)cobalt(III) Perchlorate. 4,7-dimetrien·4HCl (6.40 g, 0.02 mol) in water (60 ml) was partially neutralized by the addition of $LiOH\cdot H_2O$ (2.52 g, 0.06 mol), and $CoCl_2\cdot 6H_2O$ (4.76 g, 0.02 mol) was dissolved in the solution with slight warming. This solution was added to a flask containing $NaNO_2$ (2.90 g) and powdered charcoal (0.5 g), and after aeration for 24 hr (with some further water added periodically) the charcoal was filtered from the yellow-brown solution and solid $LiClO_4$ (4.2 g) was added in portions. The product commenced to separate immediately as fine yellow needles, and after 2 days at 6° these were filtered off and washed with ice-cold $LiClO_4$ solution, ethanol, and ether and dried at 60°; yield 6.70 g, 79%. This product was analytically pure (Table I) and no further clean product could be obtained on evaporation. Chromatography (on SP-Sephadex C-25 and Dowex 50W-X2 ion-exchange resins, and on paper[17]) of both the isolated product and the mother liquor gave only a single yellow dinitro band.

α-Dichloro(4,7-dimethyl-1,4,7,10-tetraazadecane)cobalt(III) Perchlorate. α-$[Co(4,7\text{-dimetrien})(NO_2)_2]ClO_4$ (5.00 g) was covered with concentrated HCl in an evaporating dish, and the solution was evaporated almost to dryness over a steam bath with occasional stirring. Further HCl was added, and the process was repeated to effect the complete conversion to the purple dichloro complex. At near dryness, ethanol was added and the mixture was warmed with stirring to extract some blue cobalt(II) material into solution. The solution was decanted off, and four further extractions were carried out until the ethanol was only pale purple. The large deep purple crystals of α-$[Co(4,7\text{-dimetrien})Cl_2]ClO_4$ were finally filtered off, washed with ethanol and ether, and air-dried; yield 4.36 g, 92%. See Table I for analysis.

The analogous reaction starting with α-$[Co(4,7\text{-dimetrien})(NO_2)_2]Cl\cdot 0.5H_2O$ gave α-$[Co(4,7\text{-dimetrien})Cl_2]Cl\cdot 2H_2O$, and greater reduction was evident than for the perchlorate preparation; yield 83%. See Table I for analysis.

Isolation of α-$[Co(4,7\text{-dimetrien})Cl_2]ClO_4$ from the usual aerial oxidation synthesis procedure was not successful due to substantial reduction,[6,17] and the tendency to reduction appears to be enhanced with the present tertiary amine system.

α-Carbonato(4,7-dimethyl-1,4,7,10-tetraazadecane)cobalt(III) Perchlorate. Isomerically pure α-$[Co(4,7\text{-dimetrien})Cl_2]ClO_4$ (2.02 g, 0.005 mol) was dissolved in 0.01 *M* $HClO_4$ (500 ml at 50°) and the solution was maintained at 50° for 1 hr, although this aquation time is not critical up to about 2 hr. The resulting violet solution of α-$[Co(4,7\text{-dimetrien})Cl(OH_2)]^{2+}$ was treated while warm with excess $NaHCO_3$ (3.0 g), and after cooling to room temperature the α-carbonato complex was absorbed on a short column of Dowex 50W-X2 cation-exchange resin, 200–400 mesh, Na^+ form. After all chloride and excess bicarbonate had been washed from the column with water, the complex was eluted from the resin with 0.5 *M* $NaClO_4$ solution. Under these conditions small amounts of dinitro (remaining in the starting dichloro) and diaquo complexes were retained on the resin. The eluent was concentrated in a rotary evaporator to a sludge from which the $NaClO_4$ was extracted with hot ethanol. The finely crystalline α-$[Co(4,7\text{-dimetrien})CO_3]ClO_4$ was finally filtered off from the ethanol solution, washed with ethanol and methanol, and

(16) G. H. Searle, M. Petkovic, and F. R. Keene, *Aust. J. Chem.*, 25, 2045 (1972).

(17) M. Saburi and S. Yoshikawa, *Bull. Chem. Soc. Jap.*, 45, 806 (1972).

Table I. Analytical Data

Complex (L = 4,7-dimetrien = $C_8H_{22}N_4$)	% C		% H		% N		% Cl	
	Calcd	Found	Calcd	Found	Calcd	Found	Calcd	Found
α-[CoLCl$_2$]ClO$_4$	23.8	23.8	5.5	5.6	13.9	13.8	26.4	26.3
β-[CoLCl$_2$]ClO$_4$	23.8	23.5	5.5	5.5	13.9	13.8	26.4	26.1
α-[CoLCl$_2$]Cl·2H$_2$O	25.6	25.9	7.0	6.9	14.9	15.0	28.3	28.5
β-[CoLCl$_2$]Cl·H$_2$O	26.9	26.5	6.7	6.6	15.7	15.5	29.7	29.8
α-[CoLCO$_3$]ClO$_4$	27.5	27.4	5.6	5.7	14.3	14.4	9.0	9.0
β-[CoLCO$_3$]ClO$_4$·H$_2$O	26.3	26.4	5.9	6.2	13.6	13.6	8.6	8.9
α-[CoLCO$_3$]Cl	32.9	32.7	6.7	6.7	17.0	17.0	10.8	10.6
β-[CoLCO$_3$]Cl·2H$_2$O	29.6	29.3	7.2	7.0	15.4	15.2	9.7	9.8
α-[CoL(NO$_2$)$_2$]ClO$_4$	22.6	22.8	5.2	5.2	19.8	19.9	8.4	8.5
α-[CoL(NO$_2$)$_2$]Cl·0.5H$_2$O	26.0	25.9	6.3	6.3	22.7	22.7	9.6	9.6

dried at 60°. The pmr spectrum confirmed that this crude product was isomerically pure α. The compound was recrystallized from the minimum volume of water at 80° (7 ml) by adding ethanol (50 ml) in portions as the product crystallized. The carmine red crystals were filtered off and treated as above; yield 1.72 g, 88%. See Table I for analysis.

Conversion of α-[Co(4,7-dimetrien)CO$_3$]ClO$_4$ to α-[Co(4,7-dimetrien)(NO$_2$)$_2$]ClO$_4$. α-[Co(4,7-dimetrien)CO$_3$]ClO$_4$ (0.393 g, 0.001 mol) was treated with excess 6 *M* HClO$_4$ (0.8 ml). Reaction occurred in the cold, but the solution was gently warmed over a steam bath (2 min) to ensure that conversion to the violet α-diaquo complex was complete. Water was added (40 ml), and then NaNO$_2$ (0.4 g) and LiClO$_4$ (0.2 g) were dissolved in the solution giving pH ~4. The now red-brown solution turned yellow over several hours, and the product began to separate out. The solution was evaporated in a current of air to a small volume (5 ml); then ethanol was added (30 ml) and the solution was left in a refrigerator overnight. The brown-yellow crystals were filtered off, washed with ice-cold LiClO$_4$ solution, ethanol, and ether, and dried at 60°; yield 0.407 g, 96%. *Anal.* Found: C, 22.5; H, 5.3; N, 19.8; Cl, 8.2. The pmr spectrum was identical with that of the α-dinitro product obtained from the aerial oxidation synthesis.

β-Carbonato(4,7-dimethyl-1,4,7,10-tetraazadecane)cobalt(III) Perchlorate Monohydrate. To a stirred ice-cold aqueous slurry of freshly prepared Na$_3$[Co(CO$_3$)$_3$]·3H$_2$O[18] (14.5 g in 70 ml) a solution of 4,7-dimetrien·4HCl (12.8 g in 50 ml, 0.04 mol) was added gradually. The deep red solution was then stirred and heated in a warm water bath to complete the reaction (10 min), and the hot solution was filtered. A filtered solution of excess LiClO$_4$ (6.5 g) was added and the solution was concentrated in a rotary evaporator to incipient crystallization. Some ethanol was added and the solution was left in a refrigerator to crystallize. The violet-red needles of β-[Co(4,7-dimetrien)CO$_3$]ClO$_4$·H$_2$O were filtered off, washed with a little ice-cold LiClO$_4$ solution, ethanol, and ether, and air-dried. A second fraction was obtained by further evaporating the filtrate, adding ethanol, and cooling; total yield 12.7 g, 77%. The product was fractionally recrystallized from hot water (120 ml at 95°) by cooling and evaporation and then by adding some LiClO$_4$ and ethanol to obtain the later fractions (87% recovery). All fractions had identical pmr spectra. See Table I for analysis.

β-Dichloro(4,7-dimethyl-1,4,7,10-tetraazadecane)cobalt(III) Perchlorate. Hydrogen chloride was introduced through a sintered-glass diffuser into a stirred suspension of β-[Co(4,7-dimetrien)CO$_3$]ClO$_4$·H$_2$O (2.00 g) in ethanol (40 ml) in a test tube cooled in an ice bath. The gas bubbling was continued only until the carbonato complex had dissolved to form a deep purple solution of the dichloro complex (1.5 min). LiClO$_4$ (0.5 g) was dissolved in the solution, and after filtering, the solution was evaporated to a small volume (by a current of cold air to remove much of the HCl), from which the product gradually crystallized. The violet-purple product was washed with ethanol by decantation until the solution remained essentially clear and was finally filtered off, washed with ethanol and ether, and dried in a vacuum desiccator; yield 1.83 g, 93%. See Table I for analysis. The dichloro complex tends to undergo reduction in the presence of HCl, but this is minimal under the above conditions. The pmr spectrum (D$_2$SO$_4$-D$_2$O) indicated a trace only of the α isomer (<3%).

In the analogous reaction starting with β-[Co(4,7-dimetrien)CO$_3$]Cl·2H$_2$O considerably more reduction occurred, and the β-[Co(4,7-dimetrien)Cl$_2$]Cl·H$_2$O product isolated in low yield contained ~20% of α isomer. See Table I for analysis.

(18) H. F. Bauer and W. C. Drinkard, *J. Amer. Chem. Soc.*, 82, 5031 (1960); *Inorg. Syn.*, 8, 202 (1966); M. S. Al-Obadie, A. M. Qureshi, and A. G. Sharpe, *J. Inorg. Nucl. Chem.*, 30, 3357 (1968).

α- and β-Diaquo(4,7-dimethyl-1,4,7,10-tetraazadecane)cobalt(III) Perchlorates. Samples of the respective carbonato perchlorates were each treated with a small volume of 6 *M* HClO$_4$, and the solutions were warmed gently over a steam bath to complete the hydrolysis to the diaquo products. The more reactive α-carbonato effervesced on the addition of the acid, but the β isomer required warming to initiate hydrolysis.[19] After standing in a vacuum desiccator, crystals of the diaquo perchlorates had deposited after several days (α, violet; β, deep carmine) from which the solutions were removed through a small filter tube. Despite various treatments (pumping under high vacuum or washing with ether by decantation and drying in a vacuum desiccator[6]) the crystalline products could not be obtained analytically pure, and they were very hygroscopic. Spectra of the diaquo complexes were recorded on the solutions obtained by treating samples of the carbonato perchlorates with HClO$_4$ (6 *M*, then diluted to 1 *M*, electronic spectra) or 2 *M* DClO$_4$-D$_2$O (pmr spectra).

Attempted Preparation of β-[Co(4,7-dimetrien)(NO$_2$)$_2$]ClO$_4$ and the Isomerization β → α. Method A. β-[Co(4,7-dimetrien)CO$_3$]ClO$_4$·H$_2$O (0.411 g, 0.001 mol) was treated with excess 6 *M* HClO$_4$ (0.8 ml), and the solution was warmed briefly over a steam bath to effect the conversion to the carmine β-diaquo complex. The solution was diluted (10 ml) and NaNO$_2$ was added (0.4 g). After 2 days LiClO$_4$ was added (0.2 g), the solution was evaporated to a small volume (2 ml), and then excess ethanol was added (80 ml). After the mixture stood at 6°, the brown-yellow product was filtered off, washed with ethanol and ether, and air-dried; yield 0.362 g, 84%. *Anal.* Calcd for [Co(C$_8$H$_{22}$N$_4$)(NO$_2$)$_2$]ClO$_4$: C, 22.6; H, 5.2; N, 19.8; Cl, 8.4. Found: C, 22.6; H, 5.3; N, 20.1; Cl, 8.4. The visible, infrared, and pmr spectra and X-ray powder photograph were identical with those of the α-dinitro perchlorate.

Method B. To the β-diaquo solution prepared as in method A, a small volume of water was added (2 ml), followed by LiClO$_4$ (0.2 g) and NaNO$_2$ (0.4 g). After 1 min the solution was cooled in an ice bath and ethanol was added (12 ml). The main fraction 1 (0.26 g, orange-red) was filtered off after 15 min, washed with ethanol and ether, and air-dried. Two smaller fractions (fraction 2, yellow-orange; fraction 3, yellow) were subsequently obtained after adding more ethanol and after allowing the mixture to stand in a refrigerator; total yield 0.41 g, 95%. *Anal.* Calcd for [Co(C$_8$H$_{22}$N$_4$)(ONO)$_2$]ClO$_4$: C, 22.6; H, 5.2; N, 19.8; Cl, 8.4. Found (fraction 1): C, 22.2; H, 5.1; N, 19.5; Cl, 8.6. Paper chromatography (eluent solution 4:3:2:1 1-butanol–pyridine–water–acetic acid) of such fraction 1 products isolated quickly always showed two bands, the slower moving corresponding to the α-dinitro isomer. Fractions 2 and 3 had visible and pmr spectra intermediate between those of fraction 1 and the α-dinitro complex.

Method C. β-[Co(4,7-dimetrien)Cl$_2$]ClO$_4$ (0.10 g) and excess NaNO$_2$ (0.1 g) were allowed to react in ethanol (50 ml) under reflux. The solution became orange-red and then yellow, and after 1 hr the orange solid remaining in suspension was filtered off, washed with ethanol and ether, and dried at 60°; yield 0.06 g containing a little NaCl. The pmr spectrum indicated that this was a mixture containing some α-dinitro isomer. The ethanol solution (containing the sodium salts) was evaporated to dryness, and the pmr spectrum of the yellow solid obtained was identical with that of α-[Co(4,7-dimetrien)(NO$_2$)$_2$]ClO$_4$.

The Isomerization β- → α-[Co(4,7-dimetrien)Cl$_2$]ClO$_4$ in Methanol. A solution of β-[Co(4,7-dimetrien)Cl$_2$]ClO$_4$ in methanol (0.123 g in 30 ml) was refluxed for 3 hr. The visible spectrum of the resulting methanol solution showed a shoulder (660 nm) on the higher wavelength side of band I, typical of α-dichloro isomers, which however was lacking in the visible spectrum of a freshly prepared solu-

(19) D. J. Francis and G. H. Searle, *Aust. J. Chem.*, in press.

tion of the β complex in methanol. The solution was evaporated to dryness in a current of cold air, and the purple complex was washed with ethanol and ether and dried in a vacuum desiccator; yield 0.107 g (87%). The infrared and visible spectra (maximum ϵ_{555} 151, shoulder at 660 nm) were identical with those of α-[Co(4,7-dimetrien)Cl_2]ClO_4, but the pmr spectra of transformed carbonato complex indicated that about 10% β isomer remained. No green crystals of a trans isomer were evident on microscopic examination of the isomerized dichloro product.

This isomerization also occurred during the transformation of β-[Co(4,7-dimetrien)CO_3]$ClO_4 \cdot H_2O$ to the dichloro complex with hydrogen chloride in methanol. The dichloro product was crystallized in two similar fractions and the infrared and visible spectra indicated that fraction 1 was largely α with some β, and fraction 2 was pure α.

Transformation of α-[Co(4,7-dimetrien)Cl_2]ClO_4 *to* β-[Co(4,7-dimetrien)CO_3]$ClO_4 \cdot H_2O$. α-[Co(4,7-dimetrien)Cl_2]ClO_4 (0.404 g, *0.001 mol)* was treated with Li_2CO_3 (0.4 g) in water (20 ml) over a *steam bath.* The solution changed from violet to red in a few *minutes,* and after 1 hr the excess Li_2CO_3 was filtered from the hot solution (pH ~10). The solution was reduced in volume, a little ethanol was added, and the solution was filtered again. $NaClO_4 \cdot H_2O$ (0.14 g) and more ethanol were added, and the solution was left to crystallize in a refrigerator. The fine violet-red needles were filtered off, washed with ethanol and ether, and air-dried; yield 0.371 g, 90%. The pmr spectrum indicated that this crude product was substantially β-[Co(4,7-dimetrien)CO_3]ClO_4 containing about 10% of the α isomer, and this was also demonstrated by passage of a sample of the product through a column of Dowex 50W-X2 cation-exchange resin, Na^+ form, 200–400 mesh, when the two isomers were separated on elution with 0.5 *M* $NaClO_4$ solution.

Isomerization in the Diaquo Complexes. Samples of the α- and β-carbonato perchlorates (~0.095 g) were converted to the respective diaquo complexes by adding 6 *M* $HClO_4$ (0.4 ml) and warming gently. Each solution was diluted with CO_2-free water (10 ml), then partially neutralized to pH 3.00 with carbonate-free NaOH solution, and made up to 35.0 g of solution with 0.0010 *M* $HClO_4$. This gave solutions appropriate for spectrophotometric measurements. The solutions were maintained at 50° in stoppered flasks, and to 7.0-g aliquots, withdrawn at various times, excess $NaHCO_3$ was added to convert the α- and β-diaquo complexes in the mixtures to carbonato complexes. The α- and β-carbonato isomers in each solution were separated chromatographically on a column (65 × 1.8 cm) of Dowex 50W-X2 ion-exchange resin, 200–400 mesh, Na^+ form, by elution with 0.5 *M* $NaClO_4$, and the proportions of the two isomers were determined from atomic absorption analyses (Co) of the eluted bands. Results are given in Table IV.

Results and Discussion

The preparations and reactions of the cobalt(III) complexes of 4,7-dimetrien which have been studied are set out in Figure 3. The α- and β-dichloro, α- and β-carbonato, and α-dinitro perchlorates have been isolated and were isomerically pure. The α- and β-chloroaquo and α- and β-diaquo complexes were generated in solution by treating the dichloro and carbonato perchlorates, of the corresponding α or β geometries, with appropriate solutions of perchloric acid.

Two of the complexes were synthesized, α-dinitro by the conventional aerial oxidation procedure and β-carbonato by substitution of the amine ligand in the tris(carbonato)cobaltate(III) ion. These two synthesized complexes were used to prepare the other complexes by transformation reactions which were expected to occur with full configurational retention on the basis of the retentions observed in the trien complex system.[5,6]

For all these complexes prepared, the α or β geometries were assigned largely from their pmr spectra, although electronic spectra were useful in some instances. Infrared spectra of the complexes run as perchlorate salts or as chloride salts (generally prepared from the perchlorates by ion-exchange conversions), while useful for characterization purposes, were found of no value in assigning or relating the topological configurations.[2,20]

That the α-carbonato perchlorate was isolated from the sequence α-dichloro → α-chloroaquo → α-carbonato and that α-dinitro perchlorate was obtained from α-carbonato → α-diaquo → α-dinitro constitute the main evidence that each of these four transformation steps proceeds with retention of configuration. The first three steps were also followed in solution by pmr which confirmed the full retentions. The corresponding transformations in the β system, β-dichloro → β-chloroaquo → β-carbonato → β-diaquo, were also studied in solution by pmr and each was found to occur with at least a very high degree of configurational retention. These retention reactions are analogous therefore to the observations in the trien system.[5,6]

The isomerization α-dichloro → β-carbonato occurs in alkaline carbonate solution as with α-[Co(trien)Cl_2]$^+$ [6] but the following isomerization reactions have not been observed previously in trien systems: β-dichloro → α-dichloro (in methanol), β-dichloro → α-dinitro ($NaNO_2$ in ethanol), β-chloroaquo → α-chloroaquo (in aqueous acid), β-diaquo → α-dinitro ($NaNO_2$ in aqueous acid). The occurrence of these β → α reactions has enabled the configurations of all these β complexes to be assigned as *RR,SS*-β. The β-dinitro complex could not be obtained. These various reactions and some properties of the new complexes are now discussed in some detail.

Symmetry Properties and Pmr Spectra of the Complexes. Some of the pmr spectra are shown in Figures 4–7, and the assignments of the resonances to $-CH_3$, $-CH_2-$, or NH_2 protons are listed in Table II. These assignments were based on relative peak areas (CH_3:CH_3':CH_2:NH_2 = 3:3:12:4) and the characteristic frequency regions for N–CH_3 and –NH_2 in other cobalt(III) complexes.[21] The sharp methyl resonances in the region 2.3–2.8 ppm downfield from NaTMP are particularly diagnostic of the configurations, but some sharp CH_2 signals were also useful for characterizing a particular complex isomer and for assessing isomeric purity in mixtures.

It is evident from Figure 1 that in the complexes of types α-[Co(4,7-dimetrien)X_2]$^{n+}$ and *RR-trans*-[Co(4,7-dimetrien)-X_2]$^{n+}$ the *N*-methyl substituents are related by the C_2 symmetries. In *RS-trans*-[Co(4,7-dimetrien)X_2]$^{n+}$ the methyl groups are also stereochemically equivalent by the plane of symmetry. The pmr spectra of all complexes of these types would thus be expected to show a single methyl resonance, so that α, *RR-trans*, and *RS-trans* structures may not be distinguishable by this means.

The α-dichloro, -carbonato, -diaquo, and -dinitro compounds all show a single sharp methyl pmr resonance (Table II), but only the α-carbonato complex is unequivocally assigned as α on this basis (Figure 7). The possibilities of trans structures for the three other complexes are excluded on other grounds considered below.

In all the β complexes and also in α-[Co(4,7-dimetrien)-XY]$^{n+}$ the methyl groups are stereochemically nonequivalent (Figure 1), and from the two methyl resonances obtained (3:3) (Table II) the β topologies are assigned to the β-dichloro, -carbonato, and -diaquo compounds. Although the pmr spectra would be expected to be detectably different for the *RR*-β and *RS*-β forms, at least in the methyl resonances,[10] the spectra recorded do not allow an *a priori* assignment of these two isomeric possibilities for the β complexes.

Apart from the methyl resonances, the different symmetries of the α and β structures are also reflected in the NH_2 resonances of the dichloro isomers in DMSO-d_6 (Figure 4). The

(20) J. H. Worrell and D. H. Busch, *Inorg. Chem.*, 8, 1563 (1969).

(21) D. A. Buckingham, L. Durham, and A. M. Sargeson, *Aust. J. Chem.*, 20, 257 (1967).

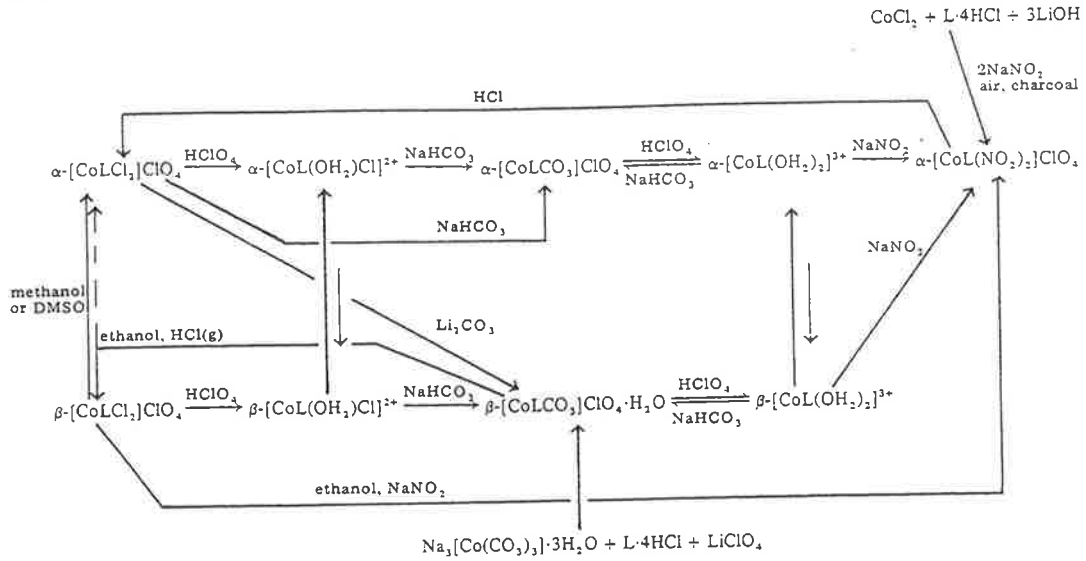

Figure 3. Reaction scheme for syntheses and interconversion reactions of $[CoLX_2]^{n+}$ complexes, L = 4,7-dimetrien.

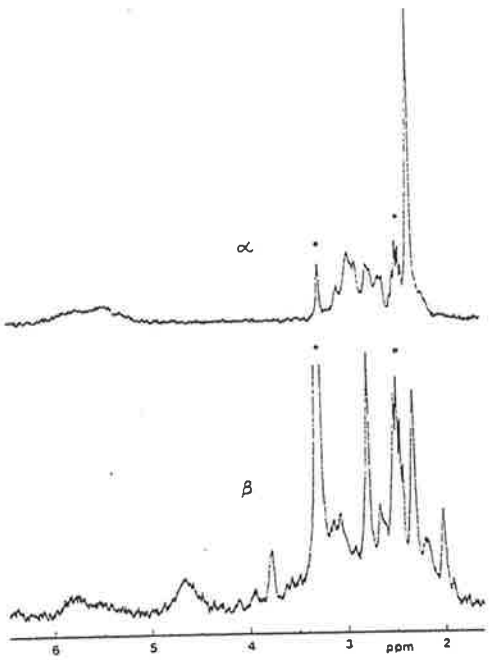

Figure 4. The 60-MHz pmr spectra of α- and β-[Co(4,7-dimetrien)Cl_2]-ClO_4 in dimethyl sulfoxide-d_6. Asterisks denote solvent signals.

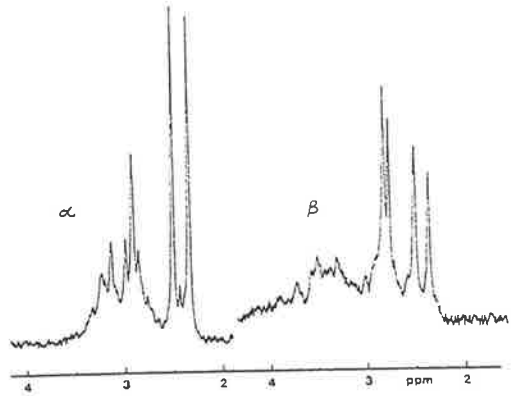

Figure 5. The 60-MHz pmr spectra of α- and β-[Co(4,7-dimetrien)-$Cl(OH_2)]^{2+}$ in 10^{-2} *M* D^+ (β run 2 min after dissolving the β-dichloro complex at room temperature).

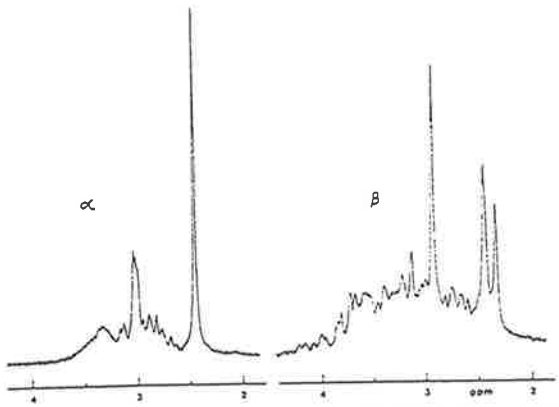

Figure 6. The 100-MHz pmr spectra of α- and β-[Co(4,7-dimetrien)-$(OH_2)_2]^{3+}$ in 2 *M* $DClO_4$.

α isomer gives two broad signals (2:2) from the nonequivalent protons within each primary amino group while three broad peaks (1:1:2) are observed from the β isomer.

Assignments of Configuration to the α Complexes. The pmr spectra do not distinguish the α and trans arrangements for the α-dichloro, -diaquo, and -dinitro complexes. However electronic spectra are usually quite different for cis and trans isomers of diacidotetraminecobalt(III) complexes,[22] so that on these two spectral bases in combination α configurations can be definitely assigned to these complexes. Table III gives visible spectral data for all the present 4,7-dimetrien complexes, along with the corresponding data for the complexes of the parent trien which offer the most relevant comparisons. In comparing these spectra it is recognized that the absorptions of the 4,7-dimetrien complexes almost in-

(22) F. Basolo, *J. Amer. Chem. Soc.*, 72, 4393 (1950).

Table II. Chemical Shifts for Pmr Spectra of α- and β-[Co(4,7-dimetrien)X_2]$^{n+}$ Complexes[a]

Complex	Solvent	CH_3	CH_2	NH_2
α-[CoLCl$_2$]$^+$	10^{-2} *M* D$^+$	2.43	2.6–3.5	~5.7
α-[CoL(OH$_2$)Cl]$^{2+}$	10^{-2} *M* D$^+$	2.35, 2.52	2.6–3.5, 2.91	~5.7
α-[CoLCl$_2$]$^+$	DMSO-d_6	2.35	2.6–3.1	5.5, 5.7
α-[CoLCO$_3$]$^+$	D$_2$O	2.68	2.97	
α-[CoL(OH$_2$)$_2$]$^{3+}$ [b]	2 *M* DClO$_4$	2.44	2.6–3.6, 3.03	5.9, 6.1
α-[CoL(NO$_2$)$_2$]$^+$	10^{-2} *M* D$^+$	2.60	2.7–3.2, 2.95, 3.00, 3.13	5.1, 5.6
β-[CoL(OH$_2$)Cl]$^{2+}$	10^{-2} *M* D$^+$	2.35, 2.50	2.7–3.9, 2.77, 2.82	~5.8
β-[CoLCl$_2$]$^+$	DMSO-d_6	2.32, 2.78	1.9–3.8, 2.02, 3.76	4.7 (mer); 5.5, 5.8 (fac)
β-[CoLCO$_3$]$^+$	D$_2$O	2.33, 2.45	2.6–3.5, 2.88 (max)	
β-[CoL(OH$_2$)$_2$]$^{3+}$ [b]	2 *M* DClO$_4$	2.33, 2.43	2.6–4.2, 2.92 (max)	~6.0
β-[CoL(ONO)$_2$]$^+$	D$_2$O	2.60, 2.70	2.2–3.5, 2.22, 2.90 (max)	

[a] 60-MHz spectra measured in ppm (δ) from sodium trimethylsilylpropanesulfonate for D_2SO_4–D_2O solutions or from tetramethylsilane for dimethyl sulfoxide, as internal references. CH_2 shifts quoted to two decimals are the sharpest or strongest resonances. [b] 100-MHz spectra.

Table III. Electronic Spectral Data[a]

Complex	L = 4,7-dimetrien				L = trien[b]			
	λ	ε	λ	ε	λ	ε	λ	ε
α-[CoLCl$_2$]ClO$_4$ [c]	560 660 sh	152	~350 sh		539 600 sh	132	381	135
α-[CoLCl$_2$]ClO$_4$ [d]	564 660 sh	156	~350 sh					
β-[CoLCl$_2$]ClO$_4$ [c]					531	131	392	118
β-[CoLCl$_2$]ClO$_4$ [d]	569	136	~365 sh					
trans-[CoLCl$_2$]ClO$_4$ [c]					621	53	446	138
α-[CoL(OH$_2$)Cl]$^{2+}$ [c]	540	116	~380 sh		526	118	376	100
β-[CoL(OH$_2$)Cl]$^{2+}$ [c]	547	127	392	112	511	126	376	95
α-[CoLCO$_3$]ClO$_4$ [f]	515	117	363	118	503	120	357	103
β-[CoLCO$_3$]ClO$_4$ [f]	525	191	372	171	507	178	358	140
α-[CoL(OH$_2$)$_2$]$^{3+}$ [e]	515	90	368	66	500	87	359	57
β-[CoL(OH$_2$)$_2$]$^{3+}$ [e]	516	122	373	108	487	122	357	85
α-[CoL(NO$_2$)$_2$]ClO$_4$ [f]	458	238	336	6500	434	212	323	4600
β-[CoL(NO$_2$)$_2$]ClO$_4$ [f]					437	241	319	4100
β-[CoL(ONO)$_2$]ClO$_4$ [f]	478	215	338	3730				

[a] Wavelengths in nm are those of band maxima. [b] Data on the trien complexes are from A. M. Sargeson and G. H. Searle, *Inorg. Chem.*, 4, 45 (1965); 6, 787 (1967). [c] Dichloro and chloroaquo spectra measured in 10^{-2} *M* $HClO_4$. [d] Measured in dimethyl sulfoxide. [e] Diaquo spectra measured in 1 *M* $HClO_4$. [f] Carbonato and dinitro spectra measured in water.

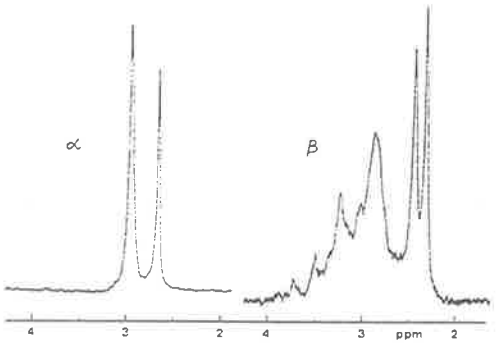

Figure 7. The 60-MHz pmr spectra of α- and β-[Co(4,7-dimetrien)-CO_3]ClO_4 in D_2O.

variably occur at higher wavelengths in accordance with the lower ligand field strength of this tertiary amine.

The visible absorption spectrum of purple α-[Co(4,7-dimetrien)Cl_2]$^+$ resembles that of α-[Co(trien)Cl_2]$^+$, not only in the position of the first band maximum allowing for the above ligand field effect but also in the splitting of the $^1A_{1g} \rightarrow {}^1T_{1g}$ (parent O_h) transition which manifests as a shoulder on the high-wavelength side of band I (Table III). This observable splitting of α-dichloro isomers (but not of corresponding β) has been a useful feature to distinguish these α and β geometries in systems of other linear tetramine[12,17,23,24] and dithiadiamine[20,25] ligands. *trans*-Dichlorotetraminecobalt(III) complexes, invariably green, show absorption bands at positions quite different from those of corresponding cis isomers (Table III), and no such green crystals could be identified in the dichloro products obtained in the present work.

For the dinitro complex isolated from the aerial oxidation of cobalt(II) chloride and 4,7-dimetrien·HCl in the presence of sodium nitrite and charcoal, the α arrangement is indicated (rather than the trans) from the similarity in positions of the second visible absorption bands of this complex, the α- and β-dinitro-trien complexes (Table III), and *cis*-dinitro complexes of some substituted trien ligands.[12,24] Band II positions appear to be relatively insensitive to N-methylation (~3 nm to higher wavelengths in the complexes of 1,3,8,10-tetrametrien[1] and 1,11-dimethyl-1,4,8,11-tetraazaundecane compared to the unmethylated situations),[24] although these band II absorptions are usually observed at about 20 nm higher wavelengths in trans than in cis isomers.[22,24] On this basis the trans arrangement may be excluded for the present dinitro-4,7-dimetrien complex.

Further evidence for the α assignment to this dinitro product is its conversion by HCl to the α-dichloro complex,[6] as a *trans*-dinitro complex would not be expected to give only α-dichloro without some evidence of a β product of the intermediate topology.

An α assignment for the α-diaquo complex can be made from the similarity of its visible spectrum to that of α-[Co-

(23) M. Goto, M. Saburi, and S. Yoshikawa, *Inorg. Chem.*, 8, 358 (1969).

(24) M. Goto, A. Okubo, T. Sawai, and S. Yoshikawa, *Inorg. Chem.*, 9, 1488 (1970).

(25) B. Bosnich, W. R. Kneen, and A. T. Phillip, *Inorg. Chem.*, 8, 2567 (1969).

(trien)$(OH_2)_2]^{3+}$ (Table III) whereas the spectrum of *RR-trans*-$[Co(trien)(OH_2)_2]^{3+}$ is quite distinct from those of the cis isomers.[7]

Assignments of Configurations to the β Complexes from the Stereochemical Relationships between Isomers. From the pmr spectra the β arrangement has been assigned to the β-dichloro, -carbonato, and -diaquo complexes, and the visible absorption spectra when compared to those of the β-trien compounds (Table III) are consistent with the β structures.

Neither method allows assignment of the conformational forms as *RR,SS*-β or *RS,SR*-β but this can be decided from the stereochemical changes which are possible when these complexes undergo any interconversion or isomerization reactions. Configurational changes at the tertiary nitrogen centers (corresponding to the secondary nitrogens in the parent trien ligand) are precluded by the methyl substituents in the cobalt(III)–4,7-dimetrien complexes unless these centers were to detach from coordination to the metal, and this possibility is considered remote. While all reactions between the 4,7-dimetrien complexes must preserve the *RR* or *RS* nitrogen configurations, topological changes may occur by edge displacements of terminal ethylene bridges (Figure 2). A complex of α topology is constrained to exist in only one conformational form Λ-*RR*-α or Δ-*SS*-α since the N-CH_3 bonds at the trigonal nitrogen centers are stereospecifically directed by the bonding of the terminal NH_2 groups in the 1 and 6 positions (Figure 1). Thus the possible stereochemical changes for this system are restricted to Λ-*RR*-α ⇄ Δ-*RR*-β ⇄ *RR*-trans and Δ-*RS*-β ⇄ *RS*-trans. This has the following implications: (1) α complexes can be formed from β complexes only with *RR,SS* configurations; (2) *RS,SR*-β complexes can be formed only in the synthesis reactions or by transformation reactions from other *RS,SR*-β complexes or from meso-trans complexes; (3) the *RR* complexes should be completely inert toward racemization, although Δ-*RS*-β complexes could racemize through the *RS*-trans(meso) structure.

The demonstration of β ⇄ α changes as discussed in later sections, involving all the present β complexes (either in transformation or isomerization reactions) thus establishes the *RR,SS*-β configurations for these β complexes.

This preclusion of nitrogen configurational change was expected to allow easier isolation of *RS*-β isomers if these were formed in the synthesis reactions, as these *RS*-β isomers of trien complexes so far studied mutarotate to the more stable[26] *RR*-β in solution.[7,11,15] The products from the synthetic preparations of the α-dinitro and β-carbonato complexes were examined therefore for the presence of *RS*-β isomers.

The pmr spectrum (D_2O) of the total dinitro product isolated from the synthesis as the perchlorate salt (79% yield) showed only a methyl singlet (Table II) with no trace of peaks which might be attributed to the methyl substituents in a β complex topology. The α isomeric purity thus indicated was consistent with only a single yellow dinitro band obtained when this product was chromatographed by various procedures.

Only two sharp methyl signals were shown by the β-carbonato perchlorate isolated from the tris(carbonato)cobaltate(III) preparation, and identical spectra were also obtained when this product was fractionally recrystallized. On this basis the isolated product was isomerically pure, and its conversion to α products (through β-dichloro to α-dichloro or through β-diaquo to α-dinitro, Figure 3) indicates its configuration must be *RR,SS*-β.

Aquation of the Dichloro Isomers. The rate constant for aquation of the α-dichloro to α-chloroaquo complex was determined spectrophotometrically to be $(1.77 \pm 0.05) \times 10^{-4}$ sec^{-1} at 25.0° in $HClO_4$ and showed no variation over the range of conditions studied ($[H^+] = 10^{-2}$–10^{-1} *M*, [Co] = (2–4) × 10^{-3} *M*, $\mu = 10^{-2}$–10^{-1} *M*). This value is closely similar to that for the corresponding α-trien complex[8] ($k = 1.56 \times 10^{-4}$ sec^{-1} at 25°).

Aquation of the β-dichloro isomer to the β-chloroaquo isomer appeared to be complete by the time first measurements of spectra after dissolution in aqueous acid solutions could be taken, so that $t_{1/2}$ is less than 1 min at room temperature giving $k > 1.2 \times 10^{-2}$ sec^{-1}. This aquation rate of the β isomer is considerably faster than the rate for the β-trien analog[8] ($k = 1.43 \times 10^{-3}$ sec^{-1} at 25°). The single pair of methyl resonances in the pmr spectrum in D^+ solution (Figure 5) was consistent with substantially only one β-chloroaquo geometric isomer being generated in the aquation as with the β-trien complex.[8]

That the β-chloroaquo was the species observed immediately on dissolution of β-dichloro in 10^{-2} *M* $HClO_4$ solution was checked in a cell $Ag|AgCl|K_2SO_4|Hg_2SO_4|Hg$ incorporating an electrode reversible with respect to chloride ion. The emf measured at 1 min, 250 mV, increased by only 5 mV over 2 hr (solution 5×10^{-3} *M* in complex). By comparison, the emf for an equimolar solution of α-$[Co(4,7\text{-dimetrien})Cl_2]ClO_4$ increased from 189 mV (1 min) to a constant value of 254 mV (14 hr), and a rate plot of the data gave $k = 1.2 \times 10^{-4}$ sec^{-1} at 21° which compares well with the spectrophotometric rate.

No satisfactory explanation is available for the difference in reactivities of the two chloro groups for aquation in β-$[Co(trien)Cl_2]^+$,[27] and we are similarly unable to account for the considerable enhancement of reactivity by N-methylation in the β isomer but not in the α. It seems likely however that the greater steric crowding introduced with the methyl substituents is one factor in accelerating the rate of aquation of the β-dichloro complex.[28,29] Reverse trends to these have been shown in acid hydrolysis of the carbonato compounds.[19] The α-carbonato is considerably more reactive than β-carbonato with both trien and 4,7-dimetrien, and N-methylation reduces the reactivity of both the α and β isomers, but other factors may be involved in these reactions.[19]

Formation of chloroaquo complexes was also examined by recording the pmr spectra of the dichloro complexes in 10^{-2} *M* D^+ (D_2SO_4-D_2O). The sharp methyl resonance at 2.43 ppm decreased as the α-dichloro complex aquated with the concurrent appearance of the α-chloroaquo methyl signals at 2.35, 2.52 ppm (Figure 5). This process was essentially complete in 2 hr at normal probe temperature, and thereafter little change was observed.

The β-chloroaquo pmr spectrum was measured immediately on dissolving the β-dichloro. Changes in the β-chloroaquo spectrum on standing were small but significant, and by 10

(26) In β,-$[Co(trien)(gly)]^{2+}$ the Δ-*RR*-β form is favored over Δ-*RS*-β by <0.1 kcal mol^{-1},[11] but for the other β trien complexes the *RR* form is considerably thermodynamically favored. The stereospecific effects of alkyl substituents on the carbon atoms of the terminal en bridges of the trien ligand may alter the relative stabilities of these isomers considerably so that Δ-*RS*-β can then become favored.[17]

(27) D. A. Buckingham, P. A. Marzilli, I. E. Maxwell, A. M. Sargeson, M. Fehlmann, and H. C. Freeman, *Chem. Commun.*, 488 (1968).

(28) D. A. Buckingham, B. M. Foxman, and A. M. Sargeson, *Inorg. Chem.*, 9, 1790 (1970).

(29) D. A. Buckingham, M. Dwyer, A. M. Sargeson, and K. J. Watson, *Acta Chem. Scand.*, 26, 2813 (1972), and private communication.

min small new peaks which were identified with α-chloroaquo CH_2 resonances had appeared. Subsequent changes were slow but at no stage could β- or α-diaquo peaks be recognized in the spectrum. Further evidence for significant β- → α-chloroaquo isomerization was adduced by transforming β-chloroaquo solutions to carbonato complexes as discussed in a later section.

Retention Reactions in the α System. α-Dichloro → α-Chloroaquo → α-Carbonato. The conversion on a preparative scale of α-[Co(4,7-dimetrien)Cl_2]ClO_4 through the α-chloroaquo to the pure α-carbonato complex with $NaHCO_3$ proves the isomeric purity of the dichloro complex and demonstrates the full retention of configuration in these two steps. If the aquation step is prolonged, some β-carbonato product can arise in this preparative procedure,[19] and the conditions necessary to form the α-carbonato isomer with the complete exclusion of the β isomer were established from a series of small-scale reactions, with the α- and β-carbonato isomers being separated by ion-exchange chromatography. For aquation times up to 2 hr in 10^{-2} *M* $HClO_4$ at 50° and complex concentration 10^{-2} *M*, the α-carbonato product was obtained exclusively after adding $NaHCO_3$. Even when the dichloro complex was dissolved in acid quickly at room temperature and treated with $NaHCO_3$ immediately, no β band was evident in the subsequent chromatography. This implies that hydrolysis of the dichloro complex in the weakly basic $NaHCO_3$ solution (pH ~8) also occurs with retention of configuration.[30] At 3-hr aquation time (50°) the carbonato-dimetrien product contained a trace of β isomer, and the proportion of final β-carbonato complex increased with longer aquation times and was substantial (~25% β) at 6 days of aquation.

These two steps were also studied by pmr. Samples of α-[Co(4,7-dimetrien)Cl_2]ClO_4 were dissolved in 10^{-2} *M* D^+-D_2O in pmr tubes and excess $NaHCO_3$ was added to the different tubes after various times. When $NaHCO_3$ was added immediately (dichloro) or when aquation to the α-chloroaquo complex was complete (2.5 hr at 40°), the resulting α-carbonato spectra showed only a trace (<4%) of β-carbonato isomer. After prolonged aquation (2.5 days at 40°) treatment with $NaHCO_3$ gave carbonato product containing about 20% of β isomer. Separate experiments established that the extent of isomerization of the α-diaquo complex is almost negligible under these conditions, so that the β isomer must arise here through some isomerization α- → β-chloroaquo.

α-Carbonato → α-Diaquo → α-Dinitro. The preparative conversion of the α-carbonato through the α-diaquo to give the α-dinitro perchlorate in high yield indicates that these steps each proceed with essentially complete retention of configuration.[5,31]

α-Diaquo → α-Carbonato. This retention was studied by pmr. α-Carbonato perchlorate was dissolved in 2 *M* D^+-D_2O in a pmr tube and the α-diaquo spectrum was recorded. Addition of excess $NaHCO_3$ regenerated the α-carbonato complex and a trace only of the β isomer was evident from the spectrum then recorded.

Retention Reactions in the β System. Reactions β-dichloro through β-chloroaquo and β-carbonato to β-diaquo were examined in solution using pmr as described for the α system. Excess $NaHCO_3$ was added to samples of β-dichloro perchlorate in 10^{-2} *M* D^+-D_2O (=β-chloroaquo) in different pmr tubes. When bicarbonate was added immediately after dissolution of the sample in the acid, the resulting β-carbonato spectrum showed only a small proportion of the α-carbonato isomer (~3%). Bicarbonate addition to the β-chloroaquo complex after standing gave increasing proportions of the α-carbonato complex with longer times (~10% after 30 min, ~30% after 1.5 days at 35°).

These experiments demonstrate that the β-chloroaquo → β-carbonato transformation proceeds with configurational retention (≥97%) as in the α case, and this provides a sensitive method for assessing the isomeric purity of any dichloro sample. Addition of excess $NaHCO_3$ immediately after dissolution in D^+ solution gives the carbonato complex, with full retention from each isomer, and the sharp α and β methyl resonances are well separated in the (mixed) pmr spectrum (Figure 7).

The significant amount of α-carbonato complex obtained after the β-chloroaquo complex had stood for 30 min is attributed to β- → α-chloroaquo isomerization, as α-chloroaquo peaks (but not β- or α-diaquo) were recognized in the pmr spectrum of a β-chloroaquo solution within this time. Significant involvement of diaquo species in the isomerization would have required the amount of aquation β-chloroaquo → β-diaquo to be substantial within 30 min and this should have been apparent in the emf experiment discussed earlier.

The sequence

$$\beta\text{-carbonato} \xrightarrow{2\ M\ D^+} \beta\text{-diaquo} \xrightarrow{NaHCO_3} \beta\text{-carbonato}$$

was followed by pmr as for the α system. About 10% isomerization to α had occurred on regeneration of the carbonato, and this isomerization in the diaquo complexes is discussed below.

Isomerization Reactions. (a) α-Dichloro → β-Carbonato. Reaction of the α-dichloro complex with Li_2CO_3 in water gave predominantly the β-carbonato complex in the isolated product, as in the trien system.[6] This isomerization α → β (Figure 2) probably occurs in an initial base hydrolysis to the chlorohydroxo complex, which is succeeded by substitution of bicarbonate ion with retention of the β configuration,[30] so that no inference can be made as to the relative carbonato isomer stabilities. For similar reasons we feel that the isolation of the β-carbonato isomer exclusively from the tris(carbonato)cobalt(III) reaction does not necessarily indicate that the β-carbonato isomer is thermodynamically favored over α.

(b) β-Diaquo → α-Diaquo. In the trien system a greater stability for a β configuration over α was demonstrated only for the diaquo complexes,[6,13] so that the α- ⇌ β-diaquo equilibrium in the present system was of some interest. However the present diaquo experiments could not be brought to a quantitative conclusion as the isomerization starting from the β complex was not a clean reaction and generated some cobalt(II), so that equilibrium was not established between the two diaquo isomers under any of the conditions used (pH 2, 3, or 6; temperature 40, 50, or 70°) within some days.

In one experiment separate solutions of the α- and β-diaquo complexes in $HClO_4$-$NaClO_4$, adjusted to pH 3.0, were allowed to isomerize at 50° and the reactions were examined by two methods. The spectrophotometric changes (band maxima are listed in Table IV) were consistent with the β form initially isomerizing to the α isomer (solution composition calculated about 30% α and 70% β after 6 hr). The spectrum of the α solution indicated the degree of isomerization of α → β as only 6% after 60 hr.

A less direct method of studying these reactions involved

(30) About 20% inversion for the reaction of *cis*-[Co(en)$_2$Cl$_2$]$^+$ with $NaHCO_3$ is reported by F. P. Dwyer, A. M. Sargeson, and I. K. Reid, *J. Amer. Chem. Soc.*, 85, 1215 (1963).

(31) F. Basolo and R. G. Pearson, "Mechanisms of Inorganic Reactions," 2nd ed, Wiley, New York, N. Y., 1967, pp 230-231, 291-294.

Table IV. Isomerization of α- and β-$[Co(4,7\text{-dimetrien})(OH_2)_2]^{3+}$ at 50°, pH 3.0, and [Co] = 0.007 *M*

	Starting soln α-diaquo			Starting soln β-diaquo					
Time, hr	pH	ϵ_{515}	ϵ_{368}	pH	λ	ε	λ	ε	% α from chromatography of carbonato isomers
0	3.00	91.4	68.4	3.00	516	124.4	373	108	23
6	2.97	91.5	68.7	2.95	516	114.5	371	98	
20		92.0	69.4		515	113.0	368	108	55
40		92.5	70.1		514	110.3	362	128	
60	2.95	93.2	71.0	2.81	511	105.8	~350 sh	~161	67

transforming the mixed α- and β-diaquo complexes in aliquots of the above solutions to the α- and β-carbonato complexes which were separated chromatographically and the proportions were assessed. This method requires that the conversion of each diaquo isomer to the corresponding carbonato isomer with bicarbonate be rapid compared to the isomerization at pH 8 (bicarbonate solution) so that the transformation occurs with retention of configuration.[5,13] This condition is essentially achieved with the present α-diaquo → α-carbonato conversion (from the pmr experiment discussed above) so that a zero-time sample of α-diaquo solution when transformed and chromatographed gave 98% recovery of α, and a β band was not detectable. The β-diaquo → β-carbonato transformation does not take place with full retention however (pmr experiment; Table IV zero-time sample chromatographed gave 23% α and 77% β, with 99% cobalt recovery from these two carbonato bands) and the isomerization probably occurs through the β-hydroxoaquo complex in the pH 8 conditions involved. The trend in the chromatography figures (Table IV) does indicate however that substantial isomerization takes place in the β-diaquo solution.

It is clear from both the above methods that while the α-diaquo complex undergoes little isomerization, the β-diaquo complex generates substantial α-diaquo isomer under similar conditions, and from these relative rates we deduce that the α-diaquo isomer is considerably favored thermodynamically.

(c) **β-Diaquo → α-Dinitro.** Substitutions of nitrite ion in the α- and β-$[Co(trien)(H_2O)_2]^{3+}$ isomers[5,6] and in α-$[Co(4,7\text{-dimetrien})(OH_2)_2]^{3+}$ produce (after standing) the corresponding dinitro complexes with retentions of configurations. However it proved impossible to prepare the β-$[Co(4,7\text{-dimetrien})(NO_2)_2]^+$ complex by this procedure from the corresponding β-diaquo complex; the final product obtained (method A, Experimental Section) was always yellow α-$[Co(4,7\text{-dimetrien})(NO_2)_2]ClO_4$, as established from comparisons of the pmr and infrared spectra and X-ray powder pattern with those of the α compound obtained from the aerial oxidation synthesis.

A red-orange complex was obtained however when conditions were arranged that the product crystallized from solution rapidly after addition of the nitrite (method B, fraction 1). Ion-exchange chromatography established the complex to be a 1+ ion, and the analysis and visible spectrum (Table III) indicated that it was (or at least contained) an intermediate nitrito complex. Stronger infrared absorption over 1000–1050 cm^{-1} (although on the side of the perchlorate band) than in all other "β" and α samples was consistent with a nitrito complex,[31] although the 820-cm^{-1} $-NO_2$ deformation band was also present. From its rapid formation[31] we propose that the β configuration was retained at this stage, and we accordingly assign this red complex as (largely) β-$[Co(4,7\text{-dimetrien})(ONO)_2]ClO_4$. We assign the two sharpest and strongest pmr peaks (Table II), which appear to be of unequal intensities, to N-CH_3 resonances (δ 2.60, 2.70 ppm), and one of these coincides with that from the α-dinitro complex (δ 2.60 ppm). The spectrum is thus consistent with a product mixture, and paper chromatography gave two bands with one corresponding to the α-dinitro complex. Other components could be any of the possible nitritonitro isomers (Figure 8). This red intermediate complex rearranged in D_2O, and after 8 hr at 50° the pmr spectrum had become identical with that of the α-dinitro complex.

(d) **β-Dichloro → α-Dinitro.** In an attempt to avoid this β → α isomerization, β-$[Co(4,7\text{-dimetrien})Cl_2]ClO_4$ was treated with nitrite in ethanol (method C). The resulting ethanol solution contained only the α-dinitro complex (identified by pmr spectrum), and the orange material remaining suspended was apparently a mixture of nitrito complexes. The pmr changed slowly with time to become identical with that of the α-dinitro complex.

Nitrito → nitro isomerizations usually occur intramolecularly with retention of the configuration about the metal center,[31] but in the present instance it seems that there is simultaneous movement of the terminal "planar" chelate ring to give the α complex topology. Competing reaction paths are then possible, with the formation of three isomeric nitritonitro complexes (Figure 8), two of which could subsequently convert directly to the α-dinitro complex. Such a scheme would then account for the varying pmr spectra observed from the different "β" samples isolated and during their subsequent rearrangement on standing in D_2O. The strong methyl resonance at 2.60 ppm was present at all stages however.

Whatever the mechanism, the fact that the β → α isomerization occurs to completion indicates that the methyl substituents exercise considerable effect in destabilizing the β complex configuration relative to the α in the dinitro complexes, and this is consistent with no β isomer being detected in the dinitro aerial oxidation synthesis in the presence of charcoal.

(e) **β- → α-Chloroaquo.** Evidence was given earlier for isomerization occurring in solutions of both the α- and β-chloroaquo isomers. From the extents of isomerization determined (β gives 30% α after 1.5 days at 35°; α gives 20% β after 2.5 days at 40°) it is clear that the β- ⇌ α-chloroaquo equilibrium favors the α isomer. Isomerizations of *cis*-chloroaquo complexes were not observed in the trien system,[8,32] although *cis*-$[Co(en)_2Cl(OH_2)]^{2+}$ isomerizes to the trans isomer.[33]

(f) **β-Dichloro → α-Dichloro.** The isomerization β- → α-$[Co(4,7\text{-dimetrien})Cl_2]ClO_4$ in methanol is a striking difference from the trien system. Methanol frequently induces isomerization in dichlorotetraminecobalt(III) complexes, but these are usually cis → trans with bis(ethylenediamine) type

(32) G. H. Searle and A. M. Sargeson, *Aust. J. Chem.*, 26, 661 (1973).
(33) A. M. Sargeson, *Aust. J. Chem.*, 16, 352 (1963).

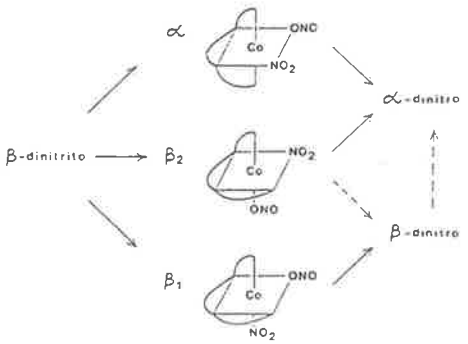

Figure 8. Possible reaction routes for nitrito–nitro isomerization and $\beta \rightarrow \alpha$ isomerization.

complexes[34] or $\beta \rightarrow$ trans with trien[6] and some carbon-methylated trien ligands.[12,23] The different solvation properties of methanol compared to water have seemed therefore to favor *trans*-dichloro configurations. With the present $[Co(4,7\text{-dimetrien})Cl_2]^+$ system, we take the observed $\beta \rightarrow \alpha$ isomerization to indicate a considerably reduced stability of the trans configuration.

This isomerization $\beta\text{-} \rightarrow \alpha\text{-}[Co(4,7\text{-dimetrien})Cl_2]ClO_4$ also occurred in dimethyl sulfoxide. The pmr spectra of the two dichloro isomers in dimethyl sulfoxide-d_6 (Figure 4) had become identical after equilibration (14 hr at 50°), and this equilibrium spectrum clearly represented an α configuration (mainly α-dichloro with a little solvent-substituted product) since the signal from the meridional NH_2 (4.7 ppm) in the β configuration was absent. Similarly the α-dichloro visible spectrum in this medium (Table III) was exactly reproducible after 20 hr at room temperature, but the spectrum of the β-dichloro complex changed slowly over several hours due largely to solvolysis.

Relative Stabilities of the α and β Isomers. Studies on the parent trien complexes showed that the relative thermodynamic stabilities of the α, β, and trans configurations depend on the substituents X and on the solvent used (water or methanol).[6] For the same acido substituents X there is a considerable dependence of these relative geometric isomer stabilities on the alkyl substitution in the tetramine chain, although the previous investigations with complexes of C- and (terminal N)-methylated trien ligands have not always allowed firm statements in this regard. Some of the dichloro and dinitro complexes which have been isolated from aqueous solutions might not be the most stable isomers (sometimes yields were low or not reported) and this is especially so if charcoal has not been present to ensure equilibration; some preparations or isolations have involved alcoholic media in which isomerizations can occur. It seems clear from aerial oxidation syntheses of dichloro and/or dinitro complexes (compared with the results of similar syntheses of the trien complexes) that the stability of the *RR,SS*-trans configuration is enhanced with the ligands 1,10-dimetrien,[24] 1,5,10-trimetrien,[24] and active 3,8-dimetrien,[17] and that the stability of the *RR,SS*-β form over the α form is enhanced with the ligands 5-metrien,[23] active 5,6-dimetrien,[23] and *meso*-3,8-dimetrien.[12] Moreover *RS,SR*-β isomers (rather than *RR,SS*-β) were obtained with the ligands active 2,9-dimetrien,[17] 2*S*,5*R*,9*S*-trimetrien,[35] and active 3,8-dimetrien.[17] These stabilizations have generally been rationalized on the basis of minimization of nonbonded atomic interactions (which is the basis of the accepted requirement that substituent methyls be equatorially disposed with respect to the chelate ring plane).[17,23,24,35]

The foregoing results for the 4,7-dimetrien complexes indicate that the α topology is thermodynamically favored over the β (and trans) in the dichloro (in methanol), chloroaquo, diaquo, and dinitro complexes. Moreover the stability of the α arrangement has become enhanced from that in the corresponding trien complexes with dichloro (where $\beta \rightarrow$ trans in methanol),[6] diaquo (where $\alpha/\beta = 0.30$ at equilibrium)[13] and dinitro (where $\alpha/\beta \approx 3$).[6] Dreiding models of the present complexes indicate that the magnitudes of the most serious nonbonded interactions, those between the methyl substituents and either the acido substituents X or the primary amine groups, are likely to be in the order $\alpha \ll RR\text{-}\beta \sim RS\text{-}\beta < RR$-trans $\sim RS$-trans. The observed relative isomer stabilities may also be rationalized on the basis that the larger *N*-methyl substituents induce greater bond angle strains at the tertiary nitrogen donor centers compared with the trien situation, so that the normal trigonal or "angular" bonding situation becomes even more preferred. While the angle strain at one "planar" nitrogen center can clearly be accommodated in the β complexes here reported, we doubt whether trans complexes of this ligand will be possible.

The effect of (secondary *N*)-methylation in favoring trigonal coordination at that nitrogen donor position is also apparent from studies on the topological isomers of $[Co(trenen)Cl]^{2+}$ (trenen = 4-(2-aminoethyl)-1,4,7,10-tetraazadecane) and $[Co(7\text{-metrenen})Cl]^{2+}$.[29] Energy minimization calculations indicate that nonbonded atomic interactions of the type mentioned account for the observed relative isomer stabilities in these trenen systems.

Acknowledgments. This work was completed while G. H. S. was a Visitor at Chemistry Department I, The H. C. Oersted Institute, University of Copenhagen, and the use of facilities and helpful discussions with Dr. Erik Larsen are gratefully acknowledged. We are grateful for microanalyses carried out by The Australian Microanalytical Service CSIRO, Melbourne; The Research School of Chemistry, Australian National University, Canberra; and Chemistry Department II, The H. C. Oersted Institute, University of Copenhagen. The work was supported by the Rask-Oersted Foundation, Copenhagen, Denmark.

Registry No. $\alpha\text{-}[CoLCl_2]ClO_4$, 42885-93-8; $\beta\text{-}[CoLCl_2]ClO_4$, 42949-46-2; $\alpha\text{-}[CoLCl_2]Cl\cdot 2H_2O$, 42885-94-9; $\beta\text{-}[CoLCl_2]Cl\cdot H_2O$, 42885-95-0; $\alpha\text{-}[CoLCO_3]ClO_4$, 42885-96-1; $\beta\text{-}[CoLCO_3]ClO_4\cdot H_2O$, 42885-97-2; $\alpha\text{-}[CoLCO_3]Cl$, 42949-47-3; $\beta\text{-}[CoLCO_3]Cl\cdot 2H_2O$, 42885-98-3; $\alpha\text{-}[CoL(NO_2)_2]ClO_4$, 42885-99-4; $\alpha\text{-}[CoL(NO_2)_2]Cl\cdot 0.5H_2O$, 42942-72-3; $\alpha\text{-}[CoL(OH_2)Cl]^{2+}$, 42893-10-7; $\beta\text{-}[CoL(OH_2)Cl]^{2+}$, 42893-11-8; $\alpha\text{-}[CoL(OH_2)_2]^{3+}$, 42893-12-9; $\beta\text{-}[CoL(OH_2)_2]^{3+}$, 42893-13-0; $\beta\text{-}[CoL(ONO)_2]ClO_4$, 42942-74-5; $Na_3[Co(CO_3)_3]\cdot 3H_2O$, 15684-40-9.

(34) D. D. Brown and C. K. Ingold, *J. Chem. Soc.*, 2680 (1953); D. D. Brown and R. S. Nyholm, *ibid.*, 2696 (1953); B. Bosnich, C. K. Ingold, and M. L. Tobe, *ibid.*, 4074 (1965); R. C. Brasted and C. Hirayama, *J. Amer. Chem. Soc.*, 80, 788 (1958).

(35) M. Saburi, T. Sawai, and S. Yoshikawa, *Bull. Chem. Soc. Jap.*, 45, 1086 (1972).

Aust. J. Chem., 1977, **30**, 1221–8

Bis(tridentate)cobalt(III) Complexes with Diethylenetriamine and 4-Methyldiethylenetriamine [2,2′-Methyliminodi(ethylamine)]: Assignment of Geometric Configurations by ^{1}H and ^{13}C N.M.R. Spectroscopy

Graeme H. Searle, Stephen F. Lincoln, F. Richard Keene, Stewart G. Teague and David G. Rowe

Department of Physical and Inorganic Chemistry,
University of Adelaide, P.O. Box 498, Adelaide, S.A. 5001.

Abstract

The new complexes *symmetrical-facial*-$[Co(medien)_2]^{3+}$ and *s-fac*-$[Co(dien)(medien)]^{3+}$ have been isolated. The ^{1}H n.m.r. spectra of these complexes, the *s-fac*, *u-fac* and *meridional* isomers of $[Co(dien)_2]^{3+}$, and *u-fac*-$[Co(daes)_2]^{3+}$ show different splittings of the NH_2 proton resonances [dien = diethylenetriamine, medien = 4-methyldiethylenetriamine or 2,2′-methyliminodi(ethylamine), daes = di(2-aminoethyl) sulphide or 2,2′-thiodi(ethylamine)]. These splittings depend on the geometries of the complexes (different numbers of stereochemically distinct NH_2 groups), the particular chelated ligands (splittings due to coupling between the two protons on each NH_2 may vary with chelate ring conformational mobility), and the counter-anions (different extents of ion-association through hydrogen bonding). Thus NH_2 proton resonance signals may not always provide a reliable method for establishing molecular geometries. In contrast, the ^{13}C n.m.r. spectra of all these complexes are completely diagnostic of the detailed geometries, and most of the resonances observed have been assigned to particular carbon atoms.

Introduction

The structures of the three geometric isomers of $[Co(dien)_2]^{3+}$ (dien = diethylenetriamine or 1,4,7-triazaheptane, $H_2NCH_2CH_2NHCH_2CH_2NH_2$), shown in Fig. 1, were initially assigned on the basis of optical resolutions and optical stabilities in alkali,[1] and by ^{1}H n.m.r. spectroscopy,[2] and were subsequently confirmed by X-ray structure analyses.[3–5] Our interest in the factors determining the relative stabilities of these isomers, and the potential value of these compounds for investigating isomerization reactions[6] prompted our examination of the cobalt(III) complexes with the ligand medien, $H_2NCH_2CH_2N(Me)CH_2CH_2NH_2$, the secondary *N*-methylated analogue of dien [medien = 4-methyldiethylenetriamine, 4-methyl-1,4,7-triazaheptane, or 2,2′-methyliminodi(ethylamine)].

The new complexes $[Co(medien)_2]^{3+}$ and $[Co(dien)(medien)]^{3+}$ have been prepared and isolated as their bromide and perchlorate salts, and the present article demonstrates the limitations of ^{1}H n.m.r. spectra in establishing the geometric configurations of these and similar kinds of complexes. It is shown that ^{13}C n.m.r. spectra are sensitive

[1] Keene, F. R., and Searle, G. H., *Inorg. Chem.*, 1972, **11**, 148.
[2] Yoshikawa, Y., and Yamasaki, K., *Bull. Chem. Soc. Jpn*, 1972, **45**, 179.
[3] Kobayashi, M., Marumo, F., and Saito, Y., *Acta Crystallogr., Sect. B*, 1972, **28**, 470.
[4] Konno, M., Marumo, F., and Saito, Y., *Acta Crystallogr., Sect. B*, 1973, **29**, 739.
[5] Sancilio, F. D., Druding, L. F., and Lukaszewski, D. M., *Inorg. Chem.*, 1976, **15**, 1626.
[6] Keene, F. R., and Searle, G. H., *Inorg. Chem.*, 1974, **13**, 2173.

functions of isomer geometry and that each of the new complexes has the *symmetrical-facial* geometry.

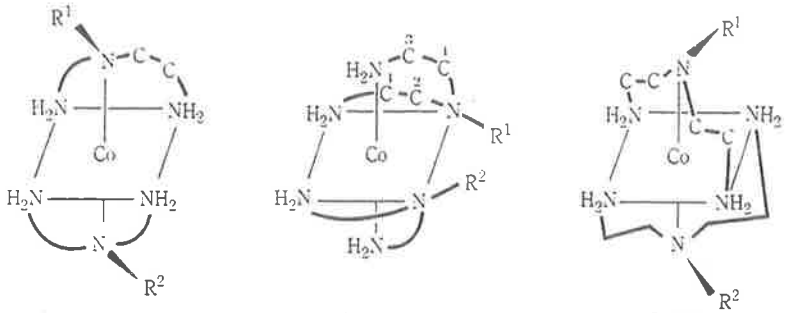

Fig. 1. Possible geometric isomers of $[Co(dien)_2]^{3+}$ ($R^1 = R^2 = H$), $[Co(medien)_2]^{3+}$ ($R^1 = R^2 = Me$), and $[Co(dien)(medien)]^{3+}$ ($R^1 = H$, $R^2 = Me$), and their point-group symmetries. The carbon atoms shown, but labelled only for the *u-fac* isomer, are one of each stereochemically distinct type.

Results and Discussion

Reaction of $[Co(NH_3)_5Cl]Cl_2$ with medien in the presence of charcoal yielded as the principal products an orange and a yellow material and these were separated chromatographically on a column of SP-Sephadex cation-exchange resin, the yellow eluting first with sodium (+)-tartrate eluent.

These isolated complexes are formulated as $[Co(medien)_2]Br_3,H_2O$ (orange) and $[Co(dien)(medien)]Br_3,H_2O$ (yellow) on the basis of ^1H n.m.r. spectra as discussed below, and microanalyses. The medien was prepared by methylation of dien, and some dien could have been carried through the ligand synthesis to give rise to the $[Co(dien)(medien)]^{3+}$ complex as the minor product. This point is being checked and the preparative work will be reported in detail in a subsequent article.

For complexes of each of these formulations three geometric isomers analogous to those of $[Co(dien)_2]^{3+}$ are possible, and these are shown in Fig. 1 along with their point-group symmetries. Chromatographic behaviour strongly suggested that the two isolated complexes were single geometric isomers, but neither material gave any indication of partial separation into optical isomers by chromatographic methods.[2,7–9]

^1H *Nuclear Magnetic Resonance Spectra*

The $[Co(dien)_2]^{3+}$ isomers have distinctive ^1H n.m.r. spectra for the amine proton resonances.[1,2] The *symmetrical-facial* isomer shows one broad symmetrical NH_2 signal, and the *unsymmetrical-facial* has two broad NH_2 signals with area ratio 1 : 1. The *meridional* compound (iodide salt) gives two broad NH_2 signals 1 : 1 (with larger separation than the *u-fac*) in dimethyl[D_6] sulphoxide,[2] but (as chloride salt) gives an

[7] Kojima, M., Yoshikawa, Y., and Yamasaki, K., *Bull. Chem. Soc. Jpn*, 1973, **46**, 1687.
[8] Yoshikawa, Y., and Yamasaki, K., *Bull. Chem. Soc. Jpn*, 1973, **46**, 3448.
[9] Searle, G. H., and Larsen, E., *Acta Chem. Scand., Ser. A*, 1976, **30**, 143.

NH_2 multiplet in D_2O/D_2SO_4.[1] These splittings of the NH_2 resonances were expected for the *u-fac* and *mer* structures since each of these structures has two non-equivalent NH_2 groups, and it has been tempting to associate each broad resonance signal with an NH_2 group in a particular stereochemical environment. It seemed therefore that the different observed splitting patterns of the NH_2 groups should be generally diagnostic of the geometries in these and analogous complexes.

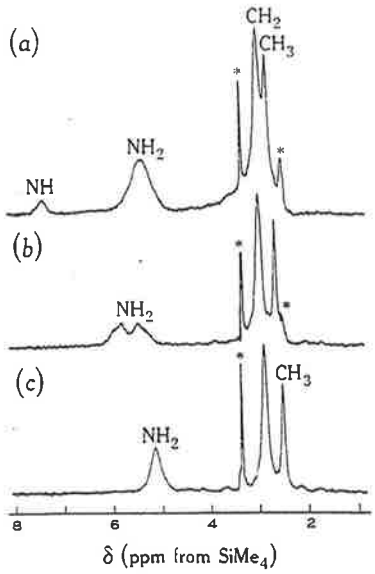

Fig. 2. 60-MHz ^{1}H n.m.r. spectra of (*a*) *s-fac*-[Co(dien)(medien)] Br_3; (*b*) *s-fac*-[Co(medien)$_2$] Br_3; (*c*) *s-fac*-[Co(medien)$_2$] $(ClO_4)_3$ in CD_3SOCD_3 with $SiMe_4$ as internal reference. Asterisks denote solvent signals.

The ^{1}H n.m.r. spectra of the new compounds run in dimethyl[D_6] sulphoxide are shown with peak assignments in Fig. 2. The spectrum of yellow *s-fac*-[Co(dien)-(medien)]Br_3 shows two broad amine signals in ratio 1 : 8, that at the lower field having a similar chemical shift (δ 7·4) to that of the secondary amine NH (7·1) in *s-fac*-[Co(dien)$_2$] I_3.[2] The formulation of this yellow complex as $[Co(dien)(medien)]^{3+}$ follows from this peak-area ratio of the signals from NH and NH_2. This mixed complex of *s-fac* geometry contains two non-equivalent NH_2 groups so that two broad NH_2 signals (1 : 1) might have been expected, but the NH_2 groups give a single broad resonance peak. Although the possible *u-fac* and *mer* isomers for [Co(dien)-(medien)]$^{3+}$ would each contain four non-equivalent NH_2 groups and would therefore be expected to show greater splitting of the NH_2 resonances than the *s-fac* isomer, the fact that no splitting of the NH_2 signal is shown by the present complex does not allow the *s-fac* geometry to be assigned with certainty.

The perchlorate salt of the same complex gives the same form of spectrum in dimethyl[D_6] sulphoxide to that of the bromide, but the chemical shifts of all the peaks are different for the two salts. Shifts (δ, ppm from $SiMe_4$) for the bromide are NH, 7·4; NH_2, 5·4; CH_2, 3·00; CH_3, 2·80, while those for the perchlorate are NH, 6·8; NH_2, 4·9; CH_2, 2·88; CH_3, 2·65, and it is evident that the shift differences are particularly significant for the amine resonances.

The spectrum of the orange *s-fac*-[Co(medien)$_2$] Br_3 shows splitting of the NH_2 resonance into four components. This greater splitting than for the corresponding

s-fac-$[Co(dien)_2]^{3+}$ complex[1,2] indicates that at least in the medien complex the two protons on the one kind of NH_2 group are non-equivalent. Coupling between these two protons should then produce an AB quartet which may be broadened due to the ^{14}N quadrupole. The observed spectrum is thus consistent with the *s-fac* geometry of the present $[Co(medien)_2]Br_3$ complex. The NH_2 resonance shows a marked anion dependence, since the spectrum of the perchlorate salt of this complex, when run in either $(CD_3)_2SO$ or $D_2O/HClO_4$, shows only a single broad NH_2 signal with no sign of splitting (Fig. 2). In the absence of the spectra of the *u-fac* and *mer* isomers, it is again not possible to assign with certainty the geometry of the *s-fac*-$[Co(medien)_2]^{3+}$ complex from these ^1H n.m.r. spectra.

The ^1H n.m.r. spectrum of the complex *u-fac*-$[Co(daes)_2]Br_3$ containing the thia ligand analogous to dien, $H_2NCH_2CH_2SCH_2CH_2NH_2$ [daes = di(2-aminoethyl) sulphide or 2,2′-thiodi(ethylamine)] also shows greatly enhanced splitting of the NH_2 resonances compared to the corresponding *u-fac*-$[Co(dien)_2]^{3+}$ isomer. Three sets of doublets at δ 4·68, 4·83 (1 : 1); 5·70, 5·82 (approx. 2 : 2); 6·33, 6·50 (1 : 1) are observed for the bromide salt of *u-fac*-$[Co(daes)_2]^{3+}$ run in $(CD_3)_2SO$ at 60 MHz, but the actual pattern observed is dependent on the anion.[9] These NH_2 splittings can be accounted for if the *u-fac* complex contains four non-equivalent protons within each of the C_2-related daes ligands in the complex molecule. Ignoring J couplings to methylene protons, coupling between the two protons of each kind of NH_2 group should in the ultimate resolution produce an AB quartet, so that up to eight NH_2 signals could be expected for this complex.

It is clear therefore that corresponding isomers of complexes of these analogous ligands may show different degrees of splitting of the NH_2 signals, and the simple correlations between NH_2 splitting and molecular geometry suggested earlier[2] from the $[Co(dien)_2]^{3+}$ complexes alone cannot be sustained as general criteria for these geometries. It is possible that the rates of ring conformational interchanges may differ in the *fac* complexes with the various ligands in the order dien > medien > daes and give rise to the varying NH_2 splitting patterns. However, from the anion dependences of NH_2 resonances from the complexes *s-fac*-$[Co(dien)(medien)]^{3+}$, *s-fac*-$[Co(medien)_2]^{3+}$ and *u-fac*-$[Co(daes)_2]^{3+}$,[9] it now seems likely that differential ion-associations between different complex cations and counter-anions may be the fundamental cause of differing NH_2 splittings, perhaps through the effect of association on rates of conformational interchange. Anion dependence of NH_2 proton resonances (in $(CD_3)_2SO$ solvent) has also been observed[10] with the complex *mer*-bis(2-aminoethylsalicylaldiminato)cobalt(III) cation, the NH_2 splitting and downfield shift increasing with different counter-anions in the order $ClO_4^- < Br^- < Cl^-$ which correlates generally with our own abovementioned observations. These progressive downfield shifts of NH and NH_2 resonances are consistent with deshielding brought about by hydrogen-bonded associations in the above anion order.

Resonances arising from methylene protons in cobalt(III)–amine complexes are usually complicated and poorly resolved due to spin–spin coupling with ^{59}Co, and are frequently not greatly informative.[9,11,12] Such is the situation with all the present complexes.

[10] Summerton, A. P., Seventh COMO Conference, Royal Australian Chemical Institute, Melbourne, 1977.

[11] Buckingham, D. A., Durham, L., and Sargeson, A. M., *Aust. J. Chem.*, 1967, **20**, 257.

[12] Jonasson, I. R., Lincoln, S. F., and Stranks, D. R., *Aust. J. Chem.*, 1970, **23**, 2267.

Carbon-13 Nuclear Magnetic Resonance Spectra

The difficulties in assigning the geometries of the new complexes *a priori* from the ^{1}H n.m.r. spectra alone prompted our examination of the carbon-13 spectra of all these complexes of medien, dien and daes.

Table 1. Carbon-13 chemical shifts for various complexes

Relative intensities are in parentheses

Compound	Solvent	δ (ppm from $SiMe_4$)				
dien,3HCl	D_2O	45·9 (1)	36·8 (1)			
medien,3HCl	D_2O	54·2 (2)	42·2 (1)	35·3 (2)		
medien	D_2O/LiOH	56·7 (2)	42·0 (1)	38·3 (2)		
s-fac-[Co(dien)$_2$] Cl_3,H_2O	D_2O	56·0 (1)	44·3 (1)			
	D_2O, 0·5 M Na_3PO_4	difference 11·8 (no reference)				
u-fac-[Co(dien)$_2$] Cl_3,$2H_2O$	D_2O	55·9 (1)	54·3 (1)	44·5 (1)	43·3 (1)	
	D_2O, 0·5 M Na_3PO_4	55·9	54·6	44·1	43·5	
u-fac-[Co(daes)$_2$] Cl_3,$2H_2O$	D_2O	46·3 (1)	45·2 (1)	39·3 (1)	38·3 (1)	
mer-[Co(dien)$_2$] Cl_3,$2·5H_2O$	D_2O	51·6 (2)	48·5 (1)	47·2 (1)		
	D_2O, 0·5 M Na_3PO_4	51·7	48·3	47·0		
	D_2O (67·89 MHz)	50·9	47·6	46·3		
	CD_3SOCD_3/10% D_2O	51·2	48·1	46·9		
mer-[Co(dien)$_2$] $(NO_3)_3$,H_2O	D_2O	51·4	48·2	46·9		
	CD_3SOCD_3	51·2	48·2	47·1		
s-fac-[Co(dien)(medien)] Cl_3	D_2O	65·9 (2)	56·3 (2)	53·1 (1)	43·8 (2)	43·0 (2)
s-fac-[Co(medien)$_2$] Cl_3,H_2O	D_2O	65·7 (2)	52·4 (1)	42·4 (2)		

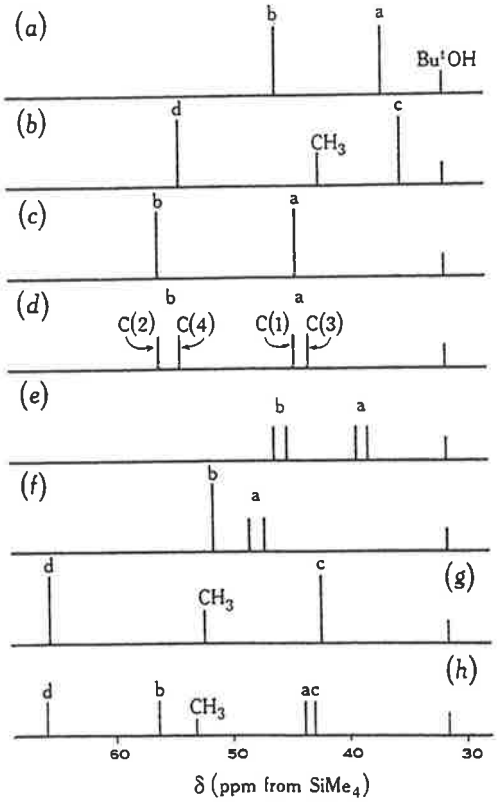

Fig. 3. The 22·625-MHz ^{13}C n.m.r. spectra in D_2O. (*a*) dien,3HCl; (*b*) medien,3HCl; (*c*) *s-fac*-[Co(dien)$_2$] Cl_3,H_2O; (*d*) *u-fac*-[Co(dien)$_2$] Cl_3,$2H_2O$; (*e*) *u-fac*-[Co(daes)$_2$] Cl_3,$2H_2O$; (*f*) *mer*-[Co(dien)$_2$] Cl_3,$2·5H_2O$; (*g*) *s-fac*-[Co(medien)$_2$] Cl_3,H_2O; (*h*) *s-fac*-[Co(dien)(medien)] Cl_3.

The numbers of stereochemically different carbon atoms present in the various $[Co(dien)_2]^{3+}$ isomers follow from the point groups as *s-fac*, two; *u-fac* and *mer*,

four each. These expectations are realized in the 22·625-MHz carbon-13 n.m.r. spectra recorded in D_2O solutions for the *s-fac* and *u-fac* isomers, and also for *u-fac*-[Co(daes)$_2$] Cl_3,2H_2O (Table 1 and Fig. 3). For the *mer* isomer of $[Co(dien)_2]^{3+}$ however the spectrum observed (Fig. 4) consists of three signals with intensity ratios 2 : 1 : 1 instead of the expected pattern of four equal resonances, and the coincidence of the resonances from two of the carbons at δ 51·6 ppm from tetramethylsilane thus indicates magnetic equivalence of these carbons. This is not due to time-averaging since conformational interconversion requires secondary-amine N–H exchange and this is quite slow even in neutral aqueous solution,[13] and such environmental averaging would in any case result in coincidence of the signals from the other two carbons also.

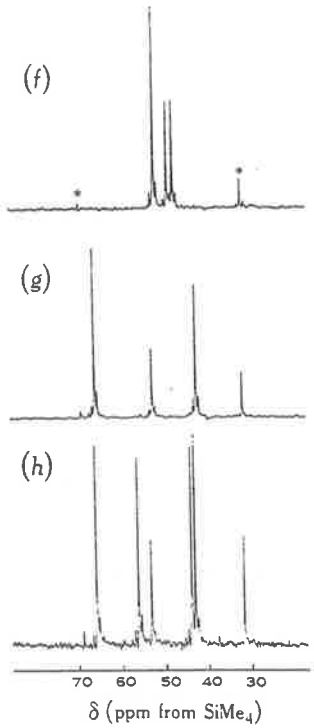

Fig. 4. The 22·625-MHz ^{13}C n.m.r. spectra for
(*f*) *mer*-[Co(dien)$_2$] Cl_3;
(*g*) *s-fac*-[Co(medien)$_2$] Cl_3;
(*h*) *s-fac*-[Co(dien)(medien)] Cl_3.
Asterisks denote Bu^{t}OH signals.

The observed spectrum can be understood from the somewhat unique symmetry properties of this molecule. The molecular symmetry is limited to C_2 because of the fixed chelate ring conformations (Fig. 1), yet each coordinated ligand exhibits (in principle) mirror image symmetry and this mirror image symmetry is confirmed in the recently reported X-ray crystal structure analysis of the racemic nitrate salt.[5] Thus the two NH_2 groups on each ligand are stereochemically non-equivalent because of their differing non-bonded interactions with the neighbouring NH_2 groups of the other coordinated dien. Magnetic non-equivalence might thus be expected for the methylene carbons adjacent to NH_2. The magnetic equivalence observed probably arises therefore with the methylene carbons adjacent to the secondary amine groups, these carbons presumably being sufficiently removed not to suffer different perturbations from the different terminal NH_2 groups. The spectrum of *mer*-[Co(dien)$_2$]-

[13] Searle, G. H., and Keene, F. R., *Inorg. Chem.*, 1972, **11**, 1006.

Cl_3 obtained at higher frequency (67·89 MHz) was identical with that at 22·625 MHz, with the C–NH–C signal remaining unsplit and confirming the magnetic equivalence of these two methylene carbons (Table 1). This result is consistent with these two methylene groups being in very similar environments stereochemically.[5]

The ^{13}C n.m.r. spectrum of *mer*-$[Co(dien)_2](NO_3)_3,H_2O$ run in dimethyl[D_6] sulphoxide (internal standard $SiMe_4$) has been reported by Sancilio, Druding and Lukaszewski[5] as showing only two peaks at frequencies δ 46·31 ppm from $SiMe_4$ (assigned as CH_2NH_2) and 47·42 ppm (assigned as CH_2NHCH_2). These authors thus concluded that only two independent types of carbon atoms were present, but our spectra do not support this view. We have obtained the spectrum of *mer*-$[Co(dien)_2]^{3+}$ under a variety of conditions: as the chloride or nitrate salts in D_2O in neutral, acidic (HCl added to pH *c.* 1) or basic ($NaHCO_3$ added to pH *c.* 9) solution; and as the chloride or nitrate salts in dimethyl[D_6] sulphoxide. The spectrum is essentially invariant under these conditions (Table 1). It seems likely that the two peaks reported by Druding and coworkers are the 1 : 1 peaks which we assign to the methylene carbons adjacent to the different NH_2 groups. The invariant 2 : 1 : 1 peak pattern we observe indicates that conformational interchange remains sufficiently slow on the n.m.r. time scale even at pH 9 that the two CH_2NH_2 carbons remain stereochemically distinct.

The carbon-13 patterns thus appear to be completely diagnostic of the geometries. The spectrum of $[Co(medien)_2]^{3+}$ shows only two methylene carbon resonances so that the geometry follows unequivocally as *s-fac*. For $[Co(dien)(medien)]^{3+}$ the four methylene carbon resonances show that this complex also has the *s-fac* geometry, and the chemical shifts of these carbons are close to those of the corresponding carbons in *s-fac*-$[Co(dien)_2]^{3+}$ and *s-fac*-$[Co(medien)_2]^{3+}$ (Fig. 3).

Fig. 3 also gives the assignments of the peaks to the particular carbon atoms, where the letters a–d are used to designate methylene carbons in the ligands as follows: for dien $N–C^a–C^b–N–C^b–C^a–N$; for medien $N–C^c–C^d–N(Me)–C^d–C^c–N$. These assignments are based on the premise that when a molecule is changed by substitution, a carbon atom nearer the point of substitution should undergo a greater change in chemical shift than will a carbon atom further removed. Comparison of the spectra of dien and medien as the free amines (protonated) thus enables the peaks at higher δ values (further downfield from $SiMe_4$) to be assigned to methylene carbons b or d of the type C–N–C. Similarly, comparison of the spectra of *u-fac*-$[Co(dien)_2]^{3+}$ and *u-fac*-$[Co(daes)_2]^{3+}$ allows the doublets further downfield to be assigned to methylene carbons b adjacent to the point of substitution. These assignments are consistent with those made previously for *mer*-$[Co(dien)_2]^{3+}$. The components of the doublets arising from these two main types of methylene carbons in the *u-fac* structures may be assigned by noting that the resonances from carbons designated 1 and 2 in Fig. 1 coincide with the a and b resonances respectively from *s-fac*-$[Co(dien)_2]^{3+}$. All of these particular carbons are in chelate rings coplanar with other chelate rings in the *u-fac* and *s-fac* complex structures.

Ion-association between phosphate anion and each of the three $[Co(dien)_2]^{3+}$ isomers has been demonstrated previously, the order of strengths being *s-fac* > *u-fac* > *mer*.[6] However, the chemical shifts for each of these isomers changed little when the spectra of the chloride salts in D_2O were rerun after Na_3PO_4 had been added to the solutions (Table 1). This insensitivity to ion-association of the resonances of the carbon atoms comprising the molecular backbone contrasts with the substantial

effects of association on the resonances of the peripheral hydrogen atoms as noted above.

It is also noted that protonation of medien causes the two different methylene resonances to be shifted downfield to similar extents, whereas the CH_3 resonance frequency remains almost constant (Table 1).

Experimental

Complexes

The isolations of $[Co(medien)_2]^{3+}$ and $[Co(dien)(medien)]^{3+}$, together with minor products, from the reaction of $[Co(NH_3)_5Cl]Cl_2$ with medien will be described in a subsequent article. Analyses of the compounds discussed in the present paper are: *s-fac*-$[Co(medien)_2]Br_3,H_2O$ (Found: C, 22·0; H, 5·6; N, 15·0; f. wt, 553. $[Co(C_5H_{15}N_3)_2]Br_3,H_2O$ requires C, 21·8; H, 5·8; N, 15·2%; f. wt, 551). *s-fac*-$[Co(dien)(medien)]Br_3,H_2O$ (Found: C, 20·2; H, 5·6; Br, 44·5; Co, 11·1; N, 15·4. $[Co(C_4H_{13}N_3)(C_5H_{15}N_3)]Br_3,H_2O$ requires C, 20·1; H, 5·6; Br, 44·6; Co, 11·0; N, 15·6%).

The isomers of $[Co(dien)_2]^{3+}$ were separated chromatographically and isolated as bromides as described previously.[1,6] A sample of each of the six complexes discussed was converted into the more water-soluble chloride salt by adsorbing the complex on a short column of Biorex-70 weak acid cation-exchange resin (50–100 mesh) in the Li^+ form, washing with water, and eluting with 0·1 M HCl. The effluent was concentrated to a small volume on a rotary evaporator, and precipitation of the chloride salt was completed by the addition of ethanol and cooling at 0°. The product was filtered off, washed with ethanol and acetone, and dried at 50° to constant weight. The chloride salts are less soluble in dimethyl sulphoxide than the bromides. *mer*-$[Co(dien)_2](NO_3)_3,H_2O$ was obtained by an analogous procedure, eluting from the resin with 0·1 M HNO_3. *s-fac*-[Co(dien)-(medien)]$(ClO_4)_3$ and *s-fac*-$[Co(medien)_2](ClO_4)_3$ were obtained from the corresponding bromides similarly, being eluted from the resins with 0·1 M $HClO_4$. The yields obtained in these conversion procedures were around 95%.

Spectra

The 60-MHz ^1H n.m.r. spectra were recorded on a Varian T60 spectrometer for *c.* 6% w/v solutions of $[Co(medien)_2]Br_3,H_2O$ and $[Co(dien)(medien)]Br_3,H_2O$ and the corresponding perchlorates in $(CD_3)_2SO$ with tetramethylsilane as internal reference.

The broad-band proton-decoupled 22·625-MHz carbon-13 n.m.r. spectra (decoupler on continuously) in D_2O were measured on a Bruker HX-90E spectrometer operating in Fourier transform mode connected to a Nicolet BNC-12 computer with 8192 data table. The spectrometer was locked to deuterium, and a capillary of t-butyl alcohol provided a reference signal (frequency 715 Hz from $SiMe_4$). Pulse angle was 45° and repetition time was 0·8 s. Solution concentrations used were 0·3 g/2 ml for the complexes as chloride salts, 1·0 g/2 ml for the ligands as hydrochloride salts, in 10 mm tubes at 28°C. Numbers of scans accumulated for the complexes were 3000, for the ligands 1000.

Acknowledgment

We are grateful for the 67·89-MHz ^{13}C n.m.r. spectrum run at the National N.M.R. Centre, Canberra.

Manuscript received 17 November 1976

Contribution from the Department of Physical and Inorganic Chemistry, The University of Adelaide, Adelaide 5001, Australia

Homogeneous and Charcoal-Catalyzed Isomerizations of the (Diethylenetriamine)(methyldiethylenetriamine)cobalt(III) and Bis(diethylenetriamine)cobalt(III) Ions

GRAEME H. SEARLE,* F. RICHARD KEENE, and STEPHEN F. LINCOLN

Received September 27, 1977

Each of the *s-fac* and *u-fac* isomers of $[Co(dien)(medien)](ClO_4)_3$ isomerizes in homogeneous aqueous solution to the same equilibrium mixture of the three geometric isomers, with no other products detectable. Proportions after 2 days at 90 °C were *s-fac*:*u-fac*:*mer* = 81:10:9. This reaction is the basis for obtaining on a preparative scale the new *u-fac* and *mer* isomers which have been characterized by ^{13}C NMR spectra. Over catalytic charcoal disproportionation occurs to a mixture of seven complexes which can be mostly separated on SP-Sephadex C-25 cation-exchange resin. Equilibrium molar proportions after 4 h at 80 °C were $Co(dien)_2^{3+}$ *s-fac*:*u-fac*:*mer*:Co(dien)(medien)$^{3+}$ *s-fac*:*u-fac*:Co(medien)$_2^{3+}$ *s-fac* = 5:~23:19 [which includes a little nonseparable *mer*-Co(dien)(medien)$^{3+}$]:~23:4:26. The charcoal reactions must involve complete dissociations of ligands, and by comparison the homogeneous reactions must involve intramolecular processes. In the homogeneous isomerizations at least two rearrangment processes must be involved, and probably three rearrangements occur. Similar experimental results have been obtained for the catalyzed and uncatalyzed reactions of the three isomers of $Co(dien)_2^{3+}$. All the homogeneous reactions are base-catalyzed and probably involve conjugate-base intermediates (deprotonated at the secondary amine nitrogens of coordinated dien). All the experimental data for the homogeneous reactions are most satisfactorily accommodated by the proposal of transient five-coordinated intermediates, formed by bond rupture, rearranging. The possibility of twisting mechanisms occurring through trigonal-prismatic transition states is also considered. Racemizations of $Co(en)_3^{3+}$ under both charcoal-catalyzed and homogeneous conditions are also base catalyzed.

Introduction

Intramolecular rearrangements in octahedral complexes,[1] manifested as isomerization or racemization processes, can occur by two major pathways: nondissociative, involving the twisting of one octahedral face relative to the opposite face about a C_3 (or a pseudo- or imaginary-C_3) axis via an idealized trigonal-prismatic transition state, and bond rupture via idealized trigonal-bipyramidal or square-pyramidal transition states. In rearrangement reactions where the processes have been established to be intramolecular, the choice between the nondissociative and bond-rupture alternatives has seldom been unambiguous, particularly for complexes of bidentate ligands on which almost all of these studies have been made.[1-3a]

Since the initial proposals of twist mechanisms[4-7] there have been considerable efforts to establish experimentally their existence, and the work has been reviewed.[1,2,8] Only recently have twist mechanisms for isomerization and racemization processes in some octahedral complexes been definitely demonstrated and several approaches have been used.

Conventional kinetic approaches involving exchange and competition rate measurements do not in general provide sufficient data to distinguish the two intramolecular alternatives. However, the complexes *cis*- and *trans*-tetracarbonyl(methoxymethylcarbene)(trialkylphosphine)chromium(0), $(CO)_4Cr(C[OCH_3]CH_3)(PR_3)$, R = C_2H_5, C_6H_{11}, provide an interesting instance where the cis–trans isomerization was assigned as a twist process.[9] For these complexes, with exclusively monodentate ligands, all possible dissociative processes were eliminated by the kinetic data leaving an intramolecular process, that is, a twist in this particular instance, as the only plausible mechanism.

Dynamic ^1H NMR spectroscopy[2] has been employed to establish twist mechanisms for the dynamic inversions $\Delta \rightleftharpoons \Lambda$ of some tris(tropolonato) complexes of cobalt(III) and aluminium by Holm and co-workers[10,11] and of some tris(dithiocarbamato) complexes of iron(III) and ruthenium(III) by Pignolet and co-workers.[12,13] Lawrance and Stranks[14] have recently demonstrated that volumes of activation, obtained from rate–pressure measurements, may provide a general criterion to distinguish the bond-rupture and twist mechanisms with some stereochemically rigid complexes. By this means the racemizations of $Cr(phen)_3^{3+}$, $Cr(bpy)_3^{3+}$, $Cr(ox)(phen)_2^+$, and $Cr(ox)(bpy)_2^+$[15] were shown to proceed by twist mechanisms, whereas $Cr(ox)_3^{3-}$, $Cr(ox)_2(phen)^-$, and $Cr(ox)_2(bpy)^-$ involved bond ruptures. These methods have limitations. The dynamic ^1H NMR method is restricted to stereochemically nonrigid complexes, and diastereotopic substituent groups on the chelate ligands are required as probes to detect the changes in chirality around the metal centers. The activation volume approach may not be easily applicable to complexes of primary and secondary amines where there is the possibility of deprotonation followed by rearrangement of a deprotonated species. Thus the generality of twist mechanisms is still unkown.

It was hoped that the use of complexes of multidentate ligands in mechanistic studies of intramolecular rearrangements might offer more opportunity of distinguishing between the bond-rupture and twist alternatives, since the coupled chelate rings restrict the number of different possible interconversions and because such molecules possess more distinguishable points of reference by which to trace the paths of specific rearrangements. We now describe experiments on the isomerizations of the geometric isomers of $[Co(dien)(medien)](ClO_4)_3$.[15] These hexamine-type complexes are useful for such mechanistic studies because the isomerizations are relatively uncomplicated by competing hydrolysis reactions and because they are closely related to other complexes like $Co(en)_3^{3+}$ for which racemization mechanisms are still unclear. Although the experiments demonstrate that the isomerizations in homogeneous solution proceed by intramolecular mechanisms, the bond-rupture and twist possibilities are not readily distinguished. However, the bond-rupture route is supported by observations on some similar systems.

Results

Identification of the Three Co(dien)(medien)$^{3+}$ Isomers by ^{13}C NMR Spectroscopy. The complexes Co(dien)(medien)$^{3+}$, $Co(dien)_2^{3+}$, and Co(medien)$_2^{3+}$ can each exist in three possible geometric isomers as shown in Figure 1. In two of these geometric forms the two secondary or tertiary amine groups are disposed trans to each other, but in the *u-fac* isomer these groups are in cis positions.

0020-1669/78/1317-2362$01.00/0

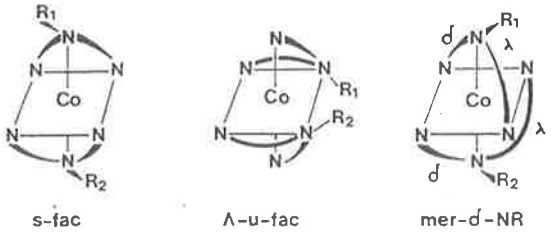

Figure 1. Possible geometric isomers of $Co(dien)_2^{3+}$ ($R_1 = R_2 = H$), $Co(medien)_2^{3+}$ ($R_1 = R_2 = Me$), and $Co(dien)(medien)^{3+}$ ($R_1 = H$, $R_2 = Me$). One optical isomer is shown for each of the *u-fac* and *mer* forms.

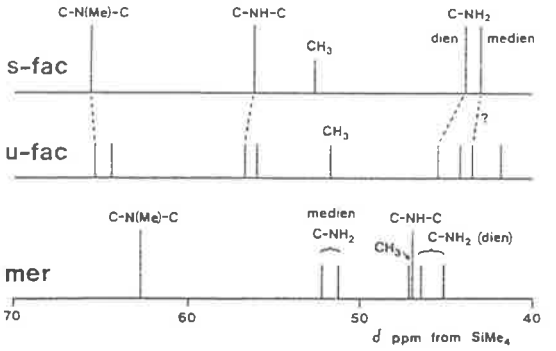

Figure 2. ^{13}C NMR spectra in D_2O of the geometric isomers of $[Co(dien)(medien)](ClO_4)_3$.

The compounds *s-fac*-$[Co(dien)(medien)]^{3+}$ and *s-fac*-$[Co(medien)_2]^{3+}$ are the major products from the reaction of $[Co(NH_3)_5Cl]Cl_2$ with dien and medien, and their geometric configurations were assigned previously from comparisons of their ^{13}C NMR spectra with the spectra of the three isomers of $Co(dien)_2^{3+}$.[16]

The *u-fac* and *mer* isomers of $Co(dien)(medien)^{3+}$ are formed by isomerization of *s-fac*-$[Co(dien)(medien)](ClO_4)_3$ in aqueous solution as described below, and their identities follow from their ^{13}C NMR spectra (Figure 2). In each of these two isomers the nine carbon atoms are, in principle, in stereochemically different environments (each isomer has symmetry C_1). However, the two methylene carbons adjacent to the secondary amine nitrogen of dien in *mer*-$[Co(dien)(medien)]^{3+}$ are evidently in closely similar environments since they give a single resonance peak (δ 47.0 ppm from $SiMe_4$) just as for *mer*-$[Co(dien)_2]^{3+}$. Similarly, the two methylene carbons adjacent to the tertiary amine group of *meridionally* coordinated medien give a single peak (δ 62.8). Thus the four methylene carbons in each ligand in a *mer* complex give a characteristic 2:1:1 peak pattern. There are no equivalences for *u-fac* isomers, so that the *u-fac*-$[Co(dien)(medien)]^{3+}$ isomer must be that which gives the nine peaks, all of similar magnitude (Figure 2).

Reactions of *s-fac*- and *u-fac*-$Co(dien)(medien)^{3+}$ in Homogeneous Aqueous Solution. When *s-fac*-$[Co(dien)(medien)](ClO_4)_3$ was heated in water at 90 °C, and the resulting solution was separated chromatographically on a column of SP-Sephadex cation-exchange resin, three bands of the geometric isomers of $Co(dien)(medien)^{3+}$ separated as the only products (Figure 3A). The rates of formation of the two new minor isomers *u-fac* and *mer* seemed to be variable in different runs in water (pH ~5–5.5). We therefore carried out two parallel reactions of the *s-fac* isomer, one in 0.01 M perchloric acid and one in sodium hydroxide solution adjusted to pH 10.5. After 2 days at 90 °C, chromatography of the solutions showed that the *s-fac* had remained completely unchanged in the perchloric acid but had substantially isomerized in the sodium hydroxide solution (pH now 7.5), so that it was clear that the isomerization reactions were inhibited by acid and were apparently base catalyzed. The reactions were subsequently carried out in a buffer solution, 0.05 M 2,4,6-trimethylpyridine–perchloric acid adjusted to pH 8.0 at 25 °C, although the actual pH at the elevated reaction temperatures would be substantially less than this, probably around 7.

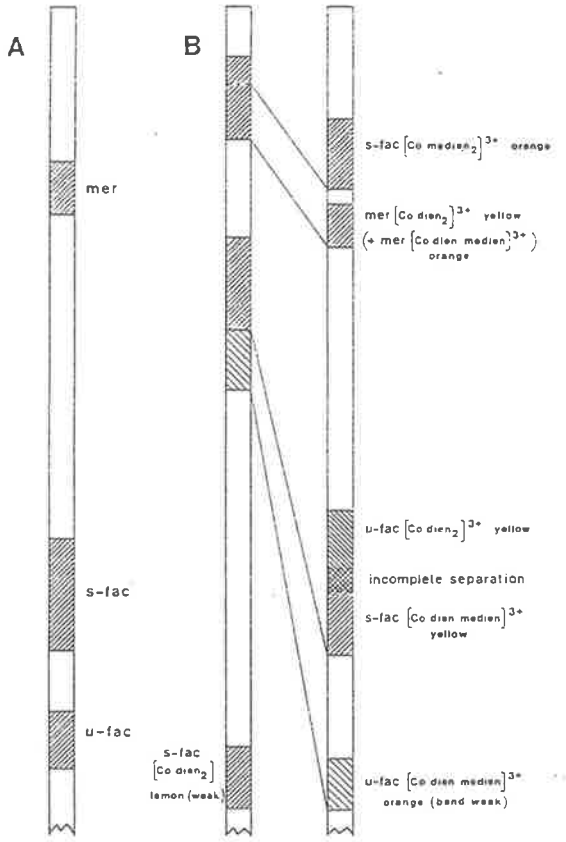

Figure 3. Chromatographic separations on Sephadex columns (Na_3PO_4 eluent): (A) equilibrium mixture of $Co(dien)(medien)^{3+}$ isomers, from *s-fac*-$[Co(dien)(medien)](ClO_4)_3$ in aqueous buffer, pH ~8; (B) products from *s-fac*-$[Co(dien)(medien)](ClO_4)_3$ on charcoal in water.

Separate solutions of *s-fac*- and *u-fac*-$[Co(dien)(medien)](ClO_4)_3$ in the buffer solution were allowed to react at 90 °C. Samples from the two solutions at this temperature gave apparently similar proportions of the three constituent isomers after 2 days so that each mixture had essentially reached equilibrium by this time. At 3 days, analysis of the proportions gave identical results from the two solutions of starting *s-fac* and *u-fac*. These equilibrium proportions of $Co(dien)(medien)^{3+}$ were *s-fac*:*u-fac*:*mer* = (81 ± 2):(10 ± 1):(9 ± 1) at 90 °C.

Chromatography of a solution of *u-fac*-$[Co(dien)(medien)](ClO_4)_3$ in 0.01 M perchloric acid, which had reacted for 2.5 days at 90 °C, showed that some isomerization to *s-fac* had occurred (*s-fac*:*u-fac* ~ 1:10 by visual estimate), but *mer* was not detectable. The formation of both of the other isomers from *u-fac* was clearly acid retarded.

The isomerization of the more stable *s-fac* isomer under the above conditions provides the most convenient means of obtaining the *u-fac* and *mer* isomers. Not only are the yields better than from other reactions we have studied (the dis-

proportionation of *s-fac*-[Co(dien)(medien)]$(ClO_4)_3$ on charcoal as described below, and $[Co(NH_3)_5Cl]Cl_2$ + dien + medien) but these other reactions produce the $Co(dien)_2^{3+}$ isomers also and it is almost impossible to separate *mer*-[Co(dien)(medien)]$^{3+}$ from *mer*-$[Co(dien)_2]^{3+}$ and difficult to separate *s-fac*-[Co(dien)(medien)]$^{3+}$ from *u-fac*-[Co-$(dien)_2]^{3+}$ by chromatography on Sephadex.[17]

Reactions of *s-fac*- and *u-fac*-[Co(dien)(medien)]$^{3+}$ over Charcoal. In water with catalytic charcoal, *s-fac*-[Co-(dien)(medien)]$(ClO_4)_3$ gave a mixture of seven complexes which were separated chromatographically into six bands on SP-Sephadex cation-exchange resin using Na_3PO_4 eluent (Figure 3B). The reaction was studied at 80 °C because some information on the equilibrium proportions of the three $Co(dien)_2^{3+}$ isomers is available for that temperature.[18] Equilibrium was established within 4 h. The identities of the six yellow or orange complexes were established from their relative orders of separation on Sephadex with Na_3PO_4, compared with those of the authentic complexes determined separately[17] and which have been characterized by ^{13}C NMR spectroscopy.[16]

The molar proportions of these six products were determined (atomic absorption) to be as follows: *s-fac*-$[Co(dien)_2]^{3+}$: *u-fac*-$[Co(dien)_2]^{3+}$:*mer*-$[Co(dien)_2]^{3+}$(+*mer*-[Co(dien)-(medien)]$^{3+}$):*s-fac*-[Co(dien)(medien)]$^{3+}$:*u-fac*-[Co(dien)-(medien)]$^{3+}$:*s-fac*-$[Co(medien)_2]^{3+}$ = 5:~23:19:~23:4:26. Clearly *s-fac*-[Co(dien)(medien)]$^{3+}$ had undergone disproportionation (in the ligand sense) so that the above proportions should represent the relative stabilities of the various species corresponding to equimolar amounts of the two ligands. Some orange *mer*-[Co(dien)(medien)]$^{3+}$ was undoubtedly formed, but this complex chromatographs with yellow *mer*-[Co-$(dien)_2]^{3+}$ in a single band[17] so that the proportions of these two species could not be directly assessed. However from the yellow color of this band and the proportion arguments below, we believe that the proportion of *mer*-[Co(dien)(medien)]$^{3+}$ was small (<4% of the total products).

The above proportions of the $Co(dien)_2^{3+}$ isomers (5:~23:~19 for perchlorates) are in accord with the previously measured equilibrium proportions at the same temperature, *s-fac*:*u-fac*:*mer* = 6:19:22 (for chlorides).[18] There is also reasonable agreement between the above proportions of the Co(dien)(medien)$^{3+}$ isomers, *s-fac*:*u-fac*:*mer* = ~23:4:small, and the equilibrium proportions of these isomers as determined for homogeneous solution (81:10:9, although these were at 90 °C). Of the three possible $Co(medien)_2^{3+}$ isomers, there has been no evidence for the formation of the *u-fac* and *mer* isomers in detectable quantities from several reactions studied.[19]

From the reaction stoichiometry

$$2Co(dien)(medien)^{3+} = Co(dien)_2^{3+} + Co(medien)_2^{3+}$$

the molar amounts of $Co(dien)_2^{3+}$ (three isomers) and $Co(medien)_2^{3+}$ were expected to be equal, but their proportion as measured above, ~47:26, shows a deficiency of medien. This proportion is only approximate because *s-fac*-[Co-(dien)(medien)]$^{3+}$ and *u-fac*-$[Co(dien)_2]^{3+}$ were incompletely separated in the chromatography (Figure 3B) and were estimated visually to be in similar amounts and because any *mer*-[Co(dien)(medien)]$^{3+}$ formed is included in the *mer*-$[Co(dien)_2]^{3+}$ figure. Nevertheless to give a 1:1 ratio of dien:medien over the total chromatographed products, proportions of *s-fac*-[Co(dien)(medien)]$^{3+}$ and *mer*-[Co(dien)-(medien)]$^{3+}$ in the respective incompletely separated bands would be required which would be too high to satisfy simultaneously the following three requirements: (1) the experimental observations (albeit approximate) of the compositions of these two bands; (2) the equilibrium proportions of the three $Co(dien)_2^{3+}$ isomers as determined separately (though for chlorides); (3) the equilibrium proportions of the three Co(dien)(medien)$^{3+}$ isomers as determined separately (though at 90 °C). Further, it is improbable that any significant amounts of *u-fac* and *mer* $Co(medien)_2^{3+}$ have escaped detection. It seems clear therefore that the amount of Co-$(medien)_2^{3+}$ formed is less than stoichiometric. This probably reflects the lower stability of the coordination between cobalt(III) and medien than between cobalt(III) and dien. This may be viewed alternatively as a greater propensity toward decomposition by $Co(medien)_2^{3+}$, probably to cobalt(II) (with charcoal, water, or OH^-[20] as possible reductants) and free ligand, than by the $Co(dien)_2^{3+}$. A significant amount of cobalt(II) was present (thiocyanate test) in the solution at 48 h despite an oxygen atmosphere being maintained above the solution. Some demethylation of *s-fac*-$[Co(medien)_2](ClO_4)_3$ to *s-fac*-[Co(dien)(medien)]$^{3+}$ on the charcoal, as observed in separate experiments,[19] would also raise the dien:medien ratio.

The *u-fac* isomer of [Co(dien)(medien)]$(ClO_4)_3$ disproportionated on charcoal to give the same products in similar proportions as from the *s-fac* isomer above. In this instance the extent of isomerization *u-fac* → *s-fac*-[Co(dien)(medien)]$^{3+}$ was considerable, and again the amount of the *mer* isomer formed was probably small.

Discussion

Isomerization Reactions of Co(dien)(medien)$^{3+}$ in Homogeneous Aqueous Solution. In aqueous solution without charcoal, isomerization of both *s-fac*- and *u-fac*-Co(dien)-(medien)$^{3+}$ occurred slowly to give the same mixture of the three Co(dien)(medien)$^{3+}$ isomers, *s-fac*:*u-fac*:*mer* = 81:10:9. That no other products were observed under these conditions implies that the reactions could not have involved ligand dissociation, since this should lead to disproportionation as in the charcoal reaction. Certainly any *s-fac*-$[Co(medien)_2]^{3+}$ would be readily detectable in the chromatographic separations (Figure 3B). Thus the isomerizations must involve entirely intramolecular pathways.

Figure 4 proposes reaction pathways between each pair of isomers. Since all three isomers are involved in the isomerizations, at least two of these three rearrangement pathways must occur, and the experimental observations give no reason to exclude any of the three interconversions between isomer pairs.

The reaction directly linking *s-fac* and *mer* involves no gross rearrangement (the secondary and tertiary amine nitrogens remain trans), and a bond rupture (one-ended dissociation) proceeding through a trigonal-bipyramid intermediate as sketched in Figure 4 is the simplest possible process for this conversion.

In the *u-fac* isomer the secondary and tertiary amine nitrogens are cis. Thus any change from *u-fac* to either of the other two isomers involves changing the relative positions of these nitrogens from cis to trans so that gross rearrangements are necessary. Two possibilities for these rearrangements can be envisaged: (1) intramolecular twists proceeding through trigonal-prismatic transition states and (2) bond ruptures to five-coordinate intermediates followed by rearrangement within each intermediate and subsequent recoordination of the $-NH_2$ group. This latter sequence is similar to the "twist-with-rupture" mechanism as described by Eaton and co-workers.[10]

Figure 4 shows the two twist processes proceeding through different trigonal-prismatic transition states which can account for the interconversions from *u-fac*. These two twists differ in that one, for *u-fac* ⇌ *s-fac*, is envisaged as a trigonal twisting of one coordinated ligand relative to the other ligand by 120° around an axis (imaginary C_3) through the centers of the faces of the octahedron containing each of the ligands as in Figure 4. The other twist, for *u-fac* ⇌ *mer*, involves the

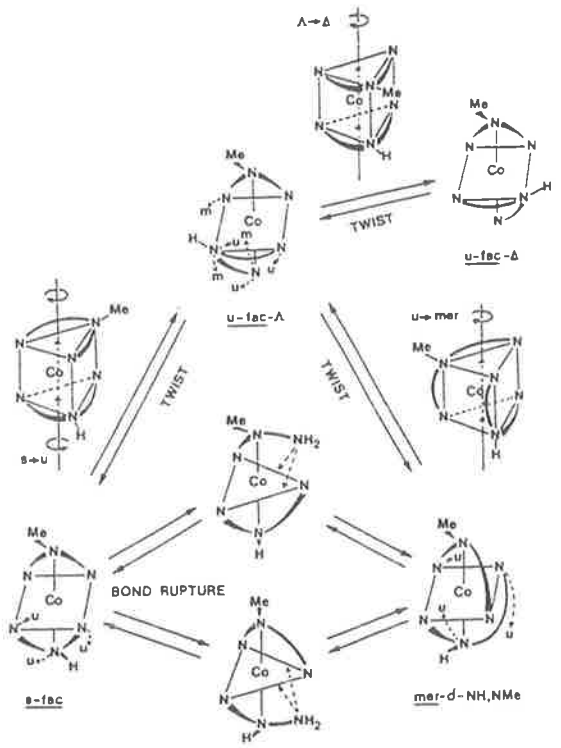

Figure 4. Possible intramolecular twist (and bond-rupture) pathways for interconversions of Co(dien)(medien)$^{3+}$ isomers. The particular enantiomers shown of the two possible geometrically different trigonal-bipyramidal intermediates linking *s-fac* and *mer* are those corresponding to the *mer*-δ optical isomer only. The trigonal-prismatic transition state for racemization of the *u-fac* is symetrical (plane). The enantiomers shown of the other two trigonal prisms correspond to the particular optical isomers drawn for *u-fac* (Λ) and *mer* (δ-NH, NMe). The small dashed arrows indicate movements of donor atoms around octahedron faces by trigonal twisting to give products designated as s (*s-fac*), u (*u-fac*), and m (*mer*).

trigonal twisting by 120° around an octahedral face of two donor nitrogen atoms of one ligand (one primary amine, one secondary or tertiary amine) and one nitrogen (primary amine) of the other ligand. Both of the trigonal-prismatic transition states are dissymmetric, so that the *u-fac* ⇌ *mer* change should be stereospecific as indicated in Figure 4. It is conceivable that in any reactions of cobalt(III), particularly those conducted at higher temperatures and in basic conditions as in the present instance, some cobalt(II) species could be formed.[20-22] Cobalt(II) was not detectable in the product solutions by the thiocyanate test, so that the concentration of any cobalt(II) must have been small (<10 ppm). Formation of any cobalt(II) would appear to provide a mechanism for the observed rearrangements by slow electron transfer between a cobalt(III) complex and labile cobalt(II),[23] but this mechanism should lead to some concomitant disproportionation, albeit at a slow rate if the cobalt(II) concentration was extremely small, and this was not observed. Such an electron-transfer mechanism for the equilibrations can thus be discarded, but this does not eliminate the possibility that the rearrangement processes (twist or bond rupture) might occur via transient labile Co(dien)(medien)$^{2+}$ intermediates. However to be consistent with the experimental observations, this mechanistic route would require that the rate of dissociation of the ligands from the transient Co(dien)(medien)$^{2+}$ be relatively slow compared with the rates of both the rearrangement and the electron-transfer acts. The electron transfer between $Co(en)_3^{3+}$ and $Co(en)_3^{2+}$ is quite slow, however,[23] and since this is a cobalt(III)–hexamine system of the same general type as Co(dien)(medien)$^{3+}$, the possibility of the above suggested cobalt(II)-rearrangement mechanism occurring without any observed dissociation of the Co(dien)(medien)$^{2+}$ seems remote. The experimental observations are therefore entirely consistent with at least one rearrangement occurring in the cobalt(III) species, *u-fac* ⇌ *s-fac* and/or *u-fac* ⇌ *mer*, and the presence of cobalt(II) need not be invoked as a participant in these slow isomerization reactions. We consider the present demonstration of an intramolecular mechanism for isomerization of Co(dien)(medien)$^{3+}$ significant because it represents one of the few cases of rearrangements of cobalt(III)–hexamine-type complexes having five-membered chelate rings where the possibility of an electron-transfer-promoted mechanism can be discounted.

The Effect of pH on the Isomerizations of Co(dien)(medien)$^{3+}$. Acid retardation is a characteristic of these intramolecular isomerization processes, which include at least two rearrangements. Acid retardation (or base catalysis) implies that the rearrangement processes might proceed through conjugate base species, and the most likely sites of the deprotonations would be the secondary amines of the coordinated dien rather than any of the coordinated primary amines. The relative acidities of the amine protons in the corresponding three isomers of $Co(dien)_2^{3+}$, based on the relative rates of N–H exchange,[24-26] are *sec*-NH (*mer*) > *sec*-NH (*s-fac* and *u-fac*) ≫ $-NH_2$ (all three isomers),[27,28] and the secondary amine protons should be the most acidic in the closely similar Co(dien)(medien)$^{3+}$ complexes also. We now consider how deprotonation might facilitate either twist or bond-rupture processes.

Twists of deprotonated species would pass through the same dissymmetric trigonal-prismatic transition-state geometries as those shown in Figure 4 (but deprotonated at the *sec*-NH), so that for the *u-fac* → *mer* change the twist act itself should remain stereospecific and optical activity should be retained. However some inversion will occur at the deprotonated *sec*-N center (coordinated dien) of the *mer* structure,[29] and under the conditions of the isomerization experiments the final *mer* product after reprotonation would not be expected to be optically active. For this *u-fac* → *mer* change we see some possibility of nitrogen to cobalt pπ–dπ bonding. Although π stabilization has not been considered to be a dominating feature in the racemization (through NH exchange) of *mer*-$[Co(dien)_2]^{3+}$ [29] nor in the base hydrolysis of *sym*-[Co(trenen)Cl]$^{2+}$ [15,26] some degree of π bonding could be the factor which promotes the *u-fac* (deprotonated) → *mer* (deprotonated) twist act.

An alternative view is that deprotonation facilitates the adjustments of the bond angles at the *sec*-amine sites which necessarily accompany stereo change. The required adjustments of bond angles would probably be greatest for the *u-fac* → *mer* twist change where a facial dien ligand becomes meridional, and this situation is analogous to the base-catalyzed isomerization *cis* → *trans*-$[Co(cyclam)(OH_2)_2]^{3+}$ [15] in which proton abstraction from a coordinated *sec*-amine group was associated with *fac* to *mer* change of coupled chelate rings in the cyclam ligand.[30] However such deprotonation requirement should be less stringent, in terms either of π bonding or of facilitating nitrogen bond angle adjustments, for the possible *s-fac* ⇌ *u-fac* twist where each ligand remains facial.

Our observations on the acid retardations of the isomerizations of Co(dien)(medien)$^{3+}$ are in accord with the suggested bond angle adjustments. After 2.5 days at 90 °C in 0.01 M perchloric acid the *u-fac* isomer had undergone some isomerization to *s-fac* (~10%) but no *mer* was detected, and this suggests that the *u-fac* → *s-fac* twist was less retarded by

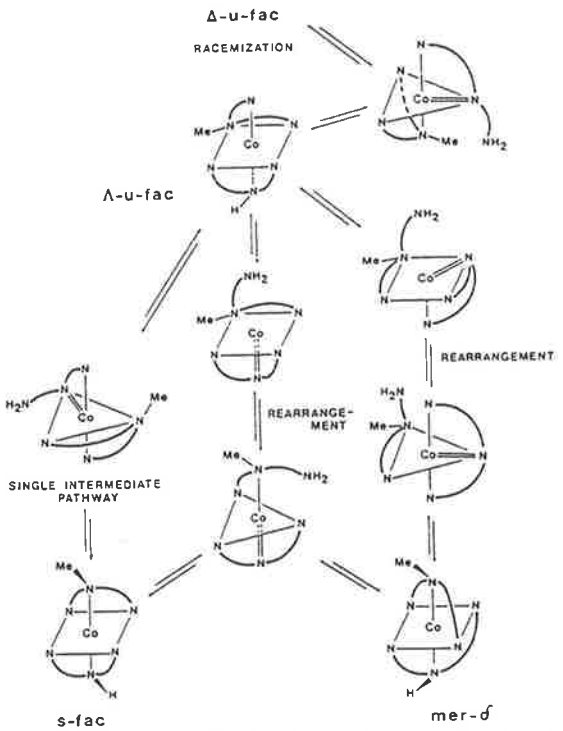

Figure 5. Possible intramolecular pathways for interconversions of Co(dien)(medien)$^{3+}$ isomers involving bond ruptures to five-coordinate intermediates. Only the central pathway may be stereospecific Λ-*u-fac* → *mer*-δ.

acidic conditions than were the other two processes. Under identical conditions the *s-fac* isomer showed no change, and the nonobservance of any *s-fac* → *u-fac* probably reflects the equilibrium position being heavily in favor of *s-fac*.

Acidic conditions may inhibit a bond-rupture process by the protonation of the dissociated amine group preventing its recoordination to the metal, as with the racemization of $Fe(bpy)_3^{2+}$.[3a] However, for the present complexes with acidic *sec*-amine sites (dien), the base catalysis of the possible bond-rupture pathways is more satisfactorily accounted for in terms of π stabilization of the five-coordinate conjugate-base intermediates (Figure 5). The apparent greater rate for *u-fac* → *s-fac* than for *u-fac* → *mer* and *s-fac* → *mer* referred to above is consistent with the single intermediate pathway for *u-fac* → *s-fac* being preferred over the others. In this single trigonal-bipyramid intermediate π-bonding overlap is likely to be more efficient as a consequence of the flexibility of the detached arm of the dien;[26] the other two pathways involve intermediates with facial dien.

Figure 4 also shows that a third twist process of the *u-fac* isomer could lead to its racemization, the transition state in this instance possessing a plane of symmetry. Similarly a bond-rupture process through a symmetrical trigonal-bipyramid intermediate (Figure 5) could lead to direct racemization of *u-fac*. The possible routes involving either twists or bond ruptures by which optical activity could be lost from the *u-fac* isomer are numerous: (1) direct racemization; (2) the symmetrical *s-fac*; (3) mutarotation to *mer* deprotonated intermediate by twist, followed by inversion of the intermediate; (4) the nonstereospecific *u-fac* → *mer* bond-rupture pathway; (5) any active *mer* product formed being subsequently racemized by hydrogen exchange at the *sec*-NH of the coordinated dien.[29] This complexity would preclude an analysis of the kinetics of loss of optical activity from active *u-fac*-[Co(dien)(medien)]$^{3+}$ in terms of possible processes, and in any case the twist and bond-rupture possibilities could probably not be distinguished. Isomerization and racemization in the isomers of Co(medien)$_2^{3+}$ should be somewhat simpler, since racemization by direct inversion of the *mer* isomer should be avoided with the two methyl substituents.

A third possible interpretation of the base catalysis of the isomerizations of Co(dien)(medien)$^{3+}$ is that OH^- is involved in the transition state in an S_N2 process. This kind of mechanism was proposed by Cooke, Im, and Busch for the base-catalyzed racemization of Co(edta)$^-$[15] by a twist process, with the OH^- suggested to be coordinated to the cobalt at a rectangular face of the trigonal prism.[31] Deprotonation is not possible with Co(edta)$^-$, and with our present amine complexes we favor the conjugate-base interpretation.

On the basis of the above conjugate-base twist and bond-rupture proposals, it becomes of considerable interest to know whether the Co(medien)$_2^{3+}$ isomers would isomerize at all in homogeneous solution, since deprotonations analogous to those at the coordinated *sec*-NH centers of the Co(dien)(medien)$^{3+}$ isomers are not possible with the Co(medien)$_2^{3+}$ compounds. A reluctance of Co(medien)$_2^{3+}$ to isomerize might confirm that deprotonations at *sec*-nitrogens are necessary preludes for twist or bond-rupture processes with cobalt(III)–amine complexes in aqueous solution and enable the S_N2 mechanism to be discounted. Unfortunately the *s-fac* is the most stable isomer of Co(medien)$_2^{3+}$, and we have not been able to obtain the *u-fac* and *mer* isomers in detectable amounts in the presence of charcoal.[19] Thus at present the crucial experiment of examining the [OH^-] dependence of the isomerization *u-fac*-[Co(medien)$_2$]$^{3+}$ → *s-fac*-[Co(medien)$_2$]$^{3+}$ cannot be carried out.

Isomerizations in the Co(dien)$_2^{3+}$ System. Isomerization experiments we have carried out with the Co(dien)$_2^{3+}$ isomers are relevant to the work already described. Due to the close similarity between the Co(dien)$_2^{3+}$ and Co(dien)(medien)$^{3+}$ complexes, we would expect that isomerizations would proceed by similar mechanisms in both systems. For the homogeneous isomerizations of Co(dien)$_2^{3+}$ the mechanisms could be confirmed as intramolecular only by comparing ligand-exchange and isomerization rates. Nevertheless intermolecular mechanisms for these homogeneous processes of Co(dien)$_2^{3+}$ and Co(dien)(medien)$^{3+}$ under the concentrations of complexes employed are considered quite unlikely, as complete dissociations of tridentate ligands would be expected to result in considerable amounts of hydrolysis products from the reactions in water, and these were not evident.

The three Co(dien)$_2^{3+}$ isomers as the acetate salts have been interconverted under a variety of conditions of solvent (water, dimethyl sulfoxide, alcohols up to *tert*-butyl alcohol, glacial acetic acid, dien), the presence or absence of charcoal for reactions in water, pH for aqueous solutions (varied by addition of 2,4,6-trimethylpyridine–hydrochloric acid buffer pH 8,[32] hydrochloric acid, or sodium hydroxide), and temperature (25 and 82 °C). The experimental methods were similar to those used for the Co(dien)(medien)$^{3+}$ compounds. Samples taken from a run at various times were chromatographed on Sephadex columns, and the proportions of the three separated isomers were determined spectrophotometrically.[18,33]

The results can be summarized as follows, one set of experimental data being given in Table I: (1) Each isomer gives a mixture of all three isomers. The reaction rates depend on the starting isomer, being greatest for the *mer* (Table I). (2) The isomerizations in water are catalyzed by base (pH range 5–9) and do not occur at pH <3. No reaction was detectable in glacial acetic acid. The complex (*s-fac*) decomposed in 0.1 M sodium hydroxide at 80 °C. (3) The *mer* equilibrium proportion is always established relatively rapidly, and the two

Table I. Isomerization Reactions of the $[Co(dien)_2](CH_3COO)_3$ Isomers in Water at 82 °C

starting isomer[a]	sampling time	isomer proportions[b] *s-fac*	*u-fac*	*mer*
s-fac	1 day	69	7	24
	3 days	32	24	44
	7 days	18	37	45
	14 days	15	41	44
u-fac	3 h	6	84	10
	1 day	7	62	31
	3 days	9	49	42
	7 days	12	45	43
	14 days	14	44	42
mer	3 h	4	7	89
	1 day	9	33	58
	3 days	13	40	47
	7 days	13	44	43
	14 days	13	43	44
proportions on charcoal at 82 °C (12 h)		15	42	43

[a] Complex concentration ~0.02 M. [b] Values given are subject to experimental error of ±2.

fac forms continue to adjust more slowly to their equilibrium proportions (Table I). The final product distribution is the same from each starting isomer under a given set of conditions and in water is identical with that obtained by the rapid equilibration of any of the isomers on activated charcoal (Table I). This confirms that charcoal effects true thermodynamic equilibration between the isomers. (4) In all instances where isomerization occurred, a small amount of a reddish purple species was detected. It is likely that this was a monoaquo species whose formation competes with isomerization in a bond-rupture process. Some cobalt(II) was evident in the reactions in alcohols, particularly in the most reducing alcohol, methanol.

The significant result here is the variation in the rates of reaction and formation of the three geometric isomers. If intramolecular mechanisms may be assumed for these processes, this observation is consistent with the reactions proceeding through three (rather than two) intramolecular pathways.

From the relative N–H exchange rates in the three isomers (given earlier), the deprotonated (at *sec*-N) *mer* species would be the most rapidly formed and would be in the greatest concentration. This probably accounts for the *mer* complex isomerizing the most rapidly and the equilibrium proportion of this isomer being attained relatively quickly.

The experimental observations on the homogeneous Co(dien)(medien)$^{3+}$ isomerizations have not allowed a decision between the twist and bond-rupture intramolecular mechanisms. However the bond-rupture route for these reactions of cobalt(III)–amine complexes is supported by the following facts: (1) decomposition of $Co(dien)_2^{3+}$ and *s-fac*-$Co(medien)_2^{3+}$ complexes in alkali at 80 °C; (2) the presence of $[Co(dien)_2OH_2]^{3+}$ or $[Co(dien)_2OH]^{2+}$ in the reaction products in small amounts; (3) a recently observed reaction of the same type with *u-fac*-$[Co(NH_2CH_2CH_2CH_2SCH_2CH_2NH_2)_2]^{3+}$ which with alkali gives $[Co(NH_2CH_2CH_2CH_2SCH_2CH_2NH_2)_2OH]^{2+}$.[34] All the data for the homogeneous systems can be rationalized by transient five-coordinate intermediates rearranging. If the twisting hypothesis is adopted the $[Co(dien)_2OH]^{2+}$ product and the decomposition have to be produced by an independent path. On the basis of the "principle of parsimony" we prefer the former analysis.

Charcoal-Catalyzed Equilibrations of Cobalt(III)–Amine Complexes, and the Catalyzed and Uncatalyzed Racemization of $Co(en)_3^{3+}$. The catalytic effect of charcoal in promoting equilibrations of cobalt(III)–amine complexes has been widely attested, but uncertainty remains as to the mechanism involved.[3b,35] Most of the kinetic and mechanistic studies have been on the racemizations of $Co(en)_3^{3+}$ salts, and since $Co(en)_3^{3+}$ and the Co(dien)(medien)$^{3+}$ isomers are all CoN_6^{3+} complexes with five-membered saturated rings, similar mechanistic features might reasonably by expected for the isomerization reactions in these two systems.

Dwyer and Sargeson demonstrated the involvement of cobalt(II) in the catalyzed racemization of $[Co(en)_3]Cl_3$ (~0.06 M complex in water)[36] and proposed[22,36] that the catalytic equilibration and racemization reactions of cobalt(III) complexes occur by two routes: (1) labilization through a high-spin activated state of cobalt(III), one suggested role of the carbon being to catalyze the conversion of a small amount of spin-paired cobalt(III) to the activated spin-free state (rearrangements and ligand dissociation would be facilitated); (2) rapid electron-transfer, charcoal catalyzed, between labile cobalt(II) species—generated by charcoal reduction of the activated high-spin cobalt(III) arising by (1)—and high-spin cobalt(III).

It has been shown subsequently[37] that with $Co(pn)_3^{3+}$[15] isomers on charcoal $\Delta \rightleftharpoons \Lambda$ interconversions occur much more rapidly than ligand exchange. In these interconversions, the major role of the charcoal thus appears to be catalysis of intramolecular processes.

Mureinik and Spiro have recently shown that in more dilute solutions (~0.002 M $[Co(en)_3]I_3$ in water) a different mechanism, which does not involve a cobalt(II) intermediate, must obtain.[35] The deduced third-order rate law implied that the reaction proceeded by interaction on the carbon surface between two adsorbed $Co(en)_3^{3+}$ ions and one adsorbed iodide. The halide apparently played a crucial although undefined role, since the perchlorate salt did not racemize at all on charcoal under similar conditions.

The mechanism for the disproportionations of the isomers of $[Co(dien)(medien)](ClO_4)_3$ over charcoal to give $Co(dien)_2^{3+}$ and $Co(medien)_2^{3+}$ clearly must involve complete dissociations of ligands, and any charcoal catalysis of intramolecular processes is obscured. In comparison with Mureinik and Spiro's work, it is significant that our present results were obtained using perchlorate salts, so that we tested the effect of our charcoal on (+)-$[Co(en)_3](ClO_4)_3$. Under a particular set of conditions (concentration, amount of charcoal, and time) in neutral water at 19 °C little if any racemization of (+)-$[Co(en)_3](ClO_4)_3$ nor of (+)-$[Co(en)_3]I_3$ was evident (percent decrease in optical rotation approximately equals decrease in visible absorption). However under similar conditions in 0.01 M sodium hydroxide we found that substantial racemization of (+)-$[Co(en)_3](ClO_4)_3$ occurred. Clearly the effects of added bases on this catalyzed reaction merit further attention.[38]

It appears therefore that different mechanisms dominate for charcoal-catalyzed equilibrations under different conditions of complex concentration. The concentrations (usually ~0.08 M) employed in our present charcoal-catalyzed isomerizations of $[Co(dien)(medien)](ClO_4)_3$ were comparable with those in Dwyer and Sargeson's work,[36] and we prefer to interpret our charcoal-catalyzed reactions as occurring essentially by electron transfer between the cobalt(III) complexes and labile cobalt(II) (both the proposed steps (1) and (2) outlined above). Our observations of significant amounts of cobalt(II) being formed in the Co(dien)(medien)$^{3+}$ reactions accords with observations on other cobalt(III) complex systems with charcoal.[22,35,36]

For the isomerization of Co(dien)(medien)$^{3+}$ in homogeneous alkaline solution, the rearrangement process might require the complex to be in an activated state as proposed

in process (1) above for the catalyzed isomerizations of cobalt(III)–amine complexes. In the homogeneous conditions the activated high-spin state of the deprotonated cobalt(III) could be attained thermally.[39] In contrast, (+)-$[Co(en)_3]^{3+}$ salts are highly optically stable, undergoing no change in neutral water (nor in dilute acid) even at 100 °C.[22,35,36,38,40] However the difference may well be associated with the higher acidities of the Co(dien)(medien)$^{3+}$ isomers due to the coordinated secondary amines, whereas (+)-$[Co(en)_3]^{3+}$ has only coordinated primary amines as sites for deprotonation.

In homogeneous solution in the presence of added $[Co(en)_3]Cl_2$ and ethylenediamine, racemization of (+)-$[Co(en)_3]Cl_3$ occurs by a second pathway in addition to the slow electron-transfer reaction.[23] The rates closely fit the proposed two-term rate law $R = k[Co(III)][Co(II)] + k'[Co(III)][en]$, and the second term has been attributed to the formation of a seven- or eight-covalent intermediate between the complex and ethylenediamine.[22,23,36,38] In the light of our finding that the rates of the homogeneous isomerizations of $[Co(dien)_2](CH_3COO)_3$ and $[Co(dien)(medien)](ClO_4)_3$ are enhanced by added base, it now seems possible that the ethylenediamine functioned as a base to abstract a proton from the thermally activated $Co(en)_3^{3+}$ species in the second pathway, so that the mechanism could be S_N1CB as with Co(dien)(medien)$^{3+}$.

Experimental Section

The complex *s-fac*-$[Co(dien)(medien)](ClO_4)_3$ was obtained from reaction of $[Co(NH_3)_5Cl]Cl_2$ with dien and medien.[16] The details of its isolation along with other products from this reaction will be described in a subsequent article.

Reactions of *s-fac*- and *u-fac*-[Co(dien)(medien)]$(ClO_4)_3$ Isomers on Charcoal. A solution of *s-fac*-$[Co(dien)(medien)](ClO_4)_3$ (0.60 g) in water (12 mL) was stirred with charcoal (0.20 g of freshly ground BDH granulated charcoal for gas absorption) in a 50-mL stoppered flask with an oxygen atmosphere and maintained at 80 °C in an oil bath. Samples (~1 mL) were removed, and the charcoal was immediately filtered off, at five different times from 4 to 48 h. These solutions were chromatographed on columns (1.2 × 40 cm) of SP-Sephadex C-25 cation-exchange resin, Na^+ form, with 0.1 M Na_3PO_4 when five clear yellow or orange bands separated (Figure 3B). The chromatographed patterns on the five columns appeared all identical. The five band effluents were collected separately and made up to standard volumes with water, and the cobalt concentrations were determined on a Varian-Techtron Model 1200 atomic absorption spectrophotometer using the emission line 240.7 nm. Values obtained for the bands (in order of their elution) from one particular aliquot were as follows: *s-fac*-$[Co(dien)_2]^{3+}$ in 25 mL, 11.6 ppm; *u-fac*-[Co(dien)(medien)]$^{3+}$ in 25 mL, 8.3 ppm; *s-fac*-[Co(dien)(medien)]$^{3+}$ + *u-fac*-$[Co(dien)_2]^{3+}$ in 200 mL, 12.8 ppm; *mer*-$[Co(dien)_2]^{3+}$ in 100 mL, 11.3 ppm; *s-fac*-$[Co(medien)_2]^{3+}$ in 100 mL, 15.6 ppm. Mean values of the cobalt ratios in the five bands, from the five separations, were (5 ± 1):(4 ± 1):(46 ± 2):(19 ± 1):(26 ± 2), respectively. The separation of the complexes *s-fac*-[Co(dien)(medien)]$^{3+}$ and *u-fac*-$[Co(dien)_2]^{3+}$ within the one band was sufficient to gauge visually that these complexes were present in roughly comparable amounts (Figure 3B), so that the molar proportions of the six complexes (in order of their elution) were 5:4:~23:~23:19:26.

u-fac-$[Co(dien)(medien)](ClO_4)_3$ was similarly equilibrated (0.10 g in 10 mL of water) over charcoal (0.04 g) for 2 days at 80 °C. Sephadex chromatography then gave a pattern of bands apparently identical in every respect (visual comparison) with the pattern starting from the corresponding *s-fac* isomer above.

Reactions of *s-fac*-and *u-fac*-[Co(dien)(medien)]$(ClO_4)_3$ Isomers in Homogeneous Solution. In test reactions, solutions of 1.00 g of *s-fac*-$[Co(dien)(medien)](ClO_4)_3$ in 20 mL of water, 0.01 M $HClO_4$, or buffer solution (0.05 M 2,4,6-trimethylpyridine–perchloric acid adjusted to pH 8.0 at 25 °C),[32] in stoppered flasks were maintained at 90 °C in an oil bath. At appropriate times, samples (~1 mL) were taken and applied directly to columns (1.2 × 40 cm) of Sephadex cation-exchange resin. On elution with 0.1 M Na_3PO_4 three bands separated as in Figure 3A from the reactions in water or buffer, but only the single band of *s-fac* was obtained from the reaction in $HClO_4$.

The effect of acid on isomerization of *u-fac*-$[Co(dien)(medien)](ClO_4)_3$ was determined by chromatographing samples from two small-scale reactions, 0.10 g of complex in 4 mL of 0.01 M $HClO_4$ or buffer solution, run concurrently at 90 °C for 2.5 days.

The determination of the equilibrium proportions of the three Co(dien)(medien)$^{3+}$ isomers was carried out on separate reactions of the *s-fac* and *u-fac* perchlorates in the buffer solution (1.00 g in 20 ml) run concurrently at 90 °C. After 3 days, samples from each reaction were chromatographed in duplicate. The three effluents containing the separated isomers from each column were collected and made up to appropriate standard volumes (*s-fac* to 250 mL, *u-fac* and *mer* each to 25 mL), and the cobalt concentrations were determined by atomic absorption. A typical result was *s-fac* 9.9 ppm, *u-fac* 11.9 ppm, and *mer* 11.3 ppm, from where the proportions follow as 81:10:9, respectively. Remaining solutions were combined and worked up for isolation of the three isomers as described below.

On a preparative scale *s-fac*-$[Co(dien)(medien)](ClO_4)_3$ (2.055 g) in the buffer solution (40 mL) was reacted at 90 °C as above. After 3 days the now orange solution was diluted (200 mL) and applied to a large Sephadex column (4.5 × 44 cm), which was then eluted with 0.1 M Na_3PO_4. The separate effluents of the three isomers were diluted threefold and adsorbed on appropriately sized columns of BIO-REX 70 weak-acid cation-exchange resin, 50–100 mesh, Li^+ form (column sizes 3 cm diameter × 2 cm for *s-fac*, 1.2 cm × 3 cm for *u-fac* and *mer*). After washing the columns with water, the complexes were eluted off with 0.1 M $HClO_4$. These effluents were evaporated to dryness or sludge on a rotary evaporator, ethanol was added, and the flasks were cooled at 0 °C. The ethanol (containing $NaClO_4$) was sucked off and each crystalline product was suspended in fresh ethanol. The ethanol suspensions of the orange *u-fac* and *mer* perchlorates were transferred to weighing bottles, most of the ethanol was sucked off, and the remaining ethanol was then removed in a vacuum desiccator. The yellow *s-fac* product was filtered off and washed with ethanol, and finally all three products were dried at 70 °C to constant weight. Amounts of the $[Co(dien)(medien)](ClO_4)_3$ isomers obtained were *s-fac* 1.556 g, *u-fac* 0.183 g, and *mer* 0.192 g, representing 94.0% recovery, and giving *s-fac*:*u-fac*:*mer* = 81:9:10 in satisfactory agreement with the proportions determined above.

Anal. Calcd for $[Co(C_4H_{13}N_3)(C_5H_{15}N_3)](ClO_4)_3$: C, 18.7; H, 4.9; N, 14.6; Cl, 18.4; $(N)CH_3$, 2.6. Found for *u-fac*: C, 18.2; H, 4.8; N, 14.8; Cl, 18.3; $(N)CH_3$, 3.1. Found for *mer*: C, 18.3; H, 4.8; N, 14.3; Cl, 18.7.

The ^{13}C NMR spectra of the $[Co(dien)(medien)](ClO_4)_3$ isomers in D_2O were obtained as described previously.[16] The methyl carbon resonances were identified by rerunning the spectra under off-resonance proton-decoupled conditions when methylene carbon resonances appeared as triplets (centered at the broad-band proton-decoupled single frequencies) and methyl carbons gave quartets. Chemical shifts δ, from $SiMe_4$, for the isomers of $[Co(dien)(medien)](ClO_4)_3$ isolated from the isomerization of the *s-fac* perchlorate in aqueous buffer solution at 90 °C are as follows: *s-fac* 65.7, 56.3, 52.7 (methyl), 43.9, 43.0 (these are almost identical with those reported previously[16] for the chloride salt); *u-fac* 65.4, 64.5, 56.7, 56.1, 51.7 (methyl), 45.5, 44.2, 43.5, 41.9; *mer* 62.8, 52.2, 51.3, 47.2 (methyl), 47.0, 46.5, 45.1. The number of scans accumulated for *u-fac* and *mer* were 63 000 for 0.10 g in 2 mL of D_2O, and for *s-fac*, 10 600 scans for 0.20 g.

$[Co(dien)_2](CH_3COO)_3$ Isomers. These were obtained by shaking the separated isomers of $[Co(dien)_2]Br_3$[33] with stoichiometric silver acetate in methanol solution, filtering, and evaporating the filtrates to dryness. The hygroscopic acetate salts were stored in a desiccator.

Registry No. *u-fac*-$[Co(dien)(medien)](ClO_4)_3$, 67049-22-3; *mer*-$[Co(dien)(medien)](ClO_4)_3$, 65608-69-7; *s-fac*-$[Co(dien)(medien)](ClO_4)_3$, 63566-67-6; $Co(dien)_2^{3+}$, 18703-28-1.

References and Notes

(1) N. Serpone and D. G. Bickley, *Prog. Inorg. Chem.*, 17, 391 (1972).
(2) R. H. Holm in "Dynamic Nuclear Magnetic Resonance Spectroscopy", L. M. Jackman and F. A. Cotton, Ed., Academic Press, New York, N.Y., 1975, pp 317–376.
(3) F. Basolo and R. G. Pearson, "Mechanisms of Inorganic Reactions", 2nd ed, Wiley, New York, N.Y., 1967: (a) p 316; (b) pp 330–332.
(4) P. C. Ray and N. K. Dutt, *J. Indian Chem. Soc.*, 20, 81 (1943).
(5) W. G. Gehman, Ph.D. Thesis, Pennsylvania State University, 1954; L. Seiden, Ph.D. Thesis, Northwestern University, 1957; J. C. Bailar, *J. Inorg. Nucl. Chem.*, 8, 165 (1958).
(6) C. S. Springer and R. E. Sievers, *Inorg. Chem.*, 6, 852 (1967).
(7) J. E. Brady, *Inorg. Chem.*, 8, 1208 (1969).
(8) J. J. Fortman and R. E. Sievers, *Coord. Chem. Rev.*, 6, 331 (1971).

(9) H. Fischer, E. O. Fischer, and H. Werner, *J. Organomet. Chem.*, 73, 331 (1974).
(10) S. S. Eaton, J. R. Hutchinson, R. H. Holm, and E. L. Muetterties, *J. Am. Chem. Soc.*, 94, 6411 (1972).
(11) S. S. Eaton, G. R. Eaton, R. H. Holm, and E. L. Muetterties, *J. Am. Chem. Soc.*, 95, 1116 (1973).
(12) D. J. Duffy and L. H. Pignolet, *Inorg. Chem.*, 11, 2843 (1972).
(13) D. J. Duffy and L. H. Pignolet, *Inorg. Chem.*, 13, 2045 (1974).
(14) G. A. Lawrance and D. R. Stranks, *Inorg. Chem.*, 16, 929 (1977).
(15) Abbreviations used: phen = 1,10-phenanthroline; bpy = 2,2′-bipyridyl; ox = oxalate; dien = diethylenetriamine = H_2N–CH_2CH_2–$NHCH_2$-CH_2–NH_2; medien = 4-methyldiethylenetriamine = 2,2′-methyliminobis(ethylamine) = H_2N–CH_2CH_2–NMe–CH_2CH_2–NH_2; en = ethylenediamine; pn = propane-1,2-diamine; trenen = 4-(aminoethyl)-1,4,7,10-tetraazadecane; cyclam = 1,4,8,11-tetraazacyclotetradecane; edta = ethylenediaminetetraacetato.
(16) G. H. Searle, S. F. Lincoln, F. R. Keene, S. G. Teague, and D. G. Rowe, *Aust. J. Chem.*, 30, 1221 (1977).
(17) G. H. Searle, *Aust. J. Chem.*, 30, 2625 (1977).
(18) F. R. Keene and G. H. Searle, *Inorg. Chem.*, 13, 2173 (1974).
(19) G. H. Searle, S. F. Lincoln, F. R. Keene, S. G. Teague, and D. G. Rowe, unpublished work.
(20) R. D. Gillard, *J. Chem. Soc. A*, 917 (1967).
(21) F. P. Dwyer and A. M. Sargeson, *J. Am. Chem. Soc.*, 81, 5269 (1959).
(22) F. P. Dwyer in "Advances in the Chemistry of the Coordination Compounds", S. Kirschner, Ed., Macmillan, New York, N.Y., 1961, p 21.
(23) F. P. Dwyer and A. M. Sargeson, *J. Phys. Chem.*, 65, 1892 (1961).
(24) M. Eigen, *Angew. Chem., Int. Ed., Engl.*, 3, 1 (1964).
(25) E. Grunwald and E. K. Ralph, *Acc. Chem. Res.*, 4, 107 (1971).
(26) D. A. Buckingham, P. A. Marzilli, and A. M. Sargeson, *Inorg. Chem.*, 8, 1595 (1969).
(27) Y. Yoshikawa and K. Yamasaki, *Bull. Chem. Soc. Jpn.*, 45, 179 (1972).
(28) F. R. Keene, Ph.D. Thesis, University of Adelaide, 1972, pp 143, 167.
(29) G. H. Searle and F. R. Keene, *Inorg. Chem.*, 11, 1006 (1972).
(30) C. K. Poon and M. L. Tobe, *Inorg. Chem.*, 7, 2398 (1968). The gross mechanism for the base-catalyzed isomerization *cis* ⇌ *trans*-$[Co(cyclam)(OH_2)_2]^{3+}$ was intermolecular involving attack of water and not intramolecular.
(31) D. W. Cooke, Y. A. Im, and D. H. Busch, *Inorg. Chem.*, 1, 13 (1962).
(32) R. M. C. Dawson, D. C. Elliott, W. H. Elliott, and K. M. Jones, "Data for Biochemical Research", 2nd ed, Oxford University Press, London, 1969, p 491.
(33) F. R. Keene and G. H. Searle, *Inorg. Chem.*, 11, 148 (1972).
(34) E. Larsen, private communication.
(35) R. J. Mureinik and M. Spiro, *J. Chem. Soc., Dalton Trans.*, 2480, 2493 (1974).
(36) F. P. Dwyer and A. M. Sargeson, *Nature (London)*, 187, 1022 (1960).
(37) S. E. Harnung, S. Kallesoe, A. M. Sargeson, and C. E. Schaffer, *Acta Chem. Scand., Ser. A*, 28, 385 (1974).
(38) W. H. Gehman and W. C. Fernelius, *J. Inorg. Nucl. Chem.*, 9, 71 (1959).
(39) D. Sen and W. C. Fernelius, *J. Inorg. Nucl. Chem.*, 10, 269 (1959).
(40) B. E. Douglas, *J. Am. Chem. Soc.*, 76, 1020 (1954).

[Reprinted from Inorganic Chemistry, 17, 2847 (1978.)]

Contribution from the Department of Inorganic Chemistry, University of Melbourne, Parkville 3052, Victoria, Australia, and Department of Physical and Inorganic Chemistry, University of Adelaide, Adelaide 5001, South Australia, Australia

Polarographic Studies of the Geometric Isomers of the Bis(diethylenetriamine)cobalt(III) and -cobalt(II) Cations in Acetone

A. M. BOND,*[1,2] F. R. KEENE,[1] N. W. RUMBLE,[1] G. H. SEARLE,[3] and M. R. SNOW[3]

Received May 18, 1978

Extensive studies have been made previously on the kinetically inert geometric isomers of $[Co^{III}(dien)_2]^{3+}$ (dien = the tridentate ligand diethylenetriamine); however, virtually no information has been available on the corresponding isomers of $[Co^{II}(dien)_2]^{2+}$. Electrochemical reduction of the cobalt(III) complexes has been studied by dc polarography, differential pulse polarography, cyclic voltammetry, and controlled-potential electrolysis. Results have enabled equilibrium constants for the redox and isomer distribution to be calculated. Two reduction waves are found for each of the meridional (*mer*), symmetrical facial (*s-fac*), and unsymmetrical facial (*u-fac*) isomers. The step (*mer*, *u-fac*, *s-fac*) $[Co^{III}(dien)_2]^{3+} + e^- \rightleftharpoons$ (*mer*, *u-fac*, *s-fac*) $[Co^{II}(dien)_2]^{2+}$ occurs with retention of geometry on the electrochemical time scale. With respect to redox behavior, the *s-fac*-$[Co^{III}(dien)_2]^{3+}$ species is the hardest to reduce and the *mer*-$[Co^{II}(dien)_2]^{2+}$ cation is the hardest to oxidize. In oxidation state II the complexes are kinetically labile and under conditions of controlled-potential electrolysis, the thermodynamically favored *mer*-$[Co^{II}(dien)_2]^{2+}$ species is the only species found. Calculations suggest that compared with oxidation state III, the stability of the meridional form is considerably enhanced with respect to the facial isomers. On further reduction no cobalt(I) complexes are found and a two-electron step leading to formation of cobalt metal occurs: (*mer*, *u-fac*, *s-fac*) $[Co^{II}(dien)_2]^{2+} + 2e^- \rightarrow Co + 2dien$. With the N-methylated complex $[Co^{III}(medien)_2]^{3+}$ (medien = $NH_2CH_2CH_2N(CH_3)CH_2CH_2NH_2$) stabilization of the *s-fac* isomer is enhanced remarkably and it is the only isomer detected in either oxidation state III or II.

Introduction

Isomerism in complexes of the type $[Co^{III}(dien)_2]^{3+}$ (dien = the tridentate ligand diethylenetriamine) has been studied extensively since Mann[4] first isolated the complex cation as the iodide salt.

The geometric isomers shown in Figure 1 may be designated in terms of the facial or meridional arrangement of the ligands. An additional specification *u-fac* (unsymmetrical) and *s-fac*

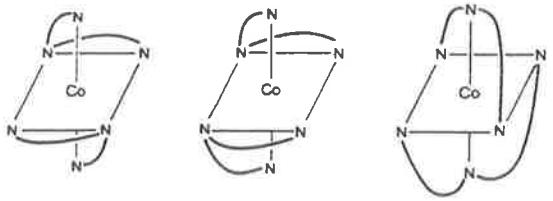

Figure 1. Geometric isomers of $[Co(dien)_2]^{2+|3+}$: left, *s-fac*; center, *u-fac*; right, *mer*.

(symmetrical) is necessary to distinguish the two facial forms. The *u-fac* and *mer* isomers have only a twofold rotation axis and can therefore also exhibit optical isomerism. Keene and Searle[5] have separated the three geometric isomers and resolved the *u-fac* and *mer* forms into optical isomers; characterization of the isomers was made from IR, NMR, and optical rotation measurements followed by chromatographic separation of the Co(III) species and spectrophotometric estimation of the relative proportions of the isomers. In a subsequent study[6] the same authors examined the factors which influence the equilibrium isomer proportions of the cobalt(III) complexes and compared the experimental data with predictions from energy-minimized conformational analysis calculations. In these investigations equilibrium proportions of the three geometric isomers of $[Co(dien)_2]^{3+}$ were generally determined from aerial oxidation of cobalt(II) salts under various conditions.

Thus, while it is apparent that considerable information is available on the $[Co^{III}(dien)_2]^{3+}$ cation, virtually no data are available on the corresponding isostructural Co(II) complexes which presumably are implicated as intermediates in the aerial oxidation studies to produce the kinetically inert $[Co^{III}(dien)_2]^{3+}$ complexes in their various isomeric forms. Since $[Co^{II}(dien)_2]^{2+}$ itself must exhibit the same isomeric forms as the well-documented Co(III) system and in this oxidation state cobalt is generally kinetically labile, the thermodynamically favored situation should be reached readily. Thus in principle equilibrium data should be easier to obtain than for the inert Co(III) cation where lengthy periods and/or addition of catalysts are required to reach the equilibrium values.

Electrochemical investigations in these laboratories of isomerization in a range of carbonyl complexes[7-9] has shown that extensive thermodynamic and kinetic data can be obtained for the isomers in different oxidation states. Since the $[Co^{III}(dien)_2]^{3+}$ geometric isomers can all be isolated in a pure form and they are known to be kinetically inert, the possibility of reducing each of them to the kinetically labile cobalt(II) state exists. Monitoring of reaction pathways following reduction should provide unambiguous data as to the thermodynamic stability of oxidation state II $[Co^{II}(dien)_2]^{2+}$ cations. Using the usual thermodynamic cycles, data applicable to both the Co(II) and Co(III) systems are therefore also easily generated. The present paper describes an investigation of the geometric isomerization of $[Co^{III}(dien)_2]^{3+}$ and $[Co^{II}(dien)_2]^{2+}$ complexes using predominantly the techniques of dc and differential pulse polarography, cyclic voltammetry, and controlled-potential electrolysis. A nonaqueous solvent, acetone, was chosen as the medium in which to carry out the investigations since all cobalt(III) and cobalt(II) complexes are soluble with the cobalt(II) complexes being stable under an inert atmosphere of nitrogen. Previous work by Sherwood and Laitinen[10] on this system has been undertaken in aqueous media and in the presence of excess dien, but the isomeric distribution was not considered in the interpretation or results.

Experimental Section

Preparations and Instrumentation. The geometric isomers of $[Co(dien)_2]^{3+}$ were prepared as their perchlorate salts using the method of Keene and Searle.[5,6] The electrolyte used for all experiments was 0.1 M tetrabutylammonium hexafluorophosphate (Bu_4NPF_6) dissolved in acetone. All solutions were degassed with nitrogen at 20 ± 1 °C prior to undertaking any measurements.

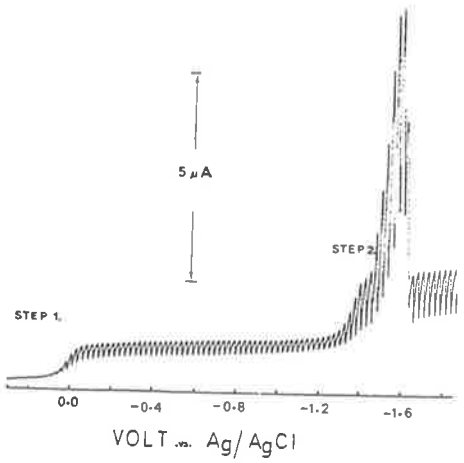

Figure 2. Dc polarogram of a 5×10^{-4} M solution of *mer*-$[Co^{III}(dien)_2](ClO_4)_3$ in acetone (0.1 M Bu_4NPF_6). Drop time = 0.5 s.

For dc and differential pulse measurements a mechanically controlled mercury drop time of 0.5 or 1.0 s was usually employed. The reference electrode was Ag|AgCl (saturated LiCl; acetone) separated from the test solution by a salt bridge containing the supporting electrolyte solution, and the auxiliary electrode was a platinum wire. For cyclic voltammetry, the scan at a rate of 500 mV/s was commenced 1 s after the commencement of the drop life. Polarographic data were obtained with a Princeton Applied Research (PAR) Corp. Model 174 polarographic analyzer.

Controlled-potential electrolysis was achieved using a PAR Model 173 potentiostat|galvanostat at a mercury pool electrode. The reference electrode was the same as used for the polarography, but the auxiliary electrode was made from platinum gauze and separated from the test solution by a salt bridge constructed from porous Vycor sinters and filled with supporting electrolyte solution. Coulometric data were obtained from the controlled-potential electrolysis experiments using a PAR Model 179 digital coulometer.

Determination of the Charcoal-Catalyzed Equilibration of the Isomers of $[Co(dien)_2]^{3+}$ in Acetone Solution. $Co(ClO_4)_2 \cdot 6H_2O$ (0.37 g, 10^{-3} mol) was dissolved in acetone (100 mL, AR), and water molecules of hydration were removed by drying the solution over molecular sieves (4-Å) for several hours. This solution was then added to another solution in acetone (200 mL) of dien (0.18 g, 1.67×10^{-3} mol), dien·3$HClO_4$ (0.14 g, 0.33×10^{-3} mol), activated charcoal (5 g), and Bu_4NPF_6 (15.7 g, 0.04 mol), and the total volume of the solution was made up to 400 mL with acetone. The mixture was aerated for 36 h, the charcoal removed by filtration, and the filtrate evaporated to near dryness (rotary evaporator). The residue was extracted with water (1 L) to remove the $[Co(dien)_2]^{3+}$ species from the sparingly soluble Bu_4NPF_6, and the filtered aqueous solution was applied to a column of SP-Sephadex C-25 cation exchanger and eluted with 0.5 M $NaClO_4$. After the removal of several brown and orange bands from the column, the slowest moving band (yellow) was collected, diluted with water, and reapplied to the column. Elution with 0.3 M sodium (+)-tartrate solution resulted in the separation of $[Co(dien)_2]^{3+}$ into its three isomers, which were collected and estimated spectrometrically as described previously.[6] The percentage figures are each considered accurate to ±1.

Results and Discussion

Figure 2 is a dc polarogram of *mer*-$[Co^{III}(dien)_2]^{3+}$ in acetone. Two reduction waves are seen. Step 1 corresponds to the one-electron reduction $Co(III) + e^- \rightleftharpoons Co(II)$ and is extremely well defined. The limiting current of this step is diffusion controlled. The second step contains an extremely pronounced maximum, but on reaching the limiting current region a well-defined diffusion-controlled plateau is obtained. The limiting current for the second wave is exactly twice that

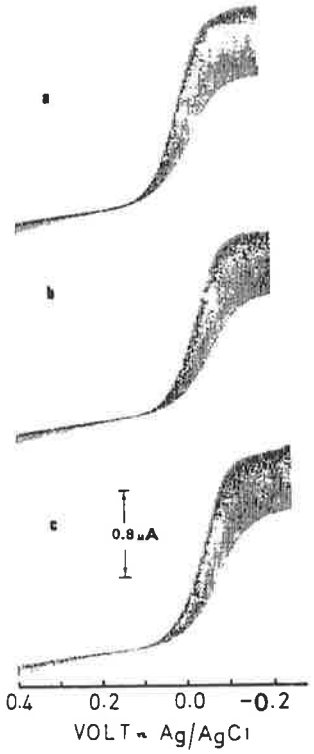

Figure 3. Expanded scale dc polarograms of the first reduction wave of 5×10^{-4} M solutions of (a) *mer*-$[Co^{III}(dien)_2](ClO_4)_3$, (b) *u-fac*-$[Co^{III}(dien)_2](ClO_4)_3$, and (c) *s-fac*-$[Co^{III}(dien)_2](ClO_4)_3$ in acetone (0.1 M Bu_4NPF_6). Drop time = 0.5 s.

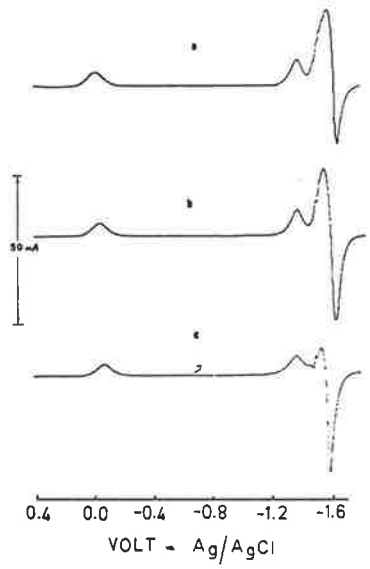

Figure 4. Differential pulse polarograms of 5×10^{-4} M solutions of (a) *mer*-$[Co^{III}(dien)_2](ClO_4)_3$, (b) *s-fac*-$[Co^{III}(dien)_2](ClO_4)_3$, and (c) *u-fac*-$[Co^{III}(dien)_2](ClO_4)_3$ in acetone (0.1 M Bu_4NPF_6). Drop time = 0.5 s, scan rate = 5 mV/s, and pulse amplitude = −25 mV.

for step 1 and is assigned to an overall two-electron step Co(II) + $2e^- \rightarrow$ Co(0).

Figure 3 displays the first Co(III)|Co(II) dc polarographic reduction step for the three geometric isomers. All three complexes are characterized by the same two-electrode processes. However, the first reduction step clearly occurs at different potentials with the *mer* complex being easiest to reduce and the *s-fac* the most difficult. Some differences in shape are also found for the more negative electrode process which includes the maximum. The amplitude and shape of the maxima were in fact found to be extremely oxygen dependent indicating that the $[Co^{II}(dien)_2]^{2+}$ species is air sensitive and reacts with oxygen on the polarographic time scale. Relevant dc polarographic data are contained in Table I.

Table I. Dc Polarographic Data for Reduction of Isomers of $[Co^{III}(dien)_2]^{3+}$ in acetone (0.1 M Bu_4NPF_6) at 20 °C

isomer	$E_{1/2}$ (V vs. Ag|AgCl) Co(III) + $e^- \rightleftharpoons$ Co(II)	$E_{1/2}$ (V vs. Ag|AgCl) Co(II) + $2e^- \rightarrow$ Co(0)
mer	+0.030	−1.350
u-fac	−0.015	−1.352
s-fac	−0.035	−1.345

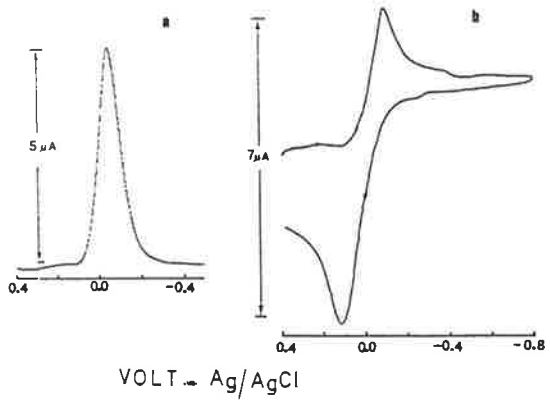

Figure 5. (a) Expanded scale differential pulse polarogram of the first reduction wave for a 5×10^{-4} M solution *u-fac*-$[Co^{III}(dien)_2](ClO_4)_3$ in acetone (0.1 M Bu_4NPF_6). Drop time = 1 s, scan rate = 5 mV/s, and pulse amplitude = −25 mV. (b) Cyclic voltammogram at a dropping mercury electrode of the same solution using a scan rate of 500 mV/s.

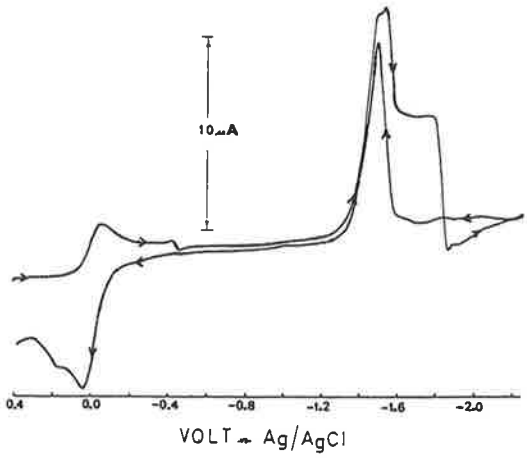

Figure 6. Cyclic voltammogram at a dropping mercury electrode of a 5×10^{-4} M solution of *mer*-$[Co^{III}(dien)_2](ClO_4)_3$ in acetone (0.1 M Bu_4NPF_6). Scan rate = 500 mV/s.

Figure 4 shows a comparison of the differential pulse polarograms for the three complexes. In the region where a sharp maximum is found in the dc polarograms, a region of negative current is found in the differential pulse curves. However, the *s-fac* complex has a markedly different shape in the second wave compared with the other isomers. The shapes of the differential pulse curves for the first wave were similar for each isomer, and the *u-fac* isomer is represented in Figure 5. Also included in Figure 5 is a cyclic voltammogram of the first reduction wave which indicates a considerable degree of chemical reversibility. Figure 6 illustrates an unusual occurrence in cyclic voltammetry where positive currents are

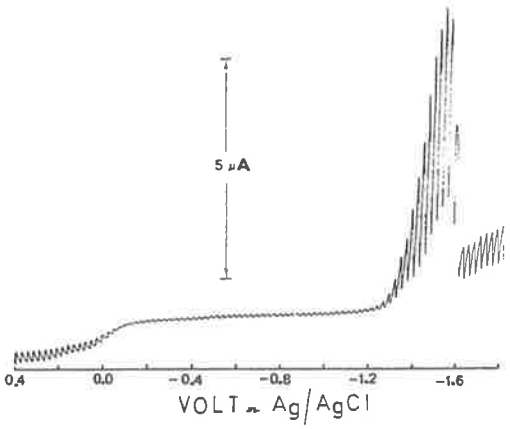

Figure 7. Dc polarogram of electrolysis products after a one-electron reduction of 5×10^{-4} M *s-fac*-$[Co^{III}(dien)_2](ClO_4)_3$ in acetone (0.1 M Bu_4NPF_6). Drop time = 0.5 s.

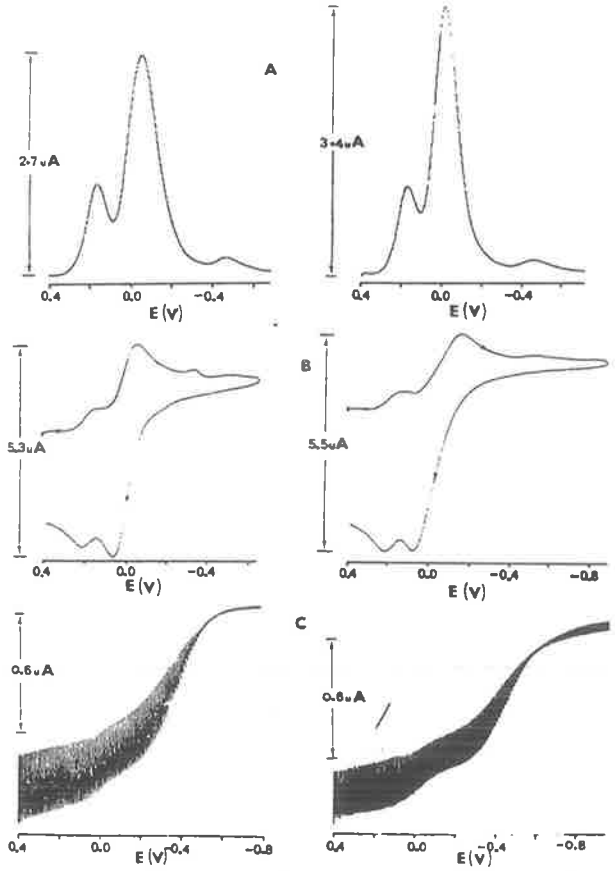

Figure 8. Voltammograms of electrolysis products resulting from one-electron reductions of 5×10^{-4} M solutions of *mer*-$[Co^{III}(dien)_2](ClO_4)_3$ (left) and *s-fac*-$[Co^{III}(dien)_2](ClO_4)_3$ (right): (A) differential pulse polarograms recorded using a scan rate of 5 mV/s, a drop time of 0.5 s, and a pulse amplitude of −25 mV; (B) cyclic voltammograms at a dropping mercury electrode using a scan rate of 500 mV/s; (C) dc polarograms recorded using a drop time of 0.5 s. All potentials are vs. the Ag|AgCl reference electrode.

obtained in both the forward and reverse sweep directions for the second step. Similar behavior was observed for all geometric isomers.

Controlled-potential electrolysis coupled with coulometry gave an n value of 1.00 ± 0.02 for the number of electrons transferred in the first reduction step for all isomers. An n value of 2.0 ± 0.1 was found for the second process confirming

Table II. Dc Polarographic Data for Electrolysis Products following a One-Electron Reduction of $[Co^{III}(dien)_2]^{3+}$ in Acetone (0.1 M Bu_4NPF_6) at 20 °C

isomer	$E_{1/2}$ (V vs. Ag|AgCl) Co(II) ⇌ Co(III) + e⁻	$E_{1/2}$ (V vs. Ag|AgCl) Co(II) + 2e⁻ → Co(0)
mer	+0.032	−1.350
u-fac	+0.034	−1.367
s-fac	+0.037	−1.342

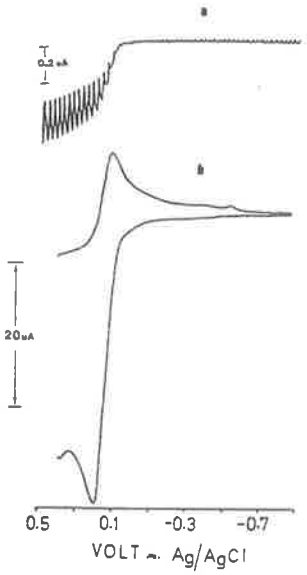

Figure 9. (a) Dc polarogram of 2.5×10^{-4} M dien in acetone (0.1 M Bu_4NPF_6), using a drop time of 0.5 s. (b) Cyclic voltammogram at a dropping mercury electrode of the same solution, using a scan rate of 500 mV/s.

the assignment of the two-electrode processes as Co(III) + e⁻ ⇌ Co(II) and Co(II) + 2e⁻ → Co(0), respectively. Polarographic monitoring of the products of electrolysis after a one-electron reduction of a 5×10^{-4} M *s-fac* solution at a potential between the two waves is shown in Figure 7. As would be expected for a chemically reversible system there is an oxidation wave corresponding to the Co(II)|Co(III) couple; however, the $E_{1/2}$ value for this wave is at a slightly more positive potential than observed for reduction of *s-fac* Co(III). In addition there is another oxidation wave, much smaller in magnitude at a slightly more positive potential than for oxidation of Co(II). This wave is just detectable in Figure 7 but quite distinct in Figure 8C. The *s-fac* electrolysis products also gave a reduction wave which showed the presence of the characteristic maxima associated with the two-electron reduction process Co(II) + 2e⁻ → Co(0). A comparison of results with those for a reduced solution of the *mer* Co(III) cation (Figure 8) shows dc and differential pulse polarograms and cyclic voltammograms are essentially identical except the magnitude of the more positive oxidation wave is less pronounced in the *mer* case. Reduction of the *u-fac* Co(III) complex produced polarograms which were also identical with those of the other reduced solutions with respect to the number of waves and their positions. After a three-electron step reduction, the only polarographic wave present was the oxidation step observed at the more positive potential after the one-electron reduction. Table II shows the relevant polarographic data after controlled-potential electrolysis experiments. These data should be compared with those in Table I.

A dc polarogram and cyclic voltammogram of the ligand (dien) is shown in Figure 9 along with curves obtained after the addition of mercuric nitrate (Figure 10). Clearly, from

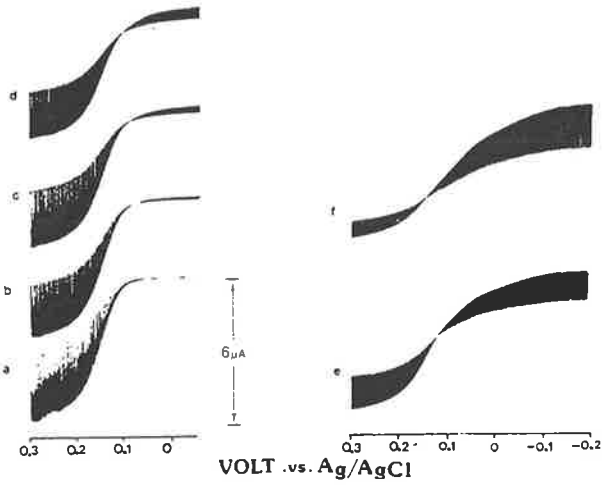

Figure 10. Dc polarograms illustrating the effect of progressively (a–f) adding mercuric nitrate to a 2.5×10^{-4} M solution of dien in acetone (0.1 M Bu_4NPF_6). Curve (a) represents the dien ligand in the absence of $Hg(NO_3)_2$.

the $E_{1/2}$ value and wave shape the additional oxidation wave obtained after the reduction of the cobalt complexes is the same as for this process, i.e., is that for the ligand. This wave is assigned to the overall electrode process of the kind

$$x\text{dien} + Hg \rightleftharpoons Hg(\text{dien})_x^{2+} + 2e^- \quad (1)$$

Roe et al.,[11] in a polarographic study of dien and mercuric complex formation, found that the bis- and tris(diethylenetriamine)mercury(II) complexes are the predominant species formed in aqueous media and that these complexes have extremely high stability constants. Therefore in eq 1, x is most likely to have the value 2 or 3. Controlled-potential electrolysis at a mercury electrode gave an n value of 1.00 ± 0.05 indicating that the bis complex is the major species formed.

Porzsolt et al.[12] also report the existence of highly stabilized complexes from reactions of $Hg(CN)_2$ with the dien ligand in aqueous media. A polarographic study by Porubsky[13] using ac techniques in aqueous media indicated stable Hg^{II}–dien complex formation with evidence of adsorption coupled to the charge-transfer step. Concentration dependence studies in acetone showed that maxima and other anomalous current–time behavior are produced at higher concentrations, and the process is complicated by adsorption. Electrocapillary curves confirmed that considerable adsorption of the neutral ligand and/or mercury complex occurs over a wide potential range. In view of the adsorption, the mechanism of the ligand wave is not completely certain but may occur via disproportionation of mercury(I) because the half-wave potential does not show

$$2\text{dien} + 2Hg \rightleftharpoons 2Hg(\text{dien})^+ + 2e^- \quad (2)$$

$$2Hg(\text{dien})^+ \rightleftharpoons Hg + Hg(\text{dien})_2^{2+} \quad (3)$$

the marked dependence on concentration predicted by eq 1 and the shape (at low concentrations) of the E vs. log $[(i_d - i)/i]$ plot has a slope close to that for a reversible one-electron step as required by eq 2. Some of the behavior at higher concentrations is consistent with the formation of $Hg_2(\text{dien})_2^{2+}$ at the electrode surface. Addition of mercury(I) nitrate to a solution of ligand also gave the same process as for mercury(II) nitrate as required by eq 2 and 3.

Plots of E vs. log $[(i_d - i)/i]$ for the one-electron reduction of the three cobalt(III) isomers were not completely linear but gave average gradients of 0.057 ± 0.005 V. These plots, other dc polarographic data, and results from differential pulse polarography and cyclic voltammetry indicate that the charge-transfer step is essentially reversible. However, a small amount of adsorption accompanies the charge transfer of the complexed ligand as is the case for the free ligand. Differential pulse polarograms are also consistent with some adsorption being coupled to the charge transfer and the complications reported in aqueous media[11] also appear to apply in acetone.

The electrochemical data obtained above demonstrate that on the polarographic time scale, isomerization of cobalt(II) does not occur. Thus the electrode processes may be described as

$$mer\text{-}[Co^{III}(\text{dien})_2]^{3+} + e^- \overset{\text{ads}}{\rightleftharpoons} mer\text{-}[Co^{II}(\text{dien})_2]^{2+} \quad (E_{1/2} = +0.030 \text{ V}) \quad (4)$$

$$u\text{-}fac\text{-}[Co^{III}(\text{dien})_2]^{3+} + e^- \overset{\text{ads}}{\rightleftharpoons} u\text{-}fac\text{-}[Co^{II}(\text{dien})_2]^{2+} \quad (E_{1/2} = -0.015 \text{ V}) \quad (5)$$

$$s\text{-}fac\text{-}[Co^{III}(\text{dien})_2]^{3+} + e^- \overset{\text{ads}}{\rightleftharpoons} s\text{-}fac\text{-}[Co^{II}(\text{dien})_2]^{2+} \quad (E_{1/2} = -0.035 \text{ V}) \quad (6)$$

The second step therefore corresponds to the reduction of the cobalt(II) isomer which is isostructural with the cobalt(III) starting material. No evidence of Co(I) is seen as an intermediate in the two-electron reduction and the ligand is released, so the product must be metallic cobalt. The overall process for step 2 is thus

$$(mer, s\text{-}fac, u\text{-}fac)\ [Co(\text{dien})_2]^{2+} + 2e^- \rightarrow Co + 2\text{dien} \quad (7)$$

Controlled-potential electrolysis experiments prove that the *mer* Co(II) complex is the complex obtained on the synthetic scale in about 10 min regardless of the starting material. The mechanism for generation of small amounts of dien in addition to the *mer*-$[Co^{II}(\text{dien})_2]^{2+}$ cation is not understood. This complex is extremely air sensitive and on aerial oxidation an unidentified cobalt(III) complex (oxo-bridged presumably) is formed. However, the oxygen reaction does not release ligand so air sensitivity is not the cause for ligand release. The adsorption process accompanying the charge transfer, which may be ligand bridging to the mercury electrode, is a plausible source of the ligand.

From the electrolysis results it can be concluded that in oxidation state II, the *mer* isomer is the thermodynamically favored structural form. The $E_{1/2}$ values given in eq 4, 5, and 6, while slightly removed from E° by adsorption, clearly indicate that in oxidation state III the *s-fac* Co(III) isomer is the hardest to reduce, i.e., the thermodynamically most stable with respect to reduction, whereas the *mer* Co(II) species is the hardest to oxidize. Setting up the usual thermodynamic cycle from E° values ($\sim E_{1/2}$) would result in the conclusion that the equilibrium constant for the reaction

$$s\text{-}fac\text{-}[Co^{II}(\text{dien})_2]^{2+} + mer\text{-}[Co^{III}(\text{dien})_2]^{3+} \overset{K_1}{\rightleftharpoons} s\text{-}fac\text{-}[Co^{III}(\text{dien})_2]^{3+} + mer\text{-}[Co^{II}(\text{dien})_2]^{2+} \quad (8)$$

lies substantially to the right.

Assuming $E_{1/2} = E^\circ$, then

$$K_1 = \frac{[s\text{-}fac\ \text{Co(III)}][mer\ \text{Co(II)}]}{[mer\ \text{Co(III)}][s\text{-}fac\ \text{Co(II)}]} = \text{antilog}\ \frac{nF\Delta E^\circ}{2.303RT} = 13 \quad (9)$$

Using the same calculation procedures for the *u-fac*|*mer* distribution gives

$$K_2 = \frac{[u\text{-}fac\ \text{Co(III)}][mer\ \text{Co(II)}]}{[mer\ \text{Co(III)}][u\text{-}fac\ \text{Co(II)}]} = 5.7 \quad (10)$$

Similarly for the *u-fac*|*s-fac* distribution:

$$K_3 = \frac{[s\text{-}fac\ \text{Co(III)}][u\text{-}fac\ \text{Co(II)}]}{[u\text{-}fac\ \text{Co(III)}][s\text{-}fac\ \text{Co(II)}]} = 2.3 \qquad (11)$$

Thus if the equilibrium constants for the isomer distribution in oxidation state III are known, those for the cobalt(II) state can be calculated.

The equilibrium isomeric distribution for $[Co^{III}(dien)_2]^{3+}$ in the presence of activated charcoal was determined under the same conditions that were used for the electrochemical measurements (acetone solution, 0.1 M Bu_4NPF_6; 20 °C).

In previous studies[6] of the equilibration of the isomers of $[Co^{III}(dien)_2]^{3+}$ on activated charcoal by synthesis using Co(II) salts, yields of the desired complex were observed to be ≥94% for both aqueous and nonaqueous solvents (viz., dimethylacetamide, dimethyl sulfoxide). For the present determination in acetone solution, the yield of $[Co(dien)_2]^{3+}$ was considerably lower (ca. 20%); this may be considered to result from condensation reactions between acetone and dien (either in the free state or while complexed to Co(II) under the conditions of the experiment) thereby modifying the amine and leading to lower yields of the desired product. Certainly, other Co(III) species (predominantly orange) were observed during the chromatographic procedures following the synthesis, but these complexes were not examined further.

Despite the low yields of $[Co^{III}(dien)_2]^{3+}$ in acetone solution, it is likely that the observed relative proportions represent the thermodynamic distribution of the isomers. The observed proportions (*s-fac*:*u-fac*:*mer* = 9:17:74) in the presence of the nonassociating anion (PF_6^-) closely resemble the proportions obtained for equilibrations in other nonaqueous solvents (DMA, Me_2SO) in the absence of added electrolytes (*s-fac*:*u-fac*:*mer* = 7:14:79) and show that the meridional isomer is the most thermodynamically favored with respect to isomer distribution in acetone for the oxidation state III system. The result is also similar to the proportions obtained in water (7:28:65).

The equilibrium constants between the three isomer pairs for $[Co^{III}(dien)_2]^{3+}$ under the present conditions are given as

$$K_4 = \frac{[mer\ \text{Co(III)}]}{[s\text{-}fac\ \text{Co(III)}]} = 8.2 \qquad (12)$$

$$K_5 = \frac{[mer\ \text{Co(III)}]}{[u\text{-}fac\ \text{Co(III)}]} = 4.3 \qquad (13)$$

$$K_6 = \frac{[u\text{-}fac\ \text{Co(III)}]}{[s\text{-}fac\ \text{Co(III)}]} = 1.9 \qquad (14)$$

Substituting eq 12 into eq 9 gives

$$K_7 = \frac{[mer\ \text{Co(II)}]}{[s\text{-}fac\ \text{Co(II)}]} = 107 \qquad (15)$$

and the conclusion is reached that in oxidation state II the *mer* Co(II) complex is relatively more stabilized with respect to isomeric form compared with results obtained in oxidation state III.

Substituting eq 13 into eq 10 gives

$$K_8 = \frac{[mer\ \text{Co(II)}]}{[u\text{-}fac\ \text{Co(II)}]} = 25 \qquad (16)$$

Again it can be seen that thermodynamic stabilization of the *mer* form with respect to the facial isomer is gained in oxidation state II.

Proceeding through the same calculation procedures and using the K_6 value of 1.75 give

$$K_9 = \frac{[u\text{-}fac\ \text{Co(II)}]}{[s\text{-}fac\ \text{Co(II)}]} = 4.4 \qquad (17)$$

Table III. Summary of Thermodynamic Data for the $[Co^{III}(dien)_2]^{3+}/[Co^{II}(dien)_2]^{2+}$ System in Acetone (0.1 M Bu_4NPF_6) at 20 °C

Set 1, *s-fac*/*mer*	
s-fac Co(II) + *mer* Co(III) $\overset{K_1}{\rightleftharpoons}$ *s-fac* Co(III) + *mer* Co(II)	$K_1 = 13$
s-fac Co(III) $\overset{K_4}{\rightleftharpoons}$ *mer* Co(III)	$K_4 = 8.2$
s-fac Co(II) $\overset{K_7}{\rightleftharpoons}$ *mer* Co(II)	$K_7 = 107$
Set 2, *u-fac*/*mer*	
u-fac Co(II) + *mer* Co(III) $\overset{K_2}{\rightleftharpoons}$ *u-fac* Co(III) + *mer* Co(II)	$K_2 = 5.7$
u-fac Co(III) $\overset{K_5}{\rightleftharpoons}$ *mer* Co(III)	$K_5 = 4.3$
u-fac Co(II) $\overset{K_8}{\rightleftharpoons}$ *mer* Co(II)	$K_8 = 25$
Set 3, *u-fac*/*s-fac*	
s-fac Co(II) + *u-fac* Co(III) $\overset{K_3}{\rightleftharpoons}$ *s-fac* Co(III) + *u-fac* Co(II)	$K_7 = 2.3$
s-fac Co(III) $\overset{K_6}{\rightleftharpoons}$ *u-fac* Co(III)	$K_8 = 1.9$
s-fac Co(II) $\overset{K_9}{\rightleftharpoons}$ *u-fac* Co(II)	$K_9 = 4.4$

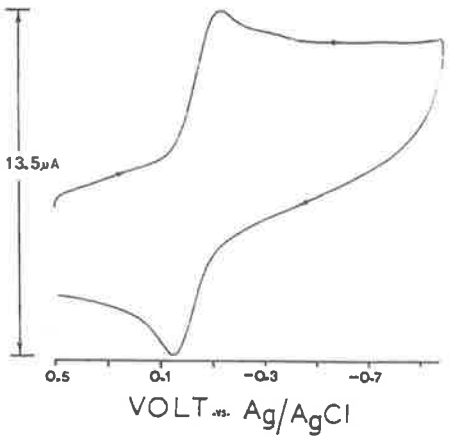

Figure 11. Cyclic voltammogram at platinum electrode of a 5×10^{-4} M solution of *mer*-$[Co^{III}(dien)_2](ClO_4)_3$ in acetone (0.1 M Bu_4NPF_6) solution. Scan rate = 500 mV/s.

This indicates that in oxidation state II the *u-fac* isomer is stabilized further relative to the *s-fac* form compared with the case of oxidation state III. Results from all the thermodynamic calculations are summarized in Table III.

The conclusion to be drawn from these results is that in oxidation state II the isomeric distribution is more discriminating than is the case for cobalt(III). That is, the *mer* isomer is heavily favored and by far the predominant species. However, the order of stability with respect to geometric distribution is the same in both oxidation states.

Voltammetry at platinum electrodes was also attempted and two reduction waves corresponding to those at mercury were found. Figure 11 shows a cyclic voltammogram of the first step at platinum. Waves were drawn out and very dependent on the surface treatment so that no quantitative data of precision comparable to that of mercury electrodes could be obtained. It appears that adsorption noted at mercury is also present at platinum and severely influences the reduction steps at platinum.

Following the study of the dien complexes, a brief investigation of the complex *s-fac*-$[Co^{III}(medien)_2](ClO_4)_3$ was undertaken, where medien is the ligand $NH_2CH_2CH_2N(CH_3)CH_2CH_2NH_2$. When this compound was synthesized, only

the *s-fac* isomer was isolated in oxidation state III.[14] Dc polarography indicated the presence of the same two reduction steps (including the maximum for the Co(II)/Co(0) step) as obtained in the previous cases. However, the $E_{1/2}$ for the Co(III) + $e^- \rightleftharpoons$ Co(II) reduction step was +0.230 V vs. Ag|AgCl, 265 mV more positive than observed in the *s-fac*-$[Co^{III}(dien)_2]^{3+}$ isomer. The half-wave potentials for the two-electron reduction step were the same for both *s-fac* complexes. Dc polarograms of the electrolysis products following a one-electron reduction were recorded. The $E_{1/2}$ values of these polarograms were the same as found for the *s-fac*-$[Co(medien)_2]^{3+}$ starting material, indicative that in oxidation state II the *s-fac* isomer is the most stable species. Free ligand was also found as with the cobalt dien system. The electrolysis products were then oxidized. Dc polarograms gave no change in half-wave potential, again indicating that in oxidation state III the *s-fac* isomer as synthesized originally is produced.

Searle, Petkovic, and Keene[15] found that the stability of the cis isomers (facial) was increased at the expense of the trans (meridional) upon N-methylation of cobalt complexes containing the triethylenetetramine ligand. Clearly the N-methylation of the dien ligand in this instance is responsible for the large enhancement of the stability of the *s-fac* isomer. So extensive is this enhancement that, in both oxidation states II and III, neither the *mer* nor the *u-fac* isomer could be detected.

Registry No. *mer*-$[Co^{III}(dien)_2]^{3+}$, 38318-06-8; *u-fac*-$[Co^{III}(dien)_2]^{3+}$, 38318-05-7; *s-fac*-$[Co^{III}(dien)_2]^{3+}$, 38318-04-6; *mer*-$[Co^{II}(dien)_2]^{2+}$, 67145-46-4; *u-fac*-$[Co^{II}(dien)_2]^{2+}$, 67145-47-5; *s-fac*-$[Co^{II}(dien)_2]^{2+}$, 67145-48-6; *s-fac*-$[Co^{III}(medien)_2]^{3+}$, 63544-39-8; *s-fac*-$[Co^{II}(medien)_2]^{2+}$, 67113-81-9.

References and Notes

(1) University of Melbourne.
(2) To whom correspondence should be addressed.
(3) University of Adelaide.
(4) F. G. Mann, *J. Chem. Soc.*, 466 (1934).
(5) F. R. Keene and G. H. Searle, *Inorg. Chem.*, **11**, 151 (1972).
(6) F. R. Keene and G. H. Searle, *Inorg. Chem.*, **13**, 2173 (1974).
(7) F. L. Wimmer, M. R. Snow, and A. M. Bond, *Inorg. Chem.*, **13**, 1617 (1974).
(8) A. M. Bond, R. Colton, and J. J. Jackowski, *Inorg. Chem.*, **14**, 274 (1975).
(9) A. M. Bond, R. Colton, and M. J. McCormick, *Inorg. Chem.*, **16**, 155 (1977).
(10) P. J. Sherwood and H. A. Laitinen, *J. Phys. Chem.*, **74**, 1751 (1970).
(11) D. K. Roe, D. B. Masson, and C. J. Nyman, *Anal. Chem.*, **33**, 1464 (1961).
(12) E. Porzsolt, M. T. Beck, and A. Bitto, *Magy. Kem. Foly.*, **80**, 127 (1974).
(13) I. Porubsky, E. Gyory-Szebenyl, and E. Gagyi Palffy, *Proc. Conf. Appl. Phys. Chem., 2nd*, **1**, 515 (1971); *Chem. Abstr.*, **76**, 101534 (1972).
(14) G. H. Searle, S. F. Lincoln, F. R. Keene, S. G. Teague, and D. G. Rowe, *Aust. J. Chem.*, **30**, 1221 (1977).
(15) G. H. Searle, M. Petkovic, and F. R. Keene, *Inorg. Chem.*, **13**, 399 (1974).

Inorganica Chimica Acta, 45 (1980) L91–L93

Isomers of the Bis(1,4,7-triazacyclodecane)cobalt(III) Ion, and the Occurrence of Higher Cyclic and Non-Cyclic Amines in the Richman–Atkins Synthesis for Cyclic Amines

MICHAEL E. ANGLEY, MARK DWYER, STEPHEN F. LINCOLN, GRAEME H. SEARLE*

Department of Physical and Inorganic Chemistry, University of Adelaide, Adelaide, S.A. 5001, Australia

RODNEY J. GEUE

Research School of Chemistry, Australian National University, Canberra, A.C.T. 2600, Australia

and F. RICHARD KEENE

Department of Chemistry and Biochemistry, James Cook University of North Queensland, Townsville, Qld. 4811, Australia

Received April 14, 1980

In seeking to prepare the two geometric isomers of $[Co(tacd)_2]^{3+}$ (Fig. 1) to continue our studies of isomerization reactions [1], we obtained the ligand tacd (tacd = 1,4,7-triazacyclodecane) through the Richman–Atkins procedure [2, 3] involving cyclization of $N\overset{+}{a}\bar{N}(Ts)CH_2CH_2CH_2\bar{N}(Ts)N\overset{+}{a}$ (I) and (Ts)-$OCH_2CH_2N(Ts)CH_2CH_2O(Ts)$ (II) (Ts = *p*-CH_3-$C_6H_4SO_2$–). The tacd·3HBr thus prepared was expected to be quite pure since: the $HN(Ts)CH_2$-$CH_2CH_2N(Ts)H$ from which (I) was prepared *in situ*, and (II), each gave clean ^{13}C n.m.r. spectra; the immediate cyclized product $tacd(Ts)_3$ was recrystallized (although melting points were variable over batches); and the tacd·3HBr from detosylation of $tacd(Ts)_3$ was crystallized in restricted yield, 55–65% (although melting points were variable over 241–250°, decomp.) The ^{13}C n.m.r. spectrum of tacd·3HBr seemed to confirm its high purity (three peaks in ratio 2:4:1; δ 45.3; 43.9, 21.4 respectively in D_2O; referenced to *t*-butyl alcohol capillary at δ 30.79 for CH_3; 20.10 MHz broad-band proton decoupled), although various batches always showed some small additional CH_2 resonances.

This tacd·3HBr was employed to synthesize the bis-complex of cobalt(III) by the standard substitution procedure

$$[Co(NH_3)_5Br]Br_2 + 2tacd\cdot3HBr + LiOH \xrightarrow[4hr]{\text{charcoal, 80 °C}} [Co(tacd)_2]^{3+}$$

*Author to whom correspondence should be addressed.

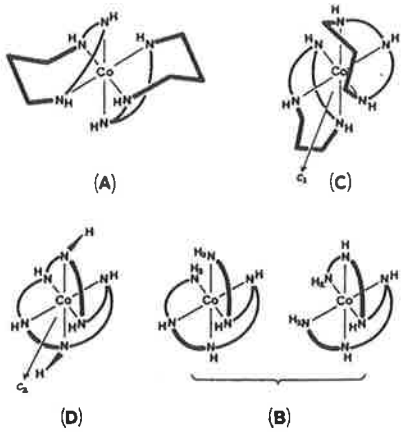

Fig. 1. Products in the synthesis of $[Co(tacd)_2]^{3+}$. (A), *trans*-$[Co(tacd)_2]^{3+}$, 96%. (C), *cis*-$[Co(tacd)_2]^{3+}$, 4%. (D), Λ-*mer*, *cis*,RR-$[Co(hace)]^{3+}$. (B), Λ-*mer*,*cis*-$[Co(dtah)]^{3+}$. Six-membered rings (tn) are shown thickened. The designations *trans* and *cis* refer to the relative geometric dispositions of the tn rings. One optical form is shown for each of the racemates (C), (D) and (B).

On cation-exchange chromatography of the product solution (SP-Sephadex with 0.1 *M* Na_3PO_4 eluent) three bands of CoN_6^{3+} complexes separated, from which the complexes were isolated by cation-exchange and crystallized as perchlorate salts. The ^{13}C n.m.r. spectra in D_2O showed that the products (A) and (B) from the first two bands respectively were pure single complex species. The product from the third eluted band gave two sets of seven resonances, showing it to be a mixture of two complexes (C) and (D) in ratio *ca.* 1:3, Table I [4]. Pure (D) was subsequently separated and isolated from this mixture (*vide infra*), and pure (C) from the equilibrium mixture formed by isomerization of (A) (*vide infra*).

Complexes (A) and (C) as perchlorate salts could be interconverted with charcoal or base (80°) to give the same equilibrium mixture (A):(C) = 96:4, in agreement with the preparative proportions, Table I (under conditions where ion-association is insignificant). These are therefore the expected geometric isomers of $[Co(tacd)_2]^{3+}$.

The clean ^{13}C n.m.r. spectra of (A) and (C) reflect the symmetries of the structures based on planar chelate rings so that the geometric configurations can be assigned unequivocally: the 2:2:2:1 peak pattern of (A) shows that it is the *trans* isomer of symmetry C_{2h}, whereas (C) gives seven equal peaks indicating C_2 symmetry and is therefore the *cis* isomer [4].

The solution spectra do not yield information on the conformations of the interconnected chelate rings (the en-rings could be δ-gauche or λ-gauche,

the tn-rings could be chair of δ-skew or λ-skew). The conformations could be locked, or could be labile within the n.m.r. time scale giving spectrum averaging, but on the basis of Dreiding models and experience with other systems [5–7] we would expect that the latter applies. The detailed conformational stereochemistry for this system is complicated: various combinations of all the ring conformations are possible, and N–H diastereoisomers are also possible in principle. However Dreiding models and energy minimization calculations indicate that the most favoured form has *trans* geometry with the tn-rings in chair conformations (Fig. 1), and the ^{13}C n.m.r. assignment of the experimentally favoured isomer (A) as *trans* with identical (averaged) ring conformations in the two ligands is consistent with this. The less favoured isomer (C) of *cis* geometry should also have chair-tn conformations.

In the presence of PO_4^{3-}, (A) becomes even more favoured over (C) due to the greater ion-association of (A) with this anion (as evidenced by its first elution in cation-exchange chromatography with Na_3PO_4 eluent [8]). Thus in Na_3PO_4 at 80 °C (but not under the conditions of the chromatography at ambient temperature) (C) isomerizes completely to (A) experimentally and this property was used to obtain pure (D), *i.e.*

$$\text{(C) + (D) mixture} \xrightarrow{Na_3PO_4,\ 80\ ^\circ C} \text{(A) + (D)},$$

these products being easily separable chromatographically.

Complex (D) has properties similar to those of *cis*-$[Co(tacd)_2]^{3+}$ (C): (D) and (C) give similar elemental analyses; they give similar ^{13}C n.m.r. spectra of seven equal resonances indicating C_2 symmetry; (C) and (D) have almost identical visible absorption spectra, which are markedly different from that of the differently coloured *trans* isomer (A), Table I; the ^1H n.m.r. spectrum (d_6-Me_2SO) of (D), like (C), shows no NH_2 resonances indicating macrocyclic ligand(s); and the two complexes elute almost together on chromatography. However (D) remained unchanged under conditions where isomerizations of CoN_6^{3+} complexes occur [1] so that it could not be another isomer of $[Co(tacd)_2]^{3+}$ (*i.e.* not a conformational isomer of NH diastereoisomer). Thus we deduce that (D) is a single diastereoisomer of $[Co(hace)]^{3+}$ (hace = 1,4,7,10,13,16-hexacycloeicosane), for which six geometrically distinct diastereoisomers are possible. This conclusion accords with the recent report by Margulis and Zompa that a particular sample of synthesized tacd·3HBr gave crystals of one diastereoisomer of $[Ni(hace)](ClO_4)_2 \cdot Me_2NCHO$, found by X-ray crystallography [9]. Our energy minimization calculations show that the lowest energy diastereoisomer of $[Co(hace)]^{3+}$ is Λ-*mer, cis*, RR/Δ-*mer, cis*, SS racemate (Fig. 1) which

TABLE I. Proportions and Properties of Complexes.

Complex	Preparative proportions, %	Colour	Visible absorption max. ϵ_{nm} in M^{-1} cm^{-1}	^{13}C n.m.r. in D_2O*	
(D) Λ-*mer,cis*,RR-$[Co(hace)]^{3+}$ (racemate)	9	Orange	$\epsilon_{349} = 105.6$, $\epsilon_{486} = 110.9$	7 equal resonances	chromatographic elution order†
(C) *cis*-$[Co(tacd)_2]^{3+}$	3	Orange	$\epsilon_{347} = 117.3$, $\epsilon_{482} = 111.0$	7 equal resonances	
(B) *mer,cis*-$[Co(dtah)]^{3+}$	<1	Orange	$\epsilon_{349} = 102.5$, $\epsilon_{485} = 109.0$	12 equal resonances	
(A) *trans*-$[Co(tacd)_2]^{3+}$	88	Yellow	$\epsilon_{341} = 84.5$, $\epsilon_{467} = 75.0$	2:2:2:1	

*20.10 MHz broad-band proton decoupled, run on a Bruker WP-80 spectrometer using 8192 data table. The spectra are referenced to the CH_3 signal δ 30.79 from a *t*-butyl alcohol capillary. Chemical shift falues are, for (D): δ 56.5, 55.6, 53.9, 53.6, 50.4, 48.5, 22.8. (C): δ 52.6, 52.0, 51.7, 49.7, 47.1, 44.7, 18.4. (B): 57.0, 55,4, 55.1, 54.0, 53.3, 50.0, 49.0, 47.6, 41.7, 39.2, 26.2, 23.0. (A): 53.5, 49.6, 44.9, 16.3 in ratio order respectively. †(C) elutes only marginally ahead of (D), insufficient for their separation.

is the analogous diastereoisomer to that isolated in the nickel(II) complex [9], and which is one of the two possibilities indicated by the ^{13}C n.m.r. spectrum (*i.e.* C_2 symmetry) and the visible absorption spectrum (*i.e. cis* topology as for (C)) and the chromatographic behaviour (*i.e. cis* topology as for (C)).

The minor complex (B) contains twelve carbons (by elemental analyses and ^{13}C n.m.r. spectrum), and the ^{1}H n.m.r. spectrum has broad peaks from NH_2 showing that the ligand is non-macrocyclic. The complex remains unchanged with charcoal or base. The visible absorption spectrum is almost identical with those of (D) and (C) (Table I). These properties indicate that (B) is one of the diastereoisomers of *mer, cis*-$[Co(dtah)]^{3+}$, Fig. 1 (dtah = 1,16-diamino-3,7,10, 13-tetraazahexadecane). Two topologies are possible for a *mer, cis* arrangement of the tn rings in $[Co(dtah)]^{3+}$ (Fig. 1), and a total of six NH diastereoisomers are possible between these two topologies (both topologies are C_1 symmetry).

These findings prompted our reexamination of the tacd·3HBr product. One batch was subjected to cation-exchange chromatography when two fractions were cleanly separated on elutions with HCl. Crystallization of the first effluent from elution with 1.5 M HCl gave pure tacd·3HCl (m. pt. 245–250 °C decomp.), which showed a clean ^{13}C n.m.r. pattern of three reasonances only (D_2O: δ 45.0, 43.5, 21.1 in ratio 2:4:1). The product from crystallization of the subsequent 4 *M* HCl effluent was in substantial amount and gave a ^{13}C n.m.r. spectrum showing ten other resonances. These correspond to the small peaks noted in the synthesized tacd·3HBr samples, and they can be attributed to hace·6HCl (three resonances, ratio 4:8:2) and dtah·6HCl (seven resonances, ratio 1:2:5:1:1:1:1). These hexamines appear to be present in comparable amounts, and the elemental analysis results of this second fraction are intermediate between the calculated figures for these two compounds. When this product was used to prepare the cobalt(III) complex, only (B) and (D) were obtained.

It is now clear that the Richman–Atkins cyclization procedure is not specific, at least for cyclic triamines. Dimeric cyclic amines (hace) and higher linear polyamines (dtah) can be co-products with the required simple cyclic amine (tacd). The condensations occur by nucleophilic attack of $-(Ts)N^-$ in (I) at the C–O(Ts) carbon centres of (II). Formation of the linear product dtah presumably results from an elimination reaction by $-(Ts)N^-$ in the linear precursor of hace. Other non-cyclized by-products, such as $NH(Ts)(CH_2)_3N(Ts)(CH_2)_2N(Ts)(CH_2)_2$-O(Ts), are also conceivable from the condensation reaction.

The tosyl derivatives and hydrobromides of the higher amine co-products will presumably have lower solubilities than $tacd(Ts)_3$ and tacd·3HBr respectively, which probably accounts for the difficulties in purifying $tacd(Ts)_3$ and tacd·3HBr by recrystallization procedures without incurring substantial losses. These losses may be minimized by carrying out only one recrystallization of $tacd(Ts)_3$. Subsequently, ion-exchange provides an efficient means of removing the higher amines from the cyclic triamine tacd·3HBr.

Acknowledgement

We acknowledge support of this work by the Australian Research Grants Committee.

References

1 G. H. Searle, F. R. Keene and S. F. Lincoln, *Inorg. Chem., 17,* 2362 (1978).
2 J. E. Richman and T. J. Atkins, *J. Am. Chem. Soc., 96,* 2268 (1974).
3 T. J. Atkins, J. E. Richman and W. F. Oettle, *Org. Synth., 58,* 86 (1978).
4 The ^{13}C n.m.r. resonances are all from CH_2 carbons in the four complexes so that peak integrations and intensities are closely proportional to numbers of carbons.
5 Y. Yoshikawa, *Chem. Letters,* 109 (1978).
6 G. H. Searle, S. F. Lincoln, F. R. Keene, S. G. Teague and D. G. Rowe, *Aust. J. Chem., 30,* 1221 (1977).
7 G. H. Searle, S. F. Lincoln, S. G. Teague and D. G. Rowe, *Aust. J. Chem., 32,* 519 (1979).
8 G. H. Searle, *Aust. J. Chem., 30,* 2625 (1977).
9 T. N. Margulis and L. J. Zompa, *J. Chem. Soc. Chem. Comm.,* 430 (1979).

Aust. J. Chem., 1981, **34**, 1331–5

Pressure Studies on the Intramolecular Isomerization Reactions of (Diethylenetriamine)-(methyldiethylenetriamine)cobalt(III) and Bis(diethylenetriamine)cobalt(III) Cations

F. Richard Keene,[A,B] *Ian A. S. McDonald*[A] *and Graeme H. Searle*[C]

[A] Department of Inorganic Chemistry, University of Melbourne, Parkville, Vic. 3052.
[B] Department of Chemistry and Biochemistry, James Cook University of North Queensland, Townsville, Qld. 4811. Author to whom correspondence should be addressed.
[C] Department of Physical and Inorganic Chemistry, University of Adelaide, P.O. Box 498, Adelaide, S.A. 5001.

Abstract

The homogeneous intramolecular isomerization reactions of all the isomers of $[Co(dien)_2](ClO_4)_3$ and $[Co(dien)(medien)](ClO_4)_3$ (dien, diethylenetriamine; medien, 4-methyldiethylenetriamine) have been studied at 90°C under atmospheric pressure and conditions of high pressure. The isomerization reactions are retarded by an increase in pressure, and for a given starting isomer of each system the various isomerization processes are affected uniformly. For each system, the same equilibrium isomer distribution was obtained regardless of starting isomer or of the pressure conditions of the experiment. The results are interpreted on the basis of a common mechanism for all isomerizations, involving Co–N bond-rupture followed by rearrangement of the resultant five-coordinate species.

Introduction

Intramolecular rearrangements of octahedral complexes have usually been rationalized in terms of either non-dissociative 'twist' processes or bond-rupture processes involving five-coordinate transition states.[1] The choice between these alternatives has seldom been unambiguous, particularly in complexes involving bidentate ligands.[1,2]

We recently reported[3] a study of the intramolecular isomerization reactions of the bis(tridentate) complexes $[Co(dien)_2]^{3+}$ and $[Co(dien)(medien)]^{3+}$ (dien = diethylenetriamine, $H_2NCH_2CH_2NHCH_2CH_2NH_2$; medien = 4-methyldiethylenetriamine = 2,2′-methyliminobis(ethylamine), $H_2NCH_2CH_2N(CH_3)CH_2CH_2NH_2$). This work indicated that the isomerization reactions are base-catalysed, and they probably involve conjugate base intermediates with deprotonation occurring at the secondary amine nitrogen of coordinated dien. The most satisfactory mechanistic scheme proposed was formation of five-coordinated intermediates by Co–N bond rupture, with subsequent intramolecular rearrangement.

The present study of these reactions under high pressure was undertaken to help clarify the details of these rearrangement mechanisms.

[1] Serpone, N., and Bickley, D. G., *Prog. Inorg. Chem.*, 1972, **17**, 391.
[2] Holm, R. H., 'Dynamic Nuclear Magnetic Resonance Spectroscopy' (Eds L. M. Jackman and F. A. Cotton) pp. 317–76 (Academic Press: New York 1975).
[3] Searle, G. H., Keene, F. R., and Lincoln, S. F., *Inorg. Chem.*, 1978, **17**, 2362.

Experimental

Materials

$[Co(dien)_2]^{3+}$ was synthesized and separated into its geometric isomers chromatographically as described previously.[4] The perchlorate salts were obtained by elution of the sorbed cation from a column of Biorex-70 weak-acid cation-exchange resin (50-100 mesh) with 0·1 M $HClO_4$, and precipitation with ethanol after concentration of the eluant. The various geometric isomers of $[Co(dien)(medien)](ClO_4)_3$ were obtained as described previously.[3]

Tris (2-amino-2-hydroxymethylpropane-1,3-diol) buffer ('THAM': Fisher) was used for these studies. Perchloric acid (Ajax Univar) and sodium perchlorate (Fluka) were used without further purification.

Apparatus

The apparatus used for conducting reactions under high pressure has been described previously.[5] The reaction solution in the sampling vessel was contained within a Lucite cylinder with a floating Teflon plunger and a Pt–Ir outlet tube. A hand-operated hydraulic pump was used to maintain the pressure of the solution up to 200 MPa.

Comparison of Isomerization Reactions at Atmospheric and at High Pressure

A sample of each isomer in turn of $[Co(dien)_2](ClO_4)_3$ (1·2 g) was dissolved in 0·1 M Tris/$HClO_4$ buffer (120 ml). The solution was divided into two equal parts, one then being maintained at 90°C under atmospheric pressure, and the other also at 90°C but under a pressure of 180 (±10) MPa. Samples (*c.* 10 ml) were taken from each solution at appropriate intervals, cooled to room temperature and sorbed on columns of SP-Sephadex C25 cation exchanger. Elution with 0·3 M sodium (+)-tartrate solution allowed separation of the geometric isomers which were collected and estimated spectrophotometrically by using a Cary 17 instrument.[4]

The isomerization reactions of the $[Co(dien)(medien)](ClO_4)_3$ isomers were performed in an analogous manner, except that the complex concentration was lower (0·5 g in 100 ml of buffer solution), and the buffer solution was adjusted to $\mu = 1$ by means of $NaClO_4$. Chromatographic separation of the samples was effected by using 0·1 M Na_3PO_4 solution as eluent.[3]

The pH of the buffer solution, and of some representative solutions, was measured at 25° and 90° by means of a Radiometer PHM62 meter and a Radiometer GK2401C combined electrode (with saturated NaCl solution in the calomel reference cell). For the determination at the higher temperature, the meter was standardized at 90° by using buffer solutions 0·05 M potassium hydrogen phthalate (pH 4·008 at 25°, 4·205 at 90°), 0·01 M borax (9·180, 8·850) and a phosphate buffer (0·025 M KH_2PO_4/0·025 M Na_2HPO_4; 6·865, 6·877).[6] The pH was determined to be 9·12 at 25° and 7·72 at 90°, and was invariant for the buffer alone and the reaction solutions.

For the buffer Tris, the effect of pressure on pH is known to be small.[5] Consequently the pH value determined at atmospheric pressure can be assumed within a small error (≤0·1 pH unit) to represent the pH under the various pressure conditions studied.

Results and Discussion

The intramolecular isomerization reactions of all the isomers of $[Co(dien)_2](ClO_4)_3$ and $[Co(dien)(medien)](ClO_4)_3$ at 90° and pH 7·72 were found to be retarded by the application of high pressure. Furthermore, the equilibrium isomer distribution obtained for each system was independent of the pressure conditions of the reaction, viz. *mer*:*u-fac*:*s-fac* 44:42:14 for $[Co(dien)_2]^{3+}$;[7] *mer*:*u-fac*:*s-fac* 9:10:81 for

[4] Keene, F. R., and Searle, G. H., *Inorg. Chem.*, 1972, **11**, 148.
[5] Stranks, D. R., Vanderhoek, N., *Inorg. Chem.*, 1976, **15**, 2645.
[6] Weast, R. C., (Ed.) 'Handbook of Chemistry and Physics' 58th Edn, p. D135 (Chemical Rubber Company: Cleveland, Ohio, 1977).
[7] Keene, F. R., and Searle, G. H., *Inorg. Chem.*, 1974, **13**, 2173: these proportions were obtained at 80°, but are consistent with the present isomer distribution obtained at 90°.

[Co(dien)(medien)]$^{3+}$.[3] The changes in isomer proportions during the isomerization of *s-fac*- and *u-fac*-[Co(dien)$_2$] (ClO_4)$_3$ are shown in Figs 1 and 2 respectively: the results for the isomerizations of *mer*-[Co(dien)$_2$] (ClO_4)$_3$, and the isomers of [Co(dien)(medien)] (ClO_4)$_3$ show similar trends.

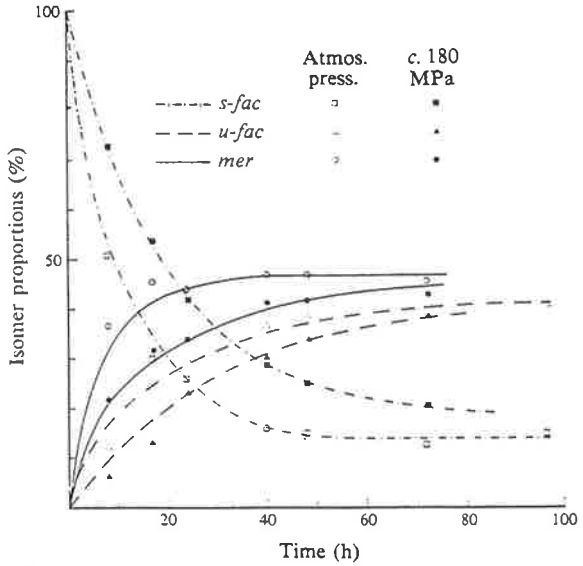

Fig. 1. Relative isomer proportions during the isomerization of *s-fac*-[Co(dien)$_2$] (ClO_4)$_3$. (Tris/$HClO_4$ buffer; pH 7·72; 90°C.)

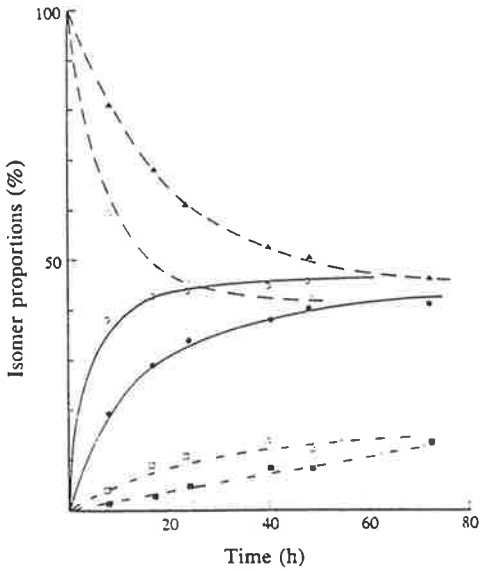

Fig. 2. Relative isomer proportions during the isomerization of *u-fac*-[Co(dien)$_2$] (ClO_4)$_3$. (Symbols as for Fig. 1.)

The possible mechanism of the intramolecular isomerization of bis(tridentate) complexes has been discussed in detail previously.[3] Since the central nitrogen atoms in the tridentate ligands are *trans* in both the *s-fac* and *mer* isomers, a Co–NH_2 bond rupture (one-ended dissociation) followed by a simple rearrangement via a trigonal-bipyramidal intermediate in which the dissociated arm of the ligand reattaches at a

different position could lead to their interconversion. On the other hand, Co–N rupture involving the central nitrogen atom of one of the tridentate ligands followed by an analogous simple rearrangement could lead to the interconversion *s-fac* ⇄ *u-fac*.[8] Non-dissociative 'twist' processes via trigonal-prismatic intermediates could allow the interconversions *s-fac* ⇄ *u-fac* and *u-fac* ⇄ *mer*. Consequently, a path for the isomerization might involve (1) only non-dissociative 'twist' rearrangements, (2) a combination of a simple bond-rupture process and the 'twist' rearrangements, (3) a combination of simple bond-rupture processes, or (4) bond-ruptures to give five-coordinate intermediates followed by a major 'twist'-type rearrangement within the intermediate, with subsequent recoordination of the amine group. This sequence (4) is essentially the 'twist-with-rupture' mechanism described earlier.[3,9]

Recent work has shown that volumes of activation, obtained from rate measurements under pressure, may provide a general criterion to distinguish between bond-rupture and twist processes in isomerization reactions of metal complexes.[10] For these two mechanistic possibilities, the bond-rupture process should lead to a positive $\Delta V^{\ddagger}$ since the trigonal-bipyramidal transition state will have a greater volume than the reactant octahedral species due to the extension of the dissociated arm of the uncharged ligand into the solvent. On the other hand, the 'twist' mechanism is assumed to occur without bond extension and with only bond angle distortion, so that the trigonal-prismatic transition state and the reactant octahedral complex should be of comparable volumes, giving $\Delta V^{\ddagger}$ essentially zero. Conversely, these values of $\Delta V^{\ddagger}$ imply that, upon application of high pressure, a process involving a bond-rupture mechanism would be retarded, whereas the rate of a 'twist' process should be virtually unaffected.

The isomerization reactions of $[Co(dien)_2]^{3+}$ and $[Co(dien)(medien)]^{3+}$ are known to be base-catalysed. If a deprotonation is required prior to any rearrangement as proposed previously,[3] a contribution to $\Delta V^{\ddagger}$ from this equilibrium prior to the rearrangement process would be expected: this contribution would be large and positive and might approach the volume change of the electrostriction of OH^- ($+22\ cm^3\ mol^{-1}$).[10] It is likely that this contribution would be approximately constant for all the interconversions. Consequently, it would be expected that, for the present reactions, a positive $\Delta V^{\ddagger}$ would be observed and that the reactions would be retarded by increased pressure. However, the activation volume of the subsequent rearrangement process must also contribute to the overall $\Delta V^{\ddagger}$.

For the present systems, isomerization reactions of $[Co(dien)(medien)]^{3+}$ are known to be intramolecular, since total dissociation of either ligand would lead to disproportionation which is not observed.[3] It can be confidently assumed that the rearrangement reactions of $[Co(dien)_2]^{3+}$ will also be intramolecular.

The present studies show that the isomerization reactions are slowed by an increase in pressure, and that the same equilibrium distribution of isomers is obtained for each of the two systems regardless of the starting isomer or of the pressure conditions under which the reaction was performed. Furthermore, in those cases where the curve of a developing isomer intersects with that of the diminishing starting isomer, the relative isomer composition corresponding to the point of intersection

[8] Hammershøi, A., and Larsen, E., *Acta Chem. Scand., Ser. A*, 1978, **32**, 485; Searle, G. H., and Angley, M. E., *Inorg. Chim. Acta*, in press.
[9] Eaton, S. S., Eaton, G. R., Holm, R. H., and Muetterties, E. L., *J. Am. Chem. Soc.*, 1973, **95**, 1116.
[10] Lawrance, G. A., and Stranks, D. R., *Acc. Chem. Res.*, 1979, **12**, 403.

of the two curves is identical (within experimental error) for both pressure conditions (see Fig. 1). This observation indicates that the separate isomerization processes involved in going from the one starting geometric form to an equilibrium mixture of the three forms are slowed uniformly.

The observed decrease in isomerization rate upon increase in pressure is expected since the reactions involve a deprotonation step (see above). Although the contribution to the overall $\Delta V^{\ddagger}$ by the rearrangement process itself (relative to the deprotonation) is not known, the present results are not consistent with three of the four mechanistic schemes given earlier. Firstly, in the case of rearrangement involving non-dissociative ('twist') processes only, a virtually constant ratio of *mer*/*s-fac* forms might be expected during the isomerization of the *u-fac* form since each of these isomers can be generated from the *u-fac* form directly by separate 'twist' processes which are likely to have similar volumes of activation. In fact, the equilibrium proportion of the *mer* isomer is established much more rapidly. Secondly, concurrent 'twist' and dissociative pathways are inconsistent with these results, since the dissociative pathway would have a more positive $\Delta V^{\ddagger}$ and this route would be slowed relative to the 'twist' processes by an increase in pressure. The observations that the equilibrium isomer proportions are identical regardless of the pressure conditions of the reaction, and that the separate isomerizations are slowed uniformly, are clearly at variance with this proposal. Similarly, a combination of bond-rupture processes seems unlikely since it is improbable that dissociations of the bonds between cobalt and both the terminal and central nitrogen atoms of the ligands would be affected equally by the pressure increase.

We believe the results suggest that there is a common mechanism for the rearrangement processes involved, and that the results are consistent with the 'twist-with-rupture' scheme of the type proposed previously.[3] This process involves initial bond rupture of the deprotonated species with subsequent major rearrangement of the resultant five-coordinate species, which would allow interconversion of each isomeric pair.

It was observed in our previous studies that small proportions of a decomposition product were formed during the isomerization reactions, and the identity of this species was assumed to be a mono-aqua or mono-hydroxo complex formed in competition with the 'twist-with-rupture' process.[3] The effect of increased pressure was an increase in the relative proportion of this product. If this were due to its formation by an associative reaction (for which $\Delta V^{\ddagger}$ would be negative) it would constitute a rather unusual reaction for a Co^{III} complex. Alternatively, if it were formed by a separate S_N1 CB process it should be retarded by increased pressure. It seems more likely to evolve from an equilibrium involving the bond-rupture five-coordinate intermediate and water, in which the formation of the aquapentamine complex is favoured by a pressure increase.

Manuscript received 2 February 1981

Inorganica Chimica Acta, *155* (1989) 125–138

Cobalt(III) Complexes with *N*-Methylethane-1,2-diamine (meen). Synthesis and Characterization of the Isomers of $[Co(meen)_3]^{3+}$, $[Co(meen)_2(en)]^{3+}$ and $[Co(meen)(en)_2]^{3+}$

GRAEME H. SEARLE*

Department of Physical and Inorganic Chemistry, University of Adelaide, Adelaide, S.A. 5001, Australia

and F. RICHARD KEENE

Department of Chemistry and Biochemistry, James Cook University of North Queensland, Townsville, Qld. 4811, Australia

(Received June 1, 1988)

Abstract

Of the twelve possible geometric isomers–diastereoisomers of $[Co(meen)_3]^{3+}$ (meen = *N*-methylethane-1,2-diamine), three isomers designated **A**, **B** and **C** according to their chromatographic elution order, have been detected from preparative mixtures. The highest yield and cleanest synthesis is $CoCl_2$ + 3meen + dimethylsulfoxide, which gives pure red **A**-$[Co(meen)_3]Cl_3$ as the crystallized product, and recrystallization of this from water or methanol gives pure orange–red **C**. Each isomer is robust in acid, but equilibrates in water to the mixture **A**:**B**:**C** = 3:1:2. These are therefore three N–H diastereoisomers of the same geometry with respect to the N–CH_3 groups, which is *mer* by ^{13}C NMR spectroscopy. This mixture can be separated by cation-exchange chromatography on SP-Sephadex by using acidic Na_2SO_4. A second synthesis method was aerial oxidation of Co(II) + 3meen + H^+ in aqueous solution with charcoal at 80 °C. The charcoal and oxygen caused some demethylation of coordinated Co–meen, and the crude yellow–orange isolated product was a mixture of isomers of $[Co(meen)_3]^{3+}$ (mostly **C**), $[Co(meen)_2(en)]^{3+}$ (three orange isomers **F**, **G**, **H**, of ten possible), $[Co(meen)(en)_2]^{3+}$ (one orange–yellow diastereoisomer **E** of two possible) and $[Co(en)_3]^{3+}$ (**D**). The en complex species were separated on Sephadex using Na_3PO_4 as eluent, and the designations **D** to **H** are in the elution order. Thus **F**, **G** and **H** are single diastereoisomers of the three different possible geometries (by ^{13}C NMR), and their ratios isolated *ca.* 5:1:36 should be approximately the equilibrium proportions.

Introduction

Complexes of *N*-methylethane-1,2-diamine (meen) have been of interest for many years, since the crude tris(meen) complexes $[Co(meen)_3]Cl_3$ and $[Ni(meen)_3]Br_2$ were first isolated by Keller and Edwards in 1952 [1]. The nickel(II) complex was further examined by Pavkovic and Meek in respect of the effect of N-substitution on spectroscopic properties [2], but the isomers of these tris(meen) complexes have never been separated or characterized. Particular isomers have, however, been isolated for several bis(meen) and mono(meen) complexes $[Co(meen)_2X_2]^+$ [3–7], $[Co(meen)(en)_2]^{3+}$ [8], $[Co(meen)(NH_3)_4]^{3+}$ [9, 10] and $[Co(meen)(CN)_4]^-$ [10], with their configurations being assigned from an X-ray crystal structure [7] and from electronic spectra, circular dichroism and NMR comparisons [6, 8], and by conformational analysis considerations [6, 10]. A prime interest in the studies with these complexes has been the effect of N-methyl substitution on various properties, including optical rotatory properties [6–8, 11, 12], kinetics of proton exchange and racemization [5, 9], conformational analysis by NMR [10], and reactivity and stabilities of some isomers [6].

Perhaps the most fundamental interest with Co–meen systems is in the stereospecificity which is imposed by the N-methyl substituent on the coordination of the ligand, which manifests in different stabilities of the isomers with some isomers being precluded [13]. The stereospecificity in the coordination of the C-methyl analogue propane-1,2-diamine (pn) and the stereochemistry of Co(pn) complex systems have been well clarified, largely through the separation, characterization and relative stabilities of the complexes $[Co(\pm pn)_3]^{3+}$, $[Co(\pm pn)_2(en)]^{3+}$ and $[Co(\pm pn)(en)_2]^{3+}$ by Corey and Bailar [14] and Dwyer and Sargeson and coworkers [15–20]. These results have played a significant role in our understanding of chelate ring conformations and in the development of conformational analysis of complex systems [14, 18].

Complex systems with meen are of comparable stereochemical interest, and in fact the stereochemistry is more complicated in these meen systems

*Author to whom correspondence should be addressed.

0020-1693/89/$3.50

because the axial-equatorial character of N-methyl substituents is less pronounced than that of C-methyl substituents which are constrained to be equatorial in Co–pn. However, there have been no systematic studies of the experimental isomer possibilities in Co(meen) complexes, so that the stereochemistry in these systems is not well understood.

Before the availability of SP-Sephadex cation-exchange chromatography and ^{13}C NMR spectroscopy we [21] and MacDermott [22] obtained a partial separation of the crude red $[Co(meen)_3]Cl_3$ materials obtained from various preparations. With paper chromatography and thin layer chromatography, only two red bands separated with acidic eluents, although there are twelve geometric and diastereoisomeric possibilities for this system. Also, from the product synthesized over charcoal (following Keller and Edwards [1]), we separated a yellow material and believed this to be another $[Co(meen)_3]^{3+}$ geometric isomer. However, these materials could not be characterized at that time and the stereochemistry in $[Co(meen)_3]^{3+}$ has remained unsolved.

We have now achieved the separation of the various components in these $[Co(meen)_3]Cl_3$ materials by SP-Sephadex chromatography, and these isolations of some of the isomers of $[Co(meen)_3]^{3+}$, $[Co(meen)_2(en)]^{3+}$ and $[Co(meen)(en)_2]^{3+}$ are now described, along with some of their properties. We have found that under preparative conditions for $[Co(meen)_3]^{3+}$ involving charcoal and oxygen, some demethylation occurs to give complexes containing en. The separation and characterization of all these species gives insight into the stereospecificity of meen coordination, as the isomer proportions found for each complex system should correspond at least roughly to the thermodynamic stabilities. The bis-(meen) and mono(meen) complexes reported previously and quoted above were not necessarily obtained under equilibrium conditions.

The stereochemistry involved in these meen complex systems is complicated, so that the isomeric possibilities for the various complexes and a nomenclature scheme are first elaborated.

Isomer Possibilities for $[Co(meen)_3]^{3+}$, and Nomenclature

There are twelve geometrically distinct forms if ring conformations are ignored, *i.e.* if the rings are taken to be flat or if the conformations are averaged. Consideration of the individual ring conformations gives a total of eightyeight conformational forms.

The isomerism arises from several sources:

(1) Alternative absolute configurations of the chelate rings about the cobalt, designated Λ and Δ according to the IUPAC scheme [23, 24], Fig. 1.

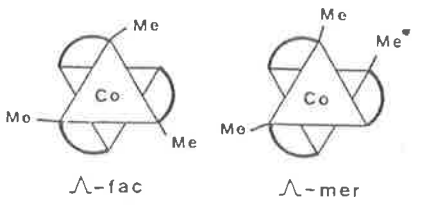

Fig. 1. Facial and meridional geometric (orientation) isomers, shown as projections down the pseudo-C_3 axes.

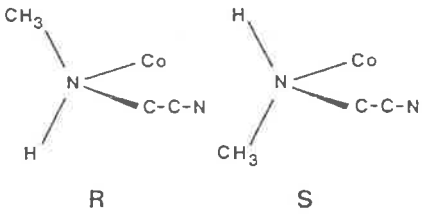

Fig. 2. Absolute configurations *R* and *S* about the coordinated *sec*-N in Co–meen.

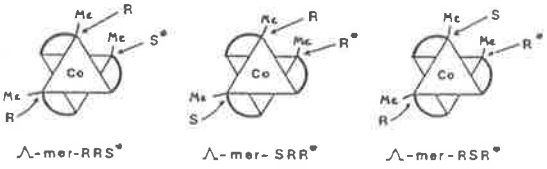

Fig. 3. Orientation isomers for Λ-*mer-RRS*-$[Co(meen)_3]^{3+}$. Stereochemistry parameters are listed for the rings clockwise around the pseudo-C_3 axis, when the single CH_3 is at the remote end of this axis. An asterisk denotes this single CH_3.

(2) The *R* or *S* absolute configuration of the substituents about the asymmetric nitrogen in each coordinated ligand, Fig. 2.

(3) Facial or meridional relative dispositions of the three methyl groups, giving rise to 'orientation isomers', Fig. 1.

(4) Further orientation isomers arise when the three chelate rings are distinguishable from each other, *i.e.* when the rings are differently orientated about the pseudo-C_3 molecular axis. This situation occurs for a *mer* arrangement of the methyl groups, where the rings are further distinguished by different absolute configurations at the nitrogens. For example the combination Λ-*mer-RRS* has three orientation isomers, Fig. 3.

The designations of such orientation isomers are not covered by the IUPAC rules [23, 24]. Further conventions are therefore necessary for specifying these isomers, and the following derive from proposals developed for the general case $[M(AB)_3]$ by MacDermott [25, 26].

(a) An asterisk is used to indicate the ligand having the single methyl at one end of the pseudo-C_3 axis [25]. This procedure distinguishes particular isomers. For example the Λ-*mer-RRS** isomer is distinguished in the *RRS* combination, Fig. 3.

(b) For complete specification of the other two *RRS* isomers Λ-*mer-SRR** and Λ-*mer-RSR**, the rings have to be described (in terms of their *R* or *S* configurations at the asymmetric nitrogen) in a particular order, say clockwise [25, 26], in which they appear when the particular isomer is viewed along the pseudo-C_3 axis such that the single methyl substituent (whose description is asterisked) is situated at the remote end of this axis. We adopt a clockwise order as our convention. An analogous situation of three orientation isomers obtains for the combination Λ-*mer-RSS*.

(5) Asymmetry of the ring conformations, designated λ or δ by the IUPAC scheme [23, 24]. In general there are eight different combinations of the conformations of the three rings (δδδ, δδλ, δλδ, λδδ, δλλ, λδλ, λλδ, λλλ), and these are superimposed on the isomers arising from the other sources. In the situations *RRR* and *SSS* however, δδλ, δλδ and λδδ are identical, as are λλδ, λδλ and δλλ.

All the subsequent consideration of the stereochemistry will be with respect to one configuration Λ of the rings about the metal, for which the eighty-eight possible isomers arising from sources (2) to (5) are listed in Table 1.

While the Λ/Δ, *R*/*S* and λ/δ parameters, and the defined order of the listing of *R*/*S* and λ/δ around the three rings, uniquely define the isomers, there are two other descriptors of the stereochemistry which highlight the geometrical relationships in these structures. Each ring may also be described in terms of the approximately parallel (lel) or oblique (ob) inclination of the C–C axis to the pseudo-C_3 axis of the molecule, and also by the equatorial (eq) or axial (ax) disposition of each methyl substituent to its respective ring. The dependences of these factors on the previous stereochemical parameters are as follows.

TABLE 1. Isomers of Λ-$[Co(meen)_3]^{3+}$

Isomer	Conformers	Ring geometries	Methyl geometries	Conformers of C_3 symmetry
Λ-*fac-RRR*	δδδ	lel, lel, lel	eq, eq, eq	C_3
	δδλ	lel, lel, ob	eq, eq, ax	
	δλλ	lel, ob, ob	eq, ax, ax	
	λλλ	ob, ob, ob	ax, ax, ax	C_3
Λ-*fac-RRS*	δδδ	lel, lel, lel	eq, eq, ax	
	δδλ	lel, lel, ob	eq, eq, eq	
	δλδ	lel, ob, lel	eq, ax, ax	
	λδδ	ob, lel, lel	ax, eq, ax	
	δλλ	lel, ob, ob	eq, ax, eq	
	λδλ	ob, lel, ob	ax, eq, eq	
	λλδ	ob, ob, lel	ax, ax, ax	
	λλλ	ob, ob, ob	ax, ax, eq	
Λ-*fac-RSS*	Eight conformers designated δ/λ and lel/ob as above			
Λ-*fac-SSS*	δδδ	lel, lel, lel	ax, ax, ax	C_3
	δδλ	lel, lel, ob	ax, ax, eq	
	δλλ	lel, ob, ob	ax, eq, eq	
	λλλ	ob, ob, ob	eq, eq, eq	C_3
Λ-*mer-RRR**	δδδ*	lel, lel, lel*	eq, eq, eq*	
	δδλ*	lel, lel, ob*	eq, eq, ax*	
	δλδ*	lel, ob, lel*	eq, ax, eq*	
	λδδ*	ob, lel, lel*	ax, eq, eq*	
	δλλ*	lel, ob, ob*	eq, ax, ax*	
	λδλ*	ob, lel, ob*	ax, eq, ax*	
	λλδ*	ob, ob, lel*	ax, ax, eq*	
	λλλ*	ob, ob, ob*	ax, ax, ax*	

For Λ-*mer*, the other seven diastereoisomeric forms are

*RRS**, *RSR**, *SRR**, *RSS**, *SRS**, *SSR**, *SSS**

Each of these has eight conformers δ/λ and lel/ob as listed above for RRR* (but the eq/ax designations will be different).

$\Lambda\delta$ or $\Delta\lambda$ gives lel

$\Lambda\lambda$ or $\Delta\delta$ gives ob

$R\delta$ or $S\lambda$ gives eq

$R\lambda$ or $S\delta$ gives ax

These secondary descriptors lel/ob abd eq/ax are useful for understanding and checking the complicated stereochemistry in this system, and they are shown for some of the isomers in Table 1. Moreover, these geometrical factors would be expected to be significant in determining the relative stabilities of the isomers and this will be considered in subsequent work.

Thus for Λ-$[Co(meen)_3]^{3+}$, twelve geometric-diastereoisomeric forms arise from orientation isomerism and nitrogen asymmetry, four *fac* and eight *mer*. For each of these twelve 'isomeric' forms either eight or four conformer combinations are possible. Experimentally, the isomers should be separable from an equilibrium mixture into their geometric 'isomeric' forms (by chromatography or fractional crystallization), each as a racemic pair.

Designations of the Enantiomers

On forming the mirror image of a molecule, the chirality descriptors Λ/Δ, R/S and λ/δ become interchanged. Also, the ordering of the three rings about the pseudo-C_3 axis becomes reversed. Thus if the clockwise ring numbering convention is retained for both Λ and Δ configurations (with molecules always viewed with the single methyl at the remote end of the axis), the order of specifying the ring parameters becomes reversed in enantiomers. For example, the enantiomer of Λ-*mer-SRR**-$\delta\lambda\delta$ is Δ-*mer-S*SR*-$\lambda\delta\lambda$, or it can alternatively be written as Δ-*mer-SRS**-$\delta\lambda\lambda$.

Stabilities of the $[Co(meen)_3]^{3+}$ Isomers

Dreiding scale models show that in a Co(III)—meen ring the equatorial or axial character of an N-methyl substituent is not greatly marked, and that accordingly there is no obvious preference for an equatorial methyl since this is not directed away from the molecule as is the equatorial methyl in a Co(III)—pn ring. It is clear from the models however, that the dominating non-bonded interactions should be those of the N-methyl groups with neighbouring rings CH_3---CH_3, CH_3---ring, and CH_3---NH_2 or CH_3---NH, and that these should significantly influence the relative stabilities of the isomers. Inter-ring H---H interactions between NH and CH_2 groups of the type causing lel conformations to be preferred in $[Co(en)_3]^{3+}$ [14] may be of relatively less importance in these Co(meen) systems.

The *fac* isomers have the three methyl groups at one end of the (pseudo)-C_3 axis, whereas two methyls are together at one end of the axis in the *mer* isomers. Dreiding models show that for many of the conformers of the twelve geometric-diastereoisomers interactions between these *cis* methyls will be severe and will probably exclude the existence of some of these twelve forms. It can thus be predicted with some confidence that the Λ-*fac-RRR* and Λ-*fac-RRS* isomers will be excluded, but such semiquantitative estimates of non-bonded interactions do not indicate great differences between the other ten geometric-diastereoisomeric forms. Moreover, molecular potential energies have contributions from bond length deformations, valence angle deformations and torsional strains, as well as from non-bonded interactions, and all four effects are interdependent. A complete energy minimization analysis is therefore necessary to predict or explain the relative stabilities of isomers and conformers in this system, and this analysis is proceeding [27].

Differences in the Λ-$[Co(meen)_3]^{3+}$ and Λ-$[Co(\pm pn)_3]^{3+}$ Systems

These systems are analogous in that they each have twelve distinct diastereoisomer species as possibilities. For a Co(meen) ring, both δ and λ conformers are possible, corresponding to axial and equatorial methyl dispositions, giving a total of eightyeight conformer possibilities (for one absolute configuration of the ligands about the metal, Δ or Λ). For any Co(pn) complex system, inter-ring non-bonded atomic interactions constrain the methyl substituent to be equatorial to its particular chelate ring, so that only the one conformational arrangement with all methyls equatorial is possible for each of the twelve 'isomeric forms' of a tris(pn) complex. Thus there is essentially complete conformational stereospecificity for a Co(pn) ring, such that the enantiomers of pn will always adopt particular chelate ring conformations on coordination, *i.e.* λ for Co-*R*(−pn) and δ for Co-*S*(+pn). The more stable isomers of $[Co(pn)_x(en)_{3-x}]^{3+}$ complexes are therefore predictable on the basis of non-bonded interactions [14]. In contrast, axial arrangements cannot necessarily be excluded from the experimental isomer possibilities for Co(meen) complexes.

Important differences experimentally between the Co(pn) and Co(meen) systems are the following:

(1) Studies of Co(pn) complexes have been aided by the use of optically resolved *R*(−)pn in the syntheses, which limits the isomeric possibilities and defines the absolute stereochemistry (as *R*) at the carbon centres. The various complexes separated are optically active, so that optical rotatory properties can be employed to characterize these species. By comparison, asymmetry in the Co(meen) complexes occurs at the methylated nitrogen centres and arises only on coordination of the ligands ('donor atom asymmetry'). It is thus not possible to use the optically active ligand to simplify elucidation

of the stereochemistry in Co(meen) complexes by restricting the isomer possibilities.

(2) Moreover, optical rotatory parameters cannot be employed to characterize the separated Co(meen) species. The separations on Sephadex are obtained by exploiting geometric differences, and the separated species are racemates.

(3) Further complications in investigations of Co(meen) systems are the possible equilibrations between the NH diastereoisomers through N–H exchange (base-catalyzed) at the asymmetric donor-nitrogen atoms, and the lower stabilities of complexes with the secondary amine meen than with pn.

Isomer Possibilities for $[Co(meen)_2(en)]^{3+}$

For $[Co(meen)_2(en)]^{3+}$ three possible geometries arise from the *cis* or *trans* relative positions of the NH_2 and CH_3 groups in the two meen ligands. Each geometry has several possible diastereoisomers, giving in all ten geometrically distinct forms for each absolute configuration of the complex. All these diastereoisomeric forms for the Λ complex configuration are shown in Fig. 4, along with their designations.

Each of these ten diastereoisomer forms has four conformer combinations for the Co(meen) rings: δδ, δλ, λδ, λλ. As previously, these different conformations of the meen rings will have different dispositions of the methyl groups, equatorial or axial, so that the non-bonded interactions from the methyl groups should differ markedly in these four conformers.

Of the forty total conformers developed so far, the following particular conformers have C_2 symmetry:

Λ-*cis*-CH_3,*trans*-NH_2-*RR*,	δδ and λλ conformers
Λ-*cis*-CH_3,*trans*-NH_2-*SS*,	δδ and λλ conformers
Λ-*trans*-CH_3,*cis*-NH_2-*RR*,	δδ and λλ conformers
Λ-*trans*-CH_3,*cis*-NH_2-*SS*,	δδ and λλ conformers

Assuming conformational mobility of all chelate rings in solution, these four diastereoisomer forms would be expected to show effective C_2 symmetry in their ^{13}C NMR spectra and give four carbon

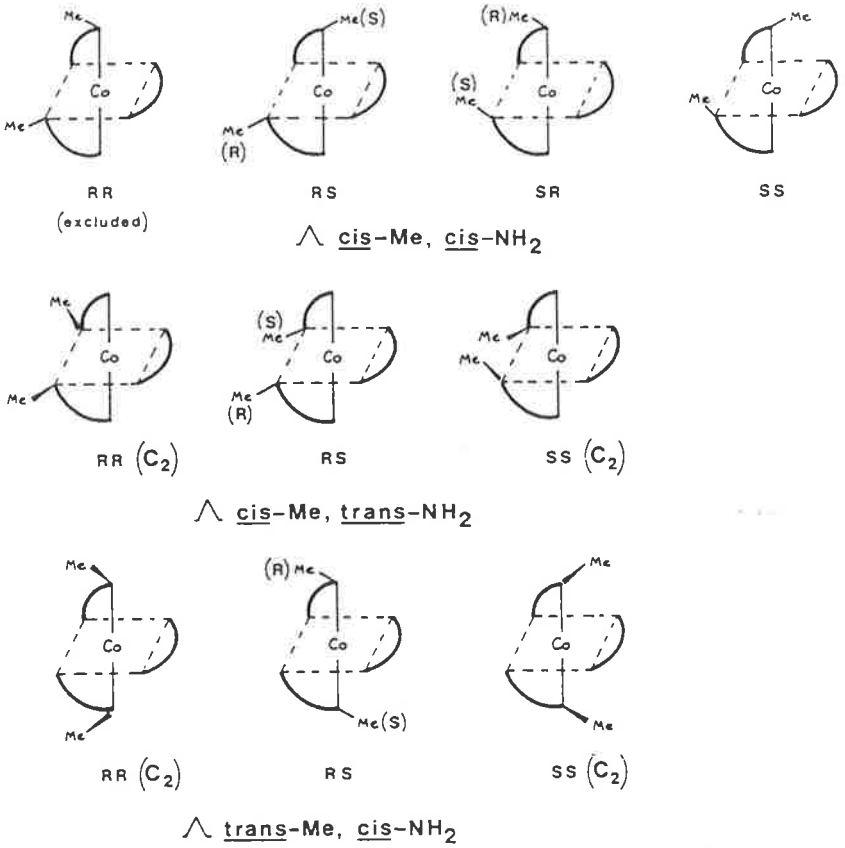

Fig. 4. Possible geometric isomers–diastereoisomers for Λ-$[Co(meen)_2(en)]^{3+}$. The four forms with effective C_2 symmetry are noted. For each of the geometries Λ-*cis*-CH_3,*trans*-NH_2 and Λ-*trans*-CH_3,*cis*-NH_2, the *RS* and *SR* forms are identical.

resonances, three from Co(meen) and one from Co(en). The other six diastereoisomer forms have C_1 symmetry and should give eight carbon resonances.

The alternative possible conformations of the Co(en) ring δ or λ will double the number of total conformer combination possibilities to eight for each diastereoisomeric form. Although the non-bonded interactions of the methyl substituents should not be greatly affected by these alternative Co(en) ring conformations, both of the en conformer possibilities will have to be considered in a complete analysis of the system. One of the diastereoisomers, Λ-*cis*-CH_3,*cis*-NH_2-*RR* (which corresponds to the least likely and excluded $[Co(meen)_3]^{3+}$ diastereoisomer), can be reasonably excluded on the basis of the methyl interactions which are indicated by models to be severe in all of the conformers. However, assessment of the stability order for the other nine forms requires a complete energy minimization analysis [27].

Isomer Possibilities for $[Co(meen)(en)_2]^{3+}$

Two diastereoisomers are possible for each configuration Λ or Δ, Fig. 5, and each diastereoisomer has alternative conformations of the Co(meen) ring. Thus the conformers are Λ-*R*-δ (eq, lel); Λ-*R*-λ (ax, ob); Λ-*S*-δ (ax, lel); Λ-*S*-λ (eq, ob).

The two diastereoisomers are in principle separable chromatographically. All the conformers have C_1 symmetry, so that with conformational averaging of all chelate rings in solution seven ^{13}C NMR resonances could be expected from each diastereoisomer in solution.

The non-bonded interactions from the methyl would seem to be lowest for the Λ-*R*-δ conformer where the methyl lies between the two en rings, suggesting that the Λ-*R* should be the more stable diastereoisomer, as considered previously by Sargeson [18].

For each diastereoisomer and Co(meen) conformer, four conformer combinations for the $Co(en)_2$ rings are possible, $\delta\delta$, $\delta\lambda$, $\lambda\delta$, and $\lambda\lambda$. Thus there are sixteen conformers in all for each configuration Λ or Δ.

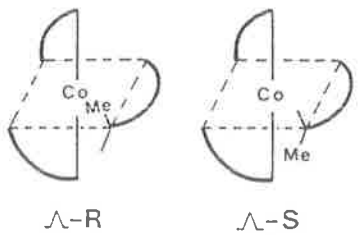

Fig. 5. Diastereoisomers of Λ-$[Co(meen)(en)_2]^{3+}$. Λ-*R* is predicted to be the more stable.

Results and Discussion

Syntheses for $[Co(meen)_3]^{3+}$

Several methods were examined for the preparation of $[Co(meen)_3]^{3+}$, in anticipation that different non-equilibrium syntheses might yield some different isomers.

Two main methods were employed. Oxidation of a mixture of $CoCl_2$ + 3meen in dimethylsulfoxide, with Me_2SO functioning as both solvent and oxidant [28], yielded a clean red product $[Co(meen)_3]Cl_3$ in high yield. This solid was one isomer **A**, but it was subsequently shown to isomerize rapidly in water to an equilibrium mixture of three isomers designated **A**, **B** and **C**. These designations refer to their chromatographic elution order. Aerial oxidation of Co(II) with meen in aqueous solution, in the presence of charcoal, was carried out at 80 °C as used by Keller and Edwards [1]. This method yielded a yellow–orange product, which was a mixture of $[Co(meen)_3]Cl_3$ as one isomer **C** (which equilibrates in water to the **A**, **B**, **C** mixture), three isomers of $[Co(meen)_2(en)]^{3+}$ designated **F**, **G** and **H**, one isomer of $[Co(meen)(en)_2]^{3+}$ **E**, and $[Co(en)_3]^{3+}$ **D**. Demethylation is thus a significant process during the aerial oxidation at 80 °C, and it must involve charcoal and probably the oxygen also.

The following syntheses did not yield any different isomers of the above complexes. From aerial oxidation carried out in methanol at 45 °C and without charcoal, the red product which precipitated was $[Co(meen)_3]Cl_3$ as isomer **C** only. Apparently **C** is the least soluble isomer as the chloride salt in water and methanol, whereas **A** is the least soluble chloride in dimethylsulfoxide, and syntheses in these different media yield these different solid isomers because of rapid equilibration. Accordingly, recrystallization of the **A** $[Co(meen)_3]Cl_3$ product from water gave pure **C** isomer, so that both of the main isomers can be readily obtained from the dimethylsulfoxide synthesis.

Substitution reactions $[Co(NH_3)_5(H_2O)]^{3+}$ + 3meen in water at 80 °C without charcoal gave $[Co(meen)_3]^{3+}$ in **A**, **B**, and **C** isomers as from the dimethylsulfoxide oxidation. However if charcoal was present this substitution reaction yielded yellow demethylated complexes. These substitution reactions produced numerous by-products and were not useful.

Sephadex Separation of the $[Co(meen)_3]^{3+}$ Isomers from the Dimethylsulfoxide Oxidation Synthesis

Sephadex chromatography indicated that all the various $[Co(meen)_3]Cl_3$ products behaved identically. With the acidic eluent 0.2 M Na_2SO_4/H_2SO_4 pH 2, two orange–red bands separated (1), first eluted, and (2), and these were in the amount ratio (1)/(2) *ca.* 2. The complexes in the eluted bands were

isolated by using a cation-exchange process: they were eluted off a resin column by either HBr or HCl, then obtained by evaporation of the HX eluent. The ^{13}C NMR spectra in D_2O/HBr (see below) showed that the band (1) product contained two isomers A and B in the mole amount ratio A/B *ca.* 3, and that the band (2) product consisted only of a single isomer C. The ratios of these $[Co(meen)_3]^{3+}$ isomers are thus A:B:C = 3:1:2, and no other isomers have been detected.

These isomers were the most satisfactorily crystallized as the bromide salts. Slow crystallization of the solutions gave large crystals of A and C. Isomer B could not be crystallized separately from the band (1) material as the bromide. However, on careful crystallization all of A could be removed pure as the bromide to leave only B in the mother liquor, from which B could be obtained as the nitrate or perchlorate salts (using conversion on Dowex resin).

With 0.1 M Na_3PO_4 eluent, the various $[Co(meen)_3]^{3+}$ isomers moved together as a pink–red band because they rapidly equilibrate in the basic conditions of the eluent. This $[Co(meen)_3]^{3+}$ band was preceded immediately by a purple smear. This purple must have contained hydrolysed species, probably $[Co(meen)_3(OH)]^{2+}$, which arose in the basic conditions, since on changing the eluent to NaCl the hydrolysis ceased and the purple was then eluted out ahead of the remaining orange $[Co(meen)_3]^{3+}$ band.

Distinction of $[Co(meen)_3]^{3+}$ Isomers by ^{13}C NMR Spectra and Chromatography

There are twelve geometrically distinct forms possible for $[Co(meen)_3]^{3+}$ (geometric isomers and N–H diastereoisomers), and each can exist in a number of conformers, giving eightyeight conformers in all for each configuration of the ligands about the cobalt as elaborated above. In solution the conformers of each 'geometric' form should rapidly equilibrate, so that the ^{13}C NMR spectra should show the highest conformational symmetry of the particular 'geometric' form by rapid conformational averaging. Two of the twelve geometric forms have C_3-symmetry conformers (Table 1) so that these geometric forms Λ-*fac-RRR* and Λ-*fac-SSS* should show effective C_3 symmetry and give three carbon resonances. All conformers of the other ten 'geometric' forms have C_1 symmetry, so that nine ^{13}C NMR resonances will be expected for each of these forms, three from each chemically distinct carbon type.

The three resonances from meen·2HCl are assigned as δ 45.9, MeN^+H_2–C; δ 35.8, C–N^+H_3; δ 33.8, CH_3. (These assignments follow from the off-resonance spectrum, and from comparisons with the spectra of en·2HCl (δ 36.9) and dien·3HCl

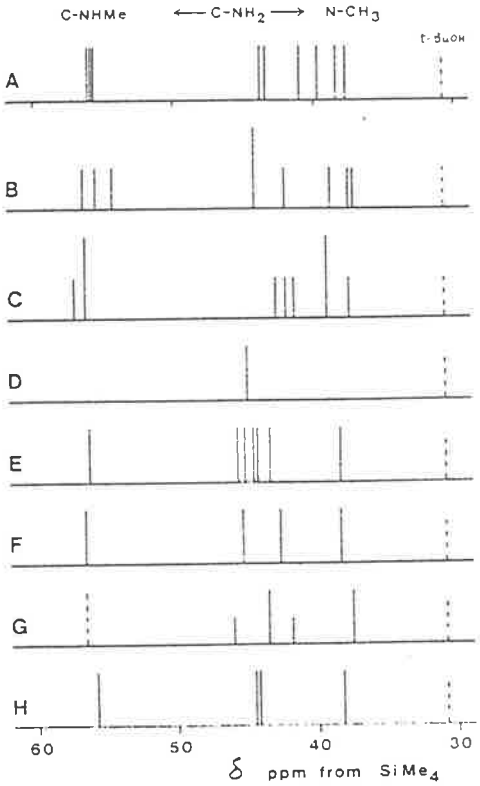

Fig. 6. 20.1 MHz ^{13}C NMR spectra of Co(meen) complexes as bromide salts in D_2O/HBr (t-butyl alcohol capillary reference, δ 30.79 ppm from $SiMe_4$). A–C, $[Co(meen)_3]^{3+}$ isomers, all C_1 symmetry: D, $[Co(en)_3]^{3+}$; E, $[Co(meen)(en)_2]^{3+}$; F and H, $[Co(meen)_2(en)]^{3+}$ isomers with C_2 symmetry; G, $[Co(meen)_2(en)]^{3+}$ isomer with C_1 symmetry.

(δ 45.0 and 35.8) [29].) The isomers of $[Co(meen)_3]^{3+}$, and also those of $[Co(meen)_2(en)]^{3+}$ and $[Co(meen)(en)_2]^{3+}$, each show resonances in three regions corresponding to these three different carbon types in meen·2HCl (Fig. 6). The signals from the complexes are downfield from those in the protonated amine, but the relative order of the chemical shifts of the three carbon types is unchanged [29, 30].

Inversions of configurations at the asymmetric nitrogens of the individual ligands of $[Co(meen)_3]^{3+}$ will be expected to occur, through proton-exchange, as in the racemization of $[Co(NH_3)_2(meen)]^{3+}$ [9]. This base-catalyzed process should lead to equilibration between diastereoisomeric forms which differ only in N-configurations, *i.e.* between the four Λ-*fac* forms, and between the eight Λ-*mer* forms. Such equilibrations are slower than the NMR time scale however, so that the NMR resonances from the individual 'geometric' forms should be recorded. This N–H isomerization has been recorded previously in some N_4 macrocycle systems with nickel(II)

[31], and with the complex system [Co(hexacyclen)]$^{3+}$, hexacyclen = 1,4,7,10,13,16-hexaazacyclooctadecane [32], and resonances of the individual NH diastereoisomers are observed from the equilibrium mixture of each system.

The ^{13}C NMR spectra of the isomers **A**, **B** and **C**, run in acid to inhibit hydrolysis, are quite similar (Fig. 6), each showing nine different carbon atoms (in 9 or 8 peaks) which give the symmetry of each as C_1.

The twelve 'geometric' forms are in principle distinguishable chromatographically, provided that the interconversions between these forms are much slower than the time required for a chromatographic separation. These interconversions should be precluded in the acidic conditions of the eluent Na_2SO_4/H_2SO_4 in chromatography. If equilibrations occur within the separation time, as in a basic eluting medium such as Na_3PO_4, only two bands corresponding to the *mer* diastereoisomer mixture and the *fac* diastereoisomer mixture would be expected if only N–H isomerizations were involved (and if both *mer* and *fac* forms could exist). If equilibration between *mer* and *fac* forms occurred during the chromatography, only one band would be obtained.

Equilibration Between the [Co(meen)$_3$]$^{3+}$ Isomers

Equilibration between the three [Co(meen)$_3$]$^{3+}$ isomers occurs readily even in neutral water. Thus the ^{13}C NMR spectra of **A** or **C** bromides in D_2O (pH *ca.* 5.5) accumulated up to one hour from dissolution showed resonances from all three isomers. The spectra obtained by further accumulations (over 2–9 h from dissolution) were essentially the same, so that equilibration must have been reached within about one hour at 25 °C. The equilibrium isomer ratio as estimated from the relative peak ratios (3:1:2) agrees with that assessed from the chromatography.

These various equilibrated solutions from the pure **A** or **C** isomers were re-separated on Sephadex with Na_2SO_4/H^+ elution into the two orange–red bands of (**A** + **B**) and **C**, to give the same ratios of the three complexes as previously. This ratio, **A**:**B**:**C** = 3:1:2, is therefore the equilibrium ratio at room temperature.

The rapid equilibration is also demonstrated in Sephadex chromatography, where elution with Na_2SO_4 in water, pH 5.5, gave less separation than with the eluent acidified to pH 2. Thus to avoid isomerization, the complexes must be chromatographed and manipulated in acidic solution, pH ⩽2.

The facility of interconversion between the 'geometric' forms of [Co(meen)$_3$]$^{3+}$ contrasts markedly with the robustness towards racemization and isomerization of other cobalt(III)–hexamine complexes such as [Co(en)$_3$]$^{3+}$ and [Co(dien)$_2$]$^{3+}$ [33]. Also, the isolated 'geometric' forms of [Co(meen)$_2$(en)]$^{3+}$ **F** and **H** are robust in base, being separated chromatographically using Na_3PO_4 (see later). Thus the isomerization of [Co(meen)$_3$]$^{3+}$ cannot involve rearrangement of chelate rings, but must be due to N–H inversions at the asymmetric nitrogen centres. This N–H isomerization, occurring in neutral conditions, is more facile however than in Ni(II)–macrocycle systems (where basic conditions 0.1 M NaOH over some hours were used to effect equilibration) [31] and in [Co(hexacyclen)]$^{3+}$ [32].

Thus the three isomers **A**, **B**, **C** must be diastereoisomers of the one geometry, and the similarity in the ^{13}C NMR spectra is consistent with this. This geometry is most probably *mer*, as some of the *fac* forms have been excluded on the basis of large non-bonded interactions, and also because the C_3 symmetries of some *fac* conformers should have reflected in the ^{13}C NMR spectra.

The two red bands separated previously by paper and thin layer chromatography [21, 22] must have been the major isomers **A** and **C**.

Aerial Oxidation Synthesis for [Co(meen)$_3$]$^{3+}$ with Charcoal at 80 °C, and Characterization of the Products

This synthesis follows the conditions as first used by Keller and Edwards [1]. With the solution stoichiometry

$$CoCl_2 + (5/2)meen + (1/2)(meen\cdot 2HCl) + (1/4)O_2 \longrightarrow [Co(meen)_3]Cl_3 + (1/2)H_2O$$

and charcoal present, aeration was carried out at 80 °C for 2 h then continued at room temperature for two days. The crude product was obtained by precipitation, and the low yield (50%) reflected the lower stabilities of complexes with N-substituted-en than those with en [34], but was due also to the high solubility of the complex mixture. This product could be fractionally crystallized from water fairly cleanly into two portions: the less soluble fraction, yellow, contained complexes with en ligands which must have arisen by demethylation of meen. The more soluble red portion predominated and contained [Co(meen)$_3$]$^{3+}$. This red material was largely complex **C** (by ^{13}C NMR in acid) as the least soluble [Co(meen)$_3$]$^{3+}$ isomer from water, with a little demethylated complex (**H**) also present.

The yellow materials were separable by Sephadex chromatography using Na_3PO_4 elution into four yellow–orange bands of CoN_6 complexes (Fig. 7). The complexes in these bands are designated **D**, **E**, **F** + **G**, and **H** according to their elution order, and were isolated using cation-exchange.

These complexes were characterized by ^{13}C NMR spectra (Fig. 6), and the chemical forms were confirmed by elemental analyses. **D** was [Co(en)$_3$]$^{3+}$,

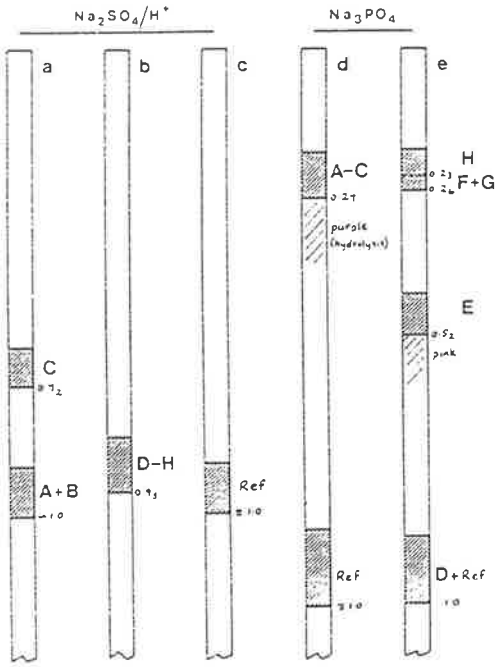

Fig. 7. Chromatographic separations on SP-Sephadex columns with different eluents 0.2 M Na_2SO_4/H_2SO_4 pH 2 and 0.1 M Na_3PO_4: columns (a) and (d), the red $[Co(meen)_3]^{3+}$ products A–C of the dimethylsulfoxide oxidation synthesis; columns (b) and (c), the less soluble yellow demethylated products **D**–**H** of the oxygen oxidation synthesis with charcoal. $[Co(en)_3]^{3+}$ has been added to columns (c), (d) and (e) as a reference. The figures are R_x values relative to $[Co(en)_3]^{3+}$.

being identical to the authentic complex (by ^{13}C NMR single resonance, and Sephadex elution).

Complex **E** showed seven approximately equal ^{13}C NMR peaks, consistent with one of the two possible diastereoisomers of $[Co(meen)(en)_2]^{3+}$.

The material from the orange third Sephadex band contained two complexes **F** and **G**, with the eight ^{13}C NMR resonances being in two sets of unequal intensities. The major component **F** was obtained pure by careful crystallization and showed four equal ^{13}C NMR peaks, identifying it as a C_2-symmetry isomer of $[Co(meen)_2(en)]^{3+}$. The other four peaks in the mixture spectrum, apparently unequal, are from **G**, which cannot be crystallized separately. The general pattern of these ^{13}C NMR resonances, together with **G** chromatographing coincidently with **F** and satisfactory elemental analyses, indicate that **G** is another $[Co(meen)_2(en)]^{3+}$ isomer. However, the three unequal resonances in the H_2N–C– region show that **G** would have C_1 symmetry and the peak assignments from the eight different carbons in $[Co(meen)_2(en)]^{3+}$ would then have to be: a resonance from two MeHN–C– carbons coincident with and obscured by the peak δ 56.5 from complex **F**; peaks 1:2:1 from H_2N–C– carbons; and the upfield peak δ 37.5 from the two methyl carbons coincidently.

H was the main yellow product. With four ^{13}C NMR peaks and eluting closely behind **F** + **G**, it is another C_2 isomer of $[Co(meen)_2(en)]^{3+}$.

The product ratios were determined semiquantitatively as **D**:**E**:**F**:**G**:**H** = 2:12:5:1:36 by visual assessment of the Sephadex bands, and from the ratio **F**/**G** determined from the ^{13}C NMR spectrum of the evaporated mixture from the orange third Sephadex band. The extent of the demethylation and hence the proportions of the different complex systems would be expected to vary with the preparative conditions (charcoal, air or oxygen, temperature, time) so there would be little significance in the ratios of these, **D**:**E**:**F** + **G** + **H** = 1:6:21, except that the ratios indicate that demethylation takes place sequentially and not stereoselectively from one of the $[Co(meen)_3]^{3+}$ complexes to give **E**. However, the ratios of the isomers within each system are meaningful as the isomers should be in equilibrium on the charcoal, and these experimental ratios can be compared with those calculated from energy minimizations. The useful figures are: for $[Co(meen)(en)_2]^{3+}$, one isomer **E** formed essentially stereospecifically; for $[Co(meen)_2(en)]^{3+}$, **F**:**G**:**H** *ca.* 5:1:36.

The ratios are also expected to vary to some extent with the manner of isolation, which was precipitation of crude total complex from the reaction mixture, followed by fractional recrystallization to obtain the less soluble yellow material. Clearly some other minor isomers which were formed would have remained in the mother liquors, but more important is the possible loss of isomers of higher solubility which might have been present in reasonable amounts in the equilibrium. We feel that the various isomers of each complex would not range so greatly in solubility as to cause the ratios obtained in the isolated solid to be markedly different from the equilibrium values, and thus we take the above ratios for the systems $[Co(meen)_2(en)]^{3+}$ and $[Co(meen)(en)_2]^{3+}$ to represent roughly the equilibrium ratios.

Equilibrations between the Demethylated Complexes and Deductions of Stereochemistry

For $[Co(meen)(en)_2]^{3+}$, the two N–H diastereoisomers possible (Fig. 5) will interconvert rapidly in base by proton exchange, so that the material isolated from the Na_3PO_4 effluent should contain these isomers in equilibrium proportions. As with the $[Co(meen)_3]^{3+}$ system, the two N–H diastereoisomers should also interconvert in neutral water, when the separate forms should be evident in the ^{13}C NMR spectrum run under such conditions. That

only one isomer **E** has been observed indicates the high stereospecificity in this mono(meen) system.

For the C_2-symmetry isomers **F** and **H** of $[Co(meen)_2(en)]^{3+}$ there are four possibilities (Fig. 4). That **F** and **H** do not interconvert in weak base (during the separation with Na_3PO_4, pH 12) shows that they are not diastereoisomers of the same geometric isomer. Thus they must be the most stable diastereoisomers in the different geometric isomer systems, *cis*-CH_3,*trans*-NH_2 and *trans*-CH_3, *cis*-NH_2. The stereospecificity within each geometry is apparently high, as only the one N–H diastereoisomer in each system has been observed, *i.e. RR* or *SS*, but not *RS*.

Complex **G** involves some uncertainty. The band (3) material containing **F** and **G** was in only small proportion, and from this only a small quantity of **F** has been isolated, and **G** has been observed only in solution with **F**. We were unable to carry out extensive equilibration trials, but a solution of **F** (pure by ^{13}C NMR in D_2O/HBr) after basifying with NaOH to pH 12.5 gave no indication of the resonances from **G** when the ^{13}C NMR spectrum was re-recorded (albeit only weak resonances expected). This suggests that **F** and **G** do not interconvert, which would exclude **G** as the **RS** diastereoisomer (C_1 symmetry) of the same geometry as **F**. Since **G** and **H** do not interconvert, **G** would then be the stable diastereoisomer of the third possible geometry for $[Co(meen)_2(en)]^{3+}$,*cis*-CH_3,*cis*-NH_2.

Work is in progress to determine the structures of these isolated complexes by single crystal X-ray analysis [35].

The Mechanism of Demethylation

Demethylation clearly occurred during the aerial oxidation synthesis of $[Co(meen)_3]^{3+}$ with charcoal at 80 °C, but the yellow demethylated complexes were not evident from a similar aerial oxidation preparation at 20 °C. Demethylated complexes were also produced in a substitution synthesis $[Co(NH_3)_5Cl]Cl_2$ + 3meen at 80 °C with charcoal, but not from a similar synthesis without charcoal. Thus demethylation occurs only with charcoal and at elevated temperatures, but the possible involvement of oxygen is unclear from these results.

Such demethylation processes have been observed previously in some other Co(III) systems. N–C cleavage was first demonstrated in the oxygen oxidation preparation at elevated temperature of $[Co(etolen)_3]^{3+}$ [etolen = 2-(2′-aminoethylamino)ethanol] when by-products $[Co(en)_3]^{3+}$, ammonia and formaldehyde were observed. No $[Co(en)_3]^{3+}$ was found from the substitution preparation $[Co(NH_3)_6]^{3+}$ + 3etolen with charcoal [36–38], but dealkylation was observed from $[Co(etolen)_3]Cl_3$ in water with charcoal and air. Thus charcoal and oxygen both have essential roles in these cleavage reactions [37–39].

Demethylation from *s-fac*-$[Co(medien)_2](ClO_4)_3$ [medien = 4-methyldiethylenetriamine] in water with charcoal (90 °C, 3 days) was substantial to give *s-fac*-$[Co(dien)(medien)]^{3+}$ as the main product (11%), and some *mer*-$[Co(dien)_2]^{3+}$ was also formed. Oxygen was shown to be necessary for this process also [40]. This work, like the $[Co(etolen)_3]^{3+}$ reactions, demonstrated that N–C cleavage is not of necessity associated with formal Co(II) + O_2 oxidation processes but can also occur from Co(III) species with charcoal present. However these Co(III) reactions may in fact involve Co(II) species behaving as catalysts, and these could presumably be generated by reduction on the charcoal. Evidence for such Co(II) involvement has been provided from detailed studies of the following systems in which demethylation occurred:

Co(II) + etolen + charcoal + O_2

$[Co(etolen)_3]Cl_3$ + charcoal + O_2

In each system the Co(II) concentration reached a steady state value, but only if charcoal was present [39].

The demethylation in the present $[Co(meen)_3]^{3+}$ system was further examined by heating solutions of pure **A**-$[Co(meen)_3]Br_3$ in D_2O at 80 °C for three hours under the following conditions:

(i) with oxygen bubbling;

(ii) with added freshly ground charcoal and oxygen bubbling;

(iii) with added charcoal, but with nitrogen bubbling.

The ^{13}C NMR spectrum from (i) showed an equilibrium mixture of the $[Co(meen)_3]^{3+}$ isomers **A**, **B** and **C**. The deep-red solutions from (ii) and (iii) after filtering off the charcoal gave similar ^{13}C NMR spectra. These were complicated, and they showed several new peaks and some peaks enhanced from (i) consistent with the appearance of demethylated products **E**, **F** and **H**, and a decrease in some peaks from (i) consistent with a decrease of **A** and **C**. The experiment (iii) is inconclusive about the role of oxygen, as traces of oxygen might be difficult to exclude. We could not detect by ^{13}C NMR any expected monocarbon products from the demethylation (HCO_2H, HCHO, MeOH), although these could have been removed with the charcoal. These product solutions were also examined by Sephadex chromatography on small columns using Na_3PO_4 and Na_2SO_4/H^+ eluents. The bands separating from reaction mixtures (ii) and (iii) were similar, and consistent with substantial demethylation to **F** and **H**, although (with sulfate elution) bands corresponding to **A** and **C** were evident. A purple band of hydrolyzed species was also present.

Similar experiments starting from meen or meen·2HCl (in D_2O with added charcoal and oxygen, 80 °C for 8 h) showed that no demethylation occurred from the uncoordinated amine.

These present results reinforce the conclusions about the demethylations in Co(III) systems observed previously. All the various observations on the three systems indicate that the oxidative N–C cleavage reactions involve free radicals. A plausible radical mechanism has been proposed (particularly for dealkylation in the oxygen oxidation synthesis of $[Co(etolen)_3]^{3+}$) in which an initial addition product of Co(II) with molecular oxygen goes to a Co(III)–superoxide intermediate. This oxide nucleophile can then attack a carbon, leading on to N–C scission [39].

Nickel peroxide is a standard free-radical oxidizing agent [41], and has been found to effect radical demethylations of *N*-methylamides [42]. However, the reagent did not effect demethylation of A-$[Co(meen)_3]Br_3$ (in D_2O at room temperature for 4 h).

Sephadex Chromatography Behaviour of the Various Complexes

The chromatographic separations on SP-Sephadex cation-exchange resin columns of the various complexes and isomers from the two main preparations are represented in Fig. 7. The separations are quantified in terms of R_x values (relative R_F) relative to $[Co(en)_3]^{3+}$ as the reference complex, obtained by using small amounts of complexes on small columns [43, 44], and these values are shown on the diagrams.

It is notable that the eluent SO_4^{2-}/H^+ gives almost no discrimination between the various demethylated products in the less soluble yellow material from the aerial oxidation synthesis $[Co(en)_3]^{3+}$ (**D**), $[Co(meen)(en)_2]^{3+}$ (**E**) and the isomers of $[Co(meen)_2(en)]^{3+}$ (**F**), (**G**), (**H**). However, with a third methyl substituent a reasonable separation between the $[Co(meen)_3]^{3+}$ isomers **A** and **C** is obtained with this eluent.

The eluent PO_4^{3-} is usually considerably more discriminating than SO_4^{2-} [43], and it effects a good separation between the differently demethylated complexes in the present work. The complexes elute progressively more slowly (lower R_x) with increasing methyl substituents:

$$[Co(en)_3]^{3+} > [Co(meen)(en)_2]^{3+} > [Co(meen)_2(en)]^{3+} \approx [Co(meen)_3]^{3+}$$

This is clearly attributable to decreasing numbers of N–H sites for association to the PO_4^{3-} anions, and perhaps also to increasing conformational rigidity caused through the steric interactions of the methyls which might hinder the optimal development of the N–H---O hydrogen bonds. There is little discrimination between the three geometric isomers of $[Co(meen)_2(en)]^{3+}$ and the single geometry (*mer*) of $[Co(meen)_3]^{3+}$, so that some saturation condition seems to be reached with two methyl substituents.

The NH diastereoisomers of the one geometry (*mer*) of $[Co(meen)_3]^{3+}$ interconvert rapidly even in neutral solution, so that they elute as one band with PO_4^{3-}, presumably corresponding to the NH diastereoisomer and conformer forming the optimum hydrogen bonding with that eluting anion [45]. The diastereoisomers of the other complexes should behave in the same manner. However SO_4^{2-} does effect separations between the NH diastereoisomers of $[Co(meen)_3]^{3+}$ (in acidic conditions), and this is surprising in view of the failure of SO_4^{2-} to separate the different methylated complexes where the differences would be expected to be less subtle.

The elution order for the three $[Co(meen)_2(en)]^{3+}$ isomers, (F + G)>H, or more precisely for the geometries of which they are the isolated diastereoisomers, can now be rationalized on the basis of the structure known for F by X-ray analysis [35] and the tentative structures deduced for G and H from the ^{13}C NMR spectra and their non-equilibrations in base. The geometry *cis*-CH_3,*cis*-NH_2, which has been assigned to G, provides one set of three primary amine groups, at one end of the pseudo-C_3 axis in each of the three diastereoisomers *RS*, *SR* and *SS*, which should be suitable for hydrogen-bonding to a PO_4^{3-} anion (diastereoisomer *RR* has been excluded). The geometry *trans*-CH_3,*cis*-NH_2, of complex F [35], has a set of three N–H bonds at each end of the pseudo-C_3 axis in the *SS* diastereoisomer, although each of these sets involves a (coordinated) secondary amine function. With the third geometry *cis*-CH_3,*trans*-NH_2, there is one set only of three N–H bonds, and one of these is from a secondary amine group. This geometry appears to present the least favourable hydrogen bonding conditions, and the assignment of this third geometry to the remaining complex H is consistent with this isomer being the slowest eluting.

Experimental

^{13}C NMR Spectra

20.1 MHz ^{13}C NMR spectra in D_2O, broad-band proton decoupled, were recorded on a Bruker WP80-DS spectrometer locked to deuterium. An S192 data table was used. For spectra in D_2O, a capillary of t-butyl alcohol provided a reference signal at 618.9 Hz, δ 30.79 ppm for CH_3 downfield from $SiMe_4$. (This reference signal was measured for a t-butyl alcohol capillary in $CDCl_3$ against $SiMe_4$ as internal reference.)

As with other cobalt(III) (3+)-charged complexes previously studied, the chemical shifts of the resonances of the $[Co(meen)_3]^{3+}$ isomers show little variation with different anions. Any such variation is similar to that found between different recordings of the same complex, generally 0.1 in δ.

The integrated intensities of proton-decoupled ^{13}C resonances may not in general be proportional to the number of carbon nuclei in each peak due to varying nuclear Overhauser enhancements and differences of the spin-lattice relaxation times [46, 47]. However, we have found that ^{13}C NMR peak areas of CH_2 and $N-CH_3$ carbons from a number of polyamine complexes of cobalt(III) do reflect carbon concentrations to within 20%, and frequently better [29, 45]. A similar situation obtains with the ^{13}C peak ratios of the complexes in the present work, and the ratios quoted have been rounded to integral values.

The amine meen (Fluka purum) was used as supplied. Its high purity was confirmed by the ^{13}C NMR spectrum run in D_2O (δ 52.9, 40.0, 34.8 ppm) when the en resonance (δ 43.2) was completely absent, and also by the spectrum of meen·2HCl (δ 45.9, 35.8, 33.8) when en·2HCl (δ 36.9) was absent.

Some of the amine was converted to meen·2HCl by addition of stoichiometric HCl in a methanol solution, filtering off the precipitated product, and washing with methanol.

Synthesis of $[Co(meen)_3]Cl_3$ by Dimethylsulfoxide Oxidation

$CoCl_2 \cdot 6H_2O$ (9.52 g, 0.04 mol) was dissolved in Me_2SO (20 ml, BDH Analar). The solution was heated to boiling and maintained for 5 min (140–160 °C) to remove much of the water, then cooled to 70 °C. A solution of meen (7.35 g, 0.10 mol) and meen·2HCl (2.94 g, 0.02 mol) in Me_2SO was prepared with warming in the minimum volume of the solvent (14 ml). The warm cobalt solution was added to the stirred amine solution whereupon reaction ensued within seconds: the temperature rose, the colour changed from blue to dark brown, a sulfide odour signified reduction of Me_2SO, and the $[Co(meen)_3]Cl_3$ product commenced to separate. The mixture was maintained at about 70 °C for 5 min, then allowed to cool to room temperature.

The fine reddish crystalline product was filtered off, washed with ethanol and acetone, and air-dried. Yields were variable, up to 14.5 g, 93%. *Anal.* Calc. for $[Co(C_3H_{10}N_2)_3]Cl_3$: C, 27.9; H, 7.8; N, 21.7. Found: C, 27.5; H, 8.0; N, 21.5%. This material was essentially pure isomer A, but on recrystallization from water with ethanol pure isomer C was obtained (^{13}C NMR spectra in D_2O/HCl). Both of these solids separated into two red components by thin layer chromatography (TLC) (sec-butanol/water/conc. HCl eluent on cellulose).

Sephadex Chromatographic Separation of the $[Co(meen)_3]^{3+}$ Isomers and their Characterization

A solution of $[Co(meen)_3]Cl_3$ from the above (1.0 g in 60 ml water) was applied to a large column (4.5 diam × 40 cm) of SP-Sephadex C-25 cation-exchange resin, and washed on with water. The column was eluted with 0.2 M Na_2SO_4/H_2SO_4 to pH 2, and the two orange–red bands which separated were collected. All samples of $[Co(meen)_3]Cl_3$, and also mother liquors, gave the same two bands only, and always in the same ratio: first eluted (1)/second eluted (2) *ca.* 2, assessed visually. (1) contained A + B, with A/B *ca.* 3 by ^{13}C NMR, and (2) contained C.

In isolation of the complexes, solutions were kept acidic to avoid isomerization. The two band effluents were diluted and applied to small columns (1.2 × 10 cm) of Dowex 50W-X2 cation-exchange resin, 200–400 mesh, H^+ form. The columns were washed first with 0.1 M HBr to remove all Na^+ (otherwise NaBr may crystallize subsequently), then the complexes were eluted off with 3 M HBr. These effluents were each rotary-evaporated to a sludge, and further HBr was removed by drawing air through the flask.

Each sludge was dissolved in 0.01 M HBr (*ca.* 4 ml) and the solution was left to crystallize in a vacuum desiccator. The mother liquor was sucked off and the deep-red crystals were air-dried on filter paper. The crystals obtained from band (1) were pure isomer A. *Anal.* Calc. for $[Co(C_3H_{10}N_2)_3]Br_3 \cdot 2H_2O$: C, 19.4; H, 6.1; N, 15.1; Br, 43.0. Found: C, 19.4; H, 6.1; N, 15.0; Br, 43.7%. ^{13}C NMR peaks: δ 56.1, 55.9, 55.7, 43.8, 43.4,* 41.0,* 39.7,* 38.4,* 37.7 ppm. A could be crystallized pure to leave B predominating in the HBr mother liquor, and further careful crystallization of A left essentially only B in the mother liquor as shown by its ^{13}C NMR spectrum: δ 56.5, 55.6, 54.4,* 44.3 (2 carbons),* 42.1, 38.9,* 37.6, 37.3,* (* are unique and distinctive peaks of the particular isomer). B could not be crystallized as bromide, but it could be isolated as the nitrate salt (from Dowex/1 M HNO_3) and as the perchlorate salt (from Dowex/3 M HCl, followed by concentrated $HClO_4$).

The crystals from band (2) were pure isomer C. *Anal.* Calc. for $[Co(C_3H_{10}N_2)_3]Br_3 \cdot H_2O$: C, 20.0; H, 6.0; N, 15.6; Br, 44.5. Found: C, 20.1; H, 6.0; N, 15.5; Br, 43.8%. ^{13}C NMR δ 57.2,* 56.4 (2 C), 42.8,* 42.1, 41.5* 39.2 (2 C),* 37.6 ppm. Resonances from the chloride salts were generally identical (±0.1 δ) to those of the bromides, except that the signals giving the double peak in the bromide of (C) (δ 56.4) were resolved into separate peaks in the chloride (δ 56.7, 56.4).

Aerial Oxidation Synthesis for $[Co(meen)_3]^{3+}$ with Charcoal

(a) At 80 °C

A solution of $CoCl_2 \cdot 6H_2O$ (19.0 g, 0.08 mol), meen·2HCl (5.9 g) and meen (14.8 g) in water (40 ml), with activated charcoal (2 g), was aerated while being heated (80 °C) over a steam bath for 2 h. Aeration was then continued at room temperature for 2 days. The charcoal was filtered off, and the volume was reduced. Ethanol was added carefully, to precipitate an orange solid. This was filtered off, washed with ethanol and acetone, and air-dried. Yield 16 g, 52%. No further tris(diamine) product crystallized on addition of $NaClO_4$ to the red–violet mother liquor, but small amounts of violet and subsequently green complexes were obtained, which were probably the isomers of $[Co(meen)_2Cl_2]$-ClO_4.

The orange hexamine complex product was fractionally recrystallized from water by addition of ethanol. The first fractions obtained were yellow, and the later more soluble fractions red, and the red material predominated. The yellowish fractions were collectively recrystallized to remove any red material; this purification was necessary as the complexes within the yellow material are not separable from those in the red material by Sephadex chromatography as used subsequently (Fig. 7).

The hexamine component complexes **D**, **E**, **F**, **G**, **H** of the yellow material were not separable by TLC. Careful fractional recrystallization gave some of the major component **H** pure (^{13}C NMR) in a first fraction. *Anal.* Calc. for $[Co(C_3H_{10}N_2)_2(C_2H_8N_2)]Cl_3 \cdot 1.5H_2O$: C, 24.0; H, 7.8; N, 21.0. Found: C, 24.1; H, 7.8; N, 21.0%. However, the subsequent yellow fractions were mixtures, so that all the complexes were best obtained by Sephadex chromatography (see below).

The red solid fractions were largely isomer **C** of $[Co(meen)_3]Cl_3$, but contained a little demethylated complex **H** (by ^{13}C NMR in acid), with **H** decreasing along the fractions. All the red fractions were chromatographically identical to the red $[Co(meen)_3]Cl_3$ product from the dimethylsulfoxide oxidation synthesis, giving two red bands by TLC, and two bands on Sephadex chromatography with Na_2SO_4/H^+.

(b) At 20 °C

A preparation similar to that above, but with aeration carried out entirely at room temperature gave only red material (*ca.* 35% yield). No discrimination was effected on fractional recrystallization, all fractions giving two red components presumably **A** and **C** on TLC or Sephadex.

Sephadex Separation of Products from the Aerial Oxidation Synthesis

The yellow material (combined fractions) from the aerial oxidation synthesis at 80 °C was applied to columns 4.5 × 40 cm of SP-Sephadex, 1.6 g over two columns. The columns were eluted with 0.1 M Na_3PO_4, when bands separated as follows: (1) pale yellow, first eluted, containing complex **D**; (2) pink–violet; (3) orange–yellow, containing **E**; (4) orange, containing **F** as major component and **G** minor; (5) orange, containing complex **H**. Bands (4) and (5) were not cleanly separated. The relative amounts of the complexes (visually estimated) were **D**:**E**:(**F** + **G**):**H** *ca.* 1:6:3:18. The complexes were isolated by applying each effluent to a column of Dowex 50W-X2 cation-exchange resin, 200–400 mesh, H^+ form. After washing with 0.1 M HBr to remove all Na^+, the complex was eluted with 3 M HBr, and the effluent was evaporated to near dryness. Bands (4) and (5) were each rechromatographed down a Sephadex column 4.5 × 40 cm when each was then obtained cleanly. To the evaporated HBr effluents ethanol was added, and the complexes were then recovered by filtration, washing with ethanol and acetone, and air-drying to constant weight. The amounts thus obtained were **D**, 0.03 g; **E**, 0.34 g; **F** + **G**, 0.13 g; **H**, 0.70 g; and these corresponded to the visually estimated relative amounts. **F** was subsequently obtained pure by recrystallization of the **F** + **G** mixture from 0.01 M HBr.

The ^{13}C NMR spectra in D_2O/HBr gave resonances as follows: **D**, $[Co(en)_3]Br_3$, δ 44.9; **E**, $[Co(meen)(en)_2]Br_3$, δ 56.2, 45.6, 45.1, 44.5, 44.2, 43.3, 38.3 (approximately equal intensities); **F**, $[Co(meen)_2(en)_2]Br_3$, δ 56.2, 45.3, 42.6, 38.3 (equal intensities); **G**, $[Co(meen)_2(en)]Br_3$, in mixture with **F**, δ 46.0, 43.5, 41.8, 37.5 (not equal), probably another resonance coincident with 56.5 of complex **F**; ratio **F**:**G** *ca.* 5:1; **H** $[Co(meen)_2(en)]Br_3$, δ 55.6, 44.0, 43.7, 38.0 (equal intensities).

Anal. Calc. for $[Co(C_3H_{10}N_2)(C_2H_8N_2)_2]Br_3 \cdot 2H_2O$: C, 15.9; H, 5.7; N, 15.9; Br, 45.3. Found for **E**: C, 15.8; H, 5.5; N, 15.2; Br, 43.9%. Calc. for $[Co(C_3H_{10}N_2)_2(C_2H_8N_2)]Br_3 \cdot H_2O$: C, 18.3; H, 5.8; N, 16.0. Found for **F** + **G**: C, 18.4; H, 5.7; N, 15.9%. Calc. for $[Co(C_3H_{10}N_2)_2(C_2H_8N_2)]Br_3 \cdot 2H_2O$: C, 17.7; H, 5.9; N, 15.5; Br, 44.2. Found for **H**: C, 17.9; H, 5.7; N, 15.3; Br, 44.6%.

The complexes were also isolated as perchlorate salts by addition of $HClO_4$ to evaporated solutions of HCl eluates from Dowex resins. *Anal.* Calc. for $[Co(C_3H_{10}N_2)(C_2H_8N_2)_2](ClO_4)_3 \cdot H_2O$: C, 14.8; H, 5.0; N, 14.7; Cl, 18.7. Found for **E**: C, 14.6; H, 5.1; N, 14.5; Cl, 18.7%. Calc. for $[Co(C_3H_{10}N_2)_2(C_2H_8N_2)](ClO_4)_3 \cdot H_2O$: C, 16.5; H, 5.2; N, 14.4; Cl, 18.2. Found for **F** + **G**: C, 16.3; H, 5.1; N, 14.1; Cl, 18.0%.

Aerial Oxidation Synthesis in Methanol

meen (1.85 g) and meen·2HCl (0.74 g) were dissolved in methanol (50 ml), and anhydrous $CoCl_2$ (1.30 g, 0.01 mol) was added. The solution was aerated at 45 °C for 6 h, then aeration was continued at room temperature for 1 day. The resulting red powder was filtered off, washed with methanol and acetone, and air-dried. Yield 2.5 g, 63%. This product was essentially pure isomer C, by the ^{13}C NMR spectrum in D_2O/HCl. Sephadex chromatography with Na_2SO_4/H^+ gave two red bands, due to equilibration of C in water during application. The methanol mother liquor gave no other bands corresponding to other CoN_6^{3+} species.

Substitution Synthesis for $[Co(meen)_3]^{3+}$

A solution of $[Co(NH_3)_5(H_2O)](ClO_4)_3$ (2.30 g, 0.005 mol) and meen (1.3 g) in water (50 ml) was heated on a steam bath with occasional stirring for 3 h. The resulting solution was first absorbed on Dowex and eluted off with 3 M HBr, then chromatographed down columns of SP-Sephadex with 0.2 M Na_2SO_4/H_2SO_4 pH 2 eluent. Hydrolysis and bromo by-products were substantial in several bands, and the $[Co(meen)_3]^{3+}$ complex eluted as two orange bands. These were collected and worked up on Dowex/3 M HCl, and they were identified by ^{13}C NMR spectra of the evaporated effluents as isomers A + B in ratio 3:1, and C. No *fac* isomers were detectable from this preparation. Elution down Sephadex with 0.1 M Na_3PO_4 gave only one band of $[Co(meen)_3]^{3+}$, and yellow bands of demethylated complexes were absent.

In another substitution synthesis charcoal was used, and the crude product was precipitated with ethanol. Yield 30%. Sephadex chromatography with Na_3PO_4 gave yellow bands corresponding to the demethylated complexes E, F and H.

References

1 R. N. Keller and L. J. Edwards, *J. Am. Chem. Soc., 74* (1952) 215.
2 S. F. Pavkovic and D. W. Meek, *Inorg. Chem., 4* (1965) 20.
3 F. Basolo, *J. Am. Chem. Soc., 75* (1953) 227.
4 E. W. Gillow and G. M. Harris, *Inorg. Chem., 7* (1968) 394.
5 D. A. Buckingham, L. G. Marzilli and A. M. Sargeson, *J. Am. Chem. Soc., 89* (1967) 3428.
6 D. A. Buckingham, L. G. Marzilli and A. M. Sargeson, *Inorg. Chem., 7* (1968) 915.
7 W. T. Robinson, D. A. Buckingham, G. Chandler, L. G. Marzilli and A. M. Sargeson, *Chem. Commun.*, (1969) 539.
8 J. A. Hearson, S. F. Mason and R. H. Seal, *J. Chem. Soc., Dalton Trans.*, (1977) 1026.
9 D. A. Buckingham, L. G. Marzilli and A. M. Sargeson, *J. Am. Chem. Soc., 89* (1967) 825.
10 T. W. Hambley, C. J. Hawkins, J. Martin, J. A. Palmer and M. R. Snow, *Aust. J. Chem., 34* (1981) 2505.
11 S. F. Mason, *Chem. Commun.*, (1969) 856.
12 S. F. Mason, *J. Chem. Soc. A*, (1971) 667.
13 G. R. Brubaker, *J. Chem. Educ., 51* (1974) 608.
14 E. J. Corey and J. C. Bailar, *J. Am. Chem. Soc., 81* (1959) 2620.
15 F. P. Dwyer, F. L. Garvan and A. Shulman, *J. Am. Chem. Soc., 81* (1959) 290.
16 F. P. Dwyer, T. E. MacDermott and A. M. Sargeson, *J. Am. Chem. Soc., 85* (1963) 2913.
17 F. P. Dwyer, A. M. Sargeson and L. B. James, *J. Am. Chem. Soc., 86* (1964) 590.
18 A. M. Sargeson, in R. L. Carlin (ed.), *Transition Metal Chemistry*, Vol. 3, Dekker, New York, 1966, p. 303.
19 T. E. MacDermott, *Inorg. Chim. Acta, 2* (1968) 81.
20 S. E. Harnung, S. Kallesoe, A. M. Sargeson and C. E. Schaffer, *Acta Chem. Scand., Ser. A, 28* (1974) 385.
21 F. R. Keene, *B.Sc. Honours Thesis*, University of Adelaide, 1967.
22 T. E. MacDermott, unpublished data, 1967.
23 IUPAC Commission on Inorganic Chemical Nomenclature, *Inorg. Chem., 9* (1970) 1.
24 IUPAC Commission on Inorganic Chemical Nomenclature, *Pure Appl. Chem., 28* (1971) 75.
25 T. E. MacDermott, *Inorg. Chim. Acta, 2* (1968) 399.
26 T. E. MacDermott, *Chem. Commun.*, (1968) 223.
27 I. M. Atkinson, F. R. Keene and G. H. Searle, unpublished work.
28 O. Bang, K. Rasmussen and F. Woldbye, *Acta Chem. Scand., Ser. A, 28* (1974) 1167.
29 G. H. Searle, S. F. Lincoln, F. R. Keene, S. G. Teague and D. G. Rowe, *Aust. J. Chem., 30* (1977) 1221.
30 G. H. Searle and T. W. Hambley, *Aust. J. Chem., 35* (1982) 1297.
31 T. A. Kaden, Lecture at 20th I.C.C.C., in D. Banerjea (ed.), *Coordination Chemistry—20*, Pergamon, Oxford, 1980, p. 71.
32 G. H. Searle, unpublished work.
33 G. H. Searle, F. R. Keene and S. F. Lincoln, *Inorg. Chem., 17* (1978) 2362.
34 R. N. Keller and L. J. Edwards, *Univ. Colorado Studies, Ser. Chem. Pharm., 3* (1961) 1; *Chem. Abstr., 56* (1962) 11178i.
35 G. H. Searle and E. R. T. Tiekink, unpublished work.
36 W. C. Drinkard, H. F. Bauer and J. C. Bailar, *J. Am. Chem. Soc., 82* (1960) 2992.
37 B. Das Sarma, G. J. Tennenhouse and J. C. Bailar, *J. Am. Chem. Soc., 90* (1968) 1362.
38 E. I. Karpeiskaya, Y. N. Kukushkin, V. A. Trofimov and I. P. Yakovlev, *Russ. J. Inorg. Chem., 16* (1971) 1042.
39 D. Huggins and W. C. Drinkard, *Adv. Chem. Ser., No. 37* (1963) 181.
40 G. H. Searle, S. F. Lincoln, S. G. Teague and D. G. Rowe, *Aust. J. Chem., 32* (1979) 519.
41 M. V. George and K. S. Balachandran, *Chem. Rev., 75* (1975) 491.
42 C. J. Easton, unpublished work.
43 G. H. Searle, *Aust. J. Chem., 30* (1977) 2625.
44 G. H. Searle, *Aust. J. Chem., 40* (1987) 375.
45 L. R. Gahan, T. W. Hambley, G. H. Searle, M. J. Bjerrum and E. Larsen, *Inorg. Chim. Acta, 147* (1988) 17.
46 G. C. Levy and G. L. Nelson, *Carbon-13 Nuclear Magnetic Resonance for Organic Chemists*, Wiley-Interscience, New York, 1972, p. 29.
47 F. W. Wehrli and Wirthlin, *Interpretation of Carbon-13 NMR Spectra*, Heyden, London, 1978, p. 7, 20, 264.

Journal of Molecular Structure, 240 (1990) 313–329
Elsevier Science Publishers B.V., Amsterdam

CONFORMATIONAL ANALYSES OF THE ISOMERS OF THE $[Co\{(\pm)pn\}_n(en)_{3-n}]^{3+}$ SYSTEMS: A REINVESTIGATION (en = ethane-1,2-diamine; pn = propane-1,2-diamine; $n = 0$–3)

IAN M. ATKINSON and F. RICHARD KEENE*

Department of Chemistry and Biochemistry, James Cook University of North Queensland, Townsville, Queensland 4811 (Australia)

GRAEME H. SEARLE

Department of Physical and Inorganic Chemistry, University of Adelaide, South Australia 5001 (Australia)

(Received 12 February 1990)

ABSTRACT

A molecular mechanics study of the isomers of $[Co(pn)_n(en)_{3-n}]^{3+}$ ($n = 0$–3) is reported. The MM2 force field has been parameterized for cobalt(III) amine complexes and the complete set of stereoisomers of the title complexes has been modelled. Detailed structural and thermodynamic comparisons are made with previous calculations on these systems and with experimental data. Structural details were satisfactorily modelled by MM2, and the correspondence between the calculated isomer ratios and those observed experimentally is excellent. The significance of statistical factors in thermodynamic comparisons of this type is discussed.

INTRODUCTION

Stereospecificity, the preference of one stereoisomer over another, has been observed widely in coordination compounds. In their classic paper in 1959, Corey and Bailar [1] particularly examined the effects induced by ligand asymmetry and the dissymmetry of chelate ring conformations on complex stability, and they attempted to quantify such effects in terms of conformational analysis methods already established for carbocyclic ring systems. This work inspired a number of experimental studies measuring relative thermodynamic stabilities of such "internal diastereoisomers", and also a development of computational methods for assessment and prediction of structural features of metal complexes.

The analysis procedure used by Corey and Bailar [1] took account only of non-bonded interactions, primarily those between hydrogen atoms in adjacent

*Author to whom correspondence should be addressed.

0022-2860/90/$03.50

chelate rings, using the potential function of Mason and Kreevoy [2]. Subsequently, Gollogly and Hawkins [3] developed a conformational analysis procedure which took account of non-bonded interactions, torsional energies of bond rotation and valence angle deformation energies, in which the atoms in the molecule were moved individually until a minimum energy was obtained. Simultaneously, an alternative approach was proposed which used more complete force fields, where a "strain energy"* (U) of the molecule included bond length distortion, valence angle distortion, torsional energy of bond rotation, and non-bonded interactions. The procedure used was originally formulated by Boyd [4], and subsequently modified by Snow [5], Sargeson and coworkers [6, 7], DeHayes and Busch [8], and recently by Hambley and co-workers [9–11]. The particular advance of these methods was the ability to minimize energies by varying all atomic coordinates simultaneously over the $(3N-6)$ variables in the potential surface of the molecule.

The most widely used molecular mechanics method was developed subsequently from the work of Allinger [12], who substantially refined the potential forms of the terms used in the previous force field, and added the contribution of dipolar interactions. These techniques have developed into the widely used MM2 package which forms the basis of many available molecular mechanics analysis programs.

In molecular mechanics, two general types of force fields (both derived from spectroscopy) are in common use: the generalized valence force fields (GVFF) and Urey–Bradley force fields (UBFF) [13], and their most significant difference relates to the consideration of 1,3-non-bonded interactions. In the Urey–Bradley approach, such interactions are included explicitly in the force field: e.g. Hambley and co-workers [9–11] have recently developed a force field which has been widely applied to cobalt(III) complexes containing amine ligands, and in which valence angle deformations are governed only by the 1,3-non-bonded interactions. The advantage of this approach is that the only bond stretching parameters required are those involving the central metal atom (which can be obtained from IR vibrational analysis), enabling the force field to be more easily transferred to systems with different central metal ions. MM2 [13] is a valence force field methodology where specific parameters are re-

*The use of the phrase "strain energy" in previous discussions of such force field calculations has not always been strictly correct. Molecular mechanics programs such as MM2 directly calculate a *steric energy* which is the final sum of the force field potential energy functions. For systems where sufficient thermodynamic data exist, empirical force field increments for discrete groups (i.e. CH_2) can be added to produce a ΔH_f^0, from which strain-free increments can be subtracted to produce a strain energy (e.g. see Clark [38] and ref. 13). Insufficient data exist for this procedure to be applied to coordination complexes, and only steric energies are quoted in this present work. Steric energies are therefore not obviously related to any real thermodynamic quantity, although they may be adjusted to be so: they are only relevant in respect of comparisons between isomers with the same number and type of interactions, i.e. bonds.

quired for bond stretching, valence angle deformations, non-bonding interactions and torsional angle deformations; the strong 1,3-non-bonding interaction is included implicitly in the parameterization process.

There has been considerable precedent in the literature of MM2 type force fields being applied to cobalt(III) amine complexes. Cobalt is a very "directional" ion, meaning that the ligands tend to coordinate close to regular octahedral geometry, so that the variations involving deformations about the metal ion are minimal and the organic component of the interactions is of major importance. Indeed, Endicott et al. [14] have shown that in comparison of cobalt(III) with cobalt(II) species, the N–Co–N angle deformation constants are of only small importance in the overall GVFF approach. For the MM2 method, the parameters for the organic components are now well refined [15]. Accordingly, the parameterization, once established for the present title complexes, should be readily applicable to cobalt(III) complexes with more complex ligand systems. Recent modifications to the minimization scheme employed by MM2, developed by Adam et al. [16] within one of our Departments (JCUNQ), have substantially improved the efficiency of these procedures.

One of the asymmetric ligands specifically addressed in the work by Corey and Bailar [1] was (±)-propane-1,2-diamine (pn). Experimental studies of the various $[Co\{(\pm)pn\}_n(en)_{3-n}]^{3+}$ ($n=0$–3) systems have been made by Dwyer and Sargeson and co-workers [17–20] and these studies have been widely quoted as classic examples of stereospecific effects in transition metal coordination compounds. Furthermore, following the initial calculations [1] of isomer stabilities, there have been a number of subsequent conformational analyses of these systems, viz. by Gollogly and Hawkins [21], Crossing and Snow [22], Laier and Larsen [23]* and Hambley and co-workers [10, 11].

We wished to undertake a molecular mechanics study of the $[Co(meen)_n(en)_{3-n}]^{3+}$ systems (meen=*N*-methylethane-1,2-diamine), for which there are a large number of isomeric forms in each case [24, 25]. Initial calculations were undertaken on the experimentally well studied tris(bidentate) $[Co(pn)_n(en)_{3-n}]^{3+}$ and bis(tridentate) $[Co(medien)_n(dien)_{2-n}]^{3+/2+}$ systems (dien=1,5-diamino-3-azapentane; medien=3-methyl-1,5-diamino-3-azapentane) to assess our computational methods. We now report these studies on the $[Co(pn)_n(en)_{3-n}]^{3+}$ complexes. The calculations on the bis(tridentate) systems and on the meen systems will be reported subsequently [26].

EXPERIMENTAL

Starting structures for the $[Co(pn)_n(en)_{3-n}]^{3+}$ species were generated from

*These calculations used the "Consistent Force Field" which is similar to the MM2 methods used in the present work, but excludes dipole–dipole interactions.

the $[Co(en)_3]^{3+}$ structure of Duesler and Raymond [27] or the Λ-$[Co(R\text{-}pn)_3]^{3+}$ structure of Saito and co-workers [28] by manipulation of crystal structure data using the CHEM 3D PLUS™ molecular modelling program.* No symmetry restrictions were placed on the minimizations, although when symmetry was present it was reflected in the final minimized coordinates.

The minimization scheme used in this work is a local adaptation [16] of the Newton–Raphson procedure used in the MM2 program of Allinger [12]. All of the organic parameters used in the force field derive from the original work by Allinger [12]. Parameters containing the metal were taken in the first instance from the work by DeHayes and Busch [8] and Brubaker and Johnson [29], and they were then adjusted to provide the best fits between MM2 minimized geometries and the available X-ray diffraction studies. The final parameters are listed below.

Non-bonding

Co^{III} van der Waals radius = 2.30 Å, $\epsilon_0 = 0.711$ kJ mol^{-1}.

Bond stretching

Co^{III}–N: $K_{str} = 195.0$ N m^{-1} molecule^{-1}, $r_0 = 1.950$ Å, bond moment = 0.0 debye, cubic stretch constant = −2.000.

Valence angle deformation

N–Co^{III}–N:Kbend = 0.400×10^{-18}N Å rad^{-2} molecule^{-1}, $\theta 1 = 90.000°$, $\theta 2 = \theta 3 = 0.000°$. Co^{III}–N–C:Kbend = 0.278×10^{-18}N Å rad^{-2} molecule^{-1}, $\theta 1 = 90.000°$, $\theta 2 = \theta 3 = 0.000°$. H–N–$Co^{III}$:$K$bend = 0.278×10^{-18}N Å rad^{-2} molecule^{-1}, $\theta 1 = 90.000°$, $\theta 2 = \theta 3 = 0.000°$.

Torsional angle deformation. (Values expressed as kJ mol^{-1}.)

C–N–Co^{III}–N:$V_1 = 0.000$, $V_2 = 0.000$, $V_3 = 0.000$. H–N–Co^{III}–N:$V_1 = 0.000$, $V_2 = 0.000$, $V_3 = 0.000$. H–C–N–Co^{III}:$V_1 = 0.000$, $V_2 = 0.000$, $V_3 = -2.174$. C–C–N–Co^{III}:$V_1 = -0.836$, $V_2 = 3.051$, $V_3 = 3.344$.

The convergence criterion for minimization was taken to be $\Delta H_{steric} < 10^{-7}$ kJ mol^{-1} between successive iterations, and this usually required between 50 and 100 cycles (generally less than 3 min CPU time on either DEC 10 or CCI Power 32 computers). Refinement to a true potential energy minimum was ensured in all cases by the use of several starting geometries: no form of $[Co(III)(pn)_{3-n}(en)_n]^{3+}$ (n=0–3) "hung" in a conformation other than that initially inputted. The numbers and types of the various interatomic potentials included in the MM2 force field calculations for the title complexes are listed in Table 1.

Tables 2–4 summarize the calculated ΔH_{steric} and "ΔG" values for the $[Co(pn)_n(en)_{3-n}]^{3+}$ (n=1–3) complexes under discussion. Complete listings of the contributing factors for these systems and $[Co(en)_3]^{3+}$ are included in the Supplementary Material (Tables S1–S4). Comparisons of bond lengths

*The computer program CHEM 3D PLUS™ (Cambridge Scientific Computing, Boston, MA) was used for editing and manipulating initial structures and viewing final output.

TABLE 1

Number of interatomic potentials included in MM2 calculations of $[Co(pn)_n(en)_{3-n}]^{3+}$

	Non-bonded	Bond stretches	Bond dipoles	Torsional angle deformations	Valence angle deformations
$Co(en)_3^{3+}$	540	391	35	84	69
$Co(pn)(en)_2^{3+}$	645	421	35	90	79
$Co(pn)_2(en)^{3+}$	759	451	35	96	89
$Co(pn)_3^{3+}$	882	481	35	102	99

and bond angles of the calculated geometries with selected crystal structure determinations are available in the Supplementary Material (Tables S5 and S7), as well as comparisons of torsional angles (Tables S6 and S8). These have been deposited with the British Library Lending Division, Boston Spa, Yorkshire, U.K., as Supplementary Publication No. SUP 26405 (15 pages).

RESULTS AND DISCUSSION

The MM2 force field can be calibrated to reproduce both structure and heats of formation, and both of these aims have been achieved for organic species because of the enormous data set that exists for these molecules. For inorganic systems, there is a paucity of thermodynamic data and so the force field has been calibrated only to reproduce structure. Therefore, the steric energies calculated can only be loosely related to heats of formation for coordination compounds. Inspection of the contributing interactions to the total steric energy of the molecules in the present study shows that the dominant contributors are the organic components, and therefore the difference between the steric energy and heat of formation should be relatively small. In the following discussion, we separately examine the correspondence between the calculated thermodynamic stabilities and the experimental isomer ratios for the various $[Co(pn)_n(en)_{3-n}]^{3+}$ systems ($n=0$–3), and between the minimized structure and the observed crystal structure in a limited number of cases.

Isomeric possibilities

For the title complexes, isomerism arises from four sources: configurational isomerism about the octahedral metal center (designated Δ/Λ [30], configurational isomerism about the chiral carbon center in the pn ligand (R/S) [30], conformational isomerism within the five-membered chelate rings formed by the bidentate pn and en ligands (δ/λ) [30], and geometric isomerism associated with the relative mutual disposition of the methyl substituents in the $[Co(pn)_3]^{3+}$ (*fac*/*mer*) and $[Co(pn)_2(en)]^{3+}$ species (*cis*/*trans*).

Within the chelate pn ring, the methyl substituent may adopt either an axial or equatorial orientation with respect to the mean plane of the ring, by analogy with the terminology used for carbocyclic ring systems. In previous work [1, 20], it has been asserted that the methyl group has a substantial energetic preference for the equatorial position, and this assumption will be maintained in this work and addressed subsequently in light of the molecular mechanics results. Because the orientation of the methyl group is directly related to the particular ring conformation, this equatorial preference limits the number of possible forms of the molecule. For a Λ absolute configuration about the central metal ion, R-pn will have the methyl group equatorial if the ring conformation is λ; correspondingly, in S-pn, the ring conformation will be constrained to be δ. To simplify comparison with previous literature, it is noted that the form R-pn has sometimes been designated (−)-pn, and S-pn as (+)-pn, where the signs refer to the rotation of plane polarized light at the sodium D line, 589.3 nm.

Although not necessary in defining the stereoisomers of the title systems, an alternative designation has been widely used to define ring conformation. When tris-(bidentate) molecules involving five-membered chelate rings of the en type are viewed down the (pseudo-)C_3 axis, the C–C bond of each ring is observed to be either roughly parallel ("lel") or oblique ("ob") to that axis. For the Λ absolute configuration of the metal, the δ conformation is "lel" and the λ conformation is "ob". (For the enantiomeric Δ absolute configuration, the λ conformation will be "lel" and the δ conformation "ob"). Consequently, whereas the reflection in a mirror plane of any of these molecules will reverse the chirality of any chelate ring (i.e. $\delta \leftrightarrow \lambda$), the "lel" or "ob" designation will not alter. This designation is included here as it is a useful way of describing and recognizing ring geometry; it has been extensively used in the experimental studies on the stabilities of the isomers of $[Co(pn)_3]^{3+}$ [20], the results of which are of direct interest to the present calculations.

The results of the calculations of the thermodynamic parameters will now be considered in turn for each of the title complexes. Discussion of the comparison of minimized structures with actual structural determinations will follow. All systems will only be discussed in terms of the Λ absolute configuration about the metal, but there are always corresponding enantiomeric forms with the Δ configuration.

Thermodynamic considerations

$[Co(en)_3]^{3+}$

This complex, in the Λ configuration, exists only in conformational isomers; viz. Λ-$\delta\delta\delta$-lel_3, Λ-$\delta\delta\lambda$-lel_2,ob, Λ-$\delta\lambda\lambda$-lel,ob_2, and Λ-$\lambda\lambda\lambda$-ob_3. (The order of designation of the rings is irrelevant in this instance.) The calculated steric energies are 31.5, 33.9, 35.2, and 34.7 kJ mol^{-1}, respectively. However, the isomers

with mixed conformations are statistically preferred in the ratio 1:3:3:1. Accordingly, if this statistical adjustment (RT ln 3 = 2.7 kJ mol^{-1} at 298 K) is applied to "ΔH_{steric}", the calculated free energy ("ΔG") values obtained are: $\delta\delta\lambda$ (31.2 kJ mol^{-1}) < $\delta\delta\delta$(31.5) < $\delta\lambda\lambda$(32.5) < $\lambda\lambda\lambda$(34.7), so that the prediction of relative percentage conformational stabilities would be $\delta\delta\delta$:$\delta\delta\lambda$:$\delta\lambda\lambda$:$\lambda\lambda\lambda$ = 32:37:22:9. Solution NMR studies have indicated that there is a significant quantity of both the $\delta\delta\delta$ and the mixed conformational forms [31]. (The validity of some of the assumptions made in these NMR studies has been questioned [32], but the broad interpretation of the presence of a mixture of conformational forms seems reasonable.) The estimation of these relative conformational stabilities indirectly from experimental studies on $[Co(pn)_n(en)_{3-n}]^{3+}$ systems [7,33] is to be treated with caution given the many different interactions present in the various systems.

$[Co(pn)en)_2]^{3+}$

In this complex, with the Λ absolute configuration about the metal, the R-pn ring conformation is constrained to be λ if the methyl group is equatorial but the en rings may adopt either a δ or λ conformation. The manner in which the forms are represented is shown in Fig. 1. Designations of the particular isomers are made according to the following arbitrary rules. Each molecule is viewed along the pseudo-C_3 axis such that the substituent methyl group is directed towards the observer (on the upper carbon of the pn ring). The rings are then listed in a clockwise order. The unique pn ring is designated by an asterisk, and is listed first. The isomeric possibilities are for R-pn: Λ-$\lambda^*\lambda\lambda$, Λ-$\lambda^*\lambda\delta$, Λ-$\lambda^*\delta\lambda$, Λ-$\lambda^*\delta\delta$; and for S-pn: Λ-$\delta^*\delta\delta$, Λ-$\delta^*\delta\lambda$, Λ-$\delta^*\lambda\delta$, Λ-$\delta^*\lambda\lambda$. There is a corresponding enantiomeric set of stereoisomers for the Δ absolute configuration.

The calculated steric energies for these isomers are listed in Table 2. For Λ-$[Co(R\text{-}pn)(en)_2]^{3+}$, the $\delta^*\delta\delta/\lambda^*\delta\delta$ comparison indicates that the axial orientation of the methyl substituent in the pn ring gives less stability than the equatorial orientation by 10.9 kJ mol^{-1}, so that only about 1% of the pn rings

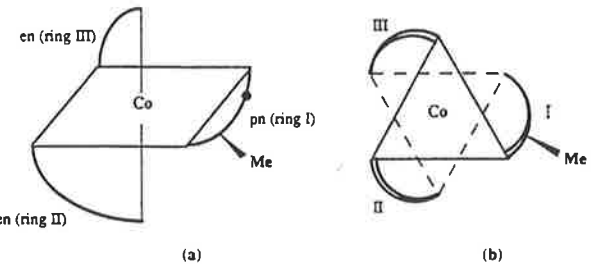

Fig. 1. Representations of the Λ-$[Co(pn)(en)_2]^{3+}$ molecule, where (b) shows the view down the pseudo-C_3 axis. (In a pn ring, CH_2 is represented as ●.)

TABLE 2

Steric energies for the isomers of Λ-[Co(pn)$(en)_2]^{3+}$

	Conformer		ΔH_{steric} (kJ mol^{-1})
For R-pn	Λ-$\lambda^*\lambda\lambda$	ob*,ob,ob	35.3
	Λ-$\lambda^*\lambda\delta$	ob*,ob,lel	35.8
	Λ-$\lambda^*\delta\lambda$	ob*,lel,ob	35.8
	Λ-$\lambda^*\delta\delta$	ob*,lel,lel	34.6
	Λ-$\delta^*\delta\delta$[a]	lel*,lel,lel	45.5
For S-pn	Λ-$\delta^*\delta\delta$	lel*,lel,lel	32.0
	Λ-$\delta^*\lambda\delta$	lel*,ob,lel	34.5
	Λ-$\delta^*\delta\lambda$	lel*,lel,ob	32.0
	Λ-$\delta^*\lambda\lambda$	lel*,ob,ob	35.8

[a]In this isomer, the CH_3 group is axial.

would have the methyl substituent in an axial orientation. Corey and Bailar's rationalization of the preference for the equatorial disposition of the methyl group was made on the basis of non-bonded interactions [1]. However, for the present model, in the breakdown of the contributions to the total steric energy (given in the Supplementary Material), the non-bonded interactions within these two conformations (Λ-$\lambda^*\delta\delta$ and Λ-$\delta^*\delta\delta$) are of similar magnitude and the difference in steric energies is reflected almost entirely in the torsional energy terms. The significant preference now calculated for the equatorial arrangement has been used in this work as the basis for the exclusive conformational preference for the pn chelate ring, the particular conformation being dependent on the chiralities of the metal and carbon centers.

The steric energy difference between the pair Λ-[Co(R-pn)$(en)_2]^{3+}$–$\lambda^*\delta\delta$-ob*,lel,lel and Λ-[Co(S-pn)$(en)_2]^{3+}$–$\delta^*\delta\delta$-lel*,lel,lel is calculated to be 2.6 kJ mol^{-1}, which represents the lel/ob difference. In this case, there are no statistical contributions to stabilities since the conformational isomers are distinct. This predicts a ratio Λ{R-pn}/Λ{S-pn} [$\equiv\Lambda${R-pn}/Δ{R-pn}] of 1:2.9 which compares well with the experimental ratio of 1:3.0 [18, 34].

Our results may be compared with previous conformational analyses of this system. Crossing and Snow [22] predicted $\Delta H = 7.7$ kJ mol^{-1} for the Λ-[Co(R-pn)$(en)_2]^{3+}$–δ^*(axial)$\delta\delta/\lambda^*$(equatorial)$\delta\delta$ pair (whence 4% of the CH_3-axial form might be observed), and calculated $\Delta H = 1.7$ kJ mol^{-1} for the Λ{R-pn}/Λ{S-pn} [$\equiv\Lambda${R-pn}/Δ{R-pn}] pair (whence the predicted ob/lel ratio would be 1:2.0). In their original paper, Corey and Bailar [1] predicted that the equatorial orientation of CH_3 would be favoured over the axial form by >8.4 kJ mol^{-1}, and that the Λ-R/Λ-S diastereoisomer ratio should be 1:2.8.

[Co(en)(pn)$_2$]$^{3+}$

To designate isomers in this system, each molecule is viewed along the pseudo-C_3 axis such that both of the substituent methyl groups are directed towards the observer (on the upper carbon atoms of the pn rings). The rings are then listed in a clockwise order. The unique en ring is designated by an asterisk, and is listed first.

The three possible geometric isomers for the Λ-[Co(en)(pn)$_2$]$^{3+}$ system are shown in Fig. 2.

As indicated above, the orientation of the methyl group is constrained to be equatorial so that R-pn will have the λ conformation only and S-pn will have the enantiomeric δ conformation. Accordingly, for the Λ configuration about the metal, we have the following possible diastereomeric possibilities, and their conformers:

[Co(en)(R-pn)$_2$]$^{3+}$ has conformers Λ-$\lambda^*\lambda\lambda$ and Λ-$\delta^*\lambda\lambda$

[Co(en)(S-pn)$_2$]$^{3+}$ has conformers Λ-$\lambda^*\delta\delta$ and Λ-$\delta^*\delta\delta$

[Co(en)(S-pn)(R-pn)]$^{3+}$ has conformers Λ-$\lambda^*\delta\lambda$ and Λ-$\delta^*\delta\lambda$

[Co(en)(R-pn)(S-pn)]$^{3+}$ has conformers Λ-$\lambda^*\lambda\delta$ and Λ-$\delta^*\lambda\delta$.

For the *cis*-CH_3, *cis*-CH_2 geometric form, all four diastereoisomers exist, and are distinct. However for the *cis*-CH_3, *trans*-CH_2 and *trans*-CH_3, *cis*-CH_2 geometric isomers with pn ligands of mixed chirality, the RS and SR forms are

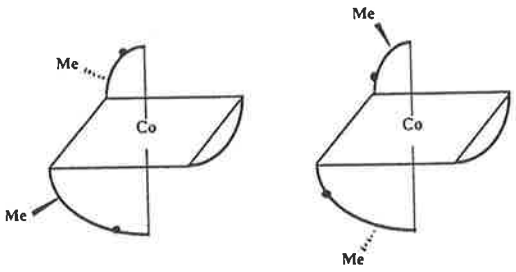

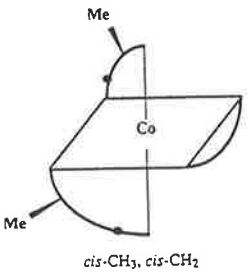

Fig. 2. Geometric isomers of Λ-[Co(en)(pn)$_2$]$^{3+}$.

equivalent; this situation arises since in each of these two geometric isomers, the chiral carbon *centers* in the two pn chelate rings bear the same relative disposition to the en chelate ring (being related by a C_2 operation).

Accordingly, there are 10 possible diastereoisomers of Λ-$[Co(en)(pn)_2]^{3+}$, each with two conformational forms (corresponding to the two conformations of the en ring). The calculated steric energies for these 20 stereoisomers are listed in Table 3. A statistical factor of $T\Delta S = 1.7$ kJ mol^{-1} ($= -RT \ln (1/2)$, $T = 298$ K) has been applied to the values of ΔH_{steric} in two separate circumstances to calculate ΔG. Firstly, for the *cis*-CH_3, *cis*-CH_2 geometric isomer, there are two equivalent forms for each of the RR and SS diastereoisomers, whereas the RS and SR forms are distinct. Secondly, since the "mixed" RS and SR combinations are equivalent in the *cis*-CH_3, *trans*-CH_2 and *trans*-CH_3, *cis*-CH_2 geometric isomers, there will be a statistical twofold preference for these forms over the RR and SS diastereoisomers; this preference will not oc-

TABLE 3

Steric energies and "free energies" (kJ mol^{-1}) for isomers of Λ-$[Co(en)(pn)_2]^{3+}$

Geometric isomer	Conformer		ΔH_{steric}	$T\Delta S$	"ΔG"
For (R-pn)$_2$					
cis-CH_3,*trans*-CH_2	Λ-$\lambda^*\lambda\lambda$	ob*,ob,ob	35.9		35.9
	Λ-$\delta^*\lambda\lambda$	lel*,ob,ob	36.4		36.4
trans-CH_3,*cis*-CH_2	Λ-$\lambda^*\lambda\lambda$	ob*,ob,ob	35.9		35.9
	Λ-$\delta^*\lambda\lambda$	lel*,ob,ob	36.4		36.4
cis-CH_3, *cis*-CH_2	Λ-$\lambda^*\lambda\lambda$	ob*,ob,ob	35.9	1.7	34.2
	Λ-$\delta^*\lambda\lambda$	lel*,ob,ob	36.4	1.7	34.7
For (S-pn)$_2$					
cis-CH_3,*trans*-CH_2	Λ-$\delta^*\delta\delta$	lel*,lel,lel	32.5		32.5
	Λ-$\lambda^*\delta\delta$	ob*,lel,lel	35.0		35.0
trans-CH_3,*cis*-CH_2	Λ-$\delta^*\delta\delta$	lel*,lel,lel	32.5		32.5
	Λ-$\lambda^*\delta\delta$	ob*,lel,lel	35.0		35.0
cis-CH_3,*cis*-CH_2	Λ-$\delta^*\delta\delta$	lel*,lel,lel	32.5	1.7	30.8
	Λ-$\lambda^*\delta\delta$	ob*,lel,lel	35.0	1.7	33.3
For (R-pn)(S-pn) or (S-pn)(R-pn)					
cis-CH_3,*trans*-CH_2	Λ-$\delta^*\delta\lambda$	lel*,lel,ob	35.1	1.7	33.4
	Λ-$\lambda^*\delta\lambda$	ob*,lel,ob	36.4	1.7	34.7
trans-CH_3,*cis*-CH_2	Λ-$\delta^*\delta\lambda$	lel*,lel,ob	35.1	1.7	33.4
	Λ-$\lambda^*\delta\lambda$	ob*,lel,ob	36.4	1.7	34.7
cis-CH_3,*cis*CH_2	Λ-$\delta^*\lambda\delta$	lel*,ob,lel	35.1		35.1
	Λ-$\lambda^*\lambda\delta$	ob*,ob,lel	36.4		36.4
	Λ-$\delta^*\delta\lambda$	lel*,lel,ob	35.1		35.1
	Λ-$\lambda^*\delta\lambda$	ob*,lel,ob	36.4		36.4

cur in the *cis*-CH_3, *cis*-CH_2 geometry where the RS and SR diastereoisomers are distinct.

The $\Lambda\{\text{R-pn}\}_2$:$\Delta\{\text{R-pn}\}_2$[$\equiv\Lambda\{\text{R-pn}\}_2$:$\Lambda\{\text{S-pn}\}_2$] equilibrium ratio was reported from experimental studies of Dwyer et al. [18] to be 1:7.5 at 25°C, although this ratio was modified from subsequent studies by MacDermott [34] to 1:3.9. The present calculations predict the same overall ratio to be 1:3.0, based on all possible isomers, or 1:3.9 based on the most stable form of each of the respective diastereoisomers. (Proportions of individual isomers are calculated in pairs by $\ln K = -\Delta G/RT$. These ratios are normalized to add to 100%, and where appropriate the ratio figures are added for isomers or conformers collected in groups.) In addition, the "mixed" species Λ-[Co(en)(R-pn)(S-pn)]$^{3+}$ would be expected to have an overall stability intermediate between the Λ-[Co(en)(R-pn)$_2$]$^{3+}$ and Λ-[Co(en)(S-pn)$_2$]$^{3+}$ forms.

A previous conformational analysis of this complex [22] has computed the Λ-RR-$\delta^*\lambda\lambda$/Λ-SS-$\delta^*\delta\delta$ steric energy difference as 3.2 kJ mol^{-1} (whence the ratio would be 1:3.6 at 25°C), whereas the original prediction of Corey and Bailar [1] for the same isomeric pair was an energy difference of 5.0 kJ mol^{-1} (whence the ratio would be 1:7.5 at 25°C).

[Co(pn)$_3$]$^{3+}$

For this system, all ring conformations are fixed by the requirement that the orientation of the methyl substituents be equatorial. However for all combinations of configurations of the pn ligands, two geometric arrangements can be identified depending on the relative disposition of the methyl substituents about the (pseudo-)C_3 axis of the molecule. These are shown in Fig. 3, and are designated ***facial*** (*fac*) when all three methyl groups are located on one octahedral face and are all *cis* to one another, and ***meridional*** (*mer*) when one of the methyl groups is located on an octahedral face opposite to the other two methyl groups.

The order of designation for the chelate rings is irrelevant for the *fac* forms. For the *mer* isomers, a caveat is required that the molecule be viewed along its

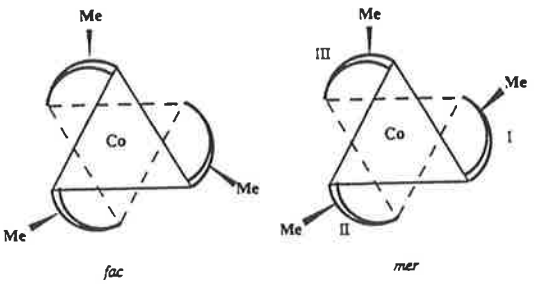

Fig. 3. Representations of geometric isomers of the Λ-[Co(pn)$_3$]$^{3+}$ cation, viewed along the (pseudo-)C_3 axis.

pseudo-C_3 axis so that two of the methyl substituents will be on the near face. The rings are then listed in a clockwise direction: the unique pn ring (methyl substituent on the remote face of the molecule) is listed first and is denoted by an asterisk.

For the *mer* isomers all of the chelate rings are distinct, whence there are eight possible internal diastereoisomers, viz. R*RR, R*RS, R*SR, R*SS, S*RR, S*SR, S*RS, S*SS, each of which can exist in only one conformational form because of the constraint that the R/S configuration predetermines the ring conformation, λ/δ.

For the *fac* isomers, there are only four possible diastereoisomeric forms; RRR, SRR, RSS and SSS.

Accordingly a total of 12 possible stereoisomers for Λ-$[Co(pn)_3]^{3+}$ can be visualized. They are summarized in Table 4, along with their calculated steric energies.

Because all three ring positions are distinct in the *mer* but are identical in the *fac* geometries, the *mer* forms should show a statistical stabilization of $-RT \ln (3)$ over the *fac* forms. Further, the "mixed" isomers (RRS, SSR) should be stabilized by a statistical factor of 3 : 1 over the RRR and SSS isomers in the *fac* (but not the *mer*) geometry. After adjustment for these statistical factors (calculated at 100 °C; $-T\Delta S = -RT \ln (3) = -3.4$ kJ mol^{-1}), the pre-

TABLE 4

Steric energies and "free energies" (kJ mol^{-1}) for the isomers of Λ-$[Co(pn)_3]^{3+}$

Conformer	ΔH_{steric}	$T\Delta S$	"ΔG"	
$[Co(R\text{-}pn)_3]^{3+}$				
fac-Λ-$\lambda\lambda\lambda$	ob_3	36.4		36.4
mer-Λ-$\lambda^*\lambda\lambda$	ob*,ob,ob	36.4	3.4	33.0
$[Co(S\text{-}pn)_3]^{3+}$				
fac-Λ-$\delta\delta\delta$	lel_3	33.0		33.0
mer-Λ-$\delta^*\delta\delta$	lel*,lel,lel	33.0	3.4	29.6
$[Co(R\text{-}pn)_2(S\text{-}pn)]^{3+}$				
fac-Λ-$\delta\lambda\lambda$	lel,ob,ob	37.0	3.4	33.6
mer-Λ-$\delta^*\lambda\lambda$	lel*,ob,ob	37.0	3.4	33.6
merΛ-$\lambda^*\lambda\delta$	ob*,ob,lel	37.0	3.4	33.6
mer-Λ-$\lambda^*\delta\lambda$	ob*,lel,ob	37.0	3.4	33.6
$[Co(S\text{-}pn)_2(R\text{-}pn)]^{3+}$				
fac-Λ-$\lambda\delta\delta$	ob,lel,lel	35.6	3.4	32.2
mer-Λ-$\lambda^*\delta\delta$	ob*,lel,lel	35.6	3.4	32.2
mer-Λ-$\delta^*\delta\lambda$	lel*,lel,ob	35.6	3.4	32.2
mer-Λ-$\delta^*\lambda\delta$	lel*,ob,lel	35.6	3.4	32.2

dicted relative stereoisomer stabilities for lel_3 : lel_2,ob:lel,ob_2 : ob_3 are 29 : 38 : 24 : 9 (Table 4). Experimental ratios at 100°C [20] are 35.7 : 41.8 : 18.4 : 4.1. (Both sets of ratios are normalized to add to 100%.)

There have been two other recent molecular mechanics calculations of the relative isomer stabilities of this system. Laier and Larsen [23] employed essentially a similar force field as used in the present calculations, with an earlier parameterization. Bond et al. [10] used a force field which replaced valence angle deformations with 1,3-nonbonded interactions, as discussed earlier. In both these previous studies, values of ΔH_{steric} were compared with the experimental results without incorporating the statistical effects discussed above. The experimental ratios have been determined for the four configurational/conformational isomer classes, viz. Λ-SSS-lel_3, Λ-SSR-lel_2,ob, Λ-SRR-lel,ob_2, Λ-RRR-ob_3, regardless of ring sequence or geometric (*mer*/*fac*) arrangement [20]. A comparison of these experimental ratios with the calculated ratios from the three studies, incorporating statistical factors in all cases, is now given in Table 5.

Clearly, when the statistical factors are included in all results, the agreement between experimental and calculated isomer ratios in the present study is particularly good. An additional point is that the calculated energies do not allow for the differential effects on the various isomers of solvation and ion-association: the correspondence between the calculated stabilities and the observed isomeric ratios indicates either that such effects are small, or that in the present system such interactions are similar for all isomers.

In earlier studies involving this system, Crossing and Snow [22] have calculated the Λ-*fac*-RRR-$\lambda\lambda\lambda$/Λ-*fac*-SSS-$\delta\delta\delta$ energy difference as 2.8 kJ mol^{-1} (whence the ratio would be 1:2.5 at 100°C; cf. 1:8.7 observed over both geometries *fac* and *mer* [20]). They also calculated a steric energy difference for the Λ-*fac*-SSS-$\delta\delta\delta$/Λ-*mer*-S*SS-$\delta^*\delta\delta$ pair of 0.3 kJ mol^{-1} (with the *fac* isomer the more stable) compared with 0 for our present calculations (Table 4): the observed ratio is 1:3 with the *mer* favoured [35], which is what would be expected from statistical considerations alone. The original calculations by Corey

TABLE 5

Comparison of molecular mechanics calculations of relative stabilities of isomers of $[Co(pn)_3]^{3+}$ with experimental ratios[a]

	lel_3	lel_2,ob	lel,ob_2	ob_3
Experimental [20]	35.7	41.8	18.4	4.1
Laier and Larsen [23]	19	42	28	11
Bond et al. [10]	25	42	24	8
Present study	29	38	24	9

[a] All calculated energies are adjusted for statistical effects.

and Bailar [1] predicted the Λ-RRR-$\lambda\lambda\lambda$-ob$_3$/Λ-SSS-$\delta\delta\delta$-lel$_3$ energy difference as 7.5 kJ mol^{-1} (whence the ratio would be 1:11.3 at 100°C; cf. 1:8.7 observed [20]).

Structural considerations

There is good agreement between the observed [27] and calculated (using MM2) structures for the Λ-[Co(en)$_3$]$^{3+}$-$\delta\delta\delta$-lel$_3$ cation (summary of comparison: RMS differences are for 15 bond lengths, 0.033 Å; for 27 bond angles, 1.33°; for 39 torsional angles, 9.39°; for all interatomic distances, 0.042 Å; Supplementary Tables S5 and S6). The crystal structure of this species is shown in Fig. 4. One feature is that the calculated minimized energy structure has true D_3 point group symmetry while the observed structure deviates slightly from that symmetry. This distortion has been rationalized by Duesler and Raymond [27] as resulting from hydrogen bonding of the axial amine protons with the HPO_4^{2-} anion. No account has been taken in the gas phase MM2 model for such ion-association or crystal packing influences. There have been a large number of X-ray crystal structure determinations for [Co(en)$_3$]$^{3+}$ complexes [11], and although there are some discrepancies between these various observed Co^{III}–N bond lengths , our calculated value is within 0.004 Å of their mean. This agreement between the observed and calculated Co–N bond lengths is slightly better than reported in recent studies on the same system by Endicott et al. [14]. However, in accordance with observations on corresponding systems containing the meen ligand [26], it is noted that the calculated C–C bond length within each of the en rings (1.531 Å) is longer than the observed value (average value 1.495 Å): this could not be changed without altering the

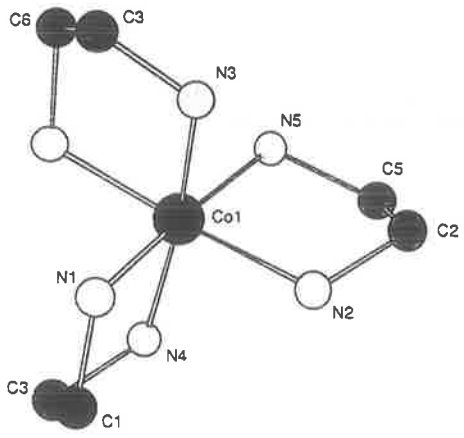

Fig. 4. Crystal structure [27] of Λ-[Co(en)$_3$]$^{3+}$-$\delta\delta\delta$-lel$_3$ (showing atom numbering scheme used in Supplementary Tables S5 and S6).

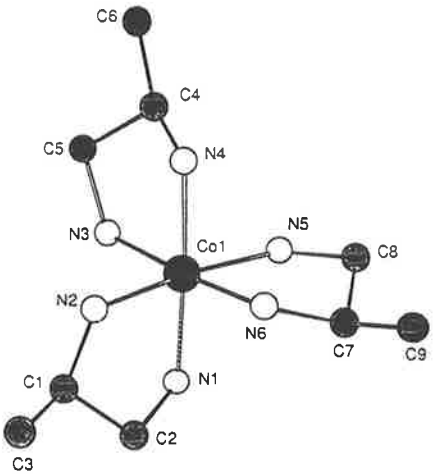

Fig. 5. Crystal structure [28] of *Λ-fac*-$[Co(R\text{-}pn)_3]^{3+}$-$\lambda\lambda\lambda$-ob_3 (showing atom numbering scheme used in Supplementary Tables S7 and S8).

carbon parameters within the MM2 force field, but this was not undertaken as it would restrict the general applicability of the parameterization.

For the comparison of the calculated and observed [28] structures for the *Λ-fac*-$[Co(R\text{-}pn)_3]^{3+}$-$\lambda\lambda\lambda$ cation, again the agreement is good (summary of comparison: RMS differences are for 18 bond lengths, 0.020 Å; for 33 bond angles, 1.37°; for 45 torsional angles, 10.77°; for all interatomic distances, 0.099 Å) although the minimized structure has an exact symmetry (C_3) in contrast to the slight distortion observed in the crystal data [28]. The crystal structure of this species is shown in Fig. 5. As with the *Λ*-$[Co(en)_3]^{3+}$ complex the C–C bonds of the chelate rings are slightly longer in the minimized structure than in the crystal structure (1.532 Å, cf. with the average value of 1.505 Å for the structure), although the (ring)C–CH_3 bond lengths are very well reproduced. The average N–Co^{III}–N angle is quite contracted in the crystal structure (84.22°) which is less than the minimized value by up to 2°. Nevertheless, we regard the overall agreement between the calculated and observed structures as satisfactory.

Clearly, in these two cases the structural parameters listed show a close correspondence for the minimized structures and the X-ray crystal structure data. Recent extensive investigations of a wide variety of cobalt(III)-amine complexes by molecular mechanics has shown that such close structural correspondence is quite general.

CONCLUSIONS

The present studies have demonstrated that the MM2 force field is capable of reproducing the structural characteristics of tris(diamine)cobalt(III) com-

plexes. This result is not unexpected due to the success of previous force fields with similar systems, and the directional nature of the metal center. However, the agreement between the calculated steric energies and the observed equilibrium isomer distributions is excellent for the isomers in all three $[Co(pn)_n(en)_{3-n}]^{3+}$ systems: in all cases the calculated and observed ratios agree within the accuracy of the experimental data and the confidence limits of the calculations.

The results also confirm that the stabilities of the complex systems are governed to a large extent by statistical factors, as suggested previously by MacDermott for the $[Co(pn)_3]^{3+}$ species [34].

Molecular mechanics methods can only produce idealized, gas phase (vacuum) minimum energy geometries. The success the current work has had in modelling the observed relative free energies of the $[Co(pn)_n(en)_{3-n}]^{3+}$ $(n=1-3)$ systems indicates that for such complexes the differential influence of ion-pairing or solvation is relatively small. For related systems, however, this is definitely not the case [36], but the calculations presented here have no direct way of incorporating these interactions. Recently, approaches combining molecular mechanics and molecular dynamics calculations have given encouraging results in the modelling of solvation of dibenzo-crown ethers with Group 1 cations in methanol solution [37], and extension of similar methods to inorganic complexes of the type studied in the present work would give more insight into these issues.

ACKNOWLEDGEMENTS

The assistance and continuing interest of Dr. K.R. Adam (James Cook University of North Queensland) in aspects of the molecular mechanics calculations is very gratefully acknowledged.

SUPPLEMENTARY MATERIAL AVAILABLE

Steric energy terms for isomers of Λ-$[Co(pn)_n(en)_{3-n}]^{3+}$ $(n=0-3)$ (Tables S1–S4; 5 pages); comparison of bond lengths/angles and torsional angles between observed and calculated structures for Λ-$[Co(en)_3]^{3+}$ and Λ-*fac*-$[Co(R\text{-}pn)_3]^{3+}$ (Tables S5–S8; 9 pages).

REFERENCES

1 E.J. Corey and J.C. Bailar, J. Am. Chem. Soc., 81 (1959) 2620.
2 E.A. Mason and M.M. Kreevoy, J. Am. Chem. Soc., 77 (1955) 5808.
3 J.R. Gollogly and C.J. Hawkins, Inorg. Chem., 8 (1969) 1168.
4 R.H. Boyd, J. Chem. Phys., 49 (1968) 2574.
5 M.R. Snow, J. Am. Chem. Soc., 92 (1970) 3610.

6 D.A. Buckingham, I.E. Maxwell, A.M. Sargeson and M.R. Snow, J. Am. Chem. Soc., 92 (1970) 3617.
7 D.A. Buckingham and A.M. Sargeson, Top. in Stereochem., 6 (1971) 219.
8 L.J. DeHayes and D.H. Busch, Inorg. Chem., 12 (1973) 1505.
9 A.M. Bond, T.W. Hambley and M.R. Snow, Inorg. Chem., 24 (1985) 1920.
10 A.M. Bond, T.W. Hambley, D.R. Mann and M.R. Snow, Inorg. Chem., 26 (1987) 2257.
11 T.W. Hambley, Inorg. Chem., 27 (1988) 2496.
12 N.L. Allinger, Adv. Phys. Org. Chem., 13 (1976) 1.
13 U. Burkert and N.L. Allinger, Molecular Mechanics, ACS Monogr. No. 177, 1982.
14 J.F. Endicott, G.R. Brubaker, T. Ramasami, K. Kumar, K. Dwarakanath, J. Cassel and D. Johnson, Inorg. Chem., 22 (1983) 3754.
15 N.L. Allinger, H.J. Geise, W. Pyckhout, L.A. Paquette and J.C. Galluci, J. Am. Chem. Soc., 111 (1989) 1106.
16 K.R. Adam, L.G. Brigden, K. Henrick, L.F. Lindoy, M. McPartlin, B. Mimagh and P.A. Tasker, J. Chem. Soc., Chem. Commun., (1985) 710.
17 F.P. Dwyer, F.L. Garvan and A. Shulman, J. Am. Chem. Soc., 81 (1959) 290.
18 F.P. Dwyer, T.E. MacDermott and A.M. Sargeson, J. Am. Chem. Soc., 85 (1963) 2913.
19 F.P. Dwyer, A.M. Sargeson and L.B. James, J. Am. Chem. Soc., 86 (1964) 590.
20 S.E. Harnung, S. Kallesoe, A.M. Sargeson and C.E. Schaffer, Acta Chem. Scand., Ser. A, 28 (1974) 385.
21 J.R. Gollogly and C.J. Hawkins, Inorg. Chem., 9 (1970) 576.
22 P.F. Crossing and M.R. Snow, unpublished work; P.F. Crossing, M.Sc. Thesis, University of Adelaide, 1973. Some of the conclusions of this study have been summarized in ref. 10.
23 T. Laier and E. Larsen, Acta Chem. Scand., Ser. A, 33 (1979) 257.
24 G.H. Searle and F.R. Keene, Inorg. Chim. Acta, 155 (1989) 125.
25 T.E. MacDermott, Inorg. Chim. Acta, 2 (1968) 399.
26 I.M. Atkinson, F.R. Keene and G.H. Searle, J. Chem. Soc., Dalt. Trans., accepted for publication.
27 E.N. Duesler and K.N. Raymond, Inorg. Chem., 10 (1971) 1486.
28 R. Kuroda, N. Shimanouchi and Y. Saito, Acta Crystallogr., Sect. B, 31 (1975) 931.
29 G.R. Brubaker and D.W. Johnson, Coord. Chem. Rev., 53 (1984) 1.
30 G.J. Leigh (Ed.), Nomenclature of Inorganic Chemistry, 3rd edn. Blackwell, Oxford, 1988.
31 J.K. Beattie, Acc. Chem. Res., 4 (1971) 253.
32 C.J. Hawkins and R.M. Peachey, Aust. J. Chem., 29 (1976) 33.
33 A.M. Sargeson, Transition Met. Chem., 3 (1966) 303.
34 T.E. MacDermott, Chem. Commun., (1968) 223.
35 M. Kojima, Y. Yoshikawa and K. Yamasaki, Inorg. Nucl. Chem. Lett., 9 (1973) 689.
36 F.R. Keene and G.H. Searle, Inorg. Chem., 13 (1974) 2173.
37 P.P.J. Grootenhuis and P.A. Kollman, J. Am. Chem. Soc., 111 (1989) 2152, and references cited therein.
38 T. Clark, A Handbook of Computational Chemistry — A Practical Guide to Chemical Structure and Energy Calculations, Wiley, New York, 1985, p. 20.

J. CHEM. SOC. DALTON TRANS. 1991

Conformational Analyses of the Isomers of the Systems $[Co(men)_n(en)_{3-n}]^{3+}$ (men = *N*-methylethane-1,2-diamine, en = ethane-1,2-diamine; *n* = 1–3)†

Ian M. Atkinson,[a] F. Richard Keene *,[a] and Graeme H. Searle *,[b]

[a] *Department of Chemistry and Biochemistry, James Cook University of North Queensland, Townsville, Queensland 4811, Australia*

[b] *Department of Physical and Inorganic Chemistry, University of Adelaide, South Australia 5001*

A molecular mechanics study of the configurational/conformational isomers of the system Λ-$[Co(men)(en)_2]^{3+}$ (men = *N*-methylethane-1,2-diamine, en = ethane-1,2-diamine) (16 isomers), and the geometric/configurational/conformational isomers of the systems Λ-$[Co(men)_2(en)]^{3+}$ (72 isomers) and Λ-$[Co(men)_3]^{3+}$ (88 isomers) has been undertaken using the MM2 force field. Calculated steric energies (adjusted for statistical factors) are used to predict isomer ratios in the three systems, which are compared with experimentally determined thermodynamic stabilities. Comparisons are also made between calculated geometries and X-ray molecular structures where these are available. For the Λ-$[Co(men)_2(en)]^{3+}$ system the calculations not only correctly predict the order of stability of the three possible geometric isomers, but also the most stable conformation for each of these cases. For the Λ-$[Co(men)_3]^{3+}$ system the two most stable forms observed experimentally are among the three forms of the molecule (of the 88 possible) calculated to be the most stable. Comparison of the geometric parameters for the two crystal structures and corresponding energy-minimized structures shows that the agreements are very good. The significance of statistical factors in thermodynamic comparisons of this type is discussed.

The classic paper in 1959 by Corey and Bailar,[1] which addressed ligand stereospecificity in metal complexes, inspired a large number of experimental studies measuring relative thermodynamic stabilities of stereoisomers of metal complex systems, and also a development of computational methods for assessment and prediction of their structural features.

One of the asymmetric ligands of particular interest has been (±)-propane-1,2-diamine (pn). Experimental studies of the various $[Co\{(\pm)pn\}_n(en)_{3-n}]^{3+}$ systems (*n* = 0–3, en = ethane-1,2-diamine) were made by Dwyer and Sargeson and co-workers[2–5] and these studies have been widely quoted to exemplify stereospecific effects in transition-metal co-ordination compounds. Furthermore, following the initial calculations of isomer stabilities,[1] there have been a number of conformational analyses of these systems, *viz.* by Gollogly and Hawkins,[6] Crossing and Snow,[7] Laier and Larsen,[8] Hambley and co-workers,[9,10] and most recently from our laboratories.[11]

In these complexes $[Co(pn)_n(en)_{3-n}]^{3+}$ isomerism arises from four sources: configurational isomerism of the chelate rings about the octahedral metal centre (Δ/Λ),[12] configurational isomerism about the chiral carbon centre in the pn ligand (*R*/*S*),[12] conformational isomerism within the five-membered chelate rings formed by the bidentate pn and en ligands (δ/λ),[12] and geometric isomerism due to the relative mutual dispositions of the methyl substituents in the $[Co(pn)_3]^{3+}$ and $[Co(pn)_2(en)]^{3+}$ species (*fac*/*mer*).[12]

Within a pn chelate ring the orientation of the substituent methyl group may be characterized as axial or equatorial to the mean plane of the ring (by analogy with the terminology used for substituted carbocyclic ring systems). This orientation is dependent on both the configuration *R*/*S* and the ring conformation: for pn in its complexes there is a substantial thermodynamic preference for the equatorial orientation.[1–11] Accordingly, the isomeric possibilities for metal complexes containing the pn ligand are limited since the absolute configuration about the chiral carbon centre predetermines the conformation of the ring: for example, *R*-pn gives a λ ring conformation for the methyl substituent to be equatorial.

In the related ligand men (*N*-methylethane-1,2-diamine) the methyl substituent is situated on one of the nitrogen atoms and this nitrogen donor becomes asymmetric only on co-ordination. However, as noted previously,[13–16] the axial/equatorial character of the *N*-methyl substituent in co-ordinated men is less pronounced than that of *C*-methyl substituents in pn, so that both conformations λ and δ may exist for a particular absolute configuration (*R*/*S*) about the chiral nitrogen centre. We have recently discussed the isomeric possibilities for the $[Co(men)_3]^{3+}$, $[Co(men)_2(en)]^{3+}$ and $[Co(men)(en)_2]^{3+}$ systems and have reported the synthesis of these complexes and characterization of the stable isomers produced,[16] and the structural details of several of the isolated isomers.[17,18]

Following the impressive predictive results of the thermodynamic stabilities of the $[Co(pn)_n(en)_{3-n}]^{3+}$ system using the MM2 force field,[11] we have calculated thermodynamic stabilities for the extended group of isomer possibilities for the analogous men complexes, along with the detailed structures of the most stable isomers of each system. These calculations are now reported and the results are compared with our experimental thermodynamics and structural results on these three systems.

The MM2 force field can only be used to study the relative thermodynamic stabilities of metal complexes in which there are the same number and type of atomic interactions (which excludes, for example, linkage isomers). The subtlety of the differences between a large number of closely related species in each of the present systems

† *Supplementary data available* (No. SUP 56800, 34 pp.): steric energy terms and calculated and observed geometric structure parameters and torsion angles. See Instructions for Authors, *J. Chem. Soc., Dalton Trans.*, 1991, Issue 1, pp. xviii–xxii.

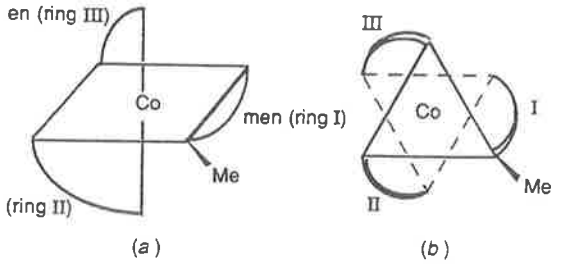

Fig. 1 Representations of the Λ-$[Co(men)(en)_2]^{3+}$ molecule, where (*b*) shows the view along the pseudo-C_3 axis

Table 1 Steric energies (kJ mol^{-1}) for the isomers of Λ-$[Co(men)(en)_2]^{3+}$; superscript * denotes the men ring

	Conformer							
Diastereoisomer	δ*δδ	δ*δλ	δ*λδ	λ*δδ	δ*λλ	λ*δλ	λ*λδ	λ*λλ
Λ-*R*	44.5	48.8	45.0	52.2	49.0	54.1	54.1	53.7
Λ-*S*	62.3	60.7	67.2	51.4	61.5	58.0	54.2	57.0

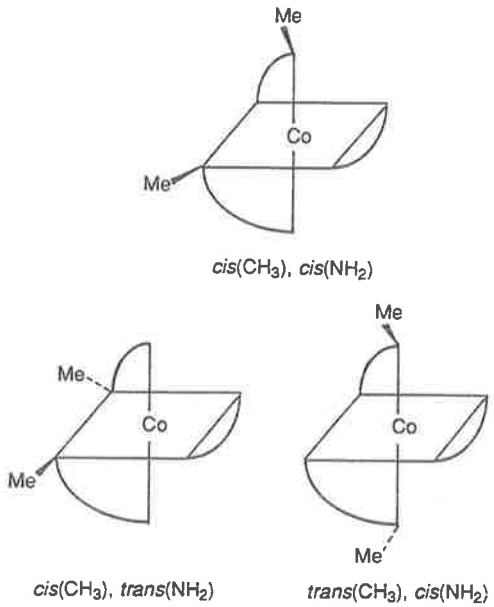

Fig. 2 Representations of the geometric isomers of the Λ-$[Co(men)_2(en)]^{3+}$ cation

provides an exceptional test of the molecular mechanics computational method.

Results and Discussion

The MM2 force field can be calibrated to reproduce both structure and heats of formation, and both of these aims have been achieved for organic molecules because of the enormous experimental data set available. The method has been applied to a substantial number of inorganic complexes:[19] however, relative to the organic systems, there is a paucity of thermodynamic data and so the force field has been calibrated only to reproduce structure. Therefore, the steric energies calculated can only be loosely related to heats of formation for co-ordination compounds. Previous studies[11] indicated that the predominant contributing interactions to the total steric energy of the $[Co(pn)_n(en)_{3-n}]^{3+}$ species were the organic components, and therefore the difference in thermodynamic energies would be expected to be closely related to the difference in steric energies. The thermodynamic and structural aspects of the calculations will be considered separately.

The isomer possibilities for $[Co(men)_3]^{3+}$, $[Co(men)_2(en)]^{3+}$ and $[Co(men)(en)_2]^{3+}$ have been elaborated previously.[16] The IUPAC nomenclature rules[12] do not allow the isomers and conformers in these complicated systems to be distinguished. This distinction requires that the stereochemical parameters (*R*/*S*, λ/δ) for the three chelate rings be specified in some definite sequence. Ring-order conventions were developed previously for the $[Co(men)_3]^{3+}$ system in particular,[16] and these conventions are extended in the present paper to the $[Co(men)_2(en)]^{3+}$ and $[Co(men)(en)_2]^{3+}$ systems to enable all possible conformers to be specified. For each complex system the discussion is limited to the Λ absolute configuration about the metal centre: there will be a corresponding enantiomeric set of stereoisomers for the Δ absolute configuration.

Thermodynamic Considerations.—$[Co(men)(en)_2]^{3+}$. Fig. 1 illustrates two representations of the Λ-$[Co(men)(en)_2]^{3+}$ molecule. The men ligand may co-ordinate to give the asymmetric *N*-methyl centre in either the *R* or *S* configuration, and as an independent factor each of the en and men rings may adopt either a δ or λ conformation.

Each molecule (Λ absolute configuration) is viewed along the pseudo-C_3 axis such that the N-*methyl group is directed towards the observer* (on the upper nitrogen of the men ring). The rings are then listed in a *clockwise order*. The parameters (δ/λ) for the unique men ring are designated with an asterisk, and are listed first. For each internal diastereoisomer Λ-*R* and Λ-*S* there are eight conformer arrangements. They are listed with their calculated steric energies in Table 1.

On the basis of these calculated energies, high stereospecificity would be expected in this complex and the Λ*R*/Δ*S* racemic pair would be preferred by a ratio >40:1 over its internal diastereoisomer (Δ*R*/Λ*S*) at 25 °C, based on the summation of the contributions of the eight conformers of each internal diastereoisomer. Since no statistical factors are present in this system, ΔH_{steric} can be equated to a 'free energy' for the species involved, so that the predicted equilibrium ratios of the most stable conformers of Λ-$[Co(men)(en)_2]^{3+}$ in equilibrium solution can then be calculated: Λ-*R*-δ*δδ, 1.00; Λ-*R*-δ*λδ, 0.82; Λ-*R*-δ*δλ, 0.18; and Λ-*R*-δ*λλ, 0.16. For the Λ configuration around the metal centre there is generally a thermodynamic preference for the δ conformation, as observed in the $[Co(en)_3]^{3+}$ and $[Co(pn)_n(en)_{3-n}]^{3+}$ systems.[11] Experimentally only one diastereoisomer was observed as explained by the calculations, but its conformational composition is at present unknown.

$[Co(men)_2(en)]^{3+}$. For $[Co(men)_2(en)]^{3+}$ there are three possible geometries arising from the *cis* and *trans* relative positions of the CH_3 and NH_2 groups in the two men ligands: the *trans*(CH_3), *cis*(NH_2), the *cis*(CH_3), *trans*(NH_2) and the *cis*(CH_3), *cis*(NH_2) forms (Fig. 2). Each geometry has three (or four) possible configuration combinations of the two asymmetric nitrogen donors of the men rings: *RR*, *SS*, *RS* (and *SR*). The *RS* and *SR* forms are identical for the two geometries with *trans* components, but for the *cis*(CH_3), *cis*(NH_2) geometry the *RS* and *SR* forms are distinct. Thus there is a total of ten stereoisomers for each configuration Λ or Δ of the complex, each of which has eight possible ring conformation combinations. Some of these conformers are equivalent by C_2 symmetry (see below) so that there is a total of 72 isomers for each configuration of this complex cation.

In designating these 72 forms, each molecule (Λ absolute configuration) is viewed along the pseudo-C_3 axis, and the rings are listed in a *clockwise order* with the parameters of the unique en ring denoted by an asterisk, and listed first. For the *trans*(CH_3), *cis*(NH_2) and *cis*(CH_3), *trans*(NH_2) geometries the orientation of the molecule along the pseudo-C_3 axis is not important since the *positions* of the two men rings will be interchanged by the two-fold symmetry of the geometry (*i.e.* ignoring *R*/*S* configurations).

For the *trans*(CH_3), *cis*(NH_2) and *cis*(CH_3), *trans*(NH_2)

Table 2 Steric energies (kJ mol^{-1}) for the isomers of Λ-[Co(men)$_2$(en)]$^{3+}$; superscript * denotes the en ring

	Conformers								
	δ*δδ	λ*δδ	δ*λδ		δ*δλ	λ*δλ		λ*λδ	δ*λλ	λ*λλ
trans(CH$_3$), *cis*(NH$_2$)										
RR	61.8[a]	67.2	⟵	*66.4*	⟶	⟵	71.8	⟶	74.7	74.6
RS	78.9	79.2	88.8		*64.9*	73.3		84.5	76.5	82.5
SS	105.6	94.0	⟵	93.8	⟶	⟵	92.2	⟶	80.1	87.0
cis(CH$_3$), *trans*(NH$_2$)										
RR	60.4[b]	58.5[b]	⟵	68.8	⟶	⟵	77.3	⟶	69.4	77.2
RS	76.8	80.3	*67.1*		85.4	86.6		85.0	79.5	78.9
SS	104.1	110.4	⟵	88.4	⟶	⟵	91.1	⟶	80.7	79.6
cis(CH$_3$), *cis*(NH$_2$)										
RR	75.9	74.7	72.3		89.0	91.3		76.5	81.8	84.0
RS	78.4	76.8	87.1		*67.6*	73.4		83.7	72.0	76.6
SR	74.3	82.4	75.6		87.2	90.0		78.0	97.0	96.5
SS	96.4	97.6	92.5		79.1	87.1		86.3	80.0	84.3

Energies within 7.5 kJ mol^{-1} of those for the isolated structures are italicized. [a] Isolated isomer **F** for which crystal structure has been determined.[17] [b] Isolated isomer **H** for which crystal structure has been determined.[18]

geometric isomers, when the two *N*-methyl centres have the same chirality, *i.e. RR* or *SS*, the molecules possess a real C_2 axis (through the centre of the en chelate). Therefore in these species the following pairs of conformers are equivalent: δ*λδ ≡ δ*δλ and λ*λδ ≡ λ*δλ (where the unique en ring is distinguished by an asterisk). For these two geometries, the forms with *N*-methyl groups of mixed chirality *RS* and *SR* are equivalent with respect to the *R* and *S* configurations, but this 'mixed configuration' does give rise to pairs of distinct conformers (since the *R* or *S* configuration does not stereospecifically determine the ring conformation). For example, for *RS* the conformations δ*λδ and δ*δλ are distinct, although these two conformations are equivalent for the *RR* and *SS* configurations.

For the *cis*(CH$_3$), *cis*(NH$_2$) geometry, in which there is no symmetry relationship between the positions of the two men rings, the caveat must be added that the molecule is viewed along the pseudo-C_3 axis with *both* N-*methyl groups directed towards the observer*.

The calculated steric energies for these isomers are listed in Table 2.

In assessing proportions of isomers, the steric energies require to be adjusted to take account of statistical inner-sphere entropy terms ($T\Delta S$). There is a statistical preference for isomers containing 'mixed' configurations of the chiral N-donors *RS* in the *trans*(CH$_3$), *cis*(NH$_2$) and *cis*(CH$_3$), *trans*(NH$_2$) forms (see above), and also for equivalent conformational forms such as δ*λδ ≡ δ*δλ. Therefore the theoretical predictions for the ratios of the most stable forms (at 80 °C, the temperature at which comparable experimental data are available) are, for the Λ absolute configuration, in order of decreasing stability (ΔG values in kJ mol^{-1}): **1** *cis*(CH$_3$), *trans*(NH$_2$)-*RR*-λ*δδ ('ΔG' = ΔH_{steric} = 58.5); **2** *cis*(CH$_3$), *trans*(NH$_2$)-*RR*-δ*δδ ('ΔG' = ΔH_{steric} = 60.4); **3** *trans*(CH$_3$), *cis*(NH$_2$)-*RR*-δ*δδ ('ΔG' = ΔH_{steric} = 61.8); **4** *trans*(CH$_3$), *cis*(NH$_2$)-*RS*-δ*δλ ['ΔG' = $\Delta H_{steric} + RT\ln(\frac{1}{2})$ = 62.9]; **5** *trans*(CH$_3$), *cis*(NH$_2$)-*RR*-(δ*λδ + δ*δλ) ['ΔG' = $\Delta H_{steric} + RT\ln(\frac{1}{2})$ = 64.4]; and **6** *cis*(CH$_3$), *cis*(NH$_2$)-*RS*-δ*δλ ('ΔG' = ΔH_{steric} = 67.6). On the presumption that conformational isomers of the same geometry/configuration would not be separated by normal crystallization and chromatographic procedures, the present calculations would predict that the ratio of the stereoisomer forms (**1** + **2**):(**3** + **5**):**4**:**6** would be 30:9:4:1 at 80 °C. In synthetic studies on the [Co(men)$_2$(en)]$^{3+}$ system[16] three isomers were obtained (designated **H**, **F** and **G**). These isomers remained distinct under basic conditions, which shows that they are of the three different geometries, since diastereoisomers *R*/*S* would interconvert in base by NH exchange, and en-type conformations are mobile in solution. Experimental ratios were obtained by chromatographic methods in basic media, where the three observed bands (**H**:**F**:**G** = *ca.* 36:5:1) would correspond to the proportions for the three possible geometries, each equilibrated to its most stable form. For comparison, it is therefore appropriate to present calculated ratios as the sums of the individual contributors within each of the three overall geometries: *i.e.* geometries *cis*(CH$_3$), *trans*(NH$_2$):*trans*(CH$_3$), *cis*(NH$_2$): *cis*(CH$_3$), *cis*(NH$_2$) = conformer forms numbered (**1** + **2**):(**3** + **4** + **5**):(**6**) = **H**:**F**:**G** = 30:13:1 at 80 °C.

Isomers **H** and **F** have been crystallized cleanly, but **G** has been characterized only in solution. The most abundant isomer **H** has been characterized by X-ray structural studies as *cis*(CH$_3$), *trans*(NH$_2$)-(Λ-*RR*-δ*δδ) + (Δ-*SS*-δ*λλ), with the unit cell containing the two different cations.[18] These molecules in **H** are pseudo-enantiomeric, differing only in the conformations of the en ring, and they correspond to the two conformers of the *cis*(CH$_3$), *trans*(NH$_2$)-Λ-*RR* diastereoisomer, δ*δδ and λ*δδ, which have the lowest calculated energies in this complete complex system. Their calculated energy difference of *ca.* 2 kJ mol^{-1} is not great, and crystal-packing forces are presumably decisive in determining the 1:1 occurrence of these conformers in the isolated material. The second most abundant isomer **F** has the structure *trans*(CH$_3$), *cis*(NH$_2$)-Λ-*RR*-δ*δδ,[17] which corresponds to the theoretically predicted next-most-stable diastereoisomer and conformation in the complete system.

The energy calculations have thus been able to predict correctly the three particular conformations (from the 72 possible) which have been isolated in the solid form, and moreover have been able to reproduce the experimental proportions of **H**:**F**:**G** with remarkable agreement.

The least-stable isomer **G** of those obtained experimentally must be of the geometry *cis*(CH$_3$), *cis*(NH$_2$). The calculated most stable conformer Λ-*RS*-δ*δλ is sufficiently lower in energy than the next most stable that this can be proposed as the structure for **G** with some confidence.

[Co(men)$_3$]$^{3+}$. Two geometry types are possible depending on the relative disposition of the *N*-methyl groups about the C_3 or pseudo-C_3 axis of the molecule. These are shown in Fig. 3, and are designated *fac* (facial) when all the *N*-methyl groups are located on one octahedral face and are all-*cis* to one another, and *mer* (meridional) when one of the *N*-methyl groups is located on an opposite octahedral face to the other two. For

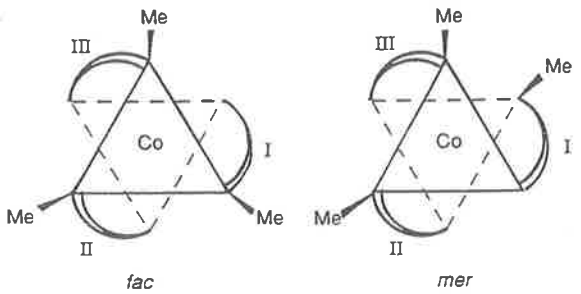

Fig. 3 Representations of the geometric isomers of the Λ-$[Co(men)_3]^{3+}$ cation, viewed down the (pseudo-)C_3 axis

designating the isomers, each molecule (Λ absolute configuration) is viewed along the (pseudo-)C_3 axis such that the *maximum number of* N-*methyl groups are directed towards the observer* on the near octahedral face (*i.e.* three for *fac* and two for *mer*). The rings are then listed in a *clockwise order*.

For the *fac* geometry there are only four possible configurational forms (diastereoisomers): *RRR*, *RRS*, *RSS* and *SSS*. In the *RRR* and *SSS* forms the ligands cannot be distinguished so that only four conformational isomers are possible for each form (δδδ, δλδ, λδλ and λλλ). In these instances with no unique men ring the order of listing the rings is irrelevant although the various types of parameter (*R*/*S* and δ/λ) must be written in the corresponding order. However the *RRS* and *SSR* isomers both have a men ring of unique configuration so that eight conformational isomers are possible: δ*δδ. δ*δλ, δ*λδ, λ*δδ, λ*λδ, λ*δλ. δ*λλ, λ*λλ. The parameters (δ/λ) for the unique men ring are designated with an asterisk, and are listed first.

For the *mer* geometry all of the chelate rings are distinct, so that there are eight possible diastereoisomer forms each of which can have eight separate conformational isomers. The ring designation commmences with the unique men ring (the *N*-methyl group on the remote octahedral face of the molecule), and the parameters (*R*/*S*, δ/λ) for this ring are designated with an asterisk, and are listed first. The eight internal diastereoisomers are therefore *R***RR*, *R***RS*, *R***SR*, *R***SS*, *S***RR*, *S***SR*, *S***RS*, *S***SS*, and each of these may exist as conformational isomers δ*δδ, δ*δλ, δ*λδ, λ*δδ, λ*λδ, λ*δλ, δ*λλ, λ*λλ.

Accordingly, there are a total of 88 possible geometric/configurational/conformational isomers for Λ-$[Co(men)_3]^{3+}$: they are listed in Table 3, along with their calculated steric energies.

Because all three ring *positions* are distinct in the *mer* but are identical in the *fac* geometries, the *mer* forms should show a statistical stabilization of $RT\ln(\frac{1}{3})$ over the *fac* forms. Further, the 'mixed' isomers (*RRS*, *SSR*) should be stabilized by a statistical factor of 3:1 over the *RRR* and *SSS* isomers for the *fac* (but not the *mer*) forms. After correction for these statistical factors (calculated at 25 °C), the most stable isomeric forms of Λ-$[Co(men)_3]^{3+}$ would be expected to be ['ΔG' = ΔH_{steric} + $RT\ln(\frac{1}{3})$, in kJ mol^{-1}]: **1** *mer*-*R***RS*-δ*δλ ('ΔG' = 83.4), **2** *mer*-*R***RR*-δ*λδ ('ΔG' = 87.1), **3** *mer*-*R***RS*-δ*λλ ('ΔG' = 87.8), **4** *mer*-*R***SR*-δ*λδ ('ΔG' = 90.6), **5** *mer*-*R***SR*-δ*δδ ('ΔG' = 90.9), **6** *mer*-*S***RR*-δ*λλ ('ΔG' = 91.8), **7** *mer*-*R***SS*-δ*λλ ('ΔG' = 92.9), **8** *mer*-*R***RS*-δ*δδ ('ΔG' = 93.6) and **9** *mer*-*R***SS*-δ*δλ ('ΔG' = 94.9). On the assumption that conformational isomers of the same geometry/configuration will not be separated experimentally (chromatography), the calculations predict that the order of geometric/configurational isomer stability will be *mer*-*R***RS* > *R***RR* > *R***SR* > *S***RR* > *R***SS* for the five most stable forms of Λ-$[Co(men)_3]^{3+}$. The experimental studies of the isomer stabilities[16] have realized three isomers (designated **A**, **B** and **C**) in the ratio 3:1:2 (at 25 °C). Isomers **A** and **C** have been determined as the *R***RR* and *R***RS* forms respectively, by X-ray structural studies.[17] While the prediction of isomer ratios in this case (**A**:**C** = 1:5) is not as satisfactory as with $[Co(men)_2(en)]^{3+}$ or for the $[Co(pn)_n(en)_{3-n}]^{3+}$ systems,[11] the selection of these two isomers (in the correct conformational form, see above) from 88 possible forms by the MM2 force field is a remarkable result. Further, the calculations allow prediction that the isolated isomer **B** should be diastereoisomer Λ-*R***SR*, and that two conformational forms δ*δδ and δ*λδ may be of comparable and highest stability. The reason for the particular stability of the *mer*-*R***RR* in complex **A** is not clear. It should be emphasized however that small changes in the free energies correspond to large changes in the relative proportions of the closely related forms of the molecule, and with these considerations the predictive value of calculations of this type within the complex systems reported here is quite striking.

Factors that are not readily accessible in calculations of this type are the differential effects on isomer stabilities of solvation and ion association. Cobalt(III) complexes containing amine ligands, like the present $[Co(men)_3]^{3+}$ and $[Co(men)_2(en)]^{3+}$ species, are known to undergo ion association with anions[20] utilizing the two groupings of three amine functions which are on opposite faces of the co-ordination octahedron. Since the CH_3 substituents are on the carbon skeleton of the rings in the $[Co(pn)_n(en)_{3-n}]^{3+}$ systems, it is possible that ion-association effects are similar for the isomers of each of these complex systems (n = 1–3) so that the relative free energies will not be greatly influenced by this factor. However, for the $[Co(men)_n(en)_{3-n}]^{3+}$ complexes the CH_3 substituent is on an N-donor atom and, dependent on its orientation, may have an influence on the interaction of the complex molecule with either solvent or anions. For this particular series of complexes such an effect is likely to become more significant in the sequence n = 1 < 2 < 3, so that its consequences may well be greatest for the $[Co(men)_3]^{3+}$ complex. Interestingly, it is only for this complex among all the $[Co(pn)_n(en)_{3-n}]^{3+}$ and $[Co(men)_n(en)_{3-n}]^{3+}$ systems studied that there is any noticeable discrepancy between the calculated and experimental thermodynamic ratios. Nevertheless, even in this least favourable case of these six systems studied, the two most stable geometric/conformational forms of the $[Co(men)_3]^{3+}$ species observed experimentally are among the three forms of the molecule calculated to be the most stable from 88 possible.

Structural Considerations.—The MM2 force-field calculations yield structural details of the minimized form of each conformer. Interconversions of ring conformations do not occur during the minimization, so that each calculation results in a lowest-energy form for the particular starting conformational isomer. The calculated and experimental structural data for the complexes are given in SUP 56800 for the complexes where X-ray crystal structures are available:[17,18] **F** = $[Co(men)_2(en)]^{3+}$, Λ-*trans*(CH_3), *cis*(NH_2)-*RR*-δ*δδ; **H** = $[Co(men)_2(en)]^{3+}$, Λ-*cis*(CH_3), *trans*(NH_2)-(*RR*-δ*δδ + *RR*-λ*δδ); **A** = $[Co(men)_3]^{3+}$, Λ-*mer*-*R***RR*-δ*λδ; and **C** = $[Co(men)_3]^{3+}$, Λ-*mer*-*R***RS*-δ*δλ. The molecular structures for the three complexes are shown in Figs. 4–7, which give the atom numbering schemes used.

Comparison of the geometric parameters for the crystal structures and minimized structures show that the correlations are very good.* Particular points of correlation are, first, the

* Summaries of comparisons: for **F**, root-mean-square (r.m.s.) differences for 17 bond lengths, 0.036 Å; for 31 bond angles, 1.60°; for 51 torsional angles, 16.08°; for all interatomic distances, 0.052 Å; for **H**, (*a*) r.m.s. differences for 17 bond lengths, 0.030 Å; for 31 angles, 1.69°; for 49 torsional angles, 2.01°; for all interatomic distances, 0.045 Å. (*b*) for 17 bond lengths, 0.022 Å; for 31 angles, 1.48°; for 49 torsional angles, 4.56°; for all interatomic distances, 0.041 Å; for **A**, r.m.s. differences for 18 bond lengths, 0.023 Å; for 33 bond angles, 0.97°; for 57 torsional angles, 7.11°; for all interatomic distances, 0.038 Å; for **C**, r.m.s. differences for 18 bond lengths, 0.027 Å; for 33 angles, 1.07°; for 57 torsional angles, *ca.* 3.00°; for all interatomic distances, 0.053 Å.

Table 3 Steric energies (kJ mol^{-1}) for the isomers of Λ-[Co(men)$_3$]$^{3+}$; superscript * designates the unique men ring

	Conformer							
Diastereoisomer	δ*δδ	δ*δλ	δ*λδ	λ*δδ	λ*λδ	λ*δλ	δ*λλ	λ*λλ
mer								
*R*RR*	96.2	111.2	89.8[a]	100.7	99.5	121.1	101.6	109.7
*R*SR*	*93.6*	108.2	*93.3*	106.5	104.0	118.7	114.8	128.9
*S*RR*	109.1	130.5	113.7	118.1	102.0	119.7	*94.5*	114.1
*R*RS*	*96.3*	86.1[b]	103.9	106.4	115.6	98.9	*90.5*	100.5
*S*RS*	125.8	135.9	111.2	109.5	117.0	100.4	111.8	104.1
*R*SS*	118.5	97.6	109.3	124.9	115.0	114.1	95.6	113.4
*S*SR*	120.5	126.6	118.2	110.3	103.0	122.8	140.0	130.1
*S*SS*	152.1	121.4	147.2	132.5	123.0	116.2	125.6	114.7
fac								
RRR	115.3	←	125.1	→	←	127.0	→	118.4
SRR	110.5	124.0	109.1	105.5	120.1	123.2	120.2	125.4
RSS	117.2	108.8	108.9	131.2	117.2	129.0	108.6	123.9
SSS	135.3	←	126.0	→	←	114.7	→	113.4

Energies within 7.5 kJ mol^{-1} of those for the isolated structures are italicized. [a] Isolated isomer **A** for which crystal structure has been determined.[17] [b] Isolated isomer **C** for which crystal structure has been determined.[17]

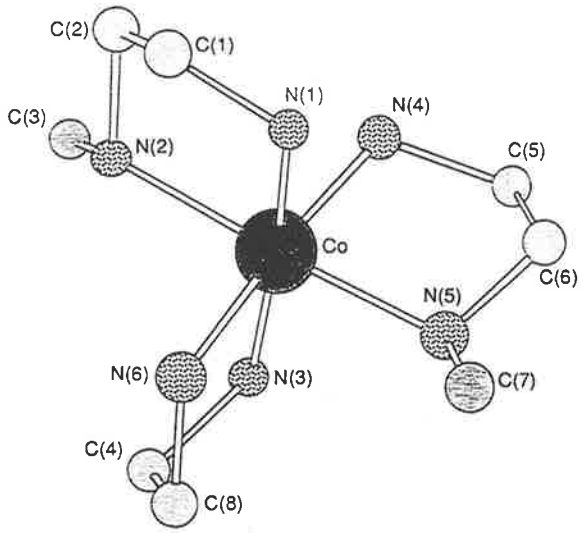

Fig. 4 Crystal structure[17] of **F**, Λ-[Co(men)$_2$(en)]$^{3+}$, *trans*(CH)$_3$, *cis*(NH$_2$)-*RR*-δ*δδ, showing atom numbering scheme used

MM2 force-field calculations have correctly accounted for the small (*ca.* 0.04 Å) Co–N bond-length increase observed for Co–NH(CH$_3$)– compared with Co–NH$_2$–. This effect is possibly caused by steric interactions involving the substituent methyl group, which elongate the Co–N bond and distort the tetrahedral geometry about the substituted N-donor atom. Restraining these N atoms to a strict tetrahedral arrangement in such calculations may reveal more about these particular interactions, but this was not undertaken in the present work.

Secondly, in the crystal structures of **A** and **C** there is a clear conformational distortion of the two δ rings, seen in Figs. 5 and 6 as a deviation from the expected parallel orientation of the C–C bonds relative to the pseudo-C_3 axis.* These distortions are duplicated in the calculated structure.

A discrepancy between the X-ray and calculated bond lengths is observed in some N–C and consistently in the (N)C–C(N) bonds, and the following factors may be involved. A deficiency of the present MM2 force field is that the parameters used for the N atoms are those of free amine groups, since MM2 force-field parameters do not exist for co-ordinated amines: undoubtedly, there will be perturbing electronic effects when amines are co-ordinated which will therefore reduce the accuracy of the parametrization. In addition, similar calculations involving O–C–C–O systems give minimized C–C bond lengths consistently longer than those observed in the same molecules in structural determinations.[21] This effect is unexplained, but it is clear that similar effects are observed in these analogous N–C–C–N systems. The correlation may be improved by adjustment of the parametrization relating to this grouping in the ligand. However, our aim in this and related studies[11] was to maintain a general force field in a comparison of its application to a variety of complex systems.

Conclusion

Where experimental thermodynamic and structural information is available for the various [Co(men)$_n$(en)$_{3-n}$]$^{3+}$ species the MM2 force-field calculations have shown a remarkable correlation. Because of the large number of closely related isomeric forms in each of these three complex systems, the results are encouraging for the predictive application of MM2 techniques to metal complex systems in which there are subtle differences between possible forms.

Experimental

The calculations used the MM2 force-field minimization program described previously.[11,22–24]

Starting structures were prepared by addition of methyl groups at standard bond lengths and angles to the cation in the [Co(en)$_3$]$_2$[HPO$_4$]$_3$·9H$_2$O structure of Duesler and Raymond.[25] The computer program CHEM 3D PLUS™ (Cambridge Scientific Computing, Boston, MA) was used for editing and manipulating initial structures and viewing final output. For each isomer minimized more than one starting geometry was used to reduce the possibility of conformations being hung in 'local energy minima'.

All of the organic parameters used in the force field derive

* When tris(bidentate) molecules involving five-membered chelate rings of the en type (*e.g.* en, pn) are viewed down the (pseudo-)C_3 axis the C–C bond of each ring is observed to be either roughly parallel ('lel') or oblique ('ob') to that axis. For the Λ absolute configuration of the metal the δ conformation is 'lel' and the λ conformation is 'ob'. For the enantiomeric Δ absolute configuration the λ conformation will be 'lel' and the δ conformation 'ob.'[11]

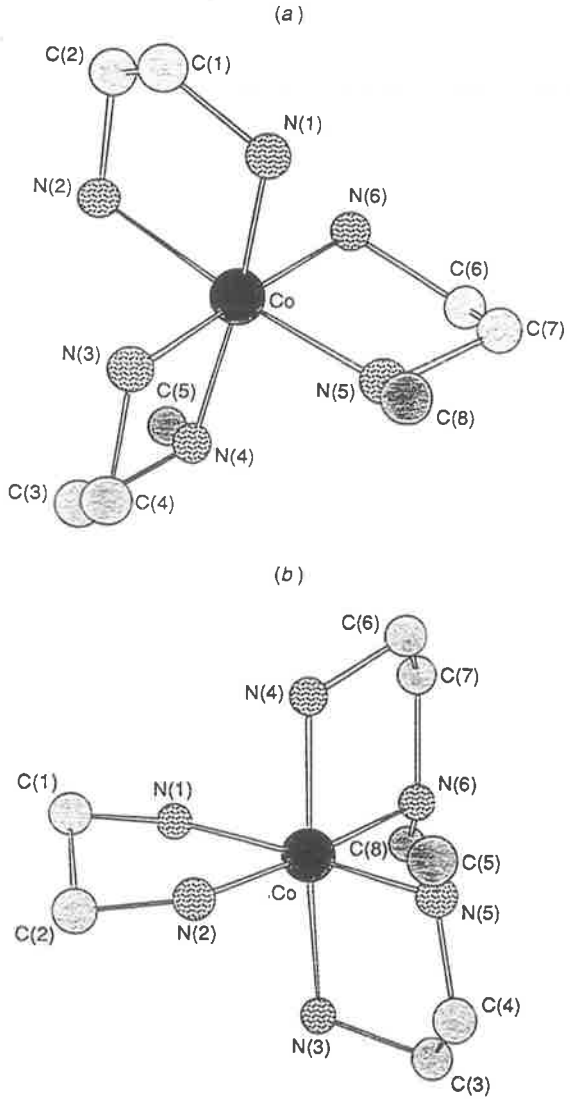

Fig. 5 Crystal structure[18] of **H**, $[Co(men)_2(en)]^{3+}$: (*a*) *cis*(CH_3), *trans*(NH_2)-Λ-*RR*-δ*δδ and (*b*) *cis*(CH_3), *trans*(NH_2)-Δ-*SS*-δ*λλ [≡ *cis*(CH_3), *trans*(NH_2)-Λ-*RR*-λ*δδ], showing atom numbering scheme used

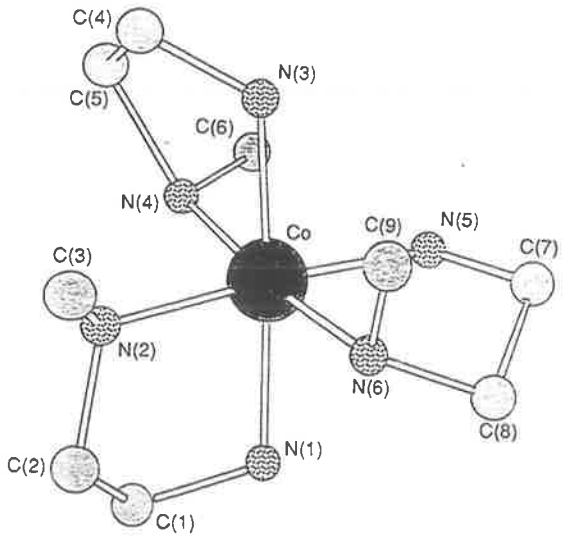

Fig. 6 Crystal structure[17] of **A**, Λ-$[Co(men)_3]^{3+}$, *mer*-*R***RR*-δ*λδ, showing atom numbering scheme used

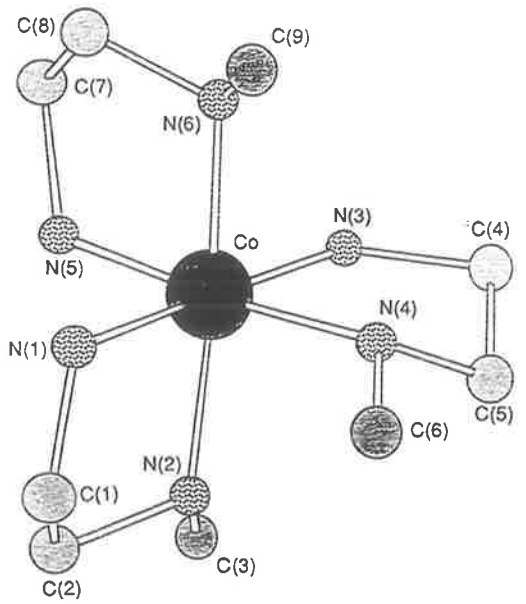

Fig. 7 Crystal structure[17] of **C**, Λ-$[(Co(men)_3]^{3+}$, *mer*-*R***RS*-δ*δλ, showing atom numbering scheme used

from the original work by Allinger.[22] Parameters containing the metal were taken in the first instance from the work by DeHayes and Busch[13] and Brubaker and Johnson,[19] and they were then adjusted to provide the best fits between MM2 minimized geometries and the available X-ray diffraction studies. The final parameters are*: non-bonding, cobalt(III) van der Waals radius, 2.30 Å; ε_0 = 0.711 kJ mol^{-1}; bond stretching, Co^{III}–N, K_{str} = 195.0 N m^{-1} molecule^{-1}, r_0 = 1.950 Å, bond moment = 0.0 D, cubic stretch constant = 2.000; valence angle deformation, N–Co^{III}–N, K_{bend} = 0.400 × 10^{-18} N Å rad^{-2} molecule^{-1}, θ_1 = 90.000°, $\theta_2 = \theta_3$ = 0.000°; Co^{III}–N–C, K_{bend} = 0.278 × 10^{-18} N Å rad^{-2} molecule^{-1}, θ_1 = 90.000°, $\theta_2 = \theta_3$ = 0.000°; H–N–Co^{III}, K_{bend} = 0.278 × 10^{-18} N Å rad^{-2} molecule^{-1}, θ_1 = 90.000°, $\theta_2 = \theta_3$ = 0.000°; torsional angle deformation, C–N–Co^{III}–N, V_1 = 0.000, V_2 = 0.000, V_3 = 0.000 kJ mol^{-1}; H–N–Co^{III}–N, V_1 = 0.000, V_2 = 0.000, V_3 = 0.000 kJ mol^{-1}; H–C–N–Co^{III}, V_1 = 0.000, V_2 = 0.000, V_3 = −2.174 kJ mol^{-1}; C–C–N–Co^{III}, V_1 = −0.836, V_2 = 3.051, V_3 = 3.344 kJ mol^{-1}.

The convergence criterion for minimization was taken to be $\Delta H_{steric} < 10^{-7}$ kJ mol^{-1} between successive iterations, and this usually required between 50 and 100 cycles (generally less than 5 min of time per isomer on either a DEC 10 or a CCI Power 32 minicomputer). For each isomer the calculations resulted in a minimum-energy geometry and the 'total steric energy', ΔH_{steric}, which is the sum of the component molecular mechanics potential-energy terms (non-bonded, bond-stretch, dipole–dipole, valence-angle bending, bend-stretch and torsional energies). Tables 1–3 summarize the calculated ΔH_{steric} values for the complexes considered. Complete listings of the contributing terms are included in SUP 56800.

Acknowledgements

The continuing interest and assistance of Dr. K. R. Adam (James Cook University of North Queensland) with aspects of

* ε_0 = Energy parameter; θ_1 = ideal bond angle, θ_2 and θ_3 are higher-order terms in the potential function; V_1, V_2 and V_3 are the first three co-efficients of the Fourier series expansion which models the torsional energy of the system.[22,23]

the molecular mechanics calculations is very gratefully acknowledged. This work was supported by the Australian Research Grants Scheme.

References

1 E. J. Corey and J. C. Bailar, *J. Am. Chem. Soc.*, 1959, **81**, 2620.
2 F. P. Dwyer, F. L. Garvan and A. Shulman, *J. Am. Chem. Soc.*, 1959, **81**, 290.
3 F. P. Dwyer, T. E. MacDermott and A. M. Sargeson, *J. Am. Chem. Soc.*, 1963, **85**, 2913.
4 F. P. Dwyer, A. M. Sargeson and L. B. James, *J. Am. Chem. Soc.*, 1964, **86**, 590.
5 S. E. Harnung, S. Kallesoe, A. M. Sargeson and C. E. Schaffer, *Acta Chem. Scand., Ser. A*, 1974, **28**, 385.
6 J. R. Gollogly and C. J. Hawkins, *Inorg. Chem.*, 1970, **9**, 576.
7 P. F. Crossing and M. R. Snow, unpublished work; P. F. Crossing, M.Sc. Dissertation, University of Adelaide, 1973; see also, D. A. Buckingham and A. M. Sargeson, *Top. Stereochem.*, 1971, **6**, 219.
8 T. Laier and E. Larsen, *Acta Chem. Scand., Ser. A*, 1979, **33**, 257.
9 A. M. Bond, T. W. Hambley, D. R. Mann and M. R. Snow, *Inorg. Chem.*, 1987, **26**, 2257.
10 T. W. Hambley, *Inorg. Chem.*, 1988, **27**, 2496.
11 I. M. Atkinson, F. R. Keene and G. H. Searle, *J. Mol. Struct.*, in the press and refs. therein.
12 *Nomenclature of Inorganic Chemistry*, 3rd edn., ed. G. J. Leigh, Blackwell, Oxford, 1988.
13 L. J. DeHayes and D. H. Busch, *Inorg. Chem.*, 1973, **12**, 1505.
14 T. W. Hambley, C. J. Hawkins, J. Martin, J. A. Palmer and M. R. Snow, *Aust. J. Chem.*, 1981, **24**, 2505.
15 D. A. Buckingham, L. G. Marzilli and A. M. Sargeson, *Inorg. Chem.*, 1968, **7**, 915.
16 G. H. Searle and F. R. Keene, *Inorg. Chim. Acta*, 1989, **155**, 125.
17 G. H. Searle and E. R. T. Tiekink, *Inorg. Chim. Acta*, 1989, **156**, 57.
18 G. H. Searle and E. R. T. Tiekink, *Acta Crystallogr., Sect. C*, 1989, **45**, 1300.
19 G. R. Brubaker and D. W. Johnson, *Coord. Chem. Rev.*, 1984, **53**, 1 and refs. therein.
20 F. R. Keene and G. H. Searle, *Inorg. Chem.*, 1974, **13**, 2173.
21 K. R. Adam, B. J. McCool and L. F. Lindoy, unpublished work.
22 N. L. Allinger, *Adv. Phys. Org. Chem.*, 1976, **13**, 1.
23 QCPE Program No. 395, The Quantum Chemistry Program Exchange. University of Indiana, Bloomington, IN, 1980.
24 K. R. Adam, L. G. Brigden, K. Henrick, L. F. Lindoy, M. McPartlin, B. Mimagh and P. A. Tasker, *J. Chem. Soc., Chem. Commun.*, 1985, 710.
25 E. N. Duesler and K. N. Raymond, *Inorg. Chem.*, 1971, **10**, 1486.

Received 14*th February* 1990; *Paper* 0/00703J

Journal of Molecular Structure, 265 (1992) 189–213
Elsevier Science Publishers B.V., Amsterdam

A molecular mechanics analysis of $[Co(medien)_n(dien)_{2-n}]^{3+}$ $\{n=0-2\}$ (dien = diethylenetriamine or 1,5-diamino-3-azapentane; medien = 3-methyl-1,5-diamino-3-azapentane), and X-ray structural studies of the *mer*- and *s-fac*-$[Co(medien)(dien)]^{3+}$ cations

Ian M. Atkinson and F. Richard Keene[1]

Department of Chemistry and Biochemistry, James Cook University of North Queensland, Townsville, Qld. 4811 (Australia)

Jacqueline M. Gulbis, Graeme H. Searle and Edward R.T. Tiekink

Department of Physical and Inorganic Chemistry, University of Adelaide, Adelaide, S.A. 5001 (Australia)

(Received 18 June 1991)

Abstract

Crystals of *mer*-$[Co(medien)(dien)]Br_2(ClO_4)\cdot H_2O$ (**1**) crystallize in the monoclinic space group $P2_1/n$ with unit cell dimensions $a=12.206(2)$, $b=12.744(1)$, $c=12.712(2)$ Å, $\beta=94.99(1)°$, $V=1969.9$ Å^3, $Z=4$; crystals of *s-fac*-$[Co(medien)(dien)](S_2O_6)_{1.5}\cdot 0.5H_2O$ (**2**) are monoclinic, space group $P2_1$ with $a=9.772(3)$, $b=10.512(2)$, $c=19.263(4)$ Å, $\beta=92.24(2)°$, $V=2014.2$ Å^3, $Z=4$. The structures were refined by a full-matrix least-squares procedure in each case. At convergence, final R 0.065, R_w 0.067 for 2578 reflections with $I \geqslant 2.5\sigma(I)$ for (**1**) and R 0.061, R_w 0.061 for 2845 reflections for (**2**). A molecular mechanics study of the isomers of the bis(tridentate)cobalt(III) complexes $[Co(medien)_n(dien)_{2-n}]^{3+}$, $n=0-2$, (dien = diethylenetriamine or 1,5-diamino-3-azapentane; medien = 3-methyl-1,5-diamino-3-azapentane) is reported. For the $[Co(dien)_2]^{3+}$ isomers, and the mer and s-fac isomers of $[Co(medien)(dien)]^{3+}$, the structural details are satisfactorily modelled by MM2. For both the $[Co(dien)_2]^{3+}$ and $[Co(medien)(dien)]^{3+}$ systems, the MM2 procedure substantially overestimates the stability of the mer geometric isomers relative to the fac forms, although the relative stabilities of the s-fac/u-fac forms correspond well with the observed isomer ratios. The calculated isomer ratios for the $[Co(medien)_2]^{3+}$ system agree with those found experimentally. The apparent variance in the capability of the MM2 procedure to predict the relative stabilities of the three geometric isomers in the three analogous systems is discussed.

[1]Author to whom correspondence should be addressed.

INTRODUCTION

The stereochemistry of the bis(tridentate)cobalt(III) complexes containing the ligands diethylenetriamine (dien=1,5-diamino-3-azapentane) and *N*-methyldiethylenetriamine (medien=3-methyl-1,5-diamino-3-azapentane) has been extensively studied, including the relative thermodynamic stabilities of the three possible geometric isomers in the systems $[Co(dien)_2]^{3+}$ [1,2], $[Co(medien)(dien)]^{3+}$ [3,4], and $[Co(medien)_2]^{3+}$ [3,4]. X-ray structural determinations of the geometrical and optical isomers of $[Co(dien)_2]^{3+}$ have also been reported [5–8].

The success of molecular mechanics methods in predicting the stable geometries and indicating the factors affecting thermodynamic stabilities of cobalt(III) complexes containing amine ligands is well established [9]. This success is due in part to the "directional" bonding characteristics of the Co(III) ion, meaning that its valence bond lengths and angles are restricted to narrow ranges. Because of the relative consistency of geometry, force fields which are parametrized for one type of complex should be reasonably applicable to different Co(III)–(amine) systems.

As part of our applications [10,11] of the MM2 force field of Allinger [12] to the prediction of thermodynamic stabilities of various $[Co(amine)_n]^{3+}$ complexes, we have carried out a comprehensive MM2 study of the stereoisomers of the title complexes. Early molecular mechanics investigations of $[Co(dien)_2]^{3+}$ had limited success [13–16]. More recently, however, Bond et al. [17] used the force field of Hambley et al. [18] to predict a relative order of the geometric isomer stabilities which correlates to that observed in solution under equilibrium conditions. The pseudo Urey–Bradley force field used in that study [17] differs from MM2 in two significant ways: valence angle deformation terms about the metal in MM2 are replaced with 1,3 non-bonded interactions in the force field of Hambley et al. [18], and torsional interactions about the metal are excluded in the original MM2 force field whereas they are implicitly included by Hambley et al. [18]. We wished to apply our MM2-based force field, unchanged from previous investigations of complexes of en, pn and men [10,11] (en=ethane-1,2-diamine; pn=propane-1,2-diamine; men=*N*-methylethane-1,2-diamine), to the three related bis(tridentate) systems $[Co(medien)_n(dien)_{2-n}]^{3+}$ (n=0–2), and determine the effectiveness of MM2-type molecular mechanics calculations for predicting the stabilities, and geometries, of the isomers of the title complexes. Comparisons with previous approaches for describing the $[Co(dien)_2]^{3+}$ system would then be possible.

The crystal structures of the *mer*- and *s-fac*-$[Co(medien)(dien)]^{3+}$ cations were also undertaken to allow comparison with the calculated structures involving the medien ligand.

EXPERIMENTAL

Molecular mechanics calculations

Our approach to the MM2 calculations using the MOLMEC suite of programs has been described previously [10,19]. The identical force field parameters were used in this work, although it was found that incorporation of a cubic bond stretch constant of −2.00 (the MM2 standard) slightly improved the geometric correlations with available X-ray structural data.

In comparisons between X-ray and MM2-calculated structures, torsional angles involving a near-linear N–Co–N segment were disregarded as they carry exaggeratedly high error [19].

Crystallography

The syntheses and separation of the isomers of the $[Co(medien)(dien)]^{3+}$ have been described previously [3,4]. *mer*-$[Co(medien)(dien)]$-

TABLE 1

Crystal data and refinement details for *mer*-$[Co(medien)(dien)]Br_2(ClO_4)\cdot H_2O$ (**1**) and *s-fac*-$[Co(medien)(dien)](S_2O_6)_{1.5}\cdot 0.5H_2O$ (**2**)

Compound	(**1**)	(**2**)
Formula	$C_9H_{30}Br_2ClCoN_6O_5$	$C_9H_{29}CoN_6O_{9.5}S_3$
Mol. wt.	556.6	528.5
Crystal system	monoclinic	monoclinic
Space group	$P2_1/n$	$P2_1$
a(Å)	12.206(2)	9.772(8)
b(Å)	12.744(1)	10.512(2)
c(Å)	12.712(3)	19.623(4)
β(deg.)	94.99(1)	92.24(2)
V(Å^3)	1969.9	2014.2
D_c(g cm^{-3})	1.887	1.743
Z	4	4
$F(000)$	1108	1072
μ(cm^{-1})	49.85	11.62
No. of data collected	3142	3049
No. of unique data	2578	2845
No. of unique reflections used with $I \geqslant 2.5\sigma(I)$	1614	1976
R	0.065	0.061
k	1.995	1
g	0.001	0.001
R_w	0.067	0.061

TABLE 2

Fractional atomic coordinates ($\times 10^4$) for *mer*-[Co(medien)(dien)]$Br_2(ClO_4)\cdot H_2O$ (**1**)

Atom	*x*	*y*	*z*
Co	2214(1)	2716(1)	4993(1)
N(1)	2309(9)	3776(9)	6128(9)
N(2)	2611(9)	3875(8)	4114(8)
N(3)	3750(9)	2318(9)	5470(9)
N(4)	2258(9)	1899(9)	3687(8)
N(5)	1790(10)	1532(10)	5882(9)
N(6)	610(8)	2942(9)	4713(10)
C(1)	2573(12)	4845(12)	5700(12)
C(2)	3210(13)	4698(11)	4765(12)
C(3)	3135(12)	3502(13)	3190(11)
C(4)	2475(13)	2576(13)	2788(10)
C(5)	3748(13)	1409(12)	6217(12)
C(6)	2735(15)	1400(18)	6690(17)
C(7)	751(17)	1803(16)	6301(19)
C(8)	−12(13)	2207(13)	5327(14)
C(9)	1670(16)	458(15)	5321(16)
Br(1)	264(1)	5255(1)	3404(1)
Br(2)	156(1)	8893(1)	7494(1)
Cl	1595(3)	2856(4)	9445(4)
O(1)	745(10)	2129(12)	9162(12)
O(2)	1818(17)	3488(15)	8631(12)
O(3)	1404(23)	3488(17)	10317(19)
O(4)	2540(14)	2304(14)	9717(22)
O(w)	5989(16)	−408(14)	6069(13)

$Br_2(ClO_4)\cdot H_2O$ was precipitated from an aqueous solution of the bromide salt by addition of $NaClO_4$: crystals were obtained by liquid diffusion of ethanol into an aqueous solution of the complex. Crystals of *s-fac*-[Co(medien)(dien)]$(S_2O_6)_{1.5}\cdot 0.5H_2O$ were obtained by liquid diffusion of an ethanolic solution of $Li_2S_2O_6$ into an aqueous solution of the bromide salt of the cation.

Intensity data for (**1**) and (**2**) were measured at room temperature on an Enraf–Nonius CAD4*F* diffractometer fitted with Mo Kα radiation, $\lambda = 0.7107$ Å. The $\omega:2\theta$ scan technique was employed in each case to measure the intensities of reflections up to θ_{max} of 22.5°. The data were corrected for Lorentz and polarization effects and an analytical absorption correction was applied in each case [20a]. Relevant crystal data are collected in Table 1.

The structures were solved by conventional heavy-atom methods and each refined by a full-matrix least-squares procedure based on *F*. Except for the C(8) atom in (**2**), which showed high thermal motion, all non-H atoms were refined with anisotropic thermal parameters. H atoms were included in the models at their calculated positions except for those associated with the water

TABLE 3

Fractional atomic coordinates ($\times 10^4$) for *s-fac*-[Co(medien)(dien)]$(S_2O_6)_{1.5}\cdot 0.5H_2O$ (**2**)

Atom	*x*	*y*	*z*
Co(1)	7857(2)	8892(-)	6094(1)
N(1)	6721(14)	7698(14)	6551(7)
N(2)	9065(12)	8779(13)	6893(6)
N(3)	6986(14)	10304(12)	6574(7)
N(4)	9048(14)	10167(13)	5662(8)
N(5)	6684(12)	8989(15)	5229(6)
N(6)	8748(12)	7498(12)	5619(7)
C(1)	7222(19)	7393(20)	7265(9)
C(2)	8737(20)	7634(18)	7293(10)
C(3)	8964(16)	10018(18)	7309(9)
C(4)	7576(19)	10468(18)	7297(9)
C(5)	8242(20)	10748(17)	5076(10)
C(6)	7467(18)	9721(19)	4717(8)
C(7)	6535(17)	7657(18)	4972(9)
C(8)	7926(17)	7012(19)	5019(9)
C(9)	5296(17)	9616(22)	5284(9)
Co(2)	2796(2)	4703(3)	8727(1)
N(1′)	1597(12)	4464(15)	9506(7)
N(2′)	3872(13)	5869(14)	9334(8)
N(3′)	1723(13)	6231(15)	8465(8)
N(4′)	4030(12)	5019(15)	7984(7)
N(5′)	1747(12)	3563(11)	8092(6)
N(6′)	3895(14)	3225(14)	9010(7)
C(21)	1827(18)	5431(21)	10032(9)
C(22)	3395(20)	5715(24)	10043(10)
C(23)	3757(19)	7141(17)	9056(12)
C(24)	2234(18)	7423(20)	8808(12)
C(25)	3830(18)	4015(23)	7441(9)
C(26)	2334(16)	3674(22)	7424(9)
C(27)	1943(18)	2253(20)	8420(9)
C(28)	3384(16)	2040(17)	8636(9)
C(29)	270(16)	3848(25)	7972(10)
S(1)	862(4)	8831(4)	3941(2)
S(2)	2918(4)	8931(5)	3607(2)
S(3)	2164(4)	−126(5)	147(2)
S(4)	2332(4)	1490(5)	796(2)
S(5)	7312(4)	2668(5)	3405(2)
S(6)	6816(7)	4411(7)	2944(5)
O(11)	343(11)	7661(11)	3651(6)
O(12)	242(11)	9962(12)	3653(6)
O(13)	964(10)	8835(13)	4668(6)
O(21)	3582(12)	7834(12)	3895(7)
O(22)	3474(11)	10110(11)	3885(7)
O(23)	2749(11)	8966(16)	2861(6)
O(31)	3597(11)	−440(14)	40(8)
O(32)	1506(11)	−1061(15)	562(6)
O(33)	1380(13)	281(16)	−428(6)

TABLE 3 (continued)

Atom	x	y	z
O(41)	3261(13)	1117(14)	1331(7)
O(42)	2844(14)	2485(13)	367(6)
O(43)	959(12)	1732(14)	1031(7)
O(51)	6255(13)	2346(14)	3848(8)
O(52)	8532(16)	3057(23)	3808(7)
O(53)	7606(29)	1832(19)	2888(9)
O(61)	7866(14)	4660(16)	2497(8)
O(62)	6113(32)	5168(26)	3269(17)
O(63)	5546(21)	3835(48)	2432(21)
O(w)	3361(12)	7968(15)	1582(7)

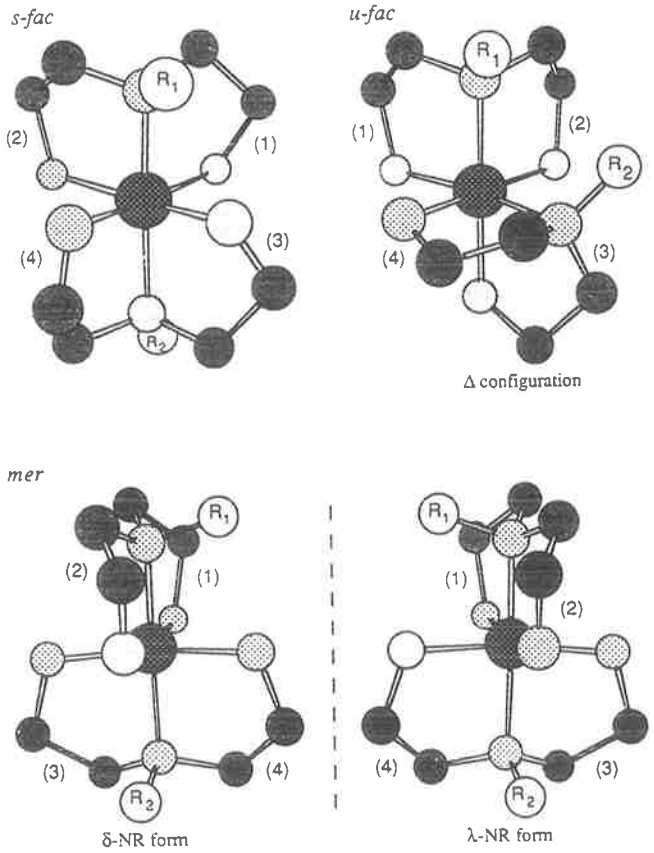

Fig. 1. Ring numbering sequence for the geometric isomers of the $[Co(medien)_n(dien)_{2-n}]^{3+}$ ($n=0$–2) systems.

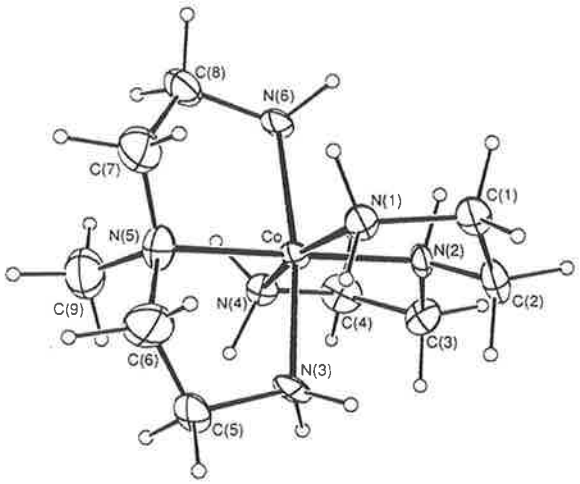

Fig. 2. Molecular structure and crystallographic numbering scheme for the cation in *mer*-[Co(medien)(dien)]$Br_2(ClO_4)\cdot H_2O$ (**1**).

molecules of crystallization. The structure of (**2**) was refined in the non-centrosymmetric space group $P2_1$ with two molecules in the asymmetric unit; attempts to refine this structure in $P2_1/m$ proved unsuccessful. The absolute configuration of (**2**) was determined on the basis of differences in Friedel pairs included in the data set. In compound **2** one of the S_2O_6 dianions was disordered such that there were several positions for the O(62) and O(63) positions. Only the positions of the major component of the disorder are reported. Each structure was refined to convergence after the inclusion of a weighting scheme of the form $w=k/[\sigma^2(F)+g|F|^2]$. Final refinement details are listed in Table 1. Fractional atomic coordinates for (**1**) and (**2**) are given in Tables 2 and 3 respectively, and the numbering schemes employed for the cations are shown in Figs. 2 and 3 respectively, which were drawn with the ORTEP program [20b]. Scattering factors for Co(III) (corrected for f' and f'') were from ref. 20c and those for the remaining atoms were as incorporated in the SHELX 76 program [20a]. Other crystallographic details, comprising thermal parameters, H-atom parameters, all bond distances and angles, and tables of observed and calculated structure factors are available from one of the authors (E.R.T.T.).

RESULTS AND DISCUSSION

Isomeric forms

A detailed description of the geometric isomerism in the title complexes has been given previously [1,3]. Three different geometric forms, designated sym-

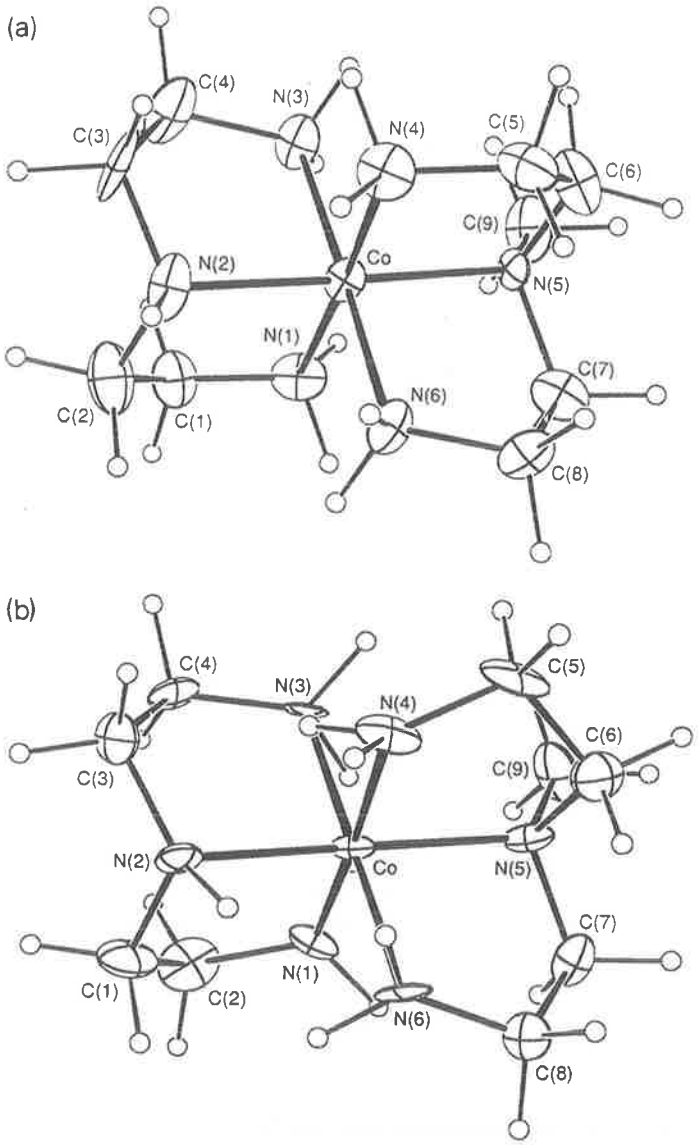

Fig. 3. Molecular structure and crystallographic numbering scheme for the cations in *s-fac*-[Co(medien)(dien)]$(S_2O_6)_{1.5}\cdot 0.5H_2O$ (**2**), conformers: (a) ($\lambda\delta,\lambda\delta$); (b) ($\delta\delta,\lambda\delta$).

metrical-facial (s-fac), unsymmetrical-facial (u-fac), and meridional (mer), exist for each of the title bis(tridentate) complexes (Fig. 1). In all cases there is a maximum number of 16 ($=2^4$) possible conformational isomers formed as a result of the possible δ and λ orientations of the four five-membered chelate

rings, but some of these may be rendered equivalent by molecular symmetry.

Configurational symmetry of the chelate ring distribution prevents a unique description of the ring order for the mer and s-fac geometric forms of the title complexes, so that an arbitrary labelling scheme must be used, and this is shown in Fig. 1. In the following discussion, for the mixed ligand system $[Co(medien)(dien)]^{3+}$ (i.e. $R_1=CH_3$, $R_2=H$), the parameters of the medien ligand are listed first.

In a configurational sense, the s-fac form is centrosymmetric when $R_1=R_2$ (point group symmetry C_{2h}), but in the mixed-ligand complex ($R_1 \neq R_2$) only the plane of symmetry is retained and the symmetry reduces to C_s. Thus, the s-fac form of each complex does not show configurational dissymmetry. Nevertheless, the various conformational forms are diastereoisomeric since the individual ring conformations are chiral, so that the molecule may show dissymmetry.

The u-fac form has configurational point group symmetry C_2 when $R_1=R_2$, while for the mixed-ligand complex ($R_1 \neq R_2$) the molecule is asymmetric. In both cases, the u-fac form has configurational dissymmetry, and the Δ configuration [1] is shown in Fig. 1.

While the mer topology does not have configurational dissymmetry, the molecule is nevertheless dissymmetic since the pseudo-D_{2d} point group symmetry is reduced to C_2 (for $R_1=R_2$) and C_1 (for $R_1 \neq R_2$) by the chelate ring conformations. The chirality of the molecule has been described in terms of the helix formed by the N–R_1 and N–R_2 bonds: a right-handed or left-handed helix is designated δ-NR and λ-NR, respectively [1]. However the chirality may be defined more directly by the helicity of the skew lines, one joining the two R groups and the other joining the central N-atoms of the two ligands, and the two descriptions give the same helicity [8]. For designating the conformational forms of the mer geometric isomer, the following arbitrary rules have been used in this discussion. The molecule is orientated in the following way.

(a) Ignoring ring conformations, one meridional ligand is positioned on the upper half of the molecule and is viewed along the ligand plane. For $[Co(medien)(dien)]^{3+}$, this ligand will be taken as medien.

(b) The N–R substituent of the lower ligand (perpendicular to the direction of observation) points toward the observer. The N–R substituent on the upper ligand will then point to the right for the δ-NR enantiomer and to the left for the λ-NR enantiomer.

The conformations of the rings are then listed in the following sequence: rings (1) and (2) are taken as those in the upper ligand, with ring (1) being distant from the observer. Rings (3) and (4) are then numbered in the lower ligand from left to right for the δ-NR enantiomer and from right to left in the λ-NR enantiomer.

Structural considerations

$[Co(dien)_2]^{3+}$

mer. Inspection of Dreiding models indicates that the conformations of the coupled chelate rings in the meridional disposition of a dien ligand will be strongly confined to a "mixed" arrangement $\lambda\delta$ or $\delta\lambda$ by the tetrahedral geometry of the coupling amine group:

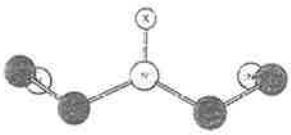

δλ-(dien)

Twisting the chelate rings into either envelope or $\delta\delta/\lambda\lambda$ conformations requires considerable distortion from the ideal 109.7° bond angle about this nitrogen atom and should therefore be energetically unfavourable. Certainly, in X-ray structure determinations of $(+)_D$-*mer*- [8] and racemic-*mer*-$[Co(dien)_2]^{3+}$ [7], only the λ-NH-$(\lambda\delta,\lambda\delta)$ and λ-NH-$(\lambda\delta,\lambda\delta)/\delta$-NH-$(\delta\lambda,\delta\lambda)$ forms (respectively) were observed.

The assertion of fixed conformations in the interlocked chelate rings of a meridional dien ligand has been addressed previously [4,20] and is corroborated by our MM2 results: calculations using any idealized conformational combinations, or perturbations of them, as initial structures all minimized to the λ-NH-$(\lambda\delta,\lambda\delta)$ conformer (Table 4). On some occasions the calculation would "hang" in a local minimum corresponding to an alternate structure; however, when these coordinates were re-minimized they resulted in the λ-NH-$(\lambda\delta,\lambda\delta)$ conformation.[a] This observation contrasts strongly with the results of Bond et al. [17] obtained by using a pseudo-Urey–Bradley force field, where minima were found for five of the mer conformers although the λ-NH-$(\lambda\delta,\lambda\delta)$ form (equivalent to δ-NH-$(\delta\lambda,\delta\lambda)$ in their study) was lower in energy by 14.8 kJ mol^{-1} than the next most stable form. We attribute this difference not to the force field differences but to the actual minimization algorithm used in our calculations [21].

There is good agreement between the minimized geometry of λ-NH-*mer*-$[Co(dien)_2]^{3+}$-$(\lambda\delta,\lambda\delta)$ and the structure determined by X-ray diffraction

[a]The minimization algorithm uses longer initial steps in geometry, which are monotonically reduced in successive iterations, allowing false minima. Re-minimizing such a structure can often, by virtue of the large initial geometry steps, take the structure out of this minimum to a "more" global form.

TABLE 4

Steric energy terms for isomers of $[Co(dien)_2]^{3+}$ (kJ mol^{-1})[a]

Isomer	$E_{N\text{-}B}$	$E_{Bond\text{-}S}$	$E_{D\text{-}D}$	E_{Bend}	$E_{Bend\text{-}S}$	E_{Tors}	E_{Total}
λ-NH-mer-$\lambda\delta,\lambda\delta$[b]	1.9	3.4	8.3	25.7	0.4	10.1	49.9
s-fac-$\lambda\delta,\lambda\delta$[b]	9.3	4.1	11.6	15.4	0.7	39.1	80.2
$\delta\delta,\delta\lambda$	17.1	5.1	10.9	16.6	0.8	41.0	91.6
$\delta\delta,\delta\delta$	18.5	5.5	10.8	16.9	0.7	41.3	93.8
$\delta\delta,\lambda\lambda$	21.4	6.0	10.6	20.5	0.8	47.4	106.7
Δ-u-fac-$\delta\lambda,\delta\lambda$[b]	8.6	4.6	11.3	16.7	0.6	38.8	80.6
$\lambda\lambda,\delta\lambda$	11.5	4.9	10.9	18.2	0.6	37.4	83.6
$\lambda\lambda,\lambda\lambda$[b]	14.1	5.2	10.3	19.2	0.6	35.6	85.3
$\delta\delta,\delta\delta$	14.2	5.5	10.6	19.2	0.6	36.4	86.4
$\delta\delta,\delta\lambda$	13.5	5.3	10.9	18.1	0.7	39.2	87.8
$\delta\delta,\lambda\lambda$	12.6	5.1	10.3	22.6	0.6	39.9	91.0

[a] $E_{N\text{-}B}$ = non-bonding energy; $E_{Bond\text{-}S}$ = bond stretch energy; $E_{D\text{-}D}$ = dipole–dipole energy; E_{Bend} = valence angle deformation energy; $E_{Bend\text{-}S}$ = bend stretch energy; E_{Tors} = torsional energy. [b] Forms have been identified in X-ray structures (ref. 5–8).

[8].[b] A comparison of the bond lengths and bond angles for the two structures is available in Supplementary Table S1, and a comparison of the torsional angles in Supplementary Table S2. No symmetry restrictions were used during the minimization, and the structure minimized to true C_2 symmetry. Chelate "bite" angles and C–C bond lengths are slightly dependent upon the ring conformation; no such discrimination by molecular mechanics has been previously reported although the differences are observed in the X-ray structures [7,8].

s-fac. There are seven possible conformers of the s-fac geometry, and only four were found to have potential energy minima in our MM2 calculations. Table 4 shows that the relative stabilities of these conformers are governed by torsional terms for those structures other than the form $(\lambda\delta,\lambda\delta)$, which is further stabilized by reduced bond-stretching and non-bonding interactions. Although the s-fac geometry does not have the conformational constraint that was present in the mer isomer, a preference for the mixed $\lambda\delta$ conformations within a dien ligand is predicted. The calculated lowest energy form is s-fac-$(\lambda\delta,\lambda\delta)$, consistent with the results of Bond et al. [17]. It is also the form identified by X-ray diffraction [5]. The C_{2h} point group symmetry of the energy-minimized

[b] Summary of comparison for λ-NH-*mer*-$[Co(dien)_2]^{3+}$-$(\delta\lambda,\delta\lambda)$: RMS differences are: for 18 bond lengths, 0.044 Å; for 33 angles, 1.50°; for 50 torsional angles, 7.8°; for all interatomic distances, 0.050 Å.

cation is higher than the C_i symmetry observed in the X-ray structure [5], presumably due to crystal packing forces distorting the cation in the solid state. There is excellent agreement between observed and calculated structures.[c]

A comparison of bond angles/bond lengths and torsional angles is given in Supplementary Tables S3 and S4 respectively. Again we found fewer stable conformers for this system than Bond et al. [17] who found minima for all seven conformational possibilities. No trend is obvious for differences in the two sets of calculations: for example, there is no symmetry correlation (we find minima for all possible combinations of conformations within a dien ligand). However, we find no minima in forms which have a large torsional energy (>35 kJ mol^{-1}) in the force field employed by Bond et al. [17].

u-fac. Six of the ten possible conformations of this geometry were found to have potential energy minima (Table 4), and in contrast to the mer and s-fac isomers they fully correspond to the six stable conformers determined by Bond et al. [17] (Table 5). Two of the three most stable conformers predicted by MM2 are those found in X-ray crystal structures, namely Δ-($\delta\lambda$,$\delta\lambda$) and Δ-($\lambda\lambda$,$\lambda\lambda$) [6]. This correspondence supports the assertion of Bond et al. [17] that intra-ligand clashes prevent the formation of Δ-($\lambda\delta$) ligand arrangements in this cation. The Δ-($\delta\lambda$,$\delta\lambda$) conformer is characterized by a substantially reduced non-bonding energy compared with the other u-fac forms.

Good agreements are again observed[d] between the minimized and X-ray structures of the Δ-($\lambda\lambda$,$\lambda\lambda$) and Δ-($\delta\lambda$,$\delta\lambda$) ions [6].

TABLE 5

Steric energies for conformers of Δ-*u-fac*-[Co(dien)$_2$]$^{3+}$

Conformer	ΔH_{Steric} (kJ mol^{-1})	
	This work	Bond et al. [17]
Δ-u-fac ($\delta\lambda$,$\delta\lambda$)[a]	80.6	79.1 (≡Λ-($\lambda\delta$,$\lambda\delta$))
($\lambda\lambda$,$\delta\lambda$)	83.6	81.1 (≡Λ-($\lambda\delta$,$\delta\delta$))
($\delta\delta$,$\delta\delta$)	86.4	81.3 (≡Λ-($\lambda\lambda$,$\lambda\lambda$))
($\lambda\lambda$,$\lambda\lambda$)[a]	85.3	81.6 (≡Λ-($\delta\delta$,$\delta\delta$))
($\delta\delta$,$\delta\lambda$)	87.8	82.0 (≡Λ-($\lambda\lambda$,$\lambda\delta$))
($\delta\delta$,$\lambda\lambda$)	91.0	85.7 (≡Λ-($\lambda\lambda$,$\delta\delta$))

[a]Forms identified in X-ray structures (ref. 6).

[c]Summary of comparison for *s-fac*-[Co(dien)$_2$]$^{3+}$-($\lambda\delta$,$\lambda\delta$): RMS differences are: for 18 bond lengths, 0.039 Å; for 33 angles, 0.99°; for 48 torsional angles, 2.10°; for all interatomic distances, 0.036 Å.

[d]Summary of comparison for Δ-*u-fac*-[Co(dien)$_2$]$^{3+}$: RMS differences are:

	($\delta\lambda$,$\delta\lambda$)	($\lambda\lambda$,$\lambda\lambda$)
for 18 bond lengths	0.026 Å	0.037 Å
for 33 angles	2.47°	2.30°
for 50 torsional angles	9.8°	9.7°
for all interatomic distances	0.063 Å	0.059 Å

A comparison of bond angles/bonds lengths and torsional angles is available in Supplementary Tables S5 and S6 respectively. The MM2 minimized structures do not well reproduce the slightly eclipsed or "envelope" conformation of one of the chelates in the observed Δ-($\lambda\lambda$,$\lambda\lambda$) structure. This result is due to the crystal structure symmetry of C_1 being lifted to C_2 by MM2 calculations.

The ranking of the conformers by steric energies is equivalent to that obtained by Bond et al. [17], apart from the reversal of the Δ-($\delta\delta$,$\delta\delta$) and Δ-($\lambda\lambda$,$\lambda\lambda$) forms (Table 5).

The observation of the Δ-($\lambda\lambda$,$\lambda\lambda$) conformation in the solid state, in preference to the Δ-($\lambda\lambda$,$\delta\lambda$) form which is calculated to be 1.7 kJ mol^{-1} more stable, indicates that the Δ-($\lambda\lambda$,$\lambda\lambda$) form may be stabilized by solid state packing. The qualitative equivalence between the data calculated by the MM2 force field and the pseudo-Urey–Bradley force field of Bond et al. [17] for the u-fac contrasts with the s-fac and mer isomers. This issue is discussed further below.

[Co(medien)(dien)]$^{3+}$

mer. In contrast to the *mer*-[Co(dien)$_2$]$^{3+}$ system, 12 of the 16 possible conformers of the *mer*-[Co(medien)(dien)]$^{3+}$ ion could be minimized, a consequence of the reduced symmetry of this mixed complex. As expected, the most stable conformers for this system have mixed ligand conformations, Table 6. However, in a majority of the minimized structures the dien ligands adopted either the $\delta\delta$ or $\lambda\lambda$ chelate forms, but these conformations were clearly less stable (the difference is about 25 kJ mol^{-1} per ligand for $\lambda\lambda$ or $\delta\delta$ compared with $\lambda\delta$ or $\delta\lambda$). Such conformations would be of insignificant proportion in equilibrium solution: however, comment is warranted as similar forms did not minimize in the calculations on the analogous [Co(dien)$_2$]$^{3+}$ system.

The molecular structure of the *mer*-[Co(medien)(dien)]$^{3+}$ cation as determined in *mer*-[Co(medien)(dien)]$Br_2(ClO_4)\cdot H_2O$ is shown in Fig. 2, and selected interatomic parameters are listed in Table 7. The Co atom is octahedrally coordinated by six N atoms with the Co–N distances lying in the narrow range 1.94(1)–1.98(1) Å. The maximum deviation from the ideal geometry is manifested in the N(1)–Co–N(4) angle of 167.6(5)°. As would be expected there is an extensive H-bonding network in the lattice involving the cation, the anions and the water molecules of crystallization. The closest contacts involving the cation are: N(4)–H(n4b)···O(w)′ (symmetry operation: $1-x$, $-y$, $1-z$) of 1.78(2) Å with an angle of 176(2)°; N(3)–H(n3b)···O(1)″ (symmetry operation: $0.5+x$, $0.5-y$, $-0.5+z$) of 2.34(2) Å and N(3)–H(n3b)···O(w)′ of 2.48 Å with angles for this bifurcated H(n3b) atom of 129(3) and 125(3)°, respectively. Other significant contacts occur between Br(1)···H(n2) of 2.35(2) Å with a Br(1)···H(n2)–N(2) angle of 170(2)° and Br(2)···H(n4a)′–N(4)′ (symmetry operation: $-x$, $1-y$, $1-z$) of 2.33(2) Å and an angle of 156(2)°.

TABLE 6

Steric energy terms for isomers of [Co(medien)(dien)]$^{3+}$ [a]

Isomer	$E_{N\text{-}B}$	$E_{Bond\text{-}S}$	$E_{D\text{-}D}$	E_{Bend}	$E_{Bend\text{-}S}$	E_{Tors}	E_{Total}
λ-NH(R)-*mer*-	23.9	8.6	6.3	28.8	1.0	24.0	92.7
λδ,λδ[b]	23.9	8.5	6.3	28.9	1.0	24.1	92.7
λδ,δλ	29.1	10.3	6.6	43.2	1.2	29.4	119.6
δδ,δλ	29.0	10.3	6.5	43.4	1.2	29.2	119.7
λλ,λδ	27.9	8.7	6.7	36.7	1.0	40.2	121.4
λδ,λλ	28.9	9.1	6.9	36.9	1.0	39.2	121.9
λδ,δδ							
δδ,λδ	29.8	10.6	6.6	43.5	1.3	30.6	122.3
λλ,δλ	29.7	10.6	6.6	43.7	1.3	30.4	122.3
δδ,δδ	27.5	9.8	7.2	48.7	1.1	46.4	140.7
λλ,λλ	31.7	9.8	7.2	46.3	1.1	47.9	144.1
δδ,λλ	32.6	10.4	7.2	51.7	1.1	44.5	147.5
λλ,δδ	33.2	10.6	7.4	47.8	1.3	48.7	149.0
s-fac-λδ,λδ[b]	23.7	8.9	8.8	22.6	1.2	38.7	104.0
δλ,δδ	28.8	9.4	8.0	22.9	1.3	40.5	110.9
δδ,λδ[b]	28.2	9.5	8.2	21.2	1.1	44.4	112.6
δδ,δδ	32.0	10.7	8.1	21.7	1.1	45.5	119.2
δδ,λλ	31.7	9.7	8.2	23.9	1.2	50.4	125.1
λλ,δδ	34.0	10.9	7.9	25.8	1.3	48.5	128.5
Δ-u-fac-λδ,δλ	28.2	10.7	9.6	26.6	1.5	39.8	116.4
δδ,δλ	27.3	11.0	9.2	25.5	1.0	43.2	117.3
λλ,δλ	26.4	10.1	9.4	28.4	1.1	46.2	121.6
λλ,λλ	30.4	10.4	9.1	33.3	1.5	43.2	127.9
λλ,δδ	30.0	9.8	9.0	32.1	1.1	47.7	128.7
δδ,δδ	40.0	12.1	8.9	32.6	1.2	44.7	131.6
δδ,λλ	32.8	12.0	8.5	31.5	1.3	46.6	132.7

[a] $E_{N\text{-}B}$ = non-bonding energy; $E_{Bond\text{-}S}$ = bond stretch energy; $E_{D\text{-}D}$ = dipole–dipole energy; $E_{Bend\text{-}S}$ = bend stretch energy; E_{Tors} = torsional energy.
[b] Forms have been identified in X-ray structures in the present work.

Although the structural determination was undertaken on the racemic form of the cation, for the sake of brevity the following discussion is phrased in terms of the λ-NH(R)- configuration, to retain consistency with the previous discussion of the analogous [Co(dien)$_2$]$^{3+}$ system.

The comparison between the X-ray and MM2-minimized structures of λ-*mer*-[Co(medien)(dien)]$^{3+}$-(λδ,λδ) (≡δ-(δλ,δλ)) reveals excellent correlation.[e] A detailed comparison of bond lengths, bond angles and torsional angles

[e] Summary of comparison for *mer*-[Co(medien)(dien)]$^{3+}$-(λ-NH(R)-(λδ,λδ)/δ-NH(R)-(λδ,λδ)): RMS differences are: for 19 bond lengths, 0.039 Å; for 36 angles, 1.44°; for 59 torsional angles, 3.49°; for all interatomic distances, 0.039 Å.

TABLE 7

Selected interatomic bond distances (Å) and bond angles (deg.) for *mer*-[Co(medien)(dien)]$Br_2(ClO_4)\cdot H_2O$ (**1**)

Parameter		Parameter	
Bond distance			
Co-N(1)	1.97(1)	Co-N(2)	1.94(1)
Co-N(3)	1.99(1)	Co-N(4)	1.97(1)
Co-N(5)	1.98(1)	Co-N(6)	1.98(1)
N(1)-C(1)	1.51(2)	N(2)-C(2)	1.49(2)
N(2)-C(3)	1.47(2)	N(3)-C(5)	1.50(2)
N(4)-C(4)	1.47(2)	N(5)-C(6)	1.49(2)
N(5)-C(7)	1.46(2)	N(5)-C(9)	1.55(2)
N(6)-C(8)	1.47(2)	C(1)-C(2)	1.49(2)
C(3)-C(4)	1.49(2)	C(5)-C(6)	1.42(2)
C(7)-C(8)	1.57(3)		
Bond angle			
N(1)-Co-N(2)	84.1(5)	N(1)-Co-N(3)	87.6(5)
N(1)-Co-N(4)	167.6(5)	N(1)-Co-N(5)	96.1(5)
N(1)-Co-N(6)	91.5(5)	N(2)-Co-N(3)	95.4(5)
N(2)-Co-N(4)	83.7(5)	N(2)-Co-N(5)	179.3(5)
N(2)-Co-N(6)	94.5(5)	N(3)-Co-N(4)	91.6(5)
N(3)-Co-N(5)	85.3(5)	N(3)-Co-N(6)	170.0(5)
N(4)-Co-N(5)	96.1(5)	N(4)-Co-N(6)	91.4(5)
N(5)-Co-N(6)	84.9(5)	Co-N(1)-C(1)	110.8(9)
Co-N(2)-C(2)	110.6(8)	Co-N(2)-C(3)	111.3(9)
Co-N(3)-C(5)	109.7(9)	Co-N(4)-C(4)	111.5(9)
Co-N(5)-C(6)	105(1)	Co-N(5)-C(7)	108(1)
Co-N(5)-C(9)	116(1)	Co-N(6)-C(8)	111.1(8)
C(2)-N(2)-C(3)	117(1)	C(6)-N(5)-C(7)	115(2)
C(6)-N(5)-C(9)	105(2)	C(7)-N(5)-C(9)	109(1)
N(1)-C(1)-C(2)	108(1)	N(2)-C(2)-C(1)	106(1)
N(2)-C(3)-C(4)	106(1)	N(4)-C(4)-C(3)	109(1)
N(3)-C(5)-C(6)	109(1)	N(5)-C(6)-C(5)	111(2)
N(5)-C(7)-C(8)	105(2)	N(6)-C(8)-C(7)	109(1)

is available in Supplementary Tables S7 and S8 respectively. The Co–N–CH_3 angle is quite extended (115.5°) in the X-ray structure and this is modelled well by MM2. The bond extension Co–N(CH_3) predicted by Kojima et al. [14] in an earlier molecular mechanics study of this complex was not observed with our force field or the structural data. On the basis of our MM2 calculations the λ-NH(R)-($\lambda\delta$,$\delta\lambda$) ($\equiv\delta$-NH(R)-($\delta\lambda$,$\lambda\delta$)) conformer was expected to be of equivalent stability to the λ-NH(R)-($\lambda\delta$,$\lambda\delta$) form, but this conformer was not observed.

The least well-modelled aspect of this structure is the "envelope" conformation of the dien ligand. Examination of the individual components of the

TABLE 8

Selected interatomic bond distances (Å) and bond angles (deg.) for *s-fac*-[Co(medien)(dien)]$(S_2O_6)_{1.5}\cdot 0.5H_2O$ (**2**)

Parameter	Molecule 1	Molecule 2
Bond distance		
Co-N(1)	1.92(1)	1.98(1)
Co-N(2)	1.93(1)	1.98(1)
Co-N(3)	1.97(1)	1.98(2)
Co-N(4)	1.99(1)	1.96(1)
Co-N(5)	2.01(1)	1.99(1)
Co-N(6)	1.96(1)	1.96(1)
N(1)-C(1)	1.50(2)	1.46(3)
N(2)-C(2)	1.48(2)	1.94(3)
N(2)-C(3)	1.54(2)	1.45(2)
N(3)-C(4)	1.52(2)	1.50(3)
N(4)-C(5)	1.50(2)	1.51(3)
N(5)-C(6)	1.50(2)	1.46(2)
N(5)-C(7)	1.49(2)	1.53(2)
N(5)-C(9)	1.52(2)	1.48(2)
N(6)-C(8)	1.49(2)	1.52(2)
C(1)-C(2)	1.50(3)	1.56(3)
C(3)-C(4)	1.44(3)	1.58(3)
C(5)-C(6)	1.48(3)	1.50(2)
C(7)-C(8)	1.52(2)	1.47(2)
Bond angle		
N(1)-Co-N(2)	85.8(6)	86.0(6)
N(1)-Co-N(3)	90.0(6)	88.9(6)
N(1)-Co-N(4)	177.4(6)	176.8(6)
N(1)-Co-N(5)	96.1(6)	95.8(5)
N(1)-Co-N(6)	90.5(6)	90.9(6)
N(2)-Co-N(3)	85.4(6)	85.3(6)
N(2)-Co-N(4)	92.2(6)	90.9(6)
N(2)-Co-N(5)	176.9(5)	178.0(6)
N(2)-Co-N(6)	94.1(5)	92.8(6)
N(3)-Co-N(4)	88.1(6)	90.2(6)
N(3)-Co-N(5)	97.0(6)	94.1(5)
N(3)-Co-N(6)	179.2(5)	178.0(6)
N(4)-Co-N(5)	86.0(6)	87.3(6)
N(4)-Co-N(6)	91.3(6)	89.9(6)
N(5)-Co-N(6)	83.4(6)	87.9(5)
Co-N(1)-C(1)	114(1)	112(1)
Co-N(2)-C(2)	110(1)	108(1)
Co-N(2)-C(3)	109.2(9)	108(1)
Co-N(3)-C(4)	112(1)	114(1)
Co-N(4)-C(5)	108(1)	110(1)
Co-N(5)-C(6)	107.6(9)	108(1)
Co-N(5)-C(7)	106(1)	103.1(9)
Co-N(5)-C(9)	116(1)	117(1)

TABLE 8 (continued)

Parameter	Molecule 1	Molecule 2
Co-N(6)-C(8)	113(1)	110(1)
C(2)-N(2)-C(3)	113(1)	115(2)
C(6)-N(5)-C(7)	108(1)	114(1)
C(6)-N(5)-C(9)	108(1)	105(1)
C(7)-N(5)-C(9)	111(1)	111(1)
N(1)-C(1)-C(2)	107(2)	106(2)
N(2)-C(2)-C(1)	111(2)	111(1)
N(2)-C(3)-C(4)	110(1)	110(1)
N(3)-C(4)-C(3)	108(2)	106(1)
N(4)-C(5)-C(6)	108(1)	106(2)
N(5)-C(6)-C(5)	109(1)	115(1)
N(5)-C(7)-C(8)	109(1)	111(2)
N(6)-C(8)-C(7)	110(1)	108(1)

strain energy reveals that within conformational isomers containing $\delta\delta$- or $\lambda\lambda$-medien, there are non-bonding interactions between the N–Me grouping and the opposite chelate ring. This distorts the medien ligand so that the N–Me group is oblique (rather than approximately parallel) to the mean plane of the dien ligand. This "twisting" stabilizes "envelope-like" ring conformations, i.e. where both the N–Co–N–C torsional angles are either quite positive (30 to 45°) or quite negative (−30 to −45°). Steric energy terms (Table 6) show this strain to be ultimately manifested in the torsion and valence angle deformation potentials. In the case of the λ-NH(R)-($\lambda\delta$,$\lambda\delta$) form, this distortion is more pronounced in the crystal structure than is predicted by the force field calculations. Distortion from regular geometries to avoid large non-bonding interactions has been observed in our previous studies [10,11].

s-fac. For this isomer, six of the ten possible conformers could be minimized. As with the mer isomer, N–methyl group interactions result in the stabilization of different conformers for *s-fac*-[Co(medien)(dien)]$^{3+}$ compared with those observed for the *s-fac*-[Co(dien)$_2$]$^{3+}$ analogue (Table 6). In both cases the most stable conformer is the ($\lambda\delta$,$\lambda\delta$) form, and the energy order of the common conformers is the same.

The molecular structure of *s-fac*-[Co(medien)(dien)]$^{3+}$ has been determined as its *s-fac*-[Co(medien)(dien)](S$_2$O$_6$)$_{1.5}$·0.5H$_2$O complex (**2**). This compound crystallizes with two formula units in the crystallographic asymmetric unit, and these differ in the conformation of one of the chelate rings within the cation, ($\lambda\delta$,$\lambda\delta$) and ($\delta\delta$,$\lambda\delta$). Selected interatomic parameters associated with the two conformers are listed in Table 8, and the numbering scheme employed is illustrated in Fig. 3. As for the Co atom geometry in (**1**), distortions from ideal octahedral geometry are minor as can be seen from Table 8. The nature of the intermolecular contacts is not symmetrical thereby precluding the centrosymmetric space group $P2_1/m$. Important contacts in the lattice

include: N(3)–H(n3b)···O(21)′ (symmetry operation: $1-x$, $0.5+y$, $1-z$) of 1.90(3) Å with an angle subtended at the H(n3b) atom of 146(2)° and N(1′)–H(1′b)···O(53)′ of 1.79(3) Å with an angle of 160(2)°. The closest contact involving the water molecule of crystallization occurs between O(w) and O(23) of 2.80(2) Å (H atoms not located).

Two conformers of this molecule found in our X-ray structural studies, ($\lambda\delta$,$\lambda\delta$) and ($\delta\delta$,$\lambda\delta$), were the first and third lowest steric energy conformers by our MM2 calculations, with the difference between them being 8.6 kJ mol^{-1} (Table 6). This is not a large differential by MM2 standards and crystal packing forces may well reduce this further. Even so, given our previous success at predicting conformer stabilities we would not have expected such a large gap between these isomers [10,11].

Comparisons between the X-ray and MM2 geometries show excellent fits for both structures.[f] Detailed comparisons of bond lengths, bond angles and torsional angles are presented separately in Supplementary Tables S9 and S10. As with the mer- isomer, large Co–N–CH_3 angles are well reproduced.

u-fac. Of 16 possible conformers, seven minimize to steric energy minima (Table 6) and five of this set correspond to forms found for the $[Co(dien)_2]^{3+}$ analogue. The lowest energy conformer for *u-fac*-$[Co(dien)_2]^{3+}$, Δ-($\delta\lambda$,$\delta\lambda$), does not appear in the *u-fac*-[Co(medien)(dien)]$^{3+}$ calculations: inter-ligand methyl group interactions destabilize this conformer. Ring conformations of the type Δ-$\lambda\delta$($\equiv\Lambda$-$\delta\lambda$) in *u-fac*-$[Co(dien)_2]^{3+}$ complexes have been previously regarded as unstable [17], and in our calculations no dien ligand in the *u-fac*-[Co(medien)(dien)]$^{3+}$ system minimizes to this arrangement although it does exist for the medien ligand. MM2 permits the medien ligand to be stabilized in envelope conformations (see above).

Crystals of *u-fac*-[Co(medien)(dien)]X_3 could not be grown: this may be a consequence of the large number of conformers very closely spaced in steric energy (Table 6).

$[Co(medien)_2]^{3+}$

mer. Although the conformers of this complex share point group symmetries with the $[Co(dien)_2]^{3+}$ analogues, the minimizations show a very different pattern. As expected, the λ-NR-*mer*-$[Co(medien)_2]^{3+}$-($\lambda\delta$,$\delta\lambda$) ($\equiv\delta$-NR-*mer*-$[Co(medien)_2]^{3+}$-($\delta\lambda$,$\lambda\delta$)) conformer is of lowest steric energy. Steric energy

[f]Summary of comparison for *s-fac*-[Co(medien)(dien)]$^{3+}$: RMS differences are:

	($\delta\delta$,$\lambda\delta$)	($\lambda\delta$,$\lambda\delta$)
for 19 bond lengths	0.044 Å	0.034 Å
for 36 angles	1.58°	1.72°
for 50 torsional angles	3.58°	8.50°
for all interatomic distances	0.049 Å	0.072 Å

minima exist for seven of the ten possible conformers. As with the *mer*-$[Co(medien)(dien)]^{3+}$ complexes, we ascribe this to stabilizing interactions of the N–Me grouping, allowing conformations to be twisted into pseudo-envelope arrangements. The possible conformers can be grouped into three categories, on the basis of their having either zero, one, or two medien ligands with the equivalent conformations $\delta\delta$ or $\lambda\lambda$: the steric energy gap between the mixed ($\delta\lambda$ or $\lambda\delta$) and each $\delta\delta$ or $\lambda\lambda$ arrangement is about 25 kJ mol^{-1} (Table 9). The minimized Co–N bond lengths are especially long (about 2 Å) and the Co–N–CH_3 bond angles are unusually large (about 120°).

s-fac. Four of the seven possible conformers were calculated to have steric energy minima for *s-fac*-$[Co(medien)_2]^{3+}$ (Table 9). The $\delta\delta$ or $\lambda\lambda$ conformational arrangements of a medien ligand are approximately 10 kJ mol^{-1} less favourable than the mixed $\delta\lambda$ combinations.

u-fac. In the *u-fac*-$[Co(medien)_2]^{3+}$ system, five conformers gave potential energy minima (Table 9), which compares with six for the $[Co(dien)_2]^{3+}$ analogue:

TABLE 9

Steric energy terms for isomers of $[Co(medien)_2]^{3+}$ [a]

Isomer	$E_{N\text{-}B}$	$E_{Bond\text{-}S}$	$E_{D\text{-}D}$	E_{Bend}	$E_{Bend\text{-}S}$	E_{Tors}	E_{Total}
λ-NR-mer-$\lambda\delta,\delta\lambda$	49.3	15.7	4.2	31.3	1.7	37.2	139.5
$\delta\delta,\lambda\delta$	51.2	16.7	4.5	47.5	1.7	42.9	164.1
$\lambda\lambda,\lambda\delta$	51.2	16.6	4.5	47.1	1.7	42.9	164.1
$\lambda\lambda,\delta\lambda$	54.1	17.5	4.5	47.0	1.8	41.4	166.4
$\lambda\lambda,\lambda\lambda$	52.1	16.7	4.7	60.4	1.6	47.1	182.6
$\delta\delta,\lambda\lambda$	56.2	18.6	4.9	61.2	1.9	47.8	190.5
$\delta\delta,\delta\delta$	59.4	20.4	5.0	61.0	2.1	49.8	197.9
s-fac-$\lambda\delta,\delta\delta$	41.7	14.8	5.2	27.1	1.7	43.3	133.8
$\delta\delta,\delta\delta$	47.7	17.1	5.2	26.8	1.8	48.1	146.6
$\delta\delta,\delta\lambda$	47.4	16.1	5.1	28.2	1.8	50.9	149.7
$\delta\delta,\lambda\lambda$	47.4	16.1	5.1	28.2	1.8	50.9	149.7
⅃-u-fac-$\delta\lambda,\lambda\delta$	43.3	17.7	8.0	42.2	2.4	38.4	151.9
$\lambda\lambda,\delta\lambda$	46.7	19.3	7.4	42.3	2.2	42.8	160.8
$\lambda\lambda,\lambda\lambda$	43.2	17.5	7.5	50.3	1.8	47.9	168.2
$\delta\delta,\delta\lambda$	48.7	20.0	7.8	49.4	2.4	41.6	169.9
$\delta\delta.\lambda\lambda$	44.5	17.5	7.7	49.6	1.8	50.2	171.4

[a] $E_{N\text{-}B}$ = non-bonding energy; $E_{Bond\text{-}S}$ = bond stretch energy; $E_{D\text{-}D}$ = dipole-dipole energy; E_{Bend} = valence angle deformation energy; $E_{Bend\text{-}S}$ = bend stretch energy; E_{Tors} = Torsional energy.

Δ-$[Co(medien)_2]^{3+}$: $(\delta\lambda,\lambda\delta) < (\lambda\lambda,\delta\lambda) < (\lambda\lambda,\lambda\lambda) < (\delta\delta,\delta\lambda) < (\delta\delta,\lambda\lambda)$

Δ-$[Co(dien)_2]^{3+}$: $(\delta\lambda,\delta\lambda) < (\lambda\lambda,\delta\lambda) < (\lambda\lambda,\lambda\lambda) < (\delta\delta,\delta\delta) < (\delta\delta,\delta\lambda) < (\delta\delta,\lambda\lambda)$

The four possible general conformational types ($\delta\lambda,\delta\lambda$ or $\delta\lambda,\lambda\delta$; $\delta\delta,\delta\lambda$ or $\lambda\lambda,\delta\lambda$; $\delta\delta,\lambda\lambda$; $\delta\delta,\delta\delta$ or $\lambda\lambda,\lambda\lambda$) have the same relative energy ordering. Given that in our MM2 calculations N–CH_3 groups tend to stabilize conformations distorted from the idealized δ and λ arrangements, the similarity between these sets is interesting.

Thermodynamic considerations

The free energy (ΔG_{calc}) values used in the following thermodynamic discussion (and quoted in Table 10) have been obtained by statistical adjustment of the appropriate steric energies. The s-fac form is destabilized by a factor of $RT\ln 2$ ($=1.7$ kJ mol^{-1} at 291 K) relative to the u-fac and mer isomers, reflecting the coordination possibilities for the second tridentate ligand once the first ligand is attached (one for s-fac compared with two for u-fac and mer).

$[Co(dien)_2]^{3+}$

The effects of ion-association on the equilibrium distribution of the isomers of $[Co(dien)_2]^{3+}$ in solution are well documented [2]: differential ion pairing can have dramatic effects on the relative equilibrium proportions of mer/s-fac/u-fac isomers in solution. For example, the mer:s-fac:u-fac ratio 62:8:30 in H_2O/ClO_4^- contrasts with the observed ratio 20:55:25 in H_2O/0.1 M PO_4^{3-} (all measurements at 291 K). This difference has been rationalized in terms of preferential hydrogen bonding of the PO_4^{3-} anion to N–H protons in the fac isomers which are favourably positioned for such interactions [2]. A correlation between the elution rates of the isomers of $[Co(dien)_2]^{3+}$ in

TABLE 10

Calculated and observed relative "Free Energies" for the geometric isomers of $[Co(dien)_2]^{3+}$

Isomer	ΔG_{calc} (kJ mol^{-1})				ΔG_{obs} (kJ mol^{-1}) at 291 K	
	Ref. 17	Ref. 15	Ref. 13	This work	PF_6^-/Acet (Ref. 23)	Cl^-/H_2O (Ref. 2)
mer	0.0	0.0	0.0	0.0	0.0	0
s-fac	9.6	1.3	−8.3	32.0	5.1	5.4
u-fac	7.3	−0.4	10.8	30.7	3.6	2.0

cation-exchange chromatography and the degree of ion association with the eluent anion has also been demonstrated [22]. Since the presence of Cl^-, NO_3^- or ClO_4^- have little differential effect on the relative isomer distribution [2], the relative ion associations of these anions with the isomers of $[Co(dien)_2]^{3+}$ are presumed to be approximately equivalent. Accordingly these experimental isomer ratios have been used in our comparisons with the MM2-calculated gas phase stabilities. Bond et al. [23] have also determined the equilibrium ratios in acetone solution containing PF_6^-, where differential ion association with the isomers of the cation would be expected to be minimal. The experimental relative isomer stabilities and those calculated by a number of molecular mechanics procedures (based on minimum energy conformers only) are listed in Table 10.

The force fields used by Bond et al. [17] and MM2 both give reasonable predictions of the relative stabilities of the u-fac and s-fac forms, especially considering the variation in the experimental values, and that no account is taken in the molecular mechanics models of solvation effects or ion-association which can be significant in these complexes [2]. Neither force field leads to accurate prediction of the relative stabilities of the mer and fac isomers, and the present MM2 result is particularly awry. Previous work on $[Co(pn)_n(en)_{3-n}]^{3+}$ (n=1–3) complexes has shown reasonable similarity between the results obtained using the pseudo-Urey–Bradley force field [17] and the MM2 force field [10]. The large discrepancy in the MM2 result for *mer*-$[Co(dien)_2]^{3+}$ requires further investigation and is discussed below.

[Co(medien)(dien)]$^{3+}$

The equilibrium distribution of the isomers of the $[Co(medien)(dien)]^{3+}$ system has been investigated in H_2O/ClO_4^- solution at 363 K [3]. Comparison of the results obtained for the equilibration of $[Co(medien)(dien)]^{3+}$ in both H_2O/ClO_4^- and H_2O/Cl^- solutions indicates little differential ion association, so that these isomer ratios may be compared to the calculated MM2 data. The experimentally determined equilibrium ratio leads to a relative order of free energies of s-fac (taken as 0 kJ mol^{-1}), u-fac (6.3 kJ mol^{-1}), and mer (6.7 kJ mol^{-1}) [3,4], while our MM2 calculations predict 0.0, 10.7, and -13.0 kJ mol^{-1} respectively. Once again the MM2 procedure provides reasonable relativities for the two fac isomers but substantially overestimates the stability of the mer isomer.

[Co(medien)$_2$]$^{3+}$

Only the s-fac isomer of this complex has been isolated from reaction mixtures [3,4]. Based on the minimum energy conformers, MM2 predicts the s-fac form to be the most stable by steric energy gaps of approximately 6 kJ mol^{-1} and 18 kJ mol^{-1} over the mer and u-fac forms respectively. At 363 K,

these relativities would predict an equilibrium ratio of s-fac:mer:u-fac=85:15:0.

The calculations are in this case in substantial agreement with the experimental results. Although in the experimental studies it was improbable that any significant formation of *u-fac-* or *mer*-$[Co(medien)_2]^{3+}$ escaped detection, the total amount of $[Co(medien)_2]^{3+}$ detected was less than stoichiometric. Within this uncertainty we regard the present results as satisfactory.

General comments

The significant steric components which lower the steric energy of λ-NH-*mer*-$[Co(dien)_2]^{3+}$-$(\lambda\delta,\lambda\delta)$ relative to the fac geometries are the non-bonding (about 6 kJ mol^{-1}) and torsional (about 30 kJ mol^{-1}) contributions.

Inspection of the individual atomic pairs contributing to the gross non-bonding energy (subtotals only are listed in Table 4) reveals a reduced hydrogen–hydrogen repulsion in the mer geometry relative to the fac forms. Specifically, hydrogen atom interactions between the separate chelate rings of the dien ligands were lessened in the mer isomer due to their spatial separation. This results in a lower relative non-bonding energy in the mer form compared with the fac forms. Such an effect is intuitive and is no doubt a contributor to the observed high thermodynamic stability of *mer*-$[Co(dien)_2]^{3+}$ relative to the fac geometries. However in our results, it is in the torsions that excessive stabilization of the mer geometry is generated.

1,3-Non-bonded interactions about the metal are used in the pseudo Urey–Bradley force field of Hambley et al. [18]. These are effectively "harder" functions than the valence angle deformation constants used in our MM2 investigations [10,11]. This has the implicit effect of increasing the steric potential about Co–N centred torsions. In this way the force field of Hambley et al. [18] indirectly accounts for N–Co–N–C and Co–N–C–C type torsions. Our parametrization of the MM2 force field explicitly included only the latter term, the former term being set to zero as is usual practice [24–26].

Including N–Co–N–C torsional parameters and/or increasing the valence angle bending parameters in the MM2 force field had a dramatic effect in reducing the steric energy differential between the *mer*-$[Co(dien)_2]^{3+}$ arrangement and the s-fac and u-fac forms. For example, when the Co–N stretch constant was stiffened by 50% to 300 N m^{-1} $molecule^{-1}$ the steric energy difference between u-fac and s-fac remained almost the same but the steric energy of the λ-NH-*mer*-$(\lambda\delta,\lambda\delta)$ form increased by 25 kJ mol^{-1}. This brings the overall predicted MM2 thermodynamic results into much better correlation with the experimental data, certainly within the range of experimental values. The including of N–Co–N–C torsional parameters had the same kind of effect, although less dramatic. In either case (using modified torsional or bending

constants), the minimized structures represented excellent correlations with the crystal structures.

Although the MM2 potentials are discussed above as if they were independent functions coupling does exist between them. Therefore, although the above discussion is presented in terms of torsions it may also be approached from the viewpoint of valence angle deformations. For example, for the mer geometric isomer of $[Co(dien)_2]^{3+}$ the N–Co–N bond angles within a dien ligand are comparatively contracted to about 84–86° (Supplementary Table S1), which contrasts strongly with the near octahedral coordination about Co in the fac forms (Supplementary Tables S3 and S5). The valence angle deformation potential has a minimum at 90°, so an increase of the bending constant will have little effect on the overall steric energy of the fac isomers as long as the N–Co–N bond angles remain close to 90°. However, the mer forms with distorted N–Co–N angles will have increased steric energy.

MM2 calculations on bis(tridentate)cobalt(II) complexes

We also investigated the stabilities of analogous complexes of dien and medien with cobalt(II). Parametrization of the MM2 force field was carried out using the X-ray crystal structures of $[Co(sep)]^{2+}$ [27], and $[Co(tacn)_2]^{2+}$ [28], where sep = sepulchrate = 1,3,6,8,10,13,16,19-octaazabicyclo[6.6.6]eicosane, and tacn = 1,4,7-triazacyclononane. Our procedure was similar to that of Endicott et al. [29], whereby we simply increased the Co–N ideal bond length (r_0) value to 2.4 Å while the N–Co–N bond bending constant was set at 350 N m^{-1} $molecule^{-1}$, and other Co parameters were unchanged. We believe this method is reasonable as the deformations of the bond angles about Co in these octahedral complexes are only small contributors to the final steric energy. The resulting MM2-minimized geometries were good fits to the crystal structures. No special account of the $[Co(sep)]^{2+}$ apical nitrogen was required in the force field to emulate the unusual angles about these atoms. Only the minimum energy conformer of each geometric isomer of $[Co(dien)_2]^{2+}$ and $[Co(medien)_2]^{2+}$ were minimized. Pleasingly, the mer arrangement of the $[Co(dien)_2]^{2+}$ complex was significantly more stable than the fac forms in comparison with the analogous Co(III) system. For the $[Co(medien)_2]^{2+}$ complex the s-fac isomer was destabilized even further with respect to the mer and u-fac geometries relative to the Co(III) analogue. Both results were in qualitative agreement with previous electrochemical observations [22].

CONCLUSIONS

Using the MM2 force field, we have calculated the relative stabilities for the isomers within each of the three $[Co(medien)_n(dien)_{2-n}]^{3+}$ (n=0–2) systems, and comparisons have been made with observed isomer ratios for the

three systems [2,3]. Discrimination between the two fac arrangements is reasonable both in the ordering and magnitude for the three title complex systems, using the force field which we have applied previously with success to $[Co(men)_n(en)_{3-n}]^{3+}$ ($n=1$–3) [11]. However, on initial application the force field has not accurately modelled the thermodynamics of the mer isomer relative to the fac forms of the $[Co(dien)_2]^{3+}$ system because of incomplete parametrization, although it is possible to adjust the parameters involving Co to improve this relativity. The force field of Hambley et al. [18] with its pseudo-Urey–Bradley character was more successful in the modelling of the mer/fac relativities for $[Co(dien)_2]^{3+}$ and in that sense is seen to be a more flexible force field.

Experimental data also exist for the total equilibrium distribution of all nine species involved in this family of complexes [3], but direct comparison of this data with our MM2 calculations is not meaningful as the zero point energy differences between complexes of different compositions are not calculable in these molecular mechanics procedures [11,15].

We believe this work has demonstrated some of the strengths and limitations of molecular mechanics as applied to metal complexes. Although good correlation with experimental data can be effected, the parametrization of the force field, even for apparently very similar systems, must be considered carefully. Very often the structural or thermodynamic information needed to enable careful parametrization of the force field is not available: indeed the absence of such data has been in many cases the reason why molecular mechanics has been applied to a problem. This work demonstrates that in cases where very different structural features exist, even within isomeric complexes, the results of MM2 calculations in a predictive manner must be interpreted with caution.

ACKNOWLEDGEMENTS

We thank Dr K.R. Adam (James Cook University of North Queensland) for his interest and assistance with aspects of the molecular mechanics calculations. The financial assistance of the Australian Research Council is gratefully acknowledged.

SUPPLEMENTARY MATERIAL AVAILABLE

Comparison of bond lengths/angles and torsional angles between observed and calculated structures for λ-NH-*mer*-$[Co(dien)_2]^{3+}$, *s-fac*-$[Co(dien)_2]^{3+}$, Δ-*u-fac*-$[Co(dien)_2]^{3+}$, *mer*-$[Co(medien)(dien)]^{3+}$ and *s-fac*-$[Co(medien)(dien)]^{3+}$ cations (Tables S1–S10; 20 pages); listings of structure factor tables, thermal parameters, hydrogen atom parameters, and a full listing of in-

teratomic parameters for (**1**) and (**2**) (Tables S11–S18; 19 pages), are all available from B.L.L.D. as Supplementary Publication number SUP 26437 (41 pages).

REFERENCES

1 F.R. Keene and G.H. Searle, Inorg. Chem., 11 (1972) 148.
2 F.R. Keene and G.H. Searle, Inorg. Chem., 13 (1974) 2173.
3 G.H. Searle, F.R. Keene and S.F. Lincoln, Inorg. Chem., 17 (1978) 2362.
4 G.H. Searle, S.F. Lincoln, F.R. Keene, S.G. Teague and D.G. Rowe, Aust. J. Chem., 30 (1977) 1221.
5 M. Kobayashi, F. Marumo and Y. Saito, Acta Crystallogr., Sect. B, 28 (1972) 470.
6 M. Konno, F. Marumo and Y. Saito, Acta Crystallogr., Sect. B, 29 (1973) 739.
7 F.D. Sancilio, L.F. Druding and D.M. Lukaszewski, Inorg. Chem., 15 (1976) 1626.
8 K. Okiyama, S. Sato and Y. Saito, Acta Crystallogr., Sect. B, 35 (1979) 2389.
9 G.R. Brubaker and D.W. Johnson, Coord. Chem. Rev., 53 (1984) 1.
10 I.M. Atkinson, F.R. Keene and G.H. Searle, J. Mol. Struct., 240 (1990) 313.
11 I.M. Atkinson, F.R. Keene and G.H. Searle, J. Chem. Soc., Dalton Trans., (1991) 45.
12 QCPE Program No. 395, (The Quantum Chemistry Program Exchange) University of Indiana, Bloomington, IN.
U. Burkert and N.L. Allinger, in Molecular Mechanics, ACS Monograph No. 177, 1982.
13 Y.J. Yoshikawa, Bull. Chem. Soc. Jpn., 49 (1976) 159.
14 M. Kojima, M. Iwagaki, Y. Yoshikawa and J. Fujita, J. Bull. Chem. Soc. Jpn., 50 (1977) 3216.
15 G.H. Searle and M. Dwyer, J. Chem. Soc. Chem. Commun., (1972) 726.
16 M. Dwyer, M.R. Snow and R.J. Geue, Inorg. Chem., 12 (1973) 2057.
17 A.M. Bond, T.W. Hambley and M.R. Snow, Inorg. Chem., 24 (1985) 1920.
18 T.W. Hambley, C.J. Hawkins, J.A. Palmer and M.R. Snow, Aust. J. Chem., 34 (1981) 45.
19 K.R. Adam, M. Antolovich, L.G. Brigden and L.F. Lindoy, J. Am. Chem. Soc., 113 (1991) 3346.
20 (a) G.M. Sheldrick, SHELX 76, Program for Crystal Structure Determination, Cambridge University, UK, 1976.
(b) J.A. Ibers and W.C. Hamilton (Eds.), International Tables for X-ray Crystallography, Vol. 4, Kynoch Press; Birmingham, 1974, pp. 99, 159.
(c) C.K. Johnson, ORTEP-II, Report ORNL-5138, Oak Ridge National Laboratory, Oak Ridge, TN, 1976.
20 G.H. Searle and F.R. Keene, Inorg. Chem., 11 (1972) 1006.
21 K.R. Adam, personal communication, 1990.
22 G.H. Searle, Aust. J. Chem., 30 (1977) 2625.
23 A.M. Bond, F.R. Keene, N.W. Rumble, G.H. Searle and M.R. Snow, Inorg. Chem., 17 (1978) 2847.
24 M.G.B. Drew, S. Hollis and P.C. Yates, J. Chem. Soc. Dalton Trans., (1985) 1829.
25 G.J. McDougall, R.D. Hancock and J.C.A. Boeyens, J. Chem. Soc., Dalton Trans., (1978) 1438.
26 L.G. Brigden, M.Sc. Thesis, James Cook University, 1989, and references cited therein.
27 I.I. Creaser, R.J. Geue, J. MacB. Harrowfield, A.J. Herlt, A.M. Sargeson, M.R. Snow and J. Springborg, J. Am. Chem. Soc., 104 (1982) 6016.
28 H.-J. Küppers, A. Neves, C. Pomp, D. Ventur, K. Wieghardt, B. Nuber and J. Weiss, Inorg. Chem., 25 (1986) 2400.
29 J.F. Endicott, G.R. Brubaker, T. Ramasami, K. Kumar, K. Dwarakanath, J. Cassel and D. Johnson, Inorg. Chem., 22 (1983) 3754.

Acta Cryst. (1993). C**49**, 13–16

Structure of the Stable Isomer of the Bis(ethane-1,2-diamine)(*N*-methylethane-1,2-diamine)cobalt(III) Cation, $[Co(meen)(en)_2]^{3+}$

BY GRAEME H. SEARLE† AND EDWARD R. T. TIEKINK

Jordan Laboratories, Department of Physical and Inorganic Chemistry, University of Adelaide, Adelaide, South Australia 5001, *Australia*

AND IAN M. ATKINSON AND F. RICHARD KEENE

Department of Chemistry and Biochemistry, James Cook University of North Queensland, Townsville, Queensland 4811, *Australia*

(*Received* 21 *October* 1991; *accepted* 5 *May* 1992)

Abstract. Bis(ethane-1,2-diamine-*N*,*N*′)(*N*-methylethane-1,2-diamine-*N*,*N*′)cobalt(III) triperchlorate monohydrate, $[Co(C_3H_{10}N_2)(C_2H_8N_2)_2](ClO_4)_3.H_2O$, $M_r = 569.6$, monoclinic, $P2_1/n$, $a = 10.280$ (1), $b = 13.905$ (2), $c = 14.533$ (2) Å, $\beta = 90.30$ (1)°, $V = 2077$ (2) Å^3, $Z = 4$, $D_x = 1.821$ g cm^{-3}, λ(Mo $K\alpha$) = 0.7107 Å, $\mu = 12.84$ cm^{-1}, $F(000) = 1176$, $T = 293$ (1) K, $R = 0.051$ for 2138 observed reflections. The Co atom in the cation is octahedrally coordinated by six N atoms from three chelating diamine ligands; Co—N 1.967 (5)–1.999 (5) Å, with Co—N(CH_3) the longest. The structure is a racemate and the conformational structure is Λ-*R*-$\delta^*\lambda\lambda$ (for one enantiomer). Comparisons are made with the structure calculated by molecular mechanics using an *MM*2 force field. The crystal lattice is held together *via* hydrogen bonds involving the cation, perchlorate anions and the water molecule of crystallization.

Introduction. The separation and isolation of a number of isomers of Co^{III} complexes of *N*-methylethane-1,2-diamine (meen) has been reported recently (Searle & Keene, 1989). Aerial oxidation of a mixture of Co^{II}, 3meen and H^+ in aqueous solution with charcoal at 353 K yields an equilibrium mixture of the complexes $[Co(meen)_3]^{3+}$, $[Co(meen)_2(en)]^{3+}$, $[Co(meen)(en)_2]^{3+}$ and $[Co(en)_3]^{3+}$, where the coordinated ethane-1,2-diamine (en) arises through demethylation of the Co^{III}–meen, brought about by the oxygen with charcoal catalysis. Each of these Co–meen complexes has a number of possible isomeric forms, arising from configurational (Λ or Δ, and *R* or *S*) and geometric (facial or meridional) isomerism.

The most stable of these complexes and isomers have been separated by cation-exchange chromatography on SP-Sephadex C25 using Na_3PO_4 as eluent, and the complexes thus detected have been labelled (*A*) to (*H*) (Searle & Keene, 1989). They were isolated in crystalline form and were characterized by their ^{13}C NMR spectra which allowed their isomeric identity to be established in most cases.

X-ray structures of several of these complexes have been reported previously: two $[Co(meen)_3]^{3+}$ isomers labelled (*A*) and (*C*), and two $[Co(meen)_2(en)]^{3+}$ isomers labelled (*F*) and (*H*) (Searle & Tiekink, 1989*a*,*b*). (*B*) is a third $[Co(meen)_3]^{3+}$ isomer which has been isolated but not yet structurally characterized.

For the complex bis(ethane-1,2-diamine)(*N*-methylethane-1,2-diamine)cobalt(III) cation, two diastereoisomers are possible, Λ-*R*/Δ-*S* and Λ-*S*/Δ-*R* (as racemic pairs). Only one of these diastereoisomers has been evident experimentally, designated as complex (*E*), and the crystal structure of this isomer is now reported.

Experimental. Complex (*E*), $[Co(meen)(en)_2]^{3+}$, was separated chromatographically and obtained as the perchlorate monohydrate salt by addition of $HClO_4$ to an HCl solution of the eluted complex. Crystals suitable for the X-ray study were grown by ethanol vapour diffusion into an aqueous solution of the complex under slight vacuum. Data were collected using an Enraf–Nonius CAD-4F diffractometer controlled by a PDP8/A computer, with graphite-monochromated Mo $K\alpha$ radiation and ω–2θ scans. Cell parameters were determined by least squares on 25 reflections ($9 \le \theta \le 14°$) (de Boer & Duisenberg, 1984) from a crystal $0.10 \times 0.25 \times 0.62$ mm. An analytical absorption correction was applied with maximum and minimum transmission factors of 0.856 and 0.640 (*SHELX*76; Sheldrick, 1976). 5575 reflections ($1.5 \le \theta \le 25.0°$) were measured in the range $-12 \le h < 12$, $0 \le k \le 16$, $-14 \le l < 5$. No significant variation was observed in the net intensity

† Deceased 24 July, 1992.

0108-2701/93/010013-04$06.00

of three reference reflections ($\bar{4}\bar{2}4$, $\bar{3}\bar{2}5$ and $\bar{4}\bar{3}6$) measured every 7200 s. 3668 unique reflections were measured ($R_{merge} = 0.021$) of which 2138 satisfied $I \geq 2.5\sigma(I)$. The structure was solved by Patterson methods, with full-matrix least-squares refinement on 292 parameters based on F (*SHELX*76; Sheldrick, 1976). Refinement included anisotropic thermal parameters for non-H atoms, and H atoms were included at their calculated positions with a common isotropic thermal parameter. The ClO_4^- anions with the Cl(2) and Cl(3) atoms were found to be disordered such that an O atom in each, *i.e.* O(8) and O(12), was situated over two positions; these were modelled with 50% site occupancy factors. At convergence $R = 0.051$, $wR = 0.060$ $\{w = 1.76/[\sigma^2(F) + 0.0008F^2]\}$, $S = 3.32$, $(\Delta/\sigma)_{max} \leq 0.02$ (for cation), $\Delta\rho_{max} = 0.75$, $\Delta\rho_{min} = -0.57$ e Å^{-3}. An extinction correction was applied such that the value of $nz = 0.0001$ (3) (*SHELX*76; Sheldrick, 1976). Scattering factors for Co^{3+} corrected for f' and f'', were taken from *International Tables for X-ray Crystallography* (1974, Vol. IV, pp. 99, 149) and for the remaining atoms as incorporated in *SHELX*76 (Sheldrick, 1976). All calculations were performed on a SUN4/280 computer system. Atomic coordinates are given in Table 1, selected interatomic parameters are in Table 2,* and the atom-numbering scheme used for the cation is shown in Fig. 1, which was drawn with *ORTEP*II (Johnson, 1976) at 25% probability levels.

Discussion. The complex (E) crystallizes as the perchlorate monohydrate salt in the space group $P2_1/n$, with two pairs of enantiomeric molecules in the unit cell. The octahedral cation geometry is defined by six N atoms derived from three chelating diamine ligands. The six Co—N bond distances are all similar, lying in the range 1.967 (5)–1.999 (5) Å; the longest distance is formed by the methylated N atom. Distortions from ideal octahedral geometry may be related to the restricted bite distance of the chelating ligands, with the maximum deviation manifested in the N(5)—Co—N(6) angle of 84.7 (2)°.

In the crystal lattice of $[Co(meen)(en)_2](ClO_4)_3.H_2O$ there are a large number of hydrogen-bonding contacts between the cation, the perchlorate anions and the water molecule of crystallization. These contacts are summarized as follows [details in

Table 1. *Fractional atomic coordinates and equivalent isotropic thermal parameters* (Å^2)

$B_{eq} = (8\pi^2/3)(U_{11} + U_{22} + U_{33})$.

	x	y	z	B_{eq}
Co	−0.01083 (7)	0.25098 (6)	0.70115 (5)	1.92
N(1)	−0.1533 (5)	0.2664 (3)	0.7897 (4)	2.66
N(2)	0.0021 (5)	0.3944 (3)	0.7048 (4)	2.74
N(3)	−0.1353 (5)	0.2586 (4)	0.5974 (3)	2.58
N(4)	0.1238 (5)	0.2397 (4)	0.6042 (4)	3.11
N(5)	0.1163 (5)	0.2356 (3)	0.8017 (4)	2.66
N(6)	−0.0242 (5)	0.1095 (3)	0.7066 (4)	2.79
C(1)	−0.1953 (6)	0.3685 (5)	0.7938 (5)	3.37
C(2)	−0.0716 (6)	0.4292 (5)	0.7867 (5)	3.34
C(3)	0.1301 (6)	0.4428 (5)	0.7015 (6)	3.92
C(4)	−0.0661 (7)	0.2741 (6)	0.5091 (5)	4.53
C(5)	0.0598 (8)	0.2235 (7)	0.5129 (6)	5.42
C(6)	0.1078 (7)	0.1362 (5)	0.8389 (5)	3.84
C(7)	0.0836 (7)	0.0691 (5)	0.7615 (6)	4.11
Cl(1)	0.2598 (2)	0.4732 (2)	0.4346 (1)	4.58
O(1)	0.2777 (8)	0.4362 (6)	0.3459 (5)	8.42
O(2)	0.1297 (7)	0.4940 (7)	0.4490 (6)	10.48
O(3)	0.3127 (8)	0.4154 (7)	0.5054 (6)	11.16
O(4)	0.3175 (10)	0.5652 (6)	0.4322 (7)	11.19
Cl(2)	0.2508 (3)	0.4707 (1)	−0.0237 (2)	5.40
O(5)	0.2749 (7)	0.4514 (5)	0.0682 (4)	6.82
O(6)	0.2225 (8)	0.3900 (6)	−0.0735 (5)	9.63
O(7)	0.2287 (12)	0.5522 (8)	−0.0498 (8)	15.08
O(8)	0.3948 (13)	0.4837 (12)	−0.0587 (13)	11.53
O(8′)	0.0956 (12)	0.4952 (11)	−0.0085 (10)	8.45
Cl(3)	−0.0201 (2)	0.2515 (1)	0.2282 (1)	3.53
O(9)	0.0875 (6)	0.2892 (7)	0.1868 (6)	9.19
O(10)	−0.0949 (9)	0.1979 (8)	0.1648 (7)	12.29
O(11)	−0.1086 (8)	0.3197 (6)	0.2558 (10)	16.06
O(12)	0.0091 (10)	0.1791 (8)	0.2973 (7)	4.74
O(12′)	0.0325 (20)	0.2774 (25)	0.3002 (14)	30.50
O(W1)	0.4565 (7)	0.2204 (5)	0.4761 (4)	7.00

Table 2. *Selected interatomic distances* (Å) *and bond angles* (°)

Co—N(1)	1.967 (5)	Co—N(2)	1.999 (5)
Co—N(3)	1.976 (5)	Co—N(4)	1.986 (5)
Co—N(5)	1.967 (5)	Co—N(6)	1.974 (5)
N(1)—C(1)	1.486 (8)	N(2)—C(2)	1.495 (9)
N(2)—C(3)	1.480 (7)	N(3)—C(4)	1.486 (8)
N(4)—C(5)	1.50 (1)	N(5)—C(6)	1.487 (8)
N(6)—C(7)	1.473 (8)	C(1)—C(2)	1.529 (8)
C(4)—C(5)	1.47 (1)	C(6)—C(7)	1.48 (1)
N(1)—Co—N(2)	85.6 (2)	N(1)—Co—N(3)	90.7 (2)
N(1)—Co—N(4)	175.5 (2)	N(1)—Co—N(5)	91.1 (2)
N(1)—Co—N(6)	91.7 (2)	N(2)—Co—N(3)	90.5 (2)
N(2)—Co—N(4)	92.9 (2)	N(2)—Co—N(5)	92.6 (2)
N(2)—Co—N(6)	176.2 (2)	N(3)—Co—N(4)	85.1 (2)
N(3)—Co—N(5)	176.5 (2)	N(3)—Co—N(6)	92.3 (2)
N(4)—Co—N(5)	93.2 (2)	N(4)—Co—N(6)	89.9 (2)
N(5)—Co—N(6)	84.7 (2)	Co—N(1)—C(1)	110.3 (4)
Co—N(2)—C(2)	108.1 (4)	Co—N(2)—C(3)	120.8 (4)
Co—N(3)—C(4)	110.8 (4)	Co—N(4)—C(5)	109.7 (4)
Co—N(5)—C(6)	109.3 (4)	Co—N(6)—C(7)	110.4 (4)
C(2)—N(2)—C(3)	109.4 (5)	N(1)—C(1)—C(2)	106.4 (5)
N(2)—C(2)—C(1)	107.5 (5)	N(3)—C(4)—C(5)	108.9 (6)
N(4)—C(5)—C(4)	110.1 (6)	N(5)—C(6)—C(7)	108.6 (5)
N(6)—C(7)—C(6)	107.1 (5)		

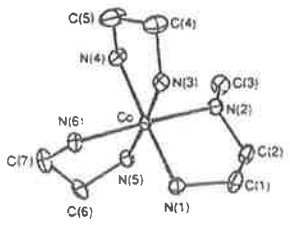

Fig. 1. Molecular structure and crystallographic numbering scheme employed for the cation in $[Co(meen)(en)_2](ClO_4)_3.H_2O$ (Johnson, 1976).

* Lists of structure factors, anisotropic thermal parameters, H-atom parameters, all interatomic parameters, hydrogen-bonding contacts and details of *MM*2 results have been deposited with the British Library Document Supply Centre as Supplementary Publication No. SUP 55430 (18 pp.). Copies may be obtained through The Technical Editor, International Union of Crystallography, 5 Abbey Square, Chester CH1 2HU, England. [CIF reference: AS0569]

supplementary table *S*(7)]:† each of the N-bound H atoms is involved in at least one contact with an O atom from either a perchlorate anion or the water molecule. The water molecule of crystallization forms two close contacts with the cation and two close contacts with the symmetry-related perchlorate groups, presumably *via* the water molecule H atoms which were not located in the difference map. Each of the perchlorate O atoms is thus involved in the hydrogen-bonding network. It is unknown how such hydrogen bonding might determine the ring conformations, although such bonding forces *acting co-operatively* must be a major factor in accounting for any differences between the detailed structures found in the solid state and those calculated by energy minimization for the cation only.

The particular diastereoisomer is the *Λ-R* isomer (as racemate), and is illustrated in Fig. 1. The conformational structure is uniquely defined as *Λ-R-δ*λλ*,‡ with the methyl substituent being equatorial (to the mean plane of its chelate ring). This diastereoisomer, which is isolated, should be the thermodynamically more stable, since the two diastereoisomers should interconvert at the asymmetric N atom in solution, *Λ-R*⇄*Λ-S*, under the basic conditions of the chromatographic separation, and these two configurations should then be fixed in their equilibrium ratio on the subsequent acidification. That only one of the diastereoisomeric pairs *Λ-R*/*Δ-S* has been observed experimentally under all conditions, indicates that *K* [equilibrium ratio of the two diasteroisomeric pairs (*Λ-R*/*Δ-S*) and (*Λ-S*,*Δ-R*)] for the two diastereoisomers must be large (say $K > 12$, for which $\Delta G > 6$ kJ mol^{-1}).

For the $[Co(meen)(en)_2]^{3+}$ system, the steric energies of the sixteen possible geometrically different conformations, eight for *Λ-R* and eight for *Δ-R*, have been calculated using the *MM*2 force field (Atkinson, Keene & Searle, 1991).§ From this recent analysis, the isomer having the lowest calculated steric energy was *Λ-R-δ*δδ* (steric energy 44.5 kJ mol^{-1}). Thus, the *MM*2 calculations correctly predicted the particular diastereoisomer and the equatorial methyl in the meen *δ** ring, but the conformations of the two en rings (*δδ*) differed from those in the observed structure (*λλ*). The calculated steric energy for this observed structure (49.0 kJ mol^{-1}) was 4.5 kJ mol^{-1} higher, which corresponds to a ratio of *K ca* 6. No specific crystal forces can be identified in the structure which might account for the *λλ* arrangement being favoured. There are two other conformers which have lower calculated steric energies than the observed structure: *Λ-R-δ*λδ* (45.0 kJ mol^{-1}) and *Λ-R-δ*δλ* (48.8 kJ mol^{-1}). Despite there being several conformers of similar energy, the complex crystallizes readily in only one form, perhaps because of the lability of the en ring conformations. In solution the conformers present are unknown and the ^{13}C NMR spectrum gives only a time average of any conformer mixture.

While the 4.5 kJ mol^{-1} steric-energy gap between the observed and calculated structures is not large by *MM*2 standards, we did observe better correlations for the $[Co(meen)_2(en)]^{3+}$ and $[Co(meen)_3]^{3+}$ systems (Atkinson, Keene & Searle, 1991). It is therefore unlikely that the origin of the discrepancy lies solely with the force field employed in the calculations. Structural comparisons between the minimized *Λ-R*-$[Co(meen)(en)_2]^{3+}$ conformations where the methyl group is equatorial reveal that the molecular shapes [as determined by the root-mean-square (r.m.s.) differences of atomic positions] are very similar irrespective of the conformations of the two en chelate rings. This situation is different from the $[Co(meen)_2(en)]^{3+}$ and $[Co(meen)_3]^{3+}$ systems, where there are additional ring substituents. It is therefore possible that in this special case of $[Co(meen)(en)_2]^{3+}$, the molecular structures are too closely related to be reliably discriminated with a general *MM*2 force field.

Comparison of the details of the determined structure with those of the calculated (minimized) structure for the *Λ-R-δ*λλ* shows close agreement between the structures: r.m.s. differences are 0.029 Å for 16 bond lengths, 1.39° for 29 bond angles, 2.41° for 40 torsional angles, and 0.042 Å for all interatomic distances [supplementary tables *S*(5) and *S*(6)].†

The energy difference from the determined structure to that calculated for the other diastereoisomer *Λ-S-λ*δδ* (51.4 kJ mol^{-1}) is only 2.4 kJ mol^{-1} (*K ca* 2.6). This does not seem sufficiently large to account for the apparent stereospecificity as the *Λ-S* isomer was not observed experimentally. It is likely, therefore, that hydrogen bonding in the solid state is important in discriminating these isomers.

The Australian Research Council is thanked for support.

† See deposition footnote.

‡ Each of the five-membered chelate rings formed by the bidentate ligands meen and en can exist in alternative conformations, *δ* or *λ*. The unique meen ring is specified first and designated with an asterisk (Atkinson, Keene & Searle, 1991). The discussion here is presented for only the *Λ* configurations of complexes, but in all cases there is an equivalent *Δ* form in the racemate that constitutes each diastereoisomeric pair.

§ An early conformational anlysis of $[Co(meen)(en)_2]^{3+}$ used non-bonded interactions only (Sargeson, 1966). Although the broad structure predicted for the more stable isomer was correct (*Λ-R-δ**), the results of such limited analyses are generally unreliable.

† See deposition footnote.

References

ATKINSON, I. M., KEENE, F. R. & SEARLE, G. H. (1991). *J. Chem. Soc. Dalton Trans.* pp. 45–51.

BOER, J. L. DE & DUISENBERG, A. J. M. (1984). Enraf–Nonius CAD-4F diffractometer software update, February 1984. Groningen and Utrecht, The Netherlands.

JOHNSON, C. K. (1976). *ORTEP*II. Report ORNL-5138. Oak Ridge National Laboratory, Tennessee, USA.

SARGESON, A. M. (1966). *Transition Met. Chem.* **3**, 303–343.

SEARLE, G. H. & KEENE, F. R. (1989). *Inorg. Chim. Acta*, **155**, 125–138.

SEARLE, G. H. & TIEKINK, E. R. T. (1989*a*). *Inorg. Chim. Acta*, **156**, 57–63.

SEARLE, G. H. & TIEKINK, E. R. T. (1989*b*). *Acta Cryst.* C**45**, 1300–1303.

SHELDRICK, G. M. (1976). *SHELX*76. Program for crystal structure determination. Univ. of Cambridge, England.

[Reprinted from the Journal of the American Chemical Society, 95, 5649 (1973).]

Base Hydrolysis of Coordinated Acetonitrile

D. A. Buckingham, F. R. Keene, and A. M. Sargeson*

Contribution from the Research School of Chemistry, Australian National University, Canberra, 2600, Australia. *Received April 13, 1973*

Abstract: The base hydrolysis of acetonitrile to acetamide is catalyzed by a factor of 2×10^6 on coordination to $Co(NH_3)_5^{3+}$. Hydroxide appears to attack the carbon atom of the nitrile group, while in a separate and concurrent process the methyl protons exchange. On addition of acid to the acetamido complex produced, protonation occurs on the carbonyl oxygen ($pK_a = 3.02$; $\mu = 1.0$ *M*, $NaClO_4$; $T = 25°$) rather than on the amide nitrogen atom.

The metal ion promoted hydrolysis of nitriles has been studied for several nitriles.[1-3] In cases where valid comparisons can be made, the corresponding N-bonded carboxamide product is formed at a rate 10^6–10^7 faster than for the base hydrolysis of the non-coordinated nitrile.[1,3]

However, in the system $[Co(en)_2X(NCCH_2NH_2)]^{2+}$ (X = Cl, Br) a different reaction occurs under basic conditions, and a tridentate amidine complex is formed by attack of a coordinated amide ion (formed by deprotonation of an amine proton of en) at the nitrile C atom.[4] Consequently, it was of interest to determine whether $[Co(NH_3)_5(N{\equiv}CCH_3)]^{3+}$ would react by direct hydroxide ion attack at the nitrile group to give the N-bonded acetamido complex, or by attack of a deprotonated ammine on the nitrile group to produce coordinated acetamidine. The present paper reports the investigation of the base hydrolysis of $[Co(NH_3)_5(N{\equiv}CCH_3)]^{3+}$, and of the properties of the hydrolysis product.

(1) R. Breslow, R. Fairweather, and J. Keana, *J. Amer. Chem. Soc.*, 89, 2135 (1967).
(2) K. Sakai, T. Ito, and K. Watanabe, *Bull. Chem. Soc. Jap.*, 40, 1660 (1967); S. Komiya, S. Suzuki, and K. Watanabe, *ibid.*, 44, 1440 (1971); P. F. D. Barnard, *J. Chem. Soc. A*, 2140 (1969).
(3) D. Pinnell, G. B. Wright, and R. B. Jordan, *J. Amer. Chem. Soc.*, 94, 6104 (1972).
(4) D. A. Buckingham, B. M. Foxman, A. M. Sargeson, and A. Zanella, *J. Amer. Chem. Soc.*, 94, 1007 (1972).

Experimental Section

Analytical reagents were used without further purification. $[Co(NH_3)_5(N{\equiv}CC_6H_5)](ClO_4)_3$ and $[Co(NH_3)_5(NHCOC_6H_5)]I_2$ (and the protonated species as the chloride salt) were obtained as described previously.[2] Electronic spectra were measured on a Cary 14 spectrophotometer, and pmr spectra on either a Varian HA-100 or a JEOL MH-100 spectrometer using TMS as external reference or *tert*-butyl alcohol as internal reference.

Preparation of $[Co(NH_3)_5(N{\equiv}CCH_3)](ClO_4)_3$ was effected as previously reported in the literature,[5] or on a larger scale by the following method. $[Co(NH_3)_5I](ClO_4)_2$[6] (9.42 g, 0.02 mol) and $AgClO_4$ (4.2 g, 0.02 mol) were stirred for 5 min in dried acetone (15 ml). Acetonitrile (50 ml) was added and the mixture stirred overnight at room temperature. Ether (50 ml) was added, and the yellow product and precipitated silver iodide were filtered off. The complex was extracted with warm water (40 ml), acidified with a few drops of acetic acid, and precipitated by the addition of $NaClO_4$ and cooling. $[Co(NH_3)_5(N{\equiv}CCH_3)](ClO_4)_3$ (8.2 g, 85%) was filtered off, washed with ethanol and ether, and air dried. The complex was recrystallized from warm acidified water. The visible spectrum of the complex in 10^{-3} *M* $HClO_4$ gave ϵ_{467}^{max} 63 and ϵ_{333}^{max} 56. *Anal.* Calcd for $CoN_6C_2H_{18}Cl_3O_{12}$: Co, 12.19; C, 4.97; H, 3.75; N, 17.38. Found: Co, 12.21; C, 5.21; H, 4.07; N, 17.06.

Isolation of Base Hydrolysis Product. $[Co(NH_3)_5(N{\equiv}CCH_3)](ClO_4)_3$ (1.21 g, 0.0025 mol) was dissolved in water (25 ml) and NaOH solution added (2.5 ml of 1.2 *M*, 0.0030 mol). After 10 sec excess $NaClO_4$ was added to precipitate the red hydrolysis product,

(5) R. B. Jordan, A. M. Sargeson, and H. Taube, *Inorg. Chem.*, 5, 1091 (1966).
(6) R. G. Yalman, *J. Amer. Chem. Soc.*, 77, 3219 (1955).

which was filtered and washed with ethanol, yield 0.82 g, 82%. Recrystallization was achieved from warm water (pH ~9, 8 ml) by the addition of $NaClO_4$ and cooling. Electronic spectra showed ϵ_{485}^{max} 73, ϵ_{351}^{max} 87, and ϵ_{252}^{max} 2.47 × 10^3 in 0.01 *M* NaOH, and ϵ_{470}^{max} 63 and ϵ_{342}^{max} 60 in 0.1 *M* $HClO_4$. *Anal.* Calcd for $CoN_6C_2H_{19}Cl_2O_9$: Co, 14.69; C, 5.99; H, 4.78; N, 20.96; Cl, 17.68. Found: Co, 14.58; C, 6.21; H, 4.92; N, 20.98; Cl, 17.60.

The complex was isolated in a protonated form (yellow) by precipitation with $NaClO_4$ from an acidified solution of the red base hydrolysis product, but the analytical results were poor and indicated some unprotonated form.

Analysis of Water Content of Base Hydrolysis Product. The base hydrolysis product was analyzed for water by the Karl Fischer method. The complex (322 mg) was dissolved in dry dimethylformamide (3 ml) and aliquots (1 ml) of this solution were added to dried methanol (10 ml) and titrated with Karl Fischer reagent. The average titer of 0.10 ml (1 ml of KF reagent ≡ 5.73 mg of H_2O) indicated <1% water content in the complex.

Kinetics of Base Hydrolysis of $[Co(NH_3)_5(N{\equiv}CCH_3)](ClO_4)_3$. A solution of the complex (2 × 10^{-4} *M*) in water was mixed with an equal volume of standard NaOH solution (μ = 2.0 *M*, $NaClO_4$) using a stopped-flow apparatus. The reaction was followed at λ 240 nm on a Cary 16K spectrophotometer at a cell temperature of 25.0°. The rate of hydrolysis was also followed by nmr techniques in a 1 *M* Tris–$DClO_4$ (D_2O) buffer (μ = 0.1 *M*; measured pH = 9.20, pD = 9.60[7]) at the probe temperature (33°).

$[Co(NH_3)_5(N{\equiv}CCH_3)](ClO_4)_3$ (*ca.* 0.1 g) and *tert*-butyl alcohol (0.02 ml) were dissolved in the buffer solution (1 ml), and pmr spectra were recorded over 4 half-lives. The methyl signals of the reactant complex (2.62 ppm) and of the product (2.12 ppm) were superimposed on the tail of the large resonance due to the buffer, and the results were plotted as the disappearance of the methyl resonance of the reactant measured in terms of peak height relative to the standard *t*-BuOH. A plot of log (peak height − peak height$_\infty$) *vs.* time was linear over 2 × $t_{1/2}$.

The extent of the proton exchange process on the CH_3 group was measured separately by recording the pmr spectrum of a solution of $[Co(NH_3)_5(N{\equiv}CCH_3)](ClO_4)_3$ in D_2O (0.1 g in 1 ml) with *tert*-butyl alcohol (0.02 ml) as a standard, then adding 0.1 ml of 1 *M* NaOD solution and recording the pmr of the base hydrolysis product. The integrals of the two methyl signals (relative to *tert*-butyl alcohol) gave the extent of proton exchange in the course of hydrolysis.

Determination of pK_a. The pK_a of the acetamide complex was obtained spectrophotometrically at 350 nm by adding aliquots of 1.0 *M* $HClO_4$ to a solution of the complex in 0.01 *M* NaOH (μ = 1.0 *M*, $NaClO_4$). The pK_a was evaluated by the procedure of Albert and Serjeant.[8]

Results and Discussion

The complex $[Co(NH_3)_5(N{\equiv}CCH_3)]^{3+}$ hydrolyzed in basic conditions according to the rate law, $v = k_{OH}\cdot$[nitrile][OH^-]. The kinetic results are given in Table I.

Table I. Kinetic Results for Base Hydrolysis of $[Co(NH_3)_5(N{\equiv}CCH_3)]^{3+}$ at 25°[a]

[OH^-], *M*	k_{obsd}, sec^{-1}	$k_{OH} = k_{obsd}/[OH^-]$, M^{-1} sec^{-1}
0.10	3.48 × 10^{-1}	3.5
0.050	1.70 × 10^{-1}	3.4
0.010	3.40 × 10^{-2}	3.4
0.0050	1.68 × 10^{-2}	3.4

[a] μ = 1.0 *M* ($NaClO_4$); [Co] = 1.2 × 10^{-4} *M*.

The hydrolysis rate (3.40 M^{-1} sec^{-1}) is 2 × 10^6 faster than base hydrolysis of free acetonitrile to acetamide (1.60 × 10^{-6} M^{-1} sec^{-1}),[9] a factor which is practically identical with the enhancement of the rate of benzonitrile hydrolysis by the $(NH_3)_5Co^{3+}$ moiety,[3] and similar to the factor of 10^7 observed for the Ni(II)–2-cyano-1,10-phenanthroline system[1] (Table II).

Table II. Comparison of the Rates of Base Hydrolysis of Nitriles

Nitrile	k_{OH}, M^{-1} sec^{-1}
$N{\equiv}CCH_3$	1.60 × 10^{-6} [a]
$(NH_3)_5CoN{\equiv}CCH_3^{3+}$	3.40[a]
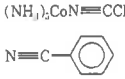	8.2 × 10^{-6} [b]
	18.8[b,c]
	2.6 × 10^{-3} [a]
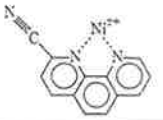	2.4 × 10^{4} [a,d]

[a] *T* = 25.0°. [b] *T* = 25.6°. [c] Reference 3. [d] Reference 1.

Before considering the mechanism of base hydrolysis, some discussion of the composition of the product is necessary to establish whether the N-bonded acetamide complex of $(NH_3)_5Co^{3+}$ or the acetamidine complex of $(NH_3)_4Co^{3+}$ is formed. The product of the base hydrolysis reaction analyzes to contain an additional hydroxyl (or water) group compared with the acetonitrile complex. Such a formulation would be consistent with the acetamido product $[(NH_3)_5Co(NH{-}COCH_3)](ClO_4)_2$ or alternatively with the acetamidino complex crystallized with one molecule of lattice water, *i.e.*, $[(NH_3)_4Co(NH{=}C(NH_2)CH_3)](ClO_4)_2\cdot H_2O$. A Karl Fischer determination of water contained in the complex showed no such water, so that the former of these two possibilities must be the product.

The nmr data obtained on this system is consistent with this assignment. The parent $[Co(NH_3)_5(N{\equiv}C{-}CH_3)]^{3+}$ ion has the pmr spectrum in D_2O–D^+ shown in Figure 1A, where the NH_3 protons are resolved by nitrogen spin decoupling into the ammine groups cis (12 protons) and trans (3 protons) to the acetonitrile ligand. The two types of ammine nitrogen atoms were also observed in the ^{14}N spectrum of the complex using the indor technique,[10] with resonances at Ξ = 7,223,269 (±10) (cis) and 7,223,207 (±10) (trans) Hz.[11]

For the base hydrolysis product, $[Co(NH_3)_5(NHCOCH_3)]^{2+}$, the pmr spectrum is given in Figure 1B, where the NH and NH_3 proton resonances are not separated. On nitrogen spin decoupling, the NH and NH_3 resonances are separated but the cis and trans ammonia proton resonances are not distinguished. The ^{14}N nmr spectrum showed the amide nitrogen atom and the five ammine nitrogen atoms at Ξ = 7,223,-247 (±10) and 7,223,217 (±10) Hz, respectively. In this respect the spectral resolution from the ^{14}N indor

(7) P. K. Glasoe and F. A. Long, *J. Phys. Chem.*, 64, 188 (1960).
(8) A. Albert and E. P. Serjeant, "Ionization Constants of Acids and Bases," Methuen, London, 1962.
(9) N. Peskoff and J. Meyer, *Z. Phys. Chem.*, 82, 129 (1913).
(10) V. J. Kowalewski, *Progr. Nucl. Magn. Resonance Spectrosc.*, 5, 1 (1969).
(11) Ξ is the resonant frequency for the particular nucleus in the same magnetic field which gives internal TMS a proton resonant frequency of 100,000,000.00 Hz.

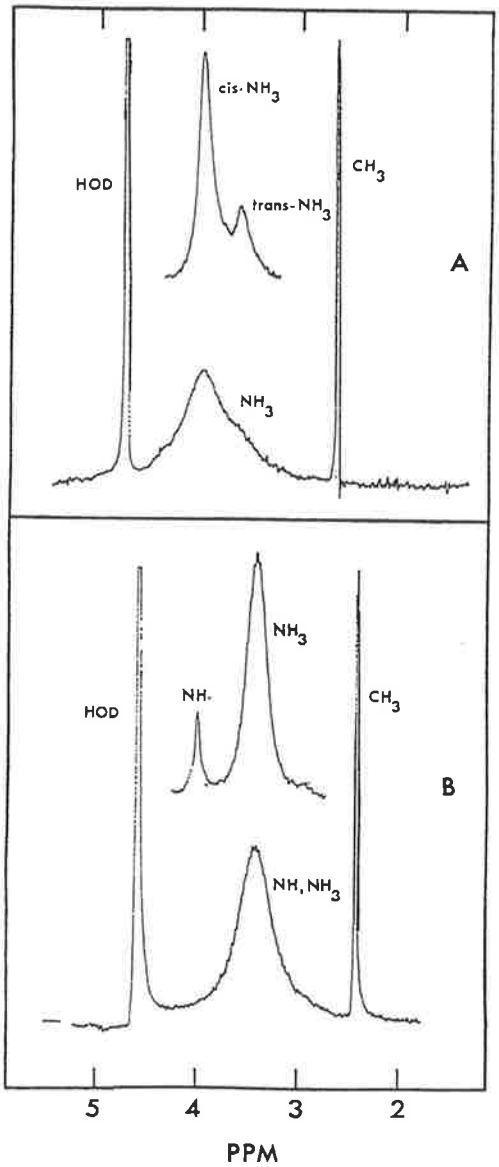

Figure 1. The 100-MHz pmr spectra, and ^{14}N decoupled ammine regions, for (A) $[Co(NH_3)_5(N{\equiv}CCH_3)](ClO_4)_3$ in 1% DCl (TMS external reference), and (B) $[Co(NH_3)_5(NHCOCH_3)](ClO_4)_2$ in 2% D_2SO_4 solution (*t*-BuOH internal reference).

technique was somewhat disappointing. Even so, the results are consistent with the acetamido formulation where three resonances were expected and two were observed, one for the ammonia residues and one for the amide moiety. For the acetamidino formulation five resonances could be expected, two involving the amide moiety and three for the ammonia residues.

The pmr spectrum of the base hydrolysis product is also shown in DMSO-d_6 (Figure 2A) where the resonances δ_{CH_3} 1.93, δ_{NH_3} 4.19, and δ_{NH} 4.77 (all relative to δ_{DMSO} centered at δ 2.51 ppm) are in agreement with the pmr of $[Co(NH_3)_5(NHCOCH_3)]^{2+}$ prepared directly from acetamide.[12] On the addition of increasing amounts of H^+ the HOD and NH signals move downfield, with the NH signal remaining at 7.25 ppm on full protonation of the complex (Figure 2B and C). The magnitude of this resonance corresponds to one

(12) R. B. Jordan, private communication.

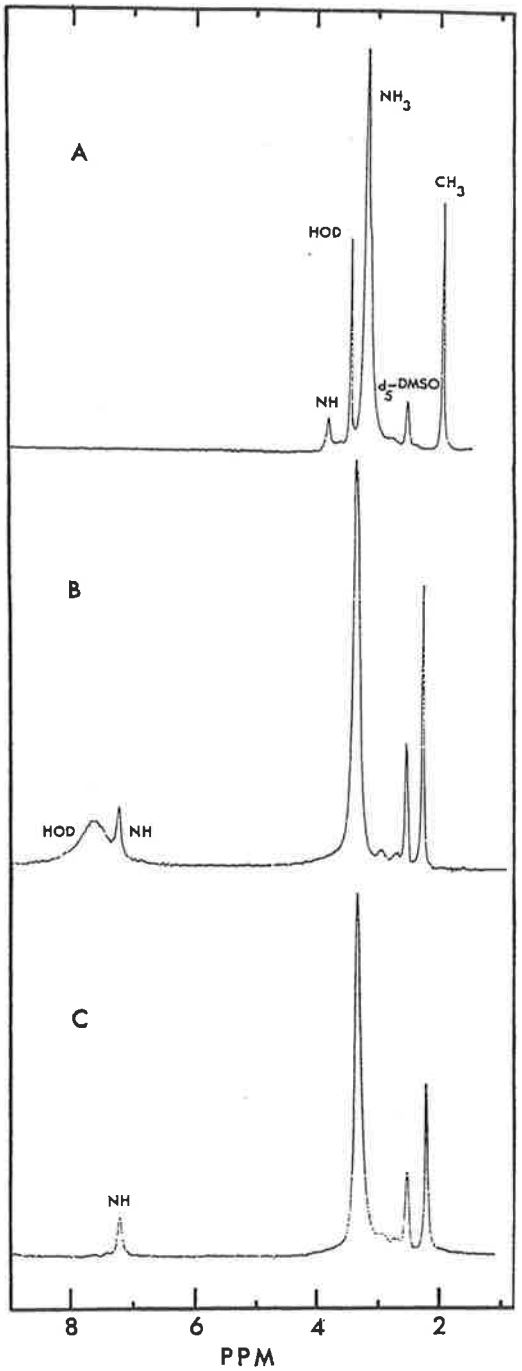

Figure 2. The 100-MHz pmr spectrum of $[Co(NH_3)_5(NHCOCH_3)](ClO_4)_2$ in DMSO-d_6 (A), and with increasing amounts of H_2SO_4 (B and C). External reference TMS.

proton throughout. This can be explained if protonation occurs on the carbonyl oxygen atom. The NH

$$CoNH{-}\overset{\overset{O}{\|}}{C}{-}CH_3 \xrightarrow{H^+} CoNH{=}\overset{\overset{OH}{|}}{C}{-}CH_3$$

proton is thereby more effectively deshielded by the anisotropy of the >C=N– compared with the >C=O double bond, and so resonates at lower field in the protonated complex. The carbonyl group, however, is weakly basic and the protonated species would be a strong acid and would exchange the proton rapidly

with H_2O in the solvent. Similar behavior has also been observed for protonation of $[Co(NH_3)_4(NH_2CH_2CONH)]^{2+}$,[13] and protonation of the carbonyl oxygen rather than the nitrogen atom is also claimed for uncoordinated acetamide.[14]

In the present case, some slow decomposition occurs in acidified DMSO with the liberation of free acetamide and the formation of $[Co(NH_3)_5(DMSO)]^{3+}$. The pmr signals associated with these products have not been included in Figure 2 for simplicity.

The pK_a of the protonated acetamide complex in aqueous solution is 3.02 (μ = 1.0 M, $NaClO_4$; T = 25°) which is slightly higher than those of the benzamide (pK_a = 1.65)[3] and formamide (pK_a = 2.16)[15] complexes of $Co(NH_3)_5^{3+}$, where protonation was indicated to be at the amide nitrogen atom. In view of the present work, it seems more likely that protonation will occur in these complexes at the carbonyl oxygen atom, and the pmr spectrum of the protonated benzamido complex in 1 M DCl solution confirms that there is only one proton at the nitrogen atom.

The rate law for the hydrolysis reaction is consistent with direct attack of hydroxide ion at the carbon atom of the nitrile group, giving rise to the acetamido complex, in the same way as proposed for the benzonitrile system.[3]

$$(NH_3)_5CoN{\equiv}CCH_3^{3+} + OH^- \longrightarrow (NH_3)_5CoNH{-}\overset{\overset{O}{\|}}{C}{-}CH_3^{2+}$$

However, unlike the nitriles previously studied,[1-3] acetonitrile has hydrogen atoms on the carbon atom α to the cyano group. Pmr studies indicate that during the hydrolysis process, exchange of about half of the methyl protons occurs. (The rate of exchange of methyl protons in the acetamido complex is extremely slow.) Consequently, the rate of disappearance of the methyl signal of $[Co(NH_3)_5(N{\equiv}CCH_3)]^{3+}$ (k_{obsd} = 1.36 × 10^{-3} sec^{-1}) exceeds that of the hydrolysis (k_{obsd} = 9.7 × 10^{-4} sec^{-1}, measured spectrophotometrically) under the same conditions (Tris–$DClO_4$ buffer in D_2O, T = 33°, pD = 9.60) since in the former case both hydrolysis and exchange are observed. It is therefore possible that deprotonation may be a prerequisite to hydrolysis.

$$\begin{array}{ccc} (NH_3)_5CoN{=}CCH_3^{3+} & \xrightarrow{OH^-} & (NH_3)_5CoN{\equiv}C\bar{C}H_2^{2+} \\ & & \uparrow \\ (NH_3)_5CoNH{-}\overset{\overset{O}{\|}}{C}{-}CH_3^{2+} & \xleftarrow{H_2O} & (NH_3)_5Co{-}\bar{N}{=}C{=}CH_2^{2+} \end{array}$$

In the present instance, the rate of exchange is such that slightly more than one exchange occurs for every hydrolysis act. Alternatively, the two processes may be independent.

For the benzonitrile analog, similar studies reveal that exchange does not occur during hydrolysis so that no deprotonation of the phenyl protons is involved, presumably as no stabilization of the carbanion is possible. Thus, hydrolysis by direct attack of hydroxide ion on the nitrile carbon atom is most likely. The similarity in catalysis of the hydrolyses of benzonitrile and acetonitrile by $(NH_3)_5Co^{3+}$ (*ca.* 2 × 10^6) suggests some identity in the mechanisms, so that hydrolysis of acetonitrile in the pentaamminecobalt(III) complex would appear to occur by direct hydroxide attack also, with exchange being an independent process.

Acknowledgments. We are grateful to Dr. R. Bramley and Mr. C. Arandjelovic for assistance with the ^{14}N indor nmr spectra, and to the Microanalytical Unit for estimations of C, H, N, Co, and Cl.

(13) D. A. Buckingham, D. M. Foster, and A. M. Sargeson, *J. Amer. Chem. Soc.*, 91, 3451 (1969).
(14) H. Benderly and K. Rosenheck, *J. Chem. Soc., Chem. Commun.*, 179 (1972).
(15) R. J. Balahura and R. B. Jordan, *J. Amer. Chem. Soc.*, 92, 1533 (1970).

Reprinted from the Journal of the American Chemical Society, 1981, *103*, 3559.

Reactivity of Coordinated Nitriles

I. I. Creaser, J. MacB. Harrowfield, F. R. Keene, and A. M. Sargeson*

Contribution from the Research School of Chemistry, Australian National University, Canberra ACT 2600, Australia. *Received July 14, 1980*

Abstract: The base hydrolysis of coordinated acrylonitrile in $[(NH_3)_5CoN{\equiv}CCH{=}CH_2]^{3+}$ to the acrylamide complex in carbonate buffers obeys the rate law $k_{obsd} = k_{OH}[OH^-] + k_c[CO_3^{2-}]$ ($k_{OH} = 35\ M^{-1}\ s^{-1}$; $k_c = 1\ M^{-1}\ s^{-1}$; 25 °C, $\mu = 1.0$), and ^{18}O tracer studies indicate the mechanism of hydrolsis by carbonate ion to involve direct nucleophilic attack at the nitrile group by CO_3^{2-} with subsequent elimination of CO_2. Coordination of malononitrile, cyanoacetic acid, and ethyl cyanoacetate to the $(NH_3)_5Co^{III}$ moiety leads to greatly increased acidity of the methylene protons (pK_a of $[(NH_3)_5CoN{\equiv}CCH_2C{\equiv}N]^{3+}$ is 5.7 ± 0.1 ($\mu = 1.0$, 25 °C) compared with 11.3 for uncoordinated malononitrile). In basic aqueous solutions, these complexes equilibrate rapidly between the original complexes and the complexes containing the deprotonated activated methylene group. The protonated complexes then hydrolyze to the coordinated amides with both hydroxide ion and water acting as nucleophiles while the coordinated carbanions undergo an intramolecular electron transfer of a single electron to yield Co(II) and the ligand radical. The C-deprotonated complexes also function as nucleophiles for appropriate substrates (such as methyl iodide, methyl pyruvate, or bromine) to form the corresponding substituted species. In nonaqueous media, generation of the ligand radical initiates polymerizations of monomers methacrylate, styrene, acrylonitrile, and methacrylonitrile by a radical (rather than an ionic) mechanism.

Increased reactivity of coordinated nitriles has been observed on a number of occasions.[1-7] Marked acceleration in the rates of hydrolysis to the amide by OH^- compared with the uncoordinated species has been recorded both for inter- and intramolecular hydrolysis processes. The acceleratory effect for coordinated acetonitrile was also accompanied by an enhancement in the rate of proton exchange for the methyl group: in fact, the latter process was slightly faster than OH^- attack at the nitrile carbon.[6] This property is in accord with some earlier observations on the treatment of $[(NH_3)_5Co(NCCH_2CN)]^{3+}$ with base.[8] A solution of this latter ion in water gave an intense red color when OH^- was added. The color faded gradually to give a yellow solution similar in appearance to the original solution, although the visible spectra were not identical. The initial observation was attributed to deprotonation of the acidic methylene group, but the second reaction was not investigated further.[8] If the interpretation of the initial reaction is correct, the acidity of coordinated malononitrile is considerably greater than that of the uncoordinated species, and this paper reports on the hydrolysis and reactivity of such nitrile complexes. Studies on several related nitriles have also been made.

Experimental Section

Electronic spectra and molar absorptivities ϵ ($M^{-1}\ cm^{-1}$) were recorded by using a Cary 118C spectrophotometer, ^1H NMR spectra by using either a Varian HA-100 or a JEOL MH-100 spectrometer, and IR spectra by using a Perkin-Elmer PE 225 spectrometer with KBr disks (ca. 5 mg of complex/200 mg of KBr).

Synthesis and Reagents. Cyanoacetic acid (Unilab), ethyl cyanoacetate (Fluka, puriss), trimethyl phosphate (Pflaum), nitrosyl tetrafluoroborate (Ozark-Mahoning), and acrylonitrile (Aldrich) were used without further purification. Malononitrile (Pfaltz and Bauer) was freshly distilled before use (76–77 °C, (1 mmHg)). $[Co(NH_3)_5N_3]Cl_2$ was converted to the tetrafluoroborate salt by using $AgOOCCH_3$/$NaBF_4$, and $[Co(NH_3)_5(OP(OCH_3)_3)](BF_4)_3$ was isolated in an analogous way to that of $[Co(NH_3)_5(OP(OC_2H_5)_3](ClO_4)_3$[8] by using the corresponding BF_4^- salts. Nitrosyl triflate was prepared by passing N_2O_3 gas (from $H_2SO_4/NaNO_2$) into purified CF_3SO_3H until crystallization was complete.

$[Co(NH_3)_5(N{\equiv}C\text{-}CH_2C{\equiv}N)](ClO_4)_3$. $[Co(NH_3)_5(OP(OCH_3)_3)](BF_4)_3$ (4.0 g) was dissolved in freshly distilled malononitrile (50 mL) and concentrated H_2SO_4 (0.5 mL) added. The mixture was maintained at ca. 50 °C until it turned yellow (ca. 3 h). Ethanol (50 mL) and ether (300 mL) were added, the solution was filtered and the product was washed with ethanol and acetone and air dried. The resultant complex (3.0 g, 80%) was purified by dissolution in 0.1 M HBr (50 mL) and adding excess LiBr (ca. 5 g) to remove any amide complex. The solution was cooled quickly and filtered, and excess solid $NaClO_4$ was added to the filtrate whereupon $[Co(NH_3)_5(N{\equiv}CCH_2C{\equiv}N)](ClO_4)_3$ crystallized out. This material was further recrystallized by precipitation using $NaClO_4$ from a 0.1 M $HClO_4$ solution and was collected as indicated above. Yield: 1.9 g, 51%.

A solution in 0.01 M $HClO_4$, measured rapidly after dissolution, gave two maxima in the visible spectrum ($\epsilon_{474} = 72$, $\epsilon_{341} = 82$). The infrared spectrum showed two absorptions at 2263 and 2330 cm^{-1}, attributed to the $-C{\equiv}N$ stretching modes of the terminal and bound –CN groups, respectively. Anal. Calcd for $[Co(NH_3)_5NCCH_2CN](ClO_4)_3$: Co, 11.6; C, 7.09; H, 3.37;, N, 19.3. Found: Co, 11.7; C, 7.3; H, 3.6; N, 19.4.

$[Co(NH_3)_5(N{\equiv}CCH_2CO_2C_2H_5)](ClO_4)_3$. $[Co(NH_3)_5N_3](BF_4)_2$ (2.0 g), ethyl cyanoacetate (30 mL), and trimethyl phosphate (10 mL, to affect dissolution) were stirred, and excess $NOBF_4$ was added slowly. The mixture was stirred for a further 2 h, and the complex (as the BF_4^- salt) was precipitated by using ether. The product was recrystallized twice by precipitation using $NaClO_4$ from solutions in slightly acidified water. It was washed with ethanol and ether and air-dried. Yield: 0.8 g, 26%.

The visible spectrum (0.01 M $HClO_4$) showed two maxima ($\epsilon_{465} = 64$, $\epsilon_{295} = 89$), and the infrared spectrum (KBr disk) indicated $\nu_{CN} = 2325\ cm^{-1}$. Anal. Calcd for $[Co(NH_3)_5(NCCH_2CO_2C_2H_5)](ClO_4)_3$: Co, 10.6; C, 10.8; H, 3.99; N, 15.1. Found: Co, 10.8; C, 10.7; H, 4.1; N, 15.1.

A much higher yield was obtained by adding NOO_3SCF_3 (8 g) to a vigorously stirred solution of $[(NH_3)_5CoN_3](CF_3SO_3)_2$ (15 g) in acetone (20 mL) and $NCCH_2COOC_2H_5$ (100 mL). Only a little complex remained undissolved in this solvent mixture. The solution rapidly turned yellow-brown as N_2 and N_2O evolution occurred, and after 15 min a copious yellow precipitate had appeared. The mixture was cooled at 0 °C for 30 min and then mixed with ether (100 mL) and the product collected. The triflate salt was recrystallized from CH_3OH by addition of ether to give fine needles (17 g).

$[Co(NH_3)_5(N{\equiv}CC(CH_3)_2CO_2C_2H_5)](NO_3)_3$. $[Co(NH_3)_5(NCCH_2CO_2C_2H_5)](ClO_4)_3$ (0.36 g) was dissolved in dry Me_2SO (10 mL), and MeI (ca. 1 mL) was added, followed immediately by imidazole (0.10 g). The mixture was shaken, stoppered, and left to stand for 10 min during which time the bright red color obtained on the addition of imidazole faded to orange. Ether (500 mL) precipitated the complex as an oil, which after two triturations with ether was solidified by the addition of isopropyl alcohol. The product was filtered and dried in vacuo. Puri-

(1) Breslow, R.; Fairweather, R.; Keana, J. *J. Am. Chem. Soc.* **1967**, *89*, 2135. Sakai, K.; Ito, T.; Watanabe, K. *Bull. Chem. Soc. Jpn.* **1967**, *40*, 1660. Watanabe, K.; Komiya, S.; Suzuki, S. *Ibid.* **1973**, *46*, 2792. Barnard, P. F. B. *J. Chem. Soc. A* **1969**, 2140.
(2) Diamond, S. E.; Grant, B.; Tom, G. M.; Taube, H. *Tetrahedron Lett.* **1974**, *46*, 4025.
(3) Balahura, R. J.; Purcell, W. L. *Inorg. Chem.* **1979**, *18*, 937.
(4) Pinnell, D.; Wright, G. B.; Jordan, R. B. *J. Am. Chem. Soc.* **1972**, *94*, 6104.
(5) Rouschais, G.; Wilkinson, G. *J. Chem. Soc. A* **1968**, 489.
(6) Buckingham, D. A.; Keene, F. R.; Sargeson, A. M. *J. Am. Chem. Soc.* **1973**, *95*, 5649.
(7) Buckingham, D. A.; Morris, P.; Sargeson, A. M.; Zanella, A. *Inorg. Chem.* **1977**, *16*, 1910.
(8) Jordan, R. B.; Sargeson, A. M.; Taube, H. *Inorg. Chem.* **1966**, *5*, 1091.

fication was achieved by anion exchange using a column of DEAE-Sephadex A-25 in the NO_3^- form (to remove ClO_4^- and I_3^- ions), evaporating the eluant to dryness and recrystallizing the residue from hot water (5 mL). The orange product was filtered, washed with ethanol and ether, and air-dried. Yield: 0.13 g, 42%.

The IR spectrum (ν_{CN} = 2330 cm^{-1}) was consistent with coordinated nitrile. Anal. Calcd for $[Co(NH_3)_5(NCC(CH_3)_2CO_2C_2H_5)](NO_3)_3$: C, 17.8; H, 5.56; N, 26.8. Found: C, 17.0; H, 5.6; N, 26.8.

$[(NH_3)_5CoNHCOCBr_2CO_2C_2H_5](ClO_4)_2$. Bromine (3 mL) was added dropwise to a stirred ice-cold solution of $[(NH_3)_5CoNCCH_2CO_2C_2H_5](CF_3SO_3)_3$ (17 g) in H_2O (100 mL). With continued cooling of the mixture, a slurry of $NaHCO_3$ (4 g) in H_2O (20 mL) was added in portions over 5 min. The solution was then stirred for 20 min at 20 °C before $HClO_4$ (20 mL, 70%) was added. On cooling of the mixture, a mass of flesh pink crystals formed which were collected and washed with ethanol and ether (yield 11 g). The product was recrystallized from water by cooling and adding $HClO_4$. Anal. Calcd for $[(NH_3)_5CoNHCOCBr_2CO_2C_2H_5](ClO_4)_2$: C, 9.52; H, 3.35; N, 13.32. Found: C, 9.3; H, 3.8; N, 13.2.

$[(NH_3)_5CoNHCOCHBr_2](ClO_4)_2$. NaOH (2 M, 5 mL) was added to a slurry of $[(NH_3)_5CoNHCOCBr_2CO_2C_2H_5](ClO_4)_2$ (1.6 g) in H_2O (15 mL). The solid rapidly dissolved to give an orange solution, and after 15 s the reaction was quenched with $HClO_4$ (12 M, 5 mL). Cooling on ice produced a minor but voluminous amount of orange precipitate which was collected and discarded. It appeared to be a mixture of $[(NH_3)_5CoNHCOCHBr_2]^{2+}$ and $[(NH_3)_5CoNHCOCBr_2COOH]^{2+}$. After 12 h at 20 °C clusters of orange needles had deposited which were collected, washed with ethanol, and dried in vacuo. Anal. Calcd for $[(NH_3)_5CoNHCOCHBr_2](ClO_4)_2$: C, 4.30; H, 3.07; N, 15.04. Found: C, 4.7; H, 3.4; N, 15.2.

$[Co(NH_3)_5(N{\equiv}CCH_2CO_2H)](ClO_4)_3$. $[Co(NH_3)_5OH_2](ClO_4)_3$ (11.6 g) and cyanoacetic acid (8.5 g, 100 mmol) were slurried in water (10 mL) in an evaporating basin, and the mixture was taken to dryness on a steam bath. Water (5 mL) was added to the resultant orange solid, and the mixture was again taken to dryness. The solid residue was cooled, dissolved in water (300 mL), and sorbed on Dowex 50W-X2 resin (200–400 mesh, H^+ form). Elution with 1 M $NaClO_4$ (pH 3) gave two bands, the first red and the second yellow. The separate eluates were reduced in volume on a rotary evaporator until crystallization occurred. After addition of methanol and cooling of the mixture, the product was collected, washed with ethanol and ether, and air-dried. The first band gave rise to pink-orange needles (0.8 g), having ν_{CN} = 2260 cm^{-1} in the infrared spectrum, indicating free C≡N, whence this compound was formulated as $[Co(NH_3)_5(O_2CCH_2CN)](ClO_4)_2$. Anal. Calcd for $CoC_3H_{17}N_6O_{10}Cl_2$: C, 8.44; H, 4.01; N, 19.68; Co, 13.80; Cl, 16.61. Found: C, 8.5; H, 3.9; N, 19.6; Co, 13.9; Cl, 16.5.

The second band resulted in bright yellow flakes (1.5 g, 11%) with ν_{CN} = 2325 cm^{-1}, indicating a coordinated nitrile group; this complex had a visible spectrum ϵ_{470} = 68 and ϵ_{336} = 66 in 0.01 M $HClO_4$ solution. Anal. Calcd for $[Co(NH_3)_5(NCCH_2CO_2H)](ClO_4)_3$: Co, 11.2; C, 6.83; H, 3.44; N, 15.9. Found: Co, 11.3; C, 6.9; H, 3.7; N, 15.7.

$[Co(NH_3)_5(N{\equiv}CCH{=}CH_2)](ClO_4)_3$. $[Co(NH_3)_5N_3](ClO_4)_2$ (10 g) was dissolved in trimethyl phosphate (30 mL) and then diluted with acrylonitrile (~75 mL). Solid $NO(CF_3SO_3)$ was added slowly until all complex had reacted and the resulting mixture left overnight at 40–50 °C. After the mixture was cooled, ether was added to precipitate the complex. It was recrystallized by dissolution in hot water at pH ~3, and the complex was precipitated by the addition of solid $NaClO_4$. The yield was >90%. ^1H NMR (D_2O, ABX spectrum): δ 6.0–7.0 relative to DSS internal reference. Anal. Calcd for $[Co(NH_3)_5(N{\equiv}CCH{=}CH_2)](ClO_4)_3$: Co, 11.9; C, 7.27; H, 3.66; N, 17.0. Found: Co, 11.8; C, 7.4; H, 3.8; N, 16.7.

Kinetics of Base Hydrolysis of $[Co(NH_3)_5(N{\equiv}CCH_2C{\equiv}N)](ClO_4)_3$. A solution of the complex in 1 M $NaClO_4$ (ca. 8 × 10^{-4} M) was maintained at the desired pH with a pH-stat apparatus and the reaction followed at 397 nm by using a Cary 16 K spectrophotometer at a cell temperature of 25.0 °C. The following Radiometer apparatus was used in the pH-stat assembly: pH meter 26, ABU1 autoburet and TTT1 titrator with a G202B glass electrode and a saturated calomel electrode coupled by a salt bridge containing 1.6 M NH_4NO_3 and 0.2 M $NaNO_3$.

Product Isolation. The resultant solutions from the above kinetic determinations were adjusted to pH 7, diluted, and sorbed on a cation-exchange resin (Dowex 50W-X2, 200–400 mesh, Na^+ form) and the products eluted with 2 M $NaClO_4$. The products of the reaction were Co^{2+}, $[Co(NH_3)_5OH_2]^{3+}$, and $[Co(NH_3)(NHCOCH_2CN)]^{2+}$ measured by atomic absorption spectroscopy.

The amide complex was isolated by evaporation of the above eluant solution but was obtained more simply by the following method. $[Co(NH_3)_5(NCCH_2CN)](ClO_4)_3$ (0.2 g) was dissolved in the minimum quantity of warm water (10 mL, acidified with CH_3COOH) and 1.0 M NaOH solution (4 mL) added. After being left to stand for 90 min, the solution was filtered to remove precipitated cobalt oxides, and the product was crystallized from the filtrate by the addition of solid $NaClO_4$. The pink-yellow solid was filtered, washed with ethanol and ether, and air-dried. Yield: 0.1 g. The complex showed ν_{CN} = 2260 cm^{-1} and ϵ_{480} = 74 and ϵ_{345} = 95 for a solution in 0.01 M NaOH. Anal. Calcd for $[Co(NH_3)_5(NHCOCH_2CN)](ClO_4)_2$: C, 8.46; H, 4.26; N, 23.0. Found: C, 8.5; H, 4.5; H, 22.8.

A yellow protonated form was also isolated by addition of 12 M $HClO_4$ to the solution obtained from the reaction of $[Co(NH_3)_5(NCCH_2CN)]^{3+}$ with OH^-, but as with protonated forms of the complexes $[Co(NH_3)_5(NHCOC_6H_5)]^{2+}$ [8] and $[Co(NH_3)_5(NHCOCH_3)]^{2+}$, [6] analytical results indicated incomplete protonation or possibly one proton shared between two of the cations via hydrogen bonding.

Base Hydrolysis of $[Co(NH_3)_5(N{\equiv}CCH{=}CH_2)]^{3+}$ and $[Co(NH_3)_5N{\equiv}CCH_3]^{3+}$. A solution of the complex perchlorate in water ((0.5–3) × 10^{-4} M) was deaerated with nitrogen and mixed with solutions of deaerated sodium hydroxide solution by using a hand-operated stopped-flow device fitted to a Cary 16K spectrophotometer. The reaction was followed at 260 and 250 nm, respectively, and constant ionic strength of 1.0 ($NaClO_4$). The amide product $[(NH_3)_5CoNHCOCH{=}CH_2]I_2$ was isolated and characterized by microanalysis and ^1H NMR spectroscopy (see paragraph in this section of tracer studies).

Catalysis of Base Hydrolysis of $[Co(NH_3)_5(N{\equiv}CCH{=}CH_2)]^{3+}$ by Carbonate Ion. In a similar method to the base hydrolysis studies above, solutions of the complex were mixed with carbonate/bicarbonate buffers of varying total carbonate concentrations (pH maintained at ca. 9.6) by using the hand-operated stopped-flow device. Ionic strength was maintained at 1.0 ($NaClO_4$), T = 25.0 °C, and all runs were followed at λ = 260 nm by using a Cary 16K spectrophotometer.

Tracer Studies of CO_3^{2-} Reaction with $[Co(NH_3)_5(N{\equiv}CCH{=}CH_2)]^{3+}$. A sample of anhydrous Na_2CO_3 (2 g) was enriched by allowing a solution in $H_2{}^{18}O$ (ca. 1.5 atom %) to stand for 14 days at 25 °C: the $H_2{}^{18}O$ was evaporated and the $Na_2C^{18}O_3$ dried for 2 h at 260 °C and then kept in an evacuated desiccator.

$Na_2C^{18}O_3$ (0.50 g) was dissolved in $H_2{}^{16}O$ (CO_2 free; 3 mL): immediately, yellow $[Co(NH_3)_5(N{\equiv}CCH{=}CH_2)](ClO_4)_3$ (0.30 g) suspended in $H_2{}^{16}O$ (2 mL) was added, whereupon the complex dissolved and the solution became pink. Excess NaI was added after a fixed period (1, 5, and 7 min) to crystallize anhydrous $[Co(NH_3)_5(NHCOCH{=}CH_2)]I_2$. The complex was washed thrice with cold 1 M NaI solution and then several times with methanol and dried overnight in vacuo over P_2O_5. Half of the solid was recrystallized from water (ca. 2 mL) containing 1 drop of glacial acetic acid. ^1H NMR (D_2O, ABX spectrum): δ 5.2–6.6 relative to DSS internal reference. Anal. Calcd for $[(Co(NH_3)_5(NHCOCH{=}CH_2)]I_2$: C, 7.70; H, 4.09; N, 18.0; Co, 12.6; I, 54.2. Found: C, 7.9; H, 4.0; N, 17.9; Co, 12.7; I, 54.1.

The analysis of the enrichment in the acrylamide product was achieved by using the Anbar and Guttman method.[9] $[Co(NH_3)_5(NHCOCH{=}CH_2)]I_2$ (0.1 g) was mixed with $HgCl_2{\cdot}Hg(CN)_2$ and heated at 400 °C for 15 h in a break-seal tube. The CO_2, separated from the other gases in a gas chromatograph, was collected by using He as the carrier gas and the ^{18}O content analyzed by using an Atlas M-86 mass spectrometer, as outlined previously.[9] The enrichment in CO_3^{2-} was determined by adding acid to the solid sample in a stream of He and trapping the CO_2 produced. In one experiment, the reaction mixture was also treated in this way to sample the enrichment of reacted CO_3^{2-}.

pK_a Determination. The pK_a values for $[Co(NH_3)_5(N{\equiv}CCH_2C{\equiv}N)]^{3+}$ and $[Co(NH_3)_5(N{\equiv}CCH_2CO_2C_2H_5)]^{3+}$ were determined by the following method. A solution (ca. 8 × 10^{-4} M) of the complex as the perchlorate salt in 1 M $NaClO_4$ (pH ca. 3) was mixed with equal volumes of various buffer solutions ([buffer] = 0.2 M; μ = 1.0, $NaClO_4$) by using a stopped-flow apparatus. The subsequent reaction was followed for ca. 3 min at a fixed wavelength (λ = 397 nm for $[Co(NH_3)_5(NCCH_2CN)]^{3+}$, λ = 527 nm for $[Co(NH_3)_5(NCCH_2CO_2C_2H_5)]^{3+}$) by using a Cary 16K spectrophotometer at a cell temperature of 25.0 °C. The pH of each solution was measured with a Radiometer 26 pH meter. In each case, the curve was extrapolated to give the optical density at the instant of mixing and the pK_a evaluated.[10]

Polymerization Studies. Acrylonitrile, methacrylonitrile, and dimethylformamide (DMF) were purified and distilled before use.[11] Styrene, methyl methacrylate, and pyridine were dried and distilled be-

(9) Anbar, M.; Guttman, S. *J. Appl. Radiation Isotopes* **1959**, *5*, 223. See: Buckingham, D. A.; Foster, D. M.; Sargeson, A. M. *J. Am. Chem. Soc.* **1968**, *90*, 6032 and references therein.

(10) Albert, A.; Serjeant, E. P. "Ionization Constants of Acids and Bases"; Methuen: London, 1962.

(11) Colebourne, N.; Collinson, E.; Dainton, F. S. *Trans. Faraday Soc.* **1963**, *59*, 886.

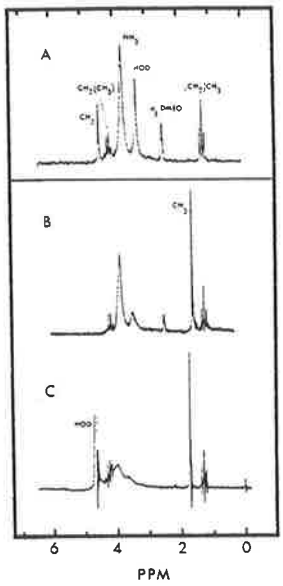

Figure 1. 100-MHz ^1H NMR spectra of $[Co(NH_3)_5(NCCH_2CO_2C_2H_5)]^{3+}$ in Me_2SO-d_6 solution (A) and of $[Co(NH_3)_5(NCC(CH_3)_2CO_2C_2H_5)]^{3+}$ in Me_2SO-d_6 solution (B) and in acidified D_2O solution (C) (sodium 4,4-dimethyl-4-silapentanesulfonate, internal reference, DSS).

fore use. All polymerizations were carried out in an all-glass vacuum line by using the following procedure. Dried and deaerated DMF (ca. 10 mL) was distilled into a 50-mL flask containing a magnetic stirrer bar and the desired complex (ca. 0.02 g). The monomer (ca. 2 mL) was then distilled into the flask, followed by pyridine (ca. 0.1 mL) if required. The flask was sealed off from the line; the contents were melted, mixed, and left for 48 h protected from the light. Subsequently, the solvent was removed and the resultant polymer recrystallized (twice) by dissolution in DMF and precipitation by the slow addition of water. The product was dried in vacuo for 3 days. The ^1H NMR spectra of samples of polymethacrylonitrile (PMAN) were measured by using a Varian HA-100 spectrometer and a 7% solution in CD_3NO_2 at 90 °C with hexamethyldisiloxane as an internal reference,[12] and trimethyl phosphate as an internal lock. The polystyrene–polymethyl methacrylate copolymer was not soluble in CD_3NO_2, and its ^1H NMR spectrum was measured in C_6D_6 solution (7%) by using a JEOL MH-100 spectrometer with tetramethylsilane as internal reference at 34 °C.

Results and Discussion

The pentaamminecobalt(III) complexes of three nitriles, malononitrile (NC–CH_2–CN), ethyl cyanoacetate (NC–CH_2–$CO_2C_2H_5$), and cyanoacetic acid (NC–CH_2–CO_2H), have been isolated and characterized analytically and spectrally. The IR spectra of the complexes all showed an absorption in the range 2315–2330 cm^{-1} attributed to the –C≡N stretching mode for the coordinated nitrile group.[4,13,14] In addition, coordinated malononitrile gave an absorption at 2260 cm^{-1}, appropriate to ν_{CN} for uncoordinated nitriles (ca. 2275 cm^{-1})[15] as did the $[(NH_3)_2CoOOCCH_2CN]^{2+}$ ion.

The ^1H NMR spectrum of $[Co(NH_3)_5(NCCH_2CO_2C_2H_5)]^{3+}$ in Me_2SO-d_6 is shown in Figure 1A. The complexes of malononitrile and cyanoacetic acid were found to have limited stability in Me_2SO, with the solvent replacing the nitrile in the coordination sphere over a period of hours at 20 °C. In all three cases, the ^1H NMR spectra measured in D^+/D_2O mixture indicated a rapid exchange of the methylene protons.

Acidified aqueous solutions of these complexes varied considerably in stability, the ethyl cyanoacetate complex being the most stable. Both the cyanoacetic acid and malononitrile complexes underwent an initial reaction, identified as hydrolysis of the coordinated nitrile group for $[Co(NH_3)_5(NCCH_2CN)]^{3+}$ (k_{obsd} = 9.6×10^{-5} s^{-1}; pH 3.0, μ = 1.0, 25 °C), followed by a slower substitution of the coordinated amide by water.

Table I. Base Hydrolysis of $[Co(NH_3)_5(N{\equiv}CCH{=}CH_2)]^{3+}$ [a]

$[OH^-]$	k_{obsd}, s^{-1}	$k_{OH} = k_{obsd}/[OH^-]$, M^{-1} s^{-1}
0.0010	3.49×10^{-2}	34.9
0.0025	8.49×10^{-2}	34.0
0.0050	1.67×10^{-1}	33.3
0.010	3.67×10^{-1}	36.7
0.010	3.70×10^{-1}	37.0
		$k_{OH}^{av} = 35.2$

[a] $[Co] = 6.70 \times 10^{-5}$ M; μ = 1.0 ($NaClO_4$); T = 25.0 °C; λ = 270 nm; all solutions deaerated.

The addition of base to solutions of the three yellow nitrile complexes resulted in the immediate formation of deep red solutions. These changed slowly to yellow solutions which differed spectrally from the initial nitrile species. The initial rapid reaction is reversible on adding acid and is attributed to the deprotonation of the acidic methylene protons. For uncoordinated malononitrile the pK_a of the methylene protons is 11.3.[16] On coordination, this value falls to 5.7 ± 0.1 (0.1 M pyridine/$HClO_4$ buffer, μ = 1.0 ($NaClO_4$), 25.0 °C). Similarly for ethyl cyanoacetate, the pK_a[16] is reduced on coordination from >9 to 7.58 (0.1 M "Tris"/$HClO_4$ buffer, μ = 1.0 ($NaClO_4$), 25.0 °C). The deprotonated complexes are presumably stabilized by extensive delocalization of the negative charge throughout the coordinated ligand. A consequence of this is the intense absorption which develops in the first ligand field band on deprotonation: the maximum molar absorptivity ϵ_{532} = 450 M^{-1} cm^{-1} for $[Co(NH_3)_5(NCCHCN)]^{2+}$ is to be compared with ϵ_{474} = 72 M^{-1} cm^{-1} for the protonated form. The former intensity is more consistent with a substantial contribution from ligand-to-metal charge transfer whereas the latter intensity is consistent with ligand field absorption and is typical in complexes of this type. A similar result was observed for the ethyl cyanoacetate complex where the deprotonated complex (ϵ_{527}^{max} = 550 M^{-1} cm^{-1}) absorbs much more strongly than the parent ion (ϵ_{465}^{max} = 64 M^{-1} cm^{-1}).

The subsequent decay of the deprotonated complex was unusually rapid for coordinated cyanoacetic acid and produced predominantly Co(II). For the other two complexes, the decay of the red solution was slower and gave both Co(II) and hydrolysis of the coordinated nitrile. Three interesting aspects arise from these properties: the mechanism of the base-hydrolysis process, the reactions of the coordinated carbanion, and the electron-transfer process from the deprotonated ligand resulting in the reduction of Co(III) to Co(II) and a ligand radical.

Base hydrolysis of coordinated nitrile in $[Co(NH_3)_5(NCR)]^{3+}$ ions has been attributed to direct attack of OH^- at the nitrile carbon atom.[4,6] For $[(NH_3)_5CoN{\equiv}CC_6H_5]^{3+}$, this seems the only feasible explanation[4] for the first-order dependence on $[OH^-]$. Although C-proton exchange occurs with coordinated CH_3CN faster than amide formation,[6] no exchange was observed on the aromatic ring of coordinated NCC_6H_5. Also, it does not seem likely that deprotonation of the ammine centers would lead to amide formation. The results for hydrolysis of $[Co(NH_3)_5NCCH{=}CH_2]^{3+}$ also support this proposal (Table I). The linear pseudo-first-order plots of log $(A_t - A_\infty)$ vs. time obtained over at least $3t_{1/2}$ demonstrate a first-order dependence of the rate on $[OH^-]$ for the production of coordinated acrylamide. Clearly OH^- adds at the nitrile carbon atom and not at the olefin β-carbon atom nor is there any proton exchange at the olefin moiety. Similar results are obtained in the presence of the CO_3^{2-} ion which also generates the acrylamide complex.

One striking feature of this study was the remarkable dependence of the base-hydrolysis rate on CO_3^{2-} concentration. The hydrolysis reaction was therefore studied at 25 °C by using carbonate/bicarbonate buffer mixtures, and the results are sum-

(12) Yamada, A.; Yanagita, M. *J. Polymer Sci., Part B* **1971**, *9*, 103.
(13) Foust, R. D.; Ford, P. C. *Inorg. Chem.* **1972**, *11*, 899.
(14) Clarke, R. E.; Ford, P. C. *Inorg. Chem.* **1970**, *9*, 227.
(15) Nakamoto, K. "Infrared Spectra of Inorganic and Coordination Compounds", 2nd ed.; Wiley-Interscience: New York, 1970; p 186.
(16) Pearson, R. G.; Dillon, R. L. *J. Am. Chem. Soc.* **1953**, *75*, 2439.

Table II. Catalysis of Base Hydrolysis of $[Co(NH_3)_5(N{\equiv}CCH{=}CH_2)]^{3+}$ by CO_3^{2-} [a]

pH	$10^3 k'_{OH}$, [b] s^{-1}	k_{obsd}, s^{-1}	$(k_{obsd} - k'_{OH})/[CO_3^{2-}]$, $M^{-1} s^{-1}$	$[carbonate]_T$, M	$[CO_3^{2-}]$, [c] M
9.64	2.59	2.78×10^{-2}	1.0	0.0455	0.0245
9.67	2.78	6.69×10^{-2}	1.0	0.1138	0.0634
9.59	2.31	7.85×10^{-2}	0.9	0.1667	0.0853
9.71	3.05	1.41×10^{-1}	1.0	0.2275	0.1319

[a] [Co] = 6.70×10^{-5} M; T = 25 °C; μ = 1.0 ($NaClO_4$); λ = 270 nm. [b] Assuming k_{OH} = 35.2 $M^{-1} s^{-1}$ (from Table I); pK_w = 13.77.[19] [c] Assuming pK_a = 9.57 for $HCO_3^- \rightleftarrows CO_3^{2-} + H^+$ at μ = 1.0.[19]

Table III. Hydrolysis of $[(NH_3)_5CoN{\equiv}CCH{=}CH_2](ClO_4)_3$ (0.12 M) with $Na_2C^{18}O_3$ (1 M) in $H_2{}^{16}O$ at 25 °C

reaction time, min	species	^{18}O label, [a] atom %	enrichment	% ^{18}O content in amide
1	CO_3^{2-}	1.4087	1.2071	
	amide [c]	1.1073	0.9057	75
5	CO_3^{2-}	1.4086	1.2070	
	amide	0.7402	0.5386	45
7	CO_3^{2-}	1.4088	1.2072	
	amide	0.5993	0.3977	33
	CO_3^{2-} [d]	1.3546	1.1530	95.5

[a] Obtained from the ion current ratios (R) using relationships atom % = $R/(2 + R)$. [b] Atom percent levels minus the normal $C^{18}O_2$ content 0.2016 atom %. [c] $[(NH_3)_5CoNHCOCH{=}CH_2]I_2$. [d] CO_2 from CO_3^{2-} in the reaction mixture.

Scheme I

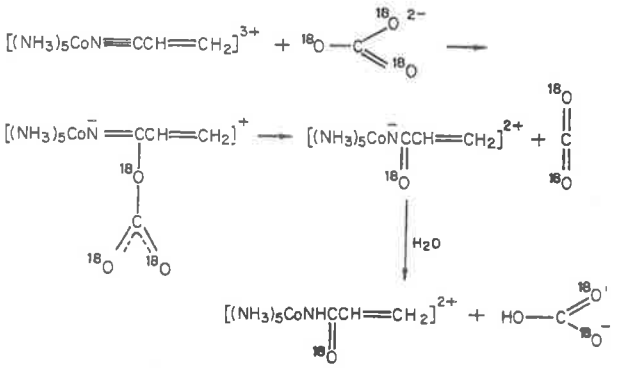

Scheme II

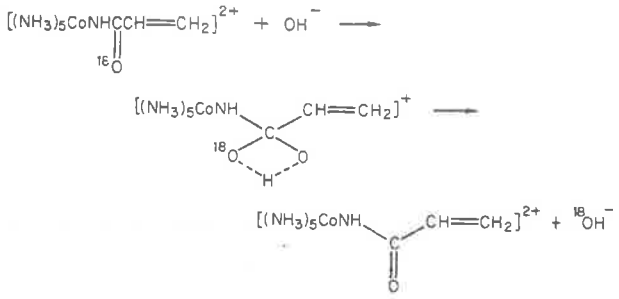

Table IV. Rates of Base Hydrolysis of $[Co(NH_3)_5NCCH_3](ClO_4)_3$ in 0.01 M NaOH [a]

temp, °C	k_{OH}, $M^{-1} s^{-1}$	temp, °C	k_{OH}, $M^{-1} s^{-1}$
15.2	0.945	35.3	8.15
24.1	2.36	40.0	12.6
30.8	4.62		

E_a = 18.8 ± 1.0 kcal mol^{-1}
$\Delta S^{\ddagger}$ = +4.4 cal deg^{-1} mol^{-1}

[a] [complex] = 2.5×10^{-4} M; λ = 250 nm; μ = 1.0 ($NaClO_4$).

marized in Table II. . The data obey the rate law $k_{obsd} = k_{OH^-}[OH^-] + k_c[CO_3^{2-}]$ with k_{OH} = 35 $M^{-1} s^{-1}$ and k_c = 1.0 $M^{-1} s^{-1}$: the carbonate ion being only a factor of 35 less efficient than OH^- in effecting hydrolysis. A question immediately arises concerning the mechanism of involvement of CO_3^{2-}. Is it by a nucleophilic mechanism or by a general-base process? The determination can be made by using ^{18}O tracer studies, since in the pH region for which the measurements shown in Table II are made, CO_3^{2-} exchanges slowly with the oxygen atoms in solvent water (for example, in 0.02 M Na_2CO_3, $t_{1/2}$ for exchange is ca. 28 h).[17] The tracer experiment was carried out by dissolving the complex in a solution of 1 M $Na_2C^{18}O_3$ of known enrichment in normal water. In different experiments, the amide product was precipitated after different intervals (1, 5, and 7 min) as the anhydrous iodide salt. (The rate constant for hydrolysis of $[Co(NH_3)_5(N{\equiv}CCH{=}CH_2)](ClO_4)_3$ in 0.25 M Na_2CO_3 is 0.28 s^{-1} at 25 °C, so hydrolysis was complete before the complex was precipitated.)

The results of the tracer experiment are given in Table III. Extrapolation of enrichment to the time required for completion of the hydrolysis process reveals that the initial product contains ca. 90% enrichment, indicating that CO_3^{2-} is involved in direct nucleophilic attack on the nitrile carbon atom, yielding an oxygen atom to the coordinated amide. The observed discrepancy from 100% enrichment in this experiment is due to concomitant hydrolysis of the nitrile by unlabeled OH^-.[18] The tracer experiments also show that the carbonate ion in the final reaction mixture is diluted in label by 4.5% compared with the expected dilution of 4.2%. The proposed mechanistic scheme for hydrolysis of coordinated acrylonitrile by CO_3^{2-} is shown (Scheme I).

Carbonate ion attacks the nitrile C atom, and either CO_2 is eliminated or a water molecule takes CO_2 off the complex as H_2CO_3. If the latter path obtained, it could be expected that this would also be a route to exchange of CO_3^{2-} oxygen atoms with solvent and that was not observed. A preference therefore exists for the path involving decarboxylation of the carbonate ester. Subsequently, protonation of the amide N generates the acrylamide complex.

A complicating feature in the reaction should be ion pairing between the parent 3^+ ion and the CO_3^{2-} anion. Analogous association constants[21] for $[Co(NH_3)_5OH_2]^{3+}$ and SO_4^{2-} are in the vicinity of $\sim 10^3$ M^{-1}. If this value holds for the present case, then all the parent complex should be ion paired and the rate law more properly formulated as $-d(CoNCR)/dt = k[(NH_3)_5CoN{\equiv}CR^{3+}{\cdot}CO_3^{2-}][Co_3^{2-}]$. A dependence of the rate of hydrolysis of coordinated nitriles on carbonate ion has been reported previously for Ru(III) and Rh(III) complexes,[20] although no direct tracer evidence was presented to distinguish between the nucleophilic and general-base mechanism. However, the involvement of CO_3^{2-} in the hydrolysis of uncoordinated nitriles does not appear to have been observed.

When these reactions were carried out for longer periods, a subsequent slower exchange process occurred with solvent water resulting in the loss of ^{18}O label from the coordinated amide (Table

(17) Mills, G. A., Urey, H. C. *J. Am. Chem. Soc.* **1939**, *61*, 534.

(18) A solution of 1 M Na_2CO_3 has a pH of ~11.8. With the assumption of pK_w = 14.17 for a solution of μ = 3.0 at 25 °C,[19] $[OH^-] = 4 \times 10^{-3}$ M. Consequently, under the conditions of the experiment, $k'_{OH} = k_{OH}[OH^-]$ = 0.14 s^{-1} and $k'_c = k_c[CO_3^{2-}]$ = 1.0 s^{-1} whence ~14% hydrolysis of the nitrile by unlabeled OH^- would be expected.

(19) *Spec. Publ.—Chem. Soc.* **1964**, *No. 17*.

(20) Zanella, A. W.; Ford, P. C. *Inorg. Chem.* **1975**, *14*, 42.

(21) Posey, F. A.; Taube, H. *J. Am. Chem. Soc.* **1956**, *78*, 15.

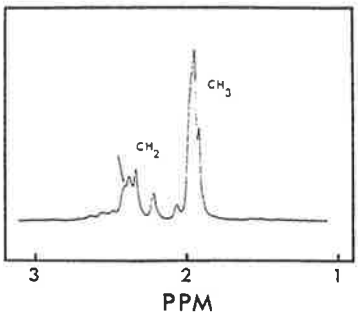

Figure 2. 100-MHz ^{1}H NMR spectrum of polymethacrylonitrile (7% in CD_3NO_2, 90 °C, hexamethyldisiloxane, internal standard).

III). In 1 M Na_2CO_3 solution, the concentrations of bicarbonate ion and carbon dioxide are low ($[HCO_3^-] \approx 6 \times 10^{-3}$ M; $[CO_2] \approx 6 \times 10^{-7}$ M)[22] so that it is unlikely that either of these species is involved in the exchange process. Neither does CO_3^{2-} lead to direct exchange, because its own exchange rate with the solvent[17] is much slower than the observed rate of amide exchange. Consequently, the most reasonable path for the loss of label from the amide would be by OH^- addition or general-base (CO_3^{2-}) catalyzed water addition, and a possible mechanism is presented in Scheme II although this exchange process has not been investigated in detail.

The base hydrolysis of $[Co(NH_3)_5(NCCH_3)]^{3+}$ has been studied at 25 °C and $\mu = 1.0$.[6] It was of interest to compare the activation parameters of the coordinated acetonitrile to those of the free ligand, and the rates were measured at five different temperatures (Table IV). From the data, the following activation parameters were calculated: $E_a = 18.8 \pm 1.0$ kcal/mol and $\Delta S^* = +4$ cal/(deg mol). The corresponding data for free acetonitrile[23] are $E_a = 19.1$ kcal/mol and $\Delta S^* = -23$ cal deg^{-1} mol^{-1}, showing that the difference in rate is reflected in the ΔS^* term while E_a is unchanged for the two reactions. Essentially the same results were observed for $[Co(NH_3)_5(NCC_6H_5)]^{3+}$ and free benzonitrile:[4] here, for the complex $E_a = 16.5$ kcal/mol and $\Delta S^* = +2.7$ cal deg^{-1} mol^{-1} compared with $E_a = 19.9$ kcal/mol and $\Delta S^* = -15.2$ cal deg^{-1} mol^{-1} for benzonitrile (in 50% acetone). The change in ΔS^* for the hydrolysis reactions from highly negative for the free nitriles to slightly positive for the coordinated nitriles may simply reflect the 3+ charge on the latter species.[24] However, it appears to be a characteristic of the coordinated ligand reactions, and there is as yet no clear correlation between charge neutralization and rate enhancement for reactions of this type.

The hydrolysis process was studied throughout the pH range 1–12 for the malononitrile complex. Continuous scans of the electronic spectra during these reactions indicated that the process was not simple. Some $[Co(NH_3)_5OH_2]^{3+}$ was detected in the reaction mixtures arising from a subsequent loss of the amide ligand. However, linear plots of log $(A_t - A_\infty)$ against time were observed for at least $3t_{1/2}$, indicating pseudo-first-order kinetics for the production of the amide and Co^{2+}. In 1 M $HClO_4$ 1% Co^{2+} was produced while the amount increased to 25% at $7 < pH < 10$. A reaction profile of the observed rate with pH for the malononitrile species is shown in Figure 2. The data and observations are consistent with Scheme III. The derived value for K (implying $pK_a \approx 5.3$) is consistent with the independently measured pK_a value of 5.7 ± 0.1 for the malononitrile complex.

The three paths are competitive but in the acid region nucleophilic attack of OH_2 at the nitrile C atom dominates the kinetics. Only ~1% Co^{2+} was produced under these conditions. However above the pK_a for coordinated malononitrile the reduction path is more dominant (25%). Presumably a unimolecular intramolecular electron transfer from the generated carbanion to the cobalt(III) ion accounts for this path ($k_{e^-} = 3.5 \times 10^{-4}$ s^{-1}). Concomitantly, the nitrile complex hydrolyzes to the amide. Either, H_2O could react with the protonated nitrile or OH^- could attack the nitrile C atom of the protonated ligand. We have argued the mechanism by the latter path primarily because it appears to be the effective route for the CH_3CN, C_6H_5CN, and $CH_2{=}CHCN$ ligands.

Scheme III

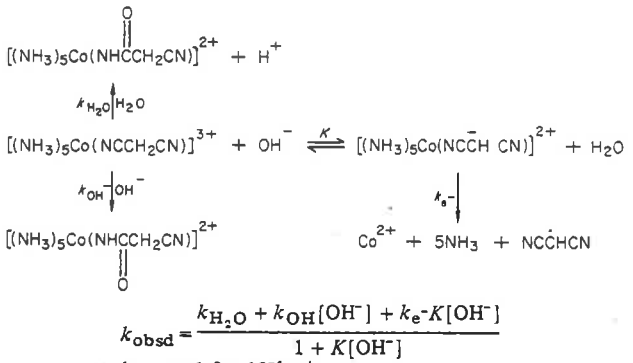

$$k_{obsd} = \frac{k_{H_2O} + k_{OH}[OH^-] + k_e\text{-}K[OH^-]}{1 + K[OH^-]}$$

$k_{H_2O} = 1.0 \times 10^{-4}$ s^{-1}
$k_{OH} = 5 \times 10^5$ M^{-1} s^{-1}
$k_{e^-} = 3.5 \times 10^{-4}$ s^{-1}
$K = 5.2 \times 10^8$ M^{-1}

The hydrolysis of coordinated malononitrile takes place under much milder conditions than the base hydrolysis of malononitrile to malonamide (NaOH/liquid NH_3 at 125 °C for 6 h).[25] Furthermore, the hydrolysis is specifically confined to one nitrile group.

Reactions of the Deprotonated Ligand. Malononitrile is a very reactive compound because of its acidic methylene group and two cyano functions and finds considerable use in industrial chemistry, particularly in the production of heterocyclic compounds.[26] The enhancement of acidity of these methylene protons on coordination means that the carbanion can be produced under milder conditions than those used for the uncoordinated case (NaH/Me_2SO or NaOEt/EtOH).[26]

For the complexes of malononitrile and ethyl cyanoacetate it was found that the addition of the substrates methyl iodide, acetone, formaldehyde, tosyl chloride, and methyl pyruvate to basified solutions (either in water or Me_2SO) led to a rapid decrease in the intensity of the color of the solution, indicating substitution at the methylene group. Bromine also rapidly reduced the color and produced $[(NH_3)_5CoNHCOCBr_2CO_2C_2H_5]^{2+}$. Bromination of the carbanion is clearly faster than hydrolysis, but the amide product is observed because the dibromo ester nitrile is very reactive and hydrolyzes as soon as it is formed. It is also worth noting that the dibromocyanoacetic ester complex hydrolyzes and decarboxylates in base to $[(NH_3)_5CoNHCOCHBr_2]^{2+}$.

For confirmation of the nucleophilic reaction of the stabilized carbanion, the product of the reaction of $[Co(NH_3)_5(NCCH_2CO_2C_2H_5)]^{3+}$ with excess MeI in Me_2SO (using imidazole as base) was isolated as $[Co(NH_3)_5(NCC(CH_3)_2CO_2C_2H_5)]^{3+}$. That the nitrile and ester moieties remained intact was shown by the IR spectrum. The ^{1}H NMR spectra in Me_2SO-d_6 (Figure 1B) and acidified D_2O (Figure 1C) indicated a single methyl resonance which integrated to give a 2:1 ratio with the CH_3 triplet of the ethyl ester group, thereby proving disubstitution. Experiments performed by using a deficiency of MeI showed only the disubstituted products, indicating that the second substitution reaction is more rapid than the first. The product also hydrolyzed in OH^- solutions with a similar rate constant (2.2 M^{-1} s^{-1} at 25 °C) to that of the acetonitrile complex ($k_{OH} = 3.40$ M^{-1} s^{-1}).[6] The products of the other reactions at the carbanion

(22) These values are calculated using the following equilibrium constants ($\mu = 3.0$, 25 °C):[19] $HCO_3^- \rightleftharpoons H^+ + CO_3^{2-}$, $pK_a = 9.56$; $CO_2 + CO_3^{2-} + H_2O \rightleftharpoons 2HCO_3^-$, log $K = 2.53$.

(23) Peskoff, N.; Meyer, J. *Z. Phys. Chem.* **1913**, *82*, 129.

(24) Wilkins, R. G. "The Study of Kinetics and Mechanism of Reactions of Transition Metal Complexes"; Allyn and Bacon: Boston, 1976; p 99.

(25) Takeda, K., Tokuyama, K. *Yakugaku Zasshi.* **1956**, *76*, 77; *Chem. Abstr.* **1956**, *50*, 13035.

(26) Freeman, F. *Chem. Rev.* **1969**, *69*, 591.

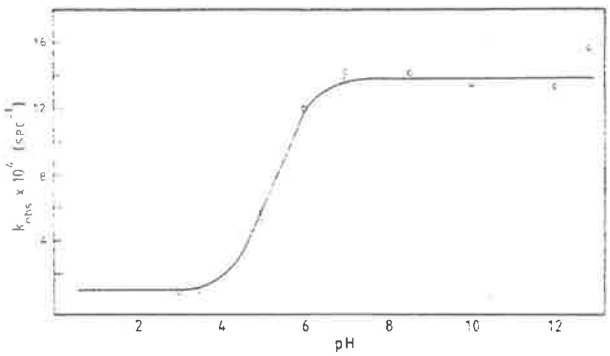

Figure 3. Reaction profile for pH dependence of observed pseudo-first-order rate constants for hydrolysis of $[Co(NH_3)_5(NCCH_2CN)]^{3+}$ (μ = 1.0 ($NaClO_4$); 25 °C).

were not isolated, but clearly the carbanion is very reactive toward these reagents and coordination of the nitrile allows the chemistry to be done in a regiospecific manner. The nitrile may be hydrolyzed without affecting the ester, and the carbanion may be alkylated without affecting the nitrile or the ester.

Polymerization Studies. Subsequent to deprotonation of the methylene proton in the $[Co(NH_3)_5(NCCH_2X)]^{3+}$ species, there is some reduction of the metal ion to Co(II) concomitant with the hydrolysis of the coordinated nitrile which increases in the order $X = CO_2C_2H_5 < CN < CO_2^-$. The reduction is enhanced at high pH. This reduction occurs by electron transfer to the metal from the delocalized carbanion and results in an organic radical, i.e.

$$(NH_3)_5Co^{3+}N{\equiv}CCH_2X \xrightarrow{OH^-} [(NH_3)_5CoN{\equiv}C\dot{C}HX]^{2+} \rightarrow$$
$$\text{“}(NH_3)_5Co^{2+}\text{”} + N{\equiv}C\dot{C}HX$$

Whether the radical remains bound to the Co(II) ion is not certain.

Such an electron transfer producing a radical organic species has been reported previously[27] for the $[Co(NH_3)_5(N{\equiv}CCH_2C_6H_5)]^{3+}$ ion, which even on dissolution in neutral H_2O yields the corresponding carbanion and then stilbene dinitrile $C_6H_5CH(CN)CH(CN)C_6H_5$ in >90% yield.

When acrylonitrile was added to the aqueous solution in which basification was carried out for the cyanoacetic acid complex, white polyacrylonitrile precipitated out. Such an observation is not new and has previously been used as evidence for free radicals in the elucidation of mechanisms of electron-transfer reactions.[28,29]

However it was decided to investigate the stereochemistry of the polymers produced by using the three complexes as initiators, because the varying lifetimes of their carbanions might lead to alternate forms of polymerization initiation.

In DMF solution, the three complexes were found to initiate the polymerization of acrylonitrile and methacrylonitrile whether or not base was added. ^1H NMR studies in CD_3NO_2 solutions of the polymethacrylonitrile (PMAN) samples obtained revealed the polymers to be identical regardless of the complex or the presence of base. Further, by comparison of these spectra with those obtained for conventional radical (azobis(isobutyronitrile), AIBN) and anionic (diethylmagnesium, $MgEt_2$) initiation of methacrylonitrile polymerization,[12] it was found that the polymers had some greater degree of isotacticity than anticipated for radical polymerization. Figure 3 shows the ^1H NMR spectrum of PMAN initiated by $[Co(NH_3)_5(NCCH_2CO_2C_2H_5)]^{3+}$, and the presence of the shoulder (arrowed) on the high-field side of the methylene signal indicates some isotacticity.[12]

A copolymerization of styrene and methyl methacrylate was thus undertaken to ascertain the mode of initiation. ^1H NMR studies of a polymer obtained by using $[Co(NH_3)_5(NCCH_2CO_2C_2H_5)]^{3+}$ as initiator revealed a 50/50 copolymer, consistent with a radical process (anionic initiation would have led to polymethyl methacrylate (PMMA) alone and cationic polymerization to polystyrene alone).[30,31] DMF is not an ideal solvent to initiate anionic polymerization (due to the availability of protons), and the carbanions generated from the complexes do not appear capable of transferring the charge to the monomers. However, the mildness of conditions for the radical polymerization and the ease of removal of the byproduct (Co^{II}) make these complexes potentially useful as radical initiators.

One interesting feature of the $[Co(NH_3)_5NCCH_2COOH]^{3+}$ ion is the prospect of inducing the radical path by varying the concentration of deprotonating base. The base concentration should govern the concentration of the carbanion produced, and thence the electron-transfer rate will control the production of radicals. Preliminary indications are that the radicals could be produced in a large burst at high base concentrations and relatively slowly over a long period at low base concentrations. In this way, the chain length of the polymer produced might be controlled.

Acknowledgment. We wish to thank the Microanalytical Service of the Australian National University and A. J. Herlt for assistance with the kinetics and equilibrium measurements.

(27) Creaser, I. I.; Sargeson, A. M. *J. Chem. Soc., Chem. Commun.* **1975**, 324. Butler, D. G.; Creaser, I. I.; Dyke, S. F.; Sargeson, A. M. *Acta Chem. Scand., Ser. A* **1978**, *A32*, 789.

(28) Collinson, E.; Dainton, F. S.; Mile, B., Tazuka, S.; Smith, D. R. *Nature (Washington, D.C.)* **1963**, *198*, 26.

(29) Kimura, K.; Sato, T. *Bull. Chem. Soc. Jpn.* **1973**, *46*, 471.

(30) Walling, C.; Briggs, E. R.; Cummings, W.; Mayo, F. R. *J. Am. Chem. Soc.* **1950**, *72*, 48.

(31) Szwarc, M. "Carbanions, Living Polymers and Electron Transfer Processes"; Interscience: New York, 1968.

[Reprinted from the Journal of the American Chemical Society, 96, 4981 (1974).]

Facile Intramolecular Hydrolysis of Dipeptides and Glycinamide

Sir:

The enzymic hydrolysis of glycinamides and peptide derivatives continues to be of considerable interest, and some debate on the source of activation remains.[1] Previously, we have demonstrated activations of 10^4–10^6 when such substrates are directly coordinated *via* the carbonyl oxygen to octahedral metal ions such as Co(III)[2] and where solvolytic hydrolysis is involved. We now report the metal ion promoted *intramolecular* hydrolysis of a simple peptide which can give rise to accelerations comparable with those observed enzymically.

Treatment of *cis*-$[Co(en)_2Br(glyglyOC_3H_7)](NO_3)_2$ with *ca.* 1 *M* HOCl at 0° for 10 min, followed by chromatography on Sephadex (SP C-25, 0.5 *M* $NaClO_4$, pH 8, 2°) resulted in the separation of a violet-red 2+ band

(1) W. P. Jencks, "Catalysis in Chemistry and Enzymology," McGraw-Hill, New York, N. Y., 1969, Chapter 5; B. L. Vallee and R. J. P. Williams, *Proc. Nat. Acad. Sci. U. S.*, **59**, 498 (1968).

(2) (a) D. A. Buckingham, C. E. Davis, D. M. Foster, and A. M. Sargeson, *J. Amer. Chem. Soc.*, **92**, 5571 (1970); (b) D. A. Buckingham, J. MacB. Harrowfield, and A. M. Sargeson, *J. Amer. Chem. Soc.*, **96**, 1726 (1974).

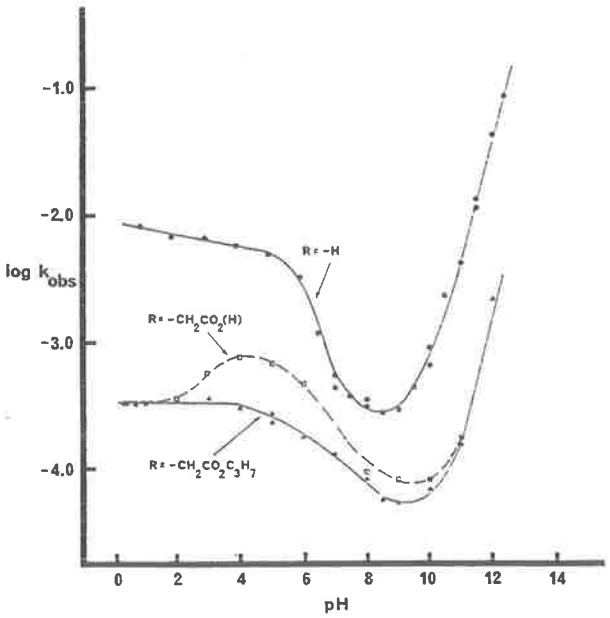

Figure 1. Plot of log k_{obsd} *vs.* pH for the intramolecular reaction of *cis*-$[Co(en)_2(NH_2CH_2CONHR)(OH)]^{2+}$ ions in the absence of buffers, 25°, μ = 1.0 *M* $NaClO_4$.

and an orange 3+ band. The 3+ species was identified as the N–O chelated dipeptide, $[Co(en)_2(glyglyOC_3H_7)]^{3+}$, by its physical properties (3+ ion; ϵ_{485} 97, pmr spectrum) and the rate and rate law

$$k_{obsd} = \frac{a[OH^-]}{b + [OH^-]} = \frac{7.5 \times 10^{-4}[OH^-]}{2.5 \times 10^{-4} + [OH^-]}$$

at 25°, (μ = 1.0 *M* $NaClO_4$), for its hydrolysis to $[Co(en)_2(glyO)]^{2+}$.[2a] The 2+ band (ϵ_{498} 103) has similar spectral properties to other *cis*-$[Co(en)_2OH(amine)]^{2+}$ ions[3,4] and has a pK_b of 7.74 (μ = 1.0 *M* $NaClO_4$). It hydrolyzes in the pH range 0–12 (pH stat) forming $[Co(en)_2(glyO)]^{2+}$ and $[Co(en)_2(glyglyOC_3H_7)]^{3+}$ (isolated by ion exchange chromatography) according to the rate law

$$k_{obsd} = k_{OH_2} + k_{OH} + k'_{OH}[OH^-]$$

(k_{OH_2} = 3.4 × 10^{-4} sec^{-1} (aquo complex), k_{OH} = 5.3 × 10^{-4} sec^{-1} (hydroxo), k'_{OH} = 0.10 M^{-1} sec^{-1} (hydroxo), μ = 1.0 *M* $NaClO_4$, 25°). The adjacent *cis* configuration of the hydroxo and dipeptide functions was established using optically pure $(+)_{589}$-*cis*-$[Co(en)_2Br(glyglyOC_3H_7)](NO_3)_2$ ($[M]_{440}$ = −1580°) which afforded $(+)_{589}$-*cis*-$[Co(en)_2(OH)(glyglyOC_3H_7)]^{2+}$ from whence optically pure $[Co(en)_2(glyO)]^{2+}$ ($[M]_{546}$ = +3400°) and $[Co(en)_2(glyglyOC_3H_7)]^{3+}$ ($[M]_{546}$ = +3270°) were obtained at pH 1. The $(+)_{589}$-*cis*-$[Co(en)_2(OH)(glyNHR)]^{2+}$ species (R = H, $CH_2CO_2^-$, $CH_2CO_2C_3H_7$) were also prepared by controlled treatment of $(+)_{589}$-*cis*-$[Co(en)_2X(glyNHR)](ClO_4)_2$ (X = Cl, Br) with alkali (pH 9–10) and chromatographic separation at 2° from $[Co(en)_2(glyNHR)]^{3+}$. However, by this method some racemic cis and trans hydroxo amide products are also formed.

Other *cis*-$[Co(en)_2(OH)(glyNHR)]^{2+}$ species (R = H, $CH_2CO_2^-$) formed in a similar manner behave similarly.

(3) F. Basolo, *J. Amer. Chem. Soc.*, 72, 4393 (1950).
(4) R. W. Hay and P. L. Cropp, *J. Chem. Soc. A*, 42 (1969).

Figure 1 gives the rate constants for the hydrolysis reactions as a function of pH (pH stat) and Table I

Table I. Product Distributions[a] for the Intramolecular Hydrolysis of *cis*-$[Co(en)_2(OH/OH_2)(glyNHR)]^{2+/3+}$ Expressed as the Ratio $[Co(en)_2(glyO)]^{2+}/[Co(en)_2(glyNHR)]^{3+}$

R	pH 1	pH 4	pH 8
H	100/0	100/0	100/0
CH_2CO_2H[b]	40/60		
$CH_2CO_2^-$[c]		77/23	76/24
$CH_2CO_2C_3H_7$[d]	46/54	44/56	45/55

[a] pH stat data in the absence of buffers. [b] pK_a = 2.9 (carboxylic acid residue). [c] pK_a = 6.3 (aquo ligand). [d] pK_a = 6.0 (aquo ligand); pK_w = 13.77 (μ = 1.0 *M* $NaClO_4$), 25°.

gives the product distributions. Above pH 9 hydrolysis of the chelated $[Co(en)_2(glyNHR)]^{3+}$ product proceeds more rapidly than does the intramolecular reaction, preventing analysis of the immediate reaction products under these conditions.

Although the cis hydroxo and aquo amide complexes are characterized here for the first time, a previous ^{18}O tracer experiment had supported their existence in one case (R = H) with subsequent hydrolysis occurring with retention of the Co–O bond.[5] The similarity in rate laws for all the hydrolyses, their rapidity, and the direct appearance of $[Co(en)_2(glyO)]^{2+}$ in the products, particularly in acid solution, is compelling evidence that they all involve the intramolecular attack of coordinated hydroxide, or water, at the adjacent carbonyl center.

Although hydrolysis is fast ($^+NH_3CH_2CONHCH_2CO_2^- + OH^-$, k = 8 × 10^{13} sec^{-1} [6]; $[Co(en)_2(NH_2CH_2CONHCH_2CO_2)(OH)]^+$, k = 2 × 10^{-4} sec^{-1}, both at pH 7), it is accelerated further by added bases. For example, in the presence of phosphate, the rate law modifies to

$$k_{obsd} = k_{OH_2} + k_{OH} + k'[OH] + k_1[H_2PO_4^-] + k_2[HPO_4^{2-}] + k_3[PO_4^{3-}]$$

over the pH range 1–12 (k_1 = 5 × 10^{-4} M^{-1} sec^{-1}, k_2 = 0.07 M^{-1} sec^{-1}, k_3 = 0.07 M^{-1} sec^{-1} for *cis*-$[Co(en)_2OH(glyglyOC_3H_7)]^{2+}$) giving k_{obsd} = 5.5 × 10^{-3} sec^{-1} at pH 7 in 0.1 *M* phosphate (μ = 1.0 *M* $NaClO_4$, 25°). This represents an acceleration of 10^{10} over the uncatalyzed hydrolysis of glycylglycine[6] and compares favorably with the Zn^{2+}–carboxypeptidase A catalyzed hydrolysis of benzoylglycyl-L-phenylalanine (V_0 = 1.2 × 10^{-6} *M* sec^{-1} at [substrate] > 10^{-2} *M*, [ZnCPA] = 10^{-8} *M*, pH 7.5, 25°)[7] and with *N*-acetyl-L-phenylalanineamide as a substrate for α-chrymotrypsin (k_{cat} = 2 × 10^{-2} sec^{-1}, pH 7, 25°).[8] The present experiments demonstrate that specific conformational effects,[1] unusual coordination geometries or active site distortions of the amide bond,[1] are not necessary to produce rapid hydrolysis. *When correctly positioned a coordinated water molecule or*

(5) D. A. Buckingham, D. M. Foster, and A. M. Sargeson, *J. Amer. Chem. Soc.*, 92, 6151 (1970).
(6) M. M. Jones, T. J. Crook, and S. Brammer, *J. Inorg. Nucl. Chem.*, 28, 1265 (1962).
(7) R. C. Davies, J. F. Riordan, D. S. Auld, and B. L. Vallee, *Biochemistry*, 7, 1090 (1968).
(8) M. L. Bender, G. E. Clement, F. J. Kézdy, and H. D'A. Heck, *J. Amer. Chem. Soc.*, 86, 3680 (1964).

Scheme I

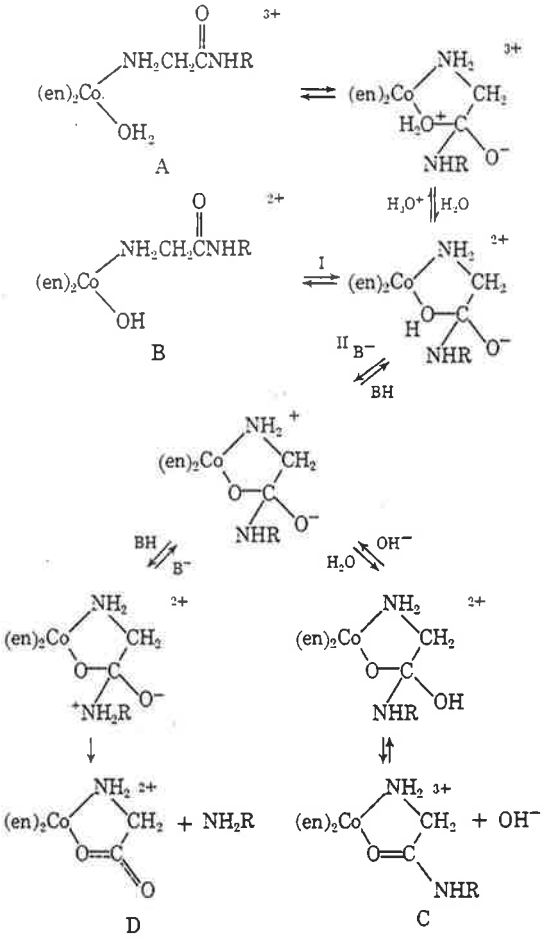

hydroxide ion can be a potent nucleophile for a carbonyl substrate even though the metal significantly reduces their basicity (~10^9 for OH^-).

The interrelation of the intramolecular hydrolysis of *cis*-$[Co(en)_2OH(glyNHR)]^{2+}$ and the intermolecular hydrolysis of $[Co(en)_2(glyNHR)]^{3+}$ by OH^-[2] is supported by the fact that the former reaction produces $[Co(en)_2(glyNHR)]^{3+}$ as well as the hydrolyzed product. A common intermediate, or set of intermediates, appears to be required. The observation of a similar Co(III) aminocarbinol intermediate which divides to chelated ester and chelated amide in the aminolysis of an amino acid ester[9] supports this claim. Amine loss follows the order $NH_3 > NH_2CH_2CO_2^- > NH_2CH_2CO_2C_3H_7$ (Table I), the order of decreasing basicity, and supports the contention that the amine leaving group is protonated. The same product ratio is found with both the aquo and hydroxo reactants in the absence of added buffer (Table I, pH 4 and 8) which supports the involvement of a single common intermediate leading to products. Also, for the hydrolysis of *cis*-$[Co(en)_2OH(glyglyOC_3H_7)]^{2+}$ in 0.1 *M* phosphate buffer at pH 7.4, 87% of $[Co(en)_2glyO]^{2+}$ is formed, compared with 45% at the same pH in the absence of buffer. This is consistent with general acid catalysis for the loss of amine and its relative absence for loss of OH. These observations are accommodated in the mechanism shown in Scheme I.

It is proposed that the rate determining step for the intramolecular hydrolysis occurs in the proton abstraction step, II. This may be concerted accompanying I, but, since most of the bases used have pK_a's outside the range spanned by the substrate hydroxo ($pK_a \sim 20$ est) and the immediate addition product ($pK_a \sim 6$ est), we contend that a stepwise process will be preferred by all but very strong bases.[10] For bases of $pK_a > 6$ proton abstraction II becomes diffusion controlled, $k = 10^9$–10^{10}[B] sec^{-1}, with every contact leading to deprotonation. Thus, HPO_4^{2-}, PO_4^{3-}, and OH^- are equally effective ($k_{obsd}/[B] \simeq 0.1\ M^{-1}\ sec^{-1}$, Brønsted $\beta = 0$) whereas for maleate, succinate, acetate, tartrate, and furoate the second-order rate constant decreases linearly with decreasing pK_a, $\beta = 0.75$. Reprotonation by BH is unfavorable and the chelated amide C hydrolyzes to D with no B being formed. This latter reaction is not general base or acid catalyzed consistent with intermolecular attack of OH^- being rate determining.

We are at present extending these mechanistic aspects and are continuing our study of the source of the large activation.

(9) D. A. Buckingham, J. Dekkers, and A. M. Sargeson, *J. Amer. Chem. Soc.*, 95, 4173 (1973).

(10) W. P. Jencks, *J. Amer. Chem. Soc.*, 94, 4731 (1972).

D. A. Buckingham,* F. R. Keene, A. M. Sargeson
Research School of Chemistry, Australian National University
Canberra, A.C.T. 2600, Australia
Received May 21, 1974

[Reprinted from Inorganic Chemistry, 18, 28 (1979).]

Contribution from the Research School of Chemistry,
Australian National University, Canberra, A.C.T., Australia 2600

Intramolecular Hydrolysis of Glycinamide and Glycine Dipeptides Coordinated to Cobalt(III). 1. Hg^{2+}, HOCl, and Base Hydrolysis of *cis*-$[Co(en)_2Br(glyNHR)]^{2+}$ (R = H, $CH_2CO_2C_3H_7$, $CH_2CO_2^-$) and Properties of *cis*- and *trans*-$[Co(en)_2(OH_2/OH)(glyNHR)]^{3+/2+}$ Ions

C. J. BOREHAM, D. A. BUCKINGHAM,* and F. R. KEENE

Received July 20, 1978

The Hg^{2+}-catalyzed removal of Br^- from *cis*-$[Co(en)_2Br(glyNHR)]^{2+}$ results in the immediate formation of $[Co(en)_2(glyNHR)]^{3+}$ containing the chelated amide or dipeptide residue; full retention of configuration about the Co(III) center obtains and no intermediate aqua complex is formed. HOCl-catalyzed oxidation of *cis*-$[Co(en)_2Br(glyglyOC_3H_7)]^{2+}$ results in the formation of some *cis*-$[Co(en)_2(OH_2)(glyglyOC_3H_7)]^{3+}$ as well as $[Co(en)_2(glyglyOC_3H_7)]^{3+}$, both with full retention of the configuration about the metal. Base hydrolysis (pH 9–14) results in the formation of some *trans*-$[Co(en)_2(OH)(glyNHR)]^{2+}$ (~6.2%) as well as *cis*-$[Co(en)_2(OH)(glyNHR)]^{2+}$ (R = H, 34% D, 20% DL; R = $CH_2CO_2C_3H_7$, 44% D, 19% DL; R = $CH_2CO_2^-$, 70% D + DL + trans) and $[Co(en)_2(glyNHR)]^{3+}$ (R = H, 20% D, 20% DL; R = $CH_2CO_2C_3H_7$, 20% D, 10% DL; R = $CH_2CO_2^-$, 30% D + DL). The *trans*-$[CO(en)_2(OH_2/OH)(glyNHR)]^{3+/2+}$ ions cyclize to $[Co(en)_2(glyNHR)]^{3+}$ according to the rate expression $R = k_{H_2O}[[Co(en)_2(OH_2)(glyNHR)]^{3+}] + (k_{OH} + k'_{OH}[OH^-])\cdot[[Co(en)_2(OH)(glyNHR)]^{2+}]$ where $k_{H_2O} = 4\ (\pm 2) \times 10^{-6}\ s^{-1}$, $k_{OH} = 2.8\ (\pm 0.1) \times 10^{-4}\ s^{-1}$, and $k'_{OH} = 5.6 \times 10^{-2}\ M^{-1}\ s^{-1}$ for R = H at 25 °C and μ = 1.0 ($NaClO_4$); this process occurs directly and not via the monodentate cis-aqua or -hydroxo ions. The *cis*-$[Co(en)_2(OH)(glyNHR)]^{2+}$ ions cyclize to $[Co(en)_2(glyO)]^{2+}$ and $[Co(en)_2(glyNHR)]^{3+}$ via a mechanism involving retention of the coordinated hydroxo oxygen atom. In acid solution the *cis*-$[Co(en)_2(OH_2)(glyNHR)]^{3+}$ ion also forms $[Co(en)_2(glyO)]^{2+}$ and $[Co(en)_2(glyNHR)]^{3+}$, but only the former retains the oxygen atom of the coordinated water molecule.

Metal ions and metal complexes have been found to accelerate the hydrolysis of esters, amides, and peptides[1] and the hydration of CO_2 and similar substrates[2] and nitriles,[3-5] and to various degrees these studies have been said to mimic the role played by metal ions in metallo enzymes. In these studies kinetically robust metal ion systems, principally those of cobalt(III), have been used to differentiate between the direct polarization mechanism represented by Scheme I and the alternate "metal–hydroxide" mechanism, Scheme II[6] (the solid oxygen atoms indicate the fate of the hydroxyl function in the product). These experiments showed that whereas Scheme I provides rate enhancements of 10^4–10^6 for all substrates independent of the leaving group,[7-12] Scheme II is effective only with the more reactive species (CO_2, anhydrides, aldehydes, and esters with good leaving groups).[6] Thus the hydrolysis of amino acid esters, amides, and simple peptides has not been observed in a bimolecular "metal–hydroxide" process. Furthermore, in the direct polarization mechanism, the rate enhancement is due entirely to entropy factors, whereas both $\Delta H^\ddagger$ and $\Delta S^\ddagger$ contribute to the latter. Also, whereas Scheme I promotes nucleophilic attack by species other than OH^- (NH_2R, ROH, H_2O),[13,14] only hydrolysis is observed with metal hydroxides,[2] and in particular general acid or general base catalysis has not been observed.

The intramolecular counterpart of Scheme II, as given by Scheme III for the hydration of aminoacetonitrile, has been observed for amino acid esters,[15,16] amides,[17] and nitriles[5,18] where five- and six-membered chelate rings result. For aminoacetonitrile, a rate enhancement of $\sim 10^{11}$ occurs at pH 7,[5,18] and this is to be compared with an acceleration of 10^6 for the Scheme I counterpart.[4] $\Delta H^\ddagger$ factors now become of great significance, and it seems that the large positive $\Delta S^\ddagger$ change found in Scheme I, and presumably arising from desolvation of solvent OH^- in the transition state, is now apparent in the metal–hydroxo reactant.[5,18]

For the amino acid ester[15,16] and amide[17] species, however, the intramolecular hydrolysis reaction has not been observed directly; it was required to occur from results of ^{18}O-tracer

*To whom correspondence should be addressed at the Department of Chemistry, University of Otago, Dunedin, New Zealand.

Scheme I

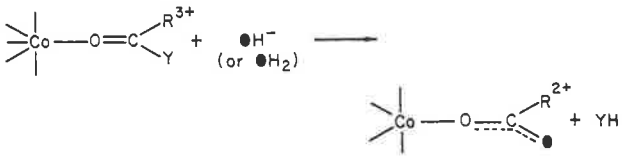

Scheme II

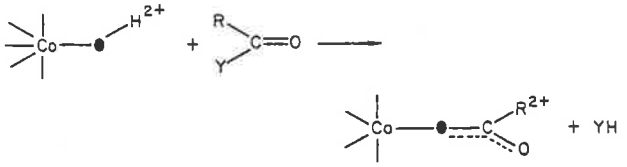

Scheme III

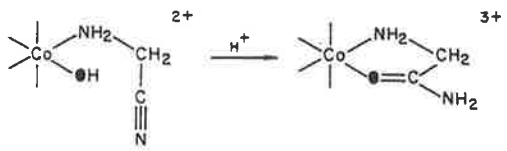

studies.[15-17] It has now been possible to isolate the cis-hydroxo and cis-aqua complexes containing glycinamide, glycylglycine, and isopropyl glycylglycinate and to study their subsequent cyclization over the pH range 0–14. This is the first time that metal-facilitated intramolecular hydrolysis of simple amides has been observed in the absence of other equilibrium processes, and the rate profiles as a function of pH, catalysis by buffers, and other mechanistic aspects are of some general significance.

In this paper we give the methods used to obtain the *cis*- and *trans*-$[Co(en)_2(OH_2/OH)(glyNHR)]^{3+/2+}$ ions (R = H, $CH_2CO_2C_3H_7$, $CH_2CO_2^-$), describe in detail the stereochemistry of these reactions, and look at the rates and products of the subsequent reactions of the trans species. A subsequent paper will consider in detail the kinetic and mechanistic aspects

of the reactions of the cis ions.[23]

Experimental Section

AnalaR reagents were used throughout without further purification. Glycylglycine (Sigma), silver perchlorate and thionyl chloride (BDH), methanol, and 2-propanol (AR) were used following recrystallization and distillation, respectively. $NaClO_4 \cdot H_2O$ (Fluka) was used as supporting electrolyte in the kinetic studies.

Electronic spectra were recorded using Cary 14 or Cary 118C spectrophotometers. ^1H NMR spectra were obtained on Varian HA-100 or JEOLCO Minimar MH-100 spectrometers using 0.1–0.3 M solutions in deuterated solvents (D_2O, Me_2SO-d_6) with NaTPS or Me_4Si as reference.

Cobalt determinations were carried out using Varian-Techtron AA-4 and AA-1000 spectrometers. Optical rotations (α_λ) were measured at 25 °C using a Perkin-Elmer P22 spectropolarimeter and in a 1-dm cell. Determinations of pH were made using a Radiometer PHM26C pH meter fitted with a G202B glass electrode and a calomel electrode protected with a NH_4NO_3 (1.6 M)/$NaNO_3$ (0.2 M) salt bridge. The meter was calibrated with 0.05 M potassium hydrogen phthalate (pH 4.01 (25 °C), 4.03 (37 °C)) or 0.01 M borax (pH 9.18 (25 °C), 9.09 (37 °C)). pH stat titrations were carried out using the above pH equipment in conjunction with a TAA_3 electrode assembly, ABU 12 and ABU 1c autoburets (2.5-mL capacity), a TT.11b titrator, and a SBR_2 titragraph. Rates of reaction were determined spectrophotometrically using a Cary 16K spectrophorometer fitted with a locally constructed thermostated cell (3.2-cm path length, 30 mL of solution) into which was inserted the electrode assembly. The titrant (1.0 or 0.1 M NaOH or $HClO_4$) was added under a nitrogen atmosphere to the magnetically stirred solution. Product separations were carried out using either BioRad Analytical Dowex 50W-X2 (200–400 mesh) or SP-Sephadex C-25 cation-exchange resins following dilution of the neutralized (pH ~4) solutions; eluents were 1–2 M HCl or 0.1–0.5 M $NaClO_4$, respectively.

Preparation of Ligands and Complexes. Methyl glycylglycinate hydrochloride was prepared by adding $SOCl_2$ (30.8 mL) dropwise to ice-cold MeOH (AR, 1.25 L) followed by glycylglycine (52.8 g). After 2-h reflux the solution volume was reduced to ca. 200 mL, and the product was crystallized by adding ether and cooling in ice. The filtered product was washed with ether and air-dried (yield 70 g (96%)). Recrystallization was effected from MeOH/ether. Anal. Calcd for $C_5H_{10}N_2O_3 \cdot HCl$: C, 32.9; H, 6.07; N, 15.3; Cl, 19.4. Found: C, 32.7; H, 6.1; N, 15.2; Cl, 19.2.

Isopropyl glycylglycinate hydrochloride was similarly prepared using $SOCl_2$ (30.8 mL), glycylglycine (52.8 g), and 2-propanol (AR, 2 L). The hot solution was filtered, cooled in ice, and the product washed with ether and air-dried (yield, 70 g (83%)). It was recrystallized from refluxing 2-propanol (90% recovery). Anal. Calcd for $C_7H_{14}N_2O_3 \cdot HCl$: C, 39.9; H, 7.18; N, 13.3; Cl, 16.8. Found: C, 40.2; H, 7.3; N, 13.6; Cl, 17.0.

$[Co(en)_2CO_3]Cl$ and *trans*-$[Co(en)_2Br_2]Br$ were prepared by the published procedures.[20,21] It was shown to be essential to convert the former to the bromide salt before making the latter complex. This was most simply done by dissolution in warm water, adding solid NaBr slowly with scratching, and finally cooling in ice. The $[Co(en)_2CO_3]Br$ was washed with MeOH and air-dried.

cis-$[Co(en)_2Br(glyNH_2)]Br_2 \cdot H_2O$ was prepared by a modification of the published method.[22] *trans*-$[Co(en)_2Br_2]Br$ (83.8 g), glycinamide hydrobromide (32 g), and $CoBr_2 \cdot 6H_2O$ (1 g) were ground to a fine paste with water (30 mL), and a solution of triethylamine (20.4 g) in MeOH (40 mL) added dropwise over 30 min with continuous mixing. Additional H_2O (60 mL in all) was added when required to keep the paste workable, and grinding was continued for a further 30 min. This mixture was dissolved in hot water (600 mL) containing glacial HOAc (5 mL) and filtered, and NaBr was added to the filtrate as it cooled until crystallization began. Following cooling in ice and filtering, the product was washed with MeOH and air-dried (yield 90 g (88%)). It was found necessary to remove a small amount of a highly charged species from the product by ion-exchange chromatography on Dowex 50W-X2 cation-exchange resin (H^+ form). The major purple 2+ band was eluted with 2 M HBr and the eluate volume reduced on a rotary evaporator until crystallization commenced. After the mixture was cooled in ice, recovered $[Co(en)_2Br(glyNH_2)]Br_2$ was recrystallized from hot water (pH ≃5) by addition of NaBr and cooling. The final product was washed on a glass filter with ice-cold MeOH and acetone and air-dried. Anal. Calcd for $[Co(en)_2Br(glyNH_2)]Br_2 \cdot H_2O$: C, 14.6; H, 4.5; N, 17.1. Found: C, 15.1; H, 4.7; N, 17.3. The product was chromatographically pure.

cis-$[Co(en)_2Br(glyglyOCH_3)]Br_2 \cdot 2H_2O$ and *cis*-$[Co(en)_2Br(glyglyC_3H_7)]Br_2 \cdot H_2O$ were prepared in a similar fashion, and it was found unnecessary to purify the products by ion-exchange chromatography.

To prepare *cis*-$[Co(en)_2Br(glyglyOCH_3)]Br_2 \cdot 2H_2O$, $glyglyOCH_3 \cdot HCl$ (36.6 g) dissolved in MeOH (AR, 400 mL) containing triethylamine (20.2 g) was added to *trans*-$[Co(en)_2Br_2]Br$ (83.4 g, 4 mL H_2O). After 4 h of standing, the product was washed with ethanol on a glass filter and recrystallized from hot 0.2 M HBr (130 mL): yield 92 g (75%); ϵ_{542} 82; ^1H NMR (CH_3) 3.66 ppm. Anal. Calcd for $[Co(en)_2Br(glyglyOCH_3)]Br_2 \cdot 2H_2O$: C, 18.0; H, 5.0; N, 14.0. Found: C, 18.1; H, 5.4; N, 14.0.

To prepare *cis*-$[Co(en)_2Br(glyglyOC_3H_7)]Br_2 \cdot H_2O$, *trans*-$[Co(en)_2Br_2]Br$ (83.8 g) and $glyglyOC_3H_7 \cdot HCl$ (42.2 g) were intimately mixed to a fine paste with H_2O (6 mL) and MeOH (AR, 60 mL), and triethylamine (20.4 g) was added dropwise over 1 h. The crude product was recovered after a further 1 h (93 g, 76%) and recrystallized twice from warm 0.2 M HBr: yield 33 g (27%); ϵ_{541} 82; ^1H NMR (C_3H_7) 1.14 (doublet) ppm. Anal. Calcd for $[Co(en)_2Br(glyglyOC_3H_7)]Br_2 \cdot H_2O$: C, 21.6; H, 5.28; N, 13.7; Br, 39.2. Found: C, 21.6; H, 5.5; N, 13.6; Br, 39.2.

cis-$[Co(en)_2Br(glyglyOH)]Br_2 \cdot 2H_2O$ was prepared from the methyl ester complex (24 g) by dissolution in water (250 mL) and addition of 48% aqueous HBr (250 mL). After overnight hydrolysis, the solution was cooled in ice and the crystalline product removed. Ethanol and acetone washing gave 16 g (68%) of the crude dipeptide acid complex. This was recrystallized from hot 0.1 M HBr (120 mL), and ^1H NMR spectra confirmed the absence of the methyl signal. Anal. Calcd for $[Co(en)_2Br(glyglyOH)]Br_2 \cdot 2H_2O$: C, 16.4; H, 4.8; N, 14.3; Br, 40.8. Found: C, 16.6; H, 5.1; N, 14.0; Br, 40.8.

Resolution of *cis*-$[Co(en)_2Br(glyglyOC_3H_7)]Br_2 \cdot H_2O$ and *cis*-$[Co(en)_2Br(glyNH_2)]Br_2$. Silver $(+)_{589}$-camphor-10-sulfonate (Ag-$(+)_{589}$-CS) was prepared by mixing equimolar quantities of $AgClO_4$ and $(+)_{589}$-camphor-10-sulfonic acid in acetone from which the product crystallized. It was washed with a little ether, air-dried, and stored in a brown bottle in the dark. To *cis*-$[Co(en)_2Br(glyglyOC_3H_7)]Br_2 \cdot H_2O$ (12.2 g) in MeOH (100 mL) was added Ag-$(+)_{589}$-CS (13.6 g) and the mixture stirred at ambient temperature for 1 h. The fine precipitate of AgBr was removed by centrifugation and the solution reduced to dryness. To the residue dissolved in MeOH (20 mL) was added acetone (500 mL), and from this solution $(+)_{589}$-$[Co(en)_2Br(glyglyOC_3H_7)]((+)_{589}\text{-CS})_2$ crystallized on scratching and cooling in an ice bath. The diastereoisomer was recovered, washed with acetone and ether, and air-dried (5.9 g). It was then recrystallized three times from MeOH/acetone to constant rotation: yield 4.6 g; $[\alpha]_{589} = +81°$, $[\alpha]_{440} = -116°$. Anal. Calcd for $CoC_{31}H_{62}N_6O_{11}S_2$: C, 41.6; H, 7.0; N, 9.4. Found: C, 41.5; H, 6.9; N, 9.7. This slightly hygroscopic diastereoisomer was stored in an evacuated desiccator. To recover the optically active cation the $(+)_{589}$-CS^- anion was removed by passing an aqueous solution down DEAE-Sephadex A-25 anion-exchange resin (NO_3^- or Br^- form). The resulting solution had $[M]_{589} = +820°$, $[M]_{440} = -1870°$ whence $[\alpha]_{589} = +134°$, $[\alpha]_{440} = -306°$ for the bromide salt monohydrate. Further impure diastereoisomer fractions were obtained from the original filtrate giving finally $(-)_{589}$-$[Co(en)_2Br(glyglyOC_3H_7)]((+)_{589}\text{-CS})_2$. However, these products were found to be contaminated with the optically active dipeptide chelate complex and were not used further.

cis-$[Co(en)_2Br(glyNH_2)]^{2+}$ was resolved as previously described[17] using ammonium $(+)_{589}$-bromocamphorsulfonate giving $(+)_{589}$- and $(-)_{589}$-$[Co(en)_2Br(glyNH_2)]Br_2$, $[\alpha]_{589} = +118, -116°$, respectively.

HOCl-Induced Hydrolysis of *cis*-$[Co(en)_2Br(glyglyOC_3H_7)]Br_2$. A ~1 M HOCl solution was prepared by saturating an ice-cold 1 M $AgClO_4$ solution with Cl_2, filtering, adding 1 M $AgClO_4$ dropwise until in slight excess, and refiltering. *cis*-$[Co(en)_2Br(glyglyOC_3H_7)]Br_2$ (ca. 0.5 g) was dissolved in the minimum volume of H_2O (~1 mL) and converted to the nitrate using DEAE-Sephadex A-25 resin (NO_3^- form). The resulting solution was concentrated to near dryness on a rotary evaporator and cooled to ca. 0 °C, the 1 M HOCl solution added (20 mL, 0 °C), and the mixture shaken periodically over 10 min at 0 °C. The pH was then adjusted to 8 (1 M NaOH), the solution was diluted with ice-water (ca. 1 L), and the complexes were sorbed onto and then eluted from SP-Sephadex C-25 resin (0.5 M, $NaClO_4$, pH 8) at ~2 °C. The resulting three bands were (in order of elution) *cis*-$[Co(en)_2(OH)(glyglyOC_3H_7)]^{2+}$ (red-violet, ϵ_{498} 103),

$[Co(en)_2(glyO)]^{2+}$ (orange, ϵ_{487} 97), and $[Co(en)_2(glyglyOC_3H_7)]^{3+}$ (orange-yellow, ϵ_{487} 98). The same procedure was used to prepare solutions of *cis*-$[Co(en)_2(OH)(glyglyO)]^+$ although $\simeq$0.2 M $NaClO_4$ was used as eluent.

Base Hydrolysis of $[Co(en)_2Br(glyNHR)]^{2+}$ Complexes. After rapid dissolution of a weighed amount of the complex in 0.10 M glycine buffer (μ = 1.0, $NaClO_4$) at 25 °C, base hydrolysis was followed by spectrophotometry or by base consumption (pH stat titration) against 0.10 M NaOH (ca. 80 mg of complex, 30 mL of 1 M $NaClO_4$, 3.2-cm thermostated cell, Cary 16K). The two major products, $[Co(en)_2OH(glyNHR)]^{2+}$ and $[Co(en)_2(glyNHR)]^{3+}$ (R = $CH_2CO_2^-$, $CH_2CO_2C_3H_7$), were separated by cation-exchange chromatography as described above. For R = H the hydroxo amide could not be obtained in a pure form, even at 2 °C, since some $[Co(en)_2(glyO)]^{2+}$ was formed on the ion-exchange resin; the $[Co(en)_2(glyNH_2)]^{3+}$ ion could, however, be isolated. Also sufficient $[Co(en)_2(OH)(glyNH_2)]^{2+}$ was obtained by this method to identify the products and stereochemistry of its subsequent reactions.[23] Normally the hydroxo products (R = $CH_2CO_2C_3H_7$, $CH_2CO_2^-$) were determined by spectrophotometry and by atomic absorption for Co. For R = H the base-hydrolyzed solution ($5t_{1/2}$) was immediately quenched with HOAc (pH 4) and the $[Co(en)_2(glyNH_2)]^{3+}$ and $[Co(en)_2(glyO)]^{2+}$ ions separated on the ion-exchange column (Dowex 50W-X2).

Isolation and Properties of the *trans*-$[Co(en)_2(OH/H_2O)(glyNHR)]^{2+/3+}$ Ions. *rac*- or $(+)_{589}$-$[Co(en)_2Br(glyNHR)]Br_2$ (R = H, $CH_2CO_2C_3H_7$) was hydrolyzed at pH 10 (6 min, pH stat). For R = H the solution was immediately quenched to pH 2 (1 M $HClO_4$) and left for 15 min after which time all the cis-aqua amide had converted to $[Co(en)_2(glyO)]^{2+}$. For R = $CH_2CO_2C_3H_7$ the hydroxo amide product was separated from the $[Co(en)_2(glyglyOC_3H_7)]^{3+}$ ion by ion-exchange chromatography at ~2 °C (pH ~8) as described earlier. This solution (0.5 M $NaClO_4$) was then treated with phosphate buffer (pH 6.64, 0.15 M, or pH 8.77, 0.07 M, 25.0 °C) for $\sim 6t_{1/2}$ for reaction of the cis ion[23] or was converted to the aqua ion (pH ~2) and allowed to stand for 4 h. For all these experiments the final solutions (R = H, $CH_2CO_2C_3H_7$) were adjusted to pH ~2 and sorbed onto Sephadex C-25 resin, and the $[Co(en)_2(glyO)]^{2+}$ product was eluted with 0.2 M $NaClO_4$ (pH ~2). The trans-aqua product remaining in the 3+ band was then removed (as the trans-hydroxo species) by first cooling the column to ~2 °C, washing the column with 0.2 M "Tris" buffer (pH ~8.1, 2 °C) until basic, and eluting with 0.2 M $NaClO_4$ at pH 8 (10^{-3} M Tris, 2 °C). The visible and ORD spectra of the trans-aqua and trans-hydroxo ions were then immediately recorded at pH ~2 and 8, respectively, and Co concentrations were measured. For R = H, ϵ_{497} is 60 ± 2 (aqua) and ϵ is 72 ± 2 (hydroxo); for R = $CH_2CO_2C_3H_7$, ϵ_{497} is 58 ± 4 (aqua) and ϵ is 78 ± 1 (hydroxo) in 1 M $NaClO_4$ at ~20 °C. The aqua and hydroxo ions (R = H, $CH_2CO_2C_3H_7$) produced from the $(+)_{589}$ bromo complexes showed no optical activity from 600 to 350 nm (~5 × 10^{-4} M solutions).

Reactions of *trans*-$[Co(en)_2(OH/OH_2)(glyNHR)]^{2+/3+}$. Rate data were obtained at 560 nm (hydroxo) or 487 nm (aqua) by continuous monitoring of the absorbance (3.2-cm cell, 25.0 °C, μ = 1.0 ($NaClO_4$), pH stat control). For pH ≥8 the solution was initially degassed and kept under a N_2 atmosphere. At the conclusion of the reaction the products were determined as follows. The solutions were quenched to pH ~2 ($HClO_4$), sorbed onto Sephadex C-25 resin, and eluted at pH ~2 with a $NaClO_4$ gradient (0.4–1.0 M). For the reactions in acid only one 3+ band was obtained, but for R = $CH_2CO_2C_3H_7$ this separated into two when eluted with 0.2 M $NaClO_4$ (pH ~8); the latter ions were identified as $[Co(en)_2(glyglyOC_3H_7)]^{2+}$ and $[Co(en)_2(glyglyO)]^{2+}$ by their rates of hydrolysis at pH 11.0; for R = H only $[Co(en)_2(glyNH_2)]^{3+}$ was found and it was similarly identified. For the products from the trans-hydroxo ions (pH ≥8.0) both 2+ and 3+ products were found and these were identified as $[Co(en)_2(glyO)]^{2+}$ and $[Co(en)_2(glyglyOC_3H_7)]^{3+}$, respectively. However, it was shown that the former derived from the latter under the conditions of the experiment.

^{18}O-Tracer Experiments. $H_2{}^{18}O$ (not normalized, 1.5 and 2.0 atom %) was obtained from Miles Laboratories Inc. (Yeda). The ^{18}O content of the CO_2 recovered from equilibration with the solvent, and from the complexes, was analyzed using an Atlas GD-150 or M-86 mass spectrometer.[24,25] In all experiments the complexes were finally obtained as $[Co(en)_2(glyO)]HgI_4$, and the glycine was recovered by pyrolysis and sublimation under vacuum as described previously.[8] The HgI_4^{2-} salt was precipitated by adding a concentrated solution of HgI_2 dissolved in aqueous NaI to the ion-exchanged product. The following experiments were carried out.

(a) $[Co(en)_2Br(glyglyOC_3H_7)]Br_2 \cdot H_2O$ (5 g) was dissolved in 50 mL of $H_2{}^{18}O$ (1.6 and 2.0 atom %) and hydrolyzed at pH 9.02 for 25 min by pH stat titration against 5 M NaOH (not enriched). A ~1-mL sample was removed for solvent determination, and the remainder was diluted to 200 mL with iced water and absorbed onto and eluted from SP-Sephadex C-25 cation-exchange resin at 2 °C using 0.5 M $NaClO_4$ at pH 8. Three major products separated: (1) a red-pink band containing $[Co(en)_2(OH)(glyglyOC_3H_7)]^{2+}$ (~60%); (2) an orange band containing $[Co(en)_2(glyO)]^{2+}$ (~25%); (3) a slow-moving brown band (~10%) which was discarded. Band (1) was flushed with N_2 and divided into two approximately equal parts which were treated as follows. The first part was diluted to 200 mL with degassed water (N_2) and pH-stated at pH 3.77 for 3 h ($\simeq 5t_{1/2}$). The second fraction in 200 mL of 0.07 M phosphate buffer was pH-stated at pH 8.77 for 31 min ($\simeq 10t_{1/2}$).[23] In a separate experiment the ^{18}O-labeled hydroxo complex was kept at pH 8.77 (pH stat control) and 25.0 °C for 15 h. The three solutions were quenched to pH 3.0 ($HClO_4$), diluted three times with H_2O, and sorbed onto CM-Sephadex C-25 exchange resin. The two reaction products $[Co(en)_2(glyO)]^{2+}$ and $[Co(en)_2(glyglyOC_3H_7)]^{3+}$ were separated with 0.2 M $NaClO_4$ and then eluted with a 0.5–1.0 M pyridinium acetate gradient. They were recovered as solids following rotary evaporation and addition of HOAc to remove pyridine. The $[Co(en)_2(glyglyOC_3H_7)]^{3+}$ products were then separately hydrolyzed at pH 11 for 53 min (pH stat, $\simeq 10t_{1/2}$), rechromatographed on CM-Sephadex C-25 (py/HOAc), and recovered as above. The various $[Co(en)_2(glyO)]^{2+}$ ions were isolated as their HgI_4^{2-} salts.

(b) $H^{18}OCl$ was prepared by adding $AgClO_4$ (20.07 g) to ice-cold $H_2{}^{18}O$ (50 ml, 1.6 atom %) and bubbling Cl_2 through the cold (~0 °C) solution for ca. 20 min. AgCl was quickly removed (Hyflo filter) and the solution rapidly back-titrated at ~0 °C to the AgCl end point. The refiltered solution was used as described below. The nitrate salt of *cis*-$[Co(en)_2Br(glyglyOC_3H_7)]^{2+}$ was prepared by ion exchange of the bromide salt (10 g in 40 mL of H_2O at 40 °C; Sephadex A-25, NO_3^-) and reducing to dryness on a rotary evaporator. This complex in 10 mL of $H_2{}^{18}O$ (1.6 atom %) at 0 °C was added over 5 min to the $H^{18}OCl$ solution, and after a further 10 min the red solution was filtered and a sample (1 mL) taken for solvent analysis. The remainder was diluted (~500 mL) and sorbed onto SP-Sephadex C-25 resin at ~2 °C. The two major products, $[Co(en)_2(glyglyOC_3H_7)]^{3+}$ and $[Co(en)_2(OH)(glyglyOC_3H_7)]^{2+}$, were then separated and collected (0.5 M $NaClO_4$, pH 8, 2 °C) and the latter was kept at pH 3.77 for 4 h (pH stat, 200 mL, 25 °C). The various $[Co(en)_2(glyglyOC_3H_7)]^{3+}$ and $[Co(en)_2(glyO)]^{2+}$ products were isolated and dealt with as described in part (a) above.

Optical Retention Experiments. (a) Hg^{2+}-Catalyzed Reaction of $(+)_{589}$-$[Co(en)_2Br(glyglyOC_3H_7)]^{2+}$. $(+)_{589}$-$[Co(en)_2Br(glyglyOC_3H_7)](CS)_2$ (0.282 g, $[\alpha]_{589}$ = +81°, CS = $(+)_{589}$-camphor-10-sulfonate) was converted to its bromide salt (Sephadex A-25) and made up to 20 mL. A 2-mL sample was removed for visible and ORD spectral analysis. $HClO_4$ (1 mL) was added to the remainder followed by a 0.2 M Hg $(ClO_4)_2$ solution (10 mL, 0.09 M $HClO_4$), and the solution stood for 30 min at ca. 25 °C. ORD and visible spectra were then recorded. The solution was then divided into two equal parts and the first was sorbed onto, and then eluted from, SP-Sephadex C-25 resin (0.2–1.0 M $NaClO_4$ gradient), and ORD and visible spectra were taken of the recovered $(+)_{589}$-$[Co(en)_2(glyglyOC_3H_7)]^{3+}$ product (1 M $NaClO_4$, pH ~6). The complex was then hydrolyzed by pH stat titration (pH 11, 50 min), the pH was adjusted to ~4 (HOAc), and the visible and ORD spectra of the $(+)_{589}$-$[Co(en)_2(glyO)]^{2+}$ product were recorded both before and following ion-exchange purification on C-25 resin (0.5 M $NaClO_4$, pH ~6). The second fraction of $(+)_{589}$-$[Co(en)_2(glyglyOC_3H_7)]^{3+}$ was immediately hydrolyzed at pH 11 (50 min), precipitated HgO removed, and the pH adjusted to ~4 (HOAc). The $(+)_{589}$-$[Co(en)_2(glyO)]^{2+}$ was then chromatographed as before, and the visible and ORD spectra of the recovered product were recorded (1.0 M $NaClO_4$, pH ~6).

(b) HOCl-Induced Reaction. The procedure was identical with that described in detail for the ^{18}O-tracer experiment: 1.39 g of $(+)_{589}$-$[Co(en)_2Br(glyglyOC_3H_7)](CS)_2$ and 40 mL of ≃1 M HOCl were used in a reaction at 0 °C. The ion-exchange-separated solution of $(+)_{589}$-$[Co(en)_2(OH)(glyglyOC_3H_7)]^{2+}$ was divided into two parts, the first being treated with 0.07 M phosphate buffer at pH 8.77 (30

Table I. Rate Data for Hg^{2+}-Promoted Removal of Bromide from the *cis*-$[Co(en)_2Br(glyNHR)]^{2+}$ Ions[a]

R	$[Hg^{2+}]$, M	$[HClO_4]$, M	$10k_{obsd}$, s^{-1}	k_{Hg},[b] M^{-1} s^{-1}
H	0.02	0.1	7.80	39
	0.01	0.1	4.00	40
	0.01	0.67	4.50	45
	0.005	0.1	2.18	41
$CH_2CO_2C_3H_7$	0.02	0.1	4.78	24
	0.01	0.1	2.31	23
	0.01	0.67	2.54	25
	0.005	0.1	1.16	23
$CH_2CO_2C_2H_5$	0.02	0.1	4.80	24
	0.01	0.1	2.36	24
	0.01	0.67	2.52	25
	0.005	0.1	1.23	25
$CH_2CO_2CH_3$	0.02	0.1	1.24	6.2
	0.01	0.1	0.63	6.3
	0.01	0.67	0.60	6.0
	0.005	0.1	0.33	6.6

[a] 25.0 °C; μ = 1.0 ($NaClO_4$). Spectrophotometric data at 560 nm; [Co] ≈ 5 × 10^{-4} M; complexes converted from Br^- salts to ClO_4^- salts using Dowex 1-X8 (50–100 mesh) anion-exchange resin. [b] $k_{Hg} = k_{obsd}/[Hg^{2+}]$.

min, 25.0 °C) and the second being held at pH 3.77 (4 h, pH stat). After being quenched to pH ~4 (HOAc) the solutions were sorbed onto, and eluted from, C-25 resin using a $NaClO_4$ gradient (0.5–1.0 M). The visible and ORD spectra of the $(+)_{589}$-$[Co(en)_2(glyO)]^{2+}$ and $(+)_{589}$-$[Co(en)_2(glyglyOC_3H_7)]^{3+}$ products were recorded in 0.5 and 1.0 M $NaClO_4$ at pH ~6, respectively.

(c) Base-Catalyzed Reaction. $(+)_{589}$-$[Co(en)_2Br(glyglyOC_3H_7)](CS)_2$ (1.39 and 1.25 g, two experiments) in water (50 mL) was hydrolyzed at pH 9.0 (21 min) and 9.5 (8 min) (pH stat control, 1 M NaOH) before adjusting the solutions to pH 8, cooling to ~0 °C, and sorbing the products onto C-25 resin packed and held at ~2 °C. The red 2+ and orange 3+ products were rapidly separated using 0.5 M $NaClO_4$ (pH 8, ~2 °C) and eluted with 0.5 M $NaClO_4$ (pH 8, 2 °C) and 1 M $NaClO_4$ (pH 5), respectively. The visible and ORD spectra were immediately recorded at pH ~2 and ~8 for the 2+ ion and at pH 5 for the 3+ ion. The solution of the former (pH 8) was then divided into two equal parts and treated at pH 8.77 (0.07 M phosphate buffer) and 3.77, respectively, as described previously. The $(+)_{589}$-$[Co(en)_2(glyO)]^{2+}$ and $(+)_{589}$-$[Co(en)_2(glyglyOC_3H_7)]^{3+}$ products were again separated, their visible and ORD spectra recorded, and the latter ion was then hydrolyzed to $(+)_{589}$-$[Co(en)_2(glyO)]^{2+}$ (pH 11, 53 min, 1.0 M $NaClO_4$, rate recorded). Visible and ORD spectra on the ion-exchange-purified product (50W-X2 resin, 1 M $NaClO_4$) were recorded.

Results and Discussion

1. Hg^{2+}-Induced Removal of Bromide. Table I gives spectrophotometric data for the reaction of Hg^{2+} with *cis*-$[Co(en)_2Br(glyNHR)]^{2+}$ (R = H, $CH_2CO_2C_3H_7$, $CH_2CO_2C_2H_5$, $CH_2CO_2CH_3$). Only one rate was observed (560 nm, maximum OD change), and plots of log k_{obsd} vs. time were linear for at least $3t_{1/2}$. The reaction is independent of $[H^+]$ and follows the rate law $R = k_{Hg}[Co(en)_2Br(glyNHR)^{2+}][Hg^{2+}]$. With the exception of the case of the dipeptide methyl ester complex, values of k_{Hg} are greater than those found for other $[Co(en)_2Br(amine)]^{2+}$ complexes, viz. (amine, k_{Hg} in M^{-1} s^{-1}): NH_3, 2.7; NH_2CH_3, 7.9; $NH_2CH_2CO_2CH_3$, 5.1; $NH_2CH_2CO_2C_2H_5$, 4.4; $NH_2CH_2CO_2C_3H_7$, 5.1; $NH_2CH_2CH_2CO_2C_3H_7$, 2.4; NH_2CH_2CN, 0.12. The reasons for this are not clear at the present time. It may arise from changes in the association constant k_{Hg} rather than from variations in the rate of loss of $HgBr^+$, but a detailed investigation of this aspect is outside the scope of the present study. Product analysis results showed that only chelated amide species, $[Co(en)_2(glyNHR)]^{3+}$, were formed and that these were produced directly and not via the intermediate aqua complex. Also, the results require the absence (<2%) of hydrolysis in the monodentate amide function prior to, or following, chelation. The former result was demonstrated by ion-exchange analysis. The *cis*- and *trans*-$[Co(en)_2(OH)glyglyOC_3H_7)]^{2+}$ ions readily separate from $[Co(en)_2(glyNHR)]^{3+}$ at pH ~8 and 2 °C, but neither was detected in the present experiments. Also *cis*-$[Co(en)_2(H_2O)(glyNHR)]^{3+}$ gives rise to appreciable amounts of $[Co(en)_2(glyO)]^{2+}$ in acidic solution and again none was found. The Hg^{2+}-promoted reaction is therefore an excellent method for preparing large amounts of the chelated amide species in a pure form.

Full retention of configuration about the metal center obtains in this reaction. Thus $(+)_{589}$-$[Co(en)_2Br(glyglyOC_3H_7)]^{3+}$ ($[M]_{589}$ = +820°) gave exclusively the chelated dipeptide ion (3+; $[M]_{589}$ = +1600°) (see eq 1).

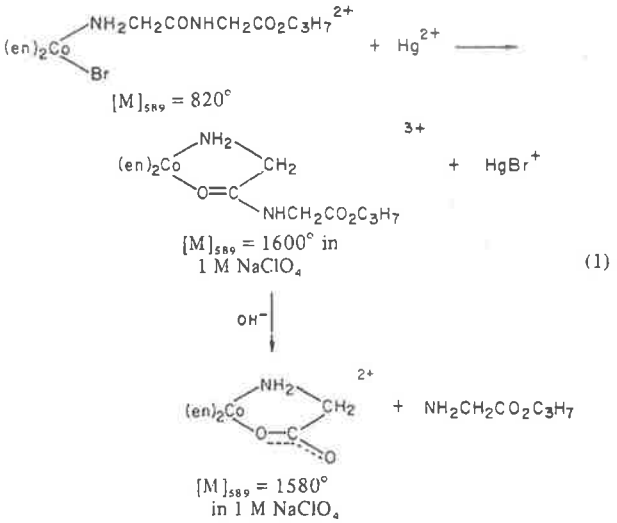

Subsequent hydrolysis at pH 11 resulted in $(+)_{589}$-$[Co(en)_2(glyO)]^{2+}$ ($[M]_{589}$ = +1580° in 0.5 M $NaClO_4$), and when this compound was compared with optically pure $(+)_{589}$-$[Co(en)_2(glyO)]I_2$ ($[M]_{589}$ = 1546° in H_2O) prepared from glycine and resolved separately,[26] it is clear that both the Hg^{2+}-catalyzed removal of Br^- and base hydrolysis of the chelated dipeptide occur with full retention. Optical rotary dispersion (ORD) and visible spectra for the two products are given in Figure 4 (supplementary material).

Similar results have been found for other *cis*-$[Co(en)_2X(NH_2R)]^{2+}$ complexes where X = Cl or Br and NH_2R = glycinamide,[17] glycine esters,[7-9] or glycinate.[27] The carbonyl or carboxylic acid function appears to be an exceedingly fine competitor for the five-coordinate intermediate generally considered to be formed in such reactions with Hg^{2+},[25,28] especially when five- and six-membered chelate rings are involved (see Scheme IV). This inability of water to compete is supported by the lack of competition by other added anions (NO_3^-, HSO_4^-),[8,9] and although a concerted process involving the simultaneous entry of the carbonyl function during loss of HgX^+ cannot be entirely eliminated, its involvement in the rate-determining transition state is unlikely since no systematic synergic increase in rate is found when the k_{Hg} values are compared with those for complexes which do not contain the >C=O grouping and which involve water (or anion) entry. The full retention of optical configuration obtained with the present complexes is entirely consistent with that found previously with *cis*-$[Co(en)_2X(NH_3)]^{2+}$ ions (X = Cl, Br).[29,30]

2. Base Hydrolysis. Table II contains rate data for the base hydrolysis of the *cis*-$[Co(en)_2Br(glyNHR)]^{2+}$ ions (R = H, $CH_2CO_2^-$, $CH_2CO_2C_3H_7$) and the product analysis results are given in Table III.

Large optical density changes were observed at 490 and 360 nm, and at these wavelengths acceptable infinity readings were

Scheme IV

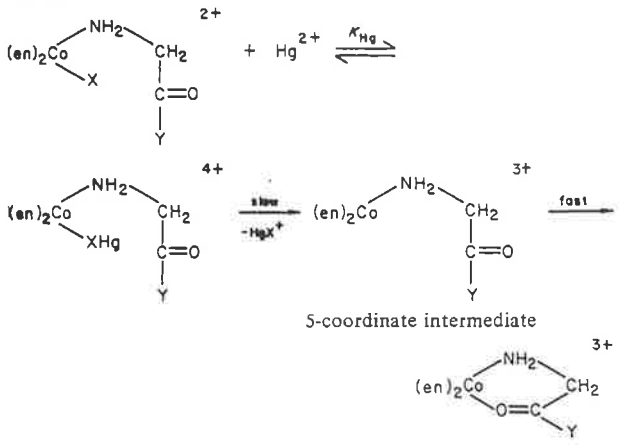

Table II. Rate Data for Base Hydrolysis of the *cis*-$[Co(en)_2Br(glyNHR)]^{2+}$ Ions[a]

R	pH	$10k_{obsd}$, s^{-1}	k_{OH},[b] M^{-1} s^{-1}
H[c]	7.84	1.80	153
	8.16	3.73	152
	9.00	25.7	151
	9.5[f]	86	160
$CH_2CO_2^-$ [d]	8.40	6.89	162
	9.09	37.3	179
	9.44	82.7	177
	9.97	275	174
$CH_2CO_2C_3H_7$[e]	8.43	8.47	191
	9.11	43.8	200
	9.57	127	201
	10.11	434	198
	9.0[f]	32.8	193
	1.5[f]	105	195
	10.0[f]	336	198

[a] 25.0 °C; μ = 1.0 ($NaClO_4$); [Co] = (1–2) × 10^{-3} M. [b] $k_{OH} = k_{obsd}/[OH^-]$, where $[OH^-]$ is calculated from pH using pK_w = 13.77. [c] 490 nm; 0.2 M Tris–$HClO_4$ buffer. [d] 360 nm; 0.1 M glycine–$HClO_4$ buffer. [e] 355 nm; 0.1 M glycine–$HClO_4$ buffer. [f] pH stat data (OH^- consumption).

obtained for the process involving removal of bromide; at other wavelengths small subsequent OD changes were observed and were shown to result from events following the removal of bromide (see below). Plots of log $(D_t - D_\infty)$ vs. time were linear for $3t_{1/2}$ in most cases, but occasionally Guggenheim plots were used to evaluate the k_{obsd} values. The pH stat data also gave linear plots of log $(V_\infty - V_t)$ vs. time for the two dipeptide complexes, but a subsequent slow uptake of acid or base (pH <9 or >9, respectively) complicated the analysis for the glycinamide complex. This again was shown to result from the subsequent reaction of the hydroxo glycinamide complex. Both methods gave data consistent with the rate expression $k_{obsd} = k_{OH}[OH^-]$ over a 10–10^2 variation in $[OH^-]$, Table II, and the second-order rate constants are similar to those obtained with other *cis*-$[Co(en)_2Br(amine)]^{2+}$ ions. Such data are consistent with the generally accepted conjugate base mechanism (S_N1cB) for hydrolysis of cobalt(III)–acido complexes of this type.[30,31]

The product analyses results, Table III, show that in addition to the chelated amide $[Co(en)_2(glyNHR)]^{3+}$ considerable amounts of the hydroxo amide are also formed, eq 2. This

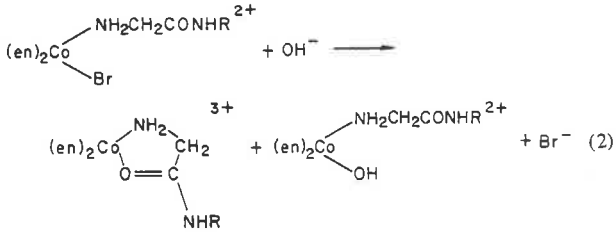

result clearly differs from that found with Hg^{2+}, and a different five-coordinate intermediate is required which competes favorably for both water and >C=O entry.[30] The product ratio is pH independent and is the same in 1 M $NaClO_4$ and 0.1 M KCl.

The occurrence of stable hydroxo amide species differs significantly from that in our previous report on the hydrolysis of the *cis*-$[Co(en)_2Br(glyNH_2)]^{2+}$ ion.[17] In the previous study it was concluded that the hydroxo glycinamide ion reacted rapidly under the conditions of base hydrolysis and that the subsequent process observed spectrophotometrically was hydrolysis of the chelated amide. Unfortunately these measurements[17] were made at wavelengths where only very small OD changes are involved for the hydroxo species and at pHs where the rate is similar to that for the chelated glycinamide ion. The earlier observation of a stable hydroxo species by Chan and Chan[32] is therefore correct, although its subsequent chemistry as reported by them is not.

For R = $CH_2CO_2C_3H_7$ and $CH_2CO_2^-$ the amount of hydroxo dipeptide is given directly by the base consumption data

Table III. Product Distributions on Base Hydrolysis of *cis*-$[Co(en)_2Br(glyNHR)]^{2+}$ Ions[a]

				% obsd prod		% cor prod[e]	
R	pH	reacn time, min	10^3k_1,[b] s^{-1}	$[Co(en)_2(glyNHR)]^{3+}$ [g]	$[Co(en)_2OH(glyNHR)]^{2+}$ or $[Co(en)_2(glyO)]^{2+}$ [g]	$[Co(en)_2(glyNHR)]^{3+}$	$[Co(en)_2(OH)(glyNHR)]^{2+}$
$CH_2CO_2^-$	9.0	30	3	33[c]	67[c]	31[f]	69[f]
	9.5	9	10	27[c]	73[c]	28[f]	72[f]
$CH_2CO_2C_3H_7$	8.06	90	0.76	32[c]	68[c]	32[f]	68[f]
	9.00	25	3.28	29[h,c]	71[h,c]	29[f]	71[f]
H	9.0	22.5	2.6	36.5	67 (53)[c]	42	58 (58)[f]
	9.0[d]	15	5.1	34	66 (55)[c]	39	61 (59)[f]
	9.5	8	8.2	34	70 (63)[c]	40	60 (60)[f]
	9.5[d]	5	16.1	32	68 (63)[c]	40	60 (60)[f]
	10.0	2.3	26	34	70 (65)[c]	39	61 (58)[f]
	10.0[d]	1.5	51	32	68 (69)[c]	38	62 (65)[f]

[a] All runs at 25.0 °C and μ = 1.0 ($NaClO_4$) unless otherwise stated, most experiments were run in duplicate on ≈0.15 g of complex. [b] k_{obsd} for Br^- removal (Table II). [c] From uncorrected base consumption data. [d] 0.1 M KCl supporting electrolyte. [e] Corrected for subsequent hydrolysis of $[Co(en)_2(glyNH_2)]^{3+}$ (k_2 = 25 M^{-1} s^{-1} (1.0 M $NaClO_4$, 0.1 M KCl)) and of $[Co(en)_2OH(glyNH_2)]^{2+}$ (k_3 (pH) = 2.2 (9.0), 3.2 (9.5), 5.4 (10.0) × 10^{-4} s^{-1} in 1.0 M $NaClO_4$; 2.6 (9.0), 4.4 (9.5), 6.5 (10.0) × 10^{-4} s^{-1} in 0.1 M KCl)[23] and for $pK_a(NH_3)$ = 9.38 (1.0 M $NaClO_4$) and 9.27 (0.1 M KCl). [f] Estimated from corrected base consumption data. [g] For R = H the observed 3+ ion (chromatographic separation) contains *trans*-$[Co(en)_2(OH_2)(glyNH_2)]^{3+}$ (5–6%) as well as $[Co(en)_2(glyNH_2)]^{3+}$. [h] Average of 10 experiments.

(pH stat). Reactions subsequent to the removal of bromide are slow so that only minor corrections to the observed base uptake were necessary. Also fair agreement was found between these data and the amount of hydroxo dipeptide separated by ion-exchange chromatography at pH 8 and 2 °C. Some small conversion (<5%) to the chelated dipeptide did appear to have occurred during absorption on or elution from the resin, but this method did provide a reliable procedure for obtaining the pure hydroxo dipeptide ions.

For *cis*-$[Co(en)_2Br(glyNH_2)]^{2+}$ the immediate products were more difficult to determine since appreciable correction is necessary for the subsequent reactions of both the chelated amide and hydroxo amide. The former consumes OH^- on hydrolysis while the latter releases it, and the amounts involved are pH dependent. Direct analysis by ion exchange proved unreliable, even at 0 °C, since the reaction of the hydroxo amide at pH ~8 appeared to be accelerated on the resin. However, this procedure did allow the recovery of sufficient $[Co(en)_2(OH)(glyNH_2)]^{2+}$ free of $[Co(en)_2(glyNH_2)]^{2+}$ (but still containing some $[Co(en)_2(glyO)]^{2+}$) to determine its products under the conditions of base hydrolysis (pH 8–10) and the subsequent analysis procedure (pH ~4). In part these results are dealt with in a subsequent paper,[23] but it is important to note here that the cis-aqua and -hydroxo glycinamide ions form only $[Co(en)_2(glyO)]^{2+}$ (pH ~4 and 8–10, respectively). The small amount of trans-hydroxo amide also formed in the base hydrolysis reaction reacts very slowly under alkaline conditions (to form $[Co(en)_2(glyNH_2)]^{2+}$, see below), and it can also be recovered unchanged from acidic solutions as the 3+ aqua ion. Alkaline hydrolysis of $[Co(en)_2(glyNH_2)]^{3+}$ (pH 8.5–12) forms only $[Co(en)_2(glyO)]^{2+}$; no $[Co(en)_2(OH)(glyNH_2)]^{2+}$ has been detected in this reaction (i.e., the chelate ring does not open up).[23] At pH ~4 the chelated amide shows no hydrolysis (<2%) over 14 days.

Using these results the immediate products of base hydrolysis of $[Co(en)_2Br(glyNH_2)]^{2+}$ were determined (see eq 3–5). Following quenching to pH ~4 after $5t_{1/2}$ for bromide

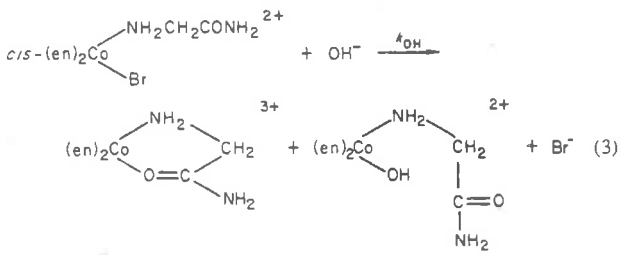

(3)

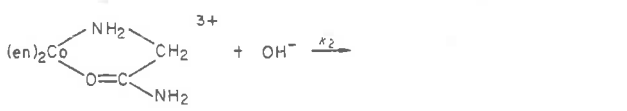

(4)

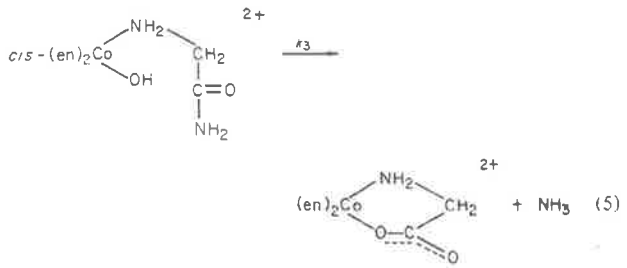

(5)

removal, the $[Co(en)_2(glyNH_2)]^{3+}$ and $[Co(en)_2(glyO)]^{2+}$ ions were separated by ion-exchange chromatography and estimated by spectrophotometry and by atomic absorption for Co. These data were then corrected for subsequent hydrolysis of the chelated amide (eq 4), and hydroxo amide (eq 5), using rate data given in the caption to Table III. The corrected product distributions are given in the last two columns of Table III. Alternatively the immediate products were determined from the base consumption data (pH stat) using the observation that reactions 3 and 4 consume OH^- while reaction 5 releases it; corrections were applied for protonation of released ammonia (pK_a = 9.38, 1.0 M $NaClO_4$, 25 °C). Acceptable agreement was found between the two methods, Table III.

It is clear from the results that entry of the >C=O function is greatest with the less bulky glycinamide complex and that ionic strength effects (1.0 M $NaClO_4$ vs. 0.1 M KCl) are unimportant.

The presence of the small amounts of the trans-hydroxo ions in the base hydrolysis products was not apparent until the detailed kinetic study of the cis-hydroxo species was well advanced.[23] For the hydroxo glycinamide ion, but not for the similar dipeptide species, this made its appearance in spectrophotometric runs at pH <11 as a small OD decrease.[23] This resulted from the presence of ~6% *trans*-$[Co(en)_2(OH)(glyNH_2)]^{2+}$ in the products of base hydrolysis and ultimately led to the isolation and characterization of all three (R = H, $CH_2CO_2C_3H_7$, $CH_2CO_2^-$) trans ions.

3. Stereochemistry of Base Hydrolysis. The stereochemistry of the base hydrolysis reaction was investigated using optically pure *cis*-$(+)_{589}$-$[Co(en)_2Br(glyglyOC_3H_7)]Br_2$ and cis-$(+)_{589}$-$[Co(en)_2Br(glyNH_2)]Br_2$. Base hydrolysis of the former (pH 9, 9.5) followed by ion-exchange separation (pH 8, 2 °C) gave the products and rotations shown in eq 6; ORD results

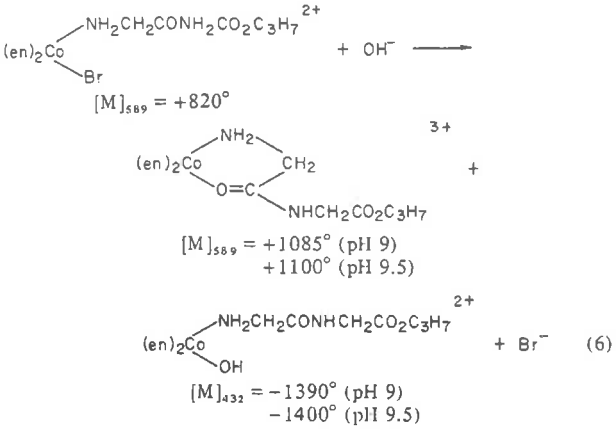

(6)

for these species are given in Figure 5 (supplementary material). The 3+ product is 66 ± 2% optically pure when compared with the same product formed in the Hg^{2+}-induced reaction, while the hydroxo dipeptide is 63 ± 2% optically pure when compared with that obtained following treatment with HOCl (see below). However, when allowance is made for 8.5% trans-hydroxo dipeptide as the 2+ ion, the retention in the cis-hydroxo species is 69 ± 2%. A similar set of results was obtained using *cis*-$(+)_{589}$-$[Co(en)_2Br(glyNH_2)]^{2+}$. In this case the 3+ ion gave $[M]_{589}$ = +842° (51% active) which is in close agreement with that obtained previously (49%).[17] However, the hydroxo glycinamide species contains 10–12% of the trans ion (Table III) which was removed (chromatographically) as a 3+ ion after allowing the cis-aqua complex to cyclize to $[Co(en)_2(glyO)]^{2+}$ at pH ~1. The latter product gave $[M)_{589}$ values of +981 and +998° (two experiments) representing at least 63% retention in the cis-hydroxo reactant. It will be shown below that the cyclization reaction in acid solution occurs with full retention of configuration so that the above value represents the retention in the cis-hydroxo ion

Table IV. Stereochemistry of Products from the Base Hydrolysis of *cis*-$(+)_{589}$-$[Co(en)_2Br(amine)]^{2+}$ Ions[a]

	products				
	$[Co(en)_2(OH)(amine)]^{2+}$			$[Co(en)_2(amine)]^{3+}$ (chelated amide)	
amine	trans	DL-cis	D-cis	DL-cis	D-cis
$NH_2CH_2CONH_2$	6.2	20	34	20	20
$NH_2CH_2CONHCH_2CO_2C_3H_7$	6.2	19	44	10	20
$NH_2CH_2CONHCH_2CO_2^-$	——70——			—30—	
NH_3[b]	23	31	46		

[a] 1 M $NaClO_4$; 25 °C. [b] Average value for bromo, chloro, and nitrato complexes.[30]

formed in the base hydrolysis of Br^-.

The overall stereochemical result for both sets of products is collected in Table IV. For the glycinamide complex the retention in the cis-hydroxo product is similar to that obtained with *cis*-$(+)_{589}$-$[Co(en)_2Br(NH_3)]^{2+}$,[30] but far less trans product is formed even when the path leading to water entry only is considered. Apparently the adjacent >C=O group competes very favorably for the part leading to trans product as well.

4. Isolation and Properties of the *trans*-$[Co(en)_2(H_2O/OH)(amide)]^{3+/2+}$ Ions. Two methods were used to obtain the trans species. Initially the hydroxo glycinamide product obtained by ion-exchange separation (pH ~8, 0.5 M $NaClO_4$, 2 °C) of the products of base hydrolysis of *cis*-$[Co(en)_2Br(glyNH_2)]^{2+}$ was immediately quenched to pH ~1 and left to stand for ~15 min to completely convert the cis-aqua ion to $[Co(en)_2(glyO)]^{2+}$. This 2+ ion was then removed from the trans-aqua 3+ ion by ion-exchange elution at pH ~2 (0.2 M $NaClO_4$, 2 °C) and the trans product recovered as a red-mauve 2+ band by elution at pH ~8 (0.4 M $NaClO_4$, 2 °C). Subsequently it was found possible to obtain the trans-glycinamide species directly from the base hydrolysis products by quenching the base-hydrolyzed (pH stat) solution to pH 1, allowing the cis-aqua ion to cyclize, and chromatographic isolation as before. Both methods were also successful in obtaining *trans*-$[Co(en)_2(H_2O/OH)(glyglyOC_3H_7)]^{3+/2+}$. When carried out with the optically pure bromo reactants, the trans ions (~5×10^{-4} M) showed no optical activity from 600 to 300 nm. Their visible spectra are compared with the cis species in Figure 1. Clearly the ϵ_{max} values for the trans-aqua and trans-hydroxo ions in the visible region are appreciably less than the corresponding cis species; a similar result obtains for the *trans*-$[Co(en)_2(H_2O)(NH_3)]^{2+}$ ion.[33] The visible and ORD spectra for *cis*-$[Co(en)_2(OH)(glyNH_2)]^{2+}$ are very similar to those for *cis*-$[Co(en)_2(OH)(glyglyOC_3H_7)]^{2+}$, but the hydroxo species of the former always contained some $[Co(en)_2(glyO)]^{2+}$ (even at 2 °C) presumably resulting from the subsequent cyclization reaction,[23] and the spectra are not recorded here.[34]

Product analysis results gave 6.0 ± 0.2% and 5.8 ± 0.2% trans-hydroxo glycinamide and dipeptide ester among the products of the base hydrolysis reactions, Table III. For the trans-dipeptide ester these results were obtained from experiments where cyclization of the cis species was accelerated by phosphate buffer. When the above values are corrected for the small loss (~8%) due to the subsequent reaction of the trans-hydroxo ions under the conditions of base hydrolysis (see below), some 6.2 ± 0.3% trans ions result from both substrates (Table IV).

It has already been noted that the trans ions were initially observed spectrophotometrically (560 nm) by their reactions at pH >11. Isolation of the trans ions allowed these processes

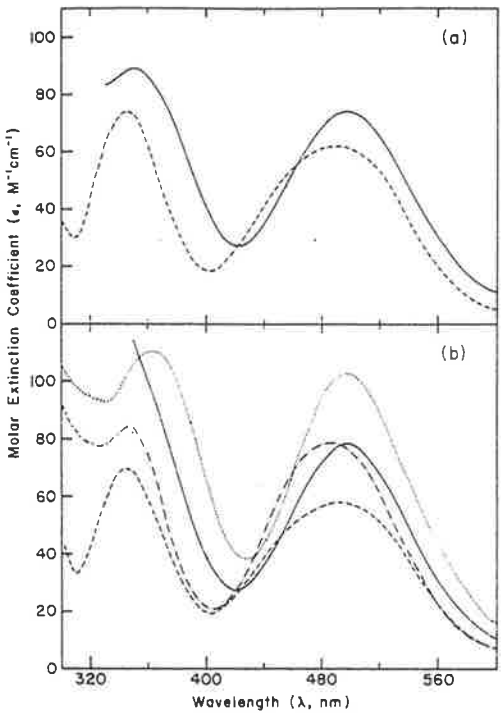

Figure 1. Visible absorption spectra for (a) *trans*-$[Co(en)_2(OH_2/OH)(glyNH_2)]^{3+/2+}$ ions [trans OH (—), trans OH_2 (---)] and (b) *cis*- and *trans*-$[Co(en)_2(OH_2/OH)(glyglyOC_3H_7)]^{3+/2+}$ ions [trans OH (—), trans OH_2 (---), cis OH (····), cis OH_2 (-·-·)] in 1.0 M $NaClO_4$, at 25.0 °C.

to be studied in detail, and Figure 2 gives a plot of k_{obsd} for *trans*-$[Co(en)_2(OH_2/OH)(glyNH_2)]^{3+/2+}$ as a function of pH. Data for the other dipeptide complexes are given in Table VI (supplementary material). Clearly three regions of reactivity occur corresponding to the acid-independent reactions of the trans-aqua and trans-hydroxo ions and to the base-dependent reaction of the trans-hydroxo ion.

$$k_{obsd} = k_{H_2O} + k_{OH} + k'_{OH}[OH^-] \quad (7)$$

The latter process involves a substantial OD change at pH >11. Values of k_{H_2O}, k_{OH}, and k'_{OH} are 4 (±2) × 10^{-6} s^{-1}, 2.8 (±0.1) × 10^{-4} s^{-1}, and 5.6 × 10^{-2} M^{-1} s^{-1} in 1 M $NaClO_4$ at 25 °C. From the limited data available (Table VI) similar rate constants are suggested for the two trans-dipeptide ions. Unlike the reaction of the cis-hydroxo ions[23] those for the trans species are unaffected by phosphate buffers. The final products at pH 2 and 8 are the racemic chelated amide complexes $[Co(en)_2(glyNHR)]^{3+}$ (R = H, $CH_2CO_2C_3H_7$). At pH 2 (14 days) only $[Co(en)_2(glyNHR)]^{3+}$ was found by ion-exchange chromatography, and this was verified by its subsequent hydrolysis to $[Co(en)_2(glyO)]^{2+}$ in basic solution (k_{obsd} = 2.3 × 10^{-2} s^{-1}, pH 12 (R = H); k_{obsd} = 6.52 × 10^{-3} s^{-1}, pH 12 (R = $CH_2CO_2C_3H_7$)). At pH 8 in the absence of buffers (pH stat) k_{obsd} approaches that for the cis-hydroxo ions,[23] and although some $[Co(en)_2(glyO)]^{2+}$ was found among the products, its presence is due entirely to subsequent hydrolysis of $[Co(en)_2(glyNHR)]^{3+}$. Thus from *trans*-$[Co(en)_2(OH)(glyNH_2)]^{2+}$, 33% $[Co(en)_2(glyO)]^{2+}$ was recovered (37% calculated) after a reaction time of 320 min (pH 8.07, 1 M $NaClO_4$) and 16.2% after 19 h in a similar experiment (pH 8) with *trans*-$[Co(en)_2(OH)(glyglyOC_3H_7)]^{2+}$ (15.7% calculated). Thus the acid-independent terms for the trans-aqua (k_{H_2O}) and trans-hydroxo (k_{OH}) ions produce only chelated amide. The immediate product of the base-dependent path of the hydroxo ion (k'_{OH}) is largely the $[Co(en)_2(glyO)]^{2+}$

ion (some decomposition occurred), and this probably results from subsequent hydrolysis of the chelated amide since hydrolysis is fast under these conditions.[23]

Since the *cis*-$[Co(en)_2(H_2O/OH)(glyglyOC_3H_7)]^{3+/2+}$ ions give rise to appreciable amounts of $[Co(en)_2(glyO)]^{2+}$ in their reactions at pH <4 and 8–9,[23] the cis species cannot be intermediates in the reactions of the trans ions. This suggests a concerted process (Scheme V) with the trans-aqua or -hydroxo ligand being synergically displaced by the >C=O group. A comparison of the rates for these reactions with those for *trans*-$[Co(en)_2(H_2O/OH)(NH_3)]^{3+/2+}$ supports this view. The latter species isomerize much more slowly than found here ($k_{H_2O} \simeq 10^{-8}$ s^{-1}, extrapolated data; $k_{OH} \simeq 1 \times 10^{-5}$ s^{-1}),[35] and in the hydroxo form at least this occurs without loss of coordinated hydroxide[35] (i.e., a different mechanism occurs).

5. Stereochemistry of the HOCl Reaction and of the Reactions of the Cis-Aqua and -Hydroxo Ions. Optical retentions were evaluated using reactants generated by base hydrolysis of *cis*-$(+)_{589}$-$[Co(en)_2Br(glyNH_2)]Br$ and *cis*-$(+)_{589}$-$[Co(en)_2Br(glyglyOC_3H_7)](NO_3)_2$ and by the HOCl-catalyzed oxidation of bromide in *cis*-$(+)_{589}$-$[Co(en)_2Br(glyglyOC_3H_7)](NO_3)_2$. The HOCl reaction is a useful method of introducing water directly into the coordination sphere[8,29] and almost certainly occurs via an oxidative interchange mechanism.[36] Treatment of *cis*-$(+)_{589}$-$[Co(en)_2Br(glyglyOC_3H_7)]^{2+}$ at ~0 °C results in a rapid violet to red-orange color change with both chelated dipeptide and aqua dipeptide ions being formed.

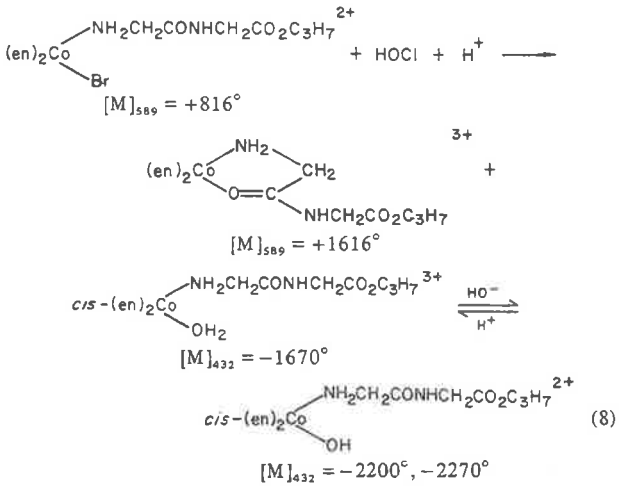

(8)

These ions were separated chromatographically on ion-exchange resin at pH ~8.5 and 2 °C, and ORD and visible spectra for the reactants and separated products are given in Figure 3. The aqua dipeptide ion exists as the hydroxo ion at pH >7.[23]

Subsequent treatment of the aqua ion at pH 3.77 and the hydroxo ion at pH 8.05 (pH stat, 21 h) and 8.77 (0.07 M phosphate buffer, 30 min) gave the two products indicated by eq 9 which, after chromatographic separation, gave the following $[M]_{589}$ values (1 M $NaClO_4$): +1680° (2+ ion), +1530° (3+ ion) at pH 3.77; +1027° (2+ ion), 1010° (3+ ion) at pH 8.05; +1630° (2+ ion), +1480° (3+ ion) at pH 8.77. ORD curves for some of the products are given in Figure 3. These data correspond to complete retention of optical configuration for the products generated from the aqua ion (by comparison with the similar optically pure species formed by treatment with Hg^{2+} (see above)), and 97% and 96% retention, respectively, in $[Co(en)_2(glyO)]^{2+}$ and $[Co(en)_2(glyglyOC_3H_7)]^{3+}$ generated from the hydroxo dipeptide in 0.07 M phosphate buffer. Corresponding retentions of 65 ± 5% and 63 ± 5% were found for the products formed in the absence of buffer at pH 8.05 (pH stat). It is clear that HOCl-induced removal of bromide occurs with full retention of configuration about the metal center, and that a similar result obtains in the hydrolyzed and chelated amide products produced in the subsequent reactions at pH 3.77 (aqua complex) and pH 8.77 in the presence of phosphate buffer (hydroxo complex). Some 35% racemization occurs at pH 8.05 in the absence of the buffer, and since this occurs with only a small amount of exchange of the bound hydroxo group with the solvent (~6%, see below), this process must occur largely via an intramolecular mechanism. A similar result has been observed by Martin and Tobe for isomerization in *trans*-$[Co(en)_2(OH)(NH_3)]^{2+}$.[35]

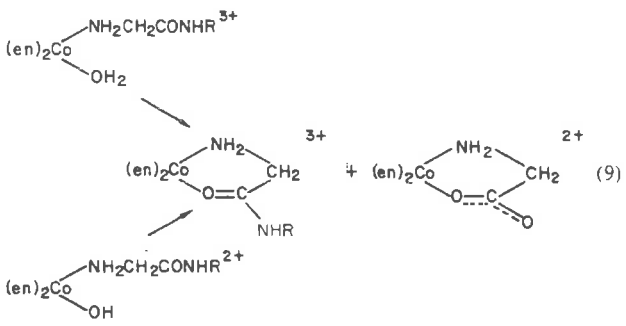

(9)

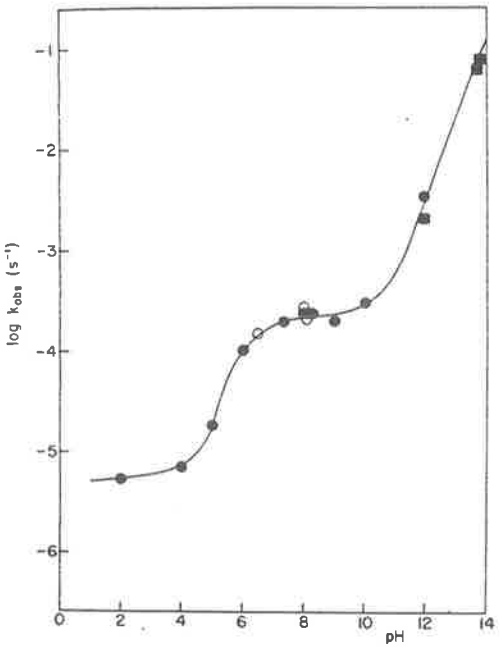

Figure 2. Plot of log k_{obsd} vs. pH for the reaction of *trans*-$[Co(en)_2(OH_2/OH)(glyNH_2)]^{3+/2+}$ to give $[Co(en)_2(glyNH_2)]^{3+}$ at 25.0 °C, μ = 1.0 ($NaClO_4$) (—). The data given by ■ are for the "slower" second reaction observed following base hydrolysis of *cis*-$[Co(en)_2Br(glyNH_2)]^{2+}$ (Figures 1 and 4 of a following paper[23]), and the O data are for the *trans*-$[Co(en)_2(OH_2/OH)(glyglyOC_3H_7)]^{3+/2+}$ under the same conditions.

Identical treatment of the aqua and hydroxo dipeptide ester ions ($[M]_{432}$ = −1160 and −1390°, respectively) isolated from base hydrolysis of *cis*-$(+)_{589}$-$[Co(en)_2Br(glyglyOC_3H_7)](NO_3)_2$ ($[M]_{589}$ = +820°) gave $[Co(en)_2(glyO)]^{2+}$ and $[Co(en)_2(glyglyOC_3H_7)]^{3+}$ products with the following $[M]_{589}$ values (three separate experiments): for the reaction at pH 3.77, +1040, +1050, +1050° (2+ ion) and +1010, +1030, +1090° (3+ ion; the first two entries contain ~13% trans-aqua ion; the third entry has had the trans ion removed); for the reaction at pH 8.77 in 0.07 M HPO_4^{2-} buffer, +1100, +1050, +1060° (2+ ion) and +925, +1000, +990° (3+ ion). ORD curves for the reactants and products are given in Figure

Scheme V

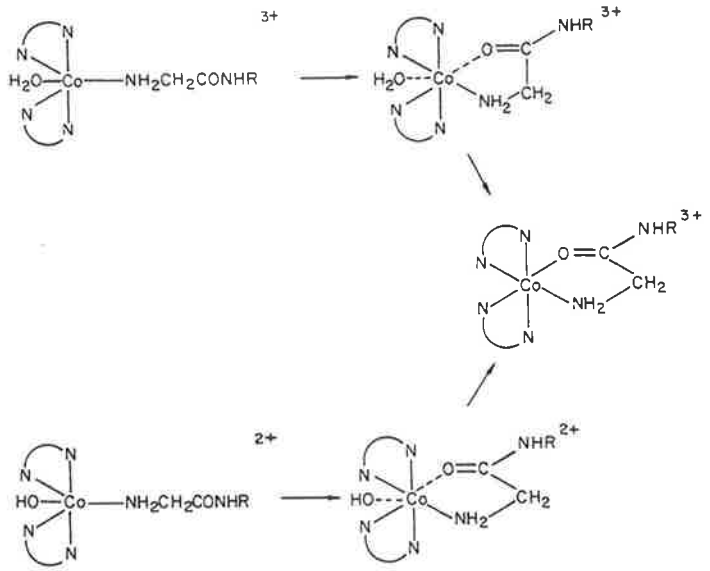

Table V. ^{18}O-Tracer Results for the Base- and HOCl-Catalyzed Hydrolyses of $[Co(en)_2Br(glyglyOC_3H_7)]^{2+}$ and for the Intramolecular Hydrolysis of $[Co(en)_2(H_2O/OH)(glyglyOC_3H_7)]^{3+/2+}$

	3+ product				2+ product	
	R values[a]					
expt	complex	solvent	blank	atom % enrichment[b]	*R* value[a] complex	atom % enrichment[b]
1[c]	0.005 596	0.025 824	0.003 434	9.8 (0.2)[f]		
2[c,g]	0.004 142	0.025 824	0.003 434	3.2	0.013 342	44.5
3[c,g]	22[e]	595[e]		3.7	274[e]	46.1
4[c,g]	0.005 100	0.033 350	0.004 840	0.9	0.017 150	43.5
5[c,h]	0.011 827	0.025 824	0.003 434	37.7	0.013 557	45.5
6[c,h]	0.011 932	0.025 820	0.003 560	37.5	0.013 415	44.1
7[c,i]	0.011 761	0.026 010	0.004 141	35.1	0.013 004	40.8
8[d]	0.005 320	0.033 24	0.004 840	1.7		
9[d,g]	0.005 070	0.033 24	0.004 840	0.8	0.016 750	42.3

[a] Observed *R* values ($R = [46]/([44] + [46])$) for CO_2. [b] Atom % enrichment = $100R/(2 + R) - 100R'/(2 + R')$ where *R* is that for CO_2 recovered from the complex and *R'* that of the normal CO_2 used as the blank. [c] Produced by base hydrolysis of $[Co(en)_2Br(glyglyOC_3H_7)]Br_2$. [d] Produced by HOCl treatment of $[Co(en)_2Br(glyglyOC_3H_7)]Br_2$. [e] Given as % enrichment above background (GD-150 mass spectrometer). [f] The value in parentheses was estimated by substracting the enrichment due to $[Co(en)_2glyglyOC_3H_7]^{3+}$ formed in the subsequent reaction of the hydroxo dipeptide in the time of the experiment (1500 s), 5.3%, and that due to reactions on the column during absorption and separation, 4.3%. [g] Products of reaction at pH 3.77 (pH stat control). [h] Products of reaction in 0.07 M phosphate buffer, pH 8.77. [i] Products of reaction at pH 8.77 (pH stat control).

5 (supplementary material). When compared with those of the optically pure species produced in the Hg^{2+}-catalyzed reaction, the rotations correspond to 68 ± 2% retention in the $[Co(en)_2(glyO)]^{2+}$ ion under the two sets of conditions (pH 3.77, 8.77 [0.07 M HPO_4^{2-}]) and a similar value (71 ± 2%) for the $[Co(en)_2(glyglyOC_3H_7)]^{3+}$ product when allowance is made for the presence of 13% *trans*-$[Co(en)_2(OH_2)(glyglyOC_3H_7)]^{3+}$ (pH 3.77) or a similar amount of racemic chelated dipeptide from the trans-hydroxo ion at pH 8.77. Since it has been shown that cyclization under these conditions occurs with full retention of configuration, it is concluded that the cis-hydroxo ion produced in the base hydrolysis reaction is 70% optically pure. This is in agreement with the value of 69 ± 2% obtained above for the isolated cis-hydroxo species (cf. section 3).

6. ^{18}O-Tracer Results. Table V contains results of reacting $[Co(en)_2Br(glyglyOC_3H_7)]^{2+}$ with OH^- (experiments 1–7) and HOCl (experiments 8 and 9) in ^{18}O-enriched water (1.6 or 2.0 atom %). Experiments 1 and 8 show that the chelated dipeptide complex $[Co(en)_2(glyglyOC_3H_7)]^{3+}$ produced directly by the two sets of conditions contains essentially no solvent label (0.2 and 1.7 atom %, respectively). The remaining data refer to the products obtained from the subsequent reactions of the ^{18}O-enriched aqua and hydroxo dipeptide ions following their separation from $[Co(en)_2(glyglyOC_3H_7)]^{3+}$. These reactions were carried out in normal unenriched water at pH 3.77 (experiments 2–4) and pH 8.77 in the presence (0.07 M, experiments 5 and 6) and absence (experiment 7) of phosphate buffer. The 3+ and 2+ products correspond to those given by eq 9 ($R = CH_2CO_2C_3H_7$), and they were separated by the normal ion-exchange procedure. The $[Co(en)_2(glyO)]^{2+}$ product was isolated and analyzed directly for its ^{18}O content. For $[Co(en)_2(glyglyOC_3H_7)]^{3+}$ it was necessary to further treat the solution at pH ~11 and recover the chelated glycine fragment as $[Co(en)_2(glyO)]HgI_4$; attempts to recover the dipeptide chelate directly proved difficult and wasteful. It has previously been shown that such a procedure involves no scrambling of glycine residues,[37] and the results given below show that little or no oxygen exchange occurs in the coordinated amide function during hydrolysis.

For the reaction at pH 3.77 the $[Co(en)_2(glyglyOC_3H_7)]^{3+}$ product contains little enrichment (3.2, 3.7 atom %), and this probably arises from a small amount of reaction during separation and isolation at pH ~8 and before quenching. The

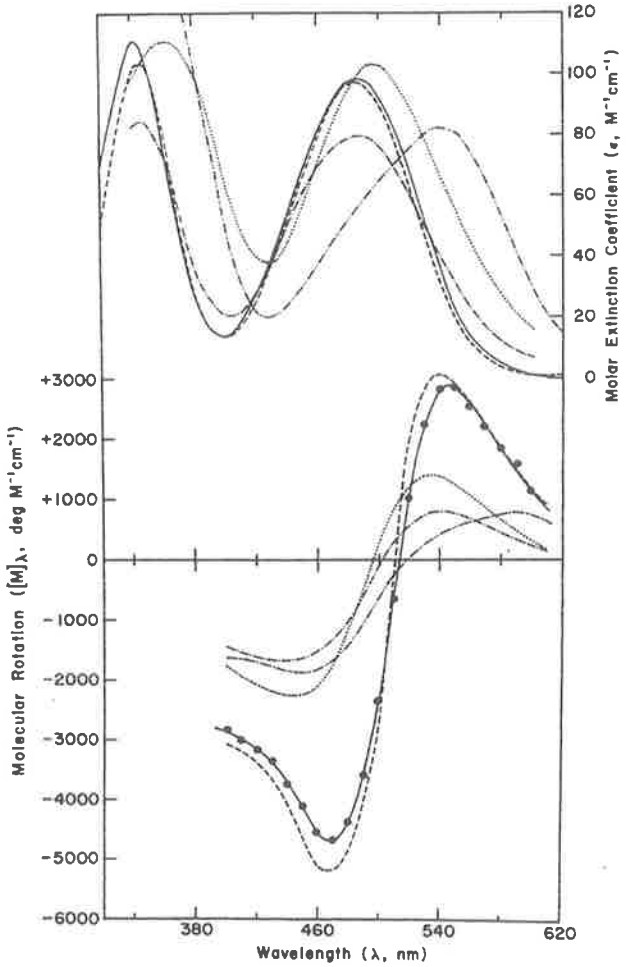

Figure 3. Visible and ORD absorption spectra for *cis*-$(+)_{589}$-$[Co(en)_2Br(glyglyOC_3H_7)](NO_3)_2$ (----), HOCl-generated *cis*-$(+)_{589}$-$[Co(en)_2(OH_2)(glyglyOC_3H_7)]^{3+}$ (pH 2) (----) and *cis*-$(+)_{589}$-$[Co(en)_2(OH)(glyglyOC_3H_7)]^{3+}$ (pH 8.5) (····), in 0.5 M $NaClO_4$, and the products of the subsequent cyclization reaction at pH 8.77 (0.07 M phosphate buffer), $(+)_{589}$-$[Co(en)_2(glyO)]^{2+}$ (---) and $(+)_{589}$-$[Co(en)_2(glyglyOC_3H_7)]^{3+}$ (—), both in 1.0 M $NaClO_4$. Data for $(+)_{589}$-$[Co(en)_2(glyglyOC_3H_7)]^{3+}$ produced in the initial HOCl reaction of the bromo complex are given by ● and clearly fall on the — curve.

3+ product produced at pH 3.77 therefore results from a process involving displacement of the coordinated aqua group. By contrast, the hydrolyzed product contains close to half of the original solvent enrichment, and one oxygen of the glycinate moiety must therefore derive from the coordinated water molecule. Similar results were obtained from aqua dipeptide produced by the HOCl and base hydrolysis reactions.

Both the 3+ and 2+ products from $[Co(en)_2(^{18}OH)(glyglyOC_3H_7)]^{2+}$ at pH 8.77 contain appreciable amounts of oxygen derived from the coordinated hydroxo group, and this is so in both the presence (experiments 5, 6) and the absence (experiment 7) of phosphate buffer. For $[Co(en)_2(glyO)]^{2+}$ produced in phosphate buffer 90% of the oxygen label is retained whereas the $[Co(en)_2(glyglyOC_3H_7)]_{3+}$ ion retains ~75% of the maximum enrichment (which is half of the solvent enrichment). The former result is similar to that found at pH 3.77, and the discrepancy from 100% probably results from some loss of the label during isolation and/or dilution during analysis. Similar lower than expected retentions have been found in other studies involving these complexes.[9,15] The extra analytical step necessary for the 3+ product may result in the larger discrepancy in this ion, but if it is remembered that ~10% of the hydroxo reactant is the trans species, then the reaction conditions and analytical procedures will result in this appearing in the 3+ product. Since this part occurs by displacement of coordinated water (or hydroxide), correction of the experimental result leads to ~90% retention of ^{18}O label in $[Co(en)_2(glyglyOC_3H_7)]^{3+}$ produced from the cis reactant in phosphate buffer. A similar correction is necessary for the 3+ ion obtained in the absence of phosphate (experiment 7), but the lower result for both the 3+ and 2+ ions in this case suggests some (~6%) water exchange in the cis-hydroxo reactant in 15 h at pH 8.77.

These results dictate the origin of the two products given by eq 9 under the different pH conditions and are of importance when the mechanistic implications are discussed. These are considered in detail in a following publication.[23]

Registry No. *cis*-$[Co(en)_2Br(glyNH_2)]Br_2$, 67784-67-2; *cis*-$[Co(en)_2Br(glyglyOCH_3)]Br_2$, 67784-68-3; *cis*-$[Co(en)_2Br(glyglyOC_3H_7)]Br_2$, 67784-69-4; *cis*-$[Co(en)_2Br(glyglyOH)]Br_2$, 67842-94-8; $(+)_{589}$-$[Co(en)_2Br(glyglyOC_3H_7)]((+)_{589}$-$CS)_2$, 67843-78-1; $(+)_{589}$-$[Co(en)_2Br(glyglyOC_3H_7)]Br_2$, 67842-95-9; $(+)_{589}$-$[Co(en)_2Br(glyNH_2)]Br_2$, 30931-80-7; $(-)_{589}$-$[Co(en)_2Br(glyNH_2)]Br_2$, 30931-81-8; $(+)_{589}$-$[Co(en)_2Br(glyglyOC_3H_7)](NO_3)_2$, 67844-45-5; *cis*-$[Co(en)_2Br(glyNHCH_2CO_2C_2H_5)]^{2+}$, 67784-70-7; *cis*-$[Co(en)_2Br(glyNHCH_2CO_2)]^+$, 67842-89-1; $[Co(en)_2(glyO)]^{2+}$, 16070-98-7; *cis*-$[Co(en)_2(OH)(glyglyOC_3H_7)]^{2+}$, 67842-90-4; $[Co(en)_2(glyglyOC_3H_7)]^{3+}$, 67844-22-8; $[Co(en)_2(glyNHCH_2CO_2)]^{2+}$, 20528-43-2; $[Co(en)_2(OH)(glyNHCH_2CO_2)]^+$, 67842-91-5; $[Co(en)_2(glyNH_2)]^{3+}$, 30931-79-4; *cis*-$[Co(en)_2(OH)(glyNH_2)]^{2+}$, 53402-85-0; *trans*-$[Co(en)_2(OH)(glyNH_2)]^{2+}$, 67842-92-6; *trans*-$[Co(en)_2(OH_2)(glyNH_2)]^{3+}$, 67842-93-7; *trans*-$[Co(en)_2(OH)(glyglyOC_3H_7)]^{2+}$, 67784-61-6; *trans*-$[Co(en)_2(OH_2)(glyglyOC_3H_7)]^{3+}$, 67784-62-7; *cis*-$[Co(en)_2(OH_2)(glyglyOC_3H_7)]^{3+}$, 67842-86-8; *cis*-$(+)_{589}$-$[Co(en)_2(OH_2)(glyglyOC_3H_7)]^{3+}$, 67842-87-9; *cis*-$(+)_{589}$-$[Co(en)_2(OH)(glyglyOC_3H_7)]^{2+}$, 67842-88-0; $(+)_{589}$-$[Co(en)_2(glyO)]^{2+}$, 19657-80-8; $(+)_{589}$-$[Co(en)_2(glyglyOC_3H_7)]^{3+}$, 67784-63-8; *cis*-$(+)_{589}$-$[Co(en)_2Br(glyNHCH_2CO_2)]^+$, 67784-64-9; D-*cis*-$[Co(en)_2(OH)(glyNH_2)]^{2+}$, 53346-40-0; D-*cis*-$[Co(en)_2(glyNH_2)]^{3+}$, 62357-85-1; *trans*-$[Co(en)_2Br_2]Br$, 15005-14-8; Hg^{2+}, 14302-87-5; $glyglyOCH_3$·HCl, 2776-60-5; $glyglyOC_3H_7$·HCl, 67784-60-5; HOCl, 7790-92-3.

Supplementary Material Available: Table VI containing spectrophotometric rate data for reactions of the isolated *trans*-$[Co(en)_2(OH)(glyNHR)]^{2+}$ ions; Figure 4 containing visible absorption and ORD spectra for optically pure $(+)_{589}$-$[Co(en)_2(glyglyOC_3H_7)]^{3+}$ and $(+)_{589}$-$[Co(en)_2(glyO)]^{2+}$; Figure 5 containing ORD curves for $(+)_{589}$-$[Co(en)_2(OH_2)(glyglyOC_3H_7)]^{3+}$, $(+)_{589}$-$[Co(en)_2(OH)(glyglyOC_3H_7)]^{2+}$, $(+)_{589}$-$[Co(en)_2(glyO)]^{2+}$, $(+)_{589}$-$[Co(en)_2(glyglyOC_3H_7)]^{3+}$, and $(+)_{589}$-$[Co(en)_2(glyO)]^{2+}$ (3 pages). Ordering information is given on any current masthead page.

References and Notes

(1) A recent review gives a summary of metal ion catalysis of amino acid esters and peptides: R. W. Hay and P. J. Morris in "Metal Ions in Biological Systems", Vol. 5, H. Sigel, Ed., Marcel Dekker, New York, 1976, p 173.

(2) (a) D. A. Buckingham and L. M. Engelhardt, *J. Am. Chem. Soc.*, 97, 5915 (1975); (b) R. B. Martin, *J. Inorg. Nucl. Chem.*, 38, 511 (1976); (c) D. A. Palmer and G. M. Harris, *Inorg. Chem.*, 13, 965 (1974), and references therein; (d) R. Breslow, D. E. McClure, R. S. Brown, and J. Eisenach, *J. Am. Chem. Soc.*, 97, 194 (1975); (e) P. Woolley, *J. Chem. Soc., Perkin Trans. 2*, 318 (1977).

(3) D. Pinnell, G. B. Wright, and R. B. Jordan, *J. Am. Chem. Soc.*, 94, 6104 (1972).

(4) D. A. Buckingham, F. R. Keene, and A. M. Sargeson, *J. Am. Chem. Soc.*, 95, 5649 (1973).

(5) D. A. Buckingham, P. J. Morris, A. M. Sargeson, and A. Zanella, *Inorg. Chem.*, 16, 1910 (1977), and references therein.

(6) See D. A. Buckingham, *Biol. Aspects Inorg. Chem.* [*Symp.*], 141 (1977).

(7) M. D. Alexander and D. H. Busch, *J. Am. Chem. Soc.*, 88, 1130 (1966).

(8) D. A. Buckingham, D. M. Foster, and A. M. Sargeson, *J. Am. Chem. Soc.*, 90, 6032 (1968).

(9) D. A. Buckingham, D. M. Foster, L. G. Marzilli, and A. M. Sargeson, *Inorg. Chem.*, 9, 11 (1970).

(10) D. A. Buckingham, C. E. Davis, D. M. Foster, and A. M. Sargeson, *J. Am. Chem. Soc.*, 92, 5571 (1970).

(11) D. A. Buckingham, J. M. Harrowfield, and A. M. Sargeson, *J. Am. Chem. Soc.*, 96, 1726 (1974).

(12) S. K. Oh and C. B. Storm, *Biochemistry*, 13, 3250 (1974).

(13) D. A. Buckingham, L. G. Marzilli, and A. M. Sargeson, *J. Am. Chem. Soc.*, **89**, 4539 (1967); D. A. Buckingham, J. Dekkers, A. M. Sargeson, and M. Wein, *ibid.*, **94**, 4032 (1972).
(14) D. A. Buckingham, D. M. Foster, and A. M. Sargeson, *J. Am. Chem. Soc.*, **92**, 5701 (1970).
(15) D. A. Buckingham, D. M. Foster, and A. M. Sargeson, *J. Am. Chem. Soc.*, **91**, 4102 (1969).
(16) E. Baraniak, Ph.D. Thesis, The Australian National University, March 1973.
(17) D. A. Buckingham, D. M. Foster, and A. M. Sargeson, *J. Am. Chem. Soc.*, **92**, 6151 (1970).
(18) D. A. Buckingham, A. M. Sargeson, and A. Zanella, *J. Am. Chem. Soc.*, **94**, 8246 (1972).
(19) D. A. Buckingham, F. R. Keene, and A. M. Sargeson, *J. Am. Chem. Soc.*, **96**, 4981 (1974).
(20) J. Springbørg and C. E. Schäffer, *Inorg. Synth.*, **14**, 63 (1973).
(21) J. Meisenheimer, *Justis Liebigs Ann. Chem.*, **438**, 217 (1924); D. A. Buckingham, C. E. Davis, and A. M. Sargeson, *J. Am. Chem. Soc.*, **92**, 6159 (1970), and references therein.
(22) See ref 17, and M. D. Alexander and D. A. Busch, *Inorg. Chem.*, **5**, 602 (1966).
(23) C. J. Boreham, D. A. Buckingham, and F. R. Keene, to be submitted for publication.
(24) M. Anbar and S. Guttman, *Int. J. Appl. Radiat. Isot.*, **5**, 223 (1959).
(25) F. A. Posey and H. Taube, *J. Am. Chem. Soc.*, **79**, 255 (1957).
(26) I. K. Reid and A. M. Sargeson, unpublished results.
(27) C. J. Boreham, D. A. Buckingham, and D. J. Francis, unpublished results.
(28) D. A. Buckingham, I. I. Olsen, A. M. Sargeson, and H. Satrapa, *Inorg. Chem.*, **6**, 1027 (1967); D. A. Loeliger and H. Taube, *ibid.*, **5**, 1376 (1966).
(29) J. F. Remar, D. E. Pennington, and A. Haim, *Inorg. Chem.*, **4**, 1832 (1965).
(30) D. A. Buckingham, I. I. Olsen, and A. M. Sargeson, *J. Am. Chem. Soc.*, **90**, 6654 (1968).
(31) J. O. Edwards, F. Monacelli, and G. Ortaggi, *Inorg. Chim. Acta*, **11**, 47 (1974).
(32) S. C. Chan and F. K. Chan, *Aust. J. Chem.*, **23**, 1175 (1970).
(33) R. S. Nyholm and M. L. Tobe, *J. Chem. Soc.*, 1707 (1956).
(34) C. J. Boreham, Ph.D. Thesis, The Australian National University, 1978.
(35) D. F. Martin and M. L. Tobe, *J. Chem. Soc.*, 1388 (1962).
(36) A. Haim and H. Taube, *J. Am. Chem. Soc.*, **85**, 3108 (1963).
(37) D. A. Buckingham, L. G. Marzilli, and A. M. Sargeson, *J. Am. Chem. Soc.*, **89**, 2772 (1967).

[Reprinted from the Journal of the American Chemical Society, 101, 1409 (1979).]

Intramolecular Hydrolysis of Glycinamide and Glycine Dipeptides Coordinated to Cobalt(III). 2. Reactions of the *cis*-$[Co(en)_2(OH_2/OH)(glyNHR)]^{3+/2+}$ Ions (R = H, $CH_2CO_2C_3H_7$, $CH_2CO_2^-$) and the Effect of Buffer Species

C. J. Boreham, D. A. Buckingham,*† and F. R. Keene†

Contribution from the Research School of Chemistry, Australian National University, Canberra, A.C.T., Australia 2600. *Received April 19, 1978*

Abstract: The intramolecular addition of cobalt(III) bound H_2O and OH^- to glycinamide, glycylglycine isopropyl ester, and glycylglycine also coordinated to Co(III) in the *cis*-$[Co(en)_2(OH_2/OH)(glyNHR)]^{3+/2+}$ ions (R = H, $CH_2CO_2C_3H_7$, $CH_2CO_2^-$) has been investigated both in the absence and presence of buffers. For the dipeptide complex (R = $CH_2CO_2C_3H_7$) both the aqua and hydroxo species form $[Co(en)_2(glyO)]^{2+}$, but loss of hydroxide also occurs resulting in the chelated amide $[Co(en)_2(glyNHR)]^{3+}$. A combination of rate and product analysis data suggests that the initial cyclization is rate determining under all conditions. Buffer species act as general bases in this rate-determining process, but they also enhance the formation of the hydrolysis product. Coordinated water is more reactive than coordinated hydroxide owing largely to a more positive $\Delta S^{\ddagger}$.

In this paper we compare the hydrolysis of glycinamide, glycylglycine, and glycylglycine isopropyl ester coordinated to Co(III) as monodentate ligands to the hydrolysis of the same substrates chelated to Co(III). In the former *cis*-$[Co(en)_2(OH_2/OH)(glyNHR)]^{3+/2+}$ species the amide or dipeptide is attached to the metal through the amino group only, whereas in $[Co(en)_2(glyNHR)]^{3+}$ the oxygen atom of the amide function is also coordinated. The two reactions are schematically represented by Schemes I and II (the oxygen atoms show the fate of hydroxide in the different situations).

^{18}O-Tracer results have established that the coordinated oxygen atom in *cis*-$[Co(en)_2(OH_2/OH)(glyNHR)]^{3+/2+}$ is retained in the hydrolyzed product $[Co(en)_2(glyO)]^{2+}$, and that under alkaline conditions the $[Co(en)_2(glyNHR)]^{3+}$ product also includes the label in the O-bound amide function.[1] These facts require hydrolysis of the monodentate and chelated amide systems **1** and **2** to be interconnected, and in this respect this study bears a close resemblance to the non-metal-catalyzed lactonization of 4-hydroxybutyramides[2,3] and 2-hydroxymethylbenzamides[4,5] where direct intramolecular participation

† Department of Chemistry and Biochemistry, James Cook University of North Queensland, Townsville, Queensland, Australia 4811 (F.R.K.), and Department of Chemistry, University of Otago, P.O. Box 56, Dunedin, New Zealand (D.A.B.).

Scheme I

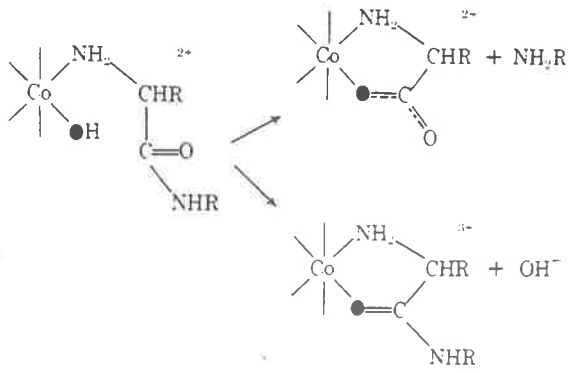

Scheme II

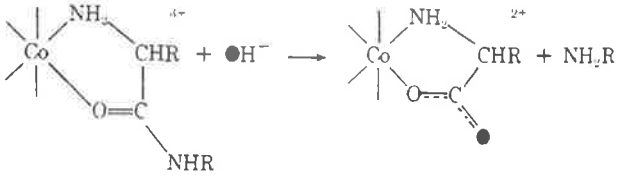

Scheme III

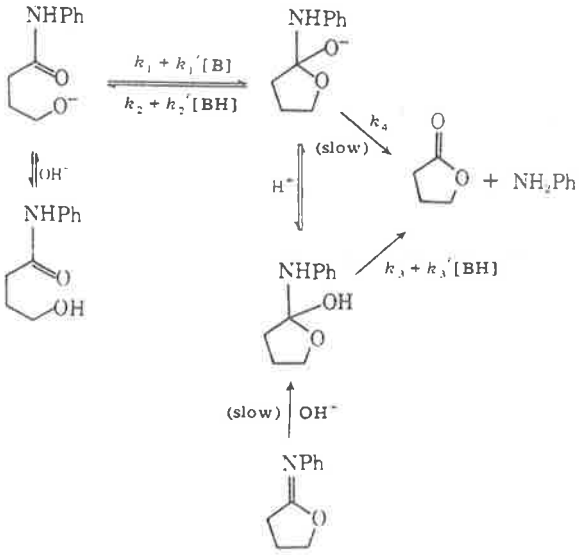

by the hydroxyl group has been suggested. The mechanistic schemes advanced in this latter study are therefore of particular relevance to this report.

For both the aliphatic 4-hydroxybutyranilides[2,3] and the more constrained 2-hydroxymethylbenzamide derivatives[4,5] the rate data in neutral and alkaline solution (pH 5–13) have been interpreted in terms of a change from rate-determining attack of alcoholate anion (k_1, $[OH^-]$ dependent) at pH <8 to rate-determining loss of amine from the neutral (k_3, overall $[OH^-]$ independent) and anionic (k_4, overall $[OH^-]$ dependent) forms of the addition intermediate (Scheme III). Phosphate and carbonate buffers were found to catalyze these processes in slightly alkaline solution (pH ~9), and the nonlinear[5] or asymptotic[3] plots of k_{obsd} vs. [buffer] were interpreted as resulting from a change from rate-determining buffer-catalyzed loss of amine from the neutral intermediate (k_3' [BH]) to cyclization of the alcoholate anion (k_1'[B][5] or k_1,[3] respectively). Parallel studies on the more rapidly hydrolyzing iminolactones[5-7] substantiated this view since the product was diverted from the hydroxy amide to amine plus lactone on addition of buffers.

The chemistry given here closely resembles the above, with i (i.e., *cis*-$[Co(en)_2(OH)(glyNHR)]^{2+}$) being the metal-

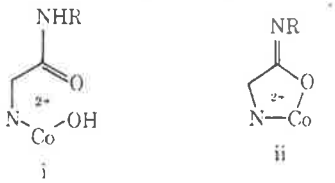

containing analogue of the 4-hydroxy amide and ii (i.e., the conjugate base form of $[Co(en)_2(glyNHR)]^{3+}$) being the metal analogue of the iminolactone. Buffers, particularly bifunctional ones (HPO_4^{2-}, HCO_3^-), also greatly accelerate the metal cyclization reactions, and saturation kinetics are approached under certain conditions. However, the presence of the metal accelerates these processes enormously compared with their organic counterparts, and this and other features have led us to a somewhat different interpretation of the mechanism.

Such differences allow interesting alternatives to the usual role found or anticipated for metal ions in hydrolytic situations.[8,9] Especially the facile intramolecular route for hydrolysis by coordinated water, and the proton tunnelling mechanism used to explain it, have not been described previously. This provides an interesting, and possibly important, alternative to previous schemes advanced for metal-containing hydrolytic enzymes such as carboxypeptidase A.[10,11] It also demonstrates that water (or a hydroxyl function such as a serine residue) in the correct environment can be a very potent nucleophile even though its intrinsic basicity may be low. This has obvious implications for proteolytic enzymes in general.

Experimental Section

Analytical quality reagents were used throughout without further purification. Other materials used are considered in the previous paper.[1] Methyl phosphate and dimethyl phosphate were prepared and recrystallized to analytical purity by the methods of Bunton[12] and Bailly,[13] respectively. Buffer pK_as (μ = 1.0, $NaClO_4$, 25.0 °C) were determined by titration against standard acid or alkali.

Preparation of the *cis*-$[Co(en)_2(OH_2/OH)(glyNHR)]^{3+/2+}$ Ions. For the dipeptide species (R = $CH_2CO_2C_3H_7$, $CH_2CO_2H/CH_2CO_2^-$) the reactant was normally prepared by base hydrolyzing *cis*-$[Co(en)_2Br(glyNHR)]Br_2$ and removing the chelated amide $[Co(en)_2(glyNHR)]^{3+}$ by ion-exchange chromatography at ~2 °C (0.5 M $NaClO_4$, pH 8).[1,14] However, some kinetic runs were carried out on the combined products of base hydrolysis (without ion-exchange separation), and some on the ion-exchange separated product obtained from the reaction with HOCl. Details of these reactions have been given previously.[1] For the glycinamide ions (R = H) kinetic measurements were carried out using the cis species generated by base hydrolysis without ion-exchange removal of $[Co(en)_2(glyNH_2)]^{3+}$. The aquaglycinamide ion reacts too rapidly ($t_{1/2} \simeq 80$ s, 25 °C) to allow it to be used following the HOCl-catalyzed removal of Br.[1]

Product analyses were carried out using the ion-exchange purified reactants (R = $CH_2CO_2C_3H_7$, H). This contains ~9% *trans*-$[Co(en)_2(OH)(glyNHR)]^{2+}$ and allowance is made for this in the results.

Other Preparations 1. $[Co(en)_2(glyglyOC_3H_7)](NO_3)_3$. *cis*-$[Co(en)_2Br(glyglyOC_3H_7)]Br_2 \cdot H_2O$ (7.55 g) and $AgClO_4$ (8.05 g) were shaken for 2 h in acetone (250 mL). AgBr was removed, and the filtrate was taken to dryness. The crude product was purified using ion-exchange chromatography (SP- Sephadex C-25 resin). Unreacted starting material was removed using 0.2 M $NaClO_4$, and the orange 3+ product recovered using 0.5 M pyridinium acetate. The eluate (ca. 2 L) was reduced to dryness and the residue dissolved in H_2O and passed through anion exchange resin (DEAE-Sephadex A-25, NO_3^- form). The eluate volume was reduced to ca. 30 mL, $LiNO_3$ and MeOH were added until crystallization commenced, and the solution was added to well-stirred 2-propanol (750 mL). The orange-yellow precipitate was washed with 2-propanol and ether and dried under

Table II. pK_a and Rate Constants for the Unbuffered Reactions of *cis*-[Co(en)$_2$(OH$_2$/OH)(glyNHR)]$^{3+/2+}$ at 25.0 ° C, μ = 1.0 ($NaClO_4$)

complex (R)		pK_a[a]	k_H,[b] s^{-1}	k'_{OH},[b] s^{-1}	k_{OH},[b] M^{-1} s^{-1}
H		6.15 ± 0.1	9.2×10^{-3}	1.5×10^{-4}	2.0
	(20 °C)	6.1 ± 0.1	5.8×10^{-3}	1.1×10^{-4}	1.6
	(30.5 °C)	6.0	1.64×10^{-2}	2.2×10^{-4}	2.8
	(36 °C)	5.8	3.0×10^{-2}	3.45×10^{-4}	3.9
	(25 °C, in D_2O)	6.6	8.25×10^{-3} [c]	1.21×10^{-4} [c]	
CH_2CO_2H		2.9[d]	3.3×10^{-4}		
$CH_2CO_2^-$		6.1	7.9×10^{-4}	7.9×10^{-5}	4.5×10^{-2}
$CH_2CO_2C_3H_7$		6.02	3.3×10^{-4}	4×10^{-5}	0.18
	(25 °C, in D_2O)		3.07×10^{-4} [c]		

[a] Acidity constant for [Co(en)$_2$(OH$_2$)(glyNHR)]$^{3+}$ species, eq 3 of text, 25.0 °C, μ = 1.0 ($NaClO_4$). [b] From computer fit of rate data (Table I, Figures 1-3) to eq 3;[18] pK_w = 13.77 (25 °C), 13.94 (20 °C), 13.58 (30.5 °C), 13.42 (36.5 °C). [c] In D_2O. Observed or calculated rate constants (see text) using pK_w = 14.94[48] and pD = pH + 0.4.[16] [d] pK_a for process *cis*-[Co(en)$_2$(OH$_2$)(glyglyOH)]$^{3+}$ ⇌ *cis*-[Co(en)$_2$(OH$_2$)(glyglyO)]$^{2+}$ + H$^+$.

vacuum: yield 3.0 g (45%); ϵ_{487} 98, ϵ_{342} 111; ^{1}H NMR (C_3H_7) 1.08 (doublet) ppm. Anal. Calcd for [Co(en)$_2$(glyglyOC$_3$H$_7$)](NO$_3$)$_3$·H$_2$O: C, 23.7; H, 5.8; N, 22.6. Found: C, 23.7; H, 5.8; N, 22.5.

2. [Co(en)$_2$(glyglyO)](ClO$_4$)$_2$·H$_2$O. $AgClO_4$ (3.2 g) was added to *cis*-[Co(en)$_2$ Br(glyglyOH)]Br$_2$·2H$_2$O (3.0 g) in acetone (100 mL). After 2 h of shaking AgBr was removed and the filtrate reduced to dryness. The product was recrystallized by dissolution in H_2O (10 mL) and adding 0.5 M LiOH solution to pH 6, followed by solid $LiClO_4$ and ethanol. The orange product was washed with ethanol and ether and air dried, yield 2.0 g (78%). Anal. Calcd for [Co(en)$_2$(glyglyO)](ClO$_4$)$_2$·H$_2$O: C, 18.2; H, 4.8; N, 15.9. Found: C, 18.3; H, 5.0; N, 15.8.

3. [Co(en)$_2$(glyNH$_2$)](NO$_3$)$_2$(ClO$_4$) was prepared as described previously.[15]

Kinetic Measurements. Solutions of [Co(en)$_2$(OH)(glyNHR)]$^{2+}$ at pH ~8 were adjusted to μ = 1.0 with $NaClO_4$, and the rate data obtained spectrophotometrically (560 nm (hydroxo), 487 (aqua)), and on occasions by acid or base uptake (0.05 M NaOH, 0.05 M $HClO_4$) using a 3.2-cm thermostated cell under pH-stat control fitted to a Cary 16 K spectrophotometer. For runs in the absence of buffer the pH was rapidly brought to the desired value by syringe or titrimeter addition of acid or base and acceptable data were obtained within 15 s of addition. For runs in the presence of buffers, the desired amount of buffer was rapidly added by syringe or pipet; and the pH maintained by pH-stat control during the remainder of the run. For all experiments at pH >6 it was found essential to use nitrogen-saturated solutions under a nitrogen atmosphere since traces of CO_2 were found to cause spurious effects.

For hydrolysis of the [Co(en)$_2$(glyNHR)]$^{3+}$ ions (R = $CH_2CO_2C_3H_7$, H) a weighed amount of the complex was dissolved in 1.0 M $NaClO_4$ or 0.1 M KCl, and rate data were obtained using the pH-stat equipment and Cary 16 spectrophotometer (280-300 nm). Buffers were added as appropriate by syringe injection.

Product Analysis Experiments. For R = $CH_2CO_2C_3H_7$, $CH_2CO_2H/CH_2CO_2^-$, the solutions from the kinetic runs (>6$t_{1/2}$) were quenched to pH ~4 (HOAc) and the products determined spectrophotometrically (487 nm) and by atomic absorption for Co following absorption on, and elution from, Dowex 50Wx2 cation exchange resin (1 M $HClO_4$/1 M $NaClO_4$ (2+ band), 1 M $HClO_4$/3 M $NaClO_4$ (3+ band)). Experiments were also carried out on larger quantities of material obtained following ion-exchange chromatography (SP-Sephadex, 0.5 M $NaClO_4$, pH 8, 2 °C), by directly quenching into acid, base, or phosphate buffer without following the reaction rates. This latter procedure was used for the R = H complex.

pK_a Measurements. pK_a values for the aqua complexes (R = $CH_2CO_2C_3H_7$, $CH_2CO_2^-$) were measured by titrating ~10^{-3} M solutions of the hydroxo complexes (1.0 M $NaClO_4$, pH (initial) ~8) with 0.1 M $HClO_4$ and following the spectral change at 560 nm. The pK_a was taken as the inflection point in the plot of OD vs. pH. For R = H the titration was carried out rapidly (2 min) since the aqua complex is rather reactive ($t_{1/2} \simeq$ 80 s). pK_a values are given in Table II. A similar procedure was used in D_2O except that the deuteroxy amide species was not isolated from the combined products of base hydrolysis. pD was estimated using the expression pD = pH + 0.4.[16] The glass electrode was standardized at 25.0 °C against borate (pH 9.18) and phosphate (pH 6.86) buffers.

Results

1. Reactions of the *cis*-[Co(en)$_2$(OH$_2$/OH)(glyNHR)]$^{3+/2+}$ Ions in the Absence of Buffers. It was found essential to use pH-stat methods to control the pH for the uncatalyzed reactions. Spectrophotometric rate data (D_t) for the three complexes were collected at 487 (aqua) and 560 nm (hydroxo) and are given in Table I for 1.0 M $NaClO_4$ and 0.1 M KCl solutions (supplementary data); similar rate data were obtained from the uptake of acid ($[V_H]_t$ pH-stat) resulting from protonation of released NH_3 or glycine isopropyl ester. For the dipeptide ester complex the optically pure (HOCl produced) and racemate ions gave identical data. For the aqua ions under acid conditions (pH <7) subsequent hydrolysis of the chelated amide ion [Co(en)$_2$(glyNHR)]$^{3+}$ formed as one of the products (R = $CH_2CO_2C_3H_7$, $CH_2CO_2H/CH_2CO_2^-$) does not occur in the times involved, but above pH 9 its rate of hydrolysis becomes comparable with, and then exceeds, that of the hydroxo amide. However, at 560 nm this hydrolysis results in only very small OD changes (<0.01) and could be ignored in the kinetic analysis. Plots of log ($D_\infty - D_t$) or log ($[V_H]_\infty - [V_H]_t$) vs. time were linear for at least 3$t_{1/2}$ for most runs and, except for the hydroxoglycinamide complex at high pH (>11), only one process was observed. For R = $CH_2CO_2C_3H_7$, $CH_2CO_2^-$, the data above pH 12 were complicated by the release of some dipeptide and the formation of a decomposition product. This was not investigated further but product analysis experiments showed that in 1 M NaOH this amounted to ~10% of the reaction.

Plots of log k_{obsd} vs. pH are given in Figures 1-3 and clearly show (except for [Co(en)$_2$(OH$_2$)(glyglyOH)]$^{3+}$ in the pH range 2.5-4.0) three regions of reactivity. From pH 0 to 4 the rate is pH independent, from pH 4 to 9 the rate decreases commensurate with ionization of the coordinated water molecule, and at pHs >9 a term first order in [OH$^-$] predominates for the hydroxo amide complex. The overall rate expression takes the form

$$v = k_H[\text{Co(en)}_2(\text{OH}_2)(\text{glyNHR})^{3+}] + k'_{OH}[\text{Co(en)}_2(\text{OH})(\text{glyNHR})^{2+}] + k_{OH}[\text{Co(en)}_2(\text{OH})(\text{glyNHR}^{2+})][\text{OH}^-] \quad (1)$$

and can be expressed

$$k_{obsd} = \frac{K_a[\text{OH}^-]}{K_w + K_a[\text{OH}^-]}\left[\frac{k_H K_w}{K_a[\text{OH}^-]} + k'_{OH} + k_{OH}[\text{OH}^-]\right] \quad (2)$$

where K_w is the dissociation constant for water (13.77, 1.0 M $NaClO_4$, 25 °C)[17] and K_a is the dissociation constant for the aqua complex.

$$[\text{Co(en)}_2(\text{OH}_2)(\text{glyNHR})]^{3+} + H_2O \overset{K_a}{\rightleftharpoons} [\text{Co(en)}_2(\text{OH})(\text{glyNHR})]^{2+} + H_3O^+ \quad (3)$$

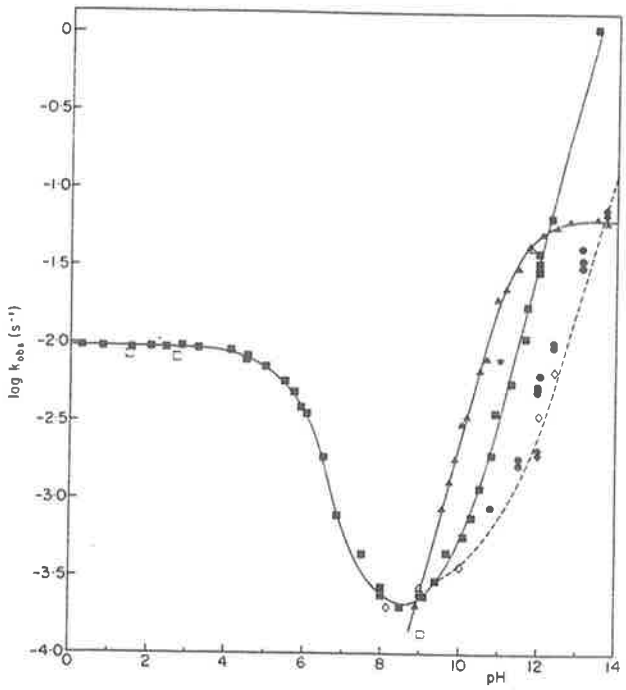

Figure 1. Log k_{obsd} values (■) vs. pH rate profile for the cyclization of *cis*-$[Co(en)_2(OH_2/OH)(glyNH_2)]^{3+/2+}$ at 25.0 °C and μ = 1.0 ($NaClO_4$). The slower reaction of the *trans*-hydroxo ion (- - - - -) observed spectrophotometrically at pH ≥10.8 is given by (●) in 0.1 M KCl and (♦) in 1.0 M KCl. Data for the isolated trans species are given by (◇), 1.0 M $NaClO_4$. Data for the cis ions in D_2O are given by (□), 1.0 M $NaClO_4$. Hydrolysis of the chelated amide $[Co(en)_2(glyNH_2)]^{3+}$ is given by (▲), and the same species obtained from the trans aqua ion by (△); data in D_2O is given by (✱). The solid lines (——) are in each case the best fit calculated curves using the rate expression given by eq 2 and 9, and the constants given in Table II and the text, respectively.

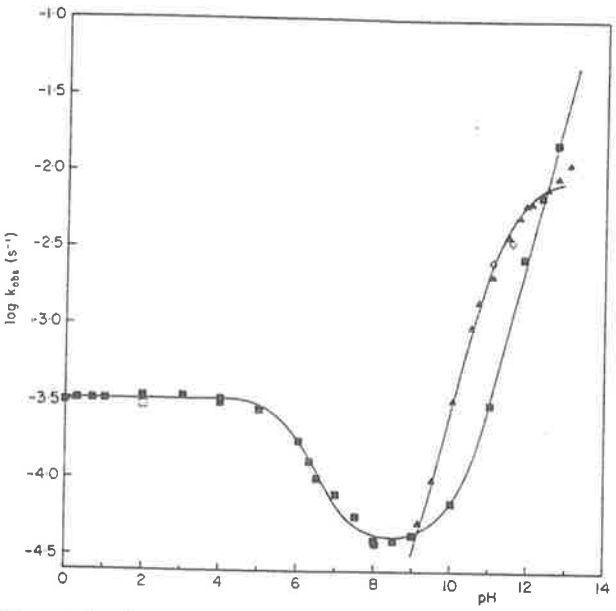

Figure 2. Log k_{obsd} values (■) vs. pH rate profile for the cyclization of *cis*-$[Co(en)_2(OH_2/OH)(glyglyOC_3H_7)]^{3+/2+}$ at 25.0 °C and μ = 1.0 ($NaClO_4$); data in D_2O is given by (□). Hydrolysis data for $[Co(en)_2(glyglyOC_3H_7)]^{3+}$ is given by (▲); the (△) and (◇) data were obtained from the similar ion produced from *trans*-$[Co(en)_2(OH_2)(glyglyOC_3H_7)]^{3+}$ and *trans*-$[Co(en)_2(OH)(glyglyOC_3H_7)]^{2+}$, respectively. The solid lines (——) are the best fit calculated curves obtained using the rate expressions of eq 2 and 9, and the constants given in Table II and the text, respectively.

The rate profile for the glycylglycinate complex (Figure 3) requires the addition of a term of the form $k_H[Co(en)_2(OH_2)(glyglyO)^{2+}]$ to accommodate the enhanced reactivity of the aquaglycylglycinate species (R = $CH_2CO_2^-$). A computer-simulated least-squares fit[18] of the data using separately measured K_a values (Table II) gives the solid curves of Figures 1–3. Values for k_H, k'_{OH}, and k_{OH} are listed in Table II.

Data obtained at 36.5, 30.5, 25.0, and 20.0 °C for $[Co(en)_2(OH_2/OH)(glyNH_2)]^{3+/2+}$ (Table I, μ = 1.0 ($NaClO_4$), supplementary data) resulted in linear Arrhenius plots for each of the three terms of eq 2 giving E_a and $\Delta S^{\ddagger}$ values of 18.3 ± 0.2 kcal mol^{-1} and −8 ± 2 cal deg^{-1} mol^{-1} for k_H, 12.5 ± 0.6 kcal mol^{-1} and −36 ± 4 cal deg^{-1} mol^{-1} for k'_{OH}, and 8.9 ± 0.3 kcal mol^{-1} and −32 ± 2 cal deg^{-1} mol^{-1} for k_{OH}. The last E_a value takes into account $\Delta H°$ for dissociation of H_2O.

Rate data in D_2O for $[Co(en)_2(OH_2)(glyNH_2)]^{3+}$ at pH (measured) 1.47 (pD 1.87[49]) and 2.63 (pD 3.03) gave k_{obsd} = 8.40×10^{-3} and 8.1×10^{-5} s^{-1}, respectively; similar data for $[Co(en)_2(OH_2)(glyglyOC_3H_7)]^{3+}$ at pH 2.0 (pD 2.4) gave $k_{obsd} = 3.07 \times 10^{-4}$ s^{-1}. For $[Co(en)_2(OH)(glyNH_2)]^{2+}$ at pH 9.0 (pD 9.4) $k_{obsd} = 1.35 \times 10^{-4}$ s^{-1}; under these conditions the aqua amide contributes 10.0% to k_{obsd}, whence k'_{OH} = 1.21×10^{-4} s^{-1}. These data (cf. Figure 1) give $k_{H/D}$ values of 1.11 for the aquaglycinamide complex and 1.24 for the hydroxoglycinamide species.

The reaction products are listed in Table III expressed as the ratio of 2+ ion (entirely $[Co(en)_2(glyO)]^{2+}$) to 3+ ion. For the dipeptide species (R = $CH_2CO_2C_3H_7$, CH_2CO_2H/$CH_2CO_2^-$) the 3+ ion is largely $[Co(en)_2(glyNHR)]^{3+}$ but contains 9 ± 1% *trans*-$[Co(en)_2(H_2O)(glyglyOR)]^{3+}$ for the reactions at pH 1–4; at pH 8 the 3+ product is entirely the chelated dipeptide but some 6% of it derives from the *trans*-hydroxo ion, the remaining 3% of the trans species being hydrolyzed to $[Co(en)_2(glyO)]^{2+}$. For the glycinamide ions (R = H) the 5–8% 3+ product is, or derives from, *trans*-$[Co(en)_2(OH_2)(glyNH_2)]^{3+}$ (pH 1.4) and, although the 3+ ion produced at pH 8 is $[Co(en)_2(glyNH_2)]^{3+}$, it similarly derives (6%) from the *trans*-hydroxo species. Thus the cis aqua- and hydroxoglycinamide ions produce very little or no chelated amide product under conditions where k_H and k'_{OH} control the rate (eq 2). The corresponding cis dipeptide ions form

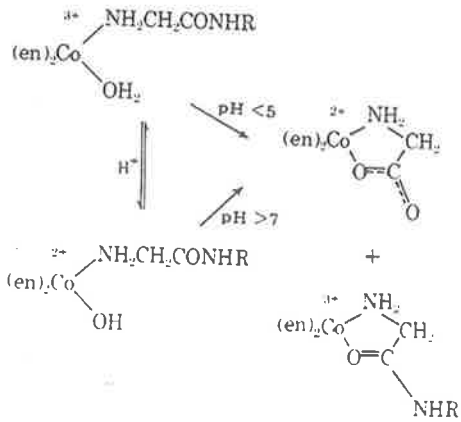

appreciable amounts of the chelated dipeptide species (≃50% for R = $CH_2CO_2C_3H_7$, ≃17% for R = $CH_2CO_2^-$) with the product ratio being little affected by pH. For R = CH_2CO_2H the aqua complex forms more chelated dipeptide (~50%) than the similar complex containing the carboxylate anion. At pH ~9 hydrolysis of $[Co(en)_2(glyNHR)]^{3+}$ becomes competitive with and then exceeds that for the hydroxo amide ion. This is shown in Figures 1–3 with k_{obsd} for the chelated amide being ~ten times that for the hydroxo amide between pH ~10 and 13. This prevents determination of the immediate reaction

Table III. Products of the Unbuffered (pH-Stat) Reactions of the [Co(en)$_2$(OH$_2$/OH)(glyNHR)]$^{3+/2+}$ Ions[a] as a Function of pH (25.0 °C, μ = 1.0 ($NaClO_4$)), Expressed as the Ratio [2+]/[3+][b]

R	pH and [2+]/[3+] ratio							
H	pH 1.0, 95/5			4.0, 94/6, 92/8			8.0[d] 90/10, 89/11	
$CH_2CO_2H/CH_2CO_2^-$ [c]	pH 0.3, 37/63	2.0, 52/48	3.0, 65/35	4.0, 77/23	5.0, 76/24	6.0, 75/25	7.0, 75/25	8.0,[d] 76/24
$CH_2CO_2C_3H_7$	pH 1.0, 46/54		3.0, 44/56	4.0, 43/57	5.0, 43/57		8.0,[d] 39/61, 40/60	

[a] Produced via base hydrolysis of the bromo complex. [b] The 2+ ion is in all cases [Co(en)$_2$(glyO)]$^{2+}$. For R = $CH_2CO_2C_3H_7$, $CH_2CO_2H/CH_2CO_2^-$ the 3+ ion is largely [Co(en)$_2$(glyglyOR)]$^{3+}$ but contains ~6% *trans*-[Co(en)$_2$(OH$_2$)(glyglyOR)]$^{3+}$ (pHs 1-4). For R = H the 3+ ion is, or derives entirely from, *trans*-[Co(en)$_2$(OH$_2$/OH)(glyNH$_2$)]$^{3+/2+}$. [c] pK_a = 2.9. [d] The ratio for the experiment at pH 8.0 is corrected for hydrolysis of the 3+ ion (to 2+) using data given in Figures 1-3.

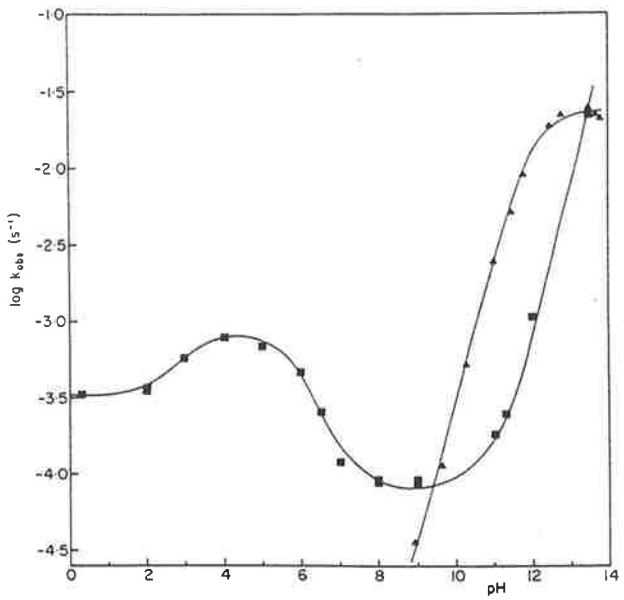

Figure 3. Log k_{obsd} values (■) vs. pH rate profile for the cyclization of *cis*-[Co(en)$_2$(OH$_2$/OH)(glyglyOH/glyglyO$^-$)]$^{3+/2+/1+}$ at 25.0 °C and μ = 1.0 ($NaClO_4$). Hydrolysis data for [Co(en)$_2$(glyglyO$^-$)]$^{2+}$ are given by (▲). The solid lines (——) are best fit calculated curves obtained using the rate expressions given by eq 2 and 9, and constants given in Table II and the text, respectively.

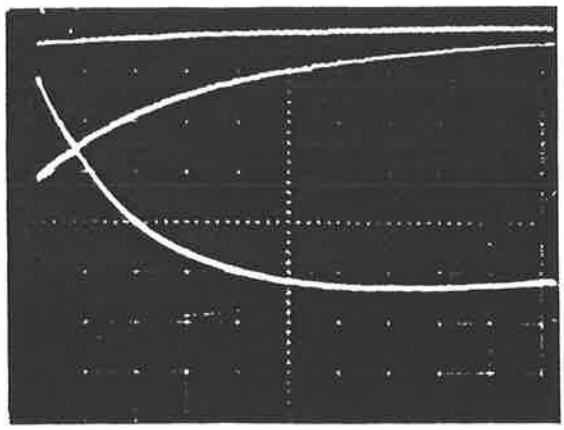

Figure 4. Stopped-flow trace of the change in OD at 560 nm for the reactants of [Co(en)$_2$(OH)(glyNH$_2$)]$^{2+}$ (generated by base hydrolysis of (+)$_{589}$[Co(en)$_2$Br(glyNH$_2$)]Br$_2$ in 0.5 M NaOH, 0.5 M KCl at 25.0 °C. The OD decreases (ordinate down) on time scale (abscissa) of 0.5 s/division, and the slower OD increase is at 5 s/division. Absorption range is 0-1.0, slit 0.1, time constant 10 ms.

products for the hydroxo amide when $k_{OH}[OH^-]$ is rate controlling (eq 2).

At pH >11 the spectrophotometric data (560 nm) for the hydroxoglycinamide complex shows two rate processes of which the first (OD decrease) agrees with that found at lower pHs and is consistent with the rate expression given by eq 2. The subsequent slower process involves an OD increase which becomes more pronounced with increasing pH. Figure 1 gives log k_{obsd} data for the process as a function of pH (1 M $NaClO_4$ and 0.1 M KCl) and Figure 4 gives a stopped-flow trace of the two processes in 0.5 M NaOH. Both reactions were observed with optically pure *cis*-(+)$_{589}$-[Co(en)$_2$Br(glyNH$_2$)]$^{2+}$ and they occurred irrespective of whether [Co(en)$_2$(glyNH$_2$)]$^{3+}$ produced in the initial base hydrolysis of bromide was present or had been previously removed by ion-exchange chromatography at 2 °C. Other experiments showed that [Co(en)$_2$(glyO)]$^{2+}$, also present with the hydroxo complex, was not involved; at the conclusion of the second reaction this species is in fact the major product (>95%). Subsequent experiments demonstrated that this "second reaction" was due to the small amount of *trans*-[Co(en)$_2$(OH)(glyNH$_2$)]$^{2+}$ (9%) present in the red 2+ band. The chemistry of this species is dealt with in a preceding paper.[1] The two rate processes were not observed for either hydroxo dipeptide species.

2. Buffer Catalysis. The addition of buffers affects both the rate and products of the reactions of the hydroxo and aqua amides; they are especially effective in alkaline solution where the hydroxo complex is involved. Tables IV-VI (supplementary data) give rate data for the three complexes [Co(en)$_2$(OH$_2$/OH)(glyNHR)]$^{3+/2+}$ (R = H, $CH_2CO_2C_3H_7$, $CH_2CO_2^-$, respectively) in various buffers, and Figure 5 gives the product analysis results for the dipeptide ester complex in acetate buffers.

The data show that the aquaglycinamide and aquadipeptide ester reactions (pH <5) are retarded by selenate (pK_a = 1.0), sulfate (1.0), phosphate (1.72), glycinate (2.42), furoate (3.16), and tartrate (3.4), with the more highly charged SeO_4^{2-} and SO_4^{2-} ions derived from the most acidic buffers being the most effective. Citrate (3.81, 4.91), succinate (5.2), maleate (5.8), and acetate (4.44) appear to catalyze the reaction slightly under conditions where appreciable amounts of the buffer anion and aqua complex are available. For these buffers the data fit the rate expression

$$v = k_H[\text{Co-OH}_2^{3+}] + k_B[\text{Co-OH}_2][B] + k'_{OH}[\text{Co-OH}^{2+}]$$

with

$$k_B = (k_{obsd} - k_{hyd})(K_a + [H^+])/[B][H^+] \qquad (5)$$

where K_a is the dissociation constant of the aqua complex and B is the basic form of the buffer. The reaction of the hydroxoglycinamide is not catalyzed by acetate (Table IV), and citrate at pH 9.5 has a retarding influence. This, and the observation of general base catalysis for other buffer anions in alkaline solution, suggests that the rate law be interpreted in

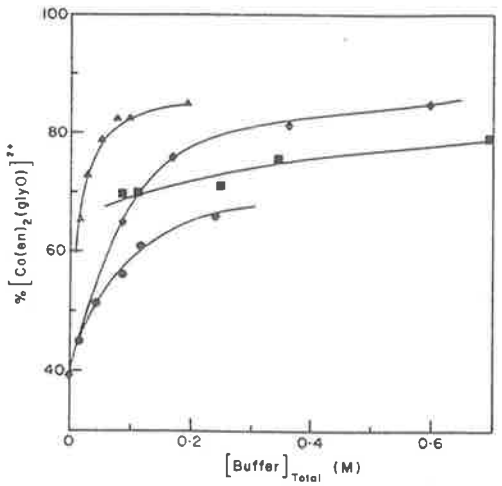

Figure 5. Products of the reaction of $[Co(en)_2(OH_2/OH)(glyglyOC_3H_7)]^{3+/2+}$ in the presence of acetate buffers at pH 4.60 (-♦-♦-♦-), and methyl phosphate buffers at pH 4.0 (-●-●-●), 6.32 (-▲-▲-▲-), and 8.20 (-■-■-■-) expressed as % $[Co(en)_2(glyO)]^{2+}$, the remainder being $[Co(en)_2(glyglyOC_3H_7)]^{3+}$ + 9% *trans*-$[Co(en)_2(OH_2)(OH_2)(glyglyOC_3H_7)]^{3+}$, μ = 1.0 ($NaClO_4$), 25.0 °C.

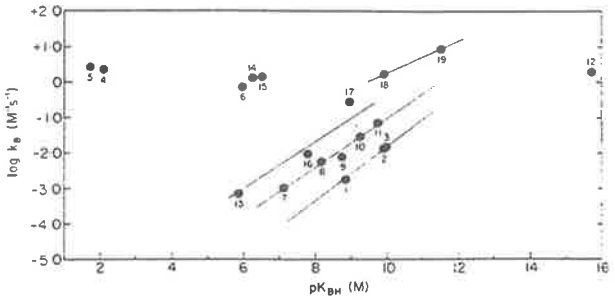

Figure 7. Brønsted plot of log k_B vs. pK_{BH} for the general-base-catalyzed reactions of *cis*-$[Co(en)_2(OH)(glyNH_2)]^{2+}$ at 25.0 ° C and μ = 1.0 ($NaClO_4$): (1) morpholine, (2) 3-quinuclidinol, (3) NEt_3, (4) $HMePO_4^-$, (5) $H_2PO_4^-$, (6) HCO_3^-, (7) *p*-nitrophenol, (8) *m*-nitrophenol, (9) $H_4BO_4^-$, (10) *p*-chlorophenol, (11) phenol, (12) OH^-, (13) $MePO_4^{2-}$, (14) $HAsO_4^-$, (15) HPO_4^{2-}, (16) SeO_3^{2-}, (17) CO_3^{2-}, (18) AsO_4^{3-}, (19) PO_4^{3-}.

terms of general base catalysis of the aqua complex rather than the alternative acid-catalyzed reaction of the hydroxo ions. The reactivity order is ($k_B < 0$, $pK_a < 3.5$) $SeO_4^{2-} \sim SO_4^{2-} < NH_3^+CH_2CO_2^- \sim$ furoate$^- \sim$ tartrate^{2-}; ($k_B > 0$, $pK_a > 4.4$) citrate^{2-} < acetate$^-$ < maleate^{2-} < succinate^{2-}. Product analysis results in the presence of acetate (Figure 5, pH 4.6) show that catalysis promotes the formation of $[Co(en)_2(glyO)]^{2+}$ at the expense of $[Co(en)_2(glyglyO\,C_3H_7)]^{3+}$ with a limiting product composition approaching 87 ± 2% 2+, 13 ± 2% 3+ at $[AcO^-] > 0.6$ M. Much of the 3+ ion derives from the trans aqua complex (see above) but some appears to be produced from the cis species by an acetate-dependent path (~5%).

Marked catalysis of the hydroxo amide reaction occurs with the more basic buffers ($pK_a > 6$), and this has been investigated in detail for $[Co(en)_2(OH)(glyNH_2)]^{2+}$ (Table IV, supplementary data); some data was also collected for the $[Co(en)_2(OH)(glyglyOC_3H_7)]^{2+}$ ion (Table V, supplementary data). For buffers with only a single protonation site (monofunctional buffers) the rate law takes the form

$$k_{obsd} = k'_{OH} + k_{OH}[OH^-] + \frac{k_B K_a[B]}{K_a + [H^+]}$$

Table VII. Second-Order Rate Constants (k_B) for the General-Base-Catalyzed Reactions of the *cis*-$[Co(en)_2(OH_2/OH)(glyNHR)]^{3+/2+}$ Ions (μ = 1.0 ($NaClO_4$), 25.0 °C)

general base B	*cis*-$[Co(en)_2(OH)(glyNH_2)]^{2+}$ 10^3k_B, M^{-1} s^{-1}	*cis*-$[Co(en)_2(OH)(glyglyOC_3H_7)]^{2+}$ 10^3k_B, M^{-1} s^{-1}	
SeO_3^{2-}	9		
p-nitrophenolate	1		
m-nitrophenolate	6		
$H_4BO_4^-$	7.8		
p-chlorophenolate	29		
phenolate	70	3.3	
3-quinuclidinolate	13	0.58	
NMe_3	14		
morpholinate	1.7		
PO_4^{3-}	9100	33[a]	(2)[b]
HPO_4^{2-}	1480	52[a]	(18.5)[b]
$H_2PO_4^-$	2700	120[a]	
$MePO_2^{2-}$	0.64	0.3	
$HMePO_4^-$	2150	81	
CO_3^{2-}	280		
HCO_3^-	730		
AsO_4^{3-}	1670		
$HAsO_4^{2-}$	1310		
$Me_2PO_4^-$	~0	0	
Gly		1.1	
n-$PrNH_2$		~0	
NEt_3		1.7	
Im		~0	
AcO^-	30[a]	2.3	
$Me_2PO_4^-$		~0	
Cit^{3-}		~0	
$HCit^{2-}$	15	~0	
H_2Cit^-	15	~0	
succinate^{2-}		5.3	
maleate^{2-}		4.6	
py		~0	

[a] 2 M $NaClO_4$. [b] Data for R = $CH_2CO_2^-$, μ = 1.0 ($NaClO_4$).

with

$$k_B = (k_{obsd} - k_{hyd})(K_a + [H^+])/K_a[B] \qquad (6)$$

where K_a is the acid dissociation constant of the complex and B is the basic component of the buffer; under conditions of pH well removed from the pK_a, $k_B = (k_{obsd} - k_{hyd})/[B]$. Values of k_{calcd} obtained using the k_B values listed in Table VII are compared with ($k_{obsd} - k_{hyd}$) in Tables IV and V (supplementary data) and it is clear that the basic form of the buffer is involved; Figure 6 (supplementary data) demonstrates this for trimethylamine and phenol. Values of k_B increase with increasing basicity and a plot of log k_B vs. pK_{BH} (Figure 7) shows separate linear correlations for the neutral, 1−, 2−, and 3− bases. The Brønsted slopes are similar for each set, $\beta \simeq 0.7$, consistent with a process involving nonlimiting general base catalysis. With the exception of phosphate and methyl phosphate, buffers of $pK_a < 6$ either retard the reaction (citrate^{3-}, SO_4^{2-}) or have no effect (AcO^-, furoate$^-$), and OH^- seems less effective than might be expected. In order to determine the immediate products of these catalyzed reactions it was necessary to use a buffer, and conditions, where no appreciable hydrolysis of the chelated dipeptide ester product could occur. Phenol (pK_a = 9.74) was chosen, and three experiments under the conditions $k_{obsd} = k_{C_6H_5O}[C_6H_5O^-]$ (1.0, 0.7, and 0.3 M phenolate ion, pH 9.8, μ = 1.0 ($NaClO_4$, 25 °C)) gave 94 ± 3% $[Co(en)_2(glyO)]^{2+}$ with the remainder being the 3+ ion. When it is remembered that some 9% of the reactant is the *trans*-hydroxo amide and that this will be largely unaffected by the conditions it is clear that the buffer diverts the products entirely to $[Co(en)_2(glyO)]^{2+}$. Similar less quantitative results were obtained with other buffers in this series.

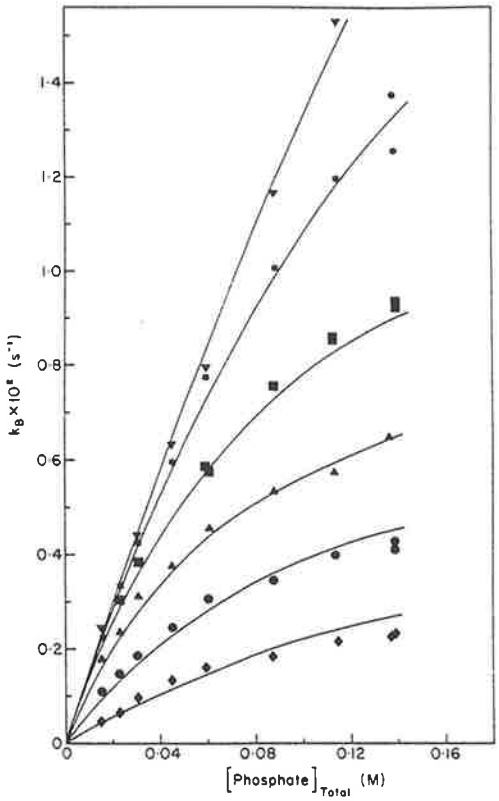

Figure 8. Plot of k_{obsd} vs. [phosphate]$_T$ for the cyclization of $[Co(en)_2(OH)(glyNH_2)]^{2+}$ as a function of pH, 25.0 °C, μ = 1.0 ($NaClO_4$): pH 5.20 (♦), 5.65 (●), 6.15 (▲), 6.70 (■), 7.28 (✱), 7.9 (▼). The solid curves are least squares fitted to eq 8 using $k_{H_2PO_4}$ = 2.7 (0.2), k_{HPO_4} = 1.44 (0.04) M^{-1} s^{-1}, and $K_1 = 2.4 \times 10^{-8}$, $K_2 = 2.06 \times 10^{-6}$. Data at higher pHs are given in Table VII.

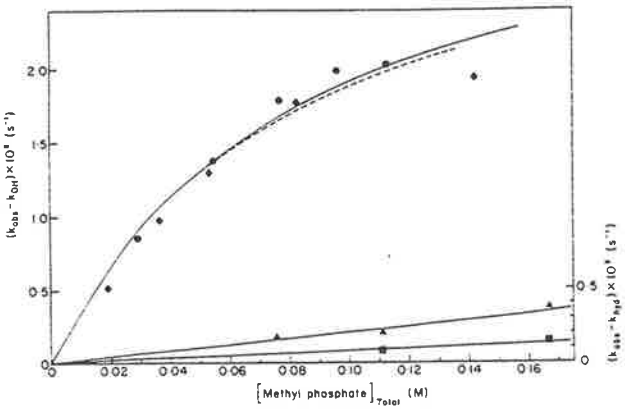

Figure 9. Plot of k_{obsd} vs. [methyl phosphate]$_T$ for the cyclization of *cis*-$[Co(en)_2(OH)(glyNH_2)]^{2+}$ as a function of pH, 25.0 °C, μ = 1.0 ($NaClO_4$): pH 5.74 (♦), 6.3 (●), 9.1 (▲), and 10.1 (■). The solid curves are least squares fitted to eq 8 using $k_{MePO_4} = 6.4 \times 10^{-4}$ M^{-1} s^{-1}, k_{HMePO_4} = 2.15 M^{-1} s^{-1}; $K_1 = 2.4 \times 10^{-8}$, $K_2 = 1.06 \times 10^{-6}$.

For phosphate, methyl phosphate, arsenate, and carbonate, which have more than one basic site, a more complex behavior was observed with both the acidic and basic forms of the buffer contributing to the rate. At pHs well removed from the pK_a of the aqua complex (pH >8.77) the data for $[Co(en)_2(OH)(glyNH_2)]^{2+}$ (Table VIII, supplementary data) and $[Co(en)_2(OH)(glyglyOC_3H_7)]^{2+}$ (Table IX, supplementary data) fit the expression

$$k_{obsd} = k' + k_{OH}[OH^-] + k_B[B] + k_{BH}[BH]$$

or

$$(k_{obsd} - k_{hyd}) = k_B[B] + k_{BH}[BH] \quad (7)$$

However, as the pH approaches the pK_a of the complex, this simple expression fails and a more complex behavior obtains. The data for $[Co(en)_2(OH)(glyNH_2)]^{2+}$ with phosphate and methyl phosphate (Figures 8 and 9, respectively), and for $[Co(en)_2(OH)(glyglyOC_3H_7)]^{2+}$ (Figures 10 and 11, supplementary data) show increasing curvature in the plots of $(k_{obsd} - k_{hyd})$ vs. [phosphate]$_T$ at low pH with a limiting rate being approached in ~0.2 M phosphate when pH $\simeq$ pK_a. The data fits expressions of the form

$$(k_{obsd} - k_{hyd}) = \frac{(k_{H_2PO_4}[H_2PO_4^-] + k_{HPO_4}[HPO_4^{2-}])[OH^-]}{K_1 + [OH^-] + K_2[HPO_4^{2-}]} \quad (8)$$

where $k_{H_2PO_4}$ (k_{HMePO_4}) and k_{HPO_4} (k_{MePO_4}) are rate constants and K_1 and K_2 are ratios of equilibrium constants. The least-squares fitted calculated curves[18] are given as solid lines in the figures ($k_{H_2PO_4}$, k_{HMePO_4}, K_2 fitted) with numerical values for the constants being given in the captions to the figures and in Table VII. It is clear that, whereas $H_2PO_4^{2-}$ and $HMePO_4^{2-}$ have similar catalytic effects, $MePO_4^{2-}$ is very much less effective than HPO_4^{2-}. The significance of this is discussed below.

The deuterium isotope effect was determined at pH 9.35 (pD 9.75)[16] using 0.0185 M phosphate buffer. The k_{obsd} value of 1.75×10^{-2} s^{-1} corresponds to k_{DPO_4} (D_2O) = 0.95 M^{-1} s^{-1}, and when compared with k_{HPO_4} (H_2O) = 1.44 M^{-1} s^{-1} gives k_H/k_D = 1.51.

The products of the phosphate and methyl phosphate catalyzed reactions also differ from those found in the presence of phenol buffers in that both $[Co(en)_2(glyO)]^{2+}$ and $[Co(en)_2(glyglyOC_3H_7)]^{3+}$ are formed. The results for phosphate are given in Figure 12 expressed as % $[Co(en)_2(glyO)]^{2+}$ with the remainder being *trans*-$[Co(en)_2(OH_2)(glyglyOC_3H_7)]^{3+}$ and $[Co(en)_2(glyglyOC_3H_7)]^{3+}$. A limiting composition of 85% $[Co(en)_2(glyO)]^{2+}$ is reached, or approached, under most conditions. Allowing for the 9 ± 1% trans aqua ion present in the initial reactant[1] the limiting composition from the *cis*-hydroxo reactant alone is 94% $[Co(en)_2(glyO)]^{2+}$. That a small amount of $[Co(en)_2(glyglyOC_3H_7)]^{3+}$ is formed by the phosphate-dependent process was confirmed in a separate experiment using $(+)_{589}$-$[Co(en)_2(OH)(glyglyOC_3H_7)]^{2+}$ prepared by base hydrolyzing the optically pure bromo complex.[1] Subsequent reaction at pH 6.64 (40 min) in the presence of 0.15 M phosphate buffer gave a recovered yield of 6.7% trans aqua free $[Co(en)_2(glyglyOC_3H_7)]^{3+}$ with $[M]_{589}$ = +634°. These conditions correspond to saturation formation of $[Co(en)_2(glyO)]^{2+}$ (Figure 12). It was calculated that of the 8.7% *trans*-hydroxo ion present in the initial reactant some 2.5% would have resulted in chelated dipeptide in the time of the experiment.[1] Thus 4.2% of the recovered $[Co(en)_2(glyglyOC_3H_7)]^{3+}$ product derives from the *cis*-hydroxo reactant, and the optical activity for this part ($[M]_{589}$ = +1011°, 62%) corresponds well with that found in the absence of buffers.[1] This suggests that full retention of configuration also obtains in the buffer-catalyzed reaction.

When modified for the trans contaminant and extrapolated to [phosphate]$_T$ = 0 the results of Figure 12 agree with those found in the absence of phosphate (cf. Table X). Finally, attention is drawn to the two other aspects of Figure 12 which will be discussed in detail below. Firstly, the limiting product composition at pH 6.7 is reached at lower phosphate concentrations than at pH 8–9. This suggests that $H_2PO_4^-$ promotes the formation of $[Co(en)_2(glyO)]^{2+}$ more effectively than does HPO_4^{2-} and this is to be contrasted with their similar k_B values

Table X. Products of the Unbuffered Reactions of *cis*-$[Co(en)_2(OH_2/OH)(glyNHR)]^{3+/2+}$ and Unimolecular Rate Constants for Hydrolysis (25 °C, μ = 1.0 ($NaClO_4$))

R	products[a] pH 1–4 (aqua complex)	products[a] pH 8 (hydroxo complex)	rate constant, s^{-1}[b] pH 1–4 (k_H')	rate constant, s^{-1}[b] pH ~9 (k'_{OH})
H	100 ± 2	97 ± 3	9.2×10^{-3}	1.5×10^{-4}
CH_2CO_2H	41 (pH 1)		1.35×10^{-4}	
$CH_2CO_2^-$	83 (pH 4)	80	6.6×10^{-4}	6.3×10^{-5}
$CH_2CO_2C_3H_7$	50 ± 2	41 ± 2	1.65×10^{-4}	1.6×10^{-5}

[a] Expressed as % $[Co(en)_2(glyO)]^{2+}$, the remainder being $[Co(en)_2(glyNHR)]^{3+}$. [b] Calculated rates using product analysis data (Table III).

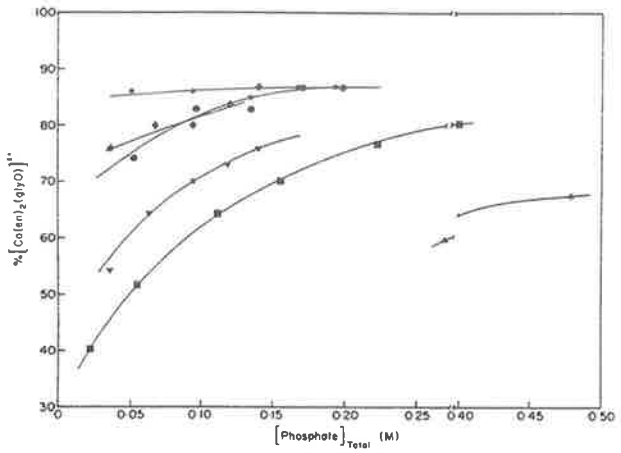

Figure 12. Product composition expressed as % $[Co(en)_2(glyO)]^{2+}$ for the phosphate-catalyzed reaction of $[Co(en)_2(OH)(glyglyOC_3H_7)]^{2+}$, 25.0 °C, μ = 1.0 ($NaClO_4$); 100 − % $[Co(en)_2(glyO)]^{2+}$ represents $[Co(en)_2(glyglyOC_3H_7)]^{3+}$ + 9% *trans*-$[Co(en)_2(OH_2)(glyglyOC_3H_7)]^{3+}$. pH 3.68 (▲), 5.76 (●), 6.64 (✱), 7.15 (♦), 7.71 (▼), 8.77 (■).

(Table VII). Secondly, the product distribution varies under conditions (pH 8.77, for example) where the rate law consists only of the $k_B[HPO_4^{2-}]$ term (eq 7). Thus the products are not decided by the composition of the rate-controlling transition state, and must result from subsequent events with differing phosphate dependencies.

A less detailed set of results for the products of the methyl phosphate catalyzed reaction of the hydroxo dipeptide are given in Figure 5. The data at pH 6.32 demonstrate that $HMePO_4^-$ also promotes the hydrolysis reaction but this again appears not to be exclusive since a limiting composition of 85% 2+, 14% 3+ is reached in 0.2 M buffer corresponding to 94% $[Co(en)_2(glyO)]^{2+}$ and 6% $[Co(en)_2(glyglyOC_3H_7)]^{3+}$ from this cis reactant. The data at pH 8.2 suggest that $MePO_4^{2-}$ either is less discriminatory than $HMePO_4^-$ or does not play as important a part in the formation of products. This is in keeping with its poor catalytic ability in a rate sense (Table VII, Figure 7) when compared with $HMePO_4^-$.

3. Hydrolysis of the Chelated Amide Ions $[Co(en)_2(glyNHR)]^{3+}$. Table XI (supplementary data) contains rate data for hydrolysis of the chelated glycinamide, dipeptide ester, and dipeptide acid complex ions at 25 °C and μ = 1.0 ($NaClO_4$); this is plotted in Figures 1–3, for comparison with the hydroxo monodentate complexes. The temperature dependence for hydrolysis of $[Co(en)_2(glyNH_2)]^{3+}$ gives a linear plot of log k_{obsd} vs. $1/T$, whence E_a = 14.3 ± 0.3 kcal mol^{-1} and $\Delta S^{\ddagger} = -7 \pm 2$ cal deg^{-1} mol^{-1}, and addition of phosphate decreases the rate slightly. For the dipeptide ester complex phosphate buffer has no effect on the rate. For $[Co(en)_2(glyNH_2)]^{3+}$ the observed rate constant in D_2O (1.0 M $NaClO_4$) at pH 11.0 (pD 11.4) was 7.86×10^{-3} s^{-1}; in H_2O at the same OH^- concentration (pH 10.23) $k_{obsd} = 3.98 \times 10^{-3}$ s^{-1} (Figure 1). Under these conditions the rate law takes the form $k_{obsd} = k_H[OH^-]$ (see below) giving k_H = 13.8 M^{-1} s^{-1} and k_D = 27.2 M^{-1} s^{-1} with k_H/k_D = 0.51. Similarly in D_2O and 0.1 M KCl, $k_{obsd} = 3.30 \times 10^{-3}$ and 1.15×10^{-2} s^{-1} at pD 10.8 and 11.41, respectively; at the same OH^- concentrations (pH 9.63, 10.24) in H_2O, $k_{obsd} = 1.10 \times 10^{-3}$ s^{-1} and 4.07×10^{-3} s^{-1}, respectively (Figure 1) whence k_H/k_D = 0.39 and 0.35. The conditions used in these experiments preclude significant ionization of the chelated amide moiety (K_b) which ensures that the effects are entirely kinetic in origin.

The plots of log k_{obsd} vs. pH (Figures 1–3) show that below pH ~11 there is a first-order dependence in $[OH^-]$. At higher pHs leveling off in k_{obsd} with increasing $[OH^-]$ occurs, and the data fit the expression[15]

$$k_{obsd} = \frac{k_H K_b [OH^-]}{K_b + [OH^-]} \qquad (9)$$

with k (M^{-1} s^{-1}) and pK_b (M^{-1}) values of 14 ± 1 and 1.4 (R = H), 1.75 ± 0.1 and 1.3 (R = $CH_2CO_2C_3H_7$), and 1.6 ± 0.2 and 1.8 (R = $CH_2CO_2^-$), respectively.[17] The pK_b values have been shown[15] to correspond to ionization of the coordinated amide group (eq 10), and for R = H (Figure 1) and $CH_2CO_2^-$

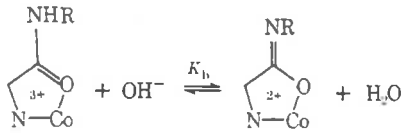

(Figure 3) a limiting rate is clearly observed at pH 13–14. While this is consistent with either solvolysis of the deprotonated amide (H_2O attack) or OH^- attack on the amide, the kinetic solvent isotope ratio (k_H/k_D = 0.3–0.5) clearly favors the latter proposal. Preequilibrium deprotonation usually favors H_2O over D_2O ($K_b(H_2O) > K_b(D_2O)$),[19] and solvolysis of the resulting imide would predict k_H/k_D values of 1.5–5.[20] The alternative mechanism of direct attack of hydroxide would be expected to have k_H/k_D ratios of 0.75,[19] in reasonable agreement with observation.

Figures 1–3 show that hydrolysis of the chelated amide is some ten times faster than the similar unbuffered reactions of the hydroxo amide in the pH range 9–12. However, the rate is little affected by buffers and in this respect it differs considerably from the related intramolecular reaction.

Hydrolysis of $[Co(en)_2(glyNH_2)]^{3+}$ in basic solution (pH 8.5–12) results only in $[Co(en)_2(glyO)]^{2+}$; no hydroxoglycinamide complex, $[Co(en)_2(OH)(glyNH_2)]^{2+}$, was detected either spectrophotometrically or by ion-exchange analysis at 2 °C (SP-Sephadex, 0.5 M $NaClO_4$, pH 8). Similar results hold for hydrolysis of $[Co(en)_2(glyglyOC_3H_7)]^{3+}$ (pH 8.3–12) and in this case the result has special significance since at pH ~ 8 the hydroxo dipeptide has been shown to form ~50% of the chelated dipeptide in the absence of buffer. Figure 13 (supplementary data) gives spectral data for the hydrolysis of $[Co(en)_2(glyglyOC_3H_7)]^{3+}$ at pH 9.14 (Figure 13a) and at pH 8.34 (Figure 13b); under the latter conditions hydrolysis

in the hydroxo ion is some five times faster, and at pH 9.14 their rates are approximately the same (Figure 2). Isosbestic points are maintained (295 nm, pH 9.14), or nearly so (305 nm, pH 8.34), and the data at pH 9.14 and 310 nm gives a linear plot ($4t_{1/2}$) of log ($D_t - D_\infty$) vs. time ($k_{obsd} = 5.35 \times 10^{-5}$ s^{-1}). The hydroxo dipeptide complex shows a large extinction coefficient at these wavelengths (Figure 13b).[1] These results preclude formation of the hydroxo amide in amounts >1% during hydrolysis of the chelated dipeptide. The $[Co(en)_2(glyNHR)]^{3+}$ ions were also shown to be stable over long periods (14 days–3 months) at pHs 1–4.

Discussion

The most significant results are (1) hydrolysis of the monodentate glycinamide and dipeptide occurs by the intramolecular addition of coordinated water or hydroxide; (2) hydrolysis by coordinated water is clearly faster than the unassisted attack by coordinated hydroxide, $k'_H > k'_{OH}$ (Table X); (3) under alkaline conditions competitive hydrolysis (loss of amine) and O-exchange to form the chelated amide (loss of hydroxide) occur with the hydroxo dipeptide complex; under these conditions hydrolysis of the chelated dipeptide fails to open the chelate ring to form the hydroxo amide species; (4) buffers act as general bases and markedly influence the rates for the hydroxo amides, but have little or no effect on the rates for the chelated amides; (5) buffers, and in particular bifunctional ones (e.g., $H_2PO_4^-$), influence the products resulting from the hydroxo amide, with loss of amine being preferred to loss of hydroxide; (6) the uncatalyzed reactions of the aqua and hydroxo amides show no significant kinetic isotope effect ($k_H/k_D = 1.1$) whereas hydrolysis of the chelated amide has a k_H/k_D ratio of 0.3–0.5.

These observations are now considered in some detail.

Hydrolysis in Dilute Acid. The overall reaction in acid solution may be represented as in eq 11, with $k_{obsd} = k_H = k_{H'}$

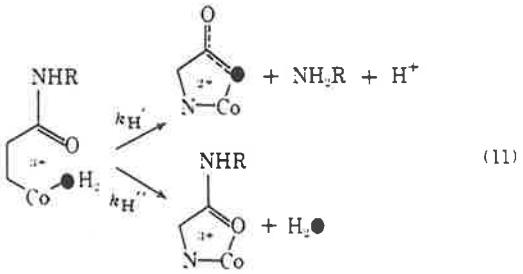

(11)

$+ k_{H''}$ (Figures 1–3, Table II). For R = H the reaction is very fast compared to that found in the absence of the metal[21] with $t_{1/2} = 75$ s, 25.0 °C, and only hydrolysis product results ($k_{obsd} = k_{H'} = 9.2 \times 10^{-3}$ s^{-1}). For the aqua dipeptide and ester systems only part is hydrolyzed with the product distributions for the cis aqua ions, corrected for that arising from the small amount of trans aqua species, being given in Table X. Thus for R = $CH_2CO_2C_3H_7$ some 50% hydrolysis occurs, with a similar amount (41%) for R = CH_2CO_2H and somewhat more (83%) for the dipeptide anion R = $CH_2CO_2^-$. The ^{18}O-tracer studies for the aqua dipeptide ester system,[1] and for *cis*-$[Co(en)_2(OH_2)(glyNH_2)]^{3+}$,[36] clearly show that the hydrolyzed product contains the coordinated solvent label, with the chelated amide arising from displacement of coordinated water. The similarity in the rates and products for the dipeptide acid system suggests a similar competitive process in this case as well.[22] Most importantly, the ^{18}O results show that the hydrolysis part is completely intramolecular in nature and this requires particularly rapid attack by coordinated water. The values of $k_{H'}$ given in Table X follow the reactivity order R = H > $CH_2CO_2^-$ > $CH_2CO_2C_3H_7 \sim CH_2CO_2H$, which is that of decreasing basicity of the amine function. This could be

Scheme IV

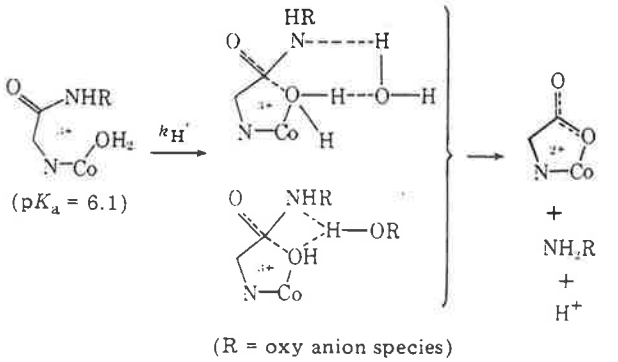

interpreted in terms of either rate-controlling addition of water or loss of NH_2R.

The rapidity of the cyclization reaction suggests assistance in the attack of water or in the loss of amine. In view of the inability of water bound to Co(III) to add to easily hydrolyzable substrates in analogous bimolecular reactions ($(NH_3)_5CoOH_2^{3+} + CO_2$, anhydrides, labile esters,[9] or in intramolecular processes in which a leaving group is not involved[46] (eq 12), we favor a proton tunnelling process (Scheme

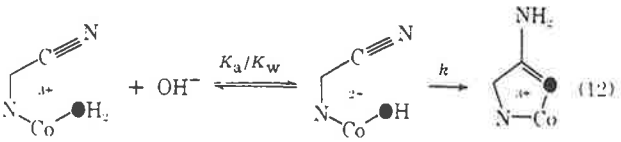

IV). A similar proposal has been made[25,29] for reactions of metal–aqua species with oxy anions (NO_2^-,[23] SO_3^{2-},[24] IO_3^-,[25] $HAsO_4^{2-}$, $H_2AsO_4^-$,[26] WO_4^{2-} and MoO_4^{2-},[27] CrO_4^{2-},[28] $HSeO_3^-$[29,30]). Leybold stereomodels suggest that transfer to the proton could occur either directly or via the help of an adjacent water molecule, and the moderate amount of catalysis by citrate, succinate, maleate, and acetate clearly supports the latter possibility.

A general base role for acetate with the aqua dipeptide complex is required by eq 5, and production of $[Co(en)_2(glyO)]^{2+}$ is also facilitated (Figure 5). This is consistent with increasing competition by the above intramolecular reaction for the alternative process involving displacement of the coordinated water molecule.[22] Also, these buffer species (H_2O, oxy anions) have basicities intermediate between those of the reactant and the direct addition product iii, and this favors a

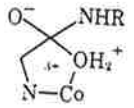

iii

concerted rather than a stepwise reaction.[31] A similar conclusion follows if the reactant takes the form iv or v and the

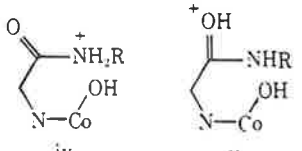

iv v

addition intermediate vi or vii, but in our view, and in the view of others,[32] it is unnecessary to postulate such high-energy species when lower energy pathways are available.[33]

The lack of an appreciable deuterium isotope effect (k_H/k_D

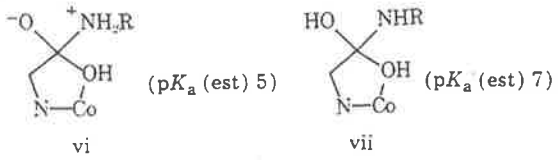

vi vii

= 1.1, Table II) also supports proton tunnelling. It can be argued that the poorer nucleophilic properties of coordinated D_2O ($k_H/k_D > 1$) would be offset by the more advanced transfer of D^+ to the departing amine ($k_H/k_D < 1$). In unassisted solvolytic reactions the former secondary isotope effect results in k_H/k_D values of ~2,[20,34] whereas the acid-catalyzed hydrolyses of esters are well-known to have inverse isotope ratios, $k_H/k_D = 0.5$–0.7.[20] Clearly an intermediate situation applies in Scheme IV with both effects being involved in the transition state.

The retarding influence of some anions (SeO_4^{2-}, SO_4^{2-}, $NH_3^+CH_2CO_2^-$, furoate$^-$, tartrate^{2-}) and the marginal effect of others (citrate$^{2-,3-}$, maleate^{2-}, succinate^{2-}) probably results from substantial ion pairing with the 3+ aqua ion. For HPO_4^{2-}, K_{ip} values of 86 and 54 are found with $[Co(en)_2(OH_2)(glyNH_2)]^{3+}$ and $[Co(en)_2(glyglyOC_3H_7)]^{3+}$ (see below), and similar values were observed by Posey and Taube[35] for the association of SO_4^{2-} with $Co(NH_3)_6^{3+}$. The retarding influence of citrate^{3-} on the rate at pH 9.5 (Table IV) suggests that such ion pairs, in this case 2+/3−, are unreactive or less reactive for buffer species of low basicity. The catalysis observed for acetate at pH 4–5 (Table IV) clearly favors the formation of $[Co(en)_2(glyO)]^{2+}$ (Figure 5, pH 4.6).

Reactions in Neutral and Alkaline Solution. At pH >6 ionization of the coordinated water molecule gives the *cis*-hydroxo amide species, and the physical properties of these ions[1] agree closely with those of *cis*-$[Co(en)_2(OH)NH_3]^{2+}$,[37] which does not have an additional reactive center or deprotonation site under these mild conditions (pH 6–14). Also, the calculated plots of log k vs. pH (Figures 1–3) agree well with the observed data implying that the equilibrium involved in the rate process is indeed the ionization of the bound water molecule. The measured pK_a values used in these calculations were determined by extrapolating the initial spectrophotometric rate data to $t = 0$ (pH 3–8), and no rapid spectrophotometric process (10 ms) was observed other than the initial (instantaneous) neutralization. Also, in more alkaline solutions, where the $k_{OH}[OH^-]$ term of eq 2 controls k_{obsd} (pH 9–13), no evidence was found for other fast reactions prior to the rate-controlling process. These facts suggest that the observed process involves the hydroxo monodentate amide complex, and that rapid prior cyclization to form an intermediate species is not involved.

The ^{18}O-tracer experiments establish that *both* the hydrolyzed *and* chelated amide products produced from *cis*-$[Co(en)_2(OH)(glyglyOC_3H_7)]^{2+}$ retain the coordinated hydroxyl oxygen for at least the k'_{OH} part of eq 2, and for the k_{HPO_4} part of eq 8. A similar result obtains for the k'_{OH} path

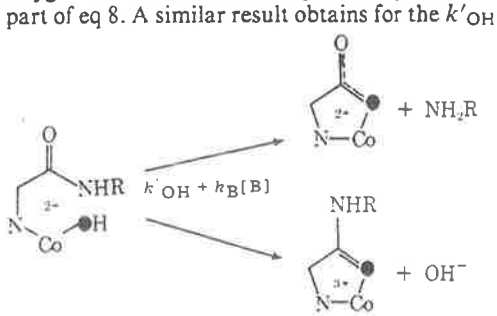

for *cis*-$[Co(en)_2(OH)(glyNH_2)]^{2+}$,[38,39] but the rapid hydrolysis of $[Co(en)_2(glyglyOC_3H_7)]^{3+}$ prevents a direct determination for the $k_{OH}[OH^-]$ part of eq 2 leading to the chelated amide. However, if OH^- behaves as other monofunctional buffers such as phenol (Figure 6) then little chelated amide is likely from this part of the rate law.

Scheme V

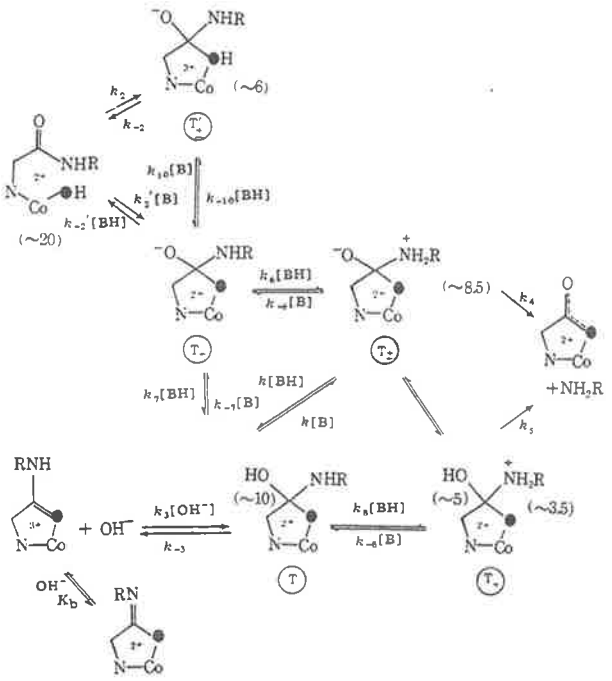

Scheme V details the proposed mechanism for the intramolecular reaction of the hydroxo amide and for hydrolysis of the chelated amide. In this scheme the addition steps k_2, k_2', and k_3 are considered to be rate determining with loss of NH_2R and OH^- occurring as rapid subsequent processes. General base catalysis occurs in the cyclization step ($k_2'[B]$), and the products are believed to result via the common intermediate T. This can decompose by a buffer-independent hydrolysis path to give $[Co(en)_2(glyNHR)]^{3+}$ (k_{-3}), or via buffer-mediated loss of amine (k_4, k_5). The results also require that opening up of the chelate ring (k_{-2}, $k_{-2}[BH]$) is not competitive with retention of the five-membered ring system.

Evidence supporting k_3 and k_2' as the rate-determining steps comes from two main sources. Firstly, the inability of phosphate (or other buffers) to influence the rate of hydrolysis of $[Co(en)_2(glyNHR)]^{3+}$ (the slight retardation observed with PO_4^{3-} for R = H, Table XI, probably results from ion pairing with the 3+ cation) is in marked contrast to the large effect buffer species have on k_2 (represented by $k_2'[B]$) and on the products of the hydroxo amide reaction. Addition of OH^- to the chelated amide forms T directly and, provided that loss of amine requires protonation (either stepwise via T_+ or $T_\pm$, or in a concerted manner without the formation of these intermediates), then the absence of terms in the rate law independent of OH^- (k_5, rate determining) or of the form $k[B]$ (rate-determining formation of T_+) or $k[B][OH^-]$ (rate-determining formation of T_-, or $T_\pm$ for bifunctional buffers) implies that addition of OH^- (k_3) is the rate-determining process for the amide chelate. For the hydroxo dipeptide, the observed variation in the product ratio in the presence of phosphate (e.g., pH 8.77, Figure 12) requires these processes to have different phosphate dependencies where the rate law is entirely of the form $k_{obsd} = k[HPO_4^{2-}]$ (Figure 9). This means that the products are decided by events subsequent to the rate-determining step. This is consistent with rate-determining cyclization to form T_- (monofunctional buffers) or T directly (bifunctional buffers, see below).

The existence of similar intermediates has been established previously and their properties are in general agreement with

those found here. Thus in the aminolysis of the chelated glycine isopropyl ester complex [Co(en)$_2$(glyOC$_3$H$_7$)]$^{3+}$ in non-aqueous solution, the intermediate viii has been observed,[40]

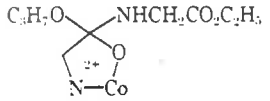

viii

and in neutral to alkaline aqueous conditions (pH >5) it forms largely [Co(en)$_2$(glyNHR)]$^{3+}$; that is, loss of $C_3H_7O^-$ competes favorably with loss of amine. In aqueous acidic solution amine is lost (presumably via T$_+$) with the eventual formation of [Co(en)$_2$(glyO)]$^{2+}$ by subsequent rapid hydrolysis of the chelated ester product. Similarly, hydrolysis of the six-membered ester chelates [Co(en)$_2$(β-alaOC$_3$H$_7$)]$^{3+}$ occurs via rate-determining loss of $C_3H_7O^-$ (or C_3H_7OH) from the neutral and anionic forms of the tetrahedral intermediate, viz.,[41] T and T$_-$. This result differs from that found here for

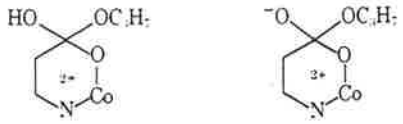

T T$_-$

the chelated amide in that k_3[OH$^-$] is not rate determining for the β-alanine ester complex under conditions where T predominates, and is consistent with the proposal[34] that protonated amine is a better leaving group than an alkoxide ion of similar or greater basicity.

The rate enhancements afforded by the monofunctional buffers show no evidence for a change in the rate-determining step. Thus the Brønsted plots for the neutral amine buffers, and for the 1−, 2−, and 3− oxy anions, are linear (Figure 7), and the individual plots of k_{obsd} vs. [B] (Figure 6) show no curvature at high buffer concentrations. The one exception to the former result is OH$^-$ (Figure 7), but this species may well have an unusual behavior in the aqueous environment and it is not uncommon to find its nucleophilic properties masked compared with its pK_a. The separate correlations for the 1−, 2−, and 3− oxy anions probably result from the overall 2+ charge on the reactant rather than from an inherent difference in catalytic ability. However, ion-pair formation was not observed spectrophotometrically (~300 nm) on addition of buffer, or from deviations in linearity in the plots of k_{obsd} vs. [B].

A concerted rather than stepwise role is envisioned for the buffer species. In this way the less stable (under alkaline conditions) intermediate T$_\pm$′ is avoided, and estimates of 20 and 6 for the pK_as of the hydroxo amide and T$_\pm$′ support a concerted role for most bases including OH$^-$.[31] However, T$_\pm$′ cannot be avoided for the uncatalyzed reaction (k'_{OH}) and this is probably why this process is comparatively slow. Certainly $\Delta H^{\ddagger}$ is reduced when the OH$^-$-catalyzed (k_{OH}, $\Delta H^{\ddagger}$ = 8.3 ± 0.3 kcal mol^{-1}) and uncatalyzed (k'_{OH}, $\Delta H^{\ddagger}$ = 11.9 ± 0.6 kcal mol^{-1}) reactions are compared. However, the observed k_H/k_D ratios of 1.1 (R = H) and 1.2 (R = CH$_2$CO$_2$C$_3$H$_7$) for the uncatalyzed reaction (k'_{OH}) are unexpected in the absence of solvent involvement in the cyclization process. Coordinated OD$^-$ might be expected to be more nucleophilic than coordinated OH$^-$ if the normal situation obtains.[19]

The remarkable catalysis shown by H$_2$PO$_4^-$, HMePO$_4^-$, HPO$_4^{2-}$, HCO$_3^-$, and HAsO$_4^-$ (Figure 7) must reside in their containing a proton since MePO$_4^{2-}$, AsO$_4^-$, CO$_3^{2-}$, and PO$_4^{3-}$ behave normally. The ability of these buffers to donate and accept protons in a concerted manner provides a direct route to T or T$_\pm$ via transition states which resemble that given in Scheme IV for the reaction in acid, viz., eq 13. This concerted general-acid/general-base property will also tend to hold

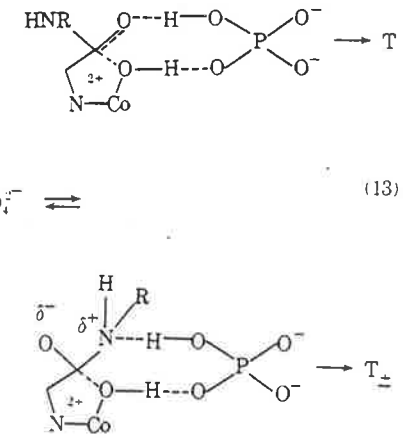

(13)

the two reacting centers together, thereby lowering the configurational free energy component.

The curvature observed at low pHs in the plots of k_{obsd} vs. [phosphate]$_T$ (Figures 8 and 10) and [Mephosphate]$_T$ (Figures 9 and 11) can be accounted for by the formation of unreactive 3+/2− ion pairs between *cis*-[Co(en)$_2$(OH$_2$)(glyNHR)]$^{3+}$

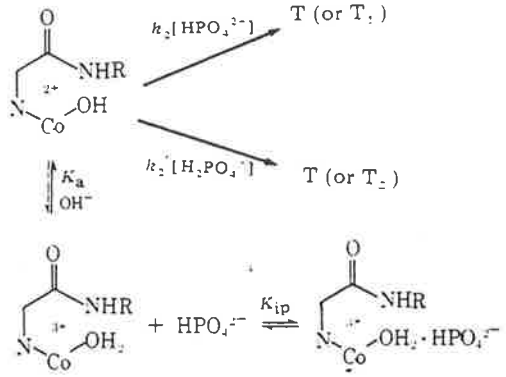

and HPO$_4^{2-}$ or MePO$_4^{2-}$. Similarly SO$_4^{2-}$, citrate^{2-}, succinate^{2-}, and maleate^{2-} retard the reaction of the aqua amide. The rate constants for H$_2$PO$_4^-$ and MeHPO$_4^-$ given in Table VII and depicted in the Brønsted plot (Figure 7) assume this mechanism. This process leads to the rate expression

$$k_{calcd} = \frac{K_a[OH^-](k_2[HPO_4^{2-}] + k'_2[H_2PO_4^-])}{K_w + K_a[OH^-] + K_{ip}K_w[HPO_4^{2-}]} \quad (14)$$

which agrees with the observed rate law (eq 8) using K_{ip} values of 86 (10) M^{-1} (R = H) and 54 (10) M^{-1} (R = CH$_2$CO$_2$C$_3$H$_7$) for HPO$_4^{2-}$ and 44 (R = H) and 65 M^{-1} (R = CH$_2$CO$_2$C$_3$H$_7$) for MePO$_4^{2-}$. The solid curves given in Figures 8–11 are for eq 14. K_{ip} values of this magnitude are not unreasonable for 3+/2− ion pairs.[35,42]

Some comment is appropriate on the existence of the intermediates given in Scheme V, and on the estimates for their pK_as.[43] The formation of the chelated amide and chelated acid from the hydroxo dipeptide requires the formation of an intermediate following the rate-determining cyclization process, and the variation in product composition with increasing or changing buffer requires the decay of such an intermediate, or intermediates, to have varying or different buffer dependencies. All three leaving groups (Co–O$^-$, RNH$^-$, and OH$^-$) are poor ones since they are all strong bases. Thus Co–O$^-$ and RNH$^-$ require protonation either prior to or in the act of departure and Co–O$^-$ is almost as poor a leaving group as RNH$^-$. The pK_a values given in parentheses in Scheme VII were estimated[43] according to the procedure of Fox and Jencks,[44] and should be accurate to ~1 pK_a unit. In the absence of buffers this allows the following estimates for the rates of interconversion.

Scheme VII

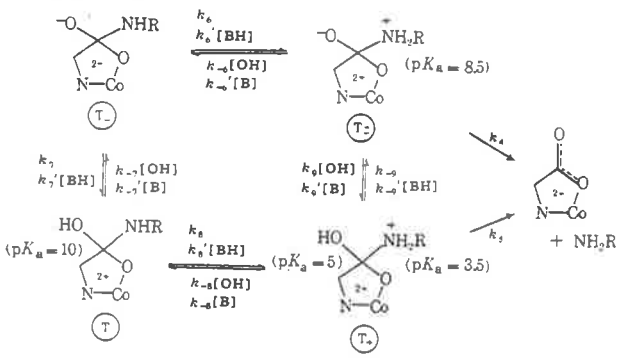

The proton transfers $T_{\pm} \rightarrow T_-$ (k_{-6}), $T_+ \rightarrow T_{\pm}$ (k_9), $T_+ \rightarrow T$ (k_{-8}), and $T \rightarrow T_-$ (k_{-7}) with the strong base OH^- are all thermodynamically favorable and will occur at or close to the diffusion-controlled limit of 10^{10} M^{-1} s^{-1} (i.e., 10^4 s^{-1} at pH 8). The reverse protonations by H_2O ($k_i = k_{-i}K_w/K_b$) will therefore have rates of $\sim 3 \times 10^4$ (k_6), 10 (k_{-9}), 0.3 (k_8), and 10^6 (k_7) s^{-1}. The similar rates for protonation by H_3O^+ (BH) will be diffusion controlled, 5×10^{10} M^{-1} s^{-1}, which at pH 8 will be of the order of 5×10^2 s^{-1}. Loss of protonated amine from $T_{\pm}$ (k_4) will be fast and, if a rate in excess of 10^9 s^{-1} occurs, as has been estimated for other alkylamine intermediates of similar constitution, e.g.,[45] eq 15, then (in the absence of buffer species) the proton transfer steps to form $T_{\pm}$ and T_+ will

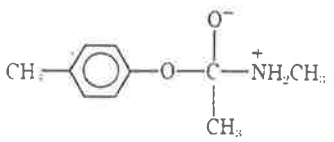

$T_{\pm}$

be the slow steps following the rate-determining formation of T_- and T. Also, since at pH 8 approximately half the product from the hydroxo dipeptide is chelated amide, then k_{-3} will have a value of $\sim 3 \times 10^4$ s^{-1} and the major route to hydrolysis product will be via $T_{\pm}$. Indeed, under these conditions T_+ will not be a major route to hydrolysis product from either the chelated amide or hydroxo amide species and will only begin to contribute at lower pHs. Also $T_{\pm}$, once formed, will prefer to decompose with loss of amine rather than interconvert to T_+ since the latter process will be slow at pH 8 ($k_{-9} = 5 \times 10^2$ s^{-1}). It can also be appreciated why the chelated amide fails to open up the chelate ring and form the hydroxo amide. An estimate of 6 for the pK_a of $T_{\pm}$'[43] (Scheme V) leads to rates for protonation of T_- of $\sim 10^2$ s^{-1} for both the H_3O^+ (at pH 8) and H_2O paths. Thus T_- will prefer to decay to $T_{\pm}$ rather than to $T_{\pm}'$ (k_{-10}) and opening up of the chelate ring becomes a real possibility only under acid conditions. However, under these conditions an alternative process comes into play for the aqua amide (Scheme IV), and the chelated amide is also unreactive.

The promotion of hydrolyzed product by buffers is also readily understandable and Scheme V suggests that this occurs via the acid-catalyzed formation of $T_{\pm}$ or T_+. Thus acetic acid (Figure 5) is more effective than phenol or methyl phosphate at the same pH (stronger acid), and the principle of microscopic reversibility requires that the formation of chelated amide from T (k_{-3}) is not catalyzed by general acids (but see below for HPO_4^{2-}).

The products of the phosphate-catalyzed reactions are also unusual in that some phosphate-promoted loss of water appears to occur in competition with phosphate-catalyzed loss of amine. This result is required by the experiment using $(+)_{589}$-$[Co(en)_2(OH)(glyglyOC_3H_7)]^{2+}$ where some 5% $[Co(en)_2(glyglyOC_3H_7)]^{3+}$ is formed under conditions (0.15 M buffer) where the product distribution has reached a limiting composition (Figure 12). Also, Figure 12 suggests that $H_2PO_4^-$ is better than HPO_4^{2-} at promoting $[Co(en)_2(glyO)]^{2+}$ formation since the maximum yields of hydrolysis product are found under the most acidic conditions consistent with reaction of the hydroxo dipeptide (pH 6–7). Thus acid-catalyzed loss of amine seems to be an important feature of these buffers at least, and it is likely that a transition state of the form ix occurs. Similar transition states have been proposed

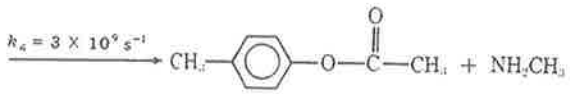

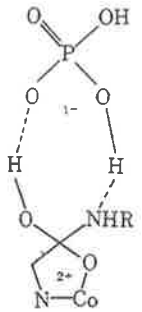

ix

for the phosphate-catalyzed hydrolysis of 4-hydroxybutyranilide.[3] $HMePO_4^-$ likewise markedly promotes the formation of $[Co(en)_2(glyO)]^{2+}$ whereas $MePO_4^{2-}$ is much less discriminating (Figure 5).

Comparison with Related Intramolecular Hydrolysis Reactions. It is appropriate that these metal-catalyzed intramolecular processes be compared with the hydrolysis of 4-hydroxybutyramides and 2-hydroxybenzamides mentioned in the introduction. The following differences are significant.

(1) The rates of reaction over the entire pH range are very much faster having the metal present. Thus the aqua dipeptide hydrolyzes 10^{11} times more rapidly than the dipeptide alone (pH 5), and a factor of 10^7 is involved for the hydroxo dipeptide complex at pH 8. The presence of phosphate enhances the latter reaction considerably so that at pH 8 in 0.1 M buffer the reaction is 10^9 times faster than the same process in the absence of the metal. For the 4-hydroxybutyramide much smaller rate increases were found in the absence of buffers (15–20 at pH $\sim$9 and 800 at pH $\sim$6),[3,7] and the OH^--promoted path for 2-hydroxymethylbenzamide is only 3500 times faster than that for benzamide itself (4×10^{-2} vs. 1.16×10^{-5} M^{-1} s^{-1}, respectively).[4] Phosphate buffers significantly catalyze both reactions but the maximum acceleration found for 4-hydroxybutyramide was only 12 600 at pH 9; under the conditions the buffer-independent cyclization process was held to be rate determining.[3] (2) For the intramolecular reaction of the metal–hydroxo complexes, formation of Co–O^- by prior deprotonation (specific OH^- catalysis) does not occur, but rather deprotonation in the transition state for addition of Co–OH (general base catalysis) occurs. For the similar reaction of 4-hydroxybutyramides, specific OH^- deprotonation of the hydroxyl function is proposed for the OH^--catalyzed reaction at least,[2,3] and general acid/general base promoted loss of amine from the tetrahedral intermediate is considered to be rate determining for all but the highest buffer concentrations.[3,5]

(3) The unusual phosphate dependence on the rate for the metal–hydroxo system (eq 8, Figures 8–11) is interpreted as

resulting from ion pairing in the reactant 3+ aqua complex rather than from a change in rate-determining step as proposed for the organic systems.[3-5]

(4) Opening up of the five-membered metal chelate ring is not competitive with loss of NH_2R or OH^-, whereas it apparently is for the nonmetal systems.[3-5]

Supplementary Material Available: Rate data for the unbuffered reactions of the $[Co(en)_2(OH_2/OH)(glyNHR)]^{1+/2+/3+}$ ions (Table I), rate data for the buffer catalyzed reactions of the *cis*-$[Co(en)_2(OH_2/OH)(glyNH_2)]^{2+/3+}$ ions (Table IV), rate data for the buffer catalyzed reactions of the *cis*-$[Co(en)_2(OH_2/OH)(glyglyOC_3H_7)]^{2+/3+}$ ions (Table V), rate data for the buffer catalyzed reactions of the *cis*-$[Co(en)_2(OH_2/OH)(glyglyO)]^{2+/1+}$ ions (Table VI), rate data for phosphate, carbonate, and arsenate catalyzed reactions of *cis*-$[Co(en)_2(OH)(glyNH_2)]^{2+}$ (Table VIII), rate data for the phosphate catalyzed reaction of *cis*-$[Co(en)_2(OH)(glyglyOC_3H_7)^{2+}$ (Table IX), rate data for hydrolysis of the $[Co(en)_2(glyNHR)]^{3+}$ ions (Table XI), plots of $(k_{obsd} - k_{hyd})$ vs. [buffer] for the reactions of $[Co(en)_2(OH)(glyNH_2)]^{2+}$ (Figure 6), plot of k_{obsd} vs. $[phosphate]_T$ for the cyclization of $[Co(en)_2(OH)(glyglyOC_3H_7)]^{2+}$ as a function of pH (Figure 10), plot of k_{obsd} vs. $[methyl\ phosphate]_T$ for the cyclization of *cis*-$[Co(en)_2(OH)(glyglyOC_3H_7)]^{2+}$ as a function of pH (Figure 11), and repetitive scans during hydrolysis of $[Co(en)_2(glyglyOC_3H_7)](NO_3)_3$ (Figure 13) (18 pages). Ordering information is given on any current masthead page.

References and Notes

(1) C. J. Boreham, D. A. Buckingham, and F. R. Keene, *Inorg. Chem.*, **18**, 28 (1978).
(2) T. C. Bruice and F.-H. Marquardt, *J. Am. Chem. Soc.*, **84**, 365 (1962).
(3) B. A. Cunningham and G. L. Schmir, *J. Am. Chem. Soc.*, **89**, 917 (1967).
(4) (a) C. J. Belke, S. C. K. Su, and J. A. Shafer, *J. Am. Chem. Soc.*, **93**, 4552 (1971); (b) K. N. G. Chiong, S. D. Lewis, and J. A. Shafer, *ibid.*, **97**, 418 (1975).
(5) T. Okuyama and G. L. Schmir, *J. Am. Chem. Soc.*, **94**, 8805 (1972).
(6) G. L. Schmir and B. A. Cunningham, *J. Am. Chem. Soc.*, **87**, 5692 (1965).
(7) B. A. Cunningham and G. L. Schmir, *J. Am. Chem. Soc.*, **88**, 551 (1966).
(8) R. W. Hay and P. J. Morris in "Metal Ions in Biological Systems", Vol. 5, H. Sigel, Ed., Marcel Dekkar, New York, N.Y., 1976, p 173.
(9) D. A. Buckingham in "Biological Aspects of Inorganic Chemistry", Proceedings of the 1976 International Symposium, A. W. Addison, R. W. Cullen, D. Dolphin, and B. R. James, Ed., Wiley-Interscience, New York, N.Y., 1977, p 141.
(10) J. J. Johansen and B. L. Vallee, *Proc. Natl. Acad. Sci. U.S.A.*, **70**, 2006 (1973); *Biochemistry*, **14**, 649 (1975).
(11) R. Breslow and D. Wernick, *Proc. Natl. Acad. Sci. U.S.A.*, **74**, 1303 (1977); *J. Am. Chem. Soc.*, **98**, 259 (1976); E. P. Kang, C. B. Storm, and F. W. Carson, *ibid.*, **97**, 6723 (1975); H. E. Van Wart and B. L. Vallee, *Biochim. Biophys. Acta*, 732 (1977); M. W. Makinen, K. Yamamura, and E. T. Kaiser, *Proc. Natl. Acad. Sci. U.S.A.*, **73**, 3882 (1976).
(12) C. A. Bunton, M. M. Mhala, K. G. Oldham, and C. A. Vernon, *J. Chem. Soc.*, 3293 (1960).
(13) O. Bailly, *C. R. Acad. Sci.*, **170**, 1061 (1920).
(14) C. J. Boreham, Ph.D. Thesis, The Australian National University, July 1978.
(15) D. A. Buckingham, C. E. Davis, D. M. Foster, and A. M. Sargeson, *J. Am. Chem. Soc.*, **92**, 5571 (1970).
(16) P. K. Glasoe and F. A. Long, *J. Phys. Chem.*, **64**, 188 (1960).
(17) Values of k and K_b are based on $pK_w = 13.77$ and $\mu = 1.0$ (KCl): H. S. Harned and W. J. Hamer, *J. Am. Chem. Soc.*, **55**, 2194 (1933). A recent value of pK_w in 1.0 M $NaClO_4$ (13.80) agrees closely with this: R. Fischer and J. Bye, *Bull. Soc. Chim. Fr.*, 2920 (1964). The data for R = H and $CH_2CO_2^-$ is taken largely from ref 15.
(18) Program written by L. M. Engelhardt for a PDP-11 computer.
(19) C. A. Bunton and V. J. Shiner, *J. Am. Chem. Soc.*, **83**, 42 (1961).
(20) C. A. Bunton and V. J. Shiner, *J. Am. Chem. Soc.*, **83**, 3207 (1961).
(21) The second-order rate for alkaline hydrolysis of glycinamide of 2×10^{-3} $M^{-1}\ s^{-1}$ gives $t_{1/2} \simeq 10^{11}$ s at pH 5: H. L. Conley and R. B. Martin, *J. Phys. Chem.*, **69**, 2923 (1965).
(22) The observation that removal of coordinated water competes for the intramolecular process requires the former reaction to also be fast, $k_{obsd} \sim 10^{-2}\ s^{-1}$ at 25 °C, $\mu = 1.0$ ($NaClO_4$).
(23) F. Basolo and G. S. Hammaker, *Inorg. Chem.*, **1**, 1 (1962).
(24) G. Basza and H. Diebler, *Proc. Int. Conf. Coord. Chem.*, **15**, 442 (1973).
(25) R. K. Wharton, R. S. Taylor, and A. G. Sykes, *Inorg. Chem.*, **14**, 33 (1975).
(26) T. A. Beech, N. C. Lawrence, and S. F. Lincoln, *Aust. J. Chem.*, **26**, 1988 (1973).
(27) R. K. Murmann and H. Taube, *J. Am. Chem. Soc.*, **78**, 4886 (1956).
(28) J. C. Sullivan and J. E. French, *Inorg. Chem.*, **3**, 832 (1964).
(29) A. D. Fowles and D. R. Stranks, *Inorg. Chem.*, **6**, 1267 (1967).
(30) These reactions are somewhat different, however, as the oxy anions themselves undergo rapid oxygen exchange in water.
(31) W. P. Jencks, *J. Am. Chem. Soc.*, **94**, 4731 (1972).
(32) W. P. Jencks, *Chem. Rev.*, **72**, 705 (1972).
(33) An estimated pK_a of −4 for the protonated amide residues gives a specific rate of $10^8\ s^{-1}$ for this species (R = H).
(34) W. P. Jencks in "Catalysis in Chemistry and Enzymology", McGraw-Hill, New York, N.Y., 1969, Chapter 4.
(35) F. A. Posey and H. Taube, *J. Am. Chem. Soc.*, **78**, 15 (1956).
(36) D. A. Buckingham, D. M. Foster, and A. M. Sargeson, *J. Am. Chem. Soc.*, **92**, 6151 (1970).
(37) D. A. Buckingham, I. I. Olsen, and A. M. Sargeson, *J. Am. Chem. Soc.*, **90**, 6654 (1968).
(38) The ^{18}O tracer result of the hydroxyglycinamide reaction is contained in ref 36. Under the conditions reported there, sufficient time was allowed following base hydrolysis of *cis*-$[Co(en)_2Br(glyNH_2)]^{2+}$ in $H_2\ ^{18}O$ to allow a large proportion of the hydroxo amide to react, and the subsequent product shows that this part retains the ^{18}O label in the chelate ring of the hydrolyzed glycinate fragment.
(39) D. A. Buckingham, D. M. Foster, and A. M. Sargeson, *J. Am. Chem. Soc.*, **91**, 3451 (1969).
(40) D. A. Buckingham, J. Dekkers, and A. M. Sargeson, *J. Am. Chem. Soc.*, **95**, 4173 (1973).
(41) E. Baraniak, Ph.D. Thesis, The Australian National University, March 1973.
(42) J. Bjerrum, *Adv. Chem. Ser.*, **No. 62**, 178 (1967).
(43) The pK_as for T, T_+, and $T_\pm$ given in Scheme VII were estimated using the method and data of Fox and Jencks[44] and others,[47] assuming that Co^{3+} attached to the phenolic oxygen of the tetrahedral intermediate has an intermediate effect to that of H^+. Thus from a $pK_a = 8.0$ for $CH_3NH_2^+CH_2CO_2Et$, that for $CH_3C(OH)_2NH_2^+CH_2CO_2Et$ and $CH_3C(OH)(O^-)NH_2^+CH_2CO_2Et$ are estimated at 4.1 and 8.9, respectively, giving a pK_a value of 6.5 for $CH_3C(OH)(OCo^{3+})^+NH_2CH_2CO_2Et$. Similarly[47] the pK_a for the alcohol function in $CH_3C(OH)(OCo^{3+})(NHCH_2CO_2Et)$ was estimated at 13.0. This intermediate polarizing ability of Co^{3+} when two atoms removed from the acidic center has been observed many times previously.[9] The influence of the Co^{3+} moiety on the aminomethyl function of the five-membered chelate was allowed for using data for $CH_3NH_3^+$ (10.7), $NH_2CH_2CH_2NH_3^+$ (9.0), and $(en)_2(Br)Co\text{–}NH_2CH_2CH_2NH_3^+$ (7.3). The Co^{3+} function has a similar property to H^+ when three atoms removed from the acidic center (viz., $CoNH_2CH_2CH_2NH_3^+$ (6.8)) and this also appears to be a common property (viz., $(NH_3)_5Co^{3+}NH_2CH_2CO_2H$ (2.3), $NH_3^+CH_2CO_2H$ (2.3) carboxylic acid functionality). Adjusting the above estimates for the tetrahedral species for this effect ~3 pK_a units) gives $pK_T \sim 10$, $pK_{T_+} \sim 3.5$, and following Jencks and Satterthwait's estimates for the related ionization[45] gives $pK_{T_\pm} \sim 8.5$ and $pK_{T_+} \sim 5$.
(44) J. P. Fox and W. P. Jencks, *J. Am. Chem. Soc.*, **96**, 1436 (1974).
(45) A. C. Satterthwait and W. P. Jencks, *J. Am. Chem. Soc.*, **96**, 7031 (1974).
(46) D. A. Buckingham, P. J. Morris, A. M. Sargeson, and A. Zanella, *Inorg. Chem.*, **16**, 1910 (1977).
(47) M. F. Aldersley, A. J. Kirby, P. W. Lancaster, R. S. McDonald, and C. R. Smith, *J. Chem. Soc., Perkin Trans. 2*, 1498 (1974).
(48) W. F. K. Wynn-Jones, *Trans. Faraday Soc.*, **32**, 1397 (1936).

[Reprinted from Inorganic Chemistry, 15, 190 (1976).]

Contribution from the W. R. Kenan, Jr., Laboratories, Department of Chemistry, University of North Carolina, Chapel Hill, North Carolina 27514

Oxidation of Coordinated Diamines in Bis(2,2'-bipyridine) Complexes of Ruthenium

GILBERT M. BROWN, THOMAS RAY WEAVER, F. RICHARD KEENE, and THOMAS J. MEYER*

Received May 28, 1975 AIC503632

A series of diaminebis(2,2'-bipyridine) complexes of ruthenium(II), e.g., $[Ru(bipy)_2(en)]^{2+}$, has been prepared and the spectral and redox properties were investigated. The ethylenediamine and *trans*-1,2-diaminocyclohexane complexes undergo net four-electron oxidations, either chemically or electrochemically, giving the corresponding α,α'-diimine complexes. The chemical and spectral properties of the α,α'-diimine complexes are similar to those of $[Ru(bipy)_3]^{2+}$. Complexes containing 2-(aminomethyl)pyridine and 1,2-diamino-2-methylpropane undergo net two-electron oxidations, in which the single CH_2–NH_2 linkage has undergone oxidative dehydrogenation to the imine. Electrochemical and titrimetric data (using Ce(IV)) in acetonitrile show that the diamine oxidative dehydrogenation reactions are initiated by oxidation of ruthenium(II) to ruthenium(III), and that the reactions probably occur in a stepwise manner via monoimine intermediates.

Introduction

Metal ions have been found to catalyze the oxidative dehydrogenation of coordinated amines to imines. The oxidation of macrocyclic amine complexes to imine complexes was investigated by Curtis[1] and Busch et al.,[2] and their studies have provided some insight into the mechanism of oxidative dehydrogenation. It was observed that the macrocyclic amine complexes of Ni^{2+}, Cu^{2+}, and Fe^{2+} undergo oxidative dehydrogenation whereas the complexes of Co^{3+} are resistant to oxidation. This indicated that the net reaction involved prior oxidation of the metal ion followed by oxidation of the ligand and reduction of the metal ion.

Elsbernd and Beattie[3] reported that $[Ru^{II}(en)_3]^{2+}$ (en is ethylenediamine) undergoes a net four-electron oxidation, and Lane, Lester, and Basolo[4] showed that the reaction involved oxidative dehydrogenation of ethylenediamine to give an α,α'-diimine (dim) complex of Ru(II)

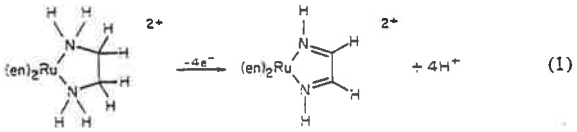

(1)

Mahoney and Beattie[5] have since reported that $[Ru(phen)_2(en)]^{2+}$ undergoes a four-electron oxidation giving $[Ru(phen)_2(dim)]^{2+}$. They also found Ru(III) intermediates in the oxidations of both $[Ru(phen)_2(en)]^{2+}$ and $[Ru(en)_3]^{2+}$. Similar oxidative dehydrogenation reactions have been observed for diamine complexes of tetracyanoferrate(II);[6] isolation of the tetracyanoethylenediamineiron(III) ion demonstrated the intermediacy of Fe(III) in the net reaction.

We have become interested in redox processes involving coordinated ligands, and in how such processes are affected by a variety of molecular features.[7–10] As part of this interest, we have studied the oxidation of a series of diaminebis(2,2'-bipyridine)ruthenium(II) complexes. In the study, evidence has been found which indicates that the oxidative dehydrogenation reactions proceed in a stepwise manner through Ru(III) intermediates.

Experimental Section

Measurements. Ultraviolet–visible spectra were obtained on Cary Model 14, Cary Model 17, or Unicam Model SP-800B spectrophotometers. Molar extinction coefficients were determined from absorbance measurements on three or more concentrations. Absorbances were checked on a Gilford Model 240 spectrometer. Infrared spectra were obtained using a Perkin-Elmer Model 421 spectrometer or a Digilab Model FTS-14 interferometer. ^1H NMR spectra were obtained on a Jeol C-60-HL spectrometer, using D_2O solutions with *t*-BuOH as an internal reference.

All electrochemical measurements were made vs. the saturated sodium chloride calomel electrode (SSCE) at 25 ± 2°C, and are uncorrected for junction potentials. All potentials reported are reduction potentials vs. the SSCE. Potential control for electrochemical experiments was obtained with a Princeton Applied Research Model 173 Potentiostat/Galvanostat. The waveform generator for voltammetric experiments was a Princeton Applied Research Model 175 Universal Programmer. Voltammograms and slow scan cyclic voltammograms were recorded on a Hewlett-Packard Model 7004B X–Y recorder. Fast scan cyclic voltammograms were obtained from photographs of the trace of a Tektronix Model 564B storage oscilloscope. Values of n, where n is the total number of equivalents of electrons transferred in exhaustive electrolyses at constant potentials, were calculated after measuring the total area under current vs. time curves for the complete reaction. Reactions were judged to be complete when the current had fallen below 1% of the initial value. All voltammetric measurements were carried out at platinum electrodes in solutions deaerated with a stream of dry, prepurified nitrogen. Platinum electrodes were cleaned by the procedure recommended by Adams.[11] Elemental analyses were carried out by Galbraith Laboratories, Inc., Knoxville, Tenn.

Materials. Tetra-*n*-butylammonium hexafluorophosphate (TBAH) was prepared by standard techniques,[12] recrystallized three times from hot ethanol–water mixtures, and vacuum dried at 80°C for 12 hr. Acetonitrile (MCB Spectrograde) was dried over Davison 4 Å molecular sieves for electrochemical measurements and used without drying for spectral measurements. Water was deionized and then distilled from alkaline permanganate. The ligands ethylenediamine, *trans*-1,2-diaminocyclohexane, 1,3-propylenediamine, 1,2-diamino-2-methylpropane, 2-(2'-aminoethyl)pyridine, and 2-(aminomethyl)pyridine were purchased commercially and used without further purification. (A list of the ligands used in this study, as well as their formulas and abbreviations, is given in Table I). The complexes $[Ru(bipy)_2Cl_2]\cdot 2H_2O$,[13] $[Ru(bipy)_3](ClO_4)_2$,[14] and $[Ru(bipy)_2(NH_3)_2](ClO_4)_2\cdot 3H_2O$[15] were prepared as previously described. All other chemicals were commercially available in reagent quality and were used without further purification.

$[Ru(bipy)_2(LL)](ClO_4)_2$ (LL = Ethylenediamine (en), *trans*-1,2-Diaminocyclohexane (dach), 1,2-Diamino-2-methylpropane (damp), 2-(2'-Aminoethyl)pyridine (AEPy), and 2-(Aminomethyl)pyridine (AMPy)). The diamine complexes were prepared by essentially the same procedure described for the preparation of the complexes $[Ru(bipy)_2(en)](ClO_4)_2$[15] and $[Ru(phen)_2(en)]I_2\cdot 2H_2O$.[16] The complex $[Ru(bipy)_2Cl_2]\cdot 2H_2O$ (0.50 g) was suspended in a 1:1 (by volume) water–methanol solution (30 ml) of the ligand (3 g). The mixture was heated at reflux on a steam bath for 1 hr under an atmosphere of nitrogen. The condenser was removed and the methanol was boiled off under a stream of nitrogen. The deep red solution was cooled and filtered. The filtrate was returned to the steam bath and warmed to 80–90°C. A saturated aqueous solution of $NaClO_4$ was added dropwise to the warm solution until the onset of precipitation. Slow cooling to room temperature gave deep red crystals which were collected by suction filtration, washed with small portions of ice cold water and methanol, and air dried. The products could be recrystallized from hot water containing a small amount of $NaClO_4$. Yields were 70% or greater.

Anal. Calcd for $[Ru(bipy)_2(en)](ClO_4)_2$: C, 39.3; H, 3.60; N, 12.5. Found: C, 39.3; H, 3.71; N, 12.3. Calcd for $[Ru(bipy)_2$-

* N. F. Curtis, *Chem. Commun.*, 881 (1966); *Coord. Chem. Rev.*, 3, 3 (1968).

Table I. Abbreviations and Chemical Formulas for Amine and Imine Ligands

Ligand	Formula	Abbreviation
Ethylenediamine	$H_2N-CH_2-CH_2-NH_2$	en
1,2-Diiminoethane	$HN=CH-CH=NH$	dim
trans-1,2-Diaminocyclohexane	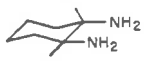	dach
1,2-Diiminocyclohexane	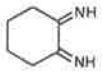	dich
1,2-Diamino-2-methylpropane	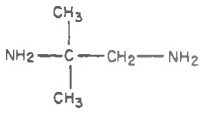	damp
2-Amino-2-methylpropanalimine	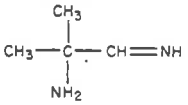	iamp
1,3-Propylenediamine (trimethylenediamine)	$NH_2-CH_2-CH_2-CH_2-NH_2$	tn
2-(Aminomethyl)pyridine	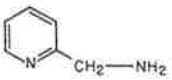	AMPy
2-(Iminomethyl)pyridine	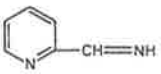	IMPy
2-(2′-Aminoethyl)pyridine	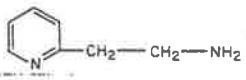	AEPy
Glyoxalbismethylimine	$CH_3N=CH-CH=NCH_3$	GMI

(dach)](ClO4)2: C, 43.0; H, 4.16; N, 11.6. Found: C, 43.0; H, 4.00; N, 11.4. Calcd for [Ru(bipy)2(damp)](ClO4)2: C, 41.2; H, 4.03; N, 12.0. Found: C, 41.0; H, 3.95; N, 11.9. Calcd for [Ru(bipy)2(AEPy)](ClO4)2: C, 44.2; H, 3.57; N, 11.4. Found: C, 43.9; H, 3.45; N, 10.8. Calcd for [Ru(bipy)2(AMPy)](ClO4)2: C, 43.3; H, 3.36; N, 11.7. Found: C, 43.5, H, 3.28; N, 11.5.

[Ru(bipy)2(tn)](PF6)2·2H2O (tn = 1,3-Propylenediamine). The complex was prepared as described above. The salt was precipitated by the addition of a filtered aqueous solution of NH_4PF_6 to a filtered, aqueous solution of the complex. The product was purified by reprecipitation from acetone–ether and vacuum dried overnight.

Anal. Calcd for [Ru(bipy)2(tn)](PF6)2·2H2O: C, 34.0; H, 3.72; N, 10.3. Found: C, 33.1; H, 3.06; N, 10.6.

[Ru(bipy)2(LL)](PF6)2 (LL = 1,2-Ethylenediimine (dim), 1,2-Diiminocyclohexane (dich), 2-(Iminomethyl)pyridine (IMPy)). The corresponding diaminebis(bipyridine)ruthenium(II) complex (100 mg) was dissolved in 1.0 *M* aqueous HCl (30 ml). The solution was oxidized by exhaustive electrolysis at constant potential which was anodic of $E_{1/2}$. It is essential that the potentials not be made so anodic that the desired diimine products are oxidized. Electrolysis was continued until the current had fallen to about 1% of the initial current. The product was precipitated from solution by the addition of a filtered, saturated, aqueous solution of NH_4PF_6 (2 ml). The product was purified by reprecipitation from acetone–ether.

Anal. Calcd for [Ru(bipy)2(dim)](PF6)2: C, 34.8; H, 2.65; N, 11.1; F, 30.0. Found: C, 34.7; H, 2.75; N, 10.9; F, 29.8. Calcd for [Ru(bipy)2(dich)](PF6)2·2H2O: C, 36.8; H, 3.56; N, 9.9; F, 26.8. Found: C, 36.9; H, 3.26; N, 9.9; F, 26.6. Calcd for [Ru(bipy)2(IMPy)](PF6)2: C, 38.6; H, 2.75; N, 10.4; F, 28.2. Found: C, 38.3; H, 2.68; N, 10.3; F, 28.0.

[Ru(bipy)2(iamp)]2+ (iamp = 2-Amino-2-methylpropanalimine). This complex was prepared in situ and not isolated. Attempts to isolate salts of the complex failed to give a pure material. Solutions of the complex were prepared from solutions of [Ru(bipy)2(damp)]2+ in 0.1 *M* TBAH–CH_3CN by exhaustive electrolysis at the $E_{1/2}$ of the [Ru(bipy)2(damp)]3+/2+ couple (0.99 V).

Conversion of perchlorate or hexafluorophosphate salts of the above cations to the chloride salt for ^1H NMR measurements was achieved by precipitation (using tetra-*n*-butylammonium chloride) from acetone solution.

Spectrophotometric Titrations with Ce(IV). Some of the oxidative dehydrogenation reactions were studied by spectrophotometric titrations in 0.1 *M* aqueous $HClO_4$ and acetonitrile solutions, using Ce(IV) as oxidant. The concentration of Ce(IV) was determined spectrophotometrically,[17] and the solutions were used immediately and protected from the light. Titrations were carried out by adding aliquots of oxidant to solutions of the complex, and monitoring the changes in absorbance in the range 600–320 nm. Some of the reactions studied required rapid mixing of the ruthenium and Ce(IV) solutions, which was accomplished by using a hand-driven device patterned after a stopped-flow syringe drive train.

Table II. Half-Wave Potentials and Electronic Spectra for Diaminebis(2,2′-bipyridine)ruthenium(II) Complexes in Acetonitrile

Compd	$E_{1/2}$, V[a]	λ_{max}, nm (ϵ)[b]
$Ru(bipy)_2(NH_3)_2^{2+}$	0.92	490 (9300)
		345 (7600)
		290 (54000)
		243 (20000)
$Ru(bipy)_2(en)^{2+}$	0.96	485 (9900)
		344 (7600)
		291 (60000)
		243 (21000)
$Ru(bipy)_2(dach)^{2+}$	0.96	488 (9900)
		344 (7600)
		292 (58000)
		244 (21000)
$Ru(bipy)_2(damp)^{2+}$	0.99	487 (10000)
		345 (7600)
		292 (58000)
		244 (21000)
$Ru(bipy)_2(tn)^{2+}$	~0.98	492 (8500)
		348 (6600)
		292 (52000)
		244 (18000)
$Ru(bipy)_2(AMPy)^{2+}$	1.12	471 (10000)
		422 (sh) (6300)
		339 (11000)
		298 (55000)
		244 (23000)
$Ru(bipy)_2(AEPy)^{2+}$	1.12	471 (9000)
		425 (sh) (5600)
		338 (9700)
		289 (54000)
		243 (23000)

[a] $E_{1/2}$ values vs. the saturated sodium chloride calomel electrode (SSCE) in 0.1 *M* $N(n\text{-}C_4H_9)_4PF_6$ at 25 ± 2°C. [b] λ_{max} values ± 2 nm; ϵ values ±5%.

Results and Discussion

Net Electrochemical Oxidation of Bound Diamine Ligands. The complex $[Ru(bipy)_2(NH_3)_2]^{2+}$ undergoes an electrochemically reversible one-electron oxidation at a platinum electrode in acetonitrile, as shown by the cyclic voltammogram in Figure 1A. Under the same experimental conditions, the complex $[Ru(bipy)_2(en)]^{2+}$ also undergoes an electrochemically reversible one-electron oxidation on the cyclic voltammetry time scale (Figure 1B).[18] The similarity in reduction potentials for the series of diamine complex 3+/2+ couples studied and that for the $[Ru(bipy)_2(NH_3)_2]^{3+/2+}$ (Table II) indicates that this oxidation occurs in all cases at the ruthenium.

Exhaustive electrolysis of acetonitrile solutions of $[Ru(bipy)_2(en)]^{2+}$ at a constant potential (1.15 V) on the diffusion plateau for the voltammetric wave gave a coulometric *n* value of 3.82. The product of the electrolytic oxidation was identified by spectral and electrochemical measurements (see below) as the α,α'-diimine complex, $[Ru(bipy)_2(dim)]^{2+}$. The net

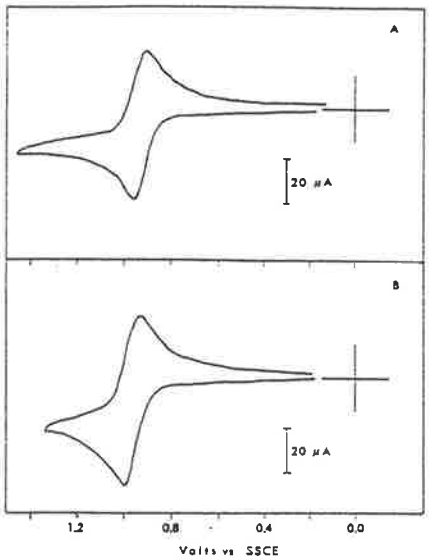

Figure 1. Cyclic voltammograms (200 mV/sec) of (A) $[Ru(bipy)_2(NH_3)_2]^{2+}$ (1.0×10^{-3} *M*), and (B) $[Ru(bipy)_2(en)]^{2+}$ (1.2×10^{-3} *M*) in acetonitrile solution (0.1 *M* TBAH).

stoichiometry of the oxidation is given by eq 2.

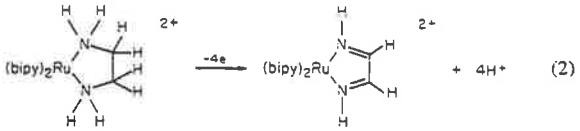

(2)

The oxidation process thus consists of two parts: initial oxidation of the metal to Ru(III)

$$[Ru(bipy)_2(en)]^{2+} \xrightarrow{-e^-} [Ru(bipy)_2(en)]^{3+} \quad (3)$$

followed by oxidation of the coordinated ligand

$$[Ru(bipy)_2(en)]^{3+} \xrightarrow{-3e^-} [Ru(bipy)_2(dim)]^{2+} + 4H^+ \quad (4)$$

In acetonitrile, for $[Ru(bipy)_2(en)]^{2+}$, and also for $[Ru(bipy)_2(dach)]^{2+}$, the initial one-electron oxidation is faster than the subsequent oxidation of the ligand. At slow voltammetry scan rates (0.2 V/sec), recapture of $[Ru(bipy)_2(en)]^{3+}$ by reduction at the electrode is more rapid than ligand oxidation, and the voltammetric waves are reversible.

In aqueous solution (1.0 *M* HCl or 1.0 *M* NaCl), electrochemical oxidation of $[Ru(bipy)_2(en)]^{2+}$ (or $[Ru(bipy)_2(dach)]^{2+}$) at a Pt electrode was irreversible, even by fast cyclic voltammetry (100 V/sec). Exhaustive electrolysis at 0.80 V (vs. SSCE) in 1.0 *M* HCl gave the corresponding α,α'-diimine complexes quantitatively and provided a convenient synthetic route to these complexes.

The ligand 2-(aminomethyl)pyridine (AMPy) contains one imine (pyridine) and one amine nitrogen atom, so that the α,α'-diimine linkage is half present initially. Exhaustive electrolysis of $[Ru(bipy)_2(AMPy)]^{2+}$ in acetonitrile at a potential on the diffusion plateau for oxidation (1.20 V) gave a coulometric *n* value of 1.96 and the α,α'-diimine complex as the sole product:

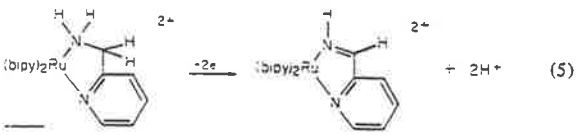

(5)

Cyclic voltammetry of $[Ru(bipy)_2(AMPy)]^{2+}$ at slow scan rates was irreversible, but at faster scan rates (≥5 V/sec) the cyclic voltammetric data were consistent with a reversible one-electron oxidation. Since the $[Ru(bipy)_2(AMPy)]^{3+/2+}$ potential (1.12 V) is higher than the potentials of the diamine complexes, the Ru(III) complex would be more strongly oxidizing and a higher rate of ligand oxidation (e.g., eq 4) is not unexpected.

Table III. Half-Wave Potentials and Electronic Spectra of Diiminebis(2,2'-bipyridine)ruthenium(II) Complexes in Acetonitrile

Compd	$E_{1/2}$, V[a]	λ_{max}, nm (ϵ)[b]
$Ru(bipy)_3^{2+}$	1.29	450 (14000)
		283 (80000)
		242 (25000)
$Ru(bipy)_2(dim)^{2+}$	1.33	454 (14000)
		280 (46000)
		242 (17000)
$Ru(bipy)_2(dich)^{2+}$	1.20	472 (16000)
		285 (48000)
		242 (18000)
$Ru(bipy)_2(iamp)^{2+}$	1.06	475 (9000)
		335 (9100)
$Ru(bipy)_2(IMPy)^{2+}$	1.27	470 (13000)
		430 (sh)
		345 (sh)
		315 (sh)
		286 (51000)
		245 (18000)
		242 (20000)

[a] Vs. the SSCE in 0.1 *M* $N(n\text{-}C_4H_9)_4PF_6$ at 25 ± 2°C. [b] λ_{max} values are ±2 nm; ϵ values ±5%.

The ligand 1,2-diamino-2-methylpropane (damp) has a skeletal framework similar to ethylenediamine, but oxidative dehydrogenation can only occur at one $-CH_2-NH_2$ group, leading to a coordinated monoimine. Cyclic voltammetry in acetonitrile solution shows that $[Ru(bipy)_2(damp)]^{2+}$ undergoes an electrochemically reversible one-electron oxidation. Exhaustive electrolysis at $E_{1/2}$ gave an *n* value of 1.76 and near-quantitative conversion to a single product whose redox and spectral properties are consistent with a monoimine complex.

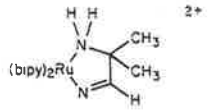

When electrolysis was carried out at potentials more anodic than $E_{1/2}$, further oxidation processes, involving the ion $[Ru(bipy)_2(iamp)]^{2+}$, occurred. The electrochemical oxidation of $[Ru(bipy)_2(damp)]^{2+}$ in aqueous solution was completely irreversible, and attempts to prepare the monoimine complex $[Ru(bipy)_2(iamp)]^{2+}$ by exhaustive electrolysis were frustrated by competitive processes involving oxidation of bound iamp. In both these cases, it is apparent that both $[Ru(bipy)_2(damp)]^{2+}$ and $[Ru(bipy)(iamp)]^{2+}$ are oxidizable, and that the oxidation rates are comparable. Because of the further ligand oxidation, a possible complicating reaction here, and in related systems, is bimolecular electron transfer giving the Ru(III) form of the ligand-oxidized complex,

$$[Ru(bipy)_2(damp)]^{3+} + [Ru(bipy)_2(iamp)]^{2+} \rightleftharpoons [Ru(bipy)_2(damp)]^{2+} + [Ru(bipy)_2(iamp)]^{3+} \quad (6)$$

Equation 6 is an equilibrium in which the forward reaction is slightly disfavored thermodynamically (using $E_{1/2}$ data in Tables II and III). From rate data on other bis(2,2'-bipyridine)ruthenium(III)–(II) electron transfer reactions,[20] the forward reaction should still be rapid, and if followed by rapid Ru(III) ligand oxidation accounts for such phenomena as the dependence of products on rates of mixing with chemical oxidants and our inability to prepare imine complexes in such systems.

The ligands 1,3-propylenediamine (tn) and 2-(2'-aminoethyl)pyridine (AEPy) contain one methylene group more than ethylenediamine and 2-(aminomethyl)pyridine, respectively, and hence cannot give conjugated α,α'-diimines upon oxidation. The complexes $[Ru(bipy)_2(tn)]^{2+}$ and $[Ru(bipy)_2(AEPy)]^{2+}$ undergo electrochemically reversible one-electron oxidations in acetonitrile solutions, as determined by cyclic voltammetry. Exhaustive electrolyses on the diffusion plateaus of the oxidation waves gave high n values and a variety of products (as shown by cyclic voltammetry), consistent with oxidation past the imine stage.

Oxidations by Ce(IV). Spectrophotometric Titrations. The oxidative dehydrogenation reactions could also be carried out chemically using Ce(IV). The Ce(IV) oxidations were studied by spectrophotometric titrations.

The spectrophotometric titration of $[Ru(bipy)_2(AMPy)]^{2+}$ with Ce(IV) in either acetonitrile or 0.1 M aqueous $HClO_4$ gave a smooth conversion to $[Ru(bipy)_2(IMPy)]^{2+}$ (isosbestic points at 388 and 513 nm) with the stoichiometry given in eq 7. The addition of more than 2 equiv of Ce(IV) per mole of

$$[Ru(bipy)_2(AMPy)]^{2+} + 2Ce(IV) \rightarrow [Ru(bipy)_2(IMPy)]^{2+} + 2Ce(III) + 2H^+ \quad (7)$$

ruthenium did not give a smooth conversion to the imine product. It appears that further oxidation of the ligand occurs, giving products which we have not characterized.

The oxidation of $[Ru(bipy)_2(damp)]^{2+}$ with Ce(IV) in acetonitrile led to the formation of $[Ru(bipy)_2(iamp)]^{2+}$, with the stoichiometry given in eq 8. The reactions were clean only

$$[Ru(bipy)_2(damp)]^{2+} + 2Ce(IV) \rightarrow [Ru(bipy)_2(iamp)]^{2+} + 2Ce(III) + 2H^+ \quad (8)$$

if the Ce(IV) and ruthenium solutions were mixed rapidly and 1 mol or less of Ce(IV) was added per mole of ruthenium. If these conditions were met, isosbestic points were observed at 477, 379, and 360 nm, and the observed spectra were consistent with the sums of the spectra of $[Ru(bipy)_2(damp)]^{2+}$ and $[Ru(bipy)_2(iamp)]^{2+}$ in the ratios expected from the stoichiometry given in eq 8. These results are understandable if the reaction of Ce(IV) with $[Ru(bipy)_2(damp)]^{2+}$ is faster than the oxidative dehydrogenation reaction, and the rate of further ligand oxidation of $[Ru(bipy)_2(iamp)]^{2+}$ is competitive with the initial oxidative dehydrogenation. The Ce(IV) oxidation of bis(2,2'-bipyridine)ruthenium(II) complexes is known to be very rapid.[20]

Titration of $[Ru(bipy)_2(dach)]^{2+}$ with Ce(IV) indicated a 4:1 stoichiometry with the formation of $[Ru(bipy)_2(dich)]^{2+}$, eq 9. Addition of 4 mol of Ce(IV) per mole of ruthenium

$$[Ru(bipy)_2(dach)]^{2+} + 4Ce(IV) \rightarrow [Ru(bipy)_2(dich)]^{2+} + 4Ce(III) + 4H^+ \quad (9)$$

gave a spectrum identical with that of an analyzed sample of $[Ru(bipy)_2(dich)]^{2+}$ prepared electrochemically. An isosbestic point occurred at 380 nm for all additions up to 4 mol of Ce(IV) per mole of ruthenium. However, the lack of an isosbestic point in the region of the 472-nm absorbance of $[Ru(bipy)_2(dich)]^{2+}$ and the 488-nm absorbance of $[Ru(bipy)_2(dach)]^{2+}$ indicated interference in this region from a third species. The likely explanation of this combination of observations is that an intermediate exists which contains one imine and one amine linkage. The addition of more than 4 mol of Ce(IV) per mole of ruthenium leads to complicated product spectra, probably due to the further oxidation of the α,α'-diimine ligand. The data indicate that the oxidative dehydrogenation leading to $[Ru(bipy)_2(dich)]^{2+}$ is faster than further oxidation of the coordinated dich ligand.

Spectrophotometric titrations of the complex $[Ru(bipy)_2(en)]^{2+}$ with Ce(IV) were extremely complicated. The data indicate that complications arise both from competitive further oxidation of the product, $[Ru(bipy)_2(dim)]^{2+}$, and from the interference of a species containing a half-oxidized ligand, with a single imine linkage ($HN{=}CHCH_2NH_2$).

Mechanism of Oxidative Dehydrogenation. These studies indicate that the diamine ligand oxidation, reaction 4, can be further broken down into two stepwise processes, the first involving oxidation to a monoimine intermediate (eq 10), and

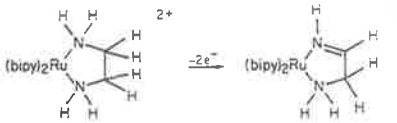

(10)

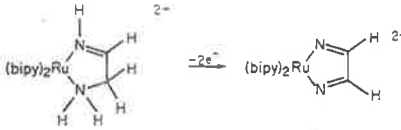

(11)

the second involving oxidation of the monoimine to the α,α'-diimine (eq 11). Analogous equations could be written for the oxidative dehydrogenation of the dach ligand.

For the complexes $[Ru(bipy)_2(AMPy)]^{2+}$ and $[Ru(bipy)_2(damp)]^{2+}$, only one of these two-electron steps is possible. On addition of a 1:1 stoichiometric quantity of Ce(IV) to a solution of either of these complexes, a clean oxidation occurs producing an equimolar mixture of the starting complex and the corresponding two-electron oxidation product, as indicated in eq 12 for the AMPy species:

$$2[Ru(bipy)_2(AMPy)]^{2+} + 2Ce(IV) \rightarrow [Ru(bipy)_2(AMPy)]^{2+} + [Ru(bipy)_2(IMPy)]^{2+} + 2Ce(III) \quad (12)$$

From the instantaneous color changes observed on the addition of Ce(IV) to solutions of the diamine complexes (spectrophotometric titrations), preliminary kinetic studies on the Ce(IV) oxidation of $[Ru(bipy)_2(en)]^{2+}$ and $[Ru(bipy)_2(AMPy)]^{2+}$,[20] and the electrochemical results, the initial step in the oxidation process involves oxidation of ruthenium(II) to ruthenium(III). Furthermore, in the Ce(IV) titration of $[Ru(bipy)_2(dach)]^{2+}$ there is clear evidence for an intermediate of a monoimine type. Detailed mechanistic information about the oxidative dehydrogenation step is not available. However, under conditions where stoichiometric amounts of oxidant are added, an overall pattern of *net* reactions can be written, and this is illustrated for $[Ru(bipy)_2(en)]^{2+}$ below:

$$2[Ru(bipy)_2(en)]^{2+} \xrightarrow{-2e^-} 2[Ru(bipy)_2(en)]^{3+} \quad (13)$$

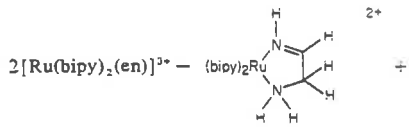

$$[Ru(bipy)_2(en)]^{2+} + 2H^+ \quad (14)$$

$$2[Ru(bipy)_2(monoimine)]^{2+} \xrightarrow{-2e^-} 2[Ru(bipy)_2(monoimine)]^{3+} \quad (15)$$

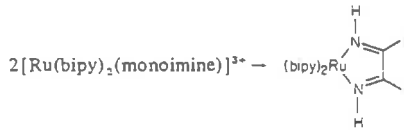

$$[Ru(bipy)_2(monoimine)]^{2+} + 2H^+ \quad (16)$$

On further oxidation,

$$[Ru(bipy)_2(dim)]^{2+} \xrightarrow{-e^-} [Ru(bipy)_2(dim)]^{3+} \quad (17)$$

$$[Ru(bipy)_2(dim)]^{3+} \rightarrow \text{further ligand oxidation} \quad (18)$$

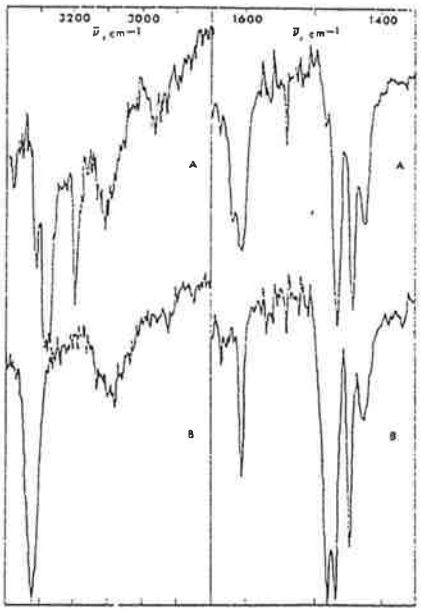

Figure 2. Infrared spectra (KBr pellets) of (A) $[Ru(bipy)_2(en)](ClO_4)_2$ and (B) $[Ru(bipy)_2(dim)](PF_6)_2$ in the regions 3400–2800 and 1650–1350 cm^{-1}.

In cases where eq 18 is sufficiently rapid, electron transfer as in eq 6 can occur giving a pathway for the depletion of the imine complexes by further ligand oxidation.

Electrochemical and Chemical Behavior of the Imine Complexes. The ruthenium(II) complexes of the α,α'-diimines reported here are stable for several hours in aqueous 1.0 *M* acid and in 0.1 *M* base solution. In neutral solution, the complexes showed little (if any) decomposition after several days. In acetonitrile solution, the complexes were also found to be unchanged after several days, even when unprotected from light.

The redox properties of the α,α'-diimine complexes were investigated by electrochemical techniques, both in aqueous solution and in acetonitrile. In aqueous solution, using 0.5 *M* *p*-toluenesulfonic acid (HTos) as the supporting electrolyte, cyclic voltammetry experiments show that the α,α'-diimine complexes $[Ru(bipy)_2(dim)]^{2+}$, $[Ru(bipy)_2(dich)]^{2+}$, and $[Ru(bipy)_2(IMPy)]^{2+}$, undergo electrochemically irreversible oxidations at a Pt electrode. However, in 0.1 *M* TBAH–CH_3CN, the complexes each undergo a reversible, or nearly reversible, one-electron oxidation at Pt, apparently involving the oxidation of Ru(II) to Ru(III).

$$[Ru^{II}(bipy)_2(\alpha,\alpha'\text{diimine})]^{2+} \xrightarrow{-e} [Ru^{III}(bipy)_2(\alpha,\alpha'\text{-diimine})]^{3+}$$

At slow scan rates (0.2 V/sec), the ratio of the cathodic to anodic peak currents (i_c/i_a) is less than one in all cases. However, at faster scan rates (10 V/sec) the ratio of i_c/i_a is one and no additional waves appeared in the cyclic voltammograms, indicating that decomposition had not occurred. Exhaustive electrolysis at controlled potentials more positive than $E_{1/2}$ gave large *n* values; the products were not characterized. Apparently, the further oxidations result in the oxidation of the α,α'-diimine ligands.

Cyclic voltammetry of the α,α'-diimine complexes in 0.1 *M* TBAH–CH_3CN also shows an electrochemically irreversible reduction in addition to the usual 2,2'-bipyridine reductions which occur at more cathodic potentials.[21] The products of the reduction waves are apparently bound, reduced radical anions in which the reduction is localized mainly on an imine linkage. Reduction of $[Ru(bipy)_2(dim)]^{2+}$ by exhaustive electrolysis gave a variety of products, as shown by cyclic voltammetry, and was not pursued further. Sodium borohydride reacts slowly with the α,α'-diimine complexes in either water or acetonitrile, but does not give well-defined products.

The α,α'-diimine complexes $[Ru(bipy)_2(dim)]^{2+}$, $[Ru(bipy)_2(dich)]^{2+}$, and $[Ru(bipy)_2(IMPy)]^{2+}$ have stability and chemical and physical properties reminiscent of $[Ru(bipy)_3]^{2+}$. On the cyclic voltammetry time scale the ruthenium(III) complexes $[Ru(bipy)_2(\alpha,\alpha'\text{-diimine})]^{3+}$ are stable (the $[Ru(bipy)_2(\alpha,\alpha'\text{-diimine})]^{3+/2+}$ couples are electrochemically reversible, or nearly reversible). However, on longer time scales, the ruthenium(III) complexes are unstable, apparently because of further oxidation processes involving the coordinated ligands. We have not investigated the subsequent reactions in detail. Chum and Krumholz[22] have investigated ligand oxidation reactions in iron(II) α,α'-diimine complexes like $[Fe(GMI)]^{2+}$ (GMI is CH_3—N=CH—CH=N—CH_3) and have found reactions such as,

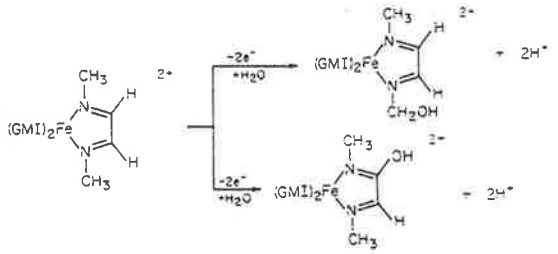

The reactions of the α,α'-diimine ligands in the coordination sphere of the ruthenium complexes may be similar.

The subsequent α,α'-diimine oxidation presents a synthetic difficulty in the conversion of diamines into α,α'-diimines. It is essential that controlled-potential electrolysis methods be used to avoid oxidation of the α,α'-diimine complexes once formed. The reaction potentials for the α,α'-diimine (1.20 to 1.33 V, Table III) and diamine couples (0.96 to 0.99 V, Table II) are sufficiently different so that electrolyses can be carried out cleanly on the diffusion plateau of the $[Ru(bipy)_2(diamine)]^{3+/2+}$ wave.

Infrared Spectra. Infrared spectra were helpful in the characterization of the α,α'-diimine complexes.

The infrared spectra of the complexes $[Ru(bipy)_2(en)](ClO_4)_2$ and $[Ru(bipy)_2(dim)](PF_6)_2$ in the regions 3400–2800 and 1650–1350 cm^{-1} are illustrated in Figure 2. For the complex $[Ru(bipy)_2(en)]^{2+}$, the absorptions at 3315, 3280, and 3195 cm^{-1} can be assigned as N–H stretching vibrations (ν_{N-H}). The absorption at 1618 cm^{-1} can be assigned as an N–H deformation (δ_{N-H}). Upon oxidation to $[Ru(bipy)_2(dim)]^{2+}$, the N–H stretching region simplifies to one absorption at 3325 cm^{-1}, as expected for an imine complex. Also as expected, the N–H deformation near 1600 cm^{-1} disappears for the imine complexes. A new absorption appears at 1480 cm^{-1} for the salt $[Ru(bipy)_2(dim)](ClO_4)_2$. A pure –C=N– stretching vibration would be expected to appear around 1600 cm^{-1}.[23,24] Nakamoto has carried out a normal coordinate analysis of the ion $[Fe(GMI)_3]^{2+}$, and has identified a band at 1530 cm^{-1} as a combination mode, which is made up predominantly of a –C=N– stretching vibration.[25] The band at 1480 cm^{-1} for $[Ru(bipy)_2(dim)](ClO_4)_2$ can reasonably be assigned to a combination mode consisting largely of the conjugated –C=N– stretch of the α,α'-diimine ligand ($\nu_{C=N}$). The characteristic ν_{N-H}, $\delta_{N=H}$, and $\nu_{C=N}$ bands for some of the ruthenium(II) amine and α,α'-diimine complexes studied are summarized in Table IV. The C=N stretching mode could not be found for the complex $[Ru(bipy)_2(IMPy)]^{2+}$. There are many strong absorptions due to the bipyridine ligands in this region, and the band of interest may well be

Table IV. Infrared Spectra of Bis(2,2'-bipyridine)ruthenium(II) Amine and Imine Complexes

Complex	ν(N–H)$_{as}$, cm^{-1}	ν(N–H)$_s$, cm^{-1}	δ(N–H), cm^{-1}	ν(C=N), cm^{-1}
[Ru(bipy)$_2$(en)](ClO$_4$)$_2$	3315 3280	3195	1618	
[Ru(bipy)$_2$(dim)](PF$_6$)$_2$	3325			1480
[Ru(bipy)$_2$(dach)](ClO$_4$)$_2$	3280 3252	3178	1615	
[Ru(bipy)$_2$(dich)](PF$_6$)$_2$	3300			1450
[Ru(bipy)$_2$(AMPy)](ClO$_4$)$_2$	3300 3267	3185	1615	
[Ru(bipy)$_2$(IMPy)](PF$_6$)$_2$	3322			

hidden. Also the intensity of the band may be diminished due to poor conjugation of the –C=N– group with the pyridine group. King and Douglas[23] observed that the –C=N– vibration was very weak in the monoalkylimine complex ((CH$_3$)$_2$C=NH)Cr(CO)$_5$.

^{1}H NMR Spectra. The ^{1}H NMR spectra of the imine complexes in D_2O solution were of limited use for characterization since the –N=CH resonance was hidden by the very complicated resonances due to the bipyridine ligands (δ = 7.0–9.0 ppm). The spectra were however consistent with the complex formulations given above; for example, the >CH$_2$ and –NH$_2$ resonances in [Ru(bipy)$_2$(en)]$^{2+}$ (centered at 2.8 and 3.5 ppm, respectively, relative to *t*-BuOH at 1.23 ppm) were absent in the spectrum of [Ru(bipy)$_2$(dim)]$^{2+}$.

Electrochemical and Electronic Spectral Data. Electronic spectra (absorption maxima and molar extinction coefficients) and half-wave potentials in acetonitrile solution are given in Table II for [Ru(bipy)$_2$(NH$_3$)$_2$]$^{2+}$ and for the diamine-bis(2,2'-bipyridine) complexes of ruthenium(II) studied here. In Table III, similar data are presented for [Ru(bipy)$_3$]$^{2+}$ and for the various imine complexes considered in this work.

Ruthenium(III)/ruthenium(II) reduction potentials are known to be dependent upon the presence of back-bonding ligands in the coordination sphere,[26-28] the potential increasing as the number of back-bonding ligands is increased. Qualitatively, this change in potential can be attributed to a stabilization of the ruthenium(II) oxidation state by increased back-bonding: back-bonding is thought to be insignificant between ruthenium(III) and pyridine-type ligands.[26] Such a trend is evident from the data in Table II: the $E_{1/2}$ values for the chelated diamine couples [Ru(bipy)$_2$(en)]$^{3+/2+}$, [Ru(bipy)$_2$(dach)]$^{3+/2+}$, [Ru(bipy)$_2$(damp)]$^{3+/2+}$, and [Ru(bipy)$_2$(tn)]$^{3+/2+}$ are close to that for [Ru(bipy)$_2$(NH$_3$)$_2$]$^{3+/2+}$, whereas the $E_{1/2}$ values for the pyridine–amine couples [Ru(bipy)$_2$(AMPy)]$^{3+/2+}$ and [Ru(bipy)$_2$(AEPy)]$^{3+/2+}$ are at considerably more anodic potentials.

If the back-bonding argument is correct, the data in Table III indicate that imine ligands undergo appreciable back-bonding with ruthenium(II) in bis(2,2'-bipyridine) complexes. The Ru(III)/Ru(II) potentials for [Ru(bipy)$_2$(dim)]$^{2+}$ and [Ru(bipy)$_2$(dich)]$^{2+}$ are at considerably higher potentials than the corresponding diamine complexes, and the potentials for all three α,α'-diimine complexes fall in the same range (1.20–1.33 V) as the potential for the [Ru(bipy)$_3$]$^{3+/2+}$ couple. The ligands 2,2'-bipyridine and 1,10-phenanthroline are high in the spectrochemical series and capable of strong back-bonding,[29] and it has been suggested[30] that it is the α,α'-diimine linkage

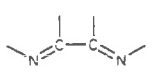

which is the important bonding feature responsible for the back-bonding. The similarities in properties between [Ru(bipy)$_3$]$^{2+}$ and the α,α'-diimine complexes reported here are consistent with this suggestion. However, it is not clear that *linked* imine systems are necessary to explain the effects observed. The linked imine system benefits from the chelate effect, and the chemical link may be the origin of the unusual chemical stability of the α,α'-diimine complexes. However, the spectral and redox properties of [Ru(bipy)$_2$(py)$_2$]$^{2+}$ are

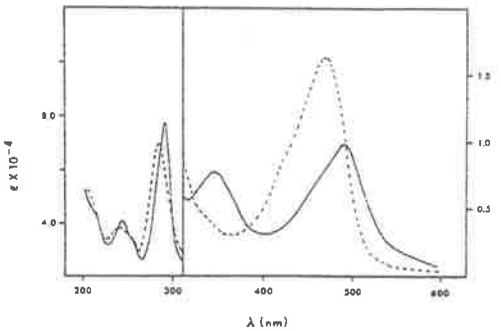

Figure 3. Electronic spectra of [Ru(bipy)$_2$(dach)]$^{2+}$ (—) and [Ru(bipy)$_2$(dich)]$^{2+}$ (- - -) in acetonitrile solution.

essentially identical with those for [Ru(bipy)$_3$]$^{2+}$.[14] The electronic effects of the α,α'-diimine ligand, particularly with regard to back-bonding, may originate primarily from the two imine linkages, irrespective of a chemical link between them.

The reduction potential for the monoimine couple [Ru(bipy)$_2$(iamp)]$^{3+/2+}$ is higher than that for its precursor diamine couple [Ru(bipy)$_2$(damp)]$^{3+/2+}$, but is similar to that for the pyridine–amine couple [Ru(bipy)$_2$(AMPy)]$^{3+/2+}$. The similarity indicates the monoimine linkage may be similar to a pyridine group in back-bonding ability.

The electronic spectra of *cis*-bis(2,2'-bipyridine)ruthenium(II) complexes are also sensitive to the presence of back-bonding ligands in the two remaining coordination positions.[15,28] The spectrum of [Ru(bipy)$_2$(NH$_3$)$_2$]$^{2+}$ has two broad maxima in the visible region, which have previously been assigned as d(Ru(II)) → π^*(bipy) MLCT transitions.[15] There are also two maxima in the uv region, which have been assigned as 2,2'-bipyridine $\pi \rightarrow \pi^*$ transitions.[15] From the data in Table II it can be seen that the electronic spectra of the diamine complexes of bis(2,2'-bipyridine)ruthenium(II) are all very similar to the spectrum of [Ru(bipy)$_2$(NH$_3$)$_2$]$^{2+}$. The spectrum of the complex [Ru(bipy)$_2$(dach)]$^{2+}$ is shown in Figure 3.

The spectra of the complexes [Ru(bipy)$_2$(AMPy)]$^{2+}$ and [Ru(bipy)$_2$(AEPy)]$^{2+}$ differ slightly from the spectra of the diamine complexes, there being additional transitions at 422 and 425 nm, respectively. An assignment of these bands as d(Ru(II)) → π^*(py) MLCT transitions is reasonable since similar transitions are known for related complexes.

As the number of back-bonding ligands in bis(2,2'-bipyridine)ruthenium(II) complexes increases, the energy of the bands in the visible region increases and for complexes with back-bonding ligands in both sites there is typically only one d(Ru(II)) → π^*(bipy) MLCT transition.[31] Distinct shoulders are also sometimes observed since the broad absorption bands are clearly a composite of allowed transitions.[15] The energy of the first d → π^* transition is observed to increase from [Ru(bipy)$_2$(NH$_3$)$_2$]$^{2+}$ (490 nm) to [Ru(bipy)$_3$]$^{2+}$ (450 nm), and those for the α,α'-diimine complexes occur between 454 and 472 nm, which again indicates considerable back-bonding from the metal to the α,α'-diimine ligand. The spectrum of [Ru(bipy)$_2$(dich)]$^{2+}$ is shown in Figure 3.

The electronic spectrum of the monoimine complex [Ru(bipy)$_2$(iamp)]$^{2+}$ is quite similar to the visible spectrum of the

pyridine–amine complex $[Ru(bipy)_2(AMPy)]^{2+}$, but lacks the d(Ru) → π*(pyridine) MLCT band at 422 nm as expected. The complex $[Ru(bipy)_2(IMPy)]^{2+}$ has a very complicated electronic spectrum, but this is expected since transitions in the MLCT region are expected to appear due to d(Ru) → π*(L) transitions, where L = 2,2'-bipyridine, pyridine, and the imine group.

The effects of back-bonding in the α,α'-diimine complexes are felt both at the metal (redox and spectral properties) and also at the ligand. For example, simple organic imines are known to be unstable with respect to hydrolysis,[32] yet coordinated α,α'-diimine ligands are remarkably stable in aqueous solution.

The complexes $[Ru(bipy)_2(AEPy)]^{2+}$ and $[Ru(bipy)_2(tn)]^{2+}$ do not have stable imine oxidation products. Because of the structures of the ligands, the imine oxidation products cannot be α,α'-diimines. It is probable that oxidation of these ligands gives first an imine intermediate, e.g.,

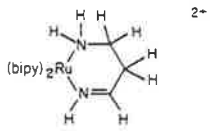

which is unstable with respect to further oxidation at the imine site. The instability of nondelocalized imines appears to be further evidence for the unusual stability of the α,α'-diimine linkage.

Acknowledgment. Acknowledgments are made to the Materials Research Center of the University of North Carolina under Grant DAHC15 73 G 9 with DARPA for support of this research.

Registry No. $[Ru(bipy)_2Cl_2]$, 19542-80-4; $[Ru(bipy)_3](ClO_4)_2$, 15635-95-7; $[Ru(bipy)_2(NH_3)_2](ClO_4)_2$, 56993-99-8; $[Ru(bipy)_2(en)](ClO_4)_2$, 31659-06-0; $[Ru(bipy)_2(dach)](ClO_4)_2$, 56889-66-8; $[Ru(bipy)_2(damp)](ClO_4)_2$, 56889-68-0; $[Ru(bipy)_2(AEPy)](ClO_4)_2$, 56889-70-4; $[Ru(bipy)_2(AMPy)](ClO_4)_2$, 56889-72-6; $[Ru(bipy)_2(tn)](PF_6)_2$, 56889-74-8; $[Ru(bipy)_2(dim)](PF_6)_2$, 56889-76-0; $[Ru(bipy)_2(dich)](PF_6)_2$, 56889-78-2; $[Ru(bipy)_2(IMPy)](PF_6)_2$, 56889-80-6; $[Ru(bipy)_2(iamp)]^{2+}$, 56889-81-7; Ce(IV), 16065-90-0.

References and Notes

(1) N. F. Curtis, *Chem. Commun.*, 881 (1966); *Coord. Chem. Rev.*, 3, 3 (1968).
(2) J. C. Dabrowiak, F. V. Lovecchio, V. L. Goedken, and D. H. Busch, *J. Am. Chem. Soc.*, 94, 5502 (1972); V. L. Goedken and D. H. Busch, *ibid.*, 94, 7355 (1972).
(3) H. Elsbernd and J. K. Beattie, *J. Chem. Soc. A*, 2598 (1970).
(4) B. C. Lane, J. E. Lester, and F. Basolo, *Chem. Commun.*, 1618 (1971).
(5) D. F. Mahoney and J. K. Beattie, *Inorg. Chem.*, 12, 2561 (1973).
(6) V. L. Goedken, *J. Chem. Soc., Chem. Commun.*, 207 (1972).
(7) J. A. Ferguson, T. J. Meyer, and D. G. Whitten, *Inorg. Chem.*, 11, 2767 (1972).
(8) G. M. Brown, F. R. Hopf, J. A. Ferguson, T. J. Meyer, and D. G. Whitten, *J. Am. Chem. Soc.*, 95, 5939 (1973).
(9) G. M. Brown, R. W. Callahan, and T. J. Meyer, *J. Am. Chem. Soc.*, 96, 7829 (1974).
(10) R. W. Callahan, G. M. Brown, and T. J. Meyer, 168th National Meeting of the American Chemical Society, Atlantic City, N.J., September 1974, Abstract No. INOR 121.
(11) R. N. Adams, "Electrochemistry at Solid Electrodes", Marcel Dekker, New York, N.Y., 1969, p 206.
(12) J. A. Ferguson, Ph.D. Dissertation, University of North Carolina at Chapel Hill, 1971.
(13) J. B. Godwin and T. J. Meyer, *Inorg. Chem.*, 10, 471 (1971).
(14) J. N. Braddock and T. J. Meyer, *J. Am. Chem. Soc.*, 95, 3158 (1973).
(15) G. M. Bryant, J. E. Fergusson, and H. K. J. Powell, *Aust. J. Chem.*, 24, 257 (1971).
(16) F. P. Dwyer, H. A. Goodwin, and E. C. Gyarfas, *Aust. J. Chem.*, 16, 544 (1963).
(17) R. W. Callahan, G. M. Brown, and T. J. Meyer, *Inorg. Chem.*, 14, 1443 (1975).
(18) Electrochemical reversibility was determined, where possible, from plots of log $([i_l - i]/i)$ vs. E from stirred solution voltammetry data. For cases where subsequent ligand oxidation was too rapid, reversibility was determined by cyclic voltammetry. In such experiments, reversibility was based on the ratio of anodic to cathodic peak currents (i_c/i_a) and the potential separation of the peaks (ΔE_p). At fast scan rates, ΔE_p was greater than the theoretical value of 59 mV which was probably due to uncompensated resistance between the working electrode and the reference electrode tip. For such cases, ΔE_p for the electrode reaction of interest was compared with ΔE_p for the couple $[Ru(bipy)_2(NH_3)_2]^{3+/2+}$, which is reversible. The half-wave potentials, $E_{1/2}$, reported here differ from formal reduction potentials by a usually small term involving differences in diffusion coefficients,[19] and refer to reactions such as $[Ru(bipy)_2(en)]^{3+} + e \rightarrow [Ru(bipy)_2(en)]^{2+}$.
(19) R. W. Murray and C. N. Reilley, "Electroanalytical Principles", Interscience, New York, N.Y., 1963, p 2175.
(20) J. N. Braddock, J. L. Cramer, E. M. Gupton, and F. R. Keene, unpublished results, University of North Carolina, 1974.
(21) N. E. Tokel-Takvoryan, R. E. Hemingway, and A. J. Bard, *J. Am. Chem. Soc.*, 95, 6582 (1973).
(22) H. L. Chum and P. Krumholz, *Inorg. Chem.*, 13, 514, 519 (1974).
(23) R. B. King and W. M. Douglas, *J. Am. Chem. Soc.*, 95, 7528 (1973).
(24) S. Patai, Ed., "The Chemistry of the Carbon-Nitrogen Double Bond", Interscience, London, 1970.
(25) K. Nakamoto, "Advances in the Chemistry of Coordination Compounds", Wiley, New York, N.Y., 1963.
(26) H. Taube, *Surv. Prog. Chem.*, 6, 1 (1973).
(27) D. A. Buckingham and A. M. Sargeson, "Chelating Agents and Metal Chelates", F. P. Dwyer and D. P. Mellor, Ed., Academic Press, New York, N.Y., 1964, p 269.
(28) G. M. Brown, R. W. Callahan, M. Cooke, E. C. Johnson, T. J. Meyer, and T. R. Weaver, manuscript in preparation; J. L. Cramer, unpublished results, University of North Carolina, 1974.
(29) F. A. Cotton and G. Wilkinson, "Advanced Inorganic Chemistry", 3rd ed, Interscience, New York, N.Y., 1972, p 577.
(30) P. Krumholz, *Struct. Bonding (Berlin)*, 9, 139 (1971).
(31) S. A. Adeyemi, Ph.D. Dissertation, University of North Carolina at Chapel Hill, 1973.
(32) J. March, "Advanced Organic Chemistry", McGraw-Hill, New York, N.Y., 1968, p 656.

[Reprinted from the Journal of American Chemical Society, 98, 1884 (1976).]

Oxidation of Primary Amines Bound to Bis(2,2′-bipyridine)ruthenium(II)

F. Richard Keene, Dennis J. Salmon, and Thomas J. Meyer*

Contribution from the W. R. Kenan, Jr., Laboratories of Chemistry, Department of Chemistry, The University of North Carolina, Chapel Hill, North Carolina 27514. *Received July 12, 1975*

Abstract: In the net sense, chemical and electrochemical oxidations of the ions $[Ru(bpy)_2(NH_2CH_2R)_2]^{2+}$ (NH_2CH_2R = allylamine, benzylamine, and *n*-butylamine) occur by dehydrogenation at the amine ligands giving the corresponding bis(nitrile) complexes, $[Ru(bpy)_2(N{\equiv}CR)_2]^{2+}$. The reactions appear to proceed by initial oxidation of Ru(II) to Ru(III), followed by a series of stepwise dehydrogenation reactions which occur via imine intermediates.

Net reactions involving the oxidative dehydrogenation of chelated amines to imines have been reported for macrocyclic amines,[1,2] and for ethylenediamine and related diamines.[3-7] For chelated amines, dehydrogenation stops at the imine stage; further oxidation gives hydroxodiimines[8] or net decomposition, rather than nitriles.[7]

There are two examples of the oxidation of monodentate primary amines to nitriles or cyanides. McWhinnie et al.[9] have reported the isolation of Ru(III) products containing the cyanide ion following the aerial oxidation of $[Ru(NH_2CH_3)_6]^{2+}$, and Diamond, Tom, and Taube[10] have shown that benzylamine bound to pentaammineruthenium(II) can be oxidized to benzonitrile.

Previous work has shown that oxidation of ligands bound to bis(2,2′-bipyridine)ruthenium(II) can be facile, and quantitative.[7,11] The reactions appear to proceed via initial oxidation of Ru(II) to Ru(III), followed by a series of rapid steps in which the net reactions involve the oxidation of a coordinated ligand.

Experimental Section

Electronic spectra were recorded on a Bausch and Lomb 210UV spectrophotometer. ^1H NMR spectra were measured on a Jeol C-60-HL spectrometer using acetone-d_6 solutions of PF_6^- salts

(Me_4Si internal reference). Ir spectra were recorded on a Perkin-Elmer 421 grating spectrophotometer using KBr disks (ca. 5 mg of complex/200 mg of KBr).

Benzylamine (Eastman), benzonitrile (MCB), allylamine (Eastman), acrylonitrile (Aldrich), *n*-butylamine (Fisher), and *n*-butyronitrile (Aldrich) were used without purification. For spectral measurements, acetonitrile (MCB, spectrograde) was used without purification and water was deionized and distilled from alkaline $KMnO_4$ before use. The complex $[Ru(bpy)_2Cl_2]\cdot 2H_2O$ was prepared as described previously,[12] and recrystallized (as the anhydrous compound) by Soxhlet extraction from methylene chloride before use. $[Ru(bpy)_2CO_3]\cdot 2H_2O$ was also prepared as described previously.[13]

Electrochemical measurements were made in acetonitrile solutions containing 0.1 M tetra-*n*-butylammonium hexafluorophosphate (TBAH) as the supporting electrolyte, or in 1.0 M HCl, vs. the saturated sodium chloride calomel electrode (SSCE) at 25 ± 2 °C, and are uncorrected for junction potentials. All potentials reported are reduction potentials vs. the SSCE. Potential control for electrochemical experiments was obtained with a Princeton Applied Research Model 173 potentiostat/galvanostat. The waveform generator for voltammetric experiments was a Princeton Applied Research Model 175 universal programmer. Voltammograms and slow scan cyclic voltammograms were recorded on a Hewlett-Packard Model 7004B x–y recorder. Fast scan cyclic voltammograms were obtained from photographs of the trace of a Tektronix Model 564B storage oscilloscope. Values of n, where n is the total number of equivalents of electrons transferred in exhaustive electrolyses at constant potentials, were calculated after measuring the total area under current vs. time curves for the complete reaction. Reactions were judged to be complete when the current had fallen below 1% of the initial value. All voltammetric measurements were carried out at platinum electrodes in solutions deaerated with a stream of dry, prepurified nitrogen.

Elemental analyses were carried out by Galbraith Laboratories Inc., Knoxville, Tenn.

Preparation of Complexes. $[Ru(bpy)_2(NH_2CH_2CH{=}CH_2)_2](PF_6)_2$. $[Ru(bpy)_2Cl_2]$ (0.46 g) was suspended in 50% aqueous MeOH (40 ml). Allylamine (5 ml) was added and the mixture kept at steam-bath temperature under N_2 for 2 h. Methanol and allylamine were evaporated off, the solution was cooled, and solid NH_4PF_6 was added slowly with stirring. The product was filtered, washed with ice-cold water and dried in vacuo, yield 0.68 g, 90%. Recrystallization was achieved by dissolution of the product in a minimum volume of CH_2Cl_2 (ca. 200 ml), filtering, and precipitating by the addition of ligroine (bp 30–60°). The red precipitate was filtered, washed with ligroine, and dried in vacuo. Anal. Calcd for $[Ru(bpy)_2(NH_2CH_2CH{=}CH_2)_2](PF_6)_2$: C, 38.2; H, 3.70; N, 10.3. Found: C, 38.0; H, 3.58; N, 10.2.

$[Ru(bpy)_2(NH_2CH_2C_6H_5)_2](ClO_4)_2$. $[Ru(bpy)_2Cl_2]$ (0.41 g) was suspended in 50% aqueous MeOH (40 ml). Benzylamine (5 ml) was added and the solution heated on a steam bath under an atmosphere of N_2 for 2 h. Methanol was evaporated off, the solution cooled, and then extracted three times with 25-ml portions of ether to remove excess benzylamine. The remaining aqueous solution was filtered, and the product precipitated by the slow addition of a filtered, saturated solution of $LiClO_4$. The red precipitate was collected, and the solid washed with ice-cold water, 2-propanol, and ether, and then dried in vacuo, yield, 0.65 g, 92%. Anal. Calcd for $[Ru(bpy)_2(NH_2CH_2C_6H_5)_2](ClO_4)_2$: C, 49.4; H, 4.15; N, 10.2. Found: C, 49.3; H, 4.09; N, 10.2.

$[Ru(bpy)_2(NH_2CH_2CH_2CH_2CH_3)_2](PF_6)_2$. $[RuB_2Cl_2]$ (0.45 g) was suspended in 50% aqueous MeOH (40 ml), *n*-butylamine (5 ml) was added, and the mixture heated on a steam bath under an N_2 atmosphere 2 h. The methanol and *n*-butylamine were evaporated off, and the last traces of the amine were removed by extraction with ether. The product was precipitated by the slow addition of solid NH_4PF_6 to a stirred solution of the complex. The solid was collected by filtration, washed with ice-cold water, and dried in vacuo. The product was recrystallized by adding a filtered CH_2Cl_2 solution to pentane, yield 0.50 g, 63%. Anal. Calcd for $[Ru(bpy)_2(NH_2CH_2CH_2CH_2CH_3)_2](PF_6)_2$: C, 39.6; H, 4.51; N, 9.9. Found: C, 39.5; H, 4.52; N, 9.7.

$[Ru(bpy)_2(N{\equiv}CR)_2](PF_6)_2$ (R is $-CH{=}CH_2$ (Acrylonitrile) and $-C_3H_7$ (*n*-Butyronitrile)). $[Ru(bpy)_2(CO_3)]\cdot 2H_2O$ (0.40 g) was suspended in acetone (15 ml) and concentrated HPF_6 (ca. 0.2 ml) added. The solution was stirred for 10 min, and anhydrous Na_2CO_3 (ca. 1 g) added. After stirring for a further 10 min the solution was filtered, the required nitrile (5 ml) added, and the mixture stirred for 2 h. The products were precipitated by adding the reaction mixtures dropwise to large volumes (300 ml) of ether, yields 0.57 g (90%) for acrylonitrile and 0.53 g (80%) for *n*-butyronitrile. Recrystallization was achieved in both cases from acetone–ether. Anal. Calcd for $[Ru(bpy)_2(N{\equiv}CCH{=}CH_2)_2](PF_6)_2$: C, 38.6; H, 2.74; N, 10.4. Found: C, 38.7; H, 2.75; N, 10.3. Calcd for $[Ru(bpy)_2(N{\equiv}CCH_2CH_2CH_3)_2](PF_6)_2$: C, 40.0; H, 3.59; N, 10.0. Found: C, 39.8; H, 3.52; N, 9.8.

$[Ru(bpy)_2(N{\equiv}CC_6H_5)_2](PF_6)_2$. The benzonitrile salt was prepared in a manner analogous to that given for the bis(benzylamine) complex, except that the complex was precipitated by the addition of NH_4PF_6 after excess benzonitrile had been removed by ether extraction. The salt was recrystallized by dissolution in CH_2Cl_2, filtering the solution, and precipitating by the addition of ligroine (bp 30–60°). The product was obtained in 71% yield. Anal. Calcd for $[Ru(bpy)_2(N{\equiv}CC_6H_5)_2](PF_6)_2$: C, 44.9; H, 2.88; N, 9.2. Found: C, 44.9; H, 2.87; N, 8.9.

Electrochemical Preparations. $[Ru(bpy)_2(N{\equiv}CC_6H_5)_2](PF_6)_2$. The salt $[Ru(bpy)_2(NH_2CH_2C_6H_5)_2](ClO_4)_2$ (120 mg) was dissolved in 1 M HCl (120 ml). The solution was electrolyzed exhaustively at 0.80 V until the current had fallen to 1% of its initial value (n = 7.9). The resulting solution was filtered and solid NH_4PF_6 added with stirring. The yellow precipitate which appeared was filtered, washed with ice-cold water, and dried in vacuo, yield 0.105 g, 87%. Recrystallization was achieved by adding ligroine (bp 30–60°) dropwise to a solution of the complex in CH_2Cl_2. Anal. Calcd for $[Ru(bpy)_2(N{\equiv}CC_6H_5)_2](PF_6)_2$: C, 44.9; H, 2.88; N, 9.2. Found: C, 44.8; H, 3.00; N, 9.2.

$[Ru(bpy)_2(NH_2CH_2C_6H_5)(N{\equiv}CC_6H_5)](PF_6)_2$. The salt $[Ru(bpy)_2(NH_2CH_2C_6H_5)_2](ClO_4)_2$ (113 mg) was dissolved in 1 M HCl (80 ml). The solution was electrolyzed exhaustively at 0.70 V until the current had fallen to 1% of its initial value (n = 3.9). The solution was filtered and solid NH_4PF_6 added slowly with stirring. The resultant precipitate was filtered, washed with ice-cold water, 2-propanol, and ether, and then air dried, yield 0.10 g, 88%. The salt was recrystallized from acetone–ether. Anal. Calcd for $[Ru(bpy)_2(NH_2CH_2C_6H_5)(N{\equiv}CC_6H_5)](PF_6)_2$: C, 44.7; H, 3.31; N, 9.2. Found: C, 44.7; H, 3.32; N, 9.2.

$[Ru(bpy)_2(NH_2CH_2R)(N{\equiv}CR)](PF_6)_2$ (R is $-CH{=}CH_2$ and $-C_3H_7$). The respective salts $[Ru(bpy)_2(NH_2CH_2CH{=}CH_2)_2](PF_6)_2$ and $[Ru(bpy)_2(NH_2CH_2CH_2CH_2CH_3)_2](PF_6)_2$ (100 mg) were dissolved in acetonitrile (30 ml; 0.1 M TBAH) and electrolyzed exhaustively at 1.10 V until the current decreased to 1% of its initial value (n = 3.8 and 3.9, respectively). The products were precipitated by filtering the solutions dropwise into stirred excesses of ether (250 ml). Recrystallization of the allylamine–(acrylonitrile) complex was achieved from CH_2Cl_2–ligroine (30–60°) (yield 0.08 g, 80%), and the *n*-butylamine–(*n*-butyronitrile) complex from acetone–ether (yield 0.03 g, 30%). Anal. Calcd for $[Ru(bpy)_2(NH_2CH_2CH{=}CH_2)(N{\equiv}CCH{=}CH_2)](PF_6)_2$: C, 38.4; H, 3.22; N, 10.3. Found: C, 38.0; H, 3.16; N, 10.2. Calcd for $[Ru(bpy)_2(NH_2CH_2CH_2CH_2CH_3)(N{\equiv}CCH_2CH_2CH_3)](PF_6)_2$: C, 39.8; H, 4.05; N, 9.9. Found: C, 39.5; H, 3.86; N, 10.0.

Results and Discussion

Electrochemical Oxidative Dehydrogenation of Bound Primary Amines. From cyclic voltammetric studies, the complexes $[Ru(bpy)_2(NH_2CH_2R)_2]^{2+}$ (R is –Ph, $-CH{=}CH_2$, $-CH_2CH_2CH_3$) undergo electrochemically reversible, one-electron oxidations in acetonitrile with $E_{1/2}$ = 1.03–1.04 V (Table I).[14] The electrochemical oxidations clearly involve reversible Ru(III)/Ru(II) couples; they are one-electron processes, and the $E_{1/2}$ values fall in the range found for the $[Ru(bpy)_2(NH_3)_2]^{3+/2+}$ ($E_{1/2}$ = 0.92 V) and related diamine couples.[7] However, exhaustive electrolysis on the diffusion plateaus of the oxidation waves indicated that n (the number of electrons passed per mole of complex) is greater than one, and is dependent (within certain limits) on the potential used for the electrolysis. At poten-

Table I. $E_{1/2}$ Values for Amine–Nitrile Complexes of Bis(2,2′-bipyridine)ruthenium(II) in Acetonitrile[a]

Complex	$E_{1/2}$, V (V vs. SSCE)
$[Ru(bpy)_2(NH_2CH_2Ph)_2]^{3+/2+}$	1.04
$[Ru(bpy)_2(NH_2CH_2Ph)(N{\equiv}CPh)]^{3+/2+}$	1.29
$[Ru(bipy)_2(N{\equiv}CPh)_2]^{3+/2+}$	1.52
$[Ru(bpy)_2(NH_2CH_2CH{=}CH_2)_2]^{3+/2+}$	1.04
$[Ru(bpy)_2(NH_2CH_2CH{=}CH_2)(N{\equiv}CCH{=}CH_2)]^{3+/2+}$	1.26[b]
$[Ru(bpy)_2(N{\equiv}CCH{=}CH_2)_2]^{3+/2+}$	1.53
$[Ru(bpy)_2(NH_2CH_2CH_2CH_2CH_3)_2]^{3+/2+}$	1.03
$[Ru(bpy)_2(NH_2CH_2CH_2CH_2CH_3)(N{\equiv}CCH_2CH_2CH_3)]^{3+/2+}$	1.24
$[Ru(bpy)_2(N{\equiv}CCH_2CH_2CH_3)_2]^{3+/2+}$	1.48

[a] At a Pt-bead electrode in 0.1 M TBAH–acetonitrile at 25 ± 2°. [b] Reversible only at scan speeds equal to or greater than 500 mV/s.

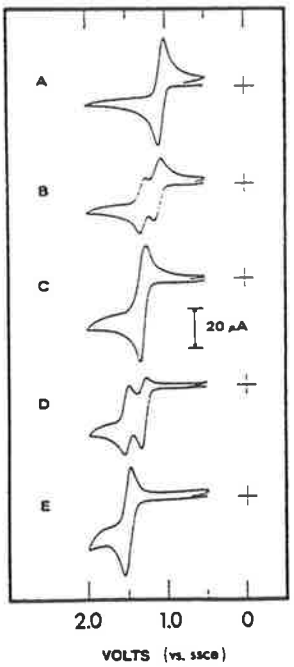

Figure 1. Cyclic voltammograms in acetonitrile of: (A) $[Ru(bpy)_2(NH_2CH_2Ph)_2]^{2+}$, (B) solution A following two-electron oxidation, (C) solution A following four-electron oxidation (giving $[Ru(bpy)_2(NH_2CH_2Ph)(N{\equiv}CPh)]^{2+}$), (D) six-electron oxidation of A, and (E) eight-electron oxidation of A (giving $[Ru(bpy)_2(N{\equiv}CPh)_2]^{2+}$). (Scan rate 200 mV/s at a Pt-bead electrode vs. the saturated sodium chloride calomel electrode at 25 ± 2°.)

tials sufficiently high on the diffusion plateau, reproducible n values of ~8.0 were obtained.

For the bis(benzylamine) complex, $[Ru(bpy)_2(NH_2CH_2Ph)_2]^{2+}$, the electrolytic oxidation was monitored in detail using cyclic voltammetry (Figure 1). Cyclic voltammograms were obtained following controlled potential electrolyses at a series of potentials. Figure 1A shows a cyclic voltammogram for the reversible $[Ru(bpy)_2(NH_2CH_2Ph)_2]^{3+/2+}$ couple. Figure 1B shows the cyclic voltammogram following electrolysis at 1.15 V until n = 2.0; there are two waves, one attributable to unreacted $[Ru(bpy)_2(NH_2CH_2Ph)_2]^{2+}$. The waves have roughly equal peak currents, indicating that there are in solution equal amounts of the starting complex, and a four-electron oxidation product with $E_{1/2}$ = 1.29 V. After complete electrolysis at 1.15 V (n = 4.0), only the four-electron oxidation product remains in solution (Figure 1C).

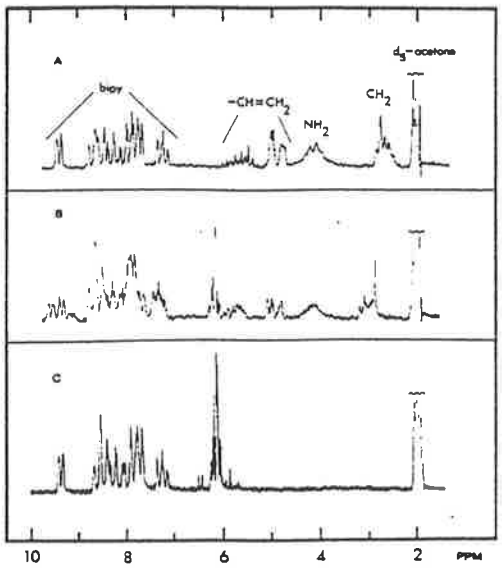

Figure 2. The 60-MHz ^1H NMR spectra in acetone d_6 of (A) $[Ru(bpy)_2(NH_2CH_2CH{=}CH_2)_2]^{2+}$, (B) four-electron oxidation product of A, and (C) eight-electron oxidation product of A ($[Ru(bpy)_2(N{\equiv}CCH{=}CH_2)_2]^{2+}$).

There are two, equally interesting, possibilities for the identity of this four-electron oxidation product. Firstly, both amine ligands might oxidize by two electrons to give the bis(monoimine) complex, $[Ru(bpy)_2(NH{=}CHPh)_2]^{2+}$ (eq 1).

$$[Ru(bpy)_2(NH_2CH_2R)_2]^{2+} \xrightarrow{-4e^-} [Ru(bpy)_2(NH{=}CHR)_2]^{2+} + 4H^+ \quad (1)$$

Reaction 1 is a likely possibility since the related four-electron oxidations of chelated diamines bound to bis(2,2′-bipyridine)ruthenium(II) have been well characterized[7] (e.g., eq 2). The second possibility is that oxidation is localized at

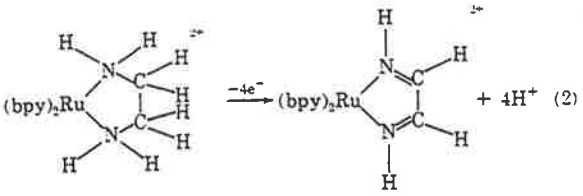

(2)

only one of the amine ligands, and the product is the amine-nitrile complex (eq 3).

$$[Ru(bpy)_2(NH_2CH_2R)_2]^{2+} \xrightarrow{-4e} [Ru(bpy)_2(NH_2CH_2R)(N{\equiv}CR)]^{2+} + 4H^+ \quad (3)$$

Predicted elemental analyses for the two possibilities are, of course, the same. However, the ^1H NMR spectrum of the complex allows a distinction to be made between them.

The effect of the four-electron oxidation on the ^1H NMR spectrum of $[Ru(bpy)_2(NH_2CH_2CH{=}CH_2)_2]^{2+}$ is shown in Figure 2. The spectrum of the bis(allylamine) complex (2A) has a typically broad and complicated region due to the 2,2′-bipyridine protons (δ 7.1–9.6 ppm, relative to Me_4Si). The $-CH{=}CH_2$ proton resonances appear at high-

er field (δ 4.7–6.1 ppm), and the $-NH_2$ and $>CH_2$ resonances are centered at δ 4.2 and 2.8 ppm, respectively.

The four-electron oxidation product has the spectrum shown in Figure 2B. An integrated spectrum indicates that the $-NH_2$ and $>CH_2$ regions are reduced to half their intensity relative to the bpy region when compared with 2A. The changes in the ^1H NMR spectra require that the four-electron oxidation product be $[Ru(bpy)_2(NH_2CH_2CH{=}CH_2)(N{\equiv}CCH{=}CH_2)]^{2+}$ and not $[Ru(bpy)_2(NH{=}CHCH{=}CH_2)_2]^{2+}$. In the latter case the imine protons would be expected to appear at lower field. Furthermore, the new resonance in the $-CH{=}CH_2$ region in 2B (δ 6.2 ppm) is an obvious characteristic of the acrylonitrile ligand, since for the bis(acrylonitrile) complex (Figure 2C) this peak constitutes the entire $-CH{=}CH_2$ resonance.

The ^1H NMR spectral changes upon oxidation for the benzylamine complex are analogous to the changes shown in Figure 2. The ^1H NMR experiment clearly shows that the four-electron oxidation product is the amine–nitrile complex, and, consequently, that the four-electron oxidation of $[Ru(bpy)_2(NH_2CH_2R)_2]^{2+}$ is described satisfactorily by eq 3.

It is worth noting that the $[Ru(bpy)_2(NH_2CH_2CH{=}CH_2)(N{\equiv}CCH{=}CH_2)]^{3+/2+}$ couple is reversible only at scan rates of > 500 mV/s. This indicates that at slower scan rates further ligand oxidation is competitive with recapture of Ru(III) at the electrode.

A further oxidation process occurs past the $n = 4.0$ stage. Continued electrolysis on the diffusion plateau of the $E_{1/2} = 1.29$ V wave (at 1.35 V) gave rise to a further oxidation. If the electrolysis is stopped at $n = 2.0$ ($n_{total} = 6.0$ based on $[Ru(bpy)_2(NH_2CH_2Ph)_2]^{2+}$ as the starting complex) there are two reversible waves in the cyclic voltammogram (Figure 1D), with equal peak currents. The wave at $E_{1/2} = 1.29$ V is clearly unreacted $[Ru(bpy)_2(NH_2CH_2Ph)(N{\equiv}CPh)]^{2+}$, and the wave at $E_{1/2} = 1.52$ V corresponds to an $n = 4.0$ ($n_{total} = 8.0$) oxidation product. Exhaustive electrolysis on the diffusion plateau of the $E_{1/2} = 1.29$ V wave gave $n_{total} = 8.0$, and the complex with $E_{1/2} = 1.52$ V as the sole product (Figure 1E). Spectral, electrochemical, and chemical isolation studies have shown that the eight-electron product is the totally oxidized, bis(nitrile) complex, $[Ru(bpy)_2(N{\equiv}CPh)_2]^{2+}$ (eq 4).

$$[Ru(bpy)_2(NH_2CH_2R)(N{\equiv}CR)]^{2+} \xrightarrow{-4e^-} [Ru(bpy)_2(N{\equiv}CR)_2]^{2+} + 4H^+ \quad (4)$$

The ^1H NMR spectrum of the bis(acrylonitrile) complex in acetone-d_6 is shown Figure 2C.

As shown by cyclic voltammetry (Figure 1E and Table I), the bis(nitrile) complexes undergo reversible one-electron oxidations at relatively high reduction potentials. It is expected that the ruthenium(III) nitrile complexes, $[Ru(bpy)_2(N{\equiv}CR)_2]^{3+}$, should undergo rapid hydrolysis at the nitrile group to give the corresponding amides,[10,15] but these reactions have not yet been investigated.

Infrared Spectra. Infrared spectra are also informative as to the nature of the four- and eight-electron oxidation products. The four-electron products of $[Ru(bpy)_2(allylamine)_2]^{2+}$ and $[Ru(bpy)_2(benzylamine)_2]^{2+}$ have bands at 2238 and 2235 cm^{-1}, respectively, indicating the presence of nitrile ligands. Both $[Ru(bpy)_2(acrylonitrile)_2]^{2+}$ and $[Ru(bpy)_2(benzonitrile)_2]^{2+}$ have $\nu_{C{\equiv}N}$ bands at 2235 cm^{-1}.

For coordinated organonitriles where little back-bonding is expected, such as in Rh(III),[16] Ru(III),[17] and Co(III)[18] complexes, the $\nu_{C{\equiv}N}$ band is found to be 50–70 cm^{-1} higher than for the uncoordinated nitrile. In the case of $[Ru(NH_3)_5(N{\equiv}CR)]^{2+}$, $\nu_{C{\equiv}N}$ was found to decrease (0–50 cm^{-1}) from the free ligand value. The decrease has been attributed to the strong back-bonding donor ability of the $(NH_3)_5Ru^{2+}$ moiety.[17] In the nitrilebis(2,2′-bipyridine) complexes of Ru(II), $\nu_{C{\equiv}N}$ increases slightly compared to the free ligand (*n*-butyronitrile, 2271 vs. 2253 cm^{-1}; acrylonitrile, 2238 vs. 2234 cm^{-1}), or is unchanged (benzonitrile, $\nu_{C{\equiv}N}$ 2235 cm^{-1} in both cases). The increases in $\nu_{C{\equiv}N}$ are small compared with related Ru(III), Rh(III), and Co(III) cases, which is reasonable and probably means that π-back-bonding in the $Ru(bpy)_2^{2+}$ complexes is present, but to a lesser extent than in $(NH_3)_5Ru^{2+}$ type complexes. The conclusion is expected, given the strongly back-bonding acceptor nature of the 2,2′-bipyridine ligands.

Table II. Electronic Spectral Data for the Amine–Nitrile Complexes of Bis(2,2′-bipyridine)ruthenium(II) in Acetonitrile

Complex	λ_{max}, nm (ϵ)[a]
$[Ru(bpy)_2(NH_2CH_2Ph)_2]^{2+}$	491 (9 200)
	348 (7 400)
	297 (54 100)
	248 (17 500)
$[Ru(bpy)_2(NH_2CH_2Ph)(N{\equiv}CPh)]^{2+}$	449 (10 000)
	291 (61 100)
	235 (29 100)
$[Ru(bpy)_2(N{\equiv}CPh)_2]^{2+}$	414 (9 500)
	286 (57 400)
	228 (38 500)
$[Ru(bpy)_2(NH_2CH_2CH{=}CH_2)_2]^{2+}$	492 (8 800)
	349 (7 100)
	296 (56 600)
	248 (17 300)
$[Ru(bpy)_2(NH_2CH_2CH{=}CH_2)(N{\equiv}CCH{=}CH_2)]^{2+}$	446 (8 300)
	290 (57 500)
	246 (22 700)
$[Ru(bpy)_2(N{\equiv}CCH{=}CH_2)_2]^{2+}$	416 (9 300)
	286 (58 000)
	256 (17 900)
	247 (17 900)
$[Ru(bpy)_2(NH_2CH_2CH_2CH_2CH_3)_2]^{2+}$	496 (8 700)
	352 (7 300)
	297 (56 800)
	248 (17 800)
$[Ru(bpy)_2(NH_2CH_2CH_2CH_2CH_3)(N{\equiv}CCH_2CH_2CH_3)]^{2+}$	450 (7 500)
	287 (53 100)
	242 (17 600)
$[Ru(bpy)_2(N{\equiv}CCH_2CH_2CH_3)_2]^{2+}$	427 (8 500)
	287 (55 300)
	246 (17 400)

[a] λ values are ±2 nm; ϵ values are ±5%.

Electronic Spectra and Reduction Potentials. Electronic spectra (Table II) and Ru(III)/Ru(II) reduction potentials (Table I) also reflect the effects of back-bonding, but at the metal rather than at the nitrile ligand. The spectra of the bis(amine) complexes are similar to the spectrum of $[Ru(bpy)_2(NH_3)_2]^{2+}$, having two maxima in the visible region (ca. 490 and 345 nm) which have previously been assigned to $d\pi(Ru(II)) \rightarrow \pi^*(bpy)$ MLCT transitions.[19] There are also two maxima in the ultraviolet region (ca. 290 and 245 nm) which have been assigned as $\pi \rightarrow \pi^*(bpy)$ transitions for $[Ru(bpy)_2(NH_3)_2]^{2+}$.[19] Upon the replacement of an amine ligand by a nitrile group, only one $d\pi(Ru(II)) \rightarrow \pi^*(bpy)$ MLCT absorption band is found in the visible region and that band is at higher energy (450 nm). Both observations are consistent with an increase in back-bonding leading to a relative stabilization of the $d\pi$ orbitals.[7,19] This trend continues for the bis(nitrile) complexes where λ_{max}

for the single $d\pi(Ru(II)) \rightarrow \pi^*(bpy)$ band is between 414 and 427 nm (Table II). The positions of the absorbance maxima and $\nu_{C\equiv N}$ stretching frequencies for the bis(nitrile) complexes are consistent with the qualitative order of back-bonding: benzonitrile > acrylonitrile > *n*-butyronitrile.

The conclusions concerning the stabilization of $d\pi(Ru)$ levels by back-bonding are borne out by $E_{1/2}$ values for the series of Ru(III)/Ru(II) couples given in Table I. From a variety of evidence, metal → ligand back-bonding is relatively unimportant in complexes of Ru(III).[20] The effect of replacing saturated amine ligands by back-bonding ligands is to stabilize the $d\pi$ levels of Ru(II) which stabilizes the Ru(II) state. In the bis(bipyridine) complexes, the Ru(II) state is already strongly stabilized by back-bonding to the 2,2′-bipyridine ligands. However, Ru(III)/Ru(II) redox potentials remain sensitive to changes in the ligands at the fifth and sixth coordination sites.[21] This can be seen clearly in the data in Table I where the redox potentials fall into three classes: bis(amines), 1.03–1.04 V amine–nitriles, 1.24–1.29 V; bis(nitriles), 1.48–1.52 V. Changes in reduction potentials follow directly from the number of back-bonding ligands in the fifth and sixth coordination positions.

Solutions of the bis(amine) complexes in acetonitrile were found to be stable over many hours in the dark. However, in normal laboratory lighting, a clean reaction occurred which exhibited well-defined isosbestic points when monitored in the uv–visible spectral region. The photochemical reactions are apparently light-induced substitutions to give amine–acetonitrile complexes. The products had spectra which were very similar to the amine–nitrile complexes (Table II). The amine–nitrile and bis(nitrile) complexes were more stable in solution, but prolonged exposure to light caused substitution of acetonitrile into the coordination sphere. Because of the light sensitivity, much of the work reported here, including the electrochemical and spectral studies, was carried out on solutions which were protected from the light.

Oxidation by Ce(IV). Mechanism of Oxidative Dehydrogenation. The bis(amine) complexes are oxidized rapidly and quantitatively by Ce(IV) in acetonitrile. Spectrophotometric experiments have shown that upon addition of 4 mol of Ce(IV) per mole of $[Ru(bpy)_2(NH_2CH_2Ph)_2]^{2+}$, the resulting product is the amine–nitrile complex (eq 5).

$$[Ru(bpy)_2(NH_2CH_2Ph)_2]^{2+} + 4Ce(IV) \rightarrow [Ru(bpy)_2(NH_2CH_2Ph)(N{\equiv}CPh)]^{2+} + 4H^+ + 4Ce(III) \quad (5)$$

When 8 mol of Ce(IV) are added, the bis(nitrile) complex is the product (eq 6).

$$[Ru(bpy)_2(NH_2CH_2Ph)_2]^{2+} + 8Ce(IV) \rightarrow [Ru(bpy)_2(N{\equiv}CPh)_2]^{2+} + 8H^+ + 8Ce(III) \quad (6)$$

The Ce(IV) oxidations were followed stepwise by spectrophotometric titrations using a fast mixing device. The titrations were followed in two stages: 0–4 mol of added Ce(IV)/mole of complex, and 4–8 mol of added Ce(IV). In neither stage were isosbestic points observed. If clean mixtures of $[Ru(bpy)_2(NH_2CH_2Ph)_2]^{2+}$ and $[Ru(bpy)_2(NH_2CH_2Ph)(N{\equiv}CPh)]^{2+}$ (0–4 mol of Ce(IV) added) or of $[Ru(bpy)_2(NH_2CH_2Ph)(N{\equiv}CPh)]^{2+}$ and $[Ru(bpy)_2(N{\equiv}CPh)_2]^{2+}$ (4–8 mol of Ce(IV)) had been present in the solutions, isosbestic points would be expected. The absence of isosbestic points indicates the existence of intermediates in the titrations. Since the overall reactions are quantitative, the most reasonable intermediates are two-electron oxidation products containing bound imine groups: $[Ru(bpy)_2(NH_2CH_2Ph)(NH{=}CHPh)]^{2+}$ and $[Ru(bpy)_2(NH{=}CHPh)(N{\equiv}CPh)]^{2+}$. This conclusion is reasonable in light of evidence obtained recently for imine intermediates in the oxidation of amines bound to $(NH_3)_5Ru(II)$[10] and in the oxidation of coordinated diamines to α,α'-diimines.[7]

Preliminary stopped-flow kinetic studies of the oxidation reaction revealed, by direct observation of the Ru(III) species, that the Ru(II) → Ru(III) oxidation step occurs very rapidly[22] so that the ligand dehydrogenation is necessarily a subsequent process. Detailed kinetic data are not available for the dehydrogenation reactions, so that proposal of a detailed mechanism is not possible. However, assuming the intermediacy of the imine species, a series of *net* reactions can be written for the oxidation process. For example, on removal of one electron per mole of complex:

$$2[Ru(bpy)_2(NH_2CH_2Ph)_2]^{2+} \xrightarrow{-2e^-} 2[Ru(bpy)_2(NH_2CH_2Ph)_2]^{3+} \quad (7)$$

$$2[Ru(bpy)_2(NH_2CH_2Ph)_2]^{3+} \rightarrow [Ru(bpy)_2(NH_2CH_2Ph)(NH{=}CHPh)]^{2+} + [Ru(bpy)_2(NH_2CH_2Ph)_2]^{2+} + 2H^+ \quad (8)$$

The two-electron oxidation of the ligand by the one-electron oxidant (Ru(III)) requires a *net* disproportionation of the type given in eq 8; furthermore, there is direct evidence for a *net* reaction of this type in the metal-assisted oxidation of $Ru(bpy)_2(2\text{-aminomethylpyridine})^{2+}$.[7] Upon removal of a second electron, a similar sequence of *net* reactions can be written:

$$2[Ru(bpy)_2(NH_2CH_2Ph)(NH{=}CHPh)]^{2+} \xrightarrow{-2e} 2[Ru(bpy)_2(NH_2CH_2Ph)(NH{=}CHPh)]^{3+} \quad (9)$$

$$2[Ru(bpy)_2(NH_2CH_2Ph)(NH{=}CHPh)]^{3+} \rightarrow [Ru(bpy)_2(NH_2CH_2Ph)(N{\equiv}CPh)]^{2+} + [Ru(bpy)_2(NH_2CH_2Ph)(NH{=}CHPh)]^{2+} + 2H^+ \quad (10)$$

Oxidation up to the eight-electron stage (the bis(nitrile) complex) can be represented by a related series of net reactions.

It should be noted that the Ru(III) imine complex is also accessible by reactions such as that given in eq 11:

$$[Ru(bpy)_2(NH_2CH_2Ph)_2]^{3+} + [Ru(bpy)_2(NH_2CH_2Ph)(NH{=}CHPh)]^{2+} \rightarrow [Ru(bpy)_2NH_2CH_2Ph)_2]^{2+} + [Ru(bpy)_2(NH_2CH_2Ph)(NH{=}CHPh)]^{3+} \quad (11)$$

Such reactions are known to be rapid in related systems.[23] We emphasize again that detailed mechanistic information is not yet available for the individual steps and that following oxidation of Ru(II) to Ru(III) a series of interrelated reactions occurs.

In the electrochemical experiments there was no evidence for either of the imine intermediates (Figure 1). This is reasonable since electrochemical oxidation processes (eq 7 and 9) are far slower than Ce(IV) oxidations, and reactions like eq 11 allow for the conversion of the imine intermediates into the amine–nitrile and bis(nitrile) products before their concentrations become appreciable.

The ligand oxidation reactions are much more rapid in acidic aqueous solution than in acetonitrile. Cyclic voltammograms of the amine complexes in 1.0 M HCl were completely irreversible at scan rates up to 50 V/s, indicating that ligand oxidation is more rapid than recapture of Ru(III) at the electrode. Electrolysis to $n = 4.0$ at potentials more anodic than E_p for the irreversible Ru(II) → Ru(III) step, gave a mixture of 0-, 4-, and 8-electron products for R = $-CH_2CH_2CH_3$ and $-CH{=}CH_2$, and the

amine–nitrile complex was obtained cleanly only for benzylamine.

Acknowledgment is made to the Materials Research Center of the University of North Carolina under Grant No. DAHC15 73 G9 with DARPA for support of this work.

References and Notes

(1) N. F. Curtis, *Chem. Commun.*, 881 (1966); *Coord. Chem. Rev.*, **3**, 3 (1968).
(2) J. C. Dabrowiak, F. V. Lovecchio, V. L. Goedken, and D. H. Busch, *J. Am. Chem. Soc.*, **94**, 5502 (1972); V. L. Goedken and D. H. Busch, *Ibid.*, **94**, 7355 (1972).
(3) H. Elsbernd and J. K Beattie, *J. Chem. Soc. A*, 2598 (1970).
(4) B. C. Lane, J. E. Lester, and F. Basolo, *Chem. Commun.*, 1618 (1971).
(5) D. F. Mahoney and J. K. Beattie, *Inorg. Chem.*, **12**, 2561 (1973).
(6) V. L. Goedken, *J. Chem. Soc., Chem. Commun.*, 207 (1972).
(7) G. M. Brown, T. R. Weaver, F. R. Keene, and T. J. Meyer, *Inorg. Chem.*, **15**, 190 (1976).
(8) H. L. Chum and P. Krumholz, *Inorg. Chem.*, **13**, 514, 519 (1974).
(9) W. R. McWhinnie, J. D. Miller, J. B. Watts, and D. Y. Wadden, *Chem. Commun.*, 629 (1971); *Inorg. Chim. Acta*, **7**, 461 (1973).
(10) S. E. Diamond, G. M. Tom, and H. Taube, *J. Amer. Chem. Soc.*, **97**, 2661 (1975).
(11) G. M. Brown, R. W. Callahan, and T. J. Meyer, *Inorg. Chem.*, **14**, 1915 (1975).
(12) J. B. Godwin and T. J. Meyer, *Inorg. Chem.*, **10**, 471 (1971).
(13) S. A. Adeyemi, Ph.D. Dissertation, University of North Carolina at Chapel Hill, 1973.
(14) Electrochemical reversibility was determined, when possible, by plots of log $(i_l - i)/i$ vs. E using stirred-solution voltammetry data. In cases where subsequent ligand reactions were too rapid, reversibility was determined using cyclic voltammetry using the ratio of anodic to cathodic peak currents (i_c/i_a). ΔE_p = 60–65 mV and the sweep rate independence of ΔE_p as criteria. The slightly greater value of ΔE_p than the theoretical value of 59 mV can be attributed to uncompensated solution resistance.
(15) A. W. Zanella and P. C. Ford, *Inorg. Chem.*, **14**, 42 (1975).
(16) R. D. Foust and P. C. Ford, *Inorg. Chem.*, **11**, 899 (1972).
(17) R. E. Clarke and P. C. Ford, *Inorg. Chem.*, **9**, 227 (1970).
(18) D. Pinnell, G. B. Wright, and R. B. Jordan, *J. Am. Chem. Soc.*, **94**, 6104 (1972); F. R. Keene and J. MacB. Harrowfield, unpublished data, Australian National University, Canberra, 1973.
(19) G. M. Bryant, J. E. Fergusson, and H. J. K. Powell, *Aust. J. Chem.*, **24**, 257 (1971).
(20) H. Taube, *Surv. Prog. Chem.*, **6**, 1 (1973).
(21) G. M. Brown, Ph.D. Dissertation, University of North Carolina, Chapel Hill, N.C., 1974.
(22) E. M. Gupton and F. R. Keene, unpublished data, University of North Carolina, Chapel Hill, 1974.
(23) J. C. Solenburger, Ph.D. Dissertation, Washington University, St. Louis, Mo., 1969; M. Chan and A. C. Wahl, 167th National Meeting of the American Chemical Society, Los Angeles, Calif., 1974, Abstract INOR 97.

Reprinted from the Journal of the American Chemical Society, 1981, *103*, 5733.

Mechanism of Oxidation of an Amine Coordinated to Ruthenium

Michael J. Ridd and F. Richard Keene*

Contribution from the Department of Chemistry and Biochemistry, James Cook University of North Queensland, Townsville, Queensland 4811, Australia. *Received November 17, 1980*

Abstract: The mechanism of the oxidative dehydrogenation of $[Ru(bpy)_2ampy]^{2+}$ (bpy = 2,2′-bipyridine; ampy = 2-(aminomethyl)pyridine) to the corresponding imine complex has been studied in aqueous media by using stopped-flow methods in association with chemical oxidation by Ce(IV), flash photolysis techniques, and electrochemical methods. Solutions to the rate laws for several possible mechanisms were obtained numerically and the spectrophotometric responses matched with the theoretical solutions by use of a nonlinear optimization program. The data were found to be consistent with a mechanism involving a Ru(IV) species in which the ampy ligand is deprotonated, and this intermediate subsequently undergoes a two-electron transfer (accompanied by deprotonation) to give the imine product. The various rate constants for the individual steps of the mechanistic scheme were consistent with values for electron-transfer reactions and proton equilibria in similar metal complex systems.

The oxidative dehydrogenation of amines to imines or nitriles is known to be catalyzed by their coordination to metal centers. Initial studies of the oxidation of macrocyclic amines were made by Curtis[1] and Busch,[2] and recent studies[3,4] have confirmed the earlier assertion[2] that such reactions involved initial oxidation of the metal center followed by an intramolecular redox process in which the ligand is oxidized and the metal reduced.

The analogous oxidation of coordinated ethylenediamine to the corresponding α,α'-diimine has also been reported,[5-7] and Meyer et al.[8] and Ford et al.[9] have studied the oxidation of a range of bidentate amines coordinated to ruthenium. The oxidative de-

(1) Curtis, N. F. *Coord. Chem. Rev.* **1968**, *3*, 3–47 and references therein.
(2) Goedken, V. L.; Busch, D. H. *J. Am. Chem. Soc.* **1972**, *94*, 7355–7363. Hipp, C. J.; Lindoy, L. F.; Busch, D. H. *Inorg. Chem.* **1972**, *11*, 1988–1994.
(3) Maruthamuthu, P.; Patterson, L. K.; Ferraudi, G. *Inorg. Chem.* **1978**, *17*, 3157–3163.
(4) Jaacobi, M.; Meyerstein, D.; Lilie, J. *Inorg. Chem.* **1979**, *18*, 429–433.
(5) Beattie, J. K.; Elsbernd, H. *J. Chem. Soc. A* **1970**, 2598–2600.
(6) Lane, B. C.; Lester, S. E., Basolo, F. *Chem. Commun.* **1971**, 1618–1619.
(7) Goedken, V. L. *J. Chem. Soc., Chem. Commun.* **1972**, 207–208.
(8) Brown, G. M.; Weaver, T. R.; Keene, F. R.; Meyer, T. J. *Inorg. Chem.* **1976**, *15*, 190–196.
(9) Alvarez, V. E.; Allen, R. J.; Matsubara, T.; Ford, P. C. *J. Am. Chem. Soc.* **1974**, *96*, 7686–7692.

hydrogenation of monodentate primary amines proceeds further and produces the corresponding nitriles.[10-12] The oxidations of coordinated alcohols to the corresponding aldehyde or ketone have also been reported.[13,14]

In all these studies of oxidative dehydrogenation reactions of coordinated ligands, limited detailed mechanistic information is available, except that the oxidation of the metal center appears to precede ligand reaction. Recent pulse radiolysis studies of nickel macrocyclic complexes[3] have been interpreted to indicate that following the initial Ni(II) → Ni(III) oxidation, a series of reactions occurs which involve a Ni(II)–radical species: the overall process is then completed by the one-electron oxidation of this radical species, yielding the dehydrogenated product. An alternative mechanism for the oxidation of an alcohol coordinated to a ruthenium center has been proposed by Tovrog et al.[14] which involves initial oxidation of the metal center from ruthenium(II) to ruthenium(III), followed by a disproportionation to form a Ru(IV) species which undergoes a two-electron reduction with concomitant two-electron oxidation of the ligand.

While it may be unlikely that the mechanism of ligand dehydrogenation is uniform throughout the range of metals and ligands for which such reactions have been observed, the general phenomenon is of considerable interest as the reactions are quantitative, in contrast to the oxidation of uncoordinated amines and alcohols. We have undertaken a detailed investigation of the oxidation of a number of amine and alcohol substrates coordinated to a variety of metal ions: we now report mechanistic studies of the oxidation of 2-(aminomethyl)pyridine (ampy) coordinated to ruthenium, using techniques of chemical oxidation, electrochemical oxidation, and flash photolysis. This particular system was chosen since the oxidation reaction (1) is well characterized[8] and yields

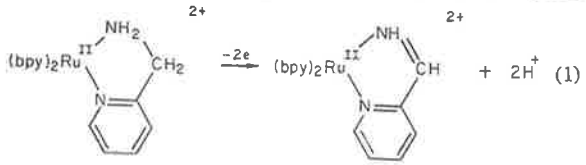

(1)

a stable product (a conjugated α,α'-diimine): furthermore, since it involves two electrons only it represents perhaps the simplest amine dehydrogenation reaction.

Experimental Section

Measurements. Electronic spectra were recorded by using a Cary 118C or Varian 634S spectrophotometer and emission spectra by using a Perkin-Elmer 3000 fluorescence spectrometer. The cell compartments were unthermostated.

All electrochemical measurements were made vs. the saturated sodium chloride calomel electrode (SSCE) at 25 ± 2 °C and are uncorrected for junction potentials. Potential control was obtained by using a Utah Electronics 0152 potentiostat and in conjunction with a Utah Electronics 0151 sweep generator for the voltammetric experiments. Slow scan cyclic voltammograms and single-sweep voltammograms were recorded by using a Houston Omnigraphic 2000 X-Y recorder. Fast scan cyclic voltammograms were obtained photographically from the trace on a Tektronix DM64 storage oscilloscope. Coulometry was performed by using a Fisher controlled potential electroanalyzer, Model 9-264-100, using platinum gauze electrodes. The charge passed was calculated by measuring the area under the i vs. t curve after the current had dropped to 1% of its initial value.

The details of the equipment used in the double-potential step experiments have been described elsewhere.[15] The pulse generator was built in the department.[16] Timing pulses were produced by a Digitimer D-4030 quartz-locked timer: current–time or charge–time responses were stored by a Biomation 805 waveform recorder, from which the output was displayed by using a Houston Omnigraphic 2000 X-Y recorder.

Elemental analyses were carried out by the Australian Microanalytical Service, CSIRO, Melbourne.

Materials. Tetra-*n*-butylammonium hexafluorophosphate (TBAH), used as an electrolyte for the electrochemical measurements, was prepared and purified by standard techniques.[17] The ligands 2,2′-bipyridine (Sigma), 2,2′:6′,2″-terpyridine (Sigma), and 2-(aminomethyl)pyridine (Aldrich) were used without purification. Propylene carbonate (Aldrich) was distilled immediately before use (90–92 °C (3.5 mmHg)) and stored over 4A molecular sieves. The complex $[Ru(bpy)_2Cl_2]\cdot 2H_2O$ was prepared as described previously.[18] Cerium ammonium sulfate (Fluka; puriss) was determined spectrophotometrically in 2 M H_2SO_4 against a standardized Ce(IV) solution and found to be $(NH_4)_4Ce(SO_4)_4\cdot 2H_2O$. All other chemicals were A.R. grade and were used without further purification.

Preparation of Complexes. (2-(Aminomethyl)pyridine)bis(2,2′-bipyridine)ruthenium(II) Perchlorate, $[Ru(bpy)_2(ampy)](ClO_4)_2$, was prepared in 72% yield by literature methods.[8] The complex was further purified by the following chromatographic procedure. An aqueous solution of the complex was sorbed on to a column of SP-Sephadex C25 cation exchanger and eluted with 1 M KNO_3. Two bands were observed, and the first (more intense) band was collected and evaporated to dryness. The residue was extracted with ethanol and the extract filtered and evaporated to dryness yielding the nitrate salt of the complex. The solid was dissolved in a minimum volume of water and the solution filtered and heated to 80–90 °C on a steam bath: addition of solid $NaClO_4$ and cooling led to crystallization of the perchlorate salt with 80% recovery. The visible spectrum in water showed $\epsilon_{471}^{max} = 10\,200$ and $\epsilon_{340}^{max} = 10\,800$, and cyclic voltammetry (propylene carbonate/0.2 M TBAH; glassy carbon electrode) gave $E_{1/2} = 1.16$ V vs. SSCE. Anal. Calcd for $RuC_{26}H_{24}N_6O_8Cl_2$: C, 33.3; H, 3.36; N, 11.7. Found: C, 33.2; H, 3.27; N, 11.4. The complex could also be obtained as the hexafluorophosphate salt by precipitation with NH_4PF_6.

(2-(Iminomethyl)pyridine)bis(2,2′-bipyridine)ruthenium(II) hexafluorophosphate, $[Ru(bpy)_2(impy)](PF_6)_2$, was prepared by literature methods,[8] and chromatographically purified as described for the corresponding ampy complex. The visible spectrum in water gave $\epsilon_{470}^{max} = 13\,600$ and cyclic voltammetry indicated $E_{1/2} = 1.33$ V vs. SSCE (propylene carbonate/0.2 M TBAH; glassy carbon electrode). Anal. Calcd for $RuC_{26}H_{22}N_6P_2F_{12}$: C, 38.6; H, 2.74; N, 10.4. Found: C, 38.8; H, 2.81; N, 10.4.

Trichloro(terpyridine)ruthenium(III), $[Ru(tpy)Cl_3]$, and (Bipyridine)chloro(terpyridine)ruthenium(II) hexafluorophosphate, $[Ru(tpy)(bpy)Cl]PF_6$, were prepared and purified by using methods supplied by Meyer et al.[19]

Aquo(bipyridine)(terpyridine)ruthenium(II) Perchlorate, $[Ru(tpy)(bpy)OH_2](ClO_4)_2$. $[Ru(tpy)(bpy)Cl]PF_6$ (0.39 g, 0.58 mmol) was suspended in water (20 mL) and $AgNO_3$ (0.39 g, 2.3 mmol) added. The mixture was protected from the light, stirred for 1 h, and then filtered. When solid $NaClO_4$ was added to the filtrate, the product crystallized (0.19 g, 51%). The visible spectrum in water gave $\epsilon_{477}^{max} = 8700$ and from cyclic voltammetry $E_{1/2} = 1.10$ V vs. SSCE (propylene carbonate/0.2 M TBAH; glassy carbon electrode).

Ammine(bipyridine)(terpyridine)ruthenium(II) Hexafluorophosphate, $[Ru(tpy)(bpy)NH_3](PF_6)_2$. $[Ru(tpy)(bpy)OH_2](ClO_4)_2$ (100 mg) was dissolved in water (10 mL) and ammonia bubbled through the solution until saturation. The solution was sealed in

(10) McWhinnie, W. R.; Miller, J. D.; Watts, J. B.; Wadden, D. Y. *Inorg. Chim. Acta* **1973**, *7*, 461–466.
(11) Diamond, S. E.; Tom, G. M.; Taube, H. *J. Am. Chem. Soc.* **1975**, *97*, 2661–2664.
(12) Keene, F. R.; Salmon, D. J.; Meyer, T. J. *J. Am. Chem. Soc.* **1976**, *98*, 1884–1889.
(13) Reichgott, D. W.; Rose, N. J. *J. Am. Chem. Soc.* **1977**, *99*, 1813–1818.
(14) Tovrog, B. S.; Diamond, S. E.; Taube, H. *J. Am. Chem. Soc.* **1979**, *101*, 5067–5069.
(15) Buess, P. Ph.D. Thesis, Université Libre de Bruxelles, 1970.
(16) Based on plans provided by Professor L. Gierst (Université Libre de Bruxelles).
(17) Ferguson, J. A.; Meyer, T. J. *Inorg. Chem.* **1972**, *11*, 631–636.
(18) Sullivan, B. P.; Salmon, D. J.; Meyer, T. J. *Inorg. Chem.* **1978**, *17*, 3334–3341.
(19) Meyer, T. J., personal communication.

a glass tube and heated at 100 °C for 2 h. After the solution was cooled, NH_4PF_6 (0.5 g) was added and the complex extracted with dichloromethane. The organic phase was dried with sodium sulfate and evaporated to dryness (75 mg, 67%). The complex was recrystallized from hot methanol with 80% recovery. Visible spectrum $\epsilon_{482}^{max} = 10000$ (water) and from cyclic voltammetry, $E_{1/2} = 1.02$ V vs. SSCE (propylene carbonate/0.2 M TBAH; glassy carbon electrode). Anal. Calcd for $RuC_{25}H_{22}N_6P_2F_{12}$: C, 37.6; H, 2.78; N, 10.5. Found: C, 37.3; H, 2.92; N, 10.4.

Chemical Oxidations. Spectrophotometric Titrations. Aliquots (10 mL) of a 1.07×10^{-4} M solution of $[Ru(tpy)(bpy)NH_3]^{2+}$ in 1 M H_2SO_4 were added to each of five 25 mL volumetric flasks. Aliquots of a 2.66×10^{-4} M solution of Ce(IV) in 1 M H_2SO_4 were added so that the Ce/Ru ratio was varied from 0 to 2, the flasks made up to the required volume with 1 M H_2SO_4, and the visible/UV spectra measured by using a Cary 118C spectrophotometer.

For $Ru(bpy)_2ampy^{2+}$, a similar procedure was followed by using 50-mL flasks with 20-mL aliquots of 7.39×10^{-5} M $Ru(bpy)_2ampy^{2+}$ solution and 1.48×10^{-4} M Ce(IV). The Ce/Ru ratio was varied from 0 to 2.5.

Kinetic Apparatus. An Aminco-Morrow stopped-flow apparatus at the Australian Atomic Energy Commission, Lucas Heights, was used to monitor the reactions: the apparatus and the computerized data acquisition system are described elsewhere.[20] Analysis of the kinetic data was undertaken on the IBM 370 computer at A.A.E.C. or on the PDP-10 system at James Cook University of North Queensland.

Oxidation of $[Ru(tpy)(bpy)NH_3]^{2+}$ by Ce(IV). The kinetics were followed under second-order conditions at $\lambda = 482$ nm. The complex and Ce(IV) solutions in H_2SO_4 solution of the appropriate concentration were thermostated to 20 °C, as was the syringe block and mixing chamber of the stopped-flow apparatus. For the oxidation reaction

$$Ce(IV) + Ru^{II}(tpy)(bpy)NH_3^{2+} \xrightarrow{k} Ce(III) + Ru^{III}(tpy)(bpy)NH_3^{3+}$$

only $Ru(tpy)(bpy)NH_3^{2+}$ absorbs at $\lambda = 482$ nm. Consequently, if A_0 and B_0 are the initial concentrations of the respective reactants, D is the absorbance at time t, and ϵ is the molar extinction coefficient of the Ru(II) species, it can easily be shown that for a second-order process

$$\frac{1}{B_0 - A_0} \log \left\{ \frac{D/\epsilon}{(B_0 - A_0 + D/\epsilon)} \right\} = kt + c$$

Oxidation of $[Ru(bpy)_2ampy]^{2+}$ by Ce(IV). The experimental conditions were as described for the oxidation of $[Ru(tpy)(bpy)NH_3]^{2+}$, with the reaction being monitored at $\lambda = 471$ nm.

The analysis of the stopped flow data for (2-(aminomethyl)pyridine)bis(2,2'-bipyridine)ruthenium(II), $Ru(bpy)_2ampy^{2+}$, is considerably more complicated than that for $[Ru(tpy)(bpy)NH_3]^{2+}$, since several steps follow the Ru^{2+}/Ru^{3+} oxidation in the overall reaction mechanism. It was not possible to obtain analytical solutions to the rate law differential equations for the reaction mechanisms considered. The differential equations were numerically solved, and the values of the rate constants resulting in the best fit between experimental and calculated responses were obtained by using nonlinear programming techniques. For a description of the numerical analysis and the nonlinear optimization techniques used, see the Appendix.

Flash Photolysis Studies. The laser photolysis and flash photolysis facilities at the University of Adelaide were used for these studies; a description of this equipment and of the data acquisition system is given elsewhere.[21]

Luminescence lifetime measurements and quenching rate measurements (by $Fe(OH_2)_6^{3+}$) were carred out by laser photolysis in 1 M H_2SO_4 and 1 M $HClO_4$, using a complex concentration of 1.00×10^{-5} M. All solutions were deaerated (using N_2) before use and thermostated at 25 °C. All runs were monitored at 629 nm.

For the flash photolysis studies of the ligand oxidation reaction, the complex concentration was maintained at 1.00×10^{-5} M, $[Fe^{3+}]$ was maintained at 2.0×10^{-3} M, and $[HClO_4]$ (or $[H_2SO_4]$) varied from 1.0 to 0.01 M. Ionic strength was maintained at $\mu = 1$ by using $NaClO_4$ or $NaHSO_4$, respectively. Each solution was deaerated before use (using N_2). Measurements were made in cylindrical 10-cm cells and conducted at room temperature (24.0 ± 0.5 °C). Each solution was used for one flash experiment only, and 3–4 determinations were conducted for each set of conditions. At an acid concentration of 1 M, a set of measurements was made in which the intensity of the flash was varied. All flash photolysis experiments were monitored at 436 nm.

Results and Discussion

The oxidation of 2-(aminomethyl)pyridine coordinated to ruthenium is given by the stoichiometric eq 1. The reaction has been reported previously[8] to be rapid and quantitative in acetonitrile solution, whether promoted chemically (by Ce(IV)) or electrochemically. Since electron exchange involving metal ions is often rapid[22] and electron-transfer processes between metal ions and electrode surfaces are likely to be rapid, it is assumed that the initial step in a reaction such as above would be a Ru(II) → Ru(III) oxidation

$$Ru^{II}(bpy)_2(ampy)^{2+} \xrightarrow{-e} Ru^{III}(bpy)_2(ampy)^{3+} \qquad (2)$$

The elucidation of the mechanism of the subsequent ligand oxidation requires a rapid method for promotion of the prior metal oxidation: we now report kinetic studies of such reactions by using flash photolysis techniques, electrochemical studies, and chemical oxidation by Ce(IV) in association with stopped-flow methods.

The oxidative dehydrogenation of the ligand is required to be a two-electron process, which may proceed via two successive one-electron transfers or by a two-electron transfer from metal to ligand. The former possibility has been proposed in the mechanistic studies of the oxidation of nickel(II) macrocycles[3] by using pulse radiolysis techniques. These data were interpreted to indicate that ligand dehydrogenation occurred by initial oxidation of the metal (Ni(II) → Ni(III)) followed by a deprotonation at the coordinated amine nitrogen group: the resultant Ni(III)–conjugate base species then underwent an intramolecular one-electron transfer to give a Ni(II)–radical species. A subsequent one-electron oxidation of the ligand radical results in the loss of a further proton from the α-carbon atom.

A second mechanistic proposal has been suggested for the ruthenium-promoted oxidation of 2-(1'-hydroxyethyl)pyridine[14] and involves a Ru(IV) intermediate formed by disproportionation of the Ru(III) species. Such disproportionation processes have been reported previously for $Ru(NH_3)_5py^{3+}$.[23] The Ru(IV) intermediate subsequently undergoes an intramolecular redox process resulting in a two-electron reduction of the metal and oxidative dehydrogenation of the ligand.

Chemical Oxidation Studies. The Ru(III)/Ru(II) couple for $[Ru(bpy)_2ampy]^{n+}$ occurs at a sufficiently anodic potential ($E_{1/2} = 1.12$ V in acetonitrile; $E_{1/2} = 1.16$ V in propylene carbonate; $E_{p,a} = 0.76$ V in 1 M H_2SO_4: all potentials relative to SSCE) that there are a limited number of appropriate chemical oxidants. Cerium(IV) was used for the present studies, and all runs were carried out at constant sulfuric acid concentration (1 M) to avoid problems with anion dependencies and hydrolysis equilibria.[24,25]

In mechanistic schemes for the ligand oxidation of $[Ru(bpy)_2ampy]^{2+}$ based on the two proposals outlined above, the

(20) Ekstrom, A. *Inorg. Chem.* **1973**, *12*, 2455–2460.
(21) Thornton, A. T.; Laurence, G. S. *Radiat. Phys. Chem.* **1978**, *11*, 311–319.
(22) Wilkins, R. G. "The Study of Kinetics and Mechanism of Reactions of Transition Metal Complexes"; Allyn and Bacon: Boston, 1976.
(23) Rudd, De F. P.; Taube, H. *Inorg. Chem.* **1971**, *10*, 1543–1544.
(24) Michaille, P.; Kikindai, T. *J. Inorg. Nucl. Chem.* **1977**, *39*, 859–864.
(25) Benson, D. "Mechanism of Oxidation by Metal Ions"; Elsevier: New York, 1976.

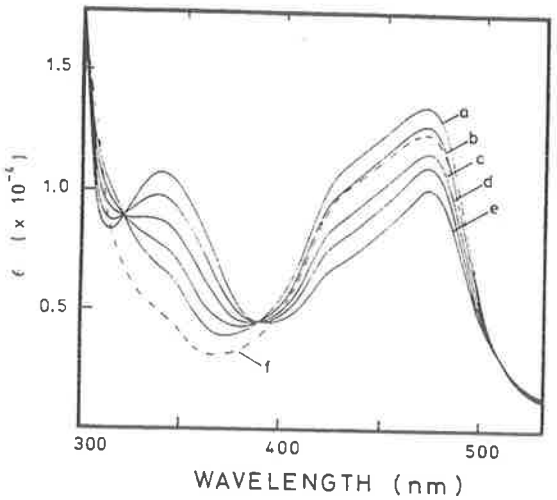

Figure 1. Spectrophotometric titration of $Ru(bpy)_2ampy^{2+}$ with Ce(IV) in 1 M H_2SO_4: Ce/Ru ratio (a) 0, (b) 0.5:1, (c) 1:1, (d) 1.5:1, (e) 2:1, (f) 2.5:1.

initial step is given by eq 2. In order to gain some insight into the rate of this reaction, we studied the oxidation of ammine(bipyridine)(terpyridine)ruthenium(II), $[Ru(tpy)(bpy)NH_3]^{2+}$. Since both $[Ru(tpy)(bpy)NH_3]^{2+}$ and $[Ru(bpy)_2ampy]^{2+}$ have five pyridine nitrogens and one amine nitrogen coordinated to a ruthenium(II) metal center, the rates of oxidation of the ruthenium(II) center to the corresponding 3+ state should be similar. The ligands in $[Ru(tpy)(bpy)NH_3]^{2+}$ are not susceptible to oxidation under the conditions of the experiment, so that the reaction may not proceed further than

$$Ce(IV) + Ru(tpy)(bpy)NH_3^{2+} \xrightarrow{k} Ce(III) + Ru(tpy)(bpy)NH_3^{3+} \quad (3)$$

for which the calculation of the rate constant is quite simple: by comparison, for $[Ru(bpy)_2ampy]^{2+}$ further ligand oxidations make the kinetic solutions complicated.

A spectrophotometric titration of $[Ru(tpy)(bpy)NH_3]^{2+}$ with Ce(IV) in 1 M H_2SO_4 shows a clean one-electron oxidation of the complex to Ru(III), with an isosbestic point at $\lambda = 354$ nm up to a Ce/Ru ratio of 1:1. In the kinetic study of reaction 3, stopped-flow measurements at $\lambda = 482$ nm gave data which showed second-order behavior and indicated $k = 6.1\ (\pm 0.2) \times 10^5\ M^{-1}\ s^{-1}$ at 20 °C.

A spectrophotometric titration of $Ru(bpy)_2ampy^{2+}$ with Ce(IV) in 1 M H_2SO_4 shows a clean two-electron oxidation of the complex to $Ru(bpy)_2impy^{2+}$.

$$2Ce(IV) + Ru(bpy)_2ampy^{2+} \rightarrow 2Ce(III) + Ru(bpy)_2impy^{2+} + 2H^+ \quad (4)$$

Figure 1 shows isosbestic points (at $\lambda = 512$, 389, and 322 nm) up to a Ce/Ru ratio of 2:1. There are further isosbestic points (at $\lambda = 239$, 251, and 286 nm). Addition of greater than 2 equiv of cerium(IV) resulted in the loss of the isosbestic points, indicating a further reaction, probably

$$Ru^{II}(bpy)_2impy^{2+} + Ce(IV) \rightarrow Ru^{III}(bpy)_2impy^{3+} + Ce(III) \quad (5)$$

A similar experiment[8] in a nonaqueous solvent (acetonitrile) revealed similar behavior.

The kinetics of the above reaction were followed in 1 M H_2SO_4 by using stopped-flow techniques, and a typical response is shown in Figure 2. An attempt was made to fit the observed responses to a number of mechanistic schemes based on the intermediacy of either a Ru(II)-free radical species or a Ru(IV) species formed by disproportionation. The programs (see Appendix) produced a numerical solution to the set of differential equations appropriate to each scheme, and a nonlinear optimization procedure then varied the rate constants for each scheme to minimize the difference between the calculated and observed transmittance–time responses. An excellent correlation was found for the mechanistic scheme shown in eq 6–9.

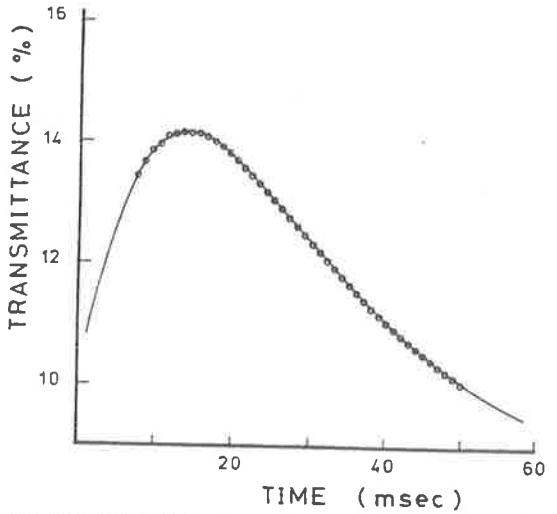

Figure 2. Calculated transmittance–time curve (—) for the oxidation of $Ru(bpy)_2ampy^{2+}$ with Ce(IV) and the observed response (O) ($[H_2SO_4] = 1$ M; $[Ru(bpy)_2ampy^{2+}] = 1.04 \times 10^{-4}$ M; $[Ce(IV)] = 8.8 \times 10^{-5}$ M).

$$(bpy)_2Ru^{II}ampy^{2+} \underset{k_{-1}}{\overset{k_1}{\rightleftharpoons}} (bpy)_2Ru^{III}ampy^{3+} \quad (6)$$

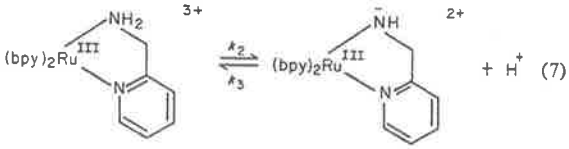

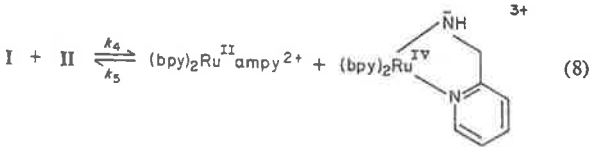

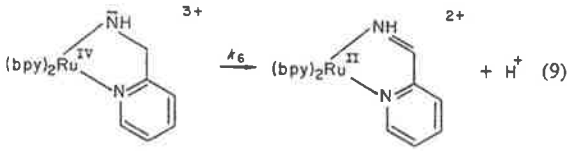

Figure 2 shows the calculated transmittance–time response based on the above mechanism and the conditions of the experimental curve shown: the calculated curves are quite sensitive to small changes in the values of the rate constants.

Much less satisfactory fits were obtained for any scheme based on the free radical proposal.

Two assumptions are made in the formulation of the differential equations and in the simulation of the absorbance–time responses. First, the oxidation of the metal center is assumed to be the initial step in the reaction. Second, it has been assumed that any Ru(III) species are optically transparent in the visible region of the spectrum: the strong visible absorption of (bipyridine)ruthenium(II) complexes is due to $d\pi[Ru(II)]-\pi^*(bpy)$ metal-to-ligand charge-transfer (MLCT) transitions,[26] and on oxidation of the metal to Ru(III), this absorption would be expected to be lost.[27] For the related complex ammine(bipyridine)(terpyridine)ruthenium(III), $[Ru(tpy)(bpy)NH_3]^{3+}$, $\epsilon < 300\ M^{-1}\ cm^{-1}$ for wavelengths greater than 425 nm. For a Ru(IV) species, however,

(26) Bryant, G. M.; Fergusson, J. E.; Powell, H. K. J. *Aust. J. Chem.* **1971**, *24*, 257–273.
(27) Bryant, G. M.; Fergusson, J. E. *Aust. J. Chem.* **1971**, *24*, 275–286.

Table I. Calculated Rate Constants for the Scheme Given in Eq 6–9 Using Data from Various Techniques

reaction[a]	Ce(IV) studies in 1 M H_2SO_4[b]	flash photolysis in 1 M H_2SO_4[c,d]	flash photolysis in $HClO_4$[c,e]
(i) k_1, M^{-1} s^{-1}	5×10^5		
k_2, s^{-1}	4×10^6	4×10^6	5×10^6
k_3, M^{-1} s^{-1}	3×10^9	2×10^9	1×10^9
k_4, M^{-1} s^{-1}	6×10^8	9×10^8	1×10^9
k_5, M^{-1} s^{-1}	4×10^6	5×10^6	5×10^6
k_6, s^{-1}	102	90	93
ϵ, M^{-1} cm^{-1}	300[f]	1100[g]	1250[g]
(ii) k_1, M^{-1} s^{-1}	5×10^5		
k_2, s^{-1}	5×10^9	3×10^9	5×10^9
k_3, M^{-1} s^{-1}	2×10^{10}	1×10^{10}	1×10^{10}
k_4, M^{-1} s^{-1}	8×10^8	1×10^9	1×10^9
k_5, M^{-1} s^{-1}	4×10^8	4×10^8	4×10^8
k_6, s^{-1}	760	910	950
ϵ, M^{-1} cm^{-1}	400[f]	950[g]	900[g]

[a] (i) and (ii) correspond to different numerical solutions to minimization. [b] 20 °C. [c] 24 °C. [d] Averaged values for $[H_2SO_4] = 1.00$ M. [e] Average values over $[HClO_4] = 0.01$–1.00 M. [f] $\lambda = 471$ nm. [g] $\lambda = 436$ nm.

absorption in this region may be somewhat larger. Comparison of the spectra of aquo(bipyridine)(terpyridine)ruthenium(II) and its two-electron oxidation product, identified by Meyer et al.[28] as oxo(bipyridine)(terpyridine)ruthenium(IV), shows the extinction coefficients at $\lambda = 471$ nm and $\lambda = 436$ nm (the wavelengths at which the present reactions were studied) to be 550 and 1150, respectively. Since ϵ for the $(bpy)_2Ru^{IV}(ampy\text{-}H)^{3+}$ species was not known, ϵ was included as a variable along with the rate constants k_1–k_6 for the numerical analysis of the mechanism given in the scheme. The only ruthenium(II) species involved are $[Ru(bpy)_2ampy]^{2+}$ and $[Ru(bpy)_2impy]^{2+}$, for which the molar extinction coefficients are known.

It was found that there were two solutions to the minimization procedure, and the values of the rate constants and extinction coefficient for each numerical solution are given in Table I. A discussion is given subsequently with the flash photolysis results.

The limitations of the use of chemical oxidation of $Ru(bpy)_2ampy^{2+}$ by Ce(IV) in a kinetic study lie in the inability to obtain information at varying acid concentrations, due to the complicated hydrolysis behavior of Ce(IV) under different pH conditions. Such data can be obtained by using flash photolysis techniques, as described subsequently.

Electrochemical Studies. Electrochemical study of the oxidation of coordinated ligands is attractive because the initial oxidation of the metal center at the electrode surface can be made to be diffusion controlled. A constraint on obtaining quantitative data from the electrochemical studies is that the theory for the analysis of relatively complex chemical reaction schemes associated with the electrode process (such as occur in this study) has not been fully developed. For this reason, much of the electrochemical data is somewhat qualitative in nature.

Previous preliminary studies on this system[8] revealed that in acetonitrile and acidic aqueous solution, a two-electron oxidation occurred on coulometry to give the imine species quantitatively. Cyclic voltammetric studies revealed that the complex had an irreversible oxidation in aqueous solution for any scan rate and an irreversible couple at slow scan rate in acetonitrile, although some evidence was obtained for the Ru(III) → Ru(II) reverse wave at high scan rates.[8]

In the course of the present study, we have reexamined the electrochemistry of this system in propylene carbonate and aqueous sulfuric acid media. The cyclic voltammetry in propylene carbonate and 1 M H_2SO_4 at low scan rates is irreversible with the reduction peak for the couple not being observed. Another reversible couple is observed at a potential anodic of the $Ru(bpy)_2ampy^{2+}$ system ($E_{1/2} = 1.33$ V vs. SSCE for propylene carbonate, $E_{1/2} = 0.97$ V vs. SSCE for 1 M H_2SO_4) corresponding to the dehydrogenated species $Ru(bpy)_2impy^{3+/2+}$ and showing that the ligand oxidation is completed in the time scale of the scan. The slow sweep cyclic voltammogram of $Ru(bpy)_2(ampy)^{3+/2+}$ in propylene carbonate is given in Figure 3.

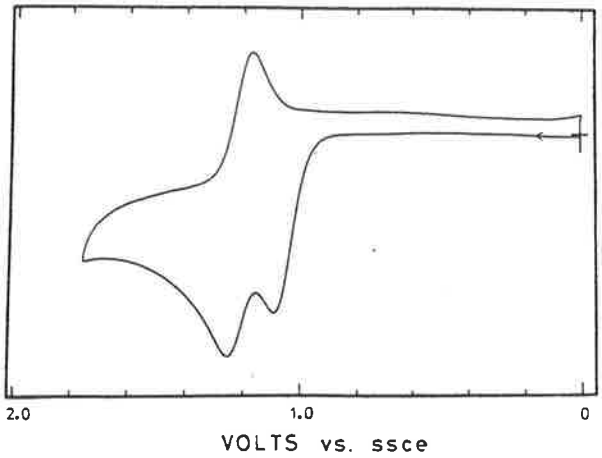

Figure 3. Slow sweep rate (50 mV/s) cyclic voltammogram of 1.07 mM $Ru(bpy)_2ampy^{2+}$ (propylene carbonate/0.2 M TBAH; glassy carbon electrode).

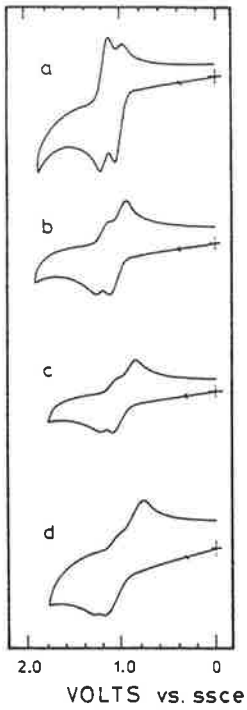

Figure 4. Effect of increasing sweep rate on the cyclic voltammetry of $Ru(bpy)_2ampy^{2+}$ in propylene carbonate/0.2 M TBAH (glassy carbon electrode): (a) sweep rate = 100 mV/s; (b) sweep rate = 1 V/s; (c) sweep rate = 5 V/s; (d) sweep rate = 10 V/s.

Figure 4 shows the effect of increasing the sweep rate of the cyclic voltammetry of $Ru(bpy)_2ampy^{2+}$ in propylene carbonate. As the sweep rate is increased, the reverse peak of the $Ru(bpy)_2ampy^{3+/2+}$ couple is observed and increases in magnitude as the sweep rate increases. Similar behavior may be observed in 5 M H_2SO_4. In 1 M H_2SO_4, it was not possible to observe the reverse peak of the $Ru(bpy)_2ampy^{3+/2+}$ couple at scan rates of up to 100 V/s: an inverse proton dependence of the rate of ligand oxidation would be expected for either of the mechanistic proposals.

Single potential step chronocoulometry studies in propylene carbonate and aqueous acidic solutions using a glassy carbon

(28) Moyer, B. A.; Meyer, T. J. *J. Am. Chem. Soc.* **1978**, *100*, 3601–3603.

working electrode reveal linear Q vs. $t^{1/2}$ plots with zero intercept after correction for the double-layer charging current. Such results indicate that there are no chemical reactions prior to the initial electrode promoted Ru(II) → Ru(III) oxidation, which is diffusion controlled, and that there is no adsorption of reactant on to the electrode surface. Hence, mass-transfer electrochemical techniques should be applicable to the present system.

It was hoped that during the course of this work, the techniques of double potential step chronocoulometry and chronoamperometry might be used in the elucidation of the mechanistic path of these oxidation reactions. Reilley et al.[29] have published calculations of electrochemical responses by using these techniques for 22 different cases of chemical reactions associated with electrochemical steps. At present, quantitative analysis of the responses from double potential step chronocoulometry or chronoamperometry is not possible for the $Ru(bpy)_2ampy^{2+}$ system because of deficiencies in the available mathematical treatment of a series of interrelated chemical and electrochemical reactions of this complexity. Work on developing the analysis of such responses for kinetic studies of coordinated ligand redox processes is currently in progress.

Preliminary double potential step chronoamperometric studies are consistent with a scheme involving a disproportionation following the initial oxidation process. Marcoux[30] has described a technique, called potential dependent chronoamperometry, in which the potential is not necessarily stepped into the region of diffusion control. Variation of the applied potential permits systematic variation of the concentration ratios within the diffusion layers adjacent to an electrode. Consequently, by variation of the upper limiting potential to a small increment (~60 mV) either side of the redox couple, Marcoux[30] found that I vs. log τ plots (where τ = time between potential steps) were dependent on the chemical reactions associated with the electrochemical step. In particular, for an electrochemical step followed by a disproportionation there was considerable variation in the position of the I vs. log τ curves, whereas for an ECE process (for example), the curves were essentially invariant with applied potential. In the present case, such studies revealed very considerable variation of the curves with applied potential, which we interpret to be more consistent with a scheme based on disproportionation rather than a free-radical process.

Flash Photolysis Studies. The technique of flash photolysis can be used for observing photochemically generated transients and for measuring their rates of reaction.[31] For example, the strongly luminescent charge-transfer excited state of $Ru(bpy)_3^{2+}$ has received considerable attention: $Ru(bpy)_3^{2+*}$ undergoes rapid quenching by a bimolecular electron-transfer process, and flash photolysis methods have been used to rapidly generate $Ru(bpy)_3^{3+}$ and to study its subsequent reactions, particularly electron transfer.[32]

The technique of flash photolysis is particularly appropriate for studies of the present system, as it allows variation of $[H^+]$ (which was not possible for the chemical oxidation studies) and [Ru(III)] (by variation of the flash intensity). This appears to be the first use of such methods for the detailed kinetic study of ligand oxidation reactions.

A solution of $Ru(bpy)_2ampy^{2+}$ in 1 M $HClO_4$ shows an emission spectrum with λ_{max} = 625 nm (excitation wavelength 471 nm). Laser photolysis studies indicate that the luminescence lifetime in the same medium is 192 ± 2 ns, and quenching studies in the presence of $Fe(OH_2)_6^{3+}$ showed the rate constant for quenching to be $(2.8 \pm 0.1) \times 10^9$ M^{-1} s^{-1}. Consequently, under the conditions used for conventional flash photolysis studies, a solution of $Ru(bpy)_2ampy^{2+}$ containing the appropriate proportion of $Fe(OH_2)_6^{3+}$ can be used to generate $Ru(bpy)_2ampy^{3+}$ very rapidly;

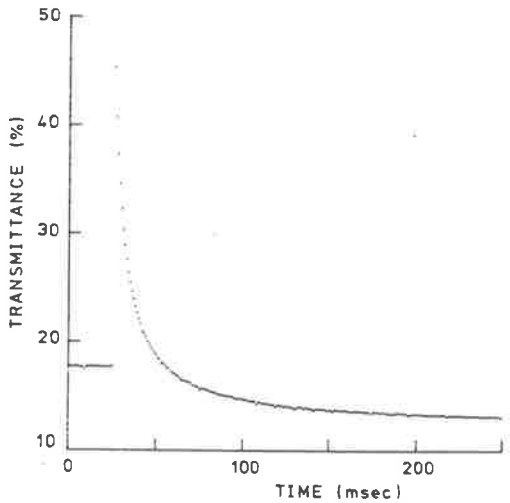

Figure 5. Typical transmittance–time response (followed at λ = 436 nm) from flash photolysis study of oxidation of $Ru(bpy)_2ampy^{2+}$ ($[HClO_4]$ = 1.0 M; T = 24.0 ± 0.5 °C).

in fact, in the lifetime of the flash used (<10 μs).

Studies were undertaken in aqueous perchloric acid media (0.01–1.00 M) by using a complex concentration of 1.01×10^{-5} M and quencher concentration $[Fe(OH_2)_6^{3+}]$ = 0.002 M. Perchlorate media were used in preference to sulfate to facilitate control of ionic strength over the range of acid concentrations used. The flash intensity was also systematically varied for a chosen set of conditions to change the [Ru(III)] produced during the flash. Conversions from Ru(II) → Ru(III) of ca. 30% were obtained, and a typical response curve is shown in Figure 5.

The responses were tested against the mechanistic schemes proposed earlier in the same manner as the chemical oxidation data. It was found that the results were entirely consistent with the scheme shown in eq 6–9, and as for the chemical oxidation data two solutions were found in the minimization procedure. The values of the rate constants and extinction coefficient for each numerical solution in both $HClO_4$ media and 1 M H_2SO_4 are given in Table I.

Calculated Rate Constants. The mechanistic scheme proposed is somewhat different to the kinetically analogous path in which the Ru(III) species formed by reaction 6 would disproportionate as shown in eq 10, with subsequent deprotonation to give the

$$2(bpy)_2Ru^{III}ampy^{3+} \underset{k_b}{\overset{k_f}{\rightleftharpoons}} (bpy)_2Ru^{II}ampy^{2+} + (bpy)_2Ru^{IV}ampy^{4+} \quad (10)$$

Ru^{IV}(ampy-H) species. This alternative scheme is identical with that proposed by Tovrog et al.[14] for the ruthenium-promoted oxidation of a coordinated alcohol. However, in both this case and that reported by Tovrog et al.,[14] the disproportionation process (k_f/k_b) would seem thermodynamically prohibited. For the system $Ru(bpy)_2Cl_2$, the $E_{1/2}$ for the Ru(III)/Ru(II) couple is 0.32 V vs. SSCE (acetonitrile solution; platinum bead electrode), whereas the corresponding Ru(IV)/Ru(III) couple occurs at 1.98 V.[33] It is a reasonable assertion that for the $Ru(bpy)_2ampy^{n+}$ system, the difference in potential between the Ru(IV)/Ru(III) and Ru(III)/Ru(II) couples is >1.0 V, so that for the disproportionation reaction (10), $K < 10^{-17}$: consequently, the formation of the Ru(IV) species by this means is unlikely. However, if the Ru(III) species were to deprotonate, the alternative path shown in eq 8 for the formation of a Ru(IV) intermediate is available.

The Ru(IV)/Ru(III) couple for the deprotonated amine species would be expected to be considerably cathodic of the couple for the nondeprotonated species. Such a reduction in potential is

(29) Hanafey, M. K.; Scott, R. L.; Ridgeway, T. H.; Reilly, C. N. *Anal. Chem.* **1978**, *50*, 116–137.
(30) Marcoux, L. *J. Phys. Chem.* **1972**, *76*, 3254–3259.
(31) Bock, C. R.; van Gustorf, E. A. K. *Adv. Photochem.* **1977**, *10*, 221–309.
(32) Bock, C. R.; Meyer, T. J.; Whitten, D. G. *J. Am. Chem. Soc.* **1974**, *96*, 4710–4712.
(33) Weaver, T. R.; Adeyemi, S. A.; Brown, G. M.; Eckberg, R. P.; Hatfield, W. E.; Johnson, E. C.; Murray, R. W.; Untereker, D.; Meyer, T. J. *J. Am. Chem. Soc.* **1975**, *97*, 3039–3048.

Table II. Rate Constants for the Scheme Given in Eq 6–9 Using Rate Data from Flash Photolysis in Perchlorate Media (λ = 436 nm; μ = 1.0, $NaClO_4$; T = 24 ± 1 °C; All Solutions Deaerated)

[H⁺], M	$10^{-6}k_2$, s^{-1}	$10^{-9}k_3$, M^{-1} s^{-1}	$10^{-9}k_4$, M^{-1} s^{-1}	$10^{-6}k_5$, M^{-1} s^{-1}	k_6, s^{-1}	ϵ, M^{-1} cm^{-1}
0.01[a]	5.1	1.4	9.0	5.1	94	1250[d]
0.01[a]	5.3	1.6	1.1	5.3	90	1250[d]
0.1	4.9	1.2	1.3	5.6	93	1250[d]
1.0[b]	5.0	1.4	1.0	5.4	92	1250
1.0[b]	5.2	1.2	1.1	5.3	93	1250
1.0[b]	5.1	1.3	1.0	5.3	93	1250
1.0[b]	5.2	1.3	1.1	5.4	94	1250
average values[c]	5.1 (±0.2)	1.3 (±0.2)	1.1 (±0.2)	5.3 (±0.2)	93 (±3)	1250

[a] Duplicate determinations. [b] These determinations were made by using different flash intensities but with all other conditions constant. [c] Errors quoted are experimental deviations. [d] ϵ set for optimum obtained from studies in 1 M $HClO_4$.

observed generally on lowering of overall complex charge[34] as, for example, in a Pt(IV) complex of a "cage" nitrogen macrocycle where a single deprotonation has been observed to stabilize the Pt(IV) state by 1.1 V.[35] Consequently, for the two couples involved in the electron-exchange reaction (8) $(Ru(bpy)_2(ampy)^{3+/2+}$ and $Ru(bpy)_2(ampy\text{-}H)^{3+/2+}$) the difference in potentials may be anticipated to be considerably less than 1 V, and possibly even negative, so that the equilibrium constant would be considerably more favorable which would allow formation of the deprotonated Ru(IV) species.

It should be noted that the stopped-flow data were obtained at 20 °C and the flash photolysis data at 24 °C, so that some care is needed in the comparison of results obtained from the two techniques. However, it is immediately clear that the results are comparable. The agreement between the calculated and experimental results is excellent for both numerical solutions, the sum of the squares of the absorbance differences between the generated curve and the data being less than 1×10^{-4} (50 points) for the flash photolysis experiments, and less than 3×10^{-4} (50 points) for the stopped-flow data.

For the stopped-flow method, six runs were taken under the same experimental conditions and the averaged run then used as data for the numerical analysis. The data obtained have limited accuracy since the observed transmittance change is relatively small, because the initial oxidation reaction (k_1) and subsequent ligand reactions are comparable in rate. All stopped-flow data were obtained in 1 M H_2SO_4 solution, as discussed earlier.

For each set of conditions using the flash photolysis technique, data were recorded in at least triplicate, and the individual runs were each analyzed. Runs were done in both sulfuric acid and perchloric acid media over the range [H⁺] = 0.01–1.00 M, and [Ru(III)] was varied by altering the intensity of the flash for solutions [H⁺] = 1.00 M. In Table I, the rate constants and extinction coefficient obtained for the two numerical solutions using data at 1 M H_2SO_4 are quoted for comparison with the stopped-flow results. The results given for perchloric acid media represent the average values obtained over the full range of conditions studied. In the following discussion, the rate constants and extinction coefficients quoted are those from the determinations in perchloric acid, since these correspond to the data of greatest precision.

k_1. The value of k_1 for the oxidation of $Ru(bpy)_2ampy^{2+}$ by Ce(IV) in 1 M H_2SO_4 was found to be $(5.0 \pm 1.0) \times 10^5$ M^{-1} s^{-1}: this is in good agreement with the rate constant for the oxidation of $Ru(tpy)(bpy)NH_3^{2+}$ under the same conditions ($k = (6.1 \pm 0.2) \times 10^5$ M^{-1} s^{-1}). Since the $E_{1/2}$ values for the Ru^{III}/Ru^{II} couples in $Ru(tpy)(bpy)NH_3^{n+}$ and $Ru(bpy)_2ampy^{n+}$ are respectively 1.02 and 1.12 V vs. SSCE in acetonitrile, it would be expected that the rate of the oxidation of $Ru(bpy)_2ampy^{2+}$ was slightly slower than that of $Ru(tpy)(bpy)NH_3^{2+}$.

k_2, k_3. For the two solutions of the numerical analysis, the values for $k_2 = 5 \times 10^6$ or 5×10^9 s^{-1} and the corresponding $k_3 = 1 \times 10^9$ or 1×10^{10} M^{-1} s^{-1}. Accordingly, the pK_a value would be either 2.4 or 0.3. The diffusion-controlled limits for the protonation of amines by the hydronium ion have been found to be in the range 10^9–10^{11} M^{-1} s^{-1},[36,37] and both solutions for k_3 are within this range. However, for the reprotonation of an analogous conjugate base complex, $[Pt(en)_2(en\text{-}H)]^{3+}$, the rate is 1.9×10^9 M^{-1} s^{-1} (at 27 °C):[36] this is consistent with $k_3 = 1.3 \times 10^9$ M^{-1} s^{-1} for numerical solution (i) (Table I) in the present system. On this basis, we are inclined to prefer solution (i) to explain the experimental observations, and a detailed summary of the results of the numerical solution (i) for the minimization procedure using data from flash photolysis experiments in perchlorate media is given in Table II.

The pK_a value for the equilibrium given in eq 7 of the scheme is therefore 2.4. For $Ru(NH_3)_6^{3+}$, the pK_a = 13.1[38] and the ammine protons are significantly more acidic for $Ru(NH_3)_5py^{3+}$ ($pK_a \approx 9$)[23], presumably because the presence of the pyridine ligand increases the Lewis acidity of the Ru(III) center. For the corresponding $Ru(bpy)_2ampy^{3+}$ complex with five pyridine-type ligands, the pK_a of the amine protons would be expected to be significantly lower, so that 2.4 would seem a reasonable value. The fact that the $-NH_2$ group is part of a chelate ring may also contribute to a lowering of the pK_a, as models of the ring system indicate that there is some strain present.

k_4, k_5. The forward rate constant (k_4) for the disproportionation in the scheme may be estimated from electron-transfer studies of similar ruthenium complexes. The disproportionation step is an electron transfer between two $Ru^{III}(bpy)_2ampy$ molecules, one of which is deprotonated. The electron-transfer rate between tris(bipyridine)ruthenium(II) and tris(1,10-phenanthroline)ruthenium(III) is 2×10^9 M^{-1} s^{-1},[39] so that the value obtained of 1×10^9 M^{-1} s^{-1} for k_4 is not unreasonable. The equilibrium constant for reaction 8 ($K \approx 208$) implies that there is a difference of ~0.14 V between the potentials of the two couples involved in the equilibrium. Since in H_2SO_4 media, $E_{1/2} \approx 0.7$ V for the $Ru(bpy)_2ampy^{3+/2+}$ couple, it can be calculated that $E_{1/2} \approx 0.56$ V for the Ru(IV)/Ru(III) couple for the deprotonated species, which is in the range expected (vide supra).

k_6. The rate constant obtained is constant on varying both acid and Ru(III) concentrations (93 s^{-1}). However, although this process has been written as a single step, it clearly involves transfer of two electrons from the ligand to the metal, together with a single deprotonation from the methylene carbon group. It is unlikely these acts would be simultaneous and it is unclear as to whether the electron transfer would involve a concerted two-electron process or two consecutive one-electron steps. To satisfy the observed kinetics, one of these processes, or the deprotonation, or a concerted process would be rate determining with any remaining steps being rapid.

ϵ. The values of the molar extinction coefficient for the $(bpy)_2Ru^{IV}$ complex of deprotonated 2-(aminomethyl)pyridine were $\epsilon_{471} = 300$ M^{-1} cm^{-1} (determined from stopped-flow measurements) and $\epsilon_{436} = 1250$ M^{-1} cm^{-1} (determined from flash

(34) Brown, G. M. Ph.D. Thesis, University of North Carolina at Chapel Hill, 1974.
(35) Lawrance, G. A.; Lay, P. A.; Sargeson, A. M., unpublished work.
(36) Eigen, M. *Angew., Chem. Int. Ed. Engl.* **1974**, *3*, 1–19.
(37) Pitner, T. P.; Martin, R. B. *J. Am. Chem. Soc.* **1971**, *93*, 4400–4405.
(38) Waysbort, D.; Navon, G. *Inorg. Chem.* **1979**, *8*, 9–13.
(39) Young, R. C.; Keene, F. R.; Meyer, T. J. *J. Am. Chem. Soc.* **1977**, *99*, 2468–2473.

photolysis measurements). These values correspond to values obtained for the analogous Ru(IV) complex $[(tpy)(bpy)Ru^{IV}{=}O]^{2+}$[28] for which $\epsilon_{471} = 550\ M^{-1}\ cm^{-1}$ and $\epsilon_{436} = 1150\ M^{-1}\ cm^{-1}$.

It seems, therefore, that the values of the rate constants are consistent with comparable electron-exchange and proton-transfer processes, and that the extinction coefficients of the proposed intermediate are consistent with those of a comparable Ru(IV) species. It should be stressed that the curve-fitting procedure produced two numerical solutions, one of which appears to be marginally more satisfactory. The consistency in the values of all variables, and particularly of k_6 on variation of both acid and Ru(III) concentration, leads us to have considerable confidence in the method. The method is quite sensitive to changes in the quoted values of the rate constants: in particular, for the fit to be maintained between the calculated and observed responses, the values of k_1, k_6, ϵ, and the ratio k_2/k_3 are critical and are required to be within 10% of the values quoted. The rate constants k_4 and k_5 are less critical (±25%). Although the ratio k_2/k_3 must be within 10%, the actual values of the individual rate constants, k_2 and k_3, may vary by a factor of 2.

Conclusions

The particular efficacy of Ru in the promotion of the oxidative dehydrogenation of an amine such as 2-(aminomethyl)pyridine seems related to its ability to readily attain an oxidation state 2 units greater than the final state, allowing a low-energy pathway for the even-electron process required in these dehydrogenation reactions. We are presently extending these methods of flash photolysis and electrochemistry to other oxidative dehydrogenation reactions to examine the generality of the scheme for ruthenium complexes containing other amines and alcohols and to assign unambigously the mechanistic schemes for such reactions involving alternative metal centers.

Acknowledgment. We wish to acknowledge the Australian Institute of Nuclear Science and Engineering for the use of stopped-flow facilities of the Australian Atomic Energy Commission, Lucas Heights. We are grateful to the Department of Physical and Inorganic Chemistry, University of Adelaide, for the use of the flash photolysis facilities, and particularly to Dr. G. S. Laurence and Ms. P. Ashwood for their assistance. We thank the Australian Research Grants Committee for supporting this research.

Appendix

Analysis of Experimental Data. In view of the complexity of the reaction mechanisms proposed in the study, analytical solution of the rate law equations was not possible: a numerical technique was required in order to analyze the experimental responses.

The numerical problem is to solve systems (up to 7) of coupled differential equations which define the rate laws. Due to the large possible variation in the magnitude of the rate constants within the proposed mechanism, the coupled differential equations are "stiff",[40] and conventional numerical differential equation algorithms such as the Runge–Kutta algorithm cannot efficiently be used. Algorithms have been specifically designed for the solution of stiff sets of equations of which the method of Gear, used in this study, is in most common use (IMSL library routine DGEAR[41]).

Kinetic information is available from the experimental responses by finding the set of rate constants for a given mechanism which minimize the sum of squares difference between the predicted and experimental response. Nonlinear programming (NLP) techniques automatically vary the rate constants such that this minimum is obtained rapidly. The two NLP techniques used were the simplex algorithm and a Marquadt Steepest Descent algorithm, the latter being the more efficient, but both were found to converge to the same solutions for certain problems, thus confirming the validity of the results.

The possibility of local rather than global optima having been reached was diminished by supplying largely varying initial values of the rate constants and observing convergence to the same optimal solution.

---

(40) Ebert, K. H.; Ederer, H. J.; Isbarn, G. *Angew. Chem., Int. Ed. Engl.* **1980**, *19*, 333–343.

(41) International Mathematical and Statistical Libraries, 1979, Vol. 7.

Reprinted from the Journal of the American Chemical Society, 1981, *103*, 6494.

Oxidation of Isopropylamine Coordinated to Ruthenium

Peter A. Adcock and F. Richard Keene*

Department of Chemistry and Biochemistry
James Cook University of North Queensland
Townsville, Queensland 4811, Australia

Received April 24, 1981

There has been much recent interest in the oxidative dehydrogenation of coordinated amines to the corresponding imines or nitriles.[1-3] Many of these studies have involved ruthenium as the metal center, and although the formation of complexes containing the α,α'-diimine moiety has been relatively common,[1] complexes containing coordinated simple monodentate imines have not been isolated.[1,2]

We have studied the oxidation of isopropylamine in the complex $[Ru(tpy)(bpy)(NH_2CHMe_2)]^{2+}$ (tpy = 2,2′:6′,2″-terpyridine; bpy = 2,2′-bipyridine). Two major processes occur: a two-electron oxidation yielding the corresponding imine complex $[Ru(tpy)(bpy)(NH{=}CMe_2)]^{2+}$, which in turn undergoes a further two-electron oxidation to yield a product characterized as $[Ru(tpy)(bpy)(NCMe_2)]^{3+}$. The nature of these two oxidation products is significant, since the two-electron oxidation product represents the first isolated monodentate imine complex of ruthenium, and the structure of the four-electron oxidation product is novel in ruthenium chemistry, as it can be formulated to contain an N-bound isopropylideneamide anion.

In their study of the oxidation of benzylamine in $[Ru(NH_3)_5(PhCH_2NH_2)]^{2+}$ to the benzonitrile complex, Diamond et al.[2] observed an intermediate which they assumed to be the imine species. In the same work, the oxidation of $[Ru(NH_3)_5(cyclohexylamine)]^{3+}$ yielded $[Ru(NH_3)_6]^{2+}$ and cyclohexanone, presumably by hydrolysis of the coordinated imine complex generated by dehydrogenation. Brown et al.[1] also claimed the generation in situ of nonconjugated chelated diimines in the oxidation of $[Ru(bpy)_2(tn)]^{2+}$ and $[Ru(bpy)_2(aepy)]^{2+}$ (tn = 1,3-propanediamine; aepy = 2-(aminoethyl)pyridine). In none of these cases could the imine complex be isolated.

A spectrophotometric titration of the oxidation of $[Ru(tpy)(bpy)(NH_2CHMe_2)]^{2+}$ by Ce(IV) in 2 M H_2SO_4 indicates an overall four-electron oxidation consisting of two separate two-electron processes which are consecutive. Spectra taken during exhaustive electrolyses (platinum gauze electrode) in 0.1 M HCl (at 0.90 V vs. SSCE) and acetonitrile (at 1.10 V vs. SSCE) indicate similar results. The overall spectrophotometric and coulometric n values were slightly less than 4.0 (viz., 3.6–3.8). The second two-electron process can be reversed electrochemically (coulometry at 0.50 V in 0.1 M HCl, 0.55 V in acetonitrile), with n for the reduction being exactly half the value for the overall oxidation. The two- and four-electron oxidation products were isolated by precipitation as the hexafluorophosphate salts and purified by ion-exchange chromatography on SP-Sephadex.

For the two-electron oxidation product, the visible spectrum (MLCT transitions) in 2 M H_2SO_4 has ϵ_{474}^{max} 8000 (cf. ϵ_{481}^{max} 8800 for the parent isopropylamine species). Cyclic voltammetry in acetonitrile solution[4] revealed $E_{p,a}$ = 1.10 V (compared with

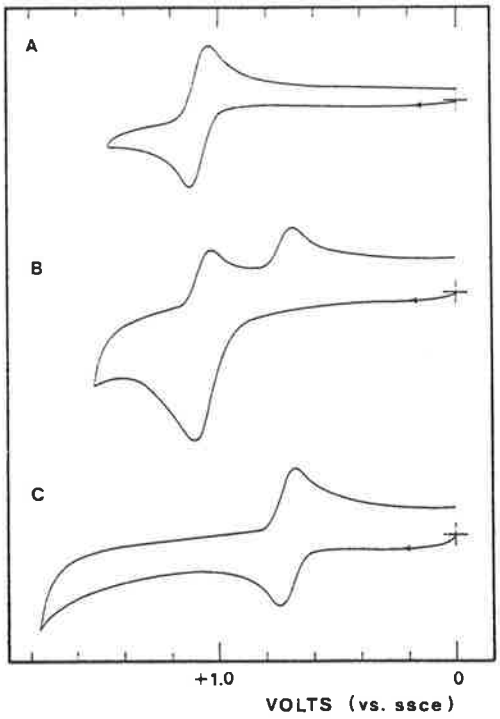

Figure 1. Cyclic voltammograms (200 mV/s) of $[Ru(tpy)(bpy)(isopropylamine)]^{2+}$ (A) and of the two-electron (B) and four-electron (C) oxidation products in acetonitrile solution.[4]

(1) Brown, G. M.; Weaver, T. R.; Keene, F. R.; Meyer, T. J. *Inorg. Chem.* **1976**, *15*, 190–196 and references therein.
(2) Diamond, S. E.; Tom, G. M.; Taube, H. *J. Am. Chem. Soc.* **1975**, *97*, 2661–2664.
(3) Keene, F. R.; Salmon, D. J.; Meyer, T. J. *J. Am. Chem. Soc.* **1976**, *98*, 1884–1889.

(4) Support electrolyte tetra-*n*-ethylammonium hexafluorophosphate; platinum bead working electrode; saturated sodium chloride calomel electrode (SSCE) as reference.

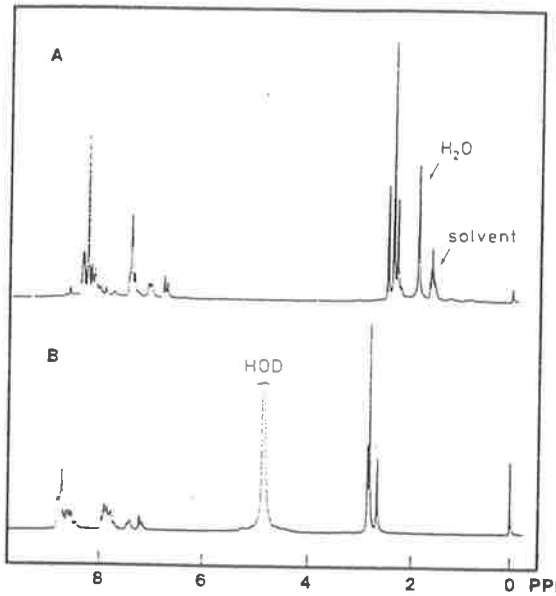

Figure 2. 100-MHz ^1H NMR spectra of $[Ru(tpy)(bpic)(C_3H_6N)]^{3+}$ in CD_3CN (A) and 0.1 M DCl (B) (Me_4Si external standard).

a reversible couple $E_{1/2} = 1.09$ V for the amine precursor), with a peak on the reverse sweep ($E_{p,c} = 0.68$ V) associated with the four-electron oxidation product, as shown in Figure 1. The ^1H NMR spectrum (in CD_3CN) showed two doublets in the aliphatic region centered at 1.12 and 1.62 ppm with very small coupling (0.73 and 1.56 Hz, respectively). This spectrum is consistent with the imine formulation, with both methyl groups being split by the adjacent NH=C moiety. On addition of a drop of D_2O, each doublet collapses to a singlet consistent with deuterium exchange at the imine NH group. We conclude therefore that the two-electron oxidation product is the isopropylimine complex $[Ru(tpy)(bpy)(NH{=}CMe_2)]^{2+}$ and that the small blue shift in the visible spectrum on going from the amine to imine ligand indicates there is a relatively small amount of back-bonding from Ru(II) to the isolated monodentate imine, compared with the large effect observed for the conjugated α,α'-diimine grouping.[1]

The four-electron oxidation product has the general formula $[Ru(tpy)(bpy)(C_3H_6N)]_z(PF_6)_{3z}$ by microanalysis,[5] and conductance measurements in acetonitrile using Feltham's method[6] show that the molecular complexity $z = 1$, so the complex is monomeric. ^1H NMR spectra of the related complex $[Ru(tpy)(bpic)(C_3H_6N)]^{3+}$ (bpic = 4,4′-dimethyl-2,2′-bipyridine) in acetonitrile-d_3 and 0.1 M DCl are shown in Figure 2. In the aliphatic region, each spectrum contains a six-proton methyl singlet due to the oxidized isopropylamine ligand, flanked by two three-proton methyl singlets arising from the dimethylbipyridine ligand. The complex shows little absorption in the visible region of the electronic spectrum, consistent with oxidation of the metal center to Ru(III)[7] or Ru(IV).[8] In dry acetonitrile solution, cyclic voltammetry shows a reversible couple, $E_{1/2} = 0.72$ V (Figure 1).

The above evidence indicates the $NCMe_2$ skeleton remains intact in the four-electron oxidation product, which can be regarded formally as a Ru(IV) complex of the coordinated isopropylideneamide anion, $(N{=}CMe_2)^-$. Such a ligand has several possible bonding modes,[9] but the ready electrochemical interconversion of this complex with the imine species leads us to believe that it functions as an N-bound mononuclear ligand in this case. Application of the 18-electron rule for the metal center suggests the ligand should be a four-electron donor, implying Ru–N multiple bonding and a linear Ru–N–C linkage. The ^1H NMR studies are in agreement with this structure, and we are undertaking an X-ray structural analysis to confirm the assignment.

The electrochemical interconversion of the two- and four-electron oxidation products of coordinated isopropylamine occurs since on oxidation of the isopropylimine species (presumably at the metal center), the acidity of the proton on the ligating imine nitrogen would be markedly increased[10] and deprotonation gives rise to the coordinated isopropylideneamide anion. It is apparent from the cyclic voltammetric behavior of the isopropylimine and isopropylideneamide complexes (Figure 1B,C) that the oxidation of the former to the latter is more rapid than the reverse process. The cathodic shift in potential for the $E_{p,a}$ of the complex of the isopropylideneamide anion relative to the isopropylimine species reflects the unusual nature of the Ru–ligand interaction in the former complex. The concept of assignment of a formal oxidation state to the metal center is clearly inappropriate for this species, and this is further evidenced by its magnetic properties, which reveal a slight paramagnetism ($\mu_{eff} = 1.2\ \mu_B$).

Details of the characterization, and chemical and electrochemical behavior of the imine and isopropylideneamide anion complexes of $Ru(tpy)(bpy)^{n+}$, will be published subsequently.

Acknowledgment. We thank Dr. T. G. Appleton (University of Queensland) for recording the 100-MHz ^1H NMR spectra. This research was supported by the Australian Research Grants Committee.

(5) Anal. Calcd. for $[Ru(tpy)(bpy)(C_3H_6N)]_z(PF_6)_{3z}$: C, 34.3; H, 2.6; N, 8.6; P, 9.4; F, 34.8. Found: C, 34.0, H, 2.7; N, 8.4; P, 9.1; F, 34.8.

(6) Feltham, R. D.; Hayter, R. G. *J. Chem. Soc.* **1964**, 4587–4591. Comparisons of equivalent conductances and slopes of Feltham plots were made with this complex and $[Ru(tpy)(bpy)(NO)](PF_6)_3$.

(7) Bryant, G. M.; Fergusson, J. E.; Powell, H. S. K. *Aust. J. Chem.* **1971**, *24*, 257–273. Bryant, G. M.; Fergusson, J. E. *Aust. J. Chem.* **1971**, *24*, 275–286.

(8) Moyer, B. A.; Meyer, T. J. *J. Am. Chem. Soc.* **1978**, *100*, 3601–3603.

(9) Chatt, J.; Dosser, R. J.; King, F.; Leigh, G. J. *J. Chem. Soc.*, Dalton *Trans.* **1976**, 2435–2440.

(10) Buhr, J. D.; Winkler, J. R.; Taube, H. *Inorg. Chem.* **1980**, *19*, 2416–2425.

J. Am. Chem. Soc. 1983, *105*, 7075–7081

Investigations of the Nature of Dehydrogenation of the α-Carbon Atom in the Oxidation of Amines Coordinated to Ruthenium

F. Richard Keene,*[1] Michael J. Ridd,[1] and Michael R. Snow[2]

Contribution from the Department of Chemistry and Biochemistry, James Cook University of North Queensland, Townsville, Australia 4811, and the Department of Physical and Inorganic Chemistry, University of Adelaide, Adelaide, South Australia 5001. *Received February 9, 1983*

Abstract: The oxidations of the amine complexes $Ru(bpy)_2(A–B)^{2+}$ (where A–B = ampy [2-(aminomethyl)pyridine], d_2-ampy [2-(1,1-dideuterioaminomethyl)pyridine], and Meampy [2-(1-aminoethyl)pyridine] and bpy = 2,2′-bipyridine) in aqueous solution to the corresponding imine species have been studied by using flash photolysis techniques. The rate-determining step of the reaction involves removal of a hydrogen from the α-carbon atom and the concomitant intramolecular transfer of two electrons from ligand to metal. Deuterium exchange and deuterium isotope effect studies, and stereochemical arguments, are consistent with a mechanism involving either (i) a hydride transfer from C to Ru or (ii) a base (solvent water)-assisted proton abstraction. Chirality studies indicate no loss of configurational integrity about the metal center during oxidation, which favors the second proposal. The X-ray crystal structure of the more rapidly oxidized diastereoisomer of $[Ru(bpy)_2(Meampy)]S_2O_6·5H_2O$ reveals it to be the $\Lambda S(\Delta R)$ form, in which the methyl substituent on the α-carbon atom is equatorial and the hydrogen substituent axial.

We recently reported[3] a detailed mechanistic study of the two-electron oxidation of 2-(aminomethyl)pyridine (ampy) coordinated to ruthenium(II) and we proposed a mechanistic scheme shown in eq 2–5.[3] The particular efficacy of Ru in the promotion

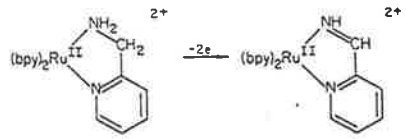

(1)

of the dehydrogenation process appears to be related in part to its ability to readily attain an oxidation state two units greater than the final state, allowing a low-energy pathway for the even-electron process required in the ligand oxidation, together with a propitious combination of redox potentials for the Ru(III)/Ru(II) and Ru(IV)/Ru(III) couples.

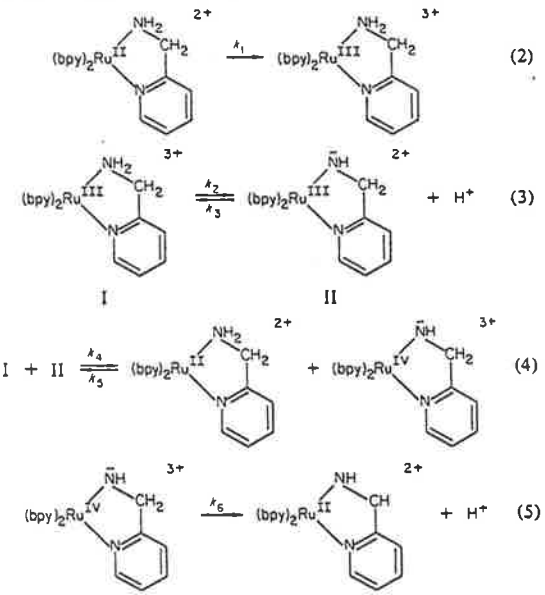

(2)

(3)

I + II

(4)

(5)

In this scheme, the reaction 5 is written as a single step, but it involves the transfer of two electrons from the ligand to the metal as well as deprotonation at the methylene carbon atom. An elucidation of the nature and sequence of these events is fundamental to the complete understanding of the dehydrogenation process. We have extended the previous studies to examine the oxidation of the analogous ruthenium(II) complexes of ligands related to ampy where (i) the methylene group is deuterated (d_2-ampy),[4] to provide mechanistic information on the deprotonation step, and (ii) the methylene group has a methyl substituent (Meampy),[4] to clarify stereochemical aspects of the reaction.

We have also extended the range of pH over which the oxidation of $[Ru(bpy)_2(ampy)]^{2+}$ was studied to verify aspects of the pH–rate profile predicted by the postulated mechanism.

Experimental Section

Measurements. Electronic spectra were recorded on a Cary 219 spectrophotometer and emission spectra on a Perkin-Elmer 3000 fluorescence spectrometer. NMR spectra were recorded on either a JEOL FX90Q (^1H) or JEOL FX60Q (^{13}C) spectrometer. Optical rotations were measured on a Perkin-Elmer 141 Polarimeter; all reported rotations were measured at λ 589 nm.

All electrochemical measurements were made vs. the saturated sodium chloride calomel electrode (SSCE) and are uncorrected for junction potentials. The cyclic voltammetric waveform was generated by use of a Utah Electronics 0152 potentiostat coupled to a Utah Electronics 0151 sweep generator. Cyclic voltammograms were recorded on a Rikadenki RW-101 X–Y recorder. Coulometry was performed on a potentiostat built in the department. Temperature control for the cyclic voltammetry was achieved with a Lauda K4RD circulating water bath.

Elemental analyses were carried out by the Australian Microanalytical Service, AMDEL, Melbourne.

Materials. Ruthenium trichloride trihydrate (Matthey-Garrett), tetra-*n*-butylammonium bromide (Fluka, puriss), 2-(aminomethyl)-pyridine (Aldrich), 2-acetylpyridine (Aldrich), ammonium hexafluorophosphate (Fluorochem), and 2,2′-bipyridine (Sigma) were used without purification. Solutions of potassium antimonyl-(+)-tartrate (BDH) were converted to the sodium form by ion exchange. $Ag_2(Sb_2(+)tart_2)$ was prepared by mixing aqueous solutions containing the appropriate molar ratios of $K_2(Sb_2(+)tart_2)$ and $AgNO_3$, filtering the precipitate, and washing the precipitate with water, ethanol, and ether. The complexes *cis*-$[Ru(bpy)_2Cl_2]·2H_2O$,[5] $[Ru(bpy)_2(ampy)](PF_6)_2$,[3] and $[Ru(bpy)_2$-

(1) James Cook University of North Queensland.
(2) University of Adelaide.
(3) Ridd, M. J.; Keene, F. R. *J. Am. Chem. Soc.* **1981**, *103*, 5733–5740 and references therein.

(4) Abbreviations for ligands: bpy = 2,2′-bipyridine; ampy = 2-(aminomethyl)pyridine; impy = 2-(iminomethyl)pyridine; d_2-ampy = 2-(1,1-dideuterioaminomethyl)pyridine; d_1-impy = 2-(1-deuterioiminomethyl)pyridine; d_4-ampy = 2-(*N*,*N*,1,1-tetradeuterioaminomethyl)pyridine; Meampy = 2-(1-aminoethyl)pyridine; hmpy = 2-(hydroxymethyl)pyridine.

0002-7863/83/1505-7075$01.50/0

(impy)](PF$_6$)$_2$[3] were prepared as described previously.

Syntheses. 2-(1-Aminoethyl)pyridine (Meampy). The oxime of 2-acetylpyridine was prepared by the standard literature procedure[6] (yield 92%; mp 118 °C). The oxime was reduced to the amine in an analogous manner to that used for 3-(1-aminoethyl)pyridine[7] (yield 81%; bp 107 °C (3 mmHg)).

(2-(1-Aminoethyl)pyridine)bis(2,2'-bipyridine)ruthenium(II) Hexafluorophosphate, [Ru(bpy)$_2$(Meampy)](PF$_6$)$_2$. This complex was prepared by an analogous method to that used for [Ru(bpy)$_2$(ampy)](PF$_6$)$_2$.[3] A solution of *cis*-[Ru(bpy)$_2$Cl$_2$]·2H$_2$O (5.0 g) and racemic Meampy (8.0 g) in deaerated 1:1 aqueous methanol (250 mL) was refluxed for 1 h. The methanol was evaporated off and NH_4PF_6 added to the filtered solution. The resultant precipitate was washed with ice-cold water, 2-propanol, and ether and dried in vacuo (yield 7.15 g, 90%).

The two diastereoisomeric pairs of [Ru(bpy)$_2$(Meampy)]$^{2+}$ were partially separated (ca. 80% enrichment) on a large scale by repeated recrystallization from aqueous solution as the iodide salt. The separation was monitored after subsequent conversion to the PF_6^- salt by ^{1}H NMR spectroscopy. The less soluble $\Lambda S(\Delta R)$ diastereoisomer shows a doublet due to the methyl resonance centered at δ 1.51 and the more soluble $\Lambda R(\Delta S)$ at δ 1.68; Me_2SO-d_6 solvent, Me_4Si internal reference.

Final purification of the enriched samples was achieved by ion-exchange chromatography using SP-Sephadex C-25 cation exchanger (60-× 8-cm column) with 0.15 M sodium (+)-antimonyl tartrate as eluent. In a typical purification 650 mg of an 80% enriched diastereoisomer was sorbed on to the column in the dark at 4 °C. The band was cycled through the column until separation of the two diastereoisomers occurred, with $\Lambda R(\Delta S)$ eluting faster than $\Lambda S(\Delta R)$. Each band was collected and precipitated as the hexafluorophosphate salt by the addition of NH_4PF_6, and diastereoisomeric purity was verified by ^{1}H NMR spectroscopy. The visible spectra in water gave $\Lambda S(\Delta R)$: ϵ_{474}^{max} 9500, ϵ_{340}^{max} 11 000; $\Lambda R(\Delta S)$: ϵ_{472}^{max} 10 200, ϵ_{343}^{max} 10 900.

Anal. Calcd for $RuC_{27}H_{26}N_6P_2F_{12}$: C, 39.3; H, 3.18; N, 10.2. Observed: $\Lambda S(\Delta R)$ C, 39.3; H, 3.13; N, 10.2. $\Lambda R(\Delta S)$ C, 39.6; H, 3.04; N, 10.3.

(2-(Aminomethyl)pyridine)bis(2,2'-bipyridine)ruthenium(II) Bromide, [Ru(bpy)$_2$(ampy)]Br$_2$. [Ru(bpy)$_2$(ampy)](PF$_6$)$_2$[3] (300 mg) was dissolved in dry 2-butanone (110 mL). Tetra-*n*-butylammonium bromide was added with stirring to produce a flocculant precipitate that yielded a filterable powder upon cooling overnight at 0 °C which was washed with 2-butanone and ether and dried in vacuo (yield 220 mg, 90%).

Bis(2,2'-bipyridine)(2-(*N*,*N*,1,1-tetradeuterioaminomethyl)pyridine)-ruthenium(II) Perchlorate, [Ru(bpy)$_2$(d$_4$-ampy)](ClO$_4$)$_2$.[4] [Ru(bpy)$_2$-(ampy)]Br$_2$ (200 mg, 3 × 10^{-4} mol) was dissolved in deaerated D_2O (9 mL). NaOD/D_2O (600 μL, 30%) was added and the solution sealed in a glass ampule under N_2. The reaction mixture was heated in the dark at 65 °C for 36 h and then acidified upon opening with 35% DCl (~1.0 mL). The product was precipitated by addition of $NaClO_4$, washed with cold D_2O, and dried in vacuo (yield 200 mg, 92%).

Bis(2,2'-bipyridine)(2-(1,1-dideuterioaminomethyl)pyridine)ruthenium(II) Hexafluorophosphate, [Ru(bpy)$_2$(d$_2$-ampy)](PF$_6$)$_2$. A solution of the cation [Ru(bpy)$_2$(d$_4$-ampy)]$^{2+}$ was prepared by stirring an aqueous suspension of the perchlorate salt (200 mg) in water (10 mL) with Dowex 1 × 8 anion exchange resin (Cl^- form). The solution was filtered, 1 M NaOH (1 mL) was added, and the solution was allowed to react in the dark for 20 min. The mixture was then acidified with HCl, and the complex was precipitated by addition of NH_4PF_6 and washed with ice cold water, 2-propanol, and ether (yield 210 mg, 94%). The visible spectrum in water gave ϵ_{471}^{max} 10 300, ϵ_{341}^{max} 10 900. Anal. Calcd for $RuC_{26}H_{22}D_2N_6P_2F_{12}$: C, 38.3; N, 10.4; H/D, 2.97. Observed: C, 38.5; N, 10.2; H, 3.06.

Bis(2,2'-bipyridine)(2-(1-deuterioiminomethyl)pyridine)ruthenium(II) hexafluorophosphate, [Ru(bpy)$_2$(d$_1$-impy)](PF$_6$)$_2$, was prepared in an analogous manner to the nondeuterated imine complex[3] except that 1 M D_2SO_4/D_2O was used as the solvent and [Ru(bpy)$_2$(d$_2$-ampy)](PF$_6$)$_2$ as the starting material. The visible spectrum in water gave ϵ_{465}^{max} 12 500.

Oxidation by Ce(IV) of [Ru(bpy)$_2$(d$_2$-ampy)]$^{2+}$. A solution of $(NH_4)_4Ce(SO_4)_4\cdot H_2O$ in 0.5 M H_2SO_4 (10 mL of 1.92 × 10^{-2} M; 1.92 × 10^{-4} mol) was added to a solution of [Ru(bpy)$_2$(d$_2$-ampy)] (PF$_6$)$_2$ in 0.5 M H_2SO_4 (95 mL of 1.012 × 10^{-3} M; 9.62 × 10^{-5} mol) slowly with stirring. NH_4PF_6 was added, the solution cooled and filtered, and the solid washed with ice-cold water and dried in vacuo.

Flash Photolysis Studies. The laser photolysis and flash photolysis facilities at the University of Adelaide were used for these studies; a description of this equipment and of the data acquisition system is given elsewhere.[8] The experimental conditions for the kinetic study of the oxidative dehydrogenation of [Ru(bpy)$_2$(d$_2$-ampy)]$^{2+}$ and the two diastereoisomers of [Ru(bpy)$_2$(Meampy)]$^{2+}$ in perchloric acid media were as described previously for the study of [Ru(bpy)$_2$(ampy)]$^{2+}$,[3] using Fe(III) as quencher. Details of the kinetic analysis of the flash photolysis data have been given previously.[3]

For the study of the rate of oxidation of Ru(bpy)$_2$(ampy)$^{2+}$ at pH 3 and pH 4 it was necessary to use Cu(II) as a quencher rather than Fe(III). The complex concentration was maintained at 1 × 10^{-5} M, but the quencher concentration increased to 0.1 M due to the slower quenching rate of the MLCT excited state by Cu(II).[9] [$HClO_4$] was varied from 10^{-2} to 10^{-4} M. No attempt at buffering was made at pH 4 to avoid possible catalytic effects on the reaction by the buffer components. A small (<0.05 pH units) decrease in the pH resulted due to the deprotonation of the complex during the reaction, but this was not significant due to the semiquantitative nature of the analysis of these particular data. The ionic strength was maintained at 1.0 by addition of $NaClO_4$. Each solution was used for one flash, and the reaction was monitored at 436 nm.

Laser photolysis indicated that the quenching rates, k_q, by Fe(III) for the diastereoisomers of [Ru(bpy)$_2$(Meampy)]$^{2+}$ are 2.8 × 10^9 M^{-1} s^{-1} for $\Lambda S(\Delta R)$ and 8.5 × 10^8 M^{-1} s^{-1} for $\Lambda R(\Delta S)$. Therefore for all the complexes studied the quenching was over within the lifetime of the flash. For the cases studied similar conversions of Ru(II) to Ru(III) as for Ru(bpy)$_2$(ampy)$^{2+}$ [3] were observed (30–40%).

Structure Determination of Diastereoisomer $\Lambda S(\Delta R)$-[Ru(bpy)$_2$-(Meampy)]S$_2$O$_6$·5H$_2$O. Collection and Reduction of X-ray Data. An aqueous solution of the complex cation as the Br^- salt (prepared in an analogous way to [Ru(bpy)$_2$(ampy)]Br$_2$) was converted to the SO_4^{2-} form by addition of a stoichiometric amount of Ag_2SO_4. After the solution was stirred and filtered, the resultant solution was passed down a column of QAE-Sephadex A-25 anion exchanger ($S_2O_6^{2-}$ form). Evaporation of water in a vacuum desiccator over silica gel yielded red crystals of [Ru(bpy)$_2$(Meampy)]S$_2$O$_6$·5H$_2$O.

A crystal plate of dimensions 0.044 × 0.13 × 0.46 mm^3 was mounted on a glass fiber and coated with cyanoacrylate super glue. Lattice parameters at 21 °C were determined by a least-squares fit to the setting angles of 25 independent reflections, measured and refined by scans performed on an Enraf-Nonius CAD-4 four-circle diffractometer employing graphite monochromated Mo Kα radiation (λ 0.7107 Å). Crystal data for $C_{27}H_{36}N_6O_{11}S_2Ru$ (formula weight 785.72): orthorhombic, space group $P2_12_12_1$ with a = 12.194 (5), b = 13.576 (7), and 19.916 (8) Å so that V = 3297.01 Å^3; Z = 4; ρ_{calcd} = 1.583, ρ_{obsd} = 1.59 g cm^{-3}; μ (Mo Kα) = 6.02 cm^{-1}; $F(000)$ = 1580 electrons.

Intensity data were collected in the range $1.5 < \theta < 24°$ using an $\omega - n\theta/3$ scan, where n (= 4) was optimized by profile analysis of a typical reflection. The ω scan angles and horizontal counter apertures employed were (1.20 + 0.35 tan θ)° and (2.40 + 0.5 tan θ) mm, respectively. Three standard reflections, monitored after every 58 min of data collection, indicated that no decomposition had occurred. Data reduction and application of Lorentz and polarization corrections were performed by using the program SUSCAD.[10] Absorption corrections were applied with the program ABSORB.[10] The maximum and minimum transmission factor were estimated to be 0.97 and 0.93, respectively. Of the 2589 reflections collected, 618 with $I < 2.5\sigma(I)$ were considered unobserved and not used in the calculations.

Solution and Refinement. The structure was solved and refined by application of the heavy-atom technique. Successive difference syntheses located all non-hydrogen atoms of the structure including five water molecules. In the full-matrix least-squares refinement, the bipyridyl ligands were refined as pairs of rigid pyridine rings and with isotropic temperature factors. Their hydrogen atoms were included as rigid groups in calculated positions (C–H, 1.00 Å). The other non-hydrogen atoms, except the oxygens of the water molecules, were refined anisotropically, and their associated hydrogens (except for those of the waters, which could not be found) were included at calculated positions assuming tetrahedral geometries around C and N (N–H, 0.95 Å). Different group temperature factors were used for the bipyridyl and other hydrogens. A weighting scheme was applied and refined, converging at $w = 2.27/(\sigma^2(F_o) + 0.0008(F_o^2))$. Refinement converged with R_1 = 0.0300 and

(5) Sullivan, B. P.; Salmon, D. J.; Meyer, T. J. *Inorg. Chem.* 1978, *17*, 3334–3341.

(6) Vogel, A. I. "Practical Organic Chemistry"; 3rd ed.; Longmans: London, 1962.

(7) La Forge, F. B. *J. Am. Chem. Soc.* 1928, *50*, 2477–2483.

(8) Thornton, A. J.; Laurence, G. S. *Radiat. Phys. Chem.* 1978, *11*, 311–319.

(9) Hoselton, M. A.; Lin, C.-T.; Schwarz, H. A.; Sutin, N. *J. Am. Chem. Soc.* 1978, *100*, 2383–2388.

(10) Programs used included SUSCAD and ABSORB "data reduction programs for the CAD-4 diffractometer", University of Sydney, 1976; SHELX, "Program for crystal structure determination", G. M. Sheldrick, 1976; and PLUTO-plotting by W. D. S. Motherwell.

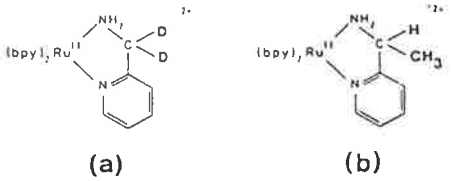

Figure 1. C-deuterated and C-monomethylated analogues of [Ru(bpy)$_2$ampy]$^{2+}$: (a) Ru(bpy)$_2$(d$_2$-ampy)$^{2+}$ and (b) Ru(bpy)$_2$(Meampy)$^{2+}$.

R_2 = 0.0306, at which stage the largest peak in the final difference map was less than 0.6 e·Å^{-3}. The absolute configuration of the crystal was confirmed by repeating the last three cycles of refinement with all coordinates inverted through the origin; the higher corresponding R values of 0.0310 and 0.0319 suggest the initial configuration was correct. All scattering factors and anomalous terms were taken from International Tables for Crystallography.[11] The final positional parameters of the non-hydrogen atoms are listed in Table I. The thermal parameters are available as supplementary material, as well as the calculated positional parameters for the hydrogen atoms, and the observed and calculated structure factors. Table II contains selected bond lengths and angles, omitting values for the rigid pyridine rings in the ligands bpy and Meampy.

Chirality Studies of Oxidation of the Diastereoisomers of [Ru(bpy)$_2$(Meampy)]$^{2+}$. Bis(2,2′-bipyridine)(2-(1-iminoethyl)pyridine)ruthenium(II) Bromide, [Ru(bpy)$_2$(Meimpy)]Br$_2$. [Ru(bpy)$_2$(Meimpy)](PF$_6$)$_2$ was prepared electrochemically in 97% yield in an analogous manner to that used for [Ru(bpy)$_2$(impy)](PF$_6$)$_2$ and was converted to the bromide salt by precipitation from an acetone solution using tetra-*n*-butylammonium bromide (ϵ_{465}^{max} 12 500 in water).

Resolution of [Ru(bpy)$_2$(Meimpy)]$^{2+}$. [Ru(bpy)$_2$(Meimpy)]Br$_2$ (3.47 g, 5.0 mmol) and Ag$_2$(Sb$_2$(+)tart$_2$) (3.80 g, 5 mmol) in water (25 mL) were stirred with glass balls for 30 min. The solution was filtered and diluted with water to 75 mL. Acetone was added to incipient crystallization (ca. 150 mL) and the solution left to stand for 1 week at 0 °C. The resulting crystals were filtered, washed with acetone/water (5:1) and acetone, and dried in vacuo (yield 1.37 g, 24% of total diastereoisomer). Two recrystallizations from water/acetone gave a product whose molecular rotation was not increased by further recrystallization (yield 0.82 g, 30% of one chiral form of the cation; $[M]_{589}^{25}$ +9700). Anal. Calcd for [Ru(bpy)$_2$(Meimpy)](Sb$_2$(+)tart$_2$)·4H$_2$O: C, 36.1; N, 7.42; H, 3.38. Observed: C, 36.1; N, 7.22; H, 3.10.

(+)-[Ru(bpy)$_2$(Meimpy)](PF$_6$)$_2$ was precipitated quantitatively by adding NH$_4$PF$_6$ to an aqueous solution of the diastereoisomer and showed $[M]_{589}^{25}$ +8500 (water).

The enantiomeric (−)-[Ru(bpy)$_2$(Meimpy)]$^{2+}$ was not isolated.

Resolution of Meampy. Meampy (4.9 g, 40 mmol) and (+)-tartaric acid (6.0 g, 40 mmol) were dissolved in water (7 mL) with slight heating. Ethanol (25 mL) was added and the solution cooled slowly to ice temperature. After standing (2 h) the crystals were filtered, washed with ethanol and ether, and air dried (yield 3.5 g, 32% of total diastereoisomer). Two recrystallizations from water/ethanol yielded the optically pure diastereoisomer ((*S*)(−)-MeampyH) ((+)Htart)·H$_2$O (2.2 g) (40% of one chiral form of the amine; $[\alpha]_{589}^{25}$ +4.7° (water); mp 162 °C (lit.[12] $[\alpha]_{589}^{25}$ +5.1°, mp 161–163 °C)). Anal. Calcd for C$_{11}$H$_{18}$N$_2$O$_7$: C, 45.5; H, 6.25; N, 9.65. Observed: C, 45.5; H, 6.20; N, 9.75.

Δ- and Λ-[Ru(bpy)$_2$((*S*)(−)-Meampy)]$^{2+}$. The ligand (*S*)(−)-Meampy was released from the tartrate diastereoisomer by basifying an aqueous solution, extracting with ether, and evaporating off the solvent. The complex cation was prepared and the internal diastereoisomers separated as detailed for the racemic ligand. For (+)-[Ru(bpy)$_2$((*S*)(−)-Meampy)]$^{2+}$, $[M]_{589}^{25}$ +6700, and for (−)-[Ru(bpy)$_2$((*S*)(−)-Meampy)]$^{2+}$, $[M]_{589}^{25}$ −6700 (water).

Chemical Oxidation of (+)- and (−)-[Ru(bpy)$_2$((*S*)(−)-Meampy)]$^{2+}$. The two diastereoisomers were separately oxidized by a two-molar ratio of Ce(IV) in 1 M H$_2$SO$_4$ solution in an analogous manner to the oxidation of [Ru(bpy)$_2$(d$_2$-impy)]$^{2+}$ described above. The resultant [Ru(bpy)$_2$(Meimpy)]$^{2+}$ products were precipitated as the PF$_6^-$ salts, which were filtered, washed with ice-cold water, 2-propanol, and ether, and dried in vacuo. Measurement of rotations (in water) showed $[M]_{589}^{25}$ 8600 for the oxidation product of (+)-[Ru(bpy)$_2$((*S*)(-)-Meampy)]$^{2+}$ and $[M]_{589}^{25}$ −8600 for the oxidation product of the levorotatory diastereoisomer.

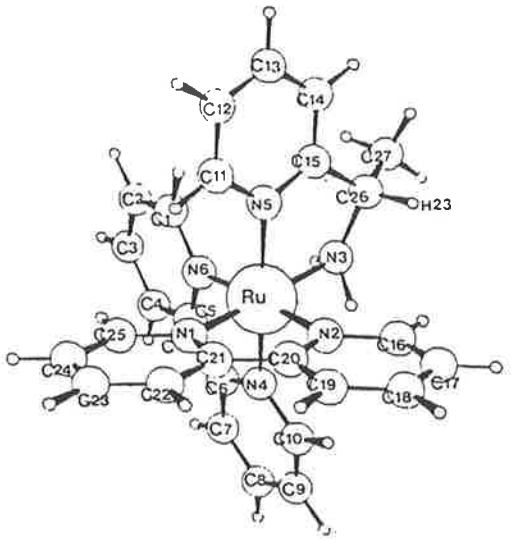

Figure 2. A PLUTO plot of ΛS(ΔR)-[Ru(bpy)$_2$(Meampy)]S$_2$O$_6$·5H$_2$O showing atom labeling.

Results and Discussion

Comments on the Synthesis and Characterization of Complexes. In the course of this study, the (bpy)$_2$Ru(II) complexes of the ampy analogues d$_2$-ampy (Figure 1a) and Meampy (Figure 1b) were developed.[4]

Dissolution of the complex [Ru(bpy)$_2$(ampy)]$^{2+}$ in D$_2$O at pD ca. 13 resulted in complete exchange of the amine protons in 20 min at 25 °C, detected by the loss of the broad NH$_2$ resonances (centered at 5.41 and 4.92 ppm relative to Me$_4$Si) in the ^{1}H NMR spectrum (PF$_6^-$ salt; Me$_2$SO-d_6 solvent), and the concomitant sharpening of the AB quartet arising from the methylene protons (4.61, 4.41, 4.19, 3.99 ppm). Exchange of the methylene protons occurs on a much slower time scale (36 h at 65 °C; pD ca. 14). The choice of appropriate conditions therefore allows selective or complete exchange of amine and methylene protons in the ampy complex.

Synthesis of the species [Ru(bpy)$_2$Meampy]$^{2+}$ (Figure 1b) realized the two diastereoisomeric forms in approximately equal amounts, which were separated by a combination of fractional crystallization and ion-exchange chromatography. ^{1}H NMR spectroscopy showed distinct methyl doublet resonances for the two diastereoisomers (ΛS(ΔR), centered at 1.51 ppm; ΛR(ΔS), 1.68 ppm; PF$_6^-$ salts, Me$_2$SO-d_6 solvent, Me$_4$Si reference). These ^{1}H NMR spectra also reveal the different chemical environments of each of the two amine protons in each of the diastereoisomers: ΛS(ΔR) shows two broad resonances centered at 5.90 ppm and 4.56 ppm and ΛR(ΔS) at 5.34 ppm and 4.82 ppm.

Description of the Structure of ΛS(ΔR)-[Ru(bpy)$_2$(Meampy)]S$_2$O$_6$·5H$_2$O. A perspective view of the structure of the cation is shown in Figure 2. The structure assigns the relative chiralities about the metal center and the methine carbon as ΛS(ΔR). The cation has normal hydrogen bonds from the amino group N(3) to a dithionate oxygen (O(1), 3.21 Å) and to a water molecule (O(10), 3.18 Å). All the dithionate oxygen atoms have a single hydrogen bond to water molecules in the range 2.76–3.07 Å. A hydrogen bond from water O(9) to both waters O(7), 2.71 Å, and O(8), 2.76 Å, completes the hydrogen bonding pattern.

The two bipyridine ligands exhibit structural features reported previously for [Ru(bpy)$_3$]$^{2+}$:[13] the chelate bite angle averages 78.7°, and the short Ru–N(bpy) bond length of 2.053 Å (average)

(11) "International Tables for Crystallography"; Kynoch Press: Birmingham, 1974; Vol. 4, pp 99 and 149.

(12) Cervinka, O.; Belovsky, O.; Rejmanova, P. *Collect. Czech. Chem. Commun.* 1973, *38*, 1358–1363.

(13) Rillema, D. P.; Jones, D. S.; Levy, H. A. *J. Chem. Soc., Chem. Commun.* 1979, 849–851.

Table I. Final Positional Parameters for Non-Hydrogen Atoms in $\Lambda S(\Delta R)$-$[Ru(bpy)_2(Meampy)]S_2O_6 \cdot 5H_2O$

atom	x	y	z
Ru(1)	0.37069 (6)	−0.04675 (5)	0.67946 (3)
S(1)	0.0831 (2)	0.4588 (2)	0.5485 (1)
S(2)	0.0122 (2)	−0.0231 (2)	0.8618 (1)
N(3)	0.3594 (6)	0.0297 (5)	0.5868 (3)
O(1)	−0.0561 (6)	0.0439 (6)	0.9924 (3)
O(2)	−0.0466 (6)	−0.1336 (5)	0.9814 (4)
O(3)	−0.1957 (5)	−0.0454 (6)	0.9291 (3)
O(4)	−0.0208 (6)	0.0699 (5)	0.8351 (4)
O(5)	0.1253 (6)	−0.0258 (5)	0.8856 (4)
O(6)	−0.0193 (6)	−0.1042 (6)	0.8204 (4)
O(7)	0.3627 (9)	0.4659 (6)	0.4713 (4)
O(8)	0.4462 (8)	0.2956 (7)	0.2771 (4)
O(9)	0.4711 (11)	0.3131 (7)	0.4145 (5)
O(10)	0.2182 (10)	0.1126 (10)	0.9693 (5)
O(11)	0.2511 (10)	0.3648 (10)	0.9305 (6)
N(1)	0.3861 (4)	−0.1060 (3)	0.7734 (2)
C(21)	0.4829 (4)	−0.0823 (3)	0.8071 (2)
C(22)	0.4996 (4)	−0.1153 (3)	0.8727 (2)
C(23)	0.4195 (4)	−0.1718 (3)	0.9046 (2)
C(24)	0.3228 (4)	−0.1955 (3)	0.8709 (2)
C(25)	0.3061 (4)	−0.1626 (3)	0.8053 (2)
N(2)	0.5290 (3)	−0.0064 (3)	0.7036 (2)
C(16)	0.6025 (3)	0.0411 (3)	0.6608 (2)
C(17)	0.7064 (3)	0.0676 (3)	0.6840 (2)
C(18)	0.7367 (3)	0.0466 (3)	0.7500 (2)
C(19)	0.6632 (3)	−0.0008 (3)	0.7928 (2)
C(20)	0.5593 (3)	−0.0274 (3)	0.7696 (2)
N(4)	0.4082 (5)	−0.1786 (4)	0.6356 (3)
C(6)	0.3195 (5)	−0.2333 (4)	0.6119 (3)
C(7)	0.3374 (5)	−0.3215 (4)	0.5778 (3)
C(8)	0.4442 (5)	−0.3551 (4)	0.5673 (3)
C(9)	0.5330 (5)	−0.3004 (4)	0.5910 (3)
C(10)	0.5150 (5)	−0.2121 (4)	0.6251 (3)
N(5)	0.3153 (4)	0.0885 (3)	0.7122 (2)
C(11)	0.2804 (4)	0.1066 (3)	0.7777 (2)
C(12)	0.2325 (4)	0.1968 (3)	0.7940 (2)
C(13)	0.2195 (4)	0.2689 (3)	0.7448 (2)
C(14)	0.2544 (4)	0.2508 (3)	0.6792 (2)
C(15)	0.3023 (4)	0.1606 (3)	0.6629 (2)
N(6)	0.2171 (4)	−0.1009 (4)	0.6580 (3)
C(1)	0.1189 (4)	−0.0515 (4)	0.6706 (3)
C(2)	0.0198 (4)	−0.0914 (4)	0.6485 (3)
C(3)	0.0190 (4)	−0.1808 (4)	0.6139 (3)
C(4)	0.1172 (4)	−0.2302 (4)	0.6014 (3)
C(5)	0.2162 (4)	−0.1902 (4)	0.6234 (3)
C(26)	0.3477 (8)	0.1365 (6)	0.5956 (4)
C(27)	0.2873 (11)	0.1822 (9)	0.5380 (6)

reflects the π back-bonding between the delocalized π^*(bpy) and t_{2g}(Ru) orbitals. For the Meampy ligand, the Ru–N(amine) bond length is longer (2.121 Å) than Ru–N(py) (2.062 Å), which demonstrates this effect. The bite angle for the Meampy chelate (N(5)–Ru–N(3)) of 79.5° is comparable with that of ampy in the complex $[Fe(ampy)_3]^{2+}$ (75.4° for high spin, 81.6° for low spin).[14,15] The bond angles within the chelate ring about the amine nitrogen N(3) (112.7°) and the methine carbon C(26) (111.4°) correspond to the equivalent angles for ampy in the complex $[Zn(ampy)_3]^{2+}$[15] (average 111.8° and 110.9°, respectively). The pyridine ring in the Meampy is planar, but the chelate ring itself is puckered. Consequently, the non-ring substituents on the methine carbon (C(26)) are distinctly either axial or equatorial, in agreement with the clearly separated methyl resonances observed in the ^{1}H NMR spectra of the two diastereoisomers. For the $\Lambda S(\Delta R)$ diastereoisomer, the methyl substituent (C(27)) is equatorial.

Kinetic Studies. Our previous study[3] of the mechanism of the oxidative dehydrogenation of coordinated 2-(aminomethyl)pyridine in $[Ru(bpy)_2(ampy)]^{2+}$ (eq 1) indicated the intermediacy of a

(14) Mikami, M.; Konno, M.; Saito, Y. *Chem. Phys. Lett.* **1979**, *63*, 566–569.

(15) Mikami-Kido, M.; Saito, Y. *Acta Crystallogr., Sect B* **1982**, *B38*, 452–455.

Table II. Selected Bond Lengths (Å) and Bond Angles (deg) for $\Lambda S(\Delta R)$-$[Ru(bpy)_2(Meampy)]S_2O_6 \cdot 5H_2O$

Distances			
N(3)–Ru(1)	2.121 (6)	N(1)–Ru(1)	2.046 (4)
N(2)–Ru(1)	2.064 (3)	N(4)–Ru(1)	2.044 (5)
N(5)–Ru(1)	2.062 (4)	N(6)–Ru(1)	2.057 (5)
O(4)–S(2)	1.427 (7)	O(5)–S(2)	1.459 (8)
O(6)–S(2)	1.429 (8)	C(26)–N(3)	1.468 (10)
C(20)–C(21)	1.409 (6)	C(5)–C(6)	1.407 (8)
C(26)–C(15)	1.486 (10)	C(27)–C(26)	1.497 (14)
Angles			
N(1)–Ru(1)–N(3)	173.7 (2)	N(2)–Ru(1)–N(3)	97.7 (2)
N(2)–Ru(1)–N(1)	78.8 (2)	N(4)–Ru(1)–N(3)	94.1 (2)
N(4)–Ru(1)–N(1)	91.5 (2)	N(4)–Ru(1)–N(2)	97.0 (2)
N(5)–Ru(1)–N(3)	79.5 (2)	N(5)–Ru(1)–N(1)	95.2 (2)
N(5)–Ru(1)–N(2)	89.8 (2)	N(5)–Ru(1)–N(4)	171.2 (2)
N(6)–Ru(1)–N(3)	86.3 (3)	N(6)–Ru(1)–N(1)	97.7 (2)
N(6)–Ru(1)–N(2)	174.4 (2)	N(6)–Ru(1)–N(4)	78.6 (2)
N(6)–Ru(1)–N(5)	94.9 (2)	O(5)–S(2)–O(4)	114.2 (4)
O(6)–S(2)–O(4)	113.1 (5)	O(6)–S(2)–O(5)	115.0 (5)
C(26)–N(3)–Ru(1)	112.7 (5)	C(21)–N(1)–Ru(1)	115.3 (1)
C(25)–N(1)–Ru(1)	124.6 (1)	C(20)–C(21)–N(1)	115.2 (2)
C(20)–C(21)–C(22)	124.8 (2)	C(16)–N(2)–Ru(1)	125.6 (1)
C(20)–N(2)–Ru(1)	114.4 (1)	N(2)–C(20)–C(21)	115.7 (2)
C(19)–C(20)–C(21)	124.1 (2)	C(6)–N(4)–Ru(1)	115.9 (2)
C(10)–N(4)–Ru(1)	124.0 (2)	C(5)–C(6)–N(4)	114.7 (3)
C(5)–C(6)–C(7)	125.2 (3)	C(11)–N(5)–Ru(1)	123.5 (1)
C(15)–N(5)–Ru(1)	116.1 (1)	C(26)–C(15)–N(5)	115.9 (4)
C(26)–C(15)–C(14)	124.0 (4)	C(1)–N(6)–Ru(1)	124.9 (2)
C(5)–N(6)–Ru(1)	114.8 (2)	N(6)–C(5)–C(6)	115.8 (3)
C(4)–C(5)–C(6)	124.2 (3)	C(15)–C(26)–N(3)	111.2 (6)
C(27)–C(26)–N(3)	111.4 (8)	C(27)–C(26)–C(15)	114.6 (8)

Ru(IV) species containing the deprotonated amine (eq 5). With the use of flash photolysis techniques developed in that work, we have now examined the oxidation of the complexes $[(Ru(bpy)_2(d_2\text{-ampy})]^{2+}$ (Figure 1a) and the diastereoisomers of $[Ru(bpy)_2(Meampy)]^{2+}$ (Figure 1b) over the pH range 0–2 to allow a detailed study of the nature of the final step in the reaction scheme (k_6; eq 5). We have also extended the pH range for the study of the oxidation of $[Ru(bpy)_2(ampy)]^{2+}$ from pH 2–4 in a semiquantitative way to test the predicted pH dependence of the mechanistic scheme[3] shown in eq 2–5.

Table III gives the observed rate constants for the oxidation of $Ru(bpy)_2(ampy)^{2+}$, $Ru(bpy)_2(d_2\text{-ampy})^{2+}$, and two diastereoisomers of $Ru(bpy)_2(Meampy)^{2+}$ studied over the pH range 0–2 in perchloric acid media and calculated by use of a computer analysis described elsewhere.[3]

Deuterium Isotope Effect and Deuterium Exchange Studies. Since the final reaction in the scheme (k_6; eq 5) is ultimately rate determining in the pH range studied, the relative importance of the electron transfer(s) and deprotonation steps involved in that reaction might be revealed by deuterium isotope effect studies.

From Table III, for the oxidations of $[Ru(bpy)_2(ampy)]^{2+}$ and $[Ru(bpy)_2(d_2\text{-ampy})]^{2+}$, the values of k_2–k_5 are within experimental error for the two systems. However, the values of k_6 (eq 5) are 93 ± 3 and 52 ± 3 s^{-1} for the nondeuterated and deuterated cases, respectively, giving $k_H/k_D = 1.78$ (±0.15). The existence of a primary isotope effect[16] for the reaction shows that the deprotonation at the methylene carbon is rate determining, and its low magnitude implies that the transition state is either linear but asymmetric[19] or nonlinear.[20]

(16) The double deuteration of the methylene carbon in $[Ru(bpy)_2(d_2\text{-ampy})]^{2+}$ could lead to a secondary isotope effect, but by comparison with studies of deuterium exchange in $PhCH_3$[17] and $PhCH_2NO_2$,[18] this would not be expected to be >1.15.

(17) Streitwieser, A.; Van Sickle, D. E. *J. Am. Chem. Soc.* **1962**, *84*, 254–258.

(18) Bordwell, F. G.; Boyle, W. J. *J. Am. Chem. Soc.* **1971**, *93*, 512–514.

(19) Westheimer, F. H. *Chem. Rev.* **1961**, *61*, 265–273.

(20) More O'Ferrall, R. A. *J. Chem. Soc. B* **1970**, 785–790.

Table III. Rate Constants for the Scheme given in Eq 3-5 Using Rate Data from Flash Photolysis in Perchlorate Media ($\lambda = 436$ nm; $\mu = 1.0$, $NaClO_4$; $T = 24 \pm 1$ °C; all solutions deaerated)[a]

complex $[Ru(bpy)_2(X-Y)]^{2+}$ X-Y =	$10^{-6}k_2$, s^{-1}	$10^{-9}k_3$, $M^{-1}\ s^{-1}$	$10^{-9}k_5$, $M^{-1}\ s^{-1}$	$10^{-6}k_5$, $M^{-1}\ s^{-1}$	k_6, s^{-1}
ampy[b,c]	5.1 ± 0.2	1.3 ± 0.2	1.1 ± 0.2	5.3 ± 0.2	93 ± 3
d_2-ampy[c]	5.2 ± 0.2	1.1 ± 0.1	1.1 ± 0.1	4.8 ± 0.3	52 ± 3
Meampy[c] diastereoisomer $\Lambda S(\Delta R)$	5.7 ± 0.1	1.4 ± 0.05	1.2 ± 0.1	2.4 ± 0.2	103 ± 2
Meampy[c] diastereoisomer $\Lambda R(\Delta S)$	13 ± 1	1.0 ± 0.1	1.3 ± 0.1	31 ± 2	76 ± 2

[a] All values are averages obtained over pH range 0–2 for 10 different runs; errors quoted are experimental deviations. [b] Values from ref 3. [c] There were two solutions to the numerical analysis, one of which has been eliminated as less reasonable in a chemical sense.

A *nonlinear transition state* would correspond to intramolecular hydride transfer from the methylene carbon atom to the ruthenium metal center, shown below.

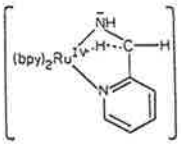

Upon the intramolecular transfer of two electrons, $Ru^{IV}-H^-$ becomes $Ru^{II}-H^+$, so that elimination of the proton would form the Ru^{II}–imine product. A mechanism of this type has been postulated previously in studies of the oxidation of monodentate amines coordinated to ruthenium, although no kinetic evidence was presented.[21] It has been suggested[22] that in $Ru^{II}-H^+$ species, the H^+ would lie on one of the faces of the coordination octahedron, and studies with molecular models reveal that such a location for the hydride bridge is appropriate in the proposed transient.

A *linear asymmetric transition state* for the final step (k_6; eq 5) would arise from base-assisted removal of a proton from the methylene carbon atom.

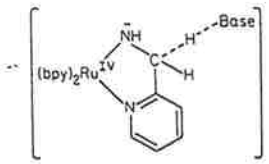

The proton abstraction and the intramolecular transfer of two electrons to the metal center result in the Ru^{II}–imine product.

The chemical oxidation of $[Ru(bpy)_2(d_2\text{-ampy})]^{2+}$ by Ce(IV) was studied in 0.5 M H_2SO_4. Figure 3 shows the proton-decoupled ^{13}C NMR spectra of the complexes $Ru(bpy)_2(impy)^{2+}$, $Ru(bpy)_2(d_1\text{-impy})^{2+}$, and the product of the Ce(IV) oxidation of $Ru(bpy)_2(d_2\text{-ampy})^{2+}$ in aqueous (H_2O) solution. A singlet in the fully protonated spectrum of the imine complex (arrowed; Figure 3A) would be expected to become a triplet in the complex deuterated at the methine carbon, due to $^2H-^{13}C$ coupling in the latter, but is of such low intensity it cannot be observed (Figure 3B). The product of the Ce(IV) oxidation of the deuterated complex shows the same spectrum (Figure 3C) as the authentic deuterated sample (Figure 3B), so that clearly no hydrogen exchange with the solvent occurs during the oxidation at the methylene carbon. Consequently, if the mechanism involves base-assisted proton removal, each act of deprotonation leads to ligand oxidation. Therefore, *either* deprotonation and intramolecular electron-transfer are concerted *or* they are consecutive with the electron transfer being very rapid (i.e., faster than the reprotonation of the carbanion). A concerted process (with OH^- as the base) has been postulated for the dehydrogenation of ethylenediamine coordinated to Os.[23]

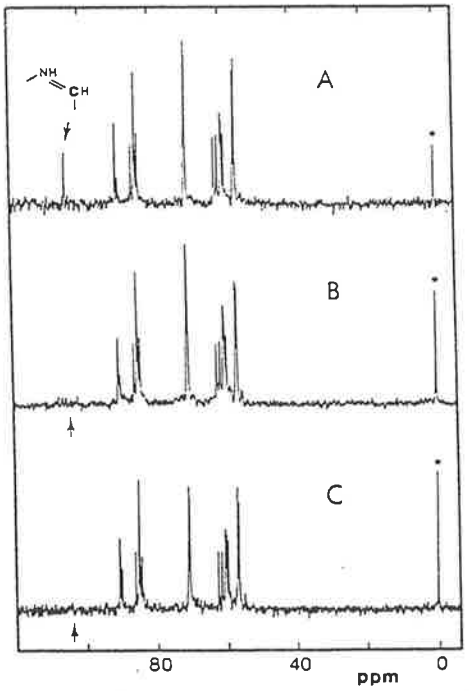

Figure 3. 60-MHz ^{13}C NMR spectra of (A) $[Ru(bpy)_2(impy)]^{2+}$; (B) $[Ru(bpy)_2(d_1\text{-impy})]^{2+}$; and (C) the product of the Ce(IV)-promoted oxidation of $[Ru(bpy)_2(d_2\text{-ampy})]^{2+}$ in 0.5 M H_2SO_4. Spectra run in D_2O with *p*-dioxane as internal reference (*). The position of resonance of the imine carbon of $[Ru(bpy)_2(impy)]^{2+}$ is indicated by an arrow in each of the spectra.

For a base-assisted proton-abstraction process, the variation of k_H/k_D with ΔpK_a (where ΔpK_a is the difference between the pK_a values of the acid and the base) is expected to exhibit a maximum at $\Delta pK_a = 0$, and k_H/k_D will become <2 when $\Delta pK_a > 12$.[24] In the present instance where H_2O is the base, pK_a for H_3O^+/H_2O is −1.74,[25] so that k_H/k_D could be <2 if the pK_a of the acid (i.e. the acidity of the methylene protons in the ampy chelate ring of the Ru(IV) transient) is >10. The methylene protons do undergo deuterium exchange in the Ru(II) species $[Ru(bpy)_2ampy]^{2+}$ under vigorous conditions (pH ~14; 65 °C for 36 h), and the pK_a would be expected to be considerably lower in a Ru(IV) complex because of the higher charge, so that a pK_a value of 10 is not unreasonable.

(21) Diamond, S. E.; Tom, G. M.; Taube, H. *J. Am. Chem. Soc.* **1975**, *97*, 2661–2664.
(22) Ford, P. C.; Kuempel, J. R.; Taube, H. *Inorg. Chem.* **1968**, *7*, 1976–1983.
(23) Lay, P. A.; Sargeson, A. M.; Skelton, B. W.; White, A. H. *J. Am. Chem. Soc.* **1982**, *104*, 6161–6164.
(24) Jones, J. R. "The Ionisation of Carbon Acids"; Academic Press: London, 1973.
(25) Jencks, W. P. "Catalysis in Chemistry and Enzymology"; McGraw-Hill: New York, 1969.

Both the deuterium exchange and deuterium isotope effect studies are therefore consistent with either of the proton-abstraction schemes, as well as with the hydride transfer proposal.

Oxidation of the Diastereoisomers of $[Ru(bpy)_2(Meampy)]^{2+}$. The nature of the final step (k_6; eq 5) of the oxidation was also probed by studying the relative rates of oxidation of the two diastereoisomeric pairs of $Ru(bpy)_2(Meampy)^{2+}$. In one of the two diastereoisomeric pairs, the methine proton removed during the oxidation is axial (and in the other it is equatorial), so that any observed deviations in the value of k_6 would reflect the difference between the two geometries. In contrast to the study of the deuterated and nondeuterated ampy complex, the rate constants for the two diastereoisomers may show deviations in both the proton transfer (k_2, k_3)[26] and electron-transfer steps (k_4, k_5),[27] as well as the final rate-determining step of the reaction (k_6), where the rate constant for the oxidation of diastereoisomer $\Lambda S(\Delta R)$ is considerably greater than that for $\Lambda R(\Delta S)$ ($103 \pm 3\ s^{-1}$ cf. $76 \pm 2\ s^{-1}$). Such an observation shows that there is a significant difference in the reactivity of the axial and equatorial methine protons.

Cyclic voltammetric studies of the two diastereoisomers of $[Ru(bpy)_2(Meampy)]^{2+}$ in acetonitrile/0.1 M tetraethylammonium perchlorate and in 5.4 M H_2SO_4 (at −16 °C) media are in accord with the kinetic observations given above. In both instances, the oxidation of diastereoisomer $\Lambda S(\Delta R)$ is observed to be considerably faster than that of $\Lambda R(\Delta S)$.

Both general mechanistic proposals are consistent with the observation that the $\Lambda S(\Delta R)$ diastereoisomer is the more readily oxidized. In this form, the axial orientation of the methine hydrogen H(23) means that it has relatively unhindered access to the nearest face of the coordination octahedron, allowing ready formation of a hydride-bridged transient. Similarly, since the methyl substituent is equatorial in this diastereoisomer, it is closer (than an axial methyl) to its ultimate position in the plane of the Meimpy chelate ring.

The ligand Meampy is chiral, and the (−)-enantiomer has previously been assigned the *S* configuration.[12] Synthesis of the complex $[Ru(bpy)_2((S)(-)\text{-Meampy})]^{2+}$ using the resolved ligand realized the two internal diastereoisomers $\Lambda(+)\text{-}[Ru(bpy)_2((S)(-)\text{-Meampy})]^{2+}$ and $\Delta(-)\text{-}[Ru(bpy)_2((S)(-)\text{-Meampy})]^{2+}$. The oxidized ligand Meimpy is achiral, so that the $[Ru(bpy)_2(Meimpy)]^{2+}$ product of the oxidation reaction may only exhibit chirality about the metal center.

The chemical oxidations by Ce(IV) in 1 M H_2SO_4 of $\Lambda(+)\text{-}[Ru(bpy)_2((S)(-)\text{-Meampy})]^{2+}$ and $\Delta(-)\text{-}[Ru(bpy)_2((S)(-)\text{-Meampy})]^{2+}$ produce $(+)\text{-}[Ru(bpy)_2(Meimpy)]^{2+}$ and $(-)\text{-}[Ru(bpy)_2(Meimpy)]^{2+}$ with equal and opposite rotatory power, identical with that obtained for independently resolved $(+)\text{-}[Ru(bpy)_2(Meimpy)]^{2+}$ (which can now be assigned the absolute configuration Λ). Thus there is no loss of configurational integrity about the metal center during the oxidation process.

The hydride transfer mechanism involves a seven-coordinate hydride transient, and configurational rearrangement about the metal might be expected to occur during oxidation. For the base-assisted proton abstraction proposal, the configuration about the metal center would be expected to be retained. On the basis of the present chirality experiments, the latter proposal would be preferred, although it is possible that because of the small size of the hydride ion and the brevity of its association with the metal that no rearrangement would result from a hydride transfer process.

Oxidation Studies at Higher pH. An essential feature of the proposed reaction mechanism is that the rate of the reaction should reach a maximum when the pH equals the pK_a of the $Ru^{III}(bpy)_2(ampy)^{3+}$ complex (eq 3; $pK_a = 2.4$[3]), since the rate of formation of the Ru(IV) intermediate (eq 4) would then be optimal. In order to compare the rate of oxidation at various pH conditions, a reaction "half-life" was computed which was defined as the time required for the imine concentration to equal one-fourth of the initial concentration of $Ru^{III}(bpy)_2(ampy)^{3+}$ generated by the flash. The pH–"half-life" profile was indeed bell shaped, but the maximum occurred at a pH between 3 and 4 (rather than between pH 2 and 3). Thus the predicted relationship between pH and rate is observed, but only in a qualitative sense. The deviation from the bell-shaped pH–rate profile with a maximum at $pH = pK_a$ for eq 3 would seem to show that an alternative mechanism is available when $pH > pK_a$. This alternative path may be the formation of Ru(IV) via the disproportionation reaction

$$2Ru^{III}\text{—}N^{-}H\text{—}CH_2\text{–} \rightarrow Ru^{IV}\text{=}N\text{—}CH_2\text{–} + Ru^{II}\text{—}NH_2\text{—}CH_2\text{–}$$

by analogy with the ruthenium aquo/hydroxo/oxo system studied by Thompson and Meyer.[28] Such a scheme would become more favorable as the pH increased and may only become significant at pH >3. Practical difficulties preclude detailed kinetic studies of the present system at pH >3; however, current studies on the oxidation of the analogous alcohol complex $[Ru(bpy)_2(hmpy)]^{2+}$[4] and of $[Ru(NH_3)_4(ampy)]^{2+}$ may elucidate this issue.

Conclusions

Our earlier studies[3] of the mechanism of the oxidative dehydrogenation of $[Ru(bpy)_2ampy]^{2+}$ revealed the intermediacy of a Ru(IV) species allowing a low-energy pathway for the two-electron ligand oxidation process.

The present work indicates that the final rate-determining step of this reaction (k_6; the decay of the Ru(IV) complex of the deprotonated amine to the Ru^{II}–imine product) can occur by *either* (i) the loss of hydrogen from the aliphatic carbon and the intramolecular transfer of two electrons from ligand to metal concomitantly via a hydride transfer from C to Ru *or* (ii) base (solvent water)-assisted proton abstraction of a hydrogen from the carbon atom with a concerted or rapid subsequent transfer of two electrons from ligand to metal. The question of simultaneous two-electron movement or consecutive (though rapid) one-electron transfers remains ambiguous for both proposals.

Both of the above proposals are consistent with the detailed kinetic studies of the oxidation, with deuterium exchange and deuterium isotope effect studies, and with stereochemical considerations. However, the observation of retention of the configurational integrity about the metal during the oxidation process favors the base-assisted proton-abstraction proposal, although the hydride transfer mechanism is by no means excluded.

Unfortunately, studies of general base catalysis of the oxidation process are excluded for this system for practical reasons since the detailed kinetics could only be studied by flash photolysis techniques at pH <3. Mechanistic studies are in progress[29] of the corresponding oxidation of the osmium analogue, $[Os(bpy)_2ampy]^{2+}$. For such a system, the optimal pH range is more compatible with general base catalysis studies, and an osmium hydride species (if formed) may be more readily observed since it would have enhanced stability compared with its ruthenium counterpart.

The semiquantitative study of the pH–rate profile for the oxidation of $[Ru(bpy)ampy]^{2+}$ indicates an optimal pH for the rate, as predicted by the mechanistic scheme.

Acknowledgment. We are grateful to the Department of Physical and Inorganic Chemistry, University of Adelaide, for the use of flash photolysis facilities, and particularly to Dr. G. S. Laurence and Mr. H. Novello for their assistance. This work was supported by the Australiam Research Grants Scheme.

Registry No. $\Lambda S(\Delta R)\text{-}[Ru(bpy)_2(Meampy)]S_2O_6\cdot 5H_2O$, 87306-04-5; $[Ru(bpy)_2(Meampy)](PF_6)_2$, 87306-05-6; $[Ru(bpy)_2(d_2\text{-ampy})](PF_6)_2$, 87306-07-8; $[Ru(bpy)_2(d_1\text{-impy})](PF_6)_2$, 87306-09-0; Ce, 7440-45-1;

(26) pK_a values are 2.4 ± 0.1 ($\Lambda S(\Delta R)$) and 2.15 ± 0.05 ($\Lambda R(\Delta S)$).

(27) Equilibrium constants determined for the electron transfer are 477 ($\Lambda S(\Delta R)$) and 42 ($\Lambda R(\Delta S)$), so that the $Ru^{IV/III}$ couple for the complex of the deprotonated amine is 0.16 and 0.09 V cathodic of the $Ru^{III/II}$ couple for the complex of the nondeprotonated amine for the respective diastereoisomers.

(28) Thompson, M. S.; Meyer, T. J. *J. Am. Chem. Soc.* **1982**, *104*, 4106–4115.

(29) Ridd, M. J.; Keene, F. R., unpublished work.

(30) Keene, F. R.; Lay, P. A.; Ridd, M. J., work in progress.

$[Ru(bpy)_2(Meimpy)]Br_2$, 87306-10-3; (+)-$[Ru(bpy)_2(Meimpy)](Sb_2$-(+)$tart_2$), 87334-87-0; (+)-$[Ru(bpy)_2(Meimpy)](PF_6)_2$, 87334-88-1; Λ-(+)-$[Ru(bpy)_2((S)(-)$-Meampy$)]^{2+}$, 87334-89-2; Δ-(−)-$[Ru(bpy)_2$-$((S)(-)$-Meampy$)]^{2+}$, 87334-90-5; $Ru(bpy)_2(ampy)^{2+}$, 56889-71-5; deuterium, 7782-39-0.

Supplementary Material Available: Tables of thermal parameters for the non-hydrogen atoms (Supplementary Table 1), calculated positional parameters for the hydrogen atoms (Supplementary Table 2), and observed and calculated structure factors (Supplementary Table 3) for the structure determination (16 pages). Ordering information is given on any current masthead page.

Contribution from the Department of Chemistry and Biochemistry, James Cook University of North Queensland, Townsville, Queensland 4811, Australia, and Department of Physical and Inorganic Chemistry, University of Adelaide, Adelaide, South Australia 5001, Australia

Oxidation of Isopropylamine and Related Amines Coordinated to Ruthenium. Formation of Monodentate Imine and Alkylideneamido Complexes of Ruthenium

PETER A. ADCOCK,[1] F. RICHARD KEENE,*[1] ROBERT S. SMYTHE,[1] and MICHAEL R. SNOW[2]

Received June 9, 1983

The chemical and electrochemical oxidation of $[Ru(tpy)(bpy)(NH_2CHR^1R^2)]^{2+}$ ($NH_2CHR^1R^2$ = isopropylamine, cyclohexylamine, or (α-methylbenzyl)amine; tpy = 2,2′:6′,2″-terpyridine; bpy = 2,2′-bipyridine) reveals two consecutive two-electron processes. The first oxidation is irreversible and yields the corresponding imine species. The second oxidation produces a complex identified as containing the N-bound alkylideneamide anion. The second process is reversible chemically or electrochemically. The X-ray crystal structure of $[Ru(tpy)(bpy)(NCMe_2)](ClO_4)_3 \cdot H_2O$ (the four-electron oxidation product of the complex containing isopropylamine) shows a linear Ru–N–C linkage with a Ru–N bond length of 1.831 (10) Å, indicating multiple bonding. The complex of formula $C_{28}H_{27}N_6Cl_3O_{13}Ru$ is orthorhombic, space group $Pna2_1$ (No. 33), with cell dimensions a = 22.034 (13) Å, b = 10.689 (6) Å, c = 14.251 (9) Å, and Z = 4.

Introduction

There has been considerable recent interest in the oxidative dehydrogenation of coordinated amines to the corresponding imines or nitriles.[3-7] Many of these studies have involved ruthenium as the metal center, and while the formation of complexes containing the α,α'-diimine moiety has been relatively common,[3,5] complexes containing coordinated simple monodentate imines had not been isolated although their intermediacy had been either observed or inferred in a few cases.[3,4]

We recently communicated[8] aspects of the oxidation of isopropylamine in the complex $[Ru(tpy)(bpy)(NH_2CHMe_2)]^{2+}$,[9] in which two major processes were observed. Initially, a two-electron oxidation yielded the corre-

(1) James Cook University of North Queensland.
(2) University of Adelaide.
(3) Brown, G. M.; Weaver, T. R.; Keene, F. R.; Meyer, T. J. *Inorg. Chem.* **1976**, *15*, 190–196 and references therein.
(4) Diamond, S. E.; Tom, G. M.; Taube, H. *J. Am. Chem. Soc.* **1975**, *97*, 2661–2664.
(5) Keene, F. R.; Salmon, D. J.; Meyer, T. J. *J. Am. Chem. Soc.* **1976**, *98*, 1884–1889.
(6) Ridd, M. J.; Keene, F. R. *J. Am. Chem. Soc.* **1981**, *103*, 5733–5740.
(7) Keene, F. R.; Ridd, M. J.; Snow, M. R. *J. Am. Chem. Soc.* **1983**, *105*, 7075–7081.
(8) Adcock, P. A.; Keene, F. R. *J. Am. Chem. Soc.* **1981**, *103*, 6494–6495.
(9) Abbreviations for ligands: bpy = 2,2′-bipyridine; tpy = 2,2′:6′,2″-terpyridine; bpic = 4,4′-dimethyl-2,2′-bipyridine.

0020-1669/84/1323-2336$01.50/0

sponding imine complex (eq 1). This product in turn un-

$$Ru(tpy)(bpy)(NH_2CHMe_2)^{2+} \xrightarrow{-2e^-} Ru(tpy)(bpy)(NH{=}CMe_2)^{2+} + 2H^+ \quad (1)$$

derwent a further reversible two-electron oxidation to yield a product characterized as $[Ru(tpy)(bpy)(NCMe_2)]^{3+}$ (eq 2).

$$Ru(tpy)(bpy)(NH{=}CMe_2)^{2+} \underset{2e^-}{\overset{-2e^-}{\rightleftharpoons}} Ru(tpy)(bpy)(NCMe_2)^{3+} + H^+ \quad (2)$$

The nature of these two oxidation products is significant, since the two-electron oxidation product represents the first isolated monodentate imine complex of ruthenium, and the suspected structure of the four-electron oxidation product is novel in ruthenium chemistry as it was formulated to contain an N-bound isopropylideneamide anion.

We now report details of the synthesis and characterization of these species, together with aspects of their chemical and electrochemical behavior.

Experimental Section

Physical Measurements. Electronic spectra were recorded with a Cary 219 spectrophotometer, and ^1H NMR spectra were obtained in CD_3CN or 0.1 M DCl solutions on a JEOL FX-100 NMR spectrometer. The DCl solutions were prepared by stirring a suspension of the PF_6^- salt of the cation in 0.1 M DCl with Dowex 1-X8 anion-exchange resin (200–400 mesh; Cl^- form) and filtering into the NMR tube. The reference signal was obtained with the aid of a capillary containing Me_4Si in CCl_4.

Magnetic susceptibilities were measured by the Faraday method. Conductance measurements in CH_3CN were performed with a Wayne Kerr Universal B221 conductance bridge. All meausrements were corrected for solvent background, and data were analyzed by the Feltham method.[10] Comparisons of equivalent conductances and slopes of Feltham plots were made with the 3:1 complex $[Ru(tpy)(bpy)(NO)](PF_6)_3$.

All electrochemical measurements were made vs. the saturated sodium chloride calomel electrode (SSCE) and are uncorrected for junction potentials. Potential control was obtained by using a Utah Electronics 0152 potentiostat, in conjunction with a Utah Electronics 0151 sweep generator for cyclic voltammetry. Cyclic voltammograms were recorded with a Rikadenki RW-101 X-Y recorder. Coulometry was performed with a potentiostat built in the department.

Elemental analyses (C, H, N, P, F) were carried out by the Australian Microanalytical Service, AMDEL, Melbourne, Australia. Ruthenium analyses were performed (0.1 M HCl solutions) on a Varian AA6 atomic absorption spectrometer using an oxidizing acetylene/air flame at $\lambda = 349.9$ nm. $K_2[RuCl_5(OH)_2]$ (Matthey-Garrett) reduced to Ru(II) (Na_2SO_3/HCl) was used as a standard.

Materials. 4-Picoline (Fluka, Prakt.) was distilled at atmospheric pressure (bp 144–146 °C) immediately before use. For electrochemical studies, acetonitrile (May and Baker, LR) was fractionated and stored over BDH 4A molecular sieves. For conductance measurements, acetonitrile (Merck, Uvasol) was used without purification. Palladium (10% on charcoal; Fluka, puriss.), ruthenium trichloride (Matthey-Garrett), 2,2′-bipyridine, and 2,2′:6′,2″-terpyridine (Sigma), and ceric ammonium sulfate (Fluka, puriss.) were used without purification. Activated alumina (507C) was obtained from Fluka.

Syntheses.[9] **4,4′-Dimethyl-2,2′-bipyridine (bpic)** was prepared by a modification of the method reported by Whitten et al.[11] Palladium (10%) on activated charcoal (4 g) was added to freshly distilled 4-picoline (100 mL). The mixture was refluxed under an N_2 atmosphere for 3 days. After boiling benzene was added (35 mL), refluxing was continued for 0.5 h. The catalyst was removed from the hot solution by vacuum filtration and the filtrate concentrated to ca. 40 mL. The crude product crystallized from the solution on cooling and was immediately recrystallized from ethyl acetate, yielding 6.91 g of almost pure product (mp 171–173 °C). This product was again recrystallized from ethyl acetate (mp 174 °C).

Trichloro(terpyridine)ruthenium(III), [Ru(tpy)Cl$_3$]. Terpyridine (1.17 g, 5 mmol) was stirred with absolute ethanol (500 mL) with gentle heating until dissolution. $RuCl_3 \cdot 3H_2O$ (1.31 g, 5 mmol) was added and the solution refluxed for 3 h with stirring. After the mixture was cooled, the brown precipitate was filtered, washed with ethanol and ether, and air-dried (yield 1.83 g, 83%).

(Bipyridine)chloro(terpyridine)ruthenium(II) Hexafluorophosphate, [Ru(tpy)(bpy)Cl]PF$_6$. [Ru(tpy)Cl$_3$] (1.76 g, 3.98 mmol) was added to a warm solution of 2,2′-bipyridine (0.62 g, 4.0 mmol) in 80% aqueous ethanol (500 mL). The mixture was refluxed for 3 h and then reduced in volume (rotory evaporator) to ca. 100 mL. The solution was diluted with distilled water (500 mL) and the complex sorbed on to a column of SP-Sephadex C25 cation exchanger. On elution with 0.2 M NaCl solution, the major brown band was collected, NH_4PF_6 added, and the solution extracted with dichloromethane. The organic extract was dried (Na_2SO_4), filtered, and evaporated to dryness. The residue was extracted with acetone (ca. 250 mL) and filtered into stirring ether (ca. 700 mL). The precipitate was collected, washed with ether, and dried in vacuo (yield 2.1 g, 83%). Anal. Calcd for $RuC_{25}H_{19}N_5ClPF_6$: C, 44.7; H, 2.85; N, 10.4. Found: C, 44.6; H, 2.99; N, 10.6.

Chloro(dimethylbipyridine)(terpyridine)ruthenium(II) hexafluorophosphate, [Ru(tpy)(bpic)Cl]PF$_6$, was prepared in a manner analogous to that for the corresponding bipyridine complex, in 35% yield.

(Bipyridine)chloro(terpyridine)ruthenium(II) chloride, [Ru(tpy)(bpy)Cl]Cl, was prepared almost quantitatively from the PF_6^- salt by addition of excess tetra-*n*-butylammonium chloride to a solution of the complex in 2-butanone. After the mixture was cooled in ice, the precipitate was collected, washed with 2-butanone and ether, and dried in vacuo.

Chloro(dimethylbipyridine)(terpyridine)ruthenium(II) chloride, [Ru(tpy)(bpic)Cl]Cl, was obtained from the PF_6^- salt in a manner similar to that for its bpy analogue.

(Bipyridine)nitro(terpyridine)ruthenium(II) Hexafluorophosphate Hydrate, [Ru(tpy)(bpy)NO$_2$]PF$_6$·H$_2$O. [Ru(tpy)(bpy)Cl]Cl (0.72 g) was dissolved in degassed distilled water (140 mL) by stirring and bubbling with nitrogen for 30 min. Excess sodium nitrite (AR, 0.72 g) was added and the solution heated on a steam bath for 2 h under nitrogen. After the solution was cooled to room temperature, ammonium hexafluorophosphate (0.50 g) was slowly added, and the mixture was then cooled in ice before collection of the orange-red precipitate, which was washed with ice-cold water, 4:1 ether/ethanol, and ether and dried in vacuo (yield 0.80 g, 89%).

The crude product (0.80 g) was recrystallized by dissolving in dichloromethane (800 mL) and filtering; the solution was stirred vigorously as petroleum ether (800 mL, X4) was slowly added. Upon settling, the precipitate was collected, washed with petroleum ether, and dried in vacuo (yield 0.69 g, 87% recovery). Anal. Calcd for $RuC_{25}H_{21}N_6O_3PF_6$: C, 42.9; H, 3.03; N, 12.0. Found: C, 42.3; H, 3.05; N, 12.1.

(Dimethylbipyridine)nitro(terpyridine)ruthenium(II) hexafluorophosphate, [Ru(tpy)(bpic)NO$_2$]PF$_6$, was prepared in 70% yield in a manner analogous to that for the corresponding bpy complex, but with three times the volume of water in the reaction mixture.

(Bipyridine)nitrosyl(terpyridine)ruthenium(II) Hexafluorophosphate, [Ru(tpy)(bpy)NO](PF$_6$)$_3$. [Ru(tpy)(bpy)NO$_2$]PF$_6$·H$_2$O (0.64 g, 0.91 mmol) was suspended in methanol (75 mL), hexafluorophosphoric acid (70%; 4 mL) added, and the mixture stirred magnetically for 1 h. The solid was then collected, washed with methanol, and dried in vacuo. The product was reprecipitated by dissolving in acetone (ca. 35 mL) and filtering into stirring ether. The precipitate was collected, washed with ether, and air-dried (yield 0.82 g, 94%).

The complex (0.200 g) was recrystallized by dissolving in dry acetone (8 mL) and filtering. To the stirring filtrate was added dry ether (2 mL). After the mixture was cooled with stirring in a closed vessel, the precipitate was collected, washed with ether, and dried in vacuo (yield 0.135 g, 67%). The IR spectrum (KBr disk) showed $\nu_{NO} = 1968$ cm^{-1}. Anal. Calcd for $RuC_{25}H_{19}N_6OP_3F_{18}$: C, 31.4; H, 2.00; N, 8.8. Found: C, 31.6; H, 2.28; N, 8.5.

(Dimethylbipyridine)nitrosyl(terpyridine)ruthenium(II) hexafluorophosphate, [Ru(tpy)(bpic)NO](PF$_6$)$_3$, was prepared in a manner analogous to that for the bpy complex, with use of half the volume of methanol (yield 92%). The crude complex was recrystallized twice by dissolving in the minimum volume of dry acetone (6 mL/100 mg of complex), filtering, adding dry ether (40–50% volume), collecting the precipitate, and washing with dry ether.

(10) Feltham, R. D.; Hayter, R. G. *J. Chem. Soc.* **1964**, 4587–4591.
(11) Sprintschnik, G.; Sprintschnik, H. W.; Kirsch, P. O.; Whitten, D. G. *J. Am. Chem. Soc.* **1977**, *99*, 4947–4954.

Aqua(bipyridine)(terpyridine)ruthenium(II) hexafluorophosphate, $[Ru(tpy)(bpy)OH_2](PF_6)_2$, was prepared by suspending $[Ru(tpy)(bpy)NO](PF_6)_3$ (1.464 g, 1.53 mmol) in distilled water (50 mL) and adding a solution of sodium azide (0.0996 g, 1.53 mmol) in distilled water (30 mL) dropwise over 0.5 h and then a further 20 mL of distilled water. The mixture was stirred for a further 3 h. The solid was filtered off, washed with ice-cold water, and dried in vacuo (yield 1.07 g, 88%).

The complex (1.07 g) was recrystallized by dissolving in hot methanol (100 mL) and filtering. To the stirring filtrate was slowly added diethyl ether (ca. 300 mL). Stirring was continued for 30 min in an ice bath. The precipitate was then collected, washed with diethyl ether, and dried in vacuo (yield 1.00 g, 93% recovery).

Aqua(dimethylbipyridine)(terpyridine)ruthenium(II) hexafluorophosphate, $[Ru(tpy)(bpic)OH_2](PF_6)_2$, was prepared in a manner analogous to that for the bpy complex in 93% yield.

(Amine)(bipyridine)(terpyridine)ruthenium(II) Hexafluorophosphate, $[Ru(tpy)(bpy)_2(NH_2R)](PF_6)_2$, Where RNH_2 = Benzylamine (NH_2Bz), (α-Methylbenzyl)amine (NH_2-α-MeBz), Isopropylamine (NH_2CHMe_2), and Cyclohexylamine (NH_2-c-Hx). $[Ru(tpy)(bpy)(OH_2)](PF_6)$ (200 mg), methanol (3 mL), and the appropriate amine (3 mL) were sealed under N_2 in glass ampule and heated at 140 °C for 48 h. When the cooled ampule was opened, methanol was removed by heating and the amine by extraction with ether. The resultant residue was solubilized in water by stirring with Dowex 1-X8 anion-exchange resin (200–400 mesh; Cl^- form) and the cation sorbed on a column of SP-Sephadex C25 cation exchanger. After elution with a 0.1 M sodium acetate/0.01 M sodium hydroxide solution to remove any aqua or chloro species, the amine complex was precipitated by the addition of solid NH_4PF_6 washed with ice-cold water and dried in vacuo. Yields were in the range 70–90%. Anal.[12] Calcd for $[Ru(tpy)(bpy)(NH_2Bz)](PF_6)_2$: C, 43.3; H, 3.18; N, 9.47. Found: C, 42.7; H, 3.24; N, 9.80. Calcd for $[Ru(tpy)(bpy)(NH_2$-α-$MeBz)](PF_6)_2$: C, 44.0; H, 3.35; N, 9.32. Found: C, 42.2; H, 3.21; N, 9.78. Calcd for $[Ru(tpy)(bpy)(NH_2CHMe_2)](PF_6)_2$: C, 40.1; H, 3.36; N, 10.0. Found: C, 40.3; H, 3.51; N, 10.0. Calcd for $[Ru(tpy)(bpy)(NH_2$-c-$Hx)](PF_6)_2$: C, 42.3; H, 3.67; N, 9.55. Found: C, 41.8; H, 3.55; N, 9.74.

(Benzonitrile)(bipyridine)(terpyridine)ruthenium(II) Hexafluorophosphate, $[Ru(tpy)(bpy)(N{\equiv}CPh)](PF_6)_2$. $[Ru(tpy)(bpy)OH_2](PF_6)_2$ (0.10 g) was dissolved in dry methanol (10 mL), and benzonitrile (2.5 mL) was added. After the mixture was refluxed for 4 h, it was poured into excess stirring ether and cooled in an ice bath. The crude product was then collected by filtration, washed with ether, and dried in vacuo (yield 0.09 g, 81%).

The complex was recrystallized by dissolving in hot absolute ethanol (100 mL) and filtering. The filtrate was cooled slowly to 0 °C, and crystals were allowed to grow for 3 days. The product was then collected, washed with 1:1 ether/absolute ethanol and then with ether, and dried in vacuo (yield 0.04 g, 44% recovery). Anal. Calcd for $RuC_{32}H_{24}N_6P_2F_{12}$: C, 43.5; H, 2.74; N, 9.51. Found: C, 43.5; H, 2.94; N, 9.21.

(Dimethylbipyridine)(isopropylamine)(terpyridine)ruthenium(II) hexafluorophosphate, $[Ru(tpy)(bpic)(NH_2CHMe_2)](PF_6)_2$, was prepared and isolated (90%) in a manner similar to that for its bpy analogue.

(Bipyridine)(isopropylideneamine)(terpyridine)ruthenium(II) Hexafluorophosphate, $[Ru(tpy)(bpy)(NH{=}CMe_2)](PF_6)_2$. Two methods were used in the synthesis of this species.

(i) $[Ru(tpy)(bpy)(NH_2CHMe_2)](PF_6)_2$ (200 mg) was solubilized in water (5 mL) with use of Dowex 1-X8 anion-exchange resin (200–400 mesh; Cl^- form) and H_2O_2 (100 volume; 12 mL) added. The mixture was heated to 60 °C for 30 min with stirring, and the product was precipitated from the filtered solution by NH_4PF_6, washed with ice-cold water (slightly acidified with HCl), and dried in vacuo (yield 190 mg, 93%). Anal. Calcd for $RuC_{28}H_{26}N_6P_2F_{12}$: C, 40.2, H, 3.13, N, 10.0; Ru, 12.1. Found: C, 40.8; H, 3.15; N, 10.3; Ru, 12.0.

(ii) $[Ru(tpy)(bpy)NH_2CHMe_2](PF_6)_2$ (0.038 g) in 0.1 M HCl (60 mL) was electrolyzed exhaustively at +0.90 V and then exhaustively at +0.51 V. Solid NH_4PF_6 was added to the stirring product solution. The precipitate was collected, washed with acidified ice-cold distilled water, and dried in vacuo (yield 0.028 g, 73%).

The product was redissolved in water and sorbed onto a column of SP-Sephadex C25 cation exchanger. The complex was eluted with 0.5 M NaCl with collection of the first (red) band. Solid NH_4PF_6 was added to the stirring eluate, and the resulting precipitate was collected, washed with ice-cold water, and dried in vacuo (79% recovery).

(Bipyridine)(isopropylideneamido)(terpyridine)ruthenium Hexafluorophosphate, $[Ru(tpy)(bpy)(NCMe_2)](PF_6)_3$. $[Ru(tpy)(bpy)(NH_2CHMe_2)](PF_6)_2$ (0.10 g) was solubilized in 0.1 M HCl (20 mL) with use of Dowex 1-X8 anion-exchange resin (Cl^-). The solution was filtered and electrolyzed exhaustively at +1.00 V (n = 3.8 electrons/Ru). The product was precipitated by the addition of solid NH_4PF_6 to the stirring solution. After settling, the precipitate was collected, washed with acidified (HCl) ice-cold distilled water, and dried in vacuo (yield 0.097 g, 83%). Anal. Calcd for $RuC_{28}H_{25}N_6P_3F_{18}$: C, 34.3; H, 2.57; N, 8.56; P, 9.47; F, 34.8. Found: C, 34.0; H, 2.71; N, 8.36; P, 9.10; F, 34.8.

(Dimethylbipyridine)(isopropylideneamine)(terpyridine)ruthenium(II) hexafluorophosphate, $[Ru(tpy)(bpic)(NH{=}CMe_2)](PF_6)_2$, was prepared in a manner identical with that detailed for the bpy complex (method ii).

(Dimethylbipyridine)(isopropylideneamido)(terpyridine)ruthenium Hexafluorophosphate, $[Ru(tpy)(bpic)(N{=}CMe_2)](PF_6)_3$. $[Ru(tpy)(bpic)(NH_2CHMe_2)](PF_6)_2$ (0.081 g) was stirred in 0.1 M HCl with Dowex 1-X8 anion-exchange resin (Cl^- form) until dissolution. After removal of the resin by filtration, the solution was electrolyzed at +0.81 V and the product sorbed on to a column of SP-Sephadex C25 cation exchanger and eluted with an aqueous 0.5 M NaCl/0.1 M HCl solution. The first ca. 95% of the only band visible was collected. Solid NH_4PF_6 was added, and after the mixture was stirred for 5 min the precipitate was collected, washed with acidified ice-cold distilled water, and dried in vacuo (yield 0.071 g).

Structure Determination of the Four-Electron Oxidation Product $[Ru(tpy)(bpy)(NCMe_2)](ClO_4)_3{\cdot}H_2O$. Collection and Reduction of X-ray Data. A concentrated solution of $[Ru(tpy)(bpy)(NCMe_2)]^{3+}$ was prepared by stirring the PF_6^- salt with Dowex 1-X8 anion-exchange resin (Cl^- form) in 0.1 M HCl. The solution was filtered, excess $NaClO_4$ added, and the mixture kept under vacuum and protected from light for several days. Initially a small amount of an unidentified green product separated (which was removed by filtration), and after ca. 2 weeks orange crystals of the desired salt were obtained from the solution.

A crystal plate of dimensions 0.035 × 0.15 × 0.40 mm^3 was mounted on a glass fiber and coated with cyanoacrylate super glue. Lattice parameters at 27 °C were determined by a least-squares fit to the setting angles of 25 independent reflections, measured, and refined by scans performed on an Enraf-Nonius CAD4 four-circle diffractometer employing graphite-monochromated radiation (λ = 0.7107 Å). Crystal data for $C_{28}H_{27}N_6Cl_3O_{13}Ru$ (formula weight 863.02): orthorhombic, space group $Pna2_1$, C_{2v}^9 (No. 33), with a = 22.034 (13) Å, b = 10.689 (6) Å, and c = 14.251 (9) Å so that V = 3356.42 Å^3; Z = 4; ρ_{calcd} = 1.688 g cm^{-3}; μ(Mo Kα) = 7.65 cm^{-1}; $F(000)$ = 1744 electrons.

Intensity data were collected in the range $1.2 < \theta < 22°$ for the $+h,+k,+l$ octant with use of an ω-$n\theta/3$ scan, where n (=2) was optimized by profile analyses of a typical reflection. The ω scan angles and horizontal counter apertures employed were $(1.20 + 0.35 \tan\theta)°$ and $(2.40 + 0.5 \tan\theta)$ mm, respectively. Three standard reflections, monitored after every 58 min of data collection, indicated that by completion of the data collection no decomposition had occurred. Data reduction and application of Lorentz and polarization corrections were performed with use of the program SUSCAD.[13] Absorption corrections were applied; the range of transmission factors was from 0.99 to 0.89. Of the 2602 reflections collected, 597 with $I < 2.5\sigma(I)$ were considered unobserved and not used in the calculations.

Solution and Refinement. The structure was solved and refined by application of the heavy-atom technique. Successive difference syntheses located all non-hydrogen atoms of the structure, including one water molecule. In the refinement by full-matrix least squares

(12) For some complexes in this study, microanalytical figures were persistently low for C and high for N. In such cases, characterization and purity assessment were made on the basis of electrochemical behavior, NMR spectra, and ion-exchange chromatography.

(13) Programs used included SUSCAD and ABSORB ("Data Reduction Programs for the CAD-4 Diffractometer", University of Sydney, 1975), SHELX ("Program for Crystal Structure Determination", G. M. Sheldrick, 1976), and ORTEP (plotting program by G. K. Johnson).

Table I. Final Positional Parameters for Non-Hydrogen Atoms in $[Ru(tpy)(bpy)(N{=}C(CH_3)_2)](ClO_4)_3 \cdot H_2O$ (Fractional Coordinates $\times 10^4$ except for Ru ($\times 10^5$))

atom	x	y	z
C(1)	2016 (3)	878 (6)	1678 (4)
C(2)	2116 (3)	151 (6)	2476 (4)
C(3)	1748 (3)	−884 (6)	2656 (4)
C(4)	1281 (3)	−1191 (6)	2038 (4)
C(5)	1181 (3)	−464 (6)	1240 (4)
C(6)	2499 (3)	3561 (7)	273 (5)
C(7)	3022 (3)	3957 (7)	739 (5)
C(8)	3218 (3)	3329 (7)	1541 (5)
C(9)	2892 (3)	2304 (7)	1878 (5)
C(10)	2369 (3)	1908 (7)	1412 (5)
C(11)	749 (4)	4242 (9)	262 (5)
C(12)	476 (4)	5253 (9)	716 (5)
C(13)	390 (4)	5224 (9)	1685 (5)
C(14)	578 (4)	4184 (9)	2201 (5)
C(15)	851 (4)	3174 (9)	1748 (5)
C(16)	1527 (3)	3036 (7)	−1824 (5)
C(17)	1404 (3)	3928 (7)	−2513 (5)
C(18)	1037 (3)	4954 (7)	−2304 (5)
C(19)	794 (3)	5089 (7)	−1406 (5)
C(20)	917 (3)	4197 (7)	−717 (5)
C(21)	1934 (3)	1951 (7)	−1867 (4)
C(22)	2308 (3)	1649 (7)	−2624 (4)
C(23)	2712 (3)	649 (7)	−2555 (4)
C(24)	2743 (3)	−48 (7)	−1729 (4)
C(25)	2369 (3)	254 (7)	−972 (4)
C(26)	318 (6)	398 (13)	−849 (8)
C(27)	−333 (6)	849 (16)	−742 (12)
C(28)	460 (8)	−819 (15)	−1374 (12)
Cl(1)	2951 (2)	2033 (4)	4824
Cl(2)	3965 (2)	972 (4)	−106 (4)
Cl(3)	4537 (2)	6351 (4)	1361 (3)
N(1)	1549 (3)	570 (6)	1060 (4)
N(2)	2173 (3)	2536 (7)	610 (5)
N(3)	936 (4)	3203 (9)	778 (5)
N(4)	1284 (3)	3171 (7)	−926 (5)
N(5)	1965 (3)	1254 (7)	−1041 (4)
N(6)	739 (4)	1010 (9)	−467 (7)
O(1)	3281 (6)	1263 (14)	5458 (9)
O(2)	2579 (5)	2885 (9)	5341 (7)
O(3)	3333 (7)	2704 (12)	4236 (12)
O(4)	2580 (9)	1275 (15)	4316 (12)
O(5)	4292 (5)	1601 (11)	10611 (7)
O(6)	3534 (8)	146 (16)	10304 (9)
O(7)	4347 (6)	289 (18)	9355 (11)
O(8)	3620 (6)	1839 (11)	−642 (10)
O(9)	4696 (7)	5053 (12)	1377 (10)
O(10)	4690 (5)	6930 (11)	2227 (8)
O(11)	3914 (5)	6464 (13)	1142 (11)
O(12)	4912 (6)	6902 (12)	657 (9)
O(13)	1245 (7)	2403 (15)	3872 (9)
Ru	13913 (4)	18674 (8)	31 (12)

the bipyridyl and terpyridyl ligands were refined as sets of rigid pyridine rings and with anisotropic temperature factors. Their hydrogen atoms were included in the rigid groups at calculated positions (C–H = 1.00 Å). The other non-hydrogen atoms were also refined anisotropically. The alternative centric symmetric space group, *Pnam*, was considered and rejected as the statistics gave mean $|E^2 - 1|$ values in the range 0.68–0.78 (centric requires 0.97 and noncentric 0.74). Also the perchlorate sites cannot be ordered in the centric space group and no evidence for disorder was found. Refinement converged with $R = 0.0357$, at which stage the largest peak in the final difference map was less than 0.3 e Å^{-3}. The absolute configuration of the crystal was tested by repeating the last three cycles of refinement with all coordinates inverted through the origin; the higher corresponding R value of 0.0374 found confirmed the initial configuration. A weighing scheme of the type $w = k/(\sigma_2(F_o) + gF_o^2)$ was refined and converged with $k = 0.82$ and $g = 0.0013$. All scattering factors and anomalous terms were taken from ref 14. The final positional parameters are listed in Table I. The thermal parameters are available as supplementary material, as well as the calculated positional parameters for the hydrogen atoms (except for the methyl hydrogens, which were not found, presumably due to free rotation), and the observed and calculated structure factors. Table II contains selected bond lengths and angles, with values omitted for the rigid pyridine rings in the ligands bpy and tpy (C–C, N–C = 1.395 Å).

(14) "International Tables for Crystallography"; Kynoch Press: Birmingham, England, 1974; Vol. 4, pp 99, 149.

Table II. Selected Bond Lengths (Å) and Bond Angles (deg) for $[Ru(tpy)(bpy)(N{=}C(CH_3)_2)](ClO_4)_3 \cdot H_2O$

Distances			
N(1)–Ru	2.076 (7)	O(3)–Cl(1)	1.388 (16)
N(2)–Ru	2.055 (6)	O(4)–Cl(1)	1.361 (18)
N(3)–Ru	2.064 (9)	O(5)–Cl(2)	1.421 (12)
N(4)–Ru	1.937 (7)	O(6)–Cl(2)	1.423 (17)
N(5)–Ru	2.060 (7)	O(7)–Cl(2)	1.353 (17)
N(6)–Ru	1.831 (10)	O(8)–Cl(2)	1.421 (14)
N(6)–C(26)	1.259 (17)	O(9)–Cl(3)	1.432 (14)
C(26)–C(27)	1.520 (20)	O(10)–Cl(3)	1.422 (13)
C(26)–C(28)	1.534 (21)	O(11)–Cl(3)	1.413 (13)
O(1)–Cl(1)	1.421 (14)	O(12)–Cl(3)	1.426 (14)
O(2)–Cl(1)	1.429 (11)		

Angles			
N(2)–Ru–N(1)	77.7 (3)	N(3)–Ru–N(1)	98.9 (3)
N(3)–Ru–N(2)	86.6 (3)	N(4)–Ru–N(1)	175.4 (3)
N(4)–Ru–N(2)	98.0 (3)	N(4)–Ru–N(3)	79.0 (3)
N(5)–Ru–N(1)	102.0 (3)	N(5)–Ru–N(2)	84.3 (3)
N(5)–Ru–N(3)	154.8 (3)	N(5)–Ru–N(4)	79.1 (3)
N(6)–Ru–N(1)	93.6 (4)	N(6)–Ru–N(2)	170.2 (4)
N(6)–Ru–N(3)	99.3 (4)	N(6)–Ru–N(4)	90.8 (4)
N(6)–Ru–N(5)	93.3 (4)	Ru–N(6)–C(26)	175.2 (10)
C(27)–C(26)–N(6)	120.7 (13)	C(28)–C(26)–C(27)	120.7 (13)
C(28)–C(26)–N(6)	120.1 (13)		

Results and Discussion

The aerial oxidation of $[Ru(NH_3)_5(NH_2Bz)]^{2+}$ has previously been reported by Diamond et al.[4] to yield the benzonitrile complex quantitatively via an observed transient, considered to be the imine species. Evidence for a coordinated imine was also inferred by the same authors from the oxidation of $[Ru(NH_3)_5(NH_2\text{-}c\text{-}Hx)]^{2+}$, where $[Ru(NH_3)_6]^{3+}$ and cyclohexanone were observed as products, presumably formed by imine hydrolysis.

For the analogous complexes in which the five innocent ligands about the metal center are pyridine-type ligands, the resultant extensive back-bonding substantially shifts the potential for the Ru(III)/Ru(II) couples anodically[3] so that the complexes are no longer oxidized aerobically. A spectrophotometric titration of the oxidation of $[Ru(tpy)(bpy)(NH_2Bz)]^{2+}$ by Ce(IV) in 2 M H_2SO_4 indicates a quantitative four-electron process yielding a single product. Cyclic voltammetric studies of this oxidation in acetonitrile solution[15] revealed an irreversible oxidation ($E_{p,a}$ = ca. 1.23 V) on the anodic sweep with a reversible couple at more anodic potentials ($E_{1/2}$ = 1.34 V). Coulometry in the same solvent at 1.27 V resulted in the loss of 3.8 electrons/Ru and the formation of a species that was electrochemically and spectroscopically identical with an authentic sample of $[Ru(tpy)(bpy)(benzonitrile)]^{2+}$ ($E_{1/2}$ = 1.34 V, λ_{max} = 449 nm in CH_3CN). Similar results were obtained in acidic aqueous solution. No evidence was obtained for the intermediacy of the two-electron oxidation product, the imine.

In an attempt to isolate an imine species, the oxidation of a number of $Ru(tpy)(bpy)^{2+}$ complexes of amines of the type $NH_2CHR^1R^2$ was undertaken (viz. (α-methylbenzyl)amine, isopropylamine, and cyclohexylamine), for which the formation of the nitrile is precluded. The results for the three complexes are ostensibly identical, and these are detailed below particularly for the isopropylamine complex, $[Ru(tpy)(bpy)(NH_2CHMe_2)]^{2+}$.

(15) (a) Tetra-*n*-butylammonium hexafluorophosphate used as supporting electrolyte; platinum-bead electrode. (b) Platinum-bead electrode.

A spectrophotometric titration of the oxidation of $[Ru(tpy)(bpy)(NH_2CHMe_2)]^{2+}$ by Ce(IV) in 2 M H_2SO_4 indicates an overall four-electron oxidation consisting of two separate two-electron processes, which are consecutive. Spectra taken during exhaustive electrolyses of the amine complex (platinum-gauze electrode) in 0.1 M HCl (at 0.90 V) and acetonitrile (at 1.10 V) indicate similar results. The overall spectrophotometric and coulometric n values were slightly less than 4.0 (typically 3.7–3.8). The second two-electron process could be reversed electrochemically (coulometry at 0.50 V in 0.1 M HCl, 0.55 V in acetonitrile), with n for the reduction being exactly half the value for the overall oxidation. The two- and four-electron products were isolated by precipitation as the hexafluorophosphate salts and could be purified by ion-exchange chromatography on SP-Sephadex.

Two-Electron Oxidation Product. The ^1H NMR spectrum (in CD_3CN) of the two-electron oxidation product revealed two doublets in the aliphatic region centered at 1.12 and 1.62 ppm, with very small coupling (0.73 and 1.56 Hz, respectively). This spectrum is consistent with the imine formulation

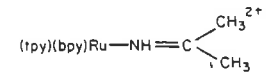

with both methyl groups being split by the adjacent NH=C moiety. On addition of a drop of D_2O, each doublet collapses to a singlet, following exchange at the imine NH group.

The visible spectrum of this species (MLCT transition) in 2 M H_2SO_4 shows $\epsilon_{474}^{max} = 8000$, compared with $\epsilon_{481}^{max} = 8800$ for the parent isopropylamine complex. For complexes of the $Ru(tpy)(bpy)^{2+}$ moiety, the position of the MLCT band in aqueous solution is virtually insensitive to the nature of the sixth ligand unless it is capable of extensive back-bonding.[16] The small blue shift in the visible spectrum on going from the amine to the imine ligand indicates there is a relatively small amount of back-bonding from Ru(II) to the coordinated monodentate imine, compared with the large effect observed for the conjugated α,α'-diimine grouping.[3] A similar conclusion is reached from electrochemical studies. The position of the Ru(II) → Ru(III) oxidation in $Ru(tpy)(bpy)X^{2+}$ complexes is also insensitive to X unless it is capable of extensive back-bonding.[17] In cyclic voltammetry, the waves of the anodic sweep corresponding to the Ru(II) → Ru(III) processes are inseparable (see below), consistent with there being little back-bonding in the case of the coordinated imine. This effect has been observed previously, where the difference between the electrode potentials for the $Ru(bpy)_2^{2+}$ complexes of 1,2-diamino-1,1-dimethylpropane and its imine is only 0.07 V in acetonitrile,[3] and the cyclic voltammetric waves of 2-(2-aminoethyl)pyridine and its imine product are indistinguishable:[18] in these cases, a monoimine or nonconjugated diimine (respectively) is seen to be only a weak π-acceptor.

Four-Electron Oxidation Product. Microanalytical data showed the product to have the general formula $[Ru(tpy)(bpy)(C_3H_6N)]_z(PF_6)_{3z}$, and conductance measurements in acetonitrile by Feltham's method[10] showed the molecular complexity $z = 1$, so that the complex is monomeric. When conductance measurements were undertaken, comparisons were made with $[Ru(tpy)(bpy)(NO)](PF_6)_3$. The values of Λ_0, the equivalent conductance at infinite dilution, were 202 ± 9 Ω^{-1} cm^2 equiv^{-1} for $[Ru(tpy)(bpy)(NO)](PF_6)_3$ and 211 ± 6 Ω^{-1} cm^2 equiv^{-1} for $[Ru(tpy)(bpy)(C_3H_6N)](PF_6)_3$. The slopes of the Feltham plots were respectively (1.02 ± 0.05) × 10^3 and (1.07 ± 0.04) × 10^3 Ω^{-1} cm^2 dm$^{3/2}$ equiv$^{-3/2}$, demonstrating clearly that the complexes are of the same ion type.

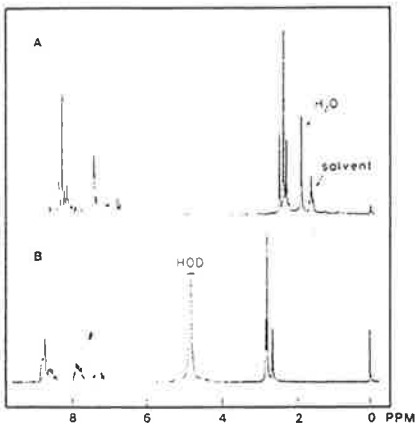

Figure 1. ^1H NMR (100 MHz) spectra of $[Ru(tpy)(bpic)(N{=}CMe_2)]^{3+}$ in CD_3CN (A) and 0.1 M DCl (B) (Me_4Si external standard).

The ^1H NMR spectra of the related complex $[Ru(tpy)(bpic)(C_3H_6N)]^{3+}$ in acetonitrile-D_3 and 0.1 M DCl are shown in Figure 1. In the aliphatic region, each spectrum contains a six-proton methyl singlet due to the oxidized isopropylamine ligand (δ = 2.31 and 2.74, respectively), flanked by two three-proton methyl singlets arising from the dimethylbipyridine ligand.

The complex showed very little absorption in the visible region of the electronic spectrum, consistent with oxidation of the metal center to Ru(III)[19] or Ru(IV).[20] There was significant absorption in the UV region, due primarily to ligand-centered $\pi \rightarrow \pi^*$ transitions, which was sufficiently distinctive to be used as a critical criterion of purity in the synthesis and purification of the complex.

In dry acetonitrile solution, cyclic voltammetric studies showed a reversible couple with $E_{1/2}$ = 0.72 V (Figure 3C).

The magnetic moment measured at 25 °C was μ_{eff} = 1.2 ± 0.1 μ_B. Since complexes of Ru(II) are invariably diamagnetic, and complexes of Ru(III) and Ru(IV) have generally exhibited magnetic behavior at room temperature consistent with one and two unpaired electrons, respectively,[21] this observation and the cathodic shift in redox potential for these species relative to the potential for the two-electron oxidation product (the isopropylideneamine complex) reflect the unusual nature of the Ru–ligand interaction.

These data were previously interpreted[8] to indicate that the $NCMe_2$ skeleton remained intact during the four-electron oxidation of coordinated isopropylamine and that the most likely structure could be considered (at least in a formal sense) as a Ru(IV) complex containing an N-bound isopropylideneamide anion:

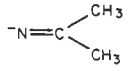

Consequently, a linear Ru–N–C linkage and Ru–N multiple bonding were predicted.

An X-ray crystal structure analysis has now confirmed that assignment and is discussed below with aspects relating to the unusual magnetic and electrochemical behavior.

(16) For example, for complexes $Ru^{II}(tpy)(bpy)X^{n+}$ in aqueous solution: X = Cl^-, λ_{max} = 479 nm; H_2O, 476 nm; NH_3, 482 nm; NO_2^-, 443 nm; py, 467 nm; benzonitrile, 448 nm.
(17) For example, for complexes $Ru(tpy)(bpy)X^{2+}$ in acetonitrile solution: X = H_2O, $E_{1/2}$ = 1.08 V; X = NH_3, $E_{1/2}$ = 1.02 V; X = benzonitrile, $E_{1/2}$ = 1.33 V.
(18) Ridd, M. J.; Keene, F. R.; unpublished results.
(19) Bryant, G. M.; Fergusson, J. E. *Aust. J. Chem.* **1971**, *24*, 275–286.
(20) Moyer, B. A.; Meyer, T. J. *Inorg. Chem.* **1981**, *20*, 436–444.
(21) Griffith, W. P. "The Chemistry of the Rarer Platinum Metals"; Interscience: London, 1967.

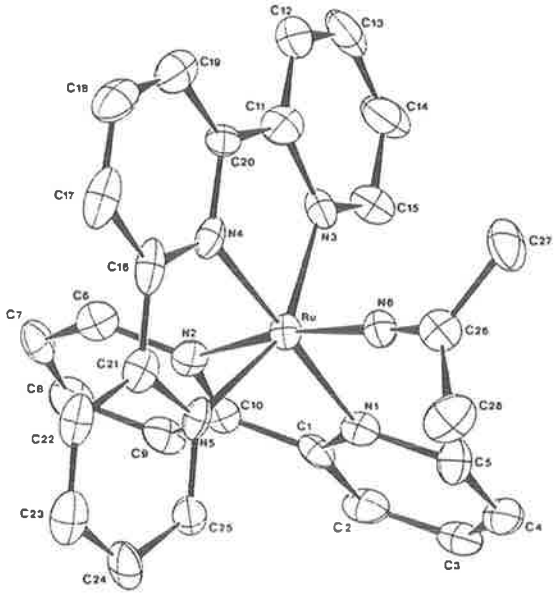

Figure 2. ORTEP plot of $[Ru(tpy)(bpy)(N{=}CMe_2)](ClO_4)_3{\cdot}H_2O$ showing atom labeling (25% probability ellipsoids).

Description of the Structures of the Four-Electron Oxidation Product, $[Ru(tpy)(bpy)(NCMe_2)](ClO_4)_3{\cdot}H_2O$. A perspective view of the structure of the cation is shown in Figure 2. The cation exhibits metal to pyridyl-type nitrogen ligand distances in the range 2.055–2.076 Å for the bipyridine and noncentral terpyridine rings. These values and the bipyridine chelate bite angles (78.0 (4), 78.5 (5)°) are similar to previous values found for other bipyridine complexes of Ru(II)[22] (where there is π-back-bonding between a delocalized π^*(bpy) and t_{2g}(Ru) orbitals) and Ru(III)[23] (where there is less extensive π-overlap[22]). The central ring of the terpyridine ligand has a Ru–N bond length of only 1.937 (7) Å: this contraction of over 0.1 Å of the metal–central N distance is tpy complexes has been noted previously in $Cr(tpy)_2^{3+}$[24] and $Cu(tpy)_2^{2+}$[25] and in mono(terpyridine) complexes of Ga,[26] Zn,[27] and Sn[28] and is presumably due to steric constraint imposed on the ligand by coordination.

The coordinated isopropylideneamide anion has a substantially linear connection to Ru, the angle at N(6) being 175.2 (1.0)°. The angles at the central carbon C(26) sum to exactly 360°, implying sp^2 hybridization: the bond length to the nitrogen atom N(6) of 1.259 (17) Å corresponds to a pure C=N double bond.[29] The Ru–N bond length of 1.831 (10) Å is particularly short: while for most Ru(II) complexes the Ru–N distances range from 2.14 Å ($[Ru(NH_3)_6]^{2+}$[30]) to 2.06 Å ($[(Ru(bpy)_3]^{2+}$[22]), only for coordinated nitrosyl is a significantly shorter Ru–N bond length observed (average Ru–NO distance 1.74 Å[31]). The analogy between nitrosyl and alkylideneamide anion species is discussed below. In Ru(III) complexes, Ru–N bond lengths are typically ca. 2.10 Å.[23,30]

The Isopropylideneamido Ligand. The potential bonding modes of the alkylideneamido (or arylideneamido) ligand, $R_2C{=}N^-$, have been discussed previously.[32] Examples of all possible linkages are known: it may function as a bridging group in polynuclear species,[33] and in mononuclear species, the M–N–C linkage can be either linear[34–36] or bent.[37] The bent linkage requires an sp^2-hybridized nitrogen donor atom, whereas for a linear M–N–C assembly, the N may be considered as sp hydridized with considerable $p_\pi(N) \rightarrow d_\pi(M)$ (and possibly $d_\pi(M) \rightarrow \pi^*(C{=}N)$) bonding giving rise to a shortened M–N bond distance. The relative involvements of p_π–d_π and d_π–π^* bonding is often ambiguous,[32] and in most cases the choice of the linear (rather than the bent) linkage could arguably be made by steric requirements.[36]

For the present structure, the nearly linear Ru–N–C linkage and short Ru–N bond indicate multiple bonding. It seems likely this is due to $p_\pi(N) \rightarrow d_\pi(Ru)$ interaction, since there is no indication of the lengthening of the C=N bond arising from $d_\pi \rightarrow \pi^*$ back-donation. Studies with molecular models indicate that the linear linkage would be strongly favored over the bent mode because of steric interaction between the methyl groups and the tpy and bpy rings in the latter case.

The magnetic and electrochemical behaviors of the four-electron oxidation product are consistent with the Ru=N=C formulation. Complexes of Ru(IV) normally exhibit magnetic moments appropriate to two unpaired electrons (d^4).[38] For oxoruthenium(IV) species, Moyer and Meyer[20] have rationalized $\mu_{eff} = 2.94\ \mu_B$ in terms of splitting of the d_π(Ru) levels into an e* set (destabilized by $p_\pi(O) \rightarrow d_\pi(Ru)$ mixing) and a b_2 nonbonding level, assuming approximately C_{4v} symmetry of the $p_\pi(O)$ orbitals. For the present complex, only one $p_\pi(N)$ orbital overlaps with $d_\pi(Ru)$ so that one MO level would be destabilized by $p_\pi(N) \rightarrow d_\pi(Ru)$ mixing, and there would be two essentially nonbonding levels. The complex might therefore be expected to be diamagnetic (as is observed also for Os(IV) complexes of deprotonated ethylenediamine):[39] however, the source of the small residual paramagnetism is unknown.

Similarly, the redox potential for the isopropylideneamido complex is considerably cathodic of the Ru(III)/Ru(II) potential for either the isopropylamine or isopropylideneamine analogue. The stabilization of the "Ru(IV)–isopropylideneamido" species is consistent with substantial charge donation from the lone pair on N to the metal center, in a way analogous to that observed for Os(IV) complexes of deprotonated ethylenediamine[39] and the oxoruthenium(IV) species.[20]

An unsuccessful attempt was made to elucidate aspects of the nature of the Ru–N and N–C bonding using infrared and Raman spectroscopy and the complex containing isopropylamine-^{15}N.

As noted earlier, the complexes of the alkylideneamide anions described here and nitrosyl complexes of ruthenium exhibit a number of similarities in physical properties, particularly with respect to shortened Ru–N bond lengths, but

(22) Rillema, D. P.; Jones, D. S.; Levy, H. A. *J. Chem. Soc., Chem. Commun.* **1979**, 849–851.
(23) Phelps, D. W.; Kahn, E. M.; Hodgson, D. J. *Inorg. Chem.* **1975**, *14*, 2486–2490.
(24) Wickramashinghe, W. A.; Bird, P. H.; Serpone, N. *Inorg. Chem.* **1982**, *21*, 2694–2698.
(25) Mathew, M.; Palenik, G. J. *J. Coord. Chem.* **1971**, *1*, 243.
(26) Beran, G.; Carty, A. J.; Patel, H. A.; Palenik, G. J. *J. Chem. Soc. D* **1970**, 222–223.
(27) Einstein, F. W. B.; Penfold, B. R. *Acta Crystallogr.* **1966**, *20*, 924–926.
(28) Einstein, F. W. B.; Penfold, B. R. *J. Chem. Soc. A* **1968**, 3019–3024.
(29) Holian, B. L.; Marsh, R. E. *Acta Crystallogr., Sect. B: Struct. Crystallogr. Cryst. Chem.*, **1970**, *B26*, 1049–1058.
(30) Stynes, H. C.; Ibers, J. A. *Inorg. Chem.* **1971**, *10*, 2304–2308.
(31) Feltham, R. D.; Enemark, J. H. *Top. Sterochem.* **1981**, *12*, 155–215.
(32) (a) Farmery, K.; Kilner, M.; Midcalf, C. *J. Chem. Soc. A* **1970**, 2279–2285. (b) Briggs, D.; Clark, D. T.; Keable, H. R.; Kilner, M. J. *J. Chem. Soc., Dalton Trans.* **1973**, 2143–2147.
(33) Kilner, M.; Midcalf, C. *J. Chem. Soc., Dalton Trans.* **1974**, 1620–1624.
(34) Collier, M. R.; Luppert, M. F.; Snaith, R.; Wade, K. *J. Chem. Soc., Dalton Trans.* **1972**, 370–373.
(35) Kilner, M.; Pinkney, J. N. *J. Chem. Soc. A* **1971**, 2887–2893.
(36) Shearer, H. M. M.; Sowerby, J. D. *J. Chem. Soc., Dalton Trans.* **1973**, 2629–2632.
(37) Alcock, N. W.; Pierce-Butler, M. *J. Chem. Soc., Dalton Trans.* **1975**, 2469–2476.
(38) Earnshaw, A.; Figgis, B. N.; Lewis, J.; Peacock, R. D. *J. Chem. Soc.* **1961**, 3132–3138.
(39) Lay, P. A.; Sargeson, A. M.; Skelton, B. W.; White, A. H. *J. Am. Chem. Soc.* **1982**, *104*, 6161–6164.

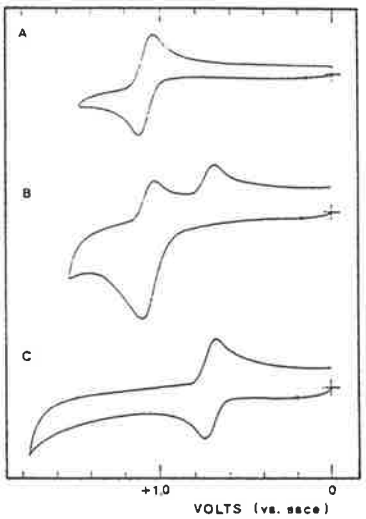

Figure 3. Cyclic voltammograms (200 mV/s) of $[Ru(tpy)(bpy)(NH_2CHMe_2)]^{2+}$ (A) and of its two-electron (B) and four-electron (C) oxidation products in acetonitrile solution.[15a]

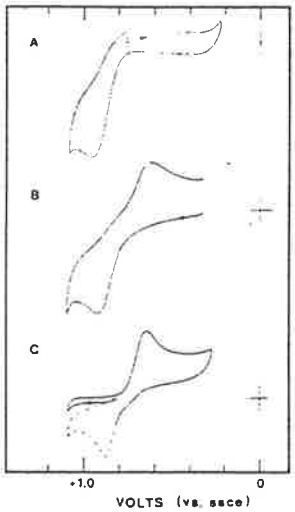

Figure 4. Cyclic voltammograms (200 mV/s) of $[Ru(tpy)(bpy)(NH_2CHMe_2)]^{2+}$ (A) and of its two-electron (B) and four-electron (C) oxidation products in 0.1 M HCl.[15b]

also their electronic spectra and redox couples (see below). The simple historical view of nitrosyl complexes as NO^+ bound to Ru(II) with extensive metal-to-ligand back-bonding[40] leads to a similar result to the concept of NCR^1R^2 bound to Ru(IV) with extensive ligand-to-metal π-donation. However, as for the nitrosyl complexes where the recognition of extensive covalent interaction has led to the formalism $\{MNO\}^n$ (where n = the total number of electrons associated with the metal d orbitals and $\pi^*(NO)$ orbitals),[31] the assignment of oxidation states to the metal and ligating atom for the (alkylideneamido)ruthenium complexes is inappropriate.

Electrochemical Studies of $[Ru(tpy)(bpy)(NH_2CHMe_2)]^{2+}$ and Its Oxidation Products. The cyclic voltammograms of $[Ru(tpy)(bpy)(NH_2CHMe_2)]^{2+}$, and of its two- and four-electron oxidation products, are shown in Figures 3 (in acetonitrile) and 4 (in 0.1 M HCl).

In acetonitrile, cyclic voltammetry (200 mV/s) of $[Ru(tpy)(bpy)(NH_2CHMe_2)]^{2+}$ reveals a reversible couple with $E_{1/2}$ = 1.08 V (Figure 3A), associated with the Ru(III)/Ru(II) couple. Under the same experimental conditions, the imine complex shows (Figure 3B) a peak on the anodic sweep ($E_{p,a}$ = 1.10 V), with two peaks ($E_{p,c}$ = 1.03 and 0.69 V) on the subsequent cathodic sweep: the relative magnitudes of these two peaks depended on the sweep rate, the proportion of the peak at more cathodic potential increasing with lower sweep rate. The isopropylideneamido species shows a reversible couple with $E_{1/2}$ = 0.72 V (Figure 3C).

In 0.1 M HCl, the cyclic voltammogram of $[Ru(tpy)(bpy)(NH_2CHMe)]^{2+}$ is completely irreversible with $E_{p,a}$ = 0.90 V, and that of the imine complex is virtually identical (Figure 4A,B). The isopropylideneamido complex shows an irreversible reduction ($E_{p,c}$ = 0.62 V), with an oxidation ($E_{p,a}$ = 0.90 V) on the subsequent anodic sweep (Figure 3C) corresponding to the imine species formed by the initial reduction.

The addition of even small amounts of water to the acetonitrile solutions used in the experiments detailed in Figure 3 gives results consistent with those for aqueous solutions.

Coulometry of the system was identical for the two solvents. Exhaustive oxidation (at 1.10 V in CH_3CN; 0.90 V in 0.1 M HCl) showed an overall four-electron oxidation (n = 3.7–3.8). This process consisted of two separate two-electron oxidations (as shown by spectrophotometric analysis during the coulometry), and the second two-electron process could be reversed electrochemically (as discussed earlier).

These electrochemical data reveal that the amine complex exhibits reversible behavior on the cyclic voltammetric time scale consistent with the Ru(III)/Ru(II) couple under anhydrous conditions but that in aqueous solution a rapid subsequent oxidation to the imine species occurs. The amine → imine conversion is irreversible. In aqueous solution, the coordinated imine → isopropylideneamido conversion is rapid and reversible: under anhydrous conditions, the imine complex undergoes ligand oxidation to the isopropylideneamido complex at a rate comparable with the cyclic voltammetric time scale, and although this reaction is reversible, the reverse process is clearly considerably slower. Because of these factors, it is difficult to synthesize electrochemically the imine complex by a two-electron exhaustive electrolysis of the amine species, since their oxidation potentials are very similar and substantial amounts of imine oxidation occur once its concentration builds up. However, since the subsequent two-electron process is reversible, following the four-electron coordinated amine → isopropylideneamide anion oxidation the imine complex may then be regenerated quantitatively by reduction at the appropriate potential.

These observations may be summarized in Scheme I, with the tpy and bpy ligands omitted from the formulas.

Scheme I

$$Ru^{II}(NH_2CHMe_2)^{2+} \underset{+e^-}{\overset{-e^-}{\rightleftharpoons}} Ru^{III}(NH_2CHMe_2)^{3+} \xrightarrow{-e^-,\ -2H^+}$$

$$Ru^{II}(NH{=}CMe_2)^{2+} \underset{+e^-}{\overset{-e^-}{\rightleftharpoons}} Ru^{III}(NH{=}CMe_2)^{3+} \underset{+H^+}{\overset{-H^+\ (fast)}{\rightleftharpoons}}$$

$$Ru^{III}(^-N{=}CMe_2)^{2+} \underset{-e^-}{\overset{+e^-}{\rightleftharpoons}} Ru{=}N{=}CMe_2^{3+}$$

The isopropylideneamido complex is relatively stable in acid solution but reverts to the imine under neutral or basic conditions, presumably with concomitant oxidation of water to hydrogen peroxide (no formation of O_2 by oxidation of OH^- has been observed). In the presence of oxidizable substrates (particularly alcohols), the isopropylideneamide → isopropylideneamine ligand reduction is relatively rapid. The potential of these cycles in the chemically catalyzed electrochemical oxidation of alcohols, or the formation of H_2O_2, may

(40) Bottomley, F. *Coord. Chem. Rev.* **1978**, *26*, 7–32.

be limited however by side reactions to as yet unidentified products.

Acknowledgment. We thank Dr. T. G. Appleton (University of Queensland) for recording the 100-MHz ^1H NMR spectra. This research was supported by the Australian Research Grants Scheme.

Registry No. $Ru(tpy)Cl_3$, 72905-30-7; $[Ru(tpy)(bpy)Cl]PF_6$, 83572-47-8; $[Ru(tpy)(bpic)Cl]PF_6$, 90412-62-7; $[Ru(tpy)(bpy)Cl]Cl$, 90412-63-8; $[Ru(tpy)(bpic)Cl]Cl$, 90412-64-9; $[Ru(tpy)(bpy)NO_2]PF_6$, 90412-65-0; $[Ru(tpy)(bpic)NO_2]PF_6$, 90412-67-2; $[Ru(tpy)(bpy)NO](PF_6)_3$, 90412-68-3; $[Ru(tpy)(bpic)NO](PF_6)_3$, 90412-70-7; $[Ru(tpy)(bpy)OH_2](PF_6)_2$, 90412-71-8; $[Ru(tpy)(bpic)OH_2](PF_6)_2$, 90412-73-0; $[Ru(tpy)(bpy)(NH_2Bz)](PF_6)_2$, 90412-75-2; $[Ru(tpy)(bpy)(NH_2\text{-}\alpha\text{-}MeBz)](PF_6)_2$, 90412-77-4; $[Ru(tpy)(bpy)(NH_2CHMe_2)](PF_6)_2$, 90412-79-6; $[Ru(tpy)(bpy)(NH_2\text{-}c\text{-}Hx)](PF_6)_2$, 90412-81-0; $[Ru(tpy)(bpy)(N{\equiv}CPh)](PF_6)_2$, 90412-83-2; $[Ru(tpy)(bpic)(NH_2CHMe_2)](PF_6)_2$, 90412-85-4; $[Ru(tpy)(bpy)(NH{=}CMe_2)](PF_6)_2$, 90412-87-6; $[Ru(tpy)(bpy)(N{=}CMe_2)](PF_6)_3$, 79361-73-2; $[Ru(tpy)(bpic)(NH{=}CMe_2)](PF_6)_2$, 90412-89-8; $[Ru(tpy)(bpic)(N{=}CMe_2)](PF_6)_3$, 90412-91-2; $[Ru(tpy)(bpy)(N{=}CMe_2)](ClO_4)_3{\cdot}H_2O$, 90412-93-4; bpic, 1134-35-6; NO_2^-, 14797-65-0; $NH_2\text{-}\alpha\text{-}MeBz$, 98-84-0; NH_2CHMe_2, 75-31-0; $NH_2\text{-}c\text{-}Hx$, 108-91-8; 4-picoline, 108-89-4.

Supplementary Material Available: Thermal parameters for the non-hydrogen atoms (supplementary Table 1), calculated positional parameters for the hydrogen atoms (supplementary Table 2), and observed and calculated structure factors (supplementary Table 3) for the structure determination (13 pages). Ordering information is given on any current masthead page.

Aust. J. Chem., 1986, **39**, 2027–35

Stabilization of Simple Imines by Coordination to Ruthenium(II), and Aspects of Their Reactivity*

Geoffrey W. Whebell[A] *and F. Richard Keene*[A,B]

[A] Department of Chemistry and Biochemistry, James Cook University of North Queensland, Townsville, Qld. 4811.
[B] Author to whom correspondence should be addressed.

Abstract

The oxidation of a number of secondary amines coordinated to ruthenium(II) was investigated. Pyrrolidine (1) and piperidine (5) formed the corresponding 1-imines [1-pyrroline (2) and 2,3,4,5-tetrahydropyridine (6)]; these complexes were stable, although spectral and electrochemical properties show there to be only minor π-back-bonding between the Ru^{II} metal centre and the imine ligands. The analogous β-unsaturated amines [3-pyrroline (3) and 1,2,3,6-tetrahydropyridine (7)] complexes also underwent oxidative dehydrogenation reactions, and in these cases produced the corresponding aromatic species [pyrrole (4) and pyridine (8), respectively]. Coordinated *N*-methylallylamine (9) was oxidized to a mixture of the two possible 1-imine species (10) and (11), and preliminary studies indicated that the 1-aza 1,3-diene (11) product would undergo a Diels–Alder reaction while attached to the metal centre.

Introduction

The oxidative dehydrogenation of coordinated amines is well documented, particularly with ruthenium as the metal centre.[1–6] While stable complexes containing the conjugated α,α'-diimine moiety are relatively common products of such reactions,[2] the observations of complexes of unconjugated or monodentate imines are few.

In their study of the aerial oxidation of benzylamine in $[Ru(NH_3)_5(NH_2CH_2Ph)]^{2+}$ to the benzonitrile complex, Diamond *et al.*[7] observed an intermediate which they assumed to be the imine species. In the same work the oxidation of cyclohexylamine in $[Ru(NH_3)_5(c\text{-}C_6H_{11}NH_2)]^{2+}$ yielded $[Ru(NH_3)_6]^{3+}$ and cyclohexanone, presumably by hydrolysis of a transient imine complex generated by dehydrogenation. Brown *et al.*[2] also claimed the generation *in situ* of a coordinated monoimine by electrochemical oxidation of the chelate ligand 2-methylpropane-1,2-diamine (damp) in the complex

* Dedicated to Bob Schoenfeld in appreciation for his contribution to Australian chemistry and chemical literature.

[1] Goto, M., Takeshita, M., Kanda, N., Sakai, T., and Goedken, V. L., *Inorg. Chem.*, 1985, **24**, 582, and references therein.
[2] Brown, G. M., Weaver, T. R., Keene, F. R., and Meyer, T. J., *Inorg. Chem.*, 1976, **15**, 190.
[3] Keene, F. R., Salmon, D. J., and Meyer, T. J., *J. Am. Chem. Soc.*, 1976, **98**, 1884, and references therein.
[4] Ridd, M. J., and Keene, F. R., *J. Am. Chem. Soc.*, 1981, **103**, 5733.
[5] Keene, F. R., Ridd, M. J., and Snow, M. R., *J. Am. Chem. Soc.*, 1983, **105**, 7075.
[6] Adcock, P. A., Keene, F. R., Smythe, R. S., and Snow, M. R., *Inorg. Chem.*, 1984, **23**, 2336.
[7] Diamond, S. E., Tom, G. M., and Taube, H., *J. Am. Chem. Soc.*, 1975, **97**, 2661.

0004-9425/86/122027$02.00

$[Ru(bpy)_2(damp)]^{2+}$ (bpy = 2,2′-bipyridine). In none of the cases could the imine complex be isolated.

The only instance in which a stable ruthenium complex of a monodentate imine has been isolated was recently reported by Adcock *et al.*;[6] the two-electron oxidation of coordinated isopropylamine yields the corresponding imine complex:

$$L_5Ru\text{–}NH_2\text{–}CH(CH_3)_2^{2+} \xrightarrow{-2e} L_5Ru\text{–}NH{=}C(CH_3)_2^{2+} + 2H^+ \qquad (1)$$

[L_5 = (tpy)(bpy), where tpy = 2,2′:6′,2″-terpyridine].

However, the imine complex may undergo subsequent oxidation to form an alkylideneamido species:

$$L_5Ru\text{–}NH{=}C(CH_3)_2^{2+} \underset{+2e}{\overset{-2e}{\rightleftharpoons}} L_5Ru{=}N{=}C(CH_3)_2^{3+} + H^+ \qquad (2)$$

Similar reactions were observed with the structurally related ligands α-methylbenzylamine and cyclohexylamine.

We sought to isolate ruthenium(II) complexes of monodentate imines in order to probe the nature of any stabilization induced by their coordination and to examine their chemical reactivity. To prevent the subsequent oxidation reaction, e.g., *(2)*, we have now studied the oxidative dehydrogenation of a number of coordinated secondary amines. This paper reports the oxidation of pyrrolidine and piperidine (and some of their congeners), and *N*-methylallylamine attached to the $Ru(tpy)(bpy)^{2+}$ moiety, and details of the resultant imine products.

Experimental

Measurements

Electronic spectra were recorded on a Cary 219 spectrophotometer, and n.m.r. spectra [in (D_6)acetone, dichloro(D_2)methane, (D_6)dimethyl sulfoxide, or D_2O solvents] on a Bruker AM-300 spectrometer with either *p*-dioxan (δ 3·53 {^1H} and 66·5 {^{13}C}) or $SiMe_4$ as internal reference. When D_2O was used as a solvent, PF_6^- salts were solubilized by stirring a suspension in D_2O with Dowex 1X8 resin (Cl^- form), and filtering prior to transfer into the n.m.r. tube.

Electrochemical measurements were made in deaerated (N_2) freshly distilled propylene carbonate (0·2 M tetrabutylammonium tetrafluoroborate), a Bioanalytical Systems (BAS) CV-27 voltammograph being used, with cyclic voltammograms output to a Linseis LY-1800 *X–Y* recorder. All potentials are reported relative to a saturated sodium chloride calomel standard electrode.

Elemental analyses were carried out by the Canadian Microanalytical Service (Vancouver).

Materials

Propylene carbonate (Aldrich) was distilled under vacuum (69–71°/0·7 mmHg). Pyrrole (Aldrich) was also distilled before use. All other chemicals and solvents were of A.R. grade (where available) and used as received. The complexes $[Ru(tpy)(bpy)(H_2O)](PF_6)_2$ and $[Ru(tpy)(bpy)Cl]PF_6$ were prepared by literature methods.[6] Argon and nitrogen used for deaeration were scrubbed of O_2 by passing through a column packed with BTS catalyst (Fluka) maintained at 180°C.

Syntheses

(Bipyridine)(pyrrolidine)(terpyridine)ruthenium(II) *hexafluorophosphate* (1) was prepared by a modification of a method described by Adcock *et al.*[6] $[Ru(tpy)(bpy)(H_2O)](PF_6)_2$ (200 mg), methanol (20 ml) and pyrrolidine (3 ml) were sealed in a glass ampoule and heated to 140° for

48 h. The ampoule was cooled, opened, and the methanol evaporated under a stream of N_2 on a steambath. The residue was washed with diethyl ether, and transferred to a separatory funnel by using dichloromethane (*c.* 50 ml). Water (100 ml) and solid NH_4PF_6 (0·5 g) were added, and the product was extracted several times with dichloromethane. The fractions were combined, evaporated to dryness, solubilized in water by stirring with Dowex 1X8 resin (200–400 mesh; Cl^- form), and sorbed onto a column of SP-Sephadex C-25 cation exchanger. After elution with 0·1 M sodium acetate/0·01 M sodium hydroxide (to remove aqua and chloro species), the amine complex was eluted from the column with 0·25 M sodium acetate solution. The eluate was extracted into dichloromethane after addition of NH_4PF_6 (*c.* 0·2 g). The combined extracts were dried with Na_2SO_4, and evaporated to dryness. The pyrrolidine complex was recrystallized from methanol/diethyl ether, and dried under vacuum. Yield 140 mg, 47% (Found: C, 41·0; H, 3·3; N, 9·8. $C_{29}H_{28}F_{12}N_6P_2Ru$ requires C, 40·9; H, 3·3; N, 9·9%).

(Bipyridine)(piperidine)(terpyridine)ruthenium(II) *hexafluorophosphate* (5) was prepared in an analogous manner to the pyrrolidine complex, in 46% yield (Found: C, 41·0; H, 3·0; N, 9·9. $C_{30}H_{30}F_{12}N_6P_2Ru$ requires C, 41·0; H, 3·1; N, 9·9%).

(Bipyridine)(pyrrole)(terpyridine)ruthenium(II) *hexafluorophosphate* (4) was prepared in a similar manner to the pyrrolidine complex, in 24% yield. In this case, because of the lower basicity of the ligand, a small amount of NaOH (*c.* 50 mg) was added to the reaction mixture (converting the brown aqua starting complex into the purple hydroxo species) and thereby facilitating the observation of the conversion into the brown pyrrole complex product.

(Bipyridine)(pyridine)(terpyridine)ruthenium(II) *hexafluorophosphate* (8) was prepared in an analogous manner to the pyrrolidine complex, in 63% yield.

(Bipyridine)(3-pyrroline)(terpyridine)ruthenium(II) *hexafluorophosphate (3).*—Standard Schlenk techniques were used when [Ru(tpy)(bpy)Cl] PF_6 (200 mg) was added to deaerated (argon) trifluoromethanesulfonic acid (2 ml), and heated (100°) with stirring while under a stream of dry argon for 5 h. The mixture was evaporated to dryness under vacuum and the residue dissolved in dry degassed sulfolane under argon. 3-Pyrroline (150 mg) in dry degassed sulfolane (5 ml) was added slowly (20 min), and the mixture stirred under argon at room temperature for 15 h. The vessel was opened to the atmosphere, and 1 M HCl (20 ml) added. The solution was washed into a separatory funnel with water, and extracted with dichloromethane after addition of NH_4PF_6 (*c.* 0·2 g). The dichloromethane extract was treated and chromatographed as for the pyrrolidine complex. The complex was recrystallized from dichloromethane/light petroleum. Yield 150 mg, 50% (Found: C, 42·1; H, 3·5; N, 9·3. $C_{29}H_{26}F_{12}N_6P_2Ru$ requires C, 41·0; H, 3·1; N, 9·9%). The ^{13}C n.m.r. spectrum of this complex indicated the presence of a small amount of aliphatic hydrocarbons (derived from the solvent) within these crystals, the impurities giving rise to the discrepancies in this analysis. The spectrum allowed clear characterization of this complex, however.

(Bipyridine)(terpyridine)(1,2,3,6-tetrahydropyridine)ruthenium(II) *hexafluorophosphate* (7) was prepared in an analogous manner to the 3-pyrroline complex in 50% yield (Found: C, 41·4; H, 3·2; N, 9·7. $C_{30}H_{28}F_{12}N_6P_2Ru$ requires C, 41·7; H, 3·3; N, 9·7%).

(Bipyridine)(N-methylallylamine)(terpyridine)ruthenium(II) *hexafluorophosphate* (9) was prepared in a similar manner to the 3-pyrroline complex, except that after addition of the ligand *N*-methylallylamine the reaction mixture was sealed under argon and stirred for 60 h. Yield 33% (Found: C, 40·7; H, 3·3; N, 9·6. $C_{29}H_{28}F_{12}N_6P_2Ru$ requires C, 40·9; H, 3·3; N, 9·9%).

Isolation of Oxidized Products

Oxidations were performed by coulometric methods in propylene carbonate. After oxidation at a potential 5–10 mV anodic of $E_{p,a}$ for the precursor amine complex until $n \approx 2$, the solution was applied to an alumina column, and eluted with dichloromethane to remove the propylene carbonate. The complex was then eluted with methanol, the eluate evaporated to a small volume, water (1–2 ml) added, and the complex precipitated with NH_4PF_6. The resultant solid was collected, and recrystallized from methanol/diethyl ether. Further purification was achieved by ion-exchange chromatography as described earlier, followed by recrystallization.

(Bipyridine)(1-pyrroline)(terpyridine)ruthenium(II) *hexafluorophosphate* (2) was obtained in 70% yield from the corresponding pyrrolidine complex (Found: C, 41·0; H, 3·0; N, 9·9. $C_{29}H_{26}F_{12}N_6P_2Ru$ requires C, 41·0; H, 3·1; N, 9·9%).

(Bipyridine)(terpyridine)(2,3,4,5-tetrahydropyridine)ruthenium(II) *hexafluorophosphate* (6) was obtained in 76% yield from the corresponding piperidine complex (Found: C, 41·7; H, 3·3; N, 9·5. $C_{30}H_{28}F_{12}N_6P_2Ru$ requires C, 41·7; H, 3·3; N, 9·7%).

The oxidation products from the *N*-methylallylamine species (9) were obtained in a similar manner by using an oxidation potential of 1·17 V and stopping the electrolysis at a coulombic *n* value of *c.* 2 electrons. The product was recrystallized from water by the addition of NH_4PF_6 after the chromatographic procedure described above.

Spectrocoulometric Determinations of the Oxidations of Coordinated Pyrrolidine (1) and Piperidine (5)

In a typical experiment, a sample of the pyrrolidine complex (1) was dissolved in dry, degassed (argon) propylene carbonate/0·2 M tetrabutylammonium tetrafluoroborate, and oxidized at 1·12 V (5 mV anodic of $E_{p,a}$) in a conventional three-compartment electrochemical cell (platinum working electrode). The solution in the working compartment was simultaneously circulated through a 0·1 cm flow cell in the spectrophotometer by means of a peristaltic pump, and the spectrum recorded at coulometric *n* values 0, 0·5, 1·0, 1·5 and 2·0 electrons.

Diels–Alder Experiments

The solid obtained from the oxidation of the *N*-methylallylamine complex (9) (15·0 mg, 17·7 nmol) was dissolved in $(CD_3)_2SO$ (0·7 ml), diethyl acetylenedicarboxylate (1·2 μl, 7·5 nmol) added, and the solution placed in an n.m.r. tube. After three cycles of freeze–thaw–degassing, the tube was sealed under argon, and the ^1H n.m.r. spectrum run immediately and again after the mixture had been maintained at 150°C for 72 h.

Results and Discussion

Synthetic Methods and Characterization

The synthesis of $[Ru(tpy)(bpy)(amine)]^{2+}$ complexes by reactions of the aqua complex with the appropriate amine in methanol solution at elevated temperature and pressure has been reported previously,[6] and was used in this work for complexes of a number of saturated and aromatic amines. However, the method proved highly unsatisfactory for amines with β-unsaturation. A new general synthetic method was therefore developed, based on procedures reported by Lay *et al.*,[8] with the $[Ru(tpy)(bpy)(CF_3SO_3)]^+$ species as a precursor: in this instance, the triflato complex was not isolated but used *in situ* where it underwent ready substitution under very mild conditions.

Identification of both amine and imine complexes was generally made by ^{13}C n.m.r. spectroscopy. The resonances arising from the bipyridine and terpyridine ligands (in the range δ 120–160) were complicated, but resonances outside this range (arising from aliphatic carbon atoms and some isolated imine carbon atoms) allowed characterization of the amine complexes and of their oxidation products.

Five-Membered Ring Systems

The electrochemical and spectral (^{13}C n.m.r. and electronic) characteristics of the pyrrolidine complex (1) are given in Table 1. Exhaustive electrolysis of this species (at 1·12 V) in propylene carbonate solution gave a coulometric *n* value of 1·98 electrons: furthermore, a coulometric titration revealed isosbestic points at 381 and 470 nm, indicating a single oxidation product. The physical properties of the product isolated from this oxidation are also given in Table 1, and the ^{13}C n.m.r. spectrum

[8] Ware, D. C., Lay, P. A., and Taube, H., *Inorg. Synth.*, 1986, **24**, 175.

Table 1. Characterization data for isolated $[Ru(tpy)(bpy)X]^{2+}$ complexes (1)–(9)

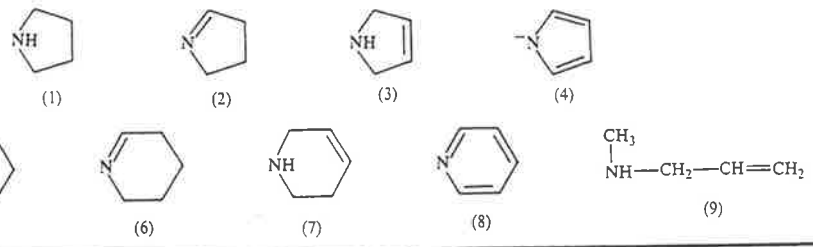

Complex	Electronic spectra[A] λ (nm)	ε (l. mol^{-1} cm^{-1})	Electrochem. data[B] $E_{1/2}$ (V)	ΔE_p (mV)	^{13}C n.m.r. data (non-aromatic resonances only)
(1)	481	10200	1·13	80	23·3, 50·2[D]
(2)	469	9090	1·15	100	20·3, 37·9, 63·0, 178·8[E]
(3)	480	10250	C		58·8[F]
(4)	485	10200	1·15	60	—
(5)	483	9800	1·08	100	22·5, 26·4, 51·1[D]
(6)	472	9040	1·13	100	17·1, 23·3, 31·4, 54·4, 177·3[E]
(7)	482	9800	1·15	80	25·6, 48·8, 49·1[F]
(8)	468	9200	1·22	80	—
(9)	477	10400	1·14	60	38·1, 57·8[E]

[A] CH_2Cl_2 solution. MLCT transition.
[B] Platinum electrode (unless otherwise indicated); scan rate 100 mV/s.
[C] $E_{p,a} = 1·26$ V (glassy carbon working electrode).
[D] D_2O solvent.
[E] CD_2Cl_2 solvent.
[F] (D_6)Acetone solvent.

of both species are presented in Fig. 1. The ^{13}C n.m.r. spectrum of the pyrrolidine complex in the aliphatic region has two resonances [δ (D_2O) 23·3 and 50·2] each representing two equivalent carbon atoms, with the peak at higher field assigned to the carbon atoms α to the amine nitrogen atom. The spectrum of the two-electron oxidation product reveals three peaks in that region [δ (CD_2Cl_2) 20·3, 37·9 and 63·0] with an additional peak downfield at δ 178·8. This is clearly consistent with the dehydrogenation of pyrrolidine to 1-pyrroline

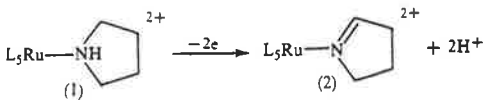

(3)

with the peak at low field assigned to the imine carbon atom, and the three higher-field resonances assigned to the three distinct saturated carbon atoms of the ring.

The visible spectrum of the 1-pyrroline complex (2) shows a small blue shift in the metal-to-ligand charge-transfer (MLCT) band when compared with the parent pyrrolidine complex (1) (Table 1). In addition, the potentials of the Ru^{III}/Ru^{II} redox couples are seen to be virtually indistinguishable. As noted previously,[6] the position of the MLCT band and redox potentials in $Ru(tpy)(bpy)X^{n+}$ complexes are relatively insensitive to the nature of X unless it is capable of substantial back-bonding. Accordingly, as for the case of coordinated propan-2-imine,[6] the monoimine 1-pyrroline is seen to be only a weak π-acceptor.

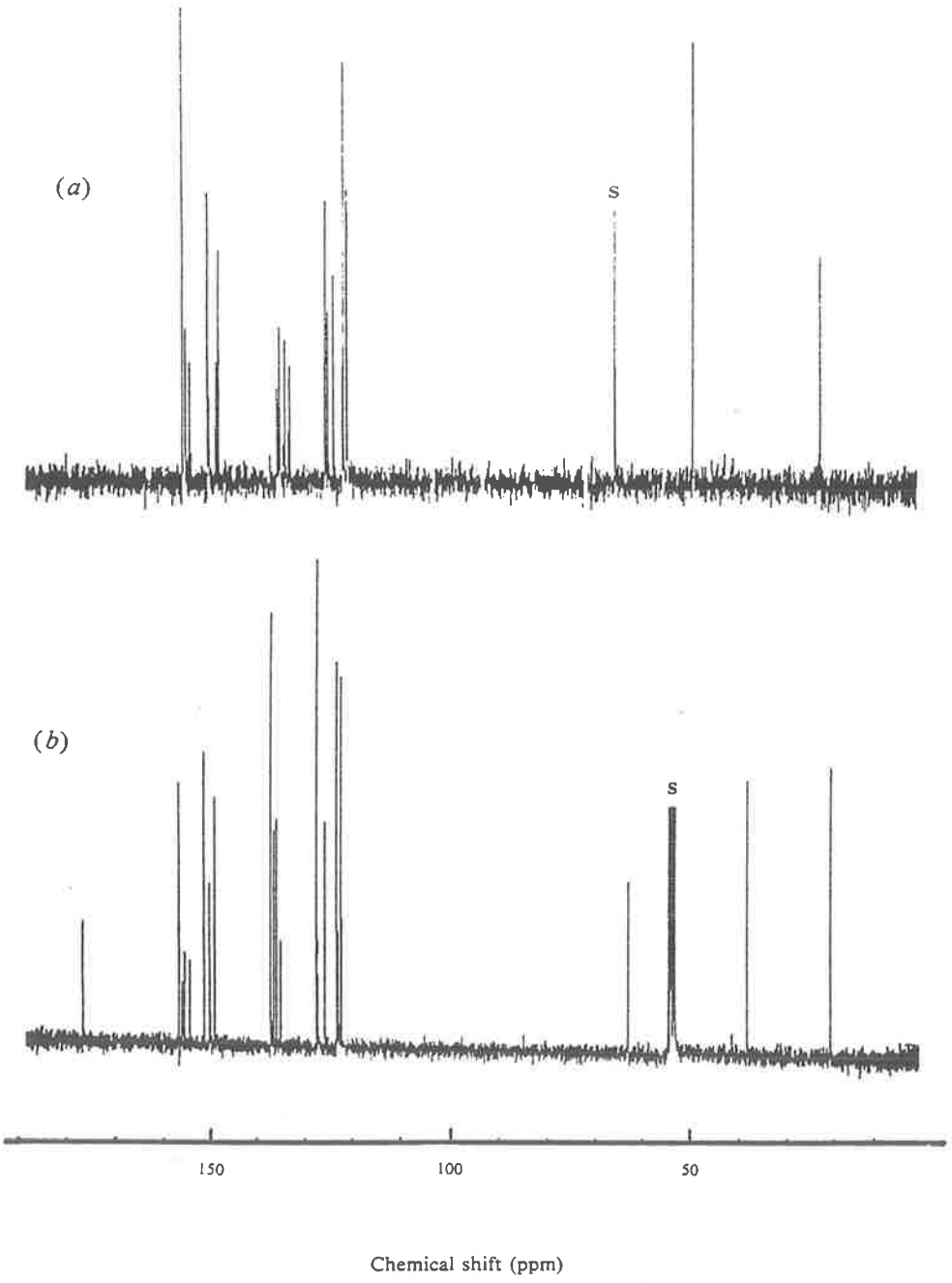

Fig. 1. Carbon-13 nuclear magnetic resonance spectra (at 75 MHz) of two ruthenium(II) complexes $[Ru(tpy)(bpy)X]^{2+}$: (*a*) X = pyrrolidine (1), in D_2O; (*b*) X = 1-pyrroline (2), in CD_2Cl_2. The S marks the standard (*p*-dioxan) resonance in (*a*), or solvent resonances in (*b*). $SiMe_4$ was used as internal reference in (*b*).

Nevertheless, the isolation of a stable complex of 1-pyrroline is significant since the free ligand has limited existance as the monomer.[9] The isolation of cobalt(III) complexes of 1-pyrroline derivatives have been reported previously,[10] although the stabilization would result from considerably different influences of the Co^{III} and Ru^{II} centres in the two instances.

The analogous complex of 3-pyrroline (3) was also synthesized (Table 1), and its oxidation attempted under similar conditions to those for the pyrrolidine species (1). Large coulometric n values (>8) were obtained, accompanied by the formation of a precipitate. Cyclic voltammetry experiments taken during the electrolysis experiment indicated the presence of a species with $E_{1/2} = 1 \cdot 15$ V, similar to the redox potential for the pyrrole complex (Table 1). It seems probable that the initial product of the dehydrogenation of coordinated 3-pyrroline is the corresponding pyrrole species:

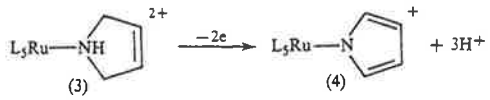

(3) (4) *(4)*

However, the charge of this complex (4) is lowered because pyrrole is deprotonated, so that the Ru^{III}/Ru^{II} redox couple is cathodic of that for the precursor complex; under the conditions of the coulometry experiment the pyrrole complex would be in the Ru^{III} form. Although the precipitate formed during this reaction was not investigated further, it is possible that subsequent condensation reactions of coordinated pyrrole may give rise to the high coulometric n values observed.

Six-Membered Ring Systems

The $Ru(tpy)(bpy)^{2+}$ complexes of piperidine (5) and 1,2,3,6-tetrahydropyridine (7) were synthesized: their physical properties are summarized in Table 1.

The exhaustive electrolysis of the piperidine complex (5) gave a coulometric n value of 1·99 electrons, and the ^{13}C n.m.r. spectrum of the product (Table 1) indicates that the product is the corresponding monoimine species:

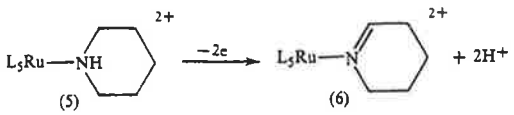

(5) (6) *(5)*

As for the five-membered ring systems, a small blue shift in the MLCT band and a small anodic shift in the Ru^{III}/Ru^{II} redox couple are observed in going from the amine to the imine complex (Table 1), and indicate that the monoimine is a weak π-acceptor ligand. However, the coordination imparts chemical stability to the monoimine heterocyclic ring system, 2,3,4,5-tetrahydropyridine (6).

The electrochemical oxidation of coordinated 1,2,3,6-tetrahydropyridine (7) proceeded with $n \simeq 4$ electrons, and the resultant major product had identical

[9] Edwards, G. B., Yamanouchi, K., Kuchitsu, K., Sugie, M., Takeo, H., Matsumara, C., Ogawa, K., and Takeuchi, Y., *J. Mol. Spectrosc.*, 1985, **111**, 301.
[10] Lawson, P. J., McCarthy, M. G., and Sargeson, A. M., *J. Am. Chem. Soc.*, 1982, **104**, 6710.

electrochemical and spectral characteristics to $[Ru(tpy)(bpy)(py)]^{2+}$ (8):

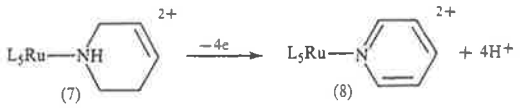

(6)

No evidence was found to indicate the presence of the intermediate two-electron oxidation product, the 1-aza 1,3-diene (2,3-dihydropyridine).

N-*Methylallylamine*

Since the stabilization of monoimines by their coordination to ruthenium(II) has been established during this and previous[6] work in these laboratories, it was partly the aim of the present studies to examine the ability of the metal centre to stabilize ligands containing the 1-aza 1,3-diene moiety (N=C–C=C). The oxidation of *N*-methylallylamine (9) was therefore investigated. The motivation for this interest was the potential value of Diels–Alder reactions of 1-aza 1,3-dienes in the synthesis of nitrogen heterocycles,[11] although few examples of this reaction are known.[11,12]

Exhaustive electrolysis of the *N*-methylallylamine complex (9) in propylene carbonate solution at 1·17 V gave a high coulometric *n* value: however, the normal isolation procedure (see Experimental) yielded a solid whose electronic spectrum and electrochemical properties were consistent with an imine species (see above). The ^{13}C n.m.r. of this solid showed two downfield resonances at δ (CD_2Cl_2) 169·0 and 179·1, indicative of two imine carbon atoms. The ^1H n.m.r. studies [$(CD_3)_2SO$ solvent] further supported the presence of the two imine complexes obtained by dehydrogenation of *N*-methylallylamine:

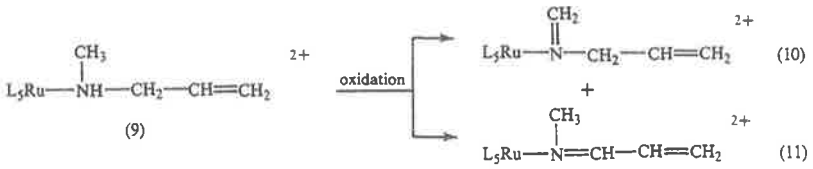

(7)

The vinyl protons in the ^1H n.m.r. spectra of both these products would be expected to show an ABX pattern in which the X proton is further coupled to vicinal proton(s). The imine product (10) showed two doublets of doublets for the terminal protons (δ 4·46, dd, 1H, *J* 17·7, 0·8 Hz; δ 4·81, dd, 1H, *J* 9·4, 0·8 Hz) and a complicated resonance for the other vinyl proton (δ 5·31, ddt, 1H, *J* 17·7, 9·4, 6·0 Hz) consistent with the assignment. The product (11) also showed two doublets of doublets for the terminal vinyl protons (δ 5·67, dd, 1H, *J* 16·6, <0·6 Hz; δ 5·88, dd, 1H, *J* 10·2, <0·6 Hz), with a complex resonance for the other vinyl proton (δ 6·70, ddd, 1H, *J* 16·6, 10·2, 10·2 Hz) and a further doublet (δ 7·12, d, 1H, *J* 5·7 Hz) attributed to the imine CH proton. Decoupling experiments with this form of the imine confirmed the structure of (11) as the 1-aza diene: irradiation at δ 7·12 simplified the non-terminal vinyl resonance to a dd pattern, and irradiation at δ 6·70 resulted in a corresponding simplification of the resonances of the two terminal vinyl protons.

[11] Cheng, Y.-S., Lupo, A. T., and Fowler, F. W., *J. Am. Chem. Soc.*, 1983, **105**, 7696.
[12] Jung, M. E., and Shapiro, J. J., *J. Am. Chem. Soc.*, 1980, **102**, 7862.

The ratio of the imines (10) and (11) formed in the oxidation reaction *(7)* was *c.* 2 : 1. The two isomers could not be readily separated, however, so that initial studies on possible Diels–Alder reactions of the 1-aza diene (11) were undertaken on the mixture of imines. On reaction [in $(CD_3)_2SO$ solution] with diethyl acetylenedicarboxylate so that the molar ratios of the 1-aza diene and the dienophile were approximately equal, ^1H n.m.r. studies indicated that the vinyl resonances of (10) remained unaltered while those of the 1-aza diene (11) disappeared, as did the ethyl resonances of the dienophile (δ 1·25, t, 3H, *J* 6·7 Hz; δ 4·27, q, 2H, *J* 7·3 Hz). However, two distinct but very similar new ethyl resonances appeared in the product spectrum (δ 1·05, t, 3H, *J* 7·2 Hz; δ 1·10, t, 3H, *J* 6·2 Hz; δ 3·44, q, 2H, *J* 7·0 Hz; δ 3·49, q, 2H, *J* 7·1 Hz) consistent with a Diels–Alder reaction occurring between the coordinated 1-aza diene and the dienophile and forming a six-membered nitrogen heterocyclic ring with two substituent $CO_2C_2H_5$ groups. These reactions are being studied further, and will be reported separately.

Acknowledgments

This research was supported by the Australian Research Grants Scheme. The assistance of Dr B. F. Bowden with the n.m.r. decoupling experiments is gratefully acknowledged.

Manuscript received 16 April 1986

J. CHEM. SOC. DALTON TRANS. 1992 1949

Mechanism of Oxidative Dehydrogenation of Alcohols co-ordinated to Ruthenium†

Michael J. Ridd,[a] David J. Gakowski,[a] Graeme E. Sneddon[b] and F. Richard Keene*[,a]
[a] *Department of Chemistry and Biochemistry, James Cook University of North Queensland, Townsville, Queensland 4811, Australia*
[b] *Department of Mathematics, James Cook University of North Queensland, Townsville, Queensland 4811, Australia*

The oxidative dehydrogenation of the complexes $[Ru(bipy)_2(NC_5H_4CH_2OH)]^{2+}$, $[Ru(bipy)_2(NC_5H_4CD_2OH)]^{2+}$ and $[Ru(bipy)_2\{NC_5H_4CH(CH_3)OH\}]^{2+}$ to the corresponding carbonyl species [bipy = 2,2'-bipyridine; $NC_5H_4CH_2OH$ = 2-(hydroxymethyl)pyridine; $NC_5H_4CD_2OH$ = 2-(dideuteriohydroxymethyl)pyridine; $NC_5H_4CH(CH_3)OH$ = 2-(1-hydroxyethyl)pyridine] has been studied in aqueous solution by kinetic and electrochemical techniques. The mechanistic scheme was found to involve the intermediacy of a ruthenium(IV)–alkoxide species, formed by disproportionaton of the ruthenium(III) complex produced in the initial step of the oxidation process. The rate-determining removal of the proton from the α-carbon atom of the chelate ring is general-base catalysed.

The oxidation of alcohols is a reaction of considerable importance. By way of two significant but disparate examples, the process is fundamental to the action of a number of dehydrogenases in living cells and to the operation of alcohol fuel cells.

Although the catalytic oxidation of alcohols by transition metals is known in a few cases, the intimate mechanistic details of the oxidative dehydrogenation reactions themselves have rarely been elucidated. For example, Gagne and Marks[1] reported the catalysis of the autoxidation and electrochemical oxidation of alcohols by [1,3-bis(4-methyl-2-pyridyl)isoindoline]trichlororuthenium(III). The essential feature of the proposed reaction path was that the catalyst underwent substitution at the metal centre by the substrate alcohol, whose oxidation took place while it was co-ordinated. By analogy with a previous stoichiometric study by Tovrog *et al.*[2] of the reaction (1), the details of the ligand oxidation process were assumed to

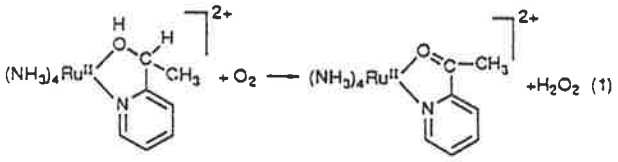

(1)

occur *via* a ruthenium(IV) intermediate, formed under basic conditions by disproportionation of the ruthenium(III) complex.

As part of a continuing general mechanistic study of ligand oxidation reactions,[3,4] we had undertaken an investigation of the oxidation [equation (2)] of a series of related alcohols co-ordinated to ruthenium.‡ **1a–1c**, reported here in detail, which verifies the intermediacy of the high-oxidation-state transient and elucidates details of the ligand dehydrogenation process.

Results and Discussion

Synthesis and Characterization of Alcohol Complexes and their Oxidation Products.—Alcohol complexes of the general

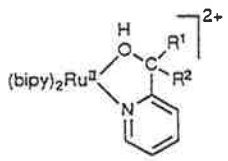

	R^1	R^2
1a	H	H
1b	D	D
1c	H	CH_3
1d	CH_3	CH_3

bipy = 2, 2'-bipyridine

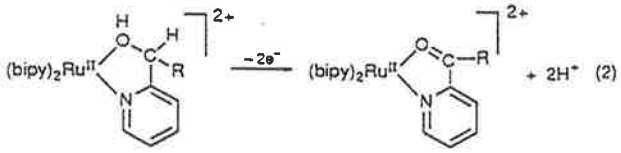

(2)

formulation **1** were synthesized in an analogous manner to the corresponding amine complexes[3,4] by reaction of the appropriate ligand with $[Ru(bipy)_2Cl_2]$ in acidic§ aqueous methanol. The ^1H NMR spectral data confirm the bidentate ligating mode of these ligands. For example, the spectrum of $[Ru(bipy)_2(NC_5H_4CH_2OH)]^{2+}$ **1a** in $(CD_3)_2SO$ reveals an AB quartet centred at δ 5.18 which is attributed to the methylene protons rendered inequivalent because of the restricted conformational flexibility of the chelate ring. There is also a singlet at δ 9.53, attributed to the proton of the co-ordinated alcohol group and which exchanges on the addition of D_2O.

Synthesis of the species $[Ru(bipy)_2\{NC_5H_4CH(CH_3)OH\}]^{2+}$ **1c** realized the two diastereoisomeric pairs in approximately equimolar amounts. They were partially separated by fractional crystallization (iodide salt), and each diastereoisomer could be enriched to *ca.* 80% isomeric purity by repeated crystallizations (monitored by the methyl doublet ^1H NMR resonances). Attempts to separate the two diastereoisomeric pairs chromatographically in the same manner as for the amine analogues[4] were unsuccessful, due to gradual oxidation of the complex under the conditions (pH 3; 4 °C) and the timescale (*ca.* 2 weeks) of the separation.

Comparative ^1H NMR nuclear Overhauser effect (NOE) difference studies of the Λ(*S*)/Δ(*R*)-$[Ru(bipy)_2\{NC_5H_4CH$-

† *Non-SI unit employed:* mmHg ≈ 133 Pa.
‡ Presented at the 187th National American Chemical Society Meeting, St. Louis, MO, April 1984, Abstract INOR 191.

§ The alcohol complexes are susceptible to aerial oxidation at higher pH.

$(CH_3)NH_2\}]^{2+}$ (for which a crystal structure has been determined)[4] and $\Lambda(R)/\Delta(S)$-$[Ru(bipy)_2\{NC_5H_4CH(CH_3)NH_2\}]^{2+}$ diastereoisomers, and the diastereoisomers **A** and **B** of the corresponding alcohol species $[Ru(bipy)_2\{NC_5H_4CH(CH_3)OH\}]^{2+}$ have allowed assignment of the stereochemistry of the latter. By observation of the enhancements resulting from the selective irradiation of the methyl protons, and separately the methine protons, in each case the higher-field methyl resonance may be associated with an equatorial orientation of the methyl group relative to the mean plane of the chelate ring.* The configuration of the less-soluble diastereoisomer of $[Ru(bipy)_2\{NC_5H_4CH(CH_3)OH\}]^{2+}$ **A** may therefore be assigned as $\Lambda(S)/\Delta(R)$. The major difference between the analogous amine and alcohol species is that in $\Lambda(R)/\Delta(S)$-$[Ru(bipy)_2\{NC_5H_4CH(CH_3)OH\}]^{2+}$ **B** the methyl group is more distinctly axial (and the methine proton more distinctly equatorial) compared with the amine counterpart. This observation may explain the greater difference in chemical shifts for the methyl groups in the alcohol (δ 1.25 and 1.73) compared with the amine (δ 1.51 and 1.68) diastereoisomers, although this effect may also be electronic in origin.

The pK_a of the alcohol proton in $[Ru(bipy)_2(NC_5H_4CH_2OH)]^{2+}$ **1a** was determined to be 7.2 ± 0.2 at 25 °C (I = 0.1 mol dm^{-3}, $LiNO_3$). For the monomethyl-substituted complex **1c** a determination of the pK_a of the diastereoisomeric mixture under the same conditions gave one value (7.6 ± 0.2). Since the method is sufficiently sensitive to detect the presence of two different acidic species if their pK_a values differ by 0.5, in the present case the two acidities must be similar. For the dimethyl-substituted species **1d** the pK_a = 8.29 ± 0.01 under the same conditions.

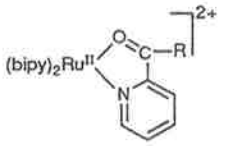

R
2a H
2b CH_3

The corresponding aldehyde **2a** and ketone **2b** complexes were synthesized by reaction of the appropriate ligand with $[Ru(bipy)_2(O_3SCF_3)_2]$ in dichloromethane under mild conditions. Under basic conditions these complexes were observed to undergo hydrate formation [equation (3)] in an analogous way to the reactions of the complexes of similar ligands with the $[Ru(NH_3)_4]^{2+}$ moiety.[5] The ^1H NMR spectrum of $[Ru(bipy)_2(NC_5H_4CHO)]^{2+}$ in $(CD_3)_2SO$ shows a singlet resonance at δ 10.38 which shifts to δ 5.99 on the addition of water due to hydrate formation of this type. The equilibrium constant for equation (3) (R = H) in aqueous solution was determined by a spectroscopic method similar to that reported by Alvarez *et al.*[5]

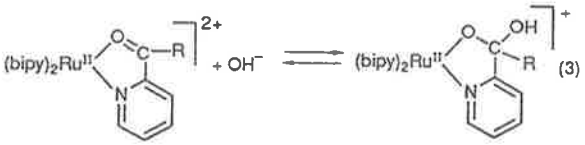

It was found that the concentrations of the aldehyde and hydrate species were equal at pH 7.95 (I = 1.00 mol dm^{-3}, NaCl; 25 °C) so that $K = 6.03 \times 10^5$ dm^3 mol^{-1}, assuming pK_w = 13.73 under these conditions.[6] This determination compares with values for pK_{hyd} (= pH where [aldehyde] = [hydrate]) of 6.5 and 6.7 obtained by Blaho and Goldsby[7] for the same system using electrochemical and spectroscopic methods respectively, although the temperature and ionic strength of the medium were not disclosed by these authors. A value of $K = 140 \pm 10$ dm^3 mol^{-1} was obtained for $[Ru(NH_3)_4(NC_5H_4CHO)]^{2+}$ under the same conditions as in the present study.[5] Accordingly, substitution of two bipy ligands for the four ammine ligands results in considerable activation of the co-ordinated aldehyde to nucleophilic attack by OH^-. Alvarez *et al.*[5] proposed that the stability of the aldehyde form in $[Ru(NH_3)_4(NC_5H_4CHO)]^{2+}$ resulted from π-back donation from the metal into the conjugated ligand system. In $[Ru(bipy)_2(NC_5H_4CHO)]^{2+}$ the extent of this back bonding from the metal to the conjugated system would be reduced due to metal-to-bipy back bonding present in the complex, resulting in decreased stability of the aldehyde form.

The complex $[Ru(bipy)_2(NC_5H_4CO_2)]^+$ **3** was prepared by reaction of pyridine-2-carboxylic acid with $[Ru(bipy)_2Cl_2]$ in an analogous manner to the syntheses of the alcohol complexes. For $[Ru(NH_3)_4(NC_5H_4CO_2H)]^{2+}$, pK_a = 0.7,[5] substitution of the ammine ligands by bipyridine would be expected to increase that acidity since back bonding from Ru^{II} to bipy enhances the Lewis acidity of the metal centre. Accordingly, $[Ru(bipy)_2(NC_5H_4CO_2)]^+$ would not be expected to be protonated, even under strongly acidic conditions.

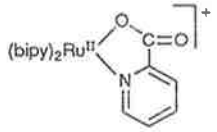

3

The visible spectra in 0.1 mol dm^{-3} HCl of $[Ru(bipy)_2(NC_5H_4CH_2OH)]^{2+}$, $[Ru(bipy)_2(NC_5H_4CHO)]^{2+}$ and its hydrate, and of $[Ru(bipy)_2(NC_5H_4CO_2)]^+$ are shown in Fig. 1.

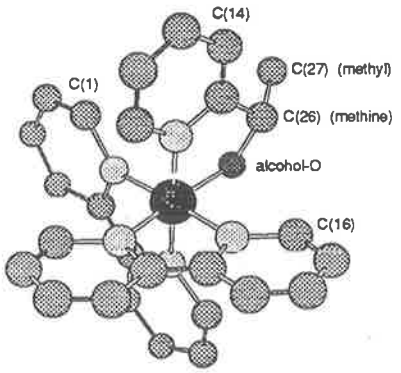

* The numbering scheme used in Fig. 2 of ref. 4 for the molecular structure of $\Lambda(S)/\Delta(R)$-$[Ru(bipy)_2\{NC_5H_4CH(CH_3)NH_2\}]^{2+}$ is adopted for the following. Irradiation of the CH_3 group resulted in enhancement (3%) of the proton attached to C(14) in the pyridine ring of $NC_5H_4CH(CH_3)NH_2$, the methine proton (2%), the proton attached to C(1) in the neighbouring bipy ring (1%) and one NH proton (1%). Irradiation of the methine proton resulted in enhancement (4%) of signals from the proton attached to C(16) in a neighbouring bipy ring, the proton attached to C(14) (2%), the methyl protons (9%), with an additional minor enhancement of the signal from the other NH proton. For the $\Lambda(R)/\Delta(S)$ diastereoisomer, irradiation of the methyl group resulted in enhancements of the proton signal on C(14) (3%), the methine proton (3%) and one NH proton (1%). Irradiation of the methine proton resulted in enhancements of the proton on C(1) (6%), the proton attached to C(14) (2%), and the other NH proton (2%). For the alcohol complexes the description of the NOE results for the $\Lambda(S)/\Delta(R)$-$[Ru(bipy)_2\{NC_5H_4CH(CH_3)OH\}]^{2+}$ diastereoisomer is essentially identical to that for the amine analogue, except for enhancements of the OH signal on irradiation of both the methyl (1%) and methine (3%) protons. However, for the $\Lambda(R)/\Delta(S)$ diastereoisomer there is a significant additional enhancement (2%) of the proton attached to C(16) when the methyl group is irradiated, and less enhancement of the signals of the protons attached to C(1) (3%) and C(14) (1%) when the methine proton is irradiated: from a study of molecular models, these observations can be rationalized in terms of a significantly greater axial orientation of the methyl group (and equatorial orientation of the methine hydrogen) relative to the mean plane of the chelate ring compared with the amine analogue.

Table 1 Electrochemical and spectral (electronic, NMR) data on ruthenium complexes reported in this study

Complex	$E_{\frac{1}{2}}$/V *vs.* SSCE	λ_{max}[a]/nm (10^{-3} ε/dm^3 mol^{-1} cm^{-1})	^{1}H NMR[b] (non-aromatic protons)
1a ($R^1 = R^2 = H$)	0.62[c]	464 (8.5), 332 (9.0)	9.53 (s, OH), 5.18 (q, CH_2)
1b ($R^1 = R^2 = D$)	0.62[c]	465 (8.7), 334 (9.1)	9.53 (s, OH)
1c ($R^1 = H$, $R^2 = CH_3$)			
isomer **A**	0.625[c]	467 (8.4), 333 (9.0)	1.25 (d, CH_3), 5.78 (q, CH), 9.39 (s, OH)
isomer **B**	0.615[c]	466 (8.5), 333 (9.0)	1.73 (d, CH_3), 5.06 (q, CH), 9.60 (s, OH)[d]
1d ($R^1 = R^2 = CH_3$)	0.50[c]	466 (8.5), 333 (9.0)	1.22 (s, CH_3), 1.84 (s, CH_3)
2a (R = H)	1.28[e]	433 (8.4)	10.38 (br, CHO)
2b ($R = CH_3$)	1.24[e]	434 (8.5)	3.66 (s, CH_3)
2c (R = D)	1.28[e]	433 (8.4)	
3	0.85[c]	469 (8.5)	

[a] In 0.1 mol dm^{-3} HCl solution. [b] In $(CD_3)_2SO$ solvent; chemical shift values quoted relative to $SiMe_4$ (internal). [c] In 0.1 mol dm^{-3} HCl solution; platinum working electrode. [d] There is a very small coupling between the methine and the alcohol protons for this diastereoisomer only. [e] In propylene carbonate–0.2 mol dm^{-3} NEt_4ClO_4; glassy carbon working electrode.

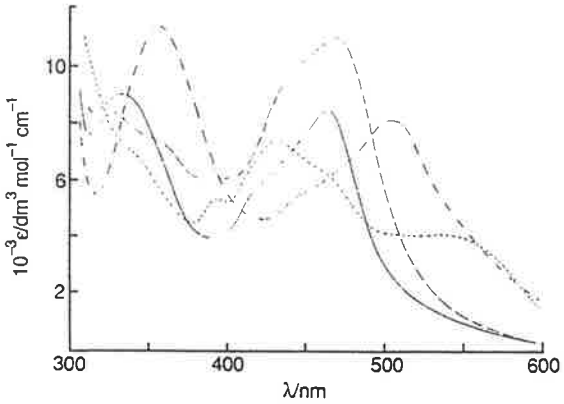

Fig. 1 Electronic spectra (in 0.1 mol dm^{-3} HCl) of $[Ru(bipy)_2(NC_5H_4CH_2OH)]^{2+}$ (——), $[Ru(bipy)_2(NC_5H_4CHO)]^{2+}$ (· · · ·), $[Ru(bipy)_2\{NC_5H_4CH(O^-)OH\}]^+$ (— · — · —), $[Ru(bipy)_2(NC_5H_4CO_2)]^+$ (– – – –)

A summary of the electrochemical and spectral (visible, ^{1}H NMR) properties for all the complexes reported in this study is given in Table 1.

Electrochemical Studies.—Cyclic voltammetry of $[Ru(bipy)_2(NC_5H_4CH_2OH)]^{2+}$ in 0.1 mol dm^{-3} HCl showed a reversible Ru^{III}–Ru^{II} couple in the anodic region, with $E_{\frac{1}{2}} = 0.62$ V. The $E_{\frac{1}{2}}$ value is pH-dependent over the range pH 1–6.5, and a plot of $E_{\frac{1}{2}}$ *vs.* pH is linear with a slope of 58 mV per pH unit. Such behaviour indicates a reversible deprotonation coupled with the electrode process, and has been observed previously for the $[Ru(L\text{–}L)_2(py)(OH_2)]^{3+/2+}$ couples (L–L = bipy[8] or 2-arylazopyridine,[9] py = pyridine), and in the present case is consistent with the reaction sequence (4) and (5). Furthermore,

$$[(bipy)_2Ru^{II}(NC_5H_4CH_2OH)]^{2+} \xrightarrow{-e^-} [(bipy)_2Ru^{III}(NC_5H_4CH_2OH)]^{3+} \quad (4)$$

$$[(bipy)_2Ru^{III}(NC_5H_4CH_2OH)]^{3+} \rightleftharpoons [(bipy)_2Ru^{III}(NC_5H_4CH_2O)]^{2+} + H^+ \quad (5)$$

the linearity of the plot throughout the pH region 1–6.5 implies the pK_a of $[Ru(bipy)_2(NC_5H_4CH_2OH)]^{3+}$ must be $\leqslant 1$.[10] In the complex $[Ru(bipy)_2(py)(OH_2)]^{2+}$ the pK_a of the aqua ligand decreases from 10.26 to 0.85 upon oxidation of the metal centre to the trivalent state.[8] The pK_a of $[Ru(bipy)_2(NC_5H_4CH_2OH)]^{2+}$ is 7.2, so that a similar decrease in the pK_a of the alcohol ligand upon oxidation of the metal centre would indicate that the pK_a of the ruthenium(III) complex may be <0, which is consistent with the electrochemical results.

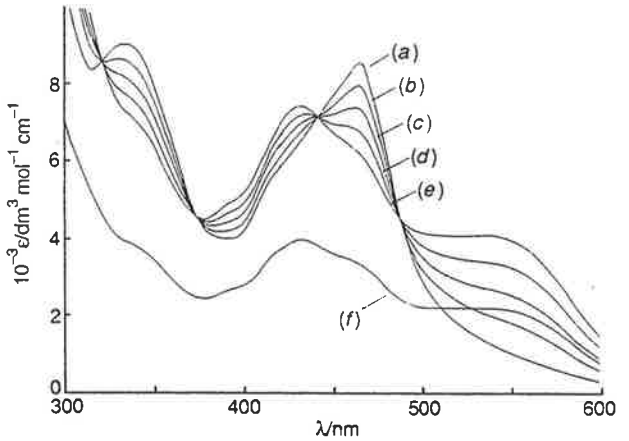

Fig. 2 Spectrocoulometric oxidation of $[Ru(bipy)_2(NC_5H_4CH_2OH)]^{2+}$ in 0.1 mol dm^{-3} CF_3SO_3H–0.9 mol dm^{-3} NaCl ($E = 0.65$ V *vs.* SSCE, platinum working electrode). Coulometric n electrons per Ru^{II}: (*a*) 0, (*b*) 0.5, (*c*) 1.0, (*d*) 1.5, (*e*) 2.0 and (*f*) 2.5

Spectrocoulometry of $[Ru(bipy)_2(NC_5H_4CH_2OH)]^{2+}$ in 0.1 mol dm^{-3} CF_3SO_3H–0.9 mol dm^{-3} NaCl solution at 0.65 V reveals a quantitative two-electron oxidation of the ligand (isosbestic points at 312, 385, 430 and 494 nm) to form the corresponding aldehyde complex $[Ru(bipy)_2(NC_5H_4CHO)]^{2+}$, identified by spectral comparisons with an authentic sample of that species (Fig. 2). The bleaching of the solution at coulometric $n > 2.0$ electrons is presumably due to formation of the ruthenium(III) species $[Ru(bipy)_2(NC_5H_4CHO)]^{3+}$.

Chemical Oxidation Studies.—The electrochemical results, and previously reported studies on the oxidation of the analogous amine complexes,[3,4] imply that the first step in the ligand oxidation reaction (2) is the one-electron oxidation of the metal centre, $Ru^{II} \longrightarrow Ru^{III}$. Of a number of chemical oxidants capable of promoting this step, $[Os(bipy)_3]^{3+}$ {$E_{\frac{1}{2}}$ for $[Os(bipy)_3]^{3+/2+} = 0.82$ V in aqueous acidic solution} was chosen because of its stability in aqueous solution over the pH range studied (0–6), and because of the presumed rapidity of reaction (6). Although the rate of this electron transfer was not

$$[Os^{III}(bipy)_3]^{3+} + [(bipy)_2Ru^{II}(NC_5H_4CH_2OH)]^{2+} \longrightarrow [Os^{II}(bipy)_3]^{2+} + [(bipy)_2Ru^{III}(NC_5H_4CH_2OH)]^{3+} \quad (6)$$

measured directly, its order of magnitude can be estimated to be $>10^9$ dm^3 mol^{-1} s^{-1}.[11] {The rate of self exchange for $[Ru(bipy)_2(NC_5H_4CH_2OH)]^{3+/2+}$ was assumed to be similar to that for $[Ru(bipy)_3]^{3+/2+}$ (2×10^9 dm^3 mol^{-1} s^{-1}).[12a] The

Table 2 Variation of the second-order rate constant k_2 for the oxidation of $[Ru(bipy)_2(NC_5H_4CH_2OH)]^{2+}$ with base strength

Base	pK_a of conjugate acid *	$10^2 k_2$/dm^3 mol^{-1} s^{-1}
Acetate	4.56	25.1
Formate	3.56	12.9
Chloroacetate	2.64	5.2
Dichloroacetate	0.98	1.1

* Values determined within this work under the conditions of the kinetic experiments [I = 1.0 mol dm^{-3} (NaCl), 25.0 °C].

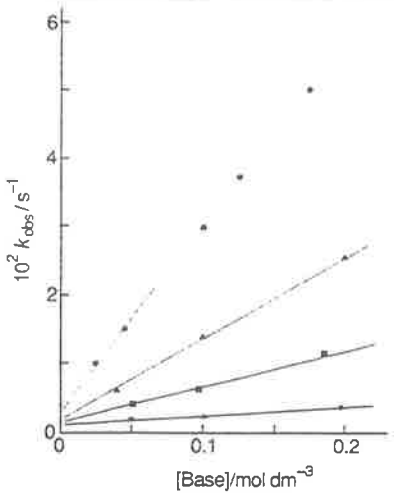

Fig. 3 Variation in pseudo-first-order rate constant (k_{obs}) with base and [base] for the base-catalysed oxidation of $[Ru(bipy)_2(NC_5H_4CH_2OH)]^{2+}$: ●, acetate buffer; ▲, formate buffer; ■, chloroacetate buffer; ★, dichloroacetate buffer

self-exchange rate for $[Os(bipy)_3]^{3+/2+}$ was also assumed to be 2×10^9 dm^3 mol^{-1} s^{-1}.[12b]

The stoichiometry of the reaction succeeding (6) is as in equation (7) and this could be followed spectrophotometrically

$$2[(bipy)_2Ru^{III}(NC_5H_4CH_2OH)]^{3+} \longrightarrow [(bipy)_2Ru^{II}(NC_5H_4CH_2OH)]^{2+} + [(bipy)_2Ru^{II}(NC_5H_4CHO)]^{2+} + 2H^+ \quad (7)$$

by monitoring the appearance of the aldehyde complex subsequent to the rapid formation of $[Ru(bipy)_2(NC_5H_4CH_2OH)]^{3+}$. The kinetics of formation of $[Ru(bipy)_2(NC_5H_4CHO)]^{2+}$ exhibited first-order behaviour, with $\log(A_\infty - A_t)$ *vs.* t plots being linear for at least 3 half-lives. The rate constant was independent of the concentration of $[Ru(bipy)_2(NC_5H_4CH_2OH)]^{2+}$, but strongly dependent on pH, base strength and base concentration.

Rate Studies in Buffer Solutions.—Variations of k_{obs} with base and base concentration. Rate studies of the oxidation reaction in the presence of a number of bases revealed general base catalysis of the process. Fig. 3 shows the dependence of k_{obs} on acetate, formate, chloroacetate and dichloroacetate concentrations in buffer solutions at pH $\approx pK_a$ in each case. A second-order rate constant (k_2) corresponding to the base-assisted process could be calculated for each set of buffers from the slope of these lines (Table 2). The variation of the intercepts with the various bases is consistent with the rate at the corresponding pH of a parallel base-independent pathway, which was studied by use of pH-stat techniques (see later).

For a general base-catalysed reaction involving the transfer of one proton the Brønsted catalysis law[13] requires the proportionality of log k_2 and pK_a: in the present case a plot of the data from Table 2 gives a straight line of slope $\beta = 0.4$, indicating general base catalysis involving an essentially symmetrical transition state.[14]

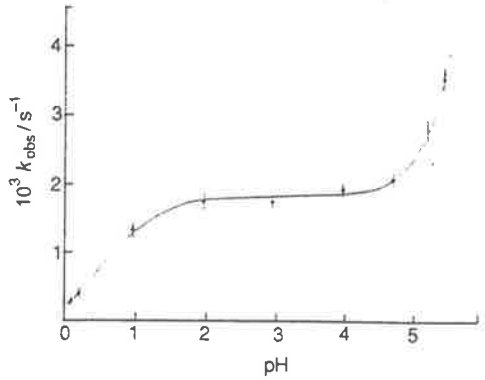

Fig. 4 Variation in pseudo-first-order rate constant (k_{obs}) with pH for the base-independent oxidation of $[Ru(bipy)_2(NC_5H_4CH_2OH)]^{2+}$

Comparative rate studies of the oxidation of $[(Ru(bipy)_2(NC_5H_4CD_2OH)]^{2+}$ reveal a kinetic isotope effect $k_H/k_D = 9$, which clearly demonstrates that the C–H bond is broken in the rate-determining step. The value of the kinetic isotope effect is sensitive to the symmetry of the transition state,[15] a large value being interpreted to indicate a symmetrical transition state, which verifies the conclusions based on the value of β.

The general base catalysis is presumed to be associated with base-assisted removal of the methylene (or methine) proton from the α-carbon atom in the rate-determining step.[4]

Variation of k_{obs} with pH.—A kinetic study of the oxidation of $[Ru(bipy)_2(NC_5H_4CH_2OH)]^{2+}$ was undertaken in the range pH 0–5.5 using pH-stat facilities (NaOH titrant) in conjunction with spectrophotometric measurements. The pH-stat results revealed that one H^+ per Os^{III} was produced during the oxidation reaction and that the uptake of NaOH was primarily associated with the mixing of the ruthenium(II) and osmium(III) reactants, and not with the subsequent slower formation of the $[Ru(bipy)_2(NC_5H_4CHO)]^{2+}$ product.

For the intramolecular redox process the spectrophotometric studies of the rate of formation of the product revealed linear log $(A_\infty - A_t)$ *vs.* t plots for 3 half-lives, and the pH-rate profile is given in Fig. 4. The curve shows an increase in k_{obs} from pH 0 to 2, followed by a pH-independent region between pH 2 and 5, with a subsequent rapid increase in rate above pH 5.

A deuterium isotope-exchange study, in which the oxidation of $[Ru(bipy)_2(NC_5H_4CH_2OH)]^{2+}$ was undertaken in D_2O solution, revealed the formation of $[Ru(bipy)_2(NC_5H_4CHO)]^{2+}$ only, so that no exchange at the methylene carbon atom occurs during the reaction.

Mechanism of Oxidative Dehydrogenation.—There have been a number of mechanistic studies of ligand oxidations, and in particular of co-ordinated amines. A common feature is that initial oxidation occurs at the metal centre with oxidative dehydrogenation of the ligand taking place in a subsequent intramolecular redox process. There are two commonly accepted alternative paths for this latter process. The first involves the intermediacy of a *ligand radical* species, and this has been identified in studies of the oxidations of nickel(II) complexes of a variety of macrocycles,[16–18] $[Fe(CN)_4(en)]^-$ (en = ethane-1,2-diamine),[19] and $[Fe(tacn)_2]^{3+}$ (tacn = 1,4,7-triazacyclononane).[20] The second alternative invokes *disproportionation* at the metal centre to form an oxidation state two units higher than the final state, allowing two-electron oxidation of the ligand with concomitant two-electron reduction of the metal. Detailed mechanistic studies of ligand oxidation in $[Ru(bipy)_2(NC_5H_4CH_2NH_2)]^{2+}$ [$NC_5H_4CH_2NH_2$ = 2-(aminomethyl)-

pyridine] and analogues (from our laboratories),[3,4] $[Os(en)_3]^{2+}$ (by Lay *et al.*[21]) and $[Ru(hbi)]^{2+}$, $[Ru(en)_3]^{2+}$ and $[Ru(tame)_2]^{2+}$ complexes {hbi = 3,6,10,13,16,19-hexaazabicyclo-[6.6.6]icosane; tame = 1,1,1-tris(aminomethyl)ethane} by Bernhard, Bull and Sargeson[22,23] have identified these disproportionation processes: the substantial stabilization of the higher oxidation states of their complexes by ligand deprotonation is a significant factor contributing to the particular ability of ruthenium and osmium to promote such reactions by this pathway.

In light of the results of the closely related studies on oxidative dehydrogenation reactions involving analogous amine complexes, the intermediacy of the ruthenium(IV)–alkoxide species, $[Ru(bipy)_2(NC_5H_4CH_2O)]^{3+}$, in the oxidation of $[Ru(bipy)_2(NC_5H_4CH_2OH)]^{2+}$ seemed likely. Two additional observations favour this hypothesis. First, the presence of a vast excess ($\times 10^4$) of the radical scavenger acrylamide had no effect on the rate of the oxidation reaction (carried out at pH 3), and no polymerization occurred. It is therefore unlikely that the oxidation mechanism involved a ligand radical species, as required for the intermediacy of a ruthenium(III) complex. Secondly, a study of the variation of the rate of the oxidation process with ionic strength (I) was undertaken at low I (< 0.04 mol dm^{-3}). According to the Brønsted–Bjerrum relationship[24] between k_{obs} and ionic strength, $\log(k_{obs}) = \log k_0 + 1.02 Z_A Z_B I^{\frac{1}{2}}$ where k_0 = rate constant at infinite dilution, Z_A and Z_B are the charges on the reacting species, a plot of $\log(k_{obs})$ *vs.* $I^{\frac{1}{2}}$ at pH 4.41 in acetate buffer solution revealed a linear relationship with a slope of -2.8. This result is interpreted to indicate that the charge on the metal complex involved in the base-catalysed reaction must be +3.

Over the range pH 2–5 the observations are consistent with the rapid formation of a ruthenium(III)–alcohol species which is immediately deprotonated, $pK_a \approx 1$. A rapid disproportionation process follows in which the intermediate $[Ru^{IV}(bipy)_2(NC_5H_4CH_2O)]^{3+}$ is formed, which then undergoes the observed first-order decay to the aldehyde product. Accordingly, the rate-determining step of the reaction may be written as in equation (8). In the absence of any other oxidizing species, the

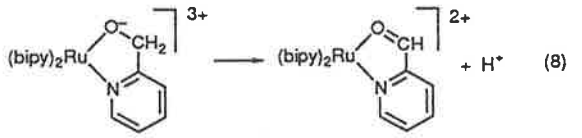

(8)

ruthenium(IV) complex may only arise from the disproportionation of two ruthenium(III) species, as described for the analogous amine species.[3,4]

Additionally, in their study of the oxidation of the alcohol complex $[Ru(NH_3)_4\{NC_5H_4CH(CH_3)OH\}]^{2+}$, Tovrog *et al.*[2] showed that on raising the pH of the solution of the ruthenium(III)–alcohol complex, equimolar amounts of the ruthenium(II)–alcohol and –ketone complexes formed. They suggested the involvement of a ruthenium(IV)–alkoxide species formed upon disproportionation of two ruthenium(III)–alcohol molecules. A similar experiment was undertaken with $[Ru(bipy)_2(NC_5H_4CH_2OH)]^{2+}$. A solution of $[Ru(bipy)_2(NC_5H_4CH_2OH)]^{2+}$ in 1.0 mol dm^{-3} was electrolysed at 650 mV [*vs.* saturated sodium chloride calomel electrode (SSCE)] to yield an essentially colourless solution of the ruthenium(III)–alkoxide complex, $[Ru(bipy)_2(NC_5H_4CH_2O)]^{2+}$. This formulation could be verified as the electrolysis corresponded to $1e^-$ per Ru^{II} and by the quantitative re-reduction of the ruthenium(III) species to the ruthenium(II) complex by electrolysis at 0.50 V (*vs.* SSCE). Additionally, there are close electronic spectral similarities between the ruthenium(III) complex (λ_{max} = 375 nm, ε = 4000 dm^3 mol^{-1} cm^{-1}) and $[Ru(bipy)_2(py)(OH)]^{2+}$ (ref. 8) (λ_{max} = 364 nm, ε = 4700 dm^3 mol^{-1} cm^{-1}). Dilution of the electrogenerated complex (20:1) with deaerated 1 mol dm^{-3} NaCl resulted in the gradual formation of an absorbance at 482 nm. A

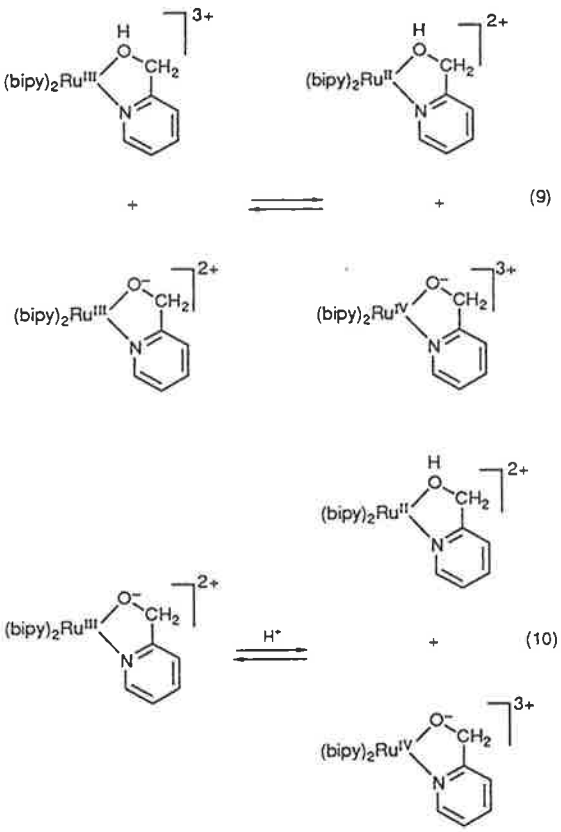

plot of $\log(A_\infty - A_t)$ *vs.* t for this reaction showed k_{obs} = 1.1×10^{-3} s^{-1} at pH 1.3, which is very similar to the observed rate for the osmium(III)-promoted oxidation of $[Ru(bipy)_2(NC_5H_4CH_2OH)]^{2+}$ at the same pH to form the same product. This behaviour is consistent with a disproportionation reaction between two ruthenium(III) species to form a ruthenium(IV) complex. The disproportionation reaction would be written either as in equation (9) or (10) depending on the pH of the solution.

The observed first-order behaviour requires that by the time the first point is recorded effectively complete formation of the ruthenium(IV) species has occurred, otherwise second-order terms in $[Ru^{III}]$ would be observed. Hence, $E_{\frac{1}{2}}$ of the redox couple $[Ru(bipy)_2(NC_5H_4CH_2OH)]^{3+/2+}$ must be anodic of that for $[Ru(bipy)_2(NC_5H_4CH_2O)]^{3+/2+}$. Such an observation is not without precedence. The Ru^{IV}–Ru^{III} couple of $[RuL_2(py)(OH)]^{n+}$ (L = 2-phenyl- or 2-tolyl-azopyridine) is cathodic of the Ru^{III}–Ru^{II} couple of $[RuL_2(py)(OH_2)]^{n+}$,[9] and in our previous studies of the oxidation of the $[Ru(bipy)_2(NC_5H_4CH_2NH_2)]^{2+}$ the $E_{\frac{1}{2}}$ of the deprotonated Ru^{IV}–Ru^{III} couple was deduced to be cathodic of the non-deprotonated Ru^{III}–Ru^{II} couple.[3] Another example of such behaviour was reported in studies of the oxidation of $[Ru(terpy)(bipy)(NH_2Pr^i)]^{2+}$ (terpy = 2,2′:6′,2″-terpyridine) where it was found that E_{pa} for the Ru^{IV}–Ru^{III} couple of $[Ru(terpy)(bipy)(N{=}CMe_2)]^{n+}$ (imine ligand deprotonated) was 0.34 V cathodic of E_{pa} for the Ru^{III}–Ru^{II} couple of $[Ru(terpy)(bipy)(NH{=}CMe_2)]^{n+}$ (imine ligand non-deprotonated).[25] The pronounced stabilization of higher oxidation states of ruthenium by ligand deprotonation is a consequence of substantial ligand-to-metal π bonding, and has been discussed previously.[3,4,25]

It is interesting that whereas the kinetics of formation of the aldehyde product is first order, the analogous formation of the imine product from the amine complex $[Ru(bipy)_2(NC_5H_4CH_2NH_2)]^{2+}$ was observed to have considerable second-order characteristics.[3] Given that the rates of the preliminary protonic

and disproportionation processes are comparable in the two cases, the difference between the amine and alcohol species is a consequence of the stability and substantially slower dehydrogenation of the ruthenium(IV)–alkoxide intermediate relative to its ruthenium(IV)–amide counterpart.

In an attempt to isolate a ruthenium(IV) complex analogous to that inferred from the kinetic considerations above, $[Ru(bipy)_2\{NC_5H_4C(CH_3)_2OH\}]^{2+}$ was synthesized. This complex would not be expected to undergo ligand dehydrogenation because of the dimethylation at the α-carbon atom. It was hoped that should the Ru^{IV}–Ru^{III} couple of the deprotonated alcohol $[Ru(bipy)_2\{NC_5H_4C(CH_3)_2O\}]^{3+/2+}$ be cathodic of the $[Ru(bipy)_2\{NC_5H_4C(CH_3)_2OH\}]^{3+/2+}$ couple, then exhaustive electrolysis of a solution of $[Ru(bipy)_2\{NC_5H_4C(CH_3)_2OH\}]^{2+}$ would yield a ruthenium(IV) complex with a coulometric $n = 2$. The alcohol complex shows a reversible cyclic voltammetric couple, but exhaustive electrolysis at a potential anodic of this couple resulted in $n = 1$ at pH 1 and 4, indicating formation of the ruthenium(III) species. The failure to produce $[Ru(bipy)_2\{NC_5H_4C(CH_3)_2O\}]^{3+}$ directly may be interpreted to show the sensitivity of the Ru^{IV}–Ru^{III} redox couple in these complexes to the variation of ligand environment around the metal centre: in this case the steric consequences of dimethylation at the α-carbon atom of the chelate ring may destabilize the ruthenium(IV)–alkoxide species.

The Relative Rate of Oxidation of the Two Diastereoisomers of $[Ru(bipy)_2\{NC_5H_4C(CH_3)OH\}]^{2+}$.—The complex $[Ru(bipy)_2\{NC_5H_4CH(CH_3)OH\}]^{2+}$ exists in two diastereoisomeric pairs, in which the α-methyl group is either axial or equatorial to the mean plane of the chelate ring. It was possible to separate the two diastereoisomers partially by repeated fractional crystallization of the iodide salt, with the ultimate ratios **A**:**B** in the final enriched samples being 86:14 and 22:78, determined by integration of the separate methyl resonances in an ^1H NMR spectrum of each of the samples.

Kinetic studies of the oxidation of the two diastereoisomers were undertaken on these enriched samples: since the ketone produced by the oxidation is non-chiral, the same product is obtained by the oxidation of both diastereoisomers **A** and **B**. The kinetics of oxidation of **A** and **B** therefore exhibited the behaviour of two competing parallel reactions, as is shown in equation (11). The rates of oxidation of the two enriched

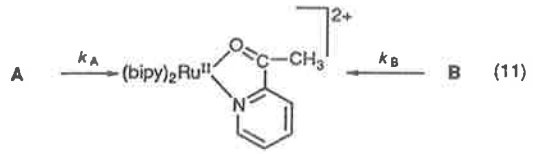

(11)

samples were measured in acetate buffer solutions, and knowing the relative proportions of **A**:**B** in the two samples the rate constants k_A and k_B were determined[26] to be 0.018 and 0.19 $dm^3\ mol^{-1}\ s^{-1}$. The ten-fold variation between **A** and **B** for the acetate-catalysed oxidation process confirms that C–H bond cleavage is involved in the rate-determining step and shows that this cleavage is sensitive to the stereochemical environment of the methine carbon.

For the corresponding amine complexes involving the ligand $NC_5H_4CH(CH_3)NH_2$ there was little difference in the rates of oxidation of the two diastereoisomers.[4] Interestingly, the relative rates of oxidation for the two diastereoisomer stereochemistries were reversed for the alcohol and amine analogues. In the present instance of the alcohol complex the origins for the different rates of oxidation of **A** and **B** are a difference in the acidity of the methine proton in the two diastereoisomers and/or stereochemical effects. If the explanation were the former and a common mechanism applies for the oxidation of the two diastereoisomers, then the acidity of the methine proton of **B** is one pK_a unit less than that of **A** given the ten-fold difference in the oxidation rates. On the other hand, the difference in rates may reflect the orientation of the methine proton (axial or equatorial) within the ruthenium(IV)–alkoxide intermediate and its accessibility to approach by the abstracting base. While it is clear that in the ruthenium(II) complexes, where the ligand is not deprotonated, the more rapidly oxidized diastereoisomer **B** has a clear equatorial orientation of the methine proton, no conclusion can be drawn for the ruthenium(IV) intermediate since in the latter case the alcohol OH group would be deprotonated and the anticipated substantial π interaction between the metal centre and the alkoxide group would lead to significant changes in the stereochemistry of the chelate ring.

Experimental

Measurements.—Electronic spectra were recorded on a Cary 219 spectrophotometer, NMR spectra using either a JEOL FX90Q or a Bruker AM-300 spectrometer; resonances are quoted relative to $SiMe_4$ as an internal reference.

All electrochemical measurements were made (and are quoted) *vs.* the SSCE and are uncorrected for junction potentials. Cyclic voltammetry experiments were performed using a Bioanalytical Systems (BAS) CV-27 Voltammograph, or a Utah Electronics 0152 potentiostat coupled to a 0151 sweep generator, and output on a Rikadenki RW-101 or a Linseis LY-1800 X-Y recorder. Coulometry experiments were made using the BAS Voltammograph. Temperature control for electrochemical experiments was achieved with a Lauda K4RD circulating water-bath (25.00 ± 0.05 °C).

Elemental analyses were carried out by the Australian Microanalytical Service, AMDEL, Melbourne.

Materials.—Tetraethylammonium perchlorate, used as an electrolyte for electrochemical measurements, was prepared and purified by standard techniques.[27] 2-Acetyl- and 2-(hydroxymethyl)-pyridine (Fluka) were used as received, and pyridine-2-carbaldehyde (Sigma) and 2-bromopyridine (Fluka) were distilled prior to use. Propylene carbonate (Aldrich) was distilled immediately before use (90–92 °C, 3–3.5 mmHg) and stored over 4 Å molecular sieves. Ammonium cerium sulfate (Fluka, puriss) was standardized and found to be $(NH_4)_4Ce(SO_4)_4\cdot H_2O$. All other chemicals were AR grade where available and were used without further purification. Tetrahydrofuran (thf) was distilled from sodium.

Syntheses.—The compounds $[Ru(bipy)_2Cl_2]\cdot 2H_2O$,[28] $[Ru(bipy)_2(CO_3)]\cdot 2H_2O$,[29] $[Os(bipy)_3][ClO_4]_2\cdot 2H_2O$,[30] pyridine-2-carboxylic acid[31] and 2-(1-hydroxyethyl)pyridine[32] were synthesized by literature methods.

2-(Dideuteriohydroxymethyl)pyridine, $NC_5H_4CD_2OH$. The compound $LiAlD_4$ (0.9 g) was suspended in freshly distilled dry thf (15 cm^3) under N_2. Pyridine-2-carboxylic acid (0.8 g) dissolved in thf (10 cm^3) was added dropwise with stirring, and the solution was refluxed for 24 h. After cooling, water (0.9 cm^3), 15% aqueous NaOH (2.5 cm^3) and water (0.9 cm^3) were sequentially added and the solution filtered. The precipitate was washed with diethyl ether, and the filtrate extracted with ether, and the combined organic extracts dried over anhydrous Na_2SO_4. After filtration, the solvent was removed by evaporation at reduced pressure to yield the crude product (0.8 g, 90%), which was used directly for complex formation.

2-(2-Pyridyl)propan-2-ol, $NC_5H_4C(CH_3)_2OH$. Freshly distilled 2-bromopyridine (3.5 cm^3, 0.030 mol) in dry ether (40 cm^3) was added rapidly dropwise to a stirred solution of $LiBu^n$ (25.5 cm^3, 1.40 mol dm^{-3}) cooled to −60 °C, giving a deep red solution. The mixture was stirred for 15 min and a solution of acetone (3.0 cm^3, 0.052 mol) in ether (20 cm^3) and thf (20 cm^3) was added dropwise. The mixture was stirred for 1 h, then allowed to warm to room temperature. The red solution was acidified (2.5 mol dm^{-3} H_2SO_4) and the ether layer extracted with 2.5 mol dm^{-3} H_2SO_4 (3 × 30 cm^3). The combined acid

extracts were basified using NaOH, and the mixture extracted with ether. The organic extract was dried over anhydrous Na_2SO_4, and the solvent evaporated. The product was distilled under reduced pressure (b.p. 77 °C, 7 mmHg); yield 2.2 g, 45%; m.p. 50 °C (lit.,[33] 50–51 °C). The ^1H NMR spectrum ($CDCl_3$) showed δ 1.55 (CH_3) and 5.00 (–OH).

Bis(2,2′-*bipyridine*)[2-(*hydroxymethyl*)*pyridine*]*ruthenium*(II) *hexafluorophosphate*, $[Ru(bipy)_2(NC_5H_4CH_2OH)][PF_6]_2$ **1a**. 2-(Hydroxymethyl)pyridine (2.2 g, 20 mmol) was added to a deaerated refluxing solution of $[Ru(bipy)_2Cl_2]\cdot 2H_2O$ (550 mg, 1.05 mmol) in water–methanol solution (1:1, 30 cm^3). After the solution had been refluxed for 40 min under a nitrogen atmosphere, 75% HPF_6 (2.5 cm^3) was added, the condenser removed, and the methanol boiled off. The solution was cooled, filtered, and the product washed with ice-cold 0.1 mol dm^{-3} HCl and dried *in vacuo*. The complex was dissolved in 0.01 mol dm^{-3} HCl and sorbed onto a column packed with SP-Sephadex C-25 cation exchanger; on elution with 0.5 mol dm^{-3} NaCl–0.01 mol dm^{-3} HCl the second (major) band was collected. The product was precipitated by the addition of NH_4PF_6, filtered off, washed with 0.1 mol dm^{-3} HCl, and dried *in vacuo*. Yield 580 mg, 68% (Found: C, 37.7; H, 2.95; N, 8.3. $C_{26}H_{23}F_{12}N_5OP_2Ru$ requires C, 38.4; H, 2.85; N, 8.6).*

Bis(2,2′-bipyridine)[2-(dideuteriohydroxymethyl)pyridine]-ruthenium(II) hexafluorophosphate, $[Ru(bipy)_2(NC_5H_4CD_2OH)][PF_6]_2$ **1b** was prepared in an analogous manner (Found: C, 38.4; H, 3.10; N, 8.7. $C_{26}H_{21}D_2F_{12}N_5OP_2Ru$ requires C, 38.3; H/D, 3.10; N, 8.5%).

Bis(2,2′-bipyridine)[2-(1-hydroxyethyl)pyridine]ruthenium-(II) hexafluorophosphate, $[Ru(bipy)_2\{NC_5H_4CH(CH_3)OH\}][PF_6]_2$ **1c**, was prepared in 70% yield by a similar method (Found: C, 37.7; H, 3.10; N, 8.4. $C_{27}H_{25}F_{12}N_5OP_2Ru$ requires C, 37.7; H, 3.25; N, 8.4%). This complex exists as two diastereoisomeric pairs which could be obtained in *ca.* 80–85% enrichment by repeated fractional crystallizations as the iodide salt. Attempts to separate the two diastereoisomers chromatographically in an analogous manner to that for the amine analogues[4] were unsuccessful because of gradual oxidation of the complex under the conditions (pH 3, 4 °C) in the time-scale of the separation (weeks). The separation of the two diastereoisomers was monitored by ^1H NMR spectroscopy in $(CD_3)_2SO$: the diastereoisomer which formed the less-soluble iodide (**A**) showed a doublet resonance centred at δ 1.25 due to the methyl group, compared with δ 1.73 observed for the more-soluble diastereoisomer (**B**). Ultimate ratios **A**:**B** in the final enriched samples were 86:14 and 22:78.

Bis(2,2′-bipyridine)[2-(2-pyridyl)propan-2-ol]ruthenium(II) hexafluorophosphate, $[Ru(bipy)_2\{NC_5H_4C(CH_3)_2OH\}][PF_6]_2$ **1d**, was prepared and purified in an analogous manner (Found: C, 40.5; H, 3.35; N, 8.1. $C_{28}H_{27}F_{12}N_5OP_2Ru$ requires C, 40.0; H, 3.25; N, 8.3%).

Bis(2,2′-*bipyridine*)*bis*(*trifluoromethanesulfonato*)*ruthenium*-(II), $[Ru(bipy)_2(O_3SCF_3)_2]$. The compound $[Ru(bipy)_2(CO_3)]\cdot 2H_2O$ (200 mg) was suspended in 1,2-dimethoxyethane (10 cm^3), trifluoromethanesulfonic acid (0.5 cm^3) was added slowly with stirring, and the solution cooled and maintained at 0 °C overnight. The precipitate was filtered off, washed with diethyl ether, and dried *in vacuo*. Yield 140 mg, 75%.

Bis(2,2′-*bipyridine*)(*pyridine*-2-*carbaldehyde*)*ruthenium*(II) *hexafluorophosphate*, $[Ru(bipy)_2(NC_5H_4CHO)][PF_6]_2$, **2a**. The compound $[Ru(bipy)_2(O_3SCF_3)_2]$ (200 mg) was suspended in a freeze-thaw-degassed solution of freshly distilled ligand (0.2 g, seven-fold molar excess) in dichloromethane (10 cm^3), and the mixture stirred in the dark on a vacuum line for 12 h. The vacuum was released, and the solution rapidly extracted with an aqueous 1% HPF_6 solution to remove the excess of ligand. The dichloromethane layer was evaporated to dryness (rotary evaporator), and the residue dissolved in 5 × 10^{-3} mol dm^{-3} HCl (25 cm^3) by stirring with Dowex 1 × 8 resin (Cl^- form). This solution was sorbed onto a column of SP-Sephadex C-25 cation exchanger and eluted with 0.5 mol dm^{-3} NaCl–5 × 10^{-3} mol dm^{-3} HCl. The second (major) band was collected and the complex precipitated by addition of NH_4PF_6. The precipitate was filtered off, washed with ice-cold 0.1 mol dm^{-3} HCl and dried *in vacuo*. Yield 183 mg, 80% (Found: C, 37.8; H, 2.70; N, 8.7. $C_{26}H_{21}F_{12}N_5OP_2Ru$ requires C, 38.5; H, 2.80; N, 8.6%).

(2-Acetylpyridine)bis(2,2′-bipyridine)ruthenium(II) hexafluorophosphate, $[Ru(bipy)_2\{NC_5H_4C(CH_3)O\}][PF_6]_2$ **2b**, was prepared and purified in an analogous manner (Found: C, 39.1; H, 2.90; N, 11.9. $C_{27}H_{23}F_{12}N_5OP_2Ru$ requires C, 39.3; H, 3.00; N, 11.8%).

Bis(2,2′-*bipyridine*)(*pyridine*-2-*carboxylato*)*ruthenium*(II) *hexafluorophosphate*, $[Ru(bipy)_2(NC_5H_4CO_2)]PF_6$ **3**. This was prepared in an analogous manner to that for $[Ru(bipy)_2(NC_5H_4CH_2OH)][PF_6]_2$. The complex was chromatographed as for $[Ru(bipy)_2(NC_5H_4CHO)][PF_6]_2$ and the first band collected (Found: C, 45.7; H, 3.00; N, 10.1. $C_{26}H_{20}F_6N_5O_2PRu$ requires C, 45.8; H, 2.95; N, 10.3%).

Stoichiometry and Equilibrium Studies.—Spectrocoulometric titration of the oxidation of $[Ru(bipy)_2(NC_5H_4CH_2OH)]^{2+}$. A solution of $[Ru(bipy)_2(NC_5H_4CH_2OH)][PF_6]_2$ (50 cm^3, 3.123 × 10^{-4} mol dm^{-3} in 0.1 mol dm^{-3} CF_3SO_3H–0.9 mol dm^{-3} NaCl) was placed in the working electrode compartment of a conventional three-compartment electrochemical cell. The solution was deaerated with Ar† and the potential of the working electrode set to 0.65 V by use of a coulometer. By taking samples, the electronic spectra of the initial solution and of the solution after oxidation corresponding to 0.5, 1.0, 1.5 and 1.99 e^- per molecule of Ru were recorded. The working electrode potential was increased to 0.80 V and a current corresponding to a further 0.5 e^- per molecule Ru was passed at which time the solution spectrum was again recorded.

Determination of the pK_a *of* $[Ru(bipy)_2(NC_5H_4CH_2OH)]^{2+}$, $[Ru(bipy)_2\{NC_5H_4CH(CH_3)OH\}]^{2+}$ *and* $[Ru(bipy)_2\{NC_5H_4(CH_3)_2OH\}]^{2+}$. The pK_a values for $[Ru(bipy)_2(NC_5H_4CH_2OH)]^{2+}$ and $[Ru(bipy)_2\{NC_5H_4CH(CH_3)OH\}]^{2+}$ in 0.1 mol dm^{-3} $LiNO_3$ solution and of $[Ru(bipy)_2\{NC_5H_4C(CH_3)_2OH\}]^{2+}$ in 0.1 mol dm^{-3} KNO_3 solution were determined at 25.0 °C by an automated titration system which has been described elsewhere.[36] In all cases the reported value is the average of two runs.

Determination of the equilibrium constant for hydrate formation of $[Ru(bipy)_2(NC_5H_4CHO)]^{2+}$. An argon-deaerated solution of $[Ru(bipy)_2(NC_5H_4CHO)][PF_6]_2$ (35 cm^3, 1.12 × 10^{-5} mol dm^{-3} in 10^{-4} mol dm^{-3} HCl–1.0 mol dm^{-3} NaCl) was placed in the titrating compartment of a Radiometer ETS 882 end-point titrating system. This solution was circulated through a 1 cm path length cell in the cell compartment of a Cary 219 spectrophotometer by use of a Gilson Minipuls 2 peristaltic pump. The pH was adjusted to the desired value over the range 5–11 by addition of 0.01 mol dm^{-3} NaOH–0.99 mol dm^{-3} NaCl, and the optical density of the solution measured at 435 and 505 nm. The equilibrium constant of the complex was calculated by a similar technique to that described by Ford and co-workers[5] for the analogous $[Ru(NH_3)_4(NC_5H_4CHO)]^{2+}$ system.

* For some complexes in this study, microanalytical features were persistently low for C. In such cases, characterization and purity assessment were made on the basis of NMR spectra, electrochemical behaviour, and ion-exchange chromatography.

† All electrochemical and kinetic measurements were conducted in argon-deaerated media due to the potential sensitivity to oxygen of the alcohol complexes. Argon was scrubbed of O_2 by passing through either a column packed with BTS catalyst (Fluka) at 180 °C[34] or a chromium(II) solution.[35]

Deuterium Exchange Studies.—A solution of $[Ru(bipy)_2(NC_5H_4CD_2OH)][PF_6]_2$ (45.3 mg, 0.056 mmol) in 0.5 mol dm^{-3} H_2SO_4 was deaerated, and a solution of $(NH_4)_4Ce(SO_4)_4 \cdot H_2O$ in the same solvent (4.67 cm^3 of 0.119 mol dm^{-3}, 0.056 mmol) was added. The solution was allowed to stand until no further reaction occurred (*ca.* 4 h) and then the complex was precipitated by the addition of excess of solid NH_4PF_6. The precipitate (a mixture of the reactant alcohol and product aldehyde complexes) was filtered off, washed with ice-cold 0.1 mol dm^{-3} HCl, and dried *in vacuo*. The ^1H NMR spectrum of the dried solid was measured in $(CD_3)_2SO$.

Kinetic Studies.—Solutions of $[Os(bipy)_3]^{3+}$ were electrogenerated immediately prior to use by exhaustive electrolysis of a solution of $[Os(bipy)_3][ClO_4]_2 \cdot 2H_2O$ in the medium to be studied (I = 1.0 mol dm^{-3}, NaCl) at 0.9 V. These solutions and $[Ru(bipy)_2(NC_5H_4CH_2OH)]^{2+}$ solutions were deaerated (Ar) and thermostatted before mixing.

Stopped-flow studies using buffer pH *control.* The ruthenium(II) and osmium(III) solutions were mixed using a hand-operated stopped-flow device constructed in the Department. The mixed solution passed into a 1 cm path length flow-through cell placed in the cell compartment of a Cary 219 spectrophotometer. The cell block was thermostatted to 25.0 °C and the cell compartment was maintained under an argon atmosphere to minimize oxygen leakage through the tubing used to connect the mixing device with the cell. The reaction was monitored at 482 and/or 467 nm.

In a typical experiment, a solution of $[Ru(bipy)_2(NC_5H_4CH_2OH)][PF_6]_2$ (4.97×10^{-5} mol dm^{-3}) dissolved in 0.1 mol dm^{-3} acetate buffer (I = 1.0 mol dm^{-3}, NaCl) was mixed with a 1.75×10^{-5} mol dm^{-3} solution of $[Os(bipy)_3]^{3+}$ in the same medium. For a given set of conditions (pH, buffer type, buffer concentration) a minimum of three runs were recorded and the average value from these runs used in the calculations. The pH values of the solutions were measured before and after the oxidation reaction with a Radiometer PHM82 standard pH meter to ensure that adequate pH control was maintained during the reaction.

Studies using pH*-stat control.* The pH was maintained using a Radiometer ETS 822 end-point titration system. An aliquot (20 cm^3) of $[Ru(bipy)_2(NC_5H_4CH_2OH)]^{2+}$ (4×10^{-5} mol dm^{-3}) in 10^{-4} mol dm^{-3} HCl–1.0 mol dm^{-3} NaCl was placed in a thermostatted titration vessel. After deaeration, a 1 cm^3 aliquot of freshly generated $[Os(bipy)_3]^{3+}$ solution (2×10^{-4} mol dm^{-3} in 10^{-4} mol dm^{-3} HCl–1.00 mol dm^{-3} NaCl) was added and the solution adjusted to the desired pH by the addition of 0.01 mol dm^{-3} NaOH–0.99 mol dm^{-3} NaCl using the titration system. The solution was maintained under a blanket of Ar and circulated through a 1 cm path length cell in the cell compartment of a Cary 219 spectrophotometer using a Gilson Minipuls 2 peristaltic pump, while the pH was maintained by the titration system.

Variation of rate with ionic strength. The stopped-flow technique used for kinetic runs studied under buffer pH-control was described earlier. A series of acetate buffer solutions ($[acetate]_{total}$ = 0.004 mol dm^{-3}, pH 4.41) was prepared in which the ionic strength was varied from 4×10^{-3} to 0.034 mol dm^{-3} by the addition of appropriate amounts of NaCl. The pH of the reaction solution was measured before and after mixing.

Acknowledgements

This work was supported by the Australian Research Council. The assistance of Mr. A. J. Leong with the measurement of the pK_a values for the alcohol complexes, and Dr. A. R. Carroll with the NOE/NMR studies, is very gratefully acknowledged.

References

1 R. R. Gagne and D. N. Marks, *Inorg. Chem.*, 1984, **23**, 65.
2 B. S. Tovrog, S. E. Diamond and F. Mares, *J. Am. Chem. Soc.*, 1979, **10**, 5067.
3 M. J. Ridd and F. R. Keene, *J. Am. Chem. Soc.*, 1981, **103**, 5733.
4 F. R. Keene, M. J. Ridd and M. R. Snow, *J. Am. Chem. Soc.*, 1983, **105**, 7075.
5 V. E. Alvarez, R. J. Allen, T. Matsubara and P. C. Ford, *J. Am. Chem. Soc.*, 1974, **96**, 7686.
6 L. G. Sillen and A. E. Martell, *Stability of Metal–Ion Complexes*, Special Publ. No. 17, The Chemical Society, London, 1963, p. 40.
7 J. K. Blaho and K. A. Goldsby, *J. Am. Chem. Soc.*, 1990, **112**, 6132.
8 B. A. Moyer and T. J. Meyer, *Inorg. Chem.*, 1981, **20**, 436.
9 S. Goswami, A. R. Chakravarty and A. Chakravarty, *Inorg. Chem.*, 1983, **22**, 602.
10 P. Zuman, *The Elucidation of Organic Electrode Processes*, Academic Press, New York, 1969, p. 22.
11 R. A. Marcus, *Annu. Rev. Phys. Chem.*, 1964, **15**, 155.
12 (*a*) R. C. Young, F. R. Keene and T. J. Meyer, *J. Am. Chem. Soc.*, 1977, **99**, 2468; (*b*) C. Creutz and N. Sutin, *Adv. Chem. Ser.*, 1978, **168**, 1.
13 W. P. Jencks, *Catalysis in Chemistry and Enzymology*, McGraw-Hill, New York, 1969, p. 173.
14 M. L. Bender, *Mechanism of Homogeneous Catalysis from Protons to Proteins*, Wiley-Interscience, New York, 1971, pp. 85–90.
15 F. H. Westheimer, *Chem. Rev.*, 1961, **61**, 265; R. A. More O'Farrell, *Proton Transfer Reactions*, Chapman Hall, London, 1965, p. 283.
16 T. J. Truex and R. H. Holm, *J. Am. Chem. Soc.*, 1972, **94**, 4529; M. Millar and R. H. Holm, *J. Am. Chem. Soc.*, 1975, **97**, 6052.
17 P. Maruthamuthu, L. K. Patterson and G. Ferraudi, *Inorg. Chem.*, 1978, **17**, 3157; P. Morliere and L. K. Patterson, *Inorg. Chem.*, 1982, **21**, 1837.
18 M. Jaacobi, D. Meyerstein and J. Lilie, *Inorg. Chem.*, 1979, **18**, 429.
19 M. Goto, M. Takeshita, N. Nanda, T. Sakai and V. Goedken, *Inorg. Chem.*, 1985, **24**, 582; Y. Kuroda, N. Tanaka, M. Goto and T. Sakai, *Inorg. Chem.*, 1989, **28**, 2163.
20 K. Pohl, K. Wieghardt, W. Kaim and S. Steenken, *Inorg. Chem.*, 1988, **27**, 440.
21 P. A. Lay, A. M. Sargeson, B. W. Skelton and A. H. White, *J. Am. Chem. Soc.*, 1982, **104**, 6161.
22 P. Bernhard and A. M. Sargeson, *J. Am. Chem. Soc.*, 1989, **111**, 597.
23 D. J. Bull, Ph.D. Thesis, Australian National University, 1992.
24 S. W. Benson, *The Foundations of Chemical Kinetics*, McGraw-Hill, New York, 1960, p. 525.
25 P. A. Adcock, F. R. Keene, R. S. Smythe and M. R. Snow, *Inorg. Chem.*, 1984, **23**, 2336.
26 C. H. Bamford and C. F. M. Tipper, *Comprehensive Chemical Kinetics*, Elsevier, London, 1969, p. 16; W. G. Jackson and J. MacB. Harrowfield, *Int. J. Chem. Kinet.*, 1977, **9**, 535.
27 D. T. Sawyer and J. L. Roberts, *Experimental Electrochemistry for Chemists*, Wiley-Interscience, New York, 1974, p. 212.
28 B. P. Sullivan, D. J. Salmon and T. J. Meyer, *Inorg. Chem.*, 1978, **17**, 3334.
29 E. C. Johnson, B. P. Sullivan, D. J. Salmon, S. A. Adeyemi and T. J. Meyer, *Inorg. Chem.*, 1978, **17**, 2211.
30 C. Creutz, M. Chou, T. L. Netzel, M. Okumura and N. Sutin, *J. Am. Chem. Soc.*, 1980, **102**, 1309.
31 A. I. Vogel, *Practical Organic Chemistry*, 3rd edn., Longmans, London, 1967, p. 343.
32 O. Cervinka, O. Belovsky and P. Rejmonova, *Collect. Czech. Chem. Commun.*, 1973, **38**, 1358.
33 E. Bordier, *Bull. Soc. Chim. Fr.*, 1973, 1549.
34 D. F. Shriver, *The Manipulation of Air Sensitive Compounds*, McGraw-Hill, New York, 1969, p. 197.
35 A. J. Gordon and R. A. Ford, *The Chemists's Companion*, Wiley, New York, 1972, p. 438.
36 K. R. Adams, A. J. Leong, L. F. Lindoy, H. C. Lip, B. W. Skelton and A. H. White, *J. Am. Chem. Soc.*, 1983, **105**, 4645.

Received 23*rd January* 1992; *Paper* 2/00364C

Aust. J. Chem., 1993, **46**, 1763–1774

Mechanism of Oxidative Dehydrogenation of an Amine Coordinated to Osmium(II)*

F. Richard Keene,[A,B] *Peter A. Lay*,[C] *Graeme E. Sneddon*[D] *and Geoffrey W. Whebell*[A]

[A] Department of Molecular Sciences, James Cook University of North Queensland, Townsville, Qld. 4811.
[B] Author to whom correspondence should be addressed.
[C] School of Chemistry, University of Sydney, Sydney, N.S.W. 2006.
[D] Department of Mathematics, James Cook University of North Queensland, Townsville, Qld. 4811.

Abstract

The synthesis and characterization of $[Os(bpy)_2(ampy)]^{2+}$ {bpy = 2,2′-bipyridine; ampy = 2-(aminomethyl)pyridine} have been studied, together with its irreversible two-electron oxidative dehydrogenation to the corresponding osmium(II) imine species in aqueous solution, by utilizing electrochemical and stopped-flow kinetic techniques. The kinetic data were analysed by using numerical integration methods to obtain solutions for the differential equations derived from mechanistic proposals. The results were consistent with the initial oxidation of the metal centre to Os^{III} and the intermediacy of a deprotonated Os^{IV} species, formed by disproportionation, in the subsequent ligand dehydrogenation.

Introduction

While examples of oxidative dehydrogenation of coordinated amines to imines and nitriles have been widely reported, particular recent attention has been directed to the elucidation of the detailed mechanism of such processes and the role of the metal centre in their promotion.[1–13]

* Dedicated to Graeme Hunter Searle, who died on 24 July 1992 in Zurich, Switzerland, after a 10 week struggle to overcome massive internal injuries sustained in a knife attack in St Petersburg, Russia. Educated in Christchurch (New Zealand) and at Australian National University, Graeme was appointed to the University of Adelaide in 1965 where he established a significant research reputation in the area of stereochemistry of cobalt complexes containing facultative polyamine ligands. His dedication as a scientist and teacher will be greatly missed by his colleagues and students.

[1] Truex, T. J., and Holm, R. H., *J. Am. Chem. Soc.*, 1972, **94**, 4529; Millar, M., and Holm, R. H., *J. Am. Chem. Soc.*, 1975, **97**, 6052.
[2] Maruthamuthu, P., Patterson, L. K., and Ferraudi, G., *Inorg. Chem.*, 1978, **17**, 3157; Morliere, P., and Patterson, L. K., *Inorg. Chem.*, 1982, **21**, 1837.
[3] Jaacobi, M., Meyerstein, D., and Lilie, J., *Inorg. Chem.*, 1979, **18**, 429.
[4] Goto, M., Takeshita, M., Kanda, N., Sakai, T., and Goedken, V. L., *Inorg. Chem.*, 1985, **24**, 582.
[5] Pohl, K., Weighardt, K., Kaim, W., and Steenken, S., *Inorg. Chem.*, 1988, **27**, 440.
[6] Ridd, M. J., and Keene, F. R., *J. Am. Chem. Soc.*, 1981, **103**, 5733.
[7] Keene, F. R., Ridd, M. J., and Snow, M. R., *J. Am. Chem. Soc.*, 1983, **105**, 7075.

↘ *References* 8–13 *on page* 1764

Manuscript received 2 March 1992

0004-9425/93/111763$05.00

In these reactions, it is clear that initial oxidation at the metal centre precedes the ligand dehydrogenation. However, in this subsequent intramolecular redox process, two general schemes have been put forward to account for the apparent dichotomy that the metal reduction would generally be a one-electron change whereas the ligand oxidation is necessarily an even-electron process. In the first of these proposals, a ligand free radical intermediate is considered to form by intramolecular transfer of one electron from the (deprotonated) ligand attached to the oxidized metal centre: the amine oxidation subsequently proceeds at the ligand. Evidence supporting this route has been presented for the oxidation of nickel complexes of a variety of macrocycles,[1-3] $[Fe(CN)_4(en)]^-$ (ref. 4) and $[Fe(tacn)_2]^{3+}$ (en = ethane-1,2-diamine; tacn = 1,4,9-triazacyclononane).[5] The second proposal involves a disproportionation of the oxidized metal centre resulting in an oxidation state two units higher than the initial state, thereby allowing a two-electron transfer from ligand to metal in the ligand dehydrogenation process: such a route has been identified in detailed mechanistic studies of ligand dehydrogenation in $[Ru(bpy)_2(ampy)]^{2+}$ {bpy = 2,2′-bipyridine; ampy = 2-(aminomethyl)pyridine}[6,7] and $[Os(en)_3]^{n+}$ (refs 8 and 9) in our laboratories, and in the $[Ru(sar)]^{2+}$, $[Ru(en)_3]^{2+}$ and $Ru(tame)_2]^{2+}$ complexes {sar = sarcophagine = 3,6,10,13,16,19-hexaazabicyclo[6.6.6]icosane; tame = 1,1,1-tris(aminomethyl)ethane}.[10-13]

It is likely, for the iron triad at least, that the latter mechanism pertains since disproportionation of $[Fe(sar)]^{3+}$ (ref. 13) and $[Fe(CN)_4(diamine)]^-$ complexes[14] to form Fe^{IV} intermediates has now been demonstrated. Ru^{IV} complexes of this type have been isolated recently in the case of $[Ru(tmen)(tmen\text{-}H)_2]^{2+}$, (ref. 15) (tmen = 2,3-dimethylbutane-2,3-diamine) and direct observation of Ru^{IV} transients have also been made in recent kinetic studies of the oxidation of $[Ru(sar)]^{3+}$ and other amine complexes.[11,13] Within studies in our laboratories, we have isolated and characterized a related species which is formally a Ru^{IV} complex containing the isopropylideneamide anion,[16] in which considerable stabilization occurs as a result of ligand-to-metal π-bonding.

A study of osmium(IV) ammines[17] has demonstrated their high acidity, and the stabilization of Os^{IV} complexes of deprotonated amines might be expected to be greater than in the case of Ru^{IV} because of the superior orbital extension for the larger metal ion.[18] Indeed, in studies of the ligand oxidation of $[Os(en)_3]^{n+}$, initially reported by Dwyer and Hogarth,[19,20] Os^{IV} complexes containing deprotonated ethane-1,2-diamine ligands were isolated and characterized. These complexes

[8] Lay, P. A., Sargeson, A. M., Skelton, B. W., and White, A. H., *J. Am. Chem. Soc.*, 1982, **104**, 6161.
[9] Lay, P. A., and Sargeson, A. M., *Inorg. Chim. Acta*, 1992, **198–200**, 449.
[10] Bernhard, P., Sargeson, A. M., and Anson, F. C., *Inorg. Chem.*, 1988, **27**, 2754.
[11] Bernhard, P., and Sargeson, A. M., *J. Am. Chem. Soc.*, 1989, **111**, 597.
[12] Bernhard, P., and Anson, F. C., *Inorg. Chem.*, 1989, **28**, 3272.
[13] Bull, D. J., Ph.D. Thesis, Australian National University, 1992.
[14] Lay, P. A., and Ludi, A., unpublished data.
[15] Biner, M., Ramseyer, S., and Ludi, A., unpublished data.
[16] Adcock, P. A., Keene, F. R., Smythe, R. S., and Snow, M. R., *Inorg. Chem.*, 1984, **23**, 2336.
[17] Buhr, J. D., Winkler, J. R., and Taube, H., *Inorg. Chem.*, 1980, **19**, 2416.
[18] Taube, H., *Surv. Prog. Chem.*, 1973, **6**, 1.
[19] Dwyer, F. P., and Hogarth, J. W., *J. Am. Chem. Soc.*, 1953, **75**, 1008.
[20] Dwyer, F. P., and Hogarth, J. W., *J. Am. Chem. Soc.*, 1955, **77**, 6152.

undergo spontaneous oxidative dehydrogenation to give the Os^{II}-monoimine species, which rapidly oxidize further in air to the Os^{II}-diimine and tetraimine complexes. The Os^{IV} complexes that are formed in the direct reaction of $Os^{IV}Br_6^{2-}$ with ethane-1,2-diamine[8,9,19,20] are also formed in the disproportionation of $[Os(en)_3]^{3+}$.[8,9] Such disproportionation is also observed in the related complex $[Os(tmen)_3]^{3+}$, where the Os^{IV} complexes are stable to oxidative dehydrogenation reactions.[21]

The present work reports a mechanistic study of the oxidative dehydrogenation of 2-(aminomethyl)pyridine in $[Os(bpy)_2(ampy)]^{2+}$, the osmium analogue of the ruthenium species studied previously in one of our laboratories.[6,7] It was undertaken on the basis that the Os^{IV} intermediate species may have considerable kinetic stability based on the Os^{IV}/en system, yet at the same time the metal centre may be a less powerful oxidant than its ruthenium counterpart,[22] so that the transient might in fact be observed rather than inferred from kinetic studies. It was felt that this complementary study would allow a more intimate understanding of the mechanism of the ligand oxidation process.

Experimental

Physical Measurements

Electronic spectra were recorded on a Cary 219 spectrophotometer, and n.m.r. spectra were recorded in D_2O by using a Bruker AM-300 spectrometer with 1,4-dioxan (δ 3·53 $\{^1H\}$ and δ 66·5 $\{^{13}C\}$, relative to Me_4Si) as internal reference. Electrochemical measurements were made with a Bioanalytical Systems (BAS) CV-27 voltammograph, with cyclic voltammograms output to a Linseis LY-1800 X-Y recorder. All potentials are reported relative to a saturated sodium chloride calomel standard electrode (s.s.c.e.).

Elemental analyses were carried out by the Canadian Microanalytical Service (Delta, B.C.).

Materials

All chemicals and solvents were of AR grade (where available) and used as received. The complexes $[Os(bpy)_2Cl_2]$[23,24] and $[Os(bpy)_3](ClO_4)_2.2H_2O$[25] were prepared by literature methods. Argon and nitrogen used for deaeration were scrubbed of O_2 by passing through a column packed with BTS catalyst (Fluka) maintained at 180°C.

Syntheses

[2-(Aminomethyl)pyridine][bis(2,2′-bipyridine)]osmium(II) *hexafluorophosphate dihydrate* $[Os(bpy)_2(ampy)](PF_6)_2.2H_2O$.—By using standard Schlenk techniques, $[Os(bpy)_2(OSO_2CF_3)_2]$ was prepared by adding $[Os(bpy)_2Cl_2]$ (200 mg) to deaerated (argon) trifluoromethanesulfonic acid (2 cm^3), and the mixture was heated (100°) with stirring for 5 h while being maintained under a stream of dry argon.[24] The mixture was evaporated to dryness under vacuum and the residue was dissolved in dry degassed sulfolane under argon. 2-(Aminomethyl)pyridine (150 mg) in dry degassed sulfolane (5 cm^3) was added slowly (20 min) and the mixture was stirred under argon at 90° for 20 min. The vessel was opened to the atmosphere and 1 M HCl (20 cm^3) was added. The solution was washed into a separating funnel with water, and extracted with dichloromethane after the addition of NH_4PF_6 (*c.* 0·2 g). After the dichloromethane extract was evaporated to

[21] Patel, A., Ludi, A., Bürgi, H.-B., Raselli, A., and Bigler, P., *Inorg. Chem.*, 1992, **31**, 3405.
[22] Takeuchi, K. J., Thompson, M. S., Pipes D. W., and Meyer, T. J., *Inorg. Chem.*, 1984, **23**, 1845.
[23] Buckingham, D. A., Dwyer, F. P., Goodwin, H. A., and Sargeson, A. M., *Aust. J. Chem.*, 1964, **17**, 325.
[24] Lay, P. A., Sargeson, A. M., and Taube, H., *Inorg. Synth.*, 1986, **24**, 291.
[25] Creutz, C., Chou, M., Netzel, T. L., Okumura, M., and Sutin, N., *J. Am. Chem. Soc.*, 1980, **102**, 1309.

dryness, the residue was dissolved in water, sorbed onto a column of SP-Sephadex C-25 cation exchanger, and eluted with 0·25 M sodium chloride solution. The major dark green fraction was collected and the eluate was extracted with dichloromethane after addition of NH_4PF_6 (*c.* 0·2 g). The combined extracts were dried with Na_2SO_4 and evaporated to dryness. The crude *product* was recrystallized from dichloromethane/light petroleum and dried under vacuum, yield 190 mg (68%) (Found: C, 33·3; H, 2·68; N, 8·6. $C_{26}H_{28}F_{12}N_6O_2OsP_2$ requires C, 33·3; H, 3·01; N, 9·0%).

[Bis(2,2′-bipyridine)][2-(iminomethyl)pyridine]osmium(II) *hexafluorophosphate [Os(bpy)$_2$(impy)](PF$_6$)$_2$.*—$[Os(bpy)_2(ampy)](PF_6)_2.2H_2O$ (31·3 mg, $3{\cdot}48\times10^{-5}$ mol) was dissolved in 0·1 M H_2SO_4 (25 cm^3) and $(NH_4)_4[Ce(SO_4)_4].H_2O$ (42·8 mg, $6{\cdot}96\times10^{-5}$ mol) in 0·1 M H_2SO_4 (10 cm^3) was slowly added over 30 min with stirring. The solution was allowed to stir for a further 30 min and the product precipitated by the slow addition of NH_4PF_6 (0·2 g). The *precipitate* was filtered off and washed several times with cold water acidified slightly with HPF_6, then with diethyl ether and then it was dried under vacuum (Found: C, 34·2; H, 2·51; N, 9·3. $C_{26}H_{22}F_{12}N_6OsP_{12}$ requires C, 34·7; H, 2·47; N, 9·3%).

Deuterium Exchange Studies

The exchange of the methylene protons during the course of the oxidation reaction was examined by undertaking the above synthesis of $[Os(bpy)_2(impy)](PF_6)_2$, but in D_2O/D^+ solution. The ^{13}C n.m.r. spectrum of the product was determined (D_2O solution).

Spectrocoulometric Determination of the Oxidation Reaction

A sample of $[Os(bpy)_2(ampy)](PF_6)_2.2H_2O$ was dissolved in 0·1 M HCl and oxidized at +0·42 V (5 mV anodic of $E_{p,a}$) in a conventional three-compartment electrochemical cell (platinum working electrode). The solution in the working compartment was simultaneously circulated through a 0·1 cm flow cell in the spectrophotometer by using a peristaltic pump, and the spectrum recorded at coulometric n values of 0, 0·5, 1·0, 1·5 and 2·0 electrons.

Kinetic Measurements

Kinetic measurements were undertaken at 25·0° by using a stopped-flow device constructed within the Department and based on the design of Carr and Tregloan.[26] In all runs, ionic strength was maintained at 1·0 M by using NaCl. In a typical experiment, a solution of $[Os(bpy)_3]^{3+}$ was generated by exhaustive electrolysis at +0·7 V of $[Os(bpy)_3](ClO_4)_2.2H_2O$ (*c.* 5×10^{-5} M in deaerated aqueous HCl or buffer solution) and this was mixed under stopped-flow conditions with a deaerated solution of $[Os(bpy)_2(ampy)](PF_6)_2.2H_2O$ (*c.* 7×10^{-5} M) in the same solvent. The concentrations of the reactant solutions were assessed spectrophotometrically. The individual solutions were stored under N_2 prior to the filling of the reactant compartments of the stopped-flow apparatus.

Kinetic data were obtained over a pH range 1–3 under unbuffered conditions, and over the range 2–5 for buffered conditions (chloroformate, formate and acetate). Absorbances (D_{obs}) were measured at $\lambda = 415$ nm and at $\lambda = 490$ nm. In each case, at least three replicate runs were made and measurements were taken at 27 time steps during the reaction. Some details of the mathematical technique used in the interpretation of the absorbance–time data are given in the Results and Discussion—a more extensive description may be obtained by request from the authors.

Results and Discussion

Synthetic Methods and Characterization

The synthesis of $[Os(bpy)_2(ampy)](PF_6)_2.2H_2O$ involved the *in situ* reaction of $[Os(bpy)_2(OSO_2CF_3)_2]$[24] with 2-(aminomethyl)pyridine, utilizing the substitutional lability of the triflato ligand. Several other preparative procedures for this complex were examined based on refluxing the $[Os(bpy)_2Cl_2]$ complex and the ligand in

[26] Carr, J. T., Ph.D. Thesis, University of Melbourne, 1981.

ethylene glycol.[27] ^1H n.m.r. and electrochemical techniques revealed that the products resulting from these extreme conditions were most likely dimers, but they were not further investigated. The synthesis via the triflato species required far milder conditions and the desired $[Os(bpy)_2(ampy)]^{2+}$ complex was obtained in good yield.

The electrochemical and spectral (^1H and ^{13}C n.m.r. $\{D_2O\}$ and electronic) characteristics of the $[Os(bpy)_2(ampy)]^{2+}$ species are given in Table 1. The ^1H n.m.r. spectrum of the cation is consistent with those of its ruthenium analogue,[6] displaying complicated aromatic resonances (δ 6·5–8·8) due to the bipyridine ligands and with an AB quartet centred at δ 4·18 in the aliphatic region assigned to the methylene protons. The amine protons were not visible in D_2O, presumably owing to rapid exchange.

The $[Os(bpy)_2(ampy)]^{2+}$ complex undergoes an irreversible two-electron oxidation (coulometric n value *c.* 2·0) on exhaustive electrolysis at +0·47 V. This is consistent

Table 1. Spectral and electrochemical data for osmium complexes

Property	$[Os(bpy)_2(ampy)]^{2+}$	$[Os(bpy)_2(impy)]^{2+}$
	Electronic spectra (0·1 M HCl)	
λ_{max} (nm)	490	488
ϵ (m^2 mol^{-1})	10200	13800
	N.m.r. spectra (D_2O) (non-aromatic only)	
δ_H	4·44, 4·34, 4·02, 3·97, q	8·94, s
δ_C		172·1
	Redox potentials (platinum working electrode)	
$E_{1/2}$ (V *v.* s.s.c.e.)	+0·42 (ΔE_p = 60 mV)	+0·70 (ΔE_p = 100 mV)

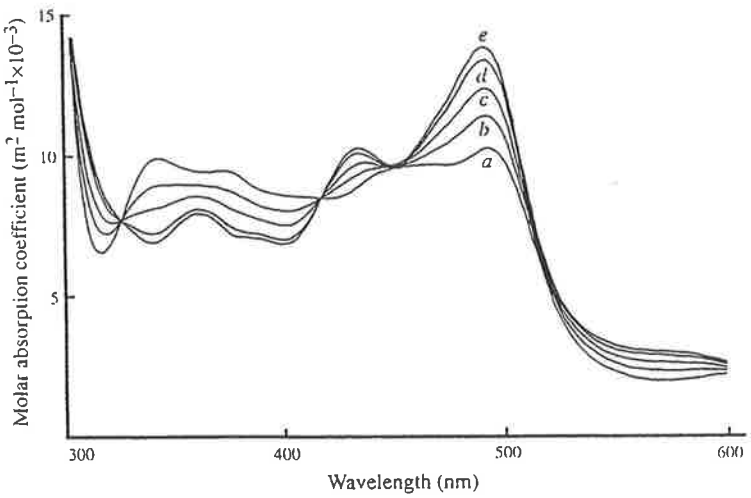

Fig. 1. Spectrocoulometric titration of $[Os(bpy)_2(ampy)]^{2+}$ in 0·1 M HCl solution (a = 0·0, b = 0·5, c = 1·0, d = 1·5, e = 1·9 electrons).

[27] Dwyer, F. P., Gibson, N. A., and Gyarfas, E. C., *J. Proc. R. Soc. N.S.W.*, 1952, **84**, 80.

with the formation of the imine product [equation *(1)*]. Spectrocoulometry (Fig. 1) revealed isosbestic points at 325 and 415 nm.

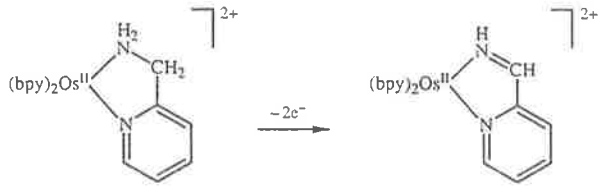

(1)

The oxidation product of $[Os(bpy)_2(ampy)]^{2+}$ is identified as the corresponding imine species and has the electrochemical and spectral characteristics shown in Table 1. The ^{13}C n.m.r. spectrum is typical of an imine complex[28] with the imine carbon resonance (δ 172·1) downfield of those assigned to the aromatic carbons; the hydrogen atom attached to the imine carbon atom is also observed in the ^1H n.m.r. spectrum as a singlet downfield of the aromatic proton resonances (δ 8·94; Table 1). If the oxidative dehydrogenation reaction is carried out in D_2O/D^+ rather than the H_2O/D^+, it is clear from ^1H n.m.r. studies that there is no observable incorporation of deuterium into the methine group (δ 8·94) of the product imine. The same observation has also been reported for the equivalent oxidative dehydrogenation reactions of $[Ru(bpy)_2(ampy)]^{2+}$,[6] $[Ru(sar)]^{2+}$ (ref. 11) and $[Os^{IV}(en{-}H)_2(en)]^{2+}$ (refs 8 and 9) to their respective imine complexes.

Electrochemistry

Cyclic voltammetry of $[Os(bpy)_2(ampy)]^{2+}$ in 0·1 M HCl in the range $0 \rightarrow +1{\cdot}0$ V revealed the characteristics of an ECE process, involving two one-electron redox couples, namely $[Os(bpy)_2(ampy)]^{3+/2+}$ with $E_{1/2} = 0{\cdot}42$ V ($\Delta E_p = 60$ mV), and $[Os(bpy)_2(impy)]^{3+/2+}$ {impy = 2-(iminomethyl)pyridine} with 0·70 V ($\Delta E_p = 100$ mV).

At fast sweep rates (>500 mV/s), only the less anodic of the two couples is observed, this corresponding to the Os^{III}/Os^{II} interconversions of the amine complex. At slow scan rates (20 mV/s), following the anodic peak of the amine complex, the Os^{III}/Os^{II} redox couple of the imine complex, is observed, with the cathodic peak of the amine species on the reverse sweep being absent because of the irreversible oxidation of the $[Os^{III}(bpy)_2(ampy)]^{3+}$ (formed in the anodic sweep) in the time scale of the cyclic voltammetry. At intermediate scan rates, ECE behaviour is observed, with the peak height of the imine couple increasing and the cathodic peak of the amine couple decreasing as the sweep rate is progressively decreased. Repeated scans also resulted in a steady increase of the imine product. These observations are consistent with the second peak on the anodic sweep being derived from the first redox couple (i.e. the Os^{III} species generated in the first oxidation undergoes a subsequent reaction to the imine species), with the rate of reaction being within the time scale of the cyclic voltammetric experiment. They also correspond to the ruthenium analogue studied by Ridd and Keene,[6,7] where the reaction following the initial oxidation of the amine complex in 1 M acid was particularly fast resulting in the redox

[28] Whebell, G. W., and Keene, F. R., *Aust. J. Chem.*, 1986, **39**, 2027.

reaction of the amine species being seen as an irreversible process for similar time scales: clearly, under equivalent conditions the osmium analogue has a slower reaction rate.

These observations are also in accordance with the oxidation of the metal centre from Os^{II} to Os^{III} being the first step in the oxidative dehydrogenation of the amine ligand.

Kinetic Studies

In order to study the kinetics of this system a chemical oxidant was sought to initiate the oxidative dehydrogenation of the amine ligand by oxidation of the metal centre. The oxidant was required to possess a redox potential intermediate between that of the Os^{III}/Os^{II} couples for the reactant amine and product imine species (to avoid subsequent oxidation of the product), and the oxidant should also not take part in any reactions subsequent to the dehydrogenation process. Further, the oxidation of the osmium metal centre would also have to be rapid so as to minimize any interference with the analysis of the data arising from subsequent ligand oxidation processes.

The oxidant chosen was $[Os(bpy)_3]^{3+}$ ($E_{1/2} = +0{\cdot}58$ V). By using Marcus theory,[29] the rate constant of electron transfer from the oxidant to the osmium(II) amine complex was calculated as 5×10^8 dm^3 mol^{-1} s^{-1}. For the purpose of this calculation, the literature value for the self-exchange rate of $[Os(bpy)_3]^{3+/2+}$ was used,[30] the self-exchange rate for the $[Os(bpy)_2(ampy)]^{3+/2+}$ complex was approximated to that of $[Os(bpy)_3]^{3+/2+}$, and the equilibrium constant for the reaction was calculated from the potentials of the respective redox couples. Prior to a kinetic experiment $[Os(bpy)_3]^{3+}$ was freshly generated by exhaustive electrolysis of the corresponding Os^{II} complex. The species is stable in solutions at low pH, but does slowly reduce back to the Os^{II} species at pH > 3.[31]

In each kinetic run, the reaction was monitored at $\lambda = 415$ nm (the isosbestic point for the overall reaction *(1)* and chosen to facilitate calculations of concentrations), and at the absorption maximum for the $[Os(bpy)_2(ampy)]^{2+}$ complex ($\lambda = 490$ nm) where maximum absorbance change occurred for the intramolecular redox process under investigation.

Mechanistic Considerations

Following the observations of Ridd and Keene relating to the oxidation of 2-(aminomethyl)pyridine and its derivatives coordinated to ruthenium(II),[6,7] and the related studies of Sargeson *et al.*[10–13] and Lay *et al.*[8,9] on amine ligand dehydrogenations in ruthenium and osmium complexes, an analogous mechanistic scheme involving disproportionation at the metal centre was considered for the osmium species.

The initial oxidation reaction [equation *(2)*] was assumed to be substantially complete within the time of mixing of the reactant $[Os(bpy)_2(ampy)]^{2+}$ and the oxidant $[Os(bpy)_3]^{3+}$, and was not considered in the calculations of the subsequent processes.

[29] Marcus, R. A., *Discuss. Faraday Soc.*, 1960, **29**, 21.
[30] Chan, M.-S., and Wahl, A. C., *J. Phys. Chem.*, 1978, **82**, 2542.
[31] Nord, G., and Wernberg, O., *J. Chem. Soc., Dalton Trans.*, 1975, 845.

$$[Os^{II}(bpy)_2(ampy)]^{2+} \xrightarrow[([Os(bpy)_3]^{3+})]{-e^-} [Os^{III}(bpy)_2(ampy)]^{3+} \quad (2)$$

The Os^{III} species formed undergoes the protonic equilibrium [equation *(3)*] because of the Lewis acidity of the oxidized metal centre:

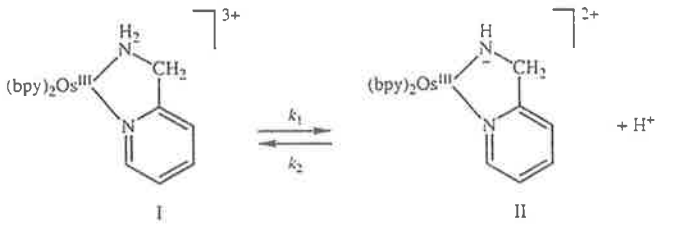

I II (3)

This is followed by a disproportionation reaction of Os^{III} involving the deprotonated form, leading to Os^{II} and Os^{IV} centres:

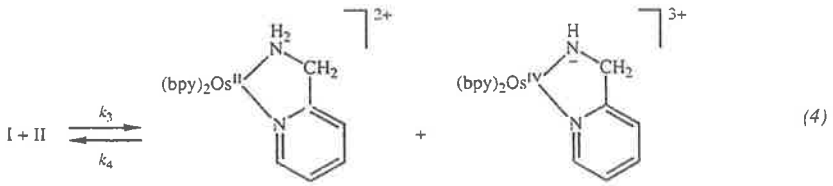

(4)

The reaction of two non-deprotonated $[Os(bpy)_2(ampy)]^{3+}$ (I) moieties as an alternative for the disproportionation process can be eliminated on similar thermodynamic grounds to that given for the ruthenium analogue[6] and other osmium(III) complexes:[8,9] the equilibrium constant in this instance would be $<1{\cdot}7\times10^{-17}$, based on a difference between the potentials of the Os^{IV}/Os^{III} and Os^{III}/Os^{II} couples of 1·0 V. Indeed, since oxidation of $[Os(NH_3)_6]^{2+}$ ($E_{1/2} = -0{\cdot}78$ V) and $[Os(NH_3)_6]^{3+}$ ($E_{p,a} = +1{\cdot}25$ V)[17] are seen to be separated by >2 V, the value for the equilibrium constant is likely to be considerably less favourable than that quoted.

The resultant Os^{IV}-amido intermediate then undergoes an intramolecular redox process in which the ligand undergoes dehydrogenation to form the imine product and the metal centre is concomitantly reduced to the Os^{II} state:

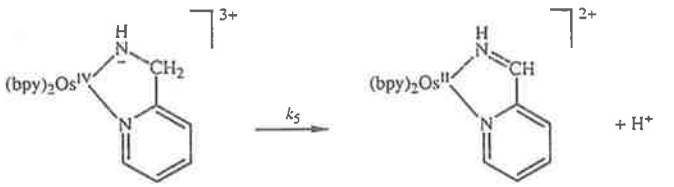

(5)

A set of three rate equations that described the proposed mechanistic scheme [equations *(3)–(5)*] was obtained. An exact analytical solution of these differential equations was not possible, and so a numerical solution was sought. For given values of the rate constants k_1, k_2, k_3, k_4 and k_5, the concentrations of all reactants could be calculated at any given time during the reaction. These

concentrations could then be used to calculate the total absorbance (D_{calc}) at any time.

In order to obtain the calculated absorbances from the concentrations, it was essential to know the values of the absorption coefficients of the species participating in the proposed scheme. In this case the absorption coefficients for $[Os(bpy)_3]^{2+}$ ($\epsilon_{415} = 9400$, $\epsilon_{490} = 12900$ m^2 mol^{-1}), $[Os(bpy)_2(ampy)]^{2+}$ ($\epsilon_{415} = 8300$, $\epsilon_{490} = 10200$ m^2 mol^{-1}) and $[Os(bpy)_2(impy)]^{2+}$ ($\epsilon_{415} = 8300$, $\epsilon_{490} = 13800$ m^2 mol^{-1}) are known. However, absorption coefficients for the $[Os(bpy)_2(ampy)]^{3+}$ species, the corresponding deprotonated form $[Os(bpy)_2(ampy-H)]^{2+}$ and the Os^{IV} complex $[Os(bpy)_2(ampy-H)]^{3+}$ are not readily obtainable. In the first instance, estimates for these species were made: for $[Os(bpy)_2(ampy)]^{3+}$ the values corresponding to those observed for $[Os(bpy)_3]^{3+}$ ($\epsilon_{415} = 860$, $\epsilon_{490} = 390$ m^2 mol^{-1}) were used. The absorption coefficients for the deprotonated $[Os(bpy)_2(ampy-H)]^{2+}$ can be estimated from the $[(bpy)(tpy)Os(OH)]^{2+}$ species ($\epsilon_{415} = 4700$, $\epsilon_{490} = 1760$ m^2 mol^{-1}),[22] while Os^{IV} complexes generally display low absorption coefficients ($\epsilon < 500$ m^2 mol^{-1}) in the region of interest (400–490 nm).[17] The numerical solutions obtained revealed that the intermediates involved in the mechanism were present in small concentrations, and consequently their contributions to the total absorbance was minimal at any given time. In addition, the absorption coefficients of the intermediates involved are significantly less (by at least an order of magnitude) than those of the major constituents $[Os(bpy)_2(ampy)]^{2+}$, $[Os(bpy)_2(impy)]^{2+}$ and $[Os(bpy)_3]^{2+}$. Consequently the results did not depend critically on the absorption coefficients chosen for these transients.

It was found that the differential equations describing the mechanistic scheme were 'stiff',* essentially because the rate constants involved differed by several orders of magnitude. For this reason, the IMSL[33] routine IVPAG was used to solve the rate equations. A simplification to the equations could be made by describing the first reaction [equation *(3)*] by an equilibrium constant K_1. Numerical solutions using reasonable values of k_1 and k_2 indicated that this assumption was valid, and its effect was to reduce the number of equations to two. Another consequence was that separate values for the rates k_1 and k_2 could not be determined: at best, only the equilibrium constant $K_1 = k_1/k_2$ could be obtained. In fact this ratio, and the rate constant k_3, appeared in the equations only in the combination

$$\bar{k}_3 = k_3(k_1/k_2')(1 + (k_1/k_2')^{-2} \qquad (6)$$

where $k_2' = k_2[H^+]$. This means that the only constants that could be determined were k_5, $\bar{k}_3$ and k_4. The IMSL[33] routine UMPOL was used to select values of k_5, $\bar{k}_3$ and k_4 that would minimize $\sum(D_{obs}-D_{calc})^2$. This routine uses the

* Because of the possible variation in the magnitudes of rate constants within the proposed mechanism, there are large differences in the time behavior of the individual reactions, and this leads to large differences in the sensitivity of the integrated solutions to the various reactions. Such systems are called 'stiff'.[32]

[32] Ebert, K. H., Ederer, H. J., and Isbarn, G., *Angew. Chem. Int. Ed. Engl.*, 1980, **19**, 333.
[33] International Mathematical and Statistical Library, 'Fortran Subroutines for Mathematical Applications' IMSL (Houston), 1987.

Simplex method and was chosen because it is quite robust, and does not rely on the derivative of the quantity to be minimized. The minimum values of $\sum(D_{obs}-D_{calc})^2$ so obtained ranged from 10^{-5} to 10^{-4}, corresponding to average differences ($D_{obs}-D_{calc}$) of about 0·002 (or less than 0·5%) in the worst case.

The value of the equilibrium constant K_1 is constrained by the data and the analysis to be within the range 10^{-3}–10^{-7} (i.e. pK_a 3–7), based on the observation that $\bar{k}_3$ proportional to 10^{-pH} in the pH region studied. From equation *(6)*, this implies that $[1+(k_1/k_2')]$ is approximately constant as the pH changes, thereby limiting the magnitude of k_1/k_2' ($= K_1$). Further, since the value of k_3 is inversely proportional to k_1/k_2' [equation *(6)*], $K_1 < 10^{-7}$ would require that the value determined for k_3 exceeded that for diffusion control (*c.* 10^9 dm^3 mol^{-1} s^{-1}). A value for K_1 within this range is consistent with the p$K_a \geq 6{\cdot}8$ determined for $[Os(tpy)(bpy)(NH_3)]^{3+}$,[34] and in fact the p$K_a$ of $[Os(bpy)_2(ampy)]^{3+}$ may be somewhat lower because of the incorporation of the amine group with the chelate ring of the ampy ligand.

The optimum values for the rate constants k_3 and k_4 equation *(4)* indicated that k_4 was less than 100 and $k_3 >> k_4$. Apart from this condition, the value of k_4 was not critical to obtaining a good fit to the data. On the other hand, the value of k_3 was critical to obtaining a minimum for each of the kinetic runs investigated and was consistently $0{\cdot}75(\pm 0{\cdot}15)\times 10^{(z+3)}$ dm^3 mol^{-1} s^{-1}, where z is the arithmetic value assumed for the pK_a of $[Os(bpy)_2(ampy)]^{3+}$. Because of the uncertainty in k_4, the equilibrium constant for this reaction is not well determined but is $\gtrsim 10^{(z+1)}$ and this would require the potential of the Os^{IV}/Os^{III} redox couple for the deprotonated species to be *cathodic* of the Os^{III}/Os^{II} couple for the non-deprotonated case (by >0·4 V if pK_a 6, >0·35 V for pK_a 5, >0·3 V for pK_a 4, or >0·25 V for pK_a 3). A similar observation has been made in investigations of the redox characteristics of $[Ru(tpy)(bpy)(isopropylimine)]^{2+}$,[16] where the imine complex underwent a two-electron oxidative dehydrogenation to an alkylideneamido species which can be regarded in a formal sense as a Ru^{IV} complex of a deprotonated imine: however, the nitrogen–ruthenium bond has significant 'double bond' character. It is this 'double bond' character of the Ru–N bond which gives stability to the oxidation state of the metal centre so that the redox couple for the Ru^{IV}/Ru^{III} species is 0·6 V cathodic of the Ru^{III}/Ru^{II} couple for the non-deprotonated parent imine species. In that example, the carbon–nitrogen–ruthenium chain was linear, but significant 'double bond' character is observed in the complexes of Os^{IV} with deprotonated ethane-1,2-diamine and 2,3-dimethylbutane-2,3-diamine ligands as evidenced by a shortening of the osmium–nitrogen bond distance and n.m.r. spectroscopy,[8,21] even though the Os–N–C chain is non-linear in those cases. Given these observations, the equilibrium constant calculated for the disproportionation therefore appears to be quite consistent with the involvement of an Os^{IV} species containing the deprotonated amine ligand ampy–H.

The calculated rate constant k_5 for reaction *(5)* was found to be pH-dependent in the absence of buffers. The pH range for these studies is of course limited, and the precision of the rate constants is considered to be ±50% as a result of uncertainties brought about by the number of experimental parameters involved

[34] Murphy, W. R., Takeuchi, K., Barley, M. H., and Meyer, T. J., *Inorg. Chem.*, 1986, **25**, 1041.

in the calculation, and the fact that the absolute value of k_5 had a limited influence on the rate constant of the overall reaction. The values obtained (from measurements at 415 and 490 nm) are $1{\cdot}2(\pm 0{\cdot}5)\ s^{-1}$ at pH 0·82, $15(\pm 5)\ s^{-1}$ at pH 1·82 and $200(\pm 100)\ s^{-1}$ at pH 2·82: accordingly there appears to be an increase in the rate constant by a factor of 10 for each unit increase in pH. This observation is in contrast with the ruthenium analogue, where the rate constant of the equivalent step of the scheme was pH-independent.[6] It is also in contrast to the oxidative dehydrogenation of $[Ru(sar)]^{2+}$, $[Ru(tame)_2]^{2+}$ and $[Ru(en)_3]^{2+}$ (refs 11 and 13) where the rate constants of the equivalent reactions of the deprotonated Ru^{IV} intermediates increased at higher acid concentrations: there is compelling evidence[13] that this effect arises from an equilibrium between singly and doubly deprotonated Ru^{IV} intermediates with the singly deprotonated species being the more powerful oxidant.

In the present case, the retardation of the rate of reaction *(5)* by acid may arise from a number of alternative effects. For example, two protonic pre-equilibria may be proposed to account for this observation: namely deprotonation at either the (*a*) amido or (*b*) methylene group, as shown in Scheme 1.

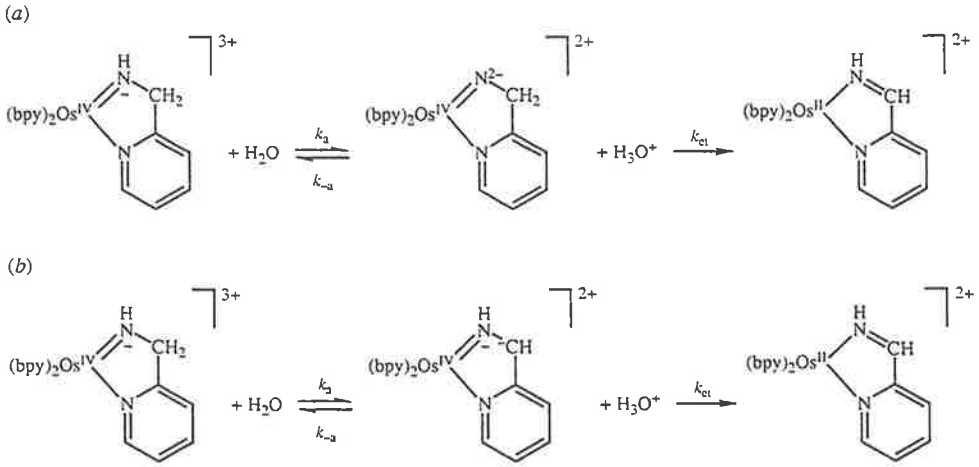

Scheme 1

In the Scheme 1*b*, the observation that no deuterium exchange is detected in the product imine species requires that the methylene deprotonation (k_a) is rate-determining and that $k_{et} >> k_{-a}$. In the $[Os^{IV}(bpy)_2(ampy{-}H)]^{3+}$ intermediate complex, the expected ligand-to-metal π-bonding[8,9,16] may be expected to lead to a labilization of hydrogen atoms attached to the α-carbon atom by a tautomeric effect.

The difference between the pH-dependencies of the ruthenium and osmium complexes can be explained readily within the proposed scheme. For ruthenium, $k_5 >> k_a$ so that no pH-dependence of the rate of ligand oxidation is observed. However, $k_5(Os) << k_5(Ru)$, which gives rise to the condition that $k_5(Os) < k_a$, and the ligand oxidation step is thus pH-dependent in the case of the osmium species. The much slower ligand oxidation step for osmium in comparison with ruthenium is consistent with the behaviour observed in the $[M(en)_3]^{n+}$ systems.[9,13]

For the oxidation of $[Os(bpy)_2(ampy)]^{2+}$, when buffered conditions were used it was found that k_5 had even less influence on the overall rate than in the unbuffered case, and no unique value could be determined from the analysis. In fact, it was observed that for various base concentrations of the same buffer at a given pH, the kinetic runs were indistinguishable. This observation was not pursued further, but is consistent with base catalysis of the final dehydrogenation of the process [equation *(5)*], under which circumstances it is no longer rate-determining. In the oxidative dehydrogenation of ruthenium complexes of the analogous alcohol ligand, $[Ru^{II}(bpy)_2(pyCH_2OH)]^{2+}$, general base catalysis of the equivalent reaction is observed.[35]

Conclusions

The present studies of the mechanism of the oxidative dehydrogenation of $[Os(bpy)_2(ampy)]^{2+}$ indicate that it is substantially consistent with that observed for the ruthenium analogue investigated by Ridd and Keene,[6,7] the related $[Ru(sar)]^{2+}$, $[Ru(tame)_2]^{2+}$ and $[Ru(en)_3]^{2+}$ systems investigated by Sargeson *et al.*,[11,13] and the $[Os(en)_3]^{n+}$ system investigated by Lay *et al.*[8,9] Following initial rapid oxidation of the metal centre, disproportionation occurs to give rise to an intermediate M^{IV} species containing a deprotonated amine ligand, which undergoes an intramolecular redox process resulting in dehydrogenation at the α-carbon atom to form the imine species.

For the present osmium system, this final reaction is observed to have an inverse dependence on acid concentration, which was not observed in the previous studies.

Acknowledgments

This research was supported by the Australian Research Council. The helpful input of Professor A. M. Sargeson (Australian National University) in the initial stages of this work is gratefully acknowledged.

[35] Ridd, M. J., Gakowski, D. J., Sneddon, G. E., and Keene, F. R., *J. Chem. Soc., Dalton Trans.*, 1992, 1949.

[Reprinted from the Journal of the American Chemical Society, 99, 2384 (1977).]

Disproportionation at the Ligand in Nitro Complexes of Ruthenium(III)

Sir:

Complexes of Ru(II) and Ru(III) are usually substitution inert and stable, and Ru(III)/Ru(II) couples have been used extensively in the study of one-electron transfer processes.[1] This is certainly true for *cis*-bis-2,2′-bipyridine (bpy) complexes where more than 100 reversible Ru(III)/Ru(II) couples are known.[2] However, oxidation to Ru(III) can lead to chemical instability because of oxidation of a bound ligand (reactions 1, 2).

$$[Ru^{III}(bpy)_2(N_3)_2]^+ + CH_3CN \rightarrow [Ru^{II}(bpy)_2(CH_3CN)N_3]^+ + \tfrac{3}{2}N_2 \quad (1)^3$$

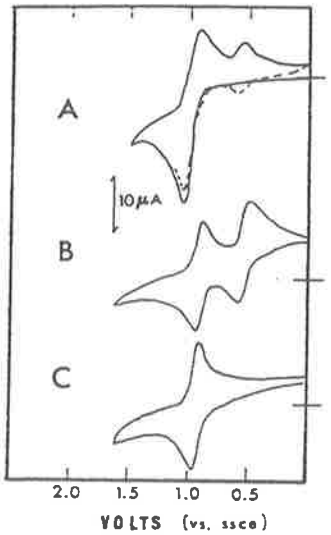

Figure 1. Cyclic voltammograms (200 mV/s) in 0.1 M $[N(C_4H_9)]PF_6$–CH_3CN vs. the SSCE at 22 ± 2 °C: A, $[Ru(bpy)_2(NO_2)py]PF_6$ (1.5×10^{-3} M); B, solution A after exhaustive electrolysis at +1.2 V (n = 1.5/Ru); C, solution A with added H_2O (1%) and 2,6-lutidine (1%) after exhaustive electrolysis at 1.2 V (n = 3.0/Ru).

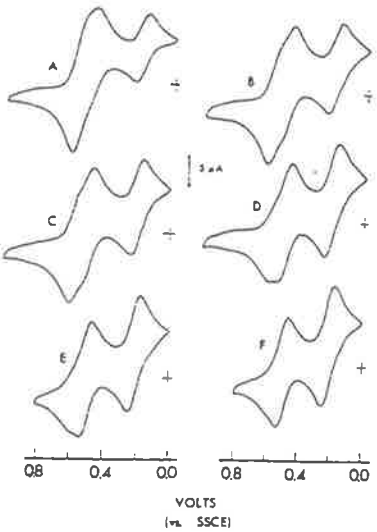

Figure 2. The 200-mV/s cyclic voltammograms in 0.2 M $[N(n\text{-}C_4H_9)_4]PF_6$–propylenecarbonate following exhaustive electrolysis of $[Ru(bpy)_2(NO_2)Cl]$ at 0.8 V: A, 1 min after completion of the electrolysis; B, 2 min; C, 4 min; D, 6 min; E, 8 min; F, 10 min. As shown in 1A, some disproportionation has occurred during the electrolysis. Rate data were obtained by monitoring the growth in peak current for the reversible reduction of $[Ru(bpy)_2(NO)Cl]^{2+}$ at $E_{p,c}$ = 0.20 V.

$$[Ru^{III}(bpy)_2(NH_2CH_2R)_2]^{3+} \xrightarrow{-7e^-} [Ru^{II}(bpy)_2(NCR)_2]^{2+} + 8H^+ \quad (2)^4$$

Attempts to prepare nitroruthenium(III) complexes by electrochemical oxidation of $[Ru^{II}(bpy)_2(NO_2)L]^{n+}$ have been unsuccessful;[5] in fact, there appear to be no known examples of stable, monomeric Ru(III)–NO_2 complexes.[6] We find that complexes like $[Ru^{III}(bpy)_2(NO_2)Cl]^+$ do exist but as kinetic transients. Their stability is limited by an unusual reaction in which intermolecular disproportionation occurs at the nitro group. The reactions are also unusual in that they utilize Ru(III)–NO_2 intermediates as oxide ion donor, two-electron acceptor oxidants in which electron acceptor sites at both metal and ligand are used.

A cyclic voltammogram of $[Ru(bpy)_2(NO_2)py]^+$ in acetonitrile (0.1 M in $[N(C_4H_9)_4](PF_6)$) is given in Figure 1A.[7] The oxidative sweep shows the expected Ru(II) → Ru(III) oxidation ($E_{p,a}$ = 1.06 V vs. SSCE at 22 ± 2 °C). The reductive sweep shows two new waves ($E_{p,c}$ = 0.90 and 0.47 V), and a further cycle shows that the two new waves are associated with reversible couples. Exhaustive electrolysis of the solution past 1.06 V gives n = 1.5 (by coulometry), and cyclic voltammetry shows that two products are formed in equal amounts both of which have reversible redox chemistry (Figure 1B). The less anodic wave ($E_{1/2}$ = 0.53 V) corresponds to the nitrosyl complex, $[Ru(bpy)_2(NO)py]^{3+}$.[8] $[Ru^{II}(bpy)_2(NO)py]^{3+}$ and related nitrosyls are known to undergo reversible reductions localized largely at the NO group (reaction 3) in the potential range 0.2–0.6 V (at 22 ± 2 °C vs. SSCE).[8] It is also known

$$[Ru^{II}(bpy)_2(NO^+)py]^{3+} \underset{-e^-}{\overset{+e^-}{\rightleftharpoons}} [Ru(bpy)_2(\dot{N}O)py]^{2+} \quad (3)^8$$

that nitrosyl and nitro groups are interconverted by simple acid–base chemistry (reaction 4).

$$[Ru(bpy)_2(NO^+)py]^{3+} \underset{H^+}{\overset{OH^-}{\rightleftharpoons}} [Ru(bpy)_2(NO_2)py]^+ \quad (4)^9$$

The second electrolysis product is apparently $[Ru^{III}(bpy)_2(NO_3)py]^{2+}$. Electrolytic redution at a potential between the waves which appear following electrolysis (Figure 1B) gave n = 0.5 per total Ru by coulometry. Electrochemical reduction gives Ru(II), presumably as $[Ru^{II}(bpy)_2(NO_3)py]^+$, which then undergoes solvolysis ($t_{1/2} \sim 10$ min) to give $[Ru(bpy)_2(CH_3CN)py]^{2+}$ ($E_{1/2}$ = 1.36 V).[2] Evaporation of the reduced solution showed the presence of free nitrate ion by IR (ν 1050 cm^{-1}).[10] We have been unable to obtain a sample of $[Ru(bpy)_2(NO_3)py]^{2+}$ free of supporting electrolyte. However, electrochemical oxidation of $[Ru^{II}(bpy)_2(NO_2)Cl]$ at 0.8 V also occurs with n = 1.5 and the products are clearly $[Ru(bpy)_2(NO)Cl]^{2+}$ [8] and $[Ru(bpy)_2(NO_3)Cl]^+$. The nitrato complex was identified by spectral and electrochemical comparisons with a known sample prepared by chemical oxidation (see below). The chloro complex differs from the pyridine complex only in that the $[Ru(bpy)_2(NO_2)Cl]^{+/0}$ couple is reversible on the cyclic voltammetry time scale, $E_{1/2}$ = 0.58 V.

As shown in reaction 5 for the chloro complex, electrochemical oxidation leads to oxidation of nitro to nitrato and of Ru(II) to Ru(III), but both in a single complex.

$$2[Ru^{II}(bpy)_2(NO_2)Cl] \xrightarrow{-3e^-} [Ru^{III}(bpy)_2(NO_3)Cl]^+ + [Ru^{II}(bpy)_2(NO^+)Cl]^{2+} \quad (5)$$

In the mechanism, $[Ru^{II}(bpy)_2(NO_2)Cl]$ is first oxidized to $[Ru^{III}(bpy)_2(NO_2)Cl]^+$ (reaction 6),

$$[Ru^{II}(bpy)_2(NO_2)Cl] \xrightarrow{-e^-} [Ru^{III}(bpy)_2(NO_2)Cl]^+ \quad (6)$$

and the subsequent chemistry is sufficiently slow so that it can be followed directly by cyclic voltammetry (Figure 2). The reaction (eq 7) is second order in [Ru(III)–NO_2] and in propylene carbonate as solvent (I = 0.2 M, $[N(n\text{-}C_4H_9)_4](PF_6)$), k(25.0 °C) = 3.0 ± 0.3 M^{-1} s^{-1}.

$$2[Ru^{III}(bpy)_2(NO_2)Cl]^+ \longrightarrow [(bpy)_2ClRu^{III}\text{—}\underset{(+)}{\overset{O}{\overset{\|}{N}}}\cdots O \cdots \overset{O}{\underset{O}{|}}N\text{—}RuCl(bpy)_2]^{2+} \longrightarrow [(bpy)_2ClRu^{II}\text{—}\dot{N}O]^+ + [(NO_3)RuCl(bpy)_2]^+ \quad (7)$$

A final n value of 3 is obtained in the electrochemical experiment (eq 5) because the reduced nitrosyl complex formed in reaction 7 is oxidized to $[Ru(bpy)_2(NO^+)Cl]^{2+}$ (eq 3) at the potential used for the electrolysis (reaction 8).[11]

$$[Ru^{II}(bpy)_2(\dot{N}O)Cl]^+ \xrightarrow{-e^-} [Ru^{II}(bpy)_2(NO^+)Cl]^{2+} \quad (8)$$

Kinetic studies using Ce(IV) as oxidant in acetonitrile show that the rate constant for disproportionation of $[Ru^{III}(bpy)_2(NO_2)py]^{2+}$ must exceed 10^7 M^{-1} s^{-1}. The reaction with Ce(IV) is first order in both Ce(IV) and $[Ru(bpy)_2(NO_2)py]^+$ (k(25.0 °C; I = 0.1 M) = 1.7×10^6 M^{-1} s^{-1}), and the disproportionation products are observed immediately. Disproportionation at the nitro group is also observed following oxidation of the complexes $[Ru(bpy)_2(NO_2)NH_3]^+$ and $[Ru(bpy)_2(NO_2)CH_3CN]^+$. There appears to be at least a qualitative correlation between the potential for oxidation of Ru(II) to Ru(III) and the rate of disproportionation at the nitro group in the four complexes $[Ru^{III}(bpy)_2(NO_2)L]^{n+}$ (L = Cl^-, NH_3, py, CH_3CN).

The key to the instability of the nitroruthenium(III) complexes is the disproportionation step (reaction 7). The reaction is unusual in that a net two-electron oxidation occurs at the nitro group of one ruthenium ($NO_2^- \rightarrow NO_3^-$) but the complementary reduction uses sites both at the metal (Ru(III) → Ru(II)) and at a ligand (Ru–NO^+ → Ru–$\dot{N}O$).

One inference that can be drawn from the mechanism is that complexes like $[Ru^{III}(bpy)_2(NO_2)Cl]^+$ can act as oxide-ion donor, two-electron acceptor oxidants. They could be facile oxidants since electron transfers to Ru(III) and Ru–NO^+ acceptor sites are known to be rapid,[8,12] and, other than oxide ion transfer, there are no major structural changes involved.[13]

Formal reduction potentials for the Ru(III)–NO_2 complexes as oxide ion donor, two-electron acceptor oxidants can be calculated by a combination of electrochemical and equilibrium measurements (Scheme I). A similar scheme using $E_{p,a}$[17] for the oxidation of $[Ru^{II}(bpy)_2(NO_2)py]^+$ gives $E \geq 0.26$ V (≥0.67 V at pH 7)[15] for the $[Ru^{III}(bpy)_2(NO_2)py]^{2+}/[Ru^{II}(bpy)_2(\dot{N}O)py]^{2+}$ couple. The reduction potential values show that the Ru(III)–NO_2 intermediates are only moderately strong as oxidants.[18]

Scheme I (in 1.0 M aqueous NaCl at 25.0 °C)

Reaction	$-\Delta G^{0\prime}$, V
$H_2O + [Ru^{II}(bpy)_2(NO_2)Cl] \rightarrow [Ru^{II}(bpy)_2(NO^+)Cl]^{2+} + 2OH^-$	-0.54[9,14]
$[Ru^{III}(bpy)_2(NO_2)Cl]^+ + e \rightarrow [Ru^{II}(bpy)_2(NO_2)Cl]^0$	0.90
$[Ru(bpy)_2(NO^+)Cl]^{2+} + e \rightarrow [Ru(bpy)_2(\dot{N}O)Cl]^+$	0.27

$$H_2O + [Ru^{III}(bpy)_2(NO_2)Cl]^+ + 2e \rightarrow [Ru^{II}(bpy)_2(\dot{N}O)Cl]^+ + 2OH^-$$

$$E(\text{NHE, 25.0 °C}) = 0.31 \text{ V (0.72 V at pH 7)}^{15}$$

The series of reactions 6–8 describes a single oxidation cycle (reaction 5) in which one Ru(II)–NO_2 complex is oxidized and the other converted into a nitrosyl. It is possible to continue through additional cycles simply by adjusting the pH. The nitrosyl–nitro interconversion (reaction 4) can be studied quantitatively by pH and spectrophotometric measurements. For reaction 9, K(1.0 M NaCl, 25.0 ± 0.1 °C) = (1.0 ± 0.3) × 10^{20} M^{-2} and for the $[Ru(bpy)_2(NO_2)Cl]$–$[Ru(bpy)_2(NO)Cl]^{2+}$ equilibrium, K(1.0 M NaCl, 25.0 ± 0.1 °C) = 1.4×10^9.[9]

$$2OH^- + [Ru(bpy)_2(NO^+)py]^{3+} \rightleftharpoons [Ru(bpy)_2(NO_2)py]^+ + H_2O \quad (9)$$

For the pyridine system, equal concentrations of nitro and nitrosyl complexes are present at pH 3.8. In an acetonitrile solution containing 1% water and 1% 2,6-lutidine, electrochemical oxidation of $[Ru(bpy)_2(NO_2)py]^+$ occurs (n = 3.0), $[Ru(bpy)_2(NO_3)py]^{2+}$ is the sole product, and the oxidation reaction is driven to completion (Figure 1C). Under these conditions, complete oxidation of $Ru^{II}NO_2$ to $Ru^{III}NO_3$ occurs because $Ru^{II}NO^+$ once formed (eq 5) is converted into $Ru^{II}NO_2$ which reenters the oxidation cycle as shown below.

$$2[Ru^{II}(bpy)_2(NO_2)py]^+ \xrightarrow{-2e^-} 2[Ru^{III}(bpy)_2(NO_2)py]^{2+}$$

$$2BH^+ \leftarrow \quad \rightarrow [Ru^{III}(bpy)_2(NO_3)py]^{2+}$$

$$2B + H_2O$$

$$[Ru^{II}(bpy)_2(\dot{N}O)py]^{3+} \xleftarrow{-e^-} [Ru^{II}(bpy)_2(\dot{N}O)py]^{2+}$$

The oxidation cycle can also be driven chemically. Using essentially the same reaction conditions but with chlorine as the oxidant and triethylamine as the base led to complete oxidation of $[Ru(bpy)_2(NO_2)Cl]$ to $[Ru(bpy)_2(NO_3)Cl]^+$. The chemical oxidation has allowed the nitrato complex to be isolated as its chloride salt which has been characterized by elemental analyses.[19]

Acknowledgments are made to the Materials Research Center of The University of North Carolina under Grant DAHC15 73 G9 and to the National Science Foundation under Grant MPS 75-11867 for support of this research.

References and Notes

(1) (a) H. Fischer, G. M. Tom, and H. Taube, *J. Am. Chem. Soc.*, **98**, 5512 (1976); (b) C. Creutz and N. Sutin, *ibid.*, **99**, 241 (1977); (c) T. J. Meyer, D. G. Whitten, and R. C. Young, *ibid.*, **98**, 286 (1976); (d) R. W. Callahan, T. J. Meyer, M. J. Powers, and D. J. Salmon, *ibid.*, **98**, 6731 (1976); (e) J. N. Braddock, J. L. Cramer, and T. J. Meyer, *ibid.*, **97**, 1972 (1975).

(2) D. J. Salmon, Ph.D. Dissertation, The University of North Carolina, 1976.

(3) G. M. Brown, R. W. Callahan, and T. J. Meyer, *Inorg. Chem.*, **14**, 1915 (1975).

(4) F. R. Keene, D. J. Salmon, and T. J. Meyer, *J. Am. Chem. Soc.*, **98**, 1884 (1976).

(5) G. M. Brown, Ph.D. Dissertation, The University of North Carolina, 1974; G. M. Brown and T. R. Weaver, unpublished results.

(6) W. P. Griffith, "The Chemistry of the Rarer Platinum Compounds", Interscience, New York, N.Y., 1967, p 159.

(7) Unless otherwise noted electrochemical results were obtained in 0.1 M $[N(n\text{-}C_4H_9)_4](PF_6)$–acetonitrile at 22 ± 2 °C using platinum electrodes. Platinum bead electrodes were used for cyclic voltammetry experiments and platinum gauze electrodes for electrolyses. $E_{1/2}$ values for chemically reversible couples were calculated as the mean of the E_p values for the anodic and cathodic waves in cyclic voltammetry experiments. Peak separations (ΔE_p) of ~70 mV were observed which were independent of sweep rate in the range 50–1000 mV s^{-1}. The reference electrode was the saturated sodium chloride calomel electrode (SSCE).

(8) R. W. Callahan and T. J. Meyer, *Inorg. Chem.*, in press; R. W. Callahan, G. M. Brown, and T. J. Meyer, *J. Am. Chem. Soc.*, **97**, 894 (1975).

(9) J. B. Godwin and T. J. Meyer, *Inorg. Chem.*, **10**, 2150 (1971).

(10) K. Nakamoto, "Infrared Spectra of Inorganic and Coordination Compounds", Wiley, New York, N.Y., 1963.

(11) Actually, given the relative potentials for the $[Ru(bpy)_2(NO)Cl]^{2+/+}$ and $[Ru(bpy)_2(NO_2)Cl]^{+/0}$ and related pyridine couples (Figures 1 and 2) and the expected rapid self-exchange rates,[8,12] reaction 7 would be followed by rapid electron transfer between $[Ru(bpy)_2(NO)Cl]^+$ and $[Ru^{III}(bpy)_2(NO_2)Cl]^+$ to give $[Ru(bpy)_2(NO^+)Cl]^{2+}$ and $[Ru^{II}(bpy)_2(NO_2)Cl]$. At the potentials used for the electrolyses, $[Ru^{II}(bpy)_2(NO_2)Cl]$ would be reoxidized to Ru(III).

(12) (a) R. W. Callahan, F. R. Keene, T. J. Meyer, and D. J. Salmon, *J. Am. Chem. Soc.*, in press; (b) R. C. Young, F. R. Keene, and T. J. Meyer, *ibid.*, in press.

(13) That they are facile oxidants is suggested by the disproportionation reactions since there is no reason to believe that a nitro group bound to Ru(III) should be especially easy to oxidize.

(14) Calculated from $-\Delta G^{0\prime} = RT \ln K$ where K refers to the nitrosyl–nitro acid–base equilibrium constant (reaction 9).

(15) Electrochemical measurements were made vs. the SCE: Values vs. NHE were calculated using a value of 0.236 V for SCE vs. NHE. The values were not corrected for junction effects which are presumably small.[16]

(16) W. H. Smyrl and J. Newman, *J. Phys. Chem.*, 72, 4660 (1968).
(17) $E_{p,a}$, the anodic peak potential for the cyclic voltammetric wave, is independent of sweep rate over the range of scan rates 50–500 mV s^{-1}.
(18) W. M. Latimer, "Oxidation Potentials", Prentice-Hall, Englewood Cliffs, N.J., 1952.
(19) Calcd for $[Ru(bpy)_2(NO_2)Cl]Cl$: C, 43.97; H, 2.95; N, 12.82. Found: C, 43.24; H, 3.36; N, 12.64.

F. Richard Keene, Dennis J. Salmon, Thomas J. Meyer*

Department of Chemistry
The University of North Carolina
Chapel Hill, North Carolina 27514

Received November 8, 1976

[Reprinted from the Journal of the American Chemical Society, 99, 4821 (1977).]

Nitro Complexes of Ruthenium(III) as Oxidation Catalysts. Chemically Catalyzed, Net Electrochemical Oxidation of Triphenylphosphine

Sir:

cis-$[Ru^{II}(bpy)_2(NO_2)Cl]$ (bpy = 2,2′-bipyridine) and related complexes can be oxidized to Ru(III), but as Ru(III) are only kinetic transients. Their stability is limited by a facile intermolecular disproportionation reaction (reactions 1 and 2), which gives both nitrosyl and nitrato complexes as products.[1] In the disproportionation reaction, a two-electron oxidation occurs at a nitro group on one ruthenium and the corresponding reduction at both metal ($Ru^{III} \rightarrow Ru^{II}$) and nitrosyl ($Ru\text{-}{}^{+}NO \rightarrow Ru\text{-}\dot{N}O$) sites. Nitrosyl complexes like $[Ru(bpy)_2(^{+}NO)Cl]^{2+}$ are known to undergo reversible electron transfer localized largely at the NO group (reaction 2).[2] In reaction 1, $[Ru^{III}(bpy)_2(NO_2)Cl]^{+}$ acts as an oxide donor, two-electron acceptor oxidant. Its formal reduction potential (eq 3) has been determined to be 0.31 V (0.72 V at pH 7) in 1.0 M aqueous NaCl at 25.0 °C vs. NHE and that for the related pyridine complex, $[Ru^{III}(bpy)_2(NO_2)py]^{2+}$, has been estimated to be ≥0.26 V (≥0.67 V at pH 7).[1]

$$2[Ru^{III}(bpy)_2(NO_2)Cl]^{+} \longrightarrow [(bpy)_2ClRu^{III}\text{-}N(O)\cdots O\cdots NRuCl(bpy)_2]^{2+} \longrightarrow [(bpy)_2ClRu^{II}\text{-}\dot{N}O]^{+} + [(NO_2)RuCl(bpy)_2]^{+} \quad (1)$$

$$[Ru^{II}(bpy)_2(\dot{N}O)Cl]^{+} \underset{+e^-}{\overset{-e^-}{\rightleftharpoons}} [Ru^{II}(bpy)_2(\dot{N}O)Cl]^{2+} \quad (2)$$

$$[Ru^{III}(bpy)_2(NO_2)Cl]^{+} + H_2O + 2e \rightarrow [Ru^{II}(bpy)_2(\dot{N}O)Cl]^{+} + 2OH^{-} \quad (3)$$

Even though disproportionation (reaction 1) is a competing pathway, in the presence of a sufficiently reactive substrate, it should be possible to capture the nitroruthenium(III) intermediates and so to exploit their properties as oxidants. Electrochemical oxidation of an acetonitrile solution (0.1 M $[N(C_4H_9)_4](PF_6)$) containing $[Ru(bpy)_2(NO_2)py]^{+}$ (1×10^{-3} M) and triphenylphosphine (3×10^{-3} M) at 1.15 V vs. the saturated sodium chloride calomel electrode (n = 2.0/Ru by coulometry)[3] gave as products $[Ru(bpy)_2(NO)py]^{3+}$ (by cyclic voltammetry; Figure 1) and triphenylphosphine oxide (by IR, ν(P=O) 1194 cm^{-1}). Oxidation of the Ru(II) complex occurs at $E_{p,a}$ = 1.06 V. The results of the experiment show that although oxidation of PPh_3 and disproportionation may be competing processes, disproportionation is unimportant under the conditions of the experiment,[4] and the net reaction is

$$[Ru^{II}(bpy)_2(NO_2)py]^{+} + PPh_3 \xrightarrow{-2e^-} [Ru^{II}(bpy)_2(^{+}NO)py]^{3+} + OPPh_3 \quad (4)$$

Electrochemical oxidation of $[Ru(bpy)_2(NO_2)Cl]$ in the presence of PPh_3 also gave $OPPh_3$ and it was possible to study the reaction in detail. The $[Ru^{III}(bpy)_2(NO_2)Cl]^{+}$–

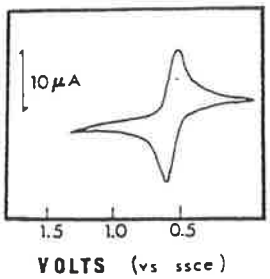

Figure 1. Cyclic voltammogram following electrolysis at 1.15 V (n = 2.0/Ru by coulometry) of a solution containing initially $[Ru(bpy)_2(NO_2)py]^{+}$ (1×10^{-3} M) and PPh_3 (3×10^{-3} M) in 0.1 M $[N(C_4H_9)_4]PF_6$–CH_3CN vs. the SSCE.

$[Ru^{II}(bpy)_2(NO_2)Cl]$ couple is reversible on the cyclic voltammetry time scale (200 mV/s; $E_{1/2}$ = 0.58 V in acetonitrile).[3] Electrochemical oxidation (at 0.80 V) of ^{18}O-enriched $[Ru(bpy)_2(NO_2)Cl]$[5] (5×10^{-4} M) in dichloromethane in the presence of a threefold excess of PPh_3 gave n = 2.0 and as products $[Ru(bpy)_2(NO)Cl]^{2+}$ and $Ph_3P{=}O$. The extent of ^{18}O labeling in the $OPPh_3$ product was identical with that in the initial nitro complex as shown by $\nu(N^{18}O)/\nu(N^{16}O)$ and $\nu(P^{18}O)/\nu(P^{16}O)$ ratios in the IR.[7] The initial step in the electrochemical experiment is oxidation of Ru(II) to Ru(III) which is followed by oxidation of PPh_3 to $OPPh_3$. The rate of the reaction between $[Ru^{III}(bpy)_2(NO_2)Cl]^{+}$ and PPh_3 was studied by chronoamperometry. The reaction is first order in both $[Ru^{III}(bpy)_2(NO_2)Cl]^{+}$ and PPh_3, and in propylene carbonate as solvent, k(25.0 °C, I = 0.2) = 200 ± 10 M^{-1} s^{-1}. The reaction is considerably more rapid than the rate of disproportionation of $[Ru(bpy)_2(NO_2)Cl]^{+}$ (reaction 1) under the same conditions (k = 3.0 M^{-1} s^{-1}),[1] which explains why Ru(III)–NO_2 once formed is captured by PPh_3 rather than by disproportionation. The rate of oxidation of PPh_3 by $[Ru^{III}(bpy)_2(NO_2)py]^{2+}$ must be even more rapid. At a PPh_3/Ru ratio of 3:1, electrochemically generated $[Ru^{III}(bpy)_2(NO_2)py]^{2+}$ is completely captured by PPh_3 (Figure 1) and yet the rate of disproportionation of the Ru(III)–nitro complex exceeds 10^7 M^{-1} s^{-1}.[1]

The electrochemical results, the ^{18}O labeling experiment, and the second-order rate law for oxidation all suggest that oxidation of PPh_3 occurs as in reactions 5–7.

$$[Ru^{II}(bpy)_2(NO_2)Cl] \xrightarrow{-e^-} [Ru^{III}(bpy)_2(NO_2)Cl]^{+} \quad (5)$$

$$[Ru^{III}(bpy)_2(NO_2)Cl]^{+} + PPh_3 \longrightarrow [(bpy)_2ClRu^{III}\text{-}N(O)\cdots O\cdots PPh_3]^{+} \longrightarrow [Ru^{II}(bpy)_2(\dot{N}O)Cl]^{+} + OPPh_3 \quad (6)$$

$$[Ru^{II}(bpy)_2(\dot{N}O)Cl]^{+} \xrightarrow{-e^-} [Ru^{II}(bpy)_2(^{+}NO)Cl]^{2+} \quad (7)$$

At the potentials used in the electrolyses, the reduced nitrosyl complexes are known to be oxidized to $[Ru(bpy)_2(^{+}NO)L]^{n+}$.[2]

The Ru(III)–nitro intermediates are weak to moderately strong oxidants as shown by their reduction potential values.

Scheme I (note Figure 2)

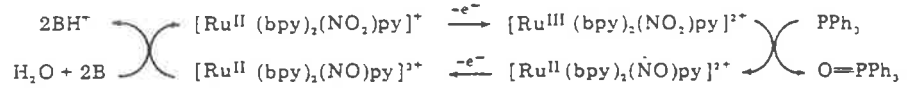

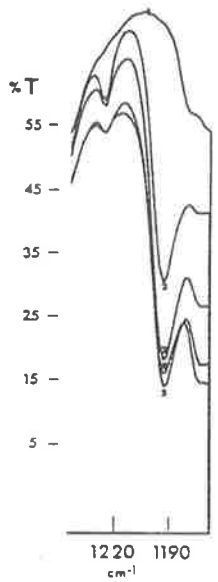

Figure 2. Infrared spectra following electrolysis of an acetonitrile solution containing initially $[Ru(bpy)_2(NO_2)py]^+$ (1.2×10^{-3} M), PPh_3 (7×10^{-3} M), 1% 2,6-lutidine, and 1% water in 0.1 M $[N(C_4H_9)_4]PF_6$. ν(PO) in $O{=}PPh_3$ occurs at 1194 cm^{-1}. The lower energy band arises from $[Ru(bpy)_2(NO_2)py]^+$: (1) before electrolysis; (2) electrolysis to 25% completion based on the initial amount of PPh_3; (3) electrolysis to 50% completion; (4) electrolysis to 60% completion; (5) electrolysis to 75% completion.

Rather than thermodynamic driving force, the origin of the relatively rapid rates of disproportionation and of PPh_3 oxidation may lie in the existence of two one-electron acceptor sites (Ru(III) and Ru-$^+$NO) in the oxidant rather than a single two-electron site and in the ability of the oxidant to donate an oxide ion. Kinetic barriers to electron transfer at both Ru(III)[8] and Ru($^+$NO)[2] sites are known to be low and there are no profound changes in coordination environment on reduction except for the loss of O^{2-}.

$[Ru(bpy)_2(NO_2)py]^+$ and $[Ru(bpy)_2(NO)py]^{3+}$ are interrelated by the acid–base equilibrium in eq 8 and in water, the two ions are present in equimolar amounts at pH 3.8.[1,9]

$$[Ru(bpy)_2(NO)py]^{3+} + 2OH^- = [Ru(bpy)_2(NO_2)py]^+ + H_2O \quad (8)[1]$$

$$K(25.0\ ^\circ C;\ 1.0\ M\ NaCl) = 1 \times 10^{20}\ M^{-2}$$

In slightly basic solution the nitrosyl complex once formed (eq 6 and 7) is converted into the nitro complex. The nitro complex reenters the oxidation sequence in reactions 5–7, which means that the oxidation of PPh_3 can be made catalytic. Exhaustive electrolysis (at 1.15 V) of an acetonitrile solution containing $[Ru(bpy)_2(NO_2)py]^+$ (1×10^{-3} M), PPh_3 (1×10^{-2} M), H_2O (1%), and 2,6-lutidine (1%) gave $n = 21.1$ by coulometry. The final ruthenium product was $[Ru(bpy)_2(NO_3)py]^{2+}$ (by cyclic voltammetry). The results are consistent with the catalytic cycle in Scheme I ($n = 20$) followed by reaction 9 ($n = 3$) when the $PPh_3 \rightarrow O{=}PPh_3$ conversion (Figure 2) is complete.

$$[Ru^{II}(bpy)_2(NO_2)py]^+ + 2B + H_2O \xrightarrow{-3e^-} [Ru^{III}(bpy)_2(NO_3)py]^{2+} + 2BH^+ \quad (9)[1]$$

The electrolytic chemistry observed here is the chemically catalyzed, net electrochemical oxidation of PPh_3 to $O{=}PPh_3$.

$$PPh_3 + H_2O + 2B \rightarrow O{=}PPh_3 + 2BH^+ + 2e^- \quad (10)$$

In an acetonitrile solution containing $[Ru(bpy)_2(NO_2)Cl]$, water, and triethylamine, the oxidation of PPh_3 is also catalytic. Under these conditions cyclic voltammetry shows only a distorted wave for the $[Ru^{II}(bpy)_2(NO_2)Cl] \rightarrow [Ru^{III}(bpy)_2(NO_2)Cl]^+$ oxidation and no rereduction wave, nor does a wave for $[Ru(bpy)_2(NO)Cl]^{2+}$ appear. The experiment shows that the chemical steps in Scheme I are rapid and that the *rate determining step in the catalyzed oxidation of PPh_3 is diffusion of $[Ru(bpy)_2(NO_2)Cl]$ to the electrode.*

The Ru(III)–nitro intermediates appear to have an extensive oxidase-like redox chemistry and their reactions with various reagents are currently under investigation. They are promising as oxidants, since in contrast to commonly used inorganic oxidants like Cr(VI) or MnO_4^-, their reactivity properties can be varied systematically by controlled chemical synthesis, and their reactions can be made catalytic.

Acknowledgment is made to the National Science Foundation under Grant MPS75-11867 and to the Materials Research Center of The University of North Carolina under Grant DAHC15 73 G9 with the National Science Foundation for support of this research.

References and Notes

(1) F. R. Keene, D. J. Salmon, and T. J. Meyer, *J. Am. Chem. Soc.*, **99**, 2384 (1977).
(2) T. J. Meyer, R. W. Callahan, and G. M. Brown, *J. Am. Chem. Soc.*, **97**, 894 (1975); R. W. Callahan and T. J. Meyer, *Inorg. Chem.*, **16**, 574 (1977).
(3) Unless otherwise noted electrochemical results were obtained in solutions 0.1 M in $[N(n\text{-}C_4H_9)_4]PF_6$ at 22 ± 2 °C vs. the saturated sodium chloride calomel eletrode (SSCE). Platinum bead electrodes were used in cyclic voltammetry and platinum gauze electrodes for electrolyses. n values were obtained by coulometry, where n is the number of electrons passed per Ru in a constant potential electrolysis.
(4) Disproportionation gives nitrosyl *and* nitrato complexes as products and $n = 3.0$ (eq 1 and 2).
(5) Ca. 7% ^{18}O-enriched $[Ru(bpy)_2(NO_2)Cl]$ was prepared by treating a suspension of $[Ru(bpy)_2(NO)Cl](PF_6)_2$ with base in ^{18}O-enriched water.[6]
(6) T. J. Meyer and J. B. Godwin, *Inorg. Chem.*, **10**, 2150 (1971).
(7) Quantitative IR experiments were carried out using a Digilab FTS-14 spectrometer.
(8) R. W. Callahan, F. R. Keene, T. J. Meyer, and D. J. Salmon, *J. Am. Chem. Soc.*, **99**, 1064 (1977); R. C. Young, F. R. Keene, and T. J. Meyer, *J. Am. Chem. Soc.*, **99**, 2468 (1977).
(9) For the $[Ru(bpy)_2(NO)Cl]^{2+}$–$[Ru(bpy)_2(NO_2)Cl]$ equilibrium, K is 1.4×10^9 under the same conditions.[6]

F. Richard Keene, Dennis J. Salmon, Thomas J. Meyer*
Department of Chemistry, University of North Carolina
Chapel Hill, North Carolina 27514
Received November 8, 1976

Inorg. Chem. 1980, *19*, 1896–1903

Contribution from the Department of Chemistry, The University of North Carolina, Chapel Hill, North Carolina 27514

Oxidation of the Ligand in Nitro Complexes of Ruthenium(III)

F. RICHARD KEENE, DENNIS J. SALMON, JERRY L. WALSH, HECTOR D. ABRUÑA, and THOMAS J. MEYER*

Received June 29, 1979

Nitro complexes of bis(bipyridyl)ruthenium(III) are unstable with respect to oxidation of the coordinated nitro ligand. For the complexes $Ru(bpy)_2(L)NO_2^+$ (L = NH_3, py (pyridine), pyr (pyrazine), CH_3CN, PPh_3) and $Ru(bpy)_2(Cl)NO_2$, electrochemical oxidation to the ruthenium(III) state results in production of the corresponding nitrosyl and nitrato complexes in a 1:1 ratio. A two-electron oxidation of the nitro ligand to nitrate occurs, and the corresponding reduction is delocalized over two sites, one at the metal ($Ru^{III} \rightarrow Ru^{II}$) and one at the ligand ($RuNO^+ \rightarrow RuNO$). For the chloro complex the rate of disappearance of $Ru^{III}(bpy)_2(Cl)NO_2^+$ is first order in Ru(III) and the rate constant, determined by monitoring the reaction by cyclic voltammetry, is 1.8×10^{-3} s^{-1} in acetonitrile at room temperature. For the pyridyl complex, variable scan-rate cyclic voltammetry experiments show the intervention of an intermediate past the initial oxidation step. A mechanism is suggested for the oxidation of coordinated nitrite which consists of an initial rearrangement of the nitro ligand from N bound to O bound. The O-bound isomer is a reactive intermediate which undergoes a bimolecular oxygen atom transfer reaction probably with the corresponding Ru^{II}-NO_2 complex to give the observed products. The acid–base properties of the $Ru(bpy)_2(py)NO_2^+$–$Ru(bpy)_2(py)NO^{3+}$ acid-base pair and formal reduction potentials for the chloro and pyridyl complexes as two-electron-acceptor, oxide ion donor oxidants have been determined. In basic solutions, oxidation of the nitro group becomes catalytic and the nitrato complex is the sole product of the oxidation.

Introduction

We are attempting to design 2,2′-bipyridyl complexes of ruthenium which can function as redox catalysts. As potential catalytic systems, the complexes are attractive because of the stability of the Ru–bpy chemical link, the availability of possible multiple electron donor or acceptor properties based either on metal[1,2] or ligand[3,4] redox sites, the existence of dimeric and oligomeric multimetallic complexes,[5] and the versatility of the background synthetic chemistry for making controlled chemical modifications.[5a,6] The complexes are also attractive from the kinetic point of view since they retain the same basic coordination number in a series of different oxidation states and, where known, the kinetic barriers to electron transfer are low as shown by electron-transfer self-exchange studies.[4a,7]

In earlier work it was shown that relatively facile oxidation of ligands coordinated to $(bpy)_2$ complexes of ruthenium can occur (eq 1 and 2). The reactions in eq 1 and 2 are known

$$Ru(bpy)_2(N_3)_2 + CH_3CN \xrightarrow{-e} Ru(bpy)_3(CH_3CN)N_3^+ + {}^3/_2N_2 \quad (1)[8]$$

$$Ru(bpy)_2(NH_2CH_2R)_2^{2+} \xrightarrow{-8e^-} Ru(bpy)_2(N{\equiv}CR)_2^{2+} + 8H^+ \quad (2)[9]$$

to occur by initial oxidation of Ru(II) to Ru(III). For the case where bound amines are oxidized (eq 2), the initial Ru(II) → Ru(III) step is followed by a series of net two-electron oxidative dehydrogenation steps at the bound amine ligands.

In this paper a third example is described where a bound ligand is oxidized following oxidation of Ru(II) to Ru(III). The chemistry involves oxidation of a bound nitro to a nitrato group. The appearance of the reaction, which was described in a preliminary communication,[10] helps explain the apparent nonexistence of stable, monomeric nitro complexes of Ru(III)[11] and more importantly suggests that Ru(III)–nitro complexes, which do exist, but as transient intermediates, may have useful properties as oxygen atom transfer catalysts.[12]

Experimental Section

Ultraviolet–visible spectra were obtained by using a Bausch and Lomb Model UV-210 spectrometer. All electrochemical measurements were at platinum electrodes, and all potentials are reported vs. the saturated sodium chloride calomel electrode (SSCE) at 22 ± 2 °C and were uncorrected for junction potentials. Potential control for electrochemical experiments was obtained by using a Princeton Applied Research Model 173 potentiostat/galvanostat. The wave-form generator for voltammetric experiments was a Princeton Applied Research Model 175 universal programmer. Slow-scan (50–500 mV/s) cyclic voltammograms were recorded on a Hewlett-Packard Model 7004B X-Y recorder. Fast-scan cyclic voltammograms were obtained from photographs of the trace from a Tektronix Model 564B storage oscilloscope. For fast-scan cyclic voltammograms, IR compensation was used. Values of n, where n is the number of equivalents of electrons transferred per complex in exhaustive electrolyses at constant potentials, were calculated from the total area under current vs. time curves. Reactions were judged to be complete when the current had fallen below 1% of the initial value.

Materials. Tetra-*n*-butylammonium hexafluorophosphate (TBAH) and tetraethylammonium perchlorate (TEAP) were prepared by standard techniques and used as the supporting electrolyte in electrochemical experiments. The acetonitrile (MCB spectrograde) used in electrochemical measurements was dried over Davidson 4-Å molecular sieves. All other chemicals were commercially available and were of reagent quality and used without further purification.

Synthesis of Complexes. $[Ru(bpy)_2(NO_2)_2]\cdot H_2O$,[13] $[Ru(bpy)_2(NO)Cl](PF_6)_2$,[13] and $Ru(bpy)_2(NO_2)Cl\cdot H_2O$[14] were prepared as described previously.

(1) (a) G. M. Brown, Ph.D. Dissertation, The University of North Carolina, Chapel Hill, 1974; (b) D. J. Salmon, Ph.D. Dissertation, The University of North Carolina, Chapel Hill, 1976.
(2) B. A. Moyer and T. J. Meyer, *J. Am. Chem. Soc.*, 100, 3601 (1978); B. A. Moyer, M. Thompson, and T. J. Meyer, *ibid.*, 102, 2310 (1980).
(3) B. P. Sullivan, H. Abruna, H. O. Finklea, D. J. Salmon, J. K. Nagle, H. Sprintschnik, and T. J. Meyer, *Chem. Phys. Lett.*, 58, 389 (1978).
(4) (a) R. W. Callahan and T. J. Meyer, *Inorg. Chem.*, 16, 574 (1977); (b) R. W. Callahan, G. M. Brown, and T. J. Meyer, *J. Am. Chem. Soc.*, 97, 894 (1975).
(5) (a) T. J. Meyer, *Ann. N.Y. Acad. Sci.*, 313, 496 (1978); (b) T. J. Meyer, *Adv. Chem. Ser.*, No. 150 (1976). (c) R. W. Callahan, E. C. Johnson, G. M. Brown, T. R. Weaver, and T. J. Meyer, *ACS Symp. Ser.*, No. 5, 66 (1975); (d) S. A. Adeyemi, E. C. Johnson, F. J. Miller, and T. J. Meyer, *Inorg. Chem.*, 12, 2371 (1973).
(6) S. A. Adeymi, F. J. Miller, and T. J. Meyer, *Inorg. Chem.*, 11, 994 (1972).
(7) (a) R. W. Callahan, F. R. Keene, D. J. Salmon, and T. J. Meyer, *J. Am. Chem. Soc.*, 99, 1074 (1977); (b) F. R. Keene, R. C. Young, and T. J. Meyer, *ibid.*, 99, 2468 (1977).
(8) G. M. Brown, R. W. Callahan, and T. J. Meyer, *Inorg. Chem.*, 14, 1915 (1975).
(9) (a) F. R. Keene, D. J. Salmon, and T. J. Meyer, *J. Am. Chem. Soc.*, 98, 1884 (1976); (b) G. M. Brown, T. R. Weaver, F. R. Keene, and T. J. Meyer, *Inorg. Chem.*, 15, 190 (1976).
(10) F. R. Keene, D. J. Salmon, and T. J. Meyer, *J. Am. Chem. Soc.*, 99, 2384 (1977).
(11) W. P. Griffith, "The Chemistry of the Rarer Platinum Metals", Interscience Publishers, New York, 1967.
(12) F. R. Keene, D. J. Salmon, and T. J. Meyer, *J. Am. Chem. Soc.*, 99, 4821 (1977); B. A. Moyer and T. J. Meyer, submitted for publication.
(13) J. B. Godwin and T. J. Meyer, *Inorg. Chem.*, 10, 471 (1971).
(14) J. B. Godwin and T. J. Meyer, *Inorg. Chem.*, 10, 2150 (1971).

$[Ru(bpy)_2(NO)(NO_2)](PF_6)_2$. $Ru(bpy)_2(NO_2)_2$ (1 g) was suspended in acetonitrile (20 mL) in subdued light. One milliliter of 70% HPF_6 was added dropwise with stirring, and the mixture was stirred for 2 min and then filtered into an excess of diethyl ether. The solid which precipitated was collected by filtration, washed with ether, and air-dried; yield 96%. The complex could be recrystallized from acetonitrile–ether solvent mixtures.

$[Ru(bpy)_2(py)(NO_2)]PF_6$. $[Ru(bpy)_2(NO)(NO_2)](PF_6)_2$ (2.425 g) was dissolved in deaerated acetone (30 mL), and a stoichiometric amount of KN_3 (0.252 g), dissolved in methanol (8 mL), was added dropwise with stirring in subdued light. The mixture was stirred for 10 min. Pyridine (5 mL) was added, and the solution was stirred for 2 h. The mixture was filtered into excess diethyl ether, giving a red-brown precipitate which was filtered, washed with ether, and dried in vacuo. Purification of the solid was achieved by chromatography on a column of alumina, using acetonitrile as an eluant under subdued light conditions. The eluant was evaporated to dryness giving a bright red product. It was recrystallized by slow addition of petroleum ether (bp 40–60 °C) to a methylene chloride solution of the complex. The electronic spectrum of the complex in water included an intense band at λ_{max} 414 nm (ϵ 7400) and in acetonitrile λ_{max} = 449 nm (ϵ 7800) and λ_{max} = 336 nm (ϵ 10000). Anal. Calcd for $[Ru(C_{10}H_8N_2)_2(C_5H_5N)(NO_2)]PF_6$: C, 43.93; H, 3.10; N, 12.30. Found: C, 44.10; H, 3.00; N, 12.15.

$[Ru(bpy)_2(py)(NO)](PF_6)_3$. $[Ru(bpy)_2(py)(NO_2)]PF_6$ (0.50 g) was suspended in acetonitrile (10 mL) in the dark, and 70% HPF_6 (1 mL) was added with stirring. The mixture was stirred for 2 min and then filtered into excess diethyl ether. The precipitated solid was collected by filtration, washed with ether, and dried in vacuo; yield 95%. The solid was recrystallized from acetone–ether. The procedure given here is a slight modification of a procedure given earlier.[4]

$[Ru(bpy)_2(CH_3CN)(NO_2)]PF_6$. This salt was synthesized by using a procedure analogous to that given for $[Ru(bpy)_2(py)(NO_2)]PF_6$ except that CH_3CN was substituted for py. The salt was purified by converting it to the nitrosyl form (by treatment with HPF_6 as mentioned above) followed by reconversion to the nitro complex. For the nitrosyl → nitro conversion, $[Ru(bpy)_2(CH_3CN)(NO)](PF_6)_3$ (0.5 g) was suspended in H_2O (20 mL) and 3 drops of a 50% NaOH solution was added. The mixture was stirred for 5 min. The solid was collected by filtration, washed with ice-cold water, and dried in vacuo.

$[Ru(bpy)_2(NH_3)(NO_2)]PF_6$. $[Ru(bpy)_2(NO)(NO_2)](PF_6)_2$ (0.110 g) was dissolved in deaerated CH_2Cl_2 (150 mL). Tetraphenylarsonium azide (0.060 g; stoichiometric) was added, and the solution was stirred in subdued light for 2 h. Ammonia was then bubbled through the solution for 2 h, after which the solution was filtered into a large excess of diethyl ether. The resulting solid was collected by filtration, washed with ether, and dried in vacuo; yield 40%.

$[Ru(bpy)_2(PPh_3)(NO_2)](PF_6)$ (Ph = Phenyl). This complex was prepared by the method given for $[Ru(bpy)_2(py)(NO_2)](PF_6)$ except that PPh_3 was substituted for py. Anal. Calcd for $[Ru(C_{10}H_8N_2)_2P(C_6H_5)_3(NO_2)](PF_6)$: C, 52.66; H, 3.61; N, 8.05. Found: C, 51.58; H, 3.41; N, 8.05.

$[Ru(bpy)_2(pyr)(NO_2)](PF_6)$ (pyr = Pyrazine). $[Ru(bpy)_2(NO)(NO_2)](PF_6)_2$ (0.40 g) was dissolved in 20 mL of deaerated acetone, and sodium azide (0.033 g) was added as a methanol solution. The resulting solution was then added to a solution of 1.02 g of pyr in acetone. This solution was stirred and gently heated for 30 min and then added to diethyl ether, and the solid product was collected by filtration. The product was purified by chromatography on a basic alumina column using acetone as eluant. The eluted product was evaporated to dryness, redissolved in a minimum amount of acetone, and precipitated with diethyl ether. Anal. Calcd for $[Ru(C_{10}H_8N_2)_2(C_4H_4N_2)(NO_2)]PF_6 \cdot 2H_2O$: C, 40.46; H, 2.26; N, 13.76. Found: C, 41.75; H, 2.73; N, 13.87.

$[Ru(bpy)_2(NO_3)Cl]Cl$. $Ru(bpy)_2(NO_2)Cl$ (0.05 g) was dissolved in CH_3CN (100 mL), and triethylamine (3 drops) and water (3 drops) were added. Chlorine was bubbled through the solution which caused a color change from red to yellow. The solution was added dropwise to 250 mL of ether and cooled to 5 °C. The solid which precipitated was collected by filtration and air-dried; yield 40%. Anal. Calcd for $[Ru(C_{10}H_8N_2)_2(NO_3)Cl]Cl$: C, 43.97; H, 2.95; N, 12.82. Found: C, 43.24; H, 3.26; N, 12.64.

Table I. Rate Constants for the Reaction $3Ru(bpy)_2(Cl)NO_2^+ \rightarrow Ru(bpy)_2(Cl)NO_2 + Ru(bpy)_2(Cl)NO_2^+ + Ru(bpy)_2(Cl)NO^{2+}$ at 22 ± 2 °C in Acetonitrile

run no.	initial concn of $Ru(bpy)_2(Cl)NO_2^+$, mM	10^3k, s^{-1}	method,[a] oxidant[b]
1	0.05	4.3	vis, $Fe(bpy)_3^{3+}$
2	0.12	4.2	vis, $Fe(bpy)_3^{3+}$
		av 4.2	
3	0.7	2.2	CV, $Fe(bpy)_3^{3+}$
4	1.8	2.3	CV, $Fe(bpy)_3^{3+}$
5	1.9	1.8	CV, $Ru(bpy)_3^{3+}$
6	3.9	0.9	CV, $Fe(bpy)_3^{3+}$
		av 1.8	

[a] vis: Rate constant values were determined from absorbance (507 nm) vs. time data after mixing $Ru(bpy)_2(Cl)NO_2$ with the oxidant. No additional electrolyte was added. CV: Rate constant values were determined by cyclic voltammetry by measuring oxidative peak currents for the $Ru(bpy)_2(Cl)NO^{2+}/Ru(bpy)_2(Cl)NO^+$ couple as a function of time following the chemical oxidation step. The region −0.2 to 1.0 volts vs. SSCE was scanned at appropriate time intervals at 200 mV/s in the cyclic voltammetry experiment. Solutions were 0.1 M in $[NEt_4](ClO_4)$. [b] $[Fe(bpy)_3](PF_6)_3$ was added as a solid directly to the solution to be oxidized. When $Ru(bpy)_3^{3+}$ was used as oxidant, it was generated electrochemically in solution immediately prior to use.

$[Ru(bpy)_2(py)(NO_3)]PF_6$. A solution of 1.42 g of $(NH_4)_2Ce(NO_3)_6$ in water (3 mL) was added to a solution of 0.589 g of $[Ru(bpy)_2(py)(NO_2)]PF_6$ in acetonitrile to give a greenish solution and a tan precipitate. After filtration, the green solution was added to diethyl ether and the resulting precipitate was collected by filtration. The solid was dissolved in water, and saturated aqueous NH_4PF_6 was added. The resulting precipitate was collected by filtration and extracted with CH_3CN. The extract was chromatographed on an alumina column with $[Ru(bpy)_2(py)(NO_3)]PF_6$ being eluted with CH_2Cl_2/CH_3CN. The eluant was rotary evaporated to small volume and precipitated by addition of diethyl ether, and the solid was collected by filtration; yield 20%. Anal. Calcd for $[Ru(C_{10}H_8N_2)_2(C_5H_5N)(NO_3)](PF_6)$: C, 42.93; H, 3.03; N, 12.07. Found: C, 42.71; H, 2.99; N, 11.52. In addition to the expected bands for bpy and py vibrations, the infrared spectrum of $[Ru(bpy)_2(py)(NO_3)]PF_6$ exhibits bands suggesting the existence of O-bound, unidentate nitrate (~1460, 1288, 1000 cm^{-1}).[15] The visible spectrum exhibits a λ_{max} at 478 nm (ϵ 8000) in acetonitrile solution. A more convenient, photochemical preparation of $[Ru(bpy)_2(py)(NO_3)]PF_6$ is described elsewhere.[16]

$[Fe(bpy)_3](PF_6)_3$. $[Fe(bpy)_3](PF_6)_2$, prepared by standard techniques,[17] was oxidized with excess $(NH_4)_2Ce(NO_3)_6$ in acetonitrile. The precipitate which formed was collected by filtration and dissolved in water, and $[Fe(bpy)_3](PF_6)_3$ was precipitated by addition of HPF_6. The precipitate was collected, dissolved in acetonitrile, and reprecipitated by addition of ether. The purity of $[Fe(bpy)_3](PF_6)_3$ was checked by cyclic voltammetry. On standing in solution or as a solid, $Fe(bpy)_3^{3+}$ is readily reduced apparently by moisture in the air or by solvent contaminants. The absence of $Fe(bpy)_3^{2+}$ in samples of $Fe(bpy)_3^{3+}$ is indicated by the absence of the intense red color of $Fe(bpy)_3^{2+}$.

Determination of the Rate Constant for Disproportionation of $Ru^{III}(bpy)_2(Cl)NO_2^+$ By Cyclic Voltammetry. For cases where $Fe(bpy)_3^{3+}$ was used as oxidant, a weighed quantity of $Ru(bpy)_2(Cl)NO_2$ was added to about 6 mL of acetonitrile (0.1 M TEAP) and the solution was stirred to dissolve at least part of the $Ru(bpy)_2(Cl)NO_2$. A slight molar deficiency of solid $[Fe(bpy)_3](PF_6)_3$ was added at which time all of the suspended material dissolved. The reaction which followed was assumed to be that shown in eq 3 based

(15) K. Nakamoto, "Infrared Spectra of Inorganic and Coordination Compounds", 2nd ed., Wiley-Interscience, New York, 1970.
(16) B. Durham, J. Walsh, C. L. Carter, and T. J. Meyer, *Inorg. Chem.*, 19, 860 (1980).
(17) F. H. Burstall and R. S. Nyholm, *J. Chem. Soc.*, 3570 (1952).

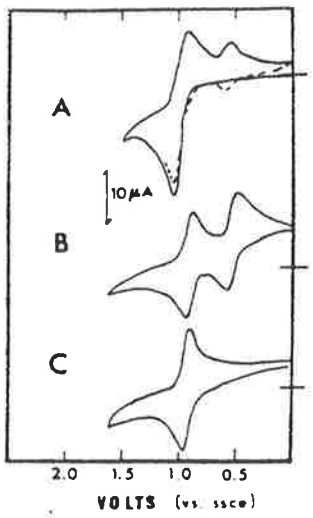

Figure 1. Cyclic voltammograms (200 mV/s) in acetonitrile (0.1 M $[NEt_4](ClO_4)$) at 22 ± 2 °C: (A) $Ru(bpy)_2(py)NO_2^{+}$; (B) solution A after exhaustive electrolysis at +1.2 V (n = 1.5); (C) solution A with added H_2O (1%) and 2,6-lutidine (1%) after exhaustive electrolysis at +1.2 V (n = 3.0).

$$3Ru(bpy)_2(Cl)NO_2^{+} \rightarrow Ru(bpy)_2(Cl)NO_2 + Ru(bpy)_2(Cl)NO_3^{+} + Ru(bpy)_2(Cl)NO^{2+} \quad (3)$$

on prior electrochemical results (see below). Cyclic voltammograms (scan rate 200 mV/s; limits −0.2 to +0.9 V vs. SSCE) were recorded as soon as possible after mixing and were recorded then at frequent intervals throughout a period of 30 min. When $Ru(bpy)_3^{3+}$ was used as oxidant, a weighed quantity of $[Ru(bpy)_3](PF_6)_2$ was exhaustively oxidized in acetonitrile (0.1 M TEAP) at 1.40 V vs. SSCE and a weighed quantity of solid $Ru(bpy)_2(Cl)NO_2$ was then added to the solution. The reaction was followed in the same fashion as when $Fe(bpy)_3^{3+}$ was used as oxidant. For each case, the rate of appearance of $Ru(bpy)_2(Cl)NO^{2+}$ was determined by the increase in the anodic peak current, i_p, for the $Ru(bpy)_2(Cl)NO^{2+}/Ru(bpy)_2(Cl)NO^{+}$ couple ($E_{p,a}$ = 0.21 V). The treatment of the kinetic data is outlined below.

By Spectrophotometry. Acetonitrile solutions of $Ru(bpy)_2(Cl)NO_2$ and $[Fe(bpy)_3](PF_6)_3$ were mixed in appropriate proportions to give a slight molar excess of $Ru(bpy)_2(Cl)NO_2$. The solution was added to a cuvette and placed in the spectrophotometer. The absorbance change at λ_{max} 507 nm for $Ru(bpy)_2(Cl)NO_2$) was monitored and absorbance vs. time data recorded. An initial rapid ($t_{1/2} \approx$ 2–4 min) increase was observed, followed by a slow decrease. The initial increase in absorbance, A, was attributed to the appearance of $Ru(bpy)_2(Cl)NO_2$ via eq 3, and the data was treated accordingly as outlined below. The origin of the slow secondary absorbance change is not clear. It should be noted that corresponding changes were not observed when the system was monitored by cyclic voltammetry but admittedly under conditions where the concentration of initial complex was higher.

Data Treatment. Kinetic data for the formation of $Ru(bpy)_2(Cl)NO^{2+}$, measured by changes in peak current (i_p) in the electrochemical experiments, or for the appearance of $Ru(bpy)_2(Cl)NO_2$, measured by changes in absorbance (A) in the spectral experiments, were analyzed by the Swinbourne method.[18] The parameter, i_p or A, at time t was plotted vs. the same parameter at time $t + \tau$, where τ is a constant time interval which was chosen as 2 min in this case. Smooth curves were drawn for the i_p or A vs. time data and then the data obtained from these plots by extrapolation were used in the Swinbourne analysis. Straight-line Swinbourne plots were obtained with slopes greater than 1 and the intersection of the straight lines with the line of slope equal to 1 were in good agreement with the infinity values either observed or obtained by extrapolation. The infinity values were used to treat the i_p or A data by standard first-order techniques, and the rate constants in Table I were obtained. The insensitivity of the observed rate constants to the concentration of $Ru(bpy)_2(Cl)NO_2^{+}$ confirms the first-order nature of the reaction.

(18) E. S. Swinbourne, *J. Chem. Soc.*, 2371 (1960).

Scheme I

$$2Ru^{II}(bpy)_2(py)NO_2^{+} \xrightarrow{-2e^-} 2Ru^{III}(bpy)_2(py)NO_2^{2+}$$

$$2Ru^{III}(bpy)_2(py)NO_2^{2+} \rightarrow Ru^{II}(bpy)_2(py)NO^{3+} + Ru^{II}(bpy)_2(py)NO_3^{+}$$

$$Ru^{II}(bpy)_2(py)NO_3^{+} \xrightarrow{-e^-} Ru^{III}(bpy)_2(py)NO_3^{2+}$$

Table II. Electrochemical Data in 0.1 M $[N(n\text{-}Bu)_4(PF_6)]$–Acetonitrile Solution at 22 ± 2 °C[a]

	couple or process		
	oxidn of $Ru(bpy)_2(L)NO_2^{+}$	$Ru(bpy)_2(L)(NO)^{3+/2+}$	$Ru(bpy)_2(L)(NO_3)^{2+/+}$
L	$E_{p,a}$ V	$E_{1/2}$, V	$E_{1/2}$, V
PPh_3	1.25	0.56	1.07[b]
CH_3CN	1.17	0.56	1.02[b]
pyr (pyrazine)	1.14	0.57	1.00[b]
py (pyridine)	1.06	0.53	0.91
NH_3	0.85	0.30	0.70[b]
Cl	0.57[c]	0.19[d]	0.45[c]

[a] Values are reported vs. the SSCE determined by cyclic voltammetry at a scan rate of 200 mV/s. [b] The nitrato complex was not isolated. The $E_{1/2}$ values were obtained by following electrolytic oxidation of solutions of $Ru(bpy)_2(L)(NO_2)^{+}$. [c] The $Ru(bpy)_2(Cl)(NO_2)^{+/0}$ couple is reversible at this scan rate, and the value quoted is the $E_{1/2}$ value. If the interpretation given below is correct for the results of scan rate dependent cyclic voltammetry experiments, it follows that $E_{1/2}$ = 1.00 V for the $Ru(bpy)_2(py)NO_2^{2+/+}$ couple in acetonitrile (I = 0.1 M). [d] The couple is $Ru(bpy)_2(Cl)(NO)^{2+/+}$. [e] The couple is $Ru(bpy)_2(Cl)(NO_3)^{+/0}$.

Measurement of K for the Equilibrium $Ru(bpy)_2(py)NO^{3+} + 2OH^- \rightleftharpoons Ru(bpy)_2(py)NO_2^{+} + H_2O$. The equilibrium constant for the nitrosyl–nitro equilibrium was determined spectrophotometrically at 25.0 ± 0.1 °C in water at I = 1.0 M (NaCl). Constant pH was maintained in the experiment by using potassium hydrogen phthalate (0.010 M) as buffer. The equilibrium constant was determined by adding an aliquot of an aqueous solution of $[Ru(bpy)_2(py)NO](PF_6)_3$ to each of ten 50-mL flasks (to give a complex concentration of ~1.2 × 10^{-4} M). In addition, NaCl (2.92 g), an aliquot of potassium hydrogen phthalate (to make the buffer concentration 0.010 M), and sufficient 0.1 M $HClO_4$ or 0.10 M NaOH to vary the pH of the solutions over the range pH 2–6 were added. The solutions were allowed to sit at 25.0 ± 0.1 °C in a water bath for 12 h. Each solution was then measured spectrophotometrically in the visible region with the absorbance at λ 414 nm [λ_{max} for $Ru(bpy)_2(py)(NO_2)^{+}$] being especially noted, and the pH of each solution was recorded. At the two extremes of pH used, only $Ru(bpy)_2(py)NO)^{3+}$ or $Ru(bpy)_2(py)(NO_2)^{+}$ were present in any appreciable amount. For the intermediate pH cases, the amounts of the two species were calculated from the absorbance at λ 414 nm. Since the nitrosyl complex is essentially transparent at this wavelength, the absorbance measurement with the known molar extinction coefficient for the nitro complex gave its concentration, and the concentration of nitrosyl complex was determined by mass balance. From the results of three separate experiments under conditions where both the nitrosyl and nitro complexes were present in appreciable amounts, an average value of K(25.0 °C, I = 1.0 M) = (1.0 ± 0.3) × 10^{20} M^{-2} was found.

Results and Discussion

Oxidation of Bound Nitrite to Nitrate. A cyclic voltammogram of a solution containing the complex $Ru(bpy)_2(py)NO_2^{+}$ in acetonitrile (0.1 M TEAP) is shown in Figure 1A. The initial oxidative sweep shows a wave at a potential which is reasonable for a Ru(II) → Ru(III) oxidation ($E_{p,a}$ = 1.06 V), but the oxidation is chemically irreversible, at least in part. On the back, reductive sweep, a new wave appears, and a second sweep through the same potential region indicates that the new wave is associated with a reversible couple. The cyclic voltammogram suggests that initial oxidation of Ru(II) to Ru(III) may occur (eq 4) but that the Ru(III) intermediate

is unstable and undergoes further chemistry following the oxidative step.

$$Ru^{II}(bpy)_2(py)(NO_2)^+ \xrightarrow{-e^-} Ru^{III}(bpy)_2(py)(NO_2)^{2+} \quad (4)$$

Figure 1B shows a cyclic voltammogram of an identical solution following exhaustive electrolysis at 1.20 V. The electrochemical stoichiometry was $n = 1.5$ by coulometry. The voltammogram shows that two new products are formed in essentially equal amounts and that both have chemically reversible redox couples in the potential region studied.

Comparisons with voltammograms for known complexes show that the wave with $E_{1/2} = 0.53$ V corresponds to the reversible nitrosyl couple $Ru(bpy)_2(py)NO^{3+}/Ru(bpy)_2(py)(NO)^{2+}$,[4] and the wave with $E_{1/2} = 0.91$ V corresponds to the $Ru^{III}(bpy)_2(py)(NO_3)^{2+}/Ru^{II}(bpy)_2(py)NO_3)^+$ couple. From the results of the voltammetry and coulometry experiments, the net electrochemical reaction which occurs is shown in eq 5. The nitrosyl and nitrato complexes are both found in the oxidized forms of their respective couples.

$$2Ru(bpy)_2(py)(NO_2)^+ \xrightarrow{-3e^-} Ru(bpy)_2(py)(NO)^{3+} + Ru(bpy)_2(py)(NO_3)^{2+} \quad (5)$$

The nature of the reaction strongly suggests that oxygen transfer occurs between nitro groups on two different ruthenium complexes following oxidation of Ru(II) to Ru(III). As discussed in the next section, the n value of 1.5 and the nature of the reaction products observed are consistent with the series of reactions shown in Scheme I.

As summarized in Table II, similar results were obtained upon oxidation of the Ru(II)–nitro complexes $Ru(bpy)_2(CH_3CN)(NO_2)^+$, $Ru(bpy)_2(NH_3)(NO_2)^+$, $Ru(bpy)_2(PPh_3)(NO_2)^+$, $Ru(bpy)_2(pyr)(NO_2)^+$ (pyr is pyrazine), and $Ru(bpy)(Cl)(NO_2)$ in acetonitrile solution. In all cases, coulometry experiments, where the potential was set at a value on the diffusion plateau of the oxidation wave, gave $n = 1.5$, and two new products appeared as shown by cyclic voltammetry. In each case, one of the products was shown to be the corresponding nitrosyl complex by voltammetric comparisons with known samples under the same conditions. For the chloro and the pyridyl complexes, the second product was shown to be $Ru^{III}(bpy)_2(Cl)(NO_3)^+$ and $Ru^{III}(bpy)_2(py)(NO_3)^{2+}$, respectively, by spectral and electrochemical comparisons with a known sample prepared as described in the Experimental Section. In each of the other cases, the assumption that the second products are the corresponding Ru^{III}–nitrato complexes seems reasonable given the similarities in the electrochemical details of the reactions.

There is a distinguishing feature in the case of the chloro complex. At scan rates of 200 mV/s or faster, the $Ru(bpy)_2(Cl)(NO_2)^{+/0}$ couple is chemically and electrochemically reversible, which shows that the reaction or reactions following the Ru(II) → Ru(III) oxidation step are relatively slow.

The Rate and Mechanism of Oxidation of the Bound NO_2^- Ligand. As mentioned in the previous section, the $Ru(bpy)_2(Cl)(NO_2)^{+/0}$ couple is chemically reversible on the cyclic voltammetry time scale ($v = 200$ mV/s). The Ru(III) form of the couple is sufficiently long-lived in solution that it can be generated by chemical means and the subsequent chemistry, which leads to the nitrosyl and nitrato complexes, eq 3, can be followed by cyclic voltammetry or spectrophotometry.

The experiments were carried out as follows. Solutions of $Ru(bpy)_2(Cl)(NO_2)$ in acetonitrile were oxidized with 1 equiv of $Fe(bpy)_3^{3+}$ or $Ru(bpy)_3^{3+}$ and the subsequent changes in spectral or electrochemical properties were observed with time.

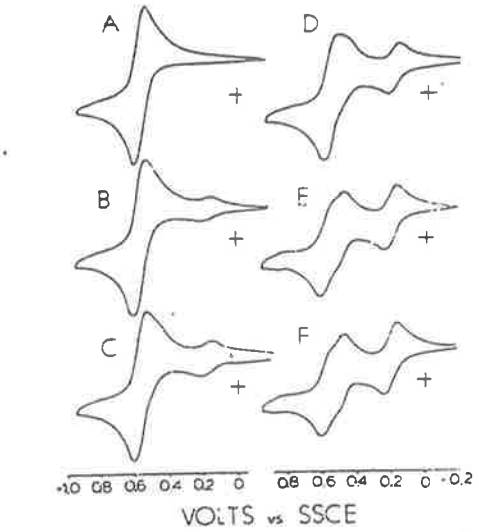

Figure 2. Reaction of $Ru(bpy)_2(Cl)NO_2^+$ according to eq 3 as followed by cyclic voltammetry in acetonitrile (0.1 M $[NEt_4](ClO_4)$ solution, 200 mV/s). Time after oxidation to Ru(III): (A) 1 min; (B) 2 min; (C) 3 min; (D) 5.5 min; (E) 12 min; (F) 16 min.

In cyclic voltammetry experiments (0.1 M TEAP), the decrease in the height of the wave due to the $Ru(bpy)_2(Cl)(NO_2)^{+/0}$ couple was accompanied by an increase in the height of the waves due to the $Ru(bpy)_2(Cl)(NO)^{2+/+}$ and $Ru(bpy)_2(Cl)(NO_3)^{+/0}$ couples (Figure 2). The initial electron-transfer step is clearly very rapid and no evidence for intermediates was observed. When 1 equiv of the oxidant was used, the final products are $Ru^{II}(bpy)_2(Cl)(NO_2)$, $Ru^{III}(bpy)_2(Cl)(NO_3)^+$, and $Ru^{II}(bpy)_2(Cl)(NO)^{2+}$ in a ratio of approximately 1:1:1. The observed ratio is consistent with the stoichiometry derived from the mechanisms shown in Scheme II and eq 3.

Scheme II

$$3Ru^{II}(bpy)_2(Cl)(NO_2) + 3M(bpy)_3^{3+} - 3Ru^{III}(bpy)_2(Cl)(NO_2)^+ + 3M(bpy)_3^{2+} \quad (M = Fe \text{ or } Ru)$$

$$2Ru^{III}(bpy)_2(Cl)(NO_2)^+ - Ru^{II}(bpy)_2(Cl)(NO_2) + Ru^{II}(bpy)_2(Cl)(NO)^{2+}$$

$$Ru^{III}(bpy)_2(Cl)(NO_2)^+ + Ru^{II}(bpy)_2(Cl)(NO_2) - Ru^{II}(bpy)_2(Cl)(NO_2) + Ru^{III}(bpy)_2(Cl)(NO_2)^+$$

Assuming that the peak current for the $Ru(bpy)_2(Cl)(NO)^{2+/+}$ couple is proportional to the concentration of $Ru(bpy)_2(Cl)(NO)^{2+}$, the disappearance of $Ru^{III}(bpy)_2(Cl)(NO_2)^+$, following its formation by the rapid oxidation of $Ru^{II}(bpy)_2(Cl)(NO_2)$ using $M(bpy)_3^{3+}$ as oxidant, follows first-order kinetics. From the stoichiometry and kinetic measurements (Table I), the rate law for the reaction is

$$\frac{d[Ru^{II}(bpy)_2(Cl)(NO)^{2+}]}{dt} = -\frac{1}{3}\frac{d[Ru^{III}(bpy)_2(Cl)(NO_2)^+]}{dt} = k[Ru^{III}(bpy)_2(Cl)(NO_2)^+] \quad (6)$$

Rate constants for this reaction were evaluated by using the Swinbourne method as described in the Experimental Section. The results of four separate experiments gave an average value of $k = 1.8 \times 10^{-3}$ s^{-1} at $I = 0.1$ M and at 22 ± 2 °C.

The reaction was also followed by monitoring changes in absorbance at 507 nm which is an absorbance maximum for $Ru^{II}(bpy)_2(Cl)(NO_2)$. A kinetic treatment of the spectral data gave 4.2×10^{-3} s^{-1} as an average value of two experiments. The value obtained spectrally is consistent with that observed in the cyclic voltammetry experiment, considering the accuracy of the data and the difference in conditions for the two types of experiments. The electrochemical experiment was carried out at $I = 0.1$ M with added TEAP while in the spectral experiment, there was no added electrolyte.

Attempts to measure the rate constant for the related reaction involving $Ru^{III}(bpy)_2(py)(NO_2)^{2+}$ were unsuccessful. Stopped-flow kinetic studies were carried out in acetonitrile by using Ce(IV) to oxidize $Ru^{II}(bpy)_2(py)(NO_2)^+$ to $Ru^{III}(bpy)_2(py)(NO_2)^{2+}$. The only reaction which could definitely be identified was the initial oxidation reaction (eq 7) which was first order both in Ce^{IV} and in $Ru(bpy)_2(py)(NO_2)^+$ and occurred with a rate constant of 1.7×10^6 M^{-1} s^{-1} at 25.0 ± 0.1 °C ($I = 0.1$ M).

$$Ru^{II}(bpy)_2(py)NO_2^+ + Ce(IV) \rightarrow Ru^{III}(bpy)_2(py)NO_2^{2+} + Ce(III) \quad (7)$$

However, following electrochemical oxidation of $Ru^{II}(bpy)_2(py)NO_2^+$ to $Ru^{III}(bpy)_2(py)NO_2^{2+}$, detailed insight into the overall mechanism can be gained by cyclic voltammetry although the interpretation of the data is intricate. In Figure 3 is shown a series of *single-sweep* cyclic voltammograms at varying sweep rates which can be interpreted on the basis of Scheme III. The critical part of the scheme is the rapid isomerization of the nitro group from N-bound, Ru^{III}–NO_2, to O-bound, Ru^{III}–ONO, following oxidation to Ru(III).

At the fastest scan rate, Figure 3A (50 V/s), oxidation of $(bpy)_2(py)Ru^{II}NO_2^+$ to Ru(III) at $E_{p,a} = 1.06$ V results in the appearance of a reduction wave for a new couple at $E_{p,c} = 0.72$ V. A following scan, returning in the oxidative direction, shows the oxidative component of the reductive wave at 0.72 V, and the reversibility of the new couple ($E_{1/2} \approx 0.80$ V) is seen clearly by low-temperature cyclic voltammetry in 0.1 M [N-(n-C_4H_9)$_4$]ClO_4-n-BuCN. The behavior described here is especially well-defined upon attachment of the [$(bpy)_2(NO_2)Ru^{II}py$~] group to a platinum electrode surface, results which will be reported in a later publication. A sample of the nitrito isomer, $(bpy)_2(py)RuONO^+$, is not available for comparison, but the potential of the wave at $E_{p,c} = 0.72$ V is consistent with potentials for other Ru(III)/Ru(II) couples which contain related ligands.[16]

At slower scan rates, a wave at $E_{p,c} = 0.95$ V grows in at the expense of the Ru–$ONO^{2+/+}$ wave at $E_{p,c} = 0.72$ V. The wave at 0.95 V appears to be the reductive component of the oxidative wave at $E_{p,a} = 1.06$ V for the Ru–$NO_2^{2+/+}$ couple. What this means in terms of Scheme III is that initial oxidation of Ru^{II}–NO_2^+ to Ru^{III}–NO_2^{2+} is followed by rapid isomerization to Ru^{III}–ONO^{2+}. The Ru^{III}–NO_2^{2+} ⇌ Ru^{III}–ONO^{2+} equilibrium lies in favor of the nitrito isomer, and at rapid scan rates it can be recaptured at the electrode by reduction to Ru^{II}–ONO^+. However, at slower scan rates, the conversion, Ru^{III}–ONO^{2+} → Ru^{III}–NO_2^{2+}, is competitive with the cyclic voltammetry time scale. Reduction of Ru(III) now occurs through Ru^{III}–NO_2^{2+} because the potential for reduction is ~0.2 V more positive than the potential for reduction of Ru^{III}–ONO.

In the interpretation given in Scheme III, at even slower scan rates, a further complication appears which leads to the nitrosyl and nitrato products. At slow scan rates, before Ru^{III}–ONO^{2+} can be reduced to Ru(II) either directly at the electrode or through Ru^{III}–NO_2^{2+}, a bimolecular reaction occurs, probably with $Ru(bpy)_2(py)NO_2^{2+}$, to give the final

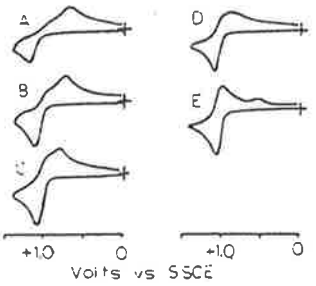

Figure 3. Scan-rate dependence of single-sweep cyclic voltammograms of solutions containing $Ru(bpy)_2(py)NO_2^+$ in acetonitrile (0.1 M [NEt_4](ClO_4)): (A) 50 V/s; (B) 20 V/s; (C) 5 V/s; (D) 3 V/s; (E) 0.5 V/s.

Scheme III

$$(bpy)_2(py)Ru^{II}NO_2^+ \underset{+e^-}{\overset{-e^-}{\rightleftharpoons}} (bpy)_2(py)Ru^{III}NO_2^{2+}$$

$$\Big\downarrow \text{fast}$$

$$(bpy)_2(py)Ru^{II}ONO \underset{+e^-}{\overset{-e^-}{\rightleftharpoons}} (bpy)_2(py)Ru^{III}ONO^{2+}$$

$$\Big\downarrow +(bpy)_2(py)Ru^{III}NO_2^{2+}$$

$$(bpy)_2(py)RuONO_2^+ + (bpy)_2(py)RuNO^{3+}$$

products. The competition is shown in Figure 3E (0.5 V/s), where, in addition to the Ru^{III}–$NO_2^{2+/+}$ wave, the reductive wave for the $Ru(bpy)_2(py)NO^{3+/2+}$ couple is clearly observed and, presumably, a wave at $E_{p,c} = 0.91$ V for the $Ru(bpy)_2(py)ONO_2^{2+/+}$ couple is present as a barely detectable shoulder on the Ru–$NO_2^{2+/+}$ wave. It should be noted that Figure 3 shows *single-sweep* cyclic voltammograms so that the oxidative components for the nitrosyl and nitrato couples do not appear.

Cyclic voltammograms at varying scan rates for the complexes $Ru(bpy)_2(PPh_3)NO_2^+$ and $Ru(bpy)_2(py)NO_2^+$ suggest that although the same net reaction and mechanism exist for the related systems, the kinetic details do vary somewhat with changes in the ligand cis to the nitro group.[19]

The electrochemical experiments suggest strongly that, unlike the chloro complex, the rate-determining step for ligand oxidation in the pyridyl complex is a bimolecular reaction involving the reactive intermediate $(bpy)_2(py)Ru^{III}ONO^{2+}$. A similar mechanism may be involved for the chloro complex as well, but because the reaction is slower and the rate-determining step first order in $Ru(bpy)_2(Cl)NO_2^+$, presumably to give $Ru^{III}(bpy)_2(Cl)ONO^+$, any information about possible reactions which occur following the rate-determining step is lost.

By combining the mechanistic information available for the chloro and the pyridyl complexes and assuming a common mechanism, it is possible to develop an overall scheme which explains the observed reactivity of the Ru^{II}–NO_2 complexes on oxidation.

For the chloro complex, initial oxidation of Ru(II) to Ru(III) is followed by a first-order reaction. The first-order nature of the process suggests that it involves an internal reorganization in the Ru(III) state, and, given the electrochemical result on the pyridyl complex, the most likely reorganization is an isomerization of the ligand from N- to O-bound, eq 8. Such a step must appear somewhere in the

$$(bpy)_2Ru^{III}(Cl)-NO_2^+ \rightarrow (bpy)_2Ru^{III}(Cl)-ONO^+ \quad (8)$$

overall mechanism since in the net reaction the oxidative conversion of an N-bound nitro to O-bound nitrato ligand occurs.

(19) R. S. Nicholson and I. Shain, *Anal. Chem.*, 36, 706 (1964).

An isomerization reaction like that in eq 8 would be expected to have substantial redox character given the usual inertia to substitution expected for complexes of Ru(III). In the limiting case the net reaction could involve an initial intramolecular electron-transfer step followed by recapture of loosely bound NO_2 before it can escape into solution

$$\left[\begin{matrix}(bpy)_2Ru^{III}-NO_2\\ |\\ Cl\end{matrix}\right]^{+} \rightarrow \left[\begin{matrix}(bpy)_2Ru^{II}\cdot NO_2\\ |\\ Cl\end{matrix}\right]^{+} \rightarrow \left[\begin{matrix}(bpy)_2Ru^{III}-ONO\\ |\\ Cl\end{matrix}\right]^{+} \quad (9)$$

Such a mechanism is entirely analogous to the proposed mechanism for the photochemical isomerization of $Co(NH_3)_5NO_2^{2+}$ following photolysis into ligand to metal charge-transfer absorption bands.[20]

The suggestion of an initial intramolecular redox step is consistent with several available facts. It fits the substantial rate enhancement for the pyridyl complex following oxidation of $Ru(bpy)_2(py)NO_2^{+}$. For the pyridyl complex $Ru(bpy)_2(py)ONO^{2+}$ is the immediately observed product even at a scan rate of 50 V/s. The origin of the rate enhancement is apparently that the pyridyl complex is a considerably stronger one-electron oxidant. Closely related chemistry has been observed for a series of complexes where there is a bound, oxidizable ligand (I^-, Br^-, NCS^-, CN^-).[1a] Electrochemically generated Ru(III) complexes rapidly produce Ru(II) and the oxidized ligand (I_2 etc). In the case of the bound azide ligand, the rate of net intramolecular ligand oxidation also follows the oxidizing strength of the metal site.[8] Although the data are limited, the suggested increase in rate constant as ionic strength decreases (Table I) is also consistent with an intramolecular redox step because of the decrease in intramolecular charge separation ($Ru^{III}-NO_2^- \rightarrow Ru^{II}-\dot{N}O_2$) in the activation process.[8]

With the pyridyl complex as the example, the initial oxidation and isomerization steps are combined with a necessary bimolecular step to complete the overall mechanism as shown in Scheme IV. When taken together, the set of reactions accounts for both the final product distribution and the appearance of an intermediate if the intermediate is $(bpy)_2(py)RuONO^{2+}$. There is a fundamental difference in reactivity between the chloro and pyridyl complexes. For the pyridyl complex, isomerization to the reactive O-bound isomer is rapid and the rate-determining step is its bimolecular reaction with a second $Ru^{II}-NO_2$ complex. For the chloro complex, isomerization is slow and becomes the rate-determining step.

The existence of a dimeric intermediate or activated complex in Scheme IV is almost demanded in the mechanism since the nature of the products suggests strongly that a net O-atom transfer occurs from one NO_2 group to the second. Although we have not carried out a labeling study on the ligand oxidation reaction, a labeling study has shown that O-atom transfer does occur in the reaction[12]

$$\begin{matrix}(bpy)_2Ru^{III}-NO_2^{+}\\ |\\ Cl\end{matrix} + PPh_3 \rightarrow \begin{matrix}(bpy)_2Ru-NO^{+}\\ |\\ Cl\end{matrix} + OPPh_3 \quad (10)$$

In terms of possible redox catalytic systems, the bimolecular redox step is of considerable interest since it is in this step that net oxygen-atom transfer occurs. The favorable reactivity of the Ru(III)–nitro system lies in its ability to donate an oxide ion in conjunction with the availability of two one-electron-acceptor sites, one at the metal ($Ru^{III} \rightarrow Ru^{II}$) and one at the nitrosyl ligand ($Ru-NO^+ \rightarrow Ru-\dot{N}O$). Chemical and electrochemical studies[4] have shown that the nitrosyl complexes are themselves mild, reversible oxidants where the electron-acceptor properties are largely localized on the nitrosyl ligand.[2]

$$\begin{matrix}(bpy)_2Ru-NO^{3+}\\ |\\ L\end{matrix} \underset{-e^-}{\overset{+e^-}{\rightleftharpoons}} \begin{matrix}(bpy)_2Ru-\dot{N}O^{2+}\\ |\\ L\end{matrix} \quad (11)$$

For the oxidation of PPh_3 by $Ru^{III}(bpy)_2(Cl)NO_2^{+}$, the results of the labeling experiment mentioned above are consistent with an O-atom transfer reactivity for the Ru(III)–nitro complex analogous to the bimolecular step shown in Scheme IV.[12] The existence of such a pathway is mechanistically appealing because the electron-acceptor properties of the oxidant are delocalized over two different sites in the molecule, and both sites are known to undergo rapid electron transfer as shown by self-exchange studies.[4a,7] Furthermore, other than loss of the oxygen atom, no major structural changes are required at the oxidant.

There are other mechanistic possibilities for some of the steps in Scheme IV, and although they cannot be ruled out, they seem less likely. One is that in the bimolecular step, O-atom transfer actually occurs to the metal to give a seven-coordinate $Ru^{IV}{=}O$ complex (eq 12). Seven-coordination

$$\begin{matrix}(bpy)_2Ru^{III}-NO_2^{+}\\ |\\ Cl\end{matrix} + \begin{matrix}(bpy)_2Ru^{III}-ONO^{+}\\ |\\ Cl\end{matrix} \rightarrow \begin{matrix}(bpy)_2Ru^{II}-NO^{2+}\\ |\\ Cl\end{matrix} + \begin{matrix}O\\ \|\\ (bpy)_2Ru-ONO\\ |\\ Cl\end{matrix}$$

$$\begin{matrix}O\\ \|\\ (bpy)_2Ru-ONO\\ |\\ Cl\end{matrix} \rightarrow \begin{matrix}(bpy)_2Ru-ONO_2\\ |\\ Cl\end{matrix} \quad (12)$$

is known for Ru(IV),[21] and the six-coordinate complex $(bpy)_2(py)Ru^{IV}{=}O^{2+}$ has been isolated and characterized.[2]

Equilibrium Constant and Reduction Potential Values. An acid–base equilibrium exists between the nitrosyl and nitro forms of the bis(bipyridyl)ruthenium(II) complexes in aqueous solution, eq 13.[14,22] For the chloro complex, an equilibrium

Scheme IV

$$2\begin{matrix}(bpy)_2Ru^{II}-NO_2\\ |\\ py\end{matrix} \xrightarrow{-e^-} 2\begin{matrix}(bpy)_2Ru^{III}-NO_2^{2+}\\ |\\ py\end{matrix}$$

$$\begin{matrix}(bpy)_2Ru^{III}-NO_2^{2+}\\ |\\ py\end{matrix} \rightleftharpoons \begin{matrix}(bpy)_2Ru^{III}-ONO^{2+}\\ |\\ py\end{matrix}$$

$$\begin{matrix}(bpy)_2Ru^{III}-ONO^{2+}\\ |\\ py\end{matrix} + \begin{matrix}(bpy)_2Ru^{III}-NO_2^{2+}\\ |\\ py\end{matrix} \rightarrow \left[\begin{matrix}(bpy)_2Ru-O-\overset{\overset{O}{\|}}{N}-O-\overset{\overset{O}{\|}}{N}-Ru(bpy)_2^{4+}\\ |\qquad\qquad\qquad\qquad\qquad |\\ py\qquad\qquad\qquad\qquad\quad py\end{matrix}\right]$$

$$\left[\begin{matrix}(bpy)_2Ru-O-\overset{\overset{O}{\|}}{N}-O-\overset{\overset{O}{\|}}{N}-Ru(bpy)_2^{4+}\\ |\qquad\qquad\qquad\qquad\qquad |\\ py\qquad\qquad\qquad\qquad\quad py\end{matrix}\right] \rightarrow \begin{matrix}(bpy)_2Ru^{II}-ONO_2^{+}\\ |\\ py\end{matrix} + \begin{matrix}(bpy)_2Ru^{II}-NO^{3+}\\ |\\ py\end{matrix} \quad \text{(fast)}$$

$$\begin{matrix}(bpy)_2Ru^{II}-ONO_2^{+}\\ |\\ py\end{matrix} \xrightarrow{-e^-} \begin{matrix}(bpy)_2Ru^{III}-ONO_2^{2+}\\ |\\ py\end{matrix}$$

(20) (a) D. A. Johnson and K. A. Pashman, *Inorg. Nucl. Chem. Lett.*, 11, 23 (1975); (b) V. Balzani, R. Ballardini, N. Sabbatini, and L. Moggi, *Inorg. Chem.*, 7, 1398 (1968).

(21) (a) B. M. Mattson and L. H. Pignolet, *Inorg. Chem.*, 16, 488 (1977); (b) K. W. Given, B. M. Mattson, and L. H. Pignolet, *Inorg. Chem.*, 15, 3152 (1976).

(22) J. B. Godwin, N. Winterton, and T. J. Meyer, *Chem. Commun.*, 872 (1970).

$$Ru(bpy)_2(Cl)(NO)^{2+} + 2OH^- \rightleftharpoons Ru(bpy)_2(Cl)(NO_2) + H_2O \quad (13)$$

constant for eq 13 of $K = (1.6 \pm 0.4) \times 10^9\ M^{-2}$ has been determined[14] by spectrophotometric titration techniques at 25.0 ± 0.2 °C in 1.0 M aqueous NaCl solution. Since quantitative information concerning the acid–base equilibrium is necessary both for the calculation of redox potentials and for the development of catalytic cycles based on the redox chemistry of the bound nitro group, we have measured the equilibrium acid–base properties of the pyridyl complex in the same medium (eq 14).

$$Ru(bpy)_2(py)(NO)^{3+} + 2OH^- \rightleftharpoons Ru(bpy)_2(py)(NO_2)^+ + H_2O \quad (14)$$

The spectrophotometric procedure was described in the Experimental Section. For eq 14, K(25.0 °C, I = 1.0 M) = $(1.0 \pm 0.3) \times 10^{20}\ M^{-2}$. In terms of relative concentrations of the nitro and nitrosyl forms in eq 13 and 14, the equilibrium constants show that the two forms are present in equal amounts at pH 9.2 for the chloro system and at pH 3.8 for the pyridyl system. The sizable increase in the acidity of the nitrosyl group for the pyridyl, compared to the chloro complex, is paralleled by an increase in the $E_{1/2}$ value for the couple $RuNO^+/RuNO$ (Table II)[4] and by an increase in the ν(NO) stretching frequency.[4] The evidence provided by such experiments suggests that the electron-deficient nature of the nitrosyl group can be systematically modulated by making variations in the cis ligand. Apparently, the differences between the chloro and pyridyl systems are due to increased electron donation to the metal from the chloro group when compared to the pyridyl group.

It is possible to determine formal reduction potential values for the chloro and pyridyl Ru(III)–nitro complexes acting as two-electron-acceptor, oxide ion donor oxidants, by using values of $\Delta G = -RT \ln K$ for the acid–base equilibria in eq 13 and 14 and formal potentials for the $RuNO^+/RuNO$ and $Ru^{III}NO_2/Ru^{II}NO_2$ couples in the same medium. The calculations for $Ru^{III}(bpy)_2(Cl)(NO_2)^+$ are shown in Scheme V. A similar calculation can be made for $Ru^{III}(bpy)_2(py)(NO_2)^{2+}$ by using $K = 1.0 \times 10^{20}\ M^{-2}$, $E_{1/2}(Ru(bpy)_2(py)(NO)^{3+/2+}) = 0.53$ V,[23] $E_{1/2} = 1.16$ V ($E_{p,a} = 1.21$ V)[23] for the $Ru(bpy)_2(py)NO_2^{2+/+}$ couple. The resulting formal potential is $E_F \simeq 0.26$ V (25.0 °C, 1 M NaCl; ≥ 0.67 V at pH 7).

The similarity in the potential values for the two complexes is worth noting. It arises because even though the oxidized forms of the pyridyl $Ru^{III}NO_2/Ru^{II}NO_2$ and $RuNO^+/RuNO$ couples are considerably more strongly oxidizing than the chloro ones, there is a compensation effect which arises from the more acidic character of the nitrosyl group in the pyridyl case (note Scheme V).

Catalytic Oxidation of the Bound Nitro Group to Nitrate. Based on the acid–base and redox chemistry of the nitro complexes, it is possible to predict that oxidation of the nitro to nitrato complexes can be made catalytic. According to eq 5, in a single cycle, a three-electron oxidation occurs to give equal amounts of $Ru(bpy)_2(py)(NO_3)^{2+}$ and $Ru(bpy)_2(py)(NO)^{3+}$. However, if the pH of the solution is maintained at a sufficiently high level, the nitrosyl complex will be converted into the nitro complex according to eq 14.

Electrolysis at 1.2 V of an acetonitrile solution containing $Ru(bpy)_2(py)(NO_2)^+$ with added water (1% by volume) and 2,6-lutidine (or collidine) (1%) results in the production of $Ru(bpy)_2(py)(NO_3)^{2+}$ as the sole product (Figure 1C), and the n value is 3. These results are consistent with the series of reactions shown in Scheme VI.

(23) These are $E_{1/2}$ values measured in water with 5% propylene carbonate added for the chloro complexes and 5% acetonitrile for the pyridyl complexes (F. R. Keene, unpublished results).

Scheme V[a]

Reaction	$-\Delta G°'$, V
$H_2O + Ru^{II}(bpy)_2(Cl)(NO_2) \rightarrow Ru^{II}(bpy)_2(Cl)(NO)^{2+} + 2OH^-$	−0.54
$Ru^{III}(bpy)_2(Cl)(NO_2)^+ + e^- \rightarrow Ru^{II}(bpy)_2(Cl)(NO_2)$	0.90[23]
$Ru(bpy)_2(Cl)(NO)^{2+} + e^- \rightarrow Ru(bpy)_2(Cl)(NO)^+$	0.27[23]
$H_2O + Ru^{III}(bpy)_2(Cl)(NO_2)^+ + 2e^- \rightarrow Ru^{II}(bpy)_2(Cl)(NO)^+ + 2OH^-$	

E_F(NHE, 25.0 °C) = 0.31 V (0.72 V at pH 7)

[a] In 1.0 M aqueous NaCl at 25 °C.

Scheme VI[a]

$$2Ru^{II}(bpy)_2(py)(NO_2)^+ \xrightarrow{-2e^-} 2Ru(bpy)_2(py)(NO_2)^{2+}$$

$$2BH^+ \quad 2B + H_2O \qquad\qquad Ru^{III}(bpy)_2(py)(NO_2)^{2+}$$

$$Ru^{II}(bpy)_2(py)(NO)^{3+} \xrightarrow{-e^-} Ru^{II}(bpy)_2(py)(NO)^{2+}$$

[a] B is collidine or 2,6-lutidine.

The existence of the catalytic scheme, which is quantitative, is worth noting since it sets the conditions for and may presage a series of applications where the $Ru^{III}NO_2$ complexes are used as net O atom transfer catalysts.

Acknowledgments are made to the Materials Research Center of The University of North Carolina under Grant DAHC15 73 G9 and the National Science Foundation under Grant MPS 75-11867 for support of this research. We also acknowledge the helpful comments of Professor R. W. Murray concerning the cyclic voltammetry data.

Registry No. $[Ru(bpy)_2(py)(NO_2)]PF_6$, 36309-80-5; $[Ru(bpy)_2(CH_3CN)(NO_2)]PF_6$, 35986-82-4; $[Ru(bpy)_2(NH_3)(NO_2)]PF_6$, 72402-33-6; $[Ru(bpy)_2(PPh_3)(NO_2)]PF_6$, 72378-54-2; $[Ru(bpy)_2(pyr)(NO_2)]PF_6$, 49734-31-8; $Ru(bpy)_2Cl(NO_2)^+$, 63771-54-0; $[Ru(bpy)_2(py)(NO)](PF_6)_3$, 29241-00-7; $[Ru(bpy)_2(CH_3CN)(NO)](PF_6)_3$, 61303-15-9; $Ru(bpy)_2(PPh_3)(NO)^{3+}$, 72378-55-3; $Ru(bpy)_2(pyr)(NO)^{3+}$, 72378-56-4; $Ru(bpy)_2(NH_3)(NO)^{3+}$, 54866-01-2; $Ru(bpy)_2Cl(NO)^{2+}$, 31847-83-3; $Ru(bpy)_2(PPh_3)(NO)^{2+}$, 72378-57-5; $Ru(bpy)_2(CH_3CN)(NO)^{2+}$, 54866-05-6; $Ru(bpy)_2(pyr)(NO)^{2+}$, 72378-58-6; $Ru(bpy)_2(py)(NO)^{2+}$, 72378-59-7; $Ru(bpy)_2(NH_3)(NO)^{2+}$, 72378-60-0; $Ru(bpy)_2Cl(NO)^+$, 54866-04-05; $[Ru(bpy)_2(NO_3)Cl]Cl$, 72402-34-7; $Ru(bpy)_2(PPh_3)(NO_3)^{2+}$, 72378-61-1; $Ru(bpy)_2(CH_3CN)(NO_3)^{2+}$, 72378-62-2; $Ru(bpy)_2(pyr)(NO_3)^{2+}$, 72390-14-8; $Ru(bpy)_2(py)(NO_3)^{2+}$, 72402-35-8; $Ru(bpy)_2(NH_3)(NO_3)^{2+}$, 72378-63-3; $[Ru(bpy)_2(py)(NO_2)]PF_6$, 72378-65-5; $Ru(bpy)_2(PPh_3)(NO_3)^+$, 72378-66-6; $Ru(bpy)_2(CH_3CN)(NO_3)^+$, 72378-67-7; $Ru(bpy)_2(pyr)(NO_3)^+$, 72390-12-6; $Ru(bpy)_2(NH_3)(NO_3)^+$, 72378-68-8; $Ru(bpy)_2Cl(NO_3)$, 72390-13-7; $[Ru(bpy)_2(NO)(NO_2)](PF_6)_2$, 58575-13-6; $Ru(bpy)_2(NO_2)_2$, 29241-01-8; $Ru(bpy)_2(NO_2)Cl$, 34398-51-1; $[Fe(bpy)_3](PF_6)_2$, 70811-29-9; $[Fe(bpy)_3](PF_6)_3$, 28190-88-7; $Ru(bpy)_3^{3+}$, 18955-01-6.

Intervalence Transfer and Electron Transfer in the Mixed-Valence Ion $[(bpy)_2ClRu(pyz)RuCl(bpy)_2]^{3+}$ [1]

Robert W. Callahan, F. Richard Keene, Thomas J. Meyer,* and Dennis J. Salmon

Contribution from the W. R. Kenan, Jr., Laboratory, Department of Chemistry, The University of North Carolina, Chapel Hill, North Carolina 27514. *Received April 23, 1976*

Abstract: The properties of the mixed-valence ion $[(bpy)_2ClRu(pyz)RuCl(bpy)_2]^{3+}$, including the appearance of a symmetric ν(pyz) stretch in the solution IR, are consistent with localized Ru(II) and Ru(III) valences and only slight delocalization between the ions. An intervalence transfer (IT) band appears in the near-infrared (near-IR), whose properties are predicted by the Hush theory. The rate of intramolecular thermal electron transfer calculated for the mixed-valence ion using the Hush theory compares favorably with the estimated rate of thermal electron transfer within the ion-pair for the outer-sphere reaction: $[(bpy)_2Ru(py)Cl]^+ + [(phen)_2Ru(py)Cl]^{2+} \rightarrow [(bpy)_2Ru(py)Cl]^{2+} + [(phen)_2Ru(py)Cl]^+$. From the solvent dependence of the IT band, λ_i and λ_o have been estimated for the intramolecular electron transfer. A prediction made by the Marcus and Hush theories of outer-sphere electron transfer has been verified for λ_i values for intramolecular electron transfer using the ions $[(bpy)_2ClRu(pyz)RuCl(bpy)_2]^{3+}$, $[(NH_3)_5Ru(pyz)RuCl(bpy)_2]^{4+}$, and $[(NH_3)_5Ru(4,4'\text{-bpy})Ru(NH_3)_5]^{5+}$. By comparing the properties of $[(bpy)_2ClRu(pyz)RuCl(bpy)_2]^{3+}$ with the properties of the Creutz and Taube ion, $[(NH_3)_5Ru(pyz)Ru(NH_3)_5]^{5+}$, it is concluded that there is a large resonance energy for the latter ion, and that it is clearly outside the weak interaction limit to which the Hush theory applies.

Hush has developed a treatment which describes the properties of intervalence transfer (IT) bands in mixed-valence compounds for cases where valences are localized and interactions between metal sites are weak.[2] An important element of the Hush theory is that the properties of IT bands can be used to obtain detailed information about intramolecular thermal electron transfer processes; information which is very seldom available using other experimental techniques.

For certain mixed-valence ions, e.g., $[(NH_3)_5Ru(pyz)RuCl(bpy)_2]^{4+}$ and $[(NH_3)_5Ru(4,4'\text{-bpy})Ru(NH_3)_5]^{5+}$, the predictions made by Hush have been verified.[3-5] However, for the closely related Creutz and Taube ion, $[(NH_3)_5Ru(pyz)Ru(NH_3)_5]^{5+}$, the properties of its near-infrared (near-IR) band are far different from the predictions made by Hush.[6,7] There is an element of confusion introduced by the latter ion which must be clarified if the Hush theory is to be used with confidence to estimate rate data for thermal electron transfer processes. It is also essential that the predictions made by the Hush theory be verified by independent experiments, and one approach is to make comparisons with closely related outer-sphere electron transfer reactions.

Experimental Section

Measurements. Infrared spectra were recorded on a Perkin-Elmer 421 spectrophotometer. Ultraviolet-visible spectra were obtained using Cary Model 14, Cary Model 17, Unicam Model SP800B, or Bausch and Lomb Spectronic 210 spectrophotometers at room temperature. Near-infrared spectra were recorded on a Cary 14 spectrophotometer.

Materials. Nitrobenzene and propylene carbonate (Reagent Grade) were passed through a column of alumina and stored over Davison 4 Å molecular sieves. Dimethyl sulfoxide (Reagent Grade), D_2O (MSD Isotopic Products), and acetonitrile (MCB, Spectrograde) were used without further purification or dried over Davidson 4 Å molecular sieves. Water (H_2O) was purified by distillation from alkaline permanganate. Ceric ammonium nitrate was obtained commercially (G. F. Smith). A solution of Ce(IV) perchlorate in 6 M $HClO_4$ was obtained from G. F. Smith ad Co. and analyzed spectrophotometrically for Ce(IV).[8] All other chemicals and solvents were reagent grade and were used without further purification.

Preparations. The complexes $[Ru(bpy)_2Cl_2]\cdot 2H_2O$, $[Ru(phen)_2Cl_2]\cdot 3H_2O$, $[Ru(bpy)_2(NO)Cl](PF_6)_2$, and $[Ru(phen)_2(NO)Cl](PF_6)_2\cdot H_2O$ were prepared and purified as described earlier.[9]

$[(bpy)_2ClRu(pyz)RuCl(bpy)_2](PF_6)_2$. The complex, $[(bpy)_2Ru(NO)Cl](PF_6)_2$ (404.6 mg, 0.526 mmol), was initially dissolved in acetone (10–15 ml) and the resulting solution was protected from light. An equimolar amount of KN_3 (42.7 mg) dissolved in methanol (10–15 ml) was added dropwise to the solution producing the desired, purple-red solvento complex. In a separate 125-ml round-bottom flask, an equimolar amount of $[(bpy)_2Ru(pyz)Cl](PF_6)$ (354.6 mg) was dissolved in acetone (10–15 ml) and protected from light. The solution of $[(bpy)_2Ru(S)Cl]^+$ (S = acetone) was then added to the solution of $[(bpy)_2Ru(pyz)Cl]^+$, and the final volume was diluted with acetone to ~70 ml. The flask was flushed with argon (10–15 min), and the solution was allowed to reflux with a continual stream of argon flowing over the mixture. After ~24 h, the solution was added dropwise to stirring anhydrous ether (~300 ml). The resulting brown-purple precipitate was collected on a glass frit and washed with CH_2Cl_2 (~60 ml) with some loss of product. The remaining product was suspended in water (10–15 ml), protected from light, and stirred for ~1 h in order to remove the potassium hexafluorophosphate by-product. The suspension was then filtered through a glass frit, and the undissolved product was dried in a vacuum desiccator over Drierite. Yield = 467 mg (70%). Anal. Calcd for $[Ru_2(C_{10}H_5N_2)_4(C_4H_4N_2)Cl_2](PF_6)_2$: C, 41.7; H, 2.86; N, 11.0. Found: C, 41.4; H, 2.80; N, 11.0.

$[(bpy)_2ClRu(pyz)RuCl(bpy)_2](PF_6)_4$. The salt, $[(bpy)_2ClRu(pyz)RuCl(bpy)_2](PF_6)_2$ (100.2 mg, 0.079 mmol), was dissolved in acetone (15–20 ml) and protected from light. The salt does not readily dissolve in acetone, but the addition of a small amount of acetonitrile (2–3 ml) speeds up dissolution considerably. Tetra-*n*-butylammonium chloride (~0.5 g) was added to the solution resulting in an immediate precipitation of $[(bpy)_2ClRu(pyz)RuCl(bpy)_2]Cl_2$. The salt was collected on a glass frit and washed with several portions (~30 ml) of acetone. The complex was then dissolved in ~1 M hydrochloric acid (10–15 ml) and protected from light. Acetonitrile (1–2 ml) was used to complete dissolution. Ceric ammonium nitrate (86.7 mg, 1.58 mmol) was added to the stirred solution which gave an immediate dark yellow color. A saturated solution of ammonium hexafluorophosphate in ~1 M hydrochloric acid (~10 ml) was quickly added giving a brown precipitate. The precipitate was collected on a glass frit and washed with several portions (~10 ml) of ~0.5 M hydrochloric acid and placed in a vacuum desiccator over Drierite overnight. Yield = 70 mg (57%). The purity of the compound was checked in the following manner. An $\sim 10^{-4}$ M solution (acetonitrile) of the complex was prepared and protected from light. One drop of 60% N_2H_4 in H_2O was added to ~10 ml of the solution. The spectrum of the resulting solution was then recorded and was essentially identical with that of the $[(bpy)_2ClRu(pyz)RuCl(bpy)_2]^{2+}$ ion ([2,2]). The characteristic absorbance maximum of the [2,2] ion appeared with ~90% of the expected intensity.

$[(bpy)_2ClRu(pyz)RuCl(bpy)_2](PF_6)_3$. The salt was prepared by the addition of the appropriate stoichiometric amounts of the fully oxidized and fully reduced complexes. The complexes $[(bpy)_2ClRu(pyz)RuCl(bpy)_2](PF_6)_2$ (48.8 mg, 0.039 mmol) and $[(bpy)_2ClRu(pyz)RuCl(bpy)_2](PF_6)_4$ (60.0 mg, 0.039 mmol), were placed in a 50-ml erlenmeyer flask and protected from light. Acetonitrile (10–15 ml) was added and the solution stirred for ~5 min. The solution was

[Reprinted from the Journal of the American Chemical Society, 99, 1064 (1977).]

added dropwise to stirred anhydrous ether (~250 ml) to produce a purple-red precipitate. The salt was collected on a glass frit and air dried. Yield = 99 mg (90%). The purity of the mixed-valence complex was checked using the hydrazine reduction method used above for the fully oxidized complex.

$[Ru(bpy)_2(py)Cl]PF_6 \cdot H_2O$. A solution of KN_3 (52.9 mg, 0.652 mmol) in methanol (5 ml) was added dropwise with stirring to a solution of $[Ru(bpy)_2(NO)Cl](PF_6)_2$ (502 mg, 0.652 mmol) in acetone (30 ml). The solution was stirred for 15 min, and pyridine (6 ml) added and the solution stirred for a further 90 min; all of the steps were carried out in subdued light. The product was precipitated by filtering the solution into a large excess (ca. 250 ml) of ether, and was filtered and dried in vacuo. The brown solid was recrystallized from methylene chloride/pentane, and then acetone/ether. Yield 300 mg, 70%. Anal. Calcd for $[Ru(C_{10}H_8N_2)_2(C_5H_5N)Cl]PF_6 \cdot H_2O$: C, 43.5; H, 3.35; N, 10.1. Found: C, 43.6; H, 3.26; N, 10.1.

Preparation of $[Ru(phen)_2(py)Cl]PF_6 \cdot H_2O$. This complex was prepared using essentially the same method as given above for the bipyridine complex, but using $[Ru(phen)_2(NO)Cl](PF_6)_2$ as the starting material. Yield, 90%. Anal. Calcd for $[Ru(C_{12}H_8N_2)_2(C_5H_5N)Cl]PF_6 \cdot H_2O$: C, 47.1; H, 3.14; N, 9.5. Found: C, 46.6; H, 2.81; N, 9.7.

Preparation of $[Ru(phen)_2(py)Cl](ClO_4)_2 \cdot 2H_2O$. The Ru(III) complex was prepared using a method developed by Johnson.[10] The salt $[Ru(phen)_2(py)Cl]PF_6 \cdot H_2O$ (300 mg, 0.406 mmol) was ground with HCl (5 ml of 0.5 M) in a mortar and pestle in the dark for 1 min. A solution of Ce(IV) in 6 M $HClO_4$ (0.32 M; 1.4 ml, 0.448 mol) was added slowly with grinding, and the total volume of the solution was brought to 10 ml by the addition of 0.50 M HCl. The mixture was ground for 10 min, $NaClO_4$ (2.8 g, 23 mmol) was added, and the mixture ground for a further minute. The green solid was filtered, washed with ice-cold 0.5 M $HClO_4$ and ether, and dried in vacuo. Yield 270 mg, 84%. Anal. Calcd for $[Ru(C_{12}H_8N_2)_2(C_5H_5N)Cl](ClO_4)_2 \cdot 2H_2O$: C, 43.0; H, 3.06; N, 8.6. Found: C, 43.0; H, 2.62; N, 8.7.

Preparation of $[Ru(bpy)_2(py)Cl](ClO_4)_2 \cdot H_2O$. The Ru(III) complex was prepared using an analogous method to that given for the phen complex. Yield, 90%. Anal. Calcd for $[Ru(C_{10}H_8N_2)_2(C_5H_5N)Cl](ClO_4)_2 \cdot H_2O$: C, 41.3; H, 2.92; N, 9.6. Found: C, 41.1; H, 3.00; N, 9.6.

Solutions. Solutions in dry acetonitrile were stable in the absence of light for several days. However, even in normal laboratory lighting, considerable decomposition (presumably substitution) occurred rapidly. Consequently, all solutions used for spectral, electrochemical or kinetic measurements were protected from the light.

Kinetic Measurements. Kinetic measurements were made using an Aminco stopped-flow apparatus with a Beckman-DU unit as a monochromator. The drive syringes and mixing chamber were thermostated using a Forma Scientific Model 2220 circulator-water bath. Condensation of atmospheric moisture at lower temperatures was prevented by passing a stream of dry nitrogen through the cell compartment.

The photomultiplier voltage output from the spectrometer was amplified, and either displayed on a Tektronix Model 564B storage oscilloscope or passed through an analog/digital converter and analyzed by a Raytheon 706 computer using the program WIGWAM 04.[11] In the second case, the data were displayed (using the computer program) on a Hewlett-Packard Model 7004B X-Y recorder.

The solutions were made up immediately prior to use, and protected from the light. All kinetic runs were obtained by mixing solutions of $Ru(bpy)_2(py)Cl^+$ and $Ru(phen)_2(py)Cl^{2+}$, and following the optical density changes at either 290 (absorbance decrease) or 266 nm (absorbance increase). The concentrations of the complexes were varied over the range $1.4–4.4 \times 10^{-6}$ M. In all cases the reaction was found to be first order to two half-lives or more. No supporting electrolyte was added since the reaction rate increases with increasing ionic strength, and the rate at the complex concentrations used was close to the limit allowed by the instrumentation.

Electrochemical Measurements. All electrochemical measurements were made at platinum electrodes vs. the saturated sodium chloride calomel electrode (ssce), and are uncorrected for junction potentials. In all experiments, standard three-electrode operational amplifier circuitry was used as described previously[12] with a PAR Model 173 potentiostat for potential control and a PAR Model 175 Universal programmer as a sweep generator for voltammetric experiments. All measurements were carried out in acetonitrile solution containing 0.1 M $[N(n\text{-}C_4H_9)_4]PF_6$ (TBAH) as the supporting electrolyte, in a thermostated cell with a Forma Scientific Model 2095 circulator-water bath for temperature control.

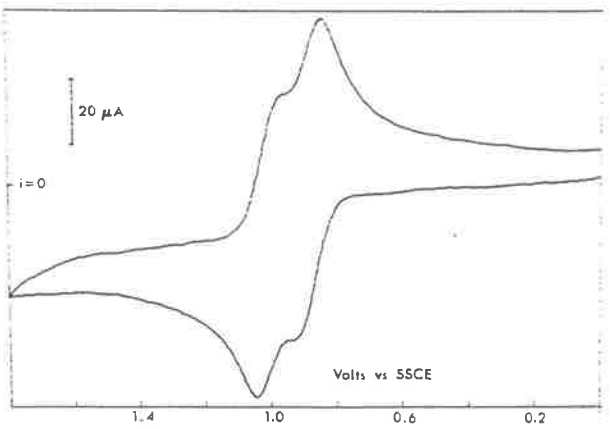

Figure 1. A 200 mV/s cyclic voltammogram of $[(bpy)_2ClRu(pyz)RuCl(bpy)_2]^{2+}$ (3.0×10^{-3} M) in 0.1 M TBAH–CH_3CN.

Half-wave potentials ($E_{1/2}$) for the Ru(III)/Ru(II) couples and electrochemical reversibility were determined by cyclic voltammetry and stirred solution voltammetry. In cyclic voltammetry, reversibility was based on the ratio of cathodic to anodic currents (i_c/i_a) and the separation in potential of the peaks (ΔE_p). A more precise criterion is obtained from a plot of potential (E) vs. $\log (i_L - i)/i$ (where i_L is the limiting current) using stirred-solution voltammetry where a slope of 59 mV indicates kinetic reversibility. The complex concentrations were $3–4 \times 10^{-3}$ M in all measurements.

Results

Electrochemistry. A cyclic voltammogram of $[(bpy)_2ClRu(pyz)RuCl(bpy)_2]^{2+}$ in 0.1 M $[N(n\text{-}C_4H_9)_4]PF_6$–acetonitrile vs. the ssce at 25 ± 2 °C is shown in Figure 1. There are two anodic waves in the potential region 0–2.0 V. $E_{1/2}$ values for the two waves are at 0.89 and 1.01 V. The $E_{1/2}$ values were calculated from the cyclic voltammograms ($E_{p,a} - E_{p,c}/2$). The peak separation for each wave is somewhat larger (ΔE_p = 75–80 mV) than theoretically predicted (ΔE_p = 58 mV) for an electrochemically reversible process. Brown has suggested that under our experimental conditions uncompensated solution resistance can cause an increase in the observed ΔE_p values.[13] It has also been suggested that the large ΔE_p values could result from the close proximity of the two waves.[13] Since the current is additive for each process, the result could be a slight apparent increase in ΔE_p. Variation of the scan rate (50–500 mV/s) showed no appreciable change in peak positions. Also, the ratio of anodic to cathodic peak currents ($i_{p,a}/i_{p,c}$) was ~1 for each of the processes.

Coulometry experiments showed that each of the two waves is a one-electron transfer process (eq 1 and 2).

$$\underset{[3,3]}{[(bpy)_2ClRu(pyz)RuCl(bpy)_2]^{4+}} + e \rightarrow \underset{[2,3]}{[(bpy)_2ClRu(pyz)RuCl(bpy)_2]^{3+}} \quad (1)$$

$$\underset{[2,3]}{[(bpy)_2ClRu(pyz)RuCl(bpy)_2]^{3+}} + e \rightarrow \underset{[2,2]}{[(bpy)_2ClRu(pyz)RuCl(bpy)_2]^{2+}} \quad (2)$$

Using the abbreviations [3,3] for the 4+ ion, [2,3] for the 3+ ion, and [2,2] for the 2+ ion, K for the conproportionation equilibrium in eq 3 is 10^2 as calculated from the $E_{1/2}$ values at 25 ± 2 °C.

$$[3,3] + [2,2] \rightleftharpoons 2[2,3] \quad (3)$$

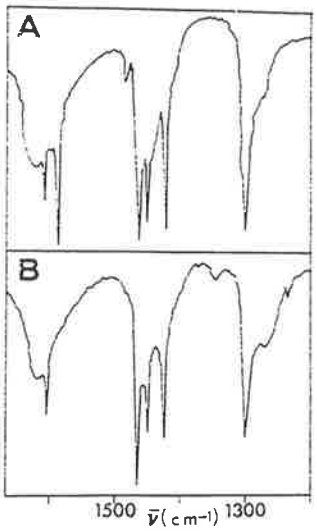

Figure 2. Solution infrared spectra (CD_3CN) of $[(bpy)_2Ru(pyz)Cl]^+$ (A) and $[(bpy)_2ClRu(pyz)RuCl(bpy)_2]^{2+}$ (B) (some absorbance by H_2O occurs in the ~1600-cm^{-1} region).

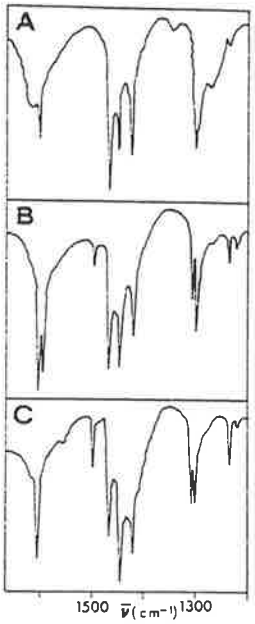

Figure 3. Solution infrared spectra (CD_3CN) of $[(bpy)_2ClRu(pyz)RuCl(bpy)_2]^{2+}$ (A), $[(bpy)_2ClRu(pyz)RuCl(bpy)_2]^{3+}$ (B), and $[(bpy)_2ClRu(pyz)RuCl(bpy)_2]^{4+}$ (C) (some absorbance by H_2O appears in the 1600-cm^{-1} region).

The equilibrium constants in 0.1 M $[N(n\text{-}C_4H_9)_4]PF_6$–acetontrile and in pure acetonitrile appear to be essentially the same, which is expected from the charge types involved in the equilibrium. Solutions of [2,3] have the same ν_{max} and ϵ values in both media (±5%).

From the value of K, solutions containing [2,3] also contain ~10% of the [2,2] and [3,3] ions. Quantitative calculations based on [2,3], which appear later in the paper, have been corrected for the equilibrium.

Ultraviolet–Visible Spectra. Table I lists λ_{max} values and extinction coefficients for the ions $[(bpy)_2ClRu(pyz)RuCl(bpy)_2]^{n+}$ (n = 2, [2,2]; n = 3, [2,3]; n = 4, [3,3]). Spectral data are also given for the parent ions $[(bpy)_2Ru(pyz)Cl]^{n+}$ (n = 1,2). The [2,3] and [3,3] ions are stable in acetonitrile with only slight decomposition (~10%) after 1–2 h if protected from light. Trace water in the solvent causes some reduction of Ru(III), but the addition of one drop of ~1 M $HClO_4$ per 50 ml of acetonitrile prevents the reaction. Solid samples of the +4 ion were stable for weeks when protected from moisture.

Table I. Electronic Spectra of the Ions $[(bpy)_2ClRu(pyz)RuCl(bpy)_2]^{n+}$ (n = 2, 3, 4) and $[(bpy)_2Ru(pyz)Cl]^{n+}$ (n = 1, 2) in Acetonitrile

Complex	λ_{max}[a]	ϵ (M^{-1} cm^{-1})[b]
$[(bpy)_2Ru(pyz)Cl]^+$	478	9.9×10^3
	384	8.4×10^3
	350 (sh)	
	292	5.0×10^4
	243	2.0×10^4
$[(bpy)_2Ru(pyz)Cl]^{2+}$ [c]	423	2.0×10^3
	312	2.8×10^4
	300	2.8×10^4
	246	2.7×10^4
$[(bpy)_2ClRu(pyz)RuCl(bpy)_2]^{2+}$	513	2.6×10^4
	497 (sh)	
	339	1.2×10^4
	292	9.2×10^4
	243	3.8×10^4
$[(bpy)_2ClRu(pyz)RuCl(bpy)_2]^{3+}$	508	1.4×10^4
	475 (sh)	
	310 (sh)	
	292	6.0×10^4
	244	4.1×10^4
$[(bpy)_2ClRu(pyz)RuCl(bpy)_2]^{4+}$	430	4.0×10^3
	310	5.0×10^4
	300	5.0×10^4
	246	4.9×10^4

[a] ±2 nm in acetonitrile. [b] Estimated error in ϵ values is ±5%. [c] Species generated in solution by suspending PbO_2 in a solution of the complex and then filtering.

Infrared Spectra. Figures 2 and 3 show the infrared spectra (CD_3CN) for $[(bpy)_2Ru(pyz)Cl]^+$ and [2,2], and the [2,2], [2,3], and [3,3] ions in the region 1200–1600 cm^{-1}. For the [2,3] ion, a band is observed at 1599 cm^{-1} which is not present for the [2,2] or [3,3] ions, but which appears for $[(bpy)_2Ru(pyz)Cl]^+$. The other bands in this region are characteristic of bis(2,2′-bipyridine) complexes of Ru(II) or Ru(III). Except for the band at 1599 cm^{-1}, the spectrum of the [2,3] ion is the sum of the spectra of the [3,3] and [2,2] ions. The estimated error in the infrared values is ±2 cm^{-1}.

Near-Infrared Spectra. The near-infrared (near-IR) spectra of the [2,2], [2,3], and [3,3] ions (~10^{-3} M) were recorded in acetonitrile using 1.0-cm matched Infrasil cells from 2200 to 800 nm. No bands were found in this region for the [2,2] or [3,3] ions, but a band was observed at 1300 nm (0.769 μm^{-1}) for the [2,3] ion (ϵ 455 M^{-1} cm^{-1}, Figure 4). In addition, the band displayed a solvent dependence as shown by the data in Table II. The near-infrared spectrum of the [2,3] ion was recorded in CD_3CN out to 2600 nm, and no new bands were found in the 2200–2600-nm region.

In a preliminary communication[14] it was reported that a near-IR band could not be observed for [2,3]. The earlier work failed to appreciate the relatively low intensity of the IT band, and the photolability of the [2,3] ion.

Data for the Self-Exchange Experiment. The half-wave potentials for the $[Ru(bpy)_2(py)Cl]^{3+/2+}$ and $[Ru(phen)_2(py)Cl]^{3+/2+}$ couples were measured in acetonitrile in the range 5–35 °C. Both couples were electrochemically reversible (ΔE_p = 59–61 mV), and the measured values are given in Table III.

For a reversible reaction, $E_{1/2}$ differs from a formal re-

Table II. Solvent Dependence of the Near-Infrared Band Maximum for $[(bpy)_2ClRu(pyz)RuCl(bpy)_2]^{3+}$

Solvent	λ_{max} (±10 nm)	$(1/n^2 - 1/D_s)^a$
Water (D_2O)	1270	0.546
Acetonitrile	1300	0.526
Propylene carbonate	1335	0.481
Dimethyl sulfoxide	1365	0.438
Nitrobenzene	1400	0.384

[a] Values calculated using indices of refraction and bulk dielectric constants found in: A. J. Gordon and R. A. Ford, "The Chemist's Companion", Interscience, New York, N.Y., 1972, pp 4–11.

Table III. $E_{1/2}$ Values for the $[Ru(bpy)_2(py)Cl]^{2+/+}$ and $[Ru(phen)_2(py)Cl]^{2+/+}$ Couples in Acetonitrile

	$E_{1/2}$ (V vs. ssce)	
T[a]	$[Ru(bpy)_2(py)Cl]^{3+/2+}$ [b]	$[Ru(phen)_2(py)Cl]^{3+/2+}$ [b]
5.0	0.776	0.785
15.0	0.777	0.784
20.0	0.777	0.782
25.0	0.785	0.778
35.0	0.784	0.788

[a] °C, ±0.1°. [b] ±0.005 V.

Table IV. Temperature Dependence of the Self-Exchange Reaction

T, °C	k_{ex}
5.7	$3.1\ (\pm0.4) \times 10^7\ M^{-1}\ s^{-1}$ [a]
15.0	$4.1\ (\pm0.4) \times 10^7\ M^{-1}\ s^{-1}$ [b]
25.0	$4.9\ (\pm0.3) \times 10^7\ M^{-1}\ s^{-1}$ [c]

[a] Mean of 42 runs: error is standard deviation. [b] Mean of 41 runs: error is standard deviation. [c] Mean of 25 runs: error is standard deviation.

duction potential by a term involving diffusion coefficients which is usually small:

$$E_{1/2} = E' - \frac{0.059}{n} \log \frac{D_{red}}{D_{ox}}$$

where E' is the formal potential, uncorrected for junction effects. Since the ratios of the diffusion coefficients, and the junction potentials at the refererce electrode should be essentially identical for the two couples, the identity of the half-wave potentials (within experimental error) for the two couples is interpreted to indicate that their formal reduction potentials are also identical.

For the net reaction studied kinetically:

$$(bpy)_2Ru(py)Cl^+ + (phen)_2Ru(py)Cl^{2+} = (bpy)_2Ru(py)Cl^{2+} + (phen)_2Ru(py)Cl^+ \quad (4)$$

$\Delta E^{\circ\prime} = 0.00 \pm 0.01$ V and $K = 1.0 \pm 0.5$. The visible–UV spectra of the Ru(II) and Ru(III) forms of the complexes $Ru(bpy)_2(py)Cl^{2+/+}$ and $Ru(phen)_2(py)Cl^{2+/+}$ in acetonitrile solution are given in Figures 5 and 6, respectively.

In one experiment, stoichiometric quantities of $Ru(bpy)_2(py)Cl^+$ and $Ru(phen)_2(py)Cl^{2+}$ were mixed and the spectrum of the resultant solution is given in Figure 7. Also shown in Figure 7 is a computed spectrum assuming equimolar concentrations for all four Ru species. The close matching between the two curves reinforces a value $K = 1.0$ for the equilibrium in eq 4.

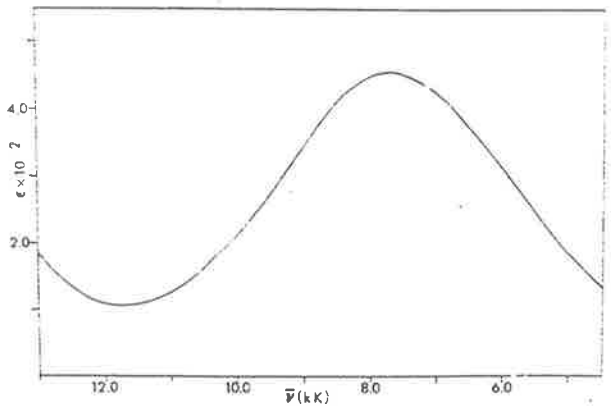

Figure 4. Near-infrared spectrum of $[(bpy)_2ClRu(pyz)RuCl(bpy)_2]^{3+}$ in acetonitrile.

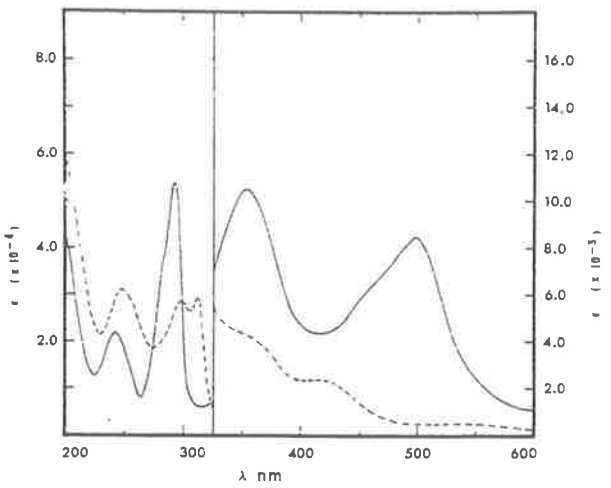

Figure 5. Visible-UV spectra of $[Ru(bpy)_2pyCl]^+$ (—), and $[Ru(bpy)_2pyCl]^{2+}$ (· · ·) in acetonitrile solution.

Kinetics. The rate of the net reaction in eq 5 was studied at three temperatures, and the results are given in Table IV.

$$[Ru(bpy)_2(py)Cl]^+ + [Ru(phen)_2(py)Cl]^{2+} \xrightarrow{k_{ex}} [Ru(bpy)_2(py)Cl]^{2+} + [Ru(phen)_2(py)Cl]^+ \quad (5)$$

The observed rate constants, k', were first order, regardless of the relative concentrations of the two solutions, and second-order rate constants, k_{ex}, were computed using the relationship developed in ref 15. The reaction rates were close to the physical limits of the instrumentation and, consequently, rate data were obtained at very low reactant concentration ($1.4–4.4 \times 10^{-6}$ M), resulting in high signal-to-noise ratios. Several runs were carried out at each concentration and temperature to allow a statistically meaningful treatment of the data. From a plot of ln k vs. $1/T$ the activation parameters for the self-exchange reactions are: $E_a = 3.9 \pm 0.6$ kcal/mol whence $\Delta H^{\ddagger} = E_a - RT = 3.3 \pm 0.6$ kcal/mol, $\Delta G^{\ddagger}$ (25°) $= 7.0 \pm 0.1$ kcal/mol, $\Delta S^{\ddagger}$ (25°) $= -12 \pm 2$ eu.

Discussion

Oxidation State Description of the Mixed-Valence Ion. Room temperature ESCA[16] and low temperature Mossbauer[17] experiments indicate that equal amounts of Ru(II) and Ru(III) exist in solid samples of the [2,3] ion. Because of the relatively long lifetime of the Mossbauer experiment the rate of electron transfer between the two metal centers must be slower than

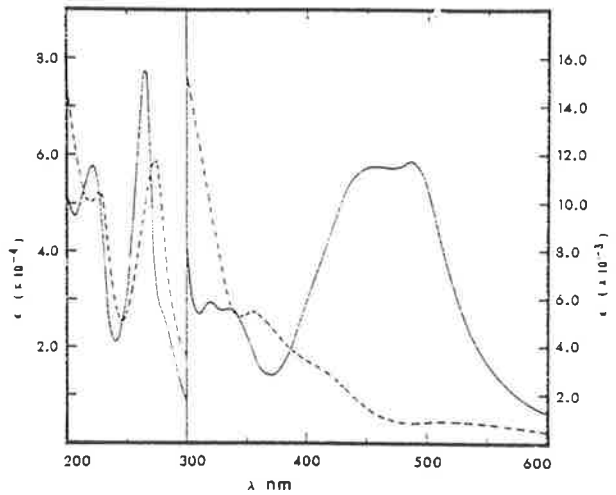

Figure 6. Visible-UV spectra of $[Ru(phen)_2pyCl]^+$ (—), and $[Ru(phen)_2pyCl]^{2+}$ (- - -) in acetonitrile solution.

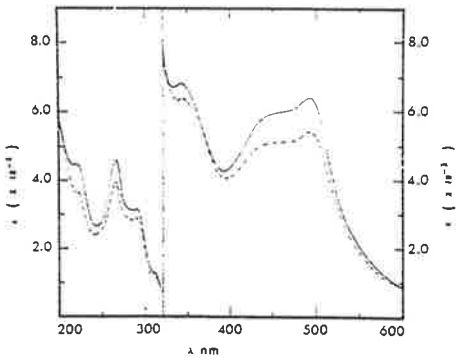

Figure 7. Visible-UV spectrum of reaction mixture after mixing equimolar quantities of $[Ru(bpy)_2pyCl]^+$ and $[Ru(phen)_2pyCl]^{2+}$ in acetonitrile solution (—), and a calculated spectrum assuming equimolar amounts of the Ru(II) and Ru(III) forms of both cations (- - -).

10^7–10^9 s^{-1} at the temperature of the experiment (~4 K).

The Mossbauer and ESCA results are not entirely conclusive. The [2,3] ion is favored only slightly in solution (eq 3), and the solid state could consist of equal amounts of [2,2] and [3,3] salts. In the solid state the Creutz and Taube system exists as the mixed-valence ion, $[(NH_3)_5Ru(pyz)Ru(NH_3)_5]^{5+}$. ESCA[16] and low temperature (~40 K) Mossbauer results[18] indicate distinct Ru(II) and Ru(III) sites, but the important observation is that solid state electronic spectra, including the appearance of the intervalence transfer band of the mixed-valence ion, are essentially the same in the solid state and in dilute aqueous solutions of the ion at 25 °C.[19] Given the pentaammine results, there is no precedence for significant disproportionation in solid samples of $[(bpy)_2ClRu(pyz)RuCl(bpy)_2]^{3+}$.

It is also conceivable that a change in electronic structure could occur upon cooling solid samples of the [2,3] ion. However, the consistency of the results at 4 K (Mossbauer experiment) and room temperature (ESCA experiment) appear to rule out this possibility. Finally, it should be noted that assignment of localized valences based on the appearance of different peaks in an ESCA spectrum has been questioned by Hush.[20] Hush has shown that for a symmetrical, delocalized ground state there are two accessible unsymmetrical photoionized states, and that the peak separation arising from the two photoionized states can be close to that for isolated M(II) and M(III) ions.

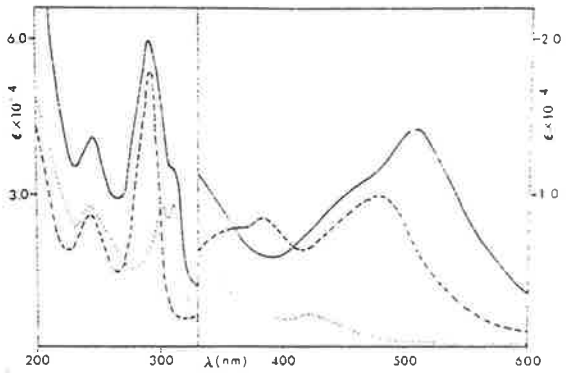

Figure 8. Electronic spectra of $[(bpy)_2ClRu(pyz)RuCl(bpy)_2]^{3+}$ (—), $[(bpy)_2Ru(pyz)Cl]^+$ (- - -), and $[(bpy)_2Ru(pyz)Cl]^{2+}$ (· · ·) in acetonitrile.

The electronic spectra of the [2,3] ion and of the parent Ru(II), $[(bpy)_2Ru(pyz)Cl]^+$, and Ru(III), $[(bpy)_2Ru(pyz)Cl]^{2+}$, complexes in acetonitrile are shown in Figure 8. The spectrum of the [2,3] ion is essentially the sum of the spectra of the monomeric Ru(II) and Ru(III) complexes both in the UV and visible. The only exception is the shift in the $t_2[Ru(II)] \rightarrow \pi^*(pyz)$ CT band from 384 nm in $[(bpy)_2Ru(pyz)Cl]^+$ to 508 nm in [2,3]. Similar shifts in related complexes have been attributed to stabilization of the MLCT excited state by the positive charge of the remote ion.[4,21]

The remaining absorption bands for [2,3] are also found in either the monomeric Ru(II) or Ru(III) complexes. The spectral similarities indicate that discrete Ru(II) and Ru(III) sites are present in the dimers and that the electronic environments at the two sites are little changed from the monomeric complexes. The pattern of $\pi \rightarrow \pi^*(bpy)$ bands at ~300 nm in bis(2,2′-bipyridine)ruthenium complexes is dependent in a systematic way upon whether the ruthenium ion is Ru(II) or Ru(III).[22-24] Evidence for both Ru(II) and Ru(III) sites in the dimer comes from the appearance of the intense band at 292 nm and the shoulder at 310 nm. Shoulders also appear in the dimer in the same spectral regions as the $t_2[Ru(II)] \rightarrow \pi^*(bpy)$ (478 nm) and $\pi(Cl) \rightarrow t_2[Ru(III)]$ (423 nm) transitions for $[(bpy)_2Ru^{II}(pyz)Cl]^+$ and $[(bpy)_2Ru^{III}(pyz)Cl]^{2+}$, respectively. The $t_2[Ru(II)] \rightarrow \pi^*(bpy)$ transition in $[(bpy)_2Ru^{II}Cl]$ type complexes is known to be sensitive to fairly slight changes in the remaining ligand.[25] The similarity in energies for the transition for the monomer and mixed-valence dimer argues that the influence of the remote Ru(III) site on the $t_2(d\pi)$ levels of Ru(II) is small, and therefore, that the metal–metal interaction cannot be appreciable. The same conclusion is reached from the electrochemical data. The potentials for the [2,3] → [2,2] and [3,3] → [2,3] couples are close to the value for the $[(bpy)_2Ru(pyz)Cl]^{2+/+}$ couple in the same medium even though the charge types involved are different.

The conclusions reached for [2,3] can be contrasted to the conclusions reached for the ion $[(bpy)_2ClRuORuCl(bpy)_2]^{2+}$.[26] For the oxo-bridged dimer the electronic spectrum and redox properties bear no resemblance to related complexes of Ru(II) or Ru(III), and the ion is apparently delocalized.

The most important aspect of the solution (CD_3CN) infrared spectrum for the [2,3] ion is the appearance of the moderately intense band at 1599 cm^{-1} since the band is not present for either the [2,2] or [3,3] ions (Figure 3). The band occurs at nearly the same energy (1589 cm^{-1}) as the band assigned as ν(pyz) in the monomeric complex $[(bpy)_2Ru(pyz)Cl]^+$.[27a] The ν(pyz) (ν_{8g}) band is a symmetrical stretch and infrared inactive in the D_{2h} symmetry of the free ligand.[27b] When bound as a monodentate ligand, the D_{2h} symmetry is

lost, the transition becomes dipole allowed, and the band appears in the infrared.[27c] In the [2,2] and [3,3] ions, effective local D_{2h} symmetry is apparently reestablished at the pyrazine and the band is absent in the IR.

In $[(bpy)_2ClRu(pyz)RuCl(bpy)_2]^{3+}$, local D_{2h} symmetry will be lost if there are discrete Ru(II) and Ru(III) sites on the lifetime of the infrared experiment. ν(pyz) appears in the IR for [2,3]. Electron transfer between the Ru(II) and Ru(III) sites must be slow on the infrared time scale and, therefore, there are localized Ru(II) and Ru(III) sites in the mixed-valence ion.

Two other explanations could account for the appearance of the ν(pyz) band. The local D_{2h} symmetry at pyrazine would be lost if there were preferred rotamers in the dimer because of the low symmetry at the ruthenium sites. This explanation seems unlikely because ν(pyz) is not observed for the [2,2] and [3,3] dimers. Also, a moderately intense 2,2′-bipyridine vibration ν(bpy), occurs in the same region as ν(pyz) (at 1604 and 1606 cm^{-1} for the [2,2] and [3,3] ions, respectively, Figure 3). The band at 1599 cm^{-1} is nearly within experimental error (± 2 cm^{-1}) of the bpy bands. The band at 1599 cm^{-1} could be ν(bpy) for Ru(II) and the 1604-cm^{-1} band ν(bpy) for Ru(III), an interpretation which is also consistent with localized valences. However, this explanation seems unlikely since in the unsymmetrical +3 and mixed-valence +4 ions, $[(NH_3)_5Ru(pyz)RuCl(bpy)_2]^{n+}$ ($n = 3, 4$), both ν(pyz) (1595 cm^{-1}) and ν(bpy) (1605 cm^{-1}) are present in CD_3CN.[27a]

Intervalence Transfer. An absorption band is observed in the near-IR spectrum of the [2,3] ion (Figure 4) which can be assigned to an IT transition (eq 6). Bands are not observed in this region for the [2,2] and [3,3] ions.

$$Ru(II)\text{-}Ru(III) \xrightarrow{h\nu} Ru(III)\text{-}Ru(II)^* \qquad (6)$$

In the [2,3] ion there appear to be localized valences and weak metal–metal interactions, and the treatment given by Hush[2] should apply to the properties of the IT band.

Assuming a Gaussian band shape, a lower limit for the bandwidth at room temperature can be calculated from eq 7 where $\bar{\nu}_{max}$ is the IT band maximum and $\bar{\nu}_{1/2}$ the bandwidth at half-height (both in μm^{-1}).

$$\bar{\nu}_{max} = (\bar{\nu}_{1/2})^2/2.31 \qquad (7)$$

Since $\bar{\nu}_{max} = 0.77$ μm^{-1} in acetonitrile, the calculated value for $\bar{\nu}_{1/2}$ is 0.42 μm^{-1} which is in good agreement with the experimental value of 0.49 μm^{-1}.

The IT band for $[(bpy)_2ClRu(pyz)RuCl(bpy)_2]^{3+}$ is essentially Gaussian with perhaps a shoulder appearing at lower energies. This distortion may affect somewhat the comparison made using eq 7. The appearance of a shoulder could conceivably mean that more than one IT band exists. Multiple IT bands could occur because of the nondegeneracies in the Ru(II) t_2 donor and Ru(III) t_2 acceptor orbitals arising from the low symmetry at the ruthenium ion sites.

The energy of the IT band, E_{op}, is shown plotted against $1/n^2 - 1/D_s$ in Figure 9 where n^2 and D_s are the optical and static dielectric constants of the solvent, respectively. The predicted linear relationship is found. The deviation of the D_2O value from the line drawn in Figure 9 may reflect the ability of the relatively small water molecule to penetrate somewhat between the planar bipyridine ligands. In that case the dielectric continuum approximation used to predict the linear relation is not fully appropriate. Strong association of water molecules with 2,2′-bipyridine complexes has been noted previously.[28-30] The sensitivity of E_{op} to changes in solvent is less for $[(bpy)_2ClRu(pyz)RuCl(bpy)_2]^{3+}$ than for $[(NH_3)_5Ru(4,4'\text{-bpy})Ru(NH_3)_5]^{5+}$,[4] which is expected given the larger size of the 2,2′-bipyridineruthenium sites (see eq 23 in the next section).

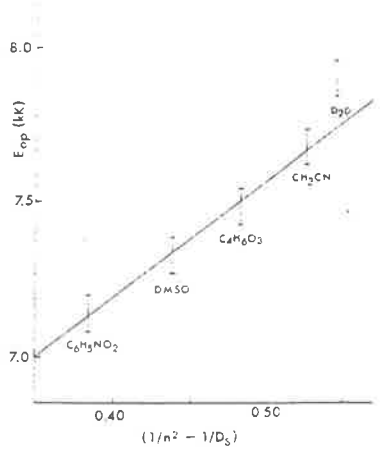

Figure 9. Plot of $(1/n^2 - 1/D_s)$ vs. E_{op} for the IT transition in $[(bpy)_2ClRu(pyz)RuCl(bpy)_2]^{3+}$.

The extent of delocalization of the exchanging electron in mixed-valence ions can be estimated from the properties of their IT bands.[2,31] A measure of delocalization in both the ground and excited states is α^2 which can be calculated from eq 8, where d is the internuclear separation between ruthenium ions (in Å) and ϵ_{max} the molar extinction coefficient at $\bar{\nu}_{max}$. The experimental α^2 value is the average of α^2 values for the ground and mixed-valence (vertical) excited states. If delocalization is small, the electronic wave functions used for overlap are relatively unperturbed, and α^2 is a direct measure of delocalization in the ground state. Using the values $d = 6.9$ Å,[32a]

$$\alpha^2 = \frac{(4.2 \times 10^{-4})\epsilon_{max}\bar{\nu}_{1/2}}{\bar{\nu}_{max}d^2} \qquad (8)$$

and in acetonitrile, $\bar{\nu}_{max} = 0.77$ μm^{-1}, $\bar{\nu}_{1/2} = 0.49$ μm^{-1}, and $\epsilon = 455$ M^{-1} cm^{-1} gives $\alpha^2 = 2.6 \times 10^{-3}$. The value for α^2 is in the same range as values calculated for the unsymmetrical dimer $[(NH_3)_5Ru^{III}(pyz)Ru^{II}Cl(bpy)_2]^{4+}$ ($\alpha^2 = 2.6 \times 10^{-3}$)[3] and for the trimer $[(NH_3)_5Ru^{III}(pyz)Ru^{II}(bpy)_2(pyz)\text{-}Ru^{III}(NH_3)_5]^{8+}$ ($\alpha^2 = 1.3 \times 10^{-3}$ per Ru(III)–Ru(II) unit)[33] in the same medium. In all three cases there is good evidence for localized valences, delocalization from Ru(II) to Ru(III) is less than 1%,[2,27a,31] and the properties of the IT bands are accounted for satisfactorily by the Hush theory.

Thermal Electron Transfer. Hush has shown that for a symmetrical complex the relationship between E_{op} for the light-induced electron transfer process (eq 6) and the energy of activation (E_{th}) for the related thermal electron transfer process (eq 9) is given by eq 10.[2]

$$[(bpy)_2ClRu^{II}(pyz)Ru^{III}Cl(bpy)_2]^{3+} \xrightarrow{k_{th}, E_{th}} [(bpy)_2ClRu^{III}(pyz)Ru^{II}Cl(bpy)_2]^{3+} \qquad (9)$$

$$E_{op} \geq 4E_{th} \qquad (10)$$

If delocalization from Ru(II) to Ru(III) is slight,

$$E_{op} \sim 4E_{th} \qquad (10a)$$

or including the effect of the resonance or delocalization energy β,

$$E_{th} \sim \frac{E_{op}}{4} - \beta \qquad (10b)^{32}$$

For reaction 9, $T\Delta S^* \sim 0$,[34] and the thermal rate constant can be written as,

$$k_{th} = \nu_{el} \exp[-(\Delta G^*/RT)] \sim \nu_{el} \exp[-(E_{th}/RT)] \qquad (11)$$

Estimates for the frequency factor, ν_{et}, of $\sim 10^{11}$ s^{-1} are available from the results of excited state quenching experiments.[35-37] A value of 10^{11} s^{-1} may be too low for reaction 9 for two reasons. Experiments using time-resolved psec. spectroscopy give a direct estimate for ν_{et}, but if $\Delta G°$ is large and favorable the measured rate constant gives only a lower limit for ν_{et} since this corresponds to electron transfer in the "abnormal free energy region".[38-40] The frequency factor for electron transfer is given very crudely by eq 12 where β is the delocalization or resonance energy and h, Planck's constant.[41]

$$\nu_{et} \sim 4\beta/h \qquad (12)^{42}$$

In the quenching experiments, electron transfer occurs by an outer-sphere mechanism and the resonance energy between quencher and excited state is probably small,[35] and certainly smaller than the resonance energy across the bridging pyrazine in $[(bpy)_2ClRu(pyz)RuCl(bpy)_2]^{3+}$.

If delocalization is small the resonance energy should be about the same in the activated complex as in the ground state. The resonance energy in [2,3] can be estimated crudely as $\beta \leq 0.049$ eV from eq 13 which gives $\nu_{et} \leq 5 \times 10^{13}$ s^{-1}.

$$\beta \leq \alpha\bar{\nu}_{max} \qquad (13)^{2b,32a}$$

Choosing the value above for β and using eq 10b gives $E_{th} \geq 4.4$ kcal/mol. Taking this value for E_{th}, the estimate of ν_{et} given above, and using eq 11 gives that $k_{th} < 3 \times 10^{10}$ s^{-1} for the [2,3] ion in acetonitrile solution at 25 °C.

The value calculated for k_{th} using the Hush approximation and eq 11 is only an estimate, but it is important to establish whether or not the value is correct even to within an order of magnitude. The direct measurement of electron transfer rates through bridging ligands has been achieved in certain unsymmetrical complexes where the rate of electron transfer is slow,[43-45] but experimental methods for measuring rates for reactions like 9 have remained elusive. For a weak interaction case where the properties of the IT band are accounted for satisfactorily by the Hush theory, the observation of an IT band demonstrates the existence of the related thermal process, and so evidence for thermal electron transfer can be obtained even through long bridging ligands.[3-5,33] If in addition, k_{th} can be estimated as described above, rate comparisons between systems can be made conveniently since measurements of E_{op} are relatively straightforward.

An upper limit for k_{th} in $[(bpy)_2ClRu(pyz)RuCl(bpy)_2]^{3+}$ can be obtained from the ν(pyz) infrared band (Figure 3). The lifetime of the IR excited state can be estimated from the uncertainty principle and the band width at half height. Using an estimated band width of 15 cm^{-1} gives $\Delta t \geq 2 \times 10^{-13}$ s and since the rate of thermal electron transfer must be slow on this time scale, $k_{th} < 5 \times 10^{12}$ s^{-1}. The estimate of Δt is only approximate since other effects may broaden the IR band,[46] but it certainly gives a reasonable estimate of an upper limit for k_{th} which is higher than the value calculated above.

An estimate for k_{th} can also be obtained from the results of the electron transfer experiment described in an earlier section. For the reaction,

$$[(bpy)_2Ru(py)Cl]^+ + [(phen)_2Ru(py)Cl]^{2+} \xrightarrow{k_{ex}} [(bpy)_2Ru(py)Cl]^{2+} + [(phen)_2Ru(py)Cl]^+ \qquad (14)$$

$\Delta G°'$ is 0, and so k_{ex} provides a reasonable estimate for the $[(bpy)_2Ru(py)Cl]^{2+/+}$ self-exchange rate. Mechanistically, the overall reaction occurs through two steps which determine the magnitude of k_{ex}. The first step involves ion-pair formation between reactants, and the second, electron transfer within the ion-pair:

Scheme I

$$Ru(bpy)_2(py)Cl^+ + Ru(phen)_2(py)Cl^{2+} \underset{k_{-1}}{\overset{k_1}{\rightleftharpoons}} Ru(bpy)_2(py)Cl^+,Ru(phen)(py)Cl^{2+}:K \qquad (15)$$

$$Ru(bpy)_2(py)Cl^+,Ru(phen)_2(py)Cl^{2+} \xrightarrow{k_2} Ru(bpy)_2(py)Cl^{2+},Ru(phen)_2(py)Cl^+ \qquad (16)$$

$$Ru(bpy)_2(py)Cl^{2+},Ru(phen)_2(py)Cl^+ \rightarrow Ru(bpy)_2(py)Cl^{2+} + Ru(phen)_2(py)Cl^+ \qquad (17)$$

The numerical value for electron transfer within the ion pair, k_2, should give a rough estimate for k_{th}. The inner- and outer-sphere reorganizational energies which largely determine the magnitudes of k_{th} and k_2[47-49] should be similar for the two reactions. The dimeric ion and the pyridine complexes have very similar chemical properties as shown by their electronic spectra and redox potentials. In both processes the electron donor and acceptor sites are held in relatively close proximity. However, k_2 is expected to be smaller than k_{th} because the resonance energy should be less in the outer-sphere case making E_{th} slightly larger (eq 10b) and ν_{et} smaller (eq 12).

The relationship between k_{ex} and the constants in Scheme I is,

$$k_{ex} = \frac{k_1 k_2}{k_{-1} + k_2} \qquad (18)$$

The experimental value for k_{ex} at 25 °C is $\sim 10^2$ below the diffusion-controlled limit calculated using the Debye–Smoluchowski equation.[50,51] The correction for diffusion effects should be negligible and assuming that $k_{-1} > k_2$ gives,

$$k_{ex} = k_2 K \qquad (19)$$

The ion-pair equilibrium constant $K = 0.41$ can be estimated from the Fuoss equation,[52-55] and using that value and eq 19 gives $k_2 = 1.2 \times 10^8$ s^{-1}.

k_2 and k_{th} are not directly comparable because the distances between the metal sites are different in the two cases (6.9 Å for [2,3] and 12.1 Å in the self-exchange reaction), and the outer-sphere reorganizational energy depends on the internuclear separation, d (see below). The correction in the outer-sphere reorganizational energy $\Delta(G_o*)$, which would make the two cases comparable can be calculated from eq 20 where n^2 and D_S were defined previously and d_1 and d_2 are the two internuclear separations.[57]

$$\Delta(\Delta G_0*) = \frac{e^2}{4}\left(\frac{1}{d_1} - \frac{1}{d_2}\right)\left(\frac{1}{n^2} - \frac{1}{D_S}\right) \qquad (20)$$

The corrected value for k_{th} using the larger internuclear separation is $k'_{th} \leq 3 \times 10^8$ s^{-1}.

It should be noted that the comparison between k'_{th} and k_2 should be valid since both the self-exchange and IT experiments were carried out in dilute solution under nearly ideal conditions. The energy of the IT band appears to be relatively insensitive to added electrolyte which is predicted theoretically.[47,48] The overall rate of outer-sphere electron transfer will of course be dependent on ionic strength because of the preequilibrium in eq 15.

The calculated values for k_{th} and k_2 are only approximate. However, the agreement found in the two values reinforces the validity of the Hush treatment for obtaining at least approximate values for thermal electron transfer rates in mixed-valence systems and demonstrates the expected close relationship between outer-sphere electron transfer processes and inner-sphere processes where delocalization between sites is small.[2,48]

The intervalence transfer experiment allows access to in-

formation about the activation process for electron transfer which is usually not available from other experiments. The IT band energy is related to the Marcus-Hush reorganizational energy term for thermal electron transfer by,

$$E_{op} = \lambda_i + \lambda_o \quad (21)$$

where λ_i and λ_o are the outer and inner sphere reorganizational contributions to λ.[47-49] In eq 21, λ is given by $\lambda = 4\Delta G^*$, where ΔG^* is the free energy of activation for thermal electron transfer, and $\lambda_i = 4\Delta G_i^*$ and $\lambda_o = 4\Delta G_o^*$ where the contribution from the resonance energy is neglected.[47-49] Since $T\Delta S^* \sim 0$ for the electron transfer step,

$$4E_{th} = \lambda \quad (22)$$

Using a dielectric continuum model, Marcus and Hush have derived eq 23 for λ_o, where r_1 and r_2 are the molecular radii of the two metal sites in the activated complex for thermal electron transfer and the remaining terms were defined previously.[47,48]

$$\lambda_o = e^2\left(\frac{1}{2r_1} + \frac{1}{2r_2} - \frac{1}{d}\right)\left(\frac{1}{n^2} - \frac{1}{D_S}\right) \quad (23)$$

λ_i is expected to be relatively independent of changes in solvent so that from eq 21 and 23 and the plot of E_{op} vs. $(1/n^2 - 1/D_S)$ in Figure 9, the intercept is equal to λ_i and λ_o in a given solvent can be calculated using eq 21. For $[(bpy)_2ClRu(pyz)RuCl(bpy)_2]^{3+}$ in acetonitrile, λ_i = 16.1 kcal/mol and λ_o = 6.0 kcal/mol, which gives ΔG_i^* = 4.0 kcal/mol and ΔG_o^* = 1.5 kcal/mol. The intervalence transfer experiment thus allows the activation barrier to electron transfer to be partitioned between inner- and outer-sphere reorganizational contributions.

The variation of IT band energies with solvent has also been measured for $[(NH_3)_5Ru(4,4'\text{-bpy})Ru(NH_3)_5]^{5+}$ [4] and for $[(NH_3)_5Ru(pyz)RuCl(BPY(_2)]^{4+}$.[5] The properties of all three ions are consistent with localized valences and small delocalization. Marcus and Hush have derived expressions for outer-sphere electron transfer between unlike ions, e.g., eq 24,[47-49] and the equations should apply to inner-sphere reactions where delocalization is small.

$$Fe(H_2O)_6^{3+} + Ru(NH_3)_6^{2+} \rightarrow Fe(H_2O)_6^{2+} + Ru(NH_3)_6^{3+} \quad (24)^{58}$$

For an inner-sphere reaction where the donor and acceptor sites are held fixed to the bridging ligand, ΔG^* is given by eq 25,

$$\Delta G^* = \frac{\lambda}{4}\left(1 + \frac{\Delta G^{\circ\prime}}{\lambda}\right)^2 \quad (25)$$

where $\Delta G^{\circ\prime}$ is the overall free energy change in the appropriate medium.

λ can be expressed in terms of λ values for the individual self-exchange reactions ($Ru(NH_3)_6^{3+/2+}$, $Fe(H_2O)_6^{3+/2+}$) as,

$$\lambda = \frac{\lambda_1 + \lambda_2}{2} \quad (26)$$

and for the inner-and outer-sphere terms,

$$\lambda_i = \frac{\lambda_{i,1} + \lambda_{i,2}}{2} \quad (27)$$

$$\lambda_o = \frac{\lambda_{o,1} + \lambda_{o,2}}{2} \quad (28)$$

λ_i for reaction 29,

$$[(NH_3)_5Ru^{III}(pyz)Ru^{II}Cl(bpy)_2]^{4+} \rightarrow [(NH_3)_5Ru^{II}(pyz)Ru^{III}Cl(bpy)_2]^{4+} \quad (29)$$

should be related to λ_i for reactions 9 ($\lambda_{i,1}$) and 30 ($\lambda_{i,2}$),

$$[(NH_3)_5Ru^{III}(4,4'\text{-bpy})Ru^{II}(NH_3)_5]^{5+} \rightarrow [(NH_3)_5Ru^{II}(4,4'\text{-bpy})Ru^{III}(NH_3)_5]^{5+} \quad (30)$$

by eq 27. The experimental value of λ_i for eq. 29 is 12.9 kcal/mol.[5] The value calculated using $\lambda_{i,1}$ = 16.1 kcal/mol and $\lambda_{i,2}$ = 10.0 kcal/mol[4] is 13.0 kcal/mol which is in excellent agreement with the experimental value. λ_o values for the three reactions should also be related but because of the difference in bridging ligands, the internuclear separations are different and the comparison cannot be made directly.

Comparisons with Other Systems. The mixed-valence ions $[(NH_3)_5Ru(4,4'\text{-bpy})Ru(NH_3)_5]^{5+}$,[4] $[(bpy)_2ClRu(pyz)RuCl(bpy)_2]^{3+}$, $[(NH_3)_5Ru(L)RuCl(bpy)_2]^{4+}$,[3,5] and $[(NH_3)_5Ru(L)Ru(bpy)_2(L)Ru(NH_3)_5]^{6+/5+}$[33]

(L is  or

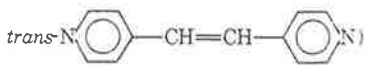

have localized valences, have only slight Ru(II) to Ru(III) delocalization, and exhibit class II behavior in the Robin and Day sense.[31] The extent of delocalization in the unsymmetrical ions is somewhat limited by the redox inequivalency of the different ruthenium ion sites.[33]

The oxo-bridged ion $[(bpy)_2ClRuORuCl(bpy)_2]^{2+}$ has multiple redox properties and is delocalized.[26] In contrast to pyrazine as a bridge, there is strong coupling between ruthenium ions across the bridging oxide ion and the redox properties are carried by orbitals which are delocalized over both ruthenium ions. Taube and his co-workers have shown that in related systems the resonance energy is sufficiently high across bridging dinitrogen (e.g., in *cis*-$[(NH_3)_4ClOs(N_2)Os(NH_3)_4Cl]^{4+}$)[59] and even across cyanogen ($[(NH_3)_5Ru(NCCN)Ru(NH_3)_5]^{5+}$)[60] to give delocalized, mixed-valence ions.

The most interesting comparison with $[(bpy)_2ClRu(PYZ(RuCl(bpy)_2]^{3+}$ is the comparison with the Creutz and Taube ion $[(NH_3)_5Ru(pyz)Ru(NH_3)_5]^{5+}$. The results of many experiments have been reported for the Creutz and Taube ion,[6,7] but a truly satisfactory description of the oxidation state properties of the ion has not been given. An absorption band has been observed for the ion in the near-IR, but the bandwidth is far narrower than predicted by eq 7, and the band energy is invariant to changes in solvent. In the IR only one $\delta(NH_3)$(sym) frequency is observed at an energy intermediate between band positions expected for Ru(II) and Ru(III) pentaammines.[6,7,21] However, both the results of Mossbauer[18] and ESCA[16] experiments have been interpreted in terms of different, chemically discrete Ru(II) and Ru(III) sites although the interpretation of the results of the latter experiment has been questioned by Hush.[20]

Some insight can be gained into the difference between $[(bpy)_2ClRu(pyz)RuCl(bpy)_2]^{3+}$ and the Creutz and Taube ion from redox potential values for the two, one-electron processes [3,3] + e → [2,3] and [2,3] + e → [2,2]. The redox potentials can be used to calculate $\Delta G^{\circ\prime}$ for the conproportionation equilibrium for both ions (eq 3).

$$[2,2] + [3,3] \rightleftharpoons 2[2,3] \quad (3)$$

In 0.10 M TBAH-acetonitrile, $\Delta G^{\circ\prime}$ = 0.12 V for the bpy system and 0.43 V for the pentaammine system. In both systems the mixed-valence ion is favored by a statistical factor of 4 or RT/nF ln 4 = 0.036 V. Both mixed-valence ions are favored slightly by an electrostatic factor which can be estimated to be ~0.028 V using a simple Coulombic model.[61] Neglecting differences arising from changes in solvation energies, the remaining value for $\Delta G^{\circ\prime}$ (0.056 V for the bpy mixed-valence

ion) must reflect the partial delocalization of the exchanging electron from Ru(II) to Ru(III). The value calculated for this effect is in the same range as the resonance energy estimated by eq 13 ($\beta \leq 0.049$ eV).

The Creutz and Taube ion is favored by an additional factor of 0.31 V (7.1 kcal/mol) over $[(bpy)_2ClRu(pyz)RuCl(bpy)_2]^{3+}$ which must come largely from the effects of greater electron donation from Ru(II) to Ru(III). An enhanced stability for the mixed-valence ion of 7.1 kcal/mol is large when it is realized that ΔG^* for intramolecular electron transfer in $[(NH_3)_5Ru(4,4'\text{-bpy})Ru(NH_3)_5]^{5+}$ is ~6–7 kcal/mol in acetonitrile from IT measurements.[4] The Creutz and Taube ion may or may not be delocalized, but it is clearly outside the weak interaction limit to which the Hush theory applies.

It has been suggested that the Creutz and Taube ion may represent an intermediate case lying between the limiting localized and delocalized descriptions,[60,62] where there is extensive delocalization but inequivalent metal sites. The same considerations may also apply in part to the mixed-valence biferrocene ion $[(C_5H_5)Fe(C_5H_4\text{-}C_5H_4)Fe(C_5H_5)]^+$ where $\Delta G^{\circ\prime}$ for eq 3 is also large and favorable and reorganizational energies are expected to be low.[63,64]

Strong Ru(II) → π*(bpy) back-bonding is an important feature in the chemistry of ruthenium complexes of 2,2′-bipyridine as evidenced by their spectral and redox properties.[23-25,65,66] Less electron donation from Ru(II) to Ru(III) is anticipated for $[(bpy)_2ClRu(pyz)RuCl(bpy)_2]^{3+}$ because competitive back-bonding to the bpy ligands must decrease the available electron density for delocalization through the π* system of the bridging pyrazine ligand. By appropriate synthetic modifications in which the nonbridging ligands are varied systematically, it will be possible to explore the region of delocalization between the bpy and pentaammine ions.

Acknowledgments are made to the Army Research Office-Durham under Grant DA-ARO-O-31-12-73-G-104 and to the Materials Research Center of the University of North Carolina under Grant DAHC15 73 G9 with DARPA for support of this research.

References and Notes

(1) A preliminary account of this work has appeared: R. W. Callahan and T. J. Meyer, *Chem. Phys. Lett.*, **39**, 82 (1976).
(2) (a) N. S. Hush, *Prog. Inorg. Chem.*, **8**, 391 (1967); (b) N. S. Hush, *Electrochim. Acta*, **13**, 1005 (1968).
(3) (a) R. W. Callahan, T. J. Meyer, and G. M. Brown, *J. Am. Chem. Soc.*, **96**, 7829 (1974); (b) *Inorg. Chem.*, **14**, 1443 (1975).
(4) G. M. Tom, C. Creutz, and H. Taube, *J. Am. Chem. Soc.*, **96**, 7827 (1974).
(5) M. J. Powers, R. W. Callahan, T. J. Meyer, and D. J. Salmon, *Inorg. Chem.*, **15**, 1457 (1976).
(6) C. Creutz and H. Taube, *J. Am. Chem. Soc.*, **91**, 3988 (1969).
(7) C. Creutz and H. Taube, *J. Am. Chem. Soc.*, **95**, 1086 (1973).
(8) J. N. Braddock, Ph.D. Dissertation, University of North Carolina, Chapel Hill, 1973.
(9) J. B. Godwin and T. J. Meyer, *Inorg. Chem.*, **10**, 471 (1971).
(10) E. C. Johnson, Ph.D. Dissertation, University of North Carolina, Chapel Hill, 1975.
(11) T. H. Ridgway, Ph.D. Dissertation, University of North Carolina, Chapel Hill, 1971; R. M. Wightman, Ph.D. Dissertation, University of North Carolina, Chapel Hill, 1974.
(12) J. A. Ferguson and T. J. Meyer, *Inorg. Chem.*, **10**, 1025 (1971).
(13) G. M. Brown, Ph.D. Dissertation, University of North Carolina, Chapel Hill, 1974, and private communication.
(14) S. A. Adeyemi, J. N. Braddock, G. M. Brown, J. A. Ferguson, and T. J. Meyer, *J. Am. Chem. Soc.*, **94**, 300 (1972).
(15) For a reaction a + b ⇌ c + d where $K = k_f/k_b = 1$, such as in the present instance, if $c_0 = d_0 = 0$ and x is the extent of reaction, the rate law is given by

$$\ln\left[1 - \frac{(a_0 + b_0)x}{a_0 b_0}\right] = -(a_0 + b_0)k_f t + \ln a_0 b_0$$

If at equilibrium $x = x_e$, then the rate law becomes

$$\ln(x_e - x) - \ln x_e = -(a_0 + b_0)k_f t$$

If A_e and A_t are absorbances at equilibrium and at time t, respectively,

$$\ln(A_e - A_t) = -(a_0 + b_0)k_f t + \text{constant}$$

Consequently, a first order rate plot yields an observed rate constant $k' = (a_0 + b_0)k_f$, so that $k_f = k'/(a_0 + b_0)$.
(16) P. Citrin, *J. Am. Chem. Soc.*, **95**, 6472 (1973).
(17) M. L. Good, private communication.
(18) M. L. Good, C. Creutz, and S. Chandra, *Inorg. Nucl. Chem. Lett.*, **9**, 171 (1973).
(19) I. M. Treitel, Ph.D. Dissertation, California Institute of Technology, 1971.
(20) N. S. Hush, *Chem. Phys.*, **10**, 361 (1975).
(21) C. Creutz, Ph.D. Dissertation, Stanford University, 1971.
(22) G. M. Bryant and J. E. Fergusson, *Aust. J. Chem.*, **24**, 275 (1971).
(23) J. N. Braddock and T. J. Meyer, *J. Am. Chem. Soc.*, **95**, 3158 (1973).
(24) G. M. Bryant, J. E. Fergusson, and H. K. Powell, *Aust. J. Chem.*, **24**, 257 (1971).
(25) W. L. Bowden, W. F. Little, T. J. Meyer, and D. J. Salmon, *J. Am. Chem. Soc.*, **97**, 6897 (1975).
(26) T. R. Weaver, T. J. Meyer, S. A. Adeyemi, G. M. Brown, R. P. Eckberg, W. E. Hatfield, E. C. Johnson, R. W. Murray, and D. Untereker, *J. Am. Chem. Soc.*, **97**, 3039 (1975).
(27) (a) R. W. Callahan, Ph.D. Dissertation, University of North Carolina, Chapel Hill, 1975; (b) R. C. Lord, A. L. Martin, and F. A. Miller, *Spectrochim. Acta*, **9**, 113 (1959); (c) M. Goldstein and W. D. Unsworth, *Spectrochim. Acta, Part A*, **27**, 1055 (1971).
(28) D. R. Gere and C. E. Meloan, *J. Inorg. Nucl. Chem.*, **25**, 1507 (1963).
(29) S. Burchett and C. E. Meloan, *J. Inorg. Nucl. Chem.*, **34**, 1207 (1972).
(30) G. N. LaMar and G. R. Van Hecke, *Inorg. Chem.*, **12**, 1767 (1973).
(31) M. B. Robin and P. Day, *Adv. Inorg. Chem. Radiochem.*, **10**, 247 (1967).
(32) (a) B. Mayoh and P. Day, *Inorg. Chem.*, **13**, 2273 (1974); (b) B. Mayoh and P. Day, *J. Am. Chem. Soc.*, **94**, 2885 (1972).
(33) M. J. Powers, R. W. Callahan, D. J. Salmon, and T. J. Meyer, *Inorg. Chem.*, **15**, 894 (1976).
(34) W. L. Reynolds and R. W. Lumry, "Mechanisms of Electron Transfer", Ronald Press, New York, N.Y., 1966, pp 128–129.
(35) D. Rehm and A. Weller, *Israel J. Chem.*, **8**, 259 (1970).
(36) D. Rehm and A. Weller, *Ber. Bunsenges. Phys. Chem.*, **72**, 257 (1968).
(37) K. B. Eisenthal, *Acc. Chem. Res.*, **8**, 118 (1975).
(38) R. A. Marcus, *J. Chem. Phys.*, **43**, 2654 (1965); **52**, 2803 (1970).
(39) S. Efrima and M. Bixon, *Chem. Phys. Lett.*, **25**, 34 (1974).
(40) R. P. VanDuyne and S. F. Fischer, *Chem. Phys.*, **5**, 183 (1974).
(41) W. Kauzmann, "Quantum Chemistry", Academic Press, New York, N.Y., 1957, pp 534–536.
(42) In Eq. 12 ν_{et} is the frequency of electron oscillation between Ru(II) and Ru(III) in the activated complex for thermal electron transfer where the coordination environments around the two sites are identical; $1/\nu_{et}$ is the lifetime of the exchanging electron initially located on Ru(II).
(43) S. S. Isied and H. Taube, *J. Am. Chem. Soc.*, **95**, 8198 (1973).
(44) D. Gaswick and A. Haim, *J. Am. Chem. Soc.*, **96**, 7845 (1974).
(45) A. Haim, *Acc. Chem. Res.*, **8**, 264 (1975).
(46) S. F. A. Kettle and I. Paul, *Adv. Organomet. Chem.*, **10**, 199 (1972).
(47) R. A. Marcus, *Annu. Rev. Phys. Chem.*, **15**, 155 (1964); *J. Phys. Chem.*, **67**, 853 (1963).
(48) N. S. Hush, *Trans. Faraday Soc.*, **57**, 557 (1961).
(49) Reference 34, Chapter 6.
(50) P. Debye, *Trans. Electrochem. Soc.*, **82**, 265 (1942).
(51) k_D was calculated from

$$k_D = \frac{2RT}{3000\eta}\left(2 + \frac{r_A}{r_B} + \frac{r_B}{r_A}\right)\frac{\delta}{e^{\delta} - 1}$$

where r_A and r_B are the "average" molecular radii of the diffusing ions taken to be 5.8 and 6.3 Å for $[Ru(bpy)_2(py)Cl]^+$ and $[Ru(phen)_2(py)Cl]^{2+}$, respectively, and $\eta = 3.45 \times 10^{-3}$ poise at 25 °C. The term δ is given by

$$\delta = Z_A Z_B E^2/dD_S kT$$

where the various terms have been defined previously or are defined below. Ionic strength corrections are negligible for the dilute solutions used.
(52) R. M. Fuoss, *J. Am. Chem. Soc.*, **80**, 5059 (1958).
(53) P. Hemmes, *J. Am. Chem. Soc.*, **94**, 75 (1972).
(54) C. T. Lin and D. B. Rorabacher, *Inorg. Chem.*, **12**, 2402 (1973).
(55) In acetonitrile at 25 °C

$$K = (2.524 \times 10^{-3})d^3 \exp\left[\frac{-9.03 Z_1 Z_2}{dRT}\right]$$

with d the internuclear separation between ions in Å and Z_1Z_2 the product of ionic charges. An ionic strength correction is unnecessary because the self-exchange rate was measured in dilute solution with no added electrolyte. Using a value for d of 12.1 Å gives $K = 0.41$ at 25 °C. Further, in the dilute solutions used, solution conductivity measurements on related complexes indicate that complications arising from ion-pairing with the negative counterions are probably unimportant.[26] If there are additional interactions between the complexes not included in the continuum treatment used by Fuoss in deriving eq 20, such as stacking interactions between the aromatic ring systems,[56] K will be larger than calculated and k_2 smaller.
(56) G. R. Cayley and D. W. Margerum, *J. Chem. Soc., Chem. Commun.*, 1002 (1974).
(57) Equation 21 was derived from eq 23. k_{th} for a given internuclear separation d is given by, $k_{th} = \nu_{et}\exp(-\lambda/4RT)$ where $\lambda/4$ is the sum of the inner- and outer-sphere reorganizational energies for thermal electron transfer. For a different value of d and λ, λ', the corrected rate constant k_2' can be calculated from: $k_{th}' = k_{th}\exp(\lambda - \lambda')/4RT$, if the resonance energy and thus ν_{et} remain the same, which is appropriate for the case considered here. If, as is also appropriate here, the inner-sphere reorganizational energy is taken to be the same for the two distances, $k_{in}' = k_{in}\exp[-(\Delta\lambda_o)/4RT]$ where $\Delta\lambda_o = \lambda_o - \lambda_o' = 4\Delta(\Delta G_o^*)$.
(58) H. Taube and T. J. Meyer, *Inorg. Chem.*, **7**, 2369 (1968).
(59) R. H. Magnuson and H. Taube, *J. Am. Chem. Soc.*, **94**, 7213 (1972).

(60) G. M. Tom and H. Taube, *J. Am. Chem. Soc.*, **97**, 5310 (1975).
(61) The electrostatic energy was estimated by a thermochemical cycle in which the [2,2] and [3,3] ions are separated as monomeric spheres of radius 6.9/2 Å (½ the Ru(pyz)Ru distance) to infinity and recombined to give [2,3]. For the individual steps in 0.1 M TBAH–CH_3CN,[55]

$$\Delta G^{\circ\prime} = \frac{9.10 Z_1 Z_2}{r}\left(\frac{1}{1 + 0.482 r I^{1/2}}\right)$$

in which r = 6.9 Å, Z_1 and Z_2 are the ionic charges, and I is the ionic strength.
(62) T. J. Meyer, *Adv. Chem. Ser.*, **No. 150**, Chapter 7 (1976).
(63) D. O. Cowan, C. LeVanda, J. Park, and F. Kaufman, *Acc. Chem. Res.*, **6**, 1 (1973).
(64) J. P. Pladziewicz and J. H. Espenson, *J. Am. Chem. Soc.*, **95**, 56 (1973); E. S. Yang, M.-S. Chan, and A. C. Wahl, *J. Phys. Chem.*, **79**, 2049 (1975).
(65) J. Cramer, Ph.D. Dissertation, University of North Carolina, Chapel Hill, 1975.
(66) D. A. Buckingham and A. M. Sargeson in "Chelating Agents and Metal Chelates", F. P. Dwyer and D. P. Mellor, Ed., Academic Press, New York, N.Y., 1964, Chapter 6.

Measurement of Rates of Electron Transfer between $Ru(bpy)_3^{3+}$ and $Fe(phen)_3^{2+}$ and between $Ru(phen)_3^{3+}$ and $Ru(bpy)_3^{2+}$ by Differential Excitation Flash Photolysis

Roger C. Young, F. Richard Keene, and Thomas J. Meyer*

Contribution from the Department of Chemistry, University of North Carolina, Chapel Hill, North Carolina 27514. *Received August 13, 1976*

Abstract: Flash photolysis of solutions containing $Fe(H_2O)_6^{3+}$, $Ru(bpy)_3^{2+}$, and $Fe(phen)_3^{2+}$ results in excitation to the CT excited state of $Ru(bpy)_3^{2+}$ followed by rapid quenching to give $Ru(bpy)_3^{3+}$ and $Fe(H_2O)_6^{2+}$. The quenching step is followed by rapid electron transfer between $Ru(bpy)_3^{3+}$ and $Fe(phen)_3^{2+}$ (k(25 °C) = 1.8×10^9 M^{-1} s^{-1} in 1.0 M $HClO_4$) and then return of the system to equilibrium by electron transfer between $Fe(phen)_3^{3+}$ and $Fe(H_2O)_6^{2+}$. Both reactions can be followed directly by observing transient spectral changes following flash photolysis. Flash photolysis of solutions containing $Ru(bpy)_3^{2+}$, $Ru(phen)_3^{3+}$, and $Fe(H_2O)_6^{3+}$ results in excitation and quenching of both the bpy and phen complexes. However, because of differences in spectral and excited state properties, in solutions in which initially there are equal amounts of $Ru(bpy)_3^{2+}$ and $Ru(phen)_3^{2+}$, an excess of $Ru(phen)_3^{3+}$ can be produced. Excitation and quenching are followed by a reaction between $Ru(bpy)_3^{2+}$ and $Ru(phen)_3^{3+}$ which takes the system to a position of transient equilibrium (see eq 12 in text), for which K = 1.0, and which is followed by the slower reductions of $Ru(phen)_3^{3+}$ and $Ru(bpy)_3^{3+}$ by $Fe(H_2O)_6^{2+}$. An appropriate analysis of the transient spectral changes following flash photolysis has given rate constant data for both the equilibration reaction and the back-reactions between $Fe(H_2O)_6^{2+}$ and $Ru(bpy)_3^{3+}$ and $Ru(phen)_3^{3+}$. At 25 °C, k_1, which is a measure of the $Ru(bpy)_3^{3+/2+}$ and $Ru(phen)_3^{3+/2+}$ self-exchange rates, is 1.2×10^9 M^{-1} s^{-1} in 1.0 M $HClO_4$. In 0.1 M $HClO_4$, $\Delta H^{\ddagger}$ = 7.7 ± 1.5 kcal/mol and $\Delta S^{\ddagger}$ = −6.6 ± 0.4 eu. It is concluded that the net reaction and, therefore, the self-exchange reactions are slightly below the diffusion-controlled limit and that a slight barrier to electron transfer exists arising from reorganization of outer coordination sphere solvent molecules.

Flash photolysis is an invaluable technique for observing photochemically generated transients and for measuring their rates of reaction. In properly designed chemical systems, flash photolysis can also be used as a kinetic device for obtaining electron transfer rate data which are otherwise inaccessible or difficult to obtain.[1-3] For example, in a solution containing $Ru(bpy)_3^{2+}$ (bpy is 2,2′-bipyridine) and $Fe(H_2O)_6^{3+}$, flash photolysis is followed by rapid quenching of the CT excited state $Ru(bpy)_3^{2+*}$ [4-6] (eq 2 in Scheme I) to give the redox products $Ru(bpy)_3^{3+}$ and $Fe(H_2O)_6^{2+}$. The subsequent back-electron transfer step (eq 3) can be followed directly using conventional flash photolysis.

Scheme I (in water)

$$Ru(bpy)_3^{2+} \xrightarrow{h\nu} Ru(bpy)_3^{2+*} \quad (1)$$

$$Ru(bpy)_3^{2+*} + Fe(H_2O)_6^{3+} \rightarrow Ru(bpy)_3^{3+} + Fe(H_2O)_6^{2+} \quad (2)$$

$$Ru(bpy)_3^{3+} + Fe(H_2O)_6^{2+} \rightarrow Ru(bpy)_3^{2+} + Fe(H_2O)_6^{3+} \quad (3)$$

When used in this way, flash photolysis becomes a relaxation technique (eq 4) in which a reaction at equilibrium is rapidly perturbed by the light absorption–quenching sequence in eq 1 and 2.

$$Ru(bpy)_3^{3+} + Fe(H_2O)_6^{2+} \underset{h\nu}{\overset{\Delta G = -0.52\ V}{\rightleftharpoons}} Ru(bpy)_3^{2+} + Fe(H_2O)_6^{3+} \quad (4)$$

The rates of very rapid reactions can be measured, including the theoretically interesting case of reactions in the "abnormal" free energy region[7-9] where the chemical driving force is large and favorable (e.g., eq 5).[1,3]

The technique can also be applied in more general ways. As shown by the sequence of reactions in Scheme II, by using two different one-electron transfer redox couples, the quenching and back-electron transfer steps can be separated and visible light used to perturb an equilibrium in which both of the reactants are transparent in the visible. The equilibrium-perturbing excited state is not involved in the net reaction.

$$P^+ + Ru(bpy)_3^{3+} \xrightarrow[CH_3CN]{\Delta G = -1.7\ V} P^{2+} + Ru(bpy)_3^{2+} \quad (5)$$

(P^{2+} is paraquat: $H_3C-N^+\bigcirc\!\!\bigcirc-\bigcirc\!\!\bigcirc N^+-CH_3$)

Scheme II (in acetonitrile)

$$Ru(bpy)_3^{2+} \xrightarrow{h\nu} Ru(bpy)_3^{2+*} \quad (6)$$

$$Ru(bpy)_3^{2+*} + P^{2+} \rightarrow Ru(bpy)_3^{3+} + P^+ \quad (7)$$

$$Ru(bpy)_3^{3+} + NPh_3 \rightarrow Ru(bpy)_3^{2+} + NPh_3^+ \quad (8)$$

$$P^{2+} + NPh_3 \underset{h\nu}{\overset{\Delta G = -1.49\ V}{\rightleftharpoons}} P^+ + NPh_3^+ \quad (9)$$

(Ph = phenyl)

The spin-paired, substitution inert polypyridine complexes of iron, ruthenium, and osmium(II) and -(III) have played an important role in testing the Marcus-Hush theory for outer-sphere electron transfer.[10-19] Previous work has shown that net reactions like eq 10 (phen is 1,10-phenanthroline),[20]

$$Ru(bpy)_3^{3+} + Fe(phen)_3^{2+} \xrightarrow{\Delta G = -0.184\ V} Ru(bpy)_3^{2+} + Fe(phen)_3^{3+} \quad (10)$$

and self-exchange reactions like eq 11,[21,22]

$$Ru(bpy)_3^{2+} + Ru'(bpy)_3^{3+} \rightarrow Ru(bpy)_3^{3+} + Ru'(bpy)_3^{2+} \quad (11)$$

are very rapid and difficult to measure using conventional

techniques. The measurement of rates of self-exchange for these systems is especially important given the usefulness of the ions as electron transfer reagents. With properly designed experiments, it should be possible to apply the flash photolysis relaxation technique to both kinds of reactions and we report here the results of such experiments using the net reaction between $Ru(phen)_3^{3+}$ and $Ru(bpy)_3^{2+}$ as a model for the self-exchange process.

Experimental Section

Chemicals. $[Ru(bpy)_3](ClO_4)_2$ and $[Ru(phen)_3](ClO_4)_2$ were prepared and purified as reported previously.[23] $Fe(ClO_4)_3 \cdot 6H_2O$ and $Fe(ClO_4)_2 \cdot 6H_2O$ were purchased from G. F. Smith and Company. Water was deionized and distilled from alkaline $KMnO_4$. Complex concentrations were determined spectrophotometrically using a Bausch and Lomb 210UV spectrophotometer and known molar extinction coefficients.[16,23]

Flash Photolysis Experiments. The flash photolysis apparatus analyzing system consisted of a Xenon Corporation Model G low ripple analyzing lamp, two lenses, a Bausch and Lomb high-intensity UV-visible monochromator, and an EMI 6256 photomultiplier tube. A nonlinear capacitor coupled dynode chain was used on the PM tube with applied potentials from 500 to 650 V and the output was measured by a Tektronix 7514 storage oscilloscope across a 1.0 kΩ load resistor. The risetime of the analyzing system was shorter than 1 μs. The photolysis system was a Xenon Corporation fast extinguishing flash tube FP-10A through which a 2.0 μF capacitor (typically charged to 4 kV) was discharged. Triggering of the flash was accomplished by use of a Xenon Corporation Model C trigger which also reproducibly triggers the oscilloscope sweep with its radio frequency noise. The output of the PM was monitored while the flash was on for each PM potential setting to ensure that the output of the PM was kept well below its maximum current rating (0.5 mA). A set of aluminum tubing light baffles painted flat black enabled PM tube voltages of up to 650 V to be used with scattered light levels insignificant at 1-mm slit widths. These precautions were necessary as the experiment required photolyzing and monitoring in the same wavelength region. UV photolyzing light was filtered out with Corning 3-73 glass filters, ensuring photolysis of only the metal chelate charge transfer bands in the visible region.

Solutions were made up containing $[Ru(bpy)_3](ClO_4)_2$ and $[Ru(phen)_3](ClO_4)_2$, $[Fe(H_2O)_6](ClO_4)_3 \cdot 6H_2O$, and $[Fe(H_2O)_6](ClO_4)_2 \cdot 6H_2O$ in 1.0 M $HClO_4$ for $\mu = 1.0$ M, or 0.076 M $HClO_4$ for $\mu = 0.1$ M. The solutions were degassed through several cycles of freezing, evacuating, and thawing, and then 1.0 atm of N_2 was added. A jacketed 12-cm cell was used for the measurements. The cell was thermostated (±0.1 °C) using a Forma Model 2095 circulator-water bath.

Changes in optical density with time following flash photolysis were recorded from the oscilloscope trace by photography and digitized manually. A computer program was developed to analyze the data according to the kinetic analysis given below.

Treatment of Kinetic Data. After excitation to give the two excited states $Ru(phen)_3^{2+*}$ and $Ru(bpy)_3^{2+*}$ and quenching by $Fe(H_2O)_6^{3+}$, which occurs during the flash, a slight excess of $Ru(phen)_3^{3+}$ is produced. The first event which occurs following the quenching step is the reaction between $Ru(bpy)_3^{2+}$ and $Ru(phen)_3^{3+}$, which leaves the system in a state of transient equilibrium (eq 12)

$$Ru(bpy)_3^{2+} + Ru(phen)_3^{3+} \underset{k_2}{\overset{k_1}{\rightleftharpoons}} Ru(bpy)_3^{3+} + Ru(phen)_3^{2+} \quad (12)$$

followed by the slower back-reactions which involve Fe^{2+} (eq 13 and 14).

$$Ru(bpy)_3^{3+} + Fe^{2+} \xrightarrow{k_3} Ru(bpy)_3^{2+} + Fe^{3+} \quad (13)$$

$$Ru(phen)_3^{3+} + Fe^{2+} \xrightarrow{k_4} Ru(phen)_3^{2+} + Fe^{3+} \quad (14)$$

From reduction potential measurements, for eq 12, $K = k_1/k_2 = 1.0$ and $k_1 = k_2$. Also, from independent studies, $k_3 \sim k_4$,[3,15] and since Fe^{2+} was present in pseudo-first-order excess in the experiments, the first-order rate constants for each of the processes (eq 13) and (eq 14) can be represented as k_3' (= $k_3[Fe^{2+}]$).

If the concentrations at time t of $Ru(bpy)_3^{2+}$ and $Ru(bpy)_3^{3+}$ are represented as B and B^+, and those of $Ru(phen)_3^{2+}$ and $Ru(phen)_3^{3+}$ as P and P^+, respectively, then $dB^+/dt = -k_1B^+P + k_2P^+B - k_3'B^+ = B^+(-k_1P - k_3') + k_1P^+B$. Similarly, $dP^+/dt = -k_1P^+B + k_2B^+P - k_4'P^+ = P^+(-k_1B - k_3') + k_1B^+P$. In terms of the total concentrations (Ru(II) + Ru(III)) of the bpy(C_T^B) and phen(C_T^P) complexes, and since $C_T^B = B + B^+$, $C_T^P = P + P^+$,

$$\frac{dB^+}{dt} = B^+(-k_1C_T^P - k_3') + k_1P^+C_T^B \quad (15)$$

$$\frac{dP^+}{dt} = P^+(-k_1C_T^B - k_3') + k_1B^+C_T^P \quad (16)$$

Equations 15 and 16 represent a linear system of differential equations, which can be solved by the use of the substitutions $B^+ = \text{constant}_1 \times e^{\lambda t}$ and $P^+ = \text{constant}_2 \times e^{\lambda t}$.[24]

The solutions of the resulting equations are $\lambda = -k_3'$ and $\lambda = -k_1(C_T^B + C_T^P) - k_3'$ which gives for the integrated forms of eq 15 and 16:

$$B^+ = C_1e^{-k_3't} + C_2e^{-[k_3' + k_1(C_T^B + C_T^P)]t} \quad (17)$$

$$P^+ = (C_T^P/C_T^B)C_1e^{-k_3't} - C_2e^{-[k_3' + k_1(C_T^B + C_T^P)]t} \quad (18)$$

If ϵ_B, ϵ_{B^+}, ϵ_P, ϵ_{P^+} represent the molar extinction coefficients of the four ions at a given wavelength ($Fe(H_2O)_6^{2+}$ and $Fe(H_2O)_6^{3+}$ are essentially transparent in the visible), then the absorbance A at any time t is given by

$$A = (\epsilon_BB + \epsilon_{B^+}B^+ + \epsilon_PP + \epsilon_{P^+}P^+)l$$

(l = path length), so that

$$A/l = (\epsilon_BC_T^B + \epsilon_PC_T^P) + B^+(\epsilon_{B^+} - \epsilon_B) + P^+(\epsilon_{P^+} - \epsilon_P)$$

or

$$(\epsilon_BC_T^B + \epsilon_PC_T^P) - A/l = B^+(\epsilon_B - \epsilon_{B^+}) + P^+(\epsilon_P - \epsilon_{P^+})$$

Since the factor $(\epsilon_BC_T^B + \epsilon_PC_T^P)l$ represents the absorbance of the reaction at completion (A_∞), the left-hand side of this equation = $(A_\infty - A_t)/l = \Delta A/l$. Substituting for B^+ and P^+ from eq 17 and 18,

$$\frac{\Delta A}{l} = C_1([\epsilon_B - \epsilon_{B^+}] + (C_T^P/C_T^B)[\epsilon_P - \epsilon_{P^+}])e^{-k_3't} + C_2([\epsilon_B - \epsilon_{B^+}] - [\epsilon_P - \epsilon_{P^+}])e^{-[k_3' + k_1(C_T^B + C_T^P)]t} \quad (19)$$

At long t, the second term on the RHS rapidly becomes small so that the reaction is dominated by the first term, i.e.

$$\Delta A \sim lC_1(\Delta\epsilon_B + (C_T^P/C_T^B)\Delta\epsilon_P)e^{-k_3't} \quad (20)$$

whence k_3' can be obtained from plots of ln ΔA vs. t. Furthermore, the contribution to ΔA at small t can be obtained by extrapolation. Consequently, rearranging eq 19 gives,

$$\Delta(\Delta A) = \Delta A - lC_1(\Delta\epsilon_B + (C_T^P/C_T^B)\Delta\epsilon_P)e^{-k_3't} = lC_2(\Delta\epsilon_B - \Delta\epsilon_P)e^{-[k_3' + k_1(C_T^B + C_T^P)]t} \quad (21)$$

so that a plot of ln ($\Delta(\Delta A)$) vs. t at the early part of the reaction should give a first-order plot with slope $k_{obsd} = k_3' + k_1(C_T^B + C_T^P)$. Since k_3' is obtained from the data at long t, and C_T^B and C_T^P are known, k_1 (the rate of electron exchange) can be calculated using the formula in eq 22.

$$k_1 = \frac{k_{obsd} - k_3'}{C_T^B + C_T^P} \quad (22)$$

For the reactions with $Fe(phen)_3^{2+}$ present, following flash photolysis and quenching, reaction 10 occurred followed by reaction 23.

$$Ru(bpy)_3^{3+} + Fe(phen)_3^{2+} \xrightarrow[\Delta G = -0.184\ V]{k_5} Ru(bpy)_3^{2+} + Fe(phen)_3^{3+} \quad (10)$$

$$Fe(phen)_3^{3+} + Fe(H_2O)_6^{2+} \xrightarrow{k_6} Fe(phen)_3^{2+} + Fe(H_2O)_6^{3+} \quad (23)$$

Under conditions where $Fe(phen)_3^{2+}$ and $Fe(H_2O)_6^{2+}$ are present in excess, the kinetic analysis simplifies to the conventional solution for a series of consecutive first-order reactions:

$$[Ru(bpy)_3^{3+}]_t = [Ru(bpy)_3^{3+}]_0e^{-k_5't} \quad (24)$$

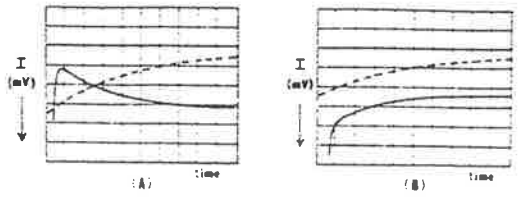

Figure 1. Oscilloscope trace following flash photolysis of a solution containing $Ru(bpy)_3^{2+}$ (3.0×10^{-6} M), $Fe(phen)_3^{2+}$ (2.5×10^{-6} M), $Fe(H_2O)_6^{3+}$ (4.0×10^{-3} M), and $Fe(H_2O)_6^{2+}$ (3.0×10^{-5} M at λ 510 nm (A) and λ 450 nm (B); - - -, 50 μs/div; —, 100 ms/div; $T = 25$ °C; $\mu = 1.0$ M.

and

$$[Fe(phen)_3^{3+}]_t = \frac{[Ru(bpy)_3^{3+}]_0 k_5'}{k_6' - k_5'}(e^{-k_5' t} - e^{-k_6' t}) \quad (25)$$

where $k_5' = k_5[Fe(phen)_3^{2+}]$ and $k_6' = k_6[Fe(H_2O)_6^{2+}]$. Accordingly, k_5' can be directly measured and k_6' calculated, or if $k_5' \gg k_6'$ the two reactions can be observed as independent first-order processes.

Analysis of Kinetic Data. The transmittance data at each wavelength were converted to changes in absorbance (ΔA) and analyzed on a Raytheon 706 computer. The kinetic analysis described above for the $Ru(bpy)_3^{2+} + Ru(phen)_3^{2+}$ system is a closed form equation describing two consecutive first-order reactions. Two important aspects of the rate law enabled analysis of the data to be accomplished without the use of Fourier transformation or the use of a Simplex program. Firstly, the two rate constants are separated into different exponential terms. Secondly, the preexponential factors are the difference and sum of two large numbers. Thus the first term appears as a small perturbation on the second term and the second reaction accounts for virtually all of the changes in absorbance after several half-lives of the first reaction have passed. In order to separate the two reactions as cleanly as possible, the experimental conditions were adjusted such that the rate of the second reaction was two or more orders of magnitude slower than the first. Thus the second reaction could be analyzed with a simple first-order ($\ln \Delta A$ vs. t) plot (eq 20). To analyze the first reaction a theoretical baseline was calculated by extrapolation of absorbance changes due to the second reaction back to time zero. The difference between the theoretical and observed changes in absorbance was analyzed with an $\ln \Delta A$ vs. t plot (eq 21). The rate constant for the first reaction is extremely sensitive to the extrapolated y intercept of the theoretical baseline. An iteration loop was written into the program which adjusted the theoretical baseline to give the best fit as determined by the correlation coefficient of a least-squares routine. In every case the standard deviation of the slope of the best fit was proportionately smaller than any other.

For the $Ru(bpy)_3^{3+} + Fe(phen)_3^{2+}$ system, the basic analysis was the same except that after extrapolation of the slower reaction (k_6') back to zero, the $\ln \Delta A$ vs. t plot of the faster reaction gave the rate constant k_5' directly.

A copy of the computer programs used is available upon request.

Results

Following flash photolysis of a solution containing $Ru(bpy)_3^{2+}$ (3.0×10^{-6} M), $Fe(phen)_3^{2+}$ (2.5×10^{-6} M), $Fe(H_2O)_6^{3+}$ (4.0×10^{-3} M), and $Fe(H_2O)_6^{2+}$ (3.0×10^{-5} M), typical transmittance–time plots at 510 and 450 nm are shown in Figure 1. Quenching of $Ru(bpy)_3^{2+*}$ and formation of redox intermediates occur during the lifetime of the flash. The signal in the first division of the fast scan is due mainly to the scattered light of the flash. At 510 nm, the 50 μs/division trace shows an absorbance decrease due to oxidation of $Fe(phen)_3^{2+}$ to $Fe(phen)_3^{3+}$ (reaction 10). The slower scan (absorbance increase) represents the back-reaction in which $Fe(phen)_3^{2+}$ is regenerated (reaction 23). The same experiment monitored at 450 nm (Figure 1) shows both reactions as absorbance increases, as at this wavelength the fast reaction is observed as mainly $Ru(bpy)_3^{3+}$ being reduced to $Ru(bpy)_3^{2+}$. The $Ru(bpy)_3^{3+}$ and $Fe(phen)_3^{3+}$ complexes are relatively transparent in the visible region. Qualitatively, the difference spectra for both processes in the region between 360 and 540 nm agreed with the difference spectra predicted by reactions 10 and 23. A solution made up without added $Ru(bpy)_3^{2+}$ showed no transient behavior following flash photolysis, indicating that the excited state or states of $Fe(phen)_3^{2+}$ arising from visible photolysis are too short-lived to undergo electron transfer quenching processes under the conditions of the experiment. Rate constants for the two processes obtained by flash photolysis are given in Table I.

Table I. Rate Constant Data for the Reactions between $Ru(bpy)_3^{3+}$ and $Fe(phen)_3^{2+}$ (k_5) and between $Fe(phen)_3^{3+}$ and $Fe(H_2O)_6^{2+}$ (k_6)

T (°C)	μ (M)	$[H^+]$ (M)	k_5[a] (M^{-1} s^{-1})	k_6[a] (M^{-1} s^{-1})
25.0	1.0	1.0	1.8×10^9	5.4×10^4
25.0	0.10	0.076	1.3×10^9	6.4×10^4

[a] Error limit estimated as ±10% from the standard deviation of the least-squares analysis at a 95% probability level.

Flash photolysis of a solution containing initially $Ru(bpy)_3^{2+}$, $Ru(phen)_3^{2+}$, $Fe(H_2O)_6^{3+}$, and $Fe(H_2O)_6^{2+}$ (Figure 2) results in electron transfer quenching of both $Ru(bpy)_3^{2+*}$ and $Ru(phen)_3^{2+*}$. However, at equal initial concentrations of $Ru(bpy)_3^{2+}$ and $Ru(phen)_3^{2+}$, an excess of $Ru(phen)_3^{3+}$ is produced and flash photolysis is followed by reaction 26.

$$Ru(phen)_3^{3+} + Ru(bpy)_3^{2+} \rightarrow Ru(phen)_3^{2+} + Ru(bpy)_3^{3+} \quad (26)$$

which takes the system to equilibrium (eq 12). Reduction potential measurements indicate that formal potentials for the $Ru(bpy)_3^{3+/2+}$ and $Ru(phen)_3^{3+/2+}$ couples are virtually the same (1.30 and 1.31 V vs. NHE at 25 °C)[25,26] so that $K_{eq} = 1.0$ and $k_1 = k_2$. The equilibration reaction is followed by the slower reductions of $Ru(bpy)_3^{3+}$ and $Ru(phen)_3^{3+}$ by $Fe(H_2O)_6^{2+}$, and as mentioned previously $k_3 \sim k_4$ from previous work.[3,15]

$$Ru(bpy)_3^{3+} + Fe(H_2O)_6^{2+} \xrightarrow{k_3} Ru(bpy)_3^{2+} + Fe(H_2O)_6^{3+} \quad (13)$$

$$Ru(phen)_3^{3+} + Fe(H_2O)_6^{2+} \xrightarrow{k_4} Ru(phen)_3^{2+} + Fe(H_2O)_6^{3+} \quad (14)$$

Evidence for the two independent processes is shown in the oscillographic trace in Figure 2.

The data treatment used to obtain k_1 and k_3 from oscillographic traces was presented in a previous section. For ease of calculation, the initial concentrations of $Ru(bpy)_3^{2+}$ and $Ru(phen)_3^{2+}$ were made the same so that after the equilibration reaction the concentrations of $Ru(bpy)_3^{3+}$ and $Ru(phen)_3^{3+}$ were the same. In a typical experiment the concentrations of reagents used were $[Ru(phen)_3^{2+}] = [Ru(bpy)_3^{2+}] = 3.0 \times 10^{-6}$ M, $[Fe(H_2O)_6^{2+}] = 3.0 \times 10^{-5}$ M and $[Fe(H_2O)_6^{3+}] = 4.0 \times 10^{-3}$ M. Rate constant data for both the equilibration reaction k_1 and for the back-electron transfer reactions are given in Table II. The data for the back-electron transfer reactions are in good agreement with the results obtained earlier by flash photolysis and reproduce the unusual feature that the rate constants decrease slightly with an increase in temperature (Table II).[1,3,15]

From the data at $\mu = 0.10$, the activation enthalpy ($\Delta H^{\ddagger}$) for the establishment of the equilibrium (eq 12) was obtained

Table II. Rate Constant Data for the Reaction between $Ru(phen)_3^{3+}$ and $Ru(bpy)_3^{2+}$ (k_1) and for the Reductions of $Ru(bpy)_3^{3+}$ and $Ru(phen)_3^{3+}$ by $Fe(H_2O)_6^{2+}$ (k_3)

T (°C)	μ (M)	$[H^+]$ (M)	k_1[a] (M^{-1} s^{-1})	k_3[b] (M^{-1} s^{-1})
50.0	0.10	0.076	9.6×10^8	1.3×10^6
35.0	0.10	0.076	7.6×10^8	1.4×10^6
25.0	0.10	0.076	4.2×10^8	1.4×10^6
15.0	0.10	0.076	2.0×10^8	1.5×10^6
5.0	0.10	0.076	1.4×10^8	1.5×10^6
25.0	1.0	1.0	1.2×10^9	1.2×10^6

[a] Error limit estimated as ±20% from the standard deviation of the least-squares analysis at a 95% probability level. [b] Estimated error ±10%.

from a plot of $\ln k_1/T$ vs. $1/T$. At each temperature the activation free energy ($\Delta G^{\ddagger}$) and activation entropy ($\Delta S^{\ddagger}$) were calculated. The activation parameters obtained were $\Delta G^{\ddagger}$(25 °C) = 5.7 ± 0.2 kcal/mol, $\Delta H^{\ddagger}$ = 7.7 ± 1.5 kcal/mol, and $\Delta S^{\ddagger}$ = −6.6 ± 0.4 eu. The error limit on $\Delta H^{\ddagger}$ is approximated by the maximum and minimum slopes that could reasonably be assigned in the plots of $\ln (k_1/T)$ vs. $1/T$. The error limit in $\Delta S^{\ddagger}$ indicates the spread of the values of $\Delta S^{\ddagger}$ calculated at all temperatures using the value $\Delta H^{\ddagger}$ = 7.7 kcal/mol.

Discussion

Application of the Flash Photolysis Relaxation Technique. The Use of Differential Excitation Flash Photolysis to Measure Rates of Self-Exchange. As mentioned above, with the proper design of chemical systems, flash photolysis can be used to measure the rates of rapid electron transfer reactions. Two different approaches were exploited here. Using low concentrations of $Ru(bpy)_3^{2+}$ and fairly high quencher concentrations, the diffusion-controlled quenching of $Ru(bpy)_3^{2+*}$ by $Fe(H_2O)_6^{3+}$ (eq 2)

$$Ru(bpy)_3^{2+*} + Fe(H_2O)_6^{3+} \rightarrow Ru(bpy)_3^{3+} + Fe(H_2O)_6^{2+} \quad (2)$$

$$k(25\ °C) = 2.9 \times 10^9\ M^{-1}\ s^{-1}\ [13]$$

occurs during the flash to give the redox products $Fe(H_2O)_6^{2+}$ and $Ru(bpy)_3^{3+}$ in low concentration. For example, with $[Fe(H_2O)_6^{3+}] = 4 \times 10^{-3}$ M the half-time for reaction 2 is 0.06 μs while the duration of the flash in a typical experiment is ~20 to ~30 μs. The back-reaction between $Fe(H_2O)_6^{2+}$ and $Ru(bpy)_3^{3+}$ is slower by a factor of 3000 and occurs on a considerably longer time scale. If $Fe(phen)_3^{2+}$ is added to the solution initially, the more rapid reaction between $Fe(phen)_3^{2+}$ and $Ru(bpy)_3^{3+}$ (eq 10) intervenes

$$Ru(bpy)_3^{3+} + Fe(phen)_3^{2+} \xrightarrow{k_5} Ru(bpy)_3^{2+} + Fe(phen)_3^{3+} \quad (10)$$

and can be followed directly. Reaction 10 goes essentially to completion (K = 1300)[25,26] and is followed by eq 23 which returns the system to equilibrium.

$$Fe(phen)_3^{3+} + Fe(H_2O)_6^{2+} \rightarrow Fe(phen)_3^{2+} + Fe(H_2O)_6^{3+} \quad (23)$$

The value obtained for k_5 in 1.0 M $HClO_4$ (k(25 °C) = 1.8 × 10^9 M^{-1} s^{-1}) is in only fair agreement with the value obtained earlier by Holzwarth and Jurgensen in 1 M H_2SO_4 (3.3 × 10^6 M^{-1} s^{-1}) using a continuous flow method which involved several numerical approximations.[20] The rate of the back-reaction between $Fe(H_2O)_6^{2+}$ and $Fe(phen)_3^{3+}$ is in reasonable agreement with data obtained earlier by stopped-flow techniques.[14]

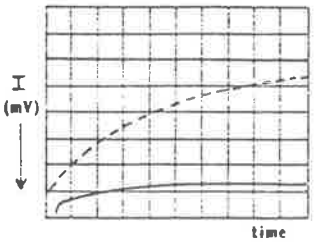

Figure 2. Oscilloscope trace following flash photolysis of a solution containing initially $Ru(bpy)_3^{2+}$ (3.0×10^{-6} M), $Ru(phen)_3^{2+}$ (3.0×10^{-6} M), $Fe(H_2O)_6^{2+}$ (3.0×10^{-5} M), and $Fe(H_2O)_6^{3+}$ (4.0×10^{-3} M) at λ 450 nm: - - -, 100 μs/div; —, 5 ms/div; T = 25 °C; μ = 1.0 M.

It is clear that the flash photolysis relaxation technique can be applied to reactions related to eq 10, where the limitations appear to include that the added reducing agent cannot itself undergo efficient visible photochemistry, and that its rate of reaction with $Ru(bpy)_3^{3+}$ must fall in the same or a shorter time range than the rate of the back-reaction with $Fe(H_2O)_6^{2+}$.

The approach taken for the estimation of the $Ru(bpy)_3^{3+/2+}$ self-exchange rate relied on differences in spectral and excited state properties between the bpy and phen systems. Electrochemical studies on a series of bpy and phen complexes have shown that in complexes which are structurally analogous, Ru(III)/Ru(II) reduction potentials are essentially identical. However, the optical spectra of the bpy and phen complexes are different and so reactions like eq 27 and 28 can be followed directly using stopped-flow techniques. Given the similarities in the bpy and phen ligand systems and the fact that K_{eq} = 1.0, rate constants for reactions like eq 27 and 28 provide a good estimate for rates of the corresponding self-exchange processes for the couples $Ru(bpy)(NH_3)_4^{3+/2+}$, $Ru(phen)(NH_3)_4^{3+/2+}$ and $Ru(bpy)_2(py)Cl^{2+/+}$, $Ru(phen)_2(py)Cl^{2+/+}$.

$$Ru(bpy)(NH_3)_4^{3+} + Ru(phen)(NH_3)_4^{2+} \rightarrow Ru(bpy)(NH_3)_4^{2+} + Ru(phen)(NH_3)_4^{3+} \quad (27)[17]$$

$$Ru(phen)_2(py)Cl^{2+} + Ru(bpy)_2(py)Cl^{+} \rightarrow Ru(phen)_2(py)Cl^{+} + Ru(bpy)_2(py)Cl^{2+} \quad (28)[27]$$

In a solution containing $Ru(bpy)_3^{2+}$, $Ru(phen)_3^{2+}$ and $Fe(H_2O)_6^{3+}$, flash photolysis in the visible gives both $Ru(bpy)_3^{2+*}$ and $Ru(phen)_3^{2+*}$ and both excited states are quenched by $Fe(H_2O)_6^{3+}$ at or near the diffusion-controlled limit.[1,3] However, molar extinction coefficients for $Ru(phen)_3^{2+}$ are greater than for $Ru(bpy)_3^{2+}$ throughout the visible. Following flash photolysis, an excess of $Ru(phen)_3^{2+*}$ over $Ru(bpy)_3^{2+*}$ can be produced when $Ru(phen)_3^{2+}$ and $Ru(bpy)_3^{2+}$ are present in equal amounts because of the higher absorptivity of $Ru(phen)_3^{2+}$. The lifetime of $Ru(phen)_3^{2+*}$ is also slightly greater than the lifetime of $Ru(bpy)_3^{2+*}$ under the conditions used in the experiments (0.8 vs. 0.6 μs).[3] The existence of both effects apparently leads to the production of an excess of $Ru(phen)_3^{3+}$ over $Ru(bpy)_3^{3+}$ following photolysis and quenching. Consequently, differential excitation and quenching leads to a situation where the Ru(III) components of the equilibrium in eq 12 are created rapidly in nonequilibrium amounts. The system then undergoes chemical relaxation to a state of transient equilibrium which is followed by the slower reduction of $Ru(phen)_3^{3+}$ and $Ru(bpy)_3^{3+}$ by $Fe(H_2O)_6^{2+}$. The latter reactions return the system to its initial state of equilibrium. The relaxation step can be followed directly because of the differences in spectral properties between the bpy and phen complexes.

The use of differential excitation flash photolysis which was exploited here should find application in related chemical problems involving rapid electron transfer.

The Self-Exchange Reaction. Earlier NMR[18] and stopped-flow[22] work by Wahl and co-workers has shown that M(II)/M(III) (Fe, Ru, Os) polypyridine self-exchange rates are in the range 3×10^6 to 3×10^7 M^{-1} s^{-1} at 25 °C in non-aqueous solvents like acetonitrile. The rate of the net reaction between $Ru(phen)_3^{3+}$ and $Ru(bpy)_3^{2+}$ in acidic aqueous solution measured by flash photolysis is considerably faster indicating that the self-exchange rates are sensitive to both the nature of the solvent and of added electrolyte which is to be expected. Using the transfer diffusion technique, Ruff and Zimonyi have reported that the self-exchange rate between $Fe(phen)_3^{2+}$ and $Fe(phen)_3^{3+}$ is $(3.3 \pm 1.4) \times 10^8$ M^{-1} s^{-1} at 25 °C in an aqueous solution saturated with Na_2SO_4.[21]

From the results of a series of electron transfer rate measurements by Holzwarth and Jurgensen[20] and from rate constants obtained for excited state quenching reactions,[1,3] a reasonable estimate for the diffusion-controlled limit in 1 M $HClO_4$ at 25 °C for the $Ru(bpy)_3^{2+}$–$Ru(bpy)_3^{3+}$ self-exchange is $k_D \sim 3 \times 10^9$ M^{-1} s^{-1}. Under the same conditions, the experimental value (measured as the net reaction between $Ru(bpy)_3^{2+}$ and $Ru(phen)_3^{3+}$ (eq 26) is 1.2×10^9 M^{-1} s^{-1} which appears to be significantly below the diffusion-controlled limit.

Corrections for diffusion effects can be made using eq 29[28]

$$\frac{1}{k_{obsd}} = \frac{1}{k_D} + \frac{1}{k_{act}} \tag{29}$$

which allows the rate constant for chemically activated electron transfer, k_{act} (the rate constant if diffusion were infinitely rapid), to be estimated. Using eq 29, k_{act} can be estimated to be 2.0×10^9 M^{-1} s^{-1} for the $Ru(bpy)_3^{3+/2+}$ self-exchange reaction.

The rate of the reaction between $Fe(phen)_3^{2+}$ and $Ru(bpy)_3^{3+}$ (k_{12}) can be estimated using the Marcus "cross reaction equation"

$$k_{12} = (k_{11}k_{22}K_{12}f)^{1/2}$$

$$\log f = \frac{(\log K_{12})^2}{4 \log (k_{11}k_{22}/Z^2)}$$

and the activated self-exchange rates for $Ru(bpy)_3^{3+/2+}$ (2.0×10^9 M^{-1} s^{-1}) and $Fe(phen)_3^{3+/2+}$ (3.3×10^8 M^{-1} s^{-1}).[21] Using these values for k_{11} and k_{22}, $K_{12} = 1300$, and assuming that Z, the collision frequency between neutral molecules of the appropriate size in the reaction medium, is 10^{11} M^{-1} s^{-1}, gives $k_{12}(act) = 2.2 \times 10^{10}$. Using this value, $k_D = 3 \times 10^9$ M^{-1} s^{-1}, and eq 29, gives $k_{calcd} = 2.6 \times 10^9$ M^{-1} s^{-1} compared to the experimental value of 1.8×10^9 M^{-1} s^{-1}. Although the discrepancy between the two values is considerable it should be noted that if the actual value for the $Fe(phen)_3^{3+/2+}$ self-exchange under our conditions were 3.3×10^7 M^{-1} s^{-1}, k_{calcd} would be 2.2×10^9 M^{-1} s^{-1} which is nearly within experimental error of the measured value.

From Marcus theory the activation barrier for outer-sphere electron transfer is given by eq 30 where $\Delta G^{\circ}_r{}'$ is the free energy change on electron transfer within the ion-pair of the reactants.

$$\Delta G^* = W_r + \frac{\lambda}{4}\left(1 + \frac{\Delta G^{\circ}_r{}'}{\lambda}\right)^2 \tag{30}$$[29]

In media of high ionic strength, the electrostatic repulsion term w_r is expected to be negligible and for a self-exchange reaction $\Delta G^{\circ}_r{}' = 0$ which gives eq 31.

$$\Delta G^* = \frac{\lambda}{4} \tag{31}$$[29]

The rate constant for reaction is given by

$$k = Z \exp[-(\lambda/4RT)] \tag{32}$$

where Z was defined above and $\lambda/4$ is the reorganizational barrier, which includes contributions from rearrangements in both the inner- and outer-coordination spheres. Using $Z \sim 10^{11}$ M^{-1} s^{-1} [29] and $k = 2 \times 10^9$ M^{-1} s^{-1}, eq 32 gives for the activation barrier for electron transfer, $\lambda/4 = 2.3$ kcal/mol.

Contributions to $\lambda/4$ from inner-sphere reorganization should be negligible. M–N bond distances in $Ru(NH_3)_6^{2+}$ and $Ru(NH_3)_6^{3+}$ are nearly the same.[30] In $Fe(phen)_3^{2+}$ [31a] and $Fe(phen)_3^{3+}$,[31b] they are identical, and differences between $Ru(bpy)_3^{2+}$ and $Ru(bpy)_3^{3+}$ or between $Ru(phen)_3^{2+}$ and $Ru(phen)_3^{3+}$ should be negligible. The activation barrier to electron transfer must arise largely from changes in orientation and polarizability in outer-sphere solvent molecules giving $\lambda/4 \sim \Delta G_0^* \sim 2.3$ kcal/mol.

Using the dielectric continuum models of Hush[32] or Marcus,[29] ΔG_0^* can be estimated using eq 33 in which r_1 and r_2 are the molecular radii of the reacting ions, n^2 and D_s are the optical and static dielectric constants of the solvent, and e is the unit electron charge. For the reaction between $Ru(phen)_3^{3+}$ and $Ru(bpy)_3^{2+}$, using $r_1 = 7.1$ and $r_2 = 6.1$ Å and the values of n^2 and D_s for water, ΔG_0^* is calculated to be 3.5 kcal/mol.

$$\Delta G_0^* = \frac{e^2}{4}\left(\frac{1}{2r_1} + \frac{1}{2r_2} - \frac{1}{d}\right)\left(\frac{1}{n^2} - \frac{1}{D_s}\right) \tag{33}$$

ΔG_0^* has also been estimated to be ~4.0 kcal/mol in water for thermal electron transfer in the slightly smaller mixed-valence ion

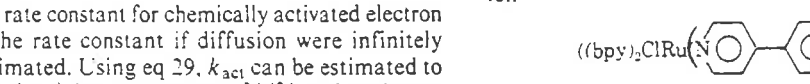

(eq 34) using intervalence transfer measurements.[33]

$$((bpy)_2ClRu^{II}(4,4'\text{-bpy})Ru^{III}Cl(bpy)_2)^{3+} \rightarrow ((bpy)_2ClRu^{III}(4,4'\text{-bpy})Ru^{II}Cl(bpy)_2)^{3+} \tag{34}$$

The slightly lower value for ΔG_0^* calculated from the rate data (eq 32) can be attributed in part to the arbitrariness of using $Z = 10^{11}$. Better agreement would have been obtained if a slightly larger value had been used. However, three different approaches suggest the same conclusion. For the self-exchange reactions there is an activation barrier to electron transfer which arises from outer-sphere reorganization. Because of the large sizes of the reacting ions, the barrier is relatively small and the reactions have rates near the diffusion-controlled limit. If the conclusions reached here are correct, eq 29, 32, and 33 predict that the rates of $Ru(bpy)_3^{3+/2+}$ and $Ru(phen)_3^{3+/2+}$ self-exchange differ from the rate of the reaction between $Ru(phen)_3^{3+}$ and $Ru(bpy)_3^{2+}$ by only a few percent with the $Ru(phen)_3^{3+/2+}$ rate fastest and the $Ru(bpy)_3^{3+/2+}$ rate slowest.

There is considerable interest in electron transfer reactions involving $Ru(bpy)_3^{2+*}$ and related excited states.[1,3,24,35] The conclusions reached here are germane to the reactivity of the excited state and in particular to the excited state self-exchange reaction (eq 35).

$$\underset{(d^5)}{Ru(bpy)_3^{3+}} + \underset{(d^5\pi^*)}{Ru(bpy)_3^{2+*}} \rightarrow \underset{(d^5\pi^*)}{Ru(bpy)_3^{2+*}} + \underset{(d^5)}{Ru(bpy)_3^{3+}} \tag{35}$$

Excited state self-exchange differs from $Ru(bpy)_3^{3+/2+}$ self-exchange in that the exchanging electron and electron hole reside in a series of closely spaced, delocalized π^*(bpy) levels rather than in t_2(Ru) levels.[4,5]

Nonetheless, the outer-sphere reorganizational barrier should be identical for both reactions (eq 33) as should Z (eq 32). In the absence of long-range electron transfer in the excited state self-exchange or of significant structural differences either in Ru–N bonds or in the bpy ligands between $Ru(bpy)_3^{3+}$ and the excited state, the two self-exchange rates should be identical.

Acknowledgments. Acknowledgments are made to the National Science Foundation (Grant CHE74-14405-A02) and to the Materials Research Center of the University of North Carolina under Grant DAHC-04-75-G-0144 with DARPA for support of this research.

References and Notes

(1) C. R. Bock, T. J. Meyer, and D. G. Whitten, *J. Am. Chem. Soc.*, **96**, 4710 (1974).
(2) R. C. Young, T. J. Meyer, and D. G. Whitten, *J. Am. Chem. Soc.*, **97**, 4781 (1975).
(3) P. C. Young, C. R. Bock, T. J. Meyer, and D. G. Whitten, *J. Am. Chem. Soc.*, **98**, 286 (1976); manuscript in preparation.
(4) G. D. Hager and G. A. Crosby, *J. Am. Chem. Soc.*, **97**, 7031 (1975).
(5) G. D. Hager, R. J. Watts, and G. A. Crosby, *J. Am. Chem. Soc.*, **97**, 7037 (1975).
(6) K. W. Hipps and G. A. Crosby, *J. Am. Chem. Soc.*, **97**, 7042 (1975).
(7) R. P. van Duyne and S. F. Fischer, *Chem. Phys.*, **5**, 183 (1974).
(8) S. Efrima and M. Bixon, *Chem. Phys Lett.*, **25**, 34 (1974); W. Schmickler, *J. Chem. Soc. Faraday Trans.*, **72**, 307 (1976).
(9) R. A. Marcus, *J. Chem. Phys.*, **43**, 2654 (1965); **52**, 2803 (1970).
(10) G. Dulz and N. Sutin, *Inorg. Chem.*, **2**, 917 (1963).
(11) J. D. Miller and R. H. Prince, *J. Chem. Soc. A*, 1370 (1966).
(12) B. M. Gordon, L. L. Williams, and N. Sutin, *J. Am. Chem. Soc.*, **83**, 2061 (1961).
(13) M. H. Ford-Smith and N. Sutin, *J. Am. Chem. Soc.*, **83**, 1830 (1961).
(14) N. Sutin and B. M. Gordon, *J. Am. Chem. Soc.*, **83**, 70 (1961).
(15) J. N. Braddock and T. J. Meyer, *J. Am. Chem. Soc.*, **95**, 3158 (1973).
(16) J. L. Cramer and T. J. Meyer, *Inorg. Chem.*, **13**, 1250 (1974).
(17) J. N. Braddock, J. L. Cramer, and T. J. Meyer, *J. Am. Chem. Soc.*, **97**, 1972 (1975).
(18) J. C. Solenberger, Ph.D. Thesis, Washington University, St. Louis, Mo., 1968.
(19) R. A. Marcus and N. Sutin, *Inorg. Chem.*, **14**, 213 (1975).
(20) J. Holzwarth and H. Jurgensen, *Ber. Bunsenges. Phys. Chem.*, **78**, 526 (1974).
(21) I. Ruff and M. Zimonyi, *Electrochim. Acta*, **16**, 515 (1973).
(22) M. Chan and A. C. Wahl, 167th National Meeting of the American Chemical Society, Los Angeles, Calif., April 1974; Inorg. 97.
(23) J. N. Braddock, Ph.D. dissertation, University of North Carolina, Chapel Hill, N.C., 1973.
(24) S. L. Ross, "Differential Equations", Xerox, Lexington, Mass., 1964, pp 230–233.
(25) A. M. Sargeson and D. A. Buckingham, "Chelating Agents and Metal Chelates", F. P. Dwyer and D. P. Mellor, Ed., Academic Press, New York, N.Y., 1964, p 269.
(26) A. A. Schilt, "Analytical Applications of 1, 10-Phenanthroline and Related Compounds", Pergamon Press, New York, N.Y., 1969, p 120.
(27) R. W. Callahan, F. R. Keene, T. J. Meyer, and D. J. Salmon, *J. Am. Chem. Soc.*, **99**, 1064 (1977).
(28) R. M. Noyes, *Prog. React. Kinet.*, **1**, 129 (1961).
(29) R. A. Marcus, *J. Phys. Chem.*, **67**, 853, 2889 (1963); *J. Chem. Phys.*, **43**, 679 (1965).
(30) H. C. Stynes and J. A. Ibers, *Inorg. Chem.*, **10**, 2304 (1971).
(31) (a) A. Zalkin, D. H. Templeton, and T. Ueki, *Inorg. Chem.*, **12**, 1641 (1973); (b) J. Baker, L. M. Engelhardt, B. N. Figgis, and A. H. White, *J. Chem. Soc., Dalton Trans.*, 530 (1975).
(32) N. S. Hush, *Trans. Faraday Soc.*, **57**, 557 (1961).
(33) M. J. Powers, D. J. Salmon, and T. J. Meyer, *J. Am. Chem. Soc.*, **98**, 6731 (1976).
(34) C. T. Lin and N. Sutin, *J. Phys. Chem.*, **80**, 97 (1976).
(35) G. S. Laurence and V. Balzani, *Inorg. Chem.*, **13**, 2976 (1974).

Inorg. Chem. 1986, *25*, 2795–2799

Contribution from the Department of Chemistry, Brookhaven National Laboratory, Upton, New York 11973, and Department of Chemistry and Biochemistry, James Cook University of North Queensland, Townsville, Queensland 4811, Australia

Coordination Mode of Tris(2-pyridyl)carbinol to Cobalt(III): Crystal Structure of $Li[Co\{(2\text{-}py)_3COH\}_2](S_2O_6)_2\cdot 10H_2O$

David J. Szalda*[1] and F. Richard Keene*[2]

Received November 4, 1985

The bis[tris(2-pyridyl)carbinol]cobalt(III) complex was isolated as either of two linkage isomers, dependent on conditions of synthesis. A symmetrical form has all donor atoms being py N (i.e. $((py)_3COH\text{-}N,N',N'')_2$), while the unsymmetrical form has one deprotonated ligand which is coordinated through two py N atoms and the alkoxy O (i.e. $((py)_3COH\text{-}N,N',N'')\text{-}((py)_3CO^-\text{-}N,N',O)$). The X-ray crystal structure of the symmetrical form as $Li[Co\{(2\text{-}py)_3COH\}_2](S_2O_6)_2\cdot 10H_2O$ is reported: the complex of formula $C_{32}H_{46}N_6O_{24}S_4LiCo$ is monoclinic, space group $C2/c$, $\beta = 109.88\ (2)°$, with cell dimensions $a = 19.177\ (6)$ Å, $b = 10.533\ (2)$ Å, $c = 23.390\ (7)$ Å, and $Z = 4$. The cation has the six pyridine N atoms coordinated to the metal center in almost perfect octahedral geometry (Co(III)–N bond distances range between 1.931 (3) and 1.944 (3) Å). Electrochemical studies of this symmetric linkage isomer reveal similarities to the $[Co(bpy)_3]^{n+}$ species, with both the Co(III)/Co(II) and Co(II)/Co(I) redox couples apparent on the cyclic voltammetric time scale.

Introduction

There have been a number of recent reports of the coordination of tripodal ligands in which the three ligating atoms belong to π-acceptor groups, such as N-heterocyclic ring systems. Boggess et al.[3-5] have synthesized first-row transition-metal complexes of the ligands

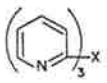

X = CH, COH, P, P=O, As, N

and have studied the spectral and electrochemical properties of these species. Canty et al.[6-8] have used a wide range of ligands of the types XY_3 (where the bridgehead atom X = CH or COH, and Y = 2-pyridyl, 1-pyrazolyl or *N*-methylimidazol-2-yl) to impose unusual coordination geometries on metal centers such as Hg(II) and Au(III).

We have been engaged on a study of the group VIII (groups 8–10[29]) complexes of these ligands, particularly with Ru[9] and Rh.[10] Within this group, reports of the coordination mode of tris(2-pyridyl)carbinol in the bis(ligand)cobalt(III) complex are conflicting. Boggess and Boberg[4] and White and Faller[11] have identified the complex to contain one deprotonated and one nondeprotonated ligand: the deprotonated ligand was considered to have an N,N',O-coordination mode (i.e. two pyridine nitrogen atoms and the deprotonated hydroxyl oxygen atom being the ligating atoms, **1**). The reports differ however as to the nature of the coordination mode of the nondeprotonated ligand, viz. N,N',O[4] or N,N',N'' (**2**).[11] We also synthesized this bis(tridentate) complex as part of our studies and observed a form of the complex whose ^{13}C NMR spectrum was inconsistent with either of the two previous assignments. We report here an X-ray crystal structure of the complex $Li[Co\{(2\text{-}py)_3COH\}_2](S_2O_6)_2\cdot 10H_2O$ in which both ligands show N,N',N''-coordination.

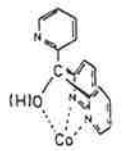

$(py)_3CO(H)$-*N,N',O*
1

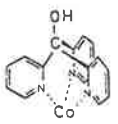

$(py)_3COH$-*N,N',N''*
2

Experimental Section

Physical Measurements. Electronic spectra were recorded with a Cary 219 spectrophotometer, and NMR spectra were obtained in CD_3CN or D_2O solutions by using a Bruker AM-300 NMR spectrometer, with *p*-dioxane ($\delta = 66.5$) as an internal standard.

All electrochemical measurements were made in acetonitrile/0.1 M tetraethylammonium perchlorate (TEAP) solution vs. an Ag/AgCl (3 M NaCl) reference electrode by using a Bioanalytical Systems Inc. (BAS) CV-27 voltammograph.

Elemental microanalyses were carried out by the Canadian Microanalytical Service, Vancouver, Canada.

Syntheses. Tris(2-pyridyl)carbinol, $(2\text{-py})_3COH$, was prepared from bis(2-pyridyl)ketone and 2-lithiopyridine as detailed previously[11,12] in 48%

(1) Brookhaven National Laboratory. Permanent address: Baruch College, New York, NY.
(2) James Cook University of North Queensland. On an approved Special Studies Program at Brookhaven National Laboratory.
(3) Boggess, R. K.; Zatko, D. A. *Inorg. Chem.* **1976**, *15*, 626–630.
(4) Boggess, R. K.; Boberg, S. J. *J. Inorg. Nucl. Chem.* **1980**, *42*, 21–26.
(5) Boggess, R. K.; Hughes, J. W.; Chew, C. W.; Kemper, J. J. *J. Inorg. Nucl. Chem.* **1981**, *43*, 939–945.
(6) Canty, A. J.; Chaichit, N.; Gatehouse, B. M.; George, E. E.; Hayhurst, G. *Inorg. Chem.* **1981**, *20*, 2414–2422.
(7) Canty, A. J.; Minchin, N. J.; Healy, P. C.; White, A. H. *J. Chem. Soc., Dalton Trans.* **1982**, 1795–1802.
(8) Canty, A. J.; Chaichit, N.; Gatehouse, B. M.; George, E. E. *Inorg. Chem.* **1981**, *20*, 4293–4300.
(9) Keene, F. R.; Szalda, D. J.; Wilson, T. A., unpublished work.
(10) (a) Keene, F. R., unpublished work. (b) Keene, F. R.; Hafeli, T. A., work in progress.
(11) White, D. L.; Faller, J. W. *Inorg. Chem.* **1982**, *21*, 3119–3122.

0020-1669/86/1325-2795$01.50/0

Table I. Experimental Details of the X-ray Diffraction Study of $Li[Co\{(C_5H_4N)_3COH\}_2](S_2O_6)_2 \cdot 10H_2O$

(A) Crystal Parameters[a] at 21 °C			
a, Å	19.177 (6)	Z	4
b, Å	10.533 (2)	M_r	1092.85
c, Å	23.390 (7)	space group	$C2/c$
β, deg	109.88 (2)	ρ(exptl),[b] g cm^{-3}	1.63 (1)
V, Å^3	4443 (3)	ρ(calcd), g cm^{-3}	1.634

(B) Measurement of Intensity Data

instrument	Enraf-Nonius Cad-4 diffractometer
radiation	Mo Kα (0.7093 Å) graphite-monochromatized
2θ limits, deg	1–55
scan type	θ(cryst)–2θ(counter)
stds	3 reflcns, (3̄14), (4̄42), and (3̄1̄8), measd after each 1 h of exposure time, showing variations of less than ±3.5% from the av value

(C) Treatment of Intensity Data[c]

reden to prelim F_o and $\sigma(F_o)$	cor for bkgd attenuators, and Lorentz–polarization effects of monochromated X-radiation in the usual manner,[c] with extinction effects not obsd in the data
abs cor[d]	μ = 6.83 cm^{-1}; max and min transmission coeff 0.8470 and 0.7730, respectively
no. of obsd data	5488 reflcns collcd; 3587 having $F_o > 3\sigma(F_o)$ used in the refinement

[a] From a least-squares fit to the settings angles of 25 reflections with $2\theta > 20°$. [b] In carbon tetrachloride and bromoform. [c] Data reduction and corrections performed by using the program KAPPA, part of the CRYSNET system at Brookhaven National Laboratory. [d] Absorption correction computed by using ABSOR, part of the CRYSNET system at Brookhaven National Laboratory.

yield; mp 127 °C (lit.[12] 127–128 °C).

Preparation of the Bis[tris(2-pyridyl)carbinol]cobalt(III) Complex. Method A. The complex was prepared as the perchlorate salt in 1:1 ethanol/dimethoxyethane as detailed previously.[4] Recrystallization was achieved by stirring a suspension of perchlorate salt in water with Dowex 1-X2 resin (Cl^- form), filtering, and precipitating with $NaClO_4$. The resultant orange complex was washed with ice-cold water and ethanol and air-dried. Yield: 80%. Anal. Calcd for $[Co\{(C_5H_4N)_3COH\}\{(C_5H_4N)_3CO^-\}](ClO_4)_2 \cdot 2H_2O$: C, 46.9; H, 3.56; N, 10.26. Found: C, 47.0; H, 3.42; N, 10.15.

The PF_6^- salt could also be obtained by precipitation with NH_4PF_6 rather than $NaClO_4$, in which case the product was washed with ice-cold water and 2-propanol.

Method B. Tris(2-pyridyl)carbinol (200 mg, 0.76 mmol) in methanol (3 mL) was added to a solution of $CoCl_2 \cdot 6H_2O$ (100 mg, 42 mmol) in water (3 mL). The solution was refluxed for 15 min and cooled, and the cation was precipitated as the PF_6^- salt by the addition of NH_4PF_6. The filtered solid was washed with cold water. The products obtained by this method contained variable mixtures of the Co(II) and Co(III) species and were sometimes a mixture of linkage isomers. Isomeric purity was obtained by refluxing the product in aqueous solution over activated charcoal (as detailed below). Recrystallization was then achieved by using techniques detailed in method A. Anal. Calcd for $[Co\{(C_5H_4N)_3COH\}_2](ClO_4)_3 \cdot 2H_2O$: C, 41.8; H, 3.29; N, 9.14. Found: C, 41.6; H, 3.31; N, 9.04.

Charcoal-Catalyzed Isomerizations of the Linkage Isomers of $[Co\{(2\text{-}py)_3COH\}_2]^{3+}$. Aqueous solutions of the complexes obtained in syntheses A and B were refluxed for 18 h in the presence of activated charcoal. The solutions were then cooled and filtered, and the products were precipitated by the addition of NH_4PF_6.

Structure Determination of $Li[Co\{(2\text{-}py)_3COH\}_2](S_2O_6)_2 \cdot 10H_2O$. Collection and Reduction of X-ray Data. Crystals of the bis[tris(2-pyridyl)carbinol]cobalt(III) dithionate complex were prepared by mixing $CoCl_2 \cdot 6H_2O$ (0.024 g; 0.1 mmol) and the ligand (0.053 g; 0.2 mmol) in distilled water (3 mL). The solution was filtered, and a solution of $Li_2S_2O_6$ (0.2 g) in ethanol (10 ml) was added without stirring. After the mixture was allowed to stand for several days, crystals formed at the diffusion layer. This compound crystallized as transparent orange prisms, which exhibited $2/m$ Laue symmetry and systematic absences hkl ($h + k = 2n + 1$) and $h0l$ ($l = 2n + 1$) consistent with the monoclinic space groups Cc (No. 9, C_s^3)[13a] and $C2/c$ (No. 15, C_{2h}^6).[13b]

Table II. Atomic Coordinates for $Li[Co\{(C_5H_4N)_3COH\}_2](S_2O_6)_2 \cdot 10H_2O$[a,b]

atom	x	y	z
Co	0.0000	0.5000	0.0000
N(1)	0.08473 (16)	0.5018 (3)	0.07457 (13)
C(12)	0.1531 (2)	0.5197 (3)	0.07177 (17)
C(13)	0.2144 (2)	0.5253 (4)	0.12365 (19)
C(14)	0.2069 (2)	0.5110 (5)	0.18090 (19)
C(15)	0.1367 (3)	0.4935 (4)	0.18287 (18)
C(16)	0.0770 (2)	0.4891 (4)	0.12992 (17)
N(2)	0.05382 (16)	0.3871 (3)	−0.03598 (13)
C(22)	0.1263 (2)	0.4102 (4)	−0.02691 (16)
C(23)	0.1681 (2)	0.3308 (4)	−0.04900 (18)
C(24)	0.1347 (3)	0.2274 (4)	−0.0828 (2)
C(25)	0.0606 (3)	0.2031 (4)	−0.0931 (2)
C(26)	0.0222 (2)	0.2830 (4)	−0.06867 (19)
N3	0.04061 (16)	0.6447 (3)	−0.02852 (13)
C(32)	0.1127 (2)	0.6448 (4)	−0.02296 (16)
C(33)	0.1434 (2)	0.7441 (4)	−0.04469 (18)
C(34)	0.0997 (2)	0.8463 (4)	−0.0714 (2)
C(35)	0.0261 (2)	0.8467 (4)	−0.0760 (2)
C(36)	−0.0018 (2)	0.7454 (4)	−0.05455 (18)
O(10)	0.23350 (14)	0.5442 (3)	0.01678 (12)
C(10)	0.15807 (19)	0.5305 (4)	0.00888 (18)
S(1)	0.19851 (6)	−0.12560 (13)	0.64092 (6)
O(11)	0.1775 (2)	−0.1945 (4)	0.58444 (17)
O(12)	0.27639 (19)	−0.1348 (4)	0.67738 (17)
O(13)	0.1497 (2)	−0.1444 (4)	0.67584 (16)
S(2)	0.18606 (9)	0.06826 (14)	0.61619 (7)
O(21)	0.2079 (3)	0.1356 (4)	0.6741 (2)
O(22)	0.1101 (3)	0.0862 (5)	0.5791 (2)
O(23)	0.2390 (3)	0.0867 (4)	0.58547 (17)
O(1)	0.3771 (2)	0.2901 (4)	0.25714 (18)
O(2)	0.0752 (4)	−0.0012 (5)	0.7842 (4)
O(3)	0.0837 (3)	0.5200 (4)	−0.1653 (2)
O(4)	0.0036 (6)	−0.2743 (11)	0.7189 (4)
O(5)	0.0000	0.3437 (6)	−0.2500
O(6)	0.3570 (7)	−0.2729 (13)	0.2195 (5)
O(7)	0.1648 (7)	−0.2652 (13)	0.8038 (5)
Li	0.1050 (16)	−0.181 (2)	0.7405 (12)

[a] Numbers in parentheses are errors in the significant digit(s). [b] The site occupancy factor for O(4), O(5), O(6), O(7), and Li is 0.5.

A crystal (0.266 × 0.400 × 0.500 mm^3) mounted in a Lindemann glass capillary was used for data collection. The reflections in the $h,k,\pm l$ octants with $h + k = 2n$ were collected. Crystal data and details of the data collection and reduction are given in Table I.

Determination and Refinement of the Structure. The coordinates of the cobalt atom were determined from a Patterson map,[14] while the other atoms were located on subsequent difference Fourier maps. Space group Cc was assumed for the solution of the structure, but after all the atoms were located $\bar{1}$ symmetry was observed in the complex and between the anions and solvent molecules, so that the space group was changed to $C2/c$ for the refinement of the structure.

Anisotropic temperature factors were used for all non-hydrogen atoms. The location of the hydrogen atoms on the ligand were calculated (C–H bond length = 0.95 Å). These hydrogen atoms were allowed to "ride"[14] on the atom to which they were attached. The hydrogen atoms on the ordered oxygen atoms were located on a difference Fourier map and fixed at these positions. A common isotropic temperature factor for all the hydrogen atoms refined to U = 0.062 (3) Å^2. The hydrogen atoms attached to oxygen atoms that were disordered (occupancy factor less than 1) were not included in the refinement.

The quantity $\sum w(|F_o| - |F_c|)^2$, where $w = 1.6085/(\sigma(F_o)^2 + 0.000563F_o^2)$, was minimized in the least-squares refinement.[15] During the final cycle of refinement the largest parameter shift was less than 0.01

(12) Wibaut, J. P.; de Jonge, A. P.; Van der Voort, H. G. P.; Otto, P. Ph. H. L. *Recl. Trav. Chim. Pays-Bas* **1951**, *70*, 1054–1060.

(13) *International Tables for X-ray Crystallography*, 3rd ed.; Kynoch: Birmingham, U.K., 1969; Vol. 1: (a) p 89; (b) p 101.

(14) Except where otherwise noted, all calculations were performed by using SHELX-76: Sheldrick, G. M. In *Computing in Crystallography*; Schenk, H., Olthof-Hazekamp, R., van Koningsveld, H., Bassi, G. C., Eds.; Delft University: Delft, Holland, 1978; pp 34–42.

(15) (a) Neutral-atom scattering factors were used in the least squares refinement: taken from: *International Tables for X-ray Crystallography*; Kynoch: Birmingham, U.K., 1974; Vol. 1, p 99. (b) Anomalous dispersion effects used in the least-squares refinement were included for all non-hydrogen atoms and were taken from: Cromer, D. T.; Liberman, D. *J. Chem. Phys.* **1970**, *53*, 1891–1898.

Table III. Bond Distances (Å) and Angles (deg) for $Li[Co\{(C_5H_4N)_3COH\}_2](S_2O_6)_2\cdot 10H_2O$

	Cobalt–Ligand Distances		
Co–N(1)	1.938 (3)	Co–N(3)	1.931 (3)
Co–N(2)	1.944 (3)		
	Cobalt–Ligand Angles		
N(1)–Co–N(2)	89.4 (1)	N(2)–Co–N(3)	89.8 (1)
N(1)–Co–N(3)	89.4 (1)	N(2)–Co–N(2′)	180.0 (1)
N(1)–Co–N(1′)	180.0 (1)	N(2)–Co–N(3′)	90.2 (1)
N(1)–Co–N(2′)	90.7 (1)	N(3)–Co–N(3′)	180.0 (1)
N(1)–Co–N(3′)	90.6 (1)		

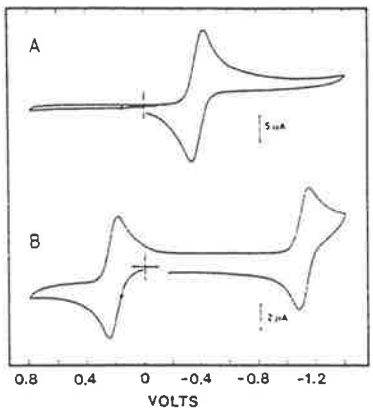

Figure 1. Cyclic voltammograms of the linkage isomers of the $[Co\{(2\text{-}py)_3COH\}_2]^{n+}$ cation in acetonitrile/0.1 M TEAP:[17] (A) unsymmetric form; (B) symmetric form. Scan rate = 100 mV/s.

of its error. The final R_1 value[16a] was 0.055, while the weighted discrepancy index R_2[16] was 0.068. The final difference Fourier map revealed a peak of 0.75 $e^-/Å^3$ near (~0.5 Å) an oxygen atom (O(2)), indicating some positional disorder, while the remaining peaks were all less than ±0.5 $e^-/Å^3$.

The non-hydrogen atomic coordinates are reported in Table II, and the Co–N distances and N–Co–N angles with their standard deviations are listed in Table III. The thermal parameters for the non-hydrogen atoms, the positional parameters for the hydrogen atoms, the interatomic distances and angles for the ligand/anions/lithium coordination sphere, the final observed and calculated structure factors, the hydrogen bonding interactions, and least-squares planes for the pyridine rings are all available as supplementary material.

Results and Discussion

Synthesis and Characterization of Linkage Isomers of the Bis[tris(2-pyridyl)carbinol]cobalt(III) Cation. Synthesis of the title cation in ethanol/dimethoxyethane using the method of Boggess and Boberg[4] yielded the Co(III) species $[Co\{(py)_3COH\}\{(py)_3CO^-\}](ClO_4)_2$. The electronic spectrum in acetonitrile showed absorption maxima at λ = 387 nm (ϵ = 340 M^{-1} cm^{-1}) and 463 nm (ϵ = 84 M^{-1} cm^{-1}). Cyclic voltammetry[17] of the complex in acetonitrile (Figure 1A) showed a quasi-reversible redox couple at $E_{1/2}$ = −0.38 V (ΔE_p = 80 mV), attributed to Co(III)/Co(II). Coulometry under inert conditions (argon) on the diffusion plateau of the reduction wave led to $n \sim 1$, however extensive decomposition of the complex occurred.

The ^{13}C NMR spectrum (75 MHz) of this Co(III) species in CD_3CN is shown in Figure 2A. Nineteen resonances are observed in the aromatic region, and the two resonances at δ = 93.1 and 83.2 associated with the aliphatic bridging carbon atoms demonstrate that the two $(2\text{-}py)_3COH$ tripod ligands are in different environments. These data are consistent with either an asymmetric bis(N,N′,O) form of the cation (the symmetric form of this coordination mode would show no more than 15 pyridine C resonances) or the (N,N′,N″)(N,N′,O) species. The magnitude of the separation of the chemical shifts for the two bridging carbon atoms favors the latter assignment, as determined by White and Faller.[11]

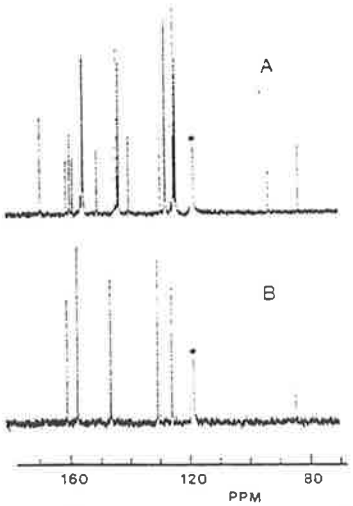

Figure 2. 75-MHz ^{13}C NMR spectra of the linkage isomers of the bis[tris(2-pyridyl)carbinol]cobalt(III) cation in CD_3CN: (A) unsymmetric form; (B) symmetric form. An asterisk indicates resonance due to solvent.

Syntheses of the complex in aqueous solution yielded products of varying composition: the species identified above is one (generally minor) component. However, an additional major product was obtained which had the following characteristics. The cyclic voltammetry[17] is shown in Figure 1B: there is a reversible one-electron couple at $E_{1/2}$ = +0.22 V and a quasi-reversible couple at $E_{1/2}$ = −1.13 V (ΔE_p = 70 mV), which are assigned to Co(III)/Co(II) and Co(II)/Co(I), respectively. Using spectrocoulometric techniques, the electronic spectrum of the Co(III) form shows ϵ_{445}^{max} = 73 M^{-1} cm^{-1} in acetonitrile solution, with the Co(II) species having ϵ_{381}^{max} = 2100 M^{-1} cm^{-1}. The variable ratio of D_{381}/D_{345} for different syntheses indicates Co(II)/Co(III) variation for individual preparations and reflects some sensitivity of the Co(II) species to oxygen. Solutions of the Co(II) species oxidize to Co(III) over a period of days.

Coulometry under inert conditions (argon) of the pink Co(II) complex in acetonitrile solution was undertaken at −1.20 V at +25 and −10 °C, and also in the presence of a tenfold excess of the ligand at both temperatures. In all cases, a rapid formation of a bright blue species was observed up to n = 0.5–1.0, whereupon the solution reverted to a pink color with the gradual formation of a fine pink precipitate as n approached ca. 2. The initial blue color was more sustained at lower complex concentrations. These data are consistent with the initial formation of the Co(I) species on reduction (which might be expected to be deep blue in color by analogy with $Co(bpy)_3^{+}$[18]), and it seems likely that it is the Co(II)/Co(I) couple that is observed at $E_{1/2}$ = −1.13 V on the CV time scale. However, in the coulometry experiment, as the concentration of Co(I) builds up, it undergoes decomposition (presumably via a disproportionation process) to unknown products.

(16) (a) $R_1 = \sum(||F_o| - |F_c||)/\sum|F_o|$; $R_2 = [\sum w(|F_o| - |F_c|)^2/\sum w(F_o)^2]^{1/2}$. (b) $\sigma_{av} = \sum_m(I_m - \bar{I})^2/(m - l)^{1/2}$.

(17) All cyclic voltammetry data were recorded by using a glassy-carbon working electrode and are quoted vs. a Ag/AlCl (3 M NaCl) reference electrode (which is 35 mV anodic of the saturated sodium chloride calomel electrode, SSCE). All coulometric measurements were performed by using a Pt-gauze working electrode.

(18) (a) Waind, G. M.; Martin, B. *J. Inorg. Nucl. Chem.* **1958**, *8*, 551–556. (b) Kaizu, Y.; Torii, Y.; Kobayashi, H. *Bull. Chem. Soc. Jpn.* **1970**, *43*, 3296–3297. (c) Willett, B. C.; Anson, F. C. *J. Electrochem. Soc.* **1982**, *129*, 1260–1266. (d) Keene, F. R.; Creutz, C.; Sutin, N., unpublished work.

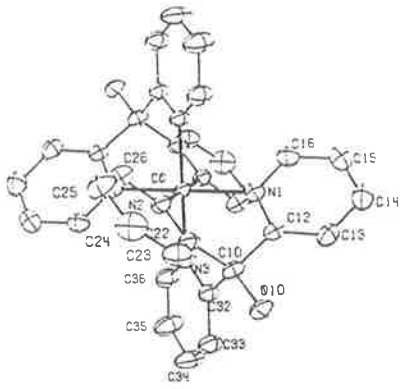

Figure 3. ORTEP drawing of the $[Co\{(C_5H_4N)_3COH\}_2]^{3+}$ cation, with thermal ellipsoids at 50% probability level. The atom-numbering scheme is shown. Hydrogen atoms are omitted for clarity.

The ^{13}C NMR spectrum of the Co(III) complex shows five resonances in the aromatic region, and one bridgehead carbon environment (δ = 84.2). This is consistent only with a stereochemistry in which all pyridine rings are equivalent (i.e. point group symmetry D_{3d}) so that the coordination mode of both ligands is necessarily N,N′,N″.

Quite clearly there are two linkage isomers for this cation, and the X-ray structural analysis of the bis(N,N′,N″) form is detailed below.

Isomerization of Linkage Isomers. Isomers of Co(III) complexes may be equilibrated in the presence of activated charcoal.[19] In this instance, after being refluxed for 18 h in aqueous solution, the symmetrical isomer is observed to be the more stable form, as the unsymmetrical isomer will isomerize almost quantitatively to it under these conditions. Such methods constitute the most satisfactory way of obtaining the isomerically pure symmetric Co(III) complex.

Description of the Structure. A view of the $[Co\{(C_5H_4N)_3COH\}_2]^{3+}$ cation and the atom-labeling scheme used are presented in Figure 3. The cobalt atom lies on a center of inversion at (0, $^1/_2$, 0), and the two tridentate ligands attached to it are related to each other by this center of inversion. The six nitrogens coordinated to the cobalt are arranged in an almost perfect octahedral geometry with the Co–N bond distances ranging from 1.931 (3) to 1.944 (3) Å, and all the N–Co–N bond angles (both intra- and interligand) are within 0.7° of either 90 or 180° (Table III). These bond lengths are normal for a Co(III)–N bond, where N is part of a pyridine ring.[20-22]

The bond lengths and angles within the ligand are normal, with the average[16b] intrapyridine C–C bond length being 1.375 (10) Å and C–N bond length being 1.325 (5) Å,[20,23,24] and with an average C–COH bond length of 1.520 (9) Å.[8]

The average S–O distance in the $S_2O_6^{2-}$ anions is 1.445 (9) Å with an S–S distance of 2.114 (2) Å.

The lithium ion has an approximately tetrahedral coordination sphere of oxygen atoms, as expected,[25] with Li–O distances ranging between 1.77 (3) and 2.31 (2) Å and O–Li–O bond angles ranging between 98° and 121° with an average value of 109 (8)°.

Crystal Packing. The crystal is held together by a network of hydrogen bonds involving the alcohol group on the ligands, the dithionate anions, and the waters of crystallization. Each cation is surrounded by six dithionate ions. The four dithionate ions closest to the Co(III) center form two sets related by a center of inversion, with the shortest Co–S distances in the sets being 5.69 and 5.85 Å. These ion–ion interactions also help stabilize the crystal. In addition, there are two $S_2O_6^{2-}$ anions which are hydrogen bonded to the cation through the alcohol group of each ligand.

Comparisons with Other Structures. Structures of FeL_2^{2+} [23] and CoL_2^{2+},[24] where L = tris(2-pyridyl)amine, are known, and the ligand is found to be coordinated to the metal atom in a tridentate manner through the three pyridyl nitrogen atoms. The two complexes each contain a center of inversion about the metal center. The immediate ligand environment in the Fe(II) complex[23] is the more octahedral (average intraligand N–Fe–N angle = 88.1°, compared with 85.6° for N–Co(II)–N in CoL_2^{2+} [24]). In the present structure of the bis[tris(2-pyridyl)carbinol]cobalt(III) cation, both ligands are also coordinated through the three pyridyl nitrogen atoms, and the ligand environment is almost perfectly octahedral (average intraligand N–Co(III)–N angle = 89.5°). This may be the result of two factors: the decrease in the metal–nitrogen bond length from 2.100 (2) – 2.152 (2) Å in CoL_2^{2+} [23] to 1.98 (2) Å in FeL_2^{2+} [24] to 1.938 Å in the present case and the longer pyridine–bridging atom bond length (1.528 (9) Å) compared with 1.44 (1) Å for the tris(2-pyridyl)amine species.

Tris(2-pyridyl)methane has also been assigned a tridentate coordination mode in the bis(ligand) complexes of Co(II) and Co(III) from NMR studies.[11]

While tris(2-pyridyl)amine and tris(2-pyridyl)methane may only coordinate through the pyridyl nitrogen atoms, the coordination mode of tris(2-pyridyl)carbinol as a tridentate is ambiguous since it may also coordinate via the alcohol group. Canty et al.[8] have reported structural studies of a methylmercury(II) complex containing tris(2-pyridyl)carbinol. In this case, the coordination mode of the tripodal ligand is tridentate with binding occurring through the three pyridyl nitrogen atoms, although the geometry is somewhat distorted with one Hg–N bond being significantly shorter than the other two. No structures of octahedral complexes of this ligand have been described in detail, although White and Faller have given preliminary results of a structural determination of the title complex in a footnote to ref 11. In previous discussions of the bis[tris(2-pyridyl)carbinol]cobalt(III) ion, Boggess and Boberg[4] have claimed from spectroscopic studies (IR, electronic) that both tris(2-pyridyl)carbinol ligands coordinate to Co(III) in an N,N′,O fashion with one of the two coordinated alcohol groups being deprotonated, while White and Faller[11,26] subsequently determined one $(py)_3CO^-$-*N,N′,O* ligand and one $(py)_3COH$-*N,N′,N″* from their structure. It seems probable from the present work that the products observed in these two previous studies were the same, and that it does have (N,N′,N″)(N,N′,O)-coordination.[27] However, the present work has also identified and characterized a new symmetrical bis(N,N′,N″) linkage isomer of the title complex.

It is noted that the (N,N′,N″)(N,N′,O)-coordination mode is observed for this ligand in the bis(ligand)ruthenium(II) analogue, details of which will be published subsequently.[9]

Electrochemistry of the $[Co\{(2\text{-py})_3COH\}_2]^{n+}$ Cation. Earlier electrochemical studies[3] of bis(ligand)cobalt(II) complexes of $(2\text{-py})_3X$ (X = N, P, P=O, As) have shown that reduction produces a stable Co(I) species when X = P, P=O, or As, whereas for X = N a direct reduction from Co(II) to metallic Co(0) occurs. Since X is capable of $d\pi$–$p\pi$ bonding in the former cases, delocalization through the ligand is possible, and their electrochemical behavior was concluded[3] to be similar to that of $Co(bpy)_3^{n+}$, with the low-valent Co(I) species being stabilized by $t_{2g} \rightarrow \pi^*$ backbonding. The relative instability of the Co(I) complex for X = N was therefore claimed to be due to the inability of the

(19) (a) Dwyer, F. P. In *Advances in the Chemistry of Coordination Compounds*; Kirschner, S., Ed.; Macmillan: New York, 1961; p 21. (b) Keene, F. R.; Searle, G. H. *Inorg. Chem.* **1974**, *13*, 2174–2180.
(20) Yanagi, K.; Ohashi, Y.; Sasada, Y.; Kaizu, Y.; Kobayashi, H. *Bull. Chem. Soc. Jpn.* **1981**, *54*, 118–126.
(21) Brunschwig, B. S.; Creutz, C.; Macartney, D. H.; Sham, T. K.; Sutin, N. *Discuss. Faraday Soc.* **1982**, *74*, 113–127.
(22) Figgis, B. N.; Kucharski, E. S.; White, A. H. *Aust. J. Chem.* **1983**, *36*, 1563–1571.
(23) Kucharski, E. S.; McWhinnie, W. R.; White, A. H. *Aust. J. Chem.* **1978**, *31*, 53–56.
(24) Kucharski, E. S.; McWhinnie, W. R.; White, A. H. *Aust. J. Chem.* **1978**, *31*, 2647–2650.
(25) Dollase, W. A. *Acta Crystallogr., Sect. B: Struct. Crystallogr. Cryst. Chem.* **1969**, *B25*, 2298–2302.
(26) Faller, J. W., personal communication to F. R. Keene.
(27) Boggess, R. K.; Heltzel, C. E. *Inorg. Chem.* **1985**, *24*, 2947–2950.

bridgehead atom to allow extensive delocalization.

However, the present study shows that for the analogous complexes where the bridgehead atom is carbon (i.e. X = COH in the title complex, and X = CH[10]) the cyclic voltammetric behavior parallels that of $Co(bpy)_3^{n+}$ and not $Co[(2\text{-}py)_3N]_2^{n+}$. Furthermore, there is evidence from the coulometric studies reported above for the transient existance of the $[Co[(2\text{-}py)_3COH]_2]^+$, and the $[Co[(2\text{-}py)_3CH]_2]^+$ complex can be synthesized by sodium amalgam reduction of the Co(II) species and shows reasonable stability (several days) under inert conditions.[10a] Since delocalization via $d\pi-p\pi$ bonding would not be anticipated in either of these ligands, the above observations argue against the necessity of extensive delocalization via the bridging atom to allow stabilization of the low-valent Co(I) species, unless there is a spatial electronic interaction between pyridine rings in these tripodal ligands.[28]

Further studies of the Co(I) and Rh(I) complexes of a number of these tripodal ligands are in progress[10b] and will be reported subsequently.

Acknowledgment. This research was performed partly at Brookhaven National Laboratory (which is operated under Contract No. DE-AC02-76CH00016 with the Department of Energy and supported in part by its Office of Basic Energy Sciences) and partly at James Cook University of North Queensland (where it was supported by the Australian Research Grants Scheme). D.J.S. thanks Baruch College for released time to do this research, and F.R.K. acknowledges the Australian-American Educational Foundation for assistance through a Fulbright Award while on a Special Studies Program at Brookhaven National Laboratory. The contribution of Tracy Wilson (an undergraduate student at James Cook University) to aspects of the solvent dependence of linkage isomer formation is also acknowledged.

Registry No. $[Co[(2\text{-}py)_3COH][(2\text{-}py)_3CO^-]](ClO_4)_2$, 73580-28-6; $[Co[(2\text{-}py)_3COH]_2](ClO_4)_3$, 102630-75-1; $Li[Co[(2\text{-}py)_3COH]_2](S_2O_6)_2 \cdot 10H_2O$, 102630-77-3.

Supplementary Material Available: Tables of thermal parameters for the non-hydrogen atoms, positional parameters for the hydrogen atoms, interatomic distances and angles for the ligand, the anions, and the lithium coordination sphere, hydrogen bonding interactions, and least-squares planes (9 pages). Ordering information is given on any current masthead page.

(28) In this case, the complex of tris(2-pyridyl)amine may be the exception because of ligand distortion induced by the relative shortness of the bridgehead (N)–pyridine bonds.

(29) The periodic group notation in parentheses is in accord with recent actions by IUPAC and ACS nomenclature committees. A and B notation is eliminated because of wide confusion. Groups IA and IIA become groups 1 and 2. The d-transition elements comprise groups 3 through 12, and the p-block elements comprise groups 13 through 18. (note that the former Roman number designation is preserved in the last digit of the new numbering: e.g., III → 3 and 13).

Inorg. Chem. 1987, *26*, 2211–2216

Contribution from the Department of Chemistry and Biochemistry, James Cook University of North Queensland, Townsville, Queensland 4811, Australia, and Department of Chemistry, Brookhaven National Laboratory, Upton, New York 11973

Mode of Coordination of Tris(2-pyridyl)methanol to Ruthenium(II): Synthetic, Spectral, and Structural Studies of the Bis(ligand) Species

F. Richard Keene,*[1] David J. Szalda,*[2] and Tracy A. Wilson[1]

Received September 4, 1986

Two forms of the cation bis[tris(2-pyridyl)methanol]ruthenium(II) have been isolated—a yellow species, $[Ru((py)_3COH)_2]^{2+}$ (**2**), and an orange form in which one ligand is deprotonated, $[Ru((py)_3COH)((py)_3CO^-)]^+$ (**1**). The pK_a for the ligand deprotonation is 3.78 (±0.02) in aqueous 0.1 M KNO_3 at 25.0 °C. X-ray structural determinations show coordination occurs in an (N,N′,N″)(N,N′,O) mode for both complexes, with the coordinated oxygen atom being the site of the acid/base reactivity. The deprotonated species (**1**) has a plane of symmetry with Ru–N bond lengths in the range 2.040–2.063 Å. The nondeprotonated form (**2**) has Ru–N bond lengths in the range 2.046–2.058 Å, except for an abnormally short Ru–N bond (2.023 (2) Å) trans to the coordinated Ru–OH. Additionally, in **2** the plane of symmetry is lost. In aqueous solution the redox potentials for the Ru(III)/Ru(II) couples are 0.40 (**2**) and 0.25 V (**1**) vs. SSCE. The electronic and ^{13}C NMR spectra are also reported. Crystals of the deprotonated form, $[Ru((py)_3COH)((py)_3CO)]Br\cdot 2C_2H_5OH$ (**1a**), are monoclinic, space group $P2_1/m$, with a = 8.096 (2) Å, b = 13.584 (2) Å, c = 15.204 (2) Å, β = 101.96 (1)°, V = 1635 (1) Å^3, and Z = 2. Crystals of $[Ru((py)_3COH)_2](CH_3SO_4)_2$ (**2a**) are triclinic, space group $P\bar{1}$, with a = 13.517 (3) Å, b = 14.458 (2) Å, c = 9.727 (2) Å, α = 104.72 (2)°, β = 108.56 (2)°, γ = 92.41 (2)°, V = 1727 (3) Å^3, and Z = 2.

Introduction

The ligation of a number of tripodal π-acceptor tridentates to a variety of metal centers has been reported. Canty et al.[3–6] have used a wide range of ligands XY_3 (X = CH, COH; Y = 2-pyridyl, 1-pyrazolyl, *N*-methylimidazol-2-yl) to impose unusual coordination geometries on metal centers such as Hg(II) and Au(III). White and Faller[7] and Szalda and Keene[8] have isolated complexes of cobalt with tris(2-pyridyl)methanol and tris(2-pyridyl)methane, and Boggess and co-workers[9–11] have reported studies of a number of complexes of first-row transition metals with ligands of the type $(2\text{-py})_3X$ (X = N, P, As, P=O, CH, COH). The zinc complexes of the trisubstituted methanols have also been noted[12] as models for the enzyme carbonic anhydrase.

Tris(2-pyridyl)methanol has been shown to be ambiguous with regard to its mode of coordination, with ligation occurring via three py N atoms (N,N′,N″), structure A, or via two py N atoms and the deprotonated alcohol O (N,N′,O$^-$), structure B. For the

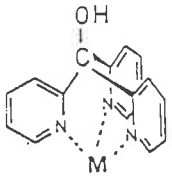

$(py)_3COH$-*N*,*N*′,*N*″
A

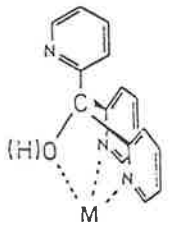

$(py)_3CO(H)$-*N*,*N*′,*O*
B

bis(ligand)cobalt(III) species, two linkage isomers were isolated:[8] viz. the symmetrical bis(N,N′,N″) form and the (N,N′,N″)-(N,N′,O$^-$) species. As part of our current general study of complexes of tripodal π-acceptor ligands with metals in Groups 8–10, we now report synthetic and structural studies of the corresponding bis(ligand)ruthenium(II) complex, which have realized only the unsymmetric (N,N′,N″)(N,N′,O$^-$) form and its nondeprotonated analogue (N,N′,N″)(N,N′,O).

Experimental Section

Physical Measurements. Electronic spectra were recorded on a Cary 219 spectrophotometer, and NMR spectra were recorded with a Bruker AM-300 spectrometer (Me_2SO-d_6 solution; Me_4Si reference).

Electrochemical measurements were made by using a Bioanalytical Systems (BAS) CV-27 voltammograph, with cyclic voltammograms

(1) James Cook University of North Queensland.
(2) Brookhaven National Laboratory. Permanent address: Baruch College, New York, NY 10010.
(3) Canty, A. J.; Chaichit, N.; Gatehouse, B. M.; George, E. E.; Hayhurst, G. *Inorg. Chem.* **1981**, *20*, 2414–2422.
(4) Canty, A. J.; Chaichit, N.; Gatehouse, G. M.; George, E. E. *Inorg. Chem.* **1981**, *20*, 4293–4300.
(5) Canty, A. J.; Minchin, N. J.; Healy, P. C.; White, A. H. *J. Chem. Soc., Dalton Trans.* **1982**, 1795–1802.
(6) Canty, A. J.; Patrick, J. M.; White, A. H. *Inorg. Chem.* **1984**, *23*, 3827–3830.
(7) White, D. L.; Faller, J. W. *Inorg. Chem.* **1982**, *21*, 3119–3122.
(8) Szalda, D. J.; Keene, F. R. *Inorg. Chem.* **1986**, *25*, 2795–2799.
(9) Boggess, R. K.; Zatko, D. A. *Inorg. Chem.* **1976**, *15*, 626–630.
(10) Boggess, R. K.; Boberg, S. J. *J. Inorg. Nucl. Chem.* **1980**, *42*, 21–26.
(11) Boggess, R. K.; Hughes, J. W.; Chew, C. W.; Kemper, J. J. *J. Inorg. Nucl. Chem.* **1981**, *43*, 939–945.
(12) Brown, R. S.; Huguet, J. *Can. J. Chem.* **1980**, *58*, 389–901.

0020-1669/87/1326-2211$01.50/0

output to a Linseis LY-1800 X-Y recorder. Both platinum and glassy-carbon working electrodes were used, and all potentials are reported relative to a saturated sodium chloride calomel electrode (SSCE).

The pK_a measurements were made by using an automated titration system, which has been described earlier.[13] Determinations were made at 25.0 °C in 95% methanol/0.1 M tetraethylammonium perchlorate by titration with tetraethylammonium hydroxide and in aqueous 0.1 M KNO_3 by titration with KOH.

Elemental analyses were carried out by the Canadian Microanalytical Service, New Westminster, Canada.

Materials. $[Ru(H)(CO_2CH_3)(PPh_3)_3]$ was purchased from Strem Chemicals, and $[Ru(H)(OH_2)_2(CH_3OH)(PPh_3)_2]BF_4$[14] and tris(2-pyridyl)methanol[8,15] were prepared by literature methods.

Syntheses. [Tris(2-pyridyl)methanol][tris(2-pyridyl)methoxo]ruthenium(II) Tetrafluoroborate Dihydrate, $[Ru((py)_3COH)((py)_3CO)]BF_4 \cdot 2H_2O$. Freshly prepared $[Ru(H)(OH_2)_2(CH_3OH)(PPh_3)_2]BF_4$ (0.39 g, 0.50 mmol) was added to thoroughly degassed (N_2) AR methanol (30 mL), tris(2-pyridyl)methanol (0.39 g; 1.5 mmol) was added, and the mixture was refluxed for ca. 18 h (until the sparingly soluble precursor complex had dissolved). The orange solution was cooled and filtered and the solvent evaporated off; the residue was triturated three times with dry ether, filtered, and washed with ether. Recrystallization was achieved from methanol/ether. Yield: 0.30 g; 84%. Anal. Calcd for $RuC_{32}H_{25}N_6O_2BF_4 \cdot 2H_2O$: C, 51.3; H, 3.90; N, 11.2. Found: C, 50.9; H, 3.81; N, 10.9.

[Tris(2-pyridyl)methanol][tris(2-pyridyl)methoxo]ruthenium(II) bromide, $[Ru((py)_3COH)((py)_3CO)]Br$, was prepared by dissolving the tetrafluoroborate salt in 2-butanone and precipitation by the addition of tetra-*n*-butylammonium bromide. The bromide was filtered and washed with 2-butanone and ether. Yield: >90%.

[Tris(2-pyridyl)methanol][tris(2-pyridyl)methoxo]ruthenium(II) Bromide–Bis(ethanol), $[Ru((py)_3COH)((py)_3CO)]Br \cdot 2C_2H_5OH$ (1a). $[Ru((py)_3COH)((py)_3CO)]Br$ (0.037 g) was dissolved in ethanol (4 mL) containing 2 drops of 2,6-lutidine. Dry diethyl ether was layered on top of this solution, and the solution was left undisturbed in the dark for several days. The resultant orange crystals were collected and washed with ether.

Bis[tris(2-pyridyl)methanol]ruthenium(II) Bis(methyl sulfate), $[Ru((py)_3COH)_2](CH_3SO_4)_2$ (2a). $[Ru((py)_3COH)((py)_3CO)]Br$ (0.040 g, 57 μmol) was dissolved in methanol (4 mL) and Ag_2SO_4 (0.010 g; 32 μmol) added. The mixture was stirred in the dark for 30 min and filtered, 2 drops of concentrated H_2SO_4 were added, and dry ether was layered on top of the solution. After several days, the resultant yellow crystals of the methyl sulfate salt[16] were collected and washed with ether.

Collection and Reduction of X-ray Data. [Tris(2-pyridyl)methanol-*N*,*N*′,*N*″][tris(2-pyridyl)methoxo-*N*′,*N*′,*O*]ruthenium(II) Bromide–Bis(ethanol) (1a). This compound crystallized as red-orange prisms. The crystals slowly lost solvent so they were coated with petroleum jelly and enclosed in Lindemann glass capillary tubes. A preliminary X-ray study indicated the crystals had monoclinic symmetry and symmetric absences $0k0$, $k = 2n + 1$, consistent with the space groups $P2_1$ (No. 4, C_2^2)[17a] and $P2_1/m$ (No. 10, C_{2h}^2).[17b] The structure was originally solved in space group $P2_1$, but because the cation exhibited mirror symmetry the space group was changed to $P2_1/m$ for the final refinement. The successful refinement of the structure confirmed that $P2_1/m$ is the correct space group.

The crystal used for data collection was a prism of dimensions 0.220 × 0.425 × 0.500 mm³ and faces (001) and (00$\bar{1}$), (100) and ($\bar{1}$00), and (100) and ($\bar{1}$00), respectively. Crystal data and details of the data collection and reduction are given in Table I.

Bis[tris(2-pyridyl)methanol-(*N*,*N*′,*N*″)(*N*,*N*′,*O*)]ruthenium(II) Bis(methyl sulfate) (2a). The crystals were yellow prisms. They were coated with petroleum jelly and sealed in Lindemann glass capillary tubes. These crystals showed $\bar{1}$ Laue symmetry consistent with the triclinic space groups $P1$ (No. 1, C_1^1)[17c] and $P\bar{1}$ (No. 2, C_i^1).[17d]

The crystal used for data collection had dimensions 0.176 × 0.400 × 0.500 mm³ and faces ($\bar{1}$10) and (1$\bar{1}$0), (110) and ($\bar{1}\bar{1}$0), and (01$\bar{2}$) and (0$\bar{2}$1), respectively. Crystal data and details of the data collection and reduction are given in Table I.

Table I. Experimental Details of the X-ray Diffraction Study of $[Ru((py)_3COH)((py)_3CO)]Br \cdot 2C_2H_5OH$ (1a) and $[Ru((py)_3COH)_2](CH_3SO_4)_2$ (2a)

(A) Crystal Parameters[a] at 22 °C

	1a	2a
a, Å	8.096 (2)	13.517 (3)
b, Å	13.584 (2)	14.458 (2)
c, Å	15.204 (2)	9.727 (2)
α, deg	90.0	104.72 (2)
β, deg	101.96 (1)	108.56 (2)
γ, deg	90.0	92.41 (2)
V, Å³	1635 (1)	1727 (3)
Z	2	2
mol wt	798.70	849.85
space group	$P2_1/m$	$P\bar{1}$
ρ(exptl), g cm^{-3}	1.57[b]	1.65[c]
ρ(calcd), g cm^{-3}	1.621	1.634

(B) Measurement of Intensity Data

	1a and 2a
instrument	Enraf-Nonius Cad 4 diffractometer
radiation	Mo Kα (λ = 0.709 26 Å) graphite monochromatized
2θ limits	2–55°
scan type	θ(crystal)–2θ(counter)
stds	3 reflcns measd after each 1 h of exposure, with no systematic variations

(C) Treatment of Intensity Data[d]

	1a	2a
reden to prelim F_o and $\sigma(F_o)$	correction for background, attenuators, and Lorentz–polarization effects of monochromatized X-radiation in the usual manner	
abs cor	μ = 18.17 cm^{-1}	μ = 6.34 cm^{-1}
transmissn coeff max	0.6859	0.8969
min	0.4792	0.7837
obsd data	7670 obsd data combined to yield 3617 unique data with a R_{av} = 0.0041 of which 2825 having $F_o > 3\sigma(F_o)$ were used in the refinement	7969 obsd data of which 5962 having $F_o > 3\sigma(F_o)$ were used in the refinement

[a] From a least-squares fit to the setting angles of 25 reflections with $2\theta > 20°$. [b] Using carbon tetrachloride and hexane. [c] Using carbon tetrachloride and bromoform. [d] Data reduction and corrections performed by using the program KAPPA and the absorption correction computed by using ABSOR, both part of the CRYSNET system at Brookhaven National Laboratory.

Determination and Refinement of Structures. Both structures were solved by heavy-atom Patterson and Fourier[18] methods. Anisotropic temperature factors were used for all non-hydrogen atoms. Corrections for anomalous dispersion[19] effects were included for all atoms. The locations of the hydrogen atoms on the pyridine rings were calculated (C–H bond lengths of 0.95 Å). These hydrogen atoms were allowed to "ride"[18] on the atom to which they were attached.

For $[Ru((py)_3COH)((py)_3CO)]Br \cdot 2C_2H_5OH$ (1a) the alcoholic hydrogen on the $(py)_3COH$-*N*,*N*′,*N*″ ligand was located on a difference Fourier map and fixed at that position. A common isotropic temperature factor for all the hydrogen atoms refined to a value of U = 0.055 (5) Å². The hydrogen atoms on the ethanol solvent molecules were not included in the refinement. The quantity $\sum w(|F_o| - |F_c|)^2$ where $w = 1.4332/(\sigma^2(F_o) + 0.002504(F_o)^2)$ was minimized in the least-squares refinement. During the final least-squares cycle, the largest parameter shift was less

(13) Adam, K. R.; Leong, A. J.; Lindoy, L. F.; Lip, H. C.; Skelton, B. W.; White, A. H. *J. Am. Chem. Soc.* **1983**, *105*, 4645–4651.
(14) Young, R. J.; Wilkinson, G. *J. Chem. Soc., Dalton Trans.* **1976**, 719–725.
(15) Wibaut, J. P.; de Jonge, A. P.; Van der Voort, H. G. P.; Otto, H. L. *Recl. Trav. Chim. Pays-Bas* **1951**, *70*, 1054–1060.
(16) The methyl sulfate anion is formed by the reaction of the solvent with sulfuric acid under the anhydrous conditions.
(17) *International Tables for X-Ray Crystallography*, 3rd ed.; Kynoch: Birmingham, U.K., 1969; Vol. I: (a) p 79; (b) p 91; (c) p 74; (d) p 75.
(18) Except where otherwise noted, all calculations were performed by using SHELX-76: Sheldrick, G. M. In *Computing in Crystallography*; Schenk, H., Olthof-Hazekamp, R., van Koningsveld, H., Bassi, G. C., Eds.; Delft University Press: Delft, Holland, 1978; pp 34–42.
(19) (a) Neutral-atom scattering factors were taken from: *International Critical Tables for X-Ray Crystallography*; Kynoch: Birmingham, U.K., 1974; Vol. IV, p 99. (b) Anomalous dispersion effects were taken from: Cromer, D. T.; Liberman, D. *J. Chem. Phys.* **1970**, *53*, 1891–1898.

Table II. $[Ru((py)_3COH)((py)_3CO)]Br\cdot 2C_2H_5OH$ Atomic Coordinates[a]

atom	x	y	z
Ru	−0.02705 (7)	0.2500	0.81196 (4)
N(1)	−0.1233 (5)	0.1468 (3)	0.7153 (3)
C(12)	−0.0669 (6)	0.1597 (4)	0.6384 (3)
C(13)	−0.1133 (7)	0.0984 (4)	0.5662 (4)
C(14)	−0.2185 (9)	0.0200 (5)	0.5718 (5)
C(15)	−0.2775 (9)	0.0060 (5)	0.6505 (5)
C(16)	−0.2271 (7)	0.0702 (4)	0.7203 (4)
N(3)	0.1018 (9)	0.2500	0.4917 (5)
C(32)	0.1688 (10)	0.2500	0.5785 (5)
C(33)	0.3388 (12)	0.2500	0.6106 (7)
C(34)	0.4440 (14)	0.2500	0.5509 (8)
C(35)	0.3767 (13)	0.2500	0.4607 (7)
C(36)	0.2092 (13)	0.2500	0.4347 (6)
O(1)	0.1512 (6)	0.2500	0.7341 (3)
C(1)	0.0529 (9)	0.2500	0.6461 (5)
N(4)	0.0920 (5)	0.1477 (3)	0.9013 (3)
C(42)	0.0949 (6)	0.1572 (4)	0.9894 (3)
C(43)	0.1754 (7)	0.0890 (4)	1.0517 (4)
C(44)	0.2591 (8)	0.0102 (4)	1.0228 (4)
C(45)	0.2593 (7)	0.0022 (4)	0.9317 (4)
C(46)	0.1755 (7)	0.0703 (4)	0.8746 (4)
N(5)	−0.2140 (7)	0.2500	0.8840 (4)
C(52)	−0.1765 (8)	0.2500	0.9742 (5)
C(53)	−0.3019 (9)	0.2500	1.0252 (5)
C(54)	−0.4698 (10)	0.2500	0.9815 (6)
C(55)	−0.5084 (9)	0.2500	0.8899 (6)
C(56)	−0.3791 (9)	0.2500	0.8435 (5)
O(2)	0.0201 (6)	0.2500	1.1118 (3)
C(2)	0.0103 (9)	0.2500	1.0187 (4)
Br	0.40808 (14)	0.2500	0.22082 (8)
O(3)	0.6167 (19)	0.0556 (9)	0.2495 (9)
C(3)	0.745 (4)	0.068 (2)	0.3171 (13)
C(4)	0.814 (9)	0.129 (3)	0.299 (4)

[a] Numbers in parentheses are errors in the last significant digit(s).

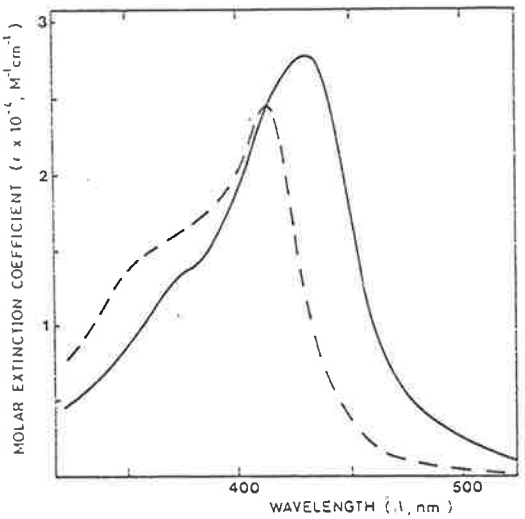

Figure 1. Visible spectra of the cations $[Ru((py)_3COH)((py)_3CO)]^+$ (**1**) in 0.2 M phosphate buffer at pH 7 (—) and $[Ru((py)_3COH)_2]^{2+}$ (**2**) in 0.1 M HCl (– –).

than 0.08 of its standard deviation. The final R_1[20] value was 0.056. The final weighted discrepency index R_2[20] was 0.069. A final difference Fourier map revealed peaks of 1–1.6 e/Å^3 near the bromide and ruthenium atoms. Other peaks were less than 0.5 e/Å^3. The final non-hydrogen atomic parameters are reported in Table II.

For $[Ru((py)_3COH)_2](CH_3SO_4)_2$ (**2a**) the space group was assumed to be $P\bar{1}$, and the successful refinement of the structure confirmed the correctness of this assignment. A common isotropic temperature factor for the pyridine hydrogen atoms refined to a value of $U = 0.059$ (4) Å^2. The positional and isotropic temperature factors for the alcoholic hydrogen atoms on the ligands were refined (Table S1). The hydrogen atoms on the anions were not located. The quantity $\sum w(|F_o| - |F_c|)^2$ where $w = 0.3307/(\sigma^2(F_o) + 0.004(F_o)^2)$ was minimized in the least-squares refinement. During the final least-squares cycle the largest parameter shift was less than 0.42 of its error. The final R_1[20] was 0.053. The final weighted discrepency index R_2[20] was 0.072. A final difference Fourier map revealed a peak of ca. 1.8 e/Å^3 near one of the anions, indicating some positional disorder, but no disordered model for this anion could be determined. Several peaks of about 1 e/Å^3 were also observed near the ruthenium atoms. The final non-hydrogen atomic positions are listed in Table III.

Table III. $[Ru((py)_3COH)_2)](CH_3SO_4)_2$ Atomic Coordinates[a]

atom	x	y	z
Ru	0.22998 (3)	0.14745 (2)	0.40747 (4)
N(1)	0.1468 (3)	0.2401 (3)	0.5094 (4)
C(12)	0.1588 (3)	0.3305 (3)	0.4966 (5)
C(13)	0.1081 (4)	0.4020 (4)	0.5562 (6)
C(14)	0.0408 (5)	0.3801 (4)	0.6285 (7)
C(15)	0.0259 (5)	0.2881 (5)	0.6380 (7)
C(16)	0.0800 (4)	0.2198 (4)	0.5782 (6)
N(2)	0.3585 (3)	0.2508 (3)	0.5316 (4)
C(22)	0.3452 (4)	0.3392 (3)	0.5142 (5)
C(23)	0.4252 (4)	0.4164 (4)	0.5860 (6)
C(24)	0.5218 (4)	0.4004 (4)	0.6764 (7)
C(25)	0.5356 (4)	0.3113 (5)	0.6929 (7)
C(26)	0.4533 (4)	0.2375 (4)	0.6208 (6)
N(3)	0.2516 (4)	0.5138 (3)	0.4424 (5)
C(32)	0.2154 (4)	0.4266 (3)	0.3447 (5)
C(33)	0.1594 (5)	0.4139 (5)	0.1937 (8)
C(34)	0.1471 (6)	0.4966 (6)	0.1456 (10)
C(35)	0.1854 (7)	0.5845 (6)	0.2422 (13)
C(36)	0.2365 (6)	0.5903 (5)	0.3887 (13)
C(1)	0.2339 (4)	0.3420 (3)	0.4102 (5)
O(1)	0.2064 (2)	0.2525 (2)	0.2882 (4)
N(4)	0.0950 (3)	0.0571 (3)	0.2694 (4)
C(42)	0.0938 (4)	−0.0390 (3)	0.2377 (5)
C(43)	0.0033 (4)	−0.1019 (4)	0.1493 (6)
C(44)	−0.0874 (4)	−0.0657 (4)	0.0883 (6)
C(45)	−0.0862 (4)	0.0339 (4)	0.1185 (6)
C(46)	0.0060 (4)	0.0920 (3)	0.2081 (6)
N(5)	0.3115 (3)	0.0589 (3)	0.2946 (4)
C(52)	0.2860 (4)	−0.0378 (3)	0.2578 (5)
C(53)	0.3376 (4)	−0.1005 (4)	0.1808 (6)
C(54)	0.4179 (4)	−0.0652 (4)	0.1420 (6)
C(55)	0.4448 (4)	0.0339 (4)	0.1831 (6)
C(56)	0.3909 (4)	0.0927 (4)	0.2582 (6)
N(6)	0.2508 (3)	0.0578 (3)	0.5408 (4)
C(62)	0.2319 (4)	−0.0390 (3)	0.4796 (5)
C(63)	0.2429 (4)	−0.1020 (4)	0.5673 (6)
C(64)	0.2735 (4)	−0.0663 (4)	0.7206 (6)
C(65)	0.2946 (4)	0.0324 (4)	0.7847 (6)
C(66)	0.2833 (4)	0.0911 (4)	0.6933 (5)
C(2)	0.1981 (4)	−0.0753 (3)	0.3063 (5)
O(2)	0.1862 (4)	−0.1759 (3)	0.2702 (5)
S(1)	0.14385 (12)	−0.31425 (10)	−0.13736 (16)
O(11)	0.2564 (5)	−0.3319 (6)	−0.0514 (8)
O(12)	0.1091 (4)	−0.2638 (5)	−0.0240 (6)
O(13)	0.0882 (5)	−0.3991 (5)	−0.2260 (9)
O(14)	0.1568 (9)	−0.2533 (7)	−0.2224 (13)
C(11)	0.3212 (8)	−0.3585 (9)	−0.1524 (15)
S(2)	0.39127 (12)	0.28945 (10)	0.09600 (17)
O(21)	0.3735 (8)	0.3873 (6)	0.0571 (12)
O(22)	0.4403 (5)	0.2349 (5)	0.0068 (8)
O(23)	0.2905 (3)	0.2425 (3)	0.0807 (5)
O(24)	0.4511 (6)	0.3368 (6)	0.2452 (8)
C(21)	0.3170 (11)	0.3860 (9)	−0.0869 (11)

[a] Numbers in parentheses are errors in the last significant digit(s).

Results and Discussion

The ruthenium(II) complex containing two tris(2-pyridyl)-methanol ligands was synthesized by using the $[Ru(H)(OH_2)_2(CH_3OH)(PPh_3)_2]BF_4$ precursor, in a manner analogous to the synthesis of $[Ru(py)_6]^{2+}$ developed by Templeton.[21] The orange cation thus obtained was found (microanalysis, ion-exchange

(20) $R_1 = \sum(||F_o| - |F_c||)/\sum|F_o|$; $R_2 = [\sum w(|F_o| - |F_c|)^2/\sum w(F_o)^2]^{1/2}$.

(21) Templeton, J. L. *J. Am. Chem. Soc.* **1979**, *101*, 4906–4917.

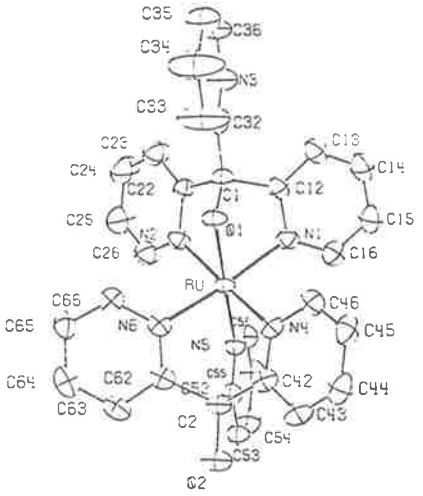

Figure 2. ORTEP drawing of a single molecule of the cation $[Ru((py)_3COH)((py)_3CO^-)]^+$ showing the atom-labeling scheme used. The thermal ellipsoids are at the 50% probability level. The molecule lies on a crystallographic mirror plane that contains the ruthenium, the uncoordinated pyridine ring (N(3)–C(36)), a coordinated pyridine ring (N(5)–C(56)), the coordinated methoxy group (C(1) and O(1)) and the uncoordinated alcohol group (C(2), O(2), H(2)). The pyridine rings labeled N(2)–C(26) and N(6)–C(66) are related to the pyridine rings N(1)–C(16) and N(4)–C(46) respectively by the mirror plane (x, $^1/_2 - y$, z). Hydrogen atoms have been omitted for clarity.

Table IV. Bond Distances (Å) and Angles (deg) for $[Ru((py)_3COH)((py)_3CO)]Br\cdot 2C_2H_5OH$

	Ruthenium–Ligand Distances		
Ru–O(1)	2.047 (5)	Ru–N(4)	2.040 (4)
Ru–N(1)	2.063 (4)	Ru–N(5)	2.044 (6)
	Ruthenium–Ligand Angles		
O(1)–Ru–N(1)	78.2 (1)	N(1)–Ru–N(5)	99.8 (2)
O(1)–Ru–N(4)	95.3 (1)	N(1)–Ru–N(6)	173.5 (2)
O(1)–Ru–N(5)	177.2 (2)	N(4)–Ru–N(5)	86.7 (2)
N(1)–Ru–N(2)	85.6 (2)	N(4)–Ru–N(6)	85.9 (2)
N(1)–Ru–N(4)	93.9 (2)		

chromatography) to have a +1 charge by virtue of deprotonation of one of the ligands. A yellow form of the cation (charge +2) could be obtained by protonation of the orange form. The visible spectra of the two complexes are shown in Figure 1.

Alternative synthetic methods using $[RuCl_5(OH_2)]^{2-}$ or $[Ru(DMF)_6]^{2+}$ as precursors have also realized the same coordination mode of the ligand.[22]

Description of the Structures. A view of the $[Ru((py)_3COH)((py)_3CO)]^+$ cation (**1**) and the atom-labeling scheme used are shown in Figure 2. The neutral tris(2-pyridyl)methanol ligand is coordinated to the ruthenium by its three pyridyl nitrogens (N,N′,N″; A), while the anionic tris(2-pyridyl)methoxide ligand is coordinated through two pyridyl nitrogens and the methoxide oxygen (N,N′,O⁻; B). Complex **1** contains a crystallographic mirror plane (see Figure 2). The neutral ligand (N,N′,N″-coordinated) has an average Ru–N bond distance of 2.042 (6) Å (Table IV) while the anionic ligand (N,N′,O⁻-coordinated) has a somewhat longer average Ru–N bond distance of 2.063 (4) Å indicating some bond stretching as a result of the oxygen coordination. The average Ru–N(pyridyl) bond length reported in $[Ru(bpy)_3]^{2+}$[25] is 2.056 Å. The Ru–O bond length is 2.047 (5) Å, which is normal for a Ru(II)–O⁻ bond.[24]

A view of the $[Ru((py)_3COH)_2]^{2+}$ cation (**2**) and the atom-labeling scheme used are presented in Figure 3. In this case the

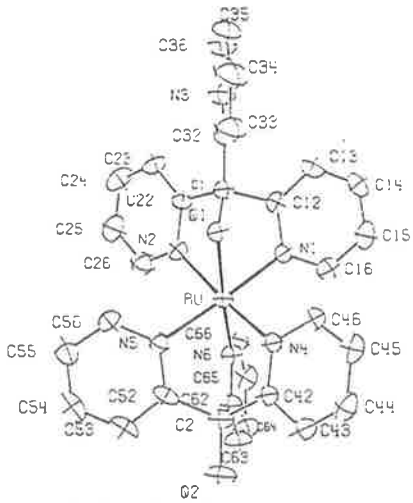

Figure 3. ORTEP drawing of the $[Ru((py)_3COH)_2]^{2+}$ cation with the atom-labeling scheme. The thermal ellipsoids are at the 50% probability level. Atom O(1) is protonated, but all the hydrogen atoms have been omitted for clarity. The pyridine rings containing N(3) and N(6) are 13.6° for coplanar.

Table V. Bond Distances (Å) and Angles (deg) for $[Ru((py)_3COH)_2](CH_3SO_4)_2$

	Ruthenium–Ligand Distances		
Ru–N(1)	2.050 (4)	Ru–N(4)	2.046 (3)
Ru–N(2)	2.058 (3)	Ru–N(5)	2.058 (4)
Ru–O(1)	2.111 (4)	Ru–N(6)	2.023 (4)
	Ruthenium–Ligand Angles		
N(1)–Ru–N(2)	85.7 (1)	N(2)–Ru–N(6)	100.0 (2)
N(1)–Ru–O(1)	76.2 (2)	O(1)–Ru–N(4)	95.6 (1)
N(1)–Ru–N(4)	91.5 (1)	O(1)–Ru–N(5)	100.2 (2)
N(1)–Ru–N(5)	176.3 (2)	O(1)–Ru–N(6)	173.8 (1)
N(1)–Ru–N(6)	98.1 (2)	N(4)–Ru–N(5)	88.2 (1)
N(2)–Ru–O(1)	77.2 (1)	N(4)–Ru–N(6)	87.0 (1)
N(2)–Ru–N(4)	172.7 (2)	N(5)–Ru–N(6)	85.5 (2)
N(2)–Ru–N(5)	94.1 (2)		

complex contains two neutral tris(2-pyridyl)methanol ligands, one ligand coordinated to the ruthenium(II) by its three pyridyl nitrogens while the other is coordinated by two pyridyl nitrogen atoms and the nondeprotonated oxygen of the alcohol. For the two ligands, the average Ru–N bond length is 2.053 (6) Å, except for the Ru–N(6) bond (trans to Ru–O(1)), which is abnormally short (2.023 (4) Å; Table V). The Ru–O bond length is 2.111 (4) Å; the average Ru–O bond length in $Ru(OH_2)_6^{2+}$ is 2.12 (2) Å.[25]

Protonation of the tris(2-pyridyl)methoxide ligand in **1** occurs at the coordinated oxygen, rather than on the uncoordinated pyridine nitrogen, to give **2**. This protonation is accompanied by an increase in the Ru–O bond length of 0.064 Å between **1** and **2** and a corresponding decrease in the Ru–N bond length trans to the coordinated oxygen from 2.044 (6) to 2.023 (4) Å, which is significantly shorter than the other Ru–N bond distances. A similar feature has been observed in the structure of *cis*-$[Ru(bpy)_2Cl_2]\cdot 3.5H_2O$:[26] the Ru(II)–Cl bond lengths are relatively long, whereas the Ru–N bond lengths trans to Cl⁻ are shorter (2.013 (2) Å) than those trans to the bpy N (2.054 (2) Å). This effect was attributed[26] to the importance of Ru → N(bpy) π-back-bonding where the trans ligand is not a back-bonding competitor for the electron density involving the same filled dπ orbitals; in the present case the effect of the –OH ligation in **2** is considered to be analogous to that of Cl⁻. In the deprotonated complex **1**, the Ru–N bond in the trans position has the slightly longer bond

(22) Keene, F. R.; Stephenson, P. J., unpublished work.
(23) Rillema, D. P.; Jones, C. S.; Levy, H. A. *J. Chem. Soc., Chem. Commun.* 1979, 849–851.
(24) Clegg, W. *Acta Crystallogr., Sect. B: Struct. Crystallogr. Cryst. Chem.* 1980, *B36*, 3112–3114.
(25) Bernhard, P.; Burgi, H.-B.; Hauser, J.; Lehmann, H.; Ludi, A. *Inorg. Chem.* 1982, *21*, 3936–3941.
(26) Eggleston, D. S.; Goldsby, K. A.; Hodgson, D. J.; Meyer, T. J. *Inorg. Chem.* 1985, *24*, 4573–4580.

Table VI. Physical Characteristics of $[Ru((py)_3COH)((py)_3CO^-)]^+$ (1) and $[Ru((py)_3COH)_2]^{2+}$ (2)

	$[Ru((py)_3COH)((py)_3CO^-)]^+$	$[Ru((py)_3COH)_2]^{2+}$
electronic spectra	ϵ_{432} = 27 800 ϵ_{253} = 30 500 (0.2 M phosphate buffer, pH 7.0)	ϵ_{415} = 24 700 ϵ_{246} = 30 600 (0.1 M H_2SO_4)
^{13}C NMR spectra	bridgehead carbon atoms δ = 81.0, 90.0 (Me_2SO-d_6 solvent; Me_4Si internal reference)	bridgehead carbon atoms δ = 81.1, 86.7 (Me_2SO-d_6 solvent/CF_3CO_2H; Me_4Si internal reference)
electrochemical chemical properties	$E_{1/2}$ = 0.25 V ($\Delta E \approx$ 80 mV) (0.05 M TRIS buffer/0.1 M KNO_3; glassy-carbon working electrode; sweep rate 100 mV/s; SSCE reference electrode)	$E_{1/2}$ = 0.40 V ($\Delta E \approx$ 90 mV) (0.05 M H_2SO_4; glassy-carbon working electrode; sweep rate 100 mV/s; SSCE reference electrode)
pK_a	3.86 (±0.01){95% MeOH/0.1 M Et_4NClO_4} 3.78 (±0.02){0.1 M KNO_3}	

length of 2.044 (6) Å. This observation may be rationalized in terms of σ-bonding effects if the energy of the e_g orbital of the metal corresponds more closely to the energy of the σ orbital of oxygen in O^- rather than the more stable –OH; in such a case, the strength of the Ru–O^- bond would be enhanced (compared with that of Ru–OH), with a resultant relative diminution of the strength of the trans Ru–N bond.

The possible role of π-bonding might also be considered in relationship to these structural observations. ^{13}C NMR data on uncoordinated tris(2-pyridyl)methanol and the tris(2-pyridyl)-methoxide anion indicate a downfield shift in the resonance of the bridgehead carbon on deprotonation, consistent with a degree of delocalization in the anion in which the C–O bond may have some double-bond character.[27] Accordingly, when the anion is coordinated via the N,N′,O mode (B), $d\pi(Ru) \rightarrow \pi^*$(ligand) back-bonding may occur, so that Ru–O^- is potentially a back-bonding competitor with the trans Ru–N bond, which therefore might be expected to have a longer bond length than in the nondeprotonated case. However, the –O^- ligand would be expected to function primarily as a π-donor, although this may not substantially influence the extent of back-bonding (and therefore, the bond length) of the trans Ru–N bond.[28] There is no structural evidence for multiple bond character in the C–O bond of coordinated tris(2-pyridyl)methoxo-*N,N′,O*$^-$ since the bond length (1.408 (8) Å) is the same as the C–O bond length in the tris(2-pyridyl)methanol-*N,N′,N″* ligand in **2** (1.401 (8) Å) and **1** (1.395 (6) Å) (Tables S6 and S7). The X-ray data do indicate that in complex **2**, for the tris(2-pyridyl)methanol-*N,N′,O* ligand the attachment of the oxygen to both the proton and the metal weakens both the Ru–O and C–O bonds, increasing both bond lengths (0.064 and 0.047 Å, respectively) in comparison with the equivalent deprotonated ligand in **1**.

The ^{13}C NMR spectral studies reveal that the resonances due to the bridgehead carbon atom are virtually identical in free tris(2-pyridyl)methanol (δ = 81.4) and in the neutral N,N′,N″-coordinated ligand (δ = ca. 81.1; Table VI and ref 27). For the neutral N,N′,O-coordinated ligand, the same resonance is shifted downfield (δ = 86.7) and is shifted further downfield on ligand deprotonation (δ = 90.0). The downfield shift observed for *both* of the N,N′,O-coordinated ligands relative to the free ligand reflects a complex metal/ligand electronic interaction in both species.

(27) ^{13}C NMR studies (Me_2SO-d_6 solvent) show the bridgehead carbon resonance of tris(2-pyridyl)methanol shifts downfield (δ = 81.4–83.4) on deprotonation by NaH.
(28) Adcock, P. A.; Keene, F. R.; Smythe, R. S.; Snow, M. R. *Inorg. Chem.* 1984, *23*, 2336–2343.

The Ru–N bond lengths in both complexes **1** and **2** are more similar to those found in $Ru(bpy)_3^{2+}$, 2.056 Å,[23] than those found in $Ru(NH_3)_6^{2+}$, 2.144 Å,[29] and $Ru(py)_6^{2+}$, 2.12 Å.[21] This indicates the presence of π-back-bonding from the metal to the ligands in both **1** and **2** and, in comparison with $[Ru(py)_6]^{2+}$,[21] provides evidence for ligand delocalization in both tris(2-pyridyl)methanol and the corresponding methoxide in all observed coordination modes for the two ligands. Delocalization of back-bonded charge density in these tripodal ligands has been observed previously in Co(I) complexes.[8,9]

In the nondeprotonated species (**2**), the uncoordinated pyridine ring and the coordinated pyridine ring trans to –OH are 13.6° from being coplanar, while the pyridine rings trans to one another are 16.9 and 14.1° from being coplanar. In the cobalt(III) complex of the same ligand (in which both ligands are N,N′,N″-coordinated), the pyridine rings trans to one another are coplanar.[8] In both complexes, **1** and **2**, the bonds and angles within the pyridine rings are normal[8,30,31] (Tables S6 and S7). The bond distances and angles for the methyl sulfate anions in **2** are also similar to those reported.[32]

Comparisons with Other Structures. There are few reports of structural studies of complexes involving the title ligand, tris(2-pyridyl)methanol. Canty et al.[4] have reported a methylmercury(II) species, $[MeHg((py)_3COH)](NO_3)$, in which the ligand is tridentate with binding occurring via the three py N atoms; the coordination geometry is irregular with one Hg–N bond being significantly shorter than the other two. For the octahedral bis(ligand)cobalt(III) complex, two linkage isomers have been reported: an (N,N′,N″)(N,N′,O^-) form in which one ligand is deprotonated (and coordinated in the N,N′,O^- mode)[33] and the symmetrical bis(N,N′,N″) form in which both ligands are nondeprotonated.[8] Consequently, in the present study, structure **2** is the first example of N,N′,O-coordination of the nondeprotonated tris(2-pyridyl)methanol ligand. For the tris(2-pyridyl)-methanol-*N,N′,N″* ligand in both complexes **1** and **2**, the angles Ru–N–C(2) and Ru–N–C(6) (see Figures 2 and 3) are approximately equal, as they are in the N,N′,N″-coordinated ligands in $Co((py)_3COH)_2^{3+}$.[8] However, for the N,N′,O-coordinated ligand in **1** and **2** these angles are asymmetric (113 (1) and 128 (1)°, respectively) as are the angles about the coordinated pyridyl nitrogens in $Co((py)_3N)_2^{2+}$[31] and $Fe((py)_3N)_2^{3+}$.[30] In these two cases the asymmetric angles are a result of the shorter bridging C–N bond length of 1.44 (1) Å; for complexes **1** and **2** this distortion may also arise from steric constraints in coordination.

Physical Characteristics of $[Ru((py)_3COH)((py)_3CO)]^+$ (1) and $[Ru((py)_3COH)_2]^{2+}$ (2). The physical characteristics of the two forms of the cation are given in Table VI. Both species show an (N,N′,N″)(N,N′,O) coordination mode, differing according to the deprotonated (**1**) or nondeprotonated (**2**) state of the coordinated alcohol O atom. The ^{13}C NMR spectra (Me_2SO-d_6 solution) of the two species show complicated resonances in the region δ = 120–170 attributed to the pyridine C atoms, and the appearance of separate resonances for the two bridgehead carbon atoms (δ = 81.1 and 86.7 for **1**; δ = 81.0 and 90.0 for **2**) consistent with the nonsymmetric coordination of the two ligands. The preference of the metal center for N_5O- rather than N_6-coordination is unexpected, given the affinity of Ru(II) for unsaturated ligands such as pyridine.[34] The bis(ligand)ruthenium(II) species with other $(py)_3X$ ligands (X = CH, N, P, P=O) have been isolated and their structures determined;[35] since no unusual features are apparent in these N_6-coordinated species, the reason for N_5O-coordination of tris(2-pyridyl)methanol is unlikely to be steric

(29) Stynes, H. C.; Ibers, J. A. *Inorg. Chem.* 1971, *10*, 2304–2308.
(30) Kucharski, E. S.; McWhinnie, W. R.; White, A. H. *Aust. J. Chem.* 1978, *31*, 53–56.
(31) Kucharski, E. S.; McWhinnie, W. R.; White, A. H. *Aust. J. Chem.* 1978, *31*, 2647–2650.
(32) Munns, A. R. I.; Low, J. N.; Tollin, P.; Young, D. W. *Cryst. Struct. Commun.* 1981, *10*, 1431–1434.
(33) Preliminary details of structure given in a footnote to ref 7.
(34) Taube, H. *Surv. Prog. Chem.* 1973, *6*, 1–46.
(35) Keene, F. R.; Stephenson, P. J.; Tiekink, E. R. T.; Snow, M. R., unpublished work.

and may reflect a kinetic effect in the synthetic process.

The pK_a for the deprotonation is 3.78 (±0.02) in aqueous solution (μ = 0.1; 25.0 °C). By comparison, the pK_a of coordinated 2-pyridinemethanol in the complex $[Ru(bpy)_2((py)CH_2OH)]^{2+}$ is 7.2 (±0.1) under the same conditions:[36] the higher acidity of coordinated tris(2-pyridyl)methanol probably reflects additional steric strain within the tripodal ligand. There is no evidence for protonation of the free py N atom in the N,N',O-coordinated ligand even at pH ca. 1. The pK_a values of the free ligand $(py)_3COH$ in 95% methanol are 4.9 (±0.1) and 1.9 (±0.1), with the third value probably slightly lower than 1.5;[12] while the pK_a of the alcohol OH is significantly lowered by coordination to the positive metal center, the nonprotonation of the free py N is clearly unusual, since the pK_a values of the uncoordinated py N atoms in a number of polypyridyl-type ligands are actually raised by their coordination in a monodentate manner to Ru(II).[35,37] In the present case, one possibility is that in solution the coordinated –OH is hydrogen-bonded to the py N in the free ring, thereby forming a five-membered ring (–O(1)–H(1)···N(3)–C(32)–C(2)–, in the numbering scheme used in Figure 3) and inhibiting protonation of N(3). This is not the case for the solid state, however, where Figure 3 reveals that the free pyridine ring is rotated so that the nitrogen atom (N(3)) points away from the O(1)–H(1), and the –OH group is in fact hydrogen bonded to an oxygen atom of a methyl sulfate anion (Table S11).

The deprotonation is also associated with a color change of the complex from yellow to orange (see Table VI and Figure 1) and a cathodic shift in the redox potential of the Ru(III)/Ru(II) couple from 0.40 to 0.25 V. A reduction in redox potential is generally observed on lowering of the overall complex charge.[38] The potential of the Ru(III)/Ru(II) couple for the nondeprotonated species **2**, $E_{1/2}$ = 0.40 V, compares with 0.62 V for $[Ru(bpy)_2((py)CH_2OH)]^{3+/2+}$[36] under the same conditions.

Studies of the photochemical properties of the ruthenium(II) complexes of a variety of tripodal π-acceptor ligands will be published subsequently, but preliminary measurements with the deprotonated complex **1** indicate a luminescence lifetime of ca. 1.4 ns.[39]

Acknowledgment. This work was performed at James Cook University of North Queensland (where it was supported by the Australian Research Grants Scheme) and at Brookhaven National Laboratory (which is operated under Contract No. DE-AC02-76CH00016 with the Department of Energy and supported by its Office of Basic Energy Sciences). D.J.S. thanks Baruch College for released time to do this research. Dr. P. Duckworth is thanked for useful comments on the manuscript, and the technical assistance of A. J. Leong (JCUNQ) with some of the pK_a measurements is gratefully acknowledged.

Registry No. **1a**, 108451-82-7; **2a**, 108451-84-9; $[Ru((py)_3COH)((py)_3CO)]BF_4$, 108451-80-5; $[Ru((py)_3COH)((py)_3CO)]Br$, 108451-81-6; $[Ru(H)(OH_2)_2(CH_3OH)(PPh_3)_2]BF_4$, 60020-13-5; tris(2-pyridyl)methanol, 73569-80-9.

Supplementary Material Available: Tables listing positional and isotropic thermal parameters for the refined hydrogen atoms in **2** (Table S1), anisotropic thermal parameters for the non-hydrogen atoms in **1** (Table S2) and **2** (Table S3), atomic coordinates for the hydrogen atoms in **1** (Table S4) and **2** (Table S5), bond distances and angles for **1** (Table S6) and **2** (Table S7), hydrogen bonding in **1** (Table S10) and **2** (Table 11), and best planes for **1** (Table S12) and **2** (Table S13) (19 pages); tables of observed and calculated structure factors for **1** (Table S8) and **2** (Table S9) (37 pages). Ordering information is given on any current masthead page.

(36) Ridd, M. J.; Keene, F. R.; Gakowski, D. J.; Sneddon, G. E., manuscript in preparation.
(37) Lavallee, D. K.; Fleischer, E. B. *J. Am. Chem. Soc.* **1972**, *94*, 2583–2599.
(38) Ridd, M. J.; Keene, F. R. *J. Am. Chem. Soc.* **1981**, *103*, 5733–5740 and references quoted therein.
(39) Winkler, J. R.; Keene, F. R., unpublished work.

Acta Cryst. (1988). C**44**, 757–758

Tris(2-pyridyl)phosphine

BY F. RICHARD KEENE

Department of Chemistry and Biochemistry, James Cook University of North Queensland, Townsville, Queensland 4811, *Australia*

AND MICHAEL R. SNOW AND EDWARD R. T. TIEKINK

Jordan Laboratories, Department of Physical and Inorganic Chemistry, University of Adelaide, South Australia 5001, *Australia*

(*Received* 30 *October* 1987; *accepted* 2 *December* 1987)

Abstract. $C_{15}H_{12}N_3P$, $M_r = 265{\cdot}3$, monoclinic, $P2_1/c$, $a = 9{\cdot}162$ (1), $b = 9{\cdot}163$ (1), $c = 16{\cdot}071$ (2) Å, $\beta = 100{\cdot}92$ (1)°, $U = 1325$ (2) Å^3, D_m (by flotation) = 1·33 (1), $D_x = 1{\cdot}330$ Mg m^{-3} for $Z = 4$, Mo $K\bar{\alpha}$ radiation, $\lambda = 0{\cdot}7107$ Å, $\mu = 0{\cdot}153$ mm^{-1}, $F(000) = 552$, $T = 293$ (2) K, $R = 0{\cdot}046$ for 2041 observed reflections. The P-atom environment is pyramidal with P—C bond distances of 1·834 (3), 1·824 (3) and 1·826 (2) Å and C—P—C angles of 102·7 (1), 101·9 (1) and 101·0 (1)°. The orientations of the rings are such that there is a significant deviation from C_{3v} symmetry; one of the N atoms is directed to the same side of the molecule as the P^{III} lone pair of electrons, while the remaining two N atoms point in the opposite direction. The P atom is almost coplanar with each of the rings [max. deviation 0·0420 (6) Å] and the dihedral angles between the planes through the N(1)—C(5), N(2)—C(10) and N(3)—C(15) groups are 87·8, 97·0 and 97·5° respectively.

Experimental. Transparent crystals were obtained from the slow evaporation of a benzene/373–393 K petroleum spirit solution of the compound (Hafeli, Keene, Stephenson & Wright, 1986). Enraf–Nonius CAD-4F diffractometer controlled by a PDP8/A computer, graphite-monochromated Mo $K\bar{\alpha}$ radiation; $\omega{:}2\theta$ scan technique. Cell parameters on crystal 0·88 × 0·48 × 0·34 mm from least-squares procedure on 25 reflections ($8 \le \theta \le 14°$). Analytical absorption correction applied (Sheldrick, 1976); max./min. transmission factors 0·9596 and 0·8797. Total of 5159 reflections ($1 \le \theta \le 27{\cdot}5°$) measured in the range $-11 \le h \le 11$, $-11 \le k \le 0$, $-20 \le l \le 9$. No significant variation in the net intensities of three reference reflections ($\bar{4}\bar{1}5$, $\bar{2}\bar{2}7$, $\bar{5}24$) measured every 3600 s. 3029 unique reflections (R_{int} 0·057), 2041 satisfied $I \ge 2{\cdot}5\sigma(I)$. Structure solved from interpretation of Patterson map, full-matrix least-squares refinement of 173 parameters based on F (Sheldrick, 1976). Anisotropic thermal parameters for non-H atoms and H atoms included in the model at their calculated positions. The

Table 1. *Fractional atomic coordinates and* B_{eq} *values* (Å^2)

$B_{eq} = 8\pi^2(U_{11} + U_{22} + U_{33})/3$.

	x	y	z	B_{eq}
P(1)	0·11758 (7)	0·28688 (7)	0·37503 (4)	3·08
N(1)	0·2973 (3)	0·1143 (3)	0·4927 (2)	4·19
N(2)	0·1697 (2)	0·5576 (2)	0·3332 (1)	3·50
N(3)	0·3809 (2)	0·2597 (2)	0·3161 (1)	3·34
C(1)	0·1700 (3)	0·1890 (3)	0·4759 (2)	3·17
C(2)	0·3292 (4)	0·0429 (3)	0·5673 (2)	4·56
C(3)	0·2360 (4)	0·0433 (3)	0·6257 (2)	4·47
C(4)	0·1068 (4)	0·1183 (4)	0·6072 (2)	5·13
C(5)	0·0721 (3)	0·1928 (3)	0·5310 (2)	4·47
C(6)	0·2046 (3)	0·4648 (3)	0·3991 (2)	3·02
C(7)	0·2231 (3)	0·6934 (3)	0·3435 (2)	4·42
C(8)	0·3128 (3)	0·7428 (3)	0·4169 (2)	4·47
C(9)	0·3486 (4)	0·6483 (3)	0·4832 (2)	4·81
C(10)	0·2925 (3)	0·5058 (3)	0·4752 (2)	3·85
C(11)	0·2417 (2)	0·2052 (2)	0·3115 (1)	2·67
C(12)	0·4634 (3)	0·1977 (3)	0·2657 (2)	3·88
C(13)	0·4189 (3)	0·0810 (3)	0·2123 (2)	3·93
C(14)	0·2792 (3)	0·0279 (3)	0·2089 (2)	3·74
C(15)	0·1879 (3)	0·0904 (3)	0·2582 (2)	3·21

Table 2. *Interatomic distances* (Å) *and bond angles* (°)

P(1)–C(1)	1·834 (3)	P(1)–C(6)	1·824 (3)
P(1)–C(11)	1·826 (2)	N(1)–C(1)	1·335 (3)
N(1)–C(2)	1·347 (3)	N(2)–C(6)	1·348 (3)
N(2)–C(7)	1·337 (4)	N(3)–C(11)	1·358 (3)
N(3)–C(12)	1·335 (3)	C(1)–C(5)	1·376 (4)
C(2)–C(3)	1·384 (4)	C(3)–C(4)	1·352 (4)
C(4)–C(5)	1·385 (4)	C(6)–C(10)	1·384 (3)
C(7)–C(8)	1·380 (4)	C(8)–C(9)	1·364 (5)
C(9)–C(10)	1·401 (4)	C(11)–C(15)	1·387 (3)
C(12)–C(13)	1·383 (4)	C(13)–C(14)	1·361 (4)
C(14)–C(15)	1·381 (4)		

C(1)–P(1)–C(6)	102·7 (1)	C(1)–P(1)–C(11)	101·9 (1)
C(6)–P(1)–C(11)	101·0 (1)	C(1)–N(1)–C(2)	117·6 (2)
C(6)–N(2)–C(7)	117·6 (2)	C(11)–N(3)–C(12)	116·4 (2)
P(1)–C(1)–N(1)	120·2 (2)	P(1)–C(1)–C(5)	117·6 (2)
N(1)–C(1)–C(5)	122·2 (3)	N(1)–C(2)–C(3)	123·0 (3)
C(2)–C(3)–C(4)	118·6 (3)	C(3)–C(4)–C(5)	119·3 (3)
C(1)–C(5)–C(4)	119·2 (3)	P(1)–C(6)–N(2)	111·6 (2)
P(1)–C(6)–C(10)	126·0 (2)	N(2)–C(6)–C(10)	122·4 (2)
N(2)–C(7)–C(8)	123·8 (3)	C(7)–C(8)–C(9)	118·4 (3)
C(8)–C(9)–C(10)	119·4 (3)	C(6)–C(10)–C(9)	118·4 (3)
P(1)–C(11)–N(3)	119·8 (2)	P(1)–C(11)–C(15)	118·1 (2)
N(3)–C(11)–C(15)	122·1 (2)	N(3)–C(12)–C(13)	124·8 (2)
C(12)–C(13)–C(14)	117·8 (2)	C(13)–C(14)–C(15)	119·7 (2)
C(11)–C(15)–C(14)	119·1 (2)		

0108-2701/88/040757-02$03.00

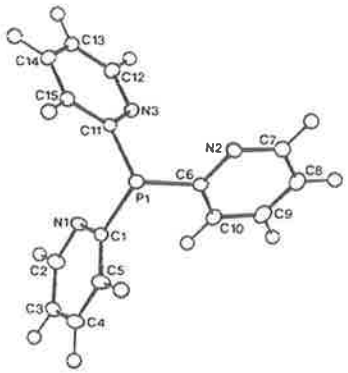

Fig. 1. Molecular structure and numbering scheme for tris-(2-pyridyl)phosphine. Hydrogen atoms are numbered according to the C atom to which they are bonded (Johnson, 1971).

reflections $\bar{5}14$, $\bar{6}14$ and $\bar{7}14$ were excluded from the final refinement owing to poor agreement. At convergence $R = 0{\cdot}046$, $wR = 0{\cdot}056$, $w = [\sigma^2(F) + 0{\cdot}0028F^2]^{-1}$, $S = 1{\cdot}47$, $(\Delta/\sigma)_{max} \leq 0{\cdot}001$, $(\Delta\rho)_{max} = 0{\cdot}94$, $(\Delta\rho)_{min} = -0{\cdot}27$ e Å^{-3}; no extinction correction. Scattering factors for all atoms given in *SHELX*76 (Sheldrick, 1976). All calculations on VAX11/785 computer system. Atomic parameters given in Table 1, bond distances and angles in Table 2;* the numbering scheme used is shown in Fig. 1.

Related literature. The title compound, $(2\text{-py})_3P$, has been shown by spectroscopic methods to function primarily as a tridentate ligand through the three N donor atoms, *e.g.* $[M\{(2\text{-py})_3P\}_2](ClO_4)_2$ for M = Mn, Co, Ni, Cu and Zn (Boggess & Zatko, 1975), for M = Co (Boggess & Zatko, 1976; Hafeli & Keene, 1987) and for M = Fe (Boggess, Hughes, Chew & Kemper, 1981). However, both monodentate P and bidentate P,N coordination have been reported for the $(2\text{-py})_3P$ ligand in a series of Ru and Rh compounds, *e.g.* $RuHCl\{(2\text{-py})_3P\}_3$ and $RhCl\{(2\text{-py})_3P\}_2$ (Kurtev, Ribola, Jones, Cole-Hamilton & Wilkinson, 1980). The only crystallographic characterization of a compound containing $(2\text{-py})_3P$ is that for the $[Ru\{(2\text{-py})_3P\}_2]^{2+}$ cation in which $(2\text{-py})_3P$ adopts the more common tridentate mode of coordination (Stephenson, Keene, Snow & Tiekink, 1988).

The Australian Research Grants Scheme is thanked for support.

* Lists of structure factors, thermal parameters, H-atom parameters and mean-plane data have been deposited with the British Library Document Supply Centre as Supplementary Publication No. SUP 44593 (13 pp.). Copies may be obtained through The Executive Secretary, International Union of Crystallography, 5 Abbey Square, Chester CH1 2HU, England.

References

BOGGESS, R. K., HUGHES, J. W., CHEW, C. W. & KEMPER, J. J. (1981). *J. Inorg. Nucl. Chem.* **43**, 939–945.

BOGGESS, R. K. & ZATKO, D. A. (1975). *J. Coord. Chem.* **4**, 217–224.

BOGGESS, R. K. & ZATKO, D. A. (1976). *Inorg. Chem.* **15**, 626–630.

HAFELI, T. A. & KEENE, F. R. (1987). Unpublished work.

HAFELI, T. A., KEENE, F. R., STEPHENSON, P. J. & WRIGHT, T. P. (1986). Unpublished work.

JOHNSON, C. K. (1971). *ORTEP*II. Report ORNL-3794. Oak Ridge National Laboratory, Tennessee, USA.

KURTEV, K., RIBOLA, D., JONES, R. A., COLE-HAMILTON, D. J. & WILKINSON, G. (1980). *J. Chem. Soc. Dalton Trans.* pp. 55–58.

SHELDRICK, G. M. (1976). *SHELX*76. Program for crystal structure determination. Univ. of Cambridge, England.

STEPHENSON, P. J., KEENE, F. R., SNOW, M. R. & TIEKINK, E. R. T. (1988). In preparation.

Acta Cryst. (1988). C**44**, 937–938

Tris(2-pyridyl)methanol

BY F. RICHARD KEENE

Department of Chemistry and Biochemistry, James Cook University of North Queensland, Townsville, Queensland 4811, *Australia*

AND MICHAEL R. SNOW AND EDWARD R. T. TIEKINK

Jordan Laboratories, Department of Physical and Inorganic Chemistry, University of Adelaide, Adelaide, South Australia 5001, *Australia*

(*Received* 15 *December* 1987; *accepted* 7 *January* 1988)

Abstract. $C_{16}H_{13}N_3O$, $M_r = 263{\cdot}3$, monoclinic, $P2_1/n$, $a = 11{\cdot}034$ (1), $b = 8{\cdot}794$ (3), $c = 14{\cdot}007$ (2) Å, $\beta = 102{\cdot}31$ (1)°, $U = 1328$ (2) Å^3, $D_x = 1{\cdot}317$ Mg m^{-3} for $Z = 4$, Mo $K\bar{\alpha}$ radiation, $\lambda = 0{\cdot}7107$ Å, $\mu = 0{\cdot}049$ mm^{-1}, $F(000) = 552$, $T = 293$ (2) K, $R = 0{\cdot}045$ for 1811 observed reflections. Within the molecule the C—C(py) distances lie in the range 1·524 (3)–1·530 (2) Å and the maximum deviation from ideal tetrahedral geometry is seen in the O(1)—C(16)—C(11) angle of 106·1 (2)°. The dihedral angles between the N(1)—C(5), N(2)—C(10) and N(3)—C(15) rings are 89·7, 100·8 and 81·5° respectively. The disposition of the N atoms is such that two point in the opposite direction of the alcohol function while the other, N(2), lies on the same side of the molecule as the C—OH group; the O—H(16)···N(2) separation of 2·19 (3) Å may be indicative of a weak intramolecular interaction between these atoms. In the crystal lattice there is also a close contact between N(2) and the centrosymmetrically related hydroxyl proton of 2·37 (4) Å.

Table 1. *Fractional atomic coordinates and* B_{eq} *values* (Å^2)

$B_{eq} = 8\pi^2(U_{11} + U_{22} + U_{33})/3$.

	x	y	z	B_{eq}
O(1)	−0·4060 (1)	0·2963 (2)	0·0612 (1)	3·71
N(1)	−0·2377 (2)	0·2679 (2)	−0·1306 (1)	3·40
N(2)	−0·3400 (1)	0·5571 (2)	−0·0155 (1)	3·13
N(3)	−0·1071 (2)	0·1391 (2)	0·0734 (1)	3·60
C(1)	−0·3106 (2)	0·2220 (2)	−0·0715 (1)	2·72
C(2)	−0·2526 (2)	0·2002 (3)	−0·2175 (2)	4·16
C(3)	−0·3376 (3)	0·0876 (3)	−0·2494 (2)	4·49
C(4)	−0·4129 (3)	0·0425 (3)	−0·1886 (2)	4·78
C(5)	−0·4002 (2)	0·1102 (2)	−0·0987 (2)	3·99
C(6)	−0·2491 (2)	0·4613 (2)	0·0232 (1)	2·71
C(7)	−0·3102 (2)	0·7031 (2)	−0·0236 (2)	3·77
C(8)	−0·1917 (2)	0·7587 (3)	0·0061 (2)	4·08
C(9)	−0·0995 (2)	0·6597 (3)	0·0470 (2)	4·22
C(10)	−0·1281 (2)	0·5084 (3)	0·0555 (2)	3·68
C(11)	−0·2003 (2)	0·2050 (2)	0·1040 (1)	2·89
C(12)	−0·0234 (2)	0·0620 (3)	0·1395 (2)	4·01
C(13)	−0·0291 (3)	0·0484 (3)	0·2355 (2)	4·53
C(14)	−0·1245 (3)	0·1169 (4)	0·2654 (2)	5·97
C(15)	−0·2130 (3)	0·1963 (3)	0·1997 (2)	4·93
C(16)	−0·2919 (2)	0·2966 (2)	0·0287 (1)	2·79

Experimental. Transparent crystals were obtained from the slow evaporation of a benzene/373–393 K petroleum spirit solution of the compound (Wibaut, De Jonge, Van Der Voort & Otto, 1951). Enraf–Nonius CAD-4F diffractometer controlled by a PDP8/A computer, graphite-monochromated Mo $K\bar{\alpha}$ radiation; $\omega/2\theta$ scan technique. Cell parameters on crystal 0·18 × 0·56 × 0·56 mm from least-squares procedure on 25 reflections ($13 \le \theta \le 19°$). Analytical absorption correction applied (Sheldrick, 1976); max./min. transmission factors 0·9919 and 0·9778. Total of 4501 reflections ($1 \le \theta \le 27{\cdot}5°$) measured in the range $-14 \le h \le 14$, $-11 \le k \le 0$, $-20 \le l \le 6$. No significant variation in the net intensities of three reference reflections (562, 253, 366) measured every 7200 s. 3049 unique reflections (R_{int} 0·056), 1813 satisfied $I \ge 2{\cdot}5\sigma(I)$. Structure solved by direct methods, full-matrix least-squares refinement of 233 parameters based on F (Sheldrick, 1976). Anisotropic thermal parameters for non-H atoms and H atoms located from difference map and refined. The reflections $\bar{2}04$ and 013 were excluded from the final refinement due to poor agreement. At convergence $R = 0{\cdot}045$, $wR = 0{\cdot}053$, $w = [\sigma^2(F) + 0{\cdot}0076F^2]^{-1}$, $S = 0{\cdot}73$, $(\Delta/\sigma)_{max} \le 0{\cdot}001$, $(\Delta\rho)_{max} = 0{\cdot}16$, $(\Delta\rho)_{min} = -0{\cdot}29$ e Å^{-3}; no extinction correction. Scattering factors for all atoms given in *SHELX*76 (Sheldrick, 1976). All calculations on VAX11/785 computer system. Atomic parameters are given in Table 1, bond distances and angles in Table 2;* the numbering scheme used is shown in Fig. 1.

Related literature. Several crystal structures have been determined for metal complexes containing the title compound, $(py)_3COH$, as a ligand. Thus symmetric

* Lists of structure factors, thermal parameters, H-atom parameters and mean-plane data have been deposited with the British Library Document Supply Centre as Supplementary Publication No. SUP 44671 (15 pp.). Copies may be obtained through The Executive Secretary, International Union of Crystallography, 5 Abbey Square, Chester CH1 2HU, England.

0108-2701/88/050937-02$03.00

Table 2. *Interatomic distances* (Å) *and bond angles* (°)

N(1)–C(1)	1·333 (3)	N(1)–C(2)	1·334 (3)
N(2)–C(6)	1·333 (2)	N(2)–C(7)	1·336 (3)
N(3)–C(11)	1·329 (3)	N(3)–C(12)	1·343 (3)
C(2)–C(3)	1·372 (4)	C(3)–C(4)	1·368 (4)
C(4)–C(5)	1·374 (4)	C(5)–C(1)	1·389 (3)
C(7)–C(8)	1·375 (3)	C(8)–C(9)	1·368 (4)
C(9)–C(10)	1·378 (3)	C(10)–C(6)	1·379 (3)
C(12)–C(13)	1·364 (4)	C(13)–C(14)	1·354 (4)
C(14)–C(15)	1·380 (4)	C(15)–C(11)	1·380 (3)
C(16)–O(1)	1·427 (2)	C(16)–C(1)	1·524 (3)
C(16)–C(6)	1·530 (2)	C(16)–C(11)	1·526 (3)
O(1)–H(16)	0·88 (3)		

C(1)–N(1)–C(2)	117·3 (2)	C(6)–N(2)–C(7)	117·2 (2)
C(11)–N(3)–C(12)	117·6 (2)	N(1)–C(1)–C(5)	122·2 (2)
N(1)–C(1)–C(16)	117·4 (2)	C(5)–C(1)–C(16)	120·4 (2)
N(1)–C(2)–C(3)	124·2 (3)	C(2)–C(3)–C(4)	118·1 (2)
C(3)–C(4)–C(5)	119·2 (2)	C(4)–C(5)–C(1)	119·0 (2)
N(2)–C(6)–C(10)	122·3 (2)	N(2)–C(6)–C(16)	113·9 (1)
C(10)–C(6)–C(16)	123·8 (2)	N(2)–C(7)–C(8)	123·4 (2)
C(7)–C(8)–C(9)	118·4 (2)	C(8)–C(9)–C(10)	119·1 (2)
C(9)–C(10)–C(6)	119·0 (2)	N(3)–C(11)–C(15)	122·3 (2)
N(3)–C(11)–C(16)	116·9 (2)	C(15)–C(11)–C(16)	120·8 (2)
N(3)–C(12)–C(13)	123·7 (2)	C(12)–C(13)–C(14)	117·9 (2)
C(13)–C(14)–C(15)	120·3 (2)	C(14)–C(15)–C(11)	118·2 (2)
O(1)–C(16)–C(1)	109·8 (1)	O(1)–C(16)–C(6)	108·7 (1)
O(1)–C(16)–C(11)	106·1 (2)	C(1)–C(16)–C(6)	110·1 (1)
C(1)–C(16)–C(11)	110·4 (2)	C(6)–C(16)–C(11)	111·6 (1)
C(16)–O(1)–H(16)	106 (2)		

tridentate N,N′,N″ coordination has been noted in the cations $[M\{(py)_3COH\}_2]^{2+}$, M = Co (Szalda & Keene, 1986) and for one ligand in M = Ru (Keene, Szalda & Wilson, 1987). Asymmetric tridentate coordination has been found in $[CH_3Hg(py)_3COH)][NO_3]$ (Canty, Chaichit, Gatehouse & George, 1981) with Hg–N bond distances in the range 2·28 (1) to 2·53 (1) Å. Tridentate coordination *via* two N atoms and the hydroxyl O atom has also been observed in one of the ligands in $[Ru\{(py)_3COH\}_2]^{2+}$ (Keene, Szalda & Wilson, 1987) and in $[Ru(NH_3)_3\{(py)_3COH\}]^{2+}$ (Diamantis, Keene, Moritz, Snow & Tiekink, 1988).

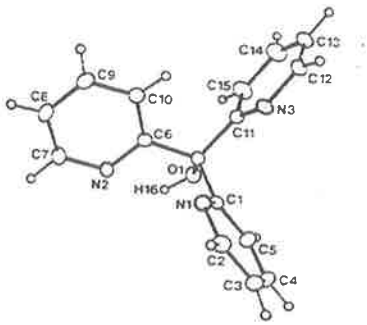

Fig. 1. The molecular structure and numbering scheme for $(C_5H_4N)_3COH$. Hydrogen atoms are numbered according to the C atom to which they are bonded (Johnson, 1971).

When deprotonated, the ligand also coordinates *via* two N atoms and the O atom as found in $[Ru\{(py)_3COH\}\{(py)_3CO\}]^+$ (Keene, Szalda & Wilson, 1987).

The Australian Research Grants Scheme is thanked for support.

References

CANTY, A. J., CHAICHIT, N., GATEHOUSE, B. M. & GEORGE, E. E. (1981). *Inorg. Chem.* **20**, 4293–4300.

DIAMANTIS, A. A., KEENE, F. R., MORITZ, P. S., SNOW, M. R. & TIEKINK, E. R. T. (1988). In preparation.

JOHNSON, C. K. (1971). *ORTEPII*. Report ORNL-3794. Oak Ridge National Laboratory, Tennessee, USA.

KEENE, F. R., SZALDA, D J. & WILSON, T. A. (1987). *Inorg. Chem.* **26**, 2211–2216.

SHELDRICK, G. M. (1976). *SHELX76*. Program for crystal structure determination. Univ. of Cambridge, England.

SZALDA, D. J. & KEENE, F. R. (1986). *Inorg. Chem.* **25**, 2795–2799.

WIBAUT, J. P., DE JONGE, A. P., VAN DER VOORT, H. G. P. & OTTO, P. PH. H. L. (1951). *Recl Trav. Chim. Pays Bas*, **70**, 1054–1066.

2040 *Inorg. Chem.* 1988, *27*, 2040-2045

Contribution from the Department of Chemistry and Biochemistry, James Cook University of North Queensland, Townsville, Queensland 4811, Australia, and Jordan Laboratories, Department of Physical and Inorganic Chemistry, University of Adelaide, Adelaide, South Australia 5001

Ruthenium(II) Complexes of the C_{3v} Ligands Tris(2-pyridyl)amine, Tris(2-pyridyl)methane, and Tris(2-pyridyl)phosphine. 1. Synthesis and X-ray Structural Studies of the Bis(ligand) Complexes

F. Richard Keene,*[1] Michael R. Snow,[2] Philip J. Stephenson,[1] and Edward R. T. Tiekink[2]

Received November 25, 1987

Bis(ligand)ruthenium(II) complexes [ligand = tris(2-pyridyl)amine, tris(2-pyridyl)methane, and tris(2-pyridyl)phosphine] were synthesized by the reaction of $[Ru(DMF)_6]^{2+}$ (DMF = *N*,*N*-dimethylformamide) with excess of the respective ligands under anaerobic conditions in propan-1-ol solution. Crystals of $[Ru\{(2\text{-py})_3CH\}_2](tosylate)_2 \cdot H_2O$ (**1**) crystallize in the monoclinic space group $C2/c$ with unit cell dimensions a = 13.205 (9) Å, b = 13.437 (6) Å, c = 23.614 (22) Å, β = 96.57 (6)°, V = 4162.5 Å^3, and Z = 4; crystals of $[Ru\{(2\text{-py})_3P\}_2](tosylate)_2 \cdot C_2H_5OH$ (**2**) are also monoclinic ($P2_1/c$) with a = 10.065 (7) Å, b = 13.008 (4) Å, c = 34.772 (22) Å, β = 92.40 (5)°, V = 4548.6 Å^3, and Z = 4. $[Ru\{(2\text{-py})_3N\}_2](S_2O_6) \cdot 4H_2O$ (**3**) crystallizes in the triclinic space group $P\bar{1}$ with a = 8.914 (3) Å, b = 9.060 (2) Å, c = 11.243 (2) Å, α = 95.52 (1)°, β = 104.19 (2)°, γ = 92.03(2)°, V = 874.6 Å^3, and Z = 1. The structures were refined by a full-matrix least-squares procedure in each case. At convergence, final R = 0.050, R_w = 0.055 for 2931 reflections with $I \geq 2.5\sigma(I)$ for **1**, R = 0.063, R_w = 0.065 for 2017 reflections for **2**, R = 0.039, R_w = 0.041 for 2582 reflections for **3**. The cations show increasing distortion in the structure from ideal D_{3d} symmetry with an increase in the bridgehead (X)–C(py) bond distance.

Introduction

There has been considerable interest in the ruthenium[3,4] and rhenium[5-7] complexes containing polypyridyl ligands such as 2,2′-bipyridyl and 1,10-phenanthroline, primarily because of their potential as photosensitizers in significant processes such as water or carbon dioxide reduction.

Studies in these laboratories[8,9] and by other workers[10,11] involving complexes of tripodal ligands of the type

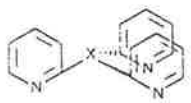

X = CH, COH, N, P, P=O

have drawn attention to the fact that such ligands stabilize the Co(I) (d^8) state, in the same manner as 2,2′-bipyridine and its congeners where such stabilization has generally been attributed[12] to the π-acceptor properties of the bidentate ligands. The synthetic versatility of the tripodal ligands[13] commends their use in the study of a number of aspects relating to bonding in complexes of polypyridyl ligands, including the structural features and the physical properties of such complexes.

As part of our continuing interest in the complexes of tripodal π-acceptor ligands with transition metals of groups 6–11, we have undertaken studies of the synthesis, structure, and physical properties of the ruthenium(II) complexes of these ligands. We have previously reported[14] investigations involving the tris(2-pyridyl)methanol ligand—we now report a new general synthetic method for this genre of RuL_2^{2+} complexes and the structural details of the bis(ligand)ruthenium(II) complexes of tris(2-pyridyl)amine, tris(2-pyridyl)methane, and tris(2-pyridyl)phosphine. Details of the spectroscopic and electrochemical behavior of these species will be published subsequently.[15]

Experimental Section

NMR spectra were recorded on a Bruker AM-400 spectrometer ($CDCl_3$ solvent; $SiMe_4$ internal reference). Elemental analysis were carried out by the Canadian Microanalytical Service (New Westminster, B.C.).

Syntheses. The ligand tris(2-pyridyl)amine[16] was prepared by literature methods in 15% yield. The complexes $[Ru(OH_2)_6](tos)_2$ (tos = 4-toluenesulfonate anion, $H_3CC_6H_4SO_3^-$) and $[Ru(DMF)_6](tos)_2$ (DMF = *N*,*N*-dimethylformamide) were prepared by methods of Bernhard et al.[17,18]

Tris(2-pyridyl)methane. Bis(2-pyridyl)methane[19] (6.40 g; 0.037 mol) in dry diethyl ether (70 mL) was added to *n*-butyllithium (23.8 mL of 1.55 M; 0.037 mol) at −60 °C and the mixture stirred for 15 min under an atmosphere of dry N_2. Freshly distilled 2-bromopyridine (3.26 mL; 0.037 mol) in dry ether (70 mL) was added over 1.5 h with continuous stirring at −60 °C: the temperature was maintained in turn at that temperature for another 30 min, at −20 °C for 1 h, and at 0 °C for 30 min. Dry benzene (170 mL) was added, the ether removed by distillation, and the mixture refluxed overnight. After cooling, water (170 mL) was added and the benzene layer separated. The aqueous layer was reextracted with benzene (3 × 50 mL) and the combined organic extracts dried with $MgSO_4$. The solvent was evaporated (rotary evaporator) and the (liquid) residue extracted with petroleum ether (300 mL). This solution was refluxed with activated charcoal, filtered hot, slowly evaporated to ca. 120 mL, and cooled, and the resultant solid was filtered, washed with cold petroleum ether, and air dried: yield 4.9 g, 53%; mp 100 °C (lit.[20] mp 99–100 °C). ^{1}H NMR ($CDCl_3$): singlet (methine proton), δ 5.98; ^{13}C NMR ($CDCl_3$): singlet (tertiary carbon), δ 64.1; five singlets (pyridine ring carbons), δ 121.6, 124.1, 136.4, 149.4, and 161.1.

Tris(2-pyridyl)phosphine was prepared by modification of a literature procedure.[21] A solution of *n*-butyllithium in hexane (39 mL; 1.44 M) in dry diethyl ether (80 mL) was cooled to ca. −100 °C. Under an atmosphere of dry N_2, freshly distilled 2-bromopyridine (5.4 mL) in dry diethyl ether (5 mL) was added dropwise with a gastight syringe, and the resultant dark red solution was stirred at −100 °C for 4 h. A solution of freshly distilled PCl_3 (1.60 mL) in diethyl ether (8 mL) was added dropwise over a period of 1 h, also with a gastight syringe. After further stirring for 2 h at −100 °C, the light tan suspension was warmed slowly to room temperature. The mixture was extracted three times with 2 M H_2SO_4 (1 × 40 mL, 2 × 20 mL), and the aqueous layer was neutralized

(1) James Cook University of North Queensland.
(2) University of Adelaide.
(3) Sutin, N.; Creutz, C. *Pure Appl. Chem.* **1980**, *52*, 2717–2738.
(4) Kalyanasundaram, K. *Coord. Chem. Rev.* **1982**, *46*, 159–244.
(5) Kutal, C.; Weber, M. A.; Ferraudi, G.; Geiger, D. *Organometallics* **1985**, *4*, 2161–2166.
(6) Sullivan, B. P.; Meyer, T. J. *Organometallics* **1986**, *5*, 1500–1502.
(7) Hawecker, J.; Lehn, J.-M.; Zeissel, R. *Helv. Chim. Acta* **1986**, *69*, 1990–2012.
(8) Szalda, D. J.; Keene, F. R. *Inorg. Chem.* **1986**, *25*, 2795–2799.
(9) Hafeli, T. A.; Keene, F. R. *Aust. J. Chem.*, in press.
(10) Boggess, R. K.; Zatko, D. A. *Inorg. Chem.* **1976**, *15*, 626–630.
(11) Boggess, R. K.; Zatko, D. A. *Inorg. Nucl. Chem. Lett.* **1976**, *12*, 7–11.
(12) Szalda, D. J.; Creutz, C.; Mahajan, D.; Sutin, N. *Inorg. Chem.* **1983**, *22*, 2372–2379.
(13) White, D. L.; Faller, J. W. *Inorg. Chem.* **1982**, *21*, 3119–3122.
(14) Keene, F. R.; Szalda, D. J.; Wilson, T. A. *Inorg. Chem.* **1987**, *26*, 2211–2216.
(15) Atkinson, I. M.; Keene, F. R.; Stephenson, P. J., unpublished work.
(16) Wibaut, J. P.; La Bastide, G. L. C. *Recl. Trav. Chim. Pays-Bas* **1933**, *52*, 493–498.
(17) Bernhard, P.; Sargeson, A. M. *J. Chem. Soc., Chem. Commun.* **1985**, *1516*–1518.
(18) Bernhard, P., personal communication to F.R.K.
(19) Canty, A. J.; Minchin, N. J. *Aust. J. Chem.* **1986**, *39*, 1063–1069.
(20) Osuch, C.; Levine, R. *J. Am. Chem. Soc.* **1956**, *78*, 1723–1725.
(21) Kurtev, K.; Ribola, D.; Jones, R. A.; Cole-Hamilton, D. J.; Wilkinson, G. *J. Chem. Soc., Dalton Trans.* **1980**, *55*–58.

0020-1669/88/1327-2040$01.50/0

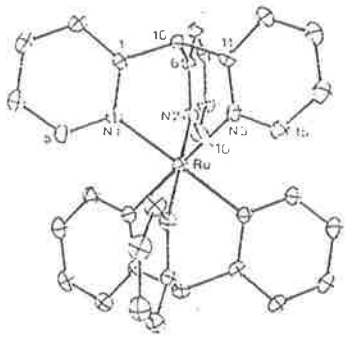

Figure 1. ORTEPII drawing of $[Ru\{(2\text{-py})_3CH\}_2]^{2+}$ (1^{2+}) showing the atom-labeling scheme used. Note that the Ru atom is situated on a crystallographic 2-fold axis. Atoms not otherwise indicated are carbons, and hydrogen atoms have been omitted for clarity.

and adjusted to pH 10–11 by using a 30% NaOH solution (with cooling). The precipitated tris(2-pyridyl)phosphine was collected, washed with water (50 mL) and petroleum ether (4 × 5 mL), dried in vacuo, and stored under N_2: yield 3.3 g, 66%; mp 111–113 °C (lit.[22,23] mp 115 °C). The product was recrystallized in 60% yield from deaerated acetone/petroleum ether.

Bis[tris(2-pyridyl)amine]ruthenium(II) Tosylate, $[Ru\{(2\text{-py})_3N\}_2](tos)_2$. $[Ru(DMF)_6](tos)_2$ (0.1 g) was added to a degassed (Ar) solution of the ligand (0.08 g) in dry propan-1-ol (60 mL). The solution was refluxed overnight, during which time it changed from a light orange color to an intense yellow-orange. The solvent was removed under reduced pressure, and the residue was recrystallized from ethanol/ether. Yield: 0.09 g, 82%. Anal. Calcd for $[Ru(C_{15}H_{12}N_4)_2](C_7H_7SO_3)_2$: C, 56.2; H, 4.08; N, 11.9. Found: C, 56.3; H, 4.23; N, 11.8. The tosylate salt was converted (100%) to the PF_6^- form by adding solid NH_4PF_6 to an ethanolic solution; the resultant crystals were washed with cold ethanol and dried in vacuo. Orange-yellow crystals of the dithionate salt were grown for X-ray structural studies by layering an ethanolic solution of $Li_2S_2O_6$ above an aqueous solution of $[Ru\{(2\text{-py})_3N\}_2](PF_6)_2$.

Bis[tris(2-pyridyl)methane]ruthenium(II) tosylate hydrate, $[Ru\{(2\text{-py})_3CH\}_2](tos)_2\cdot H_2O$, was prepared in a manner similar to that used for the amine analogue. After evaporation of the propan-1-ol solvent, the residue was chromatographed on Sephadex LH-20 (methanol solvent) giving two incompletely separated species. The leading edge of the eluted band (yellow) was collected, the solvent removed under reduced pressure, and the residue recrystallized from methanol/diethyl ether. Yield: 44%. Anal. Calcd for $[Ru(C_{16}H_{13}N_3)_2](C_7H_7SO_3)_2\cdot H_2O$: C, 57.7; H, 4.43; N, 8.8. Found: C, 57.5; H, 4.37; N, 8.6. Orange crystals of the tosylate salt for X-ray structural studies were grown by layering ether on top of a methanolic solution of the complex.

The tail of the band from the chromatography (orange) was treated in the same manner, giving a slightly lesser amount of an orange solid. The nature of this material will be addressed in a subsequent communication.[15]

Bis[tris(2-pyridyl)phosphine]ruthenium(II) tosylate ethanolate, $[Ru\{(2\text{-py})_3P\}_2](tos)_2\cdot C_2H_5OH$, was prepared in a manner similar to that used for the amine analogue, in 67% yield. Anal. Calcd for $[Ru(C_{15}H_{12}N_3P)_2](C_7H_7SO_3)_2\cdot C_2H_5OH$: C, 54.1; H, 4.35; N, 8.2. Found: C, 53.6; H, 4.38; N, 8.2. Orange-red crystals of the tosylate salt for the X-ray structural studies were grown by layering ether on top of an ethanolic solution of the complex.

Collection and Reduction of X-ray Data. Intensity data were measured at room temperature, 295 (2) K, with the use of Mo Kα (graphite monochromator) radiation (λ = 0.7107 Å) on an Enraf-Nonius CAD4F diffractometer employing the ω–2θ scan technique. Corrections were routinely applied for Lorentz and polarization effects and for absorption with an analytical procedure.[24] The net intensity values of three standard reflections (monitored after every 3600 s of X-ray exposure time) decreased to 80% of their original values for **1**, and hence the data were corrected for this variation; no such decomposition was detected during the data collection for **2** or **3**. All relevant data collection parameters and crystal data are listed in Table I.

Determination and Refinement of Structures. The structures of **1** and **2** were solved from the interpretation of the Patterson in both cases; for

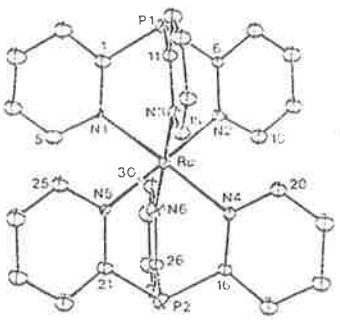

Figure 2. ORTEPII drawing of $[Ru\{(2\text{-py})_3P\}_2]^{2+}$ (2^{2+}) showing the atom-labeling scheme used. Atoms not otherwise indicated are carbons, and hydrogen atoms have been omitted for clarity.

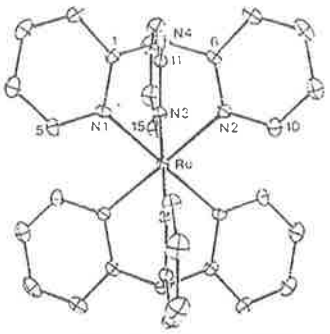

Figure 3. ORTEPII drawing of $[Ru\{(2\text{-py})_3N\}_2]^{2+}$ (3^{2+}) showing the atom-labeling scheme used. Note that the Ru atom is situated on a crystallographic center of inversion. Atoms not otherwise indicated are carbons, and hydrogen atoms have been omitted for clarity.

3 the Ru atom was at a site of symmetry $\bar{1}$ at (0, 0, 0). The structures were each refined by a full-matrix least-squares procedure in which the function $\sum w\Delta^2$ was minimized, where w was the weight applied to each reflection, and $\Delta = ||F_o| - |F_c||$.[24] The cation in **1** is situated about a crystallographic 2-fold axis as is a water molecule of crystallization. Anisotropic thermal parameters were introduced for all non-hydrogen atoms in **1** and **3**. However, due to the limited data set obtained for **2**, only Ru, N, O, P, and S atoms were refined anisotropically. Hydrogen atoms were included in each model at their calculated positions. A weighting scheme of the form $w = k/[\sigma^2(F) + gF^2]$ was introduced in the calculations, and the refinements were continued until convergence. The choice of $C2/c$ as the space group for **1**, as opposed to Cc, was vindicated by the smooth and ready convergence of the refinement as well as the distribution of the E statistics.[24] Refinement details are given in Table I.

Fractional atomic coordinates are given in Tables II–IV, selected bond distances and angles for the compounds are listed in Tables V–VII, and the numbering schemes employed are shown in Figures 1–3 (drawn with ORTEPII[25] at 15% probability ellipsoids). The scattering factors for C, H, N, O, P, and S were those incorporated in the SHELX program[24] and for central Ru were those (corrected for f' and f'') from ref 26.

Results and Discussion

Synthesis. There are a number of synthetic routes for polypyridyl complexes of ruthenium(II),[27] of which the most generally used is the reaction of $[RuCl_5(OH_2)]^{2-}$ (or similar chlororuthenate(III) species) with excess ligand either in a reducing solvent (e.g. methanol) or in aqueous solution in the presence of a reducing agent (e.g. sodium phosphinite, NaH_2PO_2). Although the former method was used satisfactorily in the preparation of the bis[tris(2-pyridyl)methanol]ruthenium(II) species,[14] these methods generally were not satisfactory for the synthesis of the

(22) Mann, F. G.; Watson, J. *J. Org. Chem.* **1948**, *13*, 502–531.
(23) Boggess, R. K.; Zatko, D. A. *J. Coord. Chem.* **1975**, *4*, 217–224.
(24) Sheldrick, G. M. "SHELX76, Program for Crystal Structure Determination"; University of Cambridge, England, 1976.
(25) Johnson, C. K. "ORTEPII"; Report ORNL-3794; Oak Ridge National Laboratory: Oak Ridge, TN, 1971.
(26) Hamilton, W. C.; Ibers, J. A. *International Tables of X-Ray Crystallography*; Kynoch: Birmingham, England, 1974; Vol. IV, pp 99, 149.
(27) Seddon, E. A.; Seddon, K. R. *The Chemistry of Ruthenium*; Elsevier: Amsterdam, 1984; pp 414–424 and references therein.

Table I. Crystal Data for 1–3

	$[Ru\{(py)_3CH\}_2](tos)_2\cdot H_2O$	$[Ru\{(py)_3P\}_2](tos)_2\cdot C_2H_5OH$	$[Ru\{(py)_3N\}_2](S_2O_6)\cdot 4H_2O$
formula	$C_{46}H_{42}N_6O_7S_2Ru$	$C_{46}H_{44}N_6O_7P_2S_2Ru$	$C_{30}H_{32}N_8O_{16}S_2Ru$
fw	956.1	1020.0	829.8
cryst syst	monoclinic	monoclinic	triclinic
space group	$C2/c$ (C_{2h}^6, No. 15)	$P2_1/c$ (C_{2h}^5, No. 14)	$P\bar{1}$ (C_i^1, No. 2)
a, Å	13.205 (9)	10.065 (7)	8.914 (3)
b, Å	13.437 (6)	13.008 (4)	9.060 (2)
c, Å	23.614 (22)	34.172 (22)	11.243 (2)
α, deg	90	90	95.52 (1)
β, deg	96.57 (6)	92.40 (5)	104.19 (2)
γ, deg	90	90	92.03 (2)
V, Å^3	4162.5	4548.6	874.6
D_{expt}, mg m^{-3}	1.52	1.52	1.54
Z	4	4	1
D_{calcd}, mg m^{-3}	1.526	1.490	1.576
$F(000)$	1968	2096	424
μ, mm^{-1}	0.490	0.514	0.584
cryst dimens,[a] mm	±(111) 0.18; ±(1$\bar{1}$1) 0.11; ±(001) 0.25	±(100) 0.25; ±(010) 0.06; ±(001) 0.06	±(011) 0.27; ±(02$\bar{1}$) 0.13; ±(110) 0.10; ±(101) 0.13
transmissn factors	0.9322; 0.8347	0.9422; 0.8931	0.8890; 0.7586
θ limits, deg	1–25	1–20	1–25
range	$\pm h,k,l$	$\pm h,k,l$	$\pm h,\pm k,+l$
no. of data collcd	5306	5547	3611
no. of unique data	3662	4248	3081
R_{anal}[b]	0.065	0.059	0.021
no. of unique data used with $I \geq 2.5\sigma(I)$	2911	3017	2582
R	0.050	0.063	0.039
k	2.73	1.37	1.0
g	0.0007	0.0026	0.0130
R_w	0.055	0.065	0.041
r_{max}, e Å^{-3}	1.41	0.89	0.96

[a] From centroid. [b] $R_{anal} = (\sum[N\{w(F_{mean} - |F_o|^2)\}]/\sum[(N-1)\sum(w|F_o|^2)])^{1/2}$, where the inner summation is over N equivalent reflections averaged to give F_{mean}, the outer summation is over all unique reflections, and the weight, w, is taken as $[\sigma(F_o)]^{-2}$.

Table II. Fractional Atomic Coordinates for $[Ru\{(2\text{-}py)_3CH\}_2](tos)_2\cdot H_2O$ (1) (×10^5 for Ru; ×10^4 for Remaining Atoms)

atom	x	y	z
Ru	0	24236 (3)	25000
N(1)	807 (3)	2427 (2)	1806 (2)
N(2)	999 (2)	1344 (2)	2851 (2)
N(3)	1031 (3)	3476 (2)	2859 (2)
C(1)	1834 (3)	2401 (3)	1895 (2)
C(2)	2421 (3)	2391 (3)	1449 (2)
C(3)	1966 (4)	2421 (3)	897 (2)
C(4)	917 (4)	2449 (3)	803 (2)
C(5)	373 (4)	2455 (3)	1263 (2)
C(6)	2000 (3)	1453 (3)	2812 (2)
C(7)	2715 (3)	778 (3)	3043 (2)
C(8)	2392 (3)	−50 (3)	3318 (2)
C(9)	1378 (4)	−188 (3)	3358 (2)
C(10)	704 (3)	529 (3)	3119 (2)
C(11)	2025 (3)	3305 (3)	2832 (2)
C(12)	2781 (3)	3928 (3)	3098 (2)
C(13)	2485 (4)	4739 (3)	3403 (2)
C(14)	1485 (4)	4919 (3)	3428 (2)
C(15)	765 (3)	4287 (3)	3147 (2)
C(16)	2302 (4)	2487 (3)	2506 (2)
S(1)	5092 (1)	2290 (1)	949 (1)
O(1)	4180 (3)	1996 (4)	596 (2)
O(2)	5078 (3)	1909 (3)	1527 (2)
O(3)	5341 (3)	3326 (3)	937 (2)
C(17)	6092 (3)	1633 (3)	676 (2)
C(18)	5923 (3)	680 (4)	469 (2)
C(19)	6703 (4)	151 (4)	255 (3)
C(20)	7666 (3)	566 (4)	251 (2)
C(21)	7821 (3)	1513 (4)	466 (2)
C(22)	7044 (3)	2062 (4)	675 (2)
C(23)	8534 (5)	5 (5)	34 (3)
O(4)	5000	6947 (5)	7500

title compounds, resulting in either very low yields or green products of uncertain composition. Similarly, the ligand substitution of $[Ru(H)(OH_2)_2(CH_3OH)(PPh_3)_2]BF_4$ in methanol solution, a method developed by Templeton for the preparation of $[Ru(py)_6]^{2+}$[28] and used subsequently in our laboratories in the synthesis of the $[Ru(L)_2]^{n+}$ species [L = tris(2-pyridyl)-methanol],[14] met with mixed success for the range of tripod ligands of the present study.

Accordingly, we have used as a general method for the synthesis of the bis(ligand)ruthenium(II) complexes the ligand substitution of a new precursor, $[Ru(DMF)_6]^{2+}$ (DMF = *N*,*N*-dimethylformamide), developed by Bernhard and Sargeson.[27] The reaction of this species with a 3 molar ratio of the respective ligand for 12 h in refluxing dry propan-1-ol under anaerobic conditions resulted in high yields of the respective $[Ru(L)_2]^{2+}$ products.

The corresponding complex of tris(2-pyridyl)methanol was also prepared by this technique and yielded a product identical with that previously obtained by other methods.[14]

Description of Structures. Views of the cations $[Ru\{(2\text{-}py)_3CH\}_2]^{2+}$ (1^{2+}), $[Ru\{(2\text{-}py)_3P\}_2]^{2+}$ (2^{2+}), and $[Ru\{(2\text{-}py)_3N\}_2]^{2+}$ (3^{2+}) and the atom-labeling schemes used are shown in Figures 1–3, respectively. In all cases, the ligands are coordinated in a tripodal manner through the three py N atoms. Complex **1** has a crystallographic 2-fold axis, whereas there is only an approximate 2-fold axis in **2**; on the other hand for **3**, the molecule possesses a center of symmetry.

For the three cations of **1**, **2**, and **3**, the average[29] Ru–N bond distances (see Tables V–VII) are 2.068 (2), 2.072 (4), and 2.066 (2) Å, respectively: the carbon- and phosphorus-bridged donors reveal significantly greater variations than the nitrogen-bridged donor in this distance. The average Ru–N(bpy) bond length reported in $[Ru(bpy)_3]^{2+}$ is 2.056 Å;[30] the similar length of the

(28) Templeton, J. L. *J. Am. Chem. Soc.* **1979**, *101*, 4906–4917.

(29) A standard procedure for obtaining weighted averages was used:

$$\bar{x} = \frac{\sum(x_i/\sigma_i^2)}{\sum(1/\sigma_i^2)} \qquad \sigma^2(\bar{x}) = \sum(1/\sigma_i^2)$$

(30) Rillema, D. P.; Jones, O. S.; Levy, H. A. *J. Chem. Soc., Chem. Commun.* **1979**, 849–851.

Table III. Fractional Atomic Coordinates for $[Ru\{(2\text{-py})_3P_{12}\}(tos)_2\cdot C_2H_5OH$ (2) (×10⁵ for Ru; ×10⁴ for Remaining Atoms)

atom	x	y	z
Ru	25985 (13)	22290 (12)	9226 (4)
P(1)	2813 (4)	4167 (4)	287 (2)
P(2)	2479 (5)	260 (4)	1555 (2)
N(1)	4284 (11)	3076 (9)	828 (4)
N(2)	1495 (12)	3560 (11)	933 (4)
N(3)	2175 (11)	2078 (11)	334 (3)
N(4)	906 (11)	1382 (10)	1033 (4)
N(5)	3711 (11)	900 (9)	897 (4)
N(6)	3017 (13)	2353 (12)	1515 (4)
C(1)	4293 (16)	3827 (14)	571 (5)
C(2)	5388 (17)	4436 (15)	514 (5)
C(3)	6617 (18)	4193 (15)	734 (6)
C(4)	6636 (17)	3435 (14)	988 (5)
C(5)	5462 (16)	2850 (15)	1031 (5)
C(6)	1595 (14)	4289 (12)	666 (5)
C(7)	814 (16)	5196 (13)	653 (5)
C(8)	51 (18)	5351 (15)	940 (6)
C(9)	171 (17)	4629 (13)	1211 (5)
C(10)	588 (16)	3715 (14)	1209 (6)
C(11)	2355 (14)	2913 (13)	101 (5)
C(12)	2152 (16)	2829 (15)	−290 (5)
C(13)	1739 (16)	1904 (13)	−449 (5)
C(14)	1516 (15)	1082 (13)	−217 (5)
C(15)	1776 (16)	1210 (15)	166 (5)
C(16)	941 (15)	596 (13)	1276 (5)
C(17)	−157 (17)	4 (14)	1352 (5)
C(18)	−1380 (17)	231 (14)	1145 (5)
C(19)	−1388 (17)	1045 (13)	890 (5)
C(20)	−235 (16)	1592 (13)	832 (5)
C(21)	3647 (15)	152 (13)	1167 (5)
C(22)	4376 (16)	−738 (14)	1151 (5)
C(23)	5265 (16)	−855 (14)	848 (5)
C(24)	5377 (16)	−134 (14)	591 (5)
C(25)	4591 (16)	772 (13)	614 (5)
C(26)	2908 (15)	1510 (14)	1747 (5)
C(27)	3106 (16)	1609 (15)	2133 (6)
C(28)	3468 (18)	2586 (15)	2297 (6)
C(29)	3568 (18)	3400 (17)	2055 (6)
C(30)	3325 (17)	3247 (16)	1669 (6)
S(1)	7399 (5)	7749 (5)	6571 (2)
O(1)	6202 (14)	7368 (11)	6724 (4)
O(2)	7203 (15)	8161 (11)	6191 (4)
O(3)	8452 (17)	7026 (13)	6608 (7)
C(31)	7878 (15)	8809 (12)	6859 (5)
C(32)	7089 (18)	9662 (14)	6837 (5)
C(33)	7516 (19)	10505 (15)	7097 (6)
C(34)	8722 (19)	10512 (17)	7295 (6)
C(35)	9482 (20)	9671 (16)	7268 (6)
C(36)	9091 (17)	8798 (14)	7065 (5)
C(37)	9152 (20)	11465 (20)	7514 (8)
S(2)	2461 (7)	7153 (6)	5078 (2)
O(4)	3762 (19)	7235 (14)	4920 (5)
O(5)	1521 (15)	7883 (12)	4900 (4)
O(6)	1981 (24)	6105 (14)	5090 (6)
C(38)	2619 (15)	7532 (12)	5566 (5)
C(39)	1686 (17)	7214 (15)	5828 (5)
C(40)	1819 (19)	7571 (14)	6211 (6)
C(41)	2821 (19)	8224 (15)	6330 (6)
C(42)	3719 (19)	8477 (15)	6078 (6)
C(43)	3689 (17)	8165 (13)	5694 (6)
C(44)	2910 (21)	8545 (18)	6739 (7)
O(7)	3246 (32)	8823 (28)	7985 (10)
C(45)	3681 (35)	9798 (28)	7962 (12)
C(46)	2509 (33)	10267 (25)	7850 (10)

metal–ligand bond in the title compounds provides some evidence for the presence of π-back-bonding, in comparison with $[Ru(py)_6]^{2+}$ where the Ru–N bond length is 2.12 Å.[28]

The average bridgehead (X)–C(py) bond distances are 1.518 (3) Å for X = CH, 1.823 (8) Å for X = P, and 1.440 (3) Å for X = N; the average bond angles about the bridgehead atoms for C(py)–X–C′(py′) are 111.1 (2)° for X = C, 100.1 (3)° for X = P, and 112.4 (2)° for X = N. Again these data reveal increasing variation within the ligand as the bridgehead–C(py) bond distance

Table IV. Fractional Atomic Coordinates for $[Ru\{(2\text{-py})_3N_{12}\}(S_2O_6)\cdot 4H_2O$ (3) (×10⁴)

atom	x	y	z
Ru	0	0	0
N(1)	1441 (3)	1299 (3)	−714 (3)
N(2)	−266 (3)	1899 (3)	1088 (3)
N(3)	1936 (3)	−294 (3)	1384 (3)
N(4)	2465 (3)	2290 (3)	1373 (3)
C(1)	2470 (4)	2256 (4)	101 (3)
C(2)	3504 (5)	3161 (4)	−246 (4)
C(3)	3508 (5)	3129 (5)	−1481 (5)
C(4)	2433 (5)	2156 (5)	−2327 (4)
C(5)	1431 (4)	1276 (4)	−1915 (3)
C(6)	1029 (4)	2767 (4)	1616 (3)
C(7)	1047 (5)	4022 (4)	2418 (4)
C(8)	−329 (6)	4419 (5)	2685 (4)
C(9)	−1651 (5)	3546 (5)	2142 (4)
C(10)	−1595 (4)	2315 (4)	1353 (4)
C(11)	2884 (4)	908 (4)	1871 (3)
C(12)	4216 (4)	889 (5)	2800 (3)
C(13)	4566 (4)	−449 (5)	3287 (4)
C(14)	3603 (5)	−1691 (5)	2806 (4)
C(15)	2289 (4)	−1587 (4)	1861 (3)
S(1)	5892 (1)	5135 (1)	4527 (1)
O(1)	5136 (3)	4756 (3)	3233 (3)
O(2)	6427 (3)	6691 (3)	4845 (3)
O(3)	7033 (3)	4114 (3)	5036 (3)
O(4)	1152 (3)	1118 (3)	4115 (3)
O(5)	8315 (5)	1367 (5)	4680 (6)

Table V. Selected Bond Distances (Å) and Angles (deg) for **1**

Ru–N(1)	2.055 (4)	N(3)–C(11)	1.341 (5)
Ru–N(2)	2.069 (3)	C(1)–C(16)	1.505 (6)
Ru–N(3)	2.075 (3)	C(6)–C(16)	1.524 (5)
N(1)–C(1)	1.349 (5)	C(11)–C(16)	1.521 (5)
N(2)–C(6)	1.344 (5)		
N(1)–Ru–N(2)	87.5 (1)	N(1)–Ru–N(3)	87.1 (1)
N(2)–Ru–N(3)	87.5 (1)	N(1)–Ru–N(1′)[a]	179.7 (1)
N(2)–Ru–N(2′)	91.0 (1)	N(2)–Ru–N(3′)	178.4 (1)
N(3)–Ru–N(3′)	94.1 (1)		
Ru–N(1)–C(1)	118.6 (3)	Ru–N(1)–C(5)	123.9 (3)
Ru–N(2)–C(6)	118.9 (3)	Ru–N(2)–C(10)	123.7 (3)
Ru–N(3)–C(11)	117.6 (3)	Ru–N(3)–C(15)	124.0 (3)
N(1)–C(1)–C(16)	116.5 (4)	N(2)–C(6)–C(16)	115.8 (3)
N(3)–C(11)–C(16)	117.2 (3)	C(1)–C(16)–C(6)	111.4 (3)
C(1)–C(16)–C(11)	112.2 (3)	C(6)–C(16)–C(11)	109.7 (3)

[a] Where the primed atom is related by a 2-fold axis.

increases. Associated with the change in bond distances and angles at the bridgehead (X) is a contraction of the bite angle N(py)–Ru–N′(py′) as the X···C′(py) distance decreases, viz. 90.6 (2)° for X = P, 87.37 (6)° for X = CH, and 86.60 (6)° for X = N.

There are, as may be expected, substantial interionic interactions in the crystal lattices of **1** and **2**. These interactions occur between the electron-rich sulfonate moieties of the tosylate anions and the hydrogen atoms of the pyridyl rings. For **1**, the closest contact occurs between H(3) and O(1), 2.29 Å, and for **2** a contact of 2.25 Å occurs between H(15) and O(6′) (where O(6′) is related by the symmetry operation x, $^1/_2 - y$, $^1/_2 + z$). The closest interionic contact in **3** occurs between O(1) and H(3′) of 2.30 Å (where H(3′) is related by the symmetry operation $1 - x$, $1 - y$, z).

Comparisons with Other Structures. There are very limited data on structural aspects of complexes containing the tris(2-pyridyl)methane ligand. In the species $[AuMe_2\{(2\text{-py})_3CH\}]NO_3$[31] the ligand coordinates in a bidentate mode with the Au(III) center having square-planar geometry. In addition, although no structures were reported, the ligand exhibits tripodal coordination, as claimed in the electrochemical studies of $[Fe\{(2\text{-py})_3CH_{12}\}]^{n+}$ by Boggess et al.[32] and in the NMR studies of $[Co\{(2\text{-py})_3CH_{12}\}]^{3+}$

(31) Canty, A. J.; Minchin, N. J.; Healy, P. C.; White, A. H. *J. Chem. Soc., Dalton Trans.* **1982**, *1795*–1802.

Table VI. Selected Bond Distances (Å) and Angles (deg) for 2

Ru–N(1)	2.06 (1)	Ru–N(2)	2.06 (1)
Ru–N(3)	2.08 (1)	Ru–N(4)	2.08 (1)
Ru–N(5)	2.06 (1)	Ru–N(6)	2.09 (1)
N(1)–C(1)	1.32 (2)	N(2)–C(6)	1.33 (2)
N(3)–C(11)	1.37 (2)	N(4)–C(16)	1.33 (2)
N(5)–C(21)	1.36 (2)	N(6)–C(26)	1.37 (2)
C(1)–P(1)	1.81 (2)	C(6)–P(1)	1.84 (2)
C(11)–P(2)	1.81 (2)	C(16)–P(2)	1.85 (2)
C(21)–P(2)	1.83 (2)	C(26)–P(2)	1.80 (2)
N(1)–Ru–N(2)	90.1 (5)	N(1)–Ru–N(3)	91.7 (5)
N(1)–Ru–N(4)	178.6 (5)	N(1)–Ru–N(5)	89.4 (5)
N(1)–Ru–N(6)	89.1 (5)	N(2)–Ru–N(3)	90.5 (5)
N(2)–Ru–N(4)	89.7 (5)	N(2)–Ru–N(5)	178.5 (5)
N(2)–Ru–N(6)	90.3 (6)	N(3)–Ru–N(4)	89.8 (5)
N(3)–Ru–N(5)	88.1 (5)	N(3)–Ru–N(6)	179.0 (6)
N(4)–Ru–N(5)	90.8 (5)	N(4)–Ru–N(6)	89.5 (5)
N(5)–Ru–N(6)	91.2 (5)		
Ru–N(1)–C(1)	122 (1)	Ru–N(2)–C(6)	122 (1)
Ru–N(1)–C(5)	120 (1)	Ru–N(2)–C(10)	121 (1)
Ru–N(3)–C(11)	119 (1)	Ru–N(4)–C(16)	122 (1)
Ru–N(3)–C(15)	124 (1)	Ru–N(4)–C(20)	119 (1)
Ru–N(5)–C(21)	122 (1)	Ru–N(6)–C(26)	120 (1)
Ru–N(5)–C(25)	120 (1)	Ru–N(6)–C(30)	120 (1)
N(1)–C(1)–P(1)	121 (1)	N(2)–C(6)–P(1)	121 (1)
N(3)–C(11)–P(1)	123 (1)	N(4)–C(16)–P(2)	121 (1)
N(5)–C(21)–P(2)	120 (1)	N(6)–C(26)–P(2)	122 (1)
C(1)–P(1)–C(6)	100.9 (8)	C(1)–P(1)–C(11)	99.6 (8)
C(6)–P(1)–C(11)	99.6 (7)	C(16)–P(2)–C(21)	100.5 (8)
C(16)–P(2)–C(26)	99.4 (8)	C(21)–P(2)–C(26)	101.0 (8)

Table VII. Selected Bond Distances (Å) and Angles (deg) for 3

Ru–N(1)	2.064 (3)	Ru–N(2)	2.069 (3)
Ru–N(3)	2.066 (3)	N(1)–C(1)	1.346 (5)
N(2)–C(6)	1.346 (4)	N(3)–C(11)	1.339 (4)
N(4)–C(1)	1.428 (5)	N(4)–C(6)	1.445 (4)
N(4)–C(11)	1.444 (4)	O(1)–S(1)	1.447 (3)
O(2)–S(1)	1.454 (3)	O(3)–S(1)	1.449 (3)
S(1)–S(2)	2.139 (2)		
N(1)–Ru–N(2)	86.9 (1)	N(1)–Ru–N(3)	86.6 (1)
N(2)–Ru–N(3)	86.3 (1)	Ru–N(1)–C(1)	116.5 (2)
Ru–N(1)–C(5)	125.8 (3)	Ru–N(2)–C(6)	116.4 (2)
Ru–N(2)–C(10)	126.2 (3)	Ru–N(3)–C(11)	117.0 (2)
Ru–N(3)–C(15)	125.1 (2)	C(1)–N(4)–C(6)	112.8 (3)
C(1)–N(4)–C(11)	112.8 (3)	C(6)–N(4)–C(11)	111.6 (3)
N(1)–C(1)–N(4)	117.5 (3)	N(2)–C(6)–N(4)	117.4 (3)
N(3)–C(11)–N(4)	117.0 (3)	O(1)–S(1)–O(2)	113.8 (2)
O(1)–S(1)–O(3)	114.3 (2)	O(2)–S(1)–O(3)	113.8 (2)

and $[Co\{(2\text{-py})_3CH\}_2]^{2+}$ by White and Faller.[13]

Structural determinations have been made for ruthenium(II) complexes of the related C-bridgehead ligand, tris(2-pyridyl)-methanol (X = COH).[14,33] Two forms of $[RuL_2]^{n+}$ were identified:[14] in both there is one $(2\text{-py})_3COH$ ligand coordinated through the three py N atoms (N, N′, N″), with the other ligand having an N,N′,O-coordination mode, but being either deprotonated or nondeprotonated. Since there is considerable distortion in the $(py)_3COH$-*N*,*N*′,*N*″ ligand in $[Ru\{(2\text{-py})_3COH\}_2]^{2+}$, the comparison of $(py)_3COH$-*N*,*N*′,*N*″ in $[Ru\{(2\text{-py})_3COH\}\{(2\text{-py})_3CO^-\}]^+$ with $(2\text{-py})_3CH$ in the present instance seems more appropriate. The structural features are very similar for X = CH and COH in these complexes: viz. the average bridgehead (X)–C(py) bond distance is 1.54 (1) Å for X = COH (cf. 1.518 (3) Å for X = CH), the C(py)–X–C′(py′) bond angle is 109.4 (3)° (cf. 111.1 (2)°), and the intraligand bite angle is 86.4° (cf. 87.37 (6)°). The $(2\text{-py})_3COH$ ligand in $[Ru(NH_3)_5\{(2\text{-py})_3COH\}]^{2+}$ exhibits an N,N′,O-coordination mode,[33] and is not relevant to the present discussion.

To our knowledge, the present structural study of $[Ru\{(2\text{-py})_3P\}_2]^{2+}$ represents the first such determination of a complex containing this ligand: the X-ray structure of the free ligand has been determined recently.[34] However, complexes containing this ligand have been reported previously: viz. $[Co\{(2\text{-py})_3P\}_2]^{2+}$[10,23] and $[Fe\{(2\text{-py})_3P\}_2]^{2+}$,[32] in which the ligand was claimed to be tridentate via the py N atoms, and a series of ruthenium(II) and rhodium(I) species (e.g. $[RuHCl\{(2\text{-py})_3P\}_2]$ and $[RhCl\{(2\text{-py})_3P\}_2]$) in which ^1H and ^{31}P NMR studies indicated tris(2-pyridyl)phosphine to be coordinated both as a monodentate ligand (via P) or as a bidentate ligand (via P and one py N).[21]

A number of structures involving the ligand tris(2-pyridyl)amine have been determined. Kucharski et al. reported the structures of $[Fe\{(2\text{-py})_3N\}_2]^{2+}$[35] and $[Co\{(2\text{-py})_3N\}_2]^{2+}$,[36] and in both cases the ligand adopted a tripodal coordination mode with the three py N atoms ligating. Ibers and co-workers[37] have also reported the structure of a cubane-like cluster $[Cu_4(OH)_4(SO_3CF_3)_2\{(2\text{-py})_3N\}](SO_3CF_3)_2\cdot C_3H_6O$, in which the tris(2-pyridyl)amine behaves in a bidentate rather than a tridentate manner.

In the only such comparison that may be made for any of the three title ligands, for the same coordination mode of the ligand on different metal centers the intraligand bite angle observed for tris(2-pyridyl)amine seems related to the metal–N(py) bond length: viz. 85.6 (5)° for N–Co–N, where the Co–N bond length is 2.12 (2) Å,[36] 88.1 (3)° for N–Fe–N (Fe–N is 1.98 (1) Å),[35] and 86.60 (6)° for N–Ru–N (Ru–N is 2.066 (2) Å) in the present case.

By comparison of intraligand bond lengths in the $[Co(bpy)_3]^{2+}$ and $[Co(bpy)_3]^+$ cations, Szalda et al.[12] were able to identify changes that were consistent with π back-bonding from the Co(I) (d^8) metal center to the bpy ligand. In the present structures involving complexes of the tripodal ligands with the Ru(II) (d^6) center, the bond distances between the respective bridgehead atom (X) and the 2-carbon atom of the pyridine rings are very similar to those determined with other metal centers. The bond distance between the bridgehead atom P and the C(py) atoms in **2** averages 1.823 (8) Å; an X-ray structural determination reveals that this bond distance is essentially identical with that in the free ligand tris(2-pyridyl)phosphine (1.827 (2) Å).[34] In a similar manner, the average N–C(py) bond length in **3** —1.440 (3) Å— is indistinguishable from the equivalent bond lengths in other complexes of the same ligand (1.44 Å in $[Fe\{(2\text{-py})_3N\}_2]^{2+}$[35] and $[Co\{(2\text{-py})_3N\}_2]^{2+}$.[36] The C–C(py) bond length in **1**—1.518 (3) Å—is also the same as that found in tris(2-pyridyl)methane coordinated to Au(III),[31] where the ligand is bidentate and the bond distances are identical for both the attached and free pyridine rings (1.52 (2) Å). The constancy of the bridgehead (X)–C(py) bond distances in all the title ligands regardless of the metal and the invariance of the bond lengths and angles in the P–C–N groupings in coordinated and uncoordinated tris(2-pyridyl)phosphine do not reveal any structural evidence of ring-to-ring delocalization through the σ-system or through d_π–p_π bonding between the bridgehead atom and the 2-carbon atom of the pyridyl ring as claimed by Boggess and Zatko[10,11] in the stabilization of Co(I) by $(2\text{-py})_3P$ and its arsine analogue. We are currently undertaking molecular mechanics and MO calculations to rationalize the nature of the π-back-bonding in the ruthenium(II) and cobalt(I) species of these ligands; these results will be published shortly, together with details of the spectral (electronic, NMR, vibrational) and photochemical properties of the title complexes and their electrochemical behavior.[15]

The progressive distortion of the title molecules from ideal D_{3d} point group symmetry as the bridgehead (X)–C(py) bond distance is lengthened is not totally understood. Interestingly, for the least symmetrical of these complexes, $[Ru\{(2\text{-py})_3P\}_2]^{2+}$, the asymmetric distortion is also seen in solution in $^1H/^{13}C$ 2D NMR studies:[15]

(32) Boggess, R. K.; Hughes, J. W.; Chew, C. W.; Kemper, J. J. *J. Inorg. Nucl. Chem.* **1981**, *43*, 939–945.
(33) Moritz, P. S.; Diamantis, A. A.; Keene, F. R.; Snow, M. R.; Tiekink, E. R. T. *Aust. J. Chem.*, in press.
(34) Keene, F. R.; Snow, M. R.; Tiekink, E. R. T. *Acta Crystallogr., Sect. C: Cryst. Struct. Commun.*, in press.
(35) Kucharski, E. S.; McWhinnie, W. R.; White, A. H. *Aust. J. Chem.* **1978**, *31*, 53–56.
(36) Kucharski, E. S.; McWhinnie, W. R.; White, A. H. *Aust. J. Chem.* **1978**, *31*, 2647–2650.
(37) Dedert, P. L.; Sorrell, T.; Marks, T. J.; Ibers, J. A. *Inorg. Chem.* **1982**, *21*, 3506–3517.

the N- and CH-bridged complexes show no such asymmetry in solution. This may well be a steric effect, and the molecular mechanics calculations[15] will hopefully provide information on this unusual observation.

Acknowledgment. The assistance of Dr Paul Bernhard (Australian National University) in providing details of synthetic procedures for the precursors used in this study is gratefully acknowledged. This work was supported by the Australian Research Grants Scheme.

Registry No. 1, 114378-75-5; 2, 114378-78-8; 3, 114378-72-2; PCl_3, 7719-12-2; $[Ru(DMF)_6](tos)_2$, 114378-79-9; tris(2-pyridyl)methane, 77429-58-4; bis(2-pyridyl)methane, 1132-37-2; 2-bromopyridine, 109-04-6; tris(2-pyridyl)phosphine, 26437-48-9; $[Ru[(2\text{-}py)_3N_2](tos)_2$, 114460-50-1.

Supplementary Material Available: Tables S1–S12, listing thermal parameters, the derived hydrogen positions, and bond distances and angles for 1–3 (12 pages); Tables S13–S15, listing calculated and observed structure factors for 1–3 (44 pages). Ordering information is given on any current masthead page.

Aust. J. Chem., 1988, **41**, 1353–62

Synthetic and Characterization Studies of the Complexes $[Ru(NH_3)_3(Py_3X)]^{2+}$ (Py = 2-Pyridyl; X = N, COH, CH, P), and the X-Ray Crystal Structure of $[Ru(NH_3)_3(Py_3COH)]Br_2.H_2O$†

Paul S. Moritz,[A] *Alex A. Diamantis,*[A,B] *F. Richard Keene,*[C] *Michael R. Snow*[A] *and Edward R. T. Tiekink*[A]

[A] Jordan Laboratories, Department of Physical and Inorganic Chemistry, University of Adelaide, S.A. 5001.
[B] Author to whom correspondence should be addressed.
[C] Department of Chemistry and Biochemistry, James Cook University of North Queensland, Townsville, Qld. 4811.

Abstract

Reaction of molar ratios of the ligands tri(2-pyridyl)amine (Py_3N), or tri(2-pyridyl)-methanol (Py_3COH) with $[Ru(NH_3)_3(OH_2)_3]^{2+}$ in aqueous solution produces the respective $[Ru(NH_3)_3(tripod)]^{2+}$ complexes. The analogous reaction with tri(2-pyridyl)methane (Py_3CH) yields $[Ru(NH_3)_2(OH_2)(Py_3CH)]^{2+}$, while the reaction with the tri(2-pyridyl)phosphine ligand produces several (unidentified) species. The N- and CH-bridged ligands appear coordinated in a tripodal manner through the three pyridine-*N* atoms of the ligand, whereas tri(2-pyridyl)-methanol is coordinated in an *N,N',O* mode through two pyridine-*N* atoms and the hydroxy group of the bridge. The X-ray crystal structure of $[Ru(NH_3)_3(Py_3COH)]Br_2.H_2O$ confirms this assignment: the complex of formula $C_{16}H_{24}Br_2N_6O_2Ru$ is monoclinic, space group $P2_1/c$, with cell dimensions *a* 13·916(6), *b* 10·300(2), *c* 15·910(7) Å, β 111·90(3)°, and *Z* 4. Full-matrix least-squares refinement on 2062 reflections with $I > 2{\cdot}5\sigma(I)$ converged to final *R* 0·030 and R_w 0·035. The coordinated OH group in the complex has a pK_a of 6·5(±0·1) at 25°C (aqueous 0·1 mol dm^{-3} KNO_3).

Introduction

Recent work in our separate laboratories has investigated the synthetic, electrochemical and acid–base behaviour of a series of complexes of the $Ru(NH_3)_3$ moiety,[1] and the synthesis and properties of complexes of the transition elements of Groups 8–10 with tripodal π-acceptor ligands.[2–6]

As a complement to both studies, and to provide further information on aspects of the electronic effects within complexes of tripodal ligands, we have undertaken the

† Dedicated to the memory of Donald R. Stranks, who died on 9 August 1986.

[1] Moritz, P. S., Ph.D. Dissertation, University of Adelaide, 1987; Moritz, P. S., and Diamantis, A. A., unpublished data.
[2] Szalda, D. J., and Keene, F. R., *Inorg. Chem.*, 1986, **25**, 2795.
[3] Keene, F. R., Szalda, D. J., and Wilson, T. A., *Inorg. Chem.*, 1987, **26**, 2211.
[4] Keene, F. R., Snow, M. R., Stephenson, P. J., and Tiekink, E. R. T., *Inorg. Chem.*, in press.
[5] Hafeli, T. A., and Keene, F. R., *Aust. J. Chem.*, 1988, **41**, 1379.
[6] Atkinson, I. M., Hafeli, T. A., Keene, F. R., Stephenson, P. J., and Wright, T. P., unpublished data.

0004-9425/88/091353$03.00

synthesis and characterization of the $[Ru(NH_3)_3(Py_3X)]^{2+}$ complexes (X = N, CH, COH, P) and a structural determination of the tri(2-pyridyl)methanol species, which we now report.

Experimental

Physical Measurements

Electronic spectra were recorded on a Varian DMS100 u.v./visible spectrophotometer. Electrochemical measurements were obtained on a Bioanalytical Systems BAS100 electrochemical analyser. A conventional single-compartment/three-electrode cell was used for the electrochemical experiments, with a glassy carbon working electrode, and a saturated calomel reference electrode. All potentials are given in volts *v.* the s.c.e. Cyclic voltammetric and differential pulse voltammetry (d.p.v.) measurements were obtained in aqueous solution by using deionized water purified by a Millipore Milli-Q water purification system: in acid solutions the electrolyte was 0·1 mol dm^{-3} methanesulfonic acid, and at higher pH the solutions were 0·02 mol dm^{-3} in the appropriate buffer and 0·1 mol dm^{-3} in sodium methanesulfonate as the supporting electrolyte.

The pK_a measurements were made by using an automated titration system, which has been described previously.[7] The determinations were made at 25·0°C in aqueous 0·1 mol dm^{-3} KNO_3 by titration with KOH.

Analyses were performed by the Canadian Microanalytical Service (New Westminster, B.C.).

Materials

$[Ru(NH_3)_3(OH_2)_3](CF_3SO_3)_3$,[1] and the ligands tri(2-pyridyl)phosphine (Py_3P),[4] tri(2-pyridyl)amine (Py_3N),[8] tri(2-pyridyl)methane (Py_3CH)[4] and tri(2-pyridyl)methanol (Py_3COH)[2,9] were prepared as described elsewhere.

Syntheses

Triamminetris(pyridine)ruthenium(II) *Diperchlorate,* $[Ru(NH_3)_3(py)_3](ClO_4)_2$

$[Ru(NH_3)_3(OH_2)_3](CF_3SO_3)_3$ (0·159 g) was dissolved in 1 mol dm^{-3} pyridine/pyridinium buffer* (10 cm^3), and the solution was deaerated with argon. Amalgamated zinc was added, and the reaction mixture stirred under argon for 6·5 h, at which time d.p.v. analysis (in 0·1 mol dm^{-3} $MeSO_3H$ containing a 0·10 cm^3 aliquot from the reaction solution) showed the reaction to be complete. The gold-coloured solution was filtered by using Schlenk techniques, and excess $NaClO_4$ added to the filtrate. The mixture was cooled in an ice bath for 1 h, the product collected by filtration, and washed with ice-cold $NaClO_4$ solution (2×5 cm^3), diethyl ether (1×5 cm^3), and air-dried. The crude product was recrystallized from hot methanol as bright yellow *cubes.* Yield 0·077 g, 48% (Found: C, 30·1; H, 4·5; N, 14·5; Cl, 12·3. $C_{15}H_{24}Cl_2N_6O_8Ru$ requires C, 30·6; H, 4·1; N, 14·3; Cl, 12·1%).

The corresponding bromide salt, $[Ru(NH_3)_3(py)_3]Br_2$, was prepared in 96% yield by adding excess tetrabutylammonium bromide to a butan-2-one solution of the perchlorate complex. After cooling in ice, the bromide salt was filtered off and washed with butan-2-one and ether.

* Prepared from pyridine/methanesulfonic acid in aqueous solution.[10]

[7] Adam, K. R., Leong, A. J., Lindoy, L. F., Lip, H. C., Skelton, B. W., and White, A. H., *J. Am. Chem. Soc.*, 1983, **105**, 4645.
[8] Wibaut, J. P., and Bastide, G. L. C., *Recl Trav. Chim. Pays-Bas*, 1933, **52**, 493.
[9] Wibaut, J. P., de Jonge, A. P., van der Voort, H. G. P., and Otto, H. L., *Recl Trav. Chim. Pays-Bas*, 1951, **70**, 1054.
[10] Ford, P. C., and Sutton, C., *Inorg. Chem.*, 1969, **8**, 1544.

Triammine{tri(2-pyridyl)methanol}ruthenium(II) *Dibromide Monohydrate, $[Ru(NH_3)_3(Py_3COH)]Br_2.H_2O$*

$[Ru(NH_3)_3(OH_2)_3](CF_3SO_3)_3$ (0·172 g, 0·26 mmol) was dissolved in water (7 cm^3), and the solution was deaerated with argon. Hydrogen gas was bubbled into the solution through a platinum black gauze for 1·5 h. Tri(2-pyridyl)methanol (0·068 g, 0·26 mmol) was added and the treatment with hydrogen continued for 45 min, and the mixture then stirred under argon until d.p.v. analysis showed the reaction to be complete (3 h). The dark golden solution was filtered by using Schlenk techniques, and excess NH_4PF_6 added to the filtrate. The mixture was stirred under argon for 15 min and stored at −10°C for 24 h. The yellow solid was collected by filtration and washed with ice-cold ethanol (2×5 cm^3), ether (1×3 cm^3), and air-dried. The crude product (0·108 g, 55%) was dissolved in butan-2-one (5 cm^3), excess tetrabutylammonium bromide added with stirring, and the mixture then cooled to −10° for 16 h. The pale yellow solid was collected by filtration and washed with butan-2-one (2×3 cm^3) and dry ether (1×5 cm^3), and air-dried. Yield 0·068 g, 46%. The crude bromide *salt* was recrystallized from methanol/butan-2-one (Found: C, 32·6; H, 3·7; N. 13·7. $C_{16}H_{24}Br_2N_6O_2Ru$ requires C, 32·4; H, 4·1; N, 14·2%).

Triammine{tri(2-pyridyl)amine}ruthenium(II) *Diperchlorate, $[Ru(NH_3)_3(Py_3N)](ClO_4)_2$*

The PF_6^- salt of the cation was prepared (60% yield) in an analogous manner to that given for the tri(2-pyridyl)methanol species, but with a reaction time of 3·5 h. The crude PF_6^- salt was then converted into the ClO_4^- salt by precipitation with excess $NaClO_4$ from a hot saturated aqueous solution. The resultant solid was filtered off, washed with ice-cold water and ether, and air-dried (Found: C, 30·5; H, 3·6; Cl, 11·7; N, 16·0. $C_{15}H_{21}Cl_2N_7O_8Ru$ requires C, 30·1; H, 3·5; Cl, 11·8; N, 16·4%).

Diammineaqua{tri(2-pyridyl)methane}ruthenium(II) *Dibromide, $[Ru(NH_3)_2(OH_2)(Py_3CH)]Br_2$*

This *complex* was prepared in 33% yield in a similar manner to the triammine{tri(2-pyridyl)methanol} species, with a reaction time of 2·5 h (Found: C, 34·5; H, 4·37; Br, 28·0; N, 12·0. $C_{16}H_{21}Br_2N_5ORu$ requires C, 34·3; H, 3·78; Br, 28·5; N, 12·5%).

Crystallography

Collection and Reduction of X-Ray Data for $[Ru(NH_3)_3(Py_3COH)]Br_2.H_2O$

Crystals of $[Ru(NH_3)_3(Py_3COH)]Br_2.H_2O$ were obtained as orange rectangular blocks from methanol solution by vapour diffusion of acetone. Intensity data for a crystal 0·13 by 0·28 by 0·18 mm were measured at room temperature on an Enraf–Nonius CAD4-F diffractometer with graphite-monochromatized Mo Kα radiation, λ 0·7107 Å. The $\omega:2\theta$ technique was employed to measure the intensities of 3532 reflections up to a maximum Bragg angle of 22·5°. No significant decomposition of the crystal occurred during the data collection, and the data set was corrected for Lorentz and polarization effects and for absorption;[11] maximum and minimum transmission factors were 0·6573 and 0·3293. There were 2766 unique reflections, and of these 2062 satisfied the $I > 2{\cdot}5\sigma(I)$ criterion of observability.

Crystal Data

$C_{16}H_{24}Br_2N_6O_2Ru$, M 593·3, monoclinic, space group $P2_1/c$ (C_{2h}^5, No. 14), a 13·916(6), b 10·300(2), c 15·910(7) Å, β 111·90(3)°, V 2115·9 $Å^3$, Z 4, D_X 1·863 g cm^{-3}, $F(000)$ 1168, μ(Mo Kα) 44·32 cm^{-1}.

Solution of the Structure

The structure was solved with the aid of the MITHRIL program,[12] and refined by a full-matrix least-squares procedure based on F with the use of the SHELX76 program.[11] Anisotropic thermal

[11] Sheldrick, G. M., SHELX76, 'Program for Crystal Structure Determination', University of Cambridge, England, 1976.
[12] Gilmore, C. J., *J. Appl. Crystallogr.*, 1984, 17, 42.

Table 1. Fractional atomic coordinates for $[Ru(NH_3)_3(Py_3COH)]\,Br_2.H_2O$ ($\times 10^5$ for Ru; $\times 10^4$ for remaining atoms)

Atom	*x*	*y*	*z*	Atom	*x*	*y*	*z*
Ru	18257(3)	25394(4)	16421(3)	C(7)	4701(5)	3528(5)	1531(4)
N(1)	552(4)	2844(5)	406(3)	C(8)	4623(5)	3337(6)	638(4)
N(2)	1703(4)	518(4)	1357(3)	C(9)	3737(5)	2852(6)	15(4)
N(3)	789(4)	2288(5)	2334(4)	C(10)	2898(5)	2597(5)	249(4)
N(4)	2113(3)	4456(4)	2038(3)	C(11)	4802(4)	3263(5)	3420(3)
N(5)	2937(3)	2817(4)	1100(3)	C(12)	5292(5)	2086(6)	3549(4)
N(6)	5244(5)	4282(5)	3918(4)	C(13)	6268(5)	1933(7)	4206(4)
O(1)	3086(3)	2362(3)	2733(2)	C(14)	6726(5)	2985(7)	4716(5)
C(1)	3114(4)	4655(5)	2571(3)	C(15)	6186(6)	4116(8)	4567(6)
C(2)	3456(5)	5851(5)	2927(4)	C(16)	3748(4)	3394(5)	2661(3)
C(3)	2749(5)	6875(6)	2726(5)	Br(1)	8695(1)	293(1)	5817(1)
C(4)	1727(5)	6660(6)	2176(5)	Br(2)	795(1)	301(1)	8960(1)
C(5)	1439(5)	5435(5)	1852(5)	O(2)	6884(4)	4857(4)	1672(3)
C(6)	3822(4)	3245(5)	1733(3)				

Table 2. Bond distances (Å) for $[Ru(NH_3)_3(Py_3COH)]\,Br_2.H_2O$

Ru–N(1)	2·124(5)	Ru–N(4)	2·065(4)
Ru–N(2)	2·124(4)	Ru–N(5)	2·053(4)
Ru–N(3)	2·132(5)	Ru–O(1)	1·963(3)
N(4)–C(1)	1·350(7)	N(4)–C(5)	1·333(7)
C(1)–C(2)	1·365(8)	C(2)–C(3)	1·395(9)
C(3)–C(4)	1·383(9)	C(4)–C(5)	1·365(8)
N(5)–C(6)	1·341(7)	N(5)–C(10)	1·354(7)
C(6)–C(7)	1·406(7)	C(7)–C(8)	1·398(7)
C(8)–C(9)	1·356(9)	C(9)–C(10)	1·378(9)
N(6)–C(11)	1·321(7)	N(6)–C(15)	1·343(9)
C(11)–C(12)	1·369(8)	C(12)–C(13)	1·380(8)
C(13)–C(14)	1·361(9)	C(14)–C(15)	1·36(1)
C(16)–O(1)	1·439(6)	C(16)–C(1)	1·546(7)
C(16)–C(6)	1·527(7)	C(16)–C(11)	1·518(7)

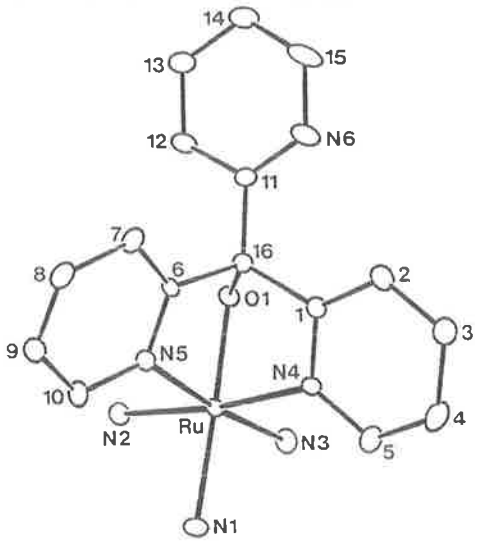

Fig. 1. Molecular structure and numbering scheme used for $[Ru(NH_3)_3(Py_3COH)]\,Br_2.H_2O$ [Py_3COH = tri(2-pyridyl)methanol]. Note that the atoms not otherwise indicated are carbon atoms.

parameters were introduced for all non-hydrogen atoms, and hydrogen atoms were included in the model at their calculated positions. A weighting scheme of the form $w = k/[\sigma^2|F| + g|F|^2]$ was introduced, and the refinement continued until convergence; R 0·030, R_w 0·035 for k 0·27 and g 0·003. The analysis of variance showed no special features, indicating an appropriate weighting scheme had been used, and the maximum residual electron density peak in the final difference map was 0·53 e $Å^{-3}$. The scattering factors for neutral Ru (corrected for f' and f'') were from ref. 13, and for the remaining atoms were those incorporated in SHELX76.[11] Final fractional atomic coordinates are listed in Table 1, and the bond distances and angles are given in Tables 2 and 3 respectively. The numbering scheme employed is shown in Fig. 1 (drawn with ORTEPII[14]). Tables of thermal parameters, hydrogen atom coordinates and the structure factors have been deposited; copies are available on application to the Australian Journal of Chemistry, 314 Albert Street, East Melbourne, Vic. 3002.

Table 3. Bond angles (deg) for $[Ru(NH_3)_3(Py_3COH)]Br_2.H_2O$

N(1)–Ru–N(2)	88·5(2)	N(1)–Ru–N(3)	90·2(2)
N(1)–Ru–N(4)	98·1(2)	N(1)–Ru–N(5)	95·2(2)
N(1)–Ru–O(1)	174·3(2)	N(2)–Ru–N(3)	88·6(2)
N(2)–Ru–N(4)	173·2(2)	N(2)–Ru–N(5)	93·4(2)
N(2)–Ru–O(1)	94·1(2)	N(3)–Ru–N(4)	92·8(2)
N(3)–Ru–N(5)	174·3(2)	N(3)–Ru–O(1)	94·9(2)
N(4)–Ru–N(5)	84·5(2)	N(4)–Ru–O(1)	79·2(2)
N(5)–Ru–O(1)	79·6(2)		
Ru–N(4)–C(1)	112·0(3)	Ru–N(5)–C(6)	110·8(3)
Ru–N(4)–C(5)	128·0(4)	Ru–N(5)–C(10)	129·9(4)
N(4)–C(1)–C(16)	110·5(4)	N(5)–C(6)–C(16)	112·6(4)
N(4)–C(1)–C(2)	121·1(5)	N(5)–C(6)–C(7)	122·0(5)
C(2)–C(1)–C(16)	128·4(5)	C(7)–C(6)–C(16)	125·4(5)
C(1)–C(2)–C(3)	118·7(6)	C(6)–C(7)–C(8)	117·3(5)
C(2)–C(3)–C(4)	119·6(6)	C(7)–C(8)–C(9)	120·0(5)
C(3)–C(4)–C(5)	118·3(6)	C(8)–C(9)–C(10)	120·2(5)
N(4)–C(5)–C(4)	122·2(6)	N(5)–C(10)–C(9)	121·1(5)
C(1)–N(4)–C(5)	120·0(4)	C(6)–N(5)–C(10)	119·3(5)
N(6)–C(11)–C(12)	121·3(5)	N(6)–C(11)–C(16)	120·1(5)
C(12)–C(11)–C(16)	118·5(5)	C(11)–N(6)–C(15)	117·6(6)
C(11)–C(12)–C(13)	120·7(5)	C(12)–C(13)–C(14)	118·0(6)
C(13)–C(14)–C(15)	118·2(6)	N(6)–C(15)–C(14)	124·1(6)
O(1)–C(16)–C(1)	105·6(4)	O(1)–C(16)–C(6)	106·2(4)
O(1)–C(16)–C(11)	109·1(4)	C(1)–C(16)–C(6)	103·7(4)
C(1)–C(16)–C(11)	119·8(4)	C(6)–C(16)–C(11)	111·5(4)
Ru–O(1)–C(16)	104·3(3)		

Results and Discussion

Synthesis of Complexes

In aqueous solution the tripodal ligands tri(2-pyridyl)amine and tri(2-pyridyl)methanol reacted with $[Ru(NH_3)_3(OH_2)_3]^{2+}$ to give bright yellow solutions of $[Ru(NH_3)_3(tripod)]^{2+}$ species; under the same conditions, tri(2-pyridyl)methane apparently produced the related $[Ru(NH_3)_2(OH_2)(tripod)]^{2+}$ complex, and the ligand tri(2-pyridyl)phosphine reacted to give a yellow solution, but electrochemical studies

[13] 'International Tables for X-Ray Crystallography' Vol. 4, pp. 58, 99, 149 (Kynoch Press: Birmingham 1974).

[14] Johnson, C. K., ORTEP, Report ORNL-3794, Oak Ridge Laboratory, Tennessee., U.S.A., 1971.

of the reaction mixture (and of a solid isolated as the PF_6^- salt) revealed a mixture of products. The precursor $[Ru(NH_3)_3(OH_2)_3]^{2+}$ was generated *in situ* by hydrogen reduction of $[Ru(NH_3)_3(OH)_3]^{3+}$ or, in the case of the tris(pyridine) complex, by zinc amalgam reduction. The solutions were oxygen-sensitive, but once precipitated (generally as the PF_6^- or ClO_4^- salts) the solid species were relatively air-stable.

In $[Ru(NH_3)_3(Py_3N)]^{2+}$ and $[Ru(NH_3)_2(OH_2)(Py_3CH)]^{2+}$ the tripodal ligands are believed to be coordinated through the three pyridyl nitrogen atoms in a facial arrangement (*N*,*N*′,*N*″). An X-ray structural determination (see below) revealed that the ligand Py_3COH is coordinated through two pyridyl nitrogen atoms and the oxygen atom of the alcohol group (*N*,*N*′,*O*). In the complex $[Ru(Py_3COH)_2]^{2+}$, both modes of coordination are observed.[3]

The reasons for the differences in the reactions of the precursor $[Ru(NH_3)_3(OH_2)_3]^{2+}$ with the ligands Py_3X (X = N, CH, P) is unclear. Significantly, however, structural and solution n.m.r. studies of the bis(ligand)ruthenium(II) complexes of these ligands reveal increasing distortion in the structures as the bridgehead (X)–C (Py) bond lengthens in the sequence N < CH < P.[4] In the present case, while the $[Ru(NH_3)(Py_3N)]^{2+}$ forms readily under the conditions used, microanalysis results indicate that one ammine ligand is replaced by an aqua ligand when X = CH. This was further supported by the determination of a pK_a value of 9·5(±0·1), which is consistent with the deprotonation of water ligated to Ru^{II}: for example, the pK_a of $[Ru(NH_3)_3(phen)(OH_2)]^{2+}$ (phen = 1,10-phenanthroline) is *c.* 11·4 at ionic strength 0·1,[1] and the pK_a of the present complex would be expected to be lower because of the additional π-acceptor properties associated with the extra pyridine ligand.

For X = P, there is no evidence during the reaction for formation of a substantial amount of a species in which Py_3P is coordinated as a tridentate through the three pyridine-*N* atoms, although a number of products are observed from electrochemical studies. In this case, either a number of deammination reactions may occur, in which case the electrochemistry of the resultant mono-, di- and tri-aqua species would be complicated, or else the tri(2-pyridyl)phosphine ligand may adopt one or more other coordination modes besides that suggested above: in a previous report of ruthenium(II) complexes containing this ligand, Wilkinson *et al.*[15] have claimed from n.m.r. studies that the ligand is bidentate through one Py(*N*) and the bridgehead(*P*)] in the complex $[RuCl(Py_3P)_2]$, and both bidentate and monodentate [through the bridgehead(*P*) atom] in the complex $[RuHCl(Py_3P)_3]$. The identification and characterization of the products formed on the reaction of $[Ru(NH_3)_3(OH_2)_3]^{2+}$ with Py_3P was not followed further in the present work.

Electronic Spectra

The u.v./visible spectra of the three complexes with tripodal ligands (X = N, CH, COH) contained bands attributable to intraligand and to MLCT transitions. The spectral features are listed in Table 4.

The spectra of $[Ru(NH_3)_3(Py_3N)]^{2+}$ and $[Ru(NH_3)_2(OH_2)(Py_3CH)]^{2+}$ are similar: MLCT bands are observed at λ 367 and 414 nm, and at λ 369 and 415 nm, respectively. The intraligand bands are at λ 249 and 280 nm in both cases, although in the case of the latter complex the lower-energy band is only evident as a shoulder. The

[15] Kurtev, K., Ribola, D., Jones, R. A., Cole-Hamilton, D. J., and Wilkinson, G., *J. Chem. Soc., Dalton Trans.*, 1980, 55.

Table 4. Spectral and electrochemical data of ruthenium(II) complexes

Ruthenium(II) complex	λ (nm)	ε (mol^{-1} dm^3 cm^{-1})	$E_{1/2}$ (V *v.* s.c.e.)
$[Ru(NH_3)_3(py)_3]^{2+}$	244	17600[A]	0·48[A]
	350	shoulder	
	393	18000	
$[Ru(NH_3)_3(Py_3COH)]^{2+}$	240	shoulder[A]	+0·07[A]
	260	14300	
	350	shoulder	
	415	450	
$[Ru(NH_3)_3(Py_3CO^-)]^{+}$	240	14500[B]	−0·09[B]
	265	15500	
	350	shoulder	
$[Ru(NH_3)_3(Py_3N)]^{2+}$	249	15700[A]	0·57[A]
	280	2600	
	367	12700	
	414	10000	
$[Ru(NH_3)_2(OH_2)(Py_3CH)]^{2+}$	249	14300[A]	0·50[A]
	280	shoulder	
	369	9060	
	415	7340	
$[Ru(Py_3COH)_2]^{2+}$ (ref. 3)	246	30600[C]	0·40[C, D]
	415	24700	
$[Ru(Py_3COH)(Py_3CO^-)]^{+}$ (ref. 3)	253	30500[E]	0·25[D, E]
	432	27800	

[A] 0·1 mol dm^{-3} $MeSO_3H$. [B] Tris/$MeSO_3H$ buffer; pH 8. [C] 0·05 mol dm^{-3} H_2SO_4. [D] $E_{1/2}$ *v.* s.s.c.e. [E] Tris/H_2SO_4 buffer; pH 8.

comparison of these N- and CH-bridged ligand species is valid since the substitution of an aqua for an ammine ligand is not expected to have a major influence on the electronic spectra: for example, in the complexes $[Ru(NH_3)_3(OH_2)(acac)]^+$ and $[Ru(NH_3)_4(acac)]^+$, the electronic spectra are very similar in both form and λ_{max} values.[16] The MLCT transitions in both the above tripodal ligand species are similar in energy and intensity to those in the spectra of $[Ru(NH_3)_3(py)_3]^{2+}$ and the respective $[Ru(tripod)_2]^{2+}$ complexes,[6] although in the latter the molar absorptivities are approximately twice as high, consistent with the presence of six pyridyl groups. A ligand-field treatment of orbital energies in *fac*-MX_3Y_3 complexes of C_{3v} symmetry[17] indicates that *fac*-$[Ru(NH_3)_3(py)_3]^{2+}$ would be expected to show only one MLCT band unless there were some distortion in the coordination sphere, where the degeneracy of the t_2 orbitals would be lifted so that a second transition to the ligand π^* orbital may become apparent. Whilst only one band is observed in $[Ru(NH_3)_3(py)_3]^{2+}$ the presence of two distinct MLCT peaks in the complexes containing the tripodal ligands suggests that there is some distortion in the latter: this may arise from the presence of the aqua ligand in the complex containing Py_3CH, and may arise from some distortion of the chromophore in the complex containing Py_3N because the three pyridyl rings in the tripodal ligand are subject to rigidity constraints imposed by the bonds to the bridgehead group.

[16] Diamantis, A. A., Moritz, P. S., Snow, M. R., and Tiekink, E. R. T., *Aust. J. Chem.*, 1988, **41**, 1251.
[17] Krishnamurthyl, R., and Schaap, W. B., *J. Chem. Educ.*, 1969, **46**, 799.

The spectrum of $[Ru(NH_3)_3(Py_3COH)]^{2+}$ was pH-dependent, due to the presence of the weakly acidic coordinated OH group. In 0·1 mol dm^{-3} $MeSO_3H$ the intraligand bands were present at 260 and at 240 nm (shoulder), and at pH 8 the band at 240 nm was resolved into a peak, and the lower-energy band was at 265 nm. The expected MLCT bands were evident as weak shoulders at 350 nm (ϵ 1500 mol^{-1} dm^3 cm^{-1}) and 415 nm (ϵ 450 mol^{-1} dm^3 cm^{-1}) in acid solution, and in base there was a shoulder at 350 nm. The intraligand bands are comparable to those in the spectrum of $[Ru(Py_3COH)_2]^{2+}$, which has one peak at 246 nm when the coordinated OH group is protonated; this shifts to 253 nm in the deprotonated case.[3] For the MLCT absorptions, the energy at which they occur in the bis(ligand) complex is comparable with the energy of the MLCT in $[Ru(NH_3)_3(Py_3COH)]^{2+}$ but their intensity is appreciably lower for the mono(ligand) than for the bis(ligand) complex.

Electrochemical Studies

The cyclic voltammogram (c.v.) of $[Ru(NH_3)_3(py)_3]^{2+}$ consisted of a single quasi-reversible wave with $E_{1/2} = +0{\cdot}48$ V. At a scan rate of 25 mV s^{-1}, the peak separation $\Delta E_p = 72$ mV, while at 900 mV s^{-1}, $\Delta E_p = 126$ mV. In 0·1 mol dm^{-3} $MeSO_3H$ solution, at a glassy carbon working electrode, the three complexes with the tripod ligands had reversible c.v. waves due to the Ru^{III}/Ru^{II} couples. The c.v. of the complex with Py_3COH is pH-dependent, because of the presence of the coordinated OH group: the pK_a value for dissociation of this proton in aqueous solution was determined to be 6·5(±0·1) at 25·0°C (in 0·1 mol dm^{-3} KNO_3). In acid solution, where the complex form is $[Ru(NH_3)_3(Py_3COH)]^{2+}$, $E_{1/2}$ is +0·07 V. At pH 8, where the complex exists as primarily as $[Ru(NH_3)_3(Py_3CO)]^{+}$, $E_{1/2}$ is −0·09 V. The pK_a of $[Ru(Py_3COH)_2]^{2+}$ is 3·78 under the same conditions, compared with a value of 7·2 for coordinated pyridine-2-methanol in $[Ru(bpy)_2(PyCH_2O)]^{2+}$.[18] The higher acidity of coordinated tri(2-pyridyl)methanol compared with pyridine-2-methanol was attributed[3] to steric strain within the tripod ligand: an intermediate value for the pK_a of the mono(tripod) species is consistent with that proposal, given that there is less π-backdonation of electron density than in the bis(tripod) complex.

The redox potentials for the $[Ru(NH_3/OH_2)_3(tripod)]^{3+/2+}$ couples are all less positive than those for the corresponding bis(tripod) complexes.[6] This reflects the difference between the π-acceptor properties of the three extra pyridyl rings in the bis(tripod) complexes and the σ-donor properties of the ammine ligands in the triammine complexes. The $E_{1/2}$ potentials for complexes involving Py_3COH as a ligand are less positive than those for $[Ru(NH_3)_2(OH_2)(Py_3CH)]^{2+}$ and $[Ru(NH_3)_3(Py_3N)]^{2+}$, because of the σ-donor ability of the OH group and the presence of only two π-accepting pyridyl groups in the coordination sphere when the ligand is in the (N,N',O) coordination mode. For $[Ru(NH_3)_2(OH_2)(Py_3CH)]^{2+}$ and $[Ru(NH_3)_3(Py_3N)]^{2+}$, the $E_{1/2}$ potentials are more positive than that of $[Ru(NH_3)_3(py)_3]^{2+}$, indicating that the rigid configuration of three pyridine rings leads to better π-acceptor ability than the non-bridged configuration of pyridine rings. However, the reverse is true in the case of $[Co(NH_3)_3(Py_3COH)]^{2+}$ which has an $E_{1/2}$ value less positive than that of *cis*-$[Ru(NH_3)_4(py)_2]^{2+}$ (0·26 V).[19]

[18] Ridd, M. J., Keene, F. R., Sneddon, G. R., and Gakowski, D. J., unpublished data.
[19] Matsubara, T., and Ford, P. C., *Inorg. Chem.*, 1976, **15**, 1107.

As was the case for the electronic spectra, the substitution of an aqua for an ammine ligand is not expected to have a major effect on the redox potential of the Ru^{III}/Ru^{II} couple: for example, the $E_{1/2}$ values for $[Ru(NH_3)_3(OH_2)(acac)]^{2+/+}$ and $[Ru(NH_3)_4(acac)]^{2+/+}$ are −0·32 and −0·38 respectively.[16]

Description of the Crystal Structure of $[Ru(NH_3)_3(Py_3COH)]Br_2.H_2O$

The crystal structure of the complex containing tri(2-pyridyl)methanol is shown in Fig. 1, which also shows the atomic numbering scheme employed. The bond lengths and angles are listed in Tables 2 and 3.

The structure comprises a distorted octahedron, with the ammine ligands arranged facially, and the tripod ligand [coordinated in the (N,N',O) mode] also occupying one face. The bond angles between Ru and the donor atoms of the tripod ligand are all less than 90°, indicating a small ligand bite. As a consequence, the angles between the atoms *trans* to each other are less than 180°, indicating that the steric constraints of the tripod ligand prevent the donor atoms from occupying the apical positions of a regular octahedron. The bond angles between Ru and the ammine N atoms are close to 90°, indicating that the facial arrangement of the ammines is nearly regular.

The Ru–N bond lengths for the ammine ligands are between 2·124(4) and 2·132(5) Å. These bond lengths are comparable to those of the Ru–N bonds in $[Ru(NH_3)_6]I_2$, where the average length is 2·144 Å.[20] The pyridyl Ru–N bond lengths are 2·065(5) and 2·053(4) Å, which are very close to the average Ru–N bond length of 2·053(6) Å in $[Ru(Py_3COH)_2]^{2+}$,[3] and 2·056 Å in $[Ru(bpy)_3]^{2+}$,[21] these results indicating that the π-backbonding to the pyridyl rings of the tripod ligands is similar to that of other polypyridyl ligands.

The Ru–O bond length in $[Ru(NH_3)_3(Py_3COH)]^{2+}$ is 1·963(3) Å, which is shorter than the average Ru–O bond length in $[Ru(H_2O)_6]^{2+}$ [2·12(2) Å].[22] In $[Ru(Py_3COH)_2]^{2+}$, the Ru–O bond distance is 2·111(4) Å.

The distortion of the coordination sphere is a feature of the (N,N',O) coordination mode, and probably arises because in Py_3COH the minimum distance between the bridgehead carbon atom and the oxygen donor atom [1·439(6) Å] is much less than the distance between the bridgehead carbon atom and the pyridyl nitrogen donor atoms (2·382 and 2·388 Å). In the structure of $[Co(Py_3COH)_2]^{3+}$, in the linkage isomer where both ligands coordinate in the (N,N',N'') mode, the six nitrogen atoms are arranged in almost perfect octahedral geometry;[2] in $[Ru(Py_3CH)_2]^{2+}$, where only the (N,N',N'') mode is possible, the bond angles and distances, while not as regular as in the case of the cobalt complex, are much closer to those of a regular octahedron than in the tri(pyridyl)methanol(N,N',O) complexes.[3,4]

Similar distortions about the (N,N',O) ligand are also apparent in the structure of $[Ru(Py_3COH)_2]^{2+}$,[3] but, in that case, the deviations from regular geometry are greater, with the N–Ru–O angles being 76·2 and 77·2° compared with 79·6 and 79·2° for the triammine complex. The bond angles between Ru and the donor atoms of the (N,N',N'') ligand are closer to 90° than those of the (N,N',O) ligand and are almost comparable with the bond angles between Ru and the ammine ligands in the triammine complex.

[20] Stynes, H. C., and Ibers, J. A., *Inorg. Chem.*, 1971, **10**, 2304.
[21] Rillema, D. P., Jones, O. S., and Levy, H. A., *J. Chem. Soc., Chem. Commun.*, 1979, 849.
[22] Bernhard, P., Burgi, H.-B., Hauser, J., Lehman, H., and Ludi, A., *Inorg. Chem.*, 1982, **21**, 3936.

A notable difference between the structures of $[Ru(NH_3)_3(Py_3COH)]^{2+}$ and $[Ru(Py_3COH_2)]^{2+}$ is the Ru–O distance. In the triammine complex this bond is shorter than the Ru–N bonds, and also shorter than the average bond length in $[Ru(H_2O)_6]^{2+}$.[22] However, in the bis(tripod) complex, the Ru–O bond length is greater than any of the Ru–N bond lengths, and longer than the same bond in $[Ru(NH_3)_3(Py_3COH)]^{2+}$. It would, perhaps, be expected that the effect of five pyridine rings on the Ru^{II} centre would be to make it more like an Ru^{III} ion, but this would tend to shorten the Ru–O bond. A plausible explanation for the shorter Ru–O bond is that the three *trans* nitrogen donor atoms in the triammine complex permit a closer approach of the tripod ligand. This is best achieved in the less crowded N,N',O mode of coordination which accommodates the smaller angle on the bridgehead carbon required by the closer approach. The oxygen atom is then in a position to donate electron density to the metal atom more effectively achieving thus a short bond distance.

Another difference between the structures of the two tri(pyridyl)methanol complexes is the orientation of the uncoordinated pyridyl ring. In $[Ru(Py_3COH)_2]^{2+}$ the planes of the three pyridine rings of the (N,N',O) ligand are inclined at 120° to each other and the uncoordinated ring is almost coplanar with the rings *trans* to the coordinated OH group.[3] However, in $[Ru(NH_3)_3(Py_3COH)]^{2+}$, the uncoordinated pyridine ring lies perpendicular to the line intersecting the planes of the other two rings of the (N,N',O) ligand. This effect may be associated with hydrogen bonding effects, which were suggested to be influential in the orientation of the free pyridine ring in the $[Ru(Py_3COH_2]^{2+}$ complex.[3]

Acknowledgments

The Australian Research Grants Scheme is thanked for financial support. P.S.M. was supported by an Australian Commonwealth Postgraduate Research Award, and a University of Adelaide Scholarship. The assistance of Mr A. J. Leong, James Cook University of North Queensland, with the pK_a measurements is appreciated.

Manuscript received 1 February 1988

Aust. J. Chem., 1988, **41**, 1379–88

Stabilization of Cobalt(I) by Tripodal π-Acceptor Ligands Py_3X (Py = 2-Pyridyl; X = N, CH, COH, P, P=O), and Preliminary Studies on the Reaction of Water and Carbon Dioxide with the Bis(ligand)cobalt(I) Complexes†

Tracy A. Hafeli[A] *and F. Richard Keene*[A, B]

[A] Department of Chemistry and Biochemistry, James Cook University of North Queensland, Townsville, Qld. 4811.
[B] Author to whom correspondence should be addressed.

Abstract

Bis(ligand)cobalt(III/II) complexes of the tripodal π-acceptor ligands Py_3X (Py = 2-pyridyl; X = N, CH, COH, P, P=O) have been synthesized and characterized. Electrochemical studies in acetonitrile (or propylene carbonate) solution reveal the Co^{III}/Co^{II} and Co^{II}/Co^{I} redox couples for all complexes on the cyclic voltammetric time scale; coulometry studies show the Co^{I} species for X = CH, P, P=O have long-term stability, while for X = N, COH the analogous complexes may be observed but are not sustained for such long periods (i.e. minutes or hours in the last two cases). Aspects relating to the stabilization of the Co^{I} state by these ligands are discussed. Preliminary studies on the reactivity of the bis(ligand)cobalt(I) species (X = CH, P) with water and HCO_3^- are also reported: water undergoes reduction to H_2 but no reduction of HCO_3^- occurs. In the water reduction reaction involving the complex with X = P, ligand dissociation does not occur, in contrast to the case for X = CH and for the analogous reaction of $[Co(bpy)_3]^+$.

Introduction

Ruthenium(II) complexes of polypyridyl ligands, and tris(2,2′-bipyridine)-ruthenium(II)—$[Ru(bpy)_3]^{2+}$—in particular, have been the focus of intense interest as potential photosensitizers in processes converting light energy into chemical energy.[1,2] On their absorption of visible light, a relatively long-lived metal-to-ligand charge transfer excited state is formed which is able to undergo very rapid electron transfer reactions with suitable quenchers to form either the reduced Ru^{I} or oxidized Ru^{III} species. Strategies have been developed whereby water may be reduced to gaseous hydrogen, based on both oxidative quenching (where the reduced quencher is the reducing agent) or reductive quenching (where the reducing agent is either $[Ru(bpy)_3]^+$ or a reduced species formed by reaction with it).[1,2] In both cases a catalyst is required: this catalyst is normally heterogeneous (e.g. colloidal platinum), but homogeneous catalysis of the reduction has been demonstrated by using cobalt

† Dedicated to the memory of Donald R. Stranks, who died on 9 August 1986: outstanding teacher and scientific colleague; valued mentor and friend.

[1] Kalyanasundaram, K., *Coord. Chem. Rev.*, 1982, **46**, 159, and references cited therein.
[2] Sutin, N., and Creutz, C., *Pure Appl. Chem.*, 1980, **52**, 2717, and references cited therein.

0004-9425/88/091379$03.00

complexes of polypyridyl ligands. For example, Sutin *et al.*[3] have reported the scheme shown below involving reductive quenching by ascorbate ion ($HAsc^-$) in the presence of bpy and Co^{II}:

$$Ru(bpy)_3^{2+} \xrightarrow{h\nu} {}^*Ru(bpy)_3^{2+}$$

$${}^*Ru(bpy)_3^{2+} + HAsc^- \rightarrow Ru(bpy)_3^{+} + HAsc^{\bullet}$$

$$HAsc^{\bullet} \rightarrow \text{products}$$

$$Ru(bpy)_3^{+} + Co(bpy)_3^{2+} \rightarrow Ru(bpy)_3^{2+} + Co(bpy)_3^{+}$$

$$Co(bpy)_3^{+} + H_2O \rightarrow Co(bpy)_3^{2+} + \tfrac{1}{2}H_2 + OH^-$$

The intermediacy of hydridocobalt species has been proposed in the final reduction reaction.[3] The particular ability of the cobalt complexes to promote homogeneous H_2 production in these schemes can be attributed to the simultaneous possession of a number of characteristics:[3,4] firstly, the strongly reducing properties of the lowest (Co^I) oxidation state; secondly, the existence of three accessible oxidation states (III/II/I) so that the reduction may occur as a two-electron process (since the one-electron reduction pathways are relatively unfavourable thermodynamically); thirdly, the capacity of the intermediate oxidation state (Co^{II}) species to be reduced by either Ru^I or $*Ru^{II}$; and fourthly, the substitutional lability of high-spin Co^I and Co^{II} (and perhaps also Co^{III} as the hydride).

Similar considerations are undoubtedly also important in the reduction of $CO_2 \rightarrow CO$ by analogous cobalt species.[5–7]

Of primary importance in these reactions is the stabilization of the Co^I state by the polypyridyl ligands; this is generally attributed to the existence of π-backbonding from the t_{2g} orbitals of the d^8 metal ion to the π^*-orbitals of the ligand. The particular π-acceptor ability of 2,2′-bipyridine or 1,10-phenanthroline has been discussed previously, and evidence has been given from structural,[8] ^1H n.m.r.[9] and visible/near-infrared spectral[10] studies to support this claim.

In their electrochemical studies of cobalt species (1) containing the tripodal π-acceptor ligands Py_3X (where Py = 2-pyridyl; X = N, P, P=O, As), Boggess and

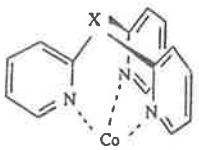

cobalt species (1)
X = N, P, P=O, As

[3] Krishnan, C. V., Creutz, C., Mahajan, D., Schwarz, H. A., and Sutin, N., *Israel J. Chem.*, 1984, **22**, 98.
[4] Creutz, C., and Sutin, N., *Coord. Chem. Rev.*, 1985, **64**, 321.
[5] Keene, F. R., Creutz, C., and Sutin, N., *Coord. Chem. Rev.*, 1985, **64**, 247.
[6] Hawecker, J., Lehn, J.-M., and Ziessel, R., *J. Chem. Soc., Chem. Commun.*, 1983, 536.
[7] Ziessel, R., Hawecker, J., and Lehn, J.-M., *Helv. Chim. Acta*, 1986, **69**, 1065.
[8] Szalda, D. J., Creutz, C., Mahajan, D., and Sutin, N., *Inorg. Chem.*, 1983, **22**, 2372.
[9] Fitzgerald, R. J., Hutchinson, B. B., and Nakamoto, K., *Inorg. Chem.*, 1970, **9**, 2618.
[10] Kaizu, Y., Torii, Y., and Kobayashi, H., *Bull. Chem. Soc. Jpn*, 1970, **43**, 3296.

Zatko[11,12] reported that the Co^{I} state was stabilized for the bis(ligand)cobalt species where X = P, P=O and As, whereas for X = N the Co^{II} state underwent a two-electron reduction: this difference in behaviour was attributed to the non-availability of d-orbitals in the bridgehead atom in the last case which precluded delocalization over the ligand of charge donated by the metal centre, in contrast to the other three cases where p_{π}–d_{π} interaction between the bridgehead atom and the attached pyridyl rings is possible.

During our own studies of complexes of the transition metals of Groups 8–10 with ligands of this type,[13–17] we noted that the Co^{I} state could be observed for the species $[Co(Py_3X)_2]^{n+}$ where X = CH and COH;[13] this is not consistent with the previous claims. We have therefore pursued the study of the $[Co(Py_3X)_2]^{n+}$ series of complexes (X = N, CH, COH, P, P=O) to clarify this ambiguity with regard to the stability of the Co^{I} species and thereby to probe the nature of the π-backdonation in cobalt complexes of polypyridyl ligands. We report those studies now, together with some preliminary observations on the reactions of water and carbon dioxide with such species.

Experimental

Physical Measurements

Electronic spectra were recorded with a Cary 219 spectrophotometer. Electrochemical experiments were conducted in an argon atmosphere, a Vacuum Atmospheres Co. glove box being used: cyclic voltammetry and controlled potential coulometry were performed by using a Bioanalytical Systems Inc. (BAS) CV27 voltammograph with a saturated sodium chloride calomel electrode (s.s.c.e.) as the reference.

Gas chromatographic determinations of H_2 and CO were made by using a Pye Unicam 304 gas chromatograph and a thermal conductivity detector, with 13X molecular sieve support (1 m column) and argon carrier gas (injection temperature 75°C; column temperature 35°C; detector temperature 50°C).

Microanalyses were carried out by the Canadian Microanalytical Service, New Westminster, B.C.

Materials

Propylene carbonate (Aldrich) was distilled immediately before use (90–92°C/3·5 mmHg) and stored over 4 Å molecular sieves. Acetonitrile (Ajax UNICHROM-210) was dried with 4 Å molecular sieves. All other chemicals were of A.R. quality (where available) and were used without further purification.

Syntheses

The ligands tri(2-pyridyl)amine (Py_3N),[18] tri(2-pyridyl)methanol (Py_3COH),[19,20] tri(2-

[11] Boggess, R. K., and Zatko, D. A., *Inorg. Chem.*, 1976, **15**, 626.
[12] Boggess, R. K., and Zatko, D. A., *Inorg. Nucl. Chem. Lett.*, 1976, **12**, 7.
[13] Szalda, D. J., and Keene, F. R., *Inorg. Chem.*, 1986, **25**, 2795.
[14] Keene, F. R., Szalda, D. J., and Wilson, T. A., *Inorg. Chem.*, 1987, **26**, 2211.
[15] Keene, F. R., Snow, M. R., Stephenson, P. J., and Tiekink, E. R. T., *Inorg. Chem.*, in press.
[16] Moritz, P. S., Diamantis, A. A., Keene, F. R., Snow, M. R., and Tiekink, E. R. T., *Aust. J. Chem.*, 1988, **41**, 1353.
[17] Keene, F. R., Atkinson, I. M., Hafeli, T. A., Stephenson, P. J., and Wright, T. P., unpublished data.
[18] Wibaut J. P., and la Bastide, G. L. C., *Recl Trav. Chim. Pay-Bas*, 1933, **52**, 493.
[19] Wibaut, J. P., de Jonge, A. P., van der Voort, H. G. P., and Otto, P. Ph. H. L., *Recl Trav. Chim. Pay-Bas*, 1951, **70**, 1054.
[20] White, D. L., and Faller, J. W., *Inorg. Chem.*, 1982, **21**, 3119.

pyridyl)methane (Py_3CH),[15] tri(2-pyridyl)phosphine (Py_3P)[15,21,22] and tri(2-pyridyl)phosphine oxide ($Py_3P{=}O$)[21] were synthesized according to literature methods.

Bis{ tri(2-pyridyl)amine} cobalt(II) *hexafluorophosphate, [Co(Py$_3$N)$_2$](PF$_6$)$_2$*. To deaerated water (5 ml) was added $CoCl_2.6H_2O$ (51 mg, 0·21 mmol), and the solution refluxed under nitrogen for 10–15 min. Tri(2-pyridyl)amine (105 mg, 0·43 mmol) dissolved in deaerated methanol (2 ml) was added, and the solution refluxed for 1 h before cooling and addition of NH_4PF_6 (0·1 g in 2 ml H_2O; adjusted to pH 7 with 0·1 M NaOH). The orange precipitate was filtered off, washed with iced water and dried under vacuum. A *sample* for microanalysis was recrystallized from acetonitrile/toluene. Yield: 0·15 g, 82% (Found: C, 42·2; H, 2·9; N, 12·9. $C_{30}H_{24}CoF_{12}N_8P_2$ requires C, 42·6; H, 2·9; N, 13·2%).

Bis{ tri(2-pyridyl)methane} cobalt(III) *hexafluorophosphate,*[20] *[Co(Py$_3$CH)$_2$](PF$_6$)$_3$*. To tri(2-pyridyl)methane (0·30 g, 1·21 mmol) dissolved in methanol (4 ml) was added $CoCl_2.6H_2O$ (0·15 g, 0·63 mmol) in water (4 ml). The orange solution was heated gently and stirred for 15 min before precipitation of the solid with NH_4PF_6 (0·30 g in 3 ml H_2O; adjusted to pH 7 with 0·1 M NaOH). The pastel pink precipitate was spun in a centrifuge and washed three times with water before filtering off and drying under vacuum. Yield: 0·52 g (84%). Part (0·38 g) of this sample was converted into pure Co^{III} form[13] by refluxing over charcoal in H_2O (30–40 ml) for 16 h, then filtering while hot and precipitating the yellow solid with NH_4PF_6. The *complex* was filtered off, washed with ice-cold water, and dried under vacuum before recrystallization from acetonitrile/toluene. Yield: 0·14 g (Found: C, 38·9; H, 2·7; N, 8·4. $C_{32}H_{26}CoF_{18}N_6P_3$ requires C, 39·0; H, 2·7; N, 8·5%).

The PF_6^- salt was converted into the corresponding Br^- salt by precipitation with excess tetrabutylammonium bromide from a 3:1 acetone/acetonitrile solution. The resultant solid was washed with acetone, diethyl ether, and dried under vacuum.

Bis{ tri(2-pyridyl)phosphine} cobalt(II) *perchlorate, [Co(Py$_3$P)$_2$](ClO$_4$)$_2$*. $Co(ClO_4)_2.6H_2O$ (29 mg, 0·078 mmol) was refluxed under nitrogen in a deaerated solution of 1:1 dimethoxypropane/ethanol for 30 min. Tri(2-pyridyl)phosphine (39 mg, 0·146 mmol) dissolved in deaerated ethanol (2 ml) was added and the solution refluxed under nitrogen for a further 2 h. The brown *solid* was filtered off, washed with ethanol, and dried under vacuum before recrystallization from acetonitrile/toluene (both nitrogen-degassed). Yield: 39·9 mg, 65% (Found: C, 45·9; H, 3·2; N, 10·2. $C_{30}H_{24}Cl_2CoN_6O_8P_2$ requires C, 45·7; H, 3·1; N, 10·7%).

The ClO_4^- salt was converted into the Br^- form as described above for the analogous complex of the ligand Py_3CH.

Bis{ tri(2-pyridyl)phosphine oxide} cobalt(II) *hexafluorophosphate, [Co(Py$_3$P=O)$_2$](PF$_6$)$_2$*. $CoCl_2.6H_2O$ (65 mg, 0·27 mmol) was dissolved in water (3 ml) with gentle warming before the addition of tri(2-pyridyl)phosphine oxide dissolved in ethanol (4 ml). The solution was refluxed for 15–30 min, cooled, and the pale yellow-orange solid precipitated with NH_4PF_6. After standing in the refrigerator overnight, the solid was filtered off, washed with iced water, and dried under vacuum. A *sample* for microanalysis was recrystallized from acetonitrile/toluene. Yield: 0·11 g, 45% (Found: C, 37·8; H, 2·9; N, 8·8. $C_{30}H_{28}CoF_{12}N_6O_4P_4$ requires C, 38·0; H, 3·0; N, 8·9%).

Bis{ tri(2-pyridyl)methanol-N,N′,N″} cobalt(III) *perchlorate, [Co(Py$_3$COH)](ClO$_4$)$_2$*,[13] *and tris(2,2′-bipyridine)cobalt*(II) *chloride, [Co(bpy)$_3$]Cl$_2$*,[3] were prepared by literature methods.

Stoichiometry Studies of [Co(Py$_3$X)$_2$]$^+$ / H$_2$O/ HCO$_3^-$ Reaction (X = CH, P) in Aqueous Solution

All manipulations were performed in the glove box under an atmosphere of argon.

Solutions of $[Co(Py_3CH)_2]^+$ and $[Co(Py_3P)_2]^+$ (*c.* 1×10^{-2} M) were generated by coulometry at the diffusion plateau of the respective Co^{II}/Co^{I} couples in ethanol/0·1 M tetrabutylammonium bromide solution at a platinum gauze working electrode: a small amount (10%) of acetonitrile was required in the former case to dissolve $[Co(Py_3CH)_2]Br_3$.

For each determination, an aliquot (500 μl) of the appropriate Co^{I} solution was transferred by syringe into 5 ml of 0·2 M Tris/H_2SO_4 buffer of required pH (I = 0·5 M; Na_2SO_4) contained

[21] Boggess, R. K., and Zatko, D. A., *J. Coord. Chem.*, 1975, 4, 217.
[22] Kurtev, K., Ribola, D., Jones, R. A., Cole-Hamilton, D. J., and Wilkinson, G., *J. Chem. Soc., Dalton Trans.*, 1980, 55.

in a Sure-Seal bottle (capacity 13 ml) fitted with a silicone serum cap; in some determinations, $NaHCO_3$ or excess of the appropriate ligand had been dissolved in the buffer. The reaction was stirred until the disappearance of the blue colour characteristic of Co^I, and the gas above the solution was analysed for H_2. For the runs containing HCO_3^- the mixture was then acidified, and the gas also analysed for carbon monoxide.

Results and Discussion

Electrochemical and Spectral Studies

Electrochemical studies of the complexes $[Co(Py_3X)_2]^{n+}$ were undertaken in propylene carbonate (for X = N) and acetonitrile (for X = CH, COH, P, P=O) solutions. The cyclic voltammograms at a platinum working electrode in the potential range *c.* $+1\cdot0 \rightarrow -1\cdot5$ V (*v.* s.s.c.e.) are shown in Fig. 1. The $E_{1/2}$ values (and their respective ΔE_p) for the Co^{III}/Co^{II} and Co^{II}/Co^I redox couples are given in Table 1. The data obtained for $[Co(bpy)_3]^{n+}$ under similar conditions are given also for comparison. Similar overall results were obtained by using a glassy carbon working electrode.

Table 1. Cyclic voltammetry data for $[Co(Py_3X)_2]^{n+}$ cations

Platinum working electrode; s.s.c.e. reference; scan rate 100 mV s^{-1}; acetonitrile/0·1 M Et_4NPF_6 solvent, unless otherwise indicated

Complex cations	Co^{III}/Co^{II}		Co^{II}/Co^I	
	$E_{1/2}$ (V)	ΔE_p (mV)	$E_{1/2}$ (V)	ΔE_p (mV)
$[Co(Py_3N)_2]^{n+}$ [A]	0·35	60	−1·11	70
$[Co(Py_3CH)_2]^{n+}$	0·22	70	−1·21	70
$[Co(Py_3P)_2]^{n+}$	0·55	100	−0·97	80
$[Co(Py_3P{=}O)_2]^{n+}$	0·99	100	−0·75	70
$[Co(Py_3COH)_2]^{n+}$ [B]	0·19	70	−1·17	80
$[Co(bpy)_3]^{n+}$	0·32	80	−1·01	70

[A] Propylene carbonate/0·2 M Et_4NPF_6. [B] Ref. 13.

For all complexes studied, both redox couples are observed and are reversible or quasi-reversible on the cyclic voltammetry time scale. The Co^{II}/Co^I couple is marginally scan-rate-dependent for X = N at very slow scan rates (e.g. 20 mV s^{-1}), with the diminution of the wave on the anodic sweep: however, reversibility is restored by the presence of excess Py_3N ligand.

Controlled potential electrolysis of the cobalt complexes in the presence and absence of excess ligand were conducted on the diffusion plateau of the respective Co^{II}/Co^I reductions in acetonitrile or propylene carbonate media, a platinum gauze working electrode being used under inert conditions (argon). A sustainable deep blue colour, characteristic of polypyridylcobalt(I) species,[10,23] formed rapidly for the complexes with tri(2-pyridyl)phosphine and tri(2-pyridyl)phosphine oxide ligands, as reported previously,[11,12] but also with the tri(2-pyridyl)methane ligand. These reductions could be readily repeated following aerial oxidation. For the $[Co(Py_3COH)_2]^{n+}$ complex, Szalda and Keene[13] have reported the limited stability of the cobalt(I) species on the coulometric time scale. For the analogous complex containing the tri(2-pyridyl)amine ligand, a blue colour formed on reduction in the presence of excess ligand: the colour

[23] Waind, G. M., and Martin, B., *J. Inorg. Nucl. Chem.*, 1958, **8**, 551.

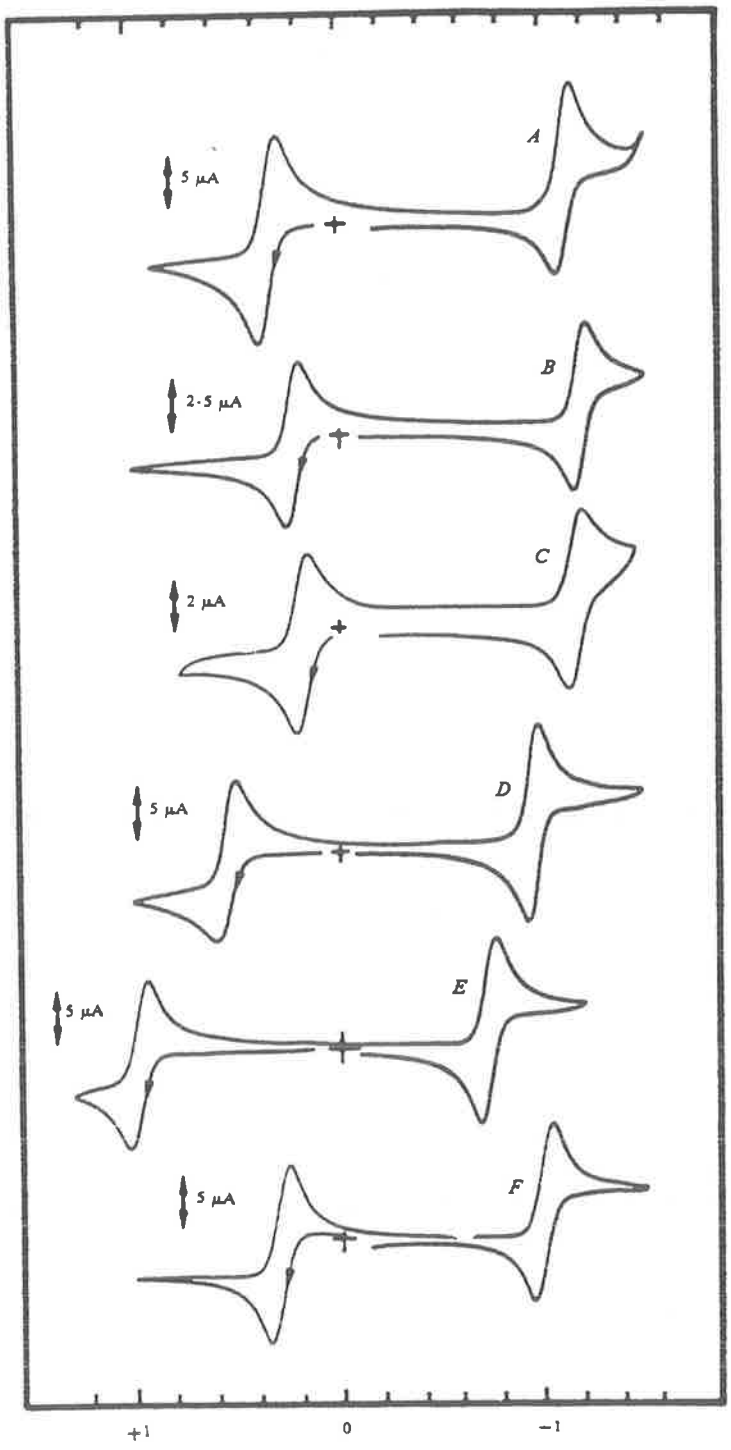

Fig. 1. Cyclic voltammograms of the complexes $[Co(Py_3X)_2]^{n+}$ where *A*, X = N; *B*, X = CH; *C*, X = COH; *D*, X = P; *E*, X = P=O; and *F*, $[Co(bpy)_3]^{n+}$. (Platinum working electrode: *B*–*F* were performed in acetonitrile/0·1 M Et_4NPF_6 at scan rate 100 mV s^{-1}; *A* was performed in propylene carbonate/0·2 M Et_4NPF_6 at scan rate 50 mV s^{-1}.)

was sustained for a considerable time (30 min) but gradually faded with the formation of a yellow solution of unknown composition. Clearly, however, tri(2-pyridyl)amine is able to stabilize cobalt(I) to some extent in propylene carbonate solution.

In their previous electrochemical studies of these complexes (X = N, P, P=O, As)[11,12] in acetonitrile solution with polarographic techniques, Boggess and Zatko observed the Co^{II}/Co^{I} couple for X = P, P=O and As, whereas for X = N a two-electron reduction of the Co^{II} species occurred to give Co^{0}. Similarly, in cyclic voltammetric experiments these authors observed a reversible Co^{II}/Co^{I} couple for the first three complexes whereas no such couple was observed for X = N. The present studies reveal that, in the less coordinating solvent propylene cabonate, the Co^{II}/Co^{I} redox couple of $[Co(Py_3N)_2]^{n+}$ can be observed on both the cyclic voltammetric and coulometric time scales, although the cobalt(I) species has limited stability.

Of greater significance, however, are the present electrochemical results obtained for the bis{tri(2-pyridyl)methane}cobalt complex. The carbon bridgehead atom, like nitrogen, is unable to take part in d_π–p_π bonding with the attached pyridyl groups. Fig. 1, curve *B*, shows the cyclic voltammetry scans of $[Co(Py_3CH)_2]^{n+}$, and demonstrates the ability of tri(2-pyridyl)methane to stabilize the cobalt(I) oxidation state. Analogous behaviour is seen for $[Co(Py_3COH)_2]^{n+}$ (see Fig. 1, curve *C*, and ref. 13). Furthermore, $[Co(Py_3CH)_2]^{+}$ can be synthesized by sodium amalgam reduction of the Co^{II} species, and both the solid and its solutions show considerable stability (several days) under inert conditions.[17]

The ability of 2,2′-bipyridine to stabilize the formal low oxidation states of cobalt is generally attributed to an ability of the ligand to accept electron density from the metal centre through d-π^* backbonding.[8] On reduction of the cobalt(II) state, the added electron enters a metal πd orbital and is partially delocalized onto the 2,2′-bipyridine ligand.[8] Evidence for the occurrence of metal-to-ligand charge transfer comes from ^{1}H n.m.r. studies,[9] visible and near-infrared spectra[10] and crystallographic data on metal-to-ligand and intraligand bond distances as a function of metal oxidation state.[8]

Pyridine, like 2,2′-bipyridine, is also a π-acceptor ligand able to receive electron density from the metal. Hexakis(pyridine)cobalt(II) seems extremely unstable, decomposing to the four-coordinate species unless stored under a pyridine atmosphere,[24] and the cobalt(I) species is not known. The stability imparted by 2,2′-bipyridine and its analogues (1,10-phenanthroline, 2,2′:6′,2″-terpyridine, etc.) therefore has been claimed to be a function of the 2,2′-diimine chromophore, which allows accepted electron density to be delocalized over more than one pyridine ring. Although the 2,2′-diimine chromophore is absent in the tripodal ligands that are the

Table 2. Visible absorbance maxima for $[Co(Py_3X)_2]^+$ complexes and $[Co(bpy)_3]^+$

Complex	Solvent/electrolyte	λ_{max} (nm)
$[Co(Py_3N)_2]^+$	propylene carbonate/0·2 M Et_4NPF_6	680, *c.* 470sh
$[Co(Py_3CH)_2]^+$	acetonitrile/0·1 M Et_4NPF_6	705, 485
$[Co(Py_3P)_2]^+$	acetonitrile /0·1 M Et_4NPF_6	685, 495
$[Co(Py_3P{=}O)_2]^+$	acetonitrile/0·1 M Et_4NPF_6	665, 415, 386
$[Co(bpy)_3]^+$	ethanol	605, 370

[24] Morrison, R. M., and Thompson, R. C., *Inorg. Nucl. Chem. Lett.*, 1976, 12, 937.

subject of the present study, quite clearly for Py_3X (X = CH, P, P=O) their behaviour resembles that of 2,2′-bipyridine and not pyridine. In this regard, the redox potentials for the various Co^{II}/Co^{I} couples (see Table 1) reveal that the Co^{I} state is destabilized for Py_3X ligands with X = N, CH by comparison with bpy, whereas with X = P it is comparable, and the complex involving $Py_3P{=}O$ is considerably stabilized.

The visible and near-infrared spectra of the cobalt(I) complex of bipyridine are characterized by intense absorptions in the visible (λ_{max} 605 nm)[10,23] and near-infrared (λ_{max} 1390 nm)[23] regions, attributed to metal-to-ligand charge transfer transitions. Solutions of $[Co(Py_3X)_2]^+$ (X = N, CH, P, P=O) were produced by coulometry, and Table 2 lists the absorbance maxima in the visible region of the spectra. By analogy with $[Co(bpy)_3]^+$,[10] the intense absorption maxima observed at 680, 705, 685 and 665 nm for $[Co(Py_3N)_2]^+$, $[Co(Py_3CH)_2]^+$,$[Co(Py_3P)_2]^+$ and $[Co(Py_3P{=}O)_2]^+$, respectively, may be tentatively assigned to d–π^* metal-to-ligand charge transfer.

Since the tripodal ligands Py_3X do appear to take part in π-backbonding from the metal centre, the question arises as to how these ligands stabilize cobalt(I) in the absence of the 2,2′-diimine chromophore. The proposal of Boggess and Zatko[11,12] that electron density is delocalized over the three pyridine rings of each ligand through the bridgehead atom is clearly not possible for those ligands with a nitrogen or carbon bridgehead. However, as pyridine and di(2-pyridyl)methane $\{Py_2CH_2\}$ ligands[17] are both unable to stabilize cobalt(I), the stability imparted to cobalt(I) by the tripodal ligands must be a function of the bridgehead atom, together with a requirement for three pyridyl rings. The α-carbon atom-to-bridgehead atom (X) bond lengths become shorter in the sequence P > CH > N. Consequently, the differing abilities of these tripodal ligands to stabilize cobalt(I) may be controlled by steric factors rather than electronic, with tri(2-pyridyl)amine simply less able to accommodate the increase in metal size occurring on reduction of cobalt(II) to cobalt(I).

The requirement for ligands containing three pyridyl rings suggests the ligand geometry imposed by the bridgehead atom may allow stabilization through some form of 'through space' electron delocalization between the pyridyl rings, although studies with space-filling models indicate that there is very little likelihood of π-overlap between the pyridyl rings of each ligand which (if the molecule is viewed down the C_3 axis) are constrained to a vertical orientation but 120° apart. Alternatively, the actual constraint of the pyridyl rings in their coordination positions by the bridgehead atom may promote overlap between the ligand p_π orbitals and the t_{2g} orbitals of the metal. The nature of the stabilization requires further study, and resolution of its origin may depend on molecular orbital and molecular mechanics calculations, and these are currently in progress.[17]

The redox potentials of the Co^{III}/Co^{II} couples are also reported in Table 1. These are not crucial to the present discussion, but the existence of this couple for $[Co(Py_3P{=}O)_2]^{n+}$ is noted as it was not observed in the previous study of this complex.[11]

Reactivity of $[Co(Py_3X)_2]^+$ Species (X = CH, P) as Reductants for Water and Carbon Dioxide

The polypyridyl complexes of cobalt(I) are known to promote the reduction of water to hydrogen,[3,5] and of carbon dioxide to carbon monoxide and formate ion.[5–7] The mechanism of water reduction by $[Co(bpy)_3]^+$ is proposed to occur through formation of a hydridocobalt species according to either of two schemes:

$$[Co(bpy)_3]^+ + H_3O^+ \rightarrow [Co(bpy)_2(H_2O)H]^{2+} + bpy$$

and/or

$$[Co(bpy)_3]^+ + 2H_2O \rightarrow [Co(bpy)_2(H_2O)_2]^+ + bpy$$

$$[Co(bpy)_2(H_2O)_2]^+ + H^+ \rightarrow [Co(bpy)_2(H_2O)H]^{2+} + H_2O$$

The $[Co(bpy)_2(H_2O)H]^{2+}$ complex subsequently reacts with a proton source to give H_2 according to the equation

$$[Co(bpy)_2(H_2O)H]^{2+} + H^+ + bpy \rightarrow [Co(bpy)_3]^{3+} + H_2$$

The reduction of CO_2, if present in aqueous media, occurs in competition with that of water, and via a common intermediate.[5] Kinetic studies are consistent with either the reaction of HCO_3^- with the hydride $[Co(bpy)_2(H_2O)H]^{2+}$, or reaction of CO_2 with $[Co(bpy)_2(H_2O)_2]^+$. The reduction of both H_2O and CO_2 therefore involves loss of a bipyridine ligand, and yields of H_2 are dramatically reduced in the presence of excess ligand. In the water reduction process, the hydride intermediate has been proposed[3] on the basis of comparison with analogous rhodium systems.[25]

In view of the stabilization of the Co^I state by the tripodal Py_3X ligands, it is of considerable interest to consider the reactivity of the title complexes with both water and carbon dioxide. Since the substitutional lability of $[Co(bpy)_3]^+$ and coordination with H^+ and CO_2 (or HCO_3^-) appear to be important to its reduction of water and carbon dioxide,[3–5] the possibility that the present tridentate ligands may be intrinsically less likely than bpy to dissociate from the metal centre could lead either to total inhibition of the reduction reaction, or to its occurrence by a modified pathway.

Preliminary semiquantitative studies reveal that for the reactions of $[Co(Py_3P)_2]^+$ and $[Co(Py_3CH)_2]^+$ in aqueous solution in the pH range 7·8–9·4

(A) both species react with water to produce H_2;

(B) the presence of HCO_3^- does not affect the yield of hydrogen and in no case could CO be detected as a product;

(C) for the former complex, the H_2 yield is not markedly affected by pH change in the limited range studied, whereas in the latter case the H_2 yield decreases rapidly with decreasing pH;

(D) the H_2 yields are not affected by the presence of excess ligand for X = P, but are decreased for X = CH, although the effect is dramatically less than that observed for equivalent reductions by $[Co(bpy)_3]^+$ in the presence of bpy.[5]

Further stoichiometric and kinetic studies are necessary to elucidate details of these reactions, but a number of general conclusions can be drawn from the present observations.

For the bis(ligand)cobalt complexes of Py_3X (X = CH, P), both Co^I species reduce water to form hydrogen, but, in contrast to the case of $[Co(bpy)_3]^+$,[5] there is no competition for the reductant by HCO_3^-. Furthermore, in the case of water reduction by $[Co(Py_3P)_2]^+$, the H_2 yield is not affected by the presence of excess

[25] Chou, M., Creutz, C., Mahajan, D., Sutin, N., and Zipp, A. P., *Inorg. Chem.*, 1982, 21, 3989.

ligand. Accordingly, for this species, complete ligand dissociation is not required, and H_2O reduction occurs through an alternative mechanism to that operating for $[Co(bpy)_3]^+$. A likely postulate is that dissociation of a single pyridyl moiety occurs, allowing formation of a hydridocobalt species. Reaction of this complex with an H^+ source would then give H_2. Since the coordination of CO_2 (or HCO_3^-) is also thought to be required for carbon dioxide reduction,[4,5] it would follow that no such reduction may occur.

On the other hand, the reduction of water by $[Co(Py_3CH)_2]^+$ is diminished by the presence of excess ligand, although the effect is far less marked than that observed for $[Co(bpy)_3]^+$.[5] This gradation in the reduction by the series of ligands bpy < Py_3CH < Py_3P could well reflect the decreasing lability of their cobalt complexes of reduced oxidation state. A difference in the lability of the ligands Py_3P and Py_3CH is not unexpected: a similar observation has been made for the analogous complexes of rhodium, $[Rh(Py_3P)_2]^{n+}$ and $[Rh(Py_3CH)_2]^{n+}$, where in the former case a reversible reduction is observed in cyclic voltammetry of the Rh^{III} species, in contrast to the latter species where the reduction is irreversible.[17] In view of the likely dissociation of Py_3CH in the reaction of its bis(ligand)cobalt(I) complex, it is perhaps surprising that no competition for water reduction by CO_2 (or HCO_3^-) is observed since their coordination might occur more readily than for the Py_3P case.

Mindful of the importance of the catalysis of the reduction of water[2,3] and of carbon dioxide[7,26–30] by activated hydrides, we have further studies in train on the mechanistic aspects of the above reactions involving $[Co(bpy)_3]^+$ [31] and the title complexes.[17]

Acknowledgments

This research was supported by the Australian Research Grants Scheme. We are grateful to Geoff Whebell and Ian Atkinson for their experimental assistance, and to Copper Refineries Pty Ltd for use of the gas chromatography facilities.

Manuscript received 3 February 1988

[26] Eisenberg, R., and Hendriksen, D, E., *Adv. Catal.*, 1979, **28**, 79.
[27] Inoue, S., and Yamazaki, N., (Eds) 'Organic and Bio-organic Chemistry of Carbon Dioxide' (John Wiley: New York 1982), and references cited therein.
[28] Darensbourg, D. J., and Kudaroski, R. A., *Adv. Organomet. Chem.*, 1983, **22**, 129, and references cited therein.
[29] Hawecker, J., Lehn, J.-M., Ziessel, R., *Helv. Chim. Acta*, 1986, **69**, 1990.
[30] Bruce, M. R. M., Megehee, E., Sullivan, B. P., Thorp, H., O'Toole, T. R., Downard, A., and Meyer, T. J., *Organometallics*, 1988, **7**, 238.
[31] Keene, F. R., Creutz, C., and Sutin, N., unpublished data.

Acta Cryst. (1990). C46, 1562–1563

Tri(2-pyridyl)methane

BY F. RICHARD KEENE

Department of Chemistry and Biochemistry, James Cook University of North Queensland, Townsville, Queensland 4811, Australia

AND EDWARD R. T. TIEKINK

Jordan Laboratories, Department of Physical and Inorganic Chemistry, University of Adelaide, South Australia 5001, Australia

(*Received* 16 *January* 1990; *accepted* 26 *February* 1990)

Abstract. $C_{16}H_{13}N_3$, $M_r = 247{\cdot}3$, monoclinic, $C2/c$, $a = 13{\cdot}998$ (1), $b = 8{\cdot}653$ (1), $c = 22{\cdot}368$ (2) Å, $\beta = 103{\cdot}15$ (1)°, $U = 2638$ (1) Å^3, $D_x = 1{\cdot}245$ Mg m^{-3}, $Z = 8$, Mo $K\bar{\alpha}$ radiation, $\lambda = 0{\cdot}7107$ Å, $\mu = 0{\cdot}042$ mm^{-1}, $F(000) = 1040$, $T = 293$ (2) K, $R = 0{\cdot}034$ for 947 observed reflections. In the title compound, $(2\text{-py})_3CH$, the central C atom exists in a slightly distorted tetrahedral geometry [tetrahedral angles range from 105 (1) to 113·8 (2)°]. The C—C(py) distances are 1·517 (4), 1·515 (4) and 1·522 (4) Å and the dihedral angles between the three pyridyl rings are 103·6, 106·8 and 88·4°, respectively. One of the pyridyl rings is disordered with a 180° rotation about the C(methane)—C(py) bond at C(1)—C(31). In the major conformation (*ca* 58%) the two N atoms are orientated as to point in the same direction as the methane H atom.

Experimental. The compound, $(2\text{-py})_3CH$, was prepared as in the literature (Keene, Snow, Stephenson & Tiekink, 1988). Suitable crystals for X-ray study were obtained from the slow evaporation of a dichloromethane/373–393 K petroleum spirit solution of the compound. Enraf–Nonius CAD-4F diffractometer controlled by a PDP8/A computer, graphite-monochromated Mo $K\bar{\alpha}$ radiation; $\omega{:}2\theta$ scan technique. Cell parameters on crystal 0·16 × 0·20 × 0·45 mm from least-squares procedure on 25 reflections ($4 \le \theta \le 12°$). No absorption correction applied (Sheldrick, 1976). Total of 2932 reflections ($1{\cdot}5 \le \theta \le 25{\cdot}0°$) measured in the range $-16 \le h \le 16$, $0 \le k \le 10$, $-26 \le l \le 3$. No significant variation in the net intensities of two reference reflections ($2\bar{2}5$, $3\bar{1}1$) measured every 7200 s. 2330 unique reflections (R_{int} 0·015) and 947 satisfied $I \ge 2{\cdot}5\sigma(I)$. Structure solved by direct methods (Sheldrick, 1986), full-matrix least-squares refinement of 229 parameters based on F (Sheldrick, 1976). Anisotropic thermal parameters for non-H atoms and H atoms refined with isotropic thermal parameters. The pyridyl ring C(31)–C(36) was found to be disordered over two sites such that N(32) and C(36) were interchanged by a 180° rotation about the C(1)—C(31) bond. Refinement of fractional site occupancies gave the major component of the disorder [58 (5)%] with N and C atoms in the N(32) and C(36) sites respectively and the minor component [42 (5)%] with C and N atoms in these sites respectively. At convergence $R = 0{\cdot}034$, $wR = 0{\cdot}037$, $w = 0{\cdot}71/[\sigma^2(F) + 0{\cdot}0018F^2]$, $S = 0{\cdot}84$, $(\Delta/\sigma)_{max} \le 0{\cdot}001$, $(\Delta\rho)_{max} = 0{\cdot}08$, $(\Delta\rho)_{min} = -0{\cdot}13$ e Å^{-3}; no extinction correction. Scattering factors for all atoms given in *SHELX*76 (Sheldrick, 1976). All calculations on SUN4/280 computer system. Atomic parameters given in Table 1, selected bond distances and angles in Table 2,* the numbering scheme used is shown in Fig. 1.

* Lists of structure factors, thermal parameters, H-atom parameters, all bond distances and angles, and mean-plane data have been deposited with the British Library Document Supply Centre as Supplementary Publication No. SUP 52830 (11 pp.). Copies may be obtained through The Technical Editor, International Union of Crystallography, 5 Abbey Square, Chester CH1 2HU, England.

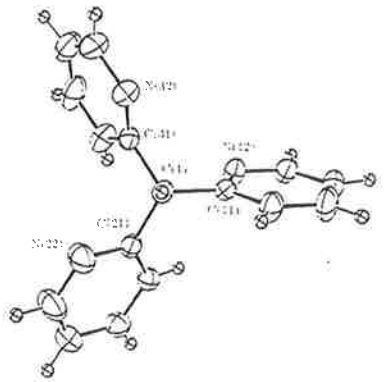

Fig. 1. Molecular structure and numbering scheme for $(2\text{-py})_3CH$ drawn at 25% probability levels (Johnson, 1971).

0108-2701/90/081562-02$03.00

Table 1. *Fractional atomic coordinates* ($\times 10^4$) *and* B_{eq} *values* (Å^2)

$B_{eq} = 8\pi^2(U_{11} + U_{22} + U_{33})/3$

	x	y	z	B_{eq}
C(1)	5100 (2)	2765 (3)	3498 (1)	4·15
C(11)	5843 (2)	1858 (3)	3968 (1)	4·11
N(12)	5568 (2)	1297 (3)	4456 (1)	5·18
C(13)	6225 (2)	495 (4)	4865 (2)	5·54
C(14)	7151 (3)	217 (4)	4808 (2)	6·46
C(15)	7436 (3)	805 (5)	4313 (2)	7·98
C(16)	6779 (2)	1641 (4)	3879 (2)	6·41
C(21)	5021 (2)	4449 (3)	3664 (1)	4·26
N(22)	4619 (2)	5353 (4)	3188 (1)	7·14
C(23)	4537 (3)	6856 (5)	3293 (2)	8·51
C(24)	4826 (3)	7520 (5)	3852 (2)	6·96
C(25)	5229 (3)	6599 (4)	4339 (2)	6·03
C(26)	5327 (2)	5043 (4)	4239 (2)	4·76
C(31)	4095 (2)	1999 (3)	3358 (2)	4·39
N(32)*	3898 (3)	1010 (4)	2873 (1)	6·43
C(33)	2979 (4)	334 (5)	2738 (3)	7·96
C(34)	2304 (4)	656 (6)	3060 (3)	8·51
C(35)	2538 (3)	1660 (7)	3543 (2)	8·42
C(36)*	3439 (2)	2343 (6)	3690 (2)	6·49

* Site occupancy factor 0·58 (5).

Related literature. The title compound was examined as part of a wider study of compounds of this type including the ligands (2-py)$_3$P (Keene, Snow & Tiekink, 1988*a*) and (2-py)$_3$COH (Keene, Snow & Tiekink, 1988*b*), and their complexes (Keene *et al.*, 1988). In complexes both bidentate and tridentate coordination have been shown by X-ray crystallography in [AuMe$_2${(2-py)$_3$CH}]NO$_3$ (Canty, Minchin, Healy & White, 1982) and [Ru{(2-py)$_3$CH}$_2$]-(tosylate)$_2$ (Keene *et al.*, 1988), respectively.

Table 2. *Selected interatomic distances* (Å) *and bond angles* (°)

C(1)—C(11)	1·517 (4)	C(1)—C(21)	1·515 (4)
C(1)—C(31)	1·522 (4)	C(1)—H(1)	1·11 (2)
C(11)—N(12)	1·329 (3)	N(12)—C(13)	1·335 (4)
C(21)—N(22)	1·338 (4)	N(22)—C(23)	1·332 (5)
C(31)—C(32)*	1·361 (5)	N(32)—C(33)	1·383 (6)
C(31)—C(36)*	1·338 (5)	C(36)—C(35)	1·363 (6)

C(11)—C(1)—C(21)	113·8 (2)	C(11)—C(1)—C(31)	111·9 (2)
C(11)—C(1)—H(1)	109 (1)	C(21)—C(1)—C(31)	110·7 (2)
C(21)—C(1)—H(1)	106 (1)	C(31)—C(1)—H(1)	105 (1)
C(1)—C(11)—N(12)	118·5 (2)	C(1)—C(11)—C(16)	119·6 (3)
C(1)—C(21)—N(22)	114·1 (3)	C(1)—C(21)—C(26)	124·8 (3)
C(1)—C(31)—N(32)	116·6 (3)	C(1)—C(31)—C(36)	120·5 (3)
C(11)—N(12)—C(13)	118·0 (3)	C(21)—N(22)—C(23)	117·9 (3)
C(31)—N(32)—C(33)	116·7 (4)		

* N(32) and C(36) have site occupancies 0·58 (5).

The Australian Research Council is thanked for support.

References

CANTY, A. J., MINCHIN, N. J., HEALY, P. C. & WHITE, A. H. (1982). *J. Chem. Soc. Dalton Trans.* pp. 1795–1802.

JOHNSON, C. K. (1971). *ORTEP*II. Report ORNL-3794, revised. Oak Ridge National Laboratory, Tennessee, USA.

KEENE, F. R., SNOW, M. R., STEPHENSON, P. J. & TIEKINK, E. R. T. (1988). *Inorg. Chem.* **27**, 2040–2045.

KEENE, F. R., SNOW, M. R. & TIEKINK, E. R. T. (1988*a*). *Acta Cryst.* C**44**, 757–758.

KEENE, F. R., SNOW, M. R. & TIEKINK, E. R. T. (1988*b*). *Acta Cryst.* C**44**, 937–938.

SHELDRICK, G. M. (1976). *SHELX*76. Program for crystal structure determination. Univ. of Cambridge, England.

SHELDRICK, G. M. (1986). *SHELXS*86. Program for the solution of crystal structures. Univ. of Göttingen, Federal Republic of Germany.

Applied Organometallic Chemistry (1990) 4 523–533

0268-2605/90/050523-11$05.50

Ambidentate coordination of the tripyridyl ligands 2,2′:6′,2″-terpyridyl, tris(2-pyridyl)-amine, tris(2-pyridyl)methane and tris(2-pyridyl)phosphine to carbonylrhenium centres: structural and spectroscopic studies*

Peter A Anderson,† F Richard Keene,†‡ Ernst Horn§ and Edward R T Tiekink§
† Department of Chemistry and Biochemistry, James Cook University of North Queensland Townsville, Queensland 4811, Australia, and § Department of Physical and Inorganic Chemistry, University of Adelaide, GPO Box 498, Adelaide, South Australia 5001, Australia

Received 12 January 1990 *Accepted 12 March 1990*

The reactions of $[Re(CO)_5Cl]$ with the ligands tpy (2,2′:6′,2″-terpyridine), py_3N {tris(2-pyridyl)-amine}, py_3CH {tris(2-pyridyl)methane}, and py_3P {tris(2-pyridyl)phosphine} in toluene solution realize compounds with the general formulation [Re(ligand)$(CO)_3$Cl] in which the tripyridyl ligands are bidentate. X-ray structural determinations of *fac*-[Re(tpy)$(CO)_3$Cl].H_2O and *fac*-[Re$(py_3N)(CO)_3$Cl] confirm these assignments. [Re(tpy)$(CO)_3$Cl].H_2O ($C_{18}H_{13}ClN_3O_4Re$) is monoclinic, space group $P2_1/n$, with cell dimensions $a=7.432(2)$ Å, $b=17.016(4)$ Å, $c=14.466(2)$ Å, $\beta=93.51(2)°$, and $Z=4$; full-matrix least-squares refinement on 2435 reflections with $I \geqslant 2.5\sigma(I)$ converged to a final $R=0.028$ and $R_w=0.029$. [Re$(py_3N)(CO)_3$Cl] ($C_{18}H_{12}ClN_4O_3Re$) is triclinic, space group $P\bar{1}$ with cell dimensions $a=13.761(2)$ Å, $b=14.636(6)$ Å, $c=11.110(2)$ Å, $\alpha=110.70(2)°$, $\beta=102.45(2)°$, $\gamma=107.48(2)°$, and $Z=4$; full-matrix least-squares refinement on 3459 reflections with $I \geqslant 2.5\sigma(I)$ converged to a final $R=0.038$ and $R_w=0.039$. If the synthetic procedure is undertaken under irradiation by visible light, for the ligand py_3N a species [Re$(py_3N)(CO)_2$Cl] (characterized by infrared spectroscopy and conductance measurements) is also formed, in which the ligand py_3N is tridentate. No analogous tridentate species is formed with the ligands tpy or py_3P, although there is evidence that it also forms for py_3CH.

* Supplementary material is lodged with the Cambridge Crystallographic Data Centre, UK.

Keywords: Rhenium, carbonyl, terpyridyl, tris(2-pyridyl)amine, tris(2-pyridyl)methane, tris(2-pyridyl)phosphine, structure

INTRODUCTION

Interest in the chemistry of the 'Greenhouse' gas carbon dioxide has increased substantially in recent years: in particular, its conversions to C_1 feedstocks for chemicals manufacture (e.g. carbon monoxide, formaldehyde, methanol) or to potential fuels (e.g. methanol, methane) have attracted particular attention. The direct electrochemical reduction of CO_2 at metal electrodes is generally non-specific and is attended by large overpotentials. However, a number of molecular electrocatalysts have been developed which mediate the electrochemical reduction and substantially reduce the overpotential.[1]

One such group of catalysts are the polypyridine complexes of rhenium of the general form [Re(L—L)$(CO)_3$X] {L—L = 2,2′-bipyridine (bpy) or 1,10-phenanthroline (phen), or their derivatives; X = Cl or Br}, which have been studied particularly by Hawecker *et al.*,[3] Meyer and Sullivan and co-workers,[3–5] and Kutal *et al.*[6] The complexes act as efficient homogeneous catalysts for the selective and sustained reduction of CO_2 to carbon monoxide (CO); furthermore, the reduction can be promoted either electrochemically or photochemically. The large turnover numbers observed are a consequence in part of

the stability of the catalyst with respect to deactivation reactions with the dominant product, CO. Despite the considerable attention directed towards the reactivity of CO_2 with such catalysts, the intimate mechanism of the reduction of CO_2 is a matter of considerable conjecture.[4] The elucidation of the key electron-, proton- and atom-transfer steps in such processes is clearly required for the rational design of effective catalysts.

With this in mind, we undertook a study of the synthesis and reactivities of a series of carbonylrhenium compounds incorporating the ligands py_3X, where py_3X represents the ligands tris(2-pyridyl)amine (py_3N), tris(2-pyridyl)methane (py_3CH), and tris(2-pyridyl)phosphine (py_3P). These tripodal π-acceptor ligands offer a greater synthetic versatility than the bidentate 2,2′-bipyridine and 1,10-phenanthroline ligands by virtue of possible variation of the bridging atom, the heterocyclic rings (e.g. 2-pyridyl, 2-methylimidazole, or 2-pyrrazolyl),[7] and the substituents on the heterocyclic rings. Such versatility might be expected to allow a subtle control over the redox chemistry which is not possible with bipyridine or phenanthroline species. Furthermore, electrochemical studies of the bis(ligand)cobalt complexes indicate the ability of these tripodal ligands to stabilize low oxidation states of metal centres to an extent comparable with 2,2′-bipyridine.[8] It was our hope that by subtle variation of the redox properties of the polypyridyl complexes of carbonylrhenium centres, a new mechanistic insight would be possible into the role of such metal species in their catalysis of CO_2 reduction processes.

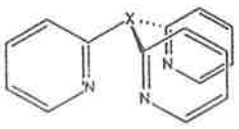

py_3X (X = N, CH, P)

The recent report by Juris *et al.*[9] of the synthesis of a related species containing the potentially tridentate ligand tpy, which was purported to be '$[Re(tpy)(CO)_2Cl]$', and of its ability to catalyse the electrochemical reduction of carbon dioxide, gave impetus to the proposal for the mechanistic studies of bis(carbonyl)rhenium species containing the tripodal ligands. However, during the synthetic aspects of this work, a number of anomalies arose relating to the characterization of these '$[Re(tridentate)(CO)_2Cl]$' complexes—in particular, the tendency of terpyridine to function as a bidentate rather than a tridentate ligand, and the ambidentate (bidentate/tridentate) ligating properties of the tripodal ligands.

The present paper reports structural and spectroscopic studies of carbonylrhenium compounds of these tripyridyl ligands, together with some initial observations on their electrochemistry and reactivity.

EXPERIMENTAL

Materials

$[Re(CO)_5Cl]$ (Pressure Chemical Co.), 2,2′-bipyridine (Strem) and 2,2′:6′,2″-terpyridine (Aldrich) were used as supplied; all other chemicals and solvents were of AR grade (where available). For the electrochemical experiments, the solvent 1-methyl-2-pyrrolidinone (NMP; Aldrich HPLC grade) was purified by fractional distillation under reduced pressure following drying over anhydrous $MgSO_4$. *N*,*N*-Dimethylformamide (DMF; BDH) was twice fractionally distilled under vacuum. Acetonitrile (BDH HIPerSolv 'Far UV'), used for the conductance measurements, was dried over calcium hydride and fractionally distilled. Tetra-n-butylammonium tetrafluoroborate ($TBA.BF_4$; Fluka; puriss) was used as the supporting electrolyte.

Instrumentation

Infrared spectra were measured in dichloromethane solution using a Perkin–Elmer 1600 Series FTIR. All electronic spectra were recorded on a Varian Cary 219 spectrophotometer. Electrochemical measurements were performed in an argon atmosphere and were recorded on a BAS 100A Electrochemical Analyzer using a glassy carbon working electrode and an Ag^+/Ag reference electrode (0.01M $AgNO_3$ in acetonitrile/0.1M $TBA.BF_4$; which is +0.31 V vs s.s.c.e.). Conductance measurements in acetonitrile (CH_3CN) were performed with Kerr Universal B221 conductance bridge. Microanalyses were performed within the Department (JCUNQ) or by the Canadian Microanalytical Service (Delta, B.C.).

Synthesis of ligands

Tris(2-pyridyl)amine,[10] tris(2-pyridyl)methane,[11] tris(2-pyridyl)methanol[12] and tris(2-pyridyl)phosphine[11] were prepared by literature methods.

Synthesis of rhenium compounds

The synthesis of the rhenium complexes was from a general method described by Juris *et al.*[9]

(2,2′-Bipyridine)tricarbonylchlororhenium(I), [Re(bpy)(CO)$_3$Cl]

2,2′-Bipyridine (72.5 mg, 0.46 mmol) was added to a solution of [Re(CO)$_5$Cl] (167.5 mg, 0.46 mmol) in toluene (80 ml, 80°C) under an argon atmosphere, which resulted in an immediate colour change from almost colourless to bright yellow and precipitation of a yellow complex within 1 min. The mixture was stirred and heated overnight. On cooling, the yellow precipitate was isolated by filtration, washed with petroleum spirit, and air-dried. Yield: 181 mg, 85%. The product was recrystallized twice from dichloromethane/petroleum spirit. Analysis: Calcd for $ReC_{13}H_8ClN_2O_3$: C, 33.8; H, 1.75; N, 6.1. Found: C, 33.7; H, 1.79; N, 6.1%.

Tricarbonylchloro(2,2′:6′,2″-terpyridine)-rhenium(I) hydrate, [Re(tpy)(CO)$_3$Cl].H$_2$O

2,2′:6′,2″-Terpyridine (56.8 mg, 0.24 mmol) was added to a solution of [Re(CO)$_5$Cl] (88.1 g, 0.24 mmol) in toluene (30 ml, 60°C) under an argon atmosphere. The solution gradually deepened in colour with a yellow precipitate forming after *ca* 20 minutes. The mixture was stirred and maintained at 80°C overnight. On cooling, the yellow precipitate was collected by filtration and recrystallized from dichloromethane/petroleum spirit. Yield: 100 mg, 80%. Analysis: Calcd for $ReC_{18}H_{11}ClN_3O_3.H_2O$: C, 38.8; H, 2.35; N, 7.5; Cl, 6.4. Found: C, 38.7; H, 2.33; N, 7.5; Cl, 6.4%.

Tricarbonylchloro{tris(2-pyridyl)amine}-rhenium(I) and Dicarbonylchloro-{tris(2-pyridyl)amine}rhenium(I), [Re(py$_3$N)(CO)$_x$Cl] (x=2,3)

Tris(2-pyridyl)amine (162 mg, 0.65 mmol) was added to a solution of [Re(CO)$_5$Cl] (235 mg, 0.65 mmol) in toluene (110 ml, 82°C) under a nitrogen atmosphere. The mixture was heated and stirred while illuminated by a 100 W tungsten floodlight for 70 h. The resultant pale orange solution was separated from a red precipitate by centrifugation. The supernatant was evaporated (rotary evaporator) to yield a pale orange compound.

For the pale orange compound, [Re(py$_3$N)(CO)$_3$Cl]: yield = 202 mg, 56% (based on total conversion of [Re(CO)$_5$Cl] to this product). Analysis: Calcd for $ReC_{18}H_{12}ClN_4O_3$: C, 39.0; H, 2.37; N, 10.1. Found: C, 39.3; H, 2.30; N, 10.0%.

For the red compound, [Re(py$_3$N)(CO)$_2$Cl]: yield = 95 mg, 28% (based on total conversion of [Re(CO)$_5$Cl] to this product). Analysis: Calcd for $ReC_{17}H_{12}ClN_4O_2 \cdot 0.25C_6H_5CH_3$: C, 41.0; H, 2.57; N, 10.2; Cl, 6.5. Found: C, 40.6; H, 2.73; N, 9.6; Cl, 7.2%.

Tricarbonylchloro{tris(2-pyridyl)phosphine}-rhenium(I), [Re(py$_3$P)(CO)$_3$Cl]

Tris(2-pyridyl)phosphine (131 mg, 0.49 mmol) was added to a solution of [Re(CO)$_5$Cl] (178 mg, 0.49 mmol) in toluene (80 ml, 70°C) under an argon atmosphere. The mixture was heated and stirred while illuminated by a 100 W tungsten floodlight for 60 h. The volume of the reaction mixture was reduced to *ca* 10 ml (rotary evaporator) and a brown–orange solid was precipitated by the addition of petroleum spirit. The collected precipitate was recrystallized twice from dichloromethane/petroleum spirit. Yield = 150 mg, 56%. Analysis: Calcd for $ReC_{18}H_{12}ClN_3PO_3$: C, 37.9; H, 2.12; N, 7.4. Found: C, 37.6; H, 2.32; N, 7.8%.

Using a similar synthetic method, a yellow–orange complex containing the ligand tris(2-pyridyl)methane (py$_3$CH) was synthesized in 85% yield (based on a product [Re(py$_3$CH)(CO)$_3$Cl]).

Crystallography

Crystals of [Re(tpy)(CO)$_3$Cl)].H$_2$O and [Re(py$_3$N)(CO)$_3$Cl] were grown by layer diffusion of petroleum spirit into solutions of the respective compounds in dichloromethane. Intensity data for [Re(tpy)(CO)$_3$Cl].H$_2$O and [Re(py$_3$N)(CO)$_3$Cl] were measured at room temperature using the ω:2θ scan technique on an Enraf–Nonius CAD4F diffractometer fitted with graphite monochromated MoKα radiation, λ = 0.7107 Å. No decomposition of either crystal occurred during its respective data collection. Data were corrected for Lorentz and polarization effects and an analytical absorption was applied in each case.[13] Crystal data are given in Table 1.

Table 1 Crystal data for *fac*-[Re(tpy)(CO)$_3$Cl].H$_2$O and *fac*-[Re(py$_3$N)(CO)$_3$Cl]

Compound	[Re(tpy)(CO)$_3$Cl].H$_2$O	[Re(py$_3$N)(CO)$_3$Cl]
Formula	$C_{18}H_{13}ClN_3O_4Re$	$C_{18}H_{12}ClN_4O_3Re$
Mol. wt	557.0	541.9
Crystal system	Monoclinic	Triclinic
Space group	$P2_1/n$	$P\bar{1}$
a, Å	7.432(3)	13.761(2)
b, Å	17.016(4)	14.636(6)
c, Å	14.466(2)	11.110(2)
α, deg	90	110.70(2)
β, deg	93.51(2)	102.45(2)
γ, deg	90	107.48(2)
V, Å^3	1826.0	1862.2
Z	4	4
D_c(g cm^{-3})	2.026	1.933
F(000)	1064	1056
μ, cm^{-1}	68.81	67.45
Transmission factors (maximum)	0.560; 0.401	0.747; 0.584
Θ limits, deg	1.5–25.0	1.5–24.0
No. of data collected	4165	5974
No. of unique data	3215	5842
No. of unique reflections used with $I \geq 2.5\sigma(I)$	2435	3459
R	0.028	0.038
g	0.002	0.003
R_w	0.029	0.039
Residual ρ_{max}, e Å^{-3}	0.98	1.85

The structure of *fac*-[Re(tpy)(CO)$_3$Cl].H$_2$O was solved from the interpretation of the Patterson synthesis whilst that of *fac*-[Re(py$_3$N)(CO)$_3$Cl] was solved by direct methods. The structures were each refined by a full-matrix least-squares procedure based on F.[13] All non-H atoms were refined with anisotropic thermal parameters in [Re(tpy)(CO)$_3$Cl].H$_2$O and the Re, Cl, carbonyl groups and amine-N atoms in [Re(py$_3$N)(CO)$_3$Cl] were refined anisotropically; the remaining non-H atoms were refined with isotropic thermal parameters for the latter structure. Hydrogen atoms were included at their calculated positions. The locations of the py-N atom in the non-coordinating pyridyl rings were confirmed by comparing the associated bond distances for both conformations. The refinements were continued until convergence after the introduction of a weighting scheme of the form $w = [\sigma^2(F) + g|F|^2]^{-1}$. Refinement details are listed in Table 1.

Fractional atomic coordinates are given in Tables 2 and 3 and the numbering schemes for both compounds are shown in Figs 2 and 3 (diagrams drawn with ORTEP[14] at 25% and 15% probability ellipsoids, respectively). Scattering factors for neutral Re (corrected for f' and f'') were from Ref. 15 and those for the remaining atoms were as incorporated in SHELX.[13] Calculations were performed on a SUN4/280 computer.

For both structures, full listings of the thermal parameters, hydrogen atom parameters, all bond distances and angles, and the observed and calculated structure factors are available on request from one of the authors (ERTT).

RESULTS AND DISCUSSION

Characterization and structural details

fac-[Re(bpy)(CO)$_3$Cl]

The [Re(bpy)(CO)$_3$Cl] species, and other [Re(bpy)(CO)$_3$X] compounds, have been characterized to have the chloro ligand *cis* to both ligating N atoms of the 2,2′-bipyridine ligand, with the three carbonyl ligands occupying a *facial* disposition in the coordination octahedron. A number of structural determinations of compounds of this type confirm the stereochemistry—

Table 2 Fractional atomic coordinates ($\times 10^5$ for Re; $\times 10^4$ for other atoms) for *fac*-[Re(tpy)(CO)$_3$Cl].H$_2$O

Atom	*x*	*y*	*z*
Re	20257(3)	5091(1)	24385(1)
Cl	4420(2)	1481(1)	2892(1)
O(1)	2296(9)	910(3)	381(3)
O(2)	−886(8)	−711(3)	1942(4)
O(3)	4886(9)	−713(3)	2073(5)
N(1)	2027(7)	305(3)	3920(4)
N(2)	228(6)	1421(3)	2952(3)
N(3)	−312(9)	2388(3)	908(4)
C(1)	2164(10)	791(4)	1148(5)
C(2)	200(10)	−247(4)	2134(5)
C(3)	3802(10)	−263(4)	2201(5)
C(4)	2833(9)	−303(4)	4351(5)
C(5)	3017(10)	−346(5)	5306(5)
C(6)	2378(11)	254(6)	5826(5)
C(7)	1525(10)	876(5)	5392(5)
C(8)	1345(9)	899(4)	4426(4)
C(9)	334(8)	1513(4)	3890(4)
C(10)	−486(10)	2137(4)	4328(5)
C(11)	−1422(10)	2684(4)	3787(5)
C(12)	−1581(10)	2596(4)	2837(5)
C(13)	−744(9)	1952(3)	2450(5)
C(14)	−1067(9)	1842(4)	1423(4)
C(15)	−2182(10)	1261(4)	1066(5)
C(16)	−2498(12)	1217(5)	117(6)
C(17)	−1733(11)	1749(5)	−430(5)
C(18)	−655(13)	2316(5)	−17(5)
O(w)	3298(10)	2976(4)	1554(5)

for example, of [Re(bpy)(CO)$_3$(PO$_2$F$_2$)],[16] [Re(bpy)(CO)$_3$(HCOO)],[17] [Re(bpy)(CO)$_3$(NCBH$_3$)],[17] and a related dimeric hydrido species [Re$_2$(bpy)$_2$(CO)$_6$(μ-H)]Cl.[17]

The electrochemical characteristics, as well as the electronic and infrared spectral properties of this compound, are listed in Table 4, together with the data for the other compounds involved in this study. The infrared spectrum in the region 2100–1800 cm^{-1} (carbonyl stretch) is shown in Fig. 1A, where three ν(CO) absorptions are observed (point group symmetry C_s).

fac-[Re(tpy)(CO)$_3$Cl]

The physical properties of the compound assigned as [Re(tpy)(CO)$_2$Cl] by Juris *et al.*[9] are virtually identical to those of [Re(bpy)(CO)$_3$Cl] (Table 4). This led us to consider an alternative formulation in which the tpy ligand was bidentate and the structure analogous to [Re(bpy)(CO)$_3$Cl]: certainly, the infrared characteristics (viz. the *three* ν(CO) absorptions, Fig. 1B) and the conductance

Table 3 Fractional atomic coordinates ($\times 10^5$ for Re; $\times 10^4$ for other atoms) for *fac*-[Re(py$_2$N)(CO)$_3$Cl]

Atom	*x*	*y*	*z*
Re(1a)	34973(4)	67200(3)	27333(5)
Cl(1a)	3623(3)	7229(3)	852(3)
O(1a)	5297(9)	8895(9)	4879(12)
O(2a)	1868(8)	7704(8)	3301(11)
O(3a)	3390(9)	6046(9)	5022(10)
C(1a)	4630(10)	8078(11)	4108(15)
C(2a)	2478(11)	7324(10)	3090(14)
C(3a)	3431(10)	6276(11)	4148(14)
C(4a)	5548(9)	6519(9)	2146(11)
C(5a)	6290(10)	6090(10)	1870(13)
C(6a)	6049(10)	5048(10)	1596(13)
C(7a)	5045(9)	4425(10)	1583(12)
C(8a)	4344(8)	4917(9)	1900(11)
N(1a)	4599(7)	5952(7)	2180(9)
C(10a)	2374(9)	4252(9)	908(11)
C(11a)	1647(10)	3272(10)	−165(13)
C(12a)	762(11)	3198(11)	−1108(14)
C(13a)	652(10)	4136(10)	−955(13)
C(14a)	1430(10)	5104(10)	83(12)
N(2a)	2282(7)	5180(7)	1040(9)
C(15a)	3138(9)	3803(9)	2680(12)
C(16a)	3984(12)	3723(12)	3494(15)
C(17a)	3712(12)	3209(12)	4327(15)
C(18a)	2636(12)	2826(12)	4267(16)
C(19a)	1860(13)	2922(12)	3399(15)
N(3a)	2113(9)	3431(9)	2616(12)
N(4a)	3303(7)	4340(8)	1858(10)
Re(1b)	80899(3)	01144(3)	26242(5)
Cl(1b)	6763(2)	8304(2)	824(3)
O(1b)	7629(9)	9554(10)	4898(11)
O(2b)	9940(8)	9400(8)	3112(10)
O(3b)	9734(9)	12349(8)	4791(11)
C(1b)	7815(11)	9810(11)	4068(14)
C(2b)	9231(10)	9675(9)	2893(13)
C(3b)	9101(11)	11518(11)	3963(14)
C(4b)	5773(9)	10055(9)	2303(12)
C(5b)	4885(10)	10318(11)	2064(13)
C(6b)	4932(11)	11067(11)	1595(13)
C(7b)	5876(9)	11601(10)	1443(12)
C(8b)	6765(9)	11324(9)	1772(11)
N(1b)	6722(7)	10564(7)	2200(10)
C(10b)	8041(9)	11155(9)	606(12)
C(11b)	8092(9)	11312(9)	−536(12)
C(12b)	8340(10)	10664(10)	−1510(13)
C(13b)	8569(11)	9822(11)	−1283(14)
C(14b)	8501(9)	9720(10)	−134(12)
N(2b)	8244(7)	10367(7)	827(9)
C(15b)	8363(9)	12926(9)	2241(12)
C(16b)	8020(11)	13638(10)	2991(13)
C(17b)	8691(12)	14715(12)	3572(16)
C(18b)	9681(13)	15058(13)	3458(16)
C(19b)	9998(12)	14320(12)	2709(15)
N(3b)	9318(9)	13240(9)	2079(12)
N(4b)	7755(8)	11815(7)	1600(10)

(indicating a zero-charged species) favoured the formulation [Re(tpy)(CO)$_3$Cl]. A similar rationalization has been made previously for the related compound [Re(tpy)(CO)$_3$(NO$_3$)].[18]

Accordingly, we undertook an X-ray crystal structure determination of the terpyridine compound to settle this ambiguity.

The molecular structure of *fac*-[Re(tpy)-$(CO)_3Cl].H_2O$ is shown in Fig. 2 and selected bond distances and angles are given in Table 5. The Re atom exists in a distorted octahedral environment defined by a *facial* arrangement of the three carbonyl groups, and a Cl atom and two N atoms which occupy the other octahedral face. The N atoms are *cis* and are derived from the tpy ligand which is functioning in the bidentate mode. The non-coordinating N atom, N(3), is directed away from the Re atom and the Re · · · N separation is 4.20 Å. The major distortion from regular octahedral symmetry arises as a result of the restricted bite angle of the chelate; N(1)–Re–N(2) 75.2(2)°. The N(1)–C(8)C(9)–N(2) torsion angle is −1.1° and the N(2)–C(13)C(14)–N(3) torsion angle is −114.9°. $[Re(tpy)(CO)_3Cl].H_2O$ was found to crystallize as a monohydrate and this water molecule is closely associated with the Cl and N(3) atoms. The Cl · · · O(w) and N(3) · · · O(w) separations are calculated to be 3.27 and 2.96 Å, respectively.

$[Re(py_3N)(CO)_xCl]$ ($x=2, 3$)

Using a synthetic procedure analogous to that for *fac*-$[Re(bpy)(CO)_3Cl]$ and *fac*-$[Re(tpy)(CO)_3Cl]$, a product was isolated which exhibited similar infrared spectral characteristics when $[Re(CO)_5Cl]$ was reacted with py_3N.

When the synthesis was repeated but under intense irradiation by visible light, two products were formed. A toluene-soluble form, which was identical to product obtained in the absence of light, has the infrared spectrum shown in Fig. 1C, and an X-ray structural determination indicates that the tripodal ligand is coordinated in a bidentate manner and the formulation of the complex is *fac*-$[Re(py_3N)(CO)_3Cl]$.

The molecular structure of *fac*-$[Re(py_3N)-(CO)_3Cl]$ is shown in Fig. 3, and selected interatomic parameters are given in Table 6. There are two molecules in the crystallographic asymmetric unit for this compound, designated **a** and **b** respectively. The numbering scheme for molecule **a** is shown in Fig. 3 and that of molecule **b** is identical. There are no major differences between molecules **a** and **b** of $[Re(py_3N)(CO)_3Cl]$, with the maximum difference occurring for the N(1)–Re–C(3) angle of 92.1(4)° for molecule **a** compared with 94.7(5)° for molecule **b**. As found for the tpy derivative, the Re atom in $[Re(py_3N)(CO)_3Cl]$ exists in a distorted octahedral environment with a *facial* arrangement of the three carbonyl groups. The remaining three positions are occupied by the Cl atom and two N atoms of the potentially tridentate py_3N ligand. The amine N atom, N(4), is 3.18 Å (3.19 Å for molecule **b**) from the central Re atom, which does not indicate a significant bonding interaction between these atoms. The N(1)–Re–N(2) chelate angle is 80.8(3)° {81.8(3)° for molecule **b**} which represents the maximum deviation from ideal octahedral symmetry in the structure. The N–Re–N chelate angles are larger here than in the $[Re(tpy)(CO)_3Cl]$ structure {75.2(2)°} which reflects the reduced steric strain in the six-membered N(1)C(8)N(4)C(10)N(2)Re ring in $[Re(py_3N)(CO)_3Cl]$ compared with the five-membered N(1)C(8)C(9)N(2)Re ring formed in $[Re(tpy)(CO)_3Cl]$.

The toluene-insoluble compound isolated from

Table 4 Spectral and electrochemical data

Compound	Electrochemistry[a] $E_{p,c}$	$E_{p,a}$	Electronic spectra[c] λ_{max} (nm)	Infrared spectra[d] ν(CO) (cm^{-1})
$[Re(bpy)(CO)_3Cl]$	−1.71	−1.62	370, 291, 233	2022, 1916, 1899
$[Re(tpy)(CO)_3Cl]$	−1.71	−1.64	374, 305, 255 sh	2022, 1918, 1897
$[Re(py_3N)(CO)_3Cl]$	−2.27[b]		300, 258, 226 sh	2023, 1916, 1897
$[Re(py_3N)(CO)_2Cl]$	−2.34[b]		450, 342, 255	1900, 1824
$[Re(py_3P)(CO)_3Cl]$				2023, 1932, 1897
$[Re(py_3CH)(CO)_2Cl]$				1896, 1819

[a] Cyclic voltammetry measurements at glassy carbon working electrode, relative to Ag/Ag^+ reference electrode; solvent NMP/0.1M $TBA.BF_4$, except for $[Re(tpy)(CO)_3Cl]$ (DMF/0.1M $TBA.BF_4$). Scan rate 100 $mV\,s^{-1}$. [b] Irreversible. [c] Acetonitrile solution. [d] Dichloromethane solution, except for $[Re(py_3P)(CO)_3Cl]$ (nujol mull), and $[Re(py_3CH)(CO)_2Cl]$ (acetonitrile solution).

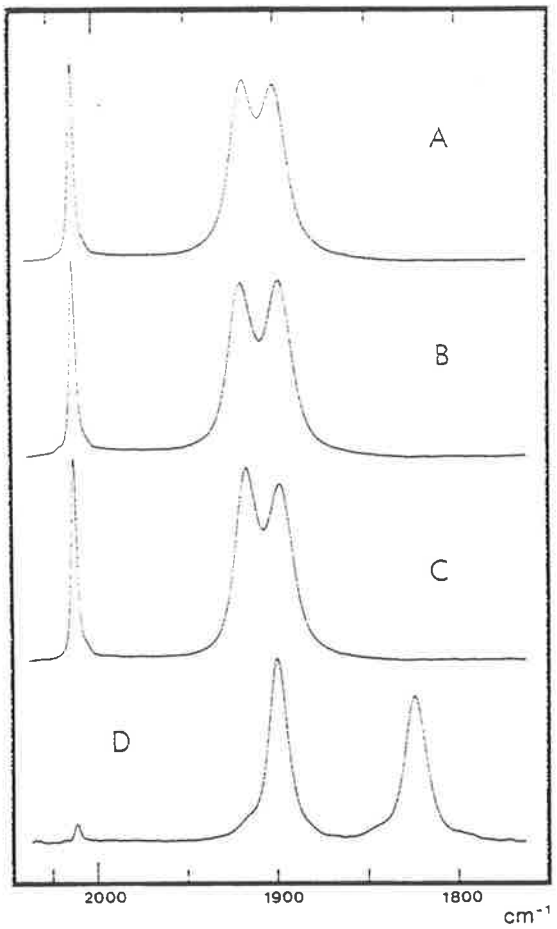

Figure 1 Infrared spectra (carbonyl stretch region) in dichloromethane solution for selected compounds: A, *fac*-[Re(bpy)(CO)$_3$Cl]; B, *fac*-[Re(tpy)(CO)$_3$Cl]; C, *fac*-[Re(py$_3$N)(CO)$_3$Cl]; D, [Re(py$_3$N)(CO)$_2$Cl].

this synthesis exhibits only two ν(CO) absorption peaks (Fig. 1D; Table 4), consistent with either [Re(py$_3$N)(CO)$_2$Cl] (C_s) or the symmetrical [Re(py$_3$N)(CO)$_3$]Cl (C_{3v}) formulations. However, conductance measurements indicate a zero-charged species. Although we have not yet been successful in growing satisfactory crystals of this compound for a structural determination, we are confident that this species is [Re(py$_3$N)(CO)$_2$Cl], where the py$_3$N ligand is now tridentate.

Accordingly, the ligand py$_3$N exhibits ambidentate behaviour with respect to its coordination with the carbonylrhenium(I) centres.

[Re(py$_3$CH)(CO)$_3$Cl] and [Re(py$_3$P)(CO)$_3$Cl]

Synthesis of the carbonylrhenium(I) compounds containing the tripodal ligands py$_3$CH and py$_3$P were carried out using the same general technique as for the py$_3$N analogue.

In the case of py$_3$P, only one product could be detected, and it exhibited three ν(CO) absorpotions in the infrared spectrum (Table 4). By analogy with the *fac*-[Re(bpy)(CO)$_3$Cl], *fac*-[Re(tpy)(CO)$_3$Cl] and *fac*-[Re(py$_3$N)(CO)$_3$Cl] compounds, it may confidently be formulated as *fac*-[Re(py$_3$N)(CO)$_3$Cl], with the ligand py$_3$P being bidentate.

For py$_3$CH, a product was isolated with a complicated infrared spectrum in the ν(CO) region. By analogy with the [Re(py$_3$N)(CO)$_3$Cl], the spectrum is consistent the isolated product being a mixture of *fac*-[Re(py$_3$CH)(CO)$_3$Cl] and [Re(py$_3$CH)(CO)$_2$Cl] in which the py$_3$CH ligand has coordinated both as a bidentate and tridentate ligand. Indeed, in a preliminary separation experiment utilizing the differing solubilities of the two components in dichloromethane, the less soluble yellow compound exhibited an IR spectrum analogous to that of [Re(py$_3$N)(CO)$_2$Cl] (Table 4); the remaining component, although slightly contaminated with the yellow less soluble species, exhibited an IR spectrum consistent with that of *fac*-[Re(py$_3$N)(CO)$_3$Cl].

It should be noted that examples are known in which py$_3$CH exhibits bidentate and tridentate

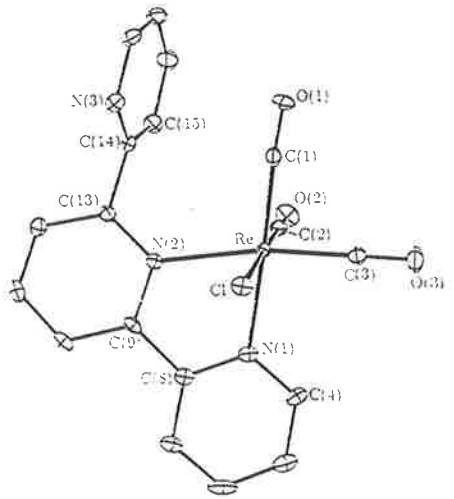

Figure 2 Molecular structure and numbering scheme for *fac*-[Re(tpy)(CO)$_3$Cl].H$_2$O. Atoms otherwise not indicated are carbons. Hydrogen atoms have been omitted for clarity.

Table 5 Selected bond distances (Å) and angles (deg) for *fac*-[Re(tpy)(CO)$_3$Cl].H$_2$O

Atoms	Distance	Atoms	Distance
Re–Cl	2.488(2)	Re–N(1)	2.170(5)
Re–N(2)	2.206(5)	Re–C(1)	1.936(7)
Re–C(2)	1.901(7)	Re–C(3)	1.908(7)
N(1)–C(4)	1.331(8)	N(1)–C(8)	1.365(9)
C(8)–C(9)	1.477(9)	N(2)–C(9)	1.362(7)
N(2)–C(13)	1.342(8)	C(13)–C(14)	1.501(9)
N(3)–C(14)	1.335(8)	N(3)–C(18)	1.35(1)
Atoms	**Angle**	**Atoms**	**Angle**
Cl–Re–N(1)	83.6(1)	Cl–Re–N(2)	83.2(1)
Cl–Re–C(1)	90.6(2)	Cl–Re–C(2)	178.0(2)
Cl–Re–C(3)	90.8(2)	N(1)–Re–N(2)	75.2(2)
N(1)–Re–C(1)	174.0(2)	N(1)–Re–C(2)	94.4(2)
N(1)–Re–C(3)	96.3(3)	N(2)–Re–C(1)	102.7(2)
N(2)–Re–C(2)	96.6(3)	N(2)–Re–C(3)	170.0(2)
C(1)–Re–C(2)	91.4(3)	C(1)–Re–C(3)	85.4(3)
C(2)–Re–C(3)	89.1(3)	Re–C(1)–O(1)	175.4(6)
Re–C(2)–O(2)	178.9(6)	Re–C(3)–O(3)	178.4(6)
Re–N(1)–C(4)	124.1(5)	Re–N(1)–C(8)	115.7(4)
N(1)–C(8)–C(9)	115.8(5)	C(8)–C(9)–N(2)	116.0(5)
Re–N(2)–C(9)	114.6(4)	Re–N(2)–C(13)	127.5(4)
N(2)–C(13)–C(14)	120.0(5)	C(13)–C(14)–N(3)	114.7(6)

coordination behaviour in the complexes $[AuMe_2(py_3CH)]^{-}$[7] and $[Ru(py_3CH)_2]^{2+}$,[11] respectively.

Comments on the synthetic method

The synthetic results are consistent with reported photochemical characteristics of $[Re(CO)_5Cl]$[19] and CO-substituted derivatives such as *fac*-$[Re(bpy)(CO)_3Cl]$.[20] The electronic transition giving rise to absorption by $[Re(CO)_5Cl]$ in the visible region (*ca* 366 nm) has been assigned mainly LF character, and photolysis in the absence of other ligands leads to the formation of

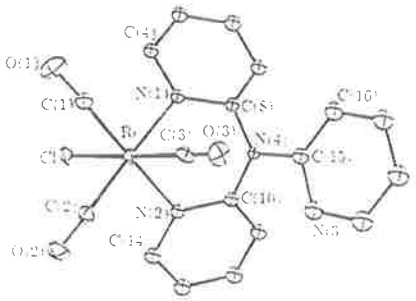

Figure 3 Molecular structure and numbering scheme for *fac*-[Re(py$_3$N)(CO)$_3$Cl] (molecule a). Atoms otherwise not indicated are carbons. Hydrogen atoms have been omitted for clarity. The numbering scheme for molecule b is identical to that shown for molecule a.

Table 6 Selected bond distances (Å) and angles (deg) for *fac*-[Re(py$_3$N)(CO)$_3$Cl]

	Distances	
Atoms	Molecule a	Molecule b
Re–Cl	2.477(3)	2.476(3)
Re–N(1)	2.208(8)	2.186(9)
Re–N(2)	2.191(9)	2.197(9)
Re–C(1)	1.92(1)	1.89(1)
Re–C(2)	1.91(1)	1.87(1)
Re–C(3)	1.91(1)	1.90(1)
N(1)–C(4)	1.34(1)	1.35(1)
N(1)–C(8)	1.35(1)	1.35(1)
N(2)–C(10)	1.36(1)	1.35(1)
N(2)–C(14)	1.35(1)	1.35(1)
N(3)–C(15)	1.33(2)	1.33(2)
N(3)–C(19)	1.37(2)	1.38(2)
N(4)–C(8)	1.41(1)	1.43(1)
N(4)–C(10)	1.41(1)	1.40(1)
N(4)–C(15)	1.41(1)	1.40(1)
	Angles	
Atoms	Molecule a	Molecule b
Cl–Re–N(1)	85.1(2)	84.4(2)
Cl–Re–N(2)	83.6(2)	82.6(2)
Cl–Re–C(1)	92.2(4)	92.8(4)
Cl–Re–C(2)	92.9(4)	93.0(4)
Cl–Re–C(3)	177.1(4)	178.2(4)
N(1)–Re–N(2)	80.8(3)	81.8(3)
N(1)–Re–C(1)	96.0(4)	94.8(4)
N(1)–Re–C(2)	176.2(4)	177.0(4)
N(1)–Re–C(3)	92.1(4)	94.7(5)
N(2)–Re–C(1)	174.9(4)	174.5(5)
N(2)–Re–C(2)	95.8(4)	96.5(4)
N(2)–Re–C(3)	95.2(5)	95.7(4)
C(1)–Re–C(2)	87.3(5)	86.7(5)
C(1)–Re–C(3)	88.8(6)	88.8(6)
C(2)–Re–C(3)	89.9(5)	87.8(5)
Re–C(1)–O(1)	177(1)	176(1)
Re–C(2)–O(2)	179(1)	177(1)
Re–C(3)–O(3)	177(1)	178(1)
Re–N(1)–C(4)	120.1(7)	121.0(8)
Re–N(1)–C(8)	121.1(7)	122.3(7)
N(1)–C(8)–N(4)	116.2(9)	116.0(9)
Re–N(2)–C(10)	120.4(7)	121.6(8)
Re–N(2)–C(14)	122.4(8)	121.4(7)
N(2)–C(10)–N(4)	117.1(9)	117(1)
C(8)–N(4)–C(10)	118.7(9)	117.4(9)
C(8)–N(4)–C(15)	123.2(9)	122.8(9)
C(10)–N(4)–C(15)	118.0(9)	119.3(9)
N(4)–C(15)–N(3)	113(1)	115(1)

the dimer, $[Re(CO)_4Cl]_2$.[19] In the presence of a ligand such as 2,2′-bipyridine, photolysis of $[Re(CO)_5Cl]$ results in the quantitative formation of $[Re(bpy)(CO)_3Cl]$,[19,20] and these photosubstitution processes are very much more rapid than thermal CO-substitution rates. On the other hand, the lowest energy absorption of *fac*-$[Re(bpy)(CO)_3Cl]$-type compounds is assigned principally to a $Re \rightarrow X(\pi^*)$ CT transition, in which the excited state is not substitutionally labilized.[20]

In the present instance, the thermal reactions of the potentially tridentate ligands tpy and py_3N with $[Re(CO)_5Cl]$ give rise to the *fac*-$[Re(ligand)(CO)_3Cl]$ species in which the tripyridyl ligands are bidentate, in a reaction which is analogous to that of the bidentate ligands bpy and phen with $[Re(CO)_5Cl]$. In the presence of light, the reaction involving the py_3N or py_3CH ligands also produces the tridentate species $[Re(py_3X)(CO)_2Cl]$ consistent with the CO-labilization of $[Re(CO)_5Cl]$ by visible light absorption. Additional observations reinforce this assertion. Firstly, two separate syntheses involving the py_3CH ligand, with identical reaction times but differing in that irradiation was maintained for the duration of the reaction in one case, but for only the first 10 minutes of reaction in the other, both gave products which were mixtures of the two components: although the ratio of the components may have varied, it is clear that the CO-labilization occurs in the initial stages of the reaction and therefore involves the reactant $[Re(CO)_5Cl]$. Secondly, attempts to promote coordination of the third N-donor of the potentially tridentate ligands tpy or py_3N in the compounds *fac*-$[Re(ligand)(CO)_3Cl]$ under irradiation were totally unsuccessful.

It is interesting to note that under the conditions used in the syntheses, neither tpy or py_3P appears to give the corresponding tridentate compound. The reason for these observations is probably steric in origin. In compounds containing coordinated tpy, it is well documented that the metal–central N distance is significantly contracted compared with the metal–outer N distances, and this is presumably due to steric constraints imposed by the tridentate tpy ligand.[21]

The ligand tpy has been shown to exhibit ambidentate coordination behaviour: Deacon *et al.*[22] have synthesized and structurally characterized the series of ruthenium(II) complexes *cis*,*cis*-$[Ru(Cl)_2(CO)_2(tpy)]$ (in which tpy is bidentate), and the related species *cis*-$[Ru(Cl)_2(CO)_2(tpyH)]^+$ in which the free pyridyl-N atom is protonated, as well as the corresponding decarbonylated species *cis*- and *trans*-$[Ru(Cl)_2(CO)(tpy)]$ (in which tpy is tridentate).

Py_3P, with its increased 'bite' angle compared with py_3CH and py_3N, also appears to prefer bidentate coordination in the present case: it is noted that in structural studies of the $[Ru(py_3X)_2]^{2+}$ complexes,[11] the cations show increasing distortion from the ideal D_{3d} symmetry with an increase in the bridgehead X–C(py) bond distance in the series $py_3N < py_3CH < py_3P$. As a further example, in the series of complexes $[Ru(py_3X)(NH_3)_3]^{2+}$ (X = N, CH, COH, P), only in the case of py_3P did a tridentate species not form.[23]

Nature of metal–ligand interaction for tripodal ligands py_3X

The title tripodal ligands are known to exhibit π-back-bonding interactions with low oxidation state metals.[8] Because of the presence of the bridging atom between the pyridyl rings the back-bonding characteristics of the tripodal ligands py_3X (X = N, CH, P), relative to ligands such as bpy or phen which possess the α,α'-di-imine chromophore, are somewhat counter-intuitive. It has been suggested that the particular stereochemical requirements of these ligands may serve to maximize the appropriate metal–ligand interaction,[8] and molecular-orbital calculations are in progress to probe the nature of the bonding.[24]

The ambidentate nature of the coordination of py_3N might therefore have been expected to provide additional insight into this issue, since in the bidentate coordination mode the chromophore is equivalent to two pyridyl rings separated by the bridging atom, in contrast with the tridentate coordination mode where the bridgehead atom may serve to constrain the three pyridyl rings in a conformation particularly favourable for overlap between the ligand p_π and metal t_{2g} orbitals. However, the ν(CO) absorptions in the infrared spectra of the series of compounds *fac*-$[Re(bpy)(CO)_3Cl]$, *fac*-$[Re(tpy)(CO)_3Cl]$, *fac*-$[Re(py_3N)(CO)_3Cl]$, and *fac*-$[Re(py_3P)(CO)_3Cl]$ are virtually identical in nature and position (Table 4; Fig. 1); it has been acknowledged for some time that in substituted metal carbonyl compounds of this type, the CO-stretching frequency shifts are not a reliable

means of assessing the π-bonding abilities of ligands.[25] Neither are the electrochemical characteristics of the compounds in this study particularly revealing, because the reduction of the compounds containing the ligand py_3N are irreversible, compared with the reversible redox behaviour exhibited by the bpy- and tpy-containing species (Table 4).

Carbon dioxide reactivity

In earlier studies, Juris *et al.*[9] reported that the compound characterized as '$[Re(tpy)(CO)_2Cl]$' chemically catalysed the electrochemical reduction of carbon dioxide in a similar manner to *fac*-$[Re(bpy)(CO)_3Cl]$.[2,6] In view of the present reassessment of the formulation of the tpy-containing species as *fac*-$[Re(tpy)(CO)_3Cl]$, in which tpy is bidentate rather than tridentate, the similarity is not unexpected.

We have observed that the *fac*-$[Re(py_3X)(CO)_3Cl]$ and $[Re(py_3X)(CO)_2Cl]$ compounds do mediate in the electrochemical reduction of CO_2. However, the initial reductions of the $[Re(py_3N)(CO)_xCl]$ ($x=2, 3$) species occur at considerably more negative potentials ($E_{p,c}=-2.34$ and -2.27 V vs Ag/Ag^+, respectively) than those of *fac*-$[Re(bpy)(CO)_3Cl]$ and *fac*-$[Re(tpy)(CO)_3Cl]$ ($E_{p,c}=-1.71$ V in both cases; Table 4). Given that for the $CO_2/CO_2^{\cdot-}$ couple in water $E^\circ=-1.90$ V (vs normal hydrogen electrode:[26] i.e. *ca* -2.5 V vs Ag/Ag^+), the compounds containing the tripodal ligands py_3X do not appear to be particularly attractive candidates for electrocatalysis of CO_2 reduction.

CONCLUSIONS

The present work has shown an apparent special stability of species of the general formula *fac*-$[Re(L—L)(CO)_3L]$ where L—L is a bidentate ligand, even in instances where L—L is potentially tridentate. If the synthetic procedure (CO-substitution of $[Re(CO)_5Cl]$) is undertaken under irradiation by visible light, for the ligands py_3N and py_3CH compounds of the general formula $[Re(L_3)(CO)_2Cl]$ containing the respective tridentate ligands are also obtained, whereas for tpy and py_3P they are not. The reason for this difference may be stereochemical in nature.

Acknowledgment Useful discussion with Professor M I Bruce in the early stages of this work is gratefully acknowledged. The Australian Research Council is thanked for financial support.

REFERENCES

1. Collin, J P and Sauvage, J-P *Coord. Chem. Rev.*, 1989, 93: 245, and references therein
2. Hawecker, J, Lehn, J-M and Ziessel, R *Helv. Chim. Acta*, 1986, 69: 1990
3. Sullivan, B P and Meyer, T J *Organometallics*, 1986, 5: 1500
4. Sullivan, B P, Bruce, M R M, O'Toole, T R, Bolinger, C M, Megehee, E, Thorp, H and Meyer, T J *Electrocatalytic Carbon Dioxide Reduction*, In *Catalytic Activation of Carbon Dioxide*, Ayres, W M ed. A.C.S Symp. Ser. No 363, Washington DC, 1988, pp 52–90
5. O'Toole, T R, Margerum, L D, Westmoreland, T D, Vining, W J, Murray, R W and Meyer, T J *J. Chem. Soc., Chem. Commun.*, 1985, 1416
6. Kutal, C, Weber, M A, Ferraudi, G and Geiger, D *Organometallics*, 1985, 4: 2161
7. Canty, A J, Minchin, N J, Healy, P C and White, A H *J. Chem. Soc., Dalton Trans.*, 1982, 1795; Byers, P K, Canty, A J, Skelton, B W and White, A H *Aust. J. Chem.*, 1985, 38: 1251
8. Hafeli, T A and Keene, F R *Aust. J. Chem.*, 1988, 41: 1379
9. Juris, A, Campagna, S, Bidd, I, Lehn, J-M and Ziessel, R *Inorg. Chem.*, 1988, 27: 4007
10. Wibaut, J P and La Bastide, G L C *Recl. Trav. Chim. Pays-Bas*, 1933, 52: 493
11. Keene, F R, Snow, M R, Stephenson, P J and Tiekink, E R T *Inorg. Chem.*, 1988, 27: 2040
12. Wibaut, J P, de Jonge, A P, Van der Voort, H G P and Otto, P Ph H L *Recl. Trav. Chim. Pays-Bas*, 1951, 70: 1054
13. Sheldrick, G M SHELX 76, Program for crystal structure determination, Cambridge University, UK, 1976
14. Johnson, C K ORTEP-II Report ORNL-3794, Oak Ridge National Laboratory, Tennessee, USA, 1971
15. Ibers, J A and Hamilton, W C *International Tables for X-Ray Crystallography*, Vol IV, Kynoch Press, Birmingham, UK, pp 99, 149
16. Horn, E and Snow, M R *Aust. J. Chem.* 1980, 33: 2369
17. Guilhem, J, Pascard, C, Lehn, J-M and Ziessel, R *J. Chem. Soc., Dalton Trans.*, 1989, 1449
18. Addison, C C, Davis, R and Logan, N *J. Chem. Soc., Dalton Trans.*, 1974, 2070
19. Wrighton, M S, Morse, D L, Gray, H B and Ottesen, D K *J. Am. Chem. Soc.*, 1976, 98: 1111
20. Wrighton, M S and Morse, D L *J. Am. Chem. Soc.*, 1974, 96: 998
21. Adcock, P A, Keene, F R, Smythe, R S and Snow, M R *Inorg. Chem.*, 1984, 23: 2336, and references therein

22. Deacon, G B, Patrick, J M, Skelton, B W, Thomas, N C and White, A H *Aust. J. Chem.*, 1984, 37: 929
23. Moritz, P S, Diamantis, A A, Keene, F R, Snow, M R and Tiekink, E R T *Aust. J. Chem.* 1988, 41: 1353
24. Anderson, P A and Keene, F R (work in progress)
25. Angelici, R J *J. Inorg. Nucl. Chem.*, 1966, 28: 2627
26. Schwarz, H A and Dodson, R W *J. Phys. Chem.*, 1989, 93: 409; Surdhar, P S, Mezyk, S P and Armstrong, D A *J. Phys. Chem.*, 1989, 93: 3360

Inorganica Chimica Acta, *187* (1991) 217–220

Coordination of bis(2-pyridyl)phosphinic acid as a tridentate ligand. Crystal structure of the {bis(2-pyridyl)phosphinato}{tris(2-pyridyl)-phosphine oxide}ruthenium(II) cation, $[Ru\{py_2P(O)O\}\{py_3PO\}]BF_4 \cdot 2H_2O$

F. Richard Keene*, Philip J. Stephenson

Department of Chemistry and Biochemistry, James Cook University of North Queensland, Townsville, Qld. 4811 (Australia)

and Edward R. T. Tiekink

Department of Physical and Inorganic Chemistry, University of Adelaide, Adelaide, SA 5001 (Australia)

(Received April 9, 1991; revised May 21, 1991)

Abstract

In the synthesis of the bis{tris(2-pyridyl)phosphine oxide}ruthenium(II) cation, $[Ru(py_3P{=}O)_2]^{2+}$, the species {bis(2-pyridyl)phosphinato}{tris(2-pyridyl)phosphine oxide}ruthenium(II), $[Ru\{py_3P{=}O\}\{py_2P(O)O\}]^+$, was also isolated. The latter cation has been characterized by a structural determination and is the first example of a tridentate phosphinate anion. The electrochemical and spectral properties of both cations are reported. Crystals of $[Ru\{py_2P(O)O\}\{py_3PO\}]BF_4 \cdot 2H_2O$ crystallize in the monoclinic space group $P2_1/n$ with unit cell dimensions $a = 16.128(7)$, $b = 11.493(6)$, $c = 17.576(11)$ Å, $\beta = 102.64(4)°$, $V = 3178.9$ Å^3, $Z = 4$. The structure was refined by a full-matrix least-squares procedure, and converged with $R = 0.107$ and $R_w = 0.108$ for 1172 reflections.

Introduction

As part of a study of the synthesis and properties of transition metal complexes containing the tripodal ligands $(py)_3X$,

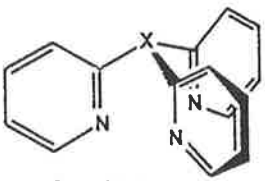

py = 2-pyridyl
X = N, CH, COH, P, P=O

we recently published details of the ruthenium(II) complexes of tris(2-pyridyl)amine, tris(2-pyridyl)-methane, tris(2-pyridyl)methanol and tris(2-pyridyl)-phosphine [1–3]. We had also undertaken the synthesis of the analogous compounds involving tris(2-pyridyl)phosphine oxide $\{py_3P{=}O\}$, a ligand reported previously [4, 5]. In the course of the work, we have indeed isolated $[Ru(py_3P{=}O)_2]^{2+}$, as well as the species $[Ru\{py_3P{=}O\}\{py_2P(O)O\}]^+$ which we have characterized by a structural determination. Details of this structure are now presented, together with electrochemical characteristics of both the isolated products.

*Author to whom correspondence should be addressed.

Results and discussion

Synthesis aspects

The synthetic route to the $[Ru(py_3P{=}O)_2]^{2+}$ cation was identical to that established in our earlier studies of the analogous $[RuL_2]^{2+}$ species containing the ligands py_3N, py_3CH and py_3P [2], which involved ligand substitution of the labile precursor $[Ru(DMF)_6]^{2+}$ (DMF = *N*,*N*-dimethylformamide) developed by Bernhard and Sargeson [6]. In addition to the desired (major) orange product, a minor amount of a sparingly soluble red product was also obtained, subsequently identified as containing $[Ru\{py_3P{=}O\}\{py_2P(O)O\}]^+$. The origin of the ligand bis(2-pyridyl)phosphinic acid in the reaction mixture is uncertain, but must arise either from a hydrolysis reaction during the synthesis of tris(2-pyridyl)-phosphine oxide, or alternatively because of the presence of small amounts of hydroxybis(2-pyridyl)-

0020-1693/91/$3.50

phosphine in the tris(2-pyridyl)phosphine precursor*. We regard the latter explanation as the more likely, and clearly the low solubility of the $[Ru\{py_3P{=}O\}\{py_2P(O)O\}]^+$ salts has allowed their ready isolation in this case.

Description of structure of the $[Ru\{py_3P{=}O\}\{py_2P(O)O\}]^+$ cation

The molecular structure of the $[Ru\{py_3P{=}O\}\{py_2P(O)O\}]^+$ cation is shown in Fig. 1 and selected interatomic parameters are given in the caption. While the structure is not of high precision owing to the poor quality of the crystals obtained, the analysis unambiguously establishes the stoichiometry of the compound and the molecular connectivity. The asymmetric unit comprises the $[Ru\{py_3P{=}O\}\{py_2P(O)O\}]^+$ cation, a BF_4^- anion and two water molecules of solvation associated with the ions via the expected hydrogen bonding contacts.

The Ru atom in the cation exists in a slightly distorted octahedral geometry comprised of an N_3 donor set derived from a $py_3P{=}O$ tripod ligand and an N_2O donor set derived from a hydrolyzed $py_3P{=}O$ ligand, i.e. $py_2P(=O)O^-$ anion. The oxidation state of the Ru atom is +II owing to the presence of a BF_4^- anion in the lattice. The Ru–N bond distances lie in the narrow range 2.04(3)–2.11(3) Å with the shorter Ru–N bond distance being *trans* to the Ru–O bond of 2.11(2) Å reflecting the *trans* influence of the O(1) atom. The maximum deviation from the ideal octahedral geometry is manifested in the O(1)–Ru–N(1) bond angle of 82.9(9)°. The Ru–P(1) separation of 2.87(1) Å is not indicative of a significant interaction between these atoms. As expected the P(1)–O(1) bond distance of 1.56(2) Å is longer than the P(1)=O(2) distance of 1.44(3) owing to the coordination of the O(1) atom to the Ru atom; the P(2)=O(3) distance is 1.48(3) Å.

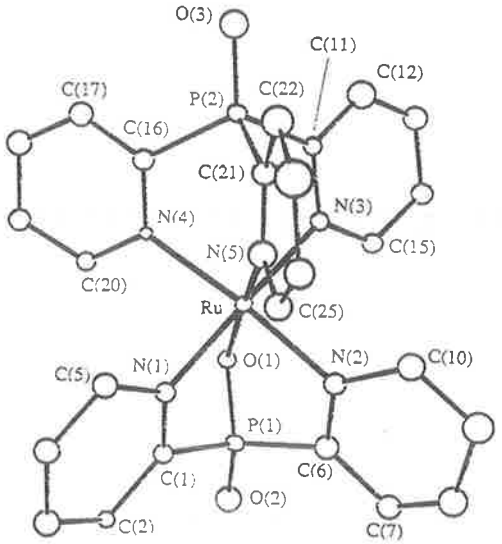

Fig. 1. The molecular structure of the $[Ru\{py_3P{=}O\}\{py_2P(O)O\}]^+$ cation showing the crystallographic numbering scheme employed. Selected interatomic parameters: Ru–O(1) 2.11(2), Ru–N(1) 2.06(3), Ru–N(2) 2.06(3), Ru–N(3) 2.11(3), Ru–N(4) 2.05(2), Ru–N(5) 2.04(3) Å; N(1)–Ru–N(3) 175(1), N(2)–Ru–N(4) 174(1) and O(1)–Ru–N(5) 176(1)°.

Ligating properties of bis(2-pyridyl)phosphinic acid

There are a limited number of examples of phosphinic acids (or their anions) acting as ligands for transition metal centers [7–11]. The bidentate coordination mode of the phosphinic acid in the species {bis(4,5-di-isopropylimidazol-2-yl)phosphinic acid}-dichlorozinc monohydrate [11] is noted, but the tridentate coordination mode observed in the title compound appears unique.

The π-backbonding characteristics of ligands coordinated to ruthenium are reflected in their ability to stabilize the Ru(II) oxidation state [12, 13]. In the present instance, the $E_{1/2}$ value of the $[Ru(py_3P{=}O)]^{3+/2+}$ redox couple ($E_{1/2}$ = 1.26 V; ΔE_p = 60 mV) in acetonitrile/0.1 M $(C_2H_5)_4NPF_6$ solution is not dissimilar to that for other $[Ru(py_3X)]^{3+/2+}$ species [14] (or indeed for $[Ru(bpy)_3]^{3+/2+}$) under the same conditions (i.e. $[Ru(py_3N)_2]^{3+/2+}$ (1.32 V; 80 mV); $[Ru(py_3CH)_2]^{3+/2+}$ (1.26 V; 60 mV); $[Ru(py_3P)_2]^{3+/2+}$ (1.37 V; 60 mV); $[Ru(bpy)_3]^{3+/2+}$ (1.29 V; 60 mV)).

For the $[Ru\{py_3P{=}O\}\{py_2P(O)O\}]^+$ species, the most valid comparison is with the ruthenium(II) complex containing the ligand tris(2-pyridyl)-methanol [1], where $[Ru(py_3COH\text{–}N,N',N'')(py_3CO^-\text{–}N,N',O)]^+$ has the same charge type and the same immediate ligand environment (N_5O) as the present complex. In this case, from the $E_{1/2}$ values for the $[Ru(py_3X)]^{3+/2+}$ species, the contribution of the $py_3P{=}O$ and $py_3COH\text{–}N,N',N''$ ligands to the stabilization of Ru(II) is assumed to be similar. Accordingly, the difference between the $E_{1/2}$ values for $[Ru\{py_3P{=}O\}\{py_2P(O)O\}]^{2+/+}$ (0.65 V) and $[Ru(py_3COH)(py_3CO^-)]^{2+/+}$ (0.25 V) (both measured in aqueous solution) reflects a significantly greater degree of backbonding by the phosphinate ligand compared with the $py_3CO^-\text{–}N,N',O$ ligand.

*The synthetic method for py_3P involves nucleophilic substitution of PCl_3 by a 3-molar ratio of the 2-pyridyl anion, with subsequent workup in aqueous solution. Clearly, incomplete substitution would lead to hydroxybis(2-pyridyl)phosphine which would give rise to bis(2-pyridyl)phosphinic acid in the subsequent oxidation.

Experimental

Measurements

Electrochemical measurements were obtained using a glassy carbon working electrode and are reported versus a saturated sodium chloride calomel (SSCE) reference electrode. Analyses were carried out by the Canadian Microanalytical Service (Delta, BC).

Materials

Tris(2-pyridyl)phosphine [5] and $[Ru(DMF)_6](tos)_2$ [6] (DMF = *N*,*N*-dimethylformamide; tos = 4-toluenesulfonate anion) were prepared as described previously.

Syntheses

Tris(2-pyridyl)phosphine oxide, $py_3P{=}O$

Tris(2-pyridyl)phosphine (200 mg; 0.75 mmol) dissolved in a minimum volume of ethanol was treated with H_2O_2 (1 ml of 30%), and the solution stirred for 2 h before drying over anhydrous Na_2SO_4. After filtering, the volume was reduced by rotary evaporation and solid tris(2-pyridyl)phosphine oxide ($py_3P{=}O$) crystallized on standing overnight in the refrigerator. The crystals were washed with diethyl ether and dried *in vacuo*. Yield 170 mg (80%); m.p. 210–211 °C (lit. 209 °C [15]).

$[Ru(py_3P{=}O)_2](PF_6)_2$ and
$[Ru(py_3P{=}O)\{py_2P(O)O\}]PF_6$

Tris(2-pyridyl)phosphine (145 mg) was dissolved in dry propan-1-ol (80 ml) under an argon atmosphere. After deaeration for 1 h, $[Ru(DMF)_6](tos)_2$ (104 mg) was added and the mixture refluxed overnight under argon. After cooling, the solvent was removed under vacuum, the residue extracted with methanol (5 ml), and the resulting orange solution was applied to a column of Sephadex LH20 and eluted with methanol. The front of the band was collected (λ_{max} = 429 nm), the eluant evaporated to dryness, the residue dissolved in water (20 ml) and converted to the PF_6^- salt by passage down a column of anion-exchange resin (Dowex 1×8–400). The water was removed by rotary evaporation and the residue recrystallized from acetone/diethyl ether. Yield 65 mg, 55%. Visible spectrum: λ_{max} (H_2O) = 429 nm. *Anal.* Calc. for $[Ru(py_3P{=}O)_2](PF_6)_2$, $C_{30}F_{12}H_{24}N_6O_2P_4Ru$: C, 37.8; H, 2.54; N, 8.8. Found: C, 38.3; H, 2.80; N, 9.1%.

The red residue remaining from the methanol extraction was collected and air dried. It was converted to the PF_6^- salt by anion exchange methods and the eluant evaporated to dryness. Yield 18 mg, 17%. Visible spectrum: λ_{max} (H_2O) = 452 nm. *Anal.* Calc. for $[Ru(py_3P{=}O)\{py_2P(O)O\}]PF_6$, $C_{25}F_6H_{20}N_5O_3P_3Ru$: C, 40.2; H, 2.70; N, 9.4. Found: C, 40.3; H, 2.94; N, 8.9%.

X-ray crystallography

$[Ru(py_3P{=}O)\{py_2P(O)O\}](tos)$ was converted to the BF_4^- salt by anion exchange methods. Crystals of $[Ru(py_3P{=}O)\{py_2P(O)O\}]BF_4 \cdot 2H_2O$ for the X-ray structural analysis were grown by liquid diffusion (ethanol/diethyl ether). Intensity data for 3844 reflections were measured at room temperature on a weakly diffracting crystal such that θ_{max} was 17°. The 3391 unique data were corrected for Lorentz and polarization effects and for absorption [16]; max. and min. transmission factors were 0.877 and 0.837.

Crystal data: $C_{25}H_{24}BF_4N_5O_5P_2Ru$, M = 724.3, monoclinic, space group $P2_1/n$, a = 16.128(7), b = 11.493(6), c = 17.576(11) Å, β = 102.64(4)°, V = 3178.9 Å^3, Z = 4, D_c = 1.513 g cm^{-3}, $F(000)$ = 1456, μ = 6.09 cm^{-1}. The structure was solved by the Patterson method and refined by a full-matrix least-squares procedure using 1172 reflections which satisfied the $I \geq 2.5\sigma(I)$ criterion of observability. Owing to severe disorder in the structure and the lack of observed data, the BF_4^- anion was refined as a regular tetrahedron and only the Ru and P atoms were refined anisotropically; H atoms were not included in the model. The refinement converged with R = 0.107 and R_w = 0.108 for $w = 1.73/[\sigma^2(F) + 0.009|F|^2]$.

Supplementary material

Listings of fractional atomic coordinates and thermal parameters, interatomic bond distances and bond angles, and tables of F and $\sigma(F)$ are available from the authors on request (Tables S1–S4; 7 pages).

Acknowledgement

The financial support of the Australian Research Council is gratefully acknowledged.

References

1 F. R. Keene, D. J. Szalda and T. A. Wilson, *Inorg. Chem., 26* (1987) 2211.
2 F. R. Keene, P. J. Stephenson, M. R. Snow and E. R. T. Tiekink, *Inorg. Chem., 27* (1988) 2040.
3 P. S. Moritz, A. A. Diamantis, F. R. Keene, M. R. Snow and E. R. T. Tiekink, *Aust. J. Chem., 41* (1988) 1353.
4 R. K. Boggess and D. A. Zatko, *J. Coord. Chem., 4* (1975) 217.

5 K. Kurtev, D. Ribola, R. A. Jones, D. J. Cole-Hamilton and G. Wilkinson, *J. Chem. Soc., Dalton Trans.*, (1980) 55.
6 P. Bernhard and A. M. Sargeson, *J. Am. Chem. Soc., 111* (1990) 597.
7 T. Glowiak and W. Sawka-Dobrowolska, *Acta Crystallogr., Sect. B, 33* (1977) 2763.
8 P. Betz and A. Bino, *Inorg. Chim. Acta, 147* (1988) 109.
9 P. Betz and A. Bino, *Inorg. Chim. Acta, 145* (1988) 11.
10 B. Deschamps, J. Fischer, F. Mathey and A. Mitschler, *Inorg. Chem., 20* (1981) 3252.
11 R. G. Ball, R. S. Brown and J. L. Cocho, *Inorg. Chem., 23* (1984) 2315.
12 H. Taube, *Survey Prog. Chem., 6* (1973) 1.
13 P. A. Adcock, F. R. Keene, R. S. Smythe and M. R. Snow, *Inorg. Chem., 32* (1984) 2336.
14 F. R. Keene and P. J. Stephenson, unpublished results.
15 F. G. Mann and J. Watson, *J. Org. Chem., 13* (1948) 502.
16 G. M. Sheldrick, *SHELX-76,* program for crystal structure determination, Cambridge University, U.K., 1976.

Zeitschrift für Kristallographie 206, 275 – 278 (1993)

Crystal structure of bis(nitrato)bis(2,2′,2″-tripyridylamine)copper(II), $C_{30}H_{24}CuN_{10}O_6$

P. A. Anderson and F. R. Keene

Department of Chemistry and Biochemistry, James Cook University of North Queensland, Townsville, Queensland 4811, Australia

and J. M. Gulbis and E. R. T. Tiekink

Department of Chemistry, The University of Adelaide, Adelaide, South Australia 5005, Australia

(Received September 10, 1992)

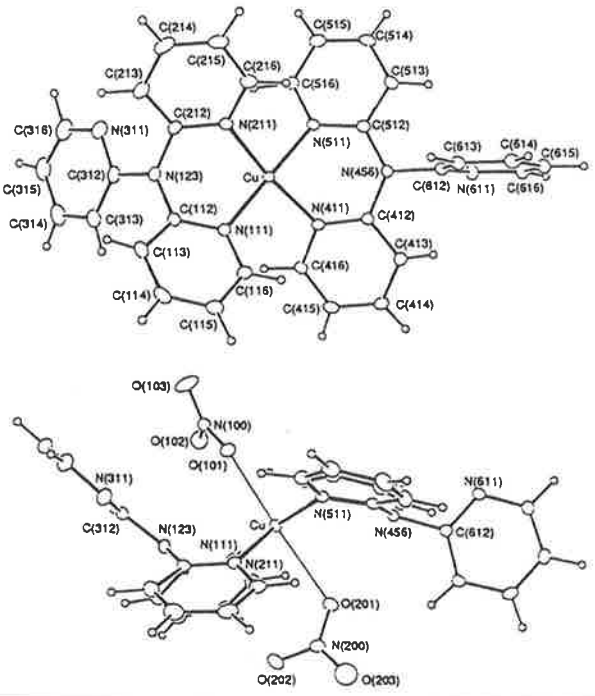

Monoclinic, $P12_1/n1$ (No. 14), $a = 9.140(2)$ Å, $b = 32.020(6)$ Å, $c = 10.006(1)$ Å, $\beta = 90.28(1)°$, $V = 2928.3$ Å^3, $Z = 4$, $R = 0.031$.

Source of material: The compound was prepared by the reaction of $Cu(NO_3)_2 \cdot 3H_2O$ and 2 x py_3N in minimal acetone (with a few drops of methanol). After heating (at 333 K) and stirring for 90 min, the deep green solution was allowed to cool slowly precipitating green crystals.

The title compound $\{Cu[py_3N]_2(NO_3)_2\}$, featuring a tetragonally distorted octahedral geometry about the Cu atom, is defined by two bidentate py_3N ligands and two axially coordinated NO_3^- anions. The Cu atom geometry is comparable to those found in the structures of $\{Cu[py_3N]_2(ClO_4)_2\}$ (see ref. 1) and $\{Cu[py_3N]_2(CH_3CN)_2\}(CF_3SO_3)_2$ (see ref. 2).

Table 1. Parameters used for the X-ray data collection

Diffractometer type:	Enraf-Nonius CAD4	Number of unique reflections:	5147
Wave length:	Mo K_α radiation (0.7107 Å)	Criterion for unobserved reflections:	$F_o < 5\,\sigma(F_o)$
Crystal characteristics:	dark green crystal, size 0.144 x 0.076 x 0.182 mm	Number of refined parameters:	497
Temperature of measurement:	293 K	Scan mode:	$\omega/2\theta$
		μ:	7.75 cm^{-1}
$2\theta_{max}$:	50°	Structure solution program used:	SHELX

Table 2. Final atomic coordinates and displacement parameters (in $Å^2$)

Atom	x	y	z	U_{11}	U_{22}	U_{33}	U_{12}	U_{13}	U_{23}
Cu(1)	0.30830(3)	0.11750(1)	0.71363(3)	0.0295(2)	0.0303(2)	0.0288(2)	0.0031(1)	-0.0043(1)	-0.0026(1)
N(111)	0.1280(2)	0.15383(7)	0.6964(2)	0.031(1)	0.032(1)	0.032(1)	-0.0004(9)	-0.0016(9)	0.002(1)
C(112)	0.1284(3)	0.19183(9)	0.7506(3)	0.034(2)	0.034(2)	0.034(1)	-0.001(1)	0.002(1)	0.003(1)
C(113)	0.0033(4)	0.2156(1)	0.7662(4)	0.050(2)	0.036(2)	0.055(2)	0.010(1)	0.008(2)	0.003(1)
C(114)	-0.1270(4)	0.2001(1)	0.7172(4)	0.036(2)	0.053(2)	0.062(2)	0.012(1)	0.007(2)	0.016(2)
C(115)	-0.1290(3)	0.1613(1)	0.6568(3)	0.031(2)	0.057(2)	0.052(2)	-0.002(1)	-0.000(1)	0.009(2)
C(116)	-0.0018(3)	0.1387(1)	0.6528(3)	0.033(2)	0.046(2)	0.041(2)	-0.005(1)	-0.004(1)	0.002(1)
N(211)	0.3382(2)	0.14356(7)	0.8959(2)	0.032(1)	0.038(1)	0.028(1)	-0.003(1)	-0.0011(9)	0.001(1)
C(212)	0.3211(3)	0.1843(1)	0.9125(3)	0.032(1)	0.042(2)	0.033(1)	-0.006(1)	0.003(1)	-0.006(1)
C(213)	0.3467(4)	0.2046(1)	1.0332(3)	0.068(2)	0.055(2)	0.041(2)	-0.010(2)	0.003(2)	-0.016(2)
C(214)	0.3916(4)	0.1805(2)	1.1406(4)	0.071(3)	0.090(3)	0.034(2)	-0.022(2)	-0.002(2)	-0.016(2)
C(215)	0.4034(4)	0.1383(1)	1.1263(3)	0.043(2)	0.086(3)	0.033(2)	-0.009(2)	-0.004(1)	0.009(2)
C(216)	0.3758(3)	0.1201(1)	1.0041(3)	0.037(2)	0.058(2)	0.033(2)	-0.003(1)	0.000(1)	0.007(1)
N(311)	0.4549(3)	0.25428(9)	0.8164(3)	0.056(2)	0.050(2)	0.076(2)	-0.018(1)	0.004(2)	-0.005(2)
C(312)	0.3303(4)	0.24388(9)	0.7547(3)	0.046(2)	0.033(2)	0.049(2)	-0.002(1)	0.013(1)	-0.007(1)
C(313)	0.2721(4)	0.2666(1)	0.6503(4)	0.062(2)	0.041(2)	0.055(2)	0.003(2)	0.014(2)	0.001(2)
C(314)	0.3473(6)	0.3012(1)	0.6072(4)	0.093(3)	0.047(2)	0.063(3)	0.011(2)	0.028(2)	0.004(2)
C(315)	0.4773(5)	0.3123(1)	0.6704(5)	0.079(3)	0.041(2)	0.096(3)	-0.015(2)	0.035(3)	0.000(2)

Table 2. (Continued)

Atom	*x*	*y*	*z*	U_{iso}/U_{11}	U_{22}	U_{33}	U_{12}	U_{13}	U_{23}
C(316)	0.5238(5)	0.2886(1)	0.7717(5)	0.067(3)	0.058(3)	0.099(3)	-0.024(2)	0.015(2)	-0.011(2)
N(123)	0.2654(3)	0.20670(7)	0.8008(2)	0.043(1)	0.029(1)	0.042(1)	-0.005(1)	-0.000(1)	-0.003(1)
H(113)	0.011(4)	0.241(1)	0.809(4)	0.050(3)					
H(114)	-0.215(4)	0.215(1)	0.720(4)	0.050(3)					
H(115)	-0.224(4)	0.150(1)	0.627(4)	0.050(3)					
H(116)	-0.006(4)	0.111(1)	0.615(4)	0.050(3)					
H(213)	0.336(4)	0.235(1)	1.047(4)	0.050(3)					
H(214)	0.400(4)	0.193(1)	1.227(4)	0.050(3)					
H(215)	0.428(4)	0.117(1)	1.202(4)	0.050(3)					
H(216)	0.382(4)	0.090(1)	0.983(4)	0.050(3)					
H(313)	0.181(4)	0.260(1)	0.605(4)	0.050(3)					
H(314)	0.296(4)	0.314(1)	0.530(4)	0.050(3)					
H(315)	0.536(4)	0.336(1)	0.654(4)	0.050(3)					
H(316)	0.624(5)	0.293(1)	0.817(4)	0.050(3)					
N(411)	0.2704(2)	0.08309(7)	0.5507(2)	0.030(1)	0.034(1)	0.026(1)	0.0019(9)	-0.0010(9)	0.001(1)
C(412)	0.2700(3)	0.04144(8)	0.5560(3)	0.026(1)	0.031(2)	0.029(1)	0.001(1)	0.002(1)	-0.000(1)
C(413)	0.1946(3)	0.0181(1)	0.4598(3)	0.043(2)	0.037(2)	0.044(2)	0.002(1)	-0.007(1)	-0.005(1)
C(414)	0.1353(4)	0.0384(1)	0.3505(3)	0.046(2)	0.052(2)	0.038(2)	0.002(1)	-0.011(1)	-0.010(1)
C(415)	0.1501(4)	0.0811(1)	0.3377(3)	0.044(2)	0.059(2)	0.031(2)	0.007(2)	-0.009(1)	0.003(1)
C(416)	0.2165(3)	0.1024(1)	0.4397(3)	0.042(2)	0.037(2)	0.032(2)	0.003(1)	-0.004(1)	0.007(1)
N(511)	0.4772(2)	0.07874(7)	0.7417(2)	0.024(1)	0.036(1)	0.028(1)	0.0018(9)	-0.0007(9)	0.0010(9)
C(512)	0.4618(3)	0.03740(9)	0.7320(3)	0.030(1)	0.040(2)	0.025(1)	0.004(1)	0.003(1)	-0.000(1)
C(513)	0.5617(4)	0.0109(1)	0.7968(3)	0.051(2)	0.038(2)	0.046(2)	0.010(1)	-0.008(1)	0.001(1)
C(514)	0.6818(4)	0.0278(1)	0.8594(3)	0.042(2)	0.065(2)	0.047(2)	0.021(2)	-0.016(2)	-0.001(2)
C(515)	0.7049(4)	0.0699(1)	0.8565(3)	0.032(2)	0.066(2)	0.048(2)	0.002(2)	-0.007(1)	-0.006(2)
C(516)	0.6002(3)	0.0945(1)	0.7987(3)	0.032(1)	0.044(2)	0.039(2)	-0.001(1)	-0.001(1)	0.000(1)
N(611)	0.3929(3)	-0.04738(8)	0.5834(2)	0.043(1)	0.033(1)	0.039(1)	0.003(1)	0.011(1)	-0.002(1)
C(612)	0.3221(3)	-0.02388(9)	0.6703(3)	0.032(1)	0.034(2)	0.030(1)	0.003(1)	0.001(1)	0.001(1)
C(613)	0.2301(3)	-0.0387(1)	0.7692(3)	0.035(1)	0.040(2)	0.033(2)	0.004(1)	0.005(1)	0.002(1)
C(614)	0.2096(3)	-0.0813(1)	0.7754(3)	0.038(2)	0.053(2)	0.038(2)	-0.008(1)	0.002(1)	0.012(1)
C(615)	0.2780(4)	-0.1067(1)	0.6846(3)	0.051(2)	0.032(2)	0.046(2)	0.000(1)	-0.004(1)	0.003(1)
C(616)	0.3685(4)	-0.0886(1)	0.5911(3)	0.051(2)	0.035(2)	0.042(2)	0.002(1)	0.005(1)	-0.004(1)
N(456)	0.3457(2)	0.02094(7)	0.6592(2)	0.032(1)	0.029(1)	0.028(1)	0.0023(9)	0.0014(9)	-0.0003(9)
H(413)	0.185(4)	-0.009(1)	0.476(3)	0.050(3)					
H(414)	0.092(4)	0.021(1)	0.283(3)	0.050(3)					
H(415)	0.114(4)	0.092(1)	0.261(3)	0.050(3)					
H(416)	0.230(3)	0.134(1)	0.433(3)	0.050(3)					
H(513)	0.543(3)	-0.019(1)	0.793(3)	0.050(3)					
H(514)	0.739(4)	0.010(1)	0.901(3)	0.050(3)					
H(515)	0.790(4)	0.084(1)	0.893(3)	0.050(3)					
H(516)	0.598(3)	0.126(1)	0.797(3)	0.050(3)					
H(613)	0.191(3)	-0.020(1)	0.833(3)	0.050(3)					
H(614)	0.149(4)	-0.094(1)	0.843(3)	0.050(3)					
H(615)	0.263(3)	-0.138(1)	0.685(3)	0.050(3)					
H(616)	0.417(4)	-0.108(1)	0.520(3)	0.050(3)					
N(100)	0.4798(3)	0.18699(8)	0.5176(3)	0.047(2)	0.033(1)	0.038(1)	0.004(1)	0.007(1)	0.004(1)
O(101)	0.4877(2)	0.16238(7)	0.6155(2)	0.049(1)	0.046(1)	0.047(1)	0.001(1)	0.006(1)	0.014(1)
O(102)	0.3608(3)	0.19382(8)	0.4629(2)	0.062(2)	0.066(2)	0.053(1)	0.001(1)	-0.015(1)	0.002(1)
O(103)	0.5901(3)	0.2037(1)	0.4756(3)	0.058(2)	0.103(2)	0.112(3)	-0.009(2)	0.014(2)	0.066(2)
N(200)	0.0849(3)	0.07104(9)	0.9422(3)	0.037(1)	0.052(2)	0.037(1)	-0.002(1)	0.004(1)	0.003(1)
O(201)	0.1393(3)	0.06460(8)	0.8316(3)	0.097(2)	0.057(2)	0.056(2)	-0.002(1)	0.040(1)	-0.008(1)
O(202)	0.0263(3)	0.10506(9)	0.9664(3)	0.055(1)	0.063(2)	0.080(2)	0.002(1)	0.023(1)	-0.023(1)
O(203)	0.0822(5)	0.0444(1)	1.0263(3)	0.187(4)	0.101(3)	0.077(2)	0.047(3)	0.027(2)	0.047(2)

Further details of the structure determination (e.g. structure factors) have been deposited within the relevant database and can be accessed as Collection No. 320542 or ordered from the Fachinformationszentrum Karlsruhe, D-7514 Eggenstein-Leopoldshafen 2, Federal Republic of Germany.

References:

1. Boys, D., Escobar, C., Zamudio, W.: Structure of diperchloratobis(2,2′,2″-tripyridylamine)-copper(II). Acta Crystallogr. **C48** (1992) 1118-1120.
2. Dedert, P.L., Thompson, J.S., Ibers, J.A., Marks, T.J.: Metal ion binding sites composed of multiple nitrogenous heterocycles. Synthesis and spectral and structural study of bis(2,2′,2″-tripyridylamine)copper(II)bis(trifluoromethanesulfonate) and its bis(acetonitrile) adduct. Inorg. Chem. **21** (1982) 969-977.

J. CHEM. SOC. DALTON TRANS. 1995

Extended X-Ray Absorption Fine Structure, Crystal Structures at 295 and 173 K, and Electron Paramagnetic Resonance and Electronic Spectra of Bis[tris(2-pyridyl)-methane]copper(II) Dinitrate†

Timothy Astley,[a] Paul J. Ellis,[b] Hans C. Freeman,*[,b] Michael A. Hitchman,*[,a] F. Richard Keene[c] and Edward R. T. Tiekink[d]

[a] *Chemistry Department, University of Tasmania, Box 252C, Hobart, Tasmania 7000, Australia*

[b] *Department of Inorganic Chemistry, University of Sydney, NSW 2006, Australia*

[c] *Department of Molecular Sciences, James Cook University of North Queensland, Townsville, Queensland 4811, Australia*

[d] *Department of Chemistry, The University of Adelaide, Adelaide, South Australia 5005, Australia*

The crystal structure of bis[tris(2-pyridyl)methane]copper(II) dinitrate, $[Cu\{(C_5H_4N)_3CH\}_2][NO_3]_2$ has been determined. At 295 K the Cu atom lies on a special position so that all six Cu–N bonds are crystallographically equivalent [Cu–N 2.103(4) Å]. The structure at 173 K is very similar [Cu–N 2.095(3) Å]. However, the electronic spectrum suggests that the Cu^{2+} ion experiences a ligand field of tetragonal symmetry. This has been confirmed by the EXAFS of the compound, which shows four nitrogen atoms at 2.04 Å and two at 2.25 Å from the copper. The apparent trigonal symmetry revealed by the X-ray analysis is thus due to disorder of the long and short Cu–N bonds about the three-fold axis. The EPR spectrum shows an isotropic signal at 295 K, but a signal characteristic of a tetragonally elongated octahedral complex at 150 K. This suggests that the directions of the long and short bonds interchange rapidly on the EPR time-scale at room temperature, but that the complexes become frozen into particular orientations on cooling.

Tripodal ligands involving nitrogen-donor heterocycles have been found to exhibit a number of useful properties in co-ordination and organometallic chemistry.[1] As part of a study of the electronic and steric characteristics of transition-metal complexes of ligands of this kind,[2–7] we have prepared the compound $[Cu\{(C_5H_4N)_3CH\}_2][NO_3]_2$, where $(C_5H_4N)_3CH$ is tris(2-pyridyl)methane. We report here the crystal structures of the compound at 295 and 173 K. These are closely similar. In both structures the metal and bridgehead carbon atoms of the $[Cu\{(C_5H_4N)_3CH\}_2]^{2+}$ complex lie on a three-fold symmetry axis, so that the six Cu–N bonds are crystallographically equivalent. Six equivalent bonds in such a complex would be highly unusual, as they would lead to an orbitally degenerate ground state, which is unstable with respect to a Jahn–Teller distortion. The electronic spectrum of the compound is also reported, and is closely similar to those of analogous complexes which have the tetragonally distorted octahedral co-ordination geometry commonly observed for Cu^{II}.[6,7] This suggests that the *local* co-ordination geometry may be a tetragonally distorted octahedron, and that the crystallographic symmetry results from disorder of the Cu–N bonds about the three-fold axis. Disorder of this kind has been observed for other Cu^{II} compounds, such as $[Cu(en)_3]SO_4$ (en = ethane-1,2-diamine).[8] The disorder model for $[Cu\{(C_5H_4N)_3CH\}_2][NO_3]_2$ is supported by the electron paramagnetic resonance (EPR) spectrum which shows an isotropic signal at 293 K but a signal characteristic of a tetragonally elongated octahedral complex at 150 K.

As an additional probe of the Cu^{II} stereochemistry in $[Cu\{(C_5H_4N)_3CH\}_2][NO_3]_2$ we have measured the extended X-ray absorption fine structure (EXAFS) of the compound. This is dominated by contributions from back-scattering atoms in the immediate vicinity of an X-ray absorber (in the present case, the Cu atom). In solids where the apparent structure revealed by X-ray diffraction may be affected by disorder, EXAFS provides a powerful means of studying the local co-ordination geometry. For example, we have recently used the EXAFS of the 3-chloroanilinium salt $[NH_3C_6H_4Cl\text{-}3]_8[CuCl_6]Cl_4$ to confirm that the tetragonally compressed geometry of the $[CuCl_6]^{4-}$ complex derived from an X-ray crystal-structure analysis[9] was in fact due to a superposition of disordered $[CuCl_6]^{4-}$ ions having the normal elongated tetragonal geometry.[10] The EXAFS data for $[Cu\{(C_5H_4N)_3CH\}_2][NO_3]_2$ likewise show that the local geometry around the Cu atom is elongated tetragonal, the Cu–N distances being in good agreement with the electronic and EPR spectra.

Experimental

Synthesis of $[Cu\{(C_5H_4N)_3CH\}_2][NO_3]_2$.—A solution of tris(2-pyridyl)methane[4] (80 mg, 0.323 mmol) in acetone (10 cm^3) was added dropwise with stirring to a solution of $Cu(NO_3)_2\cdot3H_2O$ (35 mg, 0.145 mmol) in the same solvent (15 cm^3). The mixture was cooled and the light blue product separated by centrifugation. Yield 86 mg, 87%. The solid was recrystallised from methanol–diethyl ether (Found: C, 56.4; H, 3.85; N, 16.4. Calc. for $C_{32}H_{26}CuN_8O_6$: C, 56.3; H, 3.85; N, 16.4%). Crystals suitable for diffraction measurements were obtained by evaporation of an ethanolic solution.

Spectroscopic Measurements.—Single-crystal electronic spectra were measured using a Cary 5A spectrophotometer. The procedure is described elsewhere.[11] The sample was cooled

† *Supplementary data available:* (SUP No. 57060, 7 pp.). Observed EXAFS data, final positional parameters and Debye–Waller factors. See Instructions for Authors, *J. Chem. Soc., Dalton Trans.*, 1995, Issue 1, pp. xxv–xxx.

Non-SI units employed: eV ≈ 1.60×10^{-19} J, G = 10^{-4} T.

Table 1 Crystal data for $[Cu\{(C_5H_4N)_3CH\}_2][NO_3]_2$[a]

	295 K	173 K
a/Å	11.677(3)	11.607(3)
c/Å	17.999(4)	17.906(6)
U/Å^3	2125.7(9)	2089(1)
D_c/g cm^{-3}	1.599	1.626
μ/cm^{-1}	8.35	8.49
Max., min. transmission factors	1.081, 0.794	1.084, 0.826
No. data measured	1247	1245
No. unique data	653	645
No. observed data [$I \geqslant 2.5\sigma(I)$]	496	556
R	0.046	0.035
R'	0.048	0.045

[a] Details in common: formula $C_{32}H_{26}CuN_8O_6$, M 682.2, space group $R\bar{3}$, $Z = 3$, $F(000)$ 1053; $w = 1/\sigma^2(F)$.

Table 2 Fractional atomic coordinates for the non-hydrogen atoms of $[Cu\{(C_5H_4N)_3CH\}_2][NO_3]_2$

Atom	x	y	z
295 K			
Cu[a]	1.0	0.0	1.0
O(1)	0.6667(5)	0.2275(5)	0.9787(3)
N(1)[b]	$\frac{2}{3}$	$\frac{1}{3}$	0.9705(6)
N(11)	0.9861(5)	0.1349(5)	0.9285(2)
C(1)[b]	1.0	0.0	0.8305(4)
C(12)	0.9701(6)	0.2320(7)	0.9523(3)
C(13)	0.9589(6)	0.3177(7)	0.9050(4)
C(14)	0.9648(6)	0.3015(6)	0.8288(4)
C(15)	0.9820(6)	0.2010(6)	0.8038(3)
C(16)	0.9897(5)	0.1168(5)	0.8549(3)
173 K			
Cu[a]	1.0	0	1.0
O(1)	0.5595(3)	0.2270(3)	0.9778(2)
N(1)[b]	$\frac{2}{3}$	$\frac{1}{3}$	0.9736(3)
N(11)	0.9867(3)	−0.1481(3)	0.9277(1)
C(1)[b]	1.0	0	0.8289(3)
C(12)	0.9723(4)	−0.2646(4)	0.9510(2)
C(13)	0.9601(4)	−0.3607(4)	0.9045(2)
C(14)	0.9658(4)	−0.3388(4)	0.8287(2)
C(15)	0.9828(4)	−0.2190(3)	0.8029(2)
C(16)	0.9912(3)	−0.1280(3)	0.8542(2)

[a] Atom has $\frac{1}{6}$ site occupancy factor. [b] Atom has $\frac{1}{3}$ site occupancy factor.

using a Cryodyne model 22C cryostat. The reflectance spectrum was recorded with a Beckmann DK2A spectrophotometer. The EPR spectra were measured at Q-band frequency, ≈34 GHz, using a JEOL JES-FE spectrometer equipped with a standard JEOL cryostat and temperature controller.

Crystallography.—Intensity data were measured on a Rigaku AFC6R diffractometer fitted with a graphite monochromator [λ(Mo-Kα) = 0.710 73 Å, ω–2θ mode, θ_{max} = 27.5°]. A single crystal (0.13 × 0.18 × 0.24 mm) was used to record data at 295 and 173 K. No decomposition of the crystal occurred during the data collections. Absorption corrections were applied.[12] Reflections with $I \geqslant 3.0\sigma(I)$ were used in the analyses. Crystal data are summarized in Table 1.

The structure was solved by conventional heavy-atom methods and refined by a full-matrix least-squares procedure based on F.[13] Non-hydrogen atoms were refined with anisotropic thermal parameters. Hydrogen atoms were located in a difference map during the 295 K analysis. They were included in the model at their calculated positions (C–H 0.97 Å) and were assigned plausible isotropic thermal parameters. At convergence (sigma weights) R = 0.046 and R' = 0.048 for the 295 K data, and R = 0.035 and R' = 0.045 for the 173 K data. The analysis of variance showed no special features. The highest peak in the final difference map was 0.50 e Å^{-3} for the 295 K data and 0.38 e Å^{-3} for the 173 K data. Scattering factors for all atoms were those incorporated in the TEXSAN program.[13]

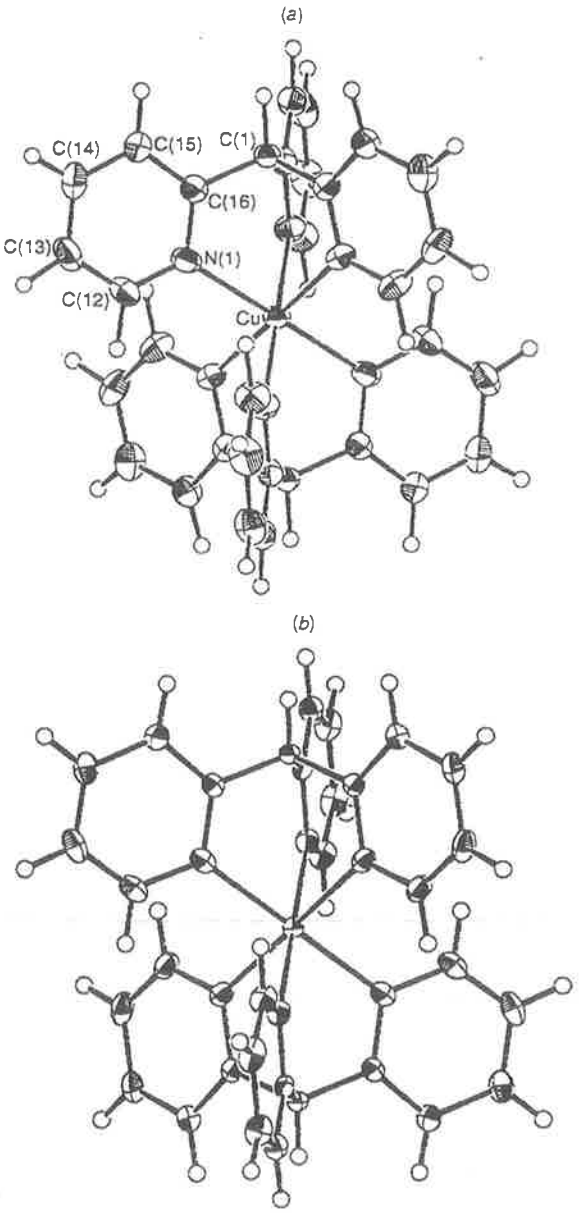

Fig. 1 Molecular structure (ORTEP[14]) and atom labelling for the $[Cu\{(C_5H_4N)_3CH\}_2]^{2+}$ complex in $[Cu\{(C_5H_4N)_3CH\}_2][NO_3]_2$ at (*a*) 295 K and (*b*) 173 K. The thermal ellipsoids are drawn at the 35% probability level

The structure and atom labelling scheme are shown in Fig. 1. The fractional atomic coordinates of the non-hydrogen atoms are listed in Table 2, bond distances and angles in Table 3 and anisotropic thermal ellipsoid parameters in Table 4.

Additional material available from the Cambridge Crystallographic Data Centre comprises H-atom coordinates and remaining bond lengths and angles.

EXAFS.—X-Ray absorption measurements were made at the Australian National Beamline Facility on bending-magnet beamline 20B at the KEK Photon Factory, Tsukuba, Japan. The storage ring delivered a current of 330–300 mA at 2.5 GeV. The monochromator was a Si(111) channel-cut double crystal.

No detuning was applied. The X-ray spectra were recorded in transmission mode using standard N_2-filled ionisation chambers. Energies were calibrated by means of a Cu-foil internal standard, the first inflection point on the Cu edge being assigned as 8980.3 eV.

The sample of $[Cu\{(C_5H_4N)_3CH\}_2][NO_3]_2$ was a finely ground powder diluted with BN (boron nitride). The mixture was pressed into a pellet (1 mm thick) supported in an Al spacer with 63.5 μm Mylar tape windows. Two scans of the X-ray absorption spectrum were recorded at ambient temperature (295 K). The scans were averaged using weights based on the signal-to-noise ratios. A background correction was applied by fitting a polynomial to the pre-edge region, extrapolating it into the EXAFS region and subtracting it from the data. A three-region spline was fitted to the EXAFS region and subtracted. The data were normalised to an edge jump of 1.0 and compensated for decreasing absorbance past the edge. The background-subtracted, normalised and compensated data were converted to k space, where k is the photoelectron wavevector $\hbar^{-1}[2m_e(E - E_0)]^{\frac{1}{2}}$ and E_0 is the threshold energy.

For the EXAFS refinement of the structure, a model comprising the non-H atoms of the $(C_5H_4N)_3CH$ ligand was constructed using the known geometry of the $(C_5H_4N)CH$ fragment in $[Cu\{(pz)_2(C_5H_4N)CH\}_2]^{2+}$ (pz = pyrazol-1-yl).[9] The geometry of the model is shown in Fig. 2. The three Cu–N(pyridyl) bonds were initially assigned lengths 2.0, 2.1 and 2.3 Å. The single-scattering Debye–Waller factors, $2\sigma^2$, were assigned typical room-temperature values [0.01 Å^2 for the N(pyridyl) atoms, increasing to 0.02 Å^2 for the most distant atoms]. In keeping with the stoichiometry of the complex, the atoms of the ligand molecule were given multiplicity 2.

In the refinement calculations (see below), the positions and Debye–Waller factors of all atoms in the model were treated as variables. The number of *independent* variables was, however,

Table 3 Selected bond distances (Å) and angles (°) for $[Cu\{(C_5H_4N)_3CH\}_2][NO_3]_2$

	295 K	173 K
Cu–N(11)	2.103(4)	2.095(3)
N(11)–C(12)	1.310(7)	1.343(4)
N(11)–C(16)	1.345(6)	1.334(4)
C(1)–C(16)	1.494(6)	1.506(4)
C(12)–C(13)	1.370(9)	1.340(5)
C(13)–C(14)	1.391(9)	1.377(6)
C(14)–C(15)	1.362(8)	1.382(5)
C(15)–C(16)	1.381(7)	1.367(4)
N(1)–O(1)	1.245(5)	1.242(3)
N(11)–Cu–N(11^i)	93.6(2)	94.1(1)
N(11)–Cu–N(11^{ii})	86.4(2)	85.9(1)
Cu–N(11)–C(12)	123.1(4)	123.8(2)
Cu–N(11)–C(16)	117.7(4)	119.0(2)
C(12)–N(11)–C(16)	119.2(5)	117.2(3)
C(16)–C(1)–C(16^{ii})	111.7(3)	111.4(2)
N(11)–C(12)–C(13)	122.4(5)	123.6(3)
C(12)–C(13)–C(14)	118.9(6)	118.9(3)
C(13)–C(14)–C(15)	118.8(6)	119.1(4)
C(14)–C(15)–C(16)	118.9(5)	118.1(4)
N(11)–C(16)–C(1)	117.1(5)	116.6(3)
N(11)–C(16)–C(15)	121.7(5)	123.1(3)
C(1)–C(16)–C(15)	121.2(5)	120.2(3)
O(1)–N(1)–O(1^{iii})	119.2(5)	119.64(7)

Symmetry operations: i, $x - y, x - 1, 2 - z$; ii, $1 - y, x - y - 1, z$; iii, $1 - y, x - y, z$.

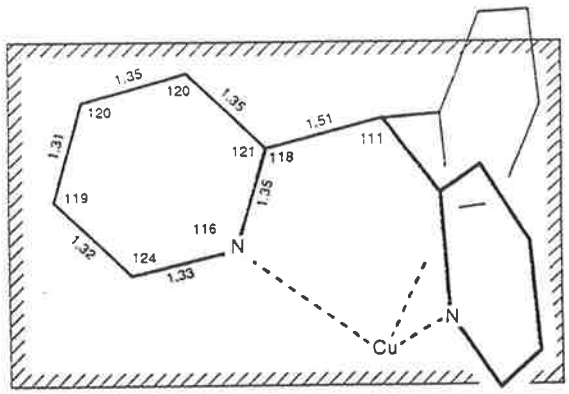

Fig. 2 Ideal EXAFS model geometry. The mirror plane is represented by the shaded rectangle

Table 4 Anisotropic thermal parameters (Å^2) for $[Cu\{(C_5H_4N)_3CH\}_2][NO_3]_2$

Atom	U_{11}	U_{22}	U_{33}	U_{12}	U_{13}	U_{23}
295 K						
Cu	0.0389(6)	0.0389(6)	0.0266(7)	0.0194(7)	0	0
O(1)	0.092(4)	0.071(4)	0.117(4)	0.043(4)	0.005(3)	−0.004(4)
N(1)	0.069(5)	0.069(5)	0.076(8)	0.035(8)	0	0
N(11)	0.049(3)	0.047(3)	0.034(2)	0.026(3)	0.001(2)	−0.005(2)
C(1)	0.037(3)	0.037(3)	0.028(5)	0.018(5)	0	0
C(12)	0.066(5)	0.049(4)	0.048(4)	0.031(4)	0.005(3)	−0.012(3)
C(13)	0.060(5)	0.045(4)	0.069(5)	0.029(4)	0.010(4)	−0.012(4)
C(14)	0.052(4)	0.035(4)	0.074(4)	0.021(3)	0.004(4)	0.006(4)
C(15)	0.045(4)	0.040(3)	0.047(3)	0.021(3)	−0.001(3)	0.003(3)
C(16)	0.033(3)	0.035(3)	0.040(3)	0.014(3)	0.001(3)	−0.003(3)
173 K						
Cu	0.0210(3)	0.0210(3)	0.0180(4)	0.0105(4)	0	0
O(1)	0.042(2)	0.057(2)	0.057(2)	0.027(2)	0.003(1)	0.001(2)
N(1)	0.040(2)	0.040(2)	0.039(3)	0.020(3)	0	0
N(11)	0.026(2)	0.029(2)	0.028(1)	0.013(1)	0.001(1)	0.006(1)
C(1)	0.022(2)	0.022(2)	0.018(2)	0.011(2)	0	0
C(12)	0.033(2)	0.037(2)	0.035(2)	0.021(2)	0.003(2)	0.012(2)
C(13)	0.033(2)	0.028(2)	0.054(2)	0.019(2)	0.006(2)	0.013(2)
C(14)	0.033(2)	0.029(2)	0.047(2)	0.020(2)	0.005(2)	0.001(2)
C(15)	0.027(2)	0.029(2)	0.031(2)	0.016(2)	0.001(2)	−0.001(2)
C(16)	0.018(2)	0.023(2)	0.025(2)	0.009(1)	0.002(1)	0.003(1)

The anisotropic thermal parameter is given by the expression: $T_{aniso} = \exp[-2\pi^2(h^2a^{*2}U_{11} + k^2b^{*2}U_{22} + l^2c^{*2}U_{33} + 2hka^*b^*U_{12} + 2hla^*c^*U_{13} + 2klb^*c^*U_{23})]$.

Table 5 Restraints and constraints used in the refinement of the $[Cu\{(C_5H_4N)_3CH\}_2][NO_3]_2$ model *versus* the observed EXAFS

	Ideal value/Å		Ideal value/Å
N(1)–C(16)	1.350	C(12)–N(1)–C(16)	116.0
N(1)–C(12)	1.330	N(1)–C(16)–C(15)	120.9
C(16)–C(15)	1.354	C(16)–C(15)–C(14)	119.5
C(12)–C(13)	1.323	C(15)–C(14)–C(13)	120.1
C(15)–C(14)	1.348	C(14)–C(13)–C(12)	119.1
C(13)–C(14)	1.308	C(13)–C(12)–N(1)	124.4
C(16)–C(1)	1.507	N(1)–C(16)–C(1)	117.6
		C(16)–C(1)–C(16)*	111.3

Debye–Waller factor restraints	Debye–Waller factor constraints
$\sigma^2_{C(16)} > \sigma^2_{N(1)}$	$\sigma^2_{C(13)} = \sigma^2_{C(14)} = \sigma^2_{C(15)}$
$\sigma^2_{C(12)} > \sigma^2_{N(1)}$	$\sigma^2_{C(13)} - \sigma^2_{C(12)} = \sigma^2_{C(13')} - \sigma^2_{C(12')}$
$\sigma^2_{C(15)} > \sigma^2_{C(16)}$	$\sigma^2_{C(13)} - \sigma^2_{N(1)} = \sigma^2_{C(12')} - \sigma^2_{N(1')}$
$\sigma^2_{C(13)} > \sigma^2_{C(12)}$	$\sigma^2_{C(16)} - \sigma^2_{N(1)} = \sigma^2_{C(16')} - \sigma^2_{N(1')}$

The same restraints are used for each of the three rings. The atoms of the ring lying on the mirror plane are indicated by primes. The σ values used in the refinement were 0.1 Å for all distance restraints, 5° for all angle restraints, and 0.002 Å² for all Debye–Waller factor restraints.

* This angle is the bond angle at the methyl carbon.

substantially reduced by applying appropriate restraints and constraints (Table 5). The bond lengths and bond angles were tightly restrained to the ideal geometry of Fig. 2. Additional restraints were applied to preserve the planarity of the pyridyl rings, to keep the Cu atom coplanar with each of the pyridyl rings, and to ensure that the single-scattering Debye–Waller factors of the ring atoms increased with increasing distance from the Cu atom. Constraints were applied to keep the Debye–Waller factors of the three atoms furthest from the Cu in each ring equal, and to make the increments between the Debye–Waller factors around the ring identical in all three rings. During the initial refinement cycles it was observed that the two shorter Cu–N(pyridyl) distances had refined to the same value. A plane of symmetry was accordingly introduced between these two pyridyl rings, resulting in a further reduction of the number of independent variables.

The EXAFS analysis was performed by means of the program XFIT[15] which uses non-linear least-squares fitting to vary the model until the agreement between the observed and calculated EXAFS is optimised. The EXAFS of the model was calculated *ab initio* using the curved-wave multiple-scattering EXAFS program FEFF 6.01.[16] The calculation included 151 unique paths with effective length < 5 Å and up to 6 legs. The Debye–Waller factors for the multiple-scattering paths were estimated from the single-scattering Debye–Waller factors using an uncorrelated isotropic vibration model.[15]

The quantity minimised during the refinements is given by equation (1), where $\chi_{calc}(k)$ and $\chi_{obs}(k)$ are the k^3-weighted and

$$\chi'^2 = \int_{k=0}^{\infty} [\chi_{calc}(k) - \chi_{obs}(k)]^2 \, dk + \sum_i w_i \Delta_i^2 \quad (1)$$

Fourier-filtered values of the calculated and observed EXAFS, respectively. The k^3 weighting was applied to each EXAFS curve prior to Fourier filtering; Δ_i is the difference between the model parameter and the value to which it is restrained in the ith restraint, and w_i is the weight of the restraint; $w_i = \sigma_i^{-2}$ where σ_i is an arbitrary variance-like parameter.

The parameters varied were the position (x, y, z) and single-scattering Debye–Waller factor $2\sigma^2$ of each atom, the threshold energy E_0 and the scale factor S_0^2. The goodness-of-fit parameter R was calculated from equation (2). The standard

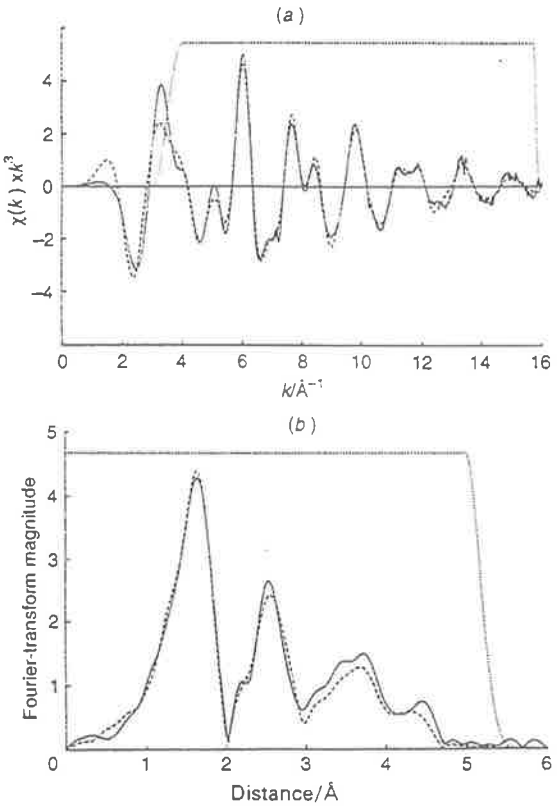

Fig. 3 (*a*) EXAFS of $[Cu\{(C_5H_4N)_3CH\}_2]^{2+}$: observed (——), calculated from refined model (- - - -), window used in Fourier filter (· · · ·). (*b*) Fourier-transform amplitude of EXAFS: observed (——), calculated (- - - -), window used in Fourier filter (· · · ·)

$$R = \int_{k=0}^{\infty} [\chi_{calc}(k) - \chi_{obs}(k)]^2 \, dk \Big/ \int_{k=0}^{\infty} \chi_{obs}(k)^2 \, dk \quad (2)$$

deviations were estimated by fitting the model to a number of EXAFS curves generated by first using a Fourier filter to smooth the observed EXAFS, and then adding random noise at the level found in the original observed EXAFS. The noise in the observed EXAFS was estimated using Fourier filtering.[15] The deviations obtained using this Monte-Carlo method were less than 0.002 Å for the Cu–N distances and 0.0005 Å² for the Cu–N Debye–Waller factors. These values represent solely the errors due to counting statistics. The fact that the values are small reflects the high quality of the EXAFS data. The systematic errors in the short and long Cu–N distances are typically estimated as *ca.* 0.01 and 0.02 Å, respectively, and these values are used in the text.

The observed and calculated EXAFS, the corresponding Fourier transforms, and the window functions used in the Fourier filter are shown in Fig. 3. The final R value was 0.168. The maximum deviation from ideal geometry was less than 0.01 Å for the bond lengths and 0.5° for the bond angles. The R value obtained by refining a model with the three-fold symmetry found in the X-ray diffraction analysis was 0.218. The Cu–N distance in the refined model with three-fold symmetry was 2.03 Å and the S_0^2 factor was low, indicating that the strong EXAFS from the two pyridine rings closer to the Cu atom had dominated the refinement. The refined Cu–N bond lengths and the first and second shell thermal parameters are shown in Table 6. The observed EXAFS data, and the final positional parameters and Debye–Waller factors for all atoms, have been deposited as SUP 57060.

Table 6 EXAFS analysis of $[Cu\{(C_5H_4N)_3CH\}_2][NO_3]_2$ at 295 K: main distances around Cu *

E_0/eV	8992.97(12)
S_0^2	1.190(10)
R factor	0.168 3

Shell	Distance/Å	$2\sigma^2$/Å^2
4N	2.038 5(5)	0.012 87(12)
2N	2.250 3(15)	0.023 6(5)

* Standard deviations are given in parentheses. The estimated *systematic* errors in the distances for the two shells are 0.01–0.02 Å.

Results and Discussion

Crystal Structure.—The dimensions of the complex (Table 3) provide little reason to suspect that they represent anything other than the true geometry. The dimensions of the pyridyl rings are similar to those of the pyridyl rings in complexes of the related ligand $(pz)_2(C_5H_4N)CH$ (pz = pyrazol-1-yl).[6] The six crystallographically equivalent Cu–N(pyridyl) bonds have precisely the length, 2.10 Å, that would be predicted from the average of the M–N(pyridyl) bond lengths in $[M\{(pz)_2(C_5H_4N)CH\}_2][NO_3]_2$, M = Ni^{II} or Zn^{II}, at 295 K.[6] The only results that might be symptomatic of an underlying problem in the crystallographic refinements are that several of the ligand dimensions in Table 3 appear to undergo highly significant changes ($\geq 3\sigma$) between 295 and 173 K, and that these changes do not seem to be correlated with one another or with other features of the structure. A facile explanation of these observations is that the estimated standard deviations of the atomic positional coordinates are too low, but this merely emphasises that the refinements may not have converged to the optimum solution.

A more serious problem is that Cu^{II} complexes almost never have six identical copper–ligand bond lengths but adopt an elongated tetragonal co-ordination geometry. For example, in the centrosymmetric complex $[Cu\{(pz)_2(C_5H_4N)CH\}_2][NO_3]_2$ formed by another tripod ligand, the copper–ligand bond lengths are Cu–N(pyridyl) 2.020(3), Cu–N(pz) 1.994(3) and Cu–N(pz) 2.385(3) Å.[6] This lowering in symmetry is explained conventionally in terms of vibronic Jahn–Teller coupling, which acts to remove the orbital degeneracy that would occur in a regular octahedral Cu^{II} complex. It should be noted that a moderate distortion of the three symmetry related N–Cu–N angles from 90° (such as ≈86° in the present complex) does *not* suffice to remove the degeneracy. These effects are the subject of a recent review.[17]

Other examples of Cu^{II} complexes that crystallise with the metal atom on a three-fold symmetry axis and with six crystallographically equivalent metal–ligand bonds have been reported.[18] Detailed analysis has in each case revealed that four short and two long bonds occur at the *local* level, the high crystallographic symmetry being due to disorder of the bonds about the three-fold axis.[19] Clues are frequently (but not always) to be found in the crystallographically determined vibrational ellipsoids. For example, in the crystal structure of $[Cu(en)_3]SO_4$ (en = ethane-1,2-diamine), the elongation of the vibrational ellipsoids along the Cu–N bond vectors was taken as evidence of disorder in the positions of the nitrogen atoms.[9] In several instances, quantitative analysis of the vibrational parameters has yielded estimates of the local Cu^{II} co-ordination geometry.[19,20] On the other hand, in a study of the compound $[Cu(C_5H_5N_3)_2][Cu(CN)_3]\cdot 2H_2O$, an analysis of the crystallographic vibrational parameters failed to detect any disorder of the ligands, although this was clearly indicated by spectroscopic data.[21]

In the case of the present complex $[Cu\{(C_5H_4N)_3CH\}_2][NO_3]_2$, the vibrational parameters of the nitrogen atoms provide no evidence for disorder. The diagonalised vibration ellipsoid parameters (Table 4) and the vibrational ellipsoids derived from them (Fig. 1) both show that the deviations from spherical symmetry are not much larger for the nitrogen atoms than for the central Cu. Even at 173 K, where the decrease in vibrational amplitudes should make any effects due to disorder more apparent, the relative elongation of the ellipsoids is at best marginal (Fig. 1). The failure of the crystallographically derived vibrational ellipsoids to give any indication of disorder is puzzling, since the evidence for disorder from the EXAFS and electronic and EPR spectra of the compound is unequivocal (see later). An explanation that would be consistent with our earlier comments on the crystallographic refinement is that the disorder extends over a sufficiently large proportion of the atoms of the ligand to let the effects become lost in the noise of the experiment or 'averaged out'.

EXAFS.—The observed EXAFS is incompatible with the EXAFS calculated for a model with six equivalent pyridines, but is well matched by the EXAFS calculated after refinement of the model with four short and two long Cu–N bonds. The weighted average of the four shorter Cu–N distances, 2.04(±0.01) Å, and the two longer ones, 2.25(±0.02) Å, is 2.11(±0.01) Å, in good agreement with the crystallographic values, 2.103(4) Å at 295 K and 2.095(3) Å at 173 K.

Electronic Spectra.—At room temperature (298 K) the electronic reflectance spectrum of $[Cu\{(C_5H_4N)_3CH\}_2][NO_3]_2$ over the range 4000–22 000 cm^{-1} shows a band centred at ≈7000 cm^{-1} and a peak at 16 000 cm^{-1} [Fig. 4(*a*)]. The weak, sharp peaks at ≈6000 cm^{-1} are due to IR overtones, as may be seen from the reflectance spectrum of the analogous Zn^{II} compound [Fig. 4(*a*)]. The spectra recorded from a single crystal at 298 K and ≈12 K over the range 12 000–25 000 cm^{-1} are shown in Fig. 4(*b*). (The near-IR region was inaccessible due to the small size of the crystals.) The single broad peak which is centred at ≈16 300 cm^{-1} at 298 K is clearly resolved into bands at ≈16 800 and ≈14 600 cm^{-1} at ≈12 K [Fig. 4(*b*)].

The large energy separation between the bands in the electronic spectrum of $[Cu\{(C_5H_4N)_3CH\}_2][NO_3]_2$ is incompatible with a complex having six identical Cu–N bond lengths and a near octahedral geometry. Such a stereochemistry is expected to produce a single broad band centred at ≈13 000 cm^{-1}, as is observed for the first electronic transition of the corresponding Ni^{II} complex. On the contrary, the observed spectrum of $[Cu\{(C_5H_4N)_3CH\}_2][NO_3]_2$ is closely similar to those of $[Cu\{(pz)_2(C_5H_4N)CH\}_2][NO_3]_2$ and $[Cu\{(pz)_3CH\}_2][NO_3]_2$. The Cu^{II} atoms in both these compounds have tetragonally elongated octahedral geometries, with Cu–N bond distances similar to those deduced from the EXAFS of $[Cu\{(C_5H_4N)_3CH\}_2][NO_3]_2$.

EPR Spectra.—At 293 K the EPR spectrum of powdered $[Cu\{(C_5H_4N)_3CH\}_2][NO_3]_2$ is characteristic of an isotropic g value. On cooling to 150 K, although the *average* g value remains unchanged, the spectrum largely changes to that expected for a complex with a tetragonally elongated octahedral geometry (Fig. 5). This behaviour is similar to that reported for the $[Cu(H_2O)_6]^{2+}$ ion in Cu^{2+}-doped $[Zn(H_2O)_6]SiF_6$,[22] and subsequently observed for several pure Cu^{2+} compounds.[23] It may be explained by assuming that each Cu^{2+} complex has a tetragonally elongated octahedral geometry, and that the long bonds are randomly distributed along the three metal–ligand bond directions. The different orientations are energetically equivalent, except for the small effects of 'strains' due to lattice defects, so that upon input of energy the direction of tetragonal elongation may switch from one bond to another. At low temperature, this switching is relatively slow and the EPR spectrum is anisotropic, as though it originated from the powder of a tetragonally elongated complex with the direction of the long axis of each complex fixed in space. At room

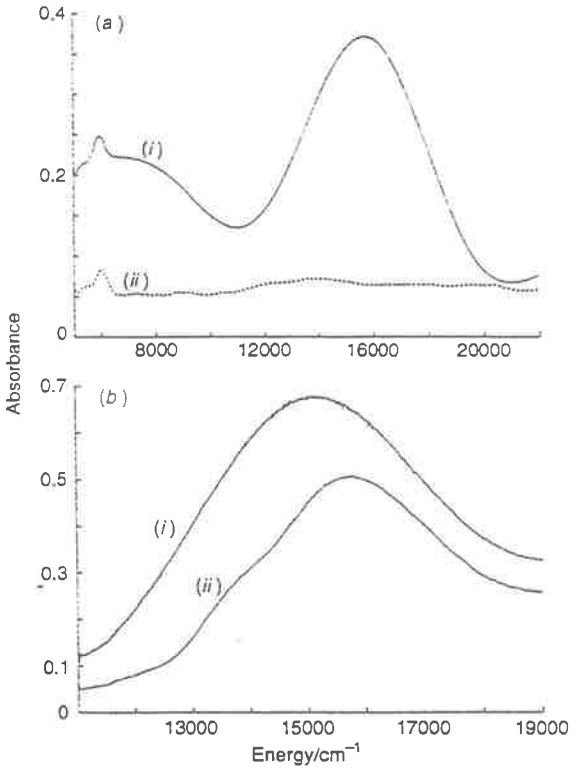

Fig. 4 (*a*) Room-temperature reflectance spectra of $[M\{(C_5H_4N)_3CH\}_2][NO_3]_2$, where M = Cu (*i*) and Zn (*ii*). (*b*) Electronic absorbance spectra (unpolarised light) from an arbitrary face of a crystal of $[Cu\{(C_5H_4N)_3CH\}_2][NO_3]_2$ at 298 K (*i*) and ≈12 K (*ii*)

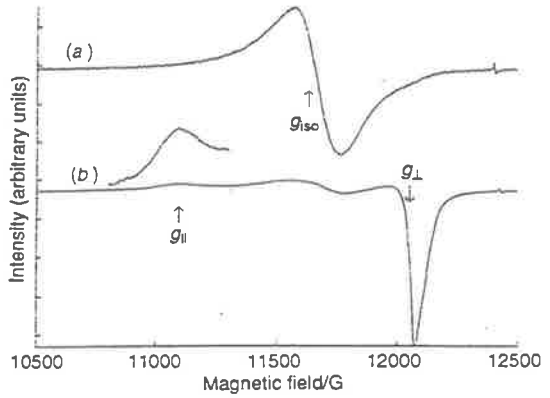

Fig. 5 The EPR spectrum of powdered $[Cu\{(C_5H_4N)_3CH\}_2][NO_3]_2$ measured at 293 K (*a*) and 150 K (*b*). The signal in the region of $g_\parallel$ at 150 K is also shown at an enhanced intensity. The weak inflections at a field of ≈12 400 G are due to a speck of powdered diphenylpicrylhydrazyl used as an internal standard (g = 2.0036)

temperature, the rate of switching is fast compared with the EPR time-scale, so that an isotropic signal is observed.

Two further aspects of the low-temperature EPR spectrum should be noted. First, a weak residual isotropic signal persists at low temperature (Fig. 5). This signal may originate from the fact that the random strains which act to localise the vibronic wave functions have a range of values, so that the rates at which the Cu–N bond lengths switch direction are not identical for all sites in the crystal. A similar behaviour has been observed in other systems of this type.[24] Secondly, the observation of a predominantly anisotropic signal at low temperature shows that the rate of *inter*molecular electron exchange in this compound is relatively slow. If the electron-exchange rate were fast enough to produce 'exchange narrowing', the random orientation of the bond axes would lead to the observation of an isotropic signal even at low temperature.

The EPR spectrum thus confirms that at the local level $[Cu\{(C_5H_4N)_3CH\}_2][NO_3]_2$ has a tetragonally elongated octahedral geometry. The g values derived from the low-temperature spectrum ($g_\parallel$ = 2.244, $g_\perp$ = 2.067) are characteristic of a ground state with the unpaired electron in the $d_{x^2-y^2}$ orbital, consistent with the complex having a tetragonally elongated octahedral geometry, as confirmed conclusively by the EXAFS. The g values are similar to those reported for the tetragonally elongated complexes formed by Cu^{2+} with analogous tripod ligands.[6,7] In the following section we show that similar values ($g_\parallel$ = 2.252, $g_\perp$ = 2.059) are also obtained by CAMMAG calculations using an isotropic orbital reduction parameter k = 0.78.

Metal–Ligand Bonding in Terms of the Angular Overlap Model.—A convenient method of parametrising the energy levels of transition-metal complexes is provided by the angular overlap model (AOM). This approach has recently been used to analyse the electronic spectra of complexes with a variety of tripod ligands.[6,7] It is of interest to see whether the transition energies of $[Cu\{(C_5H_4N)_3CH\}_2][NO_3]_2$ may be interpreted using chemically reasonable bonding parameters.

Calculations were carried out using the computer program CAMMAG developed by Gerloch and co-workers.[25] This program estimates the transition energies using a set of bonding parameters e_σ, $e_{\pi x}$, $e_{\pi y}$ to define the σ- and π-bonding characteristics of each ligand. The geometry is derived from an appropriate crystal structure. For the purposes of the calculations, the geometry of the present complex was assumed to be similar to that of $[Cu\{(pz)_2(C_5H_4N)CH\}_2][NO_3]_2$.[6] The crystallographically determined Cu–N distances in the latter complex are close to those determined for the present complex by the EXAFS analysis described above. An effective spin–orbit coupling constant of 645 cm^{-1} was used. π-Bonding in the plane of the amine ligand, represented by $e_{\pi x}$, was assumed to be negligible ($e_{\pi x}$ = 0), as found in other studies.[7] When the values used for the other bonding parameters were e_σ = 5800 cm^{-1}, $e_{\pi y}$ = 900 cm^{-1} for the four equatorial ligands, and e_σ = 2300 cm^{-1}, $e_{\pi y}$ = 350 cm^{-1} for the two axial ligands, the calculated transition energies were in reasonable agreement with those observed experimentally (see below).

Calc.: 17 350, 16 000, 14 600, 7050 cm^{-1}
Obs.: 16 800, ≈14 600, ≈7000 cm^{-1}

The bonding parameters of the closer (equatorial) nitrogen atoms are similar to those derived for other complexes with metal–ligand bond lengths comparable to the value 2.04 Å determined from the EXAFS of $[Cu\{(C_5H_4N)_3CH\}_2][NO_3]_2$.[6,7] For example, in $[Cu\{(pz)_2(C_5H_4N)CH\}_2][NO_3]_2$, e_σ = 6590 cm^{-1}, $e_{\pi y}$ = 1300 cm^{-1} for two N(pyridyl) atoms at 2.020 Å, and e_σ = 5540 cm^{-1}, $e_{\pi y}$ = 740 cm^{-1} for two N(pyrazolyl) atoms at 1.994 Å.[6]

On the other hand, if the bonding parameter e_σ varies as the inverse of the fifth or sixth power of the bond distance, as suggested by other studies,[6,7,26b] then the value predicted for the Cu–N distance of 2.25 Å determined from the EXAFS study is $e_\sigma \approx 3000$ cm^{-1}. The value obtained for the axial ligands in $[Cu\{(C_5H_4N)_3CH\}_2][NO_3]_2$ is significantly lower, e_σ = 2300 cm^{-1}. A deviation of this kind is in fact always observed for Cu^{2+} complexes with a tetragonally elongated octahedral geometry, being generally explained in terms of configuration interaction between the $a_{1g}(z^2)$ and metal $a_{1g}(4s)$ orbitals.[27] The present discrepancy corresponds to a depression of ≈1400 cm^{-1} in the energy of the $^2A_{1g}(z^2)$ excited state, which is very similar to that deduced for an axial bond length of 2.3 Å in a

study of a series of tetragonally distorted Cu^{II} amine complexes by Deeth and Gerloch.[28] Even smaller values, e_σ = 800 and 500 cm^{-1}, were obtained for the bonding parameters of the axial ligands in the complexes $[Cu\{(pz)_2(C_5H_4N)CH\}_2][NO_3]_2$ and $[Cu\{(pz)_3CH\}_2][NO_3]_2$, respectively.[6,7] The depression in e_σ is expected to increase as the tetragonal distortion increases. For the Cu^{2+} complexes of the above three tripod ligands, the decrease in the e_σ values of the axial ligands, 2300 > 800 > 500 cm^{-1}, does indeed mirror the increase in the axial bond lengths, 2.3 < 2.355 < 2.385 Å. Thus the AOM calculations are consistent with the relatively short axial bond length derived from the EXAFS analysis of $[Cu\{(C_5H_4N)_3CH\}_2][NO_3]_2$.

Conclusion

The results illustrate the differences between the information provided by the various techniques. X-Ray diffraction reveals atomic positions averaged over the lattice as a whole. In $[Cu\{(C_5H_4N)_3CH\}_2][NO_3]_2$ the ligand atoms of the tetragonally elongated $[Cu\{(C_5H_4N)_3CH\}_2]^{2+}$ complex are disordered to give a space-averaged geometry with six identical Cu–N bond lengths. It is not clear why the disorder is not apparent in the vibrational ellipsoid parameters produced by the X-ray analysis, but the *absence* of a significant asymmetry in such parameters cannot be taken as evidence that the atoms are localised at the observed positions. In contrast, the electronic spectrum and EXAFS are determined by the true local ligand geometry about each Cu^{2+}. Provided that, as in the present case, intermolecular electron exchange is slow, EPR spectroscopy lies between these two extremes. An isotropic spectrum is observed at room temperature where the ligand atoms interchange position rapidly, but at 150 K the signal becomes anisotropic because the ligand exchange rate has dropped below the EPR timescale.

Acknowledgements

The X-ray absorption data were recorded at the Australian National Beamline Facility (ANBF) at the KEK Photon Factory, Tsukuba, Japan. The research was supported by grants A29131459 (to M. A. H.), AL9132720 (to E. R. T. T.), A28415896 (to F. R. K.) and A29230677 (to H. C. F. and J. M. Guss) from the Australian Research Council, and by a travel grant from ANBF. P. J. E. was the holder of an Australian Postgraduate Research Award.

References

1 S. Trofimenco, *Chem. Rev.*, 1972, **72**, 497; *Prog. Inorg. Chem.*, 1986, **34**, 115.
2 T. A. Hafeli and F. R. Keene, *Aust. J. Chem.*, 1988, **41**, 1379.
3 P. S. Moritz, A. A. Diamantis, F. R. Keene, M. R. Snow and E. R. T. Tiekink, *Aust. J. Chem.*, 1988, **41**, 1352.
4 F. R. Keene, M. R. Snow, P. J. Stephenson and E. R. T. Tiekink, *Inorg. Chem.*, 1988, **27**, 2040.
5 P. A. Anderson, F. R. Keene, E. Horn and E. R. T. Tiekink, *Appl. Organomet. Chem.*, 1990, **4**, 523.
6 T. Astley, A. J. Canty, M. A. Hitchman, G. L. Rowbottom, B. W. Skelton and A. H. White, *J. Chem. Soc., Dalton Trans.*, 1991, 1981.
7 T. Astley, J. M. Gulbis, M. A. Hitchman and E. R. T. Tiekink, *J. Chem. Soc., Dalton Trans.*, 1993, 509.
8 D. L. Cullen and E. C. Lingafelder, *Inorg. Chem.*, 1970, **9**, 1858.
9 D. Tucker, P. S. White, K. L. Trojan, M. L. Kirk and W. E. Hatfield, *Inorg. Chem.*, 1991, **30**, 823.
10 P. J. Ellis, H. C. Freeman, M. A. Hitchman, D. Reinen and B. Wagner, *Inorg. Chem.*, 1994, **33**, 1249.
11 M. A. Hitchman, *Transition Met. Chem. (New York)*, 1985, **9**, 1.
12 N. Walker and D. Stuart, *Acta Crystallogr., Sect. A*, 1983, **39**, 158.
13 TEXSAN, Single Crystal Structure Analysis Software, Version 1.6, The Woodlands, Molecular Structure Corporation, TX, 1993.
14 C. K. Johnson, ORTEP II, ORNL Report 5136, Oak Ridge National Laboratory, TN, 1976.
15 P. J. Ellis, unpublished work.
16 J. J. Rehr and R. C. Albers, *Phys. Rev. B*, 1990, **41**, 8139; J. J. Rehr, J. Mustre de Leon, S. I. Zabinsky and R. C. Albers, *J. Am. Chem. Soc.*, 1991, **113**, 5135; J. Mustre de Leon, J. J. Rehr, S. I. Zabinsky and R. C. Albers, *Phys. Rev. B*, 1991, **44**, 4146.
17 M. A. Hitchman, *Comments Inorg. Chem.*, 1994, **15**, 197.
18 N. W. Isaacs and C. H. L. Kennard, *J. Chem. Soc. A*, 1969, 386; M. D. Joesten, M. S. Hussain, P. G. Lenhert and J. H. Veneble jun., *J. Am. Chem. Soc.*, 1968, **90**, 5623; M. D. Joesten, M. S. Hussain and P. G. Lenhert, *Inorg. Chem.*, 1970, **9**, 151.
19 D. L. Cullen and E. C. Lingafelder, *Inorg. Chem.*, 1971, **10**, 1264; J. H. Ammeter, H. B. Bürgi, E. Gamp, V. Sandrin-Meyer and W. P. Jensen, *Inorg. Chem.*, 1979, **18**, 733.
20 J. S. Wood, C. P. Keijzers, E. de Boer and A. Buttafava, *Inorg. Chem.*, 1980, **19**, 2213; M. Stebler and H. B. Bürgi, *J. Am. Chem. Soc.*, 1987, **109**, 1395.
21 P. Chaudhuri, K. Oder, K. Wieghardt, J. Weiss, J. Reedijk, W. Hinrichs, J. Wood, A. Ozarowski, H. Stratemeier and D. Reinen, *Inorg. Chem.*, 1986, **25**, 2951.
22 B. Bleaney and D. J. E. Ingram, *Proc. Phys. Soc., Ser. A*, 1950, **63**, 408.
23 D. Reinen and S. Krause, *Solid State Commun.*, 1979, **29**, 691; R. C. Koch, M. D. Joesten and J. H. Venable, *J. Chem. Phys.*, 1973, **59**, 6312.
24 M. J. Riley, M. A. Hitchman, D. Reinen and G. Steffen, *Inorg. Chem.*, 1988, **27**, 1924.
25 D. A. Cruse, J. E. Davies, M. Gerloch, J. H. Harding, D. Mackey and R. F. McMeeking, CAMMAG, a Fortran Computing Package, University of Cambridge, 1979.
26 M. Bermejo and L. Pueyo, *J. Chem. Phys.*, 1983, **78**, 854.
27 L. G. Vanquickenborne and A. Ceulemans, *Inorg. Chem.*, 1981, **20**, 796.
28 R. Deeth and M. Gerloch, *Inorg. Chem.*, 1984, **23**, 3849.

Received 16*th September* 1994; *Paper* 4/05652C

J. CHEM. SOC. DALTON TRANS. 1995

Crystal Structures and Electron Paramagnetic Resonance Spectra of $[Cu\{P(C_5H_4N)_3\}_2]Br_2\cdot 8H_2O$ and Cu^{2+}-Doped $[Zn\{P(C_5H_4N)_3\}_2]Br_2\cdot 8H_2O$, Examples of a Dynamic Jahn–Teller Effect in Two Dimensions†

Timothy Astley,[a] Henrietta Headlam,[a] Michael A. Hitchman,[a] F. Richard Keene,[b] John Pilbrow,[c] Horst Stratemeier,[a] Edward R. T. Tiekink[d] and Y. C. Zhong[c]

[a] *Chemistry Department, University of Tasmania, Box 252C, Hobart, Tasmania 7000, Australia*

[b] *Department of Molecular Sciences, James Cook University of North Queensland, Townsville, Queensland 4811, Australia*

[c] *Department of Physics, Monash University, Clayton, Victoria 3168, Australia*

[d] *Department of Chemistry, The University of Adelaide, Adelaide, South Australia 5005, Australia*

Crystals of $[Cu\{P(C_5H_4N)_3\}_2]Br_2\cdot 8H_2O$, studied at 173 K are triclinic, space group $P\bar{1}$, with unit-cell dimensions $a = 9.082(4)$, $b = 11.340(1)$, $c = 9.084(2)$ Å, $\alpha = 98.40(4)$, $\beta = 94.78(3)$, $\gamma = 98.27(7)°$ and $Z = 1$; those of $[Zn\{P(C_5H_4N)_3\}_2]Br_2\cdot 8H_2O$ studied at 293 K are monoclinic, space group $C2/m$ with $a = 12.506(6)$, $b = 13.588(7)$, $c = 11.593(7)$ Å, $\beta = 101.62(4)°$ and $Z = 2$. The structures were refined to final $R = 0.050$ for 3192 reflections with $I \geqslant 3.0\sigma(I)$, and $R = 0.033$ for 1737 reflections with $I \geqslant 3.0\sigma(I)$, respectively. The centrosymmetric copper complex has two Cu–N bonds [2.002(4) Å] considerably shorter than the other four [2.189(5) × 2, 2.191(5) Å × 2]. However, the temperature dependence of the EPR spectrum suggests that in fact the complex has a tetragonally elongated octahedral geometry with two possible orientations in the crystal lattice, these differing by interchange of the directions of the long and intermediate Cu–N bond directions. These forms are in dynamic equilibrium, with an activation energy of ≈600 cm^{-1} for the interchange. Analysis of the relative intensities of the EPR signals observed at ≈10 K suggests an energy difference between the structural isomers of ≈4 cm^{-1}. The zinc complex has crystallographic $2/m$ symmetry with two independent Zn–N distances [2.150(3) × 2; 2.187(3) Å × 4]. The temperature dependence of the EPR spectrum of this compound doped with ≈1% Cu^{2+} is similar to that of the pure copper(II) compound, but with a lower activation energy for interchange of the structural isomers. The dynamic behaviour of the copper(II) complex in the two compounds is discussed in terms of a potential surface obtained by considering the effects of Jahn–Teller coupling and lattice strain interactions. Bonding parameters derived from the electronic spectrum are consistent with the tetragonally elongated octahedral co-ordination geometry proposed.

Tripodal ligands involving nitrogen-donor heterocycles have been found to exhibit a number of useful properties in co-ordination and organometallic chemistry.[1] As part of a study of the electronic and steric characteristics of first-row transition-metal complexes of ligands of this kind[2–7] we have prepared the compounds $[M\{P(C_5H_4N)_3\}_2]Br_2\cdot 8H_2O$ (M = Cu or Zn) and report here their crystal structures. These indicate that one pair of *trans* M–N bonds is considerably shorter than the other two pairs. Such a ligand arrangement would be highly unusual for a copper(II) complex, as it implies the tetragonally compressed form of the Jahn–Teller distortion rather than the tetragonally elongated form almost invariably observed for six-co-ordinate complexes of this metal ion.[8] Although this has been previously reported for several compounds,[9] subsequent research has almost always found[10] that the compressed tetragonal geometry is in fact due to disorder of the long and one pair of short metal–ligand bonds of complexes which have the common tetragonally elongated octahedral co-ordination geometry. Electron paramagnetic resonance (EPR) spectroscopy[11] and extended X-ray absorption fine structure (EXAFS)[12] have both proved to be useful tools in resolving ambiguities of this kind, and we recently used these techniques to show[13] that the six crystallographically equivalent Cu–N bonds observed for the similar compound $[Cu\{CH(C_5H_4N)_3\}_2][NO_3]_2$ are in fact due to a three-dimensional disorder of the long and both pairs of short Cu–N bonds of a complex with a tetragonally elongated octahedral geometry.

The EPR spectrum of a complex exhibiting disorder can be particularly revealing, as the variation with temperature often provides information about the dynamics of the equilibrium between the structural isomers.[14] Recently, we developed a model to describe the potential surface of a six-co-ordinate copper(II) complex under the influence of Jahn–Teller coupling and perturbations due to the surrounding crystal lattice.[15] Initially, this was used to interpret the EPR spectra of the complexes formed when Cu^{2+} is doped into a range of diamagnetic host lattices,[16–18] though the model was later extended to treat the combined structural and EPR data available for pure copper(II) compounds,[19] and the situation where dynamic equilibria are influenced by pressure rather than temperature.[20]

The present paper reports the crystal structures and EPR spectra of $[Cu\{P(C_5H_4N)_3\}_2]Br_2\cdot 8H_2O$ and the analogous zinc(II) compound doped with ≈1% Cu^{2+}, and interprets these in terms of the potential surface and associated vibronic

† *Supplementary data available:* see Instructions for Authors, *J. Chem. Soc. Dalton Trans.*, 1995, Issue 1, pp. xxv–xxx.

Non-SI unit employed: G = 10^{-4} T.

wavefunctions of a copper(II) complex perturbed by Jahn–Teller coupling and 'strain' induced by the surrounding lattice.

Experimental

Syntheses.—The compound tris(2-pyridyl)phosphine was obtained using established methods.[4,21]

Bis[tris(2-pyridyl)phosphine]copper(II) nitrate, $[Cu\{P(C_5H_4N)_3\}_2][NO_3]_2$. A solution of $Cu(NO_3)_2\cdot 6H_2O$ (150 mg, 0.5 mmol) in acetone (5 cm^3) was added dropwise at room temperature to a stirred solution of tris(2-pyridyl)phosphine (265 mg, 1 mmol) in acetone (10 cm^3). The resulting suspension was cooled at 0 °C for 2 h, filtered, washed with acetone and air dried. Yield: 300 mg, 83%.

Bis[tris(2-pyridyl)phosphine]copper(II) bromide, $[Cu\{P(C_5H_4N)_3\}_2]Br_2\cdot 8H_2O$. The nitrate salt was converted into the bromide salt by anion-exchange chromatography using a QAE Sephadex A25 anion exchanger. Crystals grown by slow evaporation of an aqueous solution (Found: C, 40.4; H, 4.7; N, 9.4. Calc. for $C_{30}H_{40}Br_2CuN_6O_8P_2$: C, 40.1; H, 4.50; N, 9.4%).

Bis[tris(2-pyridyl)phosphine]zinc(II) nitrate, $[Zn\{P(C_5H_4N)_3\}_2][NO_3]_2$. A solution of $Zn(NO_3)_2\cdot 6H_2O$ (150 mg, 0.5 mmol) in acetone (5 cm^3) was added dropwise at room temperature to a stirred solution of tris(2-pyridyl)phosphine (250 mg, 1 mmol) in acetone (10 cm^3). The resulting suspension was cooled at 0 °C for 2 h, filtered, washed with acetone and air dried. Yield: 280 mg, 78%.

Bis[tris(2-pyridyl)phosphine]zinc(II) bromide, $[Zn\{P(C_5H_4N)_3\}_2]Br_2\cdot 8H_2O$. The nitrate salt was converted into the bromide salt by anion-exchange chromatography using a QAE Sephadex A25 anion exchanger. Crystals were grown by slow evaporation of an aqueous solution (Found: C, 40.2; H, 4.0; N, 9.6. Calc. for $C_{30}H_{40}Br_2N_6O_8P_2Zn$: C, 40.0; H, 4.5; N, 9.3%).

Spectroscopic Measurements.—The reflectance spectrum was recorded with a Beckmann DK2A spectrophotometer. The EPR spectra were measured at Q-band frequency, ≈34 GHz, over the temperature range 293–77 K using a JEOL JES-FE spectrometer equipped with a standard JEOL cryostat, crystal-rotation device and temperature controller. A crystal spectrum of the pure copper(II) compound was also measured at ≈10 K at X-band frequency (≈9.4 GHz) using a Varian E12 spectrometer. The crystal was cooled using an Oxford Instruments flow cryostat. An EPR spectrum of the powdered Cu^{2+}-doped zinc(II) compound was measured in the temperature range 4–100 K using a Bruker ESP 380E spectrometer operating at X-band. In each case the sample was prevented from losing water by covering it with a layer of EPR-inert silicone vacuum grease.

Crystallography.—Intensity data for a blue crystal of $[Cu\{P(C_5H_4N)_3\}_2]Br_2\cdot 8H_2O$ (173 K, 0.13 × 0.23 × 0.24 mm) and a pale yellow crystal of $[Zn\{P(C_5H_4N)_3\}_2]Br_2\cdot 8H_2O$ (293 K, diameter 0.5 mm) were measured on a Rigaku AFC6R diffractometer fitted with graphite-monochromatised Mo-Kα radiation, λ = 0.710 73 Å; the ω–2θ scan technique was employed to measure data such that θ_{max} was 27.5°. No decomposition of either crystal occurred during their respective data collections and only absorption-corrected data[22] which satisfied the criterion $I \geq 3.0\sigma(I)$ were used in the subsequent analyses. Crystal data are summarised in Table 1.

Each structure was solved by placing the metal atom on a crystallographic special site of symmetry and the remaining atoms were located from subsequent difference maps: the structures were refined by a full-matrix least-squares procedure based on F.[23] Non-hydrogen atoms were refined with anisotropic thermal parameters and H atoms were included in the models at their calculated positions (C–H 0.97 Å); water hydrogen atoms were not located. At convergence (σ weights, *i.e.* $1/\sigma^2(F)$ $R = 0.050$ and $R' = 0.060$ for the copper complex and $R = 0.033$ and $R' = 0.037$ for the zinc complex. The analysis of variace showed no special features in either case and the maximum peak in the final difference map was 0.71 and 0.43 e $Å^{-3}$ for the copper and zinc complexes, respectively. Scattering factors for all atoms were those incorporated in the TEXSAN program.[23] Fractional atomic coordinates are listed in Tables 2 and 5, anisotropic thermal parameters for the Cu^{2+} complex in Table 3, the numbering schemes shown in Figs. 1 and 2 which were drawn with the ORTEP program[24] with 50 and 30% probability ellipsoids, respectively and selected bond distances and angles are presented in Tables 4 and 6.

Additional material available from the Cambridge Crystallographic Data Centre comprises H-atom coordinates, thermal parameters and remaining bond lengths and angles.

Results and Discussion

Crystal Structures.—The structure of the cation in $[Cu\{P(C_5H_4N)_3\}_2]Br_2\cdot 8H_2O$ is shown in Fig. 1. The unit cell contains one formula unit of $[Cu\{P(C_5H_4N)_3\}_2]Br_2\cdot 8H_2O$, with the complex being disposed about a crystallographic centre of inversion. As expected for a structure of this type there are significant intermolecular contacts in the lattice; however, these contacts do not involve the cation but the bromide anion and the water molecules of crystallisation. The bromide atom forms three hydrogen-bonding contacts to the solvent water molecules [Br···O(2), O(4), O(3) are 3.291(4), 3.324(5), 3.326(5) Å, respectively] and, as well, there are water–water contacts involving each of the four water molecules. In the CuN_6 octahedral cation there are two classes of Cu–N contacts with the Cu–N(21) and Cu–N(31) distances of 2.189(5) and 2.191(5) Å being equal within experimental error and significantly longer than the Cu–N(11) distance of 2.002(4) Å; other parameters within the complex cation are as expected. The co-ordination geometry about the copper(II) atom, with two short and four long Cu–N distances, is thereby unusual, the compound appearing to conform to the rare *compressed* form of the tetragonal Jahn–Teller distortion.[8] Such a geometry would be remarkable, since previous reports[9] of such a stereochemistry have almost invariably been found to be fallacious;[10] as far as we are aware $KAlCuF_6$ remains the only example of a compound involving just one ligand type where all available evidence[25,26] suggests a compressed tetragonal Jahn–Teller distortion. As shown in the following section, the EPR evidence

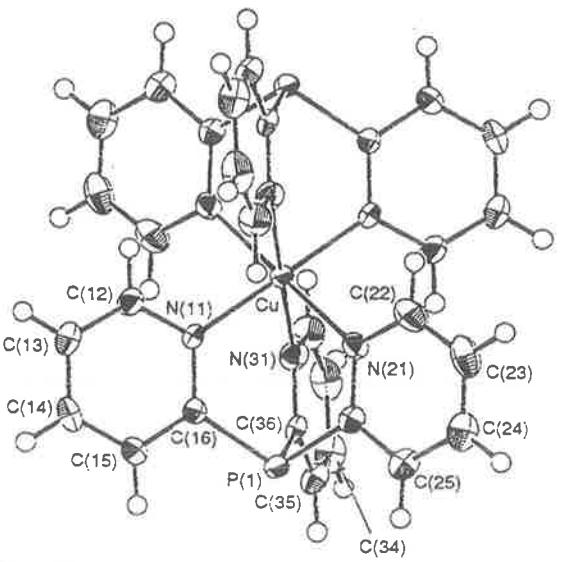

Fig. 1 Molecular structure and crystallographic numbering scheme for the cation in $[Cu\{P(C_5H_4N)_3\}_2]Br_2\cdot 8H_2O$

Table 1 Crystal data for $[M\{P(C_5H_4N)_3\}_2]Br_2\cdot 8H_2O$ (M = Cu 1 or Zn 2)

Compound	1	2
Formula	$C_{30}H_{40}Br_2CuN_8O_8P_2$	$C_{30}H_{40}Br_2N_8O_8P_2Zn$
M	898.0	899.8
Crystal system	Triclinic	Monoclinic
Space group	$P\bar{1}$	$C2/m$
a/Å	9.082(4)	12.506(6)
b/Å	11.40(1)	13.588(7)
c/Å	9.084(2)	11.593(7)
α/°	98.40(4)	
β/°	94.78(3)	101.62(4)
γ/°	98.27(7)	
U/Å^3	915.4(9)	1929(1)
Z	1	2
D_c/g cm^{-3}	1.629	1.549
μ/cm^{-1}	28.49	28.49
Maximum, minimum transmission factors	1.033, 0.948	1.153, 0.842
$F(000)$	455	912
No. data measured	4669	2417
No. unique data	4398	2313
No. observed data [$I \geqslant 3.0\sigma(I)$]	3192	1737
R	0.050	0.033
R'	0.060	0.037

Table 2 Fractional atomic coordinates for the non-hydrogen atoms of $[Cu\{P(C_5H_4N)_3\}_2]Br_2\cdot 8H_2O$

Atom	x	y	z
Br	0.616 80(6)	0.328 13(5)	0.616 77(6)
Cu*	0	0	0
P(1)	0.276 0(2)	−0.011 6(1)	0.275 9(2)
O(1)	0.846 9(4)	0.499 6(4)	0.152 2(4)
O(2)	0.888 9(4)	0.359 9(3)	0.889 3(4)
O(3)	−0.581 8(5)	0.416 8(5)	−0.108 1(6)
O(4)	0.891 5(5)	0.416 6(5)	0.418 4(5)
N(11)	0.128 8(4)	0.141 5(4)	0.128 3(5)
N(21)	0.203 6(5)	−0.079 4(4)	−0.027 3(5)
N(31)	−0.027 8(5)	−0.079 7(4)	0.203 3(5)
C(12)	0.108 3(6)	0.251 1(5)	0.108 0(6)
C(13)	0.191 4(7)	0.352 8(5)	0.191 5(7)
C(14)	0.298 6(6)	0.342 0(5)	0.298 7(6)
C(15)	0.320 8(6)	0.229 8(5)	0.320 7(6)
C(16)	0.234 3(5)	0.131 9(4)	0.235 2(5)
C(22)	0.225 9(7)	−0.135 5(6)	−0.160 3(7)
C(23)	0.341 1(7)	−0.200 2(6)	−0.180 2(7)
C(24)	0.433 2(7)	−0.208 8(6)	−0.060 1(7)
C(25)	0.413 0(6)	−0.149 7(5)	0.078 3(6)
C(26)	0.297 5(6)	−0.086 3(5)	0.089 6(6)
C(32)	−0.159 7(6)	−0.135 9(6)	0.225 8(7)
C(33)	−0.179 7(7)	−0.200 0(6)	0.340 1(8)
C(34)	−0.059 6(7)	−0.208 1(6)	0.433 8(7)
C(35)	0.077 6(6)	−0.150 1(5)	0.412 9(6)
C(36)	0.089 8(6)	−0.085 7(4)	0.298 5(6)

* Atom has site occupancy factor = 0.5.

strongly suggests that in $[Cu\{P(C_5H_4N)_3\}_2]Br_2\cdot 8H_2O$ the longer Cu–N bonds actually represent the *average* ligand positions of one pair of closely bonded pyridines (Cu–N ≈2.04 Å), and one pair of loosely bound amines (Cu–N ≈2.34 Å), so that the local co-ordination geometry about the copper(II) in fact conforms to that generally observed for this metal ion.

The Cu–N distances proposed for $[Cu\{P(C_5H_4N)_3\}_2]Br_2\cdot 8H_2O$ are quite similar to those observed for complexes of other similar tripod ligands, for instance 1.994, 2.020 and 2.385 Å in the compound $[Cu\{CH(C_5H_4N)(pz)_2\}_2][NO_3]_2$, where pz = pyrazol-1-yl.[6] However, the overall Jahn–Teller distortion is somewhat larger than that suggested by the bond lengths 2.04 (×4) and 2.25 (×2) Å revealed by EXAFS of the compound $[Cu\{CH(C_5H_4N)_3\}_2][NO_3]_2$.[13]

Although $[Zn\{P(C_5H_4N)_3\}_2]Br_2\cdot 8H_2O$ has a similar stoichiometry and co-ordination geometry to the above copper(II) compound, it crystallises in the monoclinic space group $C2/m$. The molecular structure of the cation is shown in Fig. 2. In the lattice, there are three contacts between the bromide anion and symmetry-related water molecules of solvation [*i.e.* Br ··· O(3), O(1), O(1′) 3.333(4), 3.356(4), 3.356(4) Å, respectively] and water–water interactions involving all water molecules. The geometry about the zinc atom, which is located at a crystallographic site of symmetry 2/*m*, is distorted octahedral, the Zn–N(11) distances being 2.150(3) Å (×2) and Zn–N(21) 2.187(3) Å (×4). However, the difference in bond lengths is much smaller than for the copper(II) complex (≈0.03 compared with ≈0.19 Å) because of the absence of the Jahn–Teller effect. Also, because of the higher site symmetry, the two longer Zn–N bonds are crystallographically equivalent, and this has implications for the EPR spectrum of Cu^{2+} doped into the zinc compound (see following section).

EPR Spectra.—At 293 K the EPR spectrum of powdered $[Cu\{P(C_5H_4N)_3\}_2]Br_2\cdot 8H_2O$ is characteristic of a tetragonal g tensor with $g_\parallel = 2.04$, $g_\perp = 2.165$. On cooling to 77 K, although the *average* g value remains unchanged, the $g_\perp$ signal is largely replaced by resonances corresponding to $g = 2.09$ and 2.25, so that at low temperature the overall spectrum is that expected for a complex with a tetragonally elongated octahedral geometry with a slight orthorhombic distortion. Except that the change occurs at higher temperature, this behaviour is reminiscent of that observed for the centre $[Cu(H_2O)_2Cl_4]^{2-}$ in Cu^{2+}-doped NH_4Cl.[18] Here, a 'reversed' g tensor of tetragonal symmetry is replaced by a 'normal' g tensor of orthorhombic symmetry at a temperature of ≈30 K, and this was explained by the complex having a tetragonally elongated octahedral geometry, but with the long bonds fluctuating between the Cu–Cl directions. Above ≈30 K the rate of exchange between the 'structural isomers' is more rapid than the EPR time-scale, but when the temperature drops below ≈30 K the $[Cu(H_2O)_2Cl_4]^{2-}$ complex becomes 'frozen' into one orientation.

The behaviour of $[Cu\{P(C_5H_4N)_3\}_2]Br_2\cdot 8H_2O$ can therefore be explained if the complex has an essentially tetragonally elongated octahedral geometry, though with the long bonds randomly distributed between two of the three Cu–N bond directions. The different orientations are almost energetically equivalent, so that upon input of energy the direction of tetragonal elongation may 'switch' from one bond to another. At low temperature this switching is relatively slow, and the EPR spectrum is that expected for an orthorhombically

Table 3 Anisotropic thermal parameters for $[Cu\{P(C_5H_4N)_3\}_2]Br_2\cdot 8H_2O$*

Atom	U_{11}	U_{22}	U_{33}	U_{12}	U_{13}	U_{23}
Br	0.0279(3)	0.0291(3)	0.0284(3)	0.0035(2)	0.0006(2)	0.0026(2)
Cu	0.0180(4)	0.0189(5)	0.0183(5)	0.0042(4)	0.0011(4)	0.0033(4)
P(1)	0.0207(7)	0.0219(7)	0.0209(7)	0.0057(5)	0.0005(5)	0.0048(6)
O(1)	0.034(2)	0.037(2)	0.032(2)	0.005(2)	0.011(2)	0.002(2)
O(2)	0.031(2)	0.026(2)	0.034(2)	0.008(2)	−0.000(2)	0.007(2)
O(3)	0.039(3)	0.069(4)	0.057(3)	0.017(2)	0.010(2)	−0.005(3)
O(4)	0.053(3)	0.069(4)	0.044(3)	−0.005(3)	0.010(2)	0.018(3)
N(11)	0.019(2)	0.017(2)	0.022(2)	0.006(2)	0.004(2)	0.004(2)
N(21)	0.034(3)	0.023(2)	0.018(2)	0.005(2)	0.001(2)	0.001(2)
N(31)	0.021(2)	0.026(3)	0.036(3)	0.005(2)	0.002(2)	0.004(2)
C(12)	0.029(3)	0.021(3)	0.031(3)	0.005(2)	0.001(2)	0.007(2)
C(13)	0.038(3)	0.020(3)	0.039(3)	0.007(3)	0.006(3)	0.007(3)
C(14)	0.031(3)	0.022(3)	0.027(3)	−0.004(2)	0.008(2)	−0.005(2)
C(15)	0.021(3)	0.026(3)	0.020(3)	0.002(2)	0.005(2)	0.001(2)
C(16)	0.018(2)	0.020(3)	0.018(3)	0.005(2)	0.006(2)	0.002(2)
C(22)	0.046(4)	0.042(4)	0.024(3)	0.003(3)	0.003(3)	−0.000(3)
C(23)	0.049(4)	0.034(4)	0.032(3)	0.000(3)	0.018(3)	−0.005(3)
C(24)	0.041(4)	0.034(4)	0.038(4)	0.010(3)	0.021(3)	0.007(3)
C(25)	0.030(3)	0.029(3)	0.029(3)	0.007(2)	0.010(2)	0.010(2)
C(26)	0.024(3)	0.021(3)	0.023(3)	0.003(2)	0.006(2)	0.008(2)
C(32)	0.022(3)	0.034(3)	0.050(4)	−0.000(3)	0.003(3)	0.003(3)
C(33)	0.030(3)	0.034(4)	0.052(4)	−0.003(3)	0.017(3)	−0.002(3)
C(34)	0.041(4)	0.030(3)	0.041(4)	0.006(3)	0.020(3)	0.008(3)
C(35)	0.031(3)	0.027(3)	0.032(3)	0.011(2)	0.010(2)	0.008(3)
C(36)	0.023(3)	0.016(3)	0.025(3)	0.008(2)	0.006(2)	0.002(2)

* Anisotropic thermal parameter given by the expression $T_{aniso} = \exp[-2\pi^2(h^2a^{*2}U_{11} + k^2b^{*2}U_{22} + l^2c^{*2}U_{33} + 2hka^*b^*U_{12} + 2hla^*c^*U_{13} + 2klb^*c^*U_{23})]$.

Table 4 Selected bond distances (Å) and angles (°) for $[Cu\{P(C_5H_4N)_3\}_2]Br_2\cdot 8H_2O$

Cu–N(11)	2.002(4)	Cu–N(21)	2.189(5)
Cu–N(31)	2.191(5)	P(1)–C(16)	1.813(5)
P(1)–C(26)	1.819(5)	P(1)–C(36)	1.820(5)
N(11)–C(12)	1.326(6)	N(11)–C(16)	1.334(6)
N(21)–C(22)	1.328(7)	N(21)–C(26)	1.324(6)
N(31)–C(32)	1.321(7)	N(31)–C(36)	1.334(6)
N(11)–Cu–N(21)	87.5(2)	N(11)–Cu–N(31)	87.8(2)
N(11)–Cu–N(21′)*	92.5(2)	N(11)–Cu–N(31′)	92.2(2)
N(21)–Cu–N(31)	89.7(2)	N(21)–Cu–N(31′)	90.3(2)
C(16)–P(1)–C(26)	100.9(2)	C(16)–P(1)–C(36)	100.6(2)
C(26)–P(1)–C(36)	99.9(2)	Cu–N(11)–C(12)	118.9(3)
Cu–N(11)–C(16)	123.5(3)	C(12)–N(11)–C(16)	117.6(4)
Cu–N(21)–C(22)	120.1(4)	Cu–N(21)–C(26)	121.4(4)
C(22)–N(21)–C(26)	118.0(5)	Cu–N(31)–C(32)	120.6(4)
Cu–N(31)–C(36)	121.2(4)	C(32)–N(31)–C(36)	117.8(5)

* Primed atoms are related by a centre of inversion.

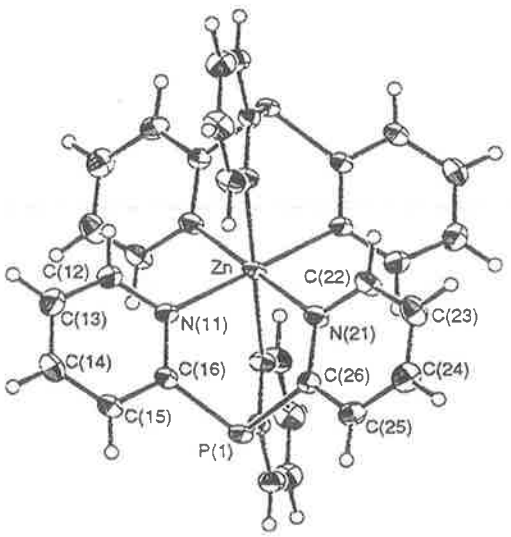

Fig. 2 Molecular structure and crystallographic numbering for the cation in $[Zn\{P(C_5H_4N)_3\}_2]Br_2\cdot 8H_2O$

distorted tetragonally elongated complex with the direction of the long axis of each complex fixed in space. However, at room temperature, the rate of switching is faster than the EPR time-scale, so that the signals associated with the long and one pair of short bonds are averaged to give the g_2 signal.

This picture was confirmed by measuring the EPR spectrum of a single crystal at 77 K. In general, two symmetry-related signals were observed, despite the fact that the triclinic cell contains only one $[Cu\{P(C_5H_4N)_3\}_2]^{2+}$ complex. The positions of the signals varied with the crystal orientation, and they coalesced at the orientation producing the minimum g value (2.04). It may be assumed that here the magnetic field is parallel to the short Cu–N(11) bond. The variation of the g values in the plane normal to this direction is shown in Fig. 3. Two similar sinusoidal curves occur, with extrema 90° apart. A hyperfine splitting of 160×10^{-4} cm^{-1} due to coupling with the copper nuclear spin was observed for the signals associated with the higher g values. The maximum and minimum g values, $g_3 = 2.25$, $g_2 = 2.09$, are identical to the molecular g values observed in the powder spectrum at 77 K. The two sets of signals thus correspond to two possible orientations of a complex having an orthorhombically distorted tetragonally elongated geometry, one having the long bond to N(21), and the other with this to N(31). For one of the curves in Fig. 3 the maximum and minimum g values occur when the magnetic field lies close to the Cu–N(21) and Cu–N(31) bond directions, respectively, while the reverse is true for the other curve.

Upon raising the temperature the signals corresponding to the two possible orientations coalesce at ≈140 K (Fig. 4). At this temperature, the energy difference between the signals, measured in frequency units, approximately equals the rate of

Table 5 Fractional atomic coordinates for the non-hydrogen atoms of $[Zn\{P(C_5H_4N)_3\}_2]Br_2\cdot 8H_2O$

Atom	x	y	z
Br(1)[a]	0.619 84(4)	0	0.328 11(5)
Zn[b]	0	0	0
P(1)[a]	0.275 52(8)	0	−0.015 1(1)
O(1)	0.155 6(2)	0.265 7(2)	0.419 1(3)
O(2)[a]	0	0.151 9(3)	0.5
O(3)[a]	0.890 8(3)	0	0.360 3(3)
N(11)[a]	0.136 1(3)	0	0.146 6(3)
N(21)	0.086 1(2)	0.112 3(2)	−0.081 2(2)
C(12)[a]	0.119 7(4)	0	0.257 7(4)
C(13)[a]	0.203 6(4)	0	0.354 9(4)
C(14)[a]	0.309 6(4)	0	0.339 4(4)
C(15)[a]	0.327 7(3)	0	0.225 1(4)
C(16)[a]	0.240 7(3)	0	0.131 7(4)
C(22)	0.032 1(2)	0.188 9(2)	−0.137 3(3)
C(23)	0.078 0(3)	0.257 5(2)	−0.199 7(3)
C(24)	0.185 2(3)	0.246 8(2)	−0.206 2(3)
C(25)	0.243 5(3)	0.168 9(2)	−0.148 2(3)
C(26)	0.192 9(2)	0.103 3(2)	−0.086 5(2)

[a] Atom has site occupancy factor = 0.5. [b] Atom has site occupancy factor = 0.25.

Table 6 Selected bond distances (Å) and angles (°) for $[Zn\{P(C_5H_4N)_3\}_2]Br_2\cdot 8H_2O$

Zn–N(11)	2.150(3)	Zn–N(21)	2.187(3)
P(1)–C(16)	1.841(4)	P(1)–C(26)	1.837(3)
N(11)–C(12)	1.344(5)	N(11)–C(16)	1.352(5)
N(21)–C(22)	1.337(4)	N(21)–C(26)	1.356(3)
N(11)–Zn–N(21)	87.73(9)	N(11)–Zn–N(21′)	92.27(9)
N(21)–Zn–N(21″)	88.5(1)	N(21)–Zn–N(21‴)	91.5(1)
C(16)–P(1)–C(26)	101.6(1)	C(26)–P(1)–C(26″)	99.6(2)
Zn–N(11)–C(12)	120.5(3)	Zn–N(11)–C(16)	122.1(3)
C(12)–N(11)–C(16)	117.4(4)	Zn–N(21)–C(22)	120.6(2)
Zn–N(21)–C(26)	122.1(2)	C(22)–N(21)–C(26)	117.0(3)

Primed atoms related by the symmetry operation $-x, -y, -z$, doubly primed ones by $x, -y, z$ and triply primed ones by $-x, y, -z$.

exchange R_{exch} between the two orientations, equation (1).[27,†]

$$R_{exch} \approx |g_2 - g_3|\beta B\pi/(\sqrt{2}h) \quad (1)$$

Here, β is the Bohr magneton and h Planck's constant, and substituting $g_2 = 2.09$, $g_3 = 2.25$ and the average magnetic field of the signals $B = 1.15$ T into equation (1) yields the rate $R \approx 5.7 \times 10^9$ s^{-1}. Since the energy difference between the structural isomers, ΔE, is clearly small compared with the energy barrier ΔE^*, the latter may be estimated from the rate expression (2)[28] where k is the Boltzmann constant, R the gas constant and T the absolute temperature. Substitution of the above exchange rate, together with the temperature of coalescence $T \approx 140$ K, into equation (2) yields the estimate $\Delta E^* \approx 607$ cm^{-1}.

$$R_{exch} \approx kT[\exp(-\Delta E^*/RT)]/h \quad (2)$$

The fact that the activation energy is so high means that at low temperature the complexes will be 'frozen' into the less-stable orientation. When the sample is cooled rapidly, as in the present case, this non-equilibrium situation will occur at approximately the temperature at which the cooling rate becomes comparable to the rate of exchange between the orientations. Assuming a cooling rate of 1 K s^{-1}, and substituting this for R_{exch} in equation (2), suggests the complex will be 'frozen' into a particular distribution of orientations at $T \approx 27$K, the estimate being quite insensitive to the rate of cooling. In agreement with this, the single-crystal EPR spectra measured at X-band frequency at ≈10 K still showed two signals for most orientations of the magnetic field, though these were no longer equal in intensity. The relative intensity of each signal is expected to be proportional to the fractional number of complexes having that orientation, so that the ratio of the intensities is equal to the ratio P of the populations of the two states. When the complexes are in equilibrium, P depends upon the energy difference ΔE between the two states *via* expression (3).[29] The spectra when the magnetic field is approximately

$$P = \exp(\Delta E/RT) \quad (3)$$

parallel to the Cu–N(21) and Cu–N(31) directions are shown in Fig. 5, from which it may be seen that the signal corresponding to $g = 2.25$ is relatively more intense than that at $g = 2.09$ for one direction of the magnetic field, while the reverse is true for

† Note that the frequency ω in ref. 27 is given in rad s^{-1}. This may be converted into the frequency in Hz, ν, *via* the relationship $\omega = 2\pi\nu$.

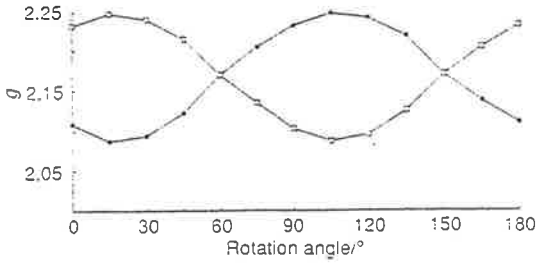

Fig. 3 Plot of g_1 (■) and g_2 (□) as a function of the rotation of the direction of the magnetic field in the plane normal to the Cu–N(11) direction in a crystal of $[Cu\{P(C_5H_4N)_3\}_2]Br_2\cdot 8H_2O$ at 77 K

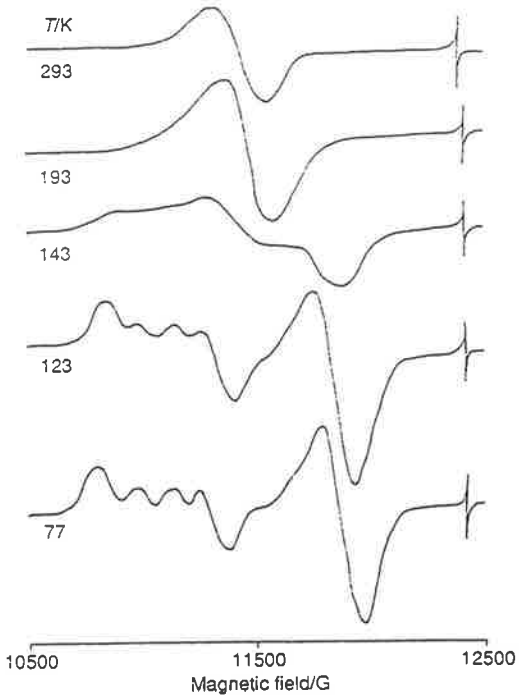

Fig. 4 Q-Band EPR spectra at various temperatures of a crystal of $[Cu\{P(C_5H_4N)_3\}_2]Br_2\cdot 8H_2O$ with the magnetic field parallel to the Cu–N(21) or Cu–N(31) direction. The weak, sharp resonance at ≈0.13 T is due to finely ground diphenylpicrylhydrazyl (dpph)

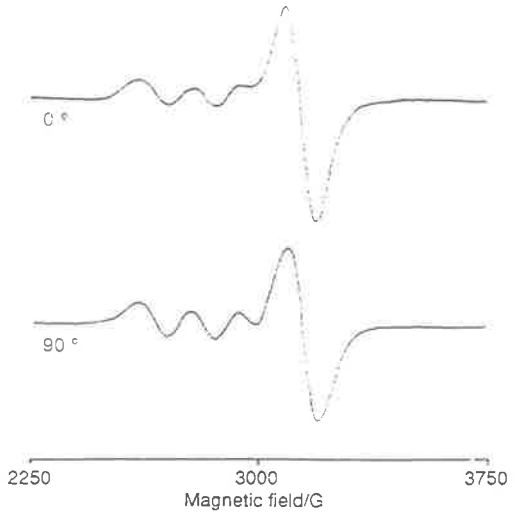

Fig. 5 X-Band EPR spectra of a crystal of $[Cu\{P(C_5H_4N)_3\}_2]Br_2 \cdot 8H_2O$ with the magnetic field parallel to the Cu–N(21) and Cu–N(31) directions (which orientation corresponds to which direction is unknown)

the other. Unfortunately, because of the poorly defined morphology of the crystals, it was not possible to determine which signal is associated with each bond direction. The ratio of the intensities was estimated to be ≈0.83:1 and substitution of this in equation (3) together with the temperature $T \approx 27$ K at which the complexes are 'frozen' into the two states yields the value $\Delta E \approx 3.5$ K for the energy difference between the orientational isomers. A similar slight intensity difference between the signals was still apparent in the spectra measured at 77 K. The ratio of signal intensities was ≈0.93:1 and substitution into equation (3) yields $\Delta E \approx 3.9$ K. Considering the rather large uncertainties involved, the self-consistency of the two estimates is pleasing.

The temperature dependence observed for the EPR spectrum of a powdered sample of $[Zn\{P(C_5H_4N)_3\}_2]Br_2 \cdot 8H_2O$ doped with ≈1% Cu^{2+} is quite similar to that of the pure compound, except that a change from the pattern associated with a 'reversed' to a 'normal' g tensor occurred at ≈50 K. The spectra observed at Q band at 293 and 77 K, and at X band over the range 120–20 K, are shown in Fig. 6. The Q-band spectra yield the values $g_{\parallel} = 2.042$, $g_{\perp} = 2.165$ for the high-temperature exchange-narrowed g tensor. For the low-temperature spectrum, only the highest g value may be resolved at $g = 2.255$; the resonances due to the other two g values presumably contribute to the broad inflection at ≈0.34 T (Fig. 6). Assuming that the $g_{\perp}$ signal in the exchange-narrowed spectrum splits symmetrically in the low-temperature spectrum, while the lowest g value is temperature independent, leads to the estimates $g_1 = 2.04$, $g_2 = 2.08$, $g_3 = 2.26$ for the molecular g values of Cu^{2+}-doped $[Zn\{P(C_5H_4N)_3\}_2]Br_2 \cdot 8H_2O$, these being virtually identical to those of the pure copper(II) complex. Hyperfine splittings of 85×10^{-4} and 160×10^{-4} cm^{-1} were observed above and below the transition temperature, the latter being identical to that seen for the pure complex, and very similar to the values observed for analogous complexes with tetragonally elongated octahedral geometries.[6,7] At low temperature additional structure was observed, presumably due to coupling with the nitrogen nuclei, but this was too poorly resolved to be worthy of analysis (Fig. 6). Substitution of the appropriate parameters $g_2 = 2.08$, $g_3 = 2.26$, $T = 50$, $B = 0.33$T into equations (1) and (2) yields the value $\Delta E^* \approx 220$ cm^{-1} for the activation energy of the interchange of the long and intermediate bond directions for the copper(II) guest complex.

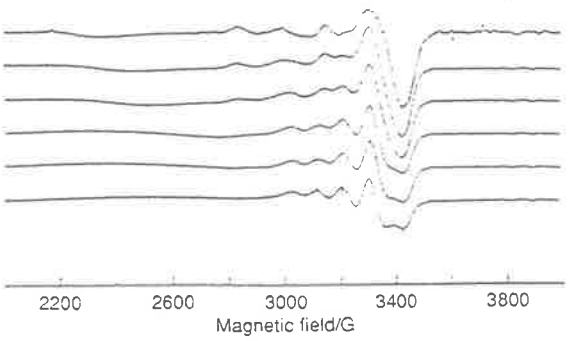

Fig. 6 X-Band EPR spectra of a powder of $[Zn\{P(C_5H_4N)_3\}_2]Br_2 \cdot 8H_2O$ doped with ≈1% Cu^{2+} measured at temperatures of (from top to bottom) 20, 40, 50, 60, 80 and 120 K

This is considerably lower than the corresponding value for the pure copper(II) compound, and the possible reasons are discussed in the following section.

Potential Surface of the Complex.—The energy levels of a six-co-ordinate copper(II) complex are conventionally described in terms of the coupling between the ^2E_g electronic state and the e_g Jahn–Teller active vibration.[15] To first order, a complex with six identical ligands undergoes a radial distortion ρ in the e_g mode to yield the 'Mexican hat' potential surface shown in Fig. 7(*a*). Here, E_{JT} represents the Jahn–Teller stabilisation energy. At this level of approximation, the Q_θ and Q_ε components of the vibration, pictured in Fig. 7(*b*), are equivalent, and the energy minimum is a circular well of radius ρ with the geometry and concomitant electronic wavefunction specified by the angle φ. Higher-order effects distort this surface, producing three minima which almost invariably occur at φ = 0, 120 and 240°, corresponding to octahedral geometries tetragonally elongated along z, x and y, respectively, and the unpaired electron in a $d_{x^2-y^2}$ type orbital. Saddlepoints corresponding to compressed tetragonal geometries, and d_{z^2} type electronic wavefunctions, occur at φ = 60, 180 and 300°, the energy difference between the minima and saddlepoints being defined as 2β. When the ligands are inequivalent, either inherently or due to interactions with the surrounding crystal lattice, this is normally expressed by a 'strain' characterised by axial and equatorial components S_θ and S_ε, respectively. The strain shifts both the positions and relative energies of the minima, and it is the dynamic equilibrium between the vibronic levels of such surfaces that gives rise to temperature-dependent effects of the kind discussed here.[15] A model based on these concepts has been able to account quantitatively for the temperature dependence of the EPR spectra and geometries of a range of dynamic copper(II) complexes,[16–20] and it is of interest to apply this to the present complex.

The procedure used to calculate the potential surface has been described in detail previously.[16–18] The basic potential surface of the $[Cu\{P(C_5H_4N)_3\}_2]^{2+}$ complex is best defined by considering the g values at low temperature. Although in principle the metal hyperfine parameters may be treated in a similar fashion, here the interpretation is complicated by the fact that these depend not only on the orbital angular momentum of the unpaired electron, but also on the 'contact' interaction between the s-electron density and the nuclear spin. Since the primary interest is in the dynamics of the system the hyperfine coupling has therefore not been considered in the present treatment.

The overall Jahn–Teller distortion is largely decided by the balance between the force constant f of the e_g mode and the linear coupling constant A_1. For the present complex the former was assumed to be similar to that reported[17] for the $[Cu(H_2O)_6]^{2+}$ ion, where $h\nu = 300$ cm^{-1}. Assuming that the distortion

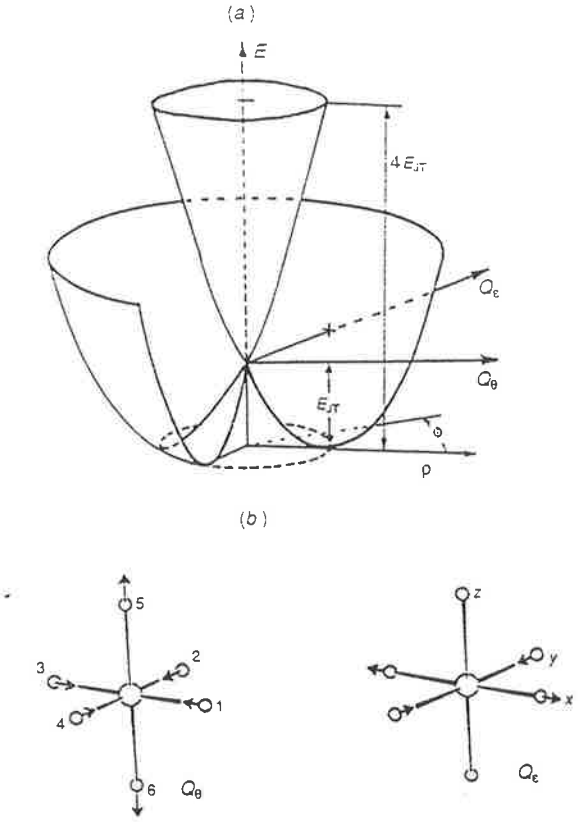

Fig. 7 (*a*) 'Mexican hat' potential surface formed by $e_g \times E_g$ Jahn–Teller coupling. (*b*) Form of the two components of the e_g Jahn–Teller active vibration

involves motion of the pyridine group as a whole, so that the effective mass M is 78, the energy of the e_g mode may be estimated as $h\nu = 140\ cm^{-1}$ from the relationship (4). The value

$$h\nu = \sqrt{(f/M)}/0.001\ 722 \qquad (4)$$

of A_1 may be obtained from the relationship (5) (see ref. 16 for a

$$A_1 = (2h\nu E_{JT})^{\frac{1}{2}} \qquad (5)$$

discussion of the units used to define the various parameters). The Jahn–Teller stabilisation energy E_{JT} [Fig. 7(*a*)] can be estimated approximately from the energy ΔE of the transition between the split levels of the ^2E_g state of the parent octahedral complex,[14] equation (6). The reflectance spectrum of

$$\Delta E \approx 4E_{JT} + 2|S_\theta| \qquad (6)$$

$[Cu\{P(C_5H_4N)_3\}_2]Br_2 \cdot 8H_2O$ is shown in Fig. 8. This consists of a band at 15 500 cm^{-1} with a shoulder at $\approx$ 17 000 cm^{-1} which may be assigned to transitions to the split components of the $^2T_{2g}$ level of the parent octahedral complex, and a shoulder at $\approx$8500 cm^{-1} which is due to the transition between the levels derived from the $d_{x^2-y^2}$ and d_{z^2} orbitals. The sharper peaks at lower energy are assigned as infrared overtones; similar peaks are observed in the reflectance spectrum of the corresponding zinc(II) compound (Fig. 8). Substitution of $\Delta E = 8500\ cm^{-1}$ into equation (6), and anticipating the value $S_\theta \approx -660\ cm^{-1}$, gives $E_{JT} = 1795\ cm^{-1}$, and substitution of this into equation (5) yields the estimate $A_1 = 700\ cm^{-1}$.

The position of the minimum in the 'trough' of the warped Mexican-hat potential surface depends upon the balance

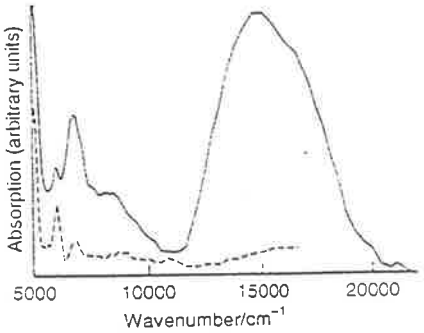

Fig. 8 Reflectance spectrum of powdered $[Cu\{P(C_5H_4N)_3\}_2]Br_2 \cdot 8H_2O$ at 293K (full line); the spectrum of $[Zn\{P(C_5H_4N)_3\}_2]Br_2 \cdot 8H_2O$ (dashed line) is shown in the lower-energy region to indicate the positions of the infrared overtones

between the lattice strain, which in the present case favours a compressed tetragonal geometry, and the warping parameter β, which is a measure of the tendency of the strain-free complex to prefer a tetragonally elongated geometry. It has been shown[30] that the former geometry will only become stable when $|S_\theta| > \approx 9\beta$. An axially symmetric strain of lower magnitude, relative to β, will produce a pair of equivalent minima each corresponding to an orthorhombic geometry.[30] The calculation of the low-temperature orthorhombic g tensor of $[Cu\{P(C_5H_4N)_3\}_2]Br_2 \cdot 8H_2O$ thus provides a means of estimating the ratio of S_θ to β reasonably accurately. The absolute values of the parameters may be obtained only approximately. For the pure complex the large activation energy for the exchange between the two lowest vibronic wavefunctions, $\approx$600 cm^{-1}, indicates a high degree of warping of the potential surface, with $\beta > \approx 300\ cm^{-1}$ (the barrier height for a warped potential surface in the absence of lattice strain effects is $\approx 2\beta$). The axial strain S_θ acts along the Cu–N(11) direction, and raises in energy the third minimum in the potential surface, that which corresponds to the long bonds of the tetragonally elongated complex lying along this direction. As thermal population of the well would cause an increase in the g value along this bond direction, its temperature invariance over the range 4–293 K provides a lower limit of $\approx -400\ cm^{-1}$ for the parameter S_θ (the negative sign corresponds to a compression). The parameter S_ε represents the amount by which lattice interactions render the other two minima in the surface inequivalent in energy. These correspond to the long Cu–N bonds occurring to N(21) and N(31), and *vice versa*, and as this energy difference is very small, $\approx 4\ cm^{-1}$, S_ε must also be quite modest, $\approx 2\ cm^{-1}$.

Reasonable agreement with the experimental data is obtained with vibronic wavefunctions calculated using the values $\beta = 507\ cm^{-1}$, $S_\theta = -660$ and $S_\varepsilon = 3\ cm^{-1}$. The g values of the lowest vibronic level, $g_1 = 2.054\ (2.04)$, $g_2 = 2.080\ (2.09)$, $g_3 = 2.251\ (2.25)$, agree well with the experimental values (in parentheses) of the more intense set of signals observed at low temperature. The effects of covalency were included by means of orbital-reduction parameters $k_1 = 0.84$, $k_2 = 0.83$, $k_3 = 0.74$. The electronic components of the vibronic wavefunctions are linear combinations of the $d_{x^2-y^2}$ and d_{z^2} orbitals $ad_{x^2-y^2} - bd_{z^2}$, and the resulting wavefunctions are of the form[31] (7). The

$$\Psi = cx^2 + ey^2 + fz^2 \qquad (7)$$

expectation values of the squares of the parameters c, e and f normalised to unity give the relative probability that the unpaired electron will be found along the x, y or z cartesian axis. For the lowest wavefunction the parameters are $\langle c^2 \rangle = 0.0026$, $\langle e^2 \rangle = 0.4664$ and $\langle f^2 \rangle = 0.5310$ so that the unpaired electron essentially occupies a $d_{z^2-y^2}$ orbital, with a slight admixture of d_{x^2}. The unconventional labelling of the orbitals

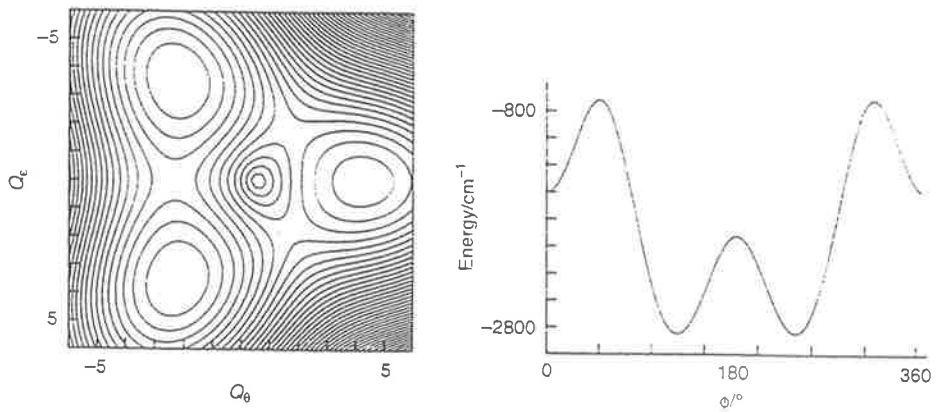

Fig. 9 Left: contour energy plot of the lower region of the potential surface calculated for $[Cu\{P(C_5H_4N)_3\}_2]Br_2\cdot 8H_2O$ (the spacing between each curve represents 100 cm^{-1} and Q_θ and Q_ϵ have dimensionless units; see ref. 18). Right: variation of the potential energy as a function of co-ordination geometry at a fixed Jahn–Teller radius (see text for details). The parameters defining the potential surface are: $A_1 = 700$ cm^{-1}, $\beta = 505$ cm^{-1}, $S_\theta = -660$ cm^{-1}, $S_\epsilon = 3$ cm^{-1}, $h\nu = 140$ cm^{-1}, $M = 78$

occurs because z defines the symmetry axis of the axial strain. Since this corresponds to a compression it is expected to coincide with the direction of the shortest Cu–N bond, Cu–N(11). The bond lengths calculated as described previously[19,20] (1.98, 2.04, 2.37 Å) represent only approximate estimates, since these depend upon the ligand mass. This was taken as that of a single pyridine group, 78, and coupling with internal vibrations of the tripod ligand was ignored. Nevertheless, the calculated value of Cu–N(11) agrees reasonably well with that observed experimentally, 2.002 Å, while the average calculated for the two longer bonds, 2.20 Å, is similar to the distances observed for Cu–N(21) and Cu–N(31), 2.189 and 2.191 Å.

The second lowest level lies at 4.8 cm^{-1}, with g values which are essentially identical to those of the lowest level, but with g_2 and g_3 reversed. These correspond to the values derived from the less-intense set of signals observed at low temperature (values in parentheses). The electronic wavefunction parameters $\langle c^2\rangle = 0.4662$, $\langle e^2\rangle = 0.0026$ and $\langle f^2\rangle = 0.5312$ conform to this pattern, with the magnitudes of $\langle c^2\rangle$ and $\langle e^2\rangle$ being interchanged, as do the calculated bond lengths.

A contour-energy plot of the lower region of the potential surface, and the variation of the energy minimum as a function of the angle φ at a constant Jahn–Teller radius $\rho = A_1/h\nu$, are shown in Fig. 9. The high value of β means that the surface is strongly warped, with the lower-energy vibronic wavefunctions highly localised in the minima. The barrier height between the lower pair of minima is very high, which is consistent with the activation energy for exchange between the two lowest wavefunctions, $\Delta E^* \approx 600$ cm^{-1}. In agreement with this, the first vibronic wavefunction to be significantly delocalised over the two lower minima occurred at ≈ 700 cm^{-1}.

The g values of the $[Cu\{P(C_5H_4N)_3\}_2]^{2+}$ complex formed when Cu^{2+} is doped into $[Zn\{P(C_5H_4N)_3\}_2]Br_2\cdot 8H_2O$ are essentially identical to those of the pure compound, implying that the lowest pair of vibronic wavefunctions are very similar in the two lattices. However, exchange between these involves a much lower activation energy, $\Delta E^* \approx 220$ cm^{-1}, for the 'doped' complex, suggesting that here delocalisation of the vibronic wavefunctions occurs at significantly lower energy. One factor contributing to this is the higher symmetry of the zinc(II) lattice. Since the Zn–N(21) and Zn–N(31) bonds are crystallographically equivalent the orthorhombic component of the lattice strain is formally zero. In the absence of random strains due to lattice imperfections, this means that even the lowest pair of vibronic wavefunctions are delocalised over the two minima. In practice, as first recognised by Ham,[32] small random strains make the wells at each lattice site inequivalent, and act to localise the vibronic wavefunctions. Little experimental evidence is available on the size of the random strains present in different lattices, and estimates have ranged from ≈ 1.5 to 10^{-5} cm^{-1}.[18,32] To investigate this point, it was assumed that the random strains could be represented by a single average value, and calculations were performed for S_ϵ ranging from 2 to 10^{-5} cm^{-1} with all other parameters identical to those used for pure $[Cu\{P(C_5H_4N)_3\}_2]Br_2\cdot 8H_2O$. For the lowest pair of levels, for all values of S_ϵ the vibronic wavefunctions were strongly localised, one in each of the two lower wells of the potential surface, and g values similar to those observed experimentally were obtained in each case. However, for very small of values the random strain, delocalisation over the two lowest minima in the potential surface occurred for quite low-lying upper vibronic levels. For $S_\epsilon = 10^{-5}$ cm^{-1}, the first significantly delocalised level occurred at 237 cm^{-1}, quite similar to the activation energy $\Delta E^* \approx 220$ cm^{-1} estimated for the rate of exchange between the lowest pair of levels in the Cu^{2+}-doped complex.

Plots of the square of the vibrational part of the vibronic wavefunctions are shown for the first, second, seventh and eighth vibronic wavefunctions, calculated on the one hand using the value of the orthorhombic strain, $S_\epsilon = 3$ cm^{-1}, estimated for pure $[Cu\{P(C_5H_4N)_3\}_2]Br_2\cdot 8H_2O$ [Fig. 10(*a*)], and on the other using an estimate of $S_\epsilon = 10^{-5}$ cm^{-1} to represent the random strains present in Cu^{2+}-doped $[Zn\{P(C_5H_4N)_3\}_2]Br_2\cdot 8H_2O$ [Fig. 10(*b*)]. For the pure copper compound, the wavefunctions are highly localised, with the maxima alternating in the two wells as the energy increases. For the doped complex, while the lower pair of levels are strongly localised, the seventh and eighth wells are significantly delocalised. Thus, the lower energy barrier to the interchange between the 'structural isomers' in the doped complex, compared with the pure compound, is most likely due to the greater delocalisation of the upper vibronic wavefunctions which occurs when the orthorhombic component of the lattice strain is very small.

It is to be expected that a broadly similar lattice strain to that which acts on the guest copper(II) complex will also be present in the zinc(II) compound. Assuming a similar energy for the e_g vibration, and correcting for the difference in average metal–ligand bond distance, the estimate $S_\theta = -660$ cm^{-1} derived from the above analysis of the EPR spectrum implies the bond lengths Zn–N 2.145 (×2), 2.190 (×4) Å for the corresponding zinc compound, in excellent agreement with the values observed crystallographically, Zn–N(11) 2.150(3) (×2), Zn–N(12) 2.187(3) (×4) Å. The same value of S_θ was derived for the pure and doped copper(II) complexes, and this confirms that despite

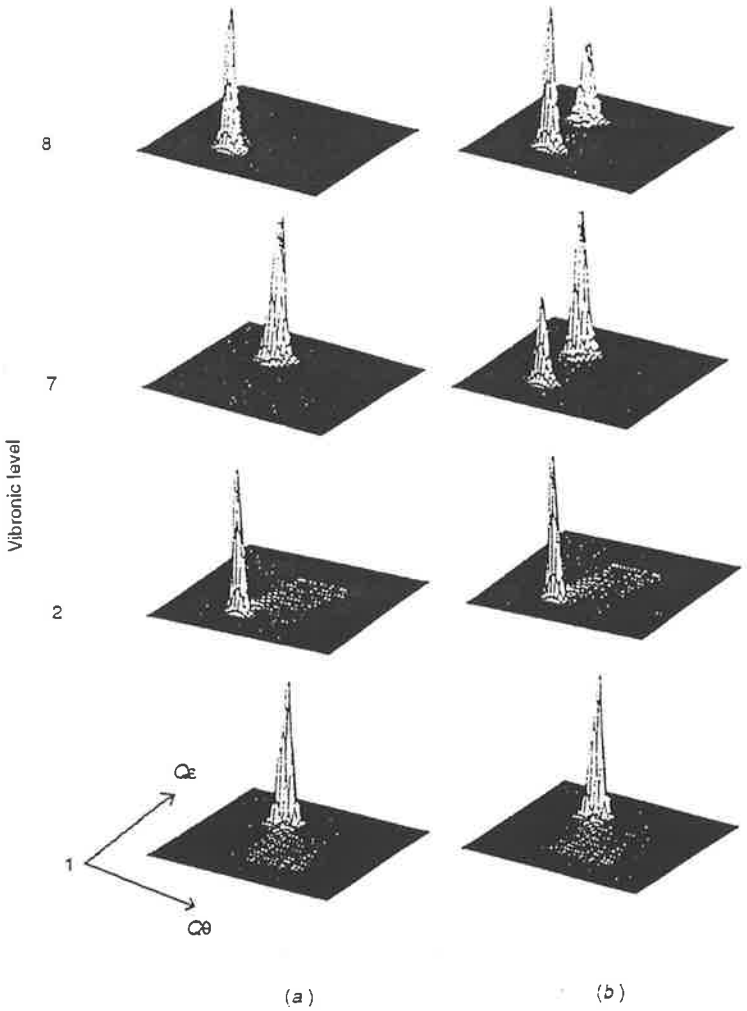

Fig. 10 Plots of the square of the vibrational part of the vibronic wavefunctions for the first, second, seventh and eighth levels of (*a*) $[Cu\{P(C_5H_4N)_3\}_2]Br_2\cdot 8H_2O$ and (*b*) the copper complex in Cu^{2+}-doped $[Zn\{P(C_5H_4N)_3\}_2]Br_2\cdot 8H_2O$

the difference in the crystal structure the lattice interactions in the copper(II) and zinc(II) compounds are very similar.

Bonding Parameters.—The above model implies that at the local level each complex in $[Cu\{P(C_5H_4N)_3\}_2]Br_2\cdot 8H_2O$ has a tetragonally elongated octahedral geometry, with a slight orthorhombic distortion, rather than the compressed tetragonal geometry indicated by the X-ray diffraction results, and it is of interest to consider the implications of this on the metal–ligand interactions. These are conveniently described using the angular overlap model of the bonding in metal complexes.[33] The transition energies expected for the complex were investigated using the computer program CAMMAG developed by Gerloch and co-workers.[34] This calculates the transition energies by assigning angular overlap model σ- and π-bonding parameters e_σ, $e_{\pi x}$, $e_{\pi y}$ to each ligand, and summing the metal–ligand interactions using an angular-overlap matrix defined by the crystal structure of the complex. In the present case, the structure was assumed to be similar to that of the complex in $[Cu\{CH(C_5H_4N)(pz)_2\}_2][NO_3]_2$, where the Cu–N bond distances[6] are quite close to those derived for $[Cu\{P(C_5H_4N)_3\}_2]Br_2\cdot 8H_2O$ in the above calculations. Bonding parameters based upon those reported[13] for the pyridine groups in the complex $[Cu\{CH(C_5H_4N)_3\}_2][NO_3]_2$, $e_\sigma = 5800\ cm^{-1}$, $e_{\pi y} = 900\ cm^{-1}$, were used in the calculation. These values relate to a Cu–N bond length of 2.04 Å, and to take into account the somewhat different geometry of the present complex it was assumed the bonding parameters are inversely proportional to the fifth power of the metal–ligand bond distance, as in other studies.[33] For the disordered Cu–N bonds, the distances derived in the calculations (2.038 and 2.365 Å) were used to make these corrections. The $e_{\pi x}$ parameter, which defines the π bonding in the plane of the pyridine ring, was assumed negligible, as in studies with other similar ligands.[6,13] An additional parameter e_{4s} to describe the configuration interaction with the metal 4s orbital,[36] was used. This was set to one quarter the value of e_σ, the approximate ratio observed for a range of planar complexes.[35] The following calculated transition energies are reasonably close to those observed experimentally (given in parentheses): 7500 (7800); 15 050 (15 500); 17 300, 18 200 (18 000) cm^{-1}. The g values $g_1 = 2.040$, $g_2 = 2.066$, $g_3 = 2.235$, calculated using an isotropic orbital reduction parameter $k = 0.80$ and effective spin–orbit coupling constant $\lambda = 590\ cm^{-1}$, are also in reasonable agreement with the experimental values ($g_1 = 2.04$, $g_2 = 2.09$, $g_3 = 2.25$). Moreover, the bonding parameters derived for the ligand are quite similar to those estimated for pyridine groups in analogous tripod ligands.[6,13] It should be noted that transition energies calculated in an analogous manner, but using the bond lengths of the compressed tetragonal geometry

implied by the crystal structure of the complex (4600; 13 600; 15 600, 16 500 cm^{-1}), are in poor agreement with those observed experimentally. The angular overlap model calculations thus confirm the conclusions of the above model, that at the local level the copper(II) complex in $[Cu\{P(C_5H_4N)_3\}_2]Br_2 \cdot 8H_2O$ has a tetragonally elongated octahedral geometry, rather than the tetragonally compressed geometry implied by the crystal-structure analysis.

Conclusion

Although the crystal structure of $[Cu\{P(C_5H_4N)_3\}_2]Br_2 \cdot 8H_2O$ measured at 173 K indicates Cu–N bond distances which imply a tetragonally compressed octahedral co-ordination geometry, the EPR spectrum suggests that at the local level each complex has a tetragonally elongated octahedral geometry with a slight orthorhombic distortion. The shortest Cu–N bonds always occur to one pair of nitrogen atoms, but the intermediate and long Cu–N bonds are randomly distributed between the other two pairs of nitrogen atoms. The two arrangements of the copper(II) complex differ in energy by only ≈ 4 cm^{-1}, so that at temperatures above ≈ 100 K the number of complexes adopting each orientation is almost equal, and it is the *average* of the two bond lengths which is observed in the crystal-structure analysis. The energy barrier to 'switching' of the two pairs of bonds is quite high, ≈ 600 cm^{-1}, so that on cooling to below ≈ 27 K complexes in the higher-energy orientation become 'frozen' into this orientation. The crystal structure of $[Zn\{P(C_5H_4N)_3\}_2]Br_2 \cdot 8H_2O$ is similar to that of the corresponding copper(II) compound in that two Zn–N bonds are shorter than the other four, but in this case the four longer bonds are crystallographically equivalent. At low temperature the g values of the copper(II) complex formed by doping $\approx 1\%$ Cu^{2+} into the zinc(II) compound are identical to those of the pure compound, suggesting a similar geometry for the 'guest' copper complex. However, the energy barrier to interchange of the two possible orientations of this guest complex is considerably smaller than that for the pure compound. This is probably because the very small energy difference between the orientations at any particular site, produced by random strains in the lattice, causes significant delocalisation of low-lying vibronic wavefunctions.

Acknowledgements

We are grateful to Mr. Richard Bowen and Dr. Sue Berners-Price (Griffith University, Brisbane) for a gift of a sample of tris(2-pyridyl)phosphine. Dr. Malcolm Gerloch of the University of Cambridge is thanked for making available the computer program CAMMAG. The assistance of Dr. Barry O'Grady of the University of Tasmania in estimating the rate of exchange between the structural isomers is gratefully acknowledged. Financial support (to M. A. H., J. P., F. R. K. and E. R. T. T.) was provided by the Australian Research Council.

References

1 S. Trofimenco, *Chem. Rev.*, 1972, **72**, 497; *Prog. Inorg. Chem.*, 1986, **34**, 115.
2 T. A. Hafeli and F. R. Keene, *Aust. J. Chem.*, 1988, **41**, 1379.
3 P. S. Moritz, A. A. Diamantis, F. R. Keene, M. R. Snow and E. R. T. Tiekink, *Aust. J. Chem.*, 1988, **41**, 1352.
4 F. R. Keene, M. R. Snow, P. J. Stephenson and E. R. T. Tiekink, *Inorg. Chem.*, 1988, **27**, 2040.
5 P. A. Anderson, F. R. Keene, E. Horn and E. R. T. Tiekink, *Appl. Organomet. Chem.*, 1990, **4**, 523.
6 T. Astley, A. J. Canty, M. A. Hitchman, G. L. Rowbottom, B. W. Skelton and A. H. White, *J. Chem. Soc., Dalton Trans.*, 1991, 1981.
7 T. Astley, J. M. Gulbis, M. A. Hitchman and E. R. T. Tiekink, *J. Chem. Soc., Dalton Trans.*, 1993, 509.
8 See B. J. Hathaway, *Struct. Bonding (Berlin)*, 1984, **57**, 55.
9 K. Knox, *J. Chem. Phys.*, 1959, **30**, 991.
10 C. Friebel and D. Reinen, *Z. Anorg. Allg. Chem.*, 1974, **407**, 193.
11 H. Stratemeier, B. Wagner, E. R. Krausz, R. Lindner, H.-H. Schmidtke, J. Pebler, W. E. Hatfield, L. ter Haar, D. Reinen and M. A. Hitchman, *Inorg. Chem.*, 1994, **33**, 2320.
12 P. J. Ellis, H. C. Freeman, M. A. Hitchman, D. Reinen and B. Wagner, *Inorg. Chem.*, 1994, **33**, 1249.
13 T. Astley, P. J. Ellis, H. C. Freeman, M. A. Hitchman, F. R. Keene and E. R. T. Tiekink, *J. Chem. Soc., Dalton Trans.*, 1995, 595.
14 D. Reinen and M. Atanasov, *Magn. Reson. Rev.*, 1991, **15**, 167.
15 M. A. Hitchman, *Comments Inorg. Chem.*, 1994, **15**, 197.
16 M. J. Riley, M. A. Hitchman and D. Reinen, *Chem. Phys.*, 1986, **102**, 11.
17 M. J. Riley, M. A. Hitchman and A. wan Mohammed, *J. Chem. Phys.*, 1987, **87**, 3766.
18 M. J. Riley, M. A. Hitchman, D. Reinen and G. Steffen, *Inorg. Chem.*, 1988, **27**, 1924.
19 J. Bebendorf, H. B. Bürgi, E. Gamp, M. A. Hitchman, D. Reinen, M. J. Riley and H. Stratemeier, unpublished work.
20 C. J. Simmons, M. A. Hitchman, H. Stratemeier and A. J. Schultz, *J. Am. Chem. Soc.*, 1993, **115**, 11304.
21 R. J. Bowen, S. Berners-Price and I. D. Jenkins, unpublished work.
22 N. Walker and D. Stuart, *Acta Crystallogr., Sect. A*, 1983, **39**, 158.
23 TEXSAN, Structure Analysis Package, Molecular Structure Corporation, Houston, TX, 1992.
24 C. K. Johnson, ORTEP II, ORNL Report 5136, Oak Ridge National Laboratory, Oak Ridge, TN, 1976.
25 G. Wingefeld and R. Hoppe, *Z. Anorg. Allg. Chem.*, 1984, **516**, 223.
26 M. Atanasov, M. A. Hitchman, R. Hoppe, K. S. Murray, B. Mourbaraki, D. Reinen and H. Stratemeier, *Inorg. Chem.*, 1993, **32**, 3397.
27 A. Carrington and A. D. McLachlan, *Introduction to Magnetic Resonance*, Harper and Row, New York, 1967, p. 207.
28 K. J. Laidler, *Chemical Kinetics*, 3rd edn., Harper and Row, New York, 1987, p. 94.
29 B. Silver and D. Getz, *J. Chem. Phys.*, 1974, **61**, 638.
30 D. Reinen and S. Krause, *Inorg. Chem.*, 1980, **20**, 2750.
31 M. A. Hitchman, *J. Chem. Soc. A*, 1970, 4.
32 F. S. Ham, *Phys. Rev. A*, 1965, **138**, 1727; 1968, **166**, 307.
33 C. E. Schäffer, *Pure Appl. Chem.*, 1970, **24**, 361 and refs. therein.
34 D. A. Cruse, J. E. Davies, M. Gerloch, J. H. Harding, D. J. Mackey and R. F. McMeecking, CAMMAG, A FORTRAN Computing Package, University Chemical Laboratory, Cambridge, 1979.
35 M. A. Hitchman, *Inorg. Chem.*, 1982, **21**, 821.
36 D. W. Smith, *Inorg. Chim. Acta*, 1977, **22**, 107.
37 R. G. McDonald and M. A. Hitchman, *Inorg. Chem.*, 1990, **29**, 3081 and refs. therein.

Received 9th May 1995; *Paper* 5/02929E

Structural, spectroscopic and angular-overlap studies of tripodal pyridine ligands with nickel(II) and zinc(II)

Timothy Astley,*[†,a] Michael A. Hitchman,[a] F. Richard Keene[b] and Edward R. T. Tiekink[c]

[a] *Chemistry Department, University of Tasmania, Hobart, Tasmania 7001, Australia*
[b] *Department of Molecular Sciences, James Cook University of North Queensland, Townsville, Queensland 4811, Australia*
[c] *Department of Chemistry, The University of Adelaide, Adelaide, South Australia 5005, Australia*

Zinc(II) and nickel(II) complexes $[M\{X(C_5H_4N)_3\}_2]^{2+}$, where $X(C_5H_4N)_3$ are symmetrical tripodal nitrogen-donor ligands with X = CH, N or P, have been prepared and examined by single-crystal X-ray diffraction and single-crystal electronic spectroscopy. The structural studies, and the application of the angular overlap model to the spectroscopic results, confirm previous results on the bonding characteristics of pyridine and provide a unique way of establishing the effect of the bridgehead atom, X. The cations are all centrosymmetric with the ligand 'bite' angles N–M–N 85.2(1)–88.5(2)°, resulting in a slight trigonal distortion from octahedral geometry. The ligand fields in the three nickel compounds are very similar and the large ligand-field splitting is consistent with the rather short metal–nitrogen bond lengths. The pyridine groups act as moderately strong σ-donor and weak π-donor ligands, with no evidence of conjugation of the π system across the bridgehead atom. The crystal structure of $[Ni\{CH(C_5H_4N)_3\}_2][NO_3]_2$ shows the complex cation to have crystallographic $\bar{3}$ symmetry such that there is one independent Ni–N interaction of 2.069(2) Å. The corresponding zinc complex, isolated as its dibromide nonahydrate salt, has crystallographic 2/*m* symmetry with two Zn–N contacts of 2.123(5) Å being shorter than the others, *i.e.* 2.141(3) Å. In the phosphine analogue, $[Zn\{P(C_5H_4N)_3\}_2]^{2+}$, isolated as its diperchlorate monohydrate salt, the Zn^{2+} cation is situated on a site of symmetry $\bar{1}$ with one Zn–N distance [2.145(4) Å] being shorter than the other two, 2.162(4) and 2.173(4) Å. Small trigonal distortions from the ideal octahedral geometry are due to the restricted bite distances of the tripodal ligands.

Recent work from our laboratories has concentrated on furthering understanding of the bonding properties of polydentate ligands containing heterocycles, especially pyridine and pyrazole.[1,2] For ligands of the type $(pz)_3CH$, where pz = pyrazol-1-yl, it was found[2] that there is no evidence of conjugation between the heterocyclic rings. The high ligand-field strength of $(pz)_3CH$ was explained using the angular overlap model (AOM) as arising from the short metal–ligand bonds imposed by the tripodal nature of the ligand. As part of this study the compounds, tris(2-pyridyl)-methane, -phosphine and -amine have been synthesized. The complexes formed by $(NC_5H_4)_3CH$ enable a comparison of the bonding characteristics of pyrazole and pyridine. In addition, the analogous complexes formed by compounds in which the bridgehead atom is altered to P or N indicate the effect on the stereochemistry and bonding properties of an alteration of this feature.

Experimental

Tris(2-pyridyl)-methane, -phosphine and -amine were prepared using published methods.[3] The purity of the complexes was checked by microanalysis performed by the Central Science Laboratory, Hobart, Tasmania and Chemical and Micro Analytical Services Pty. Ltd., Melbourne, Victoria. Single-crystal and KBr disc electronic spectra were recorded using either a Cary 17 or 5 spectrophotometer as described in detail elsewhere,[4] with the samples cooled using a Cryodyne model 22C cryostat. Absorption coefficients were estimated by measuring the crystal thickness using a microscope with a graduated eyepiece. Reflectance spectra were recorded using a Beckmann DK-2A ratio recording spectrophotometer.

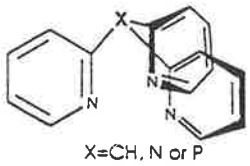

X=CH, N or P

Synthesis of metal(II) complexes

Bis[tris(2-pyridyl)methane]nickel(II) nitrate, $[Ni\{CH(C_5H_4N)_3\}_2][NO_3]_2$. A solution of $Ni(NO_3)_2{\cdot}6H_2O$ (145 mg, 0.5 mmol) in acetone (5 cm^3) was added dropwise to a stirred solution of tris(2-pyridyl)methane (250 mg, 1 mmol) in acetone (10 cm^3). The resulting suspension was cooled at 0 °C for 2 h, filtered, washed with acetone and air dried. Yield: 260 mg, 77%. Crystals were grown by liquid diffusion of a solution of the complex in acetonitrile layered on top of toluene (Found: C, 56.7; H, 3.95; N, 16.4. Calc. for $C_{32}H_{26}N_8NiO_6$: C, 56.7; H, 3.85; N, 16.5%).

Bis[tris(2-pyridyl)phosphine]nickel(II) nitrate, $[Ni\{P(C_5H_4N)_3\}_2][NO_3]_2{\cdot}H_2O$ and bis[tris(2-pyridyl)amine]nickel(II) perchlorate, $[Ni\{N(C_5H_4N)_3\}_2][ClO_4]_2{\cdot}2H_2O$. The nitrate salts were prepared in an analogous manner to that the $(NC_5H_4)_3CH$ complex (yields 73% and 70%, respectively) and the latter species was converted into the perchlorate salt by metathesis in aqueous solution (Found: C, 48.8; H, 3.15; N, 14.6. Calc. for $C_{30}H_{26}N_8NiO_2P_2$: C, 49.2; H, 3.60; N, 15.3. Found: C, 47.5; H, 3.20; N, 14.7. Calc. for $C_{30}H_{24}Cl_2N_8NiO_8$: C, 47.8; H, 3.20; N, 14.9%).

Bis[tris(2-pyridyl)methane]zinc(II) nitrate, $[Zn\{CH(C_5H_4)_3\}_2][NO_3]_2$. A solution of $Zn(NO_3)_2{\cdot}6H_2O$ (150 mg, 0.5

[†] *Present address:* Chemistry Department, University of Reading, Whiteknights Park, Reading RG6 2AD, UK.

mmol) in acetone (5 cm^3) was added dropwise to a stirred solution of tris(2-pyridyl)methane (250 mg, 1 mmol) in acetone (10 cm^3). The resulting suspension was cooled at 0 °C for 2 h, filtered, washed with acetone and air dried. Yield: 320 mg, 94%. A sample of the nitrate salt was converted into the bromide using anion-exchange chromatography, and crystals of $[Zn\{CH(C_5H_4N)_3\}_2]Br_2\cdot 9H_2O$ were grown by slow evaporation of an aqueous solution (Found: C, 43.2; H, 4.45; N, 9.2. Calc. for $C_{32}H_{44}Br_2N_6O_9Zn$: C, 43.6; H, 5.05; N, 9.5%).

The complex $[Zn\{P(C_5H_4N)_3\}_2][NO_3]_2$ was prepared in an analogous manner (yield: 340 mg, 95%). A sample of the nitrate salt was converted into the perchlorate by metathesis in aqueous solution, and crystals of $[Zn\{P(C_5H_4N)_3\}_2][ClO_4]_2\cdot H_2O$ were grown by slow evaporation of an aqueous solution (Found: C, 45.5; H, 3.00; N, 10.3.* Calc. for $C_{30}H_{24}Cl_2N_6O_8P_2Zn$: C, 45.3; H, 3.05; N, 10.6%).

Crystallography

Intensity data for a mauve crystal of $[Ni\{CH(C_5H_4N)_3\}_2][NO_3]_2$ (0.13 × 0.29 × 0.29 mm) and colourless crystals of $[Zn\{CH(C_5H_4N)_3\}_2]Br_2\cdot 9H_2O$ (0.13 × 0.24 × 0.40 mm) and $[Zn\{P(C_5H_4N)_3\}_2][ClO_4]_2\cdot H_2O$ (0.16 × 0.16 × 0.32 mm) were measured at 293 K on a Rigaku AFC6R diffractometer fitted with graphite-monochromatized Mo-Kα radiation, $\lambda = 0.710\,73$ Å; the ω–2θ scan technique was employed to measure data such that θ_{max} was 27.5°. No decomposition of the crystals occurred during their respective data collections and only absorption-corrected data [5] which satisfied the criterion $I \geqslant 3.0\sigma(I)$ were used in the subsequent analyses. Crystal data are summarized in Table 5.

Each structure was solved by heavy-atom methods and the remaining atoms located from subsequent difference maps; the structures were refined by a full-matrix least squares based on F,[6] such that the function minimized was $\Sigma w\Delta^2$ where w was the weight applied to each reflection and $\Delta = |F_o| - |F_c|$. Non-hydrogen atoms were refined with anisotropic thermal parameters, the only exception being for the isotropic refinement of the O(4) atom in $[Zn\{CH(C_5H_4N)_3\}_2]Br_2\cdot 9H_2O$; this atom was found to be disordered over the two-fold axis and was refined with 0.5:0.5 site occupancy. The H atoms were located from difference maps for the $(NC_5H_4)_3CH$ complexes and included in the models but not refined. In the case of the $P(C_5H_4N)_3$ complex the H atoms were included at their calculated positions (C–H 0.97 Å); water-bound hydrogen atoms were not located in the zinc complexes. At convergence $R = 0.043$ and $R' = 0.047$ (unit weights) for $[Ni\{CH(C_5H_4N)_3\}_2][NO_3]_2$, 0.041 and 0.051 [sigma weights, *i.e.* $1/\sigma^2(F)$] for $[Zn\{CH(C_5H_4N)_3\}_2]Br_2\cdot 9H_2O$ and 0.049 and 0.049 (unit weights) for $[Zn\{P(C_5H_4N)_3\}_2][ClO_4]_2\cdot H_2O$. No corrections were applied for extinction effects. Scattering factors for all atoms were those incorporated in the TEXSAN program. Fractional atomic coordinates are listed in Tables 6–8; structures were drawn with the ORTEP program.[7]

Complete atomic coordinates, thermal parameters and bond lengths and angles have been deposited at the Cambridge Crystallographic Data Centre. See Instructions for Authors, *J. Chem. Soc., Dalton Trans.*, 1996, Issue 1.

Results and Discussion

Crystal Structures of the complexes

The compounds are all quite different. Whilst they contain a basically similar cation $[ML_2]^{2+}$ each involves a different anion and has a varying degree of solvation, with the nickel(II) complex being unsolvated and the $[Zn\{CH(C_5H_4N)_3\}_2]Br_2$ compound having nine waters of solvation. In each case the metal lies on a crystallographic inversion centre. All structures are essentially ordered, without the disorder found in $[Cu\{CH(C_5H_4N)_3\}_2]^{2+}$ [8] and the complexes formed by bis(pyrazol-1-yl)(2-pyridyl)methane.[1]

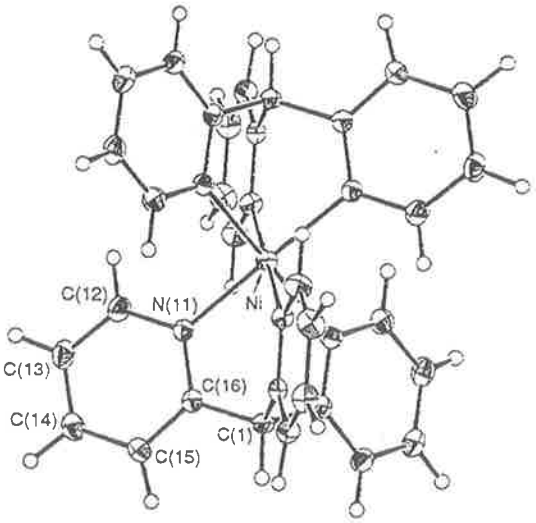

Fig. 1 Molecular structure and crystallographic numbering scheme for the cation in $[Ni\{CH(C_5H_4N)_3\}_2][NO_3]_2$

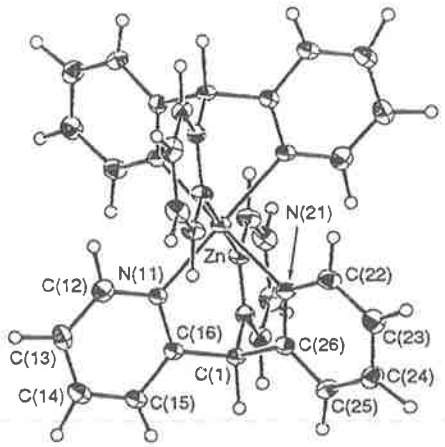

Fig. 2 Molecular structure and crystallographic numbering scheme for the cation in $[Zn\{CH(C_5H_4N)_3\}_2]Br_2\cdot 9H_2O$

The metal–pyridine bond lengths are significantly shorter than those in complexes involving monodentate pyridine ligands, 2.069(2) Å in the nickel compound for instance, compared with 2.14 Å.[9] However, they are comparable to those in $[M\{CH(C_5H_4N)(pz)_2\}_2][NO_3]_2$, where the Ni–N bond length is 2.076(5) Å.[1] For all of the complexes the 'bite' of the tripodal ligand and the ligand geometry results in an unsymmetrical orientation of each ring with respect to the M–N direction. In the $(NC_5H_4)_3CH$ complexes the M–N–C(6) angles are between 117.5(2) and 118.3(4)° and the M–N–C(2) angles are significantly larger, being between 123.2(3) and 128.8(2)°. This effect is not seen for the $P(C_5H_4N)_3$ complex [M–N–C(6) 120.4(3)–122.5(4), M–N–C(2) 120.5(4)–121.5(4)°] presumably because the larger size of the bridgehead atom allows the pyridine rings to orientate more directly along the M–N axis.

The average Zn–N bond lengths are considerably longer than those involving Ni, as expected from the ionic radii of the divalent metal ions. The planes of the amine rings make angles

* The freshly isolated crystal used in the crystal structure was the monohydrate; on a slightly longer time-scale it is clear that loss of the water of crystallization occurs from the sample, as it was analysed as the anhydrous salt.

Table 1 Selected bond distances (Å) and angles (°) for $[Ni\{CH(C_5H_4N)_3\}_2][NO_3]_2$

Ni–N(11)	2.069(2)	N(11)–C(12)	1.339(4)
N(11)–C(16)	1.335(4)	C(1)–C(16)	1.497(3)
C(12)–C(13)	1.348(5)	C(13)–C(14)	1.375(5)
C(14)–C(15)	1.370(5)	C(15)–C(16)	1.369(4)
N(1)–O(1)	1.235(3)		
N(11)–Ni–N(11^{I})	93.5(1)	Ni–N(11)–C(12)	123.8(2)
Ni–N(11)–C(16)	118.7(2)	C(12)–N(11)–C(16)	117.5(3)
C(16)–C(1)–C(16^{II})	111.3(2)	N(11)–C(12)–C(13)	123.5(3)
C(12)–C(13)–C(14)	118.9(3)	C(13)–C(14)–C(15)	118.6(3)
C(14)–C(15)–C(16)	119.4(3)	N(11)–C(16)–C(15)	122.1(3)
N(11)–C(16)–C(1)	116.6(3)	C(1)–C(16)–C(15)	121.2(3)

Symmetry operations: I $x - y, -1 + x, 2 - z$; II $1 - y, -1 + x, -y, z$.

Table 2 Selected bond distances (Å) and angles (°) for $[Zn\{CH(C_5H_4)_3\}_2]Br_2 \cdot 9H_2O$

Zn–N(11)	2.123(5)	Zn–N(21)	2.141(3)
N(11)–C(12)	1.320(8)	N(11)–C(16)	1.335(7)
N(21)–C(22)	1.320(5)	N(21)–C(26)	1.329(5)
C(1)–C(16)	1.505(8)	C(1)–C(26)	1.513(5)
C(12)–C(13)	1.366(9)	C(13)–C(14)	1.367(9)
C(14)–C(15)	1.357(9)	C(15)–C(16)	1.361(8)
C(22)–C(23)	1.358(6)	C(23)–C(24)	1.369(6)
C(24)–C(25)	1.364(6)	C(25)–C(26)	1.360(6)
N(11)–Zn–N(21)	85.3(1)	N(21)–Zn–N(21^{I})	86.1(2)
Zn–N(11)–C(12)	123.5(4)	Zn–N(11)–C(16)	118.3(4)
Zn–N(21)–C(22)	123.4(3)	Zn–N(21)–C(26)	118.1(3)
C(12)–N(11)–C(16)	118.2(5)	C(22)–N(21)–C(26)	118.4(4)
C(16)–C(1)–C(26)	111.8(3)	C(26)–C(1)–C(26^{I})	110.5(5)
N(11)–C(12)–C(13)	123.2(6)	C(12)–C(13)–C(14)	117.8(6)
C(13)–C(14)–C(15)	119.6(6)	C(14)–C(15)–C(16)	119.4(6)
N(11)–C(16)–C(1)	117.7(5)	N(11)–C(16)–C(15)	121.7(5)
C(1)–C(16)–C(15)	120.5(5)	N(21)–C(22)–C(23)	123.3(4)
C(22)–C(23)–C(24)	117.9(4)	C(23)–C(24)–C(25)	119.3(4)
C(24)–C(25)–C(26)	119.3(4)	N(21)–C(26)–C(1)	117.6(4)
N(21)–C(26)–C(25)	121.7(4)	C(1)–C(26)–C(25)	120.6(4)

Symmetry operation: I $x, -y, z$.

of ≈40° with those defined by the M–N bond vectors, resulting in a 'paddlewheel' conformation about the trigonal axis as found in the $(NC_5H_4)_3CH$ complexes.[2]

$[Ni\{CH(C_5H_4N)_3\}_2][NO_3]_2$. The structure of the cation is shown in Fig. 1 and selected interatomic parameters are listed in Table 1. The structure comprises discrete entities with the closest non-H interionic contact occurring between the O(1) and C(13) atoms of 3.290(5) Å. The structure is isomorphous with the copper(II) analogue[9] and the Ni^{2+} is situated on a crystallographic site of symmetry $\bar{3}$. The six Ni–N bonds are equivalent at 2.069(2) Å. The major distortion from the ideal octahedral geometry is found in the chelate angles of 86.5(1)° which arise as a result of the restricted bite angles of the $(NC_5H_4)_3CH$ ligand.

$[Zn\{CH(C_5H_4N)_3\}_2]Br_2 \cdot 9H_2O$. The structure of the cation is shown in Fig. 2 and selected interatomic parameters are listed in Table 2. The structure crystallizes in the monoclinic space group $C2/m$ with two complex cations, four bromides and eighteen water molecules of crystallization comprising the unit-cell contents. The Zn^{2+} cation is located on a site of symmetry $2/m$, the methine C(1) atom and pyridine ring N(11)–C(16) on a mirror plane, and the N(21)–C(26) ring in a general position. In the lattice there is, as expected, a complicated network of intermolecular contacts involving ions and water molecules. The Br atom forms four contacts with water molecules in the range 3.363(4)–3.480(5) Å and the closest contact involving water molecules, 2.734(8) Å, occurs between a pair of O(1) atoms. There are two independent Zn–N bond distances with Zn–N(11) 2.123(5) Å (× 2) being shorter than Zn–N(21) 2.141(3) Å (× 4) and the maximum deviation from octahedral geometry is manifested in the N(11)–Zn–N(21) angle of 85.3(1)°.

Table 3 Selected bond distances (Å) and angles (°) for $[Zn\{P(C_5H_4N)_3\}_2][ClO_4]_2 \cdot H_2O$

Zn–N(11)	2.162(4)	Zn–N(21)	2.145(4)
Zn–N(31)	2.173(4)	P(1)–C(16)	1.816(6)
P(1)–C(26)	1.824(6)	P(1)–C(36)	1.807(5)
N(11)–C(12)	1.326(7)	N(11)–C(16)	1.339(6)
N(21)–C(22)	1.331(7)	N(21)–C(26)	1.343(6)
N(31)–C(32)	1.313(7)	N(31)–C(36)	1.338(6)
C(12)–C(13)	1.365(8)	C(13)–C(14)	1.345(9)
C(14)–C(15)	1.365(9)	C(15)–C(16)	1.367(7)
C(22)–C(23)	1.356(8)	C(23)–C(24)	1.348(9)
C(24)–C(25)	1.367(9)	C(25)–C(26)	1.363(7)
C(32)–C(33)	1.352(8)	C(33)–C(34)	1.355(8)
C(34)–C(35)	1.363(8)	C(35)–C(36)	1.381(7)
Cl–O(1)	1.346(6)	Cl–O(2)	1.371(6)
Cl–O(3)	1.371(6)	Cl–O(4)	1.391(5)
N(11)–Zn–N(21)	87.8(2)	N(11)–Zn–N(31)	88.5(2)
N(21)–Zn–N(31)	87.8(2)	C(16)–P(1)–C(26)	99.2(2)
C(16)–P(1)–C(36)	103.0(2)	C(26)–P(1)–C(36)	100.9(2)
Zn–N(11)–C(12)	120.5(4)	Zn–N(11)–C(16)	122.1(3)
Zn–N(21)–C(22)	120.5(4)	Zn–N(21)–C(26)	122.5(4)
Zn–N(31)–C(32)	121.5(4)	Zn–N(31)–C(36)	120.4(3)
C(12)–N(11)–C(16)	117.2(5)	C(22)–N(21)–C(26)	116.9(5)
C(32)–N(31)–C(36)	117.9(5)	N(11)–C(12)–C(13)	123.1(5)
C(12)–C(13)–C(14)	118.9(6)	C(13)–C(14)–C(15)	119.6(6)
C(14)–C(15)–C(16)	118.6(6)	P(1)–C(16)–N(11)	121.4(4)
P(1)–C(16)–C(15)	116.1(4)	N(11)–C(16)–C(15)	122.5(5)
N(21)–C(22)–C(23)	122.9(6)	C(22)–C(23)–C(24)	119.7(6)
C(23)–C(24)–C(25)	118.9(6)	C(24)–C(25)–C(26)	118.9(6)
P(1)–C(26)–N(21)	121.1(4)	P(1)–C(26)–C(25)	116.2(4)
N(21)–C(26)–C(25)	122.7(5)	N(31)–C(32)–C(33)	124.1(5)
C(32)–C(33)–C(34)	118.6(6)	C(33)–C(34)–C(35)	119.1(5)
C(34)–C(35)–C(36)	119.3(5)	P(1)–C(36)–N(31)	123.2(4)
P(1)–C(36)–C(35)	115.8(4)	N(31)–C(36)–C(35)	121.0(5)

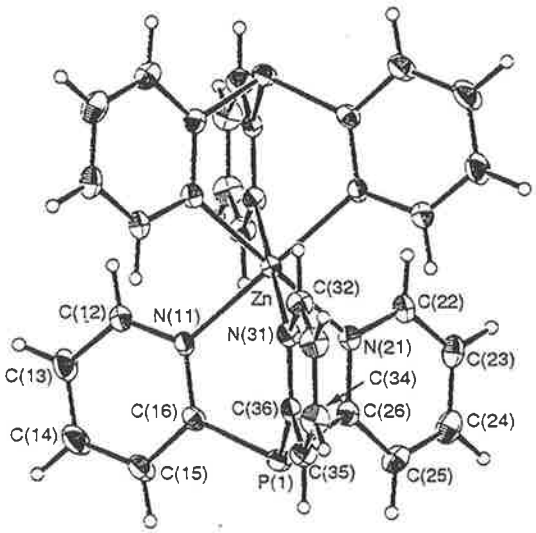

Fig. 3 Molecular structure and crystallographic numbering scheme for the cation in $[Zn\{P(C_5H_4N)_3\}_2][ClO_4]_2 \cdot H_2O$

$[Zn\{P(C_5H_4N)_3\}_2][ClO_4]_2 \cdot H_2O$. The structure of the cation is shown in Fig. 3 and interatomic parameters are listed in Table 3. The closest non-H contact in the lattice occurs between the O(5) and C(33′) atoms of 3.08(1) Å (symmetry operation: $\frac{1}{2} + x, \frac{1}{2} + y, 1 + z$). The cation is centrosymmetric with the

Zn–N(21) bond distance 2.145(4) Å being shorter than the others, *i.e.* Zn–N(11) 2.162(4) and Zn–N(31) 2.173(4) Å. The distortions from the ideal octahedral geometry are less in this complex, *i.e.* N(11)–Zn–N(21) is 87.8(2)°, owing to the longer P–C bonds.

Electronic spectra

The spectra of all complexes were recorded both as single crystals and KBr discs at room temperature (290 K) and ≈15 K. The room-temperature spectrum of $[Ni\{CH(C_5H_4N)_3\}_2]^{2+}$ (Fig. 4) consists of a highly asymmetric peak centred at ≈13 300 cm^{-1}, with a shoulder at ≈14 200 cm^{-1}, and two peaks at 21 300 and 22 370 cm^{-1}, with a shoulder at ≈19 000 cm^{-1}. At 15 K the peaks tend to move slightly to higher energy. The lowest-energy pair of peaks are assigned to the $^3T_{2g}$ level of the parent octahedral complex, split by low-symmetry components of the ligand field. The asymmetry of the peak at 13 300 cm^{-1} may be due to the close proximity of the spin-forbidden ^1E transition, which is calculated to lie very close to the ^3E level (Table 4). The shoulder at 19 000 cm^{-1} and the peak at ≈21 300 cm^{-1} are assigned to the split components of the $^3T_{1g}(F)$ level, with the remaining peaks being due to spin-forbidden transitions. The relatively high intensity of the peak at 22 370 cm^{-1} can be explained by its proximity to the neighbouring spin-allowed band. As with the $(NC_5H_4)_3CH$ complexes,[2] $[Ni\{CH(C_5H_4)_3\}_2]^{2+}$ belongs to the D_{3d} point group and thus the orbital triplet states are split into a singlet and a doublet. The selection rules indicate that polarized spectra will not differentiate the transitions, so that the assignment is based solely upon the AOM calculations. The band assignments are given in Table 4.

The spectrum of the $[Ni\{P(C_5H_4N)_3\}_2]^{2+}$ complex was measured with both nitrate and perchlorate counter anions. The spectrum of the perchlorate salt was better resolved at low temperature and is shown in Fig. 5. The spectrum consists of an asymmetric peak centred at ≈13 000 cm^{-1} with a shoulder at higher energy, and another asymmetric peak centred at ≈20 000 cm^{-1} with a shoulder at ≈18 500 cm^{-1} which is better resolved at low temperature. A weak peak can be seen at low temperature at about 20 600 cm^{-1}. The lowest-energy band is assigned to the $^3T_{2g}$ level of the parent octahedral complex, with the bands at 18 500 and ≈20 000 cm^{-1} being due to components of the $^3T_{1g}(F)$ level, the splittings being caused by the low symmetry of the ligand field. For this compound at room temperature, Holm and co-workers[10] reported peaks at 11 500, 12 600 and 19 000 cm^{-1} and a number of far more intense ($\varepsilon > 200$ dm^3 mol^{-1} cm^{-1}) transitions at higher energy.

The single-crystal spectrum of the $[Ni\{N(C_5H_4N)_3\}_2]^{2+}$ complex (Fig. 6) showed a band at ≈13 300 cm^{-1}, with shoulders at 13 000 and ≈14 200 cm^{-1}, and two peaks at 18 500 and 20 800 cm^{-1}, which are well resolved using polarized light. These may be compared with the peak energies[11] reported for the room-temperature reflectance spectra (10 700, 12 800, 19 050 and 26 800 cm^{-1}). The band assignments (Table 4) are similar to those of the other compounds studied in this work, in keeping with the proposed very similar structure, and thus it is assumed the spin-forbidden peak is at about 13 100

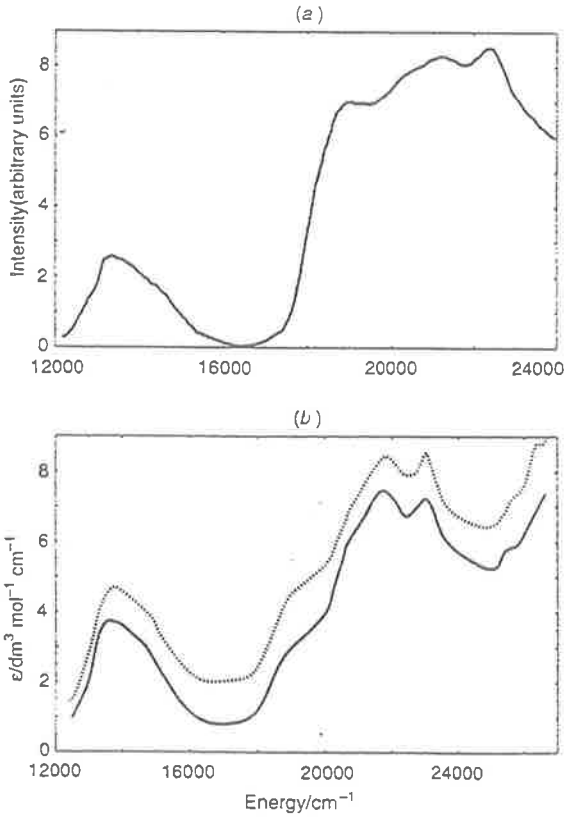

Fig. 4 Electronic spectrum of $[Ni\{CH(C_5H_4N)_3\}_2][NO_3]_2$ recorded (*a*) as a KBr disc at ≈15 K and (*b*) as a single crystal at ≈15 K with the electric vector of the polarized light along each of the two extinction directions of a crystal face of unknown morphology

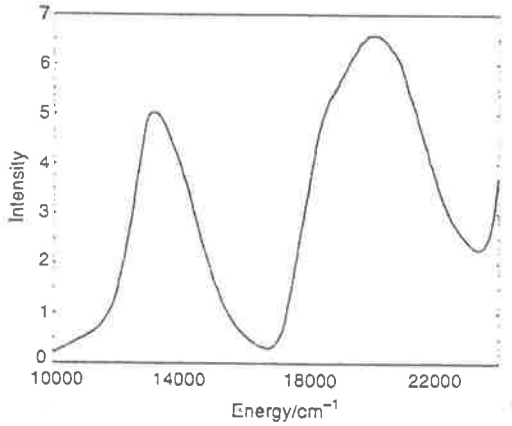

Fig. 5 Electronic spectrum of $[Ni\{P(C_5H_4N)_3\}_2][ClO_4]_2$ measured as a KBr disc at ≈15 K

Table 4 Observed and calculated transition energies (cm^{-1})

Assignment	$[Ni\{CH(C_5H_4N)_3\}_2]^{2+}$	$[Ni\{P(C_5H_4N)_3\}_2]^{2+}$	$[Ni\{N(C_5H_4N)_3\}_2]^{2+}$	Calculated
$^3A_{1g} \longrightarrow {}^3A_{2g}[^3T_{2g}(F)]$	13 300	13 000	13 000	13 250
$\longrightarrow {}^3E_g[^3T_{2g}(F)]$	14 200	14 200?	14 200	14 300
$\longrightarrow {}^1E_g$	≈13 500	Not observed	Not observed	13 100
$\longrightarrow {}^3A_{2g}[^3T_{1g}(F)]$	18 500	18 500	18 500	18 800
$\longrightarrow {}^3E_g[^3T_{1g}(F)]$	21 300	20 500	20 800	21 500
$\longrightarrow {}^1A_{1g}$	22 370	20 750	22 000	22 100

Parameters used: $e_\sigma = 5300$, $e_{\pi 1} = 1040$ and $e_{\pi 2} = 0$ cm^{-1} in all cases; $B = 750$, $C = 3675$ cm^{-1}.

Table 5 Crystal data for the complexes

	$[Ni\{CH(C_5H_4N)_3\}_2][NO_3]_2$	$[Zn\{CH(C_5H_4N)_3\}_2]Br_2\cdot 9H_2O$	$[Zn\{P(C_5H_4N)_3\}_2][ClO_4]_2\cdot H_2O$
Formula	$C_{32}H_{26}N_8NiO_6$	$C_{32}H_{44}Br_2N_8O_9Zn$	$C_{30}H_{26}Cl_2N_8O_9P_2Zn$
M	677.3	881.9	812.8
Crystal system	Trigonal	Monoclinic	Monoclinic
Space group	$R\bar{3}$	$C2/m$	$C2/c$
a/Å	11.655(3)	13.020(1)	24.041(1)
b/Å	—	13.221(1)	9.787(4)
c/Å	17.829(5)	11.053(2)	17.184(2)
β/°	90	104.22(1)	125.781(3)
U/Å^3	2097(1)	1844.3(3)	3280.2(9)
Z	3	2	4
D_c/g cm^{-3}	1.609	1.588	1.646
μ/cm^{-1}	7.59	28.98	10.74
Maximum, minimum transmission factors	1.091, 0.833	1.032, 0.963	1.204–0.890
$F(000)$	1050	900	1656
No. of data measured	1229	2407	4242
Range $h\,k\,l$	−15 to 15, 0–15, 0–23	0–17, 0–17, −15 to 15	0–32, 0–13, −23 to 23
No. unique data	1114	2307	4143
R_{int}[a]	0.049	0.059	0.034
No. observed data [$I \geqslant 3.0\sigma(I)$]	878	1621	2093
R[b]	0.043	0.041	0.049
R'[c]	0.047	0.051	0.049
Goodness of fit[d]	1.18	2.89	1.10

[a] $\sum_{i=1}^{n}\sum_{j=1}^{m}|\langle F_i^2\rangle - F_{ij}^2|/\sum_{i=1}^{n} m\langle F_i^2\rangle$ where n is the number of reflections measured more than once, m the number of times a given reflection has been measured and $\langle F_i^2\rangle$ is the average value for F^2 for the unique reflection i. [b] $\sum_{i=1}^{n}(|F_{oi}| - |F_{ci}|)/\sum_{i=1}^{n}|F_{oi}|$. [c] $[\sum_{i=1}^{n} w_i(|F_{oi}| - |F_{ci}|)^2/\sum_{i=1}^{n} w_i|F_{oi}|^2]^{\frac{1}{2}}$. [d] $[\sum_{i=1}^{n}(|F_{oi}| - |F_{ci}|)\sigma_i]/(n-m)$ where n is the number of reflections used in refinement and m the number of variables.

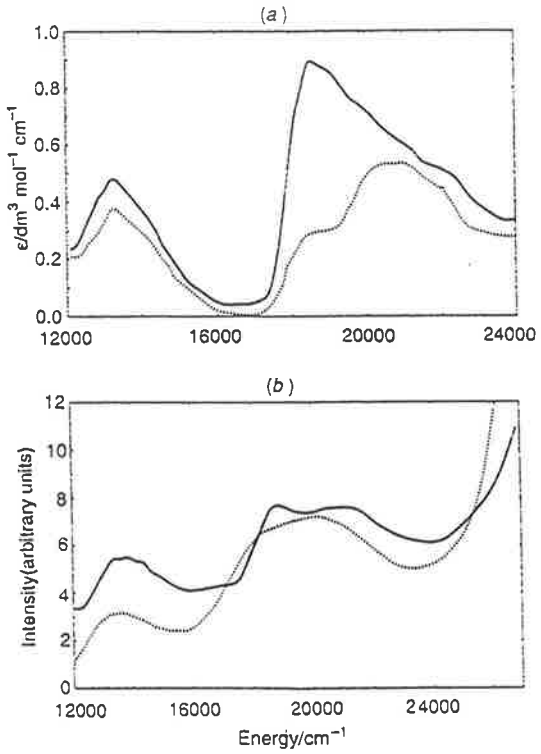

Fig. 6 Electronic spectra of $[Ni\{N(C_5H_4N)_3\}_2][NO_3]_2$ recorded (*a*) as a single crystal at ≈ 15 K with the electric vector of the polarized light along each of the two extinction directions of a crystal face of unknown morphology, and (*b*) as a KBr disc at room temperature (dashed line) and ≈ 15 K (solid line)

cm^{-1}, so that the observed band probably includes this, which may partly account for the asymmetrical nature of the first transition.

Metal–ligand bonding parameters

The relatively high energies of the 'd–d' transitions indicate the presence of a strong ligand field. This can be due either to π-acceptor character in the metal–ligand bonding, or the donor being positioned close to the metal ion. For other tripodal ligands like $(pz)_3CH$[2] and $(pz)_2(NC_5H_4)CH$[1] it has been shown that the second case is true.

To investigate the bonding characteristics of the compounds, the computer package CAMMAG, developed by Gerloch and co-workers,[12] was used to estimate the metal–ligand bonding parameters of the complexes within the framework of the AOM. The program calculates the transition energies of a complex, using as input σ- and π-bonding parameters of the ligand donor atoms and the molecular geometry indicated by the crystal structure. In the present case this involved the parameters e_σ, $e_{\pi x}$ and $e_{\pi y}$ for each pyridine group, where $e_{\pi x}$ and $e_{\pi y}$ describe the π bonding parallel and perpendicular to the plane of the amine ring, respectively. It should be noted that in mixed-ligand complexes it is impossible to determine all the bonding parameters independently, and it has usually been assumed that the $e_{\pi x}$ parameter of ligands such as pyridine is zero.[13] The present study provides an opportunity to test the validity of this assumption.

Without the crystal structures of the $[Ni\{P(C_5H_4N)_3\}_2]^{2+}$ and $[Ni\{N(C_5H_4N)_3\}_2]^{2+}$ complexes, unambiguous calculations of bonding parameters for these ligands are impossible. However, a comparison of the structures of similar complexes formed by $P(C_5H_4N)_3$ and $N(C_5H_4N)_3$ suggests[3] that the effect on the co-ordination geometry (both bond lengths and angles) is minimal, so that the $(NC_5H_4)_3CH$ structure could be used to gauge the bonding parameters. The spectra of all three compounds are similar, so it is not surprising that the same bonding parameters gave an adequate fit to the spectra. The results are shown in Table 4.

For each complex, the parameters reported[1] for the pyridine-type nitrogen of $(pz)_2(NC_5H_4)CH$, scaled as described previously to take into account the differences in bond lengths,[1] were used initially to calculate the excited-state energies of the complexes. The limited number of parameters to be determined

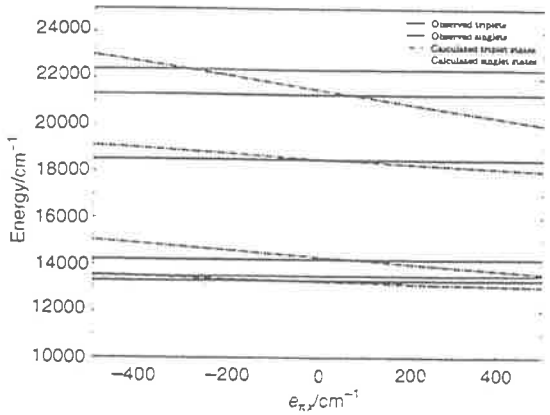

Fig. 7 Plot of the calculated transition energies as a function of $e_{\pi x}$

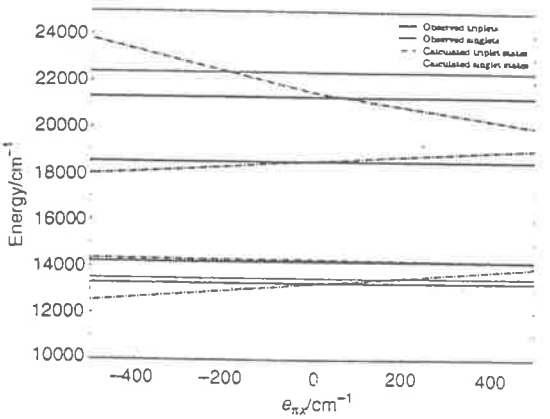

Fig. 8 Plot of the calculated transition energies as a function of $e_{\pi x}$ (with Δ constant)

Table 6 Fractional atomic coordinates for the non-hydrogen atoms in $[Ni\{CH(C_5H_4N)_3\}_2][NO_3]_2$

Atom	*x*	*y*	*z*
Ni[a]	1.0	0	1.0
O(1)	0.6668(4)	0.2279(3)	0.9775(2)
N(1)[b]	2/3	1/3	0.9709(4)
N(11)	0.9869(2)	0.1334(2)	0.9290(1)
C(1)[b]	1.0	0	0.8297(3)
C(12)	0.9726(3)	0.2345(3)	0.9528(2)
C(13)	0.9604(4)	0.3189(3)	0.9062(2)
C(14)	0.9645(3)	0.3024(3)	0.8301(2)
C(15)	0.9811(3)	0.2008(3)	0.8045(2)
C(16)	0.9901(3)	0.1172(3)	0.8551(2)

[a] Atom has site occupancy factor 1/6. [b] Atom has site occupancy factor 1/3.

Table 7 Fractional atomic coordinates for the non-hydrogen atoms in $[Zn\{CH(C_5H_4N)_3\}_2]Br_2\cdot 9H_2O$

Atom	*x*	*y*	*z*
Br[a]	0.610 45(5)	0	0.300 15(7)
Zn[b]	0	0	0
O(1)	0.653 1(3)	0.234 5(3)	0.419 9(4)
O(2)[a]	1.0	0.155 6(4)	0.5
O(3)[a]	0.885 5(4)	0	0.357 2(4)
O(4)[b]	0.5	0.072 6(19)	1.0
N(11)[a]	0.135 7(4)	0	0.152 7(4)
N(21)[a]	0.083 9(2)	0.110 6(3)	−0.079 9(3)
C(1)[a]	0.235 8(4)	0	−0.006 4(5)
C(12)[a]	0.130 8(5)	0	0.270 6(6)
C(13)[a]	0.218 5(6)	0	0.368 5(6)
C(14)[a]	0.315 6(5)	0	0.341 9(6)
C(15)[a]	0.321 9(5)	0	0.221 2(6)
C(16)[a]	0.231 2(4)	0	0.128 3(5)
C(22)	0.038 3(3)	0.191 1(3)	−0.140 9(4)
C(23)	0.090 1(4)	0.257 6(4)	−0.198 7(4)
C(24)	0.194 8(4)	0.239 7(4)	−0.192 6(4)
C(25)	0.243 1(3)	0.157 6(3)	−0.128 3(4)
C(26)	0.185 7(3)	0.094 0(3)	−0.074 0(4)

[a] Atom has site occupancy factor 0.5. [b] Atom has site occupancy factor 0.25.

Table 8 Fractional atomic coordinates for the non-hydrogen atoms of $[Zn\{P(C_5H_4N)_3\}_2][ClO_4]_2\cdot H_2O$

Atom	*x*	*y*	*z*
Zn*	0	0	0
Cl	0.3594(8)	0.0125(2)	0.0275(1)
P(1)	0.1750(7)	0.0353(1)	0.1631(1)
O(1)	0.4208(3)	0.0741(8)	0.0716(5)
O(2)	0.3489(4)	−0.0834(7)	−0.0380(5)
O(3)	0.3094(4)	0.1110(9)	−0.0159(5)
O(4)	0.3552(4)	−0.0445(6)	0.0980(4)
O(5)*	0.5	0.1605(12)	0.75
N(11)	0.0551(2)	0.1837(4)	0.0763(3)
N(21)	0.0648(2)	−0.1088(4)	0.1326(3)
N(31)	0.0767(2)	−0.0373(4)	−0.0266(3)
C(12)	0.0214(3)	0.2979(6)	0.0652(4)
C(13)	0.0531(4)	0.4142(6)	0.1162(5)
C(14)	0.1216(4)	0.4141(7)	0.1808(6)
C(15)	0.1579(3)	0.2981(6)	0.1949(5)
C(16)	0.1233(3)	0.1855(5)	0.1406(4)
C(22)	0.0383(3)	−0.1992(6)	0.1603(4)
C(23)	0.0763(4)	−0.2650(6)	0.2458(5)
C(24)	0.1440(4)	−0.2391(7)	0.3069(5)
C(25)	0.1731(3)	−0.1481(6)	0.2802(4)
C(26)	0.1326(3)	−0.0860(5)	0.1930(4)
C(32)	0.0597(3)	−0.0827(6)	−0.1097(4)
C(33)	0.1053(3)	−0.1138(7)	−0.1288(4)
C(34)	0.1730(3)	−0.0947(7)	−0.0590(5)
C(35)	0.1927(3)	−0.0476(6)	0.0284(4)
C(36)	0.1434(3)	−0.0210(5)	0.0437(4)

* Atom has site occupancy factor 0.5.

meant that there was no need to restrain $e_{\pi x}$ to 0. Initial calculations with $e_{\pi x} = 0$ and the scaled parameters provided an excellent fit, with most calculated transition energies being within 300 cm^{-1} of those observed experimentally. The Racah parameters were reduced to ≈75% of their free-ion values,[14] which is in good agreement with the results for the corresponding $(pz)_3CH$ complex.[2] The sensitivity of the calculated transition energies to the π-bonding was investigated by changing $e_{\pi x}$ while keeping the other parameters unaltered and the effect is shown in Fig. 7. While the fit to the splitting of the $^3T_1(F)$ level is best with an $e_{\pi x}$ value of about +200 cm^{-1}, the splitting of the $^3T_2(F)$ level is better with $e_{\pi x} = -200$ cm^{-1}. By keeping Δ the same (by decreasing $e_{\pi y}$ as $e_{\pi x}$ is increased) the best fit is clearly found with $e_{\pi x}$ close to zero (see Fig. 8). Variation of the other parameters was also tested and no substantially improved fit was obtained. The results of the best fit are shown in Table 4. The parameters, $e_\sigma = 5300$ and $e_{\pi y} = 1040$ cm^{-1}, found for all three complexes, compare well with those for the slightly longer nickel–pyridine interaction in $[Ni\{CH(C_5H_4)(pz)_2\}_2]^{2-}$ where $e_\sigma = 5175$ and $e_{\pi y} = 1020$ cm^{-1}.[2] The fact that different parameters were not required for the nitrogen nor phosphorus bridgehead ligands indicates that conjugation between the rings, possible in these ligands but impossible in the carbon bridgehead ligand, is not required to explain their electronic properties.

Conclusion

The molecular geometries of the complexes are very similar, and to those of other complexes formed by similar tripodal ligands.

The large ligand-field splitting observed for each complex is due to the relatively strong σ-donor and moderate π-donor capacity of the ligands, this probably being caused by the relatively short M–N bonds in the compounds. The bonding parameters of the three ligands are indistinguishable, suggesting that the nature of the bridgehead atom has little effect on the metal–ligand interaction. In particular, the π-bonding parameters provide no evidence for conjugation of the π systems in any of the ligands. In agreement with McWhinnie *et al.*[11] we find that conjugation within polypyridyl ligands is not a prerequisite for high values of Δ'. In agreement with simple theory, no notable degree of in-plane π bonding was detected.

Acknowledgements

The financial support of the Australian Research Council is acknowledged and Dr. M. Gerloch, Cambridge University Chemical Laboratory, is thanked for making available the computer package CAMMAG. The assistance of Mr. P. A. Anderson and Mr. R. J. A. Janssen in the initial stages of the syntheses is acknowledged.

References

1 T. Astley, A. J. Canty, M. A. Hitchman, G. L. Rowbottom, B. W. Skelton and A. H. White, *J. Chem. Soc., Dalton Trans.*, 1991, 1981.
2 T. Astley, J. M. Guibis, M. A. Hitchman and E. R. T. Tienkink, *J. Chem. Soc., Dalton Trans.*, 1993, 509.
3 F. R. Keene, M. R. Snow, P. J. Stephenson and E. R. T. Tiekink, *Inorg. Chem.*, 1988, **27**, 2040.
4 M. A. Hitchman, *Transition Met. Chem.*, 1985, **9**, 1.
5 N. Walker and D. Stuart, *Acta Crystallogr., Sect. A*, 1983, **39**, 158.
6 TEXSAN, Structure Analysis Package, Molecular Structure Corporation, Houston, TX, 1992.
7 C. K. Johnson, ORTEP II, Report ORNL-5136, Oak Ridge National Laboratory, Oak Ridge, TN, 1976.
8 T. Astley, P. J. Ellis, H. C. Freeman, M. A. Hitchman, F. R. Keene and E. R. T. Tiekink, *J. Chem. Soc., Dalton Trans.*, 1995, 595.
9 G. J. Long and P. J. Clarke, *Inorg. Chem.*, 1978, **17**, 1394; D. J. Hamm, J. Bordner and A. F. Schreiner, *Inorg. Chim. Acta*, 1973, **7**, 637.
10 E. Larser, G. N. La Mar, B. E. Wagner, J. E. Parks and R. H. Holm, *Inorg. Chem.*, 1972, **11**, 2652.
11 W. R. McWhinnie, G. C. Kulasingham and J. C. Draper, *J. Chem. Soc. A*, 1996, 1199.
12 D. A. Cruse, J. E. Davies, M. Gerloch, J. Harding, D. Mackey and R. F. McMeeking, CAMMAG, a FORTRAN computing package, University of Cambridge, 1979.
13 B. J. Kennedy, K. S. Murray, M. A. Hitchman and G. L. Rowbottom, *J. Chem. Soc., Dalton Trans.*, 1987, 825.
14 A. B. P. Lever, *Inorganic Electronic Spectroscopy*, 2nd edn., Elsevier, Amsterdam, 1984, p. 115.

Received 11*th September* 1995; *Paper* 5/06010I

Stabilization of cobalt(I) by the tripodal ligands tris(2-pyridyl)methane and tris(2-pyridyl)phosphine. Structural, spectroscopic and *ab initio* studies of the $[CoL_2]^{n+}$ species†

Kenneth R. Adam,[a] Peter A. Anderson,[a] Timothy Astley,[b] Ian M. Atkinson,[a] John M. Charnock,[c,d] C. David Garner,[d] Jacqueline M. Gulbis,[e] Trevor W. Hambley,[f] Michael A. Hitchman,[b] F. Richard Keene*[,a] and Edward R. T. Tiekink[e]

[a] *Department of Chemistry and Chemical Engineering, School of Molecular Sciences, James Cook University of North Queensland, Townsville, Queensland 4811, Australia*
[b] *Department of Chemistry, University of Tasmania, Hobart, Tasmania 7001, Australia*
[c] *CCLRC Daresbury Laboratory, Warrington WA4 4AD, UK*
[d] *Department of Chemistry, University of Manchester, Manchester M13 9PL, UK*
[e] *School of Chemistry, University of Sydney, Sydney, NSW 2001, Australia*
[f] *Department of Chemistry, University of Adelaide, Adelaide, South Australia 5005, Australia*

The nature of bonding in a series of complexes $[CoL_2]^{n+}$ [L = the tripodal ligand tris(2-pyridyl)methane or tris(2-pyridyl)phosphine, n = 1–3] has been investigated by single-crystal X-ray diffraction, X-ray absorption and electronic spectroscopy and density functional theory *ab initio* calculations. The structural studies reveal that the cobalt ions each exist in a distorted octahedral geometry defined by six N-donor atoms; the cations are all centrosymmetric. In both series of complexes the bond lengths Co^{I}–N ≈ Co^{II}–N > Co^{III}–N. Data from the various studies indicate that the 'cobalt(I)' state of the complex $[Co\{X(C_5H_4N\text{-}2)_3\}_2]^+$ (X = CH or P) is better described by the d^8 cobalt(I)–ligand formulation rather than as d^7 cobalt(II)–ligand radical.

The co-ordination compounds of chelating π-acceptor ligands such as bipy = 2,2′-bipyridine, phen = 1,10-phenanthroline and their analogues have been widely studied, particularly with regard to their photochemistry,[1] redox characteristics[2–4] and the stabilization of low metal oxidation states. In the last context the species $[Co(bipy)_3]^+$ has attracted considerable attention[3–6] because of its utility as a homogeneous reduction catalyst for the production of H_2 from H_2O,[7–9] CO from CO_2[10–12] and the reduction of organic substrates.[13,14] The nature of the ligand–metal interaction has been probed by electronic spectral,[15,16] magnetic moment,[16,17] NMR contact shift[18,19] and structural studies[2,6] aimed at elucidating whether the species is better described as an octahedral high-spin cobalt(I) d^8 system with substantial $Co(d_\pi)\rightarrow bipy(\pi^*)$ back donation, or alternatively as a cobalt(II) species containing a reduced $bipy^-$ ligand radical. The consensus resides with the former option. In particular, the high-spin d^8 configuration is in accord with the magnetic susceptibility values of 2.53[16] and 2.89 μ_B,[17] which compare with that found for the isoelectronic high-spin d^8 $[Ni(bipy)_3]^{2+}$, μ_{eff} = 2.88 μ_B.[20] Further, the VIS/near-IR spectrum of $[Co(bipy)_3]^+$ contains bands consistent with metal-to-ligand-charge transfer (m.l.c.t.) transitions, which Kaizu *et al.*[16] interpret as evidence that the electron furnished by reduction of $[Co(bipy)_3]^{2+}$ resides primarily on the central cobalt atom. Fitzgerald *et al.*[19] investigated NMR contact shifts in $[Co(bipy)_3]^+$, $[Co(dmbipy)_3]^+$, $[Ni(bipy)_3]^{2+}$ and $[Ni(dmbipy)_3]^{2+}$ (dmbipy = 4,4′-dimethyl-2,2′-bipyridine) on the basis that π-back bonding affects charge distribution, so that such effects would be expected to be exhibited in local changes in ^1H and ^{13}C NMR spectra.[18,21] It was shown that both σ- and

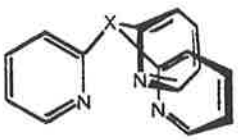

π-delocalization mechanisms were operative in $[Co(bipy)_3]^+$, and that the dominant π-delocalization mechanism most likely involved a direct overlap of the metal σ_{2e} orbitals with the highest-filled π-symmetry ligand orbitals, although other plausible mechanisms placing negative spin density in empty π^* orbitals of the ligand were not discounted.[19]

Finally, the crystal structural investigation of Szalda *et al.*[6] compared the structures of the cobalt(I) complex $[Co(bipy)_3]^+$ and its high-spin cobalt(II) d^7 $[Co(bipy)_3]^{2+}$ analogue. The similarity of the Co–N bond lengths for the cobalt-(II) (average Co–N 2.128 Å) and -(I) complexes (average Co–N 2.11 Å) is in contrast with the large difference between the cobalt-(II) and -(III) species [1.93(2) Å].[22] In addition, a shortening of the bridging C(2)–C(2′) bond lengths in the bipy ligands was observed for the reduced form (1.42 *cf.* 1.49 Å). These data were interpreted to indicate that on reduction of the species from Co^{II} to Co^{I} the extra electron enters a d_π orbital and is partially delocalized *via* $Co(d_\pi)\rightarrow bipy(\pi^*)$ back donation. The trends in the Co–N distances in the $[Co(bipy)_3]^{n+}$ cations have also been observed in extended X-ray absorption fine structure (EXAFS) studies.[2]

The tripodal compounds $X(C_5H_4N\text{-}2)_3$ (X = N, CH, COH, P, P=O or As) and their complexes raise interesting questions with regard to the rationale described above. Boggess and Zatko[23,24] reported that the ligands with X = P and As stabilized Co^{I} whereas there was no stabilization when X = N; they attributed this observation to the ability of the bridging atom to allow delocalization throughout the ligand *via* p_π–d_π interaction between the bridgehead atom X and the pyridine rings, a mech-

† *Supplementary data available* (No. SUP 57201, 4 pp.): normalized Co K-edge EXAFS spectra of complexes involved in this study and table of radial distribution of atoms about the central Co atom. See Instructions for Authors, *J. Chem. Soc., Dalton Trans.*, 1997, Issue 1.

Non-SI units employed: $\mu_B \approx 9.27 \times 10^{-24}$ J T^{-1}, eV ≈ 1.60×10^{-19} J.

anism which is only possible for the larger bridgehead atoms. However, our re-examination of the electrochemistry of the cobalt complexes for X = N, COH, CH, P or P=O showed that in all cases the $[CoL_2]^+$ species were stabilized.[25] In that work we proposed that either the geometry imposed by the bridgehead atom allowed 'through space' delocalization between the rings, or that the orientation of the pyridyl rings in their constrained co-ordination geometries permitted enhanced overlap between the ligand p_π and the metal t_{2g} orbitals.

The specific mechanism of delocalization has implications for our general understanding of the nature of the interaction of polypyridyl ligands, such as 2,2'-bipyridine, with metal centres. The present study is directed at elucidating the metal–ligand interaction between Co^I and $X(C_5H_4N\text{-}2)_3$ (X = CH or P) using structural and spectroscopic techniques, and density functional theory (DFT) *ab initio* calculations which together provide an insight into the charge distribution in the complexes $[Co\{CH(C_5H_4N\text{-}2)_3\}_2]^+$ and $[Co\{P(C_5H_4N\text{-}2)_3\}_2]^+$.

Experimental

Materials

The following reagents were used as supplied without further purification: $Co(NO_3)_2\cdot 6H_2O$ (Aldrich; 99+%), 2,2'-bipyridine (Merck, 99.5%), lithium perchlorate (Fluka, purum >98%), potassium hexafluorophosphate (Aldrich, 98%), tetra-*n*-butylammonium bromide (Fluka, 99%), tetraethylammonium bromide (Sigma) and silver nitrate (Aldrich, 99.9999%). Tetra-*n*-butylammonium hexafluorophosphate used in electrochemical measurements, was obtained from Fluka (puriss) and recrystallized twice from ethanol–water and twice from dichloromethane–diethyl ether. Acetonitrile (Aldrich, 99.9+%, HPLC grade) was used as received. Solvents used in the electrosynthesis and crystal growth of $[Co\{X(C_5H_4N\text{-}2)_3\}_2]^+$ [*viz.* diethyl ether, ethanol and light petroleum (b.p. 40–60 °C)] were rigorously purified using literature methods.[26]

Physical measurements

Electrochemistry. All electrochemical experiments were undertaken in a Vacuum Atmosphere glove-box under an argon atmosphere, using a Bioanalytical Systems BAS 100A electrochemical analyser. For cyclic voltammetry, solutions of the $[Co\{X(C_5H_4N\text{-}2)_3\}_2]^{n+}$ complexes (0.5–3 mmol dm^{-3}) were prepared in acetonitrile with $NBu^n_4PF_6$ (0.1 mol dm^{-3}) as the supporting electrolyte. A platinum-button working electrode, platinum-wire auxiliary and a $Ag–Ag^+$ reference electrode [0.01 mol dm^{-3} $AgNO_3$, 0.1 mol dm^{-3} $NBu^n_4PF_6$ in MeCN, +0.31 V *vs.* saturated calomel electrode (SCE)] were used. A sweep rate of 100 mV s^{-1} was used for cyclic voltammetry.

Electron absorption spectra. Single-crystal and potassium bromide disc electronic spectra were measured using a Cary 17 or 5 spectrophotometer fitted with a CTI Cryogenics unit, a Palm Beach 4025 cryogenic thermometer/controller or Oxford DTC2 temperature controller. Solutions of cobalt(I) complexes [$(3–30) \times 10^{-5}$ mol dm^{-3}] were prepared in ethanol under inert conditions, and their electronic spectra measured using a Cary 17 spectrophotometer.

Extended X-ray absorption fine structure. Samples used for X-ray absorption spectroscopy were ground with boron nitride using a mortar and pestle, and mounted in aluminium sample cells with Sellotape windows. The air-sensitive cobalt(I) samples were handled in a glove-box, and upon removal were immediately immersed in liquid nitrogen. Cobalt K-edge X-ray absorption spectra were recorded at ambient temperature for cobalt(II) and -(III) species, but at *ca.* 77 K for the cobalt(I) species which were mounted on the cold-finger of a liquid-nitrogen-filled cryostat in an evacuated sample chamber. The data were collected on Station 7.1 of the Daresbury Synchrotron Radiation Source, operating at 2 GeV with an average current of 150 mA. The data were analysed, including multiple scattering from the pyridine rings fixed at the geometry determined by crystallographic studies of these complexes by varying the shell distances and Debye–Waller parameters using EXCURV 92[27] to obtain optimum agreement between the experimental and simulated EXAFS and their Fourier transforms.

Syntheses

Tris(2-pyridyl)methane and tris(2-pyridyl)phosphine were obtained by literature methods.[28]

Bis[tris(2-pyridyl)methane]cobalt(II) nitrate, $[Co\{CH(C_5H_4N\text{-}2)_3\}_2][NO_3]_2$. A solution of $Co(NO_3)_2\cdot 7H_2O$ (145 mg, 0.5 mmol) in acetone (5 cm^3) was added dropwise to a stirred solution of tris(2-pyridyl)methane (250 mg, 1.01 mmol) in acetone (10 cm^3). The resulting suspension was cooled at 0 °C for 2 h, the solid filtered off, washed with acetone and air dried. Yield: 260 mg, 76% (based on an anhydrous product).‡ Orange crystals of $[Co\{CH(C_5H_4N\text{-}2)_3\}_2][NO_3]_2$ were obtained by vapour diffusion of diethyl ether into an acetonitrile solution of the complex.

For use in the synthesis of $[Co\{CH(C_5H_4N\text{-}2)_3\}_2]Br$, the nitrate salt was converted into the hexafluorophosphate by metathesis from an aqueous solution with NH_4PF_6. The hexafluorophosphate salt was converted into the bromide by metathesis in an acetone solution using tetra-*n*-butylammonium bromide.

Bis[tris(2-pyridyl)phosphine]cobalt(II) nitrate, $[Co\{P(C_5H_4N\text{-}2)_3\}_2][NO_3]_2$. This complex was prepared in an analogous manner to the $[Co\{CH(C_5H_4N\text{-}2)_3\}_2][NO_3]_2$: yield 270 mg, 76% (based on an anhydrous product).‡ Orange crystals of $[Co\{P(C_5H_4N\text{-}2)_3\}_2][NO_3]_2\cdot 8H_2O$ were obtained by slow evaporation of an aqueous solution of the complex.

Bis[tris(2-pyridyl)methane]cobalt(III) perchlorate, $[Co\{CH(C_5H_4N\text{-}2)_3\}_2][ClO_4]_3$. This complex was obtained by coulometry of a solution of $[Co\{CH(C_5H_4N\text{-}2)_3\}_2][NO_3]_2$ (*ca.* 50 mg) in HCl (0.1 mol dm^{-3}, 50 cm^3) at a platinum-gauze electrode at a potential of 0.50 V *vs.* an SCE reference electrode until the current decreased to <1% of its initial value. The resultant solution was reduced to a small volume and the complex precipitated by the addition of $LiClO_4$, filtered off, washed with ethanol and air dried. The yield was quantitative.‡ The perchlorate salt was converted into the bromide by anion-exchange chromatography. Yellow crystals of $[Co\{CH(C_5H_4N\text{-}2)_3\}_2]Br_3\cdot 14H_2O$ were obtained by slow evaporation of an aqueous solution.

Bis[tris(2-pyridyl)phosphine]cobalt(III) perchlorate, $[Co\{P(C_5H_4N\text{-}2)_3\}_2][ClO_4]_3$. This complex was prepared by coulometry as described for $[Co\{CH(C_5H_4N\text{-}2)_3\}_2][ClO_4]_3$, at a potential of 0.70 V *vs.* SCE. The yield was quantitative.† Yellow crystals of $[Co\{P(C_5H_4N\text{-}2)_3\}_2][ClO_4]_3\cdot 0.5H_2O$ were obtained by the slow evaporation of an aqueous solution.

Bis[tris(2-pyridyl)methane]cobalt(I) bromide, $[Co\{CH(C_5H_4N\text{-}2)_3\}_2]Br$. The electrosynthesis of $[Co\{CH(C_5H_4N\text{-}2)_3\}_2]Br$

‡ For this series of complexes considerable variation in the extent of hydration was experienced which rendered microanalysis difficult. In all cases but one, *viz.* $[Co\{P(C_5H_4N\text{-}2)_3\}_2]^+$, the salt ultimately obtained was characterized unambiguously by X-ray crystallography. In the latter case the established identity of the cobalt(II) precursor, the observation that its electrochemical characteristics were identical to those of the cobalt(II) species, and the close analogy with the $CH(C_5H_4N\text{-}2)_3$ counterpart were taken as sufficient verification of the assignment.

Table 1 Crystallographic data and refinement details for complexes **1–5**

	1	2	3	4	5
Formula	$C_{32}H_{34}Br_3CoN_6O_{14}$	$C_{32}H_{26}CoN_8O_6$	$C_{32}H_{28}BrCoN_6O$	$C_{30}H_{28}Cl_3CoN_6O_{14}P_2$	$C_{30}H_{40}CoN_8O_{14}P_2$
M	1045.46	677.5	651.4	923.8	857.6
Crystal size/mm	0.25 × 0.11 × 0.32	0.08 × 0.19 × 0.32	0.20 (dia.)	0.16 × 0.20 × 0.21	0.44 × 0.65 × 0.65
Colour	Orange	Orange	Blue	Orange-red	Red-orange
Crystal system	Orthorhombic	Trigonal	Orthorhombic	Orthorhombic	Monoclinic
Space group	*Pccn*	$R\bar{3}$	*Pbcn*	*Pccn*	*C*2/*c*
a/Å	21.183(6)	11.6572(7)	8.369(1)	12.634(2)	20.50(3)
b/Å	20.551(4)	11.6572(7)	19.714(1)	19.066(1)	11.00(1)
c/Å	11.480(2)	17.893(1)	19.145(4)	15.348(2)	16.83(2)
β/°					92.1(1)
U/Å^3	4997(2)	2116.4(5)	3159(1)	3697(1)	3793(8)
Z	4	3	4	4	4
D_c/g cm^{-3}	1.390	1.595	1.370	1.660	1.501
F(000)	2128	1047	1328	1880	1780
μ/cm^{-1}	28.27	6.75	17.9	8.44	6.13
Absorption correction	Numerical	Empirical	—	Analytical	Empirical
Transmission factors	0.525–0.748	0.957–1.029	—	0.766–0.900	0.900–1.028
Diffractometer	CAD4F	AFC6R	CAD4F	CAD4F	AFC6R
No. of data collected	3909	1239	2414	2791	3792
θ_{max}/°	23.0	27.5	22.5	22.5	25.0
No. unique data	3909	1123	2065	2430	3679
No. unique data [with $I \geq n\sigma(I)$]	1308 (2.5)	950 (3.0)	709 (2.5)	1502 (2.5)	2983 (3.0)
R	0.072 *	0.041	0.063	0.040	0.048
R'	0.063 *	0.049	0.065	0.057	0.059
Residual electron density/e Å^{-3}	0.4	1.26	1.26	0.36	0.70

* $R = \Sigma(||F_o| - |F_c||/\Sigma|F_o|$, $R' = [\Sigma w(|F_o| - |F_c|)^2/\Sigma wF_o^2]^{\frac{1}{2}}$.

was carried out in an inert (Ar) atmosphere. The complex $[Co\{CH(C_5H_4N\text{-}2)_3\}_2]Br_2$ (*ca.* 50 mg) was dissolved in dry ethanol–acetonitrile (5:2, 7 cm^3) and electrolyte added (NBu^n_4Br. 20 mg, producing a solution *ca.* 0.01 mol dm^{-3}). The complex was reduced coulometrically at a platinum-gauze working electrode in a three-compartment cell using an Ag–Ag$^+$ reference electrode (0.01 mol dm^{-3} $AgNO_3$). The electrolysis was conducted at −1.55 V (*vs.* Ag–Ag$^+$) over 2 h, during which time the orange solution changed to a deep blue with precipitation of a dark solid. The electrolyte solution in the platinum-auxiliary electrode side-arm was changed at regular intervals throughout the electrolysis. When the cell current had dropped to a steady value (<5% of the initial current) the product was filtered off and washed with ethanol–diethyl ether (1:3 v/v) and then diethyl ether (×3). Yield: *ca.* 20 mg.‡ Dark blue crystals suitable for structural analysis were obtained by liquid diffusion of diethyl ether into a solution of the complex in dry ethanol. A single crystal was isolated in a tapered glass capillary and sealed with the exclusion of air.

Bis[tris(2-pyridyl)phosphine]cobalt(I) perchlorate, $[Co\{P(C_5H_4N\text{-}2)_3\}_2]ClO_4$. The electrosynthesis of $[Co\{P(C_5H_4N\text{-}2)_3\}_2]ClO_4$ was carried out in a similar manner to that described for $[Co\{CH(C_5H_4N\text{-}2)_3\}_2]Br$. The complex $[Co\{P(C_5H_4N\text{-}2)_3\}_2][NO_3]_2$ (*ca.* 18 mg, 0.025 mmol) was dissolved in acetronitrile–dry ethanol (4:3, 8 cm^3) containing $LiClO_4$ as electrolyte (*ca.* 0.015 mol dm^{-3}). The electrolysis was conducted at −1.40 V (*vs.* Ag–Ag$^+$) over 3 h, during which the initially orange solution changed to a deep blue and the cell current had dropped to less than 2% of the initial value. The electrolysis solution was shaken with light petroleum (30 cm^3) giving rise to a blue layer of reduced volume (predominantly MeCN) and a clear layer (light petroleum and EtOH). Upon separation of the solvent layers, diethyl ether (20 cm^3) was added to the blue layer causing the precipitation of the blue product, which was filtered off and washed with diethyl ether.‡ Despite many attempts, no crystals were obtained which provided satisfactory X-ray diffraction for determination of the structure by crystallography.

Ab initio calculations

Density functional theory calculations were performed on an SGI Power Challenge computer system using the GAUSSIAN 94 package.[29] The local spin-density approximation (LSDA) S-VWN5[30] exchange-correlation potential was used in this work together with the 3-21G basis set, which was the largest practical with our computational facilities. This corresponded to 401, 423 and 427 basis functions for $[Co(bipy)_3]^{n+}$, $[Co\{CH(C_5H_4N\text{-}2)_3\}_2]^{n+}$ and $[Co\{P(C_5H_4N\text{-}2)_3\}_2]^{n+}$ (n = 1–3) systems, respectively.

The bonding analysis was based on the Mulliken population overlap scheme[31,32] where electron overlaps are distributed between the atoms involved. Mulliken population overlaps give fractional electron occupancies which can yield useful information regarding bond strengths, despite not being normalized to integral values. Total atomic charges are calculated as the difference between the atomic number and the gross atomic population. Despite the shortcomings of Mulliken analysis the scheme has been widely used for determining atomic charges within molecules.[33–35]

Owing to the computational expense of the optimization of the geometries of the complexes, only single-point calculations were performed using the coordinates taken from the available crystal structures. In the case of $[Co\{P(C_5H_4N\text{-}2)_3\}_2]^+$ where an X-ray determination was not available the coordinates used were those of $[Co\{P(C_5H_4N\text{-}2)_3\}_2]^{2+}$. This approximation is justified by the apparent similarity between the structures of the two complexes observed from the EXAFS data.

X-Ray crystallography

The crystallographic data are summarized in Table 1, and selected interatomic parameters for the five structures are given in Table 2.

$[Co\{CH(C_5H_4N\text{-}2)_3\}_2]Br_3\cdot 14H_2O$ 1. Cell constants were determined by a least-squares fit to the setting parameters of 25 independent reflections, measured and refined on an Enraf-Nonius CAD4-F diffractometer fitted with a graphite monochromator. Data were obtained at 21 °C with Mo-Kα radiation (λ = 0.710 69 Å).

The structure was solved by heavy-atom methods using SHELXS 86[36] and the solution was extended by Fourier-

Table 2 Selected bond lengths (Å) and angles (°) for complexes 1–5

	1 X = C	2 X = C	3 X = C	4 X = P	5 X = P
Co–N(11)	1.95(1)	2.109(2)	2.09(1)	1.967(4)	2.096(3)
Co–N(21)	1.95(1)		2.13(1)	1.984(4)	2.121(3)
Co–N(31)	1.95(1)		2.12(2)	1.978(4)	2.108(4)
N(11)–C(12)	1.36(2)	1.334(3)	1.31(2)	1.359(6)	1.322(4)
N(11)–C(16)	1.34(2)	1.330(3)	1.36(2)	1.347(6)	1.331(5)
N(21)–C(22)	1.33(2)		1.35(3)	1.355(7)	1.334(4)
N(21)–C(26)	1.37(2)		1.33(2)	1.359(6)	1.316(5)
N(31)–C(32)	1.33(2)		1.29(3)	1.349(7)	1.330(4)
N(31)–C(36)	1.32(2)		1.34(3)	1.352(6)	1.330(5)
X(1)–C(16)	1.50(2)	1.501(3)	1.51(2)	1.829(5)	1.808(4)
X(1)–C(26)	1.48(2)		1.51(3)	1.817(6)	1.821(4)
X(1)–C(36)	1.54(2)		1.52(3)	1.825(5)	1.821(4)
C(12)–C(13)	1.40(2)	1.356(4)	1.34(3)	1.360(7)	1.360(6)
C(13)–C(14)	1.37(2)	1.371(4)	1.39(3)	1.376(8)	1.350(6)
C(14)–C(15)	1.36(2)	1.363(4)	1.40(3)	1.369(8)	1.363(6)
C(15)–C(16)	1.34(2)	1.375(4)	1.40(3)	1.378(7)	1.373(5)
C(22)–C(23)	1.35(2)		1.34(3)	1.368(8)	1.367(5)
C(23)–C(24)	1.42(2)		1.39(4)	1.368(9)	1.345(7)
C(24)–C(25)	1.39(2)		1.39(3)	1.374(9)	1.356(6)
C(25)–C(26)	1.35(2)		1.42(3)	1.389(8)	1.371(5)
C(32)–C(33)	1.37(2)		1.38(4)	1.368(8)	1.360(5)
C(33)–C(34)	1.37(2)		1.32(4)	1.385(9)	1.332(6)
C(34)–C(35)	1.38(2)		1.38(4)	1.370(9)	1.360(5)
C(35)–C(36)	1.35(2)		1.43(3)	1.376(8)	1.346(5)
N(11)–Co–N(21)	88.4(4)	85.50(9)[a]	86.9(6)	91.5(2)	88.7(1)
N(11)–Co–N(31)	88.9(5)	85.50(9)[b]	86.6(6)	91.7(2)	89.3(1)
N(21)–Co–N(31)	89.6(5)	85.50(9)[a,b]	85.8(6)	91.6(2)	89.7(1)
N(11)–Co–N(21)	91.6(4)[c]	94.50(9)[d]	93.1(6)[e]	88.5(2)[f]	91.3(1)[g]
N(11)–Co–N(31)	91.1(5)[c]	94.50(9)[g]	93.4(6)[e]	88.3(2)[f]	90.7(1)[e]
N(21)–Co–N(31)	90.4(5)[c]	85.50(9)[d,g]	94.2(6)[e]	91.6(2)[e,f]	90.3(1)[e]
Co–N(11)–C(12)	121(1)	123.3(2)	125(1)	119.5(3)	120.6(3)
C(12)–N(11)–C(16)	119(1)	118.8(2)	117(1)	122.6(3)	121.5(2)
C(12)–N(11)–C(16)	119(1)	117.8(2)	118(2)	117.8(4)	117.9(3)
Co–N(21)–C(22)	123(1)		124(1)	119.4(3)	120.3(3)
Co–N(21)–C(26)	119(1)		117(1)	122.1(3)	121.5(2)
C(22)–N(21)–C(26)	118(1)		118(2)	118.6(4)	118.0(3)
Co–N(31)–C(32)	122(1)		127(1)	119.5(4)	120.4(3)
Co–N(31)–C(36)	121(1)		116(1)	121.8(3)	122.1(2)
C(32)–N(31)–C(36)	117(2)		116(2)	118.5(6)	117.4(3)
C(16)–X(1)–C(26)	109(1)	111.6(2)[a]	110(1)	97.5(2)	101.3(2)
C(16)–X(1)–C(36)	110(1)		109(1)	100.0(2)	101.8(2)
C(26)–X(1)–C(36)	111(1)		108(1)	96.9(2)	99.2(2)
N(11)–C(12)–C(13)	119(2)	123.3(3)	124(2)	122.6(6)	123.2(4)
N(11)–C(16)–X(1)	116(1)	116.8(3)	121(2)	121.0(4)	121.6(2)
N(11)–C(16)–C(15)	122(2)	122.1(3)	120(2)	121.6(5)	121.8(3)
C(15)–C(16)–X(1)	123(2)	121.1(3)	119(2)	117.3(4)	116.6(3)
N(21)–C(22)–C(23)	124(2)		124(2)	121.8(5)	122.6(4)
N(21)–C(26)–X(1)	116(1)		121(2)	121.0(4)	121.4(3)
N(21)–C(26)–C(25)	122(2)		121(2)	118.1(4)	116.8(3)
C(25)–C(26)–X(1)	123(2)		118(2)	120.9(5)	121.7(3)
N(31)–C(32)–C(33)	123(1)		125(2)	122.2(5)	122.9(4)
N(31)–C(36)–X(1)	115(1)		121(2)	121.4(4)	120.6(3)
N(31)–C(36)–C(35)	124(2)		120(2)	120.9(5)	117.5(3)
C(35)–C(36)–X(1)	121(2)		119(2)	117.7(4)	121.9(3)
C(12)–C(13)–C(14)	122(2)	118.5(3)	122(2)	119.2(6)	118.9(4)
C(13)–C(14)–C(15)	117(2)	119.2(3)	114(2)	119.0(5)	119.2(3)
C(14)–C(15)–C(16)	122(2)	119.1(3)	122(2)	119.8(5)	119.0(4)
C(22)–C(23)–C(24)	118(2)		120(2)	119.9(6)	119.0(4)
C(23)–C(24)–C(25)	119(2)		117(2)	119.1(6)	118.9(4)
C(24)–C(25)–C(26)	120(2)		119(2)	119.6(5)	119.8(4)
C(32)–C(33)–C(34)	118(2)		122(2)	119.8(6)	118.7(4)
C(33)–C(34)–C(35)	119(2)		115(2)	117.7(6)	119.4(4)
C(34)–C(35)–C(36)	119(2)		122(2)	120.9(6)	119.7(4)

Symmetry operations: [a] $1-y, -1+x-y, z$; [b] $2-x+y, 1-x, z$; [c] $1-x, -y, -z$; [d] $1+y, 1-x+y, 2-z$; [e] $-x, -y, -z$; [f] $-x, 1-y, 1-z$; [g] $x-y, -1+x, 2-z$.

difference methods. Many peaks were found in the space between the cationic complexes. Only two of these could be unequivocally assigned as being bromide sites, and even they were only partially occupied. The remaining contribution to the 1.5 bromide anions expected could not be discerned from among the many oxygen(water) sites. Hydrogen atoms were included at calculated sites (C–H 0.95 Å) with fixed isotropic thermal parameters and all other atoms, with the exception of minor solvent or anion sites, were refined anisotropically. Full-matrix least-squares methods were used for the refinement (on F) of an overall scale factor, positional and thermal parameters. Neutral atom scattering factors were taken from

Cromer and Waber.[37] Anomalous dispersion effects were included in F_c;[38] the values for $\Delta f'$ and $\Delta f''$ were those of Creagh and McAuley.[39] The values for the mass-attenuation coefficients were those of Creagh and Hubbell.[40] All calculations were performed using the TEXSAN[41] crystallographic software package and plots were drawn using ORTEP.[42]

$[Co\{CH(C_5H_4N\text{-}2)_3\}_2][NO_3]_2$ 2, $[Co\{CH(C_5H_4N\text{-}2)_3\}_2]Br\cdot H_2O$ 3, $[Co\{P(C_5H_4N\text{-}2)_3\}_2][ClO_4]_3\cdot 2H_2O$ 4 and $[Co\{P(C_5H_4N\text{-}2)_3\}_2][NO_3]_2\cdot 8H_2O$ 5. Intensity data for complexes 2–5 were measured at room temperature (20 °C) on an Enraf-Nonius CAD4F (3 and 4) or a Rigaku AFC6R diffractometer (2 and 5) fitted with graphite-monochromated Mo-Kα radiation (λ = 0.710 73 Å) employing the ω–2θ scan technique in each case. The data sets were corrected for Lorentz-polarization effects and an absorption correction was applied for 2,[43] 3[43] and 4.[44]

The structures were solved by placing the metal cation at an appropriate site of symmetry and were each refined (3 and 4;[44] 2 and 5[41]) by a full-matrix least-squares procedure based on *F*. Non-H atoms were refined with anisotropic thermal parameters and H atoms included in the models in their calculated positions (C–H 0.97 Å); the water H atoms were not located in the refinements of complexes 3–5. The refinements were continued until convergence employing a weighting scheme of the form $[\sigma^2(F) + g|F|^2]^{-1}$ for 3 ($g = 0.008$)[44] and 4 ($g = 0.002$)[44] and sigma weights $[1/\sigma^2(F)]$[41] for 2 and 5. The analysis of variance showed no special features indicating that an appropriate weighting scheme had been applied in each case; no corrections were applied for extinction effects. The numbering schemes employed for 4 and 5 are available as supplementary material. All figures are drawn with ORTEP[42] using 25% probability ellipsoids. The SHELX 76[44] program was employed for the analysis of 3 and 4 and TEXSAN[41] for 2 and 5.

Complex 1 consists of cations, disordered Br^- anions and approximately fourteen water molecules. The structure is made up of the hydrophobic cations in a close-packed arrangement with an unusually extensive solvent/anion layer occupying the intervening space, as shown in Fig. 4. In this respect the crystals resemble those of a protein and behave similarly; *i.e.* if the crystals are exposed to air for more than a few seconds they become opaque and do not diffract X-rays. Two of the solvent/anion sites could be assigned as partially occupied bromide, amounting to approximately one bromide. The remaining 0.5 bromide in the asymmetric unit could not be located and one or more of the sites assigned as oxygen must in fact be a bromide. On this basis it is estimated that there are seven water molecules comprising the asymmetric unit. Mobility and disorder of the solvent/anion atoms severely limited the quality and extent of the diffraction data and, as a consequence, a detailed analysis of the derived interatomic parameters is inappropriate.

Atomic coordinates, thermal parameters and bond lengths and angles have been deposited at the Cambridge Crystallographic Data Centre (CCDC). See Instructions for Authors, *J. Chem. Soc., Dalton Trans.*, 1997, Issue 1. Any request to the CCDC for this material should quote the full literature citation and the reference number 186/324.

Results and Discussion

X-Ray crystallography

The structures of the bis(ligand) cobalt complexes of tris(2-pyridyl)methane in three different formal oxidation states have been determined, as well as those of the analogous cobalt-(II) and -(III) complexes of tris(2-pyridyl)phosphine. The structures of a number of cobalt complexes of other tripodal π-acceptor ligands have been reported previously: for the cobalt(III) complexes of tris(2-pyridyl)amine[45] and tris(2-pyridyl)methanol,[46] and the cobalt(II) complex of tris(pyrazol-1-yl)methane.[47]

The molecular structures of the cations in complexes 1–5 are shown in Figs. 1–3 and as supplementary material, and selected interatomic parameters are collected in Table 2; details of anion/solvent geometries and intermolecular associations of interest for 2–5 have been deposited. In the structures of 1 and 3–5 the cobalt atom is located on a crystallographic centre of inversion and in 2 the metal is located at a site of symmetry $\bar{3}$. The cations each feature a slightly distorted N_6 octahedral geometry with the octahedral faces being defined by the nature of the bridgehead atom X in the tripodal ligands $X(C_5H_4N\text{-}2)_3$ where X = CH or P.

As has been noted recently,[48] coherent series of related structures are still relatively rare despite the availability of modern techniques. This arises, in part, because of the difficulty of obtaining suitable crystals for X-ray crystallographic analyses. In the present investigation structures for complexes 1–5 have been obtained, although their analysis has been less than optimal. Significant experimental difficulties were encountered with the diffraction study (see Experimental section) and hence, while the cation structures have been determined unambiguously, there are relatively high errors associated with the derived interatomic parameters in some of the structures, thereby making general comparisons of ligand parameters difficult. Nevertheless, it is still possible to determine with a measure of confidence the magnitude of the Co–N interactions as the oxidation state is changed. Thus, in the $CH(C_5H_4N\text{-}2)_3$ series the average Co–N interactions vary from 1.95(1) to 2.109(2) to 2.111(7) Å for the cobalt-(III), -(II) and -(I) complexes, respectively; *i.e.* a significant increase from Co^{III} to Co^{II} but no apparent increase from Co^{II} to Co^{I}. For the $P(C_5H_4N\text{-}2)_3$ complexes, for which the estimated standard deviations are significantly lower, the average Co–N distance in the cobalt(III) complex of 1.976(2) Å compares with 2.108(2) Å in the cobalt(II) analogue. As the Co–N distances lengthen there is a widening in the Co–N(*n*1)–C(*n*2) angles (n = 1–3) and a concomitant decrease in the Co–N(*n*1)–C(*n*6) angles, particularly for the 1–3 series. Given the limitations of the data it is only possible to compare the geometric parameters for the ligands in 2 and 5 [monitoring the effect on the cobalt(II) centre as X is varied from CH to P] and between 4 and 5 (examining the effect when the oxidation state of cobalt is changed).

Comparing the structures of complexes 2 and 5, *i.e.* changing X from CH to P in the cobalt(II) complexes, the average Co–N bond distances of 2.109(2) and 2.108(2) Å, respectively, are indistinguishable. This similarity is extended to the N–C (ring) bond distances which average 1.332(2) and 1.328(2) Å, respectively, and indeed the C–C distances. The most significant difference in the cations is found in the parameters involving the X atom, *i.e.* the expected increase in X–C and a contraction of the angles (*ca.* 10°) about the X atom in 5. From this analysis it can be concluded that the cobalt and pyridine parameters are largely independent of the nature of X.

Comparing the two $P(C_5H_4N\text{-}2)_3$ structures with the cobalt-(II) and -(III) centres, some systematic changes in the ligand parameters are noted mirroring the changes in the Co–N bond distances. As the Co–N bond distances increase in complex 5 the average N–C(ring) distances decrease, *i.e.* 1.328(2) Å for 5 *cf.* 1.354(3) Å for 4. Even allowing for the greater errors in the C–C parameters in the pyridine rings, the C–C distances in 5 are longer than the comparable distances in 4. Clearly, there is an influence on the ligand parameters as the oxidation state of the cobalt cation is varied.

EXAFS Studies

Extended X-ray absorption fine structure beyond an X-ray absorption edge arises from back scattering of the ejected photoelectron by atoms adjacent to the absorbing atom.[49,50] The intensity and frequency of the EXAFS may be interpreted in terms of the number, nature and distance of the back-scattering atoms adjacent to the absorbing atom,[50–52] and in

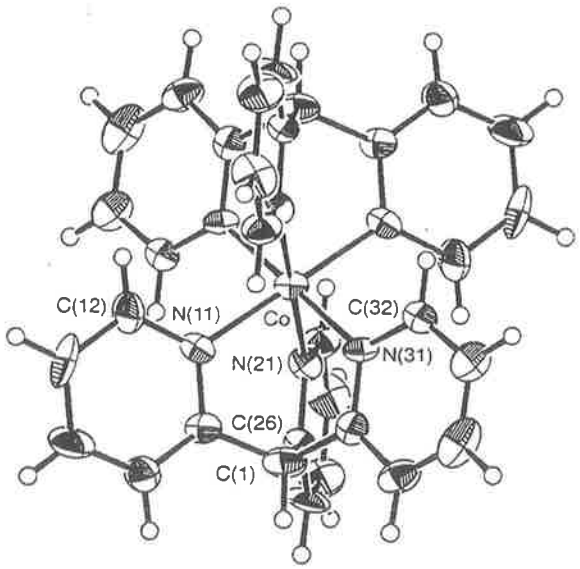

Fig. 1 Molecular structure and crystallographic numbering scheme for the cation in $[Co\{CH(C_5H_4N\text{-}2)_3\}_2]Br_3\cdot 14H_2O$ 1

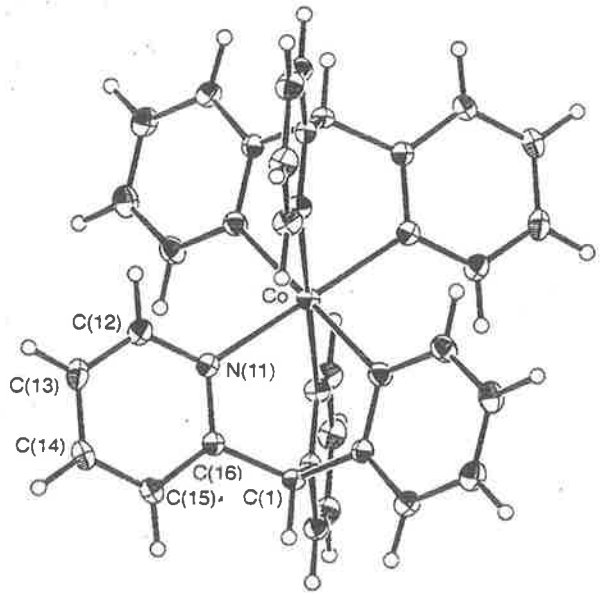

Fig. 2 Molecular structure and crystallographic numbering scheme for the cation in $[Co\{CH(C_5H_4N\text{-}2)_3\}_2][NO_3]_2$ 2

addition the edge position in the normalized near-edge spectra is indicative of the oxidation state.[53]

In the current study of the $[Co\{X(C_5H_4N\text{-}2)_3\}_2]^{n+}$ complexes structural data from the EXAFS measurements provide information complementary to the X-ray crystallographic results. The environment of the central cobalt atoms has been investigated in each complex. This allows a direct comparison of the Co–N distances obtained by cobalt K-edge EXAFS with those determined by X-ray crystallography, and in the case of $[Co\{P(C_5H_4N\text{-}2)_3\}_2]^+$ (where suitable crystals proved elusive) the cobalt K-edge EXAFS provides the only available measurement of the Co–N distances within this complex and allows other predictions regarding its likely structure to be made. Such comparisons have been made previously for the $[Co(bipy)_3]^{n+}$ system.[2,6]

The cobalt K-edge positions and cobalt-ligand distances determined by X-ray absorption spectroscopy are presented in Table 3. There is a clear shift to lower energy in edge position in going from Co^{III} to Co^{II}, with a corresponding increase in the

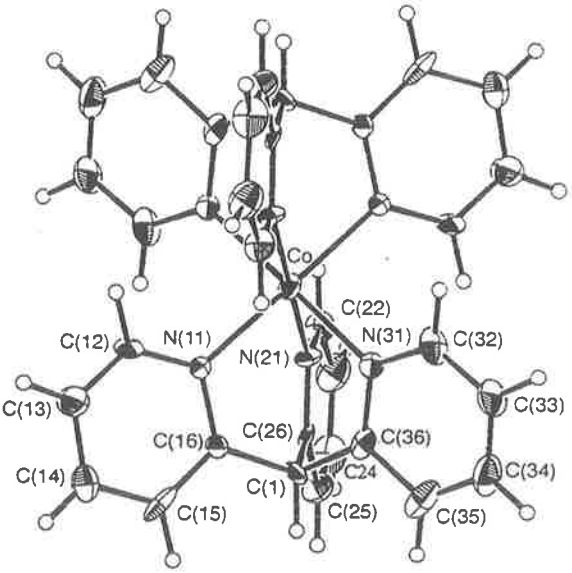

Fig. 3 Molecular structure and crystallographic numbering scheme for the cation in $[Co\{CH(C_5H_4N\text{-}2)_3\}_2]Br\cdot H_2O$ 3

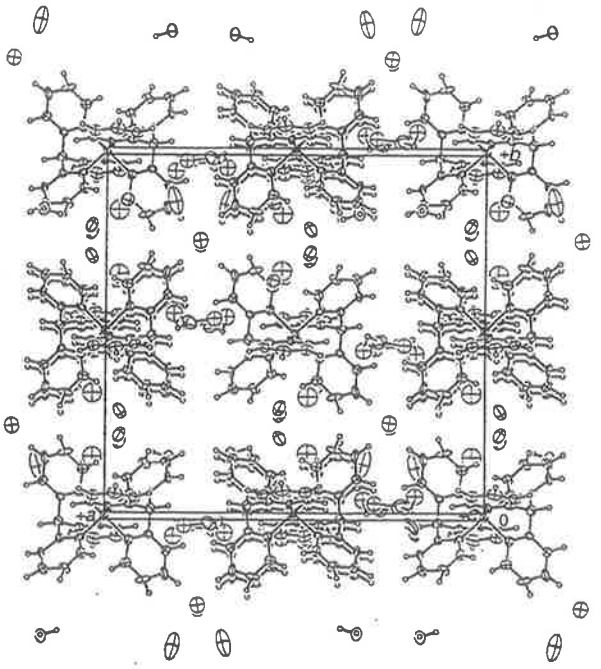

Fig. 4 Packing diagram for complex 1 showing close-packed cations with an intervening solvent–anion layer

Table 3 The K-edge positions (E_0) and Co–N distances as determined by EXAFS and single-crystal X-ray diffraction

		Co–N/Å	
Complex[a]	E_0/eV	EXAFS[b]	X-Ray[c]
$[Co\{CH(C_5H_4N\text{-}2)_3\}_2][ClO_4]_3$	7718.4	1.94	—
$[Co\{CH(C_5H_4N\text{-}2)_3\}_2]Br_3$	—	—	1.95(1)
$[Co\{CH(C_5H_4N\text{-}2)_3\}_2][NO_3]_2$	7714.7	2.12	2.109(2)
$[Co\{CH(C_5H_4N\text{-}2)_3\}_2]Br$	7713.8	2.10	2.111(7)
$[Co\{P(C_5H_4N\text{-}2)_3\}_2][ClO_4]_3$	7718.2	1.97	1.976(2)
$[Co\{P(C_5H_4N\text{-}2)_3\}_2][NO_3]_2$	7714.5	2.13	2.108(2)
$[Co\{P(C_5H_4N\text{-}2)_3\}_2][ClO_4]$	7713.9	2.10	—

[a] Anions indicated, hydration omitted for simplicity. [b] The estimated uncertainty is ±0.03 Å. [c] Average values.

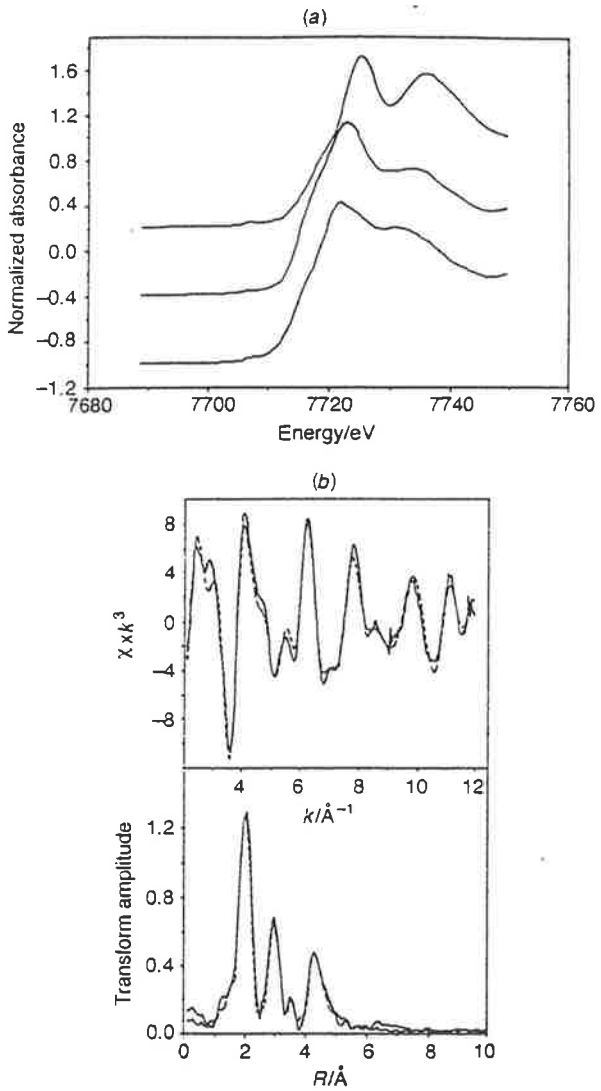

Fig. 5 (*a*) Normalized cobalt-edge XANES (X-ray absorption near-edge structure) profiles of $[Co\{P(C_5H_4N\text{-}2)_3\}_2][ClO_4]_3$ (top), $[Co\{P(C_5H_4N\text{-}2)_3\}_2][NO_3]_2$ and $[Co\{P(C_5H_4N\text{-}2)_3\}_2]ClO_4$ (bottom). (*b*) The EXAFS (top) and Fourier transform of $[Co\{P(C_5H_4N\text{-}2)_3\}_2]ClO_4$. ——, Experiment; – – –, simulation

Co–N bond length. However, there is no significant difference between the cobalt-(II) and -(I) complexes. The k^3-weighted cobalt K-edge EXAFS of $[Co\{P(C_5H_4N\text{-}2)_3\}_2]^{n+}$, together with its Fourier transform are shown in Fig. 5. The equivalent cobalt K-edge spectra for the other complexes have been deposited.

The structural information derived from the EXAFS and X-ray crystallographic determinations shows a high degree of agreement for each of the five complexes where both experiments were possible (Table 3). The EXAFS results confirm the trend in the $[Co\{CH(C_5H_4N\text{-}2)_3\}_2]^{n+}$ series where the bond lengths $Co^{I}\text{–}N \approx Co^{II}\text{–}N > Co^{III}\text{–}N$. The radial distributions of the atoms about the central cobalt up to *ca.* 5 Å (see SUP 57201) are strikingly similar for the $[Co\{CH(C_5H_4N\text{-}2)_3\}_2]^{+}$ and $[Co\{CH(C_5H_4N\text{-}2)_3\}_2]^{2+}$ cations, and for the $[Co\{P(C_5H_4N\text{-}2)_3\}_2]^{+}$ and $[Co\{P(C_5H_4N\text{-}2)_3\}_2]^{2+}$ cations.

Analysis of the structural data cannot in itself answer the principal questions raised regarding the electronic nature of the $[Co\{X(C_5H_4N\text{-}2)_3\}_2]^{n+}$ complexes and the reason for the stabilization of the formally cobalt(I) state. However, such data do establish some very important points. First, the Co–N distance for both the $[Co\{CH(C_5H_4N\text{-}2)_3\}_2]^{n+}$ series is not significantly different for the formally Co^{I}–N and Co^{II}–N species, with the Co^{III}–N bond length substantially shorter. This is exactly analogous to the crystal structure results for the $[Co(bipy)_3]^{n+}$ series.[6] Secondly, if π-back bonding is operative in these systems, the α(C)-to-X (bridgehead) bond distance does not constitute an indicator for it, as there are no significant differences in this parameter for either system. Thirdly, the bridgehead atom imposes steric constraints on the orientation of the pyridine rings, and is responsible for variations in the N–Co–N bond angles and other angles between analogous complexes. Thus the bridgehead atom potentially influences the overlap of metal- and ligand-centred orbitals.

Apart from the obvious structural differences imposed by the oxidation state of the metal centre and the bridgehead atom X, the complexes are very similar with respect to overall geometry and intraligand bond distances and angles. The structural parameters of the pyridine rings in $[Co\{CH(C_5H_4N\text{-}2)_3\}_2]^{+}$ do show some differences to those in the cobalt-(II) and -(III) complexes. However, within the limitations imposed by the accuracy of the crystal structure determinations, it is not possible to identify any significant inequivalence of the pyridine rings in the $[Co\{CH(C_5H_4N\text{-}2)_3\}_2]^{+}$ structure.

The observed pattern of Co–N bond lengths may be considered from two perspectives. On the one hand, as the occupancy of the metal d orbitals varies: Co^{III}, low spin, $(t_{2g})^6$; Co^{II}, high spin, $(t_{2g})^5(e_g)^2$; Co^{I}, high spin, $(t_{2g})^6(e_g)^2$. Thus, the cobalt-(II) and -(I) configurations have two electrons in the Co–N σ-antibonding orbitals and would be expected to have not only bond lengths longer than that for the cobalt(III) situation but also a similar bond length, as the variation in the t_{2g} population is expected to have a lesser effect on the Co–N bond lengths.

The alternative interpretation is one of 'normal' Co^{III}–N and Co^{II}–N distances, and a short Co^{I}–N distance. Two possibilities arise. The $[Co\{X(C_5H_4N\text{-}2)_3\}_2]^{+}$ complexes may be described as $[Co^{II}\{X(C_5H_4N\text{-}2)_3\}\{X(C_5H_4N\text{-}2)_3^{\bullet-}\}]^{+}$ thus essentially containing Co^{II}–N bonds, or $[Co^{I}\{X(C_5H_4N\text{-}2)_3\}_2]^{+}$ with the unusually short Co^{I}–N bond due to significant π-back donation from the Co atom to the $X(C_5H_4N\text{-}2)_3$ ligands.

This issue was pursued by magnetic and spectroscopic studies, and the electronic nature of $[Co\{X(C_5H_4N\text{-}2)_3\}_2]^{+}$ has been investigated in the current study by *ab initio* calculations, as discussed below.

Electronic spectroscopy and bonding parameters

The electronic spectra of the cobalt-(II) and -(III) complexes were measured at 290 and ≈15 K as KBr discs, and the spectra of the cobalt(I) complexes were recorded as solutions in deaerated ethanol at 290 K. The spectrum of a crystal of $[Co\{CH(C_5H_4N\text{-}2)_3\}_2][PF_6]_2$ was also measured over the range 18 000–25 000 cm^{-1}.

For the ligand $CH(C_5H_4N\text{-}2)_3$, the cobalt(III) complex shows a broad peak centred at 23 000 cm^{-1} which can be assigned as the transition to the components of the $^1T_{1g}$ excited state, with absorption to charge transfer commencing at ≈27 000 cm^{-1}. A similar assignment has been reported[48] for the $CH(pz)_3$ (pz = pyrazolyl) complex, with the transition here occurring at 21 500 cm^{-1}. The higher band energy for the $CH(C_5H_4N\text{-}2)_3$ complex is in line with the bonding parameters derived for complexes of the mixed tripod ligand $CH(C_5H_4N\text{-}2)(pz)_2$, where pyridine was found to be a stronger ligand than pyrazole.[54]

The spectrum of the cobalt(II) complex is shown in Fig. 6(*a*) and consists of a peak at 11 800 cm^{-1} with a shoulder at 13 200 cm^{-1}, a weak sharp peak due to a spin-forbidden transition at 19 735 cm^{-1} and a broad peak centred at ≈23 100 cm^{-1} with a shoulder at ≈22 300 cm^{-1}. The first two transitions may safely be assigned to the $^4A_{1g}$ and ^4E_g states derived from the $^4T_{2g}$ level of the parent octahedral complex. The pair of peaks at *ca.* 23 000 cm^{-1} probably encompass the transitions to the $^4A_{2g}$ and ^4E_g states of the $^4T_{1g}$ level and the transition to the $^4A_{2g}(P)$ state which, as noted previously,[55] gives rise to a weak band which is

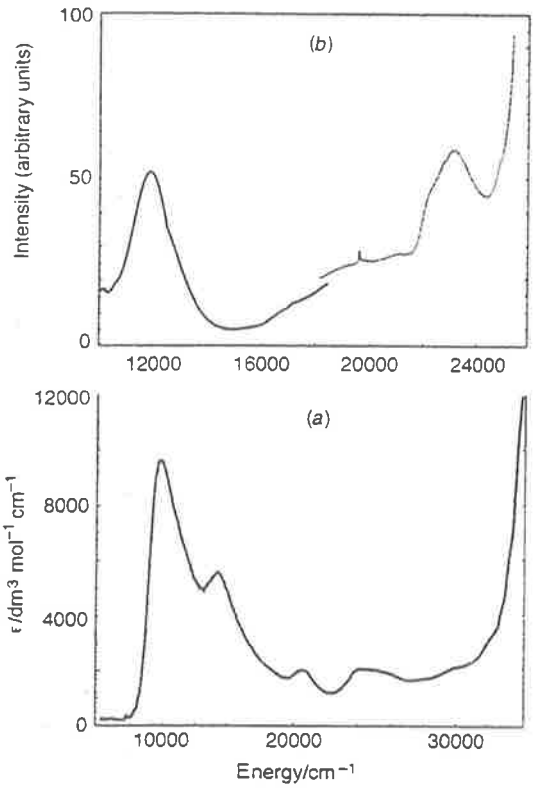

Fig. 6 The UV/VIS spectra of (*a*) $[Co\{CH(C_5H_4N\text{-}2)_3\}_2]^+$ (ethanol solution) and (*b*) $[Co\{CH(C_5H_4N\text{-}2)_3\}_2]^{2+}$ at 15 K [KBr disc and single crystal (···)]

often not resolved. The band energies and assignments are given in Table 4.

The solution spectrum of the $[Co\{CH(C_5H_4N\text{-}2)_3\}_2]^+$ species is shown in Fig. 6(*b*) and is dominated by a very intense peak at 9800 cm^{-1} ($\varepsilon = 10\,000$ dm^3 mol^{-1} cm^{-1}). This may be assigned as a metal-to-ligand charge-transfer transition, the low energy being consistent with the easy access of the cobalt(II) state, and the ready availability of low-energy empty π^* orbitals on the ligand. A peak of moderate intensity occurs at 14 200 cm^{-1}, with a weaker band at 20 600 cm^{-1}, a weak broad band centred at ≈25 000 cm^{-1} and a very weak shoulder at ≈32 000 cm^{-1} on the edge of the intense absorption due to charge transfer and/or intraligand transitions. The assignment of the bands to 'd–d' transitions can only be tentative, since additional peaks may be masked under the intense charge-transfer band at 9800 cm^{-1}; moreover, it is possible that weak charge-transfer transitions may occur in this region. Three spin-allowed transitions are expected for the d^8-electron configuration of Co^I in an approximately octahedral ligand environment, and the bands at 14 200 and 20 600 cm^{-1} may be assigned to the transitions to the $^3T_{2g}$ and $^3T_{1g}(F)$ states, respectively. The transition to the $^3T_{1g}(P)$ state may then either give rise to the very weak peak at ≈32 000 cm^{-1} or be masked under the intense absorption commencing at ≈33 000 cm^{-1}. The weak broad band at ≈25 000 cm^{-1} is assigned to several spin-forbidden transitions which are expected in this region. The band energies and tentative assignments are summarized in Table 4.

Basically similar spectra were observed for the complexes of $P(C_5H_4N\text{-}2)_3$. That of the cobalt(III) complex shows a shoulder at ≈22 000 cm^{-1} which may be assigned to the 'd–d' transition to the $^1T_{1g}$ state, occurring on the edge of an intense charge-transfer absorption. The band energies and assignments of the cobalt-(II) and -(I) complexes are given in Table 4. Those of the cobalt(II) complex are very similar to those reported for the visible region by Holm *et al.*[56] for an acetonitrile solution of this complex (11 000 and 21 800 cm^{-1}) with the observation of additional weak peaks at 18 500 and 19 450 cm^{-1} in the present work assigned to spin-forbidden transitions. The intense metal-to-ligand charge-transfer occurs at slightly lower energy for $[Co\{P(C_5H_4N\text{-}2)_3\}_2]^+$ than for $[Co\{CH(C_5H_4N\text{-}2)_3\}_2]^+$ (8600 compared with 9800 cm^{-1}). A similar change has been observed for the iron(II) complexes of these ligands[57] where the corresponding bands occur at 21 500 and 22 800 cm^{-1}. The onset of the intense absorption in the ultraviolet also occurs at slightly lower energy in the $P(C_5H_4N\text{-}2)_3$ complex, ≈33 500 cm^{-1}.

For the cobalt(II) compounds metal–ligand bonding parameters were derived using the angular overlap model (AOM) by methods identical to those described previously for the analogous $CH(pz)_3$ and $CH(C_5H_4N\text{-}2)(pz)_2$[54] complexes. The calculated transition energies and associated bonding parameters are indicated in Table 4. Note that the π-bonding parameter refers to the out-of-plane interaction, the in-plane interaction being assumed negligible, as found in other studies.[47] The three sets of parameters for the $P(C_5H_4N\text{-}2)_3$ complex refer to the three different Co–N bond distances.[47,54] For both complexes, excellent agreement with the observed transition energies is obtained, the σ- and π-bonding parameters being very similar to those reported[54] for the pyridine group in $[Co\{CH(C_5H_4N\text{-}2)(pz)_2\}_2]^{2+}$ (e_σ ≈4575 cm^{-1}, $e_\pi = 930$ cm^{-1}), and quite similar to those of the pyrazole groups in $[Co\{CH(pz)_3\}_2]^{2+}$ (e_σ ≈4540 cm^{-1}, e_π ≈585 cm^{-1}).[47] Both $P(C_5H_4N\text{-}2)_3$ and $CH(C_5H_4N\text{-}2)_3$ thus act as quite strong σ donors and moderate π donors towards Co^{II}. The close similarity between the two sets of parameters implies that any conjugation across the bridgehead atom in the former ligand has an insignificant effect upon the π interaction with the metal.

Since the assignment of the 'd–d' transitions of the cobalt(I) compounds is only tentative any discussion of the bonding parameters in these complexes must be viewed with caution. If it is assumed that the peaks at ≈14 000 cm^{-1} correspond to the first transition of the cobalt(I) ion, calculated transition energies which are consistent with the spectrum observed for $[Co\{CH(C_5H_4N\text{-}2)_3\}_2]^+$ are obtained using an average σ-bonding parameter e_σ ≈4760 cm^{-1} with e_π close to zero. As in previous studies,[47,54] the e_σ values were scaled to take into account the different Co–N bond lengths observed in the solid complex, though it is possible that these differences are smaller in solution. The calculated splittings in each excited state are quite small, and consistent with the observed band widths. A significant non-zero value of e_π would be expected to produce resolvable band splittings similar to those observed for the analogous isoelectronic nickel(II) complexes.[47,58] The Racah parameter $B = 675$ cm^{-1} used in the calculations seems acceptable, representing a reduction to ≈77% of the value of 880 cm^{-1} estimated for the free cobalt(I) ion.[59] As the crystal structure of the $[Co\{P(C_5H_4N\text{-}2)_3\}_2]^+$ complex is unknown, analysis of the spectrum is less reliable. However, assuming a structure similar to that of the $[Co\{CH(C_5H_4N\text{-}2)_3\}_2]^+$ complex, which, except for the differences in the Co–N bond lengths, appears to be reasonable from an analysis of the EXAFS data, the transition energies may be reproduced satisfactorily using similar, though marginally smaller bonding and Racah parameters.

The above interpretation implies that the σ-bonding interaction in the cobalt(I) complexes is quite similar to that in the cobalt(II) complexes. This seems reasonable, as although the lower oxidation state will cause an expansion of the d orbitals, enhancing overlap with the ligand orbitals, the concomitant increase in the energy separation between the metal and ligand σ-bonding orbitals will produce a decrease in the metal–ligand interaction energy. Apparently, the two effects approximately balance. The marked decrease in the π-donor capacity of the ligands when the metal is in the lower oxidation state also seems reasonable, as the metal t_{2g} orbitals will shift in energy away from the filled ligand π orbitals towards the empty ligand π^* orbitals. The relatively high π-acceptor character of the ligand

Table 4 Calculated and observed transition energies (in cm^{-1}) of the complexes $[Co\{X(C_5H_4N\text{-}2)_3\}_2]^{n+}$ (X = CH or P; n = 1 or 2)

$[Co\{CH(C_5H_4N\text{-}2)_3\}_2]^+$		
Transition	Calculated	Observed
c.t.[a]		9 800
$^1A_{2g} \longrightarrow {}^1T_{2g}$[b]	13 600 14 300 14 550	14 200
$^1A_{2g} \longrightarrow {}^1T_{1g}$[b]	19 950 20 700 21 200	20 600
c		≈25 000
$^1A_{2g} \longrightarrow {}^1T_{1g}$[b]	31 650 31 800 32 225	32 000
Bonding and Racah parameters (cm^{-1})		
e_σ	4500, 4650, 5135	
e_{π}	0	
$e_{\pi'}$	0	
B	675	

$[Co\{CH(C_5H_4N\text{-}2)_3\}_2]^{2+}$		
Transition	Calculated	Observed
$^4A_{2g} \longrightarrow {}^4A_{1g}$ $^4A_{2g} \longrightarrow {}^4E_g$	11 620 13 000	11 800 13 200
c		19 725
$^4A_{2g} \longrightarrow {}^4A_{1g}$ $^4A_{2g} \longrightarrow {}^4E_g$	22 520 22 920	22 300 23 100
	4850	
	950	
	0	
	810	

$[Co\{P(C_5H_4N\text{-}2)_3\}_2]^+$		
Transition	Calculated	Observed
c.t.[a]		8 600
$^1A_{2g} \longrightarrow {}^1T_{2g}$	13 950 14 000 14 030	14 025
$^1A_{2g} \longrightarrow {}^1T_{1g}$[b]	19 525 20 250 20 375	19 600
c		≈23 250
$^1A_{2g} \longrightarrow {}^1T_{1g}$[b]	30 925 31 050 31 925	≈29 500
	4700	
	0	
	0	
	625	

$[Co\{P(C_5H_4N\text{-}2)_3\}_2]^{2+}$		
Transition	Calculated	Observed
$^4A_{1g} \longrightarrow {}^4T_{2g}$	10 800 11 400 12 800	12 000
c		18 500 19 450
$^4A_{1g} \longrightarrow {}^4T_{1g}$	21 510 21 600 22 500	21 800
	4400, 4600, 4700	
	890, 930, 960	
	0	
	740	

[a] Metal-to-ligand charge-transfer transition. [b] Assignment tentative, see discussion. [c] Spin-forbidden transition, several of which are predicted in this region.

Table 5 Electrochemical data for $[Co\{X(C_5H_4N\text{-}2)_3\}_2]^{n+}$ cations and $[Co(bipy)_3]^{n+}$ [25,46]

	$E_{\frac{1}{2}}$/V	
Complex	Co^{III}–Co^{II}	Co^{II}–Co^{I}
$[Co(bipy)_3]^{n+}$	0.32	−1.01
$[Co\{N(C_5H_4N\text{-}2)_3\}_2]^{n+}$ [a]	0.35	−1.11
$[Co\{CH(C_5H_4N\text{-}2)_3\}_2]^{n+}$	0.22	−1.21
$[Co\{P(C_5H_4N\text{-}2)_3\}_2]^{n+}$	0.55	−0.97
$[Co\{OP(C_5H_4N\text{-}2)_3\}_2]^{n+}$	0.99	−0.75
$[Co\{COH(C_5H_4N\text{-}2)_3\}_2]^{n+}$	0.19	−1.17

[a] In acetonitrile–0.1 mol dm^{-3} $NBu^n_4PF_6$ solution: platinum-button working electrode; 298 K; scan rate 100 mV s^{-1}; reference, saturated sodium chloride calomel electrode (SSCE). [b] Propylene carbonate (4-methyl-1,3-dioxolan-2-one)–0.2 mol dm^{-3} $NBu^n_4PF_6$.

in the cobalt(I) complexes is in accord with the behaviour normally associated with aromatic amines.

The ligand-field-splitting parameter Δ is given by $3e_\sigma - 2e_\pi$ for an aromatic amine with negligible in-plane π bonding. Substitution of the appropriate values (Table 4) implies that Δ rises from ≈12 650 cm^{-1} for $[Co\{CH(C_5H_4N\text{-}2)_3\}_2]^{2+}$ to ≈14 200 cm^{-1} for $[Co\{CH(C_5H_4N\text{-}2)_3\}_2]^{+}$, with the increase being due entirely to the enhanced π-acceptor character of the ligand. It is generally observed that a decrease in oxidation state is accompanied by a marked *decrease* in Δ, as is indeed the case on going from $[Co\{CH(C_5H_4N\text{-}2)_3\}_2]^{3+}$, where Δ ≈ 25 000 cm^{-1}, to $[Co\{CH(C_5H_4N\text{-}2)_3\}_2]^{2+}$. However, it has been suggested[60] that the dominant cause of the decrease in Δ associated with the change from Co^{II} to Co^{III} is the marked contraction in the metal–ligand bond length, from 2.109 to 1.95 Å in the present case. The present analysis appears to support this viewpoint, suggesting that, at least where low oxidation states are concerned, a decrease in oxidation state is not always accompanied by a decrease in Δ.

It must be stressed that the above analysis is only tentative. An acceptable fit to the observed transition energies may also be obtained if the first spin-allowed transition of $[Co\{CH(C_5H_4N\text{-}2)_3\}_2]^{+}$ is at ≈10 000 cm^{-1}, masked by the charge-transfer transition at 9800 cm^{-1}, with calculated energies of the $^3T_{1g}$ states then being at 14 200 and 22 000 cm^{-1}. This would imply a Δ value of ≈10 000 cm^{-1}, considerably lower than the 12 650 cm^{-1} for the corresponding cobalt(II) complex. However, a Racah *B* parameter of ≈470 cm^{-1} is required for this assignment, which seems an unacceptably large reduction from the free-ion value of 880 cm^{-1} for Co^{I}.

Electrochemical studies

The electrochemical data for the cobalt complexes of a number of tripod ligands and bipy are given in Table 5.[25,46] The potential of the Co^{II}–Co^{I} couple can be taken as a measure of the stability of the cobalt(I) state. The data indicate that the $[Co\{X(C_5H_4N\text{-}2)_3\}_2]^{+}$ cations are stabilized to an extent comparable to $[Co(bipy)_3]^{+}$. It is expected that the reduction potentials of the unbound ligands would vary to a much greater degree than the Co^{II}–Co^{I} couples, indicating significant metal involvement in the reduction of the complexes. Unfortunately, reliable $E_{\frac{1}{2}}$ values for the ligand reductions cannot be obtained as they exhibit irreversible behaviour. The reduction potentials of the complexes infer there is a similarity in the nature of the metal–ligand interaction. The variations may well be due to the different steric constraints imposed on the ligands by the bridgehead atoms as suggested by Hafeli and Keene,[25] and elucidated by the structural studies described previously.

Ab initio studies

Single-point density functional theory *ab initio* calculations at the X-ray geometries have been performed for the $[Co\{CH(C_5H_4N\text{-}2)_3\}_2]^{n+}$ and $[Co\{P(C_5H_4N\text{-}2)_3\}_2]^{n+}$ ions (n = 1–3). For comparison similar calculations were also run on the $[Co(bipy)_3]^{n+}$ (n = 1–3) system. Mulliken population analysis has been used to obtain information about the atomic charges of these complexes. Although such population-analysis schemes are sensitive to the basis set used they generally provide good comparative results across series of closely related molecules.[33,35] In this work the population analysis was employed to provide supplementary information in support of the experimental data.

Results of the DFT calculations are summarized in Table 6. Only one spin state was considered for each of the cobalt-(I) and -(III) species, formally high and low spin respectively. The ion $[Co(bipy)_3]^{2+}$ is considered to be a high-spin species, although a low-spin form can also be postulated. The high-spin form of $[Co(bipy)_3]^{2+}$, and of the tripod species, is calculated to be the more stable spin state, which is in accord with the experimental data for $[Co(bipy)_3]^{2+}$.[20] In all species investigated the calculated bond orders (Co–N overlap populations) are of a similar magnitude and no significant differences or trends are apparent. These calculations are geometry dependent; however, the results can be interpreted as indicating no major difference exists between the strength of the Co–N bonds within the different species. Significant differences do exist in the calculated spin density of the cobalt, with the cobalt(I) and high-spin cobalt(II) species having approximately equal spin density, and the low-spin cobalt(II) species having relatively less spin (as expected); the cobalt(III) species are formally spin neutral. The similarity between the spin states on the high-spin Co^{II} and Co^{I} suggests a similarity in the local cobalt electronic environments in each case that is independent of the formal oxidation state of the species. Such a conclusion could also be drawn from the fact that relatively sharp ^1H NMR spectra can be observed for both $[Co(bipy)_3]^{+}$ and $[Co(bipy)_3]^{2+}$.[19,61]

Mulliken atomic charges for the cobalt and nitrogen atoms are presented in Table 7. The calculated charges on the cobalt atoms are somewhat less than the formal oxidation states, indicating that the charge is distributed throughout the entire systems, consistent with a π-back bonding mechanism. It is important to note that the population analysis and partitioning of charge (and spin) onto any particular centre is not unique so that the resulting total atomic charge is *not* an exact or unique measure. A more complete analysis using fully geometry-optimized structures with high-level basis sets and an atoms in molecules (AIM) description[62] of the intramolecular charge distribution of the present complexes is being investigated.[63] What is apparent from the results presented is that the cobalt(II)–radical anion ligand species model for the cobalt(I) species is not supported by these calculations, and that the spin-density and Mulliken-analysis results suggest an equivalence between the cobalt environments within the cobalt-(I) and -(II) species.

Conclusion

Although no individual experiment reported here provides an unequivocal picture of the nature of the stabilization of the cobalt(I) oxidation state in the present complexes, the accumulation of evidence from the variety of measurements obtained presents a consistent description. The X-ray and EXAFS data are in close accord, and show the Co–N bond lengths in the order $Co^{I} \approx Co^{II} < Co^{III}$, suggesting there is a similarity in the local cobalt environment for the +I and +II oxidation states. Further analysis shows that the C–X bridgehead distance can be wholly explained as a function of the bridging atom, without reference to the oxidation state of the complex. Similar observations have also been made for the $[Co(bipy)_3]^{n+}$ system. The AOM analysis of the electronic spectra yields very similar bonding parameters for the ligands $X(C_5H_4N\text{-}2)_3$ (X = CH or P) when complexed to Co^{II}. This implies that the bridgehead

Table 6 Results of SCF calculations on the cobalt polypyridyl species

System	Charge	Multiplicity	E^a	Co–N Overlap population[b]	Spin density on Co[c]
$[Co(bipy)_3]^{n+}$	1	3	−2838.0916	0.1927	2.67
	2	2	−2837.8077	0.1939	1.02
	2	4	−2837.8154	0.1950	2.85
	3	1	−2837.0196	0.1893	0.00
$[Co\{CH(C_5H_4N\text{-}2)_3\}_2]^{n+}$	1	3	−2914.7905	0.1871	2.31
	2	2	−2914.5705	0.1936	0.76
	2	4	−2914.5764	0.1897	2.77
	3	1	−2913.8383	0.1983	0.00
$[Co\{P(C_5H_4N\text{-}2)_3\}_2]^{n+}$	1	3	−3515.2157	0.2021	2.52
	2	2	−3515.0042	0.1927	0.96
	2	4	−3515.9491	0.1894	2.35
	3	1	−3514.6512	0.2041	0.00

[a] Electronic energy in Hartrees (≈4.36 × 10^{-18} J). [b] Average calculated from Mulliken population overlaps. [c] Total orbital spin condensed onto the cobalt atom; total spin multiplicity of the system = 1.

Table 7 Mulliken populations on the cobalt and nitrogen atoms of the cobalt polypyridyl species

		Charge/multiplicity			
System	Atom	1/3	2/2	2/4	3/1
$[Co(bipy)_3]^{n+}$	Co	0.884	0.907	0.937	1.451
	N	−0.646	−0.651	−0.644	−0.740
	N	−0.714	−0.721	−0.721	−0.740
	N	−0.671	−0.678	−0.679	−0.764
	N	−0.634	−0.632	−0.644	−0.749
	N	−0.650	−0.653	−0.648	−0.762
	N	−0.685	−0.682	−0.694	−0.751
$[Co\{CH(C_5H_4N\text{-}2)_3\}_2]^{n+}$	Co	0.858	0.957	0.950	1.404
	N	−0.674	−0.655	−0.660	−0.719
	N	−0.651	−0.660	−0.658	−0.715
	N	−0.672	−0.664	−0.658	−0.740
	N	−0.675	−0.655	−0.660	−0.719
	N	−0.656	−0.660	−0.656	−0.715
	N	−0.671	−0.665	−0.658	−0.740
$[Co\{P(C_5H_4N\text{-}2)_3\}_2]^{n+}$	Co	1.021	1.405	1.362	1.640
	N	−0.621	−0.633	−0.649	−0.666
	N	−0.622	−0.690	−0.696	−0.653
	N	−0.619	−0.650	−0.660	−0.663
	N	−0.639	−0.614	−0.625	−0.667
	N	−0.620	−0.679	−0.689	−0.657
	N	−0.618	−0.677	−0.672	−0.663

atom has little influence on the bonding parameters. The cobalt(I) complexes $[Co\{CH(C_5H_4N\text{-}2)_3\}_2]^+$ and $[Co\{P(C_5H_4N\text{-}2)_3\}_2]^+$ have similar bonding parameters that probably correspond to a somewhat larger ligand-field splitting than for the cobalt(II) complexes, possibly due to the influence of $Co(d_\pi)\rightarrow L(\pi^*)$ back donation. Results from the DFT calculations suggest that despite the formal oxidation state on the complexes the cobalt-(I) and -(II) species all have similar Mulliken charges and spins on the Co atom. Also, the sum of the Mulliken charges on the cobalt and co-ordinated nitrogens is ≈ −3 for the cobalt-(I) and -(II) complexes studied. This indicates that the ligand accepts a greater or lesser degree of electron density as required to maintain a stable environment around the cobalt.

Accordingly, $Co(d_\pi)\rightarrow L(\pi^*)$ back donation appears to be operative in both the present cobalt(I) complexes. However, the clear inference of the studies is that conjugation between the pyridine ligands is not a significant feature with regard to the bonding of any of these ligands with Co^I, and the back donation is not further stabilized by electron delocalization within the ligand system. If delocalization is to be discounted, the most likely option is simply that of the chelate effect stabilizing the high charge accumulation on the tripod ligands resulting from π-back donation. Such a conclusion, while not in fundamental disagreement with current thinking, widens the possible variety of ligand systems that may stabilize Co^I and therefore extend the possible catalytic actions of this metal ion.

Acknowledgements

This work was supported by the Australian Research Council (F. R. K., M. A. H., E. R. T. T. and T. W. H.). We thank the Director of the Daresbury Laboratory (UK) for the provision of facilities for the EXAFS measurements.

References

1 A. Juris, S. Barigelletti, S. Camagna, V. Balzani, P. Belser and A. von Zelewsky, *Coord. Chem. Rev.*, 1988, **84**, 85.
2 B. S. Brunschwig, C. Creutz, D. H. Macartney, T.-K. Sham and N. Sutin, *Faraday Discuss. R. Soc. Chem.*, 1982, **74**, 113.
3 C. Creutz and N. Sutin, *Coord. Chem. Rev.*, 1985, **64**, 321.
4 H. A. Schwarz, C. Creutz and N. Sutin, *Inorg. Chem.*, 1985, **24**, 433.
5 S. Margel, W. Smith and F. C. Anson, *J. Electrochem. Soc.*, 1978, **125**, 241.
6 D. J. Szalda, C. Creutz, D. Mahajan and N. Sutin, *Inorg. Chem.*, 1983, **22**, 2372.
7 C. V. Krishnan, B. S. Brunschwig, C. Creutz and N. Sutin, *J. Am. Chem. Soc.*, 1985, **107**, 2005.
8 C. V. Krishnan, C. Cruetz, D. Mahajan, H. A. Schwarz and N. Sutin, *Isr. J. Chem.*, 1982, **22**, 98.
9 C. V. Krishnan and N. Sutin, *J. Am. Chem. Soc.*, 1981, **103**, 2141.
10 F. R. Keene, C. Creutz and N. Sutin, *Coord. Chem. Rev.*, 1985, **64**, 247.
11 J. Hawecker, J.-M. Lehn and R. Ziessel, *J. Chem. Soc., Chem. Commun.*, 1983, 536.
12 J.-M. Lehn and R. Ziessel, *Proc. Natl. Acad. Sci. USA*, 1982, **79**, 701.

13 S. Margel and F. C. Anson, *J. Electrochem. Soc.*, 1978, **125**, 1232.
14 D. A. Reitsma and F. R. Keene, *Organometallics*, 1994, **13**, 1351.
15 T. Saji and S. Aoyagui, *J. Electroanal. Chem. Interfacial Electrochem.*, 1974, **60**, 1.
16 Y. Kaizu, Y. Torii and H. Kobayashi, *Bull. Chem. Soc. Jpn.*, 1970, **43**, 3296.
17 G. M. Waind and B. Martin, *J. Inorg. Nucl. Chem.*, 1958, **8**, 551.
18 D. K. Lavallee, M. D. Baughman and M. P. Phillips, *J. Am. Chem. Soc.*, 1977, **99**, 718.
19 R. J. Fitzgerald, B. B. Hutchinson and K. Nakamoto, *Inorg. Chem.*, 1970, **9**, 2618.
20 R. W. Asmussen, *Magneto Kemiske Undersogelser over Uorganiske Kompleksforbindsler*, Gjellerups, Forland, Copenhagen, 1944.
21 D. K. Lavellee and E. B. Fleischer, *J. Am. Chem. Soc.*, 1972, **94**, 2583.
22 K. Yanagi, Y. Osashi, Y. Kaizu and H. Kobayashi, *Bull. Chem. Soc. Jpn.*, 1981, **54**, 118.
23 R. K. Boggess and D. Zatko, *Inorg. Nucl. Chem. Lett.*, 1976, **12**, 7.
24 R. K. Boggess and D. Zatko, *Inorg. Chem.*, 1976, **15**, 626.
25 T. A. Hafeli and F. R. Keene, *Aust. J. Chem.*, 1988, **41**, 1379.
26 D. D. Perrin, W. L. F. Armarego and D. R. Perrin, *Purification of Laboratory Chemicals*, Permagon, London, 1980.
27 N. Binsted, J. W. Campbell, S. J. Gurman and P. C. Stephenson, SERC Daresbury Laboratory, 1991.
28 F. R. Keene, M. R. Snow, P. J. Stephenson and E. R. T. Tiekink, *Inorg. Chem.*, 1988, **27**, 2040.
29 GAUSSIAN 94, Revision B.3, M. J. Frisch, G. W. Trucks, H. B. Schlegel, P. M. W. Gill, B. G. Johnson, M. A. Robb, J. R. Cheeseman, T. Keith, G. A. Petersson, J. A. Montgomery, K. Raghavachari, M. A. Al-Laham, V. G. Zakrzewski, J. V. Ortiz, J. B. Foresman, C. Y. Peng, P. Y. Ayala, W. Chen, M. W. Wong, J. L. Andres, E. S. Replogle, R. Gomperts, R. L. Martin, D. J. Fox, J. S. Binkley, D. J. Defrees, J. Baker, J. P. Stewart, M. Head-Gordon, C. Gonzalez and J. A. Pople, Gaussian Inc., Pittsburgh, PA, 1995.
30 S. H. Vosko, L. Wilk and M. Nusair, *Can. J. Phys.*, 1980, **58**, 1200.
31 R. S. Mulliken, *J. Chem. Phys.*, 1955, **23**, 2338.
32 R. S. Mulliken, *J. Chem. Phys.*, 1955, **23**, 1833.
33 W. J. Hehre, L. Radom, P. v. R. Schleyer and J. A. Pople, *Ab Initio Molecular Orbital Theory*, Wiley, New York, 1986.
34 M. Vitale, C. K. Ryu, W. E. Palke and P. C. Ford, *Inorg. Chem.*, 1994, **33**, 561.
35 G. S. Chandler, G. A. Christos, B. N. Figgis, D. P. Gribble and P. A. Reynolds, *J. Chem. Soc., Faraday Trans*, 1992, 1953.
36 G. M. Sheldrick, in *Crystallographic Computing 3*, eds. G. M. Sheldrick, C. Krüger and R. Goddard, Oxford University Press, Oxford, 1986, pp. 175–189.
37 D. T. Cromer and J. T. Waber, *International Tables for X-Ray Crystallography*, Kynoch Press, Birmingham, 1974, vol. 4, pp. 2339–2346.
38 J. A. Ibers and W. C. Hamilton, *Acta Crystallogr.*, 1964, **17**, 781.
39 D. C. Creagh and W. J. McAuley, in *International Tables for Crystallography*, ed. A. J. C. Wilson, Kluwer Academic Publishers, Boston, 1992, vol. C, Table 4.2.6.8, pp. 219–222.
40 D. C. Creagh and J. H. Hubbell, in *International Tables for Crystallography*, ed. A. J. C. Wilson, Kluwer Academic Publishers, Boston, 1992, vol. C, Table 4.2.4.3, pp. 200–206.
41 TEXSAN, Crystal Sructure Analysis Package, Molecular Structure Corporation, Houston, TX, 1985 and 1992.
42 C. K. Johnson, ORTEP, A Thermal Ellipsoid Plotting Program, Oak Ridge National Laboratory, Oak Ridge, TN, 1965.
43 N. Walker and D. Stuart, *Acta Crystallogr., Sect. A*, 1983, **39**, 158.
44 G. M. Sheldrick, SHELX 76, *Program for Crystal Structure Determination*, Univeristy of Cambridge, 1976.
45 E. S. Kucharski, W. R. McWhinnie and A. H. White, *Aust. J. Chem.*, 1978, **311**, 2647.
46 D. A. Szalda and F. R. Keene, *Inorg. Chem.*, 1986, **25**, 2795.
47 T. Astley, J. M. Gulbis, M. A. Hitchman and E. R. T. Tiekink, *J. Chem. Soc., Dalton Trans.*, 1993, 509.
48 R. Taylor and F. H. Allen, *Structure Correlation*, eds. H.-B. Bürgi and J. D. Dunitz, VCH, Weinheim, 1994, vol. 4, pp. 111–161.
49 P. A. Lee and J. B. Pendry, *Phys. Rev. B*, 1975, **11**, 2795.
50 B. K. Teo, *EXAFS: Basic Principles and Data Analysis*, Springer, Berlin, 1986.
51 S. J. Gurman, N. Binsted and I. Ross, *J. Phys. C.*, 1986, **19**, 1845.
52 S. J. Gurman, N. Binsted and I. Ross, *J. Phys. C.*, 1984, **17**, 143.
53 C. D. Garner, *Adv. Inorg. Chem.*, 1991, **36**, 303.
54 T. Astley, A. J. Canty, M. A. Hitchman, G. L. Rowbottom, B. W. Skelton and A. H. White, *J. Chem. Soc., Dalton Trans.*, 1991, 1981.
55 A. B. P. Lever, *Inorganic Electronic Spectroscopy*, Elsevier, Amsterdam, 1984, p. 480.
56 E. Larsen, G. N. La Mar, B. E. Wagner, J. E. Parks and R. H. Holm, *Inorg. Chem.*, 1972, **11**, 2652.
57 T. Astley, Ph.D. Thesis, University of Tasmania, 1993.
58 T. Astley, M. A. Hitchman, F. R. Keene and E. R. T. Tiekink, *J. Chem. Soc., Dalton Trans.*, 1996, 1845.
59 B. N. Figgis, *Introduction to Ligand Fields*, Interscience, New York, 1964, p. 52.
60 M. A Hitchman, *Inorg. Chem.*, 1982, **21**, 821.
61 M. L. Wicholas and R. S. Drago, *J. Am. Chem. Soc.*, 1968, **90**, 2196.
62 R. F. W. Bader, *Atoms in Molecules, A Quantum Theory*, Clarendon, Oxford, 1990.
63 K. R. Adam, I. M. Atkinson, N. Green and F. R. Keene, unpublished work.

Received 29*th August* 1996; *Paper* 6/05967H

548 Zeitschrift für Kristallographie 209, 548–549

Crystal structure of bis[tris(pyrazol-1-yl)methane]cobalt(II) nitrate (redetermination at 173 K), $C_{20}H_{20}CoN_{14}O_6$

F. R. Keene

Department of Molecular Sciences, James Cook University of North Queensland, Townsville, Queensland 4811, Australia

and E. R. T. Tiekink

Department of Chemistry, The University of Adelaide, Adelaide, S.A. 5005, Australia

(Received October 4, 1993, CSD-No. 400366)

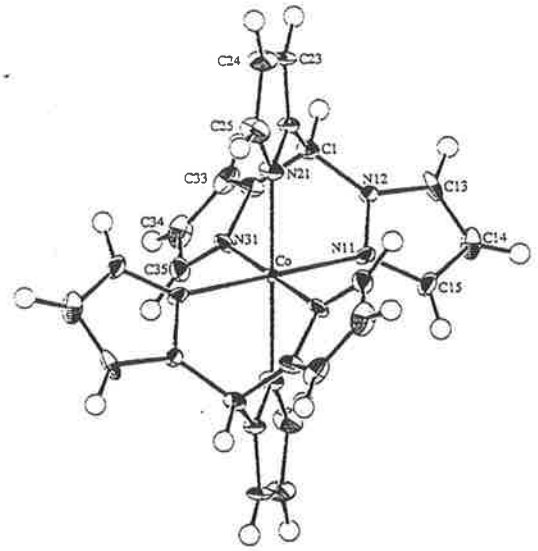

Source of material: (see ref. 1).
The structure of the title compound has been determined recently at room temperature (see ref. 1).

$C_{20}H_{20}CoN_{14}O_6$, monoclinic, $P2_1/n$ (No. 14),
$a = 9.733(2)$ Å, $b = 7.848(6)$ Å, $c = 16.848(4)$ Å,
$\beta = 103.42(2)°$, $V = 1251.8$ Å^3, $Z = 2$, $R(F) = 0.043$,
$R_w(F) = 0.049$.

Table 1. Parameters used for the X-ray data collection

Crystal:	yellow multifaceted, size 0.40 mm diameter
Wave length:	Mo K_α radiation (0.7107 Å)
μ:	7.55 cm^{-1}
Diffractometer:	Rigaku AFC6R
Scan mode:	$\omega/2\theta$
$T_{measurement}$:	173 K
$2\theta_{max}$:	50°
$N(hkl)_{unique}$:	2471
Criterion for F_o:	$F_o > 6\,\sigma(F_o)$
$N(patram)_{refined}$:	187
Program:	teXsan

Table 2. Final atomic coordinates and displacement parameters (in Å^2)

Atom	Site	x	y	z	U_{iso}
H(1)	4e	0.2114	−0.18844	0.11585	0.01473
H(13)	4e	0.06756	−0.35588	−0.00706	0.01775
H(14)	4e	0.10114	−0.41331	−0.14772	0.02066
H(15)	4e	0.31703	−0.24946	−0.15986	0.01662
H(23)	4e	0.12323	0.09877	0.15264	0.01804
H(24)	4e	0.18393	0.40226	0.12651	0.02406
H(25)	4e	0.37333	0.38857	0.04783	0.02432
H(33)	4e	0.38273	−0.3845	0.21187	0.01823
H(34)	4e	0.6442	−0.43729	0.23702	0.02458
H(35)	4e	0.73422	−0.2355	0.14428	0.02145

References

1. Astley, T., Gulbis, J.M., Hitchman, M.A., Tiekink, E.R.T.: Structure, spectroscopic and angular-overlap studies of tris(pyrazol-1-yl)methane complexes. J. Chem. Soc. Dalton Trans. (1993) 509-515.
2. Walker, N., Stuart, D.: An empirical method for correcting diffractometer data for absorption effects. Acta Crystallogr. A39 (1983) 158-166.

Table 3. Final atomic coordinates and displacement parameters (in Å^2)

Atom	Site	x	y	z	U_{11}	U_{22}	U_{33}	U_{12}	U_{13}	U_{23}
Co	2*b*	0.5	0.0	0.0	0.0073(3)	0.0058(3)	0.0114(3)	−0.0017(3)	0.0045(2)	−0.0017(3)
O(1)	4*e*	0.5049(3)	0.3573(4)	0.3248(2)	0.052(2)	0.025(2)	0.115(3)	−0.008(2)	0.035(2)	−0.021(2)
O(2)	4*e*	0.3874(3)	0.1308(3)	0.3201(2)	0.042(2)	0.021(2)	0.081(2)	0.001(2)	0.048(2)	0.016(1)
O(3)	4*e*	0.5422(3)	0.1510(4)	0.2504(2)	0.029(1)	0.056(2)	0.028(2)	0.012(1)	0.020(1)	−0.000(1)
N(1)	4*e*	0.4785(3)	0.2129(4)	0.2979(2)	0.018(2)	0.012(2)	0.028(2)	0.006(1)	0.008(1)	0.010(1)
N(11)	4*e*	0.3326(3)	−0.1689(3)	−0.0444(2)	0.014(1)	0.013(1)	0.008(1)	−0.003(1)	0.006(1)	−0.001(1)
N(12)	4*e*	0.2466(3)	−0.2065(3)	0.0061(2)	0.011(1)	0.012(1)	0.009(1)	−0.005(1)	0.005(1)	−0.001(1)
N(21)	4*e*	0.3591(3)	0.1299(3)	0.0529(2)	0.013(1)	0.008(1)	0.020(2)	−0.001(1)	0.008(1)	0.000(1)
N(22)	4*e*	0.2744(3)	0.0380(3)	0.0887(2)	0.011(1)	0.011(2)	0.015(2)	−0.000(1)	0.007(1)	−0.003(1)
N(31)	4*e*	0.5322(3)	−0.1534(3)	0.1041(2)	0.007(1)	0.018(2)	0.014(2)	−0.001(1)	0.004(1)	0.002(1)
N(32)	4*e*	0.4167(3)	−0.2044(3)	0.1292(2)	0.013(1)	0.011(2)	0.015(2)	−0.000(1)	0.008(1)	0.004(1)
C(1)	4*e*	0.2805(3)	−0.1444(4)	0.0879(2)	0.012(2)	0.013(2)	0.014(2)	−0.003(1)	0.007(1)	0.002(1)
C(13)	4*e*	0.1421(3)	−0.3110(4)	−0.0306(2)	0.009(2)	0.013(2)	0.027(2)	−0.008(2)	−0.001(1)	0.003(1)
C(14)	4*e*	0.1596(4)	−0.3422(4)	−0.1061(2)	0.022(2)	0.014(2)	0.023(2)	−0.009(2)	−0.002(2)	−0.005(2)
C(15)	4*e*	0.2784(3)	−0.2516(4)	−0.1117(2)	0.018(2)	0.015(2)	0.013(2)	−0.000(2)	0.001(1)	−0.006(1)
C(23)	4*e*	0.1925(3)	0.1368(5)	0.1233(2)	0.014(2)	0.025(2)	0.022(2)	0.003(2)	0.011(2)	−0.008(2)
C(24)	4*e*	0.2250(4)	0.2999(5)	0.1095(2)	0.021(2)	0.018(2)	0.034(2)	0.005(2)	0.011(2)	−0.013(2)
C(25)	4*e*	0.3285(4)	0.2905(4)	0.0662(2)	0.020(2)	0.011(2)	0.036(2)	−0.001(2)	0.010(2)	−0.006(2)
C(33)	4*e*	0.4485(4)	−0.3270(4)	0.1856(2)	0.030(2)	0.014(2)	0.012(2)	−0.004(2)	0.006(2)	0.002(2)
C(34)	4*e*	0.5889(4)	−0.3561(5)	0.1993(2)	0.029(2)	0.017(2)	0.018(2)	0.003(2)	−0.003(2)	0.003(2)
C(35)	4*e*	0.6365(3)	−0.2449(4)	0.1478(2)	0.013(2)	0.021(2)	0.017(2)	0.004(2)	−0.002(1)	−0.003(2)

Coordination Chemistry Reviews, 64 (1985) 247—260
Elsevier Science Publishers B.V., Amsterdam — Printed in The Netherlands

REDUCTION OF CARBON DIOXIDE BY TRIS(2,2'-BIPYRIDINE)COBALT(I)

F. RICHARD KEENE (ref. 1), CAROL CREUTZ, and NORMAN SUTIN
Department of Chemistry, Brookhaven National Laboratory, Upton, New York 11973

ABSTRACT

Preliminary stoichiometric and kinetic results bearing on the mechanism of the reduction of HCO_3^- to CO by tris(2,2'-bipyridine)cobalt(I) in aqueous media are reported. The results indicate that CO (not formate) is the dominant carbon product and that it is scavenged by $Co(bpy)_3^+$ to give insoluble $[Co(bpy)(CO)_2]_2$. At pH ~ 9, bicarbonate reduction occurs in competition with H_2O reduction. Both processes are inhibited by bpy and promoted by H^+, suggesting the common intermediate $Co(bpy)_2(H_2O)H^{2+}$. The bicarbonate reaction itself branches to give H_2 and CO in ~ 3:1 ratio.

INTRODUCTION

There has been considerable recent interest in the use of tris(2,2'-bipyridine)ruthenium(II) (2,2'-bipyridine = bpy) and its analogues as photosensitizers in photoconversion processes, primarily because of their spectral properties, the relative longevity of the MLCT excited states, and the facility of electron transfer processes involving both excited state and ground state species (refs. 2,3). A number of strategies have been developed for the reduction of water, based on either oxidative quenching of $*Ru(bpy)_3^{2+}$ (with water reduction being performed by the reduced quencher), or reductive quenching (with water reduction involving either $Ru(bpy)_3^+$ or reducing species formed by reaction with it). In most cases, a heterogeneous catalyst (e.g. colloidal platinum) is required for hydrogen formation, but particularly significant exceptions are homogeneous systems using a cobalt(II) complex as catalyst. Scheme I involves reductive quenching by ascorbate ion (HAs^-) in the presence of added Co(II) (ref. 4).

I. Reductive Quenching

$$Ru(bpy)_3^{2+} \xrightarrow{h\nu} *Ru(bpy)_3^{2+}$$
$$*Ru(bpy)_3^{2+} + HAs^- \longrightarrow Ru(bpy)_3^+ + HAs\cdot$$
$$HAs\cdot \longrightarrow \text{Products}$$
$$Ru(bpy)_3^+ + Co(bpy)_3^{2+} \longrightarrow Ru(bpy)_3^{2+} + Co(bpy)_3^+$$
$$Co(bpy)_3^+ + H_2O \longrightarrow Co(bpy)_3^{2+} + 1/2\ H_2 + OH^-$$

In Scheme II oxidative quenching by $Co(bpy)_3^{2+}$ in the presence of the electron

0010-8545/85/$04.90

donor triethanolamine (ref. 5; TEOA = triethanolamine, L = 4,7-$(CH_3)_2$phen, 50% aq. acetonitrile) yields H_2 with a quantum yield of 0.3.

II. Oxidative Quenching

$$RuL_3^{2+} \xrightarrow{h\nu} {}^*RuL_3^{2+}$$
$${}^*RuL_3^{2+} + Co(bpy)_3^{2+} \longrightarrow RuL_3^{3+} + Co(bpy)_3^{+}$$
$$RuL_3^{3+} + TEOA \longrightarrow RuL_3^{2+} + TEOA^{\cdot+}$$
$$TEOA^{\cdot+} + TEOA \longrightarrow TEOA^{\cdot\prime} + TEOAH^{+}$$
$$TEOA^{\cdot\prime} + Co(bpy)_3^{2+} \longrightarrow Prod + Co(bpy)_3^{+}$$
$$Co(bpy)_3^{+} + H_2O \longrightarrow Co(bpy)_3^{2+} + 1/2\ H_2 + OH^{-}$$

In either case the net photoinduced sequence is (Donor = TEOA or HAs^-):

$$h\nu + Donor + Co(bpy)_3^{2+} \xrightarrow{[Ru(bpy)_3^{2+}]} Prod + Co(bpy)_3^{+}$$
$$Co(bpy)_3^{+} + H_2O \longrightarrow Co(bpy)_3^{2+} + OH^{-} + 1/2H_2$$

The ability of cobalt complexes to promote homogeneous H_2 production appears unique, and the involvement of hydridocobalt species has been proposed.[4,5]

Lehn and Ziessel (ref. 6) have reported the photochemical reduction of carbon dioxide to carbon monoxide in 20% aq. acetonitrile using a system with constituents similar to II above. Reduction of ${}^*RuL_3^{2+}$ to RuL_3^{+} by triethanolamine or trialkylamines as quencher, followed by reduction of Co(II) to Co(I) (as $Co(bpy)_3^{+}$) by RuL_3^{+} was proposed. However, in light of recent results (ref. 5) characterizing H_2 formation in the triethanolamine, $Co(bpy)_3^{2+}$, $Ru(4,7\text{-}(CH_3)_2phen)_3^{2+}$ systems in aqueous acetonitrile the oxidative quenching sequence II also merits serious consideration for the CO_2 system. In related work, a 2,9-dimethyl-1,10-phenanthroline cobalt(II) complex also exhibits high CO_2-reduction activity in dimethylformamide (ref. 7).

Direct electrochemical reduction of CO_2 to produce CO, formate, or oxalate (ref. 8) is characterized by a large overpotential, and has been reported to occur at -2 V vs NHE. Chemically catalyzed electrochemical reductions on metal (ref. 9) and semiconducting (ref. 10) electrodes significantly lower the overpotential, and in some cases reduction (to CO plus CO_3^{2-}) occurs at -1.2 ± 0.1 V vs NHE in aqueous solution. Mediation of reduction of CO_2 to CO by photo- and electrogenerated $Re^0(bpy)(CO)_3Cl$ (ref. 7,11), and electrogenerated Ni^I(cyclam) (ref. 12) and (adsorbed) $Co^Ipc(H^-)$ (pc = phthalocyanine) (ref. 13) has also been found. Catalysis of the CO_2/HCO_2^- equilibrium by Pd(0) (ref. 14) and electroencapsulated Pd(0) has also been reported (ref. 15).

Activation of carbon dioxide to reduction by transition metal complexes has been attributed to insertion of CO_2 into metal-hydride bonds (producing

formate) or disproportionation of CO_2 (producing CO and CO_3^{2-}) (ref. 16): in neither case is the intimate mechanism of the process known. In view of the intrinsic interest and importance of carbon dioxide activation and its light-promoted reduction, we have begun a study of the reactions of $Co(bpy)_3^+$ with water and bicarbonate ion in aqueous solution. Preliminary results are reported here.

EXPERIMENTAL SECTION

All manipulations were performed in a Vacuum Atmospheres glove box under an argon atmosphere, unless otherwise indicated. Solid $[Co(bpy)_3]Cl.H_2O$ was prepared as described previously (ref. 4) and recrystallized (ref. 17) by dissolving the crude solid (~ 300 mg) in dry ethanol (5 mL) containing 2,2'-bipyridine (770 mg). The solution was filtered, diethyl ether was added without stirring, and the Schlenk tube was stoppered and left undisturbed for 3 days. The blue/black crystals were collected, washed with ether and dried in vacuo. In some studies stock solutions of $Co(bpy)_3^+$ in ethanol were prepared by controlled potential electrolysis (E_{app} = -1.1 V vs aq SCE) of ~ 0.03 M $[Co(bpy)_3]Cl_2$ solutions using either carbon rod or platinum gauze working electrodes. Water used for all buffers was obtained from a MILLIPORE Milli-Q water purification system, and drawn immediately before deaeration with argon to avoid contamination by atmospheric CO_2. All materials were AR grade and were used without further purification.

Stoichiometry studies. In a typical run, 4.0 mL of the appropriate buffer (secondary amines react with CO_2 and so could not be used as buffers) containing $NaHCO_3$ and/or $Co(bpy)_3^{2+}$, if required, was transferred to a glass vessel (total volume = 13 mL) fitted with a serum cap. A 200 µL aliquot of a stock solution of $[Co(bpy)_3]Cl.H_2O$ in dry ethanol (containing bpy if required) was added by syringe, and the solution was stirred until completion of the reaction. H_2 and CO were determined by GC methods (molecular sieve 4A column thermostated at 150 °C, argon carrier gas, thermal conductivity detector); acidification of the solution was required prior to CO analysis.

The Co(I) concentrations in the stock solutions for the kinetic and stoichiometry studies were determined spectrophotometrically following reaction with either methyl viologen or $Os(bpy)_3^{3+}$.

Analysis for formate and oxalate ions present in product solutions from stoichiometric and kinetic studies was performed using a DIONEX 2010 Ion Chromatograph (HPICE-AS1 column; 10^{-3} M HCl/2% acetonitrile eluent). The reactions were run in TRIS-HCl media because borate and sulfate interfered with the formate determinations.

Kinetic studies. In a typical run, a 200 uL aliquot of a stock solution of $[Co(bpy)_3]Cl.H_2O$ in dry ethanol (containing bpy if required) was added to 4.0 mL of the appropriate buffer (containing $NaHCO_3$ and/or $Co(bpy)_3^{2+}$ if required) in a 1 cm cell. The cell was immediately stoppered, removed from the glovebox, and the decay of Co(I) measured spectrophotometrically (605 nm) for 3-4 half-lives. The infinity reading was obtained after exposing the solution to air, and the pH was measured.

Formation and analysis of $[Co(bpy)(CO)_2]_2$

Reaction of $Co(bpy)_3^+$ with HCO_3^-. A solution of $[Co(bpy)_3]Cl\cdot H_2O$ (70 mg) in ethanol (1.5 mL) was added to 17.5 mL of 0.20 M boric acid buffer (pH 9.2; $[Co(bpy)_3^+]$ = 7.8 mM; $[Co(bpy)_3^{2+}]$ = 2.5 mM; μ = 0.5 M, Na_2SO_4) containing 100 mg $NaHCO_3$ (0.063 M). The blue solution was stirred until completion of the reaction was indicated by the pale yellow solution and dark precipitate. After ~ 1 hour the black precipitate was filtered under argon, washed with water and dried in vacuo. The yield was low and somewhat variable.

Reaction of $Co(bpy)_3^+$ with CO. A solution of $[Co(bpy)_3]Cl\cdot H_2O$ (90 mg) in dry ethanol (12 mL) was stirred under a CO atmosphere for 15 minutes. The black product was filtered under argon, washed with ethanol, and dried in vacuo. Yield 20 mg, 95%.

Analysis. CO was determined by acidification of a weighed sample in a closed vessel followed by GC analysis of the gas above the solution. Cobalt was determined by atomic absorption spectroscopy and x-ray fluorescence, and bpy spectrophotometrically.

RESULTS AND DISCUSSION

General Considerations

In neutral aqueous solution the overall thermodynamic requirements for reduction of water to hydrogen and of carbon dioxide to CO or formate are similar:

TWO-ELECTRON REDUCTION, pH 7, 25 °C (ref. 18), vs NHE

$$2H_2O_{(\ell)} + 2e \longrightarrow H_{2(g)} + 2OH^-_{(aq)} \qquad E^o = -0.41\ V$$

$$CO_{2(g)} + H_2O_{(\ell)} + 2e \longrightarrow CO_{(g)} + 2OH^-_{(aq)} \qquad E^o = -0.53\ V$$

$$CO_{2(g)} + H_2O_{(\ell)} + 2e = HCO^-_{2(aq)} + OH^-_{(aq)} \qquad E^o = -0.31\ V$$

Moreover, in seeking catalysts for these reactions similar issues arise. Both reductions are very difficult via one-electron processes, since the one-electron reduction products H atom and $\cdot CO_2^-$ (formate radical) are extremely energetic species. By using pulse-radiolytic methods, Schwarz and Dodson have recently determined E° for the $CO_2/\cdot CO_2^-$ couple to be -1.9 V vs NHE in water (ref. 19), and the intrinsic barrier for this one-electron reduction is estimated to be ca. 0.6 V (ref. 20). The $\cdot CO_2^-/:CO_2^{2-}$ potential has been estimated to be -1.2 V vs. NHE (ref. 21). Values for $H^+/H\cdot/H^-$ have been discussed previously (ref. 2).

ONE-ELECTRON REDUCTION, pH 7, 25 °C, vs NHE

$$H^+ \xrightarrow{-2.7\ V} H\cdot \xrightarrow{+0.03\ V} H^-$$

$$CO_2 \xrightarrow{-1.9\ V} \cdot CO_2^- \xrightarrow{-1.2\ V} :CO_2^{2-}$$

Thus in either H_2O or CO_2 reduction, paths involving the (free) one-electron reduction products are expected to be vanishingly slow and means of circumventing these paths or stabilizing the one-electron species are sought. In the H_2O/H_2 reaction, metal hydride complexes may provide catalytic routes. In the CO_2/CO or HCO_2^- reaction, catalysis by metal complexes may involve coordination of carbon dioxide (ref. 22) or insertion into a metal hydride bond to yield a formate species (ref. 23).

As will be seen, comparison of the above parameters for H_2O and CO_2 reduction is particularly appropriate in the present system because, in the presence of HCO_3^-, these reactions occur in competition with each other and even appear to involve a common intermediate. Interestingly, the presence of water is required in a number of systems when CO_2 reduction occurs. Unfortunately, the presence of water also complicates the issue of the carbon substrate undergoing reduction. In aqueous media the following equilibria must be considered:

$$CO_{2(g)} \rightleftharpoons CO_{2(aq)} \qquad K = 3 \times 10^{-2}\ M\ atm^{-1}$$

$$CO_{2(aq)} + H_2O \rightleftharpoons H_2CO_3 \qquad K = 2.6 \times 10^{-3}$$

$$H_2CO_3 \rightleftharpoons H^+ + HCO_3^- \qquad K = 2.5 \times 10^{-5}\ M$$

$$HCO_3^- \rightleftharpoons H^+ + CO_3^{2-} \qquad K = 1.6 \times 10^{-10}\ M$$

(The equilibrium constants given are appropriate to ~ 0.5 M ionic strength, 25 °C (ref. 24).) Above pH 10 and below pH 4, "CO_2" solutions contain CO_3^{2-} and H_2CO_3/CO_2, respectively. Near pH 7, the three species HCO_3^-, CO_2 and H_2CO_3 are all present and their distribution is pH dependent. Consequently pH variations carried out to assess the role of H^+ in CO_2 reduction systems may be difficult to interpret when the dominant "CO_2" form(s) change.

Furthermore, the equilibration of gaseous and aqueous CO_2 must be taken into account: Depending upon the experimental procedures (and time scales) the above equilibria may lead to substantial changes in the CO_2 partial pressure above a solution and in the concentration(s) of dissolved species.

Finally, the free-energy change for "CO_2" reduction is a function of the substrate and pH. Fig. 1 summarizes these data in graphic form.

pH	Half-Reaction	E^o, V	H^+/H_2 E^o, V
0	$CO_{2(g)} + 2H^+ + 2e = CO_{(g)} + H_2O$	-0.12	-0.00
7	$HCO_3^- + 3H^+ + 2e = CO_{(g)} + 2H_2O$	-0.48	-0.41
9	$HCO_3^- + 3H^+ + 2e = CO_{(g)} + 2H_2O$	-0.66	-0.53
11	$CO_3^{2-} + 4H^+ + 2e = CO_{(g)} + 2H_2O$	-0.87	-0.65

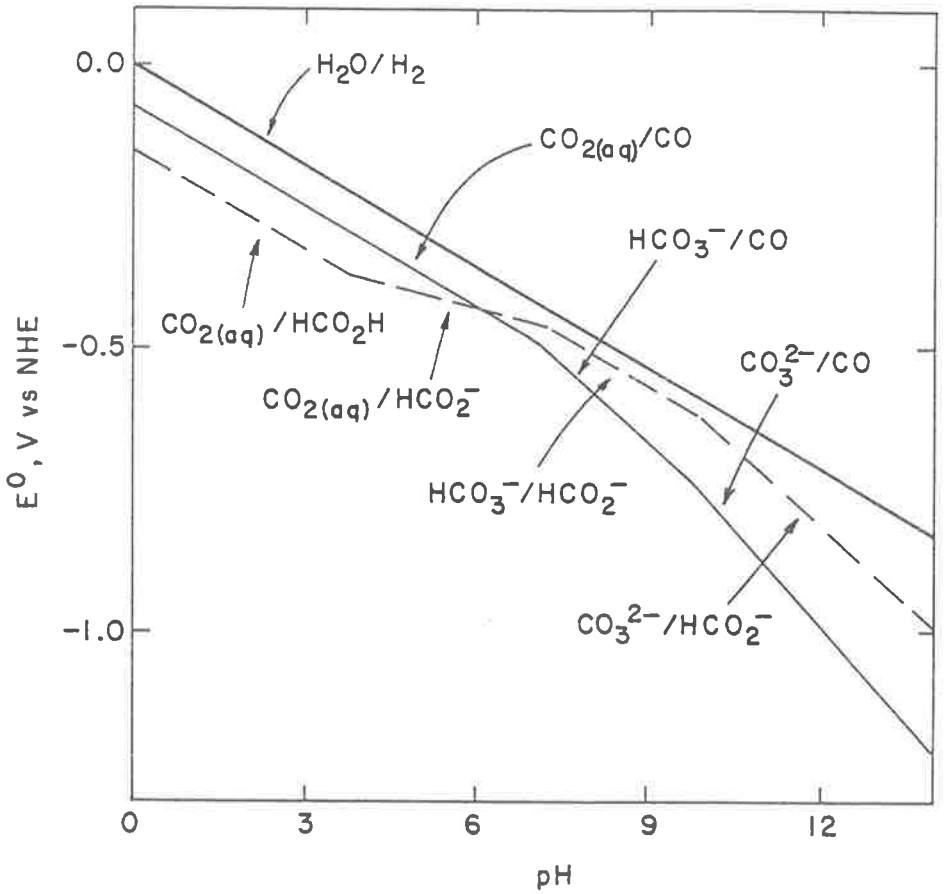

Fig. 1. E^o values (vs NHE) for two-electron reduction of H_2O and CO_2 as a function of pH and the dominant forms of reactants and products. The following standard state conventions are used: H_2O, liquid; H_2 and CO, gas (i.e., 1 atm); CO_2, HCO_2H, HCO_2^-, HCO_3^-, and CO_3^{2-}, aqueous (i.e., 1 M).

General Features of the $Co(bpy)_3^+/H_2O/HCO_3^-$ System

No reaction of $Co(bpy)_3^+$ with CO_2 is found in dry ethanol over several days. However, reaction does occur in aqueous media. This system (like others, refs. 6,9,10) is complicated by side-reactions: $Co(bpy)_3^+$ also reacts with water to yield H_2 at pH > 7 and dihydrobipyridines at lower pH (ref. 4). These products reflect the fact that $Co(bpy)_3^+$ is a strong reductant: $E^o(Co(bpy)_3^{2+/+}) = -0.95$ V and $E^o(Co(bpy)_3^{3+/+}) = -0.33$ V (ref. 5). Accordingly, in aqueous media CO_2 reduction must occur in competition with these reactions. As noted above, an additional complication is the pH-dependent $CO_3^{2-}/HCO_3^-/CO_2$ equilibria. In the pH-range considered here HCO_3^- is the dominant form with CO_3^{2-} = 1-10% and $CO_{2(aq)}$ < 3% of the total "CO_2" species and is therefore considered the reactant.

The reaction was studied spectrophotometrically by observing the disappearance of $Co(bpy)_3^+$ in aqueous buffer solutions under anaerobic conditions in the presence and absence of HCO_3^-. The competition of H_2O and HCO_3^- for $Co(bpy)_3^+$ is illustrated in Fig. 2. While it is evident that the

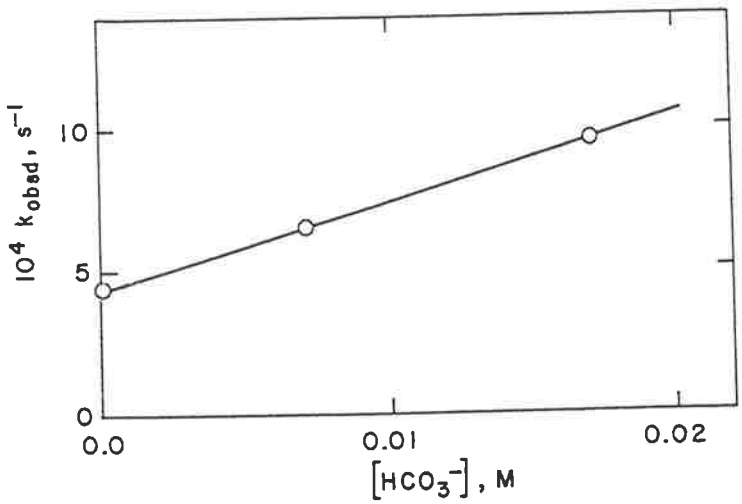

Fig. 2. Pseudo-first-order rate constants (25 °C) for the disappearance of $Co(bpy)_3^+$ in borate buffer (pH 8.8) as a function of $[HCO_3^-]$ (0.16 mM Co(I); 2.4 mM $Co(bpy)_3^{2+}$; 4.8% ethanol; ionic strength = 0.5 M, Na_2SO_4).

rate of $Co(bpy)_3^+$ consumption increases linearly with $[HCO_3^-]$, it is also evident that there is a relatively large intercept. The latter is due to the reaction with water, which gives H_2 according to eq. 1 (ref. 4) in > 70% yield.

$$Co(bpy)_3^+ + H_2O \longrightarrow Co(bpy)_3^{2+} + 1/2\ H_2 + OH^- \qquad (1)$$

Not only does HCO_3^- accelerate the rate of consumption of $Co(bpy)_3^+$, but it

also reduces the amount of H_2 formed. This is illustrated in Fig. 3 where H_2 yields are plotted as a function of $[HCO_3^-]$ for TRIS buffers at pH 8.4.

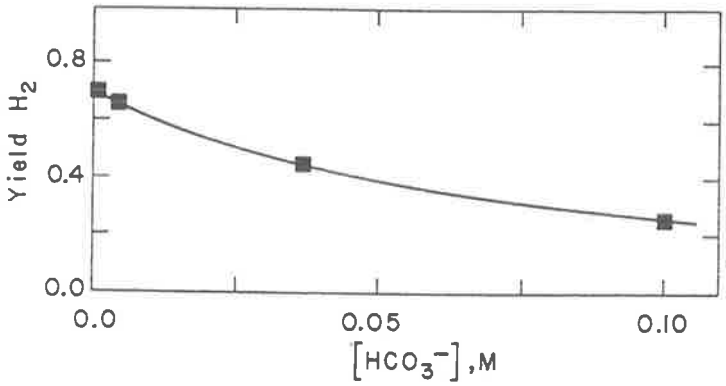

Fig. 3. Hydrogen yields (based on eq. 1) as a function of $[HCO_3^-]$ in TRIS buffer at pH 8.4 (1.4 mM Co(I); 4.8% ethanol; ionic strength = 0.5 M, Na_2SO_4).

CO_2/HCO_3^- Reduction Product

On G.C. analysis of the gas above the reaction solutions with HCO_3^- present (pH 8.4-9.5), no free CO was detected, and although formate ion was found by ion chromatographic analysis of the solution, it was not formed in significant amounts (< 1%). In the stoichiometry studies at high $[HCO_3^-]$ with high [Co(I)], small amounts of a dark solid were formed. This product showed IR absorptions at 1933, 1895 and 1717 cm^{-1}: the product obtained from similar experiments using $H^{13}CO_3^-$ gave equivalent absorptions at 1891, 1852 and 1679 cm^{-1}, respectively, indicating that the absorptions arise from carbonyl groups formed during the reduction process. A product with identical IR spectral properties and analytical data (Co/bpy = 1:1, Co/CO - 1:2) is produced by the reaction of $Co(bpy)_3^+$ with CO in ethanol. It seems clear that the product of both reactions is the same as the product formed by reduction of Co(II) by BH_4^- in the presence of bpy and CO (ref. 25), or by the reaction of $(norbornadiene)_2Co_2(CO)_4$ with bpy (ref. 26). The structure of this complex has been assigned as $[Co(bpy)(CO)_2]_2$ (C_{2v}) (as distinct from the geometric

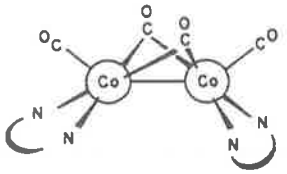

isomer (C_{2h}) with the terminal CO groups trans) on the basis of group theory

analysis of the IR spectrum. The complex is stable in contact with basic solution, but, upon acidification to pH < 1, decomposes to liberate ~ 2 mols CO per Co and ~ 1 mol H_2 per Co (eq. 2), consistent with the above formulation.

$$[Co(bpy)(CO)_2]_2 + 6H^+ \longrightarrow 4CO + 2H_2 + 2Co^{2+}_{aq} + 2bpyH^+ \quad (2)$$

Thus these results indicate that CO (rather than formate) is the major product of HCO_3^- reduction by $Co(bpy)_3^+$ (eq. 3, where the CO may be free or bound to cobalt). The CO produced is scavenged by $Co(bpy)_3^+$ to give

$$2Co(bpy)_3^+ + HCO_3^- + H_2O \longrightarrow 2Co(bpy)_3^{2+} + CO + 3OH^- \quad (3)$$

$$Co(bpy)_3^+ + CO \longrightarrow 1/4[Co(bpy)(CO)_2]_2 + bpy + 1/2\ Co(bpy)_3^{2+} \quad (4)$$

insoluble $[Co(bpy)(CO)_2]_2$ (eq. 4). Subsequent acidification of the product solution decomposes the cobalt carbonyl dimer (eq. 2) allowing determination of CO as the gas.

In Fig. 4, H_2 and CO yields are compared. The H_2 yields (based on

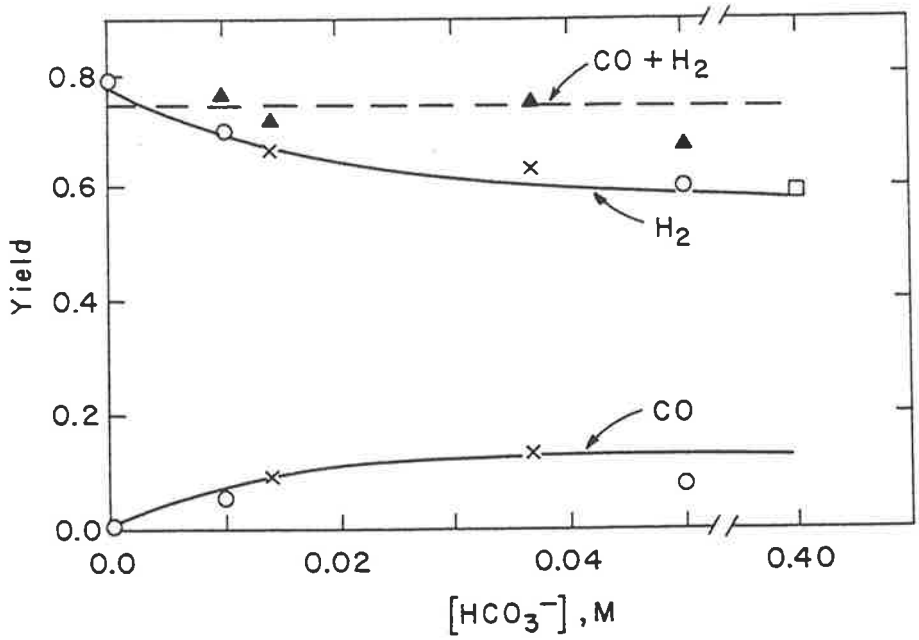

Fig. 4. Balance of yields of CO/H_2 from reaction of $Co(bpy)_3^+$ with HCO_3^- in aqueous solution: x, $[Co(I)]_0$ = 0.66 mM; 0.2 M boric acid buffer, pH 8.8; μ = 0.5 M, Na_2SO_4; no Co(II). ○ $[Co(I)]_0$ = 0.74 mM, $[Co(II)]_0$ = 0.74 mM; 0.4 M boric acid buffer, pH 8.8, μ = 0.5 M, Na_2SO_4. □ $[Co(I)]_0 = [Co(II)]_0$ = 0.74 mM, 0.4 M $NaHCO_3$, pH 8.8, μ = 0.5 M. No excess bpy, 4.8% ethanol. H_2 yield = 2 x (mols H_2 per mol Co(I) taken) (where H_2 is determined prior to acid addition) and CO yield = 3 x (mols CO per mol Co(I) taken). ▲ Sum of H_2 and CO yields.

eq. 1) were determined prior to acid addition so that H_2 from eq. 2 is not included. The CO yields are calculated on the basis of eq. 3 and eq. 4, i.e., $3Co(bpy)_3^+$ are consumed per CO detected. With the yields so defined the sum of the yields should be constant if no other products are formed. From Fig. 3 it is evident that reasonable constancy is found.

Kinetics and Product Yields

The kinetics studies were focussed primarily on the behavior of the system in the absence and presence of low added bpy in the pH range 8.4-9.5. Within the pH range studied, there is a minor contribution to the rate from a parallel pathway whose rate expression shows a square dependence on [Co(I)] and $[H^+]$ and an inverse dependence on $[Co(bpy)_3^{2+}]$ (ref. 27). The Co(II) salt was therefore added to many of the kinetic and stoichiometric runs to suppress this contribution. Some kinetic details of the pathway are known, and its involvement in the HCO_3^- reduction processes under the conditions used appears negligible. Under the present conditions the rate is first-order in $[Co(bpy)_3^+]$, first order in $[H^+]$, and first order in $[HCO_3^-]$. The rate of eq. 1 (i.e. no added HCO_3^-) is first order in both $[Co(bpy)_3^+]$ and $[H^+]$ (ref. 27). The rates of both reactions are inhibited by bpy, indicating loss of bpy prior to the rate-determining step. The observations suggest that HCO_3^- and H_2O (eq. 1) may compete for a common intermediate formed from $Co(bpy)_3^+$ and H^+ with loss of bpy -- possibly $Co(bpy)_2(H_2O)H^{2+}$ (ref. 28). [The analogous rhodium complex has also been characterized (ref. 29).] Previous studies (ref. 4) of the stoichiometry of the $Co(bpy)_3^+/H_2O$ reaction have also demonstrated inhibition of the H_2-yield by excess bpy. Stoichiometry studies show that the $Co(bpy)_3^+/HCO_3^-$ reaction is also suppressed by the presence of excess bpy, so that as the bpy concentration increases, HCO_3^- eventually does not affect the H_2-yield for the water reduction reaction. These observations also support the competition of H_2O and HCO_3^- for the same intermediate, e.g.,

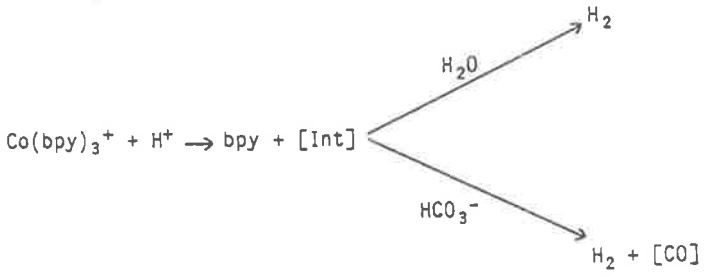

where [CO] denotes the HCO_3^-/CO_2 reduction product $[Co(bpy)(CO)_2]_2$.

Note, however, that in the pH range studied a rate law such as $-d[Co(bpy)_3^+]/dt = a[Co(bpy)_3^+][H^+][HCO_3^-]/[bpy]$ is kinetically indistinguishable from $-d[Co(bpy)_3^+]/dt = a'[Co(bpy)_3^+][CO_2]/[bpy]$. The first expression suggests rate-determining reaction of $Co(bpy)_2(H_2O)H^{2+}$ with HCO_3^- while the second suggests reaction of $Co(bpy)_2^+$ (ref. 20) with CO_2 (generated through the pre-equilibrium $H^+ + HCO_3^- = CO_2 + H_2O$) to give a CO_2 complex. Thus our data do not rule out reaction pathways such as the latter. In fact it is even possible that the two occur in parallel.

Finally, in addition to the parallel reactions with water and bicarbonate ion discussed above, there is also evidence that the HCO_3^- reaction itself gives both H_2 and CO. In Fig. 5 the ratio of HCO_3^- to H_2O paths as

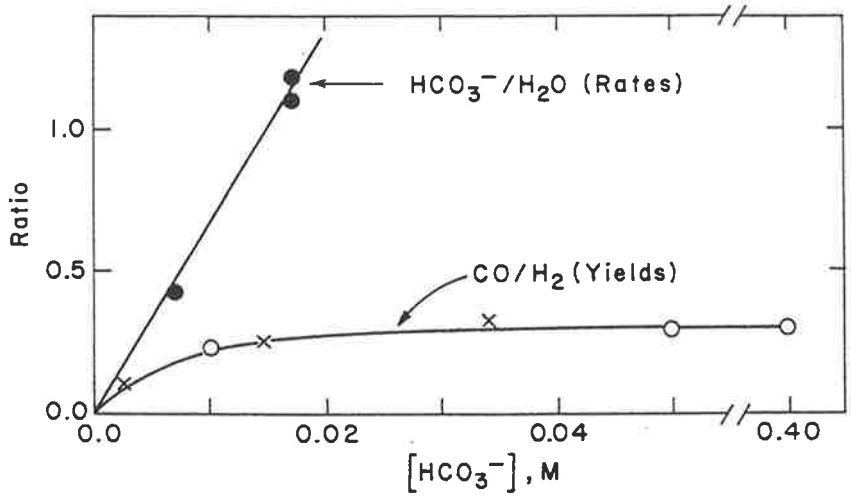

Fig. 5. $Co(bpy)_3^+/HCO_3^-$ reaction in borate buffers, pH 8.4-9.5 (no added bpy; 4.8% ethanol; ionic strength = 0.5 M, Na_2SO_4). The solid symbols are associated with kinetic measurements (see Fig. 2) and the other symbols with product measurements (see Fig. 4). The ratios are defined by (stoichiometric) $R_{HCO_3^-}/R_{H_2O} = 3(a_{H_2O} - a_{HCO_3^-})/2a_{H_2O}$ where a_{H_2O} = mols H_2 per Co(I) formed in the absence of HCO_3^- and $a_{HCO_3^-}$ = mols H_2 per Co(I) with added bicarbonate, and (kinetic) $R_{HCO_3^-}/R_{H_2O} = (k_{obsd,HCO_3^-} - k_{obsd,H_2O})/k_{obsd,H_2O}$ where k_{obsd,HCO_3^-} and k_{obsd,H_2O} are the pseudo-first-order rate constants for $Co(bpy)_3^+$ reaction in the presence and absence of bicarbonate.

evaluated from the kinetics is plotted as a function of $[HCO_3^-]$. Also shown (solid symbols) are CO-to-H_2 ratios obtained from product analysis of comparable solutions. While the CO-to-H_2 ratio rises between 0 and ~ 0.03 M HCO_3^-, it levels off at higher $[HCO_3^-]$ attaining a limiting value of ~ 0.3 at pH 9 under the conditions shown. Preliminary evidence indicates this

partitioning to be variable: for example, the ratio is higher in TRIS (Fig. 2) than in borate buffer and much lower in pH 7 phosphate buffer. Analogous changes in branching ratio have been reported by Lehn and Ziessel who noted the sensitivity of this ratio to substituents on the tertiary amines; CO production was found to be favored in the order $N(C_2H_5OH)_3 > N(n\text{-propyl})_3 > N(Et)_3 > N(CH_3)_3$ (ref. 6). The fact that the HCO_3^- reaction branches may reflect the fact that (bound) HCO_3^- may act as either a proton source (to give H_2) or a "carbon" source (to give CO), but the origin of the sensitivity of the branching ratio to the nature of the buffer is not obvious. In any case it is noteworthy that the thermodynamic ratio of H_2 to (free) CO is ~ 10^2 at pH 9. The fact that relatively high yields of CO are observed in the present $Co(bpy)_3^+$ system may be due to the $Co(bpy)_3^+$ scavenging of CO (eq. 4) which drives the reaction. Alternatively, the observed partitioning may solely reflect kinetic (as opposed to thermodynamic) factors.

Formate ion is a minor product in the $Co(bpy)_3^+$ - HCO_3^- reaction (CO: HCO_2^- ~ 10:1). Interestingly, the reduction of HCO_3^- or CO_2 to HCO_2^- is favored on thermodynamic grounds over (gaseous) CO formation above pH ~ 6 (see Fig. 1). The fact that the CO produced in the $Co(bpy)_3^+$ reaction is not free but converted to $[Co(bpy)(CO)_2]_2$ does, of course, cloud the picture somewhat; possibly the formation of the insoluble dimer does help to drive CO formation thermodynamically. In any event, we have shown that "CO" is a primary product; added formate is not converted to "CO" under the reaction conditions. Thus the fact that HCO_2^- is produced in such small yield (relative to CO) suggests kinetic control of the product distribution. Formate ion is the expected product for reaction of (molecular) CO_2 with a metal hydride (insertion into the M-H bond). In the $Co(bpy)_3^+$ system, such a pathway would be manifested as $-d[Co(bpy)_3^+]/dt = b[Co(bpy)_3^+][H^+]^2[HCO_3^-]/[bpy]$ at pH > 7. Although our kinetic data (pH $\geq$ 8.5) do not indicate an $[H^+]^2$-dependence, a small ($\leq$ 10%) contribution from this term cannot be ruled out. Thus the formate may arise from such a reaction. However, as discussed above, from the observed kinetics and product distribution, the major "bicarbonate" reaction involves either HCO_3^- attack on $Co(bpy)_2(H_2O)H^{2+}$ or CO_2 attack on $Co(bpy)_2(H_2O)_2^+$ (or both).

SUMMARY

In aqueous bicarbonate solutions (pH 8.5 - 10) $Co(bpy)_3^+$ reacts with water to give H_2 and with HCO_3^- to give H_2, CO (as the insoluble $[Co(bpy)(CO)_2]_2$), and some HCO_2^-, with the extent of reaction with HCO_3^- increasing as $[HCO_3^-]$ increases. The rate laws for reaction with H_2O and HCO_3^- are first-order in $[Co(bpy)_3^+]$ and $[H^+]$ and inverse in [bpy]. Thus both

water and HCO_3^- reactions may involve the hydride $Co(bpy)_2(H_2O)H^{2+}$ as intermediate. (Of course, kinetically equivalent pathways -- such as, for HCO_3^-, reaction of $Co(bpy)_2(H_2O)_2^+$ with CO_2 -- cannot be ruled out.) In the HCO_3^--reaction the branching between H_2 and CO depends upon the nature of the buffer and favors H_2 over CO in about a 3-to-1 ratio in borate media.

ACKNOWLEDGMENTS

This research was carried out at Brookhaven National Laboratory which is operated under contract DE-AC-02-76-CH00016 with the U.S. Department of Energy and supported by its Office of Basic Energy Sciences. FRK acknowledges financial assistance of the Australian-American Educational Foundation through a Fulbright Award. We thank Ms. E. Norton for performing the Co, Cl, and bpy analyses.

REFERENCES

1 On an approved Special Studies Program from the Department of Chemistry and Biochemistry, James Cook University of North Queensland, Townsville, Queensland 4811, Australia.
2 N. Sutin and C. Creutz, Pure and Appl. Chem., 52 (1980) 2717-2738; and references cited therein.
3 K. Kalyanasundaram, Coord. Chem. Rev., 46 (1982) 159-244; and references cited therein.
4 C.V. Krishnan, C. Creutz, D. Mahajan, H.A. Schwarz and N. Sutin, Israel J. Chem., 22 (1982) 98-106.
5 C.V. Krishnan, C. Creutz, B.S. Brunschwig and N. Sutin, J. Am Chem. Soc., in press.
6 J.-M. Lehn and R. Ziessel, Proc. Nat. Acad. Sci. USA, 79 (1982) 701-704.
7 J. Hawecker, J.-M. Lehn and R. Ziessel, J. Chem. Soc., Chem. Commun., (1983) 536-538.
8 C. Amatore and J.-M. Saveant, J. Am. Chem. Soc., 103 (1981) 5021-5023.
9 B. Fisher and R. Eisenberg, J. Am. Chem. Soc., 102 (1980) 7361-7363.
10 (a) M.G. Bradley, T. Tysak, D.J. Graves and N.A. Vlachopoulos, J. Chem. Soc., Chem. Commun., (1983) 349-350. (b) K.W. Freese, Jr. and D. Canfield, J. Electrochem. Soc., 131 (1984) 2518.
11 H. Hawecker, J.M. Lehn, and R. Ziessel, J. Chem. Soc., Chem. Commun., (1984) 328-330.
12 M. Beley, J.P. Collins, R. Rupert, and J.-P. Sauvage, J. Chem. Soc., Chem. Commun., (1984) 1315-1316.
13 C.M. Lieber and N.S. Lewis, J. Am. Chem. Soc., 106 (1984) 5033-5034.
14 C.J. Stalder, S. Chao, D.P. Summers, and M.S. Wrighton, J. Am. Chem. Soc., 105 (1983) 6318-6320.
15 C.J. Stalder, S. Chao, and M.S. Wrighton, J. Am. Chem. Soc., 106 (1984) 3673-3675.
16 S. Inune and N. Yamazaki (Eds.), Organic and Bioorganic Chemistry of Carbon Dioxide, Kodansha Ltd., Tokyo, Wiley, New York, 1982.
17 D.J. Szalda, C. Creutz, D. Mahajan and N. Sutin, Inorg. Chem., 22 (1983) 2372-2379.
18 W. M. Latimer, Oxidation Potentials, Prentice-Hall, Englewood Cliffs, NJ (1952).
19 H.A. Schwarz and R.W. Dodson, to be submitted for publication.
20 H.A. Schwarz, C. Creutz and N. Sutin, Inorg. Chem., 24 (1985) xxxx.
21 J. Lilie, G. Beck and A. Henglein, Ber. Bunsenges, Phys. Chem., 75 (1971) 458-465.

22 (a) S. Gambarotta, F. Arena, C. Floriani and P.F. Zanazzi, J. Am. Chem. Soc., 104 (1982) 5082-5092. (b) R. Eisenberg and D.E. Hendrickson, Adv. Catalysis, 28 (1979) 79-172.
23 (a) A. Yamamoto, S. Kitazume, L.S. Pu and S. Ikeda, J. Am. Chem. Soc., 93 (1971) 371-380. (b) A. Misono, Y. Uchida, M. Hidai and T. Kuse, Chem. Commun., (1968) 981. (c) B.P. Sullivan and T.J. Meyer, J. Chem. Soc., Chem. Commun., (1984) 1244-1245. (d) S. Slater and J.H. Wagenknecht, J. Am. Chem. Soc., 106 (1984) 5367-5368.
24 D. A. Palmer and R. van Eldik, Chem. Rev., 83 (1983) 651-731.
25 G. Mestroni, A. Camus and E. Mestroni, J. Organomet. Chem., 24 (1970) 775-781.
26 H. Behrens and W. Aquila, Z. Anorg. Allg. Chem., 356 (1967) 8-21.
27 F.R. Keene, D. Mahajan, S.F. Chan, C. Creutz and N. Sutin, work in progress.
28 C. Creutz, H.A. Schwarz and N. Sutin, J. Am. Chem. Soc., 106 (1984) 3036.
29 M. Chou, C. Creutz, D. Mahajan, N. Sutin and A.P. Zipp, Inorg. Chem., 21 (1982) 3989-3997.

Chapter 1

THERMODYNAMIC, KINETIC, AND PRODUCT CONSIDERATIONS IN CARBON DIOXIDE REACTIVITY

F. Richard Keene

Department of Chemistry and Biochemistry, James Cook University of North Queensland, Townsville, Australia 4811

There has been a recent upsurge in interest in the reactivity of carbon dioxide for two primary reasons. Firstly, carbon dioxide is the ultimate by-product of all processes involving oxidation of carbon compounds and its increasing presence in the atmosphere since the beginning of the Industrial Revolution has given rise to widespread concern about possible consequences (the so-called "Greenhouse Effect"). Secondly, in view of the vastness of its supply, carbon dioxide represents a possible potential source for C_1 feedstocks for the manufacture of chemicals and fuels, alternative to the current predominant use of petroleum-derived sources. Carbon reserves in the form of atmospheric carbon dioxide, carbon dioxide in the hydrosphere and carbonates in the terrestrial environment substantially exceed those of the fossil fuels such as coal and petroleum (1,2).

Of course, the conversion of carbon dioxide to fuels and chemicals is carried out in the biosphere on an enormous scale by photosynthesis. The raising of consciousness on the industrial/ecological issues of limitations to fossil fuel reserves and of the consequences of their extensive use has heightened interest in the concept of recycling carbon resources, and therefore in the activation of carbon dioxide and "artificial photosynthesis" (3).

Many of the aspects of the thermodynamics of carbon dioxide reactivity, as well as considerations of carbonate chemistry, were extensively reviewed in 1983 by Palmer and van Eldik (4). The present Chapter seeks to present a brief overview of some of the properties and reactivity of carbon dioxide, and to highlight potential means of promotion of its reactivity: many of the issues raised will be elaborated upon in subsequent chapters in this volume.

1. Physical Properties of Carbon Dioxide

1.1 ***Structure and Bonding.*** Carbon dioxide is a linear molecule for which the following canonical structures can be drawn:

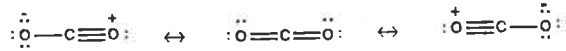

Despite the linear symmetry and overall nonpolar nature of the molecule, some chemical reactivity might be anticipated associated either with the presence of the π-electron density of the double bonds and the lone pairs of electrons on the oxygen atoms, or with the electrophilic carbon atom. The

qualitative MO energy level diagram is given in Figure 1, and the estimation of the level of the lowest unoccupied antibonding orbital {*ca.* 3.8 eV (1)} indicates a high electron affinity associated with the central carbon atom.

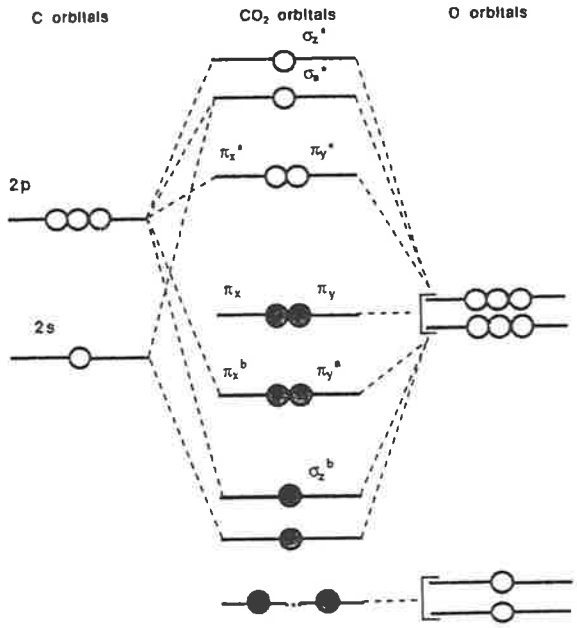

Figure 1. MO energy level diagram for the linear triatomic molecule CO_2

On the other hand, the first ionization potential is high {13.7 eV (1)}, so that the electrophilicity of the central carbon atom might be anticipated as the site of predominant reactivity.

1.2 ***Stability.*** Carbon dioxide, CO_2, is the ultimate product of oxidation of carbon and its compounds and is extremely thermodynamically stable {ΔG° = -394 kJ mol^{-1}, *cf.* -137 kJ mol^{-1} for carbon monoxide, CO (5,6)}. The bond strength of the C-O bond in carbon monoxide is the largest known {D = 1076 kJ mol^{-1} (7)}. In carbon dioxide, that bond strength is measured at D = 532 kJ mol^{-1} (7).

1.3 ***Carbon Dioxide Reduction.*** The redox potentials for the reduction of carbon dioxide have been determined:

$CO_2 \quad \rightleftarrows \quad CO_2^{\cdot-} \qquad E^\circ = -1.90V$ (8), $-1.85V$ (vs NHE (9))

$CO_2^{\cdot-} \quad \rightleftarrows \quad CO_2^{2-} \qquad E^\circ = -1.2V$ (vs NHE (10))

For the first reduction, there is a change in geometry from the linear CO_2 to a bent $CO_2^{\cdot-}$ (11): this structural change gives rise to a very slow self-exchange rate for the $CO_2/CO_2^{\cdot-}$ couple (12) and to a significant overpotential in the reduction of CO_2 (13). As noted previously by Schwarz *et al* (12), the nature of $CO_2^{\cdot-}$ may be significant in the consideration of aspects of the activation of CO_2.

2. Organic Reactions of Carbon Dioxide

Carbon dioxide has a reasonably extensive organic chemistry, which has been reviewed previously (14-16). Much of this chemistry requires catalysis in some form, and reactions are generally represented within one of the following categories -

- reductions of CO_2 by H_2: Via the water-gas-shift reaction (WGS - equation (1))

$$CO_2 + H_2 \rightleftarrows CO + H_2O \qquad [1]$$

  and technologies such as the Fischer-Tropsch processes (17), a variety of products may be produced including methanol, alkanes, alkenes, alcohols, ethers, esters, aldehydes, ketones, etc.

- carboxylation of active hydrogen compounds: e.g. carbon dioxide reacts with alkynes to produce pyrones, with 1,3-butadienes and allenes to produce esters and lactones, with methylenecyclopropanes to produce lactones, and with epoxides to produce organic carbonates.

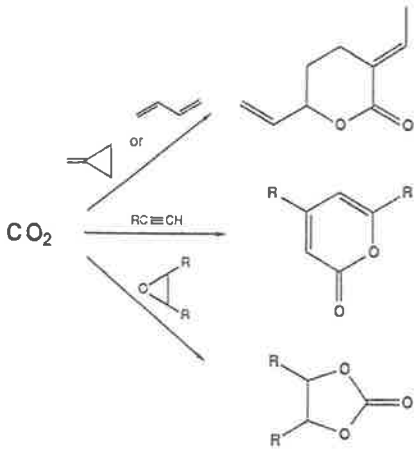

- chemistry related to the Kolbe-Schmitt reaction (i.e. the reaction of CO_2 with phenolates): e.g. alkali metal phenolates react with CO_2 to produce 2- and 4-carboxylated phenols.

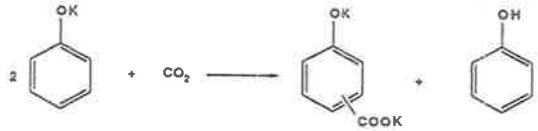

- the reaction of CO_2 with amines (including ammonia): e.g. CO_2 undergoes reaction with primary and secondary amines to yield carbamates (which may react further in the presence of appropriate substrates), and with ammonia under forcing conditions to produce urea.

$$R_2NH + CO_2 \rightleftarrows R_2NCOOH$$

$$2NH_3 + CO_2 \rightarrow H_2NC(O)NH_2 + H_2O$$

Within this diversity, there are only four major industrial chemical processes which use carbon dioxide as a carbon feedstock.

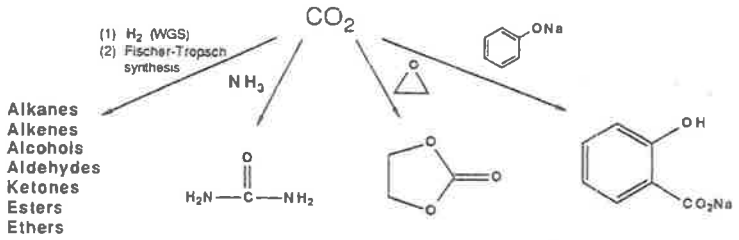

The commercial use of CO_2 is quite extensive, particularly in refrigeration and as a cryogen, in fire extinguishers and in beverages.

The reduction reactions involving molecular hydrogen are instructive in terms of the thermodynamics of carbon dioxide reactivity. The free energies on reduction of $CO_{2(g)}$ by molecular hydrogen, and in a limited number of organic reactions, are calculated and shown in the Table below (5,6).

Clearly, the thermodynamic stabilities of the CO_2 and H_2O molecules are dominant in the consideration of the reactions of CO_2 with molecular hydrogen. In cases where water acts as an "oxygen sink" the chances of a thermodynamically favorable reaction are higher. However as has been pointed out previously (16,18), molecular hydrogen is produced industrially by the involvement of the water-gas-shift reaction (equation (1)), whence CO_2 itself is the ultimate "oxygen sink". This irony illustrates the necessity for alternative reduction strategies for carbon dioxide reactivity, and carbon dioxide reduction in particular, among which the reaction of CO_2 with metal-hydride species must be of fundamental interest.

REACTION	ΔG° (kJ mol^{-1})
$CO_2 + H_2 \rightarrow CO + H_2O_{(l)}$	+19.9
$CO_2 + H_2 \rightarrow HCOOH_{(l)}$	+48.4
$CO_2 + 2H_2 \rightarrow HCHO_{(g)} + H_2O$	+47.2
$CO_2 + 3H_2 \rightarrow CH_3OH_{(l)} + H_2O$	-9.1
$CO_2 + 4H_2 \rightarrow CH_4 + 2H_2O$	-130.8
$2CO_2 + H_2 \rightarrow (COOH)_{2(s)}$	+90.9
$2CO_2 + 6H_2 \rightarrow CH_3OCH_{3(g)} + 3H_2O$	-36.8
$CO_2 + C_6H_{6(l)} \rightarrow C_6H_5COOH_{(s)}$	+18.7
$CO_2 + CH_4 \rightarrow CH_3COOH_{(l)}$	+53.2
$CO_2 + CH_4 + H_2 \rightarrow CH_3CHO_{(g)} + H_2O$	+74.4
$CO_2 + H_2 + CH_3OH_{(l)} \rightarrow CH_3COOH_{(l)} + H_2O$	-68.5
$CO_2 + 3H_2 + CH_3OH_{(l)} \rightarrow CH_3CH_2OH_{(l)} + 2H_2O$	-88.5

These values can be compared with analogous reactions for carbon monoxide: e.g.

REACTION	ΔG° (kJ mol^{-1})
$CO + 2H_2 \rightarrow CH_3OH_{(l)}$	-29.0
$CO + H_2O \rightarrow HCOOH_{(l)}$	+28.5
$CO + CH_3OH_{(l)} \rightarrow CH_3COOH_{(l)}$	-88.4

3. Biological Reactions of Carbon Dioxide

Carbon dioxide is nature's primary source of carbon, particularly through photosynthetic fixation to form carbohydrates. In terms of other chemical reactions of CO_2 in biological systems, many may be broadly classified as carboxylation reactions involving the electrophilic addition of CO_2 to a substrate anion, as for example in the enzymic conversion of phosphoenolpyruvate to oxalacetate:

(where RX is a phosphoryl acceptor such as water, a nucleoside diphosphate, or inorganic phosphate). In addition, the hydration/dehydration of CO_2 is essential in respiration and is catalyzed by the enzyme carbonic anhydrase.

$$CO_2 + H_2O \rightleftarrows H_2CO_3 \rightleftarrows HCO_3^- + H^+$$

A discussion of the variety of these biological reactions is not warranted here, but they have been reviewed elsewhere (19).

4. Equilibria and Kinetics of Aqueous Solutions Containing Carbon Dioxide

Many of the experimental studies addressing aspects of the solubility of carbon dioxide in a variety of solvents, and of the nature and kinetics of the resultant equilibria, have been extensively reviewed (4) and only a summary of some of those details will be discussed here.

On dissolution of gaseous carbon dioxide in water, a rapid $CO_{2(g)} \rightleftarrows CO_{2(aq)}$ equilibrium occurs, whereupon a slow equilibrium (equation (2)) is established between loosely hydrated $CO_{2(aq)}$ and "carbonic acid", H_2CO_3.

$$CO_{2(aq)} + H_2O \underset{k_{-1}}{\overset{k_1}{\rightleftarrows}} H_2CO_3 \qquad (K_H) \qquad [2]$$

The equilibrium constant, K_H, for this reaction can be calculated as 2.6×10^{-3} at 25°C: this value shows only minor temperature variation. Average values of k_1 and k_{-1} (25°C; zero ionic strength) are 6.2×10^{-2} s^{-1} and 23.7 s^{-1}, respectively (4).

The ionization constant for the dissociation of "carbonic acid"

$$H_2CO_3 \rightleftarrows H^+ + HCO_3^- \qquad (K_0) \qquad [3]$$

has been determined (20,21) to be 1.7×10^{-4} (25°C), and the reactions are very rapid (the rate of protonation of HCO_3^- is virtually diffusion controlled (22)). Accordingly, although the first ionization to produce the bicarbonate ion, HCO_3^-, is better expressed in the form

$$CO_{2(aq)} + H_2O \rightleftarrows H^+ + HCO_3^- \qquad (K_1) \qquad [4]$$

since <1% of the dissolved CO_2 is present as H_2CO_3, H_2CO_3 is an intermediate in reaction (3). K_1 is often referred to as the "apparent" acid dissociation constant of H_2CO_3, and should have a value (K_0K_H) of *ca.* 4×10^{-7} under the above conditions.

At higher pH values, $CO_{2(aq)}$ may react directly with OH^-

$$CO_{2(aq)} + OH^- \rightleftarrows HCO_3^- \qquad (K_{1'}) \qquad [5]$$

where the forward and back reactions determined at 7.7×10^3 M^{-1}s^{-1} (23,24) and 2.3×10^{-4} s^{-1} (25) at 25°C (respectively) lead to $K_{1'} = 3 \times 10^7$ M^{-1}.

The second dissociation reaction, viz.

$$HCO_3^- \rightleftarrows H^+ + CO_3^{2-} \qquad (K_2) \qquad [6]$$

appears normal in every respect and $K_2 = 4.7 \times 10^{-11}$ at 25°C (26).

A further equilibrium, called "carbonate catalysis" may also be present in solutions containing CO_3^{2-}:

$$CO_{2(aq)} + CO_3^{2-} + H_2O \rightleftarrows 2HCO_3^- \qquad [7]$$

however, unless a buffer containing carbonate ion were being used, rate studies indicate the contribution of such a path to be negligible by comparison with the previous equilibria (4,27).

The effect of temperature and ionic strength on the position and rates of the CO_2 equilibria have also received substantial attention particularly in view of their ubiquitous presence in the biosphere and the hydrosphere, and the presence of carbonate minerals in the earth's crust. The details of such studies are not relevant to a discussion ultimately directed towards metal activation of carbon dioxide reactivity, but are of paramount importance in the consideration of carbon dioxide storage and the ecosphere.

Finally, a comment might be made on the rate of the CO_2 equilibria in biological systems. Both the hydration of CO_2 to H_2CO_3 and the dehydration of H_2CO_3 are slow processes under normal conditions (*vide supra*) - too slow for respiratory functions - but the processes occur extremely rapidly *in vivo* through the involvement of a catalyst, the zinc-containing enzyme carbonic anhydrase. The question of activation of CO_2 in this case has received much attention: it is clear that the zinc metal does not coordinate directly to CO_2 but that the zinc ion is attached to a water molecule (or hydroxide ion) which is the source of the rapid proton transfer reactions which are essential for the rapid rate-determining step and which is involved in a nucleophilic attack on the carbon atom of CO_2 (19).

5. Thermodynamic Considerations of CO_2 Reactions in Aqueous Media

The standard $\Delta G°$ (25°C; pH = 0) and corresponding $E°$ values for the two-, four-, six-, and eight-electron reductions of $CO_{2(g)}$ in aqueous solution may be calculated (5,6) to give the values shown below:

REACTION	$\Delta G°$ (kJ mol^{-1})	$E°$ (Volts vs. NHE)
$2CO_{2(g)} + 2H^+ + 2e^- \rightarrow H_2C_2O_4$	+91.8	-0.475
$CO_{2(g)} + 2H^+ + 2e^- \rightarrow HCOOH_{(aq)}$	+38.4	-0.199
$CO_{2(g)} + 2H^+ + 2e^- \rightarrow CO_{(g)} + H_2O$	+19.9	-0.103
$CO_{2(g)} + 4H^+ + 4e^- \rightarrow HCHO_{(aq)} + H_2O$	+27.5	-0.071
$CO_{2(g)} + 6H^+ + 6e^- \rightarrow CH_3OH_{(aq)} + H_2O$	-17.3	+0.030
$CO_{2(g)} + 8H^+ + 8e^- \rightarrow CH_{4(g)} + 2H_2O$	-130.8	+0.169

As noted previously (28) in aqueous solution the nature of the carbon-containing substrate varies according to pH because of the equilibria given in equations (2), (3) and (6). Accordingly, there will be a pH-dependence of $E°$ value of the respective reactions, and these are shown in Figures 2 and 3 (5,6,29).

As expected, the reductions are more favorable at lower pH, and with the exception of the "CO_2" $\rightarrow CH_3OH$ and "CO_2" $\rightarrow CH_4$ processes all are less favored than the reduction $H_2O \rightarrow H_2$. Additionally, for the multi-electron reductions of CO_2 the reductions become more favorable in a thermodynamic sense the more reduced the product, although the difficulty of transfer of multiple electrons to the site of the reduction is a limiting factor in the feasibility of such processes.

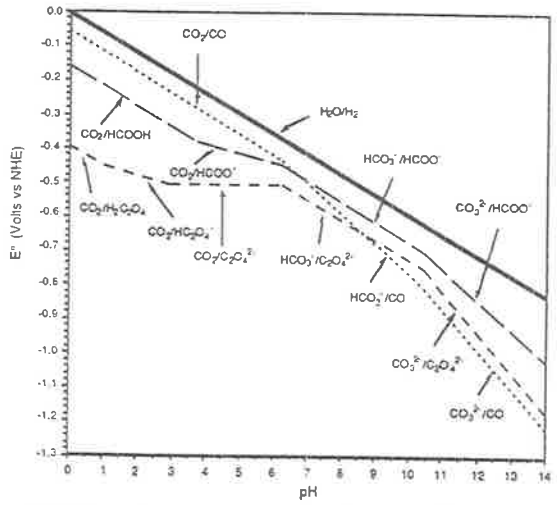

Figure 2. $E°$ values for the two-electron reductions of CO_2 and H_2O (Standard states $H_2O_{(l)}$, $CO_{(g)}$, $H_{2(g)}$, $CO_{2(aq)}$, $HCO_3^-{}_{(aq)}$, $CO_3^{2-}{}_{(aq)}$, $HCOOH_{(aq)}$, $HCOO^-{}_{(aq)}$, $H_2C_2O_{4(aq)}$, $HC_2O_4^-{}_{(aq)}$, $C_2O_4^{2-}{}_{(aq)}$)

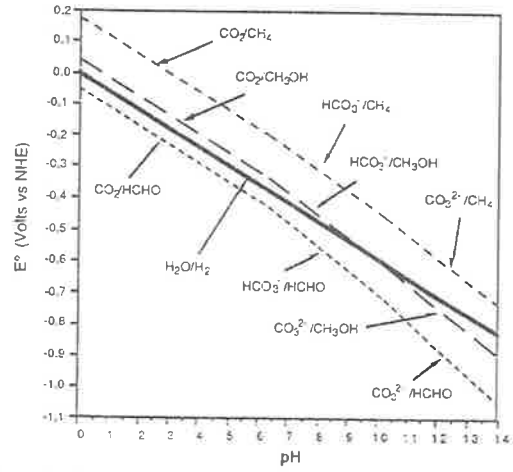

Figure 3. $E°$ values for the four-, six- and eight-electron reductions of CO_2 (Standard states $H_2O_{(l)}$, $H_{2(g)}$, $CO_{2(aq)}$, $HCO_3^-{}_{(aq)}$, $CO_3^{2-}{}_{(aq)}$, $HCHO_{(aq)}$, $CH_3OH_{(aq)}$, $CH_{4(g)}$)

By way of comparison, the E° values for the stepwise two-electron reductions "CO_2" → HCOOH → HCHO → CH_3OH → CH_4 are also given (5).

$$CO_{2(g)} \xrightarrow{-0.20} HCOOH_{(aq)} \xrightarrow{0.034} HCHO_{(aq)} \xrightarrow{0.232} CH_3OH_{(aq)} \xrightarrow{0.59} CH_{4(g)}$$

$$CO_3^{2\cdot-}{}_{(aq)} \xrightarrow{-1.01} HCOO^{\cdot}{}_{(aq)} \xrightarrow{-1.07} HCHO_{(aq)} \xrightarrow{-0.59} CH_3OH_{(aq)} \xrightarrow{-0.2} CH_{4(g)}$$

6. Electrochemical Reduction of Carbon Dioxide

The uncatalyzed electrochemical reduction of carbon dioxide is very solvent dependent. In water, the main product is formic acid, whereas in solvents with lower proton availability (such as dimethylformamide, dimethyl sulfoxide or propylene carbonate) oxalic acid and carbon monoxide are formed (13,30,31). The addition of small amounts of water (or the presence of adventitious water) in such dipolar aprotic solvents favours the formation of formic acid and promotes the further reduction of oxalic acid to glycolic acid, $HOCH_2$-CO_2H (30). Following the initial electron transfer reaction (**8**), the three reactions {self-coupling of the radical anion to form oxalate (**9**), reaction with water to form formate (**10**), and carbon-oxygen coupling leading to disproportionation producing carbon monoxide (**11**)} are competitive.

$$CO_2 + 1e \rightleftharpoons CO_2^{\cdot-} \qquad [8]$$

$$2\ CO_2^{\cdot-} \longrightarrow C_2O_4^{2-} \qquad [9]$$

$$CO_2^{\cdot-} + H_2O \longrightarrow HCO_2^{\cdot} \qquad [10]$$

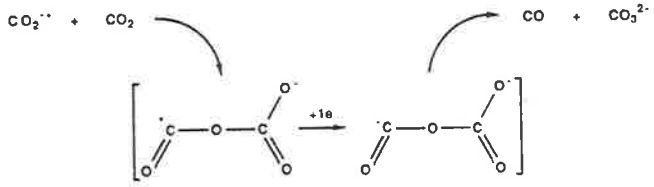

[11]

The potential of the electrochemical reduction of carbon dioxide (DMF, mercury electrode) was -2.21 V (vs. SCE) {i.e. -2.45V (*vs.* NHE)} (13), which represents a significant overpotential when compared with the reduction potential (E° = -1.90 V *vs.* NHE) for the $CO_2/CO_2^{\cdot-}$ couple (8,9). The large overpotential observed in the uncatalyzed electrochemical reduction of CO_2 arises in part because of a geometry change in the $CO_2 \rightarrow CO_2^{\cdot-}$ process (*vide supra*).

The presence of transition metal species substantially reduce the potential associated with the electrochemical reduction of carbon dioxide, to an extent dependent on the electrocatalyst, electrode and solvent used: such electrocatalysis has been the subject of a number of recent reviews (31-33).

Carbon monoxide is almost invariably the sole product of these chemically-catalyzed electrochemical reductions, and clearly such metal species substantially modify the path of the reduction since the potential of the reduction is in many cases at least 500mV anodic of E° for the $CO_2 \rightarrow CO_2^{\cdot-}$ process.

The mediation by transition metal centers of the chemical or electrochemical reduction of CO_2 has been extensively reviewed (2,4,16,18,31-39) and has been discussed in terms of

- reaction of CO_2 with oxophilic centers , where the $CO_2 \rightarrow CO$ conversion is achieved by transfer of the oxygen atom to a metal center, or to an associated ligand which has a high oxygen affinity (e.g. a phosphine).
- activation of the substrate CO_2 by direct coordination to the metal center, or
- activation of reagents that may react with the CO_2;

the latter two clearly more general in their scope and applicability to carbon dioxide activation, and are now considered in more detail.

7. Influence of Transition Metal Ions on Carbon Dioxide Reactivity

7.1 *Carbon Dioxide Coordination Chemistry.* One of the possible means of activation of carbon dioxide reactivity is the of modification of the properties of the CO_2 molecule by direct coordination to a metal center. The CO_2 molecule has three major potential modes of attachment to such a metal center - "end on" through an oxygen atom, "side on" to a C-O bond, or via the central carbon atom -

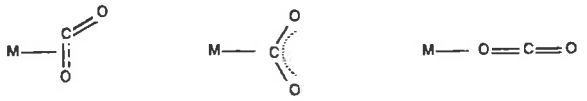

"side-on" coordination	C coordination	"end-on" coordination
η^2-CO_2	η^1-CO_2	η^1-OCO

as well as a number of less favorable modes (34). There have been a number of MO calculations of the relative stabilities of these ligating forms (40,41). The particular conclusions of Sasaki *et al* (40) were that there were two predominant interactions: π-back-donation, which stabilizes the "side-on" coordination mode (and which is generally the most favorable), and electrostatic interaction or σ-donation which favors "end-on" coordination and will be favored when the metal center is positively charged. C-coordination will be generally less favorable than side-on bonding, and would only be expected when the latter was inhibited by such effects as coordination numbers.

In fact, there are very few authenticated examples of simple transition metal complexes of carbon dioxide. Although there have been a number of claims for such species based on IR and

NMR spectral evidence, such assignments are often in question because of the similarities in such physical properties of bicarbonato-, carbonato- and carboxylato-metal species. The examples established by X-ray crystallography are listed in the Table below.

COMPLEX	REFERENCE	COORDINATION MODE
$[Ni(CO_2)(PCy_3)_2]$	(42,43)	η^2-CO_2
[Co(pr-salen)K(CO_2)THF)]	(44)	η^1-CO_2
$[Nb(\eta\text{-}C_5H_4Me)_2(CH_2SiMe)(CO_2)]$	(45)	η^2-CO_2
$[Rh(CO_2)(Cl)(diars)]$	(46)	η^1-CO_2
$[Mo(CO_2)_2(PMe_3)_3(CNR)]$ (R = Pr^i, $CH_2C_6H_5$)	(47)	η^2-CO_2
$[Mo(\eta^5\text{-}C_5H_5)_2(CO_2)]$	(48)	η^2-CO_2

In addition, there has been determined a structure of the complex $[IrCl(C_2O_4)(PMe_3)_3]$ (formed by exposure of $[IrCl(C_8H_{14})(PMe_3)_3]$ to carbon dioxide {C_8H_{14} = cyclooctene}) in which two CO_2 molecules have condensed to form a five-membered metallocycle (49):

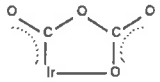

Since the promotion of the two-electron reduction of CO_2 may also be achieved by carbon dioxide activation involving two (or more) metal centers, the occurrence of binuclear (or multinuclear) species is also of considerable interest. Certainly in biological systems it appears that carbon dioxide requires acidic-basic centers for its activation, although the two roles in the bifunctional system are not played by metal centers. However, as for the case of the monofunctional species, there are few structurally authenticated examples of bifunctional metal systems. For the complex [Co(pr-salen)K(η^1-CO_2)THF)] (44), the carbon dioxide is reversibly bound and the ligand is stabilized by interaction of the acidic alkali metal cation with the oxygen atoms of the ligand. The only other authenticated examples of polynuclear species appear to be $(\eta^5\text{-}C_5H_5)Re(NO)(PPh_3)(CO_2SnPh_3)$ (50), $[(cod)Rh]_2OsH_2CO_2(PMe_2Ph)_3$ {cod = 1,5-cyclooctadiene} (51), $(\mu\text{-}CO_2)_2[Re(CO)_5][Re(CO)_4]_2$ (52), and $[Pt(CH_3)(dppp)]_2(\mu\text{-}CO_2)$ {dppp = $Ph_2P(CH_2)_3PPh_2$} (53).

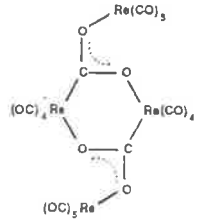

$(\mu\text{-}CO_2)_2[Re(CO)_5][Re(CO)_4]_2$ (52)

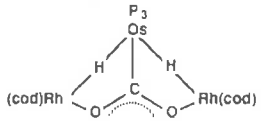

$[(cod)Rh]_2OsH_2CO_2(PMe_2Ph)_3$ (51)

7.2 *"Insertion" Reactions.* Much of the interest in the involvement of metals in the reactivity of carbon dioxide has been in the so-called "insertion" reactions of the general form

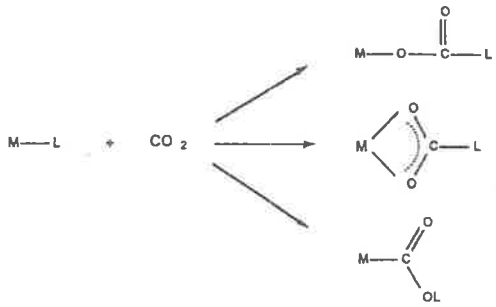

where

- L = H, giving rise to coordinated *formato* or *hydroxycarbonyl* ion;
- L = a ligand with a C ligating atom, giving rise to a *carboxylato* product;
- L = a ligand with an N ligating atom, giving rise to a *carbamato* product; and
- L = a ligand with an O ligating atom, giving rise to a *carbonato* product.

Since there is a lone pair of electrons on each of the oxygen atoms of CO_2 while the central carbon atom is relatively electron deficient, it would be the normal expectation that a positive metal atom (or M-L bond polarized in that manner) might prefer insertion to give the O-bound species, whereas insertions involving more electron-rich metal centers might result in the C-bound product. The former case would be regarded as the more likely possibility and is often referred to as the "normal" insertion mode.

There are a number of examples for each of these possible "insertion" processes, which have been extensively reviewed previously (2,4,16,34,38), but specific mention is made here of one instance in each case where the expected product has been authenticated by structural studies. Lehn *et al* (54) have recently reported the structure of the $[Re(bpy)(CO)_3(OOCH)]$, formed by a reaction which is assumed to be CO_2-insertion into the Re-H bond in $[Re(bpy)(CO)_3(H)]$ (55-57). For the case of CO_2-insertion into an M-C bond there has been structural identification of the product in the reaction (58):

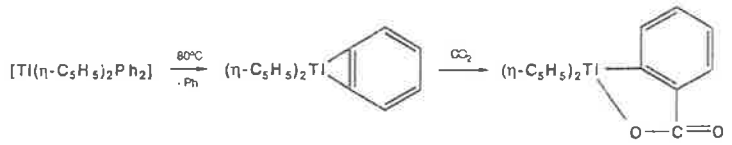

Similarly, in the reactions

$$[W(NMe_2)_6] + 3CO_2 \longrightarrow [W(NMe_2)_3(OCONMe_2)_3]$$

$$[Nb(NMe_2)_5] + 5CO_2 \longrightarrow [Nb(OCONMe_2)_5]$$

Chisholm and Extine have confirmed CO_2-insertion into M-N bonds (59,60). Finally, among examples of CO_2-insertion into M-OH or M-OR bonds is the following reaction which occurs both in the solution and solid states (61):

$$[Mo_2(OR)_6] + 2CO_2 \longrightarrow [Mo_2(OR)_4(O_2OCO)_2]$$

R = Me_3Si, Me_3C, Me_2CH, Me_3CCH_2

The path of such insertion reactions is by no means unambiguous, as there are a number of means by which the metal ion may influence such a process, as shown in the scheme below.

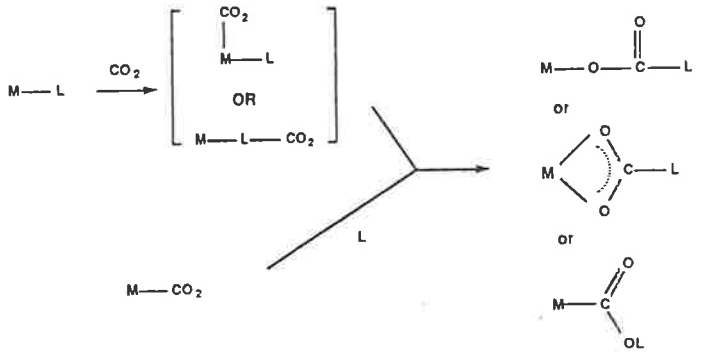

It should also be noted, however, that there is an additional path leading to the same products and which is not insertion and does not involve direct activation by the metal center:

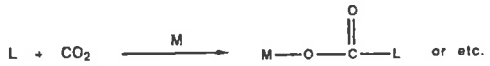

Such a path has been identified (62) for the reaction of $[Ir(depe)_2]Cl$ with CO_2 in acetonitrile solution to yield the $[Ir(depe)_2(H)(O_2CCH_2CN)]Cl$ species {depe = $Et_2PCH_2CH_2PEt_2$}, and by Chisholm *et al* in studies on CO_2 insertion into M-N (63) and M-O (64) bonds.

8. Reduction of Carbon Dioxide to Carbon Monoxide

In light of the above discussion, it is clear that the means by which metal complexes may mediate in the $CO_2 \rightarrow CO$ conversion may arise primarily from two paths:

(1) *Activation of CO_2 by coordination to a metal center,* including promotion of *reductive disproportionation:*

$$2CO_2 + 2e^- \rightarrow CO + CO_3^{2-}$$

(2) *Insertion of CO_2 into a metal-hydride bond,* with subsequent formation and decomposition of a formato or hydroxycarbonyl (carboxylato) transient species.

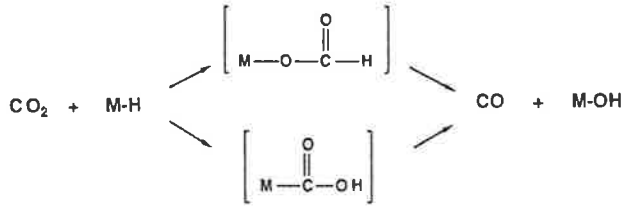

There has been no particular indication of enhanced reactivity of coordinated carbon dioxide in its isolated complexes. However, a number of recent thermodynamic and kinetic studies have provided insight into the influence of metal binding on CO_2 reactivity. For example, the binding of CO_2 with macrocyclic complexes of cobalt and nickel, which were the complexes reported in the initial studies of metal-promoted electrochemical reduction of CO_2 by Fisher and Eisenberg (65) has been assessed in terms of the effects of a number of parameters (e.g. the macrocycle, steric configuration, redox potential, solvent, etc.) (66-68). Carbonate ion does not appear to be a necessary co-product of CO_2 reduction to CO so that while there are reactions which involve reductive disproportionation, it is by no means a general path to the $CO_2 \rightarrow CO$ conversion.

The intermediacy of hydroxycarbonyl species following CO_2-insertion into M-H bonds has been postulated on a number of occasions as a pathway for CO production (69,70). The alternative possibility of the involvement of formato complexes (also formed by CO_2-insertion into M-H bonds) has also been noted and there are cases where isolated formato complexes have been reported to undergo decarbonylation processes: e.g. the acidification of $[\{P(C_6H_5)_3\}Co(HCOO)]$ (71) and the oxidation of $[Ru(NH_3)_5(HCOO)]^+$ and $[Os(NH_3)_5(HCOO)]^+$ (72).

These issues are discussed in detail subsequently in this volume.

9. Multi-electron Reduction of Carbon Dioxide

The two-electron reduction of CO_2 to either carbon monoxide or formic acid may be achieved by electrochemical, chemical and photochemical means. In many cases the reactions have involved the use of a transition metal center, although the role of the metal in the promotion of the reactivity of CO_2 is not always understood. Undoubtedly the production of carbon monoxide (especially in association with water reduction to molecular hydrogen) is a desirable aim since the technology for the utilization of "synthesis gas" is well established.

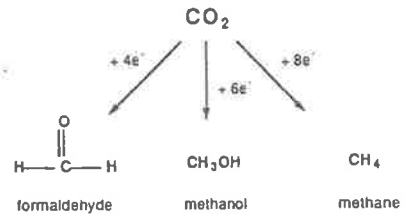

However, the direct conversion of carbon dioxide to more highly reduced products is tantalizing, not only from the point of view of the utility of the resultant products but also because the thermodynamics of such reactions are increasingly favorable (*vide supra*). While there have been reported reduction of CO_2 to formaldehyde and methanol at semiconductor electrodes (73-76) and to methanol and methane at Ru electrodes (77), there do not appear to have been any detailed reports on the selective homogeneous catalysis of multi-electron reduction of CO_2 by transition metal species.

In addition to the C_1 products of the multi-electron reduction of carbon dioxide, the C_2 and higher carbon products are also important. The coupled product oxalic acid is obtained from CO_2 reduction under certain circumstances, and oxalic acid reduction products (e.g. glycolic acid) have also been detected in the electrochemical reduction of CO_2 (30,31). Using the assumption of the additivity of bond and group properties in the various products involved in the sequential reduction of oxalic acid to ethylene glycol, the enthalpy changes for this series of reactions may be calculated (78) and are given in the Table 1 below (all results quoted refer to standard states of ideal gas at 1 atmosphere and 25°C).

For comparison , the equivalent calculated enthalpy changes for the sequential reduction of CO_2 to CH_4 are also given in the Scheme below.

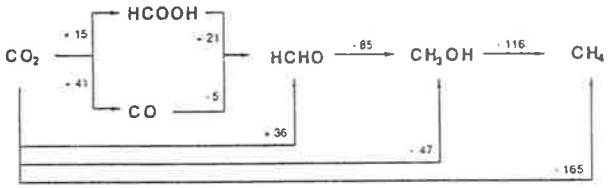

For the C_2 as well as the C_1 sequence, the multi-electron reductions of CO_2 become progressively more favorable thermodynamically as reduction is more complete, although there is the associated problem of transfer of multiple electrons. In principle at least, polynuclear coordination complexes and organometallic clusters provide a means of simultaneous delivery of multiple electrons to a catalytic metal site and this aspect of carbon dioxide activation may be expected to the subject of considerable attention in the immediate future.

REACTION	ΔH_f (kJ mol^{-1})
oxalic acid $\xrightarrow{+H_2}$ glyoxalic acid + H_2O	+ 25
glyoxalic acid $\xrightarrow{+H_2}$ glyoxal + H_2O	+ 21
glyoxalic acid $\xrightarrow{+H_2}$ glycolic acid	- 80
glyoxal $\xrightarrow{+H_2}$ glycolaldehyde + H_2O	+ 25
glycolic acid $\xrightarrow{+H_2}$ glycolaldehyde	- 75
glycolaldehyde $\xrightarrow{+H_2}$ ethylene glycol	- 67
OVERALL:	
oxalic acid $\xrightarrow{+4H_2}$ ethylene glycol + 2 H_2O	- 96

Table 1. Calculated enthalpy changes for the sequential reduction of oxalic acid
(Standard states of ideal gas at 1 atmosphere and 25°C)

10. References

1. M.E. Vol'pin and I.S. Kolomnikov, Pure Appl. Chem., 33 (1973), 567-581.
2. "Carbon Dioxide Activation by Metal Complexes", A. Behr, Ed., VCH (Weinheim, FRG), 1988.
3. T.J. Meyer, Acc. Chem. Res., 22 (1989), 163-170; D. Gust and T.A. Moore, Science, 244 (1989), 35-41; and references cited within both articles.

4. D.A. Palmer and R. Van Eldik, Chem. Rev., 83 (1983), 651-731; and references therein.
5. W.L. Latimer, "The Oxidation States of the Elements and Their Potentials in Aqueous Solutions" (2nd. Edn.), Prentice-Hall (U.S.A.), 1952.
6. "Standard Potentials in Aqueous Solution", A.J. Bard, R. Parsons, and J. Jordan, Eds., IUPAC, Physical and Analytical Chemistry Divisions, Marcel-Dekker (New York), 1985.
7. "Handbook of Chemistry and Physics", Vol. 58, R.C. Weast, Ed., CRC (Cleveland), 1978.
8. H.A. Schwarz and R.W. Dodson, J. Phys. Chem., 93 (1989), 409-414.
9. P.S. Surdhar, S.P. Mezyk, and D.A. Armstrong, J. Phys. Chem., 93 (1989), 3360-3363.
10. J. Lilie, G. Beck, and A. Henglein, Ber. Bunsenges, Phys. Chem., 75 (1971), 458-465.
11. M.V.V.S. Reddy, K.V. Lingham, and T.K.G. Rao, Mol. Phys., 41 (1980), 1493-1500.
12. H.A. Schwarz, C. Creutz, and N. Sutin, Inorg. Chem., 24 (1985), 433-439.
13. C. Amatore and J.-M. Saveant, J. Am. Chem. Soc., 103 (1981), 5021-5023; and references cited therein.
14. E. Haruki, "Organic Syntheses with Carbon Dioxide" in "Organic and Bio-organic Chemistry of Carbon Dioxide", S. Inoue and N. Yamazaki, Eds., Kodansha (Tokyo), 1982: pps 5-78.
15. B. Denise and R.P.A. Sneeden, Chemtech, (1982), 108-112.
16. R.P.A. Sneeden, "Reactions of Carbon Dioxide" in "Comprehensive Organometallic Chemistry", G. Wilkinson, F.G.A. Stone and E.W. Abel, Eds., 8 (1982), 225-283.
17. R.P.A. Sneeden, "Organic Syntheses where Carbon Monoxide is the Unique Source of Carbon" in "Comprehensive Organometallic Chemistry", G. Wilkinson, F.G.A. Stone and E.W. Abel, Eds., 8 (1982), 20-100.
18. R. Eisenberg and D.E. Hendricksen, Adv. Catal., 28 (1979), 79-172.
19. K. Asada, "Biological Carboxylations" in "Organic and Bio-organic Chemistry of Carbon Dioxide", S. Inoue and N. Yamazaki, Eds., Kodansha (Tokyo), 1982: pps 185-251.
20. G. Berg and A. Patterson, J. Amer. Chem. Soc., 75 (1953), 5197-5200.
21. K.F. Wissbrun, D.M. French, and A. Patterson, J. Phys. Chem., 58 (1954), 693-695.
22. M. Eigen, Angew. Chem., 75 (1963), 489-508.
23. B.R.W. Pinsent, F.J.W. Roughton, Trans. Farad. Soc., 47 (1951), 263-269.
24. B.R.W. Pinsent, L. Pearson, and F.J.W. Roughton, Trans. Farad. Soc., 52 (1956), 1512-1520.
25. M.J. Welch, J.F. Lifton, and J.A. Seck, J. Phys. Chem., 73 (1969), 3351-3356.
26. "Critical Stability Constants, Volume 4", R.M. Smith and A.E. Martell, Eds., Plenum (New York), 1976.
27. D.J. Poulton and H.W. Baldwin, Can. J. Chem., 45 (1967), 1045-1050.
28. F.R. Keene, C. Creutz, and N. Sutin, Coord. Chem. Rev., 64 (1985), 247-260.
29. The value for $\Delta G°$ for $HCOO^-_{(aq)}$ given in Ref.5 (-351.0 kJ mol^{-1}) is different from the value given in Ref. 6 (viz. -334.7 kJ mol^{-1}): it appears that the latter value is correct, and it was used in the calculations leading to Figure 2.
30. J.C. Gressin, D. Michelet, L. Nadjo, and J.-M. Saveant, Nouveau J. Chem., 3 (1979), 545-554.
31. I. Taniguchi, "Electrochemical and Photoelectrochemical Reduction of Carbon Dioxide" in "Modern Aspects of Electrochemistry", J. O'M. Bockris, R.E. White, and B.E. Conway, Eds., Plenum (New York), 1989: pps 327-400.
32. J.P. Collin and J.P. Sauvage, Coord. Chem. Rev., 93 (1989), 245-268; and references cited therein.
33. C. O'Connell, S.I. Hommeltoft, and R. Eisenberg, "Electrochemical Approaches to the Reduction of Carbon Dioxide" in "Carbon Dioxide as a Source of Carbon: Chemical and Biochemical Uses", M. Aresta and G. Forti, Eds., Reidel (Dordrecht), 1987; pps 33-54.
34. T. Ito and Y. Yamamoto, "Organometallic Reactions of Carbon Dioxide" in "Organic and Bio-organic Chemistry of Carbon Dioxide", S. Inoue and N. Yamazaki, eds., Wiley (New York), 1982: pps 79-151; and references cited therein.
35. D. Walther, Coord. Chem. Rev.,79 (1987), 135-174; and references therein.
36. "Catalytic Activation of Carbon Dioxide", W.M. Ayers, Ed., A.C.S. Symposium Series, Vol. 363, 1988.
37. P. Braunstein, D. Matt, and D. Nobel, Chem. Rev., 88 (1988), 747-764; and references cited therein.
38. D.J. Darensbourg and R.A. Kudaroski, Adv. Organomet. Chem., 22 (1983), 129-168.
39. S. Inoue and K. Koinuma, Rev. Inorg. Chem., 6 (1984), 291-355.
40. S. Sakaki, K Kitaura, and K. Morokuma, Inorg. Chem., 21 (1982), 760-765.
41. C. Mealli, R. Hoffman, and A. Stockis, Inorg. Chem., 23 (1984), 56-65.

42. M. Aresta, C.F. Nobile, V.G. Albano, E. Forni, and M. Manassero, J. Chem. Soc. Chem. Comm., (1975), 636-637.
43. A. Doehring, P.W. Jolly, C. Krueger, and M.J. Romao, Z. Naturforsch., B: Anorg. Chem., Org. Chem., 40B (1985), 484-488.
44. G. Fachinetti, C. Floriani, and P.F. Zanazzi, J. Am. Chem. Soc., 100 (1978), 7405-7407; S. Gambarotta, F. Arena, C. Floriani, and P.F. Zanazzi, J. Am. Chem. Soc., 104 (1982), 5082-5092.
45. G.S. Bristow, P.B. Hitchcock, and M.F. Lappert, J. Chem. Soc. Chem. Comm., (1981), 1145-1146.
46. J.C. Calabrese, T. Herskovitz, and J.B. Kinney, J. Am. Chem. Soc., 105 (1983), 5914-5915.
47. R. Alvarez, E. Carmona, E. Gutierrez-Puebla, J.M. Marin, A. Monge, and M.L. Poveda, J. Chem. Soc., Chem. Commun., (1984), 1326-1327; R. Alvarez, E. Carmona, J.M. Marin, M.L. Poveda, E. Gutierrez-Puebla, and A. Monge, J. Am Chem. Soc., 108 (1986), 2286-2294.
48. S. Gambarotta, C. Floriani, A. Chiesi-Villa, and C. Guastini, J. Am. Chem. Soc., 107 (1985), 2985-2986.
49. T. Herskovitz and L.J. Guggenberger, J. Am. Chem. Soc., 98 (1976), 1615-1616.
50. D.R. Senn, J.A. Gladysz, K. Emerson, and R.D. Larsen, Inorg. Chem., 26 (1987), 2737-2739.
51. E.G. Lundquist, J.C. Huffman, K. Folting, B.E. Mann, and K.G. Caulton, Inorg. Chem., 29 (1989), 128-134.
52. W. Beck, K. Raab, U. Nagel, and M. Steimann, Angew. Chem., Int. Ed. Engl., 21 (1982), 526-527.
53. Footnote 48 in M.A. Bennett, G.B. Robertson, A. Rokicki, and W.A. Wickramasinghe, J. Am. Chem. Soc., 110 (1988), 7098-7105.
54. J. Guilhem, C. Pascard, J.-M. Lehn, and R. Ziessel, J. Chem. Soc., Dalton Trans., (1989), 1449-1454.
55. J. Hawecker, J.-M. Lehn, and R. Ziessel, Helv. Chim. Acta, 69 (1986), 1990-2012.
56. C. Kutal, M.A. Weber, G. Ferraudi, and D. Geiger, Organometallics, 4 (1985), 2161-2166.
57. B.P. Sullivan, and T.J. Meyer, Organometallics, 5 (1986), 1500-1502.
58. I.S. Kolomnikov, T.S. Lobeeva, V.V. Gorbachevskaya, G.G. Aleksandrov, Y.T. Struchkov, and M.E. Vol'pin, Chem. Commun., (1971), 972-973.
59. M.H. Chisholm and M. Extine, J. Am. Chem. Soc., 96 (1974), 6214-6216.
60. M.H. Chisholm and M.W. Extine, J. Am. Chem. Soc., 99 (1977), 782-792.
61. M.H. Chisholm, W.W. Reichert, F.A. Cotton, and C.A. Murillo, J. Am. Chem. Soc., 99 (1977), 1652-1654.
62. A.D. English and T. Herskovitz, J. Am. Chem. Soc., 99 (1977), 1648-1649.
63. M.H. Chisholm and M.W. Extine, J. Am. Chem. Soc., 99 (1977), 792-802.
64. M.H. Chisholm, F.A. Cotton, M.W. Extine, and W.W. Reichert, J. Am. Chem. Soc., 100 (1978), 1727-1734.
65. B. Fisher and R. Eisenberg, J. Am. Chem. Soc., 102 (1989), 7361-7363.
66. M. Beley, J.-P. Collin, R. Ruppert, and J.P. Sauvage, J. Chem. Soc., Chem. Commun., (1984), 1315-1316.
67. D.A. Gangi and R.R. Durand, J. Chem. Soc., Chem. Commun., (1986), 697-69.
68. M.H. Schmidt, G.M. Miskelly, and N.S. Lewis, J. Am. Chem. Soc., 112 (1990), 3420-3426.
69. N.E. Katz, D.J. Szalda, M.H. Chou, C. Creutz, and N. Sutin, J. Am. Chem. Soc., 111 (1989), 6591-6601.
70. E. Fujita, D.J. Szalda, C. Creutz, and N. Sutin, J. Am. Chem. Soc., 110 (1988), 4870-4871.
71. L.S. Pu, A. Yamamoto, and S. Ikeda, J. Am. Chem. Soc., 90 (1968), 3896.
72. T. Kobayahi, N. Inoue, K. Shimizu, and G.P. Sato, Nippon Kag. Kaishi, 9 (1986), 1181-1186; P.A. Lay and H. Taube, unpublished results.
73. T. Inoue, A. Fujishima, S. Konishi, and K. Honda, Nature, 277 (1979), 637-638.
74. D. Canfield and K.W. Frese, J. Electrochem. Soc., 130 (1983), 1772-1773.
75. K.W. Frese and D. Canfield, J. Electrochem. Soc., 131 (1984), 2518-2522.
76. K. Ogura and H. Uchida, J. Electroanal. Chem., 220 (1987), 333-337.
77. K.W. Frese and S. Leach, J. Electrochem. Soc., 132 (1985), 260-261.
78. S.W. Benson, "Thermochemical Kinetics: Methods for the Estimation of Thermochemical Data and Rate Parameters", Wiley (New York), 1968.

Chapter 5

Mechanisms of the Electrochemical Reduction of Carbon Dioxide Catalyzed by Transition Metal Complexes

F. RICHARD KEENE and B. PATRICK SULLIVAN

1. INTRODUCTION.

Carbon dioxide is a potential source of single carbon fragments for the synthesis of future fuels and chemicals. It is a renewable resource with a chemistry that is in part responsible for the diversity of biological structures in nature. Despite the importance of this simple substrate, its reduction chemistry, both stoichiometric and catalytic, has not been explored. This situation, however, is slowly changing due to the recent extensive advances in coordination chemistry, organometallic chemistry and transition metal electrochemistry. The purpose of this chapter is to critically review the contributions that have defined our present understanding of the mechanistic steps that occur during electrochemical reduction of carbon dioxide.

Some fundamental chemical processes involving C_1 chemistry derived from CO_2 are, on the one hand, formation of new C-H bonds, and on the other, the scission of C-O bonds. This chapter focuses on the chemistry of the forward processes, while at the same time highlighting the microscopic reverse, i.e., the activation and breaking of C-O bonds with the formation of new C-H bonds. Several examples are shown in Eqs. 1 and 2.

$$M\text{-}O\text{-}\overset{O}{\overset{\|}{C}}\text{-}H \rightleftharpoons M\text{-}H + CO_2 \qquad [1]$$

$$CH_3OH \rightleftharpoons CH_4 + O\text{-}A \qquad [2]$$

In addition, examples of the formation of C-C bonds are also discussed.

In Eq. 1, the breaking of a C-H bond is coupled with the formation of a metal-hydrogen bond. As will be discussed later, both the forward and reverse reactions for this example are the subjects of mechanistic studies, so that insight on the microscopic level is available. Less is known concerning the reaction shown in Eq. 2, where a carbon-oxygen bond in methanol is replaced by a C-H bond, even though it is involved in the final stage of bacterial methanogenesis (1, 2). This chapter examines the interrelationship of CO_2 reduction and C-H activation by presenting and discussing the fundamental mechanistic steps involved. Organizationally, it covers CO_2 reduction with emphasis on the sequential mechanistic steps that could occur, and then progresses to a discussion of electrocatalytic CO_2 reduction. In each of the following sections we will highlight what we feel are important studies that contribute to the understanding of the C-H bond-making and C-O bond-breaking steps that occur during CO_2 reduction.

2. STEPWISE REDUCTION OF CARBON DIOXIDE

Scheme 1 shows the C_1 transformations that accompany the stepwise reduction of carbon dioxide to methane by either hydrogenation or electrochemical reduction.

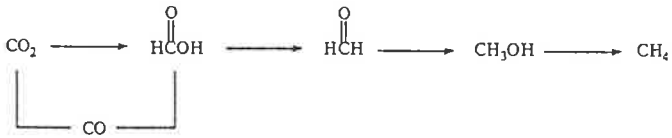

Scheme 1. Stepwise hydrogenation of CO_2.

In both chemical reduction of CO_2 using molecular H_2 or electrochemical reduction involving coupled proton/electron transfer steps, the initial conversion to formic acid or the dehydration product CO is unfavorable. Likewise, the conversion of formic acid to formaldehyde is unfavorable (see the previous chapter on thermodynamics). A point to consider here is that the direct reduction of these compounds at an electrode involves reaction conditions that are far different from the working conditions of the mechanistic organometallic chemist. For example, while the reduction from formaldehyde to methanol takes place at a potential of -0.36 V (vs. NHE) in water at pH 7 (3) this value could differ significantly in a non-aqueous solvent or water/organic mixture, for example, THF or H_2O/CH_3CN.

Although thermodynamic potentials (3) for the electrochemical reduction of CO_2 to the products shown in Scheme 1 are generally between ca. -0.24 and -0.9 V (vs. NHE at pH 7), reduction of CO_2 to its radical anion requires -2.21 V in DMF (4) and ca. -1.9 V in water (5). In this sense, chemical catalysis is necessary to achieve a significant lowering of the overpotential for the initial single electron transfer step.

While the formation of both methanol and methane by conventional hydrogenation is exergonic, substantial kinetic barriers exist here also. This is undoubtedly due to the necessity to proceed through the intermediacy of CO, formic acid, or formaldehyde, which are formed by endergonic steps. As far as electrochemical reduction is concerned, high overpotentials are also found for the formation of these products.

Transition metal catalysis, both in the homogeneous and heterogeneous sense, can achieve the desired effect of reducing the overpotential in electrochemical CO_2 reduction and to promoting rapid hydrogenation of CO_2 to methanol or methane. In recent years the sophistication of coordination and organometallic chemistry has developed to the point where it is possible to discuss the reaction chemistry of proposed intermediates on the reaction coordinate to C_1 products. In a broader sense, it might be possible to "design" catalytic reactions to realize a number of the steps in Scheme 1.

2.1 Sequential Mechanistic Steps in Carbon Dioxide Reduction.

Returning to Scheme 1, it is obvious that as one progresses from CO_2 to CH_4, or in the opposite sense from CH_4 to CO_2, C-H and C-O activation must occur. In the former case CO bonds must be broken and C-H bonds must be formed, while in the latter C-H bonds must be broken and C-O bonds formed. Furthermore, the presence of an oxygen acceptor for the hydrogenation, and an oxygen donor for the "combustion" reaction sequence, is required.

In this section we will focus on the possible transition metal intermediates that can accomplish the potentially reversible C-O and C-H activation steps involved in CO_2 reduction. Scheme 2 shows the matrix of sequential steps that convert CO_2 to CH_4.

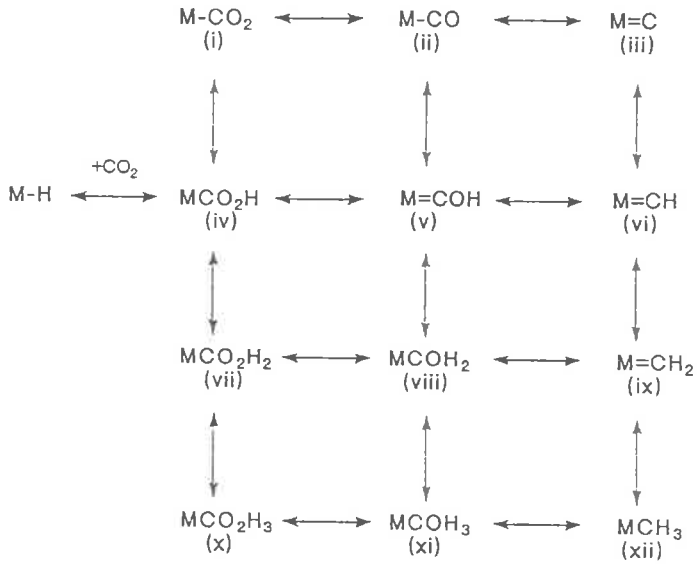

Scheme 2. Empirical formulae of possible reduction products of CO_2 upon stepwise hydrogenation or coupled proton/electron transfer reactions.

Scheme 2 is meant to convey the empirical structures of the metal coordinated carbon fragments that result from CO_2 reduction. By moving vertically in the scheme, a formal addition or subtraction of a hydrogen radical occurs, and by moving horizontally an oxygen atom addition or subtraction occurs. The skeletal formulae for the intermediates in Scheme 2 cover a number of possible isomeric metal complexes. For these, the following twelve catagories apply.

1. Structure (i) is a metal-CO_2 complex. These have been discussed in detail by Creutz in Chapter 2 of this volume.
2. Stucture (ii) is a metal carbonyl complex.
3. Structure (iii) is a metal carbide complex. Formally this would be formed (on a monomeric metal center) by deprotonation of a parent alkylidyne. Polymetallic systems have been shown to adequately support the "bare" carbon atom.
4. Structure (iv) will exist either as the metallocarboxylic acid, M-C(O)OH (also called hydroxycarbonyl), or the formato complex, M-OC(O)H.
5. Structure (v) will exist as one of two drastically different isomeric forms, the hydroxyalkylidyne complex, MC-OH, or the formyl complex, M-C(O)H.
6. Structure (vi) is the parent alkylidyne complex, MC-H.
7. Structure (vii) is a dihydroxyalkylidene complex, $MC(OH)_2$.
8. Structure (viii) is a hydroxyalkylidene complex, MC(OH)H, or a complex of formaldehyde, $M(O)CH_2$.
9. Structure (ix) is the unsubstituted alkylidene complex, MCH_2.
10. Structure (x) is a dihydroxymethyl complex, $MCH(OH)_2$.
11. Structure (xi) is a hydroxymethyl complex, $MCH_2(OH)$.
12. Structure (xii) is a methyl complex, MCH_3.

Many of the interconversions implied by Scheme 2 have been observed to occur in organometallic chemistry: in the following section we will briefly review exemplary cases which have relevance to the electrochemical reduction of CO_2.

2.1.1 Metal-CO_2 Complexes and Their Reactivity. As a ligand carbon dioxide can bind in three fundamental geometric arrangements to a monomeric transition metal center. These are: 1) η^1, bonding through oxygen; 2) η^1, bonding through carbon; and 3) a "side bonded" mode where the metal is located approximately between an oxygen and carbon atom (η^2). The first mode has never been definitively proven, but the latter two have sparse but ample crystallographic precedent (6, 7) as discussed in Chapter 2 of this volume. The binding of CO_2 to multimetal systems has been documented, and crystal structure data shows that combinations of the above modes contribute to CO_2 as multidentate ligand. These cases have been nicely summarized in several recent reviews by Behr (6, 7) and are discussed in detail in Chapter 2.

Despite this background very little is known about reactivity of metal-complexed CO_2, especially under electrochemical conditions. Although Scheme 2 shows possible CO_2 pathways in an empirical sense, Scheme 3 presents observed or likely transformations.

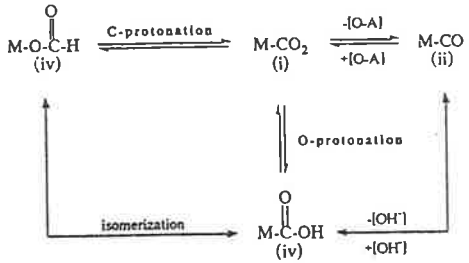

Scheme 3. Possible reactivity of M-CO_2 complexes under electrochemical conditions.

In Scheme 3, it is seen that proton attack on coordinated CO_2 can, in principle, take place via either C or O protonation to yield the isomeric complexes M-OCH or M-COH, respectively (these species could also be interconverted in the isomerization reaction shown above). Carbon-protonation evidently has not been observed, whereas O-protonation has ample precedent, as will be discussed later.

A number of studies, many of which are concisely reviewed by Culter, Hanna and Vites (8), have shown that C-bound CO_2 reacts with electrophilic reagents to form structures that are analogous to a metallocarboxylic acid. Thus silylation readily occurs to give complexes with the M-C(O)OSiR_3 unit, which is formaly a metallocarboxylate ester (9). Another mode of reaction is electrophilic attack at both CO_2 oxygen atoms to give structures containing a bidentate coordination mode. Nice illustrations of this reactivity are found in the work of Gladys et al. (10) using the presumed $[(\eta^5\text{-}C_5H_5)Re(NO)(PPh_3)(CO)_2]^-$ complex, which demonstrates that by changing the nature the electrophile from Ge to Sn bidentate is favoured over monodentate coordination (Eqs. 3 and 4: [Re] is the $(\eta^5\text{-}C_5H_5)Re(NO)(PPh_3)$ fragment).

$$[Re]CO_2^- + Ph_3GeBr \rightarrow [Re][\eta^1\text{-}CO_2GePh_3] + Cl^- \quad [3]$$

$$[Re]CO_2^- + R_3SnCl \rightarrow [Re][\eta^2\text{-}CO_2SnR_3] + Cl^- \quad [4]$$

Another reaction of note is the intramolecular "condensation" of CO_2 with an electrophilic site such as a coordinated CO or CO_2. For example, the proposed intermediate in intramolecular ^{13}C and ^{18}O scambling in $[(\eta^5\text{-}C_5H_5)Fe(CO)_2CO_2]^-$ is through the metalloanhydride intermediate (11) shown in Figure 1.

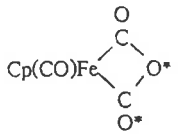

Figure 1. Proposed cyclic intermediate that equilibrates labelled oxygen in $FpCO_2^-$ (Fp is the $[(\eta^5\text{-}C_5H_5)Fe(CO)_2]$ fragment.

A unique structure is found for the Ir[complex shown in Figure 2 (12) where two CO_2 molecules have condensed.

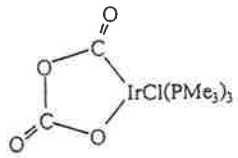

Figure 2. Head-to-tail condensation of two CO_2 molecules in the coordination sphere of formal Ir(III).

The amphoteric nature of the CO_2 ligand can be exploited to yield structures in which there exist multiple metal-CO_2 interactions. Of particular note are the cyclic structures of $[Re(CO)_4]_2(CO_2)_2[Re(CO)_5]_2$ (13) and the mixed metal system $[Os(PMe_3)_2Cl(CO_2)(H)_2][Rh(COD)]_2$ (14) shown below.

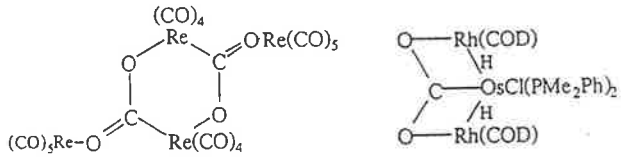

Figure 3. Two multimetallic CO_2 complexes where all atoms of the CO_2 molecule are coordinated to metal centers.

It is possible that multimetallic systems such as these will be capable of delivering more than two redox equivalents to a single coordinated CO_2.

2.1.2 Reduction of Carbon Dioxide to Carbon Monoxide Involving Metallocarboxylates or Metal Formates. Although there are many examples of metal complex catalysis of the chemical, electrochemical, and photochemical reduction of carbon dioxide to carbon monoxide (6, 15-23), the mechanism of this transformation, and in particular the role of the metal-CO_2 complexes in its promotion, is not conclusively established. In fact, it is possible that a number of general mechanistic paths may exist for this conversion - a number of proposals have been put forward for such processes. As shown in Scheme 3 a variety of pathways exist, for example protonation at carbon will yield a metal formate while protonation at oxygen gives a metallocarboxylate. Also, from a limited number of kinetic studies it is becoming clear that metallocarboxylato (formed by what has been termed an "abnormal insertion") or metal formato complexes can be intermediates. The latter product can result from insertion of CO_2 into the metal

hydride bond, is considered later in a separate section. A related reaction, the insertion of CO into a metal alkoxide bond to give formate complexes has not been proven.

$$M\text{-}OH + CO \rightarrow M\text{-}CO_2H \qquad [5]$$

Furthermore, where deliberate studies on this issue have been undertaken (24), the conclusion has been reached that formate and carbon monoxide reactivity in such systems are unrelated.

Metallocarboxylate complexes are implicated as important intermediates in processes such as the water-gas shift reaction (see earlier in this volume)

$$CO + H_2O \rightarrow CO_2 + H_2 \qquad [6]$$

where the nucleophilic attack of OH^- on the carbon atom of the carbonyl group to form the such an intermediate is seen as an important step in homogeneous catalysis (25, 26).

$$M{-}C{\equiv}O + OH^- \longrightarrow \left[M{-}\overset{\displaystyle OH}{\overset{|}{C}}{=}O \right]^- \longrightarrow M{-}H + CO_2 \qquad [7]$$

On a number of occasions, the involvement of metallocarboxylates as an intermediates or transition states has been suggested for the net transformation of $CO_2 \rightarrow CO$ (23, 24, 27-30). However, despite a number of claims for such species in organometallic chemistry (25, 26), there is little detailed information available on their chemistry (e.g., their acid/base properties) or on structural aspects.

The decomposition of metallocarboxylate complexes (generally thermally) produces CO_2 and the metal-hydride complex, which is the reverse of the reaction under discussion - however the accessibility of such an intermediate in the $CO_2 \rightarrow CO$ reduction is confirmed by the reversibility principle. The uncatalyzed reaction favors CO_2 and H_2 thermodynamically, so that the involvement of the metal center in promoting the reverse reaction would be to influence the stability of intermediates or products in the reaction.

The first structural characterization of a monondentate C-donor -COOH ligand was reported in a recent study by Bennett *et al.* (31), where the complex *trans*-$[Pt(COOH)(C_6H_5)(PEt_3)_2]$ was formed by CO insertion into a Pt-OH bond in *trans*-$[Pt(OH)(C_6H_5)(PEt_3)_2]$.

Involvement of metallocarboxylates in the interconversion of coordinated CO_2 and CO is demonstrated by the reaction of the transient $[(\eta^5\text{-}C_5H_5)Fe(CO)_2CO_2]^-$ with protons, which occurs as shown in Eqs. 8 and 9.

$$[(\eta^5\text{-}C_5H_5)Fe(CO)_2CO_2]^- + H^+ \rightarrow [(\eta^5\text{-}C_5H_5)Fe(CO)_2CO_2H] \qquad [8]$$

$$[(\eta^5\text{-}C_5H_5)Fe(CO)_2CO_2H] \rightarrow [(\eta^5\text{-}C_5H_5)Fe(CO)_3]^+ + OH^- \qquad [9]$$

Some understanding of the reactivity of the metallocarboxylate complexes is emerging as a result of the recent work of Creutz *et al.* (32, 33). In the decomposition of the cationic cobalt(III) complex $[Co(en)_2(H_2O)(CO_2H)]^{2+}$ (32), the nucleophilic elimination process

$$[Co(en)_2(H_2O)(CO_2H)]^{2+} \rightarrow [Co(en)_2(H_2O)(CO)]^{3+} + OH^- \qquad [10]$$

is suppressed substantially over reductive elimination (which yields free CO_2, or the $CO_2^{\cdot-}$ radical or its conjugate acid) and is only a significant path in strongly acidic solution where the rate shows a first order dependence on both complex and acid concentration. Furthermore, no formate ion is formed by the homolysis reaction. For the Co(III) center, the pK_a (2.5 ± 0.5) for equilibrium shown in Eq. 11 indicates that $-CO_2H$ is rather acidic.

$$[Co(en)_2(H_2O)(CO_2H)]^{2+} \leftrightarrow [Co(en)_2(H_2O)(CO_2)]^+ + H^+ \qquad [11]$$

The structural and spectroscopic studies reported in this paper also indicate that CO_2^{2-} and CO_2H^- are strong field ligands, so that it might be expected that for a more basic metal center the pK_a would be higher, and the nucleophilic elimination process might be somewhat more favorable thermodynamically and therefore more accessible.

The kinetic study by Keene, Creutz and Sutin (34) of the reduction of CO_2 to CO by $[Co(bpy)_3]^+$ in aqueous solution is also significant. The rate for water reduction (to H_2) and HCO_3^- reduction (to CO) show a common rate law:

$$\text{Rate} = k \frac{[Co(bpy)_3^+][H^+][HCO_3^-]}{[bpy]}$$

Kinetic and stoichiometric studies also indicate a common intermediate for the two processes (the cobalt-hydride species formed on dissociation of one bpy ligand was suggested). These studies were undertaken at a pH where all the "CO_2" would be expected to be present as HCO_3^-, and the data were interpreted to indicate reaction between HCO_3^- (rather than CO_2) and the hydride species. The nature of the intermediate species is not clear in this instance: certainly formate ion is not a significant product of the reaction, and a carboxylate or carboxylato species may well be involved. The related complex $[Co\{(2\text{-}py)_3P\}_2]^+$ reduces water but not HCO_3^-/CO_2 under the same conditions (35). The reason for this difference is not entirely clear at this stage, although it may be related to availability of coordination positions for reaction since the tridentate ligand in this case (unlike the bidentate bpy) does not totally dissociate.

2.1.3 Formation of CO With Oxide Ion Acceptors. The reductive disproportionation of carbon dioxide, $2CO_2 \rightarrow CO + CO_3^{2-}$, was identified by Saveant *et al.* (36) in their studies of the uncatalyzed electrochemical reduction of CO_2. In transition metal complexes, conversion of a metal-CO_2 complex to metal-coordinated carbon monoxide is a facile reactivity pathway especially in the presence of an oxide acceptor, A , which can be CO_2 itself. Examples include the reaction of metal carbonylates such as $[(\eta^5\text{-}C_5H_5)Fe(CO)_2]^-$ and $W(CO)_5^{2-}$ with CO_2

to form $[(\eta^5\text{-}C_5H_5)_2Fe(CO)_3]^+$ (11) and $W(CO)_6$ (37), respectively. In these cases a second molecule of CO_2 acts as the oxide acceptor and as a consequence gives CO_3^{2-} as a product. Another reaction that apparently occurs from complexed CO_2 is phosphine attack to give carbonyl complexes and a phosphine oxide (38).

A novel reaction is that shown in Eq. 12 where the same metal center to which CO_2 evidently coordinates, acts as the acceptor during the homolytic scission of a CO bond (39). The net result is the formation of an oxo-carbonyl complex.

$$[W(PR_3)_4Cl_2] + CO_2 \rightarrow [O{=}W(PR_3)_2(CO)Cl_2] + 2PR_3 \qquad [12]$$

The observation by Herskovitz and Guggenberger (12) of an iridium complex containing the proposed "head-to-tail" (carbon-oxygen coupled) CO_2 dimer metallocycle aroused considerable interest that the role of the metal in the $CO_2 \rightarrow CO$ transformation might well be the stabilization of this important intermediate. While a general scheme involving such an intermediate has been proposed in a number of cases (12, 40-42), it must be noted that where such a metallocyle has been isolated there is no evidence of it decomposing in this way to lead to the disproportionation (43). However, there are a number of examples that indicate the metal-promoted disproportionation process: e.g., in the reaction (43).

$$2[Mo(N_2)_2(PMe_3)_4] + 2CO_2 \rightarrow [Mo(CO_3)(CO)(PMe_3)_3]_2 \qquad [13]$$

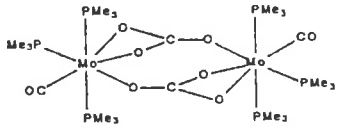

In the reductive disproportionation of $2CO_2 \rightarrow CO + CO_3^{2-}$ discussed above, CO_2 acts as an oxygen acceptor to allow the reaction to proceed, possibly via a metallocycle. An alternative mode of reduction of carbon dioxide is the involvement of "oxophilic" metal centers (e.g. Ti(III) and Zr(III)) (44, 45).

$$[Cp_2TiCl_2]_2 + CO_2 \rightarrow [Cp_2TiCl]_2O + CO \qquad [14]$$

$$3[Cp_2Zr(CO)_2] + 3CO_2 \rightarrow [Cp_2ZrO]_3 + 9CO \qquad [15]$$

or oxygen transfer to an adjacent ligand (e.g. a phosphine) which allow the $CO_2 \rightarrow CO$ by oxygen transfer (46, 47).

$$[(PBu_3)_2RhCl(CO_2)] \rightarrow [(PBu_3)RhCl(CO)(OPBu_3)] \qquad [16]$$

$$[Mo(C_2H_4)(Ph_2PCH_2CH_2PPh_2)_2] + CO_2 \rightarrow [(Ph_2PCH_2CH_2PPh_2)_2Mo(CO)_2] + \text{phosphine oxide products} \qquad [17]$$

In a study in which the following sequence (48) of reactions were proposed,

$$[Fe(PMe_3)_4 + CO_2] \rightarrow [Fe(PMe_3)_4(CO_2)] + [Fe(PMe_3)_3(CO)(CO_3)] \qquad [18]$$

$$[Fe(PMe_3)_4(CO_2)] \rightarrow [Fe(PMe_3)_4(CO)] + Me_3P{=}O \qquad [19]$$

the involvement of on oxophilic phosphine was also considered in reaction [19], although disproportionation was claimed in reaction [18].

In summary, it is apparent that evidence is becoming available for a number of paths for the metal complex catalyzed $CO_2 \rightarrow CO$ conversion. Clearly, for metal centers which have a significant "oxophilic" character (e.g. Ti(III), Zr(II)) the metal itself may play a direct role in the reduction process. The presence of other "oxophilic" centers (particularly phosphines) may also lead to the redution process. Insertion of CO_2 into metal-hydride bonds also provides a means for $CO_2 \rightarrow CO$ conversion, and although the intermediacy of formato complexes and subsequent rearrangement cannot be entirely discounted, it seems that metallocarboxylate species would appear as more likely intermediates, especially in the cases where Co(I) and Rh(I) are involved.

The observation of free (bi)carbonate ion or of (bi)carbonato complexes in the reduction of CO_2 does not necessarily indicate a disproportionation processes, particularly in the presence of water, where HCO_3^-/CO_3^{2-} may form through the normal "carbonic acid" equilibria. An example of this is the reaction is the reaction of $[RhH\{P(^iPr)_3\}]$ with CO_2 in the presence of water (27), where any one of the paths shown in the scheme below may lead to the observed product. The (bicarbonato)dihydro complex thus formed reduces CO_2 further to form a (bicarbonato)carbonyl species.

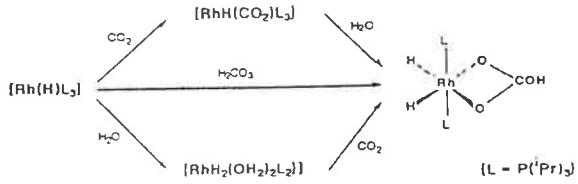

Scheme 4. Formation of a bicarbonate complex reaction of CO_2 at a Rh(I) metal center. Notice that formation of the bicarbonate complex occurs to the exclusion of insertion into the Rh-H bond of $Rh(H)\{P(^iPr)_3\}_3$.

2.1.4 Formation of Formate by Insertion into a Metal-Hydride Bond. Insertion reactions into metal-hydride bonds of the C_1 substrates CO and CO_2 may have widespread importance in a number of industrial processes, including the water-gas-shift reaction, Fischer-Tropsch-type chemistry and hydroformylation (18, 25). There have been a number of recent observations of carbon monoxide insertion into a Zr-H bond to produce a formaldehyde species (49), and evidence for insertion into a Ta-H bond (50) and an Fe-H (51) bond to form formyl species has also been presented. There have also been a substantial number of claims of observations of CO_2 insertion into M-H bonds to produce formato complexes or free formate ion (16-21). While many of the examples are difficult to rationalize in other ways, the number of examples where there has been detailed characterization of the reactant hydride species and structural authentication of the formato product are few. However, both modes of "normal' insertion are observed - the formation of the monodentate O-bound formato linkage (Figure 4a) by apparent insertion of CO_2 into a Re-H bond has been observed and studied by Lehn *et al* (24) and Sullivan and Meyer (52, 53). The reaction of CO_2 with $[(Ph_3P)_4RuH_2]$, $[(Ph_3P)_2Ru(N_2)H_2]$, and $[(Ph_3P)_3RuH_4]$ has been shown (54) to produce the O-bound bidentate species (Figure 4b).

(a) (b)

Figure 4. The two types of formate coordination, (a) monodentate and (b) bidentate.

There are few detailed kinetic investigations of the mechanism of such "insertion" reactions of CO_2 into metal-hydride bonds. Of particular interest, however, are recent mechanistic studies on the systems $[Re(bpy)(CO)_3H]$ (53, 55) and $[Os(bpy)_2(CO)H]$ (55, 56).

The insertion of CO_2 into Re-H in $[Re(bpy)(CO)_3H]$ to form the formato species is a second-order process (53)

$$\text{rate} = k[Re(bpy)(CO)_3H][CO_2]$$

with the rate showing a substantial dependence on the solvent. Isotope exchange studies revealed an inverse isotope effect ($k_H/k_D = 0.55$) (53), and activation parameters were determined to be $\Delta H^{\ddagger} = 53.5$ kJmol^{-1} and $\Delta S^{\ddagger} = -138$ Jmol^{-1}K^{-1}. A study of the rate variation with the modification of the inert bpy ligand indicated that the insertion process is facilitated by electron-donating substituent groups. These results were interpreted to indicate an associative hydride-transfer process: the inverse deuterium isotope effect is consistent with a cyclic or unsymmetrical linear transition state, and the solvent effect indicates considerable charge separation during the hydride transfer. The transition states may be envisaged as

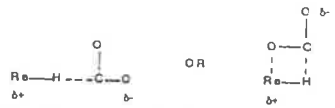

Figure 5. Two possible transition states for CO_2 insertion into a metal hydride bond

resulting from attack by the hydride ligand on the carbon atom of CO_2.

As shown in one study, electrochemical reduction of CO_2 to formate ion in the manner described above is dependent on the prior formation of a hydride complex from $[Re(bpy)(CO)_3Cl]$ under the conditions of the electrolysis (24).

The mechanism of production of formate by electrochemical reduction of CO_2 in the presence of $[Os(bpy)_2(CO)H]^+$ appears to create some contrast with the studies on the rhenium-species (40): the CO and H groups in this case are inert, as shown by isotope exchange studies. The di-reduced complex $[Os(bpy)_2(CO)H]^-$ would appear the active reductant in this reaction and undergoes a reaction with CO_2 which leads to the formation of CO and (in the presence of water) formate.

2.1.5 Stepwise Reduction Past the Two-Electron Stage. As has been demonstrated, reduction of CO_2 to CO or formate is readily observed but further reduction is rare. A strategy for obtaining reduction past the two-electron stage might involve further coupled proton/electron transfer to the intermediate formate or CO complexes. Apparently only the latter has mechanistic precedent.

A number of studies have demonstrated the reduction of metal-CO complexes to the M-CH_3 stage (57, 58, 59). A most illustrative example is that of Lapinte, Catheline and Astruc (59) where, depending upon conditions, all the intermediate reduction products can be directly detected. This is illustrated in Scheme 5.

$$Fp\text{-}CO^+ \xrightarrow{a} Fp\text{-}C(O)H \xrightarrow{b} Fp\text{-}CH_2OH \xrightarrow{c} Fp\text{-}CH_3$$

Scheme 5. Stepwise reduction of CO. Conditions are: a) $NaBH_4$, THF, -80° K; b) BH_3, THF, -60° K; c) $NaBH_4$, THF, 20° K.

A most notable achievement is the use of Fp-H as a hydride source for the reduction. Thus under conditions of excess hydride reagent a 240% yield of methyl complex can be obtained from $[Fp\text{-}CO]^+$. An important extension of this chemistry is the electrogeneration of a hydridic reagent in the presence of a metal-CO complex. Recently, this has been accomplished to give reduction to the metal-formyl stage (60). The ultimate goal here will be to devise a two-site catalytic system that reduces CO_2 to metal-bound CO at one site while generating a reactive metal hydride site that is capable of effecting multiple redox events like those shown in Scheme 5.

2.2 Carbon-Carbon Bond Formation.

Reductive coupling of two CO_2 molecules followed by sequential proton/electron transfers can result in the formation of a variety of products starting with oxalic acid through glyoxalic acid and glycolic acid and culminating with ethylene gylcol or perhaps ethane. As far as metal-catalyzed processes are concerned, only oxalate has precedent, although the studies are sparse. Another approach to carbon-carbon bond formation is to react free CO_2 with a metal alkyl or aryl complex.

2.2.1 Formation of Oxalate. Although the formation of oxalate is observed in the uncatalyzed electrochemical reduction of CO_2 in anhydrous media (36), the presence of a metal complex does not appear to favor this route. In fact only one such example has been reported (61), where the silver and palladium complexes of octaethylporphyrin, and the palladium complex of tetraphenylporphyrin, catalyzed the reduction of CO_2 to oxalate at platinum and glassy carbon electrodes in CH_2Cl_2 solution. The reason for the selectivity of the metal and ligand in this reaction is not clear.

2.2.2 CO_2 Insertion into Metal-Carbon Bonds. There have been a number of reports of insertion reactions of CO_2 into metal-carbon bonds: some specific examples have been mentioned above, and the extent of these observations has been discussed at greater length elsewhere (16-22, 62). A particular instance in which there has been structural identification of the product is in the reactions shown in equation 20 (63).

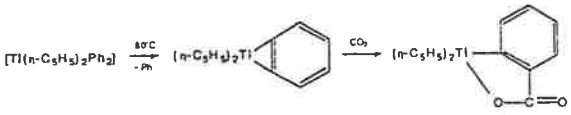

(20)

While there are no specific examples of the chemical catalysis for electrochemically-induced carboxylation of metal-alkyl bonds, the mechanistic details of the homogeneous process are outlined here by way of comparison with the insertion into metal-hydride bonds. The most detailed investigations of the intimate details of such insertion reactions have been undertaken by Darensbourg *et al.*, who have examined both the kinetic (62, 64) and stereochemical aspects (65) of CO_2 insertion into metal-carbon bonds in a series of complexes $[RM(CO)_4L]^-$ (R = alkyl or aryl; L = CO, phosphine or phosphite; M = W or Cr). These species possess the particular property of undergoing carboxylation reactions (21), as well as the migratory carbonylation insertion reactions (22) for which significant mechanistic information is available.

[21]

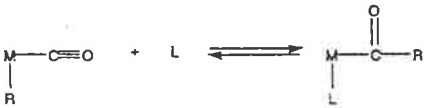

[22]

Reactions of *cis*-$[CH_3W(CO)_4L]^-$ (L = CO or phosphorus ligand) with CO_2 to form the acetato species revealed an overall second order reaction with

$$\text{rate} = k_2[CH_3W(CO)_4L^-][CO_2]$$

The value of k_2 was found to increase with the increasing electron-donating character of L (i.e., $CO<P(OMe)_3<PMe_3$), and the activation parameters [for the species with L = $P(OMe)_3$] were $\Delta H^{\ddagger} = 42.7$ kJmol^{-1} and $\Delta S^{\ddagger} = -181.2$ Jmol^{-1}K^{-1}, which were interpreted to be indicative of an I_a mechanism involving significant bond-making in the transition state, rather than a dissociative process.

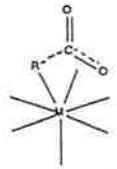

Figure 6. Proposed transition state for insertion of CO_2 into the metal-methyl bonds of $CH_3W(CO)_4L^-$ type complexes.

Consistent with that interpretation were the further observations that the rate of CO_2 insertion into the $[CH_3Cr(CO)_5]^-$ species is slower than its tungsten analogue, and that there was an insignificant dependence on the nature of R. The insertion reaction is accelerated by the presence of alkali metal ions, presumably by stabilization of the intermediate species by interaction at the distal oxygen atom of the CO_2, a situation analogous to the bifunctional stabilization proposed by Floriani (45, 66). Unfortunately, this acceleration cannot be utilized since the presence of the alkali metal ions also promotes the ultimate displacement of the carboxylate anion produced and its subsequent replacement by other ligands (solvent THF or CO). The CO_2 insertion reactions show no inverse dependence on CO although there is concurrent CO migratory insertion into the metal-carbon bond: clearly, no loss of CO is involved in the carboxylation process.

The stereochemical studies of the CO_2 insertion reaction were undertaken by investigation of the conversion of *threo*-$[W(CO)_4L(CHDCHDPh)]^-$ to *threo*-$[W(CO)_4L(O_2CCHDCHDPh)]^-$ (L = CO, PMe_3): accordingly it is clear that there is retention of configuration at the α-carbon atom during the insertion process (65). Such retention is also observed for the carbonylation process and contrasts with the SO_2-insertion process where inversion occurs at the α-carbon center (47).

On the broader issue of the possibility of uses of the combined carbon oxides (CO + CO_2) as C_1 feedstocks for chemicals synthesis, the comparison given by Darensbourg *et al.* (62, 64, 65) of the carboxylation reactions with the carbon monoxide migratory insertion reactions involving the same substrates is instructive. In the carbonylation reactions, the electron-donating ability of the R group does enhance the rate of the process, the reactions are accelerated by donating solvents, the ancillary ligands have little effect, and the rate law is mixed-order in CO (and independent of CO at high CO pressures). The striking difference in the mechanisms of the two insertion reactions is significant as it provides the selective use of the catalyst for either substrate.

3. ELECTROCATALYTIC CYCLES AND ELECTROCHEMICAL MECHANISMS.

The availability of computer-generated numerical solutions to key electrochemical relationships like the Butler-Volmer or Cottrell equations has led to the development of digital simulation techniques for applying methods like cyclic voltammetry or chronoamperometry as standard kinetic tools. At the same time, the combination of electrochemistry and in situ spectroscopy, i.e., spectroelectrochemistry, has had a powerful influence in unravelling key mechanistic steps in CO_2 reduction. In this section we consider the mechanistic steps that have been implicated in electrocatalytic CO_2 reduction.

3.1. Anatomy of a Catalytic Cycle.

In recent years the study of the electrochemical properties of transition metal complexes has led to greater understanding of the electronic structure and chemical reactivity of coordination or metal-organic complexes in different oxidation states. To understand the role of metal complexes in their functioning as electrocatalysts it is necessary to design studies to probe the chemical and electrochemical steps separately.

Based on a number of studies, the cycle shown in Figure 7 represents the simplest paradigm of electrocatalysis. For effective catalysis, the *catalyst precursor* in Fig. 7 must take up electrons at a relatively low potential to give a *reaction intermediate* that can bind one or more equivalents of substrate. Note that the substrate may be CO_2 itself or another species that is activated toward attack at CO_2. In any event, a *substrate complex* is formed. At this point direct outer-sphere reduction of substrate by the reduced catalyst precursor is subject to redox potential constaints. The substrate complex can now react with excess electrons and/or substrate,or, conceivably, with another equivalent of itself to products and regenerate either the reaction intermediate or the catalyst precursor. An important consideration is the reaction pathways that lead to catalyst deactivation. Generally, these will occur at the stage of the reaction intermediate or substrate complex. In some cases they can be as simple as physical precipitation of a complex that appears in competition with the catalysis (see later).

Although Section 2 was concerned with possible intermediates in the multielectron reduction of CO_2 to C_1 and C_2 oxycarbons and hydrocarbons, development of homogeneous solution electrocatalysts and indentification of reaction intermediates and/or substrate complexes has proceeded relatively slowly, and has yielded a mechanistic understanding only at the two electron reduction stage. In terms of products, only CO, HCO_2^- and $C_2O_4^{2-}$ have been unequivocally demonstrated. In terms of structural types, electrocatalysts can be grouped in the following categories:

1. Complexes of porphyrins, phthalocyanines and nitrogen containing macrocyclyic ligands.
2. Phosphine complexes.
3. Cyclopentadienyl complexes.

4. Complexes of 2,2'-bipyridine and related ligands.
5. Metal clusters and other polymetallic complexes.

Several of the studies on the above complexes have yielded reasonable mechanistic proposals with regard to the initial reaction intermediates produced by either one- or two-electron reduction of the catalyst precursor, or of perhaps greater importance, the substrate complex. In this latter section we will discuss the two types of substrate complex thought to be present in a number of electrocatalytic systems, namely the metal-CO_2 complex and the metal hydride complex.

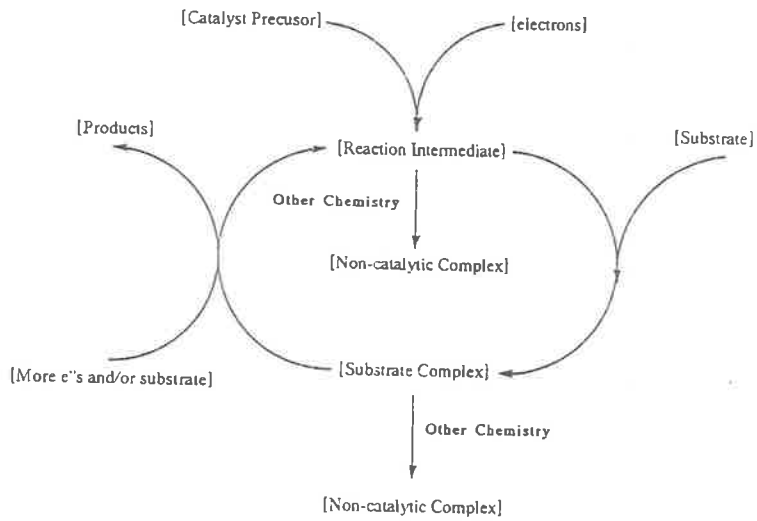

Figure 7. The simplest electrocatalytic cycle for CO_2 reduction.

3.2. Mechanisms Thought to Involve Metal-CO_2 Complexes.

Intermediates involving CO_2 complex formation are probably common in electrocatalysis although there are no reports of direct detection. Studies in which chemical evidence is in accord with complex formation are those involving *cis*-$[Ru(bpy)_2(CO)_2]^{2+}$ (67-69), $[Pd(triphos)(solvent)]^{2+}$ (where triphos is, for example, bis(dicyclohxylphosphinoethyl)phenylphosphine) and solvent is CH_3CN) (30, 60), *cis*-$[Os(bpy)_2(CO)H]^+$ (56) and of *fac*-$[Re(bpy)(CO)_3L]^{n+}$ (24, 29, 55, 70).

Tanaka et al. (67-69) have reported that *cis*-$[Ru(bpy)_2(CO)_2]^{2+}$ is a catalyst precursor for the electrocatalytic reduction of CO_2 to CO in mixed water/DMF solvent at ca. -1.5 V vs. SCE. They suggest that a CO_2 complex is formed during electrolysis which then is protonated to give a metallocarboxylate which in turn results in CO formation. A similar pathway may be involved in the formation of CO by *cis*-$[Ru(bpy)_2(CO)H]^+$ (71) under similar conditions (see later sections).

$[Pd^{II}(triphos)(solvent)]^{2+}$ (where triphos is, for example, bis(dicyclohexylphosphinoethyl)phenylphosphine) and the solvent is CH_3CN) have been shown to be efficient electrocatalysts for the reduction of CO_2 to CO in the presence of acidic aqueous DMF (30, 60). In these examples, as in the Ru complex discussed above, evidence for a CO_2 complex, in this case $[Pd^{II}(triphos)(CO_2)]^+$, and a metallocarboxylic acid, $[Pd^{II}(triphos)(CO_2H)]^+$, has been obtained. Of note is that the potential required for catalysis of -0.9 V vs. SCE is not far from the thermodynamic value (vide infra).

CO is the major product from *cis*-$[Os(bpy)_2(CO)H]^+$ in dry acetonitrile (56). Suprisingly, kinetic and labelling experiments demonstrate that both the Os-CO and Os-H bond are retained during catalysis and that formation of a CO_2 complex occurs. The intermediate CO_2 complex, which tenatively can be formulated as $[Os(bpy)_2(CO)(CO_2)H]^-$, undergoes a bimolecular reaction to give CO and CO_3^{2-} and to reform $[Os(bpy)_2(CO)H]^+$.

3.2.1 Electrocatalytic Reduction by Rhenium Polypyridine Complexes.

Electrocatalytic reduction of CO_2 by *fac*-$[Re(bpy)(CO)_3L]^{n+}$ complexes exhibits a sensitive dependence to initial conditions such as electrolysis potential, CO_2 concentration and the nature of L. The catalyst precursors are unique in the catalytic literature in that four different pathways result in CO_2 reduction. Study of Re(I) complexes has been pursued vigorously with multidisciplinary input and international efforts (24, 29, 52, 53, 55, 70-86). As discussed earlier, one pathway apparently involves the insertion of CO_2 into the metal-hydride bond of *fac*-$[Re(bpy)(CO)_3H]$ to give the corresponding metal formate and has allowed the first mechanistic study of CO_2 metal hydride insertion. Another pathway, by which the first significant amount of oxalate was produced, is found in the catalytic reduction of CO_2 by poly-[*fac*-Re(vbpy)$(CO)_3$Cl] (vbpy is 4-vinyl-4'-methyl-2,2'-bipyridine) attached to electrode surfaces. This was the first solid state polymeric film-based electrocatalyst for CO_2 reduction. Two other pathways also were found by which CO was produced from *fac*-$[Re(bpy)(CO)_3L]^{n+}$ in homogeneous solution via either a "one-electron" pathway involving the intermediate radicals $[Re(bpy)(CO)_3L]$ and $[Re(bpy)(CO)_3]$ or a "two-electron" pathway utilizing the anion $[Re(bpy)(CO)_3]^-$. In both the reactions CO_2 adducts are implied as intermediates.

Little is known concerning the reactivity and properties of the proposed CO_2 complexes $[Re(bpy)(CO)_3CO_2]$ and $[Re(bpy)(CO)_3CO_2]^-$ that are implicated in the "one" and "two" electron pathways. Understanding their reactivity should provide the mechanistic information that will allow the synthesis of new electrocatalytic complex precursors in which the reactivity of coordinated CO_2 can be controlled for use in the synthesis of fuels and chemicals.

The formation of the radical $[Re(bpy)(CO)_3CO_2]$ is possibly due to the unique nature of the redox processes in *fac*-$[Re(bpy)(CO)_3L]^{n+}$ complexes. This point is best illustrated by comparison of the electrochemical properties of bpy and non-bpy derivatives of the type *fac*-$[Re(bpy)(CO)_3L]^{n+}$ (where L is a phosphine, amine or carbonyl ligand and L' is X (n=0) or solvent (n=1) as shown in Eqs. 23-28. In the absence of CO_2 the series of reactions shown in Eqs. 23-26 occur.

$$[ReL_2(CO)_3L']^n \underset{-e^-}{\overset{+e^-}{\rightleftharpoons}} [ReL_2(CO)_3L']^{(n-1)} \qquad [23]$$

$$[ReL_2(CO)_3L']^{(n-1)} \underset{k_{-1}}{\overset{k_1}{\rightleftharpoons}} [ReL_2(CO)_3L'] + L^{(n-1)} \qquad [24]$$

$$[ReL_2(CO)_3] \underset{-e^-}{\overset{+e^-}{\rightleftharpoons}} [ReL_2(CO)_3L']^{\cdot} \qquad [25]$$

$$2[ReL_2(CO)_3] \xrightarrow{k_d} [ReL_2(CO)_3]_2 \qquad [26]$$

For *fac*-$[Re(CO)_5(CH_3CN)]^+$, where the initial reduction is a metal-based $Re^{I/0}$ process, the electrochemical scheme proceeds efficiently through Eqs. 23, 24 and 26, and should substantially bypass Eq. 25 at an overall rate that is near diffusion control. A different situation ensues for *fac*-$Re(bpy)(CO)_3(CH_3CN)]^+$ where the reduction is ligand-based. In this case the metal-metal bonded dimer $[Re(bpy)(CO)_3]_2$ forms at a rate of only ca. 10^2 M^{-1} s^{-1}, probably through the intramolecular redox equilibrium shown in Eq. 27 (55).

$$[Re^{I}(\bar{bpy})(CO)_3L'] \underset{}{\overset{K_{eq,1}}{\rightleftharpoons}} [Re^{0}(bpy)(CO)_3L'] \qquad [27]$$

Apparently, transfer of the electron from bpy to metal triggers ligand (L') loss from the metal: note that this corresponds to a 19e- to 17e- change in electron configuration (Eq. 28, $K_{eq,2}$).

$$[Re^{0}(bpy)(CO)_3L'] \underset{}{\overset{K_{eq,2}}{\rightleftharpoons}} [Re^{0}(bpy)(CO)_3] + L' \qquad [28]$$

Since $[Re(bpy)(CO)_3]$ is expected to be more reducing, and presumably more reactive than $[Re(CO)_5]$, and because of the unfavorable equilibrium constant K_{eq}, dimerization can be intercepted by rate-limiting, second order scavenging of $[Re(bpy)(CO)_3]$ by substrate. An example is found in recent electrochemical kinetic studies which have shown that formation of *fac*-$Re(bpy)(CO)_3X$ from $Re(bpy)(CO)_3(CH_3CN)]$ and RX or PhX is consistent with the direct reaction with the halocarbon (87).

Dimerization of *fac*-$[Re(bpy)(CO)_3L]^{n+}$ complexes in the coordinating solvent acetonitrile also is inhibited by reaction with CO_2. In this case, mechanistic studies by cyclic voltammetry indicate saturation kinetics that are most consistent with a dissociative-interchange mechanism.

$$[Re^{0}(bpy)(CO)_3L^{-}] + CO_2 \xrightarrow{k_{rxn}} [Re(bpy)(CO)_3CO_2] + L^{-} \qquad [29]$$

The latter mechanism also is consistent with flash photolysis/transient absorbance measurements during the generation of $[Re(bpy)(CO)_3Br]^-$ in the presence of CO_2 (81, 82).

Unfortunately, direct redox reactions of $[Re(bpy)(CO)_3CO_2]$ at the electrode are not observed, either by cyclic voltammetry or under electrocatalytic conditions. The lack of accumulation of $[Re(bpy)(CO)_3CO_2]$ can be reasonably be rationalized either by direct reduction to an anion followed by rapid reaction with a second equivalent of CO_2, or by a rapid dimerization. Hopefully future studies will distinguish between these alternatives.

CO_2 reduction by $[Re(bpy)(CO)_3]^-$ formed from the direct reduction of $[Re(bpy)(CO)_3Br]^-$ at a potential more anodic than -1.5V (vs. SCE) effectively gives CO at catalytic rates tenfold faster than the radical route discussed above, possibly via the CO_2 complex $[Re(bpy)(CO)_3CO_2]$. Another route for the production of $[Re(bpy)(CO)_3CO_2]^-$ could come from the direct electrode or mediated reduction of $[Re(bpy)(CO)_3CO_2]$, (see Eq. 25). An understanding of the chemical properties of the anion $[Re(bpy)(CO)_3CO_2]^-$ is essential before its reactivity can be exploited. For example, if this species can be considered a d^8, $18e^-$, Re(-I) species its reactivity would be considerably different from another alternative, i.e., a d^7, $17e^-$, Re(0) diradical with electrons localized on both the metal and the bpy ligand.

3.3 Mechanisms Thought to Involve Metal Hydride Complexes.

As discussed previously, a possible mechanism for formate formation would involve insertion of CO_2 into a metal-hydrogen bond followed by labilization of formate or formic acid. Several studies have now confirmed the mechanistic sequence necessary to provide a catalytic cycle based on insertion. Proposed hydrides are found for $[Rh(bpy)_2X_2]^+$ (88, 89) and $[Rh(dppe)_2]^+$ (90) although the origins of the cycles are much different. For $[Rh(bpy)_2X_2]^+$ four-electron reduction yields $[Rh(bpy)_2]^-$ which then is thought to abstract H^+ from the electrolyte. The proposed complex $[Rh(bpy)_2H]$ then inserts CO_2, releases formate, and regenerates the reaction intermediate $[Rh(bpy)_2]^+$. For $[Rh(dppe)_2]^+$ a one electron reduction gives $[Rh(dppe)_2]$ which abstracts H radical from the solvent to form $[Rh(dppe)_2H]$ that inserts CO_2 to regenerate the starting complex and formate.

3.3.1 Metal-Macrocycle Complexes. There have been a number of studies of electrochemical CO_2 reduction by complexes of macrocyclic ligands, principally those containing the nickel or cobalt. In general, CO and H_2 are the major products of such reactions and the requirement for a proton source is implied by evidence for the intermediacy of hydride species (92). The reactions appear to be metal complex dependent, as reactions in aqueous media show differing discrimination for CO_2 compared with H_2O reduction. For the $[Ni(cyclam)]^{2+}$ species (Figure 8a), CO is the only product although other similar macrocyclic species show H_2 as well in the product distribution (93). While possible variations within this class of compounds makes them attractive as potential electrocatalysts for CO_2 reduction, little is known about their role in promotion of the reactions.

The cobalt macrocycle, $[Co([14]diene)]^{n+}$ (Figure 8b), which was the first macrocyclic species observed to catalyze the electrochemical reduction of CO_2, (92) has been the subject of a recent detailed mechanistic study that has shed some light on possible paths for these reactions (34, 94, 95).

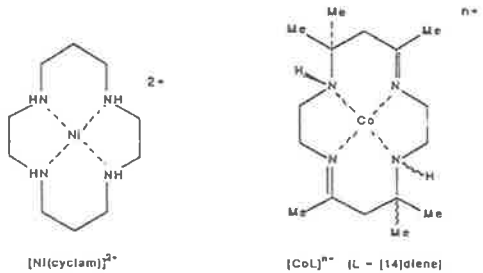

$[Ni(cyclam)]^{2+}$ (a)

$[CoL]^{n+}$ (L = [14]diene) (b)

Figure 8. Two types of metal-macrocycle complexes which are thought reduce CO_2 via metal-hydride intermediates.

The complex $[CoL]^+$ reversibly binds with CO_2 in Me_2SO solution (94). In aqueous solution, pulse radiolysis measurements indicate that CoL^+ reversibly binds with H^+, CO and CO_2 to form the adducts $[CoLH]^{2+}$, $[CoLCO]^+$, and $[CoLCO_2]^+$, respectively (95). Interestingly, no direct insertion of CO_2 into the Co-H bond is found, and the homolysis of $[CoL(CO_2)]^+$ to $[CoL]^{2+}$ and $CO_2^{\cdot-}$ is negligible. In aqueous solution, CO_2 binding is slightly favored over CO binding, although that situation is dramatically reversed in acetonitrile solution (34). Protonation studies of the CO_2 adduct gives $pK_a = 3.1$, a value similar to that reported for $[Co(en)_2(OH_2)(CO_2H)]^{2+}$ (33). In a separate study of the reduction of carbon dioxide to CO by a cobalt(I) macrocycle in acetonitrile solution (34), a second-order disappearance of the adduct, $[Co([14]diene)CO_2]^+$ was observed, which is consistent with either a disproportionation process or a binuclear intermediate. The intermediacy of a dimeric species is favored, since a complex containing a bridging carboxylato (or carbon dioxide) ligand was isolated from the reaction (structure xiii).

(xiii)

It is clear in this instance that CO_2 binding does not by itself activate CO_2 reduction, so that the single-centered two-electron reduction is not a significant pathway in acetonitrile solution.

3.3.2 Electrocatalysis by *cis*-$[Ru(bpy)_2(CO)H]^+$. This complex has been shown to be a catalyst for the reduction of CO_2 to formate in CH_3CN in the presence of H_2O (71). Also, Lehn and Ziessel have photochemically produced formate from CO_2 by using *cis*-$[Ru(bpy)_2(CO)H]^+$ as a catalytic site and $[Ru(bpy)_3]^{2+}$ as the chromophoric site (96).

The reactive intermediate is the once-reduced form of the complex $[Ru(bpy)_2(CO)H]$ where the added electron resides on a bpy ligand. This reactive intermediate is 'activated' toward insertion of CO_2 into the metal-hydride bond to give a formate complex. At this point a second electron is consumed and formate is displaced by the solvent to form $[Ru(bpy)_2(CO)CH_3CN]$. Upon reaction of this third intermediate with H_2O the starting hydride $[Ru(bpy)_2(CO)H]^+$ is regenerated. The entire process is presented in Figure 9.

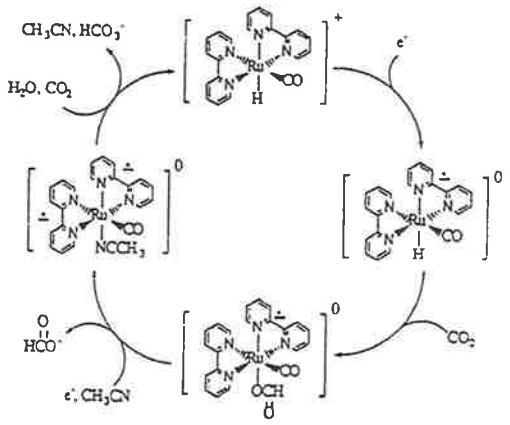

Figure 9. Proposed electrocatalytic cycle for the reduction of CO_2 to CO by $[Ru(bpy)_2(CO)H]^+$.

Key steps in the cycle are the electrochemically-induced insertion of CO_2 into the metal hydride bond and the electrochemical reformation of the metal hydride at the expense of a proton source.

Another pathway, which is competitive with the reduction to formate, resulted CO formation (71). $[Ru(bpy)_2(CO)CH_3CN]$ and perhaps other reduced species are implicated in this net transformation. The mechanisms proposed earlier by Tanaka et al., which seem to indicate the formation of Ru-CO_2 complexes, could play a role here (67-69).

3.4 Deactivation Pathways.

The preferential reaction of products of the CO_2 reduction processes with the metal centers that promote such reactivity leads to their deactivation, in the sense that the role of the metal complex is stoichiometric rather than catalytic in nature. The formation of carbonato complexes in the $CO_2 \rightarrow CO$ reduction is one such example. In view of the paucity of examples in which CO_2 is coordinated to low-valent metal centers, and by contrast the extensive chemistry associated with CO as a ligand, it might be anticipated that carbon monoxide produced in a $CO_2 \rightarrow CO$ reduction reaction could readily deactivate a metal-centered catalyst. The stability constants of the two substrates with metals does not invariably favor CO. For example, in one of the few cases where the equilibrium constants for association of CO and CO_2 with the same center are available, it is noteworthy that the stability of the CO_2 complex is the greater in water, whereas the situation is reversed in acetonitrile (95). While there are a number of examples of electrocatalyst deactivation where the particular product has not been identified, a clear example to the contrary occurs in the CO_2 (as HCO_3^-) $\rightarrow$ CO reduction by $[Co(bpy)_3]^+$ in aqueous solution. In this instance, the CO produced by reduction of CO_2 scavenges unreacted $[Co(bpy)_3]^+$ to remove the metal from the cycle by precipitation of the complex shown in structure xiv (34).

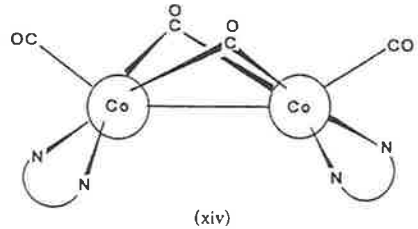

(xiv)

A requirement for a transition metal complex that functions as an effective homogeneous catalyst for the $CO_2 \rightarrow CO$ conversion (promoted chemically, electrochemically or photochemically) might be that it has little or no affinity for further CO coordination. It may be significant that two of the complexes that have received particular attention as catalysts for this conversion, *viz.*, *fac*-$[Re(bpy)(CO)_3Cl]$ and *cis*-$[Os(bpy)_2(CO)H]^+$ possess this property.

Deactivation routes involving the formation of carbonato or bicarbonato complexes also appear in several studies. For example, *fac*-$[Re(bpy)(CO)_3Cl]$ under electrocatalytic conditions in "dry" CH_3CN solution slowly deposits the extremely insoluble bicarbonate *fac*-$[Re(bpy)(CO)_3O_2COH]$ (55). The origin of the proton is unclear. For *cis*-$[Ru(bpy)_2(CO)H]^+$ catalysis is stopped by the precipitation of blue, insoluble *cis*-$[Ru(bpy)_2CO_3]$ (71).

4. FUTURE STUDIES

An understanding of the mechanistic steps available to transition metal electrocatalysts that produce the two-electron products CO or formate from CO_2 reduction is beginning to emerge. For CO formation, protonation of intermediate CO_2-metal complexes to yield CO by way of metallocarboxylate intermediates, and reaction of metal-CO_2 complexes with acceptors such as free CO_2 are both important. Formate apparently can be made by either direct protonation of a metal-CO_2 complex via uncharacterized intermediates or electrochemically-induced insertion into a metal hydride bond. In any event, future studies should be designed to precisely define these modes of reactivity, especially by direct observation of the properties of the CO_2 adduct during electrochemical conditions.

In general, the area of electrocatalytic formation of C-C bonds from CO_2 has been ignored. A specific challenge is to prepare catalysts with the ability to selectively couple CO_2 to produce oxalate. As mentioned here the only verified case of oxalate formation is found for polymeric films containing ring-modified *fac*-[Re(bpy)$(CO)_3$Cl] complexes, where ca. 7-14% current yield has been found (73, 85). In one study it was suggested that two CO_2 complexes in close proximity were able to couple via carbon to yield the product (85). If this is correct, it would indicate that a program for the study of dimeric complexes would be appropriate. Another stategy for forming C-C bonds might be the electrochemically-induced insertion of CO_2 into metal alkyl or aryl bonds, where the latter have been formed initially by electrogeneration from a halocarbon.

A great challenge will be to couple the formation of bound CO species by electrocatalytic reduction of CO_2 with the further two-electron steps that are necessary to give formaldehyde, methanol or methane. It seems likely that this can be accomplished in an environment containing two different metal sites, one functioning to produce activated CO and the other to transfer hydrogen, e.g., a metal hydride.

Finally, another future focus will be the transposition of homogeneous catalysts to polymer films (97), or self-assembled monolayers, where it has been shown that new mechanistic pathways exist that are different from those that occur in solution. Such systems could fulfil the desirable goal of achieving selectivity in the electrocatalytic reduction of CO_2 to fuels or chemicals.

Acknowledgements. BPS would like to thank the National Science Foundation under the EPSCoR program for generous support. FRK would like to acknowledge the support of the Australian Research Council.

5. REFERENCES

1 K.K. Thauer, G. Diekert, and P. Schoenheit, Trends Biochem. Sci. 5 (1980) 304.
2 J.G. Zeikus, R. Kerby, and J.A. Krzycki, Science 227 (1985) 1167.
3 I. Taniguchi, in "Modern Aspects of Electrochemistry," J. Bockris, R.E. White, B.E. Conway, Editors, Vol. 20 (1989) 327, Plenum Press, New York.
4 E. Lamy, L. Nadjo, and J.M. Saveant, J. Electrochem. Soc. 78 (1977) 403.

5 H.A. Schwarz and R.W. Dodson, J. Phys. Chem. 93 (1989) 409; P.S. Surdhar, S.P. Mezyk, and D.A. Armstrong, J. Phys. Chem. 93 (1989) 3360.
6 A. Behr, "Carbon Dioxide Activation by Metal Complexes," VCH Press, New York, 1988.
7 A. Behr and W. Keim, Angew. Chem. 97 (1985) 326.
8 A.R. Cutler, P.K. Hanna, and J.C. Vites, Chem. Rev. 88 (1988) 1363.
9 M.E. Giuseppetti and A.R. Cutler, Organometallics 6 (1987) 970.
10 D.R. Senn, J.A. Gladysz, K. Emerson, and R.D. Larsen Inorg. Chem. 26 (1987) 2739
11 G.R. Lee and N.J. Cooper, Organometallics 4 (1985) 794.
12 T. Herskovitz and L.J. Guggenberger, J. Am. Chem. Soc. 98 (1976) 1615.
13 W. Beck, K. Raab, U. Nagel, and M. Steimann, Agnew. Chem. 94 (1982) 556.
14 E.G. Lundquist, J.C. Huffman, K. Folting, B.E. Mann, and K.G. Caulton, Inorg. Chem. 29 (1990) 128.
15 R. Eisenberg and D.E. Hendricksen, Adv. Catal. 28 (1979) 119.
16 T. Ito and Y. Yamamoto, "Organometallic Reactions of Carbon Dioxide" in "Organic and Bio-organic Chemistry of Carbon Dioxide", S. Inoue and N. Yamazaki, eds., Wiley (New York), 1982: pps 79-151.
17 R.P.A. Sneeden, "Reactions of Carbon Dioxide", in "Comprehensive Organometallic Chemistry", G. Wilkinson, Ed., Vol. 8; Pergamon (Oxford), 1982; Chapter 50.4, pps 225-283.
18 D.J. Darensbourg and R.A. Kudaroski, Adv. Organomet. Chem., 22 (1983) 129-168.
19 D.A. Palmer and R. van Eldik, Chem. Rev. 83 (1983) 651-731.
20 D. Walther, Coord. Chem. Rev. 79 (1979) 135-174; and references therein.
21 "Catalytic Activation of Carbon Dioxide", W.M. Ayers, ed., A.C.S. Symposium Series, Vol. 363, Washington, DC, 1988.
22 P. Braunstein, D. Matt, and D. Nobel, Chem. Rev. 88 (1988) 747; and references therein.
23 J.P. Collin and J.P. Sauvage, Coord. Chem. Rev. 93 (1989) 245-268.
24 J. Hawecker, J.-M. Lehn, and R. Ziessel, Helv. Chim. Acta 69 (1986) 1990.
25 P.C. Ford and A. Rokicki, Adv. Organomet. Chem. 28 (1988) 139.
26 M.A. Bennett, J. Mol. Catal. 41 (1987) 1; and references therein.
27 T. Yoshida, D.L. Thorn, T. Okano, J.A. Ibers, and S. Otsuka, J. Am. Chem. Soc. 101 (1979) 4212.
28 B. Beguin, B. Denise, and R.P.A. Sneeden, J. Organometal. Chem. 208 (1981) C18.
29 R. Ziessel, J. Hawecker, and J.-M. Lehn, Helv. Chim. Acta 69 (1986) 1065.
30 D.L. DuBois and A. Miedaner, J. Am. Chem. Soc. 109 (1987) 113.
31 M.A. Bennett, G.B. Robertson, A. Rokicki, and W.A. Wickramasinghe, J. Am. Chem. Soc. 110 (1988) 7098.

32 N.E. Katz, D.J. Szalda, M.H. Chou, C. Creutz, and N. Sutin, J. Am. Chem. Soc. 111 (1989) 6591.

33 E. Fujita, D.J. Szalda, C. Creutz, and N. Sutin, J. Am. Chem. Soc. 110 (1988) 4870.

34 F.R. Keene, C. Creutz, and N. Sutin, Coord. Chem. Rev. 64 (1985) 247.

35 T.A. Hafeli and F.R. Keene, Aust. J. Chem. 41 (1988) 1379.

36 J.C. Gressin, D. Michelet, L. Nadjo, and J.-M. Saveant, Nouveau J. Chem. 3, (1979) 545; C. Amatore and J.-M. Saveant, J. Am. Chem. Soc. 103 (1981) 5021 and references therein.

37 J.M. Maher and N.J. Cooper J. Am Chem. Soc. 102 (1980) 7606.

38 K.M. Nicholas, J. Organometalal. Chem. 188 (1980) C10.

39 J.C. Bryan, S. J. Geib, A.L. Rheingold, and J.M. Mayer, J. Am. Chem. Soc. 109 (1987) 2826.

40 C. Mealli, R. Hoffman, and A. Stockis, Inorg. Chem. 23 (1984) 56.

41 J. Chatt, M. Kubota, G.J. Leigh, F.C. Marsh, R. Mason, and D.J. Yarrow, J. Chem. Soc., Chem. Commun. (1974) 1033.

42 G.O. Evans, W.F. Walter, D.R. Mills, and C.A. Streit, J. Organometal. Chem. 144 (1978) C34.

43 E. Carmona, F. González, M.L. Poveda, and J.M. Marin, J. Am. Chem. Soc. 105 (1983) 3365.

44 G. Fachinetti, C. Floriani, A. Chiesi-Villa, and C. Guastini, J. Am. Chem. Soc. 101 (1979) 1767.

45 C. Floriani, Pure & Appl. Chem. 54 (1982) 59; and references therein.

46 M Aresta and C.F. Nobile, Inorg. Chim. Acta 24 (1977) L49.

47 T. Ito and A. Yamamoto, J. Chem. Soc., Dalton Trans. (1975) 1398.

48 H.H. Karsch, Chem. Ber. 110 (1977) 2213.

49 K. Kropp, V. Skibbe, and G. Erker, J. Am. Chem. Soc. 105 (1983) 3353.

50 P.A. Delmonte, F.G.N. Cloke, and R.R. Schrock, J. Am. Chem. Soc. 105 (1983) 2643.

51 S.G. Davies and S.J. Simpson, J. Organometal. Chem. 240 (1982) C48.

52 B.P. Sullivan and T.J. Meyer, J. Chem. Soc., Chem. Commun. (1984) 1244.

53 B.P. Sullivan and T.J. Meyer, Organometallics 5 (1986) 1500.

54 I.S. Kolomnikov, A.I. Gusev, G.G. Aleksandrov, T.S. Lobeeva, Yu.T. Struchkov, and M.E. Vol'pin, J. Organometal. Chem. (1973) 349.

55 B.P. Sullivan, M.R.M. Bruce, T.R. O'Toole, C.M. Bolinger, E. Megehee, H. Thorp, and T.J. Meyer, *"Electrocatalytic Carbon Dioxide Reduction"*, in Reference 7, pps 52-.

56 M.R.M. Bruce, E. Megehee, B.P. Sullivan, H. Thorp, T.R. O'Toole, A. Downard, and T.J. Meyer, Organometallics 7 (1988) 238.

57 P.M. Treichel and R.L. Schubhin, Inorg. Chem. 6, 1328.

58 C. Lapinte and D. Astruc, J. Chem. Soc., Chem. Commun. (1983) 430.

59 C. Lapinte and D. Catheline, D. Astruc, Organometallics 7 (1988) 1683.

60 D. Dubios, personal communication.

61 J.Y. Becker, B. Vainas, R. Eger, and L. Kaufman, J. Chem. Soc., Chem. Commun. (1985) 1471.

62 D.J. Darensbourg, C.G. Bauch, and C. Ovalles, *"Metal-Induced Transformations of Carbon Dioxide"*, in Reference 7, pps. 26-41.

63 I.S. Kolomnikov, T.S. Lobeeva, V.V. Gorbachevskaya, G.G. Aleksandrov, Y.T. Struchkov, and M.E. Vol'pin, Chem. Commun. (1971) 972.

64 D.J. Darensbourg, R. K. Hanckel, C.G. Bauch, M. Pala, D. Simmons, and J.N. White, J. Am. Chem. Soc. 107 (1985) 7463.

65. D.J. Darensbourg and G. Grötsch, J. Am. Chem. Soc. 107 (1985) 7473; and references therein.

66 S. Gambrarotta, C. Floriani, A. Chiesi-Villa, and C. Guastini, J. Am. Chem. Soc. 107 (1985) 2985.

67 H. Ishida, K. Tanaka and T. Tanaka, Chem. Lett. (1985) 405.

68 H. Ishida, K. Tanaka, M. Morimoto and T. Tanaka, Organometallics 5 (1986) 724.

69 H. Ishida, K. Tanaka and T. Tanaka, Organometallics 6 (1987) 181.

70 B.P. Sullivan, C. M. Bolinger, D. Conrad, W. J. Vining, and T.J. Meyer, J. Chem. Soc., Chem. Commun. (1985) 1414.

71 J. R. Pugh, M.R.M. Bruce, B.P. Sullivan, and T.J. Meyer, Inorg. Chem. 30 (1991) 86.

72 J. Hawecker, J.-M. Lehn, and R. Ziessel, J. Chem. Soc., Chem. Commun. (1984) 328.

73 S. Cosnier, A. Deronzier, and J. C. Moutet, J. Electroanal. Chem. 207 (1986) 315.

74 N.A. Surridge and T.J. Meyer, Anal. Chem. 58 (1986) 1576.

75 A.I. Breikss and H.D. Abruna, J. Electroanal. Chem. 201 (1986) 201 347.

76 A. Juris, S. Campagna, I. Bidd, J.-M. Lehn, and Ziessel, R. Inorg. Chem. 27 (1988) 4007.

77 J. Guilhem, C. Pascard, J.-M. Lehn, and R. Ziessel, J. Chem. Soc., Dalton Trans. (1989) 1449.

78 J. Hawecker, J.-M. Lehn, and R. Ziessel, J. Chem. Soc., Chem.Commun. (1985) 56.

79 J. Hawecker, J.-M. Lehn, and R. Ziessel, J. Chem. Soc., Chem.Commun. (1983) 536.

80 B. Akermark, U. Eklund-Westlin, P. Baeckstrom, and R. Lof, Acta. Chemica Scand. 34 (1980) 27.

81 C. Kutal, M.A. Weber, G. Ferraudi, and D. Geiger, Organometallics 4 (1985) 2161.

82 C. Kutal, A.J. Corbin, and G. Ferraudi, Organometallics 6 (1987) 553.

83 H. Hukkanen and T.T. Pakkanen, Inorg. Chim. Acta 114 (1986) L43.

84 C.R. Cabrera and H.D. Abruna, J. Electroanal. Chem. 209 (1986) 101.

85 T.R. O'Toole, B.P. Sullivan, M.R.M. Bruce, L.D. Margerum, R.W. Murray, and T.J. Meyer, J. Electroanal. Chem. 259 (1989) 217.

86 T.R. O'Toole, L.D. Margerum, T.D. Westmoreland, W.J. Vining, R.W. Murray, and T.J. Meyer, J. Chem. Soc., Chem. Commun. (1985) 865.

87 T. R. O'Toole, T.J. Meyer, and B.P. Sullivan, manuscript in preparation.

88 C.M. Bolinger, B.P. Sullivan, D. Conrad, J.A. Gilbert, N. Story, and T.J. Meyer, J. Chem. Soc., Chem. Commun. 1985, 796

89 C.M. Bolinger, N. Story, B.P. Sullivan, and T.J. Meyer, Inorg. Chem. 27 (1988) 4582.

90 S. Slater and J.H. Wagenknecht, J. Am. Chem. Soc., 106 (1984) 5367.

91 C. O'Connell, S.I. Hommeltoft, and R. Eisenberg, "Electrochemical Approaches to the Reduction of Carbon Dioxide" in *"Carbon Dioxide as a Source of Carbon"*, M. Aresta and G Forti, Eds. pps.33-54.

92 B. Fisher and R. Eisenberg, J. Am. Chem. Soc. 102 (1989) 7361.

93 M. Beley, J.-P. Collin, R. Ruppert, and J.-P. Sauvage, J. Chem. Soc., Chem. Commun. (1984) 1315.

94 D.A. Gangi and R.R. Durand, J. Chem. Soc., Chem. Commun. 1986, 697.

95 C. Creutz, H.A. Schwarz, J.F. Wishart, E. Fujita, and N. Sutin, J. Am. Chem. Soc. 111 (1989) 1153.

96 J.-M. Lehn and R. Ziessel, J. Organometal. Chem. 382 (1990) 157.

97 B.P. Sullivan, Platinum Metals Rev. 33 (1989) 2.

Reprinted from Organometallics, 1994, 13.

Reduction of Terminal Alkynes Mediated by Tris(2,2′-bipyridine)cobalt(I)

David A. Reitsma and F. Richard Keene*

Department of Molecular Sciences, James Cook University of North Queensland, Townsville, Queensland 4811, Australia

Received November 17, 1993®

In buffered aqueous ethanolic solution, phenylacetylene is reduced to styrene by $[Co(bpy)_3]^+$ (bpy = 2,2′-bipyridine). In solutions of lower proton availability the predominant products were oligomeric, including coupled species such as 1,4-diphenylbutenyne.

Introduction

The tris(2,2′-bipyridine)cobalt(I) cation, $[Co(bpy)_3]^+$ (I), has previously been reported to mediate in the reduction of water (to dihydrogen),[1] carbon dioxide (to carbon monoxide),[2] and allyl chloride (to 1,5-hexadiene).[3] Stoichiometric and kinetics studies suggested that in aqueous solution the first two reactions involve a common intermediate,[1,2] which was considered to be a reactive cobalt–hydride species. A further interest of these studies was the fact that $[Co(bpy)_3]^+$ may be generated photochemically from the reduction of the corresponding cobalt(II) and cobalt(III) species,[4] so that the $[Co(bpy)_3]^{n+}$ moiety may act as a homogeneous catalyst in schemes for the photochemical reduction of water[1,5] and carbon dioxide,[2] using $[Ru(bpy)_3]^{2+}$ as a photosensitizer.

In the case of allyl chloride,[3] initial π-coordination of the substrate to the cobalt center was proposed, as in the case of similar substrates such as acrylonitrile and allyl alcohol, with the greater reactivity of allyl chloride allowing subsequent reaction to occur.

Satyanarayana and Periasamy[6] reported the reaction of $CoCl_2$, $NaBH_4$, and PPh_3 with terminal alkynes to produce *trans,trans*-1,3-dienes. The authors suggested the insertion of an alkyne into the cobalt–hydride bond of a species formed *in situ* by reduction of a (triphenylphosphine)cobalt(II) complex by BH_4^- as an initial step in the reaction. However, recent studies by Bianchini *et al.*[7] have shown that the reaction of 16-electron $[Co(PP_3)]^+$ $\{PP = P(CH_2CH_2PPh_2)_3\}$ fragments with terminal alkynes initially resulted in the π-alkyne species (as a kinetic product), which in turn isomerized to the hydride–alkynyl and ultimately to the vinylidene species, which is considered the thermodynamically stable product.

The dichotomy between the potential of $[Co(bpy)_3]^+$ as a general hydrogenation catalyst for unsaturated organic substrates and the rich chemistry of cobalt(I) centers with alkynes, prompted us to attempt a preliminary stoichiometric and kinetic study of the course of the reactions of $[Co(bpy)_3]^+$ with terminal alkynes. The results of this study are now reported.

Experimental Section

General Comments. Product determinations of H_2 were obtained by GC (molecular sieve 5A support; 35 °C; argon carrier gas; thermal conductivity detector (50 °C); injector temperature, 75 °C). Separation and purification of organic products were performed by HPLC (Si-100 7-μm column; low-boiling petroleum ether eluent), and by column chromatography under reduced pressure (silica gel adsorbent; petroleum ether or petroleum ether/ethyl acetate mixtures as eluents).[8]

Ethanol, diethyl ether, benzene, ethyl formate, and low-boiling petroleum ether were purified by the respective literature methods.[9,10] Alkyne reagents were checked for purity by ^{1}H-NMR (300-MHz) techniques and, except for phenylacetylene, required no further purification. Phenylacetylene had a 2% styrene impurity and was freshly purified by vacuum distillation as required.

All other reagents were used without further purification.

Sodium amalgam (0.9%) was prepared by the method established in the literature.[9] Solid $[Co(bpy)_3]Cl$ was prepared and recrystallized using the literature method (overall yield 80%).[2,11]

$[Co(bpy)_3]^+$ is extremely air sensitive, and consequently, all manipulations involving this reagent were performed in a Vacuum Atmospheres HE-Series glovebox under an argon atmosphere.

Buffer Solutions. Buffer solutions were obtained by addition of appropriate quantities of NaOH to aqueous solutions of acetic, chloroacetic, or formic acid. For acid catalysis studies, $[base^-]$ was maintained at 0.2 mol dm^{-3}, and the acid concentration was varied to attain the same pH (3.7) for each buffer. For all other studies an acetate buffer was used, with $[HOAc] = [OAc^-] = 0.2$ mol dm^{-3}; reaction mixtures requiring buffer contained 10% v/v of this aqueous buffer solution, unless otherwise stated.

Stoichiometry Studies. In a typical reaction, appropriate quantities of buffer (or water), ethanol, and alkyne were added to a 60-mL glass vessel, followed by addition of a 0.041 mol dm^{-3} ethanolic solution of $[Co(bpy)_3]^+$, and the vessel was sealed with a septum cap. For most reactions 2.5 mL of the cobalt solution was used to make up a total volume of 10 mL. The stoppered vessels were left until the reaction was complete, as indicated by the loss of the blue color of Co(I), or the lack of further color change after several days. The reaction mixture was acidified (1 mol dm^{-3} HCl), the organic products were extracted into low-boiling petroleum ether (3 × 10 mL) and washed with a saturated aqueous solution of NaCl, and the solvent was removed on the rotary evaporator. ^{1}H and ^{13}C NMR spectra (300 and 75 MHz,

* Abstract published in *Advance ACS Abstracts*, March 1, 1994.

(1) Krishnan, C. V.; Creutz, C.; Majahan, D.; Schwarz, H. A.; Sutin, N. *Isr. J. Chem.* 1982, 22, 98.
(2) Keene, F. R.; Creutz, C.; Sutin, N. *Coord. Chem. Rev.* 1985, 64, 247.
(3) Margel, S.; Smith, W.; Anson, F. C. *J. Electrochem. Soc.* 1978, *125*, 241. Margel, S.; Anson, F. C. *J. Electrochem. Soc.* 1978, *125*, 1232.
(4) Creutz, C.; Sutin, N. *Coord. Chem. Rev.* 1985, 64, 321.
(5) Ziessel, R.; Hawecker, J.; Lehn, J.-M. *Helv. Chim. Acta* 1986, *69*, 1065.
(6) Satyanarayana, N.; Periasamy, M. *Tetrahedron Lett.* 1986, 27, 6253.
(7) Bianchini, C.; Peruzzini, M.; Vacca, A.; Zanobini, F. *Organometallics* 1991, *10*, 3697.
(8) Bowden, B. F.; Coll, J. C. *J. Nat. Prod.* 1986, *49*, 934.
(9) Vogel, A. I. *A Textbook of Practical Organic Chemistry Including Qualitative Organic Analysis*, 3rd ed.; Longmans: London, 1962.
(10) Perrin, D. D.; Armarego, W. L. F.; Perrin, D. R. *Purification of Laboratory Chemicals*; 2nd ed.; Pergamon: Oxford, U.K., 1980.
(11) Szalda, D. J.; Creutz, C.; Majahan, D.; Sutin, N. *Inorg. Chem.* 1983, 22, 2372.

0276-7333/94/2313-1351$04.50/0

respectively) were obtained in $CDCl_3$ using dinitrobenzene, where appropriate, as an internal standard.

The concentrations of $[Co(bpy)_3]^+$ stock solutions for all studies were determined spectrophotometrically (absorption coefficient $\epsilon_{605} = 6500$ m^2 mol^{-1}).[12]

Where an estimate of the yield of H_2 was required, a sample of the gas (0.25 or 1.0 mL as appropriate) above the solution was taken: the overall gas volume above the liquid was evaluated in each sample by water displacement.

Kinetic Studies. Reaction mixtures for the following *in situ* analyses were prepared as described above, utilizing smaller reaction vessels (total volume = 13 mL), and the reaction mixture volume was varied from 1 to 5 mL as appropriate. Reaction mixtures for kinetic studies involving acid catalysis were prepared by the addition of a solution of $[Co(bpy)_3]^+$ (0.2 mL, 0.041 mol dm^{-3}) to an ethanol (4.29 mL) solution containing buffer (0.5 mL) and phenylacetylene in a 5-fold excess (0.01 mL). After preparation, the mixtures were immediately transferred to gastight 2-mm cuvettes fitted with ground glass stoppers, and the decay of $[Co(bpy)_3]^+$ was measured spectrophotometrically (at 605 nm). Infinity readings were obtained after exposing the solutions to air.

Results

The addition of the terminal alkynes phenylacetylene or 1-decyne in excess to acetate-buffered aqueous ethanol solutions containing $[Co(bpy)_3]^+$ leads to an increased rate of consumption of the blue reductant, compared with the rate in the absence of the alkyne.

The organic products of such reactions were analyzed for various alkynes and compared with the reaction products in nonbuffered aqueous ethanol solutions. The analysis of dihydrogen was performed for the reactions of phenylacetylene in buffered aqueous ethanol solutions of $[Co(bpy)_3]^+$ to investigate the extent of the competition between this substrate and water for the proposed cobalt–hydride intermediate.

Stoichiometry Studies. The reactions of phenylacetylene with $[Co(bpy)_3]^+$ were studied in aqueous ethanol solutions in which the water content was varied from 0.5 to 10%. The majority of the organic products were unidentified aromatic compounds, presumably oligomeric species. Diphenylbutadiyne and *cis*/*trans*-1,4-diphenylbutenyne were detected in the reaction mixtures with a water content up to 5%. The greatest yield of *cis*/*trans*-1,4-diphenylbutenyne was 18% (based on eq 1), obtained in mixtures containing 1% water, whereas diphenylbutadiyne was present only in trace quantities.

$$[Co(bpy)_3]^+ + 3PhC{\equiv}CH \rightarrow PhC{\equiv}C{-}CH{=}CHPh + [CoH(bpy)_2(C{\equiv}CPh]^+ \quad (1)$$

For a series of equivalent reactions conducted in aqueous ethanol with acetate buffer, the dominant feature was the hydrogenation of phenylacetylene to styrene. The greatest yield was observed for the 90% ethanol solution and was evaluated to be 44% on the basis of the reaction given in eq 2. At a lower water content the styrene yield diminished,

$$2[Co(bpy)_3]^+ + PhC{\equiv}CH + 2H^- \rightarrow PhCH{=}CH_2 + 2[Co(bpy)_3]^{2+} \quad (2)$$

(12) Keene, F. R. unpublished results.

Table 1. H_2 Yields for the Reaction of Phenylacetylene and $[Co(bpy)_3]^+$ in Buffered 90% Ethanol Solutions (Total Volume of Reaction Mixtures = 10 mL)

[PhC≡CH]/mol dm^{-3}	$[Co(bpy)_3^+]$/mol dm^{-3}	H_2/mL
0.039	0.038	0.02
0.039	0.076	0.04
0.156	0.038	0.01
0	0.038	2.44

and no styrene was detected in solutions with an H_2O content below 5%. 1,4-Diphenylbutenyne was detected in reaction mixtures with low water content, although the yields were much less than observed in the absence of buffer (see above). Unidentified aromatic oligomers were also present in these samples, and the proportion of oligomers increased with lower water content.

The reaction was examined with a number of other alkyne substrates. Addition of $[Co(bpy)_3]^+$ to separate buffered 90% ethanol solutions of 4-octyne and diphenylacetylene generated no organic products. Indeed, diphenylacetylene and 4-octyne apparently inhibited the reaction of $[Co(bpy)_3]^+$ with water, as indicated by the length of time required for the oxidation of Co(I). Reaction of 1-decyne and $[Co(bpy)_3]^+$ under the same conditions produced some hydrogenated product, although the yield was very low, suggesting that the hydrogenation reaction requires suitably activated monosubstituted alkynes.

The reactions were also analyzed to determine the effect of the presence of the alkynes on reduction of water by $[Co(bpy)_3]^+$. The addition of this reductant to similar solutions of aqueous ethanol (with and without acetate buffer) in the absence of phenylacetylene results in the reduction of water to dihydrogen (H_2). The significant finding from the present work was that the presence of phenylacetylene almost completely inhibits the reduction of water to H_2. As an example, the H_2 yields from the reaction of phenylacetylene and $[Co(bpy)_3]^+$ in buffered 90% ethanol are presented in Table 1. For samples which are equimolar in phenylacetylene and $[Co(bpy)_3]^+$, the production of H_2 was reduced by 2 orders of magnitude compared with that observed in the absence of the alkyne. Additional experiments of this type showed that increasing the water content of the buffered solution to 40% had very little effect on the inhibition of H_2 production by phenylacetylene.

Spectral Observations. The addition of phenylacetylene to a solution containing $[Co(bpy)_3]^+$ significantly modifies its electronic spectral characteristics over the region 350–650 nm. It is apparent that there is interaction between phenylacetylene and $[Co(bpy)_3]^+$.

An attempt was made to identify the nature of the interaction using IR methods. In previous studies, π-alkyne, σ-alkynyl, and vinylidene attachment to cobalt by alkynes has been reported.[7,13] In the present instance, using *in situ* studies, no bands were detected that could be assigned to linkages of π-alkyne, σ-alkynyl, or hydride to the metal center. The vinylidene and σ-alkenyl structures, although not evident, cannot be discounted, as their IR absorptions may be obscured by absorptions due to the polypyridyl ligands. It should also be noted that the nonobservance of absorptions in the region 2200–1900 cm^{-1} may not eliminate a σ-alkynyl compound, since

(13) Habadie, N.; Dartiguenave, M.; Dartiguenave, Y. *Organometallics* 1989, *8*, 2564.

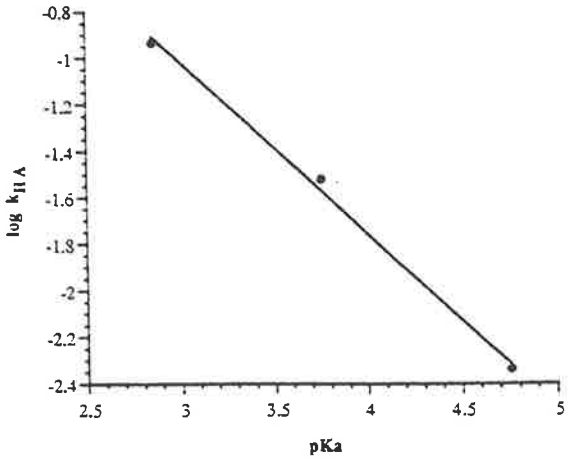

Figure 1. Plot of log k_{HA} vs buffer pK_a for the oxidation of Co(I) in buffered 90% ethanol solutions containing $[Co(bpy)_3]^+$ (1.6×10^{-3} mol dm^{-3}), phenyacetylene (18×10^{-3} mol dm^{-3}), and 10% v/v aqueous buffer. For aqueous buffer solutions: [base] = 0.2 mol dm^{-3}; pH = 3.7; total bufffer concentrations ([HA] + [A$^-$]) were 0.225 mol dm^{-3} chloroacetate, 0.4 mol dm^{-3} formate, 2.2 mol dm^{-3} acetate.

very weak $\nu_{C\equiv C}$ absorptions have been reported in compounds of phenylacetylide attached to ruthenium[14] and iron.[15]

Similarly, *in situ* NMR studies provided no information on the interaction of phenylacetylene and the metal center, primarily because of the paramagnetic nature of the metal ion, but they provided evidence for free 2,2′-bipyridine (presumably by loss from the cobalt center) in the early stages of the reaction.

Kinetics Studies. In buffered aqueous ethanol solutions, the reaction of phenylacetylene and $[Co(bpy)_3]^+$ is first order with respect to the concentration of the complex ion, and for equimolar mixtures of phenylacetylene and $[Co(bpy)_3]^+$ the rate of loss of cobalt(I) is comparable to that found for similar solutions without the alkyne present. The latter reaction produces dihydrogen from the reduction of water, while the former results in the hydrogenation of phenylacetylene to styrene. The similarity in rates for these two processes indicates that the inhibition of dihydrogen production by phenylacetylene is not due to a kinetic factor in the competition between phenylacetylene and water for the intermediate $[CoH(bpy)_2(H_2O)]^{2+}$; the similarity in rate appears to be coincidental, rather than the function of a common step in the mechanism. The initial attachment of the alkyne to the metal center is consistent with these results.

The involvement of buffer in the hydrogenation of phenylacetylene is evident from the reaction rate studies, and there is a requirement of buffer for the formation of hydrogenation products. Reaction mixtures without added buffer often remained blue for several days, compared with a half-life of minutes in the case of the buffered solutions.

The rate of loss of cobalt(I) was found to be strongly inhibited by added bpy, indicating loss of one (or more) of these ligands from the metal center prior to the rate-determining step.

For the current study, the effect of acetate, formate, and chloroacetate buffers was investigated with a view to elucidating the nature of the involvement of the buffer. A Brønsted plot[16] of $k_{HA} = k(obs)/[HA]$ vs buffer pK_a (Figure 1) for the reaction of phenylacetylene and $[Co(bpy)_3]^+$ in 90% ethanol/10% buffer indicates this reaction is general-acid catalyzed. The large value of α (0.73) obtained gives a strong indication of acid catalysis, suggesting proton donation is an important feature of the hydrogenation reaction.

Discussion

The results obtained in this study suggest that the initial reaction between $[Co(bpy)_3]^+$ (I) and alkynes is the attachment of the substrate to the metal center. The formation of a π-alkyne organometallic compound from the interaction of alkynes with transition metals is well established in the literature, and the mechanisms discussed below are based on this assumption.

Hydrogenation Mechanisms. Alkyne hydrogenations reported in the literature almost invariably proceed via a pathway involving a σ-alkenyl species.[15,17-22]

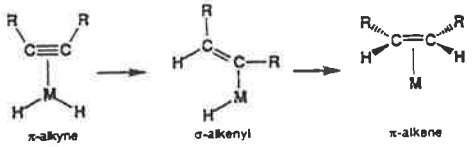

Such a mechanism requires the presence of a hydride moiety adjacent to the alkyne, with subsequent insertion of the organic species into the M–H bond. For the present system, a hydride is not generated prior to attachment of an alkyne to the cobalt center. The π-alkyne formed initially (II; Scheme 1) possibly rearranges to the vinylidene species,[7] and reaction with a proton source would produce the σ-alkenyl (III) by either ligand protonation[23,24] or metal–hydride formation and subsequent insertion of the alkyne into the Co–H bond.

Further reaction with a proton source and insertion can account for the production of styrene and complete oxidation of cobalt(I). An alternative reaction of the σ-alkenyl species, involving reaction of additional alkyne, is well documented in the literature:[14,15,25] this mechanism requires the oxidative addition of phenylacetylene and reductive elimination of styrene and results in the formation of a σ-alkynyl species (IV) which may then react with further alkyne to produce enynes, diynes, and higher

(14) Albertin, G.; Amendola, P.; Antoniutti, S.; Ianelli, S.; Pelizzi, G.; Bordignon, E. *Organometallics* **1991**, *10*, 2876.
(15) Bianchini, C.; Meli, A.; Peruzzini, M. Vizza, F.; Zanobini, F.; Frediani, P. *Organometallics* **1989**, *3*, 2080.
(16) Jencks, W. P. *Catalysis in Chemistry and Enzymology*; McGraw-Hill: New York, 1969; pp 163–173.
(17) Clark, H. C.; Ferguson, G.; Goel, A. B.; Janzen, E. G.; Ruegger, H.; Siew, P. Y.; Wong, C. S. *J. Am. Chem. Soc.* **1986**, *108*, 6961.
(18) Stolzenberg, A. M.; Muetterties, E. L. *Organometallics* **1985**, *4*, 1739.
(19) Schrock, R. R.; Osborn, J. A. *J. Am. Chem. Soc.* **1976**, *98*, 2143.
(20) Muetterties, E. L. *Inorg. Chim. Acta* **1981**, *50*, 1.
(21) Adams, R. D.; Chen, G.; Yin, J. *Organometallics* **1991**, *10*, 2087.
(22) Andriollo, A.; Esteruelas, M. A.; Meyer, U.; Oro, L. A.; Sanchez-Delgado, R. A.; Sola, E.; Valero, C.; Werner, H. *J. Am. Chem. Soc.* **1989**, *111*, 7431.
(23) Field, L. D.; George, A. V.; Purches, G. R.; Slip, I. H. M. *Organometallics* **1992**, *11*, 3019.
(24) Hughes, D. L.; Jimeneq-Tenorio, M.; Leigh, G. J.; Rowley, A. T. *J. Chem. Soc., Dalton Trans.* **1993**, 3151.
(25) Bianchini, C.; Meli, A.; Peruzzini, M.; Vizza, F.; Frediani, P. *Organometallics* **1990**, *9*, 1146.

Scheme 1. Proposed Pathway for the Reactivity of $[Co(bpy)_3]^+$ with Phenylacetylene in Buffered Aqueous Ethanolic Solution

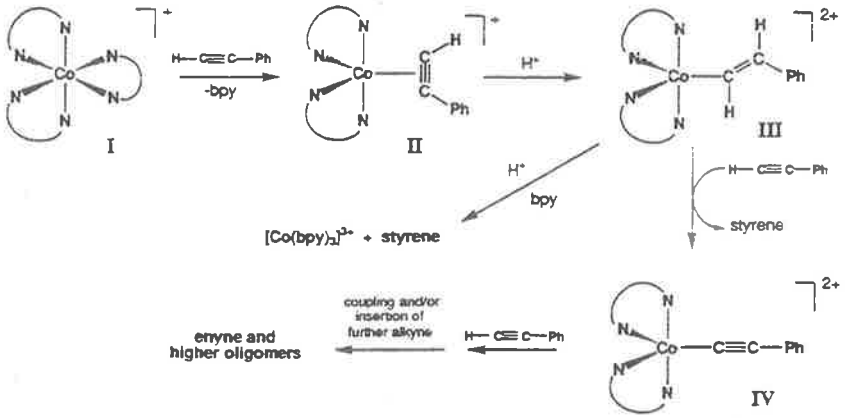

oligomers. This is consistent with the observation of these products in buffered ethanol solutions of low water content.

The conclusion that may be drawn is that there are competing reactions for the σ-alkenyl species, dependent on proton availability. In solutions of high water content, the predominant product is styrene. As the water content and proton availability is reduced, the reaction with additional phenylacetylene is favored. Although no intermediates were detected in this study, this mechanistic scheme accounts for the kinetics data and the absence of hydrogenation products at low water content (because the initial step after attachment of phenylacetylene requires reaction with a proton source) and is consistent with the literature precedents.

Oligomerization Mechanisms. Reaction of phenylacetylene with $[Co(bpy)_3]^+$ in the absence of buffers produced 1,4-diphenylbutenyne as well as oligomeric compounds. The dimerization of 1-alkynes to enynes, mediated by transition metal complexes, usually occurs through the reaction of a σ-alkynyl compound with additional alkyne.[14,25,26] In the current system, this may be rationalized by initial oxidative addition of phenylacetylene to the cobalt center (with loss of one bpy ligand) to form a σ-alkynyl/hydride compound which in turn reacts with additional phenylacetylene to produce a species containing one σ-alkynyl and one π-alkyne linkage; coupling or insertion between these two groups would produce an enynyl compound. Higher oligomers may be generated by further reactions of this type. Alternatively, and more likely according to several authors,[14,26,27] the π-alkyne rearranges to the vinylidene derivative and formation to the enynyl compound occurs through coupling of the vinylidene and σ-alkynyl moieties.[28] Both these alternatives have no proton requirement and are consistent with the greatest yield of enyne being observed in reaction mixtures with low proton availability.

(26) Jia, G.; Meek, D. W. *Organometallics* **1990**, *9*, 1444.

Conclusion

It has been established that the cobalt hydride intermediate implicated in the reduction of water and CO_2 is not involved in the hydrogenation of alkynes. The feasibility of the mediation of alkyne reductions by $[Co(bpy)_3]^+$ was investigated, and although many complications in these reductions were apparent, the selective hydrogenation of phenylacetylene was observed under conditions of ready proton availability.

Acknowledgment. We would like to acknowledge helpful discussions with Dr. George Koutsantonis (Griffith University) on aspects of this work. Queensland Nickel Pty. Ltd. (Yabulu) are thanked for allowing access to their GC facilities. The research was supported by the Australian Research Council.

OM930786S

(27) Koutsantonis, G. Ph.D. Thesis, University of Adelaide, 1989; pp 1–183; private communication, 1991.

(28) Schäfer, M.; Mahr, N.; Wolf, J.; Werner, H. *Angew. Chem., Int. Ed. Engl.* **1993**, *32*, 1315.

Contribution from the Kenan Laboratories of Chemistry, University of North Carolina, Chapel Hill, North Carolina 27599-3290

Site Dilution of Osmium Polypyridine Complexes in Three Electron-Hopping Conductive Polymer Films on Electrodes by Electrochemical Copolymerization of Osmium with Ruthenium and with Zinc Complexes

Nigel A. Surridge, F. Richard Keene,† Brent A. White,‡ John S. Facci,§ Marvin Silver,‖ and Royce W. Murray*

Received May 7, 1990

The electrochemical copolymerization of three pairs of metal complexes was investigated for utility of the copolymers for electron-transport studies. The ligands within each pair are the same, in order that polymer sites for the electron-transport-active osmium metal complexes can be isostructurally diluted with the other complex, which is based on Ru or Zn centers. The ligands include the electropolymerizable groups *N*-(4-pyridyl)cinnamamide, 4-vinylpyridine, and 4-methyl-4′-vinyl-2,2′-bipyridine. A kinetic analysis was used to estimate the degree of random copolymer formation properties of the three metal complex pairs. The pairs $[Os(bpy)_2(p\text{-cinn})_2]^{2+}/[Ru(bpy)_2(p\text{-cinn})_2]^{2+}$ and $[Os(vbpy)_3]^{2+}/[Zn(vbpy)_3]^{2+}$ formed ideal and near-ideal random copolymers, while the behavior of the $[Os(bpy)_2(vpy)_2]^{2+}/[Ru(bpy)_2(vpy)_2]^{2+}$ pair indicated a greater relative reactivity of the osmium monomer. A preliminary sandwich electrode measurement of electron transport in a $[Os(vbpy)_3]^{2+}/[Zn(vbpy)_3]^{2+}$ copolymer is given.

Polymer films that contain electron-transfer-active metal complexes affixed to the polymeric lattice exhibit changes in oxidation states[1] in electrochemical reactions when (a) the electron-hopping reactions between metal complex sites are reasonably rapid on the experimental time scale and (b) the films contain diffusively mobile charge-compensating counterions. The electrochemical behavior provides a convenient avenue to study the electron self-exchange dynamics of the immobilized metal complex, which is interesting for its own sake and for its relevance to electrocatalytic applications of the films.[1] The electron self-exchange rate is often (phenomenologically) expressed as the "electron diffusion coefficient", D_e, which is translatable into a bimolecular rate constant k_{ex}.[2]

The electron self-exchange reaction in the polymer phase differs from that familiar in homogeneous solution in that the metal complex sites are diffusively immobile (or only slowly mobile), being affixed to the polymer lattice. The rate constant k_{ex} may, accordingly, depend on the concentration of metal complex sites (donor/acceptor sites) within the polymer film. In particular, the electron-hopping rate constant may decrease as the sites are diluted, because of decreased populations of nearest neighbor D/A pairs, slow polymer-controlled translational modes of the sites, and/or increased distances of electron transfer.[3,4] Detecting and understanding site concentration depedencies of k_{ex} values is crucial to a basic appreciation of electron dynamics in electroactive polymer films.

The literature on the electrochemistry of site-dilutable polymer films[5] and their electron-transport rates[3,6] remains sparse. A difficulty is in the synthesis of polymeric films with the desired properties: (i) a sufficiently large ionic conductivity that the electron-hopping rate is a property of the chemistry of the sites and not of the mobility of the charge-compensating counterion, (ii) metal complexes substitutionally inert in both oxidation states (or stable organic donor/acceptor pair), (iii) a combination of k_{ex} and metal complex site concentration values that gives a readily measurable D_e value (i.e., D_e between 10^{-12} and 10^{-7} cm^2/s), and (iv) an ability to alter the site concentration without changing details of the polymer structure (and thus any polymer-related kinetic factors). As for factor i, theory is evolving that potentially allows accounting for electron hopping driven by bulk potential gradients that are consequences of low ionic mobility;[7,8] other theoretical and experimental approaches[9] rely on negligible ionic motions. Factors ii and iii can be anticipated on the basis of an analogy between solution- and polymer-phase chemistry.[10]

Factor iv is, on the other hand, an important constraint on polymer design. Our approach[3] to the problem has been based on forming polymeric metal polypyridine films by electrochemical *co*polymerization[11] of two metal complexes, having the same coordination shell and polymerization linkages but differing metals. One of the metal complexes has a redox couple suitable for an electron-hopping study, while the other is electrochemically silent (does not form a mixed-valent state) at electrode potentials where the first is active. Because their coordinations are identical, copolymerization from solutions containing the two complexes in different proportions yields copolymers in which electron-transfer-active complexes are controllably diluted by nonactive but *structurally equivalent* sites of the other complex. By change in

† On approved Special Studies Program from the Department of Chemistry and Biochemistry, James Cook University, Townsville, Queensland 4811, Australia.
‡ Present address: The Upjohn Co., Kalamazoo, MI 49001.
§ Present address: Xerox Corp., Webster, NY 14580.
‖ Department of Physics, University of North Carolina, Chapel Hill.

(1) (a) Murray, R. W. in *Electroanalytical Chemistry*; Bard, A. J., Marcel Dekker: New York, 1984; Vol. 13, pp 191–368. (b) Murray, R. W. *Annu. Rev. Mater. Sci.* **1984**, *14*, 145. (c) Abruna, H. D. *Coord. Chem. Rev.* **1988**, *86*, 135.
(2) (a) $D_e = 10^3\delta^2 k_{ex}C_T$; where δ = intersite separation at electron transfer and C_T = total concentration of exchanging sites.[2b,c] (b) Andrieux, C. P.; Saveant, J.-M. *J. Electroanal. Chem. Interfacial Electrochem.* **1980**, *111*, 377. (c) Laviron, E. *J. Electroanal. Chem. Interfacial Electrochem.* **1980**, *112*, 1.
(3) (a) Facci, J. S.; Schmehl, R. H.; R. W. Murray *J. Am. Chem. Soc.* **1982**, *104*, 4959. (b) Facci, J. S. Ph.D. Dissertation, University of North Carolina, Chapel Hill, NC, 1982.
(4) (a) Fritsch-Faules, I.; Faulkner, L. R. *J. Electroanal. Chem. Interfacial Electrochem.* **1989**, *263*, 237. (b) Shigehara, K.; Yama, N. C.; Anson, F. C. *J. Am. Chem. Soc.* **1981**, *103*, 2552. (c) Stolka, M.; Yanus, J. F.; Pai, D. M. *J. Phys. Chem.* **1984**, *88*, 4707.
(5) (a) Abruna, H. D.; Denisevich, P.; Umana, M.; Meyer, T. J.; Murray, R. W. *J. Am. Chem. Soc.* **1981**, *103*, 1. (b) Denisevich, P.; Abruna, H. D.; Leidner, C. R.; Meyer, T. J.; Murray, R. W. *Inorg. Chem.* **1982**, *21*, 2153. (c) Kelly, J. M.; Long, C.; O'Connell, C. M.; Vos, J. G. *Inorg. Chem.* **1983**, *22*, 2818. (d) Ohsaka, T.; Yamamoto, H.; Oyama, N. *J. Phys. Chem.* **1987**, *91*, 3775. (e) Oyama, N.; Ohsaka, T.; Yamamoto, H.; Kaneko, M. *J. Phys. Chem.* **1986**, *90*, 3850.
(6) (a) He, P.; Chen, X. *J. Electroanal. Chem. Interfacial Electrochem.* **1988**, *256*, 353. (b) Guadalupe, A. R.; Usifer, D. A.; Potts, K. T.; Hurrell, H. C.; Megstad, A.-E.; Abruna, H. D. *J. Am. Chem. Soc.* **1988**, *110*, 3462.
(7) (a) Buck, R. P. *J. Electroanal. Chem. Interfacial Electrochem.* **1987**, *112*, 23. (b) *J. Electroanal. Chem. Interfacial Electrochem.* **1987**, *219*, 23. (c) *J. Electroanal. Chem. Interfacial Electrochem.* **1986**, *210*, 1. (d) Buck, R. P. *J. Phys. Chem.* **1989**, *93*, 6212.
(8) (a) Savéant, J. M. *J. Electroanal. Chem. Interfacial Electrochem.* **1986**, *201*, 211. (b) *J. Electroanal. Chem. Interfacial Electrochem.* **1987**, *7227*, 299. (c) Savéant, J. M. *J. Phys. Chem.* **1988**, *92*, 1011. (d) *J. Phys. Chem.* **1988**, *92*, 4526. (e) Andrieux, C. P.; Savéant, J.-M. *J. Phys. Chem.* **1988**, *92*, 6761. (f) Andrieux, C. P.; Savéant, J. M. *J. Electroanal. Chem. Interfacial Electrochem.* **1980**, *111*, 377.
(9) (a) Jernigan, J. C.; Surridge, N. A.; Zvanut, M. E.; Silver, M.; Murray, R. W. *J. Phys. Chem.* **1989**, *93*, 4620. (b) Jernigan, J. C.; Murray, R. W. *J. Phys. Chem.* **1987**, *91*, 2030.
(10) White, B. A.; Murray, R. W. *J. Am. Chem. Soc.* **1987**, *109*, 2576.
(11) (a) Calvert, J. M.; Schmehl, R. H.; Sullivan, B. P.; Facci, J. S.; Meyer, T. J.; Murray, R. W. *Inorg. Chem.* **1983**, *22*, 2151. (b) Abruña, H. D.; Denisevich, P.; Umaña, M.; Meyer, T. J.; Murray, R. W. *J. Am. Chem. Soc.* **1981**, *103*, 1. (c) Meyer, T. J.; Sullivan, B. P.; Caspar, J. V. *Inorg. Chem.* **1987**, *26*, 4147.

0020-1669/90/1329-4950$02.50/0

the copolymer composition, the concentration of the active sites can thus be systematically altered without changing any dynamics of the polymer lattice that might be important in the electron-transfer chemistry. The objective is that site concentration is the sole varied parameter.

This scheme depends on identifying copolymerizable pairs of metal complexes that exhibit easily measured metal ratios in the resulting polymer film. Further, the metal ratios must be relatable to the composition of the feed electropolymerization solution. In particular, if the population of the two metal complexes in the polymer film is equal to that in the feed solution, we have a random copolymerization reaction forming an ideal solid "solution" of one metal complex in the other.

This paper deals with an analysis of the copolymerization characteristics of three pairs of metal polypyridine complexes. An osmium complex serves as the electron-transfer-active metal complex in each case; Ru and Zn complexes serve as the inactive diluents.

The three metal complex pairs are based on the electropolymerizable ligands: *N*-(4-pyridyl)cinnamamide (*p*-cinn), 4-vinylpyridine (vpy), and 4-vinyl-4′-methyl-2,2′-bipyridine (vbpy), bound in the following pairs: $[Os(bpy)_2(p\text{-}cinn)_2]^{2+}$ and $[Ru(bpy)_2(p\text{-}cinn)_2]^{2+}$, $[Os(bpy)_2(vpy)_2]^{2+}$ and $[Ru(bpy)_2(vpy)_2]^{2+}$, and $[Os(vbpy)_3]^{2+}$ and $[Zn(vbpy)_3]^{2+}$. Polymerization properties of all of these complexes, taken singly, and the ability to form copolymers during electropolymerization have been previously described.[11] Additionally, the electron-hopping properties of the poly-$[Os(bpy)_2(p\text{-}cinn)_2]^{2+}$/poly-$[Ru(bpy)_2(p\text{-}cinn)_2]^{2+}$ pair were published earlier.[3]

We will show that copolymerization of $[Os(bpy)_2(p\text{-}cinn)_2]^{2+}$ with $[Ru(bpy)_2(p\text{-}cinn)_2]^{2+}$, and of $[Os(vbpy)_3]^{2+}$ with $[Zn(vbpy)_3]^{2+}$, are nearly ideal as to randomness of osmium complex sites in the product film. We have previously presented[3] results for D_e in the poly-$[Os(bpy)_2(p\text{-}cinn)_2]^{2+}$/poly-$[Ru(bpy)_2(p\text{-}cinn)_2]^{2+}$ pair and present here a preliminary result for electron transfer in the newer poly-$[Os(vbpy)_3]^{2+}$/poly-$[Zn(vbpy)_3]^{2+}$ pair. The $[Os(vbpy)_3]^{2+}$/$[Zn(vbpy)_3]^{2+}$ pair is especially promising for solid state electron transfer studies of the kind recently described for 1:1 poly-$[Os(bpy)_2(vpy)_2]^{2+/3+}$ mixed valent films.[9]

Experimental Section

Chemicals. Acetonitrile (CH_3CN, Burdick and Jackson) was stored over molecular sieves. Tetraethylammonium perchlorate (Et_4NClO_4) electrolyte was recrystallized twice from water; tetraethylammonium tetrafluoroborate (Et_4NBF_4, Fluka) was used as received.

Electrochemistry. Experiments were performed with conventional potentiostats in three-electrode cells employing Pt auxiliary and either saturated (sodium chloride) calomel (SSCE), Ag/Ag^+ (0.01 M in CH_3CN) reference, or Ag-wire quasi-reference electrodes. Potentials are corrected to and reported vs SSCE. The copolymerizations were performed under N_2, either in an inert (dry N_2) atmosphere enclosure or in cells under N_2 purge. The former technique is more reliable.

Ligand. Preparation of the vbpy ligand was based on a literature method, where 3,4-dichloroanisole was substituted for (chloromethyl) methyl ether.[12]

Monomers. Preparations of $[(Os\text{ or }Ru)(bpy)_2(vpy)_2]^{2+}$, $[Os(vbpy)_3]^{2+}$, $[Zn(vbpy)_3]^{2+}$, and $[(Os\text{ or }Ru)(bpy)_2(p\text{-}cinn)_2]^{2+}$, were as reported in the literature.[11]

Copolymerizations of Films. Copolymeric films composed of the poly-$[Os(bpy)_2(p\text{-}cinn)_2]^{2+}$/poly-$[Ru(bpy)_2(p\text{-}cinn)_2]^{2+}$ and poly-$[Os(bpy)_2(vpy)_2]^{2+}$/poly-$[Ru(bpy)_2(vpy)_2]^{2+}$ monomer pairs were prepared from 0.1 M Et_4NClO_4/CH_3CN solutions of the complexes at concentrations in the 1–2 mM range, by cycling the Pt electrode potential at 100 mV/s between −1.0 and −1.75 V vs SSCE for the first pair[11] and between −1.0 and −1.70 V vs SSCE for the latter pair.[11] The total surface coverage of metal centers (Os plus Ru) varied between 2×10^{-9} and 9×10^{-9} mol cm^{-2} as determined by integrations of the charges under the Os(III/II) and Ru(III/II) cyclic voltammograms.

Copolymeric films containing poly-$[Os(vbpy)_3]^{2+}$ and poly-$[Zn(vbpy)_3]^{2+}$ were deposited on Pt electrodes (0.002 cm^2 for electrochemical measurements and 0.19 cm^2 for XPS experiments) by cycling the electrode potential between −1.0 and ≈−1.75 V vs SSCE at 150 or 200 mV/s in 0.1 M Et_4NBF_4/CH_3CN. The typical concentration of Os plus Zn complexes in the polymerizing feed solution was 0.2–0.5 mM. The surface coverage of poly-$[Os(vbpy)_3]^{2+}$ sites was determined by Os(III/II) cyclic voltammetry, with that of the poly-$[Zn(vbpy)_3]^{2+}$ sites determined by replacement of the metal with Fe as described in the following section.

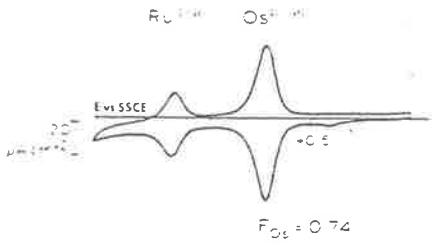

Figure 1. Cyclic voltammogram of poly-$[Os(bpy)_2(vpy)_2]^{2+}$/poly-$[Ru(bpy)_2(vpy)_2]^{2+}$ copolymer in 0.1 M Et_4NClO_4/CH_3CN. Scan rate = 20 mV/s, $\Gamma_{TOTAL} \sim 8.6 \times 10^{-9}$ mol/cm^2, $f_{Os} \sim 0.4$, $F_{Os} \sim 0.74$.

Substitution of Zn by Fe in $[Os(vbpy)_3]^{2+}$/$[Zn(vbpy)_3]^{2+}$ Copolymer Films. The copolymer-coated electrode was soaked in a degassed solution of $FeCl_2$ (≈50 mM, recrystallized from CH_3CN) in 0.1 M Et_4NBF_4/CH_3CN for 1 h (overnight gave equivalent results),[11c] rinsed with CH_3CN, and transferred to an electrochemical cell. The film was "conditioned"[11] by potential cycling at 200 mV/s between +1.5 V and the initial rising current for the first bipyridine reduction (usually ca. −1.4 V) until there was no further change in the voltammogram. The film surface coverage was then assessed by 5–10 mV/s potential scans between 0 and +1.5 V vs SSCE to observe voltammograms for the poly-$[Os(vbpy)_3]^{2+/3+}$ and poly-$[Fe(vbpy)_3]^{2+/3+}$ couples. The Os/Fe ratio thus derived has error estimated at ca. ±20% owing to the overlap of the two voltammetric waves ($E°_{Fe(II/III)} \approx 0.92$ V, $E°_{Os(II/III)} \approx 0.74$ V). The Os/Fe ratio is taken as the same as the original Os/Zn ratio, assuming complete replacement of Zn by Fe. This assumption is investigated as described in the text.

Removing Copolymer Films from Electrodes. The copolymer films were lifted off the Pt electrode by overcasting of a film of poly(vinyl alcohol).[13] A casting solution was prepared by adding 0.5 g of Aldrich Low MW PVA (average MW = 14 000; 99% hydrolyzed) to 15 mL of Nanopure water, heating (50 °C) with stirring until the solution cleared, and adding a further 0.5 g of PVA with stirring again until clear. Two or three drops of the warm solution were cast carefully onto the copolymer film surface so as to give a high-profile droplet spreading somewhat onto the Teflon shroud surrounding the Pt-disk electrode. The solution was allowed to dry for 6 h and the PVA film peeled from the electrode surface with tweezers, in most cases taking the electropolymerized film nearly quantitatively with it (vide infra). Drying the PVA film for longer periods results in a brittle film, not easily removed.

XPS Analysis of Films. Survey (BE = 0–1000 eV) and higher resolution spectra for Os, Zn, Fe, C, F, and N were obtained for the exterior surfaces of copolymer films by placing the entire electrode/film assembly in a Perkin-Elmer Physical Electronics Model 5400 XPS instrument. Mg Kα X-rays, anode energy 1253.6 eV, 300 W, were typically used with collection from an area of ≈1 mm^2 on the film surface. Binding energies are charge corrected to C 1s at 284.6 eV. The interior copolymer film surface (the side originally next to the electrode surface) was analyzed, with similar results, by observing the underside of peeled-off PVA films or, on occasion, the remnants of copolymer that sometimes remained on the Pt electrode after PVA peeling.

***D* Measurements.** A preliminary measurement of electron transport in a poly-$[Os(vbpy)_3]^{2+}$/poly-$[Zn(vbpy)_3]^{2+}$ copolymer film was performed with a "sandwich" cell, made by growing the copolymer on a Pt wire tip electrode (glass shrouded, 0.002 cm^2) and overcoating with a porous Au (ca. 300 Å) film as previously described.[9] Immersing the "sandwich" in 0.1 M Et_4NBF_4/CH_2Cl_2 and applying 0.0 V to the Au side and +1.2 V vs SSCE to the Pt side gave a limiting current for hopping electron transport via the Os(III/II) couple. The Zn(II) couple is electrochemically inactive and acts only as a diluent of osmium sites.

Results

Copolymer Films Based on *p*-cinn and vpy Ligands. As objects of electron-exchange dynamics studies, it is desirable that the active metal sites be randomly dispersed within the copolymer film. Criteria for randomness are available from comparing the composition of a two-monomer polymerization feed solution to that

(12) Abruna, H. D.; Breikess, A. I.; Collum, D. B. *Inorg. Chem.* **1985**, *24*, 987.

(13) Westmoreland, T. D.; Johnson, C.; Murray, R. W. Unpublished results.

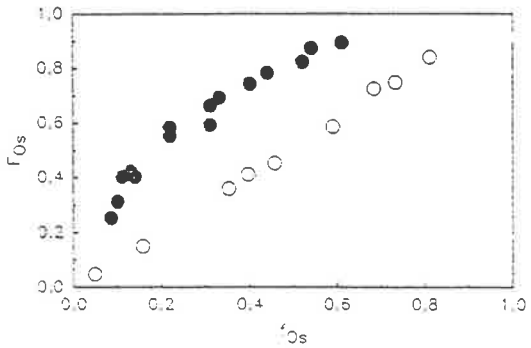

Figure 2. Plot of mole fraction of osmium in the copolymer, F_{Os}, vs that in the feed solution, f_{Os}, for copolymers containing poly-$[Os(bpy)_2(vpy)_2]^{2+}$/poly-$[Ru(bpy)_2(vpy)_2]^{2+}$ (●), and poly-$[Os(bpy)_2(p\text{-cinn})_2]^{2+}$/poly-$[Ru(bpy)_2(p\text{-cinn})_2]^{2+}$ (○).

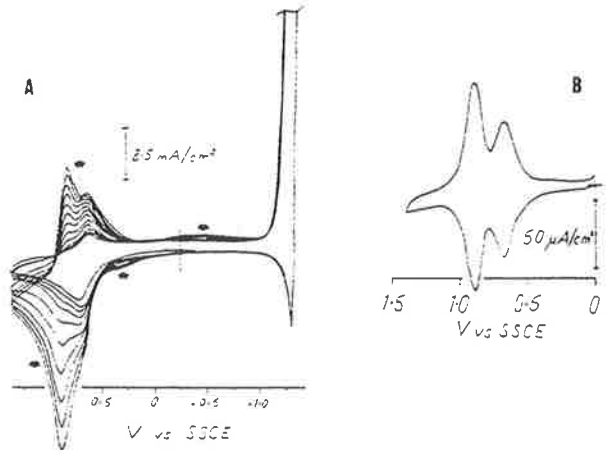

Figure 3. (A) Electrochemical conditioning of poly-$[Os(vbpy)_3]^{2+}$/poly-$[Zn(vbpy)_3]^{2+}$ copolymer, in 0.1 M Et_4NBF_4/CH_3CN after exposure to a ~50 mM solution of $FeCl_2$ for ca. 1 h. Scan rate = 200 mV/s. (B) Cyclic voltammogram in 0.1 M Et_4NBF_4, scan rate 10 mV/s, of the copolymer in part A after substitution of the Zn with Fe. $f_{Os} = 0.5$; $F_{Os} \sim 0.46$.

of the resulting copolymer.[14] Figure 1 exemplifies cyclic voltammetry of a poly-$[Os(bpy)_2(vpy)_2]^{2+}$/poly-$[Ru(bpy)_2(vpy)_2]^{2+}$ copolymer film; that for a poly-$[Os(bpy)_2(p\text{-cinn})_2]^{2+}$/poly-$[Ru(bpy)_2(p\text{-cinn})_2]^{2+}$ copolymer has nearly the same appearance. The mole fraction f_{Os} of the $[Os(bpy)_2(vpy)_2]^{2+}$ complex in the feed solution producing the film of Figure 1 was 0.4; that (F_{Os}) in the film, measured from the voltammogram charges, was 0.74. Repeating the analysis of Figure 1 for a series of f_{Os} values in the feed solution produced the results for F_{Os} vs f_{Os} shown in Figure 2. It is clear that F_{Os} vs f_{Os} is linear for the poly-$[Os(bpy)_2(p\text{-cinn})_2]^{2+}$/poly-$[Ru(bpy)_2(p\text{-cinn})_2]^{2+}$ copolymers but decidedly nonlinear for those based on copolymerization of $[Os(bpy)_2(vpy)_2]^{2+}$ with $[Ru(bpy)_2(vpy)_2]^{2+}$. The latter result shows that the poly-$[Os(bpy)_2(vpy)_2]^{2+}$/poly-$[Ru(bpy)_2(vpy)_2]^{2+}$ copolymer film contains a greater proportion of $[Os(bpy)_2(vpy)_2]^{2+}$ sites than does the feed solution; the polymerization is more selective for the Os monomer.

Copolymer Films Based on vbpy Ligands. In the previous description[11c] of $[Zn(vbpy)_3]^{2+}$ copolymerization, it was observed that the substitution of Fe for Zn by soaking in $FeCl_2$ solution required a subsequent "electrochemical cycling period of 10–20 min" to develop the redox response of the poly-$[Fe(vbpy)_3]^{2+/3+}$ couple.[11c] The voltammetric behavior during this "conditioning", conducted as in the Experimental Section, is shown in Figure 3A; initially, only the Os(III/II) response is observed (at the left),

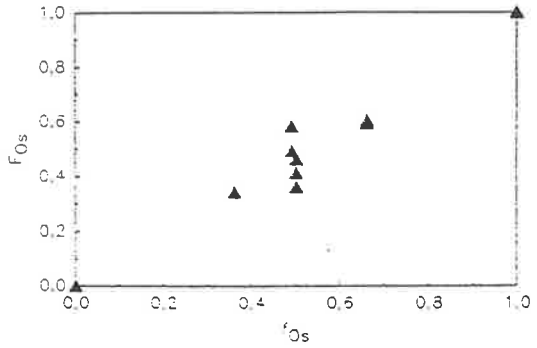

Figure 4. Plot of F_{Os} vs f_{Os} for poly-$[Os(bpy)_3]^{2+}$/poly-$[Zn(bpy)_3]^{2+}$ copolymer.

but with time peaks for the more positive Fe(III/II) couple grow in. The current at the right is for the reduction of bipyridine rings in copolymer sites; partial reduction of the bipyridine rings is essential for obtaining maximum incorporation of electroactive $[Fe(vbpy)_3]^{2+}$ into the copolymer.

Figure 3B shows the voltammetry of the copolymer film prepared in Figure 3A. The Os(III/II) and Fe(III/II) voltammetric waves are not well separated at the relatively fast potential scan rate used in Figure 3A, but are well-defined at the slow potential scan rates in Figure 3B. However, the moderate overlap of the Os(III/II) and Fe(III/II) waves is still troublesome during determination of the electrochemical charges under the two waves: this was done by assuming the Os wave to be symmetric about its $E_{p,a}$, reflecting the negative side of the wave about $E_{p,a}$, and using the resultant wave as the background current to be subtracted in order to measure the charge under the Fe(III/II) wave. Cyclic voltammograms of an undiluted poly-$[Os(vbpy)_3]^{2+}$ film are slightly asymmetric with the wave being slightly broader on the positive side,[15] so if this asymmetry occurs also in the copolymer the above procedure slightly underestimates the mole fraction F_{Os} of Os complex in the film.

For the film undergoing Zn/Fe replacement in Figure 3A, the Os mole fraction f_{Os} was 0.50 in the $[Os(vbpy)_3]^{2+}/[Zn(vbpy)_3]^{2+}$ feed solution producing the film, whereas the mole fraction F_{Os} of Os sites measured from the voltammogram of Figure 3B was 0.46. Repeating this procedure for a series of films produced the F_{Os} vs. f_{Os} results of Figure 4. The data are mainly in the middle range; although poly-$[Os(vbpy)_3]^{2+}$/poly-$[Zn(vbpy)_3]^{2+}$ copolymers are readily made at large and small f_{Os} feed ratios, the analysis of F_{Os} outside the range 0.3–0.7 is difficult owing to the Os(III/II)–Fe(III/II) wave overlap noted above. It should be stressed, however, that the points at $f_{Os} = 0$ and $f_{Os} = 1$ are known limits of the plot. The scatter in the F_{Os} results obtained for the five films grown at $f_{Os} \sim 0.5$ is suspected more to reflect variability in the Zn/Fe replacement and in quantifying the overlapping Os/Fe voltammetry of Figure 3B, rather than variability in the actual F_{Os}.

Analysis of the Copolymerization. Plots analogous to Figures 2 and 4 are commonly used in kinetic studies of monomer addition to growing polymer chains in free-radical polymerizations of two monomers.[14] Applying this theory to the present circumstance (an approximation since cross-linking may also occur), we define four propagation rate constants (where M = Os or Ru, or Os or Zn, and –M–M–Os$^{\bullet-}$ indicates a chain terminating in an activated Os complex site):

$$-M-M-Os^{\bullet-} + Os \xrightarrow{k_{11}} -M-M-Os-Os^{\bullet-}$$

$$-M-M-Os^{\bullet-} + Ru \xrightarrow{k_{12}} -M-M-Os-Ru^{\bullet-}$$

$$-M-M-Ru^{\bullet-} + Os \xrightarrow{k_{21}} -M-M-Ru-Os^{\bullet-}$$

$$-M-M-Ru^{\bullet-} + Ru \xrightarrow{k_{22}} -M-M-Ru-Ru^{\bullet-}$$

(14) (a) Ham, G. E. Copolymers. In *High Polymers Series*; Wiley-Interscience Publishers: New York, 1964; Vol. 18, Chapter 1. (b) Hiemenz, P. C. *Polymer Chemistry*; Marcel Dekker: New York, 1984, Chapter 7.

(15) Surridge, N. A.; Keene, F. R.; Zvanut, M. E.; Silver, M.; Murray, R. W. Manuscript in preparation.

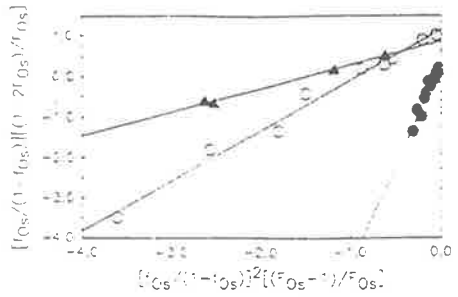

Figure 5. Analysis of data in Figures 2 and 4 according to eq 3, showing linear fits to the data. Copolymer: poly-$[Os(bpy)_2(vpy)_2]^{2+}$/poly-$[Ru(bpy)_2(vpy)_2]^{2+}$ (●); poly-$[Os(bpy)_2(p\text{-cinn})_2]^{2+}$/poly-$[Ru(bpy)_2(p\text{-cinn})_2]^{2+}$ (○); poly-$[Os(vbpy)_3]^{2+}$/poly-$[Zn(vbpy)_3]^{2+}$ (▲).

Writing kinetic equations for the ratio of the rate of incorporation of the two monomers M_1 and M_2, applying steady-state approximations for the concentrations of radical species during polymerization, and defining the reactivity ratios $r_1 = k_{11}/k_{12}$ and $r_2 = k_{22}/k_{21}$, gives

$$\frac{d[M_1]}{d[M_2]} = \frac{[M_1](r_1[M_1] + [M_2])}{[M_2](r_2[M_2] + [M_1])} = \frac{1 + r_1[M_1]/[M_2]}{1 + r_2[M_2]/[M_1]} \quad (1)$$

Accordingly, the mole fraction F_1 of M_1 (the Os complex) incorporated into the polymer can be expressed in terms of the mole fraction in the solution f_1 and of the reactivity ratios r_1 and r_2:

$$F_1 = \frac{r_1 f_1^2 + f_1 f_2}{r_1 f_1^2 + 2 f_1 f_2 + r_2 f_2^2} \quad (2)$$

We see that if the reactivity ratios are equal, i.e., $r_1 = r_2 = 1$, then $F_1 = f_1$; i.e., the polymer and feed solution compositions are equal. This satisfies the criterion $r_1 r_2 \approx 1$ required for forming a *random copolymer*;[14] i.e., the reactivities of Os and Ru (or Zn) monomers are identical whether they encounter an activated Os or a Ru site on the polymer chain (film surface). On the other hand, if r_1 and r_2 are both <1, then Os and Ru monomers are (relatively) unreactive toward Os and Ru polymer sites, respectively, which is the condition for an *alternating copolymer*. If r_1 and r_2 are > 1, then Os and Ru monomers prefer to react with Os and Ru polymer sites, respectively, which indicates a tendency for the monomers to homopolymerize. When $r_1 r_2 > 1$ with $r_1 > 1 > r_2$, the formation of a *block copolymer* is indicated.

Equation 2 can be rearranged to a form suitable for analysis of F_1 vs f_1 data

$$\frac{f_1}{1 - f_1}\,\frac{1 - 2F_1}{F_1} = r_2 + \left(\frac{f_1}{1 - f_1}\right)^2 \frac{F_1 - 1}{F_1}\, r_1 \quad (3)$$

where a plot of the expression on the left-hand side vs the coefficient of r_1 should be linear and give r_2 and r_1 from the intercept and slope.

Figure 5 shows such plots and regression lines for the three copolymer systems. The results for the poly-$[Os(vbpy)_3]^{2+}$/poly-$[Zn(vbpy)_3]^{2+}$ copolymer (▲) at $f_{Os} \approx 0.5$ in Figure 4 are averaged as a single point in Figure 5. This does not distort the obtained values of r_1 and r_2; a separate nonlinear least-squares fit of the raw unaveraged data in Figure 4 gave the same results.

Figure 5 shows that all three copolymers follow the form of eq 3, producing linear plots. The results for r_1 and r_2, and their interpretation, are as follows.

(1) For the poly-$[Os(bpy)_2(p\text{-cinn})_2]^{2+}$/poly-$[Ru(bpy)_2(p\text{-cinn})_2]^{2+}$ copolymer, $r_1 = 1.01$ and $r_2 = 1.04$ ($r_1 r_2 = 1.06$). The poly-$[Os(bpy)_2(p\text{-cinn})_2]^{2+}$/poly-$[Ru(bpy)_2(p\text{-cinn})_2]^{2+}$ pair appears to form ideal random copolymers, i.e., $r_1 r_2 = 1$. The electrochemical polymerization relies on reduction of the ligand system and activation of the reactivity of the vinyl-containing ligand (*p*-cinn) as a pseudo-radical anion, in head-to-head hydrodimerization-type couplings that would produce a linear polymer[5] and/or in the recently described[16] "living polymerization" metal complex chain reaction, which would allow for cross-linking steps. The ideal behavior of the $[Os(bpy)_2(p\text{-cinn})_2]^{2+}$/$[Ru(bpy)_2(p\text{-cinn})_2]^{2+}$ metal complex pair demonstrates the absence of any significant metal-related difference in the coupling reactivity of the *p*-cinn ligand complexes or in their lifetimes as end-units on active polymer chains.

Table I. Fraction of Os Sites Occurring in Blocks of n Sites for the $Os(vbpy)_3$–$Zn(vbpy)_3$ System[a]

	fraction of sites				
f_{Os}	$n = 1$	$n = 2$	$n = 3$	$n = 4$	$n = 5$
0.00	0.00	0.00	0.00	0.00	0.00
0.10	0.94	0.06	0.00	0.00	0.00
0.20	0.87	0.11	0.01	0.00	0.00
0.30	0.80	0.16	0.03	0.01	0.00
0.40	0.72	0.20	0.06	0.02	0.00
0.50	0.63	0.23	0.09	0.03	0.01
0.60	0.53	0.25	0.12	0.05	0.03
0.70	0.42	0.24	0.14	0.08	0.05
0.80	0.30	0.21	0.15	0.10	0.07
0.90	0.16	0.13	0.11	0.10	0.08
1.00	0.00	0.00	0.00	0.00	0.00

[a] Fraction of sites for each value of n calculated by using values for $r_1 \sim 0.58$ and $r_2 \sim 0.87$, obtained from fit in Figure 5.

(2) For the poly-$[Os(vbpy)_3]^{2+}$/poly-$[Zn(vbpy)_3]^{2+}$ copolymer, $r_1 = 0.58 \pm 0.04$ and $r_2 = 0.87 \pm 0.06$ ($r_1 r_2 = 0.51$). These results, while not far from the ideal $r_1 r_2 \approx 1$, suggest a tendency toward forming an alternating copolymer, or preferred heterocoupling. Given the uncertainties in the assay of copolymer composition (noted above, Figures 3–5), and results from XPS (vide infra), we are inclined to accept the $[Os(vbpy)_3]^{2+}$/poly-$[Zn(vbpy)_3]^{2+}$ copolymerization as "near-ideal", and as suitable for site dilution purposes in electron transport studies.

(3) For the poly-$[Os(bpy)_2(vpy)_2]^{2+}$/poly-$[Ru(bpy)_2(vpy)_2]^{2+}$ copolymer, $r_1 = 4.84 \pm 0.36$ and $r_2 = 0.26 \pm 0.05$ ($r_1 r_2 = 1.28$). By examination of the definitions of r_1 and r_2, this somewhat nonideal result suggests that the $[Os(bpy)_2(vpy)_2]^{2+}$ monomer has a greater reactivity toward electropolymerization than does the $[Ru(bpy)_2(vpy)_2]^{2+}$ monomer. This is surprising given the ideal and near-ideal copolymerization behavior of the two structurally related metal complex pairs based on *p*-cinn and vbpy ligands. The possible reasons for this variance in behavior are as follows: (i) There may be a difference in coupling reactivity of a vpy ligand attached to Os vs Ru metals or in its lifetime as an end-unit on active polymer chains. It is potentially significant that, of the three vinyl-substituted ligands, the least ideally behaved (vpy) is also the least extensive aromatic system, whose electronic structure can be expected to be most sensitive to the influence of coordinated metal.[17] Note that the most ideally behaved (*p*-cinn) involves a coupling unit more electronically remote from the metal. (ii) To some extent, films grow by precipitation of polymer formed in the diffusion layer around the electrode (as opposed to direct grafting of monomers to the polymer film surface). Thus, differing solubility properties of Os- vs Ru-containing oligomers could alter the apparent values of r_1 and r_2 by promoting incorporation of less-soluble oligomer into the film. (iii) A related factor influencing the $[Os(bpy)_2(vpy)_2]^{2+}$/$[Ru(bpy)_2(vpy)_2]^{2+}$ copolymerization may be the presence, in the particular samples of $[Os(bpy)_2(vpy)_2]^{2+}$ employed, of oligomeric poly-$[Os(bpy)_2(vpy)_2]^{2+}$ impurities (preblocks) arising from the relatively harsh reaction conditions of the $[Os(bpy)_2(vpy)_2]^{2+}$ synthesis. We have independent evidence[16b] that solutions of oligomeric forms of poly-$[Os(bpy)_2$-

(16) (a) A recent study[16b] showed that the related complex $[Fe(4\text{-methyl-}4'\text{-vinyl-}2,2'\text{-bipyridine})_3]^{2+}$ undergoes efficient electropolymerization and produces films containing average coupled ligand chain lengths of seven. (b) Elliott, C. M.; Baldy, C. J.; Nuwaysir, L. M.; Wilkins, C. L. *Inorg. Chem.* **1990**, *29*, 389.

(17) (a) Kober, E. M. Ph.D. Dissertation, University of North Carolina, Chapel Hill, 1982. (b) In the $[Os(bpy)_2(vpy)_2]^{2+}$/$[Ru(bpy)_2(vpy)_2]^{2+}$ metal complex pair, a greater degree of spin–orbit coupling in the Os monomer may yield greater stability of its reduced and or chain end-unit form and preferential incorporation of Os.

$(vbpy)_3]^{2+}$ form polymer films more efficiently during electropolymerization, but no attempt was made in the present study to further elucidate this problem.

The reactivity ratios r_1 and r_2 can be used, with a probability analysis,[14] to calculate the expected distribution of site neighbors, i.e., the fraction of Os sites (on a chain) that exist in a block length of one Os (i.e. are isolated Os sites, in the chain) or that exist in a block length of two or three or four Os sites etc. Table I shows such calculations using the r_1 and r_2 values for the nonideal $[Os(vbpy)_3]^{2+}$/poly-$[Zn(vbpy)_3]^{2+}$ pair, where, for example, in a polymer made from a growth solution with $f_{Os} = 0.5$, ca. 63% of the Os sites in a chain are bounded by Zn sites whereas ca. 23% are bounded by one Os and one Zn.

The r_1 and r_2 determinations and Table I calculations are instructive, but it is important to realize that they refer to the pattern of site distributions *on a given polymer chain*. In the context of electron-hopping events in a polymer film assembled from Os complexes, the chains of metal complexes are quite concentrated (total metal complex concentration >1 M). Electron self-exchanges undoubtedly occur between Os(III) and Os(II) sites on the same chain (*intrachain* exchange), but they will also occur between sites that are *adjacent but are on different polymer chains* (*interchain*). The literature of electron transport in redox polymers as yet offers no experimental way to distinguish between interchain and intrachain electron hopping in concentrated polymers. The analysis in Table I, strictly speaking, best applies to a dilute, *soluble* copolymer chain. As a consequence, it is possible that the effects of compositional irregularities in copolymer formation (i.e., blocking or alternation of sites) may be diminished by randomness in how adjacent chains pack together and thus randomness in the identity of nearest neighbors on adjacent chains. That is, interchain electron hops should relax to some extent the requirement that $r_1r_2 = 1$ for a useful, dilutable copolymer electron-transfer system. In the absence of a way to estimate the importance of interchain electron transfers and the randomness of interchain packing (potentially oligomer solubility-sensitive), the selection of copolymer systems with r_1 and r_2 near unity is, at present, the least ambiguous course.

XPS Experiments. The analysis of r_1 and r_2 for the poly-$[Os(vbpy)_3]^{2+}$/poly-$[Zn(vbpy)_3]^{2+}$ copolymer depends on the efficacy of replacing poly-$[Zn(vbpy)_3]^{2+}$ sites with voltammetrically active poly-$[Fe(vbpy)_3]^{2+}$ sites. Sullivan et al.[11c] indicate >95% site replacement in this chemistry; we explored this question further with XPS measurements of the exterior and interior surfaces of copolymer films deposited on Pt electrodes.[19] A PVA overcasting/peeling technique was employed to expose the film interior surface (see Experimental Section). The metal complex surface coverages (poly-$[Os(vbpy)_3]^{2+}$ plus poly-$[Zn(vbpy)_3]^{2+}$) in the films used for XPS studies, measured as in Figure 3, were typically between 5×10^{-9} and 2×10^{-8} mol/cm^2.

XPS Spectra of poly-$[Os(vbpy)_3]^{2+}$/poly-$[Zn(vbpy)_3]^{2+}$ Copolymers. Survey spectra of typical poly-$[Os(vbpy)_3]^{2+}$/poly-$[Zn(vbpy)_3]^{2+}$ copolymers (Figure 6A, $f_{Os} = 0.5$) exhibit the expected peaks for Os 4f ($4f_{7/2}$, $4f_{5/2}$ doublet, ≈52 eV), Zn 3p (≈86 eV), Zn 3s (≈136 eV), Zn Auger (≈263 eV), N 1s (≈397 eV), C 1s (≈284 eV), F 1s (≈682 eV), and F Auger (≈596 eV). The observed F 1s peak is consistent[20] with the BF_4^- counterion becoming incorporated into the film during electropolymerization. A peak at ca. 196 eV appears with highly variable intensity; this may be a Cl 2p impurity that could have arisen from the CH_2Cl_2 rinse of the films prior to XPS analysis. Peaks associated with the Pt substrate were never observed, which means that the 50–200 nm thick films were free of macroscopic pinhole defects.

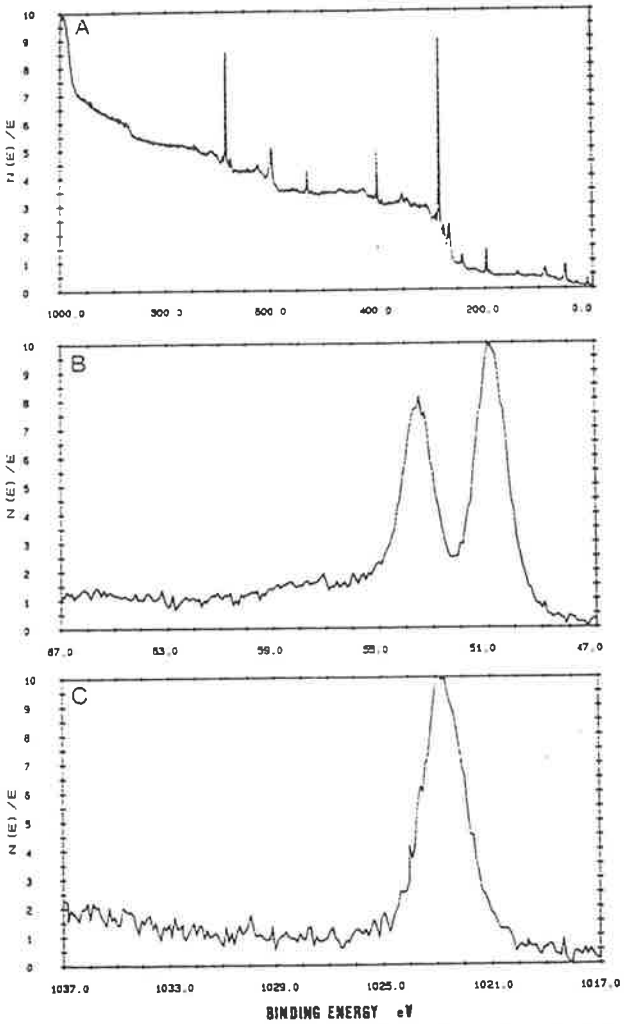

Figure 6. XPS spectra of the exterior surface of a poly-$[Os(vbpy)_3]^{2+}$/poly-$[Zn(vbpy)_3]^{2+}$ copolymer grown on a Pt electrode from a solution where $f_{Os} \approx 0.5$: (A) survey spectra; (B) Os 4f region; (C) Zn 2p region.

Spectral expansions showing the Os $4f_{7/2}$, $4f_{5/2}$ and Zn 2p regions (Figure 6B,C) reveal only one chemical form of the two elements, as expected.

XPS Spectra of poly-$[Os(vbpy)_3]^{2+}$/poly-$[Fe(vbpy)_3]^{2+}$ Copolymers. Survey spectra of films like that in Figure 6, using $f_{Os} = 0.5$ in the feed solution, and following exposure to $FeCl_2$ solutions, "conditioning" (vide supra), and rinsing, are completely free of Zn peaks and exhibit Fe 2p, 3p, and Auger peaks. Qualitatively, the signals for C, N, O, and F were unchanged.

Similar results were obtained in spectra of exterior and interior surfaces of the film. Figure 7 compares spectra of the film exterior (Figure 7A) and interior (Figure 7B) surfaces in the Os 4f/Fe 3p region. The two lower BE bands represent Os 4f and the solid lines are Gaussian fits using a linear baseline correction. Again there is no obvious multiplicity of Os and Fe chemical forms. Figure 7C shows for the same film the Zn 2p region for the interior surface; the exterior spectrum is the same. Exposure to $FeCl_2$ solution and electrochemical "conditioning" clearly completely removes Zn from the interior surface and thus presumably throughout the film. On the other hand, if the film is exposed to $FeCl_2$ but *not* conditioned, residual Zn is found at the interior film/electrode interface, as shown by Figure 7D. This demonstrates that the conditioning potential cycling *is* required for complete removal of Zn and presumably its substitution by Fe. The reduction of bipyridine rings in the films may facilitate Zn/Fe substitution both by labilizing the Zn^{2+} and by facilitating Fe^{2+}

(18) McCarley, R. L.; Thomas, R. E.; Irene, E. A.; Murray, R. W. *J. Electrochem. Soc.* **1990**, *137*, 1485.

(19) The initial experiments used copolymer films grown on Au-coated Si wafers. This procedure was satisfactory for XPS examination of the exterior film surface, but subsequent peeling of the copolymer with overcast PVA films stripped off the Au layer as well. The PVA stripping of copolymer is successful for non X-ray irradiated films, so X-ray irradiation apparently improves adhesion at the copolymer–Au interface.

(20) *Handbook of X-ray Photoelectron Spectroscopy*; G. E. Muilenburg, G. E., Ed.; Perkin-Elmer: Minneapolis, MN, 1979.

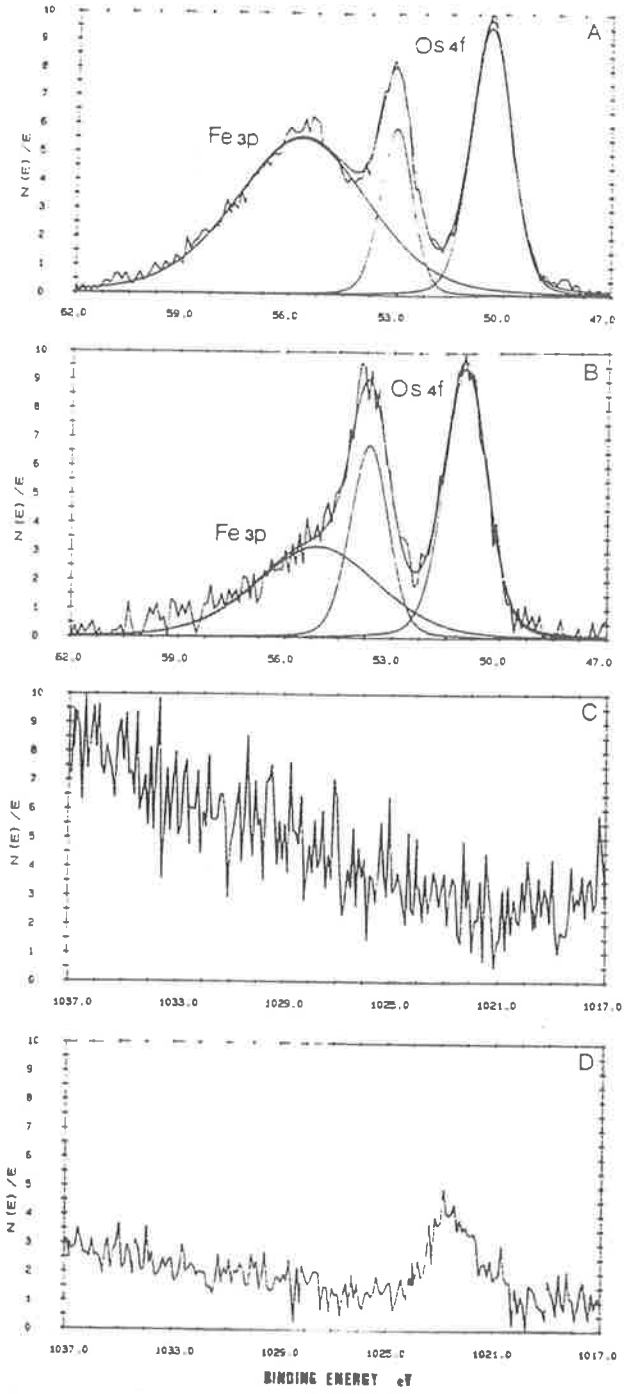

Figure 7. XPS spectra of poly-$[Os(vbpy)_3]^{2+}$/poly-$[Fe(vbpy)_3]^{2+}$ copolymer grown from a $[Os(vbpy)_3]^{2+}/[Zn(vbpy)_3]^{2+}$ solution where $f_{Os} \approx 0.5$. (A) Exterior surface of film, supported on Pt electrode, after exposure to a $FeCl_2$ solution and electrochemically "conditioned". Also shown is a least-squares fit using three Gaussian curves of the Os 4f and Fe 3p peaks. (B) Interior surface of the film in part A after removal from Pt, supported on PVA. (C and D) Zn 2p region of interior surface of PVA-supported film similar to that in part A where $f_{Os} \sim 0.5$, which was then exposed to a $FeCl_2$ solution and (C) electrochemically conditioned or (D) not electrochemically conditioned.

diffusion in the less positively charged film. Also, XPS (not shown) of the exterior surface of a $[Os(vbpy)_3]^{2+}$/poly-$[Zn(vbpy)_3]^{2+}$ copolymer film that has been soaked in Fe(II) solution but *not* conditioned, reveals a very large Fe 3p signal (obscuring that due to Os 4f). This observation shows that a large residue of uncoordinated Fe remains on the film surface, and probably within it, prior to the conditioning potential cycling. Presumably this Fe serves as a reservoir for incorporation into the Zn sites that remain after soaking and are labilized by the bipyridine reduction part of the electrochemical conditioning. The ultimate fate of any excess Fe following conditioning is unknown.

The relative areas of the Os 4f and Fe 3p bands in spectra like Figure 7A,B, accounting for elemental sensitivities,[21] yield the mole fractions of Fe on the film exterior and interior surfaces. For the example of Figure 7A,B, the XPS result for F_{Fe} was 0.54 and 0.35 for the exterior and interior, respectively. While this suggests that Fe incorporation at the film's interior may not be quantitative, we note that the reliability of the XPS quantitation is actually not very good. For example, determinations of the relative Fe and Os band intensities on a series of films polymerized in a single run from the same feed solution, which gave similar values of F_i based on the Os(III/II)–Fe(III/II) voltammetry, unfortunately varied as much as 3×. The XPS results therefore are qualitatively consistent with the voltammetric results, but the latter are quantitatively more reliable.

Determination of *D* in an Os–Zn Copolymer. To preliminarily test electron transport in the poly-$[Os(vbpy)_3]^{2+}$/poly-$[Zn(vbpy)_3]^{2+}$ copolymer, two copolymer films were grown under identical conditions on the polished tips of two Pt wire electrodes set in an insulating shroud from a solution of $[Os(vbpy)_3]^{2+}$ and $[Zn(vbpy)_3]^{2+}$ in 0.1 M Et_4NBF_4/CH_3CN where $f_{Os} = 0.61$. One of the films was assayed for F_{Os} by Fe replacement and "conditioning"; the voltammetric results were similar to those shown in Figure 3, and values of $\Gamma_{Os+Zn} = 9.2 \times 10^{-9}$ mol/cm^2 and $F_{Os} = 0.69$ were obtained. These values correspond to an approximate film thickness of 71 nm and an osmium complex site concentration of 0.9×10^{-3} mol/cm^3, taking total film concentration as 1.3 M.

A thin, porous Au film was evaporated over the other copolymer film, forming a "sandwich" electrode.[9] Application of 0.0 V to the Au electrode and +1.2 V vs SSCE to the Pt electrode, in a Et_4NBF_4/CH_2Cl_2 solution, gave a limiting current of 0.88 mA/cm^2. Assuming that the films were identical, this current corresponds to a value of $D_e = 5 \times 10^{-11}$ cm^2/s. If this result is compared to that[15] for undiluted poly-$[Os(vbpy)_3]^{2+}$ sites, where $D_e = 3.4 \times 10^{-9}$ cm^2/s, a substantially attenuated rate of electron transport through the film is indicated. The main value of the preliminary result is in showing that sandwich electrodes can be fashioned from copolymers based on these monomers for use in conductivity studies, which are on-going.

One further consideration in choosing a system for electron-transport measurements is potential interference by the diluent through its own electron self-exchange. The Zn complex used above is completely silent in terms of electron transport at potentials near that of the Os complex. The potentials of the Ru complexes are ca. 600 mV away from the Os potential, which in most circumstances ensures that Ru–Ru or Os–Ru electron-hopping activity will not contribute to the electron transport of Os(III/II) mixed-valent films. On the other hand, if the ratio of Os(III)/Os(II) sites is made quite large, and large ΔG driving energy is applied (as with a large dE/dX),[6] participation by the diluent Ru sites might become noticeable. That is, under particular circumstances, there will be constraints in Ru–Os pairs, such as in doping the Os polymer to large Os(III)/Os(II) mixed valent ratios, whereas Os–Zn pairs have no such constraints. In the present experiments, this is not a major limitation since working with large Os(III)/Os(II) ratios is experimentally difficult on other grounds, namely their large oxidizing potential.

Acknowledgment. This research was supported in part by a Materials Chemistry Initiative grant from the National Science Foundation and by the Office of Naval Research. We thank Susan Maybury for assistance with XPS spectra and instrumentation, funded by a grant from the Office of Naval Research (N0O014-86-G-0200).

(21) The atom fraction, C_x, of a species x can be expressed by: $C_x = n_x/\sum n_i = (I_x/S_x)/(\sum I_i/S_i)$, where n is the number of atoms per cubic centimeter, S is the instrument-dependent atomic sensitivity factor, and I is the signal intensity.

962 J. Phys. Chem. 1992, 96, 962-970

Effects of Mixed-Valent Composition and Bathing Environment on Solid-State Electron Self-Exchanges in Osmium Bipyridine Redox Polymer Films

Nigel A. Surridge, Mary Ellen Zvanut,† F. Richard Keene,‡ Connie S. Sosnoff, Marvin Silver,† and Royce W. Murray*

Departments of Chemistry and Physics, University of North Carolina, Chapel Hill, North Carolina 27599-3290
(Received: February 15, 1991; In Final Form: September 12, 1991)

Rate constants for the electrical gradient driven, bimolecular electron-self-exchange reaction between Os^{II} and Os^{III} sites in dry, mixed-valent films of the undiluted, polymeric metal complexes poly[$Os(bpy)_2(vpy)_2$]$(BF_4)_m$ and poly[$Os(vbpy)_3$]$(BF_4)_m$ in interdigitated array electrodes and in sandwich electrodes are measured as a function of m. Linear potential sweep and ac impedance measurements show that the reaction follows the expected, but in solid-state materials, seldom evaluated, bimolecular rate law from $C_{Os(III)}/C_{Os(II)}$ = 6 to 0.1. Comparison of rate constants for poly[$Os(bpy)_2(vpy)_2$]$(BF_4)_m$ and poly[$Os(vbpy)_3$]$(BF_4)_m$ self-exchanges driven by electrical and concentration gradients, measured in a variety of bathing environments, shows that electron hopping rates decrease in the order liquid solvent > solvent vapor > dry N_2 bathing environment, and in each environment, the rate constant for the former complex is larger. It appears that the electron hopping rate is affected by the rigidity of the polymeric matrix; matrices that are more rigid by virtue of the absence of solvent or through enhanced cross-linking (as in the vbpy complex) exhibit slower rates. The results imply that electron hopping involves (short range) nuclear displacement of the pendant osmium site from its equilibrium location in solvent-wetted polymers and is slowed when polymer rigidity inhibits such displacement.

Electron hopping between diffusively immobile donor and acceptor molecular sites embedded within (attached to) polymer films has been an active research topic in recent years. Polymer films in which the counterions of a mixture of donor and acceptor sites are mobile, making the polymers mixed (both electron and ion) conductors, can be investigated using electrochemical approaches.[1] We have been interested in comparisons of electron hopping rates in solvent-wetted vs dry mixed-valent polymers and rates in polymer films vs solutions of analogous monomers.[2] The effects of site concentration,[3] counterion mobility,[1,2,4] and reaction free energy for cross-reactions at polymer–polymer interfaces[5] have also been studied.

In films of electroreductively polymerized poly[$Os(bpy)_2(vpy)_2$]$(X)_2$ (vpy = 4-vinylpyridine, bpy = 2,2′-bipyridine), sandwiched between two electrodes, the polymer-phase electron hopping transport can be written as the bimolecular self-exchange reaction

$$\text{poly-}Os^{2+} + \text{poly-}Os^{3+} \rightarrow \text{poly-}Os^{3+} + \text{poly-}Os^{2+} \quad (1)$$

which repeated through successive layers of metal complex sites transports the electron between the electrodes. When the polymer is a mixed conductor (i.e., counterions diffuse in the film) but the electrodes are counterion-blocking, limiting concentration gradients develop by electrolysis under an applied voltage bias. The resulting limiting current measures the electron hopping rate as the phenomenological electron diffusion coefficient, D_e, and as the electron-self-exchange rate constant, k_{ex}, through the equations[2,6]

$$i_{lim} = \omega^\circ nFAD_e\frac{C_T}{d} = 10^3\omega^\circ nFAk_{ex,C}\delta^2\frac{C_T^2}{6d} \quad (2)$$

where $k_{ex,C}$ (M^{-1} s^{-1}) denotes a concentration gradient derived rate constant and C_T is the total site concentration (mol/cm³), d the film thickness ($d = \Gamma_T/C_T$ where Γ_T, mol/cm², is the electrochemically determined coverage), δ (cm) the average intersite separation, and ω° a small (1.07) numerical factor accounting for electrostatic coupling between electron and counterion motions.[6d]

Alternatively, freezing out[2a] the counterion (X^-) transport in mixed-valent films of poly[$Os(bpy)_2(vpy)_2$]$(X)_{2.5}$ by using either fast experimental time scales or low temperatures leads to electron transport (reaction 1) that is driven by sustained, 10^4–10^6 V/cm electrical (rather than concentration) gradients within the bulk polymer film. Deriving the reaction free energy for reaction 1 from the potential difference (ϕ) between adjacent sites imposed by the applied voltage ΔE is formally related to electron drift mobility in other materials[7] derived by transient measurements, in that the electron conductivity increases at higher applied voltages. Current–voltage curves for 200–500-nm-thick poly-[$Os(bpy)_2(vpy)_2$]$(BF_4)_{2.5}$ conform[2a] to the following relation, based on Marcus[8] theory

$$i = i^\circ\{\exp[-nF\rho\phi/2RT] - \exp[nF\rho\phi/2RT]\} \quad (3)$$

where[9] the average intersite voltage, ϕ, is ΔE divided by the

† Department of Physics.
‡ On Approved Special Studies Program from James Cook University, Department of Chemistry and Biochemistry, Townsville, QLD 4811 Australia.

(1) (a) Surridge, N. A.; Jernigan, J. C.; Dalton, E. F.; Buck, R. P.; Watanabe, M.; Wooster, T. T.; Zhang, H.; Pinkerton, M. L.; Facci, J. S.; Murray, R. W. *Faraday Discuss. Chem. Soc.* **1990**, *88*, 1. (b) Dalton, E. F.; Surridge, N. A.; Jernigan, J. C.; Wilbourn, K. O.; Murray, R. W. *Chem. Phys.* **1990**, *141*, 143 and references therein. (c) Murray, R. W. *Annu. Rev. Mater. Sci.* **1984**, *14*, 145.

(2) (a) Jernigan, J. C.; Surridge, N. A.; Zvanut, M. E.; Silver, M.; Murray, R. W. *J. Phys. Chem.* **1989**, *93*, 4620. (b) Jernigan, J. C.; Murray, R. W. *J. Phys. Chem.* **1987**, *91*, 2030. (c) Jernigan, J. C.; Murray, R. W. *J. Am. Chem. Soc.* **1987**, *109*, 1738. (d) Jernigan, J. C.; Chidsey, C. E. D.; Murray, R. W. *J. Am. Chem. Soc.* **1985**, *107*, 2824. (e) White, B. A.; Murray, R. W. *J. Am. Chem. Soc.* **1987**, *109*, 2576.

(3) (a) Facci, J. S.; Schmehl, R. H.; Murray, R. W. *J. Am. Chem. Soc.* **1982**, *104*, 4959. (b) Facci, J. S. Ph.D. Dissertation, University of North Carolina, Chapel Hill, NC, 1982. (c) Fritsch-Faules, I.; Faulkner, L. R. *J. Electroanal. Chem.* **1989**, *263*, 237. (d) Chidsey, C. E. D.; Murray, R. W. *J. Phys. Chem.* **1986**, *90*, 1479. (e) Hurrell, H. C.; Abruna, H. D. *Mol. Cryst. Liq. Cryst.* **1988**, *160*, 377. (f) Ofer, D.; Wrighton, M. S. *J. Am. Chem. Soc.* **1988**, *110*, 4467. (g) Kelly, J. M.; Long, C.; O'Connell, C. M.; Vos, J. G. *Inorg. Chem.* **1983**, *22*, 2818.

(4) Bruns, M. W.; Fritsch-Faules, I.; Faulkner, L. R. *J. Electrochem. Soc., Ext. Abs.* **1989**, *89*, 722.

(5) Leidner, C. R.; Murray, R. W. *J. Am. Chem. Soc.* **1984**, *106*, 1606.

(6) (a) Laviron, E. *J. Electroanal. Chem.* **1980**, *112*, 1. (b) Andrieux, C. P.; Saveant, J. M. *J. Electroanal. Chem.* **1980**, *111*, 377. (c) Buck, R. P. *J. Phys. Chem.* **1988**, *92*, 4196. (d) Saveant, J. M. *J. Electroanal. Chem.* **1988**, *242*, 1.

(7) (a) Pai, D. M.; Yanus, J. F.; Stolka, M.; Renfer, D. S.; Limburg, W. W. *Philos. Mag. B* **1983**, *48*, 505. (b) Stolka, M.; Yanus, J. F.; Pai, D. M. *J. Phys. Chem.* **1984**, *88*, 4707. (c) Pai, D. M. *J. Appl. Phys.* **1975**, *46*, 5122. (d) Mort, J.; Pai, D. M. *Photoconductivity and Related Phenomena*; Elsevier: New York, 1976.

(8) (a) Marcus, R. A. *Annu. Rev. Phys. Chem.* **1964**, *15*, 155. (b) Marcus, R. A. *J. Chem. Phys.* **1965**, *43*, 679. (c) Sutin, N. *Acc. Chem. Res.* **1982**, *15*, 275.

(9) (a) The number of monolayers is calculated from Γ_T/Γ_{mono} where Γ_{mono} is taken as 1.0 mol/cm². ϕ is taken as negative at the electrode at which a (positive) reduction current flows; i.e., electron hops in the direction of increasingly positive charge are favored.[1b] This convention was not made clear in the earlier paper.[2a]

0022-3654/92/2096-962$03.00/0

number of monolayers of osmium complex sites between the two electrodes, and the current represents the difference between forward and reverse electron hopping rates. ρ is a fitting parameter whose value is ideally one but in real samples exceeds one (vide infra). i°, the intersite exchange current density (A/cm^2) when $\Delta G_{rxn} = \Delta E = \phi = 0$, is related to the bimolecular reaction rate constant and the concentrations of donor and acceptor sites by

$$i^\circ = (10^3/6)nFC_{Os(III)}C_{Os(II)}\delta k_{ex,E} \quad (4)$$

where $k_{ex,E}$ denotes an electrical gradient derived rate constant.

The electron conductivity σ at small ϕ can be linearized

$$\sigma = d(i/\Delta E)\ (ohm^{-1}\ cm^{-1}); \quad \sigma(i^\circ) = \rho i^\circ nF\delta/RT \quad (5)$$

but at large ϕ is nonlinear given the form of eq 3. Consideration of the reverse electron hopping rate is necessary because, although the electrical gradient may be large, it amounts to a modest intersite driving force; i.e., for a 10^5 V/cm gradient and intersite spacing (δ) of 1.2 nm, ϕ is only 26 mV (210 cm^{-1}, 0.6 kcal/mol, or ca. kT_{298}).

This paper describes further studies of mixed-valent poly[Os(bpy)$_2$(vpy)$_2$](BF$_4$)$_m$ films (bpy = 2,2′-bipyridine; vpy = 4-vinylpyridine) and of a related polymer poly[Os(vbpy)$_3$](BF$_4$)$_m$ (vbpy = 4-methyl-4′-vinylbipyridine) that address the following points.

A. Equations 3–5 show that, at a fixed *total* concentration (C_T) of redox sites, σ depends on the electron acceptor and donor concentration product (i.e., $C_{Os(III)}C_{Os(II)}$ or $C_{Os(II)}[C_T - C_{Os(II)}]$), but k_{ex} should not. All previous electrochemical concentration gradient based measurements of D_e and k_{ex} in redox polymers rely[6,10] on this bimolecular model and *assume* that the electron-self-exchange rate constant k_{ex} is invariant with the product $C_{don}C_{acc}$. In our previous[2a] study, only 1:1 Os(III):Os(II) mixed-valent films were employed (i.e., $C_{Os(III)} = C_{Os(II)}$, $m = 2.5$).

There are, in fact, few data that address the validity of the bimolecular rate law assumption[1,2a,3,11] in redox polymer materials, and in all of the available data, the observed k_{ex} is relatively constant near $C_{acc} = C_{don}$ but decreases as either C_{acc} or C_{don} becomes greatly in excess. To further investigate this problem, we have carried out electrical gradient based electron transport measurements on the undiluted polymers poly[Os(bpy)$_2$(vpy)$_2$](BF$_4$)$_m$ and poly[Os(vbpy)$_3$](BF$_4$)$_m$ in films where m is varied between 2 and 2.5 in the former and between 2 and 3 in the latter. The total osmium site concentration is constant at C_T = 1.3 M. The rate law expressed in eqs 2–4 proves to be satisfactory when m is near 2.5, i.e., at mixed-valent compositions near 1:1, but as in the previous studies deviations occur at more extreme ratios. The deviations may represent experimental uncertainties at very low or high mixed-valent ratios, rather than breakdown of the bimolecular model.

B. Our previous measurements[2a] were based on current–voltage curves derived from sweeps of ΔE sufficiently fast as to be sweep rate independent, indicative of avoiding counterion motion. Here, we support those experiments with an ac impedance study of poly[Os(bpy)$_2$(vpy)$_2$](BF$_4$)$_m$ films in which both frequency and temperature are varied.

C. A fitting parameter $\rho > 1$ was necessary in the previous study[2a] to fit eq 3 to experimental current–voltage responses of poly[Os(bpy)$_2$(vpy)$_2$](BF$_4$)$_{2.5}$ films. The parameter may reflect overestimation of the interelectrode film distance and/or a dispersion in the electron-transfer barrier height.[1a,2a,7b] The problem is clarified here, in part, by defining the interelectrode dimension with an interdigitated electrode.

Equations 2 and 4 contain a geometrical factor[6c] of 6 which was unfortunately omitted in the previous studies.[2] The previous[2a,b] values of k_{ex} (not those of i° or σ) should properly be multiplied by 6. When making comparisons of present and previous electron-transfer rate constants for the polymer poly[Os(bpy)$_2$(vpy)$_2$](X)$_{2.5}$, the previous[2a] data have been corrected for the geometrical factor.

(10) In electrochemical D_e measurements, where a concentration gradient profile exists, the total $C_{don} + C_{acc} = C_T$ concentration may be constant, but the relative values of C_{don} and C_{acc} in any region of the film will vary widely.
(11) Wilbourn, K.; Murray, R. W. *J. Phys. Chem.* **1988**, *92*, 3642.

Experimental Section

The ligand 4-methyl-4′-vinyl-2,2′-bipyridine (vbpy) was synthesized in two steps based on a modification[12a] of a literature method.[12b] [Os(bpy)$_2$(vpy)$_2$][PF$_6$]$_2$ was prepared as described earlier.[13]

Synthesis of [Os(vbpy)$_3$][PF$_6$]$_2$. Vbpy (0.222 g; 1.133 mmol) was added to $(NH_4)_2OsCl_6$ (0.164 g; 0.375 mmol) in 8 mL of ethylene glycol under N_2 and the mixture heated under reflux for 3 h. The solution was cooled to room temperature, and an equal volume of water added, followed by NH_4PF_6 (0.1465 g; 0.899 mmol) to precipitate the product, which was filtered, washed with water and ether, and air-dried. The product was chromatographically purified on an alumina column using 1:1 CH_3CN:toluene as eluent. The faster moving (major) band, the desired product, was collected and the solvent evaporated to give a dark green solid: yield 0.385 g; 96%. Anal. Calcd for $OsC_{39}H_{36}N_6P_2F_{12}$: P, 5.81. Found: P, 6.03. No Cl was found by elemental analysis.

^{1}H NMR. This complex can exist as two isomers: a "facial" or cis form with C_3 symmetry and a "meridional" or trans form with C_1 symmetry. The splitting observed in both the methyl and vinyl resonances is consistent with the statistically preferred *meridional* isomer, with no evidence for the facial isomer. A slower moving second band collected from the column exhibits aliphatic NMR resonances suggestive of a polymerized complex.

Electrochemistry. Film deposition and three- and four-electrode voltammetry were performed with a Pine Instruments RD4 bipotentiostat. Acetonitrile (CH_3CN) and CH_2Cl_2 (Burdick & Jackson) solvents were used as received and stored over 4-Å molecular sieves. The electrolyte was 0.1 M tetrabutylammonium tetrafluoroborate (Bu_4NBF_4, Fluka), unless otherwise noted. Potentials were measured vs saturated sodium chloride calomel (SSCE), 0.01 M Ag^+/Ag, or Ag-wire quasi-reference electrodes and are reported vs SSCE.

Deposition of Poly[Os(bpy)$_2$(vpy)$_2$](BF$_4$)$_2$ and Poly[Os(vbpy)$_3$](BF$_4$)$_2$ Films. These were electrochemically polymerized from 0.2 to 0.8 mM monomer solutions in 0.1 M Bu_4NBF_4/CH_3CN onto polished tips of Pt wires sealed in glass or onto Pt interdigitated array electrodes (vide infra), in an inert-atmosphere enclosure (dry N_2), by cyclically scanning the electrode potential between −1.0 and −1.75 V vs SSCE at 150 or 200 mV/s. The electroactive film coverage, Γ_T, was determined by integrating the charge under the Os(III/II) voltammetric wave (20–50 mV/s) observed in monomer-free, 0.1 M Bu_4NBF_4/CH_3CN. This voltammetry is like that in our previous publication.[1,2]

Sandwich Electrodes. Films deposited on (0.002 or 0.0013 cm^2) Pt wire tip electrodes were used to prepare Pt/polymer/Au "sandwich" electrodes, as previously[14] described, by evaporation of a porous, ca. 300 Å Au film overcoat onto the polymer. Electrical contact to the Au film was made by allowing the evaporated Au film to overlap the surrounding glass insulator, and a nearby, bare Pt wire also sealed in the glass.

IDA Electrodes. Interdigitated arrays[15] consisted of 100 interdigitated, 3-μm-wide Pt fingers (50 per electrode side) separated by either 5- or 2-μm gaps, on SiO_2/Si substrate. The Pt finger height was 1700 Å as measured by a Tencor Alpha Step 100 surface profilometer. Pt tracks overcoated with an insulator lead to contact pads at the top end of the wafer slice, where contact was made with copper wire and Ag paint and insulated with a coat of quick-drying epoxy. Electropolymerization onto IDA electrodes was conducted with the two sets of fingers of the array

(12) (a) Reed, R. Unpublished results, University of North Carolina. (b) Abruna, H. D.; Breikers, A. I.; Collum, D. B. *Inorg. Chem.* **1985**, *24*, 987.
(13) (a) Kober, E. M.; Caspar, J. V.; Sullivan, B. P.; Meyer, T. J. *Inorg. Chem.* **1988**, *27*, 4587.
(14) Pickup, P. G.; Kutner, W.; Leidner, C. R.; Murray, R. W. *J. Am. Chem. Soc.* **1984**, *106*, 1991.
(15) Aoki, K.; Moritz, M.; Niwa, O.; Tabei, H. *J. Electroanal. Chem.* **1988**, *256*, 269.

shorted together as the working electrode and potential scanned in the same way as the Pt wire tip electrodes, in a solution of 0.4 mM $[Os(vbpy)_3]^{2+}$.

Preparation of Dry, Mixed-Valent Polymer Films. The metal complex polymer films, Os^{II} as-prepared, must be converted to an $Os^{III/II}$ mixed-valent form for two-electrode electron transport rate measurements as dry, N_2-bathed films. The previously described[2a,14] procedure was modified as follows: Immersing the Pt/polymer/Au sandwich or polymer-coated IDA in 0.1 M Bu_4NBF_4/CH_2Cl_2 with the two electrode terminals shorted together, a potential is applied vs reference electrode to electrolyze the polymer to the desired mixed-valent composition. The sandwich or IDA electrode assembly is raised from the solution, rinsed with pure CH_2Cl_2, and placed in a dry N_2 atmosphere for 15 min to evaporate the residual solvent, *after* which the potentiostat is disconnected. The specimen was (typically) immediately used in electron transport studies.

Sandwich electrodes containing Os^{III} states, when in CH_3CN, tend to corrode the Au contact, presumably via Os^{III}-mediated oxidation of Au in the strongly coordinating solvent. Reliable generation of mixed-valent films[2] has thus relied on a brief electrolysis period with continuous potential control until the film has been rinsed and dried, after which the Au corrosion ceases. We have found that using the less strongly coordinating CH_2Cl_2 in the electrolysis alleviates the Au corrosion problem considerably. The change to CH_2Cl_2 was crucial in the present study, permitting individual sandwich electrode specimens to be repeatedly reelectrolyzed to different mixed-valent compositions.

Electron Transport (Conductivity) Measurements. Electron transport measurements can be made[1,2] with the sandwich (or IDA) electrode immersed either in an electrolyte solution or in a dry N_2 atmosphere. In electrolyte solutions, four electrodes are employed: a reference and auxiliary electrode and the two sandwich or IDA electrodes whose potentials are each controlled vs E_{ref}. Some of the initially all-Os^{II} film undergoes electrolysis to Os^{III} states when appropriately negative, and positive potentials are applied to the two contacting electrodes (vs E_{ref}), at the positive (Pt) electrode to Os^{III} but maintaining Os^{II} at the negative (Au) electrode. Films used in dry N_2 atmosphere owing to ion budget restrictions[2d] must be first rendered mixed valent (vide supra). In both environments, after a short period, electrolysis develops linear concentration gradients of Os^{II} and Os^{III} sites across the film, and the initially large currents decrease to steady values given by eq 2, from which D_e and $k_{ex,C}$ are obtained.[2]

In two-electrode, electrical gradient based electron transport measurements on N_2-dry, mixed-valent films (vide supra), fast time scales and/or lowered temperatures are employed (based on previous work[2a]) to render interfacial electrolysis and diffusion of the film's counterions unimportant on the experimental time scale. These measurements are carried out in two ways: (a) linear cyclical voltage sweeps are made at sufficiently large rates that the current–voltage pattern *and amplitude* are sweep rate independent, or (b) an ac voltage is applied at a series of frequencies, measuring the resulting ac current amplitude and phase angle. We refer to these two procedures, the results from which will be compared, as the *fast linear sweep* and the *ac impedance* methods, respectively, and label rate constants thus derived as $k_{ex,E,LS}$ and $k_{ex,E,AC}$, respectively.

In the fast linear sweep method, ±3 to 4 V triangular wave ΔE are applied to sandwich electrodes using a PAR 174 universal programmer or a Wavetek function generator, at sweep rates up to 1000 V/s. Current measured as a voltage across a 30–2500-ohm series resistor is recorded with a Nicolet 2090 digital storage oscilloscope. In experiments using smaller amplitude triangular waves (±0.6 V) and sweep rates (<50 mV/s), a potentiostat with reference and auxiliary electrodes shorted together and an X–Y recorder are employed. In linear sweep (electrical gradient) experiments on IDA electrodes, the larger (5-μm gap) interelectrode distance requires much larger ΔE values to achieve appreciable electrical voltage gradients; a Kepco BOP 36-12M high-power bipolar amplifier driven by the PAR generates a ±36-V triangle wave at a ramp rate of ca. 8600 V/s. The current–voltage data stored on the oscilloscope were transferred to a microcomputer for further analysis using eq 3.

Ac impedances were measured for sandwich electrodes containing films of poly$[(bpy)_2Os(vpy)_2][BF_4]_m$, where $m = 2$–2.5, using a Solartron 1255 frequency response analyzer (FRA). The FRA automatically steps the frequency through a specified range, usually 1–10^6 Hz, measuring the voltage, current, and phase angle at selected frequencies and producing frequency-dependent values of in-phase (Z_{real}) and 90° out-of-phase (Z_{imag}) impedances. The ac voltage amplitude is 20 mV for samples with impedance $<10^6$ Ω and 500 mV for samples with impedance $>10^6$ Ω; in both cases, it was verified that the signal amplitude did not alter the results. Measurements between room temperature and −100 °C are made with the sandwich electrodes in a cell flooded with a precooled N_2 gas flow.

Results and Discussion

Electron Transport in Pt/Poly[Os(vbpy)$_3$](BF$_4$)$_{2.5}$/Au Sandwich Electrodes, Using Concentration Gradients. Concentration gradient driven electrode transport in this polymer has not been previously studied so initial experiments involved characterization and comparison to poly$[Os(bpy)_2(vpy)_2](BF_4)_{2.5}$. A four-electrode measurement of D_e for a Pt/poly$[Os(vbpy)_3](BF_4)_2$/Au sandwich immersed in 0.1 M Bu_4NClO_4/solvent gives a sigmoidal current–potential curve with a well-defined limiting current, much like that[2] for poly$[Os(bpy)_2(vpy)_2](ClO_4)_2$ films. Based on several batches of electrodes and taking C_T = as 1.3 M, CH_2Cl_2 and CH_3CN-wetted D_e and associated $k_{ex,C}$ values were obtained from i_{lim} using eq 2 (Table I). $k_{ex,C}$ in liquid CH_3CN is ca. 7-fold smaller than that obtained[2a] (ca. 2×10^7 M^{-1} s^{-1}) for poly$[Os(bpy)_2(vpy)_2](ClO_4)_2$ films[2] and is ca. 2-fold larger than in liquid CH_2Cl_2. The substantial scatter in the Table I D_e and $k_{ex,C}$ data for different film preparations ("batches") is common in these kinds of measurements.[1,2]

When Pt/poly$[Os(vbpy)_3](BF_4)_{2.5}$/Au (1:1 Os^{III}:Os^{II}) sandwiches immersed in CH_2Cl_2 *vapor* are examined with very slow potential sweeps, steady-state, sigmoidally shaped current–voltage curves with well-defined limiting currents are observed that resemble those[2] for 1:1 Pt/poly$[Os(bpy)_2(vpy)_2](BF_4)_{2.5}$/Au sandwiches immersed in various batching gases. This two-electrode measurement signifies that the film's counterions are sufficiently mobile to diffuse across the film during the potential sweep, which allows electrolytic generation of linear concentration gradients of Os^{III} and Os^{II} sites. In an analogous experiment, but in a *dry* N_2 bath, the evidently slower counterion diffusion[16] produced non-steady-state currents at sweep rates even as slow as 2 mV/s, so i_{lim} was measured by applying a constant potential on the plateau of the current–voltage profile until the current settled to a steady value.

Comparison of the results in Table I for batch 1 shows that the electron hopping rate for Pt/poly$[Os(vbpy)_3](BF_4)_{2.5}$/Au sandwiches in different bathing media decreases in the order liquid solvent > solvent vapor > dry N_2. The variations with bathing environment span about a factor of 10, and their order and rough magnitude are similar to[2a] that observed with Pt/poly$[Os(bpy)_2(vpy)_2](BF_4)_{2.5}$/Au sandwiches.

Electron Transport in Pt/Poly[Os(vbpy)$_3$](BF$_4$)$_{2.5}$/Au Sandwich Electrodes, Using Electrical Gradients, by Fast Linear Sweep Method. Upon imposing *fast* potential sweeps on dry, N_2-bathed Pt/poly$[Os(vbpy)_3](BF_4)_{2.5}$/Au sandwiches, the currents are much larger, are independent of potential sweep rate, and rise exponentially with voltage (out to irreversible film breakdown). Analogous responses are obtained by lowering the temperature; counterion diffusivity is more readily thermally quenched than is electron hopping.[2a,b] Figure 1A displays the 266 K current–voltage curve for a 1:1 mixed-valent Pt/poly$[Os(vbpy)_3](BF_4)_{2.5}$/Au sandwich that was cooled to 187 K and subjected

(16) Pt/poly$[Os(vbpy)_3](BF_4)_{2.5}$/Au sandwiches approach steady state much more slowly than do previously studied[1a] Pt/poly$[Os(bpy)_2(vpy)_2](BF_4)_{2.5}$/Au sandwiches. This and other current experiments[17] indicate that counterion transport is slower in the former polymer.

(17) Surridge, N. A.; Murray, R. W. Unpublished results, 1990.

TABLE I: Collected Electron Transport Data for Pt/poly[Os(vbpy)$_3$](BF$_4$)$_{2.5}$/Au Sandwiches

			in CH_2Cl_2/Bu_4NBF_4		in CH_2Cl_2 vapor		in dry N_2				
batch no.	no. of samples	$10^8\Gamma_T$,[a] mol/cm^2	10^9D_e, cm^2/s	$10^{-6}k_{ex,C}$, M^{-1} s^{-1}	10^9D_e, cm^2/s	$10^{-5}k_{ex,C}$, M^{-1} s^{-1}	10^9D_e, cm^2/s	$10^{-5}k_{ex,C}$, M^{-1} s^{-1}	10^4i°, A	ρ	$10^{-5}k_{ex,E,LS}$, M^{-1} s^{-1}
1	4	0.85	3.4	1.1 ± 1.0	2.1	6.6 ± 1.0	0.93	3.0 ± 0.8	3.3	3.0	1.3 ± 0.3
2	1	2.2	8.2	2.6			9.8	31	10.4	6.3	6.6
3	3	1.2							12.7	3.1	3.7
4	2	2.5	3.7	1.2							
5	3	1.4	4.3	1.4							
6	4	2.1	8.2[b]	2.6[b]							
7	5	1.7	10.6[b]	3.4[b]							

[a] The polymer film thickness (d) is given by Γ_T/C_T where C_T is total site concentration, 1.3 × 10^{-3} mol/cm^3. For batch 1, d = 65 nm. [b] In CH_3CN/Bu_4NBF_4.

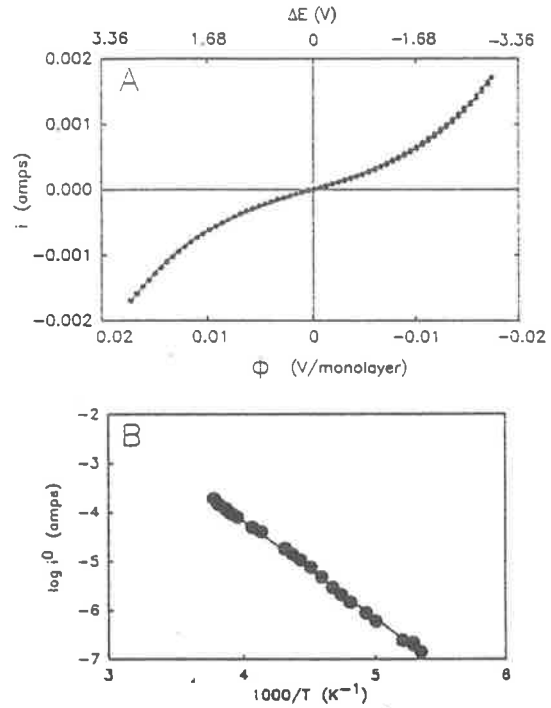

Figure 1. (A) Current–voltage curve (●) for a Pt/poly[Os(vbpy)$_3$](BF$_4$)$_{2.5}$/Au film in dry N_2 at 266 K. Γ_T = 2.2 × 10^{-8} mol/cm^2. (—) is calculated from eq 3 for $i^\circ \approx 1.9 \times 10^{-4}$ A and $\rho \approx 6.5$. (B) Arrhenius plot of similarly obtained i° values for the film in panel A; linear, least-squares fit gives E_A = 9.1 kcal/mol, $\sigma_\infty \approx 29.3\ \Omega^{-1}$ cm^{-1} (eq 5), and $k_{ex,\infty} \approx 6 \times 10^9\ M^{-1}\ s^{-1}$ (eq 4).

to ±3-V potential sweeps as the film slowly warmed. Figure 1A also shows the satisfactory fit of eq 3 to the experimental curve; similarly good fits were obtained at lower temperatures.

The current–voltage response in Figure 1A resembles that found for Pt/poly[Os(bpy)$_2$(vpy)$_2$](BF$_4$)$_{2.5}$/Au sandwiches[2a,b] and reflects electrical gradient driven electron hopping as opposed to self-exchange promoted by concentration gradients between the Os complex sites. Analysis by eq 3 produces two parameters: the exchange current i° (and through eq 4 the self-exchange rate constant $k_{ex,E,LS}$) and the fitting parameter ρ, which are shown for room-temperature experiments in Table I (batches 1–3). Comparison of the $k_{ex,E,LS}$ results with those obtained in concentration gradient experiments ($k_{ex,C}$) for the same Pt/poly-[Os(vbpy)$_3$](BF$_4$)$_{2.5}$/Au electrodes (Table I, rhs, batchs 1 and 2) shows that the latter is larger by ca. 2–4 times. Such a difference was found for Pt/poly[Os(bpy)$_2$(vpy)$_2$](BF$_4$)$_{2.5}$/Au sandwiches.[2a] Ideally, the rate of electron hopping should not depend on whether the reaction free energy is supplied by electrical or by concentration gradients. Possible reasons for the difference between $k_{ex,E,LS}$ and $k_{ex,C}$ were conjectured[2a] for Pt/poly[Os(bpy)$_2$(vpy)$_2$](BF$_4$)$_{2.5}$/Au sandwiches, and of them, as shown here (vide infra), uncertainty in the actual film thickness is at least part of the answer.

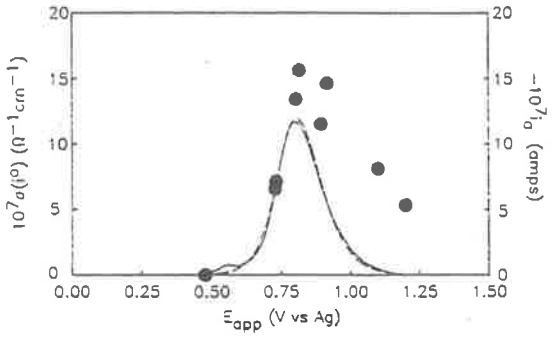

Figure 2. Anodic branch (—) of room temperature cyclic voltammogram (20 mV/s, background subtracted) of Pt/poly[Os(vbpy)$_3$](BF$_4$)$_m$/Pt film electropolymerized from 0.1 M Bu_4NBF_4/CH_2Cl_2 onto 2-μm gap IDA electrode. (The cathodic branch is a mirror image.) Total electroactive polymer on the IDA is 1.3 × 10^{-10} mol. Simulation (– – –) of the voltammetric wave; see text. (●) are conductivities derived from i° (Table II) measured with fast potential sweeps (e.g., Figure 3) after electrolyzing the film at different E_{app} to set the mixed valency (m) and drying in N_2.

Results for the temperature dependence of the exchange current parameter i° are given in Figure 1B. The Arrhenius plot is linear over the range examined and gives an activation barrier of ca. 9.1 kcal/mol (0.39 eV) for the electron hopping reaction. This barrier is similar to that obtained by ac impedance measurements described below. The fitting parameter ρ required in the current–voltage analysis with eq 3, 5.8–6.8 (average 6.3), is independent of temperature.

Electron Transport in Solvent-Wetted Pt/Poly[Os(vbpy)$_3$](BF$_4$)$_2$/Pt Films on IDA's, Using Concentration Gradients. A film of poly[Os(vbpy)$_3$](BF$_4$)$_2$ was deposited on a Pt IDA electrode (2-μm gaps) from a 0.4 mM monomer solution by potential cycling for 15 min. Loosely attached material was removed by brief sonication[18] in CH_3CN, leaving a relatively smooth film but ca. 10–20% of the finger area uncovered. Figure 2 (—) shows the anodic branch of the $Os^{III/II}$ cyclic voltammetry in 0.1 M Bu_4NBF_4/CH_1CN which gave a charge, Q, of 1.88 × 10^{-5} C. Application of 0 V vs SSCE to one set of Pt fingers and +1.37 V to the other to produce the limiting current i_{lim} for $Os^{III/II}$ transport gave D_e = 1.9 × 10^{-8} cm^2/s using the relation[19]

$$D_e = (i_{lim}Gp/Q)(N/[N-1]) \qquad (6)$$

where G is the interelectrode gap, p the (finger width + interelectrode gap), and N the number of fingers. By eq 2, this corresponds to $k_{ex,C} = 6 \times 10^6\ M^{-1}\ s^{-1}$, which is close to the sandwich result in Table I (batches 6 and 7). The ca. 0.005 cm^2 plan area of the IDA, the above charge, and 1.04 nm/monolayer indicate

(18) Both the cyclic voltammetric charge and i_{lim} were larger on the film prior to sonication, but by similar amounts (32% vs 22%), so that the value of D_e was little different, 1.9 × 10^{-8} cm^2/s.

(19) (a) Chidsey, C. E. D.; Feldman, B. J.; Lundgren, C.; Murray, R. W. *Anal. Chem.* **1986**, *58*, 601. (b) Feldman, B. J.; Murray, R. W. *Anal. Chem.* **1986**, *58*, 2844.

TABLE II: Conductivity Measurements on Pt/poly[Os(vbpy)$_3$](BF$_4$)$_m$/Pt IDA Electrode

$E_{app} - E°'$,[a] V	$C_{Os(III)}/C_{Os(II)}$	$i°$,[b] A/cm^2	ρ[b]	$\sigma(i°)$,[c] Ω^{-1} cm^{-1}	$k_{ex,E,LS}$,[c] M^{-1} s^{-1}
-3.30×10^{-1}	5.34×10^{-4}	5.7×10^{-9}	3.4	9.2×10^{-14}	(3.3)
-8.20×10^{-2}	1.56×10^{-1}	4.0×10^{-2}	3.4	6.6×10^{-7}	1.1×10^5
-7.80×10^{-2}	1.71×10^{-1}	4.0×10^{-2}	3.8	7.2×10^{-7}	0.96×10^5
-6.00×10^{-3}	8.73×10^{-1}	8.3×10^{-2}	3.4	1.3×10^{-6}	1.0×10^5
6.00×10^{-3}	1.10	9.7×10^{-2}	3.4	1.6×10^{-6}	1.2×10^5
8.40×10^{-2}	4.00	6.9×10^{-2}	3.5	1.2×10^{-6}	1.3×10^5
1.06×10^{-1}	5.75	9.1×10^{-2}	3.4	1.5×10^{-6}	2.2×10^5
2.94×10^{-1}	1.28×10^2	4.7×10^{-2}	3.6	8.1×10^{-7}	(1.9×10^6)
3.89×10^{-1}	6.12×10^2	2.9×10^{-2}	3.8	5.3×10^{-7}	(5.5×10^6)
					av $1.3 (\pm 0.3) \times 10^5$

[a] Measured from $E°'$ for the $Os^{II/III}$ couple. [b] Fitted parameters from eq 3, finger edge area = 3.5×10^{-4} cm^2. [c] Calculated from eqs 4 and 5, using $i°$ obtained by fit of eq 3 to curves like Figure 3.

an average film thickness of ca. 2000 Å, larger than the ca. 1700 Å Pt finger height. Assuming that the gaps have been adequately filled with polymer, this film was employed to study the effect of mixed-valent composition in dry films, as described next.

Electron Transport in Dry Pt/Poly[Os(vbpy)$_3$](BF$_4$)$_m$/Pt Films on IDA's, as a Function of *m*, Using Electrical Gradients, by Fast Linear Sweep Method. As noted above, our previous[2a,b] studies were exclusively of 1:1 mixed-valent Os^{III}:Os^{II} films; according to eq 4, this is the most conductive state. One objective of the present study (section A, Introduction) is to examine films containing an excess of Os^{III} or Os^{II}, at constant $C_{Os(II)} + C_{Os(III)}$, where according to eq 4 conductivity σ but no $k_{ex,E}$ should vary with the excess. Another objective (section C, Introduction) is to use an IDA with a well-defined interelectrode distance to examine the effect of interelectrode separation.

The above polymer-coated IDA was electrolyzed in 0.1 M Bu_4NBF_4/CH_2Cl_2 with the Pt finger sets shorted together, at selected potentials on the $Os^{III/II}$ wave to prepare various mixed-valent compositions. After each electrolysis, the film was withdrawn from solution, rinsed, allowed to dry in a N_2 atmosphere, and subjected to a fast cyclical potential sweep, producing current–voltage curves like that shown for a 1:1 mixed-valent film in Figure 3. Figure 3 also shows a nonlinear least-squares fit according to eq 3, which yields $\rho = 3.4$ and $i° = 8.3 \times 10^{-2}$ A/cm^2. Taking the Pt finger height as the cross-sectional area of the film through which electron transport occurs gives $k_{ex,E,LS} = 1.0 \times 10^5$ M^{-1} s^{-1} using eq 4.

Results from experiments like Figure 3 are summarized in Table II ($i°$, ρ, and conductivity $\sigma(i°)$ from eq 5) and are presented in Figure 2 (●) as a function of the electrolysis potential used to prepare the mixed-valent state. The potential axis for the electrolysis and for the cyclic voltammetry curve (—) is the same, and the film conductivity $\sigma(i°)$ and the voltammetric current both pass through a maximum at $E°'$. This agrees with eq 4 in that conductivity should be maximal when $C_{Os(III)} = C_{Os(II)}$.

Analysis of the Table II and Figure 2 data to derive values of $k_{ex,E,LS}$ from $i°$ requires converting the electrolysis potential to the actual $C_{Os(III)}$ and $C_{Os(II)}$ compositions. This is a thorny step because these films, like most redox polymers,[1c,20] do not exactly follow the Nernst equation, which predicts that the voltammetric wave should at 298 K be symmetrical with $\Delta E_{fwhm} = 90.6$ mV. The wave in Figure 2 (—) is slightly broader on the positive side and has $\Delta E_{fwhm} = 185$ mV. The electrolysis potential was converted to film composition with the modified[20] Nernst relation

$$E = E_{1/2} + \frac{RT}{gnF} \ln \frac{C_{Os(III)}}{C_{Os(II)}} \qquad (7)$$

that approximates the wave broadening with a nonideality factor g, obtainable from an experimental voltammogram as $\Delta E_{fwhm} = 3.53RT/gnF$. The Figure 2 voltammogram produced $g = 0.55$ and 0.42 for the sides of the wave negative and positive of $E°'$, respectively. The fit of eq 7, written for current due to a surface-confined species[21] (Figure 2, ---), is good over the central ca. ±80 mV region and deviates somewhat further out on the wings of the wave. Fits to the cathodic branch of the voltammogram (not shown) were similar. Values of $C_{Os(III)}/C_{Os(II)}$ from such fits are given in Table II as are values of $k_{ex,E,LS}$ calculated from eq 4.

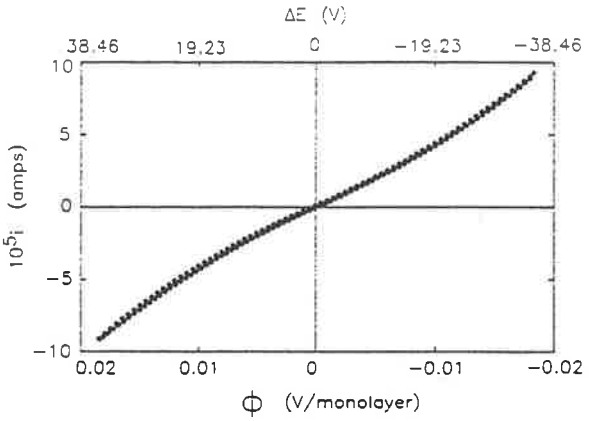

Figure 3. Example of current–voltage curve (●, shown for fast forward and reverse linear sweeps at ±36 V) analyzed with eq 3 to produce conductivity data for Pt/poly[Os(vbpy)$_3$](BF$_4$)$_m$/Pt film in Figure 2 and Table II; in N_2, $C_{Os(II)}/C_{Os(III)} = 1$ for the film shown. (—) is the theoretical curve from eq 3 for $i° \approx 2.9 \times 10^{-5}$ A and $\rho \approx 3.4$.

The results in Table II show that $k_{ex,E,LS}$ is independent of mixed-valent composition for electrolysis potentials ca. ±85 mV from $E°'$ or from $C_{Os(III)}/C_{Os(II)}$ ca. 6 to 0.1. This is an important result, showing the electron hopping rate law expressed in eq 4 to be adequately obeyed within this range. That is, these results confirm the presumption of eqs 1–3, that the electron conductivity of these materials is a solid-state, *bimolecular* reaction between diffusively immobile sites.

Further examination of the $k_{ex,E,LS}$ data in Table II shows that $k_{ex,E,LS}$ is larger at $C_{Os(III)}/C_{Os(II)} > 4$ and smaller at $C_{Os(III)}/C_{Os(II)} < 0.1$. Both these experimental regimes have difficulties. The conductivities in poly-Os^{III}-rich films are subject to several experimental problems, most notably the experimentally demonstrable (vide infra) reactivity of the poly-Os^{III} sites in the films. Reversion of even small quantities of poly-Os^{III} sites to poly-Os^{II} sites would, at large $C_{Os(III)}/C_{Os(II)}$, cause large apparent values of $\sigma(i°)$ and $k_{ex,E,LS}$ as observed. The deviation at low $C_{Os(III)}/C_{Os(II)}$ probably reflects an inaccuracy in converting electrolysis potential to film composition with eq 7 at potentials far from $E°'$.

Two other significant observations can be made by comparing the $k_{ex,E,LS}$ results in Table I vs II. Firstly, at 1:1 Os^{III}:Os^{II} composition, $k_{ex,E,LS} = 1.3 \times 10^5$ M^{-1} s^{-1} (IDA, Table II) is in very good agreement with that for the *smallest* film thickness

(20) (a) Ikeda, T.; Leidner, C. R.; Murray, R. W. *J. Electroanal. Chem.* **1982**, *138*, 343. (b) Albery, W. J.; Boutelle, M. G.; Colby, P. J.; Hillman, A. R. *Ibid.* **1982**, *133*, 135.

(21) (a) See eq 12.5.11 in: Bard, A. J.; Faulkner, L. R. *Electrochemical Methods*; Wiley: New York, 1980; p 522. (b) Ratio of activity coefficients of Os^{II} and Os^{III} is assumed to be unity.

TABLE III: Conductivity Measurements on Pt/poly[$(bpy)_2Os(vpy)_2](BF_2)_m$/Au Sandwiches

$E_{app} - E^{\circ\prime}$,[a] V	$C_{Os(III)}/C_{Os(II)}$	i°,[b] A/cm^2	ρ[b]	$k_{ex,E,LS}$, M^{-1} s^{-1}	$k_{ex,E,AC}$, M^{-1} s^{-1}	$\sigma(i^{\circ})$, Ω^{-1} cm^{-1}	σ(ac), Ω^{-1} cm^{-1}
−0.190	1.22×10^{-3}	4.6×10^{-4}	(4.8)	(1.1×10^5)	(0.5×10^5)	1.0×10^{-8}	4.4×10^{-9}
−0.157	3.92×10^{-3}	7.8×10^{-4}	(4.7)	(0.6×10^5)	(0.3×10^5)	1.8×10^{-8}	8.9×10^{-9}
−0.113	1.85×10^{-2}	3.3×10^{-3}	(7.2)	(0.6×10^5)	(0.5×10^5)	1.1×10^{-7}	8.9×10^{-8}
−0.060	1.18×10^{-1}	6.0×10^{-2}	6.4	2.0×10^5	1.8×10^5	1.8×10^{-6}	1.7×10^{-6}
−0.055	1.43×10^{-1}	2.5×10^{-2}	6.5	0.7×10^5	0.5×10^5	7.7×10^{-7}	5.9×10^{-7}
−0.038	2.57×10^{-1}	1.8×10^{-1}	6.0	3.3×10^5	2.8×10^5	5.0×10^{-6}	4.2×10^{-6}
−0.033	3.20×10^{-1}	1.9×10^{-1}	5.9	3.1×10^5	2.7×10^5	5.2×10^{-6}	4.3×10^{-6}
0.0000	1.00	4.6×10^{-1}	5.5	5.7×10^5	4.2×10^5	1.2×10^{-5}	8.8×10^{-6}
0.014	1.48	3.4×10^{-1}	5.8	4.3×10^5	3.8×10^5	9.3×10^{-6}	8.1×10^{-6}
0.016	1.60	4.1×10^{-1}	5.8	5.3×10^5	4.1×10^5	1.1×10^{-5}	8.6×10^{-6}
			av 6.0 (±0.3)	$3.5 (\pm 1.2) \times 10^5$	$2.8 (\pm 1.2) \times 10^5$		

[a] Measured from $E^{\circ\prime}$ for the $Os^{II/III}$ couple. [b] Fitted parameters from eq 3. [c] Calculated from $\sigma(ac) = d/R_{ac}A$.

samples (sandwich, Table I, batch 1, $k_{ex,E,LS} = 1.2 \times 10^5$ M^{-1} s^{-1}). The film dimension over which the applied potential ΔE drops is 2 μm in the IDA result and ca. 100 nm for the sandwich electrode result, a 20-fold difference. Changing sample thickness in conductivity measurements is a classical criterion for differentiating interfacial from bulk resistances, and the present result confirms that the *bulk* film resistance is the dominant effect.

Second, data in the tables, and other recent results,[22] show that agreement between $k_{ex,E,LS}$ and $k_{ex,C}$ is best, and the fitting parameter ρ is closest to its ideal value of one, when using sandwich electrodes that contain the thinnest polymer films (ρ = 3–4), as compared to sandwiches containing thicker polymer films, where ρ = 4–7. As discussed previously,[2a] if the amount of mixed-valent polymer that is actually present *between* the electrodes of a sandwich is less than that estimated from the voltammetric Γ_T, the underestimation of film thickness would appear as a multiplier of intersite voltage, i.e., as $\rho\phi$. Recent ellipsometric and scattering electron microscopic studies[23] of poly[$Os(bpy)_2(vpy)_2](X)_2$ films show that, while they are smooth and dense up to ca. 100 nm, deposition of further material tends to occur as a rough, fibrous layer, which in making the sandwich electrode is thus potentially penetrated by evaporated Au to yield a smaller effective Pt–Au interelectrode spacing, especially for the thicker films. In contrast, the IDA interelectrode spacing is predetermined by the microlithography, and the uncertainty there is a different one: whether the deposited film perfectly fills the interelectrode gap. Note that eqs 2 and 3, 4 have differing dependencies on the value of the interelectrode gap (d), and so that an error in it would cause measured $k_{ex,C}$ and $k_{ex,E}$ values to diverge. These combined observations lead us to surmise that the fitting parameter ρ, and the differences between $k_{ex,C}$ and $k_{ex,E}$ at least in part, is an artifact arising from underestimation of the exact dimensions of the thicker versions of the sandwich polymer films[24] employed in these studies. This observation does not, however, exclude contributions from other, additional, energy barrier dispersive factors as previously discussed.[2a]

Electron Transport in Dry Pt/Poly[$Os(bpy)_2(vpy)_2(BF_4)_m$/Au and Pt/Poly[$Os(vbpy)_3](BF_4)_{2.5}$/Au Sandwich Electrodes, as a Function of m and of Temperature, Using Electrical Gradients, by Fast Sweep and by Ac Impedance Methods. Previous[2a] electron transport measurements in dry Pt/poly[$Os(bpy)_2(vpy)_2$]-$(BF_4)_{2.5}$/Au sandwich films were confined to a 1:1 $C_{Os(III)}/C_{Os(II)}$ ratio. Extending these measurements to varied m, using the fast potential sweep method and eqs 3 and 5, gave results for i°, ρ, and $\sigma(i^{\circ})$ shown in Table III and Figure 4 (O). Film compositions with $C_{Os(III)}/C_{Os(II)} > 1$ were not studied. As anticipated from the Figure 2, results for poly[$Os(vbpy)_3](BF_4)_m$, the electron hopping conductivity rises as Os^{III} sites are introduced, to an apparent maximum at $C_{Os(III)}/C_{Os(II)} = 1$. Converting the i° data to $k_{ex,E,LS}$ values with eq 4 and the electrolysis potentials to mixed-valent composition with eq 7, as above, gives the results in Table III. The rate constant for the $C_{Os(III)}/C_{Os(II)} = 1$ film, $k_{ex,E,LS} = 5.6 \times 10^5$ M^{-1} s^{-1}, is in satisfactory agreement with the previous study,[2a] $k_{ex,E,LS} = 1.0 \times 10^6$ M^{-1} s^{-1}, for films prepared in an inert-atmosphere enclosure.

Conductivities were also measured by ac impedance for the same series of film compositions (Pt/poly[$Os(bpy)_2(vpy)_2$]-$(BF_4)_m$/Au with m = 2–2.5) and over a range of lowered temperatures for poly[$Os(vbpy)_3](BF_4)_{2.5}$ films where m = 2.5. The ac experiment had not previously been applied to electrical gradient driven electron hopping in these mixed-valent films, and the

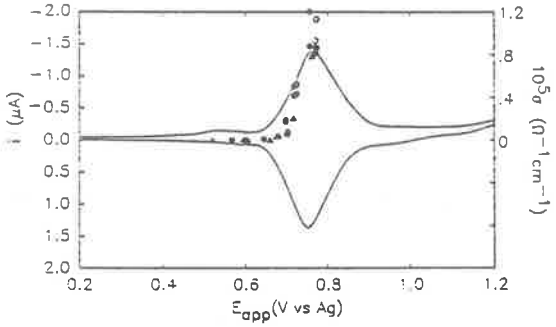

Figure 4. Cyclic voltammogram (—, 50 mV/s) for Pt/poly[$Os(bpy)_2$-$(vpy)_2(BF_4)_m$/Au sandwich, $\Gamma_T \approx 2.2 \times 10^{-8}$ mol/cm^2, in 0.1 M Bu_4NBF_4/CH_2Cl_2, and conductivities of this and a similar film after electrolyzing the film at E_{app} vs Ag and drying in N_2: (O) conductivity $\sigma(i^{\circ})$ derived from i° obtained from fast potential sweeps and fit to eq 3; (●, △, ▲) conductivity σ(ac) derived from ac impedance measurements. (O, ●, and △ are from the same film, data given in Table III.)

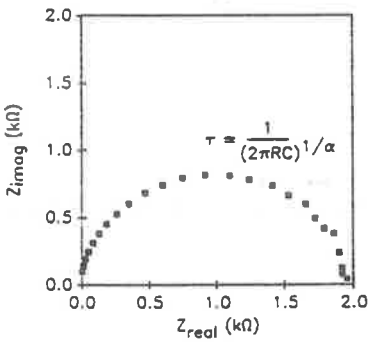

Figure 5. Cole–Cole ac impedance plot (1–10^6 Hz) for Pt/poly[$Os(bpy)_2(vpy)_2(BF_4)_{2.2}$]/Au sandwich where $\Gamma_T \approx 2.3 \times 10^{-8}$ mol/cm^2 and $C_{Os(III)}/C_{Os(II)} \approx 0.26$. The low (right-hand) frequency limit indicates an $R_b \approx 2130$ Ω, corresponding to $k_{ex,E,AC} \approx 2.8 \times 10^5$ M^{-1} s^{-1} (see entry 6, Table III), and a least-squares fit (not shown) gives C_b = 90 pF, $\alpha \approx$ 0.8, and $R_b \approx 2000$ Ω.

(22) Sosnoff, C. S. Master's Thesis, University of North Carolina, 1990.
(23) McCarley, R. L.; Thomas, R. E.; Irene, E. A.; Murray, R. W. *J. Electrochem. Soc.* **1990**, *137*, 1485.
(24) It is worth noting that error in sandwich electrode film thickness has no particular bearing on previous[2-14] investigations that depended on observing *relative* values of D_e and k_{ex} for a *given* sandwich electrode specimen as a function of environmental conditions and that emphasized a ca. 2× experimental scatter which is consistent with the present observations. These two points were made previously;[2-14] the present results serve to suggest an origin of the experimental scatter and to suggest the use of the thinnest practical film thicknesses in sandwich electrodes.

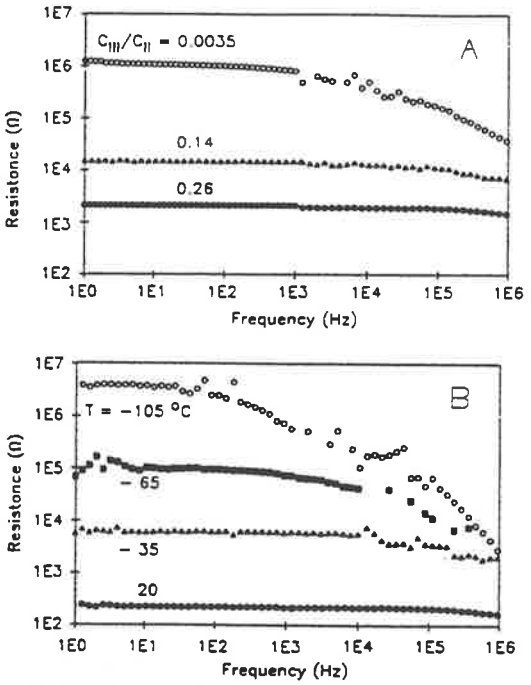

Figure 6. (A) Room temperature R_b obtained from the inverse of the real part of ac admittance (Y) of the film in Figure 5, as a function of frequency, at selected values of $C_{Os(III)}/C_{Os(II)}$; see Table III. At 20 °C, the low-frequency limiting resistance is 2200 Ω, which corresponds to $k_{ex,E,AC} \approx 2.0 \times 10^5$ M^{-1} s^{-1}. (B) R_b of a similar film ($\Gamma_T \approx 2.1 \times 10^{-8}$ mol/cm^2) at selected temperatures at $C_{Os(III)}/C_{Os(II)} \approx 1$.

purpose here was to confirm the fast potential sweep results.

Figure 5 is a representative ac impedance (Cole–Cole) plot of Z_{real} vs Z_{imag} for a room temperature Pt/poly[Os(bpy)$_2$-(vpy)$_2$](BF$_4$)$_{2.2}$/Au sandwich electrode (i.e., $C_{Os(III)}/C_{Os(II)}$ = 0.26). Results at frequencies from 1 to 10^6 Hz (increasing to the left in Figure 5) form a slightly sunken semicircle whose equivalent circuit is a parallel resistor (R_b), capacitor (C_b), and dispersive element[25] $R_b/(j\omega\tau)^{\alpha}$.[23] Following the results above, we take the resistance and capacitance to represent the bulk film properties.

The bulk resistance to electron hopping is related to conductivity by $\sigma(ac) = d/AR_b$, where d and A are film thickness and cross-section area; $\sigma(ac)$ is translated to electron-self-exchange rate constant $k_{ex,E,AC}$ with eqs 4 and 5. Values of R_b for poly-[Os(bpy)$_2$(vpy)$_2$](BF$_4$)$_m$ films are shown as a function of ac frequency in Figure 6A at room temperature and m = 2–2.62 and in Figure 6B for m = 2.5 at varied temperature. There is some decrease in the resistance at high frequency (we return to this dispersive effect below), but R_b is frequency independent at lower frequencies and strongly increases as $C_{Os(III)}/C_{Os(II)}$ becomes < 1:1 and as the film temperature decreases. The increase in R_b reflects a decrease in the electron hopping rate: the change in mixed-valent composition (presumably) effecting diminution in reactant pair population (eq 4) and the change in temperature decreasing the populations of vibronic states[2a,26] which provide the activation pathway for electron exchange.

The low-frequency R_b results, expressed as conductivity $\sigma(ac)$, are given in Table III and as (△, ▲, ●) in Figure 4. These ac data were obtained from the same poly[Os(bpy)$_2$(vpy)$_2$](BF$_4$)$_m$ films that were examined by fast potential sweeps in Table III. The $k_{ex,E,LS}$ and $k_{ex,E,AC}$ results (Table III, Figure 4) are in excellent agreement, which is gratifying in light of the different basis of

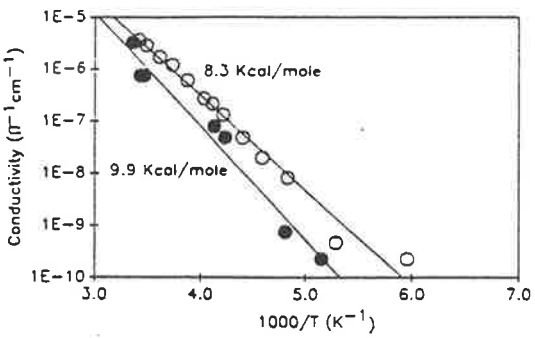

Figure 7. Arrhenius plots of $\sigma(ac)$, conductivity derived from ac impedance, in N_2 for sandwiches containing (○) poly[Os(bpy)$_2$(vpy)$_2$](BF$_4$)$_{2.5}$ at $\Gamma_T \approx 2.1 \times 10^{-8}$ mol/cm^2 ($E_A \approx 8.3$ kcal/mol (0.36 eV), $\sigma_\infty \approx 6.0$ Ω^{-1} cm^{-1}) and (●) poly[Os(vbpy)$_3$](BF$_4$)$_{2.5}$ at $\Gamma_T \approx 2.5 \times 10^{-8}$ mol/cm^2 ($E_A \approx 9.9$ kcal/mol (0.43 eV), $\sigma_\infty \approx 42$ Ω^{-1} cm^{-1}).

the two methods, one being a small-voltage-amplitude method (ac) and the other a large-amplitude one (fast potential sweep).[27]

Inspection of the Table III results for the effect of $C_{Os(III)}/C_{Os(II)}$ ratio on $k_{ex,E,AC}$ and $k_{ex,E,LS}$ for poly[Os(bpy)$_2$(vpy)$_2$](BF$_4$)$_m$ films produces much the same conclusions as drawn from the analogous Table II experiments. The electron-self-exchange rate constants seem to be independent of the $C_{Os(III)}/C_{Os(II)}$ ratio for electrolysis potentials between $E^{\circ\prime}$ and those ca. 60 mV more negative, i.e., from $C_{Os(III)}/C_{Os(II)}$ ca. 2 to 0.1. The result demonstrates that electron hopping reactions in this polymer, like poly[Os-(vbpy)$_3$](BF$_4$)$_m$, follow a bimolecular rate law over this central composition range.

As seen in Table II, the rates in Table III decrease at low $C_{Os(III)}/C_{Os(II)}$. While experiments at low $C_{Os(III)}/C_{Os(II)}$ are probably less reliable (vide supra), it is appropriate to note that analogous discrepancies are found in measurements of D_e in a poly[Os(bpy)$_2$(vpy)$_2$](ClO$_4$)$_m$ film contacted by liquid[3d] CH$_3$CN and in conductivities of films of poly(vinylferrocene)[1b,28] and of the ladder polymer[11] BBL as a function of mixed-valent composition. That is, in both solvent-wetted and dry mixed-valent polymers, the bimolecular character of the electron-self-exchange reaction is, strictly speaking, only confirmed for OX/RED values inside the range ca. 0.1–10, and thus, strictly speaking, the issue of proper bimolecular behavior outside that range remains an open question. With respect to understanding of the electronic properties of very lightly or very heavily "doped" molecular materials, this remaining issue is a significant one.

Ac results for R_b in poly[Os(bpy)$_2$(vpy)$_2$](BF$_4$)$_{2.5}$ films at low temperature (Figure 6B) show that the electron hopping rate decreases strongly at lowered temperature, are frequency-independent at low frequencies, and exhibit some dispersion at higher frequency. The low-frequency R_b results for poly[Os(vbpy)$_3$]-(BF$_4$)$_{2.5}$ and poly[Os(bpy)$_2$(vpy)$_2$](BF$_4$)$_{2.5}$ films, expressed as $\sigma(ac)$, follow Arrhenius behavior (Figure 7) as expected for thermally activated electron hopping and from previous observations[2a,b] for poly[Os(bpy)$_2$(vpy)$_2$](BF$_4$)$_{2.5}$. Figure 7 gives activation barriers $E_a \approx 8.3$ kcal/mol (0.36 eV) for poly[Os-(bpy)$_2$(vpy)$_2$][BF$_4$]$_{2.5}$, in agreement with the previous study (8.5 kcal/mol), and ≃9.9 kcal/mol (0.43 eV) for poly[Os(vbpy)$_3$]-[BF$_4$]$_{2.5}$, in agreement with the barrier (9.1 kcal/mol) derived in Figure 1B from potential sweep IDA experiments.

The ac impedance measurements also yield the bulk capacitance for poly[Os(bpy)$_2$(vpy)$_2$](ClO$_4$)$_m$ films as a function of $C_{Os(III)}/C_{Os(II)}$ = 0.003–0.26 (Figure 8A) and temperature (Figure 8B) at m = 2.5. The results show that C_b changes with mixed-valent composition and temperature, but to a quite minor degree (2–4 times) compared to the changes in R_b. (Note: R_b is displayed

(25) α measures the dispersion which can be taken as a distribution of time constants (a nondispersive element has α = 1). α in this study ranged from 0.6 to 0.8 over m = 2–2.5.

(26) (a) Holstein, T. In *Tunnelling in Biological Systems*; Chance, B., Ed.; Academic Press: New York, 1979; p 129. (b) Sutin, N. *Prog. Inorg. Chem.* **1983**, *30*, 441.

(27) While the $\sigma(i^{\circ})$ results in Table III represent the small ϕ region, they are calculated from values of i° and ρ (eqs 4 and 5) which were obtained by potential sweeps to large voltages (eq 3).

(28) Pittman, C. U.; Suryuarayanan, B.; Sasaki, Y. *Adv. Chem. Ser.* **1976**, *No. 150*, 46.

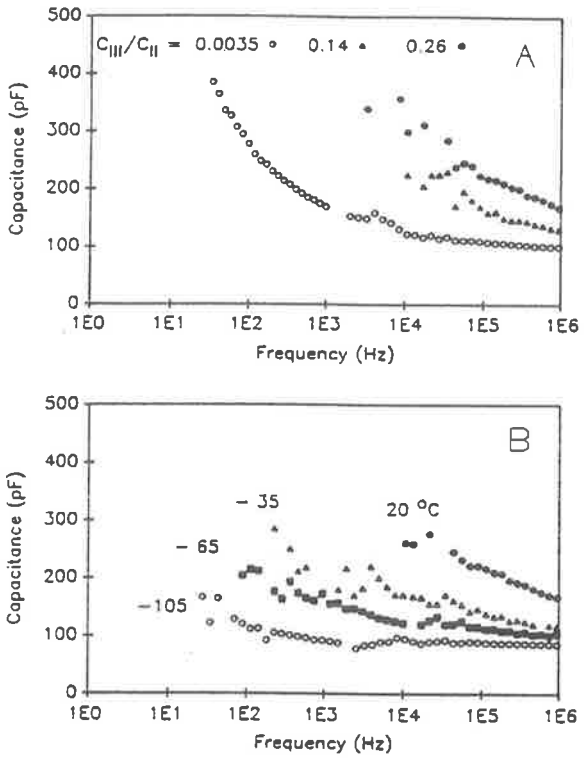

Figure 8. (A) Room temperature capacitance (Y_i/ω, where Y_i is the imaginary part of the admittance) of the film in Figure 6A, at indicated $C_{Os(III)}/C_{Os(II)}$. C_b = 90 pF, ϵ_r = 9. (B) Capacitance of the film in Figure 6B at $C_{Os(III)}/C_{Os(II)} \approx 1$ for indicated temperatures. C_b = 105 pF, ϵ_r = 10.

in Figure 6 on a log scale.) C_b approaches a high-frequency limiting value of ca. 90 pF from which the effective dielectric constant of the mixed-valent medium can be estimated as $\epsilon \approx 9$ from $\epsilon = C_b/\epsilon_0 A$, where ϵ_0 is the permittivity of free space. This value presumably represents the response of the osmium metal complex sites, and their counterions, as polarizable dipoles.

Regarding the frequency dependence in R_b and C_b seen in Figures 6 and 8, the decrease in R_b at higher frequency is most pronounced for the most resistive films, i.e., at small $C_{Os(III)}/C_{Os(II)}$ and at low temperature. Parallel electron hopping resistance and film capacitance should ideally display no such frequency dispersion, so this effect reflects some nonideal chemical process that is superimposed upon the primary dependency of R_b on composition and temperature. Given the characteristics of the ac and linear sweep methods, it appears likely that the dispersion in the ac results and the fitting parameter ρ found in the linear sweep experiments (vide supra) have common origins, such as a dispersion in the energy barrier for the electron-self-exchange reaction. As discussed before,[2a] an energy barrier dispersion could arise from structural nonidealities of the polymeric material, but until it becomes possible to systematically manipulate details of the polymer structure, it will be difficult to assess this hypothesis. Analogous dispersive effects are common in time-of-flight observations, and while they have been modeled extensively,[29] their molecular basis also remains obscure.

Conclusions

These experiments collectively show that the electron transport dynamics in Pt/poly[$Os(vbpy)_3$]$(BF_4)_m$ and poly[$Os(bpy)_2(vpy)_2$]$(BF_4)_m$ films follow a bimolecular rate law provided the film composition is within the range ca. 0.1–6 Os^{III}:Os^{II}. Further, while the electron-transfer rate behavior of Pt/poly[$Os(vbpy)_3$]$(BF_4)_{2.5}$ films is generally similar to that of the related[2a,b] poly[$Os(bpy)_2(vpy)_2$]$(BF_4)_{2.5}$ polymeric complexes, the *rates are slower in the former polymer*. The difference is by factors between 2- and 10-fold and appears in all forms of measurement: with solvent-wetted concentration gradient [$k_{ex,C} = 3 \times 10^6$ M^{-1} s^{-1} (Table I, batchs 6 and 7) vs 2×10^7 M^{-1} s^{-1},[2a] respectively, in CH_3CN], in dry N_2 with concentration gradient [$k_{ex,C} = 3 \times 10^5$ M^{-1} s^{-1} (Table I, batch 1) vs 6×10^6 M^{-1} s^{-1},[2a] respectively], or with electrical gradient [$k_{ex,E,LS} = 1 \times 10^5$ M^{-1} s^{-1} (Tables I and II) vs $k_{ex,E,LS} = 4 \times 10^5$ M^{-1} s^{-1} (Table III), $k_{ex,E,AC} = 3 \times 10^5$ M^{-1} s^{-1} (Table III), and 1×10^6 M^{-1} s^{-1},[2a] respectively]. The difference in activation barrier observed for Pt/poly[$Os(vbpy)_3$]$(X)_{2.5}$ (9.1 and 9.9 kcal/mol, Figures 1B and 7) vs poly[$Os(bpy)_2(vpy)_2$]$(X)_{2.5}$ (8.3 kcal/mol, Figure 7, and 8.3 kcal/mol[2a]) in the case of the dry films is consistent with the smaller rate constant for the ostensibly more highly cross-linked tris-vbpy polymeric complex.

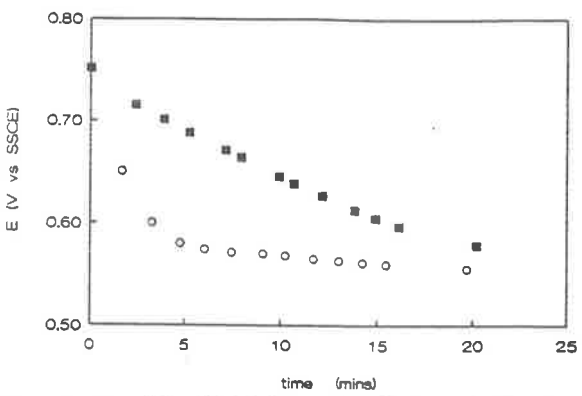

Figure 9. Potential vs SSCE of two Pt/poly[$Os(vbpy)_3$]$(BF_4)_{2.5}$/Au sandwich films, previously electrolyzed at 0.751 V vs SSCE ($E^{o\prime}$ for the $Os^{II/III}$ couple), upon exposure to 0.1 M Bu_4NBF_4/CH_2Cl_2. The areas of evaporated Au contacts exposed to the solution are 0.28 cm^2 (○) and 0.06 cm^2 (■).

Second, the environmental effects on the rate constants for both polymers, derived here and earlier,[2a-c] show that k_{ex}(liquid CH_3CN or CH_2Cl_2) > k_{ex}(vapor) > k_{ex}(dry N_2). These polymer-phase rates range from nearly equal to (in the case of poly[$Os(bpy)_2(vpy)_2$]$(BF_4)_{2.5}$ in liquid CH_3CN) to 70-fold smaller than (in the case of dry poly[$Os(vpy)_3$]$(BF_4)_{2.5}$) the k_{ex} rate constant for *monomer* $[Os(bpy)_3]^{3+/2+}$ exchange in solutions.[30] Third, we also have established[17] that the diffusivity of Cl^- counterion is smaller in acetonitrile-wetted Pt/poly[$Os(vbpy)_3$]$(BF_4)_{2.5}$, as compared to that of the, ostensibly, less highly cross-linked Pt/poly[$Os(bpy)_2(vpy)_2$]$(BF_4)_{2.5}$.

These observations are consistent with a definite influence on the electron hopping rate in the polymer of the rigidity by the polymeric matrix. Matrices which are more rigid by virtue of the absence of solvent or through enhanced cross-linking lead to slower rates. The inference drawn is that the electron-transfer hopping rate is aided by circumstances allowing some nuclear displacement of the osmium sites away from their equilibrium locations (i.e., short-range oscillations of pendant sites) and/or distortion of the vinyl polymer framework holding the sites together, and the hopping rate is slowed when polymer rigidity inhibits such displacement or distortion. That is, the polymer lattice can, under rigidified circumstances, impose an "inner-sphere"-like barrier.

Stability of Os^{III} in a Mixed-Valent Sandwich Electrode

We noted (Experimental Section) the instability of mixed-valent films when using CH_3CN rather than CH_2Cl_2 as the electrolysis solvent and when attempting to generate films where $C_{Os(III)} \gg C_{Os(II)}$. The following experiments demonstrate that Os^{III}-driven oxidation of the evaporated gold film electrode is the source of this effect. Two nominally identical Pt/poly[$Os(bpy)_2(vpy)_2$]-

(29) Abkowtiz, M.; Pai, D. M. *Philos. Mag.* **1989**, *53*, 193.

(30) Chan, M.-S.; Wahl, A. C. *J. Phys. Chem.* **1982**, *86*, 126.

$(BF_4)_{2.5}$/Au sandwiches were prepared, each containing $\Gamma_T = 2.0 \times 10^{-8}$ mol/cm^2 deposited on 0.002-cm^2 Pt wire tip electrodes, with evaporated gold overlayer contacts that covered the film and spread out onto the surrounding glass shroud to different extents (28 and 6 mm^2 of Au in area). Each sandwich was immersed in 0.1 M Bu_4NBF_4/CH_2Cl_2 and electrolyzed at $E°'$, so as to produce a mixed-valent film where $C_{Os(III)} = C_{Os(II)}$; then potentiostatic control was released, and the potential of each film (Pt electrode) vs a SSCE reference electrode was monitored vs time. In both cases, E_{film} decayed with time in a direction indicating loss of Os^{III} states (Figure 9), and the decay was *faster* for the sandwich electrode having the larger area of Au exposed to the solution. This result shows that either oxidation of Au or of some trace solution component at the Au surface occurs to discharge the Os^{III} states. The dimensions are such that less than 1×10^{-10} equiv/cm^2 of charge (less than one molecular layer) must pass across the Au/solution interface in order to completely discharge the Os^{III} layer.

Our experience indicates that effects such as Figure 9 are greatly retarded in films *dried of solvent*, which is the reason that, in preparing mixed-valent films, it is important to retain potential control of the film until it has been raised from the solution, rinsed, and dried.

Acknowledgment. This research was supported in part by grants from the National Science Foundation. We gratefully acknowledge the Pt IDA's supplied for this research by Masao Morita and Osamu Niwa of the NTT Basic Research Laboratories, Nippon Telegraph and Telephone Company, Tokai, Ibaraki, 319-11, Japan.

Registry No. Vbpy, 74173-48-1; BF_4^-, 14874-70-5; $([Os(bpy)_2(vpy)_2](BF_4)_{2-5})_x$, 138062-06-3; $([Os(vbpy)_3](BF_4)_{2-5})_x$, 138089-55-1; $[Os(vbpy)_3](PF_6)_2$, 130728-19-7; $(NH_4)_2OsCl_6$, 12125-08-5; NH_4PF_6, 16941-11-0; CH_2Cl_2, 75-09-2; CH_3CN, 75-05-8; Bu_4NBF_4, 429-42-5; $([Os(bpy)_2(vpy)_2](BF_4)_2)_x$, 138062-07-4; $([Os(vbpy)_3](BF_4)_2)_x$, 138062-08-5; Pt, 7440-06-4; Au, 7440-57-5.

Aust. J. Chem., 1995, **48**, 1425–1436

Synthesis of 4-[ω-(3-Thienyl)alkyl]pyridines and 4-[ω-(3-Thienyl)alkyl]-2,2′-bipyridines

Jiaxiong Wang,[A] *Maria Pappalardo*[A] *and F. Richard Keene*[A,B]

[A] Department of Molecular Sciences, James Cook University of North Queensland, Townsville, Qld. 4811.
[B] Author to whom correspondence should be addressed.

Abstract

The synthesis is reported of 4-[ω-(3-thienyl)alkyl]pyridine (2), 4-[ω-(3-thienyl)alkyl]-2,2′-bipyridine (3) and 4-methyl-4′-[ω-(3-thienyl)alkyl]-2,2′-bipyridine (4), where the length of the alkyl chain is varied (n = 2, 5, 7, 9, 11). The synthetic methodology involved the reaction of the 3-(ω-bromoalkyl)thiophen with the anions derived from 4-methylpyridine, 4-methyl-2,2′-bipyridine or 4,4′-dimethyl-2,2′-bipyridine by lithiation. The n.m.r. (^{1}H and ^{13}C) and electronic spectral characteristics of the compounds are discussed.

Introduction

The formation of adherent polymer films on electrode surfaces by electropolymerization of stable monomers is an important means of electrode modification.[1,2] The resultant films may vary widely in character, and be conducting (as in the case where they are derived from heterocycles such as pyrrole or thiophen) or non-conducting (for example, when they are based on a polyvinyl framework).[2] The incorporation of redox-active centres within films of both types has been achieved, with the aim of inducing specific catalytic activity, and also of probing of factors which affect the electron and ion transfer processes within the films themselves.[3–7]

Of interest in the present study was the incorporation of metallated redox-active centres in polymer-coated electrodes formed from monomers with an appended

[1] Murray, R. W., Ewing, A. G., and Durst, R. A., *Anal. Chem.*, 1987, **59**, 379A.
[2] Abruna, H. D., *Coord. Chem. Rev.*, 1988, **86**, 135.
[3] Faulkner, L. R., *Electrochim. Acta*, 1989, **34**, 1699.
[4] Garnier, F., *Angew. Chem., Int. Ed. Engl.*, 1989, **28**, 513.
[5] Surridge, N. A., Sosnoff, C. S., Schmehl, R., Facci, J. S., and Murray, R. W., *J. Phys. Chem.*, 1994, **98**, 917.
[6] Surridge, N. A., Zvanut, M. E., Keene, F. R., Sosnoff, C. S., Silver, M., and Murray, R. W., *J. Phys. Chem.*, 1992, **96**, 962.
[7] Surridge, N. A., Keene, F. R., White, B. A., Facci, J. S., Silver, M., and Murray, R. W., *Inorg. Chem.*, 1990, **29**, 4950.

Manuscript received 2 February 1995 0004-9425/95/081425$05.00

N-heterocyclic group that may act as a ligand for metal coordination. Earlier work on the introduction of redox-active centres into polymers utilized pyrrole as the basic monomer unit, and many examples of alkylated pyrroles bearing pyridyl-based ligands have been reported.[8–15] Pyrrole has proved itself to be a convenient synthetic starting point, the ease of alkylation at the nitrogen being one reason for its early popularity.

An alternative monomer unit, thiophen, has received more limited attention presumably because of the greater difficulties associated with its derivatization. Although there are a significant number of examples in the literature of thiophens alkylated at the 3-position,[16–18] there are few reports of the attachment of *N*-heterocycles to the thiophen moiety. Mirrazaei *et al.* have reported the synthesis of two 3-substituted thiophens attached to tris(2,2′-bipyridine)iron redox centres through vinyl or ether linkages between the thiophen and bipyridyl groups in the 5-position.[19] Thiophen attached to pyridine with methine and ethine linkages has recently been reported.[20]

A recent publication by Bäuerle *et al.*[21] reported the synthesis of a series of 3-(ω)-haloalkyl)thiophens (1) for $n = 4$–6, 8 and 10. These species provide access to a range of 3-substituted thiophens, including functionalization by potentially ligating species which may be attached to metal centres. We undertook the synthesis of such thiophen derivatives with *N*-heterocyclic substituent groups, where the length of the alkyl linkage between the thiophen and pyridyl (or bipyridyl) moieties was systematically varied from 2 to 11, with the ultimate aim of investigating the electrochemical characteristics of their electropolymerized films and the metallated analogues. A particular interest was the effect exerted on those properties as the alkyl bridge between the two entities was systematically lengthened. New synthetic procedures were required to produce the desirable monomers, containing either pyridyl or bipyridyl ligands attached from the 4-position of the *N*-heterocycle through a saturated alkyl chain to the 3-position of thiophen. This paper reports the synthesis of 4-[ω-(3-thienyl)alkyl]pyridine (2), 4-[ω-(3-thienyl)alkyl]-2,2′-bipyridine (3) and 4-methyl-4′-[ω-(3-thienyl)nonyl]-

[8] Mao, H., and Pickup, P. G., *J. Am. Chem. Soc.*, 1990, **112**, 1776.
[9] Cauquis, G., Cosnier, S., Deronzier, A., Galland, B., Limosin, D., Moutet, J. C., Bizot, J., Deprez, D., and Publicani, J. P., *J. Electroanal. Chem.*, 1993, **352**, 181.
[10] Collomb-Dunand-Sauthier, M.-N., Deronzier, A., and Ziessel, R., *J. Phys. Chem.*, 1993, **97**, 5973.
[11] Bidan, G., Divisia-Blohorn, B., Lapkowski, M., Kern, J.-M., and Sauvage, J.-P., *J. Am. Chem. Soc.*, 1992, **114**, 5986.
[12] Deronzier, A., and Mouet, J. C., *Acc. Chem. Res.*, 1989, **22**, 249.
[13] De Giovani, W. F., and Deronzier, A., *J. Electroanal. Chem.*, 1992, **337**, 285.
[14] De Giovani, W. F., and Deronzier, A., *J. Chem. Soc., Chem. Commun.*, 1992, 1461.
[15] Downard, A., Surridge, N., Meyer, T., Cosnier, S., Deronzier, A., and Moutet, C., *J. Electroanal. Chem.*, 1988, **246**, 321.
[16] Waltman, R. J., and Bargon, J., *Can. J. Chem.*, 1986, **64**, 76.
[17] Roncali, J., Marque, P., Garreau, R., Garnier, F., and Lemaire, M., *Macromolecules*, 1990, **23**, 1347.
[18] Grimshaw, J., and Perera, S., *J. Electroanal. Chem.*, 1990, **278**, 287.
[19] Mirrazaei, R., Parker, D., and Munro, H. S., *Macromolecules*, 1989, **23**, 1347.
[20] Efange, S. M. N., Michelson, R. H., Tan, A. K., Krueger, M. J., and Singer, T. P., *J. Med. Chem.*, 1993, **36**, 1278.
[21] Bäuerle, P., Würthner, F., and Heid, S., *Angew. Chem., Int. Ed. Engl.*, 1990, **29**, 419.

2,2′-bipyridine (4). Detailed electrochemical studies of the polymerized films will be reported subsequently.

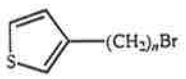

(1)

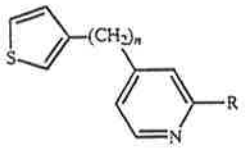

(2a–e; n = 2, 5, 7, 9, 11)

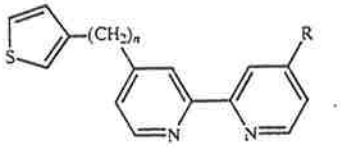

(3a–e; n = 2, 5, 7, 9, 11) R = H
(4; n = 9) R = CH_3

Results and Discussion

The key step in the syntheses of the target molecules (2)–(4) was seen to be the coupling of the thiophen and *N*-heterocyclic moieties through an alkyl chain. The decision was made to extend the chain from thiophen rather than the *N*-heterocycles after some unsuccessful preliminary Grignard and Wittig reaction trials using 4-(ω-bromoalkyl)-4′-methyl-2,2′-bipyridine. Three possible strategies were considered: (i) Wittig coupling using the triphenyl phosphonium salt derived from a ω-bromoalkyl chain extended from thiophen; (ii) catalysed coupling of Grignard reagents formed from (ω-bromoalkyl)thiophens; and (iii) coupling of (ω-bromoalkyl)thiophens with the anion formed from 4-methyl-*N*-heterocycles by lithiation.

Of these, (iii) ultimately proved the most tractable and was the preferred synthetic route. As all three strategies involved the use of a family of 3-(ω-bromoalkyl)thiophens (1) as precursors, the synthesis of (1) was an initial goal before an investigation of the coupling step was undertaken.

Synthesis of 3-(ω-Bromoalkyl)thiophen (1)

The production of (1) used the three-step synthetic pathway described by Bäuerle *et al.*[21] (Scheme 1), which allowed access to a series of homologues where the length of the alkyl chain varied with n = 4, 6, 8 or 10. Attempts were made to eliminate the protection/deprotection steps [Scheme 1, (i) and (iv)] by using α-bromo-ω-chloroalkanes in the catalysed Grignard coupling reaction [(ii) and (iii)]. It is known[22] that in haloalkanes where both bromide and chloride substituents are present, mono-Grignard formation can occur exclusively at the bromide, leaving the chloride intact, provided the alkyl chain between the halides has more than two carbon atoms. Unfortunately in the present case, the consumption of both halides was found to occur, reinforcing the utility of the protection step (i)[23] of Scheme 1 to produce (1). Both protection and deprotection steps generally proceeded with good yields (65–80%, except where n = 4), and products were easy to purify by either distillation or chromatography. A yield of 35% was obtained in the deprotection to produce 3-(ω-bromobutyl)thiophen, lower than that reported (51%) in earlier work done by Bäuerle *et al.*[21]

[22] March, J., 'Advanced Organic Chemistry' 4th Edn, (*a*) p. 623; (*b*) p. 449 (John Wiley: New York 1992).
[23] Ashley, J. N., Collins, R. F., Davis, M., and Sirett, N. E., *J. Chem. Soc.*, 1958, 3298.

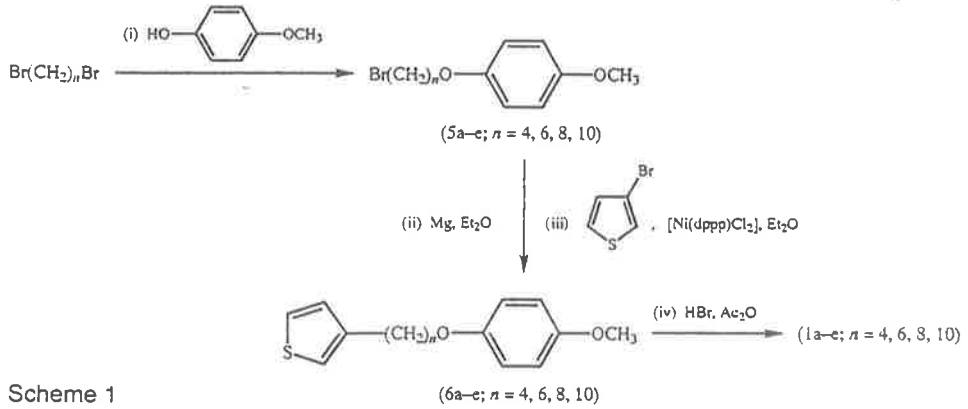

Scheme 1

The second step in Scheme 1 [the formation of the Grignard reagent (ii) and its catalysed coupling with 3-bromothiophen (iii)][21,24] gave excellent yields. Quantitative production of the Grignard reagent (based on unused magnesium) was possible as long as the magnesium had been sufficiently activated.[25] The method of activation was to rinse magnesium turnings in distilled diethyl ether, heat under vacuum to ensure dryness, and then stir overnight under an atmosphere of dry nitrogen. Slow, controlled addition of monoprotected alkyl bromide to the magnesium with constant reflux was essential to eliminate Wurtz-type[22] coupling. The second stage of the reaction (the catalysed coupling of 3-bromothiophen with the alkylmagnesium bromides) was achieved by refluxing the reagents overnight in diethyl ether in the presence of 0·1–1 mol % 1,3-bis(diphenylphosphino)propanenickel(II) chloride [Ni(dppp)Cl_2],[26] which produced the compounds (6b; $n = 4$), (6c; $n = 6$), (6d; $n = 8$) and (6e; $n = 10$) in high yields (80–97%). The lowest yield (80%) was observed for 3-[ω-(4-methoxyphenoxy)butyl]thiophen (6b), where there was a small amount of a by-product formed [ω-(4-methoxyphenoxy)but-1-ene].

The ^{1}H n.m.r. spectral data ($CDCl_3$ solvent) for the compounds (5), (6) and (1) are given in supplementary Tables S1–S3, respectively.†

It is noted that in these reactions where $n = 3$ and $n = 2$ (i.e. starting with 1,3-dibromopropane[21] and 1,2-dibromoethane), elimination was extensive during the Grignard step (ii).

An alternative strategy was used to produce the shortest alkyl chain ($n = 1$) homologue of (1). A photochemically initiated free-radical bromination of 3-methylthiophen with *N*-bromosuccinimide[27] produced the desired product (1; $n = 1$) in 78% yield. The reaction was undertaken in CCl_4, in which solvent succinimide, formed as the reaction proceeds, is insoluble and was removed by filtration. The product was found to be unstable, with slow decomposition over several days, and so was immediately used in the next stage of the synthesis.

† Copies of the supplementary Tables (Tables S1–S5) are available from the Australian Journal of Chemistry, P.O. Box 89, East Melbourne, Vic. 3002.

[24] Tamao, K., Kodama, S., Nakajima, I., Kumada, M., Minato, A., and Suzuki, K., *Tetrahedron*, 1982, **38**, 3347.
[25] Baker, K. V., Brown, J. M., Hughes, N., Skarnulis, A. J., and Sexton, A., *J. Org. Chem.*, 1991, **56**, 698.
[26] Wecke, G. R. V., and Horrocks, W. D., *Inorg. Chem.*, 1966, **5**, 1968.
[27] Futurama, S., and Zong, Z. M., *Bull. Chem. Soc. Jpn*, 1992, **65**, 345.

Synthesis of 4-Methyl-2,2′-bipyridine (Mebpy) (8)

The synthetic procedure for 4-methyl-2,2′-bipyridine (8) is shown in Scheme 2.[28–30] The principle of the method has been discussed by Kröhnke.[28] A modified method was used here, involving isolation and purification of the iodide intermediate (7)[29] as well as the addition of some water in the second step. The addition of water elevated the reflux temperature from 64 to 75–85°C and this may be a key factor in improving the yield from 10%[29] to over 50%. A further improvement was also possible for the final purification procedure through the formation of the $[Fe(Mebpy)_3]^{2+}$ complex, this facilitating the elimination of organic impurities that were otherwise difficult to remove.[30]

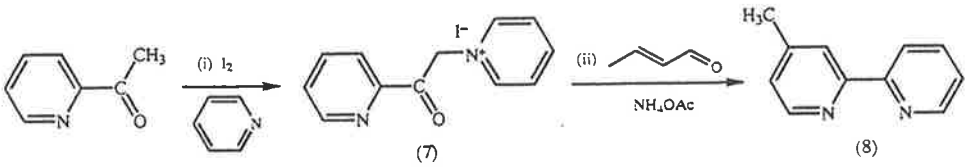

Scheme 2

Wittig Coupling of 3-(ω-Bromoalkyl)thiophens with Pyridine-4-carbaldehyde and 4′-Methyl-2,2′-bipyridine-4-carbaldehyde

Mirrazaei *et al.*[19] have utilized a Wittig coupling to produce an unsaturated bridge between thiophen and a bipyridyl moiety. In the present work, the methodology had the immediate drawback of requiring a hydrogenation step to reach the target molecule from the Wittig product. The method is shown in Scheme 3, the reaction of (1c) with pyridine-4-carbaldehyde being used as an example. Although the synthetic route was successful, yields were poor (less than 20%). The phosphonium salts proved almost intractable as they adhered to the walls of the reaction flasks, making isolation very difficult. Interestingly, in the n.m.r. spectra, the resonances for the olefinic protons were observed relatively downfield of normal olefinic protons. The proximity to the aromatic system presumably allowed delocalization of the electrons, thus causing pseudo-aromatic behaviour. Proton shifts in the n.m.r. spectra indicated that only one geometric isomer had formed, this being tentatively assigned as the *cis* isomer on the basis of the coupling values of 12 Hz.[31]

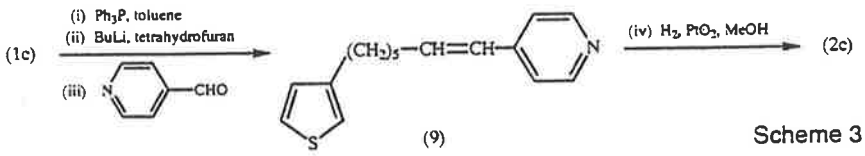

Scheme 3

[28] Kröhnke, F., *Synthesis*, 1976, 1.
[29] Treffert-Ziemelis, S. M., Golus, J., Strommen, D. P., and Kincaid, J. R., *Inorg. Chem.*, 1993, **32**, 3890.
[30] Boussie, T., personal communication.
[31] Silverstein, R. M., Bassler, G. C., and Morrill, T. C., 'Spectrophotometric Identification of Organic Compounds' 4th Edn, p. 235 (John Wiley: New York 1981).

Catalysed Coupling of the Grignard Reagent Formed from 3-(ω-Bromoalkyl)thiophens with 3-Bromopyridine

The reaction was investigated in which the Grignard reagents generated from 3-(ω-bromoalkyl)thiophens were reacted with 3-bromopyridine, in an analogous procedure to the catalysed Grignard coupling reaction in Scheme 1 [(ii) and (iii)]. Unfortunately, this method was not totally successful; ^{1}H and ^{13}C n.m.r. spectra confirmed the generation of the desired product after purification by chromatography, but the yield was very low (less than 10%) and the purification was difficult. This result was not entirely unexpected because the reactions of halopyridines with Grignard reagents generally occur in rather low yields.[32,33] Tamao *et al.* have reported the preparations of 3-butylpyridine with a yield of 47%,[24] but in the present case significantly lower yields were observed in the synthesis of 3-[ω-(3-pyridyl)butyl]thiophen. This reaction scheme was not pursued further.

Coupling of 3-(ω-Bromoalkyl)thiophens with the Carbanion Formed from 4-Methylpyridine, 4-Methyl-2,2′-bipyridine or 4,4′-Dimethyl-2,2′-bipyridine by Lithiation (Scheme 4)

This strategy proved to be the best method for coupling (1) with 4-methylpyridine, 4-methyl-2,2′-bipyridine and 4,4′-dimethyl-2,2′-bipyridine. Carbanions may be formed in high yield by deprotonation of a methyl substituent in *N*-heterocyclic ring systems by using a lithium salt of an amine anion (such as lithium diisopropylamide).[34,35] Such anions have been used extensively[35–38] for the elaboration of alkyl substituents on these systems. They react smoothly with electrophiles, and bromides are known[36] to react readily and cleanly with the lithiated methyl groups, following the mechanism of nucleophilic substitution. The highly coloured carbanions are stable for moderate periods at low temperatures. In the case of the 4,4′-dimethyl-2,2′-bipyridine, monolithiation at only one methyl group can be successfully achieved by an addition of 1 equiv. of base,[35] and allowing the reaction to stir over about 30 min. Lithiated methyl intermediates reacted readily with (1) to produce the target series of compounds.

The relative stabilities of the generated carbanions varied with the number of pyridyl rings. Whereas the 4-methylpyridine anion was stable at 0°C (orange solution), the dark purple/deep red 4-methyl-2,2′-bipyridine anions were found to require lower temperatures (−78°C) to minimize losses by adventitious quenchers before the reaction with the 3-(ω-bromoalkyl)thiophens was complete. The reaction rates of these larger carbanions were considerably slower than those of the methylpyridines. This is consistent with steric considerations[39] in a nucleophilic substitution process. There was no evidence to indicate dependence of reaction

[32] Ryang, H. S., and Sakurai, H., *J. Chem. Soc., Chem. Commun.*, 1972, 594.
[33] Wynberg, H., Van Bergan, T. J., and Kellogg, R. M., *J. Org. Chem.*, 1969, **34**, 3175.
[34] Uff, B. C., 'Comprehensive Heterocyclic Chemistry' (Eds A. R. Katritzky and C. W. Rees) Vol. 2A, p. 333 (Pergamon: Oxford 1986).
[35] Ghosh, P. K., and Spiro, T. G., *J. Am. Chem. Soc.*, 1980, **102**, 5543.
[36] Sassoon, R. E., Gershuni, S., and Rabani, J. *J. Phys. Chem.*, 1992, **96**, 4672.
[37] Griggs, C. G., and Smith, D. J. H., *J. Chem. Soc., Perkin Trans. 1*, 1982, 3041.
[38] Della, Ciana, L., Hamachi, I., and Meyer, T. J., *J. Org. Chem.*, 1989, **54**, 1731.
[39] Hartshorn, S. R., 'Aliphatic Nucleophilic Substitution' p. 33 (Cambridge University Press: London 1973).

rate on the length of the alkyl chains attached to the thiophen, again consistent with the mechanism of substitution at a primary alkyl halide. As an exception, the coupling of 3-bromomethylthiophen was markedly more rapid than the longer chained thiophens. This may be indicative of the benzylic bromide producing a cation sufficiently stabilized to allow an S_N1-type mechanism.[39] The formation of the target monomers was completed by this coupling strategy in yields that ranged from 40 to 75%.

The chemical structures of 4-[ω-(3-thienyl)alkyl]pyridines (2) and 4-[ω-(3-thienyl)alkyl]-2,2′-bipyridines (3) were analysed by ^{1}H and ^{13}C n.m.r. spectra; the resonances and their assignments are available in supplementary Tables S4 and S5. Representative data are given for the respective species with $n = 2$ and 11 in the Experimental section. The spectra of 4-[ω-(3-thienyl)undecyl]pyridine (2e; $n = 11$) are summarized as an illustrative example. In the ^{1}H spectrum, resonances at δ 8·47 and 7·07 arise from protons on the pyridine ring, and at δ 7·21, 6·92 and 6·90 from protons on the thiophen ring. In the aliphatic region, evidence of connection of thiophen to pyridine by the undecyl chain is provided by the resonances at δ 2·61 and 2·57: two close triplets are assigned to the protons attached to C 1′ (attached to thiophen) and C 11′ (attached to pyridine) of the undecyl chain, respectively. The four protons connected to C 2′ and C 10′ of the alkyl chain appear as a multiple peak centred at δ 1·61. In the ^{13}C spectrum, resonances at δ 151·5 and 143·0 are assigned to C 4″ of pyridine and C 3 of thiophen. In the undecyl chain, the C 11′ connected to pyridine ring is observed at δ 35·1, and C 1′ (connected to the thiophen ring) at δ 30·4. Signals arising from the other carbon atoms of the undecyl chain are in the range δ 29–30·1.

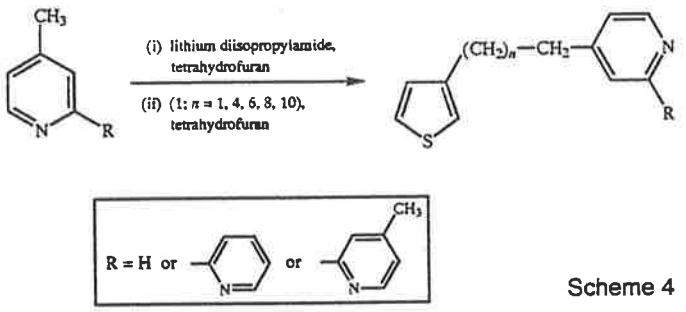

Scheme 4

In the ^{1}H n.m.r. spectrum of the analogous bipyridine derivative, (3e; $n = 11$) two protons at 6-positions of the pyridine rings appear at δ 8·69 and 8·55, downfield of the α-protons of the pyridine ring in (2e). The signal at δ 8·40, with coupling constants $^3J_{3''',4'''}$ 8·1 and $^4J_{3''',5'''}$ 0·9 Hz, is assigned to the proton at the 3‴-position. A simple peak with an insignificant split at δ 8·23 corresponds to the proton at the 3″-position of the bipyridine. These two protons are downfield of the β-protons of pyridine in (2e) because of the effect of the second pyridine ring. The resonances of the protons of the thiophen ring are similar to those observed for the 4-[ω-(3-thienyl)alkyl]pyridines. In the aliphatic region, four protons connected to C 2′ and C 10′ of the alkyl chain show a larger separation of the peaks (δ 2·69 and 2·61 respectively) compared with the equivalent protons in 4-[ω-(3-thienyl)alkyl]pyridines. The other assignments are listed in Table S4.

The ^1H and ^{13}C n.m.r. spectra of the other 4-[ω-(3-thienyl)alkyl]pyridines and 4-[ω-(3-thienyl)alkyl]-2,2′-bipyridines may be rationalized in a similar manner. $^1H,^1H$-COSY two-dimensional and $^1H,^{13}C$-correlated two-dimensional n.m.r. spectra confirmed the connectivities given in supplementary Tables S4 and S5.

Ultraviolet Spectroscopic Analysis of 4-[ω-(3-Thienyl)alkyl]pyridines (2) and 4-[ω-(3-Thienyl)alkyl]-2,2′-bipyridines (3)

In 4-[ω-(3-thienyl)alkyl]pyridines (2), absorptions arising from $\pi \rightarrow \pi^*$ transitions occur with λ_{max} at 194–196, 204–210 and 238 nm, with a shoulder at 264 nm, in acetonitrile solution. For (3), λ_{max} are observed at 212, 240 and 275 nm, with two shoulders at 194–196 and 286–288 nm. Thiophen has been reported to have λ_{max} at 204–220 and 221–260 nm (in hexane),[40–42] and pyridine at 256 and 281 nm (shoulder) in cyclohexane.[43] Because of the effect of the alkyl chain, the $\pi \rightarrow \pi^*$ bands of (2) and (3) are shifted to longer wavelengths, consistent with a previous report.[43] There do not appear to be significant dependencies of λ_{max} on the length of alkyl chain for either series, particularly (3).

Conclusions

A methodology has been developed for the synthesis of (2)–(4) with different alkyl chain lengths in the range $n = 2$–11, involving the reaction of the appropriate 3-(ω-bromoalkyl)thiophen with the carbanions derived from 4-methylpyridine, 4-methyl-2,2′-bipyridine or 4,4′-dimethyl-2,2′-bipyridine by lithiation. The products have been characterized by ^1H and ^{13}C n.m.r. spectroscopy.

Experimental

Materials

For Grignard reactions, magnesium turnings (AJAX) were washed sequentially with 1 M HCl (twice), H_2O, ethanol and dry diethyl ether (Et_2O), dried overnight under vacuum at 100°C, then stirred for 2 days under dry nitrogen at room temperatures.[25] Dry Et_2O was refluxed and distilled from sodium benzophenone ketyl prior to use. 1,3-Bis(diphenylphosphino)propanenickel(II) chloride ([Ni(dppp)Cl_2]; Strem) and ω-(*p*-methoxyphenoxy)alkyl bromides were dried under vacuum. 3-Bromothiophen (Aldrich) and 4-methylpyridine (Aldrich) were distilled and stored over 4 Å molecular sieves. *N*-Bromosuccinimide (Fluka) was recrystallized from hot water and dried under vacuum. Pyridine (AJAX; L.R.) was freshly distilled under nitrogen from KOH onto 5 Å molecular sieves. All the solvents used for recrystallization and chromatography were distilled prior to use. The light petroleum used had a boiling point range of 40–60°C. All solvents for synthesis, except CCl_4 (M & B; A.R. grade), were of laboratory grade and used without further purification. Acetonitrile (Fluka; for u.v. spectroscopy) was used without further purification. 2-Acetylpyridine (Aldrich; 99+%), crotonaldehyde (Aldrich; 99+%), iodine (Aldrich; 99·8%), ammonium acetate (BDH; A.R.), acetic anhydride (Aldrich; 99+%) and hydrobromic acid (Aldrich; 48%) were used without further purification. Butyllithium (Aldrich) and lithium diisopropylamide mono(tetrahydrofuran) (Aldrich) were purchased as solutions in cyclohexane, and the concentrations checked by titration against 2,2,2′-trimethylpropionanilide. Aluminium oxide (Fluka Type 507C, neutral; Aldrich activated basic Brockmann 1) and silica gel (Merck; Kieselgel 60H) were used for chromatography.

4-Methyl-2,2′-bipyridine (Mebpy) (8) was synthesized as described elsewhere.[29,30]

[40] Menczel, S., *Z. Phys. Chem.*, 1927, **125**, 161.
[41] Braude, E. A., *Ann. Rep. Progr. Chem.*, 1945, **42**, 105.
[42] Leandri, G., Mangini, F., Montanari, F., and Passerini, R., *Gazz. Chim. Ital.*, 1955, **85**, 769.
[43] Halverson, F., and Hirt, R. C., *J. Chem. Phys.*, 1951, **19**, 711.

Spectroscopic Measurements

^{1}H (300 MHz) and ^{13}C (75 MHz) n.m.r. spectra were recorded on a Bruker AM300 Fourier-transform spectrometer. U.v./vis. spectra were recorded by using an HP 8452A Diode Array spectrophotometer.

Syntheses

ω-(4-Methoxyphenoxy)alkyl Bromides (5b–e; n = 4, 6, 8, 10)

The syntheses followed literature procedures.[21,23] The compounds (5b) [73% yield, b.p. 129–130°C/0·3 mm, m.p. 41–42°C (lit.[23] 42–44°C)] and (5c) [80% yield, b.p. 148–150°C/0·3 mm, m.p. 49–50°C (lit.[44] 47°C)] were purified by distillation. The reaction mixtures for (5d,e) were distilled to remove the dibromides, and the residues recrystallized from n-hexane (A.R.). Filtration realized white crystals which were dried under high vacuum at 45°C for several days: (5d), yield 67%, m.p. 54–55°C; (5e), yield 72%, m.p. 62–63°C (lit.[45] 61–62°C). The ^{1}H n.m.r. spectral data of (5b–e) are available in supplementary Table S1.

3-[ω-(4-Methoxyphenoxy)alkyl]thiophens (6b–e; n = 4, 6, 8, 10)

All glassware was dried at 130° overnight and cooled in a desiccator prior to use. Reactions were performed under high purity nitrogen. Compound (5) (0·11 mol) in dry Et_2O (300 cm^3) was added to magnesium turnings (5·4 g, 0·22 mol) in dry Et_2O (50 cm^3) over 5–6 h, with stirring and gentle refluxing of the solution. The reaction mixture was then refluxed for 1 h. The Grignard solution of (5) was subsequently transferred via cannula to another dried apparatus and added dropwise at 0°C to a mixture of [Ni(dppp)Cl$_2$] (0·3 g, 0·5 mol %) and 3-bromothiophen (19·5 g, 0·12 mol) over 1 h. The reaction mixture was refluxed for 12–15 h. The resultant solution was hydrolysed with an iced aqueous solution of 0·2 M HCl (200 cm^3) at 0°C followed by extraction with several portions of Et_2O. The organic phase was washed to neutrality with water and dried with anhydrous sodium sulfate before the solvent was removed under vacuum giving a yellowish-white material which was recrystallized from hexane or methanol to give (6). Yields: (6b) (77%); (6c) (90%), (6d) (96%), (6e) (97%). The low melting point compounds were characterized by comparison of their ^{1}H n.m.r. spectra (supplementary Table S2) with those reported in the literature.[21]

3-(ω-Bromoalkyl)thiophens (1b–e; n = 4, 6, 8, 10)

The syntheses followed a method modified from that described by Bäuerle *et al.*[21] Acetic anhydride (112 g, 1·1 mol) was added to 48% HBr (76 cm^3, 0·67 mol) dropwise with stirring at 0°C. This mixture was then added to (6) (0·112 mol) under nitrogen, and the reaction mixture was heated at 100°C for 20–25 h. After dilution with water, the mixture was extracted with Et_2O. The combined organic phase was washed to neutrality with saturated $NaHCO_3$ solution and dried over anhydrous Na_2SO_4. After removal of solvent, a mixture of Et_2O and light petroleum was added until a dark green precipitate formed. After cooling, the precipitate was filtered off, and the filtrate reduced to a small volume. The crude product was purified by column chromatography [silica gel (7×10 cm); eluent light petroleum]. Removal of solvent provided white crystals [(1b) yield 35%] or colourless oils [(1c) (65%), (1d) (70%), (1e) (71%)] as the product. The compounds were characterized by comparison of their ^{1}H n.m.r. spectra (supplementary Table S3) with those reported in the literature.[21]

3-Bromomethylthiophen (1a; n = 1)

A mixture of *N*-bromosuccinimide (4·45 g, 25 mmol) and CCl_4 (80 cm^3) was added gradually over 0·5 h to a vigorously refluxed solution of 3-methylthiophen (2·03 g, 21 mmol) in CCl_4 (10 cm^3) with irradiation by a 100 W sun lamp and under an inert atmosphere. The mixture was refluxed under irradiation for 40 min until no more precipitate formed. The resultant solution was cooled in an ice bath before the succinimide was filtered off and the filtrate was dried with calcium carbonate. The product was distilled under N_2 from calcium carbonate and collected (yield 78%) at 96–99°C/2·3 mm (lit.[46] 75–78°C/1 mm). The ^{1}H

[44] Korte, H., Schumacher, H., Klein, W., and Daffertshofer, *Tetrahedron*, 1968, **24**, 5601.
[45] Ziegler, K., and Weber, H., *Chem. Ber.*, 1937, **70**, 1275.
[46] Rabjohn, N., (Ed.) *Org. Synth.*, 1963, Coll. Vol. 4, 921.

and ^{13}C n.m.r. spectra are available in supplementary Table S3. The pure product (colourless oil) may be stored under N_2 in a refrigerator for only 2–3 days.

4-[ω-(3-Thienyl)heptyl]pyridine (2c)

A solution of Ph_3P (10·1 g, 41 mmol) in toluene (30 cm^3) was added to (1c) (1·03 g, 4·2 mmol) in toluene (10 cm^3) under nitrogen. The mixture was heated to reflux overnight. The sticky phosphonium salt (1·07 g, 51%) was filtered off, washed with cold toluene and light petroleum (b.p. 60–80°C), and dried under vacuum. To a solution of this salt (0·87 g, 1·71 mmol) in dry tetrahydrofuran (40 cm^3) was added butyllithium (1·13 cm^3 of 1·2 M solution in cyclohexane; 1·71 mmol) via syringe under nitrogen at −78°C. The mixture was stirred for about 30 min, then 0·163 cm^3 (1·71 mmol) of pyridine-4-carbaldehyde was added via syringe and the reaction mixture was stirred for 1 h at −78°C before the temperature was allowed to rise to room temperature and the reaction was stirred for a further 5 h. The reaction mixture was quenched with water (40 cm^3) at 0°C and extracted with Et_2O. The organic phases were combined and dried over anhydrous Na_2SO_4 before removal of the solvent provided yellow crystals as a crude product. The crystals were purified by column chromatography (alumina, $CHCl_3$/light petroleum, 1:1). Removal of solvent provided 4-[ω-(3-thienyl)hept-1-enyl]pyridine (9) (90 mg) as a light yellow powder (19%).

A reaction flask, charged with this compound (46 mg, 0·17 mmol) and PtO_2 (1 mg) in MeOH (15 cm^3), was evacuated, purged with hydrogen and maintained under a slight positive pressure of hydrogen by using a balloon. The reaction mixture was stirred at room temperature for 10 h before being filtered through a pad of Celite to remove the catalyst. Evaporation of solvent under vacuum gave 43 mg (95%) of (2c) as light yellow crystals. The ^1H n.m.r. spectrum is reported in supplementary Table S4.

4-[ω-(3-Thienyl)alkyl]pyridines (2a,b,d,e; n = 2, 5, 9, 11)

All glassware was dried at 130°C overnight and cooled in a desiccator prior to use. To a stirred solution of lithium diisopropylamide mono(tetrahydrofuran) (10 cm^3 of 1·5 M; 15 mmol) in dry tetrahydrofuran (14 cm^3) at 0°C, 4-methylpyridine (1·4 cm^3, 14·3 mmol) was added dropwise under nitrogen over 10 min. The resultant orange mixture was stirred over 50 min at 0°C. To this solution, 3-(ω-bromoalkyl)thiophen, (1), (8·0 mmol; dried under high vacuum) in tetrahydrofuran (12 cm^3) was added dropwise at 0°C over 15 min. The resultant darker mixture was stirred at 0°C for 3–6 h before the temperature was allowed to rise gradually to room temperature. The reaction was stopped for (2a) after 3 h reaction at 0°C. With long chain 3-(ω-bromoalkyl)thiophens the solution was allowed to remain stirring at room temperature under nitrogen for longer periods (e.g. overnight). The resultant solution was hydrolysed with water (30 cm^3) added dropwise at 0°C, followed by extraction with Et_2O. The organic phases were dried with anhydrous sodium sulfate and the solvent was removed under vacuum to afford yellowish-white solids. Crude products were purified by column chromatography (neutral alumina; $CHCl_3$/light petroleum, 2:5). The R_F of the products was *c.* 0·6 on t.l.c. (alumina) with the same eluent. Removal of solvent gave yellow pure liquids of (2b) (70%), (2d) (81%) and (2e) (60%). Following solvent removal, (2a) (61%) was further purified by distillation (b.p. 102–104°C/0·2 mm) to give a yellow crystalline *solid* (m.p. 74–75°C) (Found for (2a): C, 69·7; H, 5·9; N, 7·2. $C_{11}H_{11}NS$ requires C, 69·8; H, 5·9; N, 7·4%. Found for (2b): C, 72·7; H, 7·3; N, 5·5. $C_{14}H_{17}NS$ requires C, 72·7; H, 7·4; N, 6·0%. Found for (2d): C, 75·7; H, 7·9; N, 4·5. $C_{18}H_{25}NS$ requires C, 75·2; H, 8·8; N, 4·9%. Found for (2e): C, 76·2; H, 9·3; N, 3·9. $C_{20}H_{29}NS$ requires C, 76·1; H, 9·3; N, 4·4%).

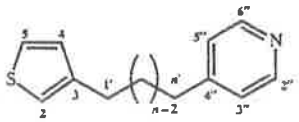

For (2a): δ_H (300 MHz, $CDCl_3$) 8·48, 2H, dd, $J_{2'',3''}$ 4·51, $J_{2'',5''}$ 1·46 Hz, H 2″,6″; 7·24, 1H, dd, $J_{5,4}$ 4·81, $J_{5,2}$ 2·91 Hz, H 5; 7·08, 2H, d, $J_{3'',2''}$ 5·89 Hz, H 3″,5″; 6·92, 1H, dd, $J_{4,5}$ 4·98, $J_{4,2}$ 1·23 Hz, H 4; 6·90, 1H, dd, $J_{2,5}$ 2·50, $J_{2,4}$ 1·28 Hz, H 2′; 2·95, 2H, t, $J_{1,2}$ 3·41 Hz, H 1′; 2·93, 2H, t, $J_{2,1}$ 3·35 Hz, H 2′.

For (2e): δ_H (300 MHz, $CDCl_3$) 8·47, 2H, d, $J_{2'',3''}$ 5·28 Hz, H 2'',6''; 7·21, 1H, dd, $J_{5,4}$ 4·77, $J_{5,2}$ 3·08 Hz, H 5; 7·07, 2H, d, $J_{3'',2''}$ 5·54 Hz, H 3'',5''; 6·92, 1H, dd, $J_{4,5}$ 5·03, $J_{4,2}$ 1·10 Hz, H 4; 6·90, 1H, dd, $J_{2,5}$ 2·51, $J_{2,4}$ 1·61 Hz, H 2; 2·61, 2H, t, $J_{1',2'}$ 7·59 Hz, H 1'; 2·57, 2H, t, $J_{11',10'}$ 8·09 Hz, H 11'; 1·61, 4H, m, $J_{2',1'}$ 6·45, $J_{10',11'}$ 7·02 Hz, H 2',10'; 1·35–1·20, 14H, m, H 3',4',5',6',7',8',9'. δ_C (75 MHz, $CDCl_3$) 151·6, C 4''; 149·4, C 2'', 6''; 143·0, C 3; 128·1, C 4; 124·9, C 5; 123·7, C 3'',5''; 119·6, C 2; 35·1, C 11'; 30·4, C 1'; 30·1, C 2',10'; 29·4, C 3',4',5',7',8',9'; 29·0, C 6'. The ^1H and ^{13}C n.m.r. spectra of (2a–e) are given in supplementary Table S4.

1-[2-Oxo-2-(2-pyridyl)ethyl]pyridinum Iodide (7)

This compound was synthesized by using a modification of literature procedures.[28] To a solution of 2-acetylpyridine (8·4 g, 0·4 mol) in dry pyridine (100 cm^3) was added a solution of iodine (101·5 g, 0·4 mol) in the same solvent (300 cm^3) at 20°C. The reaction mixture was refluxed for 3 h under nitrogen, then the heating bath was removed and the reaction mixture was allowed to stand overnight. The crude crystals were filtered off, washed with pyridine, and dried under suction. The crude crystals were recrystallized from ethanol (2·7 litre), to which active charcoal (40 g) was added; after the mixture was refluxed for 1 h, it was filtered through Celite and the filtrate was cooled (4°C) overnight, producing light yellow shining crystals (yield 58·5 g, 45%), m.p. 197–198°C (lit.[47] 198–199°C). δ_H (300 MHz, CD_3CN) 8·79, 1H, dt, $J_{6',5'}$ 4·6, $J_{6',4'}$ 1·1 Hz, H 6'; 8·73, 2H, dd, $J_{2,3}$ 5·5, $J_{2,4}$ 1·2 Hz, H 2,6; 8·64, 1H, tt, $J_{4,3}$ 7·8, $J_{4,5}$ 7·6, $J_{4,6}$ 1·2 Hz, H 4; 8·13, 2H, t, $J_{3,2}$ 7·2, $J_{3,4}$ 7·1 Hz, H 3,5; 8·06, 1H, t, $J_{4',3'}$ 2·5, $J_{4',2'}$ 1·3 Hz, H 4'; 8·04, 1H, d, $J_{3',4'}$ 1·6 Hz, H 3', 7·72, 1H, m, H 5'; 6·41, 2H, s, CH_2. δ_C (75 MHz, CD_3CN) 192·0, C=O; 151·4, C 2'; 150·6, C 6'; 147·6, C 4; 147·0, C 2,6; 138·9, C 4', 130·1, C 5'; 129·0, C 3,5; 123·2, C 3'; 67·6, CH_2.

4-Methyl-2,2'-bipyridine (Mebpy) (8)

The title compound was synthesized from (7) by using literature procedures.[29,30] The crude solid was sublimed at 80°C/0·1 mm to give a white crystalline solid (yield 51%), m.p. 65·5–66°C (lit.[29] 63–64°C) (Found: C, 77·6; H, 6·0; N, 16·6. $C_{11}H_{10}N_2$ requires C, 77·7; H, 5·9; N, 16·5%). δ_H (300 MHz, $CDCl_3$) 8·66, 1H, dt, $J_{6',5'}$ 4·96, $J_{6',4'}$ 1·15 Hz, H 6'; 8·53, 1H, d, $J_{6,5}$ 4·9 Hz, H 6, 8·39, 1H, dt, $J_{3',4'}$ 8·0, $J_{3',5'}$ 1·0 Hz, H 3', 8·23 1H, t, $J_{3,5}$ 0·9 Hz, H 3, 7·82; 1H, dt, $J_{4',3'}$ 7·7, $J_{4',5'}$ 7·6, $J_{4',6'}$ 1·7 Hz, H 4'; 7·33–7·26, 1H, m, H 5'; 7·15, 1H, dd, $J_{5,6}$ 4·8, $J_{5,3}$ 1·1 Hz, H 5; 2·44, 3H, s, CH_3. δ_C (75 MHz, $CDCl_3$) 156·5, C 2'; 155·9, C 2; 149·1, C 6'; 140·0, C 6; 148·1, C 4; 136·9, C 4'; 124·7, C 3; 123·6, C 3'; 121·9, C 5; 121·2, C 5'; 21·2, CH_3.

4-[ω-(Thienyl)alkyl]-2,2'-bipyridines (3a–e; n = 2, 5, 7, 9, 11)

Butyllithium (6·74 cm^3 of 1·9 M solution in cyclohexane, 12·8 mmol) was added dropwise via syringe to diisopropylamide (1·79 cm^3, 12·8 mmol) in dry tetrahydrofuran (15 cm^3) at −78°C under nitrogen. The mixture was stirred for 10 min at −78°C before a solution of (8) (2·0 g, 11·76 mmol) in dry tetrahydrofuran (10 cm^3) was added dropwise via syringe to the reaction mixture at −78°C. The resultant dark purple solution was stirred for 50 min at −78°C before (1a–e) (13·0 mmol) in dry tetrahydrofuran (10 cm^3) was added over 10 min. The mixture was stirred for a further 1 h at −78°C, after which the temperature was allowed to rise gradually to room temperature. After stirring for a further 1–3 days (until the mixture changed colour to yellow or light brown), the reaction was quenched with 5% aqueous NH_4Cl solution at 0°C then extracted with Et_2O (3×50 cm^3). The organic layers were combined and dried over anhydrous Na_2SO_4. Removal of solvent provided a yellow oil as the crude product, which was purified by column chromatography on basic alumina (eluent chloroform/light petroleum, 2:5). The R_F of the products was 0·58 (3c) on t.l.c. (alumina) with the same eluent. Following removal of solvent, the residue was found to contain some of the starting material (7), which was readily removed by sublimation. The pure products were obtained as crystalline materials [light yellow for (3a) (yield 71%), m.p. 72–73°C; white for (3e) (yield 59%), m.p. 41–42°C)] or colourless oils [(3b) (yield 52%), (3c) (yield 69%), (3d) (yield 74%)] (Found for (3a): C, 71·8; H, 5·0; N, 10·1. $C_{16}H_{14}N_2S$ requires C, 72·2; H, 5·3; N, 10·5%. Found for (3b): C, 74·3; H, 6·2; N, 9·4. $C_{19}H_{20}N_2S$ requires C, 74·0; H, 6·5; N, 9·5%.

[47] Kröhnke, F., and Gross, K. F., *Chem. Ber.*, 1959, **92**, 22.

Found for (3c): C, 75·2; H, 7·3; N, 7·8. $C_{21}H_{34}N_2S$ requires C, 75·0; H, 7·2; N, 8·3%. Found for (3d): C, 75·6; H, 7·8; N, 7·4. $C_{23}H_{28}N_2S$ requires C, 75·8; H, 7·70; N, 7·7%. Found for (3e): C, 76·4; H, 8·6: N, 6·9. $C_{25}H_{32}N_2S$ requires C, 76·5; H, 8·2; N, 7·1%).

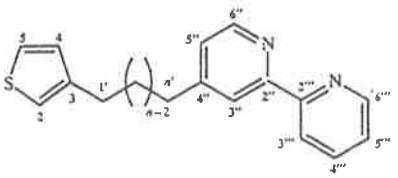

For (3a): δ_H (300 MHz, $CDCl_3$) 8·70, 1H, dt, $J_{6''',5'''}$ 4·9, $J_{6''',4'''}$ 1·1 Hz, H6‴; 8·56, 1H, d, $J_{6'',5''}$ 4·9 Hz, H6″; 8·40, 1H, dt, $J_{3''',4'''}$ 8·2, $J_{3''',5''}$ 1·0 Hz, H3‴; 8·28, 1H, t, $J_{3'',5''}$ 0·9 Hz, H3″; 7·82, 1H, td, $J_{4''',3'''}$ 7·7, $J_{4''',5'''}$ 7·7, $J_{4''',6'''}$ 1·8 Hz, H4‴; 7·34–7·29, 1H, m, H5‴; 7·28–7·25, 1H, m, H5; 7·10, 1H, dd, $J_{5'',6''}$ 4·9, $J_{5'',3''}$ 1·7 Hz, H5″; 6·96, 1H, dd, $J_{4,5}$ 4·8 Hz, H4; 6·94, 1H, dd, $J_{2,5}$ 2·8 Hz, H2; 3·03, 4H, t, H1′,2′. δ_C (75 MHz, $CDCl_3$) 156·2, C2‴; 156·1, C2″; 151·5, C4″; 149·1, C6‴; 149·1, C6″; 141·2, C3; 136·9, C4‴; 128·0, C4; 125·6, C5; 123·9, C2; 123·7, C3‴; 121·2, C5‴; 121·0, C3″; 120·6, C5″; 36·4, C2′; 31·0, C1′.

For (3e): δ_H (300 MHz, $CDCl_3$) 8·69, 1H, dt, $J_{6''',5'''}$ 4·9, $J_{6''',4'''}$ 1·0 Hz, H6‴; 8·55, 1H, dd, $J_{6'',5''}$ 5·0 Hz, H6″; 8·40, 1H, dt, $J_{3''',4'''}$ 8·1, $J_{3''',5'''}$ 0·9 Hz, H3‴; 8·23, 1H, t, H3″; 7·81, 1H, td, $J_{4''',3'''}$ 7·6, $J_{4''',5'''}$ 7·5, $J_{4''',6'''}$ 1·7 Hz, H4‴; 7·33–7·28, 1H, m, H5‴; 7·22, 1H, dd, $J_{5,4}$ 4·9, $J_{5,2}$ 3·0 Hz, H5; 7·15, 1H, dd, $J_{5'',6''}$ 4·9, $J_{5'',3''}$ 1·4 Hz, H5″; 6·94, 1H, dd, $J_{4,5}$ 6·2, $J_{4,2}$ 0·9 Hz, H4; 6·92, 1H, dd, $J_{2,5}$ 2·4, $J_{2,4}$ 1·0 Hz, H2; 2·69, 2H, t, $J_{1',2'}$ 7·5 Hz, H1′; 2·61, 2H, t, $J_{11',10'}$ 7·6 Hz, H11′; 1·70, 2H, m, H2′; 1·61, 2H, m, H10′; 1·40–1·20, 14H, m, H3′–9′. δ_C (75 MHz, $CDCl_3$) 156·3, C2‴; 155·9, C2″; 152·9, C4″; 149·1, C6″,6‴; 143·2, C3; 136·9, C4‴; 128·3, C4; 125·0, C5; 124·0, C2; 123·6, C3‴; 121·2, C5‴; 121·1, C3″; 119·7, C5″; 35·5, C11′; 30·5, C1′; 30·4, C10′; 30·2, C2′; 29·5, C6′; 29·5, C3′,9′; 29·4, C4′,8′; 29·3, C5′,7′.

The ^1H and ^{13}C n.m.r. data for (3a–e) are given in supplementary Table S5.

4-Methyl-4′-[ω-(3-thienyl)]nonyl]-2,2′-bipyridine (4)

A solution of butyllithium in hexane (11·9 cm^3, 1·5 M, 1 equiv.) was added to diisopropylamine (2·52 cm^3, 1·1 equiv.) in tetrahydrofuran (20 cm^3) at −78°C and the mixture was stirred for 10 min before being transferred slowly via cannula to a solution of 4,4′-dimethyl-2,2′-bipyridine (3·3 g, 1 equiv.) in tetrahydrofuran (100 cm^3) at −78°C. After 30 min, (1d) (5 g) dissolved in tetrahydrofuran (50 cm^3) was added, and the reaction was allowed to gradually rise to room temperature. Stirring was continued for 2 days before the reaction mixture was quenched with 10% $NaHCO_3$ solution and extracted with Et_2O. The organic extracts were washed with a saturated solution of $NaHCO_3$ before being dried with anhydrous sodium sulfate. Removal of solvent afforded a light yellow solid which was purified by column chromatography on neutral alumina (ethyl acetate eluent). Recrystallization from acetonitrile gave (4) as a white *powder* (3·3 g, 49%), m.p. 45·5–46·0°C (Found: C, 76·4; H, 7·80; N, 7·8. $C_{24}H_{30}N_2S$ requires C, 76·1; H, 8·00; N, 7·4%). δ_H (300 MHz, $CDCl_3$) 8·54, 2H, t, J 4·6 Hz; 8·2, 2H, s; 7·22, 1H, br m, J 1 Hz; 7·13, 2H, d, J 4·6 Hz; 6·93, 1H, d, $J < 1$ Hz; 6·90, 1H, d, $J < 1$ Hz; 2·68, 2H, d, J 3·5 Hz; 2·60, 2H, t, J 7·6 Hz; 2·44, 3H, s; 1·72, 2H, br t, J 6·4 Hz; 1·65, 2H, br t, J 7·3 Hz, 1·23, 10H, br m. δ_C (75 MHz, $CDCl_3$) 156·1; 152·9; 148·9; 148·1; 143·0; 128·2; 125·0; 124·6; 123·9; 122·0; 121·3; 119·7; 35·5; 30·5; 30·4; 30·2; 29·4; 29·3; 21·2.

Acknowledgments

This research was supported by the Australian Research Council. We thank Dr George Meehan and Mr Laurie Kelso for their assistance, and Dr Tom Boussie (University of North Carolina) for providing details of the improved synthesis of Mebpy (8) prior to publication. J.W. wishes to acknowledge the Australian International Development Assistance Bureau for an Australian Development Cooperation Scholarship Scheme scholarship and James Cook University for a postgraduate research award for overseas students.

ELSEVIER

Journal of Electroanalytical Chemistry 405 (1996) 59–70

JOURNAL OF ELECTROANALYTICAL CHEMISTRY

Electrochemical properties of poly[3-(ω-4-pyridylalkyl) thiophenes]

Jiaxiong Wang, F. Richard Keene *

Department of Chemistry and Chemical Engineering, School of Molecular Sciences, James Cook University of North Queensland, Townsville, Qld. 4811, Australia

Received 29 June 1995; in revised form 28 September 1995

Abstract

Poly[3-(ω-4-pyridylalkyl)thiophenes] (P{P(*n*)T}; *n* = 2, 5, 7, 9, 11) were prepared on the surfaces of Pt disk electrodes by oxidative electropolymerization of the respective monomers. Scanning electron microscopy and cyclic voltammetry were used to investigate the surface structure and electrochemical properties of the polymer-modified electrodes. Apparent diffusion coefficients D_{app} for charge transfer in the polymer matrices were measured by chronoamperometry, and revealed a dependency on both the porous structure of the polymers (which is determined by the length of the alkyl chains between thiophene and pyridyl groups), and the nature of the supporting electrolytes. A.c. impedance spectra depended on the doped state of the films and the nature of the supporting electrolytes. In oxidized polymers, the charge transfer processes within the bulk polymers and at interfaces are controlled by both kinetic factors and diffusion, while for the reduced films kinetic factors predominate.

Keywords: Poly[3-(ω-4-pyridylalkyl)thiophenes]; Electrochemical properties

1. Introduction

The electropolymerization of thiophene and its derivatives has been extensively studied because of the particular properties of the resultant films — notably, their conducting nature and the potential for structural versatility arising from functionalization of the monomer precursor [1]. The predominant electrochemical activity of such films occurs in the anodic region, although there have been recent reports of substituted polythiophenes which also exhibit activity in the cathodic region [2–7]. In this latter case, the thiophenes all possessed aromatic groups within the substituents. The details of the electrochemical behavior are still unclear, possibly as a consequence of the complexity of the charge transfer process in the reduced polymers since an electroactive group is located in the side chain.

An understanding of the charge transfer characteristics of such films is fundamental to their ultimate application. Accordingly, quantitative measurements of charge and ion transport rates, and factors controlling such transport, are of particular interest. In most films, charge transport is thought to occur both by electron self-exchange reactions between the neighboring oxidized and reduced sites ("electron hopping") and by ion transport through the film to achieve charge neutrality [8,9], and either process can be rate-controlling for overall charge transport.

A charge transport process is mathematically representable by Fick's diffusion laws, where the diffusion coefficient D_{ct} is indicative of its rate. Owing to the contribution to externally applied current from both electron hopping and ion motions, the experimentally measured apparent diffusion coefficient D_{app} in the polymer consists of a combination of electron self-exchange and physical diffusion of the counter ions. Some studies indicate that ion diffusion coefficients D_i and electron diffusion coefficients D_e can be separated in order to study the diffusion behavior of ions and electrons respectively in the films [10].

Diffusion coefficients of poly(thiophenes) and other conducting polymers have been studied [11–16] using primarily chronoamperometric, chronocoulometric and chronopotentiometric methods. It was found that counter ions exert an important influence on the diffusion coefficients of poly(3-methylthiophenes) [11].

An additional technique, a.c. impedance spectroscopy, is important for the determination of the electrical dielectric properties of conducting materials, as it can provide quantitative information on the kinetics of charge transfer

* Corresponding author.

SSDI 0022-0728(95)04386-1

within the bulk material and at interfaces [17–33]. It provides a complement to traditional electrochemical techniques for the study of the electrochemical properties at polymer-modified electrodes.

We recently reported [34] the synthesis of a series of 3-(ω-4-pyridylalkyl)thiophenes, P(n)T, with differing lengths of the alkyl chain between the thiophene and pyridyl rings ($n = 2$–11).

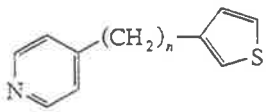

{$n = 2, 5, 7, 9, 11$}

The present paper reports studies of the electropolymerization of P(n)T, and of the structure and properties of the resultant films using scanning electron microscopy (SEM) and a variety of electrochemical methods (including cyclic voltammetry, chronoamperometric and impedance measurements). On the basis of these studies, charge transfer mechanisms within the bulk polymers and at the polymer interfaces are considered in both the anodic and cathodic regions. Details of an analogous study on electropolymerized films derived from 3-{ω-[4-(2,2′-bipyridyl)]alkyl}-thiophenes, and their metal complexes, will be published subsequently [35].

2. Experimental

2.1. Materials

The synthesis and characterization of 3-(ω-4-pyridylalkyl)thiophenes {P(n)T; $n = 2, 5, 7, 9, 11$} have been described previously [34].

Tetra-n-butylammonium perchlorate ([(n-C_4H_9)$_4$N]-ClO_4; Fluka, puriss) was recrystallized twice from a mixture of acetone and water and dried under vacuum at 50°C. Nitrobenzene (Ajax, AR grade) was distilled prior to use. Other reagents and solvents, including tetra-n-butylammonium hexafluorophosphate ([(n-C_4H_9)$_4$N]PF_6; Fluka, electrochemical grade), $LiClO_4$ (Fluka, MicroSelect), and acetonitrile (Fluka, UV grade), were used without further purification.

2.2. Measurements

2.2.1. Scanning electron microscopy

Scanning electron micrographs of P{P(2)T}, P{P(5)T} and P{P(11)T} were recorded at an electron energy of 15 kV using a scanning electron microscope (JEOL JXA-840A) in the Advanced Analytical Center at James Cook University. The polymers were deposited on a platinum disk electrode under the conditions described below.

2.2.2. Electrochemistry

Cyclic voltammetric experiments were conducted with a Bio-Analytical systems (BAS) CV-27 cyclic voltammograph connected to a Houston Model 2000 x–y recorder. Chronoamperometric experiments were performed with a BAS 100A electrochemical analyzer. Before I–t curves were recorded, a cyclic voltammogram was measured from −1.7 to +1.9 V at a scan rate of 20 mV s^{-1} so that a stable redox current could be obtained. For chronoamperometric experiments, the electrode potentials were stepped from 0 to −2.0 V or from 0 to +2.0 V. The counter electrode was a coil of platinum wire. All potentials were measured and are reported with respect to an Ag|0.01 M $AgNO_3$ in CH_3CN reference electrode. All electrochemical measurements were conducted in a three-electrode cell at room temperature under an N_2 atmosphere, and solutions were deoxygenated by bubbling with high purity N_2 prior to measurement.

2.2.3. Determination of the oxidation potentials of the monomers

The oxidation potentials of the various monomers were measured by linear sweep voltammetry from 0 to +2.0 V in an acetonitrile solution containing 0.4 M $LiClO_4$. Low monomer concentrations (0.01 M) and high scan rates (500 mV s^{-1}) were used in order to prevent polymerization. Before each experiment, the platinum disk working electrode (area $A = 0.07$ cm^2) was polished with a slurry of 0.05 μm alumina powder, and treated as described in the literature [36].

2.2.4. Electropolymerization of the monomers

Poly[3-(ω-4-pyridylalkyl)thiophenes], P{P(n)T}, were prepared on platinum disk electrodes ($A = 0.07$ cm^2) by the electrochemical oxidation of the corresponding monomers (0.1 M) in nitrobenzene solutions containing 0.02 M [(n-C_4H_9)$_4$N]ClO_4 at constant potentials ranging from 1900 mV to 2200 mV, unless otherwise indicated. The faradaic charges (Q) passed were measured from I–t curves from which the surface coverage $\Gamma (= Q/nFA$, $n = 2.25$) [37] and the film thickness d were roughly estimated, assuming no side-reactions occurred during the electrolysis process. In general, Q values were controlled between 100 and 150 mC cm^{-2} and the thickness of the P{P(n)T} films was estimated to be between 320 and 480 nm (P{P(2)T}) and 780 nm and 1.1 μm (P{P(11)T}) on the basis of a literature report [38] and the SEM results. After the polymerization, the film-modified electrodes were rinsed with acetonitrile, dried under an N_2 stream and electrochemically dedoped at a potential of 0 V for 10 min in an acetonitrile + 0.1 M [(n-C_4H_9)$_4$N]ClO_4 solution.

2.2.5. Impedance measurements

Impedance measurements of the polymer films were carried out with a Feedback TFA 607 transfer function

analyzer coupled to a Feedback PFG 505 power function generator. This system was connected to a BAS CV-27 cyclic voltammograph. The electrochemical cell and the technique used in the electropolymerization of the films on the electrodes have been described above. Before conducting the impedance measurements, a cyclic voltammogram was recorded (from -1.7 to $+1.9$ V at 20 mV s^{-1}) in order to check there was a good contact with the solution. The impedance measurements were performed at a series of fixed working potentials, and a small sinusoidal alternating voltage with an amplitude of 10 mV was superimposed on these d.c. polarizations. After each polarization, the impedance measurements were started when the d.c. components reached constant values, and a series of complex alternating voltage and current values were recorded on the basis of 10 cycle coverages for the frequency range 10 mHz–200 Hz in the form of $a + jb$ (where a indicates the real part and b the imaginary part of the voltage or current). The relatively long time constant of the BAS 27 (1 ms) placed an upper limit of 200 Hz on the frequencies used. From these data, the complex impedances of the film-modified electrodes ($Z = Z' - jZ''$), having a magnitude given by $Z = \Delta E/\Delta I$, were calculated and complex plane plots (Z' vs. $-Z''$) were obtained.

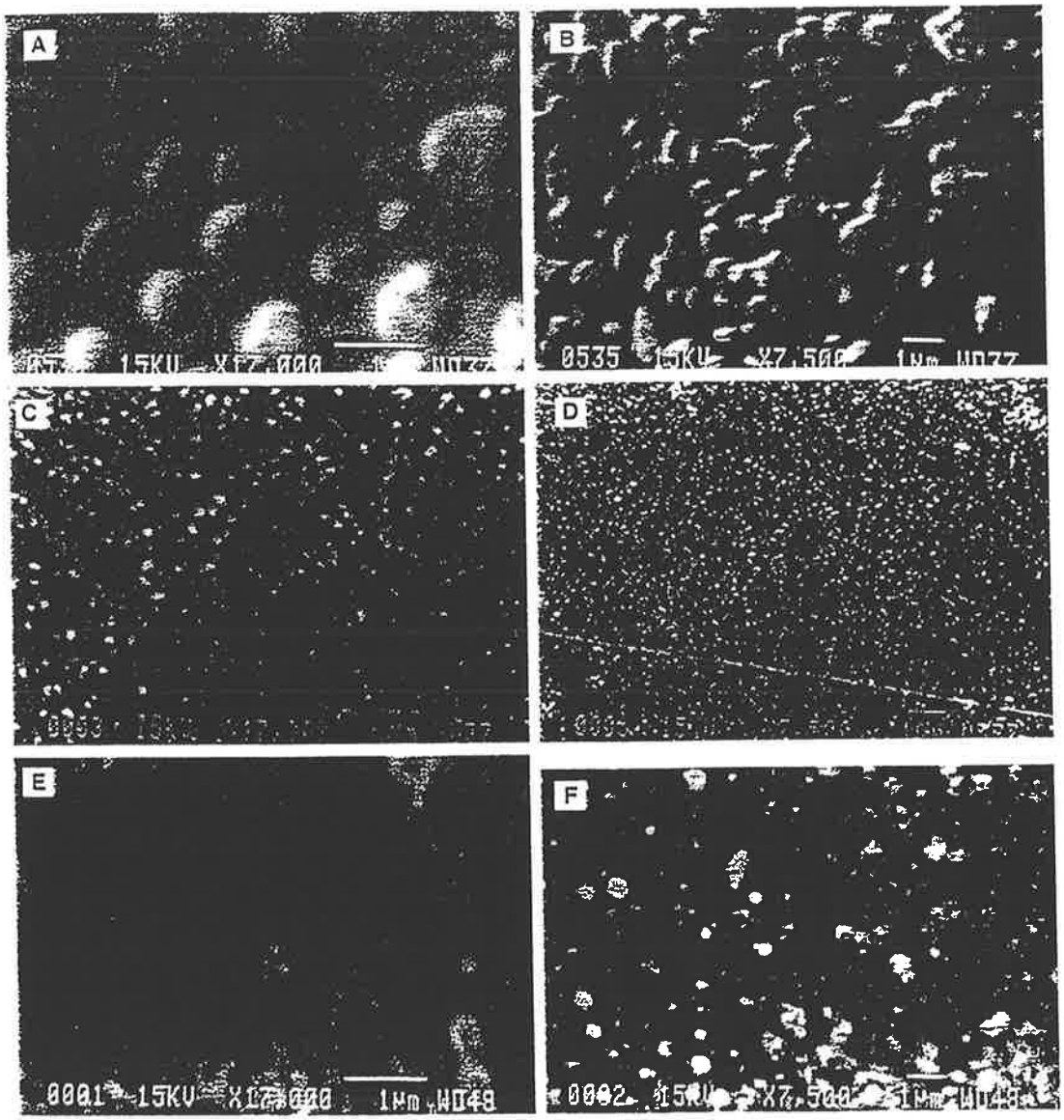

Fig. 1. Scanning electron micrographs of P(P(n)T) films. A and B: P(P(2)T); C and D: P(P(5)T); E and F: P(P(11)T). Magnifications: 17000 (A, C and E) and 7500 (B, D and F).

3. Results and discussion

3.1. Electropolymerization and structure of polymers

3.1.1. Effect of the length of the alkyl chain on the electropolymerization of the monomers

The nature of the functionalization of 3-substituted thiophene monomers, and the electropolymerization conditions, are reported to have a substantial effect on the formation, structure and properties of polymers derived from them [39–43]. The presence of the electron-withdrawing pyridine substituent might be expected to have an inhibiting effect on the electropolymerization of the thiophene. However, while long connecting alkyl chains might be expected to diminish such electronic effects within the present series of monomers, they may also impede the process because of steric hindrance. As a comparison, for poly(3-alkylthiophenes) in which the steric but not the electronic factor exists, the lengthening of linear alkyl chains has little effect on the electropolymerization reaction but does affect the structure and properties of the resulting polymers [39,40,44].

In the present study of the influence of electronic and steric effects on the polymerization of P(n)T, no profound systematic variations were observed. The polymers were produced at relatively high potentials (above 1.8 V). The monomers with intermediate lengths of alkyl chains, such as P(5)T and P(9)T, electropolymerized more readily than P(2)T and P(11)T because of lower oxidation overpotentials. The polymerization of P(2)T required the highest potential, presumably because of the electronic effect arising from the pyridyl ring.

The resulting polymer films had a metallic appearance; thin films having a silver, and thick films a golden, coloration. If neutral silver-colored films were oxidized or reduced, they became golden.

3.1.2. SEM analysis of the surface structures of the polymers

Fig. 1 shows scanning electron micrographs of P{P(2)T}, P{P(5)T} and P{P(11)T} films, and reveals a number of apertures (seen as black spots) on the surfaces of the polymers. The mean diameters of these apertures are about 0.2 μm in P{P(11)T}, 0.14 μm in P{P(5)T} and 0.1 μm in P{P(2)T}. With the lengthening of the alkyl chain, the films appear more porous and less regular: short-chain P{P(n)T}s have more compact surface structures. While P{P(5)T} has smaller surface particle sizes than P{P(11)T}, P{P(2)T} shows the largest surface particles although it has a very compact surface structure (Fig. 1B).

The increase of the porosity, and hence the surface-to-volume ratio of the polymer which occurs with the lengthening of the alkyl chain, may affect the polymer properties by way of increased mobility of the counter ions inside the films.

3.2. Electrochemical properties of polymers

3.2.1. Cyclic voltammetry of the film-modified electrodes

The cyclic voltammograms of the P{P(n)T} film-modified electrodes ($n = 2, 5, 11$) in $CH_3CN + 0.1$ M $[(n\text{-}C_4H_9)_4N]ClO_4$ solution are shown in Fig. 2. In the positive potential region, there is an oxidative wave at +1.5 V for P{P(5)T}, which is not present in the subsequent cycles. An equivalent wave is not observed for the other P{P(n)T} films. In contrast, the first oxidation wave of poly(3-methylthiophene) occurs at ca. +0.6 V [11], so that the presence of the pyridyl substituent has a significant effect on the oxidation process. A wave near −0.5 V on the first subsequent negative sweep for the P{P(5)T} film corresponds to the reduction current of the p-doped (oxidized) state.

The reduction (n-doping) process of the P{P(n)T} films and the reverse oxidation (dedoping) process are both clearly observed in the cyclic voltammetric curves, but with a large peak separation. A P{P(7)T} film exhibits a strong reduction wave at −1.55 V (scan rate 50 mV s^{-1}) and an oxidation wave of lower peak current at −0.8 V, with a peak separation ΔE_p of 0.75 V, which becomes larger with an increase in scan rate (Fig. 3). The other P{P(n)T}s exhibit similar voltammetric behavior. When the P{P(n)T} films are continuously scanned at negative potentials, the reduction current is greater in the initial than

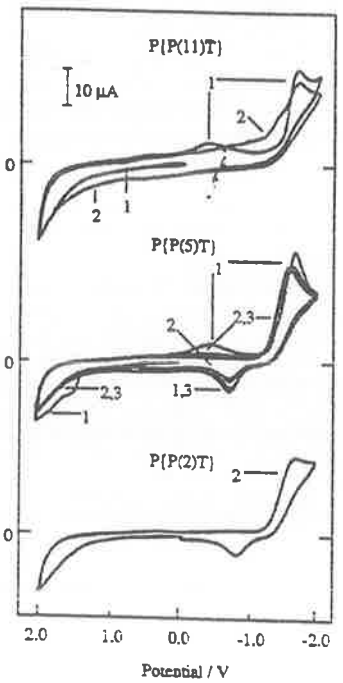

Fig. 2. Cyclic voltammograms of P{P(n)T} films in $CH_3CN - 0.1$ M $[(n\text{-}C_4H_9)_4N]ClO_4$ solution. Scan rate 50 mV s^{-1}. The numbers indicate the cycle number in a continuously scanning experiment.

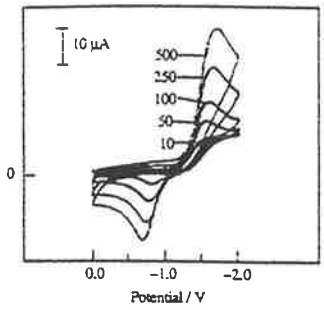

Fig. 3. Cyclic voltammogram of a reduced P{P(7)T} film at different scan rates in $CH_3CN + 0.1$ M$[(n\text{-}C_4H_9)_4N]ClO_4$ solution. The numbers indicate scan rates.

in subsequent cycles. In contrast to poly(3-alkylthiophene) films, the P{P(n)T} analogs have stable n-doped (reduced) states (i.e. a constant cyclic voltammetric response) as a consequence of the presence of the substituent pyridine groups. The current for the oxidation process on the reverse, positive sweep is higher for the shorter chain P{P(n)T} films. The peak is not observed for P{P(11)T}, which indicates that the longer alkyl chain linkages increase the irreversibility of the n-doping process. The reduction process is assumed to occur on the substituent pyridyl groups, which become increasingly isolated from the conducting polythiophene matrix as the alkyl chain linkage is lengthened. The P{P(5)T} film seems to exhibit the best redox behavior with the largest reverse current, in agreement with a literature report relating to the p-doping process of poly(alkylthiophenes) [44] where the mean conjugation length and the electrochemical reversibility were markedly improved by the introduction of alkyl chains containing seven to nine carbons, rather than either very short or very long chains.

3.2.2. *Effect of supporting electrolytes on electrochemical properties of P{P(n)T}s*

The supporting electrolyte exerts an important influence on charge transfer processes in the P{P(n)T} films. The cyclic voltammograms of P{P(2)T} and P{P(11)T} films in $CH_3CN + 0.1$ M $[(n\text{-}C_4H_9)_4N]PF_6$ solution are shown in Fig. 4: they have a similar appearance in $CH_3CN + 0.1$ M $[(n\text{-}C_4H_9)_4N]ClO_4$ solution, but the n-doping (reduction) currents are larger with PF_6^- as the anion. The cyclic voltammogram of the P{P(11)T} film (Fig. 4) shows that the film is stable after the second cycle; in contrast, the reduction currents associated with the n-doping of P{P(2)T} decay continuously up to the fifth cycle (Fig. 4), whereas its associated oxidation current grows continuously.

The cyclic voltammetric response of the P{P(n)T} films in CH_3CN solution with 0.1 M $LiClO_4$ as the electrolyte (Fig. 5) is completely different from that described above. For P{P(5)T}, there is little response on the first cycle as the potential is swept from 0 to +2.3 V. Within the negative potential region, two reductions are observed at

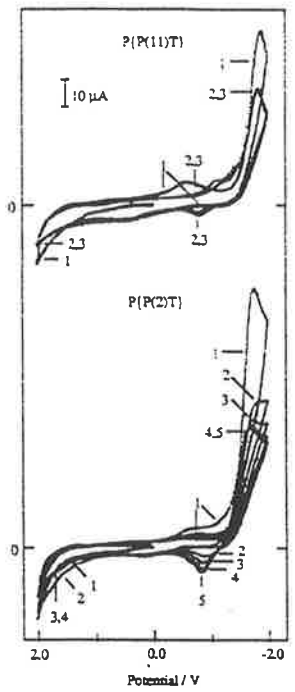

Fig. 4. Cyclic voltammograms of P{P(n)T} films in $CH_3CN + 0.1$ M$[(n\text{-}C_4H_9)_4]PF_6$ solution. Scan rate 50 mV s^{-1}. The numbers indicate the cycle number in a continuously scanning experiment.

−1.30 and −1.65 V. On the reverse sweep, an oxidation wave is observed at −1.35 V, but the peak current is much smaller than the corresponding reduction at −1.65 V; this again reflects the inhibition of charge transfer between the reduced pyridyl groups and the polythiophene matrix by the alkyl chain linkage. When the potential is

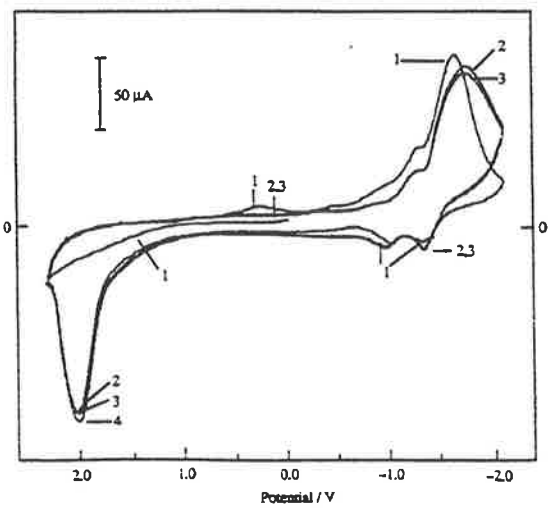

Fig. 5. Cyclic voltammogram of a P{P(5)T} film in $CH_3CN + 0.1$ M $LiClO_4$ solution. Scan rate 100 mV s^{-1}. The numbers indicate the cycle number in a continuously scanning experiment.

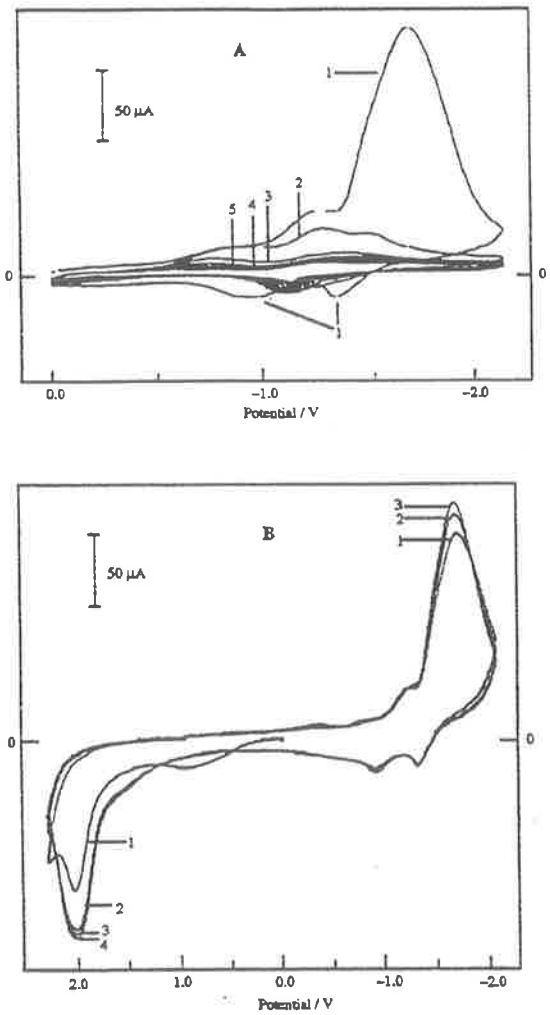

Fig. 6. Cyclic voltammograms of P{P(5)T} film in $CH_3CN + 0.1$ M $LiClO_4$ solution. Scan rate 100 mV s^{-1}. A, Continuously scanning at negative potentials; B, sweep after A.

then subsequently swept into the positive region, an oxidation wave with a high current appears at ca. +2.0 V; this phenomenon occurs as a result of the oxidation of both the thiophene ring and the reduced pyridyl ring, as it is not observed if the scan is only performed in the anodic region. The redox couple at $E_{p,c} - 1.30$ V and $E_{p,a} - 1.0$ V is presumably associated with the polythiophene matrix. In subsequent cycles, all redox waves tend to be stable with very little change in the position and magnitude over successive scans.

For the P{P(5)T} film, when the potential is cycled continuously in the negative potential region (0 to −2.1 V) in $CH_3CN + 0.1$ M $LiClO_4$ solution, the reduction wave is very large only on the first sweep and decays dramatically in the following cycles (Fig. 6A). However, the deactivated film can be reactivated if the potential is swept to +2.3 V (Fig. 6B).

The redox processes of the P{P(5)T} film may be rationalized in the following way. On a scan into positive potentials, the film is oxidized so that the thiophene conjugated chains are *p*-doped, with the electron loss being less than one per thiophene group [45,46]. At negative potentials, the primary process is reduction of the pyridyl groups, in which every pyridine acquires one electron. The small reverse waves observed following the reduction process signify that only a minority of reduced pyridine groups are oxidized in the negative potential region; however, they are subsequently reoxidized at more positive potentials.

Supporting electrolytes might be expected to affect the electrochemical behavior of conducting polymers as a consequence of a number of factors, e.g. the nature, size, concentration and magnitude of charge of counterions [34,47–52]. Anions influence primarily the polymer structure adopted in the electropolymerization process rather than its subsequent electrochemical behavior [11], whereas the nature of cations affects mainly the electrochemical doping/dedoping process of poly(3-methylthiophene) rather than its structure [11].

The present results also indicate that anions do not exert an extensive influence on the electrochemistry of the P{P(*n*)T} films. The cyclic voltammetric curves of the P{P(*n*)T}s at positive potential are analogous regardless of whether the anion is ClO_4^- ($r_i[ClO_4^-] = 0.290$ nm) or PF_6^- ($r_i[PF_6^-] = 0.301$ nm) {cf. Figs. 2 and 4}. However, significantly larger redox currents are obtained for the polymers at negative potential in $CH_3CN + 0.1$ M $[(n\text{-}C_4H_9)_4N]PF_6$ compared with $CH_3CN + 0.1$ M $[(n\text{-}C_4H_9)_4N]ClO_4$ solution: the reduction process of the P{P(*n*)T} films is accompanied by anion exclusion and the dedoping process by their reinsertion into the polymer matrixes, so that the counter ion PF_6^- appears to favor these process.

The small reverse waves observed following the reduction processes in solutions containing Li^+ merits comment. In general, reduction is most likely to occur on the pyridine rings, and the negative charge may remain there or rapid charge transfer (by tunelling through the alkyl chain, or by "electron hopping" between the redox species in the polymer) may take place to the polythiophene matrix, which would be the charge storage moiety. The free Li^+ ion has a very small size (ionic radius r_i [Li^+] = 0.068 nm) so that it may very easily penetrate the membranes due to the porosity of the P{P(*n*)T} films. Being incorporated into the reduced polymers as a counter cation, Li^+ would strongly localize the electrogenerated negative charge on the pyridine rings. (If the Li^+ ions are solvated in acetonitrile, the effective radius will be larger but such ions may be desolvated on entry into the polymer, with the negatively charged pyridine groups displacing the solvent molecules, ultimately giving rise to the same effect.) The presence of Li^+ would inhibit the transfer of the charge to

the polythiophene matrix and the electrode, as seen in the present study in the deactivation of the polymers in the cathodic region. The ambiguity of the site of electron storage is thus not critical in this instance, but this issue will be addressed subsequently in the discussion of diffusion coefficients within these polymer films. Nevertheless, the reduced films are reoxidized at +2.0 V when the exclusion of the Li^+ cations leads to reactivation of the polymers. In contrast to the P{P(*n*)T} films, the n-doping of poly(3-phenylthiophene) films was found to be very difficult in the presence of Li^+ compared with other electrolytes [7], a result confirmed by Roncali et al. using a series of polythiophenes containing substituted phenyl groups [2].

3.2.3. Apparent diffusion coefficients for charge transfer in the P{P(n)T} polymer matrixes

Chronoamperometry was used to measure apparent diffusion coefficients of charge transfer in the P{P(*n*)T} polymer matrixes. The diffusion is predicted to follow Fick's diffusion equation in conducting polymer films with the redox couple

$$O + ne^- \rightleftarrows R$$

For a potential step experiment on a polymer with a film thickness d, the finite diffusion current–time relation is [12]

$$I = \frac{nFAD^{1/2}c}{\pi^{1/2}t^{1/2}}\left[1 + 2\sum_{m=1}^{\infty}(-1)^m \exp\left(\frac{-m^2d^2}{Dt}\right)\right] \quad (1)$$

This equation describes the dependence of a transition current on time, and from it the rate of electrochemical charge transport in the polymer films can be evaluated quantitatively. At a sufficiently short time, $Dt/d^2 < 1$, diffusion is effectively semi-infinite. Under these conditions, the exponential item in Eq. (1) is small enough to be omitted. Therefore, Eq. (1) can be simplified to the Cottrell equation

$$I = \frac{nFAD_0^{1/2}c}{\pi^{1/2}t^{1/2}} \quad (2)$$

The average concentration of electroactive species in the films is given by $c = \Gamma/d$, where Γ is the surface coverage and d is the thickness of the films; Γ can be estimated from the deposit charges according to Faraday's law, so that D_0 is obtainable. The concentration c is not precisely known, nor the thickness d of the polymers, but relative charge transfer within the P{P(*n*)T}s can be compared on the basis of these calculations. The value of n was chosen as unity for the reduction process of the P{P(*n*)T} films, on the assumption that every pyridyl site acquires one electron. For an oxidation (*p*-doping) process, although the actual value is not readily determined, $n < 1$ (see above) but it is likely to be the same for all the P{P(*n*)T} films since the alkyl chain length does not exert any significant influence on the *p*-doping process in these films. For the purpose of simplifying the calculations, n was assumed to have the value of unity. This assumption means that the absolute values of D_{app} calculated for the *p*-doping processes must be treated with some caution, although they may be used for comparison between polymers of different chain lengths between the thiophene and pyridyl moieties. For large t ($Dt/d^2 \geq 1$), the exponential item in Eq. (2) is significant and the finite diffusion relationship (Eq. (1)) is applicable; then, the chronoamperometric current is less than that given by Eq. (2) and the I–$t^{-1/2}$ curve deviates from linearity.

For the potential step to negative potential (0 to −2.0 V) in CH_3CN + 0.1 M $[(n\text{-}C_4H_9)_4N]ClO_4$ solution, the chronoamperometric I–$t^{-1/2}$ curves of the P{P(*n*)T}-film-modified electrodes show reasonably linear relationships (passing through the origin), at least for low values of t. The plot for P{P(11)T} has the largest slope and that for P{P(9)T} has the same slope as P{P(2)T}. The corresponding studies with positive potential steps also revealed linear plots for short t. From the slopes D_0 of these lines the initial approximate value of D, can be evaluated on the basis of Eq. (2). By substitution of values for D around D_0 into Eq. (1), a series of I values was calculated for a certain t using an iterative computer procedure until the deviation between calculated and experimental values was less than 0.1%. This D value was selected as D_j, and a

Table 1
Apparent diffusion coefficients of charge transfer in P{P(*n*)T} films [a]

Polymer	Estimated thickness/nm	*n*-Doped film [b]		*p*-Doped film [b]	
		$10^8 D_0^{1/2}c$/ mol cm^{-2} s$^{-1/2}$	$10^{11} D_{app}$/ cm^2 s^{-1}	$10^8 D_0^{1/2}c$/ mol cm^{-2} s$^{-1/2}$	$10^{11} D_{app}$/ cm^2 s^{-1}
P{P(2)T}	340	12	7.4	9.3	4.2
P{P(5)T}	480	8.1	6.7	8.5	7.1
P{P(7)T}	590	8.7	11	10	16
P{P(9)T}	590	12	31	12	26
P{P(11)T}	800	16	72	11	31

[a] All data obtained in CH_3CN + 0.1 M $[(n\text{-}C_4H_9)_4N]ClO_4$ solution. Potential steps from 0 to −2.0 V and from 0 to +2.0 V respectively. Coverage of the films: $\Gamma = 4.8 \times 10^{-7}$ mol cm^{-2}.

[b] D_0 from Eq. (2) and D_{app} from Eq. (1).

series of D_j values obtained corresponding to every I–t data point. The average value of these D_j was taken as representing D_{app}. Although reduced P{P(2)T} provides an exception to the general trend, the P{P(n)T}s with long alkyl chains have the larger D_{app} values in CH_3CN + 0.1 M $[(n\text{-}C_4H_9)_4N]ClO_4$ solution, as shown in Table 1.

The apparent diffusion coefficient D_{app} for charge transfer through conducting polymers is considered as the sum of an electron-diffusion rate D_e and an ion-diffusion rate D_i component [10]. D_e arises from electron hopping among redox species in the polymer matrixes, and D_i is attributed to the mobility of counter ions in the films, and either of them may become predominant. In the present case, there are three factors which may affect charge transfer in the P{P(n)T} films. Firstly, the presence of the pyridyl ring will give rise to an electronic effect which will have a significant influence on the D_e values of the P{P(n)T} films in which the alkyl chain length is short. Secondly, the alkyl chain length will affect D_e, especially in the case of reduction of the polymers, as the short alkyl chains should favor the intramolecular electron transport if this transport is conducted through the alkyl chain and ultimately through the polythiophene matrix. Finally, the film structure will affect the ion-diffusion coefficients D_i. Owing to the greater porosity and larger holes in the long alkyl chain P{P(n)T} matrixes, the mobility of the counter ions in the polymers is increased and higher D_i values are predicted.

In the p-doping process within the polymers, the charge transport takes place only through the conjugated thiophene rings. As a result, the effect of alkyl chain length on D_e is unimportant and the predominant influence on D_{app} is the structure of the films. Therefore, the P{P(n)T} films with long alkyl chains exhibit larger apparent diffusion coefficients as a consequence of the larger apertures and greater porosity. The situation for the cathodic processes in the P{P(n)T} films is somewhat more complex. The observation of larger D_{app} values for the P{P(n)T}s in which n is large argues against substantial electron transport through the alkyl chains, and suggests either that electron hopping may be conducted between two aromatic rings directly because of structural flexibility, or that ion diffusion may make a determinant contribution to D_{app} when the potential is stepped to −2.0 V. The peculiarity of P{P(2)T} may be attributed to a direct electronic effect arising from the pyridyl substituent. The D_{app} values are of the same order for the p- and n-doping processes (Table 1). This may arise because of the assumption for the p-doping processes in the calculations in Eqs. (1) and (2) that n has a value of unity; actually $n < 1$ in this case, so that D_{app} for the p-doping processes should be larger than those listed in Tables 1 and 2.

The implications could have more significance, however. "Electron hopping" processes between redox centers would be expected to be slower than electron conduction through a conducting polymer chain. If the polythiophene matrix were the site of charge storage in the p-doped polymers, and the pyridyl rings the site of storage in the n-doped forms, then larger D_{app} values might be expected for the p-doped than the n-doped state. The observation that they have values of the same order may reflect that the charge transfer in both the n- and p-doping processes occurs by the same mechanism within the polythiophene matrix.

The influence of the identity of the ions in the electrolyte can be seen in the diffusion coefficients. Cations play a major role in the determination of D_{app} in the reduction and subsequent reoxidation of P{P(n)T} films. In CH_3CN + 0.1 M $LiClO_4$ solution, I–$t^{-1/2}$ curves do not pass through the origin although they are linear, so that Eqs. (1) and (2) may not be applicable to the polymers in this medium. The reason for this observation is not clear, but may arise from the rapid mobility of the small lithium cation in the negatively-charged film, or a specific interaction between Li^+ and the polymer matrix with consequent kinetic control of some aspect of the charge transfer process, as described above. The additional possibility is that the phenomenon arises from interface charging effects, and reflects differences between the Li^+ and $[(n\text{-}C_4H_9)_4N]^+$ cations.

Anions also exert quite significant effects on D_{app} in reduced P{P(n)T}s. Although the I–$t^{-1/2}$ curve has a slightly larger slope in CH_3CN + $[(n\text{-}C_4H_9)_4N]ClO_4$ than in CH_3CN + 0.1 M $[(n\text{-}C_4H_9)_4N]PF_6$ solution, the effect diminishes as the chain length becomes longer, and is negligible for the case of P{P(11)T}. However, there is a significant difference in D_{app} of the P{P(2)T} film between solutions containing the two electrolytes (Table 2). The reduction process of the P{P(n)T} films must be accompanied by insertion of cations and exclusion of anions from the polymer matrices to maintain electroneutrality. Ionic mobility may therefore be a factor in the charge transfer.

Table 2
Apparent diffusion coefficients of charge transfer in P{P(2)T} and P{P(11)T} films in the presence of different supporting electrolytes [a]

Polymer	10^{11} D_{app}/cm^2 s^{-1}, n-doped film		10^{11} D_{app} cm^2 s^{-1}, p-doped film	
	$[(n\text{-}C_4H_9)_4N]ClO_4$	$[(n\text{-}C_4H_9)_4N]PF_6$	$[(n\text{-}C_4H_9)_4N]ClO_4$	$[(n\text{-}C_4H_9)_4N]PF_6$
P{P(2)T}	7.4	15	4.2	1.5
P{P(11)T}	72	80	31	26

[a] Conditions are the same as Table 1 except that the solutions are CH_3CN + 0.1 M $[(n\text{-}C_4H_9)_4N]ClO_4$ and CH_3CN + 0.1 M $[(n\text{-}C_4H_9)_4N]PF_6$ respectively.

and might be expected to be less in the P{P(2)T} films due to their lower porosity and the smaller holes in the matrices of the polymer. However, since the ClO_4^- and PF_6^- ions are of similar size (see above), the effect would seem to arise from some inherent property of the anions.

Table 2 also shows the effects of supporting electrolytes on D_{app} in the oxidized polymers, and in a similar manner to the reduction process, the difference of D_{app} caused by anions is much more significant in the P{P(2)T} than in the P{P(11)T} film. However, $[(n\text{-}C_4H_9)_4N]ClO_4$ produces a larger slope in the I–$t^{-1/2}$ curve than $[(n\text{-}C_4H_9)_4N]PF_6$, indicating faster diffusion of ClO_4^- in the film.

3.3. Impedance analysis of the polymers

3.3.1. A.c. impedance spectra of a P{P(7)T} film-modified electrode

Fig. 7 shows the impedance complex planes of a P{P(7)T} film-coated electrode at different potentials in $CH_3CN + 0.1$ M $[(n\text{-}C_4H_9)_4N]ClO_4$ solution. When the polymer remains in a non-doped state, the spectra appear as straight lines at low and intermediate frequencies (Figs. 7A, 7B). However, they seem not to be consistent with Warburg impedance because the slope is much greater than unity. This phenomenon has been reported previously for other film-coated electrodes [24,32,53] and the spectra indicate that the neutral polymer possesses capacitive characteristics. In the oxidized polymer, a semicircle appears at intermediate frequencies corresponding to a charge transfer resistance R_{ct} (Figs. 7C–7E). In addition, there is a Warburg impedance at low frequencies and its slope becomes close to unity with increase of the p-doping level of the polymer. From these spectra, it appears that R_{ct} and Z_w are both important in the p-doping process of the P{P(7)T} film. In the case of n-doped films, a series of spectra recorded at different potentials show different diameters of semicircles in the intermediate to low frequency range, and Warburg impedance at low frequencies (Figs. 7F–7I). In these spectra, the semicircles arising from charge transfer resistance show a dependency on the potentials: at -1.2 V, which is located just at the foot of the reduction peak of the polymer, the semicircle has the smallest diameter.

The a.c. impedance spectra of a conducting polymer-modified electrode is predicted to possess two kinetic semicircles from the P|M (polymer|metal) interface (R_{ct1} in parallel with C_{dl1} for electronic charge transfer) and the

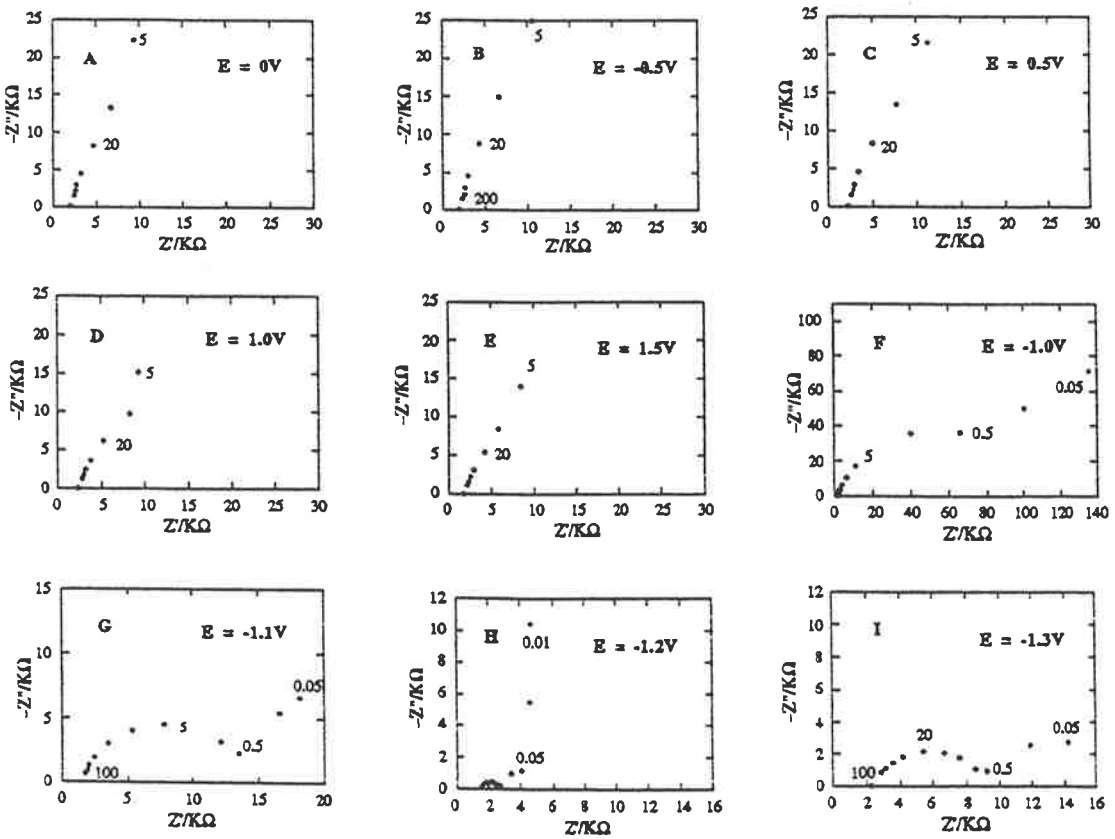

Fig. 7. Complex impedance planes for P{P(7)T} film at different potentials in $CH_3CN + 0.1$ M$[(n\text{-}C_4H_9)_4N]ClO_4$ solution. Film thickness 250 nm. The numbers indicate frequencies f in Hz.

P|S (polymer|solution) interface (R_{ct2} in parallel with C_{dl2} for ion transfer) respectively [54]. Under most circumstances, however, only one semicircle can be observed [54], and in the low frequency range a Warburg impedance often appears after the charge transfer semicircle(s). In addition, the electrode behaves as a capacitor at very low frequencies. At high frequencies, a semicircle arising from the resistance R_b of the polymer phase, in parallel with its geometric capacitance C_b, can be observed with dry films [54]. In general this semicircle is absent when the conducting polymer-modified electrode is studied in electrolyte solution. A model by Fletcher [55] interpreted this phenomenon in terms of a model where the impedance of the solid polymer can be replaced by a Randle's circuit; i.e. a parallel arrangement of a resistor R_Z and a capacitor C_Z, in series with a resistor R_Ω. At very high frequencies, this impedance can be simplified to R_Ω. Under conditions where the frequency was relatively low (less than 1 kHz), the impedance of C_Z became so large that the capacitor became blocking and the bulk polymer resistance $R_b = R_\Omega + R_Z$ [55]. If the film thickness d is known, the specific conductivity κ of the polymer can be calculated:

$$R_b = d/A\kappa \quad (4)$$

where A is the electrode area.

In the neutral P{P(7)T} film, the charge transfer resistance R_{ct} is infinite and the equivalent circuit is shown in Fig. 8A. By contrast, in the doped polymer R_{ct} is finite and depends on the potentials. The equivalent circuit is shown in Fig. 8B. For a reduced P{P(7)T} film, R_{ct} can be calculated from the impedance spectra and is at a minimum (about 70 Ω cm^2) at -1.2 V. A Warburg impedance Z_w can be observed only at low frequencies in these spectra. The experimental results suggest that the cathodic electrode reaction is controlled mainly by kinetic factors, and diffusion is only significant at low frequencies. In the case of an oxidized film, the Warburg impedance becomes very important since it covers a wide frequency range, which suggests that the electrode reaction is controlled by both kinetics and diffusion, the latter appearing to be the more important. The neutral film is nearly non-conductive due to the infinite R_{ct}, and most current flows through the capacitor C_{dl}. The high frequency semicircle is absent in

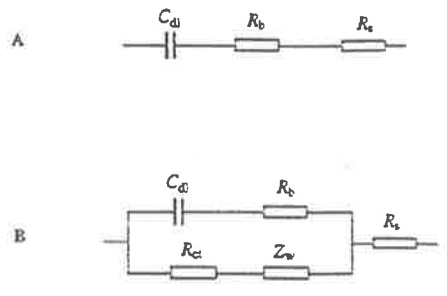

Fig. 8. Equivalent circuit of P{P(n)T} films in $CH_3CN + 0.1$ M [$(n$-$C_4H_9)_4$]ClO_4 solution. A non-doped state; B doped state.

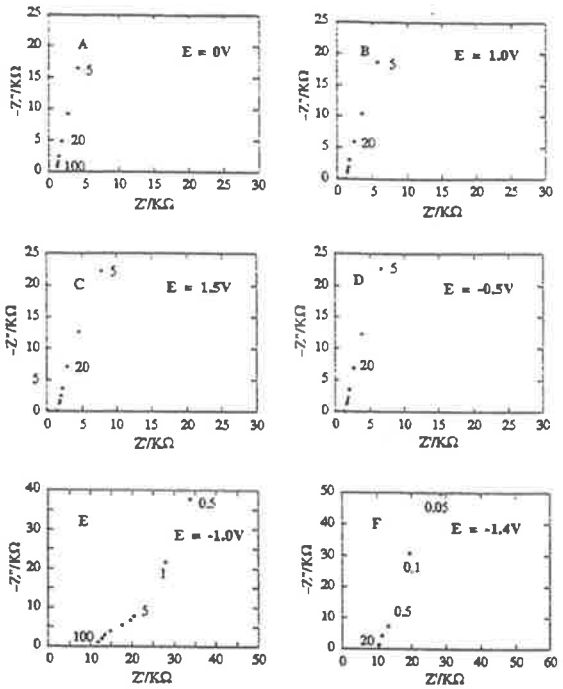

Fig. 9. Complex impedance planes of P{P(7)T} film at different potentials in $CH_3CN + 0.1$ M $LiClO_4$ solution. Film thickness 180 nm.

all the spectra and the bulk film resistance R_b is basically independent of the doped state of the polymer. In all the spectra, R_b is about 2 kΩ (140 Ω cm^2). In comparison with this value, the solution resistance R_S is negligible. The specific conductivity κ of the bulk polymer can be estimated to be about 4×10^{-7} S cm^{-1} for this P{P(n)T}-coated electrode. This value indicates a poor conductivity of the polymer.

The other P{P(n)T} films exhibit similar behavior.

The bulk film resistance R_b may be determined only by the dielectric characteristic of the polymers and the film component distribution. It seems not to be affected significantly by either the applied potentials or the length of the alkyl chains in the case of P{P(n)T} films. The spectra do not reveal any dependence of the impedance spectra of the P{P(n)T} films on the length of alkyl chains. This implies that the electron transport is conducted in various ways, such as transfer through the alkyl chains and direct hopping between thiophene and pyridine.

3.3.2. *Effect of supporting electrolytes on the impedance of P{P(n)T} films*

Fig. 9 shows the impedance spectra of the P{P(7)T} film in $CH_3CN + 0.1$ M $LiClO_4$ solution. The neutral film behaves as a capacitor at intermediate and low frequencies. Its equivalent circuit is represented by Fig. 8A. However, Fig. 9C seems to show a large charge transfer resistance semicircle at intermediate frequencies, but no Warburg

impedance in the spectrum. The kinetic semicircles for charge transfer resistance can be observed in the reduced film, as shown in Figs. 9E and 9F. R_{ct} is about 1.4 kΩ cm^2 at a potential of -1.0 V, which is smaller than that (7.35 kΩ cm^2) of the P{P(7)T} film at the same potential in $CH_3CN + 0.1$ M $[(n\text{-}C_4H_9)_4N]ClO_4$ solution. The Warburg impedance is not very significant, but low frequency capacitive properties appear in the reduced film. These features suggest that the diffusion of counter ions is fast and that the kinetic factor controls the charge transfer reaction in the P{P(7)T} film in $CH_3CN + 0.1$ M $LiClO_4$ solution. This result is consistent with those of the cyclic voltammetry and chronoamperometry studies. In the neutral and *p*-doped states, R_b resembles those values obtained in the presence of $[(n\text{-}C_4H_9)_4N]ClO_4$. However, in the reduced state R_b increases dramatically up to a value of 10 kΩ (700 Ω cm^2), which leads to a specific conductivity κ for the polymer of ca. 2.6×10^{-8} S cm^{-1}. The substantial increase of R_b may occur because the Li^+ ions which enter the film in the reduction process are immobilized by a strong association with the pyridine radical anions in the matrix.

4. Conclusions

The steric and electronic parameters exert little effect on the electrosynthetic process for P{P(*n*)T} films, but they have a substantial influence on the properties of the polymers. The SEM analysis showed that the structure of P{P(*n*)T} films becomes more porous, less regular and less compact with increase in the length of the alkyl branch chain between the thiophene and the pyridine moieties.

Chronoamperometric studies have enabled the measurement of apparent diffusion coefficients D_{app} for charge transfer processes in the polymers. They are determined to a large extent by the porous structure of the films, and are therefore dependent not only on the length of the alkyl chain, but also on the nature of the supporting electrolytes. Larger D_{app} values are obtained for those polymers with long alkyl chains. While the effect of the anion is relatively unimportant, the presence of Li^+ cations leads to unusual electrochemical behavior of the polymers.

Impedance measurements show a significant bulk film resistance R_b, which is independent of the potential and the length of the alkyl chain at higher frequencies, but is dependent on the supporting electrolytes. In the presence of the Li^+ cation, a much larger R_b value is observed than that obtained in the solution containing $[(n\text{-}C_4H_9)_4N]^+$ cation. In the presence of $[(n\text{-}C_4H_9)_4N]ClO_4$, a finite charge transfer resistance R_{ct} is observed at intermediate frequencies depending on the doped states of the polymers. This charge transfer resistance is infinite in the undoped films, which behave as capacitors. In the *p*-doped polymers, the impedance spectra show that the electrochemical processes are controlled by both kinetic and diffusion phenomena. However, the spectra of *n*-doped films indicate that the electrode processes are kinetically controlled in these films.

Acknowledgements

This research was supported by the Australian Research Council. JW wishes to acknowledge the Australian International Development Assistance Bureau for an ADCSS scholarship and James Cook University of North Queensland (JCUNQ) for a postgraduate research award for overseas students. Associate Professor A. Walton and Mr. S. Cumming (Department of Electrical and Computer Engineering, JCUNQ) are thanked for the loan of the instrumentation for the measurement of a.c. impedance spectra, and Associate Professor F.G. Thomas (Department of Molecular Sciences, JCUNQ) for helpful discussions. We also acknowledge the helpful comments of a referee regarding aspects of the charge transfer mechanism prior to revision of the manuscript.

References

[1] J. Roncali, Chem. Rev., 92 (1992) 711.
[2] J. Roncali, H.K. Youssoufi, R. Garreau, F. Garnier and M. Lemaire, J. Chem. Soc., Chem. Commun., (1990) 414.
[3] R. Mirrazaei, D. Parker and H.S. Munro, Synth. Met., 30 (1989) 265.
[4] A. Rudge, I. Raistrick, S. Gottesfeld and J.P. Perrarist, Electrochim. Acta, 39 (1994) 3793.
[5] C. Visy, J. Lukkari and J. Kankare, Macromol. 26 (1993) 3295.
[6] J. Roncali, C. Thobie-Gauter, H. Brisset, J.-F. Favart, and A.J. Guy, J. Electroanal. Chem., 381 (1995) 257.
[7] M. Onoda, H. Nakayama, S. Morita and K. Yoshino, J. Appl. Phys. 73 (1993) 2859.
[8] F.B. Kaufman, A.H. Schroeder, E.M. Engler, S.R. Kramer and J.Q. Chambers, J. Am. Chem. Soc., 102 (1980) 483.
[9] J.O'M. Bockris and F.B. Diniz, Electrochim. Acta, 34 (1989) 567.
[10] N.A. Surridge, J.C. Jernigan, E.F. Dalton, R.P. Buck, M. Watanabe, H. Zhang, M. Pinkerton, T.T. Wooster, M.L. Longmire, J.S. Facci and R.W. Murray, J. Chem. Soc., Faraday Discuss., 88 (1989) 1.
[11] P. Marque, J. Roncali and F. Garnier, J. Electroanal. Chem., 218 (1987) 107.
[12] P. Daum, J.R. Lenhard, D. Rolison and R.W. Murray, J. Am. Chem. Soc., 102 (1980) 4649.
[13] N. Oyama, S. Yamaguchi, Y. Nishiki, K. Tokuda, H. Matsuda and F.C. Anson, J. Electroanal. Chem., 139 (1982) 383.
[14] K. Shigehara, N. Oyama and F.C. Anson, J. Am. Chem. Soc., 103 (1981) 2552.
[15] K. Kanamura, S. Yonezawa, S. Yoshioka and Z.-L. Takehara, J. Phys. Chem., 95 (1991) 7939.
[16] P. Daum and R.W. Murray, J. Phys. Chem., 85 (1981) 389.
[17] T. Amamiya, K. Hashimoto and A. Fujishima, J. Phys. Chem., 97 (1993) 4192.
[18] M. Sharp, B. Lindholm-Sethson and E.-L. Lind, J. Electroanal. Chem., 345 (1993) 223.
[19] C. Deslouis, M.M. Musiani and B. Tribollet, J. Electroanal. Chem., 264 (1989) 37.
[20] G. Lang, J. Backsai and G. Inzelt, Electrochim. Acta, 38 (1993) 773.

[21] C. Gabrielli, H. Takenouti, O. Haas and A. Tsukada, J. Electroanal. Chem., 302 (1991) 59.
[22] F. Beck and P. Hulser, J. Electroanal. Chem., 280 (1990) 159.
[23] X. Ren and G. Pickup, J. Phys. Chem., 97 (1993) 5356.
[24] J. Tanguy, J.L. Baudoin, F. Chao and M. Costa, Electrochim. Acta, 37 (1992) 1417.
[25] S. Sunde, G. Hagan and R. Ødegard, J. Electroanal. Chem., 345 (1993) 43.
[26] S. Sunde, G. Hagen and R. Ødegard, J. Electroanal. Chem., 345 (1993) 59.
[27] J. Tanguy, N. Mermilliod and M. Hoclet, J. Electrochem. Soc., 134 (1987) 795.
[28] R.M. Penner and C.R. Martin, J. Phys. Chem., 93 (1989) 984.
[29] G. Lang and G. Inzelt, Electrochim. Acta, 36 (1991) 847.
[30] P. Fiordiponti and G. Pistoia, Electrochim. Acta, 34 (1989) 215.
[31] I. Rubinstein, E. Sabatini and J. Rishpon, J. Electrochem. Soc., 134 (1987) 3081.
[32] W.J. Albery and A.R. Mount, J. Electroanal. Chem., 305 (1991) 3.
[33] G. Lang, L. Kocsis and G. Inzelt, Electrochim. Acta, 38 (1993) 1047.
[34] J. Wang, M. Pappalardo and F.R. Keene, Aust. J. Chem., 48 (1995) 1425.
[35] J. Wang and F.R. Keene, J. Electroanal. Chem., 405 (1996) 71.
[36] R.N. Adams, Electrochemistry at Solid Electrodes, Marcel Dekker New York, 1969.
[37] A.F. Diaz, J.I. Castillo, J.A. Logan and W.-Y. Lee, J. Electroanal. Chem., 129 (1981) 115.
[38] J. Roncali and F. Garnier, Macromol., 22 (1989) 804.
[39] R.J. Waltman, J. Bargon and A.F. Diaz, J. Phys. Chem., 87 (1983) 1459.
[40] G. Dian, G. Barbey and B. Decroix, Synth. Met., 13 (1986) 281.
[41] R.J. Waltman, A.F. Diaz and J. Bargon, J. Electrochem. Soc., 131 (1983) 1452.
[42] J.P. Ruiz, K. Nayak, D.S. Marynick, and J.R. Reynolds, Macromol. 22 (1989) 1231.
[43] S. Tanaka, M. Sato and K. Kaeriyama, Synth. Met., 13 (1988) 281.
[44] J. Roncali, R. Garreau, A. Yassar, P. Marque, F. Garnier and M. Lemaire, J. Phys. Chem., 91 (1987) 6706.
[45] G. Tourillon and F. Garnier, J. Electroanal. Chem., 135 (1982) 173.
[46] T.F. Otero, R. Tejada and A.S. Elola, Polymer, 28 (1987) 651.
[47] N. Oyama and F.C. Anson, J. Electrochem. Soc., 127 (1980) 640.
[48] G. Inzelt, Electrochim. Acta, 34 (1989) 83.
[49] K. Imanishi, M. Satoh, Y. Yasuda, R. Tsushima and S. Aoki, J. Electroanal. Chem., 260 (1989) 469.
[50] S. Cosnier, A. Deronzier and J.-F. Roland, J. Electroanal. Chem., 310 (1991) 71.
[51] A.H. Schroeder and F.B. Kauffman, J. Electroanal. Chem., 113 (1980) 209.
[52] J.S. Miller, A.J. Epstein and W.M. Beiff, Chem. Rev., 88 (1988) 201.
[53] S. Ye, F. Girard and D. Bélanger, J. Phys. Chem., 97 (1993) 12373.
[54] B.W. Johnson, D.C. Read, P. Christensen, A. Hamnett and R.D. Armstrong, J. Electroanal. Chem., 364 (1994) 103.
[55] S. Fletcher, J. Electroanal. Chem., 337 (1992) 127.

ELSEVIER

Journal of Electroanalytical Chemistry 405 (1996) 71–83

JOURNAL OF ELECTROANALYTICAL CHEMISTRY

Synthesis and electrochemical properties of poly[3-{ω-[4-(2,2′-bipyridyl)]alkyl}thiophenes], P{B(*n*)T}, and of poly[Ru(II){B(*n*)T}$_3^{2+}$]

Jiaxiong Wang, F. Richard Keene *

Department of Chemistry and Chemical Engineering, School of Molecular Sciences, James Cook University of North Queensland, Townsville, Qld. 4811, Australia

Received 5 July 1995; in revised form 17 October 1995

Abstract

The electropolymerization of a series of ligands 3-{ω-[4-(2,2′-bipyridyl)]alkyl}thiophene (B(*n*)T; *n* = 2, 5, 7, 9, 11) and their tris(ligand)ruthenium(II) complexes, [Ru{B(*n*)T}$_3$]$^{2+}$, is reported. The electrochemical properties of the polymers were investigated using cyclic voltammetry, chronoamperometry and a.c. impedance spectroscopy. These studies reveal the dependence of the electrochemical behavior of the poly{Ru{B(*n*)T}$_3^{2+}$] films upon the length of alkyl chains between the thiophene and the bipyridyl groups, and on the supporting electrolytes; longer alkyl chains induce more irreversible voltammetric behavior and larger charge transfer resistances in the cathodic processes of the polymers. On the basis of these investigations, the mechanism of charge transfer in the polymer-modified electrodes has been evaluated, and interpreted. This shows that electrochemical processes of the polymers in the anodic region are controlled both by kinetic and diffusion factors, whereas the primary influences in the cathodic region are associated with kinetic factors arising from the alkyl chains.

Keywords: Ruthenium(II) complexes; Conducting polymer films; Electropolymerization; A.c. impedance spectroscopy

1. Introduction

The mechanism of charge transfer in conducting polymers has been extensively studied [1–18], and in polythiophenes and polypyrroles (and their derivatives) it occurs through the conjugated aromatic rings. However, in poly-[3-(ω-4-pyridylalkyl)thiophene] films, P{P(*n*)T}s, we recently showed that charge transfer processes are rendered more complex as the branch chains in the polymers exert an additional influence [19].

Our further interest was to undertake a parallel study on the synthesis and electrochemical properties of polymers derived from the related series 3-{ω-[4-(2,2′-bipyridyl)]alkyl}thiophenes, B(*n*)T.

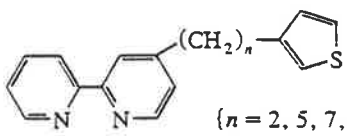

{*n* = 2, 5, 7, 9, 11}

This study was also extended to examine the polymers derived from the electropolymerization of metal complexes derived from B(*n*)T, e.g. [Ru{B(*n*)T}$_3$]$^{2+}$, to investigate the consequent effect on the charge transfer properties of the metallated films obtained by electrodeposition. The identity of the particular metal system chosen was complexes of ruthenium(II) with polypyridyl ligands, such as [Ru(bpy)$_3$]$^{2+}$ (bpy is 2,2′-bipyridine) and its analogues, which have been the subject of intense research related to their use as photosensitizers and electron transfer reagents [20]. In an extension of these properties, [Ru(bpy)$_3$]$^{2+}$ has been incorporated into Nafion® and clay-coated electrodes [21–24], which then acted as photoelectrodes under irradiation.

In poly-[Ru{B(*n*)T}$_3$](PF$_6$)$_{2x}$ films described in this paper (designated P{RuB(*n*)T}), the polythiophene polymer is fixed to the surface of the electrode and the [Ru(bpy)$_3$]$^{2+}$ units are linked to the thiophene rings by alkyl chains of different lengths. Depending on the electrode potentials, the thiophene rings may themselves be involved in redox processes or mediate in charge transfer between the electrode and the ruthenium centers. Similar systems have

* Corresponding author.

SSDI 0022-0728(95)04417-5

been investigated by Deronzier and coworkers where the metal centers were attached to polypyrroles [25–30]. The study of the P{B(n)T} films, and of films containing redox-active metal centers, was undertaken to examine the difference in the charge transfer characteristics upon variation of the bridge length.

2. Experimental

2.1. B(n)T monomers and reagents

3-{ω-[4-(2,2'-Bipyridyl)]ethyl}thiophene {B(2)T}, 3-{ω-[4-(2,2-bipyridyl)]pentyl}thiophene {B(5)T}, 3-{ω-[4-(2,2-bipyridyl)]heptyl}thiophene {B(7)T}, 3-{ω-[4-(2,2-bipyridyl)]nonyl}thiophene {B(9)T} and 3-{ω-[4-(2,2-bipyridyl)]undecyl}thiophene {B(11)T} were synthesized and chromatographically purified, as described previously [31].

N,N-Dimethylformamide (DMF; Merck, LR) was distilled from $MgSO_4$ onto 3 Å molecular sieves. Triethyl orthoformate (BDH, LR) was distilled from K_2CO_3 and stored over 3 Å and 13X molecular sieves prior to use. Propan-1-ol (M&B, LR) was dried over anhydrous K_2CO_3 and distilled under nitrogen from CaH_2 onto 3 Å molecular sieves. Dry Et_2O was refluxed and distilled from sodium benzophenone ketyl prior to use. Methanol (AJAX, AR) was used without further purification. Acetone (BDH, LR) was distilled before use. Sephadex LH 20 was obtained from Pharmacia. NH_4PF_6 (Fluka, puriss) was used without further purification.

Tetra-*n*-butylammonium hexafluorophosphate, [(n-$C_4H_9)_4N]PF_6$, and $LiClO_4$ were electrochemical grade (Fluka). Acetonitrile (Fluka, UV grade) was used for electrochemical and spectroscopic studies without further purification.

Samples of $[Ru(H_2O)_6](tos)_2$ and $[Ru(DMF)_6](tos)_2$ were synthesized by literature methods [32,33].

2.2. Syntheses of $[Ru\{B(n)T\}_3](PF_6)_2$

These complexes were prepared by a modification of the method described by Keene et al. [34]. $[Ru(DMF)_6](tos)_2$ (270 mg, 0.3 mmol) was added to a degassed (N_2) solution of B(n)T (0.97 mmol) in dry propan-1-ol (160 cm^3). The mixture was refluxed overnight during which time the color changed from orange to purple and finally to red. The solvent was removed in vacuo. The residue was dissolved in a minimum volume of MeOH, sorbed onto a column (24 × 3 cm) of Sephadex LH 20 and eluted with MeOH. The first band (orange) was collected and removal of the solvent provided red residues of $[Ru\{B(n)T\}_3](tos)_2$. This salt was dissolved in a minimum quantity of MeOH and an excess of solid NH_4PF_6 added with stirring. The resultant mixture was stored at −20°C overnight. The supernatant solution was decanted and the thick dark-red oily residue was dissolved in a minimum quantity of acetone, sorbed onto a Sephadex LH 20 column and eluted with acetone. The red band was collected, and removal of the solvent provided red crystals of $[Ru(II)\{B(n)T\}_3](PF_6)_2$. Yields of $[Ru\{B(n)T\}_3](PF_6)_2$: n = 2, 78% (m.p. 148°C); n = 5, 61% (m.p. 126°C); n = 7, 64% (m.p. 98°C); n = 9, 61% (m.p. 66°C); n = 11, 75% (m.p. 59°C). The products were characterized by ^1H NMR spectra; these data are given in Supplementary Table 1 which may be obtained from the authors on request.

2.3. Electropolymerization of the monomers

Poly[3-{ω-[4-(2,2'-bipyridyl)]alkyl}thiophenes], P{B(n)T}s, were prepared on platinum disk electrodes (area, 0.07 cm^2) by electrochemical oxidation of the corresponding monomers (0.1 M) at a constant potential of +2.3 V in acetonitrile solutions containing 0.1 M [(n-$C_4H_9)_4N]PF_6$. The faradaic charges passed Q were measured from I–t curves from which the film thickness d and the surface coverage Γ ($= Q/nFA$, $n = 2.25$ [35]) could be estimated as described previously [19], assuming no side-reactions occurred during the electrolysis processes. In general, Q values were controlled at 500 mC cm^{-2} and the thicknesses of the P{B(n)T} films were estimated to be between 2.0 (P{B(2)T}) and 3.8 μm (P{B(11)T}). The colors of the films varied according to the monomers and thickness of the polymers, with the P{B(n)T} films ($n \geq 5$) having dark colors, changing from green to a blue or purple color with increasing thickness. The P{B(2)T} films were a yellow color.

Poly-$[Ru\{B(n)T\}_3](PF_6)_{2x}$ films, P{RuB(n)T}, were prepared on platinum disk electrodes by positive potential scanning from 0 V to +2.0 V at a scan rate of 50 mV s^{-1} in an acetonitrile + 0.1 M [(n-$C_4H_9)_4N]PF_6$ solution containing 2 mM of the monomers, unless otherwise indicated. An outcome is shown in Fig. 1. The growth of the films was monitored by the increase of peak current of the Ru^{III}–Ru^{II} redox couple around 0.9 V. The oxidation peak of thiophene was observed close to 2.0 V, but the peak

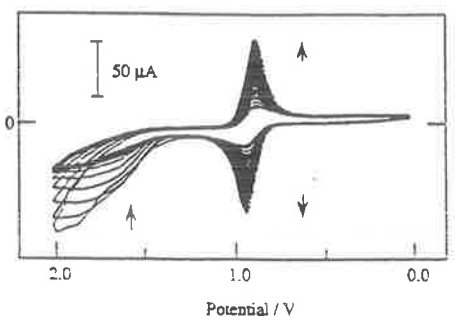

Fig. 1. Cyclic voltammograms of $[Ru\{B(5)T\}_3]^{2+}$ during an anodic electropolymerization. Solution: 2 mM $[Ru\{B(5)T\}_3]^{2+}$ + CH_3CN + 0.1 M [(n-$C_4H_9)_4N]PF_6$. Scan rate: 50 mV s^{-1}.

current decayed (rather than increased) with the polymerization process, until it reached a constant value. The alkyl chain length exerted some influence on the electropolymerization; compared with the other monomers, $[Ru\{B(5)T\}_3]^{2+}$ and $[Ru\{B(7)T\}_3]^{2+}$ exhibited a faster increase in film growth. The first cycle of $[Ru\{B(2)T\}_3]^{2+}$ showed a large oxidation peak at +1.7 V which was not clearly observable for those monomers with longer alkyl chains; instead there was a current plateau at more positive potentials. The colors of all the films were golden.

The charges passed and the surface coverages of the film-coated electrodes could be varied by controlling the number of the scans. Surface coverages, $\Gamma = Q/nFA$ (mol cm^{-2}), were determined by integrating the oxidative component of the Ru^{III}–Ru^{II} wave of cyclic voltammograms measured at a slow scan rate (10 mV s^{-1}) in CH_3CN + 0.1 M $[(n\text{-}C_4H_9)_4N]PF_6$ solution. Surface coverages were typically in the range $\Gamma_{Ru} = (1.5\text{–}2.5) \times 10^{-8}$ mol cm^{-2}, unless otherwise indicated.

Prior to electrodeposition, the working electrodes were polished to a mirror finish with a slurry of 0.05 μm alumina powder. The polished electrodes were then immersed in a concentrated $H_2SO_4 + K_2Cr_2O_7$ solution for 20 min, washed with tap water and triply distilled water, and dried with a stream of nitrogen. These cleaned electrodes were maintained at a potential of −100 mV in CH_3CN + 0.1 M $[(n\text{-}C_4H_9)_4N]PF_6$ solution for 10 min to reduce the oxidized species on the electrode surface. The electropolymerization was conducted in a three-electrode cell, with a platinum coil as the counter electrode and a Ag|0.01 M $AgNO_3 + CH_3CN$ electrode as the reference. The solutions were degassed by bubbling with high purity nitrogen prior to polymerization, and the electropolymerization was carried out at room temperature under a nitrogen atmosphere. After the polymerization, the film-modified electrodes were rinsed with acetonitrile, dried under an N_2 stream and electrochemically undoped by holding the electrodes at −100 mV for 10 min in CH_3CN + 0.1 M $[(n\text{-}C_4H_9)_4N]PF_6$ solution free of the monomers.

2.4. Electrochemical measurements of the polymer films

All the electrochemical measurements were performed with a BAS 100A electrochemical analyzer. The experiments were conducted in a standard three-electrode cell as described above. All solutions were deaerated by bubbling with high purity N_2 prior to measurement. The counter electrode was a platinum coil. All potentials were measured (and are reported) with respect to a Ag|0.01 M $AgNO_3 + CH_3CN$ reference electrode. Before chronoamperometric experiments were conducted, a cyclic voltammogram was measured from −1.7 to +1.9 V at a scan rate of 20 mV s^{-1} so that a stable redox current could be obtained. Further details of the procedure have been described previously [19].

2.5. Spectroscopic measurements of $[Ru\{B(n)T\}_3](PF_6)_2$

300 MHz ^{1}H NMR spectra (d_6–acetone solvent) were recorded on a Bruker AM 3000 FT spectrometer.

2.6. A.c. impedance measurements of the polymer-modified electrodes

The equipment and the experimental procedure have been described previously [19].

3. Results and discussion

3.1. Cyclic voltammetric behavior of P{B(n)T} and P{RuB(n)T} films

3.1.1. Cyclic voltammetric behavior of P{RuB(n)T} films in CH_3CN + 0.1 M $[(n\text{-}C_4H_9)_4N]PF_6$ solution

Fig. 2 shows cyclic voltammograms of P{RuB(n)T} films in CH_3CN + 0.1 M $[(n\text{-}C_4H_9)_4N]PF_6$ solution. The Ru^{III}–Ru^{II} redox couple appears at about 0.9 V, slightly

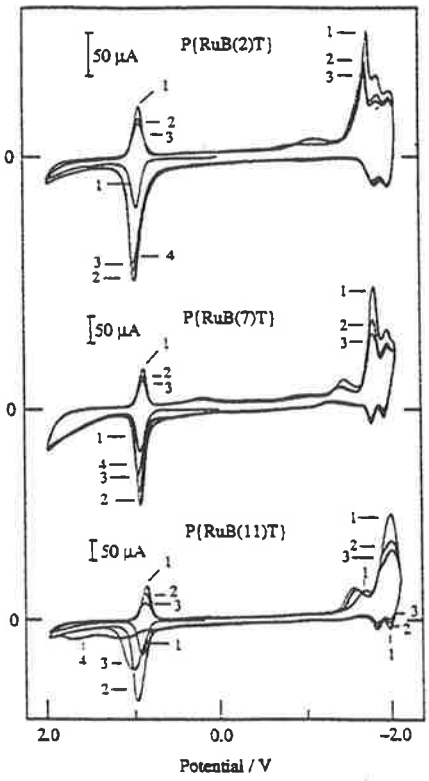

Fig. 2. Cyclic voltammograms of P{RuB(n)T} films in CH_3CN + 0.1 M $[(n\text{-}C_4H_9)_4N]PF_6$ solution. Scan rate: 0.1 V s^{-1}. Numbers indicate the cycle number in a continuously scanning experiment.

negative of the potential for the $[Ru(bpy)_3]^{2+}$ complex ($E_{1/2} = 0.95$ V vs. $Ag/AgNO_3$) [20]. Multiple redox waves appear at the more negative potentials. For a P{RuB(7)T} film, the first ligand reduction wave occurs at −1.5 V (the first cycle), the second reduction wave (the largest) is at −1.86 V accompanied by a reverse oxidation peak at −1.8 V, and the third reduction wave of the ligand is observed at −2.0 V (with a reverse oxidation peak at −1.96 V). In comparison with the reduction waves, these associated oxidation currents are very small. This suggests that most of the ligands remain in a reduced state and can be oxidized only at high potentials close to the oxidation potentials of the Ru^{III}–Ru^{II} couples. As a result, the oxidation currents of the Ru^{III}–Ru^{II} couples in the P{RuB(n)T} films increase dramatically, as shown in Fig. 2, but reduce in subsequent cycles as the ligand reduction component decays.

The variation of the alkyl chain length has a significant effect on the electrochemistry of the polymers. Compared with polymers with short alkyl chains, the ligand reduction waves of a P{RuB(11)T} film are shifted in a negative direction so that the third reduction wave cannot be seen within the lower potential limit of −2.1 V. However, in this case two reverse oxidation waves in the positive sweep are still observable at −1.82 and −1.95 V. The P{RuB(7)T} film behaves similarly, but the P{RuB(2)T} film is significantly different, presumably because of electronic factors arising from the mutual influence of thiophene and bpy moieties. Compared with the other polymers, the ligand reduction waves of the P{B(2)T} film shift negatively and occur at −1.77 (large and sharp), −1.9 and −2.04 V. Moreover, the reverse oxidation waves, with considerably larger currents, are found at −1.85 and −2.0 V.

The first (least negative) reduction wave for these films is different from the subsequent waves: it has no reverse peak and varies with the alkyl chain length (Fig. 2). The peak has $E_{p,c} \approx -1.77$ V with a sharp contour in the P{RuB(2)T} film. For the other polymers with a longer alkyl chain length, the first reduction peak is significantly more positive and the contour is broader. A peak of similar nature was also found by Deronzier et al. for analogous species based on polypyrrole [26], and in the present case it may be the n-doped current of the thiophene rings. The subsequent waves in these cases are associated with the reduction of the bpy ligand groups. For the P{RuB(2)T} film, the observation reflects the facilitated electron transport via the thiophene to the bpy groups through the short alkyl chain linkage.

Similarly, the redox waves at the Ru(III)–Ru(II) couple depend on the alkyl chain lengths. They occur at the same potential for the P{RuB(7)T} and P{RuB(11)T} films, but shift slightly in a positive direction for the P{RuB(2)T} film. Furthermore, the current decay of the Ru^{III}–Ru^{II} couple is faster after the first cycle for those polymers with longer alkyl chains, especially in the P{RuB(11)T} film where the broad oxidation waves are shifted positively. These voltammograms indicate that the lengthening of the alkyl chains of the polymers increases the irreversibility of the electrochemical reactions occurring in the P{RuB(n)T} films.

If the potential is scanned over the more positive potentials only, the P{RuB(n)T} films exhibit very stable redox behavior—their cyclic voltammograms have consistent redox potentials and there is very little current decay during a period of repeated potential cycles.

The influence of the alkyl chain lengths on the cyclic voltammetric behavior of the polymers can be rationalized as follows. The complex electron transport process between thiophene and 2,2′-bipyridine may occur in a number of ways, for instance by transport of the electrons through the alkyl chains, or by direct transfer of the electrons from the bipyridyl rings to the conjugated thiophene chains. In addition, the transfer of electrons in the reduced polymers may occur via self-exchange between different bpy rings. If the electron transport is conducted primarily through the alkyl chains, it is reasonable that the long chains would increase the irreversibility of the reduction processes of the polymers. The large reverse oxidation currents associated with the reduction of the P{Ru(2)T} films are rationalized in terms of the lower impediment to electron transport because of conduction through the shorter alkyl chain.

Intramolecular charge transfer via saturated bonds has been discussed previously [36,37]. McConnell reported a theoretical analysis of the rate of intramolecular charge transfer of the odd electron between the two phenyl groups in the mononegative ions of the α,ω-diphenylalkanes, Φ-$(CH_2)_n$-Φ [38], and a number of conclusions were drawn. The polymethylene chain can be replaced by a pseudopotential corresponding to an effective direct transfer between the rings; it was found that there is a strong tendency for self-trapping of the odd electron on one phenyl ring or the other owing to solvent polarization and bond distortions in the rings. This self-trapping greatly reduced the rate of intramolecular charge transfer. The intramolecular charge transfer occurred as an electronic resonance effect when a short-lived thermally-activated molecular state was formed in which the two rings appear equivalent to the odd electron. The activation energy was estimated to be of the order of 1000 cm^{-1}. Additionally, the rate of intramolecular charge transfer was found to decrease significantly with the length of the polymethylene chain.

Although it cannot be determined how far electrons can be transferred, the intramolecular charge transfer through a polymethylene chain is thought to be fast via short chains (3 carbon atoms or less) but slow via longer chains [38–40].

Shimada and coworkers investigated the intramolecular charge transfer in some similar systems with various lengths of alkyl chains using ESR spectroscopy [39–42]. These studies revealed that the charge transfer might not actually proceed via the chain but rather occur when the donor

approached the acceptor as a consequence of the flexibility of a long alkyl chain [42].

In the case of the P{RuB(n)T} films, while the thiophene groups are fixed onto the electrode as for the P{B(n)T} analogues, three bpy groups are connected to one another by a ruthenium center, leading to cross-linking networks among different alkyl chains and substantially decreasing the flexibility of the bpy groups. As described previously [19], the P{P(n)T} films were found to be more porous and less regular in their structure with increasing lengths of the alkyl chains; within the P{RuB(n)T} films, this tendency may well be enhanced because of the steric requirements caused by the coupling of the bpy groups with the metal centers. Although the concentration of the Ru redox sites may be relatively high in the films and the intermetal distance short, the cross-linking within the P{RuB(n)T} films would decrease the flexibility of the bpy groups to such an extent that the probability of direct electron transfer between the thiophene and the bpy groups is diminished. Similarly, the probability of electron transport through direct 'self-exchange' between the bpy groups is also low. The possibility of such direct electron transport cannot be totally excluded, but it is noted that both the above mechanisms would be favored by long alkyl chains, which increase the chain flexibility; accordingly, the polymers with longer chains should exhibit more reversible voltammetric behavior. However, cyclic voltammetry indicates that in the reduction processes of P{RuB(n)T} films, charge transfer decreases with the lengthening of the alkyl chains between the thiophene and bpy groups. As a result, the cathodic reduction waves of the polymers with longer chains possess features of kinetic control (i.e. broader contours) and these films exhibit smaller corresponding reverse oxidation waves in the cathodic region, as shown in Fig. 2. This result (and others discussed below) suggests that, in the cathodic region, charge transfer involves conduction through the alkyl chains.

The reduction characteristics of a P{RuB(7)T} film in $CH_3CN + 0.1$ M $[(n\text{-}C_4H_9)_4N]PF_6$ solution are shown in Fig. 3. Within a lower limit of -2.3 V (Fig. 3(A)), four reduction waves are observed and the response changes greatly during repeated potential sweeps (Fig. 3(B)). The first reduction wave at -1.5 V grows rapidly and the second wave decays continuously until it disappears completely. The positions of both these waves shift in a negative direction with repeated scan cycles, as does the third wave. With continuous scanning, the redox processes become more irreversible, and after a number of cycles, the extension of the scan to more positive potentials reveals that the redox waves of the Ru^{III}–Ru^{II} couple disappear completely, although the oxidation current of thiophene was still observed. Accordingly, the reduction processes result in a local deactivation of the polymer.

The disappearance of the Ru^{III}–Ru^{II} redox couple implies breakdown of the metal–ligand bonds, i.e. the partial decomposition of the polymer, although the mechanism is still unclear. However, aggregation of excess negative charges on the polymer may be an important factor. The other P{RuB(n)T} films have similar characteristics.

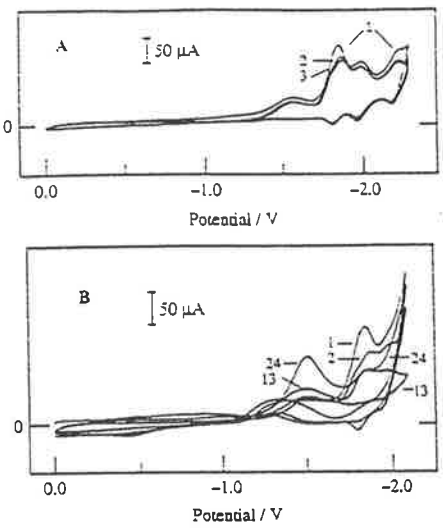

Fig. 3. Cyclic voltammograms of P{RuB(7)T} films in $CH_3CN + 0.1$ M $[(n\text{-}C_4H_9)_4N]PF_6$ solution. Scan rate: 0.1 V s^{-1}. (A) The first three cycles of scans; (B) continuous sweep cycles. The number indicates the cycle number in a continuously scanning experiment.

3.1.2. Cyclic voltammetric behavior of P{RuB(n)T} films in $CH_3CN + 0.1$ M $LiClO_4$ solution

The P{RuB(n)T} films have quite different voltammetric behavior in $CH_3CN + 0.1$ M $LiClO_4$ solution, compared with that described above, as shown in Fig. 4. At more positive potentials, the P{RuB(7)T} and P{RuB(11)T}

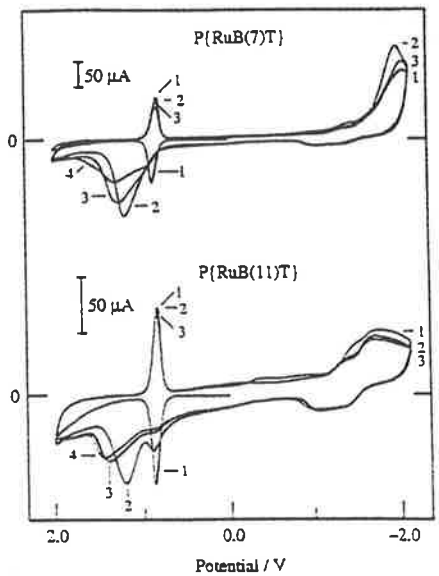

Fig. 4. Cyclic voltammograms of P{RuB(n)T} films in $CH_3CN + 0.1$ M $LiClO_4$ solution. Scan rate: 0.1 V s^{-1}. The numbers indicate the cycle numbers in a continuously scanning experiment.

films both exhibit the Ru^{III}–Ru^{II} couple at $E_{1/2} \approx +0.85$ V during the first scan cycle, but the $E_{p,a}$ shifts positively and assumes broader contours on subsequent scans. In contrast, the associated reduction peaks of the Ru^{III}–Ru^{II} couple retain the same position and shape, with little decay.

The electrochemical processes are influenced by the length of the alkyl chains. For the P{RuB(11)T} film, with a long alkyl chain, $I_{p,a}$ for the Ru^{III}–Ru^{II} couple is small in the second cycle of the scan, and although this peak decays in the subsequent cycles it is still observable. In the P{RuB(7)T} film, this peak appears only as a shoulder. The large faradaic charges observed between about +0.7 and +1.8 V are due to the contribution of the reduction processes of the polymers, as described previously for the case of the P{P(*n*)T} [19]. The broad contours signify that the charge transfer reaction is kinetically controlled.

At negative potentials, the P{RuB(7)T} film exhibits a reduction wave of the ligand at −1.95 V for the first cycle, with a broad associated oxidation wave from −1.5 to −0.8 V. For the P{RuB(11)T} film, ligand reduction peaks occur at ca. −1.35 and −1.7 V. Their broad contours signify that kinetic factors are more important in determining the cathodic electrochemical processes occurring in the polymers with longer chains; this provides further evidence for the earlier assertion that the electron transfer between the thiophene and the bpy groups may be conducted primarily through the alkyl chains linking them. The cathodic processes of the polymers are irreversible as the oxidation current of the ligand is very small compared with the reduction peak. The cathodic processes of the polymers seem to exhibit more irreversibility in $CH_3CN + LiClO_4$ than in $CH_3CN + [(n\text{-}C_4H_9)_4N]PF_6$ because of the broader contours of the redox waves and larger ΔE_p in the former case.

The residual charge retained in the cycle at more negative potentials may be estimated, based on the difference in area between the reduction waves of the bpy moiety and the corresponding oxidation waves. If this is compared with the increase in charge observed in the subsequent oxidation at more positive potentials (based on the difference between the areas of the peaks for the oxidation from +0.7 to +1.8 V and that for the Ru^{III}–Ru^{II} couple alone (obtained in the first cycle)), it is found that there is a clear correspondence. This provides further evidence that the excess negative charges, arising from the ligand reduction, are released to the electrode in a potential range from about +0.7 to +1.8 V.

Fig. 5(A) shows the cyclic voltammograms of the P{RuB(7)T} film swept continuously at more negative potentials. Very large reduction currents are observed in the first scan, which decay dramatically in subsequent cycles. However, the deactivated film can be reactivated if the potential is swept to +2.0 V, as shown in Fig. 5(B). In the continuous cycles at positive potentials, the film exhibits a large oxidation wave at $E_{p,a} = +1.08$ V and a

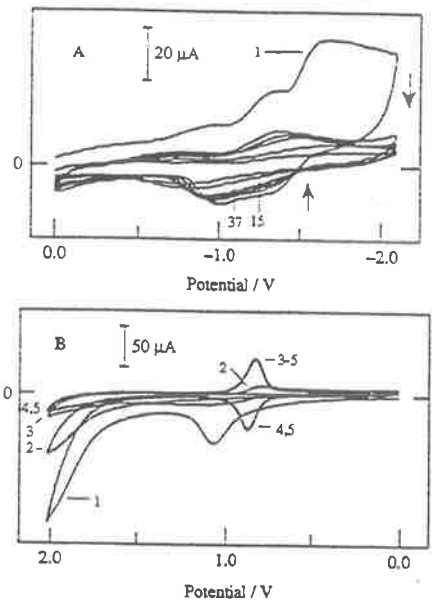

Fig. 5. Cyclic voltammograms of P{RuB(7)T} film in CH_3CN+0.1 M $LiClO_4$ solution. Scan rate: 0.1 V s^{-1}. (A) Continuously scanning at negative potentials. (B) Positive scanning for film deactivated in (A).

large oxidation current of the thiophene at potentials of +1.6 V or above. There are no corresponding reverse reduction waves in the first cycle of the sweep. In the second cycle, the oxidation wave at +1.08 V disappears but a reverse reduction wave starts to appear. After the third scan cycle, the redox waves of the Ru^{III}–Ru^{II} couple are recovered and retain stable redox currents. If the potential is swept at negative potentials, the reduction waves of the ligand are also recovered.

The Ru^{III}–Ru^{II} redox couples in the P{RuB(*n*)T} films are more irreversible in $CH_3CN + 0.1$ M $LiClO_4$ than in $CH_3CN + 0.1$ M $[(n\text{-}C_4H_9)_4N]PF_6$ solution. This phenomenon may be attributed to diffusion factors if a concentration polarization arising from non-linear diffusion of the counterions in the film results in larger ΔE_p values in $CH_3CN + 0.1$ M $LiClO_4$ solution. Additionally, some chemical irreversibility may also be involved, as discussed previously [19].

The variations in electrochemical responses in the cathodic processes of the P{RuB(*n*)T} films may be attributed to the influence of counter-cations of the electrolyte involved. Although there is some uncertainty as to the extent of solvation of Li^+ in CH_3CN, because of the smaller size of Li^+ it can diffuse into the reduced films very rapidly to maintain the electroneutrality, thus enhancing film stability. In the subsequent positive scans, the films reactivate as a result of the exclusion of the Li^+ cations. By contrast, the bulky cation Bu_4N^+ moves slowly in the films so that the reduced films are electroneutralized more slowly and gradually decompose.

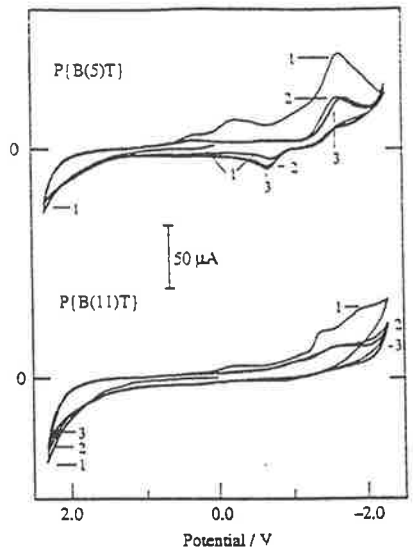

Fig. 6. Cyclic voltammograms of P{B(*n*)T} films in $CH_3CN + 0.1$ M $[(n\text{-}C_4H_9)_4N]PF_6$ solution. Scan rate: 0.1 V s^{-1}. The numbers indicate the cycle numbers in a continuously scanning experiment.

3.1.3. Cyclic voltammetric behavior of P{B(n)T} films

The cyclic voltammograms of a P{B(5)T} and a P{B(11)T} film in $CH_3CN + 0.1$ M $[(n\text{-}C_4H_9)_4N]PF_6$ solution are shown in Fig. 6. The oxidation currents of the thiophene are much larger than those observed in the corresponding P{RuB(*n*)T} films. The reduction waves of thiophene in the P{B(5)T} film appear at +0.3 and −0.25 V, although the wave at −0.25 V can be found in the first cycle only. The first scan cycle of the P{B(11)T} film shows the reduction wave of thiophene at −0.2 V, but it disappears in the following cycles. The reduction processes of the P{B(*n*)T} films are much simpler than those of the P{RuB(*n*)T}. For the P{B(5)T} film, only one large wave associated with the bpy reduction is observed at −1.68 V and it decays in subsequent cycles. The associated oxidation peak of the ligand occurs at −0.75 V (with a small accompanying peak at ca. −1.4 V), and it shifts in a positive direction in subsequent scan cycles. This peak is not observable in the P{B(11)T} film (only a small current is seen at about −0.9 V in the first cycle). This signifies that the reduction process is more irreversible in the polymers with long alkyl chains.

In a similar manner to the P{RuB(*n*)T} films, the cyclic voltammograms of the P{B(*n*)T} films exhibit a current decay at negative potentials with the continuous potential scanning in $CH_3CN + 0.1$ M $[(n\text{-}C_4H_9)_4N]PF_6$ solution. This is associated with gradual decomposition, as the deactivated films cannot be reactivated due to the damage to the polymer structure, as described in the case of the P{RuB(*n*)T} films.

The P{B(*n*)T} films exhibit similar cyclic voltammetric behavior in $CH_3CN + 0.1$ M $LiClO_4$ solution to that of the P{P(*n*)T} films reported previously [19]. The main difference is that the P{B(*n*)T} films possess slightly larger associated oxidation waves at more negative potentials. Decay of the cathodic current occurs in the reduction processes for the P{B(*n*)T} films in $CH_3CN + 0.1$ M $LiClO_4$ solution, but the films can be reactivated by means of a positive potential cycle from 0 to +2.3 V, with two large oxidation waves occurring at +0.9 and +2.1 V in the first cycle.

3.2. Apparent diffusion coefficients for charge transfer in P{B(n)T} films

The techniques used for the measurement of apparent diffusion coefficients of charge transfer in the polymers have been described previously [19]. If the potentials are respectively stepped from 0 to +2.0 V and from 0 to −2.0 V for the p- and n-doping processes of the polymers, the current decay will be described by the Cottrell equation [4,43,44]

$$I = \frac{nFAD^{1/2}c}{\pi^{1/2}t^{1/2}} \quad (1)$$

where A is the surface area of the electrode. The average concentration of electroactive species in the films is given by $c = \Gamma/d$, where Γ is the surface coverage and d is the thickness of the films; Γ can be estimated from the deposit charges according to Faraday's law, so that the apparent diffusion coefficients D_{app} for charge transfer in the polymers are obtainable on the basis of experimentally measured I–t data. The value of n is unity for the n-doping process of the polymers. However, it is difficult to determine for the p-doping process, although it can be assumed to be similar for all the polymers because the electron transport in p-doped polymers is conducted only through the conjugated polythiophene matrix and is therefore not significantly affected by the alkyl chain length. Taking into account the uncertainty in the determination of c and n, we present the results in the form of $D^{1/2}c$ and $nD^{1/2}c$ (p-doping process) values to estimate the charge transfer rates in these polymer-modified electrodes.

Table 1 shows the $D_{app}{}^{1/2}c$ values for charge transfer

Table 1
Apparent diffusion coefficients of charge transfer in P{B(*n*)T} films [a]

Polymer	Estimated thickness / μm	n-doped film [b]	p-doped film [b]
		$10^8\ D^{1/2}c$ / mol cm^{-2} $s^{-1/2}$	$10^8\ nD^{1/2}c$ / mol cm^{-2} $s^{-1/2}$
P{B(2)T}	2.0	2.3	1.1
P{B(5)T}	2.6	3.6	0.86
P{B(7)T}	3.0	2.1	1.3
P{B(9)T}	3.4	1.6	1.3
P{B(11)T}	3.8	1.4	1.4

[a] All the data obtained in $CH_3CN + 0.1$ M $[(n\text{-}C_4H_9)_4N]PF_6$ solution; potential steps from 0 to −2.0 V and from 0 to +2.0 V. [b] Surface coverage $\Gamma_{Th} \approx 2.3 \times 10^{-6}$ mol^{-1} cm^{-2}.

in the P{B(n)T} films in CH_3CN + 0.1 M[(n-C_4H_9)$_4$N]PF_6 solution. There is possibly a dependence of D_{app} on the alkyl chain length of the polymers. In the p-doping process, the $nD^{1/2}c$ values do not show a clear trend as the chain length is increased. However, if c decreases with lengthening of the alkyl chains (owing to the increase of d at a certain Γ value determined by the same Q in the polymer preparation), the D_{app} values of the polymers may increase with lengthening of the alkyl chains, with the exception of the P{B(2)T} film. The electron hopping in the p-doping process occurs in the conjugated thiophene rings, and the alkyl chain length of the polymers does not exert any significant kinetic influence on this process. Therefore, a significant factor in determining D_{app} values may be the porous structure of the polymers, since D_{app} is determined by the ion-transport rate D_i rather than the electron-transport rate D_e in this circumstance [19,45]. As described previously [19], the P{P(n)T} polymers become more porous with larger apertures as the alkyl chain length is increased. The P{B(n)T} films are assumed to exhibit the same tendency, which was also reported in the case of poly(3-alkylthiophenes) [46]. In those polymers with longer alkyl chains, the mobility of counterions is greater and larger D_{app} values are predicted. The exception of the P{B(2)T} film may be attributed to the electronic effect arising from pyridyl substitution. Although there appears to be a tendency for the $D^{1/2}c$ values for the n-doping process to decrease with increase in the alkyl chain length, it is counteracted by the decrease in c with lengthening of the alkyl chains, so that no clear trend is apparent in D_{app} itself.

3.3. Impedance analysis of the P{B(n)T} and the P{RuB(n)T} polymers

3.3.1. The predicted impedance spectra and equivalent circuits of conducting polymers

Fig. 7 shows the double layer structure, an equivalent circuit and a predicted impedance spectrum of the conducting polymers [11,47]. There are two double layers located at the metal|polymer (M|P) and the polymer|solution (P|S) interfaces respectively, as shown in Fig. 7(A). Accordingly, two kinetic semicircles can be predicted in the spectrum of Fig. 7(C). In general, the bulk polymer resistance semicircle at high frequencies is absent when the polymer-modified electrodes are studied in electrolyte solution [11]. This phenomenon may be interpreted by the Fletcher model [48] as described previously [19]. The typical a.c. impedance spectrum of a polymer-coated electrode consists of a charge transfer resistance semicircle, a Warburg impedance segment and a low frequency capacitance C_L, besides a solution resistance R_s and a bulk polymer resistance R_b [11,19,47,49–54]. The reason for the common observation of only one kinetic semicircle has been discussed by Johnson et al. [11].

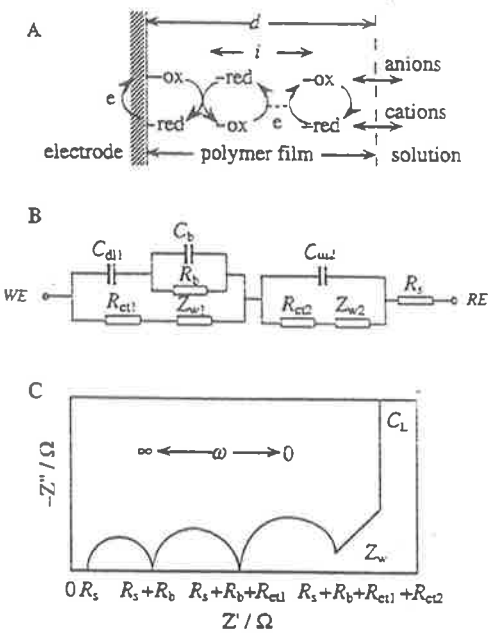

Fig. 7. Schematic representations of charge transfer in the double layers and the bulk film (A), the equivalent circuit (B) and the predicted impedance spectrum of conducting polymers (C).

The double layer capacitance can be evaluated from the spectrum on the basis of Eq. (2):

$$C_{dl} = 1/\omega^* R_{ct} \tag{2}$$

where $\omega^* = 2\pi f$ is the frequency at the top of the semicircle. The Warburg coefficient leading to $D_{app}^{1/2}c$ can be evaluated from the Warburg segment in the spectrum since

$$Z''\omega^{1/2} = \sigma = \frac{RT}{n^2F^2A\sqrt{2}\,D_{app}^{1/2}c} \tag{3}$$

where c is the concentration of the counterion in the polymer and D_{app} is its apparent diffusion coefficient [11]. A is the surface area of the electrode.

3.3.2. Impedance spectra of the P{B(n)T} films

Fig. 8 shows some impedance spectra of a P{B(5)T} film at different potentials in CH_3CN + 0.1 M [(n-C_4H_9)$_4$N]PF_6 solution. For a non-doped state of the polymer, the spectrum appears as a straight line with a slope of about 60° (Fig. 8(A)). This indicates that a non-doped polymer possesses considerable capacitance characteristics, which is consistent with the P{P(n)T} behavior [19]. At a potential of +1.5 V, an oxidized P{B(5)T} film shows a kinetic semicircle at intermediate frequencies, a Warburg impedance and a low-frequency capacitance (Fig. 8(B). This is in agreement with a report on polythiophene films [11]. However, analysis of the kinetic semicircle gives a charge transfer resistance of around 8–9 kΩ cm^2, which is much larger than that of polythiophene films (about 30 Ω

cm^2 at 1.1 V vs. SCE in CH_3CN + 0.1 M [$(n$-$C_4H_9)_4N$]ClO_4 solution [11], with a parallel capacitance of 5–10 $\mu F\ cm^{-2}$. It is not possible from this spectrum to identify which interface (M|P or P|S) is responsible for this semicircle. However, it can be confirmed that the charge transfer in an oxidized P{B(n)T} film meets a large resistance and is controlled by both kinetic and diffusion factors.

The reduction process of the P{B(5)T} film exhibits a particular impedance feature of two overlapping kinetic semicircles (Fig. 8(C)). The first semicircle, intercepting the Z' axis from 2.2 to 63 kΩ with a resistance R_{ct1} of about 4.2 kΩ cm^2 and a parallel capacitance of 10–20 $\mu F\ cm^{-2}$, is assigned to the charge transfer through the M|P interface. The other, which is assigned to the charge transfer through the P|S interface, intercepts the Z' axis from 50 to 75 kΩ and possesses a resistance R_{ct2} of around 1.7 kΩ cm^2 and a parallel capacitance of 200–250 $\mu F\ cm^{-2}$. The result suggests that the electron transport across the M|P interface is more difficult than the ion transport through the P|S interface, with a ratio of R_{ct1} to R_{ct2} equal to about 2.5. Instead of the Warburg impedance, a large arc appears at low frequencies with positive Z'', which is a feature of the generation of intermediates associated with phase changes (e.g. electrocrystallization [55–58], adsorption [59,60], and dissolution reactions [59,61,62]). In the case of the P{B(n)T} films, this self-inductive arc is attributed to the slow dissolution of the reduced polymer during the measurement. The spectra indicate that kinetic factors control charge transfer in the reduction processes of the P{B(n)T} films. The other P{B(n)T} polymers exhibit similar impedance behavior.

Owing to the large scales used in Fig. 8, the spectroscopic feature associated with R_b are not observable. The data from the spectra indicate that a bulk film resistance semicircle is absent in all the impedance spectra, but the sum of R_b and R_s values is about 100 Ω cm^2 for the p-doping process and 140–170 Ω cm^2 for the neutral and n-doped films. By comparison with the R_b values, the solution resistance (less than 10 Ω cm^2) is small and constant and may be ignored. The data signify that the R_b values are large and dependent on the doped states of the films. The incorporation of anions into the polymers may result in the decrease of the film resistance.

3.3.3. Impedance spectra of the P{RuB(n)T} films

The P{RuB(n)T} films are expected to have similar impedance behavior to those of their P{B(n)T} analogues. Fig. 9 shows some impedance spectra of the P{RuB(5)T} films in different doped states in CH_3CN + 0.1 M [$(n$-$C_4H_9)_4N$]PF_6 solution. At +0.9 V, a half-wave potential of the Ru^{III}–Ru^{II} couple, the polymer behaves as a capacitor. The curve intersects the real axis at about 30 Ω cm^2 (Fig. 9(B)), which implies a small bulk polymer resistance R_b occurring in a highly conductive polymer. The P{RuB(5)T} film shows similar impedance spectra to those of P{B(5)T} for the non-doped state and the reduction process of the polymer, and gives rise to similar R_b values. However, the P{RuB(5)T} film reveals smaller charge transfer resistances at both the M|P and the P|S interfaces.

At the M|P interface, R_{ct1} is estimated to be about 1.3 kΩ cm^2 with a parallel capacitance of around 50 μF

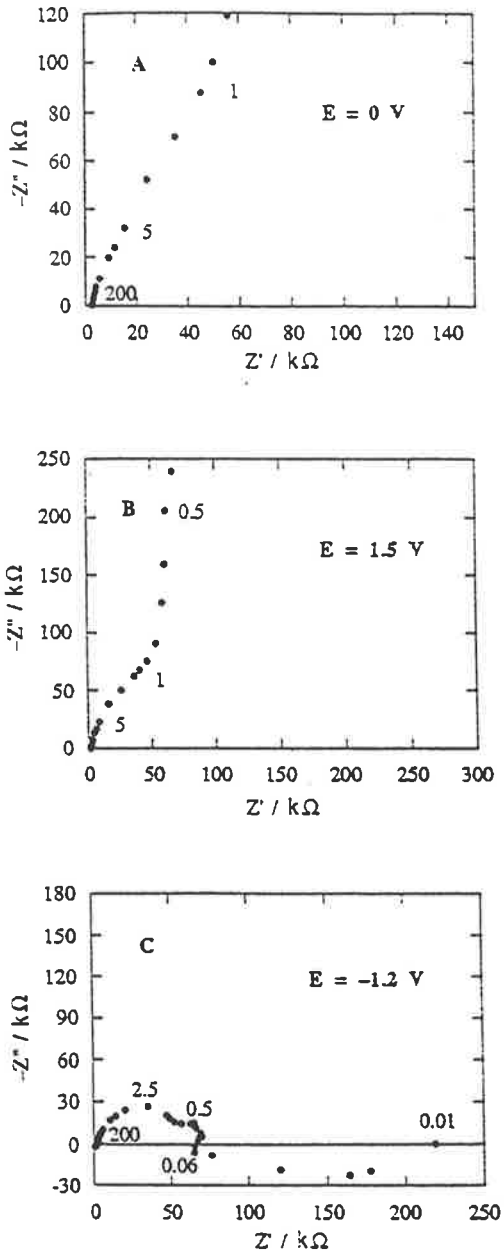

Fig. 8. Complex impedance planes for P{B(5)T} film at different potentials in CH_3CN + 0.1 M [$(n$-$C_4H_9)_4N$]PF_6 solution. Film thickness: 2.6 μm. The numbers indicate frequencies f in Hz.

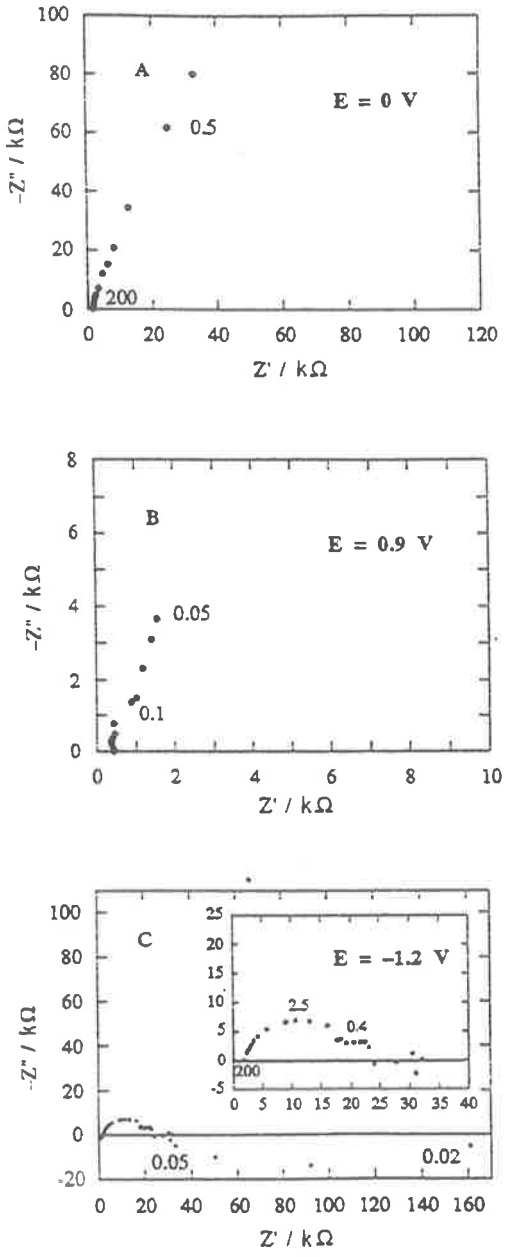

Fig. 9. Complex impedance planes for P{RuB(5)T} film at different potentials in CH_3CN + 0.1 M $[(n\text{-}C_4H_9)_4N]PF_6$ solution. $\Gamma_{Ru} = 1.6 \times 10^{-8}$ mol cm^{-2}. The numbers indicate frequencies f in Hz.

cm^{-2}. R_{ct2} is calculated to be about 420 Ω cm^2 with a parallel capacitance of around 500 μF cm^{-2} at the P|S interface. Both values are lower than those estimated for the P{B(5)T} film; this may be attributed either to the difference in surface coverages between the P{RuB(5)T} and the P{B(5)T} films, or to the influence of the metal center on the charge transfer in the polymers.

The self-inductive arc for P{RuB(5)T} and P{B(5)T} is somewhat different from the loops reported in the literature, since the Z' values increase rather than decrease for lower frequencies. It is found that a thicker P{RuB(5)T} film (where $\Gamma_{Ru} = 2.5 \times 10^{-8}$ mol cm^{-2}) exhibits a similar self-inductive loop to those reported in the literature [55–62]. This may arise from the difference in the relaxation time corresponding to the different thickness of the polymers. Fleischmann has pointed out that these phase formation and dissolution processes may occur as a result of microscopic changes in the morphology of the surface due to the nucleation, growth, and overlap at growth or dissolution centers [63]. The contribution of the inductive component was probably due to periodic changes in the morphology because of alterations in the spacing of steps generated by dislocations [63]. The response can thus be rationalized in terms of dissolution of the P{B(n)T} and P{RuB(n)T} films at negative potentials, which has been confirmed by cyclic voltammetric results as discussed above.

The impedance behavior of a P{RuB(5)T} film in CH_3CN + 0.1 M $LiClO_4$ solution is shown in Fig. 10. The non-doped polymer behaves as a capacitor (Fig. 10(A)). In addition, the intersection of the curve at the real axis gives rise to a bulk polymer resistance of about 140 Ω cm^2, similar to the value found in CH_3CN + 0.1 M $(n\text{-}C_4H_9)_4N]PF_6$ solution. This spectroscopic feature of the bulk polymer resistance is similar to that of the P{P(n)T} film, which was discussed previously [19]. At +0.82 V, a half-wave potential of the Ru^{III}–Ru^{II} couple, the polymer possesses typical capacitance characteristics. The vertical line intersects the real axis at about 30 Ω cm^2 (Fig. 10(B)); this implies a small bulk polymer resistance R_b appearing in a highly conductive polymer, a feature also observed for the film in CH_3CN + 0.1 M $[(n\text{-}C_4H_9)_4N]PF_6$ solution (see above). The spectrum of a reduced film shows a small kinetic resistance semicircle with a charge transfer resistance R_{ct} of 350 Ω cm^2 and a C_{dl} of 11 μF cm^{-2}, a Warburg impedance and a low-frequency capacitance. From the Warburg region, the $D^{1/2}c$ value is evaluated to be 7×10^{-10} mol cm^{-2} $s^{-1/2}$ on the basis of Eq. (3). This value implies a small value of D_{app} which is probably due to the network structure of the polymer. It is noted that the value of the charge transfer resistance R_{ct} is close to that of the R_{ct2} (420 Ω cm^2) for the same polymer measured in CH_3CN + 0.1 M $(n\text{-}C_4H_9)_4N]PF_6$ solution. This means that the semicircle in Fig. 10(C) may be attributed to the P|S interface, an assumption which corresponds with that presented for the polythiophene film [11]. In contrast to the spectra in CH_3CN + 0.1 M $(n\text{-}C_4H_9)_4N]PF_6$ solution, the spectroscopic feature of a self-inductance does not appear in CH_3CN + 0.1 M $LiClO_4$ solution. The spectrum suggests that both diffusion and kinetic factors control the electrochemical process in the reduced film; this is consistent with the cyclic voltammetry data, which reveal that the kinetic factor is predominant for

the P{RuB(11)T} but that diffusion is also important for the P{RuB(7)T} film. The result is different from that of the P{P(*n*)T} films [19], where kinetic control is observed in the P{P(*n*)T} films in $CH_3CN + 0.1$ M $LiClO_4$ solution. This difference may be ascribed to their respective structures: in the P{RuB(*n*)T} film, the cross-linking structure caused by the ligation of bpy groups to the metal centers inhibits the mobility of counterions so that the mass transfer becomes important. Fig. 10(C) shows a very large R_b (nearly 1.3 kΩ cm^2), which may arise because the large amount of Li^+ incorporated into the negatively charged film changes the dielectric properties of the polymer and the film resistance, as discussed in the case of the P{P(*n*)T} films [19].

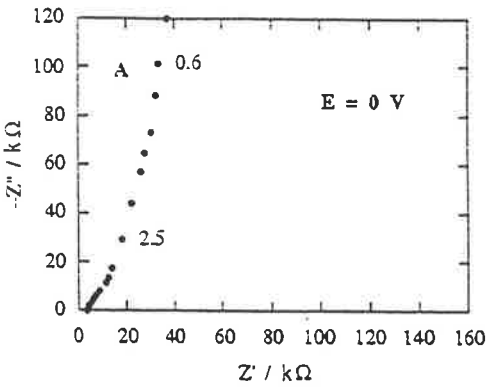

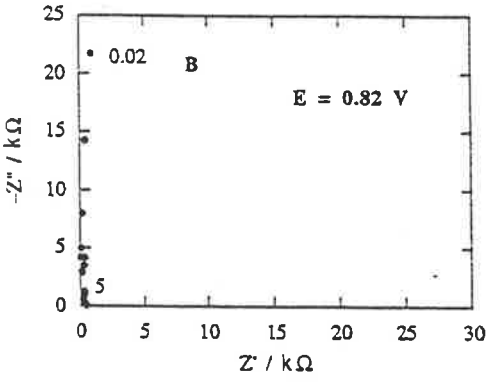

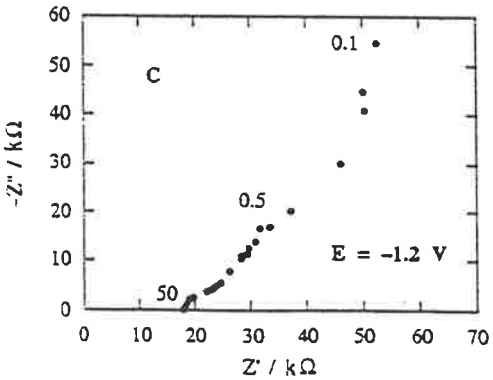

Fig. 10. Complex impedance planes for P{RuB(5)T} film at different potentials in $CH_3CN + 0.1$ M $LiClO_4$ solution. $\Gamma_{Ru} = 2.2 \times 10^{-8}$ mol cm^{-2}. The numbers indicate frequencies f in Hz.

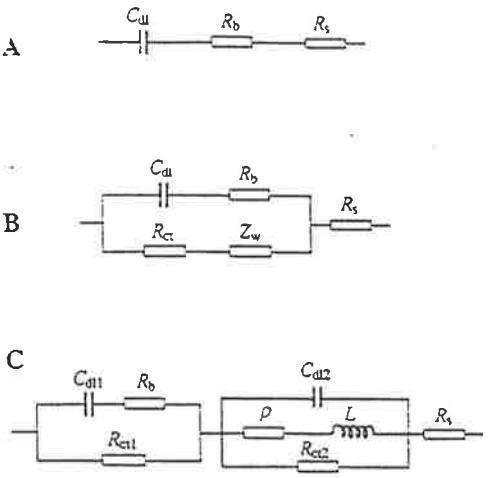

Fig. 11. Equivalent circuits of the P{B(*n*)T} and P{RuB(*n*)T} film electrodes. (A) Non-doped states and oxidation of the Ru^{III}–Ru^{II} couple; (B) p-doping process in $CH_3CN + 0.1$ M $[(n\text{-}C_4H_9)_4N]PF_6$ and n-doping process in $CH_3CN + 0.1$ M $LiClO_4$ solution; (C) n-doping process in CH_3CN0.1 M $[(n\text{-}C_4H_9)_4N]PF_6$ solution. R_s, solution resistance; R_b, bulk polymer resistance; C_{dl}, double-layer capacitance; R_{ct}, charge transfer resistance; ρ faradaic resistance; L, self-inductance.

3.3.4. Equivalent circuits of the P{B(n)T} and P{RuB(n)T} polymer electrodes

Under the different conditions, the impedance behavior of the P{B(*n*)T} and P{RuB(*n*)T} films is represented by the equivalent circuits in Fig. 11. For non-doped films, the equivalent circuit consists of a capacitance, a solution resistance and a bulk polymer resistance R_b (Fig. 11(A)). This circuit also describes the oxidation process of the Ru^{III}–Ru^{II} couple of the P{RuB(*n*)T} films.

In this case, both R_{ct} and Z_w are unimportant. The situation for oxidized films is represented by the circuit in Fig. 11(B), where the parallel circuit indicates the kinetic semicircle and Warburg impedance in the spectrum. This circuit also represents the reduction processes of the polymers in $CH_3CN + 0.1$ M $LiClO_4$ solution. A more complicated equivalent circuit is shown in Fig. 11(C) for the case of those films reduced in $CH_3CN + 0.1$ M $[(n\text{-}C_4H_9)_4N]PF_6$ solution. The series combination of an self-inductance L and a faradaic resistance ρ is associated with the partial dissolution of the polymers at the P|S interface. This part of the equivalent circuit is in agreement with that reported previously for the anodic dissolution of iron in acidic solutions [61].

Table 2
Impedance parameters of P{RuB(n)T} films at −1.2 V in CH_3CN + 0.1 M $[(n\text{-}C_4H_9)_4N]PF_6$ solution

Polymer	$10^6\ \Gamma_{Ru}$ / mol cm^{-2}	R_{ct1} / kΩ cm^2	R_{ct2} / kΩ cm^2	C_{dl1} / μF cm^{-2}	C_{dl2} / μF cm^{-2}
P{RuB(2)T}	1.9	1.0	0.35	16	900
P{RuB(5)T}	1.6	1.3	0.42	50	500
P{RuB(7)T}	2.0	2.4	0.91	13	290
P{RuB(9)T}	1.5	2.9	1.4	16	160
P{RuB(11)T}	1.6	4.6	2.1	14	150

3.3.5. Dependence of charge transfer resistances of the reduced P{RuB(n)T}-film modified electrodes on the alkyl chain length between the two functionalities

In non-doped and oxidized states, the impedance spectra of the P{B(n)T} and P{RuB(n)T} films do not exhibit any significant dependence on the alkyl chain length n. Also, the n-doping process of the P{B(n)T} films is independent of the alkyl chain lengths. However, the reduction processes of the P{RuB(n)T} films in CH_3CN + 0.1 M $[(n\text{-}C_4H_9)_4N]PF_6$ solution do show such a dependence, as shown in Table 2. Both R_{ct1} and R_{ct2} increase with lengthening of the alkyl chains, but the ratio of R_{ct1} to R_{ct2} remains between 2.5 and 3.5, which is similar to the case of P{B(5)T} films. The result confirms an earlier assertion—longer alkyl chains increase the difficulty of the charge transfer in the films, which implies that this charge transfer occurs through the alkyl chains and then the conjugated polythiophene matrix in the reduced polymers. Furthermore, the charge transfer appears to take place through the alkyl chains, even when up to 11 carbon atoms are present, in spite of the large impedance.

In addition to charge transfer resistance, it is found that R_b values are larger for those polymers with longer alkyl chains. Thus the R_b values of the polymers are dependent not only on the doped state but also the alkyl chain lengths for the n-doped films. Also, larger self-inductive arcs are observed for the polymers with longer alkyl chains, suggesting there is a larger impedance for the dissolution of these polymers.

4. Conclusions

The cyclic voltammetric behavior of the P{B(n)T} and the P{RuB(n)T} polymers is largely irreversible. This irreversibility increases with the lengthening of the alkyl chains in the reduced polymers. The polymers were found to decompose gradually upon repeated potential sweeping at negative potentials in CH_3CN + 0.1 M $[(n\text{-}C_4H_9)_4N]PF_6$ solution. These polymers exhibit quite different electrochemical behavior in CH_3CN + 0.1 M $LiClO_4$ solution, where the films deactivate quickly with repeated sweeps at negative potentials with storage of multiple electrons in the bpy groups, but may be reactivated by cycling into the anodic region.

The impedance spectra of the non-doped P{B(n)T} and P{RuB(n)T} film electrodes indicate a capacitive behavior, which is applicable to the impedance characteristics of the Ru^{III}–Ru^{II} couple of the polymers as well. The oxidation processes of the P{B(n)T} and P{RuB(n)T} films show a charge transfer resistance, a Warburg impedance and a low-frequency capacitance. The reduced polymers exhibit similar behavior in CH_3CN + 0.1 M $LiClO_4$ solution, but with a much larger bulk polymer resistance. These results are interpreted to show that the electrochemical processes are controlled by both kinetic and diffusion factors in these cases. In contrast, the impedance spectra of the reduced polymer electrodes indicate that the diffusion is unimportant in the electrochemical processes of the films in CH_3CN + 0.1 M $[(n\text{-}C_4H_9)_4N]PF_6$ solution. The charge transfer resistances at interfaces imply that electron transport through the M|P interface is more difficult than ion transport through the P|S interface. Furthermore, the impedance spectra of the reduced P{RuB(n)T} films show a dependence on the alkyl chain length of the polymers; those polymers with longer alkyl chains exhibit larger charge transfer resistances at both M|P and P|S interfaces, suggesting that charge transfer between the thiophene and bipyridine groups is conducted mainly through the alkyl chains in the reduced P{RuB(n)T} films. Accordingly, the kinetic factors caused by the alkyl chains control the charge transfer processes in the reduced films. In addition, these spectra exhibit a self-inductive impedance feature consistent with formation of soluble intermediates in CH_3CN + 0.1 M $[(n\text{-}C_4H_9)_4N]PF_6$ solution, confirming the slow decomposition of the reduced films.

Acknowledgements

This research was supported by the Australian Research Council. JW wishes to acknowledge the Australian International Development Assistance Bureau for an ADCSS scholarship and James Cook University for a postgraduate research award for overseas students. Assoc. Professor A. Walton and S. Cumming (Department of Electrical & Computer Engineering, JCUNQ) are thanked for the loan of the instrumentation for the measurement of a.c. impedance spectra. Helpful discussions with Assoc. Professor F.G. Thomas (Department of Chemistry and Chemical Engineering, JCUNQ) are also gratefully acknowledged.

References

[1] R.J. Waltman, J. Bargon and A.F. Diaz, J. Phys. Chem., 87 (1983) 1459.
[2] J.O'M. Bockris and F.B. Diniz, Electrochim. Acta, 34 (1989) 567.
[3] F.B. Kaufman, A.H. Schroeder, E.M. Engler, S.R. Kramer and J.Q. Chambers, J. Am. Chem. Soc., 102 (1980) 483.
[4] P. Daum, J.R. Lenhard, D. Rolison and R.W. Murray, J. Am. Chem. Soc., 102 (1980) 4649.

[5] A. Yassar, J. Roncali and F. Garnier, Macromolecules, 22 (1989) 804.
[6] C. Deslouis, M.M. Musiani and B. Tribollet, J. Electroanal. Chem., 264 (1989) 37.
[7] C. Gabrielli, H. Takenouti, O. Haas and A. Tsukada, J. Electroanal. Chem., 302 (1991) 59.
[8] F. Beck and P. Hulser, J. Electroanal. Chem., 280 (1990) 159.
[9] X. Ren and G.J. Pickup, J. Phys. Chem., 97 (1993) 5356.
[10] S. Sunde, G. Hagen and R. Ødegard, J. Electroanal. Chem., 345 (1993) 59.
[11] B.W. Johnson, D.C. Read, P. Christensen, A. Hamnett and R.D. Armstrong, J. Electroanal. Chem., 364 (1994) 103.
[12] N. Oyama and F.C. Anson, J. Electrochem. Soc., 127 (1980) 640.
[13] R. Mirrazaei, D. Parker and H.S. Munro, Synth. Met., 30 (1989) 265.
[14] J. Roncali, C. Thobie-Gauter, H. Brisset, J.-F. Favart and A. Guy, J. Electroanal. Chem., 381 (1995) 257.
[15] E. Buhks and I.M. Hodge, J. Chem. Phys., 83 (1985) 5976.
[16] J. Ochmanska and T.G. Pickup, J. Electroanal. Chem., 271 (1989) 83.
[17] M. Onoda, H. Nakayama, S. Morita and K. Yoshino, J. Appl. Phys., 73 (1993) 2859.
[18] G.P. Vanderlaan, M.P. Dehaas, A. Buik and B. Deruiter, Synth. Met., 57 (1993) 4930.
[19] J. Wang and F.R. Keene, J. Electroanal. Chem., 59.
[20] A. Juris, S. Barigelletti, S. Campagna, V. Balzani, P. Belser and A. von Zelewsky, Coord. Chem. Rev., 84 (1988) 85.
[21] K.V. Gobi and R. Ramaraj, J. Electroanal. Chem., 368 (1994) 77.
[22] W.E. Rudzinski and A.J. Bard, J. Electroanal. Chem., 199 (1986) 323.
[23] D. Ege, P.K. Ghosh, J.R. White, J.F. Fqucy and A.J. Bard, J. Am. Chem. Soc., 107 (1985) 5644.
[24] I. Rubinstein and A.J. Bard, J. Am. Chem. Soc., 103 (1981) 5007.
[25] A. Deronzier and J.-C. Moutet, Acc. Chem. Res., 22 (1989) 249.
[26] A. Deronzier, J.-C. Moutet and D. Zsoldos, J. Phys. Chem., 98 (1994) 3086.
[27] A. Deronzier, J.-C. Moutet and E. Saint-Aman, J. Electroanal. Chem., 327 (1992) 147.
[28] A. Deronzier, R. Devaux, D. Limosin and J.-M. Latour, J. Electroanal. Chem., 324 (1992) 325.
[29] A. Deronzier and M. Essakalli, J. Chem. Soc. Chem. Commun., (1990) 242.
[30] A. Deronzier, M. Essakalli and J.-C. Moutet, J. Electroanal. Chem., 244 (1988) 163.
[31] J. Wang, M. Pappalardo and F.R. Keene, Aust. J. Chem., 48 (1995) 1425.
[32] P. Bernhard, H.B. Bürgi, J. Hauser, H. Lehmann and A. Ludi, Inorg. Chem., 21 (1982) 3936.
[33] P. Bernhard and A.M. Sargeson, J. Am. Chem. Soc., 111 (1989) 597.
[34] F.R. Keene, M.R. Snow, P.J. Stephenson and E.R.T. Tiekink, Inorg. Chem., 27 (1988) 2040.
[35] A.F. Diaz, J.I. Castillo, J.A. Logan and W.-Y. Lee, J. Electroanal. Chem., 129 (1981) 115.
[36] K.D. Jordan and M.N. Paddon-Row, Chem. Rev., 92 (1992) 395.
[37] M.R. Wasielewski, Chem. Rev., 92 (1992) 435.
[38] H.M. McConnell, J. Chem. Phys., 35 (1961) 508.
[39] K. Shimada, G. Moshuk, H.O. Connor, P. Caluwe and M. Szwarc, Chem. Phys. Lett., 14 (1972) 396.
[40] K. Shimada and M. Szwarc, Chem. Phys. Lett., 28 (1974) 540.
[41] H.D. Connor, K. Shimada and M. Szwarc, Chem. Phys. Lett., 14 (1972) 402.
[42] K. Shimada and M. Szwarc, Chem. Phys. Lett., 34 (1975) 503.
[43] R.W. Murray, in A.J. Bard (Ed.), Electroanalytical Chemistry, Vol. 13, Marcel-Dekker, 1984, p. 208.
[44] A.J. Bard and L.R. Faulkner, Electrochemical Methods, Wiley, New York, 1980, p. 143.
[45] N.A. Surridge, J.C. Jernigan, E.F. Dalton, R.P. Buck, M. Watanabe, H. Zhang, M. Pinkerton, T.T. Wooster, M.L. Longmire, J.S. Facci and R.W. Murray, J. Chem. Soc. Faraday Discuss., 88 (1989) 1.
[46] J. Roncali, R. Garreau, A. Yassar, P. Marque, F. Garnier and M. Lemaire, J. Phys. Chem., 91 (1987) 6706.
[47] M. Sharp, B. Lindholm-Sethson and E.V. Lind, J. Electroanal. Chem., 345 (1993) 223.
[48] S. Fletcher, J. Electroanal. Chem., 337 (1992) 127.
[49] C. Gabrielli, H. Takenouti, O. Haas and A. Tsukada, J. Electroanal. Chem., 302 (1991) 59.
[50] J. Tanguy, J.L. Baudoin, F. Chao and M. Costa, Electrochim. Acta, 37 (1992) 1417.
[51] J. Tanguy, N. Mermilliod and M. Hoclet, J. Electrochem. Soc., 134 (1987) 795.
[52] S. Ye, F. Girard and D. Bélanger, J. Phys. Chem., 97 (1993) 12373.
[53] W.J. Albery and A.R. Mount, J. Electroanal. Chem., 305 (1991) 3.
[54] T. Osaka and T. Momma, Electrochim. Acta, 38 (1993) 2011.
[55] R.D. Armstrong and R.E. Firman, J. Electroanal. Chem., 45 (1973) 3.
[56] W.I. Archer and R.D. Armstrong, Electrochemistry, Chemical Society Specialist Periodical Reports, 7 (1980) 157.
[57] W. Davison, J.A. Harrison and J. Thompson, Faraday Discuss. Chem. Soc., 56 (1974) 171.
[58] I. Epelboin and R. Wiart, J. Electrochem. Soc., 118 (1971) 1577.
[59] R.D. Armstrong, R.E. Firman and H.R. Thirsk, Faraday Discuss. Chem. Soc., 56 (1974) 244.
[60] R.D. Armstrong and M. Henderson, J. Electroanal. Chem., 39 (1974) 81.
[61] I. Epelboin, M. Keddam and J.C. Lestrade, Faraday Discuss. Chem. Soc., 56 (1974) 264.
[62] I. Epelboin and M. Keddam, Electrochim. Acta, 17 (1972) 177.
[63] M. Fleischmann, Faraday Discuss. Chem. Soc., 56 (1974) 294.

Pergamon

Electrochimica Acta, Vol. 41, No. 16, pp. 2563–2569, 1996

0013–4686/96 $15.00 + 0.00

PII:S0013–4686(96)00070–9

MECHANISM OF MEDIATION OF THE ELECTROCHEMICAL OXIDATION OF $K_4Fe(CN)_6$ AT POLY-[TRIS(3-{ω-[4-(2,2′-BIPYRIDYL)] ALKYL}-THIOPHENE)IRON(II)]-FILM MODIFIED ELECTRODES IN AQUEOUS SOLUTIONS

JIAXIONG WANG and F. RICHARD KEENE*

Department of Chemistry and Chemical Engineering, School of Molecular Sciences, James Cook University of North Queensland, Townsville, Queensland 4811, Australia

(*Received* 26 *June* 1995; *in revised form* 6 *November* 1995)

Abstract—The kinetics of the electrochemical oxidation of $K_4Fe(CN)_6$ at poly-[tris(3-{ω-[4-(2,2′-bipyridyl)]alkyl}thiophene)iron(II)]-film modified electrodes have been investigated in aqueous solutions, using cyclic voltammetry and rotating disk electrode voltammetry. The retro-electrocatalytic reaction of the substrate at the polymer-coated electrodes is dependent on the alkyl chain length between the thiophene and 2,2′-bipyridine moieties and on the concentration of the substrate. The electrodes coated with the films possessing short alkyl chains exhibit more reversible voltammetric behavior and better catalytic activity to the oxidation of $[Fe(CN)_6]^{4-}$ species in aqueous solutions compared with those possessing long alkyl chains. Kinetic parameters, calculated on the basis of modified Levich equations, indicate that under most circumstances the mediated reactions are controlled by the chemical step. Copyright © 1996 Elsevier Science Ltd

Key words: modified electrode, polythiophene, tris(2,2′-bipyridine)iron(II), electrocatalysis, mechanism.

INTRODUCTION

The modification of electrode surfaces by polymer films which contain transition-metal complexes has received considerable attention due to the potential application in the areas of photo- and electrocatalysis[1–5]. By comparison with homogeneous catalysis, the heterogeneous catalysis arising from this kind of polymer-modified electrode has some particular advantages: firstly, the amount of catalyst required is markedly lower since all the active centers are concentrated on the surface of an electrode, and the regeneration of the catalyst is relatively straightforward. Secondly, since they are in different phases, the separation of products from the catalyst is facilitated. Finally, some selective catalysis may be achieved through the design of the polymer structure. On the other hand, the kinetic characteristics of such heterogeneous catalytic reactions are more complex than the homogeneous case.

Polymer-modified electrodes have been applied to various catalytic reactions, such as selective catalysis in organic synthesis[6–13], the reduction of O_2[14–18] and CO_2[19–25], and photocatalysis[26, 27]. A majority of these polymer matrixes, such as poly(vinylpyridine) (PVPy) and Nafion films, are non-conductive. Deronzier and co-workers have developed a series of electrodes modified with conducting polymers based on polypyrrole matrixes for use in catalytic processes. In these studies, 2,2′-bipyridyl groups containing transition-metal centers were attached to the *N*-atom of pyrrole *via* carbon chains and the catalytic activity of the resultant substituted polypyrrole films was investigated[11–13, 22, 24, 25, 27–34] Because of the high electronic conductivities and electrochemical activity, the electrodes coated with conducting polymers containing transition-metal complexes have considerable promise for catalytic applications. Perhaps surprisingly, reports of analogous electrode modification using polythiophene and its derivatives as the support matrix are scarce. This may be due to difficulties associated with the monomer synthesis, and the high oxidation potential required for the thiophene electropolymerization. However, polythiophene possesses more aromatic character and air stability than polypyrrole. Therefore, the catalytic electrodes based on the polythiophenes and incorporating transition-metal centers are an attractive target for development: this kind of polymer-modified electrode has recently been prepared, and their properties investigated, in particular the mechanism of charge transfer[35].

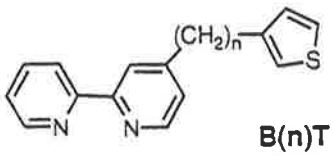

B(n)T
{n = 2, 7, 11}

* Author to whom correspondence should be addressed.

The present work aims to provide some basic kinetic information on electrocatalytic reactions occurring at the interface of such modified electrodes. For this purpose, the metal electrodes coated with poly-[Fe(II){B(*n*)T}$_3$] (designated P{FeB(*n*)T}) have been employed {B(*n*)T = 3-{ω-[4-(2,2′-bipyridyl)]alkyl}thiophene}, and $[Fe(CN)_6]^{4-}$ was chosen as the electroactive substrate because the reaction between it and the catalytic species is thermodynamically favored and the anion may easily diffuse into the oxidized films. The reactions were undertaken in aqueous solution.

The catalytic scheme can be written as

$$\begin{aligned} &Pt/P\{FeB(n)T\}^{2+} - e \rightleftharpoons Pt/P\{FeB(n)T\}^{3+} \\ &\uparrow \qquad\qquad\qquad\qquad \downarrow \\ &Pt/P\{FeB(n)T\}^{3+} \\ &+ [Fe(CN)_6]^{4-} \xrightarrow{k_{cts}} Pt/P\{FeB(n)T\}^{2+} \\ &\qquad\qquad + Fe(CN)_6]^{3-}. \quad (1) \end{aligned}$$

For the kinetics of this kind of mediated reaction, four potential current-controlling factors must be taken into account[36]:

1. The rate of mass transport of the substrate $[Fe(CN)_6]^{4-}$ in the solution to the polymer/solution interface, with a diffusion coefficient D_s;
2. The rate of electron transfer k_{cts} (mediated reaction rate $k_{cts}\Gamma$) between the catalyst and the substrate at the interface, and within the polymer films in cases where the substrate permeates the films;
3. The rate of transport of electrochemical charge through the polymer catalyst films by a diffusion-like process with a coefficient D_{ct}; and
4. The rate of permeation of the substrate, with a partition coefficient P and a diffusion coefficient $D_{s,pol}$, into and within the polymer films.

The rate of permeation of the substrate $[Fe(CN)_6]^{4-}$ is predicted to be relatively fast within the oxidized (*p*-doped) films. Therefore, the final factor (#4) was not considered to exert an important influence on the mediated process. Cyclic voltammetry and rotating disk electrode (*rde*) voltammetry were employed to investigate the kinetics of the oxidation reactions occurring at the interface of the electrodes coated with P{FeB(*n*)T}, and its dependence on the lengths of the alkyl chains between the thiophene and bipyridyl rings, and provides some insights into the catalytic properties of the polythiophene-based electrodes.

EXPERIMENTAL

B(n)*T monomers and reagents*

3-{ω-[4-(2,2′-Bipyridyl)ethyl}thiophene {B(2)T}, 3-(ω-[4-(2,2′-bipyridyl)heptyl}thiophene {B(7)T} and 3-{ω-[4-(2,2′-bipyridyl)undecyl}thiophene {B(11)T} were synthesized and chromatographically purified, as described previously[37]. Ferrous sulfate ($FeSO_4 \cdot 7H_2O$; HBS, AR) was used for the syntheses of iron complexes. Acetone (BDH, LR) was distilled prior to use. Ammonium hexafluorophosphate (NH_4PF_6; Fluka, purum) and diethyl ether (Et_2O; BDH, AR) were used without further purification.

Tetra-*n*-butylammonium hexafluorophosphate ($[n\text{-}C_4H_9)_4N]PF_6$; Fluka, electrochemical grade), acetonitrile (Sigma-Aldrich, HPLC), sulfuric acid (98%; Ajax, AR), potassium ferrocyanide (Ajax, AR) and sodium sulfate (Ajax, AR) were used without further purification. Water for electrochemistry was distilled and further purified through a Modulab Millipore apparatus.

Syntheses of $[Fe\{B(n)T\}_3](PF_6)_2$

These complexes were synthesized by a modification of the method described by Elliott *et al.*[38] To an aqueous solution (30 cm^3) of $FeSO_4 \cdot 7H_2O$ (28 mg, 0.1 mmol) was added B(*n*)T (0.3 mmol) in hot acetone (50 cm^3) with stirring. The acetone was then removed (rotary evaporator) and excess NH_4PF_6 was added to precipitate $[Fe\{B(n)T\}_3]^{2+}$ as the PF_6^- salt. The mixture was stirred and the dark red solid was filtered under vacuum before washing twice with water (10 cm^3). The crude products were reprecipitated by the dropwise addition of a solution of $[Fe\{B(n)T\}_3](PF_6)_2$ (*ca.* 100 mg) in CH_3CN (3–5 cm^3) into stirring Et_2O (400 cm^3). The mixture was stirred for about 1 h, cooled and filtered. The products were collected and washed with Et_2O and dried. Yields: 87% for $[Fe\{B(2)T\}_3](PF_6)_2$, 75% for $[Fe\{B(7)T\}_3](PF_6)_2$ and 62% for $[Fe\{B(11)T\}_3(PF_6)_2$.

Preparation of poly-$[Fe\{B(n)T\}_3]^{2+}$*-coated electrodes*

The detailed procedure of the electrode pretreatment and electropolymerization have been described elsewhere[35]. The polymers were prepared at room temperature and under an N_2 atmosphere on platinum disk electrodes (area = 0.07 cm^2) by anodic potential scanning from 0–20 V at a scan rate of 50 mV/s in an acetonitrile/$[(n\text{-}C_4H_9)_4N]PF_6$ (0.1 M) solution containing the monomer (2 mM). The growth of the films was monitored by the increase in the peak current of the Fe^{III}/Fe^{II} redox couple at *ca.* 0.7 V. The electropolymerization was conducted in a three-electrode cell, with a platinum coil as the counter electrode and an $Ag/AgNO_3$ (0.01 M in CH_3CN) electrode as the reference. For non-aqueous solutions, all potentials were measured (and are reported) with respect to a $Ag/AgNO_3$ (0.01 M in CH_3CN) reference electrode.

After a polymerization, the film-modified electrodes were rinsed with acetonitrile, dried under an N_2-stream and electrochemically undoped by holding the electrodes at −100 mV for 10 min in an acetonitrile/$[(n\text{-}C_4H_9)_4N]PF_6$ (0.1 M) solution free of the monomers.

All the resultant films possessed golden colors. Surface coverages, $\Gamma_{Fe}(mol/cm^2) = Q/nFA$, were determined by integrating the oxidative component of the Fe^{III}/Fe^{II} wave of cyclic voltammograms measured at slow scan rate (20 mV/s) in acetonitrile/$[(n\text{-}C_4H_9)_4N]PF_6$ (0.1 M) solution. Surface coverages were typically in the range $\Gamma_{Fe} = 0.8\text{–}1.2 \times 10^{-8}$ mol/cm^2.

Electrochemical measurements

All the electrochemical measurements were performed using a BAS 100 A electrochemical analyzer. The experiments were conducted in a standard three-compartment electrochemical cell at room temperature under a nitrogen atmosphere. Rotating disk electrode (*rde*) voltammetry was performed with a Metrohm 628-10 rotator. The *rde* voltammograms, recorded at a scan rate of 5 mV/s, were obtained by periodically stopping the potential scan, stirring the solution and allowing the current due to the surface wave to decay to zero. All solutions were deoxygenated by bubbling with high purity N_2 prior to measurement. The working electrode (area = 0.07 cm^2) was a teflon-sealed Pt disk and the counter electrode was a platinum coil. In aqueous solution, all the potentials were measured and reported with respect to a *sce* reference electrode which was connected to the main compartment by a Luggin capillary.

RESULTS AND DISCUSSION

Cyclic voltammetry of P{FeB(n)T} *films in the presence of* $K_4Fe(CN)_6$

Figure 1 shows the cyclic voltammograms of the P{FeB(*n*)T}-film modified electrodes in 0.5 M H_2SO_4 solution and in 10 mM $K_4[Fe(CN)_6]$/0.5 M H_2SO_4 solution. In the H_2SO_4 solution, a P{FeB(2)T} film does not exhibit reversible voltammetric behavior: the ΔE_p and i_p values of the Fe^{III}/Fe^{II} couple increase non-linearly with respect to the scan rate v. At a scan rate of 0.1 V/s, the $E'_{cat} = +0.85$ V and $\Delta E_p \approx 60$ mV (Fig. 1(A)). Irreversibility of the Fe^{III}/Fe^{II} redox couple develops with the lengthening of the alkyl chains in the polymers, as shown in Figs 1(B) and (C). In addition, the tailing of the redox waves suggests that the electrochemical reactions are kinetically controlled for those polymers possessing the long alkyl chains. This dependence of the redox reversibility of metallic centers upon the length of the alkyl chains between thiophene and bipyridine is much more significant in aqueous solution than in acetonitrile, in which solvent the ruthenium analogues were studied[35]. This implies an influence of solvent polarity on the charge transfer through the alkyl chains, a tendency theoretically predicted since a polar solvent increases the difficulty of intramolecular charge transfer *via* saturated bonds[39]. This type of charge transfer mechanism has been discussed in detail for the case of the ruthenium analogues, P{RuB(*n*)T}, in a previous paper[35]. Accordingly, in the design of new catalytic polymer-modified electrodes, short alkyl chains or conjugated linkages should be chosen to reduce the energy barrier to intramolecular charge transfer.

In Fig. 1(B), a small and broad wave was observed at about 0.52 V on the reverse (reductive) sweep. This wave appears not to be related to the Fe^{III}/Fe^{II} redox couple, but is located at the same potential as that for oxygen reduction at the P{FeB(*n*)T}-coated electrodes. However, it was not removed by additional deaeration of the solution with an inert gas. A possible explanation is that a trace of H_2O may be electrocatalytically oxidized at the polymeric film during the oxidative potential scan, forming oxygen which is absorbed at the interface then reduced at its normal potential on the modified electrode on the reverse scan.

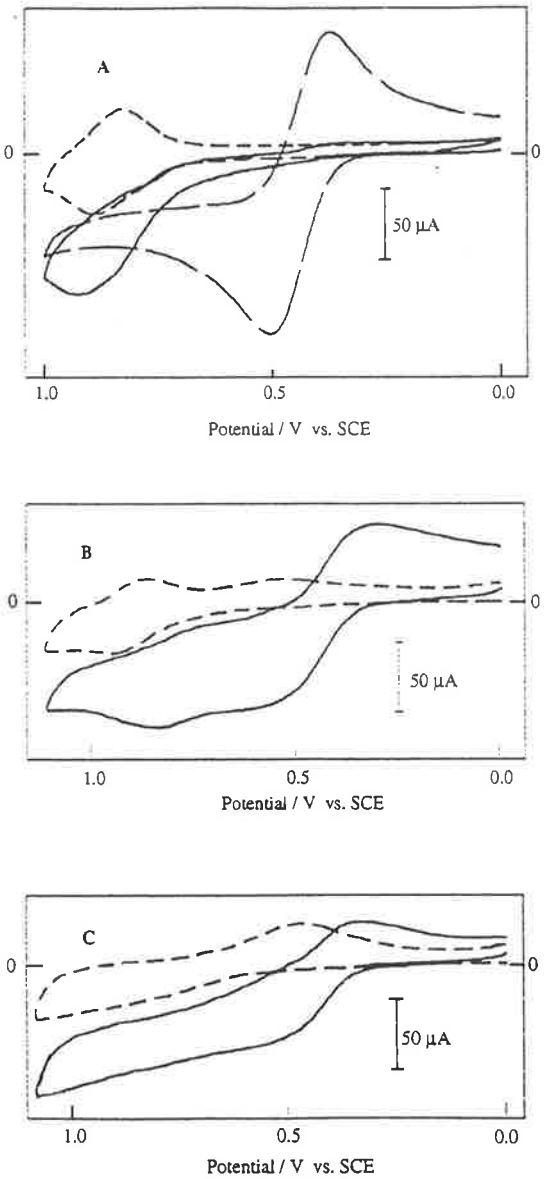

Fig. 1. Cyclic vlotammograms of Pt/P{FeB(2)T} (A), Pt/P{FeB(7)T} (B) and Pt/P{FeB(11)T} (C) films in 0.5 M H_2SO_4 (---) and 10 mM $K_4Fe(CN)_6$/0.5 M H_2SO_4 solution (——). $\Gamma_{Fe} \approx 10^{-8}$ mol/cm^2. Curve (---) in (A) represents that of a naked Pt electrode in 10 mM $K_4Fe(CN)_6$/0.5 M H_2SO_4 solution. Scan rates: 100 mV/s.

The effectiveness of these polymer-coated electrodes as electrocatalysts decreases significantly for the polymers with long alkyl chains. As shown in Fig. 1(A), for the P{FeB(2)T} film $[Fe(CN)_6]^{4-}$ is oxidized at the potential where poly-$[Fe\{B(2)T\}_3]^{2+}$ is oxidized to poly-$[Fe\{B(2)T\}_3]^{3+}$ rather than at its normal oxidation potential. Surprisingly, a very small reduction wave of $[Fe(CN)_6]^{3-}$ is observable. In a similar system, Oyama and Anson attributed such a phenomenon to the cross-linking structure of

the polymer film[40]. In the case of the P{FeB(2)T} film, the cross-linking arising from the binding together of bipyridyl groups by the metal centers, and the less porous structure of the film than these homologues with longer alkyl chains[35, 41], may make penetration by $[Fe(CN)_6]^{3-}$ into the film difficult so that its reduction wave is diminished. However, this rationale does not completely explain the present experimental results. It is noted that the magnitude of the reduction wave of $[Fe(CN)_6]^{3-}$ is inversely dependent on the efficiency of the catalytic reaction; *ie*, a strong catalytic current results in a small reduction wave of $[Fe(CN)_6]^{3-}$. When the catalytic reaction becomes very rapid, a majority of the poly-$[Fe\{B(2)T\}_3]^{3+}$ sites are reduced to poly-$[Fe\{B(2)T\}_3]^{2+}$ by a chemical rather than an electrochemical reaction, so that the film is in a non-conductive state on a reverse scan. Although poly(alkylthiophenes) are conducting polymers, they are essentially non-conductive at a potential below +0.6 V, as confirmed by *ac* impedance spectra in previous reports[35]. In a similar manner to the Ru analogues[35], the P{FeB(*n*)T} films exhibit the regular electroactivity of the polymeric backbone in non-aqueous solutions at potentials considerably anodic of the potential limitation in aqueous media. Therefore, the reduction of $[Fe(CN)_6]^{3-}$ species occurs with difficulty on the resultant non-conductive polymer. In addition, the magnitude of reduction wave of $[Fe(CN)_6]^{3-}$ depends on its concentration. In a dilute solution, the amount of $[Fe(CN)_6]^{4-}$ species is not sufficient to reduce all the poly-$[Fe\{B(2)T\}_3]^{3+}$ sites, some of which will thus be electrochemically reduced. Under these circumstances, the polymer is still conductive on the reverse cycle, and the reduction wave of $[Fe(CN)_6]^{3-}$ species is observable. In contrast to the case with the P{FeB(2)T} film, the $[Fe(CN)_6]^{4-/3-}$ couple exhibits considerably stronger peak currents at their normal potentials on the electrodes coated with polymers containing long alkyl chains. This may be attributed to the more porous structure of these polymers, which can increase the penetration of $[Fe(CN)_6]^{4-/3-}$ species into the polymers. On the other hand, the catalytic currents of the polymer-modified electrodes are smaller than those of the P{FeB(2)T} film, which may result in some of the poly-$[Fe\{B(2)T\}_3]^{3+}$ sites being electrochemically reduced, so that the polymers are still conductive at the normal reduction potential of the $[Fe(CN)_6]^{3-}$ species. The broad wave shape, which reveals a kinetically-controlled reaction, suggests a slow rate of electron exchange between the poly-$[Fe\{B(n)T\}_3]^{2+}$ and the poly-$[Fe\{B(n)T\}_3]^{3+}$ sites in the P{FeB(*n*)T} films where the alkyl chains are long.

Measurements of rate of oxidation of $[Fe(CN)_6]^{4-}$ *ions, mediated at the* P{FeB(n)T} *films using limiting currents, and dependency of the rates on alkyl chain length*

At slow scan rates, rotating disk electrode voltammetry for an electrochemical reaction results in the steady-state limiting current, i_l, which is observed as a current plateau in a voltammogram. Figure 2 shows the rotating electrode voltammograms of

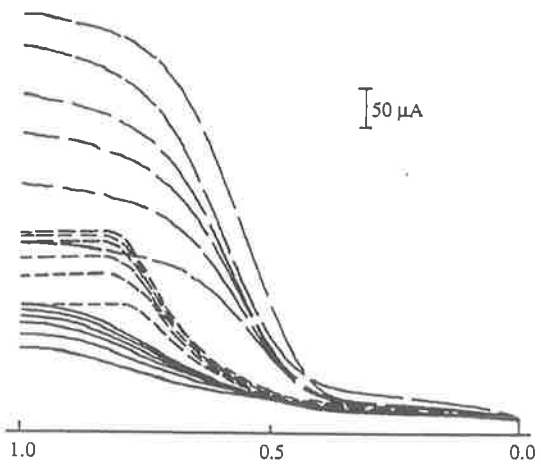

Fig. 2. Rotating disk electrode voltammograms of a naked Pt (– – –), P{FeB(2)T} (– · –) and P{FeB(7)T} (——) modified electrodes in 10 mM $K_4Fe(CN)_6$/0.5 M H_2SO_4 solution. $\Gamma_{Fe} \approx 10^{-8}$ mol/cm^2. ω of each group (from bottom to top) = 500, 1000, 1500, 2000, 2500 and 3000 rpm, respectively.

a naked Pt electrode and of electrodes modified with P{FeB(2)T} and P{FeB(7)T} in 10 mM $K_4Fe(CN)_6$/0.5 M H_2SO_4 solution. The naked Pt electrode shows the largest i_l, and the smallest i_l is observed on the P{FeB(7)T} film-coated electrode. In addition, a shoulder, which is the oxidation current of $[Fe(CN)_6]^{4-}$ species at its normal potential, is detected at *ca.* +0.45 V on this latter polymer-coated electrode. This shoulder cannot be seen on the P{FeB(2)T} electrode films, which is consistent with the result of the cyclic voltammetry experiment. On the basis of data from these voltammograms, Levich plots (i_l vs. $\omega^{1/2}$) and reciprocal Levich plots (i_l^{-1} vs. $\omega^{-1/2}$) were obtained for each of these electrodes, and they are shown in Figs 3(A) and (B), respectively. For a naked Pt electrode, the limiting current can be described by Levich equation,

$$i_d = 0.62nFAD_s^{2/3}\nu^{-1/6}\omega^{1/2}C_s \qquad (2)$$

where D_s is the diffusion coefficient of the redox substrate and C_s is its concentration, and ν is the kinematic viscosity of solution; for water and dilute aqueous solutions near 20°C, it has a value of *ca.* 0.01 cm^2/s[42]. By substituting $n = 1$, $F = 96\,485$ C/mol, $A = 0.0707$ cm^2, $\nu = 0.01$ cm^2/s and $C_s = 0.01$ M into equation (2), a value of $D_s = 6.0 \times 10^{-6}$ cm^2/s is obtained for the $[Fe(CN)_6]^{4-}$ species from the slope of the plot.

Since the rate of permeation of $[Fe(CN)_6]^{4-}$ into the oxidized P{FeB(*n*)T} film is assumed to be fast (see earlier), a proposed approximate equation[36, 43, 44] for this case is

$$\frac{1}{i_l} = \frac{1}{nFAk_{cts}\Gamma C_s} + \frac{1}{nFAD_{ct}C_s/d} + \frac{1}{0.62nFAD_s^{2/3}\nu^{-1/6}\omega^{1/2}C_s} \qquad (3)$$

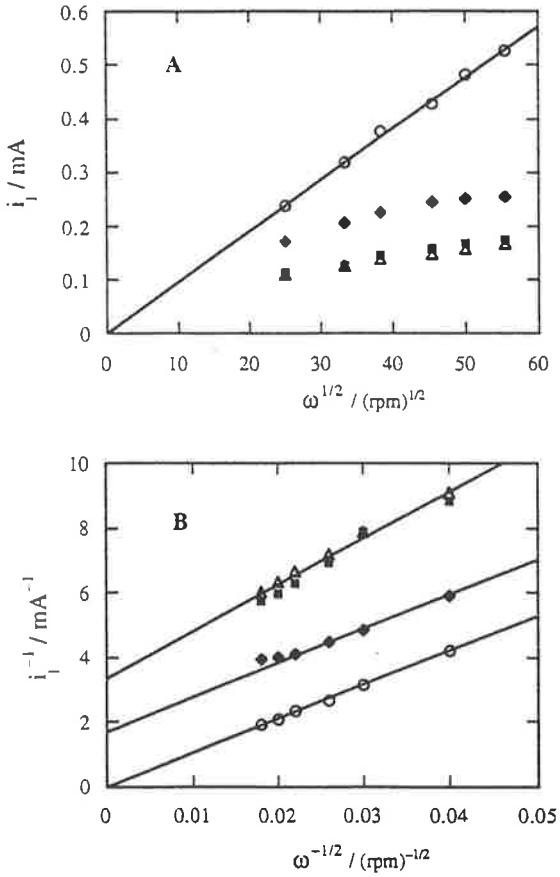

Fig. 3. Levich i_l vs. $\omega^{1/2}$ plots (A), and relative reciprocal Levich i_l^{-1} vs. $\omega^{-1/2}$ plots (B) of 10 mM $K_4Fe(CN)_6$ in 0.5 M H_2SO_4 solution at naked Pt (○), Pt/P{FeB(2)T} (◆), Pt/P{FeB(7)T} (△) and Pt/P{FeB(11)T} film (■) electrodes. $\Gamma_{Fe} \approx 10^{-8}$ mol/cm^2.

where the cross-reaction rate constant k_{cts} is in units of cm^3 mol^{-1} s^{-1}, Γ is the coverage of poly-[Fe{B(*n*)T}$_3$]$^{2+}$ sites on the surface of the electrode, D_{et} is the effective diffusion coefficient for charge transport by electron self-exchange between neighboring poly-[Fe{B(*n*)T}$_3$]$^{2+}$ and poly-[Fe{B(*n*)T}$_3$]$^{3+}$ sites in the film, C_t the concentration of poly [Fe{B(*n*)T}$_3$]$^{2+}$ sites in the film, *d* the thickness of the film, and the quantity $0.62nFAD_s^{2/3}\nu^{-1/6}\omega^{1/2}C_s$ is equal to i_d. The Levich plots of the P{FeB(*n*)T} films show a deviation from the linear relationship of i_l and $\omega^{1/2}$ at high rotation rates, a deviation which is much more significant for the P{FeB(2)T} film than for the P{FeB(7)T} and P{FeB(11)T} films, as seen in Figs 3(A) and (B). This suggests that a slow chemical step limits the current at high rotation rates[40]. At low rotation rates, the transfer of $[Fe(CN)_6]^{4-}$ species through the rather thick Levich layer controls the current so that linear *i* vs. $\omega^{1/2}$ behavior results. At higher values of ω, the thickness of the Levich layer decreases and the magnitude of the current is controlled by the rate of the redox reaction between poly-[Fe{B(*n*)T}$_3$]$^{3+}$ and $[Fe(CN)_6]^{4-}$. This chemical catalytic current is more important in the P{FeB(2)T} film: as seen from its voltammograms, the P{FeB(2)T}-film modified electrode exhibits a strong catalytic oxidation wave without a reverse reduction wave in 10 mM $K_4Fe(CN)_6$/0.5 M H_2SO_4 solution. This indicates a fast mediated reaction rate $k_{cts}\Gamma$ between poly-[Fe{B(2)T}$_3$]$^{3+}$ and the $[Fe(CN)_6]^{4-}$ species, which may be attributed to the electronic effect arising from the thiophene moieties, as discussed previously[35], allowing rapid charge transfer between the substrate and the oxidized metal centers. By contrast, such an electronic effect is not present in the polymers possessing longer alkyl chains, and consequently the P{FeB(7)T} and P{FeB(11)T} films are predicted to have the same mediated reaction rate $k_{cts}\Gamma$. However, the rate of permeation of the electroactive substrate is expected to be faster than that in the P{FeB(2)T} film due to larger apertures and increased porosity in these polymer matrixes. It is not surprising that the P{FeB(7)T} and P{FeB(11)T} films have the same Levich plots, as described in the analysis above.

The reciprocal Levich plots for the P{FeB(7)T} and the P{FeB(11)T} films have slightly larger slopes than that for the naked Pt electrode in 10 mM $K_4Fe(CN)_6$/0.5 M H_2SO_4 solution. D_s is calculated to be 3.7×10^{-6} cm^2/s for the $[Fe(CN)_6]^{4-}$ substrate at the P{FeB(7)T] and the P{FeB(11)T}-film coated electrodes, a value which is a little smaller than that calculated for the naked Pt electrode. An approximation which has been used previously[36, 40, 43, 44] is that since the rate of transport of electrochemical charge through the polymer catalyst films is rapid, equation 3 is simplified to become

$$\frac{1}{i_l} = \frac{1}{nFAk_{cts}\Gamma C_s} + \frac{1}{0.62nFAD_s^{2/3}\nu^{-1/6}\omega^{1/2}C_s} \quad (4)$$

where the intercept of the reciprocal Levich plot is equal to $1/nFAk_{cts}\Gamma C_s$. The mediated reaction rate $k_{cts}\Gamma$ between the $[Fe(CN)_6]^{4-}$ species and the catalyst sites in the P{FeB(7)T} and the P{FeB(11)T} films can be evaluated to be 4.2×10^{-3} cm/s. A corresponding value is not available for the P{FeB(2)T} film since the relationship between i_l^{-1} and $\omega^{-1/2}$ deviates significantly from the linearity, so that equation (4) may not be applicable. Unfortunately, there is no appropriate model to quantitatively describe the electrocatalytic process in the case of the P{FeB(2)T} film. However, it is clear that the catalytic reaction on the P{FeB(2)T}-coated electrode is much faster than that on the P{FeB(7)T} film (see below). By comparison with the catalytic reaction on the poly-[Ru(vbpy)$_3$]$^{2+}$ film (vbyp = 4-methyl-4'-vinyl-2,2'-bipyridine)[36], the mediated reaction rate $k_{cts}\Gamma$ between $[Fe(CN)_6]^{4-}$ species and catalyst sites in the P{B(7)T} and the P{FeB(11)T}-coated electrodes is slower due probably to the effect of the alkyl chains on the intramolecular charge transfer.

Mediated oxidation reaction rates of different concentrations of $K_4Fe(CN)_6$ at the P{FeB(2)T] modified electrode in 0.5 M H_2SO_4 solution, and measurement of electron transport rates in the polymer

The concentrations of electroactive substrates exert important influences on the catalytic reaction at the interface of the film and the solution. Figure 4

shows the Levich plots and relative reciprocal Levich plots for different concentrations of $K_4Fe(CN)_6$ in 0.5 M H_2SO_4 solution at the P{FeB(2)T}-coated electrode. All the Levich plots show linearity at a naked Pt electrode but deviation from the linearity at a P{FeB(2)T}-film modified electrode, which suggests that all the reactions at the modified electrode are controlled by chemical steps at high rotation rates. The slopes of their reciprocal Levich plots are proportional to the bulk concentrations of $[Fe(CN)_6]^{4-}$ and are essentially consistent with the values obtained at the naked electrode. The intercepts are obtained at $\omega \to \infty$. In this circumstance, equation (3) can be simplified to

$$\frac{1}{i_{1(\omega\to\infty)}} = \frac{1}{nFAk_{cts}\Gamma C_s} + \frac{1}{nFAD_{ct}C_t/d} \quad (5)$$

Equation (5) provides a convenient general method for distinguishing between currents that are limited by electron transfer through polymeric coatings on electrode surfaces and those that are controlled by the rate of a catalytic redox reaction[36, 40, 45] If the mediated reaction rate $k_{cts}\Gamma$ is slow, the plot of $i_{1(\omega\to\infty)}^{-1}$ vs. C_s^{-1} is linear. The value of $k_{cts}\Gamma$ can be obtained from the slope of this straight line, and the rate of electron transport through the polymers, D_{ct}, may be evaluated from the intercept.

By contrast, if $i_{1(\omega\to\infty)}^{-1}$ is independent of C_s^{-1}, the reaction is controlled by the rate of electron transfer and the catalytic reaction is fast. In the case of the P{FeB(2)T}-film modified electrode, the plot of $i_{1(\omega\to\infty)}^{-1}$ (intercept) vs. C_s^{-1} is linear (omitting data obtained at 10 mM substrate), indicating that the kinetics of a mediated reaction occurring at the P{FeB(*n*)T} film is dependent not only on the alkyl chain length of the polymers (compared with the polymers with long alkyl chains, P{FeB(2)T} possesses a fast electron exchange rate) but also on the concentrations of electroactive substrates in the solution. In some concentrations, *eg*, 10 mM $[Fe(CN)_6]^{4-}$, the mediated reaction rate $k_{cts}\Gamma$ is considerably faster so that the reaction is controlled by the electron transfer through the films. This result is in agreement with the cyclic voltammetric results. In most cases, the reactions are controlled by $k_{cts}\Gamma$ and equation (4) will provide a good approximation to the actual process. From the slope of the plot, the mediated reaction rate $k_{cts}\Gamma$ is calculated to be 0.11 cm s^{-1}, which is significantly larger than that for the P{FeB(7)T} and P{FeB(11)T} films obtained in 10 mM $K_4Fe(CN)_6$/0.5 M H_2SO_4 solution. The intercept gives $D_{ct}^{1/2}C_t = 4.8 \times 10^{-8}$ mol cm^{-2} $s^{-1/2}$, which is close to the value for a P{B(2)T} film (1.1×10^{-8} mol cm^{-2} $s^{-1/2}$), reported previously[35]. The calculation is made on the basis of the equation $d = \Gamma/C_t$. These data indicate that the mediated reaction rates are still fast for the retro-catalytic reaction of $K_4Fe(CN)_6$ in 0.5 M H_2SO_4 solution. Other experiments indicate the effect of coverage Γ_{Fe} is not important, which is in consistent with literature reports for similar systems[44, 45].

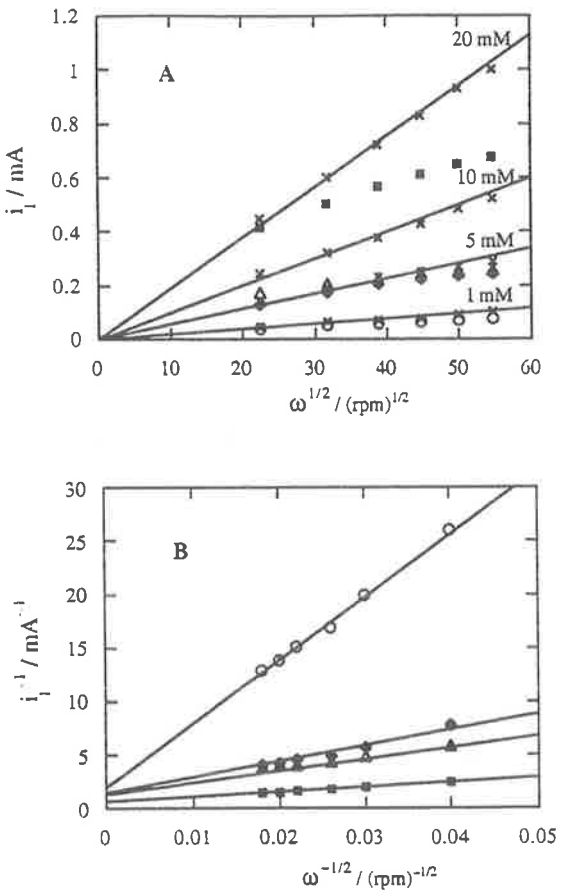

Fig. 4. (A) Levich i_l vs. $\omega^{1/2}$ plots of $K_4Fe(CN)_6$ at naked Pt (×) and the Pt/P{FeB(2)T} electrode. (B) relative reciprocal Levich i_l^{-1} vs. $\omega^{-1/2}$ plots of $K_4Fe(CN)_6$ at the Pt/P{FeB(2)T} electrode. Solution: 0.5 M H_2SO_4. $\Gamma_{Fe} \approx 10^{-8}$ mol/cm^2. Concentrations (marked above the lines in the case of naked Pt) of $K_4Fe(CN)_6$: 1 mM (○), 5 mM (◆), 10 mM (△) and 20 mM (■).

CONCLUSIONS

The results presented in this paper elucidate aspects of the retro-electrocatalytic behavior of the P{FeB(*n*)T}-film modified electrodes to $K_4Fe(CN)_6$ in aqueous solutions, and several conclusions can be drawn.

Firstly, the polymer-modified electrodes exhibit stable electrochemical behavior in acidic aqueous solutions. The reversibility of the electrochemical redox reaction of the P{FeB(*n*)T}-film coated electrodes depends on the alkyl chain length of the polymers, with less irreversible electrochemical behavior being observed when the alkyl chain is short and increasing irreversibility as the chain is lengthened.

Secondly, the kinetics of the mediated reaction at the P{FeB(*n*)T}-film modified electrodes is dependent on the concentrations of the substrate and the length of the alkyl chain between the thiophene and the bipyridyl rings of the polymers. A P{FeB(2)T}-film coated electrode shows a faster reaction rate than the polymers with longer alkyl chains.

Thirdly, the kinetic parameters of mediated oxidation of $[Fe(CN)_6]^{4-}$ species at the P{FeB(*n*)T} electrodes can be probed using rotating disk voltammetry and the Levich equation. At a substrate

concentration of 10 mM $K_4Fe(CN)_6$, the retro-electrocatalytic oxidation reaction at the P{FeB(2)T} film-coated electrode is so fast that the reaction is controlled by the electron transport through the polymer film. Under general circumstances, however, the overall reaction is controlled by the chemical step.

Acknowledgements—This research was supported by the Australian Research Council. JW wishes to acknowledge the Australian International Development Assistance Bureau for an ADCSS scholarship and James Cook University for a postgraduate research award for overseas students.

REFERENCES

1. H. D. Abruña, *Coord. Chem. Rev.* **86**, 135 (1988).
2. A. Merz, *Topics in Current Chemistry* (Edited by E. Stekhan), **152**, 49 (1990).
3. R. W. Murray, *Introduction to Molecularly Designed Electrode Surfaces* in *Molecular Design of Electrode Surfaces* (Edited by R. W. Murray), *Techniques in Chemistry* series, Wiley, New York (1992).
4. C. P. Andrieux and J.-M. Saveant, *Catalysis at Redox Polymer Coated Surfaces* in *Molecular Design of Electrode Surfaces* (Edited by R. W. Murray), *Techniques in Chemistry* series, Wiley, New York (1992).
5. M. E. G. Lyons, *Electroactive Polymer Electrochemistry—Fundamentals* (Part 1), Plenum, New York (1994).
6. R. C. McHatton and F. C. Anson, *Inorg. Chem.* **23**, 3935 (1984).
7. A. R. Guadalupe, X. H. Chen, B. P. Sullivan and T. J. Meyer, *Inorg. Chem.* **32**, 5502 (1993).
8. W. J. Vining and T. J. Meyer, *J. Electroanal. Chem.* **237**, 191 (1987).
9. G. J. Samuels and T. J. Meyer, *J. Am. Chem. Soc.* **103**, 307 (1981).
10. I. M. F. De Oliveira, J.-C. Moutet and N. Vlachopolous, *J. Electroanal. Chem.* **291**, 243 (1990).
11. W. F. De Giovani and A. Deronzier, *J. Chem. Soc., Chem. Commun.* 1461 (1992).
12. A. Deronzier, J.-C. Moutet and E. Saint-Aman, *J. Electroanal. Chem.* **327**, 147 (1992).
13. W. F. De Giovani and A. Deronzier, *J. Electroanal. Chem.* **337**, 285 (1992).
14. A. E. Hourch, S. Belcadi, P. Moisy, P. Crouigneau, J.-M. Léger and C. Lamy, *J. Electroanal. Chem.* **339**, 1 (1992).
15. A. Elzing, A. van der Putten, W. Visscher and E. Barendrecht, *J. Electroanal. Chem.* **200**, 313 (1986).
16. H.-Y. Liu, I. Abdalmuhdi, C. K. Chang and F. C. Anson, *J. Phys. Chem.* **89**, 665 (1985).
17. J. P. Collman, M. Marrocco, P. Denisevich, C. Koval and F. C. Anson, *J. Electroanal. Chem.* **101**, 117 (1979).
18. J. P. Collman, P. Denisevich, Y. Konai, M. Marrocco, C. Koval and F. C. Anson, *J. Am. Chem. Soc.* **102**, 6027 (1980).
19. H. C. Hurrell, A.-L. Mogstad, D. A. Usifer, K. T. Potts and H. D. Abruña, *Inorg. Chem.* **28**, 1080 (1989).
20. H. Tanabe and K. Ohno, *Electrochim. Acta* **32**, 1121 (1987).
21. T. R. O'Toole, L. D. Margerum, T. D. Westmoreland, W. J. Vining, R. W. Murray and T. J. Meyer, *J. Chem. Soc., Chem. Commun.* 1416 (1985).
22. M.-N. Collomb-Dunand-Sauthier, A. Deronzier and R. Ziessel, *J. Chem. Soc., Chem. Commun.* 189 (1994).
23. C. R. Cabrera and H. D. Abruña, *J. Electroanal. Chem.* **209**, 101 (1986).
24. S. Cosnier, A. Deronzier and J.-C. Moutet, *J. Mol. Cat.* **45**, 381 (1988).
25. S. Cosnier, A. Deronzier and J.-C. Moutet, *J. Electroanal. Chem.* **207**, 315 (1986).
26. M.-N. Collomb-Dunand-Sauthier, A. Deronzier and R. Ziessel, *J. Phys. Chem.* **97**, 5973 (1993).
27. A. Deronzier and M. Essakalli, *J. Chem. Soc., Chem. Commun.* 242 (1990).
28. A. Deronzier, J.-C. Moutet and D. Zsoldos, *J. Phys. Chem.* **98**, 3086 (1994).
29. A. Deronzier and J.-C. Moutet, *Acc. Chem. Res.* **22**, 249 (1989).
30. S. Cosnier, A. Deronzier and N. Vlachopoulos, *J. Chem. Soc., Chem. Commun.* 1259 (1989).
31. A. Downard, N. Surridge, T. Meyer, S. Cosnier, A. Deronzier and J.-C. Moutet, *J. Electroanal. Chem.* **246**, 321 (1988).
32. A. Deronzier, M. Essakalli and J.-C. Moutet, *J. Electroanal. Chem.* **244**, 163 (1988).
33. S. Cosnier, A. Deronzier and J.-C. Moutet, *J. Electroanal. Chem.* **193**, 193 (1985).
34. A. Deronzier, R. Devaux, D. Limosin and J.-M. Latour, *J. Electroanal. Chem.* **324**, 325 (1992).
35. J. Wang and F. R. Keene, *J. Electroanal. Chem.* in press.
36. T. Ikeda, C. R. Leidner and R. W. Murray, *J. Electroanal. Chem.* **138**, 343 (1982).
37. J. Wang, M. Pappalardo and F. R. Keene, *Aust. J. Chem.* **48**, 1425 (1995).
38. C. M. Elliott, C. J. Baldy, L. M. Nuwaysir and C. L. Wilkins, *Inorg. Chem.* **29**, 389 (1990).
39. H. M. McConnell, *J. Chem. Phys.* **35**, 508 (1961).
40. N. Oyama and F. C. Anson, *Anal. Chem.* **52**, 1192 (1980).
41. J. Wang and F. R. Keene, *J. Electroanal. Chem.* in press.
42. A. J. Bard and L. R. Faulkner, *Electrochemical Methods*; p. 283; John Wiley: New York (1980).
43. R. W. Murray, *Phil. Trans. R. Soc. Lond.* **A302**, 253 (1981).
44. R. D. Rocklin and R. W. Murray, *J. Phys. Chem.* **85**, 2104 (1981).
45. T. Ikeda, C. R. Leidner and R. W. Murray, *J. Am. Chem. Soc.* **103**, 7422 (1981).

CO_2-Laser Desorption and Multiphoton Ionization of Tris(2,2′-bipyridyl)ruthenium

Ronald Beavis,[1] Josef Lindner,[1] Jürgen Grotemeyer,[1]
Ian M. Atkinson,[2] F. Richard Keene,[2] and
Alan E. W. Knight*[,3]

Institut für Physikalische und Theoretische Chemie der Technische Universität München, D-8046 Garching Federal Republic of Germany
Department of Chemistry and Biochemistry James Cook University of North Queensland Townsville, Queensland 4811, Australia
Division of Science and Technology Griffith University Nathan, Queensland 4111, Australia

Received August 12, 1988

Elucidation of the spectroscopy of metal coordination compounds is an important ingredient in arriving at an understanding of their photophysical and photochemical properties. However, in solution and the condensed phase, most metal complexes and organometallic compounds display electronic spectra that are environmentally broadened and are therefore relatively uninformative, and the low volatility of these species usually precludes gas-phase studies.[4,5] Ideally, it would be desirable to measure spectra of metal coordination compounds under molecular beam conditions where the cooling and rarefaction afforded by expansion would assist in reducing thermal congestion in the electronic spectrum.[6] The spectroscopy of ruthenium polypyridyl complexes

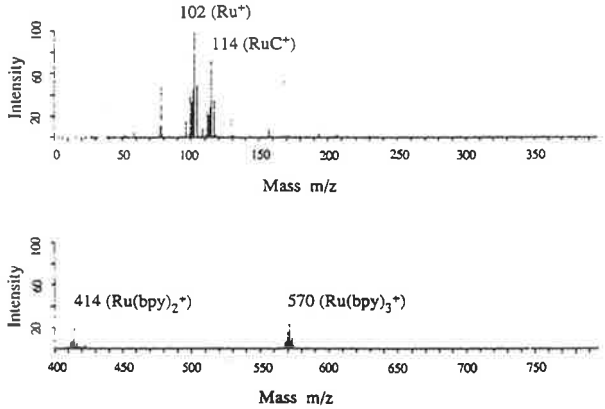

Figure 1. Resonance enhanced multiphoton ionization time-of-flight mass spectrum following CO_2-laser desorption of $[Ru(bpy)_3](CH_3COO)_2$.

is of particular interest, because of their relevance as photosensitizers for solar energy conversion schemes.[7] However, to our knowledge there have been no successful attempts to introduce such molecules into the gas phase for measurement of their spectroscopy.

We have succeeded in producing a seeded molecular beam expansion of the tris(2,2′-bipyridyl)ruthenium moiety by using a pulsed CO_2-laser desorption technique[8-10] that has been employed successfully to introduce many other involatile species into molecular beam expansions for analytical[11] purposes.

Details of the CO_2-laser desorption and multiphoton ionization technique have been described elsewhere.[8-10] In the present ap-

(1) Der Technische Universität München.
(2) James Cook University of North Queensland.
(3) Griffith University; Deutsche Forschungsgemeinschaft Guest Professor and Alexander von Humboldt Fellow, at Technische Universität München, 1987.
(4) Lever, A. B. P. "Inorganic Electronic Spectroscopy", In *Studies in Physical and Theoretical Chemistry*, 2nd ed.; Elsevier: Amsterdam, 1984; Vol. 33.
(5) Geoffroy, G. L.; Wrighton, M. S. *Organometallic Photochemistry*; Academic: New York, 1979.
(6) Levy, D. H. *Ann. Rev. Phys. Chem.* **1980**, *31*, 197.
(7) Kalyansundaram, K. *Coord. Chem. Rev.* **1982**, *46*, 159.
(8) von Weyssenhoff, H.; Selzle, H. L.; Schlag, E. W. *Z. Naturforsch.* **1985**, *40a*, 674.
(9) Grotemeyer, J.; Boesl, U.; Walter, K.; Schlag, E. W. *J. Am. Chem. Soc.* **1986**, *108*, 4233.
(10) Grotemeyer, J.; Boesl, U.; Walter, K.; Schlag, E. W. *J. Org. Mass. Spectrom.* **1986**, *21*, 645.

0002-7863/88/1510-7534$01.50/0

plication, tris(2,2′-bipyridyl)ruthenium(II) acetate is encased in a polyethylene tablet mixed with finely divided metal powder (gold or silver, 1 μm diameter). The use of such composite materials to aid desorption will be fully described in a future publication. This method of sample preparation has been found to minimize fragmentation during the desorption process. The CO_2 TEA low-pressure laser (bimodal pulse, initial spike FWHM = 1 μs, tail FWHM = 10 μs, 10 mJ pulse energy) is weakly focussed on the sample probe which is located 2–3 mm below the axis of the expansion orifice. The desorbed compound is carried downstream to the ionization region (differentially pumped) where two-photon ionization is effected by a focussed frequency doubled pulsed dye laser tuned to 290 nm. At this wavelength, the photon energy is sufficient to resonantly ionize the bipyridyl ligands via the first excited electronic state. Ions are detected with a Bruker TOF-1 reflectron time-of-flight mass spectrometer.

Figure 1 displays the multiphoton ionization mass spectrum of the tris(2,2′-bipyridyl)ruthenium complex following CO_2-laser desorption. Clearly evident is the cluster of peaks around m/z = 570 amu. This almost certainly corresponds to the $[Ru(bpy)_3]^+$ ion since there is little likelihood that clustering would lead to a doubly charged dimer ion. Indirect confirmation of this assignment is obtained from the isotopic splitting pattern (due to the seven Ru and the ^{13}C and ^{15}N isotopes in natural abundance) and from the observation of the $[Ru(bpy)_2]^+$ fragment (m/z = 414 for the most abundant Ru isotope). Ru^+ and RuC^+ fragments (m/z = 102, 114 for the most abundant ^{102}Ru isotope) are also observed. There is also evidence for some pyridine derived fragments (C_5H_4N, m/z = 78). Obviously absent from the spectrum displayed in Figure 1 are $[Ru(bpy)]^+$, (m/z = 258), $[Ru(bpy)_3]^{2+}$, (m/z = 285), and bipyridyl$^+$ (m/z = 156).

It is a little surprising at first glance, given that the original sample is a salt of the Ru(II) complex, that the $[Ru(bpy)_3]$ complex appears in the mass spectrum only as a *singly* charged cation. (Both the acetate and trifluoromethanesulfonate salts yielded the same results). In the following analysis of the mass spectrum we suggest possible reasons as to why this may be the case.

The assignment of the cluster of peaks at m/z = 570 as the $[Ru(bpy)_3]^+$ complex does not appear to be in any doubt. Because of the instrumental configuration (positively charged repeller grid), only a neutral $[Ru(bpy)_3]$ complex could enter the ionizing region. The laser photon energy (4.3 eV) is sufficient to two-photon ionize one of the bpy ligands, thus we observe $[Ru(bpy)_3]^+$ cation. The neutral $[Ru(bpy)_3]$ complex is probably formed during the desorption process as a consequence of progressive electron attachment to the $[Ru^{II}(bpy)_3]^{2+}$ cation, leading to $[Ru(bpy)_3]^+$, $[Ru(bpy)_3]^0$, and possibly $[Ru(bpy)_3]^-$. (Only the neutral species will enter the ionizing region.) Support for this mechanism comes from electrochemical and spectral studies of the reduction of $[Ru^{II}(bpy)_3]^{2+}$ in solution where sequential addition of electrons occurs, the added electrons remaining somewhat localized on the separate ligands.[12]

Other species found in the mass spectrum ($[Ru(bpy)_2]^+$, Ru^+, $C_5H_4N^+$) could appear either as a result of dissociation of the $[Ru(bpy)_3]^+$ cation during ionization or if they are formed as dissociation products during the desorption process. We favor the latter explanation since there is no evidence in the mass spectrum for the bipyridyl ligand that would be released on dissociation of $[Ru(bpy)_3]^+$. Ionization of bipyridyl, if present, would be possible with the available photon energy. During desorption, bipyridyl released due to dissociation of $[Ru(bpy)_3]^+$ presumably attaches an electron and is therefore not transmitted through the ionization region. The small yield of C_5H_4N is probably due to the dissociation $bpy^- \rightarrow C_5H_4N^- + C_5H_4N$, with the neutral fragment being transmitted and ionized via near-resonant multiphoton ionization.

This demonstration that tris(2,2′-bipyridyl)ruthenium may be introduced into a molecular beam offers immense promise for the application of laser spectroscopy to metal coordination compounds in general. We are proceeding toward applying this combination of laser desorption with resonance enhanced multiphoton ionization spectroscopy to measure the electronic spectrum of $[Ru(bpy)_3]$ under cold molecular beam conditions.

Acknowledgment. This work has been supported by the Bundesministerium für Forschung and Technologie and the Deutsche Forschungsgemeinschaft (GR 917 (1-1)). R.B. was supported by a NATO Postdoctoral Fellowship. Support was also provided by the Australian Research Grants Scheme.

(11) Grotemeyer, J.; Schlag, E. W. *Angew. Chemie, Int. Ed. Engl.* **1988**, *27*, 447.
(12) Ohsawa, Y.; Hanck, K. W.; DeArmond, M. K. *J. Electroanal. Chem.* **1984**, *175*, 229.

"Low Fragmentation Laser Desorption of Thermally Labile Molecules", I.M. Atkinson, J.A. Shorter, R.T.T. Karaiste, F.R. Keene, J.I. Steinfeld, and A.E.W. Knight, *Materials Research Society, Conference Proceedings,* **201** (Surface Chemistry. Beam-Solid Interactions), 459-461 (1991).

No copies of this paper are available

2776 Anal. Chem. 1993, 65, 2776–2783

Molecular Beam Spectroscopy of Molecules with Low Volatility via Laser Desorption from Thin Films Containing Particulate Silver

R. Timo T. Karaiste,[†,§] Ian M. Atkinson,[†,‡] Jeffrey A. Shorter,[‡,⊥] Alan E. W. Knight,[*,‡] and F. Richard Keene[*,†]

Department of Molecular Sciences, James Cook University of North Queensland, Townsville, Queensland 4811, Australia, and Molecular Dynamics Laboratory, Faculty of Science and Technology, Griffith University, Brisbane, Queensland 4111, Australia

A new polymer matrix containing particulate silver has been developed for the introduction of analytes with low or negligible volatility into molecular beams via laser desorption. These silver-containing film matrices (SCFM) permit stable desorption to proceed for extended periods (ca. ~10 h) and have been applied successfully to the nondestructive volatilization of a number of amino acids and a transition-metal compound. Analytes can be extracted directly from solution onto the SCFM surface by simply dipping the film into the solution and then air-drying the film. The laser desorption apparatus, when coupled to a supersonic molecular beam/laser ionization time-of-flight mass spectrometer, permits the detection of the analytes at femtogram levels. Furthermore, we have developed a reel-to-reel tape transport device that allows extended usage of the analyte-loaded SFCM, thereby permitting the measurement of wavelength-scanned mass-selected resonance-enhanced multiphoton ionization spectra of analytes with low or negligible volatility. We demonstrate this application with the aromatic amino acids L-tryptophan and L-phenylalanine. The degree of cooling achieved in the molecular expansion is shown to be comparable with that achieved using conventional beam sources, and the desorption yield is sufficiently stable for high-quality spectra to be measured.

INTRODUCTION

Supersonic jet methodologies are now the techniques of choice for probing electronic spectroscopy for both analytical and fundamental photophysical studies. The rarefaction and cooling afforded by molecular beams result in spectra which are dramatically simplified and are therefore significantly easier to interpret.[1] However, most spectroscopic applications of jet expansions have been directed toward relatively volatile molecules that may be introduced conveniently into gaseous flows. Molecules with low or negligible volatility present a greater challenge. While there have been numerous techniques developed for introducing nonvolatile analytes into molecular beams for mass spectrometric analysis, there has yet to be a routine application of jet methods for recording their electronic spectra, especially for thermally fragile species of appreciable molecular weight. There is significant need for the development of a general purpose method for generating stable, cold jet expansions of such species in order to permit the measurement of their electronic spectra. The analytical utility of such a technique in biochemistry and pharmacology is obvious, where the extreme sensitivity and selectivity (optical and mass) of the combined mass spectroscopic and laser ionization techniques may be exploited.[2,3] Great potential also exists in inorganic chemistry, where gas-phase methodologies have made little impact in photophysical or photochemical studies due to the involatility of the majority of the compounds of interest. However, high-resolution spectroscopic methods would be of great value in elucidating the photophysics of many potentially important transition-metal coordination and organometallic species.[4,5]

Techniques that exist for the introduction of nonvolatile molecules into the gas phase for mass spectral analysis include plasma desorption,[6] fast atom bombardment,[7,8] electrospray,[9] and supercritical fluid expansions.[8] Of these methods, only supercritical fluid expansions appear to have been coupled successfully to molecular beams for the purpose of measuring jet-cooled spectra.[10–12] However, various technical problems, including solvent clustering, limited range of solvents, vacuum pump loading, and signal instability, have restricted the widespread application of the supercritical expansion methods to spectroscopic experiments.[8,11,12]

Laser ablation methods, wherein a single laser pulse induces evaporation, fragmentation, and ionization of a solid analyte, are used in the study of refractory materials.[13,14] More recently, laser desorption (LD) methods have emerged, where the evaporation and ionization steps are accomplished

* Authors to whom correspondence should be addressed.
† James Cook University of North Queensland.
‡ Griffith University.
§ Deceased, April 1991.
⊥ Visiting Scholar from Department of Chemistry, Massachusetts Institute of Technology, Cambridge, MA 02139.

(1) Levy, D. H. *Ann. Rev. Phys. Chem.* **1980**, *31*, 197–225.
(2) Lubman, D. M. *Anal. Chem.* **1987**, *59*, 31A–40A.
(3) Hahn, J. H.; Zenobi, R.; Zare, R. N. *J. Am. Chem. Soc.* **1987**, *109*, 2842–2843.
(4) Geoffroy, G. L.; Wrighton, M. S. *Organometallic Photochemistry*; Academic Press: New York, 1979.
(5) Juris, A.; Barigelletti, S.; Campagna, S.; Balzani, V.; Belser, P.; von Zelewsky, A. *Coord. Chem. Rev.* **1988**, *84*, 85–277.
(6) Cotter, R. J. *Anal. Chem.* **1980**, *60*, 781A–793A.
(7) Ashcroft, A. E.; Chapman, J. R.; Cottrell, J. S. *J. Chromatogr.* **1987**, *394*, 15–20.
(8) Vestal, M. L. *Mass Spectrom. Rev.* **1983**, *2*, 447–480.
(9) Fenn, J. B.; Mann, M.; Meng, C. K.; Wong, S. F.; Whitehouse, C. M. *Science* **1989**, *246*, 64–71.
(10) Brennecke, J. F.; Tomasko, D. L.; Peshkin, J.; Eckert, C. A. *Ind. Eng. Chem. Res.* **1990**, *29*, 1682–1690.
(11) Sin, C. H.; Pang, H. M.; Lubman, D. M.; Zorn, J. *Anal. Chem.* **1986**, *58*, 487–491.
(12) Sin, C. H.; Linford, M. R.; Goates, S. R. *Anal. Chem.* **1992**, *64*, 233–236.
(13) Vertes, A.; DeWolf, M.; Juhasz, P.; Gijbels, R. *Anal. Chem.* **1989**, *61*, 1029–1036.
(14) Gray, A. L. *Analyst* **1985**, *110*, 551–556.

0003-2700/93/0365-2776$04.00/0

separately using different laser sources.[15] The advantage of the latter methodology is that desorption can be effected "softly", without significant fragmentation or ionization. Many reports have demonstrated the potential for analytical sensitivity and selectivity of laser desorption, particularly with fragile biomolecules.[16] Recently matrix materials have been employed to reduce fragmentation of molecules in the desorption step.[17-19]

The combination of laser desorption with supersonic jet/resonance-enhanced multiphoton ionization (REMPI)/time-of-flight mass spectrometry (TOF-MS) to record high-quality *wavelength-scanned* spectra as opposed to simple mass spectra has been explored in a few accounts.[20-25] However, much of this work has dealt with molecules which have low rather than negligible vapor pressures. Indeed, often the molecules could be volatilized into a molecular beam by sufficient heating, the desorption process being simply a means of flash heating. Two limiting mechanisms are involved in these experiments: heating of the sample via direct absorption of the desorption laser (e.g., *p*-aminobenzoic acid desorbed with 248 nm excimer radiation[22]) and absorption of the laser radiation by a substrate which mediates the heating of the analyte.[26] The advantage of the latter approach is that the desorbing laser need not be in electronic resonance with the analyte, therefore potentially reducing photofragmentation or ionization of sample molecules. However, substrate-mediated heating has been restricted in application due to the difficulties in maintaining a sufficiently stable yield of desorbing molecules for periods long enough to allow reproducible wavelength-scanned spectral measurements to be taken.

Several approaches have been applied to the problem of signal reproducibility in desorption experiments, mostly involving sample preparation. Examples include the preparation of thin films on metal blocks and polymers,[26] slurry matrices,[19] and materials such as glycerol.[27] Movement of the sample is advantageous, allowing a clean surface to be exposed to each laser shot, thus reducing sample variability with a commensurate improvement in stability, reproducibility, and experimental duration.[24,28]

Unfortunately difficulties exist with LD in the desorption of metal-containing compounds. Fragmentation of the desorbing species is facile as ligand binding energies are usually quite small. Such fragmentation has been observed for many organometallic compounds in the gas phase.[29-31] However, the use of an Ag/poly(ethylene oxide) matrix has been found to reduce fragmentation of at least one coordination compound, viz, tris(2,2'-bipyridine)ruthenium(II) {$[Ru^{II}(bpy)_3]^{2+}$}, to the point that large parent mass peaks of the parent complex are present in the LD/REMPI mass spectrum of the molecule.[19]

We present in this paper a simple methodology involving photographic emulsions containing particulate silver which can be used as matrices for laser desorption/MS, which overcome many of the problems associated with LD experiments, and which may facilitate the routine recording of the jet-cooled spectra of molecules with low or negligible volatility. An underlying principle of this method is that the desorption laser is absorbed predominantly by the optically dense silver particles, which in turn heat the remainder of the matrix (including the analyte). Hence, the desorption of the analyte is decoupled from the primary absorption step, and reduced fragmentation of the analyte results. The methodology we describe also has significant potential for analytical use in that it offers a reliable sampling procedure for introduction of nonvolatile analytes into molecular beams for subsequent spectral or mass spectral quantitation.

The aromatic amino acids L-phenylalanine, L-tyrosine, and L-tryptophan were chosen as the target substrates for this study. When conventional thermally-heated molecular beam sources have been used to measure the mass spectra of these species, significant fragmentation has been observed.[27,32-34] Nevertheless, despite the thermal lability and low vapor pressure of these amino acids, their jet-cooled electronic spectra have been measured previously using a variety of desorption methods.[27,32-34] The present paper compares mass and electronic spectral results obtained using desorption from the silver-containing film matrices (SCFM) with previous studies. In addition, the desorption of $[Ru(bpy)_3]^{2+}$, a substance with negligible vapor pressure, is also reported.

EXPERIMENTAL SECTION

Preparation of the Desorption Matrix. The flexible silver-containing film matrix (SCFM) for desorption studies was prepared from a diffusion-transfer film receiver (DTFR) material that is available from several manufacturers (e.g., AGFA copyproof film A4 0,01). The DFTR sheets do not themselves contain any silver or compounds of silver, our intention being to controllably introduce particulate silver into the film emulsion ourselves. Initially, the sheets of DTFR were conditioned by washing in a running water bath to remove any contamination of sulfur-containing image dye. Under photographic safety light, silver bromide crystals were then grown within the film by cycling the sheets alternatively through baths containing aqueous $AgNO_3$ solution (0.1–0.15 M) and aqueous KBr solution (0.5 M). Crystal growth (as measured by optical density) was gradual and reached a saturation plateau after ~8 cycles. The resultant sheets were exposed to a strong white light and reduced to metallic silver using conventional photographic development (AGFA Rodinal) and air-dried.

Water-soluble analytes were introduced into the SCFM by soaking the sheets in a solution containing about 5% by weight analyte, removing the film from the analyte bath, squeezing off the residual solution, and blow-drying the film. Experimentally, it was found that the DTFR emulsion became fully swollen on immersion in water for about 1 min, the measured weight gain being greatest at pH 12 and dropping to ~40% of this value at pH 2. It is estimated that up to about 0.5 g m^{-2} of analyte was introduced into the SCFM structure.

(15) Grotemeyer, J.; Boesl, U.; Walter, K.; Schlag, E. W. *Org. Mass Spectrom.* **1986**, *21*, 645–653.
(16) Grotemeyer, J.; Schlag, E. W. *Org. Mass Spectrom.* **1988**, *23*, 388–396.
(17) Hillenkamp, F.; Karas, M.; Beavis, R. C.; Chait, B. T. *Anal. Chem.* **1991**, *63*, 1193A–1202A.
(18) Beavis, R. C.; Lindner, J.; Grotemeyer, J.; Schlag, E. W. *Chem. Phys. Lett.* **1988**, *146*, 310–314.
(19) Beavis, R. C.; Lindner, J.; Grotemeyer, J.; Atkinson, I. M.; Keene, F. R.; Knight, A. E. W. *J. Am. Chem. Soc.* **1988**, *110*, 7534–7535.
(20) Imasaka, T.; Tashiro, K.; Ishibashi, N. *Anal. Chem.* **1989**, *61*, 1530–1533.
(21) Meijer, G.; deVries, M. S.; Hunziker, H. E.; Wendt, H. R. *J. Chem. Phys.* **1990**, *92*, 7625–7635.
(22) Meijer, G.; deVries, M. S.; Hunziker, H. E.; Wendt, H. R. *J. Phys. Chem.* **1990**, *94*, 4394–4396.
(23) Cable, J. R.; Tubergen, M. J.; Levy, D. H. *J. Am. Chem. Soc.* **1989**, *111*, 9032–9039.
(24) Cable, J. R.; Tubergen, M. J.; Levy, D. H. *J. Am. Chem. Soc.* **1987**, *109*, 6198–6199.
(25) Li, L.; Lubman, D. M. *Appl. Spectrosc.* **1989**, *43*, 543–549.
(26) Cable, J. R.; Tubergen, M. J.; Levy, D. H. *Faraday Discuss. Chem. Soc.* **1988**, *86*, 143–152.
(27) Li, L.; Lubman, D. M. *Appl. Spectrosc.* **1988**, *42*, 418–424.
(28) Cheshnovsky, O.; Yang, S. H.; Pettiette, C. L.; Craycraft, M. J.; Liu, Y.; Smalley, R. E. *Chem. Phys. Lett.* **1987**, *138*, 119–124.
(29) Leutwyler, S.; Evan, U.; Jortner, J. *J. Chem. Phys.* **1981**, *85*, 3026–3029.
(30) Hossenlopp, J. M.; Rooney, D.; Samoriski, B.; Bowen, G.; Chaiken, J. *Chem. Phys. Lett.* **1985**, *116*, 380–386.
(31) Prinslow, D. A.; Vaida, V. *J. Am. Chem. Soc.* **1987**, *109*, 5097–5100.
(32) Rizzo, T. R.; Park, Y. D.; Peteanu, L. A.; Levy, D. H. *J. Chem. Phys.* **1986**, *84*, 2534–2541.
(33) Chiarelli, M. P.; Gross, M. L. *Anal. Chem.* **1989**, *61*, 1895–1900.
(34) Martinez, S. J.; Alfano, J. C.; Levy, D. H. *J. Mol. Spectrosc.* **1992**, *156*, 421–430.

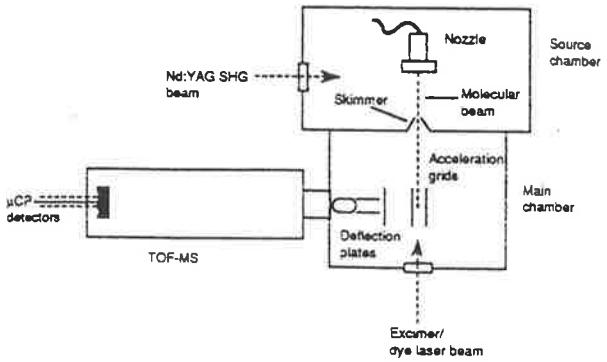

Figure 1. Schematic diagram of experimental configuration.

Each A4 SCFM sheet was cut into 3-mm-wide strips and spliced seamlessly (with motion picture splicing tape) together to form the final desired length of tape (~10 m).

Scanning Electron Microscopy. Scanning electron micrographs were recorded using a JEOL JXA-840 scanning electron microscope. The SCFM samples were Au-sputtered to allow contrasting of the polymer matrix in the SEM image. Electron energies of approximately 15 kV were used, and no surface damage was induced at these voltages.

Laser Desorption/TOF-MS Apparatus. Figure 1 shows a schematic diagram of the experimental arrangement, part of which has been described previously.[35] The tape player unit directed the DTFR film parallel to and 1–3 mm below the axis of a pulsed molecular beam valve (General Valve Series 9; ~150-μs duration, 0.8-mm-diameter orifice, Ar carrier gas at ~400 kPa) in the source region of the molecular beam apparatus (working pressure of 3×10^{-4} Torr). Laser desorption was effected by the 532-nm output of a frequency-doubled Nd:YAG laser operating in Q-switch mode (~2–6 mJ/pulse, 15 ns FWHM) weakly focused onto the SCFM through an 80-mm cylindrical lens. Power densities at the laser focus were on the order of ~3×10^8 W cm^{-2}. The tape was advanced at a rate such that the overlap between bleach spots on the film was between 10 and 50%.

The free jet expansion containing the desorbed molecules was skimmed (2-mm-diameter skimmer orifice; nozzle–skimmer separation ~ 80 mm) and directed through the DC extraction region of a Wiley–McLaren configuration TOF-MS (drift length 850 mm, working pressure ~2×10^{-6} Torr). Ionizing radiation was generated by a Lambda Physik excimer laser (EMG 101 MSC, 308 nm) pumping a Lambda Physik FL3002 dye laser. For all experiments described herein, the laser dye was C540A. Output light was frequency-doubled by an angle-tuned KDP crystal and weakly focused (by a 1000-mm lens), and the unfiltered beam was directed anticollinear with the molecular beam between the extraction plates in the source region of the TOF-MS. The laser output was attenuated using a rotating Glan–Taylor prism polarizer and/or apertures to reduce saturation of optical transitions.

Cations produced by (1 + 1) ionization of the sample were extracted (~100 V) and accelerated (~1000 V) in the source region of the TOF and directed down the flight tube toward tandem microchannel plate (MCP) detectors. Any correction for non-normal ion trajectories was achieved by adjustable low-voltage biases (≤10 V) applied to horizontal and vertical deflector plates. Output signal from the dual MCP detectors was buffered and impedance matched by a 400-MHz video amplifier (NS LH0063) before display on a digital storage oscilloscope (Tektronix 2432). The oscilloscope was interfaced with a microcomputer (Macintosh SE/30) via an IEEE-488 connection. Discrete spectra were recorded by collecting an averaged mass spectrum (16 or 32 shots) for each laser step (typically 0.0005 nm in the UV region). Custom-written graphics interface software[36] permitted individual mass/wavelength regions of interest to be selected subsequently and displayed. Either a wavelength-scanned spectrum for a selected mass range or a mass spectrum for a selected laser ionization wavelength range could be extracted. This collection strategy meant that all mass channels were measured simultaneously in a given wavelength scan, a feature that has considerable advantages in noise reduction through background subtraction. Analogue spectra were taken using a PAR 162/165 boxcar and gated integrator with output to a chart recorder. All timing and triggering for the experiment, which was run at 10 Hz, were provided by a custom-built digital delay generator, with 16 independently programmable outputs, precision ≤100 ps.[37] The optimal temporal delay between the desorption and ionizing lasers was typically 400–500 μs.

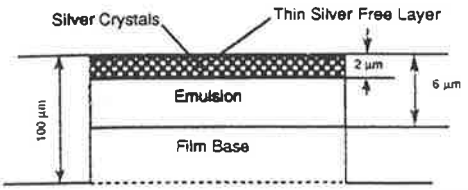

Figure 2. Cross section of silver-containing film matrix (SCFM) (not drawn to scale).

RESULTS AND DISCUSSION

Film Structure. The intent of the design of the desorption matrix was to produce a film in which the analyte was dispersed evenly in a layer in which finely divided metal particles (silver) were also present. Water-swellable materials such as conventional black-and-white photographic film were investigated but were rejected because of instability of the gelatine emulsion and a substantial gelatine-related background present in the LD-generated mass spectra of such materials.

The final choice for the matrix host was a commercially available DTFR material which contains a synthetic polymer emulsion layer. (The precise composition of the emulsion layer was considered proprietary information by the manufacturers.) Particulate silver was introduced into the emulsion layer as described above. The exact quantity of silver crystals introduced was difficult to determine due to changes in the equilibrium moisture content of the emulsion layer. However, we estimate that the silver content was in the range of 3 g cm^{-2}. From SEM studies, the silver crystal size range was evaluated to be in the range of 0.1–0.35 μm, never exceeding 0.5 μm. The effective silver crystal size in the emulsion was estimated at about 0.08 μm. (Silver particle size was calculated using the Nutting equation,[38] which relates the optical density of a silver emulsion with the number of silver particles in an observed area, and estimating that the 2.0-μm-thick emulsion layer is unlikely to contain more than 3 g/m^2 of silver.) Figure 2 shows schematically the dimensions of the SCFM.

If potassium chloride, rather than potassium bromide, is used in the preparation of the matrices, the silver particle size is reduced, never exceeding ~0.03 μm.

Volatilization of Amino Acids. Mass Spectra. Figure 3 displays the mass spectra of the three aromatic amino acids L-tryptophan, L-phenylalanine, and L-tyrosine, taken using the SCFM/LD technique. All of the spectra were measured using ionization wavelengths coincident with the $S_1 \leftarrow S_0$ electronic origin of the molecules concerned, with ionization laser energies of ~50 μJ/pulse. No contamination from the DTFR polymer matrix was ever observed in the mass spectra. This indicates that laser powers in the range ≤10 mJ, while

(35) Bieske, E. J.; Rainbird, M. W.; Atkinson, I. M.; Knight, A. E. W. *J. Chem. Phys.* **1989**, *91*, 752–61.

(36) Butz, K. W. unpublished software. Rock, A. B., Ph.D Thesis, Griffith University, 1993.

(37) Beames, S., Faculty of Science and Technology, Griffith University; information available on request.

(38) James, T. H. *The Theory of the Photographic Process*; Macmillan: New York, 1977.

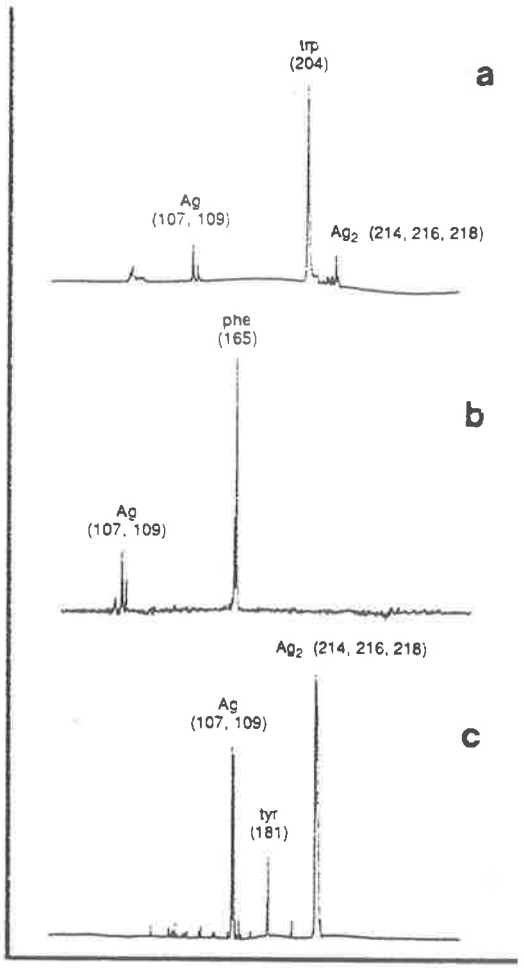

Figure 3. Mass spectrum of amino acids laser-desorbed from SCFM matrix. (a) L-Tryptophan (desorption λ = 532 nm, ionization λ = 286.755 nm); (b) L-phenylalanine (desorption λ = 532 nm, ionization λ = 266.084 nm); and (c) L-tyrosine (desorption λ = 532 nm, ionization λ = 281.350 nm).

still sufficient to induce substantial desorption of the analyte, are insufficient to produce any fragmentation of the DTFR polymer matrix. (No evidence for any DTFR composition products could be found, even when higher ionization laser powers were used (220 μJ/pulse). However, the possibility also exists that DTFR decomposition products were not ionized in the spectral region scanned.)

Evident in all of the spectra are the silver masses Ag (107, 109) and Ag_2 (214, 216, 218). Some variation in the yield of Ag, Ag_2 relative to that of the amino acid is apparent. Partial explanation of the differing Ag_n/amino acid ratios in these spectra lies with the varying absorption cross sections of the amino acid and the different loadings into the SCFM that could be achieved with each analyte. However, the primary explanation lies with the nature of the silver desorption/ionization. Ag_2 has a rich vibronic spectrum in the wavelength regions spanned in these studies,[39,40] and as each spectrum is taken at a different ionization wavelength, the magnitude of the Ag_2 signal will correlate with the proximity of the ionizing wavelength to features in the Ag_2 absorption spectrum.

Laser ablation of Ag/Ag_2 from metallic or crystalline silver has been studied previously[41-45] and may be compared with the laser desorption/molecular beam data reported here. Although there is no a priori reason to exclude the formation of Ag_n^+ clusters for $n > 2$ in a laser ablation experiment, only the monomer and dimer species have so far been reported. In accordance with the ablation data,[43] Ag_2 was the largest silver mass observed in our experiment, the dimer/monomer ratio decreasing with increasing desorption laser power. With appropriate adjustment of backing pressures, nozzle pulse width, and desorption laser intensity, $Ag_2(Ar)_n$ clusters of up to n = 20 could be observed.

We note in passing that Willey et al.[40] have measured electronic spectra of Ag_2Ar using one-color REMPI spectroscopy. The spectra reported by these authors match those collected in our own work using SCFM, although the SCFM spectra indicate that the vibrational temperatures for Ag_2Ar are higher than those obtained by Willey et al.[40]

The power dependence of the desorption signal for Ag/Ag_2 is not as sharp using the SCFM method as reported for other desorption matrices[44] and displays a fairly wide plateau (~2 mJ/pulse). The observed power dependence profile is relatively flat compared to most other desorption methods, and therefore the desorption yield of SCFM is less sensitive to laser power fluctuations than these other methods.[21,22] This single feature is a significant advantage of the SCFM approach to desorption for spectroscopic measurements, since it is the poor stability of the desorption yield that is the major limiting factor in applying most other desorption methods to measuring wavelength-resolved spectra.

There is indication that the kinetic energy distributions of Ag and Ag_2 may be different from those for the amino acids. The temporal profile of the TOF-MS signal for the organic molecules is fairly sharp, corresponding to a packet width of ~20 μs in the jet. However, Ag and Ag_2 display a temporal profile ~2–3 times as long.

Wavelength-Scanned Spectra. A sensitive test of the efficacy of the SCFM method in producing a steady and significant concentration of the desorbed analyte in a molecular beam is the recording of wavelength-scanned spectra. Figure 4a shows the REMPI spectrum of the origin region of tryptophan measured using the SCFM technology. The quality of this spectrum can be contrasted with Figure 4b, which presents the REMPI spectrum of the same molecule recorded by Levy et al.[32] using a continuous jet thermal desorption source. (In their original experiments with tryptophan, Levy et al.[45] used a thermospray source, but it was later realized that the thermospray simply coated the walls of the channel nozzle from which tryptophan was thermally desorbed.[46,47] Some slight instability may exist in such a source because of uneven or discontinuous desorption from the channel walls.) Tryptophan is sufficiently stable to permit the use of a relatively stable thermal source in its volatilization.

Comparison of the spectra in Figure 4 establishes that there is no reduction in spectral quality using our pulsed-laser desorption source compared with the intrinsically stable

(39) Beutel, V.; Bhale, G. L.; Kuhn, M.; Demtröder, W. *Chem. Phys. Lett.* **1991**, *185*, 313–318.
(40) Willey, K. F.; Cheng, P. Y.; Yeh, C. S.; Robbins, D. L.; Duncan, M. A. *J. Chem. Phys.* **1991**, *95*, 6249–6256.
(41) Herminghaus, S.; Leiderer, P. *Appl. Phys. Lett.* **1991**, *58*, 352–354.
(42) Helvajian, H.; Welle, R. *J. Chem. Phys.* **1989**, *91*, 2616–2626.
(43) Helvajian, H.; Welle, R. P. *Mater. Res. Soc. Symp. Proc.* **1989**, *129*, 359–364.
(44) Karas, M.; Bachmann, D.; Bahr, U.; Hillenkamp, F. *Int. J. Mass. Spectrom. Ion Processes* **1987**, *78*, 53–68.
(45) Rizzo, T. R.; Park, Y. D.; Levy, D. H. *J. Am. Chem. Soc.* **1985**, *107*, 277–278.
(46) Rizzo, T. R.; Park, Y. D.; Peteanu, L. A.; Levy, D. H. *J. Chem. Phys.* **1985**, *83*, 4819–4820.
(47) Park, Y. D.; Rizzo, T. R.; Peteanu, L. A.; Levy, D. H. *J. Chem. Phys.* **1986**, *84*, 6539–6549.

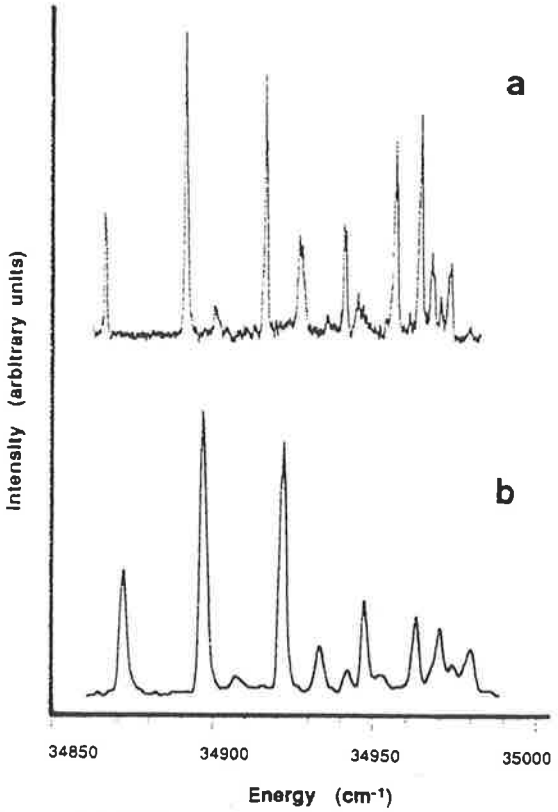

Figure 4. (a) REMPI spectrum of L-tryptophan via laser desorption from SCFM. (b) REMPI spectrum of L-tryptophan (Levy et al.[32] Reproduced with permission from the *Journal of Chemical Physics*).

continuous thermal desorption source. Temperature and/or different conformer populations may be partly responsible for the difference in some of the relative band intensities between the spectra in Figure 4. Differences in spectral saturation levels may also contribute to the differing intensities.[32]

The pulsed-LD-derived spectrum has slightly more noise, but also more structure, than the thermal desorption analogue. If the LD data are smoothed with a sliding 5-point average, the spectrum is found to display resolution and noise almost identical to that found in the spectrum of L-tryptophan in reference 32.

A scan time of ~30 min was required to measure the LD spectrum, which means that a considerable amount of data can be collected from a 10-m strip of SCFM tape (translated at ~1–1.5 m/h).

Molecular Beam Character and Cooling. The extent to which the desorbed molecules are cooled in the supersonic expansion is reflected by the rotational bandwidths of the vibronic transitions in the REMPI spectra. The FWHM peak widths of the bands in the LD-derived spectra of L-tryptophan are ~1.3 cm^{-1}, compared with those of the previously reported spectra of ~2.5 cm^{-1}.[32] This indicates that our SCFM/LD method permits cooling in the expansion at least as dramatic as that observed previously for amino acids such as tryptophan. The rotational temperature estimated from rotational contour analysis[48] of the origin band in Figure 4a indicates that the beam temperature is no higher than ~5 K.

From the absence of hot bands in the REMPI spectra of L-tryptophan and L-phenylalanine,[49] the vibrational temperature is estimated to be ≤15 K. However, in the spectrum of the latter,[49] there is indication that some conformers of L-phenylalanine may be generated in the molecular beam with higher vibrational temperatures, perhaps up to 50 K.

The position of the tape with respect to the nozzle was found to be important (but not critical) to the *cooling* achieved in the molecular beam, although the *quantity* of material entrained varied significantly. In general, the best cooling and beam flux density were obtained when the tape edge was flush with the exit face of the nozzle and located 0.5–1 mm below the axis of the nozzle orifice. With distances less than 0.5 mm, beam flux dropped as the beam quality was degraded (presumably due to physical obstruction of the Mach bottle by the tape). Moving the tape to a position further than ~3 mm from the nozzle resulted in only ~10% of the potential maximum signal obtainable. It was found that moving the tape further from the nozzle along the axis of the molecular beam was very destructive to the molecular beam profile, distances of >2 mm causing drastic signal reductions, presumably because the tape edge interfered with the sheath of the Mach bottle associated with the expansion.[50]

Desorption Signal Strength and Detection Limits. It is an important requirement that the SCFM/LD method to be able to yield a sufficient density of neutral molecules so that reasonable REMPI ion currents can be generated without the need to resort to high-power ionizing lasers. Low ionizing laser powers are advantageous in that saturation of spectral transitions can be minimized in one-color REMPI spectra, although the use of LIF or two-color REMPI would reduce the problem of spectral saturation. Quantification of the desorption flux in the present experiments is difficult because of the many variables involved, and no attempt was made to experimentally calibrate the necessary instrument-dependent parameters. However, some reasonable approximations may be made.

Peak ion signals for L-phenylalanine were ~150 mV with a 20-ns FWHM peak width (50-Ω oscilloscope input, electron multiplication ~2×10^6), which corresponds to ~100 ions detected per laser pulse. The ionization efficiency is probably ~1%,[50] while the fraction of neutral species entrained in the molecular beam passing through the 2-mm skimmer is about 0.1%.[50] Several factors are not accounted for in this estimation (e.g., losses in the TOF drift region), but the order-of-magnitude estimate of about 10^7 neutral molecules being desorbed per pulse is probably close to the real value. Although approximate, this figure reflects the high analyte loadings that can be achieved with SCFM and correlates to a minimum amount of phenylalanine required to produce detectable signal of ~1.5 fg. Phenylalanine has an extinction coefficient of about one-sixth that of tyrosine and about one-twentyfifth that of tryptophan, so the detection limits for these analytes are correspondingly lower.

Desorption Signal Stability. Several conditions must be satisfied for the successful measuring of wavelength-scanned spectra with accurate, reproducible intensities and band contours. Small fluctuations of the signal intensity can be tolerated and compensated for with smoothing; however, this increases the time required for a spectral scan and therefore places more emphasis on longer term (i.e., several hours) desorption stability. Workers who have previously applied LD to spectral collection have reported pulse-to-pulse variations in the desorption yield of ≥30% and total scan times limited to 0.5 h or less.[21,22,24] Lubman et al.[27] have reported the LD of tyrosine analogues from a glycerol matrix

(48) Atkinson, I. M. Ph.D. Thesis, James Cook University of North Queensland, 1992.

(49) Atkinson, I. M.; Shorter, J. A.; Karaiste, R. T. T.; Keene, F. R.; Knight, A. E. W., manuscript in preparation.

(50) Arrowsmith, P.; deVries, M. S.; Hunziker, H. E.; Wendt, H. R. *Appl. Phys. B* **1988**, *46*, 165–173.

(51) Li, L.; Lubman, D. M. *Anal. Chem.* **1989**, *61*, 1911–1915.

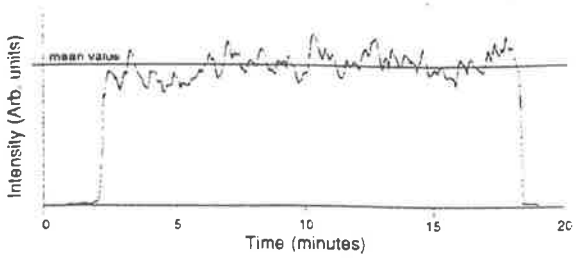

Figure 5. Stability of neutral desorption yield of L-phenylalanine laser desorbed from SCFM (desorption λ = 532 nm, ionization λ = 266.084 nm).

set on a Macor rod, but, once again, the instability of the desorption yield compromises the quality of the spectrum.

Computer averaging may be used to average spectra from several different scans, i.e., where the wavelength range for the spectrum is scanned repetitively, rather than taking a single, long scan. This procedure has the advantage of suppressing any noise due to random surface variations of the SCFM and pulse-to-pulse instabilities of the desorption laser. In this way, two separate scans of 16 shots/point can be added, for example, to produce a 32 shots/point spectrum, with a significantly smoothed desorption yield over the entire data set. However, in practice, it was found that this extra averaging was not usually necessary with our SCFM desorption source since the stability of the SCFM technology was quite sufficient for high-quality spectral scans. Pulse-to-pulse desorption stability was usually ~10%. An additional advantage of the SCFM is that a 532-nm Nd:YAG laser (which is usually considerably more stable than excimer or CO_2 sources) can be used for the desorption light source, and the desorption yield of SCFM is less sensitive to laser power fluctuations than direct desorption without matrix mediation (vide supra).

Experiments were conducted in which the laser wavelength was tuned to the $S_1 \leftarrow S_0$ origin transition of phenylalanine and the laser adjusted so that the REMPI signal was saturated, and the neutral desorption yield was monitored under these conditions. Figure 5 illustrates a typical trace of the signal stability observed. These data were taken using a boxcar gated to the mass of L-phenylalanine, and time constants were set to be much more sensitive than would be the case in a wavelength-scanned experiment, so that smoothing did not unduly influence the trace presented.

Figure 6 illustrates the $S_1 \leftarrow S_0$ origin band of L-phenylalanine scanned successively and repetitively over the sample spectral range. Desorption and ionizing laser powers differed by no more than 5% between any of these runs, which took a total of 90 min to accumulate. No smoothing or averaging has been applied to these data, so as to give a realistic impression of the reproducibility of the SCFM technology. As may be seen, all of the profiles have the same shape, and their integrated intensities vary by no more than ±10%.

Although the signal stability from SCFM technology is reasonable, it could be improved. We currently believe that attention should be focused toward removing any surface inhomogeneities that are present in the film structure.

Physical Damage to the SCFM. The physical effect of the laser on the SCFM was investigated by subsequent SEM analysis using a series of samples that had endured a single laser pulse. At low laser powers, very little effect was observed on the SCFM surface. Using a 100-mm lens to focus the desorption radiation onto the SCFM and a laser power of ~1 × 10^7 W cm^{-2}, the surface appeared physically intact to the naked eye, with the exception that a brown discoloration was apparent: SEM studies revealed the surface to be peppered with small round holes (~0.2–1.0 μm in diameter) together

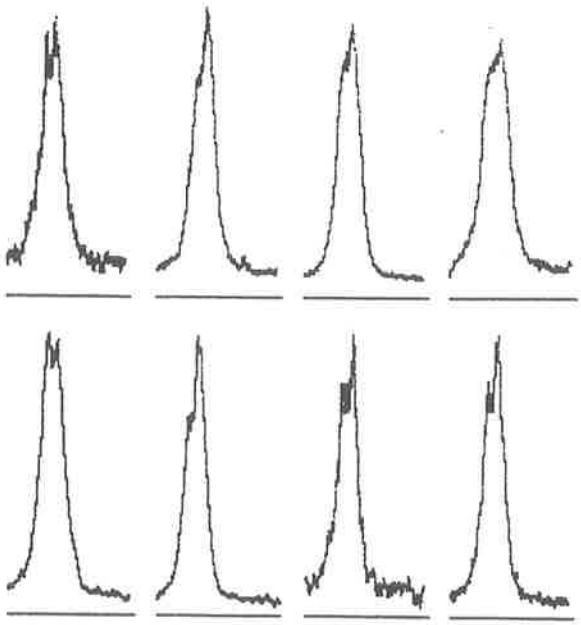

Figure 6. Repetitive scans of the $S_1 \leftarrow S_0$ origin band of L-phenylalanine laser desorbed from SCFM (desorption λ = 532 nm, ionization λ scanned 37 516.5–37 544.5 cm^{-1}, phe 0_0^0 = 37 529.7 cm^{-1}).

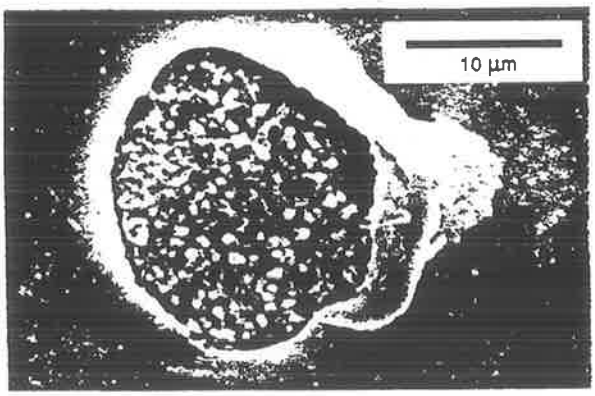

Figure 7. Single shot laser damage spot of SCFM (AgBr-derived Ag, desorption laser power ~4 × 10^7 W cm^{-2}).

with some significantly larger holes (~10 μm) that resembled burst bubbles. The overall impression was that a considerable gas or vapor pressure had developed underneath the surface layer of the SCFM. At higher laser powers (about 1.7 × 10^7 W cm^{-2}), surface damage was obvious to the naked eye. The higher power damage suggested that a thin layer of the emulsion polymer had expanded as a bubble and then burst, leaving pieces of the surface layer around the damage site (Figure 7). In this case, a large amount of gas or vapor may have been generated underneath the cool transparent surface layer of the SCFM, causing it to stretch and expand until it finally burst, releasing the analyte as a vapor into the stream of supersonic gas sweeping across the SCFM. It was apparent from desorption studies of a stationary SCFM that all of the analyte was desorbed in 5–10 laser pulses. Moreover, the desorption yield from the first laser pulse was not as high as the succeeding few pulses. This indicated that disruption of the surface layer from the SCFM enhanced the desorption process and explains why stronger signals were observed when the tape player was run with some overlap between successive laser shots. Further increases in laser power increased the surface damage. This led to an eventual loss of signal due to fragmentation/ionization of the sample molecules when the

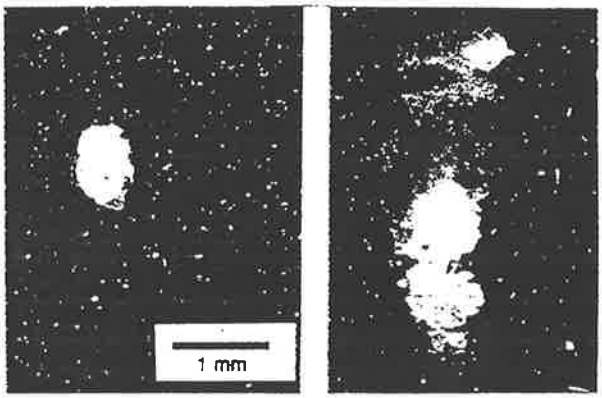

Figure 8. Single shot laser damage shot of SCFM (desorption laser power = 1.7×10^7 W cm^{-2}). (Left) AgBr-derived silver (larger particles), and (right) AgCl-derived silver (smaller particles).

onset of ionic desorption/ablation was reached, typically at desorption laser fluences of (5–6) $\times$ 10^7 W cm^{-2}.

The exposed layer of silver crystals showed no evidence of melting or fusion, but the crystals were covered with a layer of emulsion polymer adhering to the surface. In between the silver crystals, there were deep crevices and channels leading into the silver–emulsion polymer matrix structure.

Surface temperatures of the laser heated film were estimated by assuming that the silver particles were the primary photon absorber, approximating the laser pulse profile as triangular, and applying the model proposed by Ready:[52]

$$T_{max} = (1 - R)\frac{8}{3D}\left(\frac{k}{\pi}\right) I_0 \left(\frac{t_0}{4 - t_r/t_0}\right)^{1/2}$$

where $I(t)$ is the incident power as a function of time (W cm^{-2}), R is the surface reflectivity, k is the thermal conductivity (W cm^{-1} K^{-1}), and D is the thermal diffusivity (cm^2 s^{-1}) {$D = k/\rho C_p$, where ρ is the density of the surface, and C_p the heat capacity at constant pressure}. Using this equation, calculations of the rise in surface temperature of the SCFM suggest peak values around the Ag particles of ~1250 K, with the temperature in the region between Ag granules somewhat less than this value. (Calculation based upon: D_{Ag} = 1.688 cm^2 s^{-1}; k_{Ag} = 4.154 W cm^{-1} K^{-1}; t_0 = 16 ns; t_r = 18 ns; I_0 = 1×10^7 W cm^2. As the intersilver spaces are not directly heated by the desorption laser, the temperature in these regions may not reach the predicted maximum.) This figure is regarded as only a rough guide to the true peak temperature because of the difficulty in determining the exact thermal parameters of the SCFM material.

Smaller silver particles (ca. 300 nm) could be introduced into the DTFR by using AgCl-based precipitations as well as the AgBr process described previously. As illustrated in Figure 8, the laser couples more efficiently with the smaller particles, yielding a larger damage spot. However, better signal stability was observed from the AgBr-based SCFM. Nonetheless, the chloride-based film may have some advantages for specific analytical applications.

FURTHER DEVELOPMENTS

The SCFM possesses several attributes that invite further development. Firstly, the emulsion polymer, whilst not completely characterized, is amenable to modification. The degree of ionic cross-linking which binds the emulsion structure may be adjusted over a wide range by simple treatment of the emulsion during the preparation of SCFM. The moisture content in the emulsion lowers the melting temperature of the polymer, and experiment has shown that this enhances analyte release. Any moisture inside the SCFM will be rapidly vaporized during the laser pulse, and this expanding vapor may assist in "flushing" the adsorbed analyte into the molecular beam. The analyte is uniformly distributed throughout the silver-containing matrix structure, and it is possible that any analyte that is in intimate contact with the silver crystals becomes thermally fragmented during the desorption. It is probable that several desorption mechanisms are operative in SCFM-based desorption.

It is conceivable that SCFM could be produced that is swellable in solvents other than water, further extending the utility of the matrix. In principle, it is possible to manufacture matrix structures from colloidal silver powder mixed with various polymers. The main advantage envisaged of these materials would be an increased analyte loading and more control over the analyte introduction into the matrix. While these experiments are incomplete, we provide in the following paragraphs a summary of some initial results that are relevant in the present context.

One of the aims of our work was to volatilize transiton-metal compounds in preparation for their spectroscopic interrogation via molecular beam techniques. We had demonstrated previously that tris(2,2′-bipyridine)ruthenium was introduced into a molecular beam from a slurry of poly(ethylene oxide) and colloidal Ag or Au using a pulsed CO_2 laser for desorption.[19] However, the yield of parent ion was relatively low (<5% of the total ion signal) due to substantial fragmentation. Our current approach produces greater than 50% parent ion signal.

Tris(2,2′-bipyridine)ruthenium(II) acetate was mixed with an aqueous Ag colloid supported with 10% poly(vinyl alcohol) (PVA) and applied with a home-built film applicator to a Mylar backing sheet. Inspection of the resulting air-dried matrix by optical and scanning electron microscopy showed that the analyte was bound to the PVA binder, which in turn surrounded the Ag colloid granules to a depth of ~100 nm. The matrix had a void volume of 64% and provides a high surface area medium that can be heavily loaded with analyte (~1% by weight) while simultaneously serving as an optically dense medium for laser absorption. The material is flexible, as required for its use on the tape drive (described above).

Laser desorption of the coordination compound was achieved using 532-nm irradiation, with subsequent laser ionization at 290 nm, which is sufficient to two-photon-ionize the 2,2′-bipyridine ligand.[53] The desorption mass spectrum was dominated by a single broad peak centered at m/z = 570, corresponding to that expected for the singly charged monocation, $[Ru(bpy)_3]^+$. The spectrum contained no evidence for the fragments $[Ru(bpy)_2]^+$ (m/z = 414) or $[Ru(bpy)]^+$ (m/z = 258), corresponding to loss of one or two bipyridine fragments from the parent cation. In our previous work,[19] substantial fragmentation of the $[Ru(bpy)_3]^{n+}$ moiety was observed. When 270-nm irradiation was used as the ionization wavelength, the mass spectrum remained unchanged. No evidence for production of laser ablated ions (desorption and ionization within the desorbing laser pulse) could be found within the sensitivity of our apparatus, indicating that neutral $[Ru(bpy)_3]$ was the dominant desorbed species.

In our previous report,[19] we suggested that fragmentation of the parent complex may be the result of ionization-induced fragmentation of $[Ru(bpy)_3]$. However, we have used similar laser powers for ionization in both sets of experiments, so that the reduced fragmentation reported here is presumably

(52) Ready, J. F. *Effects of High Power Laser Radiation*; Academic Press: New York, 1971.

(53) Barone, V.; Cauletti, C.; Piancastell, M. N.; Ghedini, M.; Toscano, M. *J. Phys. Chem.* **1991**, *95*, 7217–7220.

a consequence of either the different sample medium or the differences in the characteristics of the desorption laser. The CO_2 laser used for desorption in our previous work[19] had a relatively long pulse width (~1-μs spike, ~10-μs tail) and a power density of $\sim 10^4$ W cm^{-2}. In our current experiments, the temporal width of the desorption signal is ~20–40 μs. Hence it is likely that the longer pulse width of the CO_2 laser could have caused secondary laser-induced fragmentation of [Ru(bpy)$_3$] following the initial desorption step.

This preliminary study demonstrates that the use of polymer-coated colloidal metals, in conjunction with short-pulse laser desorption, is a potentially useful technique for mass spectral study of transition-metal coordination and organometallic compounds. We believe that by appropriate choice of the binding polymer, the technique could be expanded for use in other solvents if required by different solubility characteristics of the analyte. At this stage, while the mass spectral results are encouraging in terms of the nondestructive volatilization of the coordination compound, the signal was not sufficiently stable for the measurement of wavelength-scanned spectra.

ACKNOWLEDGMENT

The assistance of the staff of the mechanical and electronic workshops within the Faculty of Science and Technology, Griffith University, is gratefully acknowledged. The U.S.-Australian Cooperative Research Program [DITAC (Australia) and the NSF International Division (U.S.A.)] supported the visit of J.A.S. to G.U. Financial assistance from the Australian Research Council is also acknowledged.

RECEIVED for review April 12, 1993. Accepted July 7, 1993.*

* Abstract published in *Advance ACS Abstracts*, September 1, 1993.

3004 *Inorg. Chem.* 1992, *31*, 3004–3006

Synthesis of Polypyridyl Complexes of Ruthenium(II) Containing Three Different Bidentate Ligands

Geoffrey F. Strouse,† Peter A. Anderson,‡ Jon R. Schoonover,† Thomas J. Meyer,*,† and F. Richard Keene*,‡

Department of Chemistry, Venable and Kenan Laboratories, The University of North Carolina at Chapel Hill, Chapel Hill, North Carolina 27599-3290, and Department of Chemistry and Biochemistry, James Cook University of North Queensland, Townsville, QLD 4811, Australia

Received April 10, 1992

The metal-to-ligand charge transfer (MLCT) excited states of polypyridyl complexes of Ru(II) have provided a basis for the study of photoinduced electron or energy transfer in solution and in molecular assemblies.[1-5] The properties of these excited states can be varied systematically by varying the ligands.[6-9] We describe here a general synthetic procedure which extends the coordination chemistry to heteroleptic tris-bidentate polypyridyl (pp) complexes, $[Ru(pp)(pp')(pp'')]^{2+}$, based on the ligands

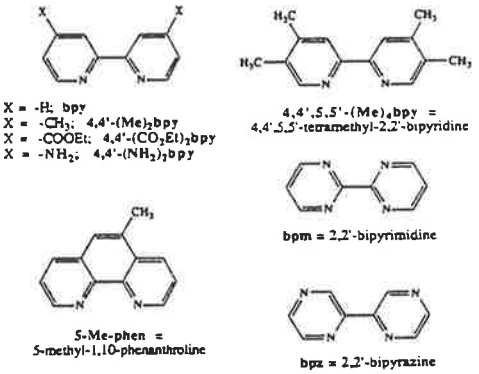

and opens new possibilities for the design of specific excited-state properties.

Earlier attempts to develop general synthetic routes to heteroleptic tris-bidentate complexes have met with limited success.[10] Our procedure was adapted from the method of Deacon and Thomas[11-13] and uses $[Ru(CO)_2(Cl)_2]_n$ as the precursor.[14] When $[Ru(CO)_2(Cl)_2]_n$ and a bidentate polypyridyl ligand (pp) were heated at reflux in EtOH or MeOH for 15 min, the yellow solids *trans*-(Cl)-$[Ru(pp)(CO)_2Cl_2]$ (pp = bpy or 4,4′-$(Me)_2$bpy) precipitated and were isolated as fine yellow crystals on recrystallization from MeOH in 80–90% yield. They were converted into the corresponding triflato species, $[Ru(pp)(CO)_2(CF_3SO_3)_2]$ by heating at 105–110 °C for 90 min in trifluoromethanesulfonic acid in a stream of N_2 and collected after precipitating the white product by the addition of ethyl ether at 0 °C. The white to pale yellow cations $[Ru(pp)(pp')(CO)_2]^{2+}$ (pp = bpy, 4,4′-$(Me)_2$bpy; pp′ = bpy, 4,4′-$(Me)_2$bpy, 4,4′-$(CO_2Et)_2$bpy, bpm, 5-Me-phen) were formed by dissolving the triflato complexes and an excess of a second polypyridyl ligand (pp′) and heating in ethanol at reflux for 90 min. They were isolated as PF_6^- salts in 70–80% yield upon addition of a saturated aqueous solution of NH_4PF_6 and recrystallization from ethanol. The tris-bidentate cations $[Ru(pp)(pp')(pp'')]^{2+}$ were formed by heating the dicarbonyl cations $[Ru(pp)(pp')(CO)_2]^{2+}$ with a 3-fold excess of the decarbonylating reagent trimethylamine *N*-oxide in 1,2-dimethoxyethane at reflux in the presence of an excess of the third polypyridyl ligand (pp″) (pp″ = bpy, 4,4′-$(Me)_2$bpy, 4,4′-$(CO_2Et)_2$bpy, bpm, 5-Me-phen, 4,4′-$(NH_2)_2$bpy, 4,4′,5,5′-$(Me)_4$bpy, bpz). Purification was achieved by Sephadex (SP-

† The University of North Carolina at Chapel Hill.
‡ James Cook University of North Queensland.

(1) (a) Chen, P. Y.; Duesing, R. D.; Graff, D.; Meyer, T. J. *J. Phys. Chem.* **1991**, *95*, 5850. (b) Danielson, E.; Elliott, C. M.; Merkert, J. W.; Meyer, T. J. *J. Am. Chem. Soc.* **1987**, *109*, 2519. (c) Westmoreland, T. D.; Schanze, K. S.; Neveux, P. E., Jr.; Danielson, E.; Sullivan, B. P.; Chen, P. Y.; Meyer, T. J. *Inorg. Chem.* **1985**, *24*, 2596.
(2) (a) Lee, E. J.; Wrighton, M. S. *J. Am. Chem. Soc.* **1991**, *113*, 8562. (b) Cooley, L. F.; Larson, S. C.; Elliott, C. M.; Kelly, D. F. *J. Phys. Chem.* **1991**, *95*, 10694. (c) Resch, U.; Fox, M. A. *J. Phys. Chem.* **1991**, *95*, 6169. (d) Haga, M.; Kiyoshi, I.; Boone, S. R.; Pierpont, C. G. *Inorg. Chem.* **1990**, *29*, 3795. (e) Perkins, T. A.; Humer, W.; Netzel, T. L.; Schanze, K. S. *J. Phys. Chem.* **1990**, *94*, 2229.
(3) (a) Ohno, T.; Yoshimura, A.; Prasad, D. R.; Hoffman, M. Z. *J. Phys. Chem.* **1991**, *95*, 4723. (b) Ohno, T.; Yoshimura, A.; Mataga, N. *J. Phys. Chem.* **1990**, *94*, 4871. (c) Kitamura, N.; Obati, R.; Kim, H.-B.; Tazuke, S. *J. Phys. Chem.* **1989**, *93*, 5764. (d) Navon, G.; Sutin, N. *Inorg. Chem.* **1974**, *13*, 2159.
(4) (a) Meyer, T. J. In *Photochemical Processes in Organized Molecular Systems*; Kitamura, N., Ed.; Elsevier: Amsterdam, 1991; p 133. (b) Balzani, V.; Scandola, F. *Supramolecular Photochemistry*; Ellis Horwood: Chichester, England, 1991. (c) Photoinduced Electron Transfer 1–3. Mattey, J., Ed. *Top. Curr. Chem.* **1990, 1991**, *156*, *158*, *159*. (d) Meyer, T. J. *Acc. Chem. Res.* **1989**, *22*, 163. (e) *Photoinduced Electron Transfer*; Fox, M. A., Chanon, M., Eds.; Elsevier: New York, 1988. (f) Balzani, V.; Sabbatini, N.; Scandola, F. *Chem. Rev.* **1987**, *86*, 319. (g) Balzani, V., Ed. *Supramolecular Photochemistry*; NATO ASI Series C214; Reidel: Dordecht, The Netherlands, 1987. (h) Peterson, J. D. *Coord Chem. Rev.* **1985**, *64*, 261.
(5) (a) Furue, M.; Yashidzumi, T.; Kinoshita, S.; Kushida, T.; Nozakura, S.; Kamachi, M. *Bull. Chem. Soc. Jpn.* **1991**, *64*, 1632. (b) Murtaza, Z.; Zipp, A. P.; Worl, L. A.; Graff, D.; Jones, W. E.; Bates, W. D.; Meyer, T. J. *J. Am. Chem. Soc.* **1991**, *113*, 5113. (c) Boyde, S.; Strouse, G. F.; Jones, W. E., Jr.; Meyer, T. J. *J. Am. Chem. Soc.* **1989**, *111*, 7448. (d) Tamilarsan, R.; Endicott, J. F. *J. Phys. Chem.* **1986**, *90*, 1027. (e) Scandola, F.; Balzani, V. J. *J. Chem. Educ.* **1983**, *60*, 814. (f) Lin, C.-T.; Böttcher, W.; Chou, M.; Creutz, C.; Sutin, N. S. *J. Am. Chem. Soc.* **1976**, *98*, 6536.
(6) (a) Juris, A.; Balzani, V.; Barigelletti, F.; Campagna, S.; Belser, P.; Von Zelwesky, A. *Coord. Chem. Rev.* **1988**, *84*, 85. (c) Krause, R. A. *Struct. Bonding (Berlin)* **1987**, *67*, 1. (d) Meyer, T. J. *Pure Appl. Chem.* **1986**, *58*, 1576. (e) Kalayanasundaram, K. *Coord. Chem. Rev.* **1982**, *46*, 159. (f) Seddon, K. R. *Coord. Chem. Rev.* **1982**, *41*, 79. (g) Ferguson, J.; Herren, F.; Krausz, E. R.; Maeder, M.; Vrbancich, J. *Coord. Chem. Rev.* **1985**, *64*, 21. (h) Sutin, N.; Creutz, C. *Pure Appl. Chem.* **1980**, *52*, 2717.
(7) (a) Johanson, S. R.; Wetmoreland, T. D.; Caspar, J. V.; Barquawi, K. R.; Meyer, T. J. *Inorg. Chem.* **1988**, *27*, 3195. (b) Kober, E. M.; Marshall, J. C.; Dressick, W. J.; Sullivan, B. P.; Caspar, J. V.; Meyer, T. J. *Inorg. Chem.* **1985**, *24*, 2755. (c) Allan, G. H.; White, R. P.; Rillema, D. P.; Meyer, T. J. *J. Am. Chem. Soc.* **1984**, *106*, 2613. (d) Kober, E. M.; Sullivan, B. P.; Dressick, W. J.; Caspar, J. V.; Meyer, T. J. *J. Am. Chem. Soc.* **1980**, *102*, 1383.
(8) (a) Kober, E. M.; Caspar, J. V.; Sullivan, B. P.; Meyer, T. J. *Inorg. Chem.* **1988**, *27*, 4587. (b) Barquawi, K. R.; Llobet, A.; Meyer, T. J. *J. Am. Chem. Soc.* **1988**, *110*, 7751. (c) Rillema, D. P.; Taghdiri, D. G.; Jones, D. S.; Keller, C. D.; Worl, L. A.; Meyer, T. J.; Levy, H. *Inorg. Chem.* **1987**, *26*, 5787.
(9) (a) Leasure, R. M.; Sacksteader, L. A.; Nesselrodt, D.; Reitz, G. A.; Demas, J. N.; Degraff, B. A. *Inorg. Chem.* **1991**, *30*, 3722. (b) Bankuch, B. J.; Lackey, D. E.; Crosby, G. A. *J. Phys. Chem.* **1980**, *84*, 2061. (c) Creutz, C.; Chou, M.; Netzel, L.; Okimura, M.; Sutin, N. S. *J. Am. Chem. Soc.* **1980**, *102*, 1309. (d) Malouf, G.; Ford, P. C. *J. Am. Chem. Soc.* **1977**, *99*, 7213.
(10) (a) Ross, H. B.; Boldaji, M.; Rillema, D. P.; Blanyon, C. B.; White, R. P. *Inorg. Chem.* **1989**, *28*, 1013. (b) Juris, A.; Campagna, S.; Balzani, V.; Gremaud, G. *Inorg. Chem.* **1988**, *27*, 3652. (c) von Zelewsky, A.; Gremaud, G. *Helv. Chim. Acta* **1988**, *71*, 1108.
(11) (a) Thomas, N. C. Ph.D. Dissertation, Monash University, 1983. (b) Black, D. St. C.; Deacon, G. B.; Thomas, N. C. *Inorg. Chim. Acta* **1982**, *65*, L75. (c) Thomas, N. C.; Deacon, G. B. *Inorg. Synth.* **1989**, *25*, 107.
(12) Thomas, N. C.; Deacon, G. B. *Synth. React. Inorg. Met.-Org. Chem.* **1986**, *16*, 85.
(13) (a) Black, D. St. C.; Deacon, G. B.; Thomas, N. C. *Polyhedron* **1983**, *2*, 409. (b) Black, D. St. C.; Deacon, G. B.; Thomas, N. C. *Aust. J. Chem.* **1982**, *35*, 2445.
(14) (a) Cleare, M. J.; Griffith, W. P. *J. Chem. Soc.* **1969**, (*A*), 372. (b) Bruce, M. I. Ruthenium Carbonyls and Related Compounds. In *Comprehensive Organometallic Chemistry*; Wilkinson, G., Stone, F. G. A., Abel, E. W., Eds.; 1982; Vol. 4, p 661 and references cited therein.

0020-1669/92/1331-3004$03.00/0

Table I. Ground and Excited State Properties in CH_3CN at 298 K

	$E_{1/2}$, V vs SSCE[a]		λ_{max}, nm (±2 nm)	λ_{em},[b]	ϕ_{em}[c]	τ,[b]	ϕ_{dec},[d]
	oxidn	redn	($\epsilon \times 10^{-3}$, M^{-1} cm^{-1})	nm (±3 nm)	±5%	ns (±5%)	(±10%)
$[Ru(bpy)_3]^{2+}$	+1.29	−1.33	285 (87.0)[e]	626	0.062	920	0.029
		−1.52	323 (6.5)				
		−1.78	345 (6.5)				
			451 (14.0)				
$[Ru(bpy)(4,4'\text{-}(Me)_2bpy)(5\text{-}Me\text{-}phen)]^{2+}$	+1.24	−1.37	268 (68.8)	627	0.069	1115	0.011
		−1.56	286 (68.5)				
		−1.81	385 (sh) (8.96)				
			429 (20.1)				
			453 (17.2)				
$[Ru(bpy)(4,4'\text{-}(Me)_2bpy)(bpm)]^{2+}$	+1.37	−1.03	269 (50.7)	665	0.007	67	<0.001
		−1.49	286 (62.9)				
		−1.74	395 (sh) (9.59)				
			429 (13.2)				
			448 (13.1)				
$[Ru(bpy)(4,4'\text{-}(Me)_2bpy)(4,4'\text{-}(CO_2Et)_2bpy)]^{2+}$	+1.35	−1.01	286 (56.7)	702	0.055	772	<0.001
		−1.48	309 (34.4)				
		−1.69	366 (9.63)				
			399 (sh) (9.19)				
			426 (10.3)				
			483 (10.7)				

[a] Acetonitrile/0.1 M $[N(n\text{-}C_4H_9)_4]PF_6$ at a Pt-button working electrode (0.4 cm^2) at a scan rate of 100 mV/s. [b] In ~1×10^{-5} M Ar-sparged CH_3CN solutions at 298 K. [c] Emission quantum yields (ϕ_{em}) by using $[Ru(bpy)_3](PF_6)_2$ in CH_3CN (ϕ_{em} = 0.062) as the standard, as described previously. Caspar, J. V.; Meyer, T. J. *J. Am. Chem. Soc.* **1989**, *111*, 7448. [d] Quantum yields for decomposition measured relative to $[Ru(bpy)_3](PF_6)_2$ (ϕ_p ~ 0.029) at ~2×10^{-5} M in a freeze–pump–thaw degassed (4×), stirred 0.2 M $[N(n\text{-}C_4H_9)_4]Cl/CH_3CN$ solution at 295 K by measuring the decrease in emission intensity as a function of time (12 h). A collimated 75-W Xe lamp was used as the source, with the intensity of irradiation measured using Reincke salt as a chemical actinometer. Durham, B.; Caspar, J. V.; Nagle, J. K.; Meyer, T. J. *J. Am. Chem. Soc.* **1982**, *104*, 4803. [e] Rillema, D. P.; Allen, G. H.; Meyer, T. J.; Conrad, D. *Inorg. Chem.* **1983**, *22*, 1617.

C25) cation-exchange chromatography with 0.2 M NaCl in H_2O as the eluent. The complexes were isolated from the eluent as PF_6^- salts by addition of a saturated aqueous solution of NH_4PF_6. The purities of the samples were established by ion-exchange HPLC on a Brownlee AX-100 "Prep 10" column following procedures described elsewhere.[15]

The compounds and salts were characterized by ^1H-NMR spectroscopy, electrochemical measurements and elemental analysis.[16] Corroborating evidence that the products were the tris-heteroleptic chelates $[Ru(pp)(pp')(pp'')]^{2+}$ (rather than a statistical mixture of complexes with varying ligand distributions) was obtained by fast atom bombardment mass spectrometry (FAB) in a 3-nitrobenzyl alcohol matrix.[17] Appearing in the spectra were the ion pairs, $\{[Ru(pp)(pp')(pp'')](PF_6)\}^+$, and fragment ions corresponding to the loss of the second PF_6^- and sequential loss of the remaining polypyridyl ligands. Parent ions for the tris-heteroleptic chelates were not observed.

The photophysical and electrochemical properties of some of these complexes have been investigated in detail; those for $[Ru(bpy)(4,4'\text{-}(Me)_2bpy)(5\text{-}Me\text{-}phen)]^{2+}$, $[Ru(bpy)(4,4'\text{-}(Me)_2bpy)(bpm)]^{2+}$, and $[Ru(bpy)(4,4'\text{-}(Me)_2bpy)(4,4'\text{-}(CO_2Et)_2bpy)]^{2+}$ are summarized in Table I. They include $E_{1/2}$ values for the $Ru^{III/II}$ and the one-electron ligand-based couples, absorption and emission spectral maxima, MLCT excited state lifetimes, and quantum yields for emission and ligand loss relative to $[Ru(bpy)_3]^{2+}$. Excitation spectra acquired at the emission maximum overlay the absorption spectra within experimental error. On the basis of transient resonance Raman spectra of the excited states, emission originates from MLCT states with the excited electron on the ligand having the most positive reduction potential.[18] For $[Ru(bpy)(4,4'\text{-}(Me)_2bpy)(bpm)]^{2+}$, where bpm has the lowest lying π^* acceptor level, intense excited-state resonance Raman signals characteristic of $4,4'\text{-}(Me)_2bpy$ in $[Ru(4,4'\text{-}(Me)_2bpy)_3]^{2+*}$ at 1202, 1321, 1445, and 1624 cm^{-1} and bpy in $[Ru(bpy)_3]^{2+*}$ at 1211, 1321, and 1624 cm^{-1} were not observed, while bands for bpm at 766, 1012, 1034, 1174, 1249, 1421, 1490, and 1560 cm^{-1} were observed. Compared with $[Ru(bpy)_3]^{2+}$, all of the mixed ligand complexes are much less prone to undergo photochemically induced ligand loss. From this observation and the fact that emission lifetimes (τ) for $[Ru(bpy)(4,4'\text{-}(Me)_2bpy)(5\text{-}Me\text{-}phen)]^{2+}$ and $[Ru(bpy)(4,4'\text{-}(Me)_2bpy)(4,4'\text{-}(CO_2Et)_2bpy)]^{2+}$ in 4:1 (v/v) EtOH:MeOH are only slightly temperature dependent over the range 160–298 K, the dd states in these complexes appear to be relatively inaccessible in these ligand environments at room temperature.[19,20]

The synthetic method described here is general. It opens new strategies for the design of molecular assemblies and visible light

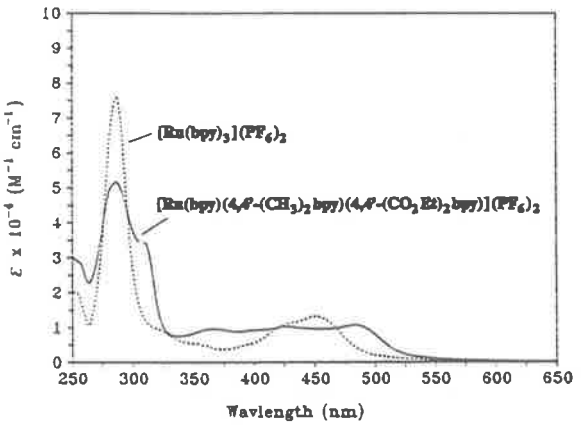

Figure 1. Absorption spectra in CH_3CN at 298 K.

(15) Strouse, G. F.; Boyde, S.; Peek, B.; Mecklenburg, S.; Erickson, B.; Meyer, T. J. Manuscript in preparation.
(16) Satisfactory elemental analysis (±0.4% for C, H, N) were found for all of the new compounds reported in this manuscript.
(17) (a) Liang, X.; Suwanrumpha, S.; Freas, R. B. *Inorg. Chem.* **1991**, *30*, 652. (b) Miller, J. M.; Balasanmugam, K.; Nye, J.; Deacon, G. B. *Inorg. Chem.* **1987**, *26*, 560. (c) Cerny, R. L.; Sullivan, B. P.; Bursey, M. M.; Meyer, T. J. *Inorg. Chem.* **1985**, *24*, 397. (d) Cerny, R. L.; Sullivan, B. P.; Bursey, M. M.; Meyer, T. J. *Anal. Chem.* **1983**, *55*, 1954.
(18) (a) Mabrouk, P. A.; Wrighton, M. S. *Inorg. Chem.* **1986**, *25*, 526. (b) Schoonover, J. R.; Strouse, G. F.; Meyer, T. J. Work in progress.
(19) (a) Lumpkin, R. S.; Kober, E. M.; Worl, L. A.; Murtaza, Z.; Meyer, T. J. *J. Phys. Chem.* **1990**, *94*, 239. (b) Danielson, E.; Lumpkin, R. D.; Meyer, T. J. *J. Phys. Chem.* **1987**, *91*, 1305.

sensitizers based on tris-bidentate complexes of Ru^{II}. For example, by proper exploitation of the substituents on the polypyridyl ligands and by taking advantage of the existence of $d\pi \rightarrow \pi^*$ transitions to the lowest two acceptor levels at the polypyridyl ligand, it is possible to "fill in" large portions of the visible spectrum of these complexes compared to $[Ru(bpy)_3]^{2+}$. This can be seen in Figure 1 where spectra for $[Ru(bpy)_3]^{2+}$ and $[Ru(bpy)(4,4'\text{-}(Me)_2\text{-}bpy)(4,4'\text{-}(CO_2Et)_2bpy)]^{2+}$ are compared. For the mixed-ligand complex bands arising from $d\pi \rightarrow \pi_1^*(4,4'\text{-}(CO_2Et)_2bpy)$ and $d\pi \rightarrow \pi_2^*(4,4'\text{-}(CO_2Et)_2bpy)$ transitions appear at 520 and 380 nm, the former extending to 580 nm with appreciable absorption. The region between 450 and 460 nm is filled in by $d\pi \rightarrow \pi_1^*$(bpy, 4,4'-$(Me)_2$bpy) absorptions while the $d\pi \rightarrow \pi_2^*$(bpy, 4,4'-$(Me)_2$bpy)) absorption appears at $\lambda < 350$ nm, overlapped with $\pi \rightarrow \pi^*$ transitions at the polypyridyl ligands.

We are currently exploring the use of multiple ligands to prepare complexes with even lower energy absorptions, with the ultimate goal of designing "black absorbers" which will exhibit high absorptivity throughout the visible and near-UV region, be photostable, and retain appreciable excited-state lifetimes.

Acknowledgment. Financial support from the Department of Energy (Grant DE-FG05-86ER13633) and the Australian Research Council is gratefully acknowledged. Travel between the two laboratories (G.F.S., P.A.A.) has been supported by the US National Science Foundation (Grant INT-9015262) and the (Australian) Department of Industry, Technology and Commerce within the Australia–US Bilateral Science and Technology Program. We would also like to thank Dr G. B. Deacon (Monash University) for his cooperation with us in the extension and development of the synthetic methodology initiated within his laboratory by N. C. Thomas.

(20) (a) Juris, A.; Barigelletti, F.; Balzani, V.; Belser, P.; Von Zelewsky, A. *Inorg. Chem.* **1985**, *24*, 202. (b) Barigelletti, F.; Juris, A.; Balzani, V.; Belser, P.; Von Zelewsky, A. *Inorg. Chem.* **1983**, *22*, 3335. (c) Wallace, W. M.; Hoggard, P. E. *Inorg. Chem.* **1980**, *19*, 2141. (d) Allsopp, S. R.; Cox, A.; Kemp, T. J.; Reed, W. J.; Carassiti, V.; Traverso, O. *J. Chem. Soc., Faraday Trans.* **1979**, *75*, 353. (e) Allsopp, S. R.; Cox, A.; Jenkins, S. H.; Kemp, T. J.; Tunstal, S. M. *Chem. Phys. Lett.* **1976**, *43*, 135. (f) Hager, C. D.; Crosby, G. A. *J. Am. Chem. Soc.* **1975**, *97*, 7031.

J. CHEM. SOC. DALTON TRANS. 1993 2859

Diastereoisomeric Forms of Ligand-bridged Dimetallic Diruthenium(II) and Ruthenium(II)–Osmium(II) Species containing Bidentate Polypyridyl Ligands

David A. Reitsma and F. Richard Keene *
Department of Molecular Sciences, James Cook University of North Queensland, Townsville, Queensland 4811, Australia

A new general synthetic route is reported for dinuclear species of the type $[(L_t)_2RuL_bRu(L_t')_2]^{4+}$ or $[(L_t)_2RuL_bOs(L_t')_2]^{4+}$ (L_t, L_t' = bidentate polypyridyl ligands, $L_t \neq L_t'$; L_b = bridging ligand), together with the chromatographic separation and characterization of the diastereoisomeric pairs of the dimers.

There is considerable interest in polymetallic 'supramolecular' assemblies containing chromophoric centres, for which polypyridyl complexes of ruthenium, osmium and rhenium have been primary targets because of the capacity for controlled variation of their ground and excited state properties, redox potentials, and electron and energy transfer characteristics.[1]

An important issue which has received little attention in these studies is that of stereoisomerism within the molecular assemblies. Even in the simplest case of a symmetrical dinuclear complex with a symmetrical bridge, *viz.* $[(bipy)_2Ru(bipym)Ru(bipy)_2]^{4+}$ (bipy = 2,2'-bipyridine; bipym = 2,2'-bipyrimidine), there will be *meso* ($\Delta\Lambda$) and *rac* ($\Delta\Delta$/$\Lambda\Lambda$) diastereoisomeric forms. The presence of different ligands on the two centres, an unsymmetrical bridge, or higher nuclearity in the assembly rapidly increase the isomeric complexity.

We reported recently the development of a general synthetic methodology for mononuclear tris(heteroleptic) ruthenium complexes of bidentate polypyridyl ligands.[2] The present communication reports the extension of this scheme to a general synthetic method for dinuclear species of the type $[(L_t)RuL_bRu(L_t')_2]^{4+}$ (L_t, L_t' = bidentate polypyridyl ligands where $L_t \neq L_t'$; L_b = bridging ligand), together with the chromatographic separation and NMR characterization of the diastereoisomeric pairs.

A variety of monomeric precursors of the general types $[Ru(L_t)_2(CO)_2]^{2+}$ and $[Ru(L_t')_2L_b]^{2+}$ may be synthesized as outlined previously.[2] Heating $[Ru(L_t)_2(CO)_2]^{2+}$ with a three-fold excess of trimethylamine *N*-oxide in acetone or methoxyethanol (*ca.* 50 cm^3 per 20 mg of the dicarbonyl species) at reflux for 3 h in the presence of a 20% excess of $[Ru(L_t')_2L_b]^{2+}$ realizes the corresponding dimer $[(L_t)_2RuL_bRu(L_t')_2]^{4+}$. Following ion-exchange chromatography (SP-Sephadex C-25 cation exchanger, 0.5 mol dm^{-3} NaCl eluent), products were isolated as the PF_6^- salts and recrystallized (acetone–diethyl ether): overall yields of the products were approximately 35%. For dimeric species containing Os centres, *i.e.* $[(L_t)_2RuL_bOs(L_t')_2]^{4+}$, two alternative synthetic schemes were utilized, either $[Ru(L_t)_2L_b]^{2+}$ was treated with $[Os(L_t')_2Cl_2]$[3] (by refluxing equimolar amounts in aqueous methanol solution, *ca.* 50 cm^3 per 20 mg of the ruthenium species), or $[Os(L_t')_2L_b]^{2+}$ (prepared by refluxing $[Os(L_t')_2Cl_2]$ with a four-fold excess of L_b in aqueous methanol) was treated with $[Ru(L_t)_2(CO)_2]^{2+}$ under the same conditions as for the analogous decarbonylation synthesis of the diruthenium species. In the present work, we have synthesized and characterized the dimeric complexes $[(bipy)_2Ru(bipym)Ru(phen)_2]^{4+}$, $[(bipy)_2Ru(bpypz)Ru(phen)_2]^{4+}$, $[(phen)_2Ru(bipym)Ru(tmbipy)_2]^{4+}$, $[(tmbipy)_2Ru(bipym)Ru(bipy)_2]^{4+}$, $[(bipy)_2Os(bipym)Ru(phen)_2]^{4+}$ and $[(bipy)_2Os(bipym)Ru(tmbipy)_2]^{4+}$ [phen = 1,10-phenanthroline; tmbipy = 4,4',5,5'-tetramethyl-2,2'-bipyridine; bpypz = 2,3-bis(2-pyridyl)pyrazine].

For all these dimeric species, there are two diastereoisomeric forms, each comprising an enantiomeric pair. The two stereoisomers may be represented schematically as shown in Fig. 1. A significant difference in the relative ligand orientations may be discerned in the two diastereoisomeric pairs: the polypyridyl ligands 'above' and 'below' the plane of the bridging ligand (Fig. 1) are approximately parallel in the $\Delta\Delta$/$\Lambda\Lambda$ form, whereas they are perpendicular in the $\Lambda\Delta$/$\Delta\Lambda$ stereoisomer.

In earlier work, Hua and von Zelewsky[4] have reported the stereoselective synthesis of similar dinuclear species using chiral monomers as precursors: while this represents a definitive solution to the problem of the stereoisomerism in such dimers, it requires that the precursors must be resolved on an individual basis. We have found that the two diastereoisomeric pairs may be separated by ion-exchange chromatography (SP-Sephadex C25 cation exchanger, 0.25 mol dm^{-3} sodium toluene-*p*-sulfonate as eluent), presumably based on the differential association of the aromatic anion with the alternative relative orientations of the heterocyclic ligands in the two forms. The method appears quite general and we have separated the diastereoisomers for the six dimeric species listed above. Variation of the bridging ligand L_b (symmetric bipym or unsymmetric bpypz) and metals (homonuclear Ru–Ru or heteronuclear Ru–Os) has little effect on the separation, although the efficacy of the procedure (and therefore the length of column required) is substantially influenced by the identity

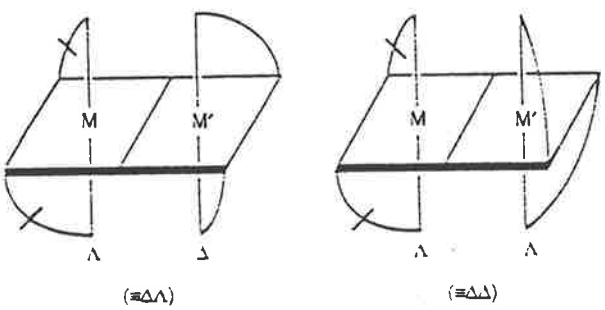

Fig. 1 Schematic view of the orientation of the non-bridging bidentate ligands in the two diastereoisomeric pairs of the general dinuclear species $[(L_t)_2ML_bM'(L_t')_2]^{4+}$ (the L_t and L_t' chelate rings are differentiated by hatch marks)

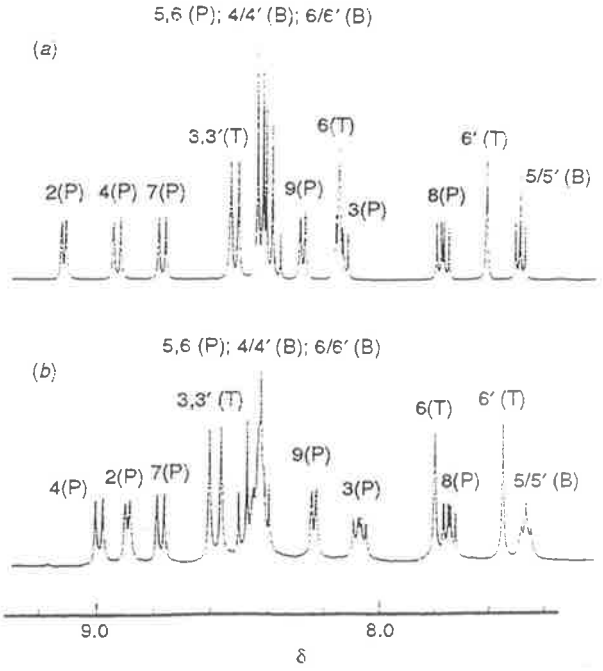

Fig. 2 Proton NMR spectra (300 MHz, 25 °C, [$^2H_6$]acetone) of (*a*) ΛΔ (≡ΔΛ) and (*b*) ΔΔ (≡ΛΛ)-[(phen)$_2$Ru(bipym)Ru(tmbipy)$_2$]$^{4+}$: protons of phen, bipym and tmbipy are indicated by P, B and T respectively

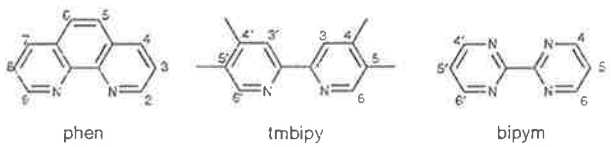

of the terminal ligands. For the systems reported, the two diastereoisomers were observed to form in comparable amounts; there was no indication of substantial stereospecificity induced by differential steric interactions in the two forms.

Proton NMR studies have been undertaken for the separated stereoisomers, and are reported below for the representative example [(phen)$_2$Ru(bipym)Ru(tmbipy)$_2$]$^{4+}$: the 300 MHz ^{1}H NMR spectra of the separated diastereoisomeric pairs of this dinuclear species are shown in Fig. 2. Full assignment of the observed resonances for both diastereoisomers has been obtained by decoupling experiments, and connectivity confirmed by heteronuclear multiple-bond correlation (HMBC) and heteronuclear multiple-quantum coherence (HMQC) two-dimensional NMR techniques. In both stereoisomeric forms, the two non-bridging ligands on each metal centre are related by a two-fold axis of symmetry, although the two ends of each individual ligand are in non-equivalent environments. Based on the conventional numbering sequences for the three ligands involved (see above), and adopting the convention that the numbering sequence in the phen ligand starts in the ring *cis* to both the ligating atoms of the bridge (and that the non-primed numbers in the tmbipy ligand also refer to the pyridine ring in that ligand *cis* to both ligating atoms of the bridge), the assignments are as indicated in Fig. 2. The stereochemistry of the two diastereoisomeric pairs has also been deduced from the NMR studies.

The most significant differences between the two spectra are the shifts in the resonances for the protons attached to the 2 position of the phen ligands, and to the 6 position of tmbipy (i.e. the protons in those ligands adjacent to a pyridyl ring co-ordinated to the other metal centre). In both cases, these protons in ΔΔ/ΛΛ-[(phen)$_2$Ru(bipym)Ru(tmbipy)$_2$]$^{4+}$ are shielded (relative to the ΛΔ/ΔΛ form) by the ring current associated with that adjacent pyridyl ring.

We are currently undertaking photophysical studies on the separated diastereoisomers to assess the effect of the stereochemistry on the electronic communication between the two metal centres. Those studies, and full details of the present synthesis and characterization of the diastereoisomeric dinuclear species, will be reported subsequently.

Acknowledgements

This work was supported by the Australian Research Council. Drs. B. F. Bowden and A. R. Carroll are thanked for helpful discussion on the NMR studies.

References

1 See, for example, S. Campagna, G. Denti, S. Serroni, M. Ciano, A. Juris and V. Balzani, *Inorg. Chem.*, 1992, **31**, 2982; S. Serroni and G. Denti, *Inorg. Chem.*, 1992, **31**, 4251; G. Denti, S. Campagna, S. Serroni, M. Ciano and V. Balzani, *J. Am. Chem. Soc.*, 1992, **114**, 2944; J. S. Bridgewater, L. M. Vogler, S. M. Molnar and K. J. Brewer, *Inorg. Chim. Acta*, 1993, **208**, 179 and refs. therein.
2 G. F. Strouse, P. A. Anderson, J. R. Schoonover, T. J. Meyer and F. R. Keene, *Inorg. Chem.*, 1992, **31**, 3004.
3 D. A. Buckingham, F. P. Dwyer, H. A. Goodwin and A. M. Sargeson, *Aust. J. Chem.*, 1964, **17**, 325.
4 X. Hua and A. von Zelewsky, *Inorg. Chem.*, 1991, **30**, 3796.

Received 14*th June* 1993; *Communication* 3/03428C

Inorg. Chem. 1994, *33*, 3863–3864

Black MLCT Absorbers

Peter A. Anderson,[†] Geoffrey F. Strouse,[§] Joseph A. Treadway,[‡] F. Richard Keene,*[,†] and Thomas J. Meyer*[,‡]

Department of Molecular Sciences, James Cook University of North Queensland, Townsville, Queensland 4811, Australia, and Department of Chemistry, The University of North Carolina CB#3290, Chapel Hill, North Carolina 27599-3290

Received June 3, 1994

Polypyridyl complexes of ruthenium(II) have been used extensively in studies of photoinduced electron and energy transfer.[1] We recently reported the development of a general procedure for synthesis of tris(heteroleptic) complexes which contain bidentate ligands,[2] e.g. $[Ru(bpy)(Me_2bpy)\{(Et_2CO_2)_2bpy\}]^{2+}$ (bpy is 2,2′-bipyridine, Me_2bpy is 4,4′-dimethyl-2,2′-bipyridine, and $(EtCO_2)_2bpy$ is 4,4′-bis(carboxyethyl)-2,2′-bipyridine), based on sequential addition of the ligands to oligomeric $[Ru(CO)_2Cl_2]_n$ and the earlier work of Deacon *et al.*[3] We report here application of this methodology to a specific target: *viz.* the systematic design of chromophores with appreciable absorption throughout the near-UV and visible spectral regions. Initial photophysical studies indicate that the metal-to-ligand charge transfer (MLCT) excited states that result can be sufficiently long-lived to undergo efficient electron and energy transfer and they tend to be photochemically inert compared with $[Ru(bpy)_3]^{2+}$.

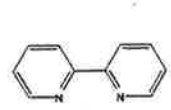
bpy

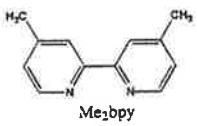
Me_2bpy

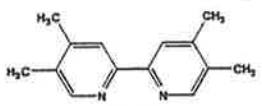
Me_4bpy

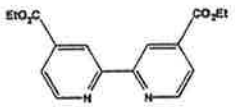
$(EtCO_2)_2bpy$

Visible light absorptivity in these complexes arises primarily from charge transfer transitions from $d\pi(Ru^{II})$ to multiple, low-lying π^*(polypyridyl) levels, e.g. eq 1.[4]

$$Ru^{II}(bpy)_3^{2+} \xrightarrow{h\nu} Ru^{III}(bpy^{-})(bpy)_2^{2+*} \qquad (1)$$

In this example, $d\pi \rightarrow \pi_1^*$ occurs at 450 nm and $d\pi \rightarrow \pi_2^*$ at 243 nm in CH_3CN.[1] Ligand-based, $\pi \rightarrow \pi^*$ transitions with absorptivities >40 000 m^2 mol^{-1} dominate the near-UV region.[5]

The MLCT transitions produce excited states that are largely singlet, e.g. $^1(d\pi^6) \rightarrow {}^1(d\pi^5\pi^{*1})$, but which possess significant triplet character due to spin–orbit coupling.[4] In mixed-chelate complexes, separate transitions occur to each of the ligands, but rapid intramolecular electron transfer leads ultimately to a triplet MLCT state in which the excited electron is localized on the ligand having the lowest π^*-acceptor orbital.[6] Our design strategy for black absorbers was to find ways to systematically shift the $d\pi \rightarrow \pi^*$ bands toward the red region of the spectrum. There are two approaches to this problem. One is to add electron-withdrawing groups to a polypyridyl ligand to lower π^*,[7] and the other is to stabilize the "hole" at Ru^{III} in the MLCT state by introducing electron-donating ligands.[8]

We have explored the effect of decreasing π^* energies in the series $[Ru(Me_2bpy)(Me_4bpy)(BL)]^{2+}$ (Me_4bpy is 4,4′,5,5′-tetramethyl-2,2′-bipyridine) where BL is 2,3-bis(2-pyridyl)pyrazine (dpp), 6,7-dimethyl-2,3-bis(2-pyridyl)quinoxaline (Me_2dpq), 2,3-bis(2-pyridyl)quinoxaline (dpq), or 2,3-bis(2-pyridyl)-1,4-diazaanthracene (dpa).[9] Electrochemical measurements show that in

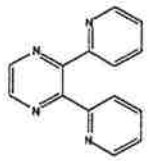
dpp

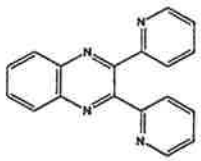
dpq

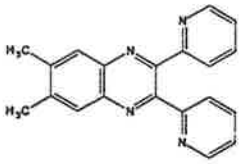
Me_2dpq

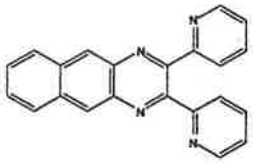
dpa

this series $E_{1/2}$ = –1.09, –0.91, –0.83, and –0.67 V, respectively (in acetonitrile versus ssce), for the first (ligand-based) reduction. Since the BL ligands are more easily reduced than either Me_2bpy or Me_4bpy, the potentials indicate the order of increasing electron-acceptor ability to be dpa > dpq > Me_2dpq > dpp. This ordering tracks the lowest-energy MLCT bands (Figure 1a), and is consistent with earlier observations on related complexes.[10]

† James Cook University of North Queensland.
‡ The University of North Carolina.
§ Present address: Institut für Anorganische Chemie, Universität Bern, Freiestrasse 3, CH3000 Bern 9, Switzerland.

(1) (a) Scandola, F.; Bignozzi, C. A.; Indelli, M. T. *Photosensitization and Photocatalysis Using Inorganic And Organometallic Compounds*; Kluwer Academic Publishers: Dordrecht, The Netherlands, 1993; pp 161–216. (b) Juris, A.; Barigelletti, S.; Campagna, S.; Balzani, V.; Belser, P.; von Zelewsky, A. *Coord. Chem. Rev.* **1988**, *84*, 85. (c) Meyer, T. J. *Pure Appl. Chem.* **1986**, *58*, 1576. (d) Kalayanasundaram, K. *Coord. Chem. Rev.* **1982**, *46*, 159. (e) Sutin, N.; Creutz, C. *Pure Appl. Chem.* **1980**, *52*, 2717.

(2) (a) Strouse, G. F.; Anderson, P. A.; Schoonover, J. R.; Meyer, T. J.; Keene, F. R. *Inorg. Chem.* **1992**, *31*, 3004. (b) Strouse, G. F.; Haarmann, K. H.; Reitsma, D. R.; Anderson, P. A.; Treadway, J. A.; Meyer, T. J.; Keene, F. R. Manuscript in preparation.

(3) (a) Black, D. S.; Deacon, G. B.; Thomas, N. C. *Aust. J. Chem.* **1982**, *35*, 2445. (b) Black, D. S.; Deacon, G. B.; Thomas, N. C. *Inorg. Chim. Acta* **1982**, *65*, L75. (c) Black, D. S.; Deacon, G. B.; Thomas, N. C. *Polyhedron* **1983**, *2*, 409. (d) Thomas, N. C.; Deacon, G. B. *Inorg. Synth.* **1989**, *25*, 107.

(4) (a) Kober, E. M.; Meyer, T. J. *Inorg. Chem.* **1982**, *21*, 3967. (b) Watts, J. *J. Chem. Educ.* **1983**, *60*, 843. (c) Demas, J.; Taylor, D. G. *Inorg. Chem.* **1974**, *18*, 3177.

(5) Lytle, F. E.; Hercules, D. M. *J. Am. Chem. Soc.* **1969**, *91*, 253.

(6) (a) Mabrouk, P. A.; Wrighton, M. S. *Inorg. Chem.* **1986**, *25*, 526. (b) Chang, Y. J.; Xiaobing, X.; Soo-Chang, Y.; Anderson, D. R.; Orman, L. K.; Hopkins, J. B. *J. Phys. Chem.* **1990**, *94*, 729. (c) Bradley, P. G.; Kress, N.; Hornberger, B. A.; Dallinger, R. F.; Woodruff, W. H. *J. Am. Chem. Soc.* **1981**, *103*, 7441. (d) Caspar, J. V.; Westmoreland, T. D.; Allen, G. H.; Bradley, P. G.; Meyer, T. J.; Woodruff, W. H. *J. Am. Chem. Soc.* **1984**, *106*, 3492. (e) Danzer, G. D.; Golus, J. A.; Kincaid, J. R. *J. Am. Chem. Soc.* **1993**, *115*, 8643. (f) Ford, W. E.; Calvin, M. *Chem. Phys. Lett.* **1980**, *76*, 105. (g) Riesen, H.; Krausz, E. R. *J. Phys. Chem.* **1993**, *99*, 7614.

(7) (a) Lever, A. B. P. *Inorg. Chem.* **1990**, *29*, 1271. (b) Sullivan, B. P.; Caspar, J. V.; Johnson, S. R.; Meyer, T. J. *Organometallics* **1984**, *3*, 1241. (c) Curtis, J. C.; Sullivan, B. P.; Meyer, T. J. *Inorg. Chem.* **1983**, *22*, 224. (d) Oshawa, Y.; Hanck, K. W.; DeArmond, M. K. *J. Electroanal. Chem.* **1984**, *175*, 229.

(8) Rillema, D. P.; Mack, K. B. *Inorg. Chem.* **1982**, *21*, 3849. (b) Rillema, D. P.; Blanton, C. B.; Shaver, R. J.; Jackman, D. C.; Boldaji, M.; Bundy, S.; Worl, L. A.; Meyer, T. J. *Inorg. Chem.* **1992**, *31*, 1600.

0020-1669/94/1333-3863$04.50/0

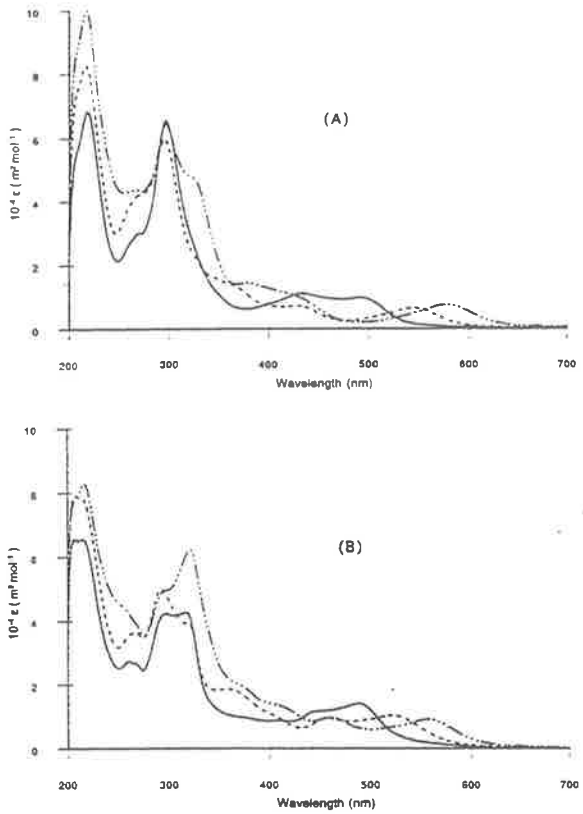

Figure 1. UV–visible absorption spectrum of (A) $[Ru(Me_2bpy)(Me_4bpy)(BL)]^{2+}$, and (B) $[Ru(Me_2bpy)\{(EtCO_2)_2bpy\}(BL)]^{2+}$ in acetonitrile solution BL = dpa (– · · · –), dpq (- - -), dpp (—).

The shift to lower energy reaches λ_{max} = 568 nm for BL = dpa, but at the expense of creating a "spectral gap" with a minimum at ~470 nm. The gap can be filled by using a ligand with an intermediate π^*-acceptor orbital. This is illustrated in Figure 1b for the series $[Ru(Me_2bpy)\{(EtCO_2)_2bpy\}(BL)]^{2+}$. With BL = dpa, bands arising from $d\pi \rightarrow \pi_1^*$ are observed at 548, ~452, and ~410 nm (to dpa, $(EtCO_2)_2bpy$, and Me_2bpy, respectively), while bands from $d\pi \rightarrow \pi_2^*$ appear at higher energy.

It is possible to extend MLCT absorption to even lower energies by incorporating an electron-donating ligand that possesses significant σ- and π-donating character; we have used diethyldithiocarbamate anion, Et_2dtc^-.[11] Anionic ligands stabilize the excited states by electron donation to Ru^{III} (eq 1) causing a general red shift in the MLCT bands. Absorption spectra for $[Ru\{(EtCO_2)_2bpy\}(dpa)(Et_2dtc)]^+$ and $[Ru(Me_2bpy)\{(EtCO_2)_2bpy\}(Et_2dtc)]^+$ are shown in Figure 2. In the former, significant visible light absorption ($\epsilon > 3000$ m^2 mol^{-1}) is extended past 700 nm. Both exhibit significant light absorption throughout the visible.

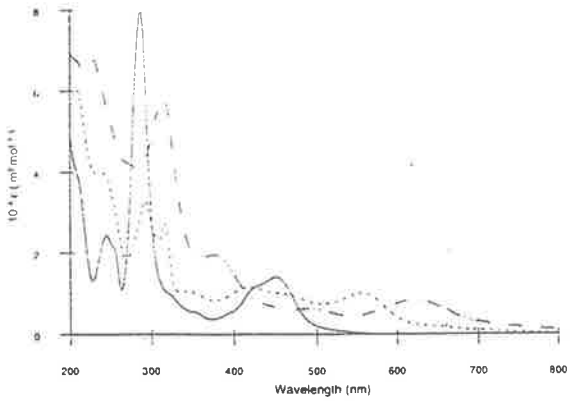

Figure 2. UV-visible absorption spectra of $[Ru\{(EtCO_2)_2bpy\}(dpa)(Et_2dtc)]^+$ (– · · · –) and $[Ru(Me_2bpy)\{(EtCO_2)_2bpy\}(Et_2dtc)]^+$ (- - -) in acetonitrile solution. The spectrum of $[Ru(bpy)_3]^{2+}$ is shown for comparison (—).

These low-energy broad-band absorbers may have useful excited state properties as well. For instance, $[Ru(Me_2bpy)\{(EtCO_2)_2bpy\}(dpa)]^{2+*}$ is a near-IR emitter ($\lambda_{max} > 850$ nm in CH_3CN at 298 K) with $\tau = 98(\pm 5)$ ns ($k = 1.02 \times 10^7$ s^{-1}),[12] as determined by transient absorption measurements (3–4 mJ/pulse). Emission from $[Ru(Me_2bpy)\{(EtCO_2)_2bpy\}(Et_2dtc)]^{+*}$ occurs at λ_{max} = 1100 nm (in CH_3CN at 298 K) with $\tau = 12(\pm 4)$ ns, as measured by transient absorption (λ_{ex} = 532 nm, <5 mJ/pulse).[13] All of these complexes are photochemically inert. In the future we will extend the overlapping band strategy and known approaches for extending excited state lifetimes to prepare a family of black absorbers which can be used as sensitizers.

Acknowledgment. Financial support from the Australian Research Council and the U.S. Department of Energy (Grant DE-FG05-86ER13633) is gratefully acknowledged. Travel between the two laboratories (G.F.S., J.A.T., P.A.A.) has been supported by the US National Science Foundation (Grant INT-9015262) and the (Australian) Department of Industry, Technology, and Regional Development within the Australia–US Bilateral Science and Technology Program.

(9) Satisfactory elemental analyses (±0.4% for C,H,N) were found for all the complexes reported in this manuscript.

(10) (a) Bianaio, J. A.; Carlson, D. L.; Wolosh, G. M.; DeJesus, D. E.; Knowles, C. F.; Szabo, E. G.; Murphy, W. R. *Inorg. Chem.* **1990**, *29*, 2327. (b) Carlson, D. L.; Murphy, W. R. *Inorg. Chim. Acta* **1991**, *181*, 61. (c) Molnar, S. M.; Neville, K. R.; Jensen, G. E.; Brewer, K. J. *Inorg. Chim. Acta* **1993**, *206*, 69.

(11) (a) Van Gaal, H. L. M.; Diesveld, J. W.; Pijpers, F. W.; van der Linden, J. G. M. *Inorg. Chem.* **1979**, *18*, 3251. (b) Bond, A. M.; Martin, R. L. *Coord. Chem. Rev.* **1984**, *54*, 23.

(12) We acknowledge Dr. S. L. Mecklenburg for this measurement.

(13) We acknowledge Dr. J. V. Caspar for this measurement.

(14) Boyde, S.; Strouse, G. F.; Jones, W. E., Jr.; Meyer, T. J. *J. Am. Chem. Soc.* **1990**, *112*, 7395.

J. CHEM. SOC. DALTON TRANS. 1994

Stereochemistry in Tris(bidentate ligand)ruthenium(II) Complexes containing Unsymmetrical Polypyridyl Ligands

Todd J. Rutherford, David A. Reitsma and F. Richard Keene*
Department of Molecular Sciences, James Cook University of North Queensland, Townsville, Queensland 4811, Australia

The synthesis and stereochemistry of monomeric ruthenium(II) complexes containing the unsymmetrical bidentate ligand pmbipy [4-(2,2-dimethylpropyl)-4'-methyl-2,2'-bipyridine] have been studied. In the complexes $[Ru(dmbipy)(pmbipy)(CO)_2]^{2+}$ (dmbipy is the symmetrical bidentate ligand 4,4'-dimethyl-2,2'-bipyridine) and $[Ru(pmbipy)_2(CO)_2]^{2+}$, the geometric isomers (two and three, respectively) have been identified and characterized by NMR techniques, and one isomer of each species has been isolated in a pure form by fractional recrystallization. The dicarbonyl species have both been used as precursors for the synthesis of $[Ru(dmbipy)(pmbipy)_2]^{2+}$ by a decarbonylation process: under certain conditions, the conversion was shown to take place with retention of the stereochemical relationship of the two ligands in the dicarbonyl precursor. Mixtures of the three geometric isomers of $[Ru(dmbipy)(pmbipy)_2]^{2+}$ were separated by cation-exchange chromatography, and the isomers characterized by NMR techniques. The complex $[Ru(pmbipy)_3]^{2+}$ was synthesized, and the two geometric isomers separated and characterized in a similar manner.

We have recently reported the utilization of a synthetic methodology for tris(heteroleptic) complexes of ruthenium(II),[1,2] which has allowed access to an extended range of compounds with increased complexity of formulation and stereochemistry. The scheme is based on the sequential addition of three bidentate polypyridyl ligands (L^1, L^2 and L^3) to the oligomer $[\{Ru(CO)_2Cl_2\}_n]$.[3-6] By incorporating potentially bridging ligands, such as 2,2'-bipyrimidine (bipym) or 2,3-bis(2-pyridyl)pyrazine (bpypz), the method may be extended to the synthesis of dinuclear (and higher nuclearity) species.[7]

Such polymetallic 'supramolecular' assemblies have evoked considerable attention because of the possibility of achieving redox charge separation within them following light absorption—with the consequent potential application to the harvesting of light energy and its conversion to chemical fuels.[8] Polypyridyl complexes of ruthenium, osmium and rhenium have been primary targets for the component centres of such assemblies because of the capacity for controlled variation of their ground and excited state properties, redox potentials, and electron and energy transfer characteristics.[9] A number of recent reports have described the spectral, photophysical and electrochemical behaviour of assemblies including such centres with nuclearities of 2–22.[10-13]

An important issue which has received little attention in these studies is that of the spatial relationship of the metal centres within the molecular assemblies, which may profoundly effect energy (and electron) migration patterns. This in turn depends on the stereochemical identity (chiral and geometric) of the component metal centres.

There have been few studies of stereoisomerism of monomeric ruthenium(II) centres with unsymmetrical ligands. For complexes of the type $[Ru(L^4)_3]^{2+}$ (L^4 is an unsymmetrical bidentate ligand), the existence of *fac* and *mer* geometric isomers has been recognized from ^1H and ^{13}C NMR studies of complexes where L^4 = unsymmetrically substituted derivatives of 2,2'-bipyridine and 1,10-phenanthroline,[14,15] 2,2'-azopyridine,[16] and 2-(2-pyridyl)thiazole and 2-(2-pyrazinyl)thiazole.[17] Similary, ^{99}Ru NMR spectroscopy has been used to identify the presence of both geometric isomers in analogous complexes where L^4 = 1-(2-pyridyl)-3,5-dimethylpyrazole,[18] 2-(2-pyridyl)oxazole[19] and 2,3-bis(2-pyridyl)pyrazine.[20] In only one report has the separation of such stereoisomers been claimed, using HPLC techniques, in the species $[Ru(apy)_3]^{2+}$ (two geometric isomers) and $[Ru(apy)_2(bipy)]^{2+}$ (two of the three possible geometric isomers) [bipy = 2,2'-bipyridine, apy = 2,2'-azopyridine].[16]

For ligand-bridged dinuclear species containing polypyridyl bidentate ligands, there is even greater paucity in reported examples of stereoisomerism. Hua and von Zelewsky[21] prepared single isomers of two dinuclear species using optically resolved mononuclear precursors, and the diastereoisomers of a range of such dimers have been separated within our own work.[7]

We are undertaking a detailed stereochemical study of monomeric tris(bidentate ligand)ruthenium(II) complexes, and the polynuclear species derived from them, with the ultimate aim of stereochemical control of metal centres in polynuclear assemblies.

Using our synthetic methodology, the dicarbonyl species $[Ru(L^1)(L^2)(CO)_2]^{2+}$ are key precursors in the syntheses of mono- and poly-nuclear systems, and we report here investigations of the mononuclear $[Ru(L^1)(L^2)(CO)_2]^{2+}$ and $[Ru(L^1)(L^2)_2]^{2+}$ systems where the two ligands L^1 and L^2 are the symmetrical ligand dmbipy [4,4'-dimethyl-2,2'-bipyridine] and the unsymmetrical ligand pmbipy [4-(2,2-dimethylpropyl)-4'-methyl-2,2'-bipyridine].

Results and Discussion

Synthesis of 4-(2,2-*Dimethylpropyl*)-4'-*methyl*-2,2'-*bipyridine* (*pmbipy*).—The ligand pmbipy was synthesized by reaction of 2-bromo-2-methylpropane with the mono anion of 4,4'-dimethyl-2,2'-bipyridine (dmbipy) (formed by its reaction with one mole equivalent of the hindered base lithium diisopropylamide). The nucleophilic substitution stage was found to be

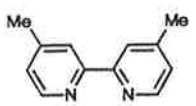

dmbipy

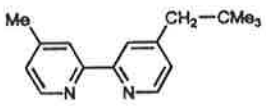

pmbipy

very slow, presumably due to the steric bulk of the *tert*-butyl substituent and the relatively poor leaving-group capabilities of Br^-. A minor yield of the disubstituted species was also obtained, but was separated from the required product by chromatographic procedures.

The ^1H and ^{13}C NMR spectral details for pmbipy are given in the Experimental section. The protons at the 3- and 5-positions of the pyridyl ring containing the neopentyl substituent are shielded (upfield) relative to those on a pyridyl ring containing a methyl group, due to the increased inductive effects of the neopentyl group. The assignment of the 5- and 6- (and 5'- and 6'-) positions to the two pairs of doublets for each ring were based on the deshielding effects of the nitrogen atoms. Peak assignments were determined by XHCORRD (CX-H shift correlation with ^1H decoupling in F1 domain), DEPT (distortionless enhancement by polarization transfer) and proton decoupling techniques.

Synthetic Methodology for Complexes.—Ruthenium complexes containing bidentate polypyridyl ligands, $[Ru(L^1)(L^2)(L^3)]^{2+}$, were synthesized by sequential addition of the ligands to the oligomer $[\{RuCl_2(CO)_2\}_n]$.[1–6]

The first step in this procedure was the addition of the first ligand (L^1) producing $[Ru(L^1)(CO)_2Cl_2]$, with the geometry *cis*-$(CO)_2$,*trans*-Cl_2.[2,22,23] The substitution of the second ligand (L^2) initially requires the replacement of chloride by trifluoromethanesulfonate ligands (which are superior leaving groups), and is achieved by reaction of the dichloro complex with trifluoromethanesulfonic acid in 1,2-dichlorobenzene solution.[24] The addition of L^2 to $[Ru(L^1)(CO)_2(CF_3SO_3)_2]$ [which has been assigned the geometry *cis*-$(CO)_2$,*cis*-$(CF_3SO_3)_2$][2,3,5] was performed in absolute ethanol at reflux yielding the dicarbonyl complex *cis*-$[Ru(L^1)(L^2)(CO)_2]^{2+}$. The final stage of the synthesis involved the decarbonylation of the $[Ru(L^1)(L^2)(CO)_2]^{2+}$ species by trimethylamine *N*-oxide in the presence of the third polypyridyl ligand (L^3) using 2-methoxyethanol as a solvent.

In the present instance, the major target complex was $[Ru(dmbipy)(pmbipy)_2]^{2+}$, which may be formed by either of two routes depending on the order of the sequential addition: *viz.* by addition of dmbipy to $[Ru(pmbipy)_2(CO)_2]^{2+}$ in the final decarbonylation step, or alternatively by addition of pmbipy to $[Ru(dmbipy)(pmbipy)(CO)_2]^{2+}$. There are stereochemical implications of syntheses of the target from these alternate dicarbonyl precursors.

Stereochemical Considerations and Characterization of Isomers.—For the complex $[Ru(dmbipy)(pmbipy)_2]^{2+}$ there are three possible geometric isomers based on the relative orientation of the two neopentyl groups (R). The two isomers in which the neopentyl groups bear a *cis* relationship to each other are differentiated by the fact that **II** has higher symmetry (sym-*cis*: point group C_2) than **III** (unsym-*cis*: C_1). For the two precursor dicarbonyl species, $[Ru(dmbipy)(pmbipy)(CO)_2]^{2+}$ has two possible geometric forms **IV** and **V**, and $[Ru(pmbipy)_2(CO)_2]^{2+}$ three **VI–VIII** {which are analogous to those for the target $[Ru(dmbipy)(pmbipy)_2]^{2+}$ species}.

Experimentally, the dicarbonyl complex $[Ru(dmbipy)(pmbipy)(CO)_2]^{2+}$ formed two geometric isomers (**IV** and **V**), which were separated by fractional recrystallization from ethanolic solution (**IV** being the less soluble) and identified by ^1H NMR spectroscopy (Table 1). The assignment of the *tert*-butyl signals at δ 1.05 and 0.88 to **IV** and **V**, respectively, is based on the upfield shift of protons orientated above the plane of an adjacent pyridyl ring, from which they experience an out-of-plane ring current effect. The integration of these two peaks indicates an isomer ratio **IV**:**V** of 1:1, which suggests there are no stereochemical or electronic preferences under the described reaction conditions and the orientation of attachment is predominantly statistical.

The complete assignment of the spectra of these isomers was based on such ring current effects.[17,25,26] The consequence of the ring currents generated by the aromatic rings is a shielding effect of up to 2 ppm on protons lying above the plane of an adjacent ring. The magnitude of this shift diminishes in protons more distant from the nitrogen: the difference in chemical shifts for the H^3 protons is only 0.1–0.2 ppm. A further effect which influences the chemical shifts of the aromatic protons is the inductive effects of the neopentyl substituent. This is observed in the resonances of the H^3 protons: in **V** the protons H^{3a} and H^{3b} have equivalent positions relative to the carbonyl substituents, but differ in their proximity to a neopentyl or methyl group (respectively), and H^{3a} is shifted upfield 0.11 ppm relative to H^{3b}. A similar shift is present in **IV** (compare H^{3a} and $H^{3'b}$). A similar effect is also observed with the H^5 protons.

Similarly, the ^1H NMR assignments of the three isomers of $[Ru(pmbipy)_2(CO)_2]^{2+}$ were based on the upfield shift observed on protons lying above the plane of an adjacent ring and the upfield inductive effect of the neopentyl substituent group. Separation of isomer **VI** was achieved by fractional recrystallization from ethanol of an isomeric mixture. The other two isomers could not be completely separated, but were identified and characterized by ^1H NMR spectroscopy (Table 1). In **VI**, both neopentyl-substituted pyridyl rings are *cis* to the two carbonyl groups, while in **VIII** only one neopentyl-substituted pyridyl ring is *cis* to the two carbonyl groups. For **VII** each neopentyl-substituted ring is *trans* to a carbonyl ligand. The three possible isomers were assigned and their relative proportions determined using the *tert*-butyl singlet ^1H NMR resonance. The *tert*-butyl signal at δ 1.05 is the most downfield *tert*-butyl resonance and is assigned to isomer **VI** as the *tert*-butyl groups on rings a and b experience no ring current effects from adjacent ligands. The differences between isomers **VII** and **VIII** are more subtle as the neopentyl-substituted pyridyl rings are orientated over the plane of the adjacent ligand and therefore both experience ring current effects. The integration of the *tert*-butyl signals at δ 1.05, 0.85 and 0.88 (2.6:1.0:1.1) does not give the isomer ratio directly since there are two *tert*-butyl environments in isomer **VIII**. By assuming that the resonance at δ 0.85 corresponds to **VII**, the isomer ratio can be determined as **VI**:**VII**:**VIII** = 1.5:1:2.2. This analysis is consistent with the ratio based on the resonances arising from the H^6,$H^{6'}$ protons, as well as similar calculations based on the methylene and methyl resonances.

The three isomers of the target complex $[Ru(dmbipy)(pmbipy)_2]^{2+}$ were separated by cation-exchange chromatography, and their ^1H NMR spectra are shown in Fig. 1 and detailed in Table 2. The resonances of the protons attached to the C^3 position of the pyridyl rings are the most downfield of the aromatic protons due to in-plane ring current effects. If adjacent to a neopentyl group there is an upfield shift by ≈ 0.14 ppm relative to the protons adjacent to a methyl group. This same effect is also observed for the protons attached to the C^5 positions of the rings. The inductive effect of the neopentyl group has only a very small influence (0.02 ppm) on protons attached at the C^6 positions.

The protons at the C^6 positions do appear to have very slight ring current effects, depending on whether they are positioned over a methyl- or neopentyl-substituted ring. Hence, for the two more symmetrical isomers of $[Ru(dmbipy)(pmbipy)_2]^{2+}$ (*trans* and sym-*cis*) there are three environments, two of which coincide in the *trans* isomer.

The symmetry of these two isomers is also evident in the protons attached at C^5. The two protons adjacent to a neopentyl group (the upfield signal) are in one environment in each of the isomers, although that environment differs between the two isomers. These two protons have different environments in the unsym-*cis* isomer.

The singlet resonance arising from the *tert*-butyl group appears at δ 0.90 for the sym-*cis* isomer and at δ 0.93 for the other two isomers. The *tert*-butyl signals of $[Ru(dmbipy)_2$-

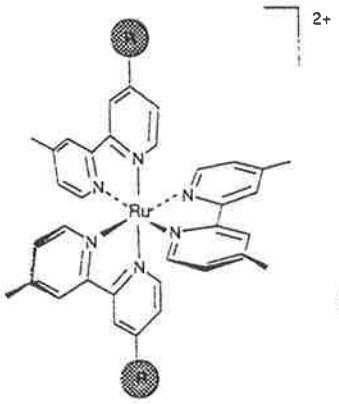

I *trans* (R)

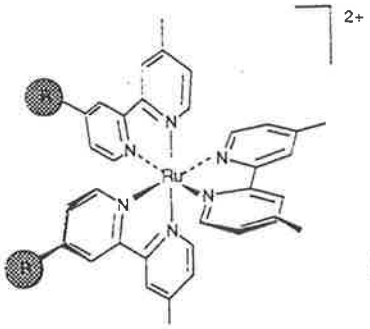

II sym-*cis* (R)

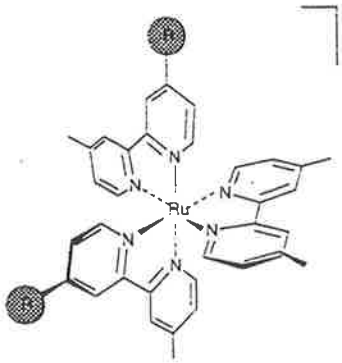

III unsym-*cis* (R)

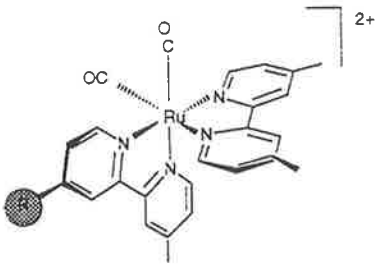

IV

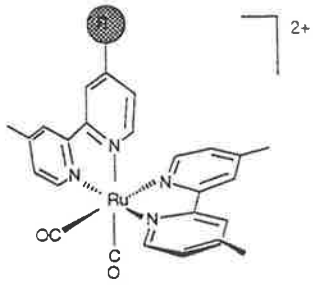

V

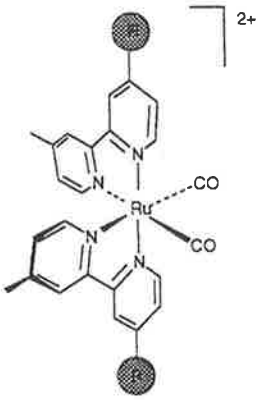

VI *trans* (R)

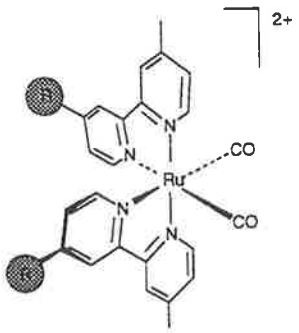

VII sym-*cis* (R)

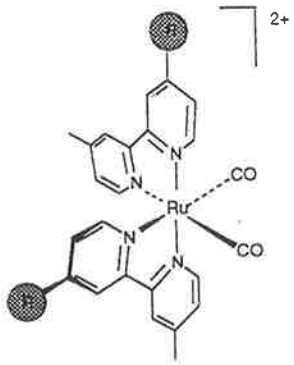

VIII unsym-*cis* (R)

(pmbipy)]$^{2+}$ and *fac*-[Ru(pmbipy)$_3$]$^{2+}$ are also observed at δ 0.93. In *mer*-[Ru(pmbipy)$_3$]$^{2+}$ there are two peaks at δ 0.90 (two protons) and 0.93 (one proton). There are two different *cis* environments in [Ru(dmbipy)(pmbipy)$_2$]$^{2+}$ (exemplified in the sym-*cis* and unsym-*cis* isomers) and it appears that the *tert*-butyl resonance occurs at δ 0.93 except in the particular *cis* environment found in the sym-*cis* isomer. In the *mer*-[Ru(pmbipy)$_3$]$^{2+}$ species, two of the *tert*-butyl groups are in such a juxtaposition and hence the ratio of peaks at δ 0.90 and 0.93 is 2:1. Interestingly, in the complex [Ru(dpbipy)$_3$]$^{2+}$ [dpbipy is the symmetrically disubstituted neopentyl ligand 4,4′-bis(2,2-dimethylpropyl)-2,2′-bipyridine], all the *tert*-butyl groups would display this special relationship, and the ^{1}H NMR spectrum does indeed show one resonance at δ 0.90.[27]

The two geometric isomers of [Ru(pmbipy)$_3$]$^{2+}$ were separated by cation-exchange chromatography, and the ^{1}H NMR spectra are shown in Fig. 2, and the peak positions are rationalized by the arguments used above for the [Ru(dmbipy)(pmbipy)$_2$]$^{2+}$ analogues (Table 2). The higher symmetry of the *fac*- (IX; point group C_3) compared with the *mer*-isomer (X; point group C_1) is clearly evident from the spectra [Fig. 2(*b*) and 2(*a*), respectively].

Stereochemical Aspects of the Decarbonylation Reaction.— There are two paths by which the target complex [Ru-

Table 1 ^{1}H NMR chemical shifts (δ_H) for $[Ru(L^1)(L^2)(CO)_2]^{2-}$ in CD_3CN solution

Complex	Isomer	Ligand[a]	H^3	$H^{3'}$	$H^{5,6}$	$H^{5',6'}$	$H^{6,6'}$	$H^{6''}$	H^{7}	$H^{7'}$	H^{8}	H^{10}
$[Ru(dmbipy)(pmbipy)(CO)_2]^{2-}$	IV	a	8.31	8.34	7.66	7.29	8.88	7.18	2.47	—	2.85	1.05
		b	8.31	8.42	7.29	7.71	7.18	8.86	2.47	2.68	—	—
	V	a	8.20	8.46	7.24	7.71	7.19	8.86	—	2.68	2.65	0.88
		b	8.31	8.42	7.29	7.71	7.19	8.86	2.47	2.68	—	—
$[Ru(pmbipy)_2(CO)_2]^{2-}$	VI	a	8.31	8.34	7.67	7.30	8.89	7.17	—	2.48	2.85	1.05
		b	8.31	8.34	7.67	7.30	8.89	7.17	—	2.48	2.85	1.05
	VII	a	8.20	8.47	7.25	7.72	7.20	8.87	—	2.68	2.65	0.85
		b	8.20	8.47	7.25	7.72	7.20	8.87	—	2.68	2.65	0.85
	VIII	a	8.31	8.34	7.67	7.30	8.89	7.17	—	2.48	2.85	1.05
		b	8.20	8.47	7.25	7.72	7.19	8.87	—	2.68	2.65	0.88

[a] See Experimental section. [b] Doublet, J 5 Hz.

Table 2 ^{1}H NMR chemical shifts (δ_H) for $[Ru(L^1)(L^2)(L^3)]^{2-}$ in CD_3CN solution

Complex	Isomer	H^3	$H^{3'}$	$H^{3''}$	H^5	$H^{5'}$	H^6	$H^{6'}$	$H^{6''}$	H^7	H^8	H^{10}
$[Ru(dmbipy)(pmbipy)_2]^{2-}$	*trans* I	8.21[a]	8.35	8.31	7.15[b]	7.19[b]	7.51[b]	7.49[b]	—	2.51	2.67	0.93
	sym-*cis* II	8.20[a]	8.35	8.32	7.12[c]	7.20[d]	7.51[b]	7.53[b]	7.50[b]	2.51	2.67	0.90
	unsym-*cis* III	8.21[a]	8.35	8.31	7.15[d]	7.20[d]	7.50[d]	—	—	2.51	2.67	0.93
$[Ru(pmbipy)_3]^{2-}$	*fac* IX	8.21	8.35	—	7.15[b]	7.19[b]	7.49[b]	7.52[b]	—	2.51	2.67	0.93
	mer X	8.22	8.35	8.20	7.13[d]	7.20[d]	7.51[c]	—	—	2.51	2.67	0.90, 0.93
$[Ru(dmbipy)_2(pmbipy)]^{2-}$		8.21	8.35	8.31	7.13[b]	7.19[b]	7.50[d]	—	—	2.50	2.66	0.93

[a] Doublet, J 1.5 Hz. [b] Doublet, J 5 Hz. [c] Doublet of doublets, J 1.5 and 5 Hz. [d] Multiplet.

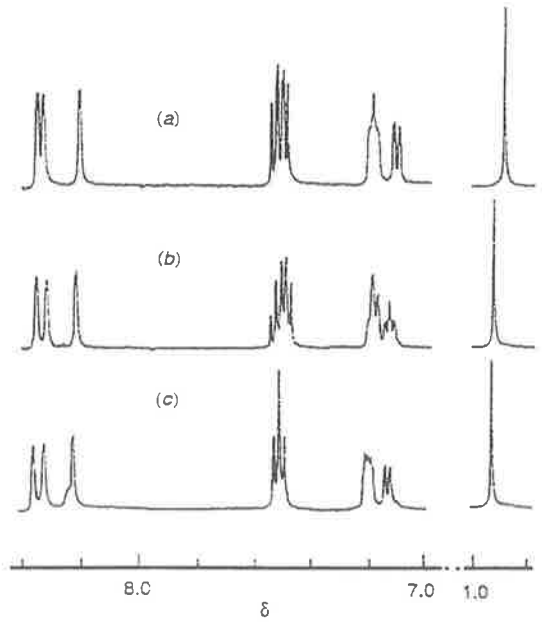

Fig. 1 Proton NMR spectra (300 MHz, CD_3CN) of the geometric isomers of $[Ru(dmbipy)(pmbipy)_2]^{2-}$: (*a*) sym-*cis* (II); (*b*) unsym-*cis* (III); (*c*) *trans* (I)

$(dmbipy)(pmbipy)_2]^{2+}$ may be obtained from the dicarbonyl precursors, equations (1) and (2). It is clear that if the

$$[Ru(dmbipy)(pmbipy)(CO)_2]^{2-} \xrightarrow[Me_3NO,pmbipy]{MeOCH_2CH_2OH} [Ru(dmbipy)(pmbipy)_2]^{2-} \quad (1)$$

$$[Ru(pmbipy)_2(CO)_2]^{2-} \xrightarrow[Me_3NO,dmbipy]{MeOCH_2CH_2OH} [Ru(dmbipy)(pmbipy)_2]^{2-} \quad (2)$$

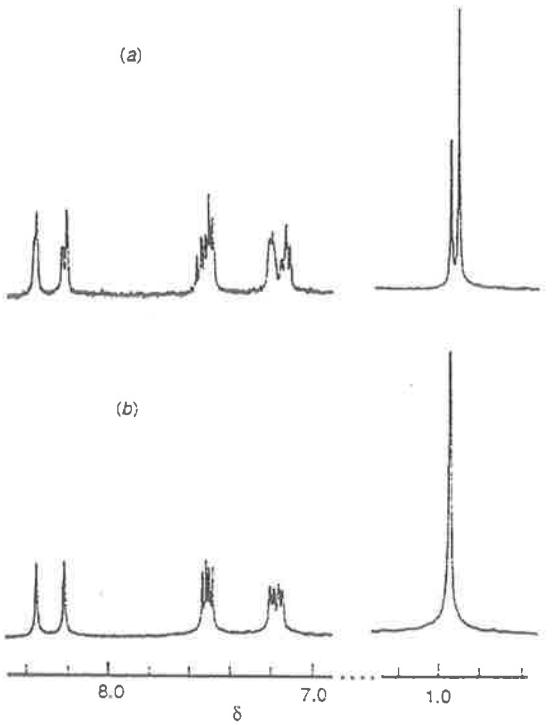

Fig. 2 Proton NMR spectra (300 MHz, CD_3CN) of the geometric isomers of $[Ru(pmbipy)_3]^{2-}$: (*a*) *mer* (X); (*b*) *fac* (IX)

decarbonylation process occurs so that the relative geometry of the two ligands in the dicarbonyl precursors is retained, the transformation of each form of $[Ru(pmbipy)_2(CO)_2]^{2-}$ would produce the corresponding geometric isomer of $[Ru(dmbipy)(pmbipy)_2]^{2-}$ (*i.e.* VI ⟶ I, VII ⟶ II, VIII ⟶ III). On the other hand, the decarbonylation reactions of each

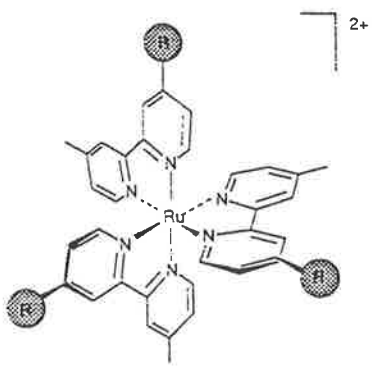

fac IX

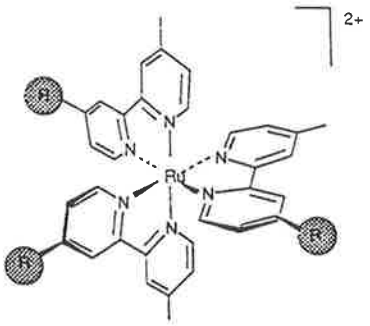

mer X

isomer of $[Ru(dmbipy)(pmbipy)(CO)_2]^{2+}$ in the presence of pmbipy would produce two isomers of the target complex $[Ru(dmbipy)(pmbipy)_2]^{2+}$, *i.e.* **IV** ⟶ **II** + **III** (because the neopentyl group must remain *cis* to the two positions of substitution) and **V** ⟶ **I** + **III**.

In previous applications of the synthetic methodology,[1–6] the incorporation of the third bidentate ligand was achieved by decarbonylation of $[Ru(L^1)(L^2)(CO)_2]^{2+}$ by Me_3NO in the presence of L^3 in refluxing 2-methoxyethanol solution. In the present studies, it was possible to determine the stereochemical course of this reaction, by use of specific geometric isomers of the $[Ru(pmbipy)_2(CO)_2]^{2+}$ and $[Ru(dmbipy)(pmbipy)(CO)_2]^{2+}$ precursors with an assessment of the isomeric distribution in the $[Ru(dmbipy)(pmbipy)_2]^{2+}$ product.

These studies indicated that at the higher temperatures associated with refluxing 2-methoxyethanol, there was some loss of stereochemical integrity and ligand scrambling during the decarbonylation process. However at lower temperatures, reactions left for a longer period underwent the decarbonylation and substitution to produce the product in which the stereochemical and ligand integrity were maintained, although the yields were lower.

By reacting a 1:1 mixture of **IV** and **V** with pmbipy at room temperature, the three isomers of $[Ru(dmbipy)(pmbipy)_2]^{2+}$ were obtained in the ratio **I**:**II**:**III** = 1:1:2. This represents a sum of the conversion **V** ⟶ **I** + **III** and **IV** ⟶ **II** + **III**, and is consistent with retention of stereochemistry in the reaction. Under the same conditions, the reaction of **IV** alone realized a 1:1 mixture of **II** and **III**, which clearly indicates the retention of the stereochemical relationship of the ligands in $[Ru(dmbipy)(pmbipy)(CO)_2]^{2+}$ during its subsequent reaction.

The reaction of **VI** with dmbipy at room temperature under decarbonylation conditions realized only isomer **I** of the product $[Ru(dmbipy)(pmbipy)_2]^{2+}$. Interestingly, when the same reaction was performed under reflux, scrambling was evident and the other isomers [sym-*cis* (16%) and unsym-*cis* (2%)] were detected, as well as the species $[Ru(dmbipy)_2(pmbipy)]^{2+}$ (3%).

Tris[4-(2,2-*dimethylpropyl*)-4′-*methyl*-2,2′-*bipyridine*]*ruthenium*(II). $[Ru(pmbipy)_3]^{2+}$.—In the course of these studies, the complex $[Ru(pmbipy)_3]^{2+}$ was synthesized and chromatographically separated into its two possible geometric isomers, which were characterized by ^1H NMR spectroscopy. This complex has been reported previously,[28] but isomeric forms were not considered. There is only one literature reference[16] of the complete separation of isomers of a complex of the type $[Ru(L^4)_3]^{2+}$.

Conclusion

The synthesis and characterization of the geometric isomers of $[Ru(dmbipy)(pmbipy)(CO)_2]^{2+}$ and $[Ru(pmbipy)_2(CO)_2]^{2+}$, and of the $[Ru(dmbipy)(pmbipy)_2]^{2+}$ product formed from their decarbonylation, have been achieved. Examination of the stereochemistry of the addition of this final ligand in a decarbonylation step have revealed that under certain reaction conditions the stereochemical relationship of the ligands in the dicarbonyl precursors is maintained in the process.

These results have a number of important consequences. Dicarbonyl species of this type may be used in the construction of polymetallic molecular assemblies,[7] and the present observations raise the possibility of predetermination of the spatial relationship of metal centres by the use of dicarbonyl species of specific geometry. The further aspect of chiral control has also been investigated in our laboratory.[29] In addition, it is noted that in previous studies of complexes incorporating quencher-functionalized ligand substituents, charge-separated excited states have been reported without consideration of the spatial effects within the possible geometric isomers.[30] Studies of the present type, in which such redox-active groups replaced the model neopentyl substituents, would allow an assessment of the spatial dependence of such processes on the relationship of such groups within isomeric forms of the same molecule. An alternative approach[31] has been taken to this problem by the attachment of redox-active groups to the separated isomers of tris(bidentate ligand)ruthenium(II) complexes containing carboxylato-substituted ligands of the 2,2′-bipyridine type. A collaborative photophysical study of the spatial dependence of electron and energy transfer processes within such isomeric species will be undertaken,[31] and reported subsequently.

Experimental

Measurements.—The NMR studies [^1H and ^{13}C NMR, XHCORRD (optimized for J 138 Hz), DEPT and decoupling experiments] were performed on a Bruker Aspect AM300 NMR spectrometer in CD_3CN solutions. Infrared spectra were measured using a Perkin-Elmer 1600 series FTIR spectrophotometer with samples prepared in Nujol mulls and placed between NaCl plates. Electronic spectra (in acetonitrile solutions) were obtained using a Hewlett Packard HP 89532K UV/VIS spectrophotometer. Microanalyses were carried out by Chemical & Micro Analytical Services Pty. Ltd. (Belmont, Victoria, Australia).

Materials.—The compounds 4,4′-dimethyl-2,2′-bipyridine (Aldrich), 2-bromo-2-methylpropane (Aldrich), butyllithium (Aldrich), $RuCl_3 \cdot 3H_2O$ (Strem), 2-methoxyethanol (Aldrich) and formic acid (BDH, 90%) were used as received without further purification. Laboratory grade solvents were used unless otherwise specified.

Diisopropylamine (Aldrich) was distilled under nitrogen and stored over 5 Å molecular sieves. Tetrahydrofuran (BDH) was doubly distilled under nitrogen from sodium wire with benzophenone as an indicator. Trifluoromethanesulfonic acid

(3 mol dm^{-3}) and 1,2-dichlorobenzene (Aldrich) were freshly distilled as required. Standardization of butyllithium was performed by titrating against 2,2,2'-trimethylpropionanilide (Aldrich). The oligomer $[\{Ru(CO)_2Cl_2\}_n]$ was synthesized by the method established in the literature.[2,32]

Thin-layer chromatography was conducted on Kiesegel 60 H F_{254} plates (Merck). Kieselgel 60 H (Merck) was used for vacuum column chromatography.[33] Sephadex LH-20 and SP-Sephadex C-25 (Pharmacia) were used for chromatographic purification of metal complexes by exclusion and cation-exchange techniques respectively.

Ligand Syntheses.—*4-(2,2-Dimethylpropyl)-4'-methyl-2,2'-bipyridine* (*pmbipy*). The reaction was carried out under an inert atmosphere of dry nitrogen at −78 °C. 4,4'-Dimethyl-2,2'-bipyridine (dmbipy; 5 g, 0.027 mol) was dried under vacuum at 60 °C overnight then dissolved in freshly distilled thf (150 cm^3). Lithium diisopropylamide (1.1 equivalents) was formed *in situ* by reacting LiBu (24.27 cm^3, 1.116 mol dm^{-3}) with diisopropylamine (3.8 cm^3) in thf (20 cm^3). The lithium diisopropylamide mixture was stirred for *ca.* 1.5 h, and the dmbipy solution added dropwise over 1 h. The resultant deep red-purple solution was allowed to stir for an additional 1 h prior to transfer by cannula to another vessel containing 2-bromo-2-methylpropane (12.49 cm^3, 5 equivalents) in thf (20 cm^3). This mixture was stirred for 1 h, warmed to room temperature and stirred for 3 d, during which time the colour changed from red through green to yellow. The reaction mixture was quenched with distilled water (100 cm^3), extracted into diethyl ether (50 cm^3) and dichloromethane (3 × 50 cm^3), and the combined organic extracts dried over anhydrous sodium sulfate and the solvent removed. Purification was accomplished by vacuum column chromatography using silica gel [eluent: 50% ethyl acetate–light petroleum (b.p. 40–60 °C)]. Thin-layer chromatography of the procedure using the same solvent showed three spots with R_f values of 0.04, 0.38 and 0.78 corresponding to the three compounds dmbipy, pmbipy and bpbipy. The pure product pmbipy was isolated as a yellow oil, yield 2.14 g, 37%. NMR (CD_3CN): ^{1}H, δ 8.50 (1 H, d, *J* 4.85,

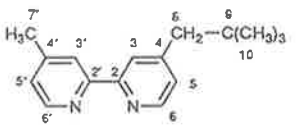

pmbipy

H^6), 8.48 (1 H, d, *J* 4.9, $H^{6'}$), 8.25 (1 H, s, $H^{3'}$), 8.18 (1 H, s, H^3), 7.20 (1 H, d, *J* 5.1, $H^{5'}$), 7.16 (1 H, d, *J* 4.9 Hz, H^5), 2.61 (2 H, s, H^8), 2.42 (3 H, s, $H^{7'}$), 0.93 (9 H, s, H^{10}); ^{13}C, δ 156.9 ($C^{2'}$), 156.3 (C^2), 150.5 ($C^{4'}$), 149.9 ($C^{6'}$), 149.4 (C^6), 149.2 (C^4), 126.7 (C^5), 125.6 ($C^{5'}$), 123.5 (C^3), 122.4 ($C^{3'}$), 49.9 (C^8), 32.2 (C^9), 29.5 (C^{10}), 21.2 ($C^{7'}$).

Complex Syntheses.—*Dicarbonyldichloro(4,4'-dimethyl-2,2'-bipyridine)ruthenium*(II), $[Ru(dmbipy)(CO)_2Cl_2]$. A solution of the ligand dmbipy (2.5 g, 13.6 mmol) in AR methanol (25 cm^3) was deaerated for 30 min before the addition of $[\{Ru(CO)_2Cl_2\}_n]$ (1.55 g, 6.8 mmol). The mixture was refluxed for 1.5 h with vigorous stirring and the precipitate collected on cooling. The yellow product was recrystallized from boiling methanol in subdued light, yield 1.96 g, 70% (Found: C, 37.5; H, 2.10; N, 7.2%. $C_{14}H_{14}Cl_2N_2O_2Ru$ requires C, 37.5; H, 2.10; N, 7.3%). IR: $\tilde{\nu}_{max}/cm^{-1}$ (Nujol) 2060 and 1988 (CO). NMR: $\delta_H(CD_3CN)$ 8.96 (2 H, d, *J* 5, H^6), 8.29 (2 H, s, H^3), 7.54 (2 H, d, *J* 5 Hz, H^5), 2.57 (6 H, s, CH_3).

Dicarbonyldichloro[4-(2,2-dimethylpropyl)-4'-methyl-2,2'-bipyridine]ruthenium(II), $[Ru(pmbipy)(CO)_2Cl_2]$. The pmbipy compound was synthesized and purified in an analogous manner to the corresponding dmbipy complex in 81% yield (Found: C, 46.0; H, 4.30; N, 5.9. $C_{18}H_{20}Cl_2N_2O_2Ru$ requires C, 46.2; H, 4.30; N, 6.0%). IR: $\tilde{\nu}_{max}/cm^{-1}$ (Nujol) 1981 and 2047 (CO). NMR: $\delta_H(CD_3CN)$ 8.98 (1 H, d, *J* 5, H^6), 8.95 (1 H, d, *J* 5, $H^{6'}$), 8.33 (1 H, s, $H^{3'}$), 8.21 (1 H, s, H^3), 7.54 (1 H, d, *J* 5, $H^{5'}$), 7.51 (1 H, d, *J* 5 Hz, H^5), 2.75 (2 H, s, H^8), 2.57 (3 H, s, $H^{7'}$), 0.98 (9 H, s, H^{10}).

Dicarbonyl(4,4'-dimethyl-2,2'-bipyridine)bis(trifluoromethanesulfonato)ruthenium(II), $[Ru(dmbipy)(CO)_2(CF_3SO_3)_2]$. This complex was synthesized by a method based on that of Sullivan *et al.*[24] in which $[Ru(dmbipy)(CO)_2Cl_2]$ (750 mg, 1.82 mmol) in 1,2-dichlorobenzene (200 cm^3) was deaerated with dry nitrogen for 30 min, resulting in a cloudy yellow solution. Trifluoromethanesulfonic acid (0.5 cm^3) was added dropwise by syringe (platinum needle) and the solution heated to 120 °C for 1.5 h. The mixture was cooled to 0 °C and the product precipitated by the addition of diethyl ether (200 cm^3). The mixture was allowed to stir for 1 h, and the complex collected by vacuum filtration under nitrogen and washed with diethyl ether (2 × 5 cm^3), cold distilled water (2 × 5 cm^3) and diethyl ether (2 × 5 cm^3), yield 990 mg, 85%. IR: $\tilde{\nu}_{max}/cm^{-1}$ (Nujol) 2099 and 2027 (CO), 1031, 893, 574 and 516 ($CF_3SO_3^-$).

Dicarbonyl[4-(2,2-dimethylpropyl)-4'-methyl-2,2'-bipyridine]bis(trifluoromethanesulfonato)ruthenium(II), $[Ru(pmbipy)(CO)_2(CF_3SO_3)_2]$. The pmbipy compound was synthesized in a similar manner to the dmbipy complex, with the exception that the 1,2-dichlorobenzene was distilled off prior to precipitation with diethyl ether. Yield was 55%. IR: $\tilde{\nu}_{max}/cm^{-1}$ (Nujol) 2033 and 2095 (CO), 1028, 895, 574 and 518 ($CF_3SO_3^-$).

Dicarbonylbis(4,4'-dimethyl-2,2'-bipyridine)ruthenium(II) *hexafluorophosphate dihydrate*, $[Ru(dmbipy)_2(CO)_2][PF_6]_2 \cdot 2H_2O$. The complex $[Ru(dmbipy)(CO)_2(CF_3SO_3)_2]$ (780 mg, 1.21 mmol) was added to a deaerated solution of dmbipy (590 mg, 2.45 mmol) in absolute ethanol (30 cm^3) and the mixture was refluxed for 1.5 h. The ethanol was removed on the rotary evaporator and the black residue extracted with boiling water (50 cm^3) and filtered. The complex was precipitated from the filtrate by addition of KPF_6 and the mixture stored at 4 °C overnight. The cream complex was collected, and washed with cold distilled water and diethyl ether. The solid was recrystallized from ethanol–acetone, yield 714 mg, 75%. The complex was purified by cation-exchange chromatography (SP-Sephadex C-25, 0.2 mol dm^{-3} NaCl eluent): the cation was precipitated from the eluent by the addition of solid KPF_6, and the resultant solid filtered off and washed with water (20 cm^3) and diethyl ether (20 cm^3) (Found: C, 38.1; H, 2.90; N, 6.7. $C_{26}H_{24}F_{12}N_4O_2P_2Ru$ requires C, 38.3; H, 2.95; N, 6.9%). IR: $\tilde{\nu}_{max}/cm^{-1}$ (Nujol) 2087 and 2034 (CO). NMR: $\delta_H(CD_3CN)$ 8.86 (2 H, d, *J* 5, H^6), 8.43 (2 H, s, H^3), 8.30 (2 H, s, $H^{3'}$), 7.72 (2 H, d, *J* 5, H^5), 7.30 (2 H, d, *J* 5, $H^{5'}$), 7.19 (2 H, d, *J* 5 Hz, $H^{6'}$), 2.67 (6 H, s, CH_3), 2.47 (6 H, s, CH_3').

Dicarbonyl(4,4'-dimethyl-2,2'-bipyridine)[4-(2,2-dimethylpropyl)-4'-methyl-2,2'-bipyridine]ruthenium(II) *hexafluorophosphate dihydrate*, $[Ru(dmbipy)(pmbipy)(CO)_2][PF_6]_2 \cdot 2H_2O$. The mixed bipyridine complex was synthesized and purified (90% yield) in an analogous manner to $[Ru(dmbipy)_2(CO)_2][PF_6]_2$, by the substitution of pmbipy into $[Ru(dmbipy)(CO)_2(CF_3SO_3)_2]$ (Found: C, 39.7; H, 3.55; N, 6.0. $C_{30}H_{36}F_{12}N_4O_4P_2Ru$ requires C, 39.7; H, 4.00; N, 6.2%). IR: $\tilde{\nu}_{max}/cm^{-1}$ (Nujol) 2099 and 2053 (CO).

The crude product was found to be a mixture of two isomers (IV and V). By fractional recrystallization from ethanol, the less soluble isomer (IV) could be obtained in pure form. The ^{1}H NMR shifts (in CD_3CN solution) of the two isomers are given in Table 1 (numbering scheme shown below).

Dicarbonylbis[4-(2,2-dimethylpropyl)-4'-methyl-2,2'-bipyridine]ruthenium(II) *hexafluorophosphate hydrate*. $[Ru(pmbipy)_2(CO)_2][PF_6]_2 \cdot H_2O$. The crude complex was synthesized and purified (62% yield) in an analogous manner to that described for $[Ru(dmbipy)_2(CO)_2][PF_6]_2$, by the substitution of pmbipy into $[Ru(pmbipy)(CO)_2(CF_3SO_3)_2]$ (Found: C, 43.2; H, 4.30; N, 5.8. $C_{34}H_{42}F_{12}N_4O_3P_2Ru$ requires C, 43.2; H, 4.50; N, 5.9%). IR: $\tilde{\nu}_{max}/cm^{-1}$ (Nujol) 2096 and 2042 (CO).

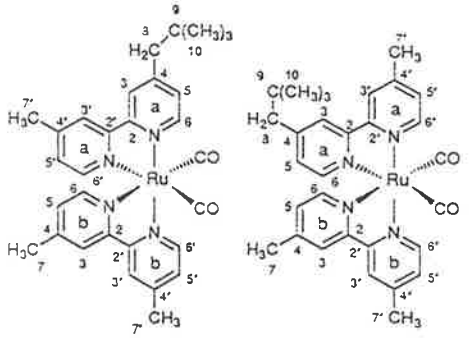

IV V

The crude product was found to be a mixture of three isomers (VI, VII and VIII), which were separated by fractional recrystallization from ethanol. The ^{1}H NMR shifts (in CD_3CN solution) of the three isomers are given in Table 1 (numbering scheme shown below).

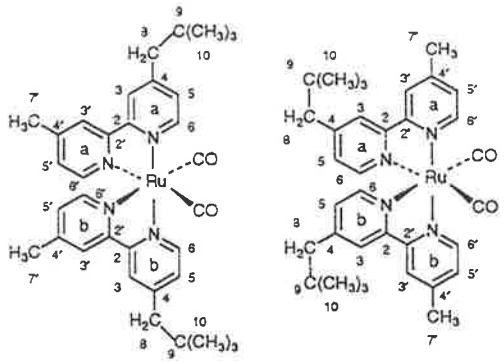

VI VII

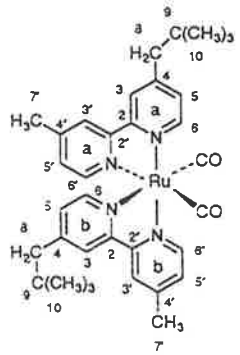

VIII

(4,4'-Dimethyl-2,2'-bipyridine)bis[4-(2,2-dimethylpropyl)-4'-methyl-2,2'-bipyridine]ruthenium(II) *hexafluorophosphate dihydrate*. [Ru(dmbipy)(pmbipy)$_2$][PF_6]$_2$·2H_2O. As an exemplar of the synthetic method, [Ru(dmbipy)(pmbipy)(CO)$_2$] (30 mg, 0.034 mmol) and pmbipy (24 mg, 0.1 mmol) were dissolved in 2-methoxyethanol (10 cm^3) and deaerated with dry nitrogen for 20 min. An excess of trimethylamine *N*-oxide (7 mg, 0.1 mmol) was added and the reaction refluxed for 3 h, during which time the solution changed from yellow to bright orange. The alternative for the reaction was that the solution was maintained at room temperature for 36 h. In both cases, the solvent was removed on the rotary evaporator, the residue dissolved in water, and the product precipitated from the filtered solution by the addition of KPF_6. This mixture was stored at 4 °C overnight, and the product collected by vacuum filtration, sorbed onto a column of SP-Sephadex C-25 cation exchanger, and eluted with 0.2 mol dm^{-3} NaCl. The single band was collected, KPF_6 added, and the orange cation extracted into dichloromethane (3 × 50 cm^3), which was dried over anhydrous sodium sulfate. The solvent was removed, the residue dissolved in water and the product re-precipitated with KPF_6. After storage at 4 °C overnight, the solid was collected by vacuum filtration, washed with diethyl ether and air dried. Yield 25 mg, 70% at reflux; 7 mg, 20% at room temperature (Found: C, 48.6; H, 4.65; N, 7.9. $C_{44}H_{56}F_{12}N_6O_2P_2Ru$ requires C, 48.4; H, 5.15; N, 7.7%). UV/VIS: λ_{max}/nm (CH_3CN) 210 (ε/dm^3 mol^{-1} cm^{-1} 79 600), 250 (25 400), 258 (24 000), 288 (70 600), 426 (sh), 458 (12 000).

The isomers were separated by cation exchange chromatography on SP-Sephadex C-25 using 0.125 mol dm^{-3} sodium toluene-4-sulfonate as the eluent.[7] The hexafluorophosphate salts were isolated by precipitation from the eluent by addition of KPF_6, and the suspension extracted using dichloromethane. The ^{1}H NMR shifts (in CD_3CN solution) of the three isomers are given in Table 2.

Bis(4,4'-dimethyl-2,2'-bipyridine)[4-(2,2-dimethylpropyl)-4'-methyl-2,2'-bipyridine]ruthenium(II) *hexafluorophosphate*. [Ru(dmbipy)$_2$(pmbipy)][PF_6]$_2$. The complex was synthesized in 57% yield in an analogous manner to that described for [Ru(dmbipy)(pmbipy)$_2$][PF_6]$_2$, by reaction of pmbipy with [Ru(dmbipy)$_2$(CO)$_2$]$^{2+}$ under decarbonylation conditions (Found: C, 48.2; H, 4.30; N, 8.3. $C_{40}H_{44}F_{12}P_2N_6Ru$ requires C, 48.1; H, 4.45; N, 8.4%). UV/VIS: λ_{max}/nm (MeCN) 208 (ε/dm^3 mol^{-1} cm^{-1} 84 000), 250 (25 000), 258 (23 300), 288 (84 200), 426 (sh), 458 (15 300). The ^{1}H NMR shifts (in CD_3CN solution) are given in Table 2.

Tris[4-(2,2-dimethylpropyl)-4'-methyl-2,2'-bipyridine]ruthenium(II) *hexafluorophosphate*, [Ru(pmbipy)$_3$][PF_6]$_2$. The complex was synthesized using an adaption of a procedure published previously,[3,4,5] *via* [Ru(dmf)$_6$]$^{2+}$ (dmf = *N*,*N*-dimethylformamide) as precursor. Yield: 25% (Found: C, 51.5; H, 4.80; N, 7.2. $C_{48}H_{60}F_{12}N_6P_2Ru$ requires C, 51.8; H, 5.45; N, 7.6%). UV/VIS: λ_{max}/nm (MeCN) 210 (ε/dm^3 mol^{-1} cm^{-1} 70 100), 250 (21 000), 258 (19 600), 288 (66 000), 426 (sh), 458 (12 000).

The isomers were separated by cation-exchange chromatography on SP-Sephadex C-25 using 0.125 mol dm^{-3} sodium toluene-4-sulfonate as the eluent.[7] The hexafluorophosphate salts were isolated by precipitation from the eluent by addition of KPF_6, and the suspension extracted using dichloromethane. The ^{1}H NMR shifts (in CD_3CN solution) of the two isomers are given in Table 2.

Acknowledgements

We are grateful to Mr. Laurie Kelso and Mr. Joe Treadway for useful discussions on aspects of the work, and the Australian Research Council for financial support.

References

1 G. F. Strouse, P. A. Anderson, J. R. Schoonover, T. J. Meyer and F. R. Keene, *Inorg. Chem.*, 1992, **31**, 3004.
2 P. A. Anderson, G. B. Deacon, K. H. Haarmann, F. R. Keene, T. J. Meyer, D. A. Reitsma, B. W. Skelton, G. F. Strouse, N. C. Thomas, J. A. Treadway and A. H. White, unpublished work.
3 D. S. Black, G. B. Deacon and N. C. Thomas, *Aust. J. Chem.*, 1982, **35**, 2445.
4 D. S. Black, G. B. Deacon and N. C. Thomas, *Inorg. Chim. Acta*, 1982, **65**, L75.
5 D. S. Black, G. B. Deacon and N. C. Thomas, *Polyhedron*, 1983, **2**, 409.
6 N. C. Thomas and G. B. Deacon, *Inorg. Synth.*, 1989, **25**, 107.
7 D. A. Reitsma and F. R. Keene, *J. Chem. Soc., Dalton Trans.*, 1993, 2859.

8 V. Balzani and F. Scandola, *Supramolecular Photochemistry*, Ellis Horwood, Chichester, 1991, p. 427.
9 A. Juris, S. Barigelletti, S. Campagna, V. Balzani, P. Belser and A. von Zelewsky, *Coord. Chem. Rev.*, 1988, **84**, 85.
10 G. Denti, S. Campagna, S. Serroni, M. Ciano and V. Balzani, *J. Am. Chem. Soc.*, 1992, **114**, 2944.
11 P. Belser, A. von Zelewsky, M. Frank, C. Seel, F. Vögtle, L. De Cola, F. Barigelletti and V. Balzani, *J. Am. Chem. Soc.*, 1993, **115**, 4076.
12 M. M. Richter and K. J. Brewer, *Inorg. Chem.*, 1993, **32**, 5762.
13 V. Balzani, R. Ballardini, F. Bolletta, M. T. Gandolfi, A. Juris, M. Maestri, M. F. Manfrin, L. Moggi and N. Sabbatini, *Coord. Chem. Rev.*, 1993, **125**, 75.
14 M. J. Cook, A. P. Lewis and G. S. G. McAuliffe, *Org. Magn. Reson.*, 1984, **22**, 388.
15 M. J. Cook, A. P. Lewis, G. S. G. McAuliffe and A. J. Thomson, *Inorg. Chim. Acta*, 1982, **64**, 25.
16 M. Krejcik, S. Zalis, J. Klima, D. Sykora, W. Matheis, A. Klein and W. Kaim, *Inorg. Chem.*, 1993, **32**, 3362.
17 G. Orellana, C. A. Ibarra and J. Santoro, *Inorg. Chem.*, 1988, **27**, 1025.
18 C. Brevard and P. Granger, *Inorg. Chem.*, 1983, **22**, 532.
19 G. Orellana, A. Kirsch-De Mesmaeker and N. J. Turro, *Inorg. Chem.*, 1990, **29**, 882.
20 G. Predieri, C. Vignali, G. Denti and S. Serroni, *Inorg. Chim. Acta*, 1993, **205**, 145.
21 X. Hua and A. von Zelewsky, *Inorg. Chem.*, 1991, **30**, 3796.
22 J. M. Kelly, C. M. O'Connell and J. G. Vos, *Inorg. Chim. Acta*, 1982, **64**, L75.
23 K. Joseph, S. S. Deshpande, S. A. Pardhy, I. R. Unny, S. K. Pandit, S. Gopinathan and C. Gopinathan, *Inorg. Chim. Acta*, 1984, **82**, 59.
24 B. P. Sullivan, J. V. Caspar, S. R. Johnson and T. J. Meyer, *Organometallics*, 1984, **3**, 1241.
25 R. Hage, J. G. Haasnoot, H. A. Nieuwenhuis, J. Reedijk, R. Wang and J. G. Vos, *J. Chem. Soc., Dalton Trans.*, 1991, 3271.
26 M. Heijden, P. M. Vanvliet, J. G. Haasnoot and J. Reedijk, *J. Chem. Soc., Dalton Trans.*, 1993, 3675.
27 D. A. Reitsma, T. J. Rutherford and F. R. Keene, unpublished work.
28 N. Kitamura, S. Rajagopal and S. Tazuke, *J. Phys. Chem.*, 1987, **91**, 3767.
29 T. J. Rutherford, M. G. Quagliotto and F. R. Keene, unpublished work.
30 L. F. Cooley, S. L. Larson, C. M. Elliott and D. F. Kelley, *J. Phys. Chem.*, 1991, **95**, 10694.
31 T. Boussie and T. J. Meyer, personal communication.
32 M. J. Cleare and W. P. Griffith, *J. Chem. Soc. A*, 1969, 372.
33 J. C. Coll and B. F. Bowden, *J. Nat. Prod.*, 1986, **49**, 934.
34 F. R. Keene, M. R. Snow, P. J. Stephenson and E. R. T. Tiekink, *Inorg. Chem.*, 1988, **27**, 2040.
35 P. Bernhard and A. M. Sargeson, *J. Am. Chem. Soc.*, 1989, **111**, 597.

Received 23rd *May* 1994; *Paper* 4/03028A

Inorg. Chem. **1995**, *34*, 3857−3858

Chiral $[Ru(pp)_2(CO)_2]^{2+}$ Species (pp = Bidentate Polypyridyl Ligand) and Their Use in the Stereoselective Synthesis of Ligand-Bridged Dinuclear Complexes

Todd J. Rutherford, Michael G. Quagliotto, and F. Richard Keene*

Department of Molecular Sciences, James Cook University of North Queensland, Townsville, Queensland 4811, Australia

Received March 15, 1995

Polymetallic supramolecular assemblies have considerable potential for application to *photochemical molecular devices* (PMDs),[1,2] and the spatial interrelationship of the component metal centers is likely to influence intramolecular energy and electron transfer processes. In photobiological systems, there is no ambiguity in the geometry of the natural assembly, as the building blocks of the enzymic matrix are chiral amino acids or phosphate sugars. By analogy, in the construction of covalent artificial polymetallic assemblies, spatial control will depend on the availability of building blocks with predetermined stereochemistry: however, this problem has rarely been addressed.

We previously reported a general synthetic methodology for tris(heteroleptic) complexes of ruthenium(II), $[Ru(pp)(pp')(pp'')]^{2+}$ (pp etc. are bidentate polypyridyl ligands), via the dicarbonyl species $[Ru(pp)(pp')(CO)_2]^{2+}$.[3,4] The scheme may be extended to dinuclear and higher polynuclear species.[5]

Significantly, we have also shown that, in cases where pp and pp′ are unsymmetrical, and therefore geometric isomers of $[Ru(pp)(pp')CO_2]^{2+}$ may exist, the stereochemical relationship of the two bidentate ligands is retained on conversion to $[Ru(pp)(pp')(pp'')]^{2+}$.[6] We have now extended those studies to demonstrate the maintenance of chirality in such reactions and the utilization of the dicarbonyl species as "building blocks" in the formation of dinuclear species in which the chirality of the two metal centers is predetermined.

The dicarbonyl precursor complexes $[Ru(bpy)_2(CO)_2]^{2+}$, $[Ru(Me_2bpy)_2(CO)_2]^{2+}$, and $[Ru(phen)_2(CO)_2]^{2+}$ (bpy = 2,2′-bipyridine; Me_2bpy = 4,4′-dimethyl-2,2′-bipyridine; phen = 1,10-phenanthroline) were synthesized and characterized as outlined previously[3,4] and resolved by the following general method: $[Ru(pp)_2(CO)_2](PF_6)_2$ was converted to $[Ru(pp)_2(CO)_2]Br_2$ by metathesis in 2-butanone solution using $[(n\text{-}C_4H_9)_4N]Br$, collected, and dissolved in distilled water. The solution was stirred in the dark for 30 min with 2 equiv of Ag[(+)-SbOtart]. The AgBr precipitate was separated from the mixture by filtration and the water removed to yield $[Ru(pp)_2(CO)_2][(+)\text{-}SbOtart]_2$, which was fractionally recrystallized from methanol.

The enantiomeric purity of the recrystallized dicarbonyl complexes was determined by ^1H NMR techniques using the chiral lanthanide-induced shift reagent tris{3-[(trifluoromethyl)-hydroxymethylene]-(+)-camphorato}europium(III), Eu(tfc)$_3$.[7] The complexes were converted to chloride salts using anion-exchange chromatography, and the ^1H NMR spectra were measured in CD_2Cl_2 solution {for $[Ru(Me_2bpy)_2(CO)_2]Cl_2$} or

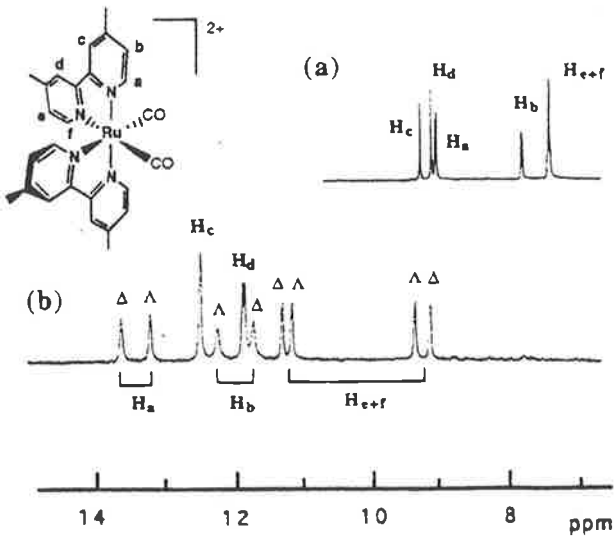

Figure 1. 300 MHz ^1H NMR spectra of $[Ru(Me_2bpy)_2(CO)_2]Cl_2$ in CD_2Cl_2 solution: (a) with no Eu(tfc)$_3$; (b) with added Eu(tfc)$_3$. [The numbering system for the Me_2bpy ligand in the complex is indicated in the structure (the two bidentate ligands are related by C_2 symmetry).]

CD_3CN {for $[Ru(bpy)_2(CO)_2]Cl_2$ and $[Ru(phen)_2(CO)_2]Cl_2$} in the presence of increasing amounts of the shift reagent. The effect of the shift reagent in discriminating between the enantiomers of $[Ru(Me_2bpy)_2(CO)_2]^{2+}$ (CH_2Cl_2 solution) is shown in Figure 1. Greater induced shifts and selectivities were observed in dichloromethane, whereas differentiation between the enantiomers in acetonitrile required increased amounts of the chiral shift reagent, probably because of greater competition for the reagent by that solvent.

The less soluble fractions in the resolutions of the dicarbonyl complexes $[Ru(bpy)_2(CO)_2]^{2+}$, $[Ru(Me_2bpy)_2(CO)_2]^{2+}$, and $[Ru(phen)_2(CO)_2]^{2+}$ exhibited molecular rotations, $[M]_{365}$, of −4820°, +44 430° and +12 080°, respectively, measured as the chloride salts. Following conversion to the hexafluorophosphate salt by metathesis, decarbonylation of (−)-$[Ru(bpy)_2CO_2](PF_6)_2$ (with 3 equiv of TMNO in 2-methoxyethanol solution containing 10 equiv of bpy, under stirring at room temperature for 3 days) yielded Δ-(−)-$[Ru(bpy)_3](PF_6)_2$,[8] establishing the Δ configuration of the dicarbonyl precursor. The Δ-$[Ru(bpy)_3](PF_6)_2$ product was converted to the iodide salt, which showed a molecular rotation $[M]_D$ of −6740°, compared to the literature value of −6750°,[9] indicating complete retention of configuration during the decarbonylation process. The decarbonylation reactions were carried out in the absence of light as a precautionary measure, although no photoracemization of the $[Ru(pp)_2(CO)_2]^{2+}$ species was observed under normal laboratory lighting conditions.

(1) Balzani, V.; Scandola, F. *Supramolecular Photochemistry*; Ellis Horwood: Chichester, U.K., 1991.
(2) Sauvage, J.-P.; Collin, J.-P.; Chambron, J.-C.; Guillerez, S.; Coudret, C. *Chem. Rev.* **1994**, *94*, 993.
(3) Strouse, G. F.; Anderson, P. A.; Schoonover, J. R.; Meyer, T. J.; Keene, F. R. *Inorg. Chem.* **1992**, *31*, 3004.
(4) Anderson, P. A.; Deacon, G. B.; Haarmann, K. H.; Keene, F. R.; Meyer, T. J.; Reitsma, D. A.; Skelton, B. W.; Strouse, G. F.; Thomas, N. C.; Treadway, J. A.; White, A. H. Submitted for publication.
(5) Reitsma, D. A.; Keene, F. R. *J. Chem. Soc., Dalton Trans.* **1993**, 2859.
(6) Rutherford, T. J.; Reitsma, D. A.; Keene, F. R. *J. Chem. Soc., Dalton Trans.* **1994**, 3659.
(7) Barton, J. K.; Nowick, J. S. *J. Chem. Soc., Chem. Commun.* **1984**, 1650.
(8) McCaffery, A. J.; Mason, S. F.; Norman, B. J. *J. Chem. Soc. A* **1969**, 1428.
(9) Dwyer, F. P.; Gyarfas, E. C. *J. Proc. R. Chem. Soc. N.S.W.* **1949**, *83*, 174.

0020-1669/95/1334-3857$09.00/0

Scheme 1

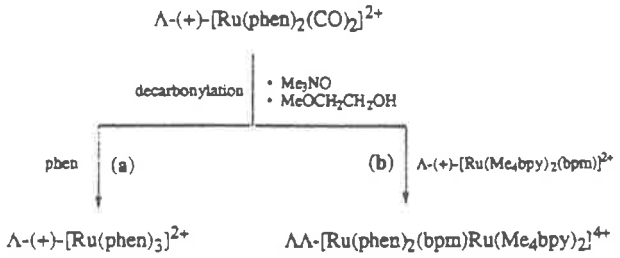

Λ-(+)-$[Ru(phen)_3]^{2+}$ [8] was formed by decarbonylation of (+)-$[Ru(phen)_2(CO)_2]^{2+}$ in the presence of excess phen, but otherwise under conditions identical to those described above for the reaction of (−)-$[Ru(bpy)_2(CO)_2]^{2+}$ with bpy (Scheme 1(a)). The product showed $[M]_{546} = +13\,100°$, indicating an optical purity of approximately 100%,[10] which was confirmed using the chiral lanthanide-induced shift reagent. The decarbonylation of (+)-$[Ru(Me_2bpy)_2(CO)_2]^{2+}$ under the same conditions in the presence of excess Me_2bpy realized (+)-$[Ru(Me_2bpy)_3]^{2+}$, for which $[M]_{546} = +6280°$ compared with $[M]_{546} = 6750°$ for the chromatographically-resolved product (see below), suggesting an optical purity of approximately 93% (96% as determined by the chiral lanthanide-induced shift experiment). These results indicate that the stereochemical integrities of Δ-$[Ru(bpy)_2(CO)_2]^{2+}$ and Λ-$[Ru(phen)_2(CO)_2]^{2+}$ are maintained during the course of the decarbonylation reaction whereas (+)-$[Ru(Me_2bpy)_2(CO)_2]^{2+}$ undergoes minor racemization.

During the course of this work, a cation-exchange chromatographic technique was developed[11] for resolution of tris(bidentate)ruthenium(II) complexes based on the differential association of the enantiomeric forms with a chiral organic counteranion.[5,12-14] The complexes $[Ru(Me_2bpy)_3]^{2+}$ and $[Ru(phen)_3]^{2+}$ were resolved on a column of SP-Sephadex C-25 cation exchanger using 0.2 mol dm^{-3} NaCl/0.125 mol dm^{-3} sodium (−)-*O*-*O*′-dibenzoyl-L-tartrate solution as the eluent. In both cases, the enantiomers were clearly separated, and following isolation from the bands by precipitation as the PF_6^- salts, the molecular rotations $[M]_{546}$ (acetonitrile solution) for $[Ru(Me_2bpy)_3](PF_6)_2$ were −6950° (eluted first) and +6750° and those for $[Ru(phen_3](PF_6)_2$ were −12 540° (eluted first) and +12 740°. The latter complex was also converted to the chloride salt, and $[\alpha]_D$ values (aqueous solution) of −1310 and +1400° were obtained (literature values of −1330 and +1340°).[10]

The chromatographic resolution technique was also extended to mononuclear ruthenium(II) complexes containing bridging ligands $[Ru(pp)(pp')(BL)]^{2+}$: $[Ru(Me_4bpy)_2(bpm)](PF_6)_2$ (bpm = 2,2′-bipyrimidine and Me_4bpy = 4,4′,5,5′-tetramethyl-2,2′-bipyridine) was synthesized and resolved in this manner, giving $[M]_{546}$ values of −4440 and +4750° for the enantiomers as PF_6^- salts in acetonitrile solution.

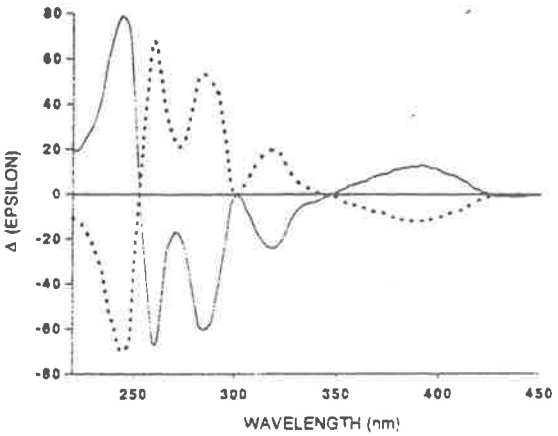

Figure 2. CD spectra of $[(phen)_2Ru(bpm)Ru(Me_4bpy)_2](PF_6)_4$ (acetonitrile solution): ΔΔ enantiomer (—); ΛΛ enantiomer (···).

The synthesis of dinuclear species may be achieved by reaction under decarbonylation conditions of a dicarbonyl precursor $\{[Ru(pp)(pp')(CO)_2]^{2+}\}$ with the tris(bidentate) complex $[Ru(pp)(pp')(BL)]^{2+}$ containing a bridging ligand.[5] In the present case (+)-$[Ru(Me_4bpy)_2(bpm)](PF_6)_2$ was added to a solution of 2-methoxyethanol containing 4 equiv of Λ-(+)-$[Ru(phen)_2(CO)_2](PF_6)_2$ and 4 equiv of TMNO, and the mixture was stirred at 30−35 °C in the dark for 14 days to yield ΛΛ-$[(phen)_2Ru(bpm)Ru(Me_4bpy)_2](PF_6)_2$ (Scheme 1(b)), confirmed by ^1H NMR measurements.[5] The NMR spectrum also indicated the presence only a very minor amount (<2%) of the ΛΔ diastereoisomer, confirming retention of chirality during the decarbonylation reaction. Accordingly, the absolute configuration of (+)-$[Ru(Me_4bpy)_2(bpm)]^{2+}$ can be confirmed as Λ, consistent with the configuration/rotatory dispersion relationship reported for $[Ru(bpy)_3]^{2+}$, $[Ru(phen)_3]^{2+}$, and their bis(heteroleptic) analogues.[8,15-17] The ΔΔ isomer was obtained by reacting Δ-(−)-$[Ru(Me_4bpy)_2(bpm)](PF_6)_2$ with 3 equiv of *rac*-$[Ru(phen)_2(CO)_2](PF_6)_2$ and 3 equiv of TMNO in 2-methoxyethanol at reflux for 3 h. The two diastereoisomers formed (ΔΔ and ΔΛ) were separated by ion-exchange chromatography (SP Sephadex C-25 cation exchanger) with 0.25 mol dm^{-3} sodium toluene-4-sulfonate as eluent.[5]

The circular dichroism of the ΔΔ and ΛΛ forms of $[(phen)_2Ru(bpm)Ru(Me_4bpy)_2]^{4+}$ are shown in Figure 2, demonstrating the enantiomeric nature of the two species.

The results reported exemplify the application of our synthetic methodology to the synthesis of an extended range of dinuclear species from the precursors $[Ru(pp)(pp')(CO)_2]^{2+}$ and $[Ru(pp)(pp')(BL)]^{2+}$, where pp and pp′ may or may not be identical. Furthermore, these building blocks enable the predetermination of the stereochemistry of the metal centers in dinuclear species, and in this sense the study is complementary to an earlier report.[18] However, the present scheme has greater versatility in terms of the variation of ligand environment and is more readily extended to the synthesis of higher nucleate assemblies.[3,4,19] The methodology will be exploited to enable us to probe the effect of stereochemical aspects on electron and energy transfer processes in such assemblies.

Acknowledgment. This work was funded by the Australian Research Council. We wish to thank Mr. D. A. Rietsma (JCUNQ) for helpful discussions.

IC9502990

(10) Dwyer, F. P.; Gyarfas, E. C. *J. Proc. R. Chem. Soc. N.S.W.* **1949**, *83*, 170.
(11) Reitsma, D. A.; Keene, F. R. Unpublished work.
(12) Keene, F. R.; Searle, G. H. *Inorg. Chem.* **1974**, *13*, 2173.
(13) Searle, G. H. *Aust. J. Chem.* **1977**, *30*, 2625.
(14) Yoshikawa, Y.; Yamasaki, K. *Coord. Chem. Rev.* **1979**, *28*, 205.
(15) Bosnich, B. *Inorg. Chem.* **1968**, *7*, 2379.
(16) Gillard, R. D.; Hill, R. E. D.; Maskill, R. *J. Chem. Soc. A* **1970**, 707.
(17) Tada, T. *J. Sci. Hiroshima Univ., Ser. A: Phys. Chem.* **1982**, *46*, 73.
(18) Hua, X.; von Zelewsky, A. *Inorg. Chem.* **1991**, *30*, 3796.
(19) Anderson, P. A.; Strouse, G. F.; Treadway, J. A.; Keene, F. R.; Meyer, T. J. *Inorg. Chem.* **1994**, *33*, 3863.

Inorg. Chem. **1995**, *34*, 6145−6157 6145

Designed Synthesis of Mononuclear Tris(heteroleptic) Ruthenium Complexes Containing Bidentate Polypyridyl Ligands

Peter A. Anderson,[†] Glen B. Deacon,[‡] Klaus H. Haarmann,[†] F. Richard Keene,*[,†] Thomas J. Meyer,[§] David A. Reitsma,[†] Brian W. Skelton,[⊥] Geoffrey F. Strouse,[§] Nicholas C. Thomas,[‡] Joseph A. Treadway,[§] and Allan H. White[⊥]

School of Molecular Sciences, James Cook University of North Queensland, Townsville, Queensland 4811, Australia, School of Chemistry, Monash University, Clayton, Victoria 3168, Australia, Department of Chemistry, University of North Carolina, Chapel Hill, North Carolina 27599-3290, and Department of Chemistry, University of Western Australia, Nedlands 6907, Australia

Received April 3, 1995[⊗]

A general synthetic methodology is reported for tris(bidentate)ruthenium(II) complexes containing three different polypyridyl ligands, based on the sequential addition of the ligands to the oligomer $[Ru(CO)_2Cl_2]_n$. The tris(heteroleptic) complexes were characterized by FAB mass spectrometry and NMR spectroscopy. An X-ray crystal structure determination was made for the complex $[Ru(Me_2bpy)(phen)(bpa)](PF_6)_2 \cdot C_6H_{14}$ [$C_{40}H_{43}F_{12}N_7P_2Ru$, M = 1062.8; Me_2bpy = 4,4′-dimethyl-2,2′-bipyridine, phen = 1,10-phenanthroline, bpa = bis(2-pyridyl)amine]: triclinic, space group $P\bar{1}$, a = 14.57(3) Å, b = 13.50(3) Å, c = 12.73(3) Å, α = 68.6(2)°, β = 63.5(1)°, γ = 79.8(2)°, V = 2082 Å^3, Z = 2. Aspects of the electrochemistry, spectroscopy, and photophysics of the tris(heteroleptic) species are discussed.

Introduction

Coordination compounds of ruthenium(II) containing polypyridyl ligands have been the subject of a wide variety of photochemical studies directed toward their use as "photosensitizers" in photochemical molecular devices (PMDs).[1,2] The complex tris(2,2′-bipyridine)ruthenium(II), $[Ru(bpy)_3]^{2+}$, is the archetype of such species and demonstrates the combined attributes of significant absorption in the visible spectral region, the relative longevity of the metal-to-ligand charge transfer (MLCT) excited states formed on light absorption, the relative inertness of the metal center in a variety of oxidation states, and the rapidity of the redox reactions involving the excited states (quenching).

The excited state properties of complexes of this genre are controlled by the pattern of low-lying electronic levels which are ligand-dependent,[3,4] as is the redox behavior.[1,3−5] Indeed there are clear correlations between aspects of these two characteristics, as they share a dependence on the π^* energies of the ligands and the $d\pi$ levels at the metal.[5] Accordingly, through a judicious choice of ligands, it is possible to "fine tune" the redox and photophysical properties of the ground and excited states of polypyridylruthenium(II) complexes. As alluded to previously,[1] with 200 bidentate ligands (pp), there are 200 homoleptic possibilities $[Ru(pp)_3]^{2+}$, ~4 × 10^4 bis(hetereoleptic) $[Ru(pp)_2(pp')]^{2+}$ species, and ~1.3 × 10^6 tris(heteroleptic) complexes $[Ru(pp)(pp')(pp'')]^{2+}$!

The lack of a generalized synthetic methodology for tris(bidentate) complexes of ruthenium(II) in which the three ligands are different {tris(heteroleptic) species} has limited the exploitation of this concept of rational control of their physical characteristics. Existing procedures are most effective for incorporation of at most two different ligands into the coordination sphere, and examples of tris(heteroleptic) complexes are very limited.[6−9] The synthetic technique described here and in preceding papers[10−16] provides a general route for the preparation of tris(heteroleptic) species of ruthenium(II). It presents new strategies for the design of visible-light sensitizers of the tris(bidentate)ruthenium(II) genre and for polymetallic molecular assemblies based on such centers.

Experimental Section

Physical Measurements. UV/visible spectra were recorded on a Hewlett-Packard 8452A diode array, CARY 219, or CARY 14 spectrophotometer (the last being interfaced to an IBM PC by On-Line Systems, Inc.). NMR spectra were recorded on a BRUKER AM300 or AC200 spectrometer. Infrared spectra were recorded on

[†] James Cook University of North Queensland.
[‡] Monash University.
[§] University of North Carolina.
[⊥] University of Western Australia.
[⊗] Abstract published in *Advance ACS Abstracts,* October 15, 1995.

(1) Juris, A.; Barigelletti, S.; Campagna, S.; Balzani, V.; Belser, P.; von Zelewsky, A. *Coord. Chem. Rev.* **1988**, *84*, 85.
(2) Balzani, V.; Scandola, F. *Supramolecular Photochemistry*; Horwood: Chichester, U.K., 1991.
(3) Johnson, S. R.; Westmoreland, T. D.; Caspar, J. V.; Barqawi, K. R.; Meyer, T. J. *Inorg. Chem.* **1988**, *27*, 3195.
(4) Kober, E. M.; Marshall, J. C.; Dressick, W. J.; Sullivan, B. P.; Caspar, J. V.; Meyer, T. J. *Inorg. Chem.* **1985**, *24*, 2755.
(5) Kober, E. M.; Caspar, J. V.; Sullivan, B. P.; Meyer, T. J. *Inorg. Chem.* **1988**, *27*, 4587.
(6) Thummel, R. P.; Lefoulon, F.; Chirayil, S. *Inorg. Chem.* **1987**, *26*, 3071.
(7) Ross, H. B.; Boldaji, M.; Rillema, D. P.; Blanton, C. B.; White, R. P. *Inorg. Chem.* **1989**, *28*, 1013.
(8) Juris, A.; Campagna, S.; Balzani, V.; Gremaud, G. *Inorg. Chem.* **1988**, *27*, 3652.
(9) von Zelewsky, A.; Gremaud, G. *Helv. Chim. Acta* **1988**, *71*, 1108.
(10) Thomas, N. C. Ph.D. Thesis, Monash University, 1983.
(11) Black, D. S.; Deacon, G. B.; Thomas, N. C. *Inorg. Chim. Acta* **1982**, *65*, L75.
(12) Thomas, N. C.; Deacon, G. B. *Inorg. Synth.* **1989**, *25*, 107.
(13) Thomas, N. C.; Deacon, G. B. *Synth. React. Inorg. Met.-Org. Chem.* **1986**, *16*, 85.
(14) Black, D. S.; Deacon, G. B.; Thomas, N. C. *Polyhedron* **1983**, *2*, 409.
(15) Black, D. S.; Deacon, G. B.; Thomas, N. C. *Aust. J. Chem.* **1982**, *35*, 2445.
(16) Strouse, G. F.; Anderson, P. A.; Schoonover, J. R.; Meyer, T. J.; Keene, F. R. *Inorg. Chem.* **1992**, *31*, 3004.

0020-1669/95/1334-6145$09.00/0

either a Perkin Elmer Series 1600 FTIR or a Nicolet 20DX FTIR spectrometer. Electrochemical measurements were made in a drybox (Ar) using a Bioanalytical Systems (BAS) 100A electrochemical analyzer, an EG&G PAR Model 175 potentiostat and Model 175 waveform generator, or an EG&G Model 273 potentiostat. Unless otherwise indicated, cyclic voltammetry was carried out by using platinum working electrodes, and all potentials were measured relative to an $Ag/AgNO_3$ (0.01 M in acetonitrile) reference electode: however, potentials are quoted relative to a saturated sodium chloride calomel electrode (SSCE) unless otherwise specified. Positive-ion fast atom bombardment mass spectra were recorded on a JEOL-DX300 probe (Ar^+ source) with samples mulled in 3-nitrobenzyl alcohol.

Prior to photophysical analysis, all metal complexes were purified by cation-exchange HPLC chromatography on a Brownlee CX-100 Prep10 column utilizing linear gradient elution with 0−400 mM KBr in 2:3 (v/v) CH_3CN/aqueous phosphate buffer (0.6 mM; pH = 7.2), controlled by a Perkin Elmer Series 4 pump control unit and monitored at a Perkin Elmer LC-95 variable UV−vis spectrophotometer detector fitted with a 4.5 μL path length flow cell.

Photophysical measurements (emission spectra and time-resolved emission studies) were carried out as described previously,[17] as were the emission quantum yields (Φ_{em}) using $[Ru(bpy)_3](PF_6)_2$ in CH_3CN (Φ_{em} = 0.062) or $[Os(bpy)_3](PF_6)_2$ in CH_3CN (Φ_{em} = 0.0046) as standards.[18] Due to limited detector response at low energies, approximately 30% of the emission band of $[Ru(Me_2bpy)\{(EtCO_2)_2bpy\}\{(Et_2N)_2bpy\}](PF_6)_2$ (**Vi**) could not be reliably measured. The full spectrum, as well as the spectrum for the $[Os(bpy)_3](PF_6)_2$ standard, was reconstructed using spectral fitting techniques described previously.[19] This method was found to reproduce the emission quantum yield for $[Ru(bpy)_3](PF_6)_2$ to within experimental error. Quantum yields for decomposition (Φ_{dec}) were measured relative to $[Ru(bpy)_3](PF_6)_2$ ($\Phi_{dec} \sim 0.029$ [20]) at $\sim 2 \times 10^{-5}$ M in a freeze−pump−thaw degassed (4×) stirred 0.2 M $[N(n\text{-}C_4H_9)_4]Cl/[CH_3CN$ solution at 295 K by measuring the decrease in emission intensity as a function of time (12 h). A collimated 75 W lamp was used as the source, with the intensity of irradiation measured using Reinicke's salt as a chemical actinometer.[20]

Materials. Hydrated $RuCl_3 \cdot 3H_2O$ (Strem), formic acid (BDH; AnalaR, 90%), and 1,2-dimethoxyethane (FLUKA; puriss) were used as supplied. Trifluoromethanesulfonic acid (3 M) was distilled under vacuum before use. Trimethylamine *N*-oxide (TMNO) was obtained by vacuum sublimation of the hydrate (FLUKA; purum) at 120 °C. The ligands (pp) were acquired as commercial reagents when available or obtained from reported synthetic routes. Reagent solvents were used without further purification. Spectral grade acetonitrile (Burdick and Jackson), methanol (Burdick and Jackson), and ethanol (freshly distilled over Mg/I_2) were used for all spectroscopic and electrochemical measurements.

Syntheses. Chemical analyses were performed by either Chemical & Micro Analytical Services Pty. Ltd. (Melbourne, Australia) or Oneida Research Services, Inc. (Whitesboro, NY). The microanalytical data for the compounds listed are available in the supplementary material (supplementary Table S1).

The ligands 5,5′-Me_2bpy and ^{i}Pr$_2$bpy (see Chart 1) were synthesized by W. H. F. Sasse (Division of Applied Organic Chemistry, CSIRO),[21,22] $(Et_2N)_2$bpy[23] (see Chart 1) was kindly donated by P. Belser (Université de Fribourg Suisse), and the ligands Me_4bpy, $(EtCO_2)_2$bpy, $(NH_2)_2$bpy,[24] bbpa,[25] qpy,[26] and daf[27] (see Chart 1), were obtained by standard methods. Metathesis of Br^- to the PF_6^- salts were carried out by the addition of an aqueous solution of NH_4PF_6.

Chart 1

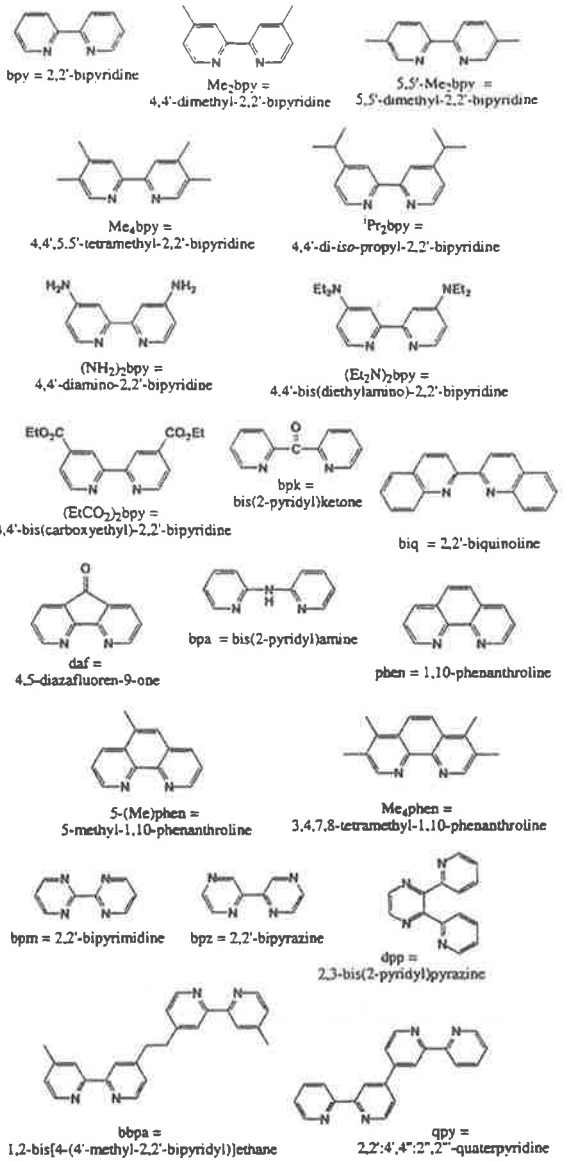

$[Ru(CO)_2Cl_2]_n$ (I). Paraformaldehyde (1 g) and $RuCl_3 \cdot 3H_2O$ (2.02 g, 9.74 mmol) were added to an Ar-sparged solution of 90% formic acid (50 mL), and the solution was then heated at reflux for 6 h. The solution changed in color from reddish-yellow to deep green over the course of 1 h. Further heating resulted in a change from green to yellow-orange in 4 h and a change to pale yellow in 6 h. The reaction vessel was cooled to room temperature and then stored at 4 °C overnight to allow complete conversion to the polymer. The solution was evaporated to dryness on a steam bath and the residue triturated with hexane and dried *in vacuo*: yield, 2.00 g (8.52 mmol, 90%). IR (Nujol): $\bar{\nu}_{CO}$ at 2074 and 2017 cm^{-1} {$\bar{\nu}_{CO}$ at 2138 cm^{-1} for the orange dimer $[Ru(CO)_3Cl_2]_2$, which may occur as an impurity}.

***trans(Cl)*-[Ru(pp)(CO)$_2$Cl$_2$] (II).** In a typical experiment, bpy (1.03 g; 6.6 mmol) was mixed with sufficient AR methanol to dissolve at

(17) Caspar, J. V.; Meyer, T. J. *J. Am. Chem. Soc.* **1989**, *111*, 7448.
(18) (a) Calvert, J. M.; Caspar, J. V.; Binstead, R. A.; Westmoreland, T. D.; Meyer, T. J. *J. Am. Chem. Soc.* **1982**, *104*, 3335. (b) Caspar, J. V.; Kober, E. M.; Sullivan, B. P.; Meyer, T. J. *J. Am. Chem. Soc.* **1982**, *104*, 630.
(19) Strouse, G. F.; Schoonover, J. R.; Duesing, R.; Boyde, S.; Jones, W. E.; Meyer, T. J. *Inorg. Chem.* **1995**, *34*, 473.
(20) Durham, B.; Caspar, J. V.; Nagle, J. K.; Meyer, T. J. *J. Am. Chem. Soc.* **1982**, *104*, 4803.
(21) Badger, G. M.; Sasse, W. H. F. *Adv. Heterocycl. Chem.* **1963**, *2*, 179.
(22) Rosevear, P. E.; Sasse, W. H. F. *J. Heterocycl. Chem.* **1971**, *8*, 483.
(23) Maerker, G.; Case, F. H. *J. Am. Chem. Soc.* **1958**, *80*, 2745.
(24) Worl, L. A.; Duesing, R.; Chen, P.; Della Ciana, L.; Meyer, T. J. *J. Chem. Soc., Dalton Trans.* **1991**, 849.
(25) Elliott, C. M.; Freitag, R. A.; Blaney, D. D. *J. Am. Chem. Soc.* **1985**, *107*, 4647.
(26) Downard, A. J.; Honey, G. E.; Phillips, L. F.; Steel, P. J. *Inorg. Chem.* **1991**, *30*, 2259.
(27) Eckhard, L. F.; Summers, L. A. *Aust. J. Chem.* **1973**, *26*, 2727.

least two-thirds of the ligand (10 mL). Following deaeration (N_2) for 30 min, $[Ru(CO)_2Cl_2]_n$ (1.0 g; 4.4 mmol) was added and the mixture heated at reflux under the inert atmosphere for 30 min with vigorous stirring (3 h for **IId**). Extra methanol was added after 15 min of the reaction to facilitate stirring of the suspension as the product precipitated. After cooling to room temperature, the pale yellow precipitate was collected and recrystallized from boiling methanol to yield fine very pale yellow feathery crystals (orange for **IId**). The absence of ligand in the complex was confirmed by thin layer chromatography (TLC) (silica gel absorbent; acetonitrile eluent).

$[Ru(bpy)(CO)_2Cl_2]$ (**IIa**); yield, 80%. IR (nujol): $\bar{\nu}_{CO}$ at 2057 and 1998 cm^{-1}. $[Ru(Me_2bpy)(CO)_2Cl_2]$ (**IIb**); yield, 50% {recrystallized from $CHCl_3$}. IR (nujol): $\bar{\nu}_{CO}$ at 2060 and 1989 cm^{-1}. $[Ru(Me_4bpy)(CO)_2Cl_2]$ (**IIc**); yield, 81%. IR (nujol): $\bar{\nu}_{CO}$ at 2063 and 1996 cm^{-1}. NMR (^1H, $CDCl_3$): δ 2.42 (s), 2.48 (s), 7.90 (s), 8.84. $[Ru\{(EtCO_2)_2bpy\}(CO)_2Cl_2]$ (**IId**); yield, 78%. IR (nujol): $\bar{\nu}_{CO}$ at 2065 and 1992 cm^{-1}. NMR (^1H, CD_2Cl_2): δ 1.46 (t), 4.51 (q), 8.23 (d), 8.91 (s), 9.31 (d). $[Ru(phen)(CO)_2Cl_2]$ (**IIe**); yield, 61%. IR (nujol): $\bar{\nu}_{CO}$ at 2060 and 2008 cm^{-1}.

***cis,cis*-[Ru(pp)(CO)$_2$(CF$_3$SO$_3$)$_2$] (III). Method A.** In a typical experiment, $[Ru(bpy)(CO)_2(Cl)_2]$ (0.290 g, 0.76 mmol) was added to an oven-dried Schlenck tube and the apparatus was purged with N_2 for 30 min. Freshly distilled trifluoromethanesulfonic acid (2.5 mL) was transferred into the apparatus (through a septum) resulting in a red-orange solution. The mixture was heated to 105−110 °C for 90 min with stirring under a continuous flow of dinitrogen bubbled through the solution. The reaction flask was cooled to 0 °C, and diethyl ether (10 mL) was injected through the septum with vigorous stirring, resulting in an off-white precipitate. The solid was collected under a constant flow of N_2 and washed with diethyl ether (5×), water (5×), and diethyl ether (5×). The white powdery product was collected, dried under vacuum, and stored under nitrogen. Recrystallization could be effected from dichloromethane/diethyl ether, although the product was generally used immediately without further purification.

$[Ru(bpy)(CO)_2(CF_3SO_3)_2]$ (**IIIa**); yield, 55%. IR (nujol): $\bar{\nu}_{CO}$ at 2082 and 2020 cm^{-1}; $\bar{\nu}_{SO}$ at 1340, 1178, 1007 cm^{-1}; $\bar{\nu}_{CF}$ at 1235 cm^{-1}. $[Ru(Me_2bpy)(CO)_2(CF_3SO_3)_2]$ (**IIIb**); yield, 39%. IR (nujol): $\bar{\nu}_{CO}$ at 2099 and 2027 cm^{-1}; $\bar{\nu}_{SO}$ at 1338, 1176, 1008 cm^{-1}; $\bar{\nu}_{CF}$ at 1238, 1205 cm^{-1}.

Method B. $[Ru(Me_2bpy)(CO)_2Cl_2]$ (0.75 g, 1.82 mmol) in 1,2-dichlorobenzene (200 mL) was deaerated with dry nitrogen for 30 min, resulting in a cloudy yellow solution. CF_3SO_3H (0.5 mL) was added dropwise by syringe (platinum needle), and the solution heated to 110 °C for 1.5 h. The mixture was cooled to 0 °C and the product precipitated by the addition of diethyl ether (200 mL). The mixture was allowed to stir for 1 h, and the complex $[Ru(Me_2bpy)(CO)_2(CF_3SO_3)_2]$ (**IIIb**) collected by vacuum filtration under nitrogen and washed with diethyl ether (2 × 5 mL), cold distilled water (2 × 5 mL), and diethyl ether (2 × 5 mL); yield, 0.99 g, 85%.

$[Ru(Me_4bpy)(CO)_2(CF_3SO_3)_2]$ (**IIIc**); yield, 60%. NMR (^1H, CD_2Cl_2): δ 7.91 (s), 7.95 (s), 8.40 (s), 8.72 (s), 2.41 (s), 2.45 (s), 2.53 (s), 2.57 (s).

Method C. $[Ru\{(EtCO_2)_2bpy\}(CO)_2(CF_3SO_3)_2]$ (IIId). Freshly distilled CH_2Cl_2 (750 mL) and $[Ru\{(EtCO_2)_2bpy\}(CO)_2(Cl)_2]$ (0.320 g, 0.61 mmol) were added to an N_2-charged reaction vessel, and the mixture was allowed to stir at room temperature for 30 min, resulting in a yellow-orange solution. In the dark, $Ag(CF_3SO_3)$ (0.32 g, 1.21 mmol) was added and the mixture refluxed for 3 h. The dark colored precipitate was filtered under N_2 through Celite (to remove AgCl), and the yellow filtrate, concentrated on a rotary evaporator. The concentrated solution (2−5 mL) was filtered dropwise into anhydrous diethyl ether (100 mL), resulting in a fine white precipitate which was collected on a medium porosity frit, washed with ether (5×), and dried under vacuum; yield, 0.10 g (1.58 mmol, 26%).

[Ru(pp)(pp′)(CO)$_2$](PF$_6$)$_2$ (IV). In a typical experiment, $[Ru(bpy)(CO)_2(CF_3SO_3)_2]$ (0.15 g, 0.31 mmol) and Me_2bpy (0.113 g, 0.61 mmol) were dissolved in 95% ethanol (25 mL) under N_2. The solution was brought to reflux, resulting in a color change from colorless to yellow within 30 min. It was then allowed to continue to reflux for an additional 60 min before it was evaporated to dryness by rotary evaporation. The gray residue was dissolved in boiling water and filtered to remove unreacted ligand (Me_2bpy) and a saturated aqueous solution of NH_4PF_6 (5 mL) added, resulting in an off-white precipitate which was collected and washed with cold water followed by copious amounts of ether. Recrystallization was achieved from hot ethanol/acetone (acetone aids in solubilization: the solution was warmed until it became cloudy as the acetone evaporated, and it was then cooled and placed in the freezer overnight).

Performing the synthesis by the alternative sequence of ligand addition for **IVa**, **c**, and **d** gave identical results.

$[Ru(bpy)(Me_2bpy)(CO)_2](PF_6)_2$ (**IVa**): yield, 55%. IR (CH_2Cl_2 solution): $\bar{\nu}_{CO}$ at 2098 and 2049 cm^{-1}. $[Ru(bpy)(Me_4bpy)(CO)_2](PF_6)_2$ (**IVb**); yield, 80%. IR (CH_3Cl solution): $\bar{\nu}_{CO}$ at 2096 and 2041 cm^{-1}. $[Ru(bpy)\{(EtCO_2)_2bpy\}(CO)_2](PF_6)_2$ (**IVc**); yield, 40%. IR (CH_2Cl_2 solution): $\bar{\nu}_{CO}$ at 2102 and 2045 cm^{-1}. $[Ru(Me_2bpy)\{(EtCO_2)_2bpy\}(CO)_2](PF_6)_2$ (**IVd**); yield, 45%. IR (CH_2Cl_2 solution): $\bar{\nu}_{CO}$ at 2099 and 2042 cm^{-1}. $[Ru(bpy)\{(NH_2)_2bpy\}(CO)_2](PF_6)_2$ (**IVe**); yield, 35%. IR (CH_2Cl_2 solution): $\bar{\nu}_{CO}$ at 2088 and 2038 cm^{-1}. $[Ru(Me_2bpy)(Me_4bpy)(CO)_2](PF_6)_2$ (**IVf**); yield, 68%. IR (Nujol mull): $\bar{\nu}_{CO}$ at 2092 and 2036 cm^{-1}. NMR (^1H, acetone-d_6): δ 2.04 (s, 3H), 2.44 (s, 3H), 2.52 (s, 3H), 2.54 (s, 3H), 2.64 (s, 3H), 2.74 (s, 3H), 7.38 (s, 1H), 7.47 (d, 1H), 7.61 (d, 1H), 7.94 (d, 1H), 8.57 (s, 1H), 8.66 (s, 1H), 8.68 (s, 1H), 8.79 (s, 1H), 9.15 (s, 1H), 9.26 (d, 1H, J = 5 Hz). $[Ru(Me_4bpy)\{(EtCO_2)_2bpy\}(CO)_2](PF_6)_2$ (**IVg**); yield, 33%. IR (Nujol mull): $\bar{\nu}_{CO}$ at 2089 and 2040 cm^{-1}. NMR (^1H, acetone-d_6): δ 1.34 (t, J = 7 Hz), 1.46 (t, J = 7 Hz), 2.06 (s), 2.43 (s), 2.56 (s), 2.66 (s), 4.42 (q, J = 7 Hz), 4.56 (q, J = 7 Hz), 7.49 (s), 8.02 (d, J = 5.8 Hz), 8.08 (dd, J = 5.8 and 1.5 Hz), 8.50 (dd, J = 5.8 and 1.5 Hz), 8.59 (s), 8.70 (s), 9.17 (s), 9.29 (s), 9.42 (s), 9.72 (d, J = 5.8 Hz). $[Ru(phen)(bpy)(CO)_2](PF_6)_2$ (**IVh**); yield, 53%. IR (Nujol mull): $\bar{\nu}_{CO}$ at 2090 and 2037 cm^{-1}). $[Ru(phen)(Me_4bpy)(CO)_2](PF_6)_2$ (**IVi**); yield, 71%. IR (KBR disk): $\bar{\nu}_{CO}$ at 2093 and 2048 cm^{-1}. $[Ru\{(EtCO_2)_2bpy\}(bpz)(CO)_2](PF_6)_2$ (**IVj**); yield, 45%. IR (Nujol mull): $\bar{\nu}_{CO}$ at 2093 and 2038 cm^{-1}.

[Ru(pp)(pp′)(pp″)](PF$_6$)$_2$ (V). Typically, 1 mol equiv $[Ru(pp)(pp')(CO)_2]^{2+}$, 3 mol equiv of pp″, and dry 2-methoxyethanol (2.5 mL/10^{-5} mole of complex) were combined in a round-bottom flask fitted with a condenser and Teflon needles to purge the solution with N_2. A 3-fold excess of freshly sublimed trimethylamine *N*-oxide was added to the yellow solution, which was heated at reflux for 3 h. The reaction took place with a color change from almost colorless to deep red with the concurrent production of trimethylamine—trapping of trimethylamine by bubbling through an HCl bubbler is strongly suggested. The reaction mixture was evaporated to dryness and redissolved in water (a minimum of acetone may be added to aid in dissolution of the product), and the product was purified by ion-exchange chromatography (SP-Sephadex C-25; eluent 0.2 M NaCl). Precipitation of the product as the PF_6^- salt was achieved by addition of a saturated aqueous solution of NH_4PF_6 to the eluant containing the major band. The solid was collected on a medium porosity frit and then washed several times with cold water and copious quantities of diethyl ether. Reprecipitation from CH_2Cl_2/ether yielded a red powder. Yields were in the range of 50−85%.

$[Ru(bpy)(Me_2bpy)(bpm)](PF_6)_2 \cdot 3H_2O$ (**Va**). NMR (^1H, acetone-d_6): δ 2.55 (s), 2.56 (s), 7.40 (d), 7.57 (dd), 7.70 (t), 7.71 (t), 7.82 (d), 8.05 (d), 8.07 (d), 8.21 (dd), 8.24 (d), 8.44 (dd), 8.45 (dd), 8.69 (s), 8.80 (d), 9.17 (dd), 9.18 (dd). $[Ru(bpy)(Me_2bpy)(5\text{-}(Me)phen)](PF_6)_2$ (**Vb**). NMR (^1H, acetone-d_6): δ 2.49 (s), 2.60 (s), 2.90 (s), 7.21 (m), 7.35 (m), 7.44 (m), 7.63 (d), 7.85 (m), 7.93 (m), 8.16 (m), 8.31 (t), 8.40 (t), 8.65 (m), 8.82 (m). $[Ru(bpy)(Me_2bpy)(dpp)](PF_6)_2 \cdot 0.25HPF_6$ (**Vc**), $[Ru(bpy)\{(EtCO_2)_2bpy\}(dpp)](PF_6)_2 \cdot 0.25HPF_6$ (**Vd**),[28] and $[Ru(bpy)(Me_2bpy)\{(EtCO_2)_2bpy\}](PF_6)_2 \cdot H_2O$ (**Ve**). NMR (^1H, acetone-d_6): δ 1.37 (t, J = 7 Hz), 1.38 (t, J = 7 Hz), 2.55 (s), 2.57 (s), 4.44 (q, J = 7 Hz), 4.45 (q, J = 7 Hz), 7.36 (d, J = 5 Hz), 7.42 (d, J = 5 H), 7.52 (t, J = 6 Hz), 7.60 (t, J = 6 Hz), 7.83 (m), 7.97 (m), 8.04 (m), 8.35 (m), 8.60 (s), 8.81 (m), 9.27 (s). $[Ru(Me_2bpy)(Me_4bpy)(4,7\text{-}Me_2phen)](PF_6)_2$ (**Vf**) and $[Ru(Me_2bpy)(Me_4bpy)(bpm)](PF_6)_2 \cdot 2H_2O$ (**Vg**). NMR (^1H, acetone-d_6): δ 2.10 (s), 2.11 (s), 2.47 (s), 2.55 (s), 7.38 (d), 7.63 (s), 7.67 (t), 7.80 (d), 7.91 (s), 8.01 (d), 8.39 (dd), 8.40 (dd), 8.56 (s), 8.65 (s), 9.14 (d). $[Ru(Me_2bpy)\{(EtCO_2)_2bpy\}(dpp)](PF_6)_2 \cdot H_2O$ (**Vh**),[28]

(28) Prepared as indicated above, but using 1,2-dimethoxyethane as the solvent.

Table 1. Crystallographic Data for $[Ru(Me_2bpy)(phen)(bpa)](PF_6)_2 \cdot C_6H_{14}$ (**Vv**)

formula	$C_{40}H_{43}F_{12}N_7P_2Ru$
MW	1062.8.
a (Å)	14.57(3).
b (Å)	13.50(3)
c (Å)	12.73(3)
α (deg)	68.6(2)
β (deg)	63.5(1)
γ (deg)	79.8(2)
V (Å^3)	2082
Z	2
crystal system/space group	triclinic, $P\bar{1}$ (C_i^1, No. 2)
T (K)	295
radiation; λ (Å)	monochromatic Mo Kα; 0.710 69
d_{calc} (g cm^{-3})	1.70
μ (Mo Kα) (cm^{-1})	4.7
min/max transmn coeff	0.86−0.91
crystal dimens	0.40 × 0.28 × 0.70 mm
no. of reflecns	5408
no. of reflecns ($I > 3\sigma(I)$)	2892
absorpn coeff (cm^{-1})	4.7
$R(F_o)^a$ (%)	6.4
$R_w(F_o)^b$ (%)	6.5

$^a R = \sum(|\Delta|F||/\sum|F_o|$. $^b R_w = (\sum\omega\Delta^2/\sum\omega F_o^2)^{1/2}$.

$[Ru(Me_2bpy)\{(EtCO_2)_2bpy\}\{(Et_2N)_2bpy\}](PF_6)_2 \cdot 2H_2O$ (**Vi**),[28] $[Ru(Me_2bpy)(Me_4bpy)(dpp)](PF_6)_2 \cdot H_2O$ (**Vj**), $[Ru(Me_2bpy)(Me_4bpy)\{(Et_2N)_2bpy\}](PF_6)_2 \cdot 2H_2O$ (**Vk**), $[Ru(Me_2bpy)(Me_4bpy)(bbpa)](PF_6)_2 \cdot 0.5HPF_6$ (**Vl**), $[Ru(Me_2bpy)\{(EtCO_2)_2bpy\}(bbpa)](PF_6)_2 \cdot 0.5HPF_6$ (**Vm**),[28] $[Ru(Me_2bpy)\{(EtCO_2)_2bpy\}(bpm)](PF_6)_2 \cdot 0.5H_2O$ (**Vn**),[27] $[Ru(Me_2bpy)(Me_4bpy)(qpy)](PF_6)_2 \cdot HPF_6$ (**Vo**),$[Ru(phen)(Me_4bpy)(bpm)](PF_6)_2 \cdot 2H_2O$ (**Vp**), $[Ru(bpy)(phen)(biq)](PF_6)_2$ (**Vq**), $[Ru(bpy)(phen)(bpa)](PF_6)_2$ (**Vr**), $[Ru(bpy)(phen)(daf)](PF_6)_2$ (**Vs**), $[Ru(bpy)(phen)(bpk)](PF_6)_2$ (**Vt**), $[Ru(Me_2bpy)(phen)(biq)](PF_6)_2$ (**Vu**), $[Ru(Me_2bpy)(phen)(bpa)](PF_6)_2$ (**Vv**), $[Ru(Me_2bpy)(phen)(5,5'\text{-}Me_2bpy)](PF_6)_2$ (**Vw**), $[Ru(Me_2bpy)(bpy)(5,5'\text{-}Me_2bpy)](PF_6)_2$ (**Vx**), $[Ru(Me_2bpy)(bpy)(^iPr_2bpy)](PF_6)_2$ (**Vy**), $[Ru(Me_2bpy)(phen)(biq)](PF_6)_2$ (**Vz**), $[Ru(bpy)\{(NH_2)_2bpy\}(bpz)](PF_6)_2$ (**Vaa**), and $[Ru(bpy)\{(EtCO_2)_2bpy\}(bpz)](PF_6)_2$ (**Vbb**).

X-ray Structure Analysis. Red-brown crystals of $[Ru(Me_2bpy)(phen)(bpa)](PF_6)_2 \cdot C_6H_{14}$ were obtained by liquid diffusion of hexane into a solution of the complex in acetonitrile. The specimen available for structure determination was oversized and aggregated: a portion was mounted in a capillary to avoid loss of hexane. Tolerable alignment was achieved on the major component of the aggregate and a unique data set measured to $2\theta_{max} = 45°$ using a Syntex $P2_1$ four-circle diffractometer in a conventional $2\theta/\theta$ mode. A set of 5408 independent reflections was obtained, 2892 with $I > 3\sigma(I)$ being considered "observed" and used in the full matrix least squares refinement. Anisotropic thermal parameter refinement was achieved successfully for all atoms except C(1,5) of the hexane solvent; C(1) was modeled as equally disordered over two sites, while thermal motion of C(5) was exceedingly high, as in fact is true of the solvent generally. (x, y, z, U_{iso})$_H$ were included, constrained at estimated values. Residuals on $|F|$ at convergence were R, $R' = 0.064$, 0.065, statistical reflection weights derived from $\sigma^2(I) = \sigma^2(I_{diff}) + 0.0001\sigma^4(I_{diff})$ being used. Neutral atom complex scattering factors[29] were employed; computation used the XTAL 2.2 program system[30] implemented by S. R. Hall. Material deposited comprises non-hydrogen atom thermal parameters, hydrogen atom parameters, ligand non-hydrogen geometries, anion and solvent non-hydrogen geometries, and structure factor amplitudes (supplementary material Tables S2−S6, respectively).

The crystal data are given in Table 1.

Results and Discussion

Synthesis. The synthetic methodology we have used for the heteroleptic tris(bidentate)ruthenium(II) complexes is based on the sequential addition of the polypyridyl ligands to the oligomeric precursor $[Ru(CO)_2Cl_2]_n$, as summarized in Scheme 1.

Scheme 1. Synthetic Strategy for Tris(heteroleptic) Complexes (pp = Bidentate Polypyridyl Ligands)

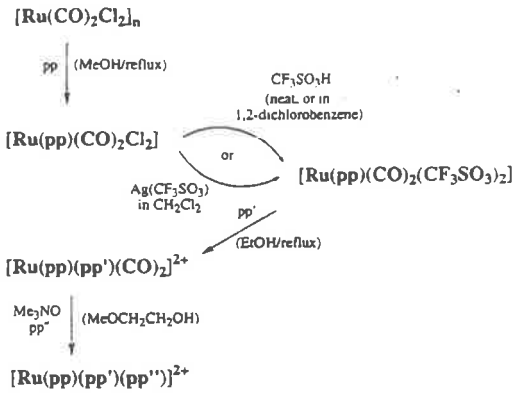

Preliminary details of the scheme were reported earlier.[10−16]

The synthetic method described for $[Ru(CO)_2Cl_2]_n$ (**I**) is formally considered a $RuCl_3$-assisted decarbonylation of formic acid, and the reaction is promoted by formaldehyde as an initial reductant of Ru(III) to Ru(II).[31,32] Two products are formed—**I** and a chloro-bridged dimer, $[Ru(CO)_3Cl_2]_2$, generated as a side product—and variable relative yields are obtained depending on the purity of the starting materials ($RuCl_3 \cdot 3H_2O$ and formic acid). The presence of formaldehyde (via decomposition of paraformaldehyde at 192 °C and sublimation into the formic acid at 0 °C or direct addition of the paraformaldehyde to the reaction mixture) favors the formation of the polymer, **I**. The dimer arises from HCl formation during the course of the reaction, and certainly the addition of HCl to the reaction mixture substantially increases the proportion of the dimer byproduct.[31,32] Conversion of the dimer to the polymer by heating or treating with formaldehyde-saturated formic acid has been unsuccessful. Over the course of the synthesis, a characteristic color change from red to green to orange to pale yellow is observed. The reaction may be stopped following the formation of the orange intermediate, and conversion to the desired yellow polymeric material is achieved by maintaining the reaction mixture at 0 °C over several hours. Successive recrystallizations from acetone/diethyl ether yield pure polymer. Contamination by $[Ru(CO)_3Cl_2]_2$ in **I** may be identified by IR studies as the dimer exhibits a characteristic $\bar{\nu}_{CO}$ stretch at 2138 cm^{-1} in the infrared spectrum.[31,32] Drying the polymer at elevated temperatures causes decomposition of the material.

The polymer reacts readily with bidentate ligands (pp) in refluxing methanol solution to yield $[Ru(pp)(CO)_2Cl_2]$ (**II**). These complexes were recrystallized from hot methanol, producing feathery, yellow crystals. Purity (primarily absence of free ligand) was checked by TLC on silica gel, using acetonitrile as a solvent. The CO stretching frequencies ($\bar{\nu}_{CO}$) in this series are observed at *ca.* 2060(±5) and 1998(±10) cm^{-1} and do not appear to show predictable dependence on the nature of the pp ligand. In general, the yields for the complexes of substituted bipyridyl ligands are lower (~50%) than for 2,2′-bipyridine itself (~80%), presumably due to solubility characteristics of the substituted-bipyridine species in methanol. Longer reaction times improved the reaction yields for prepara-

(29) Ibers, J. A.; Hamilton, W. C. *International Tables of X-ray Crystallography*; Kynoch Press: Birmingham, 1974; Vol. 4.
(30) Hall, S. R.; Stewart, J. M. *XTAL Users' Manual Version 2.2*; Universities of Western Australia and Maryland: Nedlands, Australia, and College Park, MD, 1987.
(31) Bruce, M. I. In *Comprehensive Organometallic Chemistry*; Wilkinson, G., Stone, F. G. A., Abel, E. W., Eds.; Vol. 4, p 661.
(32) Cleare, M. J.; Griffith, W. P. *J. Chem. Soc. A* **1969**, 372.

tion of $[Ru(pp)(CO)_2Cl_2]$ in which the ligand (pp) contains electron-withdrawing substituents.

In ^1H NMR studies in this work, substantial use was made of the ligand 4,4′,5,5′-tetramethyl-2,2′-bipyridine (Me_4bpy) as the particular pattern of substitution results in each ring showing only two singlet aliphatic resonances (the methyl groups) and two singlet aromatic resonances (the protons in the ring 3- and 6-positions), simplifying the spectrum. The ligand $(Et_2CO)_2bpy$ was also chosen as it is an example of an analogous derivative, but with electron-withdrawing substitutuents (rather than electron-donating for the methyl groups), and it gives rise to distinctive triplet and quartet resonances associated with the ethyl groups.

The NMR data are given for the two representative examples $[Ru(Me_4bpy)(CO)_2Cl_2]$ and $[Ru\{(EtCO_2)_2bpy\}(CO)_2Cl_2]$ (data are available for other complexes in supplementary material Table S7): they indicate the equivalence of the two sides of a symmetrical pp ligand in $[Ru(pp)(CO)_2Cl_2]$, so that the complex may only possess either the *trans*-(Cl),*cis*-(CO) or *trans*-(CO),*cis*-(Cl) geometries. From group theory calculations, the existence of two $\bar{\nu}_{CO}$ absorptions in the IR spectrum is consistent with either geometry. However, the carbonyl ligands would be expected to adopt a *cis*-relationship due to competition for π-back-bonding from the metal d-orbitals. On this basis, the stereochemistry of $[Ru(pp)(CO)_2Cl_2]$ would therefore be *trans*-(Cl),*cis*-(CO), in agreement with previous studies.[14,15,33] A recent structural determination on a sample of $[Ru(bpy)(CO)_2Cl_2]$ having an ^1H NMR spectrum identical to that of the sample obtained by our synthetic procedure confirms this assignment.[34] No evidence was obtained during the present chromatographic or spectroscopic studies for isomeric forms of these species.

The reaction of $[Ru(pp)(CO)_2Cl_2]$ with a second bidentate ligand (pp′) was accomplished by initial conversion of $[Ru(pp)(CO)_2Cl_2]$ to the corresponding bis(trifluoromethansulfonato) {"bis(triflato)"} species, $[Ru(pp)(CO)_2(CF_3SO_3)_2]$, to utilize the enhanced lability of the $CF_3SO_3^-$ ligand.[35] This conversion may be achieved by any one of three methods. In two of these, the dichloro species is heated in the presence of trifluoromethansulfonic acid, with the HCl formed being removed to drive the reaction: i.e., heating **II** in neat trifluoromethansulfonic acid[14] or in 1,2-dichlorobenzene solution in the presence of the acid (in both cases at 110 °C).[36] The reaction yields were ~65 and ~85%, respectively. For some complexes such as $[Ru\{(EtCO_2)_2bpy\}(CO)_2Cl_2]$, such reaction conditions result in decomposition of the ligand—in this case, acid hydrolysis of the ester group. This was circumvented by reaction of $[Ru\{(EtCO_2)_2bpy\}(CO)_2Cl_2]$ with $Ag(SO_3CF_3)$ at reflux in CH_2Cl_2, producing the desired bis(trifluoromethanesulfato) species, albeit in disappointingly low yields (~26%).

Decomposition of the triflato species was observed if temperatures above 110 °C were sustained in the reaction, presumably due to degradation of the complex and protonation of the polypyridyl ligands. The washing of the product with water is an important aspect in ensuring the removal of the protonated ligand impurity from the desired dicarbonyl species. The triflato species are stable for long periods of time if the residual trifluoromethanesulfonic acid is removed by washing thoroughly with water and drying *in vacuo*.

For $[Ru(pp)(CO)_2(CF_3SO_3)_2]$ species (**III**), the $\bar{\nu}_{CO}$ stretching frequencies are observed at 2082 and 2020 cm^{-1} for pp = bpy and 2099 and 2027 cm^{-1} for pp = Me_2bpy. Characteristic infrared bands assignable in the infrared spectrum for the bound trifluoromethanesulfonate can be identified for the $\bar{\nu}_{SO}$ stretches at *ca.* 1340, 1180, and 1010 cm^{-1} and the $\bar{\nu}_{CF}$ stretches at ~1240 and 1200 cm^{-1}.[14,15]

From the available IR data, we infer that the carbonyl groups remain in a *cis* disposition. Earlier reports have claimed that, in the $[Ru(pp)(CO)_2(CF_3SO_3)_2]$ complexes prepared by reaction of the dichloro species with trifluoromethanesulfonic acid, the trifluoromethanesulfonato ligands also had a *cis* disposition—i.e., the stereochemistry was *cis*-(CO),*cis*-(CF_3SO_3)—based on the inequivalence of the two halves of a symmetrical pp ligands as seen in the ^1H NMR spectrum.[14] We would concur with that analysis, on the basis of the ^1H NMR spectrum of $[Ru(Me_4bpy)(CO)_2(CF_3SO_3)_2]$, in which the ligand Me_4bpy exhibits four aromatic and four aliphatic singlet resonances (δ 7.91, 7.95, 8.40, 8.72, 2.41, 2.45, 2.53, 2.57), consistent with *cis*-(CO),*cis*-(CF_3SO_3), i.e., point group symmetry C_2. The *cis*-(CO),*trans*-(CF_3SO_3) isomer has been identified in related studies.[15]

Reaction of the bis(trifluoromethanesulfonato) species with pp′ gave the cation $[Ru(pp)(pp')(CO)_2]^{2+}$, which was precipitated as the PF_6^- salt, in *ca.* 60% yield. Purity was checked by TLC on alumina plates using H_2O (10% in NH_4Cl)/DMF/MeOH (2:1:1) or H_2O (10% in NaCl)/acetone (1:1) as the eluents. Small-scale chromatographic separations were also achieved by PLC using the same adsorbent and solvents.

The IR spectra for $[Ru(pp)(pp')(CO)_2]^{2+}$ are consistent with the retention of the *cis*-CO configuration. The ^1H NMR characteristics of the complexes $[Ru(Me_4bpy)\{(EtCO_2)_2bpy\}(CO)_2]^{2+}$ and $[Ru(Me_2bpy)(Me_4bpy)(CO)_2]^{2+}$ are provided in the Experimental Section (and data for the other complexes of this type are available in supplementary material Table S8). The ^1H NMR data indicate the inequivalence in the complex of the two halves of each of the "symmetrical" bidentate ligands, pp and pp′. For example, in $[Ru(Me_4bpy)\{(EtCO_2)_2bpy\}(CO)_2]^{2+}$, the inequivalent CH_3 protons of Me_4bpy are easily identified as four singlets occurring at δ 2.06, 2.43, 2.56, and 2.66 ppm. Magnetic inequivalency at H_3 and $H_{3'}$, and at H_6 and $H_{6'}$, in the Me_4bpy ligand is also clearly illustrated by well-resolved singlets at δ 8.59, 9.17, 9.29, and 9.42 ppm. The same rationalization can be made for the resonances of the $(Et_2CO)_2bpy$ ligand and for the resonances of the two polypyridyl ligands in $[Ru(Me_2bpy)(Me_4bpy)(CO)_2]^{2+}$. Accordingly, the NMR and IR data are consistent with a *cis* disposition of the two CO ligands.

No evidence was obtained in any of the complexes investigated for formation of *trans*-CO species.

The tris(bidentate) complexes of ruthenium(II), $[Ru(pp)(pp')(pp'')]^{2+}$, are generated by decarbonylation of $[Ru(pp)(pp')(CO)_2]^{2+}$ using trimethylamine *N*-oxide (TMNO), in the presence of the third bidentate ligand pp″.[11,37,38] This reaction was normally performed in 2-methoxyethanol as solvent, although the reaction can also be undertaken in acetone.

In cases involving the ligand $(EtCO_2)_2bpy$ it was observed that the decarbonylation reaction took place with transesterification (presumably base catalyzed by trimethylamine formed during the decarbonylation process), resulting in replacement of R = −Et by $-CH_2CH_2OMe$ as determined by NMR studies of the product. In these cases, the solvent 1,2-dimethoxyethane was successfully used as an alternative to 2-methoxyethanol.

(33) Kelly, J. M.; O'Connell, C. M.; Vos, J. G. *Inorg. Chim. Acta* **1982**, *64*, L75.
(34) Haukka, M.; Kivekäs, J.; Ahlgrén, M.; Pakkanen, T. A. *Organometallics* **1995**, *14*, 825.
(35) Lawrance, G. A. *Chem. Rev.* **1986**, *86*, 17.
(36) Sullivan, B. P.; Caspar, J. V.; Johnson, S. R.; Meyer, T. J. *Organometallics* **1984**, *3*, 1241.
(37) Black, D. S.; Deacon, G. B.; Thomas, N. C. *Inorg. Chim. Acta* **1981**, *54*, L143.
(38) Luh, T.-Y. *Coord. Chem. Rev.* **1984**, *60*, 255.

In general, where such a complication was not involved, 2-methoxyethanol was found to be a superior solvent for the reaction.

The rate of the decarbonylation reaction of $[Ru(pp)(pp')(CO)_2]^{2+}$ was observed to depend significantly on the nature of the two ligands pp and pp': *viz.*, in cases where these ligands had electron-withdrawing substituents, the rate of the reaction was more rapid. TMNO-assisted decarbonylations are generally thought to occur via oxygen atom transfer to the carbonyl carbon atom,[39] and the present observations support that assertion. The substantial partial negative charge on the oxygen atom of TMNO suggests the mechanism may involve nucleophilic attack on the carbon atom,[40,41] and its susceptibility to such attack (i.e. electrophilicity) would be enhanced by the lowering of the electron density of the metal center—such would be the case where electron-withdrawing substituents were present on the "innocent" pp-type ligands. A corollary of this rationale is that such substituents should reduce the π-back-bonding from the metal to the carbonyl ligands, thereby increasing the bond order of the C≡O bond and weakening the Ru—C bond, and indeed the propensity of carbonyl groups to such decarbonylation reactions has previously been shown to be greater when the $\tilde{\nu}_{CO}$ stretching frequencies are high.[42,43]

The complexes were examined and characterized by a number of physical methods. The following discussion briefly describes the outcomes of those studies, in each area using a limited number of examples which best illustrate the point at hand, in preference to an exhaustive coverage. Further details may be obtained from the authors on written request.

Microanalyses. Satisfactory elemental analyses (±0.4% for C, H, and N) were obtained for all the tris(heteroleptic) complexes reported. For complexes containing additional nonligating N atoms in the heterocyclic rings (e.g., in the potential bridging ligands bpm, dpp, bbpa, and qpy) it was found that there was often either water (**Vh**, **Vi**, **Vj**, **Vk**, **Vn**, **Vp**) or HPF_6 (**Vd**, **Vl**, **Vm**, **Vo**) contained in the lattice. In separate measurements made in our laboratories of the pK_a values of the species of this type, it is clear that only one protonation occurs and that the proton interacts (e.g., by hydrogen bonding) to both N atoms.[44]

Microanalytical data for the tris(heteroleptic) complexes, and the precursor species, are available in Supporting Information Table S1.

Fast Atom Bombardment Mass Spectrometry. Fast atom bombardment (FAB) has been proposed as a probe for the differentiation of mixed-ligand complexes with those that are mixtures of complexes, since no scrambling is detected in the mass spectra of species such as $[Ru(Me_2bpy)_2(phen)](PF_6)_2$.[45] Such techniques have been used previously in the identification and characterization of tris(bidentate) polypyridyl complexes of ruthenium(II).[45-47] In the present case, three tris(heteroleptic) species were studied in particular—*viz.*, $[Ru(bpy)(Me_2bpy)(5\text{-}Me)phen)](PF_6)_2$, $[Ru(bpy)(Me_2bpy)(bpm)](PF_6)_2$, and $[Ru(bpy)(Me_2bpy)\{(EtCO_2)_2bpy\}](PF_6)_2$—using a 3-nitrobenzyl alcohol matrix. In all cases, the ion pair $\{[Ru(pp)(pp')(pp'')](PF_6)\}^+$ was observed, together with the reduced species $[Ru(pp)(pp')(pp'')]^+$, and peaks due to the sequential loss of the remaining polypyridyl ligands. No peaks of the type "$[Ru(pp)_2]^{+}$" were observed, attesting to the tris(heteroleptic) assignment. Only in the case of $[Ru(bpy)(Me_2bpy)(bpm)](PF_6)_2$ is another significant peak observed, at $m/z = 460$, corresponding to the ion-pair $\{[Ru(bpy)(Me_2bpy)]\cdot F\}^+$: the presence of fluoride ion in such ion pairs, arising from reductive elimination of HF, has been observed previously in FAB spectra of hexafluorophosphate salts.[47]

NMR Studies. The NMR spectral behavior of homoleptic (point group symmetry D_3) and bis(heteroleptic) complexes (C_2) of symmetrical bidentate ligands have been discussed previously.[48-52] In the case of tris(heteroleptic) ligands, there is a further complication that the symmetry is lowered to C_1 so that the two halves of each ligand are necessarily in magnetically inequivalent environments.[52] As an example, for the complex $[Ru(Me_2bpy)(Me_4bpy)(bpm)]^{2+}$, the assignments of individual resonances in the ligands were made using the COSYRCT (relayed coherence transfer) technique, which shows the chain of coupling around each heterocyclic ring. The chemical shifts associated with the resonances at the various protons are indicated below (acetone-d_6 solution):

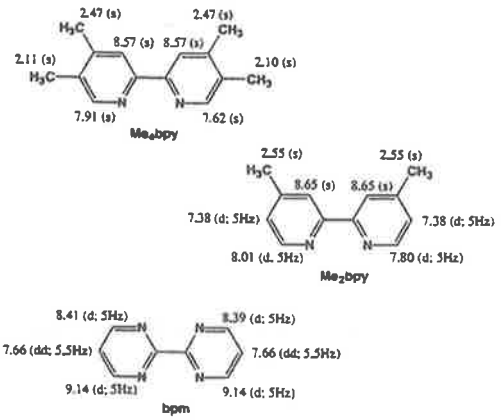

In the spectrum, the methyl groups in the 5- and 5′-positions in Me_4bpy are seen to be in different environments, and the protons in the 6- and 6′-positions in both Me_4bpy and Me_2bpy are differentiated in that one proton in each case lies over a ring of the bpm ligand and the other over a ring of the Me_4bpy ligand. In bpm, the 3- and 3′-protons are differentiated for similar reasons.

In cases where the three ligands in a tris(heteroleptic) species are different derivatives of the same bidentate ligand, the aromatic regions are relatively simplified as there is some overlap of resonances. For example, the spectrum of $[Ru(phen)(Me_2bpy)(5,5'\text{-}Me_2bpy)]^{2+}$ contains four methyl resonances (two singlets separated by 0.11 ppm assigned to the Me_2bpy and two singlets separated by 0.23 ppm assigned to 5,5′-Me_2bpy).

(39) Blumer, D. J.; Barnett, K. W.; Brown, T. L. *J. Organomet. Chem.* **1979**, *173*, 71.
(40) Chan, H. S.; Hor, T. S. A.; Leong, Y. P. *Thermochim. Acta* **1989**, *145*, 179.
(41) Gao, Y.; Shen, J.; Peng, L.; Shi, Q.; Basolo, F. *J. Indian Chem. Soc.* **1992**, *69*, 464.
(42) Koelle, U. *J. Organomet. Chem.* **1977**, *133*, 53.
(43) Blumer, D. J.; Barnett, K. W.; Brown, T. L. *J. Organomet. Chem.* **1979**, *173*, 71.
(44) Anderson, P. A.; Keene, F. R. Unpublished results.
(45) Miller, J. M.; Balasanmugam, K.; Nye, J.; Deacon, G. B.; Thomas, N. C. *Inorg. Chem.* **1987**, *26*, 560.
(46) Liang, X.; Suwanrumpha, S.; Freas, R. B. *Inorg. Chem.* **1991**, *30*, 652.
(47) Cerny, R. L.; Sullivan, B. P.; Bursey, M. M.; Meyer, T. J. *Inorg. Chem.* **1985**, *24*, 397.
(48) Orellana, G.; Ibarra, C. A.; Santoro, J. *Inorg. Chem.* **1988**, *27*, 1025.
(49) Hage, R.; Haasnoot, J. G.; Nieuwenhuis, H. A.; Reedijk, J.; Wang, R.; Vos, J. G. *J. Chem. Soc., Dalton Trans.* **1991**, 3271.
(50) Heijden, M.; Vanvliet, P. M.; Haasnoot, J. G.; Reedijk, J. *J. Chem. Soc., Dalton Trans.* **1993**, 3675.
(51) Predieri, G.; Vignali, C.; Denti, G.; Serroni, S. *Inorg. Chim. Acta* **1993**, *205*, 145.
(52) Rutherford, T. J.; Reitsma, D. A.; Keene, F. R. *J. Chem. Soc., Dalton Trans.* **1994**, 3659.

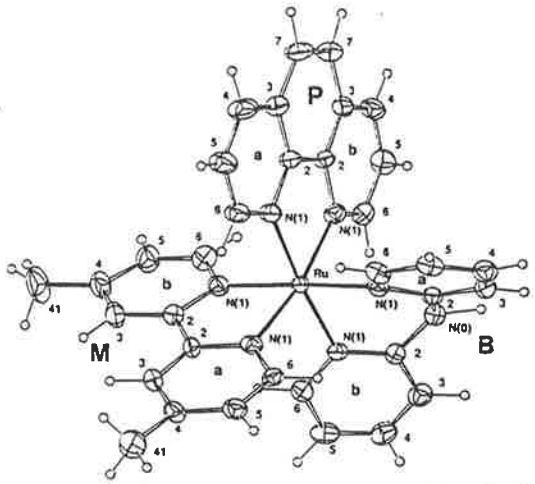

Figure 1. Projection of cation $[Ru(Me_2bpy)(phen)(bpa)]^{2+}$ {[Ru mpd]$^{2+}$} showing non-hydrogen atoms with 20% probability thermal elloipsoids and labeling. Hydrogen atoms have an arbitrary radius of 0.1 Å.

However, the spectrum of $[Ru(bpy)(Me_2bpy)(5,5'\text{-}Me_2bpy)]^{2+}$ contains only two methyl singlets. Presumably, since all the ligands contain similar 2,2′-bipyridine ring systems, the 5- and 5′-methyl groups in 5,5′-Me_2bpy experience similar magnetic environments, as do the 4- and 4′-methyl groups in Me_2bpy. The related complex $[Ru(bpy)(Me_2bpy)(^iPr_2bpy)]^{2+}$ also exhibits only one singlet for the methyl groups in the Me_2bpy ligand, and the isopropyl groups are also magnetically equivalent (one doublet at δ 1.31 and one quartet at δ 3.16).

It is noted that the precursor dicarbonyl complexes, $[Ru(pp)(pp')(CO)_2]^{2+}$, also possess C_1 point group symmetry so that the two halves of each bidentate ligand are inequivalent. By comparison with the tris(heteroleptic) complexes, the chemical shift differences observed between identical substitutents in the 4- and 4′-positions of a 2,2′-bipyridine parent ligand are greater for the dicarbonyl species. In earlier discussions, the coordination-induced shifts in the resonances of the 4- and 4′-protons of 2,2′-bipyridine were attributed to the σ-donor and π-acceptor characteristics of the ligand, as these positions were considered sufficiently isolated to preclude anisotropic interactions.[48] In the present case, it is tempting to evoke a similar rationalization for the observed shifts of substituents in these positions for the dicarbonyl and tris(heteroleptic) complexes, in view of the differences in π-acceptor characteristics of the CO and pp ligands. However, our recent NMR studies involving geometric isomers in bis(bidentate)dicarbonyl and tris(bidentate) species containing the unsymmetrical ligand 4-methyl-4′-*neo*-pentyl-2,2′-bipyridine (pmb) are inconsistent with a unilateral rationalization of substituent shifts based on bonding effects alone, and they indicate that anisotropic effects are also important;[52] i.e., there is an interaction of the magnetic fields of rings of adjacent ligands. The same situation is likely to pertain in the present series of complexes.

X-ray Structural Study. The crystal structure of $[Ru(Me_2bpy)(phen)(bpa)](PF_6)_2$ (for which tolerable single crystals were obtained) was carried out to establish the coordination of three different bidentate heterocyclic nitrogen ligands attached to ruthenium—no similar X-ray structure has been carried out on a tris(heteroleptic)ruthenium(II) species. The results of the structure determination confirm the cation formulation: however, a relatively low precision was obtained for the structure as a consequence of a high degree of thermal motion in the PF_6^- anions (which were modeled as ordered) and a solvent (hexane) residue. Nevertheless, a number of features may be noted about the cation. The structure of the cation is displayed in Figure 1, atom coordinates are listed in Table 2, and bond distances and angles relating to the ruthenium environment are given in Table 3.

Ruthenium has approximately octahedral stereochemistry from chelation of the three different bidentate ligands. The Me_2-bpy ligand is almost flat with a dihedral angle of 6.3(4)° between the two pyridine rings, with Ru lying 0.29(2) and 0.15(2) Å out of the planes of rings A and B, respectively. On the other hand, the dihedral angle between the 2-pyridyl rings of bpa is 35.5(4)° with Ru lying 0.34(2) and 0.18(2) Å out of the planes of rings A and B, respectively. The 1,10-phenanthroline ligand is very close to planar, with Ru being only 0.090(8) Å out of the $C_{12}N_2$ plane in the chelate ring formed with that ligand.

There is some suggestion of an increase in the Ru−N distance for binding the three ligands in the series Me_2bpy (2.056 Å), phen (2.083 Å), and bpa (2.100 Å), with the difference between the two Ru−N distances in any one ligand significant only for 4,4′-dimethyl-2,2′-bipyridine (2.040(8), 2.072(9) Å). The Ru−N(Me_2bpy) distances are similar to Ru−N in $[Ru(bpy)_3]X_2$ complexes, e.g., X = ClO_4 (2.056(3)−2.060(3) Å)[53] or PF_6 (2.056(2) Å at 298 [54] and 143 K;[55] 2.053(2) Å at 105 K[54]), and in $[Ru(bpy)_2L]^{2+}$, e.g., L = 2,3-bis(2-pyridyl)quinoxaline (Ru−N, 2.06 Å),[56] $[Ru(bpy)_2L]^+$ (LH = 3-methyl-5-(pyridin-2′-yl)-1,2,4-triazole,[57] 2.042(5)−2.060(4) Å; LH = 2-(2-hydroxyphenyl)-pyridine,[58] 2.022(4)−2.049(5) Å), and $[Ru(bpy)_2(NH{=}CMe_2)_2]^{2+}$ (2.035(9), 2.081(9) Å).[59] For the 1,10-phenanthroline ligand, the Ru−N bond length is at the higher end of values for reported Ru^{II}−phen complexes, e.g., $[RuL_3]^{2+}$ (L = 4,7-diphenyl-1,10-phenanthroline) (Ru−N, 2.06 Å, with a range 2.029(2)−2.079-(2) Å),[60] $[RuL_2L']^{2+}$ (L = phen, Ru−N, 2.06, 2.07 Å; L′ = 2,9-dimethyl-1,10-phenanthroline, Ru−N, 2.09 Å),[61] and *trans*-$[Ru(phen)_2(py)_2]^{2+}$ (2.096(5), 2.100(5) Å).[62] In the last example, the bonds are lengthened by steric repulsion between the *trans*-phen ligands and this factor also causes significant nonplanarity of these ligands as well as their inclination to the N_4(phen)Ru plane. For both the Me_2bpy and phen ligands, the bite angles are unexceptional and consistent with reported values.[53−55,57,58,60,62]

No structural charaterization of Ru^{II}−bpa complexes has previously been reported. However, the Ru−N(bpa) distances are very similar to those for Ru−N(py) bonds of *trans*-$[Ru(phen)_2(py)_2]^{2+}$ (2.097(5) Å)[62] and $[Ru(tpy)(bpy)(py)]^{2+}$ (tpy = 2,2′:6′,2″-terpyridine) (2.114(6) Å),[63] as might be expected for the separated 2-pyridyl units. These distances are somewhat larger than Ru−N for bis{tris(2-pyridyl)amine}ruthenium(II) (2.064(3), 2.066(3), 2.069(3) Å).[64] In contrast to the bite angles

(53) Harrowfield, J. M.; Sobolev, A. N. *Aust. J. Chem.* **1994**, *47*, 763.
(54) Biner, M.; Burgi, H. B.; Ludi, A.; Rohr, C. *J. Am. Chem. Soc.* **1992**, *114*, 5197.
(55) Rillema, D. P.; Jones, D. S.; Levy, H. A. *J. Chem. Soc., Chem. Commun.* **1979**, 849.
(56) Rillema, D. P.; Taghdiri, D. G.; Jones, D. S.; Keller, C. D.; Worl, L. A.; Meyer, T. J.; Levy, H. A. *Inorg. Chem.* **1987**, *26*, 578.
(57) Buchanan, B. G.; Vos, J. G.; Kaneko, M.; van der Putten, W. J. M.; Kelly, J. M.; Hage, R.; de Graeff, R. A. G.; Haasnoot, J. G.; Reedijk, J. *J. Chem. Soc., Dalton Trans.* **1990**, 2425.
(58) Holligan, B. M.; Jeffery, J. C.; Norgett, M. K.; Schatz, E.; Ward, M. D. *J. Chem. Soc., Dalton Trans.* **1992**, 3345.
(59) Wong, K.-Y.; Che, C.-M.; Li, C.-K.; Chiu, W.-H.; Zhou, Z.-Y.; Mak, T. C. W. *J. Chem. Soc., Chem. Commun.* **1992**, 754.
(60) Goldstein, B. M.; Barton, J. K.; Berman, H. M. *Inorg. Chem.* **1986**, *25*, 842.
(61) Ichida, H.; Tachiyashiki, S.; Sasaki, Y. *Chem. Lett.* **1989**, 1579.
(62) Bonneson, P.; Walsh, J. L.; Pennington, W. T.; Cordes, A. W.; Durham, B. *Inorg. Chem.* **1983**, *22*, 1761.
(63) Hecker, C. R.; Fanwick, P. E.; McMillin, D. R. *Inorg. Chem.* **1991**, *30*, 659.

Table 2. Non-hydrogen Atom Coordinates Data for $[Ru(Me_2bpy)(phen)(dpa)](PF_6)_2 \cdot C_6H_{14}$ (Vv)

	A			B		
atom	*x*	*y*	*z*	*x*	*y*	*z*
cation						
Ru	0.18103(6)	0.25502(6)	0.07402(8)			
bpy ligand						
N(n1)	0.2617(6)	0.3949(6)	−0.0058(6)	0.3247(6)	0.2078(6)	−0.0269(7)
C(n2)	0.3653(8)	0.3832(8)	−0.0626(8)	0.4014(8)	0.2774(9)	−0.0763(9)
C(n3)	0.4296(7)	0.4665(9)	−0.1055(9)	0.5024(8)	0.2520(9)	−0.1379(11)
C(n4)	0.3906(9)	0.5655(9)	−0.0929(9)	0.5208(9)	0.1515(11)	−0.1526(11)
C(n41)	0.4582(9)	0.6558(9)	−0.1294(12)	0.6413(9)	0.1238(11)	−0.2166(14)
C(n5)	0.2854(9)	0.5748(8)	−0.0367(9)	0.4528(10)	0.0843(9)	−0.1082(12)
C(n6)	0.2235(7)	0.4915(8)	0.0029(8)	0.3535(9)	0.1102(9)	−0.0451(11)
phen ligand						
N(n1)	0.2143(6)	0.2055(6)	0.2286(7)	0.1214(6)	0.1018(6)	0.1637(7)
C(n2)	0.1775(7)	0.1078(8)	0.3084(9)	0.1286(7)	0.0513(7)	0.2741(9)
C(n3)	0.1892(8)	0.0612(9)	0.4188(10)	0.0943(7)	−0.0522(8)	0.3469(10)
C(n4)	0.2381(10)	0.1212(10)	0.4480(10)	0.0504(8)	−0.1057(8)	0.3065(11)
C(n5)	0.2742(9)	0.2205(10)	0.3684(11)	0.0429(8)	−0.0573(9)	0.1970(12)
C(n6)	0.2617(8)	0.2581(8)	0.2599(9)	0.0801(8)	0.0460(8)	0.1259(9)
C(n7)	0.1488(9)	−0.0439(10)	0.4960(10)	0.1060(9)	−0.0985(9)	0.4600(11)
dpa ligand						
N(0)	−0.0389(6)	0.2671(6)	0.0736(8)			
N(n1)	0.0393(6)	0.3159(6)	0.1747(7)	0.1346(6)	0.2953(6)	−0.0715(7)
C(n2)	−0.0467(8)	0.3041(7)	0.1671(9)	0.0359(8)	0.2905(7)	−0.0472(9)
C(n3)	−0.1415(8)	0.3259(9)	0.2475(10)	0.0056(8)	0.3071(8)	−0.1430(11)
C(n4)	−0.1518(9)	0.3660(9)	0.3378(10)	0.0765(10)	0.3296(9)	−0.2608(11)
C(n5)	−0.0641(10)	0.3859(8)	0.3404(9)	0.1762(10)	0.3397(9)	−0.2870(9)
C(n6)	0.0291(8)	0.3600(8)	0.2611(9)	0.2032(7)	0.3202(8)	−0.1900(10)
anion						
P	0.7815(3)	0.4393(3)	−0.3173(3)	−0.2490(3)	0.0639(3)	0.1789(4)
F(1)	0.8282(7)	0.5281(6)	−0.4392(7)	−0.2999(11)	0.0839(8)	0.0931(14)
F(2)	0.7310(8)	0.3483(8)	−0.1932(7)	−0.1935(8)	0.0465(8)	0.2609(8)
F(3)	0.8383(6)	0.4766(7)	−0.2607(7)	−0.2544(8)	0.1811(6)	0.1630(12)
F(4)	0.7261(7)	0.4006(8)	−0.3734(8)	−0.2309(9)	−0.0512(8)	0.1746(12)
F(5)	0.8739(8)	0.3687(8)	−0.3669(9)	−0.1425(9)	0.0885(12)	0.0713(9)
F(6)	0.6914(7)	0.5100(8)	−0.2644(9)	−0.3464(9)	0.0367(13)	0.2827(13)
solvent						
C(n1)[a]	0.571(4)	0.068(4)	0.576(5)	0.569(2)	0.497(2)	0.405(2)
C(n2)	0.507(6)	0.165(4)	0.503(5)	0.501(6)	0.381(5)	0.474(7)
C(n3)	0.442(2)	0.264(4)	0.513(4)	0.543(8)	0.290(6)	0.491(8)

[a] C(A1) is disordered; the second component (CA1′) (both fragments populated at 0.5) is at (0.610(2), 0.169(2), 0.520(3)).

Table 3. Ruthenium Environment in Structure of $[Ru(Me_2bpy)(phen)(dpa)](PF_6)_2 \cdot C_6H_{14}$ (Vv)[a]

atom	*r*	N(mB1)	N(pA1)	N(pB1)	N(bA1)	N(bB1)
N(mA1)	2.072(9)	78.4(4)	93.3(4)	169.7(4)	96.7(4)	91.9(4)
N(mB1)	2.040(8)		89.6(4)	94.9(4)	175.0(4)	93.6(4)
N(pA1)	2.078(10)			78.7(4)	89.7(4)	174.3(3)
N(pB1)	2.088(8)				89.9(3)	96.3(4)
N(bA1)	2.095(8)					87.5(4)
N(bB1)	2.105(11)					

[a] *r* is the Ru−N distance (Å); other entries in the matrix are the angles subtended at the ruthenium by the relevant atoms at the head of the row and column. The abbreviations m, p, and b are 4,4′-dimethyl-2,2′-bipyridine, 1,10-phenanthroline, and bis(2-pyridyl)amine, respectively.

of Me_2bpy and phen (78.4(4), 78.7(4)°), the bite angle of bpa is much larger (87.5(4) Å), in keeping with the increased size of the metallocycle ring, with a concomitant effect on the ruthenium environment; e.g., the *trans* angles associated with the bpa ligand (175.0(4), 174.3(3) Å) differ considerably from that between the two other ligands (169.7(4)°). In another of the few X-ray characterized examples of a bpa ligand chelated in a six-coordinate metal atom environment, *viz.*, *trans*-$[Cd(bpa)_2(ONO)_2]$,[65] M−N is increased (2.310(4), 2.316(3) Å) with a concomitant decrease in the bite angle to 79.0(1)°. In both of these complexes it is of interest to find the ligand "folded", so that the dihedral angles between the two C_5N planes are very similar (35.5(4)° (Ru); 33.6(2)° (Cd)). These data contrast with the many examples of bpa complexes in a four-coordinated environment about copper(I) (e.g., refs 66 and 67). In the less crowded array, the ligands are more nearly planar. The interplanar dihedral angles in the ten ligands quoted in these references have a distribution of 17.2(9) (maximum), 15.7(2), 11(1), and the remainder 8° or less. Bite angles range between 92.5(2) and 94.6(3)° and Cu−N is 1.96−2.05 Å. The origin of the nonplanarity in the six-coordinate species presumably originates in the requirement for a smaller bite angle coupled with the greater steric hindrance between ligands in opposition in the *trans* disposition or because of steric interactions between *ortho*-hydrogen atoms in the tris(bidentate) array. The noncoplanarity of the two pyridine rings is reflected in the angle at the bridging nitrogen atom, C−N−C, being 128(1) and 128.8(3)° in the present ruthenium complex and the cadmium complex,[65] while in all of the copper compounds quoted (except $[bpaCuBr_2]^-$ where the precision is poor[67]) it rises above 130°.

Scrambling. One of the critical issues in the utilization of this synthetic methodology is the elimination of scrambling of the three ligands within the steps of the scheme. Clearly, by the observations given above for the FAB experiments, and the

(64) Keene, F. R.; Snow, M. R.; Stephenson, P. J.; Tiekink, E. R. T. *Inorg. Chem.* **1988**, *27*, 2040.
(65) Griffith, A. H.; Li, H.-Y.; Amma, E. L. *Inorg. Chim. Acta* **1988**, *148*, 203.
(66) Thompson, J. S.; Whitney, J. F. *Inorg. Chem.* **1984**, *23*, 2813.
(67) Bowmaker, G. A.; Healy, P. C.; Kepert, D. L.; Kildea, J. D.; Skelton, B. W.; White, A. H. *J. Chem. Soc., Dalton Trans.* **1989**, 1639.

conclusions of the NMR studies, the occurrence of bis(heteroleptic) or homoleptic species is minimal. A detailed study of this issue revealed that minor scrambling does occur, specifically during the final decarbonylation reaction. In addition, decomposition was sometimes observed in the step involving conversion of the dichloro → bis(triflato) species and was greatest in complexes containing the ligands with the highest basicity, as discussed above. Extremely pure bis(triflato) complexes could be obtained, but in reduced yield, by recrystallization from hot CH_2Cl_2/Et_2O.

A series of reactions was undertaken in which the complex $[Ru(bpy)(Me_4bpy)(CO)_2]^{2+}$ was produced by both possible alternatives of the sequential addition and the products closely examined by ^1H NMR techniques for $[Ru(Me_4bpy)_2(CO)_2]^{2+}$, which would be quite apparent if present in even small quantities. No such product was detected. Indeed, in the present studies there was only one circumstance, involving the addition of a very basic ligand pp′ to $[Ru(pp)(CO)_2(CF_3SO_3)_2]$, where a small amount (<3%) of the product $[Ru(pp')_2(CO)_2]^{2+}$ was detected as a product in this step of the scheme. The subsequent addition of the third bidentate ligand bpm to $[Ru(bpy)(Me_4bpy)(CO)_2]^{2+}$ under decarbonylation conditions in refluxing 2-methoxyethanol indicated $[Ru(Me_4bpy)_2(bpm)]^{2+}$ as a minor impurity (<5%). In this particular experiment (which is consistent with all other observations during this work), the scrambling clearly occurs in the decarbonylation step. Recrystallization of the tris(bidentate) species almost invariably allowed removal of the impurity, or purification was achieved by cation-exchange chromatographically (*vide supra*). However, detailed studies on the decarbonylation process revealed that it could be undertaken at lower temperatures (<25 °C) for longer periods, under which conditions no scrambling was detected, although yields tended to be lower. This observation is in complete agreement with associated stereochemical studies involving the decarbonylation reactions of complexes of the type $[Ru(pp)(pp')(CO)_2]^{2+}$.[52,68]

In order to probe the mechanism of the decarbonylation process, we have followed this step of the synthetic scheme by IR and NMR spectroscopic methods. In a typical case, a dicarbonyl compound was mixed with 2 equiv of TMNO and 2 equiv of *tert*-butylpyridine ((^{t}Bu)py) in CD_2Cl_2. At room temperature, the two $\bar{\nu}_{CO}$ stretching frequencies at 2100 and 2050 cm^{-1} (solution cell) gave way to two extremely closely spaced peaks (<2 cm^{-1} difference) centered around 1990 cm^{-1}. If the reaction was stopped at this point, $[Ru(pp)(pp')((^{t}Bu)py)(CO)]^{2+}$ could be isolated and characterized by ^1H NMR spectroscopy. The two possible geometric isomers were always found in a 1:1 ratio, indicating that TMNO had no preference for the two CO sites. When this species was resubmitted to a CH_2Cl_2 solution of pyridine (py) and TMNO, and the mixture heated to 35 °C, the complex $[Ru(pp)(pp')((^{t}Bu)py)(py)]^{2+}$ was produced (characterized by NMR and IR). Since the reaction could be separated into two steps—a facile one at room temperature or below and a subsequent step that required heating—the removal of the second carbonyl is apparently more difficult, an observation which has also been made for related halogenated compounds.[11,37] This observation appears entirely reasonable given our earlier analysis of the effect of electron-withdrawing groups: the replacement of one CO by a less back-bonding pyridine derivative would be expected to retard the second decarbonylation. However, while this second step may be facilitated in the case where the ligand involved is a bidentate, the opportunity for ligand scrambling clearly occurs at elevated temperatures. The precise mechanism of such a process is uncertain, and its elucidation would require further detailed studies, but this path is depressed when the entire reaction is conducted at lower temperatures.

Chromatography. The separation of mixtures of tris(bidentate)ruthenium(II) complexes of the type involved in this study was necessary for proof that the methodology realized tris(heteroleptic) species and ultimately for their purification. In earlier studies, we reported the use of cation-exchange chromatography in the separation of diastereoisomeric ligand-bridged dinuclear complexes of the type $[(pp)_2Ru(BL)Ru(pp')_2]^{4+}$ and $[(pp)_2Ru(BL)Os(pp')_2]^{4+}$ (where pp and pp′ may or may not be the same).[69] The technique involved the use of an aromatic anion (such as 4-toluenesulfonate) as the counterion in the electrolyte of the eluent: such anions appear to have different associations with the stereoisomers, allowing their chromatographic separation. In the present study, it was observed, in all cases where the chromatography of the tris(heteroleptic) complex $[Ru(pp)(pp')(pp'')]^{2+}$ was undertaken in the presence of any of the possible bis(heteroleptic) ($[Ru(pp)_2(pp')]^{2+}$) or homoleptic species ($[Ru(pp)_3]^{2+}$), that their separation was achieved under the same conditions. In other work, we have also shown that optical isomers of tris(bidentate) complexes,[70] and the geometric isomers of complexes of this genre containing unsymmetical ligands,[52] may be separated by this technique. A detailed study of the interaction of such anions with these complexes, and the consequences in the chromatographic process, is in progress and will be published subsequently.[71]

Electrochemical Studies. The electrochemical behavior of polypyridyl complexes of ruthenium(II) has been rationalized in terms of a metal-based oxidation and a series of reductions which are ligand-based and occur in a stepwise manner to each ligand π^*-system, with the order of the reduction correlating with the ease of reduction of the uncoordinated ligands.[7,8,72–74] The extensive variation of the ligand environment available through this general synthetic procedure for tris(heteroleptic) compounds allows a wider assessment of these proposals and in particular of the mutual interdependence of the ligands. The redox properties of the tris(heteroleptic) complexes were determined by cyclic voltammetry and differential pulse voltammetry, and Table 4 shows the potentials for a selection of the tris(heteroleptic) complexes synthesized in the study.

Lever and co-workers have recently proposed a scheme for the parametrization of the oxidation[75,76] and reduction potentials[77] of metal complexes, by using a ligand electrochemical series based on their Ru(III)/Ru(II) redox couples. The fundamental electrochemical parameter is $E_L(L)$, defined as one-sixth the potential for the Ru(III)/Ru(II) couple for RuL_6 in acetonitrile solution. The metal-based Ru(III)/Ru(II) couple of any complex may be calculated using the formulation

$$E_{calc}\{Ru(III)/Ru(II)\} = S_M \sum E_L(L) + I_M \qquad (1)$$

(68) Rutherford, T. J.; Quagliotto, M. G.; Keene, F. R. *Inorg. Chem.* **1995**, *34*, 3857.
(69) Reitsma, D. A.; Keene, F. R. *J. Chem. Soc., Dalton Trans.* **1993**, 2859.
(70) Rutherford, T. J.; Reitsma, D. A.; Keene, F. R. Unpublished work.
(71) Reitsma, D. A.; Keene, F. R. Unpublished work.
(72) Rillema, D. P.; Allen, G.; Meyer, T. J.; Conrad, D. *Inorg. Chem.* **1983**, *22*, 1617.
(73) Ohsawa, Y.; Hanck, K. W.; DeArmond, M. K. *J. Electroanal. Chem.* **1984**, *175*, 229.
(74) Morris, D. E.; Ohsawa, Y.; Segers, D. P.; DeArmond, M. K.; Hanck, K. W. *Inorg. Chem.* **1984**, *23*, 3010.
(75) Lever, A. B. P. *Inorg. Chem.* **1990**, *29*, 1271.
(76) Lever, A. B. P. *Inorg. Chem.* **1991**, *30*, 1980.
(77) Dodsworth, E. S.; Vlcek, A. A.; Lever, A. B. P. *Inorg. Chem.* **1994**, *33*, 1045.

Table 4. Electrochemical Characteristics of Selected Tris(heteroleptic) Complexes

complex[a]	$E_{1/2}$ values (vs SSCE)[b] oxidation	reduction	$\Delta E_{1/2}$[c]
$[Ru(bpy)_3]^{2+}$	+1.29	−1.33, −1.52, −1.78	2.62
$[Ru(bpy)(Me_2bpy)(5\text{-}(Me)phen)]^{2+}$	+1.24	−1.37, −1.56, −1.81	2.61
$[Ru(bpy)(Me_2bpy)(bpm)]^{2+}$	+1.37	−1.03, −1.49, −1.74	2.40
$[Ru(bpy)(Me_2bpy)\{(EtCO_2)_2bpy\}]^{2+}$	+1.35	−1.01, −1.48, −1.69	2.36
$[Ru(Me_2bpy)(Me_4bpy)(dpp)]^{2+}$	+1.26	−1.09, −1.61, −1.98	2.35
$[Ru(Me_2bpy)\{(EtCO_2)_2bpy\}(dpp)]^{2+}$	+1.45	−0.96, −1.19, −1.66	2.41
$[Ru(Me_2bpy)\{(EtCO_2)_2bpy\}\{(Et_2N)_2bpy\}]^{2+}$	+0.97	−1.09, −1.61, −1.88[d]	2.06
$[Ru(Me_2bpy)(Me_4bpy)\{(Et_2N)_2bpy\}]^{2+}$	+0.79	−1.55, −1.86, −2.13	2.34

[a] As PF_6^- salts. [b] Acetonitrile/0.1 M $[N(n\text{-}C_4H_9)_4]PF_6$ solution; Pt button working electrode; 298 K; scan rate 100 mV/s; measured vs Ag/Ag^+ reference electrode and quoted vs saturated sodium chloride calomel (SSCE). [c] $\Delta E_{1/2} = E_{1/2}(Ru(III)/Ru(II)) - E_{1/2}(first\ ligand\ reduction)$. [d] Estimated from shoulder on solvent decomposition.

where S_M and I_M are constants for a particular metal. For the first ligand-based reduction process, there is a similar relationship

$$E_{red} = S_L \sum E_L(L) + I_L \qquad (2)$$

An implication of the use of the paramter $E_L(L)$ in these contexts is that all ligands behave in the same way to many redox metal couples and also to the same metal center in circumstances where the other ligands may be widely varied in terms of their σ-donor and π-donor/-acceptor characteristics. Because of the paucity of tris(heteroleptic) species available, previous assessment of this hypothesis in terms of ligand variation has been rather limited,[75,77] and the present synthetic methodology allows a wider analysis. The conclusions are rather compelling.

For the metal-based Ru(III)/Ru(II) couples, the values of S_M and I_M (eq 1) were assumed in the first approximation to be equal to unity and zero, respectively, since the $E_L(L)$ values were themselves derived from the redox couples of ruthenium species.[75] For complexes as widely disparate as $[Ru(phen)(CO)_2Cl_2]$ (**IIe**; calculated, 1.75 V vs SSCE; observed, 1.73 V), $[Ru(Me_2bpy)(phen)(bpa)]^{2+}$ (**Vv**; 1.07 V *cf.* 1.06 V), $[Ru(Me_2bpy)(Me_4bpy)(dpp)]^{2+}$ [78] (**Vj**; 1.28 V *cf.* 1.26 V), $[Ru(Me_2bpy)(Me_4bpy)\{(Et_2N)_2bpy\}]^{2+}$ (**Vk**; 0.83 V *cf.* 0.79 V),[78] $[Ru(Me_2bpy)\{(EtCO_2)_2bpy\}(dpp)]^{2+}$ (**Vh**; 1.43 V *cf.* 1.45 V),[78] and $[Ru(Me_2bpy)\{(EtCO_2)_2bpy\}\{(Et_2N)_2bpy\}]^{2+}$ (**Vi**; 0.99 V *cf.* 0.97 V),[78] there is clearly a close correspondence between the calculated and observed values. Accordingly, the contributions of the ligands to the overall potential appears to be additive, with no significant synergism between the individual contributions.

For the ligand-based reduction processes, the values of S_L and I_L (eq 2) of Ru(pp) may be deduced from electrochemical data on the assumption of the assignment of the most reducible ligand. In previous studies, the values for Ru(bpy) ($S_L = 0.25$; $I_L = -1.40$)[80] and Ru(bpm) ($S_L = 0.31$; $I_L = -1.08$)[80] are provided,[77] and using similar procedures values can be calculated from previous electrochemical studies[1] as well as the present study to show for $Ru\{(EtCO_2)_2bpy\}$ ($S_L = 0.36$, $I_L = -1.10$, $R = 0.98$)[80] and Ru(dpp) ($S_L = 0.38$, $I_L = -1.20$, $R = 0.99$).[80] Again the results of application of eq 2 are impressive. The potential of the first reduction of $[Ru(bpy)(Me_2bpy)(bpm)]^{2+}$, which is isolated at the bpm ligand, is then predicted to be −1.04 V (observed −1.03 V vs SSCE), and the values obtained for the complexes $[Ru(bpy)(Me_2bpy)\{(EtCO_2)_2bpy\}]^{2+}$ (calculated, −0.98 V; observed, −1.01 V), $[Ru(Me_2bpy)(Me_4bpy)(dpp)]^{2+}$ (−1.10 V *cf.* −1.09 V), and $[Ru(Me_2bpy)\{(EtCO_2)_2bpy\}\{(Et_2N)_2bpy\}]^{2+}$ (−1.10 V *cf.* −1.09 V) are all closely comparable. For the complex $[Ru(Me_2bpy)\{(EtCO_2)_2bpy\}(dpp)]^{2+}$, the first reduction couple is calculated to be −1.04 or −0.94 V, based on the assumption of dpp or $(EtCO_2)_2bpy$, respectively, as the ligand with the lowest π^* energy; the observed value of −0.96 V would lead to the assignment of the ligand $(EtCO_2)_2bpy$ having the lower π^*-value, which is consistent with the reductions of the respective $[Ru(pp)_3]^{2+}$ complexes.[1]

Since the π^*-orbital involved in the first reduction process is the same as that involved in the lowest MLCT absorption and emission processes, linear correlations have been established between the energy difference between the $d\pi$ (HOMO) and π^* (LUMO) orbitals—established electrochemically by $\Delta E_{1/2} = [E_{1/2}(Ru(III)/Ru(II)) - E_{1/2}(Ru(II)/Ru(I))]$—and the absorption or emission maxima.[7,8,72−74] For the complexes of this study, such linear correlations were also observed, in an analogous manner to those established in an earlier study of a smaller series of tris(heteroleptic) complexes by Juris *et al.*[8]

Electronic Spectra. Visible light absorptivity in polypyridyl complexes of ruthenium(II) arises primarily from charge transfer transitions from filled $d\pi(Ru^{II})$ levels to multiple, low-lying π^*-(ligand) levels.[81] For the archetype tris(bidentate) species $[Ru(bpy)_3]^{2+}$; this can be represented as

$$Ru^{II}(bpy)_3^{2+} \xrightarrow{h\nu} Ru^{III}(bpy^{\bullet-})(bpy)_2^{2+*}$$

In this example, the $d\pi \rightarrow \pi_1^*$ transition results in an absorption at 450 nm and the $d\pi \rightarrow \pi_2^*$ transition at 243 nm in acetonitrile solution.[1] Ligand-based $\pi \rightarrow \pi^*$ transitions dominate the near-UV region.[82] The MLCT transitions produce excited states that are largely singlet, e.g., $^1(d\pi^6) \rightarrow {}^1(d\pi^5\pi^{*1})$, but possess significant triplet character due to spin−orbit coupling.[81] In mixed-chelate complexes, separate transitions may occur to each of the ligands, but rapid intramolecular charge transfer leads ultimately to a triplet MLCT state in which the excited electron is localized on the ligand having the lowest π^*-acceptor orbital:[83−89] the implications in terms of the

(78) $E_L(L)$ values for Me_4bpy and $(EtCO_2)_2bpy$ are derived from data in ref 1; the $E_L(L)$ value for $(Et_2N)_2bpy$ is derived from data in ref 79.
(79) Slattery, S. J.; Gokaldas, N.; Mick, T.; Goldsby, K. A. *Inorg. Chem.* **1994**, *33*, 3621.
(80) (a) Quoted relative to NHE in ref 74. (b) Quoted relative to NHE to be consistent with comparative values above.
(81) Kober, E. M.; Meyer, T. J. *Inorg. Chem.* **1983**, *22*, 1614.
(82) Lytle, F. E.; Hercules, D. M. *J. Am. Chem. Soc.* **1969**, *91*, 253.
(83) Bradley, P. G.; Kress, N.; Hornberger, B. A.; Dallinger, R. F.; Woodruff, W. H. *J. Am. Chem. Soc.* **1981**, *103*, 7441.
(84) Mabrouk, P. A.; Wrighton, M. S. *Inorg. Chem.* **1986**, *25*, 526.
(85) Danzer, G. D.; Golus, J. A.; Kincaid, J. R. *J. Am. Chem. Soc.* **1993**, *115*, 8643.
(86) Ford, W. E.; Calvin, M. *Chem. Phys. Lett.* **1980**, *76*, 105.

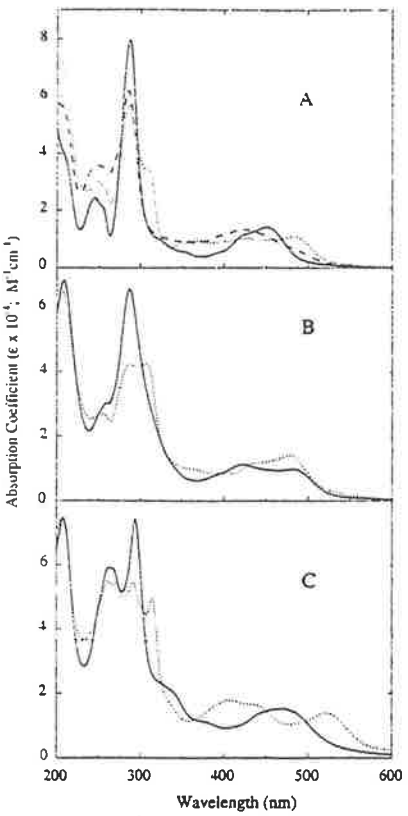

Figure 2. Electronic spectra (acetonitrile solution) of (A) $[Ru(bpy)_3]^{2+}$ (—), $[Ru(bpy)(Me_2bpy)\{(EtCO_2)_2bpy\}]^{2+}$ {**Ve**} (- -), and $[Ru(bpy)(Me_2bpy)(bpm)]^{2+}$ {**Vb**} (— —); (B) $[Ru(Me_2bpy)(Me_4bpy)(dpp)]^{2+}$ {**Vj**} (—) and $[Ru(Me_2bpy)\{(EtCO_2)_2bpy\}(dpp)]^{2+}$ {**Vh**} (- -); and (C) $[Ru(Me_2bpy)(Me_4bpy)\{(Et_2N)_2bpy\}]^{2+}$ {**Vk**} (—) and $[Ru(Me_2bpy)\{(EtCO_2)_2bpy\}\{(Et_2N)_2bpy\}]^{2+}$ {**Vi**} (- -).

photophysical properties of these tris(heteroleptic) complexes is considered below.

Figure 2A shows the electronic spectra of $[Ru(bpy)(Me_2bpy)(pp)]^{2+}$ {pp = 5-(Me)phen, bpm, and $(EtCO_2)_2bpy$}. The spectra of the series $[Ru(Me_2bpy)(Me_4bpy)(pp')]^{2+}$ and $[Ru(Me_2bpy)\{(EtCO_2)_2bpy\}(pp')]^{2+}$ are shown for pp′ = dpp (Figure 2B) and pp′ = $(Et_2N)_2bpy$ in Figure 2C.

It is apparent from these data that the MLCT transitions to the lowest π^*-levels of the individual ligands are broadly conserved within the various combinations of the bidentate ligands.[8,90] Rational design of the ligand environment therefore enables the production of "black absorbers" by systematically shifting the $d\pi \rightarrow \pi^*$ bands to the red region of the spectrum—either by using ligands with lower π^*-levels (e.g., bpm, $(EtCO_2)_2bpy$, or dpp) or by stabilization of the "hole" at Ru^{III} in the MLCT state by the introduction of electron-donating ligands. This theme has been developed elsewhere.[90]

An interesting feature in Figure 2C is the enhancement of the absorption in the region $\lambda \approx 400-440$ nm for $[Ru(Me_2bpy)\{(EtCO_2)_2bpy\}\{(Et_2N)_2bpy\}]^{2+}$. Solvent-dependent spectral studies allow assignment of this broad absorption to MLCT transitions from the $d\pi \rightarrow \pi^*$ levels of the Me_2bpy and $(Et_2N)_2$-bpy ligands, with the absorption at $\lambda \approx 522$ nm attributed to the $d\pi \rightarrow \pi^*\{(EtCO_2)_2bpy\}$ transition. On replacement of $(EtCO_2)_2bpy$ by Me_4bpy in the coordination sphere, there is a reduced $d\pi \rightarrow \pi^*$ energy gap for the Me_2bpy and $(Et_2N)_2bpy$ ligands, and a broad MLCT absorption is observed at $\lambda \approx 470$ nm for the complex $[Ru(Me_2bpy)(Me_4bpy)\{(Et_2N)_2bpy\}]^{2+}$. This reflects the relative effects induced on the $d\pi$ level in these two species by the electron-withdrawing $(EtCO_2)_2bpy$ and the electron-donating Me_4bpy ligands.

Photophysical Studies. The luminescence properties of a number of the tris(heteroleptic) complexes in CH_3CN (1×10^{-5}M) at 298 K are given in Table 5. Emission occurs from the lowest MLCT state in the tris(heteroleptic) complexes, where there are separate $d\pi \rightarrow \pi^*$(pp), $d\pi \rightarrow \pi^*$(pp′), and $d\pi \rightarrow \pi^*$(pp″) transitions: the emitting state is based on the ligand having the most positive reduction potential. Band shapes are typical of MLCT emitters—broad and structureless at room temperature and exhibiting vibronic structure at 77 K.[91] The independence of emission band shape and quantum yields on excitation wavelength from 350 to 600 nm, and excitation and absorption profiles, which are identical within experimental error, indicate that excitation into any of the three MLCT excitations leads to rapid population of the lowest ^{3}MLCT transition.

Excited state resonance Raman and transient absorbance studies[16,92-94] show that on the nanosecond time scale (<10 ns) photophysical excitation is localized on the lowest lying π^*-acceptor orbital. In the present series of complexes, by comparison of the excited state resonance Raman spectra of the tris(heteroleptic) complexes with those of each of the homoleptic complexes derived from the three ligands, the spectrum of the excited state for the tris(heteroleptic) complexes was consistent with rapid population of the lowest MLCT state, without evidence of significant population of the higher lying π^*-orbitals of the other two ancillary ligands.[16,92] For example, for $[Ru(bpy)(Me_2bpy)(bpm)]^{2+}$, where bpm has the lowest lying π^*-acceptor level, intense excited state resonance Raman bands characteristic of Me_2bpy in $[Ru(Me_2bpy)_3]^{2+*}$ at 1202, 1321, 1445, and 1624 cm^{-1} and of bpy in $[Ru(bpy)_3]^{2+*}$ at 1211, 1321, and 1624 cm^{-1} were not observed, while bands from bpm in $[Ru(bpm)_3]^{2+*}$ at 766, 1012, 1034, 1174, 1249, 1421, 1490, and 1560 cm^{-1} were observed. In a similar manner, the excited state in $[Ru(bpy)(Me_2bpy)\{(EtCO_2)_2bpy\}]^{2+*}$ could be identified as being localized on the $(EtCO_2)_2bpy$ ligand.[92]

The quantum yields (Φ_{em}) and excited state decay lifetimes are similar to those for the homoleptic analogues, although excited state lifetimes (τ) can be longer for the tris(heteroleptic) species than might be expected on the basis of the energy gap law. This is best illustrated by two examples. For $[Ru(Me_2bpy)(bpy)(5\text{-}(Me)phen)]^{2+}$ and $[Ru(bpy)_3]^{2+}$, absorption and emission maxima are nearly identical (λ_{abs} = 453 nm, λ_{em} = 627 nm and λ_{abs} = 451 nm, λ_{em} = 626 nm, respectively) and the excited state is bpy-localized in either case. The excited state lifetime and quantum yield for the former are noticeably larger (τ = 1115 ns *cf.* 920 ns; Φ_{em} = 0.069 *cf.* 0.062[18]). Calculation of the radiative (k_r) and nonradiative (k_{nr}) decay rate constants using τ and ϕ_{em} reveal that k_{nr} is less for the tris(heteroleptic) complexes than for $[Ru(bpy)_3]^{2+}$. Similarly, $[Ru(bpy)(Me_2bpy)\{(EtCO_2)_2bpy\}]^{2+}$ has a small energy gap (emitting ~1750 cm^{-1} lower in energy than $[Ru(bpy)_3]^{2+}$), but it

(87) Riesen, H.; Krausz, E. *J. Chem. Phys.* **1993**, *99*, 7614.
(88) Caspar, J. V.; Westmoreland, T. D.; Allen, G. H.; Bradley, P. G.; Meyer, T. J.; Woodruff, W. H. *J. Am. Chem. Soc.* **1984**, *106*, 3492.
(89) Chang, Y. J.; Xu, X.; Yabe, T.; Yu, S.-C.; Anderson, D. R.; Orman, L. K.; Hopkins, J. B. *J. Phys. Chem.* **1990**, *94*, 729.
(90) Anderson, P. A.; Strouse, G. F.; Treadway, J. A.; Keene, F. R.; Meyer, T. J. *Inorg. Chem.* **1994**, *33*, 3863.
(91) Kober, E. M.; Caspar, J. V.; Lumpkin, R. S.; Meyer, T. J. *J. Phys. Chem.* **1986**, *90*, 3722.
(92) Strouse, G. F.; Schoonover, J. R. Unpublished work.
(93) Schoonover, J. R.; Chen, P. Y.; Bates, W. D.; Dyer, R. B.; Meyer, T. J. *Inorg. Chem.* **1994**, *33*, 793.
(94) Bignozzi, C. A.; Argazzi, R.; Chiorboli, C.; Scandola, F.; Dyer, R. B.; Schoonover, J. R.; Meyer, T. J. *Inorg. Chem.* **1994**, *33*, 1652.

Table 5. Spectral and Photophysical Data for Selected Tris(heteroleptic) Complexes (CH_3CN Solution)

		photophysical data[a]			
complex	UV/vis spectrum λ_{max} (±2) (nm) ($\epsilon \times 10^{-3}$ (M^{-1} cm^{-1}))	λ_{em} (±3)[b] (nm)	Φ_{em} (±5%)[b]	τ (±5%)[b] (ns)	Φ_{dec} (±10%)
$[Ru(bpy)_3]^{2+}$	244 (24.4) 254 (sh) (21.4) 288 (79.5) 451 (14.0)	626	0.062	920	0.029
$[Ru(bpy)(Me_2bpy)(5\text{-}(Me)phen)]^{2+}$	268 (68.8) 286 (68.5) 385 (sh) (8.96) 429 (20.1) 453 (17.2)	627	0.069	1115	0.011
$[Ru(bpy)(Me_2bpy)(bpm)]^{2+}$	269 (50.7) 286 (62.9) 395 (sh) (9.59) 429 (13.2) 448 (13.1)	665	0.007	67	<0.001
$[Ru(bpy)(Me_2bpy)\{(EtCO_2)_2bpy\}]^{2+}$	286 (56.7) 309 (34.4) 366 (9.63) 399 (sh) (9.19) 426 (10.3) 483 (10.7)	702	0.055	772	<0.001
$[Ru(Me_2bpy)(Me_4bpy)(dpp)]^{2+}$	260 (30.3) 286 (65.7) 422 (11.2) 482 (9.77)	717	0.029	232	<0.001
$[Ru(Me_2bpy)\{(EtCO_2)_2bpy\}(dpp)]^{2+}$	250 (27.3) 256 (sh) (26.7) 288 (42.2) 308 (42.7) 441 (11.7) 479 (14.1)	678	0.037	788	<0.001
$[Ru(Me_2bpy)\{(EtCO_2)_2bpy\}\{(Et_2N)_2bpy\}]^{2+}$	206 (74.4) 260 (55.0) 270 (54.4) 292 (54.4) 314 (49.5) 408 (17.8) 432 (16.6) 522 (13.8)	810	0.0002	60	
$[Ru(Me_2bpy)(Me_4bpy)\{(Et_2N)_2bpy\}]^{2+}$	208 (74.3) 262 (59.1) 294 (74.1) 320 (sh) (23.8) 470 (15.2)	700	0.0050	154	<0.001

[a] Measured at 295 K. [b] λ_{ex} = 460 nm.

has a lifetime and quantum yield comparable with the latter. In this case, k_{nr} is less than would be predicted from the energy gap law. These differences can arise from changes in the acceptor characteristics of the ligand and in the extent of nonradiative decay by thermal activation and decay from the upper states.[95]

Upper limits for the quantum yield for ligand loss (Φ_{dec}) for the same series were measured in $[N(n\text{-}C_4H_9)_4]Cl$ (2 mM)/acetonitrile solutions. Compared with $[Ru(bpy)_3]^{2+}$ the tris(heteroleptic) complexes are much less prone to photochemically-induced ligand loss. The comparison between $[Ru(Me_2bpy)(bpy)(5\text{-}(Me)phen)]^{2+}$ and $[Ru(bpy)_3]^{2+}$ demonstrates this point. While the ground state electrochemical properties, absorption characteristics, and excited state energies of the two species are very similar, the tris(heteroleptic) species is more photoinert by a factor of ~3. Ligand-loss photochemistry in these complexes is usually associated with thermal activation to and reactivity from low-lying dd states. Temperature dependent lifetime measurements in 4:1 (v/v) ethanol–methanol between 160 and 298 K on the series of compounds $[Ru(bpy)(Me_2bpy)(pp)]^{2+}$, where pp = $\{(EtCO_2)_2bpy\}$, bpm, and 5-(Me)-phen, show only a slight temperature dependence above the glass to fluid transition. This behavior and the photolysis data are consistent with a decrease in thermally activated ligand-loss photochemistry. Similar observations have been made in $[Ru(bpy)_2(bpy\text{-}OH)]^{2+}$ and $[Ru(Me_2bpy)_2(vbpy)]^{2+}$ (vbpy = 4-methyl-4′-vinyl-2,2′-bipyridine).[96]

In the photolysis experiments there is no evidence for photochemically-induced scrambling in the tris(heteroleptic) species, and no detectable decomposition was noted either. In addition, during the time-resolved resonance Raman studies—in which the solutions were subjected to long-term intense radiation at 355 nm—there was no indication in any complex of any emission except that corresponding to the excited state involving the ligand of lowest π^*-energy: this observation also argues strongly against photochemically-induced scrambling.

The decrease in photolability and the apparent increase in the energy of the low-lying dd states may arise from the lowered

(95) Boyde, S.; Strouse, G. F.; Jones, W. E.; Meyer, T. J. *J. Am. Chem. Soc.* **1990**, *112*, 7395.

(96) Barquawi, K. R.; Murtaza, Z.; Meyer, T. J. *J. Phys. Chem.* **1991**, *95*, 47.

electronic symmetry. More electron-donating ancillary ligands have the effect of destabilizing the $d\sigma^*$-orbitals, resulting in a larger $d\pi-d\sigma^*$ energy gap: an interesting case in point is the complex $[Ru(Me_2bpy)(Me_4bpy)\{(Et_2N)_2bpy\}]^{2+}$ (for which all the ligands are "electron-donating") which is extremely photoinert (Table 5). On the other hand, electron-withdrawing substituents on the polypyridyl ligands lower π^*-acceptor levels. The combination of the two affects the energy of dd states ($d\pi^5d\sigma^*$) relative to MLCT ($d\pi^5d\pi^*$)[97] and would be responsible for the photoinertness observed in a number of other tris-(heteroleptic) species.

Significance

Application of the synthetic methodology presented here has three important consequences for future studies.

Firstly, it allows systematic control of the spectral and electrochemical characteristics of the complexes because of the ability to "tune" the π^*-levels by appropriate variation of the ligands. This may be useful in designing potential photosensitizers with broad band absorption ("black absorbers"), complexes with desired redox characteristics,[90] and complexes with controllable photophysical properties, particularly with regard to lifetimes and photoinertness.

Secondly, the scheme may be extended to the synthesis of assemblies of higher nuclearity,[69] utilizing the "complexes as ligands" approach,[98-101] in particular as described for $[Ru(pp)_2Cl_2]$ [100] and $[Ru(pp)_2(py)_2]^{2+}$ [101] species (py = pyridine). The general principle is shown in Scheme 2—the advantage of using the present dicarbonyl complexes as precursors is the added variation that mixed-ligand $[Ru(pp)(pp')]^{2+}$ moieties can be incorporated into the polynuclear compounds.

Preliminary synthetic studies have also shown that the general synthetic Scheme 1 can be used to prepare mononuclear complexes of the type $[Ru(pp)(pp')XY]^{n+}$, where X and Y are monodentate ligands containing N, O, P, or S donor atoms.[102]

Scheme 2. Synthetic Strategy for Dinuclear Species (pp = Bidentate Polypyridyl Ligands)

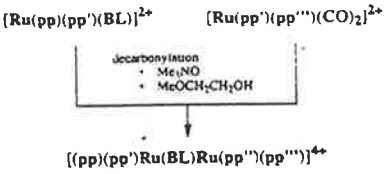

Thirdly, separate studies in our laboratory have demonstrated that decarbonylation will occur under controlled conditions with retention of the stereochemical relationship of the pp and pp′ ligands in the $[Ru(pp)(pp')(CO)_2]^{2+}$ precursor.[52,68] Accordingly, the procedure provides the possibility of the predetermining the stereochemistry of ligand-bridged polynuclear assemblies.

Acknowledgment. Financial support from the Australian Research Council (Grant No. A29130473) and the U.S. Department of Energy (Grant DE-FG05-86ER13633) is gratefully acknowledged. Travel between the laboratories at JCU and UNC (P.A.A., D.A.R., G.F.S., and J.A.T.) has been supported by the U.S. National Science Foundation (Grant INT-9015262) and the (Australian) Department of Industry, Technology and Regional Development within the Australia-U.S. Bilateral Science and Technology Program. K.H.H. acknowledges support from the Swiss National Science Foundation as a National Postdoctoral Fellow during his sojourn at JCUNQ. We are grateful to Todd Rutherford, Michael Quagliotto (JCUNQ), and John Moss (UNC) for assistance and to Dr. Jon Schoonover (Los Alamos National Laboratory) for helpful discussion.

Supporting Information Available: Tables of microanalytical and spectroscopic data for compounds reported in this work, as well as thermal parameters, hydrogen atom parameters, and non-hydrogen geometries for $[Ru(Me_2bpy)(phen)(bpa)](PF_6)_2$·hexane (15 pages). Ordering information is given on any masthead page.

IC9503794

(97) Rillema, D. P.; Blanton, C. B.; Shaver, R. J.; Jackman, D. C.; Boldaji, M.; Bundy, S.; Worl, L. A.; Meyer, T. J. *Inorg. Chem.* **1992**, *31*, 1600.
(98) Adeyemi, S. A.; Johnson, E. C.; Miller, F. J.; Meyer, T. J. *Inorg. Chem.* **1973**, *12*, 2371.
(99) Wilson, S. T.; Bondurant, R. F.; Meyer, T. J.; Salmon, D. J. *J. Am. Chem. Soc.* **1975**, *97*, 2285.
(100) Denti, G.; Campagna, S.; Serroni, S.; Ciano, M.; Balzani, V. *J. Am. Chem. Soc.* **1992**, *114*, 2944.
(101) Hua, X.; von Zelewsky, A. *Inorg. Chem.* **1991**, *30*, 3796.
(102) Treadway, J. A. Unpublished work, 1994.

2242 *Inorg. Chem.* **1996,** *35,* 2242−2246

Effect of Delocalization and Rigidity in the Acceptor Ligand on MLCT Excited-State Decay

Joseph A. Treadway,[†] Barbara Loeb,[‡] Rosa Lopez,[‡] Peter A. Anderson,[§] F. Richard Keene,[§] and Thomas J. Meyer*,[†]

Department of Chemistry, The University of North Carolina, CB#3290, Chapel Hill, North Carolina 27599-3290, Faculty of Chemistry, Pontificia Universidad Catolica de Chile, Casilla 306, Buzon 521, Santiago, Chile, and Department of Molecular Sciences, James Cook University of North Queensland, Townsville, Queensland 4811, Australia

Received July 28, 1995[⊗]

In its most simple form, the energy gap law for excited-state nonradiative decay predicts a linear dependence of ln k_{nr} on the ground- to excited-state energy gap, where k_{nr} is the rate constant for nonradiative decay. At this level of approximation, the energy gap law has been successfully applied to nonradiative decay in a wide array of MLCT excited states of polypyridyl complexes of Re^{I}, Ru^{II}, and Os^{II}. This relationship also predicts a dependence of k_{nr} on the structural characteristics of the acceptor ligand. We report here a brief survey of the literature which suggests that such effects exist and have their origin in the extent of delocalization of the excited electron in the ligand π^* framework and on acceptor ligand rigidity.

Along with the $\pi-\pi^*$ excited states of porphyrins and metalloporphyrins, metal-to-ligand charge-transfer (MLCT) excited states of polypyridyl complexes have dominated the study of photoinduced electron and energy transfer in molecular assemblies.[1] Polypyridyl complexes of Ru(II), e.g. $[Ru(bpy)_3]^{2+}$ (bpy is 2,2′-bipyridine), Os(II), and Re(I) have provided the majority of examples. The synthetic chemistry in this area (both at the metal and the ligands) has grown considerably, driven in part by the demands associated with preparing increasingly complex assemblies and model systems for refining theoretical concepts.[2] This chemistry has been used to prepare multicomponent molecular assemblies,[3] derivatized soluble polymers,[4] electropolymerized thin polymeric films,[5] photoactive DNA cleavage agents,[6] and photovoltaic cells based upon dye-sensitized, colloidal TiO_2.[7]

There is an extensive literature on MLCT excited states and much has been learned about electronic structure, coupled molecular vibrations, the role of low-lying excited states of different orbital origins, and medium effects.[8−10] Much remains to be learned if ground- and excited-state properties (*e.g.* light absorption, excited-state lifetime) are to be optimized. An important molecular feature in these excited states is the acceptor ligand, the ultimate ligand of residence for the excited electron. In heteroleptic chelates, this is the ligand having the lowest π^* acceptor level.[11] For example, in $[Ru(dmb)_2(bpy)]^{2+}$ (dmb is 4,4′-dimethyl-2,2′-bipyridine) the acceptor ligand is bpy (eq 1).

$$[Ru^{II}(dmb)_2(bpy)]^{2+} \xrightarrow{h\nu} [Ru^{III}(dmb)_2(bpy^-)]^{2+*} \quad (1)$$

In some cases the acceptor ligand has been identified directly by transient resonance Raman spectroscopic measurements on

[†] The University of North Carolina.
[‡] Pontificia Universidad Catolica de Chile.
[§] James Cook University of North Queensland.
[⊗] Abstract published in *Advance ACS Abstracts,* February 15, 1996.

(1) (a) Connolly, J. S.; Bolton, J. R. In *Photoinduced Electron Transfer*; Fox, M. A., Chanon, M., Eds.; Elsevier: Amsterdam, 1988; Part D, p 303. (b) Balzani, V.; Scandola, F. *Supramolecular Photochemistry*; Ellis Horwood: New York, 1991. (c) Gust, Moore, T. A. *Science* **1989**, *244*, 35. (d) Scandola, F.; Indelli, M. T.; Chiorboli, C.; Bignozzi, C. A. *Top. Curr. Chem.* **1990**, *158*, 73. (e) Meyer, T. J. *Acc. Chem. Res.* **1989**, *22*, 163. (f) Willner, I; Willner, B. *Adv. Photochem.* **1995**, *20*, 217. (g) Scandola, F.; Bignozzi, C. A.; Indelli, M. T. *Photosensitization and Photocatalysis Using Inorganic and Organometallic Compounds*; Kluwer Academic: Dordrecht, The Netherlands, 1993; pp 161−216. (h) Meyer, T. J. *Pure Appl. Chem.* **1986**, *58*, 1193. (i) Kalyanasundaram, K. *Coord. Chem. Rev.* **1982**, *46*, 159. (j) Sutin, N.; Creutz, C. *Pure Appl. Chem.* **1980**, *52*, 2717. (k) Johnson, S. R.; Westmoreland, T. D.; Caspar, J. V.; Barqawi, K. R.; Meyer, T. J. *Inorg. Chem.* **1988**, *27*, 3195.

(2) (a) Della Ciana, L.; Hamachi, I.; Meyer, T. J. *J. Org. Chem.* **1989**, *54*, 1731. (b) Katritzky, A. R.; Lang, H. Y.; Lan, X. F. *Tetrahedron* **1993**, *49*, 2829. (c) Geren, L.; Hahm, S.; Durham, B.; Millett, F. *Biochemistry* **1991**, *30*, 9450. (d) Luong, J. C.; Faltynek, R. A.; Wrighton, M. S. *J. Am. Chem. Soc.* **1980**, *102*, 7892. (e) Katz, N. E.; Mecklenburg, S. L.; Meyer, T. J. *Inorg. Chem.* **1995**, *34*, 1282 and references therein. (f) Kober, E. M.; Sullivan, B. P.; Dressick, W. J.; Caspar, J. V.; Meyer, T. J. *J. Am. Chem. Soc.* **1980**, *102*, 7383. (g) Sullivan, B. P.; Salmon, D. J.; Meyer, T. J. *Inorg. Chem.* **1978**, *17*, 3334. (h) Juris, A.; Baragelletti, S.; Campagna, S.; Balzani, V.; Belser, P.; von Zelewsky, A. *Coord. Chem. Rev.* **1988**, *84*, 85. (i) Ross, H. B.; Boldaji, M.; Rillema, D. P.; Blanyon, C. B.; White, R. P. *Inorg. Chem.* **1989**, *28*, 1013. (j) Juris, A.; Campagna, S.; Balzani, V.; Gremaud, G. *Inorg. Chem.* **1988**, *27*, 3652. (k) von Zelewsky, A.; Gremaud, G. *Helv. Chim. Acta* **1988**, *71*, 1108. (l) Strouse, G. F.; Anderson, P. A.; Schoonover, J. R.; Meyer, T. J.; Keene, F. R. *Inorg. Chem.* **1992**, *31*, 3004. (m) Hayoz, P.; von Zelewsky, A.; Stoecklievans, H. *J. Am. Chem. Soc.* **1993**, *115*, 5111. (n) Anderson, P. A.; Deacon, G. B.; Haarmann, K. H.; Keene, F. R.; Meyer, T. J.; Reitsma, D. A.; Skelton, B. W.; Strouse, G. F.; Thomas, N. C.; Treadway, J. A.; White, A. H. *Inorg. Chem.* **1995**, *34*, 6145−6157.

(3) (a) Opperman, K. A.; Mecklenburg, S. L.; Meyer, T. J. *Inorg. Chem.* **1994**, *33*, 5295. (b) Mecklenburg, S. L.; Peek, B. M.; Schoonover, J. R.; McCafferty, D. G.; Wall, C. G.; Erickson, B. W.; Meyer, T. J. *J. Am. Chem. Soc.* **1993**, *115*, 5479. (c) Mecklenburg, S. L.; McCafferty, D. G.; Schoonover, J. R.; Peek, B. M.; Erickson, B. W.; Meyer, T. J. *Inorg. Chem.* **1994**, *33*, 2974. (d) Peek, B. M.; Ross, G. T.; Edwards, S. W.; Meyer, T. J. *Int. J. Peptide Protein Res.* **1991**, *38*, 114. (e) Mecklenburg, S. L.; Peek, B. M.; Erickson, B. W.; Meyer, T. J. *J. Am. Chem. Soc.* **1991**, *113*, 8540. (f) Peek, B. M.; Edwards, S. W.; Erickson, B. W.; Mecklenburg, S. L.; Meyer, T. J. In *Peptides: Chemistry, Structure, and Biology*; Smith, J. A., Rivier, J. E., Eds.; ESCOM: Leiden, The Netherlands, 1992. (g) Wasielewski, M. R. *Chem. Rev.* **1992**, *92*, 435. (h) Gust, D.; Moore, T. A. *Top. Curr. Chem.* **1991**, *159*, 103. (i) Balzani, V.; Sabatini, N.; Scandola, F. *Chem. Rev.* **1987**, *86*, 319. (j) Petersen, J. D. *Coord. Chem. Rev.* **1985**, *64*, 261. (k) Krause, R. A. *Struct. Bonding (Berlin)* **1987**, *67*, 1. (l) Ferguson, J.; Herren, F.; Krausz, E. R.; Maeder, M.; Vrbrancich, J. *Coord. Chem. Rev.* **1985**, *64*, 21. (m) Creutz, C. P.; Chou, M.; Netzel, L.; Okumura, M.; Sutin, N. S. *J. Am. Chem. Soc.* **1980**, *102*, 1309. (n) Pankuch, B. J.; Lacky, D. E.; Crosby, G. A. *J. Phys. Chem.* **1980**, *84*, 2061. (o) Lee, E. J.; Wrighton, M. S.; *J. Am. Chem. Soc.* **1991**, *113*, 8562

0020-1669/96/1335-2242$12.00/0

the excited state.[12] The role of the acceptor ligand is the theme of this paper: specifically, how the manipulation of acceptor ligand structure can be used to control lifetime by exploiting *delocalization* and *rigidity* and evidence from the literature that these are general effects.

Most polypyridyl complexes of Ru(II), Os(II), and Re(I) are sufficiently weak emitters that lifetimes are dominated by nonradiative decay. In this limit, the following relationships hold.

$$\tau^{-1} = k_r + k_{nr} \tag{2a}$$

$$\Phi_{em} = \tau k_r \tag{2b}$$

$$\tau^{-1} \sim k_{nr} \tag{2c}$$

In eqs 2, k_r and k_{nr} are the rate constants for radiative and nonradiative decay, Φ_{em} is the emission quantum yield, and τ is the lifetime. Nonradiative decay can include contributions from thermal population and decay through upper excited states. This is commonly the case for complexes of Ru(II), where low-lying dd states of orbital origin $(d\pi)^5(d\sigma^*)^1$ lie close in energy to the emitting MLCT state(s).[8,12]

Nonradiative decay from MLCT states to the ground state is typically dominated by energy loss into a series of medium-frequency ring-stretching vibrations with energy spacings between 1000 and 1600 cm^{-1}.[12,13] For purposes of analysis, these vibrations can be approximated as a single averaged mode of quantum spacing $\hbar\omega_M$ and electron−vibrational coupling constant S_M. S_M is related to the change in equilibrium displacement between the ground and excited state, ΔQ_e, and the reduced mass, M, by eq 3. In the limit that $E_0 \gg$

$$S_M = \frac{1}{2}\frac{M\omega}{\hbar}(\Delta Q_e)^2 \tag{3}$$

$S_M \cdot \hbar\omega_M$ and $\hbar\omega_M \gg k_B T$. k_{nr} varies with E_0 (the energy gap) according to the energy gap law, eqs 4.[14] The first term

$$\ln k_{nr} = \ln(\beta_0) + \ln[F(\text{calc})] \tag{4a}$$

in this equation includes the vibrationally induced electronic coupling matrix element. Nonradiative decay is a transition between states whose electronic wave functions are solutions of the same Hamiltonian. To zero order, they can not mix. The states can be mixed, however, and the transition between states induced, by coupled vibrations of appropriate symmetry.

The second term in eq 4a contains the Boltzmann-weighted vibrational overlap factor, F(calc). The magnitude of k_{nr}

(4) (a) Baxter, S. M.; Jones, W. E.; Danielson, E.; Worl, L. A.; Younathan, J.; Strouse, G. F.; Meyer, T. J. *Coord. Chem. Rev.* **1991**, *111*, 47. (b) Younathan, J. N.; McClanahan, S. F.; Meyer, T. J. *J. Phys. Chem.* **1991**, *95*, 488. (c) Olmstead, J., III; McClanahan, S. F.; Danielson, E.; Younathan, J. N.; Meyer, T. J. *J. Am. Chem. Soc.* **1987**, *109*, 3297. (d) Younathan, J. N.; McClanahan, S. F.; Meyer, T. J. *Macromolecules* **1989**, *22*, 1048. (e) Margerum, L. D.; Meyer, T. J.; Murray, R. W. *J. Phys. Chem.* **1986**, *90*, 2696. (f) Jones, W. E.; Baxter, S. M.; Strouse, G. F.; Meyer, T. J. *J. Am. Chem. Soc.* **1993**, *115*, 7363. (g) Strouse, G. F.; Worl, L. A.; Younathan, J. N.; Meyer, T. J. *J. Am. Chem. Soc.* **1989**, *111*, 9101. (h) Worl, L. A.; Strouse, G. F.; Younathan, J. N.; Baxter, S. M.; Meyer, T. J. *J. Am. Chem. Soc.* **1990**, *112*, 7571.

(5) (a) Abruna, H. D. *Coord. Chem. Rev.* **1988**, *86*, 135. (b) Calvert, J. M.; Schmehl, R. H.; Sullivan, B. P.; Facci, J. S.; Meyer, T. J.; Murray, R. W. *Inorg. Chem.* **1983**, *22*, 2151. (c) Denisevich, P.; Abruna, C. R.; Leidner, C. R.; Meyer, T. J.; Murray, R. W. *Inorg. Chem.* **1982**, *21*, 2153. (d) Calvert, J. M.; Sullivan, B. P.; Meyer, T. J. In *Chemically Modified Surfaces In Catalysis and Electrocatalysis*; Miller, J., Ed.; ACS Symposium Series; American Chemical Society: Washington, DC, 1982; p 159. (e) Abruna, H. D.; Calvert, J. M.; Denisevich, P.; Ellis, C. D.; Meyer, T. J.; Murphy, W. R.; Murray, R. W.; Sullivan, B. P.; Walsh, J. L. In *Chemically Modified Surfaces In Catalysis and Electrocatalysis*; Miller, J., Ed.; ACS Symposium Series; American Chemical Society: Washington, DC, 1982; p 133. (f) Gould, S.; Gray, K.; Linton, R. W.; Meyer, T. J. *Inorg. Chem.* **1992**, *31*, 5521.

(6) (a) Neyhart, G. A.; Cheng, C.; Thorp, H. H. *J. Am. Chem. Soc.* **1995**, *117*, 1463. (b) Thorp, H. H.; Cheng, C.; Goll, J. G. *J. Am. Chem. Soc.* **1995**, *117*, 2970. (c) Thorp, H. H.; Cheng, C.; Johnson, D. H. *Inorg. Chem.* **1994**, *33*, 6388. (d) Smith, S. R.; Neyhart, G. A.; Kalsbeck, W. A. *New J. Chem.* **1994**, *18*, 397. (e) Grover, N.; Gupta, N.; Singh, P. *Inorg. Chem.* **1992**, *31*, 2014.

(7) (a) Nazeeruddin, M. K.; Kay, A.; Rodicio, I.; Humphry-Baker, R.; Müller, E.; Liska, P.; Viachopoulos, N.; Grätzel, M. *J. Am. Chem. Soc.* **1993**, *115*, 6382. (b) O'Reagan, B.; Grätzel, M. *Nature* **1991**, *353*, 737. (c) Willig, F.; Eichberger, R. *Chem. Phys.* **1990**, *141*, 159. (d) Vlachopoulos, N.; Liska, P.; Augustyynski, J.; Grätzel, M. *J. Am. Chem. Soc.* **1988**, *110*, 1216. (e) Kamat, P. V. *Chem. Rev.* **1993**, *93*, 267. (f) Heimer, T. A.; Bignozzi, C. A.; Meyer, G. J. *J. Phys. Chem.* **1993**, *97*, 11987. (g) Bignozzi, C. A.; Meyer, G. J.; Argazzi, R. *Inorg. Chem.* **1994**, *33*, 5741.

(8) (a) Durham, B.; Caspar, J. V.; Nagle, J. K.; Meyer, T. J. *J. Am. Chem. Soc.* **1982**, *104*, 4803. (b) Porter, G. B.; Sparks, R. H. *J. Photochem.* **1980**, *13*, 123. (c) Rillema, D. P.; Blanton, C. B.; Shaver, R. J.; Jackman, D. C.; Boldaji, M.; Bundy, S.; Worl, L. A.; Meyer, T. J. *Inorg. Chem.* **1992**, *31*, 1600. (d) Segers, D. P.; DeArmond, M. K. *J. Phys. Chem.* **1982**, *86*, 3768. (e) Gleria, M.; Minto, F.; Beggiato, G.; Bortolus, P. *J. Chem. Soc., Chem. Commun.* **1978**, 285. (e) Allen, G. H.; White, R. P.; Rillema, D. P.; Meyer, T. J. *J. Am. Chem. Soc.* **1984**, *106*, 2613. (f) Barqawi, K. R.; Llobet, A.; Meyer, T. J. *J. Am. Chem. Soc.* **1988**, *110*, 7751. (g) Kirchoff, J. R.; McMillan, D. R.; Marnot, P. A.; Sauvage, J. *J. Am. Chem. Soc.* **1985**, *107*, 1138. (h) Lin, C. T.; Boettcher, W.; Chou, M.; Creutz, C.; Sutin, N. *J. Am. Chem. Soc.* **1976**, *98*, 6536. (i) Pinnick, D. V.; Durham, B. *Inorg. Chem.* **1984**, *23*, 3841.

(9) (a) Chen, P.; Mecklenburg, S. L.; Meyer, T. J. *J. Phys. Chem.* **1993**, *97*, 13126. (i) Chen, P.; Danielson, E.; Meyer, T. J. *J. Phys. Chem.* **1988**, *92*, 3708. (b) Jones, W. E.; Chen, P.; Meyer, T. J. *J. Am. Chem. Soc.* **1992**, *114*, 387. (c) Castellano, F. N.; Heimer, T. A.; Tandhasetti, M. T.; Meyer, G. J. *Chem. Mater.* **1994**, *6*, 1041. (d) Ford, W. E.; Rodgers, M. A. J. *J. Phys. Chem.* **1994**, *98*, 7415. (e) Barigelletti, F.; Juris, A.; Balzani, V.; Belser, P.; von Zelewky, A. *J. Phys. Chem.* **1987**, *91*, 1095. (f) Vining, W. J.; Caspar, J. V.; Meyer, T. J. *J. Phys. Chem.* **1985**, *89*, 1095.

(10) (a) Kober, E. M.; Meyer, T. J. *Inorg. Chem.* **1982**, *21*, 3967. (b) Kober, E. M.; Goldsby, K. A.; Narayana, D. N. S.; Meyer, T. J. *J. Am. Chem. Soc.* **1983**, *105*, 4303. (c) Kober, E. M.; Meyer, T. J. *Inorg. Chem.* **1984**, *23*, 3877. (d) Goldsby, K. A.; Meyer, T. J. *Inorg. Chem.* **1984**, *23*, 3002. (e) Danielson, E.; Lumpkin, R. S.; Meyer, T. J. *J. Phys. Chem.* **1987**, *91*, 1305. (f) Crosby, G. A. *Acc. Chem. Res.* **1975**, *8*, 231. (g) Mandal, K.; Pearson, T. P. C.; Krog, W. P.; Demas, J. N. *J. Am. Chem. Soc.* **1983**, *105*, 701. (h) Crosby, G. A.; Watts, R. J.; Carstens, D. H. W. *Science* **1970**, *170*, 1195. (i) Sprouse, S.; King, K. A.; Spellane, P. J.; Watts, R. J. *J. Am. Chem. Soc.* **1984**, *106*, 6647. (j) Demas, J. N. *J. Chem. Educ.* **1983**, *60*, 803. (k) Watts, R. J. *J. Chem. Educ.* **1983**, *60*, 834. (l) Hager, G. P.; Crosby, G. A. *J. Am. Chem. Soc.* **1975**, *97*, 7031. (m) Crosby, G. A. Elfring, J. *J. Phys. Chem.* **1976**, *80*, 2206. (n) Hipps, K. W.; Crosby, G. A.; *J. Am. Chem. Soc.* **1975**, *97*, 7042.

(11) Ford, W. E.; Calvin, M. *Chem. Phys. Lett.* **1980**, *76*, 105. (b) Riesen, H.; Krausz, E. R. *J. Chem. Phys.* **1993**, *99*, 7614.

(12) (a) Mabrouk, P. A.; Wrighton, M. S. *Inorg. Chem.* **1986**, *25*, 526. (b) Chang, Y. J.; Xiaobing, X.; Soo-Chang, Y.; Anderson, D. R.; Orman, L. K.; Hopkins, J. B. *J. Phys. Chem.* **1990**, *94*, 729. (c) Bradley, P. G.; Kress, N.; Hornberger, B. A.; Dallinger, R. F.; Woodruff, W. H. *J. Am. Chem. Soc.* **1981**, *103*, 7441. (d) Caspar, J. V.; Westmoreland, T. D.; Allen, G. H.; Bradley, P. G.; Meyer, T. J.; Woodruff, W. H. *J. Am. Chem. Soc.*, **1984**, *106*, 3492. (e) Danzer, G. D.; Golus, J. A.; Kincaid, J. R. *J. Am. Chem. Soc.* **1993**, *115*, 8643.

(13) (a) Maruszewski, K.; Bajdor, K.; Strommen, D. P.; Kincaid, J. R. *J. Phys. Chem.* **1995**, *99*, 6286. (b) Van Houten, J.; Watts, J. R. *J. Am. Chem. Soc.* **1976**, *98*, 4853. (c) Kober, E. M.; Meyer, T. J. *Inorg. Chem.* **1985**, *24*, 106. (d) Caspar, J. V.; Kober, E. M.; Sullivan, B. P.; Meyer, T. J. *J. Am. Chem. Soc.* **1982**, *104*, 630. (e) Dallinger, R. F.; Woodruff, W. H. *J. Am. Chem. Soc.* **1979**, *101*, 4391. (f) Clark, R. J. H.; Turtle, P. C.; Strommen, D. P.; Streusand, B.; Kincaid, J. R.; Nakamoto, K. *Inorg. Chem.* **1977**, *16*, 84.

(14) (a) Kober, E. M.; Caspar, J. V.; Lumpkin, R. S.; Meyer, T. J. *J. Phys. Chem.* **1986**, *90*, 3722. (b) Freed, K. F. *Top. Curr. Chem.* **1972**, *31*, 105. (c) Englman, R.; Jortner, J. *Mol. Phys.* **1970**, *18*, 145. (d) Freed, K. F.; Jortner, J. *J. Chem. Phys.* **1970**, *52*, 6272. (e) Bixon, M.; Jortner, J. *J. Chem. Phys.* **1968**, *48*, 715.

$$\ln[F(\text{calc})] = -{}^1/_2 \ln\left[\frac{\hbar\omega_M E_0}{(1000\ \text{cm}^{-1})^2}\right] - S_M - \frac{\gamma E_0}{\hbar\omega_M} + \left(\frac{\gamma+1}{\hbar\omega_M}\right)^2\left[\frac{(\Delta\bar{\nu}_{0.1/2})^2}{16\ln 2}\right] \quad (4b)$$

$$\gamma = \ln\left(\frac{E_0}{S_M\hbar\omega_M}\right) - 1 \quad (4c)$$

depends on the square of the vibrational overlap integral between the initial $\upsilon_M^* = 0$ level in the excited state and the acceptor vibrational level in the ground state, υ_M. This is the origin of the energy gap term, $\gamma E_0/\hbar\omega_M$, in eq 4b. The vibrational overlap integral is a quantitative measure of the coincidence of the two states along the normal coordinate. The transition between states must occur with energy conservation. The difference between the initial excited-state energy and the energy of the acceptor level, $S_M{\cdot}\hbar\omega_M$, appears in the ground state in coupled low-frequency vibrations and in the solvent. These are included in the term containing the bandwidth, $\Delta\bar{\nu}_{0.1/2}$, in eq 4b. $\Delta\bar{\nu}_{0.1/2}$ includes low-frequency vibrations treated classically ($\chi_{i,L}$) and the solvent reorganizational energy (χ_o). E_0 is related to the 0−0 energy, $E(0-0)$, by eq 5. The relationship between k_{nr} and E_0 in eq 4 has been shown to be valid for MLCT decay in many cases.[15,16]

$$E(0-0) = E_0 + \frac{(\Delta\bar{\nu}_{0.1/2})^2}{16\ln 2\, k_B T} \quad (5)$$

Since the term linear in E_0 is the most important one in eq 4, the approximation in eq 6 is typically found to hold.[14a,16] The

$$\ln \tau^{-1} \sim \ln k_{nr} \propto -\frac{\gamma E_0}{\hbar\omega_M} \quad (6)$$

acceptor ligand appears in this relationship in two ways. One is the energy gap. The other is the extent of excited-state distortion as measured by ΔQ_e. ΔQ_e appears in S_M (eq 3) which appears in γ. As noted above, these parameters dictate the magnitude of vibrational wave function overlap between $\upsilon_M^* = 0$ levels in the excited state and $\upsilon_M = 0, 1, 2, \ldots$ levels in the ground state. In the limit that the energy gap law is valid, overlap increases as E_0 decreases. Overlap also increases as S_M increases.

The dependence of k_{nr} on E_0 and S_M has been verified experimentally. For example, the dependence on energy gap has been demonstrated in the two series $[Os(phen)(L)_4]^{2+}$ (phen is 1,10-phenanthroline) and $[Os(bpy)(L)_4]^{2+}$, where the energy gap was varied by changes in the nonchromophoric ligands L.[14a,17] A role for ligand rigidity and S_M has been found in comparing the two ligands as acceptors. For example, $[Os(bpy)_3]^{2+*}$ and $[Os(phen)_3]^{2+*}$ have comparable energy gaps ($E_0 \sim 13\,400\ \text{cm}^{-1}$), but k_{nr} for the bipyridine complex ($1.6 \times 10^7\ \text{s}^{-1}$) is approximately four times that of the phenanthroline complex ($3.8 \times 10^6\ \text{s}^{-1}$) in acetonitrile at 298 K.[18] From a Franck−Condon analysis of emission spectra, $S_{bpy} > S_{phen}$ because of enhanced rigidity in phenanthroline as the acceptor arising from the chemical link between the pyridyl rings.

An additional effect has been identified in the bridged complex $\{[Ru(dmb)_2]_2(bbpe)\}^{4+*}$ (bbpe is 1,2-bis(4-(4′-methyl)-2,2′-bipyridyl)ethene).[19] The value of k_{nr} in 4:1 ethanol:methanol at 157 K ($6.6 \times 10^5\ \text{s}^{-1}$) is much less than in $[Ru(bpy)_2(py)Cl]^{+*}$ ($9.6 \times 10^6\ \text{s}^{-1}$) even though the energy gaps are comparable. Spectral fitting shows that S_M decreases from 0.72 for $[Ru(bpy)_2(py)Cl]^{+*}$ to 0.38 in the bbpe-bridged complex. The decrease in S_M decreases excited/ground state vibrational overlap. S_M is smaller when bbpe is the acceptor ligand because the excited electron is delocalized over a larger molecular framework. This decreases displacement changes in the local C−C and C−N bonds. Ligand delocalization contributes to the fact that $[Ru(dmb)_2(bbpe)]^{2+*}$ has a longer lifetime (1150 ns) than $[Ru(dmb)_3]^{2+*}$ (950 ns in acetonitrile at 298 K) even though the energy gap in $[Ru(dmb)_2(bbpe)]^{2+}$ is much smaller (14 600 cm^{-1} compared to 16 350 cm^{-1}). Recently, Schmehl *et al.* observed a similar effect in $[Ru(dmb)_2(bphb)]^{2+*}$ and $\{[(dmb)_2Ru]_2(bphb)\}^{4+*}$, where bphb is the phenyl-bridged ligand 1,4-bis(4-methyl-2,2′-bipyridin-4-yl)benzene.[20]

We report here a brief survey of the literature which suggests that these are general effects. Data relevant to this issue are summarized in Table 1. The structures of the ligands are shown in Figure 1.

Table 1. Ground- and Excited-State Parameters for Ru^{II} and Os^{II} Polypyridyl Complexes at 298 K

complex[a]	λ_{abs} (nm)	λ_{em} (nm)	E_{em} (cm^{-1})	τ (ns)	ref
$[Ru(bpy)_3]^{2+}$	452	615	16 300	1100	26
$[Ru(dmb)(bpy(COOEt)_2)(dpp)]^{2+}$	479	678	14 700	788	2p
$[Ru(dmb)(bpy(COOEt)_2)(dpq)]^{2+}$	511	790	12 600	29	29b,c
$[Ru(dmb)(bpy(COOEt)_2)(dpb)]^{2+}$	547	>850	<11 800	98	29a,c
$[Os(bpy)_3]^{2+}$	658	746	13 400	60	17
$[Os(tpy)_2]^{2+}$	657	718	13 900	296	17
$[Os(ttpy)_2]^{2+}$ [b]	668	736	13 600	236	21
$[Os(tptpy)_2]^{2+}$ [b]	692	751	13 300	266	21
$[Os(bpy)_2(bbpe)]^{2+}$	668	810	12 300	58	19
$\{(bpy)_2Os(bbpe)Os(bpy)_2\}^{4+}$	682	>850	<11 800	52	19
$[Ru(bpy)_2(dpp)]^{2+}$	464	660	15 200	226	30
$[Ru(bpy)_2(dpp')]^{2+}$	466	678	14 700	1214	31
$[Ru(bpy)_2(dpq)]^{2+}$	516	766	13 100	71	30
$[Ru(bpy)_2(dpq')]^{2+}$	536	828	12 100	327	31

[a] Complexes in deaerated acetonitrile except where noted. [b] In deaerated 4:1 ethanol:methanol (v/v).

Analysis

Care must be taken in interpreting the lifetime data in Table 1. In Ru^{II} complexes, contributions to k_{nr} come in varying degrees from thermal population and decay through low-lying dd states and upper MLCT states.[8,18] Analysis of lifetimes based on the energy gap law is valid only for nonradiative decay from the lowest MLCT state or states. Contributions to k_{nr} from competing thermally activated processes can be assessed by temperature-dependent lifetime measurements, but even in the absence of these data there are revealing trends in the data in Table 1.

There are clear-cut examples of the delocalization effect in the series $[Ru(dmb)(bpy(COOEt)_2)(LL)]^{2+}$, where LL is 2,3-bis(2-pyridyl)pyrazine (dpp), 2,3-bis(2-pyridyl)quinoxaline (dpq), and 2,3-bis(2-pyridyl)benzoquinoxaline (dpb). As the number of rings in the dpp, dpq, or dpb acceptor ligands is increased, the energy gap (as approximated by E_{em}) decreases. The

(15) (a) Barqawi, K. R.; Murtaza, Z.; Meyer, T. J. *J. Phys. Chem.* **1991**, *95*, 47. (b) Worl, L. A.; Duesing, R.; Chen, P.; Della Ciana, L.; Meyer, T. J. *J. Chem. Soc., Dalton Trans.* **1991**, 849.
(16) (a) Caspar, J. V.; Sullivan, B. P.; Kober, E. M.; Meyer, T. J. *Chem. Phys. Lett.* **1982**, *91*, 91. (b) Caspar, J. V.; Meyer, T. J. *J. Phys. Chem.* **1983**, *87*, 952.
(17) Kober, E. M.; Marshall, J. L.; Dressick, W. J.; Sullivan, B. P.; Caspar, J. V.; Meyer, T. J. *Inorg. Chem.* **1985**, *24*, 2755.
(18) Lumpkin, R. S.; Kober, E. M.; Worl, L.; Murtaza, Z.; Meyer, T. J. *J. Phys. Chem.* **1990**, *94*, 239.
(19) Strouse, G. F.; Schoonover, J. R.; Duesing, R.; Boyde, S; Jones, W. E.; Meyer, T. J. *Inorg. Chem.* **1995**, *34*, 473.
(20) Baba, A. I.; Ensley, H. E.; Schmehl, R. H. *Inorg. Chem.* **1995**, *34*, 1198.

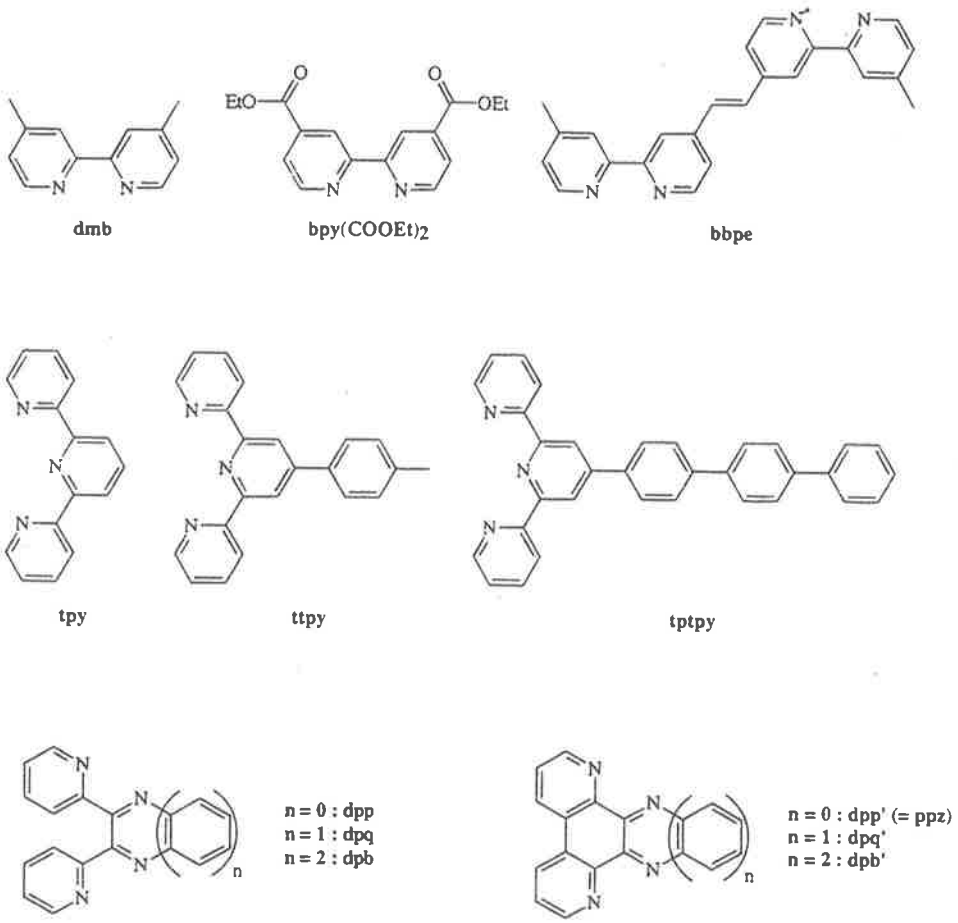

Figure 1. Ligand structures.

decrease in the energy gap occurs because of stabilization of the lowest π^* acceptor level as shown by electrochemical measurements. The $Ru^{III/II}$ potentials for the three are nearly constant at 1.44−1.47 V (versus SCE, 0.1 M $[N(n\text{-}C_4H_9)_4](PF_6)$ in acetonitrile) while the ligand-based reduction potentials are −0.96 V (dpp), −0.75 V (dpq), and −0.59 V (dpb). The excited-state lifetime does decrease from LL = dpp to LL = dpq (although less than expected based solely on the energy gap), but in a comparison of dpq and dpb as acceptor ligands, the excited-state lifetime actually increases from 29 to 98 ns even though the energy gap decreases by ~1000 cm^{-1}. In these complexes, the MLCT excited states are relatively low in energy. Ligand loss photochemistry, which usually accompanies nonradiative decay by thermal activation to dd states, is either of low efficiency or not observed, and dd states presumably play a negligible role in dictating the magnitude of τ.

Another example is shown in the Os(II) complexes containing terpyridyl derivatives as the acceptor ligands. In these ligands there are three acceptor rings compared to two for bipyridine. $[Os(tpy)_2]^{2+}$ and $[Os(bpy)_3]^{2+}$ have comparable energy gaps, but the terpyridine complex exhibits a substantially longer lifetime (296 ns compared to 60 ns).[17] In a comparison of $[Os(ttpy)_2]^{2+}$ and $[Os(tptpy)_2]^{2+}$, the latter has an energy gap 270 cm^{-1} smaller than the former yet exhibits a longer lifetime (266 ns versus 236 ns).[21] The Os(II) complexes incorporating bbpe as an acceptor ligand provide another example. $[Os(bpy)_2(bbpe)]^{2+*}$ has an energy gap that is ~1000 cm^{-1} smaller than $[Os(bpy)_3]^{2+*}$, but their lifetimes are nearly the same. $[(bpy)_2Os(bbpe)Os(bpy)_2]^{4+*}$ emits even further into the red (<11 800 cm^{-1}) but has a comparable lifetime.[19] Because $10Dq$ is ~30% larger for Os(II) compared to Ru(II), excited-state behavior for Os(II) complexes tends to be free of complicating features arising from dd states.[22]

A combination of rigidity *and* delocalization may account for the enhanced lifetimes of $[Ru(bpy)_2(dpp')]^{2+}$ and $[Ru(bpy)_2(dpq')]^{2+}$ compared to $[Ru(bpy)_2(dpp)]^{2+}$ and $[Ru(bpy)_2(dpq)]^{2+}$. Delocalization plays a role as evidenced by the decrease in emission energies, but the bipyridine versus phenanthroline comparison mentioned above suggests that the additional bond linking the ring systems in dpp′ and dpq′ may play a role as well.

There are additional examples in the literature where extended π systems and delocalization in the acceptor ligand appear to play a significant role. Examples include (Figure 2) i-biq,[23] dpop,[24] HAT,[25] dmch,[26] dppz,[27] and the series tpy(phenyl)$_n$tpy (n = 0, 1, 2).[28] A proper accounting must await a more

(21) (a) Beley, M.; Collin, J.; Sauvage, J.; Sugihara, H.; Heisel, F.; Miehé, A. *J. Chem. Soc., Dalton Trans.* **1991**, 3175. (b) Beley, M.; Chodorowski, S.; Collin, J.; Sauvage, J.; Flamigni, L.; Barigelletti, F. *Inorg. Chem.* **1994**, *33*, 2543.

(22) (a) Jorgensen, C. K. *Absorption Spectra and Chemical Bonding in Complexes*; Pergamon: London, 1962; p 114. (b) Kober, E. M.; Meyer, T. J. *Inorg. Chem.* **1983**, *22*, 1614.

(23) Juris, A.; Barigelletti, F.; Balzani, V.; Belser, P.; von Zelewsky, A. *Inorg. Chem.* **1985**, *24*, 202.

(24) (a) Ruminski, R. R.; Servies, D.; Jacquez, M. *Inorg. Chem.* **1995**, *34*, 3358. (b) Ruminski, R. R.; Freiheit, D.; Johnson, J. E. B. *Inorg. Chim. Acta* **1994**, *224*, 27.

(25) (a) Buyl, F. d.; Mesmaeker, A. K.; Tossi, A. *J. Photochem. Photobiol., A: Chem.* **1991**, *60*, 27. (b) Sahia, R.; Rillema, D. P.; Shaver, R.; Van Wallendael, S.; Jackman, D. C.; Boldaji, M. *Inorg. Chem.* **1989**, *28*, 1022.

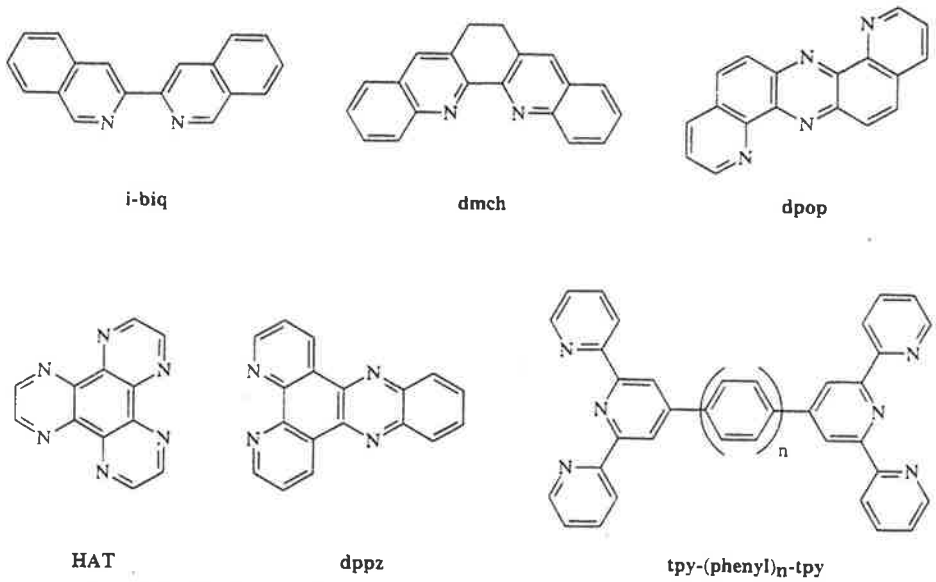

Figure 2. Ligand structures where delocalization appears to play a significant role.

comprehensive analysis including spectral fitting and temperature-dependent lifetime measurements for the Ru(II) complexes.

Conclusions

On the basis of our observations, there are important implications for nonradiative decay and for the design of MLCT excited states. They point out that the energy gap law must be applied with care. As suggested by eq 5, ln k_{nr} and ln τ^{-1} may vary with energy gap, but they also depend on γ and S_M (eqs 4). Within the series $[Os(phen)(L)_4]^{2+*}$ and $[Os(bpy)(L)_4]^{2+*}$, S_M has been found to vary linearly with E_0.[15a,16a,17] As the structure of the acceptor ligand is varied, the dependence of S_M on E_0 will vary as well. Each acceptor ligand should have its own energy gap dependence.

If applied systematically, the rigidity and delocalization effects offer new possibilities for the design of controlled excited-state properties. For example, we recently reported a synthetic approach to "black" MLCT chromophores which absorb appreciably throughout much of the near UV−vis.[29] The energy gaps of the excited states formed upon MLCT excitation are small, *e.g.* $E_{em} < 11\,800$ cm^{-1} for $[Ru(dmb)(bpy(COOEt)_2)(dpb)]^{2+*}$, which would normally lead to short lifetimes. The combination of both rigidity and delocalization in dpb as the acceptor ligand, however, leads to an excited state lifetime (τ = 98 ns in acetonitrile at 298 K) long enough for either intra- or intermolecular electron or energy transfer to compete with excited-state decay.

Acknowledgment. Financial support from the Australian Research Council, Fondecyt-CHILE (Grant 1940577), Conicyt-CHILE (Grant 2950063), and the U.S. Department of Energy (Grant DE-FG05-86ER13633) is gratefully acknowledged. Travel between the laboratories at PUC and UNC (B.L. and R.L.) has been supported by the U.S. National Science Foundation (Grant INT-9123215) and Conicyt. Travel between the laboratories at JCUNQ and UNC (J.A.T. and P.A.A.) has been supported by the U.S. National Science Foundation (Grant INT-9015262) and the Australian Department of Industry, Science, and Technology within the Australia-U.S. Bilateral Science and Technology Program.

IC950961S

(26) Juris, A.; Balzani, V; Belser, P.; von Zelewsky, A. *Helv. Chim. Acta* **1981**, *64*, 2175.

(27) (a) Amouyal, E.; Homsi, A.; Chambron, J.; Sauvage, J. *J. Chem. Soc., Dalton Trans.* **1990**, 1841. (b) Hartshorn, R. M.; Barton, J. K. *J. Am. Chem. Soc.* **1992**, *114*, 5919

(28) (a) Collin, J.; Guillerez, S.; Sauvage, J.; Barigelletti, F.; De Cola, L.; Flamigni, L.; Balzani, V. *Inorg. Chem.* **1991**, *30*, 4230. (b) Collin, J.; Guillerez, S.; Sauvage, J. *J. Chem. Soc., Chem. Commun.* **1989**, 776.

(29) (a) Anderson, P. A.; Strouse, G. F.; Treadway, J. A.; Keene, F. R.; Meyer, T. J. *Inorg. Chem.* **1994**, *33*, 3863. (b) Anderson, P. A. Ph.D. Thesis, James Cook University of North Queensland, Australia, 1995. (c) Anderson, P. A.; Keene, F. R.; Loeb, B.; Lopez, R.; Meyer, T. J.; Strouse, G. F.; Treadway, J. A. Manuscript in preparation.

(30) (a) Molnar, S. M.; Neville, K. R.; Jensen, G. E.; Brewer, K. J. *Inorg. Chim. Acta* **1993**, *206*, 69. (b) Wallace, A. W.; Murphy, W. R.; Petersen, J. D. *Inorg. Chim. Acta* **1989**, *166*, 47.

(31) (a) Lopez, L. Licentiate and Chemist Degree Thesis, Pontificia Universidad Catolica de Chile, 1994. (b) Loeb, B. L.; Lopez, R.; Lopez, L.; Treadway, J. A.; Claude, J. P.; Meyer, T. J. Work in progress.

5144 *Inorg. Chem.* 1996, *35*, 5144−5153

Spectral and Electrochemical Properties of the Diastereoisomeric Forms of Azobis(2-pyridine)-Bridged Diruthenium Species

Laurence S. Kelso, David A. Reitsma, and F. Richard Keene*

Department of Chemistry and Chemical Engineering, School of Molecular Sciences, James Cook University of North Queensland, Townsville, Queensland 4811, Australia

Received January 24, 1996[⊗]

A series of dinuclear complexes of ruthenium(II) have been synthesized in which α-azodiimines {such as azobis-(2-pyridine), apy, and azobis(4-methyl-2-pyridine), mapy} act as the bridge and 2,2′-bipyridine (bpy) or 4,4′-dimethyl-2,2′-bipyridine (Me_2bpy) as the terminal ligands. The diastereoisomeric forms of each species {ΔΛ *(meso)* and ΔΔ/ΛΛ *(rac)*} have been separated by cation-exchange chromatography and characterized by ^{1}H-NMR spectroscopy. Electronic spectral and electrochemical studies show there to be differences in inter-metal communication between the diastereoisomeric forms in each case. Comparison of the spectroelectrochemical behavior of the range of complexes has allowed unequivocal assignment of the site of the successive reduction processes observed in dinuclear complexes of this type.

Introduction

The stereoisomeric complexity of ligand-bridged polymetallic molecular assemblies based on tris(bidentate)metal centers has only recently been addressed.[1−6] The number of isomers in such species increases exponentially with nuclearity, and the consequences of this stereoisomerism may well prove significant in terms of intramolecular electron and energy transfer processes.

In the simplest case of a dinuclear species $[\{Ru(pp)_2\}_2(\mu\text{-}L)]^{4+}$ (where L is a symmetrical bridging ligand and pp is a bidentate terminal ligand), an examination of the two diastereoisomeric forms (Figure 1) shows a significant difference in the relative orientations of the terminal ligands "above" and "below" the plane of the bridging ligand. In the simplest case, where the bridging ligand is 2,2′-bipyrimidine,[1,4,6] or azobis-(2-pyridine) as in the present study, the "above plane" ligands are parallel in the ΔΔ/ΛΛ *(racemic)* and orthogonal in the ΔΛ/ΛΔ *(meso)* diastereoisomer.

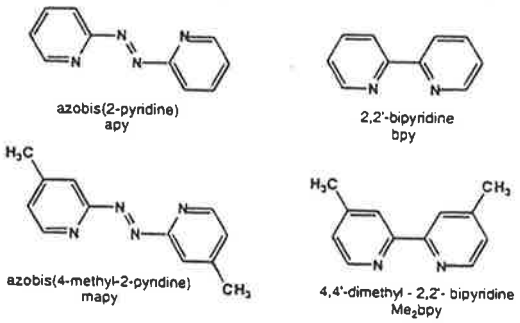

In addition to such stereochemical considerations, the bridging ligand affects the degree of metal−metal interaction in di- and oligonuclear complexes, as it determines the distance and relative orientation of the metal centers, and influences through-space electronic coupling and the degree of through-bond communication (via ligand−metal orbital overlap).[7,8]

Ligands possessing the azo functionality have extremely low-lying π^* orbitals and are strongly π-accepting.[9−15] Moreover,

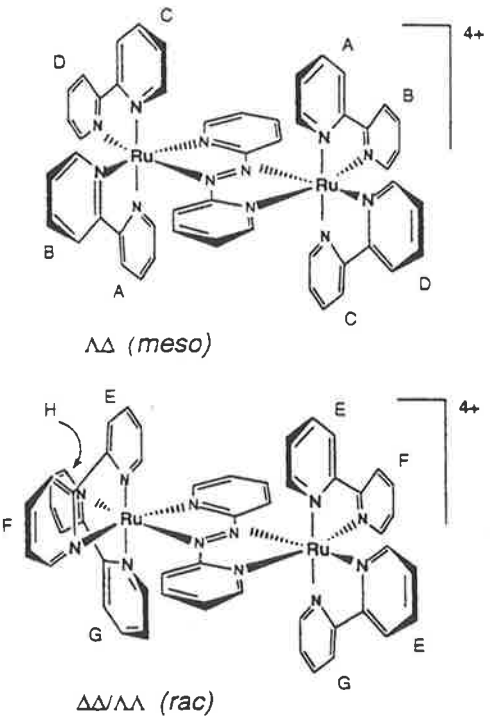

Figure 1. Diastereoisomeric forms (*meso* and *rac*) of $[\{Ru(bpy)_2\}_2(\mu\text{-apy})]^{4+}$ and ring-numbering scheme used for NMR discussion.

[⊗] Abstract published in *Advance ACS Abstracts*, August 1, 1996.

(1) Reitsma, D. A.; Keene, F. R. *J. Chem. Soc., Dalton Trans.* **1993**, 2859.
(2) Anderson, P. A.; Deacon, G. B.; Haarmann, K. H.; Keene, F. R.; Meyer, T. J.; Reitsma, D. A.; Skelton, B. W.; Strouse, G. F.; Thomas, N. C.; Treadway, J. A.; White, A. H. *Inorg. Chem.* **1995**, *34*, 6145.
(3) Rutherford, T. J.; Quagliotto, M. G.; Keene, F. R. *Inorg. Chem.* **1995**, *34*, 3857.
(4) Hua, X.; von Zelewsky, A. *Inorg. Chem.* **1991**, *30*, 3796.
(5) von Zelewsky, A. *Chimia* **1994**, *48*, 331.
(6) Hua, X.; von Zelewsky, A. *Inorg. Chem.* **1995**, *34*, 5791.
(7) Kalyanasundaram, K.; Nazeeruddin, M. K. *Inorg. Chim. Acta* **1994**, *226*, 213.
(8) Balzani, V.; Scandola, F. *Supramolecular Photochemistry*; Ellis Horwood: Chichester, U.K., 1991; p 427.
(9) Ernst, S. D.; Kaim, W. *Inorg. Chem.* **1989**, *28*, 1520.
(10) Krause, R. A.; Krause, K. *Inorg. Chem.* **1980**, *19*, 2600.
(11) Krause, R. A.; Krause, K. *Inorg. Chem.* **1982**, *21*, 1714.
(12) Krause, R. A.; Krause, K. *Inorg. Chem.* **1984**, *23*, 2195.

S0020-1669(96)00089-4 CCC: $12.00

dinuclear complexes in which ligands such as azobis(2-pyridine) function as the bridge have comproportionation constants (K_c) in excess of 10^8 for the diruthenium case and hence exhibit a very high degree of metal−metal interaction.[7,9,13,16,17] Bridging ligands of this type also are found to enhance the structural differences between the diastereoisomers of such dinuclear species.

Despite the intense interest in dimetallic polypyridyl complexes, studies of their properties have been based almost exclusively on nonseparated isomeric mixtures so that reported data may be thought of as an average of the contributions of each form. The high degree of metal−metal interaction within α-azodiimine-bridged dinuclear complexes, coupled with structural dissimilarities between the diastereoisomeric pairs, prompted an examination of the spectral and electrochemical behavior of the different forms. By subtle variation of the bridge via incorporation of ring substituents (e.g. methyl groups) the electronic character of the resulting complexes may be probed. The photophysical and electrochemical effects of variations in the terminal (nonbridging) ligands upon the bridge also warrant examination[18] and may be probed in a similar manner.

In the present work, we describe the synthesis of a series of mono- and dinuclear complexes containing α-azodiimine ligands such as azobis(2-pyridine) and azobis(4-methyl-2-pyridine) {abbreviated apy and mapy, respectively} and assess the influence of the bridge on metal−metal and also metal−ligand interactions. Significantly, differences in various properties of the separated diastereoisomers of α-azodiimine-bridged dinuclear ruthenium(II) complexes are observed.

Experimental Section

Physical Measurements. Electronic spectra were recorded using a Cary 5E UV−vis−near-IR spectrophotometer. NMR spectra were recorded on a Bruker Aspect AM3000 spectrometer. Electrochemical measurements were made in a Vacuum Atmospheres drybox (Ar) using a Bioanalytical Systems (BAS) 100A electrochemical analyzer. Cyclic and differential pulse voltammetries were carried out in a three-electrode cell using a platinum microdisk working electrode, with a platinum counter electrode. All potentials are quoted relative to an $Ag/AgNO_3$ reference electrode (0.01 M in CH_3CN), which is 0.095 V cathodic of the ferrocene/ferrocenium couple as an internal standard. Elemental analyses were performed within the School of Molecular Sciences, JCUNQ. The successive oxidized and reduced forms of the dinuclear species were selectively generated and characterized *in situ* by electronic absorption spectroscopy using a cryostatic optically transparent thin-layer electrochemical (OTTLE) cell[19] in conjuction with a Perkin-Elmer Lambda 9 UV−vis−near-IR spectrophotometer.

Materials. 2-Aminopyridine, sodium toluene-4-sulfonate, sodium ditoluoyl-(−)-tartrate, 2,2′-bipyridine, 4,4′-dimethyl-2,2′-bipyridine (all Adrich), 2-amino-4-methylpyridine (Fluka), $RuCl_3{\cdot}3H_2O$ (Strem), and commercial grade NaOCl (12.5% w/v, Swimfree pool chlorine) were used as supplied. The electrolyte tetra-*n*-butylammonium perchlorate {[(*n*-$C_4H_9)_4N]ClO_4$; purum, Fluka) was recrystallized from ethyl acetate/hexane and dried at 60 °C under vacuum. Spectral grade acetonitrile (Sigma) was used for all spectroscopic and electrochemical measurements. All other reagent grade solvents were used without further purification.

Ligand Syntheses. Azobis(2-pyridine), apy, was prepared by modification of literature methods.[20,21] The crude product was purified by vacuum chromatography on silica gel,[22] using dichloromethane as eluent. Unreacted starting material eluted first, followed by the highly colored major product band. Red needles were obtained after recrystallization from petroleum ether (600 cm³, bp 60−80 °C). Yield: 3.82 g (35%). Mp: 84.5−85 °C (lit.[23] 85−86 °C). ^{1}H-NMR (CD_3CN): δ 8.74 ($H^{6,6'}$, d), 8.00 ($H^{4,4'}$, dd), 7.80 ($H^{3,3'}$, d), 7.64 ($H^{5,5'}$, dd). The ^{1}H-NMR spectrum in $CDCl_3$ was consistent with a literature report.[13]

Azobis(4-methyl-2-pyridine), mapy. A rapidly stirred solution of sodium hypochlorite (500 cm³, 12.5% w/v) was chilled in an acetone/dry ice slush bath until solids began to precipitate. To this was added (all at once) a solution of 2-amino-4-methylpyridine {12.1 g in 1:1 CH_3CN/H_2O (120 cm³)}. Stirring and cooling were continued for 4 min, after which the resulting orange solution was extracted rapidly with diethyl ether (4 × 100 cm³). Between each extraction, the remaining aqueous layer was rechilled, since the continuing reaction of unreacted starting material with hypochlorite ion is exothermic. The organic layers were combined and dried over anhydrous Na_2SO_4, and the solvent was removed to give an orange solid. The crude product was purified as for apy. An orange crystalline product was obtained after two recrystallizations from petroleum ether (600 cm³, bp 60−80 °C). Yield 3.44 g (29%). Mp: 143.5−145 °C (lit.[23] 149−151 °C). ^{1}H-NMR ($CDCl_3$): δ 8.62 ($H^{6,6'}$, d), 7.82 ($H^{3,3'}$, d), 7.27 ($H^{5,5'}$, dd), 2.46 (CH_3, s). Anal. Calcd for $C_{12}H_{12}N_4$: C, 67.9; H, 5.70; N, 26.4. Found: C, 67.3; H, 5.67; N, 26.2.

$[Ru(pp)_2L]^{2+}$ (II). Mononuclear complexes were prepared from the appropriate $[Ru(pp)_2Cl_2]$ precursor[24] and an excess of the bridging α-azodiimine.[25] In a typical reaction, $[Ru(Me_2bpy)_2Cl_2]$ (500 mg; 0.925 mmol) and apy (511 mg; 2.77 mmol) were refluxed in 50% aqueous methanol (50 cm³) for 1h under N_2. The solvent was removed, and the solids were redissolved in methanol (5 cm³) for purification via gel permeation chromatography using a column of Sephadex LH-20 as support and methanol as eluent. The major claret-red product band eluted first, followed by a red-orange band of apy. The product band was evaporated to dryness, the residue redissolved in water, the solution filtered to remove any remaining solids, and the filtrate diluted to a total volume of 150 cm³. Saturated aqueous KPF_6 solution (8 cm³) was added dropwise to the stirred solution, and the precipitated hexafluorophosphate salt was collected via vacuum filtration, washed with diethyl ether, and air-dried. Recrystallization was achieved from acetone/diethyl ether. $[Ru(apy)(bpy)_2](PF_6)_2{\cdot}C_3H_6O$: yield 210 mg (51%). Anal. Calcd for $RuC_{33}H_{30}N_8OP_2F_{12}$: C, 41.9; H, 3.20; N, 11.9. Found: C, 41.5; H, 2.87; N, 12.0. ^{1}H-NMR (CD_3CN): δ 8.58, 8.54, 8.40, 8.26 (H^3_{bpy}, d), 8.19, 8.12, 8.15, 7.94 (H^4_{bpy}, dd), 7.52, 7.48, 7.47, 7.25 (H^5_{bpy}, dd), 7.48, 8.03, 7.26, 7.52 (H^6_{bpy}, d), 8.85, 7.52 (H^3_{apy}, d), 8.24, 7.87 (H^4_{apy}, dd), 7.67, 7.35 (H^5_{apy}, dd), 7.88, 7.89 (H^6_{apy}, d). $[Ru(apy)(Me_2bpy)_2](PF_6)_2$: yield 525 mg (60%). Anal. Calcd for $RuC_{34}H_{32}N_8P_2F_{12}$: C, 43.3; H, 3.42; N, 11.9. Found: C, 43.8; H, 3.27; N, 11.7. ^{1}H-NMR (CD_3CN): δ 8.43, 8.35, 8.24, 8.09 ($H^4_{Me_2bpy}$, s), 2.57, 2.52, 2.54, 2.44 (CH_{3Me_2bpy}, s), 7.37, 7.28, 7.27, 7.05 ($H^5_{Me_2bpy}$, d), 7.28, 7.78, 7.05, 7.28 ($H^6_{Me_2bpy}$, d), 8.79, 7.51 (H^3_{apy}, d), 8.20, 7.85 (H^4_{apy}, dd), 7.65, 7.33 (H^5_{apy}, dd), 7.86, 7.92 (H^6_{apy}, d). $[Ru(mapy)(bpy)_2](PF_6)_2{\cdot}0.5C_3H_6O$: yield 388 mg (91%). Anal. Calcd for $RuC_{33.5}H_{31}N_8O_{0.5}P_2F_{12}$: C, 42.3; H, 3.28; N, 11.8. Found: C, 42.9; H, 3.06; N, 12.0. ^{1}H-NMR (CD_3CN): δ 8.57, 8.51, 8.40, 8.24 (H^3_{bpy}, d), 8.18, 8.11, 8.16, 7.92 (H^4_{bpy}, dd), 7.57, 7.57, 7.47, 7.22 (H^5_{bpy}, dd), 7.48, 8.06, 7.27, 7.50 (H^6_{bpy}, d), 8.68, 7.31 (H^3_{mapy}, d), 2.86, 2.33 (CH_{3mapy}, s), 7.49, 7.15 (H^5_{mapy}, dd), 7.69, 7.74 (H^6_{mapy}, d). $[Ru(mapy)(Me_2bpy)_2](PF_6)_2$: yield 350 mg (78%). Anal. Calcd for $RuC_{36}H_{36}N_8P_2F_{12}$: C, 44.5; H, 3.73; N, 11.5. Found: C, 45.1; H, 3.58; N, 11.2. ^{1}H-NMR (CD_3CN): δ 8.42, 8.35, 8.24, 8.09 ($H^3_{Me_2bpy}$, s), 2.57, 2.52, 2.54, 2.43 (CH_{3Me_2bpy}, s), 7.36, 7.27, 7.26, 7.03 ($H^5_{Me_2bpy}$,

(13) Krejcik, M.; Zalis, S.; Klima, J.; Sykora, D.; Matheis, W.; Klein, A.; Kaim, W. *Inorg. Chem.* **1993**, *32*, 3362.
(14) Goswami, S.; Chakravarty, A. R.; Chakravorty, A. *Inorg. Chem.* **1982**, *21*, 2737.
(15) Bessel, C. A.; Margarucci, J. A.; Acquaye, J. H.; Rubino, R. S.; Crandall, J.; Jircitano, A. J.; Takeuchi, K. J. *Inorg. Chem.* **1993**, *32*, 5779.
(16) Ernst, S.; Kasack, V.; Kaim, W. *Inorg. Chem.* **1988**, *27*, 1146.
(17) Kaim, W.; Kohlmann, S. *Inorg. Chem.* **1987**, *26*, 68.
(18) Giuffrida, G.; Campagna, S. *Coord. Chem. Rev.* **1994**, *135*, 517.
(19) Duff, C. M.; Heath, G. A. *Inorg. Chem.* **1991**, *30*, 2528.
(20) Kirpal, A.; Reiter, L. *Chem. Ber.* **1927**, *60*, 664.
(21) Baldwin, D. A.; Lever, A. B. P.; Parish, R. V. *Inorg. Chem.* **1969**, *8*, 107.
(22) Coll, J. C.; Bowden, B. F. *J. Nat. Prod.* **1986**, *49*, 934.
(23) Campbell, N.; Henderson, A. W.; Taylor, D. *J. Chem. Soc.* **1953**, 1281.
(24) Togano, T.; Nagao, N.; Tsuchida, M.; Kumakura, H.; Hisamatsu, K.; Howell, F. S.; Mukaida, M. *Inorg. Chim. Acta* **1992**, *195*, 221.
(25) Brown, G. M.; Weaver, T. R.; Keene, F. R.; Meyer, T. J. *Inorg. Chem.* **1976**, *15*, 190.

d), 7.26, 7.83, 7.05, 7.26 ($H^6_{Me_2bpy}$, d), 8.65, 7.36 (H^5_{mapy}, d), 2.67, 2.32 (CH_{3mapy}, s), 7.49, 7.13 (H^5_{mapy}, dd), 7.67, 7.76 (H^6_{mapy}, d).

$[\{Ru(pp)_2\}_2(\mu\text{-}L)]^{4+}$ (III). Typically, 1 mol equiv of $[Ru(pp)_2Cl_2]$ and 1.5 mol equiv of $[Ru(pp)_2L]^{2+}$ were dissolved in a 50% aqueous methanol solution under N_2. The mixture was refluxed for at least 5 days. $AgNO_3$ (2 mol equiv) and $[Ru(pp)_2Cl_2]$ (1 mol equiv) were added to the solution each day. The mixture was filtered (Celite) and the filtrate concentrated on a rotary evaporator. Purification was achieved by cation-exchange chromatography (SP-Sephadex C-25; eluent 0.5 M NaCl). Separation of the diastereoisomers and resolution of the *rac* forms were achieved by cation-exhange chromatography on the same support using 0.25 M sodium toluene-4-sulfonate and 0.25 M sodium ditoluoyl-(+)-tartrate solutions as eluents, respectively.[26] The product was precipitated as the PF_6^- salt by addition of a saturated solution of KPF_6 to the green eluent. The green solid was collected and washed with a dilute KPF_6 solution. $[\{Ru(bpy)_2\}_2(\mu\text{-apy})](PF_6)_4$: yield 52%. $[\{Ru(Me_2bpy)_2\}_2(\mu\text{-apy})](PF_6)_4$: yield 41%. $[\{Ru(bpy)_2\}_2(\mu\text{-mapy})](PF_6)_4$: yield 40%, isomer ratio *meso:rac* = 3.8:1. $[\{Ru(Me_2bpy)_2\}_2(\mu\text{-mapy})](PF_6)_4$: yield 90%. $[(bpy)_2Ru(\mu\text{-mapy})Ru(Me_2bpy)_2](PF_6)_4$: yield 79%, isomer ratio *meso:rac* = 1.67:1.

Microanalytical data are provided for the two diastereoisomeric forms of one dinuclear species. $[\{Ru(Me_2bpy)_2\}_2(\mu\text{-apy})](PF_6)_4$, by way of an example. Anal. Calcd for *meso*-$[\{Ru(Me_2bpy)_2\}_2(\mu\text{-apy})](PF_6)_4$, $Ru_2C_{58}H_{56}N_{12}P_4F_{24}$: C, 40.9; H, 3.31; N, 9.8. Found: C, 41.3; H, 3.08; N, 9.4. Anal. Calcd for *rac*-$[\{Ru(Me_2bpy)_2\}_2(\mu\text{-apy})](PF_6)_4\cdot 2H_2O$, $Ru_2C_{58}H_{60}N_{12}O_2P_4F_{24}$: C, 40.0; H, 3.48; N, 9.6. Found: C, 39.8; H, 3.11; N, 9.2. In general, characterization of dinuclear species was achieved using ^{1}H-NMR and electrochemical techniques (see Results and Discussion), as microanalyses are not particularly discriminating for larger molecules.

Results and Discussion

Syntheses. The α-azodiimine ligands apy and mapy were obtained by oxidation of 2-aminopyridine and 2-amino-4-methylpyridine, respectively, in sodium hypochlorite solution. The *trans* isomer is thermodynamically preferred,[13,23] and after purification there was no evidence from ^{1}H-NMR studies of any of the *cis* form being present.

The reaction between $[Ru(pp)_2Cl_2]$ (pp = bpy or Me_2bpy) and excess L (L = apy or mapy) proceeds at reflux in 50% aqueous methanol. Mononuclear complexes of the form $[Ru(pp)_2L]^{2+}$ were isolated as hexafluorophosphate salts and were used as precursors in the synthesis of dinuclear species.

The dinuclear complexes were generally prepared by the reaction of excess $[Ru(pp)_2Cl_2]$ with $[Ru(pp)_2L]^{2+}$ in aqueous methanol in the presence of Ag^+. The attachment of the second metal center to the bridging ligand (to give $[(pp)_2Ru(\mu\text{-}L)Ru(pp)_2]^{4+}$) is not a facile step, and the typical synthesis required days of refluxing and periodic additions of both excess $[Ru(pp)_2Cl_2]$ and $AgNO_3$. The large activation barrier to the formation of apy-bridged dimers from monomeric precursors has previously been attributed to steric interactions between the 6- and 6′-protons of the bridge and the coordinating nitrogen atoms of adjacent ligands.[9,17] The azobis(2-pyridine) bridging ligands are exceptions to the "charge transfer assisted polynucleation" phenomenon, in which dimer formation is facilitated.[9,17,26] All attempts to prepare the dinuclear complexes directly from the bridging ligand and a stoichiometric excess of $[Ru(pp)_2Cl_2]$ gave diminished yields compared with the two-step route. Previous work partially addressed these synthetic difficulties by the use of higher boiling solvents (1-butanol) and extended reaction times.[16]

Separation of Diastereoisomeric Pairs. We have previously shown that the diastereoisomeric pairs of ligand-bridged dinuclear polypyridyl compounds may be separated by cation-exchange chromatography.[1] By use of this chromatographic technique, the diastereoisomers of all five dinuclear compounds were separated within a 20 cm column length, considerably less than the column length required for the separation of compounds in which 2,2′-bipyrimidine (bpm) and 2,3-bis(2-pyridyl)pyrazine (dpp) were the bridging ligands.[1]

The relative ease of separation may be rationalized in terms of the stereochemistry. As described above, the diastereoisomers differ in terms of the relative orientation of the terminal ligands.[1,4,6,27] In the case where the bridging ligand is an α-azodiimine (rather than bpm or dpp), the differences are even more pronounced, as the offset position of the metal centers places the "above plane" ligands almost coplanar in the ΔΔ/ΛΛ *(rac)* isomer (Figure S1, Supporting Information).

An interesting observation during the separation was the noticeable difference in the color of the diastereoisomers on the column. The first band was dark green and the second band olive green for all five dinuclear compounds.

Most of the dinuclear compounds investigated were found to have only a slight diastereoisomeric excess favoring the *meso* form, which was eluted first. However, for the complex $[\{Ru(bpy)_2\}_2(\mu\text{-mapy})]^{4+}$ the isomer ratio (assessed by ^{1}H-NMR integration) was 3.8:1. A preference for the *meso* diastereoisomer would be predicted on stereochemical grounds, as examination of models reveals possible inter-ligand interactions in the *rac* form.

Previous studies of α-azodiimine-bridged dinuclear compounds suggested that only one diastereoisomer is observed.[13] The current work clearly shows the presence of both isomers. In the previous studies, the reactions were performed at higher temperatures and it is possible that under such conditions one isomer may dominate. Additionally, the purification techniques used previously may have excluded one isomer due to the differences in solubilities of the diastereoisomeric forms.

Resolution of *rac* (ΔΔ/ΛΛ)-$[\{Ru(Me_2bpy)\}_2(\mu\text{-apy})]^{4+}$. The four "symmetrical" dinuclear compounds prepared in this study (i.e. those with the same terminal ligands on both metal centers) have two diastereoisomers, one *racemic* (consisting of the ΔΔ/ΛΛ enantiomeric pairs) and the other a *meso* (ΔΛ) form. Consequently, the resolution of one of the diastereoisomers would unequivocally establish its identity as *rac*. We have developed chromatographic methods for separation of enantiomers by ion-exchange chromatography, using chiral eluents.[3,28] Resolution of the species corresponding to band 1 and band 2 of $[\{Ru(Me_2bpy)\}_2(\mu\text{-apy})]^{4+}$ from the separation of the diastereoisomers was attempted by cation-exchange chromatography using an aqueous solution of sodium toluoyl-(+)-tartrate as the eluent. Band 2 was found to separate into two bands—the isolated cations of which had equal and opposite ORD curves—allowing the assignment of band 2 as the *rac* form. The ^{1}H-NMR studies described below are consistent with this assertion.

^{1}H-NMR Studies. The ^{1}H-NMR data for the mononuclear and dinuclear compounds are listed in Table 1. The notation used for the pyridine rings in the terminal ligands of the two diastereoisomeric forms is shown in Figure 1.

In each case, the H^3 to H^6 protons of each pyridyl ring show the normal coupling patterns,[29,30] and assignments were made on the basis of COSY spectra (an example is given in Figure 2

(26) Kohlmann, S.; Ernst, S.; Kaim, W. *Angew. Chem., Int. Ed. Engl.* **1985**, *24*, 684.

(27) Hage, R.; Dijkhuis, A. H. J.; Haasnoot, J. G.; Prins, R.; Reedijk, J.; Buchanan, B. E.; Vos, J. G. *Inorg. Chem.* **1988**, *27*, 2185.

(28) Reitsma, D. A.; Keene, F. R. Manuscript in preparation.

(29) Bolger, J. A.; Ferguson, G.; James, J. P.; Long, C.; McArdle, P.; Vos, J. G. *J. Chem. Soc., Dalton Trans.* **1993**, 1577.

(30) Orellana, G.; Ibarra, C. A.; Santoro, J. *Inorg. Chem.* **1988**, *27*, 1025.

Table 1. 300 MHz ^{1}H-NMR Data[a] for the Dinuclear Complexes Used in This Study (PF_6^- Salts; CD_3CN Solvent)

		$[\{Ru(bpy)_2\}_2(\mu\text{-apy})]^{4+}$	$[\{Ru(bpy)_2\}_2(\mu\text{-mapy})]^{4+}$	$[\{Ru(Me_2bpy)_2\}_2(\mu\text{-apy})]^{4+}$	$[\{Ru(Me_2bpy)_2\}_2(\mu\text{-mapy})]^{4+}$	$[Ru(bpy)_2(\mu\text{-mapy})Ru(Me_2bpy)_2]^{4+}$[c]	
						bpy	Me_2bpy
				ΔΛ Diastereoisomers			
ring A	H^3	8.57	8.50	8.38	8.35	8.51	8.36
	H^4[b]	8.28	8.22	2.58	2.58	8.23	2.59
	H^5	7.72	7.69	7.46	7.47	7.69	7.46
	H^6	7.21	7.16	7.03	6.99	7.20	6.94
ring B	H^3	8.59	8.55	8.40	8.41	8.55	8.42
	H^4[b]	8.27	8.22	2.58	2.58	8.22	2.59
	H^5	7.63	7.62	7.39	7.42	7.61	7.43
	H^6	7.83	7.83	7.50	7.57	7.83	7.57
ring C	H^3	8.64	8.60	8.42	8.43	8.60	8.45
	H^4[b]	8.28	8.22	2.58	2.58	8.20	2.59
	H^5	7.57	7.51	7.36	7.34	7.50	7.35
	H^6	7.49	7.47	7.24	7.27	7.50	7.26
ring D	H^3	8.57	8.53	8.36	8.37	8.54	8.38
	H^4[b]	8.16	8.11	2.51	2.52	8.12	2.51
	H^5	7.24	7.21	6.97	6.99	7.18	7.01
	H^6	7.24	7.16	6.92	6.93	7.18	6.90
azodiimine	H^3	8.06	7.74	8.00	7.71	7.72, 7.72	
	H^4[b]	7.77	2.06	7.70	2.06	2.06, 2.06	
	H^5	7.66	7.44	7.60	7.43	7.43, 7.43	
	H^6	7.88	7.62	7.80	7.61	7.61, 7.61	
				ΔΔ/ΛΛ Diastereoisomers			
ring E	H^3	8.45	8.42	8.28	8.29	8.42	8.26
	H^4[b]	8.12	8.09	2.56	2.58	8.07	2.58
	H^5	6.90	6.86	6.65	6.68	6.87	6.65
	H^6	6.38	6.33	6.22	6.11	6.39	6.06
ring F	H^3	8.50	8.48	8.31	8.34	8.48	8.32
	H^4[b]	8.21	8.18	2.56	2.57	8.18	2.56
	H^5	7.63	7.60	7.40	7.42	7.60	7.43
	H^6	7.84	7.86	7.56	7.62	7.88	7.62
ring G	H^3	8.76	8.69	8.54	8.52	8.68	8.54
	H^4[b]	8.30	8.22	2.59	2.58	8.22	2.58
	H^5	7.42	7.39	7.18	7.20	7.40	7.20
	H^6	7.68	7.63	7.38	7.38	7.62	7.38
ring H	H^3	8.76	8.69	8.54	8.52	8.68	8.54
	H^4[b]	8.28	8.23	2.59	2.58	8.21	2.58
	H^5	7.48	7.41	7.27	7.26	7.40	7.27
	H^6	7.10	7.09	6.84	6.88	7.08	6.86
azodiimine	H^3	8.36	8.05	8.29	8.02	8.05, 8.03	
	H^4[b]	7.89	2.18	7.80	2.15	2.18, 2.18	
	H^5	7.68	7.46	7.61	7.42	7.45, 7.43	
	H^6	7.89	7.63	7.81	7.59	7.62, 7.62	

[a] For ring designation, see Figure 3. H^3 is a doublet (d) and a singlet (s) when the terminal ligand is bpy and Me_2bpy, respectively; H^4 is dd (bpy) or s (i.e. CH_3; Me_2bpy); H^5 is dd (bpy) or d (Me_2bpy); H^6 is d in both cases. Coupling constants (Hz): $J_{3-4} = 8$, $J_{4-5} = 8$, $J_{5-6} = 5$, $J_{3-5} = 1.2$, $J_{4-6} = 1.2$. [b] For the methyl-substituted pyridyl rings the methyl instead of the H^4 chemical shift is indicated. [c] ΔΛ and ΛΔ enantiomers.

for the species ΔΛ/ΛΔ-$[(Me_2bpy)_2Ru(\mu\text{-mapy})Ru(bpy)_2]^{4+}$) and selective ^{1}H-decoupling experiments. In the case where methyl-substituted pyridyl rings were present (Me_2bpy and mapy), the chemical shift of the methyl singlet is provided in Table 1 in place of the H^4 signal. The connectivity between the two pyridyl rings of each ligand was established by NOE experiments. The H^3 protons show an NOE to the adjacent H^3 proton on the connected pyridyl ring of the same ligand. For example, in the complex *rac*-$[\{Ru(Me_2bpy)_2\}_2(\mu\text{-mapy})]^{4+}$ the H^3 proton of ring A shows an NOE to H^3 on ring B and H^3 on ring C shows an NOE to H^3 on ring D (Figure S2, Supporting Information). Connectivity was established for the *meso* (ΔΛ) dimers in an analogous manner.

For the mononuclear compounds, there are six distinguishable pyridyl rings. The coordinated apy (or mapy) ligand is unsymmetrical, and hence there are four bpy (or Me_2bpy) pyridyl environments and two apy (or mapy) pyridyl environments. In the dinuclear complexes in which the two metal centers have the same terminal ligands, the *racemic* form (ΔΔ/ΛΛ) has C_2 and the *meso* form (ΔΛ) has C_i point group symmetry—accordingly both species show five pyridyl environments. On the other hand, both diastereoisomers of the "mixed" $[(bpy)_2Ru(\mu\text{-mapy})Ru(Me_2bpy)_2]^{4+}$ species have 10 pyridyl environments.

The most notable aspect of the ^{1}H-NMR spectroscopic studies is the difference in the spectra between the diastereoisomeric pairs of each dinuclear species. As an example, the spectra for the complex $[\{Ru(Me_2bpy)_2\}_2(\mu\text{-mapy})]^{4+}$ are given in Figure 3. The *meso* isomer of all five dimers have similar spectra (allowing for the 0.2−0.3 ppm upfield shift of protons adjacent to a methyl group and the different coupling pattern of the methyl-substituted pyridyls). Likewise, the spectra of the *rac* isomers are also similar. It is apparent that the ligand geometry has a greater effect on chemical shift than methyl substitution.

In the dinuclear species, the assignment of the resonances associated with individual terminal ligands is based on the

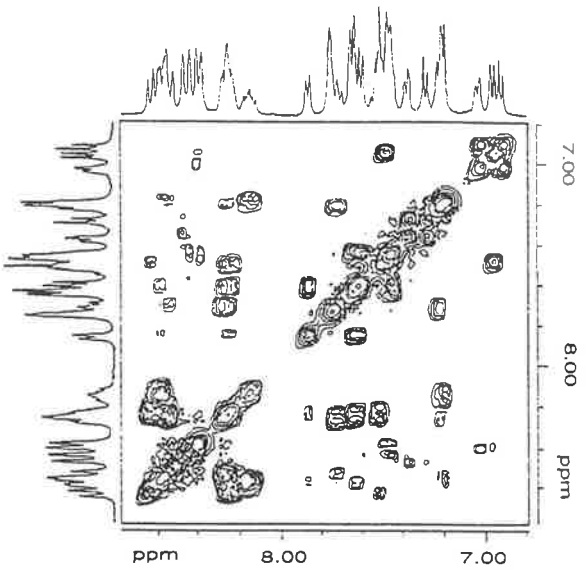

Figure 2. COSY ^{1}H-NMR spectrum for $\Delta\Lambda/\Lambda\Delta$-[(bpy)$_2$Ru($\mu$-mapy)-Ru(Me$_2$bpy)$_2$]$^{4-}$ (300 MHz in CD_3CN).

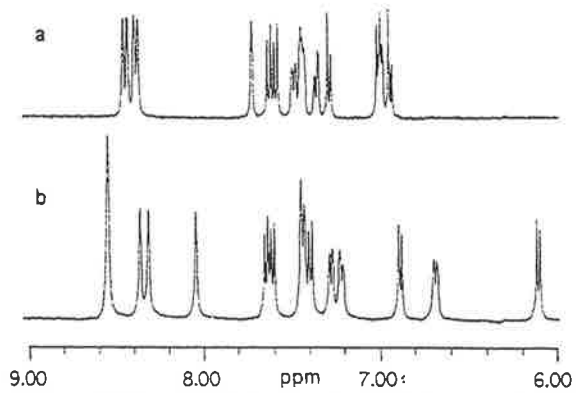

Figure 3. 300 MHz ^{1}H-NMR spectra (CD_3CN) of diastereoisomers of [{Ru(Me$_2$bpy)$_2$}$_2$(μ-mapy)]$^{4-}$: (a) *meso* ($\Delta\Lambda$); (b) *rac* ($\Delta\Delta/\Lambda\Lambda$).

differential ring current effect of the two ligands above (or below) the plane of the bridge between the two diastereoisomers (refer to Figure 1). There are four environments for the H^6 protons of the terminal ligands, two over the bridge and two directed away from it. The H^6 protons over the bridge will show the greatest change in chemical shift between the two isomers. In one environment the H^6 protons (of rings A and E) are positioned over the apy (or mapy) pyridyl rings and in the other "over bridge" environment the H^6 protons (of rings C and G) are over the azo moiety. For the complex [{Ru(Me$_2$-bpy)$_2$}$_2$(μ-apy)]$^{4+}$ the H^6 proton of ring E is 0.9 ppm upfield of the H^6 proton of ring A and the H^6 proton of ring G is 0.14 ppm downfield of the same proton in ring C. Examination of models reveals that the H^6 proton on ring E lies directly over the pyridyl ring of the ligand positioned across the bridge (the other ring E; see Figure 1) and is in a considerably shielded environment compared to the H^6 proton on ring A, which is directly in the plane of the pyridyl ring (ring C) across the bridge. The H^6 protons of rings C and G are not directly over, or in the plane of, the ligand across the bridge and experience less anisotropy. The H^6 proton of ring G is in a slightly deshielding environment compared to the H^6 proton on ring C. The assignment of the two H^6 environments over the bridge in each diastereoisomer, in association with the connectivity

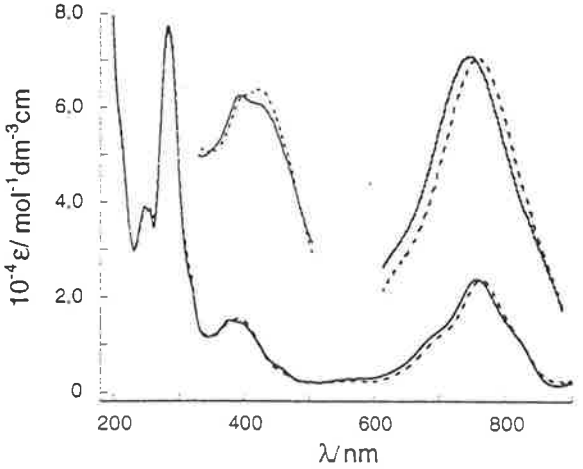

Figure 4. UV−visible absorption spectra (CH_3CN solution) of [{Ru(bpy)$_2$}$_2$(μ-apy)](PF$_6$)$_4$: *meso* (—); *rac* (- - -).

discussed above, leads to the complete assignment of all the protons in these dinuclear complexes.

The ^{1}H-NMR analysis is consistent with the designation of the band 1 eluant as the *meso* isomer.

Electronic Spectroscopy. The absorption spectra of the complexes show intense bands in the UV region, with bands in the visible region (assigned as arising from MLCT transitions) at *ca.* 510 nm for the mononuclear species and at *ca.* 380 and 770 nm for the dinuclear compounds. As an example, the absorption spectra of the two diastereoisomers of [{Ru(bpy)$_2$}$_2$-(μ-apy)]$^{4+}$ are presented in Figure 4, and in the inset the expansion of the absorption arising from the lowest energy d(Ru) → π^*(μ-apy) transition reveals a difference in MLCT energy between the two forms: i.e. there is a red shift of ~7 nm for the *rac* compared with the *meso* form. The stereochemistry also affects the d(Ru) → π^*(bpy) transition; the shoulder at 400 nm for the *meso* isomers is enhanced for the *rac* isomers. For the complex [{Ru(bpy)$_2$}$_2$(μ-apy)]$^{4+}$ the λ_{max} is at 393 nm with the shoulder at 375 nm (see inset, Figure 4). We are not aware of other reports of a significant difference in such physical properties of ligand-bridged diastereoisomers. There have been numerous assertions that stereochemistry will have little influence on physical properties in circumstances where mixtures of isomers were investigated.[9,31] It is apparent now that the stereochemistry does influence the electronic transitions and the inter-metal communication.

The difference in spectral characteristics of the diastereoisomeric forms of these complexes might also be rationalized in terms of variations in solvation. Although the data are reported in acetonitrile solution, similar trends are observed in a number of solvents, which gives less credence to this alternative explanation. In any case, the differences still originate from stereochemical factors.

As well as the stereochemical influences on the electronic transitions, there are substituent effects. The shoulder at 400 nm discussed above is enhanced for dinuclear complexes with bpy compared to complexes containing Me$_2$bpy terminal ligands. Similarly, the shoulder at 830 nm is not present for complexes with the Me$_2$bpy terminal ligands. The dimers with the mapy bridge exhibit an additional shoulder at 420 nm.

The addition of methyl substituents to terminal polypyridyl ligands raises the energy of the d(Ru) orbital, lowering the d(Ru)

(31) Denti, G.; Campagna, S.; Serroni, S.; Ciano, M.; Balzani, V. *J. Am. Chem. Soc.* **1992**, *114*, 2944.

Table 2. Electronic Spectral and Electrochemical Data for Mono- and Dinuclear Ruthenium(II) Complexes in This Study (CH_3CN Solvent)

mononuclear complex	abs max λ, nm (log ϵ)	E_{MLCT},[a] eV	$\Delta E_{ox/red}$,[b] V
$[(bpy)_2Ru(apy)]^{2+}$	244 (4.36) 280 (4.61) 508 (3.88)	2.44	1.96
$[(Me_2bpy)_2Ru(apy)]^{2+}$	278 (4.67) 512 (3.93)	2.42	1.95
$[(bpy)_2Ru(mapy)]^{2+}$	246 (4.38) 280 (4.65) 506 (3.93)	2.45	1.97
$[(Me_2bpy)_2Ru(mapy)]^{2+}$	278 (4.65) 510 (3.92)	2.43	1.93

dinuclear complex		λ, nm (log ϵ)	E_{MLCT},[a] eV	$\Delta E_{ox/red}$,[b] V	ΔE_{ox},[c] V	log K_c[d]
$[\{Ru(bpy)_2\}_2(\mu\text{-apy})]^{4+}$	$\Delta\Lambda$	247 (4.59) 283 (4.89) 375 (4.18) 757 (4.38)	1.64	1.42	0.49	8.28
	$\Delta\Delta/\Lambda\Lambda$	255 (4.58) 284 (4.88) 393 (4.19) 764 (4.37)	1.62	1.44	0.50	8.45
$[\{Ru(Me_2bpy)_2\}_2(\mu\text{-apy})]^{4+}$	$\Delta\Lambda$	282 (4.94) 376 (4.25) 768 (4.41)	1.61	1.37	0.52	8.79
	$\Delta\Delta/\Lambda\Lambda$	283 (4.92) 380 (4.19) 775 (4.42)	1.60	1.40	0.53	8.96
$[\{Ru(bpy)_2\}_2(\mu\text{-mapy})]^{4+}$	$\Delta\Lambda$	246 (4.62) 283 (4.93) 377 (4.15) 761 (4.30)	1.63	1.42	0.47	7.95
	$\Delta\Delta/\Lambda\Lambda$	255 (4.60) 284 (4.92) 382 (4.15) 767 (4.32)	1.62	1.44	0.49	8.28
$[\{Ru(Me_2bpy)_2\}_2(\mu\text{-mapy})]^{4+}$	$\Delta\Lambda$	282 (4.92) 379 (4.11) 774 (4.35)	1.60	1.37	0.49	8.28
	$\Delta\Delta/\Lambda\Lambda$	283 (4.94) 383 (4.14) 778 (4.37)	1.59	1.39	0.51	8.62
$[(bpy)_2Ru(\mu\text{-mapy})Ru(Me_2bpy)_2]^{4+}$	$\Delta\Lambda/\Lambda\Delta$	255 (4.62) 283 (4.93) 378 (4.15) 766 (4.32)	1.62	1.39	0.50	8.45
	$\Delta\Delta/\Lambda\Lambda$	258 (4.60) 284 (4.92) 382 (4.12 773 (4.31)	1.60	1.41	0.52	8.79

[a] Energy for the lowest energy MLCT absorption. [b] Difference between the first oxidation and first reduction potential. [c] Difference between the first two oxidation potentials of the dinuclear complexes. [d] K_c is calculated comproportionation constant.

$\rightarrow \pi^*(\mu\text{-apy})$ MLCT energy.[32] The presence of methyl substituents on the bridge raises the π^* level. This is demonstrated by the bathochromic shift of the d(Ru) $\rightarrow \pi^*(\mu\text{-apy})$ transition in complexes containing methyl-substituted ligands (Table 2), as for each pair of methyl substituents (either on the bridge or on the terminal ligands) the MLCT absorption is red-shifted by 3 nm.

The large (250 nm) bathochromic shift upon coordination of a second $[Ru(bpy)_2]^{2+}$ moiety has been observed previously.[9] Methyl substituents on the terminal (bpy) or bridging (μ-apy) ligands increase such a shift by 6−15 nm as a result of the increased ligand σ-donor strength, the greatest effect being observed for $[\{Ru(Me_2bpy)_2\}_2(\mu\text{-mapy})]^{4+}$.

Electrochemistry. The redox couples in both the anodic and cathodic regions were determined for each mononuclear and dinuclear species using both cyclic voltammetry (CV) and differential pulse voltammetry (DPV) methods, the latter providing the greater precision and resolution. The close proximity to each other of the successive later ligand reductions rendered difficult the determination of some $E_{1/2}$ values from cyclic voltammetry. In these cases $E_{1/2}$ was calculated using the peak potential (E_p) from DPV, since

$$E_p = E_{1/2} - (PA)/2 \qquad (1)$$

where PA is the pulse amplitude.[33]

For mononuclear complexes of the form $[Ru(pp)_2L]^{2+}$, all displayed one metal-centered oxidation ($Ru^{III/II}$) and four ligand reductions, each of which appeared to be a reversible redox process. Table 3 summarizes the electrochemical data obtained.

(32) Anderson, P. A.; Strouse, G. F.; Treadway, J. A.; Keene, F. R.; Meyer, T. J. *Inorg. Chem.* **1994**, *33*, 3863.
(33) Parry, E. P.; Osteryoung, R. A. *Anal. Chem.* **1965**, *37*, 1634.

Table 3. Redox Potentials (V vs Ag/Ag$^+$) for Mono- and Dinuclear Ruthenium(II) Complexes (CH_3CN/0.1 M $[(n\text{-}C_4H_9)_4N]ClO_4$ Solvent)[a]

	$E_{1/2ox(2)}$	$E_{1/2ox(1)}$	$E_{1/2red(1)}$	$E_{1/2red(2)}$	$E_{1/2red(3)}$	$E_{1/2red(4)}$	$E_{1/2red(5)}$	$E_{1/2red(6)}$
				Mononuclear Complexes				
$[Ru(apy)(bpy)_2]^{2+}$	+1.29	−0.67	−1.38	−2.01	−2.37			
$[Ru(apy)(Me_2bpy)_2]^{2+}$	+1.22	−0.73	−1.44	−2.11	−2.42			
$[Ru(mapy)(bpy)_2]^{2+}$	+1.26	−0.71	−1.42	−2.02	−2.36			
$[Ru(mapy)(Me_2bpy)2]^{2+}$	+1.17	−0.76	−1.46	−2.11	−2.43			
				Dinuclear Complexes				
$\Delta\Lambda$-$[\{Ru(bpy)_2\}_2(\mu\text{-apy})]^{4+}$	+1.85	+1.36	−0.06	−0.71	−1.83[b]		−2.12	−2.23
$\Delta\Delta/\Lambda\Lambda$-$[\{Ru(bpy)_2\}_2(\mu\text{-apy})]^{4+}$	+1.87	+1.37	−0.07	−0.74	−1.84[b]		−2.15	−2.24
$\Delta\Lambda$-$[\{Ru(Me_2bpy)_2\}_2(\mu\text{-apy})]^{4+}$	+1.75	+1.23	−0.15	−0.79	−1.94[b]		−2.21	−2.31
$\Delta\Delta/\Lambda\Lambda$-$[\{Ru(Me_2bpy)_2\}_2(\mu\text{-apy})]^{4+}$	+1.77	+1.24	−0.16	−0.82	−1.95[b]		−2.23	−2.33
$\Delta\Lambda$-$[\{Ru(bpy)_2\}_2(\mu\text{-mapy})]^{4+}$	+1.78	+1.31	−0.11	−0.76	−1.85[b]		−2.14	−2.23
$\Delta\Delta/\Lambda\Lambda$-$[\{Ru(bpy)_2\}_2(\mu\text{-mapy})]^{4+}$	+1.82	+1.33	−0.11	−0.77	−1.84[b]		−2.16	−2.24
$\Delta\Lambda$-$[\{Ru(Me_2bpy)_2\}_2(\mu\text{-mapy})]^{4+}$	+1.69	+1.20	−0.17	−0.82	−1.94[b]		−2.22	−2.32
$\Delta\Delta/\Lambda\Lambda$-$[\{Ru(Me_2bpy)_2\}_2(\mu\text{-mapy})]^{4+}$	+1.71	+1.20	−0.20	−0.85	−1.94[b]		−2.23	−2.34
$\Delta\Lambda/\Lambda\Delta$-$[(Me_2py)_2Ru(\mu\text{-mapy})Ru(bpy)_2]^{4+}$	+1.75	+1.25	−0.14	−0.79	−1.82	−1.95	−2.15	−2.29
$\Delta\Delta/\Lambda\Lambda$-$[(Me_2py)_2Ru(\mu\text{-mapy})Ru(bpy)_2]^{4+}$	+1.77	+1.25	−0.16	−0.82	−1.83	−1.95	−2.17	−2.32

[a] Calculated from DPV measurements (eq 1). [b] Two-electron reduction.

Table 4. Potential Differences ($\Delta E = E_{rac} - E_{meso}$) between the Diastereoisomeric Forms of the Dinuclear Species (mV vs Ag/Ag$^+$ Reference Electrode)[a]

dinuclear complex	$\Delta E_{ox(2)}$	$\Delta E_{ox(1)}$	$\Delta E_{red(1)}$	$\Delta E_{red(2)}$	$\Delta E_{red(3)}$	$\Delta E_{red(4)}$	$\Delta E_{red(5)}$	$\Delta E_{red(6)}$
$[\{Ru(bpy)_2\}_2(\mu\text{-apy})]^{4+}$	16	8	−12	−32	−4		−32	−12
$[\{Ru(Me_2bpy)_2\}_2(\mu\text{-apy})]^{4+}$	20	12	−12	−46	−8		−20	−24
$[\{Ru(bpy)_2\}_2(\mu\text{-mapy})]^{4+}$	40	24	4	−16	8		−20	−14
$[\{Ru(Me_2bpy)_2\}_2(\mu\text{-mapy})]^{4+}$	24	0	−24	−28	4		−16	−20
$[(bpy)_2Ru\{\mu\text{-mapy}\}Ru(Me_2bpy)_2]^{4+}$	20	0	−16	−24	−14	2	−18	−30

[a] Assessed from DPV measurements.

The bridging α-azodiimine ligands employed in this study are more π-accepting than the terminal ligands (bpy, Me_2bpy),[9,13] and consequently the first two electrons added to these complexes are localized on the α-azodiimine, as the second reduction process occurs at less cathodic potentials than any possible bpy-centered reduction. This has previously been confirmed using spectroelectrochemistry.[13]

The presence of methyl substituents on either the α-azodiimine or the bpy-type ligands affects the apy-centered reduction potentials. Conversely, methylation of apy ligand has no noticeable effect upon the bpy-centered reductions. The consequence of changing from bpy to Me_2bpy is to shift the two apy reductions ~50 mV more cathodic, while the third and fourth redox couples move ~100 mV. A comparison of the apy to the mapy complex shows ~40 and ~35 mV cathodic shifts (respectively) in only the first two couples. Since interchanging ligands also raises or lowers the d levels of the metal center, corresponding shifts in the oxidative $Ru^{III/II}$ couple are observed.

Previous studies have noted the correlation between $\Delta E_{ox/red}$ (the potential difference between the couples associated with the metal-based oxidation and the first ligand-based reduction—and therefore between the HOMO and LUMO energy levels) and E_{MLCT} (the energy associated with the lowest MLCT absorption) for a selection of tris(bidentate)ruthenium(II) complexes containing polypyridyl ligands.[34-36] There are some notable exceptions, including complexes containing the ligand dipyrido[3,2-*c*:2′,3′-*e*]pyridazine (taphen),[37,38] where it has been suggested the reduction involves population of the LUMO (π_1*) level while the MLCT absorption involves a transition to the SLUMO(π_2*). It is noted in passing that the present mononuclear complexes of apy and mapy do not correlate with the general trend either: a plot of $\Delta E_{ox/red}$ vs E_{MLCT} for a variety of tris(bidentate)ruthenium(II) complexes and for the mononuclear species in the present study are given as Supporting Information (Figure S3).

For dinuclear complexes of the form $[(pp)_2Ru(\mu\text{-L})Ru(pp)_2]^{4+}$, two widely separated metal-centered oxidations and five (six in the case of the "mixed-end" dimer) ligand-based reductions were observed, all of which appeared to be reversible redox couples. Previous studies undertaken in a different solvent[13] identified a sixth couple at more negative potentials for the $[\{Ru(bpy)_2\}_2(\mu\text{-apy})]^{4+}$ complex: the present investigation was undertaken using CH_3CN/0.1 M $[(n\text{-}C_4H_9)_4N]ClO_4$, which imposes a reductive limit of ~−2500 mV (vs Ag/Ag^+), but it is reasonable to predict the existence of an analogous couple at more negative potentials for the other dinuclear species studied.

One of the significant aspects of this work is that, having separated the diastereoisomeric pairs for each of the five dinuclear complexes synthesized, we observed measurable differences in the physical properties not only between the different complexes but also between the two diastereoisomers of the same complex. The net differences between the *rac* and the *meso* forms for each redox couple of the various dinuclear species are summarized in Table 4. In all the complexes, the oxidative couples are shifted to more positive potentials and the reductive couples to more negative potentials for the *rac* ($\Delta\Delta/\Lambda\Lambda$) forms relative to the *meso* ($\Delta\Lambda$) diastereoisomers. Additionally, the separation between the two metal-centered oxidations ($\Delta E_{1/2ox}$) is consistently larger for the *rac* form. This implies a slightly greater degree of metal−metal communication for one stereochemical form over the other (the comproportionation constants are given in Table 2), and we believe this to be the first observation of stereochemical influences on the electron transfer properties within dinuclear metallic complexes.

(34) Dodsworth, E. S.; Lever, A. B. P. *Chem. Phys. Lett.* **1985**, *119*, 61.
(35) Dodsworth, E. S.; Lever, A. B. P. *Chem. Phys. Lett.* **1986**, *120*, 152.
(36) Juris, A.; Barigelletti, S.; Campagna, S.; Balzani, V.; Belser, P.; von Zelewsky, A. *Coord. Chem. Rev.* **1988**, *84*, 85.
(37) Juris, A.; Belser, P.; Barigelletti, F.; von Zelewsky, A.; Balzani, V. *Inorg. Chem.* **1986**, *25*, 256.
(38) Barigelletti, F.; Juris, A.; Balzani, V.; Belser, P.; von Zelewsky, A. *Inorg. Chem.* **1987**, *26*, 4115.

Scheme 1

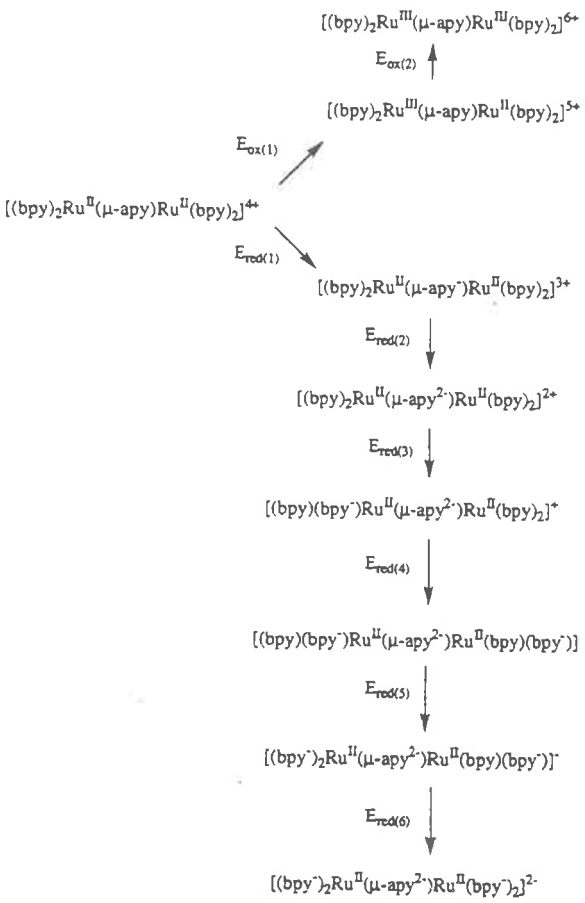

Earlier work,[9-13] which exclusively studied the $[\{Ru(bpy)_2\}_2(\mu\text{-apy})]^{4+}$ dinuclear species in DMF solution, tentatively assigned the first two reductions as bridge-centered and the next two-electron process as bpy-centered. This was then said to be followed by three further two-electron processes, the first of these again bridge-centered and the other two bpy-centered. This suggested the possibility of achieving the reversible acceptance of 10 electrons by the dinuclear complex. With the advantage of having prepared and measured a larger number of dinuclear α-azodiimine species in the present work, we prefer alternative assignments for the redox couples labeled $E_{1/2red(5)}$ and $E_{1/2red(6)}$, shown in Scheme 1, on the basis of our studies in acetonitrile solution.

The effect on the redox couples of a methyl substituent at the bridge or the peripheral ligands follows the trends observed for the mononuclear complexes. Comparison of the apy- to the mapy-bridged complexes reveals a ~40 mV and a ~30 mV cathodic shift (respectively) for the first two bridge-centered reductions. The same couples are cathodically shifted ~85 mV when methyl substituents are added to the four terminal ligands. Smaller shifts (only 50 mV) were observed for the mononuclear species, which is consistent in simplistic additive terms: i.e., there are twice as many nonbridging ligands in the dinuclear species compared with the corresponding mononuclear case. This is confirmed by examining $[(bpy)_2Ru(\mu\text{-mapy})Ru(Me_2bpy)_2]^{4+}$—the so-called "mixed-end" dimer—where the shift is ~35 mV: here Me_2bpy ligands are coordinated to only one of the two ruthenium centers.

Figure 5 shows differential pulse voltammograms of the *rac* diastereoisomers of three dimer species bridged by mapy. When

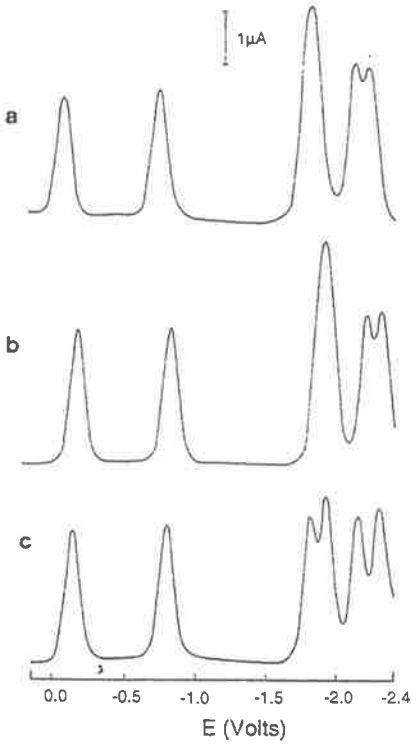

Figure 5. Differential pulse voltammograms for the *rac* (ΔΔ/ΛΛ) forms of (a) $[\{Ru(bpy)_2\}_2(\mu\text{-mapy})]^{4+}$, (b) $[\{Ru(Me_2bpy)_2\}_2(\mu\text{-mapy})]^{4+}$, and (c) $[(bpy)_2Ru(\mu\text{-mapy})Ru(Me_2bpy)_2]^{4+}$ (CH_3CN/0.1 M $[(n\text{-}C_4H_9)_4N]ClO_4$ solution; Pt working electrode; Ag/Ag^+ reference electrode).

the terminal ligands attached to both ruthenium centers in the dimer are the same, there is a broad peak ($E_{1/2red(3)}$) associated with a two-electron process (or more probably, two one-electron reductions occurring almost simultaneously at opposite ends of the molecule). For the "mixed-end" dimer (Figure 5c), there are two distinctly resolved one-electron peaks, now separated by over 100 mV. By comparison with responses shown in Figures 5a,b, the first peak can be assigned as a reduction of a bpy ligand attached to one metal center, and the second ($E_{1/2red(4)}$), as a reduction of Me_2bpy attached to the other metal. These $E_{1/2}$ values (Table 4) are consistent with those of the symmetrical dimers in which the terminal ligands are all bpy and all Me_2bpy, respectively. As with the mononuclear species, the presence of methyl substituents on the α-azodiimine bridge does not appear to affect the reduction potentials of the terminal (non-bridging) ligands.

The redox couple labeled $E_{1/2red(5)}$ was previously assigned as a two-electron bridge-centered reduction[13] for the complex $[\{Ru(bpy)_2\}_2(\mu\text{-apy})]^{4+}$. After integration of the area under the DPV response for this compound and also the four other α-azodiimine-bridged species, it now appears to be a single-electron, bpy-centered process. Similarly, $E_{1/2red(6)}$, which was also thought to involve two electrons, now appears to be a single-electron reduction. The original assignment of $E_{1/2red(5)}$ was based upon spectroelectrochemical studies and the presence of nonreduced bpy in the spectrum of what was assumed to be the $[\{Ru(bpy)_2\}_2(\mu\text{-apy})]^{2-}$ anion. This implied the presence of a $\{\mu\text{-apy}\}^{4-}$ moiety, although characteristic absorption features for this ligand could not be established. However if $E_{1/2red(5)}$ involves only a single electron transfer, then the anion investigated was actually $[\{Ru(bpy)_2\}_2(\mu\text{-apy})]^-$, which would still possess an unreduced terminal ligand. An examination of the redox potentials shows shifts of ~85 mV for these couples

between the species containing bpy and Me_2bpy as terminal ligands. Modification of the bridging ligand by methyl substitution has no effect on either the fifth or sixth reductions. If $E_{1/2red(5)}$ was bridge-centered, the electron-donating ability of a methyl substitutent would be expected to make reduction more difficult, and by analogy to the case of $E_{1/2red(1)}$ and $E_{1/2red(2)}$ (which are indeed bridge-based processes) a cathodic shift of ~35 mV might be anticipated.

Spectroelectrochemisty. Spectroelectrochemical studies of the dinuclear complexes show isosbestic points for the first oxidation process and for the first two reductions. The full oxidation of both metal centers to the trivalent state could not be achieved at −32 °C due to the electrochemical limits of the solvent ($[(n\text{-}C_4H_9)_4N]ClO_4$ in acetonitrile). Reversibility of the first oxidation and the six reduction steps was demonstrated by the coincidence of the isosbestic points during each reverse electrolysis step and ultimate recovery of the starting compound.

The first oxidation is a one-electron process producing the mixed-valence species $[(pp)_2Ru^{III}(\mu\text{-}L)Ru^{II}(pp)_2]^{5+}$, which have IVCT bands (ν_{max} 6800−6900 cm^{-1}; ϵ_{max} 800−1200 mol^{-1} dm^3 cm^{-1}; $\Delta\nu_{1/2}$ 1600−1900 cm^{-1}). The formation of these IVCT bands in a spectroelectrochemical experiment is shown for the oxidation of *meso*-$[(bpy)_2Ru^{II}(\mu\text{-mapy})Ru^{II}(bpy)_2]^{4+}$ in Figure S4 (Supporting Information). There is a small difference in the shape of the IVCT band between the two compounds $[(bpy)_2Ru^{III}(\mu\text{-mapy})Ru^{II}(bpy)_2]^{5+}$ and $[(Me_2bpy)_2Ru^{III}(\mu\text{-mapy})Ru^{II}(Me_2bpy)_2]^{5+}$. However, there is no discernible difference between diastereoisomers of the same species. The difference in communication between the metal centers observed in electrochemical measurements of the $[(bpy)_2Ru^{III}(\mu\text{-mapy})Ru^{II}(bpy)_2]^{5+}$ diastereoisomers ($E_{1/2ox}$) did not manifest itself in any detectable variation between the IVCT bands, the two band shapes (including $\Delta\nu_{1/2}$) appearing almost superimposable.

These mixed-valent dinuclear species containing the α-azodiimine bridging ligands have previously been categorized as both weakly interacting (class II)[7] and strongly interacting (class III)[39] systems, and the complexes do not clearly meet the criteria for either assignment. In the application of Hush's theory[40,41] to the IVCT band, a large discepancy is observed between the calculated $\Delta\nu_{1/2}$ and the experimental value. While a strong solvent dependency may account for this (our measurements were only carried out in a single solvent), the nonapplicability of the theory suggests a large degree of delocalization and thus strongly interacting (class III) behavior.[7,39,42]

The spectroelectrochemistry studies of the six reduction steps in the dinuclear species support our previous assertions that the first two reductions are centered on the bridge and the next four one-electron reductions are localized on the terminal ligands. The spectral changes associated with the first two reduction processes can be seen in Figure 6, where they are shown as the reverse oxidations [2+] → [3+] and [3+] → [4+]. In the first reduction, the d(Ru) → π*(bpy) MLCT absorption is red-shifted and the d(Ru) → π*(bridge) MLCT absorption undergoes a blue shift, consistent with the first electron being localized on the azobis(4-methyl-2-pyridine) bridge. The red shift is the smaller electronic effect, as bridge reduction raises the d(Ru) level. The band attributed to the d(Ru) → π*(bridge) MLCT absorption collapses completely upon addition of the second electron, while the d(Ru) → π*(bpy) MLCT absorption is further red-shifted, confirming that this second electron is also localized on the bridge.

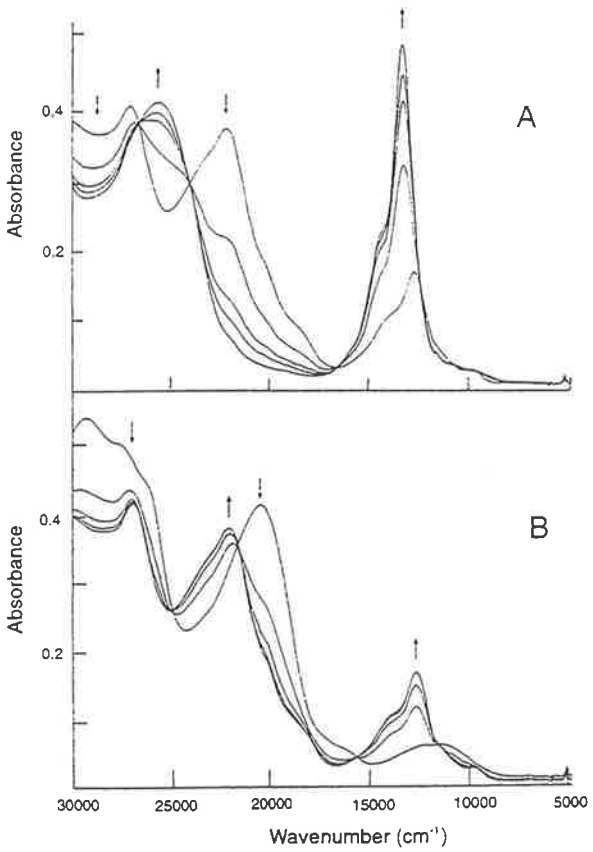

Figure 6. Spectroelectrochemical changes for the oxidation reactions (A) *meso*-$[(bpy)_2Ru^{II}(\mu\text{-}mapy^-)Ru^{II}(bpy)_2]^{3+}$ → *meso*-$[(bpy)_2Ru^{II}(\mu\text{-}mapy)Ru^{II}(bpy)_2]^{4+}$ and (B) *meso*-$[(bpy)_2Ru^{II}(\mu\text{-}mapy^{2-})Ru^{II}(bpy)_2]^{2+}$ → *meso*-$[(bpy)_2Ru^{II}(\mu\text{-}mapy^-)Ru^{II}(bpy)_2]^{3+}$ (CH_3CN/0.1 M $[(n\text{-}C_4H_9)_4N]ClO_4$ solution).

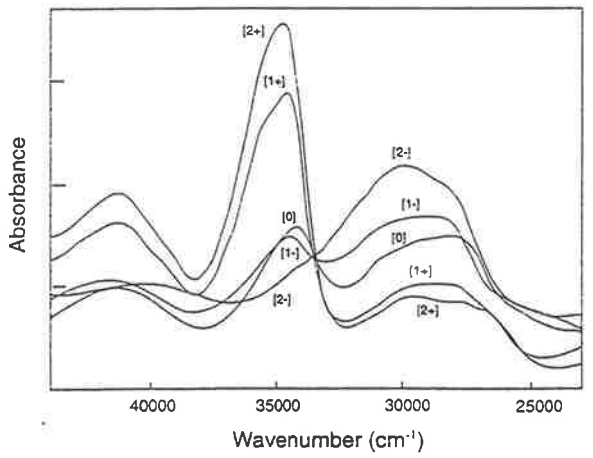

Figure 7. UV−visible absorption spectra (acetonitrile solution) of *meso*-$[(bpy)_2Ru(\mu\text{-}mapy)Ru(bpy)_2]^{n+}$: [2+], $[(bpy)_2Ru^{II}(\mu\text{-}mapy^{2-})Ru^{II}(bpy)_2]^{2+}$; [1+], $[(bpy^-)(bpy)Ru^{II}(\mu\text{-}mapy^{2-})Ru^{II}(bpy)_2]^{+}$; [0], $[(bpy^-)(bpy)Ru^{II}(\mu\text{-}mapy^{2-})Ru^{II}(bpy)(bpy^-)]$; [1−], $[(bpy^-)_2Ru^{II}(\mu\text{-}mapy^{2-})Ru^{II}(bpy)(bpy^-)]^-$; [2−], $[(bpy^-)_2Ru^{II}(\mu\text{-}mapy^{2-})Ru^{II}(bpy^-)_2]^{2-}$.

The bpy^0 and bpy^- bands located in the UV region (centered at 33 800 and 29 600 cm^{-1} respectively; Figure 7) demonstrate that the next four one-electron reductions are localized sequentially on each of the terminal bpy ligands. For each successive reduction ($E_{1/2red(3-6)}$) the bpy^0 band decreases in intensity and

(39) Crutchley, R. J. *Adv. Inorg. Chem.* **1994**, *41*, 273.
(40) Hush, N. S. *Prog. Inorg. Chem.* **1967**, *8*, 391.
(41) Allen, G. C.; Hush, N. S. *Prog. Inorg. Chem.* **1967**, *8*, 357.
(42) Poppe, J.; Moscherosch, M.; Kaim, W. *Inorg. Chem.* **1993**, *32*, 2640.

finally collapses completely, while the bpy^- band correspondingly increases with each reductive step.

Conclusions

The synthesis of a series of α-azodiimine-bridged diruthenium(II) species and their separation in each case into diastereoisomers have permitted the observation and measurement of physical differences between the *meso* and *racemic* forms. Comparisons of the electronic spectra of the two diastereoisomeric forms show a ~6 nm difference in the MLCT absorptions. Electrochemical studies reveal anodic shifts for oxidative couples and cathodic shifts for reductive couples of 0−45 mV for the *racemic* relative to the *meso* forms of each of the five dinuclear complexes investigated. Similarly, there are differences in the comproportionation constants between diastereoisomeric forms as calculated from the $E_{1/2redox}$ measurements, although no discernible differences were observed between the IVCT bands of the respective forms. Significant structural differences in the relative orientations of the terminal ligands are reflected electronically in the markedly different ^{1}H-NMR spectra. The *meso* forms always appear as the major product from the synthesis and have a much lower solubility in a wide range of organic solvents.

The first six electrochemical reductions for this series of dinuclear complexes have been unequivocally assigned. Contrary to a previous report in the literature, there are six one-electron steps—the first two are centered on the bridge and the following four localized on the four terminal ligands.

Acknowledgment. This work was supported by the Australian Research Council. We are grateful to Dr. Graham Heath for the use of the OTTLE cell facilities at the Australian National University.

Supporting Information Available: Figures S1−S4, showing CHEM 3D representations of the diastereoisomeric forms of $[\{Ru(Me_2bpy)_2\}_2(\mu\text{-apy})]^{4+}$, portions of the 300 MHz ^{1}H-NMR NOE difference spectra of *rac*-$[\{Ru(Me_2bpy)_2\}_2(\mu\text{-mapy})]^{4+}$, correlation between $\Delta E_{ox/red}$ (potential difference between the first oxidation and first reduction processes) and E_{MLCT} (the lowest energy MLCT absorption) for tris(bidentate)ruthenium complexes containing polypyridyl ligands, and spectroelectrochemical changes for the oxidation reaction *meso*-$[(bpy)_2Ru^{II}(\mu\text{-mapy})Ru^{II}(bpy)_2]^{4+}$ — *meso*-$[(bpy)_2Ru^{III}(\mu\text{-mapy})Ru^{II}(bpy)_2]^{5+}$ (CH_3CN/0.1 M $[(n\text{-}C_4H_9)_4N]ClO_4$ solution), and an Appendix giving the data used to generate Figure S3 (5 pages). Ordering information is given on any current masthead page.

IC9600893

Preparation of 7,8-diazaphencyclone and its use in the construction of rigid, space-separated 1,10-phenanthroline donor–acceptor systems: new ligands for metal complexation

Ronald N. Warrener,*[a] Mark A. Houghton,[a] Austin C. Schultz,[a] F. Richard Keene,[b] Laurence S. Kelso,[b] Robert Dash[c] and Douglas N. Butler*[c]

[a] *Centre for Molecular Architecture, Central Queensland University, Rockhampton, Queensland 4702, Australia*
[b] *School of Molecular Sciences, James Cook University, Townsville, Queensland 4811, Australia*
[c] *Department of Chemistry, York University, North York, Ontario, Canada M3J 1P3*

7,8-Diazaphencyclone 7 is used as a delivery reagent to fuse 1,10-phenanthroline groups onto alkenic centres of rigid spacer molecular racks (molracs); molrac alkenes containing redox-active donor–acceptor chromophores yield molrac diads whose metal complexes, *e.g.* 26, are suitable for mechanistic studies involving intramolecular electron transfer.

Polypyridyl ligands have a special role in modern studies of the properties of metal complexes, especially those related to electron transfer.[1] Previous work on intramolecular quenching processes within metal complexes containing such ligands has generally involved flexible spacers between the ligating entities and the redox-active groups.[2] Using rigid molecular racks (molracs) as spacers[3] between the ligand and the redox-functionality provides the means for a detailed assessment of spatial influences on intramolecular electron transfer.

The previously unknown 7,8-diazaphencyclone (DAPC) 7, prepared in dimeric form 8 as outlined in Scheme 1, is used as the delivery reagent for attaching the 1,10-phenanthroline unit to the rigid molrac.

The availability of 7 as a diene was established by generating it *in situ* from its dimer 8 (but not 9) by heating in the presence of Smith's diene 10[4] where exclusive formation of the 1:1 adduct 11‡ was observed to occur (Scheme 2). The presence of an alkenic resonance in the ^{1}H NMR of 11 at δ 6.13 showed that reaction had occurred site selectivity at the cyclobutene π centre and the stereochemistry followed from the upfield position of the ester methyl resonances which occur at δ 3.14 as a result of their proximity to the ring-current of the phenanthroline.

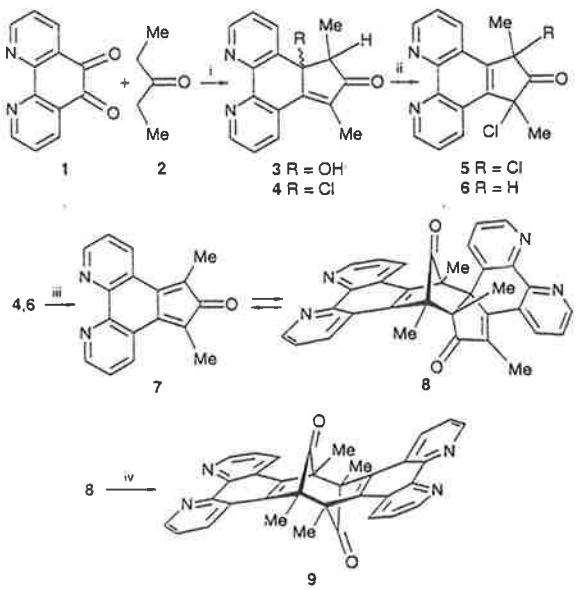

Scheme 1 *Reagents and conditions*: i, K_2CO_3 in MeOH, room temp., 24 h; ii, $SOCl_2$/pyridine (1:1); iii, NEt_3; iv, 100 °C

The ability of 7,8-diazaphencyclone 7 to react with benzonorbornene π-bonds was exploited in the conversion of the benzonorbornadiene 12 to the ligand 13 and of 14 to the phenanthroline 15. The *exo,endo*-stereochemistry of these adducts is immediately apparent from the dramatic upfield shift of the isopropylidene methyl resonances (δ −0.01) in 13 and the *syn*-related bridge methylene proton (δ −0.17) in 15.

Further members in the series of space-separated 1,10-phenanthrolines containing the dimethoxynaphthalene chromophore, *e.g.* 17, 19 and 21 were prepared in 48–75% yields by reaction of 6,7-diazaphencyclone 7 with the corresponding molrac cyclobutenes 16,[5] 18[5] and 20.[5] Spectral characteristics (^{1}H, ^{13}C NMR, *m/z*) support these structural assignments. In particular, the upfield chemical shifts of the ester methyl resonances (δ 3.22, 3.08 and 3.10 respectively) confirm the proximity of the phenanthroline ring to the ester groups in each system.

Incorporation of a naphthoquinone group can also be achieved using this reaction protocol (Scheme 3). Thus, the known quinone 22[6] was reacted with DMAD/Ru^0 under the Mitsudo conditions[7] to produce the cyclobutene diester 23, which was treated with 7,8-diazaphencyclone 7 to form the pale yellow 1:1 cycloadduct 24 in 63% yield. ^{1}H NMR data confirmed that cycloaddition had occurred at the cyclobutene preferentially to the quinone.

The complex $[Ru(bpy)_2(24)]^{2+}$ (26; bpy = 2,2′-bipyridine) was synthesised in 92% yield using an established route *via* the $[Ru(bpy)_2(CF_3SO_3)_2]$ precursor 25.[8] The structure of complex 26 is supported by electronic‡ and ^{1}H NMR spectroscopy (CD_3CN) where 26 non-equivalent proton resonances occur in the aromatic region due to the spatial interrelationship of the three bidentate ligands. Formation of 26 involves displacement of the triflato groups from the complex 25 (C_2 point group symmetry) by the phenanthroline ligand 24 (C_s symmetry), which yields a single product as there are no orientational consequences for its attachment. However, because of the disposition of the bipyridine rings, 24 loses its σ-plane on coordination, accounting for non-equivalence of the two halves of the phenanthroline entity and its attached components (*e.g.* the *C*-methyl substituents show separate singlets at δ 2.04 and 2.06; ester *O*-methyls at δ 3.11 and 3.36).

Cyclic voltammetric studies of 26, {MeCN/0.1 mol dm^{-3} $[(C_4H_9)_4N]ClO_4$ solution; Pt working electrode} show two reversible redox couples, one at $E_{1/2}$ = +1045 mV (*vs.* Ag/Ag^+)

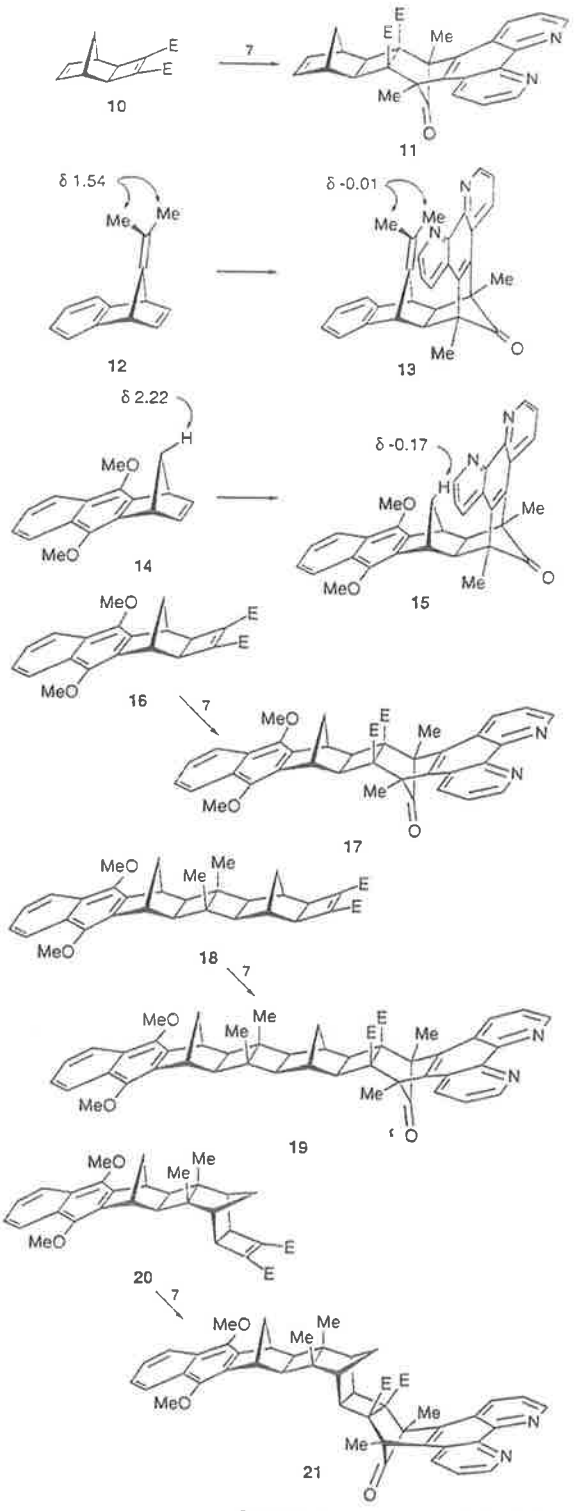

Scheme 2

associated with the metal centre ($Ru^{III/II}$) and the other at $E_{1/2}$ = −915 mV assigned as the first reduction of the quinone moiety ($Q^{0/1-}$). All further reductive events were totally irreversible, with characteristically sharp desorption peaks upon re-oxidation.

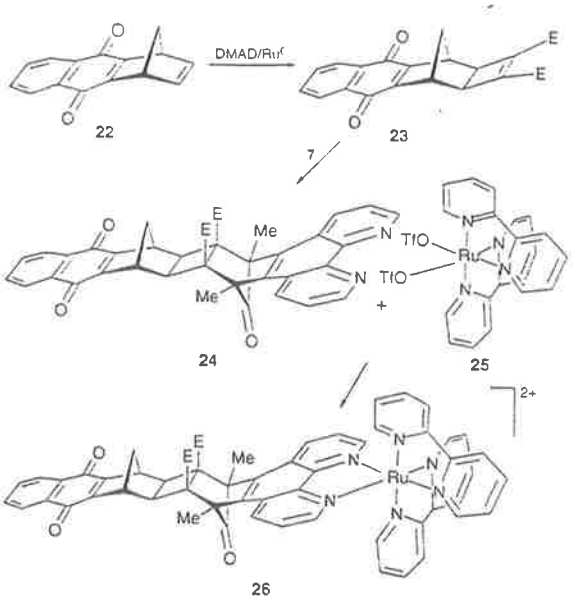

Scheme 3

Complex **26** does not luminesce at room temperature, presumably because of internal quenching following photoexcitation at the metal centre.

R. N. W. thanks the Australian Research Council for the award of an ARC Senior Research Fellowship (1992–1996). This work was funded by the ARC (R. N. W, F. R. K) and a Central Queensland University URG Grant for which we are appreciative. D. N. B thanks the Centre for Molecular Architecture, CQU for the award of a Senior Visiting Fellowship.

Footnotes

† All new compounds have been characterised by spectroscopic techniques (^{1}H NMR, ^{13}C NMR) and molecular formula established by microanalysis or mass spectrometry: representative yields and mps for **7**: 50% yield; mp > 350 °C. For **11**: 57% yield; mp 250–252 °C. For **13**: 83% yield; mp 273–275 °C (decomp.). For **24**: mp 198–200 °C.

‡ UV–VIS (MeCN) for **26** [λ_{max}/nm (ε/mol^{-1} dm^3 cm^{-1})]: 450 (MLCT) (13500); 434(sh), (12200); 276 (59700); 252 (55100) and 194 (83400).

References

1 A. Juris, S. Barigelletti, S. Campagna, V. Balzani, P. Belser and A. von Zelewsky, *Coord. Chem. Rev.*, 1988, **84**, 85.
2 J.-P. Sauvage, J.-P. Collin, J.-C. Chambron, S. Guillerez, C. Coudret, V. Balzani, F. Barigelletti, L. Decola and L. Flamigni, *Chem. Rev.*, 1994, **94**, 993; K. A. Opperman, S. L. Mecklenburg and T. J. Meyer, *Inorg. Chem.*, 1994, **33**, 5295, and references cited therein.
3 R. N. Warrener, S. Wang, L. Maksimovic, P. M. Tepperman and D. N. Butler, *Tetrahedron Lett.*, 1995, **36**, 6141; R. N. Warrener, G. M. Elsey and M. A. Houghton, *J. Chem. Soc., Chem. Commun.*, 1995, 1417 and references cited therein.
4 C. D. Smith, *J. Am. Chem. Soc.*, 1966, **88** 4273.
5 M. N. Paddon-Row, E. Cotsaris and H. K. Patney, *Tetrahedron*, 1986, **42**, 1779; R. N. Warrener and J. Strauss, ARC Grant Report, 1981, unpublished results.
6 L. A. Paquette, F. Bellamy, M. C. Bohm and R. Gleiter, *J. Org. Chem.*, 1980, **45**, 4917.
7 T. Mitsudo, K. Kokurya, T. Shinsugi, Y. Nakagawa, T. Watanabe and Y. Takegami, *J. Org. Chem.*, 1979, **44**, 4492.
8 M. J. Ridd, D. J. Gakowski, G. E. Sneddon and F. R. Keene, *J. Chem. Soc., Dalton Trans.*, 1992, 1949.

Received, 13th December 1995; Com. 5/08114I

Space-Separated 1,10-Phenanthroline, 4,5-Diazafluorene, or 3,6-Di(2-pyridyl)pyridazine Units as Ligands in Diruthenium Complexes: Preliminary Studies of Metal–Metal Interactions**

Ronald N. Warrener,* Aurélio B. B. Ferreira, Austin C. Schultz, Douglas N. Butler, F. Richard Keene,* and Laurence S. Kelso

There has been much activity in the field of intramolecular energy transfer and electron transfer in large molecular assemblies, and the next advances will clearly require sophisticated molecular design. Where metal complexes are involved as the light-harvesting chromophore[1] the design and construction of ligands becomes an important component. Studies on intramolecular electron transfer have been reported in which metal complexes have been tethered to redox-active chromophores, but almost all of these systems contain flexible linkages.[2] Elegant syntheses have been reported recently for fully conjugated diad systems incorporating the 1,10-phenanthroline moiety as the bidentate ligand,[3] and we have described the first molecular rack (molrac) in which two units of the same ligand are spatially separated.[4] We report here on the preparation of a new set of rigid bis(bidentate ligand) structures in which the individual bidentate ligands (1,10-phenanthroline, 4,5-diazafluorene, or 3,6-di(2-pyridyl)pyridazine) are fused to an alicyclic framework.

The versatile spacers in molracs permit the development of bridging ligands in which the ligating groups are placed at a set distance and relative orientation in space. These compounds should allow assessment of the factors controlling intramolecular energy- and electron-transfer processes in polymetallic species, as well as lead to new reagents for the study of self-assembly processes.[5] Rigid alicyclic frameworks have been used in molrac systems since they have proven their worth in diad and triad systems devoid of metal centers[6] and are available in an increasing range of shapes and sizes.[4, 7–10]

The typical olefinic spacers in the molracs have norbornene or cyclobutene diester end groups (or mixtures thereof), and these offer different dienophilic character. When the cycloaddition reagents 3, 2, and 1 (Scheme 1) are used to deliver the specific ligand center, it is possible to introduce 3,6-di(2-pyridyl)-pyridazine,[9] 1,10-phenanthroline,[4] and 4,5-diazafluorene groups, respectively,[10] to the norbornene end, and 1,10-phenanthroline and 4,5-diazafluorene functionalization to the cyclobutene diester end of molracs. Given that these bidentate ligands can be attached in homo or hetero pairs as shown herein, and that the 4,5-diazafluorene is linked orthogonally to the plane of the spacer whereas the other two ligands are fused in a coplanar fashion, numerous ligand and geometric variants are available by this procedure.

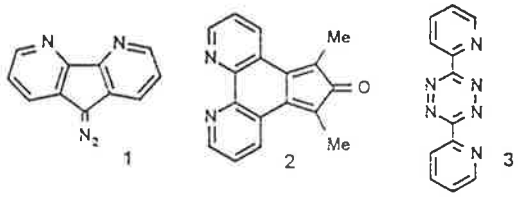

Scheme 1. Ligand-delivery agents used in this study.

For the production of molrac systems containing two diazafluorene (DAF) ligands, 9-diazo-4,5-diazafluorene (DADAF) 1 was employed as the delivery agent for 4,5-diazafluorene. Reaction of the known bis(cyclobutene) 4[11] with excess 1 (Scheme 2) produced a regiomeric pair of pyrazolines of type

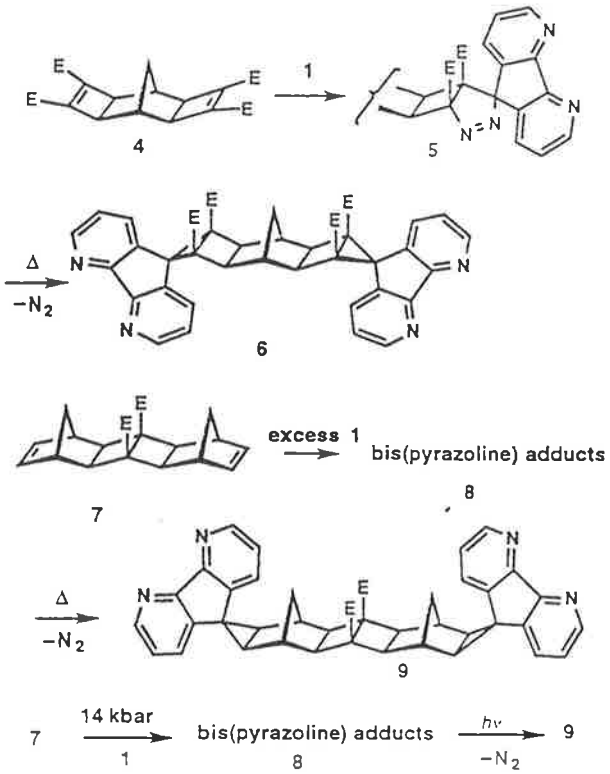

Scheme 2. Synthesis of molracs 6 and 9 in which the ligand units are coplanar with and orthogonal to the central spacer, respectively.

5, which were not separated but thermally deazotized to form the bisligand 6 (63% yield) (bisligand = a molrac having two ligand groups).[12] The ^{1}H NMR resonances[13] of the bisligand 6 are entirely in keeping with the assigned structure. This reaction is general and more extended spacer bis-DAF ligands have been produced in our laboratory.[14]

[*] Prof. Dr. R. N. Warrener, A. C. Schultz
Centre for Molecular Architecture, Central Queensland University Rockhampton, Queensland, 4702 (Australia)
Fax: Int. code +(79)309917
e-mail: r.warrener@cqu.edu.au

Dr. F. R. Keene, L. S. Kelso
Department of Chemistry and Chemical Engineering
School of Molecular Sciences
James Cook University of North Queensland
Townsville, Queensland 4811 (Australia)
Fax: Int. code +(77)814600
e-mail: richard.keene@jcu.edu.au

Dr. A. B. B. Ferreira
Departamento de Quimica, ICE
Universidade Federal Rural do Rio de Janeiro (Brazil)

Dr. D. N. Butler
Department of Chemistry, York University
North York (Canada)

[**] This work was funded by the Australian Research Council (ARC Senior Research Fellowship to R. N. W. (1992–1996), grants to R. N. W. and F. R. K.) and Central Queensland University. Dr. G. A. Heath and co-workers (Australian National University) are thanked for their assistance in undertaking spectroelectrochemical studies on the dinuclear species. D. N. B. thanks the Centre for Molecular Architecture, Central Queensland University for the award of a Senior Visiting Fellowship (1995).

Addition of DADAF 1 to the norbornene π-bonds of bis(olefin) 7[9] (Scheme 2) was sluggish and required prolonged heating (toluene, reflux, 60 h). Addition of DADAF 1 (fourfold excess) in three portions to 7, over a period of 60 h, afforded 9 in 68% yield. Alternatively, 9 could be produced by photochemical deazotization of the bis(pyrazolines) 8, themselves generated under high-pressure conditions (14 kbar, room temperature, CH_2Cl_2, from 7 and 1.

While an X-ray structure of a mono-DAF-substituted molrac has been reported,[10] the bisligand described herein has only been obtained as microcrystals unsuitable for single-crystal structure analysis. Since the results of molecular modeling (SPARTAN, AM1) are in good agreement with the X-ray derived parameters in molrac systems, computational techniques (AM1) can be used to obtain structural parameters such as separation distances and shapes.

Cyclopentadienone 2[4] was used as the delivery agent for the 1,10-phenanthroline ligand; it served as a standard electron-demand diene in Diels–Alder reactions with olefins in the order of reactivity cyclobutene-1,2-diesters > benzonorbornenes > nor-bornenes.[4] Diels–Alder addition of 2 to bis(cyclobutene) 4 occurred stereospecifically to produce first the monoadduct 10 and then the bisadduct 11 (Scheme 3). The C_s symmetry of 11

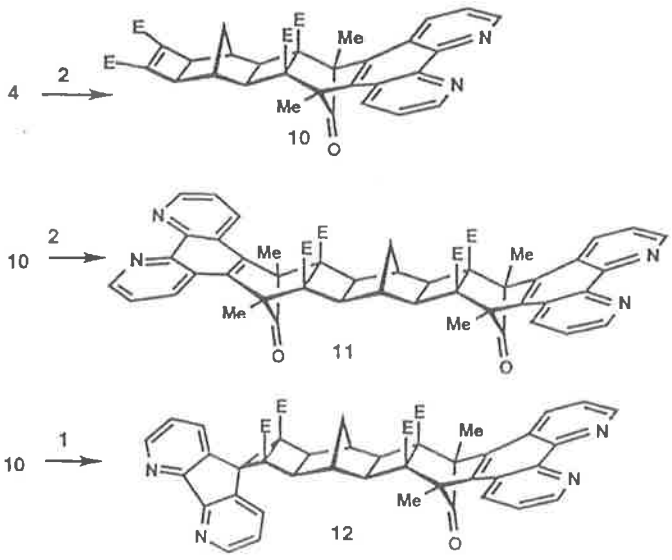

Scheme 3. Reaction of cyclopentadienone 2 with diene 4 produces the monoadduct 10; reaction with more 4 provides the bisligand 11. Reaction of 10 with DADAF 1 yields the mixed bisligand 12.

was supported by its ^1H and ^{13}C NMR spectra and the assigned stereochemistry by the upfield position of the ester methyl proton resonances ($\delta = 3.14$). Separate reaction of 10 with DADAF 1 to form 12 led to the first of the mixed ligand systems. The two ligands bear an orthogonal relationship to one another, which is reflected in the ^1H NMR shifts of the two sets of methyl ester resonances: the phenanthroline ligand shields the proximate ester groups ($\delta = 3.16$), whereas the diazafluorene ring lying orthogonal deshields the other set ($\delta = 3.60$).

Reaction of Smith's diene[15] with 3,6-di(2-pyridyl)-*s*-tetrazine/DDQ (DDQ = 2,3-dichloro-5,6-dicyanobenzoquinone) according to our reported procedure[9] occurred preferentially at the norbornene π-center to produce the fused dpp molrac 13 (Scheme 4). Treatment of 13 with 1 gives the mixed bisligand 14,

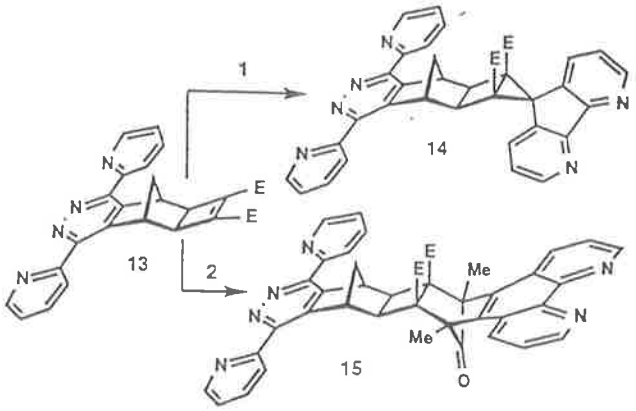

Scheme 4. Synthesis of mixed bisligands in which the two ligand units are orthogonal (14) and roughly parallel to each other (15).

where the two ligands again have an orthogonal relationship. The alternative reaction of 13 with DAPC 2 produced the bisligand 15 in which the two ligands are now parallel.

In conclusion, the versatile ligand-delivery agents 1 (for 4,5-diazafluorene), 2 (for 1,10-phenanthroline), and 3 (for 3,6-di-(2-pyridyl)pyridazine) can be attached to bis(olefins) to produce an array of doubly(bidentate ligand) molracs of varied size and geometry through simple cycloaddition reactions.

The bridged diruthenium species $[\{Ru(bpy)_2\}_2(\mu\text{-BL})]^{4+}$ (BL = 6, 9, 11; bpy = 2,2′-bipyridine) were synthesized by reaction of the respective ligands with excess $[Ru(bpy)_2(CF_3SO_3)_2]$ in chloroform/2-methoxyethanol mixtures under microwave conditions.[16, 17] In all three cases, electrochemical studies

Table 1. Selected physical data for representative compounds.

6: M.p. >340 °C (decomp); yield 63%; ^1H NMR (300 MHz, $CDCl_3$): δ = 8.86 (dd, J = 1.2, 4.8 Hz, 2H), 8.73 (dd, J = 1.4, 4.8 Hz, 2H), 8.01 (dd, J = 1.2, 8.1 Hz, 2H), 7.87 (dd, J = 1.4, 8.1 Hz, 2H), 7.41 (dd, J = 4.8, 8.1 Hz, 2H), 7.24 (dd, J = 4.8, 8.1 Hz, 2H), 3.63 (s, 12H), 3.09 (s, 4H), 2.93 (s, 2H), 2.65 (s, 2H); ^{13}C NMR (75 MHz, $CDCl_3$): δ = 165.6, 160.1, 157.2, 150.2, 150.0, 136.6, 134.9, 133.5, 131.9, 122.5, 122.3, 52.2, 46.5, 44.6, 42.2, 38.9, 38.7.

9: M.p. >340 °C (decomp); yield 68%; ^1H NMR (300 MHz, $CDCl_3$): δ = 8.66 (br. d, J = 4.7 Hz, 4H), 7.98 (dd, J = 1.2, 8.3 Hz, 2H), 7.15–7.35 (m, 6H), 3.78 (s, 6H), 2.86 (s, 4H), 2.73 (s, 4H), 2.14 (br. s, 4H), 1.95 (s, 4H).

10: M.p. 290 °C (decomp); yield 14%; ^1H NMR (300 MHz, $CDCl_3$): δ = 9.20 (dd, J = 4.2, 1.5 Hz, 2H), 8.54 (dd, J = 8.5, 1.5 Hz, 2H), 7.65 (dd, J = 8.4, 4.3 Hz, 2H), 3.81 (s, 6H), 3.16 (s, 6H), 2.69 (s, 2H), 2.65 (s, 2H), 2.15 (s, 2H), 2.07 (s, 6H), 1.85 (d, J = 12.6 Hz, 1H), 1.40 (d, J = 12.6 Hz, 1H).

11: M.p. 315 °C (decomp); yield 68%; ^1H NMR (300 MHz, $CDCl_3$): δ = 9.21 (dd, J = 4.2, 1.5 Hz, 4H), 8.54 (dd, J = 8.5, 1.6 Hz, 4H), 7.65 (dd, J = 8.4, 4.2 Hz, 4H), 3.14 (s, 12H), 3.01 (s, 2H), 2.10 (s, 4H), 2.09 (s, 12H), 1.96 (s, 2H).

12: M.p. 281 °C (decomp); yield 44%; ^1H NMR (300 MHz, $CDCl_3$): δ = 9.23 (dd, J = 4.2, 1.5 Hz, 2H), 8.85 (dd, J = 4.8, 1.0 Hz, 1H), 8.71 (dd, J = 4.7, 1.3 Hz, 1H), 8.54 (dd, J = 8.5, 1.6 Hz, 2H), 8.03 (br. d, J = 7.3 Hz, 1H), 7.84 (dd, J = 8.1, 1.3 Hz, 1H), 7.68 (dd, J = 8.4, 4.3 Hz, 2H), 7.43 (dd, J = 8.0, 4.8 Hz, 1H), 7.21 (dd, J = 8.1, 4.8 Hz, 1H), 3.60 (s, 6H), 3.16 (s, 2H), 2.87 (s, 2H), 2.85 (s, 2H), 2.73 (d, J = 12.8 Hz, 1H), 2.31 (s, 2H), 2.12 (d, J = 12.8 Hz, 1H), 2.10 (s, 6H).

14: M.p. 262–263 °C (decomp); yield 51%; ^1H NMR (300 MHz, $CDCl_3$): δ = 8.65–8.75 (m, 4H), 8.63 (br. d, J = 7.8 Hz, 2H), 7.95 (dd, J = 1.4, 8.1 Hz, 1H), 7.87 (ddd, J = 1.8, 7.8, 7.8 Hz, 2H), 7.59 (dd, J = 1.0, 8.1 Hz, 1H), 7.33 (ddd, J = 1.1, 4.8, 7.8 Hz, 2H), 7.24 (dd, J = 4.8, 8.1 Hz, 1H), 7.06 (dd, J = 4.8, 8.1 Hz, 1H), 4.70 (s, 2H), 3.70 (s, 6H), 3.03 (d, J = 10.8 Hz, 1H), 3.23 (s, 2H), 1.93 (d, J = 10.8 Hz, 1H); EI-MS: *m/z* (%): 606 (M^+, 3.1), 334 (38), 272 (86), 243 (22), 95 (25).

15: M.p. 301 °C (decomp); yield 85%; ^1H NMR (300 MHz, $CDCl_3$): δ = 9.22 (dd, J = 4.2, 1.6 Hz, 2H), 8.80 (ddd, J = 4.8, 1.8, 0.9 Hz, 2H), 8.64–8.60 (m, 4H), 7.92 (ddd, J = 7.8, 7.8, 1.8 Hz, 2H), 7.67 (dd, J = 8.5, 4.3 Hz, 2H), 7.40 (ddd, J = 7.5, 4.8, 1.1 Hz, 2H), 4.83 (s, 2H), 3.24 (s, 6H), 2.51 (s, 2H), 2.27 (d, J = 11.3 Hz, 1H), 2.11 (s, 6H), 1.73 (d, J = 11.3 Hz, 1H).

(cyclic voltammetry and differential pulse voltammetry) indicated a single oxidation (n = two electrons, by coulometry). Similarly, careful spectroelectrochemical studies at $-32\,^{\circ}C$ in acetonitrile solution provided no evidence for the transient accumulation of a Ru^{II},Ru^{III} state. Accordingly, the Ru^{II},Ru^{III} form of these complexes appears to be thermodynamically disfavored with respect to disproportionation.

These results indicate a weak interaction between the metal centers and are consistent with results reported recently for a complex in which the bridging ligand is composed of two diazofluorene units linked by an adamantane spacer.[18] As noted previously,[18, 19] such weak interactions do not preclude the existence of rapid intercomponent energy or electron transfer, and photophysical studies are in progress on Ru/Ru, Ru/Os, and Os/Os analogues of the complexes described here to assess the consequences of spatial separation on such processes.

Received: April 29, 1996 [Z 9078 IE]
German version: *Angew. Chem.* **1996**, *108*, 2651–2653

Keywords: cycloadditions · cyclopentadienones · Diels–Alder reactions · ruthenium compounds

[1] A. Juris, S. Barigelletti, S. Campagna, V. Balzani, P. Belser, A. von Zelewsky, *Coord. Chem. Rev.* **1988**, *84*, 85.

[2] a) J.-P. Sauvage, J.-P. Collin, J.-C. Chambron, S. Guillerez, C. Coudret, V. Balzani, F. Barigelletti, L. Decola, L. Flamigni, *Chem. Rev.* **1994**, *94*, 993; b) K. S. Schanze, K. Sauer, *J. Am. Chem. Soc.* **1988**, *110*, 1180; c) L. F. Cooley, S. L. Larson, C. M. Elliott, D. F. Kelley, *J. Phys. Chem.* **1991**, *95*, 10694; d) C. K. Ryu, R. Wang, R. H. Schmehl, S. Ferrere, M. Ludwikow, J. W. Merkert, C. E. L. Headford, C. M. Elliott, *J. Am. Chem. Soc.* **1992**, *114*, 430; e) S. L. Mecklenburg, B. M. Peek, J. R. Schoonover, D. G. McCafferty, C. G. Wall, B. W. Erickson, T. J. Meyer, *ibid.* **1993**, *115*, 5479; f) K. A. Opperman, S. L. Mecklenburg, T. J. Meyer, *Inorg. Chem.* **1994**, *33*, 5295.

[3] J. Bolger, A. Gourdon, E. Ishow, J.-P.-Launay, *J. Chem. Soc. Chem. Commun.* **1995**, 1799; M. J. Crossley, P. L. Burn, S. J. Langford, J. K. Prashar, *ibid.* **1995**, 1921.

[4] R. N. Warrener, M. A. Houghton, A. C. Schultz, F. R. Keene, L. S. Kelso, R. Dash, D. N. Butler, *Chem. Commun.* **1996**, 1151.

[5] M.-T. Youinou, N. Rahmouni, J. Fischer, J. A. Osborn, *Angew. Chem.* **1992**, *104*, 771; *Angew. Chem. Int. Ed. Engl.* **1992**, *31*, 733; P. N. W. Baxter, J.-M. Lehn, J. Fischer, M.-T. Youinou, *ibid.* **1994**, *106*, 2432 and **1994**, *33*, 2284.

[6] J. M. Lawson, D. C. Craig, A. M. Oliver, M. N. Paddon-Row, *Tetrahedron* **1995**, *51*, 3841; K. Kumar, R. J. Tepper, Y. Zeng, M. B. Zimmt, *J. Org. Chem.* **1995**, *60*, 4051, and references therein.

[7] a) R. N. Warrener, S. Wang, L. Maksimovic, P. M. Tepperman, D. N. Butler, *Tetrahedron Lett.* **1995**, *36*, 6141; b) R. N. Warrener, G. M. Elsey, M. A. Houghton, *J. Chem. Soc. Chem. Commun.* **1995**, 1417; c) R. N. Warrener, G. Abbenante, R. G. Solomon, R. A. Russell, *Tetrahedron Lett.* **1994**, *35*, 7639; d) R. N. Warrener, L. Maksimovic, G. M. Elsey, D. N. Butler, *J. Chem. Soc. Chem. Commun.* **1994**, 1831; e) R. N. Warrener, G. Abbenante, C. H. L. Kennard, *J. Am. Chem. Soc.* **1994**, *116*, 3645; f) R. N. Warrener, I. G. Pitt, E. E. Nunn, *Tetrahedron Lett.* **1994**, *35*, 621; g) R. N. Warrener, *Chem. Aust.* **1992**, *59*, 578; h) R. N. Warrener, P. Groundwater, I. G. Pitt, D. N. Butler, R. A. Russell, *Tetrahedron Lett.* **1991**, *32*, 1885; i) R. N. Russell, *Tetrahedron Lett.* **1991**, *32*, 1885; i) R. N. Warrener, D. A. Evans, R. A. Russell, *ibid.* **1984**, *25*, 4833; j) D. N. Butler, P. M. Tepperman, R. A. Gau, R. N. Warrener, W. H. Watson, R. P. Kashyap, *ibid.* **1995**, *36*, 6145.

[8] R. N. Warrener, I. G. Pitt, D. N. Butler, *J. Chem. Soc. Chem. Commun.* **1983**, 1340.

[9] a) R. N. Warrener, G. M. Elsey, I. V. Sankar, D. N. Butler, P. Pekos, C. H. L. Kennard, *Tetrahedron Lett.* **1994**, *35*, 6745; b) D. N. Butler, R. A. Gau, P. M. Tepperman, R. N. Warrener, *ibid.* **1996**, *37*, 2825.

[10] R. N. Warrener, A. B. B. Ferreira, E. R. T. Tiekink, *Tetrahedron Lett.* **1996**, *37*, 2161.

[11] T. Mitsudo, K. Kokurya, T. Shinsugi, Y. Nakagawa, Y. Watanabe, Y. Takegami, *J. Org. Chem.* **1979**, *44*, 4492.

[12] The monoadduct can be isolated when less DADAF is employed and added in one portion.

[13] All new compounds were characterized by spectroscopic techniques (^1H NMR, ^{13}C NMR, IR) and the molecular formula established by microanalysis or mass spectrometry (see Table 1).

[14] A. B. B. Ferreira, R. N. Warrener, unpublished results.

[15] C. D. Smith, *J. Am. Chem. Soc.* **1966**, *88*, 4273.

[16] M. J. Ridd, D. J. Gakowski, G. E. Sneddon, F. R. Keene, *J. Chem. Soc. Dalton Trans.* **1992**, 1949.

[17] $[\{Ru(bpy)_2\}_2(\mu\text{-}6)](PF_6)_4$: yield 82%; λ_{max} (metal–ligand charge transfer, MLCT) = 448 nm (ε = 25300 $mol^{-1}dm^3cm^{-1}$), CH_3CN solution; $E_{1/2}$ (Ru^{III}/Ru^{II}) = +1.04 V (vs. Ag/Ag^+, 0.1 M $[(C_4H_9)_4N]ClO_4$ in CH_3CN, Pt working electrode). $[\{Ru(bpy)_2\}_2(\mu\text{-}9)](PF_6)_4$: yield 88%; λ_{max} (MLCT) = 448 nm (ε = 26100 $mol^{-1}dm^3cm^{-1}$), CH_3CN solution; $E_{1/2}$ (Ru^{III}/Ru^{II}) = +0.97 V (vs. Ag/Ag^+, 0.1 M $[(C_4H_9)_4N]ClO_4$ in CH_3CN, Pt working electrode). $[\{Ru(bpy)_2\}_2(\mu\text{-}11)](PF_6)_4$: yield 92%; λ_{max} (MLCT) = 450 nm (ε = 31400 $mol^{-1}dm^3cm^{-1}$), CH_3CN solution; $E_{1/2}$ (Ru^{III}/Ru^{II}) = +1.06 V (vs. Ag/Ag^+, 0.1 M $[(C_4H_9)_4N]ClO_4$ in CH_3CN, Pt working electrode).

[18] L. De Cola, V. Balzani, F. Barigelletti, L. Flamigni, P. Belser, S. Bernhard, *Recl. Trav. Chim. Pays-Bas* **1995**, *114*, 534.

[19] V. Balzani, F. Scandola, *Supramolecular Photochemistry*, Ellis Horwood, Chichester, **1991**.

Synthesis and properties of mononuclear tris(heteroleptic) osmium(II) complexes containing bidentate polypyridyl ligands †

Erik Z. Jandrasics and F. Richard Keene *

Department of Chemistry and Chemical Engineering, School of Molecular Sciences, James Cook University of North Queensland, Townsville, Queensland 4811, Australia

A general synthetic methodology has been elaborated for tris(bidentate ligand)osmium(II) complexes containing three different polypyridyl ligands. The tris(heteroleptic) complexes were characterized by NMR techniques, and the ligand dependence of their electrochemistry and electronic spectroscopy examined.

We recently published details of a general synthetic methodology for tris(heteroleptic)ruthenium(II) complexes of the type $[Ru(pp)(pp')(pp'')]^{2+}$ (where pp, *etc.* are bidentate polypridyl ligands) based on the sequential addition of the pro-ligands to the oligomeric precursor $[\{Ru(CO)_2Cl_2\}_n]$.[1,2] The consequent ability to deliberately control the ligand environment has been exploited in spectral,[3] photophysical[2,4] and electrochemical[2] characteristics of the ruthenium(II) species. Furthermore, the methodology has also been utilized in the synthesis of ligand-bridged dinuclear[5,6] and higher nucleate[7] complexes, and stereochemical aspects of the scheme have been investigated.[6,8]

The osmium(II) centre is of fundamental importance in the study of d^6 polypyridyl complexes, and while earlier studies using bis(heteroleptic) species have dealt with the influence of the ligand environment on the characteristics of the metal centre,[9–14] the wider variations provided by tris(heteroleptic) complexes have not been available.

The present work details a general procedure for such species, which has close analogies with that used for the ruthenium counterparts,[1,2] and provides access to an extensive array of osmium complexes, $[Os(pp)(pp')(pp'')]^{2+}$. Preliminary studies of the physical characteristics of such species are reported.

Results and Discussion

Synthesis

In developing a synthetic methodology for the tris(heteroleptic) osmium(II) complexes a number of strategies were investigated, all necessarily involving an intermediate species of type $[Os(pp)(pp')X_2]^{n+}$. For example, the possibility of forming the precursor $[Os(pp)(pp')Cl_2]$ by reaction of $[Os(pp)Cl_4]$[15] with a second diimine (pp') was attempted: however, under forcing conditions (microwave oven using high-boiling solvents such as ethylene glycol or *N*-methylpyrrolidone)[16] the major products were bis(heteroleptic) species, *e.g.* $[Os(pp)(pp')_2]^{2+}$.

As an alternative approach, $[Os(pp)(CO)_2Cl_2]$ was sought as a possible precursor for the synthesis of $[Os(pp)(pp')(CO)_2]^{2+}$, which in turn could be transformed into the tris(heteroleptic) species. Schemes involving the carbonylation of $[Os(bipy)Cl_4]$ (bipy = 2,2'-bipyridine) in 2-methoxyethanol under an elevated CO pressure (60 psig) at 80 °C,[15] an attempted carbonylation of the same substrate by formic acid–formaldehyde (40:3 v/v) and the reaction of $OsCl_3 \cdot xH_2O$ with a 2.3-fold excess of bipy in 2-methoxyethanol solution under a CO atmosphere (60 psig)[17] all realised the target compound $[Os(bipy)(CO)_2Cl_2]$ in a very low yield (<10%). In addition, Johannsen *et al.*[18] had reported the synthesis of *cis*-$[Os(CO)_2Cl_4]^{2-}$ (as the NEt_4^+ salt) from the reaction of hexahalogenoosmate(IV) complexes with unsaturated alcohols such as propen-2-ol (allyl alcohol). While this may have provided a pathway to $[Os(pp)(CO)_2Cl_2]$, the yield was unsatisfactory and the method suffers the disadvantages of a long reaction time (7 d) and the toxicity of the alcohol.

Since none of these alternatives proved entirely satisfactory, we pursued a strategy similar to that for the ruthenium(II) species.[2] The first intermediate in that scheme was $[Ru(pp)(CO)_2Cl_2]$, formed by reaction of pp with the oligomer $[\{Ru(CO)_2Cl_2\}_n]$: however, an alternative path was required in the present case as there appears no analogue of the ruthenium oligomer in osmium chemistry. Formic acid was treated under reflux with $K_2[OsCl_6]$, and a polymeric compound of as yet uncertain composition isolated which reacted in the next step readily with a bidentate compound (pp) to produce $[Os(pp)(CO)_2Cl_2]$. It is assumed that $K_2[OsCl_6]$ reacts (like $RuCl_3$[2]) as a decarbonylating reagent of formic acid: the formation of the polymer is favoured by the presence of formaldehyde in the reaction mixture. Over the course of the reaction (2.5 d) a change from red to green to orange and (finally) light yellow was observed. A solid material (1) was isolated in high yield: its IR spectrum exhibited CO stretching frequencies at 2114, 2053, 2015, 1968 and 1927 cm^{-1}, the number of absorptions being an indication of the presence of a polymeric structure although not the same as the ruthenium equivalent, $[\{Ru(CO)_2Cl_2\}_n]$. The exact formulation of this polymer is not known although microanalysis revealed near parity in the Cl:C atom ratio (*ca.* 6:5). Characterization was not rigorously pursued as the material proved satisfactory as a precursor for the subsequent reactions.

The synthetic strategy applied for the synthesis of tris(heteroleptic)osmium(II) complexes containing diimine ligands is summarized in Scheme 1. The polymer 1 reacted readily with a bidentate polypyridyl ligand [pp = bipy or 4,4'-dimethyl-2,2'-bipyridine (dmbipy)] to form a complex $[Os(pp)(CO)_2Cl_2]$ 2, with slight modifications in the procedure described for the ruthenium analogue.[2] As osmium(II) is in general more inert than ruthenium(II), ethanol was used as a solvent rather than methanol to reach higher reaction temperatures, in conjunction with microwave heating techniques to introduce some overheating effects to accelerate the reaction.[16] Complex 2 was isolated in good yield (typically around 70%), and absence of free pro-ligand was checked by thin-layer chromatography. The reaction showed no dependence on the choice of the pp. In the IR spectrum the CO stretching frequencies ($\tilde{\nu}_{CO}$) of $[Os(pp)(CO)_2Cl_2]$ did not seem to show a predictable dependence on the nature of the ligand pp ($\tilde{\nu}_{CO}$ = 2037 and 1933 cm^{-1} for dmbipy, and 2021 and 1942 cm^{-1} for bipy). The ^1H NMR data for two complexes $[Os(pp)(CO)_2Cl_2]$ (pp = bipy or dmbipy) are given in the Experimental section: the spectra indicate the equivalence

† *Non-SI unit employed:* psi ≈ 6895 Pa.

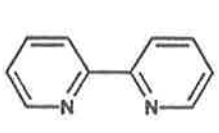

bipy = 2,2'-bipyridine

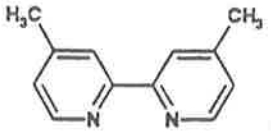

dmbipy = 4,4'-dimethyl-2,2'-bipyridine

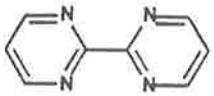

bpm = 2,2'-bipyrimidine

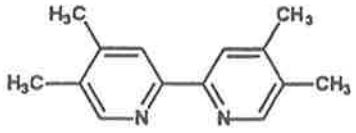

tmbipy = 4,4',5,5'-tetramethyl-2,2'-bipyridine

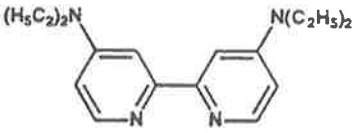

bdebipy = 4,4'-bis(diethylamino)-2,2'-bipyridine

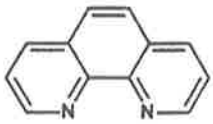

phen = 1,10-phenanthroline

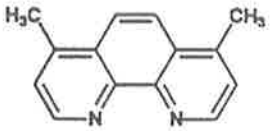

dmphen = 4,7-dimethyl-1,10-phenanthroline

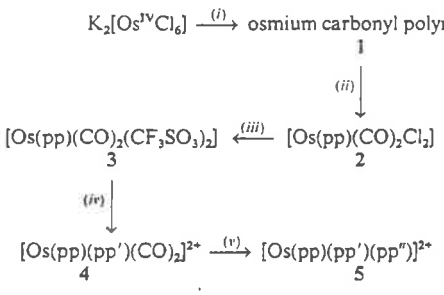

Scheme 1 Synthetic strategy for tris(heteroleptic) complexes. pp = bipy, dmbipy; pp' = bipy, dmbipy, tmbipy, phen, dmphen; pp'' = bipy, dmphen, phen, bdebipy, bpm. (*i*) Formic acid-formaldehyde, 2–3 d; (*ii*) pp, ethanol, microwave oven, 30 min; (*iii*) CF_3SO_3H, 1,2-dichlorobenzene, 3 h; (*iv*) pp', 2-methoxyethanol, 3 h; (*v*) pp'', Et_3NO, 2-methoxyethanol

of the two heterocyclic rings of the symmetrical ligand pp in the complex, consistent with either of two geometries: *viz.* *trans*(Cl),*cis*(CO) or *cis*(Cl),*trans*(CO). As previously reported for the ruthenium(II) analogue,[2] the carbonyl ligands would be expected to adopt a *cis* relationship due to competition for π back bonding from the metal d orbitals, so the stereochemistry *trans*(Cl),*cis*(CO) is assumed.

The addition of the second bidentate compound pp' to the complex $[Os(pp)(CO)_2Cl_2]$ was achieved after the conversion of **2** into the bis(trifluoromethanesulfonato) species $[Os(pp)(CO)_2(CF_3SO_3)_2]$ **3**. Compound **2** and trifluoromethaneslfonic acid were allowed to react in 1,2-dichlorobenzene at 120 °C.[19] and **3** was obtained in yields of 78 (pp = bipy) and 94% (pp = dmbipy) after purification. The grey solid material showed two CO stretching bands (2076 and 1986 cm^{-1} for pp = bipy and 2071 and 1993 cm^{-1} for pp = dmbipy) in the IR spectrum. Infrared characteristics of co-ordinated trifluoromethanesulfonate were also observed:[20,21] $\tilde{\nu}_{SO}$ at 1346 and 1163 cm^{-1} (pp = bipy) and 1330 and 1170 cm^{-1} (pp = dmbipy) as well as $\tilde{\nu}_{CF}$ at 1236 and 1200 cm^{-1} (pp = bipy) and 1237 and 1208 cm^{-1} (pp = dmbipy). According to the ^1H NMR spectra, $[Os(pp)(CO)_2(CF_3SO_3)_2]$ possesses a *cis*(CO),*cis*(CF_3SO_3) geometry, based on the inequivalence of the two pyridyl rings in the pp ligand.

The reaction of compound **3** with a second bidentate compound pp' in 2-methoxyethanol (120 °C) led to $[Os(pp)(pp')(CO)_2]^{2+}$ **4** in yields of 40–60%. The purity was checked primarily by ^1H NMR spectroscopy, and from a combination of NMR and IR spectroscopic studies there was no suggestion of the formation of the *trans*(CO) isomer: for example, in the case of $[Os(bipy)(dmbipy)(CO)_2]^{2+}$, the ^1H NMR spectrum showed two magnetically non-equivalent singlet methyl resonances, with an additional 14 distinct signals in the aromatic region.

The decarbonylation of compound **4** with trimethylamine *N*-oxide in the presence of a third bidentate compound pp'' produced tris(heteroleptic)osmium(II) complexes **5**. Purification was achieved by cation-exchange chromatography (SP Sephadex C25 absorbent; 0.2 mol dm^{-3} sodium chloride or 0.125 mol dm^{-3} sodium toluene-*p*-sulfonate solution as eluent), and $[Os(pp)(pp')(pp'')]^{2+}$ species **5** were isolated in variable yields depending on the ligand pp and pp'. The yields obtained for the osmium(II) complexes (10–40%) were generally lower than those obtained for the ruthenium(II) analogues.[2]

The microanalyses of representative examples of the intermediate species, and of the tris(heteroleptic) target compounds, are provided in the Experimental section.

The tris(heteroleptic) complexes were examined and characterized by several physical methods.

Electrospray mass spectroscopy

The ESMS measurements were undertaken on representative examples of the dicarbonyl (**4**) and tris(heteroleptic) species (**5**) to verify the characterization. For each of the complexes $[Os(dmbipy)(bipy)(CO)_2][PF_6]_2$ **4a**, $[Os(dmbipy)(dmphen)(CO)_2][PF_6]_2$ **4c** and $[Os(dmbipy)(bipy)(dmphen)][PF_6]_2$ **5a**, a *m/z* peak corresponding to the loss of one PF_6^- anion was obtained. For the complex **4a** two signals at *m/z* = 433 and 405 were also observed, corresponding to the ions $[Os(dmbipy)(CO)_2H]^+$ and $[Os(bipy)(CO)_2H]^+$, respectively.

NMR spectroscopy

Owing to the low symmetry (C_1) of the tris(heteroleptic) complexes, the ^1H NMR spectra can be relatively complicated.[2] However, in the cases where the three ligands are derivatives of the same basic ligand structure (*e.g.* bipy), the 'pseudo-symmetry' provided by the three parent bipy rings leads to a simplified spectrum because of the overlap of resonances,[2] whereas if pp' or pp'' differ from a bipy-derived structure the spectrum shows a more complex pattern. The complex [Os(dm-

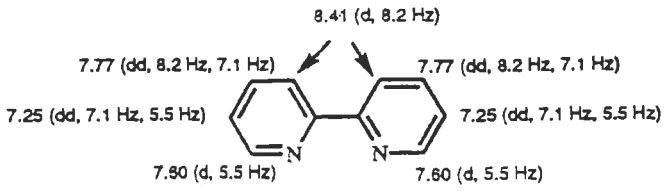

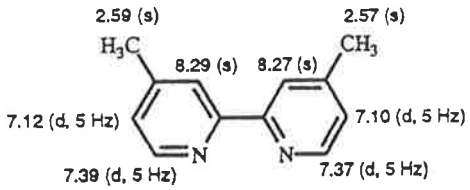

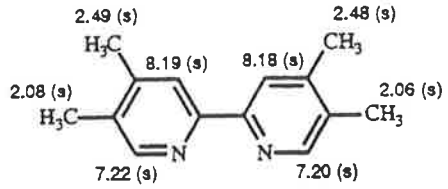

Fig. 1 Chemical shifts and coupling constants of the ligands in the tris(heteroleptic) complex [Os(dmbipy)(bipy)(tmbipy)][PF_6]$_2$ 5c

Table 1 Electrochemical properties of the tris(heteroleptic)osmium(II) complexes

	$E_{\frac{1}{2}}$[b]/V *vs.* SSCE		
Complex[a]	Oxidation	Reduction	$\Delta E_{\frac{1}{2}}$[c]
$[Os(bipy)_3]^{2+}$	+0.81	−1.29	2.10
		−1.46	
		−1.79	
5a $[Os(dmbipy)(bipy)(dmphen)]^{2+}$	+0.74	−1.33	2.08
		−1.55	
		−1.84	
5b $[Os(dmbipy)(bipy)(phen)]^{2+}$	+0.79	−1.29	2.08
		−1.51	
		−1.82	
5c $[Os(dmbipy)(bipy)(tmbipy)]^{2+}$	+0.70	−1.34	2.05
		−1.59	
		−1.93	
5d $[Os(dmbipy)(bipy)(bpm)]^{2+}$	+0.92	−0.99	1.91
		−1.42	
		−1.70	
5e $[Os(dmbipy)(bipy)(bdebipy)]^{2+}$	+0.46	−1.40	1.87
		−1.67	

[a] As PF_6^- salts. [b] Acetonitrile–0.1 mol dm^{-3} $NBu^n_4PF_6$ solution; platinum-button working electrode; 298 K; scan rate 100 mV s^{-1}; Ag–Ag^+ reference electrode (quoted *vs.* SSCE as reference, which is 0.310 V cathodic of Ag–Ag^+). [c] $\Delta E_{\frac{1}{2}} = E_{\frac{1}{2}}(Os^{III/II}) - E_{\frac{1}{2}}$(first ligand reduced).

bipy)(bipy)(tmbipy)][PF_6]$_2$ 5c is taken as an example for discussion: while in principle there are 18 different environments for the aromatic protons, only 9 signals are observed because in each ligand the two constituent rings are similar and their resonances overlap. The aromatic protons associated with the dmbipy and tmbipy ligands are shifted to high field compared with those of 2,2′-bipyridine, as a consequence of a combination of inductive and anisotropic effects.[8] The assignments were achieved by decoupling and correlation spectroscopy (COSY) experiments. Fig. 1 shows the three ligands with their respective chemical shifts and coupling constants for the complex 5c.

The separation of the magnetically non-equivalent methyl resonances for the tris(heteroleptic) complexes 5 is significantly smaller ($\Delta\delta \leq 0.02$ ppm) than that observed for the bis(heteroleptic) dicarbonyl compounds 4. For the latter series, well separated singlet resonances are observed in the aliphatic region of the spectrum ($\Delta\delta \leq 0.37$ ppm). Such phenomena are based on differences in the π-acceptor characteristics and anisotropic effects of the CO and pp″ ligands, and have also been observed for the analogous ruthenium(II) complexes.[2,8]

Electrochemical studies

Cyclic voltamograms of the tris(heteroleptic)osmium(II) complexes clearly show the metal-based oxidation and a series of reductions associated with the ligands. The ligand-based reductions occur in a stepwise manner to each ligand π* system, with the order of the reduction correlating with the ease of reduction of the unco-ordinated pro-ligands. The respective $E_{\frac{1}{2}}$ values for all tris(heteroleptic) complexes synthesized in this work are given in Table 1: in all cases, ΔE_p were in the range 70–90 mV, so that the couples are essentially reversible.

In the case of [Os(dmbipy)(bipy)(bdebipy)]$^{2+}$ 5e only two of the three reductions were observed, presumably because the π* energy level of (bdebipy) is raised so that reduction is too cathodic to be accessible under the experimental conditions. For the same complex it is also noted that the Os^{IV}–Os^{III} couple can be observed at $E_{\frac{1}{2}} \approx 1.24$ V, although the couple is only quasi-reversible ($\Delta E_p \approx 120$ mV).

There have been a number of recent proposals for the use of a 'ligand electrochemical series' in prediction of the oxidation and reduction potentials of metal complexes.[12,22] In the approach by Lever and co-workers[12] the fundamental electrochemical parameter [E_L(L)] for each ligand L is defined as one-sixth the potential for the Ru^{III}–Ru^{II} couple for RuL_6 in acetonitrile solution. The metal-based couple of any complex is postulated[12a] to obey the relationship (1) where S_M and I_M are

$$E_{obs} = S_M \sum E_L(L) + I_M \quad (1)$$

constants for a particular metal. For the first ligand-based reduction process, there is a similar relationship[12b] (2). An

$$E_{red} = S_L \sum E_L(L) + I_L \quad (2)$$

implication of the use of the parameter E_L(L) in this way is that all ligands behave in the same way when attached to different metal centres, and also to the same metal centre in circumstances where the other ligands may be widely varied in terms of their σ-donor and π-donor/acceptor characteristics. While some studies have been done using osmium complexes, the availability of tris(heteroleptic) species makes possible a much broader testing of the hypothesis.

For the metal-based Os^{III}–Os^{II} couples the values of S_M and I_M [equation (1)] have been reported as 1.01 and −0.40, respectively, in organic solvents such as acetonitrile.[12a] For the present series of complexes a plot of E_{obs} *vs.* ΣE_L(L) is a straight line ($R = 0.99$) with $S_M = 1.03$ and $I_M = -0.50$ (Fig. 2). The discrep-

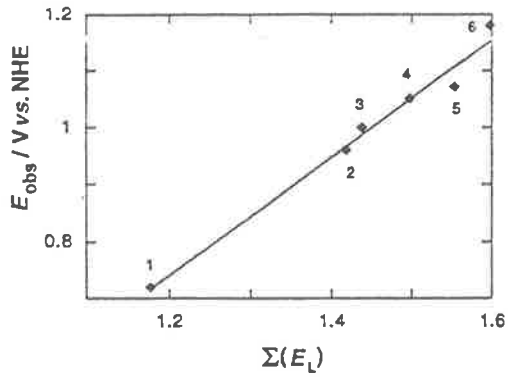

Fig. 2 Plot of E_{obs} (redox potential for Os^{III}–Os^{II} couple) as a function of $\Sigma(E_L)$ (the sum of the 'electrochemical ligand parameters'). Complexes: 1, 5e; 2, 5c; 3, 5a; 4, 5b; 5, $[Os(bipy)_3]^{2+}$; 6, 5d

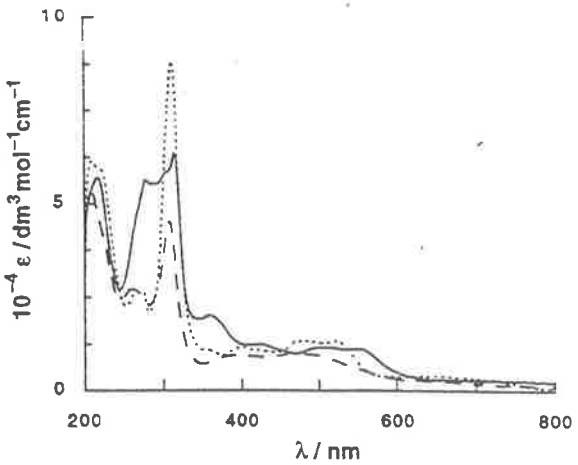

Fig. 3 The UV/VIS absorption spectra of $[Os(dmbipy)(bipy)(bpm)][PF_6]_2$ (– – –), $[Os(dmbipy)(bipy)(bdebipy)][PF_6]_2$ (——) and $[Os(dmbipy)(bipy)(tmbipy)][PF_6]_2$ (·····) in acetonitrile solution

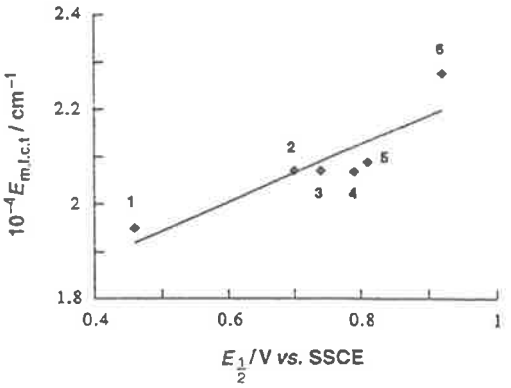

Fig. 4 Charge-transfer band energies for the lowest-energy ^{1}m.l.c.t. transition as a function of $E_{\frac{1}{2}}$ for the Os^{III}–Os^{II} couple. Data are taken from Tables 2 and 3. Complexes as in Fig. 2

ancy between this value of I_M and that previously reported is interesting as the present value actually leads to an improved predictive use of equation (1) for calculating values of the redox potential for Os^{III}–Os^{II} couples for many of the species listed in the original work.[12a] The contributions of the ligands to the overall potential appears to be additive, with no significant synergism between them.

For the ligand-based reduction processes, the values of S_L and I_L [equation (2)] of Os(pp) may be deduced from electrochemical data following the assumption of the assignment of the most reducible ligand. In previous studies the values for Os(bipy) ($S_L = 0.27$; $I_L = -1.38$)[12b] have been reported. For the present work, the bipy ligand can be assumed as the site of reduction for the complexes $[Os(bipy)_3]^{2+}$ and $[Os(dmbipy)(bipy)L]^{2+}$ (L = dmphen, tmbipy or bdebipy) and the plot is a straight line ($R = 0.994$) with $S_L = 0.29$ and $I_L = -1.33$. Again, these values lead to an improved use of equation (2) for calculating values of the redox potential for the first reduction of many of the osmium complexes listed in the original work.[12b]

Electronic spectroscopy

The archetype of tris(bidentate ligand)osmium(II) complexes of the present type is $[Os(bipy)_3]^{2+}$. A broad and weak absorption band around 580 nm is assigned to arise from a spin-forbidden ^{3}m.l.c.t. (metal-to-ligand charge-transfer) transition; ^{1}m.l.c.t. ($d_\pi \longrightarrow \pi_1^*$) absorptions are located in the domain between 370 and 480 nm as well as in the UV range ($d_\pi \longrightarrow \pi_2^*$) and further absorptions in the UV range are associated with ligand-centred $\pi \longrightarrow \pi^*$ transitions.[23–26] The UV/VIS data for the tris(heteroleptic) species synthesized in this work are presented in the Experimental section, and representative spectra are shown in Fig. 3 for the series of complexes $[Os(dmbipy)(bipy)L]^{2+}$ (where L = bpm, tmbipy or bdebipy).

In earlier studies from our laboratory it was reported that the variation of the ligand environment in analogous ruthenium complexes allowed systematic control of the spectral and electrochemical characteristics of the complexes because of the ability to 'tune' the d_π and π^* energy levels.[3] The two approaches taken to the problem of shifting absorption to the red end of the spectrum were either to add electron-withdrawing groups to a polypyridyl ligand to lower π^*,[12,19,27,28] or to stabilize the 'hole' at Ru^{III} in the m.l.c.t. state by introducing electron-donating ligands.[29,30] This strategy was useful in designing potential photosensitizers with broad-band absorption ('black absorbers'), complexes with desired redox characteristics,[3] and complexes with controllable photophysical properties, particularly with regard to lifetimes and photoinertness.

In Fig. 3 it can be observed that as the π^* level of the ligand L in the series of complexes $[Os(dmbipy)(bipy)L]^{2+}$ is raised (*i.e.* bpm < tmbipy < bdebipy) there is a bathochromic shift in the m.l.c.t. absorptions. This is in fact opposite to the trend observed for similar series of ruthenium complexes.[2,3] The contrast is interesting. For both metal centres it is observed that as the ligand L becomes more readily reducible the π^* level and the d_π level are lowered. This is seen in electrochemical studies of the respective trends in the reduction and oxidation potentials of their complexes. Furthermore, the trend in reduction potentials is closely similar for the same ligands, regardless of the identity of the metal centre. The correlation between the Os^{III}–Os^{II} potential and the energy of the lowest spin-allowed m.l.c.t. transition is shown in Fig. 4. In a manner consistent with previous observations,[11] we observe a shift of the lowest-lying ^{1}m.l.c.t. bands towards higher energies as the Os^{III}–Os^{II} couple is shifted to higher potentials, which is not consistent with the results for analogous ruthenium species. Since the directional trends of the dependence of the π^* and d_π energy levels on the identity of ligands correspond for the two metal centres, it would appear that the ligands have a more significant effect on the d_π levels in the case of Os, leading to the observed reversal of the energy of the $d_\pi \longrightarrow \pi^*$ transition as the π^* level varies. Accordingly, from the present data the d_π levels appear to determine the absorption in the visible domain of the spectra. Such a result is consistent with the notion that the osmium centre has greater orbital extension, but a wider range of the tris(heteroleptic) complexes would need to be investigated to confirm these observations.

Experimental

The UV/VIS spectra were recorded on a Cary 5E UV-visible-NIR spectrophotometer, NMR spectra on a Bruker AM3000 spectrometer, and infrared spectra on a Perkin-Elmer Series 1600 FTIR spectrometer. Electrochemical measurements were made in a dry-box (Ar) using a Bioanalytical Systems (BAS) 100A Electrochemical Analyzer. Unless otherwise indicated, cyclic voltammetry was carried out by using platinum working electrodes, and all potentials were measured relative to an Ag–$AgNO_3$ (0.01 mol dm^{-3} in acetonitrile) reference electrode. Potentials are quoted relative to a saturated sodium chloride calomel electrode (SSCE, which is 310 mV cathodic of $Ag–Ag^+$), unless otherwise specified. Electrospray mass spectra were recorded using methods previously described.[31]

Materials

The salt $K_2[OsCl_6]$ (Strem), formic acid (BDH: AnalaR, 90%), $FeCl_2·4H_2O$ (AJAX Chemicals) and 1,2-dimethoxyethanol (Fluka, puriss) were used without further purification. Trifluoromethanesulfonic acid (3 M) was distilled under vacuum before use. Trimethylamine *N*-oxide was obtained by vacuum sublimation of the hydrate (Fluka, purum) at 120 °C. The pro-ligands were used as supplied, or obtained from reported synthetic routes. Reagent solvents were used without further purification. For UV/VIS spectroscopy, HPLC-grade acetonitrile (Sigma-Aldrich) was used. The compound bdebipy was kindly donated by P. Besler (Université de Fribourg Suisse).

Syntheses

$[\{Os(CO)_xCl_y\}_n]$ 1. Formaldehyde (5 cm^3) and $K_2[OsCl_6]$ (1 g, 2.08 mmol) were added to a N_2-sparged solution of formic acid (90%, 50 cm^3). The solution was refluxed for 3 d: it changed from red-orange to brown-green within 1 h, to light green after 3 h, and ultimately to light yellow. It was allowed to cool to room temperature, then stored at 4 °C overnight. The solution was evaporated to dryness using an oil-bath (105 °C), the residue triturated with hexane and diethyl ether, and then dissolved in acetone to remove KCl. After filtration, the filtrate was evaporated to dryness, and the solid dried *in vacuo*. Yield: 840 mg; IR (Nujol): $\tilde{\nu}_{CO}$ = 2114, 2053, 2015, 1968 and 1927 cm^{-1} (Found: C, 6.2; Cl, 21.9%).

***trans*(Cl)-[Os(pp)(CO)$_2$Cl$_2$] 2.** In a typical synthesis, $[\{Os(CO)_xCl_y\}_n]$ (200 mg) and dmbipy (115 mg, 0.620 mmol) were dissolved in 95% ethanol (40 cm^3), and the reaction mixture heated for 3 × 10 min intervals in a microwave oven (Sharp Carousel, medium power level). The volume of the solution was reduced to half, and the precipitated yellow solid was filtered off and washed with cold methanol. The procedure of volume reduction of the filtrate was repeated, with separation of further fractions. The excess of free pro-ligand was removed by adding a saturated methanolic solution of $FeCl_2·4H_2O$ to the filtrate until no further red colouration was observed, followed by column chromatography (Sephadex LH20, methanol eluent). The combined light yellow, TLC-pure solid material was dried *in vacuo*. The absence of the ligand was confirmed by ^1H NMR spectroscopy and TLC [silica gel absorbent, ethanol–water–sodium chloride (1 : 1 : 0.1 mol dm^{-3}) eluent].

$[Os(dmbipy)(CO)_2Cl_2]$ **2a**: yield 70% (Found: C, 33.2; H, 2.2; N, 5.3. $C_{14}H_{12}Cl_2N_2O_2Os$ requires C, 33.5; H, 2.4; N, 5.6%); IR(Nujol) $\tilde{\nu}_{CO}$ = 2037 and 1933 cm^{-1}; ^1H NMR ($CDCl_3$): δ 8.90 [d, 2 H, H^6, $J(H^5H^6)$ = 5.5], 8.00 (s, 2 H, H^3), 7.42 [d, 2 H, H^5, $J(H^5H^6)$ = 5.5 Hz] and 2.70 (s, 6 H, CH_3). $[Os(bipy)(CO)_2Cl_2]$ **2b**: yield 60%; IR(Nujol) $\tilde{\nu}_{CO}$ = 2021 and 1942 cm^{-1}; ^1H NMR (CD_3CN): δ 9.08 [d, 2 H, H^6, $J(H^5H^6)$ = 5.6], 8.48 [d, 2 H, H^3, $J(H^3H^4)$ = 8.1], 8.27 [dd, 2 H, H^4, $J(H^3H^4)$ = 8.1, $J(H^4H^5)$ = 7.7, $J(H^4H^6)$ = 1.2] and 7.76 [dd, 2 H, H^5, $J(H^5H^6)$ = 5.6, $J(H^4H^5)$ = 7.7, $J(H^3H^5)$ = 1.2 Hz] $[Os(phen)(CO)_2Cl_2]$ **2c**: yield 70%; IR(Nujol) $\tilde{\nu}_{CO}$ = 2035 and 1978 cm^{-1}; ^1H NMR ($CDCl_3$): δ 9.44 [d, 2 H, H^2, H^9, $J(H^2H^3)$ = $J(H^9H^{10})$ = 5.5], 8.60 [d, 2 H, H^4, H^7, $J(H^3H^4)$ = $J(H^7H^8)$ = 8.3], 8.00 (s, 2 H, H^{11}, H^{12}) and 7.97 [dd, 2 H, H^3, H^8, $J(H^2H^3)$ = $J(H^8H^9)$ = 5.5, $J(H^7H^8)$ = $J(H^3H^4)$ = 8.3 Hz].

***cis*,*cis*-[Os(pp)(CO)$_2$(CF$_3$SO$_3$)$_2$] 3.** In a typical experiment, $[Os(dmbipy)(CO)_2Cl_2]$ (100 mg, 0.199 mmol) was dissolved in 1,2-dichlorobenzene (50 cm^3), the solution sparged for 40 min with N_2, trifluoromethanesulfonic acid (0.5 cm^3) added, and the solution then heated for 3 h at 120 °C. After cooling to room temperature, the solution was stirred for 1 h at 0 °C. The complex was precipitated by addition of diethyl ether, the mixture being stored overnight in a freezer before filtration. The solid product was washed with cold water and diethyl ether, and dried at room temperature *in vacuo*.

$[Os(dmbipy)(CO)_2(CF_3SO_3)_2]$ **3a**: yield 94%; IR(Nujol) 2071 and 1993 cm^{-1} ($\tilde{\nu}_{CO}$), 1330 and 1170 ($\tilde{\nu}_{SO}$), 1237 and 1208 cm^{-1} ($\tilde{\nu}_{CF}$); ^1H NMR (CD_3CN): δ 8.79 [d, 1 H, H^6, $J(H^5H^6)$ = 6.0], 8.65 [d, 1 H, $H^{6'}$, $J(H^{5'}H^{6'})$ = 6.0], 8.38 (s, 1 H, $H^{3'}$), 8.32 (s, 1 H, H^3), 7.77 [d, 1 H, $H^{5'}$, $J(H^{5'}H^{6'})$ = 6.0], 7.45 [d, 1 H, H^5, $J(H^5H^6)$ = 6.0 Hz], 2.64 (s, 3 H, CH_3) and 2.62 (s, 3 H, CH_3). $[Os(bipy)(CO)_2(CF_3SO_3)_2]$ **3b**: yield 78%; IR(Nujol) 2076 and 1986 ($\tilde{\nu}_{CO}$), 1346 and 1163 ($\tilde{\nu}_{SO}$), 1236 and 1200 cm^{-1} ($\tilde{\nu}_{CF}$); ^1H NMR (CD_3CN): δ 9.00 [d, 1 H, H^6, $J(H^5H^6)$ = 6.0], 8.85 [d, 1 H, $H^{6'}$, $J(H^{5'}H^{6'})$ = 6.0], 8.55 [d, 1 H, $H^{3'}$, $J(H^{3'}H^{4'})$ = 8.2], 8.46 [d, 1 H, H^3, $J(H^3H^4)$ = 8.2], 8.42 [dd, 1 H, $H^{4'}$, $J(H^{3'}H^{4'})$ = 8.2, $J(H^{4'}H^{5'})$ = 7.7, $J(H^{4'}H^{6'})$ = 1.6], 8.26 [dd, 1 H, H^4, $J(H^3H^4)$ = 8.2, $J(H^4H^5)$ = 7.7, $J(H^4H^6)$ = 1.6], 7.98 [dd, 1 H, $H^{5'}$, $J(H^{4'}H^{5'})$ = 7.7, $J(H^{5'}H^{6'})$ = 5.0, $J(H^{3'}H^{5'})$ = 1.6], and 7.62 [dd, 1 H, H^5, $J(H^4H^5)$ = 7.7, $J(H^5H^6)$ = 6.0, $J(H^3H^5)$ = 1.6 Hz]. $[Os(phen)(CO)_2(CF_3SO_3)_2]$ **3c**: yield 73%; IR(Nujol) 2067 and 1998 ($\tilde{\nu}_{CO}$), 1336 and 1169 ($\tilde{\nu}_{SO}$), 1240 and 1208 cm^{-1} ($\tilde{\nu}_{CF}$); ^1H NMR (CD_3CN): δ 9.36 [d, 1 H, H^2, $J(H^2H^3)$ = 5.5], 9.20 [d, 1 H, H^9, $J(H^8H^9)$ = 4.9], 8.97 [d, 1 H, H^7, $J(H^7H^8)$ = 8.2], 8.83 [d, 1 H, H^4, $J(H^3H^4)$ = 8.3], 8.33–8.20 (2s, dd, 3 H, H^5, H^6, H^8) and 7.95 [dd, 1 H, H^3, $J(H^3H^4)$ = 8.3, $J(H^2H^3)$ = 5.5 Hz].

[Os(pp)(pp′)(CO)$_2$][PF$_6$]$_2$ 4. In a typical synthesis, $[Os(dmbipy)(CO)_2(CF_3SO_3)_2]$ (50 mg, 0.068 mmol) and bipy (21.4 mg, 0.136 mmol) were dissolved in 2-methoxyethanol (20 cm^3) and the solution heated under reflux for 3 h. After evaporation to dryness, the brownish residue was dissolved in boiling water and the mixture filtered to remove the excess of pro-ligand. The complex was precipitated as the PF_6^- salt by adding a saturated solution of KPF_6 to the filtrate. The light yellow solid was filtered off and washed with water and diethyl ether. The crude product was purified by column chromatography (Sephadex LH20 absorbent, methanol eluent). Recrystallization from acetonitrile–diethyl ether led to light yellow, feathery crystals.

$[Os(dmbipy)(bipy)(CO)_2][PF_6]_2$ **4a**: yield 58% (Found: C, 33.0; H, 2.25; N, 6.2. $C_{24}H_{20}F_{12}N_4O_2OsP_2$ requires C, 32.9; H, 2.30; N, 6.4%); IR(Nujol) $\tilde{\nu}_{CO}$ = 2078 and 2009 cm^{-1}; ^1H NMR (CD_3CN): δ 9.26 [d, 1 H, $H^{6''}$, $J(H^{5''}H^{6''})$ = 5.6, $J(H^{4''}H^{6''})$ = 1.2], 9.06 [d, 1 H, $H^{6'}$, $J(H^{5'}H^{6'})$ = 5.6], 8.61 [d, 1 H, $H^{3'}$, $J(H^{3'}H^{4'})$ = 8.1], 8.52–8.43 [dd, d, s, 3 H, $H^{4''}$, $H^{3'}$, $H^{3''}$], 8.33 (s, 1 H, H^3), 8.23 [dd, 1 H, $H^{4''}$, $J(H^{3''}H^{4''})$ = 8.1, $J(H^{4''}H^{5''})$ = 7.6, $J(H^{4''}H^{6''})$ = 1.6], 7.90 [dd, 1 H, $H^{5''}$, $J(H^{4''}H^{5''})$ = 7.6, $J(H^{5''}H^{6''})$ = 5.6], 7.54 [dd, 1 H, $H^{5''}$, $J(H^{4''}H^{5''})$ = 7.6, $J(H^{5''}H^{6''})$ = 6.0, $J(H^{3''}H^{5''})$ = 1.6], 7.38 [d, 1 H, $H^{6''}$, $J(H^{5''}H^{6''})$ = 5.6], 7.34 [d, 1 H, H^5, $J(H^5H^6)$ = 6.0], 7.22 [d, 1 H, H^6, $J(H^5H^6)$ = 6.0 Hz], 2.75 (s, 3 H, CH_3') and 2.50 (s, 3 H, CH_3). $[Os(dmbipy)(dmbipy)(CO)_2][PF_6]_2$ **4b**: yield 67% (Found: C, 37.1; H, 2.90; N, 5.8%. $C_{28}H_{28}F_{12}N_4O_2OsP_2$ requires C, 36.1; H, 3.05; N, 6.0%); IR(Nujol) $\tilde{\nu}_{CO}$ = 2070 and 2005 cm^{-1}; ^1H NMR (CD_3CN): δ 9.04 [d, 1 H, $H^{6''}$, $J(H^{5''}H^{6''})$ = 5.5], 8.77 (s, 1 H, $H^{6''}$), 8.43 (s, 1 H, $H^{3'}$), 8.31

(2s, 2 H, $H^{3'}$, $H^{3''}$), 8.22 (s, 1 H, $H^{3'''}$), 7.70 [d, 1 H, $H^{5'}$, $J(H^{5'}H^{6'}) = 5.5$], 7.32 [d, 1 H, H^{5}, $J(H^{5}H^{6}) = 6.0$ Hz], 7.27 [d, 1 H, H^{6}, $J(H^{5}H^{6}) = 6.0$ Hz], 6.95 (s, 1 H, $H^{6'}$), 2.73 [s, 3 H, $CH_3(4')$], 2.60 [s, 3 H, $CH_3(4''')$], 2.50 [s, 3 H, $CH_3(4)$] 2.47 [s, 3 H, $CH_3(5''')$], 2.41 [s, 3 H, $CH_3(4'')$] and 2.04 [s, 3 H, $CH_3(5'')$]. $[Os(dmbipy)(dmphen)(CO)_2][PF_6]_2$ **4c**: yield 43%; IR(Nujol) $\tilde{\nu}_{CO} = 2083$ and 2015 cm^{-1}; ^1H NMR (CD_3CN): δ 9.45 [d, 1 H, $H^{9'}$, $J(H^{8'}H^{9'}) = 6.0$], 9.15 [d, 1 H, H^{6}, $J(H^{5}H^{6}) = 6.0$], 8.47 (s, 2 H, $H^{3'}$), 8.45 (s, 1 H, H^{12}), 8.39 (s, 1 H, H^{11}), 8.31 (s, 1 H, H^{3}), 8.04 [d, 1 H, $H^{8'}$, $J(H^{8'}H^{9'}) = 6.0$], 7.75 [d, 1 H, $H^{5'}$, $J(H^{5'}H^{6'}) = 6.0$], 7.65 [d, 1 H, $H^{3''}$, $J(H^{2''}H^{3''}) = 5.5$], 7.58 [d, 1 H, $H^{2''}$, $J(H^{2''}H^{3''}) = 5.5$], 7.12 [d, 1 H, H^{5}, $J(H^{5}H^{6}) = 6.0$], 7.02 [d, 1 H, H^{6}, $J(H^{5}H^{6}) = 6.0$ Hz], 3.11 [s, 3 H, $CH_3(7'')$], 2.90 [s, 3 H, $CH_3(4')$], 2.75 [s, 3 H, $CH_3(4'')$] and 2.41 [s, 3 H, $CH_3(4)$]. $[Os(dmbipy)(phen)(CO)_2][PF_6]_2$ **4d**: yield 63% (Found: C, 34.8; H, 2.15; N, 6.1. $C_{26}H_{20}F_{12}N_4O_2OsP_2$ requires C, 34.7; H, 2.35; N, 6.2%); IR(Nujol) $\tilde{\nu}_{CO} = 2076$ and 2008 cm^{-1}; ^1H NMR (CD_3CN): δ 9.62 [d, 1 H, $H^{9'}$, $J(H^{8'}H^{9'}) = 5.2$], 9.15 [d, 1 H, H^{6}, $J(H^{5}H^{6}) = 5.5$], 9.03 [d, 1 H, $H^{7'}$, $J(H^{7'}H^{8'}) = 8.2$], 8.79 [d, 1 H, $H^{4'}$, $J(H^{3'}H^{4'}) = 8.2$], 8.49 (s, 1 H, H^{3}), 8.40 (3s, d, dd, 5 H, H^{5}, $H^{5'}$, $H^{6'}$, $H^{3'}$, $H^{8'}$), 7.83 [dd, 1 H, $H^{3'}$, $^3J(H^{3'}H^{4'}) = 8.2$, $J(H^{2'}H^{3'}) = 5.0$], 7.75 [2d, 2 H, $H^{2'}$, H^{5}, $J(H^{2'}H^{3'}) = 5.0$, $J(H^{5}H^{6}) = 5.5$], 7.11 [d, 1 H, $H^{5'}$, $J(H^{5'}H^{6'}) = 5.1$], 7.05 [d, 1 H, $H^{6'}$, $J(H^{5'}H^{6'}) = 5.1$ Hz], 2.75 (s, 3 H, CH_3) and 2.41 (s, 3 H, CH_3).

$[Os(pp)(pp')(pp'')][PF_6]_2$ 5. The compound $[Os(dmbipy)(dmphen)(CO)_2][PF_6]_2$ (20 mg, 0.022 mmol) and bipy (10.1 mg, 0.066 mmol) were dissolved in dry 2-methoxyethanol (6 cm^3), and a six-fold excess of trimethylamine *N*-oxide (9.9 mg, 0.132 mmol) was added. The almost colourless solution turned dark green within 10 min. It was heated at reflux for 3 h. After evaporation to dryness the residue was dissolved in hot water, and the solution filtered to eliminate the excess of pro-ligand. The filtrate was applied to a column of SP-Sephadex C25 cation exchanger, eluted with 0.2 mol dm^{-3} NaCl, and the product precipitated by addition of a saturated aqueous solution of KPF_6 to the eluent containing the major band. The solid was collected on a low-porosity frit, and then washed with water (5 cm^3) and diethyl ether. Recrystallization of the green complex was achieved from acetonitrile–diethyl ether. Yield: 40%.

$[Os(dmbipy)(bipy)(dmphen)][PF_6]_2$ **5a**: yield 40% (Found: C, 41.0; H, 3.3; N, 7.6. $C_{36}H_{32}F_{12}N_6OsP_2$ requires C, 41.3; H, 3.1; N, 8.1%); ^1H NMR (CD_3CN): δ 8.45 (dd, 2 H), 8.37–8.27 (m, 4 H), 7.88–7.65 (m, 5 H), 7.75–7.38 (m, 4 H), 7.30 (dd, 1 H), 7.22 (d, 1 H), 7.15 (d, 1 H), 7.06 (dd, 1 H), 6.94 (d, 1 H), 2.98 (s, 3 H, CH_3), 2.96 (s, 3 H, CH_3), 2.70 (s, 3 H, CH_3) and 2.45 (s, 3 H, CH_3); UV/VIS [acetonitrile, λ/nm (ε/dm^3 mol^{-1} cm^{-1})] 206 (71 700), 232 (37 400), 266 (57 700), 290 (63 400), 370 (8780), 408 (12 300), 438 (15 900), 484 (15 500) and 546 (4900). $[Os(dmbipy)(bipy)(phen)][PF_6]_2$ **5b**: yield 26%; ^1H NMR (CD_3CN): δ 8.48 (d, 1 H), 8.43 (d, 1 H), 8.40–8.28 (m, 4 H), 8.21 (s, 2 H), 7.98 (d, 2 H), 7.82 (dd, 1 H), 7.74 (dd, 2 H), 7.64 (m, 2 H), 7.54 (d, 1 H), 7.40 (d, 1 H), 7.33 (dd, 1 H), 7.20 (2d, 2 H), 7.07 (dd, 1 H), 6.95 (d, 1 H), 2.62 (s, 3 H, CH_3) and 2.52 (s, 3 H, CH_3); UV/VIS [acetonitrile, λ/nm (ε/dm^3 mol^{-1} cm^{-1})] 202 (57 500), 268 (45 800), 290 (54 100), 364 (6780), 394 (8300), 434 (12 200), 484 (12 500) and 564 (3490). $[Os(dmbipy)(bipy)(tmbipy)][PF_6]_2 \cdot H_2O$ **5c**: yield 32% (Found: C, 41.0; H, 3.3; N, 7.6. $C_{36}H_{38}F_{12}N_6OsP_2$ requires C, 41.1; H, 3.45; N, 8.0%); ^1H NMR (CD_3CN): δ 8.42 [d, 1 H, H^{3}, $J(H^{3}H^{4}) = 8.2$], 8.41 [d, 1 H, H^{3I}, $J(H^{3I}H^{4I}) = 8.2$], 8.29 (s, 1 H, H^{3II}), 8.27 (s, 1 H, H^{3III}), 8.19 (s, 1 H, H^{3IV}), 8.18 (s, 1 H, H^{3V}), 7.78 [2dd, 2 H, H^{4}, $H^{4'}$, $J(H^{3}H^{4}) = J(H^{3I}H^{4I}) = 8.2$], 7.60 [d, 2 H, H^{6}, H^{6I}, $J(H^{5}H^{6}) = J(H^{5I}H^{6I}) = 5.5$], 7.38 [d, 2 H, H^{6II}, H^{6III}, $J(H^{5II}H^{6II}) = J(H^{5III}H^{6III}) = 5.5$], 7.27–7.19 [2d, 2s, H^{5}, $H^{5'}$, H^{6IV}, H^{6V}, $J(H^{5}H^{6}) = J(H^{5I}H^{6I}) = 5.5$], 7.11 [2d, 2 H, H^{5II}, H^{5III}, $J(H^{5II}H^{6II}) = J(H^{5III}H^{6III}) = 5.5$ Hz], 2.59 [s, 3 H, $CH_3(4^{II})$], 2.57 [s, 3 H, $CH_3(4^{III})$], 2.49 [s, 3 H, $CH_3(4^{IV})$], 2.48 [s, 3 H, $CH_3(4^{V})$], 2.07 [s, 3 H, $CH_3(5^{IV})$] and 2.05 [s, 3 H, $CH_3(5^{V})$]; UV/VIS [acetonitrile, λ/nm (ε/dm^3 mol^{-1} cm^{-1})] 206 (59 800), 252 (26 100), 256 (26 800), 292 (88 600), 332 (10 900), 374 (11 700), 424 (10 800), 448 (13 300), 484 (13 600) and 600 (4430). $[Os(dmbipy)(bipy)(bpm)][PF_6]_2 \cdot 2Et_2O$ **5d**: yield 10% (Found: C, 40.1; H, 3.45; N, 9.5. $C_{38}H_{46}F_{12}N_8O_2OsP_2$ requires C, 40.5; H, 3.2; N, 9.9%); ^1H NMR (CD_3CN): δ 8.98 (2d, 2 H), 8.81 (2d, 2 H), 8.67 (s, 2 H), 8.42 (2dd, 2 H), 8.,19 (d, 1 H), 8.10–7.92 (m, 5 H), 7.73 (d, 1 H), 7.64–7.46 (m, 4 H), 7.37 (d, 2 H) and 2.62 (s, 6 H, $2CH_3$); UV/VIS [acetonitrile, λ/nm (ε/dm^3 mol^{-1} cm^{-1})] 200 (52 700), 244 (27 200), 288 (45 100), 364 (9380), 438 (10 100) and 574 (3000). $[Os(dmbipy)(bipy)(bdebipy)][PF_6]_2$ **5e**: yield 33%; ^1H NMR (CD_3CN): δ 8.38 (2d, 2 H), 8.30 (s, 1 H), 8.25 (s, 1 H), 7.85 (d, 1 H), 7.72–7.56 (m, 4 H), 7.39 (d, 1 H), 7.35–7.23 (m, 3 H), 7.18 (d, 1 H), 7.14 (dd, 1 H), 7.00 (d, 1 H), 6.83 (2d, 2 H), 6.45 (m, 2 H), 3.50 (4q, 8 H, CH_2 of Et_2N), 2.63 (s, 3 H, CH_3), 2.52 (s, 3 H, CH_3) and 1.15 (4t, 12 H, CH_3 of Et_2N); UV/VIS [acetonitrile, λ/nm (ε/dm^3 mol^{-1} cm^{-1})]: 206 (57 000), 262 (56 300), 286 (58 500), 294 (63 500), 336 (20 100), 394 (12 400), 468 (11 600), 512 (11 200) and 620 (2920).

Acknowledgements

This research was supported by the Australian Research Council. We thank Dr Ray Colton (La Trobe University) for the ESMS measurements. E. Z. J. acknowledges financial support from the Swiss National Science Foundation in the form of a Postdoctoral Fellowship for his sojourn at James Cook University. We are grateful to Mr Laurie Kelso and Mr Todd Rutherford for valuable discussions, Mr Mick Henderson for his experimental contribution, and Dr Bruce Bowden and Mr David Reitsma for assistance with the COSY experiments.

References

1 G. F. Strouse, P. A. Anderson, J. R. Schoonover, T. J. Meyer and F. R. Keene, *Inorg. Chem.*, 1992, **31**, 3004.
2 P. A. Anderson, G. B. Deacon, K. H. Haarmann, F. R. Keene, T. J. Meyer, D. A. Reitsma, B. W. Skelton, G. F. Strouse, N. C. Thomas, J. A. Treadway and A. H. White, *Inorg. Chem.*, 1995, **34**, 6145.
3 P. A. Anderson, G. F. Strouse, J. A. Treadway, F. R. Keene and T. J. Meyer, *Inorg. Chem.*, 1994, **33**, 3863.
4 J. A. Treadway, B. Loeb, R. Lopez, P. A. Anderson, F. R. Keene and T. J. Meyer, *Inorg. Chem.*, 1996, **35**, 2242.
5 D. A. Reitsma and F. R. Keene, *J. Chem. Soc., Dalton Trans.*, 1993, 2859.
6 T. J. Rutherford, M. G. Quagliotto and F. R. Keene, *Inorg. Chem.*, 1995, **34**, 3857.
7 T. J. Rutherford and F. R. Keene, unpublished work.
8 T. J. Rutherford, D. A. Reitsma and F. R. Keene, *J. Chem. Soc., Dalton Trans.*, 1994, 3659.
9 J. V. Casper, B. P. Sullivan, E. M. Kober and T. J. Meyer, *Chem. Phys. Lett.*, 1982, **91**, 91.
10 E. M. Kober, J. C. Marshall, W. J. Dressick, B. P. Sullivan, J. V. Casper and T. J. Meyer, *Inorg. Chem.*, 1985, **24**, 2755.
11 E. M. Kober, J. V. Casper, B. P. Sullivan and T. J. Meyer, *Inorg. Chem.*, 1988, **27**, 4587.
12 (*a*) A. B. P. Lever, *Inorg. Chem.*, 1990, **29**, 1271; (*b*) E. S. Dodsworth, A. A. Vlcek and A. B. P. Lever, *Inorg. Chem.*, 1994, **33**, 1045.
13 A. A. Vlcek, E. S. Dodsworth, W. J. Pietro and A. B. P. Lever, *Inorg. Chem.*, 1995, **34**, 1906.
14 S. S. Fielder, M. C. Osborne, A. B. P. Lever and W. J. Pietro, *J. Am. Chem. Soc.*, 1995, **117**, 6990.
15 D. A. Buckingham, F. P. Dwyer, H. A. Goodwin and A. M. Sargeson, *Aust. J. Chem.*, 1964, **17**, 315.
16 D. M. P. Mingos and D. R. D. Baghurst, *Chem. Soc. Rev.*, 1991, **20**, 1.
17 J. P. Collins and W. R. Roper, *J. Am. Chem. Soc.*, 1966, **88**, 3504.
18 F. H. Johannsen, W. Preetz and A. Scheffler, *J. Organomet. Chem.*, 1975, **102**, 527.
19 B. P. Sullivan, J. V. Caspar, S. R. Johnson and T. J. Meyer, *Organometallics*, 1984, **3**, 1241.
20 D. S. Black, G. B. Deacon and N. C. Thomas, *Polyhedron*, 1983, **2**, 409.

21 D. S. Black, G. B. Deacon and N. C. Thomas, *Aust. J. Chem.*, 1982, 35, 2445.
22 E. C. Constable, A. M. W. Cargill Thompson, D. A. Tocher and M. A. M. Daniels, *New J. Chem.*, 1992, **16**, 855.
23 J. V. Caspar, T. D. Westmoreland, G. H. Allen, P. G. Bradley, T. J. Meyer and W. H. Woodruff, *J. Am. Chem. Soc.*, 1984, **106**, 3492.
24 S. Decurtins, F. Felix, J. Ferguson, H.-U. Güdel and A. Ludi, *J. Am. Chem. Soc.*, 1980, **102**, 4102.
25 F. Felix, J. Ferguson, H.-U. Güdel and A. Ludi, *Chem. Phys. Lett.*, 1979, **62**, 153.
26 F. Felix, J. Ferguson, H.-U. Güdel and A. Ludi, *J. Am. Chem. Soc.*, 1980, **102**, 4096.
27 J. C. Curtis, B. P. Sullivan and T. J. Meyer, *Inorg. Chem.*, 1983, **22**, 224.
28 Y. Ohsawa, K. W. Hanck and M. K. De Armond, *J. Electroanal. Chem. Interfacial Electrochem.*, 1984, **175**, 229.
29 D. P. Rillema and K. B. Mack, *Inorg. Chem.*, 1982, **21**, 3849.
30 D. P. Rillema, C. B. Blanton, R. J. Shaver, D. C. Jackman, M. Boldaji, S. Bundy, L. A. Worl and T. J. Meyer, *Inorg. Chem.*, 1992, **31**, 1600.
31 R. Colton and J. C. Traeger, *Inorg. Chim. Acta*, 1992, **201**, 153.

Received 23*rd July* 1996; *Paper* 6/05161H

ELSEVIER

Coordination Chemistry Reviews
166 (1997) 121–159

COORDINATION CHEMISTRY REVIEWS

Stereochemistry and polymetallic ligand-bridged molecular assemblies

F. Richard Keene *

School of Molecular Sciences, James Cook University of North Queensland, Townsville, Qld 4811, Australia

Received 11 November 1996

Contents

Abstract

There have been many recent developments in synthetic methodologies for polymetallic ligand-bridged molecular assemblies, encouraged by the prospect that such materials have potential application to photochemical molecular devices. The assemblies have involved

* *Corresponding author. Fax: 006177814600; e-mail: richard.keene@jcu.edu.au*

PII S0010-8545(97)00006-4

ruthenium(II) metal centers, which are invariably octahedral. However, the synthetic advances have often occurred without consideration of the problem of stereochemical ambiguity in the products. The present review examines this uncertainty and ways in which it may be addressed. In particular, it assesses approaches to the pre-determination of the stereochemistry of polynuclear assemblies incorporating Ru(II) and related centers {e.g. Os(II)} by the use of precursors with an established geometry, and the use of chromatographic techniques in the separation of stereoisomeric mixtures. Some of our own work is elaborated, where we have been able to separate stereoisomers of chromophore-quencher complexes and of dinuclear and trinuclear ligand-bridged species. Additionally, the review summarizes our preliminary studies of their physical properties as a function of the spatial arrangement of the components.

1. Introduction

1.1. Mimicry of photosynthetic systems

The concept of controlled molecular architecture – and emergence of the "nanometer technology" – has developed from an increasingly intimate understanding of properties at a molecular level. One example of its application is the rational design of supramolecular assemblies which form the basis of materials to be used in photochemical molecular devices (PMDs). Following light absorption, such materials may perform a variety of functions; e.g. conversion of light energy to chemical or electrical energy, light-activated molecular switches, etc. Artificial photosynthesis is but one obvious goal.

In nature, the process of photosynthesis originates with light-promoted electronic excitation within the "antenna system" of an organism. In a series of short range, rapid electron-transfer steps, physically-separated reducing and oxidizing centers are created which have lifetimes sufficient that subsequent chemical reactivity may take place (the reduction of carbon dioxide to carbohydrates and the oxidation of water to oxygen, respectively) [1,2]. Such an organism must necessarily contain (inter alia) two essential components: light absorbers ("chromophores") which harvest light energy allowing electronic excitation, as well as electron- and energy-transfer agents ("quenchers") which rapidly relay the absorbed electronic energy away from the chromophore to an appropriate site in the system for utilization. Further, for a photosynthetic system an additional component is also required, namely catalytic sites, at which the chemical reactions occur.

The three components are contained within an enzyme matrix which controls the spatial relationships between them and, together with the trans-membrane nature of some of the relay processes, limit the reactivity pathways. However, the precise manner in which the enzyme structure effects processes such as electron transfer remains a subject of conjecture [3].

A key issue is the rapid physical separation of the excited electron from the chromophore, and a number of elegant model studies of this process have been undertaken, albeit they are limited because the linkages between the components are covalent [4–8]. The overall principle of such studies is represented below, where

a chromophore (**C**) is attached to redox-active groups (quenchers). In the case where an electron donor (**D**) and an electron acceptor (**A**) are involved, the initial D–C–A species absorbs light energy and forms an excited state D–*C–A, which produces the redox charge-separated state D^+–C–A^- by a series of electron transfer steps.

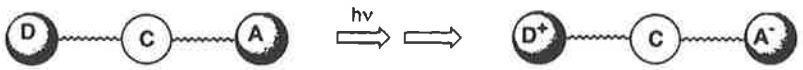

As an exemplar of such studies, the work of Gust, Moore and coworkers is cited, where photoexcitation of a carotenoid–porphyrin–diquinone tetrad (represented C–P–Q_A–Q_B) gives rise to the charge-separated state $C^{\cdot+}-P-Q_A-Q_B^{\cdot-}$, rationalized via a series of electron transfers between adjacent groups(Fig. 1)[9]. In these particular studies, the components are actually mimics of the natural system – the porphyrin as the chromophore with the carotenoid and quinone moieties being donor- and acceptor-quencher functionalities, respectively. More extended (pentad C–P_1–P_2–Q_A–Q_B) systems of the same type have also been investigated [10].

Attention is also drawn to the elegant bis(porphyrin) systems of Sauvage and coworkers [11,12] which model the function of the "reaction center" in the photosynthetic process.

Ultimately, chemical reactions in any photosynthetic scheme are multi-electron processes, although in the chromophore only one electron is excited per photon absorbed. The simultaneous supply of several electrons is achieved by the use of "antenna" systems which funnel electrons to a reaction site. To achieve artificial photosynthesis, the same elements of spatial and charge separation must occur within synthesized molecules. Although the precise chemical reactions will differ from those in the natural systems, they necessarily remain multi-electron in character, so that the artificial molecular assembly ("supramolecule") will also require several sites for light absorption and electron excitation, and be designed so that the photo-

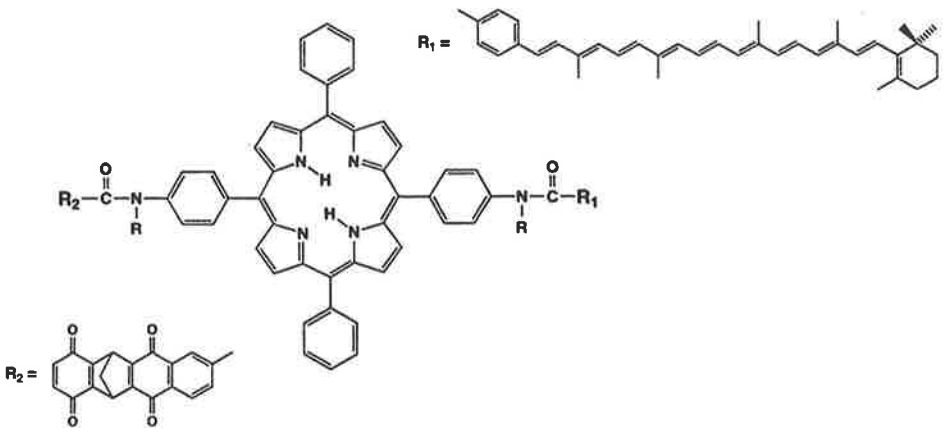

Fig. 1. Chromophore-quencher tetrad C–P–Q_A–Q_B [9].

induced electron transfer relay is directed to a spatially-separated chemically reactive (catalytic) site.

1.2. Electron and energy transfer in polymetallic assemblies

Polymetallic molecules, appropriately constructed, could conceivably provide the basis for such a supramolecular system [13,14]. For the required building blocks, mononuclear transition metal complexes of the d^6 metal centers ruthenium(II), osmium(II) and rhenium(I) with polypyridyl ligands {e.g. bpy = 2,2′-bipyridine and phen = 1,10-phenanthroline and their analogues} are of particular interest as precursors because of their extensive (and well studied!) photochemistry [15]. Of these, the ruthenium compounds have received most attention, as the synthetic versatility of osmium is comparatively limited and rhenium species tend to lack broad-band absorption in the visible spectral region.

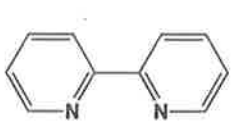

bpy = 2,2′-bipyridine

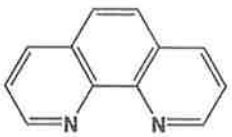

phen = 1,10-phenanthroline

The capacity for variation of the photophysical, spectral and redox characteristics by ligand control is extensive, and this has been well documented for homoleptic and bis(heteroleptic) complexes of ruthenium(II) with bidentate polypyridyl ligands [15]. As alluded to previously [15], with 200 bidentate ligands (pp), there are 200 homoleptic possibilities $[Ru(pp)_3]^{2+}$, $\sim 4 \times 10^4$ bis(hetereoleptic) $[Ru(pp)_2(pp')]^{2+}$ species and $\sim 1.3 \times 10^6$ tris(heteroleptic) complexes $[Ru(pp)(pp')(pp'')]^{2+}$: our recent reports of the synthesis of a range of tris(heteroleptic) complexes of ruthenium [16–19] and osmium [20] have served to emphasize this particularly attractive aspect of versatility in the utilization of such species as building blocks for polynuclear assemblies.

Over the last decade, significant developments have occurred in synthetic schemes for a wide range of ligand-bridged polymetallic assemblies. It is not intended to exhaustively review the area, as only a portion is of particular relevance to the subsequent discussion. However, it is noted that there is a recent comprehensive review [21] addressing the synthesis and physical properties (electrochemical and photophysical) of such complexes, and the reader is directed to that work for additional information.

The nature of the bridging moiety may have a significant influence on the properties of a polynuclear assembly. It can promote strong coupling between the centers or be effectively insulating (or anything in between). It can be flexible or it can rigidly control the spatial relationship between the attached metal centers. In terms of coupling, the concept of a "supramolecular" assembly implies that the individual components will substantially retain their individual characteristics. Very strong coupling is not consistent with this requirement, although the study of systems in

which the coupling may be systematically varied is valuable in developing our understanding of intramolecular electron and energy transfer processes that occur in polymetallic assemblies following light absorption.

The consequence of flexibility (or at least lack of rigidity) within the bridge is that the geometry of the assembly is uncertain, both in terms of the distance by which the metal centers are separated as well as their relative orientations. Under these circumstances, any theoretical treatment of electron or energy transfer is rendered difficult. Additionally, since in any applications of these materials such transfers will be over long distances and directional, the uncertainty is limiting. Such directional control, which is a feature of the framework provided by the enzyme matrix in natural systems, can only be developed when there is rigidity in the bridge and the stereochemical features of the component metal centers themselves are known and controlled.

Given these restrictions, one should note the advantages and limitations of some of the polynuclear assemblies which have been developed.

Initially, mention should be made of the self-assembled polymetallic species in which metal centers {tetrahedral such as Ag(I) or Cu(I) [22–28]; octahedral such as Fe(II), Co(II), Co(III), Ni(II), Ru(II) [24,29–31]} have been used as linking points for long chain polypyridyl ligands, forming double and triple strand helicate structures. While the helicates themselves are rod-like, there have also been examples of extending the principle to 2D structures [32–36]. The concept is extremely elegant, but is not entirely relevant to the present discussion of stereochemical variation in polynuclear species induced by tris(bidentate) ligation at octahedral centers: while such a coordination mode may be present in helicate structures, the only stereoisomeric ambiguity is the chirality which is in turn generally controlled by the helicity.

Polymetallic helical configurations are also included in the intermediate species in the formation of molecular composite knots [37], but as the Cu(I) centers involved are tetrahedral, these complexes are not germane to this review. It is primarily in cases where metal centers in a polynuclear assembly possess octahedral coordination that their individual (rather than collective) stereochemistries are of fundamental concern.

In such assemblies, simple bridges such as CN^- will produce mainly chain-like structures [38]. There is also a range of bridges, using the α,α′-diimine ligating motif in polypyridyl species, which may produce extended polynuclear systems, but in which there is considerable flexibility because of the possibility of bond rotation in the link (e.g. phenyl, polyphenyl or alkynyl) between the ligating groups [39–49]. There are a number of dendrimers (including the so-called "star-burst" and "arboral" structures) which may be put in the same category [50–53].

On the other hand, there are a number of bridges which possess sufficient rigidity to meet the criteria specified above in terms of controlling the molecular framework. As one example in this category, a series of assemblies containing up to twenty-two metal centers have been reported by the Italian groups headed by Denti and Balzani [54–68]. The syntheses involve what has been termed a "complexes as ligands" technique: this methodology dates back to early syntheses of dinuclear ligand-bridged species [69,70], but has been developed for the larger oligomers using either a convergent or divergent approach [21].

One of this series is the decanuclear species, which has been synthesized in homo- or hetero-metallic forms containing Ru(II) and/or Os(II) [56]. From photophysical studies it demonstrates that energy transfer may be directed from a number of peripheral sites (M_p) to a single central site (M_c), whereas in other cases energy is transferred in the opposite direction (Fig. 2)[56].

Structural control within such polymetallic molecules is paramount since the type and arrangement of metal centers greatly influences energy migration patterns [21,71]. But despite an extensive and rapidly growing literature on the synthesis and electronic characteristics of such compounds [21], the issue of the effects of stereoisomerism on those properties, while receiving occasional tacit acknowledgement, has rarely been addressed. An understanding of such aspects seems fundamental: photo-promoted intramolecular electron or energy transfer between chromophoric and catalytic sites are essential processes in artificial assemblies designed as photochemical molecular devices, and they will be spatially dependent. The assembly is required to provide the molecular framework which is a feature associated with the enzyme matrix in natural systems, and which controls the directional qualities of the transfer processes.

The redox charge separation described earlier in organic systems occurs also in metal-containing species, in which a metal center functions as the chromophore (**C**) and the redox active groups (**D** and **A**) are attached to the ligands. Although many examples are now known [21], two of the original examples are chosen to illustrate

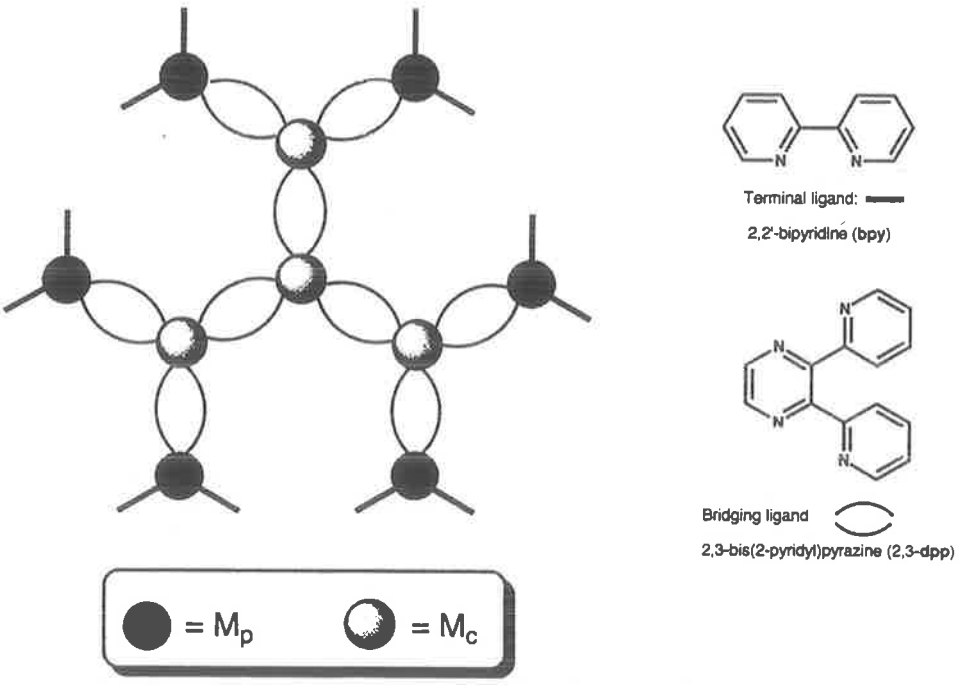

Fig. 2. The decanuclear species $[Ru_{10}(dpp)_9(bpy)_{12}]^{20+}$ [56].

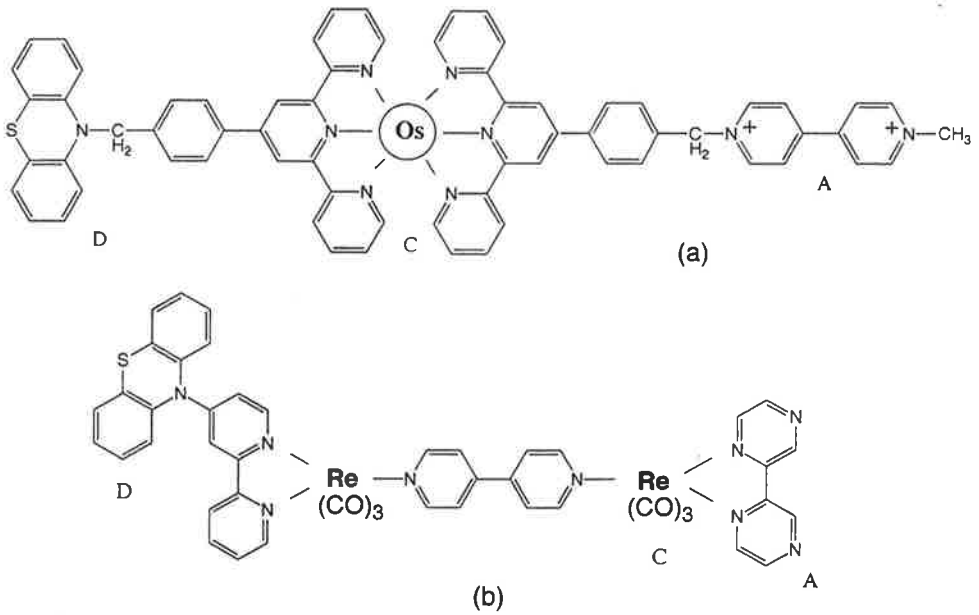

Fig. 3. Chromphore-quencher complexes exhibiting redox charge separation [72,73].

the point (Fig. 3). In system (a), following photoexcitation at the osmium center (**C**) to produce the metal-to-ligand charge transfer (MLCT) state, a sequence of redox quenching processes occur in which the donor phenothiazine (**D**) is oxidized and the acceptor 4,4′-bipyridium functionalization (**A**) reduced, forming the charge-separated state, D^+–C–$A^{\cdot -}$ [72]. Similarly in (b), charge separation can be achieved across a bridge between two metal centers: following photoexcitation of the Re^I–bpz chromophore (bpz=2,2′-bipyrazine) to form the MLCT excited state, the ultimate product has the donor phenothiazine as a radical cation and the bpz ligand as a radical anion [73]. In both of these cases, there are no isomeric uncertainties about the target molecules, but that has been an exception rather than the norm in the systems investigated.

2. Stereochemistry in polymetallic assemblies

2.1. The "stereochemical problem"

Stereoisomerism is possible in systems containing octahedral metal centers with bidentate ligands [74]. When the ligands are symmetrical (C_2 symmetry), chiral forms (Δ and Λ enantiomers) exist for the tris(bidentate) species, whereas for a bis(bidentate) complex there are geometric isomers (*cis/trans*) as well as enantiomers of the *cis* form. When ligands are non-symmetrical, extra geometrical isomerism occurs. In polynuclear species based on such centers, the stereoisomeric possibilities

increase exponentially with the number of metal centers. In such cases, the samples obtained under normal synthetic conditions will be a mixture of stereoisomers in an uncertain ratio – a product described by von Zelewsky as possessing a "fuzzy stereochemistry" [75].

A number of examples may be given involving systems where studies have been undertaken on the physical properties of isolated species which clearly have a number of stereochemical possibilities. The following cases are discussed as they are representative but are also particularly relevant to our subsequent approach to the "stereochemical problem".

In their studies of charge-separated excited states in mono-nuclear complexes containing ligands with donor- and acceptor-quencher functionalities, Elliot and coworkers have investigated the system $[Ru(44PTZ)_2(423DQ^{2+})]^{4+}$ [76,77]. An examination of stereoisomerism in such a system reveals that there are four geometric isomers, shown in Fig. 4 (**A** represents the bipyridinium acceptor quencher, and **D** the phenothiazine donor quencher). A similar number of isomers are possible in $[Ru(bpy\text{-}AQ)_2(bpy\text{-}PTZ)]^{2+}$, studied by Meyer et al. [78]. In both the above systems [77,78], the possible existence of geometric isomers was acknowledged, although there was no evidence for more than one isomer – or if more than one isomer was present there was no evidence of differences in their characteristics.

A number of examples of ligand-bridged oligomeric species have been reported

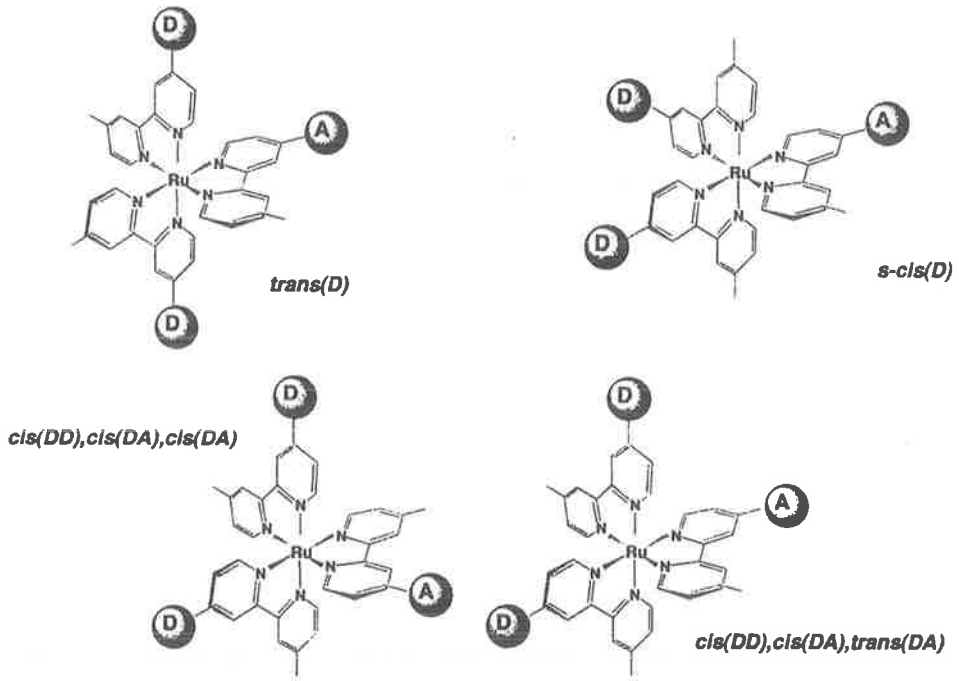

Fig. 4. Geometric isomers in a general $[Ru(bpy\text{-}D)_2(bpy\text{-}A)]^{2+}$ complex.

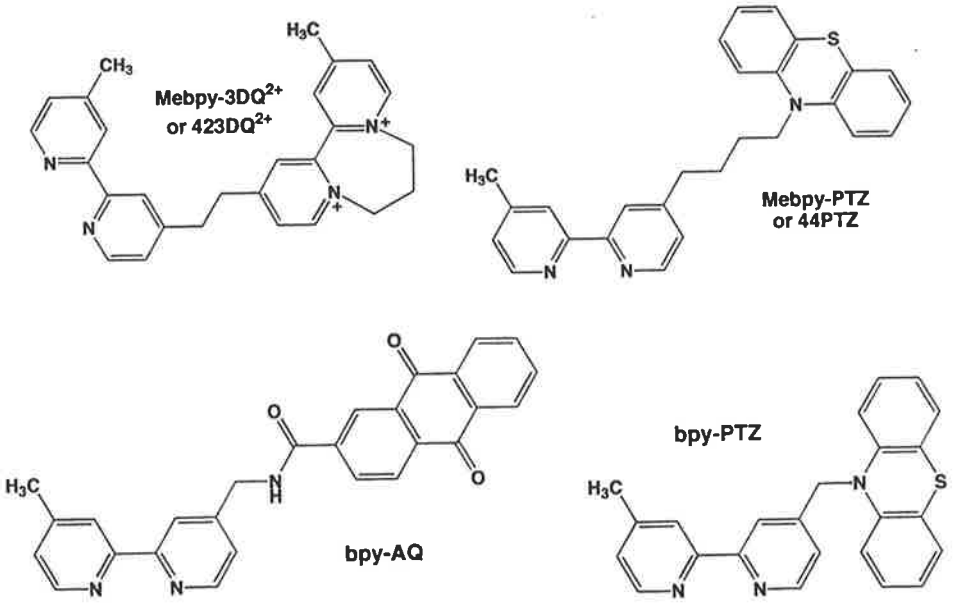

by Denti, Balzani and coworkers [54–68], as well as examples from other laboratories [21].

Of these oligomers, the decanuclear species mentioned earlier (Fig. 2) has been reported in which the bridging ligand is 2,3-bis(2-pyridyl)pyrazine (2,3-dpp) and terminal ligands 2,2-bipyridine (bpy) [56]. In such an assembly, since the internal metal centers (M_c) are $[Ru(2,3\text{-dpp})_3]^{2+}$ moieties, they all can exhibit *mer/fac* geometrical isomerism as 2,3-dpp in non-symmetrical. In addition, all ten metal centers may be chiral. As a result of this, there are in fact 6,144 diastereoisomers of this species – each with an enantiomeric form! While it is unlikely that all these stereoisomers would be represented in a synthesized mixture, it emphasizes the point that the stereochemistry of such systems is very complicated. Furthermore, the presence of a plethora of stereoisomers complicates the characterization of the complex by techniques such as NMR, the interpretation of which is rendered extremely difficult as the diastereoisomeric complexes have non-equivalent NMR spectra [58,79]. It also implies that the electrochemical and photophysical data measured represent an average of the various forms.

As another example, a study was presented by Brewer and coworkers on the electrochemical and photophysical properties of the trinuclear species $[\{Ru(bpy)_2\}_2\{Os(2,3\text{-dpp})_2Cl_2]^{4+}$ [80]. In this complex the bridging Os center may adopt a *cis(Cl)* or *trans(Cl)* geometry, and since the 2,3-dpp ligand is non-symmetrical, the *cis(Cl)* form has three geometric isomers and the *trans* isomer two. All the *cis* isomers may have chiral forms, as well as both ruthenium centers. As a result, there are actually sixteen possible diastereoisomers, all but two of which have enantiomeric forms. Of course, the full complement may not necessarily exist. However, in the representations in Fig. 5, the stereochemistry in such a linear

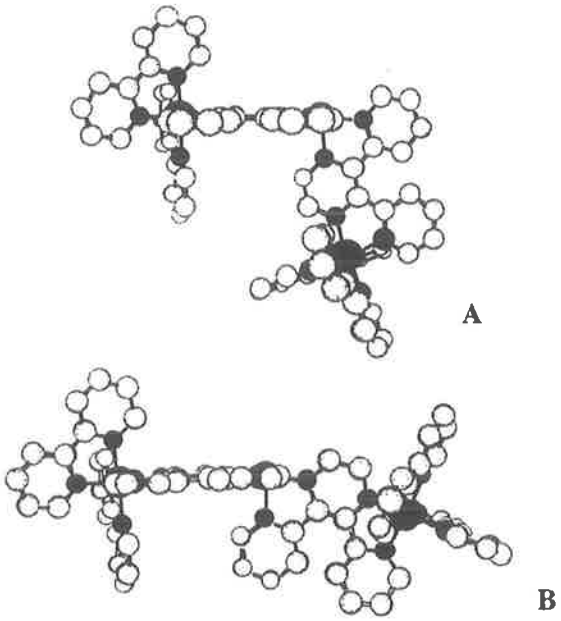

Fig. 5. Chem 3D® representation of diastereoisomers of $[\{Ru(bpy)_2\}_2\{Os(2,3\text{-}dpp)_2Cl_2]^{4+}$ (H atoms omitted for clarity) [80].

trinuclear species may be very different for a relatively small change – the species shown are both Δ(Ru)Δ(Os)Δ(Ru) forms, and differ only in that the geometric arrangement about the Os center is *cis(Cl)/cis(pyrazine)* and *cis(Cl)/trans(pyrazine)*, shown below as **A** and **B** respectively. The consequences on the relative disposition of the two "terminal" ruthenium centers is quite profound.

2.2. *Stereochemistry in ruthenium complexes with bidentate ligands*

Although an extensive literature exists on the synthesis of mononuclear complexes of ruthenium(II), there have been few studies of stereoisomerism. When non-symmetrical bidentate ligands are involved, for complexes of the type $[Ru(ab)_3]^{2+}$ the existence of *fac* and *mer* geometric isomers has been recognized from ^1H and ^{13}C NMR studies of complexes where ab = non-symmetrically-substituted derivatives of 2,2-bipyridine and 1,10-phenanthroline [81,82], azobis(2-pyridine) [83], and 2-(2-pyridyl)thiazole and 2-(2-pyrazyl)thiazole [84]. Similarly, ^{99}Ru NMR has been used to identify the presence of both geometric isomers in analogous complexes where ab = 1-(2-pyridyl)-3,5-dimethylpyrazole [85], 1-methyl-2-(2-pyridyl)imidazole, 2-(2-pyridyl)oxazole, 2-(2-pyridyl)thiazole and 2-(2-pyridyl)selenazole [86], and 2,3-bis(2-pyridyl)pyrazine [87]. Prior to our own work [88,89], there were few reports claiming the separation of such stereoisomers. Using HPLC techniques, separations were achieved for the species $[Ru(apy)_3]^{2+}$ (two geometric isomers) and $[Ru(apy)_2(bpy)]^{2+}$ (two of the three possible geometric isomers) {bpy = 2,2′-

bipyridine; apy = azobis(2-pyridine)} [83]. Structures of *mer*-$[Ru(apy)_3]^{2+}$ and *cis,trans,cis*-$[Ru(apy)_2Cl_2]$ have also been published {the order of specification of the geometry being acido ligand (Cl^-); py; azo} [90]. More recently, the separation of geometric isomers has been reported for complexes of substituted pyrazolylpyridine ligands [91].

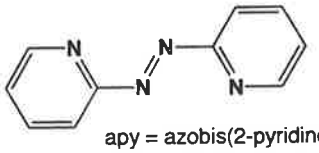

apy = azobis(2-pyridine)

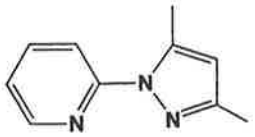

1-(2-pyridyl)-3,5-dimethylpyrazole

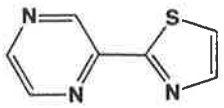

2-(2-pyrazyl)thiazole

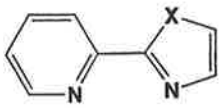

X = N-Me: 1-methyl-2-(2-pyridyl)imidazole
X = O: 2-(2-pyridyl)oxazole
X = S: 2-(2-pyridyl)thiazole
X = Se: 2-(2-pyridyl)selenazole

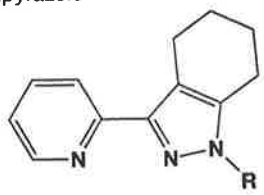

1-substituted-3-(2-pyridinyl)-
4,5,6,7-tetrahydroindazoles

Three isomers of $[Ru(pap)_2Cl_2]$ and/or $[Ru(tap)_2Cl_2]$ have been isolated [92,93], and the structures of the *cis–trans–cis*- and *cis–cis–cis*-$[Ru(pap)_2Cl_2]$ [94] and *cis–trans–cis*-$[Ru(pap)_2N_3)]$ [95] forms determined. The *cis–trans–cis, cis–cis–cis and trans–trans–trans* geometric isomers of $[Ru(npap)_2Cl_2]$ have been separated [96] and the stereochemical course investigated of the reactions of $[Ru(pap)_2Cl_2]$ and $[Ru(npap)_2Cl_2]$ species with H_2O/OH^- [97,98], and of the reaction of $[Ru(pap)_2(OH_2)_2]^{2+}$ and $[Ru(tap)_2(OH_2)_2]^{2+}$ to form $[Ru(pap)_2B_2]^{2+}$/ $[Ru(tap)_2B_2]^{2+}$ (B is a bidentate ligand) [99]. *Cis* and *trans* isomers of $[Ru(L)_2Cl_2]$ (where L are aryl(2-pyridylmethylene)amine Schiff-base ligands) have also been reported [100].

In terms of the separation of chiral forms of such molecules, the resolution of $[Ru(pp)_3]^{2+}$ [101,102], $[Ru(phen)_2(py)_2]^{2+}$ [103] and $[Os(pp)_3]^{2+}$ [104,105] (pp = phen and bpy) was achieved many decades ago.

As far as dinuclear complexes are concerned, very little stereochemical information has been available. In a number of cases, there have been claims for absolute preferences for one diastereoisomeric forms over another [83,106] and linkage isomerism has been shown in species involving the 3,4-bis(2-pyridyl)-1,2,4-triazolate (bpt) ligand (below) as a bridge [107–109]. Our own studies on the stereochemistry of ligand-bridged dimers, and those of von Zelewsky and coworkers [110,111] will be discussed in more detail below.

2.3. *Addressing the "stereochemical problem"*

2.3.1. *Using tridentate ligands.*

The stereochemical problem may be avoided by the use of tridentate ligands of the type 2,2′:6′,2″-terpyridine (tpy), which coordinate in a meridional fashion about

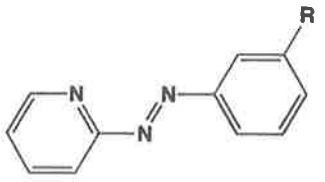

R = H: pap = 2-(phenylazo)pyridine
R = CH_3: tap = 2-(3-tolylazo)pyridine

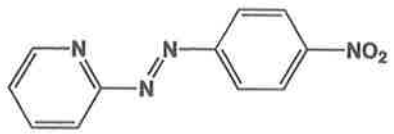

npap = 2-{(4-nitrophenyl)azo}pyridine

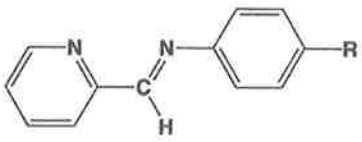

R = H, CH_3, or Cl

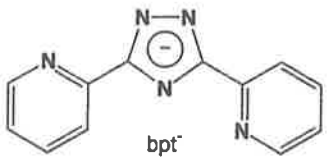

bpt$^-$

an octahedral metal center creating an achiral species of the type $[M(tpy)_2]^{n+}$ [21,39,40]. However, it should be noted that there are a number of consequences of this approach. Firstly, the lifetime of the ^{3}MLCT excited state of $[Ru(tpy)_2]^{2+}$ is some 3–4 orders of magnitude shorter at room temperature in solution than for $[Ru(bpy)_3]^{2+}$ and $[Ru(phen)_3]^{2+}$, and unlike the latter complexes $[Ru(tpy)_2]^{2+}$ does not luminesce [112–116]. This is a consequence of faster radiationless deactivation through a ^{3}MC (metal-centered) state, brought about by the weaker field strength in $[Ru(tpy)_2]^{2+}$ because of the geometric requirements of the coordinated tpy ligand and resultant distortion from the strictly octahedral environment [117,118]. At 77 K, this path is unavailable, and the luminescence and emission lifetime of $[Ru(tpy)_2]^{2+}$ is comparable with that of $[Ru(bpy)_3]^{2+}$ and $[Ru(phen)_3]^{2+}$ [119]. It has been shown that the lifetime of the $[Ru(tpy)_2]^{2+}$ chromophore is significantly increased by the incorporation of electron-withdrawing substituents at the 4′-position [39,120–122].

The second consequence is that in order to avoid further stereoisomerism (geometric), any bridging must occur through the 4′-positions of the tpy ligands, which for $[Ru(tpy)_2]^{2+}$ species have a mutually *trans* arrangement – any polynuclear species involving bridging ligands based on tpy-type ligands is therefore necessarily linear or rod-like.

Sauvage and coworkers have also examined the cyclometallated analogue on the basis that the higher σ-donating properties of the cyclometallating ligand allows some control of the spectroscopic and redox characteristics [42,43,123].

The use of these ligands and ligand-bridges has allowed a development of the

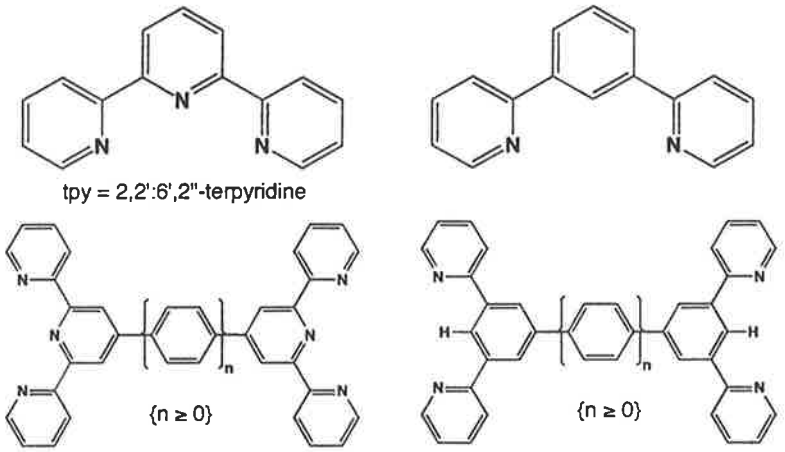

understanding of aspects of intramolecular electron and energy transfer processes [39–43,123]. However, to comprehend fully the consequences of the spatial relationship of the component metal centers on these processes – and maximize the ability to vary the characteristics of the coordination environment of those centers – the use of tris(bidentate) species is ultimately required. And therein lies a challenge.

2.3.2. Chiral building blocks and the "Chiragens"

Two separate approaches have been taken to this task by von Zelewsky and coworkers [75].

In the first, an enantiomerically pure chiral building block was sought which could be used to produce mono- and dinuclear species of predetermined stereochemistry. The complexes $[Ru(phen)_2(py)_2]^{2+}$ and $[Ru(bpy)_2(py)_2]^{2+}$ (conveniently resolved by conventional diastereoisomer formation using the O,O'-dibenzoyltartrate anion) were found to undergo stereoretentive substitution of the two monodentate pyridine ligands [110,111,124]. This important property was shown by reaction of either Δ- or Λ-$[Ru(pp)_2(py)_2]^{2+}$ (pp = bpy or phen) with the chiral bidentate ligand (R,R)-1,2-diaminocyclohexane (or its enantiomer) to give pure diastereoisomeric products [111].

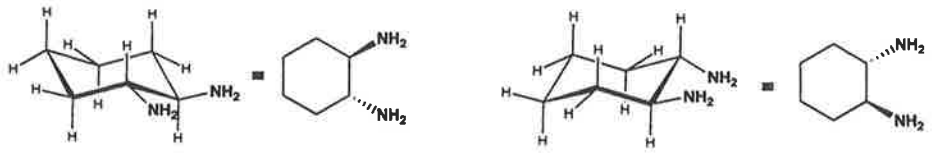

These chiral precursors were used to synthesize dinuclear species $[\{Ru(pp)_2\}_2(\mu\text{-BL})]^{4+}$ (pp = bpy or phen; BL = bridging ligands 2,2-bipyrimidine

{bpm}, 2,5-bis(2-pyridyl)pyrazine {2,5-dpp} or 4,6-bis(2-pyridyl)pyrimidine {4,6-dppm}) with predetermined stereochemistry [110,111]. In these cases the *meso*-($\Delta\Lambda$) diastereoisomer and the enantiomers ($\Delta\Delta$ and $\Lambda\Lambda$) of the *rac* diastereoisomer were separately synthesized and their stereochemical integrity confirmed using ^{1}H NMR and CD methods.

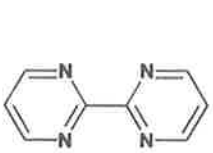

2,2'-bipyrimidine
bpm

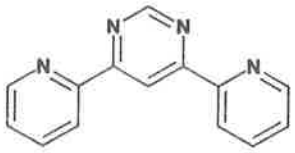

4,6-bis(2-pyridyl)pyrimidine
4,6-dppm

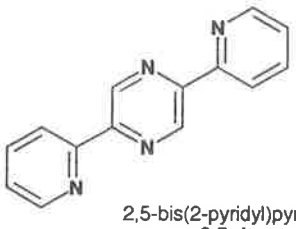

2,5-bis(2-pyridyl)pyrazine
2,5-dpp

The principle of the second strategy was to impose a chiral disposition about the metal center of a precursor, which in turn would promote the stereoselective synthesis of oligomers derived from it. Such ligands, called "Chiragens", are based on [4,5]-pineno-2,2′-bipyridine, which are derived from the naturally occurring chiral species (−)-myrtenal [125,126]. [4,5]-Pineno-2,2′-bipyridine is chiral, and undergoes regioselective deprotonation whereby two such moieties may be linked by a spacer to give the "Chiragen" series of ligands. The linkage may be an alkyl chain {denoted CG[*n*]; $n=0$, 3, 4–7} [124–127], bpy {denoted CG[bpy]} [127] or *o*-, *m*- or *p*-xylendiyl {denoted CG[*o*/*m*/*p*-xyl]} [129–131]. The Chiragens CG[*n*] where $n\geq 4$ show stereospecific coordination to octahedral metal centers ruthenium and osmium [126], and the same ligands have been used to control the stereochemistry of the general species of the type $[Ru(CG[n])Cl_2]$ and $[Os(CG[n])X_2]^{m+}$ ($X=Cl^-$, $m=0$; X=DMSO, $m=2$) [131,132], which may be used as precursors in syntheses of higher nuclearity assemblies. They have also been used to produce helicate species with predetermined chirality [129]. The ligands CG[*n*] ($n=0$, 3) and the CG[bpy] do not coordinate as tetradentate ligands: however, they coordinate to a metal center in a bidentate manner and therefore are potential bridges. They have been incorporated in di- or trinuclear species: in such systems stereospecificity was observed, but was induced by the chirality of the metal centers involved [128].

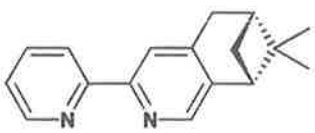

A chiragen based on the "dipineno" precursor has also been developed {designated superchiragen[0] or SGS[0]} and shows similar behavior to its CG[0] analogue [127,128].

In terms of the overall aims, by imposing stereochemistry on the primary building

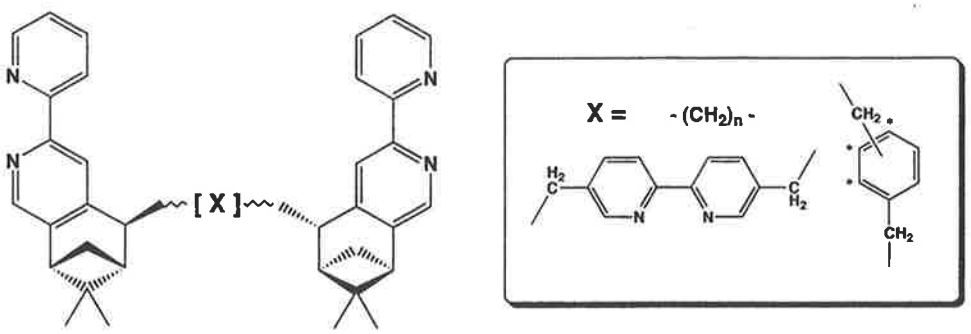

block of an assembly the "Chiragen" approach seeks to maintain stereoselectivity in the addition of further components. Furthermore, since that stereoselectivity appears to be complete, the chances of photoisomerization are minimized so that the stereochemistry is retained during photochemical processes.

The negative aspect of the approach is that since the Chiragen occupies four coordination positions about the metal center, the opportunity for versatility in terms of the coordination environment is limited.

2.3.3. Other examples of stereoselective synthesis

There are a limited number of other recent examples of controlled stereochemistry which reflect a burgeoning interest in the topic. For example, there have been a number of examples involving condensations of chiral monomers containing the 1,10-phenanthroline-5,6-dione ligand to form bridged complexes of predetermined stereochemistry. Lincoln and Nordén [133] have used this methodology to produce ΔΔ-[{Ru(phen)$_2$}$_2$(dppz(11-11′)dppz}]$^{4+}$ (Fig. 6) using resolved [Ru(phen)$_2$-

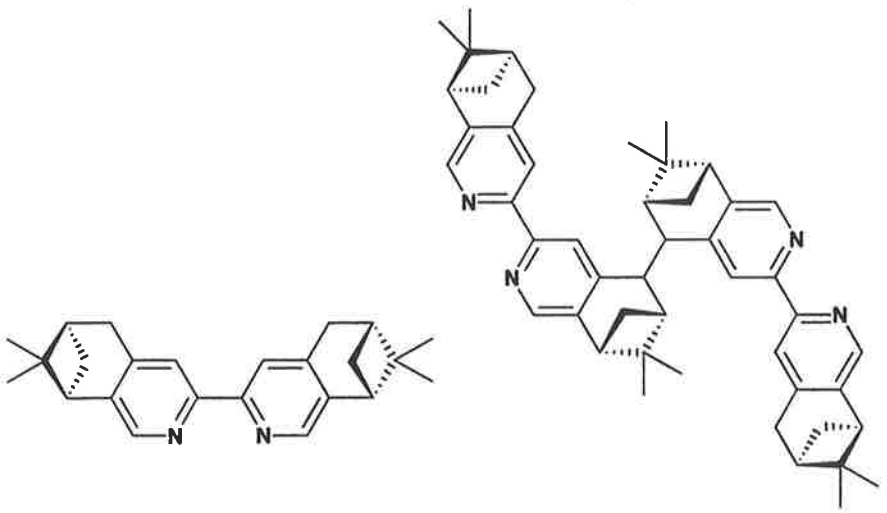

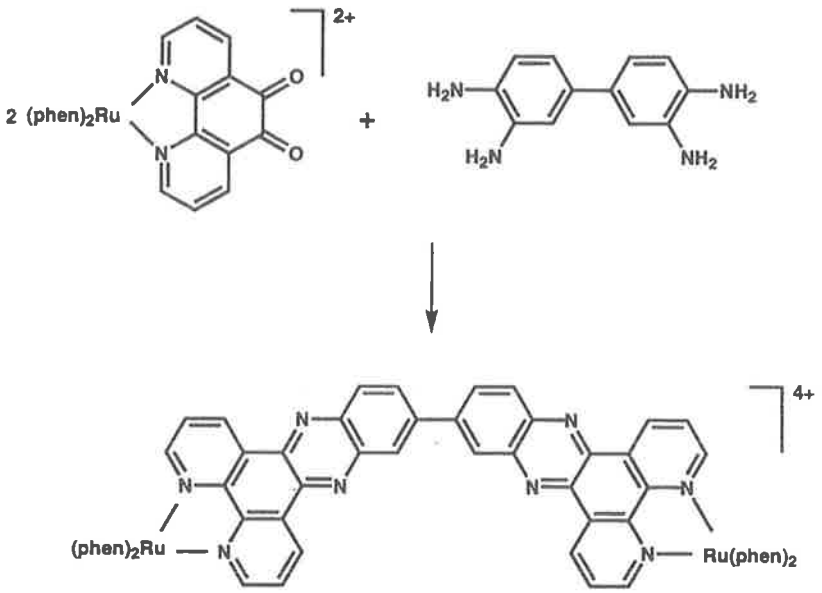

Fig. 6. Stereoselective synthesis of diastereoisomers $[\{Ru(phen)_2\}_2\{dppz(11\text{-}11')dppz\}]^{4+}$ [133].

(phen-5,6-dione)]$^{2+}$ [134] as the precursor. In a similar manner, Lehn and coworkers [135] have reported the complex shown in Fig. 7, in which the stereochemistry of the two ruthenium centers is predetermined by the use of the same Δ- or Λ-$[Ru(phen)_2$(1,10-phenathroline-5,6-dione)]$^{2+}$ precursor: Again in a related system, MacDonnell and Bodige have used resolved precursors to form a single diastereoisomer of the tpphz-bridged dimer (Fig. 8) [136]:

Tor and coworkers [137] have reported the use of the Hua and von Zelewsky precursor [111] to produce chiral complexes of functionalized phen ligands, which may be subsequently linked to form dimers with predetermined stereochemistry (Fig. 9).

Additionally, Kane-Maguire and coworkers [138] have recently reported the resolution of *cis*-$[Ru(phen)_2(CH_3CN)_2]^{2+}$, which may be used as a chiral

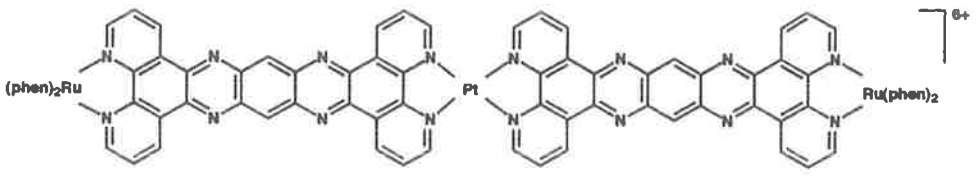

Fig. 7. Stereoselective synthesis of diastereoisomers of trimetallic species [135].

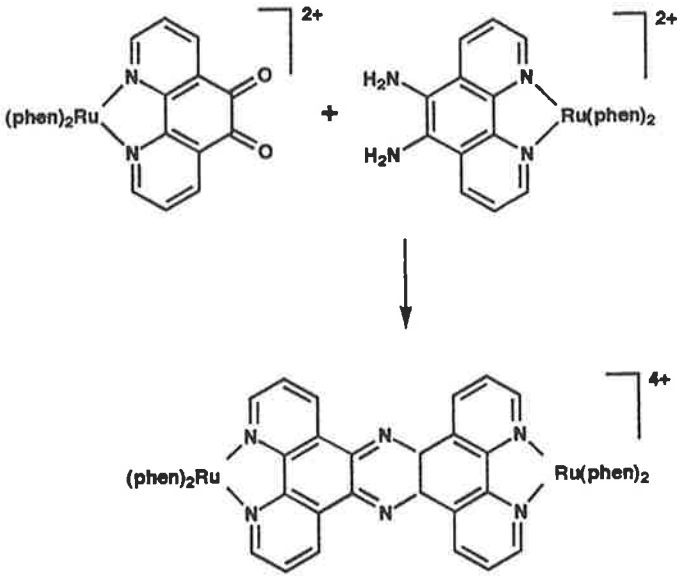

Fig. 8. Stereoselective synthesis of diastereoismers of $[\{Ru(phen)_2\}_2\{\mu\text{-tpphz}\}]^{4+}$ [136].

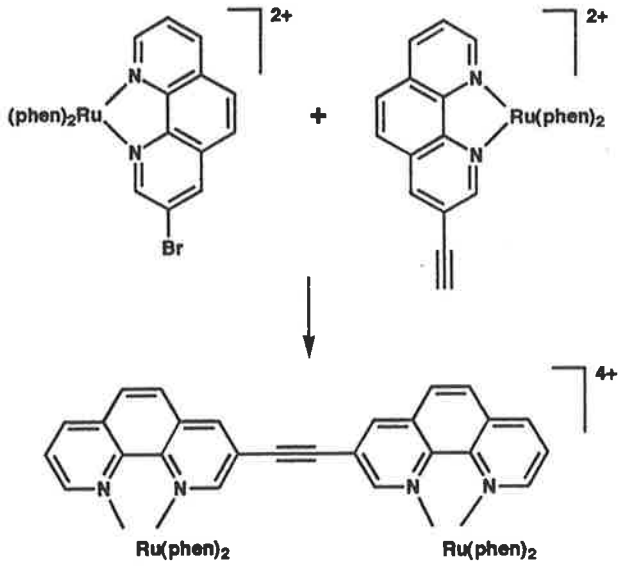

Fig. 9. Stereoselective synthesis of diastereoismers of alkyne-bridged dinuclear species [137].

precursor for further synthesis, including chiral neutral species such as *cis*-$[Ru(phen)_2X_2]$ ($X=CN^-$, Cl^-) which are difficult to obtain by other means.

While these examples show the increasing appreciation of the problem, they do not offer a general approach to its solution.

3. Stereochemistry and polynuclear assemblies

3.1. The synthesis of tris(heteroleptic) complexes

In our own approach to the stereochemical problem, we have attempted to honor three aims. Firstly, the use of metal centers in polynuclear assemblies was considered important because it provides the ability to control the photophysical and spectral characteristics of the chromophore component, as well as the redox properties (a feature important in controlling intramolecular electron and energy transfer following light absorption), and such versatility may only be achieved by the use of bidentate ligands. The second necessity was that the centers must have a substantial level of photoinertness. For complexes containing pyridyl-type ligands low levels of photolability are known [139], and in cases where stereoisomerism is possible photoisomerization and photoracemization have been reported, particularly in cases where monodentate ligands are involved [101,140,141]. In the case of the "Chiragen" ligands, one of the attractive features was that since the chiral ligand imposed a stereoselectivity on its attachment to the metal center, photoracemization would be minimized [131]. It is worth noting however from our studies that tris(heteroleptic) species proved to be at least 10^2–10^3 times more photoinert than the $[Ru(bpy)_3]^{2+}$ archetype, [17] and despite concerns to the contrary [131], we have not observed photolability in the $[Ru(pp)_2(CO)_2]^{2+}$ species.

The synthetic methodology we have used for the heteroleptic tris(bidentate)-ruthenium(II) complexes is based on the sequential addition of the polypyridyl ligands to the oligomeric precursor $[Ru(CO)_2Cl_2]_n$, as summarized in Fig. 10 [16,17].

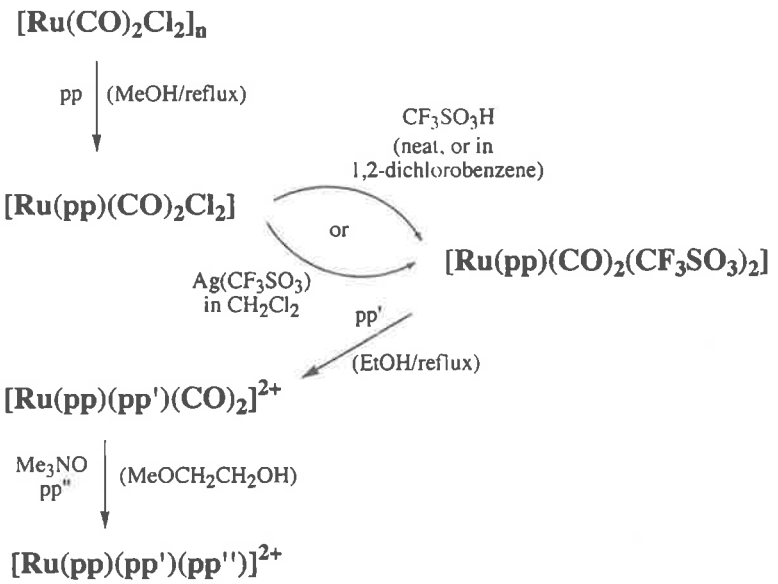

Fig. 10. Synthetic scheme for heteroleptic tris(bidentate)ruthenium(II) complexes [17].

Preliminary details of the scheme were reported earlier [142–147]. We have also recently reported a related synthetic route to produce heteroleptic tris(bidentate)osmium(II) analogues [20].

3.2. Stereochemical considerations

From a stereochemical point of view, the penultimate complex in the scheme, viz. the species $[Ru(pp)(pp')(CO)_2]^{2+}$, is pivotal as such a bis(bidentate) species is closely stereochemically related to the final product and it is at this final stage that the stereochemistry may be controlled. We undertook two separate but interrelated studies of the stereochemistry of this decarbonylation process.

In the first, the formation of the species $[Ru(Me_2bpy)(pmb)_2]^{2+}$ was studied in detail [88]. In this complex, 4,4′-dimethyl-2,2′-bipyridine (Me_2bpy) is a symmetrically-substituted ligand, and 4-methyl-4′-*neo*-pentyl-2,2′-bipyridine (pmb) is non-symmetrically substituted. The target complex in such a case has three possible geometric isomers, shown below. In terms of the synthetic scheme, there are of course two alternative approaches: the target complex can be obtained by either reaction of Me_2bpy with $[Ru(pmb)_2(CO)_2]^{2+}$ (which has three geometric isomers exactly analogous to the target), or by reaction of pmb with $[Ru(Me_2bpy)(pmb)(CO)_2]^{2+}$, which has two geometric forms. Figs. 11–13

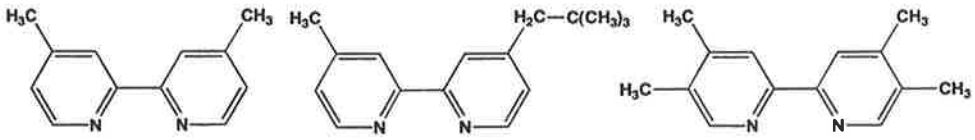

Me_2bpy **pmb** **Me_4bpy**

Clearly, in the first case, if stereochemical integrity were retained in the decarbonylation process, then a direct conversion of each of the dicarbonyl isomers to the

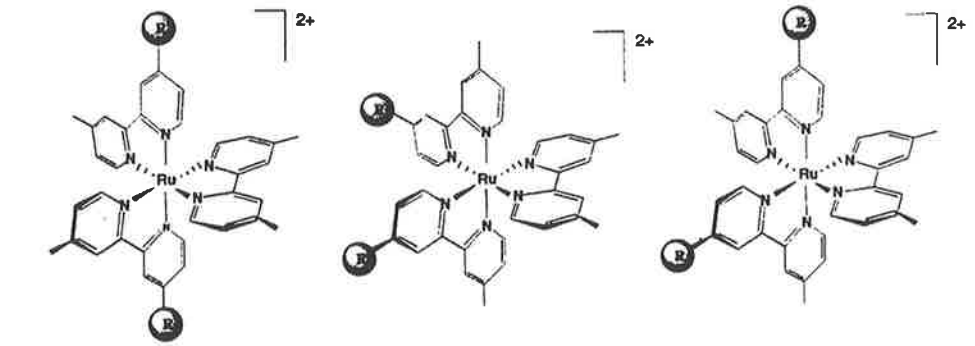

1 *trans*(R) **2** *s-cis*(R) **3** *u-cis*(R)

Fig. 11. Geometric isomers of $[Ru(pmb)_2(Me_2bpy)]^{2+}$ {R = *neo*-pentyl-).

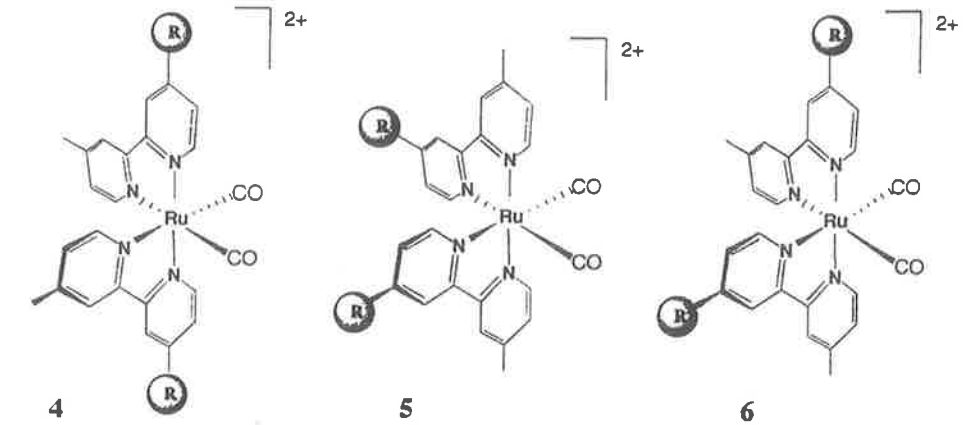

Fig. 12. Geometric isomers of $[Ru(pmb)_2(CO)_2]^{2+}$.

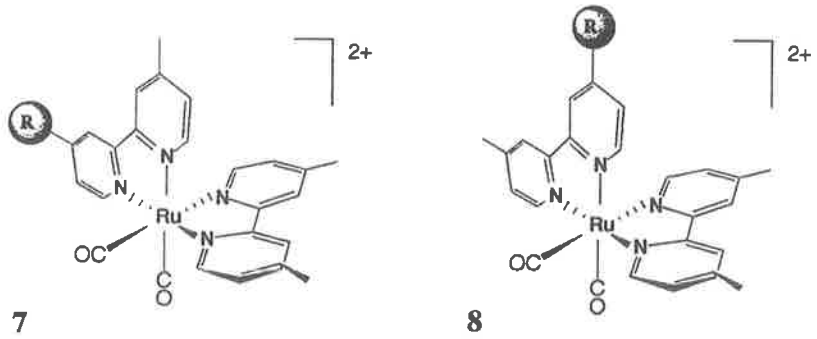

Fig. 13. Geometric isomers of $[Ru(pmb)(Me_2bpy)CO)_2]^{2+}$.

corresponding isomer of the target complex would be expected. In the second case, the addition of the second pmb ligand to either of the two geometric isomers of the dicarbonyl species could occur in two ways and so two isomers would be obtained in each case. Within our studies, the respective dicarbonyl complexes were separated into their geometric isomers and the stereochemical course of the final reaction studied. In the decarbonylation reactions, the dicarbonyl species was reacted with excess trimethylamine *N*-oxide (TM*N*O) in the presence of the third bidentate ligand. Initial studies used refluxing 2-methoxyethanol as the solvent, but careful investigations revealed that a small amount ($\sim 5\%$) of ligand scrambling occurred under those conditions: however, if the reaction was performed at $\leq 40\,^{\circ}C$, then the stereochemical integrity of the dicarbonyl species was completely retained in the manner shown in Fig. 14 [88].

In the second study, the chiral integrity of the dicarbonyl species was observed during the decarbonylation process [147]. This work involved two separate but

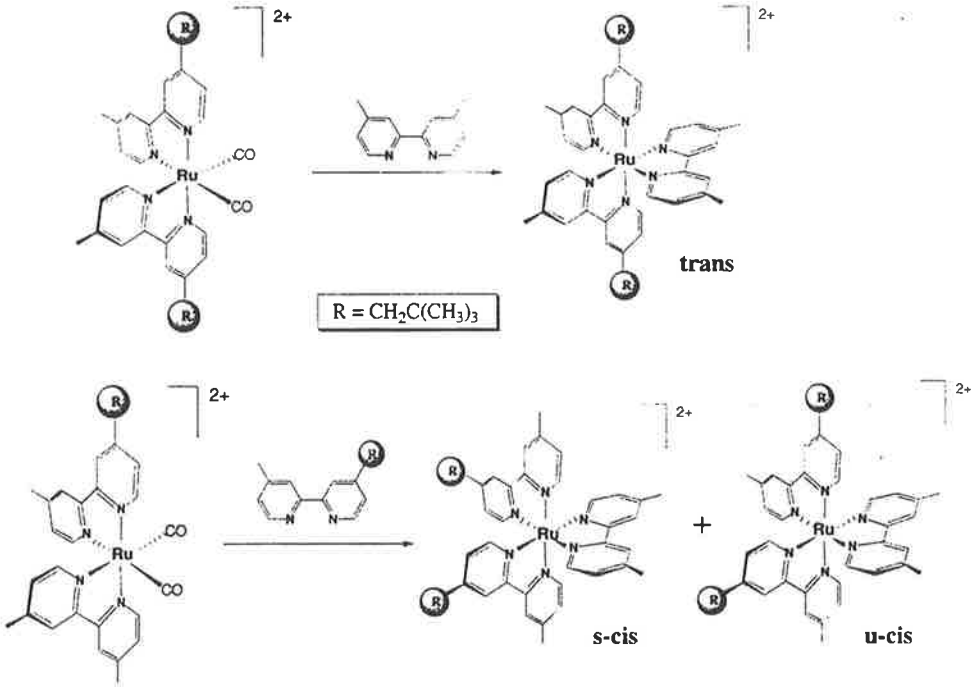

Fig. 14. Stereochemical course of the decarbonylation reactions of $[Ru(pmb)_2(CO)_2]^{2+}$ with Me_2bpy, and of $[Ru(pmb)(Me_2bpy)(CO)_2]^{2+}$ with Me_2bpy [88].

significant parts. The $[Ru(pp)(pp')(CO)_2]^{2+}$ precursor is chiral and may be resolved into Δ and Λ enantiomers. This was achieved for the cases where pp = pp' = bpy (or phen), with chiral integrity being established unequivocally by the use of ^1H NMR studies with chiral lanthanide shift reagents. The chiral $[Ru(pp)_2(CO)_2]^{2+}$ forms were then reacted under decarbonylation conditions with a third pp ligand to produce the corresponding $[Ru(pp)_3]^{2+}$ complexes, for which the chiral forms are well characterized [101,102]. The results were totally analogous with those for the $[Ru(Me_2bpy)(pmb)_2]^{2+}$ study, and showed total retention of chirality at temperatures ≤ 40 °C, with $\sim 5\%$ racemization at 120 °C.

The chiral dicarbonyl species may also be used as a precursor for dinuclear species. The synthetic methodology may be used to prepare dinuclear complexes if the dicarbonyl precursor is reacted with a complex $[Ru(pp)(pp')('pp'')]^{2+}$ in which one of the ligands in the tris(bidentate) species is a potential bridging ligand, such as 2,2′-bipyrimidine. This has been referred to earlier as the "complexes as ligands" approach to oligomer synthesis. In the present instance, the tris(bidentate) complex $[Ru(Me_4bpy)_2(bpm)]^{2+}$ {Me_4bpy = 4,4′,5,5′-tetramethyl-2,2′-bipyridine) was resolved by cation exchange column chromatogaphy (see below) and one enantiomer reacted with a chiral form of $[Ru(phen)_2(CO)_2]^{2+}$ under decarbonylation conditions. At a temperature ≤ 40 °C, it was found that the one single diastereoisomer of the dinuclear species $[(Me_4bpy)_2Ru(bpm)Ru(phen)_2]^{4+}$ was obtained(Fig. 15).

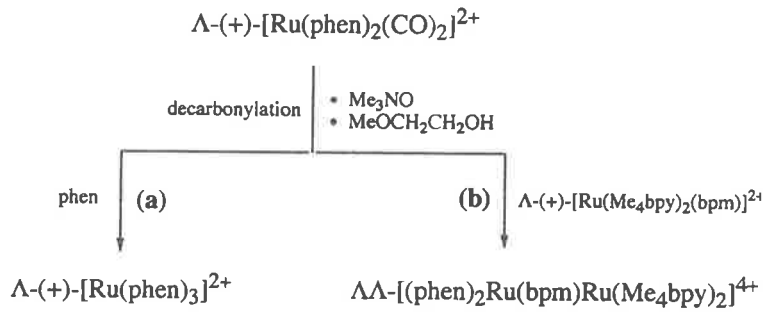

Fig. 15. Stereochemical course of decarbonylation reactions [147].

The conclusions are extremely significant. The synthetic methodology allows the extensive and controlled variation of the coordination environment of individual metal centers, and therefore of the spectral, photophysical and redox characteristics. But in addition, since the stereochemical integrity of the dicarbonyl precursor is maintained in the decarbonylation reaction, the stereochemistry may be predetermined in mononuclear and oligonuclear species by appropriate choice of the stereochemistry of the precursor. We have exploited our methodology to control the stereochemistry of ligand-bridged polymetallic assemblies, and as well as to probe the effect of the spatial relationship of the component metal centers on intramolecular electron and energy transfer within them. A number of examples are summarized below.

3.2.1. Example – a mononuclear chromophore-quencher system

Previous studies on chromophore-quencher complexes (see above) have probed the characteristics of the charge-separated state as a function of the distance of separation of the donor and acceptor groups, and the nature of the rigidity and electronic character of the bridging groups between them. However, the dependence of the electron transfer process on their stereochemical relationship has not been investigated. In some cases, the systems have been deliberately chosen to avoid this spatial ambiguity [39], while other studies of this type have investigated target compounds composed of a mixture of stereoisomers [76–78]. While the existence of the stereoisomers has been acknowledged [77,78], we are not aware of any report of the isolation of stereoisomers of a mononuclear species containing a single donor and a single acceptor functionality.

The combination of the synthetic methodology for tris(heteroleptic) complexes [17] and the confirmation of retention of stereochemical integrity during the final decarbonylation step of our scheme [88,147] allowed the isolation of a species of this type. Using variations on the earlier techniques, we have isolated the four geometric isomers of the system $[Ru(Me_2bpy)(bpy\text{-}MQ^{2+})(bpy\text{-}PTZ)]^{4+}$ (Fig. 16) {Me_2bpy = 4,4′-dimethyl-2,2′-bipyridine; $bpy\text{-}MQ^{2+}$ = ((4′-methyl-2,2′-bipyridin-4-yl)methyl)-1′-methyl-4,4′-bipyrinediium cation; bpy-PTZ = [(4′-methyl-2′,2-bipyridin-4-yl)methyl]phenothiazine} [89].

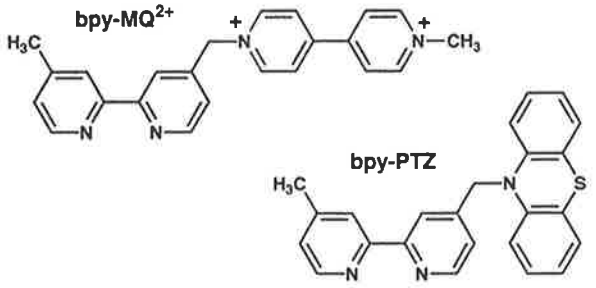

A variation in the methodology described earlier [17] was required to avoid the sensitivity of the PTZ functionality to oxidation by the decarbonylation agent TMNO. Firstly, the bpy-MQ^{2+} ligand was added to the $[Ru(Me_2bpy)(CO)_2(CF_3SO_3)_2]$ precursor. As with the pmb system, [88] the presence of the non-symmetrically-substituted bidentate ligand in $[Ru(Me_2bpy)(bpy\text{-}MQ^{2+})(CO)_2]^{4+}$ induces geometrical isomerism in its complexes: **9A** contains the MQ^{2+} substituent in a *cis/trans* orientation with respect to both carbonyl ligands, whereas in **9B** it has a *cis/cis* orientation (Fig. 17). Fractional crystallization allowed substantial but not complete separation of the geometric forms, but the separation – and the avoidance of the problem of the sensitivity of the PTZ grouping in the decarbonylation process – was achieved via an extra step introduced into the previously reported synthetic scheme [17]. The decarbonylation of **9** with TM*N*O was undertaken in the presence of pyridine (py) to produce $[Ru(Me_2bpy)(bpy\text{-}MQ^{2+})(py)_2]^{4+}$ (**10**), which was readily separated into geometric isomers by cation exchange chromatography. Such bis(pyridine) species are known to react with a third bidentate polypyridyl ligand with stereochemical retention of configuration [111].

The stereochemical consequences of the reactions of **10A** and **10B** with bpy-PTZ are shown in Fig. 18: **10A** results in a *trans*-**11** + *cis(2)*-**11** mixture and **10B** produces *cis (1)*-**11** + *cis(3)*-**11**. The two pairs of isomeric mixtures of $[Ru(Me_2bpy)(bpy\text{-}MQ^{2+})(bpy\text{-}PTZ)]^{4+}$ were separated by cation-exchange chromatography, giving the four isomers which were characterized by NMR spectroscopic techniques.

The physical characteristics of the isomers have been investigated. No significant differences were observed between the electronic absorption spectra of stereoisomers, or in their electrochemical behavior. Initial photophysical studies suggest differences are observed between the four geometric forms of the complex $[Ru(Me_2bpy)(bpy\text{-}MV^{2+})(bpy\text{-}PTZ)]^{4+}$: the lifetimes of the charge-separated state for all the *cis* isomers are different (while of the same order), with the behavior of the *trans* isomer being distinct. These details will be reported shortly [89].

3.2.2. Example – a dinuclear system with an α-azodiimine bridge

The stereochemistry of the dinuclear species $[(pp)(pp')Ru(BL)Ru(pp'')(pp''')]^{4+}$ (where pp = pp′ and pp″ = pp‴; BL is a bridging ligand) has been examined [79,110,111,147]. For all such dimeric species, there are two diastereoisomeric forms, comprised of the enantiomeric pairs ΔΔ/ΛΛ and ΔΛ/ΛΔ. In cases where the coordina-

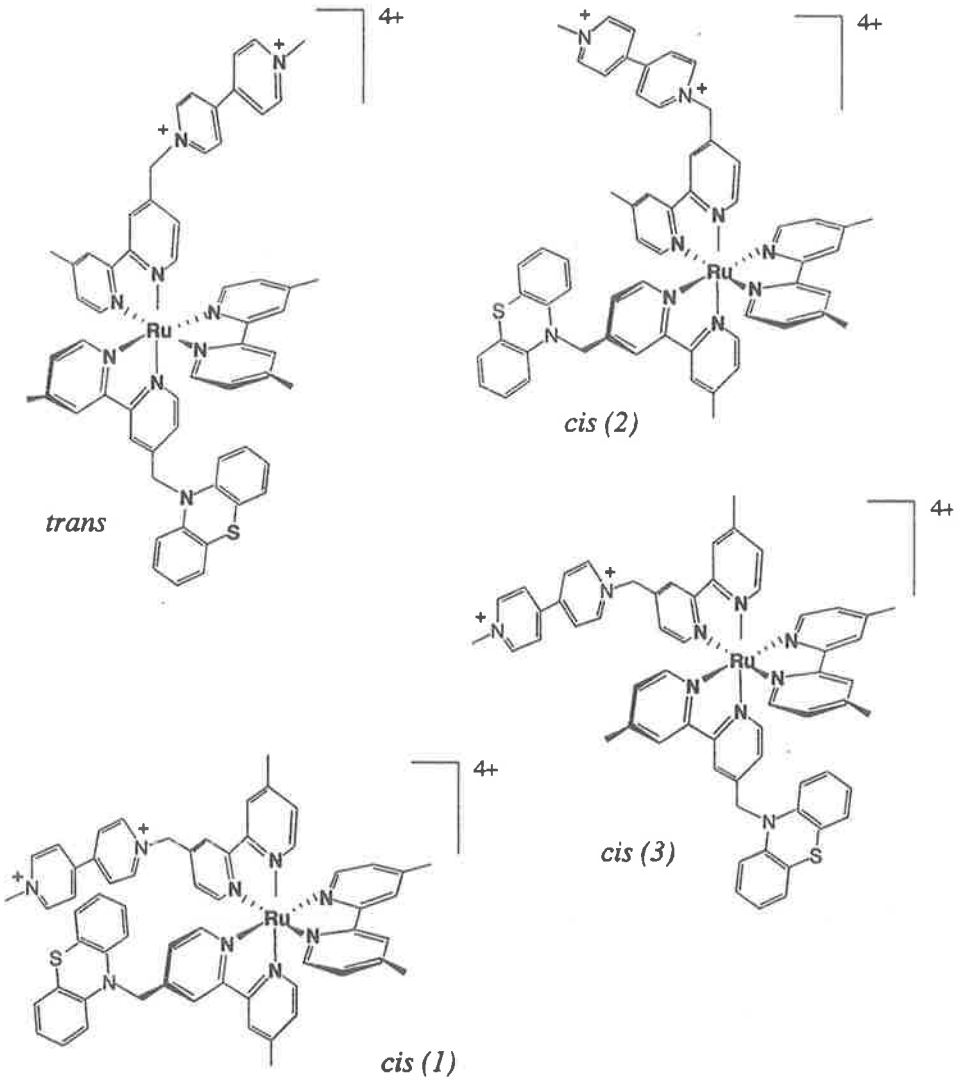

Fig. 16. Geometric isomers of the system $[Ru(Me_2bpy)(bpy\text{-}MQ^{2+})(bpy\text{-}PTZ)]^{4+}$ [89].

tion environment of the metal centers is equivalent (i.e. pp=pp′=pp″=pp‴), the ΔΛ and ΛΔ forms are identical (i.e. a *meso* form).

There is a significant difference between the *rac* and *meso* diastereoisomers as the terminal polypyridyl ligands "above" and "below" the plane of the bridging ligand bear a significantly different relationship. For the complexes where the axes of the "bites" of the two bidentate moities of the bridging ligand (BL) are linear (e.g. bpm) or have a stepped parallel relationship (e.g. apy), the terminal polypyridyl ligands "above" and "below" the plane of the bridging ligand are approximately parallel

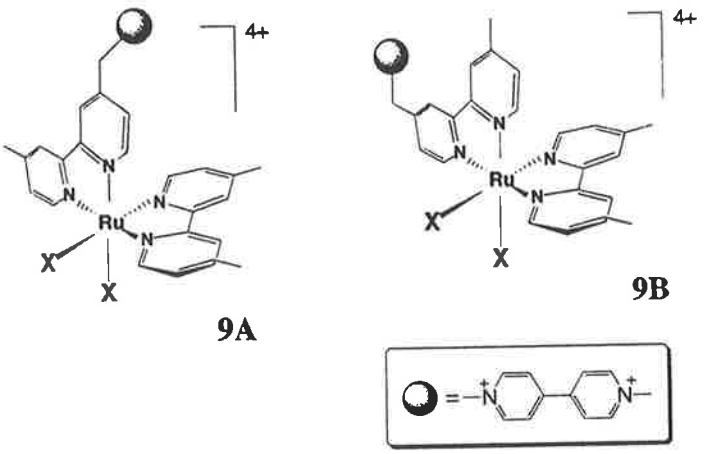

Fig. 17. Geometric isomers of the system $[Ru(Me_2bpy)(bpy\text{-}MQ^{2+})X_2]^{4+}$ {X=CO (9) or X=py (10)} [89].

in the ΔΔ/ΛΛ form, whereas they are perpendicular in the ΔΛ/ΛΔ stereoisomer. This is shown in a schematic manner in Fig. 19. It should be noted that if the relationship of the axes of the two "bites" are angular (e.g. 2,3-dpp, HAT), the above description is reversed.

We have separated the diastereoisomers for a range of dinuclear complexes by cation-exchange chromatography [79], and the synthesis of predetermined diastereoisomers of a selection of dinuclear species has been achieved using chiral precursors [110,111,147].

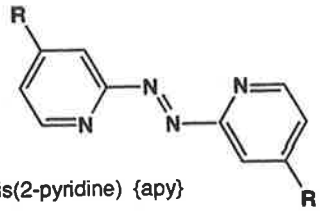

R = H: azobis(2-pyridine) {apy}

= CH_3: azobis(4-methyl-2-pyridine) {mapy}

To probe the stereochemical effects in dinuclear species, we chose to investigate the series of complexes $[(pp)_2Ru(BL)Ru(pp')_2]^{2+}$, where pp/pp′ were the terminal ligands bpy or Me_2bpy, and the bridging ligand BL was of the α-azodiimine type (apy or mapy) [148].

The bridging ligand affects the degree of metal–metal interaction in di- and oligonuclear complexes as it determines the distance and relative orientation of the metal centers, and influences through-space electronic coupling and the degree of through-bond communication (via ligand–metal orbital overlap) [14,149]. Ligands possessing the azo functionality have extremely low-lying π* orbitals and are strongly π-accepting [83,92,96,150–153]. Moreover, dinuclear complexes in which ligands

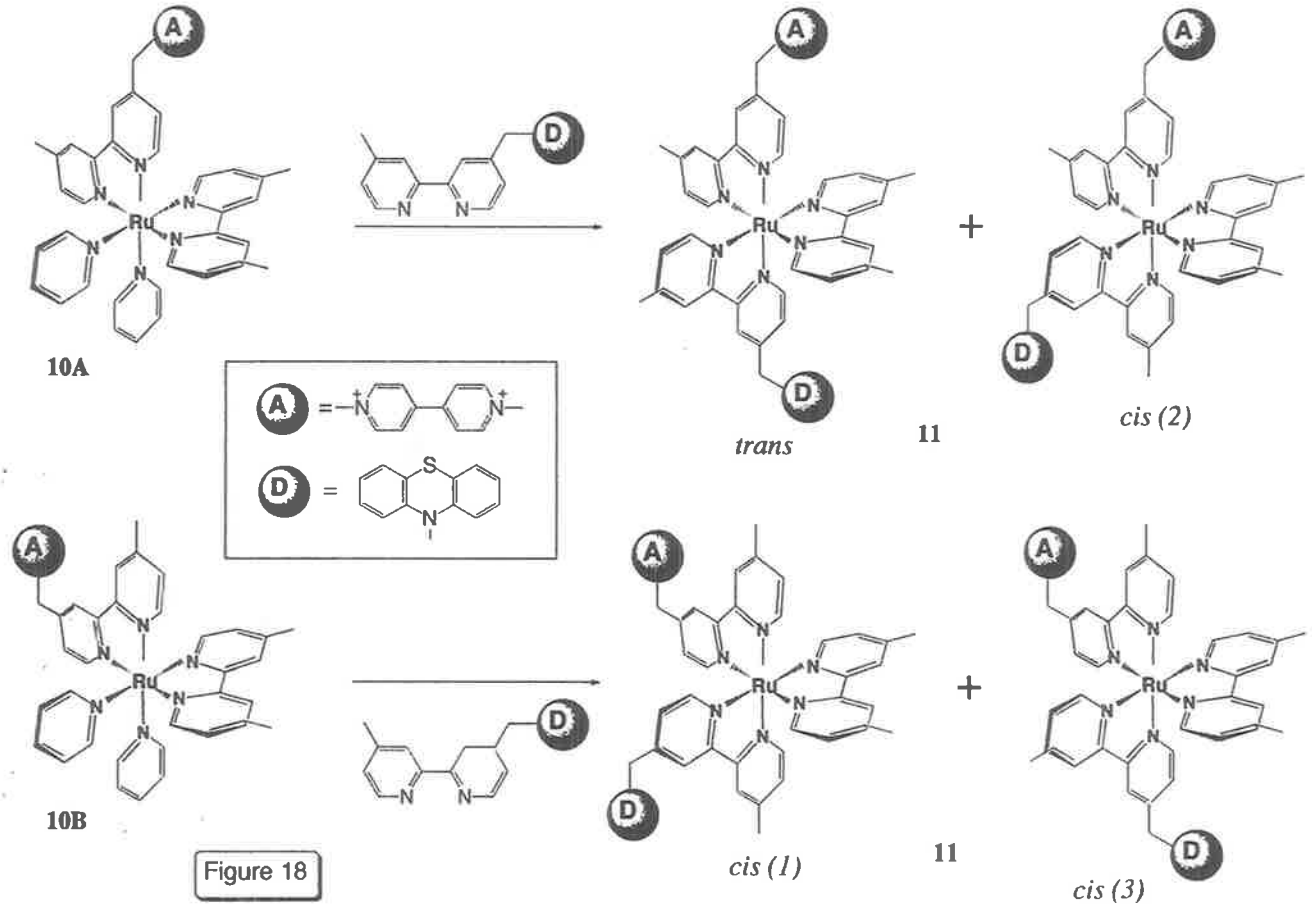

Fig. 18. Stereochemical course of the reactions of the geometric isomers (**10A** and **10B**) of $[Ru(Me_2bpy)(bpy\text{-}MQ^{2+})(py)_2]^{4+}$ with bpy-PTZ. [89].

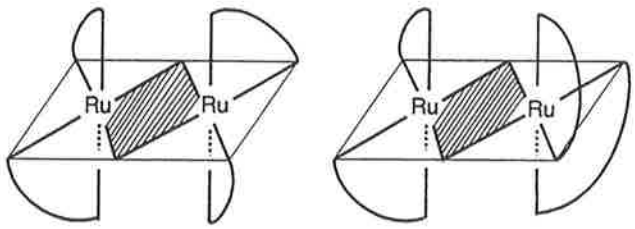

Fig. 19. Schematic representation of the diastereoisomeric forms of the dinuclear ligand-bridged species $[\{Ru(pp)_2\}_2(BL)]^{4+}$ {pp = a symmetrical bidentate ligand; BL = a symmetric bridging ligand (shown hatched) in which the axes of the two "bites" are linear}.

such as azobis(2-pyridine) function as the bridge have comproportionation constants (K_c) in excess of 10^8 for the di-ruthenium case, and hence exhibit a very high degree of metal–metal interaction [83,149,150,154,155]. Bridging ligands of this type also are found to enhance the structural differences between the diastereoisomers of such dinuclear species, because of the stepped-parallel (as opposed to linear) orientation of the axes of the bidentate chelating ligand functions in the apy-type bridging groups (Fig. 20).

The two diastereoisomeric forms were readily separated by cation-exchange chromatography, the relative ease of separation being rationalized in terms of the pronounced stereochemical differences in the relative orientation of the terminal ligands induced by the α-azodiimine bridging ligands.

Previous studies of α-azodiimine-bridged dinuclear compounds suggested that only one diastereoisomer was observed [83]: there were differences in the synthesis

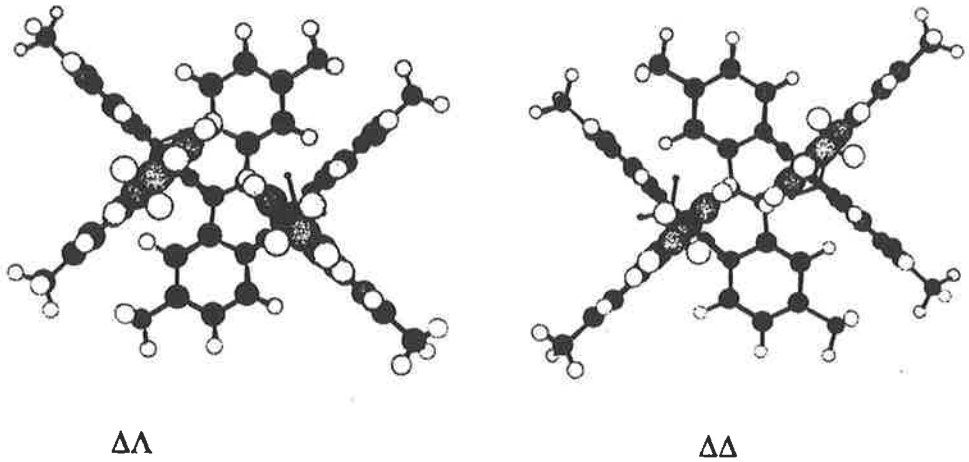

Fig. 20. CHEM 3D® representations of the diastereoisomeric forms of $[\{Ru(Me_2bpy)_2\}_2(\mu\text{-mapy})]^{4+}$ [148].

conditions in the two studies, but our work clearly shows the presence of both isomers [148].

The diastereoisomers show differences in their physical characteristics. For example, during the chromatographic separation there was a noticeable difference in the color of the diastereoisomers on the column – the first band eluted (*meso*) was dark emerald-green and the second band (*rac*) olive-green for all five dinuclear compounds involving the α-azodiimine bridging ligands. The absorption spectra of the complexes showed intense bands in the UV region, with bands in the visible region (assigned as arising from MLCT transitions) at ca. 380 and 770 nm: for the two diastereoisomers of $[\{Ru(bpy)_2\}_2(\mu\text{-apy})]^{4+}$ there was a red shift of ~7 nm in the *rac* compared with the *meso* form in the absorption arising from the lowest energy $d(Ru)\rightarrow\pi^*(\mu\text{-apy})$ transition. The stereochemistry also affected the $d(Ru)\rightarrow\pi^*(bpy)$ transition; a shoulder at 400 nm in the *meso* isomers was enhanced in the *rac* isomers. We are not aware of other reports of a significant difference in such physical properties of ligand-bridged diastereoisomers.

The differences were also reflected in the electrochemical properties of the diastereoisomers. Although the effects were relatively small, in all the α-azodiimine bridged complexes, the oxidative couples were shifted to more positive potentials and the reductive couples to more negative potentials for the *rac* (ΔΔ/ΛΛ) forms relative to the *meso* (ΔΛ) diastereoisomers. Additionally, the separation between the two metal-centered oxidations ($\Delta E_{1/2ox}$) was consistently larger for the *rac* form. This implies a slightly greater degree of metal–metal communication for one stereochemical form over the other, and we believe this to be the first observation of stereochemical influences on the electron transfer properties within dinuclear metallic complexes.

Similar differences may be even more clearly demonstrated in a related dinuclear complex, $[\{(bpy)_2Ru\}_2(\mu\text{-dpa})]^{4+}$ {dpa = 2,3-bis(2-pyridyl)-1,4-diaazaanthracene}. In this case, the separation of the oxidation waves of the two metal centers is greater {$E_{1/2}$ = 1.17 and 1.32 V cf. 1.14 and 1.32 V} for the *meso* diastereoisomer (in which the terminal ligands of the different metal centers are parallel), indicating differences in the communication induced by the stereochemistry (Fig. 21) [156].

3.2.3. *Example – mono-, di- and tri-nuclear complexes of the HAT ligand*

We have also investigated the stereochemistry of complexes containing the bridging ligand 1,4,5,8,9,12-hexaazatriphenylene (HAT) [157]: This ligand has three sites for bidentate ligation to a metal center, and may serve as a bidentate ligand in mononuclear species or as a ligand bridge in di- and tri-nuclear species. Examples are

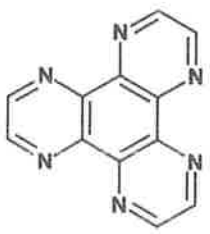

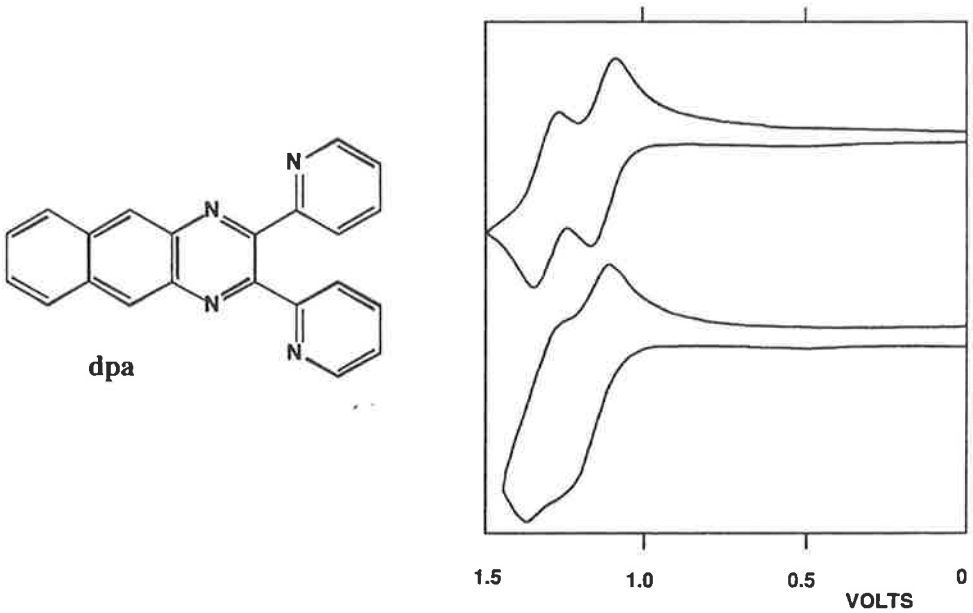

Fig. 21. Cyclic voltammetry of $[\{(bpy)_2Ru\}_2(\mu\text{-dpa})]^{4+}$ (CH_3CN/0.1M $[(C_4H_9)_4]ClO_4$ solution vs Ag/Ag^+) [156].

known in each of these categories, and studies have addressed synthetic strategies for homonuclear and heteronuclear species [158–162], photophysical properties [159,161–165] and interaction with biological species such as DNA [166–169]. In all these studies, the problem of stereoisomerism within the species of each nuclearity has not been elaborated, although it has been acknowledged [165].

The development of synthetic methodologies using stereoisomerically pure building blocks [88,147] and chromatographic techniques [79] have enabled us to isolate individual diastereoisomers (and their corresponding enantiomeric pairs) in homonuclear and heteronuclear complexes involving HAT as the bridging ligand [157,170]. This stereochemical control has allowed an investigation into the effect of stereoisomerism on physical properties such as their electrochemical and photophysical characteristics [157], and the interaction with chiral assemblies such as DNA. These investigations had previously been limited because stereoisomerically pure complexes have not been available

Our investigations of the mono-, di- and tri-nuclear complexes are discussed in succession below. The separated diastereiosomers – and when appropriate, enantiomers – have all been isolated, and were characterized by ^1H NMR spectroscopy (including studies involving the chiral lanthanide-induced shift reagent $[Eu(tfc)_3]$), CD spectra and ORD measurements).

In general, the separation of stereoisomers was achieved using cation exchange chromatographic techniques. The mononuclear complexes $[Ru(pp)_2(HAT)]^{2+}$ (HAT = bpy or phen) were resolved into enantiomeric forms using an eluent with a

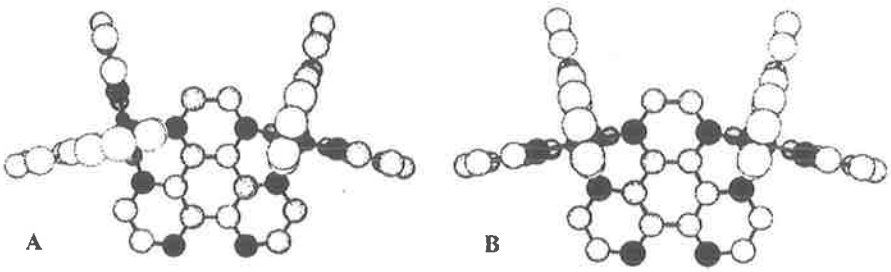

Fig. 22. Chem 3D® representation of diastereoisomeric forms of $[\{Ru(bpy)_2\}_2(\mu\text{-HAT})]^{4+}$: (A) *rac*- {ΔΔ (≡ΛΛ)}; (B) *meso*- {ΛΔ}. Hydrogen atoms are omitted for clarity.

chiral anion (see below). The dinuclear complexes $[\{Ru(pp)_2\}_2(\mu\text{-HAT})]^{4+}$ were chromatographically separated into the *rac* (ΔΔ/ΛΛ) and *meso* (ΔΛ) diastereoisomeric forms, and the *rac* form was resolved by the same technique using a chiral eluent. In a similar manner, the homometallic trinuclear complexes $[\{Ru(pp)_2\}_3(\mu\text{-HAT})]^{6+}$ were chromatographically separated into the heterochiral ($\Delta^2\Lambda/\Lambda^2\Delta$) and homochiral ($\Delta^3/\Lambda^3$) diastereoisomeric forms (determined by NMR spectroscopy), and the Δ^3/Λ^3 diastereoisomer was subsequently resolved using a chiral eluent (Figs. 22 and 23).

The resolution of the $\Delta^2\Lambda/\Lambda^2\Delta$ diastereoisomer could not be achieved chromatographically, but the two forms were isolated by separately reacting resolved ΔΔ and ΛΛ forms of $[\{Ru(pp)_2\}_2(\mu\text{-HAT})]^{4+}$ with *rac*-$[Ru(pp)_2Cl_2]$ resulting in the two diastereoisomeric complexes $\Delta^3/\Delta^2\Lambda$ and $\Lambda^3/\Lambda^2\Delta$, respectively. These diastereoisomeric mixtures were separated by cation exchange chromatography, thus realizing the $\Delta^2\Lambda$ and $\Lambda^2\Delta$ forms. Since the absolute configuration of the precursor complex $[\{Ru(bpy)_2\}_2(\mu\text{-HAT})]^{4+}$ was known, the absolute configuration assignments of $\Delta^2\Lambda$- and $\Lambda^2\Delta$-$[\{Ru(bpy)_2\}_3(\mu\text{-HAT})]^{6+}$ could be made. We have used the same methodology to isolate the stereoisomers of mixed Ru/Os trinuclear systems [170].Fig. 24

Cyclic voltammetry was performed on the separated diastereoisomers, *rac*- and *meso*-$[\{Ru(pp)_2\}_2(\mu\text{-HAT})]^{4+}$, and homochiral- and heterochiral-$\{Ru(pp)_2\}_3$-

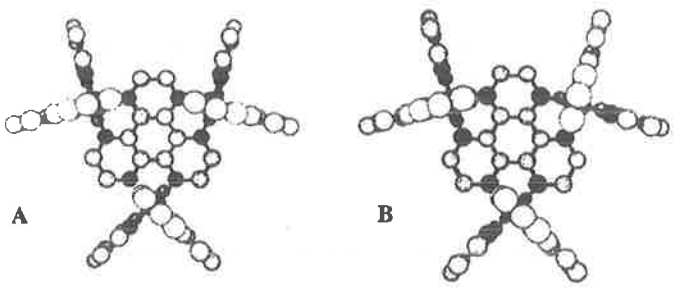

Fig. 23. Chem 3D® representation of diastereoisomeric forms of $[\{Ru(bpy)_2\}_3(\mu\text{-HAT})]^{6+}$: (A) heterochiral {ΔΔΛ}; (B) homochiral {ΔΔΔ (≡ΛΛΛ)}. Hydrogen atoms are omitted for clarity.

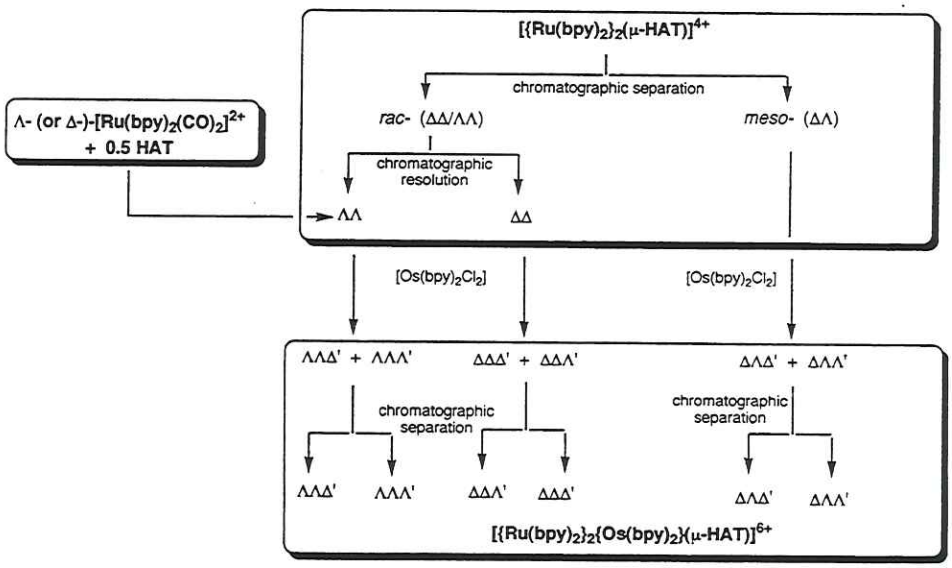

Fig. 24. Synthetic methodology for stereoisomers of $[\{Ru(bpy)_2\}_2\{Os(bpy)_2\}(\mu\text{-HAT})]^{6+}$ [170].

$(\mu\text{-HAT})]^{6+}$ (where pp = bpy or phen). The one-electron reversible oxidation waves are directly correlated with the number of coordinated metal centers [158,164], suggesting significant metal–metal electronic communication which is a characteristic of conjugated bridging ligands [171]. Comparisons of the metal–metal interaction between the second and third metal oxidation process indicated a 40 mV increase (stronger interaction) in the homochiral-$[\{Ru(phen)_2\}_3(\mu\text{-HAT})]^{6+}$ over the heterochiral-$[\{Ru(phen)_2\}_3(\mu\text{-HAT})]^{6+}$ diastereoisomer.

No significant differences were observed between the electronic absorption spectra of the diastereoisomers in the present study.

Initial photophysical results have been undertaken on these systems. For the dinuclear species at room temperature, the relative luminescence quantum yields and the emission lifetimes showed a significant drop for the *meso* compared with the *rac* diastereisomers. Moreover in a glass at low temperature (77 K), the luminescence of the lifetimes of the trinuclear heteronuclear diastereoisomer were slightly shorter than those of the homonuclear form. No significant differences were detected at room temperature in the diastereoisomeric forms of the trinuclear compounds.

3.3. Stereochemistry – does it make any difference?

There have been numerous assertions that stereochemistry will have little influence on physical properties in circumstances where mixtures of isomers were investigated [56,150]. It is apparent for these first studies of this question that the stereochemistry does influence the electronic transitions and the inter-metal communication. It would be the normal expectation that such variations would become more significant as

the size of the assembly grew, and we are currently investigating oligomers of higher nuclearity to clarify this issue.

Moreover, there have been several assertions that the use of tris(bidentate) building blocks for polynuclear assemblies will inevitably lead to a stereochemical complexity which is intractable [21,39,40]. Perhaps it is premature to impose such judgement at this point of time.

3.4. Chromatographic techniques

The chromatographic separation of stereoisomers forms an essential part of our study. The mechanism deserves some comment in the present context. Our studies of these processes are at an advanced stage and will be published in the near future [172,173].

While the technique is based on a cation exchange mechanism (SP-Sephadex C25 support), the mode of separation is profoundly influenced by a differential association between the components of the mixture and the anion of the eluent. This effect has been studied previously [174–176], particularly in relation to the separation of stereoisomers of cobalt(III) complexes containing polyamine ligands. In those instances, the association of different geometric isomers with appropriate anions via hydrogen bonding [177] was regarded as the prime operative mechanism. Optical resolution of racemates to the enantiomers has also been achieved using eluents with chiral anions, although the Sephadex support itself is chiral and is not without participation in such separations [174,175].

For the present polypyridyl complexes, the rate of elution – even for species with high charges – is rapid in the presence of certain anions by comparison with (e.g.) Cl^-, indicating that there is an association which lowers the effective charge of the complex. In addition, in these circumstances where the association is present, separations of mononuclear complexes of the same charge but different ligand composition, geometric isomers of mononuclear species, and diastereoisomeric di- and oligonuclear complexes is achieved. Clearly, the different species undergo differential association with certain anions leading to chromatographic separation in their presence. Additionally, enantiomers of mono- and oligonuclear complexes can be separated, on the basis of differential association with chiral anions and/or because of the involvement of the chiral support [172,173].

The precise nature of the associations is currently under investigation. For species containing polypyridyl ligands, a hydrogen bonding mechanism is unlikely. In our early studies involving the separation of diastereoisomeric forms of dinuclear species, toluene-4-sulfonate was used on the instinctive notion that an aromatic ion might undergo π-stacking with the diastereosiomer in which the terminal ligands were parallel (rather than orthogonal). While separation was indeed achieved, the order of elution indicated that preferential association occurred with the diastereoisomer in which the terminal rings were orthogonal. Further, the effect does not actually require an aromatic anion, and any alkyl carboxylate where $n>4$ shows an association and allows a chromatographic separation. Our studies indicate that the association appears to have components involving both π-stacking and specific hydrophobic

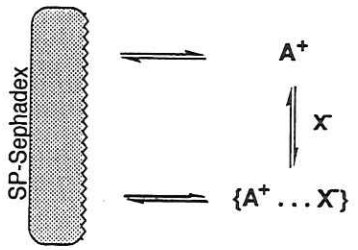

Fig. 25. Proposed mechanism for influence of anions on cation exchange processes.

interactions, as confirmed by NMR studies of the interaction of the anions and the substrates [172,173].

Studies of these chromatographic processes over the temperature range 5–50 °C reveal a temperature dependence [172,173]: since the equilibria directly involving the support are likely to have small activation energies [178], it is clear that the association equilibrium is fundamental in the process. NMR titration studies of the anions with diastereoisomeric forms of dinuclear complexes indicate differences in the association constants between pairs of diastereoisomers in dinuclear systems, so that the separations occur as a result of the association processes (Fig. 25).

We have been able to routinely resolve mononuclear, dinuclear and trinuclear complexes into their enantiomers using eluents with chiral anions [147,157,179]. The optical resolutions undoubtedly occur by similar differential associations. Again the nature of that association is uncertain at this point: interestingly, a crystal structure of Δ-$[Ru(bpy)_2(py)_2]\{(-)$-O,O′-dibenzoyl-L-tartrate$\}12.H_2O$ clearly demonstrates a specific packing of benzoyl groups of the anion between the bpy planes and py rings of the cation, allowing differential interaction of the chiral anion with enantiomers of the cation [180].

4. Stereochemistry and polynuclear assemblies – the past, present and future

There has been a major recent surge in the methodologies of synthetic chemistry of polymetallic assemblies, and also in the design of ligands and bridges required to meet specific requirements of electronic and spatial characteristics appropriate to their potential application. Polypyridyl ligands have a special importance in these developments – particularly in combination with the d^6 metal centers Ru(II), Os(II) and Re(I) – and a fundamental tenet of the work described above is that ultimately versatility is enhanced significantly by the use of bidentate ligands, although the requirement is not exclusive.

However, that condition is associated with the spectre of a proliferation of isomeric possibilities. Accordingly, a particular interest would be the symmetric functionalization of a bidentate ligating motif (such as 1,10-phenanthroline and 4,5-diazafluorene). There are recent examples of such methodologies in bridged species with adamantane-linked phen and daf ligands of C_{2v} symmetry {daf=4,5-diazafluorene}

[181–183], and the linking of the same groupings by norbonane-based "molrac" bridges (C_s symmetry) [184]. Both developments herald an ability to meet the symmetry restriction in a rigid bridge system yet provide a linkage with versatility in terms of electronic characteristics and the physical separation between ligating groups.

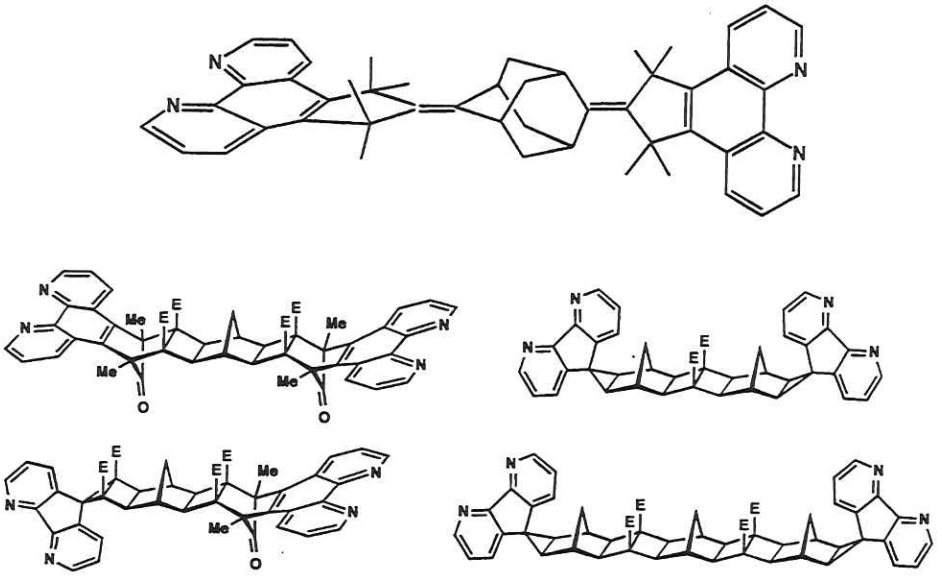

There are other consequences of the present stereochemical studies that have not been addressed in this review. There has been much recent interest in the intercalation of metal complexes into nucleotides such as DNA, and there is a relevance in terms both for their use as photoprobes and also in the design of chemotherapeutic drugs [14,185,186]. The biological activity of polypyridyl complexes of iron and ruthenium, and the stereochemical component of such interactions, have in fact been known for decades [187]. The consequences of the much wider range of complexes of this type which have now been synthesized is tantalizing, but their stereochemistry is certain to be critical in this context.

As a final reflection, it should be remembered that the synthetic techniques for large polymetallic assemblies have been acquired relatively recently (over the last decade), and in a sense this has been associated with the simultaneous development of appropriate techniques for characterization – particularly in mass spectrometry. The earlier construction of large organic assemblies was underpinned by a clear understanding of the stereochemistry of the tetrahedral carbon atom. This is not the case in coordination chemistry: over the last two or three decades the understanding and control of the stereochemistry of octahedral and tetrahedral metal centers has not always attracted attention at the cutting edge of research in inorganic chemistry. The contrast should be heeded – unless the synthetic developments are accompanied by an understanding of the detailed stereochemistry, then the products

will often remain incompletely characterized and be mixtures of stereoisomers that possess very different spatial orientations of components. The utilization of the new materials may well be critically dependent on the control of component geometry in a supramolecular assembly.

Acknowledgements

I wish to gratefully acknowledge the dedication and insight of a number of my postgraduate students and postdoctoral fellows, who have helped launch and sustain our efforts so far in this area of stereochemistry. In particular, I note the contributions of Todd Rutherford, David Reitsma, Laurie Kelso, Peter Anderson, Dr. Nick Fletcher, Dr. Erik Jandrasics, Dr. Klaus Haarmann and also Geoff Strouse (who visited my laboratory as part of a bilateral collaboration with the research group of Professor Tom Meyer at the University of North Carolina, Chapel Hill). I would also acknowledge stimulating conversations on these stereochemical issues with Professor Alex von Zelewsky during my sojourns at the Université de Fribourg Suisse. I wish to thank Dr. Nick Fletcher and Laurie Kelso for insightful comments on the manuscript. The research program has been funded by the Australian Research Council.

References

[1] J. Deisenhofer, H. Michel, Angew. Chem. Int. Ed. Engl. 28 (1989) 829.
[2] R. Huber, Angew. Chem. Int. Ed. Engl. 28 (1989) 848.
[3] R.M. Baum, Chem. Eng. News (1993) 20.
[4] I. Willner, B. Willner, Top. Curr. Chem. 159 (1991) 153.
[5] M.R. Wasielewski, Chem. Rev. 92 (1992) 435.
[6] K.D. Jordan, M.N. Paddon-Row, Chem. Rev. 92 (1992) 395.
[7] D. Gust, T.A. Moore, A.L. Moore, Acc. Chem. Res. 26 (1993) 198.
[8] M.N. Paddon-Row, Acc. Chem. Res. 27 (1994) 18.
[9] S.-J. Lee, J.M. Degraziano, A.N. Macpherson, E.J. Shin, P.K. Kerrigan, G.R. Seely, A.L. Moore, T.A. Moore, D. Gust, Chem. Phys. 176 (1993) 321.
[10] D. Gust, T.A. Moore, A.L. Moore, A.N. Macpherson, A. Lopez, J.M. Degraziano, I. Gouni, E. Bittersmann, G.R. Seely, F. Gao, R.A. Nieman, X.C.C. Ma, L.J. Demanche. S.C. Hung, D.K. Luttrull, S.-J. Lee, P.K. Kerrigan, J. Am. Chem. Soc. 115 (1993) 11141.
[11] A. Harriman, J.-P. Sauvage, Chem. Soc. Rev. (1996) 41.
[12] J.-P. Collin, A. Harriman, V. Heitz, F. Odobel, J.-P. Sauvage, Coord. Chem. Rev. 148 (1996) 63.
[13] J.-M. Lehn, Angew. Chem. Int. Ed. Engl. 29 (1990) 1304.
[14] V. Balzani, F. Scandola, Supramolecular Photochemistry, Ellis Horwood, Chichester, UK, 1991.
[15] A. Juris, S. Barigelletti, S. Campagna, V. Balzani, P. Belser, A. von Zelewsky, Coord. Chem. Rev. 84 (1988) 85.
[16] G.F. Strouse, P.A. Anderson, J.R. Schoonover, T.J. Meyer, F.R. Keene, Inorg. Chem. 31 (1992) 3004.
[17] P.A. Anderson, G.B. Deacon, K.H. Haarmann, F.R. Keene, T.J. Meyer, D.A. Reitsma, B.W. Skelton, G.F. Strouse, N.C. Thomas, J.A. Treadway, A.H. White, Inorg. Chem. 34 (1995) 6145.
[18] P.A. Anderson, G.F. Strouse, J.A. Treadway, F.R. Keene, T.J. Meyer, Inorg. Chem. 33 (1994) 3863.

[19] J.A. Treadway, B. Loeb, R. Lopez, P.A. Anderson, F.R. Keene, T.J. Meyer, Inorg. Chem. 35 (1996) 2242.
[20] E.Z. Jandrasics, F.R. Keene, J. Chem. Soc., Dalton Trans. (1997) 153.
[21] V. Balzani, A. Juris, M. Venturi, S. Campagna, S. Serroni, Chem. Rev. 96 (1996) 759.
[22] K.T. Potts, M. Keshavarz-K., F.S. Tham, H.D. Abruna, C.R. Arana, Inorg. Chem. 32 (1993) 4422.
[23] K.T. Potts, M. Keshavarz-K., F.S. Tham, H.D. Abruna, C. Arana, Inorg. Chem. 32 (1993) 4450.
[24] E.C. Constable, Prog. Inorg. Chem. 42 (1994) 67.
[25] E.C. Constable, A.J. Edwards, M.J. Hannon, P.R. Raithby, J. Chem. Soc., Chem. Commun. (1994) 1991.
[26] E.C. Constable, F.R. Heirtzler, M. Neuburger, M. Zehnder, J. Chem. Soc., Chem. Commun. (1996) 933.
[27] C.R. Woods, M. Benaglia, F. Cozzi, J.S. Siegel, Angew. Chem. Int. Ed. Engl. 35 (1996) 1830.
[28] A.T. Baker, D.C. Craig, G. Dong, Inorg. Chem. 35 (1996) 1091.
[29] R. Kramer, J.-M. Lehn, A. De Cian, J. Fischer, Angew. Chem. Int. Ed. Engl. 32 (1993) 703.
[30] K.T. Potts, M.-K. Keshavarz, F.S. Tham, H.D. Abruna, C. Arana, Inorg. Chem. 32 (1993) 4436.
[31] E.C. Constable, R. Martinez-Manez, A.M.W. Cargill Thompson, J.V. Walker, J. Chem. Soc., Dalton Trans. (1994) 1585.
[32] M.-T. Youinou, N. Rahmouni, J. Fischer, J.A. Osborn, Angew. Chem. Int. Ed. Engl. 31 (1992) 733.
[33] P.N.W. Baxter, G.S. Hanan, J.-M. Lehn, J. Chem. Soc., Chem. Commun. (1996) 2019.
[34] P.N.W. Baxter, J.-M. Lehn, J. Fischer, M.-T. Youinou, Angew. Chem. Int. Ed. Engl. 33 (1994) 2284.
[35] B. Hasenknopf, J.-M. Lehn, B.O. Kneisel, G. Baum, D. Fenske, Angew. Chem. Int. Ed. Engl. 35 (1996) 1838.
[36] F.M. Romero, R. Ziessel, A. Dupont-Gervais, A. van Dorsselaer, J. Chem. Soc., Chem. Commun. (1996) 551.
[37] R.F. Carina, C. Dietrich-Buchecker, J.-P. Sauvage, J. Am. Chem. Soc. 118 (1996) 9110.
[38] F. Scandola, R. Argazzi, C.A. Bignozzi, C. Chiorboli, M.T. Indelli, M.A. Rampi, Coord. Chem. Rev. 125 (1993) 283.
[39] J.-P. Sauvage, J.-P. Collin, J.-C. Chambron, S. Guillerez, C. Coudret, V. Balzani, F. Barigelletti, L. De Cola, L. Flamigni, Chem. Rev. 94 (1994) 993.
[40] E.C. Constable, A.M.W. Cargill Thompson, J. Chem. Soc., Dalton Trans. (1992) 3467.
[41] E.C. Constable, A.M.W. Cargill Thompson, J. Chem. Soc., Dalton Trans. (1995) 1615.
[42] F. Barigelletti, L. Flamigni, V. Balzani, J.-P. Collin, J.-P. Sauvage, A. Sour, E.C. Constable, A.M.W. Cargill Thompson, J. Am. Chem. Soc. 116 (1994) 7692.
[43] F. Barigelletti, L. Flamigni, M. Guardigli, A. Juris, M. Beley, S. Chodorowski-Kimmes, J.-P. Collin, J.-P. Sauvage, Inorg. Chem. 35 (1996) 136.
[44] V. Grosshenny, A. Harriman, R. Ziessel, Angew. Chem. Int. Ed. Engl. 34 (1995) 1100.
[45] D. Tzalis, Y. Tor, J. Chem. Soc., Chem. Commun. (1996) 1043.
[46] V. Grosshenny, A. Harriman, M. Hissler, R. Ziessel, Platinum Metals Rev. 40 (1996) 26.
[47] V. Grosshenny, A. Harriman, M. Hissler, R. Ziessel, Platinum Metals Rev. 40 (1996) 72.
[48] M.-A. Haga, M.M. Ali, R. Arakawa, Angew. Chem. Int. Ed. Engl. 35 (1996) 76.
[49] M.-A. Haga, M.M. Ali, S. Koseki, K. Fujimoto, A. Yoshimura, K. Nozaki, T. Ohno, K. Nakajima, D.J. Stufkens, Inorg. Chem. 35 (1996) 3335.
[50] G.R. Newkome, R. Guther, C.N. Moorefield, F. Cardullo, L. Echegoyen, E. Perez-Cordero, H. Luftmann, Angew. Chem. Int. Ed. Engl. 34 (1995) 2023.
[51] G.R. Newkome, F. Cardulo, E.C. Constable, C.N. Moorefield, A.M.W. Cargill Thompson, J. Chem. Soc., Chem. Commun. (1993) 925.
[52] E.C. Constable, P. Harverson, M. Oberholzer, J. Chem. Soc., Chem Commun. (1996) 1821.
[53] E.C. Constable, P. Harverson, J. Chem. Soc., Chem. Commun. (1996) 33.
[54] V. Balzani, G. Denti, S. Serroni, S. Campagna, V. Ricevuto, A. Juris, Proc. Indian Acad. Sci. 105 (1993) 421.
[55] S. Serroni, G. Denti, Inorg. Chem. 31 (1992) 4251.
[56] G. Denti, S. Campagna, S. Serroni, M. Ciano, V. Balzani, J. Am. Chem. Soc. 114 (1992) 2944.
[57] G. Denti, S. Serroni, S. Campagna, V. Ricevuto, V. Balzani, Coord. Chem. Rev. 111 (1991) 227.

[58] G. Denti, S. Serroni, S. Campagna, V. Ricevuto, A. Juris, M. Ciano, V. Balzani, Inorg. Chim. Acta 198-200 (1992) 507.
[59] S. Campagna, G. Denti, S. Serroni, M. Ciano, Inorg. Chem. 30 (1991) 3728.
[60] S. Campagna, G. Denti, S. Serroni, M. Ciano, A. Juris, V. Balzani, Inorg. Chem. 31 (1992) 2982.
[61] G. Denti, S. Campagna, L. Sabatino, S. Serroni, M. Ciano, V. Balzani, Inorg. Chim. Acta 176 (1990) 175.
[62] G. Denti, S. Serroni, S. Campagna, V. Ricevuto, V. Balzani, Inorg. Chim. Acta 182 (1991) 127.
[63] G. Denti, S. Campagna, L. Sabatino, S. Serroni, M. Ciano, V. Balzani, Inorg. Chem. 29 (1990) 4750.
[64] S. Campagna, G. Denti, L. Sabatino, S. Serroni, M. Ciano, V. Balzani, J. Chem. Soc., Chem. Commun. (1989) 1500.
[65] A. Juris, V. Balzani, S. Campagna, G. Denti, S. Serroni, G. Frei, H.-U. Güdel, Inorg. Chem. 33 (1994) 1491.
[66] S. Serroni, A. Juris, S. Campagna, M. Venturi, G. Denti, V. Balzani, J. Am. Chem. Soc. 116 (1994) 9086.
[67] S. Campagna, G. Denti, S. Serroni, A. Juris, M. Venturi, V. Ricevuto, V. Balzani, Chem-Eur. J. 1 (1995) 211.
[68] S. Serroni, S. Campagna, G. Denti, T.E. Keyes, J.G. Vos, Inorg. Chem. 35 (1996) 4513.
[69] S.A. Adeyemi, E.C. Johnson, F.J. Miller, T.J. Meyer, Inorg. Chem. 12 (1973) 2371.
[70] S.T. Wilson, R.F. Bondurant, T.J. Meyer, D.J. Salmon, J. Am. Chem. Soc. 97 (1975) 2285.
[71] V. Balzani, R. Ballardini, F. Bolletta, M.T. Gandolfi, A. Juris, M. Maestri, M.F. Manfrin, L. Moggi, N. Sabbatini, Coord. Chem. Rev. 125 (1993) 75.
[72] J.-P. Collin, S. Guillerez, J.-P. Sauvage, F. Barigelletti, L. De Cola, L. Flamigni, V. Balzani, Inorg. Chem. 31 (1992) 4112.
[73] R. Duesing, G. Tapolsky, T.J. Meyer, J. Am. Chem. Soc. 112 (1990) 5378.
[74] A. von Zelewsky, Stereochemistry of Coordination Compounds, Wiley, Chichester, UK, 1995.
[75] A. von Zelewsky, Chimia 48 (1994) 331.
[76] L.F. Cooley, S.L. Larson, C.M. Elliott, D.F. Kelley, J. Phys. Chem. 95 (1991) 10694.
[77] K. Danielson, C.M. Elliott, J.W. Merkert, T.J. Meyer, J. Am. Chem. Soc. 109 (1987) 2519.
[78] K.A. Opperman, S.L. Mecklenburg, T.J. Meyer, Inorg. Chem. 33 (1994) 5295.
[79] D.A. Reitsma, F.R. Keene, J. Chem. Soc., Dalton Trans. (1993) 2859.
[80] S.M. Molnar, G. Nallas, J.S. Bridgewater, K.J. Brewer, J. Am. Chem. Soc. 116 (1994) 5206.
[81] M.J. Cook, A.P. Lewis, G.S.G. McAuliffe, Org. Magn. Reson. 22 (1984) 388.
[82] M.J. Cook, A.P. Lewis, G.S.G. McAuliffe, A.J. Thomson, Inorg. Chim. Acta 64 (1982) 25.
[83] M. Krejcik, S. Zalis, J. Klima, D. Sykora, W. Matheis, A. Klein, W. Kaim, Inorg. Chem. 32 (1993) 3362.
[84] G. Orellana, C.A. Ibarra, J. Santoro, Inorg. Chem. 27 (1988) 1025.
[85] C. Brevard, P. Granger, Inorg. Chem. 22 (1983) 532.
[86] G. Orellana, A. Kirsch – De Mesmaeker, N.J. Turro, Inorg. Chem. 29 (1990) 882.
[87] G. Predieri, C. Vignali, G. Denti, S. Serroni, Inorg. Chim. Acta 205 (1993) 145.
[88] T.J. Rutherford, D.A. Reitsma, F.R. Keene, J. Chem. Soc., Dalton Trans. (1994) 3659.
[89] T.J. Rutherford, F.R. Keene, Inorg. Chem. (1997) to be published; T.J. Rutherford, J.A. Treadway, P.Y. Chen, F.R. Keene, T.J. Meyer, unpublished results.
[90] J. Fees, H.D. Hausen, W. Kaim, Z. Naturforsch. B 50 (1995) 15.
[91] Y. Luo, P.G. Potvin, Y.-H. Tse, A.B.P. Lever, Inorg. Chem. 35 (1996) 5445.
[92] R.A. Krauseand, K. Krause, Inorg. Chem. 19 (1980) 2600.
[93] A.K. Deb, M. Kakoti, S. Goswami, J. Chem. Soc., Dalton Trans. (1991) 3249.
[94] A. Seal, S. Ray, Acta Crystallogr. C40 (1984) 929.
[95] K. Krause, R.A. Krause, S. Larsen, B. Rasmussen, Acta Chem. Scand., Ser. A 39 (1985) 375.
[96] R.A. Krause, K. Krause, Inorg. Chem. 23 (1984) 2195.
[97] S. Goswami, A.R. Chakravarty, A. Chakravorty, Inorg. Chem. 22 (1983) 602.
[98] T. Bao, K. Krause, R.A. Krause, Inorg. Chem. 27 (1988) 759.
[99] S. Goswami, R. Mukherjee, A. Chakravorty, Inorg. Chem. 22 (1983) 2825.
[100] S. Choudhury, M. Kakoti, A.K. Deb, S. Goswami, Polyhedron 11 (1992) 3183.
[101] F.P. Dwyer, E.C. Gyarfas, J. Proc. Roy. Chem. Soc. N.S.W. 83 (1949) 174.

[102] F.P. Dwyer, E.C. Gyarfas, J. Proc. Roy. Chem. Soc. N.S.W. 83 (1949) 170.
[103] B. Bosnich, F.P. Dwyer, Aust. J. Chem. 19 (1966) 2229.
[104] F.H. Burstall, F.P. Dwyer, E.C. Gyarfas, J. Chem. Soc. (1950) 953.
[105] F.P. Dwyer, F. Lions, J. Am. Chem. Soc. 72 (1950) 1545.
[106] M.D. Ward, J. Chem. Soc., Dalton Trans. (1993) 1321.
[107] H.P. Hughes, D. Martin, S. Bell, J.J. McGarvey, J.G. Vos, Inorg. Chem. 32 (1993) 4402.
[108] L. De Cola, F. Barigelletti, V. Balzani, R. Hage, J.G. Haasnoot, J. Reedijk, J.G. Vos, Chem. Phys. Lett. 178 (1991) 491.
[109] R. Hage, A.H.J. Dijkhuis, J.G. Haasnoot, R. Prins, J. Reedijk, B.E. Buchanan, J.G. Vos, Inorg. Chem. 27 (1988) 2185.
[110] X. Hua, A. von Zelewsky, Inorg. Chem. 30 (1991) 3796.
[111] X. Hua, A. von Zelewsky, Inorg. Chem. 34 (1995) 5791.
[112] D.W. Fink, W.E. Ohnesorge, J. Am. Chem. Soc. 91 (1969) 4995.
[113] C.-T. Lin, W. Böttcher, M. Chou, C. Creutz, N. Sutin, J. Am. Chem. Soc. 98 (1976) 6536.
[114] R.C. Young, J.K. Nagle, T.J. Meyer, D.G. Whitten, J. Am. Chem. Soc. 100 (1978) 4773.
[115] J.R. Kirchoff, D.R. McMillan, P.A. Marnot, J.-P. Sauvage, J. Am. Chem. Soc. 107 (1985) 1138.
[116] J.R. Winkler, T.L. Netzel, C. Creutz, N. Sutin, J. Am. Chem. Soc. 109 (1987) 2381.
[117] J.M. Calvert, J.V. Caspar, R.A. Binstead, T.D. Westmoreland, T.J. Meyer, J. Am. Chem. Soc. 104 (1982) 6620.
[118] C.R. Hecker, P.E. Fanwick, D.R. McMillin, Inorg. Chem. 30 (1991) 659.
[119] M.L. Stone, G.A. Crosby, Chem. Phys. Lett. 79 (1981) 169.
[120] C.R. Hecker, A.K.I. Gushurst, D.R. McMillin, Inorg. Chem. 39 (1991) 538.
[121] E.C. Constable, A.M.W. Cargill Thompson, N. Armaroli, V. Balzani, M. Maestri, Polyhedron 11 (1992) 2707.
[122] M. Maestri, N. Armaroli, V. Balzani, E.C. Constable, A.M.W. Cargill Thompson, Inorg. Chem. 34 (1995) 2759.
[123] M. Beley, S. Chodorowski, J.-P. Collin, J.-P. Sauvage, L. Flamigni, F. Barigelletti, Inorg. Chem. 33 (1994) 2543.
[124] A. von Zelewsky, P. Belser, P. Hayoz, R. Dux, X. Hua, A. Suckling, H. Stoeckli-Evans, Coord. Chem. Rev. 132 (1994) 75.
[125] P. Hayoz, A. von Zelewsky, Tetrahedron Lett. 33 (1992) 5165.
[126] P. Hayoz, A. von Zelewsky, H. Stoeckli-Evans, J. Am. Chem. Soc. 115 (1993) 5111.
[127] N.C. Fletcher, F.R. Keene, M. Ziegler, H. Stoeckli-Evans, H. Viebrock, A. von Zelewsky, Helv. Chim. Acta 79 (1996) 1192.
[128] N.C. Fletcher, F.R. Keene, H. Viebrock, A. von Zelewsky, Inorg. Chem. 36 (1997) 1113.
[129] H.-R. Mürner, Ph.D. thesis, Université de Fribourg Suisse, 1996.
[130] H. Mürner, A. von Zelewsky, H. Stoeckli-Evans, Inorg. Chem. 35 (1996) 3931.
[131] H.-R. Mürner, P. Belser, A. von Zelewsky, J. Am. Chem. Soc. 118 (1996) 7989.
[132] E.Z. Jandrasics, Ph.D. thesis, Université de Fribourg Suisse, 1995.
[133] P. Lincoln, B. Nordén, J. Chem. Soc., Chem. Commun. (1996) 2145.
[134] C. Hiort, P. Lincoln, B. Nordén, J. Am. Chem. Soc. 115 (1993) 3448.
[135] K. Wärnmark, J.A. Thomas, O. Heyke, J.-M. Lehn, Chem. Commun. (1996) 701.
[136] F.M. MacDonnell, S. Bodige, Inorg. Chem. 35 (1996) 5758.
[137] D. Tzalis, Y. Tor, J. Am. Chem. Soc. 119 (1997) 852.
[138] R.T. Watson, J.L. Jackson, J.D. Harper, K.A. Kane-Maguire, L.A.P. Kane-Maguire, N.A.P. Kane-Maguire, Inorg. Chim. Acta 249 (1996) 5.
[139] B. Durham, J.V. Caspar, J.K. Nagle, T.J. Meyer, J. Am. Chem. Soc. 104 (1982) 4803.
[140] G.B. Porter, R.H. Sparks, J. Photochem. 13 (1980) 123.
[141] X. Hua, A.G. Lappin, Inorg. Chem. 34 (1995) 992.
[142] D.S. Black, G.B. Deacon, N.C. Thomas, Polyhedron 2 (1983) 409.
[143] D.S. Black, G.B. Deacon, N.C. Thomas, Inorg. Chim. Acta 65 (1982) L75.
[144] D.S. Black, G.B. Deacon, N.C. Thomas, Aust. J. Chem. 35 (1982) 2445.
[145] N.C. Thomas, G.B. Deacon, Synth. React. Inorg. Metal-Org. Chem. 16 (1986) 85.
[146] N.C. Thomas, G.B. Deacon, Inorg. Synth. 25 (1989) 107.

[147] T.J. Rutherford, M.G. Quagliotto, F.R. Keene, Inorg. Chem. 34 (1995) 3857.
[148] L.S. Kelso, D.A. Reitsma, F.R. Keene, Inorg. Chem. 35 (1996) 5144.
[149] K. Kalyanasundaram, M.K. Nazeeruddin, Inorg. Chim. Acta 226 (1994) 213.
[150] S.D. Ernst, W. Kaim, Inorg. Chem. 28 (1989) 1520.
[151] R.A. Krause, K. Krause, Inorg. Chem. 21 (1982) 1714.
[152] S. Goswami, A.R. Chakravarty, A. Chakravorty, Inorg. Chem. 21 (1982) 2737.
[153] C.A. Bessel, J.A. Margarucci, J.H. Acquaye, R.S. Rubino, J. Crandall, A.J. Jircitano, K.J. Takeuchi, Inorg. Chem. 32 (1993) 5779.
[154] S. Ernst, V. Kasack, W. Kaim, Inorg. Chem. 27 (1988) 1146.
[155] W. Kaim, S. Kohlmann, Inorg. Chem. 26 (1987) 68.
[156] L.S. Kelso, D.A. Reitsma, F.R. Keene, unpublished results.
[157] T.J. Rutherford, O. Van Gijte, A. Kirsch – De Mesmaeker, F.R. Keene, Inorg. Chem. (1997) to be published.
[158] A. Masschelein, A. Kirsch–De Mesmaeker, C. Verhoeven, R. Nasielski-Hinkens, Inorg. Chim. Acta 129 (1987) L13.
[159] P. Didier, I. Ortmans, A. Kirsch – De Mesmaeker, R.J. Watts, Inorg. Chem. 32 (1993) 5239.
[160] P. Didier, L. Jacquet, A. Kirsch – De Mesmaeker, R. Hueber, A. van Dorsselaer, Inorg. Chem. 31 (1992) 4803.
[161] L. Tan Sien Hee, A. Kirsch – De Mesmaeker, J. Chem. Soc., Dalton Trans. (1994) 3651.
[162] I. Ortmans, P. Didier, A. Kirsch – De Mesmaeker, Inorg. Chem. 34 (1995) 3695.
[163] R. Sahai, D.P. Rillema, R. Shaver, S. Van Wellendael, D.C. Jackman, M. Boldaji, Inorg. Chem. 28 (1989) 1022.
[164] L. Jacquet, A. Kirsch – De Mesmaeker, J. Chem. Soc., Faraday Trans. 88 (1992) 2471.
[165] A. Kirsch – De Mesmaeker, L. Jacquet, A. Masschelein, F. Vanhecke, K. Heremans, Inorg. Chem. 28 (1989) 2465.
[166] M. Casu, G. Saba, A. Lai, M. Luhmer, A. Kirsch– De Mesmaeker, C. Moucheron, J. Reisse, Biophys. Chem. 59 (1996) 133.
[167] J.-P. Lecomte, A. Kirsch–De Mesmaeker, J.M. Kelly, H. Gorner, Photochem. Photobiol. 55 (1992) 681.
[168] J.-P. Lecomte, A. Kirsch–De Mesmaeker, G. Orellana, J. Phys. Chem. 98 (1994) 5382.
[169] J.-P. Lecomte, A. Kirsch – De Mesmaeker, M.M. Feeney, J.M. Kelly, Inorg. Chem. 34 (1995) 6481.
[170] T.J. Rutherford, F.R. Keene, submitted for publication.
[171] G. Giuffrida, S. Campagna, Coord. Chem. Rev. 135 (1994) 517.
[172] D.A. Reitsma, F.R. Keene, unpublished results.
[173] N.C. Fletcher, I.M. Atkinson, F.R. Keene, work in progress.
[174] H. Yoneda, J. Chromatogr. 313 (1984) 59.
[175] Y. Yoshikawa, K. Yamasaki, Coord. Chem. Rev. 28 (1979) 205.
[176] G.H. Searle, Aust. J. Chem. 30 (1977) 2625.
[177] F.R. Keene, G.H. Searle, Inorg. Chem. 13 (1974) 2173.
[178] F. Helfferich, Ion Exchange, McGraw–Hill, New York, 1962.
[179] P. Pellegrini, J. Aldrich-Wright, F.R. Keene, unpublished results (1996).
[180] B. Kolp, H. Viebrock, A. von Zelewsky, D. Abeln, unpublished results.
[181] L. De Cola, V. Balzani, F. Barigelletti, L. Flamigni, P. Belser, S. Bernhard, Rec. Trav. Chim. – J. Roy. Neth. Chem. 114 (1995) 534.
[182] S. Bernhard, P. Belser, Synthesis-Stuttgart (1996) 192.
[183] V. Balzani, F. Barigelletti, P. Belser, S. Bernhard, L. De Cola, L. Flamigni, J. Phys. Chem. 100 (1996) 16786.
[184] R.N. Warrener, A.B.B. Ferreira, A.C. Schultz, D.N. Butler, F.R. Keene, L.S. Kelso, Angew. Chem. Intl. Ed. Engl. (1996) 35 (1996) 2485.
[185] A.M. Pyle, J.K. Barton, Prog., Inorg. Chem. 38 (1990) 413.
[186] A. Kirsch – De Mesmaeker, J.-P. Lecomte, J.M. Kelly, Topics in Current Chemistry 177 (1996) 25.
[187] A. Shulman, F.P. Dwyer, Metal chelates in biological systems, in: F.P. Dwyer, D.P. Mellor (eds.), Chelating Agents and Metal Chelates, Academic Press, New York, 1964, p. 383.

Separatum
1192 HELVETICA CHIMICA ACTA – Vol. 79 (1996)

103. The Synthesis and Characterization of New Optically Active 'Dimeric' 'Pineno'-[4,5]-Fused 2,2′-Bipyridines Linked without Spacer or by Small Spacer Groups

by Nicholas C. Fletcher[a]), F. Richard Keene[b]), Marco Ziegler[a]), Helen Stoeckli-Evans[c]), Heiko Viebrock[a]), and Alex von Zelewsky[a])*

[a]) Institute of Inorganic and Analytic Chemistry, University of Fribourg, CH-1700 Fribourg
[b]) School of Molecular Sciences, James Cook University of North Queensland, Townsville, Queensland 4811, Australia
[c]) Institute of Chemistry, University of Neuchâtel, Avenue de Bellevaux 51, CH-2000 Neuchâtel

(26.III.96)

Linked chiral bipyridines **2**–**4** are prepared by combining two optically active 'pineno'-[4,5]-fused 2,2′-bipyridines in a stereoselective reaction (*Scheme 1*). These potential ligands are new members of the 'chiragen' family, and are characterized by NMR spectroscopy and, in the case of **2** and **3** by single-crystal X-ray analysis. A new synthesis of 'dipineno'-[4,5;4′,5′]-fused 2,2′-bipyridine **8** is described, which, when coupled, gives additional four chiral centres to the analogous 'chiragen' series (→ **9**). Analysis of the CD spectra allowed conformational information about the solution species to be determined.

Introduction. – In the last few years, many new and interesting metal complexes of helicating and caging ligands have been described [1]. Many of these ligands lead to chiral complexes or host-guest structures. However, due to the lack of stereoselectivity of the ligands, a racemic mixture of the forms is usually produced. As such systems grow in size, the number of possible diastereoisomers and enantiomeric pairs increases exponentially [2], and consequently it is necessary to develop new systems where the chirality is predetermined prior to complexation so that the exact structure can be predicted in the supramolecular assemblies.

The so-called 'chiragen' ligands have been designed to overcome these problems; these ligands contain a rigid chirality in their bipyridine moieties, introduced by the use of a readily available natural product in their synthesis [3]. Additionally, we have developed a synthetic pathway that allows a wide variety of different linking groups between the bipyridine moieties to be incluced. 'Pineno'-[4,5]-fused 2,2′-bipyridines[1]) linked by alkanediyl groups were initially reported, which were able to control the helical chirality in octahedral metal complexes depending upon the absolute configuration of the starting pinene enantiomer [4]. Subsequently, by replacing the flexible aliphatic groups by more rigid xylenediyl groups, better coordination properties were achieved [5] (*Fig. 1*).

In reducing the size of the spacer unit, it was hoped that the potential linked ligand would have greater intramolecular steric interactions, where the relative orientation of the two bipyridine moieties would influence the average configuration. Secondly, the

[1]) The locants [4,5], [4′,5′], [5,6], and [5′,6′] refer to the numbering of the 2,2′-bipyridine moiety and indicate the fusion sides with the 'pinene' moiety; for systematic names, see *Exper. Part.*

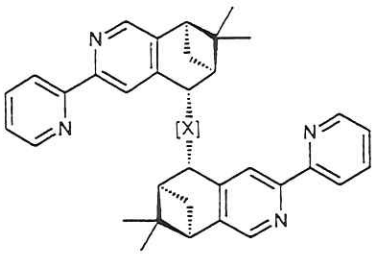

[X] = $(CH_2)_n$ with n = 4–7
= *o*-, *m*-, and *p*-xylenediyl

Fig. 1. *The 'chiragen' ligand system.* All molecules have C_2 symmetry and contain six stereogenic C-atoms.

inclusion of additional chiral centres could further direct the configuration. To this end, a new synthesis of 'dipineno'-[4,5;4′,5′]-fused 2,2′-bipyridine[1]) **8** was developed, which led to a new class of bipyridines, linked by a chiral moiety, the 'super chiragens'.

Results and Discussion. – *Synthesis.* The 'pineno'-[4,5]-fused 2,2′-bipyridine[1]) **1** can be obtained using a *Kröhnke*-type synthesis [3]. Linking **1** to a second 'pineno'-[4,5]-fused 2,2′-bipyridine moiety is readily achieved *via* a stereoselective lithiation reaction at position 5[2]) using a sterically-hindered base such as lithium diisopropylamide (LDA). Upon reaction with this lithium salt and a suitable dibromide, linking groups can be inserted in between the two chiral bipyridine moieties. It was observed, however, that if a mild oxidizing agent was present, *e.g.* O_2, a significant quantity of a by-product could be obtained. By adding I_2 to the lithium salt of **1**, it was possible to obtain this by-product in high yield. Characterization indicated it to be 'chiragen[0]' (**2**; *Scheme 1*), which is surprising by virtue of the close proximity of the two large pineno moieties. The preparation of analogous compounds with C_1- and C_2-spacer groups between the two pineno moieties was then attempted. Unfortunately, using reagents such as dibromomethane, diiodomethane, dibromoethane, and ethyl acetate, the desired target molecules were not obtained. The reaction is prevented by the large steric interactions encountered in the second approach of the lithiated species. However, successful reactions were achieved using ethyl formate and dichlorodimethylsilane which yielded the ligands **3** and **4**, respectively, containing a small spacer (*Scheme 1*).

To increase the number of chiral centres in this class of optically active bipyridines, the 'dipineno'-[4,5;4′,5′]-fused 2,2′-bipyridine **8** was synthesized. While **8** was initially prepared in eight steps from (−)-myrtenal according to an analogous reaction sequence recently elaborated by us for the synthesis of the isomeric 'dipineno'-[5,6;5′,6′]-fused 2,2′-bipyridine from (−)-pinocarvone [6], a new synthetic route was developed, taking only three steps. Again the key step of the sequence was a *Kröhnke*-type cyclization of the pyridine ring using the (cyanomethyl)pyridinium salt **5** and (−)-myrtenal to give amine **6** [7]. This amine was then converted to the bromo derivative **7** [8] which was coupled on nickel(II) to produce the desired 'dipineno'-fused bipyridine **8** [9] (*Scheme 2*). The time required and the simplicity of this reaction sequence is greatly improved as compared to the previously used method [6].

---

[2]) Systematic numbering as shown for **1** in *Scheme 1* (see also *Exper. Part*).

Scheme 1. *Preparation of the New Small 'Chiragen' Molecules*

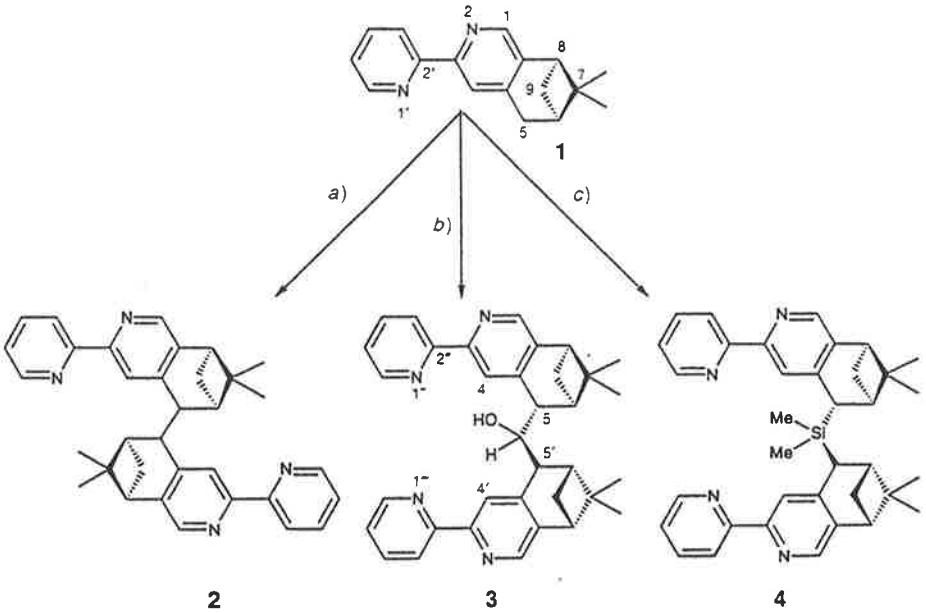

a) 1. LDA, THF, < –40.°; 2. I_2, THF. *b*) 1. LDA, THF < –40°; 2. HCOOEt. *c*) 1. LDA, THF < –40°; 2. $SiMe_2Cl_2$, THF.

The 'dipineno'-[4,5;4′,5′]-fused 2,2′-bipyridine **8** was coupled in an analogous reaction to that of the 'pineno'-[4,5]-fused 2,2′-bipyridine **1** by using 1 equiv. of LDA and then oxidizing the product with I_2. Again, a good yield was achieved, giving the product **9** with ten chiral centres.

NMR Spectroscopy. All the compounds prepared were fully characterized by both ^{13}C- and ^1H-NMR spectroscopy. While the characteristics of the starting bipyridine molecules are evident in all new 'chiragen' compounds, there were several noticeable features. While the silylene-bridged compound **4** had a spectrum very similar to that of the starting bipyridine **1**, **2**, and **9** showed a much greater downfield shift (*ca.* 1 ppm) of the proton at the linking position C(5), along with a noticeable change in peak position of the aromatic protons at C(1) and C(4)[2]. However, there is no loss in C_2 symmetry, despite the great steric hindrance in solution on an NMR time scale. However, the hydroxymethylene link in **3** renders the two bipyridine halves inequivalent. The introduction of the alcohol group removes the C_2 symmetry, which is easily seen in both the ^1H- and ^{13}C-NMR spectra of **3**. Full assignment was carried out using a combination of COSY and HETCOR techniques. It is apparent from the observed shifts that the OH group lies much closer to one of the bipyridine moieties, with protons at C(5) and C(4) being shifted much further downfield when compared to those at C(5′) and C(4′)[2]. The proton of the link, C*H*OH, is in a strongly deshielded position, with a shift of 4.71 ppm.

Structure Determinations. With the exception of **4**, the bipyridine compounds could be recrystallized from EtOH. Ligands **2** and **3** both formed crystals suitable for X-ray structure determination (see *Figs. 2* and *3*).

Scheme 2. *Preparation of the New 'Super Chiragen' Molecules*

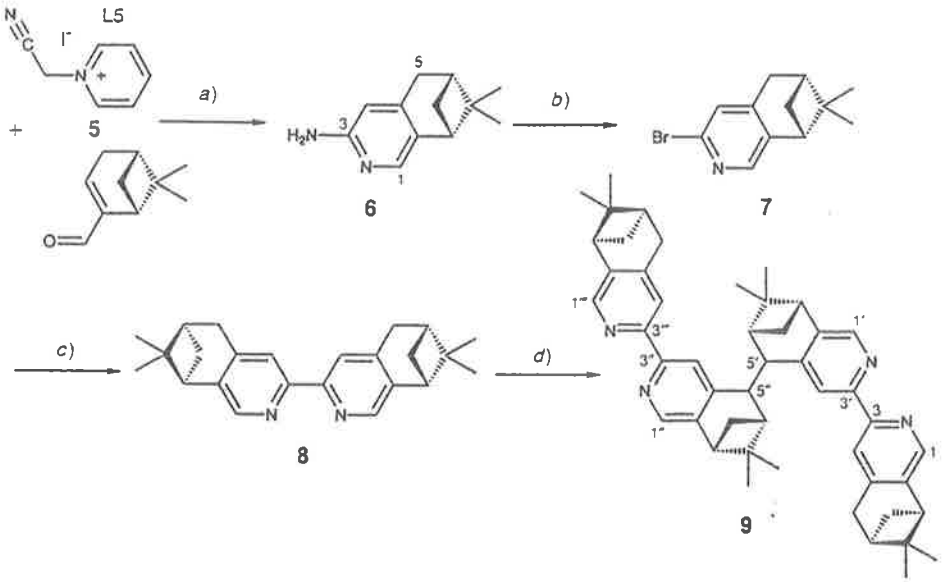

a) EtOH/AcOH NH_4OAc. *b*) 1. $NaNO_2$, HBr, 0°; 2. CuBr, HBr, 70°. *c*) Zn/[$Ni(PPh_3)_4Cl_2$], DMF. *d*) 1. LDA, THF < −40°; 2. I_2, THF.

Molecule **2** possesses crystallographic C_2 symmetry (*Fig. 2*); **3**, however, shows strong deviation from C_2 symmetry (*Fig. 3*), demonstrated by the different torsion angles C(4)–C(7)–C(14)–O(15) and C(4a)–C(7a)–C(14)–O(15), being −1.5(9) and 65.7(8)°, respectively[3]). In the solid state, the structures of both compounds **2** and **3** adopt a *trans* position of the two pyridine halves of the bipyridine unit, as is expected, with a torsion angle N(1)–C(2)–C(2′)–N(1′) of 172.5(4)° in **2** and −174.5(7)° in **3** and with N(1a)–C(2a)–C(2a′)–N(1a′) of −176.7(7)° in **3**. Both structures indicate that the alkylation at C(7)[3]) occurred from the sterically less-hindered side of the 'pineno' moiety, thus establishing the stereoselectivity of the reaction, as has been observed previously with this type of reaction [4] [5]. Additionally, it was observed that the two bipyridine units are close enough to affect each other, with the distance between C(7) and C(7a) being 1.55 and 2.59 Å in **2** and **3**, respectively. Additionally, a torsion angle C(4)–C(7)–C(7a)–C(4a) of −159.0(4)° in **2** orientates the two bipyridine moieties to superimpose one another, giving rise to possible stabilizing π–π stacking interactions. In **3**, the two bipyridine moieties adopt a more splayed conformation, with a pseudo torsion angle C(4a)–C(7a)–C(7)–C(4) of 99.8°. The solid-state structure of this compound illustrates that there is a one-dimensional linear arrangement of the molecules held together by intermolecular H-bonds between OH and N(1′) of an adjacent symmetry-related molecule. Surprisingly, the conformation adopted places the two 'pineno' units and the O-atom in an alternate configuration, placing the bulky Me groups in the same plane.

[3]) Arbitrary numbering as shown in *Figs. 2* and *3*.

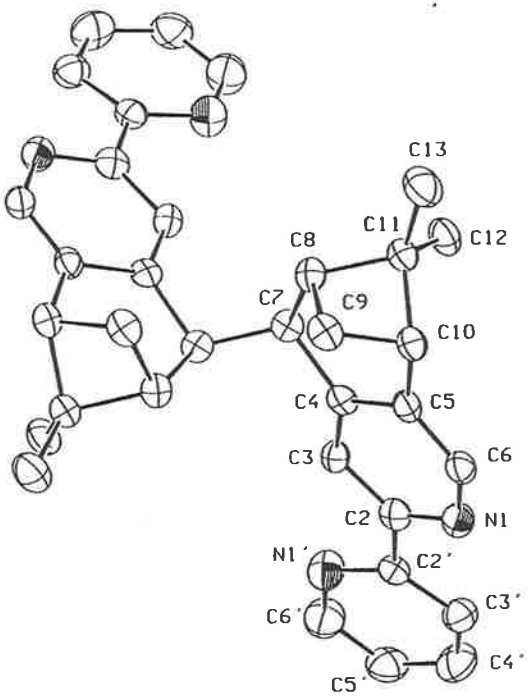

Fig. 2. *Thermal motion ellipsoid plot of* **2**, *with ellipsoids drawn at 50% probability level.* Arbitrary numbering.

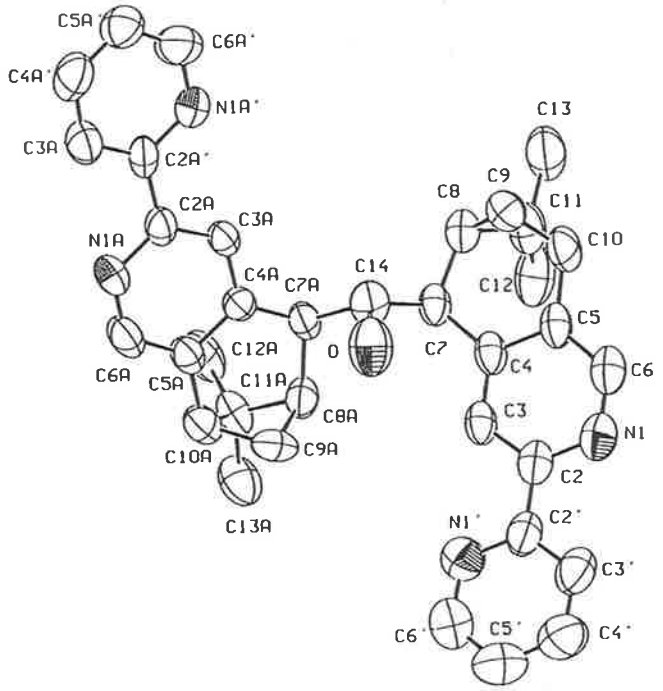

Fig. 3. *Thermal motion ellipsoid plot of* **3**, *with ellipsoids drawn at 50% probability level.* Arbitrary numbering.

Table 1. *UV/VIS Absorption Data for Ligands* **1**–**4**, **8**, *and* **9**[a])

	λ/nm	ε/M^{-1} cm^{-1}	λ/nm	ε/M^{-1} cm^{-1}
1	–	–	291	15900
2	257	12600	291	30500
3	269	11100	304	29500
4	–	–	291	34500
8	262	9900	296	19300
9	264	18600	297	33500

[a]) All spectra were recorded in $CHCl_3$ at a concentration of $2 \cdot 10^{-5}$ M.

Electronic Spectra. All bipyridine-containing ligands were investigated by UV spectroscopy (*Table 1* and *Fig. 4, a*), with the strong π–π^* transitions being evident in each case at 291 nm, except for **3** where it is red-shifted to 304 nm due to the electronegativity of the adjacent OH group. Additionally, there are strong side bands which in several cases resolved into individual peaks.

In the circular dichroism (CD) spectra of both starting bypridines **1** and **8**, very little of the chirality derived from the 'pineno' moiety is observed in the π–π^* transitions (*Fig. 4, b*). However, weak but significant CD spectra are observed for all other ligands (*Fig. 4, b*), due to the orientation of the two adjacent bipyridine groups, while the larger 'chiragens' reported previously demonstrated no effective CD activity [4–6]. It should be stated, however, that these compounds show only small $\Delta\varepsilon$'s, indicating that they adopt different conformations in solution which partially cancel each other in the CD spectrum.

Exciton theory has been used to elucidate the conformations and configurations of molecules in solution and has proved to be useful with a variety of organic compounds [10] and metal complexes [11]. With high-intensity electric dipole moment allowed transitions, exciton CD is supposed to correlate well with absolute configurations [10], as recently demonstrated by *Lightner* and coworkers [12]. An almost identical UV spectrum for the different ligands **1**–**4**, **8**, and **9** (*Fig. 4, a*) shows that the electronic transitions of the molecules containing two bipyridine moieties result from the sum of the transitions in two individual mono-bipyridines, and thus, the exciton model can be applied. ZINDO Calcu-

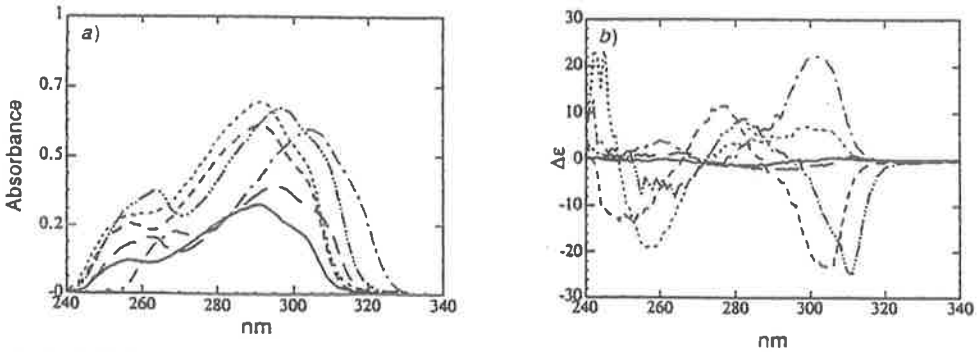

Fig. 4. a) *UV Spectra of ligands* **1**–**4**, **8**, *and* **9** ($c = 2 \cdot 10^{-5}$ M in $CHCl_3$), *and* b) *circular dichroism spectra of* **1**–**4**, **8**, *and* **9** ($c = 1 \cdot 10^{-4}$ M in $CHCl_3$). ——1; – – –2; –·–·–3; ——4; – – –8; –···–···9.

lations (INDO/1 parametrization [13]) including the orbitals from HOMO−11 to LUMO+11 in the configuration interaction (CI) active space with an INDO/1 geometry-optimized 'pineno'-[4,5]-fused 2,2′-bipyridine show that the UV/VIS bands arise primarily from long-axis polarized π–π^* transitions. The calculated spectra correspond reasonably well with those observed (*Fig. 5*). Therefore, the CD bands observed for the linked molecules arise from intramolecular electrostatic coupling of electric transition dipole moments of the two bipyridine moieties.

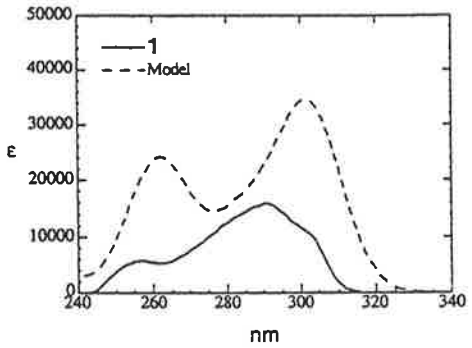

Fig. 5. *Calculated UV spectrum for 'pineno'-[4,5]-fused 2,2′-bipyridine, using geometry-optimized ZINDO(INDO/1) calculations*

The CD spectra of ligands **2** and **9** in solution (*Fig. 4, b*) indicate that the relative arrangement of the two bipyridines in the molecules are very similar. From the application of the exciton theory, the configuration adopted can be assigned as a left-handed helix (see *Fig. 6*), whereas, in the ligands **3** and **4**, a right-handed conformation is preferred. This fact is also observed in the optical rotation of the compounds, where **2** and **9** give a negative value, while **3** and **4** give positive values of [α]. This feature is due to the difference in the relative torsion angles along the link between the 'pineno' moieties, and it is apparent that only a small rotation in the angle can turn one helicity into the other thus inverting the CD transition (*Fig. 6*).

The modelled solution conformation of **3** derived from analysis of the CD spectrum agrees with the configuration observed in the X-ray-determined solid-state structure. Surprisingly, this is not the case for **2** having a link without spacer. However, in the solid state, **3** takes up a configuration where the two bipyridine units overlay each other, which would lead to a different CD spectrum as modelled with exciton theory. It can be assumed that upon crystallization, intermolecular H-bonding plays a more important role, leading to the change in average configuration.

Conclusions. – The successful synthesis of 'dipineno'-[4,5;4′,5′]-fused 2,2′-bipyridine **8** allowed us to extend the number of chiral centres appended to a bipyridine group. Using this and the previously reported 'pineno'-[4,5]-fused 2,2′-bipyridine **1**, new configurationally defined potential linked bidentate ligands of the 'chiragen' family containing up to ten chiral centres were prepared and characterized. Due to the shortness of the linking spacers between the two halves of the structure, there is helicity transferred to the relative position of the bipyridine units, since free rotation along the spacers is prevented on steric grounds. This was illustrated by both X-ray structure determinations and by circular

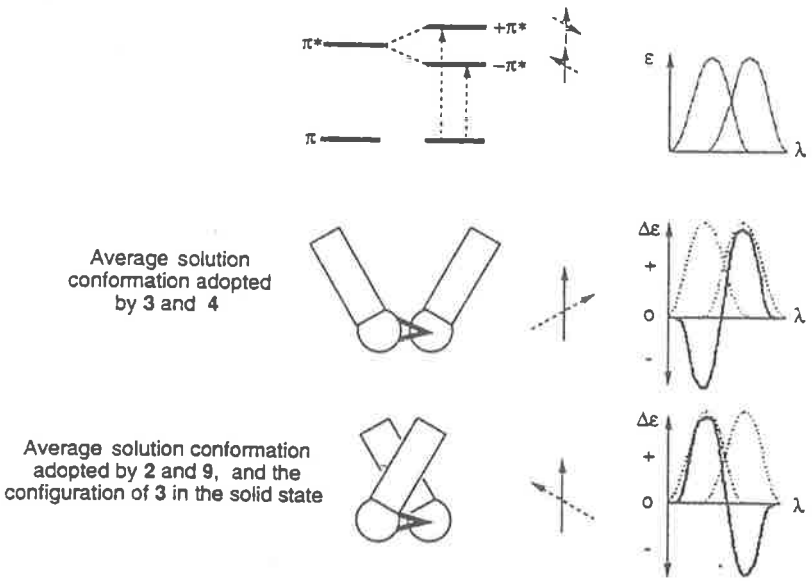

Fig. 6. The relative configurations of the two bipyridine moieties in the linked ligands **2**–**4** *and* **9** *and the expected CD spectra*

dichroism spectroscopy in solution. Additionally, it appears that only a small change in the angle between the two bipyridine moieties is required to invert the helicity of the overall molecule. These new small 'chiragens' and 'super chiragens' are believed to be able to produce chiral coordination compounds, in combination with transition metals, and currently investigations are in progress to demonstrate this.

Experimental Part

General. Unless otherwise stated, commercial-grade reagents were used without further purification. THF was pre-dried by distillation from Na. (−)-(1*R*)-Myrtenal was obtained from *Fluka* (> 97%, $[\alpha]_D^{20°} = -14.6$). Column chromatography = CC. M.p.: *Büchi-520* melting-point apparatus, uncorrected. Optical rotations: *Perkin-Elmer-MC 241* polarimeter; 10-cm cell; sample concentration *ca.* $1 \cdot 10^{-2}$ M in $CHCl_3$. UV/VIS Spectra: *Perkin-Elmer-Lambda-2* in spectrometer; λ_{max} (ε) in nm. CD Spectra: *Jobin-Yvon* spectrophotometer; λ_{max} (Δε) in nm. NMR Spectra: *Varian-Gemini-300* spectrometer (300 (^{1}H) and 75.46 MHz (^{13}C)); in $CDCl_3$; δ in ppm using the solvent as internal ref. rel. to $SiMe_4$, *J* in Hz. MS: *VG-Instruments-7070E* mass spectrometer equipped with a FAB inlet system *m/z* (rel.%). The elemental analyses were performed in the Research Centre, of *Ciba AG*, Marly.

5,6,7,8-Tetrahydro-7,7-dimethyl-3-(pyridin-2-yl)-6,8-methanoisoquinoline (**1**) was prepared according to [3] [4].

5,5′,6,6′,7,7′,8,8′-Octahydro-7,7,7′,7′-tetramethyl-3,3′-di(pyridin-2-yl)-5,5′-bi[6,8-methanoisoquinoline] ('*Chiragen(0)*'; **2**). To a soln. of **1** (504 mg, 2.01 mmol) in dry THF (10 ml) was added at −40° 1.5M lithium diisopropylamide (LDA; 1.5 ml, 2.25 mmol) in dry THF (10 ml) over 30 min. The mixture was kept at −40° for 4 h, then I_2 (254 mg, 1.0 mmol) in dry THF (10 ml) was added. At the end of the addition, the colour changed from blue to red. The mixture was stirred overnight, quenched with H_2O (2 ml), and concentrated *in vacuo*. After addition of sat. aq. $NaHCO_3$ soln. (30 ml), the mixture was extracted with CH_2Cl_2 (3 × 30 ml), the org. phase dried ($MgSO_4$) and evaporated, and the residue purified by CC (silica gel, hexane/Et_2O/Et_3N 14:6:1): 302 mg (60%) of **2**. Recrystallization from MeOH gave colourless crystals. M.p. 290–292° (dec.) $[\alpha]_D^{22°} = -115$. ^{1}H-NMR: 8.65 (*dd*, *J* = 3.9, 0.9, H–C(6″)); 8.45 (*s*, H–C(1)); 8.36 (*d*, *J* = 8.0, H–C(3″)); 8.26 (*s*, H–C(4)); 7.79 (*ddd*, *J* = 8.0, 8.0, 1.7,

H–C(4″)); 7.26 (*m*, H–C(5″)); 4.03 (*s*, H–C(5)); 2.82 (*dd*, *J* = 5.4, 5.4, H–C(8)); 2.50 (*ddd*, *J* = 9.8, 5.6, 5.6, H_b–C(9)); 2.09 (*dd*, *J* = 5.7, 5.7, H–C(6)); 1.28 (*s*, Me_a–C(7)); 1.24 (*d*, *J* = 9.6, H_a–C(9)); 0.70 (*s*, Me_b–C(7)). ^{13}C-NMR: 156.3, 154.9 (C(3), C(2″)); 149.2 (C(6″)); 147.3 (C(4a)); 145.6 (C(4)); 143.8 (C(8a)); 136.8, 123.4, 120.8, 118.4 (C(4″), C(5″), C(3″), C(1)); 43.8, 43.5, 42.2 (C(8), C(5), C(6)); 41.9 (C(7)); 28.7 (C(9)); 26.0 (*Me*–C(7)); 20.9 (Me_b–C(7)). FAB-MS: 499 (6, MH$^+$), 456 (2, [M – Me_2C]$^+$), 249 (75, 0.5 M^+), 207 (100, [249 – Me_2C]$^+$). Anal. calc. for $C_{34}H_{34}N_4$: C 81.9, H 6.8, N 11.2; found: C 81.0, H 6.7, N 11.3.

Bis[5,6,7,8-tetrahydro-7,7-dimethyl-3-(pyridin-2-yl)-6,8-methanoisoquinolin-5-yl]methanol (*'Chiragen(OH)'*; **3**). As described for **2**, using **1** (508 mg, 2.03 mmol), 1.5M LDA/THF (1.8 ml, 2.7 mmol), and HCOOEt (75.6 mg, 1.02 mmol) added in three portions over 15 min: 419 mg (78%) of **3**. Recrystallization from MeOH/CH_2Cl_2 gave colourless crystals. M.p. 245–246° $[\alpha]_D^{22°}$ = +119. ^{1}H-NMR: 8.78 (*s*, H–C(4)); 8.48 (*d*, *J* = 4.1, H–C(6″)); 8.44 (*d*, *J* = 4.1, H–C(6‴)); 8.34 (*d*, *J* = 8.0, H–C(3″)); 8.21 (*d*, *J* = 8.0, H–C(3‴)); 8.19 (*s*, H–C(1)); 8.17 (*s*, H–C(4′), H–C(1′)); 7.70–7.61 (*m*, H–C(4″), H–C(4‴)); 7.16–7.10 (*m*, H–C(5″), H–C(5‴)); 4.71 (*d*, *J* = 7.8, C*H*OH); 3.21 (*dd*, *J* = 7.8, 8.9, H–C(5)); 3.10 (*s*, H–C(5′)); 3.01 (*d*, *J* = 4.0, OH); 2.89 (*dd*, *J* = 5.2, 5.2, H–C(8′)); 2.84 (*dd*, *J* = 5.2, 5.2, H–C(18)); 2.72–2.59 (*m*, H_b–C(9), H_b–C(9′)); 2.39 (*dd*, *J* = 5.1, 5.1, H–C(6)); 2.17 (*ddd*, *J* = 5.1, 5.1, 1.7, H–C(6′)); 2.03 (*d*, *J* = 9.9, H_a–C(9)); 1.53 (*d*, *J* = 9.7, H_a–C(9′)); 1.46 (*s*, Me_a–C(7)); 1.44 (*s*, Me_a–C(7′)); 0.64 (*s*, Me_b–C(7), Me_b–C(7′)); assigned by COSY. ^{13}C-NMR: 156.7, 154.7, 156.2, 154.5 (C(3), C(3′), C(2″), C(2‴)); 148.9, 148.7 (C(6″), C(6‴)); 147.4, 146.7 (C(4a), C(4′a)); 145.8, 145.4 (C(1), C(1′)); 143.8, 142.2 (C(8a), C(8′a)); 136.7, 136.6, 123.2, 123.0, 122.3, 120.9, 120.8, 118.1 (C(4‴), C(4″), C(5‴), C(5″), C(4), C(3″), C(3‴), C(4′)); 75.9 (CHOH); 45.1, 44.7, 43.8, 42.6, 42.6 (C(8), C(8′), C(5), C(6), C(5′)); 42.2, 41.4 (C(7′), C(7)); 40.1 (C(6′)); 29.1, 28.2 (C(9′), C(9)); 26.7, 26.2 (Me_a–C(7′), Me_a–C(7)); 21.0, 20.7 (Me_b–C(7′), Me_b–C(7)); assigned by DEPT and HETCOR. FAB-MS: 551 (24, [M + Na]$^+$), 529 (100, MH$^+$), 279 (72, [0.5 M + CH_2OH]$^+$). Anal. calc. for $C_{34}H_{34}N_4 \cdot H_2O$: C 76.9, H 7.0, N 10.2; found: C 77.4, H 7.1, N 10.3.

5,5′-(Dimethylsilylene)bis[5,6,7,8-tetrahydro-7,7-dimethyl-3-(pyridin-2-yl)-6,8-methanoisoquinoline] (*'Chiragen(SiMe$_2$)'*; **4**). As described for **2** using **1** (502 mg, 2.01 mmol), 1.5M LDA/THF (1.5 ml, 3.00 mmol), and dichlorodimethylsilane (128 mg, 0.99 mmol), added over 5 min: 256 mg (46%) of **4** (50% of **1** was recovered from the 1st fraction of CC). M.p. 72–75° (dec.). $[\alpha]_D^{22°}$ = +146. ^{1}H-NMR: 8.55 (*dd*, *J* = 4.8, 0.9, H–C(6″)); 8.25 (*d*, *J* = 7.8, H–C(3″)); 8.19 (*s*, H–C(1)); 8.15 (*s*, H–C(4)); 7.67 (*ddd*, *J* = 8.0, 7.4, 0.9, H–C(4″)); 7.17 (*dd*, *J* = 4.8, 7.3, H–C(5″)); 3.07 (*s*, H–C(5)); 2.83 (*dd*, *J* = 5.5, 5.5, H– C(8)); 2.68 (*ddd*, *J* = 9.8, 5.5, 5.5, H_b–C(9)); 2.63 (*dd*, *J* = 5.6, 5.6, H–C(6)); 1.38 (*s*, Me_a–C(7)); 1.29 (*d*, *J* = 9.6, H_a–C(9)); 0.64 (*s*, Me_b–C(7)); 0.12 (*s*, Me_2Si). ^{13}C-NMR: 156.4, 154.2 (C(3), C(2″)); 148.9 (C(6″)); 147.8 (C(4a)); 145.7 (C(4)); 142.3 (C(8a)); 136.5, 123.0, 120.5, 119.7 (C(4″), C(5″), C(3″), C(1)); 44.2, 42.7 (C(8), C(6)); 38.9 (C(7)); 32.9 (C(5)); 29.3 (C(9)); 25.7 (Me_a–C(7)); 21.0 (Me_b–C(7)); 0.6 (Me_2Si). FAB-MS: 579 (17, MNA$^+$), 557 (100, MH$^+$), 399 (97, [M – 2Py]$^+$). Anal. calc. for $C_{34}H_{34}N_4 \cdot H_2O$: C 75.1, H 7.4, N 9.7; found: C 74.7, H 7.3, N 9.4.

(Cyanomethyl)pyridinium Iodide (**5**). For 4 h, 2-chloroacetonitrile (42.69 g, 565 mmol) and KI (100.00 g, 602 mmol) were refluxed in MeOH (100 ml). The mixture was cooled to r.t. and evaporated. The residual yellow oil was taken up in CH_2Cl_2 (100 ml) and filtered to remove inorg. residues. The filtrate was dried ($MgSO_4$) and filtered, and pyridine was added dropwise (200 ml) over 1 h. The mixture was stirred at r.t. for 16 h. The resulting precipitate was collected by filtration, washed with Et_2O (3 × 50 ml), and dried *in vacuo*: 105.85 g (76%) of **5**. Yellow crystalline solid. M.p. 162–163°. ^{1}H-NMR ((D_6)DMSO): 9.19 (*d*, *J* = 6.5, H–C(2), H–C(6)); 8.75 (*t*, *J* = 7.4, H–C(4)); 8.27 (*dd*, *J* = 6.5, 7.5, H–C(3), H–C(5)); 6.01 (*s*, CH_2). ^{13}C-NMR ((D_6)DMSO): 147.6, 145.4, 128.6 (C(2), C(3), C(4), C(5), C(6)); 114.2 (CN); 47.8 (CH_2). FAB-MS: 365 (100, [2 M + I]$^+$).

5,6,7,8-Tetrahydro-7,7-dimethyl-6,8-methanoisoquinolin-3-amine (**6**) [7]. A soln. of **5** (10.03 g, 38.0 mmol), (–)-myrtenal (5.09 g, 33.9 mmol), and NH_4OAc (15.67 g, 203.4 mmol) in 50% EtOH/AcOH (50 ml) was refluxed for 6 h. The resulting black soln. was allowed to stand overnight and then the volume reduced to *ca.* 15 ml. H_2O (50 ml) was added and the soln. taken to pH 14 with sat. NaOH soln. The mixture was extracted with Et_2O (10 × 100 ml) and the org. phase dried ($MgSO_4$) and concentrated to *ca.* 250 ml. This was then extracted with 2M HCl (5 × 100 ml), the aq. phase made basic with sat. NaOH soln., the alkaline soln. extracted with CH_2Cl_2 (5 × 100 ml), and the org. phase dried ($MgSO_4$) and evaporated. The resulting black oil was then further purified by CC (silica gel, gradient CH_2Cl_2/MeOH containing 2% of Et_3N): 2.42 g (38%) of **6**. Yellow oily solid. To avoid decomposition, **6** was stored under N_2 at –30° and used as quickly as possible after preparation. ^{1}H-NMR: 7.42 (*s*, H–C(1)); 6.22 (*s*, H–C(4)); 4.26 (br., NH_2); 2.70 (*d*, *J* = 2.2, H–C(5)); 2.51 (*dd*, *J* = 5.4, 5.4, H–C(8)); 2.47 (*m*, H_b–C(9)); 2.06 (*m*, H–C(6)); 1.21 (*s*, Me_a–C(7)); 1.00 (*d*, *J* = 8.5, H_a–C(9)); 0.47 (*s*, Me_b–C(7)). ^{13}C-NMR: 157.0 (C(3)); 146.5 (C(4a)); 142.9 (C(1)); 132.8 (C(8a)); 108.1 (C(4)); 43.8, 39.7 (C(8), C(6)); 39.6 (C(7)); 32.5, 32.3 (C(5), C(9)); 25.9 (Me_a–C(7)); 21.3 (Me_b–C(7)). EI-MS: 188 (15, M^+), 173 (19, [M – NH_2]$^+$), 145 (100, [M – Me_2C]$^+$).

3-Bromo-5,6,7,8-tetrahydro-7,7-dimethyl-6,8-methanoisoquinoline (**7**) [8]. A soln. of **6** (3.44 g, 0.222 mol) in 33% HBr soln. (60 ml) was cooled to below 0°. To this was added dropwise $NaNO_2$ (1.70 g, 0.246 mol) in H_2O

(10 ml) over 15 min, and the mixture was stirred for a further 15 min. CuBr (5.00 g, 0.349 mol) was added over 30 min and the mixture heated at 70° for 3 h. After cooling to r.t., the soln. was taken to pH 14 by the addition of 3M aq. NaOH. The resulting precipitate was extracted with Et_2O (5 × 100 ml), the extract dried ($MgSO_4$) and evaporated, and the resulting brown oil purified by CC (silica gel, hexane containing 5% of Et_3N): 1.27 g (28%) of **7**. Yellow oil. ^{1}H-NMR: 7.82 (*s*, H–C(1)); 7.18 (*s*, H–C(4)); 2.87 (*d*, *J* = 2.8, H–C(5)); 2.72 (*dd*, *J* = 5.5, 5.5, H–C(8)); 2.61 (*m*, H_b–C(9)); 2.22 (*m*, H–C(6)); 1.32 (*s*, Me_a–C(7)); 1.09 (*d*, *J* = 9.8, H_a–C(9)); 0.54 (*s*, Me_b–C(7)). ^{13}C-NMR: 147.8 (C(4a)); 145.8 (C(1)); 141.8 (C(3)); 139.1 (C(8a)); 127.0 (C(4)); 43.9, 39.5 (C(8), C(6)); 38.7 (C(7)); 32.4, 31.4 (C(5), C(9)); 25.9 (Me_a–C(7)); 21.3 (Me_b–C(7)). EI-MS: 251/253 (10/9, M^+), 236/238 (5/4, $[M - Me]^+$), 208/210 (100/96, $[M - Me_2C]^+$).

5,5',6,6',7,7',8,8'-Octahydro-7,7,7',7'-tetramethyl[6,8-methanoisoquinoline] (*'Super Chiragen(0)'*; **8**) [9]. To a soln. of $NiCl_2 \cdot 6H_2O$ (0.372 g, 1.56 mmol) and PPh_3 (1.640 g, 6.25 mmol) in degassed DMF (8 ml) was added Zn powder (0.130 g, 1.99 mmol). The mixture was heated at 60° for 2 h, during which time the colour changed from blue to red. Then **7** (0.393 g, 1.57 mmol) in DMF 810 ml) was added. The mixture was heated for a further 18 h and then poured into 10% NH_3/H_2O (50 ml). The resulting precipitate was extracted with CH_2Cl_2 (6 × 50 ml), dried ($MgSO_4$), and evaporated . The resulting orange oil was purified by CC (silica gel, CH_2Cl_2 containing 1% of MeOH): PPh_3, then crude product containing a significant amount of PPh_3. The latter mixture was taken up in

Table 2. *Experimental Crystallographic Data for Compounds* **2** *and* **3**

	2	**3**
Molecular formula	$C_{34}H_{34}N_4$	$C_{35}H_{36}N_4O$
Molecular weight	498.65	528.68
Crystal system	Monoclinic	Orthorhombic
Space group	*I*2	$P2_12_12_1$
Cell parameters *a* [Å]	11.880(5)	11.307(4)
b [Å]	6.360(2)	14.594(7)
c [Å]	17.828(10)	17.762(14)
α	90°	90°
β	93.43(3)°	90°
γ	90°	90°
Volume [Å^3]	1344.6(10)	2931.0(28)
Z	2	4
Calculated density [gcm^{-3}]	1.232	1.198
Diffractometer used	*Stoe AED* 4-circle	*Syntex P2$_1$* [14]
Radiation and wavelength [Å]	MoK_α 0.71073	MoK_α 0.71073
Temp. [°C]	193(2)	293(2)
Linear absorption coefficient	0.073	0.073
Scan mode	$\omega/2\theta$	$\omega/2\theta$
Max./Min. value of θ	$2.01 < \theta < 24.99$	$2.28 < \theta < 22.57$
Method used to solve / refine structure	direct methods using SHELXS-86 / SHELXL-93 with calculated H-positions using a 'riding model' for H [15] removed 'for H'	
No. of reflections measured	2599	2946
No. of independent reflections	2362	2676
No. of unique reflections	1334	1717
Criterion for classification of observed reflections	$> 2\sigma(I)$	$> 2\sigma(I)$
No. of parameters refined	175	368
Final refinement on F^2:		
Final *R*	0.0733	0.0700
Final *wR*	0.1599	0.1523
Goodness of fit	1.097	1.231
Max.+/-electron density in *Fourier* synthesis [eÅ^{-3}]	0.176/–0.158	0.509/–0.203
Plotting software used	PLUTON and PLATON [16]	

25% CH_2Cl_2/Et_2O (50 ml) and extracted with 2M HCl (4 × 50 ml). The acidic soln. was taken to pH 13 with sat. aq. NaOH soln., the resulting basic soln. extracted with CH_2Cl_2 (4 × 200 ml), and the organic soln. dried ($MgSO_4$) and evaporated. The final acid/base extraction was repeated to remove traces of P-containing impurities: 0.204 g (76%) of **8**. Further purification can be achieved by CC (silica gel, hexane containing 5% of Et_3N). M.p. 179–180°. $[\alpha]_D^{22} = -104$. ^{1}H-NMR: 8.17 (*s*, H–C(1)); 8.14 (*s*, H–C(4)); 3.03 (*d*, *J* = 2.7, H–C(5)); 2.84 (*dd*, *J* = 5.5, 5.5, H–C(8)); 2.67 (*m*, H_b–C(9)); 2.29 (*m*, H–C(6)); 1.39 (*s*, Me_a–C(7)); 1.23 (*d*, *J* = 9.8, H_a–C(9)); 0.62 (*s*, Me_b–C(7)). ^{13}C-NMR: 154.8 (C(4a)); 145.5 (C(3)); 145.2 (C(1)); 142.6 (C(8a)); 120.3 (C(4)); 44.5, 40.1 (C(8), C(6)); 39.3 (C(7)); 3.29, 31.8 (C(5), C(9)); 26.0 (Me_a–C(7)); 21.3 (Me_b–C(7)). EI-MS: 344 (11, M^+), 301 (86, $[M - Me_2C]^+$). Anal. calc. for $C_{24}H_{28}N_2 \cdot 1/2\,H_2O$: C 81.5, H 8.3, N 7.9; found: C 81.9, H 8.5, N 7.5.

4,4′,4″,4‴,5,5′,5″,5‴,6,6′,6″,6‴,7,7′,7″,7‴-Hexadecahydro-7,7′,7″,7‴,7″,7‴,7‴,7‴-octamethyl-3,3′:5′,5″:3″,3‴-quater[6,8-methanoisoquinoline] (**9**). As described for **2**, using **8** (602 mg, 1.742 mmol) in dry THF (20 ml), 1.5M LDA/THF (1.2 ml, 1.8 mmol), and I_2 (227 mg, 0.89 mmol) in dry THF (15 ml). The crude product was purified by CC (silica gel, hexane/Et_3N 20:1): 400 mg (67%) of **9** and 192 mg (32%) of recovered **8**. **9**: $[\alpha]_D^{22} = -138$. M.p. 200–204°. ^{1}H-NMR: 8.41 (*s*, H–C(1′)); 8.19 (*s*, H–C(1)); 8.22 (*s*, H–C(4′)); 8.14 (*s*, H–C(4)); 4.03 (*s*, H–C(5)); 3.04 (*d*, *J* = 1.0, H–C(5′)); 2.86 (*t*, *J* = 5.7, H–C(8′)); 2.78 (*t*, *J* = 5.5, H–C(8)); 2.76 (*m*, H_b–C(9)); 2.48 (*m*, H_b–C(9′)); 2.31 (*t*, *J* = 5.6, H–C(6)); 2.07 (*t*, *J* = 5.6, H–C(6′)); 1.41, 1.28 (*s*, Me_a–C(7), Me_a–C(7′)); 1.24 (*m*, H_a–C(9)); 1.22 (*m*, H_a–C(9′)); 0.68, 0.66 (*s*, Me_b–C(7), Me_b–C(7′)). ^{13}C-NMR: 155.6, 154.9 (C(3), C(3′)); 147.1 (C(4′a)); 145.5, 145.4 (CH(1), CH(1′)); 145.3 (C(4a)); 143.2, 142.5 (C(8a), C(8′a)); 120.1, 118.1 (CH(4), CH(4′)); 44.5, 43.7, 43.4, 42.2 (CH(8), CH(8′), CH(5′), CH(6′)); 41.8 (C(7′)); 40.1 (CH(6)); 39.3 (C(7)); 32.9, 31.9, 28.8 (CH_2(9), CH_2(9′), CH_2(5)); 26.0 (Me_a–C(7), Me_a–C(7′)); 21.3, 20.9 (Me_b–C(7), Me_b–C(7′)). FAB-MS (NBA): 688 (100, MH^+). Anal. calc. for $C_{48}H_{54}N_4 \cdot 1\,H_2O$: C 81.8, H 8.0, N 7.9; found: C 81.9, H 8.7, N 7.9.

Single Crystal Structure Determinations see *Table 2*.

The authors would like to thank *Dirk Abeln*, University of Hamburg, for the acquisition of the crystallographic data set for **3**. The work was supported by the *Swiss National Science Foundation*.

REFERENCES

[1] R. Krämer, J.-M. Lehn, A. Cian, J. Fischer, *Angew. Chem.* **1993**, *105*, 764; R. Ziessel, M.-T. Youinou, *ibid.* **1993**, *105*, 929; M. Albrecht, S. Kotila, *ibid.* **1995**, *107*, 2285; C.D. Eisenbach, U.S. Schubert, G.R. Baker, G.R. Newkome, *J. Chem. Soc., Chem. Commun.* **1995**, 69; C. Piguet, G. Hopfgartner, A.F. Williams, J.C.G. Bünzli, *ibid.* **1995**, 491; P.D. Beer, F. Szemes *ibid.* **1995**, 2245.

[2] S. Serroni, G. Denti, *Inorg. Chem.* **1992**, *31*, 4251; M.M. Richter, K.J. Brewer, *ibid.* **1993**, *32*, 5762; V. Balzani, *Tetrahedron* **1992**, *48*, 10443.

[3] P. Hayoz, A. von Zelewsky, *Tetrahedron Lett.* **1992**, *33*, 5165.

[4] P. Hayoz, A. von Zelewsky, H. Stoeckli-Evans, *J. Am. Chem. Soc.* **1993**, *115*, 5111.

[5] H.-R. Mürner, A. von Zelewsky, *Inorg. Chem.* **1996**, in press.

[6] S. Rupprecht, P. Collomb, P. Belser, A. von Zelewsky, H. Viebrock, P. Burger, in preparation.

[7] F. Kröhnke, *Synthesis* **1976**, 1.

[8] K.L. Rinehart Jr., J. Kobayashi, G.C. Harbourg, J. Gilmore, M. Mascal, T.G. Holt, L.S. Shield, F. Lafargue, *J. Am. Chem. Soc.* **1987**, *109*, 3378.

[9] M. Tiecco, L. Testaferri, M. Tingoli, D. Chianelli, M. Montanucci, *Synthesis* **1984**, 737.

[10] N. Harada, K. Nakanishi, 'Circular Dichroic Spectroscopy, Exciton Coupling in Organic Chemistry', University Science Books, Mill Valley, CA, 1983.

[11] B.J. Bosnich, *J. Am. Chem. Soc.* **1968**, *90*, 627.

[12] R.V. Person, B.R. Peterson, D.A. Lighter, *J. Am. Chem. Soc.* **1994**, *116*, 42.

[13] W.P. Anderson, T.R. Cundarai, R.S. Drago, M.C. Zerner, *Inorg. Chem.* **1990**, *29*, 1.

[14] Program P21: Programm P21, D. Abeln, J. Kopf, ECM 15 Lund 1995, Abstracts p. 132 (P21–10).

[15] 'SHELXS-86: Program for Crystal Structure Determination', University of Göttingen, Germany, 1986; G.M. Sheldrick, 'SHELXL-93; Program for Crystal Structure Refinement', University of Göttingen, Germany, 1993.

[16] PLATON: A.L. Spek, *Acta Crystallogr., Sect. A* **1990**, *46*, C34; PLUTON: molecular graphics program, Utrecht University, Utrecht, The Netherlands.

Inorg. Chem. 1997, *36*, 1113−1121

Molecular Architecture of Polynuclear Ruthenium Bipyridyl Complexes with Controlled Metal Helicity

Nicholas C. Fletcher,[†] F. Richard Keene,[‡] Heiko Viebrock,[†] and Alex von Zelewsky*[,†]

Institute of Inorganic and Analytical Chemistry, University of Fribourg, Pérolles, CH-1700 Fribourg, Switzerland, and School of Molecular Sciences, James Cook University of North Queensland, Townsville, Queensland 4811, Australia

Received August 8, 1996[⊗]

The synthesis of di- and trinuclear ruthenium(II) complexes is reported, where each metal center has a tris-(bidentate) octahedral coordination sphere with predetermined stereochemistry. New members of the "Chiragen" ligand series, consisting of two linked chiral 4,5-pineno-2,2′-bipyridine groups, have been prepared, with small spacer units between the coordination centers ($-(CH_2)_n$ {$n = 0, 3$} and $-CH_2(bpy)CH_2-$). X-ray structural data were obtained for the ligand Chiragen[3]. (Crystal data: orthorhombic, space group $P2_12_12_1$, $a = 12.229(1)$ Å, $b = 12.790(1)$ Å, $c = 20.215(1)$ Å, $V = 3161.8(4)$ Å^3, $Z = 4$.) Combination of the ligands with $Ru(bpy)_2Cl_2$ (where bpy is 2,2′-bipyridine) led to a mixture of diastereomers, while the use of enantiomerically pure Δ- or Λ-$[Ru(bpy)_2(py)_2]$(dibenzoyltartrate) or Δ-Ru(CG[*m*-xyl])Cl_2 led to almost complete stereoselectivity in the products. Circular dichroism spectra show that the complexes are composed of one helical diastereomer, with the expected absolute configuration predetermined by the chiral building block used. Additionally, ^{1}H-NMR spectroscopy indicates C_2 point group symmetry for the structures in solution, confirming the absence of ΔΛ diastereomers.

Introduction

Ruthenium complexes of polypyridyl ligands, in particular 2,2′-bipyridyl (bpy), have been extensively studied during the last few decades, due to their unique combination of chemical stability, redox properties, reactivity, and luminescence emission from the metastable excited triplet state.[1,2] As a consequence, they have been applied to such areas as photocatalysis,[3] molecular recognition (host guest) chemistry,[4−6] DNA intercalation,[7,8] and artificial photosynthesis/charge separation.[9−12]

By nature of tris(bidentate) octahedral six-coordinate (*OC*-6) species, such as $[Ru(bpy)_3]^{2+}$, there is an inherent helical chirality at the metal center (Δ or Λ), which until recently was significantly overlooked. Much attention has been devoted to the synthesis of polynuclear transition metal complexes, stimulated by attempts to design and construct multicomponent (supramolecular) species.[13] With the inclusion of more six-coordinate octahedral (*OC*-6) centers, the number of possible diastereomers that are theoretically possible increases exponentially. This is especially true for the larger species recently reported,[14−18] where it would be expected that the diastereomers would have different photophysical and electrochemical behaviors. In addition, the wide range of diastereomers typically prepared greatly hampers the characterization of the compounds by techniques such as NMR, while preventing the simple growth of crystals suitable for X-ray structural determination.

Over recent years we attempted to prepare suitable chiral building blocks to allow the synthesis of supramolecular species, where the chirality of the metal center is predetermined. To this end, we have published the separation of $[Ru(bpy)_2(py)_2]^{2+}$ into its two enantiomers by crystallization with dibenzoyltartrate, providing access to both the Δ and Λ forms, which do not undergo racemization upon replacement of the two pyridyl groups.[19,20] Similar units were recently used to prepare dinuclear[21] and linear polymetallic species.[22]

Additionally, we have found that, by using the specially designed chiral polypyridyl ligands from the "Chiragen" series, the helicity on the metal center can be predetermined from the

† University of Fribourg.
‡ James Cook University of North Queensland.
⊗ Abstract published in *Advance ACS Abstracts*, February 15, 1997.

(1) Balzani, V.; Scandola, F. *Supramolecular Photochemistry*; Ellis Horwood: Chichester, U.K., 1991.
(2) Juris, A.; Barigelletti, S.; Campagna, S.; Balzani, V.; Belser, P.; von Zelewsky, A. *Coord. Chem. Rev.* **1988**, *84*, 85.
(3) Ohkubo, K.; Hamada, T.; Ishida, H. *J. Chem. Soc., Chem. Commun.* **1993**, 1423.
(4) Beer, P. D.; Szemes, F. *J. Chem. Soc., Chem. Commun.* **1995**, 2245.
(5) Beer, P. D.; Fletcher, N. C.; Wear, T. *Polyhedron* **1996**, *15*, 1339.
(6) Beer, P. D.; Dent, S. W.; Wear, T. J. *J. Chem. Soc., Dalton Trans.* **1996**, 2341.
(7) Naing, D.; Takahashi, M.; Taniguchi, M.; Yamagishi, A. *Inorg. Chem.* **1995**, *34*, 350.
(8) Haq, I.; Lincoln, P.; Suh, D. C.; Norden, B.; Chowdhry, B. Z.; Chaires, J. B. *J. Am. Chem. Soc.* **1995**, *117*, 4788.
(9) Durr, H.; Schwarz, R.; Andreis, C.; Willner, I. *J. Am. Chem. Soc.* **1993**, *115*, 12362.
(10) Mecklenburg, S. L.; McCafferty, D. G.; Schoonover, J. R.; Peek, B. M.; Erickson, B. W.; Meyer, T. J. *Inorg. Chem.* **1994**, *33*, 2974.
(11) Seiler, M.; Durr, H.; Willner, I.; Joselevich, E.; Doron, A.; Stoddart, J. F. *J. Am. Chem. Soc.* **1994**, *116*, 3399.
(12) Yonemoto, E. H.; Saupe, G. B.; Schmehl, R. H.; Hubig, S. M.; Riley, R. L.; Iverson, B. L.; Mallouk, T. E. *J. Am. Chem. Soc.* **1994**, *116*, 4786.
(13) Balzani, V.; Juris, A.; Venturi, M.; Campagna, S.; Serroni, S. *Chem. Rev.* **1996**, *96*, 759.
(14) Molnar, S. M.; Nallas, G.; Bridgewater, J. S.; Brewer, K. J. *J. Am. Chem. Soc.* **1994**, *116*, 5206.
(15) Jacquet, L.; Kirsch-De Mesmaeker, A. *J. Chem. Soc., Faraday Trans.* **1992**, *88*, 2471.
(16) Campagna, S.; Denti, G.; Serroni, S.; Ciano, M. *Inorg. Chem.* **1991**, *30*, 3728.
(17) Denti, G.; Campagna, S.; Serroni, S.; Ciano, M.; Balzani, V. *J. Am. Chem. Soc.* **1992**, *114*, 2944.
(18) Campagna, S.; Denti, G.; Serroni, S.; Juris, A.; Venturi, M.; Ricevuto, V.; Balzani, V. *Chem—Eur. J.* **1995**, *1*, 211.
(19) Hua, X.; von Zelewsky, A. *Inorg. Chem.* **1995**, *34*, 5791.
(20) Hua, X.; von Zelewsky, A. *Inorg. Chem.* **1991**, *30*, 3796.
(21) Rutherford, T. J.; Quagliotto, M. G.; Keene, F. R. *Inorg. Chem.* **1995**, *34*, 3857.
(22) Wanmark, K.; Thomas, J. A.; Heyke, O.; Lehn, J. M. *Chem. Commun* **1996**, 701.

S0020-1669(96)00948-2 CCC: $14.00

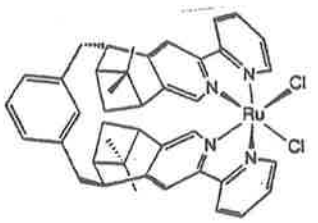

Figure 1. The chiral building block, prepared with Chiragen[*m*-xyl] (CG[*m*-xyl]).

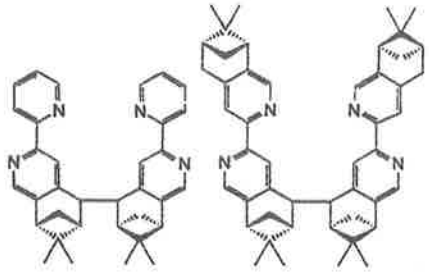

Figure 2. The tetradentate "Chiragen" ligand series. All molecules have C_2 symmetry, with six stereogenic carbon atoms.

chirality of readily available naturally-occurring terpenes.[23-25] These tetradentate ligands, when combined with ruthenium trichloride, give only one diastereomer (Figure 1), with the further advantage that they are unable to undergo photoracemization due to steric constraints.[24] Subsequent replacement of the two chloride ligands facilitates the preparation of octahedral complexes with predetermined chirality.

In this paper we illustrate how these building blocks can be applied to chiral bridging ligands of the "Chiragen" series, to produce diastereomerically and enantiomerically pure di- and trinuclear ruthenium complexes of polypyridyl ligands.

Experimental Section

(a) Measurements and Materials. NMR spectra were obtained on a Varian Gemini-300 spectrometer operating at 300 MHz for ^{1}H and 75.46 MHz for ^{13}C and on a Bruker Avance DRX500 operating at 500 MHz for ^{1}H, using the solvent as internal reference relative to TMS. UV/vis spectral data were recorded on a Perkin-Elmer Lambda 2 spectrometer, and CD spectra, on a Jobin Yvon spectrophotometer [λ_{max}, nm ($\Delta\epsilon$)]. Optical rotation values were obtained with a Perkin-Elmer MC 241 polarimeter using a 10 cm cell, with a sample concentration of approximately 1×10^{-2} M in chloroform. FAB MS data were obtained with a VG Instruments 7070E mass spectrometer (*m/z*), and electrospray MS data, with a Bruker BioApex 30e FT ion cyclotron mass spectrometer, with the samples dissolved in MeOH (0.1 mg/mL) (*m/z*). Melting points were recorded using a Büchi 520 melting point apparatus and are uncorrected. The elemental analyses were performed in The Research Center, Marly, Ciba AG. Emission spectra were recorded on a Perkin-Elmer LS 50B spectrometer. Emission quantum yields (Φ_{em}) were calculated by using [Ru(bpy)$_3$](PF$_6$)$_2$ as a standard in CH_3CN (0.062).[26-28] Electrochemical measurements were carried out at room temperature using a PAR 273A electrochemical analysis system with 270 research electrochemistry software. Cyclic voltammograms were obtained in CH_3CN, using a microcell equipped with a stationary platinum disk electrode with tetra-*n*-butylammonium hexafluorophosphate (0.1 M) as base electrolyte. [Ru(bpy)$_3$](PF$_6$)$_2$ was used as the standard, taking the oxidation potential as +1.26 V, vs SCE.[29-31] Half-wave potentials were calculated as an average of the cathodic and anodic peaks.

Unless otherwise stated, commercial grade reagents were used without further purification. Tetrahydrofuran (THF) was predried by distillation from sodium. (1*R*)-(−)-Myrtenal was obtained from Fluka, >97%, $[\alpha]^{20}_D$ −14.6°.

5,5′-Bis(bromomethyl)-2,2′-bipyridine,[32] 4,5-pineno-2,2′-bipyridine,[25,33] the 4,5-pineno-2,2′-bipyridine dimer (Chiragen-[0]), the 4,5:4′,5′-dipineno-2,2′-bipyridine dimer (SuperChiragen-[0]),[34] Ru(bpy)$_2$Cl$_2$,[35] Δ-/Λ-[Ru(bpy)$_2$(py)$_2$](dibenzoyltartrate),[19] and Δ-RuCG[*m*-xyl]Cl$_2$[24] were prepared according to the literature methods.

(b) Ligand Syntheses. (i) The 4,5-Pineno-2,2′-bipyridine Dimer (CG[3]). To a solution of 4,5-pineno-2,2′-bipyridine (602 mg, 2.41 mmol) in dry THF (10 mL) was added lithium diisopropylamine (LDA) solution (1.5 M; 1.5 mL, 2.25 mmol) in dry THF (10 mL) over 30 min at −40 °C. The reaction mixture was kept below −40 °C for 3 h; then 1,3-dibromopropane (220 mg, 1.09 mmol) dissolved in dry THF (10 mL) was added. During the addition, the color changed from blue to red. The mixture was stirred overnight, and the reaction was quenched with water (2 mL). The solution was concentrated *in vacuo*. After addition of a saturated aqueous solution of sodium hydrogen carbonate (30 mL), the mixture was extracted with dichloromethane (3 × 30 mL). The organic phase was dried over magnesium sulfate and filtered. Following removal of the solvent, the residue was purified by column chromatography on silica gel with hexane/ether/triethylamine (14:6:1) as eluent. Yield: 511 mg (79%). Recrystallization from methanol/dichloromethane gave colorless crystals. Mp: 120.5−121.5 °C. ^{1}H-NMR ($CDCl_3$, 300 MHz): δ 8.64 (dd, 1H, J = 4.8, 0.9 Hz, H-6′), 8.35 (d, 1H, J = 8.0 Hz, H-3′), 8.29 (s, 1H, H-6), 8.20 (s, 1H, H-3), 7.77 (ddd, 1H, J = 7.7, 7.7, 1.7 Hz, H-4′), 7.25 (m, 1H, H-5′), 3.01 (d, 1H, J = 9.9Hz, H-7), 2.87 (dd, 1H, J = 5.4, 5.4 Hz, H-10), 2.60 (ddd, 1H, J = 9.9, 5.8, 5.8 Hz, H-9b), 2.30 (ddd, J = 5.8, 5.8, 2.2 Hz, 1H, H-8), 2.03 (m, 1H, H-15), 1.60 (m, 2H, H-14), 1.44 (s, 3H, H-13), 1.30 (d, 1H, J = 9.7 Hz, H-9a), 0.61 (s, 3H, H-12). ^{13}C-NMR ($CDCl_3$, 300 MHz): δ 156.7, 154.9, 149.7, 148.9, 145.4, 142.6, 136.8, 123.2, 120.8, 119.6, 45.1, 43.2, 41.2, 40.9, 33.5, 28.3, 26.4, 26.2, 21.0. MS (FAB (NBA), *m/z*): 563 (16, MNa$^+$), 541 (100, MH$^+$). Anal. Calcd for $C_{37}H_{40}N_4$·MeOH: C, 79.7; H, 7.7; N, 9.8. Found: C, 80.1; H, 7.7; N, 9.8. Optical rotation: $[\alpha]^{22}_D$ = −70°.

(23) Mürner, H.; von Zelewsky, A.; Stoeckli-Evans, H. *Inorg. Chem.* **1996**, *35*, 3931.
(24) Mürner, H.; Belser, P.; von Zelewsky, A. *J. Am. Chem. Soc.* **1996**, *118*, 7989.
(25) Hayoz, P.; von Zelewsky, A.; Stoeckli-Evans, H. *J. Am. Chem. Soc.* **1993**, *115*, 5111.
(26) Strouse, G. F.; Anderson, P. A.; Schoonover, J. R.; Meyer, T. J.; Keene, F. R. *Inorg. Chem.* **1992**, *31*, 3004.
(27) Anderson, P. A.; Deacon, G. B.; Haarmann, K. H.; Keene, F. R.; Meyer, T. J.; Reitsma, D. A.; Skelton, B. W.; Strouse, G. F.; Thomas, N. C.; Treadway, J. A.; White, A. H. *Inorg. Chem.* **1995**, *34*, 6145.
(28) Caspar, J. V.; Meyer, T. J. *J. Am. Chem. Soc.* **1989**, *111*, 7448.
(29) Lin, C. T.; Boettcher, W. J.; Chou, M.; Creutz, C.; Sutin, N. *J. Am. Chem. Soc.*, **1976**, *98*, 6536.
(30) Juris, A.; Balzani, V.; Belser, P.; von Zelewsky, A. *Helv. Chim. Acta* **1981**, *64*, 2175.
(31) Sutin, N.; Creutz, C. *Adv. Chem. Ser.* **1978**, *168*, 1.
(32) Eaves, J.; Munro, H.; Parker, D. *J. Chem. Soc., Chem. Commun.* **1985**, *684*.
(33) Hayoz, P.; von Zelewsky, A. *Tetrahedron Lett.* **1992**, *33*, 5165−5168.
(34) Fletcher, N. C.; Keene, F. R.; Ziegler, M.; Stoeckli-Evans, H.; Viebrock, H.; von Zelewsky, A. *Helv Chim Acta* **1996**, *79*, 1192.
(35) Lay, P. A.; Sargeson, A. M.; Taube, H. *Inorg. Synth.* **1986**, *24*, 291.

(ii) The 4,5-Pineno-2,2′-bipyridine Dimer (CG[bpy]). A procedure analogous to that for CG[3] was followed, using 4,5-pineno-2,2′-bipyridine (500 mg, 2.00 mmol) in dry THF (10 mL), 1.5 M LDA solution (1.4 mL, 2.10 mmol), and 5,5′-bis-(bromomethyl)-2,2′-bipyridine (341 mg, 0.99 mmol) dissolved in dry THF (10 mL). Yield: 212 mg (32%). Recrystallization from methanol/dichloromethane gave colorless crystals. Mp: 217.5−218.5 °C. ^{1}H-NMR ($CDCl_3$, 300 MHz): δ 8.62 (dd, 1H, J = 4.8, 0.8 Hz, H-6′), 8.48 (d, 1H, J = 1.92 Hz, H-6″), 8.42 (s, 1H, H-6), 8.34 (d, 1H, J = 8.0 Hz, H-3′), 8.31 (d, 1H, J = 8.4 Hz, H-3″), 8.21 (s, 1H, H-3), 7.75 (ddd, 1H, J = 7.6, 7.6, 1.8, Hz, H-4′), 7.64 (dd, 1H, J = 8.2, 2.2 Hz, H-4″), 7.23 (m, 1H, H-5′), 3.46 (dd, 1H, J = 3.6, 13.8 Hz, H-14a), 3.26 (dd, 1H, J = 11.3 Hz, H-7), 2.84 (dd, 1H, J = 5.5, 5.5 Hz, H-10), 2.75 (dd, 1H, J = 11.2, 14.0 Hz, H-14b), 2.54 (ddd, 1H, J = 9.9, 5.5, 5.5 Hz, H-9b), 1.95 (dd, J = 5.8, 5.8 Hz, 1H, H-8), 1.36 (d, 1H, J = 10.0 Hz, H-9a), 1.28 (s, 3H, H-13), 0.53 (s, 3H, H-12). ^{13}C-NMR ($CDCl_3$, 300 MHz): δ 156.4, 154.8, 154.3 149.8, 149.0 148.0, 145.7, 142.7, 137.6, 136.9, 135.3 123.4 (CH-5′), 120.9, 120.6, 119.3, 45.0, 42.8, 42.4, 41.0, 36.4, 28.0, 26.2, 20.9. MS (FAB (NBA), *m/z*): 703 (9, MNa^+), 681 (48, MH^+), 432 (20, M − pineno − bpy$^+$). Anal. Calcd for $C_{46}H_{46}N_6 \cdot 2.5H_2O$: C, 76.1; H, 6.8; N, 11.6. Found: C, 76.1; H, 6.8; N, 11.6. Optical rotation: $[\alpha]^{22}_D = +133°$.

(c) Complex Syntheses Using Ru(bpy)$_2$Cl$_2$. (i) Diastereomeric Mixture of [{(bpy)$_2$Ru}$_2$-μ-CG[3]](PF$_6$)$_4$. In a typical experiment, CG[3] (53.4 mg, 0.10 mmol) and $Ru(bpy)_2Cl_2$ (106 mg, 0.20 mmol) were heated in ethylene glycol (10 mL; 10% water) at 100 °C for 20 h, after which the volume was reduced to 1 mL by vacuum distillation, and the product was precipitated with the addition 10% aqueous ammonium hexafluorophosphate solution. The red solid was filtered, dried at 50 °C, and purified by repeated passage down a Sephadex LH20 column (50% methanol/acetonitrile eluent), collecting the first fraction. Yield: 165 mg (85%). MS (FAB (NBA), *m/z*): 1804 ([M − PF_6]$^+$), 1656 ([MH − 2PF_6]$^+$), 1513 ([MH_2 − 3PF_6]$^+$). Anal. Calcd for $C_{77}H_{72}N_{12}F_{24}P_4Ru_2 \cdot H_2O$: C, 47.1; H, 3.8; N, 8.5. Found: C, 47.1; H, 3.8; N, 8.5.

(ii) Diastereomeric Mixture of [{(bpy)$_2$Ru}$_2$-μ-CG[0]](PF$_6$)$_4$. Yield: 74%. MS (FAB (NBA), *m/z*): 1761 ([M − PF_6]$^+$), 1615 ([MH − 2PF_6]$^+$). Anal. Calcd for $C_{74}H_{66}N_{12}F_{24}P_4Ru_2 \cdot 2H_2O$: C, 45.8; H, 3.6; N, 8.7. Found: C, 45.8; H, 3.8; N, 8.4.

(iii) Diastereomeric Mixture of [{(bpy)$_2$Ru}$_2$-μ-SCG[0]](PF$_6$)$_4$. Yield: 82%. MS (FAB (NBA), *m/z*): 1947 ([M − PF_6]$^+$), 1806 ([MH − 2PF_6]$^+$). Anal. Calcd for $C_{88}H_{85}N_{12}F_{24}P_4Ru_2 \cdot 1.5H_2O$: C, 49.8; H, 4.2; N, 7.9. Found: C, 49.9; H, 4.3; N, 7.7.

(iv) Diastereomeric Mixture of [{(bpy)$_2$Ru}$_3$-μ-CG[bpy]](PF$_6$)$_6$. Yield: 57%. MS (FAB (NBA), *m/z*): 2648 ([M − PF_6]$^+$), 2500 ([MH − 2PF_6]$^+$). Anal. Calcd for $C_{106}H_{92}N_{18}F_{36}P_6Ru_3 \cdot 1.5H_2O$: C, 44.9; H, 3.6; N, 8.7. Found: C, 44.8; H, 3.7; N, 8.5.

(d) Complex Syntheses Using Δ-/Λ-[Ru(bpy)$_2$(py)$_2$](dibenzoyltartrate). (i) [{(bpy)$_2$-Δ-Ru}$_2$-μ-CG[3]](PF$_6$)$_4$. In a typical experiment, CG[3] (21.6 mg, 40.0 μmol) and Δ-[Ru(bpy)$_2$(py)$_2$](dibenzoyltartrate) (101.8 mg, 89.0 μmol) were heated in ethylene glycol (10 mL; 10% water) at 100 °C for 20 h, after which the volume was reduced to 1 mL by vacuum distillation, and the product was precipitated with the addition 10% aqueous ammonium hexafluorophosphate solution. The red solid was filtered off, dried at 50 °C, and purified by preparative thick-layer plate silica chromatography using *N,N*-dimethylformamide (DMF)/water (4:1) containing 10% ammonium chloride as eluent (SCG[0]: DMF/water (10:1)). The product was extracted from the lowest fraction with acetone containing 10% ammonium hexafluorophosphate. Yield: 37 mg (41%). MS (electrospray, *m/z*): 1803 ([M − PF_6]$^+$), 829 ([M − 2PF_6]$^{2+}$), 504 ([M − 3PF_6]$^{3+}$).

(ii) [{(bpy)$_2$-Λ-Ru}$_2$-μ-CG[3]](PF$_6$)$_4$. Yield: 85%. MS (electrospray, *m/z*): 1803 ([M − PF_6]$^+$), 829 ([M − 2PF_6]$^{2+}$), 504 ([M − 3PF_6]$^{3+}$).

(iii) [{(bpy)$_2$-Δ-Ru}$_2$-μ-CG[0]](PF$_6$)$_4$. Yield: 46%. MS (electrospray, *m/z*): 1761 ([M − PF_6]$^+$), 1125 ([2M − 3PF_6]$^{3+}$), 808 ([M − 2PF_6]$^{2+}$), 490 ([M − 3PF_6]$^{3+}$).

(iv) [{(bpy)$_2$-Λ-Ru}$_2$-μ-CG[0]](PF$_6$)$_4$. Yield: 88%. MS (electrospray, *m/z*): 1761 ([M − PF_6]$^+$), 1125 ([2M − 3PF_6]$^{3+}$), 808 ([M − 2PF_6]$^{2+}$), 490 ([M − 3PF_6]$^{3+}$).

(v) [{(bpy)$_2$-Δ-Ru}$_2$-μ-SCG[0]](PF$_6$)$_4$. Yield: 22%. MS (electrospray, *m/z*): 1948 ([M − PF_6]$^+$), 902 ([M − 2PF_6]$^{2+}$), 553 ([M − 3PF_6]$^{3+}$).

(vi) [{(bpy)$_2$-Λ-Ru}$_2$-μ-SCG[0]](PF$_6$)$_4$. Yield: 55%. MS (electrospray, *m/z*): 1948 ([M − PF_6]$^+$), 1251 ([2M − 3PF_6]$^{3+}$), 902 ([M − 2PF_6]$^{2+}$), 553 ([M − 3PF_6]$^{3+}$), 378 ([M − 4PF_6]$^{4+}$).

(vii) [{(bpy)$_2$-Δ-Ru}$_3$-μ-CG[bpy]](PF$_6$)$_6$. Yield: 37%. MS (electrospray, *m/z*): 1251 ([M − 2PF_6]$^{2+}$), 785 ([M − 3PF_6]$^{3+}$), 553 ([M − 4PF_6]$^{4+}$), 413 ([M − 5PF_6]$^{5+}$), 384 ([M − 5PF_6 − HPF_6]$^{5+}$).

(viii) {(bpy)$_2$-Λ-Ru}$_3$-μ-CG[bpy]](PF$_6$)$_6$. Yield: 39%. MS (electrospray, *m/z*): 1251 ([M − 2PF_6]$^{2+}$), 785 ([M − 3PF_6]$^{3+}$), 553 ([M − 4PF_6]$^{4+}$), 413 ([M − 5PF_6]$^{5+}$), 384 ([M − 5PF_6 − HPF_6]$^{5+}$).

(e) Complex Syntheses Using Δ-RuCG[*m*-xyl]Cl$_2$. (i) [{CG[*m*-xyl]-Δ-Ru}$_2$-μ-CG[3]](PF$_6$)$_4$. In a typical experiment, CG[3] (17.5 mg, 32.4 μmol) and Δ-[Ru(CG[*m*-xyl])Cl$_2$] (50.8 mg, 65.6 μmol) were heated in ethylene glycol (10 mL; 10% water) at 100 °C for 20 h, after which the volume was reduced to 1 mL by vacuum distillation, and the product was precipitated with the addition 10% aqueous ammonium hexafluorophosphate solution. The red solid was filtered off, dried at 50 °C, and purified by preparative thick-layer plate silica chromatography with acetonitrile/butan-1-ol/water (4:1:1) containing 10% potassium nitrate as eluent. The product was extracted from the lowest fraction with acetone containing 10% ammonium hexafluorophosphate. Yield: 62 mg (76%). MS (FAB (NBA), *m/z*): 2385 ([M − PF_6]$^+$), 2239 ([MH − 2PF_6]$^+$), 2089 ([MH_2 − 3PF_6]$^+$). Anal. Calcd for $C_{121}H_{124}N_{12}F_{24}P_4Ru_2 \cdot 4MeOH$: C, 56.5; H, 5.3; N, 6.3. Found: C, 56.7; H, 5.4; N, 5.9.

(ii) [{CG[*m*-xyl]-Δ-Ru}$_2$-μ-CG[0]](PF$_6$)$_4$. Yield: 50%. MS (FAB (NBA), *m/z*): 2341 ([M − PF_6]$^+$), 2196 ([MH − 2PF_6]$^+$), 2053 ([MH_2 − 3PF_6]$^+$). Anal. Calcd for $C_{118}H_{118}N_{12}F_{24}P_4Ru_2 \cdot 5H_2O$: C, 55.0; H, 5.0; N, 6.5. Found: C, 54.5; H, 5.3; N, 5.5.

(iii) [{CG[*m*-xyl]-Δ-Ru}$_2$-μ-SCG[0]](PF$_6$)$_4$. Yield: 39%. MS (electrospray, *m/z*): 1193 ([M − 2PF_6]$^{2+}$), 764 ([M − 3PF_6]$^{3+}$), 524 ([M − 4PF_6]$^{4+}$). Anal. Calcd for $C_{132}H_{138}N_{12}F_{24}P_4Ru_2 \cdot 7H_2O$: C, 56.6; H, 5.5; N, 6.0. Found: C, 56.4; H, 5.4; N, 5.9.

(iv) [{CG[*m*-xyl]-Δ-Ru}$_3$-μ-CG[bpy]](PF$_6$)$_6$. Yield: 29%. MS (electrospray, *m/z*): 1687 ([M − 2PF_6]$^{2+}$), 1076 ([M − 3PF_6]$^{3+}$), 771 ([M − 4PF_6]$^{4+}$), 588 ([M − 5PF_6]$^{5+}$), 465 ([M − 6PF_6]$^{6+}$). Anal. Calcd for $C_{172}H_{170}N_{18}F_{36}P_6Ru_3 \cdot 7H_2O$: C, 54.5; H, 4.9; N, 6.7. Found: C, 54.6; H, 5.1; N, 6.5.

All of the complexes were fully characterized by ^{1}H-NMR, details of which are supplied in the Supporting Information. Additionally, see Table 1 and Figures 4 and 5.

(f) X-ray Structural Determination of CG[3]. The data set was collected on a Stoe AED2 four-circle diffractometer, using the $\omega/2\theta$ scan mode and Mo Kα graphite-monochromated radiation (λ 0.7107 3 Å) at room temperature. The crystals are

Table 1. Numbers and Positions of the Pineno Methyl Signals in the ^{1}H-NMR Spectra

complex	no. of methyl peaks obsd	ppm (rel integration ± 10%)												
[{(bpy)$_2$Ru}$_2$-μ-CG[3]]$^{4+}$	6	1.38 (2)	1.32 (2)	0.70 (1)	0.69 (1)	0.29 (1)	0.28 (1)							
[{(bpy)$_2$-Δ-Ru}$_2$-μ-CG[3]]$^{4+}$	2	1.38 (2)			0.69 (1)									
[{(bpy)$_2$-Λ-Ru}$_2$-μ-CG[3]]$^{4+}$	2		1.31 (2)			0.29 (1)								
[{CG[*m*-xyl]-Δ-Ru}$_2$-μ-CG[3]]$^{4+}$	5	1.42 (1)	1.28 (1)	1.27 (1)	0.77 (1)	0.59 (2)								
[{(bpy)$_2$Ru}$_2$-μ-CG[0]]$^{4+}$	8	1.29 (1)	1.23 (1)	1.19 (1)	1.12 (1)	0.82 (1)	0.79 (1)	0.41 (1)	0.38 (1)					
[{(bpy)$_2$Ru}$_2$-μ-CG[0]]$^{4+}$	2	1.29 (1)					0.79 (1)							
[{(bpy)$_2$-Δ-Ru}$_2$-μ-CG[0]]$^{4+}$	2			1.19 (1)				0.41 (1)						
[{(bpy)$_2$-Λ-Ru}$_2$-μ-CG[0]]$^{4+}$	4	1.28 (2)	0.91 (1)	0.60 (1)	0.58 (2)									
[{CG[*m*-xyl]-Δ-Ru}$_2$-μ-CG[0]]$^{4+}$	15	1.35 (1)	1.34 (1)	1.29 (2)	1.28 (1)	1.22 (1)	1.18 (1)	1.12 (1)	0.83 (1)	0.80 (1)	0.73 (1)	0.71 (1)	0.41 (1)	0.39 (1)	0.35 (1)	0.33 (1)
[{(bpy)$_2$Ru}$_2$-μ-SCG[0]]$^{4+}$	4	1.36 (1)					1.19 (1)			0.81 (1)	0.74 (1)					
[{(bpy)$_2$-Δ-Ru}$_2$-μ-SCG[0]]$^{4+}$	2			1.29 (1)	1.28 (1)								0.42 (1)		0.34 (1)	
[{(bpy)$_2$-Λ-Ru}$_2$-μ-SCG[0]]$^{4+}$	4			1.29 (1)	1.28 (1)											
[{CG[*m*-xyl]-Δ-Ru}$_2$-μ-SCG[0]]$^{4+}$	8	1.39 (1)	1.28 (1)	1.28 (1)	1.26 (1)	0.93 (1)	0.81 (1)	0.59 (1)	0.58 (1)							
[{(bpy)$_2$Ru}$_2$-μ-CG[bpy]]$^{6+}$	8	1.22 (1)	1.16 (1)	1.15 (1)	1.09 (1)	0.79 (1)	0.61 (1)	0.49 (1)	0.21 (1)	0.09 (1)						
[{(bpy)$_2$-Δ-Ru}$_2$-μ-CG[bpy]]$^{6+}$	2			1.16 (1)				0.50 (1)								
[{(bpy)$_2$-Λ-Ru}$_2$-μ-CG[bpy]]$^{6+}$	2		1.17 (1)						0.21 (1)							
[{CG[*m*-xyl]-Δ-Ru}$_2$-μ-CG[bpy]]$^{6+}$	8	1.26 (1)	1.26 (1)	1.16 (1)	1.01 (1)	0.62 (1)	0.58 (1)	0.55 (1)	0.39 (1)							

Scheme 1. Preparation of Additional "Chiragen" Ligands[a]

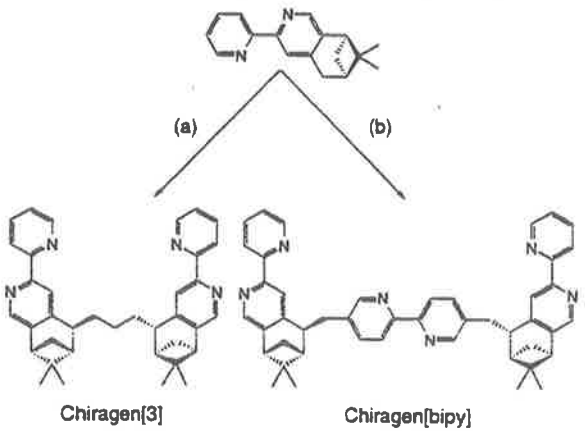

[a] Route a: (i) LDA, THF, <−40 °C; (ii) 1,3-dibromopropane. Route b: (i) LDA, THF, <−40 °C; (ii) 5,5′-bis(bromomethyl)-2,2′-bipyridine.

orthorhombic, of space group $P2_12_12_1$. Cell dimensions: a = 12.229(1) Å, b = 12.790(0) Å, c = 20.215(1) Å, and V = 3161.8(4) Å^3. D_{calc} = 1.170 g cm^{-3}; Z = 4; R = 0.0554. Additionally, a disordered molecule of water was located in the unit cell.

Results and Discussion

Synthesis. We previously published the preparation of the "Chiragen" ligand system consisting of two linked 4,5-pineno-2,2′-bipyridines.[23−25,33] To ensure unambiguous characterization of the bridged coordination complexes of this type of system by techniques such as NMR, it was necessary to design new analogues where the link between the two bipyridyl coordination sites is as small as possible. As a consequence, it would be possible to identify the diastereomers present following coordination to an octahedral transition metal center. To this end we recently described the synthesis of "Chiragen[0]" (CG[0]) and "SuperChiragen[0]" (SCG[0]), with a direct linkage between two pinene moieties. Due to the close proximity of the bulky pinene groups, a severely hindered rotation around the linkage was demonstrated, as indicated by a significant effect observed by both polarimetry and circular dichroism (CD) spectroscopy.[34]

To extend the series, "Chiragen[3]" (CG[3]), with a propylene spacer, was prepared in high yield (Scheme 1) by following the previously described procedure. Disappointingly, similar procedures to prepare the analogous ligands Chiragen[1] and Chiragen[2] (with a methylene and an ethylene spacer, respectively) were unsuccessful. Crystals of CG[3] suitable for X-ray structure determination were produced by slow evaporation from methanol/dichloromethane, giving the structure illustrated in Figure 3. The structure indicates that the coupling reaction occurs with the introduction of a pair of chiral centers on C7 and C7a, as previously described.[23−25,33]

To increase the possible number of coordination sites to three, 5,5′-bis(bromomethyl)-2,2′-bipyridine was used to form a bridge between the two pinenobipyridine groups (Scheme 1), giving "Chiragen[bpy]" (CG[bpy]). This new ligand provides three bidentate coordination sites, suitable for the preparation of trinuclear species.

Ligands CG[0], SCG[0], and CG[3] were subsequently coordinated to ruthenium(II), using an excess of the transition metal precursors, by heating in ethylene glycol containing 10% water. Ru(bpy)$_2$Cl$_2$ gave a mixture of all the possible dinuclear diastereomers in over 70% yield. In the case of the trinuclear ligand (CG[bpy]), 57% of the desired product was obtained as

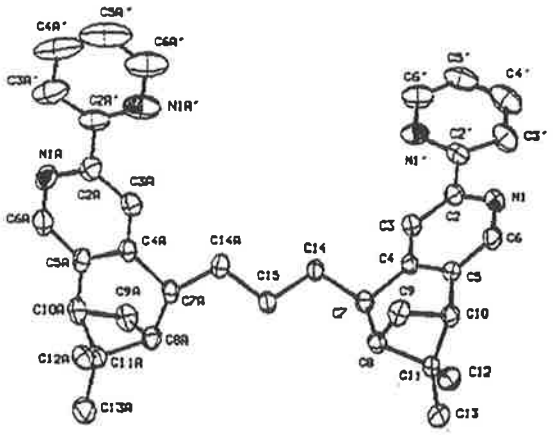

Figure 3. Thermal motion ellipsoid plot of Chiragen[3], with ellipsoids drawn at 30% probability.

a mixture of diastereomers, with a small but significant amount of a dinuclear species being observed during the purification. The complexes were purified by repeated passage of the hexafluorophosphate salt down a Sephadex LH20 column, eluting with 50% acetonitrile/methanol, giving the larger desired species first.

Using the resolved chiral building blocks Δ- and Λ-[Ru(bpy)$_2$-(py)$_2$](dibenzoyltartrate), only one of the possible diastereomers was obtained following purification by preparative plate silica chromatography eluting with a DMF/water (4:1) mixture containing 10% ammonium chloride. The complexes derived from SCG[0] indicated a greater hydrophobicity, due to the increased number of pinene groups as compared to CG[0], and were eluted with a mixture containing a higher proportion of DMF (10:1). In all cases, the slowest moving fraction was collected, while species of lower nuclearity were observed to travel much faster on the plate. The products were characterized by CD and ^{1}H-NMR spectroscopy, as described below. Additionally, electrospray mass spectroscopy gave a number of assignable peaks in accordance with the proposed species; this observation is the subject of further study. The yields proved to be disappointingly lower than that obtained with the use of Ru(bpy)$_2$Cl$_2$ due to retention of the product on the silica during purification.

The precursor, Δ-RuCG[*m*-xyl]Cl$_2$, with a predetermined helicity due to the nature of the supplementary tetradentate Chiragen[*m*-xylyl] ligand, gave only one of the possible diastereomers. Again, these were purified by preparative plate silica chromatography, eluting with acetonitrile/butan-1-ol/water (4:1:1) containing 10% potassium nitrate. It was noted that an appreciable amount of the product was retained on the silica. Compounding this, lower yields were obtained than expected for the species with the smaller bridges, CG[0], SCG[0], and CG[bpy], which we assume to be due to unfavorable steric interactions of the bulky pinene groups, preventing the formation of dinuclear (trinuclear) species. Due to the natural chirality of the ligands and the control of helicity at the ruthenium metal centers, only one diastereomer was prepared, indicated by ^{1}H-NMR and CD spectroscopy (see below). This is even the case with the complex [{CG[*m*-xyl]-Δ-Ru}$_3$-*μ*-CG[bpy]](PF$_6$)$_6$ containing 27 stereogenic sites, including three chiral metal centers.

^{1}H-NMR Spectroscopy. The dinuclear species prepared from Ru(bpy)$_2$Cl$_2$ contains all three diastereomers, ΔΔ, ΛΛ, and ΔΛ, in the expected statistical ratios (from integration). While each of these possesses either C_2 or C_s symmetry, a very complex spectrum occurs as a consequence of the diastereomeric mixture, where definite identification of individual peaks is extremely difficult. In each case, the pineno methyl peaks gave a good indication of the number of isomers present (Table 1). Using the chirally resolved precursor, either Δ- or Λ-[Ru(bpy)$_2$-

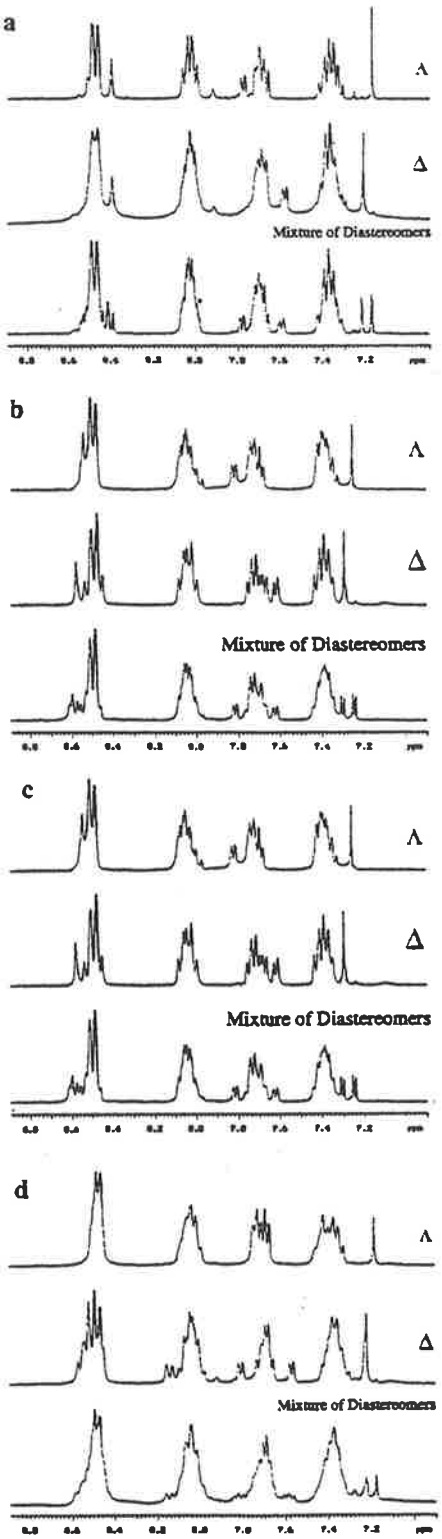

Figure 4. The aromatic region of the ^{1}H-NMR for the di- and trinuclear Λ, Δ and mixed ruthenium species of the ligands (a) [{(bpy)$_2$Ru}$_2$-*μ*-CG[3]](PF$_6$)$_6$, (b) [{(bpy)$_2$Ru}$_2$-*μ*-CG[0]](PF$_6$)$_6$, (c) [{(bpy)$_2$Ru}$_2$-*μ*-SCG[0]](PF$_6$)$_6$, and (d) [{(bpy)$_2$Ru}$_3$-*μ*-CG[bpy]](PF$_6$)$_6$.

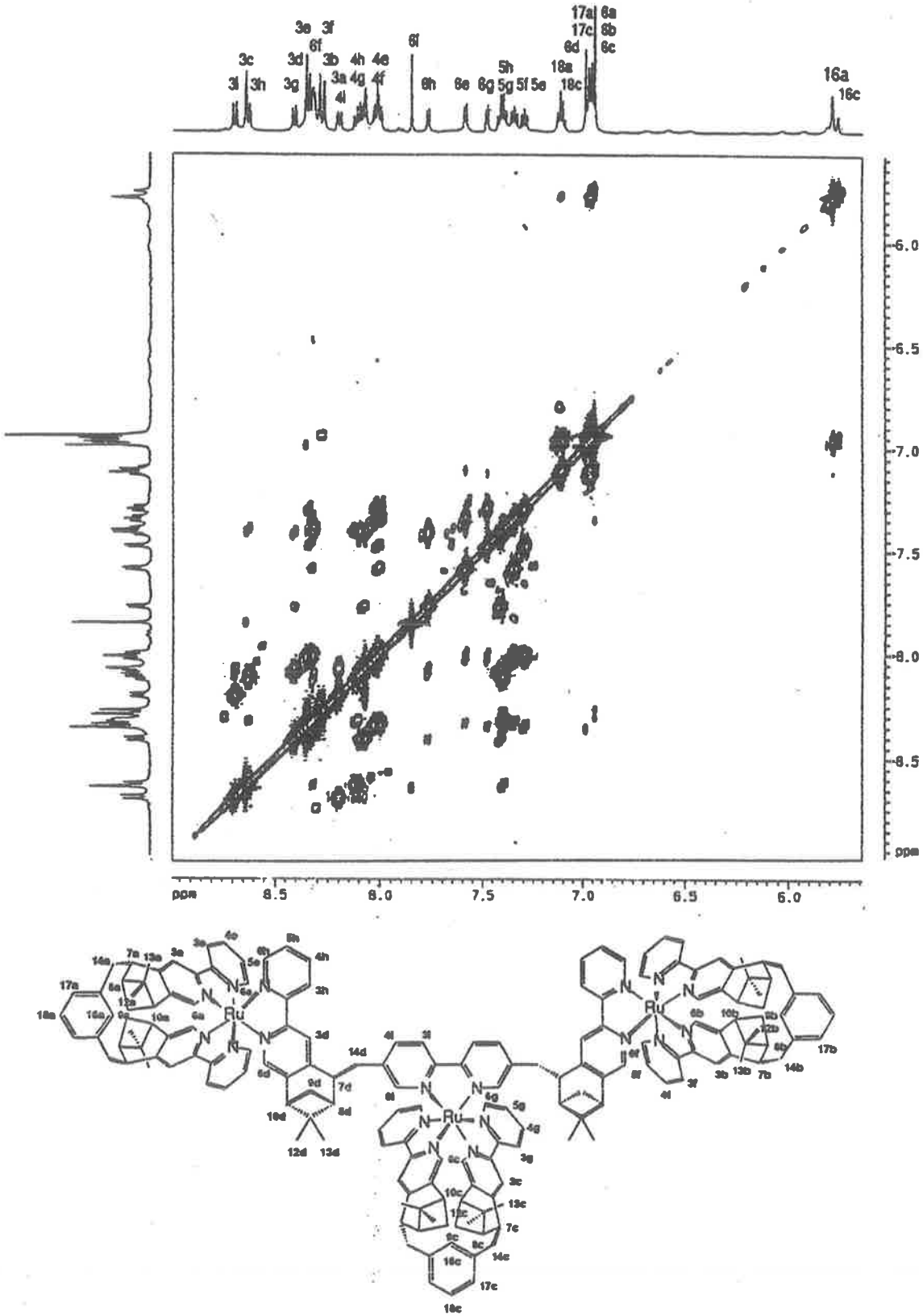

Figure 5. An H,H-COSY spectrum of $[\{CG[m\text{-xyl}]\text{-}\Delta\text{-}Ru\}_3\text{-}\mu\text{-}CG[bpy]](PF_6)_6$, with assignments shown below, run in CD_3CN (500 MHz).

$(py)_2$](dibenzoyltartrate), the ^{1}H-NMR spectrum indicates that only one of the three diastereomers was present in the product (see CD spectra), with an estimated ee of over 95%, as determined from the integration of the methyl peaks. The

Table 2. Electrochemical and Photophysical Properties in CH_3CN at 298 K

complex	$E_{1/2}$, V vs SCE oxidn	$E_{1/2}$, V vs SCE redn	E_{red}, V vs SCE redn	LC $\lambda_{max} \pm 2$, nm	LC $10^{-3}\epsilon$	MLCT $\lambda_{max} \pm 2$, nm	MLCT $10^{-3}\epsilon$	emission $\lambda_{em} \pm 2$, nm	emission $\Phi_{em} \pm 5\%$
$[Ru(bpy)_3]^{2+}$	1.26	−1.37	−1.59	286	102.3	452	16.1	610	0.062
$[\{(bpy)_2Ru\}_2\text{-}\mu\text{-}CG[3]]^{4+}$	1.21	−1.38	−1.63	288	175.1	452	37.8	613	0.049
$[\{(bpy)_2\text{-}\Delta\text{-}Ru\}_2\text{-}\mu\text{-}CG[3]]^{4+}$				288	169.6	452	36.1	615	0.052
$[\{(bpy)_2\text{-}\Lambda\text{-}Ru\}_2\text{-}\mu\text{-}CG[3]]^{4+}$				288	174.0	452	36.6	615	0.048
$[\{CG[m\text{-xyl}]\text{-}\Delta\text{-}Ru\}_2\text{-}\mu\text{-}CG[3]]^{4+}$	1.13	−1.48	−1.69	295	155.4	450	30.0	610	0.018
$[\{(bpy)_2Ru\}_2\text{-}\mu\text{-}CG[0]^{4+}$	1.23	−1.37	−1.60	288	154.5	452	31.1	611	0.053
$[\{(bpy)_2\text{-}\Delta\text{-}Ru\}_2\text{-}\mu\text{-}CG[0]]^{4+}$				288	153.5	452	34.7	614	0.055
$[\{(bpy)_2\text{-}\Lambda\text{-}Ru\}_2\text{-}\mu\text{-}CG[0]]^{4+}$				288	157.6	452	36.7	612	0.055
$[\{CG[m\text{-xyl}]\text{-}\Delta\text{-}Ru\}_2\text{-}\mu\text{-}CG[0]]^{4+}$	1.14	−1.48	−1.69	296	144.3	452	29.2	610	0.013
$[\{(bpy)_2Ru\}_2\text{-}\mu\text{-}SCG[0]]^{4+}$	1.16	−1.40	−1.64	288	158.9	452	29.9	618	0.043
$[\{(bpy)_2\text{-}\Delta\text{-}Ru\}_2\text{-}\mu\text{-}SCG[0]]^{4+}$				288	143.9	452	31.1	618	0.044
$[\{(bpy)_2\text{-}\Lambda\text{-}Ru\}_2\text{-}\mu\text{-}SCG[0]]^{4+}$				288	133.6	452	26.1	623	0.044
$[\{CG[m\text{-xyl}]\text{-}\Delta\text{-}Ru\}_2\text{-}\mu\text{-}SCG[0]]^{4+}$	1.10	−1.49	−1.75	298	143.1	438	29.2	611	0.019
$[\{(bpy)_2Ru\}_3\text{-}\mu\text{-}CG[bpy]]^{6+}$	1.22	−1.38	−1.63	288	244.9	452	56.3	614	0.061
$[\{(bpy)_2\text{-}\Delta\text{-}Ru\}_3\text{-}\mu\text{-}CG[bpy]]^{6+}$				288	230.0	452	54.1	614	0.064
$[\{(bpy)_2\text{-}\Lambda\text{-}Ru\}_3\text{-}\mu\text{-}CG[bpy]]^{6+}$				288	237.5	452	52.2	612	0.060
$[\{CG[m\text{-xyl}]\text{-}\Delta\text{-}Ru\}_3\text{-}\mu\text{-}CG[bpy]]^{6+}$	1.15	−1.48	−1.67	298	213.3	451	38.3	604	0.016

spectrum in each case simplifies considerably when compared to those of the diastereomeric mixtures (Figure 4).

Using the potential trinuclear ligand CG[bpy], the number of possible diastereomers increases to 6; *viz.*, ΔΔΔ, ΔΔΛ, ΔΛΔ, ΔΛΛ, ΛΔΛ, and ΛΛΛ. This leads to a very complex spectrum (Figure 4d). However, because the two extreme coordination centers are unable to sense each other's presence, the number of isomers observed is reduced to 3 (while in reality all six are present). By using the Δ- or Λ- $[Ru(bpy)_2(py)_2]$-(dibenzoyltartrate) precursor, only one of the respective stereoisomers is produced (see CD spectra), as with the dinuclear complexes.

Using the predetermined building block Δ-RuCG[*m*-xyl]Cl_2, only one of the possible diastereomers is observed by ^{1}H-NMR. While this series of complexes demonstrate extremely intricate ^{1}H-NMR spectra, especially for the trinuclear $[\{CG[m\text{-xyl}]\text{-}\Delta\text{-}Ru\}_3\text{-}\mu\text{-}CG[bpy]]^{6+}$, they can be assigned using H,H-COSY techniques (Figure 5) and comparison with previously characterized species such as $[\Delta\text{-}Ru(CG[m\text{-xyl}])(bpy)]^{2+}$.[24]

Cyclic Voltammetry. The complexes all gave similar CV spectra, with a quasi-reversible Ru(II/III) couple in the range 1.13−1.22 V. The first reduction wave demonstrated reversibility, at approximately −1.4 V. The subsequent wave was irreversible, and consequently the peak potential for reduction ($E_{p,c}$) is given in Table 2. The pinenobipyridyl ligands shift all redox potentials to a more negative (cathodic) potential, when compared to the case of $[Ru(bpy)_3](PF_6)_2$, as illustrated in Table 2, where larger shifts are given for complexes with a greater number of pinene groups per coordination center. No difference between the pairs of diastereomers was observed electrochemically, despite there being considerable structural differences between them.

UV/Vis Absorption and Emission Spectra. The complexes of the type $[\{(bpy)_2\text{-}Ru\}_n\text{-}\mu\text{-}L](PF_6)$ ($n = 2$, L = CG[0], SCG[0], CG[3]; $n = 3$, L = CG[bpy]) each demonstrated spectra similar to that of $[Ru(bpy)_3]^{2+}$, where the absorption is proportional to the number of chromophoric centers (Table 2). Additionally, they exhibit strong luminescence at approximately the same wavelength (610 nm) and quantum yield (0.06) (within experimental error) as those of $[Ru(bpy)_3]^{2+}$ per chromophoric center. Again, in each case, it was observed that the individual orientations at the metal centers of the ΛΛ and ΔΔ complexes did not demonstrate any significant difference in behavior.

The complexes prepared from RuCG[*m*-xyl]Cl_2 did not conform to the above observations however (Figure 6). The

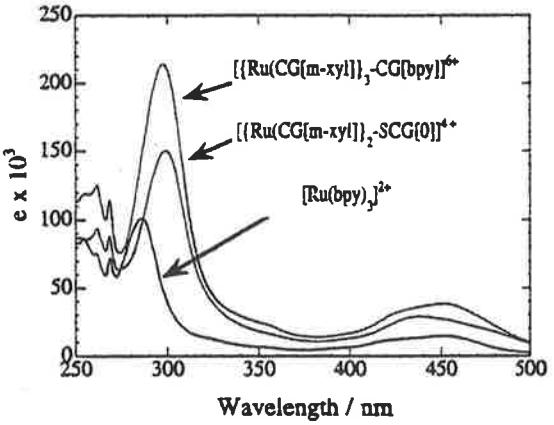

Figure 6. UV/vis absorption spectra of $[Ru(bpy)_3](PF_6)_2$, $[\{CG[m\text{-xyl}]\text{-}\Delta\text{-}Ru\}_2\text{-}\mu\text{-}SCG[0]](PF_6)_6$, and $\Delta\Delta\Delta\text{-}[\{CG[m\text{-xyl}]\text{-}\Delta\text{-}Ru\}_3\text{-}\mu\text{-}CG[bpy]](PF_6)_6$.

ligand-centered (LC) absorption is bathochromically shifted by 10 nm to 298 nm. A strong shoulder is evident in the metal-to-ligand charge transfer band (MLCT) at approximately 430 nm. With the complex $[\{CG[m\text{-xyl}]\text{-}\Delta\text{-}Ru\}_2\text{-}\mu\text{-}SCG[0]]^{4+}$ the shoulder and the maxima are inverted resulting in a hypsochromic shift of 18 nm (Table 2). Additionally, the emission is much weaker than those of the above complexes, though still at 610 nm. It is assumed that these effects are a result of additional steric constraints caused by the larger number of bulky pinene groups, forcing a deviation from the ideal octahedral coordination ligand arrangement.

Circular Dichroism Spectra. All the ligands, except CG[3], exhibit a significant Cotton effect, observed by circular dichroism (CD) spectroscopy in the LC $\pi-\pi^*$ transitions at approximately 300 nm.[34] It has been assumed that this is due to steric constraints in the rotation along the linkage, leading to a dominant solution conformation. With the mixture of diastereomers prepared using the racemic precursor $Ru(bpy)_2Cl_2$, a weak Cotton effect is evident in the solution, despite the NMR indicating a statistical mixture of the diastereomers, with small $\Delta\epsilon$ values being observed only on the LC transitions. While for the CG[3] complex the effect is small, and could be caused by a slight excess of the ΛΛ diastereomer, the effect is much more evident for the other complexes, with a pattern that does not resemble those of the single diastereomers discussed below. Thus, this observed signal is a consequence of the ligand

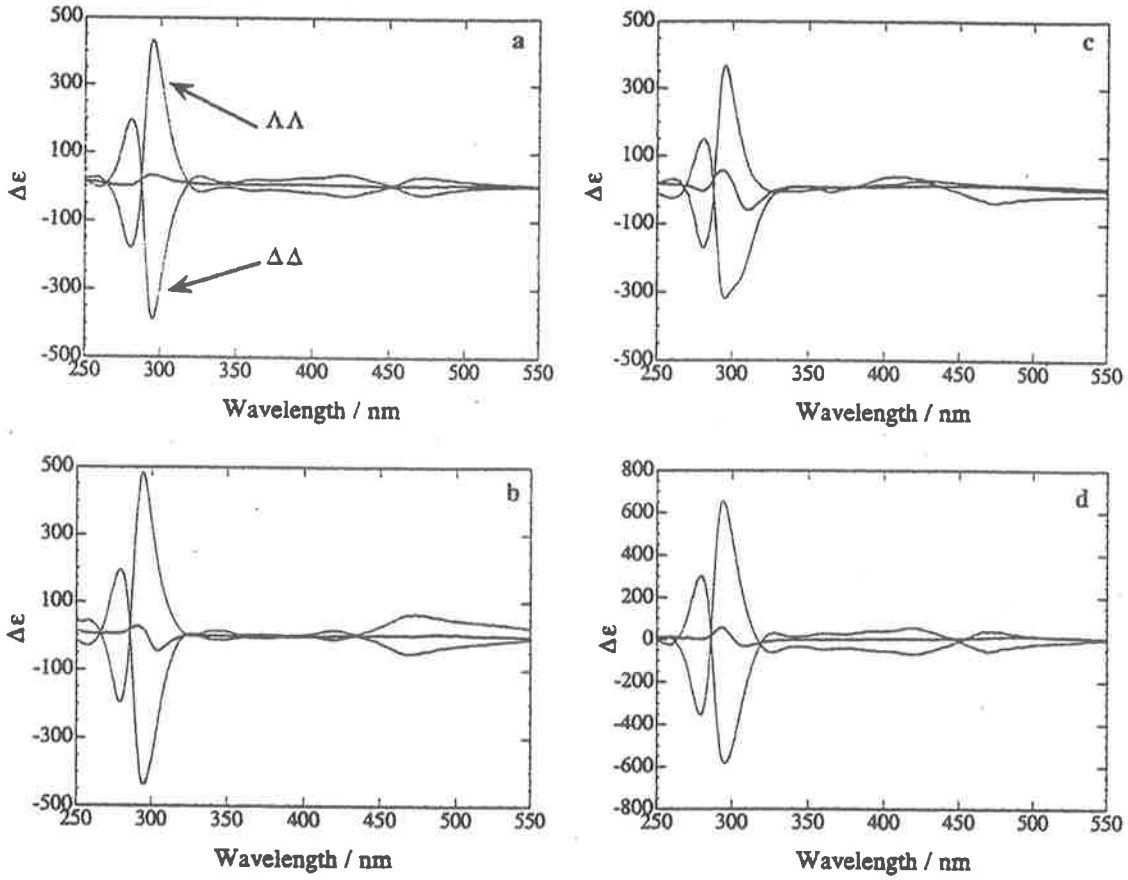

Figure 7. CD spectra of ΛΛ, ΔΔ, and mixed ruthenium species of the ligands (a) CG[3], (b) CG[0], (c) SCG[0], and (d) the trinuclear ΛΛΛ, ΔΔΔ, and mixed ruthenium species CG[bpy].

Table 3. CD Maxima Observed in Acetonitrile at 298 K

complex	$\lambda \pm 3$, nm ($\Delta\epsilon$)					
[{(bpy)$_2$Ru}$_2$-μ-CG[3]]$^{4+}$	281 (2)	294 (35)				
[{(bpy)$_2$-Δ-Ru}$_2$-μ-CG[3]]$^{4+}$	281 (197)	295 (−389)	326 (31)		419 (39)	470 (−22)
[{(bpy)$_2$-Λ-Ru}$_2$-μ-CG[3]]$^{4+}$	281 (−181)	295 (435)	327 (−15)		420 (−24)	472 (30)
[{CG[*m*-xyl]-Δ-Ru}$_2$-μ-CG[3]]$^{4+}$	286 (266)	304 (−380)	335 (21)	352 (5)	425 (26)	475 (−3)
[{(bpy)$_2$Ru}$_2$-μ-CG[0]]$^{4+}$	277 (5)	290 (30)	305 (−45)			
[{(bpy)$_2$-Δ-Ru}$_2$-μ-CG[0]]$^{4+}$	279 (198)	295 (−439)	326 (5)		420 (17)	468 (−53)
[{(bpy)$_2$-Λ-Ru}$_2$-μ-CG[0]]$^{4+}$	279 (−197)	294 (485)	328 (−1)		420 (11)	473 (66)
[{CG[*m*-xyl]-Δ-Ru}$_2$-μ-CG[0]]$^{4+}$	287 (212)	305 (−291)	335 (5)	351 (−6)	422 (10)	475 (−12)
[{(bpy)$_2$Ru}$_2$-μ-SCG[0]]$^{4+}$	280 (−5)	294 (56)	310 (−60)			
[{(bpy)$_2$-Δ-Ru}$_2$-μ-SCG[0]]$^{4+}$	281 (149)	296 (−320)	327 (−8)		422 (26)	476 (−37)
[{(bpy)$_2$-Λ-Ru}$_2$-μ-SCG[0]]$^{4+}$	281 (−174)	296 (369)	310 (sh)		363 (−7)	407 (40)
[{CG[*m*-xyl]-Δ-Ru}$_2$-μ-SCG[0]]$^{4+}$	288 (271)	307 (−415)	337 (12)	354 (−1)	429 (22)	485 (−15)
[{(bpy)$_2$Ru}$_3$-μ-CG[bpy]]$^{6+}$	280 (1)	294 (58)	309 (−31)			
[{(bpy)$_2$-Δ-Ru}$_3$-μ-CG[bpy]]$^{6+}$	279 (301)	295 (−585)	327 (+31)		417 (58)	469 (−56)
[{(bpy)$_2$-Λ-Ru}$_3$-μ-CG[bpy]]$^{6+}$	279 (−356)	294 (657)	326 (−60)		419 (−69)	471 (43)
[{CG[*m*-xyl]-Δ-Ru}$_3$-μ-CG[bpy]]$^{6+}$	286 (384)	307 (−520)	335 (30)	352 (−17)	417 (33)	471 (−1)

conformation by nature of restricted rotation along the linkage. This confirms the NMR data indicating that a statistical distribution of the diastereomers is present.

With the complexes prepared from the chiral building block, Δ- or Λ-[Ru(bpy)$_2$(py)$_2$]$^{2+}$, strong signals were obtained in the CD spectra, where in the majority of cases the ΔΔ and ΛΛ diastereomers were almost exact mirror images of each other (Table 3 and Figure 7). Only the complexes of SCG[0] deviated significantly. It is assumed that the greater number of chiral centers on the ligand play a more important role with the additional bulky pinene moieties, which force two different average solution conformations for the ΔΔ and ΛΛ isomers, thus giving distinctively different patterns (Figure 7).

Complexes prepared from RuCG[*m*-xyl]Cl$_2$ all demonstrated strong signals in the CD spectra, as has been observed with previously described mononuclear species,[24] with the $\Delta\epsilon$ in proportion to the number of metal centers present in the complex (Figure 8).

Comparison of Building Blocks and Conclusions

The successful synthesis of two new members of the "Chiragen" ligand series, CG[3] and CG[bpy], illustrates the

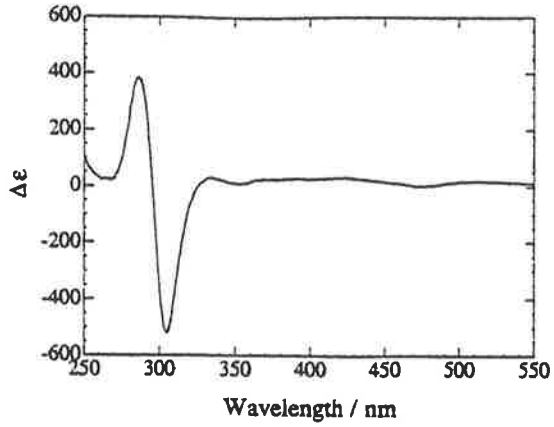

Figure 8. CD spectrum of ΔΔΔ-[{CG[*m*-xyl]-Δ-Ru}$_3$-*μ*-CG[bpy]]-$(PF_6)_6$.

great versatility of this stereospecific route to chiral bridging ligands. These can then be readily coordinated to ruthenium using $Ru(bpy)_2Cl_2$; however, this leads to a large number of diastereomers, which are clearly evident by ^{1}H-NMR spectroscopy. Using one of the enantiomerically pure precursors Δ- and Λ-$[Ru(bpy)_2(py)_2]^{2+}$, only one of the possible diastereomers is obtained, with high stereoisomeric purity in a known configuration. While in these examples all the isolated diastereomers exhibit the same electrochemical and photophysical behavior within the limits of experimentation, systems can be envisaged where the helicity of the metal center will play a greater role in the overall structure and relative distances between individual components in a supramolecular assembly. Additionally, the prepared individual diastereomers were not observed to photoracemize, despite being left in the daylight for a number of weeks. However, it must be stated that similar systems have been observed to undergo photoracemization.[36,37]

Using the building block RuCG[*m*-xyl]Cl_2, optically pure polynuclear complexes of a well-defined stereochemistry have been obtained. Due to the chiral nature of the tetradentate CG-[*m*-xyl] ligand, these complexes will not undergo the possible photoracemization alluded to above. Unfortunately, as a consequence of these same steric constraints, the photoemission is reduced, when compared to the analogous species previously described.

In conclusion, the results indicate that by the use of preprepared chiral starting materials, it is possible to design and build polynuclear transition metal complexes containing octahedral coordination sites with controlled stereochemistry, high optical purity, and a predetermined configuration. These methods are general and invaluable as the size of supramolecular assemblies expand.

Acknowledgment. We wish to thank Helen Stoekli-Evans, University of Neuchâtel, for acquiring the crystallographic data set, Hans-Ruedi Mürner and Brunhilde Kolp for kindly supplying some starting materials, Dr. G. Baykut at Bruker-Franzen Analytic GmbH for running the electrospray mass spectra, Felix Fehr for acquiring the 500 MHz NMR spectra, and the Swiss National Science Foundation for financial support.

Supporting Information Available: Textual presentation of the ^{1}H-NMR data for all complexes described (6 pages). Ordering information is given on any current masthead page

IC960948N

(36) Porter, G. B.; Sparks, R. H. *J. Photochem.* **1980**, *13*, 123.
(37) Ashby, M. T.; Govindan, G. N.; Grafton, A. K. *Inorg. Chem.* **1993**, *32*, 3803

3580 *Inorg. Chem.* 1997, *36*, 3580–3581

Isolation of the Stereoisomers of $[\{Ru(bpy)_2\}_2\{Os(bpy)_2\}(\mu\text{-HAT})]^{6+}$ (HAT = 1,4,5,8,9,12-Hexaazatriphenylene; bpy = 2,2′-Bipyridine)

Todd J. Rutherford and F. Richard Keene*

School of Biomedical and Molecular Sciences, James Cook University of North Queensland, Townsville, Queensland 4811, Australia

Received March 5, 1997

The synthesis and physical properties of polymetallic ligand-bridged molecular assemblies have been topics of intense interest,[1] motivated by their possible application to photochemical molecular devices.[2] An aspect receiving limited (but increasing) attention is the existence of stereoisomerism within such assemblies and its influence on intramolecular energy and electron transfer processes.[3]

The ligand bridge 1,4,5,8,9,12-hexaazatriphenylene (HAT) possesses three bidentate coordination sites, and a series of trimetallic species have been synthesized and studied,[4–7] including homonuclear (Ru_3[4,5]) and heteronuclear ($RuRe_2$[6] and Ru_2Rh[7]) systems. In earlier studies,[5] the stereochemical ambiguities were addressed but no separation of the isomeric possibilities was attempted. However, recent work in our laboratory has elucidated the stereochemistry of di- and trinuclear ruthenium complexes of this ligand, including investigations of the spatial dependence of the photophysical properties.[4]

In the present work, we report the synthesis of the heterometallic complex $[\{Ru(bpy)_2\}_2\{Os(bpy)_2\}(\mu\text{-HAT})]^{6+}$ and, most significantly, the isolation of its stereoisomeric forms by a strategy involving a combination of stereoselective synthetic procedures and chromatographic techniques[3] (Scheme 1: chromatographic procedures are indicated by single arrows; synthetic procedures, by double arrows). Previous stereochemical studies of ligand-bridged polynuclear species have generally selectively targeted one specific isomeric form. The stereoisomers of the title complex were characterized by ^{1}H NMR and CD spectroscopy, and their electrochemical and electronic spectroscopic properties were examined.

The stereoisomerically pure dinuclear complexes ΔΔ-, ΛΛ-, and ΔΛ-$[\{Ru(bpy)_2\}_2(\mu\text{-HAT})]^{4+}$ [4] were each reacted with *rac*-$[Os(bpy)_2Cl_2]\cdot H_2O$[8] in ethylene glycol/10% water at 120 °C for 11 h to form specifically the diastereoisomeric mixtures ΔΔΔ′/ΔΔΛ′ and ΛΛΔ′/ΛΛΔ′ (respectively) in the first two cases and the enantiomeric pair of one diastereoisomer ΔΛΛ′/ΛΔΔ′ in the final case {the configuration of the osmium center is designated with a prime; the diastereoisomers are shown in Figure 1, and their ^{1}H NMR spectra are provided in the Supporting Information, Figure S1). In all cases, the yields were *ca.* 70%, and the ratio of the stereoisomers was *ca.* 1:1. Using cation exchange chromatographic techniques recently developed for the separation of diastereoisomeric oligomeric species,[3] we separated the ΔΔΔ′/ΔΔΛ′ and ΛΛΛ′/ΛΛΔ′ mixtures (SP-25 Sephadex C-25; aqueous 0.3 M sodium toluene-4-sulfonate eluent). As the configurations of the two ruthenium centers in the precursors were known, the CD (Figure 2) and NMR spectra allowed the assignment of the absolute configurations of the four forms. The chiral resolution of the ΔΛΛ′/ΛΔΔ′ racemic mixture by similar chromatographic methods is more difficult than the previous separations of diastereoisomeric mixtures, but at least partial separation has been achieved (aqueous 0.2 M sodium toluoyl-D-tartrate solution eluent).

Scheme 1

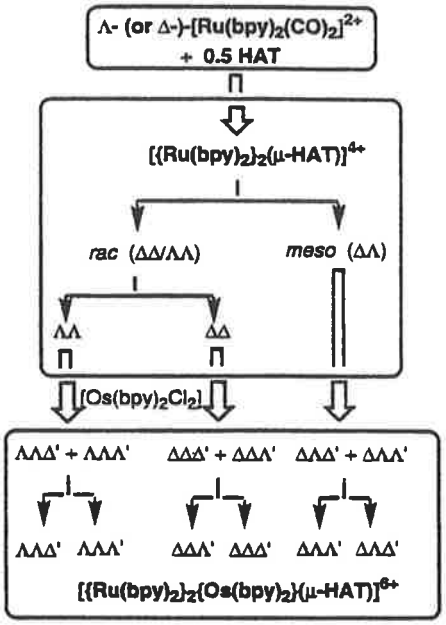

The diastereoisomers have been studied in detail by NMR spectroscopy (300 MHz), with the benefit of comparison with their homometallic (Ru_3) analogues.[4] However, because of the complexity of the present systems, certain assignments are difficult at this frequency and require pulse relay NMR techniques and/or a higher frequency spectrometer (500 MHz measurements are currently in progress).

The ΔΔΔ′/ΛΛΛ′ and ΔΔΛ′/ΛΛΔ′ forms both possess C_2 point group symmetry (Figure 1) and therefore may exhibit 27 nonequivalent proton environments (six AMJX and one AX coupled systems). Because the former diastereoisomer possesses a pseudo-C_3 symmetry axis (*cf.* the homometallic analogue $[\{Ru(bpy)_2\}_3(\mu\text{-HAT})]^{6+}$), a number of coincidental equivalences occur. The six AMJX coupled systems were identified by ^{1}H COSY and ^{1}H decoupling experiments, although connectivity between three pairs of AMJX coupled systems (allowing differentiation of the three nonequivalent bpy ligands) was not achievable at the frequency used (300 MHz).

The ΔΔΛ′/ΛΛΔ′ diastereoisomer also possesses C_2 point group symmetry, but its NMR spectrum was more complex (as

(1) Balzani, V.; Juris, A.; Venturi, M.; Campagna, S.; Serroni, S. *Chem. Rev.* **1996**, *96*, 759.
(2) Balzani, V.; Scandola, F. *Supramolecular Photochemistry*; Ellis Horwood: Chichester, U.K., 1991.
(3) Keene, F. R. *Coord. Chem. Rev.*, in press.
(4) Rutherford, T. J.; Van Gijte, O.; Kirsch-De Mesmaeker, A.; Keene, F. R. *Inorg. Chem.*, in press.
(5) (a) Jacquet, L.; Kirsch-De Mesmaeker, A. *J. Chem. Soc., Faraday Trans.* **1992**, *88*, 2471. (b) Kirsch-De Mesmaeker, A.; Jacquet, L.; Masschelein, A.; Vanhecke, F.; Heremans, K. *Inorg. Chem.* **1989**, *28*, 2465. (c) Masschelein, A.; Kirsch-De Mesmaeker, A.; Verhoeven, L.; Nasielski-Winkens, R. *Inorg. Chim. Acta* **1987**, *129*, 213.
(6) Sahai, R.; Rillema, D. P.; Shaver, R.; Van Wellendael, S.; Jackman, D. C.; Boldaji, M. *Inorg. Chem.* **1989**, *28*, 1022.
(7) Ortmans, I.; Didier, P.; Kirsch-De Mesmaeker, A. *Inorg. Chem.* **1995**, *34*, 3695.
(8) Kober, E. M.; Caspar, J. V.; Sullivan, B. P.; Meyer, T. J. *Inorg. Chem.* **1988**, *27*, 4587.

S0020-1669(97)00253-X CCC: $14.00

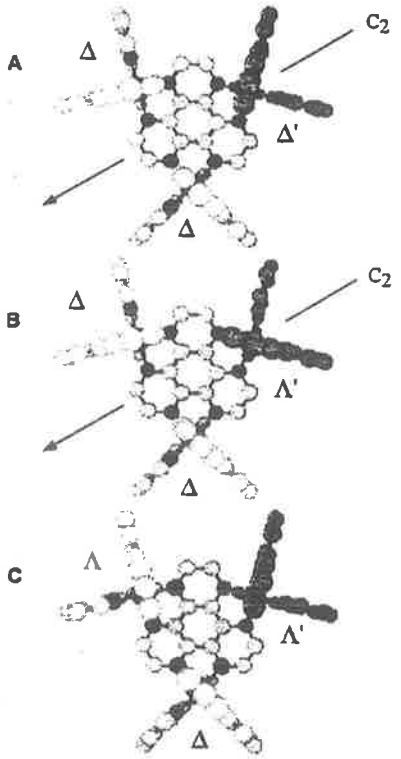

Figure 1. CHEM 3D representations of the diastereoisomeric forms of $[\{Ru(bpy)_2\}_2\{Os(bpy)_2\}(\mu\text{-HAT})]^{6+}$. Hydrogen atoms are omitted for clarity; bpy rings about the Os center are darkened to allow identification.

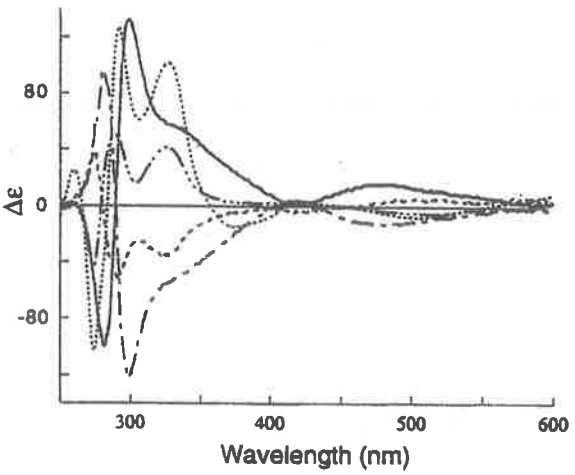

Figure 2. CD spectra (acetonitrile solution) for ΛΛΛ-$[\{Ru(bpy)_2\}_3(\mu\text{-HAT})]^{6+}$ (···) and stereoisomers of $[\{Ru(bpy)_2\}_2\{Os(bpy)_2\}(\mu\text{-HAT})]^{6+}$: ΔΔΛ′ (- - -), ΛΛΔ′ (— - - - —), ΛΛΛ′ (—), and ΔΔΔ′ (— - —).

the pseudo-C_3 symmetry axis is lacking), exhibiting six AMJX and one AX coupled proton systems, which together with a singlet resonance (two equivalent HAT protons) gave a possible total of 27 magnetically nonequivalent proton environments. A complete assignment of this diastereoisomer was possible because of the well-dispersed proton resonances and the reduced point group symmetry. The assignments were obtained using ^{1}H COSY spectra (provided in the Supporting Information, Figure S2), coupling constant values, and NOE effects.

The ΔΛΛ′/ΛΔΔ′ diastereoisomer has C_1 symmetry, resulting in a complicated ^{1}H NMR spectrum comprising 12 AMJX and 2 AX coupling systems and a singlet resonance (two protons from an AB system on the HAT ligand which are accidentally equivalent), totaling 53 magnetically nonequivalent proton environments. A full assignment of these proton environments by ^{1}H COSY spectra, decoupling effects, or NOE effects was not achievable at 300 MHz, although integration confirmed 54 proton resonances.

The CD spectra for the separated forms are comparable with those of the homometallic analogues.[4] The "heterochiral" enantiomers ΔΔΛ′- and ΛΛΔ′-$[\{Ru(bpy)_2\}_2\{Os(bpy)_2\}(\mu\text{-HAT})]^{6+}$ exhibit $\Delta\epsilon$ values about one-third those of the homochiral ΔΔΔ′- and ΛΛΛ′-enantiomers, presumably due to attentuation between Δ and Λ centers.

Electrochemical studies were undertaken on the diastereoisomers of the Ru_2Os trinuclear species. As suggested by Kirsch-de Mesmaeker *et al.*,[5a] and confirmed in this study, the one-electron reversible oxidation waves are directly correlated with the number of coordinated metal centers, suggesting significant metal−metal electonic communication which is a characteristic of conjugated bridging ligands.[9] As expected (and characteristic of osmium complexes), the first oxidation wave of $[\{Ru(bpy)_2\}_2\{Os(bpy)_2\}(\mu\text{-HAT})]^{6+}$ occurred at +1.27 V (*vs* the saturated calomel electrode, SCE; CH_3CN solvent) compared with +1.63 V for $[\{Ru(bpy)_2\}_3(\mu\text{-HAT})]^{6+}$ as a result of the raised $d\pi$ level of Os compared to Ru.[10] The oxidations of the two ruthenium centers (at 1.81 and 2.06 V *vs* SCE) in the Ru_2Os species are slightly cathodic of those for subsequent oxidations in the Ru_3 analogue (1.86 and 2.09 V *vs* SCE). The electronic spectrum of $[\{Ru(bpy)_2\}_2\{Os(bpy)_2\}(\mu\text{-HAT})]^{6+}$ {λ_{max}/nm (ϵ/M^{-1} cm^{-1}): 288 (104 000), 416 (15 750), 520 (21 000), 588 (27 000)} shows a slight bathochromic shift in the MLCT transitions in comparison with that of $[\{Ru(bpy)_2\}_3(\mu\text{-HAT})]^{6+}$ for the same reason.[11] The electronic spectra of the Ru_3 and Ru_2Os trinuclear species are provided in the Supporting Information, Figure 3.

While the redox and electronic absorption spectral characteristics of the diastereoisomeric forms of $[\{Ru(bpy)_2\}_2\{Os(bpy)_2\}(\mu\text{-HAT})]^{6+}$ were indistinguishable, we seek to study photophysical characteristics in view of the differences observed in the homometallic analogues.[4] It is our contention that the variation of physical properties between stereoisomers of such complexes will be magnified in larger polymetallic systems with increased stereochemical differences.

Acknowledgment. This work was supported by the Australian Research Council.

Supporting Information Available: ^{1}H NMR, COSY, and electronic spectra (Figures S1−S3) (3 pages). Ordering information is given on any current masthead page.

IC9702532

(9) Giuffrida, G.; Campagna, S. *Coord. Chem. Rev.* **1994**, *135*, 517.
(10) Kober, E. M.; Meyer, T. J. *Inorg. Chem.* **1983**, *22*, 1614.
(11) Richter, M. M.; Brewer, K. J. *Inorg. Chem.* **1993**, *32*, 5762.

Inorg. Chem. 1997, *36*, 4465−4474

Stereoisomers of Mono-, Di-, and Triruthenium(II) Complexes Containing the Bridging Ligand 1,4,5,8,9,12-Hexaazatriphenylene and Studies of Their Photophysical Properties

Todd J. Rutherford,[†] Olivier Van Gijte,[‡] Andrée Kirsch-De Mesmaeker,[‡,§] and F. Richard Keene*[,†]

Department of Chemistry and Chemical Engineering, School of Molecular Sciences, James Cook University of North Queensland, Townsville, Queensland 4811, Australia, and Laboratoire de Chimie Organique Physique, CP 160/08, Université Libre de Bruxelles, 1050 Bruxelles, Belgium

Received November 18, 1996[⊗]

A combination of synthetic methods involving mononuclear precursors of predetermined chirality {Δ- or Λ-[Ru(pp)$_2$(CO)$_2$]$^{2+}$; pp = 2,2′-bipyridine or 1,10-phenanthroline} and chromatographic techniques has allowed the isolation of the *meso* (ΔΛ) and *rac* (ΔΔ/ΛΛ) diastereoisomers of the dinuclear complexes [{Ru(pp)$_2$}$_2$(μ-HAT)]$^{4+}$ {HAT = 1,4,5,8,9,12-hexaazatriphenylene}. The enantiomers of the *rac* forms have been separated, and characterization of all species has been achieved by NMR and CD studies. Additonally, the homochiral (Δ^3/Λ^3) and heterochiral ($\Delta^2\Lambda/\Lambda^2\Delta$) diastereoisomers of the trinuclear complexes [{Ru(pp)$_2$}$_3$(μ-HAT)]$^{6+}$, and the enantiomers of both forms, have been isolated and identified. Emission studies of all the dinuclear species at room temperature indicate the relative luminescence quantum yields and the emission lifetimes significantly decrease for the *meso* compared with the *rac* diastereoisomers. No significant differences were detected at room temperature in the diastereoisomeric forms of the trinuclear compounds. However, in a glass at low temperature (80 K), the luminescence lifetimes of the trinuclear heterochiral diastereoisomer were slightly shorter than those of the homochiral form.

Introduction

Complexes of the d^6 metals ruthenium(II), osmium(II), and rhenium(I) containing polypyridyl ligands have received considerable recent attention because of their potential use in photochemical molecular devices and as light-sensitive probes in biological systems.[1−3] This interest is related to their spectral properties, photophysical characteristics (particularly in terms of the longevity of the excited states), inertness in a variety of oxidation states, and the redox characteristics of both the ground and excited states.[4]

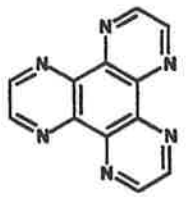

One ligand of this genre which has been investigated is 1,4,5,8,9,12-hexaazatriphenylene (HAT), where there are three sites for bidentate ligation to a metal center. It may serve as a bidentate ligand in mononuclear complexes or as a ligand bridge in di- and trinuclear species. Examples are known in each of these categories, and studies have addressed synthetic strategies for homo- and heterometallic polynuclear species,[5−9] photophysical properties,[6,9−12] and their interaction and photoreactions with various polynucleotides.[13−16]

In the studies of polynuclear complexes, the inherent problem of stereoisomerism has not been elaborated, although it has been acknowledged.[5,12] In recent studies, we have reported the separation of stereoisomers of ligand-bridged dinuclear species[17,18] and the synthesis of mononuclear and dinuclear complexes with predetermined stereochemistry.[19,20] In the present work, these techniques were applied to obtain all the stereoisomers of the mono-, di-, and triruthenium(II) complexes incorporating the ligand HAT, and studies of the photophysical characteristics are reported. Studies of the stereochemical

[†] James Cook University of North Queensland.
[‡] Université Libre de Bruxelles.
[§] Director of Research at the FNRS (Belgium).
[⊗] Abstract published in *Advance ACS Abstracts*, September 1, 1997.

(1) Balzani, V.; Scandola, F. *Supramolecular Photochemistry*; Ellis Horwood: Chichester U.K., 1991.
(2) Pyle, A. M.; Barton, J. K. *Prog. Inorg. Chem.* **1990**, *38*, 413.
(3) Kirsch-De Mesmaeker, A.; Lecomte, J. P.; Kelly, J. M. *Top. Curr. Chem.* **1996**, *177*, 25−76.
(4) Juris, A.; Barigelletti, S.; Campagna, S.; Balzani, V.; Belser, P.; von Zelewsky, A. *Coord. Chem. Rev.* **1988**, *84*, 85.
(5) Masschelein, A.; Kirsch-De Mesmaeker, A.; Verhoeven, C.; Nasielski-Hinkens, R. *Inorg. Chim. Acta* **1987**, *129*, L13.
(6) Didier, P.; Ortmans, I.; Kirsch-De Mesmaeker, A.; Watts, R. *J. Inorg. Chem.* **1993**, *32*, 5239.
(7) Tan Sien Hee, L.; Kirsch-De Mesmaeker, A. *J. Chem. Soc., Dalton Trans.* **1994**, 3651.
(8) Didier, P.; Jacquet, L.; Kirsch-De Mesmaeker, A.; Hueber, R.; van Dorsselaer, A. *Inorg. Chem.* **1992**, *31*, 4803.
(9) Ortmans, I.; Didier, P.; Kirsch-De Mesmaeker, A. *Inorg. Chem.* **1995**, *34*, 3695.
(10) Sahai, R.; Rillema, D. P.; Shaver, R.; Van Wellendael, S.; Jackman, D. C.; Boldaji, M. *Inorg. Chem.* **1989**, *28*, 1022.
(11) Jacquet, L.; Kirsch-De Mesmaeker, A. *J. Chem. Soc., Faraday Trans.* **1992**, *88*, 2471.
(12) Kirsch-De Mesmaeker, A.; Jacquet, L.; Masschelein, A.; Vanhecke, F.; Heremans, K. *Inorg. Chem.* **1989**, *28*, 2465.
(13) Lecomte, J.-P.; Kirsch-De Mesmaeker, A.; Kelly, J. M.; Tossi, A.; Gorner, H. *Photochem. Photobiol.* **1992**, *55*, 681.
(14) Casu, M.; Saba, G.; Lai, A.; Luhmer, M.; Kirsch-De Mesmaeker, A.; Moucheron, C.; Reisse, J. *Biophys. Chem.* **1996**, *59*, 133.
(15) Lecomte, J.-P.; Kirsch-De Mesmaeker, A.; Orellana, G. *J. Phys. Chem.* **1994**, *98*, 5382.
(16) Lecomte, J.-P.; Kirsch-De Mesmaeker, A.; Feeney, M. M.; Kelly, J. M. *Inorg Chem.* **1995**, *34*, 6481.
(17) Reitsma, D. A.; Keene, F. R. *J. Chem. Soc., Dalton Trans.* **1993**, 2859.
(18) Kelso, L. S.; Reitsma, D. A.; Keene, F. R. *Inorg. Chem.* **1996**, *35*, 5144.
(19) Rutherford, T. J.; Reitsma, D. A.; Keene, F. R. *J. Chem. Soc., Dalton Trans.* **1994**, 3659.
(20) Rutherford, T. J.; Quagliotto, M. G.; Keene, F. R. *Inorg. Chem.* **1995**, *34*, 3857.

S0020-1669(96)01374-2 CCC: $14.00

influence of interactions of such complexes with mononucleotides and DNA will be reported subsequently, as well as investigations of analogous polynuclear heterometallic species.

Experimental Section

Physical Measurements. ^{1}H, selective ^{1}H decoupling, NOE difference, and COSY experiments were performed on a Bruker Aspect 300 MHz NMR spectrometer using CD_3CN as the solvent. Electronic spectra were recorded in acetonitrile solution on a Hewlett Packard HP-89532K spectrophotometer using quartz cells.

All electrochemical experiments were performed under argon in an inert-atmosphere drybox using a Bioanalytical Systems BAS 100A electrochemical analyzer. Measurements were made in acetonitrile/0.1 M $[(n\text{-}C_4H_9)_4N]PF_6$ solution using a platinum button working electrode and a Ag/Ag^+ (0.01 M $AgClO_4$/0.1 M $[(n\text{-}C_4H_9N]ClO_4$ in acetonitrile) reference electrode (+0.31 V vs SSCE). Cyclic voltammetry was performed with a sweep rate of 100 mV/s; differential pulse voltammetry was run with a sweep rate of 4 mV/s and a pulse amplitude, width, and period of 50 mV, 60 ms, and 1 s, respectively. Elemental analyses were performed within the Department of Chemistry and Chemical Engineering at James Cook University of North Queensland.

ORD (optical rotary dispersion) spectra were recorded on a Perkin-Elmer 141 polarimeter in a 1 dm cell. Specific rotation at λ: $[\alpha]_\lambda = 100\alpha/cl$, where α = absolute rotation (deg), c = concentration in g/100 cm^3, and l = cell path length (in dm). Molecular rotation at λ: $[M]_\lambda$ = molecular weight $\times$ $[\alpha]_\lambda/100$. CD (circular dichroism) spectra were recorded in acetonitrile solution at concentrations of $1-3 \times 10^{-5}$ M at the University of Wollongong using a Jobin Yvon Dichrograph 6 instrument. All CD spectra are presented as $\Delta\epsilon$ vs λ (nm).

Photodecomposition/Photoracemization Studies. All solutions were prepared under argon in an inert atmosphere drybox and their UV−visible spectra recorded using stoppered 1 cm quartz cells. Samples were irradiated with a low-pressure mercury lamp: the irradiation time was 7.5 h, which corresponded to the time for 50% photodecomposition of a reference complex $[Ru(phen)_3(PF_6)_2$ in acetonitrile/0.2 M $[(C_2H_5)_4N]Cl$ solution. Photodecomposition studies were carried out in acetonitrile, water, or aqueous phosphate buffer (pH 7) solutions and monitored by variations in the UV−visible spectra, with photoracemization tested by cation exchange chromatography (SP-Sephadex C25) using sodium toluene-4-sulfonate solution as the eluent.

Luminescence Spectra and Lifetimes. The noncorrected relative emission spectra of the *meso* and *rac* dinuclear compounds were recorded with a Shimadzu RF-5001 PC spectrometer equipped with a Hamamatsu R-928 red-sensitive photomultiplier (PM) tube. The corrected emission spectra were obtained using an Edinburgh Instruments FL/FS 900 spectrofluorimeter equipped with a red-sensitive Hamamatsu R-928 PM tube and an ultrasensitive liquid-nitrogen-cooled Ge detector (spectral response 0.8−1.7 μm).

The emission lifetimes were determined from decays following single-shot pulsed-laser excitation, and also by time-resolved single photon counting (SPC). The use of the two different techniques confirmed the reproducibility of the measurements and reliability of the data treatment: it was undertaken because the luminescence is far into the long-wavelength region of the spectrum where detector response is lower, so that artifacts may appear during the measurements. The data in Table 2 correspond to average values obtained from the two techniques.

Under pulsed-laser excitation, the emission lifetimes were determined with a modified Applied Photophysics laser kinetics spectrometer equipped with a Hamamatsu R-928 PM tube. The excitation source was composed of a frequency-doubled neodymium YAG laser (Continuum NY 61-10) coupled with a dye laser (Continuum ND 60; dye DCM; λ_{exc} = 640 nm) and with the mixing option (Continuum UVX), producing a 400 nm beam (10 ns pulse width, maximum of 27 mJ/pulse; measurements at ca. 8 mJ/pulse). Kinetic analyses of the luminescence decays were performed by nonlinear least-squares regressions using a modified Marquardt algorithm.[21,22]

The SPC measurements were performed with an Edinburgh Instruments FL-900 spectrofluorimeter equipped with a nitrogen-filled discharge lamp and a Peltier-cooled Hamamatsu R-928 PM tube. The emission decays were analyzed with the Edinburgh Instruments software (version 3.0), based on nonlinear least-squares regressions using a modified Marquardt algorithm.

Microwave Techniques. Reactions were performed in a modified Sharp microwave oven (Model R-2V55; 600 W, 2450 MHz) on medium-high power.[23] Reactions were carried out in a round-bottom flask filled with a condenser, using ethylene glycol as the solvent.

Materials. 1,4,5,8,9,12-Hexaazatriphenylene (HAT) was supplied by Professor D. P. Rillema (University of North Carolina, Charlotte, NC).[10] Ethylene glycol (Ajax, 95%), $RuCl_3 \cdot xH_2O$ (Strem, 99%), 1,10-phenanthroline (phen; aldrich, 99+%), 2,2′-bipyridine (bpy; Aldrich, 99+%), potassium hexafluorophosphate (KPF_6; Aldrich 98%), ammonium hexafluorophosphate (NH_4PH_6; Aldrich, 99.99%), tris{3-[(trifluoromethyl)hydroxymethylene]-*d*-camphorato}europium(III) {[Eu(tfc)$_3$]; Fluka, 97%}, and laboratory reagent (LR) solvents were used without further purification unless specified. Trimethylamine *N*-oxide dihydrate (Fluka) was purified by sublimation at 120 °C under vacuum. $[Ru(bpy)_2Cl_2]\cdot 2H_2O$,[24] $[Ru(phen)_2Cl_2]\cdot 2H_2O$,[25] Δ- and Λ-$[Ru(phen)_2(CO)_2](PF_6)_2$,[20] and Δ- and Λ-$[Ru(bpy)_2(CO)_2](PF_6)_2$[20] were prepared according to literature methods. Sodium toluene-4-sulfonate (Sigma, 98%), (−)-*O*,*O*′-dibenzoyl-L-tartaric acid (Fluka, >99%, $[\alpha]^{20} = -117°$), and di-4-toluoyl-D-tartaric acid (Aldrich, 97%, $[\alpha]^{19} = +138°$) were used without further purification: aqueous solutions of sodium (−)-*O*,*O*′-dibenzoyl-L-tartrate and sodium (+)-di-4-toluoyl-D-tartrate were prepared by neutralization of the respective acids with sodium hydroxide.

Chromatography. All chromatographic procedures were carried out using SP-Sephadex C25 cation exchanger as the support and aqueous sodium toluene-4-sulfonate, sodium (−)-*O*,*O*′-dibenzoyl-L-tartrate, or sodium (+)-di-4-toluyl-D-tartrate as the eluent. The support was contained in a column approximately 100 cm long × 2 cm in diameter. When necessary, the column was sealed, enabling the complex to be recycled several times down its length with the aid of a peristaltic pump: in these cases, an "effective column length" (ECL) for the separation represents the total length of support traveled by the sample. All chromatography was carried out in subdued light.

Syntheses. **$[Ru(bpy)_2(HAT)](PF_6)_2$** was synthesized by the literature method[5] as well as by the alternative method described below.

A suspension of HAT (100 mg, 0.4 mmol) in ethylene glycol (20 cm^3) was heated in the microwave oven for 2 min to complete dissolution, and $[Ru(bpy)_2Cl_2]\cdot 2H_2O$ (74 mg, 0.14 mmol) was added in three portions over 4 min. The resultant red-brown solution was heated for a further 2 min and the reaction mixture allowed to cool and then filtered to remove excess ligand. The crude product was purified by the method described by Masschelein *et al.*[5] The complex was rechromatographed (SP-Sephadex C25 cation exchanger with 0.125 M sodium toluene-4-sulfonate as eluent) and the product precipitated from the major band by the addition of KPF_6 and reprecipitated from acetone/water solution by the addition of KPF_6. Yield: 96 mg (70%).[26]

Resolution of $[Ru(bpy)_2(HAT)](PF_6)_2$ was achieved by cation exchange chromatography using 0.1 M sodium di-4-toluoyl-D-tartrate as the eluent (ECL ~ 400 cm). The two bands were collected and precipitated with KPF_6 and reprecipitated as above. By comparisons with similar complexes of known configuration,[20] band 1 (the first band eluted) was assigned as Δ-(−)-$[Ru(bpy)_2(HAT)](PF_6)_2$ and band 2 (the second band) as Λ-(+)-$[Ru(bpy)_2(HAT)](PF_6)_2$.

$[\{Ru(bpy)_2\}_2(\mu\text{-}HAT)](PF_6)_4$ was synthesized by the literature method[5] as well as by the alternative method described below.

A suspension of HAT (50 mg, 0.21 mmol) in ethylene glycol (50 cm^3) was heated for ca. 2 min in the microwave oven to complete

(21) Bevington, P. R. *Data Reduction and Errors Analysis for the Physical Sciences*; McGraw Hill: New York, 1969.

(22) Demas, J. M. *Excited State Lifetime Measurements*; Academic Press: New York, 1983.

(23) Mingos, D. M. P.; Baghurst, D. R. D. *Chem. Soc. Rev.* **1991**, *20*, 1.

(24) Togano, T.; Nagao, N.; Tsuchida, M.; Kumakura, H.; Hisamatsu, K.; Howell, F. S.; Mukaida, M. *Inorg. Chim. Acta* **1992**, *195*, 221.

(25) Sullivan, B. P.; Salmon, D. J.; Meyer, T. J. *Inorg. Chem.* **1978**, *17*, 3334.

(26) Microanalyses (C, H, N) on these compounds were within acceptable limits (±0.4%), after allowance was made in some cases for inclusion of hydration in the crystal.

dissolution, and $[Ru(bpy)_2Cl_2]\cdot 2H_2O$ (218 mg, 0.42 mmol) was added in four portions over 8 min, during which time the solution changed color from red/brown to purple/black. The mixture was refluxed for a further 4 min and allowed to cool. The crude mixture was purified according to the method described by Masschelein *et al.*[5] The complex was rechromatographed (SP-Sephadex C25 cation exchanger with 0.15 M sodium (−)-*O,O'*-dibenzoyl-L-tartrate as eluent), during which procedure diastereoisomeric separation was achieved (ECL ~ 15 cm). The two bands were collected and each was precipitated by addition of a saturated solution of KPF_6. The separated diastereoisomers were dissolved in acetone/water, reprecipitated by the addition of a saturated solution of KPF_6, filtered off, and washed with distilled water and diethyl ether. The products were separately dissolved in acetone and loaded onto a short column of silica gel, washed with acetone, water, and acetone, and then eluted with acetone containing 5% NH_4PF_6. The acetone was removed and the brown-black product collected by filtration and washed with cold distilled water and diethyl ether. Total yield: 240 mg (70%); diastereoisomeric proportions were *meso* {band 1}/*rac* {band 2} = 54/46.[26]

Resolution of *rac*-[{Ru(bpy)$_2$}$_2$(μ-HAT)](PF$_6$)$_4$. The sample from band 2 of the above synthesis was resolved chromatographically (SP-Sephadex C25 cation exchanger) using 0.15 M sodium (−)-*O,O'*-dibenzoyl-L-tartrate was the eluent (ECL ~ 400 cm). The resolved products were collected and isolated as described above. Bands 1 and 2 were assigned as the ΔΔ and ΛΛ enantiomers, respectively. The CD {CH_3CH; λ_{max}, nm ($\Delta\epsilon$)} data are as follows. ΔΔ: 269 (51), 288 (−162), 319 (−94), 397 (23). ΛΛ: 269 (−51), 288 (158), 319 (91), 397 (−20).

[{Ru(bpy)$_2$}$_3$(μ-HAT)](PF$_6$)$_6$ was synthesized according to the literature method[5] and by the alternative method described below.

HAT (50 mg, 0.21 mmol) and $[Ru(bpy)_2Cl_2]\cdot 2H_2O$ (450 mg, 0.854 mmol) were added to a solution of ethylene glycol (30 cm^3), and the mixture was refluxed in the microwave oven (medium-high) for 8 min. On cooling, distilled water (ca. 150 cm^3) was added and then a saturated solution of KPF_6 until precipitation was complete. The mixture was stored overnight at 4 °C and the product collected by filtration and purified according to the method described by Masschelein *et al.*[5] As a further purification step, the product was rechromatographed (SP-Sephadex C25 cation exchanger using 0.3 M sodium toluene-4-sulfonate as the eluent). Diastereoisomeric separation also achieved (ECL ~ 10 cm), the two products were collected following the addition of saturated KPF_6 to the separated bands and repreciptated as described above for the dinuclear species. Total yield: 430 mg (86%); diastereoisomeric proportions were heterochiral ($\Delta^2\Lambda/\Lambda^2\Delta$) {band 1}/homochiral ($\Delta^3/\Lambda^3$) {band 2} = 83/17.[26]

Resolution of [{Ru(bpy)$_2$}$_3$(μ-HAT)](PF$_6$)$_6$. The sample isolated from band 2 of the above synthesis, (Δ^3/Λ^3)-[{Ru(bpy)$_2$}$_3$(μ-HAT)](PF$_6$)$_6$, was resolved by cation exchange chromatography using 0.2 M sodium (+)-di-4-toluoyl-D-tartrate as the eluent. Bands 2a (eluted first) and 2b were collected and the diastereoisomers isolated as described above and assigned as Δ^3 and Λ^3, respectively (see Discussion). The CD {CH_3CN; λ_{max}, nm ($\Delta\epsilon$)} data are as follows. Δ^3: 261 (−23), 275 (87), 291 (−136), 327 (−103), 374 (14). Λ^2: 261 (25), 275 (−102), 291 (127), 327 (101), 374 (−15).

[Ru(phen)$_2$(HAT)](PF$_6$)$_2$ was synthesized and purified under conditions identical to those described for [Ru(bpy)$_2$(HAT)](PF$_6$)$_2$, but using $[Ru(phen)_2Cl_2]\cdot 2H_2O$ as the starting material. Yield: 80%.[26]

Resolution of [{Ru(phen)$_2$(HAT)](PF$_6$)$_2$ was achieved by cation exchange chromatography using 0.1 M sodium (−)-*O,O'*-dibenzoyl-L-tartrate as the eluent (ECL ~ 300 cm). The two bands were collected and precipitated with KPF_6 and reprecipitated as above. By comparisons with similar complexes of known configuration,[20] band 1 was assigned as Δ-(−)-[Ru(phen)$_2$(HAT)](PF$_6$)$_2$ {$[\alpha]_{546} = -973°$ ($[M]_{546} = -9582°$), $[\alpha]_{578} = -1104°$ ($[M]_{578} = -10872°$); CH_3CN solution} and band 2 as Λ-(+)-[Ru(phen)$_2$(HAT)](PF$_6$)$_2$ {$[\alpha]_{546} = +987°$ ($[M]_{546} = +9719°$), $[\alpha]_{578} = +1142°$ ($[M]_{578} = +11246°$); CH_3CN solution}. The CD {CH_3CN; λ_{max}, nm ($\Delta\epsilon$)} data are as follows: Δ: 254 (150), 264 (−186), 294 (−118), 399 (16). Λ: 254 (−152), 264 (183), 295 (118), 399 (−16).

Enantiomeric purity was confirmed by ^{1}H NMR using the chiral lanthanide-induced shift reagent tris{3-[(trifluoromethyl)hydroxymethylene]-*d*-camphorato}europium(III), [Eu(tfc)$_3$]. [Ru(phen)$_2$(HAT)](PF$_6$)$_2$ was converted to the Cl^- salt by anion exchange chromatography and ^{1}H NMR experiments performed in CD_3CN.

[{Ru(phen)$_2$}$_3$(μ-HAT)](PF$_6$)$_4$ was synthesized and purified under conditions identical to those described for [{Ru(bpy)$_2$}$_2$(μ-HAT)](PF$_6$)$_4$, but using $[Ru(phen)_2Cl_2]\cdot 2H_2O$ as the starting material. Total yield: 71%; diastereoisomeric proportions were *meso* {band 1}/*rac* {band 2} = 51/49.[26]

Resolution of [{Ru(phen)$_2$}$_2$(μ-HAT)](PF$_6$)$_4$ was carried out in a manner identical to that described for [{Ru(bpy)$_2$}$_2$(μ-HAT)](PF$_6$)$_4$. The CD {CH_3CN λ_{max}, nm ($\Delta\epsilon$)} data are as follows. ΔΔ: 255 (304), 270 (−210), 296 (−257), 399 (19). ΛΛ: 255 (−298), 270 (214), 296 (247), 399 (−17).

[{Ru(phen)$_2$}$_3$(μ-HAT)](PF$_6$)$_6$ was synthesized and purified under conditions identical to those described for [{Ru(bpy)$_2$}$_3$(μ-HAT)](PF$_6$)$_6$, but using $[Ru(phen)_2Cl_2]\cdot 2H_2O$ as the starting material. Total yield: 90% diastereoisomeric proportions were heterochiral {band 1}/homochiral {band 2} = 80/20.[26]

Resolution of homochiral [{Ru(phen)$_2$}$_3$(μ-HAT)](PF$_6$)$_6$ was achieved by cation exchange chromatography using 0.2 M sodium (−)-*O,O'*-dibenzoyl-L-tartrate as the eluent (ECL ~ 330 cm). The two bands were collected and precipitated with KPF_6 and reprecipitated as described above. Bands 1 and 2 were assigned to Δ^3 and Λ^3, respectively (see Discussion). The CD {CH_3CN; λ_{max}, nm ($\Delta\epsilon$)} data are as follows. Δ^3: 217 (91), 259 (336), 278 (−220), 295 (−236). Λ^3: 217 (−94), 260 (−326), 277 (220), 295 (226).

Stereoselective Syntheses of ΔΔ-[{Ru(bpy)$_2$}$_2$(μ-HAT)](PF$_6$)$_4$ and Δ^3-[{Ru(bpy)$_2$}$_3$(μ-HAT)](PF$_6$)$_6$. A suspension of HAT (5 mg, 0.0213 mmol) in 2-methoxyethanol (5 cm^3) was degassed with dry N_2 for 15 min. Δ-(−)-[Ru(bpy)$_2$(CO)$_2$](PF$_6$)$_2$[19] (64 mg, 0.0852 mmol) and trimethylamine *N*-oxide (40 mg, 0.51 mmol) were added, and the reaction mixture was stirred at room temperature in subdued light for 11 days. A further addition of trimethylamine *N*-oxide (15 mg, 0.2 mmol) was made after approximately 6 days. The reaction produced both dinuclear and trinuclear products, which were separated by SP-Sephadex C25 cation exchange chromatography; ΔΔ-[{Ru(bpy)$_2$}$_2$(μ-HAT)]$^{4+}$ was eluted with a solution 0.3 NaCl in water/acetone (5:3) and Δ^3-[{Ru(bpy)$_2$}$_3$(μ-HAT)]$^{6+}$ with a solution 0.5 M NaCl in water/acetone (5:3). ΔΔ-[{Ru(bpy)$_2$}$_2$(μ-HAT)]$^{4+}$ and Δ^3-[{Ru(bpy)$_2$}$_3$(μ-HAT)]$^{6+}$ were further purified separately by cation exchange chromatography with elution by 0.2 and 0.3 M sodium toluene-4-sulfonate solution, respectively. The products were collected as described above. Yield: ΔΔ-[{Ru(bpy)$_2$}$_2$(μ-HAT)](PF$_6$)$_4$, 23% (8 mg); Δ^3-[{Ru(bpy)$_2$}$_3$(μ-HAT)](PF$_6$)$_6$, 24% (12 mg).[26] The CD data are as follows. ΔΔ {CH_3CN; λ_{max}, nm ($\Delta\epsilon$)}: 269 (69), 288 (−156), 319 (−96), 397 (20). Δ^3 {λ_{max}, nm ($\Delta\epsilon$)}: 261 (−23), 275 (89), 291 (−126), 327 (−96), 374 (13).

Stereoselective Syntheses of ΛΛ-[{Ru(phen)$_2$}$_2$(μ-HAT)](PF$_6$)$_4$ and Λ^3-[{Ru(phen)$_2$}$_3$(μ-HAT)](PF$_6$)$_6$. The syntheses and purification were performed under conditions similar to those described for ΔΔ-[{Ru(bpy)$_2$}$_2$(μ-HAT)](PF$_6$)$_4$ and Δ^3-[{Ru(bpy)$_2$}$_3$(μ-HAT)](PF$_6$)$_6$, but using Λ-(+)-[Ru(phen)$_2$(CO)$_2$](PF$_6$)$_2$ rather than Δ-(−)-[Ru(bpy)$_2$(CO)$_2$](PF$_6$)$_2$; the reaction mixture was stirred for a further 3 days. Yield: ΛΛ-[{Ru(phen)$_2$}$_2$(μ-HAT)](PF$_6$)$_4$, 19% (7 mg); Λ^3-[{Ru(phen)$_2$}$_3$(μ-HAT)](PF$_6$)$_6$, 28% (15 mg).[25] The CD data are as follows. ΛΛ {CH_3CN; λ_{max}, nm ($\Delta\epsilon$)}: 255 (−267), 270 (195), 296 (260), 399 (−21). Λ^3 {λ_{max}, nm ($\Delta\epsilon$)}: 218 (−93), 260 (−309), 277 (210), 295 (224).

Results and Discussion

Synthesis. The various $[\{Ru(pp)_2\}_n(HAT)]^{(2n)+}$ species {pp = 2,2'-bipyridine (bpy) or 1,10-phenanthroline (phen)} have been synthesized previously by the reaction of *n* equiv (*n* = 1−3) of $[Ru(pp)_2Cl_2]$ with HAT in methanol/water (1/1) under reflux.[5] In the first of two alternative synthetic methods developed in the present work, the reaction of the same starting materials in ethylene glycol solution under microwave conditions[23] produced reaction yields equivalent to or increased over those produced by the conventional method, but with a ca. 50-fold decrease in reaction time. The second method involved decarbonylation of chiral Δ- or Λ-$[Ru(pp)_2(CO)_2]^{2+}$ in 2-methoxyethanol solution in the presence of the ligand HAT. Such

decarbonylation reactions are known to proceed with retention of stereochemical integrity of the metal center when undertaken at room temperature and subdued light.[19,20] In the present case, due to the low solubility of HAT in the 2-methoxyethanol solvent at low temperatures, the mixture was stirred for 8−10 days, after which time both the di- and trinuclear complexes were isolated in ca. 20% yield.

Stereochemistry. The development of synthetic methodologies involving enantiomerically pure building blocks[19] and chromatographic techniques[17] has enabled us to isolate individual stereoisomers (diastereoisomers, enantiomers, and/or geometric isomers) in these and related systems.[27] This has allowed assessment of the effect of stereoisomerism on physical properties such as electrochemical and photophysical characteristics, and on the interaction with chiral assemblies such as mononucleotides and DNA. Such studies have previously been limited because stereoisomerically pure polynuclear complexes were not available. In addition, in earlier investigations of polynuclear polypyridyl complexes of ruthenium,[5,28,29] the existence of stereoisomerism complicated structural determinations and characterization: for example, NMR spectroscopy has been of limited value because the diastereoisomeric complexes have nonequivalent NMR spectra.[17,30]

The chromatographic separation of stereoisomers forms a most important part of this study. Cation exchange chromatography was employed, using SP-Sephadex C25 as the support, with aqueous sodium toluene-4-sulfonate, sodium (−)-*O,O′*-dibenzoyl-L-tartrate, or sodium (+)-di-4-toluoyl-D-tartrate solutions as the eluents. While the technique is based on a cation exchange mechanism, the mode of isomer separation is influenced by a differential association between the stereoisomers of the complex with both the anion of the eluent and the chiral support. The precise nature of the associations is currently under investigation and appears to have components involving specific π-stacking and hydrophobic interactions.[31]

Mononuclear Complexes. $[Ru(bpy)_2(HAT)]^{2}$ and $[Ru(phen)_2(HAT)]^{2+}$ were each chromatographically resolved into enantiomeric forms using the chiral eluents 0.1 M sodium (+)-di-4-toluoyl-D-tartrate and 0.1 M sodium (−)-*O,O′*-dibenzoyl-L-tartrate, respectively. The enantiomers of each compound showed equal and opposite ORD and CD spectra (shown for $[Ru(phen)_2(HAT)]^{2+}$ in Figure S1, Supporting Information), and ^{1}H NMR studies of Δ- and Λ-$[Ru(phen)_2(HAT)]^{2+}$ in the presence of the chiral lanthanide-shift reagent $[Eu(tfc)_3]$ confirmed optical purity. The absolute configurations were determined by comparisons of the CD spectra with related complexes with known absolute configurations (Figure 1).[20]

Dinuclear Complexes. $[\{Ru(bpy)_2\}_2(\mu\text{-HAT})]^{4+}$ was chromatographically separated into the *rac* (ΔΔ/ΛΛ) and *meso* (ΔΛ) diastereoisomeric forms (Figure 2) using 0.15 M sodium (−)-*O,O′*-dibenzoyl-L-tartrate as eluent, the separation being observed within 15 cm of travel. Bands 1 (eluted first) and 2 (eluted second) were determined to be the *meso* and *rac* diastereoisomers, respectively, as established by NMR characterization and comparison with an authentic sample of the ΔΔ isomer deliberately synthesized using Δ-$[Ru(bpy)_2(CO)_2]^{2+}$ as the precursor. In addition, band 2 could be chromatographically resolved (ECL ~ 400 cm) using 0.15 M sodium (−)-*O,O′*-dibenzoyl-L-tartrate as eluent, thereby confirming it as the *rac* form: bands 2a and 2b were assigned as the ΔΔ and ΛΛ enantiomers, respectively. The absolute configurations of the two bands were established by comparison of the CD spectra with that of the stereoselectively synthesized ΔΔ-$[\{Ru(bpy)_2\}_2(\mu\text{-HAT})]^{4+}$.

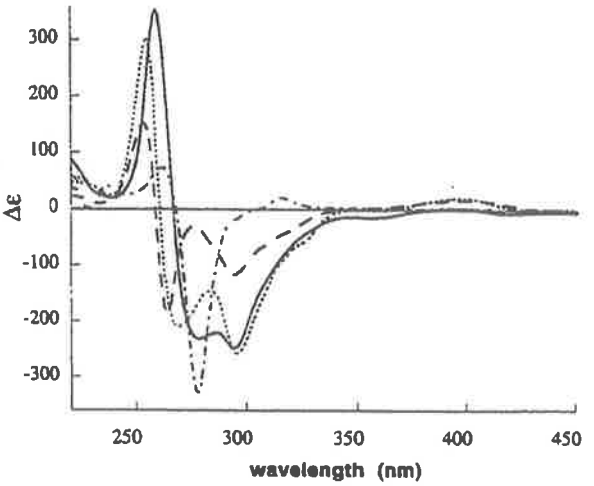

Figure 1. CD spectra of Δ-$[\{Ru(phen)_2\}_3(\mu\text{-HAT})]^{6-}$ (—), Δ-$[\{Ru(phen)_2\}_2(\mu\text{-HAT})]^{4+}$ (- - -), Δ-$[Ru(phen)_2(HAT)]^{2-}$ (— — —), and Δ-$[Ru(phen)_2(CO)_2]^{2+}$ (—·—·).

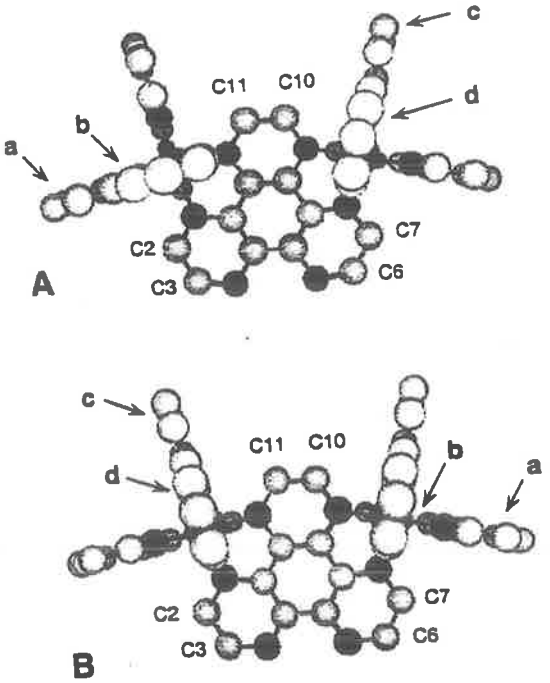

Figure 2. Chem 3D representation of diastereoisomeric forms of $[\{Ru(bpy)_2\}_2(\mu\text{-HAT})]^{4+}$: (A) *rac* {ΔΔ (≡ΛΛ)}; (B) *meso* {ΛΔ}. Hydrogen atoms are omitted for clarity; the notation shown is the same for the phen analogues and is used in the discussion of the ^{1}H NMR spectra.

Diastereoisomeric separation, resolution, and the assignment of absolute configurations of $[\{Ru(phen)_2\}_2(\mu\text{-HAT})]^{4+}$ were achieved as described above for $[\{Ru(bpy)_2\}_2(\mu\text{-HAT})]^{4+}$. The diastereoisomeric separation (ECL ~ 8 cm) and the subsequent resolution of the *rac* form into its enantiomers (ECL ~ 300 cm) were achieved, with the elution order (ΔΛ, ΔΔ, and ΛΛ) being identical to that of the bpy analogue above. The CD

(27) Keene, F. R. *Coord. Chem. Rev.*, in press.
(28) Denti, G.; Campagna, S.; Serroni, S.; Ciano, M.; Balzani, V. *J. Am. Chem. Soc.* **1992**, *114*, 2944.
(29) Denti, G.; Serroni, S.; Campagna, S.; Ricevuto, V.; Juris, A.; Ciano, M.; Balzani, V. *Inorg. Chim. Acta* **1992**, *198−200*, 507.
(30) Hua, X.; von Zelewsky, A. *Inorg. Chem.* **1995**, *34*, 5791.
(31) Fletcher, N. C.; Atkinson, I. M.; Reitsma, D. A.; Keene, F. R. Unpublished results.

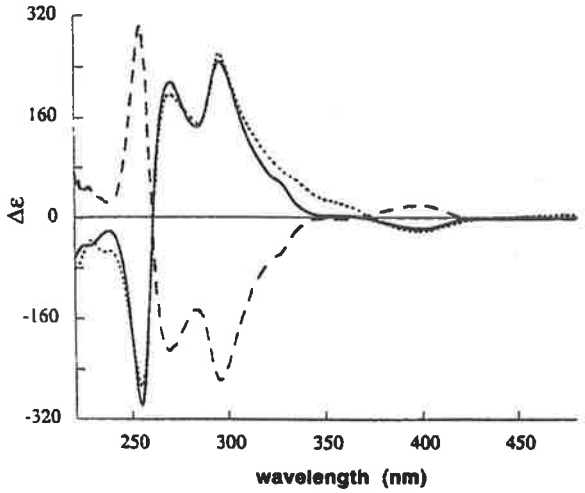

Figure 3. CD spectra for stereoisomeric forms of $[\{Ru(phen)_2\}_2(\mu\text{-HAT})]^{4+}$: ΛΛ synthesized from Λ-$[\{Ru(phen)_2\}_2(CO)_2]^{2+}$ (- - -); ΛΛ (—) and ΔΔ (— — —) from chromatographic separation.

spectra of the chromatographically separated ΔΔ- and ΛΛ-$[\{Ru(phen)_2\}_2(\mu\text{-HAT})]^{4+}$ forms, and the ΔΔ enantiomer stereoselectively synthesized from Δ-$[Ru(phen)_2(CO)_2]^{2+}$, are shown in Figure 3, and for the bpy analogues in Figure S2 (Supporting Information).

Trinuclear Complexes. $[\{Ru(bpy)_2\}_3(\mu\text{-HAT})\}^{6+}$ was chromatographically separated into the homochiral (Δ^3/Λ^3) and heterochiral ($\Delta^2\Lambda/\Lambda^2\Delta$) diastereoisomeric forms (Figure 4) using 0.3 M sodium toluene-4-sulfonate as eluent. Bands 1 and 2 were determined to be the $\Delta^2\Lambda/\Lambda^2\Delta$ and Δ^3/Λ^3 diastereoisomers, respectively, by NMR spectroscopy (the D_3 symmetry of Δ^3/Λ^3, compared to the C_2 symmetry of $\Delta^2\Lambda/\Lambda^2\Delta$, resulting in a simplified spectrum for Δ^3/Λ^3 (see below), and comparisons with the spectrum of the stereoselectively synthesized Δ^3 form). The Δ^3/Λ^3 diastereoisomer (band 2) was chromatographically resolved using 0.2 M sodium (+)-di-4-toluoyl-D-tartrate as the eluent. Bands 2a and 2b were assigned as the Δ^3 and Λ^3 enantiomers, respectively, by comparisons of the CD spectra ($\Delta\epsilon$ values) with the CD spectrum of the stereoselectively synthesized Δ^3 form.

Resolution of the $\Delta^2\Lambda/\Lambda^2\Delta$ diastereoisomer was attempted using a range of eluents at varying concentrations, but without success. However, the $\Delta^2\Lambda$ and $\Lambda^2\Delta$ enantiomers may be obtained by a combination of chromatographic separations and stereoselective syntheses: the resolved ΔΔ and ΛΛ forms of $[\{Ru(bpy)_2\}_2(\mu\text{-HAT})]^{4+}$ were separately reacted with *rac*-$[Ru(bpy)_2Cl_2]$, resulting in the two diastereoisomeric mixtures $\Delta^3/\Delta^2\Lambda$ and $\Lambda^3/\Lambda^2\Delta$, respectively, which were separated chromatographically, thus realizing the $\Delta^2\Lambda$ and $\Lambda^2\Delta$ forms. Since the absolute configuration of the precursor complex $[\{Ru(bpy)_2\}_2(\mu\text{-HAT})]^{4+}$ is known, the absolute configuration assignments of $\Delta^2\Lambda$- and $\Lambda^2\Delta$-$[\{Ru(bpy)_2\}_3(\mu\text{-HAT})]^{6+}$ may be made. The same technique has been used to isolate the stereoisomers of mixed Ru/Os trinuclear systems.[32]

$[\{Ru(phen)_2\}_3(\mu\text{-HAT})]^{6+}$ was chromatographically separated into the Δ^3/Λ^3 and $\Delta^2\Lambda/\Lambda^2\Delta$ diastereoisomeric forms using 0.3 M sodium toluene-4-sulfonate as eluent (ECL ~ 8 cm). Band 1 (eluted first) and band 2 (eluted second) were determined to be $\Delta^2\Lambda/\Lambda^2\Delta$ and Δ^3/Λ^3 in a manner similar to that described for $[\{Ru(bpy)_2\}_3(\mu\text{-HAT})]^{6+}$. The Δ^3/Λ^3 diastereoisomer (band 2) was resolved using 0.2 M sodium (−)-*O*,*O*′-dibenzoyl-L-tartrate as eluent (ECL ~ 250 cm). Bands 2a and 2b were assigned as the Δ^3 and Λ^3 enantiomers, respectively. Enantiomer assignment and purity were achieved by comparisons of the CD spectra ($\Delta\epsilon$ values) with the CD spectrum of the stereoselectively synthesized Λ^3 form. The CD spectra of the Λ^3- and Δ^3-$[\{Ru(phen)_2\}_3(\mu\text{-HAT})]^{6+}$ enantiomers are shown in Figure 5, and the bpy analogues in Figure S3 (Supporting Information).

(32) Rutherford, T. J.; Keene, F. R. *Inorg. Chem.* **1997**, *36*, 3580.

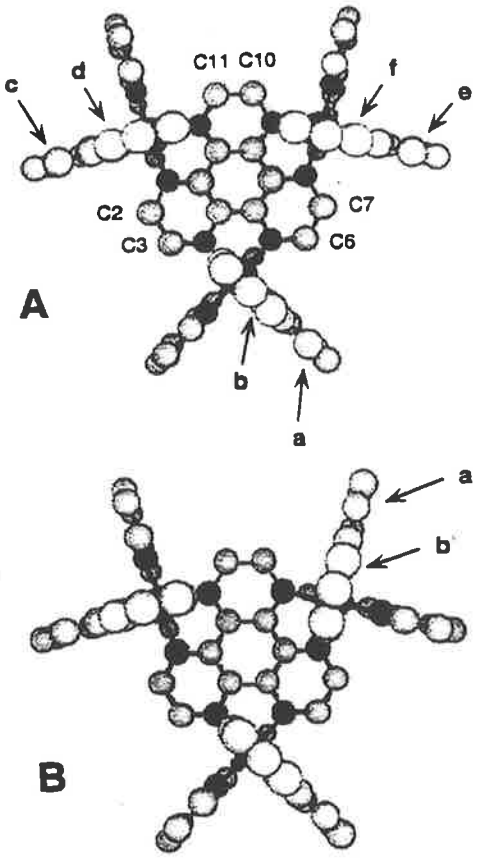

Figure 4. Chem 3D representation of diastereoisomeric forms of $[\{Ru(bpy)_2\}_3(\mu\text{-HAT})]^{6+}$: (A) heterochiral $\{\Delta^2\Lambda\}$; (B) homochiral $\{\Delta^3 (\equiv\Lambda^3)\}$. Hydrogen atoms are omitted for clarity; the notation shown is the same for the phen analogues and is used in the discussion of the ^1H NMR spectra.

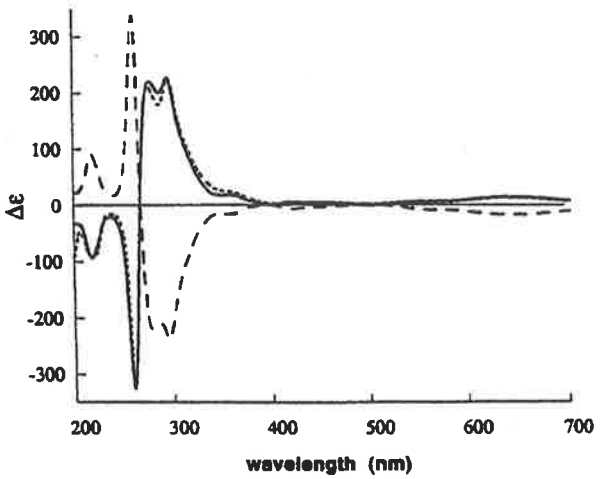

Figure 5. CD spectra for stereoisomeric forms of $[\{Ru(phen)_2\}_3(\mu\text{-HAT})]^{6+}$: Λ^3 synthesized from Λ-$[\{Ru(phen)_2\}_2(CO)_2]^{2+}$ (- - -); Λ^3 (—) and Δ^3 (— — —) from chromatographic separation.

With the characterization of the separated diastereoisomers achieved, the stereochemical features of the synthetic procedures may be revisited. No difference was observed in the diastereoisomeric ratios (*rac/meso* in $[\{Ru(pp)_2\}_2(\mu\text{-HAT})]^{4+}$ and homochiral/heterochiral in $[\{Ru(pp)_2\}_3(\mu\text{-HAT})]^{6+}$) between the conventional heating and microwave heating methods. The diastereoisomeric ratios were approximately 50/50 (*rac/meso*) for $[\{Ru(pp)_2\}_2(\mu\text{-HAT})]^{4+}$ and 17/83 (homochiral/heterochiral) for $[\{Ru(pp)_2\}_3(\mu\text{-HAT})]^{6+}$, which compare with the respective statistical ratios of 50/50 and 25/75 and suggest that electronic or steric influences play little part in the determination of diastereoisomer proportions.

^{1}H NMR Studies. The ^{1}H NMR data for the mononuclear complex and the diastereoisomeric forms of the di- and trinuclear complexes containing 1,10-phenanthroline (phen) terminal ligands and the HAT bridging ligand are shown in Table 1. The ^{1}H NMR data for the analogous series of complexes containing 2,2′-bipyridine as the terminal ligands are given in Table S1 (Supporting Information). The notation for the phen and HAT ligands for the above complexes is indicated in Figures 2 and 4.

In all cases, the phen ligands exhibited the expected coupling constant values[28] $\{J_{2,3} = J_{8,9} = 5$ Hz, $J_{2,4} = J_{7,9} = 1.5$ Hz, $J_{3,4} = J_{7,8} = 8$ Hz, and $J_{5,6} = 9$ Hz ($J_{5,6}$ variable due to second-order effects)$\}$ and coupling patterns based on the symmetry requirements of the above complexes (i.e., $[\{Ru(phen)_2(HAT)]^{2+}$ (C_2 point group symmetry), $\Lambda\Lambda/\Delta\Delta$-$[\{Ru(phen)_2\}_2(\mu\text{-HAT})]^{4+}$ (C_2) and $\Delta\Lambda$-$[\{Ru(phen)_2\}_2(\mu\text{-HAT})]^{4+}$ (C_s), Δ^3/Λ^3-$[\{Ru(phen)_2\}_3(\mu\text{-HAT})]^{6+}$ (D_3) and $\Delta^2\Lambda/\Lambda^2\Delta$-$[\{Ru(phen)_2\}_3(\mu\text{-HAT})]^{6+}$ (C_2).

The ^{1}H NMR chemical shifts listed in Tables 1 and S1 were determined by ^{1}H COSY spectra, selective ^{1}H decoupling, and NOE experiments and were assigned as described below. Connectivity between the H4 and H5, H5 and H6, and H6 and H7 protons in the individual ligands of complexes containing two or more nonequivalent phen ligands was confirmed by NOE experiments. The complete assignment of chemical shifts to the ligands in the structure (given in Table 1) was based on the relative degree of diamagnetic anisotropic interactions between adjacent ligands (these anisotropic interactions may occur between the phen and HAT ligands, the two phen ligands on the same metal center, the phen ligands on the adjacent metal centers, or combinations of these interactions).

$[Ru(phen)_2(HAT)]^{2+}$. The C_2 symmetry of $[\{Ru(phen)_2(HAT)]^{2+}$ results in an AMX, A′M′X′, and AX spectrum with three additional singlet resonances. The two AMX coupled systems were assigned to the chemical shifts seen in Table 1, by the reduced diamagnetic anisotropic interaction (less shielding influence) between H9 (8.18 ppm) and the electron deficient ligand HAT relative to H2 (8.00 ppm) and phen. The electron density (and therefore the degree of anisotropic interactions) in these polypyridyl ligands has been shown to be influenced significantly more by the incorporation of nitrogen donor atoms than by the number of aromatic rings (aromaticity).[19] Selective ^{1}H decoupling of the H9 and H2 resonances and NOE effects between H4 and H5 confirmed the subsequent assignments in Table 1. The expected coupling pattern was observed from the HAT ligand with H2/H11 assigned to 8.26 ppm (d, $J = 3$ Hz) on the basis of increased diamagnetic anisotropic interactions with the phen ligands.

$[\{Ru(phen)_2\}_2(\mu\text{-HAT})]^{4+}$. The C_2 symmetry of the *rac* diastereoisomer requires two nonequivalent phen ligands with each phen exhibiting a spectrum consisting of AMX, A′M′X′, and AB coupling patterns, and an AX coupled system and a singlet resonance from the HAT (see Figure 6). The two nonequivalent phen ligands are orientated in a pseudoorthogonal geometry on the same face of the HAT bridging ligand (see Figure 2). The assignment of the HAT proton resonances for both diastereoisomers was based on coupling constants and the relative degree of diamagnetic anisotropic interactions with the phen ligands. The singlet resonance (H10 and H11; see Table 1) in both isomers was the most shielded due to the anisotropic interaction with the four phen ligands.

Ring b (see Figure 2) is orientated over the plane of two ligands, the phen across the bridge and the HAT bridging ligand, resulting in increased diamagnetic anisotropic effects (shielding effect) in the H8 and H9 protons. As H8 is affected significantly more by the phen across the bridge relative to that with HAT (see influence of HAT on H8 and H3 in $[Ru(phen)_2(HAT)]^{2+}$ complex, Table 1), H8 ring b can be assigned to the most shielded H8/H3 resonance (dd, $J = 5$, 8 Hz) at 7.48 ppm. The subsequent assignments for rings a and b were achieved as described above. The upfield shift of H9 ring b (7.92 ppm) relative to H9 (8.18 ppm) of $[Ru(phen)_2(HAT)]^{2+}$ is attributed to the diamagnetic anisotropic interactions with the phenanthroline across the bridge as H9 ring b experiences a less shielding influence from the HAT with two coordinated metal centers. The assignment of H9 ring d to 8.28 ppm (most downfield dd, $J = 5$, 1.5 Hz) is in agreement with the above argument as H9 ring d is orientated over the plane of the electon deficient HAT ligand (two metal centers coordinated) and not in the shielding cone of the phen across the bridge and thus is deshielded relative to H9 (8.18 ppm) of $[Ru(phen)_2(HAT)]^{2+}$. The assignments based on this discussion are shown in Table 1.

The C_s symmetry of the *meso* diastereoisomer also requires the nonequivalence of two phen ligands (similar coupling patterns to *rac* isomer above and the ^{1}H NMR spectrum observed in Figure 6), which are orientated on the opposite faces of the HAT bridging ligand and the same ruthenium center (see Figure 2). The ^{1}H chemical shifts of the nonequivalent phen ligands and the HAT bridging ligand were assigned in a similar manner to those of the *rac* isomer (shown above) and are listed in Table 1.

H9 (ring b) was assigned to the most deshielded H2/H9 proton resonance at 8.45 ppm (dd, $J = 5$, 1.5 Hz) due to the diamagnetic anisotropic interactions with the HAT ligand and the equivalent phen ligand across the bridge (see Figure 2). As suggested above, H9 and H8 (ring b) are orientated in the deshielding cone of the equivalent phen, which is illustrated by their downfield shift relative to H9 and H8 (ring b) of the *rac* isomer (compare Figure 2 and Table 1). The subsequent assignments of rings b and a were achieved as described above.

As expected, the ^{1}H chemical shifts of ring a between the two diastereoisomers are near identical due their similar environments. H9 (ring d) was assigned to 8.19 ppm (dd, $J = 5$, 1.5 Hz) due the reduced diamagnetic anisotropic interactions with the HAT bridging ligand. The upfield shift H9 and H8 (ring d) relative to the *rac* isomer (ring d) is a result of anisotropic interactions between the equivalent phen ligands across the bridge. This shielding influence is also observed in the minor differences between H9 and H8 (ring d) of the *rac* isomer and H9 and H8 (ring b) of $[\{Ru(phen)_2(HAT)]^{2+}$, as H9 and H8 (ring d) should experience an increased deshielding influence from the more electron deficient HAT bridge (coordinated to two metal centers).

$[\{Ru(phen)_2\}_3(\mu\text{-HAT})]^{6+}$. The D_3 symmetry of the homochiral (Δ^3/Λ^3) diastereoisomer requires the equivalence of the six phen ligands (see Figure 4). As the two halves of the phen ligands are nonequivalent, the ^{1}H spectrum consists of AMX,

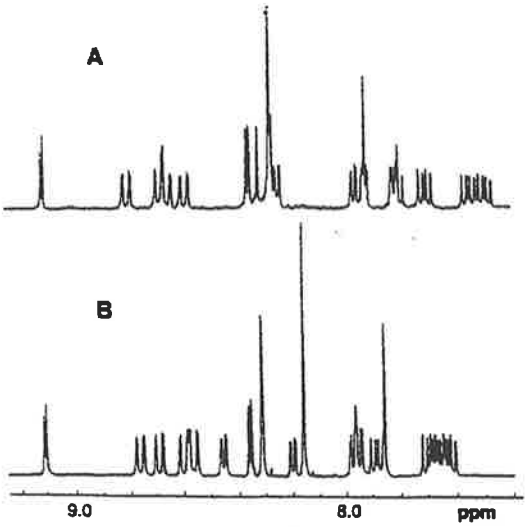

Figure 6. ^{1}H NMR spectra (300 MHz; CD_3CN solution) of the *rac* (A) and *meso* (B) diastereoisomers of $[\{Ru(phen)_2\}_2(\mu\text{-HAT})]^{4+}$.

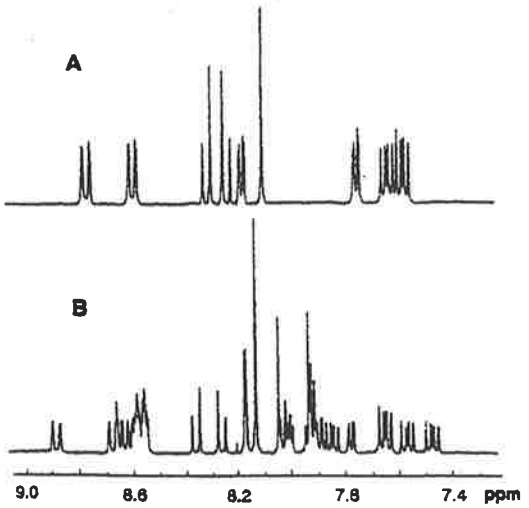

Figure 7. ^{1}H NMR spectra (300 MHz; CD_3CN solution) of the homochiral (A) and heterochiral (B) diastereoisomers of $[\{Ru(phen)_2\}_3(\mu\text{-HAT})]^{6+}$.

A′M′X′, and AB coupling patterns with an additional singlet resonance from the HAT bridging ligand (see Figure 7). The ^{1}H chemical shift assignments were achieved as described above and are shown in Table 1.

The assignment of H9 (ring b) and H2 (ring a) to 8.18 and 7.75 ppm (dd, J = 5, 1.5 Hz) was based on the following argument: H9 (ring b) is orientated over the HAT ligand with three coordinated metal centers (reduced shielding environment compared with two coordinated metal centers) and over the plane of the phen ligand across the bridge (shielding environment, similar to the *rac* dinuclear species). These comparisons suggest that the chemical shift of H9 (ring b) is downfield relative to H9 (ring b) of the *rac* dinuclear complex and is thus assigned to 8.18 ppm. Comparison between the chemical shift of H2 (ring a) (7.75 ppm) and the *rac* dinuclear H2 (ring c) (7.80 ppm) (similar relative environment with respect to other terminal ligands) is also in agreement with the above assignment.

The C_2 symmetry of the heterochiral ($\Delta^2\Lambda/\Lambda^2\Delta$) diastereoisomer requires three nonequivalent phen ligands (see Figure

Table 1. Chemical Shifts (ppm) from 300 MHz ^{1}H NMR Spectra of the Diastereoisomeric Forms of $[\{Ru(phen)_2\}_n(HAT)]^{2n+}$ Complexes (PF_6^- Salts; CD_3CN Solvent)

				$[\{Ru(phen)_2\}_2(\mu\text{-HAT})]^{4+}$		$[\{Ru(phen)_2\}_3(\mu\text{-HAT})]^{6+}$	
		$[Ru(phen)_3]^{2+}$	$[Ru(phen)_2(HAT)]^{2+}$	$\Lambda\Lambda/\Delta\Delta$	$\Delta\Lambda$	Δ^3/Λ^3	$\Delta^2\Lambda/\Lambda^2\Delta$
phen ring a (over phen)[a]	H2	8.05	8.00	7.96	7.98	7.75	7.89
	H3	7.65	7.65	7.70	7.70	7.61	7.65
	H4	8.61	8.66	8.68	8.68	8.58	8.56
	H5	8.28	8.27	8.26	8.30	8.22	8.13
phen ring b (over HAT)[a]	H6		8.27	8.26	8.31	8.30	8.13
	H7		8.66	8.64	8.76	8.77	8.56
	H8		7.68	7.48	7.87	7.61	7.48
	H9		8.18	7.92	8.45	8.18	8.01
phen ring c (over phen)[a]	H2			7.80	7.94		7.78
	H3			7.53	7.65		7.57
	H4			8.59	8.55		8.61
	H5			8.24	8.15		8.25
phen ring d (over HAT)[a]	H6			8.31	8.15		8.35
	H7			8.80	8.59		8.87
	H8			7.80	7.65		8.01
	H9			8.28	8.19		8.66
phen ring e (over phen)[a]	H2						7.93
	H3						7.65
	H4						8.57
	H5						8.17
phen ring f (over HAT)[a]	H6						8.17
	H7						8.68
	H8						7.85
	H9						8.59
HAT							
H			8.26 (H2/H11; d, J = 3 Hz)	7.91	7.85 (H11/H10; s)	8.10 H2/H3/H6/H7/H10/H11; s)	8.05 (H2/H3; s)
H			9.01 (H3/H10; d, J = 3 Hz)	8.34	8.34 (H2/H7; d, J = 3 Hz)		7.94 (H6/H11; s)
H			9.39 (H6/H7; s)	9.10	9.10 (H3/H6; d, J = 3 Hz)		7.92 (H7/H10; s)

[a] H2, H9 (dd, J = 5, 1.5 Hz); H3, H8 (dd, J = 5, 8 Hz); H4, H7 (dd, J = 8, 1.5 Hz).

4), thus producing a complicated ^{1}H NMR spectrum comprising six AMX, possibly three AB coupling systems from the phen ligands, and three singlet resonances from the HAT ligand (see Figure 7). The three singlet HAT resonances were assigned by comparison with the *meso* and *rac* dinuclear complex and the homochiral trinuclear complex (Table 1).

H9 (ring d) and H9 (ring f) are assigned to the two most downfield H2/H9 resonances (dd, $J = 5$, 1.5 Hz) at 8.66 and 8.59 ppm, respectively, on the basis of reduced diamagnetic anisotropic interactions described for the *meso* dinuclear complex (ring b) discussed above, and further information gained by comparisons between the *rac* and *meso* isomers (i.e., the H9 (ring d) of the *rac* isomer is downfield (8.28 ppm) relative to H9 (ring d) of the *meso* isomer (8.19 ppm)). For ring d of the *rac* isomer the phen ligand is in a similar perpendicular orientation to ring d of the heterochiral form. This results in a downfield shift relative to H9 (ring f), which contains the phen ligands in a parallel orientation (similar to ring d in the *meso* isomer). The subsequent assignments for rings d and f were achieved as describe above. The third phen ligand was assigned by comparisons with the homochiral isomer (see above) which indicate that the H9 proton orientated over the HAT bridge is downfield relative to the H2 orientated over a phen; thus H9 (ring b) and H2 (ring a) were assigned to 8.01 and 7.89 ppm, respectively. The relative shifts of H2 and H9 (rings a and b) in comparison with H2 and H9 (rings a and b) of the homochiral isomer can also be rationalized in a manner similar to the above on the basis of the relative chemical shifts of the *rac* and *meso* isomers.

Electrochemistry and Electronic Absorption Spectroscopy. Cyclic voltammetry and differential pulse voltammetry were performed on the separated diastereoisomers, *rac*- and *meso*-$[\{Ru(pp)_2\}_2(\mu\text{-HAT})]^{4+}$, and homochiral and heterochiral $\{Ru(pp)_2\}_3(\mu\text{-HAT})]^{6+}$ (where pp = bpy or phen), with the data reported in Table S2 (Supporting Information) and are in agreement with those reported previously.[5] The absorption spectra of $[\{Ru(pp)_2\}_n(HAT)]^{(2n)+}$ ($n = 1-3$ and pp = bpy or phen) were also measured and are in agreement with those described previously.[5,11]

No significant differences were observed in the electrochemical and spectral properties of the diastereoisomers in the dinuclear and in the trinuclear series.

Photoinduced Stereoisomerism. The photoracemization of mononuclear tris(bidentate) complexes of the type $[Ru(bpy)_3]^{2+}$ is known.[33] The related phenomenon may occur in polynuclear species, but is more appropriately designated as "photoinduced stereoisomerism" since the complexes may exist in diastereoisomeric and enantiomeric forms.

In a semiquantitative investigation, the complexes $\Delta\Lambda$-, $\Delta\Delta$-, and $\Lambda\Lambda$-$[\{Ru(pp)_2\}_2(\mu\text{-HAT})]^{4+}$ and Δ^3-, Λ^3-, and $\Delta^2\Lambda/\Lambda^2\Delta$-$[\{Ru(pp)_2\}_3(\mu\text{-HAT})]^{6+}$ (pp = bpy and phen) were irradiated in acetonitrile, aqueous or buffered aqueous solution, with decomposition being monitored by spectroscopy and photoinduced stereoisomerism by chromatography. In each system, the diastereoisomers are readily separated and even very minor interconversion would be detected because of the high absorption coefficients of the complexes involved. There was no detectable photoinduced stereoisomerism, although the chromatography suggested photodecomposition of approximately 1−2% in trimetallic complexes.

Luminescence Spectra and Lifetimes. Figure 8 shows the uncorrected emission spectra of the three stereoisomers ($\Delta\Lambda$, $\Delta\Delta$, and $\Lambda\Lambda$) of $[\{Ru(phen)_2\}_2(\mu\text{-HAT})]^{4+}$ in buffered aqueous (A) and in CH_3CN (B) solutions, recorded for comparable excitation intensities (at 500 nm) and for comparable percentages of absorbed light at the same excitation wavelength. There were no significant differences in intensities for the enantiomers of the *rac* form, whereas the *meso* diastereoisomer behaved as a slightly weaker emitter both in water and in CH_3CN. Moreover, as is generally observed, the intensity of emission was higher in the organic solvent than in aqueous solution.

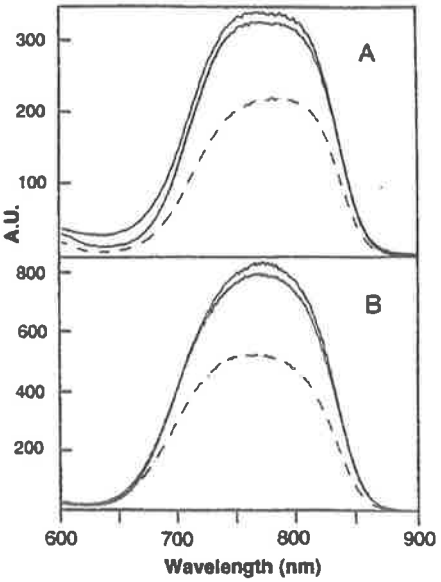

Figure 8. Noncorrected emission spectra of the three stereoisomers of $[\{Ru(phen)_2\}_2(\mu\text{-HAT})]^{4+}$ for the same % of absorbed light, in (A) TRIS buffer at pH 7 and (B) CH_3CN solutions: the enantiomers of the *rac* form (—), and the *meso* form (- - -). Excitation at 500 nm. Shimadzu spectrofluorimeter, Hamamatsu R-928 PMT.

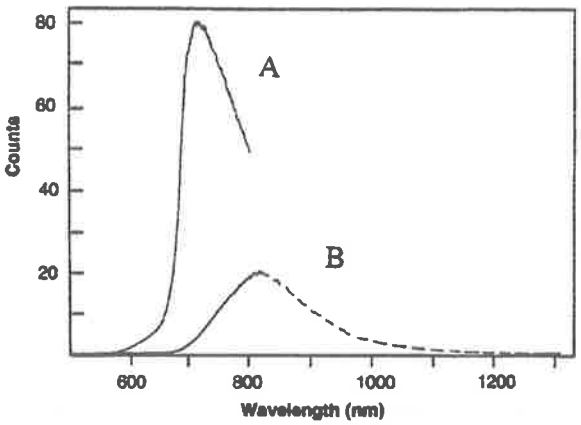

Figure 9. Corrected emission spectra in H_2O solution of (A) $[Ru(phen)_2(HAT)]^{2+}$ and (B) $[\{Ru(phen)_2\}_2(\mu\text{-HAT})]^{4+}$, measured with the Hamamatsu R-928 PMT (—) and with the Ge detector (- - -). For comparable absorbance at the excitation wavelength (432 nm) and comparable intensities of excitation at that wavelength, an intensity ratio of 15/1 can be estimated for the mono-/dinuclear compound.

Comparison of the uncorrected spectra of Figure 8 (measured with a red-sensitive PM detector) with the corrected emission spectrum of the dinuclear complex in Figure 9 (where the emission at $\lambda > 800$ nm was measured with an IR-sensitive Ge detector) illustrates the experimental problems encountered in determining reliable quantum yields of emission for the bimetallic species. Indeed, an adjustment had to be made between the two portions of the emission spectrum measured with the two different detectors under different optical conditions. Therefore,

(33) Porter, G. B.; Sparks, R. H. *J. Photochem.* **1980**, *123*, 13.

Table 2. Luminescence Lifetimes of the Diastereoisomers of the Dinuclear and Trinuclear HAT-Bridged Species in Water and CH_3CN Solutions under Air at Room Temperature, Determined by SPC and under Pulsed Laser Excitation[a]

complexes	τ (ns)	
	H_2O	CH_3CN
$\Delta\Delta$-[{Ru(bpy)$_2$}$_2$(μ-HAT)]$^{4+}$	200	458
$\Lambda\Lambda$-[{Ru(bpy)$_2$}$_2$(μ-HAT)]$^{4+}$	200	455
$\Lambda\Delta$-[{Ru(bpy)$_2$}$_2$(μ-HAT)]$^{4+}$	135	405
Δ^3-[{Ru(bpy)$_2$}$_3$(μ-HAT)]$^{6+}$	40	120
Λ^3-Δ[{Ru(bpy)$_2$}$_3$(μ-HAT)]$^{6+}$	40	110
Λ^3/Δ^3-[{Ru(bpy)$_2$}$_3$(μ-HAT)]$^{6+}$	40	105
$\Lambda^2\Delta/\Delta^2\Lambda$-[{Ru(bpy)$_2$}$_3$($\mu$-HAT)]$^{6+}$	34	110
$\Delta\Delta$-[{Ru(phen)$_2$}$_2$(μ-HAT)]$^{4+}$	310	690
$\Lambda\Lambda$-[{Ru(phen)$_2$}$_2$(μ-HAT)]$^{4+}$	306	680
$\Lambda\Delta$-[{Ru(phen)$_2$}$_2$(μ-HAT)]$^{4+}$	225	635

[a] See Experimental Section. In water, the decays are single exponentials. For the complexes in CH_3CN, the lifetimes given correspond to the highest % of contribution in the decays varying from 80 to 100% (see text). Error: ~3%, estimated from the reproducibility of the lifetime values determined by SPC and pulsed laser methods.

Φ_{em} values are not given, nor the λ_{max} of emission,[5] which cannot be easily differentiated for the three stereoisomers.

When the emissions of the trinuclear compounds [{Ru(pp)$_2$}$_3$(μ-HAT)]$^{6+}$ (pp = bpy or phen) were measured under the same conditions as those for the dinuclear species which gave the data presented in Figure 8, no significant differences in luminescence intensity were detected between the different diastereoisomers.

The emission lifetimes at room temperature in water and CH_3CN solutions for the stereoisomers of [{Ru(pp)$_2$}$_2$(μ-HAT)]$^{4+}$ and [{Ru(bpy)$_2$}$_3$(μ-HAT)]$^{6+}$ are given in Table 2. For the dinuclear compounds, the emission lifetimes were significantly shorter for the *meso* complexes than for the enantiomers of the *rac* form. However, no differences were observed for the trinuclear compounds, in accordance with the measurements of the relative emission intensities given above. For these measurements, the lifetimes were longer in CH_3CN than in water, as is generally the case.

The decay analyses for the data in Table 2 require additional comment. Problems were encountered for the measurements in CH_3CN solutions, where for the same compound single-exponential decays were not consistently observed, but were contaminated by other emitting species which contributed up to 20% to the total decays when analyzed according to biexponential functions. This effect appeared under laser excitation or in the SPC measurements (see Experimental Section) and probably originated from some (photo/dark) decomposition in CH_3CN which produced monometallic species with a much higher Φ_{em} (e.g., see the comparison between the mono- and dinuclear compounds in Figure 9). This problem of decomposition in organic solvents was mentioned previously,[11] but does not occur in water.

In order to detect possible differences of luminescence lifetimes between the diastereoisomers of the trinuclear complexes, the measurements were performed in a MeOH/EtOH (1/4) glass at low temperature (80 K). Under those experimental conditions, all the decays were observed as single exponentials and, as shown in Table 3, the emission lifetimes of the heterochiral [{Ru(pp)$_2$}$_3$(μ-HAT)]$^{6+}$ were slightly shorter than those of the homochiral forms.

Photophysics of the Diastereoisomers. Conclusions. It was shown previously[11] that thermal activation from the emitting ^{3}MLCT states to the ^{3}MC states of the bi- and trimetallic HAT complexes does not take place at room temperature because the ^{3}MLCT→^{3}MC energy gap is too large. The expected photostability is confirmed by the experimental observation that photoinduced stereoisomerism does not occur for the diastereoisomers of either nuclearity. The problems of contamination of the luminescence decays by other luminescent species under pulsed excitation in CH_3CN should thus be attributed to some dark thermal decomposition, which is inhibited in a glass at low temperature, as single-exponential decays were observed under such conditions. The absence of detectable photoisomerization establishes the accuracy of the emission quantum yields and lifetimes for the individual diastereoisomers. Although the photophysical differences between the stereoisomers are not large, this paper demonstrates their existence. They are therefore considered significant. For the first time there is evidence for inherent differences in such properties between diastereoisomers, and not differences arising from interactions with a chiral partner such as DNA or a luminescent quencher.

Table 3. Luminescence Lifetimes of the Diastereoisomeric Forms of [{Ru(pp)$_2$}$_3$(μ-HAT)]$^{6+}$ in a MeOH/EtOH 1/4 Glass at 80 K, Determined under Pulsed Laser Excitation[a]

complexes	τ (ns), MeOH/EtOH (1/4) at 80 K
Λ^3-[{Ru(phen)$_2$}$_3$(μ-HAT)]$^{6+}$	1676
Δ^3/Λ^3-[{Ru(phen)$_2$}$_3$(μ-HAT)]$^{6+}$	1655
$\Delta^2\Lambda/\Lambda^2\Delta$-[{Ru(phen)$_2$}$_3$($\mu$-HAT)]$^{6+}$	1517
Λ^3-[{Ru(bpy)$_2$}$_3$(μ-HAT)]$^{6+}$	1855
Δ^3/Λ^3-[{Ru(bpy)$_2$}$_3$(μ-HAT)]$^{6+}$	1800
$\Delta^2\Lambda/\Lambda^2\Delta$-[{Ru(bpy)$_2$}$_3$($\mu$-HAT)]$^{6+}$	1428

[a] All of the decays correspond to single exponentials. Error: ~3%, estimated from the reproducibility of the lifetime values determined by SPC and pulsed laser methods.

On the other hand, it was also concluded previously[11] that the nonradiative deactivation rate constants, k_{nr}, of the ^{3}MLCT states of the polynuclear HAT complexes are dramatically smaller than those for the corresponding mononuclear HAT compound.[11] This indicates that the vibration modes are very different in the mono- and polynuclear HAT complexes,[12] an origin of which may be the symmetry differences between each species. As the symmetries of the *rac* and *meso* forms of [{Ru(pp)$_2$}$_2$(μ-HAT)]$^{4+}$ differ (as they do also for the homo- and heterochiral forms of [{Ru(pp)$_2$}$_3$(μ-HAT)]$^{6+}$), different vibration modes would participate in the deactivation. This would explain the difference observed in the excited state lifetimes between the diastereoisomers.

It is noted also that the absence of significant shifts of λ_{max} for absorption and emission in the *meso* and *rac* diastereoisomers of the dinuclear species is in accordance with the electrochemical data, where the potentials of the first oxidation (related to the dπ level) and reduction waves (related to the π^* level) are not significantly shifted for the different diastereoisomers.

Summary

By the use of a combination of chromatographic techniques and stereoselective synthetic methods, all stereoisomers of the mononuclear [{Ru(pp)$_2$(HAT)]$^{2+}$, dinuclear [{Ru(pp)$_2$}$_2$(μ-HAT)]$^{4+}$, and trinuclear [{Ru(pp)$_2$}$_3$(μ-HAT)]$^{6+}$ species {pp = 2,2′-bipyridine or 1,10-phenanthroline} have been isolated and characterized. While the existence of such isomers had been recognized in earlier studies on the latter two systems,[5,12] their isolation in the present work has allowed investigation of the dependence of physical characteristics on the stereochemistry. Photophysical studies revealed small but significant differences between luminescence behavior of diastereoisomeric pairs in both the di- and trinuclear cases. While the differences between stereoisomers of such complexes are relatively subtle for these

small oligomers, it is clear that they will be magnified in larger polymetallic systems with increased stereochemical complexity.

Acknowledgment. F.R.K. wishes to acknowledge the Australian Research Council, and A.K.-D. and O.V.G. are grateful to the "Communauté Française de Belgique" (ARC91/96-149) and to the SSTC (PAI-IUAP 4/11 program) for financial support. O.V.G. thanks the IRSIA-FRIA for a Ph.D. fellowship. The ligand HAT was kindly donated by Professor D. Paul Rillema (University of North Carolina, Charlotte, NC). We thank David Reitsma and Laurie Kelso for useful discussion, Sue Butler (University of Wollongong) for the measurements of the CD spectra, and Fabien Dubois (Université Libre de Bruxelles) for luminescence measurements.

Supporting Information Available: Tables listing ^{1}H NMR chemical shifts (300 MHz) for the stereoisomeric forms of $[\{Ru(bpy)_2\}_n(HAT)]^{2n+}$ $\{n = 1-3\}$ complexes (CD_3CN solvent) and redox potentials for diastereoisomers of $[\{Ru(pp)_2\}_2(\mu\text{-HAT})]^{4+}$ and $[\{Ru(pp)_2\}_3(\mu\text{-HAT})]^{6+}$ {pp = 2,2′-bipyridine or 1,10-phenanthroline} and plots of CD spectra for the enantiomers of $[\{Ru(phen)_2(HAT)]^{2+}$, the enantiomers of *rac*-$[\{Ru(bpy)_2\}_2(\mu\text{-HAT})]^{4+}$, and the enantiomers of homochiral $[\{Ru(bpy)_2\}_2(\mu\text{-HAT})]^{4+}$ (5 pages). Ordering information is given on any current masthead page.

IC961374P

2872 *Inorg. Chem.* 1997, *36*, 2872−2878

Stereochemical Control of Donor and Acceptor Groups in a Monomeric Chromophore−Quencher Complex of Ruthenium(II)

Todd J. Rutherford and F. Richard Keene*

Department of Chemistry and Chemical Engineering, School of Molecular Sciences, James Cook University of North Queensland, Townsville, Queensland 4811, Australia

Received December 27, 1996[⊗]

The chromophore−quencher complex $[Ru(Me_2bpy)(bpy\text{-}MV^{2+})(bpy\text{-}PTZ)]^{4+}$, containing one donor (phenothiazine, PTZ) and one acceptor (methyl viologen, MV^{2+}) functionality, has been synthesized and separated into its four geometric isomers. This was achieved through the intermediacy of $[Ru(Me_2bpy)(bpy\text{-}MV^{2+})(py)_2]^{4+}$, the two isomers of which were separated and each reacted stereoselectively with bpy-PTZ to produce two distinct isomer pairs of the target molecule. Cation-exchange chromatography allowed separation to realize the four forms. The isomers of the product and of the intermediates were characterized by NMR spectroscopy. This is the first example of the isolation of geometric isomers of a mononuclear system containing a single donor and single acceptor functionality.

Introduction

Redox charge separation is a fundamental process in the utilization of absorbed light energy, both in natural photobiological processes such as photosynthesis[1,2] and also in artificial systems designed as photochemical molecular devices.[3]

In both contexts, intramolecular electron and/or energy transfer processes which follow light-absorption are undoubtedly influenced by the nature and relationship of the light absorbing centers (chromophores) and the redox-active groups (quenchers). In particular, their spatial relationship may control the directional characteristics of the relay processes and determine reactivity pathways.

Charge separation processes have been studied in a number of model systems,[4−12] including chromophore−quencher complexes involving polypyridyl complexes of the d^6 metal centers Ru^{II}, Os^{II}, and Re^{I}, which are of particular interest because of their particular physical characteristics.[3,13−22]

All natural and artificial systems share a common principle: a chromophore (C) with associated redox-active quenchers which may accept (A) or donate (D) electrons. In the model, the initial D−C−A species absorbs light energy and forms an excited state D−*C−A, which produces the charge-separated species D^+−C−A^- by a series of electron transfer steps. Previous studies on chromophore−quencher complexes have probed the influence of the separation distance of the donor and acceptor groups and the nature of the rigidity and electronic character of the bridging groups. However, the dependence of the electron transfer process on the stereochemical relationship among the components of the complex has not been addressed. In some cases, the systems have been deliberately chosen to avoid this spatial ambiguity,[15,16] while other studies of this type have investigated target compounds which were mixtures of stereoisomers. As a representative example of the latter scenario, it is noted that, in their studies of charge-separated excited states in mononuclear complexes containing ligands with donor− and acceptor−quencher functionalities, Elliott and coworkers have investigated the system $[Ru(44PTZ)_2(423DQ^{2+})]^{4+}$,[17−19] in which there are four possible stereoisomers (geometric).

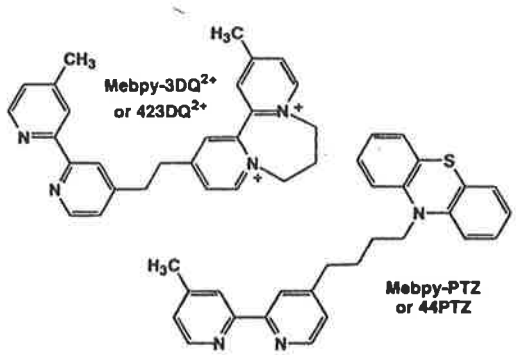

A similar number of forms exist for $[Ru(bpy\text{-}AQ)_2(bpy\text{-}PTZ)]^{2+}$,

[⊗] Abstract published in *Advance ACS Abstracts*, June 1, 1997.

(1) Deisenhofer, J.; Michel, H. *Angew. Chem., Int. Ed. Engl.* **1989**, *28*, 829.
(2) Huber, R. *Angew. Chem., Int. Ed. Engl.* **1989**, *28*, 848.
(3) Balzani, V.; Scandola, F. *Supramolecular Photochemistry*; Ellis Horwood: Chichester, U.K., 1991.
(4) Willner, I.; Willner, B. In *Artificial Photosynthetic Model Systems Using Light-Induced Electron Transfer Reactions in Catalytic and Biocatalytic Assemblies*; Willner, I., Willner, B., Eds.; Springer-Verlag: Heidelberg, 1991; Vol. 159, p 153.
(5) Wasielewski, M. R. *Chem. Rev.* **1992**, *92*, 435.
(6) Jordan, K. D.; Paddon-Row, M. N. *Chem. Rev.* **1992**, *92*, 395.
(7) Gust, D.; Moore, T. A.; Moore, A. L. *Acc. Chem. Res.* **1993**, *26*, 198.
(8) Paddon-Row, M. N. *Acc. Chem. Res.* **1994**, *27*, 18.
(9) Gust, D.; Moore, T. A.; Moore, A. L.; Macpherson, A. N.; Lopez, A.; Degraziano, J. M.; Gouni, I.; Bittersmann, E.; Seely, G. R.; Gao, F.; Nieman, R. A.; Ma, X. C.C.; Demanche, L. J.; Hung, S. C.; Luttrull, D. K.; Lee, S.-J.; Kerrigan, P. K. *J. Am. Chem. Soc.* **1993**, *115*, 11141.
(10) Lee, S.-J.; Degraziano, J. M.; Macpherson, A. N.; Shin, E. J.; Kerrigan, P. K.; Seely, G. R.; Moore, A. L.; Moore, T. A.; Gust, D. *Chem. Phys.* **1993**, *176*, 321.
(11) Harriman, A.; Sauvage, J.-P. *Chem. Soc. Rev.* **1996**, 41.
(12) Collin, J.-P.; Harriman, A.; Heitz, V.; Odobel, F.; Sauvage, J.-P. *Coord. Chem. Rev.* **1996**, *148*, 63.
(13) Lehn, J.-M. *Angew. Chem., Int. Ed. Engl.* **1990**, *29*, 1304.
(14) Juris, A.; Barigelletti, S.; Campagna, S.; Balzani, V.; Belser, P.; von Zelewsky, A. *Coord. Chem. Rev.* **1988**, *84*, 85.
(15) Sauvage, J.-P.; Collin, J.-P.; Chambron, J.-C.; Guillerez, S.; Coudret, C.; Balzani, V.; Barigelletti, F.; De Cola, L.; Flamigni, L. *Chem. Rev.* **1994**, *94*, 993.
(16) Coe, B. J.; Friesen, D. A.; Thompson, D. W.; Meyer, T. J. *Inorg. Chem.* **1996**, *35*, 4575.
(17) Cooley, L. F.; Larson, S. L.; Elliott, C. M.; Kelley, D. F. *J. Phys. Chem.* **1991**, *95*, 10694.
(18) Danielson, K.; Elliott, C. M.; Merkert, J. W.; Meyer, T. J. *J. Am. Chem. Soc.* **1987**, *109*, 2519.
(19) Larson, S. L.; Elliott, C. M.; Kelley, D. F. *J. Phys. Chem.* **1995**, *99*, 6530.
(20) Schoonover, J. R.; Strouse, G. F.; Chen, P.; Bates, W. D.; Meyer, T. J. *Inorg. Chem.* **1993**, *32*, 2618.
(21) Opperman, K. A.; Mecklenburg, S. L.; Meyer, T. J. *Inorg. Chem.* **1994**, *33*, 5295.
(22) Strouse, G. F.; Schoonover, J. R.; Duesing, R.; Meyer, T. J. *Inorg. Chem.* **1995**, *34*, 2725.

S0020-1669(96)01527-3 CCC: $14.00

studied by Meyer *et al.*[21]

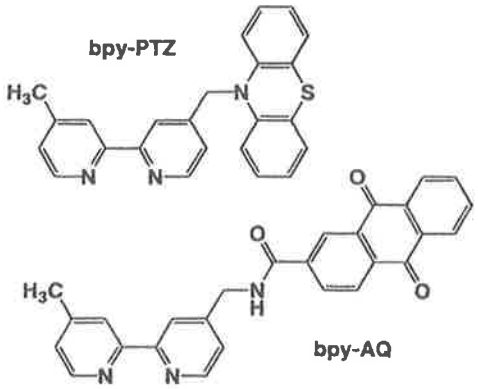

In both of these studies,[17−19,21] the possible existence of geometric isomers was acknowledged. Indeed in one case[18] it was evoked as a possible explanation for the observations of broadening in the transient absorption spectrum of the charge transfer excited state, and the possible existence of more than one component in its decay.

The spatial dependence of the photophysical behavior is unknown, as we are not aware of any report of the isolation of stereoisomers of a mononuclear species containing a single donor and a single acceptor functionality.

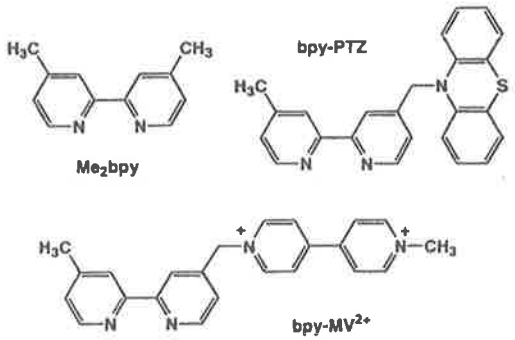

We have recently reported the synthesis of tris(heteroleptic)-ruthenium(II) complexes of bidentate polypyridyl ligands,[23] as well as the stereochemical aspects of such systems.[24,25] As an extension of the above studies, we now report a synthetic and stereochemical study in which we have isolated the four geometric isomers of the system $[Ru(Me_2bpy)(bpy\text{-}MV^{2+})(bpy\text{-}PTZ)]^{4+}$ (Figure 1) {Me_2bpy = 4,4′-dimethyl-2,2′-bipyridine; $bpy\text{-}MV^{2+}$ = 1-[(4′-methyl-2,2′-bipyridin-4-yl)methyl]-1′-methyl-4,4′-bipyridinediium cation (MV^{2+} is an acceptor quencher); bpy-PTZ = 10-[(4′-methyl-2,2′-bipyridin-4-yl)methyl]phenothiazine (PTZ is a donor quencher)}.

Charge separation processes have previously been investigated in a system based on the the tridentate ligand tpy (2,2′:6′,2″-terpyridine), $[Ru(tpy\text{-}A)(tpy\text{-}B)]^{2+}$, involving the same quencher groups. In that case there was no stereochemical ambiguity as the two functionalities were attached to the central pyridine ring in the respective tpy moieties, constraining the substituents to a "*trans*" relationship.[15,26]

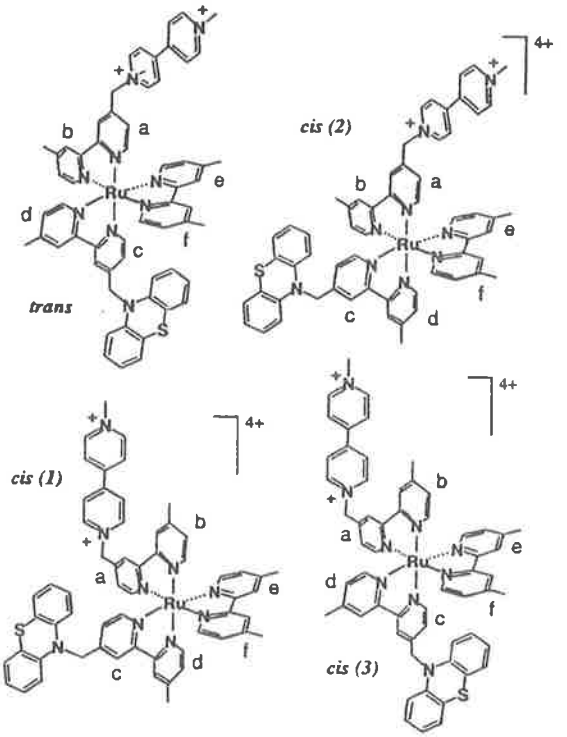

Figure 1. Geometric isomers of $[Ru(Me_2bpy)(bpy\text{-}MQ^{2+})(bpy\text{-}PTZ)]^{4+}$. Ring notation is used in discussion of NMR spectra.

A detailed comparative photophysical study of the four isomers of the present title system is in progress and will be reported subsequently.[27]

Experimental Section

Instrumentation. $^1H,^1H$-decoupling, NOE-difference, and COSY experiments were performed on a Bruker Aspect 300 MHz NMR spectrometer (CD_3CN solutions). UV−visible spectra were recorded in acetonitrile solution on a Hewlett Packard HP-89532K spectrophotometer using quartz cells.

All electrochemical experiments were performed under argon in an inert-atmosphere drybox using a Bioanalytical Systems BAS 100A electrochemical analyzer. Measurements were made in acetonitrile/0.1 M $[(n\text{-}C_4H_9)_4N]PF_6$ solution using a platinum button working electrode and a Ag/Ag^+ (0.01M $AgClO_4$/0.1 M $[(n\text{-}C_4H_9)_4N]ClO_4$ in acetonitrile) reference electrode (+0.31 V *vs* SCE). Cyclic voltammetry was performed with a sweep rate of 100 mV/s; differential pulse voltammetry was run with a sweep rate of 4 mV/s and a pulse amplitude, width, and period of 50 mV, 60 ms, and 1 s, respectively.

Elemental analyses were performed within the Department of Chemistry and Chemical Engineering at James Cook University of North Queensland and were within acceptable limits (0.4%) after allowance was made in some cases for inclusion of hydration within the crystal. In addition, the characterization of the complexes was achieved unequivocally by a combination of NMR and electrochemical data, as described herein.

Materials. Ruthenium(III) chloride trihydrate (Strem, 99.9%), cesium carbonate (Aldrich, 99.9%), potassium carbonate (Ajax), acetonitrile (Aldrich, 99.9+%), potassium hexafluorophosphate (Aldrich, 99%), sodium toluene-4-sulfonate (Aldrich, 95%), and iodomethane (Ajax) were used without further purification. 4,4′-Dimethyl-2,2′-bipyridine (Adrich, 98%), 4,4′-bipyridine (Aldrich, 98%), and selenium(IV) oxide (Aldrich, 99.9+%), were dried *in vacuo* overnight. Phenothiazine (Fluka) was recrystallized from refluxing

(23) Anderson, P. A.; Deacon, G. B.; Haarmann, K. H.; Keene, F. R.; Meyer, T. J.; Reitsma, D. A.; Skelton, B. W.; Strouse, G. F.; Thomas, N. C.; Treadway, J. A.; White, A. H. *Inorg. Chem.* **1995**, *34*, 6145.
(24) Rutherford, T. J.; Quagliotto, M. G.; Keene, F. R. *Inorg. Chem.* **1995**, *34*, 3857.
(25) Rutherford, T. J.; Reitsma, D. A.; Keene, F. R. *J. Chem. Soc., Dalton Trans.* **1994**, 3659.
(26) Collin, J.-P.; Guillerez, S.; Sauvage, J.-P.; Barigelletti, F.; De Cola, L.; Flamigni, L.; Balzani, V. *Inorg. Chem.* **1991**, *30*, 4230.
(27) Treadway, J. A.; Chen, P.; Rutherford, T. J.; Keene, F. R.; Meyer, T. J. Submitted for publication.

toluene and then from benzene. Dimethylformamide (M&B), pyridine (Ajax), 2-methoxyethyl ether (Aldrich), and standard laboratory solvents were dried and distilled prior to use. Trimethylamine *N*-oxide dihydrate (TMNO; Fluka) was sublimed under vacuum at 120 °C, yielding the anhydrous form. The complex $[Ru(Me_2bpy)_3](PF_6)_2$ was synthesized according to literature procedures.[28]

Syntheses. 4-Methyl-2,2′-bipyridine-4′-carbaldehyde (bpy-CHO) was synthesized on a 33 mmol scale using a method described by Furue *et al.*,[29] with the following modifications.[30] 2-Methoxyethyl ether was the solvent, and upon isolation of the initial product the residue was dissolved in ethyl acetate (*ca.* 750 mL) and stirred with 0.5 M K_2CO_3 solution (100 mL). The mixture was extracted with 0.2 M sodium bisulfite solution (3 × 300 mL), and the aqueous extracts were adjusted to pH 9 with K_2CO_3 and re-extracted with dichloromethane (3 × 100 mL), with the remaining aqueous layer being continually extracted with dichloromethane overnight. The organic extracts were combined and dried (Na_2SO_4), and the solvent was evaporated, giving a white solid. Physical data were identical to those described by Furue *et al.*[29] Yield: 42%.

4-(Hydroxymethyl)-4′-methyl-2,2′-bipyridine (bpy-CH_2OH)[27] and 4-(bromomethyl)-4′-methyl-2,2′-bipyridine dihydrobromide (bpy-CH_2Br·2HBr)[31] were prepared as described in the literature.

10-[(4′-Methyl-2,2′-bipyridin-4-yl)methyl]phenothiazine (bpy-PTZ). Phenothiazine (398 mg, 1.99 mmol) and Cs_2CO_3 (970 mg, 2.985 mmol) were dissolved in a degassed (N_2) solution of DMF (30 mL) and the mixture stirred for 0.5 h. Bpy-CH_2Br·2HBr (280 mg, 0.66 mmol) and Cs_2CO_3 (845 mg, 2.6 mmol) were then added, and the reaction mixture was stirred for 48 h in subdued light. The DMF was removed under vacuum and the residue purified by vacuum column chromatography[32] (silica; diethyl ether), yielding white-cream crystals. Physical data were identical to those described by Meyer *et al.*[31] using an alternative synthetic procedure. Yield: 127 mg, 50%.

1-Methyl-4,4′-bipyridinium iodide (MQ^+I^-) was synthesized (yield, 70%) as described by Yonemoto *et al.*[33]

1-[(4′-Methyl-2,2′-bipyridin-4-yl)methyl]-1′-methyl-4,4′-bipyridinediium hexafluorophosphate [(bpy-MV^{2+})$(PF_6)_2$] was synthesized using methods similar to those used by Yonemoto *et al.*[33] bpy-CH_2-Br·2HBr (1.2 g, 2.8 mmol) was dissolved in H_2O (15 mL) and excess K_2CO_3 added with stirring to liberate the free base, which was extracted with $CHCl_3$ (3 × 30 mL) and dried under vacuum. Yield: 0.75 g. A portion (250 mg, 1.07 mmol) was dissolved in acetonitrile (50 mL), the solution degassed for 20 min, MQ^+I^- (365 mg, 2.14 mmol) added, and the mixture refluxed for 28 h in subdued light. Acetonitrile was removed under vacuum, the residue dissolved in a minimum amount of water, the solution filtered, and the product precipitated by the addition of a saturated solution of KPF_6. After the suspension was cooled overnight at 4 °C, the product was filtered, washed with H_2O, $CHCl_3$, and Et_2O, and air-dried. Physical data were in agreement with those described for the same product obtained by Yonemoto *et al.*[33]

Dicarbonyl(4,4′-dimethyl-2,2′-bipyridine)bis(trifluoromethanesulfonato)ruthenium(II) [$Ru(Me_2bpy)(CO)_2(CF_3SO_3)_2$] was synthesized by the literature procedure.[23]

Dicarbonyl(4,4′-dimethyl-2,2′-bipyridine)[1-((4′-methyl-2,2′-bipyridin-4-yl)methyl)-1′-methyl-4,4′-bipyridinediium]ruthenium(II) Hexafluorophosphate [[$Ru(Me_2bpy)$(bpy-MV^{2+})$(CO)_2$]$(PF_6)_4$, I]. The ligand bpy-MV^{2+} (321 mg, 0.5 mmol) was dissolved in absolute ethanol (30 mL) and the solution degassed with N_2 for 20 min. $[Ru(Me_2bpy)(CO)_2(CF_3SO_3)_2]$ (300 mg, 0.468 mmol) was added and the reaction refluxed for 90 min, during which time the mixture turned a blue color. The reaction mixture was cooled, the solvent removed under vacuum, the residue dissolved in hot water, KPF_6 added to the filtered solution and the mixture stored at 4 °C overnight. The precipitate was collected by filtration. Fractional recrystallization from ethanol allowed the isolation of one geometric isomer. Alternatively, purification could be achieved by cation-exchange chromatography (SP-Sephadex C25): the ligand was eluted using 0.2 M NaCl/10% acetone and the complex with 0.5 M NaCl/10% acetone. The complex was precipitated with KPF_6 and collected by filtration. This latter method retained the original isomer ratio. Yield: 405 mg, 68%. IR: $\bar{\nu}_{CO}$ 2084 and 2034 cm^{-1}.

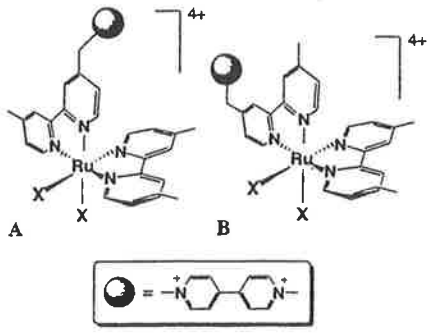

Figure 2. Geometric isomers of $[Ru(Me_2bpy)$(bpy-MQ^{2+})$(monodentate)_2]^{4+}$: I, X = CO; II, X = py.

(4,4′-Dimethyl-2,2′-bipyridine)[1-((4′-methyl-2,2′-bipyridin-4-yl)methyl)-1′-methyl-4,4′-bipyridinediium]bis(pyridine)ruthenium(II) Hexafluorophosphate [[$Ru(Me_2bpy)$(bpy-MV^{2+})$(py)_2$]$(PF_6)_4$, II]. Pyridine (200 mg, 2.5 mmol) was added to 2-methoxyethanol (10 mL) and the mixture degassed (N_2) for 20 min. $[Ru(Me_2bpy)$(bpy-MV^{2+})$(CO)_2](PF_6)_4$ (500 mg, 0.39 mmol) was added and the mixture heated to 50 °C. TMNO (68 mg, 0.905 mmol) was dissolved in 2-methoxyethanol (*ca.* 30 mL) and added dropwise over 2−3 h. The mixture was stirred at 60 °C in subdued light for 8 h, then diluted with water, and purified by cation exchange chromatography (SP-Sepahdex C25; 0.5 M NaCl eluent). The product was precipitated by the addition of a saturated solution of KPF_6. Yield: 140 mg, 27%.

The two geometric isomers (A and B, Figure 2) were separated by cation-exchange chromatography (SP-Sephadex C25; 0.25 M sodium toluene-4-sulfonate eluent), and the products were precipitated by the addition of a saturated solution of KPF_6. The two isomers were collected and separately dissolved in a minimum volume of acetone, and distilled water was added followed by a saturated solution of KPF_6. In each case the product was filtered, washed with water and ether, and air-dried.

(4,4′-Dimethyl-2,2′-bipyridine){1-[(4′-methyl-2,2′-bipyridin-4-yl)methyl]-1′-methyl-4,4′-bipyridinediium}{10-[(4′-methyl-2,2′-bipyridin-4-yl)methyl]phenothiazine}ruthenium(II) Hexafluorophosphate [[$Ru(Me_2bpy)$(bpy-MV^{2+})(bpy-PTZ)]$(PF_6)_4$, III]. bpy-PTZ (21 mg, 0.0543 mmol) was added to ethylene glycol (15 mL, containing 10% H_2O) and the mixture degassed with N_2 for 20 min. A (or B) $[Ru(Me_2bpy)$(bpy-MV^{2+})$(py)_2](PF_6)_4$ (25 mg, 0.0181 mmol) was added and the mixture heated at 110−120 °C in subdued light for 3.5 h. The solution was added to water (*ca.* 50 mL) and the excess bpy-PTZ removed by filtration. The product was purified by cation-exchange chromatography (SP-Sephadex C25, 0.3 M sodium toluene-4-sulfonate eluent) and precipitated by addition of a saturated solution of KPF_6. The single geometric isomers A and B yielded the two geometric forms *trans/cis(2)* and *cis(1)/cis(3)*, respectively (see Figure 3). Total yield: 20 mg, 70%.

The two isomeric mixtures were each separated by cation-exchange chromatography (SP-Sephadex C25; 0.25 M sodium toluene-4-sulfonate/5% acetone eluent) and the separated isomers [*trans* and *cis(2)*, *cis(1)* and *cis(3)*] precipitated by the addition of KPF_6. The products were twice reprecipitated and collected as described above.

Bis(4,4′-Dimethyl-2,2′-bipyridine){1-[(4′-methyl-2,2′-bipyridin-4-yl)methyl]-1′-methyl-4,4′-bipyridinediium}ruthenium(II) Hexafluorophosphate [[$Ru(Me_2bpy)_2$(bpy-MV^{2+})]$(PF_6)_4$, IV]. bpy-MV^{2+} (55 mg, 0.086 mmol) was added to 50% aqueous ethanol (10 mL) and the solution degassed for 20 min with N_2. $[Ru(Me_2bpy)_2Cl_2]$·H_2O (25 mg, 0.045 mmol) was added and the mixture refluxed for 1.5 h. The product was purified by cation-exchange chromatography (SP-Sephadex C-25; 0.3 M sodium toluene-4-sulfonate eluent) and precipitated by the addition of a saturated solution of KPF_6. The product was then reprecipitated as described above. Yield: 42 mg, 70%.

(28) Togano, T.; Nagao, N.; Tsuchida, M.; Kumakura, H.; Hisamatsu, K.; Howell, F. S.; Mukaida, M. *Inorg. Chim. Acta* **1992**, *195*, 221.
(29) Furue, M.; Yoshidzumi, T.; Kinoshita, S.; Kushida, T.; Nozakura, S.; Kamachi, M. *Bull. Chem. Soc. Jpn.* **1991**, *64*, 1632.
(30) Strouse, G. F. Ph.D. Thesis, University of North Carolina, Chapel Hill, 1994. Kelso, L. S., unpublished work.
(31) Della Ciana, L.; Hamachi, I.; Meyer, T. J. *J. Org. Chem.* **1989**, *54*, 1731.
(32) Coll, J. C.; Bowden, B. F. *J. Nat. Prod.* **1986**, *49*, 934.
(33) Yonemoto, E. H.; Riley, R. L.; Kim, Y. I.; Atherton, S. J.; Schmehl, R. H.; Mallouk, T. E. *J. Am. Chem. Soc.* **1992**, *114*, 8081.

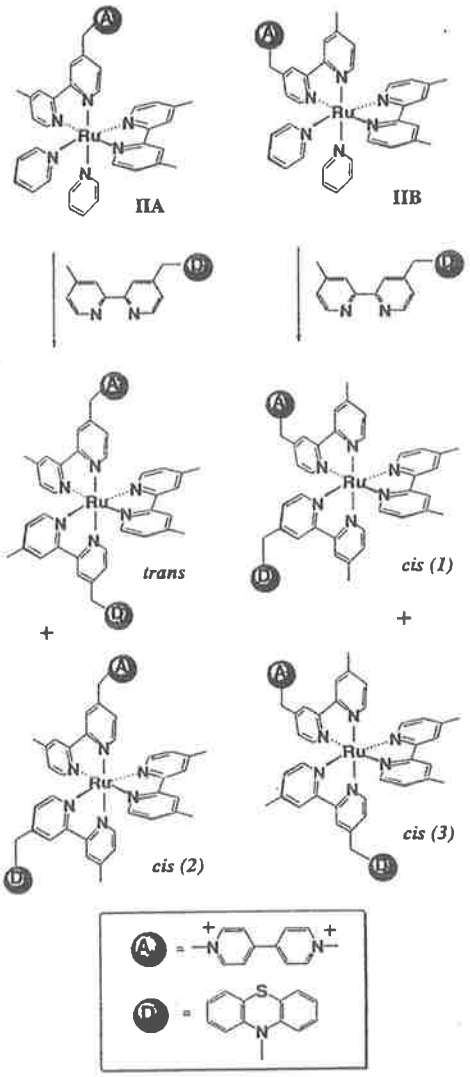

Figure 3. Stereochemistry of the conversion II → III.

Bis(4,4′-Dimethyl-2,2′-bipyridine){10-[(4′-methyl-2,2′-bipyridin-4-yl)methyl]phenothiazine}ruthenium(II) Hexafluorophosphate [[Ru(Me$_2$bpy)$_2$(bpy-PTZ)](PF$_6$)$_2$, V]. The reaction was performed under conditions similar to those used for Ru(Me$_2$bpy)$_2$(bpy-MV^{2+})(PF$_6$)$_4$, but using bpy-PTZ instead of bpy-MV^{2+}. Yield: 75%.

Results and Discussion

Syntheses. The ligand bpy-MV^{2+} was prepared by a slight modification of literature procedures, and bpy-PTZ was obtained by reaction of the PTZ anion with bpy-CH$_2$Br in DMF solution for 48 h.

The synthetic strategy for the target complex, [Ru(Me$_2$bpy)(bpy-MV^{2+})(bpy-PTZ)]$^{4+}$ (**III**), required that the ligands bpy-PTZ and bpy-MV^{2+} be added sequentially to the [Ru(Me$_2$bpy)(CO)$_2$(CF$_3$SO$_3$)$_2$] precursor. However, the PTZ functionalization is sensitive to oxidation by TMNO, which is used in the decarbonylation procedure in the final stages of the synthetic scheme. Accordingly, bpy-MV^{2+} was added first: [Ru(Me$_2$bpy)(bpy-MV^{2+})(CO)$_2$]$^{4+}$ (**I**) was prepared by the reaction of [Ru(Me$_2$bpy)(CO)$_2$(CF$_3$SO$_3$)$_2$] with bpy-MV^{2+} in refluxing ethanol.

The presence of the unsymmetrically-substituted bpy-MV^{2+} may induce stereoisomerism in its complexes: in the synthetic scheme, **I** is the first complex in which geometric isomerism is observed and can therefore be controlled. Figure 2 shows the two possible geometric forms: **IA** contains the MV^{2+} substituent in a *cis/trans* orientation with respect to the carbonyl ligands whereas in **IB** it has a *cis/cis* orientation.

The stereochemical predetermination and structural identification of one of the precursors greatly simplifies the stereochemical characterization of the target complex. The separation of the two geometric forms **I** is possible by fractional recrystallization from ethanol, with **IB** being the less soluble form. However, the stereochemical control of the reaction sequence at this point was not pursued for a number of reasons, as the more soluble form **IA** always contained traces of **IB**, and to retain stereochemical integrity the subsequent decarbonylation reactions of **I** must be undertaken at low temperatures, leading to low yields.[24,25] In addition, the lack of visible absorption by **I** renders the separation of the geometric isomers by chromatography more difficult.

To avoid the problem of the sensitivity of the the PTZ grouping in the decarbonylation process, an extra step was introduced into the previously reported synthetic scheme,[23] involving the decarbonylation of **I** with TMNO and substitution with pyridine. The conditions were varied from those described by Anderson *et al.*[23] as it was observed that any excess TMNO also led to slow decomposition of the bpy-MV^{2+} ligand. The reaction was performed in 2-methoxyethanol, and a solution of TMNO in 2-methoxyethanol was added dropwise over several hours while the reaction mixture was heated at *ca.* 60−70 °C for a total of 7−8 h. These conditions allowed the formation of [Ru(Me$_2$bpy)(bpy-MV^{2+})(py)$_2$]$^{4+}$ (**II**) in *ca.* 30% yield.

The complex **II** proved a very useful precursor to **III**. The two geometric isomers were easily distinguished by NMR spectroscopy; the complex was colored (due to MLCT absorptions in the visible spectral region) facilitating chromatographic separation procedures; and the reaction of **II** with a third bidentate polypyridyl ligand is known to proceed with stereochemical retention of configuration at high temperatures.[34] The two geometric isomers, **IIA** and **IIB** (Figure 2), were separated by cation-exchange chromatography (approximately equal proportions) and characterized by NMR spectroscopy (see below). The separation of the two geometric forms is thought to result from their differential association with the toluene-4-sulfonate anion of the eluent.[25,35]

The stereochemical consequences of the reactions of **IIA** and **IIB** with bpy-PTZ are shown in Figure 3. In ethylene glycol/10% water at 120 °C (subdued light), the substitution of pyridine reaction occurs with retention of the stereochemical integrity of the metal center,[31] so that **IIA** yields a *trans*-**III** + *cis(2)*-**III** mixture and **IIB** produces *cis(1)*-**III** + *cis(3)*-**III**. The two pairs of isomeric mixtures of [Ru(Me$_2$bpy)(bpy-MV^{2+})(bpy-PTZ)]$^{4+}$ were separated by cation-exchange chromatography on SP-Sephadex C25 with sodium toluene-4-sulfonate as the eluent. Interestingly, the separation of *cis(1)* and *cis(3)* was significantly more efficient than the separation of the *trans* and *cis(2)* forms: this observation and the order of elution are consistent with previous studies involving the separation of the geometric forms of [Ru(Me$_2$bpy)(pmb)$_2$]$^{2+}$ (pmb = 4-methyl-4-neopentyl-2,2′-bipyridine).[25] In that earlier work the *s-cis* [corresponding to *cis(1)*-**III** in the present case] and *u-cis* mixtures [corresponding to *cis(2)*- + *cis(3)*-**III** in the present case] were more easily separated than *trans* and *u-cis* mixtures, and the chromatographic elution order was *u-cis* > *s-cis* > *trans*, which is analogous to the orders observed in the present separations (*viz. cis (3)* > *cis(1)* and *cis(2)* > *trans*).[25]

(34) Hua, X.; von Zelewsky, A. *Inorg. Chem.* **1995**, *34*, 5791.
(35) Fletcher, N. C.; Atkinson, I. M.; Reitsma, D. A.; Keene, F. R., work in progress.

Table 1. Electrochememical Data (Acetonitrile Solution) for Complexes Used in This Study and Related Species

complex (as PF_6^- salts)	$E_{1/2}$ values (vs SSCE)					
	$Ru^{III/II}$	$PTZ^{0/+}$	$MV^{+/0}$	$MV^{2+/+}$	$pp^{0/-1}$	$pp^{0/-1}$
$[Ru(bpy)_3]^{2+}$	+1.29				−1.33	−1.52
$[Ru(Me_2bpy)_3]^{2+}$	+1.09				−1.44	−1.62
$[Ru(Me_2bpy)(bpy\text{-}MV)(py)_2]^{4+}$	+1.23		−0.35	−0.74	−1.39	−1.63
$[Ru(Me_2bpy)_2(bpy\text{-}MV)]^{4+}$	+1.21		−0.33	−0.73	−1.39	−1.62
$[Ru(Me_2bpy)_2(bpy\text{-}PTZ)]^{2+}$	+1.19	+0.79			−1.40	−1.59
$[Ru(Me_2bpy)(bpy\text{-}MV)(bpy\text{-}PTZ)]^{4+}$	+1.22	+0.80	−0.34	−0.74	−1.37	−1.57

Table 2. Chemical Shifts (ppm) for the Two Geometric Isomers of $[Ru(Me_2bpy)(bpy\text{-}MV^{2+})(py)_2]^{4+}$ and $[Ru(Me_2bpy)_2(py)_2]^{2+}$ [a]

	MV^{2+}				bpy-MV^{2+}								Me_2bpy							
	H2′	H3′	H3	H2	H6	H5	H3	H3′	H5′	H6′	CH_2	CH_3	H6	H5	H3	H3′	H5′	H6′	CH_3(c)	CH_3(d)
$[Ru(Me_2bpy)_2(py)_2]^{2+}$													8.68	7.57	8.19	8.10	7.18	7.67	2.42	2.57
IIA[b]	8.90	8.42	8.35	8.83	7.96	7.31	8.20	8.20	7.61	8.71	5.86	2.56	8.68	7.59	8.20	8.10	7.19	7.66	2.42	2.56
IIB[b]	9.10	8.49	8.39	8.90	8.93	7.70	8.30	8.13	7.22	7.69	6.01	2.41	8.68	7.59	8.20	8.13	7.15	7.69	2.41	2.57

[a] All spectra were recorded in CD_3CN. Pyridine chemical shifts are equivalent in the above compounds: H2, H6 = 8.23 ppm (d, 5 Hz); H3, H5 = 7.26 ppm (dd, 5, 8 Hz); H4 = 7.81 ppm (t, 8 Hz). H6 and H5 are doublets with J = 5 Hz. H2, H2′, H3, and H3′ are doublets with J = 7 Hz. N^+-CH_3 = 4.40−4.38 ppm (s). [b] $[Ru(Me_2bpy)(bpy\text{-}MV^{2+})(py)_2]^{4+}$.

Electrochemistry. The cyclic voltammetry of complexes involved in this study are given in Table 1, and the data provide valuable information regarding their electronic nature and also an electronic means of characterization. Cyclic voltammetry (acetonitrile/0.1 M $[(n\text{-}C_4H_9)_4]PF_6$ solution) indicated that $Ru^{III/II}$ redox couples ranged from $E_{1/2}$ = +1.09 V to +1.29 V, showing a small variation in that couple for the complexes—as expected from the small varations in the ligand environment. As observed by Lever *et al.*,[36,37] the electronic environment of any ligand is relatively unaffected by the other ligands present, which is apparent in the small variations in the $pp^{0/-1}$ redox potentials, and to a much lesser extent in the redox potentials of the MV^{2+} and PTZ substituents.

The above complexes exhibit electrochemical characteristics expected for complexes of the respective formulations and are in agreement with those previously reported for related species containing these ligands.[17,21,26,33] It is also noted that all redox couples were quasi-reversible with ΔE_p values between 87 and 126 mV. Cyclic voltammetry was performed on the geometric isomers of $[Ru(Me_2bpy)(bpy\text{-}MV)(py)_2]^{4+}$ (**II**) and $[Ru(Me_2bpy)(bpy\text{-}MV)(bpy\text{-}PTZ)]^{4+}$ (**III**) and no significant differences were observed between the stereoisomeric forms. The cyclic voltammogram for the target complex **III** is provided as Supporting Information (Figure S1).

Electronic Spectroscopy. As anticipated, the electronic absorption spectra of the complexes listed in Table 1 are closely similar, being dominated in the visible region by ^{1}MLCT transitions, $d\pi(Ru^{II}) \rightarrow \pi^*$(bpy), and in the UV region by bpy-ligand $\pi \rightarrow \pi^*$transitions and those arising from the PTZ and MV^{2+} substituents.[14] No differences were observed between the spectra of stereoisomers of the same complex.

^{1}H NMR Studies. The geometric isomers of $[Ru(Me_2bpy)(bpy\text{-}MV^{2+})(CO)_2]^{4+}$ (**I**), $[Ru(Me_2bpy)(bpy\text{-}MV^{2+})(py)_2]^{4+}$ (**II**), and the target species $[Ru(Me_2bpy)(bpy\text{-}MV^{2+})(bpy\text{-}PTZ)]^{4+}$ (**III**) were assigned by ^{1}H NMR spectroscopy. Chemical shifts were determined by ^{1}H COSY, selective decoupling and NOE experiments, and their assignments based on the relative degree of diamagnetic anisotropic interactions between the adjacent ligands, coupling constant values, and comparisons with structurally similar complexes $[Ru(Me_2bpy)_3]^{2+}$, $[Ru(Me_2bpy)_2(bpy\text{-}PTZ)]^{2+}$, and $[Ru(Me_2bpy)_2(bpy\text{-}MV^{2+})]^{4+}$. The NMR data for all of these complexes are discussed below.

$[Ru(Me_2bpy)(bpy\text{-}MV^{2+})(CO)_2]^{4+}$ (I). The geometric isomers **IA** and **IB** were not separated. Both possess C_1 point group symmetry so that the ^{1}H NMR spectrum of the mixture will consist of resonances due to 42 distinct protons (21 from each isomer, allowing for free rotation about the methylene group). Nevertheless, the two isomers were easily identified in the spectrum due to the different relative degrees of diamagnetic anisotropic interactions arising from the carbonyl and polypyridyl ligands:[25] isomers **IA** and **IB** were most clearly distinguished by the methylene proton (H4) resonance, which was observed at 5.93 ppm and 6.11 ppm, respectively. These shifts are explained by the reduced anisotropic interactions between the methylene-substituted pyridyl ring and carbonyl ligands in **IB** relative to its interaction with the Me_2bpy ligand in **IA**.

$[Ru(Me_2bpy)(bpy\text{-}MV^{2+})(py)_2]^{4+}$ (II). The separated geometric isomers **IIA** and **IIB** both possess C_1 point group symmetry, so that their ^{1}H NMR spectra were each composed of 24 proton resonances, the assignments of which are given in Table 2. The atom- and ring-numbering sequences used are shown in Figure 4. These two isomeric forms exhibited well-dispersed proton resonances (shown in Figure 5) resulting from the different relative degrees of anisotropic interaction between the bidentate (bpy-based) and the pyridine ligands. The assignment of **IIA** and **IIB** to the two NMR spectra shown in parts A and B, respectively, of Figure 5 was based on the differential anisotropic interactions.

In isomer **IIA**, ring a is situated over the plane of the adjacent Me_2bpy ligand, whereas in **IIB** ring a is orientated over the plane of the monodentate pyridine ligand (Figure 2). The consequent anisotropic interactions result in the ring a protons (H6, H5, and H3) being more shielded in **IIA** relative to **IIB** (see Table 2). This shielding influence is clearly observed in the methylene resonances of **IIA** compared to **IIB** (5.86 ppm and 6.01 ppm, respectively). The relative differences in the anisotropic interactions are most significant in the H6 protons, which are manifested as increased induced chemical shift differences; for example, the difference in chemical shifts of H6 (ring a) in **IIA** and **IIB** is approximately 1 ppm, compared with a difference of 0.2 ppm in the chemical shifts of H3 (ring a).

$[Ru(Me_2bpy)_3]^{2+}$. Because of the D_3 symmetry of this complex, a spectrum composed of one AX coupling system and one singlet resonance is observed in the aromatic region. The protons H6, H5, H3, and H4 were assigned to the resonances at 7.48 ppm, 7.17 ppm, 8.31 ppm, and 2.48 ppm, respectively, on the basis of coupling constant values and NOE experiments.

$[Ru(Me_2bpy)_2(bpy\text{-}PTZ)]^{2+}$ (V). With C_1 point group symmetry, this complex has a ^{1}H NMR spectrum consisting of 29

(36) Lever, A. B. P. *Inorg. Chem.* **1990**, *29*, 1271.
(37) Dodsworth, E. S.; Vlcek, A. A.; Lever, A. B. P. *Inorg. Chem.* **1994**, *33*, 1045.

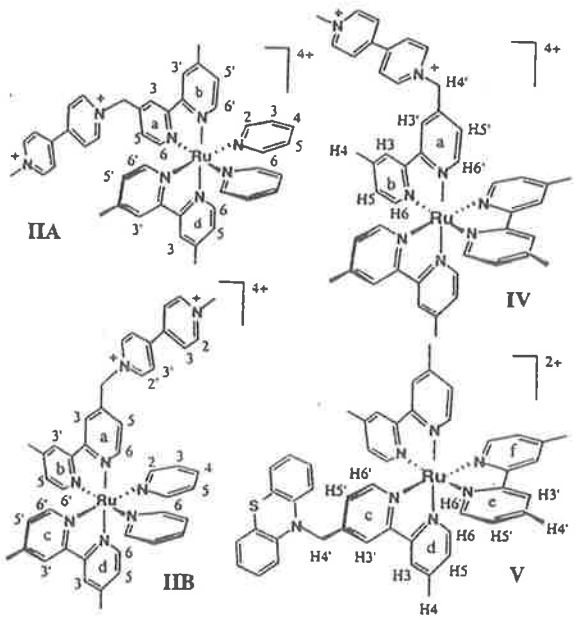

Figure 4. Atom- and ring-numbering sequences used in NMR discussion for the geometric isomers of $[Ru(Me_2bpy)(bpy\text{-}MV^{2+})(py)_2]^{4+}$ (**IIA** and **IIB**) and for the complexes $[Ru(Me_2bpy)_2(bpy\text{-}MV^{2+})]^{4+}$ (**IV**) and $[Ru(Me_2bpy)_2(bpy\text{-}PTZ)]^{2+}$ (**V**).

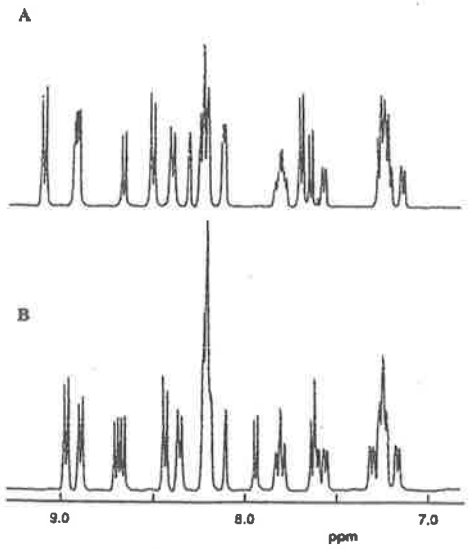

Figure 5. ^1H spectra (300 MHz; CD_3CN solvent) of the geometric isomers of $[Ru(Me_2bpy)(bpy\text{-}MV^{2+})(py)_2]^{4+}$ (**II**).

proton resonances, some of which are equivalent due to the similarity of the magnetic environments of the "base" Me_2bpy polypyridyl ligands. The atom- and ring-numbering sequences used are shown in Figure 4. The methylene proton resonance of bpy-PTZ at 5.27 ppm exhibited NOE effects to protons at 6.75 ppm (PTZ substituent), 7.28 ppm (H5′ on the PTZ-substituted ring or ring c), and 8.48 ppm (H3′ of the PTZ-substituted ring or ring c). Selective decoupling and NOE experiments enabled the complete assignment of chemical shifts in the bpy-PTZ ligand. The remaining chemical shifts were assigned to the two Me_2bpy ligands, which showed minor variations compared with protons in the $[Ru(Me_2bpy)_3]^{2+}$ complex (discussed above) with one significant exception: a resonance (d, $J = 5$Hz) at 7.32 ppm which was determined to originate from a H6 proton (>1 ppm upfield compared to other H6 and H6′ proton resonances). Models suggest that the most probable H6 proton experiencing the increased anisotropic interactions (shielding influence) is the H6 proton associated with the pyridyl ring (ring e) orientated over the plane of the PTZ-substituted pyridyl ring (ring c).

$[Ru(Me_2bpy)_2(bpy\text{-}MV^{2+})]^{4+}$ (IV). The C_1 symmetry results in a ^1H NMR spectrum showing 29 proton resonances. The atom- and ring-numbering sequences used are shown in Figure 4. The methylene resonance at 5.96 ppm (deshielded relative to the resonance of the methylene bridge in the analogous bpy-PTZ species due to inductive influences) showed NOE effects to the proton at 9.06 ppm (H3, MV^{2+} substituent), 7.33 ppm (H5′, MV^{2+}-substituted ring or ring a), and 8.44 ppm (H3′, MV^{2+}-substituted ring or ring a). ^1H COSY spectra confirmed coupling between the protons resonating at 7.33 ppm and 7.76 ppm. The H6′ (ring a) and H6 (ring b) protons of bpy-MV^{2+} are deshielded by 0.2 and 0.05 ppm, respectively, relative to the H6/H6′ proton resonances of the Me_2bpy ligand.

In the above two tris(bidentate) polypyridyl complexes, attention is drawn to two significant results: the shielding influence in the H6 protons orientated over the plane of the PTZ-substituted pyridyl ring and the relative deshielding influence experienced by the H6/H6′ protons on the bpy-MV^{2+} ligand. By comparison of isomers **IIA** and **IIB**, a small deshielding influence is experienced in the H6 protons orientated over the plane of the MV^{2+}-substituted pyridyl rings of the bpy ligands.

$[Ru(Me_2bpy)(bpy\text{-}MV^{2+})(bpy\text{-}PTZ)]^{4+}$ (III). A complete assignment of all chemical shifts for the four isomers of **III** was not possible due to the equivalence of several proton resonances, and this might only be addressed by subsequent measurement at higher frequency or with the aid of pulse-relay NMR experiments. However, chemical shift data was used in conjunction with the known stereochemical possibilities (Figure 1) to make the isomeric assignments discussed below. The ^1H NMR assignments for the four isomeric forms [*trans, cis(1), cis(2),* and *cis(3)*] were simplified by the predetermination of the stereochemistry of the precursor complex **II**, thus reducing the number of isomeric options to two [*trans/cis(2)* or *cis(1)/cis(3)*] as previously described (Figure 3). The assignment of the ^1H NMR spectra between each of these pairs was achieved by comparisons of the chemical shifts with structurally similar complexes [such as $[Ru(Me_2bpy)_2(bpy\text{-}MV^{2+})]^{4+}$ and $[Ru(Me_2bpy)_2(bpy\text{-}PTZ)]^{2+}$] and the relative degree of diamagnetic anisotropic interactions between the ligands within the particular stereochemistry.

These assignments were further confirmed by comparison of the chromatographic elution order for the four isomeric forms with previous studies involving the separation and characterization of the three isomeric forms of $[Ru(Me_2bpy)(pmb)_2]^{2+}$.[25] The ring-numbering sequences used for the various isomers are shown in Figure 1.

For the *cis(3)* isomer, the ^1H NMR spectrum consisted of 27 proton resonances and is shown in Figure 6C. The two singlet resonances at 5.93 ppm and 5.29 ppm are assigned to the methylene resonances H4′ (bpy-MV^{2+}) and H4′ (bpy-PTZ), respectively, based on NOE experiments and comparisons with $[Ru(Me_2bpy)_2(bpy\text{-}MV^{2+})]^{4+}$ and $[Ru(Me_2bpy)_2(bpy\text{-}PTZ)]^{2+}$. ^1H COSY, NOE, and selective decoupling experiments confirmed connectivity between the methylene resonance H4′ (bpy-MV^{2+}) and H3′ of ring a (8.42 ppm), H5′ of ring a (7.33 ppm), and H6′ of ring a (7.66 ppm). Similarly, connectivity between the upfield methylene resonance H4′ (bpy-PTZ) and H3′ of ring c (8.48 ppm), H5′ of ring c (7.30 ppm) and H6′ of ring c (7.54 ppm), was established. Further chemical shift assigments were

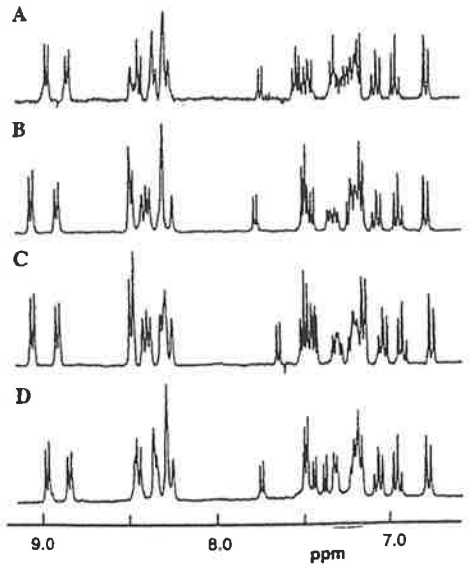

Figure 6. ^{1}H spectra (300 MHz; CD_3CN solvent) of the geometric isomers of $[Ru(Me_2bpy)(bpy\text{-}MV^{2+})(bpy\text{-}PTZ)]^{4+}$ (III): (A) *cis(2);* (B) *cis(1);* (C) *cis(3);* (D) *trans.*

possible but had little significance with respect to the stereoisomer assignment.

The stereochemistry of the *cis(3)* isomer (see Figure 1) suggests that the MV^{2+}-substituted pyridyl ring (ring a) is orientated over the plane of the PTZ-substituted pyridyl ring (ring c). As previously discussed for the $[Ru(Me_2bpy)_2(bpy\text{-}PTZ)]^{2+}$ complex, this relative orientation results in an upfield shift in the proton H6 (ring a) associated with the MV^{2+}-substituted pyridyl ring. This upfield influence of approximately 0.1 ppm is observed for H6′ (7.66 ppm, ring a) relative to the H6′ (ring a) protons in the other isomeric forms and the $[Ru(Me_2bpy)_2(bpy\text{-}MV^{2+})]^{4+}$ complex.

In the *cis(1)* isomer, some overlapping of signals may be expected in the ^{1}H NMR spectrum as a result of its "pseudo-C_2" symmetry in this isomeric form. The spectrum is shown in Figure 6B. The two singlet resonances at 5.93 ppm and 5.29 ppm were assigned to the methylene resonances H4′ (bpy-MV^{2+}) and H4′ (bpy-PTZ), respectively, on the basis of arguments similar to those discussed above. By methods similar to those described for the *cis(3)* isomer, the H6′, H5′, and H3′ protons on ring a were assigned to resonances at 7.79, 7.38, and 8.42 ppm and those on ring c to resonances at 7.52, 7.34, and 8.48 ppm, respectively.

The stereochemistry of the *cis(1)* form (see Figure 1) indicates that a pyridyl ring (ring f) of the Me_2bpy ligand is orientated over the plane of the PTZ-substituted pyridyl ring (ring c). This accounts for the H6′ (ring f) resonance upfield at 7.24 ppm relative to H6 protons on the other methyl-substituted pyridyl rings, for reasons discussed above. This resonance is slightly shielded relative to the equivalent H6 resonance in the $[Ru(Me_2bpy)_2(bpy\text{-}PTZ)]^{2+}$ complex (7.32 ppm), presumably due to a trans influence from the MV^{2+}-substituted pyridyl ring.

The ^{1}H NMR spectrum of the *cis(2)* isomer is shown in Figure 6A and reveals 27 proton resonances, with overlap of several proton resonances resulting from the C_1 symmetry. By anology with the isomers discussed above, the two methylene singlet resonances at 5.93 ppm and 5.29 ppm may be assigned to H4′ (bpy-MV^{2+}) and H4′ (bpy-PTZ), respectively, enabling the assignment of H6′, H5′, and H3′ protons on ring a to resonances at 7.73, 7.30, and 8.39 ppm and on ring c to resonances at 7.53, 7.28, and 8.48 ppm, respectively.

The stereochemistry of this isomeric form indicates that the pyridyl ring of the Me_2bpy (ring f) is orientated over the plane of the PTZ-substituted pyridyl ring (see Figure 1). For reasons discussed above, the H6′ (Me_2bpy) proton in this geometry is shifted upfield to 7.32 ppm, which is in good agreement with the H6′ (Me_2bpy) proton (at 7.32 ppm), which has a similar geometry in the $[Ru(Me_2bpy)_2(bpy\text{-}PTZ)]^{4+}$ complex.

For the *trans* isomer, the ^{1}H NMR spectrum is shown in Figure 6D; similar to observations for *cis(1)*, a number of overlapping resonances are observed due to its "pseudo-C_2" symmetry. As discussed above, the two methylene singlet resonances at 5.93 ppm (H4′, bpy-MV^{2+}) and 5.29 ppm (H4′, bpy-PTZ) enabled the assignment of H6′, H5′, and H3′ protons on ring a to resonances at 7.75, 7.32, and 8.37 ppm, and on ring c to resonances at 7.48, 7.32, and 8.47 ppm, respectively. As shown in Figure 1, the H6 proton on ring b is orientated over the plane of the PTZ-substituted pyridyl ring. This H6 proton resonance is thus observed upfield (relative to remaining H6/H6′ protons) at 7.36 ppm, by comparison with the H6′ (ring f) in the *cis(2)* isomer where it is shifted downfield by approximately 0.05 ppm. This may be rationalized using the NMR spectrum of $[Ru(Me_2bpy)_2(bpy\text{-}MV)]^{4+}$, which shows a deshielding influence (approximately 0.05 ppm) of H6 (methyl-substituted ring of the bpy-MV^{2+} ligand) relative to the H6/H6′ protons on the Me_2bpy ligands.

Conclusions

Our ability to synthesize and control the stereochemistry of complexes with a variety of ligand types has enabled us to isolate the stereoisomers of a mononuclear chromophore−quencher species of the type D−C−A. Importantly, this will now enable us to probe the influence that the spatial relationship of the donor and acceptor groups have on intramolecular electron transfer processes. Initial photophysical studies suggest that differences are observed between the four geometric forms of the complex $[Ru(Me_2bpy)(bpy\text{-}MV^{2+})(bpy\text{-}PTZ)]^{4+}$. Details of our current comparative photophysical study of the four isomers of the present title system will be reported subsequently,[27] and an investigation of analogues in which the linkages between the bpy ligating group and the MV^{2+} and PTZ functionalities are extended from the methylene group to larger alkyl chains is in progress.

Acknowledgment. This research was supported by the Australian Research Council. We would like to thank Dr. Bruce Bowden and Mr. David Reitsma for assistance with the COSY experiments and Mr. Laurie Kelso for helpful discussions. The involvement of Mr. Joe Treadway (University of North Carolina, Chapel Hill) in the initial stages of the project is acknowledged.

Supporting Information Available: Cyclic voltammogram of $[Ru(Me_2bpy)(bpy\text{-}MV^{2+})(bpy\text{-}PTZ)]^{4+}$ (1 page). Ordering information is given on any current masthead page.

IC9615279

6824 *J. Phys. Chem. A* **1997**, *101*, 6824−6826

Mapping Electron Transfer Pathways in a Chromophore−Quencher Triad

Joseph A. Treadway,[†] Pingyun Chen,[†] Todd J. Rutherford,[‡] F. Richard Keene,[‡] and Thomas J. Meyer*[,†]

Department of Chemistry, The University of North Carolina CB#3290, Chapel Hill, North Carolina 27599-3290, and Department of Chemistry and Chemical Engineering, James Cook University of North Queensland, Townsville, Queensland 4811, Australia

Received: May 16, 1997; In Final Form: July 10, 1997[⊗]

A comparative study of the photophysics of the four positional isomers (one *trans* and three *cis*) of the chromophore−quencher triad $[Ru^{II}(dmb)(bpyCH_2PTZ)(bpyCH_2MV^{2+})]^{4+}$ (dmb is 4,4′-dimethyl-2,2′-bipyridine, $bpyCH_2PTZ$ is (4′-methyl-4-(2,2′-bipyridin-4-yl)methyl)phenothiazine, and $bpyCH_2MV^{2+}$ is (4′-methyl-4-(2,2′-bipyridin-4-yl)methyl)-1′-methyl-4,4′-bipyridinium cation) has been undertaken. Following metal-to-ligand charge transfer (MLCT) excitation by laser flash photolysis at 460 or 532 nm, the redox-separated states $[Ru^{II}(dmb)(bpyCH_2PTZ^{+\bullet})(bpyCH_2MV^{+\bullet})]^{4+}$ are formed rapidly (< 5 ns). Quenching of MLCT emission occurs with near unit efficiency for all four isomers. For the *trans* and *cis3* isomers, formation of the redox-separated state is ~25% efficient. For back electron transfer from $-MV^{+}$ to $-PTZ^{+}$, $\Delta G^0 = -1.14$ eV for all four isomers from electrochemical measurements and yet k_{ET} varies from 4.5×10^6 to 8.7×10^6 s^{-1} in acetonitrile at 25 °C.

The coordination of unsymmetrically-substituted bidentate ligands to an octahedral center such as ruthenium(II) gives rise to stereoisomerism based on the relative positions of the substituents. Such geometrical isomerism, positional isomerism, has been recognized in the past, but little was known about what effect it might have on chemical and physical properties since there was no means for obtaining isomerically pure samples.[1] For instance, Opperman *et al.*[2] prepared a series of Ru(II) polypyridyl complexes containing linked phenothiazine electron transfer donors and anthraquinone acceptors. Although it was recognized that the chromophore−quencher existed in different isomeric forms, it was not possible to discern whether or not all of the four possible isomers were present in the sample and, therefore, if electron transfer kinetics observed following laser flash photolysis were of a single isomer or an average. This issue has been raised by others as well.[3] Positional isomerism is illustrated in Figure 1 for the four isomers of the chromophore−quencher complex $[Ru^{II}(dmb)(bpyCH_2PTZ)(bpyCH_2MV^{2+})]^{4+}$ (**1**) in which dmb is 4,4′-dimethyl-2,2′-bipyridine, $bpyCH_2PTZ$ is (4′-methyl-4-(2,2′-bipyridin-4-yl)methyl)phenothiazine, and $bpyCH_2MV^{2+}$ is (4′-methyl-4-(2,2′-bipyridin-4-yl)methyl)-1′-methyl-4,4′-bipyridinium cation.[4] We report here the development of techniques for the separation of these isomers and their use in mapping the various electron transfer pathways that they provide.

The synthesis of the target chromophore−quencher complex was based on a synthetic strategy for tris(heteroleptic) complexes reported previously[5] and is described in detail elsewhere.[6] It involves stepwise addition first of dmb to $[Ru(CO)_2Cl_2]_n$ to give $[Ru(dmb)(CO)_2Cl_2]$, followed by $bpyCH_2MV^{2+}$ and pyridine to give $[Ru(dmb)(bpyCH_2MV^{2+})(py)_2]^{4+}$ as the hexafluorophosphate salt. The two isomers of this complex (in which the MV^{2+} as a substituent is *trans* to one pyridine or *cis* to both) were separated by cation exchange chromatography (SP-Sephadex C25; aqueous sodium 4-toluenesulfonate eluent) by using a previously developed method.[7] The pyridyl ligands were displaced in refluxing ethylene glycol with an excess of $bpyCH_2$-

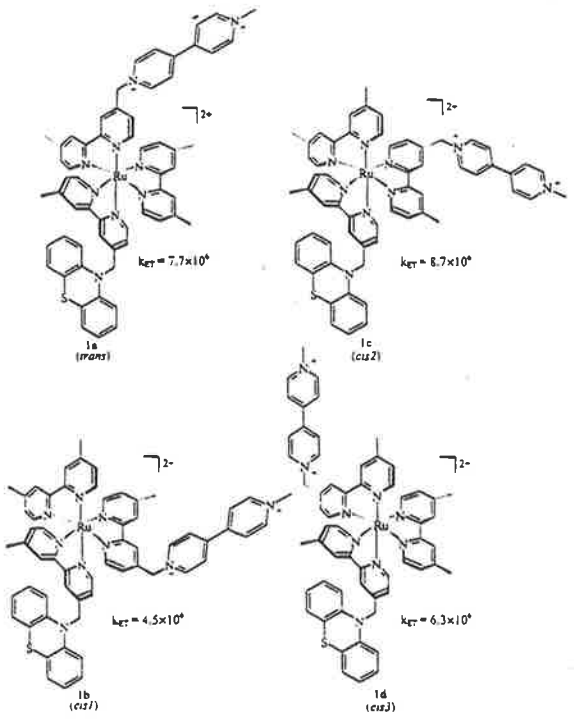

Figure 1. Geometrical isomers for $[Ru^{II}(dmb)(bpyCH_2PTZ)(bpyCH_2MV^{2+})]^{4+}$ (**1**) with rate constants for back electron transfer (k_{ET}); see text. Each of these isomers exists as a pair of Δ/Λ enatiomers.

PTZ, which gave separate sets of the binary mixtures of geometrical isomers **1a/1b** and **1c/1d** with the stereochemistry from the first separation maintained.[8] These isomeric mixtures were also separated by cation exchange chromatography by utilizing aqueous sodium 4-toluenesulfonate as eluent. Precipitation from water with KPF_6 (2×) led to the isolation of pure PF_6^- salts of the one *trans* and three *cis* isomers. The structures of **1a**, **1b**, **1c**, and **1d** were established by ^{1}H-NMR spectroscopy by utilizing ^{1}H COSY, as well as homonuclear decoupling and NOE measurements.[6] Extensive use was made

[†] The University of North Carolina.
[‡] James Cook University of North Queensland.
[⊗] Abstract published in *Advance ACS Abstracts*, August 15, 1997.

S1089-5639(97)01638-1 CCC: $14.00

SCHEME 1[a]

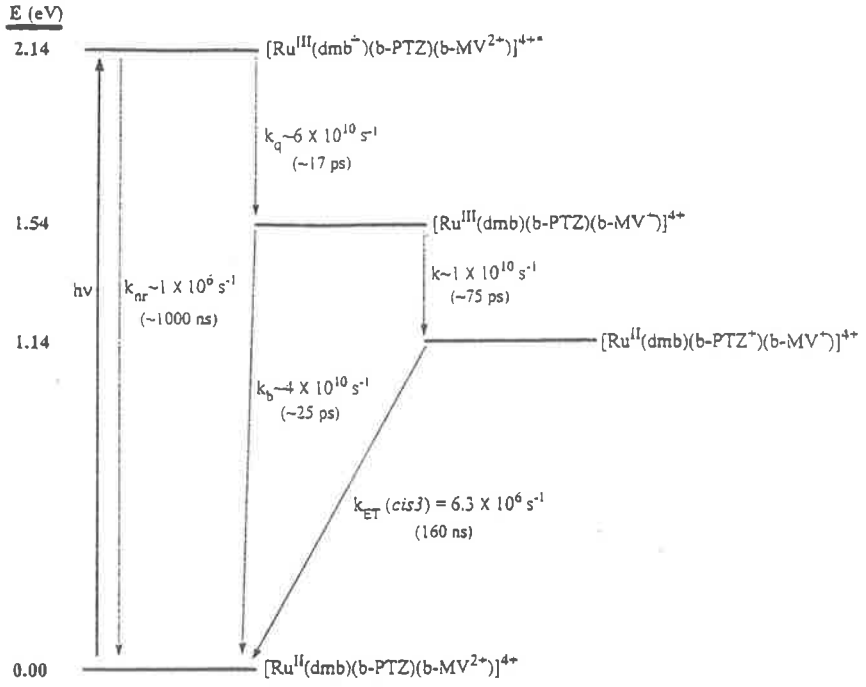

[a] In acetonitrile, b-MV^{2+} is bpyCH_2MV^{2+}, b-PTZ is bpyCH_2PTZ.

of the anisotropic interactions caused by differing degrees of shielding provided by the ring currents in differently substituted pyridyl rings as described previously.[9]

UV−visible absorption spectra of the four isomers are identical with an MLCT absorption band in acetonitrile appearing at λ_{max} = 460 nm (ϵ = 18 600 cm^{-1} M^{-1}), which is the λ_{max} for $[Ru(dmb)_3]^{2+}$. In cyclic voltammograms in acetonitrile 0.1 M in $[(n\text{-}C_4H_9)_4N]PF_6$ versus SSCE, waves appear for the couples $Ru^{III/II}$ ($E_{1/2}$ = +1.22 V), $-PTZ^{+/0}$ ($E_{1/2}$ = 0.80 V), $-MV^{2+/+}$ ($E_{1/2}$ = −0.34 V), and $MV^{+/0}$ ($E_{1/2}$ = −0.74 V). Polypyridyl-based reductions appeared at −1.37 and −1.57 V.

$$[Ru^{III}(dmb^{\bullet-})(bpyCH_2PTZ)(bpyCH_2MV^{2+})]^{4+*}$$

$$1 \xrightarrow{h\nu} [Ru^{III}(dmb)(bpy^{\bullet-}CH_2PTZ)(bpyCH_2MV^{2+})]^{4+*} \longrightarrow$$

$$[Ru^{III}(dmb)(bpyCH_2PTZ)(bpy^{\bullet-}CH_2MV^{2+})]^{4+*}$$

$$[Ru^{II}(dmb)(bpyCH_2PTZ^{\bullet+})(bpyCH_2MV^{\bullet+})]^{4+} \xrightarrow{k_{ET}} 1 \quad (1)$$
$$2$$

Compared to $[Ru(dmb)_3]^{2+}$ with an emission quantum yield of ϕ_{em} = 0.060 in acetonitrile at 25° ± 2 °C, MLCT emission from **1** is >95% quenched and short on the ~5 ns time scale.[10] Laser flash excitation at 460 or 532 nm (2.0−4.5 mJ/pulse) with absorbance monitoring from 350−700 nm under the same conditions with an apparatus described elsewhere[11] resulted in the <5 ns loss of the MLCT absorption at 460 nm, no evidence for the characteristic MLCT bleach at 460 nm, and the appearance of bands at λ_{max} = 517 nm[12] for $-PTZ^{\bullet+}$ and λ_{max} = 397 and 610 nm[13] for $-MV^{\bullet+}$ at the earliest observation times (~5 ns). These observations are consistent with initial MLCT excitation followed by a series of rapid electron transfers to give redox-separated state, **2**, in eq 1. The quantum yields for appearance of **2** for the *trans* and *cis3* isomers (η_{rss}), Table 1, were measured relative to the efficiency of reaction 2.[14] Back electron transfer ($-MV^{\bullet+} \rightarrow -PTZ^{\bullet+}$), k_{ET} in eq 1, was studied

TABLE 1: $k_{ET}(\tau)$ and Efficiencies (η_{rss}) for Intramolecular Redox Separation in Deaerated Acetonitrile at 25° ± 2 °C

isomer	*trans* (**1a**)	*cis 1* (**1b**)	*cis 2* (**1c**)	*cis 3* (**1d**)
$k_{ET} \times 10^6$ s^{-1} [a]	7.7 (130 ns)[b]	4.5 (220 ns)	8.7 (115 ns)	6.3 (160 ns)
η_{rss}	0.20, 0.22, 0.25[c]			0.25

[a] Values reproducible to ±3%. [b] Weighted average of biexponential fits or best fit to exponential decay (ref 15). [c] Measured at concentrations of 3.4 × 10^{-6}, 2.4 × 10^{-5}, and 6.5 × 10^{-5} M, respectively, ±0.05. The slight variation in η_{rss} may be real but is within the experimental error.

by transient absorption measurements throughout the visible region from 350 to 690 nm. The results are summarized in Table 1. In all cases the variation in k_{ET} with observation wavelength was <3%, and the values in the table represent an average of measurements at 10−65 wavelengths.[15]

$$[Ru(bpy)_3]^{2+*} + PTZ \rightarrow [Ru(bpy)_3]^{+} + PTZ^{\bullet+} \quad (2)$$

The kinetic scheme for formation of **2** is shown in Scheme 1. The first step is expected to be electron transfer to $-MV^{2+}$. On the basis of picosecond transient absorbance measurements in acetonitrile at 23 °C, Yonemoto *et al.*[16] concluded that MLCT excitation in $[Ru^{II}(bpy)_2(bpyCH_2MV^{2+})]^{4+}$ is followed by $bpy^{\bullet-} \rightarrow -MV^{2+}$ electron transfer to give $[Ru^{III}(bpy)_2(bpyCH_2MV^{\bullet+})]^{4+}$ with $k_q = 5.9 \times 10^{10}$ s^{-1} (τ = 17 ps) and that back electron transfer to give the ground state occurs with $k_b = 4.0 \times 10^{10}$ s^{-1} (τ = 25 ps). If the initial MLCT excited state(s) is reached with unit efficiency, $\eta_{rss} = k/(k + k_b)$ and if the rate constants measured by Yonemoto *et al.* are comparable in the *trans* and *cis3* isomers, k for $-PTZ \rightarrow Ru^{III}$ electron transfer is $\sim 1.3 \times 10^{10}$ s^{-1} (τ = 75 ps).

Initial electron transfer from −PTZ to Ru^{III*} is slow. In the model $[Ru^{II}(dmb)_2(bpy\text{-}CH_2PTZ)]^{2+}$, reductive quenching, eq 3, is uphill thermodynamically by ~0.1 eV[17] and quenching is only partly complete as shown by the decrease in the luminescence quantum yield compared to $[Ru(dmb)_3]^{2+*}$ (ϕ_{em} = 0.044

compared to $\phi_{em} = 0.060$) and a decrease in MLCT excited state lifetime from 900 to 680 ns.

$$[Ru^{III}(dmb^{\bullet-})(dmb)(bpyCH_2PTZ)]^{2+*} \rightarrow [Ru^{II}(dmb^{\bullet-})(dmb)(bpyCH_2PTZ^{\bullet+})]^{2+} \quad (3)$$

The data for k_{ET} in Table 1 map four distinct pathways for back electron transfer in the isomeric series. From the electrochemical measurements, $\Delta G^0 = -1.14$ eV for all four isomers, but k_{ET} varies from 4.5×10^6 to 8.7×10^6 s^{-1}. This is an important finding for earlier results on related systems where there were unresolved mixtures of isomers and, in retrospect, k_{ET} values were most likely averaged quantities for a series of isomers and not for a single isomeric assembly.

Given the known self-exchange rate constants for couples related to $-PTZ^{+/0}$ and $-MV^{2+/+}$, back electron transfer occurs in the inverted region since $\lambda \sim 0.9$ eV.[18] These reactions are remarkably slow given the small energy gap of 1.14 eV.[11] This must be a consequence of weak electronic coupling through the extended bond system at least for the *trans* isomer where, on the basis of molecular modeling,[19] the closest distance of through space $-MV^{\bullet+}/-PTZ^{\bullet+}$ approach is 16.5 Å (center to center). For the *cis* isomers there are accessible rotamers that bring them into edge to edge contact (7.0 Å center to center). The solvent and vibrational barriers to electron transfer for the *cis* isomers should be nearly the same. The differences in k_{ET} probably reflect differences in electronic coupling for them and subtle differences in their orbital pathways for electron transfer.

Acknowledgment. Financial support from the Australian Research Council and the U.S. National Science Foundation (Grant CHE-9321413) is gratefully acknowledged. Travel between the laboratories at JCUNQ and UNC (JAT and TJR) has been supported by the U.S. National Science Foundation (Grant INT-9015262) and the Australian Department of Industry, Science, and Technology and Tourism within the Australia-US Bilateral Science and Technology Program.

References and Notes

(1) Keene, F. R. *Coord. Chem. Rev.*, in press.

(2) Opperman, K. A.; Mecklenburg, S. L.; Meyer, T. J. *Inorg. Chem.* **1994**, *33*, 5295.

(3) Larson, S. L.; Elliott, C. M.; Kelley, D. F. *J. Phys. Chem.* **1995**, *99*, 6530.

(4) For each positional isomer there is a Δ, Λ enantiomeric pair. Each separate Λ "isomer" illustrated in Figure 1 has a corresponding Δ isomer present in equal amount in the isolated samples.

(5) (a) Anderson, P. A.; Deacon, G. B.; Haarmann, K. H.; Keene, F. R.; Meyer, T. J.; Reitsma, D. A.; Skelton, B. W.; Strouse, G. F.; Thomas, N. C.; Treadway, J. A.; White, A. H. *Inorg. Chem.* **1995**, *34*, 6145. (b) Strouse, G. F.; Anderson, P. A.; Schoonover, J. R.; Meyer, T. J.; Keene, F. R. *Inorg. Chem.* **1992**, *31*, 3004. (c) Anderson, P. A.; Strouse, G. F.; Treadway, J. A.; Keene, F. R.; Meyer, T. J. *Inorg. Chem.* **1994**, *33*, 3863.

(6) Rutherford, T. J.; Keene, F. R. *Inorg. Chem.* **1997**, *36*, 2872.

(7) (a) Rutherford, T. J.; Quagliotto, M. G.; Keene, F. R. *Inorg. Chem.* **1995**, *34*, 3857. (b) Rutherford, T. J.; Reitsma, D. A.; Keene, F. R. *J. Chem. Soc., Dalton Trans.* **1994**, 3659.

(8) Hua, X.; von Zelewsky, A. *Inorg. Chem.* **1995**, *34*, 5791.

(9) Rutherford, T. J.; Reitsma, D. A.; Keene, F. R. *J. Chem. Soc., Dalton Trans.* **1994**, 3659.

(10) There is evidence in the emission decay data for a small contribution (<3%) from an emissive impurity with $\tau \sim 1$ μs.

(11) (a) Chen, P.; Duesing, R.; Graff, D. K.; Meyer T. J. *J. Phys. Chem.* **1991**, *95*, 5850. (b) Duesing, R.; Tapolsky, G.; Meyer, T. J. *J. Am. Chem. Soc.* **1990**, *112*, 5378.

(12) Hester, R. E.; Williams, K. P. J. *J. Chem. Soc., Perkin Trans. 2* **1981**, 852.

(13) Watanabe, T.; Honda, K. *J. Phys. Chem.* **1982**, *86*, 2617.

(14) (a) The yield of $[Ru(bpy)_3]^+$ and PTZ^+ following reductive quenching of $[Ru(bpy)_3]^{2+*}$ by PTZ is ~1.0 relative to the $[Ru(bpy)_3]^{2+} + MV^{2+}$ actinometer in water (refs 14b,c). The measurements were made by measuring transient absorption changes at 10 wavelengths between 500 and 640 nm and known extinction coefficients with sufficient PTZ added (38 mM) to achieve >98% quenching. (b) Hoffman, M. Z. *J. Phys. Chem.* **1988**, *92*, 3458. (c) Hoffman, M. Z. *J. Phys. Chem.* **1991**, *95*, 2606.

(15) Kinetic decay of the *trans* form of **2** derived from **1a** is exponential with monitoring at 600−690 nm ($\lambda_{max} = 610$ nm for $-MV^{\bullet+}$). The decay kinetics are better fit as biexponentials from 360 to 590 nm possibly because of the presence of a small amount of impurity in which there is not a redox active MV^{2+}.

(16) (a) Yonemoto, E. H.; Saupe, G. B.; Schmehl, R. H.; Hubig, S. M.; Riley, R. L.; Iverson, B. L.; Mallouk, T. E. *J. Am. Chem. Soc.* **1994**, *116*, 4786. (b) Yonemoto, E. H.; Riley, R. L.; Kim, Y. I.; Atherton, S. J.; Schmehl, R. H.; Mallouk, T. E. *J. Am. Chem. Soc.* **1992**, *114*, 8081.

(17) (a) Excited state potentials were calculated from the free energy content of the excited state above the ground state, ΔG^0_{ES}, by $\Delta G^0_{ES} = \lambda_{O\perp} + E_o$. E_o is the $v^* = 0 \rightarrow v = 0$ energy gap and $\lambda_{O\perp}$ the solvent reorganizational energy including low-frequency modes treated classically. They were determined by emission spectra fitting techniques described elsewhere (refs 17b,c). (b) Claude, J. P.; Meyer, T. J. *J. Phys. Chem.* **1995**, *99*, 51. (c) Kober, E. M.; Caspar, J. V.; Lumpkin, R. S.; Meyer, T. J. *J. Phys. Chem.* **1986**, *90*, 3722.

(18) (a) As estimated from $\lambda = 4k_BT \ln(k_BT/hk_{ET})$ with $k_{ex} = k_{ET}K_A$, where K_A is the association constant (ref 18b). With $k_{ex} = 2.2 \times 10^9$ M^{-1} s^{-1} for 10-$(CH_3)PTZ^{+/0}$ (ref 18c) and $K_A \sim 0.69$ M^{-1} (ref 18e), $\lambda = 0.78$ eV. Given $k_{ex} = 8.4 \times 10^6$ M^{-1} s^{-1} for $MV^{2+/+}$ (ref 18d), $\lambda = {}^1/_2(\lambda_{11} + \lambda_{22}) \sim 0.90$ eV for k_{ET}. (b) Marcus, R. A.; Sutin, N. *Biochim. Biophys. Acta* **1985**, *811*, 265. (c) Kowert, B. A.; Marcoux, L.; Bard, A. J. *J. Am. Chem. Soc.* **1972**, *94*, 5538. (d) Bock, C. R.; Connor, J. A.; Gutierrez, A. R.; Meyer, T. J.; Whitten, D. G.; Sullivan, B. P.; Nagle, J. K. *Chem. Phys. Lett.* **1979**, *61*, 252. (e) From the Eigen-Fuoss equation (refs 18b,f,g), $K_A = (4\pi N d^3/3000)\cdot\exp(-w_r/RT)$ with $w_r = (z_A z_B e^2)/(D_S d(1 + \beta d\sqrt{\mu}))$ and $\beta = ((8\pi Ne^2)/(1000 D_S k_B T))^{1/2}$. The separation distance $d_{PTZ} = r_{PTZ} + r_{PTZ^+} \sim 6.5$ Å, and $d_{MV} = r_{MV^{2+}} + r_{MV^{\bullet+}} \sim 3.3$ Å. Radii were calculated by using the formula $r = {}^1/_2(d_x d_y d_z)^{1/3}$, in which d_x, d_y, d_z are the lengths of the three molecular axes. (f) Eigen, M. Z. *J. Phys. Chem. (Munich)* **1954**, *1*, 176. (g) Fuoss, R. M. *J. Am. Chem. Soc.* **1958**, *80*, 5059.

(19) Molecular mechanics optimization utilized a MM2 force field. The initial positions were determined by rotating around the bond between the 4-carbon and the benzylic carbon until the $-MV^{2+}$ and $-PTZ$ were in close proximity. The distances are quoted as the separations between the geometric centers of the redox pairs.

DALTON
FULL PAPER

Chromatographic separation of stereoisomers of ligand-bridged diruthenium polypyridyl species

Nicholas C. Fletcher, Peter C. Junk, David A. Reitsma and F. Richard Keene*

School of Biomedical and Molecular Sciences, James Cook University of North Queensland, Townsville, Queensland 4811, Australia

Cation-exchange chromatographic techniques have been developed to separate stereoisomers of polymetallic complexes, using SP Sephadex C-25 as support. Through the example of the ligand-bridged dinuclear cation $[\{Ru(dmbpy)_2\}_2(\mu\text{-bipym})]^{4+}$ (dmbpy = 4,4′-dimethyl-2,2′-bipyridine, bipym = 2,2′-bipyrimidine), the isolation and characterisation of the *meso* and *rac* diastereoisomers by elution with aqueous sodium toluene-4-sulfonate solution are demonstrated. The effects of variation in salt concentration and temperature on the efficacy of the separation are discussed. The enantiomeric pair of the *rac* diastereoisomer (ΔΔ and ΛΛ) was subsequently chromatographically resolved on SP Sephadex C-25, relying upon the inherent chirality of the support. Optical resolutions using eluents with chiral anions [aqueous sodium (+)-*O*,*O*′-dibenzoyl-D-tartrate and sodium (−)-*O*,*O*′-dibenzoyl-L-tartrate] were investigated, with the (−)-enantiomer demonstrating a positive [the (+)-enantiomer a negative] synergistic effect in combination with the Sephadex support. Crystals of the *meso* form were isolated, allowing an X-ray structural determination.

The study of polymetallic 'supramolecular' assemblies is a rapidly expanding field of chemistry, largely because of their potential application in materials for such diverse purposes as photochemical molecular devices,[1–4] and as photoprobes of structure and function of polynucleotides such as DNA.[5–9] In particular, much attention has been focused upon the polypyridyl complexes of ruthenium and osmium as the basis for such assemblies as a result of their favourable photochemical and redox characteristics.[1] When bidentate ligands are involved in such centres, stereoisomerism is inherent in the resultant assemblies, but surprisingly this problem has until recently received only tacit attention.

In general, studies of chirality in octahedral tris(bidentate ligand)ruthenium(II) centres have been limited to mononuclear species, and isolation of enantiomers has relied on the sometimes inefficient technique of diastereoisomer formation using chiral auxiliary anions.[10–13] Such complexes can then be used as chiral building blocks for larger assemblies,[12] but this approach requires tedious synthetic procedures where care must be taken to preserve the chiral integrity at each metal centre during every reaction step. Additionally, in the vast majority of the targets studied, crystallisation has proved the most favourable method of diastereoisomeric discrimination. Our aim was to develop general chromatographic techniques for the separation of stereoisomers not only of mononuclear complexes, but also of oligomeric transition-metal assemblies containing polypyridyl ligands. In the latter case the simplest example is that of a dinuclear complex of the type $[\{Ru(pp)_2\}_2(\mu\text{-}L_b)]^{n+}$ [pp is a symmetrical bidentate ligand, L_b is a bis(bidentate) bridging ligand]. There are the possibilities of the *meso* (ΛΔ) and the *rac* diastereoisomers, the *rac* form consisting of an enantiomeric pair (ΛΛ and ΔΔ), as illustrated in Fig. 1.

In these studies, SP Sephadex C-25 was chosen as the cation-exchange support, rather than the more commonly used polystyrene-based resins for which we had previously observed significant absorptions by some complexes containing polypyridyl ligands. This material has been extensively used in the separation of stereoisomers of various octahedral cobalt(III) species,[14–16] but surprisingly it appears not to have been widely applied to ruthenium(II) complexes containing polypyridyl ligands until our recent studies. SP Sephadex is composed of a cross-linked dextran matrix, functionalised with strongly acidic propanesulfonate groups. The cations to be separated are adsorbed onto the anionic stationary phase, and separation is achieved as a result of differential ion-exchange equilibria involving the components of the mixture and the cations of the eluting electrolytic solution (typically a Na^+ salt).[13]

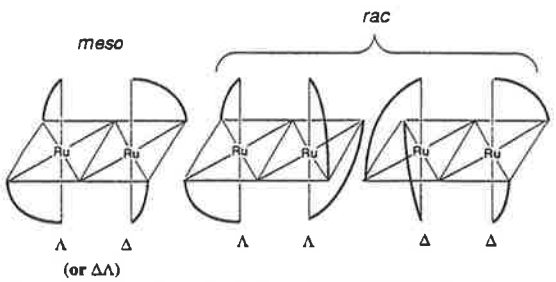

Fig. 1 Schematic view of the isomeric possibilities for the general dinuclear species $[\{M(pp)_2\}_2(\mu\text{-}L_b)]^{4+}$

To date we have successfully achieved the chromatographic separation of a wide variety of stereoisomers of mono-, di- and tri-metallic species using SP Sephadex C-25 as the support with aqueous sodium toluene-4-sulfonate solution as eluent.[17–23] Further, chiral resolution of monomeric species such as $[Ru(tmbpy)(phen)(py)_2]^{2+}$ and $[Ru(tmbpy)_2(py)_2]^{2+}$ (where tmbpy = 4,4′,5,5′-tetramethyl-2,2′-bipyridine, phen = 1,10-phenanthroline, py = pyridine) have been achieved by using an eluent containing the chiral anion (−)-di-4-toluoyl-L-tartrate.[17,24] In addition, we have described the separation and isolation of the ΛΛ and ΔΔ forms of the dinuclear complexes $[\{Ru(dmbpy)_2\}_2(\mu\text{-apy})]^{4+}$ (where dmbpy = 4,4′-dimethyl-2,2′-bipyridine, apy = 2,2′-azopyridine),[22] as well as the stereoisomers of the dinuclear species $[\{Ru(pp)_2\}_2(\mu\text{-hat})]^{4+}$ (ΔΛ, ΔΔ and ΛΛ) and of the trinuclear complexes $[\{Ru(pp)_2\}_2(\mu\text{-hat})]^{6+}$ (ΔΔΔ and ΛΛΛ, ΔΔΔ and ΛΛΛ) [where pp = bpy (2,2′-bipyridine) or phen; hat = 1,4,5,8,9,12-hexaazatriphenylene].[19]

Results and Discussion

Diastereoisomer synthesis, isolation and characterisation

The ligand-bridged dinuclear complex $[\{Ru(dmbpy)_2\}_2(\mu\text{-}$

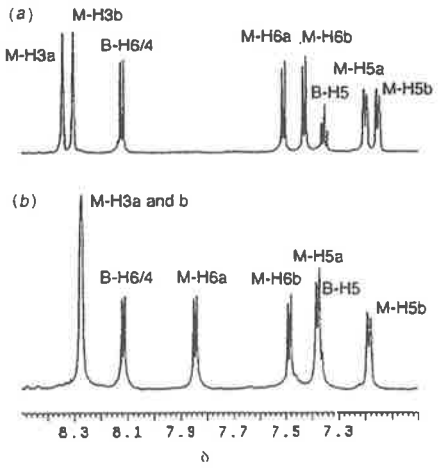

Fig. 2 Proton NMR spectra (500 MHz, 25 °C, D_2O) of (*a*) ΔΔ/ΛΛ- and (*b*) ΔΛ-[{Ru(dmbpy)$_2$}$_2$(μ-bipym)]Cl$_4$

bipym)]$^{4+}$ (where bipym = 2,2′-bipyrimidine) was synthesized by the reaction under reflux of [Ru(dmbpy)$_2$Cl$_2$] with bipym in a 2:1 stoichiometric ratio for 10 min in a microwave oven. After initial chromatographic purification on SP Sephadex C-25 cation exchanger (eluted with 0.5 mol dm^{-3} NaCl, discarding the first red monomeric fraction) and conversion into the hexafluorophosphate salt, the product was obtained in 90% yield.

The diastereoisomeric separation of this complex was achieved by cation-exchange chromatography on the same support by using 0.25 mol dm^{-3} sodium toluene-4-sulfonate solution as eluent, within a passage of 50 cm of the column length. The diastereoisomers were isolated from the eluted bands as the hexafluorophosphate salts. Since the complete removal of the toluene-4-sulfonate anion proved difficult, the complexes were converted into the chloride salts by passage through an anion-exchange resin (Amberlite) for characterisation. The purity of the two forms was confirmed by ^{1}H NMR spectroscopy: the differences between the two forms are clearly illustrated in Fig. 2. Assignment of the spectra (M-H6a and M-H5a) was achieved using ^{1}H–^{1}H correlation spectroscopy (COSY) techniques. The H6 and H5 protons of the dmbpy ligand situated over the bridge show the greatest differences in chemical shifts between the two isomers, as previously observed.[22] From examination of molecular models, a greater anisotropic effect from the ring current of the adjacent dmbpy should be observed by the *meso* form, indicated by resonances M-H6a and M-H3a being shifted downfield in comparison to the corresponding protons of the *rac* diastereoisomer. Accordingly, the first fraction was assigned as the *meso*, and the second as the *rac* diastereoisomer, which were subsequently confirmed by other results (as described below).

Similar synthetic procedures were used to obtain the analogous complexes [{Ru(tmbpy)$_2$}$_2$(μ-bipym)]$^{4+}$, [{Ru(bpy)$_2$}$_2$(μ-bipym)]$^{4+}$ and [{Ru(phen)$_2$}$_2$(μ-bipym)]$^{4+}$.[21] For all complexes the separation of the *meso*/*rac* diastereoisomers was possible by the same technique, although there was a variation in length of passage down the column before a definite resolution was observed. It was found that the identity of terminal ligands effected the isomeric separation; *e.g.* [{Ru(tmbpy)}$_2$(μ-bipym)]$^{4+}$ was resolved in approximately half the column distance required for [{Ru(dmbpy)}$_2$(μ-bipym)]$^{4+}$. Separation has been observed for other dinuclear species involving the bridge apy,[22] and in the case of [{Ru(dmbpy)$_2$}$_2$(μ-apy)]$^{4+}$ it was achieved in approximately a tenth of the distance required for [{Ru(dmbpy)}$_2$(μ-bipym)]$^{4+}$. Dinuclear complexes involving the bridges 2,3-bis(2-pyridyl)pyrazine (dpp), 2,3-bis(2-pyridyl)-quinoxaline (dpq), 3,4-bis(2-pyridyl)-1,2,4-triazolate (bpt$^-$) and hat[1] all demonstrate similar behaviour under the same conditions, and in each case the *meso* isomer (as indicated by ^{1}H NMR spectroscopy) was the fastest moving band on the column, despite the differing geometries.[25] The evidence clearly indicates that this method for diastereoisomeric separation is general for a wide variety of dinuclear species of this type.

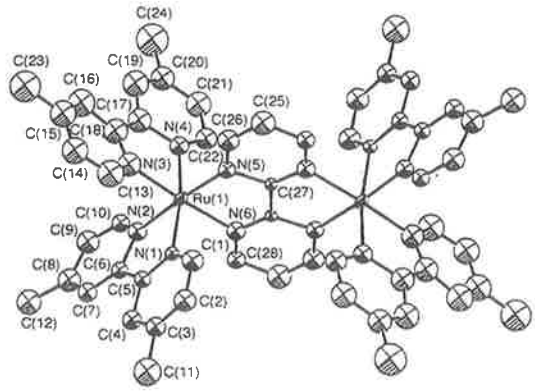

Fig. 3 Thermal ellipsoid plot of *meso*-(ΛΔ)-[{Ru(dmbpy)$_2$}$_2$(μ-bipym)]$^{4+}$, with ellipsoids drawn at 50% probability. All carbon atoms are isotropic and protons are omitted for clarity

A sample of the first major fraction (*meso*) of [{Ru(dmbpy)$_2$}$_2$(μ-bipym)]Cl$_4$ was repurified by gel permeation chromatography on Sephadex LH20 support (methanol eluent) to remove inorganic impurities. Following removal of the solvent and redissolution in water, oily crystals were grown by slow evaporation from the aqueous solution which were suitable for X-ray analysis. To date, very few crystals of dinuclear ruthenium polypyridyl complexes have been obtained. Ward and co-workers[26,27] describe an alkoxide-bridged species, where only the *rac* form was isolated, the *meso* form being excluded on steric grounds. Two examples of dinuclear species containing unsymmetrical polypyridyl ligands have been reported, where the crystals have preferentially grown in the *meso* form.[28,29] One of the problems in the growth of crystals of such species may well be the existence of a mixture of stereoisomers, and we present here for the first time the selective isolation of one of the various components prior to crystal growth.

The crystals themselves proved to be of poor quality, crumbling easily and being extremely prone to solvent evaporation. However, a data set was obtained and the structure solved, illustrating the connectivity of the complex (Fig. 3). Assuming that the crystal is representative of the bulk solution, this first major band is confirmed as the *meso* (ΛΔ) form. The clefts between the bipyridine rings contained several water molecules, while there are planes of water and chloride anions between the predominantly organic layers of the complex (Fig. 4). These distinct layers are probably the cause of the extreme brittleness and solvation dependence of the material, and another possible reason for the extremely small number of structures of these complexes existing in the literature. The selected bond lengths and angles are given in Table 1. The molecule possesses crystallographic symmetry along the bipyrimidine bridge (the second half of the molecule being generated from the first). The average Ru–N bond lengths (2.04 Å) and N–Ru–N angles correlate with those published for previous structures.[26–29]

Effect of eluent concentration on the diastereoisomeric separation

The variation of eluent concentration by a small amount can have a great influence on the observed separation. To illustrate this, a series of quantitative small-column experiments were undertaken using [{Ru(dmbpy)$_2$}$_2$(μ-bipym)]$^{4+}$ as the target, with aqueous sodium toluene-4-sulfonate solutions as eluent at concentrations between 0.05 and 1.0 mol dm^{-3}: the relative

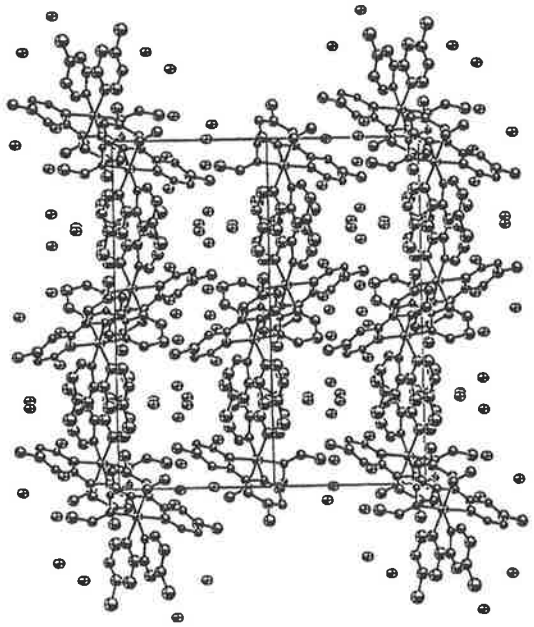

Fig. 4 Packing diagram of *meso*-(ΛΔ)-[{Ru(dmbpy)$_2$}$_2$(μ-bipym)]Cl$_4$·10H$_2$O

Table 1 Selected bond lengths (Å) and angles (°) for [{Ru(dmbpy)$_2$}$_2$(μ-bipym)]Cl$_4$·10H$_2$O

Ru(1)–N(1)	2.094(2)	Ru(1)–N(4)	2.00(2)
Ru(1)–N(2)	1.96(1)	Ru(1)–N(5)	2.01(2)
Ru(1)–N(3)	2.09(2)	Ru(1)–N(6)	2.11(2)
N(1)–Ru(1)–N(2)	79.6(9)	N(2)–Ru(1)–N(6)	95.1(10)
N(1)–Ru(1)–N(3)	94.7(8)	N(3)–Ru(1)–N(4)	78.5(9)
N(1)–Ru(1)–N(4)	171.3(8)	N(3)–Ru(1)–N(5)	94.0(10)
N(1)–Ru(1)–N(5)	97.2(8)	N(3)–Ru(1)–N(6)	175.7(10)
N(1)–Ru(1)–N(6)	86.9(7)	N(4)–Ru(1)–N(5)	88.7(9)
N(2)–Ru(1)–N(3)	89.1(10)	N(4)–Ru(1)–N(6)	100.2(8)
N(2)–Ru(1)–N(4)	94.8(10)	N(5)–Ru(1)–N(6)	81.8(9)
N(2)–Ru(1)–N(5)	175.8(9)		

rates of passage of the two bands down the column of SP Sephadex C-25 were recorded.

To ensure consistency in the results, care was taken to pre-equilibrate the column in the desired eluent, overcoming the problems of contraction of the support upon change of the salt concentration. Further, care was taken to monitor the rate of flow by recording the volume of eluent passed and the time. In order to give comparable results from each column, where slight discrepancies in flow rate were observed the data were corrected by calculating the distance travelled (cm) by the passage of 1 cm^3 of eluent down the column. A typical flow rate of 0.5 cm^3 min^{-1} was used in all cases to ensure comparable values, although the rate of flow was noted to have little effect on the column behaviour (in a range of 0.2–2.0 cm^3 min^{-1}), provided an equilibrated system had been achieved. (Exact details are given in the Experimental section.)

The relative rates of passage of the two diastereoisomers down the column using varying eluent concentrations are displayed in Fig. 5, giving the data for two forms (*rac* and *meso*) as well as those of the combined bands. At higher concentrations no resolution was observed over the length of column used in these experiments and consequently there are no data for the individual forms. Predictably, as the concentration increases the rate of travel of the two fractions increases. While the relative separation of the two bands did not change, the bands broadened with increased rate of passage due to a loss of the equi-

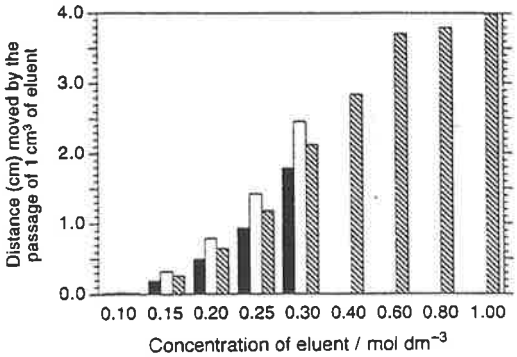

Fig. 5 Relative rate of travel of the diastereoisomers of [{Ru(dmbpy)$_2$}$_2$(μ-bipym)]$^{4+}$ down a 9 mm (inside diameter) column as a function of eluent concentration (aqueous sodium toluene-4-sulfonate) at 30 °C: *rac* (filled), *meso* (blank), combined forms (hatched)

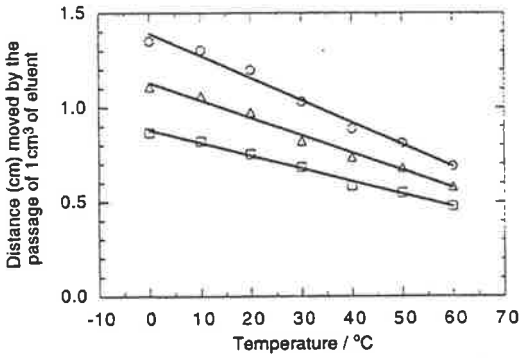

Fig. 6 Relative rate of travel of the diastereoisomers of [{Ru(dmbpy)$_2$}$_2$(μ-bipym)]$^{4+}$ down a 9 mm (inside diameter) column as a function of temperature (eluent: aqueous 0.25 mol dm^{-3} sodium toluene-4-sulfonate solution): *meso* (○), combined forms (△), *rac* (□)

librium between the stationary phase and the mobile phase. As a consequence of this the separation of the bands takes a greater length of the column to be achieved. Further, with concentrations over 0.5 mol dm^{-3}, the rates of passage of the combined fractions did not increase significantly, implying that there is a maximum possible rate of passage of the compound down the column.

From the observations made, it is apparent that the optimum concentration for efficient separation of the diastereoisomers of [{Ru(dmbpy)$_2$}$_2$(μ-bipym)]$^{4+}$ appears to be *ca.* 0.25 mol dm^{-3}.

Effect of temperature on the diastereoisomeric separation

All previous stereoisomeric separations have been carried out at room temperature, and so investigations were made into the temperature dependence of the process, while maintaining the eluent concentration at 0.25 mol dm^{-3}. The small pre-equilibrated column described above was fitted with an external water-jacket, and the temperature of the SP Sephadex C-25 controlled using a circulating thermostatted bath.

As illustrated in Fig. 6, the rate of passage of [{Ru(dmbpy)$_2$}$_2$(μ-bipym)]$^{4+}$ down the column decreases as the temperature increases. The data indicate a linear relationship, with the relative resolution of the two bands staying approximately constant. At lower temperature greater broadening of the bands was observed, associated with the faster passage through the support and loss of the equilibria.

The association between the SP Sephadex C-25 support and the cationic substrate should be essentially temperature independent, being between a solid and solute phase.[30] Since coulombic forces dominate the rate of passage of species down

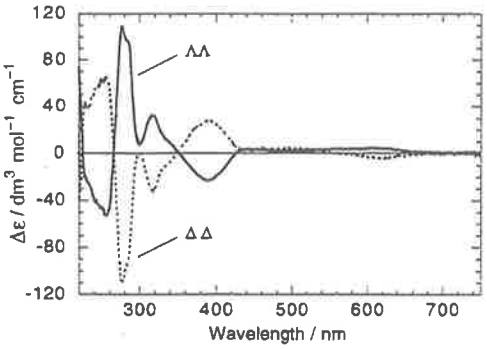

Fig. 7 Circular dichroism spectra of ΛΛ- (solid line) and ΔΔ-$[\{Ru(dmbpy)_2\}_2(\mu\text{-bipym})]^{4+}$ (dashed line)

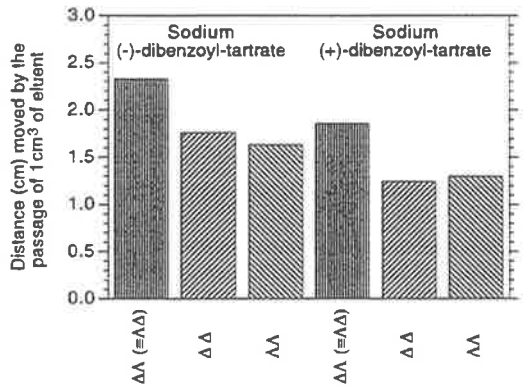

Fig. 8 Relative rate of travel of the three stereoisomers of $[\{Ru(dmbpy)_2\}_2(\mu\text{-bipym})]^{4+}$ down a 9 mm (inside diameter) column, eluted with aqueous 0.154 mol dm^{-3} sodium (+ or −)-dibenzoyltartrate solutions at 30 °C

the SP Sephadex C-25 support.[14] it can be assumed that the observed temperature dependence can be attributed to changes in the effective charges of the species travelling down the column. Tris(bipyridine)ruthenium(II)-type species associate with organic anions, and it is the differences in relative associations between the anion of the eluent and the various stereoisomers that lead to their separation by cation-exchange chromatography (the nature of these associations will be the subject of a subsequent publication).[31] From the temperature-dependence studies it may be concluded that the degree of association is higher at lower temperatures. This stronger association effectively reduces the charge on the cations, lowering the affinity with the cation-exchange resin so that the rate of travel down the column is faster at lower temperatures.

Chiral resolution of the racemic diastereoisomer with an achiral eluent

Previously, we have established that the ΔΔ and ΛΛ enantiomers of the complex $[\{Ru(dmbpy)_2\}_2(\mu\text{-apy})]^{4+}$ can be separated chromatographically using the chiral eluent sodium (−)-*O*,*O*′-di-4-toluoyl-L-tartrate.[22] However, during our studies on the $[\{Ru(dmbpy)_2\}_2(\mu\text{-bipym})]^{4+}$ system, the observation was made that there was considerable spreading of the slower-moving (*rac*) band on the column during the separation of the *meso* and *rac* diastereoisomers using sodium toluene-4-sulfonate as the eluent. To investigate whether chiral resolution could be achieved using this achiral salt, the slower-moving band from the diastereoisomer separation was reintroduced onto the top of the SP Sephadex C-25 column, and allowed to recycle several times down the length of the column (1 m). After it had travelled an effective column length (ECL) of *ca.* 2.5 m there was a clear separation of the two chiral forms of the *rac* diastereoisomer. These were collected and isolated as the hexafluorophosphate salts, and the resolution into the individual enantiomers confirmed by CD measurements (Fig. 7).

By comparison with the CD enantiomer assignment for stereoselectively synthesized ΔΔ- and ΛΛ-$[\{Ru(bpy)_2\}_2(\mu\text{-bipym})]^{4+}$ by Hua and von Zelewsky,[12] the first band off the column was assigned as the ΔΔ isomer, followed by the ΛΛ form. Importantly, we have achieved for the first time a separation of the two enantiomers using an achiral eluent on the SP Sephadex C-25 cation exchanger. The inference is clearly that the inherent structure of the dextran support itself must provide the chiral environment responsible for this process. The individual units of SP Sephadex are composed of propanesulfonate-functionalised cross-linked α-D-glucopyranoside, and there are five chiral centres in each subunit.

While coulombic forces dominate the cation-exchange chromatographic process, the charge densities or polarities of the cations[14] also exert an influence for species of the same charge. The use of a suitable counter anion in the eluent also has an effect on the second-sphere interactions between cation and anion.[14,32] Since isomers may differ in their relative interactions with the counter anion, the resultant slight variations in the effective charge and polarity of the species facilitate separation on the column. However, with the chiral resolution observed with an achiral eluent, the effective charge and polarity of the two associated enantiomers must be the same. Hence the separation must be a consequence of the support material itself, where the mechanism has elements of exclusion on the basis of shape.

The significance of this observation is that chiral eluents such as sodium (+)-*O*,*O*′-ditoluoyl-D-tartrate and sodium (−)-dibenzoyl-L-tartrate are not always necessary in the separation of simple enantiomeric pairs on the Sephadex support. It is however expected that the efficiency of such resolutions will be synergistically enhanced by the correct choice of chiral eluent.

Chiral resolution of the racemic diastereoisomer with a chiral eluent

Since the support material has such a significant effect on the two enantiomers, it can be assumed that the use of chiral counter anions in the eluent will either oppose or enhance the effect observed above. The rate of passage down the small pre-equilibrated column was therefore investigated to examine the effect of the eluents sodium (−)-dibenzoyl-L-tartrate and (+)-dibenzoyl-D-tartrate (0.154 mol dm^{-3}) on the rate of elution of the three individual stereoisomers down the column. The results are displayed in Fig. 8.

Sodium (−)-*O*,*O*′-dibenzoyl-L-tartrate behaved in a similar fashion to sodium toluene-4-sulfonate as an eluent, in that the *meso*-ΔΛ form moved the fastest, with the *rac*-ΔΔ next and the *rac*-ΛΛ slowest on the column. The chiral resolution of the *rac* form was however achieved in a much shorter distance, demonstrating a positive synergistic effect between the chiral eluent with the Sephadex support. On the other hand, with sodium (+)-*O*,*O*′-dibenzoyl-D-tartrate as eluent, the order of travel of the two enantiomers was reversed with the ΛΛ form travelling faster than the ΔΔ. Similar behaviour has also been observed using simple monomers such as $[Ru(bpy)_3]^{2+}$ and $[Ru(phen)_3]^{2+}$ and is currently undergoing intense study to try to rationalise this observation.[24]

von Zelewsky and co-workers[33] have shown by X-ray crystallography that there is a specific association between Λ-$[Ru(bpy)_2(py)_2]^{2+}$ and (−)-*O*,*O*′-dibenzoyl-L-tartrate, and between Δ-$[Ru(bpy)_2(py)_2]^{2+}$ and (+)-*O*,*O*′-dibenzoyl-D-tartrate. While in this case the possible π-stacking interactions between the aromatic benzoyl groups and the ligand pyridyl groups cause selective crystallisation, the same type of associations appear to dictate the order of travel down the column.

A comparison of the use of sodium (−)-*O*,*O*′-dibenzoyl-L-tartrate with sodium (+)-*O*,*O*′-dibenzoyl-D-tartrate as eluent indicates that there is much slower passage down the column for the latter electrolyte (1.25 times slower for the *meso* diastereoisomer). Additionally, the distance required to achieve chiral resolution between the enantiomeric pairs is larger with (+)-*O*,*O*′-dibenzoyl-D-tartrate. The implication is that the effect of the chirality of (+)-*O*,*O*′-dibenzoyl-D-tartrate opposes that of the Sephadex itself, slowing the rate of travel down the column and hindering the chiral resolution. Accordingly, care must be observed in the choice of chiral eluent to use this synergistic behaviour to enhance the separation.

Conclusion

In order to characterise simple ligand-bridged dinuclear polypyridyl species by standard techniques such as NMR spectroscopy the isolation of the individual diastereoisomers must first be achieved. Further, the isolation of stereochemically pure samples is likely to facilitate the growth of crystals appropriate for X-ray structural analysis. Such separations of diastereoisomers has been achieved using SP Sephadex C-25 cation exchanger and elution with sodium toluene-4-sulfonate. The variable-temperature experiments clearly indicate that there must be a significant degree of association of the eluent anion and cation which affects the interaction of the cation with the support. For the first time, chiral resolution of the racemic form has been achieved with the use of this achiral counter anion, rather than by using a chiral auxiliary. The respective bands from the column have been identified by a combination of a single-crystal X-ray determination and CD spectroscopy. Using the chiral auxiliaries (+)-*O*,*O*′-dibenzoyl-D-tartrate and (−)-*O*,*O*′-dibenzoyl-L-tartrate, it has become apparent that the choice of chirality of the counter anion becomes important, since it may either enhance or oppose the inherent chirality of the support material itself, and can prove critical in achieving a simple resolution of enantiomers.

Experimental

Instrumentation

The NMR spectra were recorded on a Varian Unity Inova-500 spectrometer using the solvent as the internal reference, CD spectra in acetonitrile solution using a Jobin Yvon spectrophotometer (λ_{max}/nm) and high-resolution mass spectra on a Bruker BioApex 47e ICR spectrometer with an electrospray source, using solutions *ca.* 2 μg cm^{-3} in methanol. Microanalyses were carried out on a Carlo Erba EA 1108 CHNS analyser. For the column chromatography studies, preparative columns C16/100 and C26/100 were from Pharmacia Biotech. The semiquantitative column K9 (Pharmacia Biotech) was fitted with an external water-jacket, temperature regulated with a Talabo F10 circulatory thermostatted water-bath. Column flow rates were regulated with a Gilson minipulse 2 peristaltic pump.

Materials

The compounds 4,4′-dimethyl-2,2′-bipyridine (Aldrich), 2,2′-bipyrimidine (Lancaster), 1,10-phenanthroline, 2,2′-bipyridine and sodium toluene-4-sulfonate (Aldrich) and ruthenium trichloride hydrate (Strem) were used as received without further purification. Aqueous sodium (−)-*O*,*O*′-dibenzoyl-L-tartrate and sodium (+)-*O*,*O*′-dibenzoyl-D-tartrate solutions were prepared by the addition of sodium hydroxide solution to the corresponding acids (Fluka), until a pH of 8–9 was obtained. SP Sephadex C-25 and Sephadex LH20 in anhydrous form were from Pharmacia Biotech. Amberlite IRA 400 from Aldrich. The precursors $[RuL_2Cl_2]$ (L = dmbpy, phen or bpy) were prepared according to the literature method.[34] Laboratory-grade solvents were used unless otherwise specified.

Complex syntheses

$[\{Ru(dmbpy)_2\}_2(\mu\text{-bipym})][PF_6]_4$. 2,2′-Bipyrimidine (0.137 g, 0.86 mmol) and $[Ru(dmbpy)_2Cl_2]$ (1.00 g, 1.73 mmol) in ethylene glycol (10 cm^3) were heated on 'medium heat' for 10 min in a microwave oven, fitted with an external condenser. The crude mixture was diluted with water (200 cm^3) and adsorbed on the top of a SP Sephadex C-25 column (dimensions 40 × 300 mm). On elution with 0.2 mol dm^{-3} NaCl solution the first red band was removed and discarded. The second green band was eluted with 0.5 mol dm^{-3} NaCl solution. The complex was precipitated with saturated KPF_6 solution, the solid collected by vacuum filtration and washed with water (5 × 50 cm^3). The dark green solid was dried *in vacuo*, yield 1.31 g (90%). A sample for elemental analysis was purified by passage through a short Sephadex LH20 column (eluent 50% methanol–acetone) (Found: C, 40.0; H, 3.5; N, 9.5. $C_{56}H_{54}F_{24}N_{12}P_4Ru_2$·2MeOH requires C, 40.0; H, 3.6; N, 9.6%). Further characterisation was made after diastereoisomeric isolation.

Diastereoisomeric separation

The diastereoisomeric mixture of $[\{Ru(dmbpy)_2\}_2(\mu\text{-bipym})][PF_6]_4$ (250 mg) were converted into the chloride salts by metathesis with LiCl in acetone solution. The solid was collected by filtration through Celite®, and extracted with water. The resulting dark green solution (200 cm^3) was introduced onto a SP Sephadex C-25 column (dimensions 26 × 1000 mm). Eluent flow was regulated by the use of a peristaltic pump. On elution with 0.25 mol dm^{-3} sodium toluene-4-sulfonate solution the initial fast-moving pale red and green bands were rejected, while the first (*meso*) and second (*rac*) major dark green fractions were collected and the complexes precipitated by the addition of saturated aqueous KPF_6 solution. The solids were extracted with dichloromethane, and the organic extracts dried with anhydrous Na_2SO_4. Following filtration, the solvent was evaporated and the residues dried *in vacuo*. Yields: *meso*, 80 mg, 32%; *rac*, 100 mg, 40%. These products were then converted into the chloride salt by passage of an aqueous solution down an Amberlite IRA 400 column for characterisation. *meso*: observed *m/z* 274.5663 (M^{4+}; most abundant isotope peak within cluster) ($C_{56}H_{54}N_{12}Ru_2$ requires 274.5675); ^{1}H NMR δ(D_2O) 8.28 (4 H, s, dmbpy H3a and H3b), 8.12 (2 H, d, *J* 5.5, bipym H6), 7.84 (2 H, d, *J* 6.0, dmbpy H6a), 7.49 (2 H, d, *J* 6.0, dmbpy H6b), 7.38 (2 H, d, *J* 6.0, dmbpy H5a), 7.37 (2 H, d, *J* 6.0, bipym H5), 7.19 (2 H, d, *J* 6.0 Hz, dmbpy H5b), 2.47 [6 H, s, dmbpy CH_3(4a)] and 2.43 [6 H, s, dmbpy CH_3(4b)]. *rac*: observed *m/z* 274.5663 (M^{4+}; most abundant isotope peak within cluster) ($C_{56}H_{54}N_{12}Ru_2$ requires 274.5675); ^{1}H NMR δ(D_2O) 8.35 (2 H, s, bpy H3a), 8.31 (2 H, s, dmbpy H3b), 8.12 (2 H, d, *J* 5.5, bipym H6), 7.51 (2 H, d, *J* 6.0, dmbpy H6a), 7.43 (2 H, d, *J* 6.0, dmbpy H6b), 7.36 (2 H, d, *J* 6.0, bipym H5), 7.20 (2 H, d, *J* 6.0, dmbpy H5a), 7.16 (2 H, d, *J* 6.0 Hz, dmbpy H5b), 2.53 [6 H, s, dmbpy CH_3(4a)] and 2.44 [6 H, s, dmbpy CH_3(4b)].

Resolution of the racemic form

Using a similar method to that described above, $[\{Ru(dmbpy)_2\}_2(\mu\text{-bipym})]Cl_4$ (*ca.* 50 mg) was introduced onto a column (dimensions 16 × 1000 mm). To increase the effective length of the column, once the Sephadex had equilibrated to the eluent a plunger was lowered onto the surface of the support and the system allowed to recycle. After the third passage down the column definite resolution had been achieved, and the two individual bands were collected and isolated as the hexafluorophosphate salts. Band 1, ΔΔ complex: CD λ_{max}/nm (CD_3CN) 256 (Δε/dm^3 mol^{-1} cm^{-1} +65.4), 278 (−110.8), 300 (0.4), 318 (−32.5), 392 (+28.2) and 623 (−4.3). Band 2, ΛΛ complex: CD λ_{max}/nm (CD_3CN) 256 (Δε/dm^3 mol^{-1} cm^{-1} −53.2), 278 (+109.1), 300 (7.1), 318 (+32.5), 392 (−22.6) and 607 (+4.6).

The complexes $[\{Ru(tmbpy)\}_2(\mu\text{-bipym})]^{4+}$, $[\{Ru(phen)_2\}_2(\mu\text{-bipym})][PF_6]_4$ and $[\{Ru(bpy)_2\}_2(\mu\text{-bipym})][PF_6]_4$ were prepared in an analogous fashion, and gave characterisations in accordance with the literature.[12]

Quantitative column techniques

A small Perspex column (dimensions 9 × 600 mm), fitted with an insulated water-jacket connected to a circulating thermostatted water-bath, was set to a constant temperature (30 °C for all measurements, unless otherwise stated). SP Sephadex C-25 was equilibrated in the eluent solution [aqueous 0.1–1.0 mol dm^{-3} sodium toluene-4-sulfonate for the variable-concentration data and 0.25 mol dm^{-3} for the temperature-dependent measurements; 0.154 mol dm^{-3} in the case of the investigations using sodium (+ or −)-*O*,*O*′-dibenzoyl-(D or L)-tartrate solutions], and allowed to settle in the column at a constant eluent flow rate of approximately 0.5 cm^3 min^{-1}. Once equilibration was obtained, the head of salt solution was reduced on the top of the support, and the compound to be separated was carefully introduced, dissolved in the eluent (0.25 mg of each isomer in 250 μl), so as not to disturb the Sephadex surface. With the sodium (+ or −)-*O*,*O*′-dibenzoyl-(D or L)-tartrate eluents, each isomer/enantiomer was added separately, since separation down the column was not always possible. The rate of flow through the column was carefully monitored as was the rate of travel of the individual bands. To ensure standardised results, the data are given in the volume of solvent required to move the individual bands by unit length (cm^3 cm^{-1}).

Crystallography

A sample of the first major fraction (*meso*) of $[\{Ru(dmbpy)_2\}_2(\mu\text{-bipym})]^{4+}$ was repurified by chromatography, using Sephadex LH20 as support with methanol as eluent to remove any excess of inorganic impurities. Following removal of the solvent, and redissolution of the residue in water, slow evaporation of the solution realised oily crystals which were suitable for X-ray determination.

A unique room-temperature diffractometer data set (Enraf-Nonius CAD-4 diffractometer; $T \approx 295$ K; monochromatic Mo-Kα radiation, $\lambda = 0.7107_3$ Å; 2θ–θ scan mode) was measured, yielding N_o independent reflections, N_o with $I > 3\sigma(I)$ being considered 'observed' and used in the large-block least-squares refinements. The crystal structure determination is of rather low precision as crystals of higher quality were elusive, and consequently the data were broad and weak from a poorly diffracting, decomposing specimen. Anisotropic thermal parameters were refined for Ru(1), Cl(1), Cl(2) and O(1) to O(5) only, due to limited data, and all other non-H atoms were refined isotropically. Hydrogen atoms were placed in calculated positions and not refined. Conventional residuals R, R' on $|F|$ are quoted, statistical weights derivative of $\sigma^2(I) = \sigma^2(I_{diff}) + 0.0004\sigma^4(I_{diff})$ being used. Neutral atom complex scattering factors were employed, and computation was by the XTAL 3.4 program system, implemented by S. R. Hall.[35] Specific details are as follows: $[\{Ru(dmbpy)_2\}_2(\mu\text{-bipym})]Cl_4 \cdot 10H_2O$, $C_{56}H_{74}Cl_4N_{12}O_{10}Ru_2$, M 1419.24, monoclinic, space group $P2_1/n$ (no. 14), $a = 10.87(1)$, $b = 22.67(1)$, $c = 13.88(1)$ Å, $\beta = 111.37(9)°$, $U = 3187$ Å^3, D_c ($Z = 2$) 1.48 g cm^{-3}, $F(000)$ 1460, $2\theta_{max}$ 45°, N 4473, N_o 1446, $R = 0.107$, $R' = 0.106$.

CCDC reference number 186/767.

Acknowledgements

This work was supported by the Australian Research Council. We are grateful to Mr. Brian Foster for performing the microanalyses, and Dr. Ian Atkinson (James Cook University) and Mr. Rick Willis (Australian Institute of Marine Science) for undertaking the electrospray mass spectral measurements. Andreas Beyeler and Bruni Kolp (University of Fribourg, Switzerland) are thanked for their help with the acquisition of the CD spectra.

References

1 V. Balzani, A. Juris, M. Venturi, S. Campagna and S. Serroni, *Chem. Rev.*, 1996, **96**, 759 and ref. therein.
2 V. Balzani and F. Scandola, *Supramolecular Photochemistry*, Ellis Horwood, Chichester, 1991.
3 J.-P. Sauvage, J.-P. Collin, J. C. Chambron, S. Guillerez, C. Coudret, V. Balzani, F. Barigelletti, L. De Cola and L. Flamigni, *Chem. Rev.*, 1994, **94**, 993.
4 J.-M. Lehn, *Angew. Chem., Int. Ed. Engl.*, 1990, **29**, 1304.
5 A. M. Pyle and J. K. Barton, *Prog. Inorg. Chem.*, 1990, **38**, 413.
6 A. Kirsch-De Mesmaeker, J. P. Lecomte and J. M. Kelly, *Top. Curr. Chem.*, 1996, **177**, 25.
7 E. D. A. Stemp, M. R. Arkin and J. K. Barton, *J. Am. Chem. Soc.*, 1997, 2921.
8 P. Lincoln and B. Nordén, *Chem. Commun.*, 1996, 2145.
9 P. Lincoln, A. Broo and B. Nordén, *J. Am. Chem. Soc.*, 1996, **118**, 2644.
10 J. K. Barton, A. Danishefsky and J. Goldberg, *J. Am. Chem. Soc.*, 1984, **106**, 2172.
11 C. Hiort, P. Lincoln and B. Nordén, *J. Am. Chem. Soc.*, 1993, **115**, 3448.
12 X. Hua and A. von Zelewsky, *Inorg. Chem.*, 1995, **34**, 5791.
13 T. J. Rutherford, M. G. Quagliotto and F. R. Keene, *Inorg. Chem.*, 1995, **34**, 3857.
14 G. H. Searle, *Aust. J. Chem.*, 1977, **30**, 2625.
15 H. Yoneda, *J. Chromatogr.*, 1984, **313**, 59.
16 Y. Yoshikawa and K. Yamasaki, *Coord. Chem. Rev.*, 1979, **28**, 205.
17 B. T. Patterson and F. R. Keene, 1997, *Inorg. Chem.*, in the press.
18 T. J. Rutherford and F. R. Keene, *Inorg. Chem.*, 1997, **36**, 3580.
19 T. J. Rutherford, O. Van Gijte, A. Kirsch-De Mesmaeker and F. R. Keene, *Inorg. Chem.*, 1997, **36**, 4465.
20 T. J. Rutherford, D. A. Reitsma and F. R. Keene, *J. Chem. Soc., Dalton Trans.*, 1994, 3659.
21 D. A. Reitsma and F. R. Keene, *J. Chem. Soc., Dalton Trans.*, 1993, 2859.
22 L. S. Kelso, D. A. Reitsma and F. R. Keene, *Inorg. Chem.*, 1996, **35**, 5144.
23 F. R. Keene, *Coord. Chem. Rev.*, 1997, in the press.
24 T. J. Rutherford and F. R. Keene, unpublished work.
25 D. A. Reitsma and F. R. Keene, unpublished work.
26 D. A. Bardwell, J. C. Jeffery, L. Joulié and M. D. Ward, *J. Chem. Soc., Dalton Trans.*, 1993, 2255.
27 D. A. Bardwell, L. Horsburgh, J. C. Jeffery, L. F. Joulié, M. D. Ward, I. Webster and L. J. Yellowlees, *J. Chem. Soc., Dalton Trans.*, 1996, 2527.
28 R. Hage, J. G. Haasnoot, H. A. Nieuwenhuis, J. Reedijk, D. J. A. De Ridder and J. G. Vos, *J. Am. Chem. Soc.*, 1990, **112**, 9245.
29 V. Balzani, D. A. Bardwell, F. Barigelletti, F. L. Cleary, M. Guardigli, J. C. Jeffery, T. Sovrani and M. D. Ward, *J. Chem. Soc., Dalton Trans.*, 1995, 3601.
30 F. Helfferich, *Ion Exchange*, McGraw-Hill, New York, 1962.
31 N. C. Fletcher, P. C. Junk and F. R. Keene, unpublished work.
32 F. R. Keene and G. H. Searle, *Inorg. Chem.*, 1974, **13**, 2173.
33 B. Kolp, H. Viebrock, A. von Zelewsky and D. Abeln, personal communication.
34 P. A. Lay, A. M. Sargeson and H. Taube, *Inorg. Synth.*, 1986, **24**, 291.
35 S. R. Hall, G. S. D. King and J. M. Stewart, *Xtal3.4 User's Manual*, University of Western Australia, Lamb, Perth, 1995.

Received 13*th August* 1997; *Paper* 7/05947G

Inorg. Chem. 1998, *37*, 645–650

Isolation of Geometric Isomers within Diastereoisomers of Dinuclear Ligand-Bridged Complexes of Ruthenium(II)

Bradley T. Patterson and F. Richard Keene*

School of Biomedical and Molecular Sciences, James Cook University of North Queensland, Townsville, Queensland 4811, Australia

Received August 22, 1997

The individual diastereoisomeric forms [*meso* ($\Delta\Lambda$) and *rac* ($\Delta\Delta$ and $\Lambda\Lambda$)] of the ligand-bridged dinuclear species $[\{Ru(phen)(Me_4bpy)\}_2(\mu\text{-bpm})]^{4+}$ [phen = 1,10-phenanthroline; Me_4bpy = 4,4′,5,5′-tetramethyl-2,2′-bipyridine; bpm = 2,2′-bipyrimidine] have been synthesized using chiral forms of the precursors $[Ru(phen)(Me_4bpy)(bpm)]^{2+}$ and $[Ru(phen)(Me_4bpy)(py)_2]^{2+}$. The *cis* and *trans* geometric isomers of both diastereoisomeric forms have been separated by cation exchange chromatography and characterized by NMR spectroscopy. We also report the first chiral resolutions of a heteroleptic tris(bidentate)ruthenium(II) complex, $[Ru(phen)(Me_4bpy)(bpm)]^{2+}$, and a heteroleptic bis(bidentate)bis(pyridine)ruthenium(II) complex, $[Ru(phen)(Me_4bpy)(py)_2]^{2+}$, in both cases using cation exchange chromatography.

Introduction

Ligand-bridged polymetallic molecular assemblies have potential application to photochemical devices,[1] and tris(bidentate)-ruthenium(II) centers involving polypyridyl ligands have frequently formed the basis of such assemblies by virtue of their favorable redox, spectral, and photophysical characteristics.[2] However, these moieties also introduce stereoisomerism, and there has been considerable interest by ourselves and others regarding stereochemical control in oligomeric assemblies.[3–18] Further, our initial studies have revealed that intramolecular electron and energy transfer processes depend on the spatial relationship of the components within such species.[16–20]

Dinuclear ligand-bridged complexes represent the simplest example of the genre, and stereochemical studies thus far have generally sought the stereoselective synthesis of individual diastereoisomeric or enantiomeric forms[3,4,6,7,9–14,16] or the separation of these individual stereoisomeric forms from a mixture.[5,6,16,18] However, in all such studies the individual metal centers have possessed two identical terminal (i.e. nonbridging) ligands; i.e., $[\{Ru(pp)_2\}_2(\mu\text{-BL})]^{n+}$ or alternatively $[\{Ru(pp)_2\}\{Ru(pp')_2\}(\mu\text{-BL})]^{n+}$ {pp and pp′ are symmetrical bidentate ligands such as 2,2′-bipyridine (bpy) or 1,10-phenanthroline (phen) (Chart 1); BL is a bis-bidentate bridging ligand}. In the first case, only *meso* [$\Delta\Lambda$ (=$\Lambda\Delta$)] and *racemic* ($\Delta\Delta/\Lambda\Lambda$) diastereoisomeric forms exist (with the latter being an enantiomeric pair; Figure 1), while in the second case there are analogous diastereoisomeric possibilities but with the $\Delta\Lambda$ and $\Lambda\Lambda$ forms becoming enantiomeric.[5]

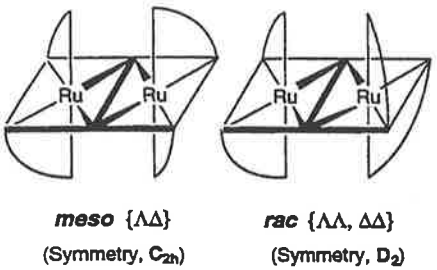

Figure 1. Schematic representation of the diastereoisomeric forms of the ligand-bridged dinuclear species $[\{Ru(pp)_2\}_2(\mu\text{-BL})]^{n+}$.

Chart 1

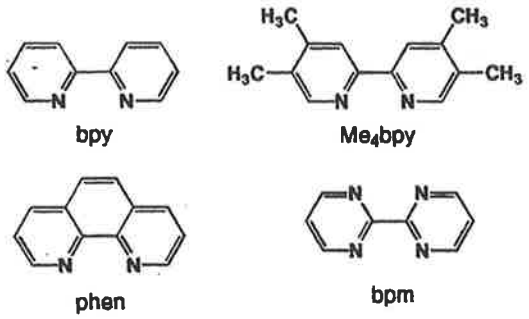

(1) Balzani, V.; Scandola, F. *Supramolecular Photochemistry*; Ellis Horwood: Chichester, U.K., 1991.
(2) Juris, A.; Barigelletti, S.; Campagna, S.; Balzani, V.; Belser, P.; von Zelewsky, A. *Coord. Chem. Rev.* **1988**, *84*, 85.
(3) Hua, X.; von Zelewsky, A. *Inorg. Chem.* **1991**, *30*, 3796.
(4) Hua, X.; von Zelewsky, A. *Inorg. Chem.* **1995**, *34*, 5791.
(5) Reitsma, D. A.; Keene, F. R. *J. Chem. Soc., Dalton Trans.* **1993**, 2859.
(6) Rutherford, T. J.; Quagliotto, M. G.; Keene, F. R. *Inorg. Chem.* **1995**, *34*, 3857.
(7) Lincoln, P.; Nordén, B. *Chem. Commun.* **1996**, 2145.
(8) Wärnmark, K.; Thomas, J. A.; Heyke, O.; Lehn, J.-M. *Chem. Commun.* **1996**, 701.
(9) Tzalis, D.; Tor, Y. *J. Am. Chem. Soc.* **1997**, *119*, 852.
(10) MacDonnell, F. M.; Bodige, S. *Inorg. Chem.* **1996**, *35*, 5758.
(11) Mürner, H.; Belser, P.; von Zelewsky, A. *J. Am. Chem. Soc.* **1996**, *118*, 7989.
(12) Mürner, H.; von Zelewsky, A.; Stoeckli-Evans, H. *Inorg. Chem.* **1996**, *35*, 3931.
(13) Fletcher, N. C.; Keene, F. R.; Ziegler, M.; Stoeckli-Evans, H.; Viebrock, H.; von Zelewsky, A. *Helv. Chim. Acta* **1996**, *79*, 1192.
(14) Fletcher, N. C.; Keene, F. R.; Viebrock, H.; von Zelewsky, A. *Inorg. Chem.* **1997**, *36*, 1113.
(15) Rutherford, T. J.; Keene, F. R. *Inorg. Chem.* **1997**, *36*, 3580.
(16) Rutherford, T. J.; Van Gijte, O.; Kirsch-De Mesmaeker, A.; Keene, F. R. *Inorg. Chem.* **1997**, *36*, 4465.
(17) Rutherford, T. J.; Keene, F. R. *Inorg. Chem.* **1997**, *36*, 2872.
(18) Kelso, L. S.; Reitsma, D. A.; Keene, F. R. *Inorg. Chem.* **1996**, *35*, 5144.

S0020-1669(97)01080-X CCC: $15.00
Published on Web 02/03/1998

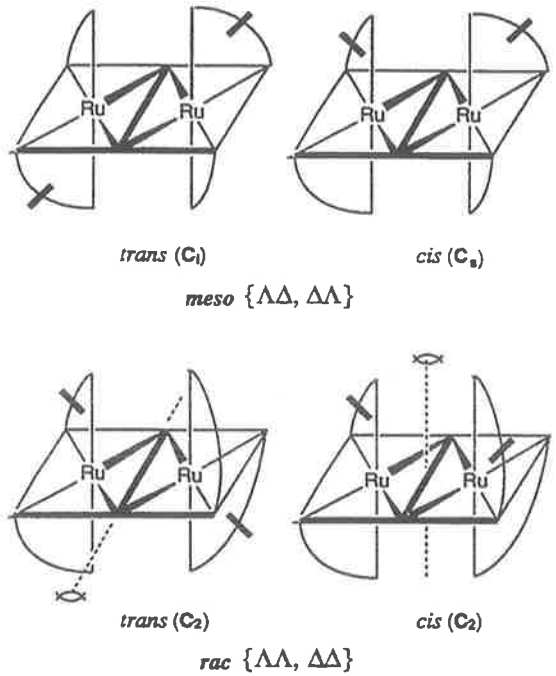

Figure 2. Schematic representation of the geometric isomers of the *meso*- and *rac*-$[\{Ru(pp)_2\}_2(\mu\text{-BL})]^{n+}$. For the *rac* forms, the C_2 axes are shown.

Clearly, the complexity in such dinuclear species may rapidly increase if the two terminal ligands on each center are not identical and/or the bridging ligand is not symmetrical. However, investigation of such systems has not been possible as the synthetic methodologies for such species have not been available. Recently reported synthetic schemes for tris(heteroleptic)ruthenium(II) centers via dicarbonyl precursors of the type $[Ru(pp)(pp')(CO)_2]^{2+}$ [21] allow extensive variation of the ligand environment, and together with the development of appropriate stereochemical techniques,[20] they provide the means to investigate these more complicated systems.

As a model for these studies, we chose the dinuclear complex $[\{Ru(phen)(Me_4bpy)\}_2(\mu\text{-bpm})]^{4+}$, in which the two terminal ligands (phen = 1,10-phenanthroline and Me_4bpy = 4,4′,5,5′-tetramethyl-2,2′-bipyridine) and the bridging ligand (bpm = 2,2′-bipyrimidine) are symmetrical. In such a case, there are again two possible diastereoisomeric forms (*meso* and *rac*), but each diastereoisomer may also possess two geometric forms (called *cis* and *trans*) in which the equivalent ligands on each metal center are disposed either on the same or on opposite sides of the plane of the bridge, respectively (Figure 2).

We report here the isolation and characterization (using NMR techniques) of all possible stereoisomeric forms of this complex by a combination of stereoselective syntheses and chromatographic separation methods.

Experimental Section

Materials. 1,10-Phenanthroline (phen; Aldrich), 2,2′-bipyrimidine (bpm; Lancaster), (1*R*,2*R*)-(−)-1,2-diaminocyclohexane (*R*,*R*′-dach; Aldrich), potassium hexafluorophosphate (Aldrich), sodium toluene-4-sulfonate (Aldrich), ethylene glycol (Aldrich), 2-methoxyethanol (Fluka), and acetonitrile (Aldrich, 99.8%) were used as received. Trimethylamine *N*-oxide (TMNO) was obtained by vacuum sublimation at 120 °C of the dihydrate (Fluka). Aqueous solutions of sodium (−)-*O*,*O*′-dibenzoyl-L-tartrate and sodium (−)-*O*,*O*′-di-4-toluoyl-L-tartrate were obtained by neutralization of the corresponding acids (Fluka) using sodium hydroxide. Pyridine (Ajax) and 3,4-lutidine (BDH) were dried (KOH) and distilled before use; all other solvents were of laboratory grade.

Measurements. ^1H and COSY experiments were performed on a Bruker Aspect 300 MHz NMR spectrometer (CD_3CN solutions). ORD (optical rotatory dispersion) curves were recorded using a Perkin-Elmer 141 polarimeter in a 1 dm cell. Specific rotation at λ: $[\alpha]_\lambda = 100\alpha/cl$, where α = absolute rotation (deg), c = concentration in g/100 cm^3, and l = cell path length (in dm). CD (circular dichroism) spectra were recorded in acetonitrile solution at concentrations of $\sim(1-3) \times 10^{-5}$ M at the University of Wollongong using a Jobin Yvon Dichrograph 6 instrument. CD spectra are presented as $\Delta\epsilon$ vs λ (nm). High-resolution mass spectra were obtained on a Brucker BioApex 47e ICR mass spectrometer with an electrospray source, using a ca. 2 μg/mL solution in methanol.

Elemental microanalyses were performed within the Department of Chemistry and Chemical Engineering at James Cook University of North Queensland.

Syntheses. The complexes $[Ru(phen)(CO)_2Cl_2]$, $[Ru(phen)(CF_3SO_3)_2(CO)_2]$ and $[Ru(phen)(Me_4bpy)(CO)_2](PF_6)_2$ were prepared using literature methods.[21]

4,4′,5,5′-Tetramethyl-2,2′-bipyridine (Me_4bpy) was synthesized by an adaption of a literature procedure.[22,23] Freshly distilled 3,4-lutidine (40 mL, 0.356 mol) was stirred with Pd/C (10%; 4 g) and the mixture refluxed for 13 days. The resulting solid was extracted (Soxhlet) with dichloromethane and decolorized with activated carbon (3 g) in refluxing dichloromethane. The solution was filtered through Celite, which was washed with several portions of hot toluene. The filtrate was evaporated to dryness, and the yellow residue was recrystallized from toluene to give a white crystalline product (22.5 g; 60%). ^1H NMR ($CDCl_3$): δ 2.28 (s), 2.33 (s), 8.11 (s), 8.36 (s).

$[Ru(phen)(Me_4bpy)(bpm)](PF_6)_2$. $[Ru(phen)(Me_4bpy)(CO)_2](PF_6)_2$ (30 mg; 0.0357 mmol) and 2,2′-bipyrimidine (22.6 mg; 0.143 mmol) were dissolved in 2-methoxyethanol (10 mL) and the solution deaerated with N_2 for 30 min. TMNO (27 mg; 0.36 mmol) was added, causing a rapid change from colorless to orange. The solution was refluxed for 3 h under subdued light and cooled, and the product was precipitated by the addition of a saturated aqueous solution of KPF_6 and collected. Further purification was achieved by cation exchange chromatography (SP Sephadex C-25; eluent 0.2 M NaCl). The major orange band was collected and the complex precipitated using KPF_6: it was reprecipitated twice by the addition of KPF_6 to an acetone/water solution of the complex, collected, washed with cold water (2 × 5 mL) and diethyl ether (2 × 10 mL), and dried in vacuo. Yield: 21 mg; 61%. Anal. Calcd for $RuC_{34}H_{30}F_{12}N_8P_2 \cdot C_3H_6O \cdot 2H_2O$: C, 43.4; H, 4.20; N, 10.7. Found: C, 43.5; H, 3.80; N, 10.5.

Chiral Resolution of $[Ru(phen)(Me_4bpy)(bpm)]^{2+}$. $[Ru(phen)(Me_4bpy)(bpm)](PF_6)_2$ was resolved into its Δ and Λ enantiomeric forms using cation exchange chromatography (SP Sephadex C-25; eluent 0.075 M sodium (−)-*O*,*O*′-dibenzoyl-L-tartrate; effective column length (ECL) of 1.5 m). The two bands were collected, and the complexes were precipitated as their PF_6^- salts and purified as described above: band 1 (Δ), $\alpha_{589} = -3550°$; band 2 (Λ), $\alpha_{589} = +3680°$.

$[Ru(phen)(Me_4bpy)(py)_2](PF_6)_2$. $[Ru(phen)(Me_4bpy)(CO)_2](PF_6)_2$ (166 mg; 0.198 mmol) and pyridine (3 mL; excess) were dissolved in 2-methoxyethanol (30 mL), and the solution was deaerated with N_2 for 30 min. TMNO (55 mg; 0.73 mmol) was added causing a change from almost colorless to orange within 30 min. The solution was refluxed in subdued light under a nitrogen atmosphere for 3 h before cooling and precipitation with a saturated aqueous KPF_6 solution. The

(19) Treadway, J. A.; Chen, P.; Rutherford, T. J.; Keene, F. R.; Meyer, T. J. *J. Phys. Chem. A* **1997**, *101*, 6824.
(20) Keene, F. R. *Coord. Chem. Rev.* **1997**, in press.
(21) Anderson, P. A.; Deacon, G. B.; Haarmann, K. H.; Keene, F. R.; Meyer, T. J.; Reitsma, D. A.; Skelton, B. W.; Strouse, G. F.; Thomas, N. C.; Treadway, J. A.; White, A. H. *Inorg. Chem.* **1995**, *34*, 6145.
(22) Sasse, W. H. F.; Whittle, C. P. *J. Chem. Soc.* **1961**, 1347.
(23) Della Ciana, L.; Dressick, W. J.; Sandrini, D.; Maestri, M.; Ciano, M. *Inorg. Chem.* **1990**, *29*, 2792.

precipitate was purified using cation exchange chromatography (SP Sephadex C-25; eluent 0.2 M NaCl) and the product collected as described above. Yield: 130 mg; 70%. Anal. Calcd for $RuC_{36}H_{34}F_{12}N_6P_2$: C, 45.9; H, 3.61; N, 8.9. Found: C, 45.8; H, 3.59; N, 8.8.

Chiral Resolution of [Ru(phen)(Me$_4$bpy)(py)$_2$]$^{2+}$. [Ru(phen)(Me$_4$bpy)(py)$_2$](PF$_6$)$_2$ (130 mg) was converted to the chloride salt by anion exchange chromatography and applied to a column of SP Sephadex C-25 cation exchanger; the two enantiomers were separated using 0.075 M sodium (−)-*O*,*O*′-di-4-toluoyl-L-tartrate solution as eluent (ECL ~ 2 m). Each band was collected, and the complexes were precipitated as their PF_6^- salts and purified (3×) as described above. Approximately 30 mg of each enantiomer was obtained: band 1 (Δ), $[\alpha]_{589} = -940°$; band 2 (Λ), $[\alpha]_{589} = +1000°$.

[Ru(phen)(Me$_4$bpy)(*R*,*R*′-dach)](PF$_6$)$_2$. The following reactions were carried out as a test for chiral purity of Δ- and Λ-[Ru(phen)(Me$_4$bpy)(py)$_2$]$^{2+}$, based on a method detailed previously.[4] In a typical experiment, [Ru(phen)(Me$_4$bpy)(py)$_2$](PF$_6$) (13.5 mg; 0.0143 mmol) and (1*R*,2*R*)-(−)-1,2-diaminocyclohexane (*R*,*R*′-dach; 5 mg; 0.044 mmol) were dissolved in 50% aqueous ethylene glycol (2 mL), and the mixture was heated at 120 °C for 5 h under an inert atmosphere (N_2). The solution was cooled and the product precipitated using a saturated aqueous solution of KPF_6. The precipitate was collected and washed with copious amounts of diethyl ether and air-dried. Yield: 11.6 mg; 89%.

***meso*-[{Ru(phen)(Me$_4$bpy)}$_2$(μ-bpm)](PF$_6$)$_4$.** Δ-[Ru(phen)(Me$_4$bpy)(bpm)](PF$_6$)$_2$ (15.6 mg; 0.0166 mmol) and Λ-[Ru(phen)(Me$_4$bpy)(py)$_2$](PF$_6$)$_2$ (19.4 mg; 0.0206 mmol) were dissolved in ethylene glycol (2 mL), and the solution was deaerated with N_2 and heated for 5 h at 100−110 °C. Upon cooling, water (3 mL) and saturated KPF_6 solution (2 mL) were added and the green precipitate was collected. Purification was achieved by cation exchange chromatography (SP Sephadex C-25; eluent 0.4 M NaCl). The green band was collected, and the complex was precipitated as the PF_6^- salt and purified as described above. Yield: 22.2 mg; 78%. As is the case in many dinuclear species of this type, microanalyses indicated the inclusion of acetone and water molecules in the crystals, rendering the data of dubious use in characterization. However, associated NMR and mass spectral data provided unambiguous assignment. Mass spectrum: observed *m*/*z* 1580.1702 (M^+: most abundant isotope peak within cluster); $[C_{60}H_{54}N_{12}Ru_2](PF_6)_3^-$ requires *m*/*z* 1580.1632.

Separation of Geometric Isomers of *meso*-[{Ru(phen)(Me$_4$bpy)}$_2$(μ-bpm)]$^{4+}$. *meso*-[{Ru(phen)(Me$_4$bpy)}$_2$(μ-bpm)](PF$_6$)$_4$ (40 mg) was converted to the chloride salt by anion exchange chromatography and the solution sorbed on to SP Sephadex C-25 cation exchanger. The complex was eluted using 0.25 M sodium toluene-4-sulfonate as eluent, and after continual recycling two bands were collected (ECL ~ 12 m). Each band was collected, and the complexes were precipitated as the PF_6^- salts and purified (3×) as described above.

ΔΔ-[{Ru(phen)(Me$_4$bpy)}$_2$(μ-bpm)](PF$_6$)$_4$. Λ-[Ru(phen)(Me$_4$bpy)(bpm)](PF$_6$)$_2$ (18 mg; 0.0191 mmol) and Λ-[Ru(phen)(Me$_4$bpy)(py)$_2$](PF$_6$)$_2$ (22.4 mg; 0.023 mmol) were dissolved in ethylene glycol (2 mL), and the solution was deaerated with N_2 and heated for 5 h at 100−110 °C. Upon cooling, water (3 mL) and saturated KPF_6 solution (2 mL) were added and the precipitate was collected. The green-brown solid was purified by cation exchange chromatography (SP Sephadex C-25; eluent 0.4 M NaCl). The resulting green band was collected, and the complex was precipitated as the PF_6^- salt and purified (3×) as described above. Yield: 27.2 mg; 83%.

Separation of Geometric Isomers of ΔΔ-[{Ru(phen)(Me$_4$bpy)}$_2$(μ-bpm)]$^{4+}$. ΔΔ-[{Ru(phen)(Me$_4$bpy)}$_2$(μ-bpm)](PF$_6$)$_4$ (60 mg) was converted to the chloride salt by anion exhange chromatography, sorbed onto SP Sephadex C-25 cation exchanger, and eluted using 0.25 M sodium toluene-4-sulfonate solution. On continual recycling of the samples, (ECL ~ 20 m), two bands were collected, and the respective complexes precipitated as the PF_6^- salts and purified (3×) as described above.

Results and Discussion

Synthetic and Stereochemical Aspects. In developing a target dinuclear species of the type [{Ru(pp)(pp′)}$_2$(μ-BL)]$^{4+}$, we selected the system [{Ru(phen)(Me$_4$bpy)}$_2$(μ-bpm)]$^{4+}$. The particular identity of the ligands was chosen for several reasons: the ^{1}H NMR spectrum of the Me$_4$bpy ligand comprises only singlets in the aromatic region, simplifying the spectral interpretation of its complexes; from earlier studies,[5,24] we have observed that the presence of phen and methyl-substituted "bpy"-type ligands facilitates chromatographic separation of the stereoisomers. Finally, bpm is a rigid symmetrical bridging ligand.

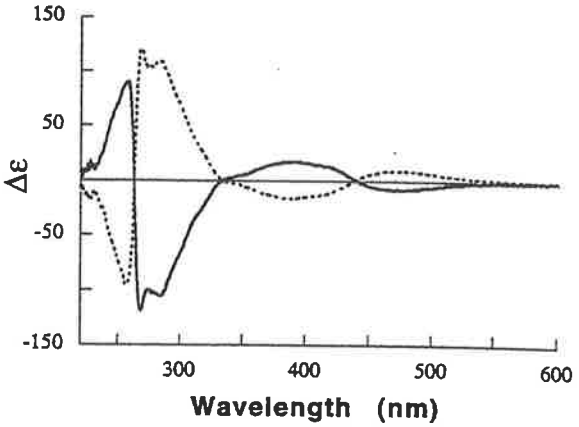

Figure 3. CD of [Ru(phen)(Me$_4$bpy)(bpm)]$^{2+}$ (CH_3CN solution): Δ (—); Λ (- - -).

Because of the potential isomeric complexity in the system, we directed our initial attention to the synthesis of the individual enantiomers of the two diastereoisomeric forms [i.e. ΔΔ and ΛΛ, ΔΛ (≡ΛΔ)], so that subsequent separation of the two geometric isomers (*cis* and *trans*) of each form was unencumbered by any uncertainty of the chiral identity. Such a stereoselective synthesis requires two chiral precursors: viz. the individual enantiomeric forms of the tris(heteroleptic) species [Ru(phen)(Me$_4$bpy)(bpm)]$^{2+}$, as well as the enantiomers of a [Ru(phen)(Me$_4$bpy)X$_2$]$^{2+}$ species (X = CO or py). In both instances, this posed an interesting challenge as there are no reported resolutions of either type of complex.

We have recently reported a general synthetic methodology for hetereoleptic tris(bidentate)ruthenium(II) complexes,[21,25] and the target complex [Ru(phen)(Me$_4$bpy)(bpm)]$^{2+}$ was conveniently obtained by this technique. We have also recently reported the routine resolution of mononuclear tris(bidentate)-ruthenium(II) species by cation exchange chromatographic methods,[20] and the complex was readily resolved using these techniques. The CD spectra of the two enantiomers are given in Figure 3. This is the first reported example of the chiral resolution of a hetereoleptic tris(bidentate)ruthenium(II) complex.

The second of the precursors was chosen as [Ru(phen)(Me$_4$bpy)(py)$_2$]$^{2+}$, rather than the dicarbonyl analogue. While both [Ru(pp)$_2$(py)$_2$]$^{2+}$ [3,4] and [Ru(pp)$_2$(CO)$_2$]$^{2+}$ [6] species have been shown to undergo the addition of a third bidentate ligand with retention of absolute configuration, the former complex reacts in higher yield, and our own studies have led to consistent resolution of bis(pyridine) complexes of this type into enantiomers by chromatographic methods. In the present instance, [Ru(phen)(Me$_4$bpy)(py)$_2$]$^{2+}$ was synthesized by decarbonylation

(24) Fletcher, N. C.; Junk, P. C.; Keene, F. R. *J. Chem. Soc., Dalton Trans.* **1998**, 133.
(25) Strouse, G. F.; Anderson, P. A.; Schoonover, J. R.; Meyer, T. J.; Keene, F. R. *Inorg. Chem.* **1992**, *31*, 3004.

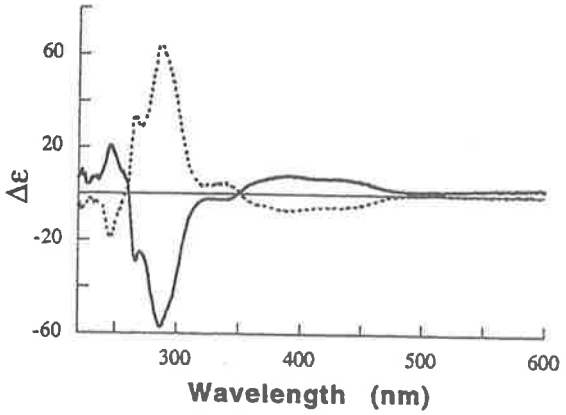

Figure 4. CD of $[Ru(phen)(Me_4bpy)(py)_2]^{2+}$ (CH_3CN solution): Δ (—); Λ (- - -).

of $[Ru(phen)(Me_4bpy)(CO)_2]^{2+}$ in the presence of pyridine, and it was chromatographically resolved. The CD spectra of the two enantiomers are shown in Figure 4. While complexes of the type $[Ru(pp)_2(py)_2]^{2+}$ (pp = a bidentate ligand) have been resolved into enantiomeric forms by diastereoisomeric formation involving chiral anions,[3,4] this is the first reported example of the resolution of a complex $[Ru(pp)(pp')(py)_2]^{2+}$ ($pp \neq pp'$), although we have previously reported the separation of geometrical isomers of such species in cases where pp and pp′ are unsymmetrical.[17]

The absolute configurations of (−)-$[Ru(phen)(Me_4bpy)(bpm)]^{2+}$ and (−)-$[Ru(phen)(Me_4bpy)(py)_2]^{2+}$ were assigned to the Δ form, using predictions made by the exciton theory[26-28] and comparisons of CD spectra with those of related species.[3,4]

The availability of the enantiomers of each of the precursors enables all diastereoisomers to be generated selectively, and route A in Scheme 1 is an example of a specific synthesis of one stereoisomer. In fact two specific diastereoisomers were obtained in this way: viz. ΛΛ and ΔΔ. In each case, cation exchange chromatography allowed the separation of two geometrical isomers, and these were characterized by a combination of 1D and 2D ^1H NMR studies, as described below.

It is noted that in the chromatographic studies, the diastereoisomer separation occurred very much more easily than the separation of geometric isomers. Consequently, once that had been established, it was found more convenient to react either Δ- or Λ-$[Ru(phen)(Me_4bpy)(bpm)]^{2+}$ with *rac*-$[Ru(phen)(Me_4bpy)(py)_2]^{2+}$ producing a ΔΔ/ΔΛ (or ΛΔ/ΛΛ) mixture, which could then be readily separated into the individual diastereoisomers prior to the isolation of the geometric components (Scheme 1B).

The separation of the geometric isomers of the *meso* and *rac* diastereoisomeric forms of an analogous species $[\{Ru(Me_2bpy)(Me_4bpy)\}_2(\mu\text{-bpm})]^{4+}$ (Me_2bpy = 4,4′-dimethyl-2.2′-bipyridine) has also been achieved by similar techniques.[29]

NMR Studies. In the discussion of the NMR spectra, the conventional numbering schemes are used with the ligands phen, Me_4bpy, and bpm. In all four species, the two phen ligands are related by symmetry (as are the two Me_4bpy ligands), but in both cases the two halves of each ligand type are not equivalent (see below). While the assignments of resonances

Scheme 1. Synthetic Scheme for Isolation of Geometric Isomers of Diastereoisomeric Forms of $[\{Ru(phen)(Me_4Bpy)\}_2(\mu\text{-bpm})]^{4+}$ (A) through Stereoselective Synthesis of Individual Diastereoisomers of the Target Complex and (B) through a Combination of Partial Stereoselective Synthesis and Cation Exchange Chromatography[a]

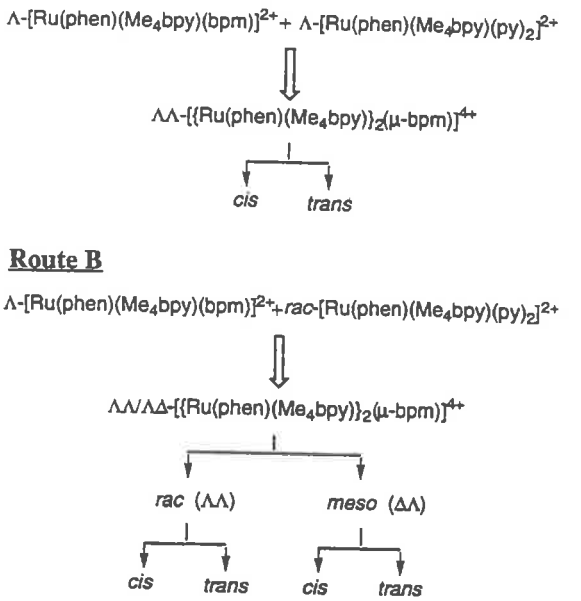

[a] Synthetic procedures are indicated by double arrows, and chromatographic separations, by single arrows.

arising from these ligands can be made unambiguously, the actual ligand orientation is not specified. In principle, such additional assignments may be deduced by a detailed consideration of anisotropic effects,[5,6,16-18,30] but in the present case it was not necessary for the isomer characterization and was therefore not undertaken. For bpm, the nonprimed protons are positioned under the phen ligands in the *meso-cis* and *rac-trans* forms. In the *meso-trans* and *rac-cis* cases, the distinction between the rings is not important (as a consequence of symmetry), but the additional convention is adopted that the 4-positions are nearer the phen ligand.

For the bis(homoleptic) complex $[\{Ru(pp)_2\}_2(\mu\text{-BL})]^{4+}$, the point group symmetries of the *meso* and *rac* forms are C_{2h} and D_2, respectively (Figure 1). In the case of the bis(heteroleptic) species $[\{Ru(pp)(pp')\}_2(\mu\text{-BL})]^{4+}$ (Figure 2), for the *meso* diastereoisomer, the *trans* geometrical form adopts C_i point group symmetry, but that of the *cis* isomer is reduced to C_s. For the *rac* diastereoisomer, the symmetries of both the *cis* and *trans* geometrical isomers are C_2 but differ with respect to the orientation of the C_2 axis. However, the two halves of each nonbridging ligand are nonequivalent. In the case of the Me_4-bpy, this gives rise to four (4) singlet resonances in the aromatic region and four (4) $-CH_3$ aliphatic resonances. The phen ligands exhibit AMX and A′M′X′ coupling systems, with the expected coupling constants:[4] $J_{2,3} = J_{8,9} \sim 5$ Hz, $J_{2,4} \sim J_{7,9} = 1.5$ Hz, and $J_{3,4} = J_{7,8} \sim 8$ Hz. An AB-type coupling pattern, due to second-order effects ($J_{5,6} \sim 9$ Hz), was observable only in the *rac* (ΔΔ/ΛΛ) diastereoisomer.

(26) Bosnich, B. *Inorg. Chem.* **1968**, *7*, 178.
(27) Bosnich, B. *Inorg. Chem.* **1968**, *7*, 2379
(28) McCaffery, A. J.; Mason, S. F.; Norman, B. J. *J. Chem. Soc. A* **1969**, 1428.
(29) Reitsma, D. A.; Keene, F. R. Unpublished work.
(30) Rutherford, T. J.; Reitsma, D. A.; Keene, F. R. *J. Chem. Soc., Dalton Trans.* 1994, 3659.

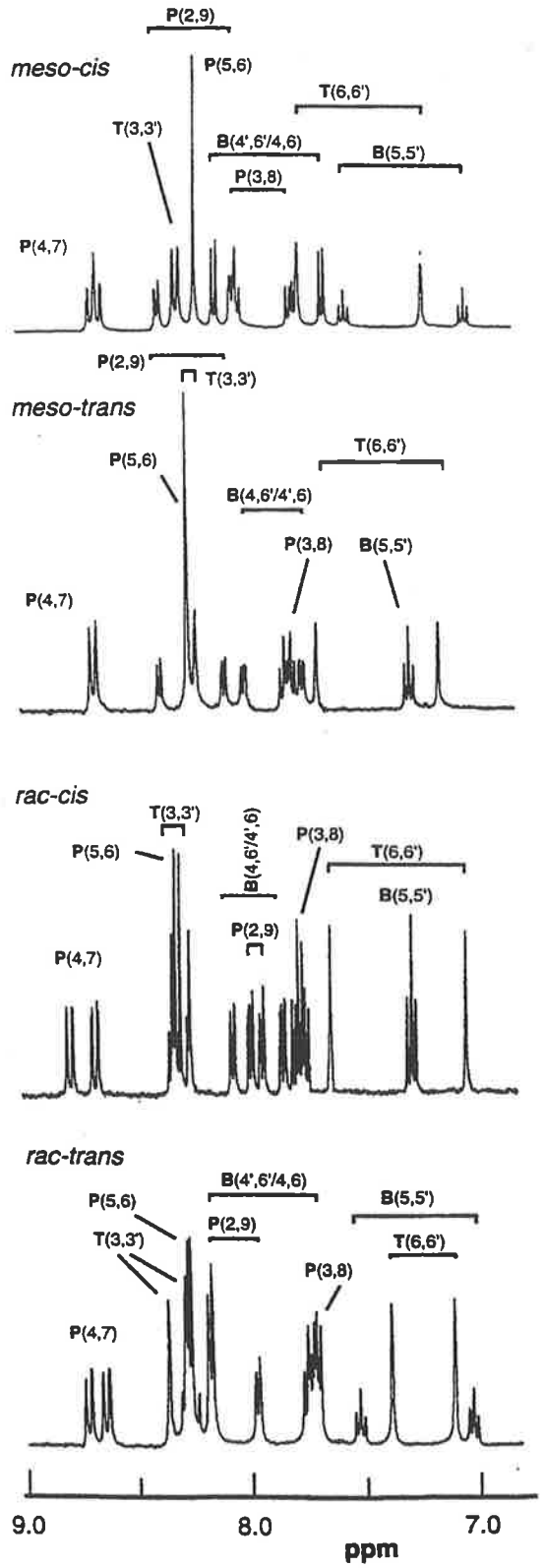

Figure 5. 300 MHz ^{1}H NMR spectra of [{Ru(phen)(Me$_4$bpy)}$_2$(μ-bpm)]$^{4+}$: (a) $\Delta\Delta$-*cis*; (b) $\Delta\Lambda$-*trans*; (c) $\Lambda\Lambda$-*cis*; (d) $\Lambda\Lambda$-*trans*.

The ^{1}H NMR spectra of the four stereoisomers in the aromatic region are given in Figure 5. For each of the diastereoisomeric forms, the assignment of its geometric isomers as *cis* or *trans* was achieved using purely symmetry arguments, which could be applied as the precise form of the diastereoisomer was known from the synthetic route using enantiomerically pure precursors. The assignment is explained below for each specific isomer.

In *meso*-[{Ru(phen)(Me$_4$bpy)}$_2$(μ-bpm)]$^{4+}$, the *trans* isomer (point group symmetry C_i) may be identified as the form that shows only one triplet (J = 5.7 Hz) since the center of symmetry renders the H5 and H5′ protons of the bpm bridge equivalent. The H4 and H6′ protons of the bpm bridge are also equivalent because of the inversion center, as are the H4′ and H6 protons. The resonances observed from these two sets of equivalent protons comprise two doublets of doublets arising from the $J_{4,5/4',5'}$ and the $J_{4,6/4',6'}$-type coupling (J = 5.7, 1.4 Hz; Figure 5b).

In the *meso-cis* form, the point group symmetry is lower (*viz.* C_s). The H5 and H5′ protons are no longer equivalent so that two triplets (J = 5.7 Hz) are observed. This nonequivalence of the two ends of the bpm ligand, along with the plane of symmetry which is orientated perpendicular to the plane of the bpm bridge incorporating the C5 and C5′ positions of the bpm and relates the H4/H6 and the H4′/H6′ protons, means that they each show only show a doublet (J = 4.3 Hz), arising from coupling to the H5 and H5′ protons, respectively. The comparison of the ^{1}H NMR spectra of the *meso-cis* and *meso-trans* forms are shown in Figure 5a,b, respectively.

For the *rac* diastereoisomer, both geometric isomers possess C_2 point group symmetry; however, in the *cis* isomers the C_2 axis is perpendicular to the plane of the bridging bpm ligand whereas in the *trans* isomer it is in the plane of the bpm ligand running through the long C5−C2−C2′−C5′ axis. In the former case, the axis renders the H5 and H5′ protons of the bridge equivalent, as well as the two pairs of protons H4/H6′ and H4′/H6. These equivalences are observed in the NMR spectrum as triplet (J = 5.7 Hz) and two doublets of doublets (J = 5.7, 1.4 Hz) resonances.

For the *trans* geometrical isomer, the C_2 axis renders the H4/H6 and the H4′/H6′ protons equivalent, giving rise to two doublets (J = 5.7 Hz). On the other hand, the H5 and H5′ protons are nonequivalent, resulting in a pair of triplets (J = 5.7 Hz). The comparison of the ^{1}H NMR spectra of the *rac-cis* and *rac-trans* forms are shown in Figure 5c,d, respectively.

Isomer Proportions. As the geometric isomers of each of the diastereoisomeric forms can be identified by ^{1}H NMR spectroscopy, the topic of stereospecificity in the synthesis may be revisited. The *cis*:*trans* ratios in the production of *meso*- and *rac*-[{Ru(phen)(Me$_4$bpy)}$_2$(μ-bpm)]$^{4+}$ are 1:2 and 1:1, respectively, assessed from NMR studies by spectral integration. A study of models shows little difference in the interactions of the methyl groups of the Me$_4$bpy ligands in the two geometric forms of the *rac* diastereoisomer. However, in the *meso* form, there appears significant interaction of these groups specifically in the *cis* geometrical isomer, consistent with the observed proportions.

Conclusions

The *cis* and *trans* geometric isomers of both the *meso* and *rac* diastereoisomeric forms of the ligand-bridged dinuclear species [{Ru(phen)(Me$_4$bpy)}$_2$(μ-bpm)]$^{4+}$ have been separated by cation exchange chromatography and characterized by NMR spectroscopy. This is the first example of the isolation of geometric isomers of this type.

The individual diastereoisomers of the target complex were also synthesized stereoselectively. In developing the appropriate precursors, we have also achieved the first chiral resolutions of

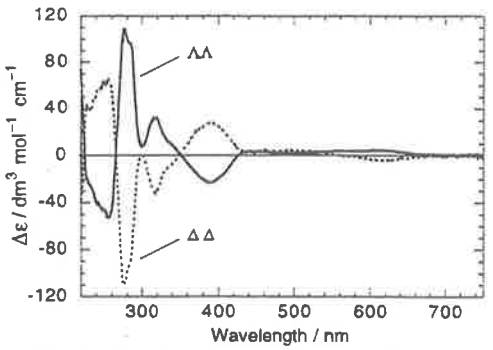

Fig. 7 Circular dichroism spectra of ΛΛ- (solid line) and ΔΔ-[{Ru(dmbpy)$_2$}$_2$(μ-bipym)]$^{4+}$ (dashed line)

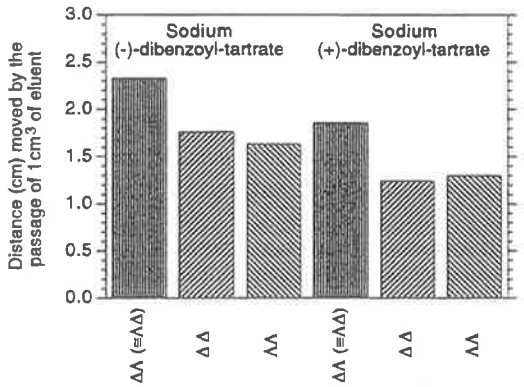

Fig. 8 Relative rate of travel of the three stereoisomers of [{Ru(dmbpy)$_2$}$_2$(μ-bipym)]$^{4+}$ down a 9 mm (inside diameter) column, eluted with aqueous 0.154 mol dm^{-3} sodium (+ or −)-dibenzoyltartrate solutions at 30 °C

the SP Sephadex C-25 support,[14] it can be assumed that the observed temperature dependence can be attributed to changes in the effective charges of the species travelling down the column. Tris(bipyridine)ruthenium(II)-type species associate with organic anions, and it is the differences in relative associations between the anion of the eluent and the various stereoisomers that lead to their separation by cation-exchange chromatography (the nature of these associations will be the subject of a subsequent publication).[31] From the temperature-dependence studies it may be concluded that the degree of association is higher at lower temperatures. This stronger association effectively reduces the charge on the cations, lowering the affinity with the cation-exchange resin so that the rate of travel down the column is faster at lower temperatures.

Chiral resolution of the racemic diastereoisomer with an achiral eluent

Previously, we have established that the ΔΔ and ΛΛ enantiomers of the complex [{Ru(dmbpy)$_2$}$_2$(μ-apy)]$^{4+}$ can be separated chromatographically using the chiral eluent sodium (−)-*O*,*O*′-di-4-toluoyl-L-tartrate.[22] However, during our studies on the [{Ru(dmbpy)$_2$}$_2$(μ-bipym)]$^{4+}$ system, the observation was made that there was considerable spreading of the slower-moving (*rac*) band on the column during the separation of the *meso* and *rac* diastereoisomers using sodium toluene-4-sulfonate as the eluent. To investigate whether chiral resolution could be achieved using this achiral salt, the slower-moving band from the diastereoisomer separation was reintroduced onto the top of the SP Sephadex C-25 column, and allowed to recycle several times down the length of the column (1 m). After it had travelled an effective column length (ECL) of *ca.* 2.5 m there was a clear separation of the two chiral forms of the *rac* diastereoisomer. These were collected and isolated as the hexafluorophosphate salts, and the resolution into the individual enantiomers confirmed by CD measurements (Fig. 7).

By comparison with the CD enantiomer assignment for stereoselectively synthesized ΔΔ- and ΛΛ-[{Ru(bpy)$_2$}$_2$(μ-bipym)]$^{4+}$ by Hua and von Zelewsky,[12] the first band off the column was assigned as the ΔΔ isomer, followed by the ΛΛ form. Importantly, we have achieved for the first time a separation of the two enantiomers using an achiral eluent on the SP Sephadex C-25 cation exchanger. The inference is clearly that the inherent structure of the dextran support itself must provide the chiral environment responsible for this process. The individual units of SP Sephadex are composed of propanesulfonate-functionalised cross-linked α-D-glucopyranoside, and there are five chiral centres in each subunit.

While coulombic forces dominate the cation-exchange chromatographic process, the charge densities or polarities of the cations[14] also exert an influence for species of the same charge. The use of a suitable counter anion in the eluent also has an effect on the second-sphere interactions between cation and anion.[14,32] Since isomers may differ in their relative interactions with the counter anion, the resultant slight variations in the effective charge and polarity of the species facilitate separation on the column. However, with the chiral resolution observed with an achiral eluent, the effective charge and polarity of the two associated enantiomers must be the same. Hence the separation must be a consequence of the support material itself, where the mechanism has elements of exclusion on the basis of shape.

The significance of this observation is that chiral eluents such as sodium (+)-*O*,*O*′-ditoluoyl-D-tartrate and sodium (−)-dibenzoyl-L-tartrate are not always necessary in the separation of simple enantiomeric pairs on the Sephadex support. It is however expected that the efficiency of such resolutions will be synergistically enhanced by the correct choice of chiral eluent.

Chiral resolution of the racemic diastereoisomer with a chiral eluent

Since the support material has such a significant effect on the two enantiomers, it can be assumed that the use of chiral counter anions in the eluent will either oppose or enhance the effect observed above. The rate of passage down the small pre-equilibrated column was therefore investigated to examine the effect of the eluents sodium (−)-dibenzoyl-L-tartrate and (+)-dibenzoyl-D-tartrate (0.154 mol dm^{-3}) on the rate of elution of the three individual stereoisomers down the column. The results are displayed in Fig. 8.

Sodium (−)-*O*,*O*′-dibenzoyl-L-tartrate behaved in a similar fashion to sodium toluene-4-sulfonate as an eluent, in that the *meso*-ΔΛ form moved the fastest, with the *rac*-ΔΔ next and the *rac*-ΛΛ slowest on the column. The chiral resolution of the *rac* form was however achieved in a much shorter distance, demonstrating a positive synergistic effect between the chiral eluent with the Sephadex support. On the other hand, with sodium (+)-*O*,*O*′-dibenzoyl-D-tartrate as eluent, the order of travel of the two enantiomers was reversed with the ΛΛ form travelling faster than the ΔΔ. Similar behaviour has also been observed using simple monomers such as [Ru(bpy)$_3$]$^{2+}$ and [Ru(phen)$_3$]$^{2+}$ and is currently undergoing intense study to try to rationalise this observation.[24]

von Zelewsky and co-workers[33] have shown by X-ray crystallography that there is a specific association between Λ-[Ru(bpy)$_2$(py)$_2$]$^{2+}$ and (−)-*O*,*O*′-dibenzoyl-L-tartrate, and between Δ-[Ru(bpy)$_2$(py)$_2$]$^{2+}$ and (+)-*O*,*O*′-dibenzoyl-D-tartrate. While in this case the possible π-stacking interactions between the aromatic benzoyl groups and the ligand pyridyl groups cause selective crystallisation, the same type of associations appear to dictate the order of travel down the column.

A comparison of the use of sodium (−)-*O*,*O*′-dibenzoyl-L-tartrate with sodium (+)-*O*,*O*′-dibenzoyl-D-tartrate as eluent indicates that there is much slower passage down the column for the latter electrolyte (1.25 times slower for the *meso* diastereoisomer). Additionally, the distance required to achieve chiral resolution between the enantiomeric pairs is larger with (+)-*O*,*O*′-dibenzoyl-D-tartrate. The implication is that the effect of the chirality of (+)-*O*,*O*′-dibenzoyl-D-tartrate opposes that of the Sephadex itself, slowing the rate of travel down the column and hindering the chiral resolution. Accordingly, care must be observed in the choice of chiral eluent to use this synergistic behaviour to enhance the separation.

Conclusion

In order to characterise simple ligand-bridged dinuclear polypyridyl species by standard techniques such as NMR spectroscopy the isolation of the individual diastereoisomers must first be achieved. Further, the isolation of stereochemically pure samples is likely to facilitate the growth of crystals appropriate for X-ray structural analysis. Such separations of diastereoisomers has been achieved using SP Sephadex C-25 cation exchanger and elution with sodium toluene-4-sulfonate. The variable-temperature experiments clearly indicate that there must be a significant degree of association of the eluent anion and cation which affects the interaction of the cation with the support. For the first time, chiral resolution of the racemic form has been achieved with the use of this achiral counter anion, rather than by using a chiral auxiliary. The respective bands from the column have been identified by a combination of a single-crystal X-ray determination and CD spectroscopy. Using the chiral auxiliaries (+)-*O*,*O*′-dibenzoyl-D-tartrate and (−)-*O*,*O*′-dibenzoyl-L-tartrate, it has become apparent that the choice of chirality of the counter anion becomes important, since it may either enhance or oppose the inherent chirality of the support material itself, and can prove critical in achieving a simple resolution of enantiomers.

Experimental

Instrumentation

The NMR spectra were recorded on a Varian Unity Inova-500 spectrometer using the solvent as the internal reference. CD spectra in acetonitrile solution using a Jobin Yvon spectrophotometer (λ_{max}/nm) and high-resolution mass spectra on a Bruker BioApex 47e ICR spectrometer with an electrospray source, using solutions *ca.* 2 μg cm^{-3} in methanol. Microanalyses were carried out on a Carlo Erba EA 1108 CHNS analyser. For the column chromatography studies, preparative columns C16/100 and C26/100 were from Pharmacia Biotech. The semiquantitative column K9 (Pharmacia Biotech) was fitted with an external water-jacket, temperature regulated with a Talabo F10 circulatory thermostatted water-bath. Column flow rates were regulated with a Gilson minipulse 2 peristaltic pump.

Materials

The compounds 4,4′-dimethyl-2,2′-bipyridine (Aldrich), 2,2′-bipyrimidine (Lancaster), 1,10-phenanthroline, 2,2′-bipyridine and sodium toluene-4-sulfonate (Aldrich) and ruthenium trichloride hydrate (Strem) were used as received without further purification. Aqueous sodium (−)-*O*,*O*′-dibenzoyl-L-tartrate and sodium (+)-*O*,*O*′-dibenzoyl-D-tartrate solutions were prepared by the addition of sodium hydroxide solution to the corresponding acids (Fluka), until a pH of 8–9 was obtained. SP Sephadex C-25 and Sephadex LH20 in anhydrous form were from Pharmacia Biotech, Amberlite IRA 400 from Aldrich. The precursors [RuL_2Cl_2] (L = dmbpy, phen or bpy) were prepared according to the literature method.[34] Laboratory-grade solvents were used unless otherwise specified.

Complex syntheses

[{Ru(dmbpy)$_2$}$_2$(μ-bipym)][PF$_6$]$_4$. 2,2′-Bipyrimidine (0.137 g, 0.86 mmol) and [Ru(dmbpy)$_2$Cl$_2$] (1.00 g, 1.73 mmol) in ethylene glycol (10 cm^3) were heated on 'medium heat' for 10 min in a microwave oven, fitted with an external condenser. The crude mixture was diluted with water (200 cm^3) and adsorbed on the top of a SP Sephadex C-25 column (dimensions 40 × 300 mm). On elution with 0.2 mol dm^{-3} NaCl solution the first red band was removed and discarded. The second green band was eluted with 0.5 mol dm^{-3} NaCl solution. The complex was precipitated with saturated KPF_6 solution, the solid collected by vacuum filtration and washed with water (5 × 50 cm^3). The dark green solid was dried *in vacuo*, yield 1.31 g (90%). A sample for elemental analysis was purified by passage through a short Sephadex LH20 column (eluent 50% methanol–acetone) (Found: C, 40.0; H, 3.5; N, 9.5. $C_{56}H_{54}F_{24}N_{12}P_4Ru_2$·2MeOH requires C, 40.0; H, 3.6; N, 9.6%). Further characterisation was made after diastereoisomeric isolation.

Diastereoisomeric separation

The diastereoisomeric mixture of [{Ru(dmbpy)$_2$}$_2$(μ-bipym)][PF$_6$]$_4$ (250 mg) were converted into the chloride salts by metathesis with LiCl in acetone solution. The solid was collected by filtration through Celite®, and extracted with water. The resulting dark green solution (200 cm^3) was introduced onto a SP Sephadex C-25 column (dimensions 26 × 1000 mm). Eluent flow was regulated by the use of a peristaltic pump. On elution with 0.25 mol dm^{-3} sodium toluene-4-sulfonate solution the initial fast-moving pale red and green bands were rejected, while the first (*meso*) and second (*rac*) major dark green fractions were collected and the complexes precipitated by the addition of saturated aqueous KPF_6 solution. The solids were extracted with dichloromethane, and the organic extracts dried with anhydrous Na_2SO_4. Following filtration, the solvent was evaporated and the residues dried *in vacuo*. Yields: *meso*, 80 mg, 32%; *rac*, 100 mg, 40%. These products were then converted into the chloride salt by passage of an aqueous solution down an Amberlite IRA 400 column for characterisation. *meso*: observed *m*/*z* 274.5663 (M^{4+}; most abundant isotope peak within cluster) ($C_{56}H_{54}N_{12}Ru_2$ requires 274.5675); ^{1}H NMR δ(D_2O) 8.28 (4 H, s, dmbpy H3a and H3b), 8.12 (2 H, d, *J* 5.5, bipym H6), 7.84 (2 H, d, *J* 6.0, dmbpy H6a), 7.49 (2 H, d, *J* 6.0, dmbpy H6b), 7.38 (2 H, d, *J* 6.0, dmbpy H5a), 7.37 (2 H, d, *J* 6.0, bipym H5), 7.19 (2 H, d, *J* 6.0 Hz, dmbpy H5b), 2.47 [6 H, s, dmbpy CH_3(4a)] and 2.43 [6 H, s, dmbpy CH_3(4b)]. *rac*: observed *m*/*z* 274.5663 (M^{4+}; most abundant isotope peak within cluster) ($C_{56}H_{54}N_{12}Ru_2$ requires 274.5675); ^{1}H NMR δ(D_2O) 8.35 (2 H, s, bpy H3a), 8.31 (2 H, s, dmbpy H3b), 8.12 (2 H, d, *J* 5.5, bipym H6), 7.51 (2 H, d, *J* 6.0, dmbpy H6a), 7.43 (2 H, d, *J* 6.0, dmbpy H6b), 7.36 (2 H, d, *J* 6.0, bipym H5), 7.20 (2 H, d, *J* 6.0, dmbpy H5a), 7.16 (2 H, d, *J* 6.0 Hz, dmbpy H5b), 2.53 [6 H, s, dmbpy CH_3(4a)] and 2.44 [6 H, s, dmbpy CH_3(4b)].

Resolution of the racemic form

Using a similar method to that described above, [{Ru(dmbpy)$_2$}$_2$(μ-bipym)]Cl$_4$ (*ca.* 50 mg) was introduced onto a column (dimensions 16 × 1000 mm). To increase the effective length of the column, once the Sephadex had equilibrated to the eluent a plunger was lowered onto the surface of the support and the system allowed to recycle. After the third passage down the column definite resolution had been achieved, and the two individual bands were collected and isolated as the hexafluorophosphate salts. Band 1, ΔΔ complex: CD λ_{max}/nm (CD_3CN) 256 (Δε/dm^3 mol^{-1} cm^{-1} +65.4), 278 (−110.8), 300 (0.4), 318 (−32.5), 392 (+28.2) and 623 (−4.3). Band 2, ΛΛ complex: CD λ_{max}/nm (CD_3CN) 256 (Δε/dm^3 mol^{-1} cm^{-1} −53.2), 278 (+109.1), 300 (7.1), 318 (+32.5), 392 (−22.6) and 607 (+4.6).

The complexes $[\{Ru(tmbpy)\}_2(\mu\text{-bipym})]^{4+}$, $[\{Ru(phen)_2\}_2(\mu\text{-bipym})][PF_6]_4$ and $[\{Ru(bpy)_2\}_2(\mu\text{-bipym})][PF_6]_4$ were prepared in an analogous fashion, and gave characterisations in accordance with the literature.[12]

Quantitative column techniques

A small Perspex column (dimensions 9 × 600 mm), fitted with an insulated water-jacket connected to a circulating thermostatted water-bath, was set to a constant temperature (30 °C for all measurements, unless otherwise stated). SP Sephadex C-25 was equilibrated in the eluent solution [aqueous 0.1–1.0 mol dm^{-3} sodium toluene-4-sulfonate for the variable-concentration data and 0.25 mol dm^{-3} for the temperature-dependent measurements; 0.154 mol dm^{-3} in the case of the investigations using sodium (+ or −)-*O*,*O*′-dibenzoyl-(D or L)-tartrate solutions], and allowed to settle in the column at a constant eluent flow rate of approximately 0.5 cm^3 min^{-1}. Once equilibration was obtained, the head of salt solution was reduced on the top of the support, and the compound to be separated was carefully introduced, dissolved in the eluent (0.25 mg of each isomer in 250 μl), so as not to disturb the Sephadex surface. With the sodium (+ or −)-*O*,*O*′-dibenzoyl-(D or L)-tartrate eluents, each isomer/enantiomer was added separately, since separation down the column was not always possible. The rate of flow through the column was carefully monitored as was the rate of travel of the individual bands. To ensure standardised results, the data are given in the volume of solvent required to move the individual bands by unit length (cm^3 cm^{-1}).

Crystallography

A sample of the first major fraction (*meso*) of $[\{Ru(dmbpy)_2\}_2(\mu\text{-bipym})]^{4+}$ was repurified by chromatography, using Sephadex LH20 as support with methanol as eluent to remove any excess of inorganic impurities. Following removal of the solvent, and redissolution of the residue in water, slow evaporation of the solution realised oily crystals which were suitable for X-ray determination.

A unique room-temperature diffractometer data set (Enraf-Nonius CAD-4 diffractometer; $T \approx 295$ K; monochromatic Mo-Kα radiation, $\lambda = 0.7107_3$ Å; 2θ–θ scan mode) was measured, yielding N_o independent reflections, N_o with $I > 3\sigma(I)$ being considered 'observed' and used in the large-block least-squares refinements. The crystal structure determination is of rather low precision as crystals of higher quality were elusive, and consequently the data were broad and weak from a poorly diffracting, decomposing specimen. Anisotropic thermal parameters were refined for Ru(1), Cl(1), Cl(2) and O(1) to O(5) only, due to limited data, and all other non-H atoms were refined isotropically. Hydrogen atoms were placed in calculated positions and not refined. Conventional residuals R, R' on $|F|$ are quoted, statistical weights derivative of $\sigma^2(I) = \sigma^2(I_{diff}) + 0.0004\sigma^4(I_{diff})$ being used. Neutral atom complex scattering factors were employed, and computation was by the XTAL 3.4 program system, implemented by S. R. Hall.[35] Specific details are as follows: $[\{Ru(dmbpy)_2\}_2(\mu\text{-bipym})]Cl_4 \cdot 10H_2O$, $C_{56}H_{74}Cl_4N_{12}O_{10}Ru_2$, M 1419.24, monoclinic, space group $P2_1/n$ (no. 14), $a = 10.87(1)$, $b = 22.67(1)$, $c = 13.88(1)$ Å, $\beta = 111.37(9)°$, $U = 3187$ Å^3, D_c ($Z = 2$) 1.48 g cm^{-3}, $F(000)$ 1460, $2\theta_{max}$ 45°, N 4473, N_o 1446, $R = 0.107$, $R' = 0.106$.

CCDC reference number 186/767.

Acknowledgements

This work was supported by the Australian Research Council. We are grateful to Mr. Brian Foster for performing the microanalyses, and Dr. Ian Atkinson (James Cook University) and Mr. Rick Willis (Australian Institute of Marine Science) for undertaking the electrospray mass spectral measurements. Andreas Beyeler and Bruni Kolp (University of Fribourg, Switzerland) are thanked for their help with the acquisition of the CD spectra.

References

1 V. Balzani, A. Juris, M. Venturi, S. Campagna and S. Serroni, *Chem. Rev.*, 1996, **96**, 759 and ref. therein.
2 V. Balzani and F. Scandola, *Supramolecular Photochemistry*, Ellis Horwood, Chichester, 1991.
3 J.-P. Sauvage, J.-P. Collin, J. C. Chambron, S. Guillerez, C. Coudret, V. Balzani, F. Barigelletti, L. De Cola and L. Flamigni, *Chem. Rev.*, 1994, **94**, 993.
4 J.-M. Lehn, *Angew. Chem., Int. Ed. Engl.*, 1990, **29**, 1304.
5 A. M. Pyle and J. K. Barton, *Prog. Inorg. Chem.*, 1990, **38**, 413.
6 A. Kirsch-De Mesmaeker, J. P. Lecomte and J. M. Kelly, *Top. Curr. Chem.*, 1996, **177**, 25.
7 E. D. A. Stemp, M. R. Arkin and J. K. Barton, *J. Am. Chem. Soc.*, 1997, 2921.
8 P. Lincoln and B. Nordén, *Chem. Commun.*, 1996, 2145.
9 P. Lincoln, A. Broo and B. Nordén, *J. Am. Chem. Soc.*, 1996, **118**, 2644.
10 J. K. Barton, A. Danishefsky and J. Goldberg, *J. Am. Chem. Soc.*, 1984, **106**, 2172.
11 C. Hiort, P. Lincoln and B. Nordén, *J. Am. Chem. Soc.*, 1993, **115**, 3448.
12 X. Hua and A. von Zelewsky, *Inorg. Chem.*, 1995, **34**, 5791.
13 T. J. Rutherford, M. G. Quagliotto and F. R. Keene, *Inorg. Chem.*, 1995, **34**, 3857.
14 G. H. Searle, *Aust. J. Chem.*, 1977, **30**, 2625.
15 H. Yoneda, *J. Chromatogr.*, 1984, **313**, 59.
16 Y. Yoshikawa and K. Yamasaki, *Coord. Chem. Rev.*, 1979, **28**, 205.
17 B. T. Patterson and F. R. Keene, 1997, *Inorg. Chem.*, in the press.
18 T. J. Rutherford and F. R. Keene, *Inorg. Chem.*, 1997, **36**, 3580.
19 T. J. Rutherford, O. Van Gijte, A. Kirsch-De Mesmaeker and F. R. Keene, *Inorg. Chem.*, 1997, **36**, 4465.
20 T. J. Rutherford, D. A. Reitsma and F. R. Keene, *J. Chem. Soc., Dalton Trans.*, 1994, 3659.
21 D. A. Reitsma and F. R. Keene, *J. Chem. Soc., Dalton Trans.*, 1993, 2859.
22 L. S. Kelso, D. A. Reitsma and F. R. Keene, *Inorg. Chem.*, 1996, **35**, 5144.
23 F. R. Keene, *Coord. Chem. Rev.*, 1997, in the press.
24 T. J. Rutherford and F. R. Keene, unpublished work.
25 D. A. Reitsma and F. R. Keene, unpublished work.
26 D. A. Bardwell, J. C. Jeffery, L. Joulié and M. D. Ward, *J. Chem. Soc., Dalton Trans.*, 1993, 2255.
27 D. A. Bardwell, L. Horsburgh, J. C. Jeffery, L. F. Joulié, M. D. Ward, I. Webster and L. J. Yellowlees, *J. Chem. Soc., Dalton Trans.*, 1996, 2527.
28 R. Hage, J. G. Haasnoot, H. A. Nieuwenhuis, J. Reedijk, D. J. A. De Ridder and J. G. Vos, *J. Am. Chem. Soc.*, 1990, **112**, 9245.
29 V. Balzani, D. A. Bardwell, F. Barigelletti, F. L. Cleary, M. Guardigli, J. C. Jeffery, T. Sovrani and M. D. Ward, *J. Chem. Soc., Dalton Trans.*, 1995, 3601.
30 F. Helfferich, *Ion Exchange*, McGraw-Hill, New York, 1962.
31 N. C. Fletcher, P. C. Junk and F. R. Keene, unpublished work.
32 F. R. Keene and G. H. Searle, *Inorg. Chem.*, 1974, **13**, 2173.
33 B. Kolp, H. Viebrock, A. von Zelewsky and D. Abeln, personal communication.
34 P. A. Lay, A. M. Sargeson and H. Taube, *Inorg. Synth.*, 1986, **24**, 291.
35 S. R. Hall, G. S. D. King and J. M. Stewart, *Xtal3.4 User's Manual*, University of Western Australia, Lamb, Perth, 1995.

Received 13*th August* 1997; *Paper* 7/05947G

Inorg. Chem. 1998, *37*, 645−650

Isolation of Geometric Isomers within Diastereoisomers of Dinuclear Ligand-Bridged Complexes of Ruthenium(II)

Bradley T. Patterson and F. Richard Keene*

School of Biomedical and Molecular Sciences, James Cook University of North Queensland, Townsville, Queensland 4811, Australia

Received August 22, 1997

The individual diastereoisomeric forms [*meso* ($\Delta\Lambda$) and *rac* ($\Delta\Delta$ and $\Lambda\Lambda$)] of the ligand-bridged dinuclear species $[\{Ru(phen)(Me_4bpy)\}_2(\mu\text{-bpm})]^{4+}$ [phen = 1,10-phenanthroline; Me_4bpy = 4,4′,5,5′-tetramethyl-2,2′-bipyridine; bpm = 2,2′-bipyrimidine] have been synthesized using chiral forms of the precursors $[Ru(phen)(Me_4bpy)(bpm)]^{2+}$ and $[Ru(phen)(Me_4bpy)(py)_2]^{2+}$. The *cis* and *trans* geometric isomers of both diastereoisomeric forms have been separated by cation exchange chromatography and characterized by NMR spectroscopy. We also report the first chiral resolutions of a heteroleptic tris(bidentate)ruthenium(II) complex, $[Ru(phen)(Me_4bpy)(bpm)]^{2+}$, and a heteroleptic bis(bidentate)bis(pyridine)ruthenium(II) complex, $[Ru(phen)(Me_4bpy)(py)_2]^{2+}$, in both cases using cation exchange chromatography.

Introduction

Ligand-bridged polymetallic molecular assemblies have potential application to photochemical devices,[1] and tris(bidentate)-ruthenium(II) centers involving polypyridyl ligands have frequently formed the basis of such assemblies by virtue of their favorable redox, spectral, and photophysical characteristics.[2] However, these moieties also introduce stereoisomerism, and there has been considerable interest by ourselves and others regarding stereochemical control in oligomeric assemblies.[3−18] Further, our initial studies have revealed that intramolecular electron and energy transfer processes depend on the spatial relationship of the components within such species.[16−20]

Dinuclear ligand-bridged complexes represent the simplest example of the genre, and stereochemical studies thus far have generally sought the stereoselective synthesis of individual diastereoisomeric or enantiomeric forms[3,4,6,7,9−14,16] or the separation of these individual stereoisomeric forms from a mixture.[5,6,16,18] However, in all such studies the individual metal centers have possessed two identical terminal (i.e. nonbridging) ligands; i.e., $[\{Ru(pp)_2\}_2(\mu\text{-BL})]^{n+}$ or alternatively $[\{Ru(pp)_2\}\{Ru(pp')_2\}(\mu\text{-BL})]^{n+}$ {pp and pp′ are symmetrical bidentate ligands such as 2,2′-bipyridine (bpy) or 1,10-phenanthroline (phen) (Chart 1); BL is a bis-bidentate bridging ligand}. In the first case, only *meso* [$\Delta\Lambda$ (=$\Lambda\Delta$)] and *racemic* ($\Delta\Delta/\Lambda\Lambda$) diastereoisomeric forms exist (with the latter being an enantiomeric pair; Figure 1), while in the second case there are analogous diastereoisomeric possibilities but with the $\Delta\Lambda$ and $\Lambda\Delta$ forms becoming enantiomeric.[5]

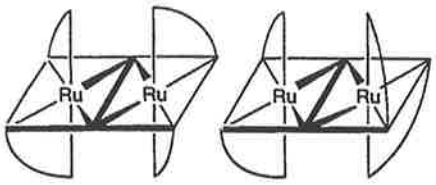

Figure 1. Schematic representation of the diastereoisomeric forms of the ligand-bridged dinuclear species $[\{Ru(pp)_2\}_2(\mu\text{-BL})]^{n+}$.

Chart 1

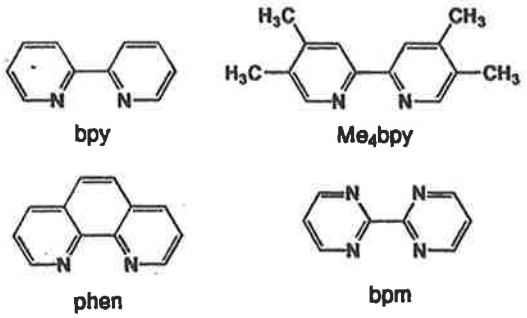

(1) Balzani, V.; Scandola, F. *Supramolecular Photochemistry*; Ellis Horwood: Chichester, U.K., 1991.
(2) Juris, A.; Barigelletti, S.; Campagna, S.; Balzani, V.; Belser, P.; von Zelewsky, A. *Coord. Chem. Rev.* **1988**, *84*, 85.
(3) Hua, X.; von Zelewsky, A. *Inorg. Chem.* **1991**, *30*, 3796.
(4) Hua, X.; von Zelewsky, A. *Inorg. Chem.* **1995**, *34*, 5791.
(5) Reitsma, D. A.; Keene, F. R. *J. Chem. Soc., Dalton Trans.* **1993**, 2859.
(6) Rutherford, T. J.; Quagliotto, M. G.; Keene, F. R. *Inorg. Chem.* **1995**, *34*, 3857.
(7) Lincoln, P.; Nordén, B. *Chem. Commun.* **1996**, 2145.
(8) Wärnmark, K.; Thomas, J. A.; Heyke, O.; Lehn, J.-M. *Chem. Commun.* **1996**, 701.
(9) Tzalis, D.; Tor, Y. *J. Am. Chem. Soc.* **1997**, *119*, 852.
(10) MacDonnell, F. M.; Bodige, S. *Inorg. Chem.* **1996**, *35*, 5758.
(11) Mürner, H.; Belser, P.; von Zelewsky, A. *J. Am. Chem. Soc.* **1996**, *118*, 7989.
(12) Mürner, H.; von Zelewsky, A.; Stoeckli-Evans, H. *Inorg. Chem.* **1996**, *35*, 3931.
(13) Fletcher, N. C.; Keene, F. R.; Ziegler, M.; Stoeckli-Evans, H.; Viebrock, H.; von Zelewsky, A. *Helv. Chim. Acta* **1996**, *79*, 1192.
(14) Fletcher, N. C.; Keene, F. R.; Viebrock, H.; von Zelewsky, A. *Inorg. Chem.* **1997**, *36*, 1113.
(15) Rutherford, T. J.; Keene, F. R. *Inorg. Chem.* **1997**, *36*, 3580.
(16) Rutherford, T. J.; Van Gijte, O.; Kirsch-De Mesmaeker, A.; Keene, F. R. *Inorg. Chem.* **1997**, *36*, 4465.
(17) Rutherford, T. J.; Keene, F. R. *Inorg. Chem.* **1997**, *36*, 2872.
(18) Kelso, L. S.; Reitsma, D. A.; Keene, F. R. *Inorg. Chem.* **1996**, *35*, 5144.

S0020-1669(97)01080-X CCC: $15.00
Published on Web 02/03/1998

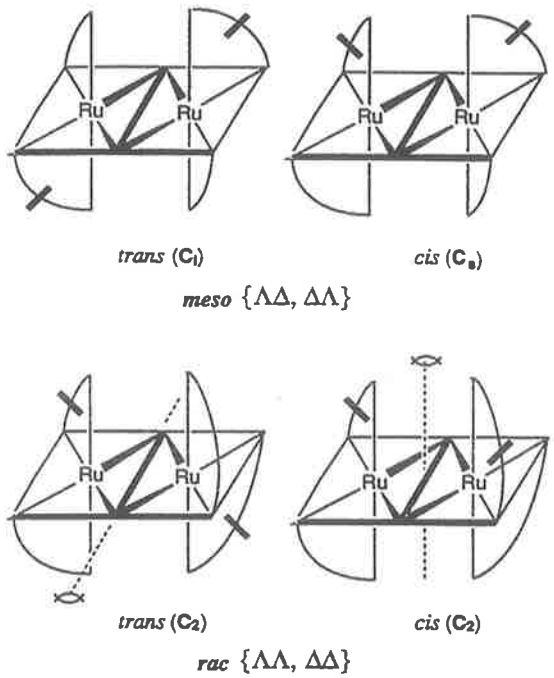

Figure 2. Schematic representation of the geometric isomers of the *meso*- and *rac*-$[\{Ru(pp)_2\}_2(\mu\text{-BL})]^{n+}$. For the *rac* forms, the C_2 axes are shown.

Clearly, the complexity in such dinuclear species may rapidly increase if the two terminal ligands on each center are not identical and/or the bridging ligand is not symmetrical. However, investigation of such systems has not been possible as the synthetic methodologies for such species have not been available. Recently reported synthetic schemes for tris(heteroleptic)ruthenium(II) centers via dicarbonyl precursors of the type $[Ru(pp)(pp')(CO)_2]^{2+}$ [21] allow extensive variation of the ligand environment, and together with the development of appropriate stereochemical techniques,[20] they provide the means to investigate these more complicated systems.

As a model for these studies, we chose the dinuclear complex $[\{Ru(phen)(Me_4bpy)\}_2(\mu\text{-bpm})]^{4+}$, in which the two terminal ligands (phen = 1,10-phenanthroline and Me_4bpy = 4,4′,5,5′-tetramethyl-2,2′-bipyridine) and the bridging ligand (bpm = 2,2′-bipyrimidine) are symmetrical. In such a case, there are again two possible diastereoisomeric forms (*meso* and *rac*), but each diastereoisomer may also possess two geometric forms (called *cis* and *trans*) in which the equivalent ligands on each metal center are disposed either on the same or on opposite sides of the plane of the bridge, respectively (Figure 2).

We report here the isolation and characterization (using NMR techniques) of all possible stereoisomeric forms of this complex by a combination of stereoselective syntheses and chromatographic separation methods.

Experimental Section

Materials. 1,10-Phenanthroline (phen; Aldrich), 2,2′-bipyrimidine (bpm; Lancaster), (1*R*,2*R*)-(−)-1,2-diaminocyclohexane (*R*,*R*′-dach; Aldrich), potassium hexafluorophosphate (Aldrich), sodium toluene-4-sulfonate (Aldrich), ethylene glycol (Aldrich), 2-methoxyethanol (Fluka), and acetonitrile (Aldrich, 99.8%) were used as received. Trimethylamine *N*-oxide (TMNO) was obtained by vacuum sublimation at 120 °C of the dihydrate (Fluka). Aqueous solutions of sodium (−)-*O*,*O*′-dibenzoyl-L-tartrate and sodium (−)-*O*,*O*′-di-4-toluoyl-L-tartrate were obtained by neutralization of the corresponding acids (Fluka) using sodium hydroxide. Pyridine (Ajax) and 3,4-lutidine (BDH) were dried (KOH) and distilled before use; all other solvents were of laboratory grade.

Measurements. ^1H and COSY experiments were performed on a Bruker Aspect 300 MHz NMR spectrometer (CD_3CN solutions). ORD (optical rotatory dispersion) curves were recorded using a Perkin-Elmer 141 polarimeter in a 1 dm cell. Specific rotation at λ: $[\alpha]_\lambda = 100\alpha/cl$, where α = absolute rotation (deg), c = concentration in g/100 cm^3, and l = cell path length (in dm). CD (circular dichroism) spectra were recorded in acetonitrile solution at concentrations of $\sim(1-3) \times 10^{-5}$ M at the University of Wollongong using a Jobin Yvon Dichrograph 6 instrument. CD spectra are presented as $\Delta\epsilon$ vs λ (nm). High-resolution mass spectra were obtained on a Brucker BioApex 47e ICR mass spectrometer with an electrospray source, using a ca. 2 μg/mL solution in methanol.

Elemental microanalyses were performed within the Department of Chemistry and Chemical Engineering at James Cook University of North Queensland.

Syntheses. The complexes $[Ru(phen)(CO)_2Cl_2]$, $[Ru(phen)(CF_3SO_3)_2(CO)_2]$ and $[Ru(phen)(Me_4bpy)(CO)_2](PF_6)_2$ were prepared using literature methods.[21]

4,4′,5,5′-Tetramethyl-2,2′-bipyridine (Me_4bpy) was synthesized by an adaption of a literature procedure.[22,23] Freshly distilled 3,4-lutidine (40 mL, 0.356 mol) was stirred with Pd/C (10%; 4 g) and the mixture refluxed for 13 days. The resulting solid was extracted (Soxhlet) with dichloromethane and decolorized with activated carbon (3 g) in refluxing dichloromethane. The solution was filtered through Celite, which was washed with several portions of hot toluene. The filtrate was evaporated to dryness, and the yellow residue was recrystallized from toluene to give a white crystalline product (22.5 g; 60%). ^1H NMR ($CDCl_3$): δ 2.28 (s), 2.33 (s), 8.11 (s), 8.36 (s).

$[Ru(phen)(Me_4bpy)(bpm)](PF_6)_2$. $[Ru(phen)(Me_4bpy)(CO)_2](PF_6)_2$ (30 mg; 0.0357 mmol) and 2,2′-bipyrimidine (22.6 mg; 0.143 mmol) were dissolved in 2-methoxyethanol (10 mL) and the solution deaerated with N_2 for 30 min. TMNO (27 mg; 0.36 mmol) was added, causing a rapid change from colorless to orange. The solution was refluxed for 3 h under subdued light and cooled, and the product was precipitated by the addition of a saturated aqueous solution of KPF_6 and collected. Further purification was achieved by cation exchange chromatography (SP Sephadex C-25; eluent 0.2 M NaCl). The major orange band was collected and the complex precipitated using KPF_6: it was reprecipitated twice by the addition of KPF_6 to an acetone/water solution of the complex, collected, washed with cold water (2 × 5 mL) and diethyl ether (2 × 10 mL), and dried in vacuo. Yield: 21 mg; 61%. Anal. Calcd for $RuC_{34}H_{30}F_{12}N_8P_2 \cdot C_3H_6O \cdot 2H_2O$: C, 43.4; H, 4.20; N, 10.7. Found: C, 43.5; H, 3.80; N, 10.5.

Chiral Resolution of $[Ru(phen)(Me_4bpy)(bpm)]^{2+}$. $[Ru(phen)(Me_4bpy)(bpm)](PF_6)_2$ was resolved into its Δ and Λ enantiomeric forms using cation exchange chromatography (SP Sephadex C-25; eluent 0.075 M sodium (−)-*O*,*O*′-dibenzoyl-L-tartrate; effective column length (ECL) of 1.5 m). The two bands were collected, and the complexes were precipitated as their PF_6^- salts and purified as described above: band 1 (Δ), $\alpha_{589} = -3550°$; band 2 (Λ), $\alpha_{589} = +3680°$.

$[Ru(phen)(Me_4bpy)(py)_2](PF_6)_2$. $[Ru(phen)(Me_4bpy)(CO)_2](PF_6)_2$ (166 mg; 0.198 mmol) and pyridine (3 mL; excess) were dissolved in 2-methoxyethanol (30 mL), and the solution was deaerated with N_2 for 30 min. TMNO (55 mg; 0.73 mmol) was added causing a change from almost colorless to orange within 30 min. The solution was refluxed in subdued light under a nitrogen atmosphere for 3 h before cooling and precipitation with a saturated aqueous KPF_6 solution. The

(19) Treadway, J. A.; Chen, P.; Rutherford, T. J.; Keene, F. R.; Meyer, T. J. *J. Phys. Chem. A* **1997**, *101*, 6824.
(20) Keene, F. R. *Coord. Chem. Rev.* **1997**, in press.
(21) Anderson, P. A.; Deacon, G. B.; Haarmann, K. H.; Keene, F. R.; Meyer, T. J.; Reitsma, D. A.; Skelton, B. W.; Strouse, G. F.; Thomas, N. C.; Treadway, J. A.; White, A. H. *Inorg. Chem.* **1995**, *34*, 6145.
(22) Sasse, W. H. F.; Whittle, C. P. *J. Chem. Soc.* **1961**, 1347.
(23) Della Ciana, L.; Dressick, W. J.; Sandrini, D.; Maestri, M.; Ciano, M. *Inorg. Chem.* **1990**, *29*, 2792.

precipitate was purified using cation exchange chromatography (SP Sephadex C-25; eluent 0.2 M NaCl) and the product collected as described above. Yield: 130 mg; 70%. Anal. Calcd for $RuC_{36}H_{34}F_{12}N_6P_2$: C, 45.9; H, 3.61; N, 8.9. Found: C, 45.8; H, 3.59; N, 8.8.

Chiral Resolution of $[Ru(phen)(Me_4bpy)(py)_2]^{2+}$. $[Ru(phen)(Me_4bpy)(py)_2](PF_6)_2$ (130 mg) was converted to the chloride salt by anion exchange chromatography and applied to a column of SP Sephadex C-25 cation exchanger; the two enantiomers were separated using 0.075 M sodium (−)-*O*,*O*′-di-4-toluoyl-L-tartrate solution as eluent (ECL ~ 2 m). Each band was collected, and the complexes were precipitated as their PF_6^- salts and purified (3×) as described above. Approximately 30 mg of each enantiomer was obtained: band 1 (Δ), $[\alpha]_{589} = -940°$; band 2 (Λ), $[\alpha]_{589} = +1000°$.

$[Ru(phen)(Me_4bpy)(R,R'\text{-dach})](PF_6)_2$. The following reactions were carried out as a test for chiral purity of Δ- and Λ-$[Ru(phen)(Me_4bpy)(py)_2]^{2-}$, based on a method detailed previously.[4] In a typical experiment, $[Ru(phen)(Me_4bpy)(py)_2](PF_6)$ (13.5 mg; 0.0143 mmol) and (1*R*,2*R*)-(−)-1,2-diaminocyclohexane (*R*,*R*′-dach; 5 mg; 0.044 mmol) were dissolved in 50% aqueous ethylene glycol (2 mL), and the mixture was heated at 120 °C for 5 h under an inert atmosphere (N_2). The solution was cooled and the product precipitated using a saturated aqueous solution of KPF_6. The precipitate was collected and washed with copious amounts of diethyl ether and air-dried. Yield: 11.6 mg; 89%.

***meso*-$[\{Ru(phen)(Me_4bpy)\}_2(\mu\text{-bpm})](PF_6)_4$.** Δ-$[Ru(phen)(Me_4bpy)(bpm)](PF_6)_2$ (15.6 mg; 0.0166 mmol) and Λ-$[Ru(phen)(Me_4bpy)(py)_2](PF_6)_2$ (19.4 mg; 0.0206 mmol) were dissolved in ethylene glycol (2 mL), and the solution was deaerated with N_2 and heated for 5 h at 100−110 °C. Upon cooling, water (3 mL) and saturated KPF_6 solution (2 mL) were added and the green precipitate was collected. Purification was achieved by cation exchange chromatography (SP Sephadex C-25; eluent 0.4 M NaCl). The green band was collected, and the complex was precipitated as the PF_6^- salt and purified as described above. Yield: 22.2 mg; 78%. As is the case in many dinuclear species of this type, microanalyses indicated the inclusion of acetone and water molecules in the crystals, rendering the data of dubious use in characterization. However, associated NMR and mass spectral data provided unambiguous assignment. Mass spectrum: observed *m*/*z* 1580.1702 (M^+: most abundant isotope peak within cluster); $[C_{60}H_{54}N_{12}Ru_2](PF_6)_3^-$ requires *m*/*z* 1580.1632.

Separation of Geometric Isomers of *meso*-$[\{Ru(phen)(Me_4bpy)\}_2(\mu\text{-bpm})]^{4+}$. *meso*-$[\{Ru(phen)(Me_4bpy)\}_2(\mu\text{-bpm})](PF_6)_4$ (40 mg) was converted to the chloride salt by anion exchange chromatography and the solution sorbed on to SP Sephadex C-25 cation exchanger. The complex was eluted using 0.25 M sodium toluene-4-sulfonate as eluent, and after continual recycling two bands were collected (ECL ~ 12 m). Each band was collected, and the complexes were precipitated as the PF_6^- salts and purified (3×) as described above.

ΔΔ-$[\{Ru(phen)(Me_4bpy)\}_2(\mu\text{-bpm})](PF_6)_4$. Λ-$[Ru(phen)(Me_4bpy)(bpm)](PF_6)_2$ (18 mg; 0.0191 mmol) and Λ-$[Ru(phen)(Me_4bpy)(py)_2](PF_6)_2$ (22.4 mg; 0.023 mmol) were dissolved in ethylene glycol (2 mL), and the solution was deaerated with N_2 and heated for 5 h at 100−110 °C. Upon cooling, water (3 mL) and saturated KPF_6 solution (2 mL) were added and the precipitate was collected. The green-brown solid was purified by cation exchange chromatography (SP Sephadex C-25; eluent 0.4 M NaCl). The resulting green band was collected, and the complex was precipitated as the PF_6^- salt and purified (3×) as described above. Yield: 27.2 mg; 83%.

Separation of Geometric Isomers of ΔΔ-$[\{Ru(phen)(Me_4bpy)\}_2(\mu\text{-bpm})]^{4+}$. ΔΔ-$[\{Ru(phen)(Me_4bpy)\}_2(\mu\text{-bpm})](PF_6)_4$ (60 mg) was converted to the chloride salt by anion exhange chromatography, sorbed onto SP Sephadex C-25 cation exchanger, and eluted using 0.25 M sodium toluene-4-sulfonate solution. On continual recycling of the samples, (ECL ~ 20 m), two bands were collected, and the respective complexes precipitated as the PF_6^- salts and purified (3×) as described above.

Results and Discussion

Synthetic and Stereochemical Aspects. In developing a target dinuclear species of the type $[\{Ru(pp)(pp')\}_2(\mu\text{-BL})]^{4+}$, we selected the system $[\{Ru(phen)(Me_4bpy)\}_2(\mu\text{-bpm})]^{4+}$. The particular identity of the ligands was chosen for several reasons: the ^1H NMR spectrum of the Me_4bpy ligand comprises only singlets in the aromatic region, simplifying the spectral interpretation of its complexes; from earlier studies,[5,24] we have observed that the presence of phen and methyl-substituted "bpy"-type ligands facilitates chromatographic separation of the stereoisomers. Finally, bpm is a rigid symmetrical bridging ligand.

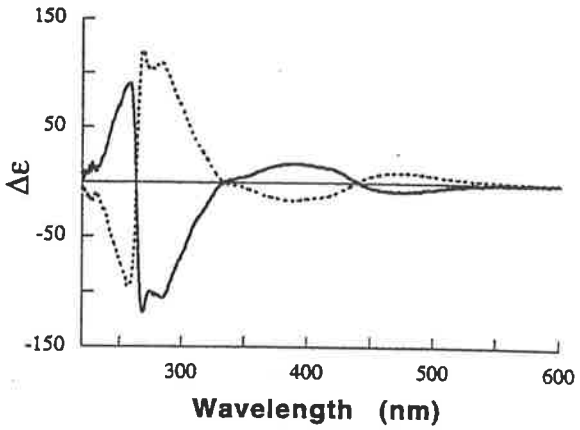

Figure 3. CD of $[Ru(phen)(Me_4bpy)(bpm)]^{2+}$ (CH_3CN solution): Δ (—); Λ (- - -).

Because of the potential isomeric complexity in the system, we directed our initial attention to the synthesis of the individual enantiomers of the two diastereoisomeric forms [i.e. ΔΔ and ΛΛ, ΔΛ (≡ΛΔ)], so that subsequent separation of the two geometric isomers (*cis* and *trans*) of each form was unencumbered by any uncertainty of the chiral identity. Such a stereoselective synthesis requires two chiral precursors: viz. the individual enantiomeric forms of the tris(heteroleptic) species $[Ru(phen)(Me_4bpy)(bpm)]^{2+}$, as well as the enantiomers of a $[Ru(phen)(Me_4bpy)X_2]^{2+}$ species (X = CO or py). In both instances, this posed an interesting challenge as there are no reported resolutions of either type of complex.

We have recently reported a general synthetic methodology for hetereoleptic tris(bidentate)ruthenium(II) complexes,[21,25] and the target complex $[Ru(phen)(Me_4bpy)(bpm)]^{2+}$ was conveniently obtained by this technique. We have also recently reported the routine resolution of mononuclear tris(bidentate)-ruthenium(II) species by cation exchange chromatographic methods,[20] and the complex was readily resolved using these techniques. The CD spectra of the two enantiomers are given in Figure 3. This is the first reported example of the chiral resolution of a hetereoleptic tris(bidentate)ruthenium(II) complex.

The second of the precursors was chosen as $[Ru(phen)(Me_4bpy)(py)_2]^{2+}$, rather than the dicarbonyl analogue. While both $[Ru(pp)_2(py)_2]^{2+}$ [3,4] and $[Ru(pp)_2(CO)_2]^{2+}$ [6] species have been shown to undergo the addition of a third bidentate ligand with retention of absolute configuration, the former complex reacts in higher yield, and our own studies have led to consistent resolution of bis(pyridine) complexes of this type into enantiomers by chromatographic methods. In the present instance, $[Ru(phen)(Me_4bpy)(py)_2]^{2+}$ was synthesized by decarbonylation

(24) Fletcher, N. C.; Junk, P. C.; Keene, F. R. *J. Chem. Soc., Dalton Trans.* **1998**, 133.
(25) Strouse, G. F.; Anderson, P. A.; Schoonover, J. R.; Meyer, T. J.; Keene, F. R. *Inorg. Chem.* **1992**, *31*, 3004.

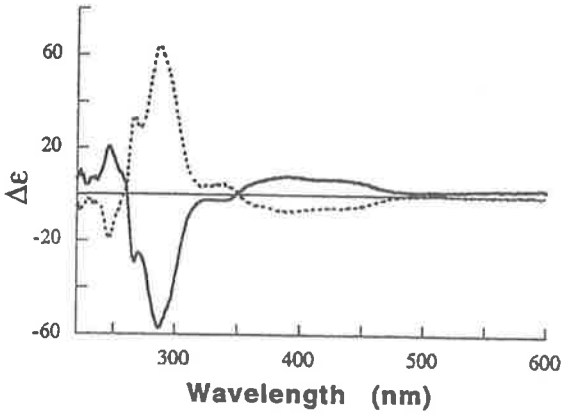

Figure 4. CD of $[Ru(phen)(Me_4bpy)(py)_2]^{2+}$ (CH_3CN solution): Δ (—); Λ (- - -).

of $[Ru(phen)(Me_4bpy)(CO)_2]^{2+}$ in the presence of pyridine, and it was chromatographically resolved. The CD spectra of the two enantiomers are shown in Figure 4. While complexes of the type $[Ru(pp)_2(py)_2]^{2+}$ (pp = a bidentate ligand) have been resolved into enantiomeric forms by diastereoisomeric formation involving chiral anions,[3,4] this is the first reported example of the resolution of a complex $[Ru(pp)(pp')(py)_2]^{2+}$ ($pp \neq pp'$), although we have previously reported the separation of geometrical isomers of such species in cases where pp and pp′ are unsymmetrical.[17]

The absolute configurations of (−)-$[Ru(phen)(Me_4bpy)(bpm)]^{2+}$ and (−)-$[Ru(phen)(Me_4bpy)(py)_2]^{2+}$ were assigned to the Δ form, using predictions made by the exciton theory[26-28] and comparisons of CD spectra with those of related species.[3,4]

The availability of the enantiomers of each of the precursors enables all diastereoisomers to be generated selectively, and route A in Scheme 1 is an example of a specific synthesis of one stereoisomer. In fact two specific diastereoisomers were obtained in this way: viz. ΛΛ and ΔΛ. In each case, cation exchange chromatography allowed the separation of two geometrical isomers, and these were characterized by a combination of 1D and 2D ^1H NMR studies, as described below.

It is noted that in the chromatographic studies, the diastereoisomer separation occurred very much more easily than the separation of geometric isomers. Consequently, once that had been established, it was found more convenient to react either Δ- or Λ-$[Ru(phen)(Me_4bpy)(bpm)]^{2+}$ with *rac*-$[Ru(phen)(Me_4bpy)(py)_2]^{2+}$ producing a ΔΔ/ΔΛ (or ΛΔ/ΛΛ) mixture, which could then be readily separated into the individual diastereoisomers prior to the isolation of the geometric components (Scheme 1B).

The separation of the geometric isomers of the *meso* and *rac* diastereoisomeric forms of an analogous species $[\{Ru(Me_2bpy)(Me_4bpy)\}_2(\mu\text{-bpm})]^{4+}$ (Me_2bpy = 4,4′-dimethyl-2.2′-bipyridine) has also been achieved by similar techniques.[29]

NMR Studies. In the discussion of the NMR spectra, the conventional numbering schemes are used with the ligands phen, Me_4bpy, and bpm. In all four species, the two phen ligands are related by symmetry (as are the two Me_4bpy ligands), but in both cases the two halves of each ligand type are not equivalent (see below). While the assignments of resonances

Scheme 1. Synthetic Scheme for Isolation of Geometric Isomers of Diastereoisomeric Forms of $[\{Ru(phen)(Me_4Bpy)\}_2(\mu\text{-bpm})]^{4+}$ (A) through Stereoselective Synthesis of Individual Diastereoisomers of the Target Complex and (B) through a Combination of Partial Stereoselective Synthesis and Cation Exchange Chromatography[a]

Route A

Λ-$[Ru(phen)(Me_4bpy)(bpm)]^{2+}$ + Λ-$[Ru(phen)(Me_4bpy)(py)_2]^{2+}$

⇓

ΛΛ-$[\{Ru(phen)(Me_4bpy)\}_2(\mu\text{-bpm})]^{4+}$

cis *trans*

Route B

Λ-$[Ru(phen)(Me_4bpy)(bpm)]^{2+}$ + *rac*-$[Ru(phen)(Me_4bpy)(py)_2]^{2+}$

⇓

ΛΛ/ΛΔ-$[\{Ru(phen)(Me_4bpy)\}_2(\mu\text{-bpm})]^{4+}$

rac (ΛΛ) *meso* (ΔΛ)

cis *trans* *cis* *trans*

[a] Synthetic procedures are indicated by double arrows, and chromatographic separations, by single arrows.

arising from these ligands can be made unambiguously, the actual ligand orientation is not specified. In principle, such additional assignments may be deduced by a detailed consideration of anisotropic effects,[5,6,16-18,30] but in the present case it was not necessary for the isomer characterization and was therefore not undertaken. For bpm, the nonprimed protons are positioned under the phen ligands in the *meso-cis* and *rac-trans* forms. In the *meso-trans* and *rac-cis* cases, the distinction between the rings is not important (as a consequence of symmetry), but the additional convention is adopted that the 4-positions are nearer the phen ligand.

For the bis(homoleptic) complex $[\{Ru(pp)_2\}_2(\mu\text{-BL})]^{4+}$, the point group symmetries of the *meso* and *rac* forms are C_{2h} and D_2, respectively (Figure 1). In the case of the bis(heteroleptic) species $[\{Ru(pp)(pp')\}_2(\mu\text{-BL})]^{4+}$ (Figure 2), for the *meso* diastereoisomer, the *trans* geometrical form adopts C_i point group symmetry, but that of the *cis* isomer is reduced to C_1. For the *rac* diastereoisomer, the symmetries of both the *cis* and *trans* geometrical isomers are C_2 but differ with respect to the orientation of the C_2 axis. However, the two halves of each nonbridging ligand are nonequivalent. In the case of the Me_4-bpy, this gives rise to four (4) singlet resonances in the aromatic region and four (4) $-CH_3$ aliphatic resonances. The phen ligands exhibit AMX and A′M′X′ coupling systems, with the expected coupling constants:[4] $J_{2,3} = J_{8,9} \sim 5$ Hz, $J_{2,4} \sim J_{7,9} = 1.5$ Hz, and $J_{3,4} = J_{7,8} \sim 8$ Hz. An AB-type coupling pattern, due to second-order effects ($J_{5,6} \sim 9$ Hz), was observable only in the *rac* (ΔΔ/ΛΛ) diastereoisomer.

(26) Bosnich, B. *Inorg. Chem.* **1968**, *7*, 178.
(27) Bosnich, B. *Inorg. Chem.* **1968**, *7*, 2379
(28) McCaffery, A. J.; Mason, S. F.; Norman, B. J. *J. Chem. Soc. A* **1969**, 1428.
(29) Reitsma, D. A.; Keene, F. R. Unpublished work.
(30) Rutherford, T. J.; Reitsma, D. A.; Keene, F. R. *J. Chem. Soc., Dalton Trans.* **1994**, 3659.

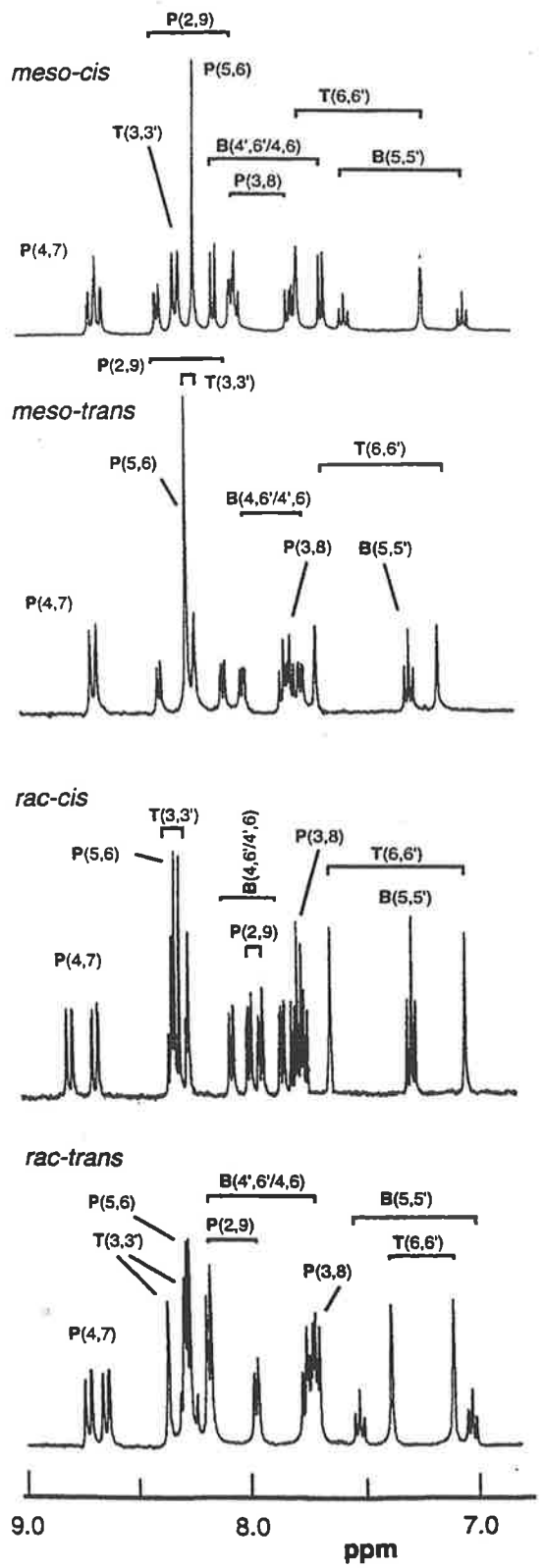

Figure 5. 300 MHz ^{1}H NMR spectra of [{Ru(phen)(Me$_4$bpy)}$_2$(μ-bpm)]$^{4+}$: (a) $\Delta\Delta$-*cis*; (b) $\Delta\Lambda$-*trans*; (c) $\Lambda\Lambda$-*cis*; (d) $\Lambda\Lambda$-*trans*.

The ^{1}H NMR spectra of the four stereoisomers in the aromatic region are given in Figure 5. For each of the diastereoisomeric forms, the assignment of its geometric isomers as *cis* or *trans* was achieved using purely symmetry arguments, which could be applied as the precise form of the diastereoisomer was known from the synthetic route using enantiomerically pure precursors. The assignment is explained below for each specific isomer.

In *meso*-[{Ru(phen)(Me$_4$bpy)}$_2$(μ-bpm)]$^{4+}$, the *trans* isomer (point group symmetry C_i) may be identified as the form that shows only one triplet (J = 5.7 Hz) since the center of symmetry renders the H5 and H5′ protons of the bpm bridge equivalent. The H4 and H6′ protons of the bpm bridge are also equivalent because of the inversion center, as are the H4′ and H6 protons. The resonances observed from these two sets of equivalent protons comprise two doublets of doublets arising from the $J_{4,5/4',5'}$ and the $J_{4,6/4',6'}$-type coupling (J = 5.7, 1.4 Hz; Figure 5b).

In the *meso-cis* form, the point group symmetry is lower (*viz.* C_s). The H5 and H5′ protons are no longer equivalent so that two triplets (J = 5.7 Hz) are observed. This nonequivalence of the two ends of the bpm ligand, along with the plane of symmetry which is orientated perpendicular to the plane of the bpm bridge incorporating the C5 and C5′ positions of the bpm and relates the H4/H6 and the H4′/H6′ protons, means that they each show only show a doublet (J = 4.3 Hz), arising from coupling to the H5 and H5′ protons, respectively. The comparison of the ^{1}H NMR spectra of the *meso-cis* and *meso-trans* forms are shown in Figure 5a,b, respectively.

For the *rac* diastereoisomer, both geometric isomers possess C_2 point group symmetry; however, in the *cis* isomers the C_2 axis is perpendicular to the plane of the bridging bpm ligand whereas in the *trans* isomer it is in the plane of the bpm ligand running through the long C5−C2−C2′−C5′ axis. In the former case, the axis renders the H5 and H5′ protons of the bridge equivalent, as well as the two pairs of protons H4/H6′ and H4′/H6. These equivalences are observed in the NMR spectrum as triplet (J = 5.7 Hz) and two doublets of doublets (J = 5.7, 1.4 Hz) resonances.

For the *trans* geometrical isomer, the C_2 axis renders the H4/H6 and the H4′/H6′ protons equivalent, giving rise to two doublets (J = 5.7 Hz). On the other hand, the H5 and H5′ protons are nonequivalent, resulting in a pair of triplets (J = 5.7 Hz). The comparison of the ^{1}H NMR spectra of the *rac-cis* and *rac-trans* forms are shown in Figure 5c,d, respectively.

Isomer Proportions. As the geometric isomers of each of the diastereoisomeric forms can be identified by ^{1}H NMR spectroscopy, the topic of stereospecificity in the synthesis may be revisited. The *cis*:*trans* ratios in the production of *meso*- and *rac*-[{Ru(phen)(Me$_4$bpy)}$_2$(μ-bpm)]$^{4+}$ are 1:2 and 1:1, respectively, assessed from NMR studies by spectral integration. A study of models shows little difference in the interactions of the methyl groups of the Me$_4$bpy ligands in the two geometric forms of the *rac* diastereoisomer. However, in the *meso* form, there appears significant interaction of these groups specifically in the *cis* geometrical isomer, consistent with the observed proportions.

Conclusions

The *cis* and *trans* geometric isomers of both the *meso* and *rac* diastereoisomeric forms of the ligand-bridged dinuclear species [{Ru(phen)(Me$_4$bpy)}$_2$(μ-bpm)]$^{4+}$ have been separated by cation exchange chromatography and characterized by NMR spectroscopy. This is the first example of the isolation of geometric isomers of this type.

The individual diastereoisomers of the target complex were also synthesized stereoselectively. In developing the appropriate precursors, we have also achieved the first chiral resolutions of

a heteroleptic tris(bidentate)ruthenium(II) complex, $[Ru(phen)(Me_4bpy)(bpm)]^{2+}$, and a heteroleptic bis(bidentate)bis(pyridine)ruthenium(II) complex, $[Ru(phen)(Me_4bpy)(py)_2]^{2+}$, in both cases using cation exchange chromatography.

Acknowledgment. This work was supported by the Australian Research Council. We thank Mr. Ian Norris and Ms. Sue Butler for assistance with the CD measurements, Dr. Ian Atkinson (JCUNQ) and Mr. Rick Willis (Australian Institute of Marine Science) for undertaking the ES-MS measurements, and Dr. Todd Rutherford, Mr. Laurie Kelso, and Dr. Nick Fletcher for helpful discussion.

IC971080J

PUBLICATIONS IN PRESS

(no pre-prints provided)

86. "'Black Absorbers" and Fuzzy Stereochemistries'", F.R. Keene, in *"Electrochemistry at the Edge"* {Proceedings of 10th Australasian Electrochemistry Conference (Surfers Paradise, 1997)}, in the press.

87. "Stereoisomers in Heterometallic (Ru_2Os) and Heteroleptic Homometallic (RuRu'Ru") Trinuclear Complexes Incorporating the Bridging Ligand HAT (1,4,5,8,9,12-hexaazatriphenylene), T.J. Rutherford and F. Richard Keene, *J. Chem. Soc., Dalton Trans.,* in the press.

88. "Isolation and Characterisation of Stereoisomers in Di- and Tri-nuclear Complexes", F.R. Keene, *Chem. Soc. Rev.,* in the press *(Invited contribution).*

MANSCRIPTS SUBMITTED FOR PUBLICATION

(no pre-prints provided)

89. "Synthesis of Mixed-Metal Dinuclear Complexes via the Stereoselective Coupling of Alicyclic Mononuclear Ru(II) and Os(II) Complexes", R.N. Warrener, A.C. Schultz, L.S. Kelso, M.R. Johnston, D. Margetic, and F.R. Keene, submitted to *Angew. Chem. Intl. Edn. Eng.*

90. "The Importance of Second-Sphere Anion Interactions in the Separation of Stereoisomers of Ligand-Bridged Polymetallic Assemblies", N.C. Fletcher and F.R. Keene, submitted to *J. Amer. Chem. Soc.*

91. "Isolation of Enantiomers of a Range of Tris(bidentate)ruthenium(II) Species using Chromatographic Resolution and Stereoretentive Synthetic Methods", T.J. Rutherford, P.A. Pellegrini, J. Aldrich-Wright, P.C. Junk, and F.R. Keene, submitted to *Eur. J. Inorg. Chem.*

92. "A New Synthetic Route to Monocarbonyl Polypyridyl Complexes of Ruthenium: Their Stereochemistry and Reactivity", N.C. Fletcher and F.R. Keene, submitted to *J. Chem. Soc., Dalton Trans.*

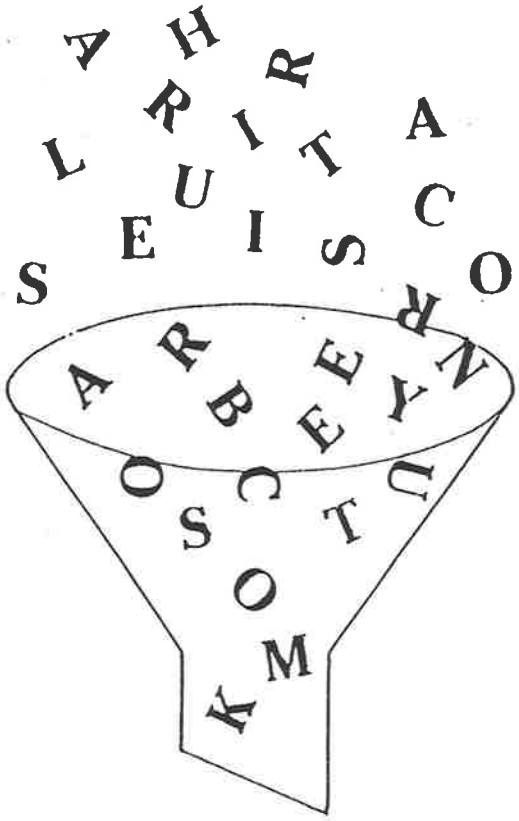

AUSTRALIAN NATIONAL CHEMISTRY WEEK

AUSTRALIAN CHEMISTRY RESOURCE BOOK

Edited by C.L. Fogliani

Vol. 11, 1992

QUEENSLAND BRANCH
SCHOOLS' CHEMISTRY LECTURE 1991

ENERGY AND CHEMISTRY

Richard Keene
Department of Chemistry
and Biochemistry
James Cook University of
North Queensland

1. INTRODUCTION

Some years ago as an 11th or 12th grade student puzzling over a particularly difficult physics or chemistry problem, I used to wonder whether the study of science was so important. I guess many of you ask yourselves the same question regularly. The decision I made is obvious, but I believe that the question is even more critical to you in the early 1990's. In the world we live in, study of the central sciences such as chemistry, physics and mathematics is of crucial importance. And I affirm that statement, regardless of whether those studies finish at the end of matriculation, or they continue for additional years at University in specific areas of science or in applied areas such as engineering or medicine. By way of illustration, I want to take a (rather light-hearted) look at aspects of a topic often dealt with in the media, and about which you probably feel you have some knowledge. Let me give you a rather different perspective.....

2. WORLD'S ENERGY RESOURCES

Figure 1 gives some predictions (1) as to the production and consumption of a few of our energy resources over the next millennium. In such a long time scale there are naturally many uncertainties involved, but the overall picture is probably reasonable. For example, a resource such as petroleum (oil) is clearly non-renewable - a certain amount is relatively easy to access, but ultimately the cost will rise in response to scarcity, the cost of exploration and the increasing difficulty of access. In this particular case, it is certain that during your lifetimes we will reach the point where our use of this resource rapidly declines and it is replaced as an energy source. We are often told that coal will provide much of the replacement - that is probably true in the short term, but ultimately the same scenario holds for coal as it did for oil, and while the peak in the curve is perhaps two centuries away it may come sooner if the environmental consequences of burning coal (namely, the production of carbon dioxide and sulphur oxides) become unacceptable.

Three points might be made from the Figure 1:

- The total human consumption of energy resources is marked on the graph. Clearly in the short term there is no "shortage" of energy and our choice is more to which is the most appropriate to use from economical and environmental viewpoints. As the population and the energy use rises, in

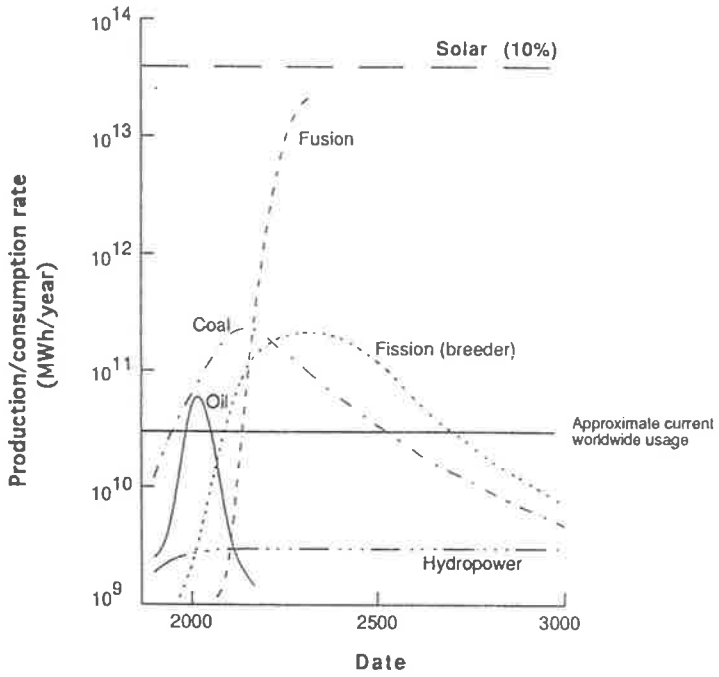

FIGURE 1: Production and Consumption of Our Energy Resources

the medium and longer term decisions will need to be made on the basis of resource availability.

- **Nuclear fusion**, the process that goes on in the Sun and in the hydrogen bomb, is the subject of intense research by physicists. If we are able to confine that reaction it would provide us with a clean and plentiful supply of energy - while there have been some very promising recent advances, realistically the technology may be some three decades away. The extraordinary debate that went on two years ago about "cold fusion" gave some indication of the importance of fusion (2); if that claim were true it would arguably be the most important scientific discovery this century, but so far it is unsubstantiated.
- The amount of **solar energy** hitting the earth's surface is enormous. In Figure 1, a level corresponding to only 10% of that resource is shown, and it is approximately 1000x greater than our current total usage of energy (the vertical scale is logarithmic).

The nuclear fusion and solar options are our only long term alternatives as providers of energy resources. The fusion technology is not yet 'accessible. Despite the fact that the solar energy is available, it has not been extensively used. There are reasons for that. Firstly, the supply is diffuse - in Queensland, a square kilometre of the earth's surface receives radiation with the energy equivalent of *ca.* 2000 tonnes of coal in one average 24 hour day. The coal, however, is relatively compact and can be moved to wherever it is needed - clearly the solar energy is spread over the wide area and cannot be transported in the same way. Moreover, it is spasmodic because of the day/night sequence and changes in weather. Secondly, the location of the majority of the world's population is to be found in temperate regions of the earth whereas the greatest solar irradiation occurs between the tropical zones. A solution to that problem would be the conversion of solar energy to an appropriate fuel, allowing the energy to be stored and transported as required to where it was needed. And that is the proposition I want to examine - what are the chemical principles involves in the concept of harvesting the sun's energy?

3. ENERGY AND CHEMISTRY - "HOT" REACTIONS

There is an intimate relationship between energy and chemistry. Each substance has its own energy content, and so any chemical reaction in which two or more substances are combined to form a product will take place with either a surplus or shortage of energy. We call these **endothermic** and **exothermic** reactions, where (respectively) energy will either be absorbed from the environment to make up the energy balance or energy will be released into the surroundings, as shown in Figure 2.

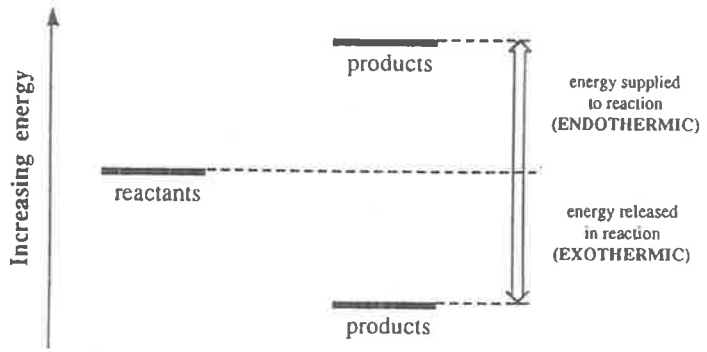

FIGURE 2: Energy Charge in Endothermic and Exothermic Reactions.

A dramatic example of an endothermic process is the reaction of the two solids barium hydroxide octahydrate $Ba(OH)_2.8H_2O$ and ammonium thiocyanate NH_4NCS (3a). The chemical equation is

$$\underset{\text{ammonium ion}}{NH_4^+} + \underset{\text{hydroxide ion}}{OH^-} + \text{energy} \rightarrow \underset{\text{ammonia}}{NH_3} + \underset{\text{water}}{H_2O}$$

and sufficient energy is absorbed from the immediate surroundings that the temperature in the reaction vessel drops by *ca.* 40°C in less than a minute. If a flask containing the reaction mixture is placed on a wooden block wetted with a few drops of water, the flask freezes to the wood and the two can be lifted together.

An example of an exothermic process is the burning (or combustion) of magnesium in oxygen to produce magnesium oxide (3b,4).

$$\underset{\text{magnesium}}{2Mg} + \underset{\text{oxygen}}{O_2} \rightarrow \underset{\text{magnesium oxide}}{2MgO} + \text{energy}$$

The excess energy is seen as an intense flash of light, and this reaction was used extensively in the old replaceable flash bulbs and is still used in flares and pyrotechnics. Another spectacular example comes from a series of reactions known as the "Thermite" processes (3c): the most common example is the reaction of powdered ferric (iron) oxide and aluminium, which react to produce aluminium oxide ("alumina") and iron. The reaction releases considerable energy so that the temperature rises within seconds to ca. 2000° and the iron that is formed is actually molten. The reaction was used by railway crews in isolated areas as a means of welding railroad tracks!

$$\underset{\text{iron oxide}}{Fe_2O_3} + \underset{\text{aluminium}}{2Al} \rightarrow \underset{\text{aluminium oxide}}{Al_2O_3} + \underset{\text{iron}}{2Fe} + \text{energy}$$

4. 'COLD' REACTIONS

Those of you who watched the recent TV series by Sir David Attenborough entitled "Trials of Life" will no doubt have been fascinated by the program on animals that emit light (such as glow-worms, fire-flies and luminescent fish). Quite clearly these organisms rely on chemistry to produce that light, but equally as obvious is the fact that the respective reactions occur at biological temperatures and are not subject to the wild fluctuations characteristic of the reactions in the previous section. There must be another link between chemistry and energy....

To give an idea of what is happening, let me introduce you to a character held in great affection by all chemists, whom I will call "Mr Molecule". In the cartoon shown in Figure 3, we can follow the sequence from 1, where our relaxed character is in his "ground state". In our story we give him energy in the form of a hot potato. On receiving it he is clearly no longer relaxed and is said to be in an "excited state"2. Since he would obviously prefer to be in the ground state, let us examine the means by which he can achieve that. Of course he can

immediately drop the hot potato. However, let us suppose that he has slow reflexes or is a particularly thoughtful character and survives the initial panic of the first excited state to reach a more rational state 3, in which he is still excited but is at a slightly lower energy than the original excited state since some loss of energy occurs in the time it took reaching the second excited state. He now has three distinctive choices:

(a) He can now throw away the hot potato - he then goes to the ground state, and importantly the potato he discards is not as hot as it was when he received it because of the loss of heat that occurred in going from the first to second excited states;

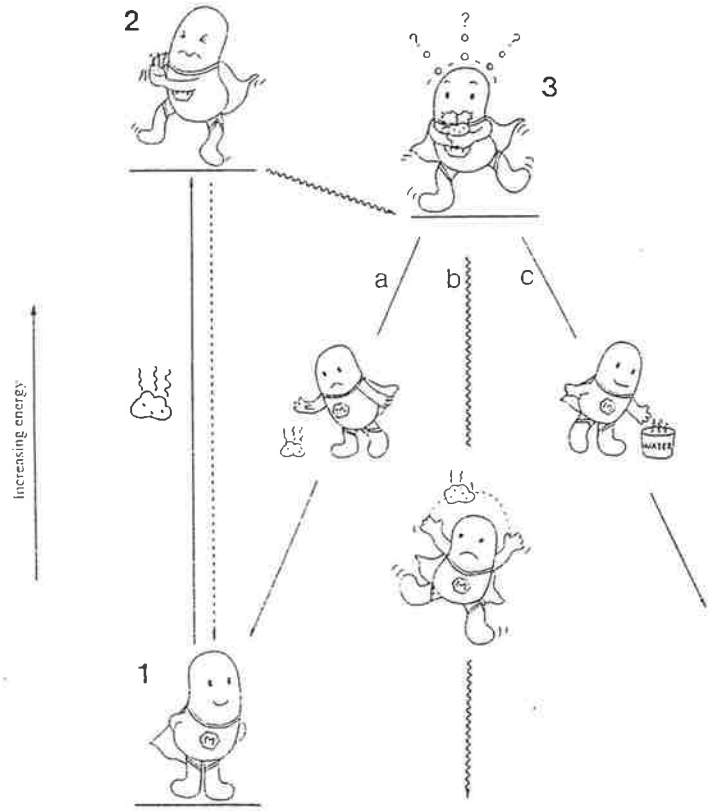

FIGURE 3: Energy State of "Mr Molecule"

(b) He can dissipate the energy into the surroundings by juggling the potato; and

(c) He can pass the energy on to something else - for example, if there is a bucket of water handy and he put the hot potato into it, he would return to the ground state and the water in the bucket would have become hot.

Three choices - throw the energy away, dissipate the energy into the immediate environment, or pass the energy on to something else.

The cartoon series is of somewhat more than passing significance - it turns out that a real molecule absorbing light energy has a similar set of options. Following absorption of the light, the "ground state" molecule goes to the excited state, 2, from where it can immediately release the absorbed energy. However, it may rapidly convert to a lower energy but longer-lived excited state, 3, from which it can undergo one or more of three processes:

- Luminescence - this is equivalent to (a) in Figure 3 where the cartoon character throws away the (slightly cooled) hot potato, and in an analogous way the radiated light (luminescence) is always lower in energy than the absorbed light.

$$*M \rightarrow M + light$$ (*represents an excited state)

You will be familiar with luminescence (phosphorescence and fluorescence are sub-categories of the general phenomenon): e.g. if we shine a beam of blue laser light (5) through a solution of the red dye Rhodamine we see an intense yellow fluorescence. The same light on a solution of the orange-coloured metal compound $[Ru(bpy)_3]^{2+}$ (bpy = 2,2'-bipyridine) produces a red luminescence (3d). You will also be familiar with the fluorescent materials put in soap powders so that on absorption of ultraviolet light they luminescence white light - the glow of a white shirt or dress under the "black light" (UV) at a disco is quite spectacular. And if someone at the disco has a glass of gin and tonic which develops an eerie blue glow under the same "black light", it's not the effect of the gin - the quinine in the tonic water is luminescing.

- **Non-radiative decay** - this is equivalent to (b) in Figure 3 where the cartoon character dissipates the absorbed energy into his own movement and into the surrounding atmosphere. An example of this is the reaction between the gases hydrogen and chlorine. Chlorine is yellow-green in colour due to absorption of light in the blue-UV region: on such absorption, the energy promotes vibration of the Cl-Cl bond to the extent that dissociation takes place to produces chlorine atoms, whereupon the following sequence occurs

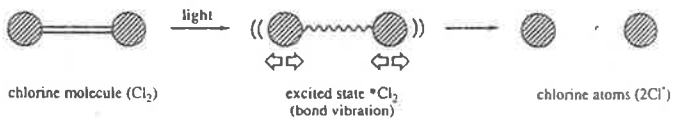

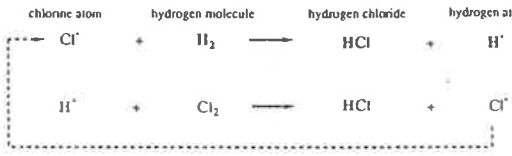

so that the cycle becomes more and more rapid and a violent explosion occurs (3e).

- **Quenching:** this is equivalent to (c) in Figure 3 where the cartoon character passes the absorbed energy on to something else. In the case of quenching, the absorbed energy is used to drive a chemical reaction of the excited state. As an example, the intense red luminescence of $[Ru(bpy)_3]^{2+}$ obtained on irradiation by the blue light (see earlier) is totally stopped by the addition of Fe(III) to the solution, due to the sequence shown below in which an electron is transferred from the excited state to the "quencher" (in this case ferric ion):

$$[Ru(bpy)_3]^{2+} \xrightarrow{light} *[Ru(bpy)_3]^{2+}$$
$$*[Ru(bpy)_3]^{2+} + Fe(III) \rightarrow [Ru(bpy)_3]^{3+} + Fe(II)$$

The question may be asked as to whether one can manipulate this sequence. For example, in terms of the cartoon character, can "Mr Molecule" pick up the hot potato from the bucket of hot water, go to an excited state, and throw the hot potato away? Or in real terms, can a chemical reaction occur in which a molecule is raised to the excited state from which it releases the energy in the form of radiation (i.e. luminescence)? The answer is yes, and the phenomenon is known as "chemiluminescence".

$$\text{chemical reaction} \rightarrow *M \rightarrow M + light$$

Again you will be familiar with examples of chemiluminescence - it explains the biological luminescence of fire-flies, glow-worms, luminous fish (which generally arise from chemical reactivity with oxygen within bacteria) but without the temperature changes that were a feature of some of the reactions I showed earlier. You may also be familiar with the emergency torches used in diving and boating in which two chemicals are mixed to form an excited state of a dye contained in the mixture which then luminesces brightly: the reactions may be summarized as follows –

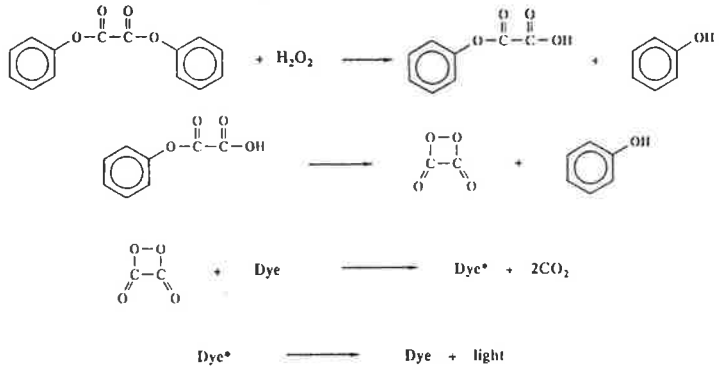

where the dye 9,10-bis(phenylethynyl)anthracene is used for a yellow chemiluminescence (3f).

5. USING THE RELATIONSHIP OF LIGHT AND CHEMISTRY

This interrelationship between light and chemistry means that chemistry may be used to harvest light energy. A graphic example of this is an experiment where one shines light on a solution containing a mixture of $[Ru(bpy)_3]^{2+}$ and $[Co(NH_3)_5Cl]^{2+}$: the ruthenium complex goes to the excited state (as we saw earlier) but undergoes quenching by the cobalt species and oxidises to form $[Ru(bpy)_3]^{3+}$- the cobalt species falls apart after the reaction and takes no further part. As a result of absorbing the light energy and undergoing oxidation, the ruthenium species changes in colour from orange to green. By doing a chemiluminescence experiment (in this case adding sodium borohydride solution) the green ruthenium species goes to the excited state and luminesces red light, demonstrating that the absorbed light energy had been stored within the chemical system (3d).

$$[Ru(bpy)_3]^{2+} \xrightarrow{\text{light}} *[Ru(bpy)_3]^{2+}$$

$$*[Ru(bpy)_3]^{2+} + [Co(NH_3)_5Cl]^{2+} \rightarrow [Ru(bpy)_3]^{3+} + [Co(NH_3)_5Cl]^{+}$$

$$[Ru(bpy)_3]^{3+} + BH_4^- \rightarrow *[Ru(bpy)_3]^{2+} + BH_3 + {}^1/_2H_2$$

$$*[Ru(bpy)_3]^{2+} \rightarrow [Ru(bpy)_3]^{2+} + \text{light}$$

One of the interesting things about science is that often, when you think you have a good idea, you find nature has already developed it to a very sophisticated level on an enormous scale. In the present case, the use of chemistry to harvest solar energy is done in nature by a process known as "photosynthesis". Many of us think of photosynthesis as the conversion of carbon dioxide and water to carbohydrates (sugars, starch and cellulose) and oxygen by plants using energy

from the sun. Well, let us look in a little more detail at that process.....;

In the cartoon of Figure 4, we see that sunlight impinges on the plant and is absorbed within the organism by a molecule (chlorophyll) which goes to the excited state. When a molecule does this, an electron is relocated from one energy level to a higher energy level. In the absence of anything else happening, the excited electron will decay back to its initial state - but in the photosynthetic scheme the excited electron is rapidly moved from the site where the light was absorbed to somewhere else in the organism. The net result is called **charge separation** and is manifested in the organism having a region with an electron excess and a physically separated region with an electron deficiency; you will recognise that those centres will be potential sites for chemical reactions called **reductions** and **oxidations**, respectively. In the case of photosynthesis, the reduction is of carbon dioxide to carbohydrates and the oxidation is of water to oxygen.

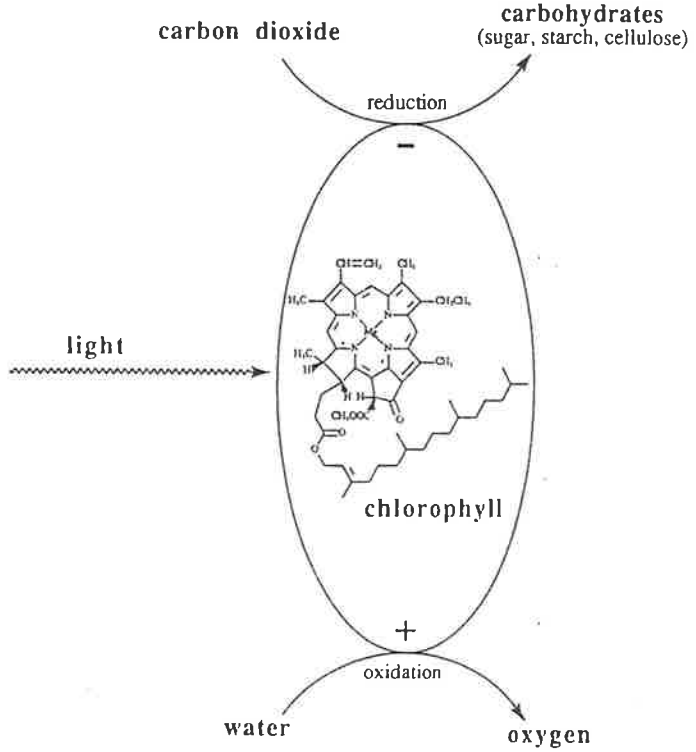

FIGURE 4: Photosynthesis

The photosynthesis process is indeed the harvesting of sunlight, the conversion of light energy to a chemical fuel. If you are in doubt about that consider that all our coal and oil reserves are derived from decayed plant matter whose origin is in photosynthesis! Despite the immensity of the scale however, the efficiency of that conversion is relatively low, being of the order of 1% even for the most efficient plant systems (e.g. sugar cane). The question one may ask is whether modern chemistry and physics can provide more efficient schemes for conversion of light to chemical fuels.

Let me give one simple example. As shown in Figure 5, if a p-type semiconductor is placed in a beaker of water containing a little acid, and connected via an external circuit to a metal or carbon electrode immersed in the same solution, then on shining light on the semiconductor bubbles of gas will be evolved at both electrodes; hydrogen at the semiconductor and oxygen at the inert electrode. In this case, the semiconductor is acting as the "Mr Molecule", absorbing the light energy and directing excited electrons to its surface where they reduce water to hydrogen. The other electrode is left with a positive potential and it oxidises water to oxygen. This simple example shows the conversion of light energy to a fuel, in this case hydrogen.

Importantly, the conditions of the experiment may be maximised so that the efficiency of light conversion to the fuel is in excess of 15%.

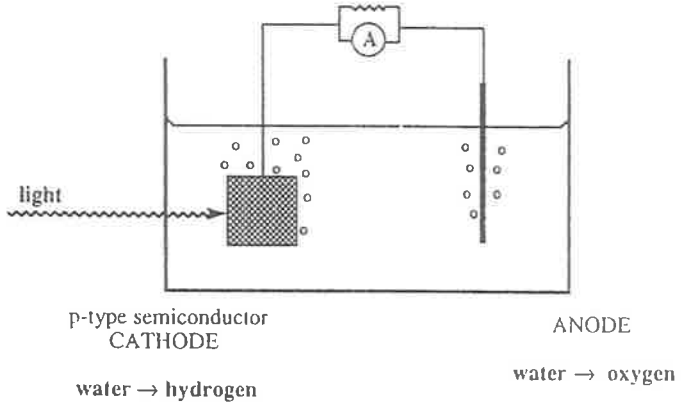

FIGURE 5: A Semiconductor Absorbing Light Energy

The use of a solar panel to generate a potential difference between two electrodes is really no different in principle, except that the light-absorbing medium is external from the solution. The solar panel fills the role of absorbing the light and allowing the "charge separation" of the excited electrons which are used in promoting chemistry in an electrolysis cell. Among a number of examples

that demonstrate this is the electrolysis (using carbon electrodes) of a solution containing potassium iodide and the pH-indicator phenolphthalein (6). While the light is shining on the panel, at the electrode to which the electrons are directed (cathode) the reaction

$$\underset{\text{water}}{2H_2O} + 2e^- \rightarrow \underset{\text{hydroxide ion}}{2OH^-} + \underset{\text{hydrogen}}{H_2}$$

occurs and the gas hydrogen is evolved, while the region around the electrode goes pink because the hydroxide ions produced make the solution alkaline and the indicator turns pink. At the other electrode (anode), iodide ions are oxidised to iodine which is seen as a brown colour developing at the electrode.

$$2I^- \rightarrow I_2 + 2e^-$$

Quite clearly, the principle of conversion of light energy to a usable fuel is achievable using the relationship between light and chemistry. If we were to take the earlier cartoon of photosynthesis (Figure 4) and modify it, we might envisage

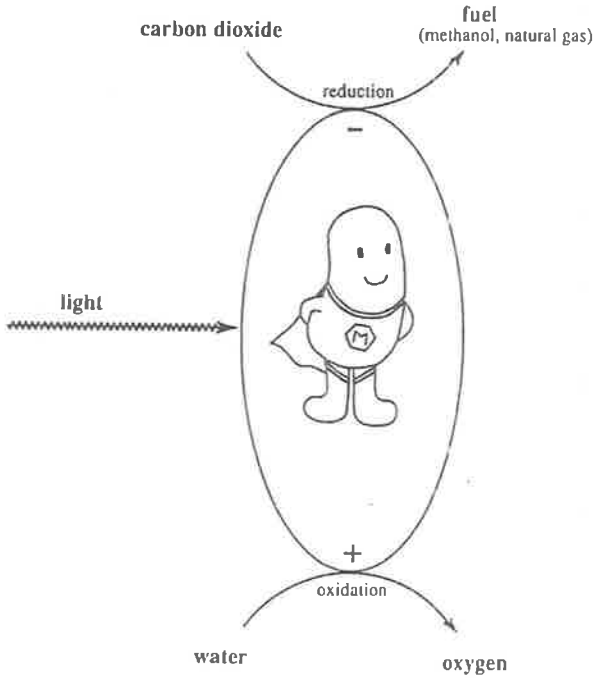

FIGURE 6: "Artificial Photosynthesis"

some sort of "artificial photosynthesis" in which some "Mr Molecule", yet to be identified or developed, is used to absorb light within a system designed to separate the excited electrons to a site where they might reduce carbon dioxide to the fuels methanol or methane (natural gas) or reduce water to hydrogen (see Figure 6). At the oxidising centre, as in photosynthesis, water might by oxidised to oxygen.

As we have seen from these discussions, this is a workable hypothesis. And the challenge to modern science? The identity of the "Mr Molecule" in such a scheme, and research proceeds in many chemistry and physics laboratories around the world to design better molecules for this purpose.

6. THE FUTURE?

We have looked at perceived problem of modern society - the availability of energy sources to generate electrical power to supply our industries and to maintain and develop our way of life. Undoubtedly science will find solutions, as it will to other problems such as the control of pollution, the protection of our environment, the production of food, the development of medicines and many others.

But why is the particular scientific discipline of chemistry so important in that context? The answer is related to the central position of chemistry among the sciences. Chemistry impinges on so much of our lives - energy, medicine, mining, agriculture, food, the environment, industry (for example textiles, soaps and detergents, paint, cement, semiconductors, cosmetics), forensic science, etc....

The community must come to an increasing understanding that many of the problems I mentioned above have a scientific basis and so the answers are to be found in science. Unfortunately, there is often a tendency to look on science as their cause, rather than the means to their solution - arguably many of the problems that exist have been caused by commercial rather than scientific decisions on alternative choices. Nevertheless, increasingly the community needs to be informed to be able to understand the basis of these issues. And it is there that the knowledge of science in the general community is important. But in this day and age of the 30-second sound-bite on the TV and the ready acceptance of a trendy phrase we often have a problem with the level of scientific insight required: the possession of a little knowledge can be dangerous.

Advances in science will obviously come from those with particular scientific training, but the public and those in positions of responsibility will increasingly need to be discerning about what is science and what is populist phraseology. I asked you earlier whether your studies in science at secondary school were important - my answer is that more than ever we will need people trained and informed in science. I offer you every encouragement to continue with your studies - they are important for you, for the society in which we live, and for the future of this country.

REFERENCES

1. McMullan, J.T., Morgan, R., and Murray, R.B., "Energy, Resources and Supply". Wiley (London), 1976. Figure 1 is adapted from Fig. 1.3 of this reference (p.6).
2. Clark, R.W., J Chem Ed., 1991, 68, 277-279
3. Adapted from Shakhashiri, B.Z., "Chemical Demonstrations - A Handbook for Teachers of Chemistry", Volume 1, University of Wisconsin Press, 1983: (a) p.10-12, (b) p.38-39, (c) p.85-89, (d) p.194-199, (e) p.121-123, (f) p.146-152.
4. Adapted from Shakhashiri, B.Z., "Chemical Demonstrations - A Handbook for Teachers of Chemistry", Volume 2, University of Wisconsin Press, 1985: p.162.
5. In the lecture series an argon laser unit, designed for use in forensic science, was loaned to the author by COHERENT SCIENTIFIC PTY LTD. (Adelaide) for these demonstrations. The company is thanked for its generosity.
6. Adapted from Summerlin, L.R., Borgford, C.L., and Ealy, J.B., "Chemical Demonstrations - A Source book for Teachers", Volume 2, 2nd Edition, American Chemical Society (Washington), 1988; p.201.

ABOUT THE AUTHOR

Richard Keene studied at the University of Adelaide and completed his PhD in 1972, after which he spent two years doing postdoctoral work at the Australian National University and three years at the University of North Carolina (Chapel Hill). He then returned to Australia where he taught briefly at the University of Melbourne before accepting a position at James Cook University of North Queensland, where he is currently an Associate Professor in the Department of Chemistry and Biochemistry. He was the recipient of the Rennie Medal of the Royal Australian Chemical Institute in 1979.

Richard has enjoyed periods of study leave, including twelve months (as a Fulbright Scholar) at Brookhaven National Laboratory in New York investigating activation of carbon dioxide reactivity. He has also spent time at Stanford University (California) and the University of North Carolina (Chapel Hill), where a particular interest was the modification of electrode surfaces for catalysis.

Richard has had a wide ranging interest in the chemistry of transition metals, but his current research thrusts are concentrated on what may be broadly defined as "artificial photosynthesis". These studies are directed to the design of metal-containing molecular assemblies in which absorbed light energy may be directed to catalytic centres at which useful chemical reactions may occur (e.g. the reduction of carbon dioxide to potential fuels such as methanol and methane).

F. R. KEENE

APPENDICES

CONFERENCE PAPERS - F.R. Keene

75. "Stereochemical Influences on Intramolecular Electron Transfer in Polymetallic Supramolecular Assemblies", F.R. Keene, IC'98, National Conference of Inorganic Chemistry Division, Royal Australian Chemical Institute, Wollongong, February 1998. Abstract SL31. ***(Invited Lecture)***

74. "The Importance of Second-Sphere Anion Interactions in the Separation of Stereoisomers of Ligand-Bridged Diruthenium(II) Complexes", N.C. Fletcher, F.R. Keene and D.A. Reitsma, IC'98, National Conference of Inorganic Chemistry Division, Royal Australian Chemical Institute, Wollongong, February 1998. Abstract PT83.

73. "Controlling the Stereochemistry of Oligonuclear Complexes of Ruthenium(II) and Osmium(II) with a Tris-chelating Bridging Ligand", T.J. Rutherford and F.R. Keene, IC'98, National Conference of Inorganic Chemistry Division, Royal Australian Chemical Institute, Wollongong, February 1998. Abstract PT80.

72. "Separation of the Geometric Isomers of a Dinuclear Polypyridyl Complex of Ruthenium", B.T. Patterson and F.R. Keene, IC'98, National Conference of Inorganic Chemistry Division, Royal Australian Chemical Institute, Wollongong, February 1998. Abstract PT81.

71. "Synthesis of d^6 Metal Complexes via the Cycloaddition of Pre-formed Mononuclear Building Blocks", L.S. Kelso, F.R. Keene, A.C. Schultz, and R.N. Warrener, IC'98, National Conference of Inorganic Chemistry Division, Royal Australian Chemical Institute, Wollongong, February 1998. Abstract PT82.

70. "Protonation Studies of Reduced and Excited States in Ruthenium(ii) Complexes", P.A. Anderson, R.F. Anderson, M. Furue, M.Z. Hoffman, F.R. Keene, and B.D. Yeomans, IC'98, National Conference of Inorganic Chemistry Division, Royal Australian Chemical Institute, Wollongong, February 1998. Abstract PT84.

69. "The Design of Rigid Space-Separated Metal Complex Dyads", A.C. Schultz, R.N. Warrener, D.N. Butler, L.S. Kelso, and F.R. Keene, Queensland Regional Conference, Inorganic Chemistry Division, Royal Australian Chemical Institute, Rockhampton, July 1997. Abstract L3.

68. "Azobis(2-pyridine)-Bridged Diruthenium Species", L.S. Kelso, D.A. Reitsma and F.R. Keene, Queensland Regional Conference, Inorganic Chemistry Division, Royal Australian Chemical Institute, Rockhampton, July 1997. Abstract L6.

67. "Second-Sphere Anion Interactions and their Importance in the Stereoisomeric Separation of Ligand-Bridged Diruthenium(II) Complexes", N.C. Fletcher, D.A. Reitsma and F.R. Keene, Queensland Regional Conference, Inorganic Chemistry Division, Royal Australian Chemical Institute, Rockhampton, July 1997. Abstract L4.

66. "Stereochemical Control of a Chromophore-Quencher Triad and the Influence on Intramolecular Electron Transfer", T.J. Rutherford and F.R. Keene, Queensland Regional Conference, Inorganic Chemistry Division, Royal Australian Chemical Institute, Rockhampton, July 1997. Abstract L1.

65. "Strongly Interacting Ruthenium(III/II) Dinuclear Species", L.S. Kelso and F.R. Keene, Queensland Regional Conference, Inorganic Chemistry Division, Royal Australian Chemical Institute, Rockhampton, July 1997. Abstract P5.

64. "Separation of the Geometric Isomers of a Simple Ruthenium Dinuclear Polypyridyl Complex", B.T. Patterson and F.R. Keene, Queensland Regional Conference, Inorganic Chemistry Division, Royal Australian Chemical Institute, Rockhampton, July 1997. Abstract L9.

63. "'Black Absorbers' and "Fuzzy Stereochemistries'", F.R. Keene, Symposium on *"Electrochemistry of Inorganic and Biological Compounds"*. 10th Australasian Electrochemistry Conference, Surfers Paradise, February 1997. ***(Invited lecture).***

62. "Multinuclear Polypyridyl Complexes of Ruthenium(II) and Osmium(II) with the Bridging Ligand 1,4,5,8,9,12-Hexaazatriphenylene (HAT)", T.J. Rutherford and F.R. Keene, 31st International Conference on Coordination Chemistry, Vancouver, August 1996. Abstract 5L21.

61. "Inherently Chiral 'Chiragen [0]' Complexes of Ruthenium(II)", N.C. Fletcher, F.R. Keene, and A. von Zelewsky, 31st International Conference on Coordination Chemistry, Vancouver, August 1996. Abstract 5P94.

60. "Influence of the Spacer on Electron and Energy Transfer in Chromophore-Quenchers Monomers and Ligand-Bridged Dimers", L.S. Kelso, M.S. Henderson, and F.R. Keene, IC'96, National Conference of Inorganic Chemistry Division, Royal Australian Chemical Institute, Townsville, July 1996. Abstract P76/B.

59. "Influence of the Anion in Cation-Exchange Chromatography", D.A. Reitsma and F.R. Keene, IC'96, National Conference of Inorganic Chemistry Division, Royal Australian Chemical Institute, Townsville, July 1996. Abstract P117/B.

58 "Stereochemical Control of Redox-Active Groups in Chromophore-Quencher Complexes", T.J. Rutherford and F.R. Keene, IC'96, National Conference of Inorganic Chemistry Division, Royal Australian Chemical Institute, Townsville, July 1996. Abstract P123/B.

57. "Stereoselective Synthesis of Bridged Binuclear Ruthenium(II) Bipyridyl Complexes", N.C. Fletcher, F.R. Keene, P. Belser, A. von Zelewsky, and H. Stoekli-Evans, R.S.C. Macrocylic Group Meeting, Sheffield, Jan. 1996.

56. "Spatial dependence of photo-promoted electron and energy transfer in polymetallic assemblies", F.R. Keene, presented at symposium on *"Inorganic Photochemistry: Applications in Bioinorganic Chemistry, Energy Conversion and Catalysis"*, International Chemical Congress of Pacific Basin Societies, Honolulu, December 1995. Abstract INOR 392. ***(Invited lecture).***

55. "Stereochemical and Substituent Effects in α-Diimine-bridged Diruthenium Species", L.S. Kelso, D.A. Reitsma and F. R. Keene, 10th National Convention, Royal Australian Chemical Institute, Adelaide, September-October 1995. Abstract P69 (Inorg.).

54. "Inorganic Stereochemistry - trying to catch up with nature", F.R. Keene, Scientific Meeting of the North Queensland Section of the Royal Australian Chemical Institute, Townsville, August 1995. ***(Invited lecture).***

53. "Stereoselective Synthesis of Bridged Binuclear Ruthenium(II) Bipyridyl Complexes", N.C. Fletcher, F.R. Keene, P. Belser, A. von Zelewsky, and H. Stoekli-Evans, Autumn Meeting of the Swiss Chemical Society, Bern, October 1995. Abstract: *Chimia* 1995, *285,* #145.

52. "Black MCLT Absorbers', P.A. Anderson, G.F. Strouse, J.A. Treadway, T.J. Meyer, and F.R. Keene, IC94' (National Conference of the Division of Inorganic Chemistry, R.A.C.I.), Perth, July 1994. Abstract B8. ***(Invited lecture).***

51. "Separation and Structural Characterisation of Diastereoisomeric Forms of Ligand-Bridged Dimetallic Species {M = Ru(II), Os(II)} Containing Bidentate Polypyridyl Ligands", D.A. Reitsma and F.R. Keene, 'IC94' (National Conference of the Division of Inorganic Chemistry, R.A.C.I.), Perth, July 1994. Abstract D27.

50. "Stereochemistry in Tris(bidentate)ruthenium(II) Complexes containing Unsymmetrical Bidentate Polypyridyl Ligands", T.J. Rutherford, D.A. Reitsma, and F.R. Keene, 'IC94' (National Conference of the Division of Inorganic Chemistry, R.A.C.I.), Perth, July 1994. Abstract C71.

49. "Artificial Photosynthesis: controlling properties and stereochemistries at metal centres in polymetallic supramolecules", F.R. Keene, 'Mini Symposium on Molecular Architecture', Central Queensland University (Rockhampton), October 1993. ***(Invited lecture).***

48. "Symmetical Functionalisation of Ligating N-Heterocycles", L.S. Kelso and F.R. Keene, Southern Highlands Conference on Heterocyclic Chemistry, Bowral (NSW), September 1993.

47. "'Designer' Photophysical Properties in Tris(heteroleptic) Complexes of Ruthenium Containing Bidentate N-Heterocyclic Ligands", G.F. Strouse, P.A. Anderson, T.J. Meyer, and F.R. Keene, Southern Highlands Conference on Heterocyclic Chemistry, Bowral (NSW), September 1993.

46. "Polymetallic Supramolecular Assemblies: Controlling the Properties and Stereochemistries of the Metal Centres", F.R. Keene, Scientific Meeting of the North Queensland Section of the Royal Australian Chemical Institute, Townsville, August 1993. ***(Invited lecture).***

45. "Electrochemical and Photophysical Studies of Heteroleptic Tris(bidentate) Polypyridyl Complexes of Ru(II)", P.A. Anderson, G.F. Strouse, T.J. Meyer, F.R. Keene, and K.H. Haarmann, 44th Southeastern/2th Middle Atlantic Regional Meeting, American Chemical Society, Washington (D.C.), December 1992. Abstract 256.

44. "Hydrogenation of Terminal Alkynes Mediated by Tris(2,2'-bipyridine)cobalt(I)",D.A. Reistma and F.R. Keene , Queensland Regional Joint Conference, Divisions of Inorganic and Organic Chemistry, Royal Australian Chemical Institute, Rockhampton, July 1992.

43. "Beyond $[Ru(bpy)_3]^{2+}$: Designed Synthesis of Heteroleptic Tris(bidentate) Polypyridyl Complexes of Ruthenium(II)", P.A. Anderson, F.R. Keene, T.J. Meyer, J.R. Schoonover, and G.F. Strouse, Queensland Regional Joint Conference, Divisions of Inorganic and Organic Chemistry, Royal Australian Chemical Institute, Rockhampton, July 1992.

42. "'Heteroleptic' $[Ru^{II}(AA)(BB)(CC)](PF_6)_2$ Complexes. Building Assemblies Containing Three Different Functionalized Moieties", G.F. Strouse, P.A. Anderson, F.R. Keene and T.J. Meyer, 203rd National A.C.S. Meeting (San Francisco, April, 1992). Abstract INOR486.

41. "Artificial Photosynthesis", F.R. Keene, Scientific Meeting of the North Queensland Section of the Royal Australian Chemical Institute, Townsville, October 1991. ***(Invited lecture).***

40. "Electrode Modification by Polythiophene Films", M. Pappalardo and F.R. Keene, Inaugural Queensland Regional Conference, Inorganic Chemistry Division, Royal Australian Chemical Institute, Rockhampton, July 1991.

39. "The Electropolymerization of Vinyl-Substituted Polypyridyls Promoted by Transition Metal Centres: Studies of the Nature of the Polymer Films Using Laser Desorption Techniques", L.S. Kelso, I.M. Atkinson, A.E.W. Knight, and F.R. Keene, Inaugural Queensland Regional Conference, Inorganic Chemistry Division, Royal Australian Chemical Institute, Rockhampton, July 1991.

38. "Reduction of Unsaturated Organic Species Using Tris(2,2'-bipyridine)cobalt(I)", D.A. Reitsma and F.R. Keene, Inaugural Queensland Regional Conference, Inorganic Chemistry Division, Royal Australian Chemical Institute, Rockhampton, July 1991.

37. "Design of Chromophore-Quencher Complexes", A.C. Schultz, G.V. Meehan, and F.R. Keene, Inaugural Queensland Regional Conference, Inorganic Chemistry Division, Royal Australian Chemical Institute, Rockhampton, July 1991.

36. "Artificial Photosynthesis", F.R. Keene, Inaugural Queensland Regional Conference, Inorganic Chemistry Division, Royal Australian Chemical Institute, Rockhampton, July 1991. ***(Invited lecture).***

35. "Laser Desorption/Time-of-Flight Mass Spectrometry and Spectroscopy of Involatile Complexes", R.T.T. Karaiste, I.M. Atkinson, J.A. Shorter, A.E.W. Knight, and F.R. Keene, 'IC91' (National Conference of the Division of Inorganic Chemistry, R.A.C.I./N.Z.I.C.), Hamilton, New Zealand, January 1991. Abstract P2/7.

34. "Electropolymerization of 4-Methyl-4'-vinyl-2,2'-bipyridine Promoted by Transition Metal Centres: Studies of the Nature of the Polymer Films Using Laser Desorption Techniques", L.S. Kelso, I.M. Atkinson, and F.R. Keene, 'IC91' (National Conference of the Division of Inorganic Chemistry, R.A.C.I./N.Z.I.C.), Hamilton, New Zealand, January 1991. Abstract P2/6.

33. "Ambidentate Coordination of the Tri-pyridyl Ligands 2,2':6',2"-Terpyridyl, Tris(2-pyridyl)amine, Tris(2-pyridyl)methane, and Tris(2-pyridyl)phosphine to Carbonylrhenium Centres", P.A. Anderson, F.R. Keene, E. Horn, and E.R.T. Tiekink, 'IC91' (National Conference of the Division of Inorganic Chemistry, R.A.C.I./N.Z.I.C.), Hamilton, New Zealand, January 1991. Abstract P2/2.

32. "Low Fragmentation Laser Desorption of Thermally Labile Molecules", I.M. Atkinson, J.A. Shorter, R.T.T. Karaiste, F.R. Keene, and A.E.W. Knight, 4th Australian Conference on Chemical Reaction Dynamics, Division of Physical Chemistry, R.A.C.I., McLaren Vale (S.A.), Nov. 1990.

31. "Low Fragmentation Laser Desorption of Thermally Labile Molecules", I.M. Atkinson, J.A. Shorter, R.T.T. Karaiste, F.R. Keene, J.I. Steinfeld, and A.E.W. Knight, Conference of the Materials Research Society, Boston, Nov/Dec 1990.

30. "Transition Metal Complexes containing the Tripodal π-Acceptor Ligands, Tris(2-pyridyl)X {X = N, CH, COH, P}: Bonding, Reactivity and Redox Properties", F.R. Keene, 199th National A.C.S. Meeting (Boston, April, 1990). Abstract INOR119. ***(Invited Lecture)***.

29. "Chemical Modification of Electrode Surfaces", F.R. Keene, Scientific Meeting of the North Queensland Section of the Royal Australian Chemical Institute, Townsville, November 1989.

28. "Cobalt(III) Complexes with N-Methylenediamine: Stereochemistry and Isolation of Isomers", G.H. Searle, F.R. Keene, and E.R.T. Tiekink, XXVII International Conference on Coordination Chemistry, Broadbeach, July 1989. Abstract T65. ***(Invited Oral Poster Presentation to Minisymposium MS9 - Chiral Complexes)***.

27. "The Application of Molecular Beam Time-of-Flight Mass Spectrometry and Laser Ablation to Coordination Complexes", I.M. Atkinson, F.R. Keene and A.E.W. Knight, XXVII International Conference on Coordination Chemistry, Broadbeach, July 1989. Abstract M32.

26. "Polypyridyl Complexes of Cobalt(I): Their Stabilization and Reactivity as Reducing Agents", F.R. Keene, 'Inorganic Chemistry '87'/8th National Convention R.A.C.I., Sydney, August 1987. Abstract p.18. ***(Invited lecture).***

25. "Synthetic and Electrochemical Studies of Rhodium Complexes of Tripodal Ligands of the Type $(2\text{-py})_3X$ (X = N, CH, COH, P, P=O)", T.A. Hafeli, F.R. Keene, and T.P. Wright, 'Inorganic Chemistry '87'/8th National Convention R.A.C.I., Sydney, August 1987. Abstract K5.

24. "Oxidation of Secondary Amines Coordinated to Ruthenium(II)", G.W. Whebell and F.R. Keene, 'Inorganic Chemistry in Australia '86', R.A.C.I., Melbourne, January 1986. Abstract W4.

23. "Mode of Coordination of Tris(2-pyridyl)carbinol to Cobalt(III)", F.R. Keene and D.J. Szalda, 'Inorganic Chemistry in Australia '86', R.A.C.I., Melbourne, January 1986. Abstract K2.

22. "Reduction of Carbon Dioxide by Cobalt(I) Complexes Containing 2,2'-Bipyridine", F.R. Keene, C. Creutz and N. Sutin, presented at "Symposium on Photochemistry and Photophysics of Metal Complexes: Applications to Solar Energy Conversion", 1984 International Chemical Congress of Pacific Basin Societies, Honolulu, December 1984. Abstract 07J19. ***(Invited lecture).***

21. "Carbon Dioxide: Is There Life after Death for Carbon?", F.R. Keene, R.A.C.I. (North Queensland Section) Conference, Townsville, July 1984.

20. "Mechanism of Oxidation of an Alcohol Coordinated to Ruthenium", F.R. Keene and M.J. Ridd, 187th A.C.S. National Meeting, St. Louis (Missouri) April 1984. Abstract INOR191.

19. "Role of the Metal in the Oxidative Dehydrogenation of Coordinated Amines", F.R. Keene and M.J. Ridd, 186th A.C.S. National Meeting, Washington D.C., August 1983. Abstract INOR316.

18. "Mechanistic Studies of the Role of the Metal in Coordinated Amine Oxidative Dehydrogenation Using Flash Photolysis Techniques", F.R. Keene and M.J. Ridd, 11th AINSE Radiation Chemistry Conference, Lucas Heights, November 1982. Abstract 4.

17. "Mechanistic Studies of Coordinated Amine Dehydrogenation using Flash Photolysis Techniques", M.J. Ridd and F.R. Keene, 11th Conference COMO Division, 7NC, R.A.C.I., Canberra, August 1982. Abstract P 55.

16. "Metal Ion Promotion of Alcohol Oxidation", F.R. Keene and M.J. Ridd, 11th Conference, COMO Division, 7NC, R.A.C.I., Canberra, August 1982. Abstract P 54.

15. "Time-Resolved Resonance Raman Studies of the Luminescent Excited States of Polypyridyl Complexes of Ruthenium", J.C. Dyason, F.R. Keene, and A.E.W. Knight, 11th Conference COMO Division, 7NC, R.A.C.I., Canberra, August 1982. Abstract P53.

14. "Fuel Hydrogen and Solar Energy", F.R. Keene, R.A.C.I. (North Queensland Section) Conference, Townsville, July 1982.

13. "Oxidation of *Iso* -Propylamine Coordinated to Ruthenium", P.A. Adcock and F.R. Keene, 10th Conference COMO Divison, R.A.C.I., Queenstown, N.Z., May 1981. Abstract PI-15.

12. "Metal-Ion Catalysis of Amine and Alcohol Oxidation", F.R. Keene and M.J. Ridd, 10th Conference COMO Division, R.A.C.I., Queenstown, N.Z., May 1981. Abstract Sl-10. ***(Invited lecture).***

11. "Metal Ion Catalysis of Oxidation Reactions", F.R. Keene, R.A.C.I. (North Queensland Section) Conference, Townsville, August 1980. ***(Rennie Medal lecture).***

10. "The Mechanism of the Oxidation of Amines Coordinated to Ruthenium", M.J. Ridd and F.R. Keene, 9th Conference COMO Division, R.A.C.I., University of New South Wales, February 1980. Abstract PP28.

9. "Oxidation of Coordinated Ligands", F.R. Keene, R.A.C.I. (North Queensland Section) Conference, Townsville, July 1978.

8. "Oxidation of Organic Molecules using Nitroruthenium(III) Complexes", F.R. Keene, T.J. Meyer, and D.J. Salmon, 7th Conference COMO Division, R.A.C.I., La Trobe University 1977. Abstract R11.

7. "The Application of Mixed-Valence Ions to Electron Transfer Theory", M.J. Powers, R.W. Callahan, F.R. Keene, T.J. Meyer, and D.J. Salmon, 172nd A.C.S. National Meeting, San Francisco (California), September 1976. Abstract INOR 224.

6. "Oxidation of Organics by Ruthenium(III) Nitrite Complexes", F.R. Keene, B.A. Moyer, D.J. Salmon, and T.J. Meyer, 171st A.C.S. National Meeting, New York, April 1976. Abstract INOR 130.

5. "The Oxidation of Coordinated Primary Amines", F.R. Keene, D.J. Salmon, and T.J. Meyer, 170th A.C.S. National Meeting, Chicago (Illinois), August 1975. Abstract INOR 024.

4. "The Facile Intramolecular Hydrolysis of Coordinated Dipeptides and Glycine Amides", D.A. Buckingham, F.R. Keene, and A.M. Sargeson, 168th A.C.S. National Meeting, Atlantic City (New Jersey), September 1974. Abstract INOR 092.

3. "The Intramolecular Hydrolysis of Coordinated Glycine Amides", F.R. Keene, 5th Conference COMO Division, R.A.C.I., Broadbeach 1974. Abstract W1G4.

2. "Isomerisation Reactions in the Bis(diethylenetriamine)-cobalt(III) System", F.R. Keene and G.H. Searle, 4th Conference COMO Division, R.A.C.I., Camden 1972. Abstract H3.

1. "The Isomers of the Bis(diethylenetriamine)cobalt(III) Ion", F.R. Keene and G.H. Searle, 3rd Conference Coordination and Metal-Organic (COMO) Chemistry Division, R.A.C.I., Canberra 1970. Proceedings p.22.

CURRICULUM VITAE

NAME: **FRANK RICHARD KEENE**

DATE OF BIRTH: October 9, 1946

NATIONALITY: Australian; born in Adelaide, South Australia

MARITAL STATUS: Married, three children

UNIVERSITY ADDRESS: Department of Chemistry & Chemical Engineering
School of Biomedical & Molecular Sciences
James Cook University of North Queensland
Townsville, Queensland 4811, AUSTRALIA
{Telephone: (07) 4781-4343; FAX: (07) 4781-4600;
E-Mail (Internet): Richard.Keene@jcu.edu.au}

HOME ADDRESS: 10 Egret Crescent
Condon, Queensland 4815
AUSTRALIA
{Telephone: (077) 73-3353}

PRESENT POSITION: Professor in Inorganic Chemistry (Personal Chair)
Head, Department of Chemistry & Chemical Engineering

PROFESSIONAL SOCIETIES: Fellow of Royal Australian Chemical Institute
Member of American Chemical Society

ACADEMIC QUALIFICATIONS: BSc. (Hons I) - University of Adelaide (1968)
PhD - University of Adelaide (1973)

CAREER DETAILS:

1968-71: Postgraduate student, Department of Physical & Inorganic Chemistry, University of Adelaide, under the supervision of **Dr Graeme H. Searle**. The research topic dealt with stereochemical aspects of complexes of cobalt containing multidentate amine ligands.

1972-74: Postdoctoral Fellow, Research School of Chemistry at Australian National University, Canberra working with **Professor Alan M. Sargeson** and **Dr David A. Buckingham**. Research dealt with mechanistic aspects of the reactions of coordinated nitriles, and the influence of metal ions on the cleavage of polypeptides.

1974-76: Research Associate, Department of Chemistry, University of North Carolina at Chapel Hill, working with **Professor Thomas J. Meyer**. Research centered on aspects of the chemistry of ruthenium, in particular the dehydrogenation of coordinated amines, the reactivity of coordinated nitrites, and the mechanism of electron exchange processes.

1977: Senior Tutor in Inorganic Chemistry in the School of Chemistry, University of Melbourne.

1978-present: Accepted position of Lecturer in Inorganic Chemistry, James Cook University of North Queensland, 1978. Promoted to Senior Lecturer, 1983. Promoted to Associate Professor, 1988. Awarded Personal Chair, 1997.

1983: Awarded Fulbright Fellowship, and spent twelve months study leave at the Brookhaven National Laboratory, New York working with **Drs Norman Sutin** and **Carol Creutz** on mechanistic aspects of the reduction of water and carbon dioxide by polypyridyl complexes of cobalt(I).

1988: Spent six months study leave at Stanford University with **Professor Henry Taube** and at the University of North Carolina at Chapel Hill working with **Professors Royce W. Murray** and **Thomas J. Meyer**. These studies primarily addressed aspects of modification of electrode surfaces using transition metal complexes.

1992: Invited Troisième Cycle Lecturer and Visiting Professor, Université de Fribourg (Switzerland).

1994-95: Professeur Invité, Université Louis Pasteur de Strasbourg (France), and Visiting Professor, Université de Fribourg Suisse.

1998: Awarded Commonmealth Fellowship, Bede Moris Fellowship Scheme. To spend 6 weeks as Professeur Invité, Université Louis Pasteur de Strasbourg (France).

SELECTED ADMINISTRATIVE ACTIVITIES AT UNIVERSITY, AND IN PROFESSIONAL CAPACITY OUTSIDE UNIVERSITY

Science Faculty Representative, Teaching Practices Committee, James Cook University of North Queensland, 1985.
Deputy Dean, Faculty of Science, JCUNQ; 1985-86. {Acting Dean - Feb./March, May 1986}.
Science Faculty Representative, Library Liaison Committee, JCUNQ, 1987.
Convenor, Schools' Information Service Advisory Group, JCUNQ; 1986-89, 1995.
Acting Head, Department of Chemistry and Biochemistry, JCUNQ; April/May 1989, Feb. 1990, Feb. 1993.
Member, Industrial Chemistry Advisory Committee, Department of Chemistry and Biochemistry, JCUNQ; 1990-91.
Chairman, Steering Committee for Open University 1991; Member, Steering Committee for Open University 1993.
Member, Promotions Committee, JCUNQ, 1995-97.
Science Faculty Representative, Research Committee, JCUNQ; 1996-1997.
Member, Research Committee, Faculty of Health, Life & Molecular Sciences, JCUNQ, 1997-present.
Member, Vice Chancellor's Steering Committee on University Marketing; 1996-present.
Elected Member (Faculty of Health, Biomedical & Molecular Sciences), Academic Board, JCUNQ, 1997-98
Elected Member (Faculty of Health, Biomedical & Molecular Sciences), Standing Committee of Academic Board, JCUNQ, 1997-98
Head of Department of Chemistry & Chemical Engineering. JCUNQ, 1997-present.

Honorary Secretary, Royal Australian Chemical Institute (North Queensland Section); 1978-82, 1985-87.
Member of Committee, RACI (North Queensland Section); 1982-85, 1989-present.
Chairman, RACI (North Queensland Section); 1987-89.
Queensland Representative, National Division of Inorganic Chemistry, RACI: 1989-1997.
Secretary, IC'96, National Conference of Inorganic Chemistry Division, Royal Australian Chemical Institute, Townsville, July 1996.
National Secretary, Division of Inorganic Chemistry, RACI, 1996-present.
Member, Organizing Committee, Inaugural Queensland Regional Conference, Division of Inorganic Chemistry, RACI (Rockhampton, 1991); Member Organising Committee, Queensland Regional Conference, Division of Inorganic Chemistry, RACI (Rockhampton, 1997).

Inaugural Secretary, CSIRO's Double Helix Science Club (Townsville Chapter), 1990-91.
Secretary, XIV International Symposium on Macrocyclic Chemistry (Townsville, 1989).
Member, Program Committee, XXVII International Conference on Coordination Chemistry (Gold Coast, 1989).
Member, National Advisory Committee, International Conference on Organometallic Chemistry, Brisbance, July 1996.
Australian Representative, Inorganic Chemistry Organising Committeee, International Chemical Congress of Pacific Basin Societies, to be held in Honolulu, December 2000.

OTHER INTERESTS AND ACTIVITIES

Sub-Deacon, St. James' Anglican Cathedral Townsville (1978-present); member of Parochial Council, 1978-87, 1990, 1993-95; Warden, 1981; Chairman, Pastoral Care Committee, 1980-82, Synod representative, 1994-present; Co-editor, "Anglican Visitor" (Parish magazine of St. James' Anglican Cathedral, Townsville, 1981-present). Photography, carpentry, golf.

PROFESSIONAL AWARDS AND FELLOWSHIPS

(i) Recipient of 1979 **Rennie Medal of Royal Australian Chemical Institute**.

The Rennie Medal is an annual national award made to the individual under 33 years of age who has contributed most to their chosen field of chemical science as judged by research publications.

(ii) Recipient of **Fulbright Award** for period June 1983-May 1984 (Brookhaven National Laboratory, New York).

(iii) Elected **Fellow of Royal Australian Chemical Institute**, November 1986.

(iv) Recipient of **Prestige Reseach Award**, James Cook University of North Queensland, 1996.

(v) **Commonwealth Fellow, Bede Morris Scheme** for period May-June 1998 (Université Louis Pasteur de Strasbourg, France).

AFFILIATIONS WITH OTHER INSTITUTIONS

Visiting Scientist, Brookhaven National Laboratory, New York; 1983-84.

Visiting Scholar, Stanford University, California; July - August, 1988.

Visiting Professor, University of North Carolina at Chapel Hill; August 1988 - January 1989.

Recipient of Bilateral Collaborative research grant {DIST (Australia)/NSF (U.S.A)}, jointly with Professor T.J. Meyer, University of North Carolina at Chapel Hill; 1991-94.

Invited Troisième Cycle Lecturer and Visiting Professor, Université de Fribourg (Switzerland); September - November, 1992.

Honorary Senior Fellow, University of Central Queensland (Rockhampton); 1993-2000.

Professeur Invité, Université Louis Pasteur de Strasbourg (France); 1994.

Visiting Professor, Université de Fribourg (Switzerland); 1994-95.

Professeur Invité, Université Louis Pasteur de Strasbourg (France); invited 1998.

RESEARCH AREAS.

Since my appointment to James Cook University, my research activities have been directed towards six major areas:

- Oxidative dehydrogenation of coordinated amines and alcohols.
- Tripodal π-acceptor ligands and their complexes with metals in groups 6-10.
- Transition-metal catalysis of reduction processes.
- Photocatalysis using molecular assemblies ("artificial photosynthesis").
- Chemical modification of electrodes.
- Spectroscopy of transition metal compounds using molecular beam techniques.

SELECTED INVITATIONS TO SCHOLARLY MEETINGS AND CONFERENCES

Invited Section Lecturer, 10th National Conference of Coordination and Metal-Organic Division, Royal Australian Chemical Institute, Queenstown, New Zealand, May 1981.

Invited Lecturer, symposium on *"Photochemistry and Photophysics of Metal Complexes: Applications to Solar Energy Conversion"*, 1984 International Chemical Congress of Pacific Basin Societies, Honolulu, December 1984.

Invited Section Lecturer, "Inorganic Chemistry '87"/8th National Convention of Royal Australian Chemical Institute, Sydney, August 1987.

Invited as a Section Lecturer (Photochemistry) at XXVII International Conference on Coordination Chemistry, held at Gold Coast, Australia, July 1989, but unable to accept for personal reasons.

Invited Lecturer, 199th National A.C.S. Meeting (Boston, April, 1990).

Invited Section Lecturer, Inaugural Queensland Regional Conference of the Inorganic Chemistry Division, Royal Australian Chemical Institute, Rockhampton, July 1991.

Invited Lecturer, IC'94 (National Conference of the Division of Inorganic Chemistry, R.A.C.I.), Perth, July 1994.

Invited Lecturer, symposium on*""Inorganic Photochemistry: Applications in Bioinorganic Chemistry, Energy Conversion and Catalysis"*, International Chemical Congress of Pacific Basin Societies, Honolulu, December 1995.

Invited Lecturer, symposium on *"Electrochemistry of Inorganic and Biological Compounds"*, 10th Australasian Electrochemistry Conference, Surfers Paradise, February 1997.

Invited Section Lecturer, IC'98 (National Conference of the Division of Inorganic Chemistry, R.A.C.I.), Wollongong, February 1998.

R.A.C.I. Queensland Schools' Chemistry Lecturer, 1991

Invited research lectures and seminars have been delivered at the following institutions -

University of North Carolina at Chapel Hill {4}, University of North Carolina at Charlotte, North Carolina State University (Raleigh), Duke University (Durham, NC), Wake Forest University (Winston-Salem, NC), Brown University (Providence, RI), State University of New York (Stonybrook campus), S.U.N.Y. (Brockport campus), S.U.N.Y. (Cortland campus), Columbia University (NY), Brookhaven National Laboratory (NY), Brandeis University (Boston, MA), University of California at Santa Barbara, Stanford University (CA) {3}, University of Kansas, University of Wyoming; University of Fribourg (Switzerland), Universität Basel (Switzerland), University of Bern (Switzerland) {3}, University of Neuchâtel (Switzerland), Eidg. Technische Hochschule (Zurich, Switzerland); Université Louis Pasteur (Strasbourg, France) {4}; Technische Hochschule Darmstadt (West Germany); Victoria University (Wellington, N.Z.), University of Waikato (Hamilton, N.Z.), University of Auckland (Auckland, N.Z.); University of Adelaide {10}, Australian National University {5}, University of Melbourne {5}, University of Queensland {2}, University of Central Queensland {2}, Griffith University {3}, La Trobe University, Monash University {3}, Deakin University, University of Tasmania, University of New South Wales, University of Wollongong, University of Sydney, Flinders University, CSIRO Division of Applied Organic Chemistry (Melbourne).